厚生労働科学研究費補助金
地球規模保健課題推進研究事業
（国際医学協力研究事業）

寄生虫疾患の病態解明及び
その予防・治療をめざした研究

（H22－国医－指定－004）

平成22年度　総括・分担研究報告書

研究代表者　　平　山　謙　二

平成23（2011）年３月

目　次

Ⅰ．総括研究報告

寄生虫疾患の病態解明及びその予防・治療をめざした研究

平山謙二　…… 1

Ⅱ．分担研究報告

１．　寄生虫症感受性の宿主因子の検討に関する研究

平山謙二　…… 10

２．　原虫症治療標的分子の機能解析

北　潔　…… 13

３．　アジアの三日熱マラリア原虫の遺伝的集団構造の解明

狩野繁之　…… 18

４．　ワクチン分子の無細胞系合成システムの確立

坪井敬文　…… 20

５．　赤痢アメーバの病原機構の解明

野崎智義　…… 27

６．　フィラリア症の疫学研究（診断法の開発と野外応用）

木村英作　…… 31

７．　フィラリア線虫と媒介節足動物の相互関係の解明

辻　尚利　…… 36

８．　日本住血吸虫症の病態発現分子解析

太田伸生　…… 38

９．　寄生蠕虫の寄生適応および免疫修飾機構の研究

金澤　保　…… 42

１０．　リーシュマニア症対策疫学研究

我妻ゆき子　…… 45

１１．　マラリア原虫の宿主細胞認識と侵入機序の解析

鳥居本美　…… 47

１２．　寄生虫感染宿主内で誘導される好塩基球の感染制御能の証明

中西憲司　…… 50

１３．　遺伝子導入ハマダラカを作成し空飛ぶ注射器としての実用性を探る

松岡裕之　…… 54

１４．　マラリアにおける宿主病原体相互関係の解析

久枝　一　…… 55

１５．　マラリア感染における T 細胞免疫応答の研究
由井克之　……57
１６．　マラリア原虫のリガンドおよび赤血球侵入関連分子の解析
金子　修　……60
１７．　マラリア原虫に有効な新規阻害剤の探索
金　惠淑　……63
１８．　住血原虫症の病態と創薬に関する研究
片倉　賢　……68
１９．　トリパノソーマの防御応答回避メカニズムの解析
嶋田淳子　……70
２０．　人獣共通寄生虫病の血清診断システムの開発と幼虫移行症の病態解明
丸山治彦　……71
２１．　住血原虫症の診断学
五十嵐郁男　……76
２２．　住血吸虫症の検査・診断・対策に関する研究
大前比呂思　……80
２３．　人獣共通寄生原虫・嫦虫症の寄生適応に関する分子生物学的解析
奈良武司　……85
２４．　人獣共通幼条虫症（脳嚢虫症、エキノコックス症）の病態、診断、治療、
予防に向けた研究
伊藤　亮　……87

Ⅲ．研究成果の刊行に関する一覧表　……93

Ⅳ．研究成果の刊行物・別刷り　……109

厚生労働科学研究費補助金（地球規模保健課題推進研究事業（国際医学協力研究事業））
総括研究報告書

寄生虫疾患の病態解明及びその予防・治療をめざした研究

研究代表者　平山謙二　長崎大学熱帯医学研究所教授

研究要旨　アジア地域は多様な地理的環境と多様な民族により構成されているが、東南アジアを中心に熱帯地域が拡がっている。これらの地域ではいまだに寄生虫感染症の患者が多数存在し、住民の健康に重大な影響を与えているばかりでなく、社会経済学的な影響も大きい。これら主要な寄生虫疾患の制圧を目指した新たな治療・予防法の開発を最終目標として、疾患別にグループを組み、各疾患の制圧を目指した基礎研究から応用研究を幅広く行い、真に地域の健康増進に資する研究を推進した。対象とした寄生虫疾患あるいは領域は以下のものである。（１）マラリア、（２）住血吸虫症、（３）フィラリア症、（４）住血原虫症（トリパノソーマ、リーシュマニア症など）、（５）新興・再興感染症（腸管寄生原虫症、腸管寄生ぜん虫症、エキノコッカス症、人獣共通感染症など）、（６）媒介昆虫領域である。上記の対象疾患の制圧に資する学術的な知見を得るために以下のようなアプローチで多様な研究を展開した。a) 保有宿主や媒介動物を含めた感染動態や伝播経路に関わる基礎研究、b) 病原体の寄生適応の分子メカニズム、c) ヒトの防御免疫および病態生理。

研究分担者名
北　潔　　東京大学大学院・医学系研究科・教授
狩野繁之　国立国際医療センター研究所・部長
坪井敬文　愛媛大学無細胞生命科学工学研究センター・教授
野崎智義　国立感染症研究所・部長
木村英作　愛知医科大学医学部・教授
辻　尚利　独立行政法人 農業・食品産業技術総合研究機構・動物衛生研究所・主任研究員
太田伸生　東京医科歯科大学・大学院医歯学総合研究科・教授
金澤　保　産業医科大学・教授
我妻ゆき子　筑波大学大学院人間総合科学研究科・教授
鳥居本美　愛媛大学大学院医学系研究科・教授
中西憲司　兵庫医科大学・教授
松岡裕之　自治医科大学・教授
久枝　一　群馬大学大学院医学研究科・教授
由井克之　長崎大学大学院医歯薬学総合研究科・教授
金子　修　長崎大学熱帯医学研究所・教授
金　恵淑　岡山大学大学院医歯薬学総合研究科・准教授
片倉　賢　北海道大学大学院獣医学研究科・教授
嶋田淳子　群馬大学医学部・教授
丸山治彦　宮崎大学医学部・教授
五十嵐郁男　帯広畜産大学原虫病研究センター・教授
大前比呂思　国立感染症研究所・室長
奈良武司　順天堂大学大学院医学研究科・准教授
伊藤　亮　旭川医科大学・教授

A. 研究目的

アジアに拡がる寄生虫疾患に関する基礎研究を推進し、その制圧、予防、治療に資する革新的な知見を集積することを目的とする。
多くの寄生虫疾患は「見捨てられた病気」として分類され、途上国や研究環境の貧弱な地域で流行し、たくさんの命が奪われ、あるいは脅かされ続けている。この分野に光を当て、現地の研究者も含めて新しくより効率的な制圧法を開発することは日本や欧米先進国の役割である。本研究課題を推進することにより、アジア地域の研究者を巻き込んだ共同研究を活性化することが可能となる。また、寄生虫疾患という環境に密着した感染症に関する研究に日本やアジア地域の若手研究者が参加することで、新たな医科学領域の後継者を育成することが可能となる。

B．研究方法

マラリア、住血吸虫症、フィラリア症、住血原虫症、新興再興感染症、媒介昆虫の６つの疾患において、以下のような観点から分子レベルでの研究を行った。

A） 感染伝播メカニズム　　B） 寄生虫の宿主適応　　C） ヒト防御免疫および病態生理

（倫理面への配慮）
本研究計画においてはアジアの流行地域での疫学調査の実施も含まれるので、ＷＨＯの基準に従った倫理基準に基づいて実施された。血液などの試料提供者には研究主旨を説明した上で自由意思による同意を書面で得た。また、ヒト資料については匿名化を行った。今年度実施分については各分担研究者が所属機関とカウンターパートの機関において倫理審査を得た上で研究を開始するべく準備中である。動物実験についても各所属機関の動物実験審査の承認を得てから実施した。なお、計画にはヒトゲノム・遺伝子解析も含んでいる

- ヒトゲノム・遺伝子解析研究に関する倫理指針
- 疫学研究に関する倫理指針
- 遺伝子治療臨床研究に関する指針
- 臨床研究に関する倫理指針
- 疫学・生物統計学の専門家の関与有
- 臨 床 研 究 登 録 予 定 無

C．研究結果

（1） マラリア

狩野はアジアの三日熱マラリア原虫の遺伝的集団構造の研究を行い、Pv mtDNA 全塩基配列に基づく分子系統解析の結果、以下のことを明らかにした。1）韓国の Pv 集団は、中国南部の Pv 集団と近縁の２つの集団からなること。2）フィリピンの Pv 検体（３検体）は、インドシナ半島の Pv 集団と遺伝的に近縁である。3）輸入三日熱マラリア患者検体は、渡航先由来の Pv 集団に含まれた。マラリアの移動が地域的に限られていることを認識した輸入症例の治療方法の選択が必要であることを示唆するものである。
坪井は無細胞系合成システムによるワクチン分子探索を継続し、114 種類のプロテインアレイと、熱帯熱マラリアに対する防御抗体を含有するヒト血清を用いてスクリーニングを行った。その結果、PfMSPDBL1 という分子が選択された。PfMSPDBL1 はメロゾイト表面に局在し、さらに抗 PfMSPDBL1 抗体は、培養熱帯熱マラリア原虫の赤血球への侵入を阻害した。新たなワクチン候補分子を発見することができ、今後の臨床開発への道をひらいた。
鳥居はマラリア原虫の宿主細胞認識と侵入機序に重要な分子である赤血球結合リガンドEBLの構造変換による機能の変化を観察した。、Py17XNL株原虫EBLの領域６の８個のシステインを、それぞれアラニンに置換した遺伝子組換え原虫を作成して、EBLの局在を間接蛍光抗体法で観察したところ、１、４、５、７番目のCys組換え原虫においてはEBLの局在がPy17XNLのマイクロネームから強毒株のPy17XLに見られる局在パターンへと変化した。第６領域がPyEBL分子の細胞内輸送に重要であること、さらにその立体構造と、分子表面の特定の領域が細胞内輸送に関わっていることが示唆され、この分子が治療薬開発の標的として重要であることが示唆された。
久枝はマウスマラリアにおける CD8Ｔ細胞の赤血球ステージマラリアに対する防御機能を明らかにした。これまで肝細胞期に有効であろうとされていた CD8T 細胞の機能が拡大され今後のワクチン開発に重要な基礎研究情報となる。
由井はマウスマラリアにおいて $CD4^+$ T 細胞は感染により非特異的に産生される IL-2 により IFN-g を産生することが明らかになった。他の感染症との重複感染の際の影響を示唆するものである。
金子修は、三日熱マラリア原虫の PvSTP2 という細胞内タンパクの細胞内での局在を間接蛍

光抗体法により観察し、原虫感染赤血球膜上シュフナー斑点によく似ることが判明した。マラリアの赤血球内での膜タンパク輸送に重要なタンパク質であることが示唆されたことから抗マラリア薬の標的となることが期待できる。

（2） 住血吸虫症

平山は、フィリピンの若年性の日本住血吸虫性肝線維症を憎悪させる要因として50の免疫応答関連遺伝子近傍に設置したマイクロサテライトマーカーのうち、IL12B　MS*241(OR=2.48)、MS*245(OR=0.45)とIL2　MS*383(OR=10.3)の3つの感受性あるいは抵抗性アレルを同定した。これらはいずれもTh1型のT細胞応答性と関連しているので、今後の肝線維症予防薬開発のための基礎的な情報として重要であると考えられる。
金澤は、マウスに慢性感染する腸管寄生蠕虫*Heligmosomoides polygyrus*(Hp)を感染させた1型糖尿病モデルマウスの発症を抑制することを発見したが、この機序にTh2偏倚が関与しないことをSTAT6KOマウスで明らかにした。ぜん虫感染による他の疾患感受性への影響は寄生虫撲滅後の保健衛生対策にも重要であり、フィールド研究へと発展するテーマである。
太田はアジアに蔓延する日本住血吸虫症がアフリカのマンソン住血吸虫症に比べ肝病変が強いことに着目し、マウスモデルにおいても肝臓の好中球と好酸球浸潤パターンの顕著な違いがあることや、Th2反応を阻害した条件下で炎症性のTh17応答性が日本住血吸虫で上昇することを突き止めた。免疫制御剤による治療モデルの開発に資する重要な研究である。
大前はフィリピンで新たに確認された２つの日本住血吸虫症浸淫地の疫学調査により、両地域が、従来から日本住血吸虫症浸淫地であることを明らかにした。腹部超音波検査と免疫血清検査の結果を組み合わせることで流行の期間や流行密度を推測することが可能であることを示したことから、今後対策の地方分権が進むフィリピンにおけるサベイランス政策立案に貢献することが期待される。

（3） フィラリア症

木村は尿サンプルを用いた簡便で乳幼児に適用可能なフィラリア症の診断法の開発と野外応用研究を推進し、スリランカの調査で尿ELISA陽性率は、血清のICT testの約5倍高く1,505人中、21人（1.4%）が陽性となった。陽性者の29%が10歳未満であったことは最近の流行を示唆しており、この方法が集団治療による対策後のサーベイランスに非常に有用な方法であることを証明した。さらにこれを改良したビーズ法の確認や環境調査に重要なLAMP法の開発も進展した。
辻はフィラリア線虫由来の抗血液凝固物質であるロンギスタチンは媒介者であるマダニの寄生維持に深く関与することを発見した。新規抗寄生虫薬の標的分子として有効であると考えられる。

（4） 住血原虫症（トリパノソーマ、リーシュマニア）

北はマラリア原虫細胞をParr homogenizerで破砕し、パーコールを用いてミトコンドリアとアピコプラストを分離できる最終的な条件を確立した。トリパノソーマのシアン耐性酸化酵素は膜結合性2核鉄タンパク質であるがその立体構造を明らかにした。アメリカリーシュマニアの新奇なミトコンドリア呼吸鎖の複合体II（コハク酸-ユビキノン還元酵素複合体）の精製法を確立した。これら抗原虫薬の標的分子候補の立体構造の解明によりインシリコあるいは化合物ライブラリーからの医薬品開発が促進されることが期待される。
片倉はネパールやインドで蔓延するカラアザールの病原原虫であるリーシュマニア原虫がNF-・B inducing kinaseを遺伝的に欠いている*aly/aly*マウスでは長期間（7か月）にわたって肝臓に存続し慢性期に原虫数が増加することを見出し、原虫のマウス体内における存続機構として$CD4^+Foxp3^+$T細胞の関与が強く示唆された。Treg細胞の抑制活性を調節する薬剤の開発により慢性感染を制御できる可能性を示唆した。またResveratrolというミヤンマーの薬用植物由来の物質に強い抗リーシュマニア活性があることを見出した。
嶋田はトリパノソーマ感染細胞のアポトーシスを抑制する宿主由来の遺伝子であるc-FLIPおよびc-IAPを培養細胞に導入し、高発現させた株を樹立することに成功した。アポトーシス抑制因子と相互作用する原虫側因子の探索が可能となったので、この因子を単離することで細胞内感染を阻止するための標的分子を決定することができる。
五十嵐はウシバベシアのスフェリカルボデ

ィ４（BbSBP4）組換え抗原を用いたELISA および膜抗原遺伝子 BV5650 および BV8970 を用いた nPCR を開発した。人獣共通寄生原虫症の診断法の開発に資するものと考えられる。

奈良は解糖系酵素であるアルドラーゼ ALD 等を用いたキネトプラスチダ類とディプロネマ類の分子進化に着目し、ALD では分子系統解析でトリパノソーマ類および *D. papillatum* の ALD の単系統性を示し、免疫蛍光染色（IFA）によって、ALD は両者において同様のドット状の蛍光パターンを示すことを証明した。このことから、*D. papillatum* の ALD は PTS を持ち、細胞内小胞に局在することが明らかとなった。これは、解糖系酵素のペルオキシソームへの移行がキネトプラスチダ類とディプロネマ類との分岐以前に既に成立していたことを示唆する最初の報告である。

キネトプラスチダ類に特異的と考えられてきたグリコソームの成立背景について、近縁群のディプロネマ類との共通祖先段階ですでに解糖系酵素の一部がペルオキシソームに移行しており、グリコソームのプロトタイプがすでに成立していた可能性が示唆された。

（５） 新興・再興感染症（腸管寄生原虫症、腸管寄生ぜん虫症、エキノコッカス症、人獣共通感染症など）

中西は好塩基球を欠損したマウスにぜん虫を感染させた場合、排虫時期が野生型マウスに比べて著しく遅延するが、腸間膜リンパ節T細胞からのサイトカイン産生、血清中IgE産生誘導、粘膜型肥満細胞の誘導に好塩基球の有無で変化は認められなかったことから新たな好塩基球依存性の排虫メカニズムの存在を明らかにした。アジア地域に広く蔓延する腸管寄生虫症の制御薬の開発に資する研究である。

野崎は酸化ストレス負荷環境下での赤痢アメーバの遺伝子発現を網羅的に計測し、システイン飢餓が原虫の遺伝子発現、特に代謝に関与する酵素遺伝子 L-cysteine-regulated NADPH-dependent oxidoreductases に影響することを明らかにした。これらの酵素活性の病原性との関連が今後の南アジアに広く蔓延するアメーバ赤痢対策のための抗原虫剤や治療薬の開発のシーズとなる可能性が高い。

丸山はブタ回虫組換え抗原 As16 が幼虫分泌排泄抗原（ES 抗原）と相関が強く、診断用抗原として優れていること、As16 とイヌ回虫の組換え抗原 TES32 との組み合わせによる幼虫移行症の病原体診断が可能であることを示した。ベネズエラ糞線虫のゲノム解析ではペアエンドライブラリの作製とフォスミドライブラリの構築が進行中で、またトランスクリプトーム解析では、虫卵、感染幼虫、肺移行期幼虫、および寄生世代成虫の cDNA を作製し、454 GS-FLX で塩基配列を決定した。総計 2,483,165 のリードが得られ、アセンブルによって計 14,016 のアイソティグ（トランスクリプトに相当）を得、7,560 に何らかのアノテーションを付けることができ、約 3,000 個はベネズエラ糞線虫特異的と考えられた。寄生性線虫ゲノム情報としては世界的に貴重なものとなることが期待される。

伊藤は有鉤条虫（*Taenia solium*）をアジア型とアメリカ・アフリカ型を区別できる新しい核遺伝子を見出した。エキノコックス属条虫も含めてアジアではさらに国や地域ごとに特徴的なハプロタイプの存在し感染した地域を特定することが可能であることを明らかにした。人体寄生テニア属条虫３種の遺伝子鑑別法としてミトコンドリアならびに核遺伝子を用いる Loop-mediated isothermal amplification（LAMP）法による糞便内遺伝子検査法を確立し、流行の現場で実施可能であることをほぼ確認した。*Taenia asiatica* と *Taenia saginata* の交雑個体がタイのみならず中国でも確認された。インドで有鉤条虫に感染し、年余にわたる虫卵排出と、自家感染による嚢虫症を引き起こした日本人症例を発見した。流行地住民から血清検査により嚢虫症患者を確認。遺伝子組み換え Em18（RecEm18）, Antigen B（Rec AgB）を用いるエキノコックス症に関する血清診断法に関する外部評価研究を展開した。この検査法（RecEm18-ELISA、RecEm18-Immunoblot）は、世界最高水準との国際評価を得、米国疾病情報対策センター（CDC）が採用を決めている。さらに、昨年度にアドテック（株）と共同で簡便な迅速イムノクロマト診断キットを開発した。国内外での活用が期待される。

（６） 媒介昆虫

松岡は、唾液腺にマラリア抗原ペプチドを発現・分泌し、口吻から放出できる遺伝子導入蚊を作製し、その蚊を繰り返しマウスに吸血させた。その結果マウスは注入されたマラリア抗原ペプチドに対して抗体を産生したので、

これを今後より実用性の高いものへと発展させてゆくことにしている。

D．考察

本年度の事業活動はほぼ計画通りに遂行された。研究計画全体の４年目にあたり、特にアジア地域に流行する寄生虫疾患とりわけ、以下にあげた、住血吸虫症、フィラリア症、マラリア、新興再興寄生虫病、ベクターの各研究領域で研究を遂行した。昨年度米国サンディエゴで免疫部会と合同で会議を開催したが、今年度は国立感染研で野崎部会員の主催で合同会議を開催し、日米のパネルおよび研究員に加えて、多数の研究協力者さらには若手のポスドク研究員や大学院学生が成果を発表し(口頭発表演題数 56)、最終日の赤痢アメーバの研究会を含め、133 名が参加し、そのうち 18 名がアジアアメリカからの招待研究者であった。これまでに確立された日本とアジアの連携にさらに日米、あるいは米アジアを加えた３角協力による優れた共同研究の新たな発展がなされつつあり、その結果としての論文の産出が顕著にみられた。米国 NIH の進めるアジア地域での米国機関とアジアとの拠点間研究が今年度から大きく前進しており、日本とアジアの枠組みを並行して発展させることにより、次期の日米５年計画ではアジアにおける３角協力推進のための新たな日米医学協力事業の存在意義を明らかにできると考えられる。

E．結論

アジアに蔓延する広範囲な寄生虫疾患を対象にした分子レベルから公衆衛生レベルまでの活発な研究が行われ、本プログラムが日米における各研究グループの間の情報交換や新しいプロジェクトの提案、若手研究者の育成に重要な役割を果たした。

F．健康危険情報

なし。

G．研究発表

1. マラリア

1. Moritoshi Iwagami, Seung-Young Hwang, Megumi Fukumoto, Toshiyuki Hayakawa, Kazuyuki Tanabe, So-Hee Kim, Weon-Gyu Kho, Shigeyuki Kano. Geographical origin of *Plasmodium vivax* in the Republic of Korea: haplotype network analysis based on the parasite's mitochondrial genome. Malaria Journal 9:184-188, 2010.
2. Tsuboi T, Takeo S, Arumugam TU, Otsuki H, Torii M. The wheat germ cell-free protein synthesis system: a key tool for novel malaria vaccine candidate discovery. Acta Trop. 2010, 114: 171-176.
3. Imai T, et al: Involvement of CD8+ T cells in protective immunity against murine blood-stage infection with *Plasmodium yoelii* 17XL strain. Eur. J. Immunol. 40: 1053-1061, 2010.
4. Ishida H, et al: Development of experimental cerebral malaria is independent of IL-23 and IL-17. Biochem. Biophys. Res. Commun. 402: 790-795, 2010.
5. Ozeki Y, et al: Transient role of CD4+CD25+ regulatory T cells in mycobacterial infection in mice..Int. Immunol. 22: 179-189, 2010.
6. Chou B, et al: Genetic immunization based on the ubiquitin-fusion degradation pathway against *Trypanosoma cruzi*. Biochem. Biophys. Res. Commun. 392: 277-282, 2010.
7. Kimura D., Miyakoda M., Honma K., Yuda M., Chinzei Y., and Yui K., Production of IFN-□□by $CD4^+$ T cells in response to malaria antigens is IL-2-dependent. Int. Immunol., 22 (12) ; 941-952, 2010.
8. Complete abrogation of sporozoite-induced sterile immunity by blood stage parasites of homologous and heterologous malaria parasites, M. Inoue, J. Tang, O. Kaneko, K. Yui, R. Culleton, Malaria J., 9 (suppl)O19, 2010
9. Wang Y, Kaneko O, Sattabongkot J, Chen J-H, Lu F, Chai J-Y, Takeo S, Tsuboi T, Ayala FJ, Chen Y, Lim CS, Han ET Genetic Polymorphism of *Plasmodium vivax* msp1p, a Paralog of Merozoite Surface Protein 1, from Worldwide Isolates. *Am J Trop Med Hyg* 84(2), 292-297 (2011/Feb).
10. Pandey BD, Pun SB, Kaneko O, Pandey K, Hirayama K. Expansion of Visceral Leishmaniasis to Western Hilly Part of Nepal. *Am J Trop Med Hyg* 84(1):107-8. (2011/Jan)
11. Pandey K, Pandey BD, Mallik AK, Kaneko O, Uemura H, Kanbara H, Yanagi T, Hirayama K. Diagnosis of visceral leishmaniasis by polymerase chain reaction of DNA extracted from Giemsa's solution-stained slides. *Parasitol Res* 107(3):727-30 (2010/Aug)

2. 住血吸虫症

1. Kohama H, Harakuni T, Kikuchi M, Nara T, Takemura Y, Miyata T, Sato Y, Hirayama K, Arakawa T. Intranasal Administration of *Schistosoma japonicum* Paramyosin Induced Robust Long-Lasting Systemic and Local Antibody as well as Delayed-Type Hypersensitivity Responses, but Failed to Confer Protection in a Mouse Infection Model. Jpn J Infect Dis. 63(3):166-72. 2010.
2. Shimizu S, Osada Y, Kanazawa T, Tanaka Y, Arai M. Suppressive effect of azithromycin on *Plasmodium berghei* mosquito stage development and apicoplast replication. *Malar J.* 9:73.2010
3. Kumagai T, Furushima-Shimogawara R, Ohmae H, Wang TP, Lu S, Chen R, Wen L, Ohta N. Detection of early and single infections of *Schistosoma japonicum* in the intermediate host snail, *Oncomelania hupensis*, by PCR and Loop-Mediated Isothermal Amplification (LAMP) assay Am J Trop. Med Hyg 2010, 83:542-548.

3. フィラリア症

1. Kimura E.The Global Programme to Eliminate Lymphatic Filariasis: History and achievements with special reference to annual single-dose treatment with diethylcarbamazine in Samoa and Fiji. Tropical Medicine and Health (in press).
2. Anisuzzaman, Islam MK, Miyoshi T, Alim MA, Hatta T, Yamaji K, Matsumoto Y, Fujisaki K, Tsuji N.(2010). Longistatin, a novel EF-hand protein from the ixodid tick *Haemaphysalis longicornis*, is required for acquisition of host blood-meals.Int J Parasitol. 40, 721-729.

4. 住血原虫症（トリパノソーマ、リーシュマニア）

1. Kido, Y., Shiba, T., Inaoka, D. K. Sakamoto, K., Nara, K., Aoki, T., Honma, T., Tanaka, A., Inoue, M., Matsuoka, S., Moore, A., Harada, S. and Kita, K.Crystallization and preliminary crystallographic analysis of cyanide-insensitive alternative oxidase from *Trypanosoma brucei brucei.* Acta Crystallographica (2010) F66, 275-278
2. Hikosaka, K., Watanabe, Y., Tsuji, N., Kita, K., Kishine, H., Arisue, N., Palacpac, N. M. Q., Kawazu, S., Sawai, H., Horii, T., Igarashi, I. and Tanabe, K. Divergence of mitochondrial genome structure in the apicomplexan parasites, *Babesia* and *Theileria*. Mol. Biol. Evolution (2010) 27, 1107-1116
3. Balogun, O. E., Inaoka, D. K., Kido, Y., Shiba, T., Nara, T., Aoki, T., Honma, T., Tanaka, A., Inoue, M., Matsuoka, S., Michels, P. AM,. Harada, S. and Kita, K. Overproduction, purification, crystallization and preliminary X-ray diffraction analysis of *Trypanosoma brucei gambiense* glycerol kinase. Acta Crystallographica (2010) F66, 304-308
4. Kido,Y., Sakamoto, K., Nakamura, K., Harada, M., Suzuki, T., Yabu, Y., Saimoto, H., Yamakura, F., Ohmori, D., Moore, A., Harada, S. and Kita, K.Purification and kinetic characterization of recombinant alternative oxidase from *Trypanosoma brucei brucei.* Biochim Biophys. Acta (Bioenergetics) (2010) 1797, 443-450
5. Masuda, I., Matsuzaki, M. and Kita, K Extensive frameshift at all AGG and CCC codons in the mitochondrial cytochrome *c* oxidase subunit 1 gene of *Perkinsus marinus* (Alveolata; Dinoflagellata).. Nucleic Acids Research. (2010) 38, 6186-6194
6. Nakamura, K., Fujioka, S., Fukumoto, S., Inoue, N., Sakamoto, Hirata, H., Kido, Y., Yabu, Y., Suzuki, T., Watanabe, Y., Saimoto, H., Akiyama, H. and Kita, K. Trypanosome alternative oxidase, a potential therapeutic target for sleeping sickness, is conserved among *Trypanosoma brucei* subspecies. Parasitol. Int. (2010) 59, 560-564
7. Hikosaka, K., Nakai, Y., Watanabe, Y., Tachibana, S., Arisue, N., Palacpac, N. M., Toyama, T., Honma, H., Horii, T., Kita, K. and Tanabe, K.Concatenated mitochondrial DNA of the coccidian parasite *Eimeria tenella.* Mitochondrion, (2010) 11, 273-278
8. Kawamura Y, Yoshikawa I, Katakura K: Imported leishmaniasis in dogs, US military bases, Japan. *Emerg Infect Dis* 16, 2017-2019, 2010
9. Bawm S, Tiwananthagorn S, Lin KS, Hirota J, Irie T, Htun LL, Maw NN, Myaing TT, Phay N, Miyazaki S, Sakurai T, Oku Y, Matsuura H, Katakura K: Evaluation of Myanmar medicinal plant extracts for antitrypanosomal and cytotoxic activities. *J Vet Med Sci* 72, 525－528, 2010
10. Mizukami C, Spiliotis M, Gottstein B, Yagi K, Katakura K, Oku Y: Gene silencing in *Echinococcus multilocularis* protoscoleces using RNA interference. *Parasitol Int* 59, 647-652, 2010

11. Armua-Fernandez MT, Nonaka N, Sakurai T, Nakamura S, Gottstein B, Deplazes P, Phiri IGK, Katakura, K, Oku Y: Development of PCR/dot blot assay for specific detection and differentiation of taeniid cestode eggs in canids. *Parasitol Int* in press
12. Nakajima-Shimada J., Hatabu T. *Trypanosoma cruzi* infection in-duces nitric oxide production and S-nitrosylation of cellular FLIP in host cell. Medimond S.r.l, Italy, 2011, in press.
13. Hikosaka K, Watanabe YI, Tsuji N, et al., K. Divergence of the mitochondrial genome structure in the apicomplexan parasites, *Babesia* and *Theileria*. Mol Biol Evol. 27(5):1107-1116, 2010.
14. Aboulaila M, Sivakumar T, Yokoyama N, Igarashi I. Inhibitory effect of terpene nerolidol on the growth of *Babesia* parasites. Parasitol Int. 59(2):278-282, 2010.
15. Iseki H, Zhou L, Kim C, Inpankaew T, Sununta C, Yokoyama N, Xuan X, Jittapalapong S, Igarashi I. Seroprevalence of *Babesia* infections of dairy cows in northern Thailand. Vet. Parasitol. 170(3-4):193-196, 2010.
16. Aboulaila M, Yokoyama N, Igarashi I. Development and evaluation of two nested PCR assays for the detection of *Babesia bovis* from cattle blood. Vet. Parasitol. 172(1-2):65-70 2010.
17. Iseki H, Kawai S, Takahashi N, Hirai M, Tanabe K, Yokoyama N, Igarashi I. Evaluation of a loop-mediated isothermal amplification method as a tool for diagnosis of infection by the zoonotic simian malaria parasite *Plasmodium knowlesi*. J Clin Microbiol. 48(7):2509-2514, 2010.
18. Goo YK, Terkawi MA, Jia H, Aboge GO, Ooka H, Nelson B, Kim S, Sunaga F, Namikawa K, Igarashi I, Nishikawa Y, Xuan X. Artesunate, a potential drug for treatment of *Babesia* infection. Parasitol Int. 59(3):481-486, 2010.
19. Ooka H, Terkawi MA, Goo YK, Luo Y, Li Y, Yamagishi J, Nishikawa Y, Igarashi I, Xuan X. *Babesia microti*: Molecular and antigenic characterizations of a novel 94-kDa protein (BmP94). Exp Parasitol. 127(1):287-293 201 1 .
20. Terkawi MA, Huyen NX, Wibowo PE, Seuseu FJ, Aboulaila M, Ueno A, Goo YK, Yokoyama N, Xuan X, Igarashi I. Spherical body protein 4 is a new serological antigen for the global detection of *Babesia bovis* infection in cattle. Clin Vaccine Immunol. 18(2):337-342, 2011.
21. Tajima K, Miura K, Ishiwata T, Takahashi F, Yoshioka M, Minakata K, Murakami A, Sasaki S, Iwakami S, Annoura T, Hashimoto M, Nara T, Takahashi K. Sex hormones alter Th1 responses and enhance granuloma formation in the lung. *Respiration, in press*
22. Makiuchi T, Annoura T, Hashimoto M, Hashimoto T, Aoki T, Nara T. Compartmentalization of a glycolytic enzyme in *Diplonema*, a non-kinetoplastid Euglenozoan. *Protist, in press*
23. Kido Y, Shiba T, Inaoka DK, Sakamoto K, Nara T, Aoki T, Honma T, Tanaka A, Inoue M, Matsuoka S, Moore A, Harada S, Kita K. Crystallization and preliminary crystallographic analysis of cyanide-insensitive alternative oxidase from *Trypanosoma brucei brucei. Acta Cryst Section F,* 66: 275-278, 2010
24. Balogun EO, Inaoka DK, Kido Y, Shiba T, Nara T, Aoki T, Honma T, Tanaka A, Inoue M, Matsuoka S, Michels PAM, Harada S, Kita K. Overproduction, purification, crystallization and preliminary X-ray diffraction analysis of *Trypanosoma brucei gambiense* glycerol kinase. *Acta Cryst Section F,* 66: 304-308, 2010
25. Tajima K, Ohashi R, Sekido Y, Hida T, Nara T, Hashimoto M, Iwakami S, Minakata K, Yae T, Takahashi F, Saya H, Takahashi K. Osteopontin-mediated enhanced hyaluronan binding induces multidrug resistance in mesothelioma cells. *Oncogene* 29(13): 1941-1951, 2010
26. Kohama H, Harakuni T, Kikuchi M, Nara T, Takemura Y, Miyata T, Sato Y, Hirayama K, Arakawa T. Intranasal administration of *Schistosoma japonicum* paramyosin induced robust long-lasting systemic and local antibody as well as delayed-type hypersensitivity responses, but failed to confer protection in a mouse infection model. *Jap J Inf Dis*, 63(3): 166-172, 2010

5. 新興・再興感染症（腸管寄生原虫症、腸管寄生ぜん虫症、エキノコッカス症、人獣共通感染症など）

1. Nakanishi K. Basophils are potent antigen-presenting cells that selectively induce Th2 cells. Eur J Immunol. 2010 ;40(7):1836-42.
2. Satoh T, Takeuchi O, Vandenbon A, Yasuda K, Tanaka Y, Kumagai Y, Miyake T, Matsushita K, Okazaki T, Saitoh T, Honma K, Matsuyama T, Yui K, Tsujimura T, Standley DM, Nakanishi K, Nakai K, Akira

S. The Jmjd3-Irf4 axis regulates M2 macrophage polarization and host responses against helminth infection. Nat Immunol 2010;11: 936-944.
3. Nakanishi K. Basophils as APC in Th2 response in allergic inflammation and parasite infection. Curr Opin Immunol 2010.22(6):814-20.
4. Jeelani, G., Husain, A., Sato, D., Ali, V., Suematsue, M., Soga, T., and Nozaki, T. (2010) Two Atypical L-cysteine-regulated NADPH-dependent oxidoreductases involved in redox maintenance, L-cystine reduction, and metronidazole activation in the enteric protozoon Entamoeba histolytica. J. Biol. Chem., 285, 26889-26899.
5. Yousuf, M. A., Mi-ichi, F., Nakada-Tsukui, K., and Nozaki, T. (2010) Localization and targeting of unusual pyridine nucleotide transhydrogenase in Entamoeba histolytica. Eukaryot. Cell 9, 926-933.
6. Yoshida A, Nagayasu E, Nishimaki A, Sawaguchi A, Yanagawa S, Maruyama H (2011): Transcriptsanalysis of infective larvae of an intestinal nematode, *Strongyloides venezuelensis* Parasitol Int. 60: 75-83.
7. Gurbadam A et al. Mongolian and Japanese Joint Congress on "Echinococcoses: diagnosis, treatment and prevention in Mongolia" June 4, 2009. *Parasites and Vectors* 2010; 3: 1/8-3/8.
8. Li T et al. Specific IgG Responses to Recombi- nant Antigen B and Em18 in Cystic and Alveolar Echinococcosis in China. *Clinical and Vaccine Immunology* 2010; 17: 40-475.
9. Ito A et al. Histopathological, Serological and Molecular Confirmation of Indigenous Alveolar echinococcosis cases in Mongolia. *American Journal of Tropical Medicine and Hygiene* 2010; 82: 266-269.
10. Li T et al. Widespread co-endemicity of human cystic and alveolar echinococcosis on the eastern Tibetan plateau, northwest Sichuan/southeast Qinghai, China. *Acta Tropica* 2010; 113: 248- 256.
11. Brunetti E et al. Expert consernsus for the diagnosis and treatment of cystic and alveolar echinococcosis in humans. *Acta Tropica* 2010;114: 1-16.
12. Yanagida T et al. Neurocysticercosis: Assessing where the infection was acquired from. *Journal of Travel Medicine* 2010; 17:206-208.
13. Nakao M et al. Genetic polymorphisms of *Echinococcus* tapeworms in China as determined by mitochondrial and nuclear DNA sequences. *International Journal for Parasitology* 2010; 40: 379-385.
14. Okamoto M et al. Evidence of hybridization between *Taenia saginata* and *Taenia asiatica*. *Parasitology International* 2010; 59: 70-74.
15. Anantaphruti MT et al. Molecular and serological survey on taeniasis and cysticercosis in Kanchanaburi Province, Thailand. *Parasitology International* 2010; 59: 326-330.
16. Nkouawa A et al. Evaluation of a loop-mediated isothermal amplification method using fecal specimens for differential detection of *Taenia* species from humans. *Journal of Clinical Microbiology* 2010a; 48: 3350-3352.
17. Nkouawa A et al. Serological studies of neurologic helminthic infections in rural areas of Southwest Cameroon: toxocariasis, cysticercosis and paragonimiasis. *PLoS Neglected Tropical Diseases* 2010b; 4: e732.
18. Nakao M et al. State-of-the-art *Echinococcus* and *Taenia*: Phylogenetic taxonomy of human- pathogenic tapeworms and its application to molecular diagnosis. *Infection, Genetics and Evolution* 2010; 10:444-452.(総説)
19. Tappe D et al. Immunoglobulin G subclass responses to recombinant Em18 in the follow- up of patients with alveolar echinococcosis in different clinical stages. *Clinical Vaccine Immunology* 2010; 17: 944-948.
20. Sato MO et al. A possible nuclear DNA marker to differentiate the two geographic genotypes of *Taenia solium* tapeworms. *Parsitology International* 2011; 60: 108-110.
21. Sako Y et al. *Echinococcus multilocularis:* identification and functional characterization of cathepsin B-like peptidases from metacestode. *Experimental Parasitology* 2011; in press.

6. 媒介昆虫

Matsuoka H, Ikezawa T, Hirai M: Production of a transgenic mosquito expressing circumsp orozoite protein, a malarial protein, in the sal ivary gland of *Anopheles stephensi* (Diptera: Culicidae). Acta Med Okayama 64(4): 233-24 1, 2010

H．知的財産権の出願・登録状況（予定を含む）

１．特許取得
なし

２．実用新案登録
なし

３．その他
なし

地球規模保健課題推進研究事業（国際医学協力研究事業）

「寄生虫疾患の病態解明及びその予防・治療をめざした研究」

分担研究概要報告書

寄生虫症感受性の宿主因子の検討に関する研究

長崎大学・熱帯医学研究所・免疫遺伝学　平山　謙二

研究要旨

フィリピン国ルソン島南端ソルソゴン州は 10 歳代においてネットワークパターン(NW)を示す肝線維化症患者が 12.3%、20 歳以上では 55.3%が存在する浸淫地である。この対象集団で肝線維化症を憎悪させる要因に関わる免疫関連遺伝子を探索する目的で、免疫応答に関わる遺伝子等の近傍に設定したマイクロサテライトマーカー多型を用いて相関解析を行った。対象群は 15～35 才の肝線維化症群 54 名と 36 才以上の非肝線維化症群 40 名で、50 の免疫応答関連遺伝子近傍に設置したマイクロサテライトマーカーのうち、7 マーカーに、有意差を認めるアレルを検出した。このうち、特に有意差及び発現頻度が高く、住血吸虫性肝線維化症の感受性と強い相関を示したマーカーは D3S3561　MS*214 （OR=3.21）、IL12B MS*241(OR=2.48)とＩＬ２　MS*383 (OR=10.3)であった。IL12B マーカーには抵抗性に相関する MS*245(OR=０.45)が観察された。これらの感受性・抵抗性アレルのホモ接合体を持つ患者が、線維化症群では MS*241 (31.5%)、MS*245 (23.1%)、正常群では MS*241 (61.5%)、MS*245 (27.8%) で MS*241 ホモ接合体は正常群で有意に増加していたことから、抵抗性に相関したと考えられた（p＜0.002、OR＝0.24）。これらのマイクロサテライトマーカーと HLA-DRB1*1501 との相互作用は認められず、独立に肝線維化症の感受性に関与したと考えられた。抵抗性アレルを 2 個以上持つ場合あるいは、感受性アレルを 2 個以上持つ場合でそれぞれ、線維化症群と正常群で比較したところ、感受性アレルを持つ場合に有意差が認められたことから、感受性アレルの存在が肝線維化症に対して優性に働いた事が示唆された。

A. 研究目的

フィリピン国ルソン島南端ソルソゴン州は高度信淫地で、これまで住血吸虫症に対する十分な治療や防圧対策が取られていない。千種らが 2005～6 年に渡って行われた 1500 名(3～84 歳)に及ぶ住血吸虫症の現地調査の結果、虫卵陽性率(Kato-Katz)は全体の 6.3%程度であったが、虫卵に対する抗体陽性率は 61.4%、10 歳代においてネットワークパターン (NW) を示す肝線維化症患者が 12.3%、20 歳以上では 55.3%が存在する浸淫地であることが報告されている。

本研究においては、フィリピン国ソルソゴン州で観察された若年性肝線維化症発症に関わる免疫応答分子を網羅的に解析することにより、発症機序の本態を明らかにし発症の予防・治療法の開発、あるいは高リスク患者の早期発見に寄与することを目的とする。

B. 研究方法

肝線維化症を憎悪させる要因には HLA だけではなく他の免疫関連分子も関係することが報告されていることから、発症に関わる免疫関連遺伝子を探索する目的で、フィリピン国ルソン島南端ソルソゴン州の住血吸虫浸淫地で収集した 288 名のうち、15～35 才の肝線維化症群 54 名と 36 才以上の非肝線維化症群 40 名で、免疫応答に関わる遺伝子である、各種サイトカイン、サイトカインレセプター、シグナル伝達に関わる遺伝子、文献等から選択した遺伝子 100 について遺伝

子座内あるいは近傍（200K 以内）にマイクロサテライトマーカーを設置した。このマイクロサテライトマーカーを用いて相関解析を行った。また、感受性を示した DRB1*1501 との関連や相関を示した免疫応答遺伝子発現レベルの解析の為に、フィリピン国ルソン島南端ソルソゴン州で住血吸虫症患者を対象とし、共同研究を行う独協大・千種教授ら、フィリピン大学・寄生虫学レオナルド教授、及びソルソゴン州保険チームらと超音波診断、血清抗体価、Kato-Katz を施行し 30 歳以下での肝線維化症患者 10 名と、40 歳以上非肝線維化症対象者 10 名の 10ml 程度の EDTA 採血を行い、mRNA 発現解析用の試料を採取した。

現地調査及び採血、遺伝子解析等については、長崎大学・熱帯医学研究所・研究倫理委員会及びフィリピン大学での承認を得て行った。「フィリピンにおける住血吸虫性肝線維化症の遺伝的調節機構の解析」承認番号 04031002　長崎大学・熱帯医学研究所・研究倫理委員会。

C. 結果

設置した 160 のマイクロサテライトマーカーのうち IL6R, IL10, IL20, IL20.2, CR1L,CR1L.2, IL19, IRF6, IRF6.2, IL1F6, IL1F8, IL1F9, IL1B, STAT1, STAT4, D3S3561, IL5RA, CD86, CD86.2, SOD3, SOD3.2, IL8, JNK3, JNK3.2, IL2, IRF2, IL4, IL4.2, IL5, IL12B, NFKB1, NFKB1.2, SOD2, SOD2.2, IL6, IL6.2, IL7, IL18, STAT6, IFNG, IL26, IL4R, STAT3, FCER2, IL10RB, IL2RB, IL17RA, IL2RG 50 マーカーについて解析が終了し、7 マーカーに、有意差を認める 7 アレルを検出した。

表 1.　対象住血吸虫症患者

Subjects	Mean age ± SD	M	F
Liver net work pattern (NW)	26.0 ± 6.1	47	7
Normal liver	51.9 ± 12.4	20	19

特に有意差及び発現頻度が高く、住血吸虫性肝線維化症の感受性と強い相関を示したマーカーは D3S3561　MS*214（OR=3.21）、IL12B　MS*241(OR=2.48)と IL2 MS*383 (OR=10.3)であった。IL12B マーカーには抵抗性に相関する MS*245(OR=０.45)が観察された。これらの感受性・抵抗性アレルのホモ接合体を持つ患者が、線維化症群では MS*241（31.5%）、MS*245（23.1%）、正常群では MS*245（61.5%）、MS*241（27.8%）で MS*245 ホモ接合体は正常群で有意に増加していた（p＜0.002、OR＝0.24）。

表 2　相関を示したマイクロサテライトマーカーの頻度

IL10	Nor.	(%)	NW	(%)	Pv	OR
MS*172	5	(6.4)	14	(13.0)		
MS*174	**45**	**(57.7)**	45	(41.7)	<0.04	**0.52**
MS*176	16	(20.5)	25	(23.1)		
MS*182	1	(1.3)	**13**	**(12.0)**	<0.01	**10.5**
D3S3561						
MS*214	8	(10.3)	**29**	**(26.9)**	<0.01	**3.21**
MS*220	52	(66.7)	62	(57.4)		
IL12B						
MS*241	23	(29.5)	**54**	**(50.9)**	<0.01	**2.48**
MS*245	**52**	**(66.7)**	50	(47.2)	<0.01	**0.45**
IL2						
MS*383	2	(2.6)	**23**	**(21.7)**	<0.01	**10.3**
MS*385	15	(19.2)	14	(13.2)		
MS*387	30	(38.5)	28	(26.4)		
MS*389	11	(14.1)	12	(11.3)		
MS*391	10	(12.8)	14	(13.2)		

これらのマイクロサテライトマーカーと HLA-DRB1*1501 との相互作用は認められず、独立に肝線維化症の感受性に関与したと考えられた。抵抗性アレルを 2 個以上持つ場合あるいは、感受性アレルを 2 個以上持つ場合でそれぞれ、線維化症群と正常群で比較した。肝線維化症群では感受性アレルを 2 個以上持った対象者は 69.1%で正常群では２７.5%で有意差が認められた（P<0.0001）反対に肝線維化症群で抵抗性アレルを 2 個以上持つ対象者は 85.0%で、正常群では 85.0%で有意差は認められなかった。このことは、感受性アレルの存在が肝線維化症に対して優性に働いた事が示唆された。

D. 考察

有意差が検出されたマイクロサテライトマーカーのうち、IL12 は IFN-γ 産生を誘導するとともに、NK 細胞の細胞傷害活性を亢進させる活性を示し、いわゆる Th1/Th2 バランスの上で重要なサイトカインである。

IL12B-MS*241 の連鎖する多型が IL12 発現量に関連するとすれば、このことが、直接的に線維化症発症に影響するかもしれない。相関を示すようなマーカーの多くはサイトカインやＴ細胞応答に関わる遺伝子であった。今後、さらに近傍のマイクロサテライト解析を進めるとともに、遺伝子近傍のＳＮＰについて検討を進める。

E. 結論

肝線維化症を憎悪させる要因に関わる免疫関連遺伝子を探索する目的で、免疫応答に関わる遺伝子等の近傍に設定したマイクロサテライトマーカー多型を用いて相関解析を行った結果、相関を示すいくつかのサイトカイン遺伝子が検出された。

G. 研究発表

1. 論文発表

和文論文

平山謙二. 今日の診断指針 第 6 版 医学書院 金澤一郎、永井良三 総編集 住血吸虫症・消化器吸虫症 pp 1373-7, 2010 (2010 年 1 月発刊)

平山謙二. 今日の治療指針 医学書院 山口徹、北原光夫、福井次矢 総編集 リーシュマニア症 pp 254-5, 2011 (2010 年発刊)

英文論文

Kohama H, Harakuni T, Kikuchi M, Nara T, Takemura Y, Miyata T, Sato Y, Hirayama K, Arakawa T. Intranasal Administration of *Schistosoma japonicum* Paramyosin Induced Robust Long-Lasting Systemic and Local Antibody as well as Delayed-Type Hypersensitivity Responses, but Failed to Confer Protection in a Mouse Infection Model. Jpn J Infect Dis. 63(3):166-72. 2010.

Shuaibu M.N. Kikuchi M, Cherif M.S, Helegbe G.K., Yanagi T, Hirayama K., Selection and identification of malaria vaccine target molecule using bioinformatics and DNA vaccination. Vaccine, 28(42): 6868-75, 2010.

Del Puerto F., Nishizawa JE., Kikuchi M, Iihoshi N, Roca Y, Avilas C, Gianella A, Lora J, Velarde FUG., Renjel LA, Miura S, Higo H, Komiya N, Maemura K, Hirayama K. Lineage Analysis of Circulating *Trypanosoma cruzi* Parasites and their Association with Clinical Forms of Chagas Disease in Bolivia. PLoS Neglected Tropical Diseases 4(5);e687, 2010.

2. 学会発表

Mihoko Kikuchi and Kenji Hirayama. Microsatellite markers of immune responses gene as a tool for immunogenetic analysis of parasitological disease. 1st Conference on Cadmium in Food and Human Health. Phitsanulok, Thailand, January 15-17, 2010

Florencia Del Puerto Rodas, Eiki J. Nishizawa, Mihoko Kikuchi, Keiko Iihoshi, Freddy U. G. Velarde, Luis A. Renjel, Jelin Roca, Norihiro Komita. Kouji Maemura, Sachio Miura, Michio Yasunami, Kenji Hirayama Immunogenetic analysis of chronic Chagas disease in Bolivia. 第 79 回日本寄生虫学会大会、旭川市、2010 年 5 月 20-21 日

菊池三穂子, EDELWISA M. S.-MERCADO, LYDIA R LEONARDO, 千種雄一, 林尚子, 亀井香里, 井上哲, NAPOLEON L AREVALO, RONALD R LIM, LEA M AGSOLID, 吾妻健、平山謙二フィリピンの若年性住血吸虫症性肝線維化症についての考察 第 4 回蠕虫研究会 宮崎 11 月 26~27 日

菊池三穂子, Edelwisa M. Segubre-Mercado, Lydia R. Leonardo , 千種雄一, 林 尚子, 亀井香里, 井上 哲, Napoleon L. Arevalo , Ronald R. Lim , Lea M. Agsolid , 吾妻 健, 平山謙二 フィリピンにおける若年性住血吸虫性肝線維化症の発症に関わる免疫関連遺伝子の探索
第 51 回熱帯医学会大会 仙台市 2010 年 12 月 3～４日

H. 知的財産権の出願・登録状況

1. 特許取得
   なし
2. 実用新案登録
   なし

厚生科学研究費補助金（地球規模保健課題推進研究事業）
分担研究報告書

原虫症治療標的分子の機能解析

分担研究者　北　潔　東京大学大学院医学系研究科

研究要旨　寄生原虫のミトコンドリア呼吸鎖は宿主哺乳類のミトコンドリアと大きく異なった性質を持ち、しかもその増殖に必要不可欠である事から特異的阻害剤による抗寄生虫薬の重要な標的となる事が明らかになりつつある。我々はマラリア原虫およびトリパノソーマのミトコンドリアを薬剤標的として捉え、特に呼吸鎖電子伝達系に関して、その特異的な性質を明らかにした。

A.　研究目的

われわれは寄生適応に必須な基本的要素である各種代謝系のなかでも特にエネルギー代謝系に焦点を絞り、寄生虫ミトコンドリアが宿主と極めて異なったエネルギー代謝系を作動させることによって宿主内の環境に適応していることを明らかにしてきた。この成果をふまえマラリア原虫やトリパノソーマのミトコンドリア電子伝達系の特異性を解析することにより、最終的に化学療法の標的として捉えたいと考えている。そこで、熱帯熱マラリア原虫におけるエネルギー代謝系を先端的なエネルギー転換系研究の視点から追求し、さらにトリパノソーマなど他の寄生原虫も含め寄生現象全般に共通する適応戦略の分子基盤とその多様性を明らかにする事を目的として研究を進めている。

B. 研究方法

赤血球内型マラリア原虫ミトコンドリアの呼吸鎖電子伝達系は化学療法剤の標的として期待されている。しかしマラリア原虫ミトコンドリアに関する情報は非常に限られたものであり、これが研究の進展を妨げている。そこで活性を保持したミトコンドリアの単離法検討し、その結果ネズミマラリア原虫の系を用いて生化学的な解析が可能な量のミトコンドリアの調製法を確立した。またマラリア原虫にはアピコプラストと呼ばれる 35 kb の環状 DNA を持つオルガネラが存在し、マラリア原虫の増殖に必須な機能を有している。電子顕微鏡による観察から両者が細胞の中で常に近傍に局在している事が報告されている。そこでこの２つのオルガネラの相互作用を調べ、さらにそれぞれの機能を独立に解析する目的で細胞分画における挙動を調べて来た。昨年度は熱帯マラリア原虫の培養系から単離した粗ミトコンドリア画分を用い、ミトコンドリアとアピコプラストの相互作用を調べる目的で Percoll による分離に対する細胞破砕条件などを含む、種々の処理、薬剤の効果の検討を進めた結果、ミトコンドリアとアピコプラストのそれぞれを異なった画分に分離する事ができた。そこで本年度はこの分離法の最終的なプロトコールを確立すべく、種々の条件を比較し最適化を試みた。

また、アフリカトリパノソーマに関しては、極めて低濃度で効果を示す抗トリパノソーマ薬アスコフラノンの標的であるシアン耐性酸化酵素のタンパク質としての性質を調べる目的で、これまでに組換え酵素を用い高純

度で高活性の酵素の精製法を確立した。昨年度はこの精製標品を用いて、その結晶を得る事ができた。そこで今年度はその解像度を上げ、またアスコフラノンやその誘導体との共結晶を得てその結合様式を明らかにする事を試みた。

（倫理面への配慮）

本研究はほとんどがin vitroの実験系であり、またネズミマラリア原虫の実験は東京大学医学部の動物実験指針に従って行ったもので、倫理面の問題はない。

C. 研究結果

【マラリア原虫】

昨年までの結果を踏まえ、ヒト赤血球を用いて培養した熱帯熱マラリア原虫のオルガネラ分離法の最適化を試みた。すなわち N2 cavitation法とPercoll密度勾配遠心分離法の改良を行ない、核DNA由来と思われる凝集の除去や、細胞骨格の阻害剤による処理により、ヘモゾインを含む食胞を取り除くことによって、ミトコンドリアとアピコプラストを部分的に精製することが可能となった。ミトコンドリアの純度の指標としてのジヒドロオロト酸還元酵素の比活性は約 60 nmol/min/mg と、他の報告に比べて約 4-5 倍高い値を示した。最終的なプロトコールを以下に示す。

1. トロホゾイト期の熱帯熱マラリア原虫（3D7株など）を360 mLの培養から回収する。
2. 0.075%サポニン処理により赤血球膜を可溶化する。
3. 10 μM Nocodazoleを添加したMSEバッファーに懸濁し、Parr homogenizerにより300 psiにて細胞を破砕する。
4. 800 x g、5分の遠心で核画分を除く。
5. 上清を5,000 x g、20分で遠心し、粗ミトコンドリア画分を沈殿として得る。
6. 粗ミトコンドリア画分を28% Percoll PLUSにて100,000 x g、1時間遠心を行なう。
7. 上層部付近の凝集塊をピペットで除き、混和後さらに100,000 x g、1時間遠心を行なう。
8. ペリスタポンプにて350 μLずつ回収する。

以上の方法により、同一容量の培地から高島、見市らの以前の方法で調製した熱帯熱マラリア原虫ミトコンドリア（約 1 mg）に比べ3 倍以上の粗ミトコンドリアを得る事が可能となり、複合体IIのコハク酸-ユビキノン還元酵素の比活性も3倍以上に上昇した。これは河原らによるネズミマラリア原虫（*P. yoelii*）の場合のマウス 5 匹分に相当し、熱帯熱マラリア原虫ミトコンドリアの生化学的な解析に充分な高活性の粗ミトコンドリア調製法が確立できた。また、Percoll による分離の後のWestern ブロットおよび各種酵素活性の解析からミトコンドリアとアピコプラストを再現性良く分離している事が明らかとなった。実際にこのミトコンドリア画分を用いる事によって初めて複合体 II の Clear native electrophoresisが可能となり、コハク酸脱水素酵素活性による染色でウシ心筋複合体IIと同様なサイズを示す事が判った。

【アフリカトリパノソーマ】

アフリカ睡眠病の病原体アフリカトリパノソーマのシアン耐性酸化酵素に関しては、昨年度までに大腸菌の発現系を用い、高純度、高活性の酵素の精製法を確立し、1 分子の酵素が 2 分子の鉄を含む事を示し、酵素学的な解析から還元型ユビキノン-1 に対する K_m が 338 μM であり、特異的阻害剤であるアスコフラノンによる阻害形式は非競合混合型であることが明らかにして来た。さらにこの標品を用いて結晶化を試み、膜結合性の 2 核鉄タンパク質として初めての結晶を得る事ができ

た。本年度は結晶化の条件をさらに検討し、またアスコフラノンとの結合様式を明らかにする目的でアスコフラノンやその誘導体との共結晶を試みた。TAO の結晶化は最終的に界面活性剤存在下で PEG400 を結晶化剤に用いて行った。位相決定は、TAO 中の二核鉄原子の異常分散効果を利用した単波長異常分散法（SAD 法）で行ない（3.2 Å 分解能、波長=1.739 Å）、2.85 Å 分解能で精密化した立体構造を得ることができた。TAO は 6 本の長いヘリックスと 4 本の短いヘリックスから構成され、長い 6 本のヘリックスが逆平行なバンドル構造を形成した。N 末端には、非常に長いループがあり、隣の分子と相互作用しており結晶中では、ダイマーを形成していた。バンドルを形成している 4 本の長いヘリックス中に存在するグルタミン酸残基が二核鉄に配位していた。また、TAO の分子表面には疎水性アミノ酸残基が集中しているところがあり、そこが膜結合領域と考えられる。さらに、アスコフラノンの阻害機構を明らかにするために、その誘導体との複合体結晶を soaking 法で調製し、2.6 Å 分解能で複合体構造を明らかにした。複合体結晶では、二核鉄に近傍に存在する 1 つのヒスチジン残基が新たに配位結合を形成していた。アスコフラノン誘導体は、二核鉄の近くに結合し、近傍のアミノ酸残基と水素結合及び疎水性相互作用を形成することによって認識されていた

【アメリカトリパノソーマ】

中南米のトリパノソーマ症 Chagas 病の病原体である *Trypanosoma cruzi* のレドックス調節に関わる酵素群の立体構造に基づく薬剤の分子設計を進めているが、ミトコンドリアの複合体 II（SQR）に関して精製を試みたところ *T. cruzi* 酵素は 12 種類のサブユニット（7.3～62 kDa）で構成される二量体酵素（286.5 kDa x 2）で、哺乳類や出芽酵母の 4 サブユニット型酵素（約 130 kDa）とは大きく異なっていた。また本酵素は複合体 II の特異的阻害剤に対する感受性が哺乳類の酵素と大きく異なっており、実際に酵素活性を最も強く阻害するアトペニンは原虫の増殖を抑制する事から、薬剤標的として極めて有望と考えられた。そこでその立体構造を解析する目的で大量培養が可能でヒトへの感染の危険性がないトリパノソーマ科鞭毛虫類の一種で爬虫類に寄生する *Leishmania. Tarentolae* を用いる事とした。*L. tarentolae* の培養において液体培地 10 L 当たりから 3 g 以上の大量のミトコンドリアが得られた。これは *T. cruzi* の 10 倍ほどの収量である。次に、このミトコンドリアからの複合体Ⅱの可溶化を試みた。種々の界面活性剤や可溶化条件を検討した結果、スクロースモノラウレート（SML）が高い効果を示す事が判った。この可溶化画分から各種クロマトグラフにより複合体 II を精製を試みたところ *T. cruzi* 同様に 12 のサブユニットの精製標品を得る事ができた。

D. 考察

マラリア原虫ミトコンドリアは大量調製法が確立されていなかった事から生化学的解析が遅れていた。特に熱帯熱マラリア原虫は培養系のスケールアップが困難な事からこの点が大きな問題となっていた。しかし今回、一回の実験で 3 mg 以上の粗ミトコンドリアを再現性良く調製する方法を確立できた事は、今後マラリア原虫の研究の新しい展開に大いに貢献すると考えられる。さらにマラリア原虫のミトコンドリアとアピコプラストの分離条件を見出した事は、これらのオルガネラ間の相互作用の解析、またそれぞれの機能を独立に調べる事が可能になったと言う点で大きな前進である。実際に熱帯熱マラリア原虫ミト

コンドリアの DNA ポリメラーゼの局在や酵素学的な性質の解析に今回確立した方法が大いに貢献している。

我々が見出し、開発中のアスコフラノンは、現在最も強力な抗トリパノソーマ薬とされ、その標的はトリパノソーマのミトコンドリアに局在するシアン耐性酸化酵素である。しかしそのタンパク質としての性質は酵素が極めて不安定であるため、ほとんど判っていなかった。酵素学的な解析に加え、結晶を得る事ができた事は鉄を 2 分子含む膜結合性の 2 核鉄 (di-iron) タンパク質としては初めての報告である。さらに今回アスコフラノン誘導体との共結晶からその相互作用が明らかになった事は、今後のより低コストの誘導体あるいは阻害剤の分子設計に大いに役立つと考えられる。

複合体 II（コハク酸-ユビキノン還元酵素）は TCA 回路の酵素中唯一の膜結合性の酵素であり、ミトコンドリアのマーカー酵素として知られている。本酵素は呼吸鎖の脱水素酵素としてコハク酸からの還元力を呼吸鎖のユビキノンに伝達し、TCA 回路と呼吸鎖を直接結ぶ重要な酵素であり、宿主哺乳類ばかりでなく、寄生虫においてもそのエネルギー代謝に大きな役割を果たしている。これまで、そのサブユニット構造はヒトから細菌まで基本的には 4 つとされていたが、今回 *T. cruzi* の複合体 II が 12 サブユニットから構成される事が明らかになり、寄生虫の持つ多様性がさらに明確になった。この構造はアフリカトリパノソーマやリーシュマニアにも共通しており、12 サブユニットの複合体 II に対する特異的阻害剤を探索する事によって、極めて作用スペクトルの広い抗原虫薬の開発が期待される。ミトコンドリアの大量調製法を確立し、精製法を検討中の *L. tarentolae* に関してはすでに次世代シーケンサーを用いて全ゲノムの塩基配列の情報を得ている。この解析結果からも *L. tarentolae* の複合体 II は *T. cruzi* の複合体 II 同様に 12 のサブユニットを持ち、さらに極めて類似したアミノ酸配列を持つ事を確認している。*L. tarentolae* の複合体 II の新規な立体構造を解析する事によって、これまで我々が *T. cruzi* のジヒドロオロト酸脱水素酵素で行なって来たのと同様に薬剤の分子設計が可能になると考えられる。

E. 結論

マラリア原虫やトリパノソーマなど寄生原虫のミトコンドリア呼吸鎖は宿主哺乳類のミトコンドリアと大きく異なった性質を持ち、特異的阻害剤による抗寄生虫薬の重要な標的となる事が明らかになった。

F. 健康危険情報

特になし

G. 研究発表

論文発表

1) Crystallization and preliminary crystallographic analysis of cyanide-insensitive alternative oxidase from *Trypanosoma brucei brucei*. Kido, Y., Shiba, T., Inaoka, D. K. Sakamoto, K., Nara, K., Aoki, T., Honma, T., Tanaka, A., Inoue, M., Matsuoka, S., Moore, A., Harada, S. and Kita, K. Acta Crystallographica (2010) F66, 275-278

2) Divergence of mitochondrial genome structure in the apicomplexan parasites, *Babesia* and *Theileria*. Hikosaka, K., Watanabe, Y., Tsuji, N., Kita, K., Kishine,

H., Arisue, N., Palacpac, N. M. Q., Kawazu, S., Sawai, H., Horii, T., Igarashi, I. and Tanabe, K. Mol. Biol. Evolution (2010) 27, 1107-1116

3) Overproduction, purification, crystallization and preliminary X-ray diffraction analysis of *Trypanosoma brucei gambiense* glycerol kinase. Balogun, O. E., Inaoka, D. K., Kido, Y., Shiba, T., Nara, T., Aoki, T., Honma, T., Tanaka, A., Inoue, M., Matsuoka, S., Michels, P. AM,. Harada, S. and Kita, K. Acta Crystallographica (2010) F66, 304-308

4) Purification and kinetic characterization of recombinant alternative oxidase from *Trypanosoma brucei brucei.* Kido,Y., Sakamoto, K., Nakamura, K., Harada, M., Suzuki, T., Yabu, Y., Saimoto, H., Yamakura, F., Ohmori, D., Moore, A., Harada, S. and Kita, K. Biochim Biophys. Acta (Bioenergetics) (2010) 1797, 443-450

5) Extensive frameshift at all AGG and CCC codons in the mitochondrial cytochrome *c* oxidase subunit 1 gene of *Perkinsus marinus* (Alveolata; Dinoflagellata). Masuda, I., Matsuzaki, M. and Kita, K. Nucleic Acids Research. (2010) 38, 6186-6194

6) Trypanosome alternative oxidase, a potential therapeutic target for sleeping sickness, is conserved among *Trypanosoma brucei* subspecies. Nakamura, K., Fujioka, S., Fukumoto, S., Inoue, N., Sakamoto, Hirata, H., Kido, Y., Yabu, Y., Suzuki, T., Watanabe, Y., Saimoto, H., Akiyama, H. and Kita, K. Parasitol. Int. (2010) 59, 560-564

7) Concatenated mitochondrial DNA of the coccidian parasite *Eimeria tenella.* Hikosaka, K., Nakai, Y., Watanabe, Y., Tachibana, S., Arisue, N., Palacpac, N. M., Toyama, T., Honma, H., Horii, T., Kita, K. and Tanabe, K. Mitochondrion, (2010) 11, 273-278

学会発表

1）畑 昌幸、佐藤 恵春、北 潔 「熱帯熱マラリア原虫からの生化学的解析を目的としたミトコンドリア調製法の確立」第 66 回日本寄生虫学会西日本支部大会平成 22 年 11 月

2）志波智生、城戸康年、稲岡ダニエル健、坂元君年、奈良 武司、青木孝、本間光貴、田仲昭子、井上将行、松岡 茂、Anthony Moore、原田繁春、北潔 「Trypanosome Alternative Oxidase (TAO)の結晶構造解析」第 33 回日本分子生物学会年会・第 83 回日本生化学会大会 合同大会 平成 22 年 12 月

3）Balogun, Emmanue Oluwadare, Inaoka Daniel Ken, Kido, Yasutoshi, Tomoo Shiba, Harada, Shigeharu, Kita, Kiyoshi「Structure of glycerol kinase from human African trypanosomes」第 33 回日本分子生物学会年会・第 83 回日本生化学会大会 合同大会 平成 22 年 12 月

H. 知的財産権の出願・登録状況

特になし

厚生労働科学研究費補助金(地球規模保健課題推進研究事業(国際医学協力研究事業))
分担研究報告書

アジアの三日熱マラリア原虫の遺伝的集団構造の解明

研究分担者　狩野　繁之　国立国際医療研究センター研究所部長
研究協力者　石上　盛敏　国立国際医療研究センター研究所上級研究員

研究要旨　本研究では、三日熱マラリア原虫(Pv)ミトコンドリア(mt)DNA 塩基配列に基づく分子系統解析を行い、現生Pv集団の起源と拡散の過程を明らかにすることを目的とした。同ゲノム塩基配列に関して、すでにGenBankデータベースに世界各地の検体のデータが報告されているが、韓国やフィリピンなど、まだ報告がない国や地域が残されている。そこで本研究では、アジアの三日熱マラリア原虫のゲノムを解析し、すでに報告された検体のデータと共に分子系統解析を行うことで、これまでにないより精度の高い現生 Pv 集団の分子系統樹の構築を目指した。本解析の結果、同原虫集団は、地理的に非常に分化していることが明らかになった。韓国のPv集団は遺伝的に異なる2つの集団からなり、それらは遺伝的に異なる2つの中国南部のPv集団と近縁であった。フィリピンのPv集団は、インドシナ半島の Pv 集団と近縁であった。上記の結果より、韓国並びにフィリピンの Pv 集団はヒトの移動に伴って拡散したものと推定された。さらに本解析方法の応用として、国立国際医療研究センターを訪れた輸入三日熱マラリア患者検体を解析した結果、どの検体も患者の渡航先由来の Pv 集団を含むクラスターに含まれた。したがって本解析方法は、患者の感染地推定にも有効であると考えられた。

A. 研究目的

近年、地球規模のマラリア対策により熱帯熱マラリア患者数は減少傾向にあり、特にアジア、中南米諸国では、三日熱マラリアの重要性が増している。しかし、三日熱マラリア原虫(Pv)に関する研究は非常に遅れている。本研究では、現生 Pv 集団の起源と拡散の過程を明らかにすることを目的として、Pv の分子系統解析を行った。特に GenBank にまだ DNA 情報が報告されていな韓国、フィリピンといったアジア地域との国際医学協力を行いながら、それぞれの地域の検体を解析し、Pv 集団の進化遺伝学的な位置の推定を試みた。次に同解析によって得られた成果を応用して、三日熱マラリア患者検体がどの地域由来の株であるかを推定し、治療ならびに治療後のフォローアップを行う医師に、その患者が感染したと推定される地域の三日熱マラリアの疫学情報を提供し、臨床管理に役立てることを試みた。

B. 研究方法

1)材料は分担研究者の所属する国立国際医療研究センター研究所で保管している韓国の三日熱マラリア(Pv)検体(11 検体)、フィリピン(パラワン島)の検体(18 検体)、その他、同部局で保管する輸入マラリア患者検体(20検体)を用いた。

(倫理面への配慮)

患者からの検体の採取の際は、必要なインフォームド・コンセントの取得や、事前の倫理審査など、適切な作業と研究内容の正当性を確実に保つことに最大限の注意を払った。また赤血球に感染したマラリア原虫の遺伝子解析は行ったが、宿主であるヒトの遺伝子解析は行っていないので、文部科学省・厚生労働省・経済産業省が共同作成した「ヒトゲノム・遺伝子解析研究に関する倫理指針」に抵触する研究は行っていない。

2)患者血球から PvDNA を抽出し、PCR 法で検体の mtDNA 全領域(約 6Kb)を増幅後、

DNA シークエンサーを用いて mtDNA 全塩基配列を決定した。
3) GenBank データベースに報告されている世界各地の Pv 検体(約 280 検体)の mtDNA 塩基配列情報と共に、近隣結合法、及びハプロタイプネットワーク法を用いて分子系統樹を作成した。

C. 研究結果

Pv mtDNA 全塩基配列に基づく分子系統解析の結果、世界の Pv 集団は、それぞれの流行地域毎のクラスターに分かれることが明らかとなった。1) 韓国の Pv 集団は、遺伝的に異なる2つの集団からなることが本研究ではじめて明らかとなった。そしてそれら2つの Pv 集団は、それぞれ遺伝的に異なる2つの中国南部の Pv 集団と近縁であった(Iwagami ら, Malar J, 2010)。2) フィリピンの Pv 検体(3検体)は、タイをはじめとするインドシナ半島の Pv 集団と遺伝的に近縁であることが明らかとなった。3) 分担研究者の部局で保管する輸入三日熱マラリア患者検体は、全て患者の渡航先由来の Pv 集団を含むクラスターに含まれた。

D. 考察

結果1) より、韓国の Pv 集団の起源は中国南部の Pv 集団にあると推定された。恐らく同地域間でのヒトの移動に伴って Pv が拡散したと推察された。結果 2) より、フィリピンのパラワン島の Pv は、地理的に近いインドネシアの Pv よりも、インドシナ半島の Pv と遺伝的に近縁であったことから、船によるヒトの移動が盛んになってから同地域にもたらされた可能性が示唆された。なお GenBank に登録されているフィリピン株(1検体)は、パプアニューギニアの Pv 集団と近縁であったことから、フィリピンの Pv 集団はヘテロジニアスな集団である可能性が高いと推察された。結果 3) より、複数の流行地域を渡航して感染地が不明な患者でも、感染地推定が可能であると考えられた。実際、そのような患者由来の2検体を解析し、患者の渡航先と矛盾のない感染地の推定結果が得られた。

E. 結論

韓国やフィリピンとの国際医学協力研究をとおして、Pv mtDNA 塩基配列に基づく分子系統解析を行い、アジアに流行する現生 Pv 集団は生物地理学的に非常に多様な集団であることが明らかとなった。また同集団は、ヒトの移動に伴って世界中に拡散したと推定され、地球規模保健課題である「人口移動と再興感染症の拡散」という問題を包含していることが明らかとなった。さらに本解析方法を応用することで、三日熱マラリア患者の臨床管理に役立つ情報を医師に提供出来ることが明らかになり、わが国の厚生労働行政上問題となる輸入マラリアの管理に関して、有用な解析手法であることが渡航医学的にも明らかとなった。

F. 研究発表

1. 論文発表

Moritoshi Iwagami, Seung-Young Hwang, Megumi Fukumoto, Toshiyuki Hayakawa, Kazuyuki Tanabe, So-Hee Kim, Weon-Gyu Kho, Shigeyuki Kano. Geographical origin of *Plasmodium vivax* in the Republic of Korea: haplotype network analysis based on the parasite's mitochondrial genome. Malaria Journal 9:184, 2010.

2. 学会発表

1) Moritoshi Iwagami, Megumi Fukumoto, Weon-Gyu Kho, Pilarita T. Rivera, Shigeyuki Kano. Phylogeographic Analysis of Mitochondrial DNA Sequences of *Plasmodium vivax* and its Application to Travel Medicine. 第8回アジア太平洋渡航医学会大会, 奈良新公会堂 (2010 年 10 月 20–23 日)

2) 石上盛敏, 福本恵, Weon-Gyu Kho, 狩野繁之. ハプロタイプネットワーク法による韓国の三日熱マラリア原虫の起源の推定. 第79回日本寄生虫学会大会, 大雪クリスタルホール(2010 年 5 月 20–21 日)

G. 知的財産権の出願・登録状況

なし

厚生労働科学研究費補助金(国際医学協力研究事業)

分担研究報告書

ワクチン分子の無細胞系合成システムの確立

分担研究者　坪井敬文　愛媛大学無細胞生命科学工学研究センター　教授

研究要旨：　コムギ胚芽無細胞タンパク質合成系を用いることにより、熱帯熱マラリア原虫遺伝子をコドン改変することなく原虫ゲノムワイドなプロテインアレイを作製した。この中からメロゾイト期に特異的な組換えタンパク質 114 種をモデルに用いて、我々が確立したハイスループット抗原スクリーニング法により、タイから得られたマラリア免疫血清を用いて熱帯熱マラリア原虫の新規抗原タンパク質のスクリーニングを試行した結果、機能未知の原虫分子の中に、マラリア免疫ヒト血清と反応有する分子を検出することに成功した。さらにこれらの内、PfMSPDBL1 と呼ばれている機能未知分子がマラリア赤血球期ワクチン候補となりうるか検討し、PfMSPDBL1 は熱帯熱マラリア原虫メロゾイトの赤血球侵入に重要な役割を果たすこと、さらに新規赤血球期ワクチン候補となる可能性が示唆された。以上の結果から、本法のハイスループット免疫スクリーニング系としての有用性が確認された。

A．研究目的

マラリア撲滅が 2007 年に再度宣言されて依頼、マラリアワクチン開発は緊急の課題として再認識された。そのためには、既知のワクチン候補のみの研究では限界に達しており、新たなワクチン候補分子の探索が、緊急の課題となっている。申請者らは、マラリア原虫組換えタンパク質の合成に優れているコムギ胚芽無細胞タンパク質合成法を用いて熱帯熱マラリア原虫のゲノムワイドに組換えタンパク質を発現し、その中から新規抗原を同定することを目的に本研究を実施した。

B．研究方法

1) 熱帯熱マラリア原虫メロゾイト期組換えタンパク質の合成

コムギ胚芽無細胞タンパク質合成系を用いて、熱帯熱マラリア原虫タンパク質の内、マラリアゲノム情報データベース（PlasmoDB）より、メロゾイト期にのみ発現が示唆されている遺伝子を選択し、コムギ胚芽無細胞タンパク質合成系を用いて熱帯熱マラリア原虫赤血球期プロテインアレイを作製した。これを用いて、以下のスクリーニングを実施した。

2) ハイスループット抗原抗体アッセイ

これらのプロテインアレイとマラリア感染者血清との抗原抗体反応を検出するために、これまでに確立したアルファスクリーン法を応用した。

3)　タイ国におけるマラリア流行地からの血清試料の入手

なお、用いたマラリアに対する防御免疫を保有していると考えられる血清はタイ国カンチャナブリ県のマラリア流行地コンモンタ村において一

昨年度入手し、また防御免疫を保有していないと考えられる血清は、タイ国タ－ク県のマラリア患者から入手した。

（倫理面への配慮）

タイ国におけるマラリア患者血液の採取に当たってはタイ国保健省の許可を得、患者への説明を十分行なった上で同意を得て実施した。また、本血清試料の利用は愛媛大学ヒトゲノム・遺伝子解析研究倫理委員会の許可を得ている。

C．研究結果および考察

1) 熱帯熱マラリア原虫メロゾイト期組換えタンパク質の合成

コムギ胚芽無細胞タンパク質合成系を用いて昨年度樹立した熱帯熱マラリア原虫メロゾイト期分子114種類からなるプロテインアレイを免疫スクリーニングに用いた。

2) ハイスループット抗原抗体アッセイの実施

昨年度、上記のプロテインアレイを用いて、タイのコンモンタ村から得られた熱帯熱マラリアに対する防御抗体を含有している可能性の高いヒト免疫血清 22 人分と、タイ国タ－ク県のマラリア患者から入手した患者血清 22 人分の反応性をアルファスクリーン法を用いて検討し、患者血清よりも免疫血清と有意に高く反応した防御抗体の誘導に関連する可能性のある分子が７種類選択された。その内訳は、これまでにワクチン候補抗原として研究されてきた既知分子が５種類、機能未知の分子が２種類であった。そこで今年度は、これらの機能未知分子の内、PfMSPDBL1 と呼ばれている分子がマラリア赤血球期ワクチン候補となりうるかを検討した。PfMSPDBL1 は一次構造上、既知の赤血球結合タンパク質EBA175等の分子が有するDBL（Duffy Binding Like)ドメインに類似したドメインを有するため、赤血球侵入において重要な機能を果たすことが予測された。全長および部分長PfMSPDBL1組換えタンパク質をコムギ胚芽無細胞系により合成し動物抗血清を作製した。これら抗血清を用いた間接蛍光抗体法により、PfMSPDBL1 は赤血球への侵入型であるメロゾイト表面への局在が確認された。また、原虫のPfMSPDBL1はヒト赤血球表面に結合し、さらに抗PfMSPDBL1 抗体は、培養熱帯熱マラリア原虫の赤血球への侵入を阻害することが明らかとなった。以上の結果から、PfMSPDBL1 は熱帯熱マラリア原虫メロゾイトの赤血球侵入に重要な役割を果たすこと、さらに新規赤血球期ワクチン候補となる可能性が示唆された。以上の結果から、本法のハイスループット免疫スクリーニング系としての有用性が確認された。

3）今後の課題

同定されたその他の新規の抗原に関しては、PfMSPDBL1 同様個別の研究を進めてゆき、ワクチン活性の同定にすすめてゆく予定である。

D．結論

コムギ胚芽無細胞タンパク質合成系を用いたハイスループット抗原抗体反応スクリーニングにより、新規マラリアワクチン候補抗原のスクリーニングがゲノムワイドに可能となると考えられた。

E．研究発表

１．論文発表

1) Tsuboi T, Takeo S, Arumugam TU, Otsuki H, Torii M. The wheat germ cell-free protein synthesis system: a key tool for novel malaria vaccine candidate discovery. Acta Trop. 2010, 114: 171-176.

2) Miyata T, Harakuni T, Tsuboi T, Sattabongkot J, Kohama H, Tachibana M, Matsuzaki G, Torii M, Arakawa T. *Plasmodium vivax* ookinete surface protein, Pvs25, linked to cholera toxin B subunit induces potent transmission-blocking immunity by intranasal as well as subcutaneous immunization. Infect Immun. 2010, 78: 3773-3782.

3) Blagborough AM, Yoshida S, Sattabongkot J, Tsuboi T, Sinden RE. Intranasal and intramuscular immunization with baculovirus dual expression system-based Pvs25 vaccine substantially blocks *Plasmodium vivax* transmission. Vaccine. 2010, 28: 6014-6020.

２．学会発表

1) Takeo S, Sakamoto H, Kaneko T, Tachibana M, Miura K, Varma S, Sattabongkot J, Torii M, Tsuboi T. Identification of novel blood-stage vaccine candidates against *Plasmodium falciparum* by high-throughput immunoscreening. Adaptive and Innate Immune Responses to Neglected Tropical Diseases, San Diego, USA, January 9-11, 2010.

2) Miura K, Takeo S, Sakamoto H, Kaneko T, Varma S, Torii M, Sirima SB, Tsuboi T. Identification of *Plasmodium falciparum* blood-stage potential vaccine candidates: high-throughput immunoscreening approach with Burkina Faso children sera. Adaptive and Innate Immune Responses to Neglected Tropical Diseases, San Diego, USA, January 9-11, 2010.

3) Takeo S, Sawasaki T, Torii M, Sattabongkot J, Endo Y, Tsuboi T. Functional production of malarial parasites' proteins with wheat germ cell-free system. Keystone Symposium, Structural Genomics: Expanding the Horizons of Structural Biology, Breckenridge, USA, January 8-13, 2010.

4) Tsuboi T, Tachibana M, Takeo S, Sattabongkot J, Wu Y, Torii M.
Sexual stage parasites and transmission-blocking antibodies.
Keystone Symposium, Malaria: New Approaches to Understanding Host-Parasite Interactions, Copper Mountain, USA, April 11-16, 2010.

5) Chen JH, Jung JW, Wang Y, Lu F, Ha KS, Tsuboi T, Han ET.
Evaluation of putative immunogenic proteins from vivax malaria blood stage by high-throughput screening assays.
Keystone Symposium, Malaria: New Approaches to Understanding Host-Parasite Interactions, Copper Mountain, USA, April 11-16, 2010.

6) Tsuboi T, Tachibana M, Takeo S, Sattabongkot J, Wu Y, Torii M.
(Invited speaker)
Wheat germ cell-free system-expressed Pfs230 is an effective transmission-blocking vaccine candidate antigen.
12th International Congress of Parasitology, Melbourne, Australia, August 16-20, 2010.

7) Miura T, Takeo S, Otsuki H, Torii M, Tsuboi T.
Erythrocyte proteome screening for interaction partners of malarial merozoite RhopH complex.
12th International Congress of Parasitology, Melbourne, Australia, August 16-20, 2010.

8) Ito D, Han ET, Takeo S, Thongkukiatkul A, Otsuki H, Torii M, Tsuboi T.
Characterization of putative rhoptry neck protein 3 (PfRON3) in *Plasmodium falciparum* merozoite.
12th International Congress of Parasitology, Melbourne, Australia, August 16-20, 2010.

9) Arumugam TU, Takeo S, Thonkukiatkul A, Miura K, Otsuki H, Zhou H, Long CA, Thompson J, Healer J, Crabb B, Cowman A, Torii M, Tsuboi T.
A new Pf merozoite micronemal protein is a novel blood-stage vaccine candidate antigen.
12th International Congress of Parasitology, Melbourne, Australia, August 16-20, 2010.

10) Sakamoto H, Takeo S, Kaneko T, Sattabongkot J, Torii M, Tsuboi T.
A novel blood-stage malaria vaccine candidate with human erythrocyte binding capacity.
The 10th Awaji International Forum on Infection and Immunity, Awaji, Japan. September 7-10, 2010.

11) Arumugam TU, Takeo S,

Thonkukiatkul A, Miura K, Otsuki H, Zhou H, Long CA, Sattabongkot J, Torii M, Tsuboi T.
Wheat germ cell-free system facilitated the identification of a novel malaria vaccine candidate.
The 10th Awaji International Forum on Infection and Immunity, Awaji, Japan. September 7-10, 2010.

12) Miura T, Takeo S, Otsuki H, Sawasaki T, Endo Y, Torii M, Tsuboi T.
RhopH complex from mouse malaria parasite interacts with erythrocyte calmyrin.
ASTMH 59th annual meeting, Atlanta, USA, November 3-7, 2010.

13) Arumugam TU, Takeo S, Thonkukiatkul A, Miura K, Otsuki H, Zhou H, Long CA, Sattabongkot J, Torii M, Tsuboi T.
Identification of a novel blood stage vaccine candidate for *Plasmodium falciparum*.
ASTMH 59th annual meeting, Atlanta, USA, November 3-7, 2010.

14)坪井 敬文(シンポジスト)
マラリアワクチン研究の最前線-我が国発の技術による国際貢献
厚生労働省主催、平成 21 年度 地球規模保健課題推進研究事業シンポジウム、東京、3/30、2010。

15) 原國哲也、宮田 健、坪井敬文、Sattabongkot Jetsumon、橘 真由美、鳥居本美、李 長春、渡部久実、松崎吾朗、新川 武
酵母 *Pichia pastoris* 発現ネズミマラリアメロゾイト表面蛋白質 MSP1-19 のワクチン効果
第 79 回日本寄生虫学会大会、旭川市、5/20-21、2010。

16) 新川 武、宮田 健、池原 歩、原國哲也、坪井敬文、Sattabongkot Jetsumon、橘 真由美、鳥居本美、松崎吾朗
新たなワクチンプラットフォーム創製のための三部構成四価免疫賦活複合体(TITs)
第 79 回日本寄生虫学会大会、旭川市、5/20-21、2010。

17) 宮田 健、原國哲也、池原 歩、坪井敬文、Sattabongkot Jetsumon、橘真由美、鳥居本美、松崎吾朗、新川武
新たなワクチンプラットフォーム創製のための三部構成五価免疫賦活複合体(TIPs)
第 79 回日本寄生虫学会大会、旭川市、5/20-21、2010。

18) 橘真由美、石野智子、Jenwithisuk Rachaneeporn、Kangwanrangsan Niwat、横内ゆき、Sattabongkot Jetsumon、坪井敬文、鳥居本美
コムギ胚芽無細胞タンパク質合成法を用いた三日熱マラリア伝搬阻止ワク

チン候補抗原 Pvs230 の作製
第 79 回日本寄生虫学会大会、旭川市、5/20-21、2010。

19) Jenwithisuk Rachaneeporn、Kangwanrangsan Niwat、橘真由美、石野智子、坪井敬文、鳥居本美
A novel protein is targeted to the crystalloids of *Plasmodium yoelii* ookinetes
第 79 回日本寄生虫学会大会、旭川市、5/20-21、2010。

20) 大槻 均、入子英幸、石野智子、金子 修、福本宗嗣、坪井敬文、鳥居本美
ネズミマラリア原虫赤血球結合タンパク(EBL)の細胞内輸送ドメインの機能解析
第 79 回日本寄生虫学会大会、旭川市、5/20-21、2010。

21) 伊藤大輔、韓 銀澤、竹尾 暁、Thongkukiatkul Amporn、大槻 均、鳥居本美、坪井敬文
熱帯熱マラリア原虫メロゾイト rhoptry neck protein 3 の性状解析
第 79 回日本寄生虫学会大会、旭川市、5/20-21、2010。

22) 北村 圭、熊谷 貴、Bentum Bethel K、三田村俊秀、坪井敬文、太田信生
熱帯熱マラリア原虫におけるオートファジーの役割
第 79 回日本寄生虫学会大会、旭川市、5/20-21、2010。

23) 金子 明、Taleo George、Chaves Luis F、Perlmann Hedvig、江藤秀顕、竹尾 暁、橘 真一郎、Troye-Blomberg Marita、坪井敬文、Drakeley Chris、田邉和裕
島嶼マラリア根絶 10 年後の三日熱マラリア再燃
第 79 回日本寄生虫学会大会、旭川市、5/20-21、2010。

24) 大前比呂思、伊藤 誠、中澤 港、亀井喜世子、Bakotee Bernard、Suraj Eka、長岡史晃、坪井敬文、木村英作
ソロモン諸島のマラリア調査における尿診断法の試み
第 79 回日本寄生虫学会大会、旭川市、5/20-21、2010。

25)坪井敬文(招待講演)
マラリアワクチン研究の最前線
第 9 回四国免疫フォーラム、東温市、6/19、2010。

26)坪井敬文(招待講演)
マラリアと人類:歴史は物語る
第 114 回日本医学放射線学会中国・四国地方会、今治市、6/26、2010。

27) 坂本寛和、竹尾 暁、坪井敬文
熱帯熱マラリア原虫メロゾイトの機能未知抗原 PfMSPDBL1 は赤血球侵入に関与するか?
第18回分子寄生虫学ワークショップ、草津町、8/2-5、2010。

戸市、12/7-10、2010。

28) 垰本竜宏、竹尾 暁、坪井敬文
熱帯熱マラリア原虫メロゾイト抗原タンパク質 H103 の機能解明に向けて
第18回分子寄生虫学ワークショップ、草津町、8/2-5、2010。

29) Thangavelu U. Arumugam、竹尾 暁、Amporn Thonkukiatkul、三浦憲豊、大槻 均、Carole A Long、Jetsumon Sattabongkot、鳥居本美、坪井敬文
マイクロネームに局在する新規熱帯熱マラリア赤血球期ワクチン候補抗原の同定
第 9 回分子寄生虫・マラリア研究フォーラム、長崎市、10/8-9、2010。

30) 加藤晶、竹尾 暁、Jetsumon Sattabongkot、鳥居本美、坪井敬文
熱帯熱マラリア原虫の各侵入型原虫における新規内膜複合体関連分子の同定
第 9 回分子寄生虫・マラリア研究フォーラム、長崎市、10/8-9、2010。

31) 三浦豊和、竹尾 暁、坪井敬文
赤血球寄生期マラリア原虫の RhopH タンパク質複合体:相互作用する宿主赤血球分子の探索
第 33 回日本分子生物学会年会、神戸市、12/7-10、2010。

32) 垰本竜宏、竹尾 暁、坪井敬文
マラリア原虫メロゾイトにおける抗原タンパク質 H103 の機能解明
第 33 回日本分子生物学会年会、神

厚生科学研究費補助金（国際医学協力研究事業）
分担研究報告書

赤痢アメーバの病原機構の解明

分担研究者　野崎　智義　国立感染症研究所　部長

研究要旨　赤痢アメーバ症はアジア・アフリカ等の開発途上国を中心として蔓延する重要な腸管寄生原虫症である。本研究は赤痢アメーバの特殊な病原機構と代謝の一端を明らかにすることを目的としている。本年度は、昨年度に引き続き、赤痢アメーバの酸化ストレスに対する応答を、エネルギー代謝等を中心に解析した。

Ａ．研究目的

赤痢アメーバ症（アメーバ赤痢）は熱帯・亜熱帯の開発途上国を中心として世界の人口の約1%が感染する腸管感染症である。一方、我が国を含む一部先進諸国においても、知的障害者および男性同性愛者において重度の感染浸淫を引き起こしている。赤痢アメーバの遺伝子情報は、全ゲノムの読了(Lofus Nature 2005)により明らかにされ、本原虫の病原性、寄生性等の重要な生物機構の青写真が明らかにされつつある。しかしながら原虫が生存の過程で曝される様々なストレスに対する応答等に関する個別の研究に関しては、依然未解明なものが多く、オミクス研究に代表されるポストゲノムアプローチが不可欠である。

我々は赤痢アメーバのエネルギー産生の解明に主眼をおいて研究を継続している。赤痢アメーバは一般の原核・真核生物と異なり、主要な抗酸化物質であるグルタチオン並びに、グルタチオン生合成並びに代謝の能力を持たなず、NADPH依存性酸化還元酵素などに代表される特殊な酸化ストレス防御機構を有している。しかしながら、酸化ストレスが赤痢アメーバの中心代謝に与える影響に関してはほとんど未解明である。そこで本研究では、酸化ストレスが赤痢アメーバの中心代謝に与える影響をトランスクリプトーム解析による網羅的遺伝子発現プロファイリングにより解析した。

Ｂ．研究方法

1.　培養

赤痢アメーバ株HM-1: IMSS cl6(Louis Buddy Diamondの分離による)の培養は常法の無菌培養法に従った。

2.　トランスクリプトーム解析

Affymetrix社製のカスタム合成されたE. histoltyica/E. invadensマイクロアレイを用いた。プローブのデザイン、cRNAの作成、ハイブリダイゼーション、スキャンなどは常法に従った。トリプリケートで得られたデータの優位性はANOVAにて検定した。

（倫理面への配慮）本研究に関わる病原体の取扱に関する許可は当該研究機関にて得られている。

Ｃ．研究結果

1.　酸化ストレスによる遺伝発現変化

赤痢アメーバの栄養型をシステイン枯渇の環境で3, 6, 12, 24, 或は48 時間培養を行ったところ、9327遺伝子のうち290遺伝子が少なくとも1点以上で3倍以上の発現変化を示した(3.1%)。290遺伝子のうち、129遺伝子は発現上昇を示し、167遺伝子は発現抑制を示した。残り6遺伝子は時点により上昇あるいは下降を示した（図1)。

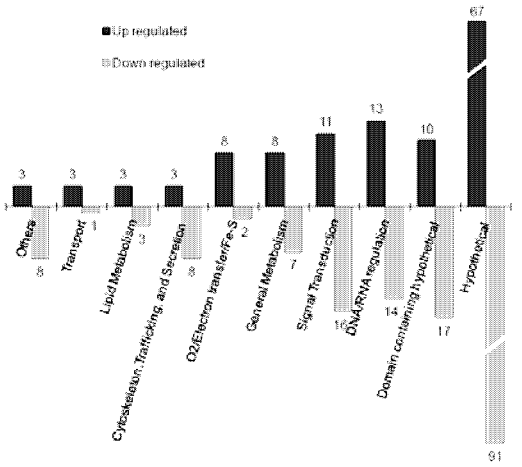

図 1 トランスクリプトーム解析により 3 倍以上変化の見られた遺伝子の分類

2. 発現変化した遺伝子の分類

129 の上昇遺伝子のうち 39%にあたる 50 遺伝子は GO(gene ontology)分類により、分類可能であった。これらは、シグナル伝達、代謝、DNA/RNA 調節、電子伝達、ストレス応答、輸送、トラフィック／分泌／細胞骨格などに分類された（図 1)。残りの 77 遺伝子(59)は"hypothetical protein"或は保存された領域を有するタンパク質と分類された。抑制された 167 遺伝子のうち 60 (38 %) は GO 分類された。一方 108 遺伝子(62 %)は"hypothetical protein"或は保存された領域を有するタンパク質と分類された。

3. qRT-PCR 法によるトランスクリプトームデータの確認

トランスクリプトーム解析の結果を確認することを目的として、発現上昇の見られた 2 遺伝子 (EHI_173950; EHI_138480)、発現低下の見られた 2 遺伝子(EHI_045340; EHI_052890)、ならびに変化のなかった 1 遺伝子(EHI_056690)に関して qRT-PCR による確認を行った。トランスクリプトームのデータと qRT-PCR のデータは良く整合していた（表 1)。

Verification of the array data by qRT-PCR

Common Name	Accession Number	Fold Change				
		3h	6h	12h	24h	48h
Major facilitator superfamily (MFS) transporter	XM_647413	2.0 (4.1)	12.8 (14.6)	7.2 (9.9)	4.2 (4.7)	2.8 (2.6)
Iron sulfur flavoprotein (Isf)	XM_650036	1.8 (3.9)	4.4 (6.8)	14.9 (9.8)	5.5 (5.4)	2.8 (4.2)
NADPH-dependent oxidoreductase (EhNOD)	XM_648481	-3.0 (+1.9)	-3.0 (+1.9)	-6.0 (+3.0)	-6.4 (+10.5)	-7.8 (8.3)
Hypothetical protein	XM_646389	-2.2 (-1.1)	-6.4 (+6.3)	-12.9 (+11.1)	-3.4 (+3.0)	-2.7 (+2.6)
RNA polymerase II 15kDa subunit	XM_643999	1.0 (1.4)	-1.2 (1.2)	1.1 (1.2)	-1.3 (1.1)	-1.3 (1.2)

表 1 マイクロアレイ解析と qRT-PCR データの整合性

4. システイン飢餓の含硫アミノ酸代謝関連遺伝子に対する影響

図 2 に含硫アミノ酸の代謝概要を示す。図 3 に示すように、一つの例外を除き、含硫アミノ酸代謝に関与すると現時点で強く示唆・予測される遺伝子の>3 倍の発現変化は見られなかった。フォスフォセリンアミノ転移酵素(phosphoserine amino transferase: PSAT)は 3-phosphohydroxypyruvate と L-phosphoserine の両方向性の反応を触媒する酵素であり、解糖経路からのセリン生合成に関与するリン酸化経路と呼ばれる経路の第二段の酵素である。PSAT の発現は 48 時間後に 3.3 倍して減少していた。3 倍の変化には満たないが、methionine adenosyl transferase (MAT)や phosphoglycerate dehydrogenase (PGDH)がそれぞれシステイン枯渇の早期、後期にそれぞれ変化していることが示された。

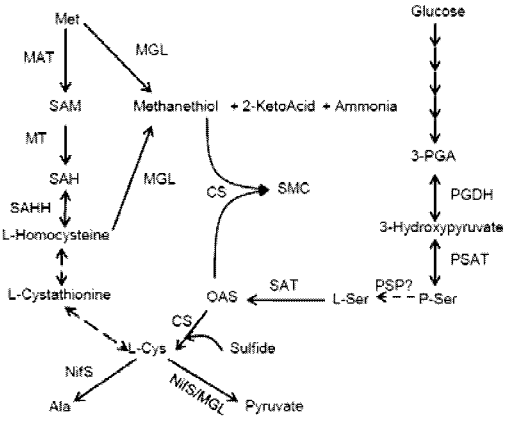

図 2 赤痢アメーバにおける含硫アミ

ノ酸代謝経路

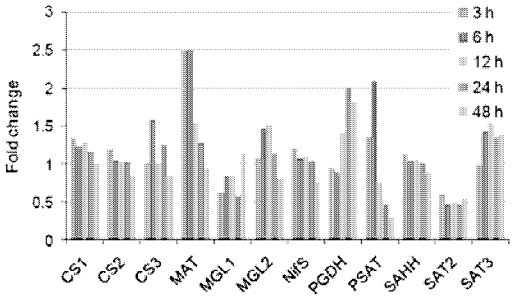

図 3 システイン飢餓による含硫アミノ酸代謝関連酵素遺伝子発現への影響

D．考察及び結論

酸化ストレスへの応答は原虫の宿主内でのサバイバルに必須である。原虫は組織侵入の際に高い酸化ストレスに暴露される。我々は本研究においてシステイン飢餓にともなう酸化ストレスに伴う原虫の遺伝子発現調節を網羅的に理解することを目的として、トランスクリプトーム解析を開始した。我々の予想に反して、システイン飢餓にも関わらず、含硫アミノ酸代謝経路のほとんどの遺伝子は転写レベルの調節を受けなかった。我々のこれまでのメタボローム解析ではシステイン飢餓で解糖経路などが大きく影響を受けることが示されており、[Husein, J Biol Chem, 2010]. 一方他種生物では、システインの availability は細胞内含硫アミノ酸代謝に大きく影響することが知られている [Lee J-in, 2008]。例えば、HepG2/C3A 細胞では、システイン飢餓により cysteinyl-tRNA synthetase, glutamate-cysteine ligase, L-cystine-glutamate transporter, cystathionine γ-lyase, glutamate-cysteine ligase などの発現が上昇し、3-phosphoadenosine 5-phosphosulfate synthase と sulfite oxidase の発現が抑圧されることが知られている[Lee J-in, 2008]。従って、赤痢アメーバのシステイン飢餓に対する遺伝子発現応答は特殊であると言える。

嫌気原虫におけるエネルギー合成系は哺乳動物と大きく異なり、本研究により明らかにされた、酸化ストレスによる中心代謝経路の調節機構は前例がない。したがって本研究成果は、赤痢アメーバに対する新規創薬の観点からも、重要な示唆を与えたと言える。

E．健康危険情報

該当せず

F．研究発表

1. 論文発表

(i) Jeelani, G., Husain, A., Sato, D., Ali, V., Suematsue, M., Soga, T., and Nozaki, T. (2010) Two Atypical L-cysteine-regulated NADPH-dependent oxidoreductases involved in redox maintenance, L-cystine reduction, and metronidazole activation in the enteric protozoon *Entamoeba histolytica*. J. Biol. Chem., 285, 26889-26899.

(ii) Yousuf, M. A., Mi-ichi, F., Nakada-Tsukui, K., and Nozaki, T. (2010) Localization and targeting of unusual pyridine nucleotide transhydrogenase in *Entamoeba histolytica*. Eukaryot. Cell 9, 926-933.

2. 学会発表

(i) J Sato, D., Husain, A., Jeelani, G., Suematsu, M., Soga, T., and Nozaki, T. Metabolic analysis of the human enteric parasite *Entamoeba histolytica*: Discovery of unique pathways and potential targets for chemotherapeutics. Metabolomics 2010, June 27-July 1, 2010, Amsterdam, The Netherlands

(ii) Jeelani, G., Sato, D., Jusain, A., Suematsu, M., Soga, T., and Nozaki, T. Metabolomics of parasite differentiation: metabolomic profiling of the human enteric protozoan parasite *Entamoeba histolyitca* revealed activation of unpredicted pathways during differentiation of the proliferative into dormant stage. Metabolomics 2010, June 27-July 1, 2010, Amsterdam, The Netherlands

なし

G. 知的所有権の出願・登録状況

1. 特許取得
   該当せず。
2. 実用新案登録
   該当せず

厚生労働科学研究費補助金（国際医学協力研究事業）
分担研究報告書

フィラリア症の疫学研究（診断法の開発と野外応用）

分担研究者　木村英作　愛知医科大学医学部教授

研究要旨
(1)頻回の集団治療（MDA）を受けたスリランカの2村において、尿ELISAとICT testの感度を比較した。Sentinel groupとされる10歳以下の小児において、前者はより高い感度を示した。尿ELISAは感染率が低いpost-MDA stageにおいても有用であることが再確認された。
(2)フィラリア症が存在しないとされていた地域の2村（スリランカ）で尿ELISAによる疫学調査を実施した。感染率は共に2%以下であったが、2村で10歳以下の小児の感染パターンが大きく異なるという興味深い結果が得られた。追跡を要する。
(3)尿を検体とするビーズ法（目視判定可能）と尿ELISAをバングラデシュで比較検討した。両者とも十分な感度と特異度を示し、住民にも良く受け入れられた。
(4)フィラリア感染蚊を効率よく発見するためのLAMP法を開発した。

A. 研究目的

本研究は、2020年までに世界からリンパ系フィラリア症を制圧するというWHOの計画に寄与することを目的とする。流行地では、年1回、5回の集団治療（MDA）を実施することになっているが既にそれを完了した国が少なくない。Post-MDA期にはフィラリア症の<征圧確認>と<再燃の早期発見>が重要で、いずれの場合も非常に低い感染レベルを見逃さない感度の高い診断法が必須となる。

我々は尿を検体とする免疫診断法（尿ELISA）を開発したが、引き続きその有用性を流行地の現場において確認する作業を行っている。また、我々は目視判定ができる新たな尿診断法（ビーズ法）を開発したが、バングラデシュにおける野外応用を目指した基礎研究（感度テストなど）を実施した。さらにビーズ法を疫学調査に応用した。

実験室の研究として、フィラリア感染蚊を発見するLAMP法をほぼ完成させた。

B. 研究方法

1. Post-MDA期における尿ELISAとICT testの比較（スリランカ）

尿ELISAの有用性を確認するため、MDAが5～13回実施されたUnawatuna, Hamugewattaの2村で、現時点で最も信頼されているICT test（抗原検出キット）

と比較研究を行った。

2. フィラリア症非流行地における尿ELISAの応用（スリランカ）

非流行地でも陰嚢水腫・象皮病が発見される。通常、流行地住民の移動によるものであるが、例数が多い時には流行の有無を検証する必要がある。このような地域にあるRatunapura村（R村：子供と若者が検査対象）とBelihul-oya村（B村:全住民が対象)で尿ELISAを実施した。

3. バングラデシュにおけるビーズ法の有用性の検討（尿ELISA、ICTとの比較）

尿診断法をバングラデシュに応用することを目的に、基礎実験として尿EISAおよびビーズ法の感度、特異性を検討した。さらに、小学生を対象とする感染調査を実施し尿診断とICT testの結果を比較した。

4. LAMP法による媒介蚊調査の簡便化

フィラリアの伝搬が起きているか否かの判定に、多数の媒介蚊を解剖してフィラリア幼虫を検出する方法がある。手技が煩雑で時間を要するため、近年PCR法が導入された。我々はさらなる簡便化をめざしてLAMP法の開発を試みた。

（倫理面の配慮）

本研究は、愛知医科大学倫理委員会の審査を経て実施されている。スリランカにおける共同研究者は、その所属機関（ルフナ大学医学部）において同様の審査・承認を得ている。バングラデシュでの研究はBangladesh Medical Research Council (BMRC)の承認を得た。被検者には十分な説明を行い同意を得ている。

C. 研究結果

1. 尿ELISAとICT testの比較

2村で計1,300人以上が尿ELISAとICTによる検査を受けた。結果を表1に示す。

表 1	尿ELISA	ICT
陽性者数/検査数*	285/1360	51/1317
陽性率（%）	21.0	3.9
陽性者数/検査数**	5/192	1/180
陽性率（%）	2.6	0.6

*全年齢　　**10歳以下のみ

尿ELISAは、新しい感染（或いは抗原曝露）を示す10歳以下の陽性率においてICT testより高値をしめした。

2. 非流行地における尿ELISAの応用

アンケート調査とGISによる分析の結果、非流行地とされる地域内に陰嚢水腫の罹患率が高い村が発見されたため尿ELISAを実施した。R村で817人中13人（1.6%)、B村では688人中8人（1.2%）が陽性であった。興味深いことに、R村では陽性者の6/13 (46%)が10歳未満なのに対し、B村では0/8 (0%)であった（最年少陽性者は19歳)。 図1に抗体価の分布を示す。

図 1-a　Belihul-oya 村

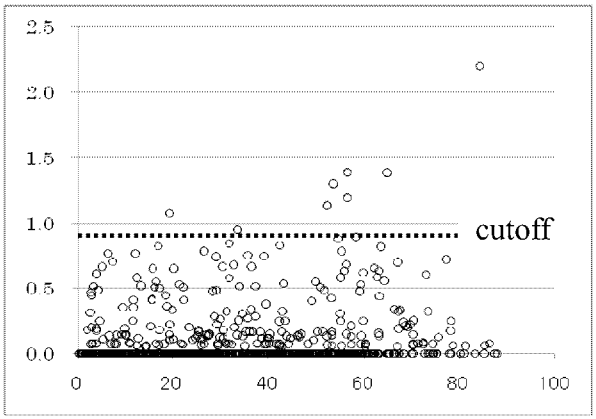

縦軸：抗体価（log 値）、横軸：年令

図 1-b　Ratunapura 村

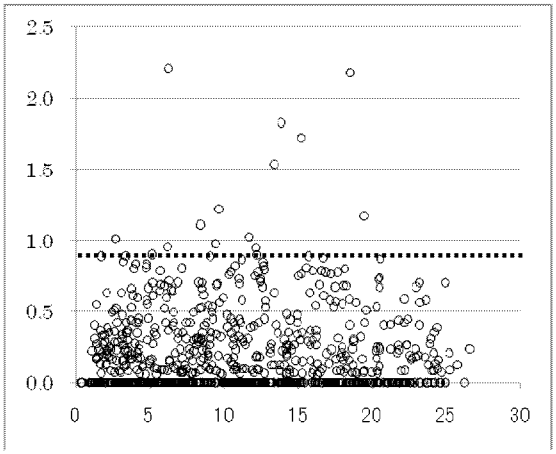

3. ビーズ法/尿 ELISA の検討

バングラデシュにおいて尿診断法の感度、特異度を検討した（表 2）。

表 2-a　　感度（％）

Gold Std.*	尿 ELISA	ビーズ法
N = 105	84.8	81.0

*ICT(+)サンプル

表 2-b　　特異度（％）

Gold Std.**	尿 ELISA	ビーズ法
N = 104	100	100

**ICT(-)サンプル

Post-MDA 期の小学校で 5-10 歳の学童 319 人を対象に尿 ELISA、ビーズ法、ICT test の結果を比較した。陽性率は、尿 ELISA 2.2%（7/319）、ビーズ法 1.6%（5/319）、ICT 0.3%（1/319）であった。

4. 媒介蚊のフィラリア感染を検出する LAMP 法の開発

様々な数のネッタイイエカ成虫プールにバンクロフト糸状虫ミクロフィラリア（mf）1 匹を加えてホモジェネートし、DNA 抽出後に PCR、LAMP を実施した。

両方法で 1 mf/40 mosquitoes までの検出が可能となった。

D. 考察

尿 ELISA　vs.　ICT

ICT test は感度、特異度が高く 10 分間でフィラリア抗原を検出できることから診断の世界標準とみなされることがあるが、almighty ではない（例えば+/-のみの定性検査である）。我々は、post-MDA 期にはむしろ抗体検出が有利と考えている。今回の比較実験で、尿 ELISA は ICT よりはるかに多くの感染者を検出することが確認された（再燃の発見に優れている）。

ELISA は技術的に煩雑であるが、定量的データを得られることから情報量が多く、フィラリア伝搬の解析に有利である。

非流行地での尿 ELISA の応用

“非流行地”の中に隠れた流行地が存在する可能性は少なくない。しかし、感

染がない地域の住民は採血を好まないことがある。今回そのような状況下での調査で、尿 ELISA が有用であることが示された。R 村では 10 歳未満の小児に抗体陽性者が発見されたが、限局的な伝搬が起きているのかもしれない。疑陽性の可能性も含めて今後検討する必要がある。

ビーズ法の野外応用

ビーズ法の感度、特異度が尿 ELISA と同様であったこと、学童の調査で ICT より高い陽性率が得られたことより、疫学調査に応用できることが示された。今後は、現地人スタッフによる目視判定を行うなど、より実際的な研究を行う必要がある。

E. 結論

(i) Post-MDA 期における尿 ELISA の有用性が ICT test との比較で確かめられた。
(ii) 尿 ELISA は非流行地でも住民に受け入れられるので、隠れた流行地の発見に利用できる。
(iii) ビーズ法が、十分に野外応用できることが示された。
(iv) フィラリア感染蚊を発見するための LAMP 法がほぼ完成した。

G. 研究発表

1. 論文発表

(1) The Global Programme to Eliminate Lymphatic Filariasis: History and achieve -ments with special reference to annual single-dose treatment with diethylcarbama -zine in Samoa and Fiji. Kimura E. Tropical Medicine and Health 39(1); 2011: 1-14

2. 学会発表

(1) Diagnosis of a mosquito-borne disease: Use of urine samples for detecting filarial infection in a monitoring program after successful mass drug administration. Kimura E, Itoh M, Weerasooriya MV, Yahathugoda TC, Samad MS, Takagi H, Nagaoka F, Moji K, Hossain M. The 2nd International Conference on Climate Change and Neglected Tropical Diseases. 29-30 Sep, 2010 (Dhaka, Bangladesh).

(2) Evaluation of two monitoring schemes after one year of community home-based care (CHBC) programme of morbidity control in lymphatic filariasis in three suburbs of Matara, Sri Lanka. Yahathugoda TC, Weerasooriya MV, Kimura E. The XIIth International Congress of Parasitology. 15-20 Aug, 2010 (Melbourne, Australia).

(3) Effects of repeated rounds of anti-filarial Mass Drug Administration (MDA) with diethylcarbamazine (DEC) plus albendazole on soil transmitted helminths (STHs) in Sri Lanka. Yahathugoda TC, Weerasooriya MV, Kimura E. The XIIth International Congress of Parasitology. 15-20 Aug, 2010 (Melbourne, Australia).

(4) A rapid assessment procedure (RAP) to assess distribution of lymphatic filariasis

using geographical information systems (GIS). Yahathugoda TC, Weerasooriya MV, Kimura E. The XIIth International Congress of Parasitology. 15-20 Aug, 2010 (Melbourne, Australia).

(5) Evaluation of urine-based IgG4 ELISA for detecting lymphatic filarial infection and the development of a visual diagnostic method with urine samples. Kimura E, Itoh M, Weerasooriya MV, Yahathugoda TC, Samad MS, Takagi H, Nagaoka F, Moji K, Hossain M. 45th Annual Japan-US Joint Conference on Parasitic Diseases. 10-11 Jan, 2011 (NIH, Tokyo).

(6) 年一回の集団治療が尿中のフィラリア特異的 IgG4 抗体に及ぼす影響：スリランカにおける 7 年間の追跡調査結果. 伊藤誠, Weerasooriya MV, Yahathugoda CT, 高木秀和, Samarawickrema WA, 木村英作. 第 66 回日本寄生虫学会西日本支部大会. 6-7 Nov, 2010（岡山大学）.

(7) バンクロフト糸状虫リコンビナント抗原 SXP1 の尿診断への応用と評価. 伊藤誠, 高木秀和, 長岡史晃, Weerasooriya MV, Wamae N, 木村英作. 第 66 回日本寄生虫学会西日本支部大会. 6-7 Nov, 2010（岡山大学）.

(8) Confirming the usefulness of ELISA to detect urinary IgG4 for the diagnosis of lymphatic filariasis in Bangladesh. Samad MS, Itoh M, Moji K, Hossain M, Mondal D, Alam MS, Kimura E. 第66回日本寄生虫学会西日本支部大会. 6-7 Nov, 2010（岡山大学）.

(9) バングラデシュにおける HDL ビーズを用いたリンパ系フィラリア症疫学調査. 長岡史晃, Samad MS, 伊藤誠, 高木秀和, 木村英作. 第66回日本寄生虫学会西日本支部大会. 6-7 Nov, 2010（岡山大学）.

H. 知的財産権の出願・登録状況

該当無し

厚生労働科学研究費補助金（国際医学協力研究事業）
分担研究報告書
フィラリア線虫と媒介節足動物の相互関係の解明
分担研究者　辻　尚利　動物衛生研究所主任研究員

病原体媒介性節足動物（ベクター）由来生物活性分子の機能探索の結果、マダニの唾液腺より、multiple coagulation factor deficiency 2 様分子ロンギスタチンを分離した。ロンギスタチン遺伝子の発現は宿主への付着時に増強されることから、マダニ吸血行動に関与すると考えられた。組換えロンギスタチンは、宿主の血液凝固を阻害することが示された。また、ロンギスタチン遺伝子の発現を抑制したマダニでは、吸血時に宿主皮下における blood pool の形成が阻害された。これらの知見より、ロンギスタチンはマダニ吸血行動に深く関与することが示唆された。

A．研究目的

本研究では、宿主体内への寄生（内部寄生虫）及び体表への寄生（外部寄生虫）に適応した巧妙な生残戦略を備えていると想定される線虫類と媒介節足動物が産生する遺伝子産物の機能解明を実施する。これによって、線虫及び媒介者の生存・侵入・存続に不可欠な分子機構を阻害することのできる新しい寄生虫感染及び伝搬防除技術を確立する。

B．研究方法

病原体媒介者であるマダニを用いて、マダニが産生する生物活性分子（TBM）の機能を生化学・細胞生物学的及び *in vivo* での内在機能を明らかにするため組換え TBM とマダニ−哺乳類宿主系を用いた解析を行った。

1) 国内最優占種であるフタトゲチマダニの TBM をコードする EST データベースよりロンギスタチン遺伝子を分離した。
2) 宿主ウサギに付着・吸血させたマダニを経時的に回収し、定量 PCR 法を用いて内在性ロンギスタチンの発現動態を検討した。
3) 分離した cDNA 配列のうち、成熟蛋白質をコードする領域をプラスミドベクター（pTrcHisB）に挿入し、大腸菌発現系にて組換えロンギスタチンを作製した。
4) 上記の組換え体を精製し、マウスに免疫して抗血清を作製した。
5) 吸血したマダニおよびマダニ吸血部位の宿主皮膚組織を固定・包埋して薄切し、免疫組織化学及び免疫蛍光抗体法を用いて、内在性ロンギスタチンのマダニ個体・宿主皮下での局在を、細胞生物学的に検討した。
6) ロンギスタチンの血液凝固阻害活性はウシ由来フィブリノゲン標品を用いて実施した。
7) ロンギスタチンのプラスミノゲンアクティベーター活性は、ヒト由来プラスミノゲン標品を用いて検討した。
8) ロンギスタチンをコードする cDNA より逆転写反応を用いて 2 本鎖 RNA を合成し、マダニ個体へ注入することによって、ロンギスタチン遺伝子の発現が抑制されたノックダウンマダニを作製した。

C．研究結果

1) フタトゲチマダニより 156 アミノ酸残基・分子量 17.7kDa からなるロンギスタチンをコードする cDNA を分離した。
2) 大腸菌で作製した組換えロンギスタチンを用いてが確認された。
3) 定量 PCR による解析の結果、ロンギスタチン遺伝子は、共に吸血開始後より発現が増強されており、吸血開始 96 時間後から吸血完了（飽血）時において最も高い発現レベルを示した。
4) 免疫蛍光抗体法を用いて検討したところ、ロンギスタチンの陽性反応は唾液腺腺房内に確認され、さらに、マダニ吸着時に宿主皮下に形成される血液貯蔵部位（blood pool）内にも免疫陽性反応が確認された。
5) 組換えロンギスタチンは、フィブリノゲン α・β・γ 鎖を分解することによって、フィブリン塊の形成を阻害することが確認された。
6) ロンギスタチンノックダウンマダニを付着させた宿主においては、皮下の blood pool の形成が阻害されるとともに、ノックダウン

マダニ自体の飽血時体重が有意に減少していることが確認された。

D．考察

ロンギスタチンは吸血時の宿主血液凝固の阻害に関与していることが示唆された。また、ロンギスタチンは宿主の吸血部位の皮下に分泌されており、効率的な吸血の持続に不可欠な blood pool の形成にも不可欠な役割を持っていることが考えられた。このような抗血液凝固因子は他の媒介節足動物や住血性寄生線虫類も保持していることが想定され、媒介昆虫を含めベクター制御に貢献できると同時にベクター由来の新規抗寄生虫薬の標的としても有効であると考えられた。

E．結論

本知見はマダニをはじめとした外部寄生性節足動物の生存戦略の根幹である、付着および吸血に関与する分子を標的とした新規寄生虫防圧法の開発に有効な知見であると考えられた。また、ロンギスタチンは住血寄生線虫や他の媒介性節足動物の寄生戦略にも関与することが考えられ、これら分子を標的とする新規の抗寄生線虫薬、抗マダニ薬及び外部寄生虫薬の開発が期待される。

G．研究発表

1. 論文発表

Anisuzzaman, Islam MK, Miyoshi T, Alim MA, Hatta T, Yamaji K, Matsumoto Y, Fujisaki K, Tsuji N.(2010). Longistatin, a novel EF-hand protein from the ixodid tick *Haemaphysalis longicornis*, is required for acquisition of host blood-meals. Int J Parasitol. 40, 721-9.

2. 学会発表

Anisuzzaman、Islam Khyrul、三好猛晴、Alim Adul、八田岳士、山地佳代子、松本安喜、藤崎幸蔵、辻尚利 Longistatin plays vital roles in blood pool formation and successful feeding by ixodid tick, *Haemaphysalis longicornis* 第79回日本寄生虫学会学術集会 P.65

Anisuzzaman, Islam MK, Miyoshi T, AlimMA, Hatta T, Yamaji K, Matsumoto Y, Fujisaki K, Tsuji N. Longistatin, a potent salivary-gland plasminogen activator from ixodid tick, is critical for blood pool development and successful blood-feeding by the ticks. The XII International Congress of Parasitology. abs#121 in CD.

H．知的財産権の出願・登録状況（予定を含む）

1. 特許取得
2. 実用新案登録
3. その他

以上なし

厚生労働科学研究費補助金（国際医学協力研究事業）

分担課題：日本住血吸虫症の病態発現分子解析

分担研究者　太田伸生
（東京医科歯科大学大学院医歯学総合研究科国際環境寄生虫病学分野）
研究協力者　熊谷 貴、関 丈典　（同上）

研究要旨

住血吸虫症の病態発現に IL-4/IL-13 の Th2 サイトカインが関与する事実がマンソン住血吸虫(Sm)の感染実験系で証明されてきたが、感染プロフィールが異る日本住血吸虫(Sj)感染においても同様の現象が起こるのか、検証がなされていなかった。Sj を感染させた IL-4$^{-/-}$IL-13$^{-/-}$マウス(DKO)の肝臓では対照マウス(WT)と比較して、好酸球浸潤は低下したが好中球浸潤が増加し、肉芽腫性炎症所見はむしろ悪化した。さらに、DKO マウスの肝臓では IL-5 の mRNA 発現が低下し、好中球浸潤や炎症性疾患に関わる Th17 関連サイトカインの mRNA 発現が上昇していた。しかし、DKO マウスでも IFN-γ の mRNA 発現上昇はなかった。以上の結果より Sj 感染病態発現には IL-4/IL-13 が Th17 関連サイトカインの産生を抑制する事によって、虫卵性肉芽腫性炎症の過度の進行や過剰な好中球の浸潤を抑制していると考えられ、Sm 感染とは異なる免疫学的機序が機能していることがわかった。

A. 研究目的

住血吸虫に対するほ乳類宿主の免疫反応の発現と調節機構の本態はなお不明であるが、マウスの実験的感染データからはマンソン住血吸虫(Sm)感染時の応答と日本住血吸虫感染時のそれとは大きな違いも存在することが示されるようになった。住血吸虫が宿主体内に産下する虫卵は毛細血管で塞栓し、宿主免疫システムは肉芽腫性炎症を引き起こす。これが Th2 系細胞による応答であることがマンソン住血吸虫感染実験で明らかにされた「一般常識」となりつつある。しかし、日本住血吸虫(Sj)感染においても同様であるのか、詳細な追跡実験で証明されたとは言えない状況である。

IL-4/13 ダブルノックアウト(DKO)マウスでは Th2 応答がほぼ完全に抑制されてしまうので、Th2 応答が肉芽腫形成を促進することが証明されているマンソン住血吸虫感染でも DKO マウスは虫卵肉芽腫形成が明らかに縮小されてくることが示されている。

Sj 虫卵や Sm 虫卵は共に肝臓に蓄積し、虫卵性肉芽腫の形成を誘導する。しかし、Sj と Sm 虫卵性肉芽腫の間には構成細胞に違いがあり、Sm では好酸球優位の、Sj では好酸球だけでなく多数の好中球も浸潤

した肉芽腫を形成する。また、Sj と Sm 虫卵は IL-4 や IL-13 など宿主 Th2 サイトカインの産生を強く誘導する。宿主応答の共通性の一方で、Sj と Sm 虫卵性肉芽腫では構成する細胞などに違いがあることは、Sj 虫卵性肉芽腫形成における Th2 応答が果たす役割は Sm とは異なる可能性を示唆する。本実験は Sj 虫卵性肉芽腫形成における IL-4/IL-13 の機能を明らかにする事を目的として行った。

B. 研究方法

1. IL-4/13 DKO マウス：英国 A. McKenzie らが創出した BALB/c バックグラウンドの IL-4/13 ダブルノックアウトマウスを入手して実験に用いた。

2. 住血吸虫感染：山梨株の日本住血吸虫 30 隻を DKO マウスおよび野生型(WT)BALB/c マウスに感染させ、６週後に安楽死処理の上、肝臓と血清を回収した。肝臓は虫卵肉芽腫を観察するために病理標本として HE 染色をおこなった。肝機能障害を評価するのに ALT を測定した。

3. フローサイトメトリー解析：感染宿主肝臓の構成細胞をフローサイトメトリーにて解析した。

4. サイトカインアッセイ：肝細胞を回収して局所のサイトカインをリアルタイム PCR で測定した。IL-4, IL-5, IL-6, IL-13, IL-17, IFNγ, IL-22, TNFα, CXCL2 等を測定した。

倫理面への配慮：本研究は東京医科歯科大学の動物実験委員会による承認を得て実施した。

C. 研究結果

1. DKO マウスにおける日本住血吸虫感染に対する病理の変化

肝臓に形成された肉芽腫サイズは、WT マウスと比較して DKO 群で増加した(図 1A)。この結果は、Sm 感染とは逆の現象であった。さらに、肝臓の好中球と好酸球浸潤を調べると、DKO マウスでは好酸球浸潤が抑制されていた一方で、好中球が多数浸潤していた(図 1B, C)。また、血清中の ALT 活性は DKO マウスで有意に増加した(図 1D)。以上の結果より DKO マウスでは好中球主体の肉芽腫が形成され、さらに肉芽腫性炎症が悪化して肝機能障害が進んだ事がわかった。

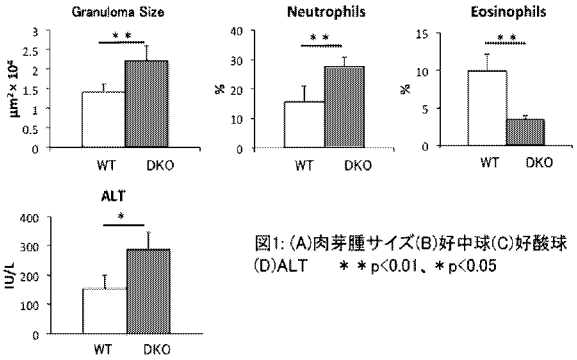

図1: (A)肉芽腫サイズ(B)好中球(C)好酸球 (D)ALT ＊＊p<0.01、＊p<0.05

2．DKO マウスにおけるサイトカイン産生プロフィール

感染６週における肝細胞を用いてサイトカイン産生を調べた所、WT マウスでは、IL-4、IL-5、IL-13 等 Th2 サイトカインの mRNA 発現が上昇していたが、DKO 宿主では IL-4 や IL-13 の mRNA 発現は検出されず、また IL-5 の mRNA 発現上昇もなかった(図 2A, B, C)。また、Th1 サイトカインである IFNγ の mRNA 発現では WT と DKO マウス間で有意差はなかった(図 2D)。

好中球浸潤や炎症性サイトカインの産生を誘導するTh17に注目すると、Th17刺激で産生されるIL-17AやIL-22のmRNA発現が、DKOではWTと比べて上昇していた(図3A,B)。また、Th17の分化を誘導するIL-6のmRAN発現も上昇していた(図3C)。さらにTh17により産生が誘導される、好中球の遊走に関与するCXCL2のmRNA発現もDKOマウスではWTマウスと比較して上昇していた(図3D)。

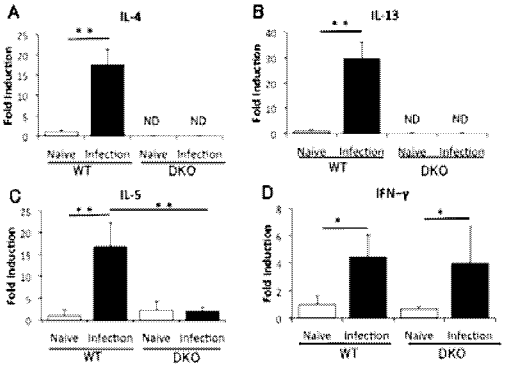

図2: 肝臓におけるTh2、Th1サイトカインmRNA発現(A)IL-4、(B)IL-5、(C)IL-13、(D) IFN-γ　＊＊p<0.01、＊p<0.05

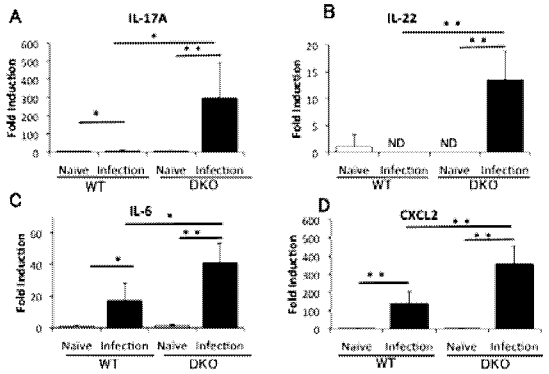

図3: 肝臓におけるTh17関連サイトカインmRNA発現
(A)IL-17A(B)IL-22(C)IL-6(D)CXCL2　＊＊p<0.01、＊p<0.05

D. 考察と結論

日本住血吸虫とマンソン住血吸虫はともにintestinal schistosomiasisとされるものであり、主病変も肝臓に見られる点で免疫病因論にも共通性があるものとの推測がなされる。それが正しいのか否かについては、これまで十分な検証はなされてこなかった。

本実験の結果より、IL-4/IL-13はSj虫卵周囲への過剰な好中球浸潤と、肉芽腫性炎症を抑制している事が示唆された。さらに肉芽腫のサイズはSm感染DKOマウスと異なり、Sj感染DKOマウスでは増加したが、これはSj虫卵性肉芽腫ではSm虫卵性肉芽腫よりも多数の好中球が浸潤している事が影響していると考えられる。これら結果より、IL-4/IL-13が肉芽腫形成において果たす役割はSjとSm虫卵性肉芽腫では異なる事がわかった。

好酸球増多はIL-4/IL-13が好酸球の分化・増殖に関与すIL-5の産生を誘導することにより誘導される事が示唆された。また、Th1/Th2バランスを考慮してIFN-γのmRNA発現を調べたが、WTとDKOマウスで差がなかったことより、IFN-γはDKOマウスでの好中球浸潤や肉芽腫性炎症の悪化には関与していないと考えられる。一方でTh17から産生されるIL-17AやIL-22のmRNA発現が増加していた。またTh17の分化に関与するIL-6やTh17により産生が誘導される好中球遊走に関与するCXCL2のmRNA発現も上昇していた。したがって、Sj感染マウスの肝臓ではIL-4/IL-13はTh17関連サイトカインを抑制して過剰な好中球浸潤や肉芽腫性炎症を抑制している可能性が示唆された。

今回の観察結果をもとに、日本住血吸虫感染時の病態発現に影響する因子の特定と解明が進み、将来の治療的応用にむけて研究が進むことが期待される。

E. 健康危険情報

該当せず

G. 研究発表

論文発表

なし

学会発表

関　丈典、熊谷　貴、Anyan WK、Kwansa-Bentum Bethel、宮沢悠樹、下河原理江子、太田伸生. 日本住血吸虫感染マウスにおける IL-4/IL-13 による炎症性サイトカインの産生抑制、第 79 回日本寄生虫学会総会、2010 年 5 月、旭川市

・関　丈典、熊谷　貴、Anyan WK、Kwansa-Bentum Bethel、宮沢悠樹、下河原理江子、太田伸生. 日本住血吸虫感染マウスにおける IL-4/IL-13 を介した炎症性サイトカインの産生抑制、第 21 回日本生体防御学会学術総会、2010 年 7 月、仙台市

・T. Seki, Kumagai T, Kwansa-Bentum B, Anyan WK, Shimogawara R, Ohta N: The role of IL-4/IL-13 in *Schistosoma japonicum* infected mice, 59th Annual Meeting of American Society of Tropical Medicine and Hygiene, 2010 年 11 月, Atlanta, USA.

・

H. 知的財産権の出願・登録状況

該当なし

厚生労働科学研究費補助金(国際医学協力研究事業)
2010(平成22)年度 (分担)研究報告書

寄生蠕虫の寄生適応および免疫修飾機構の研究

分担研究者 金澤 保(産業医科大学・免疫学寄生虫学)

研究要旨
我々は以前より、寄生蠕虫が Th17 型自己免疫疾患モデルに対し抑制作用を持つ場合があることを、住血吸虫を感染させたマウスにおける関節炎の実験系で証明してきた。今年度は誘発型1型糖尿病モデルに対する蠕虫感染の影響について検討した。マウスの腸管寄生蠕虫である *Heligmosomoides polygyrus* (Hp) をあらかじめ感染させたマウスでは、ストレプトゾトシンを多回低用量投与して誘発する1型糖尿病における血糖値上昇が、対照群に比べ抑制された。Hp 感染により脾細胞IL－4 産生能の上昇および IFNγ産生能の低下が観察されたが、Hp による血糖値上昇抑制効果は STAT6KO マウスにおいても観察されたため、本線虫のもつ抗糖尿病作用は、感染マウスにおけるTh2 への偏位に依存しないことが示唆された。

[研究協力者]
長田 良雄

A. 研究目的

微生物や寄生虫の感染によってアレルギーや自己免疫などの免疫異常疾患が予防あるいは改善するという現象が、疫学的証拠あるいは実験的証拠により示唆されている(衛生仮説)。住血吸虫を含む蠕虫の感染に関しても、種々のアレルギーおよび自己免疫疾患の発症を抑制するという実験的報告がある。我々は、寄生虫の抗炎症効果のメカニズムを解明し、炎症・アレルギー性疾患の治療法開発に貢献することを目的として研究を行っている。昨年度までに、住血吸虫感染が実験的関節炎および Th17 応答の抑制作用をもつことを報告してきた。本年度我々は、I 型糖尿病(T1D)モデルを利用し、その発症に対する蠕虫感染の影響を検討することにした。今回、住血吸虫と同様に慢性感染を起こす蠕虫として腸管寄生線虫である *Heligmosomoides polygyrus* を選択した。本虫の抗糖尿病作用は既にNODマウス(T1D 自然発症モデル)における報告があるが、NODマウスの系では種々の遺伝子欠損マウスとの比較実験が不可能なため、サイトカインの関与などについての詳細な解析が困難である。そこで我々は C57BL/6 マウスに対してストレプトゾトシン(STZ)を投与することで T1D を誘発するモデルを用いて Hp 感染実験を行うこととした。STZによる T1D の誘発には2つの方法がある。一つは単回高用量投与モデル、もう一つは多回低用量投与モデルである。後者におけるβ細胞破壊には免疫学的機序の関与が示唆されているため、ヒトにおける自己免疫性の T1D により近いモデルと考えられる。

B. 研究方法

実験系として、免疫学的機序の関与があると思われる多回低用量投与モデルを採用した。まず STZ 投与開始1週前に Hp200 隻を経口感染させた。STZ は 50mg/kg で連続 5 日間腹腔内投与し、1 週毎に血糖値を測定した。実験終了時に脾細胞を刺激培養し、サイトカイン産生を ELISA で測定した。また、膵臓はホルマリン固定後HE染色し、病理像の解析(ランゲルハンス島の面積の評価)を行った。さらに、Hp 感染の影響を野生型(WT)マウスと STAT6KO マウスや IFNγKO マウスの間で比較する実験を行い、サイトカインの関与を検証した。また、Hp 感染がマウスの糖吸収や代謝に影響を与えている可能性について検証するため、糖尿病を誘発していない感染マウ

スにおいて経口的にグルコース負荷試験を行い、非感染マウスの血糖値の動態と比較した。

[倫理面への配慮]

実験動物処置の際は必ず麻酔を使用した。産業医科大学動物実験及び飼育倫理審査において承認を受けている(承認番号:AE08-005、AE06-003)。なお本研究では人体材料は用いていない。

C. 研究結果

Hp感染はSTZ投与による血糖値上昇を抑制した。また、膵ランゲルハンス島の面積減少に対して若干の抑制傾向を示した。Hp感染により脾細胞のIFNγ産生能は低下し、IL-4やIL-10産生能は上昇した。非感染STAT6KOマウスやIFNγKOマウスではWTマウスと同様に血糖値が上昇したが、いずれのKOマウスにおいてもHp感染はWTと同様に血糖値上昇抑制効果を示した。また、経口グルコース負荷後の血糖値の動態は感染マウスと非感染マウスにおいて差は認められなかった。

D. 考察

IFNγKOマウスにおいても発症がみられたことから、本糖尿病モデルはTh1依存性モデルではないことが判明した。Hp感染はTh2応答の増強とTh1応答の抑制をもたらしたが、STAT6KOおよびIFNγKOマウスにおいてもHpによる血糖値上昇抑制が見られたことにより、Th2偏位自体は本虫の血糖値上昇抑制効果に必須ではないと考えられた。また、Hp感染は経口グルコース負荷後の血糖値の動態には影響を与えなかったことにより、血糖値の上昇抑制は、寄生虫の腸管寄生による「グルコース吸収阻害」や虫体による「グルコースの大量消費」による影響ではないことが示唆された。

E. 結論

マウスにおけるストレプトゾトシン誘発1型糖尿病の血糖値上昇に対して、HpはTh2偏位に依存しない機構により抑制効果を示した。

F. 健康危険情報

なし

G. 研究発表

1. 論文発表

[総説]

長田良雄.
寄生虫とアレルギーの親密な関係
Medical Practice. 27 (9): 1541-1542.

[原著]

Shimizu S, Osada Y, Kanazawa T, Tanaka Y, Arai M.
Suppressive effect of azithromycin on *Plasmodium berghei* mosquito stage development and apicoplast replication.
Malar J. 9:73. 2010.

2. 学会発表

長田良雄、金澤保.
住血吸虫によるThサイトカイン修飾に関与する因子の解析
第79回 日本寄生虫学会大会
旭川(2010年3月)

長田良雄、清水少一、熊谷貴、山田壮亮、金澤保.
住血吸虫による関節炎抑制には、炎症性サイトカインの産生抑制が伴う
第75回日本インターフェロン・サイトカイン学会
北九州(2010年6月)

Osada Y, Shimizu S, Kumagai T, Yamada S, Kanazawa T.
Schistosoma mansoni has anti-arthritic effects accompanied with IL-17's down-modulation dependent on viable eggs.
XIIth International Congress of Parasitology
メルボルン (2010年8月)

Osada Y.
Experimental *Schistosoma mansoni* infection suppresses autoimmune arthritis in mice.
EPS Global-Shanghai 1st International Biomedicine Forum.
上海 (2010年9月)

長田良雄、黒田悦史、金澤 保.
コラーゲン関節炎に対する蠕虫感染の影響
－ *Heligmosomoides polygurys* の場合 －
第 63 回 日本寄生虫学会南日本支部大会・第 60 回日本衛生動物学会南日本支部大会・合同大会
鹿児島(2010 年 11 月)

H. 知的財産権の出願・登録状況
該当なし

厚生労働科学研究費補助金（国際医学協力研究事業）

分担研究報告書

－寄生虫疾患の病態解明及びその予防・治療をめざした研究－

リーシュマニア症対策疫学研究

分担研究者　氏名　筑波大学大学院人間総合科学研究科　教授　我妻ゆき子

研究要旨

目的：本研究では、ニームオイルを家屋内散布することによって、リーシュマニア症コントロールが可能であるかを効果判定することを目的とした。

研究方法：バングラデシュにおいてリーシュマニア症が蔓延している地域において、その標準化家屋内散布介入をする世帯とコントロール世帯をランダム割り当てし、各世帯から１人のインデックスケースに対して、患者発生が減少したかをモニタリングして評価した。

結果とまとめ：散布家屋内において、サシチョウバエの総数は変化しなったが、吸血しているサシチョウバエの割合の減少がみられた。介入世帯とコントロール世帯において、抗体陽性化率では統計学的に有意な差はなかった。

ニームオイルの有効成分については近年、有機栽培使用に奨励されたこともあり、殺虫効果についてのエビデンスが蓄積されてきている。本研究で、サシチョウバエの総数はあまり変動せず、吸血している数が減少したことは、低濃度での散布の特性を示しているのかもしれない。さらに有効成分純度の高いニームオイルを使用することにより、予防効果を向上することができると考える。農薬問題のない天然植物素材のニームオイルが、リーシュマニア症制圧に役立つことが示せれば、世界のリーシュマニア症患者を減らすことができるばかりでなく、他の媒介昆虫による重要疾患、たとえば、マラリアやデング熱への応用が示唆される。

Ａ．研究目的

本研究の分担研究者である我妻は、ニームオイルの散布がサシチュウバエの減少に効果があることを予備実験で確かめ、その成果を日本熱帯医学会や国際リーシュマニア症シンポジウム会議にて発表してきた。リーシュマニア症は世界保健機構（WHO）の薦める重要感染症疾患に入っているにもかかわらず、人体投与薬物治療薬は非常に副作用の高い重金属アンチモニ製剤の注射薬で20日から60日の連続投与が必要である。小児や妊婦での使用が難しく、治療成績もばらばらで、治療後致死率はバングラデシュでは10%以上もあることを報告した(Bern et al, 2005)。本研究では、農薬問題のない天然植物素材であるニームオイルを家屋内散布することによって、リーシュマニア症コントロールが可能であるかを効果判定することを目的とした。

Ｂ．研究方法

ニームオイル中の有効成分であるアザルデイクチンの含有度を正確に測り、その濃度と散布回数の標準化を図り、バングラデシュのリーシュマニア症蔓延フィールドにおいて、その標準化家屋内散布介入をする家とそうでない家とをランダムに割り当て(各群約750世帯)、2年間の観察評価をして、媒介昆虫が家屋内で減少したか、また、さらには、患者発生が減少したかを評価した。2年間の介入後、最終評価のための血液検査とCDC ライトトラップによるサシチョウバエの収集を行った。並行して、ニームオイルの人々への受け入れと使用に関して、社会調査(formative study)を実施した。

（倫理面への配慮）

国際下痢症研究センター（ICDDR,B）の倫理委員会に研究プロトコールを提出し、承認を受けた。研究参加者にはインフォームド・コンセントを行い、同意書を得た。

Ｃ．研究結果

コミュニテイサーベイランス人口(1700世帯；人口8,500人)のうち、3歳以上を対象にニーム介入1年後の疾病発生血液検査(セロサーベイ）を実施し、データ解析を行った。介入１年後、2年後の評価で、罹患率に有意な差を認めな

かった。しかし、介入群において吸血しているサシチョウバエの減少に有意な差がみられた(Wagatsuma Y, 2009)。また、ニームオイルの人々への受け入れ度に関しては、比較的高く、現行の価格であっても、51%の住民が購入使用を希望していた（Fukushige M, 2009）。

D．考察

サシチョウバエの総数はあまり変動せず、吸血している数が減少したことは、この濃度散布におけるニームオイルの効果の特性を示しているかもしれない。散布濃度が低すぎた可能性があり、さらに有効成分純度の高いニームオイルを使用することにより、予防効果を向上することができるかもしれない。

環境残留有害物質の検出技術が向上するにつれ、農薬問題はその加速度を増して難しくなっている。地球環境を考慮し、将来にわたって持続性ある安全な衛生動物制御が求められている。農薬問題のない天然素材のニームオイルが、もしリーシュマニア症制圧に役立つことが示せれば、世界中のリーシュマニア症患者を減らすことができるばかりでなく、他の媒介昆虫による重要疾患、たとえば、マラリアやデング熱へも天然素材の応用が可能である道が開けるかもしれない。

E．結論

ニーム介入群において、吸血しているサシチョウバエの割合の低下がみられた。罹患率まで影響を与えるためには、さらに有効成分純度の高いものを使用して、介入試験を実施する必要がある。また、リペラント、防虫シーツやカーテンなど予防ツールの多様化を図ってゆくことにより、人々の受け入れ効果を見る必要があろう。

F．健康危険情報

該当せず。

G．研究発表

1．論文発表

Khan MGM, Alam MS, Podder MP, Itoh M, Jamil KM, Haque R, Wagatsuma Y. Evaluation of rK-39 strip test using urine for diagnosis of visceral leishmaniasis in an endemic area in Bangladesh. *Parasites and Vectors* 2010; 3:114.

2．学会発表

Ferdousi F, Alam MS, Ma E, Ito M, Haque R, Wagatsuma Y. Community-based intervention study using neem extract to control visceral leishmaniasis in Bangladesh. The 45th U.S.-Japan Joint Conference on Parasitic Diseases U.S.-Japan Cooperative Medical Science Program, Tokyo, Japan, January 10, 2011.

H．知的財産権の出願・登録状況（予定も含む）

該当せず。

厚生労働科学研究費補助金(国際医学協力研究事業)

分担研究報告書

マラリア原虫の宿主細胞認識と侵入機序の解析

分担研究者　鳥居本美　愛媛大学大学院医学系研究科教授

研究要旨：　マラリア原虫メロゾイトの赤血球結合分子 EBL (EBL : Erythrocyte Binding-Like) は赤血球侵入に必須とされる分子である。ネズミマラリア原虫（*Plasmodium yoelii*）の弱毒株である Py 17X NL (non-lethal) の EBL 分子内のアミノ酸置換をおこなって EBL 分子の局在の変化および病原性の変化について検討した。Py17XNL 株原虫 EBL の領域６に存在する８個のシステインのうち１、３、４、５、７、８番目のものを、それぞれアラニンに置換した遺伝子組換え原虫を作成して、EBL の局在を間接蛍光抗体法で観察したところ、１番目、４番目、５番目、７番目の Cys 組換え原虫においては EBL の局在が Py17XNL のマイクロネームから強毒株の Py17XL に見られるデンスグラニュール局在パターンへと変化した。３番目、８番目の Cys 組換え原虫では EBL の局在の変化が見られなかった。また、領域６の Cys 以外の表面アミノ酸の中でも置換によって PyEBL の局在が変化させるアミノ酸部位が見出された。以上の結果から、第６領域が PyEBL 分子の細胞内輸送に重要であること、また、第６領域の中に PyEBL の局在を決定するサブドメインが存在する事が示唆された。

A．研究目的

マラリア原虫メロゾイトの赤血球結合分子（EBL : Erythrocyte Binding-Like）はメロゾイトの赤血球侵入に重要な機能を果たすことから、赤血球ステージ原虫に対するワクチン候補抗原として注目されている。我々は EBL 分子を標的とするワクチン開発のモデルとして、ネズミマラリア原虫 *Plasmodium yoelii* の EBL (PyEBL) の解析を行っている。感染後の急激な原虫感染率の上昇により致死的となる強毒株（17XL）と致死的でない弱毒株（17XNL）の PyEBL 分子の塩基配列を解析し、その結果から予想されるアミノ酸配列を比較したところ、オープンリーディングフレーム内での相違は、C 末端部のシステイン（Cys）に富む領域（第６領域）内の Cys の一つが、17XL 株では Arg に置換されていることのみであった。この Cys の変異に着目し、Py17XL 株と Py17XNL 株におけるアミノ酸置換と分子の局在の差異および病原性の差違との関連性を検討した。免疫電子顕微鏡法を用いて PyEBL の詳細な局在をみると、17XNL 株では PyEBL は原虫先端部のマイクロネームに局在するのに対し、17XL 株では先端部より後方に位置するデンスグラニュールに局在することが判明した。そこで、PyEBL の第６領域のアミノ酸を置換した遺伝子改変原虫を作成して検討した結果、第６領域が PyEBL 分子の細胞内輸送に重要であること、第６領域のアミノ酸変異がマラリア原虫の赤血球侵入動態に影響し、さらには病原性の変化をもたらすことを明らかにすることが

できた。本年度は、Py17XL と Py17XNL 株における EBL 分子の局在の差が領域６の他のアミノ酸を置換しても起こりうるか否かについて、領域６内のシステインと分子表面に位置することが予想され種間で保存されているアミノ酸に着目して検討を行った。

Ｂ．研究方法および結果

遺伝子改変によって 17XNL 株の PyEBL の 726 番目のアミノ酸（第６領域の２番目の Cys）を Arg に置換した原虫 17XNL (Cys-Arg) を作成して、間接蛍光抗体法によって観察したところ、原虫における EBL の局在が Py17XNL 株特有のマイクロネーム局在パターンから Py17XL 株特有のデンスグラニュール局在パターンに変化した。そこで、17XNL 株の PyEBL の同じ 726 番目のアミノ酸（を Ara に置換した原虫を作製して観察すると、Arg 置換と同様のデンスグラニュール局在パターンへの変化が認められた。PyEBL の 726 番目のアミノ酸をそれぞれ Cys から Arg と Ara に置換した原虫の間で特に EBL の局在に差が見出されなかったので、以下の研究では領域６内のシステインをそれぞれ Ara へ置換して、アミノ酸置換による局在に及ぼす影響を検討した。また、アミノ酸を置換せず PyEBL の C 末端に緑色蛍光タンパク質（GFP）を付加するコンストラクトを作成して、組換え原虫における EBL の局在を観察したところ、GFP による蛍光の局在はマイクロネーム局在パターンを示した。これによって GFP 付加が EBL の局在に影響しないことを確認した。そこで、PyEBL の C 末端に GFP を付加する組換え用コンストラクトに、Stratagene 社の QuikChange® Site-Directed Mutagenesis Kits を用いて目的の部位の Cys を置換するための変異を挿入した。このコンストラクトを Xho I で切断して直鎖化し、Amaxa 社の Nucleofector II で P. yoelii 17XNL 株にトランスフェクションした。ピリメサミンで組換え原虫を選択し、GFP の蛍光と、抗 EBL 抗体による間接蛍光抗体法で EBL の局在を確認した。

Withers-Martinezらは熱帯熱マラリア原虫のEBLのひとつPfEBA-175の構造解析によって、領域６で保存されている８個のシステインの１番目と５番目、２番目と４番目、３番目と８番目、６番目と７番目がＳ-Ｓ結合によって架橋されることを予測している。そこで、Py17XNL株原虫EBLの領域６内の全Cysを、それぞれAraに置換した組換え原虫を作成した。観察の間に合わなかった6番目のCys置換原虫を除く全ての組換え原虫で、間接蛍光抗体法でEBLの細胞内局在を観察した。３番目と８番目のCysを置換した原虫を除く全ての組換え原虫において、EBLの局在は本来のマイクロネーム局在からデンスグラニュール局在パターンへと変化した。３番目と８番目を組換えた原虫は、ワイルドタイプと同じマイクロネーム局在パターンを示し、局在は変化しなかった。以上の結果から、Ｓ-Ｓ結合によって形成される領域６の立体構造がPyEBLの細胞内輸送に重要であるが、領域６内部にはより重要なサブドメインが存在する事が示唆された。また、変化が生じなかったCysの組み合わせ(３番目と８番目)は、

Withers-Martinezらが熱帯熱マラリア原虫のEBL (PfEBA175) において予測したS-S結合のCysの組合わせと一致していた。

次いで、PyEBLの細胞内輸送に重要なサブドメインを特定するため、種間で保存された領域6のCys以外のアミノ酸を同様にAraに置換した原虫を作製した。Withers-Martinezらにより提唱された領域6表面の KIX 類似ドメインに含まれるアミノ酸残基と、これに含まれないが保存されたアミノ酸複数を置換して同様に間接蛍光抗体法で観察した所、765番目のTyrを置換した原虫でのみPyEBLの局在がデンスグラニュール局在パターンに変化した。なお、隣接する766番目のTyrを置換した原虫では局在は変化しなかった。以上から領域6表面に PyEBL の細胞内輸送に重要なアミノ酸が存在する事、そのサブドメインは非常に限られたアミノ酸によって構成されている事が示唆された。

E. 結論

弱毒株の Py17XNL と致死株の Py17XL で PyEBL 分子のC末端部のCysに富む第6領域内の Cys の一つが、17XL 株では Arg に置換されていることに着目して検討を行った。Py17XNL株原虫EBLの領域6に存在する8個のシステインのうち、1番目のCys、4番目のCys、5番目のCys、7番目のCysを、それぞれ Ara に置換した組換え原虫を作成して間接蛍光抗体法で観察したところ、これら全ての組換え原虫において EBL の局在はマイクロネーム局在パターンからデンスグラニュール局在パターンへと変化した。しかし、3番目のCysと8番目のCysを置換した原虫ではマイクロネーム局在パターンから変化しない事を見出した。また、Cys以外の種間で保存されたアミノ酸の中に、置換するとマイクロネーム局在パターンからデンスグラニュール局在パターンへ変化するものがある事を見出した。以上の結果から、第6領域がPyEBL分子の細胞内輸送に重要であり、さらにその立体構造と、分子表面の特定の領域が細胞内輸送に関わっていることが明らかになった。

G. 研究発表

2. 学会発表

1) 大槻 均、入子英幸、石野智子、金子 修、福本宗嗣、坪井敬文、鳥居本美. ネズミマラリア原虫赤血球結合タンパク(EBL)の細胞内輸送ドメインの機能解析
第79回日本寄生虫学会大会、旭川市、5/20-21、2010.

H. 知的財産権の出願・登録状況

特記すべきものはない

厚生労働省科学研究費補助金　地球規模保健課題推進研究事業（国際医学協力研究事業）
分担報告書

寄生虫感染宿主内で誘導される好塩基球の感染制御能の証明

中西憲司 兵庫医科大学

研究要旨

蠕虫が感染すると、Th2 型の免疫応答が誘導されるとともに、好塩基球が著明に増加する。昨年度までに我々は好塩基球が抗原提示細胞として Th2 細胞を誘導できることを明らかにした。しかし、蠕虫感染に対して好塩基球がどのような役割を果たしているのかは不明である。そこで、本研究では好塩基球欠損マウスを用いて、蠕虫排除における好塩基球の働きを検討した。その結果、好塩基球がいないと、感染が著しく遷延することを明らかにした。

A. 研究目的

好塩基球は全顆粒白血球の１％弱を占める少数派細胞である。好中球あるいは好酸球と異なり、好塩基球は細菌あるいは寄生虫が感染しても末梢血中での細胞数が増加することはない。しかし、寄生虫が感染した動物では Th2 型免疫応答が誘導され、特に肝臓や脾臓において好塩基球の数が著明に増加する。好塩基球は、肥満細胞とともに、IgE 媒介性のアレルギー性炎症のエフェクター細胞として重要である。しかし、両者の特筆すべき違いは、肥満細胞が組織に固着するのに対し、好塩基球は末梢血中を巡回することである。本研究で、好塩基球の Th2 型免疫応答誘導能と蠕虫排除における役割を解明することを目的に研究した。

B. 研究方法

好塩基球欠損マウスの作製：
①正常マウスに抗 FcεRIα抗体(MAR-1)を投与し、好塩基球を除去する。あるいは、好塩基球特異的 Diphthelia toxin(DT) receptor 発現マウス(Bas-TRECK)に DT を投与し、好塩基球を除去する。
*Strongyloides venezuelensis(Sv)*排虫実験：
野生型マウス、または好塩基球欠損マウスに *Sv* の３型幼虫を経皮感染させたマウスから糞便を連日採取し、この中に現れる虫卵数を計測する。虫卵が検出されなくなった時点を排虫完了日とする。この実験によりマウスの *Sv* 排虫能における好塩基球の必要性を明らかにする。
Th2 型免疫応答誘導に対する好塩基球の影響：
１）*Sv* 感染７日目の野生型マウス、または好塩基球欠損マウスの腸間膜リンパ節細胞を採取し、抗 CD3/抗 CD28 抗体で刺激をして細胞内 IFNγ/IL-4 を染色して FACS で調べる。
２）*Sv* 感染前後の野生型マウス、または好塩基球欠損マウスの血清を経時的に採取し、血清中 IgE と粘膜型肥満細胞マーカーmMCP-1 の値を ELISA にて測定する。
１）、２）より蠕虫感染に伴う Th2 細胞誘導、IgE 産生、粘膜型肥満細胞誘導における好塩基球の役割を明らかにす

る。

(倫理面の配慮)

動物実験は、関係法令を遵守し、「兵庫医科大学動物委員会」、「兵庫医科大学遺伝子組換え委員会」の承認・許可された実験を行なっている。

C. 研究結果

MAR-1 処置マウス、Bas-TRECK マウスのいずれの好塩基球を欠損したマウスでも、*Sv* を感染させた場合、排虫時期が野生型マウスに比べて著しく遅延した。このときの腸間膜リンパ節 T 細胞からのサイトカイン産生、血清中 IgE 産生、粘膜型肥満細胞の誘導には好塩基球の有無で変化は認められなかった。

D. 考察

好塩基球欠損マウスでは感染が著しく遷延したことから、蠕虫感染防御における好塩基球の重要性が明らかとなった。しかし、そのメカニズムは蠕虫特異的 Th2 細胞の誘導よりも、むしろ腸管での効果相で作用していることが考えられる。そのメカニズムとして、IgE/FcεRIα を介した好塩基球の活性化が考えられ、今後、この関連を明らかにしていきたい。

E. 結論

今回の研究で、*Sv*感染時に好塩基球は、Th2/IgE誘導する抗原提示細胞としての役割よりも、寄生虫の排除機構に、大きく関与することが明らかになった。

F. 健康危険情報

該当せず。

研究発表

■著書■

安田好文, 中西憲司. 寄生虫に対する粘膜免疫. 清野宏 編. 臨床粘膜免疫学. 東京:シナジー, 2010:522-529

■学術論文■

[総説]

中西憲司. IL-18 とユニークなアレルギー. ファルマシア 2010;46:55-59.

中平雅清, 中西憲司. Super Th1 細胞/IL-18 による非 IgE 炎症と気管支喘息. 呼吸 2010;29:37-43.

松本真琴, 中西憲司. IL-18 と免疫疾患. Fronti Rheumatol Clin Immunol4 2010:37-43.

中西憲司. 好塩基球によるアレルギー性炎症の誘導と憎悪. アレルギー 2010;59:251

筒井ひろ子, 中西憲司. 自然型アレルギー. 侵襲と免疫 2010;19:85-86.

善本知広, 中西憲司. アレルギーと IL-18/IL-33. 実験医学 2010;28:1975-1981.

小坂久, 善本知宏, 中西憲司, 藤元治朗. 腹腔内術後癒着形成における IFN-γ の重要性. 炎症と免疫 2010;18:531-537.

中平雅清, 中西憲司. アレルギー憎悪機構. 臨床免疫・アレルギー科 2010;54:224-233.

安田好文, 中西憲司. IL-33 と好塩基球、

マスト細胞-免疫応答と疾患における役割-. 炎症と免疫 2010;18:585-591.

中平雅清, 中西憲司. Super Th1 細胞/IL-18 による非 IgE 炎症と気管支喘息. 呼吸 2010;29(2):115-121.

松本真琴, 中西憲司. IL-18と免疫疾患. Frontiers in Rheumatology & Clinical Immunology 2010;4(1):37-43.

中西憲司
好塩基球:新たな視点からみたアレルギー性炎症の誘導, 序. 炎症と免疫, 18(1) : 1-2, 2010.

[原著]

Kawa K, Tsutsui H, Uchiyama R, Kato J, Matsui K, Iwakura Y, Matsumoto T, Nakanishi K. IFN- γ is a master regulator of endotoxin shock syndrome in mice primed with heat-killed Propionibacterium acnes. Int Immunol 2010;22(3):157-66.

Nakanishi K, Tsutsui H, Yoshimoto T. Importance of IL-18-Induced Super Th1 Cells for the Development of Allergic Inflammation. Allergol Int 2010;59(2):137-141.

Kuroda-Morimoto M, Tanaka H, Hayashi N, Nakahira M, Imai Y, Imamura M, Yasuda K, Yumikura-Futatsugi S, Matsui K, Nakashima T, Sugimura K, Tsutsui H, Sano H, Nakanishi K. Contribution of IL-18 to eosinophilic airway inflammation induced by immunization and challenge with Staphylococcus aureus proteins. Int Immunol 2010;561-570.

Matsuba-Kitamura S, Yoshimoto T, Yasuda K, Futatsugi-Yumikura S, Taki Y, Muto T, Ikeda T, Mimura O, Nakanishi K. Contribution of IL-33 to induction and augmentation of experimental allergic conjunctivitis. Int Immunol 2010;22(6):479-489.

Nakanishi K. Basophils are potent antigen-presenting cells that selectively induce Th2 cells. Eur J Immunol. 2010 ;40(7):1836-42.

Yoshikawa S, Iijima H, Saito M, Tanaka H, Imanishi H, Yoshimoto N, Yoshimoto T, Futatsugi-Yumikura S, Nakanishi K, Tsujimura T, Nishigami T, Kudo A, Arii S, Nishiguchi S. Crucial role of impaired Kupffer cell phagocytosis on the decreased Sonazoid-enhanced echogenicity in a liver of a nonalchoholic steatohepatitis rat model. Hepatol Res 2010;40(8):823-831.

Tsutsui H, Imamura M, Fujimoto J, Nakanishi K. The TLR4/TRIF-Mediated Activation of NLRP3 Inflammasome Underlies Endotoxin-Induced Liver Injury in Mice. Gastroenterol Res Pract 2010:641865.

Satoh T, Takeuchi O, Vandenbon A, Yasuda K, Tanaka Y, Kumagai Y, Miyake T, Matsushita K, Okazaki T, Saitoh T, Honma K, Matsuyama T, Yui K, Tsujimura T, Standley DM,

Nakanishi K, Nakai K, Akira S. The Jmjd3-Irf4 axis regulates M2 macrophage polarization and host responses against helminth infection. Nat Immunol 2010;11: 936-944.

Nakanishi K. Basophils as APC in Th2 response in allergic inflammation and parasite infection. Curr Opin Immunol 2010.22(6):814-20.

■学会発表■

［国際学会］

Kenji Nakanishi. Innate and acquired immunity in expulsion of intestinal nematode. 14th International Congress of Immunology 2010.8 Kobe

Makoto Matsumoto, Koubun Yasuda, Masato Kubo, Tomohiro Yoshimoto, Kenji Nakanishi. Basophils play a pivotal role in the expulsion of gastrointestinal nematode *Strongyloides venezuelensis*. 14th International Congress of Immunology 2010.8 Kobe

Koubun Yasuda, Yuki Sasaki, Yuichi Kondo, Makoto Matsumoto, Tomohiro Yoshimoto, Kenji Nakanishi. IL-33 mediated expulsion of *Nippostrongylus brasiliensis* in the absence of adaptive immune system. 14th International Congress of Immunology 2010.8 Kobe

Nakahira M, Nakanishi K. Involvement of Gata3 in transcriptional regulation of *Il13* gene expression in IL-18-stimulated Th1 cells. 14th International Congress of Immunology 2010. 8 Kobe

Koubun Yasuda, Yuki Sasaki, Makoto Matsumoto, Yuuko Taki, Tomohiro Yoshimoto, Kenji Nakanishi. IL-33 mediated expulsion of *Nippostrongylus brasiliensis* and *Strongyloides venezuelensis*. The 10th Awaji International Forum on Infection and Immunity 2010. 9 Hyogo

［国内学会］

中西憲司. IL-1 ファミリーサイトカインと炎症. 第43回日本痛風・核酸代謝学会総会 2010.2 大阪

安田好文, 松葉沙織, 善本知広, 弓倉静英, 高城ゆう子, 武藤太一朗, 池田誠宏, 三村治, 中西憲司. Contribution of IL-33 to induction and augment tion of experimental allergic conjunctivis. 第75回日本インターフェロン・サイトカイン学会学術集会 2010.6 北九州

松本真琴、安田好文、久保允人、善本知広、中西憲司. *Strongyloides venezuelensis* の感染防御における好酸球と好塩基球の役割について. 第６６回日本寄生虫学会西日本支部大会 2010.11 岡山

厚生労働科学研究費補助金分担研究報告書

遺伝子導入ハマダラカを作成し空飛ぶ注射器としての実用性を探る

分担研究者　　松 岡 裕 之　自治医科大学・教授

研究要旨　遺伝子導入技術により人類に有用なワクチン蛋白を蚊につくらせ、吸血とともにワクチン蛋白を注入してくれる蚊のモデルをつくるため、蚊の唾液腺特有蛋白遺伝子のプロモーターに、マラリア抗原ペプチド遺伝子をつないでハマダラカ受精卵に注射、遺伝子導入蚊を作成した。唾液腺にはマラリア抗原ペプチドが発現し、唾液腺細胞から唾液腺腔に分泌された。またマラリア抗原ペプチドは蚊の口吻から放出された。その蚊をマウスに頻回に吸血させると、マウスはマラリア抗原ペプチドに対する抗体を産生した。

A.　研究目的

マラリアをはじめ各種疾病を媒介するために嫌悪されている蚊であるが、見方を変えると吸血相手に唾液を打ち込んで抗唾液抗体をつくらせる働きをしている。遺伝子導入技術により人類に有用なワクチン蛋白を蚊につくらせ、吸血とともにワクチン蛋白を注入してくれる有益な蚊がつくれないかと考えた。今回は外来性蛋白のモデルとしてマラリア抗原ペプチドを唾液腺に発現させることを試みた。

B.　研究方法

当ラボで新規に発見したハマダラカ唾液腺特有蛋白遺伝子のプロモーター領域に、マラリア抗原ペプチド遺伝子をつないでハマダラカ受精卵に注射し、遺伝子導入蚊を作成した。

C.　研究結果

唾液腺にマラリア抗原ペプチド産生する遺伝子導入蚊の作成に成功した。マラリア抗原ペプチドは唾液腺細胞から唾液腺腔に分泌されること、蚊の口吻からマラリア抗原ペプチドが放出されることを確認した。この蚊群を繰り返しマウスに吸血させたところ、マウスはマラリア抗原ペプチド抗体をわずかであるが産生した。

D.　考察

遺伝子導入蚊の唾液腺において、外来性蛋白であるマラリア抗原ペプチドを産生させることに成功した。今後はこの遺伝子導入蚊の刺咬により、マウスに効率よく抗体を産生させられる工夫が必要である。

E.　結論

遺伝子導入蚊の作成に成功した。マラリア抗原ペプチドが唾液腺に発現し、唾液腺腔へ分泌された。このペプチドは蚊の口吻から放出され、マウスに若干の抗体を誘導した。

G.　研究発表

1. 論文発表　Matsuoka H, Ikezawa T, Hirai M: Production of a transgenic mosquito expressing circumsporozoite protein, a malarial protein, in the salivary gland of *Anopheles stephensi*. Acta Medica Okayama 64(4): 233-241, 2010

2. 学会発表　**山本大介, 南雲浩志, 吉田栄人, 松岡裕之**:ワクチン抗原を唾液成分として発現・分泌するトランスジェニックハマダラカの作製 第 79 回日本寄生虫学会大会 2010 年 5 月 20-21 日(旭川市)(抄録集 p46)

H.　知的財産権の出願・登録状況

1. 特許取得　　なし
2. 実用新案登録　なし

厚生労働科学研究費補助金（国際医学協力研究事業）
分担　研究報告書

マラリアにおける宿主病原体相互関係の解析

分担研究者　久枝　一　群馬大学医学系研究科教授

研究要旨　マラリアに対する防御免疫を詳細に解析することは有効なワクチン開発に重要である。本報告では、マウスモデルを用いて CD8Ｔ細胞の赤血球ステージマラリアに対する防御的役割を詳細に検討した。赤血球には MHC 分子を発現しないことからその関与は否定的であった。しかしながら、CD8Ｔ細胞は IFN-γ依存的に抗マラリア原虫作用を発揮することが明らかになった。

Ａ．研究目的

マラリアが今なお問題となっている理由の一つに有効なワクチンがないことが挙げられる。ワクチンの開発には有効な免疫応答を詳細に解析することが必須である。肝臓ステージマラリアに対しては、感染肝細胞を破壊することで CD8Ｔ細胞は防御免疫に関与していることが知られている。その際には肝細胞表面にある MHC クラスⅠ分子に提示されたマラリア原虫の抗原を認識する。一方で、赤血球は MHC 分子を発現していないことから、CD8Ｔ細胞は赤血球ステージマラリアに対する防御には貢献しないとされてきた。実際に赤血球ステージマラリアに対するワクチンは抗体が認識する抗原を標的に開発されてきた。近年、脳マラリアの発症への関与等、CD8Ｔ細胞の赤血球ステージマラリアでの役割が示唆されてきた。本研究では、ネズミマラリアモデルを用いて CD8Ｔ細胞の防御的役割を詳細に検討した。

Ｂ．研究方法

近交系マウスにネズミマラリア原虫 *Plasmodium yoelii* 17XNL（PyNL），17XL（PyL）を腹腔内に接種して感染させた。感染後の経過を末梢血中の感染赤血球の割合である虫血症率と致死率で評価した。CD8Ｔ細胞は脾臓より MACS 法により精製し、Ｘ線を照射したマウスに移入した。

全ての動物実験は群馬大学倫理委員会の承認を得た後、ガイドラインに従って行われた。

Ｃ．研究結果

１．マラリア生ワクチンモデルの樹立

PyNL の感染を受けたマウスでは一過性に原虫血症が認められた後、最終的に原虫は排除される。一方、PyL を感染したマウスでは急激な原虫の増殖が見られ、全てが１０日前後で死に至る。弱毒株の感染を治癒したマウスは PyL による致死性感染に対して抵抗性となる。このように、弱毒性の PyNL は致死性の PyL に対して生ワクチンとして作用する。

２．生ワクチンモデルにおける CD8Ｔ細胞の防御的役割の検討

PyNL を耐過したマウス（免疫マウス）に抗 CD8 抗体を投与することで CD8Ｔ細胞を除去した後に PyL を感染させた。CD8Ｔ細胞を除去しても、PyL に対する抵抗性に変化なく全てのマウスが生き残った。また、免疫マウスから CD8Ｔ細胞を精製し、通常マウスに移入した後に PyL を感染させても、抵抗性を賦与することが出来なかった。これらの結果は、CD8Ｔ細胞の防御的役割を否定するものであった。

３．PyL の追加免疫による CD8Ｔ細胞応答の活性化

免疫マウスに PyL を感染させ、さらにもう一度 PyL を感染させた。依然として抵抗性であるが、これらのマウス（追加免疫マウス）から CD8Ｔ細胞を精製し、通常マウスに移入した後に PyL を感染させた。これらのマウスは PyL に対する抵抗性を獲得したことから、CD8Ｔ細胞は防御に貢献していることが明らかとなった。追加免疫マウスの CD8Ｔ細胞は $CD44^{hi}CD62L^{lo}$ のいわゆるエフェクターメモリー細胞が増加していた。

４．CD8Ｔ細胞の抗マラリア作用の解析１

CD8Ｔ細胞に免疫応答は IFN-γの分泌と細胞傷害活性に大別できる。それら抗マラリア応答への寄与を検討するために、IFN-γノックアウトマウス(GKO)、細胞傷害活性に必須である perforin を欠損するマウス(PKO)に PyNL 生ワクチン、PyL２回追加免疫を行なった。これらの変異マウスは PyNL

感染でも半分が死に至ったが、生存したマウスはPyLに対しても抵抗性を示した。これらのマウスからCD8T細胞を精製し、通常マウスに移入した後にPyLを感染させた。GKOマウスのCD8T細胞を移入したマウスでは全てのマウスで抵抗性が得られず死亡した。一方、PKOマウスのCD4T細胞は野生型マウスのCD4T細胞同様、防御的であったが、PKOCD8T細胞を移入したマウスでは高い原虫血症を認め、一匹のマウスが死亡した。

5．CD8T細胞の抗マラリア作用の解析2

CD8T細胞の防御効果にはIFN-γが必須であるが、このサイトカインの主な作用はマクロファージの活性化である。そこで、マクロファージの重要性についても検討した。追加免疫マウスのCD8T細胞を移入したマウスに、マクロファージを無力化するカラギーナンを接種し、PyLを感染させた。対照群で認められたCD8T細胞による抵抗性は、カラギーナン投与群で完全に解除された。野生型マウスの追加免疫群からのCD8T細胞を移入したマウスのマクロファージは感染赤血球を選択的に貪食していたが、GKOマウスのCD8T細胞を移入したマウスのマクロファージでは著しく貪食能力が弱まっていた。

D．考察

CD8T細胞の赤血球ステージマラリアに対する防御における関与が明らかになった。CD8T細胞の活性化にはPyNLの単独免疫では不十分であった。PyLの追加免疫はエフェクターメモリー細胞を誘導するのに必要であろう。

CD8T細胞の防御機能としては、IFN-γを分泌しマクロファージを活性化させ感染赤血球を取り込ませることがメインストリームであると思われる。予想外に、細胞傷害に関わるメカニズムも部分的にではあるが関与していることも明らかとなった。赤血球はMHCクラスIを発現しないので標的とはなり得ない。しかしながら、網状赤血球では一部MHCクラスIが残っており、この細胞が標的となる可能性がある。また、さらに未熟な赤芽球が感染を受けた場合にも破壊の対象となる。もう一つの可能性は感染赤血球を貪食したマクロファージへの細胞傷害活性であるが、これらの標的細胞の検索はこれからの課題であろう。

E．結論

これまでは否定的であった赤血球ステージマラリアに対するCD8T細胞の防御的役割を明らかにした。この知見は抗マラリアワクチンの開発に大きなインパクトを与えることが期待できる。これまでの抗体を基盤としたワクチン戦略では、多様性に富む原虫表面上の抗原を標的とする必要性があり、その開発には困難を極めている。CD8T細胞が認識する抗原は原虫のどこに発現していてもよいはずであり、保存された配列を持つ標的抗原を見つけることで幅広く効果を発揮するワクチンの開発が可能となる。

G．論文発表

Imai T, Shen J, Chou B, Duan X, Tu L, Tetsutani K, Moriya C, Ishida H, Hamano S, Shimokawa C, Hisaeda H, and Himeno K: Involvement of $CD8^+$ T cells in protective immunity against murine blood-stage infection with Plasmodium yoelii 17XL strain. **Eur. J. Immunol.** 40: 1053-1061, 2010.

Ishida H, Matsuzaki-Moriya C, Imai T, Yanagisawa K, Nojima Y, Suzue K, Hirai M, Iwakura Y, Yoshimura A, Hamano S, Shimokawa C, and Hisaeda H: Development of experimental cerebral malaria is independent of IL-23 and IL-17. **Biochem. Biophys. Res. Commun.** 402: 790-795, 2010.

Ozeki Y, Sugawara I, Udagawa T, Aoki T, Osada-Oka M, Tateishi Y, Hisaeda H, Nishiuchi Y, Harada N, Kobayashi K, and Matsumoto S: Transient role of $CD4^+CD25^+$ regulatory T cells in mycobacterial infection in mice.**Int. Immunol**. 22: 179-189, 2010.

Chou B, Hiromatsu K, Hisaeda H, Duan X, Imai T, Murata S, Tanaka K, and Himeno K: Genetic immunization based on the ubiquitin-fusion degradation pathway against Trypanosoma cruzi. **Biochem. Biophys. Res. Commun.** 392: 277-282, 2010.

H．知的財産権の出願・登録状況

該当なし

厚生労働科学研究費補助金（国際医学協力研究事業）
分担研究報告書

マラリア感染におけるT細胞免疫応答の研究

研究分担者　由井　克之　長崎大学大学院医歯薬学総合研究科教授

研究要旨

マラリア感染赤内型においては、$CD4^+$ Ｔ細胞が感染防御に重要な役割を担っている。一方マラリア感染においてＴ細胞機能が修飾されることが報告されているが、その詳細は十分に明らかではない。ワクチン等により宿主側の感染防御対策を行う場合、マラリア感染と宿主感染防御機構との相互作用を十分理解した上で行うことが重要である。そのため、我々はマウスモデルを用いて宿主感染防御機構、特にＴ細胞反応系について研究を行った。本年度は、マラリア感染中の$CD4^+$ T細胞活性制御に関する研究を行い、感染マウス$CD4^+$ T細胞のIFN-γ産生がIL-2依存性であるという新たな仕組みを明らかにしたので報告する。

Ａ．研究目的

マラリアは、感染ハマダラ蚊の吸血に伴いヒトをはじめとする哺乳動物への感染が成立する。最初は肝細胞に感染し（肝細胞期）、引き続き赤血球期へと移行して発症する。赤血球期の防御免疫は主として$CD4^+$Ｔ細胞とＢ細胞によって担われている。マラリア感染においては、樹状細胞機能の低下や免疫抑制などの免疫機能修飾が知られているが、その詳細は明らかではない。

我々は、モデル抗原としてマラリア原虫に卵白アルブミン（ovalubumin, OVA）を導入した組換えマラリア原虫（OVA-PbA）とOVA特異的T細胞受容体（TCR）トランスジェニックマウスT細胞の組み合わせを用いた実験系により、マラリア感染におけるT細胞の機能制御と感染防御における役割について研究を行ってきた。本研究では、$CD4^+$Ｔ細胞のサイトカイン産生に対するマラリア原虫感染の影響について明らかにすることを目的とした。

Ｂ．研究方法

１．OVA特異的Ｔ細胞受容体トランスジェニックマウスOT-II の$CD4^+$ T細胞を精製してC57BL/6（B6）マウスに受け身移入を行った。

２．OVA-PbA或いは野性型PbAを感染させた。

３．原虫血症上昇後、$CD4^+$ T細胞を精製し、OT-II細胞を含む$CD4^+$ T細胞の反応を細胞表面マーカー、ELISA法、細胞内サイトカイン染色、リアルタイムRT-PCR

等により解析した。
4.必要に応じて、細胞をソーティングにより精製して、抗原やリコンビナントIL-2などの刺激に対するIFN-γ産生をELISA法などで調べた。

C．研究結果
モデルマラリア抗原を用いた研究から、以下の点が明らかになった。
１． PbA感染マウスのCD4$^+$ T細胞はIL-2受容体を発現し、TCRの刺激が無くてもIL-2の刺激だけでIFN-γ、IL-4及びIL-10を産生することが明らかになった。また、IL-2と同じファミリーであるIL-7やIL-15に対して増殖反応はあるもののIFN-γ産生を行わなかった。IL-2刺激伝達系が何らかの経路でIFN-γ産生に結びついていると考えられた。
２．感染マウスのCD4$^+$ T細胞は、マラリア粗抗原に反応してIFN-γを産生することができる。この反応は抗CD25（IL-2受容体）抗体で完全に阻止されることから、CD4$^+$ T細胞のマラリア抗原に対するIFN-γ産生反応はIL-2依存性であることが明らかになった。一方抗T細胞受容体に対するIFN-γ産生反応は抗IL-2抗体で阻止されず、IL-2非依存性であると考えられた。

D．考察
マラリア感染中のマウスCD4$^+$ T細胞は、常に抗原刺激を受けているためかIL-2受容体を発現し、IL-2刺激に対してIFN-γを産生することが明らかになった。このことは、マラリア感染時においては、他の細胞が産生したIL-2にも原虫特異的T細胞が傍観者的に反応することを示している。この仕組みがマラリアと他感染症との重複感染における病態に影響する可能性が十分に考えられる。また、T細胞受容体刺激に対するCD4$^+$ T細胞のIFN-γ産生には、IL-2依存性の反応と非依存性の反応があることが明らかになった。どのような場合にIL-2依存性・非依存性になるのか、両者の違いの分子基盤は何か、今後の研究が必要である。

E. 結語
本年度は、昨年に引き続きマラリア赤血球期におけるCD4$^+$ T細胞の免疫応答の特徴について検討した。IL-2依存性と非依存性のIFN-γ産生があることを初めて明らかにする事ができた。本研究はマウスマラリアモデルを用いた実験系であり、マラリア感染患者のリンパ球でも同様なのか検討が必要である。さらに、これらの成果を治療法の開発やワクチン開発へと発展させたい。

G．研究発表
１．論文発表
Kimura D., Miyakoda M., Honma K., Yuda M., Chinzei Y., and Yui K., Production of IFN-γ by CD4$^+$ T cells in response to malaria antigens is IL-2-dependent. Int. Immunol., 22 (12) ; 941-952, 2010.

Complete abrogation of sporozoite-induced sterile immunity by blood stage parasites of

homologous and heterologous malaria parasites, M. Inoue, J. Tang, O. Kaneko, K. Yui, R. Culleton, Malaria J., 9 (suppl) O19, 2010.

２．学会発表

Production of IFN-γ by $CD4^+$ T cells in response to malaria antigen is IL-2 dependent during infection with *Plasmodium berghei*, D. Kimura, M. Miyakoda, K. Honma, K. Kimura, M. Yuda, Y. Chinzei, K. Yui, p105, April 11-16, 2010, Keystone Symposia, Colorado, USA

モデル抗原組換えマラリア原虫を用いた肝細胞期防御免疫応答の解析、木村一美、木村大輔、都田真奈、本間季里、田村隆彦、油田正夫、由井克之、2D-ML29 第７９回日本寄生虫学会大会　旭川　２０１０年５月２０日２１日

$CD4^+$ T 細胞のマラリア原虫抗原特異的 IFN-γ産生は IL-2 依存的である。木村大輔、都田真奈、本間季里、木村一美、油田正夫、鎮西康雄、由井克之、2D-ML30 第７９回日本寄生虫学会大会　旭川　２０１０年５月２０日２１日

マラリア感染における特異的記憶 $CD8^+$ T 細胞反応性の解析、都田真奈、木村大輔、本間季里、木村一美、油田正夫、鎮西康雄、由井克之、2D-ML31 第７９回日本寄生虫学会大会　旭川　２０１０年５月２０日２１日

Flt3 ligand 発現による実験的脳マラリア発症の抑制、田村隆彦、八木田秀男、由井克之、2D-ML48 第７９回日本寄生虫学会大会　旭川　２０１０年５月２０日２１日

Expansion of dendritic cells by Flt3 ligand modifies T cell responses during infection with *Plasmodium berghei* ANKA and prevents the development of cerebral malaria, T. Tamura, K. Yui, 14th International congress of Immunology Kobe August 22-27, 2010

Reduction of the memory $CD8^+$ T cell responses during infection with *Plasmodium berghei* ANKA, M. Miyakoda, D. Kimura, K. Honma, K. Kimura, M. Yuda, Y. Chinzei, K. Yui, 14th International congress of Immunology Kobe August 22-27, 2010

Prevention of cerebral malaria by Flt3 ligand during infection with *Plasmodium berghei* ANKA, T. Tamura, K. Kimura, M. Yuda, K. Yui, 45th annual Japan-US joint conference on parasitic diseases, Jan. 10-11, 2011.

H. 知的所有権の出願・登録状況

該当なし

厚生労働科学研究費補助金（国際医学協力研究事業）
分担研究報告書

マラリア原虫のリガンドおよび赤血球侵入関連分子の解析

分担研究者 金子 修 長崎大学熱帯医学研究所 教授

研究要旨
マラリアは熱帯地方において、いまだ重篤な感染症である。マラリア原虫はヒト体内では赤血球への再侵入を繰り返すことで増殖するため、赤血球認識リガンドはワクチン開発の標的となる。我々は赤血球侵入型原虫メロゾイトと原虫感染赤血球表面に発現している SURFIN の三日熱マラリア原虫における相同体 PvSTP について、転写とタンパク質発現を明らかにすることを目的に研究を進めた。

A．研究目的

三日熱マラリア原虫には、熱帯熱マラリア原虫の感染赤血球表面と赤血球侵入型原虫表面に発現している SURFIN と呼ばれる分子の相同体 PvSTP がゲノム上に見出される。原虫種を越えて保存されている分子は原虫の生存にとって共通する重要な役割を担っている可能性が高いと考え、PvSTP について、その転写とタンパク質発現を明らかにすることとした。

B．研究方法

三日熱マラリア原虫 PvSTP には PvSTP1 と PvSTP2 の二種類が存在するため、両者について転写解析を行う。分子の発現および局在を明らかにするために、両者に対して特異抗体を作成しウェスタンブロット解析および間接蛍光抗体法を行う。
（倫理面への配慮）三日熱マラリア原虫は、共同研究を行ったタイのマヒドン大学が、タイでの倫理審査を経たうえで得た原虫標本を分与してもらうことで入手した。

C．研究結果

転写解析の結果、PvSTP2 は PvSTP1 に比べて数倍-数百倍多く転写されていることが分かった。各分子に対して３つづつの組換えタンパク質を作成し、抗血清を作成したが原虫との反応が認められなかった。そのため、さらに各分子のアミノ酸配列を用いたペプチド抗体を作成したところ、ELISA にて両者ともペプチドに対する抗体価が 128,000 以上のウサギ抗血清を得ることが出来た。ウェスタン解析では、両者ともに予想分子量周囲に反応が見られたが、明瞭なバンドが検出できる PvSTP2 に対して、PvSTP1 のバンドは非常に薄かった。間接蛍光抗体法により局在を観察すると、原虫感染赤血球膜上の多数の小さな点として反応が見られたが、このようなパターンは、三日熱マラリア原虫感染赤血球をギムザ染色した際に見られるシュフナー斑点に似るため、蛍光抗体反応後にさらにギムザ染色を行い、PvSTP2 の局在をシュフナー斑点の局在と比較したところ、両者の局在は良く一致した。

D．考察

シュフナー斑点は、電子顕微鏡では赤血球表面から内側に陥凹したポケット状構造物として観察され、熱帯熱マラリア原虫でギムザ染色ではモーラー斑点として見られるモーラー・クレフトと相同の構造物と考えられる。SURFIN や PfEMP-1 はモーラー・クレフトに原虫から輸送された後に、赤血球表面に発現すると考えられているため、PvSTP2 とシュフナー斑点との共局在は、三日熱マラリア原虫にも熱帯熱マラリア原虫と似た赤血球分子輸送機構が存在し、PvSTP2 もシュフナー斑点を経由して感染赤血球表面に輸送される可能性を示唆する。このようなユニークな輸送機構は生物学的にも興味深いと共に、創薬の標的となりうるのではないかと考えている。

E．研究発表

１．論文発表

1. Wang Y, **Kaneko O**, Sattabongkot J, Chen J-H, Lu F, Chai J-Y, Takeo S, Tsuboi T, Ayala FJ, Chen Y, Lim CS, Han ET Genetic Polymorphism of *Plasmodium vivax* msp1p, a Paralog of Merozoite Surface Protein 1, from Worldwide Isolates. ***Am J Trop Med Hyg*** 84(2), 292-297 (2011/Feb).
2. Pandey BD, Pun SB, **Kaneko O**, Pandey K, Hirayama K. Expansion of Visceral Leishmaniasis to Western Hilly Part of Nepal. ***Am J Trop Med Hyg*** 84(1):107-8. (2011/Jan)
3. Pandey K, Pandey BD, Mallik AK, **Kaneko O**, Uemura H, Kanbara H, Yanagi T, Hirayama K. Diagnosis of visceral leishmaniasis by polymerase chain reaction of DNA extracted from Giemsa's solution-stained slides. ***Parasitol Res*** 107(3):727-30 (2010/Aug)

２．学会発表

1. **Kaneko O.** "*Plasmodium* SURFIN: evolution, polymorphism, and human sera reactivity." Nagasaki Singapore Symposium, Singapore (2010. Apr. 15-17)
2. Yahata K, Treeck M, Culleton R, Inoue M, Gilberger T-W, **Kaneko O**. "Time-lapse imaging of red blood cell invasion by rodent malaria parasites." The 6th annual BioMalPar conference, Heidelberg, Germany (2010. May. 3-5)
3. 矢幡一英、リチャード・カレトン、井上愛美、金子修. 「1A-ML09: 熱帯熱マラリア原虫とローデントマラリア原虫を用いた赤血球侵入時の動態観察」 (oral) 第 79 回日本寄生虫学会大会、旭川 (2010. May. 20-22)
4. 大槻均、入子英幸、石野智子、金子修、福本宗嗣、坪井 敬文、鳥居本美. 「1A-ML10: ネズミマラリア原虫赤血球結合タンパク(EBL)の細胞内輸送ドメインの機能解析」 (oral) 第 79 回日本寄生虫学会大会、旭川 (2010. May. 20-22)
5. Mutungi JK, Kaewthamasorn M, Culleton R, Sakaguchi M, Yahata K, **Kaneko O**. "1A-ML11: Characterisation of PyRON5, A *Plasmodium yoelii* rhoptry neck protein." (oral) 第 79 回日本寄生虫学会大会、旭川 (2010. May. 20-22)
6. 井上愛美、砂原俊彦、神田萌、金子修、カレトン・リチャード. "2D-ML51: Intra-host dynamics of mixed species malaria parasite infections in mice and mosquitoes." (oral) 第 79 回日本寄生虫学会大会、旭川 (2010. May. 20-22)
7. リチャード・カレトン、津守陽子、ヌデゥンガ・マセユ、砂原俊彦、五十棲理恵、上村春樹、金子修、田邉和裕. "2A-ML26: Selection for drug resistance in malaria parasites differs between urban and suburban areas of Brazzaville, Republic of Congo." (oral) 第 79 回日本寄生虫学会大会、旭川 (2010. May. 20-22)
8. Sungkapong T, 矢幡一英, Chotivanch K, 金子修 "三日熱マラリア原虫 PvSTP の解析" (oral) 第 18 回分子寄生虫学ワークショップ、草津 (2010. Aug. 2-5)
9. Yahata K, Treeck M, Culleton R, Inoue M, Gilberger TW, **Kaneko O**. "Time-lapse imaging of red blood cell invasion by rodent malaria parasites" (poster) The 12th International Conference of Parasitology, Melbourne, Australia (2010. Aug. 15-20)
10. Inoue M, Tang J, **Kaneko O**, Yui K, Culleton R "Complete abrogation of sporozoite-induced sterile immunity by blood stages of homologous and heterologous malaria parasite species" (poster) The 12th International Conference of Parasitology, Melbourne, Australia (2010. Aug. 15-20)
11. **Kaneko O**. "*Plasmodium vivax* subtelomeric transmembrane protein 2 (PvSTP2), a homolog of *P. falciparum* SURFIN: transcription and localization" (oral) XII Brazilian Meeting on Malaria Research, Ouro Preto, Brazil (2010. Oct. 3-6)
12. 佐倉孝哉・矢幡一英・金子修 "マラリア原虫EBLの細胞内輸送の解析" (oral) 第 9 回分子寄生虫・マラリア学研究フォーラム、長崎 (2010. Oct. 8-9.)
13. 矢幡一英, Treeck M, Culleton R, 井上愛美, Gilberger T-W, 金子修 "熱帯熱マラリア原虫とローデントマラリア原虫を用いた赤血球侵入時の動態観察" (oral) 第 9 回分子寄生虫・マラリア学研究フォーラム、長崎 (2010. Oct. 8-9.)
14. Inoue M, Tang J, **Kaneko O**, Yui K, Culleton R "Complete abrogation of sporozoite-induced sterile immunity by blood stage parasites of homologous and

heterologous malaria species." (oral) Parasite to prevention: Advances in the understanding of malaria, Edinburgh, UK (2010 Oct. 20-22) [on-line abstract]

15. Tang J, Inoue M, Sunahara T, Kanda M, **Kaneko O**, Culleton R "Intra-host dynamics of mixed species malaria parasite infections in mice and mosquitoes" (oral) Parasite to prevention: Advances in the understanding of malaria, Edinburgh, UK (2010 Oct. 20-22) [on-line abstract]
16. Nakazawa S, Maeno Y, Culleton R, Quang NT, **Kaneko O**, Marchand RP "*Plasmodium knowlesi* frequently infects *Anopheles dirus* and human with P. vivax and *P. falciparum* in Khanh Phu, Khan Hoa, Vietnam" (poster) Asian-African Research Forum on Emerging and Reemerging Infections, Hanoi, Vietnam (2010 Nov. 11-12)
17. Sungkapong T, Yahata K, Culleton R, Tsuboi T, Torii M, Ruengveerayuth R, Sattabongkot J, Udomsangpetch R, **Kaneko O**, Chotivanich K "Antibody response to *Plasmodium vivax* Subtelomeric Transmembrane Protein (PvSTP), a homolog of *Plasmodium falciparum* SURFIN, in *P. vivax*-infected patients" (poster) Joint International Tropical Medicine Meeting 2010 and International Malaria Colloquium 2010, Bangkok, Thailand, (2010. Dec. 1-3)
18. 佐倉孝哉、矢幡一英、**金子修** "マラリア原虫赤血球結合リガンド EBL の細胞内輸送" (oral) 第 9 回感染症沖縄フォーラム、宜野湾市（2011. Feb. 10-12）

Ｆ．知的財産権の出願・登録状況
特記すべきものはない

厚生労働科学研究費補助金・地球規模保健課題推進研究事業
分担研究報告書

マラリア原虫に有効な新規阻害剤の探索

研究分担者　金　惠淑　岡山大学大学院医歯薬学総合研究科　准教授

研究要旨

熱帯熱マラリア原虫に有効な新規抗マラリア薬の候補化合物を探索するために、分子内にペルオキシドを有する化合物の中から環状過酸化化合物・N-89 を見出した。この化合物は in vitro, in vivo の両実験系で優れた抗マラリア活性と完治効果を併せ持つことが判った。今年度はN-89 の体内動態の改善と作用機序の解析研究に重点を置いて研究を進めた。マウスを用いたN-89 の体内動態の改善を目的に投与量・投与回数の減少を目的に添加剤の検討を行った。懸濁化剤として Hydroxymethylcellulose (CMC) を用いた時の血漿中濃度推移を検討した。その結果、従来の CMC では化合物の懸濁化は出来きたものの、体内動態値の改善は見られなかった。一方、CMC 構造ベースに OH 残基を付加した誘導体ではN-89 の懸濁化の効率が改善されたが、血漿中濃度の長時間維持には至らなかった。上記に示した添加剤の検討結果、これら化合物はN-89 の抗マラリア活性に影響しない事が明らかになった。以上の結果より、一つの固体分散剤の添加では体内動態の改善が難しいので、今後、他のオイル製剤を数種混合して最適の添加条件を検討する必要がある。また、N-89 作用機序の解析研究で特定のマラリア原虫関連タンパク質（詳細は構造解析後に明らかにする）の関わりを示す予備的な結果を得た。今後標的分子とこれらタンパク質の相互作用を検討する。

A.　研究目的

近年 Artemisinin をベースに他の抗マラリア薬を併用したACT (Artemisinin-Conbination Therapy) 療法がWHOを中心に展開されているが、カンボジア国境を中心にこれら ACT 耐性の熱帯熱マラリア原虫が報告され、新しい抗マラリア薬の開発の重要性が急務になっている。

私は抗マラリア新薬開発研究で得られた分子内ペルオキシド構造を含む有機合成化合物に優れた抗マラリア活性を見出し、将来抗マラリア薬として臨床の現場で使用することを念頭において研究を進めた。そこで、マラリア流行地の状況を考慮し、安価で大量に有機合成しやすい化合物を選抜する。また、服用しやすい製剤の検討と投与回数の減少を目指した製剤の検討を行った。また、薬剤耐性マラリアを克服するためには作用機序の解析研究を同時に行い、もし、薬剤耐性のマラリア原虫が出現しても回避できる。

B.　研究方法

1.N-89 の体内動態解析

LC/MS/MS を用いたN-89 の検出条件をもとに懸濁化剤（CMC, CMC-OH など）を有機溶媒に溶解したN-89 に配合率を0～10%まで上げて、懸濁した。そして、凍結乾燥方法を行い、得られた化合物の粉末を生理食塩水に再懸濁した。マウスに従来のオイル溶解した N-89 を投与する群をコントロールとして、懸濁条件の異なる N-89 懸濁液を実験群として経口投与して体内動態の推移を解析した。

2. N-89 の抗マラリア作用機序の解析

N-89 の分子標的の探索のため、２次元電気泳動法を用いたプロテオーム解析、及びトランスクリプトーム解析法を駆使

して抗マラリア候補化合物処理時に変動する遺伝子群、及びタンパク質を解析する。標的分子と思われる分子について、MALDI-TOF/MS および nano-LC/MS/MS を用いてマラリア原虫のタンパク質を同定した。一部の標的候補タンパク質については大腸菌内で大量発現して結晶構造解析を行うとともに、組換えタンパク質標的分子候補を用いて他のマラリア原虫タンパク質と分子間相互作用を示すかどうかについても解析した。

C. 研究結果

N-89 の体内動態の解析の結果、従来のオイル製剤の値と比較して懸濁化剤(CMC)を10%含むN-89の体内動態のパラメータを比較した。40mg/kg 単回経口投与時の血漿中濃度は、従来のオイル溶解時の血漿中半減期（1.1 時間）と比較して変化は無く、逆にこれら化合物の抗マラリア活性検討の結果でも相違が見られない事から懸濁化剤を添加しても抗マラリア活性に影響品子とが判った。CMC の誘導体である CMC-OH を用いた実験でも体内動態の値は従来のオイル溶解 N-89 の値と相違がなく、これら懸濁単剤では体内動態の改善が見られない事が明らかとなった。

N-89 の作用機序の解析研究を行った。当研究室で3年間以上N-89の薬剤プレッシャを与えた原虫株よりN-89耐性株と元の株（抗マラリア活性が10倍異なる）を用いて株価のマラリア原虫遺伝子の網羅的解析を行った。株間比較の結果、N-89 耐性株で 1.5 倍以上発現量に変化が見られた遺伝子は 58 個、耐性株で発現量に減少が見られた遺伝子は41個あった。タンパク質変動を見るために両株のプロテオーム解析の結果、N-89 処理で Protein A, Protein B（仮称）の2種が共通の動きを示した。Protein A の組換えタンパク質を作成し、結晶構造解析を行っている。一方、このタンパク質の変動を western Blot で解析した結果、N-89 処理時間に伴い、Protein A の減少が見られ、また、これに付随してマラリア原虫特有のタンパク質が逆にレベルが上昇する事が割ったか。現在、これらタンパク質と Protein A との案錬成について複合体形成有無を検出している。

D. 考察

分子内のペルオキシド構造を有する化合物は抗マラリア活性と安全性を同時に有しており、アルテミシニンと比較して単剤で完治能力を示した。現在 WHO はアルテミシニンを主とした併用法(Artemisinin-Combination Therapy (ACT))を推奨しているが、既にカンボジアを中心とした東南アジアで ACT に耐性を示す熱帯熱マラリア原虫の出現が報告されている。従って、ACT 耐性の克服にも N89 は力を発揮すると考えられる。今後、高等動物を用いた N-89 の抗マラリア活性の評価と安全性試験を行い、実際マラリア流行地で使用しやすい新規抗マラリア薬として開発していく必要がある。また、マラリア流行地でこれら環状過酸化化合物が新規抗マラリア薬として使用されるためには、現地の劣悪な環境での化合物の安定性が必須である。そのため、安定性を含めた解析研究も平行していく。N-89 の作用機序解析の研究で数種のマラリア原虫タンパク質を見出したので、これらタンパク質の結晶構造の解析と機能解析研究を現在行っている。それに付随して溶解性の改善を目的に新しい溶解性と抗マラリア活性を併せ持つ新規シーズの探索も併行していく事で、いち早くマラリア流行地で必要とする新規抗マラリア薬を提供できるように最大限に努力する。

E. 結論

安全で簡単な構造を有する環状過酸化化合物（N-89）をマラリアコントロールのためには流行地の状況を考慮した製剤の検討が必要で、今回の結果では体内動態

改善出来る懸濁化剤は見出せなかった。今後懸濁化剤を含む種々の添加剤の検討し、さらに配合等の膨大な組み合わせを行い、最適の製剤条件を見出す必要が有る。

F. 研究発表

1. 論文発表

1. Morisaki, D., Kim, H.-S., Inoue, H., Terauchi, H., Kuge, S., Naganuma, A., Wataya, Y., Tokuyama, H., Ihara, M. and Takasu, K. Selective accumulation of rhodacyanine in plasmodial mitochondria is related to the growth inhibition of malaria parasites. *Chemical Science*, 1 (2): 206-209, 2010.

2. Nishiyama, Y., wasa, K., Okada, S., Takeuchi, S., Moriyasu, M., Kamigauchi, M., Koyama, J., Takeuchi, A., Tokuda, H., Kim, H.-S., Wataya, Y., Takeda, K., Liu, YN., Wu, PC., Bastow, KF., Akiyama, T. and Lee, KH. Geranyl derivatives of isoquinoline alkaloids show increased biological activities. *Heterocycles*, 81 (5): 1193-1229, 2010.

3. Sato, A .,Naito, T., Hiramoto, A., Goda, K., Omi, T., Kitade, Y., Sasaki, T., Matsuda, A., Fukushima, M., Wataya, Y. and Kim, H.-S. Association of RNase L with a Ras GTPase- activating-like protein IQGAP1 in mediating the apoptosis of a human cancer cell-line. *FEBS Journal*, 277 (21), 4464-4473, 2010.

4. Sato, A., Satake, A., Hiramoto, A., Wataya, Y. and Kim, H.-S. Protein expression profiles of necrosis and apoptosis induced by 5-fluoro-2 '-deoxyuridine in mouse cancer cells. *Journal of Proteome Research*, 9 (5): 2329-2338, 2010.

2. 学会発表

1. 鎌井一気, 平本晃子, 森田将之, 秀野勇人, 小山貴彦, 江 文, 林 孝輔, 佐藤聡, 平岡 修, 野島正朋, 金 惠淑, 綿矢有佑. 新規抗マラリア薬・環状過酸化化合物の作用機序解析. 第33回日本分子生物学会年会・第83回日本生化学会大会合同大会, 2010年12月7-10日, 神戸, 兵庫.

2. 岡田和朗, 脇本達也, 松本雅弘, 小林明日香, 森田将之, 野島正朋, 川合 覚, 平本晃子, 佐藤 聡, 金 惠淑, 綿矢有佑. 新規抗マラリア薬の開発研究～環状過酸化化合物の抗マラリア活性と体内動態～第33回日本分子生物学会年会・第83回日本生化学会大会合同大会, 2010年12月7-10日, 神戸, 兵庫.

3. 金 惠淑, 平本晃子, 佐藤 聡, 森田将之, 熊谷 貴, 下河原理江子, 谷口斎恵, 太田伸生, 綿矢有佑. 新規抗住血吸虫薬の開発研究. 第33回日本分子生物学会年会・第83回日本生化学会大会合同大会, 2010年12月7-10日, 神戸, 兵庫.

4. 中間健太郎, 佐藤 聡, 山本朗央, 平本晃子, 金 惠淑, 綿矢有佑. 5-Fluoro-2'-deoxyuridine が誘導する細胞死分子機構の解析研究 ～ネクローシスとアポトーシスを制御する因子の探索～. 第33回日本分子生物学会年会・第83回日本生化学会大会合同大会, 2010年12月7-10日, 神戸, 兵庫.

5. 山本朗央, 佐藤 聡, 中間健太郎, 平本晃子, 金 惠淑, 綿矢有佑. 5-Fluoro-2'-deoxyuridine (FUdR)が誘導する細胞死分子機構の解析研究 ～ネクローシスとアポトーシスの制御因子としてのHSP90機能～. 第33回日本分子生物学会年会・第83回日本生化学会大会合同大会, 2010年12月7-10日, 神戸, 兵庫.

6. 大見拓也, 内藤智春, 佐藤 聡, 平本晃子, 松田 彰, 佐々木琢磨, 福島正和, 北出幸夫, 金 惠淑, 綿矢有佑. 抗腫瘍性ヌクレオシドアナログ 3-Ethynylcytidine (ECyd)によるアポトーシス誘導機構の解明. 第33回日本分子生物学会年会・第83回日本生化学会大会合同大会, 2010年12月7-10日, 神戸, 兵庫.

7. Yusuke Wataya, Akira Sato, Tomoharu Naito, Takuya Omi, Akiko Hiramoto, Yukio Kitade, Takuma Sasaki, Akira Matsuda, Masakazu Fukushima, Hye-Sook Kim. Molecular mechanisms of cell death induced

by 3′-ethynylcytidine. The 37th International Symposium on Nucleic Acids Chemistry 2010, November 10-12, 2010, Yokohama, Japan.

8. Akira Sato, Kentaro Nakama, Akihiro Yamamoto, Akiko Hiramoto, Hye-Sook Kim, Yusuke Wataya. Association of intermediate filament proteins with necrosis and apoptosis in cell death induced by 5-fluoro-2′-deoxyuridine. The 37th International Symposium on Nucleic Acids Chemistry 2010, November 10-12, 2010, Yokohama, Japan.

9. 脇本達也, 岡田和朗, 松本雅弘, 小林明日香, 森田将之, 野島正明, 川合 覚, 平本晃子, 佐藤 聡, 金 惠淑, 綿矢有佑. 新規抗マラリア薬の開発研究～環状化酸化化合物の抗マラリア活性と体内動態～第６６回日本寄生虫学会西日本支部大会, 2010 年 11 月 6-7 日, 岡山.

10. 鎌井一気, 森田将之, 小山貴彦, 秀野勇人, 江 文, 林 孝輔, 平本晃子, 佐藤聡, 平岡 修, 平本一幸, 野島正朋, 綿矢有佑, 金 惠淑. 環状過酸化化合物の抗マラリア作用機序の解析. 第６６回日本寄生虫学会西日本支部大会, 2010 年 11 月 6-7 日, 岡山.

11. Akiko Hiramoto, Hye-Sook Kim, Akira Sato, Masayuki Morita, Kazuki Okada, Tatsuya Wakimoto, Kazuki Kamai, Wen Jiang, Osamu Hiraoka, Satoru Kawai, Yusuke Wataya. NEW antimalarial drug developmental research – Antimalarial synthetic endoperoxides –. 8th Asia-Pacific Travel Health Conference, October 20-23, 2010, Nara, Japan.

12. 森田将之, 小山貴彦, 平本晃子, 鎌井一気, 秀野勇人, 江 文, 林 孝輔, 佐藤 聡, 平岡 修, 平本一幸, 益山新樹, 野島正朋, 綿矢有佑, 金 惠淑. 環状過酸化化合物の抗マラリア作用機序の解析. 第９回分子寄生虫・マラリア研究フォーラム, 2010年10月8-9日, 長崎.

13. 山本朗央, 佐藤 聡, 金 惠淑, 綿矢有佑. 5-Fluoro-2'-deoxyuridineが誘導する細胞死分子機構の解析研究～ネクローシスとアポトーシスの制御因子の探索研究～. 日本がん分子標的治療学会第14回学術集会, 2010年7月6-8日, 東京.

14. 大見拓也, 佐藤 聡, 松田 彰, 佐々木琢磨, 福島正和, 金 惠淑, 綿矢有佑. 新規抗腫瘍ヌクレオシドアナログ 3'-Ethynylcytidine(ECyd; TAS-106)によるアポトーシス誘導機構の解明. 日本がん分子標的治療学会第14回学術集会, 2010年7月6-8日, 東京.

15. 森田将之, 平本晃子, 笹岡健二, 小山貴彦, 佐藤 聡, 益山新樹, 野島正朋, 綿矢有佑, 金 惠淑. 環状過酸化化合物の抗マラリア作用機序の解析. 第７９回日本寄生虫学会大会, 2010年5月20-21日, 札幌, 北海道.

16. 鎌井一気, 小山貴彦, 森田将之, 平本晃子, 佐藤 聡, 平岡 修, 益山新樹, 野島正朋, 金 惠淑, 綿矢有佑. 新規抗マラリア薬・環状過酸化化合物の作用機序解析. 第130年会日本薬学会, 2010年3月28 – 30日, 岡山.

17. 金 惠淑, 平本晃子, 佐藤 聡, 熊谷 貴, 下河原理江子, 谷口斎恵, 太田伸生, 綿矢有佑. 新規抗住血吸虫薬の開発研究. 第130年会日本薬学会, 2010年3月28 – 30日, 岡山.

18. 松本雅弘, 岡田和朗, 脇本達也, 笹岡健二, 森田将之, 小山貴彦, 鎌井一気, 益山新樹, 野島正明, 川合 覚, 平岡 修, 平本一幸, 平本晃子, 佐藤 聡, 金 惠淑, 綿矢有佑. 新規抗マラリア薬の開発研究―環状過酸化化合物の抗マラリア活性と体内動態―. 第130年会日本薬学会, 2010年3月28 – 30日, 岡山.

19. 和田 憲幸, 谷口 抄子, 佐藤 聡, 綿矢 有佑, 伊東 秀之, 波多野 力. 花椒の抗リーシュマニア活性成分. 第130年会日本薬学会, 2010年3月28 – 30日, 岡山.

20. 中間 健太郎, 佐藤 聡, 岡松 朗子, 山本 朗央, 平本 晃子, 金 惠淑, 綿矢 有佑. 5-Fluoro-2'-deoxyuridineが誘導する細胞死分子機構の解析研究 ～ネクローシスとアポトーシスの制御因子の探索～. 第130年会日本薬学会, 2010年3月28 – 30日, 岡山.

21. 山本 朗央, 佐藤 聡, 中間 健太郎, 岡松 朗子, 平本 晃子, 金 惠淑, 綿矢 有佑. 5-Fluoro-2'-deoxyuridineが誘導する細胞死分子機構の解析研究 ～ネクローシスとアポトーシスの制御因子としてのHSP90の機能～. 第130年会日本薬学会, 2010年3月28 – 30日, 岡山.
22. 大見 拓也, 内藤 智春, 佐藤 聡, 平本 晃子, 松田 彰, 佐々木 琢磨, 福島 正和, 北出 幸夫, 金 惠淑, 綿矢 有佑. 抗腫瘍性ヌクレオシドアナログ 3'-Ethynylcytidine (ECyd, TAS-106)によるアポトーシス誘導機構の解明. 第130年会日本薬学会, 2010年3月28 – 30日, 岡山.

厚生労働科学研究費補助金（国際医学協力研究事業）

分担研究報告書

住血原虫症の病態と創薬に関する研究

分担研究者　片倉　賢　北海道大学大学院獣医学研究科教授

研究要旨

内臓リーシュマニア症のマウスモデルとして、NF-κB inducing kinase を遺伝的に欠損している *aly/aly* マウスに *Leishmania donovani* の前鞭毛期型虫体を感染させ免疫病理学的解析を行なった。その結果、*aly/aly* の肝臓内の原虫数は 4 週目にコントロールの *aly/+* よりは小さいピークを示したのち、8 週目には減少したが、その後原虫数は維持され感染後数ヶ月経ても肝臓内に原虫が存続していた。肝臓内の Foxp3 mRNA 発現量と $CD4^+Foxp3^+T$ 細胞数は感染経過に伴って増加した。そこで、感染 26 週目の *aly/aly* マウスに抗 CD25 抗体または抗 FR4 抗体を投与したところ、いずれの抗体を投与したマウスにおいても抗体投与後 10 日目の肝臓内原虫数は対照抗体を投与した感染マウスに比べ有意に減少した。このことから、*aly/aly* マウスにおけるリーシュマニア原虫の存続機構として $CD4^+Foxp3^+$ T cells の関与が強く示唆された。

ミャンマー産薬用植物のブドウ科の *Vitis repens* のエチルアセテート抽出画分について抗 *Trypanosoma evansi* 血流型虫体活性について検討したところ、抗酸化物質として知られる resveratrol にその活性のあることが判明した。

A．研究目的

住血性原虫（トリパノソーマ、リーシュマニア、バベシア）の発症や病態に関わる宿主側ならびに原虫側の要因を明らかにする。アジア産薬用植物資源から抗住血性原虫活性物質を探索し，有効成分を同定するとともに、作用機序と細胞毒性について検討し、住血原虫症の創薬開発に貢献する。

B．研究方法

（1）内臓リーシュマニア症における原虫存続のメカニズム

内臓リーシュマニア症は人と犬で世界的に問題となっている人獣共通原虫症である。原虫は肝臓、脾臓、骨髄などのマクロファージ細胞内に寄生し、慢性の経過を辿る。発病機転は宿主の免疫機能と深く関わるが、宿主体内からの原虫の完全排除は困難である。内臓リーシュマニア症のマウスモデルにおいては、肝臓が感染初期の原虫増殖の場となり、免疫が誘導（肉芽腫形成）されると肝臓から原虫は排除される。感染後期になると脾臓ではその構造が破壊され、免疫不全状態となり、脾臓が原虫増殖の場となる。皮膚リーシュマニア症は、内臓リーシュマニア症の原因虫種とは異なるリーシュマニア種によって引き起こされるが、そのマウスモデルでは、抑制性 T 細胞 (T reg)が原虫の皮膚における存続に関与することが知られている。しかし、内臓リーシュマニア症のマウスモデルにおける T reg の役割についてはまだ確実な報告はない。

本研究では、NF-κB inducing kinase を遺伝的に欠いている *aly/aly* マウスに *Leishmania donovani* の promastigotes 5 x 10^7 を感染させ、肝臓、脾臓、骨髄の原虫数の算定（realtime PCR）、各種サイトカイン・ケモカインの転写量の定量（RT-PCR）、肝臓の肉芽腫の組織学的解析、および抗 T reg 抗体の原虫数に与える影響などを検討した。

（2）抗トリパノソーマ活性を有する薬用植物の探索

これまでの研究により、ミャンマー産薬用植物の中から民間療法として用いられている 60 種の薬用植物のアルコール粗抽出物について、エバンストリパノソーマ *(Trypanosoma evansi)*の血流型虫体を標的として、抗原虫活性を有する植物をスクリーニングし、*Vitis repens* に高い抗トリパノソーマ活性があることを突き止めた。そこで本研究では、*Vitis repens* のエチルアセテート画分の抗トリパノソーマ活性物質について検討した。

（倫理面への配慮）

動物実験にあたっては、北海道大学および北海道大学大学院獣医学研究科の動物実験指針を遵守した。

C．研究結果

（1）内臓リーシュマニア症における原虫存続のメカニズム

コントロールの *aly/+* マウスの肝臓内の原虫数は 4 週目にピークが認められたが、感染後 8 週では原虫は排除されていた。*aly/aly* マウスでは感染

4 週目に *aly/+*マウスよりは少ない肝臓内原虫数のピークを示し、その後 8 週目には減少したが、その原虫数は維持され感染後数ヶ月を経過しても肝臓内に原虫が存続していた。肝臓の肉芽腫を組織学的に観察したところ、*aly/aly* マウスでは類上皮細胞や単核球の浸潤の少ないは未熟な肉芽腫が多く認められた。*aly/aly* マウスの肝臓内の IFN-γ、TNF-α、iNOS、TGF-β、MAP-1、および IP10 の mRNA 発現量は感染 4 週目ではいずれも *aly/+*マウスより低値を示したが、8 週目からはコントロールマウスよりも高い値を維持した。

肝臓内の Foxp3 mRNA 発現量と $CD4^+Foxp3^+$T 細胞数は感染経過に伴って増加した。そこで、感染 26 週目の *aly/aly* マウスに、T reg 活性を抑えることが知られている抗 CD25 抗体または抗 FR4 抗体を投与したところ、いずれの抗体を投与したマウスも抗体投与後 10 日目の原虫数は対照抗体を投与したマウスに比べ有意に減少した。

aly/aly マウスの脾臓や骨髄の原虫数は感染 8 週目から著しく増加したが、抗 CD25 抗体または抗 FR4 抗体を投与すると脾臓と骨髄内原虫数も有意に減少した。

（2）抗トリパノソーマ活性を有する薬用植物の探索

ブドウ科の *Vitis repens* のエチルアセテート画分の抗トリパノソーマ活性について検討したところ、抗酸化物質として知られる resveratrol に活性のあることが判明した。

D．考察

aly/aly マウスでは原虫が長期間（7 か月）にわたって肝臓に存続すること、また、脾臓や骨髄では慢性期に原虫数が増加することを見出した。原虫のマウス体内における存続機構として $CD4^+Foxp3^+$T 細胞の関与が強く示唆されたが、T reg の組織内局在と細胞数の関係は興味深い。

ミャンマー産薬用植物のなかで強い抗トリパノソーマ活性を示した薬用植物の成分の 1 つは抗酸化物質として知られる resveratrol であることが示唆されたが、原虫に対する直接的障害性の作用機序についてさらに解析する必要がある。

E．結論

内臓リーシュマニア症における原虫存続には抑制性 T 細胞が関与することが明らかとなった。一方、住血原虫症に対する創薬の天然資源として薬用植物の有用性が示された。

F．健康危険情報

該当せず

G．研究発表

1．論文発表

1) Kawamura Y, Yoshikawa I, Katakura K: Imported leishmaniasis in dogs, US military bases, Japan. *Emerg Infect Dis* 16, 2017-2019, 2010
2) Bawm S, Tiwananthagorn S, Lin KS, Hirota J, Irie T, Htun LL, Maw NN, Myaing TT, Phay N, Miyazaki S, Sakurai T, Oku Y, Matsuura H, Katakura K: Evaluation of Myanmar medicinal plant extracts for antitrypanosomal and cytotoxic activities. *J Vet Med Sci* 72, 525－528, 2010
3) Mizukami C, Spiliotis M, Gottstein B, Yagi K, Katakura K, Oku Y: Gene silencing in *Echinococcus multilocularis* protoscoleces using RNA interference. *Parasitol Int* 59, 647-652, 2010
4) Armua-Fernandez MT, Nonaka N, Sakurai T, Nakamura S, Gottstein B, Deplazes P, Phiri IGK, Katakura, K, Oku Y: Development of PCR/dot blot assay for specific detection and differentiation of taeniid cestode eggs in canids. *Parasitol Int* in press

2．学会発表

1) 片倉賢, Bawm S, Tiwananthagorn S, Lin KS, Hirota J, Irie T, Htun LL, Maw NN, Myaing TT, Phay N, Miyazaki S, Sakurai T, Oku Y, Matsuura H: 抗トリパノソーマ活性を有するミャンマー産薬用植物の探索. 第 79 回日本寄生虫学会, 2010 年 5 月（旭川）
2) Tiwananthagorn S, Iwabuchi K, Ato M, Sakurai T, Oku Y, Katakura K: Immunopathology of *Leishmania donovani* infection in alymphoplasia (*aly/aly*) mice, ICOPA XII. 2010 年 8 月（Melbourne, オーストラリア）
3) Tiwananthagorn S, Iwabuchi K, Ato M, Sakurai T, Oku Y, Katakura K: Immunopathological response to *Leishmania donovani* infection in alymphoplasia (*aly/aly*) mice. 10th Awaji international Forum on Infection and immunity, 2010 年 9 月（兵庫）
4) Tiwananthagorn S, Iwabuchi K, Ato M, Sakurai T, Katakura K: Persistent *Leishmania donovani* infection in alymphoplasia (*aly/aly*) mice. Keystone Symposia on Molecular and Cellular Biology "Immunologic Memory, Persisting Microbes and Chronic Disease, 2011 年 2 月 (Calgary, カナダ)

H．知的財産権の出願・登録状況

なし

厚生労働科学研究費補助金（国際医学協力研究事業）

分担課題：トリパノソーマの防御応答回避メカニズムの解析

分担研究者　嶋田　淳子　群馬大学医学部　教授

研究要旨

Trypanosoma cruzi 感染により発現上昇がみられる宿主アポトーシス抑制因子 c-FLIP および c-IAP と相互作用する原虫側因子を探索するため、yeast two hybrid 用 bait ベクターを構築した。また、pull down 用の c-IAP BIR 高発現細胞株を樹立した。

A．研究目的

*Trypanosoma cruzi*感染により宿主アポトーシス 抑制因子c-FLIPおよびc-IAPの発現上昇機構を解明する。また、これらのタンパク質と相互作用する原虫側因子の探索を行う。

B．研究方法

Yeast two hybrid法によりc-FLIPおよびc-IAPと相互作用する原虫側因子を探索するため、baitベクターの作製を行った。また、pull down法を行うため、tag付き発現ベクターの作製を行った。
（倫理面への配慮）組み換えDNA実験は群馬大学で承認されている。

C．研究結果

c-FLIP全長をbaitベクターに組み込んだが、目的とするものが得られなかった。そこで、c-FLIP分子をDED領域とpseudecaspase領域に分割し、ベクターに連結した。c-IAPの全長もベクターへ組み込むことが困難であったため、BIR領域とCARD-RING領域に分けてベクターに挿入した。このBIR領域を含むベクターを培養細胞に導入し、高発現させた株を樹立することができた。

D．考察と結論

c-FLIP、c-IAPの全長の遺伝子は両者ともyeast two hybridのbaitベクターに連結するのが難しく、これらの遺伝子が発現すると大腸菌の生育に影響を与える可能性が考えられた。それぞれの遺伝子を断片化したところ、コロニーが得られたので、酵母を用いて解析を進める予定である。また、pull down用の細胞株ができ、ようやく準備が整った。

E．結論

c-FLIPおよびc-IAP遺伝子全長の発現ベクターの構築は困難であったため、分割して連結したベクターを作製した。またこれらの分割した遺伝子を発現する培養細胞株を樹立することができた

F．健康危険情報

G．研究発表

1.　論文発表

なし

2.　学会発表

日本生薬学会大会、徳島、2010
The XIIth International Congress of Parasitology、Melbourne、2010

H．知的財産権の出願・登録状況
（予定を含む。）

1. 特許取得

特許出願（2010-163039）
抗トリパノソーマ剤およびトリパノソーマ症治療薬

2. 実用新案登録

なし

3.その他

なし

厚生労働科学研究費補助金　地球規模保健課題推進研究事業（国際医学協力研究事業）

分担研究者報告書

人獣共通寄生虫病の血清診断システムの開発と幼虫移行症の病態解明

分担研究者　丸山治彦　宮崎大学医学部教授

研究要旨　宮崎大学医学部寄生虫学で施行した血清診断では、2010 年においても肺吸虫症と回虫類の幼虫による内臓幼虫移行症が多数を占めた。血清診断の重要度が高い幼虫移行症の組換え診断抗原を得るために、ブタ回虫およびイヌ回虫の体内移行期幼虫に発現している As16 と TES32 の組換えタンパク質を用いて患者血清との反応を調べた。それぞれの組換え抗原に対する血清の反応は、ブタ回虫 ES とイヌ回虫 ES 抗原との反応と相似であり、病原体診断に使用できると考えられた。また、幼虫移行症の病態解明では、虫卵、感染幼虫、肺ステージの幼虫および成虫のトランスクリプト解析をおこない、約 14,000 の isotig にアセンブルした。その中に、細菌からの水平伝播により獲得されたが推測される ferrochelatase 遺伝子を同定し、Blast2GO を用いて 53.9%の配列にアノテーション付与した。

A. 研究目的

われわれは、multiple-dot ELISA 法による抗体スクリーニングと 96-well microtiterplate ELISA 法による精査を基本とした寄生虫症診断システムを構築し、多くの寄生虫病の診断に関わってきた。2000 年以降、総検体数は年間 500 前後で推移し、毎年 100-200 例を寄生虫症と診断している（下表）。

原因寄生虫	2004	2005	2006	2007	2008	2009	2010
イヌ回虫・ブタ回虫	100	103	82	101	77	52	45
アニサキス	0	4	4	6	3	2	2
イヌ糸状虫	7	1	5	1	1	0	0
顎口虫	11	0	0	6	7	6	3
鉤虫	0	1	0	1	0	0	0
マンソン孤虫	5	4	3	6	4	3	1
有鉤嚢虫	4	0	0	0	0	1	0
肺吸虫	45	30	37	46	38	40	43
肝蛭	5	6	2	3	0	3	2
住血吸虫	5	5	6	6	4	5	3
肝吸虫	1	0	0	0	0	0	2
糞線虫	11	2	1	1	1	6	2
回虫	0	1	1	1	2	0	0
日本海裂頭条虫	1	0	2	0	1	0	4

これらの血清診断は、ほとんどの場合虫体の粗抗原を用いておこなわれているが、いくつかの問題点が明らかになっている。その第 1 は、多くの寄生虫が実験室内での維持ができないので、抗原の入手には常に困難がともなうことである。第 2 に、いくつかの疾患において粗抗原では擬陽性と真の陽性の判別が必ずしも容易でないことがあげられる。病歴や検査所見などから総合的に判断しているが、とくに動物由来の回虫類による幼虫移行症および糞線虫症では、あきらかに感染の可能性がないと考えられる症例でも抗体高値を示すことがある。

そこで、とくに幼虫移行症について、血清診断における抗原入手の問題を解決すると同時に擬陽性を排除し、さらに抗原の一定した品質を確保して体外診断薬として一般医療機関でも使用できるように、組換え抗原を作製し、患者血清との反応性をしらべ有用性を検討する。

基礎的な研究として、幼虫移行症の病態を解明するために、モデル寄生虫であるベネズエラ糞線虫の発現遺伝子解析をおこない、寄生線虫の体内移行という寄生虫の謎の解明のメカニズムを明らかにする。具体的には、虫卵、感染幼虫、体内移行期幼虫、成虫の cDNA ライブラリを作製し、高速シーケンサの 454 GS-FLX Titanium で網羅的に塩基配列を決定してステージ特異的な遺伝子発現を定量的に検討する。

B. 研究方法

1. 診断用組換え抗原の作製

幼虫移行症ではブタ回虫について組換え抗原を作製した。沖縄県および宮崎県内で採取されたブタ回虫のメスから虫卵を分離して幼虫包蔵卵を形成させた。これをウサギに投与し、感染5-6日後にウサギ肺から幼虫を回収した。

次いで肺から回収した幼虫から polyA+ RNA を抽出・精製して逆転写反応をおこない、cDNA ライブラリを作製した。得られた cDNA クローンの塩基配列を決定して、成虫や虫卵では発現の報告がないものを診断用抗原の候補とし、組換えタンパク質を作製した。このうち、予備的な実験により As16 を以下の実験にもちいた。

イヌ回虫の組換え抗原は、国立感染症研究所寄生動物部の山崎浩博士から TES32 を供与いただき、実験に使用した。

以上の研究課題は、宮崎大学動物実験委員会、宮崎大学遺伝子組換え実験安全委員会、宮崎大学病原体等安全管理委員会、の審査を受け、機関承認を得ている。

以上により組換えタンパク質を得た上で、宮崎大学医学部寄生虫学分野において 2005 年以前に動物由来の回虫類による幼虫移行症と診断された患者、およびどの寄生虫にも感染していないと判定された患者の血清を用い、前項で作製した組換え抗原の診断抗原としての有用性を酵素抗体法で検討した。

患者血清の使用に際しては、ヘルシンキ宣言の趣旨に則り、臨床研究に関する倫理指針等を遵守した。本研究は、宮崎大学医学部医の倫理委員会による審査を受け、宮崎大学医学部の承認を受けている。

2. ベネズエラ糞線虫のトランスクリプト解析

ベネズエラ糞線虫の虫卵、感染幼虫、肺ステージの幼虫および成虫から cDNA を作製し、高速シーケンサ 454 GS-FLX Titanium によって塩基配列を決定する。次いで Newbler (v. 2.3)を用いてアセンブルし isotig を得る。大規模アノテーションを Blast2GO プログラムでおこなうとともに、各 isotig がどれくらいのリードを背景にしているか、各 isotig に相当する *Caenorhabditis elegans* タンパク質は何かについて検討した。

また、*C. elegans* の NAS-34 に類似した Zinc-metalloprotease 遺伝子が何種類ゲノム上に存在するのかを明らかにするため、ベネズエラ糞線ゲノム DNA をテンプレートに PCR をおこない塩基配列を決定した。

C. 研究結果

1. ブタ回虫組換え抗原の作製と患者血清との反応性

ブタ回虫の体内移行期幼虫の cDNA ライブラリを作製しランダムに 1722 クローンの塩基配列を決定した。得られた 175 種類のユニークな配列のうち、イヌ回虫の C-タイプレクチンのブタ回虫ホモログと考えられるタンパク質 As-CTL-1 と、ブタ回虫感染に対するワクチン候補 As16 に特に注目して組換え抗原を作製し、解析を進めた。このふたつを選んだ理由は、両者とも肺から回収した幼虫の cDNA ライブラリ中のクローンの出現頻度が高く、患者の免疫系が強く感作されている可能性が高いと考えたからである。

最初に両者の幼虫移行症患者血清との反応を検討したところ、As16 の方がブタ回虫感染と考えられる患者血清と強く結合した。よって、以降の実験には、組換えブタ回虫抗原として As16 を用いた。

最初に 40 種類の幼虫移行症患者血清についてイヌ回虫幼虫 ES と As16 を反応させた。吸光度の比をとりどちらに強く結合したかを表したのが図 1 である。

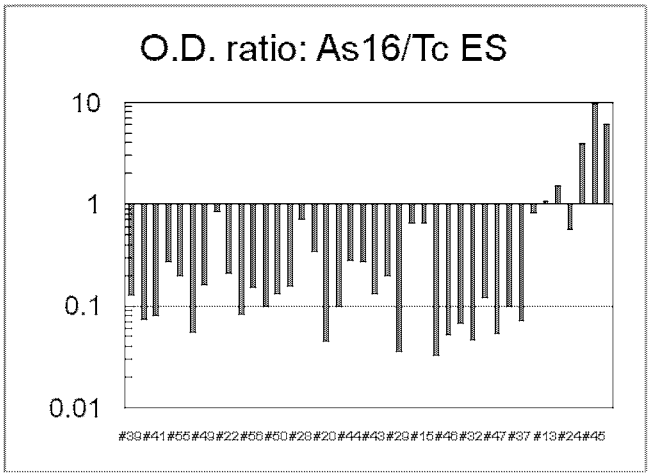

図 1　幼虫移行症患者血清の As16/イヌ回虫 ES 抗原結合比

40 検体のうち 3 検体がイヌ回虫幼虫 ES に比べて As16 に強く反応しており、これらの血清はブタ回虫感染血清と考えられた。次にイヌ回虫幼虫 ES の代わりに組換え ES 抗原である TES32 を用いて同様の実験をおこなった。結果は図 2 の通りで、イヌ回虫幼虫 ES と完全にパラレルではないものの、両者は同様の結合傾向を示した。以上より、どちらも組換え抗原である As16 と

TES32 により、幼虫移行症の病原体診断が可能であることが示唆された。

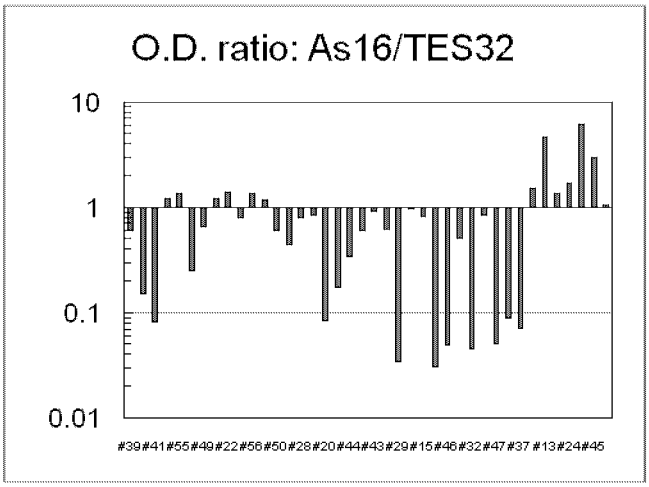

図 2　幼虫移行症患者血清の As16/TES32 結合比

2. ベネズエラ糞線虫ゲノム解析

ベネズエラ糞線虫のゲノムに関しては、昨年度のデータに SOLEXA のデータを加えた。現在ではベネズエラ糞線虫のゲノムサイズは 100Mb 程度と推定されている。今後さらにゲノムフラグメントの塩基データを追加する。ペアエンドライブラリの作製と解析、フォスミドライブラリの構築が進行中である。

3. ベネズエラ糞線虫トランスクリプトーム解析

虫卵、感染幼虫、肺移行期幼虫、および寄生世代成虫から cDNA ライブラリをそれぞれ作製し、454 GS-FLX で塩基配列を決定した。

2 回のランにより総計 2,483,165 のリードが得られた。リード数の内訳は、虫卵/L1 が 543,713、感染幼虫が 622,248、肺移行期幼虫が 679,257、成虫が 638,728 リードであった。これらを Newbler v.2.3 によりアセンブルし、計 14,016 のアイソティグ（トランスクリプトと考えられるもの）を得た。

この中で、7,560 に何らかのアノテーションを付けることができ、1,591 については酵素活性を推定することができた。*C. elegans* タンパク質にヒットしたものは 10,569 個、*Brugia malayi* は 9,779 個、統合線虫 EST データベースである NEMABASE4 には 11,367 個がヒットした。つまり、約 3,000 個のトランスクリプトはベネズエラ糞線虫特異的と考えられた。

ベネズエラ糞線虫のトランスクリプトと *C. elegans* タンパク質の比較において、単一の *C. elegans* タンパク質に多数のベネズエラ糞線虫トランスクリプトがヒットするという現象が頻繁にみられた（下表）。

contig/isotig ID	*C. elegans*	tentative annotation	occurrence
Contig02305...	F40E10.1	zinc-dependent metalloprotease, NAS-34 like	117
Isotig00079...	F37C12.1	-	79
Isotig00692...	T04D1.4	-	64
Isotig03977...	Y44E3A.2	acetylcholinesterase	45
Isotig00155...	Y69H2.3e	similar to scavenger receptor cysteine-rich protein	45
Isotig00765...	ZK1098.1	WW domain containing protein	36
Isotig00570...	ZC434.7b	-	32
Isotig00502...	C39D10.7	Chitin binding Peritrophin-A domain containing protein	30
Isotig08694...	T16H12.5b	similar to roadkill, isoform A	30
Isotig11169...	C04F6.5	Dehydrogenase	25

この中で特に注目されたのが、*C. elegans* の亜鉛結合性メタロプロテアーゼ NAS34 と相同なものが 117 個も認められたことである。NAS34 は線虫のアスタシン様メタロプロテアーゼのひとつで、*C. elegans* ではゲノム中に 39 個の NAS が存在する。そこで、他の NAS についても調べたところ、ベネズエラ糞線虫のトランスクリプトには総計 161 種類の NAS 相同配列が存在することがわかった。この中には肺移行期においてのみ発現がみられるものがあり、体内移行メカニズム研究の突破口になることが期待される。

糞線虫類では NAS34 に相同なアスタシン様メタロプロテアーゼは感染幼虫の経皮侵入に関与するとされている。そこで、本当にベネズエラ糞線虫がこのように多数のアスタシン様メタロプロテアーゼ遺伝子を持っているのかを調べる目的で、ベネズエラ糞線虫ゲノムを NAS34 相同プロテアーゼ配列を標的に PCR をおこない、PCR 産物をクローニングして、各コロニーについてサンガー法により塩基配列を決定した。

その結果、約 140 クローンの塩基配列から 87 種類のアスタシン様メタロプロテアーゼが得られた。これらはすべて活性中心やモチーフ、システインの位置が共通であり、すべてが機能的なプロテアーゼとして転写されることを示していた。

トランスクリプト解析でので他の注目点は、

細菌からの水平伝播によって獲得されたと推測される Ferrochelatase 遺伝子を同定できたことである。この遺伝子は自由生活線虫では失われているが *B. malayi* は持っており、動物寄生によって再び獲得されたことが示唆された。

D. 考察

当教室で実施している寄生虫病血清診断の結果陽性と判定される症例の大多数は、食品媒介性の人獣共通寄生虫症である。具体的には肺吸虫症とイヌ回虫やブタ回虫による内臓幼虫移行症である。例年、両者で全体の 80%を超えている。

現行の血清診断では、抗原として虫体粗抗原と一部分泌排泄抗原（ES 抗原）を用いているが、抗原の供給が安定していないこと、品質が一定の抗原を大量に準備することができないこと、抗体陽性と判定される場合でも、それが真の感染によるのか、あるいは何らかの原因で産生された抗体が偶然結合しただけなのか判断できない場合があることである。

以上のような問題点を解決するために、われわれは診断用組換え抗原を調製することとした。組換えタンパク質であれば一定の品質の抗原を大量に準備することが可能であり、供給は安定する。さらに、用いるタンパク質を注意深く選ぶことで、真の感染のみを検出する系を確立することも可能であると考えられるからである。

ブタ回虫の体内移行幼虫の cDNA ライブラリから得られた As16 と、イヌ回虫症において一定の信頼性が証明されている TES32 をもちいて患者血清との結合を精査した結果、両者の結合特性は、分泌排泄抗原（ES 抗原）と似通っていることが示された。これは、組み立て、組換え抗原を用いた幼虫移行症診断システムの開発が可能であることを示す。

一方、基礎的な研究として取り組んでいる幼虫移行症の病態解明でも、今年度はきわめて重要な知見が得られた。すなわち、モデル腸管寄生線虫であるベネズエラ糞線虫のトランスクリプトを次世代型シーケンサで解析し、これまでまったく報告のなかった発現情報を得ることができたのである。

現在までの解析において特筆すべき点は、*C. elegans* の NAS34 と相同な亜鉛結合性メタロプロテアーゼが、巨大なファミリーを形成していることが示されたことがあげられる。では 1 個しかないものが、少なくとも 117 個も認められたことは、この遺伝子群がベネズエラ糞線虫にとって、きわめて重要な機能を担っていると考えられる。

さらに、まだ予備的なデータしか得られていないが、NAS34 相同アスタシン様メタロプロテアーゼは発現のタイミングが分子によりいろいろで、虫卵から成虫まで一貫して発現がみられるもの、肺移行期以降に発現しているもの、成虫でのみ見られるものなどがある。

腸管寄生線虫の体内移行との関係で興味を引くのは、肺ステージのみで発現しているアスタシン様メタロプロテアーゼがあることである。このような分子は体内移行の key mokecule である可能性が高く、今後詳しく検討する価値がある。

E. 結論

ブタ回虫の体内移行期に発現している ES 抗原の組換えタンパク質 As16 とイヌ回虫の組換え診断抗原 TES32 の組み合わせで、幼虫移行症診断システムの開発が可能であることが示された。

モデル腸管寄生線虫であるベネズエラ糞線虫を用いた幼虫移行症のメカニズム解明のブレイクスルーとなるような、肺ステージのみで発現しているアスタシン様メタロプロテアーゼを特定することができた。

F. 研究発表

著書

1. 丸山治彦　その他の吸虫症（肺吸虫症、肝吸虫症、横川吸虫症、肝蛭症）（今日の治療指針 2011、山口徹、北原光夫、福井次矢編）、pp.263-264、医学書院（東京）（2011 年 1 月 1 日）

総説

1. 木村幹男、丸山治彦、三浦聡之：熱帯病・寄生虫症に対する研究班保管国内未承認薬 Medical Practice 27: 1565-1568, 2010
2. 丸山治彦：腹部症状（腹痛、下痢、下血など）（寄生虫の標的臓器別症状からすすめる実地診療－疑い、問診・診断から治療まで－） Medical Practice 27: 1496-1550, 2010

原著論文

1. Yoshida A, Nagayasu E, Nishimaki A, Sawaguchi

A, Yanagawa S, Maruyama H.: Transcripts analysis of infective larvae of an intestinal nematode, *Strongyloides venezuelensis* Parasitol Int. 2010 Nov 5. [Epub ahead of print]

症例報告

1. Uni S, Boda T, Daisaku K, Ikura Y, Maruyama H, Hasegawa H, Fukuda M, Takaoka H, Bain O: Zoonotic filariasis caused by *Onchocerca dewittei japonica* in a resident of Hiroshima Prefecture, Honshu, Japan, Parasitol Int. 2010 Sep;59(3):477-80. Epub 2010 May 31.
2. 安東加恵、楢原真由美、徳安彰子、明石哲彦、高谷恵子、丸山治彦：気胸・胸水から診断された肺吸虫症の 1 例　大分市医師会医学雑誌 アルメイダ医報 37: 2-6. 2010

学会発表

1. 長安英治、伊藤武彦、小椋義俊、吉田彩子、林哲也、丸山治彦、ベネズエラ糞線虫のゲノム・トランスクリプトーム解析、第 79 回日本寄生虫学会大会（旭川）
2. 長安英治、吉田彩子、丸山治彦、ベネズエラ糞線虫トランスクリプトームシーケンシング、第１８回分子寄生虫ワークショップ（草津）
3. 長安英治、小椋義俊、伊藤武彦、吉田彩子、林哲也、丸山治彦、第９回分子寄生虫・マラリア研究フォーラム（長崎）
4. Eiji Nagayasu, Ayako Yoshida, Haruhiko Maruyama, A bioinformatics approach to identify immunodiagnostic antigens for strongyloidiasis, 8th Asia-Pacific Travel Health Conference (Nara)
5. 長安英治、伊藤武彦、小椋義俊、吉田彩子、林哲也、丸山治彦ベネズエラ糞線虫のゲノム・トランスクリプトーム解析から見えてきたもの、第 4 回蠕虫研究会（宮崎）
6. Eiji Nagayasu, Yoshitoshi Ogura, Takehiko Ito, Ayako Yoshida, Tetsuya Hayashi and HaruhikoMaruyama, 45th Annual Japan-US Joint Conference on Parasitic Diseases (Tokyo)
7. 吉田彩子、長安英治、堀井洋一郎、丸山治彦 ブタ回虫肺移行期幼虫 cDNA ライブラリーの解析から得られた新規 C-type レクチン 第 79 回日本寄生虫学会大会（旭川）
8. Ayako Yoshida, Nobuo Ohta, Haruhiko Maruyama: Depletion of $CD4^+CD25^+FOXP3^+$ regulatory T cells down-regulates parasite clearance during early phase of *Plasmodium chabaudi* AS infection in A/J mice. The 14th International Congress of Immunology, Kobe, Japan, August 22-27, 2010
9. Yoshida A, Nagayasu E, Yoichiro Horii, Naotoshi Tsuji, Hiroshi Yamasaki, Maruyama H: Serological diagnosisis of Visceral Larva Migrans with recombinant antigens from Toxocara and Ascaris. 8th Asia-Pacific Travel Health Conference, Nara, Japan, October 20-23, 2010
10. 吉田彩子、堀井洋一郎、丸山治彦. ブタ回虫症血清診断用抗原候補分子のファージディスプレイ法を用いた網羅的検索 第 63 回日本寄生虫学会南日本支部大会・第 60 回日本衛生動物学会南日本支部大会
11. Eiji Nagayasu, Ayako Yoshida, Haruhiko Maruyama: Large-scale gene expression analysis of different developmental stages of Strongyloides venezuelensis, a rodent intestinal nematode. 10th Awaji International Forum on Infection and Immunity, Sep. 7-10, 2010, Awaji Yumebutai International Conference Center, Awaji, Japan
12. Haruhiko Maruyama, Ayako Yoshida, Eiji Nagayasu: Not only Fish: Japanese Delicacies and Eosinophilia. 8th Asia-Pacific Travel Health Conference, Nara, Japan, October 20-23, 2010
13. 吉田彩子、長安英治、丸山治彦 幼虫移行症の診断における局所液の有用性第 63 回日本寄生虫学会南日本支部大会・第 60 回日本衛生動物学会南日本支部大会（鹿児島市）

G. 知的財産権の出願・登録状況

1. 特許取得

なし

2. 実用新案特許

なし

3. その他

なし

分担研究報告書

住血原虫症の診断学

分担研究者　五十嵐郁男　帯広畜産大学教授

研究要旨

バベシア病は、バベシア原虫がダニの媒介により動物に感染し、世界的規模で畜産業に莫大な経済的被害を与えている。また、人獣共通原虫病としても重要である。本研究では、バベシア病に対する新規遺伝子を用いた診断法と新たな薬剤開発について検討を行った。その結果、血清診断法として *Babesia bovis* の SBP4組換え抗原を用いた ELISA がこれまで報告されている抗原の中で最も感度及び特異性が優れている事が明らかとなった。また、遺伝子診断法として *Babesia bovis* の2種類の膜抗原遺伝子を標的とした nPCR を確立した。更に、これらの方法を用いた疫学調査をアジア、アフリカで行った。また、人に感染する *B. microti* の BM94 組換え抗原を用いた ELISA 法を確立し、マウス感染実験において長期間にわたり抗体検出が可能であった。人に感染するサルマラリア原虫の遺伝子診断法についても検討を行った。更に、バベシア原虫に対する有効薬剤候補のスクリーニングを行い、trepen nerolidol 及び artesunate が牛、馬、犬及びマウスのバベシアに対して増殖抑制効果を有する事を示した。これらの研究成果は、バベシア病に対する有効診断法や治療法の実用化に向け、今後の更なる検討が必要である。

A. 研究目的

バベシア病は、ダニの媒介によりバベシアが動物に感染し、世界的規模で畜産業に莫大な経済的被害を与えている。また、人におけるバベシア感染も報告されている。バベシア病を制圧し経済的な損失を最小するためには、早期の診断と治療・予防策の開発が重要である。本研究では、バベシア病に対する新規遺伝子及び組換え抗原を用いた診断法と新たな薬剤開発について検討を行った。

B. 研究方法

(1)バベシア症に対する診断法の検討

最初に血清診断法としてウシバベシア *Babesia bovis* のスフェリカルボディ4(BbSBP4)組換え抗原を用いたELISAについて検討を行った。次に、ウシバベシア *Babesia bovis* の膜抗原遺伝子 BV5650 および BV8970を用いたnPCRについて検討を行った。また、*Plasmodium knowlesi* の LAMP 法および *B. microti* の BM94 組換え抗原を用いた ELISA 法についても検討を行った。

(2)バベシア症に対する治療薬の検討

バベシアに対する新たな治療薬を開発する目的で、植物由来で芳香剤として使用されている trepen nerolidol および抗マラリア剤といて使用されている artesunate のバベシアに対する増殖抑制効果について、培養原虫及びネズミバベシアモデル系を用いて検討を行った。

C. 研究結果

(1)バベシア症に対する診断法の検討

Babesia bovis のスフェリカルボディ4(BbSBP4)遺伝子は最近その配列が明らかとなった。そこで、本遺伝子がコードする蛋白質を作製し、この組換え抗原とこれまで報告されている抗原を用いてELISAについて検討を行った。その結果、BbSBP4を用いた ELISA は BbMSA-2c、BbRAP-1/CT、

BbTRAP-T、BbSBP-1を用いたELISAに比較して、優れた感度と特異性を有している事がアジアやアフリカの試料を用いて明らかとなった。

次に、ウシバベシア *Babesia bovis* の膜抗原遺伝子BV5650およびBV8970を用いたnPCRについてRAP-1遺伝子との比較検討を行った。その結果、BV5650遺伝子を用いたnPCRが一番感度が高い事がアジア・アフリカの試料を用いて明らかとなった。

次に第5の人マラリア原虫として注目されて来ている *Plasmodium knowlesi* のLAMP法について検討を行った。*P. knowlesi* のb-tubulin遺伝子情報を基にプラーマーを設計し、LAMP法を確立した。本LAMP法は、特異性が高く他の人マラリア原虫遺伝子と判別可能であり、また感度も通常のPCR法よりも100倍高い事が明らかとなった。

さらに、*B. microti* のBM94組換え抗原を作製し、ELISAについて検討した。その結果、BMN1-17組換え抗原を用いたELISAは、特異性が高く、マウス感染実験において、感染後約90日まで抗体検出が可能であった。

(2)バベシア症に対する治療薬の検討

trepen nerolidol のウシ及びウマバベシア原虫に対する増殖抑制効果について培養原虫を用いて検討を行った。その結果、培養を用いた実験系では、3種類のウシバベシア原虫及び1種類のウマバベシア原虫に対して、trepen nerolidolはで増殖抑制効果を示したが、マウスのバベシア原虫を用いた感染実験系では、エポキソマイシン接種により、対照よりもて低い赤血球寄生率が観察された。また、artesunate のウシ、イヌ及びウマバベシア原虫に対する増殖抑制効果について検討を行ったところ、濃度依存的に、バベシアの増殖を抑制した。

D. 考察

Spherical body(SB)はバベシアに特異的な細胞小器官である。これまで、*B. bovis* に関し3種類のSB遺伝子が報告されている。最近4番目のSB遺伝子配列が報告されているが、その機能等詳細については検討されていない。本研究により、BbSBP-4 は世界的に広く保存されている遺伝子であり、コードする蛋白質は、赤血球内発育の後期に強く発現される事が明らかとなった。また、BbSBP-4 蛋白質を用いた ELISA はこれまで報告されている抗原よりも感度特性が高い事がアジア・アフリカの試料を用いて明らかとなり、今後、世界的な疫学調査に有用であることが示唆された。

次に、ウシバベシア *Babesia bovis* の膜抗原遺伝子BV5650 およびBV8970を用いたnPCRについて検討を行ったところ、これまで報告されているRAP-1遺伝子を用いたnPCR よりも感度が高い事が明らかとなった。今後遺伝子診断法についても、ELISAと同様にこれまで報告されている多くの遺伝子との比較検討を行い、どの遺伝子が世界的な疫学調査に適しているか検討する事が期待される。

Plasmodium knowlesi のLAMP法は、特異性が高く、またサルを用いた実験感染により従来のPCRおよび nPCRよりも感度が高い事が明らかとなった。今後、流行地での人及びサルの試料により本法の有用性について検討を行う必要が有る。

さらに、*B. microti* のBM94組換え抗原を用いた ELISA は、特異性が高く、マウスの感染実験において、長期間にわたり抗体検出が可能であった。今後、流行地の人患者血清を用いて、ELISAの有用性について更に検証することが必要である。

trepen nerolidol は、マラリア原虫やリーシュマニアのイソプロテノイド合成の阻害剤である。本研究においても、ウシ及びウマの培養バベシア原虫に対して増殖抑制効果が認められた。しかし、マウスのバベシア感染実験では、trepen nerolidol により有為な原虫増殖抑制効果は示されなかった。また、抗マラリア剤といて使用されている

artesunate がバベシアに対する増殖抑制効果を示した事から、今後、マラリアも治療で行われているように artesunate と他の薬剤等の併用等について検討する事により、ベシア感染に対する新たな治療効果の薬剤の開発が期待される。

E. 結論

本研究では、血清診断法として *Babesia bovis* の SBP4 組換え抗原組み換え抗原を用いたELISA、遺伝子診断法として *Babesia bovis* の BV5650 遺伝子を標的としたnPCRを確立した。また、人獣共通原虫症として重要なサルマラリア原虫とネズミバベシアに対する遺伝子診断法及び血清診断法を開発した。更にバベシアに対する trepen nerolidol および artesunate の増殖抑制効果について検討を行った。今後これらの研究成果を、バベシア病やマラリアに対する有効診断法や治療法として実用化について更に検討する事が重要である。

G. 研究発表

1)論文発表

1. Hikosaka K, Watanabe YI, Tsuji N, Kita K, Kishine H, Arisue N, Palacpac NM, Kawazu SI, Sawai H, Horii T, Igarashi I, Tanabe K. Divergence of the mitochondrial genome structure in the apicomplexan parasites, *Babesia* and *Theileria*. Mol Biol Evol. 27(5):1107-1116, 2010.
2. Aboulaila M, Sivakumar T, Yokoyama N, Igarashi I. Inhibitory effect of terpene nerolidol on the growth of *Babesia* parasites. Parasitol Int. 59(2):278-282, 2010.
3. Iseki H, Zhou L, Kim C, Inpankaew T, Sununta C, Yokoyama N, Xuan X, Jittapalapong S, Igarashi I. Seroprevalence of *Babesia* infections of dairy cows in northern Thailand. Vet. Parasitol. 170(3-4):193-196, 2010.
4. Aboulaila M, Yokoyama N, Igarashi I. Development and evaluation of two nested PCR assays for the detection of *Babesia bovis* from cattle blood. Vet. Parasitol. 172(1-2):65-70 2010.
5. Iseki H, Kawai S, Takahashi N, Hirai M, Tanabe K, Yokoyama N, Igarashi I. Evaluation of a loop-mediated isothermal amplification method as a tool for diagnosis of infection by the zoonotic simian malaria parasite *Plasmodium knowlesi*. J Clin Microbiol. 48(7):2509-2514, 2010.
6. Goo YK, Terkawi MA, Jia H, Aboge GO, Ooka H, Nelson B, Kim S, Sunaga F, Namikawa K, Igarashi I, Nishikawa Y, Xuan X. Artesunate, a potential drug for treatment of *Babesia* infection. Parasitol Int. 59(3):481-486, 2010.
7. Ooka H, Terkawi MA, Goo YK, Luo Y, Li Y, Yamagishi J, Nishikawa Y, Igarashi I, Xuan X. *Babesia microti*: Molecular and antigenic characterizations of a novel 94-kDa protein (BmP94). Exp Parasitol. 127(1):287-293 2011.
8. Terkawi MA, Huyen NX, Wibowo PE, Seuseu FJ, Aboulaila M, Ueno A, Goo YK, Yokoyama N, Xuan X, Igarashi I. Spherical body protein 4 is a new serological antigen for the global detection of *Babesia bovis* infection in cattle. Clin Vaccine Immunol. 18(2):337-342, 2011.

2)学会発表

1. ウシバベシア2種を同時に診断可能なプロテインアレイの開発。玉城志穂他6名。第149回日本獣医学会学術集会、平成22年3月26-28日、武蔵野市。
2. 小型ピロプラズマを人工感染させたウシの病態解析。横山直明他8名。第149回日本獣医学会学術集会、平成22年3月26-28日、武蔵野市。
3. Apical membrane antigen-1 (AMA-1): new aspects towards babesia vaccine candidate。Mohamad Alaa Terkawi 他4名。平成22年3月26-28日、武蔵野市。
4. Apicomplexa 生物群におけるミトコンドリアゲノムの進化と多様性。彦坂健児他8名。第79回日本寄生虫学会大会、平成22年5月20-21日、旭川市。
5. Validation and evaluation of recombinant antigens for serdiagnosis of *Babesia bovis* infection。M. Alaa Terkawi 他7名。第79回日本寄生虫学会大会、平成22年5月20-21日、旭川市。
6. Molecular characterization of a new spherical body protein of *Babesia bovis* and evaluation of its potential use for serdiagnosis. Ikuo Igarashi 他5名。The XIIth International Congress of Parasitology、平成22年8月 15-20 日、シドニー。
7. A novel molecular diagnostic tool for zoonotic simian malaria parasites *Plasmodium knowlesi* infection. S. Kawai 他6名。The XIIth International Congress of Parasitology、平成22年8月 15-20 日、シドニー。
8. LAMP による *Plasmodium cynomolgi* 遺伝子検出法の開発.高橋延之他4名。第56回日本寄生虫学会・日本衛生動物学会北日本支部合同大会、平成22年10月 2-3 日、札幌。
9. 世界に分布する小型ピロプラズマ。Khukhuu Altangerel 他9名。第56回日本寄生虫学会・日本衛生動物学会北日本支部合同大会。平成22年10月 2-3 日、札幌。
10. LAMP による *Plasmodium cynomolgi* 遺伝子検出法の開発.高橋延之他4名。第51回日本熱帯医学会大会、平成22年12月3-4日、仙台。
11. Spherical body protein 4 is a new serological antigen for the global detection of *Babesia bovis* infection in cattle. M. Alaa Terkawi 他 9 名。45th Annual Japan-US Joint Conference on Parasitic Diseases、平成23年1月 10-11 日、東京。

H. 知的財産権の出願・登録状況

特になし

厚生労働科学研究費補助金（地球規模保健課題推進研究事業（国際医学協力研究事業））
分担研究報告書

寄生虫疾患の病態解明及びその予防・治療をめざした研究
住血吸虫症の検査・診断・対策に関する研究

分担研究者　大前比呂思　国立感染症研究所・寄生動物部　室長
研究協力者　千種　雄一　獨協医科大学・熱帯病寄生虫病室　教授

研究要旨　2000年代になってフィリピンで新しく報告された日本住血吸虫症の浸淫地で行われた疫学調査の結果を、従来から調査されてきた高度浸淫地での調査結果と比較した。フィリピンでは、2002年に、Gonzaga, CAGAYAN州、2005年に、Calatrava, NEGROS州と、複数の日本住血吸虫症の浸淫地が新しく報告された。その両地域で行われた免疫血清検査と腹部超音波検査を中心とする疫学調査の結果を、従来から高度浸淫地として知られる同国、SORSOGON州の浸淫地での結果と比較・分析した。虫卵抗原を用いたELISA検査では、陽性率が20歳程度まで年齢とともに増加していく傾向が、CAGAYAN州とSORSOGON州でみられた。また、年齢が進むにつれて、進行した肝線維化を示す腹部超音波所見:Network patternの比率が増加していく傾向は、３つの浸淫地全てでみられた。2000年代になって新たに確認されたフィリピンの２つの日本住血吸虫症浸淫地の気候は、日本住血吸虫の媒介貝である*Oncomelania quadrasi*が生息できる条件にあっている。また、疫学調査の結果、両地域、特にCAGAYAN州の浸淫地では、従来から日本住血吸虫症浸淫地であったと推測された。

A. 研究目的

住血吸虫症は現在でも世界的に重要な寄生虫性疾患であり、有病地においては住民の健康被害のみならず、社会経済的な問題ともなっている。また近年は、地球温暖化や水源開発に伴う環境変化による、媒介貝生息地の拡大に伴う浸淫地の拡大も懸念されている。

上記のような現状を考えると、新しく確認された住血吸虫症浸淫地については、２つの可能性、１）住血吸虫症浸淫地の拡大２）従来認知されていなかった住血吸虫症浸淫地の発見 を、区別することが重要である。そこで、免疫血清診断や腹部超音波検査を利用した疫学調査で、両地域を区別する方法について検討した。

B. 研究方法

2008 年から 2010 年にかけて、Gonzaga, CAGAYAN州と、Calatrava, NEGROS州の新しく発見された日本住血吸虫症浸淫地で行った調査の結果を、2005 年から 2007 年にSORSOGON州の日本住血吸虫症の高度浸淫地で行った調査結果と比較して分析した。

総計3,355人の対象者について、10歳間隔に、対象地域毎に７グループに分けた（0-9歳, 10-19歳, 20-29歳, 30-39歳, 40-49歳, 50-59 歳, 60 歳－ ）。Kato-katz 法による糞便検査を行う一方、採取した血清を用いて、日本住血吸虫卵抗原による ELISA 抗体価を求めた。また、あわせて腹部超音波検査を行って、肝線維化の進行について評価した。

被験者には、研究目的・方法について充分説明し、成人であれば本人から、未成年者であれば保護者から書面での承諾を得た。また、糞便中の虫卵陽性者はもちろん、血清診断のみでの陽性者に対しても、検査結果の情報を提供し、プラジカンテル投与を行うよう試みた。

C. 研究結果

虫卵抗原を用いたELISA検査では、10歳以降での陽性率が、SORSOGON州では70%程度、CAGAYAN州では50%前後となり、年齢群間の差がみられなかった(図1-A, 図1-B)。一方、NEGROS州では、各年齢群で全体的に陽性率が低いうえ、陽性率もばらばらであった(図1-C)。

一方、腹部超音波検査の結果では、年齢が進むにつれて、進行した肝線維化と判断される腹部超音波所見：Network patternを示す比率が増加していく傾向が、3つの浸淫地でみられ、特にSORSOGON州とCAGAYAN州の50歳くらいまでの年齢層で、明らかだった(図2-A, B, C)。また、SORSOGON州では、10代でも進んだ線維化を示す例がみられたのに対し、Network patternの検出例は、CAGAYAN州では20歳以降、NEGROS州では30歳以降で増加する傾向がみられた。

D. 考察

2000年代になって新たに確認されたフィリピンの2つの日本住血吸虫症浸淫地は、日本住血吸虫媒介貝である *Oncomelania quadrasi* の生息に適した気候環境で、毎月の月間降水量がほぼ100mmを超え、明瞭な乾季がない。また、疫学調査の結果、CAGAYAN州で新しく発見された日本住血吸症浸淫地では、虫卵抗原によるELISAの陽性率が、一定の年齢層以上では、ほぼ一定となる傾向を示した。この傾向は、従来から日本住血吸虫症の高度浸淫地として知られてきたSORSOGON州でみられる傾向と同じである。

また、腹部超音波検査の結果では、3つの浸淫地全てで、年齢が進むにつれ、進行した肝線維化を示す例の割合が増加する傾向が確認された。住血吸虫症の浸淫地では、長期間にわたり感染と治療を繰り返す結果、加齢とともに、次第に不可逆的な肝線維化を示す例が増加すると考えられている。新しく発見されたCAGAYAN州、NEGUROS州の浸淫地でも、この年齢と肝線維化の関係が確認されたことから、両地域ではかなり前から、住血吸虫の感染が繰り返し起こっていたことが示唆された。また、CAGAYAN州では、超音波検査で進行した肝線維化を示しながら、ELISAの結果が陰性となった例も確認されたが、一般的にこのような例は、10年以上前に日本住血吸虫に感染し、その後の治療が不十分であった例と考えられる。

E. 結論

2000年代になって新たに確認されたフィリピンの2つの日本住血吸虫症浸淫地は、日本住血吸虫の媒介貝である *Oncomelania quadrasi* が生息できる気候環境にある。また、疫学調査の結果を解析した結果、両地域、特にCAGAYAN州の浸淫地では、従来から日本住血吸虫症浸淫地であったと判断された。

F．健康危険情報

特になし

G．研究発表

1．論文発表

1) Shimada M, Kirinoki M, Shimizu K, Kato-Hayashi N, Chigusa Y, Kitikoon V, Pongassakulchoti P, Matsuda H. Characteristics of granuloma formation and liver fibrosis in murine schistosomiasis mekongi: a morphological comparison between *Schistosoma mekongi* and S. japonicum infection.

Parasitology 2010 ; 137:1781-1789.

2) Kumagai T, Furushima-Shimogawara R, Ohmae H, Wang TP, Lu S, Chen R, Wen L, Ohta N. Detection of early and single infections of *Schistosoma japonicum* in the intermediate host snail, *Oncomelania hupensis*, by PCR and Loop-Mediated Isothermal Amplification (LAMP) assay

Am J Trop. Med Hyg
2010, 83:542-548.

3) Kirinoki M, Chigusa Y, Ohmae H, Matsumoto J, Kitikoon V, Sinuon M, Saem C, Socheat D, Matsuda H. Application of whole-blood ELISA (WB-ELISA) for a field survey of schistosomiasis mekongi

Parasitology 2011 (in press)

4) Kirinoki M, Chigusa Y, Ohmae H, Matsumoto J, Kitikoon V, Sinuon M, Saem C, Socheat D, Matsuda H. Efficacy of sodium metaperiodate (SMP)-ELISA for the serodiagnosis of schistosomiasis mekongi.

Southeast Asi J Trop Med Pub Hlth
(in press)

2. 学会発表

1) 桐木雅史、林尚子、Muth Sinuon、Doung Socheat、Viroj Kitikoon、千種雄一、松田肇. カンボジア・クラチェ県におけるメコン住血吸虫症疫学調査.
第 79 回 日本寄生虫学会大会 旭川市 2010 年 5 月 20 日～21 日

2) 福原一磨、桐木雅史、千種雄一、尾藤伴行、井上真理、中村哲、松田肇、石川洋文. ラオス・コーン島村落間ネットワークモデルに基づくメコン住血吸虫症対策の評価. 第 79 回 日本寄生虫学会大会 旭川市 2010 年 5 月 20 日～21 日

3) Ohmae H, Kirinoki M, Suniko LS, Boldeero NP, Viacorte EA, Solon AA, Leonard LR, Leshem E, Chigusa Y. Surveys on newly found endemic foci in Southeast Asian countries 2.
The 45th Japan-US Joint Conference on Parasitic Diseases.
Tokyo, Japan January 10-11, 2011

図 1-A Sorsogon 州における日本住血吸虫卵抗原による ELISA 陽性率と年齢の関係

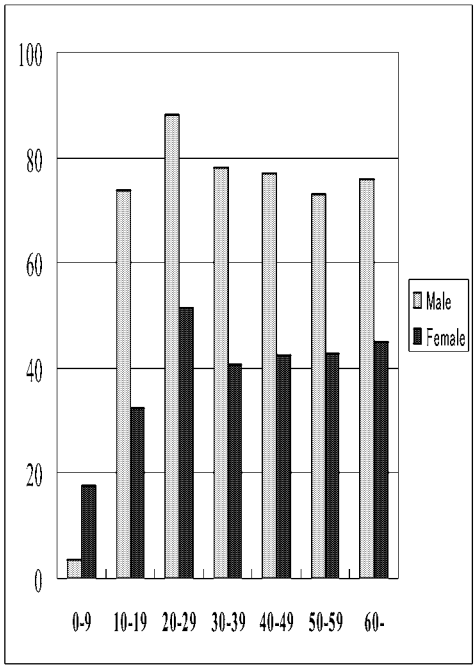

図 1-B Kagayan 州における日本住血吸虫卵抗原による ELISA 陽性率と年齢の関係

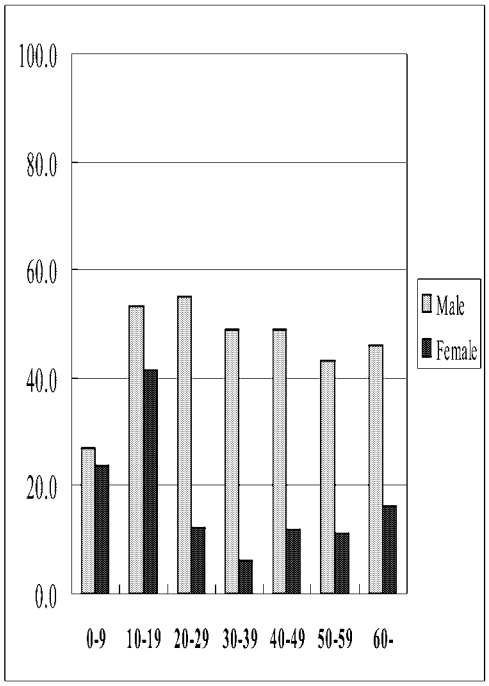

図 1-C Negro s 州における日本住血吸虫卵抗原による ELISA 陽性率と年齢の関係

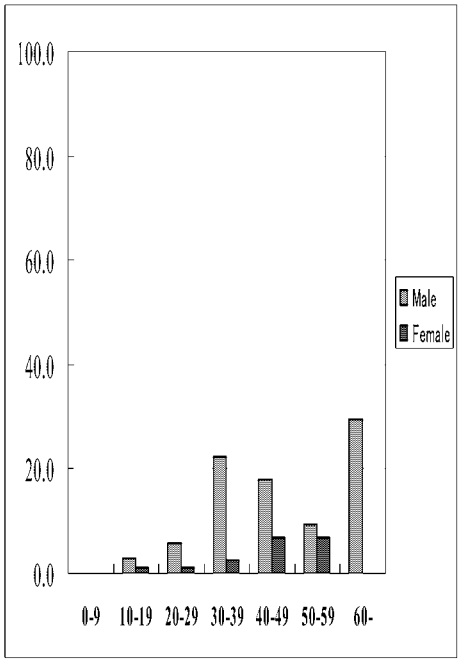

図 1-A Sorsogon 州における超音波検査による肝線維化の評価と年齢の関係

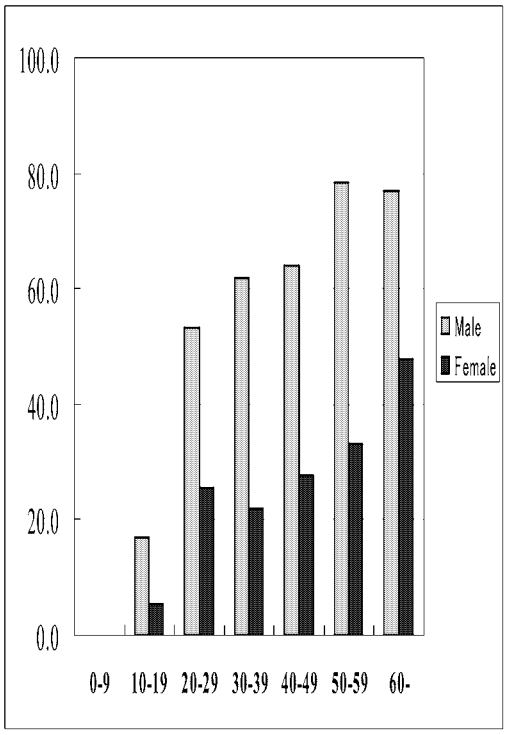

図 1-C Negros 州における超音波検査による肝線維化の評価と年齢の関係

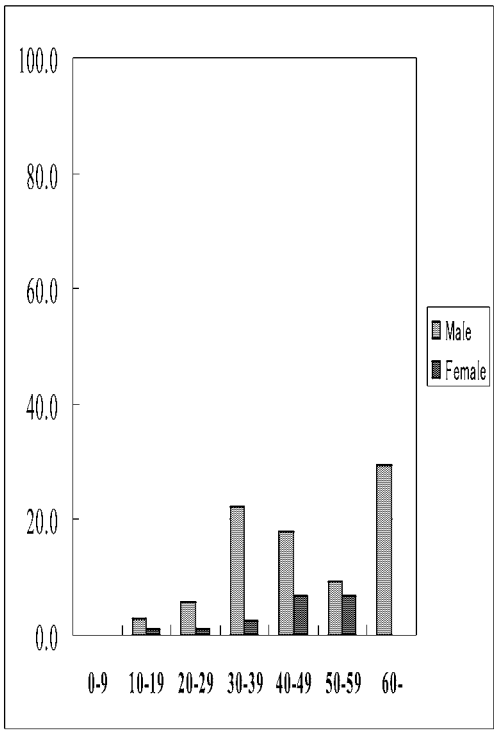

図 1-B Kagayan 州における超音波検査による肝線維化の評価と年齢の関係

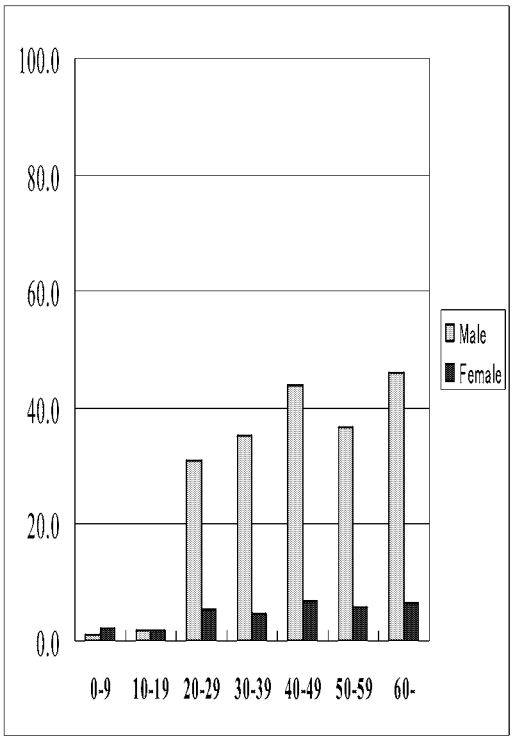

厚生労働科学研究費補助金（地球規模保健課題推進研究事業（国際医学協力研究事業）
（分担）研究報告書

人獣共通寄生原虫・蠕虫症の寄生適応に関する分子生物学的解析

分担研究者　　奈良武司　順天堂大学大学院医学研究科　准教授

研究要旨:トリパノソーマ類を含むキネトプラスチダ類の生存に必須な特異オルガネラ、グリコソームの成立背景について解析した。その結果、近縁群のディプロネマ類では一部の解糖系酵素のペルオキシソーム移行が認められ、両生物群の共通祖先においてすでにグリコソームの原型が成立していた可能性が示唆された。

A．研究目的

本研究は、アメリカトリパノソーマ症（シャーガス病）や日本住血吸虫症など、人獣共通寄生虫症を引き起こす病原体の特異な分子機構を同定し、新規治療薬開発およびワクチン開発を行なうことを目的とする。

トリパノソーマ類の生存に必須な特異オルガネラ、グリコソームは、移行シグナルの共通性などからペルオキシソームを起原とすることが示唆されているとともに、解糖系酵素や核酸代謝経路酵素の局在など、他の真核生物には無い特徴を示す。これら酵素は、ヒト酵素とは異なる局在性や生化学的性状を持つことから有望な薬剤標的と考えられる。本年度は、グリコソームの成立背景と生理的意義について解析した。ユーグレノゾア生物門のユーグレナ類、ディプロネマ類、およびトリパノソーマ類とボド類からなるキネトプラスチダ類は、進化上この順序で分岐したと考えられている。グリコソームはキネトプラスチダ類に存在する一方、ユーグレナ類には見出されていない。そこで、ユーグレナ類の分岐以降に出現したディプロネマ類について、解糖系酵素のアルドラーゼ（ALD）、およびピリミジン生合成経路のオロチジン酸脱炭酸酵素（OMPDC、トリパノソーマ類ではオロト酸フォスフォリボシルトランスフェラーゼ（OPRT）との融合酵素OMPDC-OPRTとしてグリコソームに局在する）の遺伝子クローニングと細胞内局在の解析を行なった。

B．研究方法

ディプロネマ*Diplonema papillatum*（ATCC 50162）のALDについて、すでに報告されているEST部分配列に基づいてプライマーを設計し、ORF全長をコードするcDNAをクローニングした。*D. papillatum*のOMPDCについてはすでにcDNAクローニングを終えている（Makiuchi, *et al.*, *Protist*, 159: 459-470, 2008）。ALD、OMPDCそれぞれの組換えタンパクを大腸菌で発現させ、これを用いて特異抗体を作製した。

ALDおよびOMPDCの細胞内局在について、生化学的解析および組織化学的解析を行なった。培養した*D. papillatum*を破砕後、遠心分離によって核画分、膜画分、および細胞質画分を調製し、ALDおよびOMPDC特異抗体を用いたウエスタンブロットを行ない、ALDおよびOMPDCの細胞内局在を分析した。また、ALDおよびOMPDC特異抗体を用いた免疫蛍光染色（IFA）を行ない、ALDおよびOMPDCが局在する小胞の存在を解析した。

C．研究結果

D. papillatum ALDにはグリコソーム局在タンパク同様、ペルオキシソーム移行シグナル（PTS）が存在した。分子系統解析はトリパノソーマ類および*D. papillatum*のALDの単系統性を示し、トリパノソーマ類と*D. papillatum*の共通祖先段階ですでにALDがペルオキシソームに局在していた可能性を強く示唆した。免疫蛍光染色（IFA）を行なったところ、ALDはトリパノソーマ類（*Trypanosoma cruzi*）および*D. papillatum*の両者においてドット状の蛍光パターンとして検出された。一方、*D. papillatum* OMPDCはトリパノソーマ類のOMPDCとは異なる起原を持ち（Makiuchi, *et al.*, *Protist*, 159: 459-470, 2008）、PTSを持たない。免疫蛍光染色（IFA）を行なったところ、シグナルは細胞中に一様に観察さ

れ、OMPDCは細胞質局在性であることが示唆された。

D．考 察

本研究から、*D. papillatum*のALDはPTSを持ち、細胞内小胞に局在することが明らかとなった。これは、解糖系酵素のペルオキシソームへの移行がキネトプラスチダ類とディプロネマ類との分岐以前に既に成立していたことを示唆する最初の報告である。また、*D. papillatum*ではOMPDCとALDの細胞内局在は異なることから、ディプロネマ類のグリコソーム様オルガネラは核酸合成酵素群を欠いている可能性が高い。これは、ディプロネマ類とキネトプラスチダ類が分岐した後に系統群特異的な進化を遂げた結果、現在のような特殊化したペルオキシソーム（グリコソーム）が成立したことを示している。今後、ディプロネマ類におけるグリコソーム様オルガネラの単離および性状解析を行うことによって、難治病原体であるトリパノソーマ類が持つグリコソームの成立背景および寄生適応に果たした役割を明らかにしていきたい。

E．結 論

これまでトリパノソーマ類を含むキネトプラスチダ類に特異的と考えられてきたグリコソームの成立背景について解析した結果、近縁群のディプロネマ類との共通祖先段階ですでに解糖系酵素の一部がペルオキシソームに移行しており、グリコソームのプロトタイプがすでに成立していた可能性が示唆された。

G．研究発表

1．論文発表

Tajima K, Miura K, Ishiwata T, Takahashi F, Yoshioka M, Minakata K, Murakami A, Sasaki S, Iwakami S, Annoura T, Hashimoto M, **Nara T**, Takahashi K. Sex hormones alter Th1 responses and enhance granuloma formation in the lung. *Respiration, in press*

Makiuchi T, Annoura T, Hashimoto M, Hashimoto T, Aoki T, **Nara T**. Compartmentalization of a glycolytic enzyme in *Diplonema*, a non-kinetoplastid Euglenozoan. *Protist, in press*

Kido Y, Shiba T, Inaoka DK, Sakamoto K, **Nara T**, Aoki T, Honma T, Tanaka A, Inoue M, Matsuoka S, Moore A, Harada S, Kita K. Crystallization and preliminary crystallographic analysis of cyanide-insensitive alternative oxidase from *Trypanosoma brucei brucei. Acta Cryst Section F,* 66: 275-278, 2010

Balogun EO, Inaoka DK, Kido Y, Shiba T, **Nara T**, Aoki T, Honma T, Tanaka A, Inoue M, Matsuoka S, Michels PAM, Harada S, Kita K. Overproduction, purification, crystallization and preliminary X-ray diffraction analysis of *Trypanosoma brucei gambiense* glycerol kinase. *Acta Cryst Section F,* 66: 304-308, 2010

Tajima K, Ohashi R, Sekido Y, Hida T, **Nara T**, Hashimoto M, Iwakami S, Minakata K, Yae T, Takahashi F, Saya H, Takahashi K. Osteopontin-mediated enhanced hyaluronan binding induces multidrug resistance in mesothelioma cells. *Oncogene* 29(13): 1941-1951, 2010

Kohama H, Harakuni T, Kikuchi M, **Nara T**, Takemura Y, Miyata T, Sato Y, Hirayama K, Arakawa T. Intranasal administration of *Schistosoma japonicum* paramyosin induced robust long-lasting systemic and local antibody as well as delayed-type hypersensitivity responses, but failed to confer protection in a mouse infection model. *Jap J Inf Dis*, 63(3): 166-172, 2010

H．知的財産権の出願・登録状況

特になし

厚生労働科学研究補助金（地球規模保健課題推進研究事業（国際医学協力研究事業））
「寄生虫疾患の病態解明及びその予防・治療を目めざした研究」
分担研究報告書

人獣共通幼条虫症（脳嚢虫症、エキノコックス症）の病態、診断、治療、予防に向けた研究

研究分担者　伊藤　亮　旭川医科大学寄生虫学講座

研究要旨

人獣共通寄生虫疾患である脳嚢虫症とエキノコックス症は、地球規模で環境汚染と流行拡大が年々深刻化しており、WHO によって狂犬病その他とともに Neglected Tropical Diseases にリストアップされている。本研究では、これらの寄生虫疾患についての免疫、遺伝子診断法の改善と、病原体である寄生虫の遺伝子多型解析ならびに解析結果に基づく感染地域の特定についての研究を前年度からの継続研究として実施した。1) 世界各地で嚢虫症を引き起こしている有鉤条虫(*Taenia solium*)は、ミトコンドリア DNA の遺伝子解析により大きくアジア型とアメリカ・アフリカ型に分けることができるが、アジア型とアメリカ・アフリカ型を区別できる新しい遺伝子を見出した(業績 15)。アジアではさらに国や地域ごとに特徴的なハプロタイプが存在することが判明してきた。このような寄生虫の遺伝子情報と患者の旅行歴とを照らし合わせることにより、患者が感染した地域を特定することができた(業績 7; Jongwutiwes et al. in press) 。2) 人体寄生テニア属条虫 3 種の遺伝子鑑別法としてミトコンドリアならびに各遺伝子を用いる Loop-mediated isothermal amplification (LAMP) 法を確立しているが、本年度の研究で、LAMP 法による糞便内遺伝子検査法を確立し(業績 11)、さらに流行地でのリアルタイム検査への導入条件の検討を試み、流行の現場で実施可能であることをほぼ確認した(Nkouawa et al. unpublished)。3) 上記 1)、2) の研究から、アジア各地に分布している人体寄生テニア条虫、*Taenia asiatica* と *Taenia saginata* の交雑個体がタイ(業績 9、10)のみならず中国でも確認された(業績 11; Okamoto et al. in prep; Nkouawa et al. in prep)。4) インドで有鉤条虫に感染し、年余にわたる虫卵排出と、自家感染による嚢虫症を引き起こした日本人症例に遭遇し、患者の家族ならびに会社の同僚について嚢虫症の 2 次感染の有無を血清検査、テニア症について LAMP 検査その他を実施し、国内での 2 次感染予防、阻止に向けた基礎資料を準備している(Ito et al. unpublished)。5) 血清検査により流行地住民から嚢虫症患者を確認できることができた(業績 10,12)。6) エキノコックス属条虫について、ミトコンドリアと核の遺伝子解析に基づく分子系統学ならびに系統地理学的研究行い、有鉤条虫同様ハプロタイプ解析により、感染地の特定が可能なことを報告した(業績 4、8)。7) 遺伝子組み換え Em18 (RecEm18), Antigen B(Rec AgB) を用いるエキノコックス症に関する血清診断法に関する外部評価研究を展開し(業績 3、5、14)、すでに確立されている迅速イムノクロマト診断法

を用いる海外の代表的研究機関との外部評価を実施している(Knapp J et al. in prep)。8)多包虫症に関する新しい化学療法の開発基礎研究として新規のシステインペプチターゼのクローニングと生理活性解析を行った(業績 16)。以上、患者確認に必要な血清抗体検査法、遺伝子検査法の改善、開発に取り組み、感染者と感染動物の検出精度が大きく向上し、流行の現場においてリアルタイムで役立つ検査法ならびに調査指針(業績 1、6)をほぼ確立することができた。さらに流行地における継続的な啓発と技術革新に向けた会議を主催し(業績 2)、総説 4 篇を専門書、専門誌に発表した(業績 1、2、6、13)。今後は、抗体応答解析や遺伝子多型解析に基づいて、致死的な人獣共通幼条虫症を引き起こす一群の条虫による国内での突発的な流行（脳嚢虫症）等が発生する場合にもリアルタイムで対応し、対策を講じることが可能と期待される。また、北海道の地方病であるエキノコックス症について我々が確立した検査法(RecEm18-ELISA、RecEm18-Immunoblot)は、世界最高水準との国際評価を得ている。さらに、我々は昨年度にアドテック(株)と共同で簡便な迅速イムノクロマト診断キットを開発している。このキットは特別な経験や施設を必要とせず、受診時間内にリアルタイムで結果を出せる。30 年前に 1 度だけ 1 週間のバスツアーで北海道を訪問し、昨年、確定診断がつかずに外科治療を受け、多包虫症と確定された症例がある(Amano et al. in prep)。国内では北海道の地方病として知られているが、このような北海道以外からの観光客が北海道内で感染する症例は日本人、外国人を問わず、今後も増えることが懸念される。それゆえ、北海道外の全国病院で診断が確定しない肝疾患では多包虫症の確定あるいは除外の目的で、全国病院のベッドサイドでの迅速キットの利用が推奨される。さらに 2010 年 1 月に米国疾病情報対策センター（CDC）から米国内でのエキノコックス症住民健診、確定検査法として旭川医科大学で開発した血清診断用抗原(RecEm18、RecAgB8/1)を正式採用したいという協力要請を受けていることからも、国内での住民健診に積極的に応用すべきであろう。

A. 研究目的

人獣共通幼条虫症として地球規模で深刻な問題を提示している疾患は、脳嚢虫症とエキノコックス症（単包虫症ならびに多包虫症）である。人体寄生テニア属条虫として 3 種(*Taenia solium*、*Taenia saginata*、*Taenia asiatica*)が知られているが、これらの中で人体脳嚢虫症を引き起こすのは *T. solium* 1 種である。本研究では 1）これら 3 種が同所的に分布している地域（タイ、中国）の発見と、3 種鑑別法の改善および開発、2）*T. solium* と他の 2 種の分子系統学的評価、3）嚢虫症流行地での患者検出方法の改善と新しい抗原精製法の開発、4）遺伝子解析により患者の感染地域を特定する試みについて研究を展開した。エキノコックス症に関しても同様な遺伝子解析による分類の再検討、種内変異解析、病原性と病態転換（内生出芽と外生出芽）、宿主転換（イヌ科動物とネコ科動物）と血清診断法の改良と評価を試みた。

B. 研究方法

材料：テニア属条虫症：テニア条虫感染者

から駆虫された虫体、糞便、血清
嚢虫症：摘出病巣（嚢虫）、血清、髄液
エキノコックス症：世界各国において画像診断ならびに外科手術により確定診断がついた単包虫症、多包虫症、その他の包虫症患者から得られたエタノール固定原頭節、血清、ならびに野生動物から得られたエタノール固定原頭節、虫卵と成虫
方法：寄生虫体（虫卵、幼虫、成虫）ならびに宿主糞便からDNAを抽出し、ミトコンドリアDNAと核の遺伝子を解析した。また、新たにLAMP法の導入を試みた。抗体検査についても各種遺伝子組み換え抗原を用いてイムノブロット、ELISA、さらに迅速キットを用いる迅速検査を実施した。

C. 研究結果

1. テニア症・嚢虫症研究

1) すでに確立されているLAMP法を用い、寄生虫タイの確認なしの糞便検査への応用の可能性を解析し、従来法のMultiplex PCRよりも感度が格段に高くなることを明らかにした(業績11)。

2) 遺伝子解析に基づくテニア条虫の雑種の確認：タイならびに中国で採集されたテニア条虫から無鉤条虫とアジア条虫の交雑個体が確認された(業績 9,10;Okamoto et al. in prep; Nkouawa et al. in prep)。

3) 遺伝子解析に基づく感染地の特定:国内で外科治療を受けた症例において、大脳から摘出された病理標本を用いた遺伝子解析の結果と患者の旅行歴と照らし合わせることにより、感染地域を特定できた(業績 7; Jongwutiwes et al. in press)。

4) アジア型とアフリカ・アメリカ型の識別に有用な新規の遺伝子を発見した(業績15)。

5) 嚢虫症の流行地域住民検診に血清検査法を導入し、カメルーン(業績12)、タイ(業績10)、インドネシア(Swastika et al. in prep)、中国(Li et al. in prep)で患者の確認に成功した。

2. エキノコックス症研究

1) 分子系統学的、分子検査学的研究：中国に分布している3種のエキノコックス条虫のミトコンドリア遺伝子ハプロタイプ解析から、単包条虫、多包条虫は最近チベット高地に侵入したものであり、新種 *E. shiquicus* はチベット固有種であると結論された(業績8、13)。

2) 血清診断法の開発、診断学的研究：①ドイツのKern教授（2009年からWHO informal working group on Echinococcosis 代表）との共同研究から、多包虫症の病態、病勢と完全に一致する血清検査法は旭川医科大学のEm18-ELISAであると結論する追加論文が発表された(業績14)。②フランスにおいて約20年経過観察してきた多包虫症症例の病勢、病態のフォローアップにEm18- ELISAが役立つことが判明した(Bresson- Hadni et al. Liver Transplantation in press)。③中国におけるエキノコックス症に関する画像診断と血清診断成績が報告された(業績3,5)。

3. 疫学研究

①モンゴルにおいて、多包虫症患者と多包条虫の遺伝子多型が確認された(業績 4)。②カメルーン、タイの嚢虫症流行地で血清疫学研究を展開し、感染者の特定に成功した(業績10,12)。

4. 研究指針等の総説

上記の研究に関する総説(業績 1、13)、ガイドライン(業績 6)を発表した。

D. E. 考察・結論

人獣共通幼条虫症（脳嚢虫症、エキノコックス症）ならびに条虫症（テニア症）に関する分子、遺伝子から流行の現場までを網羅する総合的な研究を展開してきた。病理標本が入手できる症例では感染地の特定が可能であった。アジアを中心に、テニア症感染の実態が判明し始めており、我々が開発した免疫学的検査法、遺伝子検査法が流行地の特定、感染者の発見、患者特定に非常に大きく役立ってきていると評価できよう。さらにエキノコックス症（多包虫症、単包虫症）迅速診断キットの開発は、治療を要する活性病巣を有している患者の 96%を 20 分以内に 1 度の検査でほぼ 100%間違いなく確認できることから、病院での外来患者の診断や治癒経過の観察のみならず、地域住民検診にも大きく役立つことが期待される。

米国疾病情報対策センターより、旭川医科大学で開発されたエキノコックス症に関する血清検査法（RecEm18、RecAgB8/1 を用いる ELISA 法）を米国民に対する住民スクリーニング、確認検査法として採用したいので協力してほしいという要請が届いている。またフランス、フレンチコムテ大学病院（WHO collaboration center for clinical echinococcosis）からも RecEm18、RecAgB8/1 の提供を要請されている。さらに、フレンチコムテ大学と迅速診断キットの外部評価研究が現在展開されており、フランス、ドイツからヨーロッパでの市販の可能性について問い合わせが来ている。

F. 健康危険情報

特になし

G. 研究発表

著書

1. Flisser A, Craig PS, Ito A. Chapter 51: Cysticercosis and Taeniosis: *Taenia solium*, *Taenia saginata* and *Taenia asiatica*. In: Oxford Textbooks of Zoonoses (eds. By Palmer SR, Lord Soulsby, Torgerson PR, Brown DWG), 627-644. Oxford University Press, 2011.

論文

2. Gurbadam A et al. Mongolian and Japanese Joint Congress on "Echinococcoses: diagnosis, treatment and prevention in Mongolia" June 4, 2009. *Parasites and Vectors* 2010; 3: 1/8-3/8.
3. Li T et al. Specific IgG Responses to Recombinant Antigen B and Em18 in Cystic and Alveolar Echinococcosis in China. *Clinical and Vaccine Immunology* 2010; 17: 40-475.
4. Ito A et al. Histopathological, Serological and Molecular Confirmation of Indigenous Alveolar echinococcosis cases in Mongolia. *American Journal of Tropical Medicine and Hygiene* 2010; 82: 266-269.
5. Li T et al. Widespread co-endemicity of human cystic and alveolar echinococcosis on the eastern Tibetan plateau, northwest Sichuan/southeast Qinghai, China. *Acta Tropica* 2010; 113: 248-256.
6. Brunetti E et al. Expert consensus for the diagnosis and treatment of cystic and alveolar echinococcosis in humans. *Acta Tropica*

2010;114: 1-16.

7. Yanagida T et al. Neurocysticercosis: Assessing where the infection was acquired from. *Journal of Travel Medicine* 2010; 17:206-208.
8. Nakao M et al. Genetic polymorphisms of *Echinococcus* tapeworms in China as determined by mitochondrial and nuclear DNA sequences. *International Journal for Parasitology* 2010; 40: 379-385.
9. Okamoto M et al. Evidence of hybridization between *Taenia saginata* and *Taenia asiatica*. *Parasitology International* 2010; 59: 70-74.
10. Anantaphruti MT et al. Molecular and serological survey on taeniasis and cysticercosis in Kanchanaburi Province, Thailand. *Parasitology International* 2010; 59: 326-330.
11. Nkouawa A et al. Evaluation of a loop-mediated isothermal amplification method using fecal specimens for differential detection of *Taenia* species from humans. *Journal of Clinical Microbiology* 2010a; 48: 3350-3352.
12. Nkouawa A et al. Serological studies of neurologic helminthic infections in rural areas of Southwest Cameroon: toxocariasis, cysticercosis and paragonimiasis. *PLoS Neglected Tropical Diseases* 2010b; 4: e732.
13. Nakao M et al. State-of-the-art *Echinococcus* and *Taenia*: Phylogenetic taxonomy of human-pathogenic tapeworms and its application to molecular diagnosis. *Infection, Genetics and Evolution* 2010; 10:444-452.(総説)
14. Tappe D et al. Immunoglobulin G subclass responses to recombinant Em18 in the follow-up of patients with alveolar echinococcosis in different clinical stages. *Clinical Vaccine Immunology* 2010; 17: 944-948.
15. Sato MO et al. A possible nuclear DNA marker to differentiate the two geographic genotypes of *Taenia solium* tapeworms. *Parsitology International* 2011; 60: 108-110.
16. Sako Y et al. *Echinococcus multilocularis:* identification and functional characterization of cathepsin B-like peptidases from metacestode. *Experimental Parasitology* 2011; in press.

3. 学会発表

省略

H. 知的財産権の出願・登録状況

なし

研究成果の刊行に関する一覧表

研究成果の刊行に関する一覧表

雑　誌

発表者氏名	論文タイトル名	発表誌名	巻号	ページ	出版年
Kohama H, Harakuni T, Kikuchi M, Nara T, Takemura Y, Miyata T, Sato Y, Hirayama K, Arakawa T.	Intranasal Administration of *Schistosoma japonicum* Paramyosin Induced Robust Long-Lasting Systemic and Local Antibody as well as Delayed-Type Hypersensitivity Responses, but Failed to Confer Protection in a Mouse Infection Model.	Jpn J Infect Dis	63(3)	166-72	2010
Kido,Y., Sakamoto, K., Nakamura, K., Harada, M., Suzuki, T., Yabu, Y., Saimoto, H., Yamakura, F., Ohmori, D., Moore, A., Harada, S. and Kita, K.	Purification and kinetic characterization of recombinant alternative oxidase from *Trypanosoma brucei brucei.*	Biochim Biophys. Acta (Bioenergetics)	1797	443-450	2010
Kido, Y., Shiba, T., Inaoka, D. K. Sakamoto, K., Nara, K., Aoki, T., Honma, T., Tanaka, A., Inoue, M., Matsuoka, S., Moore, A., Harada, S. and Kita, K.	Crystallization and preliminary crystallographic analysis of cyanide-insensitive alternative oxidase from *Trypanosoma brucei brucei*	Acta Crystallographica	F66	275-278	2010
Hikosaka, K., Watanabe, Y., Tsuji, N., Kita, K., Kishine, H., Arisue, N., Palacpac, N. M. Q., Kawazu, S., Sawai, H., Horii, T., Igarashi, I. and Tanabe, K.	Divergence of mitochondrial genome structure in the apicomplexan parasites, *Babesia* and *Theileria*	Mol. Biol. Evolution	27	1107-1116	2010

発表者氏名	論文タイトル名	発表誌名	巻号	ページ	出版年
Balogun, O. E., Inaoka, D. K., Kido, Y., Shiba, T., Nara, T., Aoki, T., Honma, T., Tanaka, A., Inoue, M., Matsuoka, S., Michels, P. AM,. Harada, S. and Kita, K. Acta Crystallographica	Overproduction, purification, crystallization and preliminary X-ray diffraction analysis of *Trypanosoma brucei gambiense* glycerol kinase	Acta Crystallographica	F66	304-308	2010
Masuda, I., Matsuzaki, M. and Kita, K.	Extensive frameshift at all AGG and CCC codons in the mitochondrial cytochrome *c* oxidase subunit 1 gene of *Perkinsus marinus* (Alveolata; Dinoflagellata)	Nucleic Acids Research	38	6186-6194	2010
Nakamura, K., Fujioka, S., Fukumoto, S., Inoue, N., Sakamoto, Hirata, H., Kido, Y., Yabu, Y., Suzuki, T., Watanabe, Y., Saimoto, H., Akiyama, H. and Kita, K.	Trypanosome alternative oxidase, a potential therapeutic target for sleeping sickness, is conserved among *Trypanosoma brucei* subspecies	Parasitol. Int.	59	560-564	2010
Hikosaka, K., Nakai, Y., Watanabe, Y., Tachibana, S., Arisue, N., Palacpac, N. M., Toyama, T., Honma, H., Horii, T., Kita, K. and Tanabe, K.	Concatenated mitochondrial DNA of the coccidian parasite *Eimeria tenella*.	Mitochondrion,	11	273-278	2010

発表者氏名	論文タイトル名	発表誌名	巻号	ページ	出版年
Moritoshi Iwagami, Seung-Young Hwang, Megumi Fukumoto, Toshiyuki Hayakawa, Kazuyuki Tanabe, So-Hee Kim, Weon-Gyu Kho, Shigeyuki Kano	Geographical origin of *Plasmodium vivax* in the Republic of Korea: haplotype network analysis based on the parasite's mitochondrial genome	Malaria Journal	9巻	184-188	2010
Tsuboi T, Takeo S, Arumugam TU, Otsuki H, Torii M	The wheat germ cell-free protein synthesis system: a key tool for novel malaria vaccine candidate discovery	Acta Trop.	114	171-176	2010
Miyata T, Harakuni T, Tsuboi T, Sattabongkot J, Kohama H, Tachibana M, Matsuzaki G, Torii M, Arakawa T	*Plasmodium vivax* ookinete surface protein, Pvs25, linked to cholera toxin B subunit induces potent transmission-blocking immunity by intranasal as well as subcutaneous immunization	Infect Immun.	78	3773-3782	2010
Blagborough AM, Yoshida S, Sattabongkot J, Tsuboi T, Sinden RE	Intranasal and intramuscular immunization with baculovirus dual expression system-based Pvs25 vaccine substantially blocks *Plasmodium vivax* transmission	Vaccine	28	6014-6020	2010
Jeelani, G., Husain, A., Sato, D., Ali, V., Suematsue, M., Soga, T., and Nozaki, T.	Two Atypical L-cysteine-regulated NADPH-dependent oxidoreductases involved in redox maintenance, L-cystine reduction, and metronidazole activation in the enteric protozoon Entamoeba histolytica.	J. Biol. Chem.	285	26889-26899	2010

発表者氏名	論文タイトル名	発表誌名	巻号	ページ	出版年
Yousuf, M. A., Mi-ichi, F., Nakada-Tsukui, K., and Nozaki, T.	Localization and targeting of unusual pyridine nucleotide transhydrogenase in Entamoeba histolytica..	Eukaryot. Cell	9	926-933	2010
Kimura E.	The Global Programme to Eliminate Lymphatic Filariasis: History and achievements with special reference to annual single-dose treatment with diethylcarbamazine in Samoa and Fiji.	Tropical Medicine and Health	39	1-14	2011
Anisuzzaman, Islam MK, Miyoshi T, Alim MA, Hatta T, Yamaji K, Matsumoto Y, Fujisaki K, Tsuji N.	Longistatin, a novel EF-hand protein from the ixodid tick *Haemaphysalis longicornis*, is required for acquisition of host blood-meals.	Int J Parasitol.	40	721-729.	2010
Kumagai T, Furushima-Shimogawara R, Ohmae H, Wang TP, Lu S, Chen R, Wen L, Ohta N.	Detection of early and single infections of Schistosoma japonicum in the intermediate host snail, Oncomelania hupensis, by PCR and loop-mediated isothermal amplification (LAMP) assay.	Am J Trop Med Hygiene	83:(3)	542-8	2010
長田良雄	寄生虫とアレルギーの親密な関係	Medical Practice	27 (9)	1541-1542	2010
Shimizu S, Osada Y, Kanazawa T, Tanaka Y, Arai M.	Suppressive effect of azithromycin on *Plasmodium berghei* mosquitostage development and apicoplast replication.	Malaria Journal	9:73.	-	2010
Khan MGM, Alam MS, Podder MP, Itoh M, Jamil KM, Haque R, Wagatsuma Y	Evaluation of rK-39 strip test using urine for diagnosis of visceral leishmaniasis in an endemic area in Bangladesh.	Parasites and Vectors	3	114	2010

発表者氏名	論文タイトル名	発表誌名	巻号	ページ	出版年
Kawa K, Tsutsui H, Uchiyama R, Kato J, Matsui K, Iwakura Y, Matsumoto T, Nakanishi K	IFN-γis a master regulator of endotoxin shock syndrome in mice primed with heat-killed Propionibacterium acnes.	Int Immunol	22(3)	157-166	2010
Nakanishi K, Tsutsui H, Yoshimoto T	Importance of IL-18-Induced Super Th1 Cells for the Development of Allergic Inflammation	Allergol Int	59(2)	137-141	2010
Kuroda-Morimoto M, Tanaka H, Hayashi N, Nakahira M, Imai Y, Imamura M, Yasuda K, Yumikura-Futatsugi S, Matsui K, Nakashima T, Sugimura K, Tsutsui H, Sano H, Nakanishi K.	Contribution of IL-18 to eosinophilic airway inflammation induced by immunization and challenge with Staphylococcus aureus proteins	Int Immunol	22(7)	561-570	2010
Matsuba-Kitamura S, Yoshimoto T, Yasuda K, Futatsugi-Yumikura S, Taki Y, Muto T, Ikeda T, Mimura O, Nakanishi K	Contribution of IL-33 to induction and augmentation of experimental allergic conjunctivitis	Int Immunol	22(6)	479-489	2010
Nakanishi K	Basophils are potent antigen-presenting cells that selectively induce Th2 cells.	Eur J Immunol	40(7)	1836-1842	2010

発表者氏名	論文タイトル名	発表誌名	巻号	ページ	出版年
Yoshikawa S, Iijima H, Saito M, Tanaka H, Imanishi H, Yoshimoto N, Yoshimoto T, Futatsugi-Yumikura S, Nakanishi K, Tsujimura T, Nishigami T, Kudo A, Arii S, Nishiguchi S	Crucial role of impaired Kupffer cell phagocytosis on the decreased Sonazoid-enhanced echogenicity in a liver of a nonalchoholic steatohepatitis rat model.	Hepatol Res	40(8)	823-831	2010
Tsutsui H, Imamura M, Fujimoto J, Nakanishi K.	The TLR4/TRIF-Mediated Activation of NLRP3 Inflammasome Underlies Endotoxin-Induced Liver Injury in Mice.	Gastroenterol Res Pract			2010
Satoh T, Takeuchi O, Vandenbon A, Yasuda K, Tanaka Y, Kumagai Y, Miyake T, Matsushita K, Okazaki T, Saitoh T, Honma K, Matsuyama T, Yui K, Tsujimura T, Standley DM, Nakanishi K, Nakai K, Akira S.	The Jmjd3-Irf4 axis regulates M2 macrophage polarization and host responses against helminth infection.	Nat Immunol	11	936-944	2010
Nakanishi K	Basophils as APC in Th2 response in allergic inflammation and parasite infection.	Curr Opin Immunol	22(6)	814-820	2010
Matsuoka H Ikezawa T Hirai M	Production of a transgenic mosquito expressing circumsporozoite protein, a malarial protein, in the salivary gland of Anopheles stephensi (Diptera: Culicidae).	Acta Medica Okayama	64巻 4号	233-241	2010

発表者氏名	論文タイトル名	発表誌名	巻号	ページ	出版年
Imai T, et al	Involvement of CD8+ T cells in protective immunity against murine blood-stage infection with Plasmodium yoelii 17XL strain.	Eur. J. Immunol	40	1053-1061	2010
Ishida H, et al	Development of experimental cerebral malaria is independent of IL-23 and IL-17.	Biochem. Biophys. Res. Commun..	402	790-795	2010
Ozeki Y, et al	Transient role of CD4+CD25+ regulatory T cells in mycobacterial infection in mice	Int. Immunol	22	179-189	2010
Chou B, et al	Genetic immunization based on the ubiquitin-fusion degradation pathway against Trypanosoma cruzi	Biochem. Biophys. Res. Commun..	392	277-282	2010
Kimura D., Miyakoda M., Honma K., Yuda M., Chinzei Y., and Yui K	Production of IFN-γby CD4+ T cells in response to malaria antigens is IL-2-dependent.	Int. Immunol.	22 (12)	941-952	2010
M. Inoue, J. Tang, O. Kaneko, K. Yui, R. Culleton	Complete abrogation of sporozoite-induced sterile immunity by blood stage parasites of homologous and heterologous malaria parasites	Malaria J.	9 (suppl)	O19	2010
Wang Y, Kaneko O, Sattabongkot J, Chen J-H, Lu F, Chai J-Y, Takeo S, Tsuboi T, Ayala FJ, Chen Y, Lim CS, Han ET	Genetic Polymorphism of Plasmodium vivax msp1p, a Paralog of Merozoite Surface Protein 1, from Worldwide Isolates.	American Journal of Tropical Medicine and Hygiene	84(2)	292-297	2011
Pandey BD, Pun SB, Kaneko O, Pandey K, Hirayama K.	Expansion of Visceral Leishmaniasis to Western Hilly Part of Nepal.	American Journal of Tropical Medicine and Hygiene	84(1)	107-108	2011

発表者氏名	論文タイトル名	発表誌名	巻号	ページ	出版年
Pandey K, Pandey BD, Mallik AK, Kaneko O, Uemura H, Kanbara H, Yanagi T, Hirayama K.	Diagnosis of visceral leishmaniasis by polymerase chain reaction of DNA extracted from Giemsa's solution-stained slides.	Parasitology Reserch	107(3)	727-730	2010
Morisaki, D., Kim, H.-S., Inoue, H., Terauchi, H., Kuge, S., Naganuma, A., Wataya, Y., Tokuyama, H., Ihara, M. and Takasu, K.	Selective accumulation of rhodacyanine in plasmodial mitochondria is related to the growth inhibition of malaria parasites.	Chemical Science,	1 (2)	206-209,	2010.
Nishiyama, Y., wasa, K., Okada, S., Takeuchi, S., Moriyasu, M., Kamigauchi, M., Koyama, J., Takeuchi, A., Tokuda, H., Kim, H.-S., Wataya, Y., Takeda, K., Liu, YN., Wu, PC., Bastow, KF., Akiyama, T. and Lee, KH.	Geranyl derivatives of isoquinoline alkaloids show increased biological activities.	Heterocycles,	81 (5)	1193-1229,	2010.
Sato, A , Naito, T., Hiramoto, A., Goda, K., Omi, T., Kitade, Y., Sasaki, T., Matsuda, A., Fukushima, M., Wataya, Y. and Kim, H.-S.	Association of RNase L with a Ras GTPase-activating-like protein IQGAP1 in mediating the apoptosis of a human cancer cell-line.	FEBS Journal,	277 (21)	4464-4473,	2010.
Sato, A., Satake, A., Hiramoto, A., Wataya, Y. and Kim, H.-S.	Protein expression profiles of necrosis and apoptosis induced by 5-fluoro-2 '-deoxyuridine in mouse cancer cells.	Journal of Proteome Research,	9 (5):	2329-2338,	2010.

発表者氏名	論文タイトル名	発表誌名	巻号	ページ	出版年
Kawamura Y, Yoshikawa I, Katakura K	Imported leishmaniasis in dogs, US military bases, Japan.	Emerg Infect Dis	16	2017-2019	2010
Bawm S, Tiwananthagorn S, Lin KS, Hirota J, Irie T, Htun LL, Maw NN, Myaing TT, Phay N, Miyazaki S, Sakurai T, Oku Y, Matsuura H, Katakura K	Evaluation of Myanmar medicinal plant extracts for antitrypanosomal and cytotoxic activities	J Vet Med Sci	72	525-528	2010
Mizukami C, Spiliotis M, Gottstein B, Yagi K, Katakura K, Oku Y	Gene silencing in Echinococcus multilocularis protoscoleces using RNA interference	Parasitol Int	59	647-652	2010
Armua-Fernandez MT, Nonaka N, Sakurai T, Nakamura S, Gottstein B, Deplazes P, Phiri IGK, Katakura K, Oku Y	Development of PCR/dot blot assay for specific detection and differentiation of taeniid cestode eggs in canids	Parasitol Int			In press
Yoshida A, Nagayasu E, Nishimaki A, Sawaguchi A, Yanagawa S, Maruyama H	Transcripts analysis of infective larvae of an intestinal nematode, Strongyloides venezuelensis	Parasitol Int	ahead of print		
Uni S, Boda T, Daisaku K, Ikura Y, Maruyama H, Hasegawa H, Fukuda M, Takaoka H, Bain O	Zoonotic filariasis caused by Onchocerca dewittei japonica in a resident of Hiroshima Prefecture, Honshu, Japan	Parasitol Int	59	477-80	2010

発表者氏名	論文タイトル名	発表誌名	巻号	ページ	出版年
Hikosaka K, Watanabe YI, Tsuji N, Kita K, Kishine H, Arisue N, Palacpac NM, Kawazu SI, Sawai H, Horii T, Igarashi I, Tanabe K.	Divergence of the mitochondrial genome structure in the apicomplexan parasites, Babesia and Theileria	Mol Biol Evol.	27(5)	1107-1116	2010
Aboulaila M, Sivakumar T, Yokoyama N,Igarashi I.	Inhibitory effect of terpene nerolidol on the growth of *Babesia* parasites	Parasitol Int.	59().	278-282	2010.
Iseki H, Zhou L, Kim C, Inpankaew T, Sununta C, Yokoyama N, Xuan X, Jittapalapong S, Igarashi I.	Seroprevalence of *Babesia* infections of dairy cows in northern Thailand.	Vet. Parasitol.	170	193-196	2010
Aboulaila M, Yokoyama N, Igarashi I.	Development and evaluation of two nested PCR assays for the detection of *Babesia bovis* from cattle blood.	Vet. Parasitol.	172	65-70	2010
Iseki H, Kawai S, Takahashi N, Hirai M, Tanabe K, YokoyamaN, Igarashi I.	Evaluation of a loop-mediated isothermal amplification method as a tool for diagnosis of infection by the zoonotic simian malaria parasite *Plasmodium knowlesi*.	J Clin Microbiol.	48(7)	2509-2514	2010
Goo YK, Terkawi MA, Jia H, Aboge GO, Ooka H, Nelson B, Kim S, Sunaga F, Namikawa K, Igarashi I, NishikawaY, Xuan X.	Artesunate, a potential drug for treatment of *Babesia* infection.	Parasitol Int.	59(3):	481-486	2010.

発表者氏名	論文タイトル名	発表誌名	巻号	ページ	出版年
Ooka H, Terkawi MA, Goo YK, Luo Y, Li Y, Yamagishi J, Nishikawa Y, Igarashi I, Xuan X.	*Babesia microti*: Molecular and antigenic characterizations of a novel 94-kDa protein (BmP94).	Exp Parasitol.	127(1).	278-293	2011
Terkawi MA, Huyen NX, Wibowo PE, Seuseu FJ, Aboulaila M, Ueno A, Goo YK, Yokoyama N, Xuan X, Igarashi I.	Spherical body protein 4 is a new serological antigen for the global detection of *Babesia bovis* infection in cattle.	Clin Vaccine Immunol.	18(2)	337-342,	2011
Tajima K, Miura K, Ishiwata T, Takahashi F, Yoshioka M, Minakata K, Murakami A, Sasaki S, Iwakami S, Annoura T, Hashimoto M, Nara T, Takahashi K.	Sex hormones alter Th1 responses and enhance granuloma formation in the lung	Respiration			In press
Makiuchi T, Annoura T, Hashimoto M, Hashimoto T, Aoki T, Nara T	Compartmentalization of a glycolytic enzyme in Diplonema, a non-kinetoplastid Euglenozoan	Protist			In press
Tajima K, Ohashi R, Sekido Y, Hida T, Nara T, Hashimoto M, Iwakami S, Minakata K, Yae T, Takahashi F, Saya H, Takahashi K	Osteopontin-mediated enhanced hyaluronan binding induces multidrug resistance in mesothelioma cells	Oncogene	29(13)	1941-1951	2010

発表者氏名	論文タイトル名	発表誌名	巻号	ページ	出版年
Gurbadam Aet al	Mongolian and Japanese Joint Congress on "Echinococcoses: diagnosis, treatment and prevention in Mongolia" June 4, 2009	Parasites and Vectors	3	1/8-3/8	2010
Li TY et al	Specific IgG Responses to Recombinant Antigen B and Em18 in Cystic and Alveolar Echinococcosis in China	Clinical and Vaccine Immunology	17	470-475	2010
Ito A et al	Histopathological, Serological and Molecular Confirmation of Indigenous Alveolar echinococcosis cases in Mongolia	American Journal of Tropical Medicine and Hygiene	82	266-269	2010
Li TY et al	Widespread co-endemicity of human cystic and alveolar echinococcosis on the eastern Tibetan plateau, northwest Sichuan/southeast Qinghai, China	Acta Tropica	113	248-256	2010
Brunetti E et al	Expert consernsus for the diagnosis and treatment of cystic and alveolar echinococcosis in humans	Acta Tropica	114	1-16	2010
Yanagida T et al	Neurocysticercosis: Assessing where the Infection Was Acquired From	Journal of Travel Medicine	17	206-208	2010
Nakao M et al	Genetic polymorphisms of *Echinococcus* tapeworms in China as determined by mitochondrial and nuclear DNA sequences	International Journal for Parasitology	40	379-385	2010

発表者氏名	論文タイトル名	発表誌名	巻号	ページ	出版年
Okamoto Met al	Evidence of hybridization between *Taenia saginata* and *Taenia asiatica*	Parasitology International	59	70-74	2010
Anantaphruti MT et al	Molecular and serological survey on taeniasis and cysticercosis in Kanchanaburi Province, Thailand	Parasitology International	59	326-330	2010
Nkouawa Aet al	Serological Studies of Neurologic Helminthic Infections in Rural Areas of Southwest Cameroon: Toxocariasis, Cysticercosis and Paragonimiasis	PLoS Neglected Tropical Diseases	4	E732	2010
Nkouawa Aet al	Evaluation of a Loop-Mediated Isothermal Amplification Method Using Fecal Specimens for Differential Detection of Taenia Species from Humans	Journal of Clinical Microbiology	48	3350-3352	2010
Nakao M et al	State-of-the-art Echinococcus and Taenia: Phylogenetic taxonomy of human-pathogenic tapeworms and its application to molecular diagnosis	Infection, Genetics and Evolution	10	444-452	2010
Tappe D et al	Immunoglobulin G Subclass Responses to Recombinant Em18 in the Follow-up of Patients with Alveolar Echinococcosis in Different Clinical Stages	Clinical and Vaccine Immunology	17	944-948	2010

発表者氏名	論文タイトル名	発表誌名	巻号	ページ	出版年
Sato MO et al	A possible nuclear DNA marker to differentiate the two geographic genotypes of Taenia solium tapeworms	Parasitology International	60	108-110	2011
Sako Y et al	Echinococcus multilocularis: identification and functional characterization of cathepsin B-like peptidases from metacestode	Experimental Parasitology In press			2011

書　籍

著者氏名	論文タイトル名	書籍全体の編集者名	書　籍　名	出版社名	出版地	出版年	ページ
平山謙二	住血吸虫症・消化器吸虫症	金澤一郎、永井良三	今日の診断指針　第6版	医学書院	東京	2010	1373-7
安田好文, 中西憲司.	寄生虫に対する粘膜免疫	清野宏	臨床粘膜免疫学	シナジー	東京	2010	522-529
片倉　賢	リーシュマニア症	木村　哲 喜田　宏	改訂版 人獣共通感染症	医薬ジャーナル社	大阪	2011	431-436
丸山治彦	その他の吸虫症（肺吸虫症、肝吸虫症、横川吸虫症、肝蛭症）	山口徹、北原光夫、福井次矢	今日の治療指針2011	医学書院	東京	2011	263-264
Mohamad AlaaTerkawi and Ikuo Igarashi*	Drug Discovery discovery against *Babesia* and *Toxoplasma*	Katja Becker	Apicomplexan Parasites: MolecularApproaches toward Targeted Drug Development (Drug Discovery inInfectious Diseases)	Wiley-Blackwell	Oxford	2011	Chapter 24
Flisser A, Craig PS, Ito A	Chapter 51: Cysticercosis and Taeniosis: Taenia solium, Taenia saginata and Taenia asiatica	Palmer SR, Lord Soulsby, Torgerson PR, Brown DWG	Oxford Textbooks of Zoonoses	Oxford University Press	Oxford	2011	627-644

研究成果の刊行物・別刷り

Jpn. J. Infect. Dis., 63, 166-172, 2010

Original Article

Intranasal Administration of *Schistosoma japonicum* Paramyosin Induced Robust Long-Lasting Systemic and Local Antibody as well as Delayed-Type Hypersensitivity Responses, but Failed to Confer Protection in a Mouse Infection Model

Hideyasu Kohama[1], Tetsuya Harakuni[1], Mihoko Kikuchi[2], Takeshi Nara[3], Yasunori Takemura[1,4], Takeshi Miyata[1], Yoshiya Sato[4], Kenji Hirayama[2], and Takeshi Arakawa[1,5]*

[1]Molecular Microbiology Group, Department of Tropical Infectious Diseases, COMB, Tropical Biosphere Research Center, University of the Ryukyus, Okinawa 903-0213; [2]Department of Immunogenetics, Institute of Tropical Medicine, Nagasaki University, Nagasaki 852-8523; [3]Department of Molecular and Cellular Parasitology, Juntendo School of Medicine, Tokyo 113-8424; and [4]Department of Parasitology and [5]Division of Host Defense and Vaccinology, Graduated School of Medicine, University of the Ryukyus, Okinawa 903-0215, Japan

(Received November 5, 2009. Accepted March 31, 2010)

SUMMARY: To investigate intranasal (i.n.) immunization efficacy of *Schistosoma japonicum* 97-kDa myofibrillar protein paramyosin (PM), a vaccine candidate for Asian schistosomiasis, BALB/c mice were i.n. immunized with *Escherichia coli*-expressed recombinant PM (rPM). I.n. immunization using rPM mixed with cholera toxin (CT) was more potent than subcutaneous (s.c.) immunization with rPM emulsified in incomplete Freund's adjuvant for induction of serum (IgG, IgE, and IgA) and mucosal (IgA in nose, lung, and intestine) antibody and delayed-type hypersensitivity (DTH) responses. The second i.n. immunization was sufficient to induce maximal serum IgG and DTH responses, which were almost completely maintained for more than 6 months. Next, to evaluate protective efficacy of the rPM against *S. japonicum* infection, immunized mice were infected with *S. japonicum* cercariae at 2 weeks after the second immunization. At 7 weeks after infection, we observed no reduction in worm burden or fecundity in both i.n. and s.c. immunized groups. Results showed that i.n. immunization with rPM/CT failed to provide protection against parasite infection, albeit the antigen was a very potent mucosal immunogen. These results may emphasize the need to innovate new mucosal adjuvants or delivery molecules to overcome such hurdles in the construction of a mucosal antiparasite vaccine platform.

INTRODUCTION

Schistosomiasis is the most significant human helminth infection caused by trematode blood fluke worms belonging to the genus *Schistosoma*; five species are known to infect humans, i.e., *Schistosoma mansoni* (intestinal schistosomiasis), *S. haematobium* (urinary schistosomiasis), *S. intercalatum*, *S. mekongi*, and *S. japonicum* (Asian intestinal schistosomiasis). This parasitic disease, which is one of the 14 neglected tropical diseases (NTDs) currently listed by the World Health Organization (WHO), is endemic in remote, rural areas and urban slums in 74 countries in Africa, South America, and Asia, infecting more than 200 million people, with approximately 650 million people estimated to be living in endemic areas (1-3). There are continual reports of transmission of schistosomiasis japonica, a zoonosis, in southern China and the Philippines (3,4). Since *S. japonicum*, unlike *S. mansoni* and *S. haematobium*, infects nonhuman vertebrates (e.g., cattle, water buffalo, sheep, goats, pigs), a transmission blocking veterinary vaccine development, for example for water buffaloes in southern China, should provide an additional and a unique approach to *S. japonicum* control (4-8). Therefore, human vaccines and/or veterinary transmission blocking vaccines targeting worm numbers, parasite fecundity, or egg viability would constitute an indispensable component for future control campaigns of schistosomiasis japonica, while vaccine-linked drug chemotherapy is believed to become a basis for future Asian schistosomiasis control campaigns (9). Although, praziquantel (PZQ) is effective against all forms of schistosomiasis with few side effects, a total eradication of the parasite solely based on PZQ chemotherapy is considered difficult and impractical for the following reasons: (i) chronic infection and frequent reinfection are observed in people living in endemic areas even after successful drug chemotherapy (3,8), and (ii) increasing concern has been raised over the emergence of PZQ-resistant parasite strains in endemic regions where large-scale use of the drug is practiced (10).

Despite the existence of various practical difficulties regarding the control of schistosomiasis, there is considerable support concerning the possibility that anti-schistosome vaccines can be developed, based on several reasons; (i) radiation-attenuated cercariae con-

*Corresponding author: Mailing address: Molecular Microbiology Group, Department of Tropical Infectious Diseases, COMB, Tropical Biosphere Research Center, University of the Ryukyus, 1 Senbaru, Nishihara, Okinawa 903-0213, Japan. Tel & Fax: +81-98-895-8974, E-mail: tarakawa@comb.u-ryukyu.ac.jp

fers significant levels of prophylactic protection from reinfection in experimental animals (11,12); (ii) age-related resistance to infection was observed in humans and also in animals such as buffaloes (13–15); (iii) naturally resistant individuals are seen in endemic populations despite years of exposure to the parasites (16).

To date, several vaccine candidates against *S. japonicum* have demonstrated their potential to reduce worm burden and/or egg numbers in infected mice and other animal models (7,8). These candidates include: (i) 26-kDa glutathione S-transferase (Sj26GST), an enzyme isoform that catalyzes redox reaction; (ii) paramyosin (Sj97 or PM), a 97-kDa myofibrillar protein with a coiled-coil structure found only in invertebrates; (iii) calpain, a calcium-activated neutral proteinase found in the tegument of adults and penetration glands of cercariae; (iv) triose-phosphate isomerase (SjTPI), an enzyme in the glycolytic pathway; (v) a 23-kDa tetraspanin integral membrane protein (Sj23); (vi) SjFABP (Sj14), a fatty acid binding protein, an essential parasite protein in the take up of fatty acids from host blood as nutrients. Among these *S. japonicum* antigens, PM, a leading candidate for the schistosomiasis japonica vaccine (17–23), was first cloned as a full-length cDNA and then recombinantly expressed in *Escherichia coli* (20), with pilot-scale production recently reported (19). The PM is located on the surface of the tegument and in the secretory glands of the larvae (24–26), and can induce protective immunity, for example, in domestic pigs, conferring 40–50% reduction in worm recovery when immunized intradermally with recombinant PM (rPM) (18). Its vaccine efficacy for egg reduction in the liver of immunized water buffaloes was also reported (17). Further, its potential has also been demonstrated in other immunization methods including DNA vaccine (27).

The potent mucosal adjuvanticity of cholera toxin (CT) and its related heat-labile enterotoxin from *E. coli* (LT) in inducing systemic and mucosal antibody responses against otherwise weakly immunogenic antigens have been demonstrated in experimental animal models for parasitic diseases such as malaria (28–30). However, it has been well documented that recombinantly expressed nonreplicating inert antigens with mucosal adjuvants often induced immune responses with a clear tendency of bias toward Th2-type in mice, inducing primary IgG1 in serum and antigen-specific IL-13 in local draining lymph nodes without induction of IFN-γ (31). Therefore, if the induction of Th2-type of immunity is able to provide protective immunity against the target infectious diseases without any particular risk, recombinant antigens with a mucosal adjuvant administered through the nasal route would be free from any disadvantages. Internasal (i.n.) immunization frequently induces an antigen-specific IgE response, therefore, such an immunization regimen would be expected to be suitable for a PM-based vaccine. Furthermore, the recent trend to search for safer and more effective new mucosal adjuvants devoid of toxicity problems, a serious concern in the clinical use of CT, may add another promising dimension to anti-parasitic mucosal vaccine development research (21,22,24).

In this study we investigated an *E. coli*-expressed rPM-based i.n. immunization regime in a mouse model. rPM antigen administered with a potent mucosal adjuvant CT induced both mucosal and systemic immune responses of mixed Th1/Th2-type with PM-specific serum IgG, IgE as well as secretory IgA. We also examined the effects of immunization on the worm burden and/or the fecundity of female worms.

MATERIALS AND METHODS

Mice and immunization with rPM: Full-length rPM was expressed and purified as described previously (18). Six-week-old female BALB/c mice were purchased from Japan SLC (Shizuoka, Japan). Five mice per group were immunized with rPM subcutaneously (s.c.) or by i.n. route. For s.c. immunization, 30 μg of rPM emulsified with incomplete Freund's adjuvant (IFA), 100 μl in total, was administered to the dorsal skin using a 28-gauge needle syringe. Mice were administered three times at weeks 0, 3, and 5. The same volume of phosphate-buffered saline (PBS) emulsified with IFA was administered to mice as a negative control. For i.n. immunization, 30 μg of rPM with or without 1 μg of CT (Sigma-Aldrich, St. Louis, Mo., USA) was administered three times at weeks 0, 3, and 5 to external nares using a micropipet. As a negative control, a group of mice was i.n. immunized with 1 μg of CT or PBS only. Mice were bled from the tip of the tail at weeks 2, 4, and 6 for antibody analysis. All animal experimental protocols were approved by the Animal Ethical Committee of the University of the Ryukyus and Nagasaki University.

ELISA: A flat-bottom 96-well microtiter plate (Immulon 4; Dynex Technology Inc., Chantilly, Va., USA) was coated with 50 μl of the rPM (3 μg/ml in bicarbonate buffer, pH 9.6) at 4°C overnight. The plate was blocked with 1% (or 5% for IgE antibody detection) bovine serum albumin (BSA) (Sigma-Aldrich) in PBS at 37°C for 2 h. Fifty microliters of mouse antisera diluted 50-fold (or 20-fold for IgE antibody detection) with PBS containing 0.5% BSA were applied to wells in duplicates and incubated for 2 h at 37°C. Secondary antibodies (i.e., specific for mouse IgG, IgG subclasses, IgM, and IgA) conjugated with alkaline-phosphatase were added to wells followed by its substrate. Plates were measured by microplate reader (Bio-Rad Laboratories, Redmond, Wash., USA) with the OD_{405} after 20 min incubation. For measurement of serum IgE, secondary (rat anti-mouse IgE monoclonal antibody [IM2992; Immunotech, Marseille, France]) and tertiary (rabbit anti-rat IgG conjugated with horseradish peroxidase [HRP] [SAB-200; Stressgen Biotechnologies, Victoria, Canada]) antibodies were applied followed by HRP substrate. Plates were measured with the OD_{405} after 20 min incubation. For analysis of secretory antibodies in nasal secretions, the nasal cavities of sacrificed animals were washed several times with 200 μl of PBS. Intestinal antibodies were collected by extensively washing 3-cm long intestinal tubes excised from the ileal region with 500 μl of PBS containing protease inhibitor cocktail (Sigma-Aldrich). Bronchoalveolar lavage fluid (BALF) was collected by repeated injections and withdrawal of fluid several times from the trachea into the lungs using an 18-gauge needle. The collected mucosal fluids were directly analyzed by ELISA as described above. Statistical significance of differences be-

tween antibody levels was determined by Student's t test ($P < 0.05$).

Delayed-type hypersensitivity (DTH) measurements: DTH responses were measured at weeks 6 and 36 (i.e., 1 week and 31 weeks after the third immunization) by injecting 2 μg of the full-length rPM into the footpad of a hind leg of immunized mice, with swelling measured after 24 h. The DTH response was calculated from the differences in thickness between the left and the right, administered with PBS and the rPM, respectively. Statistical significance of differences was determined by the Mann-Whitney U test ($P < 0.05$).

Experimental infection: Cercariae of *S. japonicum* Chinese strain (obtained from Jiangsu Provincial Institute of Parasitic Diseases in Wuxi, People's Republic of China) were released from the infected snails using light source. The cercariae which climbed up to the surface of the water were scooped up using a cover slide glass, and cercariae numbers were counted under a light microscope. The parasites were immediately used for infection experiments to avoid any reduction in infectivity. For experimental infection, 8-12 female BALB/c mice immunized twice at weeks 0 and 2 were challenged at week 4 through the abdominal skin with 30 cercariae per mouse. Briefly, mice were anesthetized by intraperitoneal injection of pentobarbital and the abdominal hair was shaved to expose the skin for infection. Animals were returned to cages after confirming the penetrations of all cercariae into the skin. At 7 weeks after the cercariae infection, mice were sacrificed and portal vein perfusion was conducted to count eggs in the liver and adult worms in the mesenteric veins. The eggs were isolated from the livers according to the standard procedure (32). Briefly, the chopped liver from each mouse was homogenized in 0.1% actinase in PBS, and digested at 37°C for 1 h. The digested sample was centrifuged (1,500 rpm, 5 min) and the pellet was resuspended in 0.01% actinase and 0.05% collagenase mixture in PBS, and additionally digested at 37°C for 1 h. After incubation, the digested sample was centrifuged again (1,500 rpm, 5 min), and the pellet was resuspended in PBS. The eggs were sieved with a steel mesh and counted under the light microscope. Adult worms were divided into male and female worms, and their numbers counted.

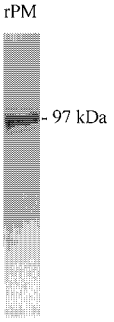

Fig. 1. Full-length recombinant *Schistosoma japonicum* paramyosin (rPM) expressed in *Escherichia coli* was detected by SDS-PAGE/CBB stain.

RESULTS

Detection of antibody levels after immunizations: The full-length rPM was expressed in *E. coli* and purified as previously described (18) (Fig. 1). To evaluate its immunogenicity, BALB/c mice were immunized through s.c. or i.n. route at weeks 0, 3, and 5, and specific antisera were collected at 1 week after the second and the third immunization, respectively. I.n. immunization with rPM/CT, but not with the antigen alone, induced robust serum IgG, which was higher than the response induced by s.c. immunization with

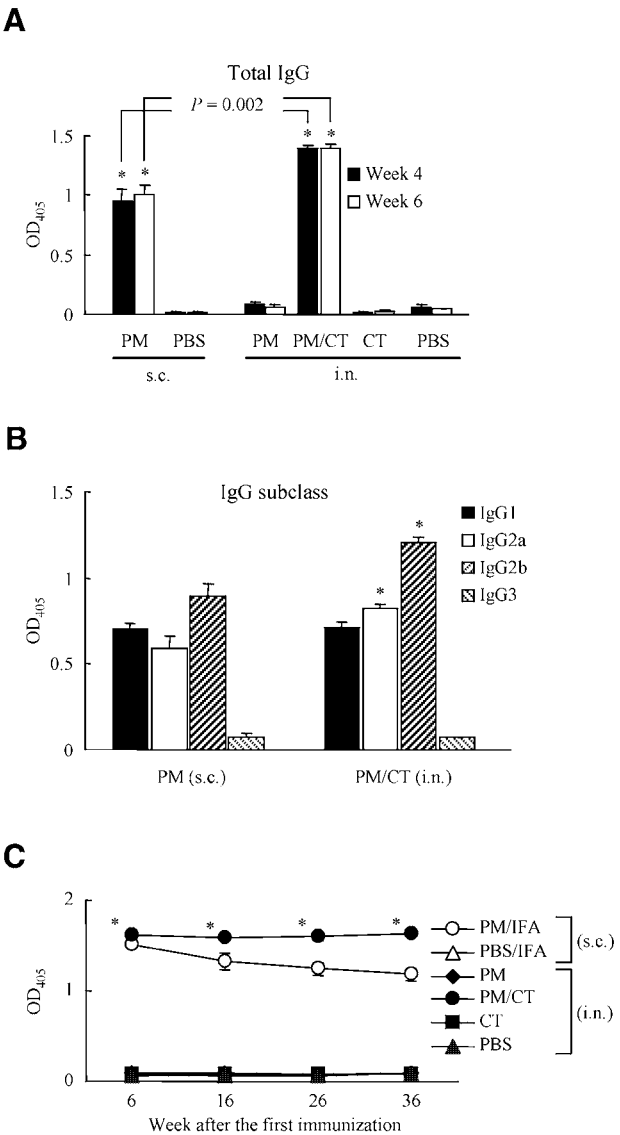

Fig. 2. Female BALB/c mice were immunized with rPM through subcutaneous (s.c.) or internasal (i.n.) route three times at weeks 0, 3, and 5, and antisera were collected at weeks 4 and 6. (A) For total serum IgG analysis, 50-fold diluted antisera collected at weeks 4 and 6 were reacted with rPM, and analyzed by ELISA. *, $P < 0.0001$ (as compared with PBS). (B) For serum IgG subclass analysis, 50-fold diluted antisera collected at week 6 were reacted with rPM. *, $P = 0.01$ (as compared with PM [s.c.]). (C) PM-specific serum IgG levels were monitored for up to 36 weeks from the first immunization. Levels of PM-specific antibodies were shown as average OD_{405} ± standard error of the mean. Statistical significance of differences was determined by the Student's t test.

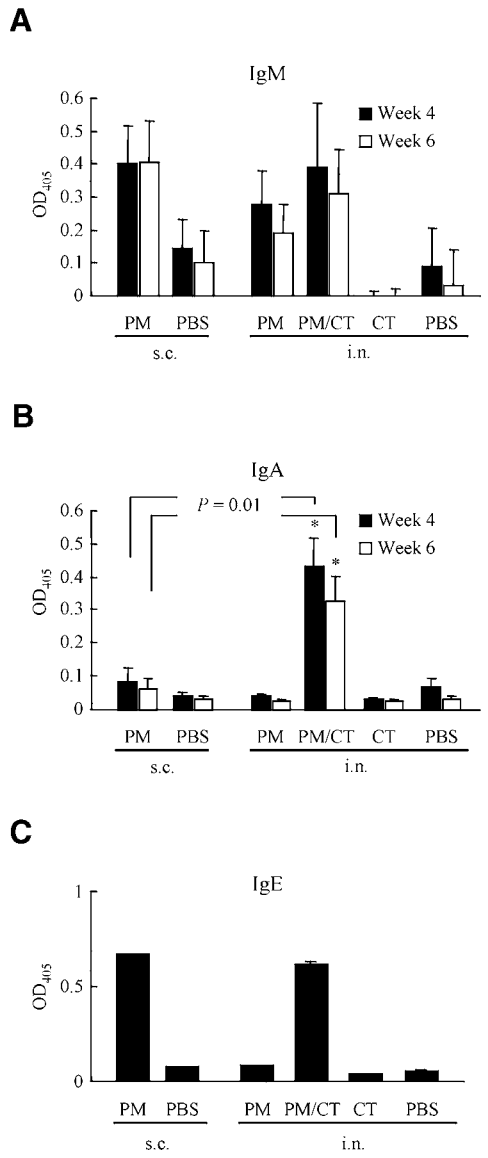

Fig. 3. Serum IgM (A) and IgA (B) levels were measured using antisera collected at weeks 4 and 6. *, $P < 0.01$ (as compared with PBS). (C) Serum IgE levels were measured using antisera collected at week 6. Levels of PM-specific antibodies were shown as average OD_{405} ± standard error of the mean. Statistical significance of differences was determined by the Student's *t* test.

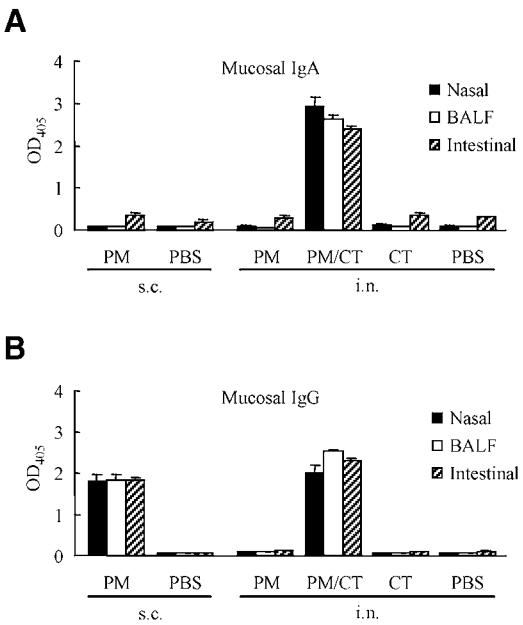

Fig. 4. Mucosal IgA (A) and IgG (B) levels were measured using mucosal samples (nasal washings, bronchoalveolar lavage fluid [BALF], and intestinal washings) collected at week 6. Data are shown as average OD_{405} ± standard error of the mean.

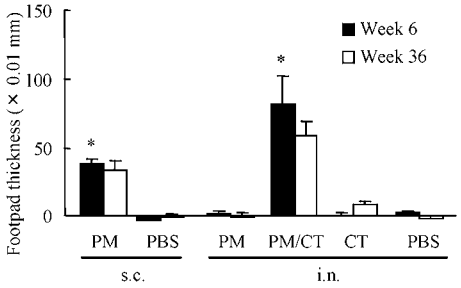

Fig. 5. A long term maintenance of PM-specific immune response was analyzed by measuring DTH. PM-specific DTH response elicited by rPM immunization by s.c. or i.n. route was analyzed at weeks 6 and 36 (i.e., 1 week and 31 weeks after the third immunization) by injecting 2 μg of rPM protein into the footpad of hind legs of immunized mice, and footpad thickness increments were measured after 24 h. Data are shown as average differences ± standard error of the mean in the thickness between the right and the left footpad injected with rPM and PBS, respectively.

rPM/IFA (Fig. 2A). The second immunization with each route was sufficient to induce the maximal levels of IgG. IgG subclass levels indicated that IgG1, IgG2a, and IgG2b were significantly elevated in rPM/CT and rPM/IFA groups (Fig. 2B). To determine the duration of antibody levels in serum, antigen-specific IgG levels were monitored for more than 6 months after the final immunization without additional booster immunization. IgG levels in serum were completely maintained in mice immunized with rPM/CT, but IgG levels in mice immunized with rPM/IFA gradually declined over the course of time (Fig. 2C). Weak but detectable serum IgM was also induced in rPM/CT and rPM/IFA groups (Fig. 3A), however, only rPM/CT immunization induced IgA in serum (Fig. 3B). Further, PM-specific serum IgE were detected in both rPM/CT and rPM/IFA immunizations (Fig. 3C).

Mucosal antibody levels in nasal, intestinal, and BALF were measured at 1 week after the third immunization. Mucosal IgA was induced only by i.n. rPM/CT immunization (Fig. 4A), but IgG was induced in both s.c. rPM/IFA and i.n. rPM/CT groups (Fig. 4B). With a clear contrast with serum IgG levels, which were found to last for at least 7 months (Fig. 2C), mucosal antibodies were completely diminished at week 40 post-immunization (data not shown), indicating much less efficient maintenance of the mucosal antibody response than that of the serum antibody response.

DTH measurement and IFN-γ production: PM-specific DTH was measured, and we found that the response was well maintained in mice immunized with both i.n. rPM/CT and s.c. rPM/IFA, up to 7 months (Fig. 5). rPM i.n. immunization without CT showed no

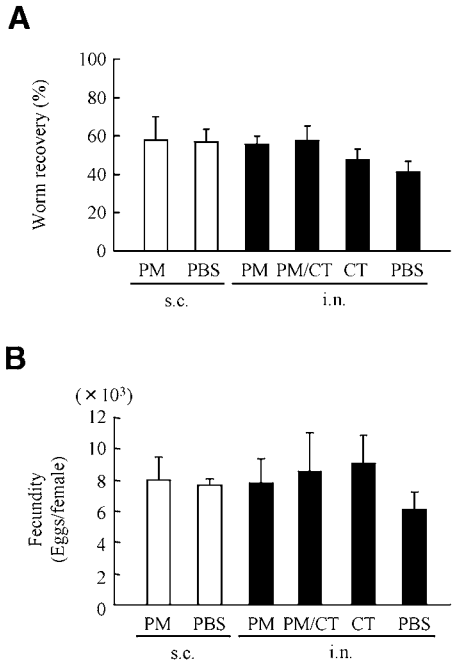

Fig. 6. Female BALB/c mice were immunized with rPM through s.c. (8 mice/group) or i.n. (12 mice/group) route twice at weeks 0 and 2. Mice were infected with approximately 30 *S. japonicum* cercariae per animal at week 4, and mice were sacrificed for parasite counts at week 11 for adult worms in the mesenteric veins and for eggs in the liver. (A) Worm recovery percents were calculated by the equation [(no. of adults recovered/no. of cercariae used for infection) × 100], and (B) fecundities were calculated by the equation (no. of eggs recovered from the liver/no. of female worms recovered/mouse). Data are shown as average numbers of adult worms or eggs ± standard error of the mean.

response at all, indicating a clear correlation between humoral and DTH responses. Despite strong humoral and DTH responses, no increment of antigen-specific IFN-γ production was observed in spleen or local draining lymph nodes collected from i.n. rPM/CT or s.c. rPM/IFA immunized mice (data not shown).

Vaccine trial against *S. japonicum*: Since the second immunization was sufficient to elicit the maximal antibody response (Fig. 2A), mice were infected with approximately 30 cercariae per animal through the abdominal skin at 2 weeks after the second immunization, and at 7 weeks post-infection mice were sacrificed and the parasite number was counted. We observed no reduction in the number of adult worms (Fig. 6A) or egg production from female worms (Fig. 6B).

DISCUSSION

PM has been demonstrated for its potential as a vaccine target, and thereby selected as one of several schistosomiasis vaccine candidates by the WHO (7). In this study we prepared the full-length rPM antigen in *E. coli* and evaluated its vaccine efficacy in a mouse infection model. The rPM induced robust humoral and DTH responses when administered mucosally or parenterally, however, the use of adjuvant was found to be essential for both immunization regimens. Although there is a report indicating that the combinations of adjuvants and routes in immunization influence the profile of immune response induction in the case of *S. mansoni* (33), we did not observe any significant difference in the quality of the response between i.n. and s.c. routes of immunization except for IgA induction by mucosal immunization (Figs. 3B and 4A). Furthermore, we found that the intensity of the immune response tends to be higher for i.n. than the s.c. route of immunization.

Humoral immunity, in addition to various inflammatory immune cells such as eosinophils, macrophages, and T-lymphocytes, may have a major importance in protection from schistosome infection (34). Although, T-cell-dependent cell-mediated immunity was found to be important for protection (34), IgE also appears as a major protective effector arm for resistance (21,22,24), and protective monoclonal IgE which recognizes B cell epitopes was determined to be located within the PM molecule (24,35). Analyses of IgG isotype profile indicated that relatively high IgG1, IgG2a, and IgG2b without noticeable levels of IgG3 were induced (Fig. 2B), suggesting the induction of mixed Th1/Th2 profile. These results were unexpected, particularly the observation of high IgG2b induction, because IgG1 is usually the only primary serum Ig isotype induced by i.n. immunization of recombinant antigens mixed with CT in mouse models (28,30). We do not have clear evidence to explain this observation, but it may suggest very high immunogenicity of recombinant PM/adjuvant vaccine formulation, and this notion is strongly supported by our observation that long-lasting serum IgG and DTH responses were induced in immunized mice (Figs. 2C and 5). We concluded that this strong immunogenicity was a result of the combination of PM and CT, because PM administration alone only induced weakly immunogenic effects.

Vaccine-induced IgA affects parasite fecundity in *S. mansoni* (36,37), and PM was determined as a target molecule of human IgA against *S. japonicum* in an epidemiological study conducted in the Philippines (13). Our results showed that antigen-specific IgA in serum and mucosa was induced only by mucosal immunization, not parenteral immunization, and this immunity may affect the migration of schistosomula in mucosal tissues such as the lungs. The advantage of mucosal administration was previously suggested by other researchers, who showed that oral administration of *S. japonicum* proteins induced specific anti-parasite antibodies and damaged adult worms (38). Given the fact that i.n. immunization is usually more effective in inducing secretory IgA than oral immunization, i.n. vaccine protocol is expected to provide better mucosal immunity than an oral vaccination regime.

After invasion by the free-swimming cercariae into the host skin of humans and animals, cercariae shed their tails and become schistosomula that migrate to the lungs. Therefore we proposed that the mucosal immunization may block larval migration into the lung and prevent them from reaching the portal vein. Furthermore, serum IgE and mucosal IgA responses induced only by i.n. immunization were expected to provide a reduction in worm burden and/or fecundity. A previous report by McManus et al. clearly demonstrated consistent protective effects of PM when immunized mice (both inbred and outbred) were challenged with *S. japonicum* cercariae (17). Further, the same study demonstrated PM's

vaccine effect on reducing liver egg numbers in water buffaloes. We supposed that their differences from our results were caused by the used mouse strains and adjuvants.

Effective antischistosome immunity seems to be dependent on a balance between protective and susceptibility-enhancing immune responses elicited by a particular vaccination regimen, rather than a mere induction of a high level of both types of immunity; for example, high IgE/IgG4 ratio to parasite antigens correlates to resistance to reinfection (21,39). Thus, it is presumably correct to draw a conclusion from our present study that the particular vaccination regime that we employed in our mouse study did not favor a protective immune response over a susceptibility-promoting immune response, though we do not know what factors critically contributed to the latter response. In humans, IgE and IgG4 responses were important in protection against *S. japonicum* infection (8,39). High IgG4 response causes sensitivity to *S. japonicum* (21). In our result, not only the IgE antibody but also all IgG subclasses apart from IgG3 increased. As one of the possibilities, the augmentation of IgG antibodies have masked an effect of IgE protection (40,41). Additionally, in our recent unpublished study with a swine infection model using miniature pigs, i.n. rPM/CT immunization failed to protect the immunized animals even though the immunization induced substantial levels of serum and mucosal antibody responses. Therefore, a failure to induce protective immunity in our i.n. immunization model may not be a host-specific phenomenon.

To reemphasize the comments made by Bergquist et al. (9) and McManus (5) in their review articles, antiparasite vaccines present a formidable challenge and might not be possible without careful selection of a suitable adjuvant to promote stimulation to the desired levels of protective immunity. Further studies are strongly encouraged, as such new mucosal adjuvants or delivery molecules should be innovated and tested for their efficacy to be included as important components of PM-based vaccine platform technologies targeting Asian schistosomiasis.

Acknowledgments This work was supported by the Program of Founding Research Centers for Emerging and Reemerging Infectious Diseases of the Ministry of Education, Culture, Sports, Science and Technology (MEXT) of Japan.

REFERENCES

1. World Health Organization (2007): Shistosomiasis. Fact sheet N°115.
2. Chitsulo, L., Engels, D., Montresor, A., et al. (2000): The global status of schistosomiasis and its control. Acta Trop., 77, 41-51.
3. Ross, A.G., Bartley, P.B., Sleigh, A.C., et al. (2002): Schistosomiasis. N. Engl. J. Med., 346, 1212-1220.
4. Gray, D.J., Williams, G.M., Li, Y., et al. (2008): Transmission dynamics of *Schistosoma japonicum* in the lakes and marshlands of China. PLoS One, 3, e4058.
5. McManus, D.P. (2005): Prospects for development of a transmission blocking vaccine against *Schistosoma japonicum*. Parasite Immunol., 27, 297-308.
6. Gray, D.J., Williams, G.M., Li, Y., et al. (2009): A cluster-randomised intervention trial against *Schistosoma japonicum* in the People's Republic of China: bovine and human transmission. PLoS One, 4, e5900.
7. McManus, D.P. and Bartley, P.B. (2004): A vaccine against Asian schistosomiasis. Parasitol. Int., 53, 163-173.
8. McManus, D.P. and Loukas, A. (2008): Current status of vaccines for schistosomiasis. Clin. Microbiol. Rev., 21, 225-242.
9. Bergquist, N.R., Leonardo, L.R. and Mitchell, G.F. (2005): Vaccine-linked chemotherapy: can schistosomiasis control benefit from an integrated approach? Trends Parasitol., 21, 112-117.
10. Fenwick, A., Savioli, L., Engels, D., et al. (2003): Drugs for the control of parasitic diseases: current status and development in schistosomiasis. Trends Parasitol., 19, 509-515.
11. Shi, Y.E., Jiang, C.F., Han, J.J., et al. (1990): *Schistosoma japonicum*: an ultraviolet-attenuated cercarial vaccine applicable in the field for water buffaloes. Exp. Parasitol., 71, 100-106.
12. McManus, D.P. (1999): The search for a vaccine against schistosomiasis—a difficult path but an achievable goal. Immunol. Rev., 171, 149-161.
13. Hernandez, M.G., Hafalla, J.C., Acosta, L.P., et al. (1999): Paramyosin is a major target of the human IgA response against *Schistosoma japonicum*. Parasite Immunol., 21, 641-647.
14. Kurtis, J.D., Friedman, J.F., Leenstra, T., et al. (2006): Pubertal development predicts resistance to infection and reinfection with *Schistosoma japonicum*. Clin. Infect. Dis., 42, 1692-1698.
15. Wang, T., Zhang, S., Wu, W., et al. (2006): Treatment and reinfection of water buffaloes and cattle infected with *Schistosoma japonicum* in Yangtze River Valley, Anhui province, China. J. Parasitol., 92, 1088-1091.
16. Correa-Oliveira, R., Caldas, I.R., and Gazzinelli, G. (2000): Natural versus drug-induced resistance in *Schistosoma mansoni* infection. Parasitol Today, 16, 397-399.
17. McManus, D.P., Wong, J.Y., Zhou, J., et al. (2002): Recombinant paramyosin (rec-Sj-97) tested for immunogenicity and vaccine efficacy against *Schistosoma japonicum* in mice and water buffaloes. Vaccine, 20, 870-878.
18. Chen, H., Nara, T., Zeng, X., et al. (2000): Vaccination of domestic pig with recombinant paramyosin: against *Schistosoma japonicum* in China. Vaccine, 18, 2142-2146.
19. Jiz, M., Wu, H. W., Meng, R., et al. (2008): Pilot-scale production and characterization of paramyosin, a vaccine candidate for schistosomiasis japonica. Infect. Immun., 76, 3164-3169.
20. Kalinna, B.H., Becker, M.M. and McManus, D.P. (1997): Engineering and expression of a full length cDNA encoding *Schistosoma japonicum* paramyosin. Purification of the recombinant protein and its recognition by infected patient sera. Acta Trop., 65, 111-115.
21. Jiz, M., Friedman, J.F., Leenstra, T., et al. (2009): Immunoglobulin E (IgE) responses to paramyosin predict resistance to reinfection with *Schistosoma japonicum* and are attenuated by IgG4. Infect. Immun., 77, 2051-2058.
22. Kojima, S., Niimura, M. and Kanazawa, T. (1987): Production and properties of a mouse monoclonal IgE antibody to *Schistosoma japonicum*. J. Immunol., 139, 2044-2049.
23. Kojima, S. (2004): Overview: from the horse experimentation by Prof. Akira Fujinami to paramyosin. Parasitol. Int., 53, 151-162.
24. Nara, T., Matsumoto, N., Janecharut, T., et al. (1994): Demonstration of the target molecule of a protective IgE antibody in secretory glands of *Schistosoma japonicum* larvae. Int. Immunol., 6, 963-971.
25. Matsumoto, Y., Perry, G., Levine, R.J., et al. (1988): Paramyosin and actin in schistosomal teguments. Nature, 333, 76-78.
26. Gobert, G.N., Stenzel, D.J., Jones, M.K., et al. (1997): *Schistosoma japonicum*: immunolocalization of paramyosin during development. Parasitology, 114 (Pt 1), 45-52.
27. Yang, W., Waine, G.J. and McManus, D.P. (1995): Antibodies to *Schistosoma japonicum* (Asian bloodfluke) paramyosin induced by nucleic acid vaccination. Biochem. Biophys. Res. Commun., 212, 1029-1039.
28. Arakawa, T., Tsuboi, T., Kishimoto, A., et al. (2003): Serum antibodies induced by intranasal immunization of mice with *Plasmodium vivax* Pvs25 co-administered with cholera toxin completely block parasite transmission to mosquitoes. Vaccine, 21, 3143-3148.
29. Arakawa, T., Komesu, A., Otsuki, H., et al. (2005): Nasal immunization with a malaria transmission-blocking vaccine candidate, Pfs25, induces complete protective immunity in mice against field isolates of *Plasmodium falciparum*. Infect. Immun., 73, 7375-7380.
30. Arakawa, T., Tachibana, M., Miyata, T., et al. (2009): Malaria ookinete surface protein-based vaccination via the intranasal

route completely blocks parasite transmission in both passive and active vaccination regimens in a rodent model of malaria infection. Infect. Immun., 77, 5496–5500.
31. Marinaro, M., Staats, H.F., Hiroi, T., et al. (1995): Mucosal adjuvant effect of cholera toxin in mice results from induction of T helper 2 (Th2) cells and IL-4. J. Immunol., 155, 4621–4629.
32. Smithers, S.R. (1960): The isolation of viable schistosome eggs by a digestion technique. Trans. R. Soc. Trop. Med. Hyg., 54, 68–70.
33. Comoy, E.E., Capron, A. and Thyphronitis, G. (1998): Adjuvant is the major parameter influencing the isotype profiles generated during immunization with a protein antigen, the *Schistosoma mansoni* Sm28-GST. Scand. J. Immunol., 47, 444–452.
34. Pearce, E.J., James, S.L., Hieny, S., et al. (1988): Induction of protective immunity against *Schistosoma mansoni* by vaccination with schistosome paramyosin (Sm97), a nonsurface parasite antigen. Proc. Natl. Acad. Sci. USA, 85, 5678–5682.
35. Nara, T., Tanabe, K., Mahakunkijcharoen, Y., et al. (1997): The B cell epitope of paramyosin recognized by a protective monoclonal IgE antibody to *Schistosoma japonicum*. Vaccine, 15, 79–84.
36. Lebens, M., Sun, J.B., Sadeghi, H., et al. (2003): A mucosally administered recombinant fusion protein vaccine against schistosomiasis protecting against immunopathology and infection. Vaccine, 21, 514–520.
37. Sun, J.B., Mielcarek, N., Lakew, M., et al. (1999): Intranasal administration of a *Schistosoma mansoni* glutathione S-transferase-cholera toxoid conjugate vaccine evokes antiparasitic and antipathological immunity in mice. J. Immunol., 163, 1045–1052.
38. Yang, W., Gobert, G.N. and McManus, D.P. (1997): Oral vaccination of mice with recombinant *Schistosoma japonicum* proteins induces specific anti-parasite antibodies and damage to adult worms after a challenge infection. Int. J. Parasitol., 27, 843–853.
39. Li, Y., Sleigh, A.C., Ross, A.G., et al. (2001): Human susceptibility to *Schistosoma japonicum* in China correlates with antibody isotypes to native antigens. Trans. R. Soc. Trop. Med. Hyg., 95, 441–448.
40. Strait, T.R., Morris, C.S. and Finkelman, D.F. (2006): IgG-blocking antibodies inhibit IgE-mediated anaphylaxis in vivo through both antigen interception and FcgRIIb cross-linking. J. Clin. Invest., 116, 833–841.
41. Garcia B.E., Sanz, M.L., Gato, J.J., et al. (1993): IgG4 blocking effect on the release of antigen-specific histamine. J. Investig. Allergol. Clin. Immunol., 3, 26–33.

Biochimica et Biophysica Acta 1797 (2010) 443–450

Contents lists available at ScienceDirect

Biochimica et Biophysica Acta

journal homepage: www.elsevier.com/locate/bbabio

Purification and kinetic characterization of recombinant alternative oxidase from *Trypanosoma brucei brucei*

Yasutoshi Kido [a], Kimitoshi Sakamoto [a], Kosuke Nakamura [a], Michiyo Harada [a], Takashi Suzuki [b], Yoshisada Yabu [b], Hiroyuki Saimoto [c], Fumiyuki Yamakura [d], Daijiro Ohmori [d], Anthony Moore [e], Shigeharu Harada [f], Kiyoshi Kita [a,*]

[a] *Department of Biomedical Chemistry, Graduate School of Medicine, The University of Tokyo, Tokyo 113-0033, Japan*
[b] *Department of Molecular Parasitology, Graduate School of Medical Sciences, Nagoya City University, Nagoya 467-8601, Japan*
[c] *Department of Materials Science, Faculty of Engineering, Tottori University, Tottori, Japan*
[d] *Department of Chemistry, School of Medicine, Juntendo University, Tokyo, Japan*
[e] *Biochemistry and Biomedical Sciences, School of Life Sciences, University of Sussex, Falmer, Brighton, UK*
[f] *Department of Applied Biology, Graduate School of Science and Technology, Kyoto Institute of Technology, Kyoto 606-8585, Japan*

ARTICLE INFO

Article history:
Received 24 September 2009
Received in revised form 23 December 2009
Accepted 25 December 2009
Available online 4 January 2010

Keywords:
Alternative oxidase
Membrane-bound diiron protein
Trypanosoma brucei
Ascofuranone
Chemotherapy

ABSTRACT

The trypanosome alternative oxidase (TAO) functions in the African trypanosomes as a cytochrome-independent terminal oxidase, which is essential for their survival in the mammalian host and as it does not exist in the mammalian host is considered to be a promising drug target for the treatment of trypanosomiasis. In the present study, recombinant TAO (rTAO) overexpressed in a haem-deficient *Escherichia coli* strain has been solubilized from *E. coli* membranes and purified to homogeneity in a stable and highly active form. Analysis of bound iron detected by inductively coupled plasma-mass spectrometer (ICP-MS) reveals a stoichiometry of two bound iron atoms per monomer of rTAO. Confirmation that the rTAO was indeed a diiron protein was obtained by EPR analysis which revealed a signal, in the reduced forms of rTAO, with a *g*-value of 15. The kinetics of ubiquiol-1 oxidation by purified rTAO showed typical Michaelis–Menten kinetics (K_m of 338 μM and V_{max} of 601 μmol/min/mg), whereas ubiquinol-2 oxidation showed unusual substrate inhibition. The specific inhibitor, ascofuranone, inhibited the enzyme in a mixed-type inhibition manner with respect to ubiquinol-1.

1. Introduction

Trypanosoma brucei is a parasite that causes African sleeping sickness in humans and Nagana in livestock and is transmitted by the tsetse fly. There is an urgent need for further development of chemotherapy against African trypanosomiasis since current chemotherapeutic drugs are not entirely satisfactory [1].

Trypanosomal parasites are equipped with a unique energy metabolism, they live as the bloodstream form in the mammalian host and as the procyclic form in the vector. The procyclic form of *T. brucei* fulfills its ATP requirement from a cyanide-sensitive and cytochrome-dependent respiratory chain comparable to that observed in the host mitochondria, whereas in the bloodstream form, trypanosomes use the glycolytic pathway, which is localized in a unique organelle the glycosome, as their major source of ATP [2–5]. Once the parasites invade the mammalian host in the bloodstream form, both its cytochrome-dependent respiratory chain and ATP synthesis by oxidative phosphorylation disappear [2,5]. Instead a cyanide-resistant and cytochrome-independent trypanosomal alternative oxidase (TAO) functions as the sole terminal oxidase to re-oxidize NADH accumulated during glycolysis [5].

TAO is generally considered to be a good target for the anti-trypanosomal drugs because this oxidase is essential for their survival, since it reoxidises cytosolic NADH, and mammalian hosts do not possess this protein [5,6]. Indeed, we found that ascofuranone, isolated from the pathogenic fungus *Ascochyta visiae*, specifically inhibits the quinol oxidase activity of TAO and rapidly kills the parasites [7]. In addition, we have confirmed the chemotherapeutic efficacy of ascofuranone *in vivo* [8,9].

The alternative oxidase (AOX) is a non-protonmotive ubiquinol oxido-reductase catalyzing the 4-electron reduction of dioxygen to water [5,10–12]. Genes encoding AOX have been found in higher

Abbreviations: AOX, alternative oxidase; DM, *n*-dodecyl-β-D-maltopyranoside; EPR, electron paramagnetic resonance; ICP-MS, inductively coupled plasma-mass spectrometer; IPTG, isopropyl, β-D-1-thiogalactoside; k_{cat}, molecular activity; C10E8, octaethylene glycol-monododecylether; OG, *n*-octyl-β-D-glucopyranoside; rTAO, recombinant trypanosome alternative oxidase; SHAM, salycylhydroxamic acid; TAO, trypanosome alternative oxidase; Ubiquinol, reduced form ubiquinone

* Corresponding author. Department of Biomedical Chemistry, Graduate School of Medicine, The University of Tokyo, Hongo, Bunkyo-ku, Tokyo 113-0033, Japan. Tel.: +81 3 5841 3526; fax: +81 3 5841 3444.
E-mail address: kitak@m.u-tokyo.ac.jp (K. Kita).

0005-2728/$ – see front matter © 2009 Elsevier B.V. All rights reserved.
doi:10.1016/j.bbabio.2009.12.021

plants, algae, yeast, slime molds, free-living amoebae, eubacteria and nematodes [13–16]. Moreover, recent bioinformatic searches have broadened the taxonomic distribution of AOX to some members of the animal kingdom [17]. The primary role of AOX in non-thermogenic plants is to regulate cellular redox balance and to protect against reactive oxygen species particularly when the cytochrome pathway is inhibited [18–20]. In addition to this role, many other physiological roles have been described for AOXs in other organisms and these have been discussed in detail elsewhere [13,21]. The ubiquitous occurrence of AOX may suggest that the metabolic flexibility that the alternative pathway confers upon an organism allows it to respond to a wide range of developmental and environmental conditions [22].

Despite universal conservation of the gene and diversified physiology, the molecular features of AOX have not yet been well characterized. Although no high-resolution AOX structure has been determined to date, current structural models predict that it is an integral interfacial membrane protein that interacts with a single leaflet of the lipid bilayer, and contains a non-haem diiron carboxylate active site [23,24]. This model is supported by extensive site-directed mutagenesis studies [18,25–29] and furthermore both EPR and FTIR spectroscopies have confirmed the presence of a binuclear iron center in both the plant and trypanosomal enzymes [30–32].

Further detailed structural and biochemical analyses of AOXs, however, requires further development of purification protocols to produce sufficiently purified and highly active protein to enable crystallization trials and kinetic analyses to proceed. In this paper, we report on the further refinement of our previous protocol through over-expressing rTAO in an *E. coli ΔhemA* mutant (FN102) strain, which lacks quinol oxidase activity of cytochrome *bo* and *bd* complexes [33–35]. Purified rTAO protein is highly active and exhibits an exceptional stability upon storage. The analysis of the prosthetic groups by inductively coupled plasma-mass spectrometer (ICP-MS) and electron paramagnetic resonance (EPR) reveals the presence of two ferric ions stoichiometrically bound per rTAO monomer. To our knowledge this is the first direct confirmation of two ferric irons per AOX. Furthermore we show that purified rTAO is potently inhibited by ascofuranone with mixed function kinetics.

2. Materials and methods

2.1. Preparation of membrane sample

The strain FN102/pTbAO carrying cDNA for *T. b. brucei* TAO [36] was pre-cultured at 37 °C in 100 ml of LB medium containing 10 mg ampicillin, 5 mg kanamycin, and 5 mg 5-aminolevulinic acid for 4–6 h. The pre-cultured cells were aerobically grown at 30 °C in 10 l of S-medium containing 100 g tryptone peptone, 50 g yeast extract, 50 g casamino acid, 104 g K_2HPO_4, 30 g KH_2PO_4, 7.5 g trisodium-citrate·$2H_2O$, 25 g $(NH_4)_2SO_4$, 0.5 g $MgSO_4 \cdot 7H_2O$, 0.25 g $FeSO_4 \cdot 7H_2O$, 0.25 g $FeCl_3$, 0.2%(w/v) glucose, and 1 g carbenicillin. The culture was initiated at O.D.$_{600}$ = 0.01 and expression of rTAO was induced by the addition of isopropyl β-D-1-thiogalactoside (IPTG) (25 μM) at O.D.$_{600}$ = 0.1. Cells were harvested 8–10 h following induction and were resuspended in 50 mM Tris–HCl (pH 7.5) containing 20%(w/w) sucrose, 0.1 mM phenylmethane sulfonyl fluoride (PMSF) and protease inhibitor cocktail (Sigma) and broken by a French Pressure Cell (Ohtake, Tokyo). Unbroken cells were removed by centrifugation at 8000 *g* for 10 min (Hitachi 21G). Inner membranes of FN102/pTbAO were fractionated in high density sucrose after ultracentrifugation at 200,000 *g* for 1 h at 4 °C (Hitachi 85H) (35 ml of supernatant was overlaid over 35 ml of 50 mM Tris–HCl pH 7.5 containing 40%(w/w) sucrose per ultracentrifuge tube). Buoyant inner rich membranes upon 40%(w/w) sucrose layer were fractionated and the inner membrane pellet was separated by further ultracentrifugation at 200,000 *g* for 1 h (HITACHI 85H). The membrane pellet was resuspended in 50 mM Tris–HCl (pH 7.5) containing 20%(w/w) sucrose.

2.2. Solubilization

Membranes were treated with solubilization buffer (6 mg/ml protein in 50 mM Tris–HCl, 1.4%(w/v) *n*-octyl-β-D-glucopyranoside (OG), 200 mM $MgSO_4$, 20%(v/v) glycerol, pH 7.3) at 4 °C and immediately ultracentrifuged at 200,000 *g* for 1 h at 4 °C. The quinol oxidase activities of the samples before centrifugation, as well as that of supernatant and pellet were determined.

2.3. Purification of rTAO

Hybrid batch/column procedure described in the manufacturer's instruction was used as stated below. Ten milliliter of the resin (BD Bioscience, TALON Metal Affinity Resin) was equilibrated in a batch format by 100 ml of equilibration buffer (20 mM Tris–HCl, 1.4%(w/v) OG, 100 mM $MgSO_4$, 20%(v/v) glycerol, pH 7.3). Twenty milliliter of OG extract was mixed with the resin for 20 min at 4 °C. The resin was washed twice with 100 ml of wash buffer (20 mM Tris–HCl, 20 mM imidazole, 0.042%(w/v) *n*-dodecyl-β-D-maltopyranoside (DM), 50 mM $MgSO_4$, 20%(v/v) glycerol pH 7.3) and the resin bound rTAO was transferred to a column for additional washing with 20 ml of second wash buffer (20 mM Tris–HCl, 165 mM imidazole, 0.042%(w/v) DM, 50 mM $MgSO_4$, 20%(v/v) glycerol pH 7.3; flow rate 1 ml/min) and protein elution. Finally, rTAO was eluted with elution buffer (20 mM Tris–HCl, 200 mM imidazole, 0.042%(w/v) DM, 50 mM $MgSO_4$, 60 mM NaCl, 20%(v/v) glycerol pH 7.3; flow rate 1 ml/min). Fractions (4 ml each) were collected.

2.4. Quantitative analysis of metals and EPR spectroscopy

Three independent preparations of rTAO were analyzed (details in Section 3). Each sample solution containing 0.1 g of rTAO was added to 1 ml of nitric acid and 7 ml of water. Organic compounds were hydrolyzed by microwave-assisted protein digestion system (Ethos Pro, Milestone General). Fe, Mn, Cu, Zn and Co in each sample were quantified by inductively coupled plasma-mass spectrometer (ICP-MS, ELAN DRC PerkinElmer Japan). Analysis was performed by the Sumika Chemical Analysis Center (Osaka, Japan). Protein concentration was determined by the Lowry method.

EPR spectra were recorded on a JEOL X-band JES-FA300 spectrometer equipped with an ES-CT470 Heli-Tran cryostat system and a Scientific Instruments digital temperature indicator/controller model 9700a. For EPR analysis of rTAO, 13 mg/ml purified rTAO was frozen in EPR tubes in liquid nitrogen. The purified rTAO was reduced by 2 mM dithionite and 1 mM phenazine methosulfate prior to freezing.

2.5. Ubiquinol oxidase assay

Ubiquinol oxidase activity was measured by recording the absorbance change of ubiquinol-1 at 278 nm (Shimadzu spectrophotometer UV-3000). Reactions were started by the addition of ubiquinol-1 (final concentration 150 μM, $\varepsilon_{278} = 15{,}000\ M^{-1}\,cm^{-1}$) after 2 min preincubation at 25 °C in the presence of rTAO and 50 mM Tris–HCl (pH 7.4). For the enzyme kinetics of purified rTAO, the reaction was initiated by the addition of ubiquinol-1 after 2 min preincubation at 25 °C in the presence of rTAO and 50 mM Tris–HCl (pH 7.4) containing 0.05%(w/v) octaethylene glycol-monododecylether detergent (C10E8).

2.6. Chemicals

All chemicals were biochemistry grade. Ubiquinone-1 and protease inhibitor cocktail were purchased from Sigma-Aldrich. The other detergents were purchased from Dojin Chemicals (Tokyo, Japan).

3. Results

3.1. Purification of fully active TAO

Although we previously established a protocol for the overproduction of rTAO in *E. coli* FN102 (*ΔhemA*) lacking cytochrome *bo* and *bd* complexes of the bacteria, the yield of the active enzyme was too low to analyze its prosthetic group [36]. Such a preparation also hampered the determination of kinetic parameters of rTAO such as its molecular activity. Therefore, conditions for the expression of rTAO and purification protocols were optimized to obtain large quantities of active and stable rTAO to enable such determinations. Three factors were critical to obtain large amounts of active rTAO, namely, growth time of the culture prior to addition of IPTG, absolute concentration of IPTG, and the use of purified inner membranes as the starting material.

After extensive screening of detergents and additives to establish the procedure for efficient extraction of active rTAO from the inner membranes, we found that *n*-octyl-β-D-glucopyranoside (OG) specifically solubilized rTAO as shown in Table 1 (specific activity increased from 23.3 to 63.2 μmol/min/mg after solubilization). Approximately 60% of the membrane quinol oxidase activity was recovered with 1.4%(w/v) OG in the extract (Sup. Fig. 1). Thus, recovery of the activity was significantly higher than that of previously reported digitonin extraction (17%) [36]. Following solubilization, it was possible to maintain enzymatic activity for at least 1 month at 20 °C.

Since rTAO was fused with N-terminal histidine tag, solubilized rTAO was purified by cobalt affinity chromatography. Although the enzyme solubilized by OG was bound to the cobalt affinity resin in the presence of OG, it was not possible to elute bound rTAO from the resin with buffer containing OG. Interestingly, however, we found that 100% of the rTAO activity could be recovered from the column when OG in the washing and elution buffers was exchanged with *n*-dodecyl-β-D-maltopyranoside (DM). In the final step, purified rTAO was obtained by a two-step elution with 165 mM and 200 mM imidazole, which resulted in a very efficient purification of active rTAO in the presence of DM. A typical elution profile of quinol oxidase activity with increasing imidazole concentration is shown in Sup. Fig. 1B. Purified rTAO, with a molecular mass of 34 kDa, was estimated to be 95% pure by SDS-PAGE (Fig. 1A, lane 5). In addition to the 34 kDa band, it is apparent that other bands are also present including two with a smaller size than rTAO and one band with an approximate molecular mass of 74 kDa. Since all of these bands were recognized in Western blot using a monoclonal antibody against TAO (Fig. 1B), the smaller protein bands possibly represent proteolytic breakdown products whilst the 74 kDa band most likely represents the dimeric form of rTAO. The specific activity of purified rTAO was more than 200 μmol/min/mg protein when 150 μM of ubiquinol-1 was used as a substrate, which had a five-fold higher activity than that of the previously purified rTAO (approximately 40 μmol/min/mg) [36]. Quinol oxidase activity of purified rTAO was insensitive to 5 mM KCN but was completely inhibited by 10 nM ascofuranone. A greater than 35-fold increase in purification was achieved using the techniques described above, and 13.2% of the total activity was recovered from the lysate of FN102/pTAO cells as summarized in Table 1. Such procedures resulted in approximately 10 mg of highly purified rTAO from a 10 l culture.

Table 1
Purification of rTAO.

Fractions	Total activity (μmol/min)	Protein (mg)	Specific activity (μmol/min/mg)	Recovery (%)
E. coli lysate	14100	2410	5.85	100
Inner membrane	3500	150	23.3	24.8
OG extract	2400	37.9	63.2	17.0
Co-column	1860	8.95	207	13.2

The activities listed here were measured using 150 μM of ubiquinol-1. Fractions (eluate numbers 6–13 in Supplemental Fig. 1B) were collected as purified rTAO after co-column.

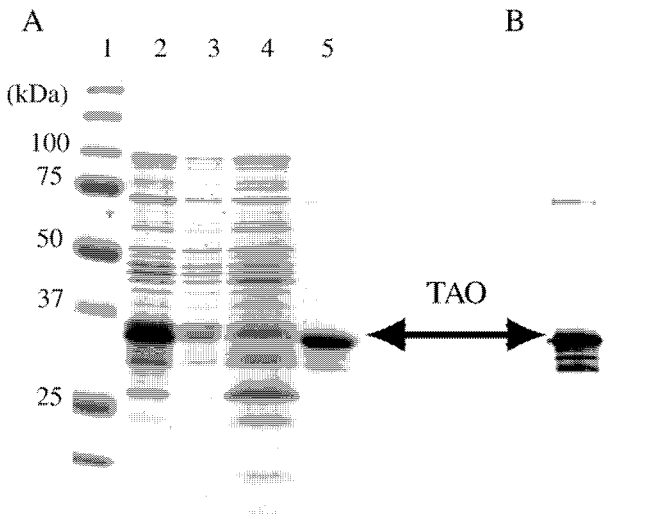

Fig. 1. SDS-PAGE and Western blotting of rTAO in purification steps. A: CBB-staining 12.5% SDS-PAGE of each fraction from the cobalt column chromatography. Lane 1, marker; lanes 2 and 3, each 5 ml of OG extract and flow through fraction; lane 4, 500 ml of wash fraction; and lane 5, 60 ml of eluted fraction collected from fractions 6–12. Loading samples on lanes 2 to 5 were precipitated with acetone. B: Western blot of purified rTAO. The same sample to lane 5 in panel B was electrophoresed on 12.5% polyacrylamide gel. Monoclonal antibodies were used against highly purified rTAO obtained by a nickel column in the presence of guanidine. Epitope recognized by this antibody is the C-terminal domain of the enzyme. The arrow indicates rTAO with an apparent molecular mass of 34 kDa.

3.2. Iron content in purified TAO

Since a highly active and stable purified rTAO could be obtained by the protocol described above, the metal content of purified rTAO was measured by ICP-MS. On the basis that TAO has a diiron center as previously proposed [23,24], then two equivalents of iron should be detected per monomer of rTAO. To this end we analyzed the iron content of purified native rTAO, inactive rTAO, denatured rTAO, and iron within the buffer eluted from the cobalt-column. Purified native rTAOs derived from three independent *E. coli* cultures were precipitated by PEG 3350 and resuspended in the elution buffer at three different concentrations as shown in Sup. Table 1. To prepare inactive rTAO, precipitated rTAO was resuspended in 50 mM Tris–HCl pH 7.4, which resulted in complete loss of enzyme activity. Denatured rTAO was prepared by resuspending the precipitant in elution buffer containing 6 M guanidine–HCl and 0.3 M EDTA. Metal contents in these preparations were 9000 ng/ml, 2900 ng/ml and 1800 ng/ml of Fe respectively for the native rTAO (3.71, 1.19 and 0.80 mg/ml), 230 ng/ml, 100 ng/ml and 28 ng/ml of Fe for inactive rTAO, denatured rTAO and the elution buffer, respectively (Sup. Table 1). From these results, the stoichiometry of bound iron per rTAO monomer can be deduced as indicated below, based on the following parameters namely, a molecular mass of rTAO of 39,391 Da (including the 6× histidine tag), purity of 95% based on SDS-PAGE gels, and the atomic weight of Fe being 55.85. Thus the ratio of iron atoms per rTAO is 1.76 for native rTAO and 0.2 and 0.08 in inactive rTAO and denatured rTAO, respectively (Table 2). This data indicates that one monomer of TAO possesses two atoms of iron which are released during inactivation or denaturation of the enzyme. To our knowledge, this is the first direct measurement of iron in purified AOX and the stoichiometry is consistent with the active site of AOX being a diiron carboxylate-center.

Other metals including Mn, Cu and Zn were also analyzed (Sup. Table 1). In all cases, these metals were below their detection limit (10 ng/ml sample solution) or background level. Although cobalt was

Table 2
Ratio of metals to purified rTAO.

	Fe/rTAO	Zn/rTAO	Mn/rTAO	Cu/rTAO
	Mean ± S.D.			
Native rTAO	1.76 ± 0.077	0.03 ± 0.013	N.D.[a]	N.D.
Inactive rTAO	0.22[b]	N.D.	N.D.	N.D.
Denatured rTAO	0.08[b]	N.D.	N.D.	N.D.

Stoichiometric ratio of metals to one molecular TAO was calculated using data in Supplemental Table 1.
[a] N.D. represents Not Detected (below 0.01).
[b] The value is an average of two independent experiments.

detected in purified rTAO, its concentration was comparable to that of cobalt in the elution buffer derived from the resin (data not shown). Similarly although 130 ng/ml, 66 ng/ml and 61 ng/ml of Zn were detected in native rTAO, these amounts of Zn were not commensurate with that of the enzyme stoichiometry. The detected Zn might be derived from the Zn-substituted form of rTAO, which was suggested to be possible from structural analysis [37]. In addition, at least 90% of the purified rTAO retained its prosthetic group in its active form.

In addition to measuring the stoichiometry of iron in purified rTAO, EPR analysis of purified rTAO was also performed in order to confirm that purified rTAO was indeed a diiron carboxylate protein and whether the detected iron originated from a diiron binding center. As shown in Fig. 2, a low field EPR signal at approximately $g = 15$ in the perpendicular EPR mode was observed with the reduced form of rTAO when the enzyme was reduced by 2 mM of dithionite and 1 mM of phenazine methosulfate (PMS), although the intensity of the signal was low. Importantly the signal disappeared in the oxidized form of rTAO. This low field EPR signal is characteristic for diiron proteins and is ascribed to an exchange-coupled high spin ferrous iron [38]. Although this signal is not normally observed in the perpendicular mode, it can be detected under certain conditions as outlined in this report [39]. The effective g-value of 15 observed in the perpendicular mode is slightly lower than the value of 16 previously observed by us [31] but this is probably due to the fact that parallel-mode EPR spectroscopy is a much more sensitive probe than the perpendicular mode. Nevertheless the finding of a low field signal when the purified enzyme is reduced is further confirmation that the purified rTAO we report here is indeed a diiron carboxylate protein. It should be noted however that we were unable to observe the $g = 15$ signal when the enzyme was reduced by more physiological reductants such as ubiquinol-1 the reasons for which are, at present, unclear.

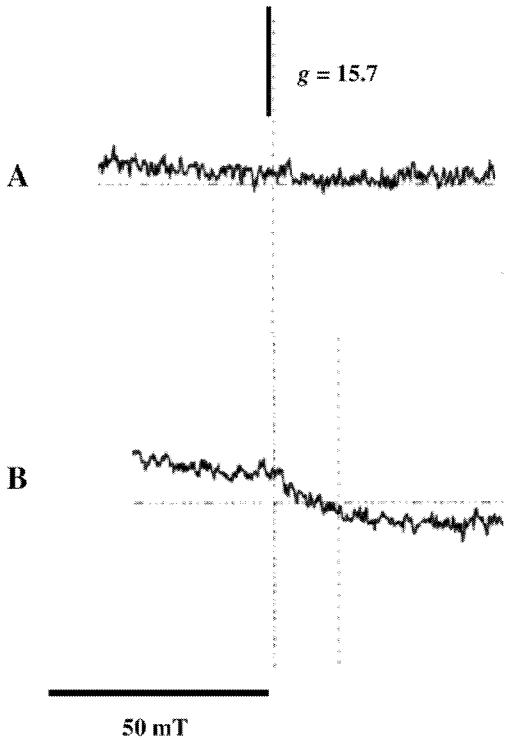

Fig. 2. EPR spectra of rTAO. A: Oxidized form of rTAO (360 μM). B: Reduced form of rTAO (360 μM), which was treated by 2 mM of dithionite and 1 mM phenazine methosulfate for 30 min on ice. Instrument parameters: microwave frequency, 9.02 GHz; microwave power, 1 mW; modulation frequency, 100 kHz; modulation amplitude, 0.6 mT; and temperature of 5 K.

3.3. Kinetic properties of purified TAO

Kinetic analysis of purified rTAO (or AOX) using ubiquinone analogs has previously proved difficult because: 1) the enzyme, following solubilization, was extremely unstable, 2) the natural substrate of trypanosome AOX is ubiquinol-9 [4], which is too hydrophobic to use as the substrate in the assay and 3) the enzymatic activity was not saturated at the maximum concentration of ubiquinol-1 (approximately 300 μM). Since we have purified rTAO in a fully active form and confirmed the stoichiometric presence of the diiron center, the purified rTAO was well-suited to a kinetic analysis.

As noted in our earlier study [36] and in AOXs from other organisms [40] non Michaelis–Menten kinetics is observed when ubiquinol-1 is used as a substrate. Hoefnagel et al. [40], however, observed that the addition of a specific detergent (0.025% EDT-20) during the assay increased the activity by 3- to 4-fold close to saturation. Although the addition of 0.025%(w/v) of EDT-20 equally enhanced the activity of purified rTAO by approximately 2-fold, it did have a deleterious effect upon the long term stability of the enzyme (Sup. Fig. 2).

In an attempt to overcome this problem, various detergents were therefore screened to determine if they could enhance activity without affecting enzyme stability. When the effect of the detergents on enzyme activity was evaluated by monitoring the activity of rTAO in the presence of detergent (Sup. Fig. 3), most activity was retained in the presence of 0.05%(w/v) of C10E8 (Sup. Fig. 4A). Light scattering at 400 nm confirmed that at least 600 μM of ubiquinol-1 was soluble in the assay system (Sup. Fig. 4B). The kinetics of ubiquinol-1 oxidation by purified rTAO in the presence of 0.05%(w/v) of C10E8 showed typical Michaelis–Menten kinetics (Fig. 3, K_m of 338 ± 23.2 μM and V_{max} of 601 ± 27.0 μmol/min/mg). In contrast, activity was linearly dependent upon substrate concentration in the absence of detergent indicating unsaturation in agreement with previous studies [36,40] (Fig. 4). Enzymatic analysis was performed with a wide range of

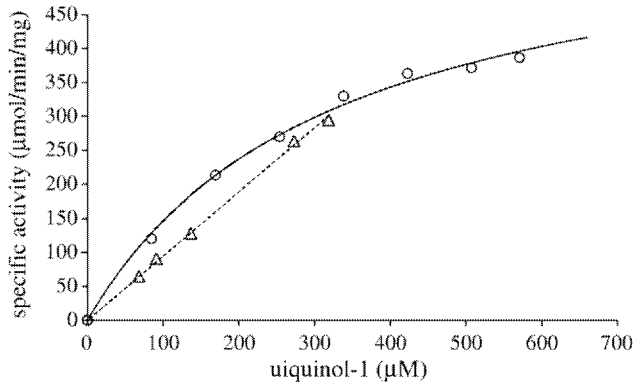

Fig. 3. Kinetics of ubiquinol-1 oxidation by purified rTAO. S–V plot of ubiquinol oxidase activity is shown using 75 ng of purified rTAO in 50 mM Tris-HCl (pH 7.4) and ubiquinol-1 (80–580 μM) with (○) and without (△) 0.05%(w/v) C10E8 at 25 °C. The solid line indicates the fitted Michaelis–Menten kinetics with the detergent (K_m of 338 ± 23.2 μM and V_{max} of 601 ± 27.0 μmol/min/mg), whereas the dashed line indicates the linear relationship between the substrate concentration and the activity without the detergent.

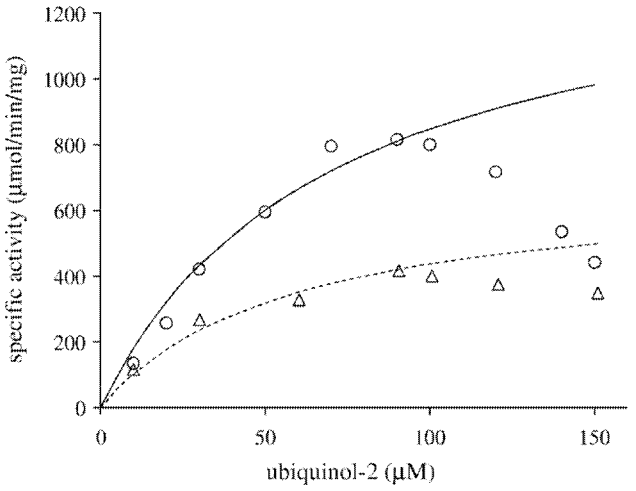

Fig. 4. Kinetics of ubiquinol-2 oxidation by purified rTAO. S–V plot of ubiquinol oxidase activity is shown using 75 ng of purified rTAO in 50 mM Tris–HCl (pH 7.4) and ubiquinol-2 (10–150 μM) with (△) 0.05%(w/v) C10E8 and with (○) 0.025%(w/v) EDT-20 at 25 °C. The solid line indicates the fitted Michaelis–Menten kinetics in the concentration range below 90 μM of ubiquinol-2 with 0.025%(w/v) EDT-20, whereas the dashed line does with 0.05%(w/v) C10E8 (K_m of 71 ± 1.2 μM and V_{max} of 1,460 ± 53.2 μmol/min/mg with 0.025%(w/v) EDT-20, whereas K_m of 57 ± 8.5 μM and V_{max} of 691 ± 28.0 μmol/min/mg with 0.05%(w/v) C10E8).

substrate concentrations (80–570 μM), which corresponded to 0.4 K_m–1.7 K_m.

To investigate whether the length of the side chain of the substrate affected the kinetic properties of rTAO, a kinetic analysis using ubiquinol-2 in the presence of EDT-20 and C10E8 (Fig. 4) was performed. Fig. 4 indicates that during the oxidation of ubiquinol-2, enzyme activity decreased above 100 μM substrate even in buffers containing either detergent. Although kinetic parameters using ubiquinol-2 could not be obtained due to substrate inhibition, S–V plots in the concentration range below 90 μM of ubiquinol-2 could be used to qualitatively analyze the effects of side chain on enzyme activity. Calculated values from such plots revealed that in the presence of 0.025%(w/v) EDT-20 the K_m (ubiquinol-2) was 71 ± 1.2 μM and V_{max} = 1460 ± 53.2 μmol/min/mg whereas with, 0.05%(w/v) C10E8 the K_m was 57 ± 8.5 μM and V_{max} = 691 ± 28.0 μmol/min/mg.

Ascofuranone is a highly specific and potent inhibitor of TAO [7] and it was therefore of importance to determine its inhibitory effect on ubiquinol-1 oxidation by purified rTAO in the presence of 0.05%(w/v) of C10E8 (Sup. Fig. 5A). From the data presented in Sup. Fig. 5A the apparent kinetic parameters of ubiquinol-1 oxidation in the presence of 0.5 nM and 2 nM of ascofuranone were estimated to be respectively $K_m^{0.5\,nM}$ = 368 ± 6.4 μM; $V_{max}^{0.5\,nM}$ = 490 ± 22.4 μmol/min/mg and $K_m^{2\,nM}$ = 492 ± 7.2 μM; and $V_{max}^{2\,nM}$ = 309 ± 60.5 μmol/min/mg. The increased K_m and decreased V_{max} values (Sup. Fig. 5B) indicate that ascofuranone inhibits purified rTAO in a mixed-type non-competitive manner with respect to ubiquinol-1.

4. Discussion

The overall goal of the present study was to obtain a highly pure and stable rTAO protein with maximum specific activity which could be used to investigate the kinetic properties of the enzyme. The quality of the purified rTAO obtained in this study has resulted in three important aspects with respect to the structure of AOX namely, the first direct evidence of stoichiometrically bound iron within the diiron center of rTAO, secondly reliable measurements of kinetic parameters and thirdly that a sample of sufficient purity and yield could be produced that has resulted in the formation of crystals [41].

4.1. Overexpression and purification of rTAO

The difficulties in isolating stable AOXs in an active form have hampered the biochemical and structural analyses of the enzyme including identification of its prosthetic groups, tertiary structural analysis and the definition of enzyme kinetic parameters. The present study reports on the overexpression and purification of active rTAO, which has enabled us to study biochemical and protein chemistry properties of this enzyme. The protocol described in this paper results in the purification of large amounts of stable rTAO with high specific activity. Two factors appeared critical to functionally express highly active rTAO. Firstly, the optimization of culture conditions, including culture duration and IPTG concentration, was crucial for the successful overexpression of rTAO with high specific activity. Secondly, activity was maximized when rTAO was purified from *E. coli* inner membranes—activity decreased substantially when it was isolated from an unpurified membrane fraction. Additionally, changing the detergent from OG to DM following solubilization, also appeared important to maximize yield and activity. Purified rTAO produced in this manner retained complete activity for more than 6 months at 4 °C and for more than 1 month at 20 °C. Furthermore, we have also been able to purify *Sauromattum guttatum* rAOX by this procedure showing the universality of the purification protocol (Elliott, C.E., Kido, Y., Kita, K. and Moore, A.L. unpublished observations).

It is anticipated that highly purified and active AOX will open a new direction with respect to the investigation of the structure and reaction mechanisms of AOXs and contribute to further progress on the study of this novel terminal oxidase. Indeed we recently took advantage of the exceptional stability and purity of the rTAO by performing the first FTIR spectroscopic investigation of any diiron protein [32]. Stepwise reduction of the fully oxidized resting state of rTAO revealed two distinct IR redox difference spectra. The first of these, "signal 1", contained clear features that could be assigned to protonation of at least one carboxylate group, further perturbations of carboxylic and histidine residues, bound ubiquinone and a negative band that might arise from a radical in the fully oxidized protein. A second IR redox difference spectrum, "signal 2", appeared more slowly (within approximately 1 h) once signal 1 had been reduced and is quite distinct from the components which comprise signal 1. The exact identity of the components which result in signal 2 await further investigations. Such a study has not previously been possible with AOX preparations because of protein instability at room temperature.

4.2. Prosthetic group analysis

Prosthetic group analysis summarized in Table 2 revealed that in highly stable and purified rTAO there are two equivalents of iron per rTAO monomer with no other metals, including Cu, Mn and Zn, being detected. EPR spectroscopy confirms that the irons are part of a diiron center since an EPR signal at $g = 15$ could be detected (Fig. 2) when rTAO is reduced by dithionite in the presence of PMS. The fact that this signal can be detected in all AOXs examined to date suggests that the signal is a characteristic signature of AOXs [30,31] and in agreement with mutational analyses [18,25–29] is further confirmation that TAO, similar to AOXs in other organisms, is a diiron carboxylate protein. Furthermore the data summarized in Table 2 revealed that when the protein was either inactivated or denatured iron was released indicating it is essential for TAO activity. Moreover, this data has established biochemically the validity of predicting the presence of a diiron center from amino acid sequence data, not only in AOX but also in other membrane-bound diiron carboxylate proteins including 5-demethoxyquinone hydroxylase (CLK-1/Coq7) (which also has the diiron binding motif EXXH). It is of interest to note that both AOX and CLK-1/Coq7 utilize ubiquinol as substrate and both are involved in respiration [42–44].

4.3. Kinetic analysis

The inclusion of C10E8 in the assay was found to be critical for the kinetic analysis of TAO and the evaluation of inhibitors. In Table 3, we have calculated fundamental kinetic parameters of TAO and compared them to those of *E. coli* cytochrome *bo* oxidase complex and *S. cerevisiae* ubiquinol–cytochrome *c* reductase [45]. These kinetic constants provide a molecular rationale on how the alternative pathway can effectively compete with other terminal oxidases, although caution must be exercised in the interpretation of this data as it is derived from experiments performed under non-physiological conditions and substrates. Nevertheless Table 3 indicates that TAO has a calculated k_{cat} of $415 \pm 19\ s^{-1}$ (on the basis that the purity of rTAO is 95%), which is slightly higher than that of the cytochrome *bo* oxidase complex ($313\ s^{-1}$), yeast ubiquinol–cytochrome *c* reductase ($153\ s^{-1}$) and previous values reported for the plant AOX ($186\ s^{-1}$), but considerably less than that calculated for cytochrome *c* oxidase ($770\ s^{-1}$) [45–48]. Taking into account that the value of the specificity constant (k_{cat}/K_m) of enzymatic reactions is known to be less than $10^9\ M^{-1}\ s^{-1}$ (from the perspective of diffusion limited access of substrates [49]), it is apparent from Table 3 that both cytochrome *bo* oxidase and TAO have quite high and comparable catalytic activities. These values suggest that the activation energy of both quinol oxidase reactions are similar and furthermore that the quinol oxidase activity of TAO is thermodynamically "alternative" to that of the cytochrome *bo* complex. In contrast however, TAO does not appear to compete effectively with the bc_1 complex in terms of specificity constant and, if the plant AOX possesses a similar specificity constant to that of TAO, it would suggest that plant alternative oxidase activity would be severely curtailed unless the conventional respiratory chain is limited either through inhibition (which appears to be the case under 'stressed conditions') or through down regulation as appears to be the case in thermogenic tissues [12,50,51].

Interestingly ubiquinol-2 oxidation by rTAO showed substrate inhibition at concentrations above 100 μM in a manner similar to that observed when the heterodimeric terminal ubiquinol oxidase of *E. coli*, cytochrome *bd* oxidized ubiquinol-2 as substrate [52]. A lower K_m value of ubiquinol-2 than that of ubiquinol-1 might be related not only to its hydrophobicity but also could be a function of the isoprenoid chain. The peculiar kinetics of ubiquinol-2 might be attributed to the following two points; 1) competition for the ubiquinol-2 oxidation site between the substrate and the product, and 2) the presence of inactive intermediates of the enzyme related to the precise catalytic mechanism.

Kinetic analysis of the mechanism of inhibition by the specific TAO inhibitor ascofuranone (Sup. Fig. 5) indicates that it is a mixed-type inhibitor with respect to ubiquinol-1. The discrepancy between the mixed inhibition observed in this report and competitive inhibition as reported in our previous study [36] might be due to the different assay conditions used in the experiments described in this paper. In the previous study, the kinetic parameters were based on apparent values because enzymatic activity was calculated without detergents and hence only low ranges of ubiquinol-1 concentrations (0.01 K_m–0.3 K_m) could be used. In contrast, the kinetic parameters reported in the current study were determined with much higher reliability since in the presence of C10E8, a much wider range of ubiquinol-1 (0.4 K_m–1.7 K_m) could be used.

Table 3
Kinetic parameters of quinol oxidases (with respect to ubiquinol-1).

	K_m (μM)	V_{max} (μmol/min/mg protein)	k_{cat} (s^{-1})	k_{cat}/K_m ($\mu M^{-1}\ s^{-1}$)
TAO[a]	338 ± 23.2	601 ± 27.0	415 ± 19	1.2
Cyt *bo* oxidase[b]	61	–	313	5.2
Ubiquinol-cyt *c* reductase[c]	13	–	220	16.9

The k_{cat} value of cytochrome *c* oxidase is $k_{cat} = 770\ (s^{-1})$ [46].
All the k_{cat} values listed here were obtained by dividing the V_{max} by the concentration of the enzymes (mol/mg protein).
[a] This study.
[b] *E. coli* cytochrome *bo* oxidase as in Sakamoto et al. [47].
[c] Ubiquinol–cytochrome *c* reductase from bovine heart as in Fato et al. [45].

4.4. Unique feature of AOX

AOX is found in various organisms and recent genome database searches have also identified AOX in different phyla of the Animalia kingdom (Mollusca, Nematoda and Chordata) [17]. It has been suggested that since AOX is absent from mammalian tissues TAO could be a chemotherapeutic target, since it functions in the bloodstream form of *T. brucei* as the only terminal oxidase and hence is essential for the survival of trypanosomes [5,6]. As an AOX protein has also been identified in *Cryptosporidium parvum* [53,54], which causes diarrheal disease cryptosporidiosis, and the recombinant *C. parvum* AOX is also sensitive to ascofuranone and as a result suggests that not only could AOX be a potential drug target in a number of parasites but furthermore ascofuranone could be used to treat a number of infections since this compound shows potent, broad-spectrum antimicrobial activity [53].

In addition to this clinical application, there is considerable interest in the unique characteristics of the enzyme since the functions and properties of TAO are clearly distinct from those of other bacterial quinol oxidases. TAO is a cytochrome-independent and cyanide-insensitive quinol oxidase, whereas cytochrome *bo* and *bd* complexes are cytochrome-dependent and cyanide-sensitive quinol oxidases [34,35]. Furthermore, TAO has various other physiological roles in *T. brucei*; the cytochrome and alternative pathways are both active and functional in the procyclic forms [55] in addition to the bloodstream form, thereby possibly providing metabolic flexibility under changing environmental conditions. TAO activity also appears to regulate the expression of one of the major surface coat proteins, GPEET, in the procyclic form [56], and in addition may regulate the observed programmed cell death-like phenomena in the bloodstream forms [57].

5. Conclusions

The primary aim of our research on TAO is to elucidate the interaction between the enzyme and its substrate or inhibitor, which hopefully could act as a structural guide for ongoing drug development. In addition to the knowledge obtained from this study, further studies on the inhibitory kinetics and structure–activity relationship of ascofuranone derivatives, along with mutational analyses of TAO [27,29] and X-ray structure analysis will undoubtedly have considerable implications with respect to our understanding of how the enzyme interacts with its substrate and inhibitors. A three-dimensional structure of TAO with and without ascofuranone should also shed light on the inhibitory mechanism of this potent drug, which according to this study occurs via a mixed-type inhibition. Such further insights about the interaction between ascofuranone and the enzyme will hopefully lead to a more rational design of more potent and safe anti-trypanosomal drugs.

Acknowledgements

This work was supported in part by Grant-in-aid for Young Scientists (B) 21790402 (to YK), Grant-in-Aid for Scientific Research (C) 21590467 (to YY), Creative Scientific Research Grant 18GS0314 (to KK), Grant-in-aid for Scientific Research on Priority Areas 18073004 (to KK) from the Japanese Society for the Promotion of Science, and Targeted Proteins Research Program (to KK) from the

Japanese Ministry of Education, Science, Culture, Sports and Technology (MEXT) and a grant for research to promote the development of anti-AIDS pharmaceuticals from the Japan Health Sciences Foundation (to KK). ALM gratefully acknowledges BBSRC for financial support and with KK the Prime Ministers Initiative 2 (Connect) fund for collaborative twinning.

Appendix A. Supplementary data

Supplementary data associated with this article can be found, in the online version, at doi:10.1016/j.bbabio.2009.12.021.

References

[1] WHO, Control and surveillance of African trypanosomiasis, Report of a WHO Expert Committee, World Health Organ Tech Rep Ser, vol. 881, 1998, pp. 1–114, I–VI.
[2] C.E. Clayton, P. Michels, Metabolic compartmentation in African trypanosomes, Parasitol. Today 12 (1996) 465–471.
[3] F.R. Opperdoes, P. Borst, S. Bakker, W. Leene, Localization of glycerol-3-phosphate oxidase in the mitochondrion and particulate NAD+-linked glycerol-3-phosphate dehydrogenase in the microbodies of the bloodstream form to *Trypanosoma brucei*, Eur. J. Biochem. 76 (1977) 29–39.
[4] A.B. Clarkson Jr., E.J. Bienen, G. Pollakis, R.W. Grady, Respiration of bloodstream forms of the parasite *Trypanosoma brucei brucei* is dependent on a plant-like alternative oxidase, J. Biol. Chem. 264 (1989) 17770–17776.
[5] M. Chaudhuri, R.D. Ott, G.C. Hill, Trypanosome alternative oxidase: from molecule to function, Trends Parasitol. 22 (2006) 484–491.
[6] C. Nihei, Y. Fukai, K. Kita, Trypanosome alternative oxidase as a target of chemotherapy, Biochim. Biophys. Acta 1587 (2002) 234–239.
[7] N. Minagawa, Y. Yabu, K. Kita, K. Nagai, N. Ohta, K. Meguro, S. Sakajo, A. Yoshimoto, An antibiotic, ascofuranone, specifically inhibits respiration and in vitro growth of long slender bloodstream forms of *Trypanosoma brucei brucei*, Mol. Biochem. Parasitol. 84 (1997) 271–280.
[8] Y. Yabu, A. Yoshida, T. Suzuki, C. Nihei, K. Kawai, N. Minagawa, T. Hosokawa, K. Nagai, K. Kita, N. Ohta, The efficacy of ascofuranone in a consecutive treatment on *Trypanosoma brucei brucei* in mice, Parasitol. Int. 52 (2003) 155–164.
[9] Y. Yabu, T. Suzuki, C. Nihei, N. Minagawa, T. Hosokawa, K. Nagai, K. Kita, N. Ohta, Chemotherapeutic efficacy of ascofuranone in *Trypanosoma vivax*-infected mice without glycerol, Parasitol. Int. 55 (2006) 39–43.
[10] M. Chaudhuri, W. Ajayi, S. Temple, G.C. Hill, Identification and partial purification of a stage-specific 33 kDa mitochondrial protein as the alternative oxidase of the *Trypanosoma brucei brucei* bloodstream trypomastigotes, J. Eukaryot. Microbiol. 42 (1995) 467–472.
[11] A.L. Moore, J.N. Siedow, The regulation and nature of the cyanide-resistant alternative oxidase of plant mitochondria, Biochim. Biophys. Acta 1059 (1991) 121–140.
[12] A.L. Moore, M.S. Albury, Further insights into the structure of the alternative oxidase: from plants to parasites, Biochem. Soc. Trans. 36 (2008) 1022–1026.
[13] J.N. Siedow, A.L. Umbach, The mitochondrial cyanide-resistant oxidase: structural conservation amid regulatory diversity, Biochim. Biophys. Acta 1459 (2000) 432–439.
[14] T. Joseph-Horne, D.W. Hollomon, P.M. Wood, Fungal respiration: a fusion of standard and alternative components, Biochim. Biophys. Acta 1504 (2001) 179–195.
[15] A. McDonald, G. Vanlerberghe, Branched mitochondrial electron transport in the Animalia: presence of alternative oxidase in several animal phyla, IUBMB Life 56 (2004) 333–341.
[16] A.E. McDonald, G.C. Vanlerberghe, Alternative oxidase and plastoquinol terminal oxidase in marine prokaryotes of the Sargasso Sea, Gene 349 (2005) 15–24.
[17] A.E. McDonald, G.C. Vanlerberghe, J.F. Staples, Alternative oxidase in animals: unique characteristics and taxonomic distribution, J. Exp. Biol. 212 (2009) 2627–2634.
[18] D.A. Berthold, M.E. Andersson, P. Nordlund, New insight into the structure and function of the alternative oxidase, Biochim. Biophys. Acta 1460 (2000) 241–254.
[19] C. Affourtit, M.S. Albury, P.G. Crichton, A.L. Moore, Exploring the molecular nature of alternative oxidase regulation and catalysis, FEBS Lett. 510 (2002) 121–126.
[20] D.P. Maxwell, Y. Wang, L. McIntosh, The alternative oxidase lowers mitochondrial reactive oxygen production in plant cells, Proc. Natl. Acad. Sci. U. S. A. 96 (1999) 8271–8276.
[21] A.L. Moore, M.S. Albury, P.G. Crichton, C. Affourtit, Function of the alternative oxidase: is it still a scavenger? Trends Plant Sci. 7 (2002) 478–481.
[22] S. Mackenzie, L. McIntosh, Higher plant mitochondria, Plant Cell 11 (1999) 571–586.
[23] J.N. Siedow, A.L. Umbach, A.L. Moore, The active site of the cyanide-resistant oxidase from plant mitochondria contains a binuclear iron center, FEBS Lett. 362 (1995) 10–14.
[24] M.E. Andersson, P. Nordlund, A revised model of the active site of alternative oxidase, FEBS Lett. 449 (1999) 17–22.
[25] M.S. Albury, C. Affourtit, A.L. Moore, A highly conserved glutamate residue (Glu-270) is essential for plant alternative oxidase activity, J. Biol. Chem. 273 (1998) 30301–30305.
[26] M. Chaudhuri, W. Ajayi, G.C. Hill, Biochemical and molecular properties of the *Trypanosoma brucei* alternative oxidase, Mol. Biochem. Parasitol. 95 (1998) 53–68.
[27] W.U. Ajayi, M. Chaudhuri, G.C. Hill, Site-directed mutagenesis reveals the essentiality of the conserved residues in the putative diiron active site of the trypanosome alternative oxidase, J. Biol. Chem. 277 (2002) 8187–8193.
[28] M.S. Albury, C. Affourtit, P.G. Crichton, A.L. Moore, Structure of the plant alternative oxidase. Site-directed mutagenesis provides new information on the active site and membrane topology, J. Biol. Chem. 277 (2002) 1190–1194.
[29] K. Nakamura, K. Sakamoto, Y. Kido, Y. Fujimoto, T. Suzuki, M. Suzuki, Y. Yabu, N. Ohta, A. Tsuda, M. Onuma, K. Kita, Mutational analysis of the *Trypanosoma vivax* alternative oxidase: the $E(X)_6Y$ motif is conserved in both mitochondrial alternative oxidase and plastid terminal oxidase and is indispensable for enzyme activity, Biochem. Biophys. Res. Commun. 334 (2005) 593–600.
[30] D.A. Berthold, N. Voevodskaya, P. Stenmark, A. Graslund, P. Nordlund, EPR studies of the mitochondrial alternative oxidase. Evidence for a diiron carboxylate center, J. Biol. Chem. 277 (2002) 43608–43614.
[31] A.L. Moore, J.E. Carre, C. Affourtit, M.S. Albury, P.G. Crichton, K. Kita, P. Heathcote, Compelling EPR evidence that the alternative oxidase is a diiron carboxylate protein, Biochim. Biophys. Acta 1777 (2008) 327–330.
[32] A. Maréchal, Y. Kido, K. Kita, A.L. Moore, P.R. Rich, Identification of three redox states of recombinant *Trypanosoma brucei* alternative oxidase by FTIR spectroscopy and electrochemistry, J. Biol. Chem. 284 (2009) 31827–31833.
[33] Y. Fukai, H. Amino, H. Hirawake, Y. Yabu, N. Ohta, N. Minagawa, S. Sakajo, A. Yoshimoto, K. Nagai, S. Takamiya, S. Kojima, K. Kita, Functional expression of the ascofuranone-sensitive *Trypanosoma brucei brucei* alternative oxidase in the cytoplasmic membrane of *Escherichia coli*, Comp. Biochem. Physiol. C Pharmacol. Toxicol. Endocrinol. 124 (1999) 141–148.
[34] K. Kita, K. Konishi, Y. Anraku, Terminal oxidases of *Escherichia coli* aerobic respiratory chain. I. Purification and properties of cytochrome b_{562}-*o* complex from cells in the early exponential phase of aerobic growth, J. Biol. Chem. 259 (1984) 3368–3374.
[35] K. Kita, K. Konishi, Y. Anraku, Terminal oxidases of *Escherichia coli* aerobic respiratory chain. II. Purification and properties of cytochrome b_{558}-*d* complex from cells grown with limited oxygen and evidence of branched electron-carrying systems, J. Biol. Chem. 259 (1984) 3375–3381.
[36] C. Nihei, Y. Fukai, K. Kawai, A. Osanai, Y. Yabu, T. Suzuki, N. Ohta, N. Minagawa, K. Nagai, K. Kita, Purification of active recombinant trypanosome alternative oxidase, FEBS Lett. 538 (2003) 35–40.
[37] O. Maglio, F. Nastri, V. Pavone, A. Lombardi, W.F. DeGrado, Preorganization of molecular binding sites in designed diiron proteins, Proc. Natl. Acad. Sci. U. S. A. 100 (2003) 3772–3777.
[38] M.P. Hendrich, E. Munck, B.G. Fox, J.D. Lipscomb, Integer-spin Epr studies of the fully reduced methane monooxygenase hydroxylase component, J. Am. Chem. Soc. 112 (1990) 5861–5865.
[39] W.A. van den Berg, A.A. Stevens, M.F. Verhagen, W.M. van Dongen, W.R. Hagen, Overproduction of the prismane protein from *Desulfovibrio desulfuricans* ATCC 27774 in *Desulfovibrio vulgaris* (Hildenborough) and EPR spectroscopy of the [6Fe–6S] cluster in different redox states, Biochim. Biophys. Acta 1206 (1994) 240–246.
[40] M. Hoefnagel, P.R. Rich, Q. Zhang, J.T. Wiskich, Substrate kinetics of the plant mitochondrial alternative oxidase and the effects of pyruvate, Plant Physiol. 115 (1997) 1145–1153.
[41] Y. Kido, T. Shiba, D.K. Inaoka, K. Sakamoto, T. Nara, T. Aoki, T. Honma, A. Tanaka, M. Inoue, S. Matsuoka, A. Moore, S. Harada, K. Kita, Crystallization and preliminary crystallographic analysis of cyanide-insensitive alternative oxidase from *Trypanosoma brucei brucei*, Acta. Crystallogr. Sect. F Struct. Biol. Cryst. Commun, doi:10.1107/S1744309109054062.
[42] H. Miyadera, H. Amino, A. Hiraishi, H. Taka, K. Murayama, H. Miyoshi, K. Sakamoto, N. Ishii, S. Hekimi, K. Kita, Altered quinone biosynthesis in the long-lived clk-1 mutants of *Caenorhabditis elegans*, J. Biol. Chem. 276 (2001) 7713–7716.
[43] P. Stenmark, J. Grunler, J. Mattsson, P.J. Sindelar, P. Nordlund, D.A. Berthold, A new member of the family of di-iron carboxylate proteins. Coq7 (clk-1), a membrane-bound hydroxylase involved in ubiquinone biosynthesis, J. Biol. Chem. 276 (2001) 33297–33300.
[44] D.A. Berthold, P. Stenmark, Membrane-bound diiron carboxylate proteins, Ann. Rev. Plant Biol. 54 (2003) 497–517.
[45] R. Fato, M. Cavazzoni, C. Castelluccio, G. Parenti Castelli, G. Palmer, M. Degli Esposti, G. Lenaz, Steady-state kinetics of ubiquinol–cytochrome *c* reductase in bovine heart submitochondrial particles: diffusional effects, Biochem. J. 290 (1993) 225–236 K.
[46] H. Witt, F. Malatesta, F. Nicoletti, M. Brunori, B. Ludwig, Tryptophan 121 of subunit II is the electron entry site to cytochrome-*c* oxidase in *Paracoccus denitrificans*. Involvement of a hydrophobic patch in the docking reaction, J. Biol. Chem. 273 (1998) 5132–5136.
[47] Sakamoto, H. Miyoshi, M. Ohshima, K. Kuwabara, K. Kano, T. Akagi, T. Mogi, H. Iwamura, Role of the isoprenyl tail of ubiquinone in reaction with respiratory enzymes: studies with bovine heart mitochondrial complex I and *Escherichia coli bo*-type ubiquinol oxidase, Biochemistry 37 (1998) 15106–15113.
[48] M.H.N. Hoefnagel, J.T. Wiskich, S.A. Madgwick, Z. Patterson, W. Oettmeier, P.R. Rich New, Inhibitors of the ubiquinol oxidase of higher plant mitochondria, Eur. J. Biochem. 233 (1995) 531–537.
[49] R.A. Alberty, G.G. Hammes, Application of the theory of diffusion-controlled reactions to enzyme kinetics, J. Phys. Chem. 62 (1958) 154–159.
[50] R. Clifton, A.H. Millar, J. Whelan, Alternative oxidases in Arabidopsis: a comparative analysis of differential expression in the gene family provides new insights into function of non-phosphorylating bypasses, Biochim. Biophys. Acta 1757 (2006) 730–741.
[51] A.M. Wagner, K. Krab, M.J. Wagner, A.L. Moore, Regulation of thermogenesis in flowering Araceae: the role of the alternative oxidase, Biochim. Biophys. Acta 1777 (2008) 993–1000.

[52] K. Sakamoto, H. Miyoshi, K. Takegami, T. Mogi, Y. Anraku, H. Iwamura, Probing substrate binding site of the *Escherichia coli* quinol oxidases using synthetic ubiquinol analogues, J. Biol. Chem. 271 (1996) 29897–29902.
[53] T. Suzuki, T. Hashimoto, Y. Yabu, Y. Kido, K. Sakamoto, C. Nihei, M. Hato, S. Suzuki, Y. Amano, K. Nagai, T. Hosokawa, N. Minagawa, N. Ohta, K. Kita, Direct evidence for cyanide-insensitive quinol oxidase (alternative oxidase) in apicomplexan parasite *Cryptosporidium parvum*: phylogenetic and therapeutic implications, Biochem. Biophys. Res. Commun. 313 (2004) 1044–1052.
[54] C.W. Roberts, F. Roberts, F.L. Henriquez, D. Akiyoshi, B.U. Samuel, T.A. Richards, W. Milhous, D. Kyle, L. McIntosh, G.C. Hill, M. Chaudhuri, S. Tzipori, R. McLeod, Evidence for mitochondrial-derived alternative oxidase in the apicomplexan parasite *Cryptosporidium parvum*: a potential anti-microbial agent target, Int. J. Parasitol. 34 (2004) 297–308.
[55] R. Walker Jr., L. Saha, G.C. Hill, M. Chaudhuri, The effect of over-expression of the alternative oxidase in the procyclic forms of *Trypanosoma brucei*, Mol. Biochem. Parasitol. 139 (2005) 153–162.
[56] E. Vassella, M. Probst, A. Schneider, E. Studer, C.K. Renggli, I. Roditi, Expression of a major surface protein of *Trypanosoma brucei* insect forms is controlled by the activity of mitochondrial enzymes, Mol. Biol. Cell 15 (2004) 3986–3993.
[57] A. Tsuda, W.H. Witola, K. Ohashi, M. Onuma, Expression of alternative oxidase inhibits programmed cell death-like phenomenon in bloodstream form of *Trypanosoma brucei rhodesiense*, Parasitol. Int. 54 (2005) 243–251.

Acta Crystallographica Section F
Structural Biology and Crystallization Communications
ISSN 1744-3091
Editors: **H. M. Einspahr and M. S. Weiss**

Crystallization and preliminary crystallographic analysis of cyanide-insensitive alternative oxidase from *Trypanosoma brucei brucei*

Yasutoshi Kido, Tomoo Shiba, Daniel Ken Inaoka, Kimitoshi Sakamoto, Takeshi Nara, Takashi Aoki, Teruki Honma, Akiko Tanaka, Masayuki Inoue, Shigeru Matsuoka, Anthony Moore, Shigeharu Harada and Kiyoshi Kita

Acta Cryst. (2010). F**66**, 275–278

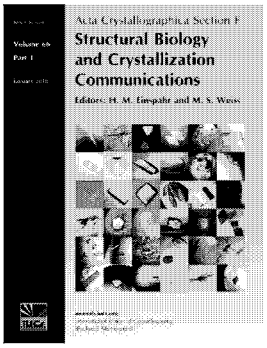

Acta Crystallographica Section F
Structural Biology and Crystallization Communications
ISSN 1744-3091

Crystallization and preliminary crystallographic analysis of cyanide-insensitive alternative oxidase from *Trypanosoma brucei brucei*

Yasutoshi Kido,[a] Tomoo Shiba,[a] Daniel Ken Inaoka,[a] Kimitoshi Sakamoto,[a] Takeshi Nara,[b] Takashi Aoki,[b] Teruki Honma,[c] Akiko Tanaka,[c] Masayuki Inoue,[d] Shigeru Matsuoka,[d] Anthony Moore,[e] Shigeharu Harada[f]* and Kiyoshi Kita[a]*

[a]Department of Biomedical Chemistry, Graduate School of Medicine, The University of Tokyo, Tokyo 113-0033, Japan, [b]Department of Molecular and Cellular Parasitology, Juntendo University School of Medicine, Tokyo 113-8421, Japan, [c]Systems and Structural Biology Center, RIKEN, Tsurumi, Yokohama 230-0045, Japan, [d]Graduate School of Pharmaceutical Sciences, The University of Tokyo, Tokyo 113-0033, Japan, [e]Biochemistry and Biomedical Sciences, School of Life Sciences, University of Sussex, Falmer, Brighton, England, and [f]Department of Applied Biology, Graduate School of Science and Technology, Kyoto Institute of Technology, Kyoto 606-8585, Japan

Correspondence e-mail: harada@kit.ac.jp, kitak@m.u-tokyo.ac.jp

Received 6 September 2009
Accepted 15 December 2009

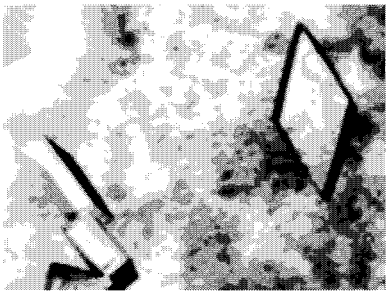

Cyanide-insensitive alternative oxidase (AOX) is a mitochondrial membrane protein and a non-proton-pumping ubiquinol oxidase that catalyzes the four-electron reduction of dioxygen to water. In the African trypanosomes, trypanosome alternative oxidase (TAO) functions as a cytochrome-independent terminal oxidase that is essential for survival in the mammalian host; hence, the enzyme is considered to be a promising drug target for the treatment of trypanosomiasis. In the present study, recombinant TAO (rTAO) overexpressed in haem-deficient *Escherichia coli* was purified and crystallized at 293 K by the hanging-drop vapour-diffusion method using polyethylene glycol 400 as a precipitant. X-ray diffraction data were collected at 100 K and were processed to 2.9 Å resolution with 93.1% completeness and an overall $R_{\rm merge}$ of 9.5%. The TAO crystals belonged to the orthorhombic space group $I222$ or $I2_12_12_1$, with unit-cell parameters $a = 63.11$, $b = 136.44$, $c = 223.06$ Å. Assuming the presence of two rTAO molecules in the asymmetric unit (2 × 38 kDa), the calculated Matthews coefficient ($V_{\rm M}$) was 3.2 Å^3 Da^{-1}, which corresponds to a solvent content of 61.0%. This is the first report of a crystal of the membrane-bound diiron proteins, which include AOXs.

1. Introduction

Cyanide-insensitive respiration in plants has been recognized since the 1920s (Moore & Siedow, 1991). Intensive biochemical studies have revealed that the mitochondrial membrane enzyme alternative oxidase (AOX) is responsible for cyanide-insensitive respiration (Moore & Siedow, 1991; Siedow & Umbach, 2000; Moore & Albury, 2008). AOX, which is cyanide-insensitive and sensitive to salicyl hydroxamic acid (SHAM), is a non-proton-pumping ubiquinol oxidase that catalyzes the four-electron reduction of dioxygen to water (Moore & Albury, 2008). AOX has been found in higher plants, algae, yeast, slime moulds, free-living amoebae, eubacteria and nematodes, as well as in protozoa, including trypanosomes (McDonald *et al.*, 2009).

Trypanosoma brucei, which causes African sleeping sickness in humans and nagana in livestock, which are serious health and economic problems in sub-Saharan Africa (World Health Organization, 2006), is known to show cyanide-insensitive respiration (Opperdoes *et al.*, 1977; Chaudhuri *et al.*, 2006). In the African trypanosomes, trypanosome alternative oxidase (TAO) functions in cyanide-insensitive respiration as a cytochrome-independent terminal oxidase (Clarkson *et al.*, 1989) that is essential for survival in the mammalian host (Clayton & Michels, 1996; Chaudhuri *et al.*, 2006).

TAO is thought to be a good target for antitrypanosomal drugs because mammalian hosts do not possess this protein (Nihei *et al.*, 2002; Chaudhuri *et al.*, 2006). Indeed, we found that ascofuranone, which is isolated from the pathogenic fungus *Ascochyta visiae*, specifically inhibits the quinol oxidase activity of TAO (Minagawa *et al.*, 1997) and rapidly kills the parasites. In addition, we have confirmed the chemotherapeutic efficacy of ascofuranone *in vivo* (Yabu *et al.*, 2003, 2006).

Although TAO and other alternative oxidases (AOXs) contain diiron-binding motifs (E*XX*H) in their amino-acid sequences, their three-dimensional structures have not yet been elucidated (Berthold

& Stenmark, 2003; Moore & Albury, 2008). The high-resolution structure of TAO will undoubtedly have considerable implications with respect to their physicochemical mechanism, enzyme reaction and structure–function relationship, including the interaction between the enzyme and ascofuranone, which may lead to the rational design of more potent and safer antitrypanosomal drugs. Here, we describe the crystallization and preliminary crystallographic analysis of TAO.

2. Materials and methods

2.1. Preparation of rTAO

To construct the host strain FN102 for the expression of rTAO, the Δ*hemA*::Km^R mutation was introduced into *Escherichia coli* strain BL21 (DE3) by P1 transduction as described in a previous study (Nihei *et al.*, 2003). The strain FN102/pTbAO (Nihei *et al.*, 2003) carrying the cDNA for *T. brucei brucei* TAO was precultured at 310 K in 100 ml LB medium (containing 10 mg ampicillin, 5 mg kanamycin and 5 mg 5-aminolevulinic acid) for 4–6 h. The precultured cells were grown aerobically at 303 K in 10 l S-medium [100 g tryptone peptone, 50 g yeast extract, 50 g casamino acids, 104 g K_2HPO_4, 30 g KH_2PO_4, 7.5 g trisodium citrate.$2H_2O$, 25 g $(NH_4)_2SO_4$, 0.5 g $MgSO_4.7H_2O$, 0.25 g $FeSO_4.7H_2O$, 0.25 g $FeCl_3$, 20 g glucose and 0.1 g carbenicillin]. The culture was started at an OD_{600} of 0.01 and expression of His_6-tagged rTAO was induced by the addition of isopropyl β-D-1-thiogalactopyranoside (IPTG; 25 μ*M*) when the OD_{600} reached 0.1. The cells were harvested 8–10 h after induction (about 40 g wet weight). The cells were then resuspended in 200 ml 50 m*M* Tris–HCl pH 7.5 containing 20%(*w*/*w*) sucrose, 0.1 m*M* phenylmethanesulfonylfluoride and protease inhibitor cocktail (Sigma) and broken using a French pressure cell at 200 MPa (Ohtake, Tokyo). Unbroken cells were removed as a pellet by centrifugation at 8000*g* for 10 min (Hitachi 21G). The supernatant (35 ml) was loaded onto 35 ml 50 m*M* Tris–HCl pH 7.5 containing 40%(*w*/*w*) sucrose and ultracentrifuged at 200 000*g* for 1 h at 277 K (Hitachi 85H); the fraction of inner membranes buoyant on the 40%(*w*/*w*) sucrose layer was recovered. The inner-membrane pellet was separated by further ultracentrifugation at 200 000*g* for 1 h (Hitachi 85H) and was resuspended in 30 ml 50 m*M* Tris–HCl pH 7.5 containing 20%(*w*/*w*) sucrose. To solubilize rTAO from the membranes, the membrane suspension (35 ml) was diluted with buffer [50 m*M* Tris–HCl, 200 m*M* $MgSO_4$, 20%(*v*/*v*) glycerol pH 7.3] at 277 K to give a 6 mg ml^{-1} solution and 14%(*w*/*v*) *n*-octyl β-D-glucopyranoside (OG) was added to a final concentration of 1.4%(*w*/*v*). The solution was immediately ultracentrifuged at 200 000*g* for 1 h at 277 K to recover the supernatant containing the solubilized rTAO.

Cobalt-affinity chromatography was performed by a hybrid batch/column procedure using the manufacturer's instructions as stated below. 10 ml BD TALON Metal Affinity Resin (BD Bioscience) equilibrated in a batch format with 100 ml equilibration buffer [20 m*M* Tris–HCl, 1.4%(*w*/*v*) OG, 100 m*M* $MgSO_4$, 20%(*v*/*v*) glycerol pH 7.3] was mixed with 20 ml of the OG extract for 20 min at 277 K. The resin was washed twice with 100 ml of the first wash buffer [20 m*M* Tris–HCl, 20 m*M* imidazole, 0.042%(*w*/*v*) *n*-dodecyl β-D-maltopyranoside (DM), 50 m*M* $MgSO_4$, 20%(*v*/*v*) glycerol pH 7.3] and then transferred to a column for additional washing with 20 ml of the second wash buffer [20 m*M* Tris–HCl, 165 m*M* imidazole, 0.042%(*w*/*v*) DM, 50 m*M* $MgSO_4$, 20%(*v*/*v*) glycerol pH 7.3; flow rate 1 ml min^{-1}]. After washing, rTAO was eluted with elution buffer [20 m*M* Tris–HCl, 200 m*M* imidazole, 0.042%(*w*/*v*) DM, 50 m*M* $MgSO_4$, 60 m*M* NaCl, 20%(*v*/*v*) glycerol pH 7.3; flow rate 1 ml min^{-1}] and the fractions containing rTAO as judged by activity measurements and SDS–PAGE were pooled (Kido *et al.*, 2010).

The fused N-terminal His_6 tag was removed from the purified rTAO using biotinylated thrombin and the tag-free rTAO was separated using streptavidin agarose (Biotinylated Thrombin Cleavage Capture Kit, Novagen) according to the manufacturer's instructions. Incubation with 10 U thrombin for 16 h at 293 K was required for the complete cleavage of 10 mg protein.

The molecular weight of the enzyme in solution was estimated by gel-filtration chromatography using a HiLoad 16/60 Superdex 200 pg column (GE Healthcare). Elution was carried out at a flow rate of 0.3 ml min^{-1} using 50 m*M* Tris–HCl pH 7.4, 0.1 *M* NaCl, 0.042%(*w*/*v*) DM and 20%(*v*/*v*) glycerol.

2.2. Crystallization and X-ray data collection

The purified rTAO was concentrated to 5 mg ml^{-1} in 20 m*M* Tris–HCl, 0.042%(*w*/*v*) DM, 50 m*M* $MgSO_4$, 20%(*v*/*v*) glycerol pH 7.3 using an Amicon Ultra centrifugal filter device (Millipore, 30 kDa molecular-weight cutoff) and used for initial screening of crystallization conditions. Crystallization was performed by the sitting-drop vapour-diffusion technique in 96-well Corning CrystalEX microplates with a conical flat bottom (Hampton Research). In the screening, 0.5 μl rTAO solution was mixed with an equal volume of reservoir solution and the droplet was equilibrated against 100 μl reservoir solution at 277 and 293 K. Commercially available screening kits purchased from Hampton Research (Crystal Screen, Crystal Screen II, Crystal Screen Lite, SaltRx and MembFac), Emerald BioStructures (Wizard I, Wizard II, Cryo I and Cryo II) and Fluidigm (OptiMax-5 Membrane), together with homemade grid-screen reagents containing 100 m*M* buffer (pH 5.0–9.0), 10–40%(*w*/*v*) polyethylene glycol (PEG 400, PEG 1000, PEG 3350, PEG 6000 and PEG 10 000) and 200 m*M* salts (NaCl and KCl), were used as reservoir solutions. However, crystals of rTAO did not appear.

Subsequently, screening was carried out at 277 K using various detergents (DM, OG, *n*-decyl β-D-maltopyranoside, *n*-octyl β-D-maltopyranoside, *n*-nonanoyl *N*-methyl-D-glucamine, octaethylene glycol monododecylether, tetraethylene glycol monooctylether and hexaethylene glycol monodecylether). rTAO samples dissolved in different detergents were subjected to free-interface diffusion in a TOPAZ 8.96 Screening Tip against reservoir solutions purchased from TOPAZ (OptiMax-1, OptiMax-2, OptiMax-3, OptiMax-4 PEG and OptiMax-5 Membrane) using a Fluidigm TOPAZ system (Segelke, 2005). When OG was used as a detergent, several reservoir solutions containing low-molecular-weight PEGs as precipitants gave tiny crystals. The conditions were further optimized by varying the PEG (PEG 200, PEG 400 and PEG 1000) concentration (10–40%), the buffer pH (6.0–8.0), the salt type (48 salts found in PEG/Ion Screen kit from Hampton Research) and the temperature (277 and 293 K) using the sitting-drop vapour-diffusion method. However, crystals larger than 30 μm could not be obtained and moreover they only diffracted X-rays to 7 Å resolution at most.

Next, the effects of additive detergents on crystal growth and X-ray diffraction were examined using reservoir solutions [25–40%(*w*/*v*) PEG 400, 100 m*M* imidazole buffer pH 6.2–7.8 and 200 m*M* potassium formate] supplemented with 0.1–0.5%(*w*/*v*) additive detergents. A dramatic improvement in crystal size was achieved using tetraethylene glycol monooctylether (C8E4) and the conditions, including the concentration of C8E4, were finally optimized.

Currently, crystals with average dimensions of approximately 0.1 × 0.07 × 0.03 mm can be reproducibly obtained at 293 K from reservoir solution consisting of 28–34%(*w*/*v*) PEG 400, 100 m*M*

imidazole buffer pH 7.4, 500 m*M* potassium formate and 0.4%(*w*/*v*) C8E4 using rTAO dissolved in 20 m*M* Tris–HCl pH 7.3, 0.8%(*w*/*v*) OG, 20 m*M* $MgSO_4$ and 20%(*v*/*v*) glycerol.

X-ray diffraction experiments were performed using synchrotron radiation on BL44XU and BL41XU at SPring-8 (Harima, Japan), BL5A and BL17A at Photon Factory and NW12A at Photon Factory Advanced Ring (Tsukuba, Japan). A crystal mounted in a nylon loop was frozen by rapidly submerging it in liquid nitrogen and X-ray diffraction patterns were recorded at 100 K. The best crystals diffracted X-rays to better than 3.0 Å resolution and a total of 180 images were recorded with an oscillation angle of 1°, an exposure time of 5 s per image and a crystal-to-detector distance of 280 mm. The data were processed and scaled using the *HKL*-2000 software package (Otwinowski & Minor, 1997).

3. Results and discussion

His_6-tagged rTAO was solubilized from inner membranes using OG and was purified by cobalt-affinity chromatography in the presence of DM. After removal of the fused N-terminal His_6 tag, about 10 mg of enzyme was obtained from a 10 l culture. The purified rTAO, consisting of 329 amino-acid residues (38 kDa), was >95% pure as estimated by SDS–PAGE (Fig. 1) and its molecular weight in solution was estimated to be 110 kDa by gel-filtration chromatography. As rTAO was prepared as a water-soluble rTAO–DM complex, the complex is probably composed of a homodimer of rTAO with DM molecules bound to the hydrophobic surface of the homodimer. A homodimeric structure of TAO has also been suggested by Chaudhuri *et al.* (2005). The molecular weight of the rTAO–OG complex could not be estimated because elution of rTAO from the gel-filtration column was only successful in the presence of DM as a detergent.

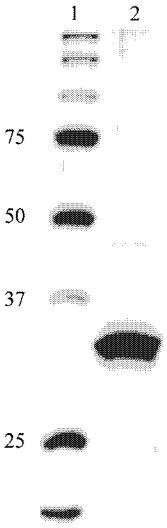

Figure 1
12.5% SDS–PAGE of rTAO with Coomassie Brilliant Blue R-250 staining. Lane 1, molecular-weight markers (kDa); lane 2, rTAO purified by affinity chromatography using BD TALON Metal Affinity Resin.

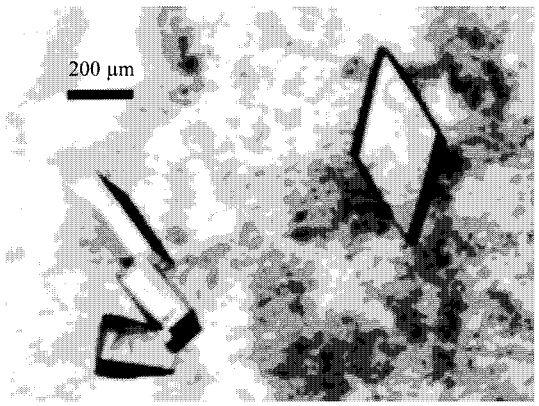

Figure 2
Rhombic plate-shaped crystals of rTAO obtained by the sitting-drop vapour-diffusion method using PEG 400 as a precipitant.

Table 1
Diffraction data statistics.

Values in parentheses are for the outermost resolution shell.

Space group	$I222$ or $I2_12_12_1$
Unit-cell parameters (Å)	a = 63.11, b = 136.44, c = 223.06
Beamline	SPring-8 BL41XU
Wavelength (Å)	1.000
Temperature (K)	100
Resolution (Å)	50.0– 2.90 (2.95–2.90)
Total reflections	135535
Unique reflections	21720
Completeness (%)	93.1 (63.2)
$R_{merge}(I)$† (%)	9.5 (57.3)
$\langle I/\sigma(I)\rangle$	9.8 (1.7)

† $R_{merge}(I) = \sum_{hkl}\sum_i |I_i(hkl) - \langle I(hkl)\rangle| / \sum_{hkl}\sum_i I_i(hkl)$, where $I_i(hkl)$ is the ith measurement of reflection hkl.

After extensive screening and optimization of crystallization conditions, crystals with average dimensions of approximately 0.1 × 0.07 × 0.03 mm could be obtained within 10 d at 293 K using rTAO dissolved in 20 m*M* Tris–HCl pH 7.3, 0.8%(*w*/*v*) OG, 20 m*M* $MgSO_4$ and 20%(*v*/*v*) glycerol with a reservoir solution containing 28–34%(*w*/*v*) PEG 400, 100 m*M* imidazole buffer pH 7.4, 100 m*M* potassium formate and 0.4%(*w*/*v*) C8E4 (Fig. 2).

Analyses of the symmetry and systematic absences in the recorded diffraction patterns indicated that the crystals belonged to the orthorhombic space group $I222$ or $I2_12_12_1$, with unit-cell parameters a = 63.11, b = 136.44, c = 223.06 Å. Assuming the presence of two rTAO molecules in the asymmetric unit (2 × 38 kDa), the calculated Matthews coefficient (V_M) is 3.2 $Å^3\ Da^{-1}$, which corresponds to a solvent content of 61.0%. If the molecular weight of the rTAO–OG complex is presumed to be comparable to that of the rTAO–DM complex, the presence of one molecule of the rTAO–OG complex in the asymmetric unit gives a V_M value of 2.2 $Å^3\ Da^{-1}$ and a solvent content of 44.1%. A data set to 2.9 Å resolution (21 720 unique reflections) was obtained after merging 135 535 reflections recorded on 180 images, with 93.1% completeness and an overall R_{merge} of 9.5%. Statistics of data collection and processing are shown in Table 1. Currently, data collection for phasing using the anomalous dispersion effect of iron is in progress. This is the first report of the crystallization of membrane-bound diiron proteins, which include AOXs.

We thank all staff members of beamlines BL44XU and BL41XU at SPring-8, BL5A and BL17A at Photon Factory and NW12 at Photon Factory Advanced Ring for their help with X-ray diffraction data collection. This work was supported in part by grant-in-aid for Young Scientists (B) 21790402 (to YK), Creative Scientific Research Grant 18GS0314 (to KK), grant-in-aid for Scientific Research on Priority Areas 18073004 (to KK) from the Japanese Society for the Promotion of Science and the Targeted Proteins Research Program (to KK) of the Japanese Ministry of Education, Science, Culture, Sports and Technology (MEXT). ALM gratefully acknowledges the BBSRC for

financial support and, together with KK, the Prime Minister's Initiative 2 (Connect) fund for collaborative twinning.

References

Berthold, D. A. & Stenmark, P. (2003). *Annu. Rev. Plant Biol.* **54**, 497–517.
Chaudhuri, M., Ott, R. D. & Hill, G. C. (2006). *Trends Parasitol.* **22**, 484–491.
Chaudhuri, M., Ott, R. D., Saha, L., Williams, S. & Hill, G. C. (2005). *Parasitol. Res.* **96**, 178–183.
Clarkson, A. B. Jr, Bienen, E. J., Pollakis, G. & Grady, R. W. (1989). *J. Biol. Chem.* **264**, 17770–17776.
Clayton, C. E. & Michels, P. (1996). *Parasitol. Today*, **12**, 465–471.
Kido, Y., Sakamoto, K., Nakamura, K., Harada, M., Suzuki, T., Yabu, Y., Saimoto, H., Yamakura, F., Ohmori, D., Moore, A., Harada, S. & Kita, K., (2010). *Biochim. Biophys. Acta*, doi:10.1016/j.bbabio.2009.12.021.
McDonald, A. E., Vanlerberghe, G. C. & Staples, J. F. (2009). *J. Exp. Biol.* **212**, 2627–2634.
Minagawa, N., Yabu, Y., Kita, K., Nagai, K., Ohta, N., Meguro, K., Sakajo, S. & Yoshimoto, A. (1997). *Mol. Biochem. Parasitol.* **84**, 271–280.
Moore, A. L. & Albury, M. S. (2008). *Biochem. Soc. Trans.* **36**, 1022–1026.
Moore, A. L. & Siedow, J. N. (1991). *Biochim. Biophys. Acta*, **1059**, 121–140.
Nihei, C., Fukai, Y., Kawai, K., Osanai, A., Yabu, Y., Suzuki, T., Ohta, N., Minagawa, N., Nagai, K. & Kita, K. (2003). *FEBS Lett.* **538**, 35–40.
Nihei, C., Fukai, Y. & Kita, K. (2002). *Biochim. Biophys. Acta*, **1587**, 234–239.
Opperdoes, F. R., Borst, P., Bakker, S. & Leene, W. (1977). *Eur. J. Biochem.* **76**, 29–39.
Otwinowski, Z. & Minor, W. (1997). *Methods Enzymol.* **276**, 307–326.
Segelke, B. (2005). *Expert Rev. Proteomics*, **2**, 165–172.
Siedow, J. N. & Umbach, A. L. (2000). *Biochim. Biophys. Acta*, **1459**, 432–439.
World Health Organization (2006). *Wkly Epidemiol. Rec.* **81**, 71–80.
Yabu, Y., Suzuki, T., Nihei, C., Minagawa, N., Hosokawa, T., Nagai, K., Kita, K. & Ohta, N. (2006). *Parasitol. Int.* **55**, 39–43.
Yabu, Y., Yoshida, A., Suzuki, T., Nihei, C., Kawai, K., Minagawa, N., Hosokawa, T., Nagai, K., Kita, K. & Ohta, N. (2003). *Parasitol. Int.* **52**, 155–164.

Molecular Biology and Evolution

Divergence of the Mitochondrial Genome Structure in the Apicomplexan Parasites, Babesia and Theileria

Kenji Hikosaka,[1] Yoh-ichi Watanabe,[2] Naotoshi Tsuji,[3] Kiyoshi Kita,[2] Hiroe Kishine,[4] Nobuko Arisue,[5] Nirianne Marie Q. Palacpac,[5] Shin-ichiro Kawazu,[6] Hiromi Sawai,[1] Toshihiro Horii,[5] Ikuo Igarashi,[6] and Kazuyuki Tanabe[1,*]

[1]Laboratory of Malariology, International Research Center of Infectious Diseases, Research Institute for Microbial Diseases, Osaka University, Suita, Osaka, Japan

[2]Department of Biomedical Chemistry, Graduate School of Medicine, The University of Tokyo, Bunkyo-ku, Tokyo, Japan

[3]Laboratory of Parasitic Diseases, National Institute of Animal Health, National Agriculture and Food Research Organization, Tsukuba, Ibaraki, Japan

[4]Department of Molecular Biology, Research Institute for Microbial Diseases, Osaka University, Suita, Osaka, Japan

[5]Department of Molecular Protozoology, Research Institute for Microbial Diseases, Osaka University, Suita, Osaka, Japan

[6]National Research Center for Protozoan Diseases, Obihiro University of Agriculture and Veterinary Medicine, Obihiro, Hokkaido, Japan

***Corresponding author:** E-mail: kztanabe@biken.osaka-u.ac.jp.
Associate editor: Richard Thomas

Abstract

Mitochondrial (mt) genomes from diverse phylogenetic groups vary considerably in size, structure, and organization. The genus Plasmodium, causative agent of malaria, of the phylum Apicomplexa, has the smallest mt genome in the form of a circular and/or tandemly repeated linear element of 6 kb, encoding only three protein genes (*cox1*, *cox3*, and *cob*). The closely related genera Babesia and Theileria also have small mt genomes (6.6 kb) that are monomeric linear with an organization distinct from Plasmodium. To elucidate the structural divergence and evolution of mt genomes between Babesia/Theileria and Plasmodium, we determined five new sequences from *Babesia bigemina*, *B. caballi*, *B. gibsoni*, *Theileria orientalis*, and *T. equi*. Together with previously reported sequences of *B. bovis*, *T. annulata*, and *T. parva*, all eight Babesia and Theileria mt genomes are linear molecules with terminal inverted repeats (TIRs) on both ends containing three protein-coding genes (*cox1*, *cox3*, and *cob*) and six large subunit (LSU) ribosomal RNA (rRNA) gene fragments. The organization and transcriptional direction of protein-coding genes and the rRNA gene fragments were completely conserved in the four Babesia species. In contrast, notable variation occurred in the four Theileria species. Although the genome structures of *T. annulata* and *T. parva* were nearly identical to those of Babesia, an inversion in the 3-kb central region was found in *T. orientalis*. Moreover, the *T. equi* mt genome is the largest (8.2 kb) and most divergent with unusually long TIR sequences, in which *cox3* and two LSU rRNA gene fragments are located. The *T. equi* mt genome showed little synteny to the other species. These results suggest that the Theileria mt genome is highly diverse with lineage-specific evolution in two Theileria species: genome inversion in *T. orientalis* and gene-embedded long TIR in *T. equi*.

Key words: mitochondrion, mitochondrial genome, Babesia, Theileria, Plasmodium, Apicomplexa.

Introduction

Mitochondria, organelles essential for energy transduction and cellular functions, are present in almost all eukaryotes. Like nuclear genomes of eukaryotes, mitochondrial (mt) genomes from diverse phylogenetic groups vary considerably in size, structure, and organization as well as in the number of genes (Gray et al. 2004). The largest mt genome is found in land plants, in which the size ranges from 180 to 2,400 kb (Ward et al. 1981; Palmer et al. 1992), and the smallest is the 6-kb genome of the genus Plasmodium, causative agents of malaria. Plasmodium belongs to the phylum Apicomplexa, which includes >5,000 species, all of which are parasites of clinical or economic importance (Levine 1988). Veterinary and opportunistic pathogens include Babesia, which causes babesiosis in ruminants and humans; Theileria, causal agents for tropical theileriosis and East Coast fever in cattle; Cryptosporidium, responsible for cryptosporidiosis in humans and animals; and Toxoplasma, causing toxoplasmosis in immunocompromised patients and congenitally infected fetuses.

Relatively few apicomplexan mt genomes have been studied, and available data suggest that they are remarkably diverse in structure and genome organization. In Plasmodium, the mt genome is in the form of a circular and/or tandemly repeated, predominantly linear 6-kb element (Preiser et al. 1996; Wilson and Williamson 1997). The 6-kb element encodes only three mt protein-coding genes (cytochrome *c* oxidase subunits I and III: *cox1* and *cox3* and cytochrome *b*: *cob*) in addition to large subunit (LSU) and small subunit (SSU) ribosomal RNAs (rRNAs). The two rRNA genes are extensively fragmented and rearranged with 20 identified rRNA pieces, and curiously, no transfer RNA genes have

yet been identified (Feagin et al. 1997). The mt genomes of closely related apicomplexan parasites Babesia and Theileria (Lau 2009) are 6.6 kb in size and monomeric linear molecules with terminal inverted repeats (TIRs), indicative of telomeres (Kairo et al. 1994; Brayton et al. 2007). Similar to Plasmodium, mt genomes of Babesia and Theileria contain the three protein-coding genes, but gene order and transcriptional direction are clearly different from Plasmodium (Kairo et al. 1994; Brayton et al. 2007). Thus, the mt genomes of Plasmodium and Babesia/Theileria are structurally highly divergent regardless of their close relatedness (Kuo et al. 2008). For *Toxoplasma gondii*, the mt genome remains to be isolated and analyzed, although multiple copies of partial mt genes (*cox1* and *cob*) were found to be scattered throughout the nuclear genome (Ossorio et al. 1991). In *Cryptosporidium parvum*, the mitochondrion is degenerative and lacks any DNA (Abrahamsen et al. 2004). Clearly, the phylum Apicomplexa provides interesting materials to further understand the evolution of mt genomes.

It remains unknown how the remarkable structural divergence between Plasmodium and Babesia/Theileria mentioned above was generated. Gathering enough data set will also help provide further insights on the extent at which the mt genomes have evolved in the different genera as well as in the phylum. In this study, we determined five new mt genome sequences from Babesia and Theileria species. Analyses of the genome structures show that although the mt genome structure is conserved in Babesia species, it varies notably in both size and genome organization in Theileria species, with lineage-specific evolution in two Theileria species: genome inversion in *T. orientalis* and gene-embedded long TIR in *T. equi*.

Materials and Methods

Parasite Species

Mitochondrial genome sequences were determined from the following seven parasite species: *Babesia bigemina* (Kochinda stock) (Fujinaga et al. 1980), *B. caballi* (USDA strain) (Avarzed et al. 1997), *B. gibsoni* (National Research Center for Protozoan Diseases strain) (Ishimine et al. 1978), *B. bovis* (Miyama stock) (Fujinaga et al. 1980), *Theileria orientalis* (Ikeda stock) (Kim et al. 2004), *T. equi* (USDA strain) (Avarzed et al. 1998), and *T. parva* (Muguga stock) (Kairo et al. 1994). Their host animals are cattle for *B. bigemina*, *B. bovis*, *T. orientalis*, and *T. parva*; horses for *B. caballi* and *T. equi*; and dogs for *B. gibsoni* (supplementary table S1, Supplementary Material online).

DNA Sequencing

Parasite genomic DNA was extracted from animal bloods infected with *B. bigemina*, *B. gibsoni*, *B. bovis*, *T. orientalis*, and *T. parva*, and from cultures of *B. caballi* and *T. equi*, using QIAamp DNA Blood Mini Kit (QIAGEN, Hilden, Germany) according to the manufacturer's instructions. Nucleotide sequences of the mt genomes were determined by direct sequencing of polymerase chain reaction (PCR) products using specific primers (supplementary table S2a, Supplementary Material online). The primers were designed by aligning reported mt genome sequences of *B. bovis* (DDBL/EMBL/GenBank accession number EU075182), *T. parva* (Z23263), and *T. annulata* (NW_001091933). Amplification was carried out in a 20 μl reaction mixture containing 0.2 μM each of forward and reverse primers, 400 μM each of deoxynucleotide triphosphate (dNTP), 1 U of LA-Taq (Takara, Shiga, Japan), 2 μl of 10× PCR buffer, 2.5 mM of $MgCl_2$, and 1 μl of genomic DNA. PCR conditions were as follows: initial denaturation at 94 °C for 1 min and amplification for 40 cycles at 94 °C for 30 s, 55–68 °C (depending on primers used) for 30 s, and 72 °C for 1–6 min (depending on amplicon size, 1 min/kb), followed by a final extension at 72 °C for 10 min.

Sequences of the *T. equi* mt telomeric regions were determined by using the terminal deoxynucleotidyl transferase (TdT) tailing method (Bah et al. 2004) with some modifications. Briefly, the 3′ end was tailed with cytosine by initial denaturation of genomic DNA (150 ng) for 5 min at 95 °C and then incubated for 30 min at 37 °C in a reaction mixture containing 200 μM deoxycytidine triphosphate, 1 U of TdT (Takara), 20 mM Tris–HCl (pH 8.4), 50 mM KCl, and 1.5 mM $MgCl_2$, followed by heat inactivation of TdT at 65 °C for 10 min. The first PCR was done in a 50 μl reaction mixture containing 2 μl of the tailed DNA fragments, 1.25 U of AmpliTaq DNA Polymerase (Applied Biosystems, Foster City, CA), 2.5 mM $MgCl_2$, 200 μM dNTPs, 0.4 μM of an mt genome–specific primer (supplementary table S2b, Supplementary Material online), and a selective anchor primer (5′-CTACTACTACTAGGCCACGCGTCGACTAGTACGGGGGGGGGGGGGGG-3′). Initial denaturation was at 95 °C for 2 min, followed by 40 cycles at 94 °C for 30 s and 62 °C for 3 min, and with a final extension step at 72 °C for 10 min. The second PCR was performed using 1 μl of the first PCR product in a 50 μl reaction mixture mentioned above, containing a nested primer (supplementary table S2b, Supplementary Material online) and a universal amplification primer (5′-CTACTACTACTAGGCCACGCGTCGACTAGTAC-3′). The second PCR amplification was at 95 °C for 2 min, and 25 cycles of 94 °C for 30 s, 62 °C for 2 min, followed by an extension step at 72 °C for 10 min. This method would not work for the other Babesia and Theileria samples. It can be surmised that relatively high (A + T) content in TIRs of the other samples may have caused some problems. Multiple palindromes in TIR reported for *T. parva* (Shukla and Nene 1998) may also be contributing factors in the difficulty to determine telomeric sequences. In *T. equi*, unlike other Babesia and Theileria species, the TIR has a relatively low (A + T) content with no apparent multiple palindromes and, surprisingly, contains *cox3* and two fragments of rRNA gene (see Results).

TIR sequences of other Babesia and Theileria species were determined using an "inverted PCR," in which primers leading toward telomere ends (supplementary table S2b, Supplementary Material online) were used. We assumed that small inverted sequences, probably present in TIRs as reported for *T. parva* (Shukla and Nene 1998), could

self-anneal in opposite direction, enabling amplification of two telomeric regions encompassed by two outward primers when *Taq* polymerase with an exonuclease activity, that could excise unpaired bases (such as LA-Taq), was used. This inverted PCR successfully amplified specific DNA bands for all (Babesia and Theileria) but one species (i.e., *T. equi*) examined here.

PCR products were purified using QIAquick PCR Purification Kit (QIAGEN). DNA sequencing was performed directly from two independent PCR products using the BigDye Terminator v3.1 Cycle Sequencing Kit (Applied Biosystems) and an ABI 3130 Genetic Analyzer (Applied Biosystems). Sequencing primers were designed to cover target regions in both directions. DDBL/EMBL/GenBank accession numbers of sequences obtained in this study are given in supplementary table S1 (Supplementary Material online). The *T. parva* sequence obtained here has a 24-bp inconsistency with the reported *T. parva* sequence (Z23263). The *B. bovis* sequence in this study has a 7-bp difference from the reported *B. bovis* sequence (EU075182). These differences may be due to polymorphism because uncloned stock (*T. parva*) and different parasite strains (*B. bovis*) were used. We used our sequences of *T. parva* and *B. bovis* for analysis.

Gene Annotation

Nucleotide sequences of obtained mt genomes from Babesia and Theileria species and their deduced amino acid sequences were aligned together with reported sequences from *B. bovis* (EU075182), *T. parva* (Z23263), and *T. annulata* (NW_001091933) by ClustalW (Thompson et al. 1994). Alignment was manually corrected. Protein-coding genes were predicted using previously annotated sequences from *T. parva* and *B. bovis*.

To identify putative rRNA genes, mitochondrial DNA (mtDNA) sequences or annotated rRNA gene fragments from *B. bovis* (EU075182) and *T. parva* (Z23263) were used as queries under the suggested algorithm parameters (Freyhult et al. 2007) in NCBI BLAST 2.2 (Altschul et al. 1990). In silico analysis was also done with Probalign beta version 1.2 (Roshan et al. 2008) and SSEARCH 3.5 (Pearson 1991) using known rRNA gene fragments and suggested advanced search options (Freyhult et al. 2007; Roshan et al. 2008). Newly identified candidate rRNA genes were, likewise, used as input sequences. The information from sequence alignments using ClustalW (Thompson et al. 1994) and putative base-pairings between fragments proposed for *T. parva* mitochondrial ribosomal RNA fragments (Kairo et al. 1994) were considered in assigning the termini of the candidate genes. Similar searches using some of the rRNA fragment sequences from *Plasmodium falciparum* (Feagin et al. 1997) detected additional candidate gene regions.

Southern Blot Hybridization

Genomic DNA of *B. gibsoni*, *T. orientalis*, and *T. equi*, either undigested or digested with *Pvu*II, *Hind*III, or *Xho*I, was electrophoresed on 0.8% agarose gels in Tris–acetate–ethylenediaminetetraacetic acid (40 mM Tris–acetate and 1 mM ethylenediaminetetraacetic acid) and then transferred to a positively charged nylon membrane (Amersham Hybond-N+; GE Healthcare, Little Chalfont, England). PCR products amplified specifically from *B. gibsoni*, *T. orientalis*, and *T. equi* genomic DNA (supplementary table S2c, Supplementary Material online) were labeled with digoxigenin-deoxyuridine triphosphate using the DIG High Prime DNA Labeling and Detection Starter Kit II (Roche Diagnostics, Rotkreuz, Switzerland). The digoxigenin-labeled DNA probes were used for overnight hybridization. Blots were washed twice with 2× saline–sodium citrate (SSC) and 0.1% sodium dodecyl sulfate (SDS) and twice with 0.5× SSC and 0.1% SDS at 65 °C for 15 min. Hybridization signals were detected using the Detection Starter Kit II.

RNA Preparation and Analysis

Transcription of *cox1*, *cox3*, and *cob* in *B. gibsoni*, *T. orientalis*, and *T. equi* was analyzed by reverse transcriptase-PCR (RT-PCR). Total RNA was extracted with RNeasy Mini Kit (QIAGEN). DNase I treatment was done to remove any residual DNA before cDNA synthesis. Using specific primers (supplementary table S2d, Supplementary Material online), cDNA synthesis and DNA amplification were carried out using PrimeScript High Fidelity RT-PCR Kit (Takara). RNA extracts that were not treated with reverse transcriptase gave no PCR products.

For northern blot analysis, total RNA including short RNAs from *B. gibsoni* was prepared with mirVana miRNA Isolation Kit (Ambion, Austin, TX). Total RNA (10 μg) was subjected to 8.3 M urea-12% (w/v) polyacrylamide gel electrophoresis. After electrophoresis, the gel was stained with ethidium bromide and photographed. RNA was electroblotted on Biodyne Plus (Pall, Glen Cove, NY) using a semi-dry blotter NA-1515B (Nihon Eido, Tokyo, Japan) according to the manufacturer's protocol. The blotted membrane was ultraviolet treated for cross-linking (Brown et al. 2004) and incubated in hybridization solution (200 mM sodium phosphate [pH 7.2]-7% [w/v] SDS) for 30 min at 37 °C. The oligo probe was 5′ labeled with T4 polynucleotide kinase and [γ-^{32}P] adenosine triphosphate according to the enzyme supplier's instruction (Takara) and purified based on Brown et al. (2004). After overnight hybridization at 37 °C, the membrane was then washed twice with 2× SSC-0.5% (w/v) SDS at 37 °C, twice at 47 °C, and finally twice with 0.2× SSC-0.5% (w/v) SDS at 47 °C. The membrane was exposed to an Imaging Plate (Fujifilm, Tokyo, Japan), and the plate was scanned with a BAS2500 Bioimaging Analyzer (Fujifilm).

Phylogenetic Analysis

The concatenated amino acid sequences of *cox1* and *cob* were used for phylogenetic analysis. (Sequences of *cox3* were not used due to very high divergence in Babesia/ Theileria species [see Results].) The data set of 834 amino acid positions, comprising 474 COX1 and 360 COB amino acids, was analyzed using the PROML program in PHYLIP version

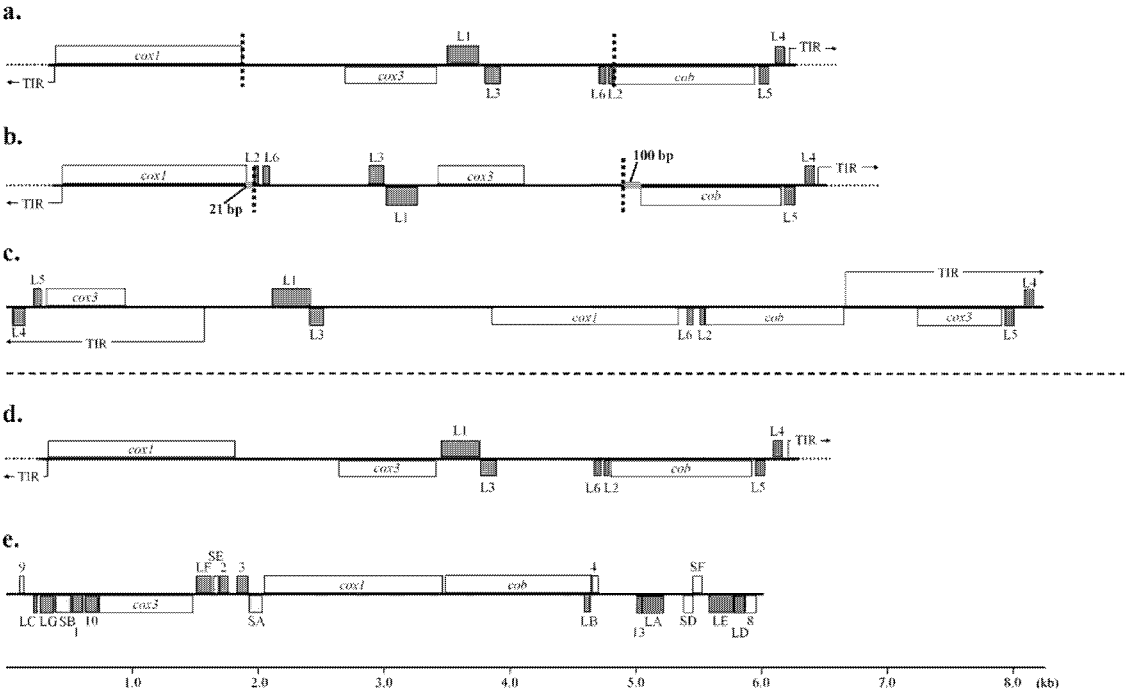

FIG. 1. Structure of the mitochondrial genomes of *Babesia gibsoni* (*a*), *Theileria orientalis* (*b*), and *T. equi* (*c*). Mitochondrial (mt) genome structure was completely conserved among *B. gibsoni*, *B. bigemina* (not shown), *B. caballi* (not shown), *B. bovis* (not shown), and *T. parva* (*d*). The *T. orientalis* mt genome has an inversion in the 3-kb central region. The *T. equi* mt genome has a relatively long TIR and contains a *cox3* gene and rRNA gene fragments. Shown for comparison is the mt genome of *Plasmodium falciparum* (*e*) (Feagin et al. 1997). Genes shown above the bold line in each genome are transcribed left to right and those below are transcribed from right to left. Two small gray lines in the *T. orientalis* genome indicate an inversion. Vertical broken lines indicate the boundaries of the 3-kb inversion. Dark and light gray boxes indicate fragments of LSU and SSU rRNA genes, respectively. *cox1*, cytochrome *c* oxidase subunit I; *cox3*, cytochrome *c* oxidase subunit III; *cob*, cytochrome *b*.

3.68 (Felsenstein and Churchill 1996) under the Jones, Taylor, and Thornton model (Jones et al. 1992) with the amino acid frequencies of the data set used to infer the maximum likelihood (ML) tree. Corresponding sequence of *P. falciparum* was used as an outgroup. To take the evolutionary rate heterogeneity, the R option was set to utilize discrete Γ distribution with eight categories for approximating the site rate distribution. CODEML program in PAML version 4.2 (Yang 2007) was used to estimate the Γ shape parameter value α. Bootstrap analysis was done by applying PROML to 100 resampled data sets produced by SEQBOOT program in PHYLIP. Bootstrap proportion (BP) values were calculated for internal branches of the inferred ML tree using CONSENSE in PHYLIP.

LSU sequences (592 sites in total: 265 bp for LSU1; 35 bp for LSU2; 111 bp for LSU3; 82 bp for LSU4; 64 bp for LSU5; and 35 bp for LSU6) were analyzed using the ML method performed with PAUP* 4.0 b10 (Swofford 2002). The appropriate nucleotide substitution model was first determined using the Modeltest (version 3.7) estimations, including both the proportion of invariable sites and the Γ shape parameter (Posada and Crandall 1998). For branch support of the ML tree, bootstrap probability was estimated from 1,000 heuristic replicates with single random addition replicates. All trees were reconstructed with TreeView 1.6.6 (Page 1996). For statistical comparisons among the ML best tree and its alternatives, *P* values of Kishino–Hasegawa (KH) test (Kishino and Hasegawa 1989) and Simodaira–Hasegawa (SH) test (Shimodaira and Hasegawa 1999) were obtained.

Results

Mitochondrial Genome Organization

We obtained 5.8- to 5.9-kb sequences from each of *B. bigemina*, *B. caballi*, *B. gibsoni*, and *B. bovis*, in which three protein-coding genes, *cox1*, *cox3*, and *cob*, and five fragments of the LSU rRNA gene were identified (fig. 1*a*). TIR sequences were also found on both ends of the predicted linear mt genomes. Although full-length sequences of TIRs were not successfully determined, the size of the TIR was inferred to be 440–450 bp from results of Southern blot hybridization analysis (see below). Additionally, we identified one LSU fragment of rRNA gene, LSU6, that showed a high sequence similarity to the 3′ part of RNA10 of the *P. falciparum* rRNA gene fragment (Feagin et al. 1997) (underlined sequence in the following *B. gibsoni* LSU sequence are identical nucleotides to *P. falciparum*

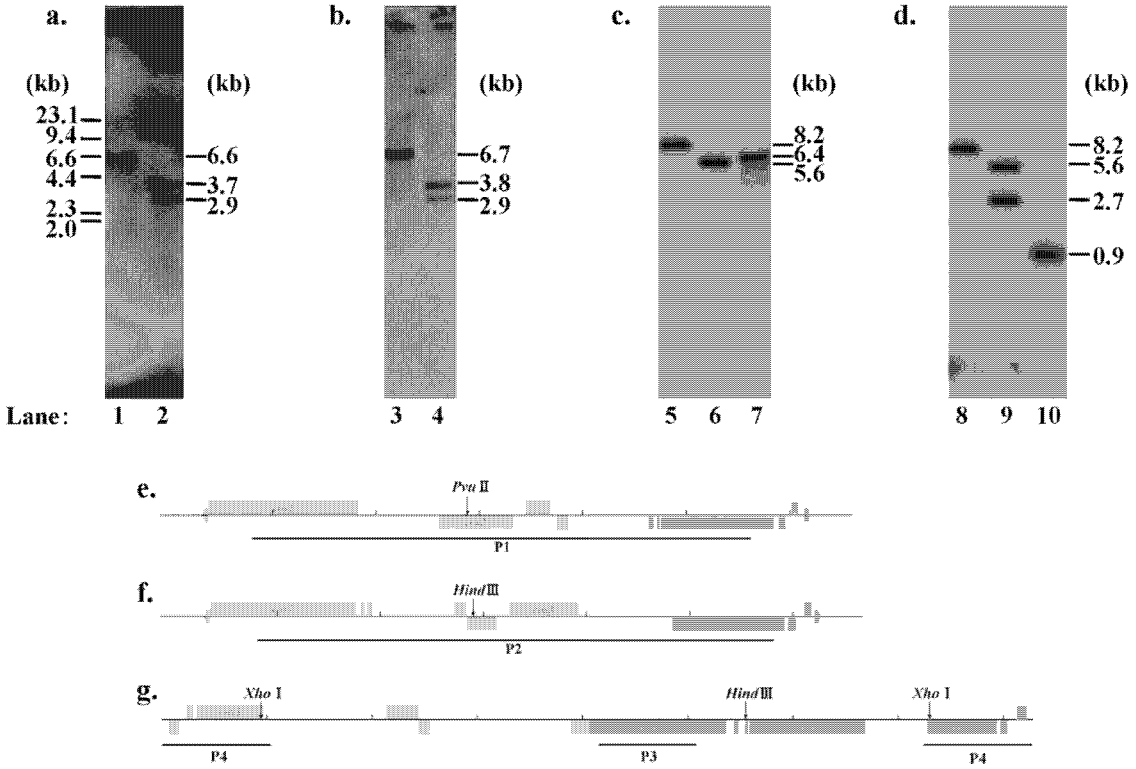

FIG. 2. Monomeric linear structure of the mitochondrial genomes of *Babesia gibsoni*, *Theileria orientalis*, and *T. equi*. Genomic DNA of *B. gibsoni* (*a*), *T. orientalis* (*b*), and *T. equi* (*c* and *d*) was hybridized with a *B. gibsoni* probe P1 (*e*), a *T. orientalis* probe P2 (*f*), and *T. equi* probes P3 and P4 (*g*), respectively. Undigested DNA (lanes 1, 3, 5, and 8) or DNA digested with *Pvu*II (lane 2), *Hind*III (lanes 4, 6, and 9), or *Xho*I (lanes 7 and 10) was fractionated on 0.8% agarose gels.

RNA10: 5′-ATAGCCGGAGTACGTAAGGAATAGGAAA-GATTAACCGCTATCA-3′). The organization and predicted transcriptional direction of the three protein-coding genes and the six LSU rRNA gene fragments were completely conserved among *B. bigemina*, *B. caballi*, *B. gibsoni*, *B. bovis*, *T. parva*, and *T. annulata* (fig. 1*a*). Southern blots probed with a 4.9-kb portion (P1) of the *B. gibsoni* mt genome produced a clear signal at 6.6 kb against *B. gibsoni* genomic DNA and two bands at 3.7 and 2.9 kb against DNA digested with *Pvu*II (fig. 2*a* and *e*). The sizes of the two bands were identical to those predicted from the sequence. These results confirm the monomeric linear 6.6 kb of *B. gibsoni* mt genome similar to that reported for *T. parva* and *T. annulata* (Hall et al. 1990; Kairo et al. 1994).

Interestingly, the *T. orientalis* mt genome, aside from having three protein-coding genes, six rRNA gene fragments, and TIRs similar to four Babesia species, *T. parva*, and *T. annulata* (fig. 1*b*) showed an inversion at the 3.0-kb central region containing *cox3*, LSU1, LSU3, LSU6, and LSU2. No sequences that potentially form secondary structures such as a hairpin structure were apparent near the boundaries of this inverted sequence, but instead, unique insertions of 21–22 and 84–102 bp were noted (fig. 1*b*), making the *T. orientalis* mt genome slightly longer (112–168 bp) than the other six Babesia and Theileria mt genomes (supplementary table S3, Supplementary Material online). As predicted from the sequence, southern hybridization using a *T. orientalis* probe (P2) that spans the central 5.0-kb region yielded a band at 6.7 kb against undigested DNA and two bands at 3.8 and 2.9 kb against *Hind*III-digested DNA (fig. 2*b* and *f*). From these results, the *T. orientalis* mt genome shows a 6.7-kb monomeric linear structure.

Strikingly distinctive from all other mt genomes described above is *T. equi*. First, the size of the *T. equi* genome is 8.2 kb, that is, 1.6–1.7 kb longer than that of other species. Second, TIR sequences are large (1,563 bp), compared with the 440–450 bp TIRs of the other seven species, and, interestingly, contained *cox3* and two LSU rRNA gene fragments, LSU4 and LSU5. TIR sequences on both ends showed complete identity. Third, the protein-coding genes and rRNA gene fragments showed little synteny to other species (fig. 1*c*). Hybridization with a probe corresponding to a 1.0-kb region in *cox1* (P3) produced a band at 8.2 kb against undigested DNA, a band at 5.6 kb against *Hind*III-digested DNA, and a band at 6.4 kb against *Xho*I-digested DNA (fig. 2*c* and *g*). Another *T. equi* probe using a 1-kb region in the TIR (P4) produced a band at 8.2 kb against undigested DNA, two bands at 5.6 and 2.7 kb against *Hind*III-digested DNA, and a band at 0.9 kb against

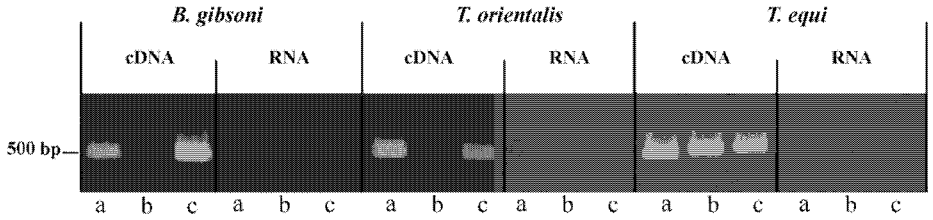

FIG. 3. Transcription of the three protein-coding genes *cox1* (*a*), *cox3* (*b*), and *cob* (*c*) in the mitochondrial genome of *Babesia gibsoni*, *Theileria orientalis*, and *T. equi*. See Materials and Methods for details.

*Xho*I-digested DNA (fig. 2*d* and *g*). The sizes of these bands match the predicted *T. equi* sequence, indicating an 8.2-kb monomeric linear structure of the *T. equi* mt genome.

Transcription

RT-PCR using three separate primer sets targeting about 500-bp sequences of *cox1*, *cox3*, and *cob* of *B. gibsoni* gave the expected transcript size using cDNA but not using RNA (fig. 3). Similarly, expected PCR sized fragments were obtained using primers specific to *T. orientalis* or *T. equi* for *cox1*, *cox3*, and *cob*. Results confirm the transcription of the three protein-coding genes, including *cox3* in the 3-kb inverted region of *T. orientalis* and *cox3* in TIR of *T. equi*.

Transcription of LSU6 was confirmed by northern blot analysis. Probing with two oligonucleotides (18-mer and 23-mer at the 5′ and 3′ end, respectively) complementary to LSU6 against *B. gibsoni* total RNA produced approximately 90-nt RNA signal (fig. 4), suggesting that the LSU6 was actually transcribed and the corresponding stable transcript existed as a short RNA fragment. Due to extreme difficulties in obtaining an adequate amount of parasites from infected hosts and/or in vitro culture limitations for *B. bigemina*, *B. caballi*, *T. orientalis*, and *T. equi*, we were unable to perform additional northern blot analyses. Together with the report of Kairo et al. (1994) on the transcription of the three protein-coding genes and five known LSU rRNA gene fragments (LSU1–LSU5) in *T. parva*, however, these results suggest that both protein genes and rRNA gene fragments are transcribed in Babesia and Theileria.

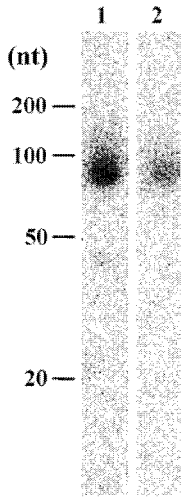

FIG. 4. Transcription of the *Babesia gibsoni* mt genome LSU6. *B. gibsoni* total RNA was probed with oligonucleotides complementary to the putative LSU6 fragment. Probe sequences: lane 1, TGATAGCGGTTAATCTTTCCTAT; lane 2, CTTACGTACTCCGGCTAT. Positions and sizes (in nucleotides [nt]) of marker RNAs (DynaMarker RNA Low II; BioDynamics Laboratory) are shown.

Sequence Similarity and Phylogeny

cox1 and *cob* pairwise sequence similarity scores among *B. bovis*, *B. bigemina*, *B. caballi*, *B. gibsoni*, *T. parva*, *T. orientalis*, *T. annulata*, and *T. equi* were comparable: 67–88% for *cox1* and 60–85% for *cob* at the amino acid sequence level (supplementary table S4, Supplementary Material online). Conserved sequence regions in COX1 and COB correspond to the 12 and 9 transmembrane domains as inferred from bovine COX1 (SWISS-PROT protein database accession number P00396) and COB (P00157), respectively, in which multiple heme-binding histidine residues that form catalytic sites are perfectly conserved (Widger et al. 1984; Yun et al. 1991; Castresana et al. 1994; Ferguson-Miller and Babcock 1996). For *cox3*, pairwise sequence similarity was relatively low, and *T. equi cox3* in particular has considerably low similarity to *cox3* of other species (37–41% compared with the 57–80% similarity of other *cox3* in Babesia and Theileria species). Nevertheless, the predicted *T. equi* COX3 amino acid sequence shows seven transmembrane domains (from I to VII) and the C-terminal hydrophobic domain VII (P00415) that are highly conserved among a wide variety of organisms from prokaryotes to plants (Haltia et al. 1991). In contrast to these protein-coding genes, pairwise sequence similarity of six LSUs was very high, 75–96% among all the Babesia and Theileria species examined here (supplementary table S5, Supplementary Material online).

The ML tree was inferred from concatenated COX1 and COB amino acid sequences using *P. falciparum* as an outgroup (fig. 5). Monophyletic relationships were observed with high BP values (98%) for 1) *B. bovis*, *B. bigemina*, *B. caballi*, and *B. gibsoni* and 2) *T. annulata*, *T. parva*, and *T. orientalis*. *Theileria equi* was located at the branch

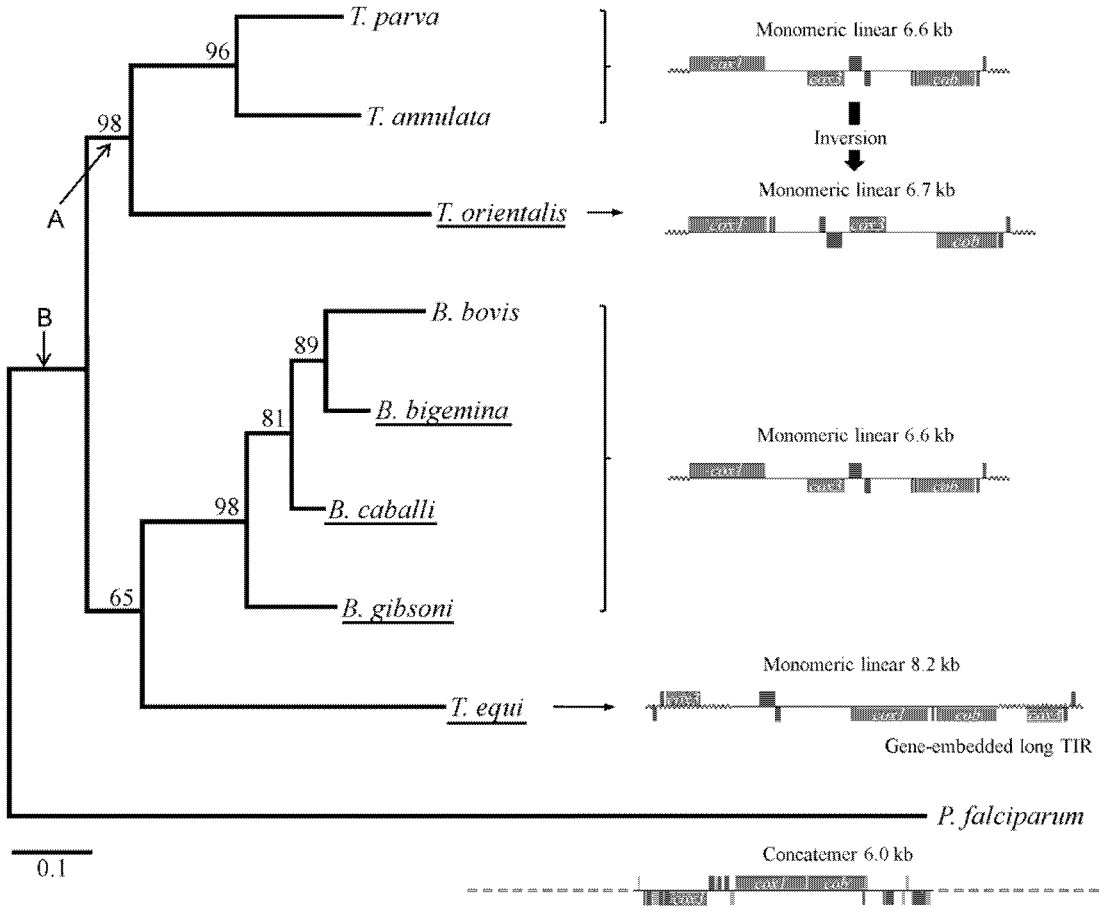

FIG. 5. The ML phylogenetic tree of the two mitochondrial protein-coding genes, *cox1* and *cob*, from eight Babesia and Theileria species. *Plasmodium falciparum* was used as an outgroup. Concatenated amino acid sequences (834 sites) were used with 1,000 heuristic replicates under a Jones, Taylor, and Thornton model ($\alpha = 0.72$). The numbers shown along nodes represent bootstrap values. Arrows, A and B, indicate alternative positions of the *Theileria equi* sequence, whose possibilities were statistically compared by the SH and KH tests. Five parasite sequences obtained in this study are underlined.

leading to the common ancestor of Babesia species with moderate BP value (65%). The other possible branching positions of *T. equi* at the ancestral branch of Theileria (arrow A in fig. 5) or at the ancestral branch of Theileria and Babesia (arrow B in fig. 5) were, however, not rejected by either the KH or the SH tests (supplementary table S6, Supplementary Material online), thus indicating that the evolutionary position of *T. equi* is yet unclear with the present data set.

The ML tree constructed using LSU sequences was basically the same as that of *cox1* and *cob* (supplementary fig. S1, Supplementary Material online), although, in this case, unrooted trees were compared because an appropriate outgroup species is not available for LSU. Monophyletic relationships of the four Babesia species and of *T. annulata*, *T. parva*, and *T. orientalis* were supported with high BP values. Within the clade of Babesia, however, the relationship between *B. bovis*, *B. bigemina*, and *B. caballi* was not supported with high BP values and not highly consistent to that in the *cox1/cob* tree. Notably, when the data set of LSU was applied to the two topologies, one for the *cox1/cob* tree and the other for the LSU tree, the two trees were not significantly different (data not shown), suggesting that the relationship of the three Babesia species was not clearly separable using the LSU sequences.

Partial TIR sequences (47–1,563 bp) (supplementary table S3, Supplementary Material online) were highly divergent among all eight Babesia and Theileria species examined here. In noncoding regions excluding TIR, we identified 14 sequence regions that were highly similar among all the Babesia and Theileria species (fig. 6 and supplementary tables S7 and S8, Supplementary Material online). Pairwise sequence similarity of these 14 regions ranged from 81% to 97%, values comparable with LSUs. The array and direction of the 14 regions were well conserved among (including the inverted region of *T. orientalis*), but one, species. *Theileria equi* was the exception, in which case the 14 regions were extensively

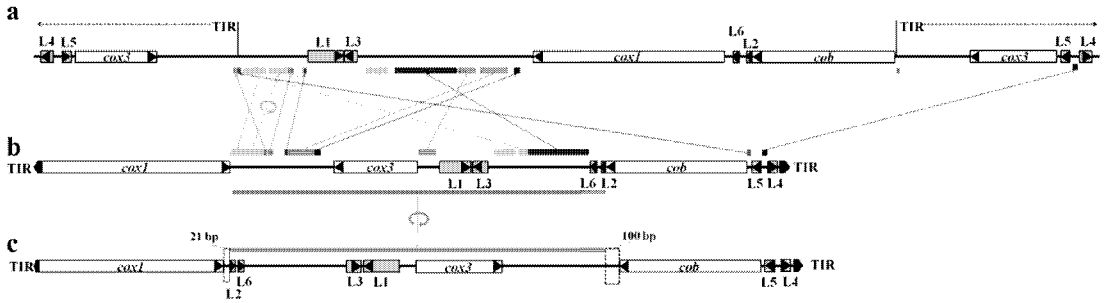

FIG. 6. Arrangement of small noncoding sequence regions in the mitochondrial genome highly conserved between *Theileria equi* (*a*), *Babesia gibsoni* (*b*), and *T. orientalis* (*c*). Those sequences are indicated by matched colored bars and arrows. A 3.0-kb inversion in the *T. orientalis* mt genome is shown by green bars with a circular arrow in (*b*) and (*c*). *cox1*, cytochrome *c* oxidase subunit I; *cox3*, cytochrome *c* oxidase subunit III; *cob*, cytochrome *b*.

rearranged (fig. 6). Within species, these 14 regions did not show sequence similarity to each other.

Discussion

This study presents for the first time evidence of the highly divergent mt genomes in the genus Theileria and a high conservation in the genus Babesia. *Theileria annulata* and *T. parva* have an mt genome structure nearly identical to that of Babesia, whereas the mt genomes of *T. orientalis* and *T. equi* were clearly distinctive: a large genomic region is inverted in *T. orientalis*, and in *T. equi*, there occurs an unusually long TIR, containing *cox3* and two LSU rRNA gene fragments. The phylogenetic tree of *cox1*/*cob* showed two separate clades: one for three Theileria species (*T. parva*, *T. annulata*, and *T. orientalis*) and another for four Babesia species. The mt genome structures of these Theileria species are highly conserved. This suggests that an inversion event occurred specifically in the *T. orientalis* lineage after divergence from a common ancestor of *T. annulata*, *T. parva*, and *T. orientalis*. The phylogenetic position of *T. equi* was not clearly determined in the *cox1*/*cob* tree. This unclear positioning of *T. equi* is consistent with the tree based on 18S rRNA gene, a nuclear genome gene (Criado-Fornelio et al. 2003). Thus, it remains to be solved whether a common ancestor of *T. equi*, the Theileria clades, and Babesia clades possessed an mt genome with gene-embedded long TIR. Phylogenetic separation of *T. equi* from Theileria clade as well as the identical life cycle, namely, the presence of schizogony in lymphocytes and lack of transovarial transmission by vector (Uilenberg 2006), suggests that, most likely, the mt genome of the common ancestor contained a long TIR.

Compared with moderate sequence similarity in *cox1* and *cob* of Theileria and Babesia species, *cox3* is highly divergent. Similarly, *cox3* is more divergent than *cox1* and *cob* in Plasmodium species (Wilson and Williamson 1997; Perkins 2008). COB is a subunit of complex III, essential for electron transfer in the mitochondrial respiratory chain (Xia et al. 1997). COX1 (subunit I) (and also COX2 [subunit II]), which contains heme and copper and is essential for electron transfer, is 1 of 13 subunits of cytochrome *c* oxidase (complex IV), a terminal oxidase in the respiratory chain (Castresana et al. 1994). COX3, which is not directly involved in the electron transport, is considered to stabilize the complex of COX1 and COX2 (Haltia et al. 1991; Tsukihara et al. 1996). Such an accessory role of COX3 in the function of cytochrome *c* oxidase may relax constraints, causing acceleration of evolutionary rate and low sequence similarity.

In addition to the five previously known LSU rRNA gene fragments (LSU1–LSU5) (Kairo et al. 1994; Brayton et al. 2007), we newly identified an LSU fragment, LSU6, in all Babesia and Theileria species, whose transcription was confirmed by northern blot analysis. Kairo et al. (1994) have previously mapped LSU1–LSU5 (by comparative secondary structure modeling) to the 3′ half of *Escherichia coli* 23S (LSU) rRNA. LSU5 and 5′ region of LSU1 form the domain IV of LSU, whereas 3′ region of LSU1, LSU2, LSU3, and LSU4 forms the domain V of the LSU, which contains the peptidyl transferase center. We mapped the newly identified LSU6 to positions 2640–2670, which forms a part of the domain VI (alpha-sarcin/ricin stem loop) of the LSU. Contrary to the other LSU fragments, the borders of LSU6 were unclear because the flanking sequences have no recognizable complementarities to other fragments. In addition to LSU6, we found a small sequence region in all Babesia and Theileria mtDNA, which showed a high sequence similarity to a small subunit fragment (SSUF) of the *P. falciparum* rRNA gene. We were not, however, able to confirm transcription of the SSUF (data not shown), although the region is regarded as one of the highly similar noncoding regions (supplementary table S7, Supplementary Material online). The mtDNA of Babesia/Theileria still contains large unannotated sequence regions (about one-third sequence regions of the genome), and those sequences are highly conserved among parasite species of the two genera (supplementary table S8, Supplementary Material online). It is thus likely that unidentified rRNA gene fragments as well as other genes exist in these regions. Comprehensive and detailed mtDNA transcript analysis of Babesia/Theileria would be required for further identification of genes and gene fragments as was done for *P. falciparum* (Feagin et al. 1997).

The observed high divergence of TIR sequences among Babesia and Theileria species was not surprising because no universal signature has been reported for TIR sequences of linear mt genomes from several unicellular flagellates: *Polytomella capuana*, *Po. parva*, and *Chlamydomonas reinhardtii* in the Reinhardtii clade of chlorophycean green algae (Smith and Lee 2008). Inverted complementary sequences at both ends of a linear mt genome are believed to play important roles in replication and stabilization (Nosek and Tomaska 2003). In TIR, small repeats with forward and reverse directions frequently occur, which are likely to form secondary structure. In general, sequence regions containing small repeats diverge rapidly compared with nonrepeat sequences. As a consequence, little sequence conservation is expected in TIR of a linear mt genome. An exception is *T. equi* TIR, in which sequence regions of *cox3* and two LSU rRNA gene fragments are relatively conserved, perhaps due to functional constraints.

In conclusion, our studies show the remarkable structural diversity in the mt genomes of Theileria species, in contrast to the highly conserved genome among Babesia species. The finding of a high structural divergence of the *T. equi* mt genome from other Babesia and Theileria species suggests the occurrence of lineage-specific evolution of mt genomes within the closely related Babesia and Theileria genera. Further investigations into mt genomes of other Theileria species and other related genera, such as those that belong to the Archaeopiroplasmids group, should provide insights into the evolutionary origin of a major structural divergence between Plasmodium (circular/concatemer genome) and Babesia/Theileria (linear genome) in the same phylum Apicomplexa.

Supplementary Material

Supplementary material, tables S1–S8, and figure S1 are available at *Molecular Biology and Evolution* online (http://www.mbe.oxfordjournals.org/).

Acknowledgments

We wish to thank T. Toyama for technical advice and H. Inokuma for kindly providing parasite samples. This work was supported by Grant-in-Aids for Scientific Research from the Ministry of Education, Culture, Sports, Science and Technology of Japan (18073013) and from Japan Society for Promotion of Sciences (18GS03140013 and 20390120).

References

Abrahamsen MS, Templeton TJ, Enomoto S, et al. (20 co-authors). 2004. Complete genome sequence of the apicomplexan, *Cryptosporidium parvum*. *Science* 304:441–445.

Altschul SF, Gish W, Miller W, Myers EW, Lipman DJ. 1990. Basic local alignment search tool. *J Mol Biol.* 215:403–410.

Avarzed A, Igarashi I, De Waal DT, et al. (12 co-authors). 1998. Monoclonal antibody against *Babesia equi*: characterization and potential application of antigen for serodiagnosis. *J Clin Microbiol.* 36:1835–1839.

Avarzed A, Igarashi I, Kanemaru T, Hirumi K, Omata Y, Saito A, Oyamada T, Nagasawa H, Toyoda Y, Suzuki N. 1997. Improved in vitro cultivation of *Babesia caballi*. *J Vet Med Sci.* 59:479–481.

Bah A, Bachand F, Clair E, Autexier C, Wellinger RJ. 2004. Humanized telomeres and an attempt to express a functional human telomerase in yeast. *Nucleic Acids Res.* 32:1917–1927.

Brayton KA, Lau AO, Herndon DR, et al. (28 co-authors). 2007. Genome sequence of *Babesia bovis* and comparative analysis of apicomplexan hemoprotozoa. *PLoS Pathog.* 3:1401–1413.

Brown T, Mackey K, Du T. 2004. Analysis of RNA by northern and slot blot hybridization. *Curr Protoc Mol Biol.* 4.9:1–19.

Castresana J, Lubben M, Saraste M, Higgins DG. 1994. Evolution of cytochrome oxidase, an enzyme older than atmospheric oxygen. *Embo J.* 13:2516–2525.

Criado-Fornelio A, Martinez-Marcos A, Buling-Sarana A, Barba-Carretero JC. 2003. Molecular studies on *Babesia*, *Theileria* and *Hepatozoon* in southern Europe. Part II. Phylogenetic analysis and evolutionary history. *Vet Parasitol.* 114:173–194.

Feagin JE, Mericle BL, Werner E, Morris M. 1997. Identification of additional rRNA fragments encoded by the *Plasmodium falciparum* 6 kb element. *Nucleic Acids Res.* 25:438–446.

Felsenstein J, Churchill GA. 1996. A hidden Markov model approach to variation among sites in rate of evolution. *Mol Biol Evol.* 13:93–104.

Ferguson-Miller S, Babcock GT. 1996. Heme/copper terminal oxidases. *Chem Rev.* 96:2889–2908.

Freyhult EK, Bollback JP, Gardner PP. 2007. Exploring genomic dark matter: a critical assessment of the performance of homology search methods on noncoding RNA. *Genome Res.* 17:117–125.

Fujinaga T, Minami T, Ishihara T. 1980. Serological relationship between a large *Babesia* found in Japanese cattle and *Babesia major*, *B. bigemina* and *B. bovis*. *Res Vet Sci.* 29:230–234.

Gray MW, Lang BF, Burger G. 2004. Mitochondria of protists. *Annu Rev Genet.* 38:477–524.

Hall R, Coggins L, McKellar S, Shiels B, Tait A. 1990. Characterisation of an extrachromosomal DNA element from *Theileria annulata*. *Mol Biochem Parasitol.* 38:253–260.

Haltia T, Saraste M, Wikstrom M. 1991. Subunit III of cytochrome *c* oxidase is not involved in proton translocation: a site-directed mutagenesis study. *Embo J.* 10:2015–2021.

Ishimine T, Makimura S, Kitazawa S, Tamura S, Suzuki N. 1978. Pathophysiological findings on blood of beagles experimentally infected with *B. gibsoni*. *Jpn J Trop Med Hyg.* 6:15–26.

Jones DT, Taylor WR, Thornton JM. 1992. The rapid generation of mutation data matrices from protein sequences. *Comput Appl Biosci.* 8:275–282.

Kairo A, Fairlamb AH, Gobright E, Nene V. 1994. A 7.1 kb linear DNA molecule of *Theileria parva* has scrambled rDNA sequences and open reading frames for mitochondrially encoded proteins. *Embo J.* 13:898–905.

Kim JY, Yokoyama N, Kumar S, Inoue N, Inaba M, Fujisaki K, Sugimoto C. 2004. Identification of a piroplasm protein of *Theileria orientalis* that binds to bovine erythrocyte band 3. *Mol Biochem Parasitol.* 137:193–200.

Kishino H, Hasegawa M. 1989. Evaluation of the maximum likelihood estimate of the evolutionary tree topologies from DNA sequence data, and the branching order in hominoidea. *J Mol Evol.* 29:170–179.

Kuo CH, Wares JP, Kissinger JC. 2008. The apicomplexan whole-genome phylogeny: an analysis of incongruence among gene trees. *Mol Biol Evol.* 25:2689–2698.

Lau AO. 2009. An overview of the *Babesia*, *Plasmodium* and *Theileria* genomes: a comparative perspective. *Mol Biochem Parasitol.* 164:1–8.

Levine ND. 1988. Progress in taxonomy of the apicomplexan protozoa. *J Protozool.* 35:518–520.

Nosek J, Tomaska L. 2003. Mitochondrial genome diversity: evolution of the molecular architecture and replication strategy. *Curr Genet.* 44:73–84.

Ossorio PN, Sibley LD, Boothroyd JC. 1991. Mitochondrial-like DNA sequences flanked by direct and inverted repeats in the nuclear genome of *Toxoplasma gondii*. *J Mol Biol.* 222:525–536.

Page RD. 1996. TreeView: an application to display phylogenetic trees on personal computers. *Comput Appl Biosci.* 12:357–358.

Palmer JD, Soltis D, Soltis P. 1992. Large size and complex structure of mitochondrial DNA in two nonflowering land plants. *Curr Genet.* 21:125–129.

Pearson WR. 1991. Searching protein sequence libraries: comparison of the sensitivity and selectivity of the Smith-Waterman and FASTA algorithms. *Genomics* 11:635–650.

Perkins SL. 2008. Molecular systematics of the three mitochondrial protein-coding genes of malaria parasites: corroborative and new evidence for the origins of human malaria. *Mitochondrial DNA.* 19:471–478.

Posada D, Crandall KA. 1998. MODELTEST: testing the model of DNA substitution. *Bioinformatics* 14:817–818.

Preiser PR, Wilson RJ, Moore PW, McCready S, Hajibagheri MA, Blight KJ, Strath M, Williamson DH. 1996. Recombination associated with replication of malarial mitochondrial DNA. *Embo J.* 15:684–693.

Roshan U, Chikkagoudar S, Livesay DR. 2008. Searching for evolutionary distant RNA homologs within genomic sequences using partition function posterior probabilities. *BMC Bioinformatics.* 9:61.

Shimodaira H, Hasegawa M. 1999. Multiple comparisons of log-likelihoods with applications to phylogenetic inference. *Mol Biol Evol.* 16:1114–1116.

Shukla GC, Nene V. 1998. Telomeric features of *Theileria parva* mitochondrial DNA derived from cycle sequence data of total genomic DNA. *Mol Biochem Parasitol.* 95:159–163.

Smith DR, Lee RW. 2008. Mitochondrial genome of the colorless green alga *Polytomella capuana*: a linear molecule with an unprecedented GC content. *Mol Biol Evol.* 25:487–496.

Swofford DL. 2002. PAUP*: phylogenetic analysis using parsimony (and other methods). Sunderland (MA): Sinauer Associates.

Thompson JD, Higgins DG, Gibson TJ. 1994. CLUSTAL W: improving the sensitivity of progressive multiple sequence alignment through sequence weighting, position-specific gap penalties and weight matrix choice. *Nucleic Acids Res.* 22:4673–4680.

Tsukihara T, Aoyama H, Yamashita E, Tomizaki T, Yamaguchi H, Shinzawa-Itoh K, Nakashima R, Yaono R, Yoshikawa S. 1996. The whole structure of the 13-subunit oxidized cytochrome c oxidase at 2.8 A. *Science* 272:1136–1144.

Uilenberg G. 2006. Babesia—a historical overview. *Vet Parasitol.* 138:3–10.

Ward BL, Anderson RS, Bendich AJ. 1981. The mitochondrial genome is large and variable in a family of plants (Cucurbitaceae). *Cell* 25:793–803.

Widger WR, Cramer WA, Herrmann RG, Trebst A. 1984. Sequence homology and structural similarity between cytochrome *b* of mitochondrial complex III and the chloroplast b_6-*f* complex: position of the cytochrome *b* hemes in the membrane. *Proc Natl Acad Sci USA.* 81:674–678.

Wilson RJ, Williamson DH. 1997. Extrachromosomal DNA in the Apicomplexa. *Microbiol Mol Biol Rev.* 61:1–16.

Xia D, Yu CA, Kim H, Xia JZ, Kachurin AM, Zhang L, Yu L, Deisenhofer J. 1997. Crystal structure of the cytochrome bc_1complex from bovine heart mitochondria. *Science* 277:60–66.

Yang Z. 2007. PAML 4: phylogenetic analysis by maximum likelihood. *Mol Biol Evol.* 24:1586–1591.

Yun CH, Crofts AR, Gennis RB. 1991. Assignment of the histidine axial ligands to the cytochrome $b_H$and cytochrome $b_L$components of the bc_1complex from *Rhodobacter sphaeroides* by site-directed mutagenesis. *Biochemistry* 30:6747–6754.

Acta Crystallographica Section F
Structural Biology and Crystallization Communications
ISSN 1744-3091

Overproduction, purification, crystallization and preliminary X-ray diffraction analysis of *Trypanosoma brucei gambiense* glycerol kinase

Emmanuel Oluwadare Balogun,[a,b] Daniel Ken Inaoka,[a] Yasutoshi Kido,[a] Tomoo Shiba,[a] Takeshi Nara,[c] Takashi Aoki,[c] Teruki Honma,[d] Akiko Tanaka,[d] Masayuki Inoue,[e] Shigeru Matsuoka,[e] Paul A. M. Michels,[f] Shigeharu Harada[g]* and Kiyoshi Kita[a]*

[a]Department of Biomedical Chemistry, Graduate School of Medicine, The University of Tokyo, 7-3-1 Hongo, Bunkyo-ku, Tokyo 113-0033, Japan, [b]Department of Biochemistry, Ahmadu Bello University, Zaria, Nigeria, [c]Department of Molecular and Cellular Parasitology, Juntendo University School of Medicine, Tokyo 113-8421, Japan, [d]Systems and Structural Biology Center, RIKEN, Tsurumi, Yokohama 230-0045, Japan, [e]Graduate School of Pharmaceutical Sciences, The University of Tokyo, Tokyo 113-0033, Japan, [f]Research Unit for Tropical Diseases, de Duve Institute and Laboratory of Biochemistry, Université Catholique de Louvain, Avenue Hippocrate 74, B-1200 Brussels, Belgium, and [g]Department of Applied Biology, Graduate School of Science and Technology, Kyoto Institute of Technology, Sakyo-ku, Kyoto 606-8585, Japan

Correspondence e-mail: harada@kit.ac.jp, kitak@m.u-tokyo.ac.jp

Received 7 September 2009
Accepted 5 January 2010

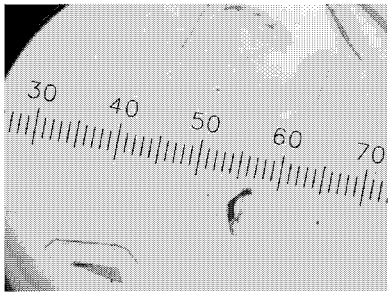

In the bloodstream forms of human trypanosomes, glycerol kinase (GK; EC 2.7.1.30) is one of the nine glycosomally compartmentalized enzymes that are essential for energy metabolism. In this study, a recombinant *Trypanosoma brucei gambiense* GK (rTbgGK) with an N-terminal cleavable His_6 tag was overexpressed, purified to homogeneity and crystallized by the sitting-drop vapour-diffusion method using PEG 400 as a precipitant. A complete X-ray diffraction data set to 2.75 Å resolution indicated that the crystals belonged to the orthorhombic space group $P2_12_12_1$, with unit-cell parameters a = 63.84, b = 121.50, c = 154.59 Å. The presence of two rTbgGK molecules in the asymmetric unit gives a Matthews coefficient (V_M) of 2.5 Å^3 Da^{-1}, corresponding to 50% solvent content.

1. Introduction

Human African trypanosomiasis (HAT) is a neglected haemoparasitic disease caused by species of the protozoan genus *Trypanosoma* and transmitted by tsetse flies. Over 20 000 new cases are reported annually; it is also a threat to 60 million human lives (World Health Organization, 2006). The human pathogens for the disease are *T. brucei gambiense* and *T. b. rhodesiense*, which cause West and East African trypanosomiasis, respectively, with animals serving as their reservoirs (Njiokou *et al.*, 2006), while the animal pathogens include *T. b. brucei*, *T. vivax*, *T. congolense* and *T. evansi* (Stevens & Brisse, 2004). HAT occurs in two forms: an acute form caused by *T. b. rhodesiense* and a chronic form caused by *T. b. gambiense*. Both agents of the disease present an early haemolymphatic stage and a late meningoencephalitic phase and are deadly at the second stage if left untreated. Unfortunately, only a few drugs are available and problems such as narrow spectrum, treatment failures owing to resistance, high cost and cases of toxicity have been reported (Brun *et al.*, 2001). Therefore, the need to search for new, safer, affordable and more effective drugs with a broader spectrum of action cannot be overemphasized.

Interestingly, the bloodstream forms (BSFs) of these parasites possess several structural and metabolic features that are absent in the mammalian hosts. Such distinctive features, which provide valid drug targets, include compartmentalization of their glycolysis into microbody-like organelles called glycosomes, their sole dependence on glycolysis for their energy needs (Haanstra *et al.*, 2008) and the presence of a rudimentary mitochondrion that houses an indispensable cytochrome-independent alternative oxidase (AOX; Chaudhuri *et al.*, 2006). AOX is not found in the host and its inhibition by salicylhydroxamic acid (SHAM) or ascofuranone (AF) has been reported to cause parasite death as a result of impaired ATP metabolism (Minagawa *et al.*, 1997; Michels *et al.*, 2000; Hannaert *et al.*, 2003; Guerra *et al.*, 2006; Yabu *et al.*, 2006; Singha *et al.*, 2008). In addition, trypanosomes contain a unique glycerol kinase (GK) in their glycosomes. Unlike the host GK, which only catalyses the forward reaction, *i.e.* ATP-dependent glycerol phosphorylation, trypanosomal GK can also catalyze the reverse reaction (Kralova *et al.*, 2000).

Our laboratory has found AF to be an excellent inhibitor of trypanosomal AOX (TAO): its K_i against TAO is 2.38 n*M* (Minagawa *et al.*, 1997) compared with 10 µ*M* for the previously discovered TAO inhibitor SHAM (Njogu *et al.*, 1980). However, *in vitro* and *in vivo* experiments have revealed that AF-induced or SHAM-induced killing of trypanosomes is considerably enhanced when they are co-administered with 5 m*M* glycerol (Fairlamb *et al.*, 1977; Van der Meer & Versluijs-Broers, 1979; Minagawa *et al.*, 1997; Yabu *et al.*, 2006). This synergistic effect of glycerol is most likely to be mediated *via* an expected mass-action-induced inhibition of GK by the added glycerol, thereby blocking the anaerobic ATP generation of glycolysis in the parasites. Unfortunately, this nonphysiologically high concentration of glycerol required for co-administration with AF is toxic to the host. Although GK in conjunction with TAO is thus a promising target for chemotherapy, an effective and selective parasite GK inhibitor has not yet become available.

GK is ubiquitous in archaea, bacteria and eukaryotes, where it belongs to the sugar kinase/heat-shock protein 70/actin superfamily (Hurley, 1996). To date, prokaryotic GKs have been the most widely studied. Of the eukaryotes, structural information is only available on *Plasmodium falciparum* GK, but GK is not essential for growth of the asexual blood stages in this organism (Schnick *et al.*, 2009). Kinetic studies also revealed a striking difference between the GKs of trypanosomes and those of other organisms (Kralova *et al.*, 2000). In *T. b. brucei* GK is encoded by five identical tandemly arranged genes (Colasante *et al.*, 2006) and plays an essential role in the survival of the parasite, especially in the absence of oxygen or in the presence of TAO inhibitors (Minagawa *et al.*, 1997), owing to its ability to catalyze the reverse reaction leading to the production of ATP required by the parasites. One may wonder whether the ability of the trypanosomal GK to catalyze the reverse reaction, in contrast to the human enzyme, is purely a consequence of the compartmentalization in glycosomes of the former or whether structure-based catalytic differences also make a contribution. We therefore perceive the parasite GK to be an interesting subject for structural investigation in terms of fundamental enzymology as well as drug-target exploitation. Here, we report the preliminary X-ray diffraction analysis of GK from *T. b. gambiense*, which may lead us to the design of parasite-specific GK inhibitors that spare the host enzyme. Since *T. b. brucei* TAO has also been crystallized recently (Kido *et al.*, 2010), X-ray structure analysis of both enzymes will aid us in the search for a new generation of chemotherapeutic agents against BSFs.

2. Materials and methods

2.1. Cloning and expression of TbgGK

Complementary DNA (cDNA) libraries were prepared from stocks of the bloodstream forms of *T. b. gambiense* (IL2343) and *T. b. rhodesiense* (Tbr; IL1501J21) using Toyobo reverse transcriptase. The cDNAs served as templates for the amplification of their GK-encoding genes (*gk*) by PCR using 5′-CACCATGAAGTACGTCGGATCCATT-3′ and 5′-CTACAACTTTGCCCACTTCGTCCTC-3′ as forward and reverse primers, respectively, with *PfuUltra* II Fusion HS DNA polymerase (Stratagene). The amplicons were gel-purified using the Toyobo gel-purification method. Plasmid constructs were obtained by cloning the blunt-ended gene into the pET151/D-TOPO plasmid vector (Invitrogen) by a ligation-independent cloning procedure. Cloning in this vector leads to the addition of an N-terminal tag containing a His_6 sequence, a V5 epitope and a tobacco etch virus (TEV) protease cleavage site (for removal of the fused 4 kDa tag) to the expressed recombinant protein.

One Shot TOP10 *Escherichia coli* cells were transformed with the Tbg or Tbr *gk*-pET151/D-TOPO plasmid construct by heat shock. Colonies were grown on Luria–Bertani (LB) plates containing 100 µg ml^{-1} carbenicillin and positive clones carrying the inserted gene were confirmed by colony PCR and selected for liquid culturing in LB media for construct amplification. Plasmid extraction from the cultured TOP10 cells was achieved using a Toyobo MagExtractor kit and was subjected to further confirmation by a combination of nested PCR and digestion with *Nco*I. Gene sequencing using the construct and designed sequencing primers was conducted using the dye-terminator method with an ABI Prism310 genetic analyzer (Applied Biosystems). The nucleotide sequence of *gk* revealed that the Tbg and Tbr GKs were exactly identical at the protein level; hence, Tbg *gk* was picked and used in this study. The recombinant plasmid was transformed into the JM109 (DE3 + pRARE2) *E. coli* strain (Novagen) for protein expression. Colonies of the transformants grown on an LB plate containing 100 µg ml^{-1} carbenicillin and 50 µg ml^{-1} chloramphenicol were selected and grown aerobically in LB medium containing the same concentrations of antibiotics.

The expression conditions were optimized for the amount and the activity of GK in the cytosolic fractions using activity measurements and SDS–PAGE by varying the concentration of the expression inducer isopropyl β-D-1-thiogalactopyranoside (IPTG), the temperature and the post-induction time before transformant harvest. The best yield was achieved with 25 µ*M* IPTG, growth at 293 K and post-induction for 8 h.

2.2. Assay of GK activity

The TbgGK activity was assayed using the reverse reaction of TbgGK (glycerol 3-phosphate + ADP → glycerol + ATP). To 1.0 ml of the reaction mixture (1 m*M* EDTA, 5 m*M* $MgSO_4$, 0.5 m*M* $NADP^+$, 50 m*M* glucose, 2 m*M* ADP, 10 m*M* glycerol 3-phosphate and one unit of hexokinase and glucose-6-phosphate dehydrogenase), TbgGK was added at 300 K. Using the ATP produced by TbgGK, hexokinase converts glucose to glucose 6-phosphate and finally glucose-6-phosphate dehydrogenase produces NADPH from glucose 6-phosphate and $NADP^+$. The rate of NADPH accumulation was spectrophotometrically monitored at 340 nm using a Jasco V-660 spectrophotometer.

2.3. Purification of recombinant TbgGK

For large-scale preparation, the transformant was grown at 293 K in 10 l LB medium for 8 h after induction and was harvested by centrifugation at 10 000*g*. The *E. coli* pellet was washed twice in 50 m*M* Tris–HCl buffer pH 7.6 containing 0.1 m*M* phenylmethylsulfonyl fluoride (PMSF) and was resuspended in 300 ml lysis buffer [100 m*M* phosphate buffer pH 6.8, 300 m*M* NaCl, 10 m*M* $MgSO_4$, 0.1 m*M* PMSF, 1 mg ml^{-1} lysozyme and 10%(*v*/*v*) glycerol]. The cell suspension was kept on ice for 30 min, passed twice through a French pressure cell operated at 140 MPa to break the cells and then subjected to centrifugation at 26 000*g* to remove unbroken cells and inclusion bodies. The supernatant was further centrifuged at 146 000*g* to remove residual undissolved material and then applied onto an Ni–NTA Agarose column (Qiagen; 1.5 × 15 cm) pre-equilibrated with 100 m*M* phosphate buffer pH 6.8 containing 20 m*M* imidazole, 300 m*M* NaCl, 10 m*M* $MgSO_4$ and 1%(*v*/*v*) glycerol. After washing the column with 100 ml of the same buffer, rTbgGK was eluted with 500 ml of buffer containing a linear gradient of 20–500 m*M* imidazole. Fractions containing active rTbgGK of higher purity as assessed

by SDS–PAGE (Laemmli, 1970) were pooled, concentrated to approximately 40 mg ml^{-1} using a centrifugal ultrafiltration tube (Amicon Ultra-15, 30 kDa cutoff; Millipore) and stored at 253 K in the presence of 50%(*v*/*v*) glycerol until the next purification step. About 5 mg of the affinity-purified protein was further purified by gel-filtration chromatography using a Superdex 200 (1 × 30 cm) column (GE Healthcare Biosciences) equilibrated with 100 m*M* phosphate buffer pH 6.8 containing 0.3 *M* NaCl and 1%(*v*/*v*) glycerol. Elution was carried out at a flow rate of 0.5 ml min^{-1} on a high-performance liquid-chromatography (HPLC) instrument. Each fraction (0.5 ml) was analyzed by SDS–PAGE and fractions containing highly pure rTbgGK were pooled. After buffer exchange to 10 m*M* MOPS buffer pH 6.8, 10 m*M* $MgSO_4$ and 1%(*v*/*v*) glycerol, the purified rTbgGK was concentrated to about 10 mg ml^{-1} for crystallization experiments. The addition of $MgSO_4$ and glycerol was crucial for preservation of the rTbgGK activity. The concentration of rTbgGK was estimated using the calculated molar extinction coefficient at 280 nm (ε_{280} = 81 080), giving an A_{280} of 1.0 for the pure rTbgGK solution at 0.74 mg ml^{-1}.

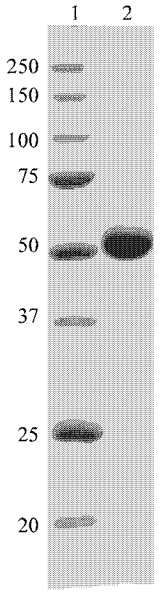

Figure 1
12.5% SDS–PAGE gel stained with Coomassie Brilliant Blue R-250 showing the apparent homogeneity of the purified rTbgGK. Lane 1, molecular-weight markers (kDa); lane 2, rTbgGK purified by Ni–NTA affinity chromatography and Superdex 200 gel filtration.

2.4. Crystallization and X-ray diffraction data collection

Crystallization conditions were initially screened at 277 and 293 K using the sitting-drop vapour-diffusion method in a 96-well Corning CrystalEX microplate with conical flat bottom (Hampton Research). A 0.5 µl droplet containing about 10 mg ml^{-1} rTbgGK dissolved in 10 m*M* MOPS buffer pH 6.8, 10 m*M* $MgSO_4$ and 1%(*v*/*v*) glycerol was mixed with an equal volume of reservoir solution and the droplet was allowed to equilibrate against 100 µl reservoir solution. In the initial screening experiment, commercially available screening kits from Hampton Research (Crystal Screen, Crystal Screen II, Grid Screen Ammonium Sulfate, Grid Screen PEG 6000, Grid Screen MPD and Quick Screen) and from Emerald BioStructures (Wizard Screen I and II) were used as the reservoir solutions. However, most of the conditions gave only heavy protein precipitates and the screening was unsuccessful. Screening was then carried out using a 5 mg ml^{-1} rTbgGK solution and twice-diluted reservoir solutions. Out of 290 conditions screened, tiny crystals and their aggregates appeared at 277 and 293 K from reservoir solutions containing 2.5–5%(*w*/*v*) PEG 6000 in the pH range 6.0–8.0. The conditions were further optimized by varying the buffer pH (5.6–8.4), the molecular weight of the PEG and its concentration [1–10%(*w*/*v*) for PEG 3350 and PEG 6000; 10–30%(*w*/*v*) for PEG 400]. Finally, single crystals suitable for X-ray diffraction experiments were obtained using a reservoir solution consisting of 30%(*w*/*v*) PEG 400 and 100 m*M* HEPES pH 7.0 within 24 h.

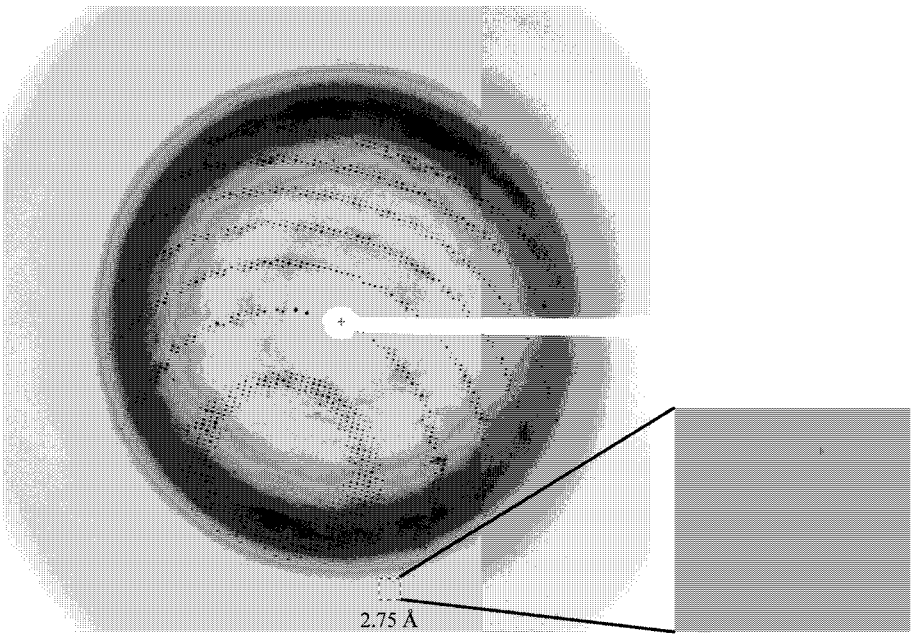

Figure 2
A typical X-ray diffraction pattern of an rTbgCK crystal. The detector edge corresponds to 2.4 Å resolution and an enlarged image of the indicated area around 2.75 Å resolution is shown. The exposure time was 1 s, with an oscillation angle of 1.0°.

X-ray diffraction experiments were performed under cryocooled conditions (100 K) on the BL41XU (λ = 1.000 Å; Rayonix MX225HE CCD detector) and BL44XU (λ = 0.900 Å; Bruker DIP-6040 detector system) beamlines at SPring-8 (Harima, Japan) and the BL17A (λ = 1.000 Å; ADSC Quantum 270 detector) beamline at the Photon Factory (Tsukuba, Japan). A crystal mounted in a nylon loop was transferred to and soaked briefly in reservoir solution containing 40%(*w*/*v*) PEG 400 and then flash-frozen at 100 K in a stream of nitrogen gas. A total of 180 images were recorded with an oscillation angle of 1.0°, an exposure time of 1 s per image and a crystal-to-detector distance of 200 mm. The diffraction data were processed and scaled with the *HKL*-2000 software package (Otwinowski & Minor, 1997).

3. Results and discussion

Gene-sequence analyses for the cDNAs of *T. b. gambiense* and *T. b. rhodesiense gks* revealed a total of seven point differences when compared with the *gk* sequence from *T. b. brucei* (TREU927; accession No. XM_822408); only one of these differences (T212 in *T. b. brucei* to C in *T. b. gambiense* and *T. b. rhodesiense*) resulted in a change of a single amino acid (Phe71 in TbbGK to Ser71 in TbgGK and TbrGK) in the 512 amino-acid residues of TbgGK. The nucleotide-sequence data for the cDNAs of *T. b. gambiense* and *T. b. rhodesiense gks* have been deposited in the DDBJ/EMBL/GenBank nucleotide-sequence databases with accession Nos. AB517984 and AB517985, respectively.

His_6-tagged rTbgGK with 545 amino-acid residues (60.4 kDa) was overexpressed and purified to homogeneity by a combination of Ni–NTA affinity chromatography and Superdex 200 gel-filtration chromatography (Fig. 1). About 80 mg purified enzyme with a specific activity of 31.7 µmol min^{-1} mg^{-1} was obtained from a 10 l culture. The rTbgGK protein eluted from the Superdex 200 column with a retention time corresponding to a molecular weight of about 119 kDa, indicating that the enzyme exists as a homodimer in solution.

In a screening of 290 crystallization conditions, crystals of rTbgGK were obtained using PEGs as precipitant. After optimization of the crystallization conditions, the best crystals, which diffracted X-rays to a resolution of 2.75 Å (Fig. 2), were grown at 293 K using a reservoir solution containing 30%(*w*/*v*) PEG 400 and 0.1 *M* HEPES buffer pH 7.0. The crystals attained typical dimensions of about 0.25 × 0.1 × 0.05 mm in 2 d (Fig. 3). Analysis of the symmetry and systematic absences in the recorded diffraction patterns revealed that the crystals of rTbgGK belonged to the orthorhombic space group $P2_12_12_1$, with unit-cell parameters a = 63.84, b = 121.50, c = 154.59 Å. Assuming the presence of two rTbgGK molecules (2 × 60.4 kDa) in the asymmetric unit, the V_M value was calculated to be 2.5 $Å^3$ Da^{-1}, with an estimated solvent content of 50% (Matthews, 1968); these values are within the range commonly observed for protein crystals. A total of 135 987 observed reflections recorded on 180 images were merged to 31 848 unique reflections in the 50.0–2.75 Å resolution range with an R_{merge} of 5.5%. The data-collection and processing statistics are shown in Table 1.

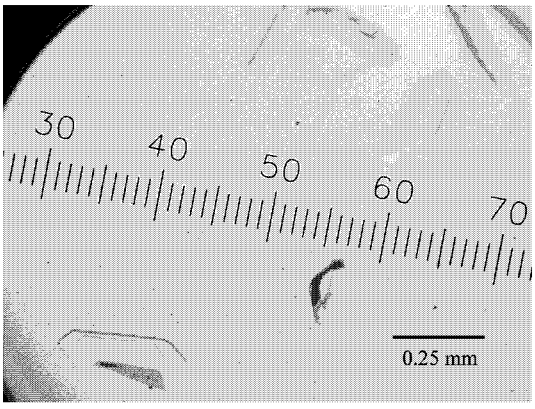

Figure 3
Crystals of rTbgGK obtained by the sitting-drop vapour-diffusion method using PEG 400 as a precipitant.

Table 1
Diffraction data statistics for the crystal of rTbgGK.

Values in parentheses are for the highest resolution shell.

Space group	$P2_12_12_1$
Unit-cell parameters (Å)	a = 63.84, b = 121.50, c = 154.59
V_M† ($Å^3$ Da^{-1})	2.5
Solvent content† (%)	50
X-ray source	BL41XU, SPring8
Wavelength (Å)	1.000
Temperature (K)	100
Resolution (Å)	50–2.75 (2.85–2.75)
Total reflections	135987
Unique reflections	31848
Completeness (%)	97.1 (95.7)
$R_{merge}(I)$‡ (%)	5.5 (46.1)
$\langle I/\sigma(I)\rangle$	18.4 (3.0)

† Assuming the presence of two molecules in the asymmetric unit. ‡ $R_{merge}(I) = \sum_{hkl}\sum_i |I_i(hkl) - \langle I(hkl)\rangle| / \sum_{hkl}\sum_i I_i(hkl)$, where $I_i(hkl)$ is the intensity of the ith observation of reflection hkl and $\langle I(hkl)\rangle$ is their average.

An attempt to solve the structure using the molecular-replacement method with the *MOLREP* program (Vagin & Teplyakov, 1997) from the *CCP*4 suite (Collaborative Computational Project, Number 4, 1994) was carried out using the refined coordinates of GK from *P. falciparum* (PDB code 2w41; 40% amino-acid sequence identity to rTbgGK; Schnick *et al.*, 2009). A promising solution with a homodimeric structure was obtained (correlation coefficient and R factor of 0.406 and 51.6%, respectively). Using the molecular-replacement solution, the structure is being subjected to refinement. In parallel with the refinement, we are now trying to obtain crystals of rTbgGK complexed with ligands, including substrates and substrate analogues. *In silico* screening of potential inhibitors from a compound library of the Chemical Biology Research Initiative at the University of Tokyo is also under way.

It should be noted that the amino-acid sequence of TbgGK was identical to that of TbrGK and showed only one difference from that of TbbGK. Therefore, inhibitors of TbgGK should also be effective against other trypanosome GKs. Since TbgGK provides a greater potential as the primary target of chemotherapy, detailed structures of TbgGK complexed with inhibitors will help structure-based drug design aimed at African trypanosomiasis.

We thank all the staff members of beamlines BL41XU and BL44XU at SPring-8 and BL17A at the Photon Factory for their help with the X-ray diffraction experiments. This work was supported by a grant from the Targeted Proteins Research Program (TPRP) and was supported in part by a Grant-in-Aid for Creative Scientific Research (18GS0314 to KK) from the Japan Society for the Promotion of Science and a Grant-in-Aid for Scientific Research on Priority Areas (18073004 to KK) from the Ministry of Education, Culture, Sports, Science and Technology, Japan. EOB is supported by a Japanese

Government Scholarship from the Ministry of Education, Science, Culture, Sports, Science and Technology.

References

Brun, R., Schumacher, R., Schmid, C., Kunz, C. & Burri, C. (2001). *Trop. Med. Int. Health*, **6**, 906–914.

Chaudhuri, M., Ott, R. D. & Hill, G. C. (2006). *Trends Parasitol.* **22**, 484–491.

Colasante, C., Ellis, M., Ruppert, T. & Voncken, F. (2006). *Proteomics*, **6**, 3275–3293.

Collaborative Computational Project, Number 4 (1994). *Acta Cryst.* D**50**, 760–763.

Fairlamb, A. H., Opperdoes, F. R. & Borst, P. (1977). *Nature (London)*, **265**, 270–271.

Guerra, D. G., Decottignies, A., Bakker, B. M. & Michels, P. A. (2006). *Mol. Biochem. Parasitol.* **149**, 155–169.

Haanstra, J. R., van Tuijl, A., Kessler, P., Reijnders, W., Michels, P. A., Westerhoff, H. V., Parsons, M. & Bakker, B. M. (2008). *Proc. Natl Acad. Sci. USA*, **105**, 17718–17723.

Hannaert, V., Bringaud, F., Opperdoes, F. R. & Michels, P. A. (2003). *Kinetoplastid Biol. Dis.* **2**, 1–30.

Hurley, J. H. (1996). *Annu. Rev. Biophys. Biomol. Struct.* **25**, 137–162.

Kido, Y., Shiba, T., Inaoka, D. K., Sakamoto, K., Nara, T., Aoki, T., Honma, T., Tanaka, A., Inoue, M., Matsuoka, S., Moore, A., Harada, S. & Kita, K. (2010). *Acta Cryst.* F**66**, 275–278.

Kralova, I., Rigden, D. J., Opperdoes, F. R. & Michels, P. A. (2000). *Eur. J. Biochem.* **267**, 2323–2333.

Laemmli, U. K. (1970). *Nature (London)*, **227**, 680–685.

Matthews, B. W. (1968). *J. Mol. Biol.* **33**, 491–497.

Michels, P. A., Hannaert, V. & Bringaud, F. (2000). *Parasitol. Today*, **16**, 482–489.

Minagawa, N., Yabu, Y., Kita, K., Nagai, K., Ohta, N., Meguro, K., Sakajo, S. & Yoshimoto, A. (1997). *Mol. Biochem. Parasitol.* **84**, 271–280.

Njiokou, F., Laveissière, C., Simo, G., Nkinin, S., Grébaut, P., Cuny, G. & Herder, S. (2006). *Infect. Genet. Evol.* **6**, 147–153.

Njogu, R. M., Whittaker, C. J. & Hill, G. C. (1980). *Mol. Biochem. Parasitol.* **1**, 13–29.

Otwinowski, Z. & Minor, W. (1997). *Methods Enzymol.* **276**, 307–326.

Schnick, C., Polley, S. D., Fivelman, Q. L., Ranford-Cartwright, L. C., Wilkinson, S. R., Brannigan, J. A., Wilkinson, A. J. & Baker, D. A. (2009). *Mol. Microbiol.* **71**, 533–545.

Singha, U. K., Peprah, E., Williams, S., Walker, R., Saha, L. & Chaudhuri, M. (2008). *Mol. Biochem. Parasitol.* **159**, 30–43.

Stevens, J. R. & Brisse, S. (2004). *The Trypanosomiases*, edited by I. Maudlin, P. Holmes & M. Miles, pp. 1–23. Wallingford: CAB International.

Van Der Meer, C. & Versluijs-Broers, J. A. (1979). *Exp. Parasitol.* **48**, 126–134.

Vagin, A. & Teplyakov, A. (1997). *J. Appl. Cryst.* **30**, 1022–1025.

World Health Organization (2006). *African trypanosomiasis*. http://www.who.int/mediacentre/factsheets/fs259/en/.

Yabu, Y., Suzuki, T., Nihei, C., Minagawa, N., Hosokawa, T., Nagai, K., Kita, K. & Ohta, N. (2006). *Parasitol. Int.* **55**, 39–43.

6186–6194 *Nucleic Acids Research, 2010, Vol. 38, No. 18* *Published online 27 May 2010*
doi:10.1093/nar/gkq449

Extensive frameshift at all AGG and CCC codons in the mitochondrial cytochrome *c* oxidase subunit 1 gene of *Perkinsus marinus* (Alveolata; Dinoflagellata)

Isao Masuda, Motomichi Matsuzaki* and Kiyoshi Kita

Department of Biomedical Chemistry, Graduate School of Medicine, The University of Tokyo, 7-3-1 Hongo, Bunkyo-ku, Tokyo 113-0033, Japan

Received December 14, 2009; Revised and Accepted May 7, 2010

ABSTRACT

Diverse mitochondrial (mt) genetic systems have evolved independently of the more uniform nuclear system and often employ modified genetic codes. The organization and genetic system of dinoflagellate mt genomes are particularly unusual and remain an evolutionary enigma. We determined the sequence of full-length cytochrome *c* oxidase subunit 1 (*cox1*) mRNA of the earliest diverging dinoflagellate *Perkinsus* and show that this gene resides in the mt genome. Apparently, this mRNA is not translated in a single reading frame with standard codon usage. Our examination of the nucleotide sequence and three-frame translation of the mRNA suggest that the reading frame must be shifted 10 times, at every AGG and CCC codon, to yield a consensus COX1 protein. We suggest two possible mechanisms for these translational frameshifts: a ribosomal frameshift in which stalled ribosomes skip the first bases of these codons or specialized tRNAs recognizing non-triplet codons, AGGY and C CCCU. Regardless of the mechanism, active and efficient machinery would be required to tolerate the frameshifts predicted in *Perkinsus* mitochondria. To our knowledge, this is the first evidence of translational frameshifts in protist mitochondria and, by far, is the most extensive case in mitochondria.

INTRODUCTION

Mitochondria, the energy-producing organelles in eukaryotic cells, possess their own genomes. Mitochondrial (mt) genomes have been reduced relative to those of their bacterial ancestors by a series of evolutionary events, including massive gene transfers to the nuclear genome and gene loss (1). Most of the mt genomes sequenced to date are single, circular, double-stranded DNA molecules that typically encode dozens of genes for respiratory electron-transport chain proteins, ATP synthase proteins, ribosomal RNA (rRNA) and transfer RNA (tRNA). However, due to independent evolutionary events across eukaryotic taxa, mt genomes are very diverse with regard to physical structure, genome size and gene content. For example, mt genomes of land plants are highly expanded (up to 2.4 Mbp in muskmelon) (2), and the smallest mt genome reported is a 6-kb long linear molecule in apicomplexan parasites (3). An mt genome with unusual organization—several hundred linear DNA molecules coding one or a few genes—is found in the icthyosporean *Amoebidium* (4). In Euglenozoan flagellate *Diplonema*, one mt gene is separated into multiple fragments, each encoded on a different mini circlular molecule (5,6).

mt gene expression is distinct from that in the nucleus, and mitochondria are notable for having alternative genetic codes. One well-known code alteration is codon reassignment in which codons are not decoded as designated in the standard codon table. For example, the UGA codon in mitochondria of many eukaryotes (other than land plants) codes for tryptophan rather than a stop (7); AGR codons (R = A or G) in inchordata mitochondria code for glycine rather than arginine (8); and CUN codons (N = A, U, G or C) in yeast mitochondria code for threonine instead of leucine (9). Some codon reassignments, even those that result in the same coding change, are suggested to have evolved independently in separate taxa; one example is the reassignment of UAG codon to leucine in chlorophycean and in fungal mitochondria (7,10–12).

Dinoflagellate mt genomes are known for their remarkable organization and genetic systems. Although the overall mt genome structure is not yet determined, these are suggested to be composed of a number of heterogeneous DNA molecules that resulted from rampant homologous recombination (13,14). The entire mt genome size

*To whom correspondence should be addressed. Tel: +81 3 5841 8202; Fax: +81 3 5841 3444; Email: mzaki@m.u-tokyo.ac.jp

is estimated to be at least 30 kb but is probably much larger (15). The genome encodes a strictly limited set of genes: three protein-coding genes, *cox1*, *cox3* and *cob*, and several fragmented rRNA genes. Curiously, the three protein-coding genes lack canonical start (AUG) and stop (UAA, UAG and UGA) codons in the 5′ and 3′ terminal regions, respectively (13–17). Transfer RNA genes have not been detected in any of the dinoflagellate mt genomes, and most of these dinoflagellate mt genomes comprise non-coding and pseudogene sequences (13,17,18). Recent studies on two basally-branching dinoflagellates have further highlighted the complexity of these mt genomes; the mt genomes of both *Oxyrrhis marina* and *Amphidinium carterae* are comprised of a number of DNA molecules bearing multiple copies of the three protein-coding genes with different intergenic contexts to one another (15,19). Particularly in the latter species, long intergenic sequences containing extensive inverted repeats are predicted to form many stem-loop structures (15).

Some of the unusual characteristics of dinoflagellate mt genomes are shared with those of parasitic apicomplexans, albeit with significant differences in mt genome organization (14,20). Apicomplexa is the sister lineage to dinoflagellates and is composed of a variety of protozoan parasites, including the malaria parasites *Plasmodium* spp. Generally, the mt genomes of apicomplexans are linear and ~6 kb long, the smallest of the known mt genomes (3). The genomes are tightly packed and have the same three protein-coding genes as dinoflagellates, as well as fragmented rRNA genes; the protein-coding genes also lack canonical start and stop codons (21,22). Although the mt genomes of these two sister lineages, which share unusual features, have not been fully characterized for the mechanisms of gene expression, the shared gene content suggests that the drastic gene reduction in genome content occurred before the divergence of these lineages. In contrast, the significant difference in dinoflagellate and apicomplexa mt genome structures indicates that drastic mt genome reorganization events occurred after the two lineages split and independently diverged from their common ancestor (14).

To further understand the uniformity and diversity of mt genomes of dinoflagellates and apicomplexans, we are characterizing the mt genome of *Perkinsus* spp., which are well-known, aquatic unicellular parasites of various commercially important bivalve mollusks. In particular, the most studied species, *P. marinus*, parasitizes the eastern oyster, *Crassostrea virginica*, causing mass mortality in the host species (23). Genus *Perkinsus* is assumed to be the most basal of the dinoflagellate lineages discovered to date, branching just after the split between dinoflagellates and apicomplexans (24). Molecular studies on this organism are currently limited, but due to its industrial and phylogenetical significance, the genome project for *P. marinus* is being undertaken by scientists at the J. Craig Venter Institute (JCVI; formerly, The Institute for Genomic Research, TIGR) and scientists at the Department of Microbiology and Immunology, University of Maryland School of Medicine/Institute of Marine and Environmental Technology (IMET; formerly, at the Center of Marine Biotechnology, UMBI) (25). Although we have observed DNA in the mitochondria of *P. marinus* using DNA- and mitochondria-specific dyes (26), critical molecular data and annotated mt gene sequences are not been available from either the National Center for Biotechnology Information (NCBI) database or the previously available TIGR draft genome database (note that the *P. marinus* genomic data set is currently being curated at JCVI).

In this article, we report the first cloning and characterization of a *Perkinsus* mt gene. We used PCR with degenerate primers, ultracentrifugal isolation both of mitochondria and mt genome, and pulsed-field gel electrophoresis. Although these initial attempts detected neither the partial nor whole mt genome, we identified short fragments of mt gene remnants inserted into the nuclear genome of *P. marinus* in the previous TIGR database. We obtained the full-length mRNA sequence for *cox1*, which codes for mt cytochrome *c* oxidase subunit 1, by PCR and RACE. The primary sequence of this mRNA shared several features with orthologs from related species, and together with Southern hybridization data, the codon usage suggested that this gene resides in the *P. marinus* mt genome. Unexpectedly, multiple sequence alignments and a three-frame translation indicated that the translation of this mRNA employs a modified decoding system. We discussed the primary sequence features of this mRNA and further described the possibility of a unique, modified translational decoding system in *Perkinsus* mitochondria.

MATERIALS AND METHODS

Strains and culture conditions

The *P. marinus* strain CRTW-3HE was purchased from the American Type Culture Collection (ATCC, no. 50439) and maintained at 26°C in ATCC medium 1886. Discontinued products were substituted as follows: Lipid Mixture (1000×; L5146; Sigma) replaced Lipid Concentrate (100×; 21900-014; Gibco) and Instant Ocean Sea Salt (Aquarium Systems) replaced artificial seawater (S1649; Sigma). Strains of *P. honshuensis* and *P. olseni* were provided by Dr Tomoyoshi Yoshinaga (The University of Tokyo) and maintained in the same manner.

Nucleic acid preparation

Perkinsus cells were collected by centrifugation at 800*g* for 5 min and re-suspended in extraction buffer [100 mM Tris, 100 mM boric acid and 50 mM ethylenediamine tetraacetic acid (EDTA), pH 8.0]. Cell suspensions were treated with sodium dodecyl sulfate at 60°C for 30 min. Total DNA was purified using standard phenol–chloroform extraction and ethanol precipitation methods. Total RNA was prepared using TRIzol Reagent (Invitrogen) according to the manufacturer's protocols, followed by the poly(A)$^+$-RNA enrichment with PolyATract mRNA Isolation System III (Promega). Complementary DNA (cDNA) was synthesized with SMART RACE cDNA amplification kit (Clontech) following manufacturer's instruction.

PCR, RACE, cloning and sequencing

PCR was performed using Takara Ex *Taq* (Takara Bio) or *PfuUltra* II HS DNA polymerase (Stratagene). We prepared reaction mixtures according to the manufacturers' instructions. Amplification was performed as follows: denaturation at 94°C for 4 min followed by 35 cycles of 94°C for 30 s, a primer annealing gradient from 40 to 50°C for 30 s, and extension at 72°C for 1 min, followed by a final extension at 72°C for 7 min. Primer set Pmcox1F1 and Pmcox1R3, based on the *cox1*-like sequences of nuclear DNA of mt origin (Numt) found in database ('Results' section), was used to amplify the partial sequence of the *Perkinsus* mt *cox1* (Supplementary Figure S1). Pmcox1R3 was then used in combination with a degerenate primer cox1-3f, which was designed based on *cox1* orthologs from related species (Supplementary Figure S1), to additionally sequence the upstream region of *Perkinsus* mt *cox1*. After determining the full *P. marinus cox1* (*Pmcox1*) mRNA sequence, we designed the primer set Pmcox1fullF and Pmcox1fullR for use in PCR of the nearly full-length *Pmcox1* both from genomic DNA (gDNA) and cDNA. Primer sequences are listed in Supplementary Table S1.

We performed RACE experiments using Takara Ex *Taq* with *P. marinus* cDNA as the template. Reaction mixtures were prepared according to the instructions of the cDNA synthesis kit manufacturer. Reaction conditions were 35 cycles of 94°C for 30 s, 48°C for 30 s, and 72°C for 3 min, and a final extension at 72°C for 7 min. Primers for 5′ and 3′ RACE were Pmcox1-5RACE and Pmcox1-3RACE, respectively (Supplementary Table S1).

PCR and RACE products were separated by electrophoresis on 1.2% agarose gel containing 1× Tris–Borate EDTA (TBE) buffer and target products were extracted with the MagExtractor PCR & Gel Clean up kit (Toyobo). The gel-purified products were then cloned using the TOPO TA cloning kit for Sequencing (Invitrogen). The recombinant plasmids containing PCR or RACE products were extracted from transformed *E. coli* (strain DH5α) using MagExtractor Plasmid (Toyobo). Both strands of cloned products were sequenced with the DYEnamic ET Terminator Cycle Sequencing kit (GE Healthcare) on an ABI310 automatic sequencer (Applied Bioscience). Sequences were determined from more than three clones, unless otherwise stated. For nearly full-length gene fragments, direct sequencing was performed on four independently obtained PCR products. Consensus sequences were determined from the alignments of multiple sequences. The assembled full-length mRNA sequence was deposited to the DNA Data Bank of Japan (accession no. AB513789).

Sequence analysis

Sequences were aligned with Clustal X 1.83 (27) and amino acid sequences were predicted using the ExPASy translate tool (http://www.expasy.org/tools/dna.html). Codon usage in several *P. marinus* genes was calculated using the Countcodon program (Kazusa DNA Res. Inst., http://www.kazusa.or.jp/codon/countcodon.html).

Accession numbers for *P. marinus* nuclear genes are as follows: *ispC* (AB284362), *sod1* (AY095212), *sod2* (AY095213) and *act1* (AY436364).

Southern hybridization

DNA fragments for use as probes were amplified by PCR using the following primer sets (for primer sequences, see Supplementary Table S1): Pmcox1pF and Pmcox1pR for *Pmcox1*, nucLSU-7f and nucLSU-7r for large subunit ribosomal DNA (LSU rDNA), PmNumt1F and PmNumt1R for *cox1*-like Numt1 and its flanking regions, and PmNumt2F and PmNumt2R for Numt2 and its flanking regions. The amplified fragments were cloned as described earlier. The extracted plasmids were digested with EcoRI overnight except for two Numt-plasmids, which were digested with both NotI and PstI, and the fragments were purified, labeled and hybridized to *P. marinus* genomic DNA with or without restriction enzyme digestion. The probes were used for detection with the AlkPhos Direct Labelling and Detection System with CDP-Star (GE Healthcare) as follows. First, 1 μg of *P. marinus* genomic DNA was digested with each restriction enzyme overnight at 37°C. Digested and uncut DNA was subjected to electrophoresis on a 0.3% agarose gel and transferred onto Hybond N^+ nylon membrane (GE Healthcare) overnight. Purified probe (100 ng) was labeled with alkaline phosphatase and hybridized to the membrane-linked genomic DNA overnight at 42°C. The membrane was washed and incubated with the substrate CDP-Star, and the chemiluminescence signal was detected using LAS-4000 (Fujifilm).

RESULTS

Primary sequence of *P. marinus cox1*

Preliminary searches for mt genome fragments of *P. marinus* in the NCBI databases of May 2008 and the *P. marinus* draft genome database at TIGR using mt gene sequences of dinoflagellates and apicomplexans as queries did not produce any sequences that were supported with statistical significance ($E < 0.01$). The identified sequences were checked carefully by eye while referring to the amino acid alignment of COX1 from related species to identify highly conserved amino acid residues in the partial sequences, and two contigs were found to harbor *cox1*-like fragments, albeit these were only partial and tiny fragments (Supplementary Figure S1). Contig no. 22713 (available as part of AAXJ01000589 in Genbank/EMBL/DDBJ) contained a fragment with 75.0% AT, that showed 68% predicted-amino acid identity (17/25 residues) with *O. marina* COX1 (ABK57983) and was found to include functionally essential amino acid residues His276 and Glu278 [amino acid numbers according to Iwata *et al.* (28)]. Another fragment in contig no. 22822 (available as part of AAXJ01000147) had 70.7% AT and showed 52% predicted-amino acid identity (20/38 residues) with *O. marina* COX1 and conserved His325 and His326 (Supplementary Figure S1A). We realized that the base composition of these *cox1*-like fragments differed from those of the flanking regions

(<55% AT). The flanking regions did not show sequence similarity to *cox1* and were discovered to harbor nuclear genes like RNA helicase gene and clathrin-associated protein gene, the former of which contained the *cox1*-like fragment in one of its intronic regions (Supplementary Figure S1B). These observations imply that these *cox1*-like, AT-rich fragments are nuclear DNA of mt origin (Numts), which are DNA fragments that had been transferred from mt genomes into the nucleus and, in many cases, have become transcriptionally inactive.

Because the *cox1*-like Numts and the true mt *cox1* are likely to have similar sequences, we used two primer sets for PCR: (i) Pmcox1F1 and Pmcox1R3, both of which were derived from the Numt sequences and (ii) Pmcox1R3 and a degenerate primer cox1-3f, which was designed based on *cox1* sequences of closely related species. In each case, there was a distinct single DNA amplification from total *P. marinus* DNA template. Sequencing of these PCR products confirmed the lengths at 167 and 434 bp, respectively, with the former being completely included in the latter. To obtain the full-length sequence of this gene, we performed 5′ and 3′ RACE using internal primers Pmcox1-5RACE and Pmcox1-3RACE, respectively, with *P. marinus* cDNA as the template. After cloning and sequencing five clones for each of the RACE products (~700 bp each), we amplified the nearly full-length sequence (~1400 bp) of both gDNA and cDNA using specific primer sets (Pmcox1fullF and Pmcox1fullR) followed by direct sequencing of multiple independent PCR products. The sequences of the RACE products and the nearly full-length sequence were manually assembled to determine the full-length mRNA sequence (1434 bp) of this gene, which was confirmed to contain sequences identical to the PCR and RACE fragments obtained above. Conversely, this mRNA contained regions which are similar to, but not identical to Numt sequences, and their flanking regions were completely different from each other (Supplementary Figure S1C). There were no substitutions, insertions and deletions between sequences from gDNA and cDNA, suggesting that RNA editing does not occur in this gene. The overall AT content of this gene was 80.9%. As a whole, this gene was similar to *cox1* of dinoflagellates and apicomplexans with an $E < 10^{-70}$; hereafter, we refer to this sequence as *Pmcox1* mRNA.

Genomic localization of *Pmcox1*

To determine the localization of *Pmcox1* in *P. marinus* genomes (nucleus or organelles), we conducted Southern hybridization using total DNA because it was difficult to isolate pure mt DNA or intact mitochondria from *P. marinus*. *Pmcox1* signals constituted a smear in the low molecular-weight region (<10 kb) of uncut genomic DNA, which is far lower than the expected position for chromosomal DNA (Figure 1). Similarly, *Pmcox1* signals formed a smear for the digestion of total DNA with BamHI, EcoRI or HindIII. A distinct signal was only observed (1–2 kb region) for the digestion of total DNA with AccI. Given the high AT content of *Pmcox1*, it is

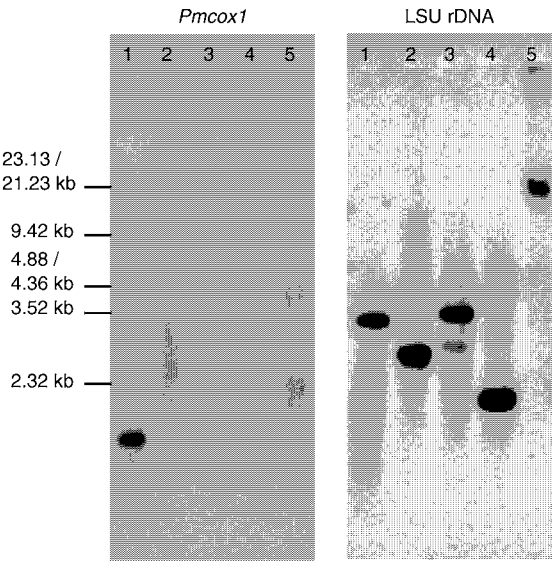

Figure 1. Southern hybridization with *Pmcox1* and a nuclear control probe. Southern hybridization using *Pmcox1* (left) and nuclear LSU rDNA (right) probes. Lanes 1–4, *P. marinus* genomic DNA digested with AccI (1), BamHI (2), EcoRI (3) and HindIII (4); lane 5, uncut genomic DNA.

natural that AccI was the only restriction enzyme tried here which cut *P. marinus* mt genome sequences around *Pmcox1*.

In sharp contrast to the *Pmcox1* probe, the probe for the nuclear LSU rDNA hybridized to the stacked, high molecular-weight, chromosomal DNA in the uncut DNA sample (Figure 1). Moreover, one or two distinct LSU rDNA band(s) were detected in genomic DNA digested with AccI, BamHI, EcoRI or HindIII. The LSU rDNA signals indicate the high quality of genomic DNA and that the restriction digests were complete. The smear signals from the *Pmcox1* probe suggest that *Pmcox1* resides on small (<10 kb) heterogeneous non-chromosomal DNA. Like the LSU rDNA probe, probes for Numts and its flanking regions hybridized to the undigested chromosomal DNA without a smear signal, indicating that they reside on chromosomal DNA (Supplementary Figure S2).

Prediction of amino acid sequence

The amino acid sequence predicted to be encoded by the primary *Pmcox1* mRNA sequence unexpectedly could not be translated in its entirety using the standard codon table in a single reading frame; several stop codons appeared in all three frames (Figure 2A). Performing Blastx-based search using the entire *Pmcox1* mRNA sequence as a query identified several partial COX1-like amino acid sequences that appeared separately in all three reading frames (gray boxes in Figure 2A). In total, we found eleven COX1-like 'coding-blocks' (gray boxes numbered I–XI in Figure 2B) that cover almost the entire sequence of *Pmcox1*, though discontinuously.

To understand the discontinuity in the COX1-like amino acid sequences, we aligned the *Pmcox1* mRNA

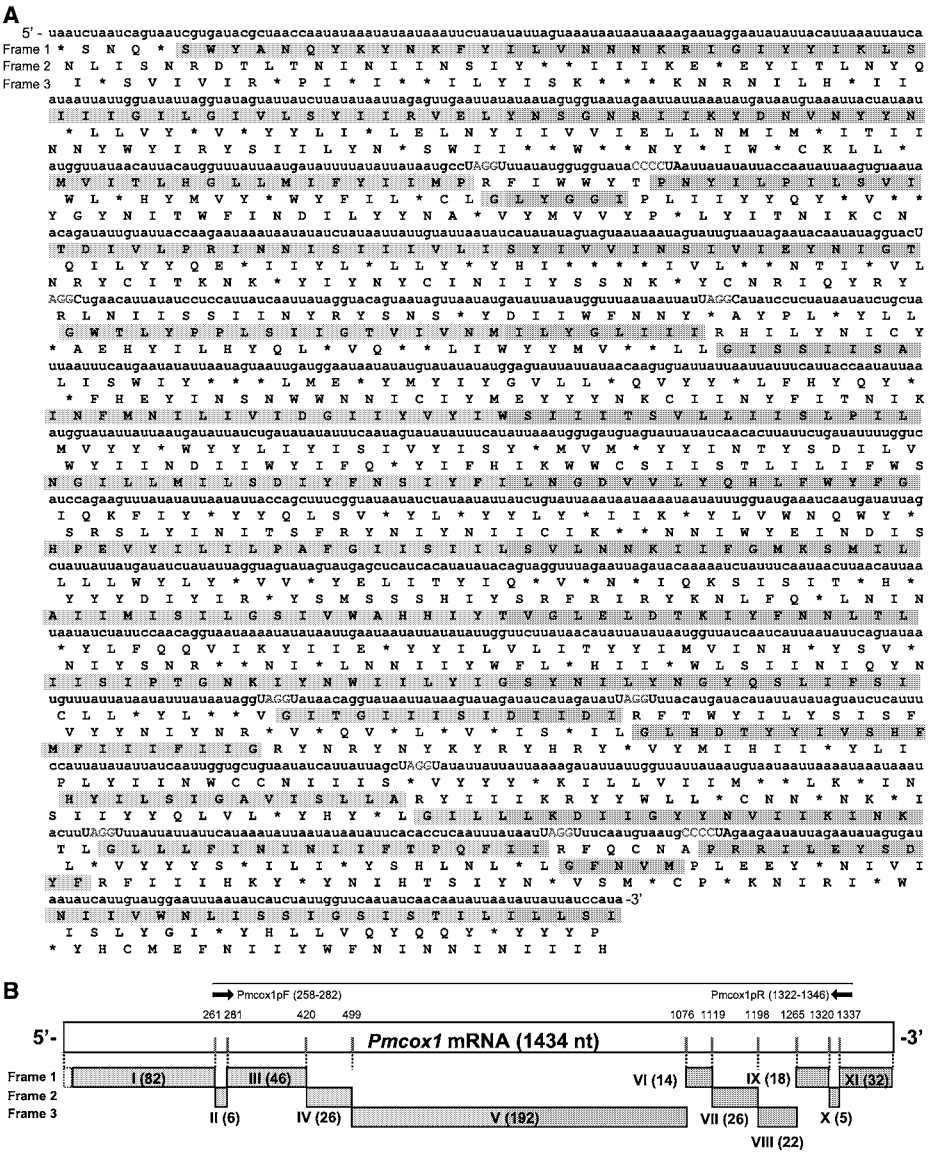

Figure 2. (**A**) Nucleotide sequence of *Pmcox1* and its three frame translation. Gray boxes denote COX1-like amino acid sequences. Nucleotides in uppercase represent the sequence motifs found in transition areas of the reading frame where COX1-like amino acid sequences are deduced. AGG and CCC codons in the motifs are highlighted in red and blue, respectively. (**B**) Schematic model of *Pmcox1* mRNA and the COX1-like blocks. COX1-like amino acid sequences distributed across three reading frames are represented by gray boxes labeled with Roman numerals. Numbers in parenthesis adjacent to the Roman numerals indicate the number of the amino acid residues. Red bars at the end of COX1-like blocks indicate UAGGY motifs containing in-frame AGG, and blue bars indicate CCCCUA motifs including in-frame CCC. Numbers above the open box indicate the positions of the first nucleotide in each motif. The uppermost bar indicates the probe region used for Southern hybridization with arrows indicating the primer locations.

sequence with *cox1* sequences of related species (Supplementary Figure S3). Among the four *cox1* sequences, *Pmcox1* was the most divergent and contained the largest number of insertions and deletions (indels). Curiously, there were 10 one- or two-base indels specifically in the *Pmcox1* mRNA that occurred in the context of UAGGY (8 of 10) or CCCCUA (2 of 10) motifs (shown on a black background in Supplementary Figure S3). Most intriguingly, these 10 regions appear to coincide with the transitions between coding-blocks, and AGG and CCC appear in-frame preceded by the predicted COX1-coding blocks (Figure 2).

Based on these observations, we postulated that modified decoding, which could shift the reading frame, occurs in the translation of *Pmcox1* mRNA. In our hypothesis, specifically, when an in-frame AGG or CCC

appears, the reading frame should be shifted forward by one or two bases, respectively. Accordingly, we prepared a putative PmCOX1 amino acid sequence in the following manner. We eliminated the A residues of the UAGGY motifs and made a +1 frameshift, making GGY instead of AGG in-frame. We also deleted the first two C residues of CCCCUA motifs and made a +2 frameshift, making CCU instead of CCC in-frame. This model accounts for all the *Perkinsus*-specific one- and two-base indels and connects the 11 'blocks' into one consecutive coding sequence. The alignment of our putative PmCOX1 sequence with counterparts from related organisms shows the conservation of functionally important amino acid residues (Figure 3, black boxes). This sequence also conserves the glycine and proline residues, which are most common in the proximity of the UAGGY and CCCCUA motifs. The potential mechanisms for these frameshifts will be further discussed later.

Based on this amino acid sequence, we identified the following characteristics of codon usage in *Pmcox1*. Around the 5′ terminal regions, no AUG codon that is likely to act as start codon was identified. Canonical stop (UAA, UAG and UGA) codons were not observed in 3′ terminal regions, as is often the case with mt genes of dinoflagellates and apicomplexans. Comparison of the COX1 amino acid alignment and nucleotide sequence also showed well-conserved tryptophan residues among related species that appeared to be coded by UGA codons in *Pmcox1* (Figure 2A and open boxes in Figure 3). On the whole, *Pmcox1* utilizes only 35 different codons whereas nuclear genes use 53–60 (Supplementary Table S2).

DISCUSSION

Pmcox1 is located in the mt genome

Using the newly determined sequence of *Pmcox1* mRNA and nearly the full-length of its genomic counterpart, we find evidence to suggest that this gene is located in the mt genome. First, Southern hybridization of total DNA from *P. marinus* shows the localization of the *Pmcox1* gene that is distinct from that of the nuclear LSU rDNA. Signal from a *Pmcox1* probe formed a smear in the relatively low molecular-weight regions of uncut total DNA, while LSU rDNA probe hybridized to stacked, uncut DNA with high molecular weight, i.e. chromosomal DNA (Figure 1). These results indicate that *Pmcox1* resides on the relatively small DNA molecules distinct from chromosomal, nuclear DNA. The present hybridization data (Figure 1) is congruent with previously reported results on other dinoflagellates (16,29,30), suggesting that *Pmcox1* is encoded on multiple heterogeneous DNA molecules, which is similar to the structure found for other dinoflagellate mt genomes.

Second, canonical start and stop codons are not found in the terminal regions of *Pmcox1* (Figure 2A). As the mt

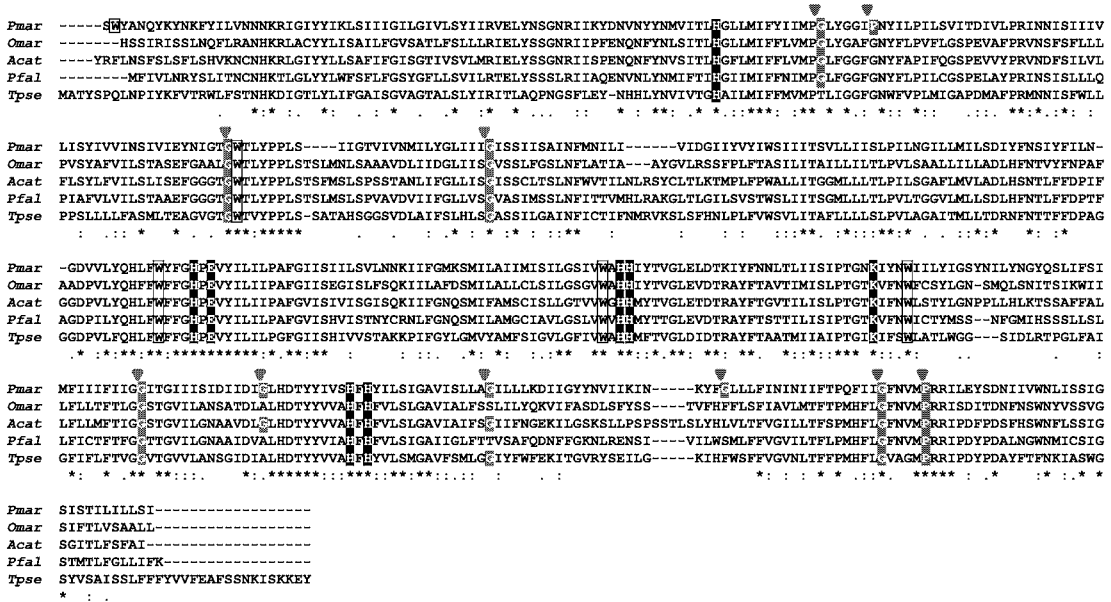

Figure 3. Alignment of multiple COX1 amino acid sequences of *P. marinus* and related protists. The sequence for *Perkinsus* was predicted based on the frameshift model. Asterisks, colons and dots indicate identical residues, conserved and semi-conserved substitutions, respectively. Residues highlighted in black are conserved amino acid essential for cytochrome *c* oxidase function: His94 (ligand for heme a), His276 (ligand for CuB), Glu278 (D-channel), His 325, His326 (ligand for CuB), Lys354 (for K-channel), His411 (ligand for heme a3) and His413 [ligand for heme a; numbers are according to *Paracoccus denitrificans* homolog, (28)]. The red and blue arrowheads indicate the motifs (UAGGY and CCCCUA, respectively) where the reading frame is hypothetically shifted. Note that the glycine and proline residues at the frameshift sites are often highly conserved (highlighted in red and blue, respectively). The open boxes indicate tryptophans coded by UGA codons in *Pmcox1* and those conserved at the homologous positions in related species. *cox1* sequences were obtained from the NCBI database for *Oxyrrhis marina* (*Omar*, EF680822), *Alexandrium catenella* (*Acat*, AB374235), *Plasmodium falciparum* (*Pfal*, AY282930) and *Thalassiosira pseudonana* (*Tpse*, DQ186202). Note that the ciliate genes are not included because they are highly divergent and the gene length also differs greatly from those of related alveolates.

genes of dinoflagellates and apicomplexans do not possess AUG start codon and stop codons, these are assumed to utilize alternative start and stop mechanisms (16,17,22,29,30). All of the *Perkinsus* nuclear genes examined here had AUG start and stop codons in the expected positions based on comparisons to orthologs from related species. These observations support that *Pmcox1* resides in the mt genome.

Lastly, overall codon usage showed significant differences between *Pmcox1* and *Perkinsus* nuclear genes (Supplementary Table S2). Moreover, several UGA codons, which typically function as stop codons in nuclear genes but often code for tryptophan in mt genes, were present in the *Pmcox1* mRNA and appeared to code for tryptophan (Figures 2A and 3). While we have no direct evidence that *Pmcox1* is located in the mt genome, these multiple lines of evidence strongly support the conclusion that this gene is not located in the nuclear but in the mt genome.

mt gene translation of *Perkinsus* involves multiple frameshifts

Surprisingly, the *Pmcox1* mRNA is apparently not translated in a single reading frame. Because we detected the cyanide-sensitive enzyme activity of cytochrome *c* oxidase according to the method described previously (31), functional COX1 protein most likely exists in *Perkinsus* mitochondria. Furthermore, we obtained partial sequences of *Pmcox1* orthologs from two other *Perkinsus* species, *P. olseni* and *P. honshuensis* (Supplementary Figure S4). Their nucleotide sequence identity to *Pmcox1* was >96%, and the UAGGY motif was conserved. There were no gaps in the alignment and all substitutions were synonymous, indicating the selective pressure to conserve the amino acid sequence in *Pmcox1* and these orthologs. Taken together with there being no *cox1*-like sequence other than *Pmcox1*, these results further emphasize that *Pmcox1* is functional and is translated with the aid of an unusual mechanism that requires multiple frameshifts (Figures 2 and 3).

At present, we are unable to show direct evidence that translation of *Pmcox1* mRNA requires frameshifts because we have not directly sequenced the PmCOX1 protein. However, the predicted PmCOX1 amino acid sequence reinforces the validity of our frameshift model. As a major functional component of mt cytochrome *c* oxidase, COX1 reduces molecular oxygen to water using electrons from cytochrome *c* and transports protons from the mt matrix to the intermembrane space. The amino acid sequence of PmCOX1 predicted by the frameshift model retains the conserved residues that are essential for these reactions (see Figure 3 and its legend) (28). The reading frame is possibly shifted back by one base (−1 frameshift) at the CCCCUA motif, but this is less likely because it would require the insertion of one extra amino acid residue into the alignment.

Moreover, this frameshift motif may be conserved in another mt gene. We identified a *cob*-like fragment from *P. marinus* whole-genome shotgun assemblies (AAXJ01022806) in a Blast-based search using dinoflagellate mt gene sequences. This fragment included four conserved UAGGY motifs and one GAGGY motif where the reading frame appeared to be shifted forward by one base to connect discontinuous COB-like amino acid sequences to form a plausible COB protein (Supplementary Figure S5). In contrast, the deduced amino acid sequences for *Perkinsus* nuclear genes shown in Supplementary Table S1 did not include such translational frameshifts. These observations strongly indicate that an unconventional event occurred during translation, specifically in mitochondria of *P. marinus*, and also of other *Perkinsus* species. Our data are the first evidence of a frameshift-dependent translation system in protist mitochondria.

Possible mechanisms suggested for frameshift in *Perkinsus* mt genes

If *Pmcox1* mRNA is read in all three frames to generate PmCOX1, an unconventional mechanism must exist in the *Perkinsus* mt translation system to shift the reading frame systematically. One possible mechanism is a ribosomal frameshift, a phenomenon observed in a wide range of organisms which results in a shift forward or backward in the reading frame during translation (32). In the case of +1 ribosomal frameshift, a rarely used codon or a stop codon in the ribosome A site is suggested to induce the ribosome to stall and allow the reading frame to be subsequently shifted forward by skipping one base (33,34). Ribosomal frameshifts have also been found in mt genes from various animals, and a +1 frameshift is suggested at specific codons (35–40). Based on previous studies, we hypothesized that ribosomes in *Perkinsus* mitochondria skip the A residue in the first position of the in-frame AGG in the shared UAGGY motif and the first two C residues in the CCCCUA motif by shifting forward by one base at in-frame CCC (Figure 4A). These two types of frameshifts at the rarely used AGG and CCC codons change the reading frame and allow the discontinuous COX1-like amino acid sequences to be joined, which produces the preferred amino acid residues at the frameshift sites (Figure 3).

Alternatively, specialized tRNAs that recognize non-triplet codons may be utilized at frameshift sites during translation. Naturally occurring deviant tRNAs recognize four-base codons and act as suppressors of non-sense mutations, and artificial tRNAs bearing modified loops can recognize quadruplet and even quintuplet codons (41–44). In the case of *Pmcox1*, specialized tRNAs may recognize AGGY (for glycine) and CCCCU (for proline) to enable the proposed frameshifts (Figure 4B). With these tRNAs, the reading frame would be shifted by one and two base(s), respectively, and one contiguous COX1 protein would be translated. Specialized tRNAs with altered decoding capacity may be used in *Perkinsus* mitochondria, although such mt tRNAs have not yet been identified from any organism.

Regardless of the mechanism, it should be noted that the efficiency of translational frameshift depends on the nucleotide sequence and the abundance of tRNAs, but 100% efficiency has never been observed (45). Lower

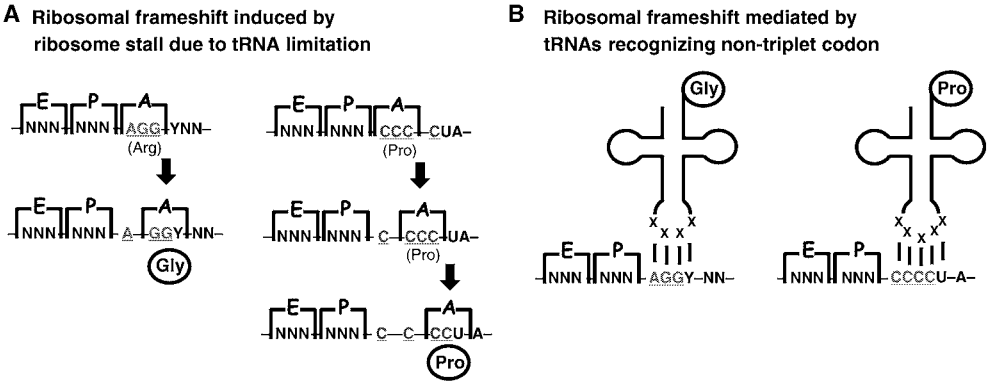

Figure 4. Possible mechanisms of frameshift-dependent translation at AGG and CCC codons of *Perkinsus* mt genes. (**A**) A ribosome stalled by tRNA limitation induces a ribosomal frameshift. When an in-frame AGG or CCC moves into the ribosome A site during translation, the ribosome stalls due to the limitation of the corresponding tRNA molecules, and the reading frame is subsequently shifted to the +1 frame. Translation then restarts in the new frame. In the case of CCCCUA, two consecutive frameshifts occur. (**B**) Specialized tRNAs recognize non-triplet codons, AGGY and CCCCU, and the reading frame shifts forward by one (AGGY) or two (CCCCU) bases.

frameshift efficiencies are not lethal to organisms known to have frameshift-dependent genes because there is only one (most cases) or at most two [for nuclear genes of some ciliates like *Euplotes* (46)] ribosomal frameshifts per gene. In contrast, frameshift must occur at as many as 10 sites to produce a complete COX1 protein in *Perkinsus*, which is a surprisingly high number. If one frameshift failure occurs at any of the 10 sites due to low efficiency, only a truncated COX1 protein, and not the full-length protein, will be synthesized to deleterious effect on respiratory function of *Perkinsus*. It is known that 'stimulatory' elements such as upstream Shine-Dalgarno-like sequences or downstream pseudoknot structures promote efficient frameshifts (47,48). There are, however, no such sequences associated with the frameshift in *Pmcox1*.

Based on these observations, we suggest that the complete translation of *Pmcox1*, a *Perkinsus* mt gene, requires a mechanism that is quite accurate for high frequency and high efficiency frameshifts. 'Ten times per gene' is by far the highest frequency among the reported ribosomal frameshifts. We suggest that the function of the frameshift mechanism in *Perkinsus* mitochondria is far more efficient and active than that of the frameshifts in other organisms. Elucidation of the amino acid sequence of *Pmcox1* is still ongoing and is required to confirm the frameshift model and also to identify the start and stop codons within *Pmcox1* mRNA. We will also investigate the translational machinery in *Perkinsus* mitochondria to understand the mechanisms that promote these 'extensive' frameshifts.

ACCESSION NUMBER

AB513789.

SUPPLEMENTARY DATA

Supplementary Data are available at NAR Online.

ACKNOWLEDGEMENTS

We thank Dr Y. Watanabe (The University of Tokyo) for helpful comments and discussions about codon recognition, Dr T. Mogi (The University of Tokyo) for valuable information on COX1, and Dr R. Kamikawa (University of Tsukuba) for providing critical comments on mt genomes of dinoflagellates. We are also grateful to Dr T. Yoshinaga (The University of Tokyo) for providing the isolates of *P. honshuensis* and *P. olseni*.

FUNDING

Grants-in-Aid for Creative Scientific Research (18GS0314 to K.K.) and for JSPS Fellows (2105920 to I.M.) from the Japan Society for the Promotion of Science (JSPS). I. M. is a JSPS research fellow. Funding for open access charge: Grants-in-Aid for JSPS Fellows (2105920 to I.M.) from the Japan Society for the Promotion of Science (JSPS).

Conflict of interest statement. None declared.

REFERENCES

1. Burger,G., Gray,M.W. and Lang,B.F. (2003) Mitochondrial genomes: anything goes. *Trends Genet.*, **19**, 709–716.
2. Ward,B.L., Anderson,R.S. and Bendich,A.J. (1981) The mitochondrial genome is large and variable in a family of plants (cucurbitaceae). *Cell*, **25**, 793–803.
3. Feagin,J.E. (1992) The 6-kb element of *Plasmodium falciparum* encodes mitochondrial cytochrome genes. *Mol. Biochem. Parasitol.*, **52**, 145–148.
4. Burger,G., Forget,L., Zhu,Y., Gray,M.W. and Lang,B.F. (2003) Unique mitochondrial genome architecture in unicellular relatives of animals. *Proc. Natl Acad. Sci. USA*, **100**, 892–897.
5. Marande,W., Lukes,J. and Burger,G. (2005) Unique mitochondrial genome structure in diplonemids, the sister group of kinetoplastids. *Eukaryot. Cell*, **4**, 1137–1146.
6. Marande,W. and Burger,G. (2007) Mitochondrial DNA as a genomic jigsaw puzzle. *Science*, **318**, 415.
7. Sengupta,S., Yang,X. and Higgs,P.G. (2007) The mechanisms of codon reassignments in mt genetic codes. *J. Mol. Evol.*, **64**, 662–688.

8. Kondow,A., Suzuki,T., Yokobori,S., Ueda,T. and Watanabe,K. (1999) An extra $tRNA^{Gly}$(U*CU) found in ascidian mitochondria responsible for decoding non-universal codons AGA/AGG as glycine. *Nucleic Acids Res.*, **27**, 2554–2559.
9. Osawa,S., Collins,D., Ohama,T., Jukes,T.H. and Watanabe,K. (1990) Evolution of the mitochondrial genetic code. III. Reassignment of CUN codons from leucine to threonine during evolution of yeast mitochondria. *J. Mol. Evol.*, **30**, 322–328.
10. Ohama,T., Inagaki,Y., Bessho,Y. and Osawa,S. (2008) Evolving genetic code. *Proc. Jpn. Acad. Ser. B Phys. Biol. Sci.*, **84**, 58–74.
11. Kück,U., Jekosch,K. and Holzamer,P. (2000) DNA sequence analysis of the complete mitochondrial genome of the green alga *Scenedesmus obliquus*: evidence for UAG being a leucine and UCA being a non-sense codon. *Gene*, **253**, 13–18.
12. Laforest,M.J., Roewer,I. and Lang,B.F. (1997) Mitochondrial tRNAs in the lower fungus *Spizellomyces punctatus*: tRNA editing and UAG 'stop' codons recognized as leucine. *Nucleic Acids Res.*, **25**, 626–632.
13. Nash,E.A., Nisbet,R.E., Barbrook,A.C. and Howe,C.J. (2008) Dinoflagellates: a mitochondrial genome all at sea. *Trends Genet.*, **24**, 328–335.
14. Waller,R.F. and Jackson,C.J. (2009) Dinoflagellate mt genomes: stretching the rules of molecular biology. *Bioessays*, **31**, 237–245.
15. Nash,E.A., Barbrook,A.C., Edwards-Stuart,R.K., Bernhardt,K., Howe,C.J. and Nisbet,R.E. (2007) Organization of the mitochondrial genome in the dinoflagellate *Amphidinium carterae*. *Mol. Biol. Evol.*, **24**, 1528–1536.
16. Jackson,C.J., Norman,J.E., Schnare,M.N., Gray,M.W., Keeling,P.J. and Waller,R.F. (2007) Broad genomic and transcriptional analysis reveals a highly derived genome in dinoflagellate mitochondria. *BMC Biol.*, **5**, 41.
17. Kamikawa,R., Nishimura,H. and Sako,Y. (2009) Analysis of the mitochondrial genome, transcripts, and electron transport activity in the dinoflagellate *Alexandrium catenella* (Gonyaulacales, Dinophyceae). *Phycol. Res.*, **57**, 1–11.
18. Norman,J.E. and Gray,M.W. (2001) A complex organization of the gene encoding cytochrome oxidase subunit 1 in the mitochondrial genome of the dinoflagellate, *Crypthecodinium cohnii*: homologous recombination generates two different *cox1* open reading frames. *J. Mol. Evol.*, **53**, 351–363.
19. Slamovits,C.H., Saldarriaga,J.F., Larocque,A. and Keeling,P.J. (2007) The highly reduced and fragmented mitochondrial genome of the early-branching dinoflagellate *Oxyrrhis marina* shares characteristics with both apicomplexan and dinoflagellate mt genomes. *J. Mol. Biol.*, **372**, 356–368.
20. Gray,M.W., Lang,B.F. and Burger,G. (2004) Mitochondria of protists. *Annu. Rev. Genet.*, **38**, 477–524.
21. Conway,D.J., Fanello,C., Lloyd,J.M., Al-Joubori,B.M., Baloch,A.H., Somanath,S.D., Roper,C., Oduola,A.M., Mulder,B., Povoa,M.M. *et al.* (2000) Origin of *Plasmodium falciparum* malaria is traced by mitochondrial DNA. *Mol. Biochem. Parasitol.*, **111**, 163–171.
22. Rehkopf,D.H., Gillespie,D.E., Harrell,M.I. and Feagin,J.E. (2000) Transcriptional mapping and RNA processing of the *Plasmodium falciparum* mitochondrial mRNAs. *Mol. Biochem. Parasitol.*, **105**, 91–103.
23. Villalba,A., Reece,K.S., Ordás,M.C., Casas,S.M. and Figueras,A. (2004) Perkinsosis in molluscs: a review. *Aquat. Living. Resour.*, **17**, 411–432.
24. Saldarriaga,J.F., McEwan,M.L., Fast,N.M., Taylor,F.J. and Keeling,P.J. (2003) Multiple protein phylogenies show that *Oxyrrhis marina* and *Perkinsus marinus* are early branches of the dinoflagellate lineage. *Int. J. Syst. Evol. Microbiol.*, **53**, 355–365.
25. Joseph,S.J., Fernández-Robledo,J.A., Gardner,M.J., El-Sayed,N.M., Kuo,C.-H., Schott,E.J., Wang,H., Kissinger,J.G. and Vasta,G.R. (2010) The alveolate *Perkinsus marinus*: biological insights from EST gene discovery. *BMC Genom.*, **11**, 228.
26. Matsuzaki,M., Kuroiwa,H., Kuroiwa,T., Kita,K. and Nozaki,H. (2008) A cryptic algal group unveiled: a plastid biosynthesis pathway in the oyster parasite *Perkinsus marinus*. *Mol. Biol. Evol.*, **25**, 1167–1179.
27. Thompson,J.D., Gibson,T.J., Plewniak,F., Jeanmougin,F. and Higgins,D.G. (1997) The CLUSTAL_X windows interface: flexible strategies for multiple sequence alignment aided by quality analysis tools. *Nucleic Acids Res.*, **25**, 4876–4882.
28. Iwata,S., Ostermeier,C., Ludwig,B. and Michel,H. (1995) Structure at 2.8 A resolution of cytochrome *c* oxidase from *Paracoccus denitrificans*. *Nature*, **376**, 660–669.
29. Chaput,H., Wang,Y. and Morse,D. (2002) Polyadenylated transcripts containing random gene fragments are expressed in dinoflagellate mitochondria. *Protist*, **153**, 111–122.
30. Norman,J.E. and Gray,M.W. (1997) The cytochrome oxidase subunit 1 gene (*cox1*) from the dinoflagellate, *Crypthecodinium cohnii*. *FEBS Lett.*, **413**, 333–338.
31. Matsumoto,J., Sakamoto,K., Shinjyo,N., Kido,Y., Yamamoto,N., Yagi,K., Miyoshi,H., Nonaka,N., Katakura,K., Kita,K. *et al.* (2008) Anaerobic NADH-fumarate reductase system is predominant in the respiratory chain of *Echinococcus multilocularis*, providing a novel target for the chemotherapy of alveolar echinococcosis. *Antimicrob. Agents Chemother.*, **52**, 164–170.
32. Farabaugh,P.J. (2000) Translational frameshifting: implications for the mechanism of translational frame maintenance. *Prog. Nucleic Acid Res. Mol. Biol.*, **64**, 131–170.
33. Belcourt,M.F. and Farabaugh,P.J. (1990) Ribosomal frameshifting in the yeast retrotransposon Ty: tRNAs induce slippage on a 7 nucleotide minimal site. *Cell*, **62**, 339–352.
34. Vimaladithan,A. and Farabaugh,P.J. (1994) Special peptidyl-tRNA molecules can promote translational frameshifting without slippage. *Mol. Cell. Biol.*, **14**, 8107–8116.
35. Härlid,A., Janke,A. and Arnason,U. (1997) The mtDNA sequence of the ostrich and the divergence between paleognathous and neognathous birds. *Mol. Biol. Evol.*, **14**, 754–761.
36. Mindell,D.P., Sorenson,M.D. and Dimcheff,D.E. (1998) An extra nucleotide is not translated in mitochondrial ND3 of some birds and turtles. *Mol. Biol. Evol.*, **15**, 1568–1571.
37. Beckenbach,A.T., Robson,S.K. and Crozier,R.H. (2005) Single nucleotide +1 frameshifts in an apparently functional mitochondrial cytochrome *b* gene in ants of the genus *Polyrhachis*. *J. Mol. Evol.*, **60**, 141–152.
38. Russell,R.D. and Beckenbach,A.T. (2008) Recoding of translation in turtle mitochondrial genomes: programmed frameshift mutations and evidence of a modified genetic code. *J. Mol. Evol.*, **67**, 682–695.
39. Milbury,C.A. and Gaffney,P.M. (2008) Complete mitochondrial sequence of the eastern oyster *Crassostrea virginica*. *Mar. Biotechnol.*, **7**, 697–712.
40. Rosengarten,R.D., Sperling,E.A., Moreno,M.A., Leys,S.P. and Dellaporta,S.L. (2008) The mitochondrial genome of the hexactinellid sponge *Aphrocallistes vastus*: evidence for programmed translational frameshifting. *BMC Genomics*, **9**, 33.
41. Magliery,T.J., Anderson,J.C. and Schultz,P.G. (2001) Expanding the genetic code: selection of efficient suppressors of four-base codons and identification of "shifty" four-base codons with a library approach in *Escherichia coli*. *J. Mol. Biol.*, **307**, 755–769.
42. Atkins,J.F. and Björk,G.R. (2009) A gripping tale of ribosomal frameshifting: extragenic suppressors of frameshift mutations spotlight P-site realignment. *Microbiol. Mol. Biol. Rev.*, **73**, 178–210.
43. Anderson,J.C., Wu,N., Santoro,S.W., Lakshman,V., King,D.S. and Schultz,P.G. (2004) An expanded genetic code with a functional quadruplet codon. *Proc. Natl Acad. Sci. USA*, **101**, 7566–7571.
44. Wang,L., Xie,J. and Schultz,P.G. (2006) Expanding the genetic code. *Annu. Rev. Biophys. Biomol. Struct.*, **35**, 225–249.
45. Sundararajan,A., Michaud,W.A., Qian,Q., Stahl,G. and Farabaugh,P.J. (1999) Near-cognate peptidyl-tRNAs promote +1 programmed translational frameshift in yeast. *Mol. Cell.*, **4**, 1005–1015.
46. Klobutcher,L.A. (2005) Sequencing of random *Euplotes crassus* macronuclear genes supports a high frequency of +1 translational frameshifting. *Eukaryot. Cell*, **4**, 2098–2105.
47. Gesteland,R.F. and Atkins,J.F. (1996) Recoding: dynamic reprogramming of translation. *Annu. Rev. Biochem.*, **65**, 741–768.
48. Giedroc,D.P. and Cornish,P.V. (2009) Frameshifting RNA pseudoknots: structure and mechanism. *Virus Res.*, **139**, 193–208.

Parasitology International 59 (2010) 560–564

Contents lists available at ScienceDirect

Parasitology International

journal homepage: www.elsevier.com/locate/parint

Trypanosome alternative oxidase, a potential therapeutic target for sleeping sickness, is conserved among *Trypanosoma brucei* subspecies ☆

Kosuke Nakamura [a,b,*,1], Sunao Fujioka [a], Shinya Fukumoto [c,d], Noboru Inoue [d], Kimitoshi Sakamoto [a], Haruyuki Hirata [c], Yasutoshi Kido [a], Yoshisada Yabu [e], Takashi Suzuki [e], Yoh-ichi Watanabe [a], Hiroyuki Saimoto [f], Hiroshi Akiyama [b], Kiyoshi Kita [a,*]

[a] *Department of Biomedical Chemistry, Graduate School of Medicine, The University of Tokyo, 7-3-1, Hongo, Tokyo 113-0033, Japan*
[b] *National Institute of Health Sciences, Tokyo 158-8501, Japan*
[c] *Center for Disease Biology and Integrative Medicine, Faculty of Medicine, The University of Tokyo, Tokyo 113-0033, Japan*
[d] *National Research Center for Protozoan Diseases, Obihiro University of Agriculture and Veterinary Medicine, Obihiro, Hokkaido 080-8555, Japan*
[e] *Department of Molecular Parasitology, Nagoya City University, Graduate School of Medical Sciences, Nagoya 467-8601, Japan*
[f] *Department of Chemistry and Biotechnology, Graduate School of Engineering, Tottori University, Tottori 680-8552, Japan*

ARTICLE INFO

Article history:
Received 26 June 2010
Received in revised form 17 July 2010
Accepted 23 July 2010
Available online 3 August 2010

Keywords:
Human African Trypanosomiasis
Sleeping sickness
Trypanosome alternative oxidase
Chemotherapy

ABSTRACT

Trypanosoma brucei rhodesiense and *T. b. gambiense* are known causes of human African trypanosomiasis (HAT), or "sleeping sickness," which is deadly if untreated. We previously reported that a specific inhibitor of trypanosome alternative oxidase (TAO), ascofuranone, quickly kills African trypanosomes *in vitro* and cures mice infected with another subspecies, non-human infective *T. b. brucei*, in *in vivo* trials. As an essential factor for trypanosome survival, TAO is a promising drug target due to the absence of alternative oxidases in the mammalian host. This study found TAO expression in HAT-causing trypanosomes; its amino acid sequence was identical to that in non-human infective *T. b. brucei*. The biochemical understanding of the TAO including its 3 dimensional structure and inhibitory compounds against TAO could therefore be applied to all three *T. brucei* subspecies in search of a cure for HAT. Our *in vitro* study using *T. b. rhodesiense* confirmed the effectiveness of ascofuranone (IC_{50} value: 1 nM) to eliminate trypanosomes in human infective strain cultures.

1. Introduction

Trypanosoma brucei, comprising three subspecies, *brucei*, *rhodesiense* and *gambiense*, causes African trypanosomiasis in mammalian hosts. *T. b. brucei* is known to cause *nagana* disease in wild and domestic animals but is non-infective to humans due to the lytic action in normal human serum [1]. On the other hand, *T. b. rhodesiense* and *T. b. gambiense* are known to cause human African trypanosomiasis (HAT), or "sleeping sickness," which currently afflicts 50,000–70,000 people and threatens over 50 million people in Africa according to a recent estimation from the World Health Organization (http://www.who.int/en/) [2]. Because African trypanosomes can escape the host's immune system by switching their cell surface antigen, variant surface glycoprotein (VSG), development of a vaccine against HAT is difficult [3]. Current chemotherapeutic treatment differs depending on the *T. brucei* subspecies and the developmental stage of the disease [4], thereby complicating diagnosis for proper treatment. Adverse events from long-term treatment, serious toxicity due to side effects, relapse and increasing prevalence of drug resistance all hamper efficient treatment of HAT [1]. Hence, there is an urgent need for a new chemotherapeutic drug therapy that can treat all disease developmental stages of different *T. brucei* subspecies.

Parasites have exploited unique energy metabolic pathways by adapting to the natural host habitat. Mitochondria in the bloodstream form of African trypanosomes are considered to be a promising chemotherapeutic target because of their unique properties not found in mammals but which are critical for parasite survival [3]. That is, these trypanosomes lack cytochromes and utilize glucose as the sole source of energy through the glycolytic pathway [3]. Trypanosome alternative oxidase (TAO) is the essential terminal enzyme for reoxidization of NADH produced during glycolysis by these parasites, and in addition to glycerol-3-phosphate dehydrogenase, it is a primary mitochondrial electron transport protein [3]. Because there

Abbreviations: HAT, Human African Trypanosomiasis; TAO, trypanosome alternative oxidase.

☆ New nucleotide sequences for alternative oxidase derived from *Trypanosoma brucei rhodesiense* and *Trypanosoma brucei gambiense* reported in this paper are available in the EMBL, GenBank and DDBJ databases under the accession nos. AB261994 and AB261993, respectively.

* Corresponding authors. Tel.: +81 3 5841 3526; fax: +81 3 5841 3444.
E-mail addresses: kosnakamura@nihs.go.jp (K. Nakamura), kitak@m.u-tokyo.ac.jp (K. Kita).
[1] Present address: National Institute of Health Sciences, 1-18-1 Kamiyoga, Setagaya-ku, Tokyo 158-8501, Japan. Tel./fax: +81 3 3700 9397.

1383-5769/$ – see front matter © 2010 Elsevier Ireland Ltd. All rights reserved.
doi:10.1016/j.parint.2010.07.006

is no alternative oxidase in the mammalian host, specific inhibitor against TAO would cause no side effects, unlike the currently available anti-trypanosomiasis drugs. In this context, TAO from *T. b. brucei* has thus been extensively studied as a possible drug target against African trypanosomiasis [3,5–9].

Ascofuranone, an antibiotic isolated from a phytopathogenic fungus (*Ascochyta visiae*), was found to specifically target TAO based on biochemical analyses and structure–activity relationship studies using derivatives of ascofuranone, indicating the site of inhibition to be the same or close to its quinol binding pocket [6,10]. It should be noted that this antibiotic was also found to cure *T. b. brucei*-infected mice *in vivo* by oral administration as well as intraperitoneal administration [11]. For further biochemical study including 3 dimensional structure analysis, *E. coli* expression system for the recombinant TAO was established [7,12]. During this study, we have recognized a strain-specific difference in amino acid sequences, particularly around the C-terminus, between our *T. b. brucei* strain (TC221) [13] and a strain analyzed by another group (EATRO110) [14]. Furthermore, we examined TAO from animal infectious strains using TC221 and two other *T. b. brucei* strains, ILTat1.4 and GUTat3.1, and concluded that these strains have completely identical amino acid sequences [13]. Subsequently, the genome sequencing project using *T. b. brucei* strain (TREU927) revealed a single copy number of the TAO gene coding for identical sequences with our strains analyzed [15].

In this study, amino acid sequences of TAO from verified human infective *T. b. rhodesiense* and *T. b. gambiense* strains were deduced from their cDNA sequences. The therapeutic efficacy of the TAO inhibitor was also analyzed *in vitro* using cultures of a human infective strain, *T. b. rhodesiense*.

2. Materials and methods

2.1. Trypanosome strains

T. b. rhodesiense (IL1501) and *T. b. gambiense* (IL3253) strains were originally provided by the International Livestock Research Institute (ILRI), Nairobi, Kenya.

(i) IL1501: This parasite was originally isolated from a human patient with HAT in Kenya in 1980 [16], subsequently subcloned *in vitro* for experimental use by the limiting dilution method at the Department of Biomedical Chemistry, the University of Tokyo. This strain was confirmed as *T. b. rhodesiense* in this study.
(ii) IL3253: This parasite was isolated from a human patient with HAT in South Sudan [16]. This strain was confirmed as *T. b. gambiense* in this study.

2.2. Trypanolytic assay for human serum resistance

Human serum resistance was investigated based on a modification of the original *in vitro* trypanolytic assay established by Rifkin [17,18] as reported previously [19]. Briefly, *in vitro* grown trypanosomes in HMI-9 medium were harvested during the exponential phase, 1×10^6/ml trypanosomes were suspended in HMI-9 medium containing 10% (v/v) heat-inactivated human serum, and the suspension was cultured in a CO_2 incubator at 37 °C. Human serum was obtained from a volunteer with no history of African trypanosome infection after overnight fasting. The medium was partly changed (>50%) every 2 days. End-point survival of the parasites was determined after at least 8 days by microscopy (200× magnification) and scored as "human serum resistance" [20].

2.3. Total genome extraction

Total genomic DNA was extracted from trypanosomes by the eukaryotic genomic DNA extraction method [21]. Briefly, phosphate-buffered saline (PBS) (pH 7.4)-washed cell pellet was lysed by lysis buffer (100 mM Tris–HCl (pH 8.0), 10 mM EDTA, 0.2% (w/v) SDS, 200 mM NaCl) and then incubated with the addition of 100 μg/mL proteinase K at 56 °C overnight. After cooling to room temperature, salt solution (3 M NaCl, 0.5 M KCl, 10 mM Tris–HCl, pH 8.0) and phenol–chloroform–isoamyl alcohol (25:24:1) were added to the sample and mixed. Genomic DNA was precipitated from the aqueous supernatant by adding isopropanol and washed with 70% (v/v) ethanol. The purified DNA was dissolved in sterilized distilled water and utilized as a template for PCR identification.

2.4. Identification of HAT-causing T. brucei subspecies by PCR

PCR for the identification of *T. brucei* subspecies was carried out using *Taq* DNA polymerase (Invitrogen, Tokyo, Japan) according to the manufacturer's instructions. Specific primers used are indicated in Table 1. PCR products were separated by 1% (w/v) agarose gel electrophoresis containing ethidium bromide (0.2 μg/ml) and visualized by an ultraviolet transilluminator.

2.5. Sequence analysis of alternative oxidase from the identified T. brucei subspecies

Total RNA of trypanosomes was extracted using TRIzol (Invitrogen) and subsequently reverse-transcribed with ReverTra Ace (Toyobo, Osaka, Japan) using the following oligo(dT) primer with an adaptor sequence, [5′-GACTCGAGTCGACATCGAT$_{17}$-3′]. The resulting cDNA was used as a template for PCR. PCR was performed using *PfuTurbo* DNA polymerase (Agilent Technologies, Inc., Santa Clara, CA). Highly conserved sequences between the TAO genes of *T. b. brucei* (GenBank accession no. AB070614) and *T. vivax* (GenBank accession no. AB070521) were used to design primers to amplify the TAO gene from different subspecies. The forward and reverse primers used were [5′-CTGGAGCCTTCC-3′] and [5′-TCGATGTCGACTCGAGTC-3′], respectively. The terminal open reading frame sequence was analyzed by 5'- and 3'-RACE using a spliced leader sequence and the oligo(dT) primer adapter sequence as the primers, respectively. Table 1 summarizes the primers used for the primary PCR for RACE. Amplified PCR products were sequenced using BigDye Terminator v3.0 Cycle Sequencing Kit (Applied Biosystems, Foster City, CA) according to the manufacturer's instructions. Sequences were determined by ABI PRISM 310 Genetic Analyzer (Applied Biosystems).

2.6. In vitro ascofuranone sensitivity assay

Ascofuranone was isolated directly from fermentation of the filamentous fungus, *A. visiae*, and handled as previously described [5]. Stock

Table 1
Oligonucleotides used in this study.

Target[a]	Primer sequence	Remarks
SRA	5′-ATAGTGACAAGATGCGTACTCAACGC-3′ 5′-AATGTGTTCGAGTACTTCGGTCACGCT-3′	Ref. [22]
R-ES	5′-GTGGCGGCAGCAAAAGTATCATC-3′ 5′-ACACTCCAACACTCTCCTATC-3′	Ref. [22]
TgsGP	5′-GCTGCTGTGTTCGGAGAGC-3′ 5′-GCCATCGTGCTTGCCGCTC-3′	Ref. [23]
TAO	5′-AACGCTATTATTAGAACAGTTTCTG-3′ 5′-AAGGTGGCGCAACATKCC-3′	For 5′ RACE
TAO	5′-GACTCGAGTCGACATCGAT$_{17}$-3′ 5′-GACCTYATCAACGTGATYC-3′	For 3′ RACE

[a] Abbreviations used are: SRA, human serum resistance-associated protein; R-ES, expression site of SRA; TgsGP, *T. b. gambiense*-specific glycoprotein; and TAO, trypanosome alternative oxidase.

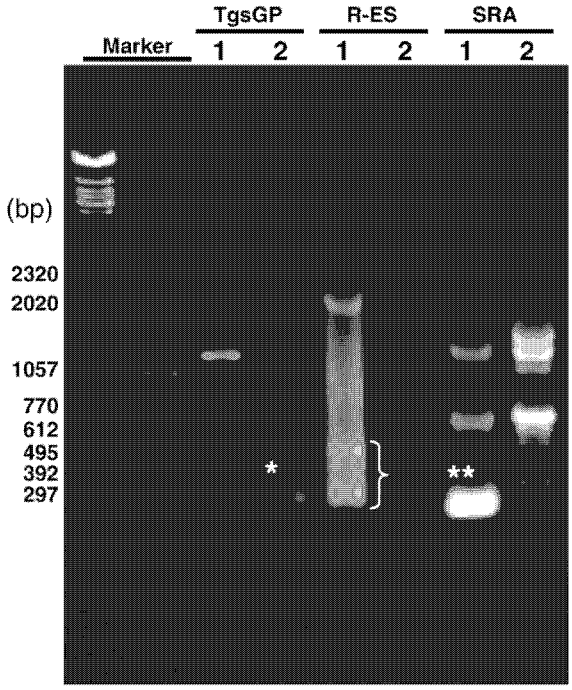

Fig. 1. Genotypical identification of *T. brucei* subspp. *rhodesiense*, *gambiense* and *brucei*. PCR was performed using genomic DNA as the template and the primers indicated in Table 1. Single asterisk indicates the 308-bp band positive for the *T. b. gambiense*-specific glycoprotein (TgsGP) gene; bracket indicates the bands positive for the human serum resistance-associated gene (SRA) expression site (R-ES) at 290, 370, 450, 530 bp; and double asterisks indicate the 284-bp SRA positive band. Lane 1, IL1501; lane 2, IL3253.

solution of ascofuranone was prepared in 100% dimethylsulfoxide (DMSO; Nacalai Tesque, Kyoto, Japan) at 10 mM and stored at −20 °C until use. Human infective *T. b. rhodesiense* at the exponential phase were centrifuged at 700×g for 5 min at room temperature and gently suspended in fresh medium to 500 cells/μl. Assays were performed in sterile 96-well microtiter plates with non-coated surface, with each well containing 100 μl parasite culture (5×10^4 bloodstream form). The first row of wells was filled with 150 μl cell suspension of the test sample at the initial concentration, and subsequent one-third serial dilutions were prepared by transferring 50 μl of the first row samples to the next row containing 100 μl cell suspension. After 18 h incubation, 10 μl Alamar Blue (Invitrogen) was added to each well and incubated for another 6 h. Absorbances of Alamar Blue in reduced (570 nm) and oxidized (600 nm) states were measured by Benchmark Plus Microplate Spectrophotometer (Bio-Rad Laboratories, Inc., Tokyo, Japan). Plates were inspected under an inverted microscope to confirm no growth changes in the controls with the same concentration of DMSO as the solvent, for determination of the MIC values, the lowest drug concentration showing no trypanosomes with normal morphology and motility compared to controls. Each sample was tested in triplicate for three independent assays.

3. Results

3.1. Identification of human infective trypanosome subspecies

A human infective form of *T. brucei* subspecies was genotypically identified by PCR using primers shown in Table 1. Genotypical identification of the trypanosome parasite was necessary since the spread of trypanosomes to new endemic areas in Africa through a movement of infected livestock and refugee as carriers has been reported [24]. One of the distinctive characteristics between *T. b. rhodesiense* and *T. b. gambiense* is human serum resistance [25]. *T. b. rhodesiense* can be differentiated by the presence of the human serum resistance-associated gene, SRA, whereas no mechanism of resistance against human serum lysis has been reported for *T. b. gambiense* [26,27]. Thus, genomic PCR targeting gene for SRA and related gene were conducted to specifically identify the *T. b. rhodesiense* strain. As shown in Fig. 1, SRA- and its expression site (R-ES)-positive PCR bands at 284 bp and at 290, 370, 450, 530 bp, respectively, were observed. This result clearly confirmed the trypanosome strain IL1501 to be *T. b. rhodesiense*. The trypanolytic assay further confirmed that a cultured IL1501 clone is resistant to lysis in the presence of human serum allowing propagation (data not shown). Moreover, as the PCR of the *T. b. gambiense*-specific glycoprotein (TgsGP) gene is reportedly unique for *T. b. gambiense* strains [23], this method was also performed for the IL3253 strain. The results were positive for TgsGP, producing a product at 308 bp, but negative for SRA or R-ES (Fig. 1), verifying IL3253 to be *T. b. gambiense*. These results are summarized in Table 2.

3.2. TAO in three T. brucei subspecies

Two positions of nucleotide polymorphism in the coding sequence of TAO are present among *T. b. brucei* strains, TC221 (GenBank accession no. AB070617.1), ILTat1.4 (GenBank accession no. AB070614.1) and EATRO 110 (GenBank accession no. U52964.2), at the 246th position (thymine in EATRO110 and cytosine in TC221 and ILTat1.4) and at the 984th position (thymine in TC221 and cytosine in ILTat1.4 and EATRO110). Importantly, the deduced amino acid sequences of TAO among all *T. b. brucei* strains analyzed are identical. Using identified *T. b. rhodesiense* and *T. b. gambiense* strains, open reading frame sequences for their TAO genes were verified from cDNA. As shown in Fig. 2, the open reading frame of TAO was 987 nucleotides in length. In comparison with the non-human infective *T. b. brucei* strain (TC221), nucleotide polymorphism was observed at the 246th position (cytosine in TC221 and IL3253 and thymine in IL1501) and 984th position (thymine in TC221 and cytosine in IL3253 and IL1501). The coding sequences of TAO in IL1501 and IL3253 were deposited in GenBank with accession numbers AB261994 and AB261993, respectively. The deduced amino acid sequence was found to be completely conserved having a length of 329 amino acids for all *T. brucei* subspecies.

3.3. In vitro ascofuranone sensitivity assay using human serum-resistant trypanosomes

Effects of ascofuranone were analyzed using the human serum-adapted IL1501 strain (*T. b. rhodesiense*). The 24-h drug sensitivity assay using the growth indicator, Alamar Blue, at 10% (v/v) showed

Table 2
Characterization of trypanosome strains.

Strain	Host origin	Subspecies	Human serum trypanolytic assay (bloodstream form)	PCR genotype analysis			GenBank accession no.
				SRA	R-ES	TgsGP	
IL1501[a]	Human (Kenya)	*T. b. rhodesiense*	R	+	+	−	AB261994
IL3253	Human (South Sudan)	*T. b. gambiense*	R	−	−	+	AB261993
TC221	Wild animal	*T. b. brucei*	S	−	−	−	AB070617

[a]A sub-culture of the original strain underwent limited dilution and was used for analysis.
R, resistant; S, sensitive.

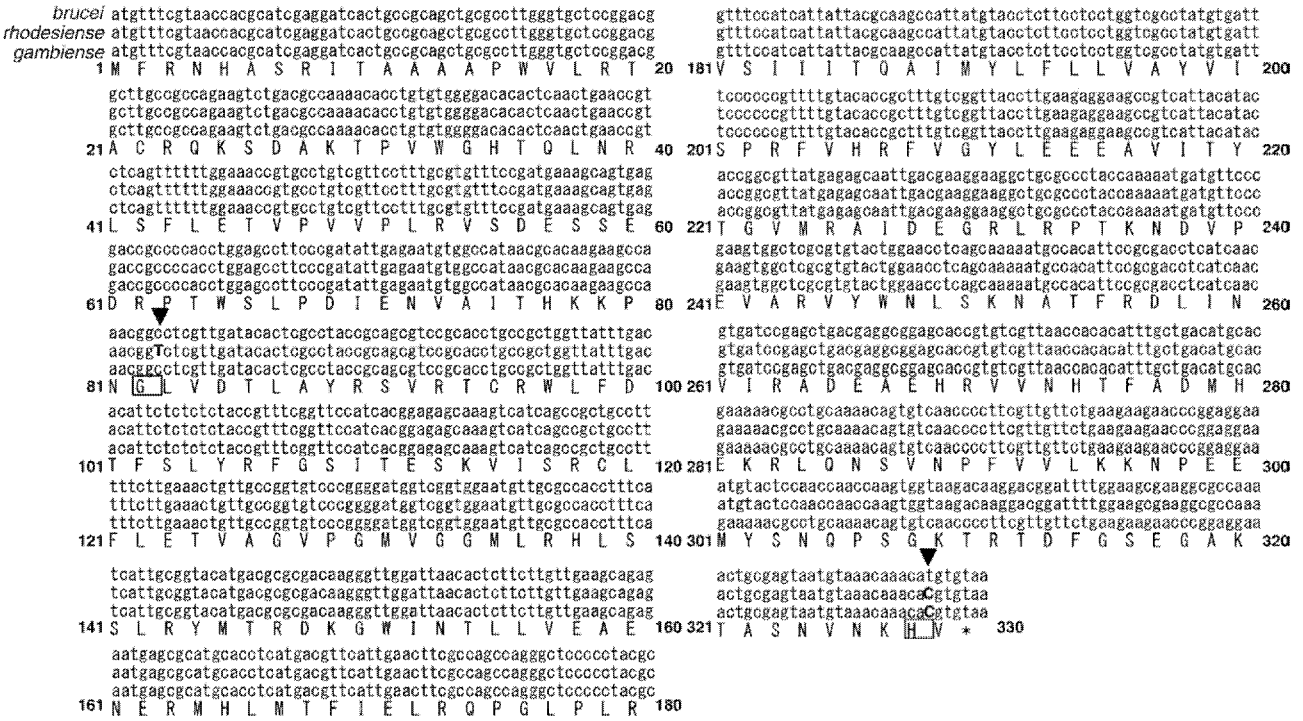

Fig. 2. Coding sequence alignment of TAO in *T. brucei* subspecies. The 987-nucleotide open reading frame sequence was translated to 329 amino acids by the universal genetic code using GENETYX-WIN program. Two positions of the amino acid sequence, which differs in the nucleotide coding sequence, are indicated in the box. Nucleotide sequence at the 246th position was cytosine in TC221 and IL3253 or thymine in IL1501 and at the 984th position was thymine in TC221 or cytosine in IL3253 and IL1501.

ascofuranone to have a dose-dependent trypanocidal effect (Fig. 3). The IC_{50} value was about 1 nM, and the MIC value was about 0.1 μM for this strain of *T. b. rhodesiense*.

4. Discussion

Sleeping sickness has a devastating impact on human health and prosperity in Africa. African trypanosome infection is always fatal unless treated. However, the currently available drugs for African trypanosomiasis have a limited effectiveness due to subspecies specificity, severe side effects and drug resistance [1,28–30]. In the past 30 years, the failure of control measures and treatment regimes has allowed this parasite to drastically increase, making it the biggest killer in certain areas of Africa, even surpassing HIV/AIDS in the provinces of Angola, Congo and Southern Sudan [31]. Currently, the choice of available drugs is limited due to the prohibitively high cost of developing new compounds showing a broad spectrum of activity [32]. Indeed, the appearance of a drug-resistant phenotype has been reported to lead to a growing number of resistant-type isolates [29,33]. Hence, a new chemotherapeutic drug that is effective at low doses, has no side effects, and is a potential treatment against all disease developmental stages of different *T. brucei* subspecies is needed.

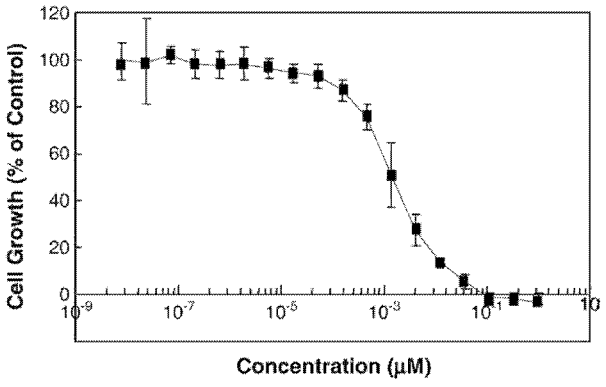

Fig. 3. *In vitro* ascofuranone sensitivity assay using human serum resistant strain, *T. b. rhodesiense*. A 24-h drug sensitivity assay was performed in sterile 96-well microtiter plates at a concentration of 500 cells/μl in the HMI-9 medium. The first row of wells was filled with 150 μl cell suspension of the test sample at the initial concentration and subsequent rows were filled with one-third serial dilutions by transferring 50 μl cell suspension from the first row to the next row of wells containing 100 μl cell suspension. After 18 h incubation, 10 μl Alamar Blue was added to each well and incubated for another 6 h. The relative difference in the reduction of Alamar Blue between the test and control samples was calculated according to the manufacturer's instructions by measuring absorbance at 570 nm and 600 nm. Data are means ± standard error of three independent experiments performed in triplicate.

Unique aspects of the parasitic mitochondria present promising chemotherapeutic targets [3], as seen by the action of the anti-malarial drug atovaquone on the mitochondrial respiratory chain [34]. Atovaquone is effective against chloroquine-resistant strains, and is already being used for treatment [35]. The specific target is thought to be complex III (ubiquinol-cytochrome *c* reductase), and analysis using resistant mutants has shown that the drug acts on the ubiquinone oxidation site in the cytochrome *b* of complex III [36–38]. Along these lines, our previous screening for such inhibitors discovered two anthelmintic compounds in adult *Ascaris suum* mitochondria: nafuredin, which inhibits at the quinone-binding domain in complex I [39], and atpenin, which inhibits the quinol-fumarate reductase activity of complex II [40]. In the case of trypanosomes found in the bloodstream of mammalian hosts, glucose is their sole energy source used in the glycolytic pathway [3]. Therefore, a respiratory enzyme, such as TAO in African trypanosome mitochondrion, could be a potential chemotherapeutic target, as it is essential for reoxidizing NADH produced during glycolysis. Ascofuranone is a potent and specific TAO inhibitor [5,6,10]. Our previous studies have characterized ascofuranone as a novel trypanocidal compound that cures mice infected with *T. b. brucei* (ILTat1.4 strain) [11] and *T. vivax* (ILDat 1.2 strain) [41].

This study deduced for the first time the amino acid sequences of TAO from human infective strains of *T. b. rhodesiense* and *T. b. gambiense* using their cDNA. The sequences were found to be

completely identical to that of TAO found in non-human infective *T. b. brucei*. Another *T. brucei* strains registered as *gambiense*, IL2343 and Wellcome, were also deduced for the amino acid sequences of TAO. It was found that they all had identical amino acid sequences. Therefore, the amino acid sequences of the TAO are highly conserved among *T. brucei* subspecies. Quite recently, we have established a protocol to prepare a highly purified TAO and crystallize the enzyme [6,7]. Recent mutational analyses on the alternative oxidase from other species provided more information on the catalytic site for the target of inhibition [42]. These data allows us to understand an inhibitory mechanism of ascofuranone and to design more effective and safe derivatives of ascofuranone from in silico analysis. We are able to apply all of the result and information from the study on *T. b. brucei* TAO to combat against HAT. In fact, the drug sensitivity assay confirmed ascofuranone as a potent inhibitor for human infective trypanosome strain, *T. b. rhodesiense*, at the IC_{50} value of about 1 nM while 0.1 μM ascofuranone completely eliminates trypanosomes. We are further investigating the inhibitory effect of ascofuranone on different strains of *T. brucei*.

In summary, the therapeutic efficacy of TAO inhibitors like ascofuranone could extend to all three subspecies of *T. brucei*, including those that cause HAT. Further studies are underway to develop a derivative of ascofuranone that can treat all developmental stages of the African trypanosomiasis.

Acknowledgements

This work was supported in part by Grant-in-aid for Creative Scientific Research Grant 18GS0314, Grant-in-aid for Scientific Research on Priority Areas 18073004 from the Japanese Society for the Promotion of Science, Targeted Proteins Research Program from the Japanese Ministry of Education, Science, Culture, Sports and Technology (MEXT) and for research on emerging and re-emerging infectious diseases from the Japanese Ministry of Health and Welfare.

References

[1] Baral TN, Magez S, Stijlemans B, Conrath K, Vanhollebeke B, Pays E, et al. Experimental therapy of African trypanosomiasis with a nanobody-conjugated human trypanolytic factor. Nat Med 2006;12:580–4.
[2] Bacchi CJ. Chemotherapy of human African trypanosomiasis. Interdiscip Perspect Infect Dis 2009;2009:195040.
[3] Kita K, Nihei C, Tomitsuka E. Parasite mitochondria as drug target: diversity and dynamic changes during the life cycle. Curr Med Chem 2003;10:2535–48.
[4] Barrett MP. The rise and fall of sleeping sickness. Lancet 2006;367:1377–8.
[5] Minagawa N, Yabu Y, Kita K, Nagai K, Ohta N, Meguro K, et al. An antibiotic, ascofuranone, specifically inhibits respiration and *in vitro* growth of long slender bloodstream forms of *Trypanosoma brucei brucei*. Mol Biochem Parasitol 1997;84: 271–80.
[6] Kido Y, Sakamoto K, Nakamura K, Harada M, Suzuki T, Yabu Y, et al. Purification and kinetic characterization of recombinant alternative oxidase from *Trypanosoma brucei brucei*. Biochim Biophys Acta 2010;1797:443–50.
[7] Kido Y, Shiba T, Inaoka DK, Sakamoto K, Nara T, Aoki T, et al. Crystallization and preliminary crystallographic analysis of cyanide-insensitive alternative oxidase from *Trypanosoma brucei brucei*. Acta Crystallogr F Struct Biol Cryst Commun 2010;66:275–8.
[8] Ott R, Chibale K, Anderson S, Chipeleme A, Chaudhuri M, Guerrah A, et al. Novel inhibitors of the trypanosome alternative oxidase inhibit *Trypanosoma brucei brucei* growth and respiration. Acta Trop 2006;100:172–84.
[9] Clarkson Jr AB, Bienen EJ, Pollakis G, Grady RW. Respiration of bloodstream forms of the parasite *Trypanosoma brucei brucei* is dependent on a plant-like alternative oxidase. J Biol Chem 1989;264:17770–6.
[10] Nihei C, Fukai Y, Kawai K, Osanai A, Yabu Y, Suzuki T, et al. Purification of active recombinant trypanosome alternative oxidase. FEBS Lett 2003;538:35–40.
[11] Yabu Y, Yoshida A, Suzuki T, Nihei C, Kawai K, Minagawa N, et al. The efficacy of ascofuranone in a consecutive treatment on *Trypanosoma brucei brucei* in mice. Parasitol Int 2003;52:155–64.
[12] Fukai Y, Nihei C, Kawai K, Yabu Y, Suzuki T, Ohta N, et al. Overproduction of highly active trypanosome alternative oxidase in *Escherichia coli* heme-deficient mutant. Parasitol Int 2003;52:237–41.
[13] Fukai Y, Nihei C, Yabu Y, Suzuki T, Ohta N, Minagawa N, et al. Strain-specific difference in amino acid sequences of trypanosome alternative oxidase. Parasitol Int 2002;51:195–9.
[14] Chaudhuri M, Ajayi W, Hill GC. Biochemical and molecular properties of the *Trypanosoma brucei* alternative oxidase. Mol Biochem Parasitol 1998;95:53–68.
[15] Berriman M, Ghedin E, Hertz-Fowler C, Blandin G, Renauld H, Bartholomeu DC, et al. The genome of the African trypanosome *Trypanosoma brucei*. Science 2005;309:416–22.
[16] Inoue N, Narumi D, Mbati PA, Hirumi K, Situakibanza NT, Hirumi H. Susceptibility of severe combined immuno-deficient (SCID) mice to *Trypanosoma brucei gambiense* and *T. b. rhodesiense*. Trop Med Int Health 1998;3:408–12.
[17] Rifkin MR. Identification of the trypanocidal factor in normal human serum: high density lipoprotein. Proc Natl Acad Sci USA 1978;75:3450–4.
[18] Rifkin MR. *Trypanosoma brucei*: some properties of the cytotoxic reaction induced by normal human serum. Exp Parasitol 1978;46:189–206.
[19] Ortiz-Ordonez JC, Sechelski JB, Seed JR. Mechanism of lysis of *Trypanosoma brucei gambiense* by human serum. J Parasitol 1994;80:924–30.
[20] Brun R, Jenni L. Human serum resistance of metacyclic forms of *Trypanosoma brucei brucei, T. brucei rhodesiense* and *T. brucei gambiense*. Parasitol Res 1987;73: 218–23.
[21] Sambrook J, Russell DW. Molecular cloning: a laboratory manual 3rd ed. Cold Spring Harbor, NY: Cold Spring Harbor Laboratory Press; 2001.
[22] Radwanska M, Chamekh M, Vanhamme L, Claes F, Magez S, Magnus E, et al. The serum resistance-associated gene as a diagnostic tool for the detection of *Trypanosoma brucei rhodesiense*. Am J Trop Med Hyg 2002;67:684–90.
[23] Radwanska M, Claes F, Magez S, Magnus E, Perez-Morga D, Pays E, et al. Novel primer sequences for polymerase chain reaction-based detection of *Trypanosoma brucei gambiense*. Am J Trop Med Hyg 2002;67:289–95.
[24] Picozzi K, Fevre EM, Odiit M, Carrington M, Eisler MC, Maudlin I, et al. Sleeping sickness in Uganda: a thin line between two fatal diseases. BMJ 2005;331: 1238–41.
[25] Ortiz JC, Sechelski JB, Seed JR. Characterization of human serum-resistant and serum-sensitive clones from a single *Trypanosoma brucei gambiense* parental clone. J Parasitol 1994;80:550–7.
[26] Raper J, Portela MP, Lugli E, Frevert U, Tomlinson S. Trypanosome lytic factors: novel mediators of human innate immunity. Curr Opin Microbiol 2001;4:402–8.
[27] Jackson AP, Sanders M, Berry A, McQuillan J, Aslett MA, Quail MA, et al. The genome sequence of *Trypanosoma brucei gambiense*, causative agent of chronic human African trypanosomiasis. PLoS Negl Trop Dis 2010;4:e658.
[28] Peregrine AS. Chemotherapy and delivery systems: haemoparasites. Vet Parasitol 1994;54:223–48.
[29] Boda C, Enanga B, Courtioux B, Breton JC, Bouteille B. Trypanocidal activity of methylene blue. Evidence for *in vitro* efficacy and *in vivo* failure. Chemotherapy 2006;52:16–9.
[30] Fairlamb AH. Chemotherapy of human African trypanosomiasis: current and future prospects. Trends Parasitol 2003;19:488–94.
[31] Matthews KR. The developmental cell biology of *Trypanosoma brucei*. J Cell Sci 2005;118:283–90.
[32] Simonite T. Protists push animals aside in rule revamp. Nature 2005;438:8–9.
[33] Dolan RB, Stevenson PG, Alushula H, Okech G. Failure of chemoprophylaxis against bovine trypanosomiasis on Galana Ranch in Kenya. Acta Trop 1992;51:113–21.
[34] Srivastava IK, Rottenberg H, Vaidya AB. Atovaquone, a broad spectrum antiparasitic drug, collapses mitochondrial membrane potential in a malarial parasite. J Biol Chem 1997;272:3961–6.
[35] Looareesuwan S, Viravan C, Webster HK, Kyle DE, Hutchinson DB, Canfield CJ. Clinical studies of atovaquone, alone or in combination with other antimalarial drugs, for treatment of acute uncomplicated malaria in Thailand. Am J Trop Med Hyg 1996;54:62–6.
[36] Kessl JJ, Lange BB, Merbitz-Zahradnik T, Zwicker K, Hill P, Meunier B, et al. Molecular basis for atovaquone binding to the cytochrome bc_1 complex. J Biol Chem 2003;278:31312–8.
[37] Syafruddin D, Siregar JE, Marzuki S. Mutations in the cytochrome *b* gene of *Plasmodium berghei* conferring resistance to atovaquone. Mol Biochem Parasitol 1999;104:185–94.
[38] Siregar JE, Syafruddin D, Matsuoka H, Kita K, Marzuki S. Mutation underlying resistance of *Plasmodium berghei* to atovaquone in the quinone binding domain 2 (Qo_2) of the cytochrome *b* gene. Parasitol Int 2008;57:229–32.
[39] Omura S, Miyadera H, Ui H, Shiomi K, Yamaguchi Y, Masuma R, et al. An anthelmintic compound, nafuredin, shows selective inhibition of complex I in helminth mitochondria. Proc Natl Acad Sci USA 2001;98:60–2.
[40] Miyadera H, Shiomi K, Ui H, Yamaguchi Y, Masuma R, Tomoda H, et al. Atpenins, potent and specific inhibitors of mitochondrial complex II (succinate-ubiquinone oxidoreductase). Proc Natl Acad Sci USA 2003;100:473–7.
[41] Yabu Y, Suzuki T, Nihei C, Minagawa N, Hosokawa T, Nagai K, et al. Chemotherapeutic efficacy of ascofuranone in *Trypanosoma vivax*-infected mice without glycerol. Parasitol Int 2006;55:39–43.
[42] Crichton PG, Albury MS, Affourtit C, Moore AL. Mutagenesis of the *Sauromatum guttatum* alternative oxidase reveals features important for oxygen binding and catalysis. Biochim Biophys Acta 2010;1797:732–7.

Mitochondrion 11 (2011) 273–278

Contents lists available at ScienceDirect

Mitochondrion

journal homepage: www.elsevier.com/locate/mito

Concatenated mitochondrial DNA of the coccidian parasite *Eimeria tenella*

Kenji Hikosaka [a], Yutaka Nakai [b], Yoh-ichi Watanabe [c], Shin-Ichiro Tachibana [a], Nobuko Arisue [d], Nirianne Marie Q. Palacpac [d], Tomoko Toyama [a,d], Hajime Honma [a,e], Toshihiro Horii [d], Kiyoshi Kita [c], Kazuyuki Tanabe [a,*]

[a] *Laboratory of Malariology, International Research Center of Infectious Diseases, Research Institute for Microbial Diseases, Osaka University, Suita, Osaka 565-0871, Japan*
[b] *Laboratory of Sustainable Environmental Biology, Graduate School of Agricultural Science, Tohoku University, Osaki, Miyagi 989-6711, Japan*
[c] *Department of Biomedical Chemistry, Graduate School of Medicine, The University of Tokyo, Bunkyo-ku, Tokyo 113-0033, Japan*
[d] *Department of Molecular Protozoology, Research Institute for Microbial Diseases, Osaka University, Suita, Osaka 565-0871, Japan*
[e] *Japan Society for the Promotion of Science, Japan*

ARTICLE INFO

Article history:
Received 28 June 2010
Received in revised form 12 October 2010
Accepted 25 October 2010
Available online 31 October 2010

Keywords:
Mitochondrion
Mitochondrial genome
Eimeria
Plasmodium
Apicomplexa
Nuclear mitochondrial DNA

ABSTRACT

Apicomplexan parasites of the genus *Plasmodium*, pathogens causing malaria, and the genera *Babesia* and *Theileria*, aetiological agents of piroplasmosis, are closely related. However, their mitochondrial (mt) genome structures are highly divergent: *Plasmodium* has a concatemer of 6-kb unit and *Babesia/Theileria* a monomer of 6.6- to 8.2-kb with terminal inverted repeats. Fragmentation of ribosomal RNA (rRNA) genes and gene arrangements are remarkably distinctive. To elucidate the evolutionary origin of this structural divergence, we determined the mt genome of *Eimeria tenella*, pathogens of coccidiosis in domestic fowls. Analysis revealed that *E. tenella* mt genome was concatemeric with similar protein-coding genes and rRNA gene fragments to *Plasmodium*. Copy number was 50-fold of the nuclear genome. Evolution of structural divergence in the apicomplexan mt genomes is discussed.

1. Introduction

Mitochondria, organelles essential for a range of cellular processes and cellular signaling, are ubiquitous in all eukaryotes. Mitochondrial (mt) genomes exhibit remarkable variation in structure and size (Gray et al., 2004), from the 6-kb genome in the malaria parasite *Plasmodium* (Feagin, 1992) to the large (180 to 2400 kb) mt genome in land plants (Ward et al., 1981; Palmer et al., 1992). *Plasmodium* belongs to the phylum Apicomplexa, with more than 5000 species, all clinically and/or economically important pathogens (Levine, 1988): *Eimeria*, responsible for the diseases of intestinal coccidiosis in intensively reared livestock; *Toxoplasma*, etiological agent of toxoplasmosis in immune-compromised patients and congenitally infected fetuses; *Cryptosporidium*, pathogens for cryptosporidiosis in humans and animals; *Babesia*, causing babesiosis in ruminants and humans; and *Theileria*, causal agents of tropical theileriosis and East Coast fever in cattle.

Mt genomes of a few apicomplexan genera have been studied, and available data suggest that they are remarkably diverse in structure and genome organization. The minuscule 6-kb tandemly repeated linear or concatenated mtDNA of *Plasmodium* encodes only three protein-coding genes (cytochrome *c* oxidase subunits I [*cox1*] and III [*cox3*] and cytochrome *b* [*cob*]) in addition to large subunit (LSU) and small subunit (SSU) ribosomal RNA (rRNA) genes (Preiser et al., 1996). The two rRNA genes are highly fragmented with 19 identified rRNA pieces (Feagin et al., 1997). The arrangement of these mt genes is completely conserved in the genus (Perkins, 2008). In the genera of *Babesia* and *Theileria*, known as piroplasms, closely related to *Plasmodium* (Lau, 2009), the mt genomes are monomeric linear, from 6.6 kb to 8.2 kb, with terminal inverted repeats on both ends (Kairo et al., 1994; Hikosaka et al., 2010). Although the *Babesia/Theileria* mt genomes encode the same three protein-coding genes, gene array and transcriptional direction are different. Furthermore, only six fragmented LSU have been identified in the *Babesia/Theileria* mt genomes, with fragmentation different from that of *Plasmodium*. Thus, the mt genomes of *Plasmodium* and *Babesia/Theileria* are structurally highly divergent regardless of their close relatedness. Although the mt genome of *Toxoplasma gondii* has yet to be sequenced, multiple copies of partial mt genes (*cox1* and *cob*) were found to be scattered throughout the nuclear genome (Ossorio et al., 1991). In *Cryptosporidium*, the mitochondrion is reduced to mitosome and has no DNA (Mogi and Kita, 2010). The phylum Apicomplexa, therefore, encompasses a large number of interesting genera to further understand the evolution of mt genomes.

* Corresponding author. Laboratory of Malariology, International Research Center of Infectious Diseases, Research Institute for Microbial Diseases, Osaka University, 3-1 Yamadaoka, Suita, Osaka 565-0871, Japan. Tel.: +81 6 6879 4260; fax: +81 6 6879 4262.
E-mail address: kztanabe@biken.osaka-u.ac.jp (K. Tanabe).

1567-7249/$ – see front matter © 2010 Elsevier B.V. and Mitochondria Research Society. All rights reserved.
doi:10.1016/j.mito.2010.10.003

In Apicomplexa, *Plasmodium* and *Babesia/Theileria* belong to the class Haematozoea, and *Eimeria* and other intestinal coccidian parasites including *Toxoplasma* belong to the class Coccidea (Hausmann and Hülsmann, 1996). The genus *Eimeria* undergoes all of its developmental stages in one host, whereas parasites belonging to the class Haematozoea require two hosts to complete their life cycles, namely, the sexual development in invertebrate vectors and the asexual development in vertebrate host. Coccidian parasites have, nevertheless, complex developmental cycles: first, oocysts excreted from the hosts undergo differentiation (sporulation) in the environment and become infective. When ingested by a host animal, oocysts undergo rounds of discrete, expansive asexual reproduction (merogony and schizogony) in the intestine, followed by sexual differentiation, fertilization and shedding of unsporulated oocysts (Jeurissen et al., 1996). *Eimeria tenella* is one of the most important *Eimeria* species, as it causes intestinal coccidiosis in domestic fowls (*Gallus gallus*), imposing enormous economic losses (Shirley et al., 2004). In *E. tenella*, two extrachromosomal DNAs have been demonstrated by pulsed-field gel electrophoresis (Dunn et al., 1998): one is the 35 kb apicoplast genome (Cai et al., 2003) and the other is a smaller size mt genome. The primary structure and the gene organization of *E. tenella* mt genome, however, remain undetermined. In this study, we report the mt genome sequence of *E. tenella*, and show that the *E. tenella* mt genome has the form of a tandemly repeated linear element or concatemer structure, and contains 19 rRNA fragments as well as three protein-coding genes. This finding indicates that the mt genomes of both *Eimeria* and *Plasmodium* retain common structural features. We discuss evolution of structural divergence in the apicomplexan mt genomes. Additionally, we identified nuclear genome DNA fragments that are shared by the mt genome of *E. tenella*.

2. Materials and methods

2.1. Blast search for mt genome sequence

A contig of *Eimeria tenella* (Houghton strain), containing mtDNA, was retrieved from *Eimeria tenella* GeneDB (http://www.genedb.org/Homepage/Etenella) using the following gene names: cytochrome *c* oxidase subunit 1, cytochrome *c* oxidase subunit 3 and cytochrome *b*. Two unfinished genomic sequences (EIMER_contig_00018071 and EIMER_contig_00018452), encoding putative COX1 and putative COB, respectively, were obtained from the Wellcome Trust Sanger Institute (http://www.sanger.ac.uk/Projects/E_tenella/).

2.2. DNA sequencing

E. tenella NIAH strain was maintained at Tohoku University by routine passage through chickens. Oocyst stage parasites were collected from feces of infected chickens and purified by the centrifugation method (Nakai et al., 1993). Purified oocysts were subjected to 5 times repeated freeze–thawing. Parasite genomic DNA was isolated using QIAamp DNA Blood Mini Kit (QIAGEN, Hilden, Germany). Genomic DNA of *Plasmodium gallinaceum* (8A strain) was kindly provided by the late M. Shahabuddin (NIAID/NIH, USA). Nucleotide sequences of the *E. tenella* mt genome; small subunit (SSU) and large subunit (LSU) rRNA genes of the *E. tenella* apicoplast genome; *cox1* and *cob* of the *P. gallinaceum* mt genome were determined by direct sequencing of polymerase chain reaction (PCR) products using specific primers (Supplementary Table 1A) designed from retrieved sequences. Amplification conditions, PCR product purification (QIAquick PCR purification kit, QIAGEN) and DNA sequencing of two independent PCR products were carried out as previously described (Hikosaka et al., 2010). Sequencing primers were designed to cover target regions in both directions. The sequences obtained in this study have been deposited in DDBJ/EMBL/GenBank with the following accession numbers: AB564272 to AB564276.

2.3. Gene annotation

Nucleotide sequences of *E. tenella* were aligned with reported sequences from *P. falciparum* (GenBank accession # M76611), *P. mexicanum* (EF079653), *B. bovis* (AB499088), *T. parva* (AB499089) and *T. annulata* (NW_001091933) by CLUSTAL W (Thompson et al., 1994) with manual corrections. Protein-coding genes were predicted using previously annotated sequences from the five parasite species. Putative rRNA genes were identified essentially as described (Hikosaka et al., 2010). MtDNA sequence or annotated rRNA gene fragments from *P. falciparum* (M76611) were used as query under suggested algorithm parameters (Freyhult et al., 2007) in NCBI BLAST 2.2 (Altschul et al., 1990). The termini of the candidate genes were assigned using aligned sequences and putative base-pairings between fragments proposed for *P. falciparum* mt rRNA fragments, and secondary structure predicted by CentroidHomfold (Hamada et al., 2009).

2.4. Southern blot hybridization

Genomic DNA of *E. tenella*, either undigested or digested with *Hind*III or *Pvu*II, were electrophoresed on 1.0% agarose gels in TAE (40 mM Tris–acetate, 1 mM EDTA) and transferred to a positively charged nylon membrane (Amersham Hybond-N+, GE Healthcare, Little Chalfont, England). PCR products specifically amplified for target regions of the *E. tenella* mt genome were labeled with digoxigenin-dUTP using the DIG High Prime DNA Labeling and Detection Starter Kit II (Roche Diagnostics, Rotkreuz, Switzerland). After overnight hybridization with the DIG-labeled DNA probes, blots were washed twice with 2× SSC, 0.1% SDS and twice with 0.5× SSC, 0.1% SDS, at 65 °C for 15 min. Hybridization signals were detected using Detection Starter Kit II. Southern blot hybridization was also done in parallel with *P. falciparum*, whose mt genome structure is known to be circular or linear concatenated with numerous branching off (Preiser et al., 1996).

2.5. Phylogenetic analysis

The concatenated amino acid sequences of COX1 and COB (755 sites) from 15 apicomplexan parasites (Supplementary Table 2) were used for phylogenetic analysis. A free-living ciliate, *Tetrahymena thermophila* (Brunk et al., 2003), was included as an outgroup. COX3 was not used, since *cox3* of *T. thermophila* is present in the nuclear (but not mt) genome. We constructed the maximum likelihood (ML) phylogenetic trees by the PROML program in PHYLIP version 3.68 (Felsenstein and Churchill, 1996). CODEML program in PAML version 4.2 (Yang, 2007) was used to estimate the Γ shape parameter value α. Bootstrap analysis was done by applying PROML to 100 re-sampled datasets produced by SEQBOOT program in PHYLIP.

A phylogenetic tree of LSU sequences of the mt genomes (LSUE, LSUF, LSUG and RNA10, 379 sites in total) was constructed using the ML method implemented in PAUP* 4.0 b10 (Swofford, 2002). SSU/LSU sequences of the apicoplast genomes (3045 sites) (Supplementary Table 2) were also used for phylogenetic analysis. The non-photosynthetic flagellate, *Astasia longa*, was included as an outgroup instead of *T. thermophila* which lacks a plastid genome. Bootstrap probability was estimated from 1000 heuristic replicates. For statistical comparisons among the best-tree and its alternatives, p-values of the KH test (Kishino and Hasegawa, 1989), the SH test (Shimodaira and Hasegawa, 1999) and the AU test (Shimodaira, 2002) were obtained.

2.6. Search for nuclear mitochondrial DNA in E. tenella

In some eukaryotes, nuclear genomes contain DNA segments which have a high sequence similarity to mtDNA (Caro et al., 2010; Hazkani-Covo et al., 2010). These sequences are considered to have been derived from mtDNA and thus designated as nuclear mtDNAs

(NUMTs) (Richly and Leister, 2004). The contigs (File version; assembly 2007_05_08.gz) of *E. tenella* were retrieved from the Wellcome Trust Sanger Institute, and the whole mt sequence obtained in this study was used as query under cut-off conditions of >50 nucleotides and >95% identity. We identified 21 NUMTs and confirmed these by direct sequencing (Supplementary Table 3). Two NUMTs, Emt3 and Emt4 occurring in contigs 00028951 and 00029260, respectively (Supplementary Table 1B), were used for Southern blot hybridization analysis against *E. tenella* DNA. Copy number of *E. tenella* mt genome was estimated using dot blot hybridization. Briefly, DNA fragments of the mt genome and the contig (contig_00029260) were amplified by PCR using specific primers (Supplementary Table 1C), and DNA amount was measured. Serial known dilutions of control PCR products were dot-blotted onto a nylon membrane, following heat denaturation (99 °C, 10 min). Genomic DNA were electrophoresed on agarose gels and then transferred to a nylon membrane. A PCR product specifically amplified from target regions of the *E. tenella* mt genome (Supplementary Table 1B) was labeled as described. Chemiluminescence signals were quantitated using LAS-4000mini.

3. Results and discussion

3.1. Mitochondrial genome organization

We obtained a mt genome sequence (6213 bp) from *E. tenella*, in which three protein-coding genes, *cob*, *cox1* and *cox3*, and 12 fragments of the large subunit (LSU) rRNA gene and 7 fragments of the small subunit (SSU) rRNA gene were identified (Fig. 1A). These genes and rRNA gene fragments are also present in the *P. falciparum* (Fig. 1B) (Feagin et al., 1997), although gene arrangements greatly differ between the two mt genomes.

Southern blot hybridization with a *cox3* probe (Emt1) against undigested DNA produced a smeared signal from around 4 kb to 20 kb. Hybridization against DNA digested with *Hind*III gave a major band at 6.2 kb which tailed-off to lower contiguous fragments. Hybridization against DNA digested with *Pvu*II yielded a clear signal at 2.6 kb. These signal sizes matched to those predicted from the *E. tenella* mt sequence (Fig. 2A and C). A *cox1* probe (Emt2) gave similar results (not shown). Southern blot hybridization using a *P. falciparum* probe (Pmt1) revealed a smeared signal from 6 kb to 23 kb against *P. falciparum* undigested DNA, a distinct band at 1.3 kb against *Hind*III-digested DNA, and a predominant 6.0 kb single band which tailed-off to a smear against *Pvu*II-digested DNA (Fig. 2B and D); yielding a similar hybridization pattern to *E. tenella*. This suggests that the *E. tenella* mt genome structure is similar to that of *P. falciparum*. The long tailing-off smears observed in both *E. tenella* and *P. falciparum* were not found in the mt genomes of *Babesia* and *Theileria* (Hikosaka et al., 2010), which have monomeric linear structures. The tailing-off smears probably reflect DNA fragments of various sizes branching off from polydispersed linear DNA molecules with various length termini (Preiser et al., 1996), which seems to be characteristics of a polydispersed concatenated mtDNA. In *E. tenella*, this tailing was somewhat longer than in *P. falciparum*, probably due to fragmentation caused by repeated freeze–thawing to disrupt the oocyst wall, which is highly rigid and not permeable to common solvents used for disruption. The absence of specific restriction fragments smaller than 6.2 kb after digestion with single-site enzymes suggests that the ends of the linear concatemers are not defined by telomere-like unique sequences, as seen in *Babesia* and *Theileria* (Kairo et al., 1994; Hikosaka et al., 2010). These results strongly suggest that the bulk of *E. tenella* mtDNA consist of polydisperse head-to-tail tandem arrays of the 6.2 kb element as in *P. falciparum*.

3.2. Phylogeny

The ML tree of concatenated COX1 and COB amino acid sequences revealed monophyly of the genera *Babesia* and *Theileria*, and of the genus *Plasmodium* with high BP values of 98 and 89%, respectively (Fig. 3A). *E. tenella* was positioned close to *Plasmodium* with a moderate BP value (75%). The ML tree of LSU sequences showed the same topology to that of the *cox1+cob* tree (Supplementary Fig. 1): *E. tenella* positioned close to *Plasmodium* with a low BP value (55%). ML tree using SSU and LSU sequences of the apicoplast genome, however, yielded a topology with *E. tenella* and *T. gondii* branching off from a common ancestor of *Plasmodium* and *Babesia/Theileria* with 100% BP (Fig. 3B). Thus, topologies of the mt trees and the apicoplast tree are not consistent. The inconsistency was not due to differences in the number of taxa used for tree construction because BP value changed little (76%) even when the number of taxa in the *cox1+cob* tree was reduced to the same as the apicoplast tree (data not shown).

The two mt tree topologies are also not consistent with phylogenetic trees constructed using 18S rRNA gene or hundreds of protein-coding nuclear genes (Morrison and Ellis, 1997; Philippe et al., 2004; Kuo et al., 2008), whereas the apicoplast tree is consistent with trees of nuclear genes. Since the positions of *E. tenella* in the two mt trees were not well supported with high BP values, we tested other possibilities of *E. tenella* position. The KH, the SH or the AU tests did not reject these alternative positions of *E. tenella* placed at a common ancestor of *Plasmodium* and *Babesia/Theileria* (arrow a in Fig. 3A) or at a common ancestor of *Babesia/Theileria* (arrow b in Fig. 3A) (Supplementary Table 4). Phylogenetic position of *E. tenella*, thus, remains unresolved with the mt dataset. *Eimeria* and other intestinal coccidians belong to the class Coccidea, and *Plasmodium* and *Babesia/Theileria* belong to the class Haematozoea. The two classes show remarkably different life cycles (Hausmann and Hülsmann, 1996). This taxonomical classification is consistent with phylogenetic trees

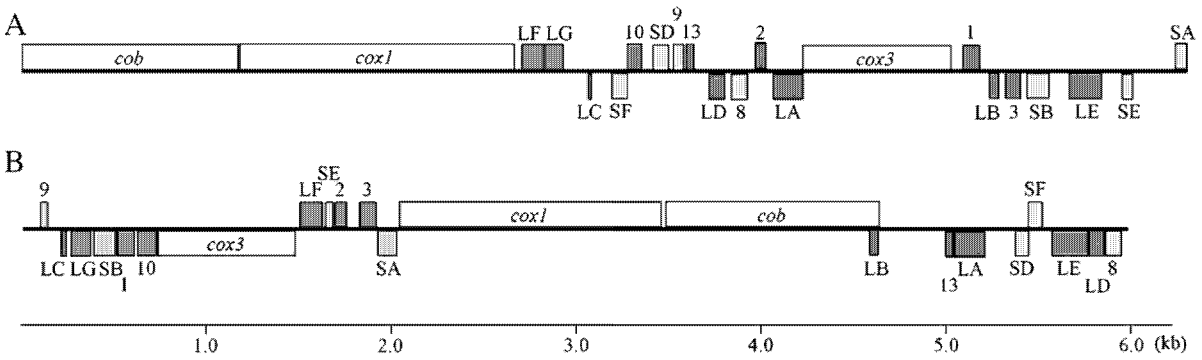

Fig. 1. Mitochondrial genome structure of *Eimeria tenella* (A) and *Plasmodium falciparum* (B). Genes shown above the bold line in each genome have predicted transcriptional directions from left to right; and those below, from right to left. Because the 6.2 kb element of *E. tenella* mt genome is tandemly repeated, both termini are arbitrary. For details refer to GenBank accession numbers AB564272 and M76611. White boxes indicate protein-coding genes (*cox1*, *cox3* and *cob*); fragments of LSU (LA–LG, 1, 2, 3, 10 and 13) and SSU (SA, SB, SD–SF, 8 and 9) rRNA genes are shown by dark and light gray boxes, respectively.

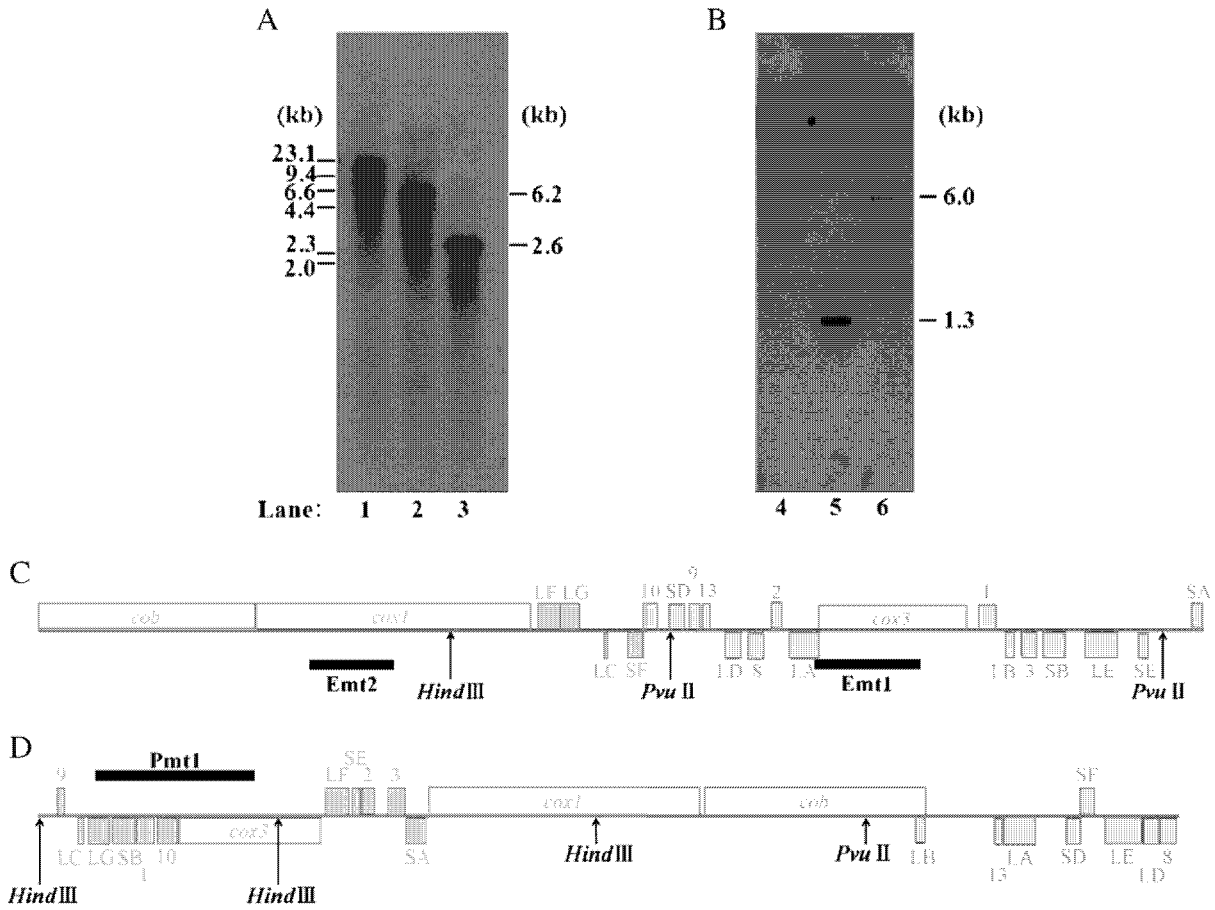

Fig. 2. Southern blot hybridization showing the mitochondrial (mt) genomes of *Eimeria tenella* (A) and *Plasmodium falciparum* (B). *E. tenella* probes (Emt1 and Emt2) and a *P. falciparum* probe (Pmt1), whose positions are shown in (C) and (D), were hybridized against undigested DNA of *E. tenella* and *P. falciparum*, respectively (lanes 1 and 4) and DNA digested with *Hind*III (lanes 2 and 5) or *Pvu*II (lanes 3 and 6).

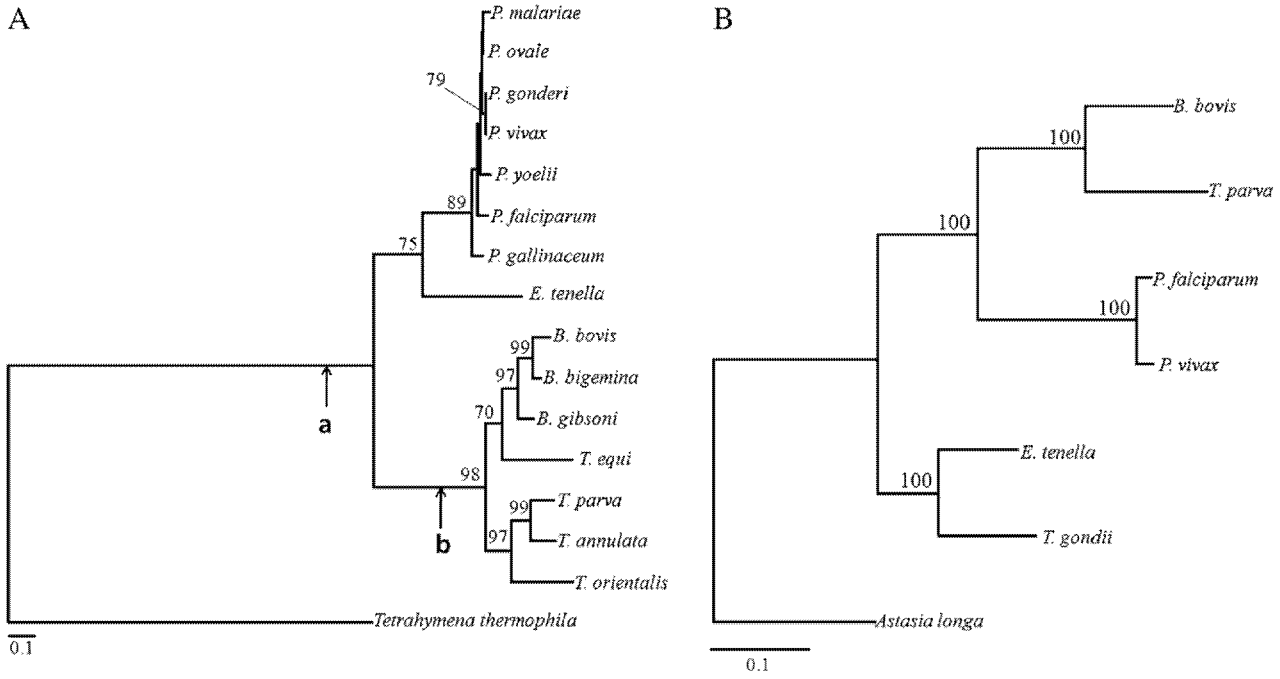

Fig. 3. Maximum likelihood phylogenetic trees of mitochondrial genes, *cox1* and *cob*, from *Plasmodium*, *Eimeria tenella*, *Babesia* and *Theileria* with *Tetrahymena thermophila* as an outgroup (A); and of apicoplast small and large subunits (SSU and LSU) of rRNA genes from six apicomplexan species with *Astasia longa* as an outgroup (B). For *cox1*+*cob* tree, concatenated amino acid sequences (755 sites) were used with 1000 heuristic replicates under a Jones, Taylor, and Thornton model (Jones et al., 1992) ($\alpha = 0.86$). For apicoplast SSU+LSU tree, concatenated nucleotide sequences (3045 sites in total: 1037 bp for SSU; 2008 bp for LSU) were used with 1000 heuristic replicates under a GTR+Γ model ($\alpha = 1.22$). Numbers shown along nodes represent bootstrap values. Arrows a and b indicate alternative positions of *E. tenella*. Both possibilities were statistically compared by the SH, KH and AU tests.

constructed using nuclear genes (Morrison and Ellis, 1997; Philippe et al., 2004; Kuo et al., 2008) and the apicoplast genome tree (Fig. 3B). We therefore consider it likely that *E. tenella* branched off from a common ancestor of *Plasmodium* clade and *Babesia/Theileria* clade.

Adopting this phylogenetic relationship allows us to infer a scenario for evolutionary trajectory of the mt genome structure of apicomplexans. Since both *Eimeria* and *Plasmodium* possess concatenated mtDNA, a common ancestor of these two parasites might have had a concatenated form of the mt genome, and the monomeric linear mt genomes of *Babesia/Theileria* were generated in the lineage. The present finding that *Eimeria* has the same 19 rRNA gene fragments as seen in the *Plasmodium* mt genome supports this scenario. Although we favor this scenario, we cannot completely rule out the possibility that a monomeric linear structure was an ancestral form and concatenated genome structures of *Eimeria* and *Plasmodium* evolved independently in each lineage. The likelihood is supported by *Tetrahymena* which has linear mt genomes, similar to those found in mt genomes of *Babesia/Theileria*. However, evolutionary distance between *Tetrahymena* and Apicomplexa is too far to gain insights into an ancestral form of the apicomplexan mt genome and, likewise, changes in molecular architecture of mt genomes are very frequent (Nosek and Tomaska, 2003). Nevertheless, it should be noted that mt genome architecture is conserved and does not change frequently within genus of the phylum: thus, in apicomplexan mt genome sequences available to date, all eight *Babesia/Theileria* species have the form of linear structure (Hikosaka et al., 2010), and all 23 *Plasmodium* species have the form of concatemer structure (Hikosaka et al., unpublished data). This within-genus stability of mt genome structure should allow us to infer an ancestral form of the apicomplexan mt genomes. In order to clarify evolutionary trajectory of the mt genome of Apicomplexa, further analysis of mt genomes of algae, closely related to apicomplexans such as *Chromera velia* and CCMP3155 (an undescribed species) would be required (Janouskovec et al., 2010).

3.3. Nuclear mitochondrial DNAs (NUMTs) in E. tenella

Blast search identified 21 sequence segments similar to the *E. tenella* mtDNA with lengths from 51 to 146 nucleotides in the *E. tenella* contigs (Supplementary Table 5). In contigs containing multiple NUMTs, several NUMTs were found arrayed in direct junction or in close proximity. Southern blot hybridization using probes Emt3 and Emt4, which contain NUMTs, gave signals derived from the *E. tenella* mt genome. We were, however, unable to detect signals derived from the nuclear genome by a similar procedure (Supplementary Fig. 2). In contrast, a probe specific to the nuclear genome (Enu1) hybridized at predicted sizes against either undigested DNA or DNA digested with *HindIII* or *Eco*RI, when a large amount of gDNA was used (data not shown). Copy number estimation analysis using Southern hybridization showed that *E. tenella* cells contained around 50 copies of the 6.2 kb element per haploid nuclear genome. The failure of detecting NUMTs in the nuclear genome with Emt3 and Emt4 was thus likely due to this copy number difference, with potential signals from the nuclear genome being masked in a smear of mtDNA.

4. Conclusion

This study suggests that the mt genome of ancestral apicomplexan parasites had a concatenated structure containing 19 rRNA gene fragments as well as three protein-coding genes and that the monomeric linear mt genome of *Babesia/Theileria* was generated in the lineage of the genera. Elucidation of a molecular mechanism, by which a linear mt genome with terminal inverted repeats on both ends was established, should help to further understand the evolution and divergence of mt genomes.

Supplementary data to this article can be found online at doi:10.1016/j.mito.2010.10.003.

Acknowledgements

This work was supported by Grant-in-Aids for Scientific Research from the Ministry of Education, Culture, Sports, Science and Technology of Japan (18073013) and from Japan Society for Promotion of Sciences (18GS03140013 and 20390120). We would like to thank the *Eimeria tenella* genome project at the Sanger Institute, UK (http://www.sanger.ac.uk/Projects/E_tenella) for partial sequences in the design of some PCR primers.

References

Altschul, S.F., Gish, W., Miller, W., Myers, E.W., Lipman, D.J., 1990. Basic local alignment search tool. J. Mol. Biol. 215 (3), 403–410.
Brunk, C.F., Lee, L.C., Tran, A.B., Li, J., 2003. Complete sequence of the mitochondrial genome of *Tetrahymena thermophila* and comparative methods for identifying highly divergent genes. Nucleic Acids Res. 31 (6), 1673–1682.
Cai, X., Fuller, A.L., McDougald, L.R., Zhu, G., 2003. Apicoplast genome of the coccidian *Eimeria tenella*. Gene 321, 39–46.
Caro, P., Gomez, J., Arduini, A., Gonzalez-Sanchez, M., Gonzalez-Garcia, M., Borras, C., Vina, J., Puertas, M.J., Sastre, J., Barja, G., 2010. Mitochondrial DNA sequences are present inside nuclear DNA in rat liver and increase with age. Mitochondrion 10 (5), 479–486.
Dunn, P.P., Stephens, P.J., Shirley, M.W., 1998. *Eimeria tenella*: two species of extrachromosomal DNA revealed by pulsed-field gel electrophoresis. Parasitol. Res. 84 (4), 272–275.
Feagin, J.E., 1992. The 6-kb element of *Plasmodium falciparum* encodes mitochondrial cytochrome genes. Mol. Biochem. Parasitol. 52 (1), 145–148.
Feagin, J.E., Mericle, B.L., Werner, E., Morris, M., 1997. Identification of additional rRNA fragments encoded by the *Plasmodium falciparum* 6 kb element. Nucleic Acids Res. 25 (2), 438–446.
Felsenstein, J., Churchill, G.A., 1996. A Hidden Markov Model approach to variation among sites in rate of evolution. Mol. Biol. Evol. 13 (1), 93–104.
Freyhult, E.K., Bollback, J.P., Gardner, P.P., 2007. Exploring genomic dark matter: a critical assessment of the performance of homology search methods on noncoding RNA. Genome Res. 17 (1), 117–125.
Gray, M.W., Lang, B.F., Burger, G., 2004. Mitochondria of protists. Annu. Rev. Genet. 38, 477–524.
Hamada, M., Kiryu, H., Sato, K., Mituyama, T., Asai, K., 2009. Prediction of RNA secondary structure using generalized centroid estimators. Bioinformatics 25 (4), 465–473.
Hausmann, K., Hülsmann, N., 1996. Protozoology, 2nd Edition. Georg Thieme Pub.
Hazkani-Covo, E., Zeller, R.M., Martin, W., 2010. Molecular poltergeists: mitochondrial DNA copies (numts) in sequenced nuclear genomes. PLoS Genet. 6 (2), e1000834.
Hikosaka, K., Watanabe, Y., Tsuji, N., Kita, K., Kishine, H., Arisue, N., Palacpac, N.M., Kawazu, S., Sawai, H., Horii, T., Igarashi, I., Tanabe, K., 2010. Divergence of the mitochondrial genome structure in the apicomplexan parasites, Babesia and Theileria. Mol. Biol. Evol. 27 (5), 1107–1116.
Janouskovec, J., Horak, A., Obornik, M., Lukes, J., Keeling, P.J., 2010. A common red algal origin of the apicomplexan, dinoflagellate, and heterokont plastids. Proc. Natl Acad. Sci. USA 107 (24), 10949–10954.
Jeurissen, S.H., Janse, E.M., Vermeulen, A.N., Vervelde, L., 1996. *Eimeria tenella* infections in chickens: aspects of host–parasite: interaction. Vet. Immunol. Immunopathol. 54 (1–4), 231–238.
Jones, D.T., Taylor, W.R., Thornton, J.M., 1992. The rapid generation of mutation data matrices from protein sequences. Comput. Appl. Biosci. 8 (3), 275–282.
Kairo, A., Fairlamb, A.H., Gobright, E., Nene, V., 1994. A 7.1 kb linear DNA molecule of *Theileria parva* has scrambled rDNA sequences and open reading frames for mitochondrially encoded proteins. EMBO J. 13 (4), 898–905.
Kishino, H., Hasegawa, M., 1989. Evaluation of the maximum likelihood estimate of the evolutionary tree topologies from DNA sequence data, and the branching order in hominoidea. J. Mol. Evol. 29 (2), 170–179.
Kuo, C.H., Wares, J.P., Kissinger, J.C., 2008. The Apicomplexan whole-genome phylogeny: an analysis of incongruence among gene trees. Mol. Biol. Evol. 25 (12), 2689–2698.
Lau, A.O., 2009. An overview of the *Babesia*, *Plasmodium* and *Theileria* genomes: a comparative perspective. Mol. Biochem. Parasitol. 164 (1), 1–8.
Levine, N.D., 1988. Progress in taxonomy of the Apicomplexan protozoa. J. Protozool. 35 (4), 518–520.
Mogi, T., Kita, K., 2010. Diversity in mitochondrial metabolic pathways in parasitic protists *Plasmodium* and *Cryptosporidium*. Parasitol. Int. 59 (3), 305–312.
Morrison, D.A., Ellis, J.T., 1997. Effects of nucleotide sequence alignment on phylogeny estimation: a case study of 18S rDNAs of apicomplexa. Mol. Biol. Evol. 14 (4), 428–441.
Nakai, Y., Edamura, K., Kanazawa, K., Shimizu, S., Hirota, Y., Ogimoto, K., 1993. Susceptibility to *Eimeria tenella* of chickens and chicken embryos of partly inbred lines possessing homozygous major histocompatibility complex haplotypes. Avian Dis. 37 (4), 1113–1116.
Nosek, J., Tomaska, L., 2003. Mitochondrial genome diversity: evolution of the molecular architecture and replication strategy. Curr. Genet. 44 (2), 73–84.
Ossorio, P.N., Sibley, L.D., Boothroyd, J.C., 1991. Mitochondrial-like DNA sequences flanked by direct and inverted repeats in the nuclear genome of *Toxoplasma gondii*. J. Mol. Biol. 222 (3), 525–536.
Palmer, J.D., Soltis, D., Soltis, P., 1992. Large size and complex structure of mitochondrial DNA in two nonflowering land plants. Curr. Genet. 21 (2), 125–129.

Perkins, S.L., 2008. Molecular systematics of the three mitochondrial protein-coding genes of malaria parasites: corroborative and new evidence for the origins of human malaria. Mitochondrial DNA 19 (6), 471–478.
Philippe, H., Snell, E.A., Bapteste, E., Lopez, P., Holland, P.W., Casane, D., 2004. Phylogenomics of eukaryotes: impact of missing data on large alignments. Mol. Biol. Evol. 21 (9), 1740–1752.
Preiser, P.R., Wilson, R.J., Moore, P.W., McCready, S., Hajibagheri, M.A., Blight, K.J., Strath, M., Williamson, D.H., 1996. Recombination associated with replication of malarial mitochondrial DNA. EMBO J. 15 (3), 684–693.
Richly, E., Leister, D., 2004. NUMTs in sequenced eukaryotic genomes. Mol. Biol. Evol. 21 (6), 1081–1084.
Shimodaira, H., 2002. An approximately unbiased test of phylogenetic tree selection. Syst. Biol. 51 (3), 492–508.
Shimodaira, H., Hasegawa, M., 1999. Multiple comparisons of log-likelihoods with applications to phylogenetic inference. Mol. Biol. Evol. 16 (8), 1114–1116.
Shirley, M.W., Ivens, A., Gruber, A., Madeira, A.M., Wan, K.L., Dear, P.H., Tomley, F.M., 2004. The *Eimeria* genome projects: a sequence of events. Trends Parasitol. 20 (5), 199–201.
Swofford, D.L., 2002. PAUP*. Phylogenetic analysis using parsimony (and other methods). Sinauer Associates, Sunderland, MA.
Thompson, J.D., Higgins, D.G., Gibson, T.J., 1994. CLUSTAL W: improving the sensitivity of progressive multiple sequence alignment through sequence weighting, position-specific gap penalties and weight matrix choice. Nucleic Acids Res. 22 (22), 4673–4680.
Ward, B.L., Anderson, R.S., Bendich, A.J., 1981. The mitochondrial genome is large and variable in a family of plants (cucurbitaceae). Cell 25 (3), 793–803.
Yang, Z., 2007. PAML 4: phylogenetic analysis by maximum likelihood. Mol. Biol. Evol. 24 (8), 1586–1591.

MALARIA JOURNAL

RESEARCH Open Access

Geographical origin of *Plasmodium vivax* in the Republic of Korea: haplotype network analysis based on the parasite's mitochondrial genome

Moritoshi Iwagami[†1], Seung-Young Hwang[†2], Megumi Fukumoto[1,3], Toshiyuki Hayakawa[4], Kazuyuki Tanabe[4], So-Hee Kim[5], Weon-Gyu Kho[*2,5] and Shigeyuki Kano[*1,3]

Abstract

Background: The Republic of Korea (South Korea) is one of the countries where vivax malaria had been successfully eradicated by the late 1970s. However, re-emergence of vivax malaria in South Korea was reported in 1993. Several epidemiological studies and some genetic studies using antigenic molecules of *Plasmodium vivax* in the country have been reported, but the evolutionary history of *P. vivax* has not been fully understood. In this study, the origin of the South Korean *P. vivax* population was estimated by molecular phylogeographic analysis.

Methods: A haplotype network analysis based on *P. vivax* mitochondrial (mt) DNA sequences was conducted on 11 *P. vivax* isolates from South Korea and another 282 *P. vivax* isolates collected worldwide.

Results: The network analysis of *P. vivax* mtDNA sequences showed that the coexistence of two different groups (A and B) in South Korea. Groups A and B were identical or close to two different populations in southern China.

Conclusions: Although the direct introduction of the two *P. vivax* populations in South Korea were thought to have been from North Korea, the results of this analysis suggest the genealogical origin to be the two different populations in southern China.

Background

Malaria is distributed not only in tropical and subtropical areas but also in some temperate areas of the world. *Plasmodium falciparum*, which is distributed in tropical and subtropical areas, accounts for 90% of malaria cases. Like *P. falciparum*, *Plasmodium vivax* is distributed in tropical and subtropical areas, but its range extends to some temperate areas. In Asian and South American countries, the proportion of *P. falciparum* cases is gradually decreasing due to global malaria controls programmes, such as The Roll Back Malaria Partnership and The Global Fund. On the other hand, the proportion of *P. vivax* cases is gradually increasing [1]. Therefore, *P. vivax* should be given greater attention than it has received.

The Republic of Korea (South Korea) is one of the countries where vivax malaria had been successfully eradicated by the late 1970s. This was due to an effective national eradication programme conducted by the National Malaria Eradication Service under the operation of the South Korean government with the support of the WHO [2-4]. However, in 1993, the first case of indigenous vivax malaria after the eradication program was reported from the border area between North and South Korea in the western Demilitarized Zone (DMZ) [5]. The number of cases steadily increased until 2000 (4,142 cases), at which point they began to gradually decrease until 2004 (864 cases). However, in 2005, 2006 and 2007, the number of reported cases increased again (1,311, 2,019 and 2,203 cases, respectively) [6]. Initially, the patients were South Korean soldiers or veterans that had served in the western DMZ. However, the numbers of vivax cases among civilians living in the area were also

* Correspondence: wgkho@inje.ac.kr, kano@ri.imcj.go.jp
[2] Department of Parasitology, Inje University, College of Medicine, 633-165 Gaegum-dong, Busanjin-gu, Busan 614-735, Korea
[2] Department of Tropical Medicine and Malaria, Research Institute, National Center for Global Health and Medicine, 1-21-1 Toyama, Shinjuku, Tokyo 162-8665, Japan
† Contributed equally
Full list of author information is available at the end of the article

gradually increasing [6]. According to the WHO, vivax malaria in the Democratic People's Republic of Korea (North Korea), with 99,582 reported cases in 1999; 298,058 cases in 2001; and 34,485 cases in 2004, was more prevalent than in South Korea [7,8].

Plasmodium vivax in South and North Korea has unique characteristics, such as a long incubation period (maximum 13 months), seasonal transmission (only the summer season) and it is adapted to a cold climate [3,9-15]: the endemic areas are covered with snow in winter season. Although the evolutionary history of *P. vivax* from other countries has recently been addressed, thus far the history of *P. vivax* in the Korean peninsula (South and North Korea) has not been clearly understood [16-18]. Several epidemiological data showed that the re-emergence of vivax malaria in South Korea would be the introduction from North Korea through the DMZ [3-8]. However, the geographical origin of *P. vivax* population in the Korean peninsula has not been determined so far. In the present study, in order to estimate geographical origin of the *P. vivax* population in the Korean peninsula, phylogeographic analysis of the *P. vivax* population in South Korea and the other populations worldwide (including a North Korean isolate) was conducted.

Materials

Sample collection

Ten blood samples were collected from vivax malaria patients who were South Korean soldiers that served in the DMZ in 1999. One blood sample was collected from a Korean visitor to Japan in 2002. He was a veteran in the Korean army who had served in the DMZ before he visited Japan and had never been abroad before his visit [19,20]. The patient blood samples were preserved at -30°C until use. These patients were also diagnosed by microscopic examination of peripheral blood smears. This study was performed according to the ethical guidelines for epidemiological studies provided by the Ministry of Education, Culture, Sports, Science and Technology and the Ministry of Health, Labour and Welfare of Japan.

DNA extraction, Polymerase chain reaction (PCR) and DNA sequencing

The parasite DNA was extracted from the frozen whole blood samples by phenol-chloroform extraction after proteinase K digestion [21]. The whole mitochondrial (mt) DNA sequences (approx. 6 Kb) of the *P. vivax* isolates form South Korea were amplified by PCR using three pairs of primer sets:

Pv-mt1 F (5'-TTCCACTACCAAAATATAATCTCCT-3')

Pv-mt1 R (5'-CACACAAAATCACCGTTCTTATAA A-3')

Pv-mt2 F (5'-TAAATGTGCTTTAATATTATTATAG-3')

Pv-mt2 R (5'-CATAATTCCATAAGAAATTAATATT-3')

Pv-mt3 F (5'-ATCAACAATGACTTTATTTGGTTTA-3')

Pv-mt3 R (5'-ACTATAAAACATGTGATCTAATTAC-3'), which were designed form the mt sequence of the *P. vivax* af20012 isolate [GenBank: AY791517]. Three amplified DNA fragments (approx. 2 Kb) overlapped with each other. Sequencing of the PCR products was performed using an Applied Biosystems 310 Genetic Analyzer (Applied Biosystems Inc, Foster City, CA, USA), using ABI PRISM Big Dye Terminator v.3.1 (Applied Biosystems Inc, Foster City, CA, USA).

Phylogenetic analysis

MtDNA sequences (approx. 6 Kb) of the 11 *P. vivax* isolates from South Korea (present study) [DDBJ: AB550270-AB550280] and another 282 *P. vivax* isolates collected worldwide that had been deposited in the GenBank database, were used for phylogenetic analysis [16,17]. Mu *et al* [16] deposited 176 sequences [GenBank: AY791517.1-AY791692.1]. Jongwutiwes *et al* [17] deposited 106 sequences [GenBank: AY598035.1-AY598140.1]. DNA alignment of the whole mtDNA sequences of the *P. vivax* isolates was performed by the DNA Alignment version 1.3.0.1 computer software (Fluxus Technology Ltd.) [22]. A haplotype network was constructed based on polymorphic sites of the whole mtDNA sequences of the isolates using the Median-Joining method in the NETWORK version 4.5.1.6 computer software (Fluxus Technology Ltd.) [23].

Results and Discussion

A haplotype network was inferred by the 282 mtDNA sequences of *P. vivax* populations that had been collected worldwide, together with the 11 South Korean isolates (Figure 1). The network tree indicated that two groups of *P. vivax* populations coexist in South Korea (i.e. SK group A and B). The isolates of the SK group A (shown in green) were genetically identical or close to some isolates from southern China (shown in red), and those of the SK group B (shown in green) were also genetically identical or close to other isolates from southern China (shown in red). A neighbour-joining (NJ) tree (Additional File 1a, b) using the same data set for the network analysis were clearly demonstrated that the isolates of the SK group A were clustered with some isolates from southern China, and those of the SK group B were also clustered with other isolates from southern China. Therefore, the two clusters as defined in the NJ tree were named group A complex and group B complex, respectively. The boundaries of the two group complexes were shown in red boxes.

In a previous report, Kho *et al* [24] also noted the observation of two types of genotypes (i.e. SK type A and B) in some antigenic molecules of *P. vivax* in South

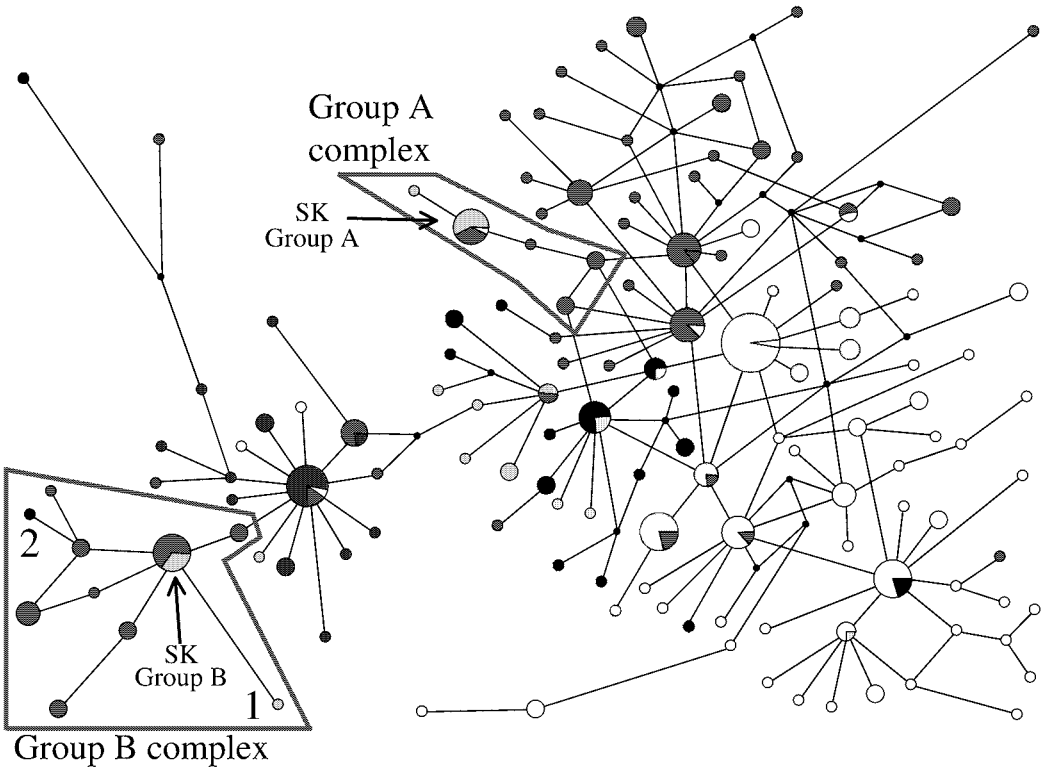

Figure 1 A haplotype network using mitochondrial genome of *P. vivax* populations. A haplotype network inferred by a median-joining method, using the 293 mitochondrial (mt) DNA sequences of *P. vivax* populations of which 11 are South Korean isolates (present study) and the other 282 are worldwide isolates that were deposited the GenBank database [16-18]. The size of the each circle represents the frequencies of the haplotype, with each color showing the geographical origin of the isolates. Green indicates isolates from South Korea (present study) and dark green indicates North Korea (the GenBank database). Red indicates isolates from southern China. Blue indicates isolates from Indonesia. Gray indicates isolates from Thailand, Vietnam and Bangladesh. White indicates isolates from Papua New Guinea, Vanuatu and the Solomon Islands. Black indicates isolates from India, Pakistan and Iran. Yellow indicates isolates from Central and South America. Light blue indicates isolates from Africa. No. 1 and 2 in the group B complex indicate isolates from South Korea (the first imported case into Japan from South Korea) and an isolate from North Korea, respectively.

Korean populations. In the present study, 91% of the isolates (10/11) were correlated to the results of the previous studies on the antigenic molecules: the South Korean isolates in the group A complex had SK type A antigenic molecules, and the South Korean isolates in the group B complex had SK type B antigenic molecules (Additional File 2).

The group A complex was genetically close to Southeast Asian populations (shown in gray); most of them were isolates from Thailand and Vietnam, or close to the South Asian population (shown in black); they were isolates from India, Pakistan and Iran (Figure 1). The group B complex was genetically close to the Indonesia population (shown in blue). Generally, old (or ancestral) populations are more genetically diverged than young populations. In this context, the Southeast Asian populations (shown in gray) and Papua New Guinean populations (shown in white) seemed old populations. Considering a possible population expansion, the group B complex seemed to have diverged from the Indonesian population (Figure 1). The genetic divergence of the extant *P. vivax* populations in the world is presumably a result of ancient hominid geographic expansion [17]. Therefore, the relationships between the group B complex and the Indonesian population suggests a possibility that the expansion of *P. vivax* population(s) from Indonesia to southern China was brought about with the migration(s) of ancient hominids. Another possible scenario is that the group B complex has directly diverged from the Southeast Asian populations because some isolates from Southeast Asia are identical to those from Indonesia. In this scenario, the expansion of *P. vivax* population(s) from Southeast Asia to Indonesia was also brought about with the migration(s) of ancient hominids. Although the present South Korean *P. vivax* populations are believed to have recently derived from North Korea via the DMZ, this study suggests that the *P. vivax* lineages in the Korean

peninsula have their genealogical ancestor in *P. vivax* populations from southern China.

One of the remarkable characteristics of *P. vivax* in Korean peninsula is its evolutionary adaptation to the cold climate. The long incubation period of Korean *P. vivax* is the key to the adaptation, because the parasites in the liver cells of the human host appears in the blood streams from the liver cells mainly between June and September (around the summer season) when mosquitoes are highly prevalent, but the parasites remain in the liver cells in the other colder seasons when mosquitoes are not present [3,9,15]. In this phenomenon, it seems as if the parasites are waiting for the mosquitoes within the host liver cells by regulating the duration of the incubation period.

Several workers reported that there seem to be two types of *P. vivax* strains (or populations) in the Korean peninsula: one with a short incubation period and the other with a long incubation period. The incubation period of the former type of North Korean strain is 14 days to 1 month, and the incubation period of the latter type of strain is 8 months to 13 months, as determined by experimental infection to humans through bites of the infected mosquitoes [25]. The proportion of strains (or populations) showing the short incubation period was 26.0%, whereas the proportion of strains (or populations) showing the long incubation period was 74.0% [25]. One mtDNA sequence of a North Korean isolate deposited in the GenBank database was included in the present study. The North Korean isolate was shown as No. 2 (shown in dark green) in the group B complex in the haplotype network in Figure 1. The information of the incubation period of the North Korean isolate was not obtained.

One isolate from the imported patient in Japan [19,20] with a long incubation period (at least eight months) was also grouped in the group B complex shown as No. 1 in the haplotype network (Figure 1). The information on the duration of the incubation period of the other 10 South Korean isolates used in this study has not been obtained thus far, but the branching patterns in the network tree appear to be related to the phenotypic characteristics of the parasites within the host.

Further study is needed to demonstrate whether the two groups of South Korean isolates (groups A and B) correlate with some clinical or epidemiological differences in the endemic areas. Haplotype network analysis using the mtDNA sequences of *P. vivax* is a useful tool for estimating the geographical origin of isolates as well as for the prediction of probable phenotypes.

Conclusion

The direct introduction of the present *P. vivax* populations to South Korea is thought to be from North Korea via the DMZ, but the true origin of the *P. vivax* populations in the Korean peninsula is now suggested to be from the two different *P. vivax* populations in southern China.

Additional material

Additional file 1 A neighbour-joining (NJ) tree inferred by mitochondrial DNA sequences of *P. vivax*. The NJ tree was constructed by MEGA version 3.1 (Kumar S, Tamura K, Nei M: MEGA3: Integrated Software for Molecular Evolutionary Analysis and Sequence Alignment. *Bioinformatics* 2004, **5**:150-163) using Kimura's 2-parameter model for calculating genetic distance. Additional File 1a continued to Additional File 1b. The isolate (AY598125 Vietnam) with Asterisk (*) at the bottom of the Additional File 1a is identical to the isolate with Asterisk at the top of the Additional File 1b. The eleven South Korean isolates (present study) were clustered into either Group A complex or Group B complex in the Additional File 1b.

Additional file 2 Genotype of antigenic molecules and mitochondria of the eleven South Korean *P. vivax* isolates. PvCSP: *P. vivax* circumsporozoite protein, PvDBP: *P. vivax* Duffy binding protein, PvMSP-1: *P. vivax* merozoite surface protein-1, Conditions of PCR and DNA sequencing for antigenic molecules have been previously reported elsewhere [24]. *Genotype of the antigenic molecules of the isolate South Korea B1 was not consistent with that of the mitochondorial genome.

Competing interests

The authors declare that they have no competing interests.

Authors' contributions

MI and SYH carried out the molecular genetic studies, performed the phylogenetic analysis and drafted the manuscript. MF and SHK helped the molecular genetic studies and helped with the writing of the manuscript. TH and KT helped the phylogenetic analysis and helped with the writing of the manuscript. WGK collected the patients' blood samples, participated in the design of the study, acquisition of funding, coordination and writing of the manuscript. SK participated in the design of the study, acquisition of funding, coordination and writing of the manuscript. All authors read and approved the final manuscript.

Acknowledgements

The authors wish to thank Dr. Pannapa Susomboon, Research Institute, International Medical Center of Japan, for her technical assistance in this study. This work was supported by a Grant-in-Aid for Scientific Research (B) (19406013) from the Ministry of Education, Culture, Sports, Science, and Technology of Japan.

Author Details

[1]Department of Tropical Medicine and Malaria, Research Institute, National Center for Global Health and Medicine, 1-21-1 Toyama, Shinjuku, Tokyo 162-8665, Japan, [2]Department of Parasitology, Inje University, College of Medicine, 633-165 Gaegum-dong, Busanjin-gu, Busan 614-735, Korea, [3]Graduate School of Comprehensive Human Sciences, University of Tsukuba, 1-1-1 Tennodai, Tsukuba, Ibaraki 305-8577, Japan, [4]Laboratory of Malariology, Research Institute for Microbial Diseases, Osaka University, Suita, Osaka 565-0871, Japan and [5]Department of Malariology, Paik Institute of Clinical Research, Inje University, College of Medicine, 633-165 Gaegum-dong, Busanjin-gu, Busan 614-735, Korea

Received: 30 March 2010 Accepted: 25 June 2010
Published: 25 June 2010

References

1. World Health Organization (WHO): **World Malaria Report.** Geneva: WHO; 2008.
2. Chai JY: **Re-emerging *Plasmodium vivax* malaria in the Republic of Korea.** *Korean J Parasitol* 1999, **37**:129-143.
3. Ree HI: **Unstable vivax malaria in Korea.** *Korean J Parasitol* 2000, **38**:119-138.
4. Shin EH, Guk SM, Kim HJ, Lee SH, Chai JY: **Trends in parasitic diseases in the Republic of Korea.** *Trends Parasitol* 2008, **24**:143-150.

5. Chai IH, Lim GI, Yoon SN, Oh WI, Kim SJ, Chai JY: **Occurrence of tertian malaria in a male patient who has never been abroad.** *Korean J Parasitol* 1994, **32**:195-200. (in Korean, English abstract available)
6. Park JW, Jun G, Yeom JS: ***Plasmodium vivax* malaria: status in the Republic of Korea following reemergence.** *Korean J Parasitol* 2009, **47(Suppl)**:S39-50.
7. Han ET, Lee DH, Park KD, Seok WS, Kim YS, Tsuboi T, Shin EH, Chai JY: **Reemerging vivax malaria: changing patterns of annual incidence and control programs in the Republic of Korea.** *Korean J Parasitol* 2006, **44**:285-294.
8. Choi YK, Choi KM, Park MH, Lee EG, Kim YJ, Lee BC, Cho SH, Rhie HG, Lee HS, Yu JR, Lee JS, Kim TS, Kim JY: **Rapid dissemination of newly introduced *Plasmodium vivax* genotypes in South Korea.** *Am J Trop Med Hyg* 2010, **82**:426-432.
9. Hasegawa Y: **Malaria in Korea.** *J Chosun Med Soc* 1913, **4**:53-69. (in Japanese. No English abstract available)
10. Eddleman EE, Hale WH, Snowden WM: **Vivax malaria with long incubation period, Report of seven cases.** *US Armed Forces Med J* 1951, **2**:1693-1698.
11. Hall WH, Loomis GW: **Vivax malaria in veterans of the Korean war. A preliminary report of 25 cases.** *New Engl J Med* 1952, **246**:90-93.
12. Brunetti R: **Outbreak malaria with prolonged incubation period in California, a nonendemic area.** *Science* 1954, **119**:74-75.
13. Brunetti R, Fritz RF, Hollister AC: **An outbreak of malaria in California, 1952-1953.** *Am J Trop Med Hyg* 1954, **3**:779-788.
14. Tiburskaja NA, Sergiev PG, Vrublevskaja OS: **Dates of onset of relapses and the duration of infection in induced tertian malaria with short and long incubation periods.** *Bull World Health Organ* 1968, **38**:447-457.
15. NMES: **Malaria pre-eradication programme in Korea.** *Progress report, 1961-1965 Ministry of Health and Social Affairs of Korea* 1966:75. (in Korean)
16. Mu J, Joy DA, Duan J, Huang Y, Carlton J, Walker J, Barnwell J, Beerli P, Charleston MA, Pybus OG, Su XZ: **Host switch leads to emergence of *Plasmodium vivax* malaria in humans.** *Mol Biol Evol* 2005, **22**:1686-1693.
17. Jongwutiwes S, Putaporntip C, Iwasaki T, Ferreira MU, Kanbara H, Hughes AL: **Mitochondrial genome sequences support ancient population expansion in *Plasmodium vivax*.** *Mol Biol Evol* 2005, **22**:1733-1739.
18. Cornejo OE, Escalante AA: **The origin and age of *Plasmodium vivax*.** *Trends Parasitol* 2006, **22**:558-63.
19. Itoda I, Kaneko Y, Yasunami T, Kikuchi K, Yamaura H, Totsuka K: **A case of imported *Plasmodium vivax* malaria from the demilitarized zone in South Korea.** *Kansenshogaku Zasshi* 2003, **77**:42-44. (in Japanese. No English abstract available)
20. Iwagami M, Itoda I, Hwang SY, Kho WG, Kano S: ***Plasmodium vivax* PCR genotyping of the first malaria case imported from South Korea into Japan.** *J Infect Chemother* 2009, **15**:27-33.
21. Sambrook J, Russell DW: **Molecular Cloning: A Laboratory Manual.** 3rd edition. New York: Cold Harbor Laboratory Press; 2001.
22. **DNA Alignment version 1.3.0.1** 2008 [http://www.fluxus-engineering.com/align.htm]. Fluxus Technology Ltd
23. **Network version 4.5.1.6** 2009 [http://www.fluxus-engineering.com/netwinfo.htm]. Fluxus Technology Ltd
24. Hwang SY, Kim SH, Kho WG: **Genetic characteristics of polymorphic antigenic markers among Korean isolates of *Plasmodium vivax*.** *Korean J Parasitol* 2009, **47(Suppl)**:S51-58.
25. Tiburskaja NA, Vrublevskaja OS: **The course of infection caused by the North Korean strain of *Plasmodium vivax*.** *WHO/MAL/77* 1977, **895**:1-19.

doi: 10.1186/1475-2875-9-184
Cite this article as: Iwagami *et al.*, Geographical origin of *Plasmodium vivax* in the Republic of Korea: haplotype network analysis based on the parasite's mitochondrial genome *Malaria Journal* 2010, **9**:184

Acta Tropica 114 (2010) 171–176

Contents lists available at ScienceDirect

Acta Tropica

journal homepage: www.elsevier.com/locate/actatropica

The wheat germ cell-free protein synthesis system: A key tool for novel malaria vaccine candidate discovery

Takafumi Tsuboi[a,b,*], Satoru Takeo[a], Thangavelu U. Arumugam[a], Hitoshi Otsuki[c], Motomi Torii[c]

[a] Cell-free Science and Technology Research Center, Ehime University, Matsuyama, Ehime 790-8577, Japan
[b] Venture Business Laboratory, Ehime University, Matsuyama, Ehime 790-8577, Japan
[c] Department of Molecular Parasitology, Ehime University Graduate School of Medicine, Toon, Ehime 791-0295, Japan

ARTICLE INFO

Article history:
Received 24 August 2009
Received in revised form 13 October 2009
Accepted 28 October 2009
Available online 11 November 2009

Keywords:
Malaria
Plasmodium falciparum
Post-genome
Vaccine candidate discovery
Wheat germ cell-free protein synthesis

ABSTRACT

Malaria kills more than a million people a year, causes malady in about three hundred million people and poses risk to approximately 40% of the world's population living in malarious countries. This disease is re-emerging mainly due to the development of drug-resistant parasites and insecticide-resistant mosquitoes. Therefore, we are now forced to resort to remedy through vaccination. Until now, not even a single licensed malaria vaccine has been developed despite intensive efforts. Even the efficacy of RTS,S, the most advanced and promising vaccine candidate in the pipeline of malaria vaccine development, was only around 50% based on a number of clinical trials. These facts urge malaria researchers to urgently enrich this pipeline, as much as possible, with potential vaccine candidates. With the availability of malaria genome database, the enrichment of this pipeline is possible if we could now employ an efficient protein expression technology to decode the malaria genomic data, without any codon optimization, into quality recombinant proteins. Then, these synthesized recombinant proteins can be characterized and screened for discovering novel potential vaccine targets. The wheat germ cell-free protein synthesis system will be a promising tool to this end. This review highlights the recent successes in synthesizing quality malaria proteins using this tool.

1. Introduction

Malaria kills more than a million people a year, causes malady in about three hundred million people and poses risk to around 3.3 billion people (WHO, 2008). Despite the parasite's complex life cycle, high level of antigenic diversity and mechanism of immune evasion, naturally acquired immunity to malaria does develop after repeated exposure over a period of several years and this immunity confers protection, against symptomatic disease, high-density parasitemia and death (Doolan et al., 2009; Genton, 2008; Gupta et al., 1999; Marsh and Kinyanjui, 2006), through protective antibodies (Cohen et al., 1961; McGregor, 1964). In addition to the naturally acquired immunities, sterile, long-lasting protective immunity has been convincingly proved in many studies, such as vaccination with radiation-attenuated sporozoites (Clyde, 1975; Hoffman et al., 2002; Nussenzweig et al., 1967), and inoculation of infective sporozoites to human volunteers under a prophylactic regimen of chloroquine (Roestenberg et al., 2009). These facts strongly support the reasoning of incorporating malaria vaccines as one of the components of malaria control measures.

2. Malaria vaccine development

The efficacy of malaria control through current interventions that employs drugs and insecticides may not be sustained too long since they rely on too few compounds (Genton, 2008). In fact, the disease is re-emerging mainly due to the emergence of drug-resistant parasites (Greenwood and Mutabingwa, 2002). Very recently, parasites have developed resistance even to the hitherto-promising artemisinin (Dondorp et al., 2009). Therefore, we have to develop and employ malaria vaccines as one of the essential components towards the malaria eradication (Greenwood, 2009). The fact that, in spite of intensive efforts, not even a single licensed malaria vaccine has been developed, urges malaria research community to employ efficient post-genomic approaches (Richie and Saul, 2002). Malaria vaccines are generally divided into three groups based on stages of the parasite life cycle targeted by the vaccine. They are pre-erythrocytic vaccines, asexual blood-stage vaccines, and transmission-blocking vaccines. Fig. 1 gives a quick description about vaccine categories, the stages they target, along with malaria vaccine candidates in clinical trials. Detailed descriptions about

* Corresponding author at: Ehime University, Cell-Free Science and Technology Research Center, 3 Bunkyo-cho, Matsuyama, Ehime 790-8577, Japan.
Tel.: +81 89 927 8277; fax: +81 89 927 9941.
E-mail address: tsuboi@ccr.ehime-u.ac.jp (T. Tsuboi).

0001-706X/$ – see front matter © 2009 Elsevier B.V. All rights reserved.
doi:10.1016/j.actatropica.2009.10.024

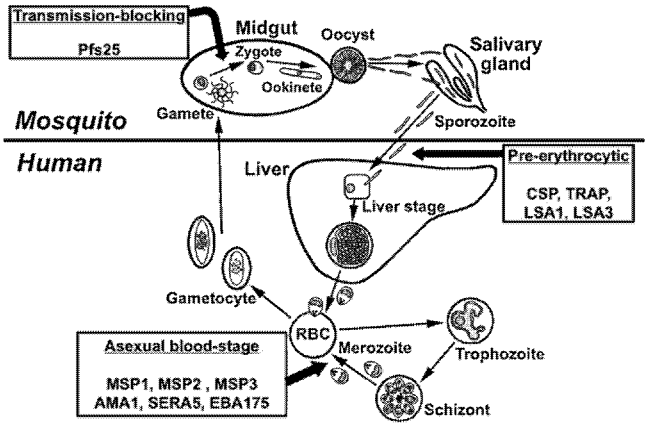

Fig. 1. Malaria vaccines in clinical trials mapped on the parasite life cycle. Malaria vaccines are categorized into three groups based on the target stages of the parasite life cycle. They are pre-erythrocytic, asexual blood-stage, and transmission-blocking vaccines. RBC: red blood cell, CSP: circumsporozoite protein, TRAP: thrombospondin-related adhesion protein, LSA1: liver stage antigen 1, LSA3: liver stage antigen 3, MSP1: merozoite surface protein 1, MSP2: merozoite surface protein 2, MSP3: merozoite surface protein 3, AMA1: Apical membrane antigen 1, SERA5: Serine repeat antigen 5, and EBA175: erythrocyte binding antigen 175. Detailed descriptions about these vaccines were given in other published reviews (Genton, 2008; Richards and Beeson, 2009).

these vaccines are given in other published reviews (Genton, 2008; Richards and Beeson, 2009).

2.1. Pre-erythrocytic vaccines

Pre-erythrocytic vaccines have been designed to prevent entry of sporozoites into hepatocytes and the development of liver stage parasites (Greenwood et al., 2008; Waters, 2006).

2.2. Asexual blood-stage vaccines

Asexual blood-stage vaccines are designed to reduce merozoite invasion, multiplication and growth in order to protect against clinical symptoms and particularly severe disease. It is widely understood that this vaccine induces antibodies that may have roles in prevention of merozoite invasion, clearance of infected erythrocytes, prevention of adhesion and sequestration of parasitized erythrocytes in the vasculature. It is also possible that, in addition to preventing clinical illness, an effective blood-stage vaccine may also contribute to malaria eradication by reducing the efficiency of the transmission of parasites from human host to mosquito by interrupting the blood-stage life cycle in the human body (Duffy, 2007; Genton, 2008; Moll et al., 2007; Richards and Beeson, 2009).

2.3. Transmission-blocking vaccines

Transmission-blocking vaccines are aimed at interrupting the parasite life cycle in the mosquito blood meal. These vaccines elicit antibodies against antigens that are expressed by the sexual stages of the parasite and, thus, stop their subsequent development in the mosquito midgut (Carter, 2001; Tsuboi et al., 2003). These transmission-blocking vaccines, if used in combination with pre-erythrocytic or asexual blood-stage vaccines, might play a key role in finally breaking the transmission of parasites, leading to eradication of the diseases (Targett and Greenwood, 2008).

It is an accepted view that an effective malaria vaccine need to target several stages of parasite and several components of the different stages of parasite (Lasonder et al., 2002) and it must induce protective immune responses equivalent to, or better than, those provided by naturally acquired immunity or immunization with attenuated whole parasite (Gardner et al., 2002). In order to accelerate the discovery of such vaccine candidates, it is indispensable now to establish and exploit two things. One is the optimal recombinant protein synthesis system for synthesizing malaria proteins on a whole-proteome scale and other is the efficient post-genomic high-throughput approaches for sifting potential vaccine candidates out from this whole malaria proteome.

3. Post-genome approaches for novel malaria vaccine candidate discovery research

As described in Fig. 1, decades of research in the pre-genomic era have identified only a handful of vaccine candidates. With the recent completion of the genome projects of human malaria parasites, *Plasmodium falciparum* (Gardner et al., 2002), *P. vivax* (Carlton et al., 2008), primate malaria parasite, *P. knowlesi* (Pain et al., 2008), and rodent malaria parasite, *P. yoelii* (Carlton et al., 2002), we are now in the post-genome era. However, to tangibly reap the benefits from these genomic data, it is indispensable to thoroughly analyze these data using at least two post-genomic high-throughput approaches. One is the functional approach (otherwise called as reverse vaccinology (Flower, 2008)), and the other is the immunoscreening approach.

3.1. Functional approach

In the functional approach, initially putative vaccine candidates are selected from the genome database based on either patent or latent functional criteria. Then these putative candidates are expressed *in vitro* using effective and efficient protein synthesis system to obtain quality proteins for further downstream vaccine candidate assessment studies (Hall et al., 2005). For example, the genes that are essential for the parasite's survival revealed by gene knockout studies (Cowman and Crabb, 2006), or the genes with signatures of strong immune selective pressure revealed by polymorphisms and diversity studies (Mu et al., 2007), or the genes involved in host cell invasion, or the genes whose products are localized on the cell surface or in the apical organelles of the sporozoite, merozoite, and ookinete could be putative vaccine candidates.

3.2. Immunoscreening approach

In the immunoscreening approach, initially putative vaccine candidates are selected based on their immuno-reactivity with the protective antibodies that are elicited in humans, after natural or experimental infection or after vaccination with attenuated organisms (Hoffman et al., 2002; VanBuskirk et al., 2009). Here extensive set of quality recombinant malaria proteins are synthesized, in small scale, using protein synthesis system and are screened intensively, using immunoassays such as enzyme-linked immunosorbent assay, protein microarray, with a large number of human serum samples obtained from non-immune and immune individuals (Doolan et al., 2008). Then, these immuno-reactive putative vaccine candidates that correlate with protection will be synthesized, in large scale, for further downstream vaccine research.

4. What is the optimal recombinant protein synthesis system for malaria proteins?

Whatever may be the approach employed for novel vaccine candidate discovery research, we do need to have an effective and

efficient recombinant protein synthesis system not only for the initial synthesis, characterization, and downstream assessment of putative vaccine candidates, but also for the mass production of vaccine antigens for vaccination purpose in the later stage. Therefore, the choice of the recombinant protein synthesis method is the most crucial factor. One of the main obstacles in malaria vaccine discovery research is the lack of an optimal protein expression system that can decode A/T-rich, low-complexity-region-containing (i.e., repeated stretches of amino acid sequences) malaria genes into high quality (i.e., properly folded) recombinant proteins that are amenable for malaria vaccine research (Gardner et al., 2002). These obstacles pose major limitation to express *P. falciparum* genes not only in conventional *E. coli* cell-based systems (Aguiar et al., 2004; Mehlin et al., 2006; Vedadi et al., 2007), but also in eukaryotic cell-based expression systems such as yeast, baculovirus, or Chinese hamster ovary cell (Tsuboi et al., 2008).

Since the rate of peptide growth on ribosomes is 5–10 times slower in eukaryotes than in prokaryotes, this slow rate of peptide growth in eukaryotic protein expression system contributes greatly towards correct conformational folding of multidomain proteins and their solubility (Hartl and Hayer-Hartl, 2002; Netzer and Hartl, 1997). Therefore eukaryotic proteins with multiple domains, such as malaria parasite proteins, when expressed either in *E. coli* cell-free or cell-based system, tend to fold incorrectly, and become insoluble (Netzer and Hartl, 1997). After all, the correct folding and solubility of malaria proteins are indispensable critical factors that directly affect the success in our genome-wide search for potential vaccine antigens. From the correct folding point of view, the eukaryotic-based system is greatly advantageous over *E. coli* based prokaryotic system. The eukaryotic-based systems have been widely used to synthesize eukaryotic multidomain proteins in active forms. However, they all suffer from low throughput and low productivity (Endo and Sawasaki, 2006; Goshima et al., 2008). For example, it is well known that the rabbit reticulocytes lysate system has been employed for the production of quality eukaryotic recombinant proteins. However, the yield of this system is very low, and moreover this system has post-translational modification machinery, i.e., glycosylation (Endo and Sawasaki, 2006). Therefore it is disadvantageous to express malaria genes in rabbit reticulocyte system and other eukaryotic cell-based protein expression systems that posses glycosylation machinery, for these systems can produce inappropriately glycosylated recombinant malaria proteins, resulting in incorrect immune responses (Gowda and Davidson, 1999; Kedees et al., 2002). The fact that both the wheat germ system and the malaria parasite do not have glycosylation machinery (Samuelson et al., 2005) is an additional advantage for expressing malaria proteins without any inadvertent glycosylation in wheat germ system. (Endo and Sawasaki, 2006). Among all eukaryotic protein expression systems, wheat germ cell-free translation system is the most suitable for easy handling and achieving high-throughput, high-solubility, and high-productivity in the synthesis of recombinant proteins (Endo and Sawasaki, 2006; Goshima et al., 2008).

From our experience in expressing around five hundred malaria genes using wheat germ cell-free system, we have found that the wheat germ cell-free system can surmount almost all of the above stumbling blocks in the path of post-genome malaria vaccine candidate discovery and therefore can be used for synthesizing high level of soluble malaria recombinant proteins (an important prerequisite for vaccine candidate assessment and large scale vaccine production), and accelerate malaria vaccine discovery (Tsuboi et al., 2008). Some of the successes that have been published by our collaborators and us have been described in the subsequent sections. Therefore we believe that the wheat germ system is the optimal system for synthesis of malaria proteins.

5. Synthesis of malaria proteins using prokaryotic protein synthesis system

There were several trials to achieve genome-wide expression of *P. falciparum* genes using the conventional *E. coli* based protein synthesis system. Aguiar et al. (2004) using *E. coli* cells, were able to express only 39 out of 292 malaria genes cloned in GST-fusion vector. Mehlin et al. (2006) tried to express 1000 genes encoding relatively small (<450 amino acids) malaria cytosolic proteins, in *E. coli*, for the structural analysis. In that study, only 30% of the genes were expressed and only 6.3% of the proteins were soluble, yielding 0.9–406 mg of protein per liter of culture medium. Vedadi et al. (2007) tried to express 182 malaria genes, for the structural analysis, utilizing genetically engineered *E. coli* strain supplemented with tRNAs that allows reading of high number of A/U codons in malaria mRNA. They achieved marginal improvement in protein solubility, i.e., 38 out of 182 (20.9%) proteins tested were soluble. Using an *E. coli* cell-free rapid expression system, Mu et al. attempted to express 108 polymorphic malaria genes that are considered to be under immune selection pressure to find potential vaccine candidates. Expression of proteins was verified via protein blot using antibodies to the histidine tags incorporated into the C-terminus of the expressed proteins. In their study, they found that, out of 108 genes, 65 genes (i.e., 60.2%) could be expressed (Mu et al., 2007). Recently, Doolan et al. (2008) reported the construction of the *P. falciparum* protein microarrays using *E. coli* cell-free protein synthesis system for high-throughput immunoscreening for vaccine candidate discovery. In their study, they obtained >90% efficiency in their effort to express 250 *P. falciparum* genes using *E. coli* cell-free *in vitro* transcription and translation reactions. And they have attributed their high success rate in this system, at least in part, to the fact that the system is supplemented with rare transfer RNAs to help translate A/T-rich genes. However, in the *E. coli* cell-free system, the rate of protein expression reported by Mu et al. (2007) was lower than the rate reported by Doolan et al. (2008). The above experiments proved that *E. coli* cell-free system is better in productivity and throughput than *E. coli* cell-based system, however, these experiments did not prove that the quality of proteins synthesized in *E. coli* cell-free system is amenable enough for vaccine candidate discovery research.

6. A cursory glance at wheat germ cell-free protein synthesis system

Recently, the wheat germ cell-free protein synthesis system was established for high-throughput synthesis of soluble recombinant proteins (Madin et al., 2000) and is now commercially available as simple protein synthesis kits (CFS Co., Ltd., Matsuyama, Japan). Basically there are two protocols established for practical use in this system (Endo and Sawasaki, 2006). The first one is for small scale, high-throughput or parallel synthesis of proteins. It can be applied for initial testing of gene expression and solubility of proteins. This will facilitate genome-wide biochemical annotation of gene products (Sawasaki et al., 2002). The second protocol is for the large scale production of interested proteins (Endo and Sawasaki, 2006; Kamura et al., 2005; Sawasaki and Endo, 2008). This protocol can produce hundreds of micrograms of protein, and also, offer scope for scale up (Sawasaki and Endo, 2008). These two protocols have already been acknowledged as advantageous for producing high quality eukaryotic proteins for structural and functional genomics studies (Goshima et al., 2008; Vinarov et al., 2004). Taken together, this system is versatile for both small and large scale synthesis of quality eukaryotic proteins.

Table 1
The recent successes in the synthesis of biologically active malaria proteins using wheat germ cell-free expression system[a].

Gene ID[b]	Gene name	Species[c]	Results[d]	References
Enzymes				
PFD0830w	Dihydrofolate reductase–thymidylate synthase	*Pf*	Enzyme activities (DHFR, and TS)	Mudeppa et al. (2007)
PVX_087680	Chitinase	*Pv*	Enzyme activities	Takeo et al. (2009)
PF10_0363	Pyruvate kinase 2	*Pf*	Ab (WB, IFA)	Maeda et al. (2009)
Sporozoite antigens				
PFC0210c	Circumsporozoite protein	*Pf*	Ab (WB, IFA)	Tsuboi et al. (2008)
PFD0215c	P52	*Pf*	Ab (IFA)	VanBuskirk et al. (2009)
PKH_121770	thrombospondin-related adhesion protein	*Pk*	T cell	Jiang et al. (2009)
Merozoite antigens				
PF11_0344	Apical membrane antigen 1	*Pf*	Ab (WB, IFA)	Tsuboi et al. (2008)
PF14_0495	Rhoptry neck protein 2	*Pf*	Ab (IP, WB, IFA, IEM)	Cao et al. (2009)
PY04764	Erythrocyte binding ligand	*Py*	Ab (WB, IFA, IEM)	Otsuki et al. (2009)
PKH_072850	Merozoite surface protein 1	*Pk*	T cell	Jiang et al. (2009)
Ookinete antigen				
PF10_0303	Pfs25	*Pf*	Ab (WB, IFA, TBA)	Tsuboi et al. (2008)

[a] The individual articles may be consulted for further details.
[b] Detailed information is available at the PlasmoDB website. (http://plasmodb.org/plasmo/).
[c] Plasmodium species, Pf: *Plasmodium falciparum*, Pv: *P. vivax*, Py: *P. yoelii*, and Pk: *P. knowlesi*.
[d] Results obtained by the contribution of recombinant proteins synthesized by the wheat germ cell-free system. Ab, antibody; IP, immunoprecipitation; WB, Western blot, IFA, immunofluorescence microscopy, IEM, immunoelectron microscopy. T cell, *in vitro* T cell studies; TBA, transmission-blocking activity.

7. Synthesis of malaria proteins using eukaryotic wheat germ protein synthesis system

Initially, in order to test the suitability of wheat germ cell-free system for high-throughput synthesis of malaria recombinant proteins, we attempted to express 124 genes encoding asexual blood-stage parasite proteins, selected from malaria genome database, PlasmoDB (http://plasmodb.org/plasmo/). Out of 124 genes, 93 of them (i.e., around 75%) yielded soluble protein products. However, the magnitude/extent of solubility among these 93 soluble proteins is on an average 65% and ranges from 26% to 100% (Tsuboi et al., 2008). The average yield of full size recombinant proteins was 1.9 μg per 150 μl of reaction mixture and this amount is sufficient for high-throughput screening of antigens that correlates with protection using hyper-immune serum.

The experimental results published by our collaborators and us (Table 1) confirm that wheat germ cell-free protein synthesis system is very suitable for decoding A/T-rich malaria genes without any codon optimization into biologically active malaria proteins. Firstly, the system was able to synthesize active malaria enzymes that are recalcitrant to expression in other systems, such as *P. falciparum* dihydrofolate reductase–thymidylate synthase (Mudeppa et al., 2007), a chitinase of *P. vivax* (Takeo et al., 2009) and pyruvate kinase type-II isozyme of *P. falciparum* (Maeda et al., 2009). Secondly, the system was able to produce a sufficient amount of good quality malaria proteins, such as repeat-rich circumsporozoite protein (Tsuboi et al., 2008), cysteine-rich P52 (VanBuskirk et al., 2009), thrombospondin-related adhesion protein (Jiang et al., 2009), rhoptry neck protein 2 (Cao et al., 2009), erythrocyte binding ligand (Otsuki et al., 2009), merozoite surface protein 1 (Jiang et al., 2009), apical membrane antigen 1 and highly cysteine-rich Pfs25 (a promising transmission-blocking vaccine candidate) (Tsuboi et al., 2008).

Recently, we attempted to express 567 of *P. falciparum* cDNA clones belonging to sporozoite, merozoite, and gametocyte stages in a high-throughput format by the wheat germ cell-free system. Out of 567 genes, 478 of them (i.e., around 84%) yielded soluble protein products (unpublished). Our biochemical, immunocytochemical, and biological analyses have revealed that the recombinant malaria proteins synthesized by this system are of high quality and therefore amenable for the assessment and discovery of potential vaccine targets (Tsuboi et al., 2008). Thus, we indeed believe that the wheat germ cell-free protein synthesis system is a key tool for decoding malaria genome for malaria proteome and vaccine research.

8. Conclusion

From a malaria vaccine perspective, wheat germ cell-free system is the most suitable system to date for easily achieving high-throughput, high-solubility, and high-productivity in the whole-proteome-scale synthesis of malaria proteins and construction of microarrays of malaria proteins that will accelerate post-genomic novel malaria vaccine candidate discovery.

Acknowledgments

We thank Kana Kato, Aya Tamai, and Mai Tasaka for their technical assistance. This work was supported in part by Grants-in-Aid for Scientific Research 19406009 (TT), Scientific Research on Priority Areas 21022034 (TT) from the Ministry of Education, Culture, Sports, Science, and Technology, Japan; and, in part, by a Grant-in-Aid from the Ministry of Health, Labour, and Welfare (H21-Chikyukibo-ippan-005) (TT), Japan.

References

Aguiar, J.C., LaBaer, J., Blair, P.L., Shamailova, V.Y., Koundinya, M., Russell, J.A., Huang, F., Mar, W., Anthony, R.M., Witney, A., Caruana, S.R., Brizuela, L., Sacci Jr., J.B., Hoffman, S.L., Carucci, D.J., 2004. High-throughput generation of *P. falciparum* functional molecules by recombinational cloning. Genome Res. 14, 2076–2082.

Cao, J., Kaneko, O., Thongkukiatkul, A., Tachibana, M., Otsuki, H., Gao, Q., Tsuboi, T., Torii, M., 2009. Rhoptry neck protein RON2 forms a complex with microneme protein AMA1 in *Plasmodium falciparum* merozoites. Parasitol. Int. 58, 29–35.

Carlton, J.M., Angiuoli, S.V., Suh, B.B., Kooij, T.W., Pertea, M., Silva, J.C., Ermolaeva, M.D., Allen, J.E., Selengut, J.D., Koo, H.L., Peterson, J.D., Pop, M., Kosack, D.S., Shumway, M.F., Bidwell, S.L., Shallom, S.J., van Aken, S.E., Riedmuller, S.B., Feldblyum, T.V., Cho, J.K., Quackenbush, J., Sedegah, M., Shoaibi, A., Cummings, L.M., Florens, L., Yates, J.R., Raine, J.D., Sinden, R.E., Harris, M.A., Cunningham, D.A., Preiser, P.R., Bergman, L.W., Vaidya, A.B., van Lin, L.H., Janse, C.J., Waters, A.P., Smith, H.O., White, O.R., Salzberg, S.L., Venter, J.C., Fraser, C.M., Hoffman, S.L., Gardner, M.J., Carucci, D.J., 2002. Genome sequence and comparative analysis of the model rodent malaria parasite *Plasmodium yoelii yoelii*. Nature 419, 512–519.

Carlton, J.M., Adams, J.H., Silva, J.C., Bidwell, S.L., Lorenzi, H., Caler, E., Crabtree, J., Angiuoli, S.V., Merino, E.F., Amedeo, P., Cheng, Q., Coulson, R.M., Crabb, B.S., Del Portillo, H.A., Essien, K., Feldblyum, T.V., Fernandez-Becerra, C., Gilson, P.R., Gueye, A.H., Guo, X., Kang'a, S., Kooij, T.W., Korsinczky, M., Meyer, E.V., Nene, V., Paulsen, I., White, O., Ralph, S.A., Ren, Q., Sargeant, T.J., Salzberg, S.L., Stoeckert, C.J., Sullivan, S.A., Yamamoto, M.M., Hoffman, S.L., Wortman, J.R.,

Gardner, M.J., Galinski, M.R., Barnwell, J.W., Fraser-Liggett, C.M., 2008. Comparative genomics of the neglected human malaria parasite *Plasmodium vivax*. Nature 455, 757–763.
Carter, R., 2001. Transmission blocking malaria vaccines. Vaccine 19, 2309–2314.
Clyde, D.F., 1975. Immunization of man against falciparum and vivax malaria by use of attenuated sporozoites. Am. J. Trop. Med. Hyg. 24, 397–401.
Cohen, S., Mc, G.I., Carrington, S., 1961. Gamma-globulin and acquired immunity to human malaria. Nature 192, 733–737.
Cowman, A.F., Crabb, B.S., 2006. Invasion of red blood cells by malaria parasites. Cell 124, 755–766.
Dondorp, A.M., Nosten, F., Yi, P., Das, D., Phyo, A.P., Tarning, J., Lwin, K.M., Ariey, F., Hanpithakpong, W., Lee, S.J., Ringwald, P., Silamut, K., Imwong, M., Chotivanich, K., Lim, P., Herdman, T., An, S.S., Yeung, S., Singhasivanon, P., Day, N.P., Lindegardh, N., Socheat, D., White, N.J., 2009. Artemisinin resistance in *Plasmodium falciparum* malaria. N. Engl. J. Med. 361, 455–467.
Doolan, D.L., Mu, Y., Unal, B., Sundaresh, S., Hirst, S., Valdez, C., Randall, A., Molina, D., Liang, X., Freilich, D.A., Oloo, J.A., Blair, P.L., Aguiar, J.C., Baldi, P., Davies, D.H., Felgner, P.L., 2008. Profiling humoral immune responses to *P. falciparum* infection with protein microarrays. Proteomics 8, 4680–4694.
Doolan, D.L., Dobano, C., Baird, J.K., 2009. Acquired immunity to malaria. Clin. Microbiol. Rev. 22, 13–36.
Duffy, P.E., 2007. *Plasmodium* in the placenta: parasites, parity, protection, prevention and possibly preeclampsia. Parasitology 134, 1877–1881.
Endo, Y., Sawasaki, T., 2006. Cell-free expression systems for eukaryotic protein production. Curr. Opin. Biotechnol. 17, 373–380.
Flower, D., 2008. Bioinformatics for Vaccinology. John Wiley & Sons, Chichester, West Sussex, UK.
Gardner, M.J., Hall, N., Fung, E., White, O., Berriman, M., Hyman, R.W., Carlton, J.M., Pain, A., Nelson, K.E., Bowman, S., Paulsen, I.T., James, K., Eisen, J.A., Rutherford, K., Salzberg, S.L., Craig, A., Kyes, S., Chan, M.S., Nene, V., Shallom, S.J., Suh, B., Peterson, J., Angiuoli, S., Pertea, M., Allen, J., Selengut, J., Haft, D., Mather, M.W., Vaidya, A.B., Martin, D.M., Fairlamb, A.H., Fraunholz, M.J., Roos, D.S., Ralph, S.A., McFadden, G.I., Cummings, L.M., Subramanian, G.M., Mungall, C., Venter, J.C., Carucci, D.J., Hoffman, S.L., Newbold, C., Davis, R.W., Fraser, C.M., Barrell, B., 2002. Genome sequence of the human malaria parasite *Plasmodium falciparum*. Nature 419, 498–511.
Genton, B., 2008. Malaria vaccines: a toy for travelers or a tool for eradication? Expert Rev. Vaccines 7, 597–611.
Goshima, N., Kawamura, Y., Fukumoto, A., Miura, A., Honma, R., Satoh, R., Wakamatsu, A., Yamamoto, J., Kimura, K., Nishikawa, T., Andoh, T., Iida, Y., Ishikawa, K., Ito, E., Kagawa, N., Kaminaga, C., Kanehori, K., Kawakami, B., Kenmochi, K., Kimura, R., Kobayashi, M., Kuroita, T., Kuwayama, H., Maruyama, Y., Matsuo, K., Minami, K., Mitsubori, M., Mori, M., Morishita, R., Murase, A., Nishikawa, A., Nishikawa, S., Okamoto, T., Sakagami, N., Sakamoto, Y., Sasaki, Y., Seki, T., Sono, S., Sugiyama, A., Sumiya, T., Takayama, T., Takayama, Y., Takeda, H., Togashi, T., Yahata, K., Yamada, H., Yanagisawa, Y., Endo, Y., Imamoto, F., Kisu, Y., Tanaka, S., Isogai, T., Imai, J., Watanabe, S., Nomura, N., 2008. Human protein factory for converting the transcriptome into an in vitro-expressed proteome. Nat. Methods 5, 1011–1017.
Gowda, D.C., Davidson, E.A., 1999. Protein glycosylation in the malaria parasite. Parasitol. Today 15, 147–152.
Greenwood, B., Mutabingwa, T., 2002. Malaria in 2002. Nature 415, 670–672.
Greenwood, B., 2009. Can malaria be eliminated? Trans. R. Soc. Trop. Med. Hyg. 103 (Suppl. 1), S2–S5.
Greenwood, B.M., Fidock, D.A., Kyle, D.E., Kappe, S.H., Alonso, P.L., Collins, F.H., Duffy, P.E., 2008. Malaria: progress, perils, and prospects for eradication. J. Clin. Invest. 118, 1266–1276.
Gupta, S., Snow, R.W., Donnelly, C.A., Marsh, K., Newbold, C., 1999. Immunity to non-cerebral severe malaria is acquired after one or two infections. Nat. Med. 5, 340–343.
Hall, N., Karras, M., Raine, J.D., Carlton, J.M., Kooij, T.W., Berriman, M., Florens, L., Janssen, C.S., Pain, A., Christophides, G.K., James, K., Rutherford, K., Harris, B., Harris, D., Churcher, C., Quail, M.A., Ormond, D., Doggett, J., Trueman, H.E., Mendoza, J., Bidwell, S.L., Rajandream, M.A., Carucci, D.J., Yates 3rd, J.R., Kafatos, F.C., Janse, C.J., Barrell, B., Turner, C.M., Waters, A.P., Sinden, R.E., 2005. A comprehensive survey of the *Plasmodium* life cycle by genomic, transcriptomic, and proteomic analyses. Science 307, 82–86.
Hartl, F.U., Hayer-Hartl, M., 2002. Molecular chaperones in the cytosol: from nascent chain to folded protein. Science 295, 1852–1858.
Hoffman, S.L., Goh, L.M., Luke, T.C., Schneider, I., Le, T.P., Doolan, D.L., Sacci, J., de la Vega, P., Dowler, M., Paul, C., Gordon, D.M., Stoute, J.A., Church, L.W., Sedegah, M., Heppner, D.G., Ballou, W.R., Richie, T.L., 2002. Protection of humans against malaria by immunization with radiation-attenuated *Plasmodium falciparum* sporozoites. J. Infect. Dis. 185, 1155–1164.
Jiang, G., Shi, M., Conteh, S., Richie, N., Banania, G., Geneshan, H., Valencia, A., Singh, P., Aguiar, J., Limbach, K., Kamrud, K.I., Rayner, J., Smith, J., Bruder, J.T., King, C.R., Tsuboi, T., Takeo, S., Endo, Y., Doolan, D.L., Richie, T.L., Weiss, W.R., 2009. Sterile protection against *Plasmodium knowlesi* in rhesus monkeys from a malaria vaccine: comparison of heterologous prime boost strategies. PLoS ONE 4, e6559.
Kamura, N., Sawasaki, T., Kasahara, Y., Takai, K., Endo, Y., 2005. Selection of 5′-untranslated sequences that enhance initiation of translation in a cell-free protein synthesis system from wheat embryos. Bioorg. Med. Chem. Lett. 15, 5402–5406.
Kedees, M.H., Azzouz, N., Gerold, P., Shams-Eldin, H., Iqbal, J., Eckert, V., Schwarz, R.T., 2002. Plasmodium falciparum: glycosylation status of *Plasmodium falciparum* circumsporozoite protein expressed in the baculovirus system. Exp. Parasitol. 101, 64–68.
Lasonder, E., Ishihama, Y., Andersen, J.S., Vermunt, A.M., Pain, A., Sauerwein, R.W., Eling, W.M., Hall, N., Waters, A.P., Stunnenberg, H.G., Mann, M., 2002. Analysis of the *Plasmodium falciparum* proteome by high-accuracy mass spectrometry. Nature 419, 537–542.
Madin, K., Sawasaki, T., Ogasawara, T., Endo, Y., 2000. A highly efficient and robust cell-free protein synthesis system prepared from wheat embryos: plants apparently contain a suicide system directed at ribosomes. Proc. Natl. Acad. Sci. U.S.A. 97, 559–564.
Maeda, T., Saito, T., Harb, O.S., Roos, D.S., Takeo, S., Suzuki, H., Tsuboi, T., Takeuchi, T., Asai, T., 2009. Pyruvate kinase type-II isozyme in *Plasmodium falciparum* localizes to the apicoplast. Parasitol. Int. 58, 101–105.
Marsh, K., Kinyanjui, S., 2006. Immune effector mechanisms in malaria. Parasite Immunol. 28, 51–60.
McGregor, I.A., 1964. The passive transfer of human malarial immunity. Am. J. Trop. Med. Hyg. 13 (Suppl.), 237–239.
Mehlin, C., Boni, E., Buckner, F.S., Engel, L., Feist, T., Gelb, M.H., Haji, L., Kim, D., Liu, C., Mueller, N., Myler, P.J., Reddy, J.T., Sampson, J.N., Subramanian, E., Van Voorhis, W.C., Worthey, E., Zucker, F., Hol, W.G., 2006. Heterologous expression of proteins from *Plasmodium falciparum*: results from 1000 genes. Mol. Biochem. Parasitol. 148, 144–160.
Moll, K., Pettersson, F., Vogt, A.M., Jonsson, C., Rasti, N., Ahuja, S., Spangberg, M., Mercereau-Puijalon, O., Arnot, D.E., Wahlgren, M., Chen, Q., 2007. Generation of cross-protective antibodies against *Plasmodium falciparum* sequestration by immunization with an erythrocyte membrane protein 1-duffy binding-like 1 alpha domain. Infect. Immun. 75, 211–219.
Mu, J., Awadalla, P., Duan, J., McGee, K.M., Keebler, J., Seydel, K., McVean, G.A., Su, X.Z., 2007. Genome-wide variation and identification of vaccine targets in the *Plasmodium falciparum* genome. Nat. Genet. 39, 126–130.
Mudeppa, D.G., Pang, C.K., Tsuboi, T., Endo, Y., Buckner, F.S., Varani, G., Rathod, P.K., 2007. Cell-free production of functional *Plasmodium falciparum* dihydrofolate reductase-thymidylate synthase. Mol. Biochem. Parasitol. 151, 216–219.
Netzer, W.J., Hartl, F.U., 1997. Recombination of protein domains facilitated by co-translational folding in eukaryotes. Nature 388, 343–349.
Nussenzweig, R.S., Vanderberg, J., Most, H., Orton, C., 1967. Protective immunity produced by the injection of x-irradiated sporozoites of *Plasmodium berghei*. Nature 216, 160–162.
Otsuki, H., Kaneko, O., Thongkukiatkul, A., Tachibana, M., Iriko, H., Takeo, S., Tsuboi, T., Torii, M., 2009. Single amino acid substitution in *Plasmodium yoelii* erythrocyte ligand determines its localization and controls parasite virulence. Proc. Natl. Acad. Sci. U.S.A. 106, 7167–7172.
Pain, A., Bohme, U., Berry, A.E., Mungall, K., Finn, R.D., Jackson, A.P., Mourier, T., Mistry, J., Pasini, E.M., Aslett, M.A., Balasubrammaniam, S., Borgwardt, K., Brooks, K., Carret, C., Carver, T.J., Cherevach, I., Chillingworth, T., Clark, T.G., Galinski, M.R., Hall, N., Harper, D., Harris, D., Hauser, H., Ivens, A., Janssen, C.S., Keane, T., Larke, N., Lapp, S., Marti, M., Moule, S., Meyer, I.M., Ormond, D., Peters, N., Sanders, M., Sanders, S., Sargeant, T.J., Simmonds, M., Smith, F., Squares, R., Thurston, S., Tivey, A.R., Walker, D., White, B., Zuiderwijk, E., Churcher, C., Quail, M.A., Cowman, A.F., Turner, C.M., Rajandream, M.A., Kocken, C.H., Thomas, A.W., Newbold, C.I., Barrell, B.G., Berriman, M., 2008. The genome of the simian and human malaria parasite *Plasmodium knowlesi*. Nature 455, 799–803.
Richards, J.S., Beeson, J.G., 2009. The future for blood-stage vaccines against malaria. Immunol. Cell Biol. 87, 377–390.
Richie, T.L., Saul, A., 2002. Progress and challenges for malaria vaccines. Nature 415, 694–701.
Roestenberg, M., McCall, M., Hopman, J., Wiersma, J., Luty, A.J., van Gemert, G.J., van de Vegte-Bolmer, M., van Schaijk, B., Teelen, K., Arens, T., Spaarman, L., de Mast, Q., Roeffen, W., Snounou, G., Renia, L., van der Ven, A., Hermsen, C.C., Sauerwein, R., 2009. Protection against a malaria challenge by sporozoite inoculation. N. Engl. J. Med. 361, 468–477.
Samuelson, J., Banerjee, S., Magnelli, P., Cui, J., Kelleher, D.J., Gilmore, R., Robbins, P.W., 2005. The diversity of dolichol-linked precursors to Asn-linked glycans likely results from secondary loss of sets of glycosyltransferases. Proc. Natl. Acad. Sci. U.S.A. 102, 1548–1553.
Sawasaki, T., Ogasawara, T., Morishita, R., Endo, Y., 2002. A cell-free protein synthesis system for high-throughput proteomics. Proc. Natl. Acad. Sci. U.S.A. 99, 14652–14657.
Sawasaki, T., Endo, Y., 2008. The wheat germ cell-free protein synthesis system. In: Spirin, A.S., Swartz, J.R. (Eds.), Cell-free protein synthesis, methods and protocols. Wiley-VCH Verlag GmbH & Co. KGaA, Weinheim, Germany, pp. 111–139.
Takeo, S., Hisamori, D., Matsuda, S., Vinetz, J., Sattabongkot, J., Tsuboi, T., 2009. Enzymatic characterization of the *Plasmodium vivax* chitinase, a potential malaria transmission-blocking target. Parasitol. Int. 58, 243–248.
Targett, G.A., Greenwood, B.M., 2008. Malaria vaccines and their potential role in the elimination of malaria. Malar. J. 7 (Suppl. 1), S10.
Tsuboi, T., Tachibana, M., Kaneko, O., Torii, M., 2003. Transmission-blocking vaccine of vivax malaria. Parasitol. Int. 52, 1–11.
Tsuboi, T., Takeo, S., Iriko, H., Jin, L., Tsuchimochi, M., Matsuda, S., Han, E.T., Otsuki, H., Kaneko, O., Sattabongkot, J., Udomsangpetch, R., Sawasaki, T., Torii, M., Endo, Y., 2008. Wheat germ cell-free system-based production of malaria proteins for discovery of novel vaccine candidates. Infect. Immun. 76, 1702–1708.
VanBuskirk, K.M., O'Neill, M.T., De La Vega, P., Maier, A.G., Krzych, U., Williams, J., Dowler, M.G., Sacci Jr., J.B., Kangwanrangsan, N., Tsuboi, T., Kneteman, N.M., Heppner Jr., D.G., Murdock, B.A., Mikolajczak, S.A., Aly, A.S., Cowman, A.F., Kappe,

S.H., 2009. Preerythrocytic, live-attenuated *Plasmodium falciparum* vaccine candidates by design. Proc. Natl. Acad. Sci. U.S.A. 106, 13004–13009.
Vedadi, M., Lew, J., Artz, J., Amani, M., Zhao, Y., Dong, A., Wasney, G.A., Gao, M., Hills, T., Brokx, S., Qiu, W., Sharma, S., Diassiti, A., Alam, Z., Melone, M., Mulichak, A., Wernimont, A., Bray, J., Loppnau, P., Plotnikova, O., Newberry, K., Sundararajan, E., Houston, S., Walker, J., Tempel, W., Bochkarev, A., Kozieradzki, I., Edwards, A., Arrowsmith, C., Roos, D., Kain, K., Hui, R., 2007. Genome-scale protein expression and structural biology of *Plasmodium falciparum* and related Apicomplexan organisms. Mol. Biochem. Parasitol. 151, 100–110.
Vinarov, D.A., Lytle, B.L., Peterson, F.C., Tyler, E.M., Volkman, B.F., Markley, J.L., 2004. Cell-free protein production and labeling protocol for NMR-based structural proteomics. Nat. Methods 1, 149–153.
Waters, A., 2006. Malaria: new vaccines for old? Cell 124, 689–693.
WHO, 2008. World Malaria Report 2008. WHO Press, Geneva, Switzerland.

INFECTION AND IMMUNITY, Sept. 2010, p. 3773–3782 Vol. 78, No. 9
0019-9567/10/$12.00 doi:10.1128/IAI.00306-10

Plasmodium vivax Ookinete Surface Protein Pvs25 Linked to Cholera Toxin B Subunit Induces Potent Transmission-Blocking Immunity by Intranasal as Well as Subcutaneous Immunization▽

Takeshi Miyata,[1] Tetsuya Harakuni,[1] Takafumi Tsuboi,[2] Jetsumon Sattabongkot,[3] Hideyasu Kohama,[1]† Mayumi Tachibana,[4] Goro Matsuzaki,[1,5] Motomi Torii,[4] and Takeshi Arakawa[1,5]*

Molecular Microbiology Group, Department of Tropical Infectious Diseases, COMB, Tropical Biosphere Research Center, University of the Ryukyus, 1 Senbaru, Nishihara, Okinawa 903-0213, Japan[1]; Cell-Free Science and Technology Research Center, Ehime University, Matsuyama, Ehime 790-8577, Japan[2]; Department of Entomology, Armed Forces Research Institute of Medical Sciences, Bangkok 10400, Thailand[3]; Department of Molecular Parasitology, Ehime University Graduate School of Medicine, Shitsukawa, Toon, Ehime 791-0295, Japan[4]; and Division of Host Defense and Vaccinology, Graduate School of Medicine, University of the Ryukyus, 207 Uehara, Nishihara, Okinawa 903-0213, Japan[5]

Received 26 March 2010/Returned for modification 20 April 2010/Accepted 16 June 2010

The nontoxic cholera toxin B subunit (CTB) was evaluated as a potential delivery molecule for the *Plasmodium vivax* ookinete surface protein, Pvs25. Recombinant Pvs25 was expressed as a secreted protein in the yeast *Pichia pastoris*, as a mixture of isoforms including multimers and the A and B monomers. The A isoform with the presumed native protein fold was the most abundant, accounting for more than 40% of all expressed protein. The molecularly uniform A isoform was chemically conjugated to CTB via its primary amines, and the fusion protein, retaining GM1-ganglioside affinity, was administered to BALB/c mice by the subcutaneous (s.c.) or intranasal (i.n.) route. Immunization of mice with conjugated Pvs25 without supplemental adjuvant induced antisera that specifically recognized *P. vivax* ookinetes *in vitro*. Furthermore, the antisera, when mixed with parasitized blood isolated from *P. vivax* patients from Thailand, was found to reduce parasite transmission to mosquitoes, conferring a 93 to 98% (s.c.) or a 73 to 88% (i.n.) decrease in oocyst number. Unconjugated Pvs25 alone conferred only a 23 to 60% (s.c.) or a 0 to 6% (i.n.) decrease in oocyst number. Coadministration of extraneous adjuvants, however, further enhanced the vaccine efficacy up to complete blockade. Taken together, we conclude that a weakly immunogenic Pvs25 by itself, when linked to CTB, transforms into a potent transmission-blocking antigen in both i.n. and s.c. routes. In addition, the present study is, to the best of our knowledge, the first demonstration of the immune potentiating function of CTB for a vaccine antigen delivered by the s.c. route.

Malaria is one of the most serious infectious diseases, with high mortality and morbidity, especially in tropical regions of the world. The disease causes 350 to 500 million clinical cases every year, and the estimated annual mortality exceeds 1.1 million (28). Implementation of many malaria control measures, including chemotherapy and insecticide-treated bed nets, have made a significant contribution to the reduction of malaria cases worldwide; however, these control measures are suboptimal, and hence new tools, particularly vaccines, should be used for local elimination and the ultimate eradication of malaria from the globe (9, 10, 24). The development of effective and affordable malaria vaccines is therefore likely to benefit global public health (Malaria Vaccine Technology Roadmap [MVTR], 2006 [http://www.malariavaccineroadmap.net/pdfs/Malaria_Vaccine_TRM_Final.pdf]).

Although *Plasmodium falciparum* causes the highest mortality rates among the four *Plasmodium* species known to infect humans (18), *P. vivax* malaria has the highest morbidity and is an important cause of recurrent malaria. This species is therefore an important target of malaria control efforts (4–6; MVTR). Furthermore, because global malaria eradiation is the ultimate goal, the value of developing vaccines against *P. vivax* cannot be underestimated (4–6; MVTR). Several promising vaccine candidates have been intensively investigated, such as those targeting the asexual stages, i.e., the sporozoite, hepatic and erythrocytic stages, which are designed to prevent infection and to reduce disease severity. On the other hand, transmission-blocking vaccines (TBVs) that target the sexual stage, in which the parasite undergoes sporogonic development in anopheline mosquitoes, prevent parasite transmission from mosquitoes to humans (7, 14, 25). TBVs induce antibodies that react with the ookinete surface proteins (OSPs) of malaria parasites within the mosquito midgut, and as such they do not directly protect vaccinated individuals from infection. They could, however, contribute to elimination of the disease by lowering the parasite transmission frequency below the threshold at which the parasite can maintain its life cycle (4, 6). In addition, TBVs, when combined with vaccines targeting other stages of the infection, could prevent transmission of parasites that have escaped the immune response. Furthermore, TBVs could also prevent transmission of drug-resistant

* Corresponding author. Mailing address: Molecular Microbiology Group, Department of Tropical Infectious Diseases, COMB, Tropical Biosphere Research Center, University of the Ryukyus, 1 Senbaru, Nishihara, Okinawa 903-0213, Japan. Phone and fax: 81-98-895-8974. E-mail: tarakawa@comb.u-ryukyu.ac.jp.

† Present address: Japan BCG Laboratory, 3-1-5 Matsuyama, Kiyose, Tokyo 204-0022, Japan.

▽ Published ahead of print on 28 June 2010.

parasites, which will likely to emerge when mass administration of primaquine is initiated. Therefore, TBVs might function as a "safety net" for pre-erythrocytic and erythrocytic vaccines, as well as other nonvaccine interventions.

We have recently tested whether a mucosal vaccination regime can be applied to TBVs, on the premise that noninvasive and easy-to-administer mucosal vaccines are advantageous in a mass vaccination campaign in a region where malaria is endemic (1–3). In these animal studies, we have demonstrated the potential of mucosal vaccines to block parasite transmission, but enhancement of the mucosal immunogenicity of recombinant antigens was found to be critically dependent upon the use of cholera toxin (CT) adjuvant. CT is well known for its high immune potentiating function for admixed antigens administered through the mucosal, particularly the intranasal (i.n.), route (13). However, its clinical application is hampered by its severe toxicity (26). Thus, alternative vaccine formulations not using the CT holotoxin are highly desirable.

Here, we extended our previous studies to test our hypothesis that the immunogenicity of a *Plasmodium vivax* malaria OSP, Pvs25, becomes substantially augmented when physically linked to the nontoxic B subunit of CT (CTB), even without supplementation with extraneous adjuvants. This should, in theory, effectively reduce parasite transmission to mosquitoes. Furthermore, we tested the TBV efficacy of the engineered fusion complex in a subcutaneous (s.c.) immunization regimen to test the immune potentiating function of CTB with this particular immunization route.

MATERIALS AND METHODS

Expression of Pvs25H protein from the methylotrophic yeast *Pichia pastoris*. The Pvs25 coding region (Ala_{23} to Leu_{195}) was amplified by PCR from plasmid Pvs25#26_SalI_pEU3, which harbors the coding region for the extracellular domain of the Pvs25 protein (12), with a sense primer (5′-GCCGTCACGGTA GACACC-3′) and an antisense primer containing an EcoRI site, a hexahistidine-coding sequence and a termination codon (5′-GGGAATTCTTAATGATGGT GATGGTGATGTGGTCCAAGGCATACATTTTTCTCTTTGTC-3′). The DNA fragment was amplified by using *Vent* DNA polymerase (New England Biolabs, Beverly, MA), was purified by using a PCR Purification Kit (Qiagen, Inc., Valencia, CA), and then digested with EcoRI. The fragment was subcloned into the SnaBI and EcoRI sites of the *P. pastoris* expression vector pPIC9K (Life Technologies, Carlsbad, CA) to construct the plasmid pPvs25H, which was designed to express an α-factor signal–Pvs25–hexahistidine fusion protein (see Fig. 1a).

P. pastoris recombination was performed according to the manufacturer's instructions (Life Technologies). Approximately 10 μg of linearized pPvs25H plasmid digested with SalI was electroporated into *P. pastoris* strain GS115 by using a Gene Pulser (1.5 kV, 200 Ω, 25 μF; Bio-Rad Laboratories, Inc., Redmond, WA). Immediately after electroporation, the cells were plated on minimal dextrose medium and incubated for 72 h at 29°C. Colonies were transferred to yeast extract-peptone-dextrose (YPD) medium containing increasing concentrations of Geneticin (G418; 1 to 5 mg/ml; Nacalai Tesque, Inc., Kyoto, Japan) for the selection of clones containing multiple copies of the desired gene. Clones that acquired a phenotype resistant to the highest level of G418 (5 mg/ml) were analyzed for production of the Pvs25H protein. Selected clones were cultured in BMGY medium with vigorous shaking in a baffled flask at 30°C until the optical density at 600 nm (OD_{600}) reached 2.0; the cultured cells were then transferred to BMMY medium containing 0.5% methanol to induce gene expression. Cells were cultured for an additional 72 h, with supplementation with 0.5% methanol for every 24 h of continued induction. The culture supernatant was collected by two rounds of centrifugation (9,600 × *g*) for 10 min, followed by filtration (FastCap filter with a 0.2-μm pore size; Nalgene Nunc International, Inc., Rochester, NY) to remove residual cells completely. Proteins secreted into the supernatant were separated by sodium dodecyl sulfate polyacrylamide gel electrophoresis (SDS-PAGE) and stained with Coomassie brilliant blue or subjected to immunoblot analysis with anti-Pvs25 antiserum or anti-histidine tag monoclonal antibody (Roche, Basel, Switzerland). The supernatant was supplemented with 20 mM imidazole and applied to an immobilized metal ion affinity chromatography column (HisTrap FF Ni Sepharose 6 Fast Flow; GE Healthcare, Little Chalfont, United Kingdom). After a washing step with a buffer containing 20 mM imidazole, the Pvs25H protein was eluted with phosphate-buffered saline (PBS) containing 500 mM imidazole. The affinity-purified protein was used for size exclusion chromatography with a flow rate of 0.2 ml/min (HiLoad 16/60 Superdex 75-pg column; GE Healthcare) to separate the monomeric from the multimeric isoforms. The monomeric isoforms that were a mixture of A and B isoforms were then subjected to hydrophobic interaction chromatography (HIC; HiTrap Phenyl Sepharose HP; GE Healthcare), in which both the A and the B isoforms bound to the hydrophobic ligand by adjusting the concentration of ammonium sulfate in the solution to 2 M. Then, a two-step elution process was performed, using 1 M ammonium sulfate for elution of the A isoform, followed by PBS elution of the B isoform.

This highly purified A isoform (Pvs25H-A) was used for all immunization experiments. The endotoxin content of the Pvs25H-A protein was measured by the *Limulus* amebocyte lysate test (Pyrogent Single Test Vials; Cambrex, East Rutherford, NJ), and the endotoxin content was found to be <0.05 endotoxin unit (EU)/μg of protein.

Immobilized *tris*[2-carboxyethyl]phosphine hydrochloride on a beaded agarose support (TCEP; Pierce, Rockford, IL) was used to generate a reduced form of the sulfhydryl groups for recombinant protein samples. In addition, 5,5′-dithio-*bis*-(2-nitrobenzoic acid) (Ellman's reagent; Pierce) and a cysteine hydrochloride monohydrate standard were used to estimate the amounts of free sulfhydryls.

The N-terminal protein sequences were analyzed by the Edman degradation method as described elsewhere, using a protein sequencer (Shimadzu, Kyoto, Japan).

All recombinant DNA experiments were conducted according to the Safety Guidelines for Gene Manipulation Experiments of the University of the Ryukyus.

Chemical conjugation between Pvs25H-A and CTB. Recombinant CTB was expressed and purified as described previously (11), and purified Pvs25H-A was chemically conjugated to CTB by using the heterobifunctional cross-linker *N*-succinimidyl 3-(2-pyridyldithio) propionate (SPDP; Thermo Scientific, Inc., Rockford, IL). One milligram of Pvs25H-A (2 mg/ml in PBS-EDTA) was incubated with SPDP (0.6 mM, final concentration) for 1 h at room temperature to add pyridyl disulfide groups to the primary amines of the protein. The reaction mixture was then desalted and buffer exchanged to PBS by a size exclusion membrane filter (Amicon Ultra-15, MWCO 10,000; Millipore, Billerica, MA) to remove excess reagent and by-products (pyridine 2-thione). Similarly, 1 mg of CTB (2 mg/ml in PBS-EDTA) was incubated with SPDP (0.6 mM, final concentration) for 1 h at room temperature and then desalted and buffer exchanged to PBS. Pyridyldithiol-activated CTB was then incubated with dithiothreitol (DTT; 50 mM, final) for 30 min at room temperature to expose the sulfhydryl groups and then desalted and buffer exchanged to PBS as before. Finally, equal amounts of pyridyldithiol-activated Pvs25H-A and sulfhydryl-activated CTB were mixed, followed by incubation at room temperature overnight for conjugation. The conjugated sample was desalted as before, and the endotoxin content was measured to confirm that there had been no significant contamination during the conjugation process.

To evaluate the conjugation efficiency, untreated Pvs25H-A was separately incubated either with untreated CTB or pyridyldithiol-activated CTB (CTB^{SPDP}). Similarly, pyridyldithiol-activated Pvs25H-A ($Pvs25H\text{-}A^{SPDP}$) was separately incubated with either untreated or DTT-treated CTB (CTB^{DTT} or $CTB^{SPDP/DTT}$, respectively) (see Results and Fig. 2a for details). Each conjugation sample was analyzed by GM1–enzyme-linked immunosorbent assay (GM1-ELISA) as described previously (11). Briefly, 5 μg of monosialoganglioside GM1 (Sigma-Aldrich, St. Louis, MO)/ml, a receptor for CT, diluted with bicarbonate buffer (15 mM Na_2CO_3, 35 mM $NaHCO_3$ [pH 9.6]; 50 μl/well) was coated onto a 96-well microtiter plate (Sumitomo Bakelite Co., Ltd., Tokyo, Japan), and the plate was incubated at 4°C overnight. After washing the plate twice with PBS containing 0.05% Tween 20 (PBS-T) and once with PBS, the plate was blocked with PBS containing 10% skim milk for 2 h at 37°C. Each conjugation sample (2 μg of total protein/well) was then applied to the wells, and the plate was incubated for 2 h at 37°C, followed by incubation with rabbit anti-CT antiserum (1/4,000; Sigma-Aldrich) or mouse anti-Pvs25 antiserum (1/500) for 2 h at 37°C. This was followed by the addition of anti-rabbit or anti-mouse IgG conjugated to alkaline phosphatase (1/4,000; Sigma-Aldrich). Finally, *p*-nitrophenylphosphate (Bio-Rad) was added, and the plate was incubated for 20 min at 37°C. The OD_{415} was measured by using a microplate reader (Bio-Rad).

To evaluate the conjugation state of the fusion complex, 1 mg of conjugation sample was subjected to size exclusion chromatography (HiLoad 16/60 Superdex

75-pg column; GE Healthcare). Molecular weight standards (Gel Filtration Calibration kits LMW; GE Healthcare) were used to estimate the molecular weights of CTB, Pvs25H-A, and their fusion complex by calculating the partition coefficient (K_{av}) values for each protein standard and sample protein.

Immunization with CTB-Pvs25H-A fusion protein and analysis of induced antibodies. Eight-week-old female BALB/c mice were purchased from Japan SLC (Shizuoka, Japan). Mice (four or eight mice per group) were immunized via the s.c. or the i.n. route with 30 μg of Pvs25H-A, a mixture of CTB and Pvs25H-A (30 μg each) or 60 μg of CTB-Pvs25H-A fusion protein. Where indicated, incomplete Freund's adjuvant (IFA; Difco Laboratories, Detroit, MI) or 0.1 to 1.0 μg of CT (List Biological Laboratories, Campbell, CA) was used for s.c. or i.n. adjuvants, respectively. The mice were immunized three times, at weeks 0, 2, and 3.

Mice were anesthetized 1 week after the third immunization (week 4) by intraperitoneal injection of pentobarbital sodium salt (Nacalai Tesque, Inc.) and were sacrificed by exsanguination to collect serum. For specific serum antibody analysis, ELISA plates (Sumilon; Sumitomo Bakelite Co.) were coated with Pvs25H-A (5 μg/ml) in bicarbonate buffer by incubating the plate at 4°C overnight. The plate was washed twice with PBS-T and once with PBS. The plate was blocked with 1% bovine serum albumin (BSA) in PBS for 2 h at 37°C. Twofold serial dilutions of the antisera starting with 50-fold dilution with 0.5% BSA in PBS were applied to the wells in duplicate, which were then incubated for 2 h at 37°C. The plate was then incubated with anti-mouse IgG conjugated to alkaline phosphatase (1/4,000; Sigma-Aldrich) for 2 h at 37°C. *p*-Nitrophenylphosphate (Bio-Rad) was added to the plate for color development, and the absorbance at OD_{415} was measured after 20 min of incubation at 37°C, using a microplate reader (Bio-Rad). The antibody titer was defined as the serum dilution that gave an OD_{415} value equal to 0.1 or as the serum dilution where a one magnitude higher dilution gave an OD_{415} value of <0.1.

All animal experimental protocols were approved by the Institutional Animal Care and Use Committee of the University of the Ryukyus, and the experiments were conducted according to the Ethical Guidelines for Animal Experiments of the University of the Ryukyus.

Mosquito membrane feeding assay. Heparinized syringes were used for peripheral blood collection, with written informed consent, from *P. vivax* patients who came to a malaria clinic in the Mae Sod district in the Tak province of northwestern Thailand. Single species infection with *P. vivax* was confirmed by Giemsa stain of thick and thin blood smears. The levels of parasitemias and the gametocytemias were 0.22 and 0.02%, respectively, for the volunteer *P. vivax* patient 1, and 0.23 and 0.01%, respectively, for the volunteer *P. vivax* patient 2. Collected blood was aliquoted into tubes (300 μl/tube), and the plasma was removed after brief centrifugation. Pooled mouse antisera were mixed with an equal volume of heat-inactivated normal human AB serum prepared from malaria-naive donors. The test antiserum sample was mixed and incubated with *P. vivax*-infected blood cells (1:1 [vol/vol] ratio) for 15 min at room temperature. The mixture was then applied to a membrane feeding apparatus kept at 37°C to allow starved *Anopheles dirus* A mosquitoes (Bangkok colony, Armed Forces Research Institute of Medical Sciences) to feed on the blood meals for 30 min. Fully engorged mosquitoes were separated from unfed mosquitoes, maintained for a week in an insectary kept at 26°C, and provided with 10% sucrose water. For each blood sample-serum mixture, 20 mosquitoes were dissected, and the number of oocysts in the midgut was counted under a microscope after 0.5% mercurochrome staining.

All human subject research conducted in the present study was reviewed and approved by the Ethics Committee of the Thai Ministry of Public Health and the Institutional Review Board of the Walter Reed Army Institute of Research.

Detection of native Pvs25 in antisera from immunized mice. Peripheral blood from *P. vivax*-infected patients was collected as described above. The gametocytemic patient blood was used to grow zygotes and ookinetes *in vitro*, as described previously (23). They were spotted onto slides and fixed with acetone as described previously (1–3). The slides were blocked with 5% nonfat milk in PBS and incubated with mouse antisera derived from immunization with CTB-Pvs25H-A fusion protein emulsified with IFA or with the fusion protein supplemented with CT (1 μg), after dilution of the antisera 100-fold with 5% nonfat milk in PBS. The samples were washed with ice-cold PBS and incubated with Alexa 488-conjugated anti-mouse antibody (Invitrogen, Carlsbad, CA). After a wash with ice-cold PBS, the slides were viewed by confocal scanning laser microscopy (LSM5 Pascal; Carl Zeiss MicroImaging, Thornwood, NY).

Statistical analysis. The Wilcoxon-Mann-Whitney test was used to compare antibody titers or the number of oocysts per mosquito between the nonimmune and an indicated immunization group or between indicated two immunization groups. The Kruskal-Wallis test was used to compare antibody titers or the number of oocysts per mosquito among three groups (i.e., S, M, and L). The chi-square test was used to analyze the difference in the proportion of parasite-free mosquitoes out of the total number of mosquitoes examined between the nonimmune and an indicated immunization group or between indicated two immunization groups. All statistical analysis were conducted by using JMP software version 8.0 (SAS Institute, Inc., Cary, NC).

RESULTS

Expression and purification of recombinant Pvs25H-A isoform from *P. pastoris*. Ookinete surface proteins (OSPs) contain several intramolecular disulfide bonds, e.g., the 11 disulfide bonds in Pvs25, which are important for overall structural integrity and native antigenicity. For this reason, *E. coli* expression systems are unsuitable, and therefore yeast *Saccharomyces cerevisiae* expression systems are used (12, 15, 19, 22). We explored other, more efficient recombinant protein expression systems for Pvs25 and found a higher production efficiency in the yeast *P. pastoris*. We constructed a plasmid for secretory expression of Pvs25 as a C-terminal hexahistidine-tagged protein (Pvs25H) (Fig. 1a). The culture supernatant of recombinant *P. pastoris* was found to contain several protein species that were not present in the culture supernatant of vector-transformed clones (Fig. 1b), and these protein bands specifically reacted with anti-Pvs25 antiserum, as well as with an anti-hexahistidine tag monoclonal antibody (data not shown). Secreted Pvs25H was affinity purified on a nickel Sepharose column and further separated into large (fractions 16 to 19) and small (fractions 21 to 23) protein species by size exclusion chromatography (Fig. 1c and d). At least five protein bands were identified on SDS-PAGE (Fig. 1b) and their corresponding peaks by size exclusion chromatography (fractions 16, 17, 18-19, 21-22, and 22-23 in Fig. 1c and d). The apparent molecular masses of these protein species based on gel mobility on SDS-PAGE were estimated to be 63.2, 47.3, 33.2, 16.1, and 28.3 kDa, respectively. The calculated molecular mass of Pvs25H (based on its deduced amino acid sequence) is 20.2 kDa, to which the fraction 21 and 22 protein species corresponded most closely. We therefore concluded that this was monomeric Pvs25H. Furthermore, the apparent molecular masses of protein species found in fractions 18 and 19, 17, and 16 corresponded very well to multiples of the molecular mass of the apparent monomer, so we concluded that they represented the dimer, trimer and tetramer of Pvs25H, respectively. The protein species that appeared in fractions 22 and 23 exhibited markedly different gel mobility (28.3 kDa) from that of the monomeric protein (16.1 kDa) (Fig. 1d), although these two showed extensively overlapping chromatographic peaks on size exclusion chromatography (Fig. 1c). We concluded that the protein species in fractions 22 and 23 was a monomeric protein with a distinct hydrophobic character, and thus decided to further separate these two monomers based on hydrophobicity profile by HIC. HIC clearly separated the two monomeric isoforms (Fig. 1f), and we named the less hydrophobic isoform and the more hydrophobic isoform the A and B monomeric isoforms, respectively (19). The observed lower gel mobility for the A isoform than the B isoform on SDS-PAGE under nonreducing conditions (Fig. 1d) was consistent with the results of HIC: the more hydrophilic the molecule, the fewer SDS molecules bind, and the protein becomes less negatively charged, resulting in reduced gel mobility on SDS-PAGE.

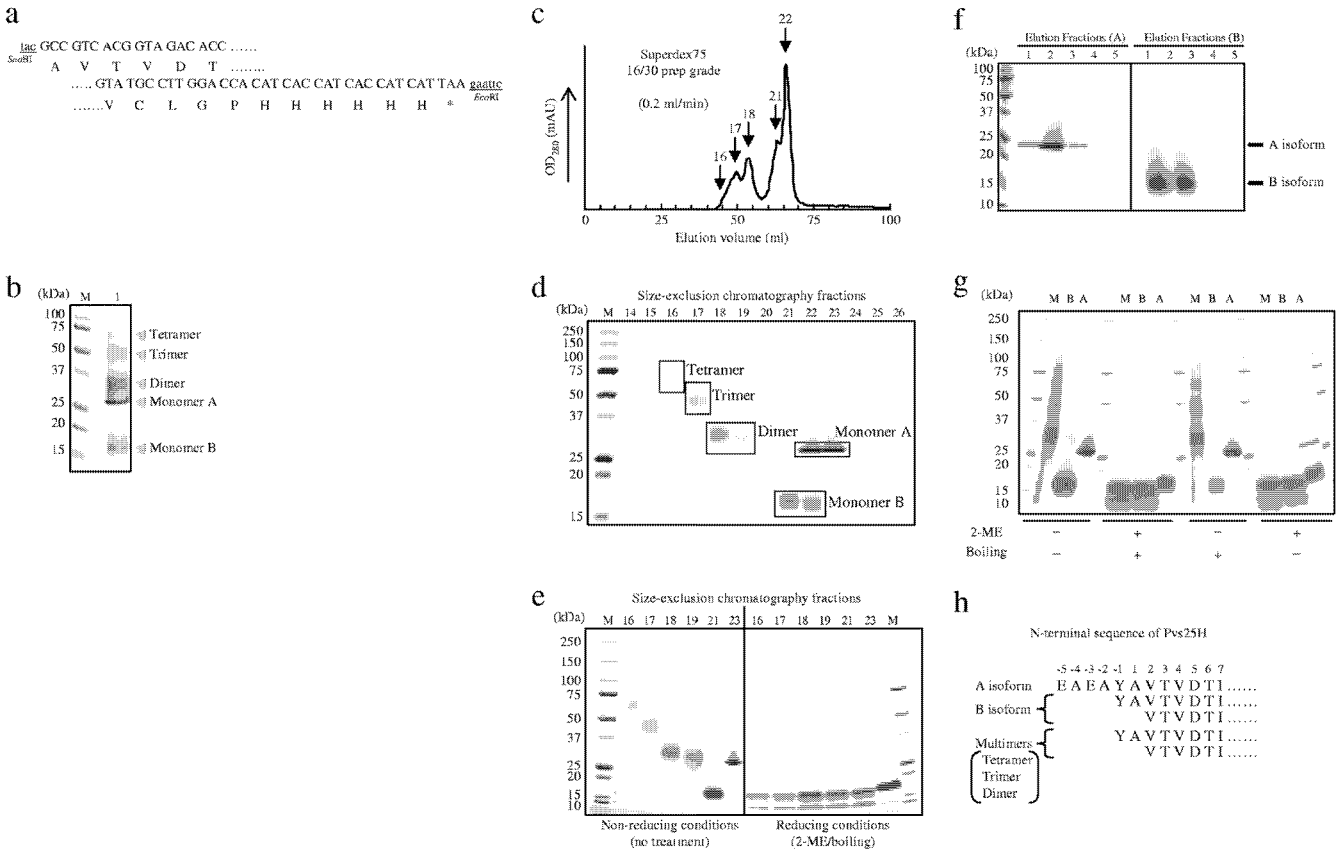

FIG. 1. Construction and expression analysis of Pvs25H in *Pichia pastoris*. (a) The 5′- and 3′-coding regions of the *Pvs25* gene sequence with its predicted amino acid sequence (Ala_{23} to Leu_{195}). The *Pvs25* gene fused to a hexahistidine tag at its C terminus was inserted into the SnaBI and EcoRI sites of pPIC9K, and the gene was integrated into the chromosomal DNA of *P. pastoris* strain GS115 by homologous recombination. (b) After selection of a high-producer clone that secreted the recombinant protein, nickel-affinity chromatography-purified Pvs25H was analyzed by SDS-PAGE (lane 1). M, molecular marker. (c) The affinity-purified Pvs25H was fractionated by size exclusion chromatography from which at least five chromatographic peaks were observed. (d) Size exclusion chromatography fractions 14–26 were subjected to SDS-PAGE (15% acrylamide). Based on the apparent molecular mass of each protein band, the fractions 16, 17, 18-19, 21-22, and 22-23 were defined as the tetramer, trimer, dimer, monomer B, and monomer A, respectively. (e) Selected chromatography peaks were subjected to 5 to 20% acrylamide gradient SDS-PAGE under nonreducing or reducing (10% 2-ME and boiling) conditions. (f) Hydrophobic interaction chromatography of the Pvs25H-A and Pvs25H-B monomeric isoforms. Elution fractions (A) are eluates of 2 M NH_4SO_4 (Pvs25H-A) and elution fractions (B) are eluates of PBS (Pvs25H-B). (g) Each isoform (M, a mixture of dimer, trimer and tetramer; B, B isoform; A, A isoform) was subjected to 15% acrylamide SDS-PAGE under various conditions, as indicated. (h) The N-terminal protein sequence of each isoform. Positively numbered amino acid residues (Ala_1 and the following) are residues of the Pvs25 protein; negatively numbered amino acids are derivatives of the pPIC9K α-factor secretion signal. The A monomer revealed a single, unique sequence, but the B monomer and the multimers showed a mixture of different N termini.

Molecular characterization of Pvs25H isoforms. The A isoform appeared as a single sharp band, but the other isoforms, including the multimers and the B monomer, appeared as diffuse bands on SDS-PAGE (Fig. 1b and d to g), indicating that the A isoform is constrained to a more uniform molecular configuration than the other isoforms. In addition, all of the isoforms, except the A isoform, generated at least three identical protein bands when samples were heat treated in the presence of SDS and β-mercaptoethanol (2-ME) prior to SDS-PAGE. The A isoform appeared as a single protein band with a slightly higher molecular mass than that for the largest protein band among the three bands observed for the other isoforms (Fig. 1e).

To characterize the molecular configuration of each isoform furthermore, mixtures of the multimers, including dimers, trimers, and tetramers and the A and B monomers, were subjected to SDS-PAGE after various treatments, as indicated in Fig. 1g. The gel mobility of all of the isoforms did not show any noticeable changes after boiling (100°C, 2 min), but 2-ME treatment (10% [vol/vol]) resulted in a banding pattern very similar to the pattern observed for complete denaturation (2-ME and boiling), except that the A isoform seemed to be slightly more resistant to the reducing agent than the other isoforms. This became particularly notable when lower concentrations of the reducing agent were used (data not shown). These results suggest that the multimers comprised B monomers self-cross-linked by intermolecular disulfide bonds and that the A isoform has a higher molecular rigidity than the other isoforms. Because all of the isoforms exhibited a strong resistance to the boiling and SDS, but not to the 2-ME and SDS treatment, it is plausible that the physical integrity of the protein is critically, if not completely, maintained by disulfide bonds.

Next, to evaluate the status of the covalent disulfide bonds in

the Pvs25H protein, Ellman's test was conducted for each isoform. No isoform reacted with the Ellman's reagent, suggesting either that no reduced sulfhydryls were present or that the molecules were inaccessible to the reagent. However, treatment with TCEP immobilized on agarose prior to the Ellman's test resulted in the detection of 4 to 6 molecules of reduced sulfhydryls per molecule of B monomer or multimeric isoforms, but fewer than 0.3 molecules of reduced sulfhydryls were detected per molecule of A monomer. These results indicated that the B and multimeric isoforms have disulfide bonds that are more accessible to surface-immobilized TCEP than those of the A isoform, indicating that the A isoform has more deeply buried disulfide bonds than the other isoforms. It is indicative of the higher molecular flexibility of the B isoform and the multimers than of the A isoform. Interestingly, however, denaturation of proteins with 2% SDS or 6 M guanidine hydrochloride, or TCEP agarose treatment in the presence of these denaturants prior to the Ellman's test, did not further increase the level of free sulfhydryls. These results strongly support the notion that all of the isoforms are tightly packed molecules and that their rigidity is maintained by intramolecular disulfide bonds and other noncovalent interactions.

Finally, the N-terminal protein sequences determined by the Edman degradation method for each isoform supported the results of SDS-PAGE, in that the multimers and the B isoform contain a mixture of polypeptide species with multiple N termini; however, the A isoform comprises a single polypeptide with a longer, unique N terminus (Fig. 1h). These results suggested that the multimers and the B isoform contain the same set of polypeptide species, with multiple primary structures and presumably various folding configurations. By using different combinations of structurally heterologous polypeptides, different isoforms might be generated.

Taken together, we concluded that the A isoform, which has a more uniform protein configuration, is less hydrophobic and has higher molecular rigidity than the B isoform, and perhaps it most closely resembles the native Pvs25 protein at the structural level. The proportions of each isoform expression were estimated to be 42% (A isoform), 27% (B isoform), 16% (dimer), 10% (trimer), and 5% (tetramer). Thus, the A isoform was produced most abundantly among all of the isoforms. The final protein yields of the total Pvs25H and the A isoform using our expression and purification method were 30 to 50 mg and 12 to 20 mg/liter of culture medium, respectively. We confirmed that the purified Pvs25H-A contained endotoxin at levels less than 0.05 EU/μg of protein. Based on these observations, we decided to use the A isoform (Pvs25H-A) as a TBV antigen to be linked to CTB.

Chemical conjugation of Pvs25H-A to CTB and its molecular evaluation. Recombinant CTB was expressed by *P. pastoris* strain GS115 and purified as previously reported (11). Pvs25H-A was chemically conjugated to CTB by using the heterobifunctional cross-linker SPDP (Fig. 2). Because CTB contains two cysteine residues per monomeric subunit, which, in the native form, are involved in an intramolecular disulfide bond, the existence of reduced sulfhydryls in our recombinant CTB was determined by using Ellman's reagent, and none was detected (data not shown).

Various conjugation schemes were evaluated for efficiency of linking Pvs25H-A to CTB via SPDP (Fig. 2a and b). Consistent with the results of Ellman's test for Pvs25H-A and CTB, SPDP modification of only one protein failed to generate the CTB-Pvs25H-A fusion complex (Fig. 2b). Thus, at least one partner protein had to be treated with the reducing agent to expose free sulfhydryls and make it reactive toward the pyridyldithiol groups added to the partner protein. Because intact disulfide bonds might be important for the overall structural integrity and native antigenicity of Pvs25 (12, 15, 19, 22), we avoided treating it with reducing agents. Therefore, the CTB or SPDP-modified CTB (CTB^{SPDP}) was treated instead with DTT (designated as CTB^{DTT} or $CTB^{SPDP/DTT}$ in Fig. 2a). Although both CTB^{DTT} and $CTB^{SPDP/DTT}$, when reacted with SPDP-modified Pvs25H-A ($Pvs25H\text{-}A^{SPDP}$), generated substantial levels of fusion complex with retained affinity for GM1-ganglioside, sequential treatment of CTB with SPDP and then with DTT resulted in an even higher specific reactivity toward Pvs25 antiserum (Fig. 2b).

Second, to evaluate the homogeneity of the fusion complex and the stoichiometry of each component within the complex, proteins before and after the conjugation process were analyzed by size exclusion chromatography (Fig. 2c). The two chromatographic peaks for Pvs25H-A and CTB in a mixed sample disappeared, and a new single peak emerged with an apparent molecular mass of 97.2 kDa. Because the molecular masses of Pvs25H-A and CTB are 29.8 and 53.4 kDa, respectively, based on the K_{av} values of chromatography standard proteins, the average stoichiometric ratio for CTB and Pvs25H-A was calculated to be 1:1.5, indicating that one CTB pentamer molecule carries one to two molecules of Pvs25H-A on its surface. Alternatively, if it is assumed that the fusion complex is highly homogeneous and its stoichiometric ratio is 1:1, the 14-kDa discrepancy between the observed and calculated fusion complex mass may be explained by irregularities in the molecular shape, resulting in a higher apparent molecular mass.

Taking all of the results together, we decided to use the $Pvs25H\text{-}A^{SPDP}$ + $CTB^{SPDP/DTT}$ conjugation method (Fig. 2d) to generate the fusion complex for all immunization experiments.

Immunogenicity in mice of Pvs25H-A and its fusion protein with CTB when administered by the s.c. or the i.n. route. BALB/c mice were immunized with Pvs25H-A (designated as "S" in Fig. 3 and 4), a mixture of Pvs25H-A and CTB (designated as "M" in Fig. 3 and 4), or CTB-Pvs25H-A fusion protein (designated as "L" in Fig. 3 and 4), by the s.c. or the i.n. route, with or without the indicated adjuvants, at weeks 0, 2, and 3. Antisera were collected at week 4, and the Pvs25H-A-specific IgG titers were determined (Fig. 3a). We demonstrated that: (i) s.c. immunization tended to induce a higher response than i.n. immunization in both the absence and the presence of adjuvants; (ii) the fusion protein (L) consistently induced a higher response than antigen alone (S) or the mixture of proteins (M), regardless of adjuvant supplementation; (iii) supplementation with adjuvants was required for substantial augmentation of the IgG response for both immunization routes; (iv) IFA significantly augmented the response elicited by unfused or CTB-mixed antigen, but CT only marginally affected the response elicited by these antigens; and (v) CT did not exhibit a dose-dependent augmentation effect on the IgG response in the dose range used in the present study (0.1 to 1.0

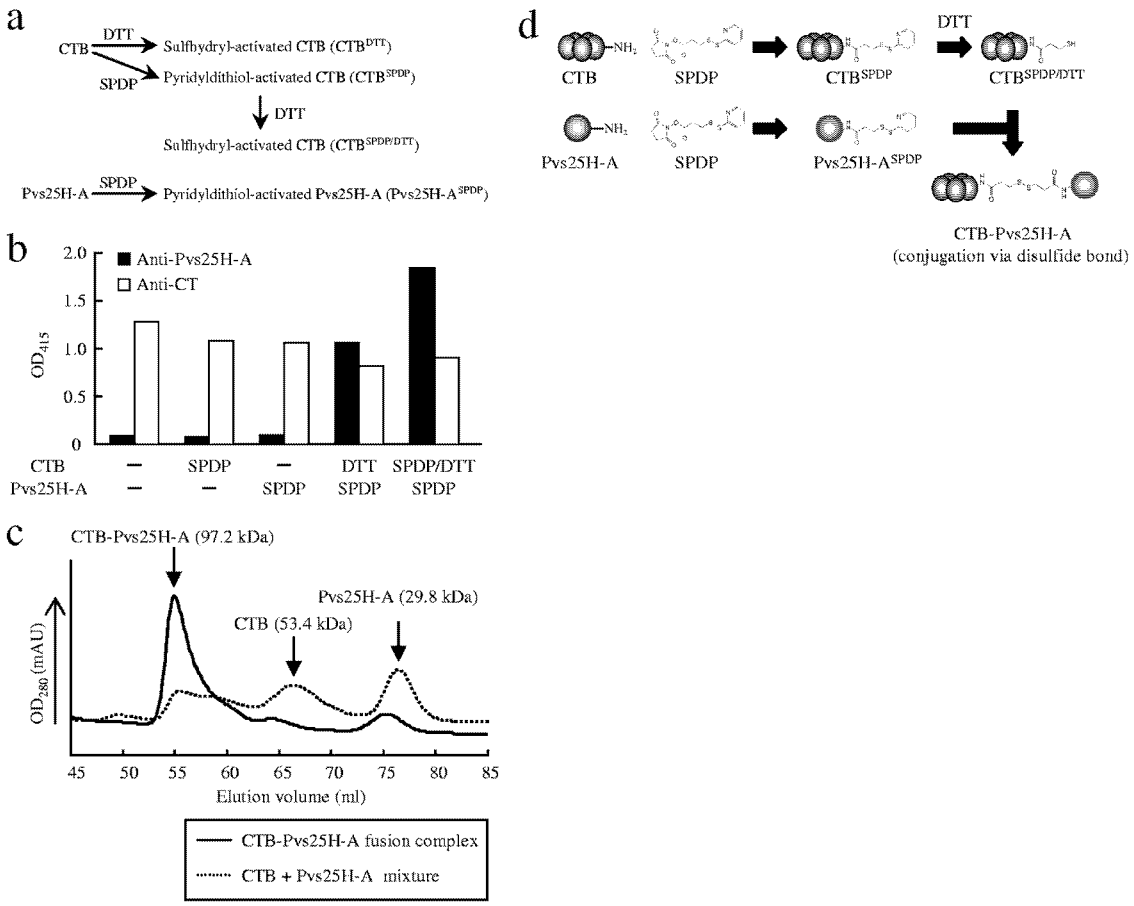

FIG. 2. Chemical conjugation of Pvs25H-A to cholera toxin B subunit (CTB). Various conjugation methods were evaluated for the generation of the CTB-Pvs25H-A fusion complex. The heterobifunctional cross-linker *N*-succinimidyl 3-(2-pyridyldithio) propionate (SPDP) was used to link Pvs25H-A to CTB via the primary amines. (a) Either CTB or SPDP-modified CTB (CTB^{SPDP}) was first treated with DTT to expose free sulfhydryls (designated as CTB^{DTT} and $CTB^{SPDP/DTT}$, respectively), and then SPDP-modified Pvs25H-A ($Pvs25H\text{-}A^{SPDP}$) was separately mixed with each of them to generate the fusion complex. (b) The CTB-Pvs25H-A fusion complex was analyzed by GM1-ELISA using anti-cholera toxin (CT) (□) or anti-Pvs25H-A (■) antiserum. (c) The CTB-Pvs25H-A fusion protein (solid line) or a mixture of CTB and Pvs25H-A (dotted line) was subjected to size exclusion chromatography. For the fusion protein, the peaks for CTB and Pvs25H-A disappeared, and a new peak emerged, indicating generation of the fusion complex. (d) The conjugation scheme chosen for production of the CTB-Pvs25H-A fusion complex. See Materials and Methods for the detailed conjugation method.

μg). Finally, we confirmed that the antisera specifically recognized the *P. vivax* ookinete surface by immunofluorescence (Fig. 3b).

Transmission-blocking effect of the induced mouse antisera against field strains of *P. vivax* parasites. The TBV efficacy of the induced mouse antisera against *P. vivax* parasites in infected blood samples from patients was evaluated by the membrane feeding assay. The same experiments were performed twice, using blood samples from two volunteer donors (Fig. 4). The average number of oocysts observed per mosquito fed on patient blood mixed with antisera induced by s.c. immunization of mice with Pvs25H-A/IFA was reduced by >99.9% compared to the naive control serum (N). Omission of the adjuvant significantly abated the effect down to 20 to 60% reduction; however, conjugating the antigen to CTB resulted in a dramatic restoration of the vaccine efficacy back to >90%. A similar tendency, albeit with significantly lower efficacy, was observed for i.n. immunization, in that antisera induced by i.n. immunization with the fusion protein decreased the oocyst number by 70 to 90%, whereas unfused antigen conferred only a 0 to 6% blocking effect. As expected, CT supplementation augmented the effect for i.n.-administered antigens, in that both unfused and CTB-fused antigens conferred a blocking effect of >90%. Interestingly, however, addition of CTB to the mixture of antigen and CT significantly abated the vaccine efficacy down to 40 to 50%. The reason for this is unknown, and it could not have been predicted from the antibody titers (Fig. 3a). Taken together, we concluded that chemical coupling of Pvs25 to CTB is a potentially promising strategy to enhance the transmission-blocking efficacy in i.n. and s.c immunization regimes.

DISCUSSION

Pvs25 is one of the top-priority *P. vivax* TBV candidates, and the production of stable and functional forms of the antigen in the most appropriate formulation is crucial (4; MVTR). In the present study, we investigated the methylotrophic yeast *P. pas-*

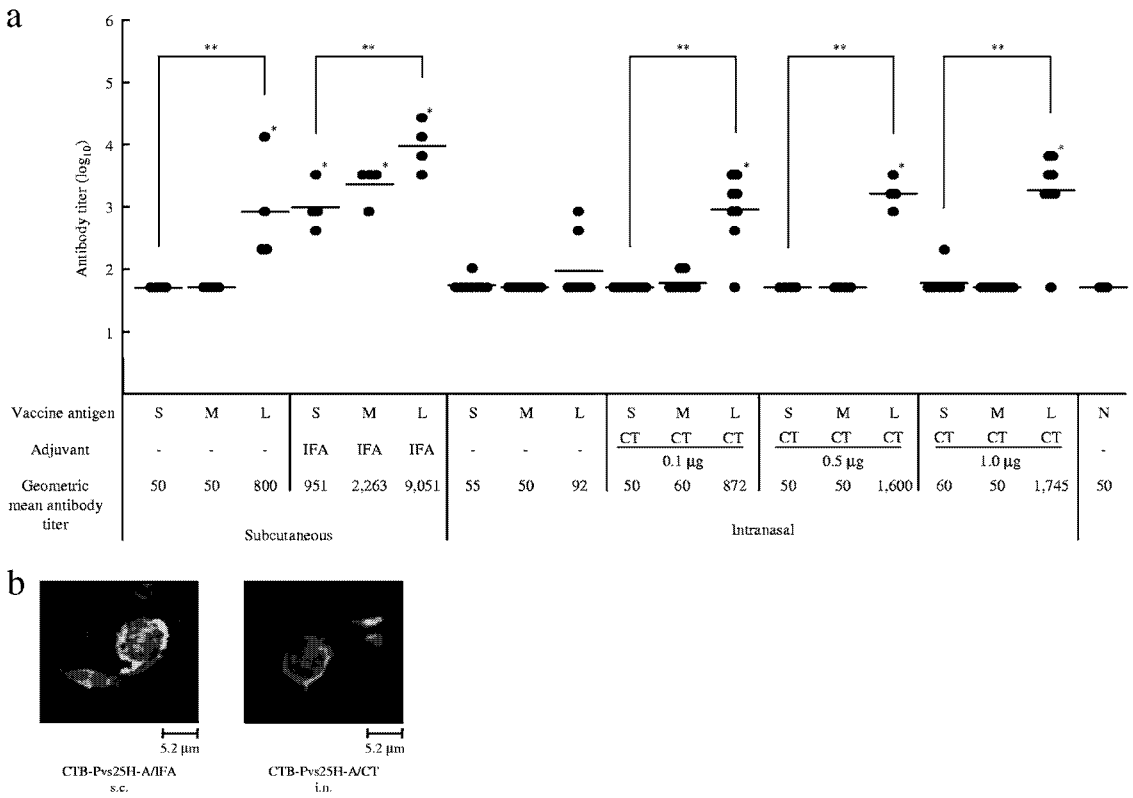

FIG. 3. Immunogenicity of the CTB-Pvs25H-A fusion protein for induction of a Pvs25-specific serum IgG response. (a) Female BALB/c mice (four or eight mice per group) were immunized with Pvs25H-A alone (30 μg) (S), a mixture of cholera toxin B subunit (CTB; 30 μg) and Pvs25H-A (30 μg) (M), or the CTB-Pvs25H-A fusion protein (60 μg), by the subcutaneous (s.c.) or the intranasal (i.n.) route (L), three times, at weeks 0, 2, and 3. Serum samples were collected a week after the third immunization and were evaluated for Pvs25-specific IgG titers. All mice received the same amount of Pvs25H-A antigen, i.e., 30 μg per injection. IFA and CT at various doses (0.1 to 1.0 μg) were used as s.c. and i.n. vaccine adjuvants, respectively. Nonimmune serum (N) was used as a negative control. Antibody titers were defined as the serum dilution that gave an OD_{415} of 0.1 or the serum dilution for which a one-point-higher dilution (2-fold) gave an OD_{415} of <0.1. *, Significantly different from nonimmune serum as determined by the Wilcoxon-Mann-Whitney test ($P < 0.05$); **, significantly different among the three groups (S, M, and L) as determined by the Kruskal-Wallis test ($P < 0.001$). (b) Ookinete-specific reactivity of induced antisera analyzed by immunofluorescence. The antisera derived from s.c. immunization with the CTB-Pvs25H-A fusion protein emulsified with IFA (CTB-Pvs25H-A/IFA), or the fusion protein administered i.n. with CT (1 μg) (CTB-Pvs25H-A/CT) specifically recognized native Pvs25 protein expressed on the surface of *Plasmodium vivax* ookinetes. Scale bar, 5.2 μm.

toris as a production host for Pvs25. The yield of Pvs25H was comparable to that reported previously for its expression in *S. cerevisiae* (19). When expressed in *S. cerevisiae*, this protein was also produced as a mixture of various isoforms (19). Although we observed a similar protein expression pattern, i.e., multimers and the A and B monomers, higher proportions of the molecularly homogeneous A isoform than the heterogeneous B and multimeric isoforms were produced when Pvs25H was expressed in *P. pastoris* and not in *S. cerevisiae*. This might present an advantage of using *P. pastoris* expression system for Pvs25 vaccine production rather than *S. cerevisiae* system. The *P. pastoris*-derived A isoform could be as conveniently and efficiently purified from the culture supernatant as reported for *S. cerevisiae*-derived A isoform, by a combination of affinity, size exclusion, and hydrophobic interaction chromatographies.

The next critical step in vaccine generation is the optimization of vaccine antigen formulations; a search for the optimal antigen formulation is often considered to be as important as choosing the best antigen among many vaccine candidate antigens. Pvs25H antigen adsorbed onto Alhydrogel (Brentag Biosector, Frederilssund, Denmark) has recently been shown to induce antibody effectively in human volunteers in a phase 1 clinical trial, and the antigen was found to be efficacious, as evidenced by significant transmission-blocking activity observed in the membrane feeding assay (17). That study confirmed that Pvs25 is a very promising TBV candidate; however, it is highly desirable to induce higher levels of transmission-blocking immunity for practical vaccine development (17). Another phase 1 clinical trial using Montanide ISA 51, a water-in-oil emulsion, has recently been completed; however, due to an unexpected frequent local reactogenicity, the vaccine efficacy has not been verified (29). Therefore, there seems to be an increasing demand for the development of a new immune-enhancing vaccine platform technology for malaria OSPs, because they are low-molecular-weight proteins that are by themselves not sufficiently immunogenic.

There have been several reports showing examples of chemical conjugation of *Plasmodium falciparum* OSPs with potential antigen carrier molecules such as the outer membrane protein of *Neisseria meningitidis* (30), exoprotein A of *Pseudomonas*

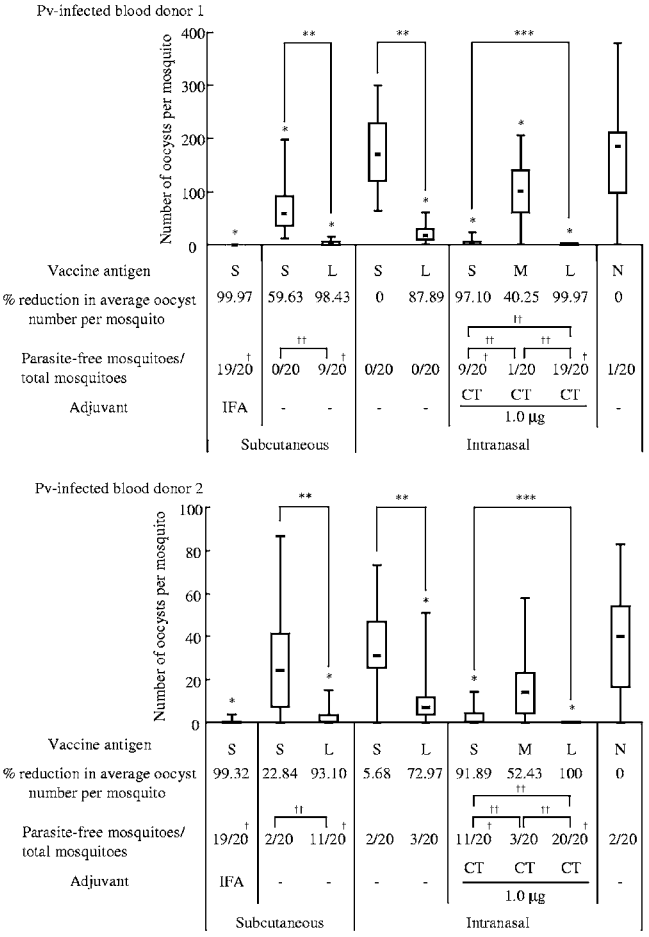

FIG. 4. Transmission-blocking vaccine (TBV) effects of the induced mouse antisera on *Plasmodium vivax* oocyst development in the *Anopheles dirus* A mosquito midgut. TBV effects on oocyst numbers induced by antisera (1/2 dilution) obtained from mice immunized with each antigen formulation (S, M, and L) as described in Fig. 3. N, nonimmune serum. Either IFA or CT was used as an adjuvant, as indicated. The data are expressed as the median values of oocyst number found per mosquito (bar within the box) with the 25 and 75% quartiles (the box) and ranges (whiskers above and below the box). The percent reduction was calculated as the reduction in the average oocyst number for each immunization group compared to the average oocyst number for the unimmunized control group (N). The number of parasite-free mosquitoes per total number of mosquitoes examined (20 mosquitoes) is provided. The analysis was performed twice, using different blood samples, as indicated in the upper panel (*P. vivax* [Pv]-infected blood donor 1) and the lower panel (Pv-infected blood donor 2). M groups without adjuvant supplementation, M and L groups with IFA supplementation, and all groups with 0.1- and 0.5-μg CT supplementation were excluded from membrane feeding analysis. *, $P < 0.001$ versus the nonimmune (N) group as determined by the Wilcoxon-Mann-Whitney test; **, $P < 0.001$ between the S and L groups as determined by the Wilcoxon-Mann-Whitney test; ***, $P < 0.001$ among the three groups (S, M, and L) as determined by the Kruskal-Wallis test; †, $P < 0.005$ versus the nonimmune (N) group as determined by the chi-square test; ††, $P < 0.005$ between the indicated two groups as determined by the chi-square test.

aeruginosa (16), ovalbumin (16), and a *P. falciparum* OSP itself by chemical crosslinking (16). All of these were demonstrated to increase TBV efficacy, but no attempts have yet been made to enhance the immunogenicity of *P. vivax* OSPs by coupling them to other proteins. In the present study we evaluated CTB as a potential carrier for Pvs25. First, to extend our previous study where CT was used as adjuvant (1–3), we tested our hypothesis that the mucosal immunogenicity of Pvs25 would increase when the protein was coupled to the nontoxic CTB subunit, even in the absence of CT supplementation. Second, to explore CTB's less-characterized immune potentiating properties for s.c.-delivered antigens, we immunized mice with the CTB-Pvs25H-A fusion protein by an s.c. route, in the presence or absence of IFA. Our principal finding was that the coupling of the antigen to CTB profoundly enhanced its immunogenicity in i.n. as well as in s.c. immunization regimes, without supplementation with extraneous adjuvants. However, the membrane feeding assay revealed that there was still much room for improvement (Fig. 4). For instance, although i.n. administration of the fusion protein alone conferred a relatively high transmission-blocking immunity (88 and 73% decreases in oocyst number for blood samples from donors 1 and 2, respectively) compared to unfused antigen alone or the unimmunized control group, only a few mosquitoes (0/20 to 3/20) were free of parasites. Supplementation of CT to the fusion protein increased the efficacy close to complete blockade (>99.9%), significantly increasing the number of mosquitoes free of parasites (19/20 to 20/20). Because supplementation of CT to unfused antigen resulted in an intermediate level of protection (97% [9/20] and 92% [11/20] decrease in oocyst number for blood samples from donors 1 and 2, respectively), we concluded that both the CT supplementation and the CTB-coupling strategies contributed to the increased vaccine efficacy, although the former was more efficient than the latter. A similar tendency was observed for the s.c. immunization regime: s.c. administration of the fusion protein alone conferred a more than 90% decrease in oocyst number, in which approximately half of the mosquitoes were free of parasites (9/20 to 11/20); however, the use of IFA with unfused antigen contributed more than the fusion method. We observed that the efficacy of the fusion protein administered alone by the s.c. route was almost equal to that attained by the unfused antigen administered i.n. with CT supplementation, in terms of the average numbers of oocyst per mosquito (>90%) as well as the number of mosquitoes free of parasites (9/20 to 11/20). Similarly, the vaccine efficacy for unfused antigen administered s.c. with IFA was almost equal to the level attained by the fusion protein administered i.n. with CT in terms of the average number of oocysts per mosquito (>99%) as well as the number of mosquitoes free of parasites (19/20 to 20/20). Although we did not assess the vaccine efficacy of the fusion protein emulsified in an oil adjuvant such as IFA, IFA was very effective in that almost complete blockade was observed for unfused antigen. It is likely that a combination of oil adjuvant and the CTB-coupling strategy would further enhance the efficacy. Taken together, we conclude that (i) s.c. immunization is more efficacious than i.n. immunization, inducing "one-level-higher" immunity than i.n. immunization, and (ii) a CTB-coupling strategy is substantially effective in enhancing transmission-blocking immunity, but supplementation with extraneous adjuvants is expected to induce an even higher immunity (Fig. 5).

The clinical use of CT, particularly as a nasal adjuvant, is hampered by its toxicity (26). Furthermore, the nontoxic CTB has yet to be proven a safe nasal vaccine delivery molecule.

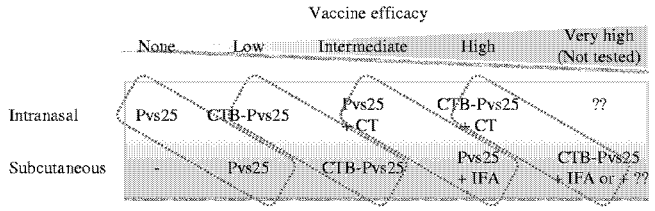

FIG. 5. Schematic summary of the observed or expected (but not tested) transmission-blocking vaccine (TBV) efficacy induced by each immunization regime. s.c. immunization tended to induce "one-level-higher" immunity than i.n. immunization in our experimental model. Identical or similar vaccine formulations are encircled by a dotted line. CTB, cholera toxin B subunit; CT, cholera toxin; IFA, incomplete Freund's adjuvant.

Therefore, an alternative approach for using CTB as a vaccine antigen carrier is highly desirable. Although there have been numerous reports demonstrating enhanced mucosal immunogenicity of various antigens by coupling to CTB (13), very few systematic studies have been conducted to assess CTB's antigen carrier capacity for s.c.-delivered antigens. Our present study clearly demonstrated the potential of CTB in s.c. vaccine platform design. Furthermore, it is notable that, unlike antigens emulsified with oil adjuvant such as IFA or antigens administered with an aluminum hydroxide adjuvant, the protein-only CTB-coupled antigens are likely to be much less reactogenic. It is believed that recent innovations in effective but much less locally reactogenic and safer oil adjuvants such as MF59 (Chiron Corp., Emeryville, CA) (20, 21), the Montanide ISA series (Seppic, Inc., Fairfield, NJ) (20, 29), and the GlaxoSmithKline adjuvant systems (GlaxoSmithKline, Brentford, United Kingdom) (8, 27), will expedite malaria vaccine development. It is also possible that protein delivery molecules will ultimately be combined with effective oil or other adjuvants, including aluminum hydroxide. This is supported by our recent unpublished study in which a recombinant malaria antigen administered with an alum adjuvant only marginally enhanced its immunogenicity, whereas the same antigen loaded onto carrier molecules became highly immunogenic when applied together with the alum.

In the present study, we did not assess the molecular mechanisms of the immune potentiating function of CTB. However, our observation that simple mixing of Pvs25H-A with CTB did not produce a profound immune enhancement implies that its immunogenicity results from the antigen delivery, rather than a physiological cell activation, as occurs for CT. Further experiments are ongoing to characterize the immune potentiating function of CTB using the C-terminal 19-kDa fragment of merozoite surface protein 1 from *Plasmodium yoelii*. The results of these studies will help us judge whether CTB could contribute to a new platform technology for the design of s.c.-delivered subunit vaccines against infectious diseases such as malaria.

ACKNOWLEDGMENTS

We thank the staff of the Department of Entomology, Armed Forces Research Institute of Medical Sciences, Bangkok, Thailand, for their technical assistance.

This study was supported by the following grants: the Program of Founding Research Centers for Emerging and Reemerging Infectious Diseases from the Ministry of Education, Culture, Sports, Science and Technology, Japan (MEXT); Grants-in-Aid for Scientific Research (19406009 and 20590425) and Scientific Research on Priority Areas (21022034) from MEXT; a grant from The Okinawa Industry Promotion Public Corp. (Naha, Okinawa, Japan); and a Cooperative Research Grant from NEKKEN, 2010.

REFERENCES

1. **Arakawa, T., A. Komesu, H. Otsuki, J. Sattabongkot, R. Udomsangpetch, Y. Matsumoto, N. Tsuji, Y. Wu, M. Torii, and T. Tsuboi.** 2005. Nasal immunization with a malaria transmission-blocking vaccine candidate, Pfs25, induces complete protective immunity in mice against field isolates of *Plasmodium falciparum*. Infect. Immun. **73:**7375–7380.
2. **Arakawa, T., M. Tachibana, T. Miyata, T. Harakuni, H. Kohama, Y. Matsumoto, N. Tsuji, H. Hisaeda, A. Stowers, M. Torii, and T. Tsuboi.** 2009. Malaria ookinete surface protein-based vaccination via the intranasal route completely blocks parasite transmission in both passive and active vaccination regimens in a rodent model of malaria infection. Infect. Immun. **77:**5496–5500.
3. **Arakawa, T., T. Tsuboi, A. Kishimoto, J. Sattabongkot, N. Suwanabun, T. Rungruang, Y. Matsumoto, N. Tsuji, H. Hisaeda, A. Stowers, I. Shimabukuro, Y. Sato, and M. Torii.** 2003. Serum antibodies induced by intranasal immunization of mice with *Plasmodium vivax* Pvs25 co-administered with cholera toxin completely block parasite transmission to mosquitoes. Vaccine **21:**3143–3148.
4. **Arevalo-Herrera, M., C. Chitnis, and S. Herrera.** 2010. Current status of *Plasmodium vivax* vaccine. Hum. Vaccin. **6:**124–132.
5. **Bill and Melinda Gates Foundation.** 2009. Global health program. Bill and Melinda Gates Foundation, Seattle, WA. http://www.gatesfoundation.org/global-health/Documents/malaria-strategy.pdf.
6. **Birkett, A. J.** 2010. PATH Malaria Vaccine Initiative (MVI): perspectives on the status of malaria vaccine development. Hum. Vaccin. **6:**139–145.
7. **Carter, R.** 2001. Transmission blocking malaria vaccines. Vaccine **19:**2309–2314.
8. **Garcon, N., P. Chomez, and M. Van Mechelen.** 2007. GlaxoSmithKline adjuvant systems in vaccines: concepts, achievements and perspectives. Expert Rev. Vaccines **6:**723–739.
9. **Genton, B.** 2008. Malaria vaccines: a toy for travelers or a tool for eradication? Expert Rev. Vaccines **7:**597–611.
10. **Greenwood, B. M., D. A. Fidock, D. E. Kyle, S. H. Kappe, P. L. Alonso, F. H. Collins, and P. E. Duffy.** 2008. Malaria: progress, perils, and prospects for eradication. J. Clin. Invest. **118:**1266–1276.
11. **Harakuni, T., H. Sugawa, A. Komesu, M. Tadano, and T. Arakawa.** 2005. Heteropentameric cholera toxin B subunit chimeric molecules genetically fused to a vaccine antigen induce systemic and mucosal immune responses: a potential new strategy to target recombinant vaccine antigens to mucosal immune systems. Infect. Immun. **73:**5654–5665.
12. **Hisaeda, H., A. W. Stowers, T. Tsuboi, W. E. Collins, J. S. Sattabongkot, N. Suwanabun, M. Torii, and D. C. Kaslow.** 2000. Antibodies to malaria vaccine candidates Pvs25 and Pvs28 completely block the ability of *Plasmodium vivax* to infect mosquitoes. Infect. Immun. **68:**6618–6623.
13. **Holmgren, J., J. Adamsson, F. Anjuere, J. Clemens, C. Czerkinsky, K. Eriksson, C. F. Flach, A. George-Chandy, A. M. Harandi, M. Lebens, T. Lehner, M. Lindblad, E. Nygren, S. Raghavan, J. Sanchez, M. Stanford, J. B. Sun, A. M. Svennerholm, and S. Tengvall.** 2005. Mucosal adjuvants and anti-infection and anti-immunopathology vaccines based on cholera toxin, cholera toxin B subunit and CpG DNA. Immunol. Lett. **97:**181–188.
14. **Kaslow, D. C.** 1997. Transmission-blocking vaccines: uses and current status of development. Int. J. Parasitol. **27:**183–189.
15. **Kaslow, D. C., I. C. Bathurst, T. Lensen, T. Ponnudurai, P. J. Barr, and D. B. Keister.** 1994. *Saccharomyces cerevisiae* recombinant Pfs25 adsorbed to alum elicits antibodies that block transmission of *Plasmodium falciparum*. Infect. Immun. **62:**5576–5580.
16. **Kubler-Kielb, J., F. Majadly, Y. Wu, D. L. Narum, C. Guo, L. H. Miller, J. Shiloach, J. B. Robbins, and R. Schneerson.** 2007. Long-lasting and transmission-blocking activity of antibodies to *Plasmodium falciparum* elicited in mice by protein conjugates of Pfs25. Proc. Natl. Acad. Sci. U. S. A. **104:**293–298.
17. **Malkin, E. M., A. P. Durbin, D. J. Diemert, J. Sattabongkot, Y. Wu, K. Miura, C. A. Long, L. Lambert, A. P. Miles, J. Wang, A. Stowers, L. H. Miller, and A. Saul.** 2005. Phase 1 vaccine trial of Pvs25H: a transmission blocking vaccine for *Plasmodium vivax* malaria. Vaccine **23:**3131–3138.
18. **Mendis, K., B. J. Sina, P. Marchesini, and R. Carter.** 2001. The neglected burden of *Plasmodium vivax* malaria. Am. J. Trop. Med. Hyg. **64:**97–106.
19. **Miles, A. P., Y. Zhang, A. Saul, and A. W. Stowers.** 2002. Large-scale purification and characterization of malaria vaccine candidate antigen Pvs25H for use in clinical trials. Protein Expr. Purif. **25:**87–96.
20. **Peek, L. J., C. R. Middaugh, and C. Berkland.** 2008. Nanotechnology in vaccine delivery. Adv. Drug Deliv. Rev. **60:**915–928.
21. **Sachdeva, S., A. Mohmmed, P. V. Dasaradhi, B. S. Crabb, A. Katyal, P. Malhotra, and V. S. Chauhan.** 2006. Immunogenicity and protective efficacy

of *Escherichia coli* expressed *Plasmodium falciparum* merozoite surface protein-1_{42} using human compatible adjuvants. Vaccine **24:**2007–2016.
22. **Saxena, A. K., K. Singh, H. P. Su, M. M. Klein, A. W. Stowers, A. J. Saul, C. A. Long, and D. N. Garboczi.** 2006. The essential mosquito-stage P25 and P28 proteins from *Plasmodium* form tile-like triangular prisms. Nat. Struct. Mol. Biol. **13:**90–91.
23. **Suwanabun, N., J. Sattabongkot, T. Tsuboi, M. Torii, N. Maneechai, N. Rachapaew, N. Yim-amnuaychok, V. Punkitchar, and R. E. Coleman.** 2001. Development of a method for the in vitro production of *Plasmodium vivax* ookinetes. J. Parasitol. **87:**928–930.
24. **Targett, G. A., and B. M. Greenwood.** 2008. Malaria vaccines and their potential role in the elimination of malaria. Malar. J. **7**(Suppl. 1)**:**S10.
25. **Tsuboi, T., M. Tachibana, O. Kaneko, and M. Torii.** 2003. Transmission-blocking vaccine of vivax malaria. Parasitol. Int. **52:**1–11.
26. **van Ginkel, F. W., R. J. Jackson, Y. Yuki, and J. R. McGhee.** 2000. Cutting edge: the mucosal adjuvant cholera toxin redirects vaccine proteins into olfactory tissues. J. Immunol. **165:**4778–4782.
27. **Waitumbi, J. N., S. B. Anyona, C. W. Hunja, C. M. Kifude, M. E. Polhemus, D. S. Walsh, C. F. Ockenhouse, D. G. Heppner, A. Leach, M. Lievens, W. R. Ballou, J. D. Cohen, and C. J. Sutherland.** 2009. Impact of RTS,S/AS02(A) and RTS,S/AS01(B) on genotypes of *P. falciparum* in adults participating in a malaria vaccine clinical trial. PLoS One **4:**e7849.
28. **World Health Organization.** 2005. World health report. World Health Organization, Geneva Switzerland.
29. **Wu, Y., R. D. Ellis, D. Shaffer, E. Fontes, E. M. Malkin, S. Mahanty, M. P. Fay, D. Narum, K. Rausch, A. P. Miles, J. Aebig, A. Orcutt, O. Muratova, G. Song, L. Lambert, D. Zhu, K. Miura, C. Long, A. Saul, L. H. Miller, and A. P. Durbin.** 2008. Phase 1 trial of malaria transmission blocking vaccine candidates Pfs25 and Pvs25 formulated with montanide ISA 51. PLoS One **3:**e2636.
30. **Wu, Y., C. Przysiecki, E. Flanagan, S. N. Bello-Irizarry, R. Ionescu, O. Muratova, G. Dobrescu, L. Lambert, D. Keister, Y. Rippeon, C. A. Long, L. Shi, M. Caulfield, A. Shaw, A. Saul, J. Shiver, and L. H. Miller.** 2006. Sustained high-titer antibody responses induced by conjugating a malarial vaccine candidate to outer-membrane protein complex. Proc. Natl. Acad. Sci. U. S. A. **103:**18243–18248.

Editor: J. H. Adams

Vaccine 28 (2010) 6014–6020

Contents lists available at ScienceDirect

Vaccine

journal homepage: www.elsevier.com/locate/vaccine

Intranasal and intramuscular immunization with Baculovirus Dual Expression System-based Pvs25 vaccine substantially blocks *Plasmodium vivax* transmission

Andrew M. Blagborough[a,*], Shigeto Yoshida[b,**], Jetsumon Sattabongkot[c], Takafumi Tsuboi[d], Robert E. Sinden[a]

[a] *Division of Cell and Molecular Biology, Department of Life Sciences, Sir Alexander Fleming Building, Imperial College London, Imperial College Road, London SW7 2AZ, UK*
[b] *Division of Medical Zoology, Department of Infection and Immunity, Jichi Medical University, Tochigi 329-0498, Japan*
[c] *Department of Entomology, Armed Forces Research Institute of Medical Sciences, Bangkok 10400, Thailand*
[d] *Cell-Free Science and Technology Research Center, Ehime University, Matsuyama, Ehime 790-8577, Japan*

ARTICLE INFO

Article history:
Received 31 March 2010
Received in revised form 28 June 2010
Accepted 29 June 2010
Available online 14 July 2010

Keywords:
Malaria
Plasmodium vivax
Baculovirus
Transgenic

ABSTRACT

We have recently developed a new experimental vaccine vector system based on *Autographa californica* nucleopolyhedrosis virus (AcNPV) termed the "Baculovirus Dual Expression System", which drives expression of vaccine candidate antigens by a dual promoter that consists of tandemly arranged baculovirus-derived polyhedrin and mammalian-derived CMV promoters. The present study used this system to generate a *Plasmodium vivax* transmission-blocking immunogen (AcNPV-Dual-Pvs25). AcNPV-Dual-Pvs25 not only displayed Pvs25 on the AcNPV envelope, exhibiting aspects of its native three-dimensional structure, but also expressed appropriately immunogenic protein upon transduction of mammalian cells. Both intranasal and intramuscular immunization of mice with AcNPV-Dual-Pvs25 induced high Pvs25-specific antibody titres, notably of IgG1, IgG2a and IgG2b isotypes, indicating a mixed Th1/Th2 response. Importantly, sera obtained from subcutaneously immunized rabbits exhibited a significant transmission-blocking effect (96% reduction in infection intensity, 24% reduction in prevalence) when challenged with human blood infected with *P. vivax* gametocytes using the standard membrane feeding assay. Additionally, active immunization (both intranasal and intramuscular routes) of mice followed by challenge using a transgenic *P. berghei* line expressing Pvs25 in place of native Pbs25 and Pbs28 (clone Pvs25DR3) demonstrates a strong transmission-blocking response, with a 92.1% (intranasal) and 83.8% (intramuscular) reduction in oocyst intensity. Corresponding reductions in prevalence of infection were observed (88.4% and 75.5% respectively). This study offers a novel tool for the development of malarial transmission-blocking vaccines against the sexual stages of the parasite, using the Baculovirus Dual Expression System that functions as both a subunit, and DNA based vaccine.

1. Introduction

Malaria is a serious, acute and sometimes relapsing disease, caused by protozoan parasites of the genus *Plasmodium*. It is responsible for high morbidity and mortality in tropical and subtropical regions, causing approximately 1 million deaths per year, the majority of whom are African children under the age of five [25]. Given the complex life cycles of the different plasmodial species and the distinct host immune responses to each developmental stage, *Plasmodium* provides many potential targets for the development of prophylactic vaccines against the parasite.

An anti-malarial transmission-blocking vaccine (TBV) that prevents fertilization and/or ookinete/oocyst development within the mosquito is an attractive strategy to limit the transmission of malaria. The ookinete proteins Pvs25 and Pvs28 which are expressed on the surface of the sexual and early sporogonic forms of *Plasmodium vivax* are presently lead targets for the development of a *P. vivax* TBV [15–18]. A variety of expression vectors (e.g., *Escherichia coli*, *Pichia pastoris* and DNA) have been used to express Pvs25 protein which has been administered alone or in combination with adjuvants (e.g., Freund's adjuvant, aluminum hydroxide and cholera toxin) [19,20,26,33,34]. To date these studies suggest that the recombinant protein currently requires both not only linear, but conformation dependent epitopes, and a strong adjuvant to induce transmission-blocking antibodies. Phase I human trials with a clinical-grade recombinant Pvs25 produced by *P. pastoris* administered with an alum adjuvant produced antibodies that inhibit transmission of the parasite by ~80% (intensity) and 20–30% (prevalence) [19].

* Corresponding author at: Imperial College Road, London SW7 2AZ, UK. Tel.: +44 0 20 7594 5350.
** Corresponding author at: 3311-1 Yakushiji, Shimotsuke, Tochigi 329-0498, Japan. Tel.: +81 285 58 7339; fax: +81 285 44 6489.
E-mail addresses: andrew.blagborough@imperial.ac.uk (A.M. Blagborough), shigeto@jichi.ac.jp (S. Yoshida).

0264-410X/$ – see front matter © 2010 Elsevier Ltd. All rights reserved.
doi:10.1016/j.vaccine.2010.06.100

To improve the safety and efficacy of current Pvs25-based TBV candidates, new vaccine vehicles and/or delivery systems (e.g., needle- and adjuvant-free, long-lasting and cost-effective) need to be considered. In addition, a suitable small-animal model for the *in vivo* assessment of *P. vivax* TBV-induced functional immune responses might provide a useful tool for evaluating its TBV efficacy before proceeding to human clinical trials. Recently, we have developed a new vaccine vector system based on the baculovirus *Autographa californica* nucleopolyhedrosis virus (AcNPV) termed the "Baculovirus Dual Expression System", which drives expression of vaccine candidate antigens by a dual promoter that consists of tandemly arranged baculovirus-derived polyhedrin and mammalian-derived CMV promoters. It has been shown that AcNPV, an enveloped double-stranded DNA virus that naturally infects insects, possesses strong adjuvant properties that can activate dendritic cell-mediated innate immunity through MyD88/TLR9-dependent and -independent pathways [30]. When applied to *P. berghei* circumsporozoite protein (PbCSP) as a model for malaria pre-erythrocytic stage vaccine, this immunogen elicited high PbCSP-specific antibody titres and PbCSP-specific $CD8^+$ T-cell responses without extraneous immunological adjuvants in mice, and conferred complete protection against sporozoite challenge [8]. The Baculovirus Dual Expression System therefore constitutes an innate immunostimulating complex, and functions as a subunit and DNA vaccine that generates strong humoral and cellular immune responses. In addition, the AcNPV-based vaccine has another great potential for adjuvant-free intranasal (i.n.) administration. For blood-stage malaria vaccine development, we have also shown that i.n. immunization with AcNPV-based vaccine expressing *P. yoelii* merozoite surface protein 1 19 kDa fragment ($PyMSP1_{19}$) induced not only strong systemic humoral immune responses with high titre of $PyMSP1_{19}$-specific antibody but also natural boosting of $PyMSP1_{19}$-specific antibody responses at a short time following challenge, and conferred complete protection [28].

Here we evaluate a second-generation transmission-blocking Pvs25 immunization protocol based on the Baculovirus Dual Expression System (AcNPV-Dual-Pvs25). We show that the AcNPV-Dual-Pvs25 elicits highly effective Pvs25-specific humoral immune responses, and confers significant transmission-blocking activity, assessed by the standard membrane feeding assay (SMFA) on peripheral blood from *P. vivax* infected patients, and by active immunization of mice challenged with *P. berghei* expressing Pv25 (Pvs25DR3), which has been specifically generated as a murine model for the *in vivo* assessment of Pvs25-based TBV-induced functional immune responses [12].

The data reported here demonstrates the successful implementation of the Baculovirus Dual Expression System using both i.n. and intramuscular (i.m.) methods of delivery, giving equivalent responses for each method of immunization. Our results show that the Baculovirus Dual Expression System provides a simple, non-toxic, safe and adjuvant-free vaccine delivery platform, and as such could be considered as a powerful tool for the development of future TBVs against *Plasmodium* spp.

2. Materials and methods

2.1. Cell lines, mice and parasites

Sf9 cells were maintained at 27 °C in SF900-II medium (Invitrogen, San Diego, CA) supplemented with antibiotics. HepG2 cells were maintained at 37 °C in Dulbecco's modified Eagle's medium (Invitrogen) supplemented with 10% (v/v) heat-inactivated fetal bovine serum, 2 mM L-glutamine, and antibiotics. Female BALB/c or Theiler's Original (TO) mice, 7–8 weeks of age at the start of the experiment, were purchased from Harlan (UK). *P. berghei* clones ANKA 2.34 and Pvs25DR3 [12] were used for challenge infections. General parasite maintenance was carried out as described previously [24].

2.2. Recombinant baculovirus

The DNA sequence corresponding to amino acids Ala_{23}-Leu_{195} of Pvs25 (*P. vivax* Salvador I strain) was amplified from pEU3-Pvs25 [27] using the primers pPvs25-F1 (5′-GAATTCATGGCTAGCGCCGTCACGGTAGACACC-3′) and pPvs25-R1 (5′-CCCGGGGCCCAAGGCATACATTTTTCTCTTT-3′). The PCR product was ligated into the *Eco*RI/*Sma*I sites of pTriEx–PbCSP–gp64 [8] to construct a baculovirus transfer vector, pTriEx–Pvs25–gp64 (Fig. 1). The recombinant baculovirus AcNPV-Dual-Pvs25 was generated in Sf9 cells by co-transfection of the recombinant transfer plasmids pTriEx–Pvs25–gp64, with BacVector-2000 DNA (Novagen), according to the manufacturer's protocol. Purification of viral particles was performed as described previously [8]. The purified baculovirus particles were free of endotoxin (<0.01 endotoxin units/10^9 PFU), as determined by the Endospecy® endotoxin measurement kit (Seikagaku Co., Tokyo, Japan).

2.3. Recombinant proteins

A 0.5-kb fragment of the *Pvs25* gene (encoding amino acids 23–159) was excised from pTriEx–Pvs25–gp64 by digestion with *Eco*RI and *Sma*I, and inserted into the *Eco*RI/*Sma*I sites of pGEX-4T-1 (GE Healthcare) to construct the recombinant expression plasmid, pGEX-Pvs25. Recombinant Pvs25, created as a fusion protein with glutathione S-transferase (GST-Pvs25), was expressed in *E. coli* and purified using a GST affinity column (GE Healthcare) as described previously [1]. Resultant protein was used as an immunogen for vaccination of mice and as antigen for isotype analysis.

2.4. Western blotting and indirect immunofluorescence assay (IFA)

Western blotting was carried out as described previously [2]. HepG2 cells were seeded at a density of 5×10^4 cells/well in collagen-type-I-coated eight-well chamber slides (BD Biosciences) and transduced with purified baculovirus particles at an m.o.i. of 10. After 48 h incubation, cells were fixed for 15 min in acetone/methanol [6,4] at −20 °C, and incubated with anti-Pvs25 mAb N1-1H10 (MR4, Manassas, VA) and then with FITC-conjugated goat anti-mouse IgG (Biosource International, Camarillo, CA).

For preparation of *P. vivax* ookinetes, peripheral blood was collected in heparinized syringes under written informed consent from patients who attended malaria clinics within the Mae Sod district in the Tak province of northwestern Thailand. The use of all human materials in this study was reviewed and approved by the Institutional Ethics Committee of the Thai Ministry of Public Health and the Human Subjects Research Review Board of the Walter Reed Army Institute of Research, USA. For IFA, cultured *P. vivax* parasite preparations rich in zygotes and small numbers of ookinetes were spotted on slides and fixed with acetone. Sera obtained from immunized mice were tested by IFA on the fixed parasite material. To confirm the position of all parasites in the IFA, the slides were stained with DAPI (4′,6-diamidino-2-phenylindole) (Wako Pure Chemical, Osaka, Japan). Bound antibodies and labeled nuclei were recorded by confocal scanning laser microscopy (LSM5 PASCAL; Carl Zeiss MicroImaging, Thornwood, NY).

2.5. Immunization

Mice were immunized four times at 3-week intervals with 5×10^7 PFU of AcNPV-Dual-Pvs25 either by the i.m. or i.n. routes.

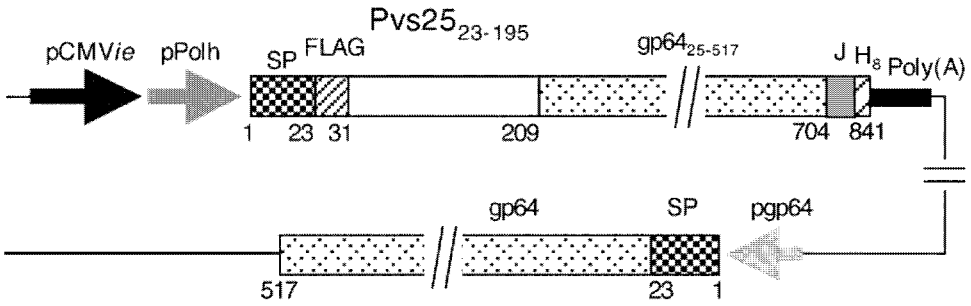

Fig. 1. Schematic representation of AcNPV-Dual-Pvs25 genome structure. A gene cassette that consisted of the gp64 signal sequence (SP), the *Pvs25* gene (Pvs25$_{25-195}$) fused to the N terminus of the AcNPV major envelope protein *gp64* gene (gp64$_{25-517}$), and the rabbit β-globlin poly(A) signal [poly(A)]. Expression of the gene cassette was driven by a dual promoter that consisted of the CMV immediate early enhancer/promoter (pCMV*ie*) and the polyhedrin promoter (pPolh). AcNPV-Dual-Pvs25 also possessed the endogenous *gp64* gene. Numbers indicate the amino acid positions of Pvs25–gp64 fusion protein and endogenous gp64. FLAG, FLAG epitope tag; Pvs25$_{25-195}$, Pvs25 corresponding to amino acids 25–195; gp64$_{25-517}$, gp64 corresponding to amino acids 25–517; J, junction consisting of 29 unrelated amino acid residues; H8, His-tag; pgp64, gp64 promoter.

For i.n. immunization, a total of 50 μl, divided into three doses delivered at 5-min intervals, was inoculated dropwise with a 20 μl pipette. As a comparative (negative) control, mice were immunized i.n. with 1×10^8 PFU of AcNPV-CMV-EGFP. Sera were collected two weeks after the final immunization prior to infection with *P. berghei* (either ANKA 2.34 or Pvs25DR3) to evaluate anti-Pvs25 response by ELISA. Immunized mice were kept for a total of 5 months following final immunization to quantify immune response over a longer time period. Serum was harvested from each mouse on a monthly basis, and ELISA performed as described below.

To prepare antibodies for use in standard membrane feeding assays using vivax patient blood, rabbits were immunized subcutaneously three times at 3-week intervals with 1×10^8 PFU of AcNPV-Dual-Pvs25. Two weeks after the final immunization, sera were collected and IgG purified using HiTrap™ Protein G HP chromatography (GE Healthcare) together with pre-immune rabbit sera.

2.6. ELISA for antibody titres and isotypes

Sera obtained from immunized mice were collected by tail bleeds prior to challenge. For some mice, sera were also collected periodically after final immunization. ELISA plates pre-coated with 100 ng/well GST-Pvs25 were incubated with serial dilutions of sera. Specific IgGs were detected using HRP-conjugated goat anti-mouse IgG (H + L) (Bio-Rad, Hercules, CA). For isotype determination, HRP-conjugated rabbit anti-mouse IgG1, IgG2a, IgG2b, and IgG3 (Zymed Laboratories, San Francisco, CA) antibodies were used. The plates were developed with peroxidase substrate solution [H_2O_2 and 2,2′-azino-bis(3-ethylbenzthiazoline-6-sulphonic acid)]. The OD at 414 nm of each well was measured using a plate reader. Endpoint titres were expressed as the reciprocal of the highest sample dilution for which the OD was equal or greater than the mean OD of non-immune control sera.

2.7. Transmission-blocking assay (standard membrane feeding assay)

Peripheral blood was collected from four volunteer patients infected only with *P. vivax* as described above. Purified anti-AcNPV-Dual-Pvs25 rabbit IgG was diluted (1-, 4- and 16-fold) with IgG from pre-immune rabbits, then 75 μl of each rabbit IgG mixture was mixed with 105 μl of heat-inactivated normal human AB serum prepared from malaria naive Thai donors. Diluted IgG was mixed with *P. vivax*-infected blood cells (1:1, v/v ratio) and incubated for 15 min at room temperature. The mixture was placed in a membrane feeding apparatus at 37 °C. *Anopheles dirus* A mosquitoes (Bangkok colony, Armed Forces Research Institute of Medical Sciences) were allowed to feed for 30 min. Unfed mosquitoes were removed after blood feeding, and fully engorged mosquitoes were maintained on 10% sucrose for seven days. For each diluted IgG, at least 20 mosquitoes were dissected and analyzed by staining with 0.5% mercurochrome and subsequent microscopy to count the number of oocysts that developed on the mosquito midguts.

2.8. Transmission-blocking assay (active immunization)

In three separate experiments, mice immunized i.m. or i.n. with AcNPV-Dual-Pvs25 were divided into two groups (three mice per group), PH treated, and three days later infected i.p. with 10^6 parasites of *P. berghei* ANKA 2.34 or *P. berghei* Pvs25DR3. As a negative control, mice were immunized i.n. with AcNPV-CMV-EGFP, divided into two groups and infected as above. Three days post-infection, starved *A. stephensi* mosquitoes were allowed to feed on the infected mice. In all pots, >50 fed mosquitoes were fed per mouse. 24 h after feeding, mosquitoes were briefly anesthetized with CO_2, and unfeds removed. Mosquitoes were then maintained on fructose [8% (w/v) fructose, 0.05% (w/v) *p*-aminobenzoic acid] at 19–22 °C and 50–80% relative humidity. Day 10 post-feeding, mosquito midguts were dissected, and oocyst prevalence and intensity recorded. All care and handling of animals was in accordance with the Guidelines for Animal Care and Use prepared by Jichi Medical University and Imperial College London.

2.9. Statistical analyses

Statistical analysis was performed with Graphpad Prism Software (Graphpad Software Inc.). For the membrane feeding assay, The Kruskal–Wallis test was used to examine the difference in oocyst counts per mosquito between pre-immune IgG and immune IgG groups. For long-term anti-Pvs25 ELISA responses, significant variations of titres over time were evaluated using Spearman's rank correlation ($p < 0.05$). For active immunization, significance was assessed using Mann–Whitney *U* test (to examine the difference in oocyst counts per mosquito between AcNPV-Dual-Pvs25 or AcNPV-CMV-EGFP immunized groups) and the Fisher's exact probability test (to examine the difference in infection prevelance between AcNPV-Dual-Pvs25 or AcNPV-CMV-EGFP immunized groups) *P* values less than 0.05 were considered statistically significant.

3. Results

3.1. Construction of baculovirus-based Pvs25 vaccine

To examine the expression of conformation-dependent epitopes, AcNPV-Dual-Pvs25 viral particles were analyzed by

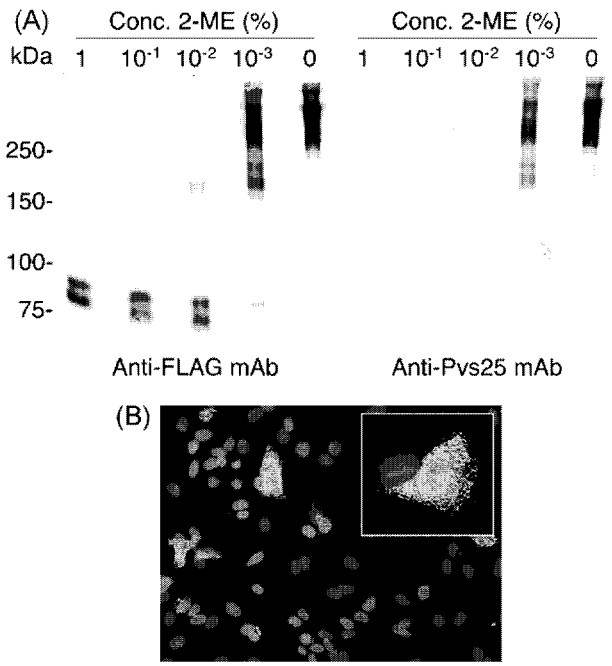

Fig. 2. Expression of Pvs25–gp64 fusion protein. (A) Western blotting of AcNPV-Dual-Pvs25 in the presence of various concentrations of 2-ME. AcNPV-Dual-Pvs25 was treated with the loading buffer containing descending concentrations of 2-ME. Reactivity of $Pvs25_{25-195}$ fusion protein was examined using either anti-FLAG mAb or anti-Pvs25 mAb, N1-1H10. The concentrations of 2-ME are shown above the gel. (B) *In vitro* expression analysis of Pvs25 by transducing AcNPV-Dual-Pvs25 in mammalian cells. HepG2 cells were transduced with AcNPV-Dual-Pvs25 at an m.o.i. of 10. Forty-eight hours later, cells were fixed with 5% paraformaldehyde followed by permeabilization with 0.1% Triton X in PBS, and incubated with anti-Pvs25 mAb 1H10. Bound antibodies were detected by FITC-labeled anti-mouse IgG by fluorescence microscopy (green). Cell nuclei were visualized by DAPI staining (blue). Original magnification, ×400.

Western blotting in the absence or presence of 10^{-3}% to 1% 2-mercaptoethanol (2-ME) (Fig. 2A). Anti-FLAG mAb, which recognizes a linear epitope within the N-terminal tag, reacted with doublet bands at all 2-ME concentrations, with relative molecular masses (M_r) of 80 and 90 kDa. The 80 kDa band corresponded to the predicted M_r of the Pvs25–gp64 fusion protein (Fig. 2A, left panel). We hypothesise the 90 kDa band may have resulted from post-translational modification within the insect cells. When 2-ME is added at concentrations above 10^{-3}%, recognition by anti-Pvs25 mAb N1-1H10, which has previously been shown to recognize a conformation-dependent epitope [29], is not detectable. In contrast, reducing of the concentration of 2-ME to below 10^{-3}% increased the reactivity of Pvs25–gp64 fusion protein with the mAb (Fig. 2A, right panel). These results suggest that the Pvs25–gp64 fusion protein on the virus envelope retains components of the three-dimensional structure of native Pvs25 protein, important to antibody recognition.

We also examined by IFA the ability of AcNPV-Dual-Pvs25 to drive Pvs25 expression in mammalian cells. Strong immunofluorescence signals were detected with N1-1H10 mAb in HepG2 cells infected with AcNPV-Dual-Pvs25 48 h after transfection (Fig. 2B). Thus AcNPV-Dual-Pvs25 not only expressed appropriately folded Pvs25 on viral particles, but also in mammalian cells.

3.2. Immunization with AcNPV-Dual-Pvs25 induces high Pvs25-specific antibody titres

I.n. and i.m. immunization with AcNPV-Dual-Pvs25 induced high antibody titres (>1:15,000) (Fig. 3A). Pvs25 antibodies were predominately IgG1, IgG2a and IgG2b (IgG1:IgG2a ratio ≅0.12 and 0.29 for i.m. and i.n. immunizations, respectively), indicating a mixed Th1/Th2-type immune response. IgG2b, which is inducible by mucosal immunization, was significantly higher in the i.n. group than the i.m. group. As demonstrated by the IFA test, these immune sera strongly reacted with Pvs25 in its native location on the parasite surface, circumferential staining of the *P. vivax* retort-form ookinete was prominent (Fig. 3B). Pvs25-specific antibody titres in sera obtained from both the i.m. and i.n. AcNPV-Dual-Pvs25 groups were sustained without any significant reduction over 5 months following the final immunization (Fig. 4).

3.3. Evaluation of transmission-blocking activity (SMFA)

Following subcutaneous immunization with AcNPV-Dual-Pvs25, IgG purified from immune rabbit serum reduced the intensity and prevalence of oocyst infection on the mosquito midgut profoundly (Fig. 5), in a dose-dependent manner. At an immune IgG concentration of 0.17 mg/ml, the mean intensity observed was 73.9 oocysts/midgut, and at 2.67 mg/ml, intensity was reduced to just 1.5 oocysts/midgut (a 98% inhibition of intensity when compared to pre-immune IgG at 2.67 mg/ml). Prevalence of infection was reduced by 70% from 94% in the pre-immune control, to give an overall reduction of 25.5% (with respect to pre-immune IgG). At lower concentrations of immune IgG tested, no significant reduction of prevalence was observed.

3.4. Evaluation of transmission-blocking activity (in vivo evaluation)

To examine transmission blockade *in vivo*, immunized mice were infected with transgenic *P. berghei* expressing Pv25 (Pvs25DR3), *A. stephensi* mosquitoes were fed directly on the immunized and challenged hosts (Table 1). AcNPV-Dual-Pvs25 was administered either by i.m. or i.n. route into six mice each. Six control mice were also immunized i.n. with AcNPV-CMV-EGFP as a negative control. For each immunization method, three mice were challenged with *P. berghei* ANKA 2.34 (to determine whether there was a direct but unexpected anti-*P. berghei* response), and three were immunized with *P. berghei* Pvs25DR3. WT *P. berghei* 2.34 does not express Pvs25, and any TB effect observed would be due to non-specific phenomenon. *P. berghei* Pvs25DR3 expresses Pvs25 on the zygote and ookinete surface [12]. Mosquitoes that fed on control (AcNPV-CMV-EGFP) mice immunized by the intranasal route displayed an, average intensity of infection of 2.16 oocysts/midgut (±S.E.M.), whereas following mucosal delivery of AcNPV-Dual-Pvs25 and subsequent challenge, the average intensity was significantly reduced to 0.17 oocysts/midgut (±S.E.M.). Following intramuscular delivery, intensity was 0.25 oocysts/midgut (±S.E.M.); thus achieving a 92.1% and an 88.4% inhibition of intensity of infection with intranasal and intramuscular deliveries, respectively. Prevalence was similarly reduced, by 83.8% and 75.5% respectively.

4. Discussion

The Baculovirus Dual Expression System aims to facilitate the development of multifunctional vaccines capable of inducing strong humoral and cellular immune responses without the need for extraneous immunological adjuvants. In the present study, we applied this system to generation of a novel *P. vivax* TBV (AcNPV-Dual-Pvs25), which possesses a single gene cassette that consists of the Pvs25–gp64 fusion gene under the CMV-polyhedrin dual promoter. AcNPV-Dual-Pvs25 not only displayed Pvs25 on the viral envelope but also expressed following transduction of mammalian cells. Immunization of mice with AcNPV-Dual-Pvs25 induced high Pvs25-specific antibody titres with predominant IgG1, IgG2a and

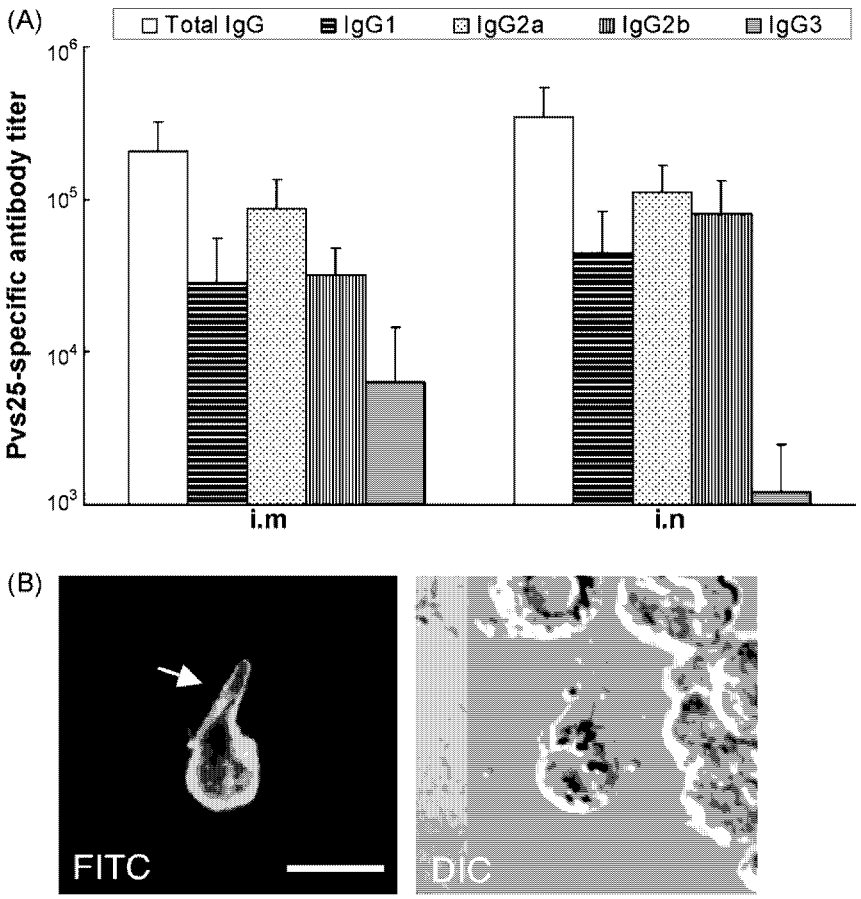

Fig. 3. Pvs25-specific antibody responses. Sera were collected from individual mice (6 mice/group) three weeks after the final immunization. (A) The individual sera were tested for total IgG, IgG1, IgG2a, IgG2b and IgG3 specific for Pvs25 by ELISA. The data represent one of two experiments, which had similar results. Data are the mean ± S.E.M. of groups. Significant differences of total IgG titres between different groups were evaluated using the two-tailed Fisher's exact probability test. *, $p < 0.01$. (B) Confocal fluorescence microscopy of sera obtained from mice immunized with AcNPV-Dual-Pvs25. The entire surface of cultured retorts/zygotes was clearly stained (green) by serum (1:500 dilution) obtained from a mouse immunized i.n. with AcNPV-Dual-Pvs25. Cell nuclei were visualized by blue DAPI staining (arrow) (immunofluorescence assay [IFA]). Right panel represents image obtained by differential interference contrast (DIC) microscopy. Scale bar, 10 μm.

IgG2b isotypes, indicating induction of both a mixed Th1/Th2 response.

We evaluated the transmission-blocking immunogenicity of AcNPV-Dual-Pvs25 using two methods. One was SMFA on peripheral blood from *P. vivax* infected patients. It has widely been accepted that malaria transmission-blocking immunity is mediated by antibodies that inhibit parasite development in the mosquito midgut [15,23,31,32]. The SMFA has provided valuable insights into functional transmission-blocking activities of sera from immunized animals. However, blood from *P. vivax*-infected patients as a source of SMFA is an unpredictable, and uncontrollable source of parasites and useful *in vitro* gametocyte culture has not been established. The other method was active immunization of mice followed by challenge with transgenic *P. berghei* Pvs25DR3. Compared with SMFA, active immunization/challenge method can assess the *in vivo* transmission-blocking potential of all immune factors including not only antibodies but also cytokine, complement and antibody-dependent cell cytotoxity. The approach of using transgenic rodent malarial parasites to assess the immune system's response to targets from a human malarial parasite has been described in previous studies [12–14]. Whilst the infectivity of all Pvs25DR3 transgenic lines tested to date is low compare to WT *P. berghei*, oocyst intensities are close to that seen *in vivo* for both *P. vivax* (and *P. falciparum*), and provide a very sensitive context to measure any transmission-blocking effect. Importantly, the transmission-blocking assays used clearly demonstrated that immunization with AcNPV-Dual-Pvs25 induced a strong transmission-blocking response, namely >90% reduction in oocyst number, and a corresponding fall in prevalence of 25.5% (SMFA) and 83.8% (i.n.)/75.5% (i.m.) (active immunization). These results provide support for this novel strategy for the delivery of a malarial TBV.

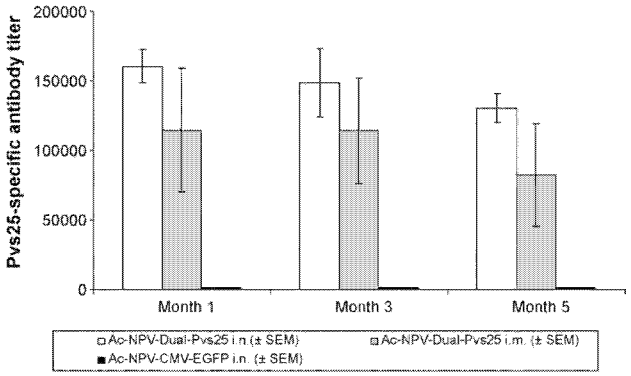

Fig. 4. Long-term ELISA titres following immunization with AcNPV-Dual-Pvs25. Sera were collected from individual mice three weeks following final immunization, and then at monthly intervals for 5 months. Six mice were examined for each immunogen. The individual sera were tested for total IgG specific for recombinant Pvs25 by ELISA. Samples shown are mean titres observed from six mice. Error bars show S.E.M. Significant variations of titres over time were evaluated using Spearman's rank correlation ($p < 0.05$). No statistically significant variation was observed in groups over 5 months.

Table 1
Evaluation of transmission-blocking activity by active immunization.

		Mean intensity (±S.E.M.)	Mean prevalence (% mosquitoes infected) (±S.E.M.)
AcNPV-Dual-Pvs25 immunized mice—i.n. delivery			
Mice 1–3: Pvs25DR3 challenged (±S.E.M.)		0.17 (0.1)	10.7 (3.1)
Mice 4–6: WT 2.34 challenged (±S.E.M.)		112.9 (8.43)	93.8 (3.46)
AcNPV-Dual-Pvs25 immunized mice—i.m. delivery			
Mice 7–9: Pvs25DR3 challenged (±S.E.M.)		0.25 (0.06)	16.2 (1.27)
Mice 10–12: WT 2.34 challenged (±S.E.M.)		88.8 (11.2)	89.6 (4.7)
AcNPV-CMV-EGFP immunized mice—i.n. delivery (negative control)			
Mice 13–15: Pvs25DR3 challenged (±S.E.M.)		2.16 (0.2)	66(4.23)
Mice 16–18: WT 2.34 challenged (±S.E.M.)		87.41 (15.6)	82.6 (10.9)
		Mean change in intensity	Mean change in prevalence
Overall Transmission blockade in AcNPV-Dual-Pvs25 immunised mice			
I.n.	Pvs25DR3	−92.10%[a]	−83.80%[b]
	P. berghei 2.34	+29.70%	+13.60%
I.m.	Pvs25DR3	−88.40%[a]	−75.50%[b]
	P. berghei 2.34	+1.60%	+8.50%

Mice were immunized four times with AcNPV-Dual-Pvs25 (i.m. and i.n.) or AcNPV-CMV-EGFP (i.n. only, negative control). Three groups of immunized mice were sub-divided into two groups, each containing three mice. Each group was then and challenged with WT *P. berghei* 2.34 (3 mice) or *P. berghei* Pvs25DR3 (3 mice), and used to assess transmission to mosquitoes via direct gametocyte feed. 10^6 parasites were injected per mouse. Mosquito midguts were dissected 10–12 days post feed. Mean intensities and prevalence were calculated from triplicate mice. Overall transmission blockade (in terms of both infection intensity and prevelance) was calculated by comparison to AcNPV-CMV-EGFP immunized mice. Significance was assessed using Mann–Whitney *U* test (to examine the difference in oocyst counts per mosquito between AcNPV-Dual-Pvs25 or AcNPV-CMV-EGFP immunized groups) and the Fisher's exact probability test (to examine the difference in infection prevelance between AcNPV-Dual-Pvs25 or AcNPV-CMV-EGFP immunized groups) ($p < 0.05$). Following challenge with WT *P. berghei* 2.34, no significant change in either intensity or prevalence was observed with either intranasal or intramuscular immunization. Significant inhibition was only observed following challenge with Pvs25DR3.

[a] $P < 0.05$, Mann–Whitney *U* test.

[b] $P < 0.05$, Fisher's exact probability test.

Mucosal vaccines have several attractive features compared with parenteral vaccines (e.g., safety, cost-effectiveness and ease of administration), but studies on their use have been limited almost exclusively to protection against mucosally transmitted pathogens. We provide evidence that i.n. immunization is a feasible alternative for preventing malaria, which is transmitted through non-mucosal routes. Compared with i.m. immunization, i.n. immunization led to higher Pvs25-specific antibody titres and potent transmission-blocking activity (i.n.:i.m.; intensity = 92.1%:88.4%, prevalence = 83.8%:75.5%). These results are consistent with our previous work showing that intranasal immunization with the baculovirus-based vaccine induced strong systemic humoral immune responses with high titres of antigen-specific antibodies and conferred complete protection against malaria blood-stage challenge [8,9,28]. It has previously been reported that intranasal immunization with recombinant Pvs25, using cholera toxin (CT) as an adjuvant, induced a systemic immune response with transmission-blocking activity [21]. Additionally, the mucosal immunogenicity and protective efficacy of recombinant Pfs25 and Pys25 have been thoroughly described [10,11]. CT, whilst a strong immune potentiator [10,11,21], which can induce immunological memory against heterologous antigens in a rodent model; however, it is precluded from clinical use due to its enterotoxicity and potential hazardous effects on olfactory nerves [22]. In contrast, a baculovirus-based delivery system may offer an attractive immunization method, as AcNPV exhibits low cytotoxicity and is incapable of replication in mammalian cells [8,9].

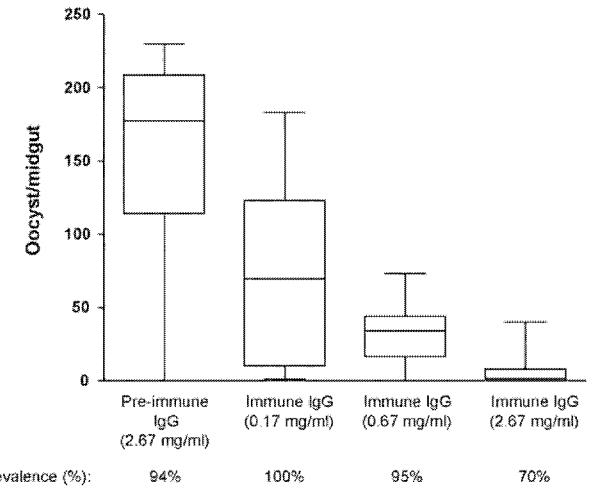

Fig. 5. Transmission-blocking efficacy against Thai *P. vivax* isolates by membrane feeding assay. Rabbits were immunized subcutaneously with AcNPV-Dual-Pvs25 vaccine. The purified rabbit IgG was evaluated by membrane feeding of *P. vivax*-infected blood from patients in Thailand. The IgG effectively inhibited oocyst formation in the mosquito midguts in a dose-dependent manner. Experiments were performed using blood from four volunteers naturally infected with *P. vivax*. The data presented was obtained from one volunteer. Data are expressed as the median numbers of oocysts per mosquitoes (lines in boxes), quartiles (boxes), and ranges (lines above and below boxes). Stastistically significant differences in oocyst counts per mosquito between pre-immune IgG and immune IgG groups were confirmed by the Kruskal–Wallis test ($P < 0.0001$).

Anti-malarial transmission-blocking vaccines based on the surface of the sexual and other sporogonic stages of *Plasmodium* inhibit further development of the parasite within the mosquito host, and have a significant potential to reduce malarial transmission in endemic areas. The data described here adds to previously presented data showing the significant potential of the baculovirus dual expression system against the blood stages of the parasite [8,9,28], but also demonstrates clearly its ability to induce antibodies against the ookinete surface protein Pvs25, and to elicit a transmission-blocking immune response against the *P. vivax* isolates from endemic areas, and a transgenic rodent malaria parasite model in preliminary studies.

Acknowledgments

We would like to thank Hitomi Araki for excellent assistance with the ELISAs and handling of the mice. We also thank Ken

Baker and Mark Tunnicliff for mosquito rearing (Imperial College, London). This work was supported by grants from the Ministry of Education, Culture, Sports and Science of Japan (21390126) (Jichi Medical University), and Biomalpar, Transmolbloc and BBSRC (award number LDAD_P15820) (Imperial College, London).

References

[1] Daly TM, Long CA. A recombinant 15-kilodalton carboxyl-terminal fragment of *Plasmodium yoelii yoelii* 17XL merozoite surface protein 1 induces a protective immune response in mice. Infect Immun 1993;61:2462–7.
[2] Davies AH. "Baculophage": a new tool for protein display. Biotechnology (N Y) 1995;13:1046.
[4] Jin R, Lv Z, Chen Q, Quan Y, Zhang H, Li S, et al. Safety and immunogenicity of H5N1 influenza vaccine based on baculovirus surface display system of *Bombyx mori*. PLoS ONE 2008;3:e3933.
[6] Matsuura Y, Possee RD, Overton HA, Bishop DH. Baculovirus expression vectors: the requirements for high level expression of proteins, including glycoproteins. J Gen Virol 1987;68(Pt 5):1233–50.
[8] Yoshida S, Kawasaki M, Hariguchi N, Hirota K, Matsumoto M. A baculovirus dual expression system-based malaria vaccine induces strong protection against *Plasmodium berghei* sporozoite challenge in mice. Infect Immun 2009;77:1782–9.
[9] Yoshida S, Kondoh D, Arai E, Matsuoka H, Seki C, Tanaka T, et al. Baculovirus virions displaying *Plasmodium berghei* circumsporozoite protein protect mice against malaria sporozoite infection. Virology 2003;316:161–70.
[10] Arakawa T, Tachibana M, Miyata T, Harakuni T, Kohama H, Matsumoto Y, et al. Malaria ookinete surface protein-based vaccination via the intranasal route completely blocks parasite transmission both in passive and active vaccination regimes in a rodent malaria infection model. Infect Immun 2009. E-pub ahead of print 14th Sep.
[11] Arakawa T, Komesu A, Otsuki H, Sattabongkot J, Udomsangpetch R, Matsumoto Y, et al. Nasal immunization with a malaria transmission-blocking vaccine candidate, Pfs25, induces complete protective immunity in mice against field isolates of *Plasmodium falciparum*. Infect Immun 2005;73(11):7375–80.
[12] Ramjanee S, Robertson JS, Franke-Fayard B, Sinha R, Waters AP, Janse CJ, et al. The use of transgenic *Plasmodium berghei* expressing the *Plasmodium vivax* antigen P25 to determine the transmission-blocking activity of sera from malaria vaccine trials. Vaccine 2007;25(January (5)):886–94.
[13] Mlambo G, Maciel J, Kumar N. Murine model for assessment of *Plasmodium falciparum* transmission-blocking vaccine using transgenic *Plasmodium berghei* parasites expressing the target antigen Pfs25. Infect Immun 2008;76(May (5)):2018–24.
[14] Kumar KA, Oliveira GA, Edelman R, Nardin E, Nussenzweig V. Quantitative *Plasmodium* sporozoite neutralization assay (TSNA). J Immunol Methods 2004;292(September (1–2)):157–64.
[15] Kaslow DC. Transmission blocking vaccines. In: Hoffman SL, editor. Malaria vaccine development. Washington, DC: ASM Press; 1996. p. 181–228.
[16] Hisaeda H, Collins WE, Saul A, Stowers AW. Antibodies to *Plasmodium vivax* transmission-blocking vaccine candidate antigens Pv25 and Pvs28 do not show synergism. Vaccine 2001;20(5–6):763–70.
[17] Peiris JS, Premawansa S, Ranawaka MB, Udagama PV, Munasinghe YD, Nanayakkara MV, et al. Monoclonal and polyclonal antibodies both block and enhance transmission of human *Plasmodium vivax* malaria. Am J Trop Med Hyg 1988;39(July (1)):26–32.
[18] Carter R. Transmission blocking malaria vaccines. Vaccine 2001;19(March (17–19)):2309–14.
[19] Malkin EM, Durbin AP, Diemert DJ, Sattabongkot J, Wu Y, Miura K, et al. Phase I clinical trial of Pvs25H: a transmission blocking vaccine for *Plasmodium vivax* malaria. Vaccine 2005;23:3131–8.
[20] Stowers A, Carter R. Current developments in malaria transmission-blocking vaccines. Expert Opin Biol Ther 2001;1:619–28.
[21] Arakawa T, Tsuboi T, Kishimoto A, Sattabongkot J, Suwanabun N, Rungruang T, et al. Serum antibodies induced by intranasal immunization of mice with *Plasmodium vivax* Pvs25 co-administered with cholera toxin completely block parasite transmission to mosquitoes. Vaccine 2003;21(July (23)):3143–8.
[22] Hagiwara Y, Iwasaki T, Asanuma H, Sato Y, Sata T, Aizawa C, et al. Effects of intranasal administration of cholera toxin (or Escherichia coli heat-labile enterotoxin) B subunits supplemented with a trace amount of the holotoxin on the brain. Vaccine 2001;19(February (13–14)):1652–60.
[23] Tirawanchai N, Winger LA, Nicholas J, Sinden RE. Analysis of immunity induced by the affinity-purified 21-kilodalton zygote-ookinete surface antigen of *Plasmodium berghei*. Infect Immun 1991;59(January (1)):36–44.
[24] Sinden RE. Molecular interactions between Plasmodium and its insect vectors. Cell Microbiol 2002;4:713–24.
[25] Aregawi M, Cibulskis R, Otten M, Williams R, Dye C. World Health Organisation, World Malaria Report; 2008.
[26] Wu Y, Ellis RD, Shaffer D, Fontes E, Malkin EM, Mahanty S, et al. Phase 1 trial of malaria transmission blocking vaccine candidates Pfs25 and Pvs25 formulated with montanide ISA 51. PLoS ONE 2008;3(7):e2636.
[27] Tsuboi T, Takeo S, Iriko H, Jin L, Tsuchimochi M, Matsuda S, et al. Wheat germ cell-free system-based production of malaria proteins for discovery of novel vaccine candidates. Infect Immun 2008;76(April (4)):1702–8.
[28] Yoshida S, Araki H, Yokomine T. Baculovirus-based nasal drop vaccine confers complete protection against malaria by natural boosting of vaccine-induced antibodies in mice. Infect Immun 2010;78(February (2)):595–602.
[29] Hisaeda H, Collins WE, Saul A, Stowers AW. Antibodies to *Plasmodium vivax* transmission-blocking vaccine candidate antigens Pvs25 and Pvs28 do not show synergism. Vaccine 2001;20(December (5–6)):763–70.
[30] Abe T, Hemmi H, Miyamoto K, Morhhshi S, Tamura H, Takaku S, et al. Imvolvement of the Toll-like receptor 9 signalling pathway in the induction of innate immunity by baculovirus. J Virol 2005;79:2847–58.
[31] Kaslow DC, Bathurst IC, Barr PJ. Malaria transmission-blocking vaccines. Trends Biotechnol 1992;10(11):388–91.
[32] Vermeulen AN, Ponnudurai T, Beckers PJ, Verhave JP, Smits MA, Meuwissen JH. Sequential expression of antigens on sexual stages of *Plasmodium falciparum* accessible to transmission-blocking antibodies in the mosquito. J Exp Med 1985;162(5):1460–76.
[33] LeBlanc R, Vasquez Y, Hannaman D, Kumar N. Markedly enhanced immunogenicity of a Pfs25 DNA-based malaria transmission-blocking vaccine by in vivo electroporation. Vaccine 2008;26(January (2)):185–92.
[34] Lobo CA, Dhar R, Kumar N. Immunization of mice with DNA-based Pfs25 elicits potent malaria transmission-blocking antibodies. Infect Immun 1999;67(April (4)):1688–93.

THE JOURNAL OF BIOLOGICAL CHEMISTRY VOL. 285, NO. 35, pp. 26889–26899, August 27, 2010

Two Atypical L-Cysteine-regulated NADPH-dependent Oxidoreductases Involved in Redox Maintenance, L-Cystine and Iron Reduction, and Metronidazole Activation in the Enteric Protozoan *Entamoeba histolytica*[*] [S]

Received for publication, January 24, 2010, and in revised form, June 28, 2010 Published, JBC Papers in Press, June 30, 2010, DOI 10.1074/jbc.M110.106310

Ghulam Jeelani[‡§1], Afzal Husain[‡], Dan Sato[¶], Vahab Ali[‖], Makoto Suematsu[**], Tomoyoshi Soga[¶], and Tomoyoshi Nozaki[‡1,2]

From the [‡]Department of Parasitology, National Institute of Infectious Diseases, 1-23-1 Toyama, Shinjuku-ku, Tokyo 162-8640, Japan, the [§]Center for Integrated Medical Research, School of Medicine, Keio University, Shinjuku, Tokyo 160-8582, Japan, the [¶]Institute for Advanced Biosciences, Keio University, Tsuruoka, Yamagata 997-0052, Japan, the [‖]Department of Biochemistry, Rajendra Memorial Research Institute of Medical Sciences, Agamkuan, Patna-800007, India, and the [**]Department of Biochemistry and Integrative Medical Biology, School of Medicine, Keio University, Shinjuku, Tokyo 160-8582, Japan

We discovered novel catalytic activities of two atypical NADPH-dependent oxidoreductases (EhNO1/2) from the enteric protozoan parasite *Entamoeba histolytica*. EhNO1/2 were previously annotated as the small subunit of glutamate synthase (glutamine:2-oxoglutarate amidotransferase) based on similarity to authentic bacterial homologs. As *E. histolytica* lacks the large subunit of glutamate synthase, EhNO1/2 were presumed to play an unknown role other than glutamine/glutamate conversion. Transcriptomic and quantitative reverse PCR analyses revealed that supplementation or deprivation of extracellular L-cysteine caused dramatic up- or down-regulation, respectively, of EhNO2, but not EhNO1 expression. Biochemical analysis showed that these FAD- and 2[4Fe-4S]-containing enzymes do not act as glutamate synthases, a conclusion which was supported by phylogenetic analyses. Rather, they catalyze the NADPH-dependent reduction of oxygen to hydrogen peroxide and L-cystine to L-cysteine and also function as ferric and ferredoxin-NADP$^+$ reductases. EhNO1/2 showed notable differences in substrate specificity and catalytic efficiency; EhNO1 had lower K_m and higher k_{cat}/K_m values for ferric ion and ferredoxin than EhNO2, whereas EhNO2 preferred L-cystine as a substrate. In accordance with these properties, only EhNO1 was observed to physically interact with intrinsic ferredoxin. Interestingly, EhNO1/2 also reduced metronidazole, and *E. histolytica* transformants overexpressing either of these proteins were more sensitive to metronidazole, suggesting that EhNO1/2 are targets of this anti-amebic drug. To date, this is the first report to demonstrate that small subunit-like proteins of glutamate synthase could play an important role in redox maintenance, L-cysteine/L-cystine homeostasis, iron reduction, and the activation of metronidazole.

Glutamate synthase (glutamine:2-oxoglutarate amidotransferase, GOGAT[3]) is an iron sulfur flavoprotein that catalyzes the transfer of the amide group of L-glutamine to 2-oxoglutrate to yield L-glutamate and is a key enzyme in the nitrogen assimilation pathway. In eubacteria, this enzyme is dependent on the pyridine nucleotide NAD(P)H for its reducing equivalents and is composed of large 150-kDa (α) and small 50-kDa (β) subunits that together form the active $\alpha\beta$ protomer (1). The structural genes encoding the α and β subunit polypeptides are commonly designated *gltB* and *gltD*, respectively, and lie adjacent on the chromosome with the α subunit preceding the β subunit, except in γ-proteobacteria, where the gene order is reversed. The small subunit of eubacterial glutamate synthase shows sequence similarity to several other protein domains and enzyme subunits (2, 3) and is, therefore, proposed to represent a prototype domain used in many different cellular processes to transfer electrons from NAD(P)H to an acceptor protein or protein domain of unknown function (4). In concord with this view, numerous organisms have been recently identified to possess glutamate synthase β subunit-like genes based on DNA sequence homology (4, 5); however, the organisms often lack a gene encoding the corresponding α subunit, or the β subunit is not present adjacent to the α subunit and is, therefore, transcribed independently (5, 6). To our knowledge, among the organisms lacking a putative GOGAT α subunit, only the GOGAT β subunit from *Thermococcus kodakaraensis* (renamed from *Pyrococcus* sp. KOD1) has been functionally associated with independent GOGAT activity (7).

* This work was supported by Grants-in-aid for Scientific Research 18GS0314, 18050006, and 18073001 (to T. N.) from the Ministry of Education, Culture, Sports, Science, and Technology of Japan, a grant for research on emerging and re-emerging infectious diseases from the Ministry of Health, Labour, and Welfare of Japan (H20-Shinkosaiko-016), and a grant for research to promote the development of anti-AIDS pharmaceuticals from the Japan Health Sciences Foundation (to T. N.).

[S] The on-line version of this article (available at http://www.jbc.org) contains supplemental Figs. S1–S3.

The nucleotide sequence(s) reported in this paper has been submitted to the GenBank™/EBI Data Bank with accession number(s) AB521132 and AB521133.

[1] Supported in part by the Global Center of Excellence Program for Human Metabolomic System Biology of the Ministry of Education Culture, Sports, Science, and Technology.

[2] To whom correspondence should be addressed. Tel.: 81-3-5285-1111 (ext. 2600); Fax.: 81-3-5285-1219; E-mail: nozaki@nih.go.jp.

[3] The abbreviations used are: GOGAT, glutamine:2-oxoglutarate amidotransferase; EhNO, *E. histolytica* NADPH-dependent oxidoreductase; rEhNO, recombinant EhNO; INT, iodonitrotetrazolium; CE, capillary electrophoresis; SoFd, *S. oleracea* ferredoxin; EhFd1, *E. histolytica* ferredoxin.

Entamoeba histolytica, the causative agent of human amebiasis, is an enteric protozoan parasite responsible for amebic colitis and extraintestinal abscesses in approximately 50 million inhabitants of endemic areas (8). As is the case with other microaerophilic parasitic infections, such as giardiasis and trichomoniasis, the 5-nitroimidazole drug metronidazole has been established as the most effective treatment of amebiasis. Because of the high prevalence of these infections (9) and because of its role as a second-line defense against *Helicobacter pylori* infections (10), metronidazole has been included in the list of "essential medicines" by the World Health Organization (11). Metronidazole is a prodrug that requires reduction of the nitro group to generate the cytotoxic nitroradical anion that undergoes further reduction resulting in the generation of nitrosoimidazole (12, 13). This active form can then react with sulfhydryl groups (14) and DNA (15) while being further reduced to an amine via a hydroxylamine intermediate. Here, we report for the first time multiple novel roles of two GOGAT β subunit-like proteins in *E. histolytica*. We demonstrated that they are not associated with glutamate synthase activity but instead exhibit robust reductase activities against L-cystine, ferredoxin, and ferric ion and are also involved in the response to oxidative stress. In addition, we showed that these enzymes can be capable of reducing and activating metronidazole and, thus, are responsible for its observed toxicity against *E. histolytica*. We designated the novel NADPH-dependent oxidoreductases as EhNO1 and -2.

EXPERIMENTAL PROCEDURES

Chemicals and Reagents—L-Cysteine, L-cystine, *trans*-epoxysuccinyl-L-leucylamido-(4-guanidino) butane, cytochrome *c*, iodonitrotetrazolium (INT), and metronidazole were purchased from Sigma. Nickel-nitrilotriacetic acid-agarose was purchased from Merck. All other chemicals of analytical grade were purchased from Wako Pure Chemical (Osaka, Japan) unless otherwise stated.

Microorganisms and Cultivation—Trophozoites of the *E. histolytica* clonal strain HM1:IMSS cl 6 were maintained axenically in Diamond's BI-S-33 medium at 35.5 °C as described previously (16, 17). Trophozoites were harvested in the late logarithmic growth phase for 2–3 days after inoculation of 1/30 to 1/12 of the total culture volume. After the cultures were chilled on ice for 5 min, trophozoites were collected by centrifugation at 500 × *g* for 10 min at 4 °C and washed twice with ice-cold PBS (pH 7.4). *Escherichia coli* BL21 (DE3) strain was purchased from Invitrogen.

Quantitative Real-time PCR—Trophozoites were cultured in BI-S-33 medium supplemented with or without 10 mM L-cysteine (18 or 8 mM final, respectively). After placing the culture on ice for 5 min, the trophozoites were harvested by centrifugation at 500 × *g* for 5 min at 4 °C. Polyadenylated RNA was extracted from ~6×10^6 tropozoites with an mRNA isolation kit (Stratagene, La Jolla, CA) and then treated with deoxyribonuclease I (Invitrogen). cDNA was reverse-transcribed with 4 μg of isolated polyadenylated RNA, the SuperScript III First-Strand Synthesis System, and an oligo$(dT)_{20}$ primer (Invitrogen). PCR was performed with the resulting cDNA as a template and specific oligonucleotide primers using the ABI PRISM 7300 Sequence Detection System (Applied Biosystems, Japan). The primers used were 5′-AGCTGCACCAGTTCCAATTC-3′ and 5′-CAATCCCCAGCTGCATATAA-3′ (EhNO1), 5′-CAGTTCCAATTCCAGGCAGT-3′ and 5′-TTGGTCCTGTAACACAATCTCCT-3′ (EhNO2), and 5′-GATCCAACATATCCTAAAACAACA-3′ and 5′-TCAATTATTTTCTGACCCGTCTTC-3′ (RNA polymerase II 15-kDa subunit, GenBank™ accession number XM_643999). The parameters for PCR were as follows: an initial step of denaturation at 95 °C for 9 min followed by 40 cycles of denaturation at 94 °C for 30 s, annealing at 50 °C for 30 s, and extension at 65 °C for 1 min and a final step at 95 °C for 9 s, 60 °C for 9 s, and 95 °C for 9 s was used to remove primer dimers.

Amino Acid Comparison and Phylogenetic Analysis—Amino acid sequences of the GOGAT β subunit and β subunit-like proteins from 40 other organisms were obtained from the DDBJ/EBI/GenBank™ data base using BLASTP searches with the novel amebic NADPH-dependent oxidoreductases (EhNO1 and EhNO2) described in this paper as queries. Sequence alignments of these proteins were generated using the ClustalW program (18). The alignments obtained by ClustalW were inspected and manually corrected using the Genedoc program (19). After the removal of all gaps, 326 unambiguously aligned residues were selected for phylogenetic analyses. The neighbor-joining and maximum parsimony methods were used to construct a final phylogenetic tree for 32 sequences using the MEGA4.1 program (20). The branch lengths and bootstrap values of 1000 replicates (in percentage) in these trees were obtained from the neighbor-joining analysis.

Construction of Plasmids—Standard techniques were used for cloning and plasmid construction, as previously described (21). Genes encoding EhNO1 and EhNO2 were cloned to produce a fusion protein containing a histidine tag (provided by the vector) at the amino terminus. The cDNA corresponding to the open reading frames of EhNO1 and EhNO2 was amplified by PCR using an *E. histolytica* cDNA library (22) as a template and oligonucleotide primers. The sense and antisense oligonucleotide primers used to amplify EhNO1 and EhNO2 were 5′-CTTATAA**GGATCC**ATGAAGAGTTTCAACATTA-3′ and 5′-ATA**GTCGAC**TTAATCTTGTTCCATTGGG-3′ (EhNO1) and 5′-CTTATAA**GGATCC**ATGGCTGCTAATTATAATA-3′ and 5′-ATA**GTCGAC**TTATTCTTCATTTTTTTTACCC-3′ (EhNO2) (bold letters indicate BamHI and SalI restriction sites). PCR was performed with Platinum *Pfx* DNA polymerase (Invitrogen) and the following parameters: an initial incubation at 94 °C for 2 min followed by 30 cycles of denaturation at 94 °C for 15 s, annealing at 45 °C for 30 s, and elongation at 68 °C for 2 min and a final extension at 68 °C for 10 min. The PCR fragments were digested with BamHI and SalI, subjected to gel electrophoresis, excised, purified with the Gene clean kit II (BIO 101, Vista, CA), and then ligated into BamHI- and SalI-digested pCOLD I (Takara Bio, Otsu, Japan) in the identical orientation as the T7 promoter to generate pCOLD1-EhNO1 and pCOLD1-EhNO2. The nucleotide sequences of the cloned EhNO1 and EhNO2 genes were verified by sequencing to be identical to the putative protein coding

regions of XP_656997 and XP_653573, respectively, in *E. histolytica*.

Bacterial Expression and Purification of Recombinant EhNO (rEhNO)—The pCOLD1-EhNO1 and pCOLD1-EhNO2 expression constructs were introduced into competent *E. coli* BL21 (DE3) cells by heat shock at 42 °C for 30 s, and the resulting transformants were grown at 37 °C in 100 ml of Luria Bertani medium in the presence of 50 μg/ml ampicillin. The overnight culture was then used to inoculate 500 ml of fresh medium, which was further cultured at 37 °C with shaking at 180 rpm. When the A_{600} reached 0.6, 1 mM isopropyl β-D-thiogalactopyranoside was added to induce protein expression, and cultivation was continued for 24 h at 15 °C. The *E. coli* cells were then harvested by centrifugation at 4050 × *g* for 20 min at 4 °C, and the resulting cell pellet was washed with PBS (pH 7.4) and re-suspended in 20 ml of lysis buffer (50 mM Tris-HCl (pH 8.0), 300 mM NaCl, and 10 mM imidazole) containing 0.1% Triton X-100 (v/v), 100 μg/ml lysozyme, and 1 mM phenylmethylsulfonyl fluoride. After a 30-min incubation at room temperature, the cells were sonicated on ice and centrifuged at 25,000 × *g* for 15 min at 4 °C. The supernatant was mixed with 1.2 ml of a 50% nickel-nitrilotriacetic acid His-bind slurry (Qiagen, Tokyo, Japan) and incubated for 1 h at 4 °C with gentle shaking. The rEhNO-bound resin was washed three times with buffer A (50 mM Tris-HCl (pH 8.0), 300 mM NaCl, and 0.1% Triton X-100, v/v) containing 10–50 mM imidazole, and bound proteins were then eluted with buffer A containing 100–300 mM imidazole. After the integrity and purity of the rEhNO proteins were confirmed by 12% SDS-PAGE analysis and Coomassie Brilliant Blue staining, they were extensively dialyzed twice against a 300-fold volume of 50 mM Tris-HCl, 150 mM NaCl, pH 8.0, containing 10% glycerol (v/v) and the Complete Mini Protease Inhibitor Mixture (Roche Applied Science) for 18 h at 4 °C. The concentrations of the dialyzed proteins were spectrophotometrically determined by the Bradford method using bovine serum albumin as a standard as previously described (23). The rEhNO proteins were stored at −80 °C in 20% glycerol in small aliquots until needed.

Analysis of Prosthetic Groups—UV-visible absorption spectra of rEhNO1 (400 μg) and rEhNO2 (200 μg) were measured under both non-reducing and sodium dithionite-reducing conditions. The purified recombinant proteins were reduced with a 10-fold molar excess of sodium dithionite in 200 μl. Flavin was liberated from the recombinant enzymes by boiling samples for 10 min and then separated from proteins by centrifugation at 14,000 × *g* for 10 min. To determine whether FAD or FMN formed a prosthetic group, the fluorescence with excitation and emission wavelengths of 450 and 535 nm, respectively, was measured at pH 2.6 and 7.7 according to the method of Faeder and Siegel (24) using a fluorescence spectrophotometer (model F-2500; Hitachi).

Iron Assay—The iron content of EhNOs was determined by the *O*-phenanthroline method as previously described (25). Briefly, 60 μl samples of rEhNO1 and rEhNO2 were mixed with 4 μl of concentrated HCl and then diluted with distilled water to 0.2 ml. After the resulting mixtures were heated to 80 °C for 10 min and cooled to room temperature, they were then mixed with 0.6 ml of water, 40 μl of 10% hydroxylamine hydrochloride, and 0.2 ml of 0.1% *O*-phenanthroline and further incubated at room temperature for 30 min. The absorbances at 512 nm (A_{512}) were then measured, and the iron concentrations were determined by comparison to a standard curve generated with 0–100 μM ferrous sulfate.

Enzyme Assays—Glutamate synthase activity was assayed spectrophotometrically by measuring the rate of NADPH or NADH oxidation at 340 nm with slight modifications of the procedure described by Jongsareejit *et al.* (7). The 200-μl assay mixture contained 20 mM potassium phosphate buffer, pH 7.5, 5 mM concentrations each of L-glutamine and 2-oxoglutarate, 0.4 mM cofactor (NADPH or NADH), and varying concentrations of rEhNO proteins. The reaction was initiated by the addition of cofactor and was performed at 37 °C. To test for ammonia-dependent activity, glutamine was replaced with 100 mM NH_4Cl.

Oxidoreductase Activity—The NADPH-dependent reduction of menadione was monitored in a coupling assay under aerobic conditions. The rate of reduction of cytochrome *c* by menadione was monitored by the absorbance at 550 nm (ϵ_{550} = 21.1 mM^{-1} cm^{-1}). Measurements were made in 50 mM Tris-HCl (pH 7.5), 200 μM NADPH, 1 μM menadione, and 30 μM cytochrome *c*. The reactions were initiated by the addition of 2 μg of rEhNO1/2.

For the other electron acceptors tested, a standard mixture containing 0.1 mM NADPH, 50 mM Tris-HCl (pH 7.5), and either 0.5 mM INT, 1 mM potassium ferricyanide, or 10 mM paraquat was used. The reactions were initiated by the addition of 2 μg of rEhNO1/2 enzyme, and the reduction of the acceptors was monitored spectrophotometrically at 490 nm for INT (ϵ = 18.5 mM^{-1} cm^{-1}), 410 nm for potassium ferricyanide (ϵ = 1 mM^{-1} cm^{-1}), and 340 nm for paraquat (NADPH oxidation, ϵ = 6.22 mM^{-1} cm^{-1}). One unit of enzyme activity was defined as the formation of 1 μmol of product/min/mg of protein.

Metronidazole reduction activity was determined by measuring the oxidation of NADPH at 340 nm (ϵ_{340} = 6.22 mM^{-1} cm^{-1}) or the reduction of metronidazole at 360 nm (ϵ_{360} = 9.2 mM^{-1} cm^{-1}), as described by Chen and Blanchard (26). Assays were conducted at room temperature under strict anaerobic conditions. The reactions were initiated by the addition of 2 μg of rEhNO protein to a mixture comprising 50 mM Tris-HCl (pH 8.0), 0.5 mM metronidazole, and 0.2 mM NADPH.

The cystine reductase activity was calculated as μmol of NADPH oxidized per min at 340 nm. The assay mixture contained 0.1 M potassium phosphate (pH 7.5), 2 mM EDTA, 0.05–0.2 mM NADPH, and 0.1–5 mM L-cystine. Approximately 2 μg of rEhNO1/2 was added to initiate the reaction, and the change in absorbance at 340 nm was monitored. The effects of sulfydryl-dependent inhibitors were examined by preincubation of 2 μg of rEhNO1 and rEhNO2 with 0.1–5 mM *N*-ethylmaleimide for 10 min before the various assays. All sample reactions were performed in triplicate at a minimum.

NAD(P)H:flavin oxidoreductase activity was assayed by measuring the initial rate of NAD(P)H oxidation at 340 nm (ϵ = 6.22 $mM^{-1}cm^{-1}$) at 25 °C as described by Lo and Reeves (27). One unit of NAD(P)H:flavin oxidoreductase activity was defined as the amount of enzyme that catalyzed the oxidation of 1 μmol of NAD(P)H/min.

Ferric reductase activity was determined by measuring the difference of NAD(P)H consumption at 340 nm in the presence and absence of Fe(III) ammonium citrate. Reaction mixtures containing 0.2 mM NADPH, 100 mM Tris-HCl (pH 7.5), 0.005–1 mM ferric ammonium citrate, and 2 μg of rEhNO1 and -2 were used for the assays.

Ferredoxin-$NADP^+$ reductase activity was determined by measuring ferredoxin-dependent reduction of cytochrome *c* (28). Activity was measured by monitoring cytochrome *c* reduction at 550 nm ($\epsilon = 21.1\ mM^{-1}\ cm^{-1}$) in a reaction mixture containing 0.1 mM NADPH, 0.01–0.5 μM ferredoxin, 10 μM cytochrome *c*, and 50 mM Tris-HCl buffer (pH 7.5). The reactions were initiated by the addition of 1 μg of rEhNO1 and -2.

Determination of H_2O_2 Formation—The ferrithiocyanate method (29) was used to measure H_2O_2 formation at various time points (1–30 min) during the NADPH:favin oxidoreductase reaction. After the reactions were terminated by the addition of 0.125 volumes of 50% trichloroacetic acid, the samples were centrifuged at 12,000 × *g*, and 0.2 volumes of 10 mM ferrous ammonium sulfate and 0.1 volumes of 2.5 M potassium thiocyanate were then added. In the presence of H_2O_2, Fe^{2+} is oxidized, resulting in a colored thiocyanate-Fe^{3+} complex that can be measured by its absorption at 480 nm. The quantity of H_2O_2 formed was determined by comparison of the A_{480} values to standard curves generated using known amounts of H_2O_2.

Metabolite Extraction—Approximately 1.5×10^6 *E. histolytica* cells were harvested after 48 h of cultivation and washed twice with 5% mannitol. The cells were then resuspended in 1.6 ml of methanol containing 20 μM concentrations of the internal standard methionine sulfone acid and mixed with 1.6 ml of chloroform and 640 μl of deionized water. After vortexing, the mixture was centrifuged at 4600 × *g* at 4 °C for 5 min, and the aqueous layer (1.6 ml) was filtrated using an Amicon Ultrafree-MC ultrafilter (Corporation, Billerica, MA) by centrifugation at 9100 × *g* at 4 °C for ~2 h. The filtrate was dried and preserved at −80 °C until mass spectrometric analysis.

Instrumentation and Capillary Electrophoresis (CE)-Time of Flight Mass Spectrometry (TOFMS) Conditions—CE-TOFMS was carried out using an Agilent CE Capillary Electrophoresis System equipped with an Agilent 6210 Time-of-Flight mass spectrometer, Agilent 1100 isocratic HPLC pump, Agilent G1603A CE-MS adapter kit, and Agilent G1607A CE-ESI-MS sprayer kit (Agilent Technologies, Waldbronn, Germany). The system was controlled by Agilent G2201AA ChemStation software for CE. Data acquisition was performed by Analyst QS Build: 7222 software for Agilent TOF (Applied Biosystems/MDS Sciex, Ontario, Canada). Instrumental conditions for the separation and detection of metabolites were as follows. The metabolites were separated on a fused silica capillary (50 μm × 100 cm) using 1 M formic acid as the electrolyte, and the applied voltage was set at +30 kV. A solution of 50% (v/v) methanol-water was delivered as the sheath liquid at 10 μl/min (30, 31). Electrospray ionization-TOFMS was conducted in the positive ion mode (4000 V). The pressure of dry nitrogen gas was maintained at 10 p.s.i. Exact mass data were acquired over a 50–1000 *m/z* range (32, 33). Before analysis, the sample was dissolved in 20 μl of deionized water containing 200 μM concentrations of the internal standard 3-aminopyrrolidine.

Generation of E. histolytica Transformants Overexpressing EhNO—The protein coding regions of EhNO1 and EhNO2 were amplified by PCR from cDNA using sense and antisense oligonucleotides containing appropriate restriction sites at the 5′ end. The sense and antisense oligonucleotide primers used for EhNO1 and EhNO2 were 5′-CTA**CCCGGG**ATGAAGAG-TTTCAACATTACA-3′ and 5′-CAA**CTCGAG**TTAATCTT-GTTCCATTGGGGT-3′ (EhNO1) and 5′-CTA**CCCGGG**AT-GGCTGCTAATTATAATAGA-3′ and 5′-CAA**CTCGAG**TT-ATTCATTTTTTTTACC-3′ (EhNO2) (bold letters indicate restriction sites). The PCR-amplified DNA fragments were digested with SmaI and XhoI and ligated into SmaI and XhoI sites of the expression vector pKT-MR (34) to produce pKT-MR-NO1 and pKT-MR-NO2. Wild-type trophozoites were transformed with pKT-MR by liposome-mediated transfection as previously described (35). Transformants were initially selected in the presence of 3 μg/ml Geneticin (Invitrogen), which was then gradually increased to 6–20 μg/ml during the subsequent 2 weeks before subjecting the transformants to analyses.

Assay for Metronidazole Sensitivity of E. histolytica Trophozoites—To determine sensitivity to metronidazole, *E. histolytica* transfectants harboring pKT-MR-NO1, pKT-MR-NO2, or pKT-MR (control) were cultured at 37 °C in BI-S-33 medium containing 20 μg/ml Geneticin. For the assay, varying concentrations (0–16 μM) of metronidazole were added to samples containing an initial density of 10^4 cells/ml. After 48 h, the number of viable cells was counted on a hemocytometer using trypan blue to identify dead cells. The assays were performed five times in duplicate.

In Vitro Interaction of EhNO1/2 with Ferredoxin—Protein cross-linking was performed as described previously (36). Briefly, EhNO1/2 and ferredoxin (4 and 20 μM, respectively) were cross-linked by treatment with 5 mM *N*-ethyl-3-(3-dimethylaminopropyl)carbodiimide in 25 mM sodium phosphate, pH 7.5. The resulting complexes were analyzed by SDS-PAGE and Western blotting using anti-His antibody.

Immunoblot Analysis—Cell lysates and culture supernatants were separated on 12% (w/v) SDS-PAGE gels and subsequently electro-transferred onto nitrocellulose membranes (Hybond-C Extra; Amersham Biosciences) as previously described (37). Nonspecific binding was blocked by incubating the membranes for 1.5 h at room temperature in 5% nonfat dried milk in TBST (50 mM Tris-HCl (pH 8.0), 150 mM NaCl, and 0.05% Tween 20). The blots were then reacted with primary antibodies specific for EhNO1 and EhNO2 and mannose 6-phosphate receptor 1 (38) and cysteine synthase 1 (22) as controls for the membrane and cytosolic fractions, respectively, at dilutions of 1:500 to 1:100. Antisera against purified rEhNO1 and rEhNO2 were raised in rabbits commercially (Operon, Tokyo, Japan). The membranes were washed with TBST and further reacted with horseradish peroxidase-conjugated anti-rabbit or anti-mouse IgG antisera (1:20,000) (Invitrogen) at room temperature for 1.5 h. After further washing with TBST, specific proteins were visualized and measured with a chemiluminescence detection

system (Millipore) using Scion Image software (Scion Corp., Frederick, MD) (39).

RESULTS

Identification of a GOGAT Small β Subunit Gene in E. histolytica upon L-Cysteine Supplementation—Upon analysis of the transcriptome of *E. histolytica* trophozoites cultured in medium supplemented with L-cysteine, a highly up-regulated gene (XM_648481) was previously identified.[4] Although the entire transcriptome data is described elsewhere, we attempted to characterize this gene in detail in the present study. The identified gene and a gene (XM_651905) that appeared to be very closely related in the *E. histolytica* genome data base (40) were predicted to encode proteins showing high similarity to the small β subunit of GOGAT from bacteria. The genes were designated as *E. histolytica* NADPH-dependent *o*xidoreductase 1 and 2 [EhNO1 (XM_651905) and EhNO2 (XM_648481)] because although the encoded proteins lacked glutamate synthase activity, they showed robust NADPH-dependent oxidoreductase activity (described below). The EhNO1 and EhNO2 genes consisted of 1347- and 1338-bp open reading frames, respectively, which were predicted to encode proteins of 448 and 445 amino acids with predicted molecular masses of 49.3 and 49.0 kDa and isoelectric points of 6.31 and 7.02, respectively.

Features of the Deduced Protein Sequence of EhNOs—The predicted amino acid sequences of the two EhNOs shared 80% mutual identity and demonstrated 20–60% identities to the small β subunit of GOGAT from Archaea, bacteria, animals, and plants. EhNO1 had the highest amino acid identities to the GOGAT β subunit-like proteins of *Chlorobium tepidum* (green sulfur bacteria) and *Methanosarcina mazei* (Archaea) (62 and 59%, respectively), whereas EhNO2 showed 61–62% identities to the small subunit of *Pyrococcus abyssi* GOGAT and the β subunit chain of formate dehydrogenase from *Moorella thermoacetica* (Archaea). Although a multiple alignment of 32 GOGAT and GOGAT-like sequences was generated using ClustalW, the comparisons of representative sequences from *E. coli*, *Clostridium saccharobutylicum*, *Azospirillum brasilense*, and *E. histolytica* were sufficient to highlight the important similarities and differences among GOGAT proteins from these organisms and between the two EhNO isotypes (supplemental Fig. S1).

All of the functional domains characteristic of GOGAT β subunits were conserved between these β subunit-like proteins (supplemental Fig. S1). Two amino-terminal cysteine clusters, $CX_2CX_4CX_3CP$ (residues 40–53 for EhNO1 and residues 41–54 for EhNO2) and $CX_3CX_3CX_3C$ (residues 87–99, EhNO1; 88–100, EhNO2), matched the conserved cysteine-rich patterns proposed to be involved in the formation of [4Fe-4S] clusters (2). Similarly, two regions (residues 137–165 and 264–293 of EhNO1, labeled "FAD-I" and "NAD(P)H", respectively) matched the conserved sequences of an ADP binding fold for the binding of FAD and NAD(P)H. Both EhNO1 and -2 shared features in the NAD(P)H binding domain with the *A. brasilense* GOGAT β-protein (41), which has been proposed to confer

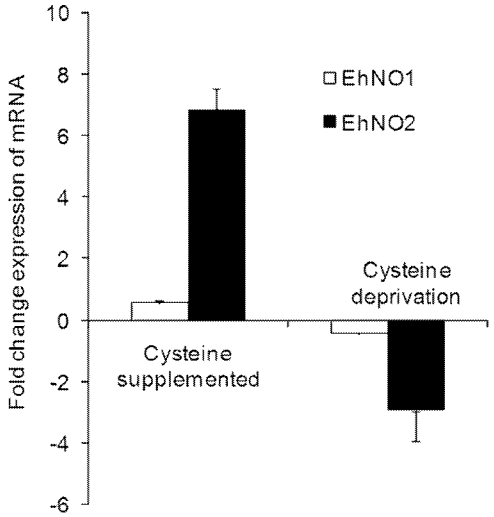

FIGURE 1. **Regulation of gene expression of EhNO isotypes in *E. histolytica* by extracellular L-cysteine concentration.** *E. histolytica* trophozoites were cultured in normal (8 mM), L-cysteine-supplemented (18 mM), or deprived medium. The expression levels of the EhNO transcripts under L-cysteine-supplemented or -deprived conditions were normalized against those of RNA polymerase II and are shown as the -fold change expression of mRNA relative to that of trophozoites from the control (normal) culture. *Error bars* represent the S.E. of three independent experiments.

specificity for NADPH, rather than NADH. The presence of alanine in place of glycine in the last residue of the motif $GXGXX$(G/A/P) (residues 269–274 of EhNO1 and 270–275 of EhNO2, shown in bold in supplemental Fig. S1) and a conserved arginine in the NAD(P)H binding domain (Arg-293 of EhNO1 and Arg-294 of EhNO2) (42) suggested that the two EhNOs prefer NADPH to NADH as a cofactor. Furthermore, a region in the carboxyl terminus (residues 401–411 of EhNO1 and 402–412 of EhNO2) matched the second FAD binding consensus sequence (TX_8GD).

Phylogenetic Analysis—Phylogenetic reconstruction was performed using neighbor-joining and maximum parsimony programs using 32 GOGAT β subunit or β subunit-like protein sequences from various organisms. The phylogenetic tree constructed using the neighbor-joining method revealed (supplemental Fig. S2) that EhNOs are more closely related to other β subunit-like homologs (supplemental Fig. S2, Group I) than to known GOGAT β subunit proteins (supplemental Fig. S2, Group II). This conclusion was also supported by the phylogenetic reconstruction using the maximum parsimony method (data not shown). Although these data did not clearly indicate the origin of the amebic GOGAT-like proteins, they suggested that EhNOs were most likely obtained by lateral gene transfer from an ancestral organism possessing a Group I-type gene, as reported previously for several other glutamate synthase β subunit-like genes (43).

Regulation of Gene Expression of EhNO Isotypes by L-Cysteine Concentration—To verify the transcriptomic data and confirm that the expression of EhNO1 and -2 was regulated by L-cysteine, the relative steady-state mRNA levels of the EhNO isotypes in *E. histolytica* trophozoites cultivated under L-cysteine-enriched or deprived conditions were measured by quantitative real-time PCR (Fig. 1). Using the RNA polymerase II 15-kDa subunit as an internal control, EhNO2 mRNA increased by

[4] A. Husain, D. Sato, G. Jeelani, M. Suematsu, T. Soga, and T. Nozaki, unpublished information.

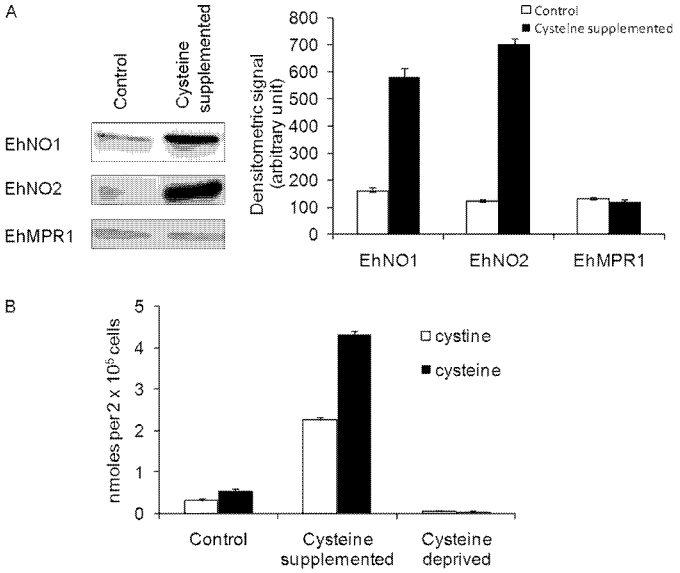

FIGURE 2. **Effects of extracellular L-cysteine concentrations on the amount of EhNO isotypes and intracellular L-cystine/L-cysteine concentrations.** *A*, an immunoblot analysis of EhNO1 and -2 is shown. After trophozoites were cultured under normal or L-cysteine-supplemented conditions for 48 h, ~15 μg of total cell lysate was electrophoresed on a 12% SDS-PAGE gel and subjected to an immunoblot assay with antibodies raised against EhNO1, EhNO2, or EhMPR1 as a control. The densitometric quantification of the reacted bands, shown in the *right graph*, was performed by Scion Image software, and the level of EhNO1, EhNO2, and EhMPR1 proteins was expressed in arbitrary units. *Error bars* represent the S.E. of three independent experiments. *B*, shown is intracellular L-cystine/cysteine concentrations under normal, L-cysteine-supplemented, and deprived conditions. L-Cystine/cysteine concentrations of the trophozoites cultivated for 48 h under the indicated conditions were analyzed by CE-MS. *Error bars* represent the S.E. of three independent experiments.

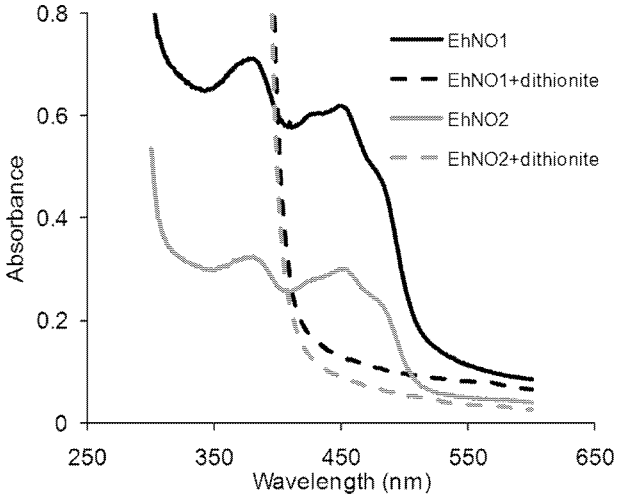

FIGURE 3. **Absorption spectra of rEhNO1 and rEhNO2 proteins.** UV-visible absorption spectra of rEhNO1 (400 μg of protein) and rEhNO2 (200 μg) under non-reducing (*solid lines*) and sodium dithionite-reducing conditions (*broken lines*) are shown. The samples were reduced with a 10-fold molar excess of sodium dithionite.

7-fold when cultured in the presence of 18 mM L-cysteine for 48 h compared with the control condition (8 mM L-cysteine), whereas it was down-regulated by 4-fold when cultured in the absence of L-cysteine. In contrast, the level of EhNO1 remained unchanged in either the presence or absence of L-cysteine.

Expression of EhNO Proteins under L-Cysteine-supplemented and -deprived Conditions—To confirm the changes of *EhNO* transcripts determined by the transcriptomic and real-time PCR analyses, we also examined EhNO expression at the protein level under L-cysteine-supplemented conditions. Immunoblot analysis using anti-rEhNO2 antibody showed that EhNO2 was induced by 6-fold when *E. histolytica* cultures were supplemented with L-cysteine (Fig. 2*A*). Although the RT-PCR results indicated that EhNO1 was not up-regulated under this condition, the protein recognized by anti-EhNO1 antibody was also found to be induced by 3.5-fold. Because anti-EhNO1 and anti-EhNO2 antibodies exhibited cross-reactivity (data not shown), the increased signal of the band recognized by anti-EhNO1 antibody was likely due to cross-reactivity with EhNO2. Alternatively, the level of EhNO1 may have increased by post-transcriptional mechanisms.

Changes in Intracellular L-Cysteine/Cystine Concentrations under L-Cysteine-supplemented and -deprived Conditions—To examine changes in intracellular L-cysteine and L-cystine concentrations caused by L-cysteine supplementation and deprivation, we quantitated their levels using a CE-MS-based approach in trophozoites maintained under normal (8 mM L-cysteine), enriched (18 mM L-cysteine), or deprived conditions. Under normal conditions, the L-cysteine to L-cystine ratio (1.70 ± 0.08) was deviated toward the reduced status. Upon L-cysteine supplementation, the intracellular levels of L-cysteine and L-cystine increased 8.1- and 7.3-fold, respectively, whereas under L-cysteine deprivation, both L-cysteine and L-cystine decreased to undetectable levels (Fig. 2*B*). Under L-cysteine-enriched conditions, the L-cysteine to L-cystine ratio (1.90 ± 0.14) slightly shifted toward the more reduced status (p = 0.031). Because several systems regulate the cellular redox reactions and electrochemical potential of the cell, the observed changes in the L-cysteine/cystine ratio were considered small. Taken together, these data clearly showed that although the extracellular L-cysteine concentration largely affects intracellular L-cysteine/L-cystine levels, its redox equilibrium is not severely affected. Furthermore, it appeared that a significant proportion of the L-cysteine incorporated into the cell was oxidized to L-cystine, which is supported by a previous finding (44). Alternatively, extracellular L-cysteine may be oxidized before uptake and reduced to L-cysteine intracellularly.

Expression and Purification of Recombinant EhNO Isotypes—To determine the biochemical properties of the two EhNO isoenzymes, recombinant proteins were first produced in *E. coli*. SDS-PAGE of the purified rEhNO1 and -2 proteins showed apparently single homogenous bands with molecular weights of 52.2 and 51.9 kDa, respectively, under reducing conditions (supplemental Fig. S3). The observed mobilities of rEhNO1 and -2 were consistent with the predicted sizes of the monomeric EhNO proteins with an extra 3.0-kDa histidine tag added at the amino terminus. The purity of the rEhNOs was estimated to be greater than 95% as judged by densitometric scanning of the stained gel. The rEhNO proteins were stable and retained their full activity for at least 3 months when stored in 10–15% glycerol at -30 or −80 °C.

Prosthetic Groups of rEhNOs—The UV-visible spectra of the purified rEhNOs showed absorbance maxima at 484, 450, 430, 378, and 280 nm (Fig. 3), which are characteristic of iron sulfur

flavoproteins (45). The dithionite-reduced rEhNOs showed, in contrast, a relatively featureless spectrum, with the increased absorbance at shorter wavelengths attributable to dithionite. Denaturation of the rEhNOs by boiling resulted in the release of flavin, indicating that it formed a non-covalent association with the protein. The fluorescence intensity of the free flavin at pH 2.6 was ~4-fold higher than that at pH 7.7 (data not shown). This indicates that FAD, rather than FMN, formed the prosthetic group in rEhNOs. It was calculated that 1.13 ± 0.32 mol of FAD (ϵ of FAD at 450 nm = 11.4×10^3 M^{-1} cm^{-1}) is associated per molecule of rEhNO1, whereas 0.89 ± 0.21 mol of FAD bound per molecule of rEhNO2. The iron analysis using the *O*-phenanthroline method indicated that rEhNO1 contained 7.8 ± 0.62 irons per molecule of rEhNO1, whereas rEhNO2 contained 7.4 ± 0.71 irons per molecule of rEhNO2. These results indicate that two [4Fe-4S] clusters are present per subunit, which is consistent with the $CX_2CX_4CX_3CP$ and $CX_3CX_3CX_3C$ motifs present in EhNO1 and -2. These data together with the stability of the enzymatic activity of rEhNOs also support the premise that rEhNOs retain most, if not all, of the features of the native EhNOs.

Kinetics Properties of rEhNO—The rEhNOs were devoid of glutamate synthase and glutamate dehydrogenase activity in both directions at either pH 7.5 or 9.5. However, both proteins oxidized NADPH and transferred electrons to several alternative electron acceptors, including INT, ferricyanide, and menadione (Table 1). In the presence of NADPH, the reduction rate of INT by rEhNO1 (specific activity 19.42 ± 3.25 μmol min^{-1} mg^{-1}) was >30-fold higher than that by rEhNO2 (0.62 ± 0.10 μmol min^{-1} mg^{-1}), whereas rEhNO2 showed a 2.8-fold higher ferricyanide reducing activity (86.64 ± 8.33 μmol min^{-1} mg^{-1}) than rEhNO1 (31.50 ± 6.21 μmol min^{-1} mg^{-1}). The menadione-reducing activities of rEhNO1 and -2 were comparable (2.48 ± 0.39 and 2.25 ± 0.41 μmol min^{-1} mg^{-1}, respectively). Both rEhNO1 and -2 were highly specific toward NADPH and did not reduce the above-tested electron acceptors with NADH as the electron donor. In the NADPH:flavin oxidoreductase reaction under aerobic conditions, rEhNO1 and -2 produced H_2O_2 at comparable levels (Table 1). Significantly, the two enzymes were also capable of reducing the anti-amebic drug metronidazole and the herbicide paraquat.

In addition to these properties, rEhNO1 and -2 could catalyze the reduction of disulfides, such as L-cystine, which was also dependent on NADPH. The K_m and k_{cat}/K_m values of rEhNO1 and -2 for L-cystine and NADPH were significantly different (Table 2). At substrate-saturating concentrations, the K_m values of rEhNO1 for L-cystine and L-NADPH were 3.3- and 2.3-fold higher, respectively, than those of rEhNO2. The k_{cat}/K_m value of rEhNO2 for L-cystine (measured at saturating concentrations of NADPH) was ~4-fold higher than that of rEhNO1. The addition of *N*-ethylmaleimide, which is commonly used to inhibit sulfydryl-dependent reactions, inhibited the disulfide reducing activities of both rEhNO1 and rEhNO2 (0.5 mM *N*-ethylmaleimide caused 50% inhibition), whereas the presence of up to 5 mM *N*-ethylmaleimide had no effect on the reduction of INT. These results indicate that the two EhNOs contain thiol(s) groups that are involved in disulfide reduction but are not required for their observed oxidoreductase activity (46, 47).

We also found that rEhNO1 and -2 catalyzed the reduction of ferric to ferrous ion. In the presence of NADPH, the reduction rate of Fe(III) by rEhNO1 (k_{cat}/K_m 15.1 ± 3.20 min^{-1} μM^{-1}) was ~116-fold higher than that by rEhNO2 (k_{cait}/K_m 0.12 ± 0.01 min^{-1} μM^{-1}) (Table 2). In addition, both rEhNOs also acted as ferredoxin:$NADP^+$ reductases capable of catalyzing the reduction of $NADP^+$ to NADPH through the utilization of the electrons provided by reduced ferredoxin, although the observed activity of EhNO1 was again higher (7.8-fold) than that of EhNO2. These data suggest that EhNO1 is mainly involved in the reduction of ferric ion and ferrodoxin:$NADP^+$, whereas EhNO2 primarily catalyzes the reduction of L-cystine. The uncatalyzed reaction rate (without enzyme) of each reaction was as follows: 22.5 ± 2.4 pmol/min, INT; 250 ± 32 pmol/min, ferricyanide; 29.2 ± 6.1 pmol/min, menadione; 307 ± 66 pmol/min, paraquat; 22.5 ± 7.8 pmol/min, cystine; 28.9 ± 6.9 pmol/min, ferric ammonium citrate; 6.16 ± 2.7 pmol/min, ferredoxin.

Binary Complexes of EhNO1/2 with Ferredoxins—To examine whether electron transfer between reduced ferredoxin and $NADP^+$ by EhNO1 was dependent on the physical interaction between these two proteins (48), as reported for the spinach leaf redox couple (36), we investigated whether EhNO1 and -2

TABLE 1
Specific activity of purified EhNO1 and EhNO2 with various electron acceptors
Values are expressed as the means ± S.D. of three independent experiments as described under "Experimental Procedures"

Substrate	Specific activity	
	rEhNO1	rEhNO2
	μmol/min/mg	
INT	19.42 ± 3.25	0.62 ± 0.10
Ferricyanide	31.50 ± 6.21	86.64 ± 8.33
Menadione	2.48 ± 0.39	2.25 ± 0.41
Metronidazole	1.75 ± 0.42	1.41 ± 0.46
Paraquat	19.73 ± 4.23	10.60 ± 2.12
Oxygen	8.31 ± 2.12	3.42 ± 0.81

TABLE 2
Kinetic parameters for cystine, ferric, and ferredoxin $NADP^+$ reductase reactions catalyzed by EhNO1 and EhNO2
Values are expressed as the means ± S.D. of three independent experiments.

Substrate	rEhNO1				rEhNO2			
	K_m	V_{max}	k_{cat}	k_{cat}/K_m	K_m	V_{max}	k_{cat}	k_{cat}/K_m
	μM	*μmol/min/mg*	min^{-1}	$min^{-1}\cdot\mu M^{-1}$	*μM*	*μmol/min/mg*	min^{-1}	$min^{-1}\cdot\mu M^{-1}$
Cystine	910 ± 20	0.88 ± 0.06	45.86 ± 7.52	0.05 ± 0.01	276 ± 23	1.15 ± 0.17	59.36 ± 3.81	0.22 ± 0.13
NADPH (cystine)	9.2 ± 2.1	1.70 ± 0.13	88.38 ± 5.83	9.61 ± 1.34	4.2 ± 0.8	1.33 ± 0.43	68.62 ± 5.40	16.33 ± 2.12
Fe(III) citrate	31.3 ± 3.4	9.10 ± 2.51	471.2 ± 17.5	15.1 ± 3.20	98.4 ± 4.5	0.26 ± 0.09	12.18 ± 2.81	0.12 ± 0.01
NADPH (ferric)	70.3 ± 4.9	10.12 ± 3.16	526.6 ± 21.2	7.49 ± 2.12	66.7 ± 8.3	0.72 ± 0.31	37.06 ± 6.28	0.56 ± 0.23
Ferredoxin	0.16 ± 0.05	2.28 ± 0.46	118.8 ± 7.4	742.5 ± 34.1	0.23 ± 0.07	0.43 ± 0.18	21.71 ± 4.51	94.39 ± 8.91

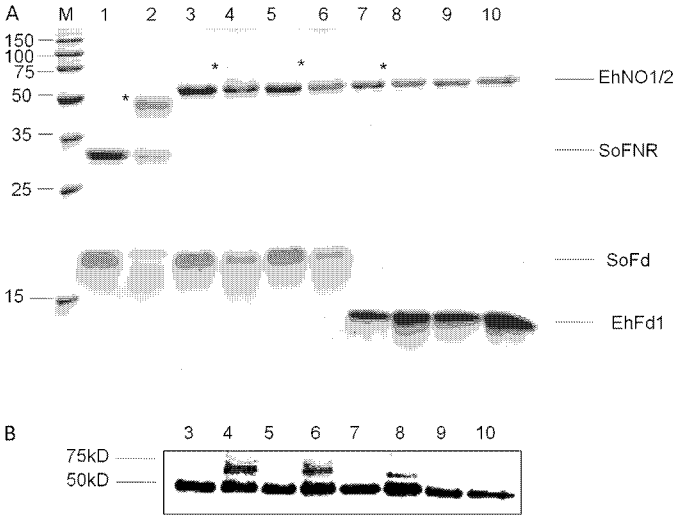

FIGURE 4. ***In vitro* interactions of EhNO with ferredoxin.** *A*, SDS-PAGE analysis of the complex of EhNO and ferredoxin is shown. Protein mixtures were incubated for 30 min with (*even lane numbers*) and without (*odd lane numbers*) 5 mM carbodiimide, electrophoresed on a 15% SDS-PAGE gel under reducing conditions, and then stained with Coomassie Brilliant Blue R250. The examined protein mixtures were as follows: *lanes 1* and *2*, spinach (*S. oleracea*) ferredoxin:NADP$^+$ reductase (*SoFNR*) + spinach ferredoxin (*SoFd*); *lanes 3* and *4*, *EhNO1*+*SoFd*; *lanes 5* and *6*, *EhNO2*+*SoFd*; *lanes 7* and *8*, *EhNO1*+*EhFd1*; *lanes 9* and *10*, *EhNO2*+*EhFd1*. Protein bands corresponding to the cross-linked proteins are indicated by an *asterisk*. The positions of the purified proteins are indicated on the *right side of the gel*. *B*, shown is an immunoblot analysis of the cross-linked samples using an anti-His antibody.

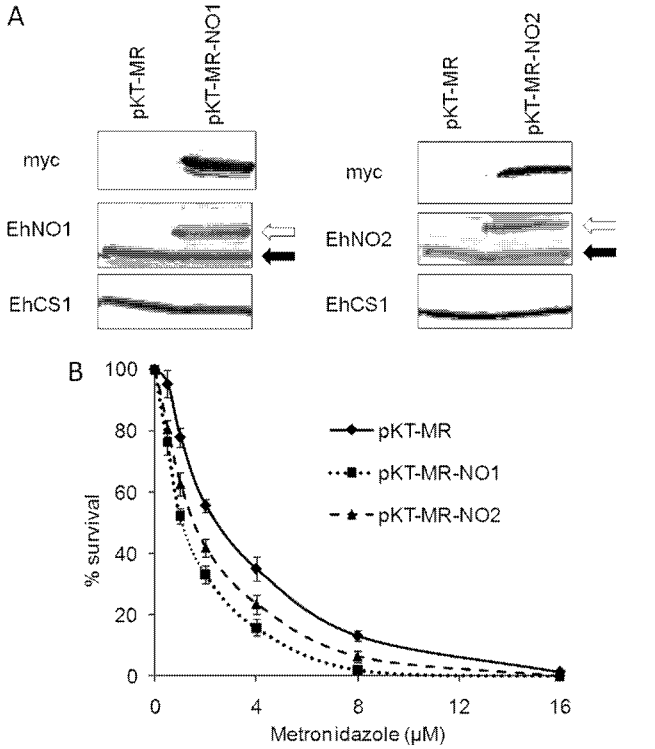

FIGURE 5. **Changes in the sensitivity of *E. histolytica* to metronidazole by overexpression of EhNOs.** *A*, shown is an immunoblot analysis of EhNOs in the transformants expressing Myc-tagged EhNO1 and -2. Approximately 40 μg of total lysate from the pKT-MR (control), EhNO1 (*pKT-MR-NO1*), and EhNO2 (*pKT-MR-NO2*)-overexpressing transformants was electrophoresed on a SDS-PAGE gel under reducing conditions and subjected to immunoblot analysis using anti-EhNO1, anti-EhNO2, anti-Myc, and anti-EhCS1 (*control*) antibodies. *Black* and *white arrows* indicate endogenous and Myc-tagged EhNO1 and -2, respectively. *B*, susceptibility of transformed trophozoites to metronidazole is shown. Trophozoites (10^4 cells/ml) were cultivated in the presence of 0–16 μM metronidazole for 48 h, and the number of viable cells was then counted. The percentages of living cells are shown relative to those of unexposed control cells. *Error bars* represent the S.E. of five independent experiments.

physically interacted with homologous and heterologous (*Spinacia oleracea*) ferredoxin (SoFd) using a carbodiimide-promoted cross-linking (50). We first cloned and purified a representative [3Fe4S] ferredoxin found in the *E. histolytica* genome data base (EhFd1; TIGR ID 128.m00136). For the assay, rEhNO1 and -2 were mixed with either purified EhFd1 or SoFd, cross-linked, and then analyzed by SDS-PAGE (Fig. 4*A*). It was observed that both rEhNO1 and -2 formed a complex with spinach ferredoxin, as shown by the appearance of a large 60-kDa band in the gel and more easily observed in the Western blot analysis using an anti-histidine antibody (Fig. 4*B*, *lanes 4* and *6*). However, only EhNO1 formed a complex with *E. histolytica* ferredoxin (EhFd1) (Fig. 4, *A* and *B*, *lanes 8* and *10*).

Cellular Distribution of EhNO—We also examined the cellular distribution of EhNO1 and -2 in trophozoites. The immunofluorescence imaging using antiserum raised against the corresponding recombinant protein revealed that the two isotypes were distributed throughout the cytosol (data not shown). We also verified the localization of EhNOs by immunoblotting using lysates produced by a Dounce glass homogenizer followed by sonication and centrifugation at 100,000 × *g* at 4 °C for 1 h. Both EhNO1 and -2 fractionated into the soluble fraction (data not shown).

Increased Metronidazole Sensitivity by EhNO Overexpression—To confirm that EhNO is the target of metronidazole in *E. histolytica*, stable transformants that overexpressed Myc-tagged EhNO1 or 2 were generated. Both the transformants expressing Myc-tagged EhNO1 or EhNO2 expressed ~2-fold higher levels of the corresponding enzymes than the control (Fig. 5*A*) and were more sensitive to metronidazole. The 50% growth inhibitory concentrations (IC_{50}) of metronidazole for the Myc-EhNO1- and Myc-EhNO2-overexpressing transformants were 1.03 ± 0.05 and 1.42 ± 0.12 μM, respectively (Fig. 5*B*), whereas the control showed an IC_{50} of 2.24 ± 0.33 μM.

DISCUSSION

In the present study we demonstrated novel enzymatic reactions catalyzed by a new class of FAD- and 2[4Fe-4S]-containing NADPH-dependent oxidoreductases from *E. histolytica*, which had been initially discovered by virtue of tightly regulated gene expression in correlation with L-cysteine concentrations. Although the two EhNOs characterized in this study had been annotated before this study based on their high degree of homology with GOGAT β subunit and β subunit-like genes from a variety of organisms, their biochemical function was unknown. The fact that the two EhNOs shared significant similarity with homologs from archaeal organisms raised the question of whether they represented a prototype GOGAT protein, similar to the β subunit protein from *Pyrococcus*, which was reported to possess NADPH-dependent GOGAT activity and be capable of both glutamine and ammonia-dependent synthesis in the absence of the α subunit (7). However, we were unable to observe glutamate synthase activity of the EhNOs under similar conditions used for the *Pyrococcus* glutamate synthase. Fur-

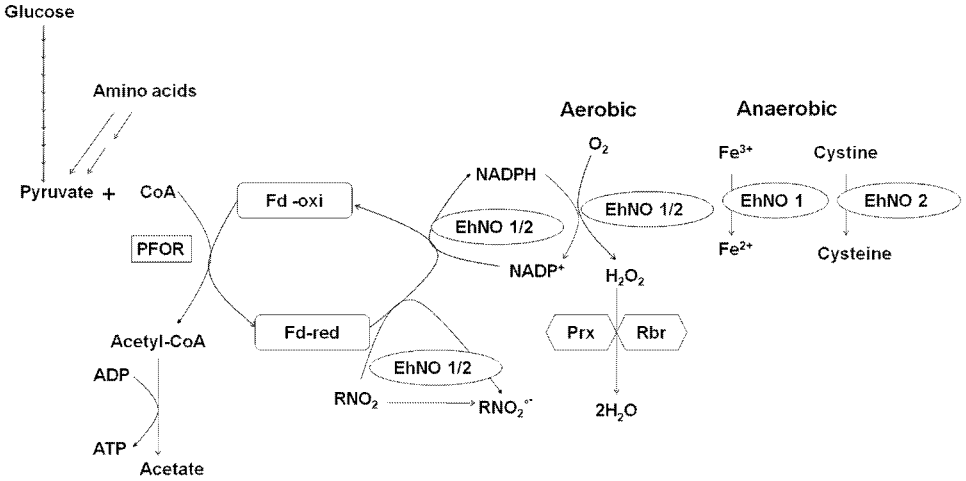

FIGURE 6. **Proposed *in vivo* reactions catalyzed by EhNO1 and -2.** *PFOR*, pyruvate:ferredoxin oxidoreductase; *Fd-red* and *Fd-oxi*, reduced and oxidized form of ferredoxin; *Prx*, peroxiredoxin; *Rbr*, rubrerythrin; RNO_2/RNO_2°, metronidazole/reduced metronidazole.

thermore, the expression of the GOGAT β subunit failed to restore glutamate auxotrophy in an *E. coli* GOGAT α subunit-deficient strain (5, 51). In addition, it was somewhat puzzling how the *Pyrococcus* GOGAT β subunit functioned in substrate binding and catalysis without the α subunit, which has been shown to be responsible for substrate recognition (52). Thus, it was thought that the EhNO β subunit-like proteins may be involved in reactions other than glutamate synthesis.

The physiological roles of EhNO1 and EhNO2 have not been unequivocally demonstrated because our attempt to repress EhNO expression by gene silencing (53) failed (data not shown), and gene knock-out has not been accomplished in *E. histolytica*. Nevertheless, our present enzymological characterization revealed the physiological significance of the presence of the two isotypes of EhNOs. EhNO2 appears to play an important role in the reduction of cystine to L-cysteine. Because L-cysteine is partially present in the oxidized form inside cells (CE-MS analysis, Fig. 2*B*), L-cystine reduction is necessary before the utilization of L-cysteine, which has been implicated in the attachment to matrix, elongation, motility, growth, and anti-oxidative defense (35, 54, 55). Transcriptomic analysis demonstrated that the transcription of EhNO2, but not EhNO1, is tightly regulated by extracellular L-cysteine concentrations. Furthermore, the measured kinetic parameters indicate that EhNO2 possesses 4-fold higher L-cystine reduction efficiency than EhNO1.

The acquisition of iron and subsequent assimilation into cellular proteins are ubiquitously essential for life. However, at physiological pH under aerobic conditions, iron is present as Fe^{3+} hydroxides and oxyhydroxides or in a complex with ferric-specific chelators, *e.g.* siderophores (56). Subsequent reduction of complexed Fe^{3+} is accomplished by ferric reductases using NAD(P)H as the electron donor (57), with the resulting Fe^{2+} being subsequently released and incorporated into iron-containing proteins (58). We showed that rEhNO1 catalyzes the reduction of ferric ion >100-fold more efficiently than rEhNO2 (Table 2), suggesting that EhNO1 is mainly involved in ferric reduction. We also confirmed that EhNO1 functions as a ferredoxin:$NADP^+$ reductase, similar to the recently reported ferric reductase from *Pseudomonas putida* (59), by catalyzing reversible electron transfer between one molecule of $NADP^+$/NADPH and two molecules of ferredoxin. *In vitro* cross-linking of the two EhNOs with ferredoxin indicate that only EhNO1 forms a stable complex with *E. histolytica* ferredoxin (EhFd1), whereas both EhNO1 and EhNO2 physically interact with spinach ferredoxin (Fig. 4*B*), indicating that the specificity toward ferredoxin differs between these two proteins. The *E. histolytica* genome encodes four types of ferredoxins which are highly divergent at the primary sequence level and also in the Fe-S clusters. We, therefore, hypothesize that EhNO2 interacts with a ferredoxin(s) other than EhFd1 in *E. histolytica*, a speculation that is supported by the observed differential binding of photosynthetic and non-photosynthetic maize ferredoxins to root *Zea mays* ferredoxin:$NADP^+$ reductase (60).

E. histolytica is anaerobic/microaerophilic and possesses highly degenerated mitochondria that are incapable of oxidative phosphorylation and ATP generation. A crucial step in energy production via glycolysis and fermentation in *E. histolytica* involves the decarboxylation of pyruvate to acetyl CoA that is catalyzed by pyruvate:ferredoxin oxidoreductase (61). Concomitant with the decarboxylation of pyruvate, an electron is transferred to oxidized ferredoxin. Generally, reduced ferredoxin subsequently donates an electron to NAD(P) by the action of ferredoxin:NADP reductase, which serves to regenerate the intracellular pools of NAD(P)H and oxidized ferredoxin. However, as the *Entamoeba* genome does not contain an ferredoxin:NADP reductase homolog, it was unclear how NAD(P)H was regenerated. Our enzymological study indicates that EhNOs, and EhNO1 in particular, function as ferredoxin:NADP reductases and are involved in the regeneration of NADPH and oxidized ferredoxin required for continuous energy production.

As stated above, *E. histolytica* possesses highly divergent mitochondria (62) and lacks a functional tricarboxylic acid cycle, cytochromes, and a conventional respiratory electron transport chain terminating in the reduction of oxygen to water. However, amebae can still tolerate up to 5% of oxygen in the gas phase (63, 64) and consume oxygen (65). As shown here, EhNOs are flavoproteins containing 1 mol of FAD as a prosthetic group per mol of enzyme. During the NADPH:flavin oxidoreductase reaction, NADPH binds to EhNOs, and two electrons are transferred to FAD to yield $FADH_2$, which is immediately dissociated from the enzyme (66). Under aerobic conditions, $FADH_2$ is rapidly oxidized by molecular oxygen to yield H_2O_2 and FAD (67). As *E. histolytica* amebae do not produce detectable amounts of H_2O_2 (27), it is possible that H_2O_2 is further converted to water by peroxiredoxin (68) and rubrerythrin (69) to overcome oxidative stress. Under anaero-

bic conditions, EhNO1 catalyzes ferric ion reduction, whereas EhNO2 catalyzes cystine reduction. Based on the demonstrated reactions catalyzed by the two EhNOs, we have proposed functional roles for these two proteins in *E. histolytica* that are summarized in Fig. 6.

Metronidazole is a prodrug currently used to treat a number of microbial infections, and its activation requires intracellular reduction to produce cytotoxic short-lived radicals and other reactive species (70). *Entamoeba* electron transport proteins, which have been reported to provide the source of electrons for the reductive activation of metronidazole, include ferredoxin (71), thioredoxin reductase (72), and nitroreductase (49). We demonstrated that both EhNO1 and -2 catalyze metronidazole reduction *in vitro* (Table 1), and their overexpression confers increased sensitivity to this drug (Fig. 5*B*). This finding suggests that in addition to ferredoxin (71), pyruvate:ferredoxin oxidoreductase (71), thioredoxin (72), and nitroreductase (49), EhNO1 and -2 are also involved in metronidazole activation in *E. histolytica*.

In conclusion, we have demonstrated for the first time that two novel NADPH-dependent GOGAT small subunit-like proteins of *E. histolytica* function, at least *in vitro*, as cystine/ferric/ferredoxin:$NADP^+$ reductase. We propose that they play a role in maintaining intracellular redox potential and may be responsible for metronidazole activation in this parasite. The physiological substrates and biological roles of the majority of oxidoreductases discovered by genome mining remain largely unknown. Vigorous attempts to discover the substrates and functions of individual oxidoreductases should unveil novel cellular metabolic processes in pathogens and cancer cells that may lead to the development of new chemotherapeutics.

Acknowledgments—We thank Kumiko Nakada-Tsukui, Fumika Michi, Takashi Makiuchi, and all other members of our laboratory for technical assistance and valuable discussions.

REFERENCES

1. Ratti, S., Curti, B., Zanetti, G., and Galli, E. (1985) *J. Bacteriol.* **163,** 724–729
2. Rosenbaum, K., Jahnke, K., Curti, B., Hagen, W. R., Schnackerz, K. D., and Vanoni, M. A. (1998) *Biochemistry* **37,** 17598–17609
3. Tóth, A., Takács, M., Groma, G., Rákhely, G., and Kovács, K. L. (2008) *FEMS Microbiol. Lett.* **282,** 8–14
4. Vanoni, M. A., and Curti, B. (1999) *Cell Mol. Life Sci.* **55,** 617–638
5. Stutz, H. E., and Reid, S. J. (2004) *Biochim. Biophys. Acta* **1676,** 71–82
6. Saum, S. H., Sydow, J. F., Palm, P., Pfeiffer, F., Oesterhelt, D., and Müller, V. (2006) *J. Bacteriol.* **188,** 6808–6815
7. Jongsareejit, B., Rahman, R. N., Fujiwara, S., and Imanaka, T. (1997) *Mol. Gen. Genet.* **254,** 635–642
8. World Health Organization (1997) *WHO/PAHO/UNESCO Report: A consultation with experts on amebiasis. Mexico City, Mexico 28–29 January, 1997. Epidemiol. Bull* **18,** 13–14
9. Upcroft, P., and Upcroft, J. A. (2001) *Clin. Microbiol. Rev.* **14,** 150–164
10. Hoffman, J. S., and Cave, D. R. (2001) *Curr. Opin. Gastroenterol.* **17,** 30–34
11. World Health Organization (2007 March) *WHO Model List of Essential Medicines*, 15th Ed.
12. Müller, M. (1983) *Surgery* **93,** 165–171
13. Moreno, S. N., and Docampo, R. (1985) *Environ. Health Perspect.* **64,** 199–208
14. West, S. B., Wislocki, P. G., Fiorentini, K. M., Alvaro, R., Wolf, F. J., and Lu,, A. Y. (1982) *Chem. Biol. Interact.* **41,** 265–279
15. Ludlum, D. B., Colinas, R. J., Kirk, M. C., and Mehta, J. R. (1988) *Carcinogenesis* **9,** 593–596
16. Diamond, L. S., Harlow, D. R., and Cunnick, C. C. (1978) *Trans. R. Soc. Trop. Med. Hyg.* **72,** 431–432
17. Clark, C. G., and Diamond, L. S. (2002) *Clin. Microbiol. Rev.* **15,** 329–341
18. Thompson, J. D., Higgins, D. G., and Gibson, T. J. (1994) *Nucleic Acids Res.* **22,** 4673–4680
19. Leão-Helder, A. N., Krikken, A. M., Gellissen, G., van der Klei, I. J., Veenhuis, M., and Kiel, J. A. (2004) *FEBS Lett.* **577,** 491–495
20. Kumar, S., Tamura, K., Jakobsen, I. B., and Nei, M. (2001) *Bioinformatics* **17,** 1244–1245
21. Sambrook, J., and Russell, D. W. (2001) *Molecular Cloning: A Laboratory Manual*, 3rd Ed., Cold Spring Harbor Laboratory Press, Cold Spring Harbor, NY
22. Nozaki, T., Asai, T., Kobayashi, S., Ikegami, F., Noji, M., Saito, K., and Takeuchi, T.. (1998) *Mol. Biochem. Parasitol.* **97,** 33–44
23. Bradford, M. M. (1976) *Anal. Biochem.* **72,** 248–254
24. Faeder, E. J., and Siegel, L. M. (1973) *Anal. Biochem.* **53,** 332–336
25. Olson, J. W., Agar, J. N., Johnson, M. K., and Maier, R. J. (2000) *Biochemistry* **39,** 16213–16219
26. Chen, J. S., and Blanchard, D. K. (1979) *Anal. Biochem.* **93,** 216–222
27. Lo, H., and Reeves, R. E. (1980) *Mol. Biochem. Parasitol.* **2,** 23–30
28. Ichikawa, Y., Hiwatashi, A., Yamano, T., Kim, H. J., and Maruya, N. (1980) in *Flavins and Flavoproteins* (Yagi, K., and Yamano, T., eds) pp. 677–691, University Park Press, Baltimore, MD
29. Thurman, R. G., Ley, H. G., and Scholz, R. (1972) *Eur. J. Biochem.* **25,** 420–430
30. Soga, T., and Heiger, D. N. (2000) *Anal. Chem.* **72,** 1236–1241
31. Soga, T., Ohashi, Y., Ueno, Y., Naraoka, H., Tomita, M., and Nishioka, T. (2003) *J. Proteome Res.* **2,** 488–494
32. Soga, T., Baran, R., Suematsu, M., Ueno, Y., Ikeda, S., Sakurakawa, T., Kakazu, Y., Ishikawa, T., Robert, M., Nishioka, T., and Tomita, M. (2006) *J. Biol. Chem.* **281,** 16768–16776
33. Ohashi, Y., Hirayama, A., Ishikawa, T., Nakamura, S., Shimizu, K., Ueno, Y., Tomita, M., and Soga, T. (2008) *Mol. Biosyst.* **4,** 135–147
34. Nakada-Tsukui, K., Okada, H., Mitra, B. N., and Nozaki, T. (2009) *Cell. Microbiol.* **11,** 1471–1491
35. Nozaki, T., Asai, T., Sanchez, L. B., Kobayashi, S., Nakazawa, M., and Takeuchi, T. (1999) *J. Biol. Chem.* **274,** 32445–32452
36. Zanetti, G., Morelli, D., Ronchi, S., Negri, A., Aliverti, A., and Curti, B. (1988) *Biochemistry* **27,** 3753–3759
37. Tokoro, M., Asai, T., Kobayashi, S., Takeuchi, T., and Nozaki, T. (2003) *J. Biol. Chem.* **278,** 42717–42727
38. Nakada-Tsukui, K., Saito-Nakano, Y., Ali, V., and Nozaki, T. (2005) *Mol. Biol. Cell* **16,** 5294–5303
39. Srivastava, M., Ahmad, N., Gupta, S., and Mukhtar, H. (2001) *J. Biol. Chem.* **276,** 15481–15488
40. Loftus, B., Anderson, I., Davies, R., Alsmark, U. C., Samuelson, J., Amedeo, P., Roncaglia, P., Berriman, M., Hirt, R. P., Mann, B. J., Nozaki, T., Suh, B., Pop., M., Duchene, M., Ackers, J., Tannich, E., Leippe, M., Hofer, M., Bruchhaus, I., Willhoeft, U., Bhattacharya, A., Chillingworth, T., Churcher, C., Hance, Z., Harris, B., Harris, D., Jagels, K., Moule, S., Mungall, K., Ormond, D., Squares, R., Whitehead, S., Quail, M. A., Rabbinowitsch, E., Norbertczak, H., Price, C., Wang, Z., Guillén, N., Gilchrist, C., Stroup, S. E., Bhattacharya, S., Lohia, A., Foster, P. G., Sicheritz-Ponten, T., Weber, C., Singh, U., Mukherjee, C., El-Sayed, N. M., Petri, W. A., Jr, Clark, C. G., Embley, T. M., Barrell, B., Fraser, C. M., and Hall, N. (2005) *Nature* **433,** 865–868
41. Morandi, P., Valzasina, B., Colombo, C., Curti, B., and Vanoni, M. A. (2000) *Biochemistry* **39,** 727–735
42. Pelanda, R., Vanoni, M. A., Perego, M., Piubelli, L., Galizzi, A., Curti, B., and Zanetti, G. (1993) *J. Biol. Chem.* **268,** 3099–3106
43. Andersson, J. O., and Roger, A. J. (2002) *Eukaryot. Cell* **1,** 304–310
44. Gillin, F. D., and Diamond, L. S. (1981) *Exp. Parasitol.* **51,** 382–391
45. Latimer, M. T., Painter, M. H., and Ferry, J. G. (1996) *J. Biol. Chem.* **271,** 24023–24028
46. Fontecave, M., Eliasson, R., and Reichard, P. (1987) *J. Biol. Chem.* **262,** 12325–12331

47. Jablonski, E., and DeLuca, M. (1978) *Biochemistry* **17,** 672–678
48. Foust, G. P., Mayhew, S. G., and Massey, V. (1969) *J. Biol. Chem.* **244,** 964–970
49. Pal, D., Banerjee, S., Cui, J., Schwartz, A., Ghosh, S. K., and Samuelson, J. (2009) *Antimicrob. Agents Chemother.* **53,** 458–464
50. Zanetti, G., Aliverti, A., and Curti, B. (1984) *J. Biol. Chem.* **259,** 6153–6157
51. Deane, S. M., and Rawlings, D. E. (1996) *Gene* **177,** 261–263
52. Vanoni, M. A., Fischer, F., Ravasio, S., Verzotti, E., Edmondson, D. E., Hagen, W. R., Zanetti, G., and Curti, B. (1998) *Biochemistry* **37,** 1828–1838
53. Bracha, R., Nuchamowitz, Y., Anbar, M., and Mirelman, D. (2006) *PLoS Pathog.* **2,** e48
54. Gillin, F. D., and Diamond, L. S. (1981) *Exp. Parasitol.* **52,** 9–17
55. Gillin, F. D., and Diamond, L. S. (1980) *J. Protozool.* **27,** 474–478
56. Barchini, E., and Cowart, R. E. (1996) *Arch. Microbiol.* **166,** 51–57
57. Lesuisse, E., Crichton, R. R., and Labbe, P. (1990) *Biochim. Biophys. Acta* **1038,** 253–259
58. Guerinot, M. L. (1994) *Annu. Rev. Microbiol.* **48,** 743–772
59. Yeom, J., Jeon, C. O., Madsen, E. L., and Park, W. (2009) *J. Bacteriol.* **191,** 1472–1479
60. Onda, Y., Matsumura, T., Kimata-Ariga, Y., Sakakibara, H., Sugiyama, T., and Hase, T. (2000) *Plant Physiol.* **123,** 1037–1045
61. Kerscher, L., and Oesterhelt, D. (1982) *Trends Biol. Sci.* **7,** 371–374
62. Tovar, J., Fischer, A., and Clark, C. G. (1999) *Mol. Microbiol.* **32,** 1013–1021
63. Band, R. N., and Cirrito, H. (1979) *J. Protozool.* **26,** 282–286
64. Reeves, R. E. (1984) *Adv. Parasitol.* **23,** 105–142
65. Weinbach, E. C., and Diamond, L. S. (1974) *Exp. Parasitol.* **35,** 232–243
66. Inouye, S. (1994) *FEBS Lett.* **347,** 163–168
67. Gibson, Q. H., and Hastings, J. W. (1962) *Biochem. J.* **83,** 368–377
68. Bruchhaus, I., Richter, S., and Tannich, E. (1997) *Biochem. J.* **326,** 785–789
69. Maralikova, B., Ali, V., Nakada-Tsukui, K., Nozaki, T., van der Giezen, M., Henze, K., and Tovar, J. (2010) *Cell Microbiol.* **12,** 331–342
70. Goldman, P., Koch, R. L., Yeung, T. C., Chrystal, E. J., Beaulieu, B. B., Jr., McLafferty, M. A., and Sudlow, G. (1986) *Biochem. Pharmacol.* **35,** 43–51
71. Müller, M. (1986) *Biochem. Pharmacol.* **35,** 37–41
72. Leitsch, D., Kolarich, D., Wilson, I. B. H., Altmann, F., and Duchene, M. (2007) *PLoS Biol.* **5,** e211

EUKARYOTIC CELL, June 2010, p. 926–933 Vol. 9, No. 6
1535-9778/10/$12.00 doi:10.1128/EC.00011-10

Localization and Targeting of an Unusual Pyridine Nucleotide Transhydrogenase in *Entamoeba histolytica*▽

Mohammad Abu Yousuf,[1,2] Fumika Mi-ichi,[1] Kumiko Nakada-Tsukui,[1] and Tomoyoshi Nozaki[1]*

Department of Parasitology, National Institute of Infectious Diseases, Tokyo 162-8640, Japan,[1] and Department of Parasitology, Gunma University Graduate School of Medicine, 3-39-22 Showa-machi, Maebashi 371-8511, Japan[2]

Received 17 January 2010/Accepted 3 April 2010

Pyridine nucleotide transhydrogenase (PNT) catalyzes the direct transfer of a hydride-ion equivalent between NAD(H) and NADP(H) in bacteria and the mitochondria of eukaryotes. PNT was previously postulated to be localized to the highly divergent mitochondrion-related organelle, the mitosome, in the anaerobic/microaerophilic protozoan parasite *Entamoeba histolytica* based on the potential mitochondrion-targeting signal. However, our previous proteomic study of isolated phagosomes suggested that PNT is localized to organelles other than mitosomes. An immunofluorescence assay using anti-*E. histolytica* PNT (*Eh*PNT) antibody raised against the NADH-binding domain showed a distribution to the membrane of numerous vesicles/vacuoles, including lysosomes and phagosomes. The domain(s) required for the trafficking of PNT to vesicles/vacuoles was examined by using amoeba transformants expressing a series of carboxyl-terminally truncated PNTs fused with green fluorescent protein or a hemagglutinin tag. All truncated PNTs failed to reach vesicles/vacuoles and were retained in the endoplasmic reticulum. These data indicate that the putative targeting signal is not sufficient for the trafficking of PNT to the vesicular/vacuolar compartments and that full-length PNT is necessary for correct transport. PNT displayed a smear of >120 kDa on SDS-PAGE gels. PNGase F and tunicamycin treatment, chemical degradation of carbohydrates, and heat treatment of PNT suggested that the apparent aberrant mobility of PNT is likely attributable to its hydrophobic nature. PNT that is compartmentalized to the acidic compartments is unprecedented in eukaryotes and may possess a unique physiological role in *E. histolytica*.

Pyridine nucleotide transhydrogenase (PNT) participates in the bioenergetic processes of the cell. PNT generally resides on the cytoplasmic membranes of bacteria and the inner membrane of mammalian mitochondria (3, 16) and utilizes the electrochemical proton gradient across the membrane to drive NADPH formation from NADH (14, 15, 39) according to the reaction H^+out + NADH + $NADP^+ \leftrightarrow H^+$in + NAD^+ + NADPH, where "out" and "in" denote the cytosol and the matrix of the mitochondria, or the periplasmic space and the cytosol of bacteria, respectively.

PNT has been identified in several protozoan parasites, including *Entamoeba histolytica* (8, 51), *Eimeria tenella* (17, 47), *Mastigamoeba balamuthi* (11) *Plasmodium falciparum* (10), *Plasmodium yoelii* (6), and *Plasmodium berghei* (12). In general, PNT contains conserved structural units consisting of three domains, the NAD(H)-binding domain (domain I [dI]) and the NADP(H)-binding domain (domain III [dIII]), both of which face the matrix side of the eukaryotic mitochondria or the cytoplasmic side in bacteria, and the hydrophobic domain (domain II [dII]), containing 11 to 13 transmembrane regions. PNT from *E. tenella* and *E. histolytica* exists as a single polypeptide in an unusual configuration consisting of dIIb-dIII-dI-dIIa, with a 38-amino-acid-long linker region between dIII and dI (48).

E. histolytica, previously considered an "amitochondriate" protist, is currently considered to possess a mitochondrion-related organelle with reduced and divergent functions, the mitosome (1, 21, 23a, 26, 42). Our recent proteomic study of isolated mitosomes identified about 20 new constituents (26), together with four proteins previously demonstrated in *E. histolytica* mitosomes: Cpn60 (8, 19, 21, 42), Cpn10 (46), mitochondrial Hsp70 (2, 44), and mitochondrion carrier family (MCF) (ADP/ATP transporter) (7). Despite the early presumption of PNT being localized in mitosomes (8), based on the amino-terminal region rich in hydroxylated (five serines and threonines) and acidic (three glutamates) amino acids, which slightly resembles known mitochondrion- and hydrogenosome-targeting sequences (8, 35), PNT was not discovered in the mitosome proteome. We also doubted this premise because PNT was one of the major proteins identified in isolated phagosomes (32, 33). Thus, the intracellular localization and trafficking of PNT remain unknown.

In this report, we showed that *E. histolytica* PNT (*Eh*PNT) is localized to various vesicles and vacuoles, including lysosomes and phagosomes, using wild-type amoebae and antiserum raised against recombinant *Eh*PNT and an *E. histolytica* line expressing *Eh*PNT with a carboxyl-terminal hemagglutinin (HA) epitope tag and anti-HA antibody. We also showed that all domains of *Eh*PNT are required for its trafficking to the acidic compartment by using amoeba transformants expressing the HA tag or green fluorescent protein (GFP) fused with a region containing various domains of *Eh*PNT.

MATERIALS AND METHODS

Cells, cultures, and reagents. Trophozoites of *E. histolytica* strain HM-1:IMSS cl6 were maintained axenically in Diamond's BI-S-33 medium (9) at 35.5°C.

* Corresponding author. Mailing address: Department of Parasitology, National Institute of Infectious Diseases, 1-23-1 Toyama, Shinjuku, Tokyo 162-8640, Japan. Phone: 81 3 5285 1111, ext. 2600. Fax: 81 3 5285 1219. E-mail: nozaki@nih.go.jp.

▽ Published ahead of print on 9 April 2010.

Chinese hamster ovary (CHO) cells were maintained in F12 medium (Invitrogen, San Diego, CA) supplied with 10% fetal calf serum (Medical Biological Laboratory International, Woburn, MA) at 37°C with 5% CO_2. *Escherichia coli* strains DH5α and BL21(DE3) were purchased from Life Technologies (Tokyo, Japan) and Novagen (Madison, WI), respectively. LysoTracker Red DND-99 and CellTracker Orange CMTMR [5-(and-6)-((((4-chloromethyl)benzoyl)amino)tetramethylrhodamine] were purchased from Molecular Probes (Eugene, OR). All other chemicals of analytical grade were purchased from Sigma-Aldrich unless otherwise stated.

Plasmid construction. Standard techniques were used for routine DNA manipulation, subcloning, and plasmid construction as previously described (38). To produce *E. coli* recombinant proteins, a coding region corresponding to dI (amino acids [aa] 565 to 960) of *Eh*PNT (*Eh*PNTdI) was amplified from an *E. histolytica* cDNA library by using a pair of appropriate primers designed on the basis of the nucleotide sequences in the GenBank database (accession number L39933) (8), with BamHI and XhoI restriction enzyme sites. The sense and antisense primers were 5′-CGA**GGATCC**GATGTTATTTATTGGTATTCCAA AAG-3′ and 5′-CGTT**CTCGAG**TCATTCTTCTTCAGTTGAAAGA-3′, respectively, where boldface type indicates the BamHI or XhoI site. The PCR products were cloned into the BamHI- and XhoI-digested vector pET47b (Novagen, Madison, WI), and the resulting plasmid was designated pHisPNTdI. To generate vectors to express either full-length or truncated forms of *Eh*PNT fused to HA in the amoeba, a protein-coding region corresponding to full-length *Eh*PNT (GenBank accession number AAC41577) (aa 1 to 1083), the 14-aa amino-terminal region encompassing the putative targeting sequence (TS)+dIIb (aa 1 to 330), TS+dIIb+dIII (aa 1 to 525), TS+dIIb+dIII+linker (aa 1 to 564), and TS+dIIb+dIII+ linker+dI (aa 1 to 960) was amplified from an *E. histolytica* cDNA library by using a pair of appropriate primers and cloned into the BglII site of pEhExHA (29). The antisense primers were 5′-CGT**GGATCC**ATGAAA CATTTTCAACATTCTG-3′, 5′-CGT**GGATCC**GAATGATCTATTCATAGCT TTACAC-3′, 5′-CGT**GGATCC**TTCTTCATTTAATTCTTCAAATCCTTTC-3′, 5′-CGT**GGATCC**ATCTTCTGCAAGAACTTTTGTTGGA-3′, and 5′-CGT**GG ATCC**TTCTTCTTCAGTTGAAAGAGT-3′, respectively, where boldface type represents the BamHI site. The sense primer described above was used for these full-length or truncated forms of *Eh*PNT to express in the amoeba. To generate a plasmid to express GFP fused to the *Eh*PNT TS, a pair of oligonucleotides corresponding to the TS were generated, self-annealed, and cloned into the BglII site of pEhExGFP. The oligonucleotides were 5′-**GATCT**ATGAGCACAAGTT CTAGTATTGAAGAAGAAGTGTTCAATTATA-3′ and 5′-**GATCT**ATAATT GAACACTTCTTCTTCAATACTAGAACTTGTGCTCATA-3′, where boldface type represents the truncated BglII site. pEhExGFP was generated by the ligation of the GFP protein-coding region of pKT-MG (29) into the BglII-XhoI site of pEhEx (31). These constructs allowed the expression of PNT with the three tandem copies of the HA tag or GFP at the carboxyl terminus. The resulting plasmids were designated pPNTFL-HA, pTS/IIb-HA, pTS/IIb/III-HA, pTS/dIIb/dIII/L-HA, pTS/IIb/III/L/I-HA, and pPNTTS-GFP. The production of the Cpn60-HA transformant was previously described (26).

Amoeba transformation. Plasmids generated as described above were introduced into amoeba trophozoites by lipofection as previously described (30). Geneticin (Invitrogen, San Diego, CA) was added at a concentration of 1 μg/ml at 24 h after transfection, and the Geneticin concentration was gradually increased for approximately 2 weeks until it reached 10 μg/ml.

Recombinant protein production. pHisPNTdI was introduced into BL21(DE3) cells. The expression of the histidine-tagged *Eh*PNTdI protein was induced with 1 mM isopropyl-β-thiogalactoside at 37°C for 3 h. After harvesting and washing three times with phosphate-buffered saline (PBS) (pH 7.4), the bacteria were lysed in B-PER reagent (Pierce, Rockford, IL) containing Complete Mini EDTA-free protease inhibitor cocktail (Roche Diagnostic, Mannheim, Germany) and mixed with 1.0 ml of a 50% slurry of Ni^{2+}-nitrilotriacetic acid (NTA) His-Bind resin. The recombinant *Eh*PNTdI-bound resin was washed in a column three times with 25 ml of buffer A (50 mM NaH_2PO_4, 300 mM NaCl [pH 8.0]) containing 20 mM imidazole. Bound proteins were eluted with buffer A containing 1 M imidazole and dialyzed against PBS.

Antibodies. Anti-*Eh*PNT antibody was raised against purified *Eh*PNTdI in rabbit commercially (Operon, Tokyo, Japan). Anti-HA 11MO mouse monoclonal antibody was purchased from Berkeley Antibody (Berkeley, CA). Anti-*Eh*Sec61 α-subunit and anti-*E. histolytica* dolicol-*P*-mannose synthase (*Eh*DPMS) antibodies were a gift from Rosana Sánchez-López (37). Anti-galactose/*N*-acetylgalactosamine inhibitable lectin (Hgl) monoclonal antibody (3F4) (23) was a gift from Barbara J. Mann and William A. Petri, Jr. Alexa Fluor 488- or 568-conjugated anti-mouse and anti-rabbit IgGs were purchased from Invitrogen. Alkaline phosphatase-conjugated goat anti-rabbit and goat anti-mouse IgGs were bought from Jackson ImmunoResearch Laboratories (Bar Harbor, ME). Anti-GFP rabbit antibody was purchased from Medical Biological Laboratory International.

Immunoprecipitation. Approximately 3×10^6 cells of *Eh*PNT-HA- and Cpn60-HA-expressing amoebae were lysed in lysis buffer (50 mM Tris-HCl [pH 7.5], 150 mM NaCl, 1% Triton X-100, and 0.5 mg/ml E-64). The soluble lysate, after centrifugation at 15,000 × *g*, was incubated with protein G-Sepharose beads (30 μl of a 50% slurry) (Amersham Biosciences, Uppsala, Sweden) premixed with anti-HA antibody (0.5 μl) or anti-HA and anti-Hgl antibodies, respectively.

Immunoblot analysis. Whole-cell lysate and immunoprecipitated samples were separated on either a 12% or 15% (wt/vol) SDS-polyacrylamide gel and subsequently electrotransferred onto nitrocellulose membranes (Hybond-C Extra; Amersham Biosciences, Little Chalfont, Bucks, United Kingdom) as described previously (41). The membranes were blocked by incubation in 5% nonfat dried milk in TBST (50 mM Tris-HCl [pH 8.0], 150 mM NaCl, and 0.05% Tween 20) for 1.5 h at room temperature. The blots were reacted with primary anti-*Eh*PNT rabbit or anti-HA mouse antibody at a dilution of 1:500 to 1:1,000. The membranes were washed with TBST and further reacted with alkaline phosphatase-conjugated anti-rabbit or anti-mouse IgG antibody (1:1,000) at room temperature for 1.5 h. After further washing with TBST, specific proteins were visualized with an alkaline phosphatase conjugate substrate kit (Bio-Rad, Hercules, CA).

Deglycosylation of PNT. The *Eh*PNT-HA-expressing transformant was cultured with 3 μg/ml of tunicamycin (Sigma, St. Louis, MO) for 24 h to inhibit asparagine-linked glycosylation according to a protocol described previously (22). For the chemical deglycosylation of *Eh*PNT, *Eh*PNT and fetuin were dried in a Speed Vac. Ice-cold trifluoromethanesulfonic acid (TFMS)-anisol (3:2, vol/vol [100 μl]) was added, and the samples were incubated for 4 h at 4°C under N_2 according to a method described previously (13). The reaction was stopped by slowly adding 200 μl ice-cold H_2O-pyridine (73:10, vol/vol) containing 0.1% SDS to the mixture. Anisol was extracted three times with 250 μl ethyl ether. Dialysis was performed against 2 mM pyridine acetate buffer. After dialysis, the samples were subjected to SDS-PAGE and silver staining. Immunoprecipitated *Eh*PNT was also digested with PNGase F (New England Biolabs, Ipswich, MA), an amidase that cleaves between the innermost *N*-acetylglucosamine and asparagine residues of asparagine-linked glycoproteins, according to the manufacturer's instructions.

Immunofluorescence assay and organelle staining. Amoeba transformant or wild-type amoebae in a logarithmic growth phase were harvested, transferred into 8-mm round wells on glass slides, and incubated for 30 min at 35°C to let trophozoites attach to the glass surface. An indirect immunofluorescence assay was performed as previously described (36). Briefly, amoebae were fixed with 3.7% paraformaldehyde in PBS for 10 min at room temperature. The cells were then permeabilized with 0.05% Triton X-100 in PBS for 5 min. The samples were reacted with anti-*Eh*PNT (1:100), anti-*Eh*Sec61 α-subunit (1:30), anti-*Eh*DPMS antibody (1:30), anti-GFP (1:1,000) rabbit antibody, anti-HA (1:1,000) mouse antibody, or preimmune rabbit serum (1:100). The samples were then reacted with Alexa Fluor 488- or 568-conjugated anti-mouse or anti-rabbit IgG (1:1,000).

For the staining of endosomes or late endosomes/lysosomes, amoebae were incubated with BI-S-33 medium containing 2 mg/ml rhodamine isothiocyanate (RITC)-dextran for 10 to 60 min (for endosomes) or LysoTracker Red DND-99 (Molecular Probes, Eugene, OR) (1:500) for 12 h (for late endosomes/lysosomes), respectively. To visualize phagosomes, CHO cells prestained with 10 μM CellTracker Orange or 20 μM CellTracker Blue were added to *E. histolytica* trophozoites in 8-mm wells on a glass slide and incubated for 10 to 60 min. The samples were examined on an LSM 510 Meta confocal laser scanning microscope (Carl Zeiss, Thornwood, NY). Images were further analyzed by using LSM510 software.

RESULTS

Identification of two isotypes of PNT in *E. histolytica*. Two isozymes of PNT have been identified in the *E. histolytica* genome database at Pathema (http://pathema.tigr.org/tigr-scripts/pathema/) (EHI_055400 and EHI_014030, corresponding to GenBank accession numbers XP_001914099 and AAC41577, respectively). They showed 90% mutual amino acid identity. The latter *Eh*PNT isotype (EH_014030) is 1,083 aa long with a predicted molecular mass of 117.0 kDa and a pI of 5.39. This predicted protein is identical to the PNT protein previously reported (GenBank accession number AAC41577)

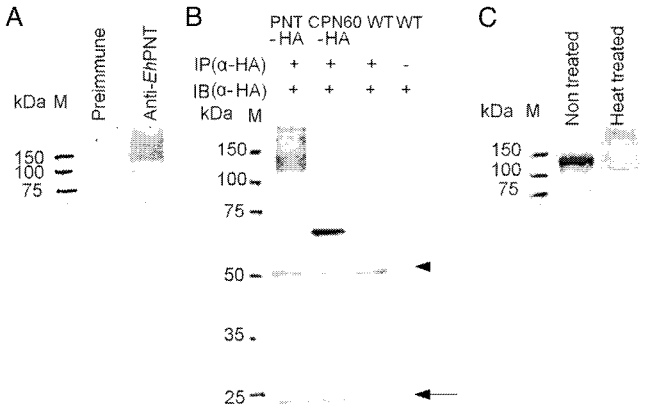

FIG. 1. Expression of PNT in *E. histolytica*. (A) Immunoblot analysis of native *Eh*PNT. Approximately 10 μg of total lysate was electrophoresed on a 12% SDS-polyacrylamide gel and subjected to an immunoblot assay with anti-*Eh*PNT antibody or preimmune serum. M, molecular mass marker. (B) Immunoprecipitation of *Eh*PNT. The lysates derived from the transformant expressing either *Eh*PNT-HA ("PNT-HA") or *Eh*Cpn60-HA ("CPN60-HA") and the wild-type strain ("WT") were subjected to immunoprecipitation with anti-HA antibody, followed by immunoblot analysis with anti-HA antibody. Lysate derived from the wild-type amoebae was also used directly for immunoblot analysis as a control. An arrowhead and an arrow indicate heavy and light chains of anti-HA antibody, respectively. IP, immunoprecipitation; IB, immunoblot. (C) Effect of heat treatment on the mobility of *Eh*PNT on an SDS-PAGE gel. Approximately 10 μg of total lysate was electrophoresed on a 12% SDS-polyacrylamide gel and subjected to an immunoblot assay with anti-*Eh*PNT antibody. M, molecular mass marker.

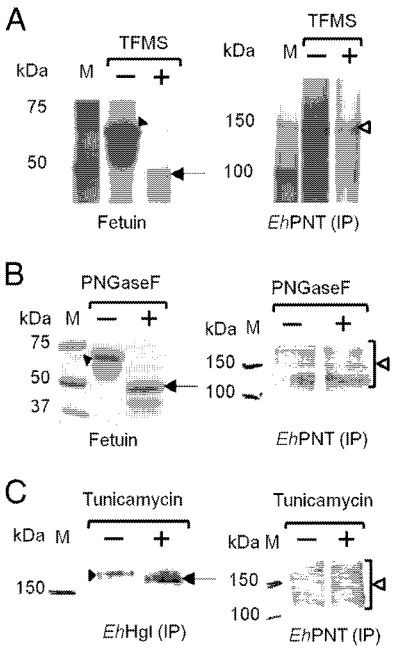

FIG. 2. Deglycosylation of *Eh*PNT. (A and B) Deglycosylation by TFMS or PNGase F. The lysates obtained from the transformant expressing *Eh*PNT-HA were subjected to immunoprecipitation (IP) with anti-HA antibody, followed by TFMS or PNGase F treatment and immunoblot detection with anti-HA antibody (right). Fetuin was used as a control, and gels were stained with silver (A) or Coomassie brilliant blue (B) (left). Filled arrowheads indicate untreated fetuin. Arrows indicate fetuin deglycosylated by TFMS (A) or PNGase F (B). Open arrowheads indicate *Eh*PNT. (C) Deglycosylation by tunicamycin. Lysates from the transformant expressing *Eh*PNT-HA cultured with tunicamycin were subjected to immunoprecipitation with either anti-*Eh*Hgl or anti-HA antibody, followed by immunoblot analysis with either anti-*Eh*Hgl or anti-HA antibody, respectively. A filled arrowhead or an arrow indicates untreated or deglycosylated *Eh*Hgl, respectively. An open arrowhead indicates *Eh*PNT.

(8). The dIII, dI, and dIIa regions of EHI_055400 (1,098 aa) are conserved except for a single amino acid substitution in dIII. EHI_055400 also contains a 5-aa extension at the amino terminus (MSLLL) and 9 aa substitutions in the putative TS (aa 1 to 14 of EHI_014030) (data not shown). In addition, dIIb of EHI_055400 contained 65 aa substitutions and two (4- and 6-aa-long) block insertions; the linker region also contains 24 aa substitutions. Since the domains involved in catalysis in EHI_055400 and EHI_014030 are totally conserved, and the two genes are expressed at comparable levels as steady-state mRNA by quantitative reverse transcriptase PCR (data not shown), we further studied only EHI_014030 in the present work. EHI_001930 (GenBank accession number XP_653216), which is annotated as the PNT β-subunit, showed no significant homology to either of the two *Eh*PNTs described above, while this sequence showed similarity with the β-subunit from other organisms and, thus, was excluded from this study.

Expression of PNT in *E. histolytica* trophozoites. Immunoblot analysis of the trophozoite lysate using anti-*Eh*PNT antibody showed a smear of >120 kDa (Fig. 1A). The size of the smear was unexpected because the predicted molecular masses of EHI_055400 and EHI_014030 were 119.0 and 117.0 kDa, respectively. To verify that this was not due to the cross-reactivity of anti-*Eh*PNT antibody, we immunoprecipitated *Eh*PNT from the *Eh*PNT-HA-expressing transformant with anti-HA antibody, followed by immunoblotting with anti-HA (Fig. 1B) or anti-*Eh*PNT (data not shown) antibody. Immunoprecipitated *Eh*PNT-HA was also recognized as a smear of >120 kDa, similar to that of endogenous *Eh*PNT.

To examine whether the smear was due to posttranslational modifications such as glycosylation, we treated immunoprecipitated *Eh*PNT-HA with TFMS or PNGase F. The pattern of immunoblots with anti-HA antibody was not affected, while the apparent molecular mass of control fetuin decreased (Fig. 2A and B). In addition, the treatment of the trophozoites with tunicamycin did not affect the mobility of *Eh*PNT, while the mobility of control Hgl increased (Fig. 2C). These data are consistent with the notion that *Eh*PNT is not glycosylated. We next examined whether aberrant mobility is due to unusual tertiary structures. We compared the patterns of the amoebic lysates, mixed with a one-third volume of 4× SDS-PAGE sample buffer (0.25 M Tris-HCl [pH 6.8], 8% SDS, and 8% 2-mercaptoethanol) and either incubated at 95°C for 5 min or left unheated, on SDS-PAGE gels. When the sample was electrophoresed without heating, *Eh*PNT was observed as a polypeptide of the predicted size (Fig. 1C). The exclusion of 2-mercaptoethanol did not affect mobility (data not shown). A similar observation was previously reported for membrane proteins, including serotonin transporter (24) and severe acute respiratory syndrome (SARS)-associated coronavirus mem-

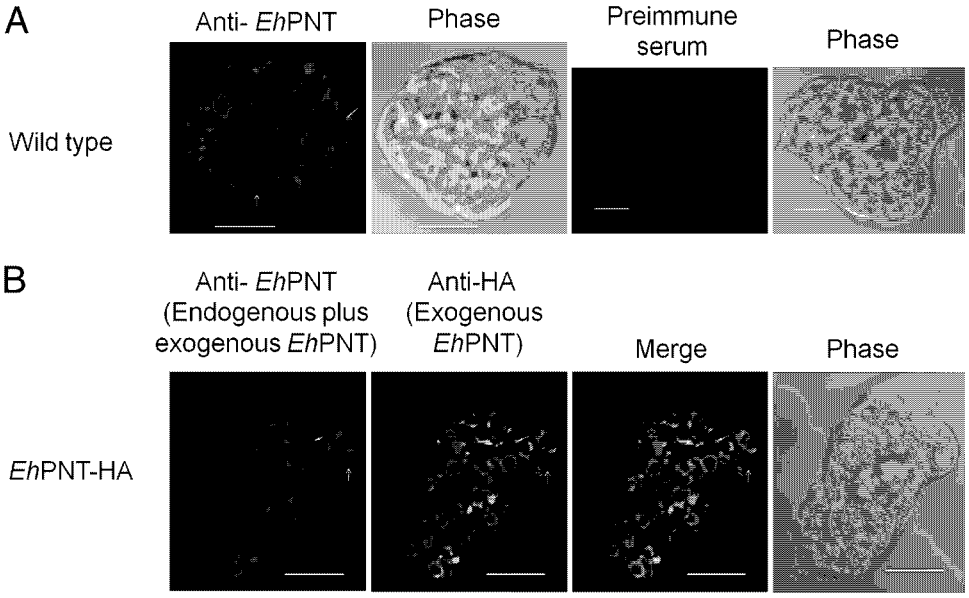

FIG. 3. (A) Subcellular localization of *Eh*PNT in wild-type amoebae. Wild-type amoebae were fixed, and an immunofluorescence assay was performed by using anti-*Eh*PNT (red) and preimmune sera. Bar, 10 μm. Arrows and arrowheads indicate representative vacuolar and dot-like structures of *Eh*PNT, respectively. (B) Colocalization of endogenous and exogenous epitope-tagged PNT in *E. histolytica*. *Eh*PNT-HA-overexpressing amoebae were fixed, and an immunofluorescence assay was performed by using anti-*Eh*PNT (red) and anti-HA (green) antibodies.

brane protein (18). In the latter case, three hydrophobic regions of 10 to 35 aa were shown to be responsible for the heat-induced aggregation of the membrane protein (18), suggesting that the heat-induced change of mobility of *Eh*PNT on SDS-PAGE is likely due to the hydrophobic nature of the protein.

Subcellular distribution of *Eh*PNT. An immunofluorescence assay using anti-*Eh*PNT antibody showed that *Eh*PNT is associated with the membranes of vesicles and vacuoles varying in size, or sometimes dot-like structures, scattered throughout the cytosol (Fig. 3A). We also examined the intracellular distribution of *Eh*PNT using the amoebic transformant that expressed *Eh*PNT (EHI_014030) with the carboxyl-terminal HA tag. The pattern of exogenous *Eh*PNT-HA (EHI_014030) and that of endogenous *Eh*PNT (a sum of EHI_055400 and EHI_014030) plus exogenous *Eh*PNT (EHI_014030) were indistinguishable (Fig. 3B). Since *Eh*PNT was previously postulated to be localized to mitosomes (8), we next examined the localization of *Eh*PNT and *Eh*Cpn60, the authentic marker of mitosomes, in the amoebic transformant expressing *Eh*Cpn60-HA (26) using anti-*Eh*PNT and anti-HA antibodies. No colocalization of *Eh*PNT and *Eh*Cpn60 was observed (Fig. 4).

Since *Eh*PNT was previously detected in isolated phagosomes (32, 33), we examined the localization of *Eh*PNT during the phagocytosis of CHO cells. Wild-type amoebae were incubated with CellTracker Orange-loaded CHO cells for 10 to 60 min to allow the ingestion of CHO cells. An immunofluorescence assay using anti-*Eh*PNT antibody (Fig. 5A) showed that the phagocytosed CHO cells were associated with *Eh*PNT at all time points (10, 20, and 60 min; only the images at 60 min are shown). The percentage of association gradually increased during the course of phagocytosis (65% ± 6%, 79% ± 9%, and 80% ± 8% at 10, 30, and 60 min, respectively). We then examined whether *Eh*PNT is localized to lysosomes using LysoTracker Red, a membrane-diffusible probe accumulated in acidic organelles (5). We found that the LysoTracker-labeled acidic compartment, the size and number of which were consistent with previous findings (28, 36), was associated with *Eh*PNT under steady-state conditions (79% ± 6% association) (Fig. 5B). To see whether *Eh*PNT is also associated with endosomes, we examined the localization of an endocytosed

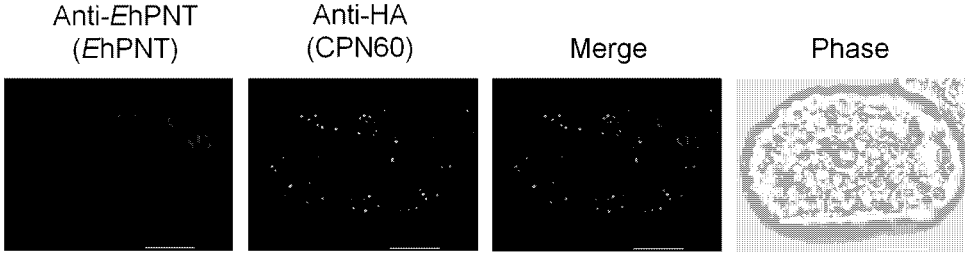

FIG. 4. Lack of association of *Eh*PNT with mitosomes. The amoebic transformant expressing *Eh*Cpn60-HA was stained with anti-HA (green) and anti-*Eh*PNT (red) antibodies to visualize *Eh*Cpn60 and *Eh*PNT, respectively. Bar, 10 μm.

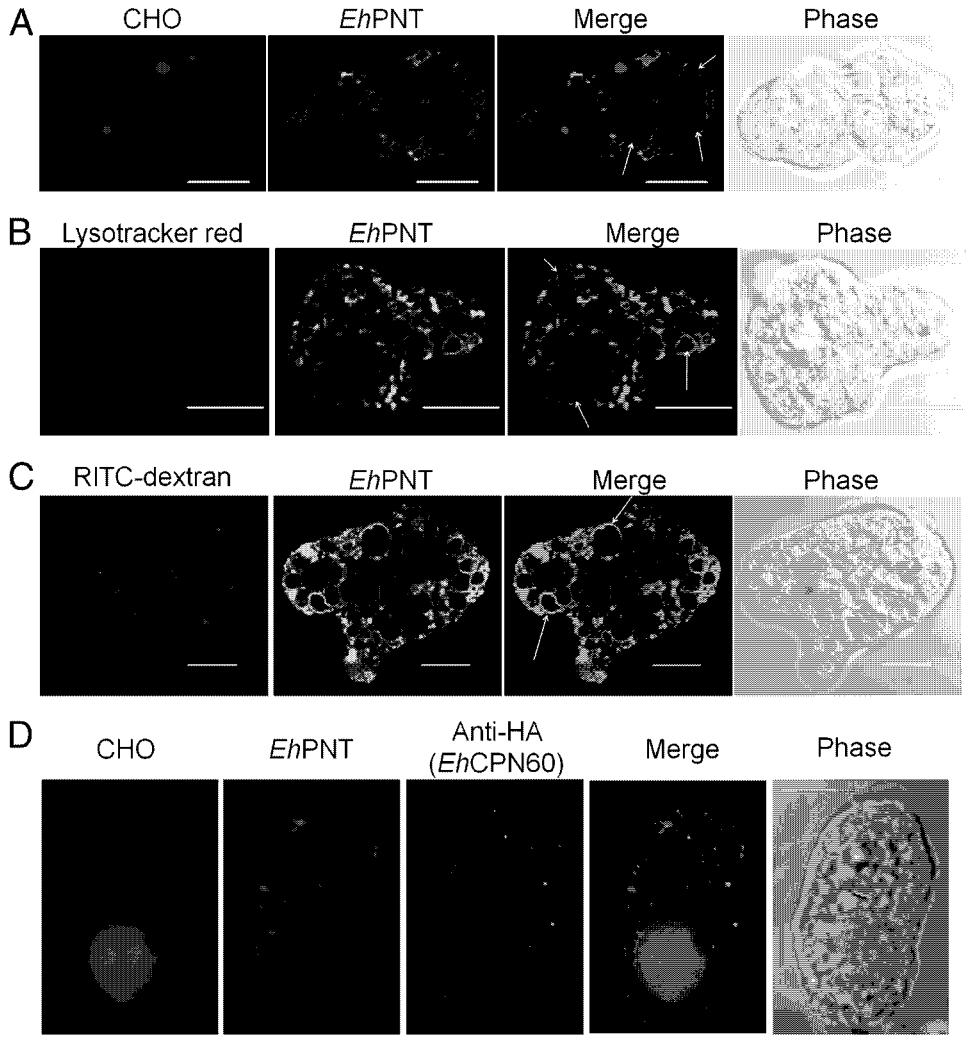

FIG. 5. Localization of *Eh*PNT to phagosomes, lysosomes, and endosomes. (A) Association of *Eh*PNT with phagosomes. Amoebae were incubated with CellTracker Orange-loaded CHO cells (red) for 60 min, fixed, and reacted with anti-*Eh*PNT antibody (green). Arrows indicate representative phagocytosed CHO cells associated with *Eh*PNT. (B) Association of *Eh*PNT with lysosomes. Amoebae were labeled with LysoTracker (red) and subjected to an immunofluorescence assay with anti-*Eh*PNT antibody (green). Arrows indicate representative lysosomes associated with *Eh*PNT. (C) Association of *Eh*PNT with the fluid-phase marker. Amoebae were incubated with medium containing RITC-dextran (red) for 1 h. The cells were fixed and reacted with anti-*Eh*PNT antibody (green). Arrows indicate representative endocytosed RITC-dextran associated with *Eh*PNT. (D) Subcellular localization of phagosomes, mitosomes, and *Eh*PNT. The amoebic transformant expressing *Eh*Cpn60-HA was incubated with CellTracker Blue-loaded CHO cells (blue) for 60 min, fixed, and reacted with anti-*Eh*PNT (red) and anti-*Eh*Cpn60 (green) antibodies. Bar, 10 μm.

fluid-phage marker, RITC-dextran. *Eh*PNT was only partially associated with RITC-dextran-containing endosomes, which were observed as tiny dot-like structures or a multivesicular body as previously shown (29), at each time point (10, 30, or 60 min; only the images at 60 min are shown) (Fig. 5C). We also examined whether *Eh*PNT is associated with mitosomes during the phagocytosis of CHO cells. An immunofluorescence assay using the amoebic transformant expressing *Eh*Cpn60-HA, CellTracker Blue-loaded CHO cells, anti-*Eh*PNT, and anti-HA antibody showed no colocalization of mitosomes and *Eh*PNT (Fig. 5D).

All domains are essential for the vesicular/vacuolar distribution of *Eh*PNT. To define the domain necessary for vesicular/vacuolar targeting of *Eh*PNT, we created amoeba transformants expressing the HA-tagged or GFP-fused protein containing various domains of PNT (Fig. 6A). The amoebic transformant expressing GFP fused with the 14-aa amino-terminal putative TS showed a cytoplasmic distribution (Fig. 6B), although the sequence MSTSSSIEEEVFNY appeared to contain the elements implicated for the TS (rich in hydroxylated and hydrophobic amino acids). The transformants expressing TS+dIIb-HA, TS+dIIb+dIII-HA, TS+dIIb+dIII+L-HA, or TS+dIIb+dIII+L+dI-HA showed a distribution that overlapped that of the endoplasmic reticulum (ER), visualized with anti-*Eh*Sec61 α-subunit antibody (27). The ER pattern was also confirmed with anti-*Eh*DPMS antibody (Fig. 6B). Full-length *Eh*PNT-HA did not overlap the ER visualized with either anti-*Eh*Sec61 α-subunit or anti-*Eh*DPMS antibody. Fractionation of the amoeba lysate followed by immunoblot analysis with anti-HA or anti-GFP an-

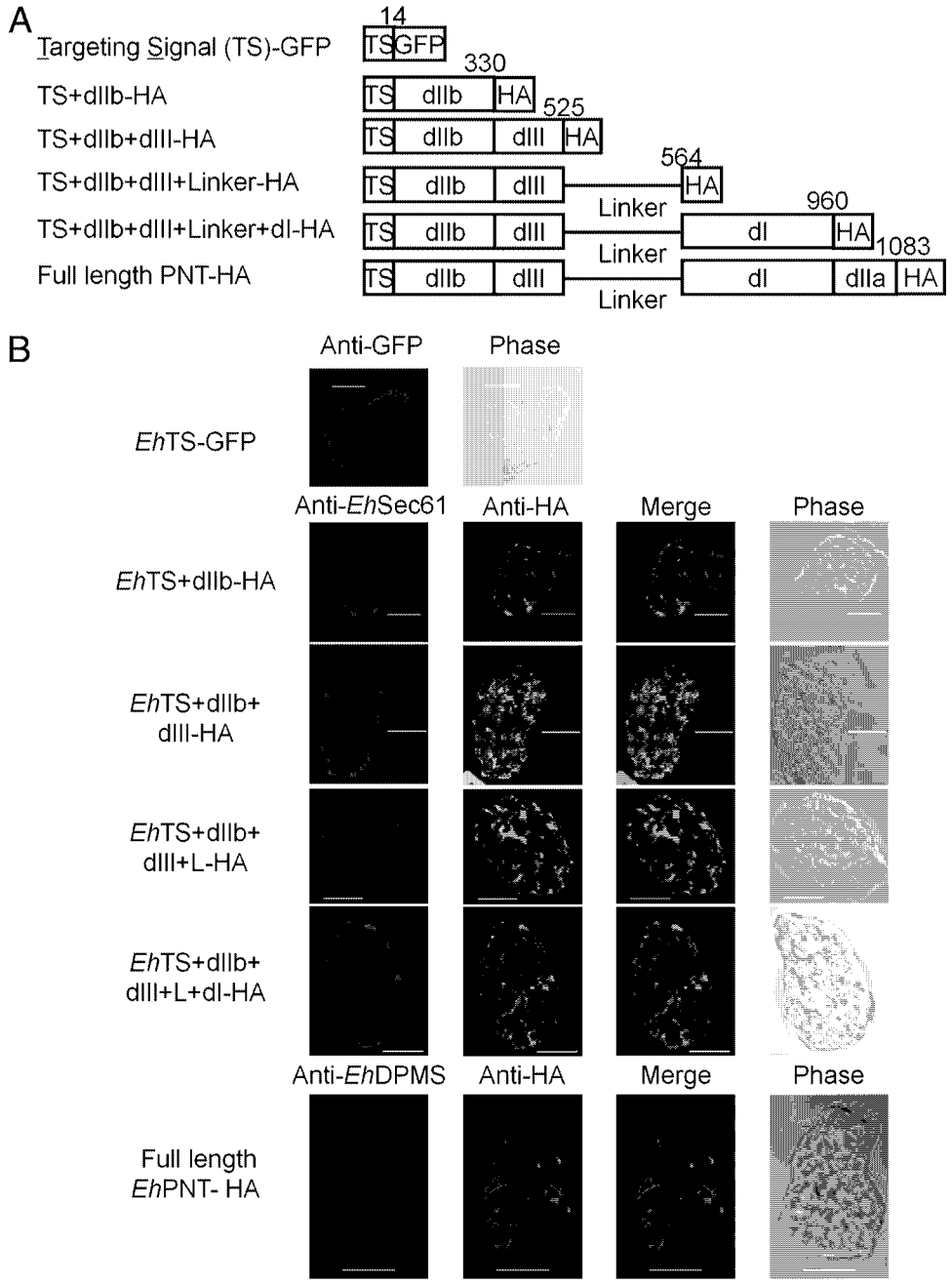

FIG. 6. Localization of a series of truncated *Eh*PNT proteins. (A) Schematic representation of HA epitope-tagged or GFP-fused recombinant *Eh*PNT used in the study. Domains, epitope (or GFP), and amino acid numbers are shown. (B) Localization of epitope-tagged or GFP-fused carboxyl-terminally truncated *Eh*PNT recombinant proteins. The transformants expressing *Eh*TS-GFP, *Eh*TS+dIIb-HA, *Eh*TS+dIIb+dIII-HA, *Eh*TS+dIIb+dIII+L-HA, and *Eh*TS+dIIb+dIII+L+dI-HA and *Eh*PNT-HA were subjected to an immunofluorescence assay using anti-HA (or anti-GFP for *Eh*TS-GFP) and anti-*Eh*Sec61 α-subunit (or anti-*Eh*DPMS for the *Eh*PNT-HA transformant) antibodies. Bar, 10 μm.

tibodies showed that all truncated forms of *Eh*PNT except for TS-GFP were partitioned into the 5,000 × *g* and 100,000 × *g* pellet fractions, while TS-GFP was fractionated into the 100,000 × *g* supernatant fraction (data not shown).

DISCUSSION

Mitosomes have been identified in several parasitic protozoan lineages such as *E. histolytica*, *Giardia intestinalis*, *Trachipleistophora hominis*, and *Cryptosporidium parvum* (21, 34, 42, 43, 50). *E. histolytica* was previously considered to be an early-branching "amitochondriate," as it lacks conventional mitochondria as well as other organelles typically found in most eukaryotes, such as peroxisomes, the rough ER, and the Golgi apparatus. However, the discovery of genes encoding the mitochondrial proteins Cpn60, PNT, mt-hsp70, ADP/ATP transporter, and Cpn10 (2, 7, 8, 21, 46) indicated that *E. histolytica* is the secondary "amito-

chondriate." While only a half-dozen proteins were shown to be localized to mitosomes (1, 2, 7, 8, 19, 21, 42, 44, 46), we recently discovered by proteomic analysis of isolated mitosomes that sulfate activation is the major pathway compartmentalized in mitosomes. Three enzymes consisting of the pathway and additional proteins required for the pathway, including sodium/sulfate symporter, mitochondrion carrier family protein, and chaperons, were identified in the mitosomal proteome. Although PNT was not discovered in the proteome, it was previously postulated to be mitosomal based on the resemblance of the amino-terminal region of *Eh*PNT to the potential mitochondrion-targeting peptide. However, it is important that the putative TS of *Eh*PNT is certainly not a canonical mitochondrion-targeting peptide because it lacks basic residues such as arginine or lysine.

Despite the premise, we showed, in this study, that *Eh*PNT was distributed to the membrane of vesicles and vacuoles, including lysosomes, phagosomes, and endosomes, but not to mitosomes. In addition, we showed that GFP fused with the amino-terminal putative TS of *Eh*PNT was distributed to the cytosol, which disproved the premise that the amino-terminal domain of *Eh*PNT functions as a putative organelle-targeting sequence. The 15-aa-long amino terminus of Cpn60 was not sufficient for the targeting of either luciferase or GFP to mitosomes (1; our unpublished data), although the removal of the first 15 aa of Cpn60 caused a mislocalization of the protein in the cytoplasm (42). Therefore, a role of the amino-terminal transit peptide for mitosomal transport remains obscure.

The association of PNT with the acidified compartments (lysosomes and phagosomes) (Fig. 5) is unprecedented in eukaryotes, where PNT is usually localized to the inner membrane of mitochondria (48). The dependence of transhydrogenase activity of *Eh*PNT on pH was demonstrated; the rate of transhydrogenation was higher at an acidic pH (5.5) than at a neutral pH (7.0 to 8.0) (49). The generation of NADPH by membrane-associated PNT (49) depends upon a proton-motive force, which is likely generated by V-ATPase localized to the acidified compartment and also the nonacidified compartment. While the colocalization of V-ATPase and *Eh*PNT has not been directly demonstrated, phagosomes contained major components of V-ATPase, as shown by the proteomic analysis of purified phagosomes (32, 33). Therefore, it is conceivable that amebic PNT localized in the acidic environment possesses enzymological properties suitable for acidic environments. Since our attempt to repress *Eh*PNT expression by gene silencing failed (our unpublished data), the physiological role of *Eh*PNT has not been elucidated. However, *Eh*PNT may be involved in the detoxification of reactive oxygen and nitrogen species by supplying NADPH as a reducing power by using a proton gradient across the lysosomal and phagosomal membranes. During tissue invasion, *E. histolytica* adapts to changing oxygen tensions as it goes from the anaerobic colonic lumen to an oxygen-rich environment in the tissue (40). Additionally, the parasite must cope with cytotoxic reactive oxygen and nitrogen species that are produced and released by activated phagocytes that are attracted to the site of infection (4, 20, 40).

Although we cannot exclude the possibility that truncated *Eh*PNT was misfolded and aggregated in the cell, our immunofluorescence and cellular fractionation data are consistent with the premise that all truncated *Eh*PNT was retained in the ER, which is suggestive of the default mechanisms of retention of multiple transmembrane proteins in the ER. The possibility that truncated *Eh*PNT is retained in the heavy microsomal fraction was previously suggested (1), where the majority (93%) of luciferase activity of the recombinant protein consisted of the 67-aa-long amino-terminal portion of PNT fused to firefly luciferase was associated with the mixed membrane fraction and was as susceptible to trypsin degradation as cytosolic luciferase from control parasites. Our present data also support the interpretation of the study that the fusion protein is embedded in the ER membrane and not targeted to mitosomes. We also showed that the aberrant mobility of PNT on SDS-PAGE gels (Fig. 1) was not likely due to either N-linked or O-linked glycosylation but was due to the hydrophobic nature of *Eh*PNT. Altogether, *E. histolytica* PNT represents a novel class of PNT localized to lysosomes and appears to have evolved uniquely in this organism.

ACKNOWLEDGMENTS

We thank Rosana Sánchez-López, Universidad Nacional Autónoma de México, for anti-*Eh*Sec61 α-subunit and anti-*Eh*DPMS antibodies and Barbara J. Mann and William A. Petri, Jr., University of Virginia Health System, for anti-Hgl antibody (3F4). We also thank Takashi Makiuchi for helpful discussions.

This work was supported by a grant-in-aid for creative scientific research (grant 18GS0314) and a grant-in-aid for scientific research (grants 18GS0314, 18050006, and 18073001) from the Ministry of Education, Culture, Sports, Science, and Technology of Japan to T.N.; a grant for Research on Emerging and Re-Emerging Infectious Diseases from the Ministry of Health, Labor, and Welfare of Japan (grant H20-Shinkosaiko-Ippan-016); and a grant for research to promote the development of anti-AIDS pharmaceuticals from the Japan Health Sciences Foundation to T.N. (grant KAA1551).

REFERENCES

1. **Aguilera, P., T. Barry, and J. Tovar.** 2008. *Entamoeba histolytica* mitosomes: organelles in search of a function. Exp. Parasitol. **118:**10–16.
2. **Bakatselou, C., C. Kidgell, and C. C. Clark.** 2000. A mitochondrial-type hsp70 gene of *Entamoeba histolytica*. Mol. Biochem. Parasitol. **110:**177–182.
3. **Bizouarn, T., O. Fjellstrom, J. Meuller, M. Axelsson, A. Bergkvist, C. Johansson, G. Karlsson, and J. Rydstrom.** 2000. Proton translocating nicotinamide nucleotide transhydrogenase from *E. coli*. Mechanism of action deduced from its structural and catalytic properties. Biochim. Biophys. Acta **1457:**211–228.
4. **Bogdan, C., M. Rollinghoff, and A. Diefenbach.** 2000. Reactive oxygen and reactive nitrogen intermediates in innate and specific immunity. Curr. Opin. Immunol. **12:**64–76.
5. **Bucci, C., P. Thomsen, P. Nicoziani, J. McCarthy, and B. van Deurs.** 2000. Rab7: a key to lysosome biogenesis. Mol. Biol. Cell **11:**467–480.
6. **Carlton, J. M., S. V. Angiuoli, and D. J. Carucci.** 2002. Genome sequence and comparative analysis of the model rodent malaria parasite *Plasmodium yoelii*. Nature **419:**512–519.
7. **Chan, K. W., D. J. Slotboom, S. Cox, T. M. Embley, O. Fabre, M. van der Giezen, M. Harding, D. S. Horner, E. R. Kunji, G. Leon-Avila, and J. Tovar.** 2005. A novel ADP/ATP transporter in the mitosome of the microaerophilic human parasite *Entamoeba histolytica*. Curr. Biol. **15:**737–742.
8. **Clark, C. G., and A. J. Roger.** 1995. Direct evidence for secondary loss of mitochondria in *Entamoeba histolytica*. Proc. Natl. Acad. Sci. U. S. A. **92:** 6518–6521.
9. **Diamond, L. S., D. R. Harlow, and C. C. Cunnick.** 1978. A new medium for the axenic cultivation of *Entamoeba histolytica* and other *Entamoeba*. Trans. R. Soc. Trop. Med. Hyg. **72:**431–432.
10. **Gardner, M. J., and B. Barrell.** 2002. Genome sequence of the human malaria parasite *Plasmodium falciparum*. Nature **419:**498–511.
11. **Gill, E. E., S. Diaz-Triviño, M. J. Barberà, J. D. Silberman, A. Stechmann, D. Gaston, I. Tamas, and A. J. Roger.** 2007. Novel mitochondrion-related organelles in the anaerobic amoeba *Mastigamoeba balamuthi*. Mol. Microbiol. **66:**1306–1320.
12. **Hall, N., M. Karras, and R. E. Sinden.** 2005. A comprehensive survey of the *Plasmodium* life cycle by genomic, transcriptomic, and proteomic analyses. Science **307:**82–86.
13. **Hiltpold, A., M. Frey, A. Hulsmeier, and P. Kohler.** 2000. Glycosylation and

palmitoylation are common modifications of *Giardia* variant surface proteins. Mol. Biochem. Parasitol. **109:**61–65.
14. **Hoek, J. B., and J. Rydstrom.** 1988. Physiological roles of nicotinamide nucleotide transhydrogenase. Biochem. J. **254:**1–10.
15. **Jackson, J. B.** 1991. The proton-translocating nicotinamide adenine dinucleotide transhydrogenase. J. Bioenerg. Biomembr. **23:**715–741.
16. **Jackson, J. B., S. J. Peake, and S. A. White.** 1999. Structure and mechanism of proton-translocating transhydrogenase. FEBS Lett. **464:**1–8.
17. **Kramer, R. A., L. A. Tomchak, S. J. McAndrew, K. Becker, D. Hug, L. Pasamontes, and M. Humbelin.** 1993. An *Eimeria tenella* gene encoding a protein with homology to the nucleotide transhydrogenases of *Escherichia coli* and bovine mitochondria. Mol. Biochem. Parasitol. **60:**327–331.
18. **Lee, Y.-N., L.-K. Chen, H.-C. Ma, H.-H. Yang, H.-P. Li, and S.-Y. Lo.** 2005. Thermal aggregation of SARS-CoV membrane protein. J. Virol. Methods **129:**152–161.
19. **Leon-Avila, G., and J. Tovar.** 2004. Mitosomes of *Entamoeba histolytica* are abundant mitochondrion-related remnant organelles that lack a detectable organeller genome. Microbiology **150:**1245–1250.
20. **MacMicking, J., Q. W. Xie, and C. Nathan.** 1997. Nitric oxide and macrophage function. Annu. Rev. Immunol. **15:**323–350.
21. **Mai, Z., S. Ghosh, M. Frisardi, B. Rosenthal, R. Rogers, and J. Samuelson.** 1999. Hsp60 is targeted to a cryptic mitochondrion-derived organelle ("crypton") in the microaerophilic protozoan parasite *Entamoeba histolytica*. Mol. Cell. Biol. **19:**2198–2205.
22. **Mann, B. J., B. E. Torian, T. S. Vedvick, and W. A. Petri, Jr.** 1991. Sequence of a cysteine-rich galactose-specific lectin of *Entamoeba histolytica*. Proc. Natl. Acad. Sci. U. S. A. **88:**3248–3252.
23. **Mann, B. J., C. Y. Chung, J. M. Dodson, L. S. Ashley, L. L. Braga, and T. L. Snodgrass.** 1993. Neutralizing monoclonal antibody epitopes of the *Entamoeba histolytica* galactose adhesin map to the cysteine-rich extracellular domain of the 170-kilodalton subunit. Infect. Immun. **61:**1772–1778.
23a. **Maralikova, B., V. Ali, K. Nakada-Tsukui, T. Nozaki, M. van der Giezen, K. Henze, and J. Tovar.** 2010. Bacterial-type oxygen detoxification and iron-sulfur cluster assembly in amoebal relict mitochondria. Cell. Microbiol. **12:**331–342.
24. **McLane, M. W., G. Hatzidimitriou, J. Yuan, U. McCann, and G. Ricaurte.** 2007. Heating induces aggregation and decreases detection of serotonin transporter protein on Western blots. Synapse **61:**875–876.
25. **Meza, I.** 1992. *Entamoeba histolytica*: phylogenetic consideration. Arch. Med. Res. **23:**1–5.
26. **Mi-ichi, F., M. A. Yousuf, K. Nakada-Tsukui, and T. Nozaki.** 2009. Mitosomes in *Entamoeba histolytica* contain a sulphate activation pathway. Proc. Natl. Acad. Sci. U. S. A. **106:**21731–21736.
27. **Mitra, B. N., Y. Saito-Nakano, K. Nakada-Tsukui, D. Sato, and T. Nozaki.** 2007. Rab11B small GTPase regulates secretion of cysteine proteases in the enteric protozoan parasite *Entamoeba histolytica*. Cell. Microbiol. **9:**2112–2125.
28. **Nakada-Tsukui, K., Y. Saito-Nakano, V. Ali, and T. Nozaki.** 2005. A retromerlike complex is a novel Rab7 effector that is involved in the transport of the virulence factor cysteine protease in the enteric protozoan parasite *Entamoeba histolytica*. Mol. Biol. Cell **16:**5294–5303.
29. **Nakada-Tsukui, K., H. Okada, B. N. Mitra, and T. Nozaki.** 2009. Phosphatidylinositol-phosphates mediate cytoskeletal reorganization during phagocytosis via a unique modular protein consisting of RhoGEF/DH and FYVE domains in the parasitic protozoon *Entamoeba histolytica*. Cell. Microbiol. **11:**1471–1491.
30. **Nozaki, T., T. Asai, L. B. Sanchez, S. Kobayashi, and M. Nakazawa.** 1999. Characterization of the gene encoding serine acetyltransferase, a regulated enzyme of cysteine biosynthesis from the protist parasites *Entamoeba histolytica* and *Entamoeba dispar*. Regulation and possible function of the cysteine biosynthetic pathway in *Entamoeba*. J. Biol. Chem. **274:**32445–32452.
31. **Nozaki, T., T. Asai, S. Kobayashi, F. Ikegami, M. Noji, K. Saito, and T. Takeuchi.** 1998. Molecular cloning and characterization of the genes encoding two isoforms of cysteine synthase in the enteric protozoan parasite *Entamoeba histolytica*. Mol. Biochem. Parasitol. **97:**33–44.
32. **Okada, M., C. D. Huston, B. J. Mann, W. A. Petri, Jr., K. Kita, and T. Nozaki.** 2005. Proteomic analysis of phagocytosis in the enteric protozoan parasite *Entamoeba histolytica*. Eukaryot. Cell **4:**827–831.
33. **Okada, M., C. D. Huston, M. Oue, B. J. Mann, W. A. Petri, Jr., K. Kita, and T. Nozaki.** 2006. Kinetics and strain variation of phagosome proteins of *Entamoeba histolytica* by proteomic analysis. Mol. Biochem. Parasitol. **145:**171–183.
34. **Riordan, C. E., J. G. Ault, S. G. Langreth, and J. S. Keithly.** 2003. *Cryptosporidium parvum* Cpn60 targets a relict organelle. Curr. Genet. **44:**138–147.
35. **Roger, A. J., S. G. Svard, J. Tovar, C. G. Clark, M. W. Smith, F. D. Gillin, and M. L. Sogin.** 1998. A mitochondrial-like chaperonin 60 gene in *Giardia lamblia*: evidence that diplomonads once harboured an endosymbiont related to the progenitor of mitochondria. Proc. Natl. Acad. Sci. U. S. A. **95:**229–234.
36. **Saito-Nakano, Y., T. Yasuda, K. Nakada-Tsukui, M. Leippe, and T. Nozaki.** 2004. Rab5-associated vacuoles play a unique role in phagocytosis of the enteric protozoan parasite *Entamoeba histolytica*. J. Biol. Chem. **279:**49497–49507.
37. **Salgado, M., J. C. Villagómez-Castro, R. Rocha-Rodríguez, M. Sabanero-López, M. A. Ramos, A. Alagón, E. López-Romero, and R. Sánchez-López.** 2005. *Entamoeba histolytica*: biochemical and molecular insights into the activities within microsomal fractions. Exp. Parasitol. **110:**363–373.
38. **Sambrook, J., and D. W. Russell.** 2001. Molecular cloning: a laboratory manual, 3rd ed. Cold Spring Harbor Laboratory Press, Cold Spring Harbor, NY.
39. **Sazanov, L. A., and J. B. Jackson.** 1994. Proton-translocating transhydrogenase and NAD- and NADP-linked isocitrate dehydrogenases operate in a substrate cycle which contributes to fine regulation of the tricarboxylic acid cycle activity in mitochondria. FEBS Lett. **344:**109–116.
40. **Stanley, S. L., Jr.** 2003. Amoebiasis. Lancet **361:**1025–1034.
41. **Tokoro, M., T. Asai, S. Kobayashi, T. Takeuchi, and T. Nozaki.** 2003. Identification and characterization of two isoenzymes of methionine γ-lyase from *Entamoeba histolytica*: a key enzyme of sulfur-amino acid degradation in an anaerobic parasitic protist that lacks forward and reverse trans-sulfuration pathways. J. Biol. Chem. **278:**42717–42727.
42. **Tovar, J., A. Fischer, and C. G. Clark.** 1999. The mitosome, a novel organelle related to mitochondria in the amitochondrial parasite *Entamoeba histolytica*. Mol. Microbiol. **32:**1013–1021.
43. **Tovar, J., G. Leon-Avila, L. B. Sanchez, R. Sutak, J. Tachezy, and M. van der Giezen.** 2003. Mitochondrial remnant organelles of *Giardia* function in iron-sulphur protein maturation. Nature **426:**172–176.
44. **Tovar, J., S. S. E. Cox, and M. van der Giezen.** 2007. A mitosome purification protocol based on Percoll density gradients and its use in validating the mitosomal nature of *Entamoeba histolytica* mitochondrial Hsp70. Methods Mol. Biol. **390:**167–177.
45. **van der Giezen, M.** 2009. Hydrogenosomes and mitosomes: conservation and evolution of functions. J. Eukaryot. Microbiol. **56:**221–231.
46. **van der Giezen, M., G. Leon-Avila, and J. Tovar.** 2005. Characterization of chaperonin 10 (Cpn10) from the intestinal human pathogen *Entamoeba histolytica*. Microbiology **151:**3107–3115.
47. **Vermeulen, A. N., J. J. Kok, P. Van Den Boogart, R. Dijkema, and J. A. J. Claessens.** 1993. *Eimeria* refractile body proteins contain two potentially functional characteristics: transhydrogenase and carbohydrate transport. FEMS Microbiol. Lett. **110:**223–229.
48. **Weston, C. J., J. D. Venning, and J. B. Jackson.** 2002. The membrane-peripheral subunits of transhydrogenase from *Entamoeba histolytica* are functional only when dimerized. J. Biol. Chem. **277:**26163–26170.
49. **Weston, C. J., S. A. White, and J. B. Jackson.** 2001. The unusual transhydrogenase of *Entamoeba histolytica*. FEBS Lett. **488:**51–54.
50. **Williams, B. A., R. P. Hirt, J. M. Lucocq, and T. M. Embley.** 2002. A mitochondrial remnant in the microsporidian *Trachipleistophora hominis*. Nature **418:**865–869.
51. **Yu, Y., and J. Samuelson.** 1994. Primary structure of an *Entamoeba histolytica* nicotinamide nucleotide transhydrogenase. Mol. Biochem. Parasitol. **68:**323–328.

Tropical Medicine and Health Vol. 39 No. 1, 2011, pp. 1-14

Review

The Global Programme to Eliminate Lymphatic Filariasis: History and achievements with special reference to annual single-dose treatment with diethylcarbamazine in Samoa and Fiji

Eisaku Kimura

Abstract: Diethylcarbamazine (DEC), first introduced in 1947, was shown to have strong efficacy and safety for treatment of human lymphatic filariasis, which is caused mostly by a species *Wuchereria bancrofti*. Many studies to optimize the dosage and treatment schedule of DEC followed, and, based on the results, control programs with various regimens were implemented in different endemic areas/countries. By the mid 1970s, with endorsement by the WHO Expert Committee on Filariasis (3rd report, 1974), the standard DEC regimen for *W. bancrofti* infection in mass treatment had been established in principle: a total dose of 72 mg/kg of body weight given in 12 divided doses, once weekly or monthly, at 6 mg/kg each. Not long after the committee report, the efficacy of annual single-dose treatment at 6 mg/kg, which is only one twelfth of the WHO-recommended dose in a year, was reported effective in French Polynesia (study period: 1973-78), and later in Samoa (study period: 1979-81). These results were published between 1978 and 1985 in the Bulletin of WHO but received little attention. In the mid 1980s, the efficacy of ivermectin, the first-choice drug for onchocerciasis, against lymphatic filariae came to light. Since the effect at a single dose was remarkable, and often better than DEC, it was predicted that the newly introduced drug would replace DEC. Treatment experiments with ivermectin increased quickly in number. Meanwhile, annual single-dose mass drug administration (MDA) with DEC at 6 mg/kg was under scrutiny in Samoa and Fiji. In the early 1990s, the Samoan study, which covered the entire population of 160,000 with 3 annual MDAs, reported a significant reduction in microfilaria (mf) prevalence and mean mf density, while in Fiji, the efficacy of 5 rounds of annual MDA (total dose, 30 mg/kg) was shown to be as effective as 28 multi-dose MDA spread over 2 years (6 weekly plus 22 monthly treatments at 5 mg/kg; total dose, 140 mg/kg). Several additional studies carried out in Samoa in relation to the annual single-dose MDAs revealed that low density mf carriers, who have a very low mf count of 1-20/ml of venous blood, could not play a significant role in filariasis transmission.

From around 1990, studies on spaced low-dose DEC treatments and various types of combination chemotherapy with DEC and ivermectin increased. Albendazole, a well-known anti-intestinal helminths agent, was later added to the combination. The main findings of these studies with *W. bancrofti* are: (i) a single dose of DEC at 6 mg/kg reduced mean mf density by ca. 90% 1 year after treatment; (ii) the same dose could damage/kill adult worms; (iii) a single dose of ivermectin at ca. 400 μg/kg was more effective than DEC in reducing mf density during the first year and was similarly or less effective in the second year; (iv) ivermectin probably could not kill adult worms; (v) a single combined dose of albendazole (400 mg) and DEC (6 mg/kg) was effective to reduce mf density by 85 to nearly 100% 12-24 months after treatment; and (vi) ivermectin or albendazole included in the combination chemotherapy produced "beyond-filariasis" benefits: clearance/reduction of intestinal helminths, and, additionally, in the case of ivermectin, skin-dwelling ectoparasites.

The Global Programme to Eliminate Lymphatic Filariasis (GPELF) started its worldwide activities in 2000, with the target of elimination by 2020. The basic strategy is to conduct annual single-dose MDAs for 4-6 years. In 2000-2007, a minimum of 570 million individuals were treated in 48 of 83 endemic countries. The drugs used are DEC 6 mg/kg plus albendazole 400 mg in most countries, or ivermectin 200-400 μg/kg plus albendazole 400 mg particularly in onchocerciasis endemic countries in Africa. (MDAs with DEC alone had been used in India.)

The GPELF achieved impressive results in terms of parasitological cure/improvement, clinical benefits, social and economic impacts, etc. However, the most impressive result of all was the programme's success in mobilizing hundreds of millions of local people, who not only took drugs but many of them actively supported MDAs as drug distributors and volunteers. Beyond filariasis, the role people can play in supplementing rural health services is now a topic of discussion and a source of hope for a new sustainable system.

Keywords: Lymphatic filariasis, global programme for elimination, diethylcarbamazine, albendazole, ivermectin, annual single-dose, mass drug administration, Samoa, Fiji

Department of Parasitology, Aichi Medical University, 21 Karimata, Yazako, Aichi-gun, Aichi-ken, Japan
Tel: 0561-62-3311
Fax: 0561-63-3645
Email: kimura@aichi-med-u.ac.jp

A. Introduction

a-1. *Parasite and disease*

Human lymphatic filariae, which are characterized by the parasitism of their adult worms in the lymphatic system, include 3 species, *Wuchereria bancrofti*, *Brugia malayi* and *Brugia timori*. Female adults reproduce offspring or microfilariae (mf) which are carried into blood circulation by the lymph flow and accumulate in the lungs. Mf are released from the lungs into the circulation at night (nocturnal periodicity of mf), synchronizing with the circadian biting cycle of mosquitoes that transmit the parasite between humans. In some Pacific islands, where *Aedes* mosquitoes bite humans in the daytime, the release from the lungs is mainly in the afternoon (diurnally subperiodicity). The detection of mf in blood is a basic method of diagnosis. After being ingested by mosquito vectors, mf develop to the infective stage of larvae in about 10-14 days. When mosquitoes with infective larvae bite humans, filarial parasites have an opportunity to enter the host. Infective larvae, males and females, penetrate the human skin, migrate in the body and reach the lymphatic system where they mature, mate and reproduce mf in about 6-12 months after skin invasion. Adult worms will damage and dilate lymphatic vessels, and cause lymphostasis often in the lower limb and around the testes and kidney. This is the basic pathology of chronic filariasis characterized by lymphedema, hydrocele, and chyluria. Lymphedema often triggers secondary bacterial infections resulting in acute fever attacks (acute dermatolymphangioadenitis [1]), which aggravate lymphedema/inflammation. In some people, the edematous skin gradually thickens, hardens and may grow to wart-like lesions. The word 'elephantiasis' refers to this condition with the often serious deformities that have caused enormous suffering among affected people worldwide for thousands of years (Fig. 1) [2].

a-2. *Epidemiology and global efforts to eliminate lymphatic filariasis*

The total number of lymphatic filariasis cases in the world, as estimated in 1996 [3], was 120 million, about 90% of which were caused by *W. bancrofti*. The total figure includes 16 million lymphedema (including elephantiasis) and 27 million hydrocele cases, the rest being cases with microfilaremia only. The infection was more prevalent among males, and adults. By region/country, India and sub-Saharan Africa had more than 40 million cases each, followed by other Asia and Islands (ca. 20 mil.) and China (ca. 10 mil.). With the swollen leg and/or scrotum, lymphatic filariasis was ranked as the 4th leading cause of permanent and long-term disability [4]. Most of the patients have been neglected and suffer from mental distress, social isolation, and economic misery due to the stigma of the disfiguring disease [5]. The estimated disability-adjusted life years (DALYs) lost in 1999 was 4.92 million [6]. As for economic loss, in India alone, the cost of treatment for acute fever attacks and chronic symptoms reached an estimated US$ 31.1 million per year, and the loss of productivity US$ 811 million per year [7].

These gloomy statistics have changed rapidly for the better since the Global Programme to Eliminate Lymphatic Filariasis (GPELF) started in 2000 (details in Section F). The Global Alliance to Eliminate Lymphatic Filariasis (GAELF) was formed the same year to support the unprecedented global program. The alliance includes health ministries of endemic countries, UN agencies (especially WHO as the secretariat), the private sector, NGDOs, academia, and government bodies (including JICA). Particularly noteworthy are the contributions of two pharmaceutical companies: GlaxoSmithKline donates albendazole free of charge and Merck & C., Inc. ivermectin. Both drugs are essential for the Mass Drug Administration (MDA) carried out annually in endemic countries. In 2007, 48 out of 81 endemic countries conducted MDAs, and 546 million people in the world were treated for lymphatic filariasis. The same year, China declared the elimination of filariasis, which was followed by Korea's declaration in 2008 [8].

B. The "new" anti-filarial drug diethylcarbamazine (DEC): Early studies to find the optimal dosage

b-1. *Trials with multi-dose treatment*

The anti-filarial effect of 1-diethylcarbamyl-4-methylpiperazine hydrochloride (DEC hydrochloride) was first reported in 1947 by Hewitt et al. [9] using naturally acquired filarial parasites in cotton rats (*Litomosoides carinii*) and dogs (*Dirofilaria immitis*). The same drug was tried for human bancroftian filariasis and its microfilaricidal and possible adulticidal effects were confirmed the following year [10]. A series of experimental treatments was conducted using DEC citrate for DEC hydrochloride to determine suitable dosage and treatment schedule. Many important studies were carried out in the South Pacific islands, where more than 10,000 American soldiers suffered clinical filariasis due to diurnally subperiodic *W. bancrofti* during World War II [11].

In American Samoa, 5 different multi-dose trials with DEC (3-9 mg/kg of body weight per day for 7-30 days, total dosage 21-270 mg/kg) confirmed rapid microfilaricidal effects, but the treatments could not prevent the reappearance of mf in 2-year follow-up studies (reported in 1953 [12]). Using 111-175 mf positives, Mahoney & Kessel [13] reported in 1971 that DEC given at 6 mg/kg daily for 6 days

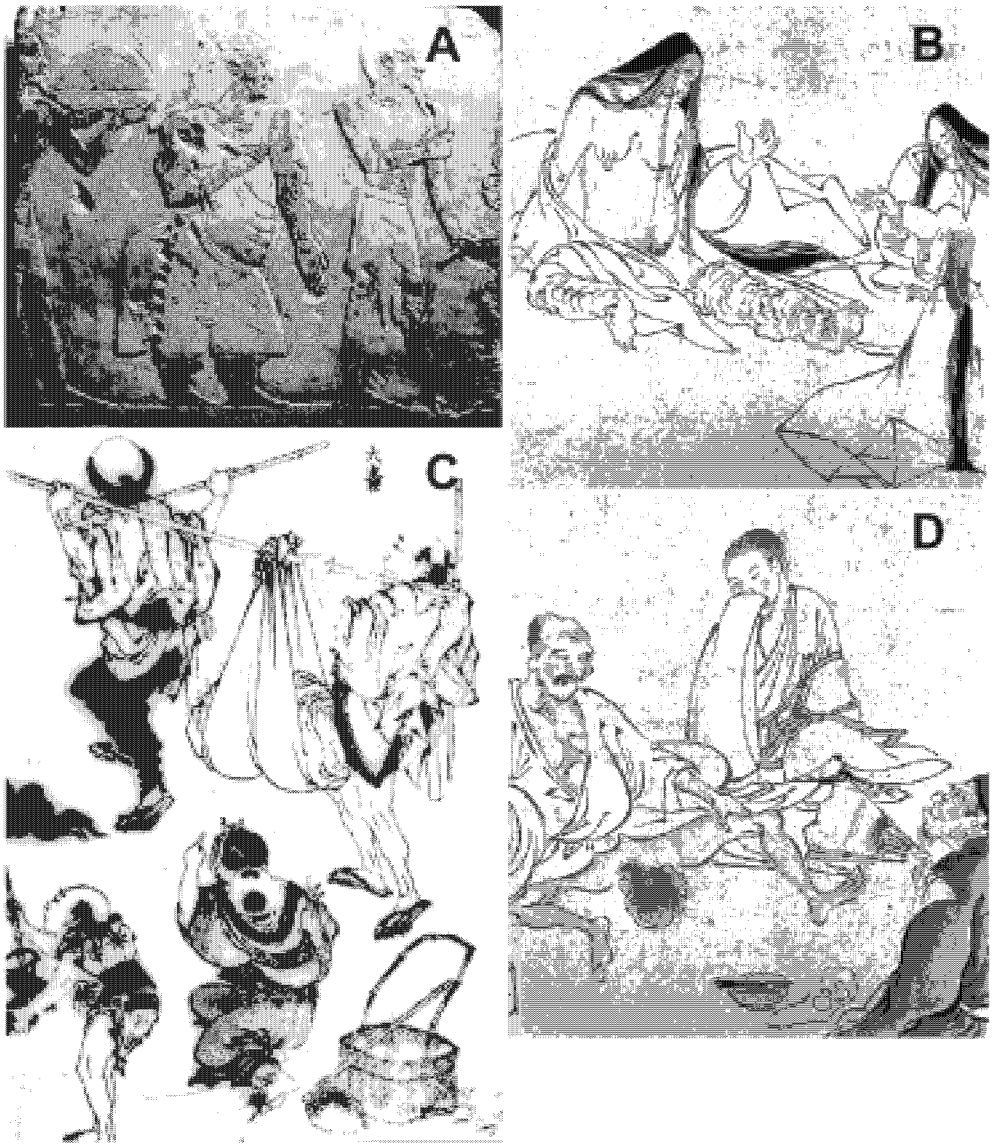

Fig. 1 Chronic symptoms of lymphatic filariasis
A: An Egyptian relief from Queen Hatshepsut's temple, Luxor, depicting the Princess of Punt, a possible elephantiasis case. (The Queen's reign: 1503-1482 B.C.); B and D: Elephantiasis of the legs and scrotum, described some 1,000 years ago in "Strange Diseases Picture Scroll." (Kyoto National Museum, Japan); C: Huge elephantiasis of the scrotum, painted by Hokusai Katsushika (1760-1849). Manga in the Edo era of Japan. {From Ref. [2], courtesy of Prof. Yoshihito Otsuji}

resulted in 32% persistence (rate of mf positive 1 week after treatment) and that the recurrence rate was 24% (rate of mf reappearance within 1 year of treatment). In this study, the diagnosis of infection was made by the detection of mf in 20 μl capillary blood obtained by the finger-prick (F-P) method.

In Fiji, Manson-Bahr (1952) [14] conducted treatment experiments with Hetrazan (DEC) at 100-300 mg daily for 15 to over 70 days and concluded that treatment must be continuous for at least two months. This conclusion was based on a finding that, even after multi-dose treatments cleared mf in 20 μl of F-P blood, mf were still positive when 1 ml of venous blood was examined by Knott's method. Burnet & Mataika (1961) [15] administered 6 weekly doses of DEC at 400 mg (ca. 5-8 mg/kg) each and repeated the same regimen half a year later (total dosage 4,800 mg). The treatment reduced mf rate, determined with 60 μl of F-P blood, from 12.2% to 2.7%. However, they noted that over 40% of mf negatives (who had been positive before treatment) were in fact positive by Knott's method

using 1 ml of venous blood.

In French Polynesia, Kessel (1957) [16] compared 3 different dosages and reported that 6 mg/kg once a month for 24 months showed the best result in terms of mf prevalence and density (mf/20 µl of blood) reductions. In Japan, among various dosage schemes tested by different workers, Sasa (1976) [17] stressed the importance of the size of total dosage given, rather than the schedule of daily, weekly or monthly treatment, and recommended a total dosage of 72 mg/kg at 6 mg/kg daily for 12 days.

The WHO Expert Committee on Filariasis analyzed the accumulated data on DEC dosage and reported in 1967 [18] that "an adequate amount seems to be a total dose of about 72 mg of diethylcarbamazine citrate per kg body weight". Spaced doses of 6 mg/kg once a week or once a month (12 times) were preferred to daily doses to reduce adverse reactions. The next WHO Expert Committee Report (1974) [19] confirmed the same total dose of 72 mg/kg for *W. bancrofti* infections and 30-40 mg/kg for *B. malayi* infections. Daily treatment was considered impractical for mass treatment. In 1984, the 4th Committee Report [20] reiterated the same total dosage for *W. bancrofti*.

b-2. *Effect of low-dose treatments: results from a "minority" group*

Several studies with *W. bancrofti* reported the remarkable effectiveness of DEC at low dosages. Rachou & Scaff (1958) in Brazil (quoted by Hawking, 1962 [21]) reported that only one dose at 6 mg/kg reduced the mf prevalence rate from 100% (pretreatment level) to 62%, and mf density by 91.4% when assessed 12 months after treatment. The authors recommended annual or biannual mass treatments without prior blood tests for mf. In Gambia, McGregor & Gilles (1960) [22] observed that a total dose of 12.5 mg/kg (2.5 mg/kg daily for 5 days) reduced microfilarial load by 90-98% 43 months after treatments and left the noteworthy comment that "mass-treatment campaigns aimed at dosing all inhabitants at spaced intervals (2-4 years) might in the long run prove to be the most effective and economical way." Nearly 2 decades later, in French Polynesia, Laigret et al. (1978) [23] reported that DEC 6 mg/kg (400 mg for males and 300 mg for females) given once per year for 3 years successfully reduced the mf rate from 100% (pretreatment level) to 12% and the average mf density from 15 per 20 µl of blood to 0.3. The annual single-dose treatment was applied to ca. 50,000 people for 4 years and succeeded in reducing the mf prevalence from 4.4% to 1.9%. In practice, not all of the people took 4 doses; the result was obtained with the average of 2.76 doses in 4 years [24].

It is surprising to find that the dosages recommended for DEC treatment differed so widely in range. Understandably, researchers seemed to focus more on the cure of infection in the early stage of dosing trials. Due to the reappearance of mf after treatments, adulticidal effect was considered a key issue in judging the efficacy of a drug. Thus, the necessity of multi-dose treatment with a high total dosage must be stressed. On the other hand, it seems that a small number of researchers, especially those working in less-developed settings, paid more attention to the applicability of a treatment scheme. Also, the experience of difficulty in conducting multi-dose treatments and the recognition of adverse effects in such treatments must have convinced researchers to accept regimens not ideally effective but operationally feasible. The realization that very light infections had been missed previously when conventional blood tests (with 20-60 µl of F-P blood) were used for diagnosis called for a more suitable means of large-scale mass treatment. In 1984, the WHO Expert Committee on Filariasis, for the first time, mentioned the effectiveness of yearly treatments at 6 mg/kg [20].

C. Filariasis control in Samoa and Fiji with annual single-dose MDA using diethylcarbamazine

c-1. *Countries and their filariasis situations*

Samoa, an independent country in the South Pacific, had a population of 160,000 (1990) in the 2 main islands of Upolu and Savaii. Diurnally subperiodic *W. bancrofti*, transmitted by *Aedes polynesiensis* and *Aedes samoanus*, is endemic. The prevalence study in 1965 revealed a mf rate of 19.1% (n = 10,129) by the 20 µl F-P blood smear method. The first nationwide MDA in 1965/66 using DEC (5 mg/kg once a week for 6 weeks, followed by the same dosage once a month for 12 months) reduced the mf rate to 1.63% (n = 42,697) in 1967, and the second MDA in 1971 (6 mg/kg once a month for 12 months) further reduced the rate – assessed by the 60 µl F-P method in 1972 – to 0.24% (n = 6,361). Despite continuing treatment of known mf positives, the prevalence increased gradually, and in 1979, reached 3.8% (n = 8,385) by 60 µl blood smear and 4.5% (n = 8,385) by the nuclepore filtration method using 1 ml of venous blood (1 ml NP method). The situation was alarming, because mf rate (by 1 ml NP method) of adult males aged ≧30 years had already reached the 20% level [25].

Fiji is the largest island country in the region, with a total population of 726,400 (1990) scattered over 100 islands. The two main islands are Viti Levu and Vanua Levu. Diurnally subperiodic type *W. bancrofti*, transmitted by *Ae. polynesiensis*, *Ae. pseudoscutellaris* and several other mosquito species, is endemic. In 1958, the mf prevalence determined by 60 µl F-P method in the delta area of the Rewa River, Viti Levu, was 12.2% (n = 1,200), which decreased

to 2.7% (n = 1,123) in 1959 after 2 rounds of MDA with DEC (400 mg once, 6 times weekly). However, by 1963, the rate increased to a level of 5% [26]. The 1968-69 studies in Taveuni and Koro islands, and Vanua Levu revealed a mf prevalence of 23% (n = 947) and 13% (n = 3,538) by the 60 μl F-P method, respectively (computed from the data by Mataika et al., 1971 [27]). A nationwide MDA campaign was commenced in 1969 using DEC at 5 mg/kg weekly for 6 weeks, followed by 22 monthly treatments (totally 28 doses, 140 mg/kg). The whole country was covered in 5 stages, and the campaign, which reached completion in 1975, successfully reduced the mf prevalence to 1% or less, but subsequent blood surveys suggested a gradual increase in infection [28]. The surveys in 1983-84 in the 2 remote islands of Lau and Rotuma revealed mf rates of 7.9% (n = 2,329) and 21.2% (n = 1,689) by the 60 μl F-P method, respectively [29]. In a 1985 survey in Kadavu island, the mf rate was 6.9% by the same method (n = 4,686) [30].

Table 1. Comparison of the effects of 3 different DEC dosages given as a single dose and assessed 12 months after treatment

	Dosages		
	4 mg/kg	6 mg/kg	8 mg/kg
No. examined (mf carriers)	51	41	45
No. mf negative after treatment	15	22	18
(% cure rate)	(29.4)	(53.7)	(40.0)
Decrease in mf count, expressed as mean of log (mf +1)			
Pre-treatment (A)	2.117	2.003	2.198
Post-treatment (B)	1.384	0.751	1.010
Change	0.733	1.251	1.188
% decrease*	81.5	94.4	93.5

* Calculated as 100 x [antilog (A) - antilog (B)]/antilog (A).
{Source: Partially adopted from Ref. [31]}

c-2. *WHO/Samoa Filariasis Research Project: Confirmation of efficacy of annual single-dose treatment*

In 1976, when the WHO/Samoa Filariasis Research Project started, it had become standard practice in the treatment of bancroftian filariasis to give a total DEC dose of 72 mg/kg in 12 treatments at 6 mg/kg each. However, difficulties in multi-dose treatment had been encountered in many endemic countries. Especially in Samoa, where a year-long multi-dose MDA was conducted twice in 1965/66 and 1971 utilizing limited health resources, the government was reluctant to repeat the procedure. In the midst of this situation, a report from French Polynesia that annually spaced single-dose DEC at 6 mg/kg was effective in reducing mf rate and density [23] brought encouraging news. Although the regimen was not popular in those days, the Research Project in Samoa decided to evaluate the efficacy of DEC single dose 12 months after treatment.

In the study in 1979-81, a single DEC dose of 4 mg/kg, 6 mg/kg or 8 mg/kg was administered to mf positive persons and the change in mf was assessed at 12 months by the 1 ml NP method (Table 1). The cure rate (% mf negative after treatment) was 29.4%, 53.7% and 40.0%, and the % decrease in geometric mean mf count was 81.5%, 94.4% and 93.5%, respectively for 4 mg/kg, 6 mg/kg and 8 mg/kg regimens. There was no significant difference among the cure rates, but the % decrease obtained with 4 mg/kg regimen was less than that of the 6 mg/kg or 8 mg/kg regimen ($P < 0.01$). Side reactions were studied by questioning people between 5 and 15 days after treatment. The occurrence of reactions (all types combined) was significantly higher in the 8 mg/kg regimen (77.9%) than in the other regimens (57-59%). It was concluded that annual single-dose DEC treatment at 6 mg/kg was suitable for the nationwide treatment for filariasis [31]. In 1981, upon completion of the study, the government of Samoa in collaboration with the Western Pacific Regional Office of WHO decided to implement a national MDA program based on this treatment.

c-3. *Nationwide MDA in Samoa with once-a-year treatment: Long-term efficacy*

A national MDA using a single dose of DEC at 6 mg/kg was started in 1981. All Samoans, except infants under the age of 1 year, pregnant women, sick people, and the very old, were the targets. After completion of the census in every village and town in the country with assistance of village Women's Committees, 3 MDAs were carried out under the supervision of medical staff by members of Women's Committees in 1982, 1983, and 1986, with a treatment coverage of 86.3%, 83.8% and 82.6%, respectively. The total population in 1986 was 159,199. The evaluation blood surveys were carried out 4 times, before and after each MDA, using 60 μl blood smears from some 9,600-13,700 people in 26-34 villages on each occasion. The MDAs reduced the mf prevalence gradually from 8.0% to 3.8% (52% reduction) in males, and from 3.2% to 1.3% (59% reduction) in females. The mf densities (geometric mean of positive counts per 60 μl) decreased from 23.1 to 9.1 (61% reduction) in males and from 14.6 to 9.4 (36% reduction) in females. The change in mf prevalence is summarized in Fig. 2, before and after 3 MDAs according to sex and age [32].

The transmission potential or infectivity index (%) of total population (IIT), which is an estimated mosquito in-

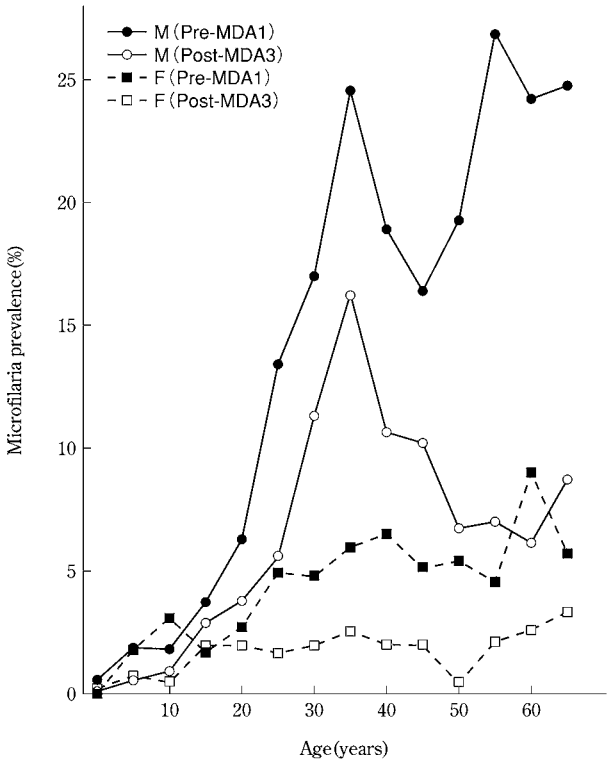

Fig. 2 Change in microfilaria prevalence before and after 3 annual single-dose MDAs with DEC at 6 mg/kg, analyzed by sex and age group (study in Samoa) {Figure redrawn from Ref. [32]}

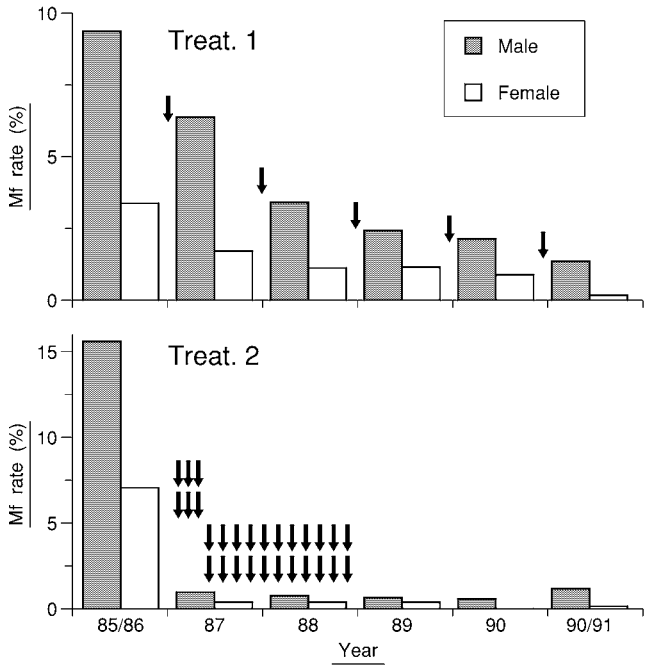

Fig. 3 Comparison of 2 MDA schemes with DEC: 5 rounds of annual single-dose treatment at 6 mg/kg (Treat. 1) and 28-dose treatment at 5 mg/kg given weekly for 6 weeks and monthly for 22 months (Treat. 2). Each arrow indicates a single treatment. {Figure redrawn from Ref. [35]}

fection rate [33], was reduced from 2.18 before MDA to 0.67 (70% reduction) after 3 MDAs. Entomological studies were also conducted at Vailu'utai village on Upolu Island. A total of 1,758 *Ae. polynesiensis* were dissected before MDA and 5,206 after the 2nd MDA. The results revealed a decrease in mosquito infection rate from 0.97% to 0.06% and the infective rate (% of mosquitoes having the infective stage of larvae) from 0.28% to 0.02% [32].

These findings indicated the remarkable long-term efficacy of annually spaced single-dose MDAs, given in fact 3 times in 6 years, and at the same time, the feasibility of a nationwide control program in which people are the major players.

c-4. *Fiji study for confirmation of efficacy of 5 rounds of annual single-dose treatment with DEC: comparison with 28 multi-dose MDA*

Mataika et al. (1993) [34] carried out an extensive study comparing DEC efficacy between 5 annual single-dose MDAs at 6 mg/kg (total 30 mg/kg) and very intensive 28-dose MDA (5 mg/kg once a week for 6 weeks, then monthly for 22 months; total 140 mg/kg). The results are shown in Fig. 3 [35]. The annual scheme reduced the mf rate year by year from 6.5% before treatment (average of males and females) to 0.9% after 5 treatments (87% reduction), while in the multi-dose scheme, the rate dropped sharply from 11.6% to 0.8% in 1987, and to 0.9% at 5 years (93% reduction). However, without treatment for more than 2 years after completion of the intensive 2-year regimen, a slight but significant increase in mf rate was observed in 1990/91 compared with the previous year. This indicates the advantage of continued annual doses rather than a concentrated multi-dose treatment. This study reconfirmed the effectiveness of annual single-dose MDAs. It was obvious that the annual scheme was much easier and more practical than the multi-dose scheme.

D. Low-density microfilaremia in Samoa and its significance in filarial transmission

d-1. *What is low-density microfilaremia?*

There are mf densities that are too low to be detected by conventional blood smears with 20-60 μl of F-P blood. The employment of nuclepore/millipore filtration of 1 ml venous blood has facilitated the detection of low density mf carriers. Low mf density was defined variously by re-

searchers. A mf range of 1-10 mf/ml was cited but often proved inconvenient for analytical studies as not many cases fell into this category. Comparing the 60 µl F-P method and 1 ml nuclepore filtration method, 1-20 mf/ml was defined as low-density microfilaremia (l.d.m.) for studies in Samoa [36]. The prevalence of l.d.m. in all mf positives was 23.6% (90/381), which led to an estimate of 1,700 low-density mf carriers in 1979 throughout the country. L.d.m was proportionally more frequent in villages with lower mf prevalences and in people < 20 years of age. By sex, there was no difference.

Since low-density mf carriers were recognized to occupy a substantial proportion of all mf carriers in Samoa, and *Ae. polynesiensis* were known to ingest more mf than estimated (up to 4.7 times) while having a blood meal on low-density mf carriers [37], the significance of l.d.m. as a source of transmission was seriously discussed, especially because it was suspected that annual single-dose DEC would not exert a sufficient adulticidal effect and therefore produce more low-density carriers than multi-dose treatment.

d-2. *Significance of low-density mf carriers in filariasis transmission: Quantitative assessment*

Based on the mosquito "infectivity index" concept proposed by Sasa [33], the significance of l.d.m. in transmission can be determined by estimating the proportion of mosquito infectivity produced by the l.d.m. group as compared to the total mosquito infectivity produced by all levels of mf carriers in an endemic community. Assuming that all people are exposed evenly to mosquito bites, the latter can be computed as follows:

Total mosquito infectivity = Σ (infection rate when mosquitoes feed on a carrier with mf density of k) x (No. of carriers with mf density of k in a community)

where k is from 1 to the maximum mf density (/1 ml of venous blood) observed in the community. Mosquito infectivity produced by low-density mf carriers will be obtained using the same formula with k value from 1 to 20.

To study the rate of mosquito infection, Samarawickrema et al. (1985) [37] conducted a detailed transmission experiment using *Ae. polynesiensis*, a main vector in Samoa, and 14 mf carriers with different mf densities ranging from 0 to 5,290 mf/ml. The results showed that the percentage of mosquitoes infected and the average number of larvae found in each infected mosquito were directly proportional to the mf densities in the carrier at the time of feeding. Based on the data from this transmission experiment, it was possible to obtain theoretical mosquito infection rates when mf carriers with different mf densities were blood sucked by mosquitoes [36]. To estimated the numbers of mf carriers with certain mf densities, a negative binomial distribution was fitted following the method of Pichon et al. (1980) [38] to the 1979 mf data from Samoa (n = 358 mf positives) [25].

The computation of mosquito infectivity is shown in Table 2. The infectivity produced by l.d.m. was 251.2 (B) and that by all levels of mf density was 11645.8 (A), and the contribution of l.d.m. to the total (B)/(A) was 0.0216 or only 2.16%. This would suggest a minor role of l.d.m. in the transmission of filariasis in Samoa [36].

E. Re-evaluation of low-dose DEC treatment, introduction of new drugs and their combination therapy

e-1. *New evidences supporting the efficacy of low-dose DEC treatments*

After around 1990, a variety of low-dose DEC treatments were tested in various countries where *W. bancrofti* is endemic. In Tahiti, a single dose of 3 mg/kg was reported effective in reducing geometric mean mf count by 95% when assessed 180 days after treatment [39]; in Papua New Guinea, 2 annual single doses at 6 mg/kg reduced the mf rate from 41% to 17%, and mf density from 71 mf/20 µl to 20 [40]; in Brazil, the efficacy of 6 mg/kg given only once was reported equally effective to 12 daily doses at 6 mg/kg when measured 12 months after treatment, although the single dose was significantly less effective than the multi doses during the first 6 months [41]; and in Tanzania, two 6-monthly treatments at 6 mg/kg reduced the geometric mean mf intensity by 92.2%, while 12 daily doses at 6 mg/kg reduced it by 98.6%, when assessed 1 year after the start of treatment. The former regimen was considered more suitable for MDAs than the standard 12-dose treatment [42]. The single dose treatment with DEC at 6 mg/kg was also applied to *Brugia malayi* infections. In Kerala, India, 2 annual mass treatments reduced the mf prevalence from 4.9% to 1.2%, and the mean mf count by 81%. In addition, clinical benefits such as a reduction in acute manifestations and recent edema cases were reported [43].

A single dose DEC at 6 mg/kg reduced not only the mf level by 90.5% but circulating filarial antigen by 39.7% 18 months after treatment, suggesting that the treatment was effective against adult parasites [44]. Brazilian researchers successfully studied the adulticidal effect of low-dose DEC treatment by direct observation of live adults using ultrasonography. The adults live in a dilated lymph vessel in the scrotal area, making a "nest" and moving actively. Amaral et al. (1994) [45] named the movement "filaria dance sign" ([46] for video image). Norões et al. (1997) [47] reported

Table 2. Mosquito infectivity produced by the low-density microfilaria (mf) carriers (B) and all levels of mf carriers (A)

Microfilaria density (mf/ml)	Theoretical % of infected fed mosquitoes (I)*	Theoretical No. of mf positive persons in each mf density group (II)	(I) x (II)	
1	0.492	13.214	6.5	
2	1.152	8.584	9.9	
-4	2.102	11.999	25.2	
-6	2.842	8.774	24.9	
-8	3.473	7.074	24.6	
-10	4.032	6.000	24.2	
-20	6.254	21.729	135.9	
			Subtotal 251.2	...(B)
-30	7.985	15.076	120.4	
-40	9.458	11.854	112.1	
-50	10.766	9.892	106.5	
-60	11.954	8.550	102.2	
-70	13.052	7.565	98.7	
-80	14.078	6.805	95.8	
-90	15.045	6.198	93.2	
-100	15.963	5.700	91.0	
-200	23.456	41.077	963.5	
-300	29.292	26.579	778.6	
-400	34.259	19.642	672.9	
-500	38.666	15.443	597.1	
-600	42.673	12.589	537.2	
-700	46.374	10.511	487.4	
-800	49.834	8.925	444.8	
-900	53.094	7.675	407.5	
-1000	56.187	6.666	374.5	
-2000	81.449	36.479	2971.2	
-3000	100 (101.123)	13.242	1324.2	
-4000	100 (117.869)	5.524	552.4	
≥4001	100 (--)	4.634	463.4	
			Subtotal 11394.6	
Total		358.000	11645.8	...(A)

* Estimated from $\log (Y + 1) = 0.5278 \log X + 0.1739$, where Y = % infected, X = mf density of a carrier.
{Source: Adopted from Ref. [36]}

that within a week after treatment at 6 mg/kg single dose, the dance sign became undetectable in 7 of 14 nests, and scrotal nodules became palpable at each site of the 7 nests. Biopsy specimens from these nodules revealed "nests" of degenerating adults, confirming the adulticidal effect. A separate histopathological study with DEC-induced nodules reported that even a single dose of 1 mg/kg could damage adult worms. However, it should be noted that, even after repeated high dose DEC treatments, some worms in the same nest remained intact [47, 48].

Fortunately, no drug resistance has been reported so far with DEC.

e-2. *Ivermectin as a new drug against lymphatic filariae*

On the other hand, ivermectin, the drug of choice for onchocerciasis that is also effective against intestinal helminths and ectoparasites such as lice, was reported in 1988 [49] to be effective against *W. bancrofti*. Since it is effective with a single oral dose at 25-200 μg/kg, ivermectin was cited as a candidate to replace DEC. The efficacy was further confirmed: when assessed at 6 months, a single dose at 21.3 μg/kg and 126 μg/kg reduced mf to 18.3% and 19.5% of the original levels, respectively, while 13 daily DEC treatments (one 3 mg/kg dose, followed by 12 daily doses at 6 mg/kg) reduced the level to 6.0% [50]. With a

higher dosage of 420 μg/kg (20 μg/kg at day 1 plus 400 μg/kg at day 5), the geometric mean mf density was reduced to 0.9% of the pretreatment level 1 year after treatment, while DEC at 6 or 7 mg/kg reduced the mean to 9.3% ($P < 0.006$) [51]. Another study with 420 μg/kg of ivermectin reported a mean mf reduction of 86.3% after 18 months, while it was 90.5% with a single dose of DEC at 6 mg/kg ($P > 0.05$). In this study, the efficacy of ivermectin was much stronger than DEC in the first 30 days after treatment, but by 18 months, the latter took over the lead and resulted in a slightly higher reduction [44]. The stronger effect of DEC as opposed to ivermectin in the second year was also reported in Brazil [52]. To study adulticidal effect of ivermectin, Dreyer et al. (1995) [53] treated 15 *W. bancrofti*-infected Brazilian men with a single dose of ivermectin at 400 μg/kg and observed the filaria dance sign by ultrasound for 3-9 months. Contrary to all expectations, there was no observable change in the dance sign, and it was concluded that ivermectin had no effect on adult worms.

e-3. *Combination chemotherapies*

Having two potent anti-filarial drugs, DEC and ivermectin, researchers tested the efficacy of their use in combination. More recently, the effectiveness of albendazole, an established antiparasitic agent, against filarial parasites was reported, and various combinations of these 3 drugs have been evaluated.

A possible additive or synergistic effect of DEC and ivermectin was reported in Haiti based on a finding that 20 μg/kg ivermectin given as a clearing dose at day 1, followed by a single 6 mg/kg dose of DEC at day 5 resulted in higher efficacy in reducing mf density than DEC alone 1 year after treatment [50]. The same regimen tested in Brazil produced the best results among different combinations of the 2 drugs: reduction of microfilaremia to 2.4% of the pretreatment level (100%) at 2 years [51]. In Tahiti, 2 annual single dose MDAs were conducted using 4 different regimens: (i) ivermectin 400 μg/kg plus DEC 6 mg/kg, (ii) ivermectin 400 μg/kg alone, (iii) DEC 6 mg/kg alone, and (iv) ivermectin 400 μg/kg plus DEC 3 mg/kg [54]. After 1 year, regimens (i) and (iv) resulted in the same 32% reduction in mf prevalence, while the reduction was only 11-14% using regimens (ii) and (iii). As for mf density, the former 2 regimens brought about a 95-96% reduction from the pretreatment level, and the latter 2 regimens 80-82%. To clarify the effect of combination therapy on adult worms, a single dose of DEC at 6 mg/kg was co-administered with either 200 μg/kg or 400 μg/kg of ivermectin, and filaria dance sign was observed with ultrasonography [55]. Interestingly, the dance sign was evident in all of the 30 nests studied, suggesting that the co-administration interfered with the already established adulticidal effect of DEC.

Other studies have looked at the combination of albendazole and DEC or ivermectin. A review by Ottesen et al. (1999) [56] summarized the role of albendazole for lymphatic filariasis elimination. Ismail et al. (1998) [57], working with *W. bancrofti*, showed more reduction in geometric mean mf density with a combined single dose of albendazole (600 mg) plus ivermectin (400 μg/kg) than with a combination of albendazole (600 mg) plus DEC (6 mg/kg) up to 12 months after treatment. At 15 months, however, there was no significant difference between the two (reduction of > 98% in both regimens). As for circulating filarial antigen, the latter combination resulted in significantly more reduction (77%) than the former at 15 months. A combined single dose of albendazole (400 mg) plus DEC (6 mg/kg) reduced mean mf density by 85.7-99.6% 12-24 months after treatment [58-61]. On the other hand, several studies could not confirm the benefit of albendazole in various combinations with ivermectin/DEC [62-65]. Dreyer et al. (2006) [66] compared the adulticidal effect of DEC (6 mg/kg) alone and DEC (6 mg/kg) plus albendazole (400 mg), and reported that the combination resulted in a much lower effect on filaria dance sign. The authors concluded that co-administration appeared to reduce the adulticidal effect of DEC. Further studies are necessary to confirm or refute anti-filarial effects of albendazole in combined use with the other anti-filarials [67].

The role of albendazole in the global program for filariasis elimination has to be emphasized for its "beyond-filariasis" benefits [55]. The drug is very effective against intestinal helminths such as *Ascaris*, *Trichuris* and hookworm, which have inflicted a tremendous burden on the health of poor people in developing countries. In Haiti, 2 annual single-dose MDAs with DEC (6 mg/kg) and albendazole (400 mg) reduced *Ascaris*, *Trichuris* and hookworm prevalences from 20.9% to 14.1%, 34.0% to 14.6%, and 11.2% to 2.0%, respectively, 9 months after the second MDA [68]. In India, the same treatment reduced the prevalence of *Ascaris* by 83%, *Trichuris* by 63% and hookworm by 69%, 11 months after the second MDA [69]. These "beyond-filariasis" benefits will not only give the anti-filariasis campaign a broader public health significance but also help to improve compliance among people and sustain the elimination program. The combination of drugs is also said to be effective in preventing the acquirement of drug resistance by filarial parasites.

F. Global Programme to Eliminate Lymphatic Filariasis (GPELF)

f-1. *Strategies/activities*

The World Health Assembly made a resolution in 1997 to eliminate lymphatic filariasis from the world as a public health problem by 2020. To execute the resolution, the GPELF was organized with a main strategy of conducting annual single-dose MDA for 4-6 years. Under MDA, all people living in endemic areas with or without filarial infection are expected to be treated, meaning that the number in 83 endemic countries will reach some 13 billion people. The drugs used for MDA are the combination of DEC (6 mg/kg) and albendazole (400 mg) in onchocerciasis-free areas, and ivermectin (200-400 μg/kg) and albendazole (400 mg) in onchocerciasis-endemic areas of Africa. The reason for the use of 2 separate regimens is that DEC could cause severe reactions if administered to *Onchocerca*-infected individuals. The biggest barrier to financing the drug supply was removed by the donation of albendazole and ivermectin by the 2 pharmaceutical giants. The GPELF has also put particular emphasis on the care of existing clinical cases of lymphedema/elephantiasis and hydrocele. Simple procedures for lymphedema management have been established [70], in which the cure and prevention of bacterial/fungal infections by maintaining good hygiene of the affected skin is the basic concept. Daily washing with soap and water, together with exercise and elevation of the affected limb to drain accumulated lymph fluid, is the most essential part of the "care" for which family members and volunteers have been trained [71].

In the beginning, many researchers/clinicians were suspicious about the success of such a huge program. Some rejected the idea outright because they considered filariasis a low-priority disease. However, a tectonic shift was already underway: the idea of DALY had changed disease priority in favor of filariasis that produces permanent or long-lasting disability, and non-profit activities for the underprivileged by a variety of voluntary groups/citizens had matured. People suffering from lymphatic filariasis, one of the world's most neglected diseases, have gained global attention for the first time in history.

f-2. *Achievements*

Ottesen et al. (2008) [72] described in detail the results of 8 years of global effort (2000-2007). More than 740 million albendazole tablets and 590 million ivermectin tablets were donated by the partner drug companies of the GAELF, while 4.7 billion DEC tablets were purchased by endemic countries. A minimum of 570 million individuals were treated in 48 of the 83 endemic countries. In 68 pre-fixed sentinel sites to monitor treatment effects, 5 rounds of MDA reduced mf prevalence by ca. 85% and cleared mf in 63% of the sites. The WHO report in 2008 [8] listed 5 countries which no longer have active transmission foci, and 2 countries (China and Korea) where the elimination of filariasis was declared.

The benefits of the MDAs conducted in 2000-2007 include the following: 6.6 million newborns were protected from filarial infection, of whom 1.4 million and 0.8 million individuals will escape hydrocele and lymphedema, respectively, in their lifetimes; 9.5 million asymptomatic parasite carriers were protected from developing hydrocele (6.0 mil.) or lymphedema (3.5 mil.). The DALYs averted in 8 years were estimated to reach 32 million, for which US$ 190 million was spent to cover MDA-related costs. Thus, the cost per DALY averted was US$ 5.90 (excluding donated drugs), which is one of the most cost effective programs in the world [73].

In addition to the benefits of the 2000-07 MDAs relating to filariasis, 56.6 million children and 44.5 million women of childbearing age were treated with albendazole for intestinal parasitic infections, and in onchocerciasis endemic countries of Africa, more than 45 million were treated with ivermectin for various skin diseases caused by *Onchocerca volvulus*, scabies mites and lice, although DALYs averted by these treatments were not quantified. It can readily be said that the global filariasis program has already established new precedents: collaboration in combating neglected diseases, single-dose treatment for different diseases, and confidence of local people in maintaining a public health program, all on a global scale.

f-3. *The future*

The progress made by the GPELF has been remarkable so far. However, the elimination program is not necessarily proceeding satisfactorily in all endemic countries. Problems arise when compliance to MDAs is not sufficient, pretreatment endemicity levels are high, the species of vector mosquito is an efficient transmitter, MDA drug dosage is not sufficient (particularly with ivermectin), etc. [74]. A more serious question will be the endpoint for the elimination program in each endemic country. The variability of biological, human-behavioral and socio-economic factors make it difficult to clarify a threshold at which filariasis transmission disappears spontaneously. With strong continuous global cooperation as a precondition, each endemic country needs to carry out well-organized and effective MDAs. The drug administration may have to be repeated if necessary. Vector control measures may become an essential part of the program in some areas [75]. And it is expected that mathematical models will play a more important

role in planning future operations [76].

G. Expansion of intervention activities by people: Community-directed treatment (ComDT)

In many endemic areas where health manpower is running short, it is difficult to carry out a large scale MDA. In Okinawa, Japan, in the 1960s, senior high school graduates living in the endemic areas were trained as "ad hoc" laboratory technicians [77]. In Sri Lanka, the MDA in 2003 achieved 80% drug coverage of 9.8 million endemic population, and more than half of the drug coverage (55.2%) was executed by volunteers making door-to-door visits [78].

In West Africa, when the Onchocerciasis Control Programme started employing annual mass treatment with ivermectin, they faced the same problem of manpower shortage. Then in 1995, WHO/TDR conducted a landmark study in 5 African countries to clarify how well local people can plan and execute the distribution of ivermectin by themselves [79]. In the study, 2 different treatment schemes were compared: community-designed treatment and program-designed treatment. In the former, after a minimal essential health education/information session, the community was invited to decide who in the community would be drug distributers and when and how the drugs would be distributed, while in the latter, experienced program staff pre-designed the criteria for selecting drug distributers and detailed procedures for drug distribution. The results were rather unexpected: the former achieved as good a treatment coverage as the latter. This was a clear indication that local people can be a reliable player in public health activities. A similar study with lymphatic filariasis followed in Ghana and Kenya [80], where community-directed treatment with some input from health services (ComDT/HS) was compared with the treatment planned and executed by the regular care system (HST). The results: ComDT/HS achieved a high treatment coverage of 75.7% - 88.0%, whereas HST obtained only 43.6% - 46.5%.

The African Programme for Onchocerciasis Control (APOC), which was set up in 1995 covering 16 countries, adopted the idea of community-designed treatment from the above 1995 TDR study and implemented the community-directed treatment with ivermectin (CDTI). The program was so successful in reducing the burden of onchocerciasis that, in the year 2007, close to 1 million DALYs could be averted [81]. For CDTI, "community drug distributers" (CDDs) play an essential role. After training, they take a census, distribute drugs, monitor adverse reactions and keep records. In 2006, there were 429,385 trained CDDs in APOC countries. These batteries of manpower with health care knowledge have become involved as a matter of course in other intervention programs. In Nigeria, successful integration of insecticide-treated bed net distribution for malaria control with lymphatic filariasis/onchocerciasis MDA was reported [82]. WHO/TDR, in 2005, launched a study to investigate whether the concept and experience of CDTI can be applied to other interventions such as delivering vitamin A supplement, insecticide treated nets, DOTS treatment for tuberculosis, and home management of malaria. The results showed that all 5 interventions (including CDTI) could be done simultaneously by the community [83].

Community-directed treatment, which was invented as a measure necessary to conduct a large scale MDA for onchocerciasis in areas where health infrastructures were poor, has been transformed into a new sustainable way of delivering therapeutic and preventive measures for rural people suffering from a variety of neglected diseases. The MDAs for lymphatic filariasis, which have been conducted side by side with APOC, can be expected to strengthen the new development synergistically.

Acknowledgment

In compiling this paper, I remembered many people: mentors, colleagues, friends, and even village people, to whom I owe a great deal. They gave me the lessons and experiences that shaped me as a parasitologist. Particularly in relation to this paper, I must mention with hearty thanks several names who guided me when I worked in Samoa and Fiji as an inexperienced WHO Medical Officer: Dr. L. Penaia, Mr. P.F. Sone, Dr. S. Pelenatu, Dr. S.T. Faaiuaso (Filariasis Office, Ministry of Health, Samoa); Dr. J.U. Mataika, Dr. J. Koroivueta, Dr. M.V. Mataitoga (Former Wellcome Virus Laboratory, Fiji); Dr. W.A. Samarawickrema, Dr. K.I. Singh (WPRO/WHO, Samoa); Dr. G.F.S. Spears (WHO Consultant, University of Otago, New Zealand); and Dr. L.S. Self, and Dr. B.C. Dazo (WPRO/WHO, Philippines).

References

1. Dreyer G, Piessens WF. In: Nutman TB (editor). *Lymphatic Filariasis*. London: Imperial College Press; 2000: 245-264.
2. Otsuji Y. In: Kimura E, Rim H-J, Sun D, Weerasooriya MV (editors). *Asian Parasitology Vol. III Filariasis in Asia and Western Pacific Islands*. Chiba: AAA Committee/Federation of Asian Parasitologists; 2005: 81-92.
3. Michael E, Bundy DAP, Grenfell BT. Re-assessing the global prevalence and distribution of lymphatic filariasis. *Parasitology* 1996; 112: 409-428.
4. WHO. World Health Report 1998 – Life in the 21st century: A vision for all.
5. Perera M, Whitehead M, Molyneux D, Weerasooriya M,

Gunatilleka G. Neglected patients with a neglected disease? A qualitative study of lymphatic filariasis. *PLoS Negl Trop Dis* 2007; 1: 2 (e128).
6. WHO. World Health Report 2000 – Health systems: improving performance.
7. Ramaiah KD, Das PK, Michael E, Guyatt H. The economic burden of lymphatic filariasis in India. *Parasitol Today* 2000; 16: 251-253.
8. WHO. Weekly Epidemiological Record 2008; 83: 333-347.
9. Hewitt RI, Kushner S, Stewart HW, White E, Wallace WS, SubbaRow Y. Experimental chemotherapy of filariasis. III. Effect of 1-diethylcarbamyl-4-methylpiperazine hydrochloride against naturally acquired filarial infections in cotton rats and dogs. *J Lab Clin Med* 1947; 32: 1314-1329.
10. Santiago-Stevenson D, Oliver-Gonzalez J, Hewitt RI. The treatment of filariasis bancrofti with 1-diethylcarbamyl-4-methylpiperazine hydrochloride (Hetrazan). *Ann N Y Acad Sci* 1948; 50: 161-170.
11. Trent SC. Reevaluation of World War II veterans with filariasis acquired in the South Pacific. *Am J Trop Med Hyg* 1963; 12: 877-887.
12. Otto GF, Jachowski Jr LA, Wharton JD. Filariasis in American Samoa III. Studies on chemotherapy against the nonperiodic form of *Wuchereria bancrofti. Am J Trop Med Hyg* 1953; 2: 495-516.
13. Mahoney LE, Kessel JF. Treatment failure in filariasis mass treatment programmes. *Bull World Health Organ* 1971; 45: 35-42.
14. Manson-Bahr P. The action of hetrazan in Pacific filariasis. *J Trop Med Hyg* 1952; 55: 169-173.
15. Burnett GF, Mataika JU. Mass-administration of diethylcarbamazine citrate in preventing transmission of aperiodic human filariasis. *Trans Roy Soc Trop Med Hyg* 1961; 55: 178-187.
16. Kessel JF. An effective programme for the control of filariasis in Tahiti. *Bull World Health Organ* 1957; 16: 633-664.
17. Sasa M. *Human filariasis – a global survey of epidemiology and control*. Tokyo: University of Tokyo Press; 1976: 500-501.
18. WHO. WHO Expert Committee on Filariasis (*Wuchereria* and *Brugia* Infections): Second Report 1967.
19. WHO. WHO Expert Committee on Filariasis: Third Report 1974.
20. WHO. Lymphatic Filariasis: Fourth report of the WHO Expert Committee on Filariasis 1984.
21. Hawking F. A review of progress in the chemotherapy and control of filariasis since 1955. *Bull World Health Organ* 1962; 27: 555-568.
22. McGregor IA, Gilles HM. Further studies on the control of bancroftian filariasis in West Africa by means of diethylcarbamazine. *Ann Trop Med Parasitol* 1960; 54: 415-418.
23. Laigret J, Fagneaux G, Tuira E. Progrès dans l'emploi de la diéthylcarbamazine en chimiothérapie de la filariose lymphatique à *Wuchereria bancrofti* var. *pacifica*: la méthode des doses espacées. *Bull World Health Organ* 1978; 56: 985-990.
24. Laigret J, Fagneaux G, Tuira E. Chimiothérapie de masse par la diéthylcarbamazine en doses espacées: effets obtenus à Tahiti sur la microfilarémie à *Wuchereria bancrofti*, var. *pacifica. Bull World Health Organ* 1980; 58: 779-783.
25. Kimura E, Penaia L, Spears GFS. Epidemiology of subperiodic bancroftian filariasis in Samoa 8 years after control by mass treatment with diethylcarbamazine. *Bull World Health Organ* 1985; 63: 869-880.
26. Burnett GF and Mataika JU. Mass administration of diethylcarbamazine citrate in preventing transmission of aperiodic human filariasis II. Results of a blood survey made four years after drug administration. *Trans Roy Soc Trop Med Hyg* 1964; 58: 545-551.
27. Mataika JU, Dando BC, Spears GFS, MacNamara FN. Mosquito-borne infections in Fiji I. Filariasis in northern Fiji: epidemiological evidence regarding factors influencing the prevalence of microfilaraemia of *Wuchereria bancrofti* infections. *J Hyg Camb* 1971; 69: 273-286.
28. Sasa M. *Human filariasis – a global survey of epidemiology and control*. Tokyo: University of Tokyo Press; 1976: 536-540.
29. Mataika JU, Mataitoga MV, Kimura E. Recent situation of filariasis in Lau and Rotuma provinces in Fiji. *Fiji Med J* 1985; 13: 211-214.
30. Mataika JU, Kimura E, Koroivueta J. Shimada M. Efficacy of five annual single doses of diethylcarbamazine for treatment of lymphatic filariasis in Fiji. *Bull World Health Organ* 1998; 76: 575-579.
31. Kimura E, Penaia L, Spears GFS. The efficacy of annual single-dose treatment with diethylcarbamazine citrate against diurnally subperiodic bancroftian filariasis in Samoa. *Bull World Health Organ* 1985; 63: 1097-1106.
32. Kimura E, Spears GFS, Singh KI, Samarawickrema WA, Penaia L, Sone PF, Pelenatu S, Faaiuaso ST, Self LS, Dazo BC. Long-term efficacy of single-dose mass treatment with diethylcarbamazine citrate against diurnally subperiodic *Wuchereria bancrofti*: eight years' experience in Samoa. *Bull World Health Organ* 1992; 70: 769-776.
33. Sasa M. *Human filariasis – a global survey of epidemiology and control*. Tokyo: University of Tokyo Press; 1976: 700-705.
34. Mataika J, Kimura E, Koroivueta J. Kaisuva JN, Brown M, Tuivaga J, Bikai S, Govind SR. Comparison of the efficacy of diethylcarbamazine between 5 rounds of annual single-dose treatment and an intensive 28-dose treatment spread over 2 years against diurnally subperiodic *Wuchereria bancrofti* in Fiji. *Fiji Med J* 1993; 19: 2-6.
35. Kimura E & Mataika JU. Control of lymphatic filariasis by annual single-dose diethylcarbamazine treatments. *Parasitol Today* 1996; 12: 240-244.
36. Kimura E, Penaia L, Samarawickrema WA, Spears GFS. Low-density microfilaremia in subperiodic bancroftian filariasis in Samoa. *Bull World Health Organ* 1985; 63: 1089-1096.
37. Samarawickrema WA, Spears GFS, Sone F, Ichimori K, Cummings RF. Filariasis transmission in Samoa I. Relation between density of microfilariae and larval density in laboratory-bred and wild-caught *Aedes (Stegomyia) polyne-*

siensis (Marks) and wild-caught *Aedes (Finlaya) samoanus* (Gruenberg). *Ann Trop Med Parasitol* 1985; 79: 89-100.
38. Pichon G, Merlin M, Fagneaux G, Riviére F, Laigret J. Etude de la distribution des numérations microfilariennes dans les foyer de filariose lymphatique. *Tropenmed Parasitol* 1980; 31: 165-180.
39. Cartel JL, Celerier P, Spiegel A, Burucoa C, Roux JF. A single diethylcarbamazine dose for treatment of *Wuchereria bancrofti* carriers in French Polynesia: efficacy and side effects. *Southeast Asian J Trop Med Public Health* 1990; 21: 465-470.
40. Schuurkamp GJ, Kereu RK, Bulungol PK, Kawereng A, Spicer PE. Diethylcarbamazine in the control of bancroftian filariasis in the Ok Tedi area of Papua New Guinea: Phase 2 – annual single-dose treatment. *PNG Med J* 1994; 37: 65-81.
41. Andrade LD, Medeiros Z, Pires ML, Pimentel A, Rocha A, Figueredo-Silva J, Coutinho A, Dreyer G. Comparative efficacy of three different diethylcarbamazine regimens in lymphatic filariasis. *Trans Roy Soc Trop Med Hyg* 1995; 89: 319-321.
42. Meyrowitsch DW, Simonsen PE, Makunde WH. Mass diethylcarbamazine chemotherapy for control of bancroftian filariasis: comparative efficacy of standard treatment and two semi-annual single-dose treatments. *Trans Roy Soc Trop Med Hyg* 1996; 90: 69-73.
43. Panicker KN, Krishnamoorthy K, Sabesan S, Prathiba J, Abidha. Comparison of effects of mass annual and biannual single dose therapy with diethylcarbamazine for the control of Malayan filariasis. *Southeast Asian J Trop Med Public Health* 1991; 22: 402-411.
44. Kazura J, Greenberg J, Perry R, Weil G, Day K, Alpers M. Comparison of single-dose diethylcarbamazine and ivermectin for treatment of bancroftian filariasis in Papua New Guinea. *Am J Trop Med Hyg* 1993; 49: 804-811.
45. Amaral F, Dreyer G, Figueredo-Silva J, Norões J, Cavalcanti A, Samico SC, Santos A, Coutinho A. Live adult worms detected by ultrasonography in human bancroftian filariasis. *Am J Trop Med Hyg* 1994; 50: 753-757.
46. Mand S, Marfo-Debrekyei Y, Dittrich M, Fischer K, Adjei O, Hoerauf A. Animated documentation of the filaria dance sign (FDS) in bancroftian filariasis. *Filaria J* 2003; 2: 3.
47. Norões J, Dreyer G, Santos A, Mendes VG, Medeiros Z, Addiss D. Assessment of the efficacy of diethylcarbamazine on adult *Wuchereria bancrofti* in vivo. *Trans Roy Soc Trop Med Hyg* 1997; 91: 78-81.
48. Figueredo-Silva J, Jungmann P, Norões J, Piessens WF, Coutinho A, Brito C, Rocha A, Dreyer G. Histological evidence for adulticidal effect of low doses of diethylcarbamazine in bancroftian filariasis. *Trans Roy Soc Trop Med Hyg* 1996; 90: 192-194.
49. Kumaraswami V, Ottesen EA, Vijayasekaran V, Devi U, Swaminathan M, Aziz MA, Sarma GR, Prabhakar R, Tripathy SP. Ivermectin for the treatment of *Wuchereria bancrofti* filariasis. Efficacy and adverse reactions. *JAMA* 1988; 259: 3150-3153.
50. Ottesen EA, Vijayasekaran V, Kumaraswami V, Perumal Pillai SV, Sadanandam A, Frederick S, Prabhakar R, Tripathy SP. A controlled trial of ivermectin and diethylcarbamazine in lymphatic filariasis. *New Eng J Med* 1990; 322: 1113-1117.
51. Addiss DG, Eberhard ML, Lammie PJ, McNeeley MB, Lee SH, McNeeley DF, Spencer HC. Comparative efficacy of clearing-dose and single high-dose ivermectin and diethylcarbamazine against *Wuchereria bancrofti* microfilaremia. *Am J Trop Med Hyg* 1993; 48: 178-185.
52. Dreyer G, Coutinho A, Miranda D, Norões J, Rizzo JA, Galdino E, Rocha A, Medeiros Z, Andrade LD, Santos A, Figueredo-Silva J, Ottesen EA. Treatment of bancroftian filariasis in Recife, Brazil: a two-year comparative study of the efficacy of single treatments with ivermectin or diethylcarbamazine. *Trans Roy Soc Trop Med Hyg* 1995; 89: 98-102.
53. Dreyer G, Norões J, Amaral F, Nen A, Medeiros Z, Coutinho A, Addiss D. Direct assessment of the adulticidal efficacy of a single dose of ivermectin in bancroftian filariasis. *Trans Roy Soc Trop Med Hyg* 1995; 89: 441-443.
54. Moulia-Pelat JP, Nguyen LN, Hascoët H, Luquiaud P, Nicolas L. Advantages of an annual single dose of ivermectin 400 micrograms/kg plus diethylcarbamazine for community treatment of bancroftian filariasis. *Trans Roy Soc Trop Med Hyg* 1995; 89: 682-685.
55. Dreyer G, Addis D, Santos A, Figueredo-Silva J, Norões J. Direct assessment in vivo of the efficacy of combined single-dose ivermectin and diethylcarbamazine against adult *Wuchereria bancrofti. Trans Roy Soc Trop Med Hyg* 1998; 92: 219-222.
56. Ottesen EA, Ismail MM, Horton J. The role of albendazole in programmes to eliminate lymphatic filariasis. *Parasitol Today* 1999; 15: 382-386.
57. Ismail MM, Jayakody RL, Weil GJ, Nirmalan N, Jayasinghe KSA, Abeyewickrema W, Rezvi Sheriff MH, Rajaratnam HN, Amarasekera N, de Silva DCL, Michalski ML, Dissanaike AS. Efficacy of single dose combinations of albendazole, ivermectin and diethylcarbamazine for the treatment of bancroftian filariasis. *Trans Roy Soc Trop Med Hyg* 1998; 92: 94-97.
58. Ismail MM, Jayakody RL, Weil GJ, Fernand D, de Silva MSG, de Silva GAC, Balasooriya WK. Long-term efficacy of single-dose combinations of albendazole, ivermectin and diethylcarbamazine for the treatment of bancroftian filariasis. *Trans Roy Soc Trop Med Hyg* 2001; 95: 332-335.
59. El Setouhy M, Ramzy RMR, Ahmed ES, Kandil AM, Hussain O, Farid HA, Helmy H, Weil GJ. A randomized clinical trial comparing single- and multi-dose combination therapy with diethylcarbamazine and albendazole for the treatment of bancroftian filariasis. *Am J Trop Med Hyg* 2004; 70: 191-196.
60. Gyapong JO, Kumaraswami V, Biswas G, Ottesen EA. Treatment strategies underpinning the global programme to eliminate lymphatic filariasis. *Expert Opin Pharmacother* 2005; 6: 179-200.
61. Sunish IP, Rajendran R, Mani TR, Munirathinam A, Reuben R, Dash AP. Impact of single dose of diethylcar-

bamazine and other antifilarial drug combinations on bancroftian filarial infection variables: assessment after 2 years. *Parasitol Int* 2006; 55: 233-236.
62. Dunyo SK, Nkrumah FK, Simonsen PE. A randomized double-blind placebo-controlled field trial of ivermectin and albendazole alone and in combination for the treatment of lymphatic filariasis in Ghana. *Trans Roy Soc Trop Med Hyg* 2000; 94: 205-211.
63. Dunyo SK, Nkrumah FK, Simonsen PE. Single-dose treatment of *Wuchereria bancrofti* infections with ivermectin and albendazole alone or in combination: evaluation of the potential for control at 12 months after treatment. *Trans Roy Soc Trop Med Hyg* 2000; 94: 437-443.
64. Pani SP, Reddy GS, Das LK, Vanamail P, Hoti SL, Ramesh J, Das PK. Tolerability and efficacy of single dose albendazole, diethylcarbamazine citrate (DEC) or co-administration of albendazole with DEC in the clearance of *Wuchereria bancrofti* in asymptomatic microfilaraemic volunteers in Pondicherry, South India: a hospital-based study. *Filaria J* 2002; 1: 1.
65. Rizzo JA, Belo C, Lins R, Dreyer G. Children and adolescents infected with *Wuchereria bancrofti* in Greater Recife, Brazil: a randomized, year-long clinical trial of single treatments with diethylcarbamazine or diethylcarbamazine-albendazole. *Ann Trop Med Parasitol* 2007; 101: 423-433.
66. Dreyer G, Addiss D, Williamson J, Norões J. Efficacy of co-administered diethylcarbamazine and albendazole against adult *Wuchereria bancrofti*. *Trans Roy Soc Trop Med Hyg* 2006; 100: 1118-1125.
67. Addiss D, Gamble CL, Garner P, Gelband H, Ejere HOD, Critchley JA, International Filariasis Review Group. Albendazole for lymphatic filariasis. *Cochrane Database Syst Rev* 2005; (4): CD003753.
68. Beau de Rochars M, Direny AN, Roberts JM, Addiss DG, Radday J, Beach MJ, Streit TG, Dardith D, Lafontant JG, Lammie PJ. Community-wide reduction in prevalence and intensity of intestinal helminths as a collateral benefit of lymphatic filariasis elimination programs. *Am J Trop Med Hyg* 2004; 71: 466-470.
69. Mani TR, Rajendran R, Sunish IP, Munirathinam A, Arunachalam N, Satyanarayana K, Dash AP. Effectiveness of two annual, single-dose mass drug administrations of diethylcarbamazine alone or in combination with albendazole on soil-transmitted helminthiasis in filariasis elimination programme. *Trop Med Int Health* 2004; 9: 1030-1035.
70. Dreyer G, Addiss D, Dreyer P, Norões J. *Basic Lymphoedema Management: Treatment and prevention of problems associated with lymphatic filariasis*. Hollis: Hollis Publishing Company; 2002: 1-112.
71. Addiss DG, Brady MA. Morbidity management in the Global Programme to Eliminate Lymphatic Filariasis: a review of the scientific literature. *Filaria J* 2007; 6: 2.
72. Ottesen EA, Hooper PJ, Bradley M, Biswas G. The global programme to eliminate lymphatic filariasis: Health impact after 8 years. *PLoS Negl Trop Dis* 2008; 2: 10 (e317).
73. Laxminarayan R, Mills AJ, Breman JG, Measham AR, Alleyne G, Claeson M, Jha P, Musgrove P, Chow J, Shahid-Salles S, Jamison DT. Advancement of global health: key messages from the Disease Control Priorities Project. *Lancet* 2006; 367: 1193-1208.
74. Kyelem D, Biswas G, Bockarie MJ, Bradley MH, El-Setouhy M, Fischer PU, Henderson RH, Kazura JW, Lammie PJ, Njenga SM, Ottesen EA, Ramaiah KD, Richards FO, Weil GJ, Williams SA. Determinants of success in national programs to eliminate lymphatic filariasis: A perspective identifying essential elements and research needs. *Am J Trop Med Hyg* 2008; 79: 480-484.
75. Sunish IP, Rajendran R, Mani TR, Munirathinam A, Dash AP, Tyagi BK. Vector control complements mass drug administration against bancroftian filariasis in Tirukoilur, India. *Bull World Health Organ* 2007; 85: 138-145.
76. Gambhir M, Michael E. Complex ecological dynamics and eradicability of the vector borne macroparasitic disease, lymphatic filariasis. *PLoS ONE* 2008; 3: 8 (e2874).
77. Yoshida C. In: Kimura E, Rim H-J, Sun D, Weerasooriya MV (editors). *Asian Parasitology Vol. III Filariasis in Asia and Western Pacific Islands*. Chiba: AAA Committee/Federation of Asian Parasitologists; 2005: 109-118.
78. Weerasooriya MV, Yahathugoda CT, Wickremasinghe D, Gunawardena KN, Dharmadasa RA, Vidanapathirana KK, Weerasekara SH, Samarawickrema WA. Social mobilisation, drug coverage and compliance and adverse reactions in a Mass Drug Administration (MDA) Programme for the Elimination of Lymphatic Filariasis in Sri Lanka. *Filaria J* 2007; 6: 11.
79. WHO/TDR. Community directed treatment with ivermectin: Report of a multi-country study (TDR/AFR/RP/96.1), 1996.
80. WHO/TDR. Community-directed treatment of lymphatic filariasis in Africa: Report of a multi-centre study (TDR/IDE/RP/CDTI/00.2), 2000.
81. WHO/APOC. Revitalising health care delivery in sub-Saharan Africa: The potential of community-directed interventions to strengthen health systems, 2007.
82. Blackburn BG, Eigege A, Gotau H, Gerlong G, Miri E, Hawley WA, Mathieu E, Richards F. Successful integration of insecticide-treated bet net distribution with mass drug administration in Central Nigeria. *Am J Trop Med Hyg* 2006; 75: 650-655.
83. WHO/TDR. Community-directed interventions for major health problems in Africa: A multi-country study. Final Report, 2008.

International Journal for Parasitology 40 (2010) 721–729

Contents lists available at ScienceDirect

International Journal for Parasitology

journal homepage: www.elsevier.com/locate/ijpara

Longistatin, a novel EF-hand protein from the ixodid tick *Haemaphysalis longicornis*, is required for acquisition of host blood-meals ☆

Anisuzzaman [a,b], M. Khyrul Islam [b,1], Takeharu Miyoshi [b], M. Abdul Alim [b], Takeshi Hatta [b], Kayoko Yamaji [b], Yasunobu Matsumoto [a], Kozo Fujisaki [c,d], Naotoshi Tsuji [a,b,*]

[a] *Department of Global Agricultural Sciences, School of Agricultural and Life Sciences, The University of Tokyo, Japan*
[b] *Laboratory of Parasitic Diseases, National Institute of Animal Health, National Agricultural and Food Research Organization, Tsukuba, Ibaraki 305-0856, Japan*
[c] *National Research Centre for Protozoan Diseases, Obihiro University of Agriculture and Veterinary Medicine, Obihiro, Hokkaido 080-8555, Japan*
[d] *Laboratory of Emerging Infectious Diseases, School of Frontier Veterinary Medicine, Kagoshima University, Korimoto, Kagoshima 890-0065, Japan*

ARTICLE INFO

Article history:
Received 4 November 2009
Received in revised form 18 November 2009
Accepted 19 November 2009

Keywords:
Arthropods
Ixodid ticks
Haemaphysalis longicornis
Longistatin
EF-hand domain
Blood-feeding

ABSTRACT

Calcium and the EF-hand Ca^{++}-binding proteins have been undisputedly recognised as the key players in almost all aspect of cell functions, starting from the cell's birth, during mitosis to its end with apoptosis. But in a few exceptional cases the EF-hand proteins are secreted from the cells and play their crucial roles extracellularly. Here, to our knowledge for the first time, we have identified and characterised an EF-hand Ca^{++}-binding protein from the salivary glands of the ixodid tick, *Haemaphysalis longicornis*, herein called longistatin. Longistatin possesses two EF-hand domains which conserve canonical structure and bind with Ca^{++}. Both the recombinant and endogenous proteins were stained with Rutheninum red. Reverse-transcription PCR data showed that longistatin-specific transcript was expressed in all life-cycle stages of *H. longicornis* and was up-regulated only in blood-fed ticks. Organ-specific transcription analysis revealed a salivary gland-specific expression of the gene which peaked at 96–120 h of feeding when ticks acquired full blood-meals and become engorged but its expression declined sharply as they detached and dropped off the host. Consistently, endogenous protein was localised in the salivary glands of adult ticks and in the lumen of the functional acini of the salivary glands. Furthermore, longistatin was detected in feeding lesions at the site of attachment of ticks on the host. These results suggest that longistatin is synthesised in, and is secreted from, the salivary glands and may have functional roles in the feeding process of ixodid ticks.

1. Introduction

Ticks are obligate haematophagous ectoparasites and all of their motile life-cycle stages are exclusively dependent on the blood-meals from host animals. Ticks are broadly classified into three families such as Ixodidae (hard ticks), Argasidae (soft ticks) and Nuttalliellidae. *Haemaphysalis longicornis* Neumann 1901, commonly known as Bush Tick or New Zealand Cattle Tick, is a hard tick and is widely distributed in many countries from the Far East to Australia (Fujisaki et al., 1994; Hoogstraal et al., 1968). In addition to direct severe adverse effects on health and productivity of infested animals, *H. longicornis* acts as vector of many bacterial, viral, protozoan and rickettsial diseases (Hoogstraal et al., 1968). Among these diseases, babesiosis, anaplasmosis, theileriosis and Q fever have both veterinary and medical importance. These diseases are associated with human suffering, and are a major constraint to animal production as they may cause morbidity or mortality in affected animals (Fujisaki et al., 1994; Ho et al., 1995).

Control of ticks may be an effective strategy to eradicate tick-borne diseases. But tick control is a herculean task as they have a wide host range. In addition, ticks are able to spend about 95% of their life-time away from the host, especially during the period of starvation (Needham and Teel, 1991). Even in this post-genomic era, various controversial methods are being used to control ticks, including the application of chemical acaricides which are very hazardous for human and animal health as they have direct toxic effects. Due to their residual effects, the acaricides are not environmentally friendly and furthermore, repeated usages of acaricides lead to the development of resistance in ticks (Zaim and Guillet, 2002). These obstacles in controlling ticks necessitate the

☆ Nucleotide sequence data has been deposited in the GenBank database under the Accession No. AB519820.

* Corresponding author. Address: Laboratory of Parasitic Diseases, National Institute of Animal Health, National Agricultural and Food Research Organization, Kannondai 3-1-5, Tsukuba, Ibaraki 305-0856, Japan. Tel.: +81 29 838 7749; fax: +81 29 838 7780.
E-mail address: tsujin@affrc.go.jp (N. Tsuji).
[1] Present address: Animal Functional Genomics Laboratory, Biosciences Research Division, Department of Primary Industries, 475 Mickleham Road, Attwood, Victoria 3049, Australia.

0020-7519/$36.00 © 2009 Australian Society for Parasitology Inc. Published by Elsevier Ltd. All rights reserved.
doi:10.1016/j.ijpara.2009.11.004

development of sustainable therapeutic interventions. Therefore, identification and characterisation of potential vaccine candidate and drug target bioactive molecules from the blood-feeding ixodid ticks are of considerable interest.

EF-hand proteins have been reported from a variety of sources such as bacteria, protozoa, helminths, arthropods and mammals including humans (Nelson and Chazin, 1998; Kawasaki et al., 1998). Calcium and the EF-hand Ca^{++}-binding proteins have been undisputedly recognised as the key players in almost all aspects of cell functions, starting from the cell's birth, through mitosis to its end with apoptosis (Berridge et al., 1998; Kahl and Means, 2003). EF-hand Ca^{++}-binding proteins modulate various biochemical reactions within the cell and in a few exceptional cases they are secreted from the cells and play their crucial roles extracellularly. For example, Osteonectin, a glycoprotein with EF-hand Ca^{++}-binding domains, is secreted from the cell and exerts versatile functions in the extracellular matrix including, a vital role as a morpho-regulatory element (Pottgiesser et al., 1994). Similarly, acetylcholinesterase, having two EF-hand domains, functions extracellularly in cell surface associations (Tsigelny et al., 2000).

Here, we have identified and cloned a full-length cDNA from the salivary glands of the ixodid tick, *H. longicornis*, which encodes a protein (longistatin) containing two functional EF-hand Ca^{++}-binding domains and is able to bind calcium. We also show that longistatin is secreted from the salivary glands and may function in the feeding process of the blood-meals from host animals by ixodid ticks. To our knowledge, longistatin is the first characterised EF-hand protein isolated from the salivary glands of ticks.

2. Materials and methods

2.1. Ticks

Parthenogenetic Okayama strains of *H. longicornis* were propagated at the Laboratory of Parasitic Diseases, National Institute of Animal Health (NIAH), Tsukuba, Japan, by feeding on the ear of specific pathogen-free (SPF) Japanese White rabbits according to the methods described previously (Alim et al., 2007) to obtain different life-cycle stages of ticks at different feeding intervals. Briefly, the ears of rabbits were cleaned by hair clipping; ticks were attached and given support with ear bags and an Elizabethan collar. Ear bags were changed at 24 h intervals. Ticks were collected after detachment following full engorgement or after the indicated period of attachment. Rabbits used in these experiments were acclimatised to the experimental laboratory conditions for 2 weeks prior to the commencement of the experiment. Animal care was conducted according to the protocols approved by the Animal Care and Use Committee, NIAH (Approval Nos. 441, 508, 578).

2.2. Cloning and sequencing of longistatin cDNA

The gene coding for longistatin was identified from the expressed sequence tags (ESTs) constructed from the salivary gland cDNA libraries of *H. longicornis* following the methods described previously (Boldbaatar et al., 2006). Briefly, the plasmid containing the gene coding for longistatin was extracted using a Qiagen DNA Purification kit (QIAGEN Science, Germantown, MA, USA). The nucleotide sequences of the cDNA were determined using the big dye terminator method on an ABI PRISM 3100 automated sequencer (Applied Biosystem, Foster City, CA, USA). The GENETYX-WIN DNA analysis software system (Software Inc.) was used to deduce the amino acid sequence of longistatin. Sequence similarity searches were performed using the BLAST programme (Altschul et al., 1997). Alignment with the previously reported similar protein sequences, available in GenBank (Benson et al., 2002), were done using CLUSTALW. The putative signal sequence was analysed using the prediction server SignalP V2.0.b2 (http://www.cbs.dtu.dk/services/SignalP) (Nielsen et al., 1997). Theoretical mol. wt and pI were determined using PeptideMass (http://us.expasy.org/tools/peptidemass.html) (Wilkins et al., 1997). Domains were searched using ExPASy-PROSITE (http://au.expasy.org/prosite/). N-linked glycosylation sites were searched using NetNGlyc 1.0 (http://www.cbs.dtu.dk/services/NetNGlyc).

2.3. Expression of longistatin

The open reading frame (ORF) of longistatin was amplified by PCR from PBS/longistatin using a set of primers, 5′ CCG CTC GAG CGG GCA GGC CGG CGA CCA GCA G 3′ and 5′ GGA ATT CCC TAA ATT TGG TTG GTC AGG TC 3′, which contained XhoI and EcoRI restriction sites, respectively. PCR was performed for 3 min at 95 °C followed by 35 cycles of 30 s at 95 °C, for 30 s at 57 °C and 1.5 min at 72 °C with a final elongation at 72 °C for 5 min. Both the PCR product and the vector pTrcHisB (Invitrogen, Carlsbad, CA, USA) were digested by XhoI and EcoRI restriction enzymes. The purified PCR product was inserted into the XhoI and EcoRI sites of the vector pTrcHisB (Invitrogen). The resultant plasmid was transformed into competent cells of *Escherichia coli* Top10F′strain (Invitrogen) following the conventional method. The expression of longistatin in *E. coli* with a Polyhistidine-tag was performed according to the procedure described by Tsuji et al. (2001). Briefly, the transfected cells were allowed to grow in SOB medium (Tryptone 20.0 g, Yeast extract 5.0 g, Sodium chloride 0.5 g, Magnesium sulphate anhydrous 2.4 g and Potassium chloride 0.186 g per litre) containing 50 μg ampicillin/ml at 37 °C under vigorous shaking (200 rpm) until the OD of 1 at 600 nm (OD_{600}) was achieved. To induce recombinant protein expression, isopropyl-β-D-thiogalactopyranoside (IPTG) was added to 1 mM concentration and the culture was grown for an additional 4 h at 37 °C on a shaking incubator. The culture was then centrifuged at 10,000*g* and 4 °C for 20 min and the pellet was resuspended in 10 ml of lysis buffer (20 mM sodium phosphate and 500 mM sodium chloride, pH 7.8). Egg white lysozyme (100 μg/ml) was added to the cell suspension and incubated in ice for 15 min. The suspension was sonicated for 2 min on ice with an ultrasonic processor (VP-15S, TAITEC, Japan) followed by immediate freezing at −80 °C and then thawing at 37 °C for 15 min in each case. After three cycles of sonication, freezing and thawing, the *E. coli* lysate was centrifuged at 23,900*g* and 4 °C for 30 min and supernatant was collected. The recombinant protein was purified using ProBond™ resin (Invitrogen) under native conditions as described by the manufacturer and subsequently eluted with a stepwise gradient of imidazole (25–500 mM). The eluted recombinant protein was concentrated using Centrisart® (Sartorius, Goettingen, Germany) having a mol. wt cut-off of 10 kDa. The concentrated protein was dialysed extensively at 4 °C with successive changes of 20 mM Tris–HCl (pH 7) and a decreasing concentration of NaCl (500–250 mM) using a Slide-A-Lyser Dialysis Cassette (Pierce, Rockford, IL, USA) with a mol. wt cut-off of 10 kDa. Purified recombinant longistatin was electrophoresed on 12.5% SDS–PAGE gel under reducing conditions. The gel was treated with 50% methanol in 10% acetic acid for 10 min at room temperature. The protein was subjected to silver staining (Daiichi Pure Chemicals, Tokyo, Japan) following the manufacturer's instructions. Finally, protein concentration was determined using micro-BCA reagent (Pierce) and stored at −20 °C until further use.

2.4. Western blot analysis

Crude *E. coli* lysate was electrophoresed through 12.5% SDS–PAGE gel under reducing conditions and the proteins were trans-

ferred onto nitrocellulose membrane. The membrane was incubated with 5% skim milk for 30 min at room temperature. Polyhistidine-tagged longistatin was probed with the anti-His monoclonal antibody (1:1000) (Anti-6 X His (Mouse IgG1-K), Monoclonal (HI192) AS, Nacalai Tesque,Inc., Kyoto, Japan). The membrane was washed with Tris-buffered saline-Tween 20 (TBS-T) and incubated with alkaline phosphate conjugated goat anti-mouse IgG (H + L) (ZYMED, San Francisco, CA, USA) as a secondary antibody for 1 h. The membrane was washed again with TBS-T and the bound protein was visualised with nitroblue tetrazolium/5-bromo-4-chloro-3-indolyl phosphate (BCIP/NBT, Promega, Medison, WI, USA).

2.5. N-terminal sequencing of longistatin

Purified recombinant protein was subjected to electrophoresis on a 12.5% SDS–PAGE gel under reduced conditions. After electrophoresis, the protein was electro-blotted onto a polyvinylidene difluoride (PVDF) membrane (Millipore, Bedford, MA, USA) in 10 mM 3-(cyclohexylamino)-1-propanesulfonic acid (CAPS) buffer (pH 11) containing 10% methanol. The blotted protein was stained with coomassie blue, followed by destaining with 50% methanol. The target protein band was excised from the blot and was subjected to N-terminal sequencing using the Procise 494 cLC Protein Sequencing System (Applied Biosystem) (Furuse et al., 1998).

2.6. Generation of mouse polyclonal antibody

BALB/c mice were immunized by s.c. injection of 50 μg of recombinant protein emulsified with FCA (DIFCO, Detroit, MI, USA) followed by booster immunizations 2 weeks apart using the same route. The immunized mice were sacrificed 1 week after the last booster and sera were collected and stored at −20 °C for further use.

2.7. Reverse transcription-PCR (RT-PCR) analysis

Unfed and fed adult ticks (24 h, 48 h, 72 h, 96 h and engorged (120 h)), and post-engorged ticks (day 0, day 1 and day 2) were washed with 70% ethanol and rinsed in PBS. Then ticks were dissected under a dissecting microscope (Olympus, SZ7, Japan) using ice-cool PBS and different organs were collected. Shortly after collection, the tissues were submerged in RNA*later*, a RNA Stabilization Reagent (QIAGEN). The total RNA was isolated by using an RNeasy Mini Kit (QIAGEN) according to the manufacturer's protocol. Total RNA was also collected from all life-cycle stages (egg, larva and nymph) of *H. longicornis*. Five hundred nanograms of total RNA was used for RT before PCR. Single stranded cDNA was prepared by using a Takara RNA PCR Kit (AMV) Ver.3.0 (Takara, Shiga, Japan) following the manufacturer's instructions. A series of PCRs were carried out using 500 ng of cDNA from each sample and longistatin-specific oligonucleotides (5′ GCT ATC TCG GCT CCT GTG TC 3′ and 5′ ATC TTC GCC AGG TCC TTC TT 3′) or oligonucleotides specific for a control cDNA encoding β-actin in a final volume of 20 μl. PCR was performed for 5 min at 95 °C followed by 35 cycles of 30 s at 95 °C, 30 s at 54 °C and 1.5 min at 72 °C and finally elongation at 72 °C for 5 min. The PCR product was subjected to electrophoresis in a 1% agarose gel.

2.8. Immunohistochemistry

Immunohistochemistry was performed as previously described (You et al., 2001). Briefly, ticks were fixed overnight in 4% paraformaldehyde in 0.1 M phosphate buffer (pH 7.2) and embedded in paraffin. Thin transverse sections were cut from paraffin-embedded well-fixed ticks. Sections were fixed on glass slides and deparaffinized with xylene. The sections were rehydrated with graded series of alcohol washes, followed by inactivation of endogenous peroxidase with 1% H_2O_2 in PBS containing 10% ethanol for 1 h and blocked with 10% goat serum (Wako, Osaka, Japan) in PBS. They were then incubated overnight at 4 °C with mouse anti-longistatin serum (1: 200). Sections treated with pre-immune mouse sera (1: 200) were used as a control. Slides were rinsed thoroughly with ice-cool PBS by placing those on a rotator (40 rpm). The sections were then reacted with peroxidase-labelled anti-mouse IgG secondary antibody and the substrate 3′,3′-diaminobenzidine tetrahydrochloride (Fast™ DAB set, Sigma, St. Luis, Mo, USA). After colour development, the slides were dehydrated with graded series of alcohol washes, cleared in xylene and then covered with cover slips and examined under a microscope (Leica Microsystem, Wetzlar, Germany).

2.9. Cell separation

Salivary gland cells were collected from partially fed (96 h) adult ticks by teasing the freshly obtained salivary glands through a stainless steel mesh in PBS containing complete protease inhibitors. The cells were washed in PBS to remove cellular debris and centrifuged at 4400*g* for 10 min at room temperature. Finally, 200 μl PBS were added and sediments were resuspended. A thin smear was prepared on a glass slide using 10 μl of cell-suspension. Cells were then fixed with 4% paraformaldehyde in PBS (0.1 M, pH 7.4) for 20 min at room temperature and were treated with 0.1% Triton X-100 in PBS for 20 min under the same conditions. The slides were washed with PBS and blocked with 10% goat serum (Wako) for 30 min at room temperature and then incubated overnight with mouse anti-longistatin serum (1: 100) at 4 °C. The cells were washed in PBS and reacted with green fluorescent-labelled secondary antibody (Alexa Flour® 488 goat anti-mouse IgG (H + L), Invitrogen) for 1 h at room temperature. The slides were then washed thoroughly with PBS and mounted with VECTASHIELD® mounting medium containing DAPI (Vector Laboratories, Burlingame, CA, USA) and examined under a fluorescent microscope (Leica).

2.10. Detection of longistatin in secretory pathways of salivary glands and in host tissues

Immunofluorescent staining was performed using thin sections from partially fed (72 h) adult ticks following the methods described previously (Miyoshi et al., 2007). Sections were treated with mouse anti-longistatin sera and bound antibodies were detected using green fluorescent-labelled secondary antibody (Alexa Flour® 488 goat anti-mouse IgG (H + L), Invitrogen). Slides were mounted with VECTASHIELD® mounting medium containing DAPI (Vector Laboratories) and examined under a fluorescent microscope (Leica). We also employed immunofluorescent staining for the detection of longistatin in the feeding lesions of the host. Thin sections were prepared from tissue samples collected from the feeding lesions developed on a rabbit ear at the site of attachment of the tick, as previously described (Islam et al., 2009). Tissues were fixed overnight in 4% paraformaldehyde and embedded in paraffin. Immunofluorescent staining was performed using mouse anti-longistatin sera as described above.

2.11. Ca^{++}-binding assays

Purified longistatin was electrophoresed using 10% SDS–PAGE gel in the presence of 3 mM $CaCl_2$ or 3 mM EDTA. BSA was used as a control. Additionally, both the endogenous and recombinant proteins were transferred onto nitrocellulose membranes and were stained with 25 mg/L Ruthenium red (Calbiochem) in 60 mM KCl,

5 mM $MgCl_2$ and 10 mM Tris–HCl (pH 7) for 15 min at room temperature.

3. Results

3.1. Molecular characterisation of longistatin

Sequence analysis revealed that the full-length longistatin cDNA consisted of 750 bases which included the complete coding region together with 5′ and 3′ non-coding regions. The in-frame start codon is located at nucleotides 133–135 and the stop codon is at 601–603. The ORF consisting of 471 nucleotides, extends from residues 133–603 which codes for a protein of 156 amino acid (aa) residues having a calculated molecular mass of 17,788 Da and a pI of 4.84. From the analysis of the N-terminus of the polypeptide with the SignalP programme (http://www.cbs.dtu.dk/services/SignalP), it was determined that the molecule has a signal peptide and is predicted to be cleaved at Ala^{21}–Gln^{22}. The mature protein has a predicted molecular mass of 15,541 Da with theoretical pI of 4.59. No potential site for N-glycosylation was predicted in the putative polypeptide encoded by the longistatin cDNA. Longistatin consists of two EF-hand Ca^{++}-binding domains (http://au.expasy.org/prosite/) at residues 83–94 and 135–146 (Fig. 1A). Alignment of longistatin EF-hand domains-I and -II (LongEFd-I and -II) with the EF-hand domains from diversified sources revealed that LongEFd-I and -II has conserved canonical structures. The loop region of each domain consists of 12 aa residues and is arranged in the pattern of X · Y · Z · –Y · –X · –Z, where X, Y, Z, –X, –Y and –Z are the Ca^{++} coordinating ligands and the dot represents the intervening residues. In the case of both domains, LongEFd-I and -II, *X* and –Z positions are occupied by aspartic acid and glutamic acid, respectively (Fig. 1B). Despite a few radical departures from the general liganding rule, the loop region of the most common canonical EF-hands usually consists of 12 aa residues which starts with aspartic acid and ends with glutamic acid (Kretsinger and Nockolds, 1973). These negatively charged aas play important roles in the binding of positively charged Ca^{++}. In conjunction, the bidentate glutamic acid at the –Z position is indispensible for the formation of pentagonal bipyramid coordination geometry (Grabarek, 2006). Furthermore, LongEFd-I and LongEFd-II contain several bulky hydrophobic residues (Fig. 1B), and are predicted to form a hydrophobic core, which is a salient characteristic of helix-loop-helix proteins (Gariépy and Hodges, 1983). The aa sequence of LongEFd-II represents the conserved glycine residue at position 6 in the loop, which plays an important role in the proper folding of ligands around the metal ion (Gariépy et al., 1983). In the LongEFd-I, the glycine residue has been substituted by asparagine. The substitution of glycine at position 6 with other aa residues is not unexpected and has been detected in some well-recognised Ca^{++}-binding proteins like, carp parvalbumin, rabbit parvalbumin, S-100a, S-100b, porcine intestinal Ca^{++}-binding protein (PICBP), bovine intestinal Ca^{++}-binding protein (BICBP) and rabbit skeletal muscle alkali light chain (Gariépy and Hodges, 1983). Results of BLAST (NCBI, National Institute of Animal Health, http://www.ncbi.nlm.nih.gov/BLAST) searches revealed that longistatin has the highest identity with multiple coagulation factor deficiency 2-like protein of *Ixodes scapularis* (51% identity).

3.2. Production of recombinant longistatin

To determine the biochemical properties, longistatin was expressed in *E. coli*, strain TOP10F′, using a pTrcHisB™ vector and was harvested as soluble protein from bacterial cultures. Translation of recombinant longistatin was detected with anti-His monoclonal antibody (Nacalai Tesque, Inc.) (Fig. 2B). One litre of bacterial culture, on average, yielded 3.15 mg purified longistatin. The purity of recombinant longistatin was confirmed by SDS–PAGE analysis followed by silver staining, and a single band was detected (Fig. 2A). The calculated molecular mass of longistatin is 15.54 kDa (excluding signal peptide). Longistatin migrated on SDS–PAGE gels as a 24 kDa fusion protein with a polyhistidine tag (Fig. 2A and B). This unexpected mobility of prokariotically expressed longistatin to 24 kDa instead of its calculated molecular mass of 15.54 kDa on SDS–PAGE analysis was not due to N-linked glycosylation, as longistatin does not contain any potential N-glycosylation sites. However, this type of mobility of the recombinant protein over the expected size has been observed in other cases. Thrombostasin, a thrombin inhibitor isolated from horn fly saliva, showed a significantly higher molecular mass (16.7 kDa) on SDS–PAGE instead of its calculated molecular mass of 9.2 kDa, which was predicted to be due to its acidic characteristics (Zhang et al., 2002). Longistatin is also acidic in nature (pI 4.59) and it is assumed that the higher molecular mass band of longistatin on SDS–PAGE is due to its acidic characteristics. Sequence analysis of the purified recombinant longistatin (24 kDa protein) was performed. The representative first 10 aa residues were QAGDQQQMQP which exactly corresponds to the 22–31 aa residues of longistatin (GenBank Accession No. AB519820), confirming that the 24 kDa protein is true longistatin.

3.3. Transcription profiling of longistatin

For transcription profiling of longistatin, total RNA was extracted from the unfed and fed different life-cycle stages and organs of ticks and was subjected to RT-PCR analysis. Longistatin-specific transcripts were expressed at a level which corresponded well to its expected size (246 bp). The transcript was detected in all life-cycle stages including eggs but its expression was highly up-regulated after feeding (Fig. 3A). Furthermore, the gene was specifically expressed in salivary glands and completely absent in other organs (Fig. 3B), suggesting its salivary gland specificity. RT-PCR data also revealed that the gene was dramatically up-regulated with the feeding process of ticks. The highest expression was detected at 96 h of feeding and in fully engorged (120 h) adult ticks (Fig. 3C). Expression of the longistatin-specific gene decreased abruptly after detachment from the host following full engorgement (Fig. 3D), implying that longistatin may have some potential roles in the blood-feeding process of hard ticks.

3.4. Detection of endogenous longistatin in salivary glands and in the blood pool in hosts' tissues

To detect the endogenous form of longistatin, both immunohistochemistry and immunofluorescent staining were performed using thin sections of partially fed (72 h) adult *H. longicornis*. Immunohistochemical examination showed that the endogenous longistatin, which reacted with mouse anti-longistatin sera, was localised only in the salivary glands, further indicating its salivary gland-specific expression. No positive reaction was detected in either the internal or external tissues of ticks treated with pre-immune mouse sera (Fig. 4A). Using immunofluorescent staining, longistatin was detected within the cells as well as in the lumen of the functional acini of salivary glands (Fig. 4A, arrow), suggesting that longistatin is synthesised and secreted by the salivary cells.

To determine the intracellular localisation of the endogenous protein, salivary gland cells from partially fed (96 h) adult ticks were isolated and were subjected to immunofluorescent staining. Cells treated with mouse anti-longistatin sera showed intense reactivity with the entire cytoplasm, however, the longistatin-specific reaction was slightly more intense near the periphery of the

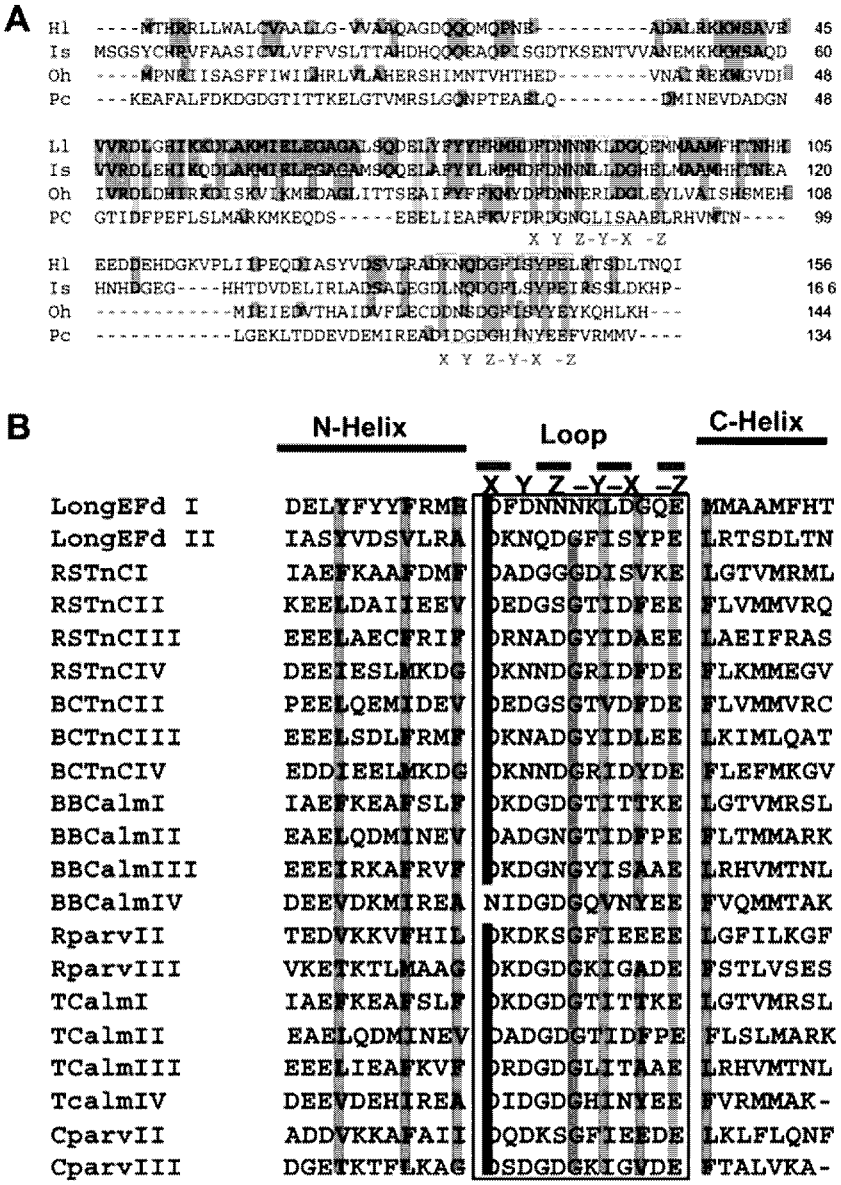

Fig. 1. Sequence alignment of longistatin. (A) Comparison of the deduced amino acid (aa) sequence of longistatin (Hl) with the aa sequences of homologous molecules. Sequences were selected from (GenBank Accession Nos. are indicated in parentheses): Is, *Ixodes scapularis* (AAY66924), Oh, *Ornithoctonus huwena* (ACH48184) and Pc, *Paramacium* calmodulin (Guy et al., 2008). Loop regions of EF-hand domains are boxed. Amino acid residues in yellow are conserved in all sequences and those in green, are identical to longistatin only. *X*, *Y*, *Z*, *−Y*, *−X* and *−Z* represent calcium coordinating positions of the loop. (B) Alignment of longistatin EF-hand domains-I and -II with EF-hand domains of proteins with known structures such as rabbit skeletal troponin C (RSTnC I, II, III and IV), bovine cardiac troponin C (BCTnC II, III and IV), bovine brain calmodulin (BBCalm I, II, III and IV), rabbit parvalbumin (Rparv II and III), *Tetrahymena* calmodulin (TCalm I, II, III and IV) and carp parvalbumin (Cparv II and III) (Gariépy and Hodges, 1983). Yellow denotes the omnipresence of glutamic acid in *−Z* position and dark red indicates commonly occurring aspartic acid in the *X* position of canonical EF-hands. Amino acid residues in green are involved in the formation of the hydrophobic core of the EF-hand domain. Violet indicates the frequently occurring glycine residue at position 6 of the loop region of standard EF-hands.

cell (Fig. 4A). These results suggest that endogenous longistatin is distributed throughout the cytoplasm of the salivary gland cells.

To ensure the presence of longistatin in the feeding lesions, thin histological sections prepared from rabbit ear tissues containing blood pools following a successful blood-feeding by adult ticks were also subjected to immunofluorescent staining. Intense longistatin-specific reactions were detected by using mouse anti-longistatin sera (1:100) in the feeding lesions (Fig. 4Bc), especially in areas where massive haemorrhages were observed by H&E staining (Fig. 4Bb), implying that longistatin is secreted and is injected through saliva into the blood pools.

3.5. Ca^{++}-binding affinity of longistatin

To verify the Ca^{++}-binding affinity of longistatin, a gel mobility shift assay was performed using 10% SDS–PAGE gel under reducing condition in the presence of 3 mM Ca^{++} or 3 mM EDTA. Data showed that migration of longistatin was relatively faster in the presence of 3 mM Ca^{++} than in the presence of a metal chelator, EDTA, under the same conditions, suggesting that longistatin is capable of binding with Ca^{++}. Longistatin appeared at the level of 21 kDa on SDS–PAGE containing 3 mM Ca^{++}. But the longistatin-specific band was observed at the level of about 24 kDa in the presence of 3 mM EDTA while the control protein BSA appeared at the

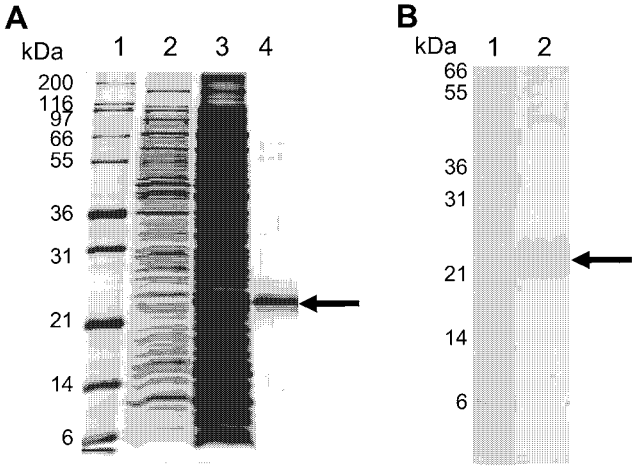

Fig. 2. Detection and purification of recombinant longistatin. (A) Detection of purity of longistatin by SDS–PAGE analysis. Purified longistatin together with *Escherichia coli* lysate was electrophoresed on 12.5% SDS–PAGE under reducing conditions. The gel was stained with silver stain. Lane 1, molecular weight marker; lane 2, *E. coli* lysate before induction; lane 3, *E. coli* lysate 3 h after induction with isopropyl-β-D-thiogalactopyranoside (IPTG) and lane 4, purified longistatin. (B) Western blot analysis to detect the His-tagged recombinant longistatin using anti-His monoclonal antibody. Crude *E. coli* lysate was electrophoresed on 12.5% SDS–PAGE gel under reducing conditions and proteins were transferred onto nitrocellulose membrane. The membrane was probed with anti-His monoclonal antibody as described in the Materials and methods section. Lane 1, molecular weight marker and lane 2, longistatin.

same level in both of the gels (Fig. 5A). We hypothesised that the binding of Ca^{++} with longistatin induces some significant conformational changes rendering the molecule to migrate rapidly during electrophoresis. A similar pattern of electrophoretic mobility was observed in several other well-studied Ca^{++}-binding proteins such as Calmodulin, Calcineurin B, Troponin C (Klee et al., 1979). For further confirmation of Ca^{++}-binding affinity, both endogenous and recombinant proteins were electrophoretically transferred onto nitrocellulose membranes and stained with Ruthenium red (Fig. 5B), which is a specific stain for Ca^{++}-binding proteins. Ruthenium red inhibits the binding of Ca^{++} with the Ca^{++}-binding proteins and specifically stains them. The interaction between Ruthenium red and Ca^{++}-binding sites is extremely specific and sensitive (Charuk et al., 1990). It is therefore widely used for the detection of Ca^{++}-binding proteins and in this case suggests the specific interaction with the Ca++ binding sites of longistatin.

4. Discussion

Tick saliva contains a wide array of pharmacologically active bio-molecules having diversified functions which help ticks to feed persistently (Nuttall et al., 2006; Islam et al., 2009), modify host defense mechanisms (Brossard and Wikel, 2004), inhibit angiogenesis (Francischetti et al., 2005; Islam et al., 2009) or modulate coagulation cascades by altering one or more of the steps of coagulation pathways (Maritz-Olivier et al., 2007). Here, we describe that longistatin, a novel EF-hand protein isolated from the salivary glands of *H. longicornis*, binds with calcium and is thought to be closely linked to the feeding process of ticks.

Sequence alignment reveals that both of the Ca^{++}-binding sites of longistatin conserve the general rules of arrangement of ligands of standard EF-hand domains with the most noteworthy, at the Ca^{++}-binding loop region at positions 8 and 10, occupied by hydrophobic aas. This ligand pattern is identical to the classical arrangement of aas in the historical consensus sequence of EF-hand first described by Kretsinger and Nockolds (1973), which is also seen in the Ca^{++}-binding sites of other well-known standard EF-hand proteins such as bovine brain calmodulin (Watterson et al., 1980), *Tetrahymena* calmodulin (Yazawa et al., 1981) and in rabbit skeletal troponin C (van Eerd and Takahashi, 1975). In the LongEFd-I, positions 8 and 10 of the loop contain leucine and glycine, respectively, but in the LongEFd-II leucine has been replaced with isoleucine, and glycine with tyrosine. Although position 8 and to a lesser extent position 10 of the EF-hand loop region are conserved hydrophobic sites, but more precisely, position 8 is most frequently occupied by the residues isoleucine, leucine or valine (Grabarek, 2006). These two well-conserved sites of the loop region, together with the C- and N-terminal hydrophobic surface, are involved in the metal dehydration process (Gariépy and Hodges, 1983).

Localisation studies strongly support the salivary gland-specific expression of longistatin. It is suggested that longistatin is

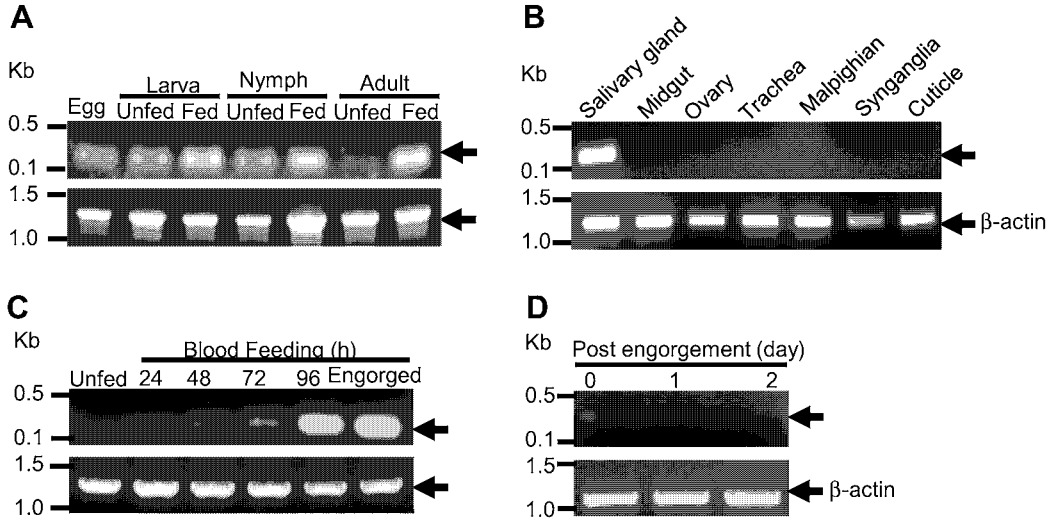

Fig. 3. Transcription profiling of longistatin in *Haemaphysalis longicornis*. (A) Expression of the longistatin-specific gene in all life-cycle stages of *H. longicornis* (arrow). Reverse transcription-PCR (RT-PCR) was performed using total mRNA extracted from all developmental stages, including eggs. (B) Organ-specific expression of longistatin gene (arrow). Total mRNA was collected from various organs of partially fed (72 h) adult ticks and subjected to RT-PCR analysis. (C) Expression profile of the gene in salivary glands of adult ticks at different blood-feeding stages (arrow). RT-PCR analysis was performed using total mRNA collected from salivary glands of adult *H. longicornis* at different blood-feeding stages. (D) Expression of the longistatin-specific gene in the post-engorgement period (arrow). Total mRNA was collected from salivary glands of adult ticks in the post-engorgement period (day 0, day 1 and day 2) and was subjected to RT-PCR analysis. Actin is shown as an internal control.

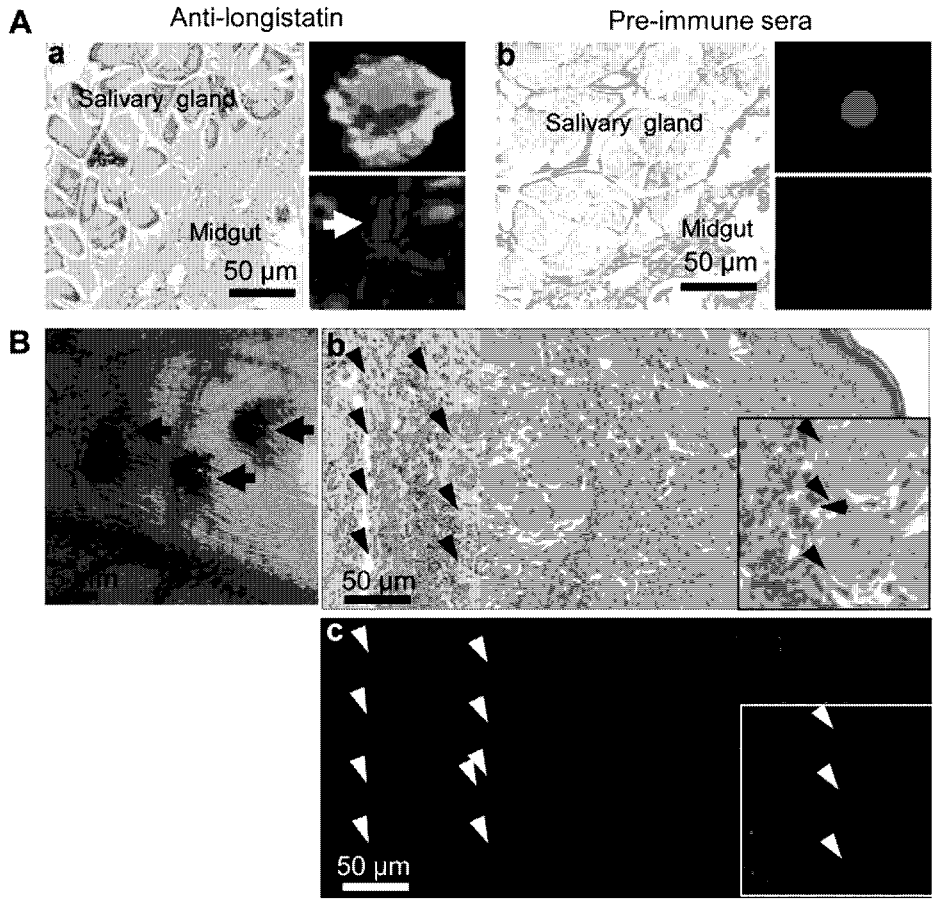

Fig. 4. Endogenous longistatin detected in the tick, *Haemaphysalis Longicornis*, and in host tissues. (A) Endogenous localisation of longistatin in partially fed (72 h) adult ticks. Ticks were fixed in paraformaldehyde and embedded in paraffin. Sections were treated with either immune (1: 100, Aa) or pre-immune mouse serum (1: 100, Ab). The longistatin-specific reaction was detected in the salivary glands and in the lumen of the functional acini (arrow). Salivary gland cells were collected from partially fed (96 h) adult ticks and reacted with mouse anti-longistatin (1: 100, Aa)/pre-immune sera (1: 100, Ab) followed by the treatment with green fluorescent-labelled secondary antibody (Alexa Flour® 488 goat anti-mouse IgG (H + L), Invitrogen). (B) Longistatin detected in the feeding lesions in vivo. A rabbit's ear showing blood pools (arrows) at the site of attachment of ticks (Ba). The area of haemorrhage in the blood pool (arrowheads), H&E staining (Bb, 10× objective). Detection of longistatin in the feeding lesions of a rabbit's ear (arrowheads; Bc, 10× objective). Rabbit's ear tissues were collected from a euthanised rabbit as described in the Materials and methods section and were fixed in 4% paraformaldehyde and embedded in paraffin. Sections were treated with mouse anti-longistatin sera (1:100) followed by the treatment with green fluorescent-labelled secondary antibody (Alexa Flour® 488 goat anti-mouse IgG (H + L), Invitrogen). The area marked by the square is at 40× objective.

synthesised and accumulated in the cytoplasm, finally secreted out of the salivary gland cells and takes part in the feeding process after reaching the blood pools, the feeding lesions on the host. Usually EF-hand Ca^{++}-binding domains are prevalent among the cytoplasmic proteins (Tsigelny et al., 2000) and act as a calcium buffer in the cytosol of the cell (Lewit-Bentley and Réty, 2000) engaging in various biological functions such as ciliary beating, muscle contraction, membrane excitability, cell proliferation and cell death through signalling of multiple physiobiochemical pathways (Skelton et al., 1994; Berridge et al., 1998). In some rare cases EF-hand Ca^{++}-binding proteins are secreted from the cells and exert their function extracellularly (Pottgiesser et al., 1994; Tsigelny et al., 2000). RT–PCR data also demonstrated that the gene coding for longistatin is expressed in all life-cycle stages, including eggs. Notably, the longistatin-specific gene is dramatically up-regulated in pre-engorged (96 h) and engorged (120 h) adult ticks but declines sharply in the post-feeding period, suggesting its vital roles in the blood-feeding processes of ixodid ticks. Feeding patterns of ixodid ticks are not like the vessel feeder haematophagous insects that suck blood directly and rapidly from the blood vessel. Ixodid ticks usually take blood over a long period of time extending from 4 to 10 days depending on the species (Nuttall, 1998), making a large blood pool under the skin. During the process of piercing the skin of mammalian hosts, ticks tear the dermis, lacerate the surrounding tissues and disrupt the continuity of the smaller blood vessels with their specialised mouth parts. Thus, they produce a blood pool under the skin from which they suck blood and fluid that are drained into the resulting wound (Maritz-Olivier et al., 2007). Tick-feeding lesions on a non-immune host are characterised by cavities filled with unclotted blood (Binnington and Kemp, 1980). While feeding, ixodid ticks inject large amounts of fluid into the host at the site of attachment which is a mixture of salivary cocktail and the regurgitated fluid component of the ingested blood. In ixodid ticks, the total blood-feeding period is distinctly divided into two phases such as the slow feeding period (up to 3 days post-attachment) and the rapid feeding period (further 2–3 days). During the slow feeding period, the size of the blood pool is relatively smaller, contains scanty blood and exudates and the tick imbibes very little blood. On the contrary, during the rapid feeding period, the blood pool becomes voluminous, contains a considerable amount of blood and exudates and the tick takes the blood-meal very rapidly (Kemp et al., 1982). Therefore, the high level of expression of the longistatin-specific gene in the pre-engorged (96 h) and engorged ticks together with the sharp declination of expression after detachment of ticks following full engorgement, clearly indicates that longistatin modulates the feeding process of host blood.

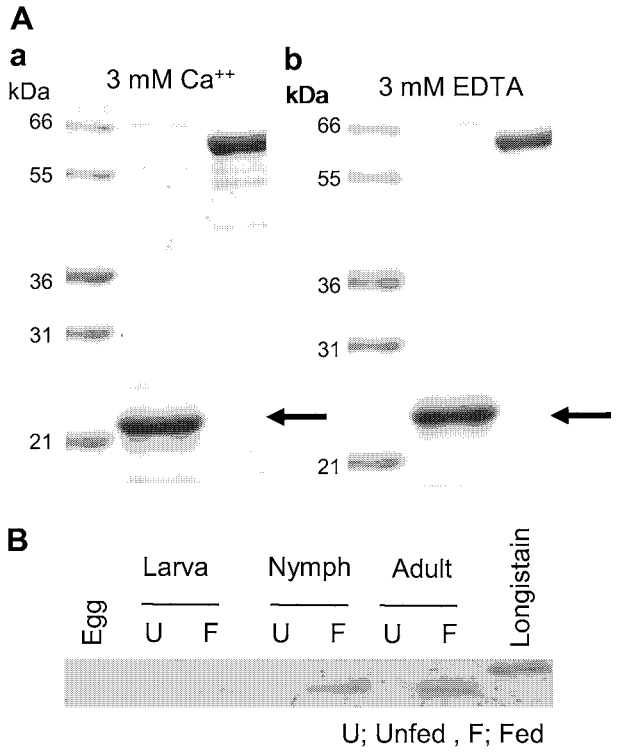

Fig. 5. Ca^{++}-binding specificity of longistatin. (A) Gel mobility shift assay. Longistatin was electrophoresed in the presence of 3 mM Ca^{++} (Aa) or 3 mM EDTA (Ab) through a 10% SDS–PAGE gel. Lane 1, molecular weight marker; lane 2, longistatin (arrow); lane 3, BSA (control). Longistatin migrated rapidly in the presence of Ca^{++}. (B) Ruthenium red staining of longistatin. Purified recombinant and endogenous forms of longistatin at different life-cycle stages were subjected to SDS–PAGE analysis followed by blotting onto nitrocellulose membranes. Nitrocellulose membranes were then stained with Ruthenium red for 15 min at room temperature. U, unfed; F, fed.

In conclusion, longistatin, an EF-hand protein, is synthesised in the salivary glands of *H. longicornis*. Our data show that longistatin is secreted with the saliva into the blood pool of hosts' tissues and is able to bind with calcium. Furthermore, our transcriptional data strongly suggest that longistatin contributes to the feeding success of blood-meals from host animals by ixodid ticks.

Acknowledgements

We thank H. Shimada and M. Kobayashi for their generous help in preparing histological sections. This work was supported by Grant-in-Aids (to N.T. and K.F.) from the Ministry of Education, Culture, Sports, Science, and Technology of Japan. This work was also supported by a grant (to N.T. and K.F.) for Promotion of Basic Research Activities for Innovative Biosciences from the Bio-oriented Technology Research Advancement Institution.

References

Alim, M.A., Tsuji, N., Miyoshi, T., Islam, M.K., Huang, X., Motobu, M., Fujisaki, K., 2007. Characterization of asparaginyl endopeptidase, legumain induced by blood feeding in the ixodid tick *Haemaphysalis longicornis*. Insect Biochem. Mol. Biol. 37, 911–922.

Altschul, S.F., Madden, T.L., Schaffer, A.A., Zhang, J., Zhang, Z., Miller, W., Lipman, D.J., 1997. Gapped BLAST and PSI-BLAST: a new generation of protein database search programs. Nucleic Acid Res. 25, 3389–3402.

Benson, D.A., Karsch-Mizrachi, I., Lipman, D.J., Ostell, J., Rapp, B.A., Wheeler, D.L., 2002. GenBank. Nucleic Acid Res. 30, 17–20.

Berridge, M.J., Bootman, M.D., Lipp, P., 1998. Calcium – a life and death signal. Nature 395, 645–648.

Binnington, K.C., Kemp, D.H., 1980. Role of tick salivary glands in feeding and disease transmission. Adv. Parasitol. 18, 315–339.

Boldbaatar, D., Sikasunge, C.S., Battsetseg, B., Xuan, X., Fujisaki, K., 2006. Molecular cloning and functional characterization of an aspartic protease from the hard tick *Haemaphysalis longicornis*. Insect. Biochem. Mol. Biol. 36, 25–36.

Brossard, M., Wikel, S.K., 2004. Tick immunobiology. Parasitology 129 (Suppl), S161–S176.

Charuk, J.H., Pirraglia, C.A., Reithmeier, R.A., 1990. Interaction of Ruthenium red with Ca^{2+}-binding proteins. Anal. Biochem. 188, 123–131.

Francischetti, I.M., Mather, T.N., Ribeiro, J.M., 2005. Tick saliva is a potent inhibitor of endothelial cell proliferation and angiogenesis. Thromb. Haemost. 94, 167–174.

Fujisaki, K., Kawazu, S., Kamio, T., 1994. The taxonomy of the bovine *Theileria* spp.. Parasitol. Today 10, 31–33.

Furuse, M., Fujita, K., Hiiragi, T., Fujimoto, K., Tsukita, S., 1998. Claudin-1 and -2: novel integral membrane proteins localizing at tight junctions with no sequence similarity to occludin. J. Cell Biol. 141, 1539–1550.

Gariépy, J., Hodges, R.S., 1983. Primary sequence analysis and folding behavior of EF hands in relation to the mechanism of action of troponon C and calmodulin. FEBS Lett. 160, 1–6.

Gariépy, J., Sykes, B.D., Hodges, R.S., 1983. Lanthanide-induced peptide folding: variations in lanthanide affinity and induced peptide conformation. Biochemistry 22, 1765–1772.

Grabarek, Z., 2006. Structural basis for diversity of the EF-hand calcium-binding proteins. J. Mol. Biol. 359, 509–525.

Guy, J.E., Wigren, E., Svärd, M., Härd, T., Lindqvist, Y., 2008. New insights into multiple coagulation factor deficiency from the solution structure of human MCFD2. J. Mol. Biol. 381, 941–955.

Ho, T., Htwe, K.K., Yamasaki, N., Zhang, G.Q., Ogawa, M., Yamaguchi, T., Fukushi, H., Hirai, K., 1995. Isolation of *Coxiella burnetii* from dairy cattle and tick, and some characteristics of isolates in Japan. Microbiol. Immunol. 39, 663–671.

Hoogstraal, H., Roberts, F.H., Kohls, G.M., Tipton, V.J., 1968. Review of *Haemaphysalis (Kaiseriana) longicornis* Neumann (resurrected) of Australia, New Zealand, New Caledonia, Fiji, Japan, Korea, and northeastern China and USSR, and its parthogenetic and bisexual populations (Ixodoidea, Ixodidae). J. Parasitol. 54, 1197–1213.

Islam, M.K., Tsuji, N., Miyoshi, T., Alim, M.A., Huang, X., Hatta, T., Fujisaki, K., 2009. The Kunitz-like modulatory protein, Haemangin, is vital for hard tick blood feeding success. PLoS Pathog. 5, e1000497.

Kahl, C.R., Means, A.R., 2003. Regulation of cell cycle progression by calcium/calmodulin-dependent pathways. Endocr. Rev. 24, 719–736.

Kawasaki, H., Nakayama, S., Kretsinger, R.H., 1998. Classification and evolution of EF-hand proteins. BioMetals 11, 277–295.

Kemp, D.H., Stone, B.F., Binnington, K.C., 1982. Tick attachment and feeding: role of the mouthparts, feeding apparatus, salivary gland secretions, and the host response. In: Obenchain, F.D., Galun, R. (Eds.), Physiology of Ticks. Pergamon Press Inc., New York, pp. 119–168.

Klee, C.B., Crouch, T.H., Krinks, M.H., 1979. Calcineurin: a calcium- and calmodulin-binding protein of the nervous system. Proc. Natl. Acad. Sci. USA 76, 6270–6273.

Kretsinger, R.H., Nockolds, C.E., 1973. Carp muscle calcium-binding protein. II. Structure determination and general description. J. Biol. Chem. 248, 3313–3326.

Lewit-Bentley, A., Réty, S., 2000. EF-hand calcium-binding proteins. Curr. Opin. Struct. Biol. 10, 637–643.

Maritz-Olivier, C., Stutzer, C., Jongejan, F., Neitz, A.W., Gaspar, A.R., 2007. Tick anti-hemostatics: targets for future vaccines and therapeutics. Trends Parasitol. 23, 397–407.

Miyoshi, T., Tsuji, N., Islam, M.K., Huang, X., Motobu, M., Alim, M.A., Fujisaki, K., 2007. Molecular and reverse genetic characterization of serine proteinase-induced hemolysis in the midgut of the ixodid tick *Haemaphysalis longicornis*. J. Insect Physiol. 53, 195–203.

Nelson, M.R., Chazin, W.J., 1998. Structure of EF-hand Ca^{++}-binding proteins: diversity in the organization, packing and response to Ca^{++} binding. BioMetals 11, 297–318.

Needham, G.R., Teel, P.D., 1991. Off-host physiological ecology of ixodid ticks. Annu. Rev. Entomol. 36, 659–681.

Nielsen, H., Engelbrecht, J., Brunak, S., Heijne, G., 1997. Identification of prokaryotic and eukaryotic signal peptides and prediction of their cleavage site. Protein Eng. Des. Sel. 10, 1–6.

Nuttall, P.A., 1998. Displaced tick–parasite interactions at the host interface. Parasitology 116, 65–72.

Nuttall, P.A., Trimnell, A.R., Kazimirova, M., Labuda, M., 2006. Exposed and concealed antigens as vaccine targets for controlling ticks and tick-borne diseases. Parasite Immunol. 28, 155–163.

Pottgiesser, J., Maurer, P., Mayer, U., Nischt, R., Mann, K., Timpl, R., Krieg, T., Engel, J., 1994. Changes in calcium and collagen IV binding caused by mutations in the EF hand and other domains of extracellular matrix protein BM-40 (SPARC, osteonectin). J. Mol. Biol. 238, 563–574.

Skelton, N.J., Kördel, J., Akke, M., Forsén, S. Chazin, W.J., 1994. Signal transduction versus buffering activity in Ca^{2+}-binding proteins. Nat. Struct. Biol. 1, 239–245.

Tsigelny, I., Shindyalov, I.N., Bourne, P.E., Südhof, T.C., Taylor, P., 2000. Common EF-hand motifs in cholinesterases and neuroligins suggest a role for Ca^{2+} binding in cell surface associations. Protein Sci. 9, 180–185.

Tsuji, N., Kamio, T., Isobe, T., Fujisaki, K., 2001. Molecular characterization of a peroxiredoxin from the hard tick *Haemaphysalis longicornis*. Insect. Mol. Biol. 10, 121–129.

Watterson, D.M., Sharief, F., Vanaman, T.C., 1980. The complete amino acid sequence of the Ca^{2+}-dependent modulator protein (calmodulin) of bovine brain. J. Biol. Chem. 255, 962–975.

Wilkins, M.R., Lindskog, I., Gasteiger, E., Bairoch, A., Sanchez, J.C., Hochstrasser, D.F., Appel, R.D., 1997. Detail peptide characterization using PEPTIDE MASS – a world Wide Web accessible tool. Electrophoresis 18, 403–408.

Yazawa, M., Yagi, K., Toda, H., Kondo, K., Narita, K., Yamazaki, R., Sobue, K., Kakiuchi, S., Nagao, S., Nozawa, Y., 1981. The amino acid sequence of the *Tetrahymena* calmodulin which specifically interacts with guanylate cyclase. Biochem. Biophys. Res. Commun. 99, 1051–1057.

You, M., Xuan, X., Tsuji, N., Kamio, T., Igarashi, I., Nagasawa, H., Mikami, T., Fujisaki, K., 2001. Molecular characterization of a troponin I-like protein from the hard tick *Haemaphysalis longicornis*. Insect. Biochem. Mol. Biol. 32, 67–73.

Zaim, M., Guillet, P., 2002. Alternative insecticides: an urgent need. Trends Parasitol. 18, 161–163.

Zhang, D., Cupp, M.S., Cupp, E.W., 2002. Thrombostasin: purification, molecular cloning and expression of a novel anti-thrombin protein from horn fly saliva. Insect. Biochem. Mol. Biol. 32, 321–330.

van Eerd, J.P., Takahashi, K., 1975. The amino acid sequence of bovine cardiac tamponin-C. Comparison with rabbit skeletal troponin-C. Biochem. Biophys. Res. Commun. 64, 122–127.

Am. J. Trop. Med. Hyg., 83(3), 2010, pp. 542–548
doi:10.4269/ajtmh.2010.10-0016

Detection of Early and Single Infections of *Schistosoma japonicum* in the Intermediate Host Snail, *Oncomelania hupensis*, by PCR and Loop-Mediated Isothermal Amplification (LAMP) Assay

Takashi Kumagai,* Rieko Furushima-Shimogawara, Hiroshi Ohmae, Tian-Ping Wang, Shaohong Lu, Rui Chen, Liyong Wen, and Nobuo Ohta

Section of Environmental Parasitology, Department of International Health Development, Division of Public Health, Graduate School of Medical and Dental Sciences, Tokyo Medical and Dental University, Tokyo, Japan; Department of Parasitology, National Institute of Infectious Diseases, Tokyo, Japan; Anhui Institute of Parasitic Diseases, Wuhu, China; Institute of Parasitic Diseases, Zhejiang Academy of Medical Sciences, Hangzhou, China

Abstract. Polymerase chain reaction (PCR) with the specific primer set amplifying 28S ribosomal DNA (rDNA) of *Schistosoma japonicum* was able to detect genomic DNA of *S. japonicum*, but not *S. mansoni*, at 100 fg. This procedure enabled us to detect the DNA from a single miracidium and a snail infected with one miracidium at just 1 day after infection. We compared these results with those from loop-mediated isothermal amplification (LAMP) targeting 28S rDNA and found similar results. The LAMP could amplify the specific DNA from a group of 100 normal snails mixed with one infected snail A PCR screening of infected snails from endemic regions in Anhui Province revealed schistosomal DNA even in snails found negative by microscopy. PCR and LAMP show promise for monitoring the early infection rate in snails, and they may be useful for predicting the risk of infection in the endemic places.

INTRODUCTION

Schistosomiasis japonica is a relatively neglected tropical disease, and it is a chronic zoonotic parasitic disease in China, the Philippines, and small pockets of Indonesia.[1] In China, the causative organism, *Schistosoma japonicum*, and its intermediate snail host, *Oncomelania hupensis*, are distributed along the Yangtze River valley and recently, in the hilly and mountainous regions of Sichuan Province.[2] Since the mid-1950s, the People's Republic of China has markedly decreased the prevalence of schistosomiasis through mass-chemotherapeutic treatment and the control of the intermediate snails.[3,4] However, a complete eradication of this disease is difficult in endemic areas. The estimated prevalence in the provinces of Hunan, Hubei, Jiangxi, Anhui, Yunnan, Sichuan, and Jiangsu was 4.2%, 3.8%, 3.1%, 2.2%, 1.7%, 0.9%, and 0.3%, respectively, in 2004.[5] A total of 564, 207, 83, and 57 acute cases of *S. japonicum* infection were reported nationwide in 2005, 2006, 2007, and 2008, respectively.[6] These findings suggest that control measures must be improved among at-risk populations, especially in lake and marshland regions. A new integrated strategy was tested for the control of schistosomiasis in China.[7,8] It involved the reduction of infectious sources by the replacement of water buffaloes with tractors for agricultural work, improved access to clean water and general sanitation, better livestock management through fencing to isolate schistosomal egg sites, and better feces management using newly constructed latrines on-shore. These strategies markedly reduced the infection rate in both humans and intermediate snails in the pilot areas. Remarkably, the prevalence of infected snails reportedly decreased to almost 0% in some areas.[8] To maintain these successes, it may be useful to use new snail-monitoring systems in such areas.

*Address correspondence to Takashi Kumagai, Section of Environmental Parasitology, Department of International Health Development, Division of Public Health, Graduate School of Medical and Dental Sciences, Tokyo Medical and Dental University, 1-5-45, Yushima, Bunkyo-ku, Tokyo, 113-8519, Japan. E-mail: tkuma.vip@tmd.ac.jp

Molecular tools such as conventional polymerase chain reaction (PCR) and improved DNA amplification methods have been shown capable of detecting schistosome DNA in a variety of samples. A highly repetitive, 121-base pair (bp) sequence has been used to detect DNA from *S. mansoni* and *S. haematobium* in stool, serum, urine, and plankton samples.[9–13] Because no similar repetitive sequence has been found in the *S. japonicum* genome, the repetitive non-long terminal repeat (LTR) retrotransposon SjR2[14] was used for DNA detection as a target sequence.[15] In an experimental rabbit model, the SjR2 sequence was detected in serum (1 week after infection) and stool samples using a PCR assay, and the 230-bp band of SjR2 was absent at 10 weeks after treatment with praziquantel,[16] and real-time PCR was applied to the detection of SjR2 gene from cercaria in an environmental water sample.[17] Alternatively, real-time PCR was also applied to the detection of a mitochondrial nicotinamide adenine dinucleotide (NADH) dehydrogenase I gene at low intensity in an infected pig model.[18] Another highly repeated sequence, 28S ribosomal DNA (rDNA), was used for multiplex PCR to detect a distinct *Schistosoma* sp. from human urine samples.[19]

Loop-mediated isothermal amplification (LAMP) is a simple, sensitive, and rapid DNA detection method.[20] The LAMP reaction requires only a single enzyme, *Bst* DNA polymerase, that can synthesize a new strand of DNA while simultaneously displacing the former complementary strand, thereby enabling DNA amplification at a single temperature. The LAMP reaction can be achieved using four primers (FIP, BIP, F3, and B3), two of which (F3 and B3) contribute to the formation of a stem-loop structure, whereas the other two (FIP and BIP), designed complementary to the inner sequence of the stem-loop structure, are used for amplification of the target sequence. This provides a higher specificity to the reaction than conventional PCR methods.[20] The LAMP assay has been widely applied for diagnosis and detection against several infectious diseases, including *Plasmodium*,[21] *Trypanosoma*,[22] *Leishmania*,[23] and *Taenia*.[24] In the present application, LAMP targeting to SjR2 for detecting the DNA from *S. japonicum* was also reported.[25]

In the present study, we evaluated the performance of the PCR method by comparing SjR2 and 28S rDNA from

S. japonicum. Next, we detected the schistosomal DNA from experimentally infected snails at 1 day after infection and detected schistosomal DNA from wild snails collected from endemic areas of Anhui Province in China. We also applied a LAMP assay to detect infected snails on-site in endemic local areas. Finally, we developed a simple, rapid, and safe screening method for determining the infection rate of snails in endemic areas after implementation of the above-described integrated strategy and detected infections using the LAMP assay with DNA extracted from a large number of snails.

MATERIALS AND METHODS

Parasites and snails. *S. japonicum* was maintained using ICR mice as a final host and *O. hupensis nosophora* from a non-endemic area (Yamanashi strain) as an intermediate host. The livers from infected mice were digested with 1 mg/mL collagenase and 0.5 mg/mL actinase, and then, purified eggs were put into water to hatch the miracidia. The collected miracidia were experimentally infected to each snail in a 96-well plate. Wild snails from endemic areas in China (*O. hupensis hupensis*) were collected from three places in Anhui Province as follows: (1) Shankou-city (30.52° N, 116.93° E) in marshland regions of Anquine county, (2) Shun'an town (30.56° N, 117.54° E) in the sand regions of the Yangtze River in Tongling county, and (3) Guanghui City (30.56° N, 117.45° E) in the marshland regions of the Yangtze River in Tongling county. Figure 1 presents detailed locations about each area. The snails were picked up in Anquine in March 2007 and in Tongling in September 2007. The collected snails were crushed and checked for infection under microscopy before preparation for DNA extraction.

DNA extraction. To detect schistosomal DNA by PCR and LAMP assay, we applied the DNA extraction method using heated NaOH.[26] Briefly, the counted miracidium was put into a 200-μL volume of 50 mM NaOH and heated at 95°C for 30 minutes. After centrifugation, the 50-μL supernatant was recovered and then mixed to an equal volume of 1 M Tris-HCl (pH 8.0). This solution was directly used as a template (1 μL) for the PCR and LAMP methods. For direct extraction from a single infected snail (non-endemic area), each snail was also put into a distinct tube, and 200 μL of 50 mM NaOH solution was added to the tube. After crushing the snail with tweezers, the DNA was extracted using the above procedures. A large-scale DNA extraction from different numbers (100, 50, 25, 10, 5, and 1) of snails from non-endemic area was also performed with 10 mL of 50 mM NaOH in a 50-mL tube that was heated at 95°C for 60 minutes. After neutralization with 1 M Tris-HCL (pH 8.0), 1 μL of the solutions was directly used as a template. Genomic DNA of *S. japonicum* was purified from adult worms using the Get-pure DNA Kit (Dojindo, Kumamoto, Japan), and the concentration of DNA was measured with a spectrometer.

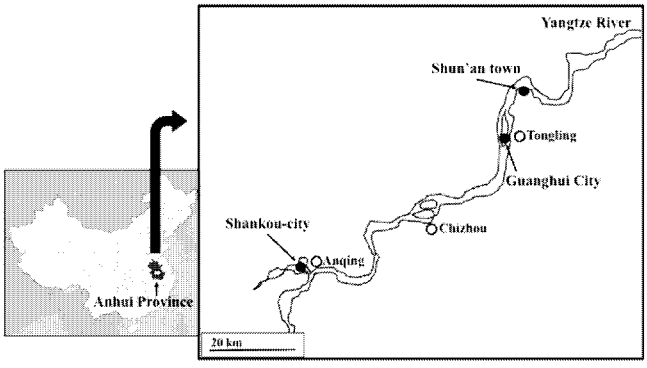

FIGURE 1. Schema of the selective areas for snail sampling in Anhui Province of China. Three points located along the Yangtze River in Anhui Province are shown as closed circles, and the capital of each country is shown as an open circle. Shankou-city in Anquine county and Guanghui City in Tongling county were marshland regions, and Shun'an town in Tongling county was in the sand regions.

Primer sets. To amplify the specific DNA of *S. japonicum*, the 28S rDNA gene (GenBank Accession No. Z46504) was selected as a target sequence. For the conventional PCR and LAMP methods, we designed specific primer sets (Table 1). As in the previous report, SjR2 (GenBank Accession No. AF412221) primers were generated for conventional PCR[16] and the LAMP assay[25] (Table 1). The LAMP primer sets were prepared to be high performance liquid chromatography (HPLC) purification grade.

PCR and LAMP assay. The PCR solution (20 μL) was prepared with a standard procedure using Top polymerase (BIONEER, Daejeon, Korea). The reaction consisted of 35 cycles each at 95°C for 30 seconds, 55°C for 30 seconds, and 72°C for 30 seconds. The PCR products were resolved by agarose gel electrophoresis and stained in ethidium bromide. The LAMP method was performed according to the manufacturer's instructions (Eiken Sci, Tokyo, Japan), except for use of the 20-μL total reaction mixture. The LAMP reaction was performed at a constant 65°C. The amplification of the target gene was confirmed based on the turbidity of magnesium pyrophosphate and by gel electrophoresis.

RESULTS

Sensitivity and specificity of PCR and LAMP assay. To determine the sensitivity of the PCR and LAMP methods, we performed the reactions using *S. japonicum* genomic DNA from 10 pg to 10 fg, respectively, by serial dilution. As shown in Figure 2, PCR using specific primers amplified the band of 405 bp from 28S rDNA, and the PCR method was able to detect more than 100 fg of genomic DNA (Figure 2A). The LAMP assay had the same level of sensitivity as the conventional PCR assay (Figure 2B). Furthermore, both methods amplified only DNA from *S. japonicum* and none from *S. mansoni*. Thus, our methods distinguished the *S. japonicum* species from others. However, PCR using SjR2 primers detected DNA at the level of 1 pg (Figure 2A), whereas LAMP did not detect the SjR2 gene at all, contrary to a recent report[25] (data not shown). Taken together with these results, we performed the following experiments using 28S rDNA primers as the appropriate targeting genes because of higher sensitivity.

Detection of the schistosomal DNA from miracidia and infected snails. To confirm whether a single miracidium DNA could be detected by the PCR and LAMP assay using 28S rDNA primers, we extracted DNA using the heated NaOH method from one miracidium and performed both methods with 10 independent samples. The PCR and LAMP detected the DNA from one miracidium in all samples (Figure 3A and B), indicating that the total DNA included in a single miracidium was enough to be amplified by both the PCR and LAMP methods. Furthermore, we performed the infection experiment with the intermediate snail with a different number

TABLE 1
Specific primer sets used in this study

PCR	Sj28S
	Forward primer; 5′-GGTTTGACTATTATTGTTGAGC-3′
	Reverse primer; 5′-TCTCACCTTAGTTCGGACTGA-3′
	SjR2[16]
	Forward primer; 5′-TCTAATGCTATTGGTTTGAGT-3′
	Reverse primer; 5′-TTCCTTATTTTCACAAGGTGA-3′
LAMP	Sj28S
	F3 primer; 5′-GCTTTGTCCTTCGGGCATTA-3′
	B3 primer; 5′-GGTTTCGTAACGCCCAATGA-3′
	FIP primer; 5′-ACGCAACTGCCAACGTGACATACTGGTCGGCTTGTTACTAGC-3′
	BIP primer; 5′-TGGTAGACGATCCACCTGACCCCTCGCGCACATGTTAAACTC-3′
	SjR2[25]
	F3 primer; 5′-GCCGGTTCCTTATTTTCACAAGG-3′
	B3 primer; 5′-CTAACATAATTTTATCGCCTTGCG-3′
	FIP primer; 5′-CTACGACTCTAGAATCCCGCTCCGCGAATGACTGTGCTTGGATC-3′
	BIP primer; 5′-CCTACTTGATATAACGTTCGAACGTATTGGTTTGAGTTCACGAAACGT-3′

of miracidia and extracted total DNA from each snail at 1 day after the infection. As a result, we found four positive samples out of a total of five samples infected with one miracidium, although all samples were positive in the five samples infected with 5 or 10 miracidia, respectively (Figure 3C). We considered that one negative snail was not penetrated by a miracidium, because not all miracidia could enter the snail. These results showed that the PCR detected the schistosome-specific band

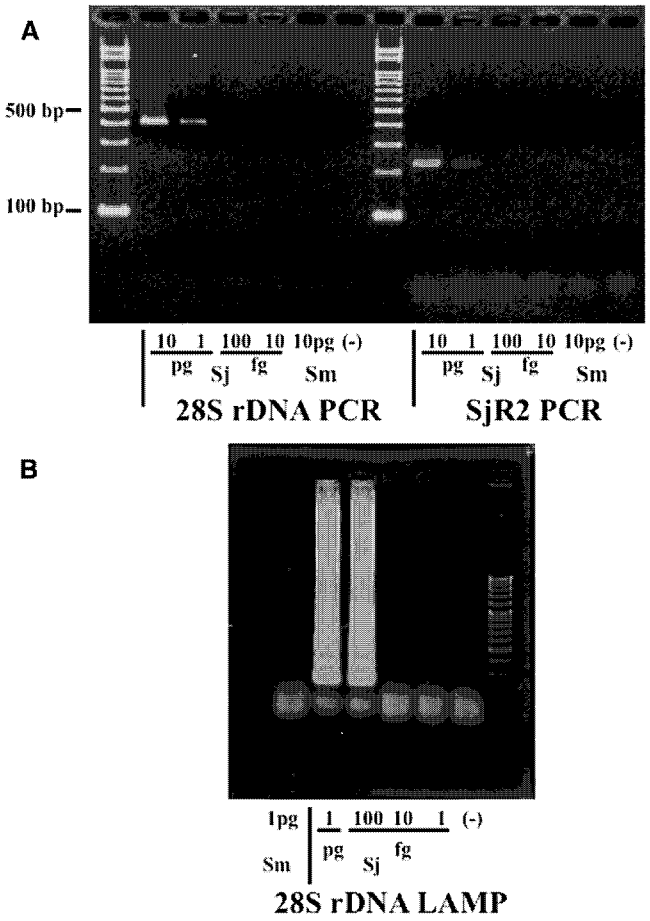

FIGURE 2. Sensitivity of the PCR and LAMP methods using genomic schistosomal DNA comparing 28S rDNA with SjR2 primers. (**A**) PCR was performed with different weights of genomic DNA, and the 28S rDNA primer set was able to detect 100 fg of DNA from *S. japonicum* but none from *S. mansoni*; the SjR2 primer set was able to detect just 1 pg of DNA. (**B**) The LAMP assay method showed the same sensitivity (100 fg) as the PCR method. Neither method reacted to DNA from *S. mansoni*, and no template (-) was the negative control.

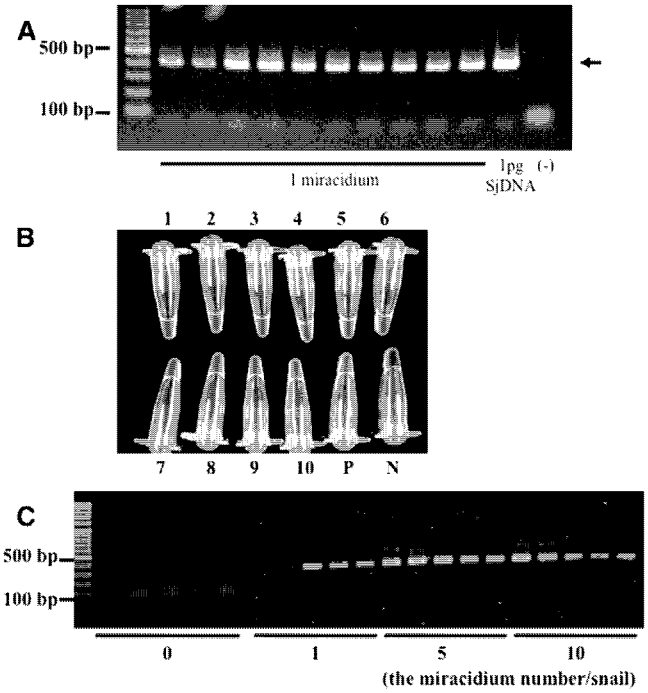

FIGURE 3. Detection of a schistosome-specific band in genomic DNA extracted from naked miracidia and the experimentally infected snail by PCR and LAMP. (**A**) The DNA extracted from one miracidium was amplified by PCR. PCR detected the specific band (arrow) in each of 10 samples extracted distinctly from one miracidium but not the no-template sample (-). Genomic DNA (1 pg) of *S. japonicum* was used for the positive control. (**B**) The DNA extracted from one miracidium was amplified by LAMP assay. LAMP showed the positive results as the white turbidity of magnesium pyrophosphate in all 10 samples extracted distinctly from one miracidium (1–10) and Sj DNA (1 pg) as positive control (P) but not the no-template sample (N). (**C**) Each snail from the non-endemic area was experimentally infected with a different number of miracidia (0, 1, 5, and 10 miracidia/snail), and genomic DNA was extracted from each snail at 1 day after infection. The PCR method detected the schistosome-specific band in DNA from a snail infected with just one miracidium without amplifying DNA from non-infected snails. Each lane represents a distinct snail infected with the same number of miracidia.

TABLE 2
The comparison of detection rate between the PCR assay and microscopy method in wild snails from Anhui Province

	Shankou-city in Anquine		Shun'an town in Tongling		Guanghui city in Tongling	
	Microscopy positive	Microscopy negative	Microscopy positive	Microscopy negative	Microscopy positive	Microscopy negative
PCR positive	10	13	2	0	0	0
PCR negative	0	217	0	72	0	48
Positive rate of microscopic examination	4.2%		2.7%		0%	
PCR positive rate	9.6%		2.7%		0%	

in the DNA extracted from the infected snail with a single miracidium. Furthermore, using the same DNA prepared from the snails infected with a single miracidium of *S. japonicum*, the result of the LAMP method was consistent with that of the PCR method (data not shown). Thus, the PCR and LAMP methods have the high specificity and sensitivity and detect schistosomal DNA immediately after the infection to the snail host.

Detection of the schistosomal DNA in wild snails collected from endemic areas. To evaluate whether the PCR assay could detect schistosomal DNA from the infected snails in the endemic areas, we collected wild snails from three points, Shankou-city, Shun'an town, and Guanghui City of Anhui Province in China (Figure 1), in which the human infection rate is 4%, 0%, and 1.6%, respectively. As shown in Table 2 in snails collected from Shankou-city during the spring, the PCR method detected more positive snails than did the microscopy method with the observation of *S. japonicum* cercaria. Although all positive snails by microscopy were also positive by PCR, PCR also amplified the DNA of *S. japonicum* in the snails negative by microscopy. This indicates that PCR could detect the infection not only in the matured cercaria but also in the early sporocyst. However, in snails from Tongling collected in the autumn, PCR detected DNA only from the snails positive by microscopy.

Screening with large-scale DNA extraction from the infected snail by LAMP assay. The PCR method is difficult to use in the field in endemic areas because of the expense of the thermal cycler and the impracticality of performing gel electrophoresis and staining. To amplify the specific DNA without such problems, we applied the LAMP method, which can be performed at a constant temperature and the result can be determined without gel electrophoresis. The LAMP detected schistosomal DNA from a single miracidium of *S. japonicum* (Figure 2B) and the snail infected with a single miracidium (data not shown). Thus, the LAMP method should be useful for the detection of specific DNA in the field without the need for a thermal cycler or gel electrophoresis. We also screened the rate of infected snails in local areas using large-scale DNA extraction. Different numbers (99, 49, 24, and 4) of non-infected snails from non-endemic areas were prepared, and a single infected snail (1 day after infection with 10 miracidia) was mixed in each group. The snails were crushed together, genomic DNA was extracted in one tube, and each sample was assayed by the LAMP method. LAMP detected 28S rDNA of *S. japonicum* from all infected groups but not non-infected groups (Figure 4), indicating that it is useful for detecting schistosomal DNA from a large number of snails in the field in endemic areas.

DISCUSSION

Schistosomiasis-control activities in China since the mid-1950s have decreased the prevalence of human infection with *S. japonicum* to less than 10%.[27,28] Furthermore, a new integrated strategy was developed and proven effective in endemic areas.[7,8] However, the complete eradication of schistosomiasis japonica and the prevention of its reemergence remain difficult. To monitor the infection rate and distribution of infected snails, we developed molecular detection tools based on the amplification of nucleic acid.

PCR targeting 28S rDNA amplified 100 fg of genomic DNA from only *S. japonicum* and none from *S. mansoni*. The ribosomal DNA was known to have a highly repetitive sequence in the genome,[18,29,30] and each region has been shown to be useful for molecular diagnosis and identification of species

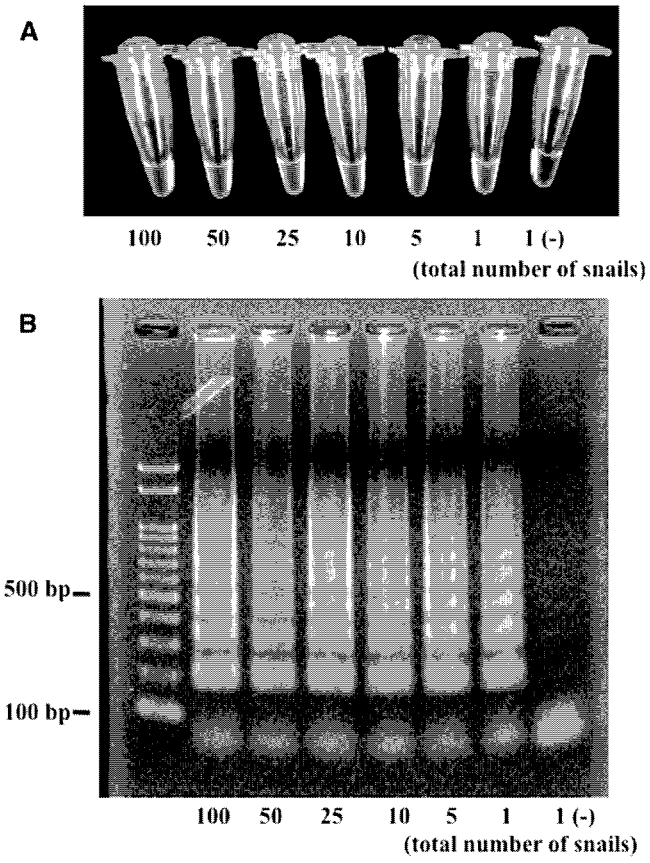

FIGURE 4. Detection of 28S rDNA from *S. japonicum* by LAMP assay in the total DNA from different numbers of non-infected snails artificially contaminated with a single infected snail. The snails infected with 10 miracidium were prepared and mixed with different numbers of snails (99 + 1, 49 + 1, 24 + 1, 9 + 1, 4 + 1, 0 + 1; normal + infected snails). Total DNA was extracted from each group and one non-infected snail (-), and the LAMP assay was performed. The 28S rDNA was amplified from all samples contaminated with the infected snail but not from non-infected snails by the LAMP assay. The results were confirmed based on the white precipitation (**Upper**) and gel electrophoresis (**Lower**).

in other infectious diseases.[31,32] Our designed primer set was suitable for detection of the 28S ribosomal region from *S. japonicum*, and it performed better than had been previously reported, indicating that the sensitivity was 15 pg.[19] Non-LTR retrotransposon, SjR2, was also detected by PCR at a sensitivity of 1 pg, nearly coinciding with the previous result (0.8 pg).[16] Our results indicated that the sensitivity of 28S rDNA is higher than that of SjR2, because R2 sequences were specifically inserted into the 28S ribosomal region and the copy numbers of SjR2 were restricted by that of the target 28S ribosomal DNA.[33]

The LAMP assay is a rapid, specific, and convenient assay employing four primers and isothermal DNA polymerase, and this tool can be applied as a new molecular diagnosis in the field in endemic areas. Our results showed that the sensitivity of LAMP was the same as that of conventional PCR. In general, the LAMP method is more sensitive than the PCR method,[20,22,34,35] although similar sensitivities between the two have also been reported.[24] This may reflect the fact that the sensitivity is dependent on the designed primers. However, the present study found that the sensitivity of PCR assay was sufficient to amplify the 28S ribosomal DNA from a single miracidium, and the results between the LAMP and PCR assays were completely consistent. Therefore, the LAMP assay seems capable of detecting a single miracidium rapidly and inexpensively in the field. Recently, Xu and others[25] investigated LAMP targeting SjR2 and found that its sensitivity was 0.08 fg. We repeated their experiment using the reported primers,[25] but we found that the DNA from *S. japonicum* was not adequately amplified, because each sequence of the reported primers was not identical to the SjR2 regions.

By contrast, PCR, using 28S rDNA primer sets amplifying the *S. japonicum* DNA from the snails infected with a single miracidium at 1 day after infection, was able to detect a single individual of *S. japonicum* throughout the snail stages, whereas conventional microscopy can detect only mature cercaria of *S. japonicum*. Furthermore, PCR is useful for beginners without skill and knowledge, because this method can be specific to *S. japonicum* and can distinguish it from the other species. To evaluate whether our PCR method could be applied in endemic areas, we collected wild snails from endemic areas in Anhui province of China. After crushing the snails and checking for infection by microscopy, total DNA extracted from each snail underwent PCR using 28S rDNA primer sets. PCR amplified the product band from not only snails including the matured cercariae of *S. japonicum* but also snails where cercaria could not be seen by microscopy. This is further support for our hypothesis that PCR could detect the potential infection in the snails with early sporocysts. However, PCR never detected schistosomal DNA from cercaria-negative snails collected from Tongling in the autumn (September). It may be that the differences in the findings between the two areas reflect differences in the timing of new infections in snails as a function of the season and local factors. These areas were part of the marshlands of the Yangtze River where water levels fluctuate markedly because of rainfall and flooding. In autumn, domestic animals exit the marshlands because of the rising water level, which usually reaches the highest level of the year. Thus, transmission of miracidia to snails may be the most difficult in autumn, although domestic animals known to contain hosts of *S. japonicum* were found to be repeatedly infected throughout the year.[36,37] These data suggested that the PCR method has the potential to monitor the timing of the infection of snails in endemic areas.

Several previous reports have suggested that LAMP is useful for the detection of the infections in pathogen-carrying vectors.[38,39] To evaluate the efficiency of the LAMP method for detecting infected snails, a large number of snails contaminated with a single infected snail were crushed together, and the total DNA was extracted in one tube. We then investigated whether LAMP could amplify the schistosomal DNA alone and found that LAMP could detect infection from a snail infected with *S. japonicum* in a group of 100 non-infected snails, indicating its use for detecting infection at a 1% infection rate. If snails (1,000–10,000 individuals) collected from several locations (e.g., 10–100 locations) were assayed, we expect that this method could precisely identify the infection rate in that area. The LAMP assay using 28S rDNA primers may be an effective tool, having the benefits of being rapid, easy, and inexpensive. Although the microscopy method is inexpensive, it is difficult to crush and observe a large number of snails. In particular, the novel LAMP method will make it possible to easily monitor very low infection rates of snails in endemic areas, where the new integrated strategy will be implemented.[7,8]

In the present study, we evaluated PCR and LAMP assay targeting to 28S rDNA from *S. japonicum*. We found that PCR amplifying 28S rDNA could detect 100 fg of DNA from *S. japonicum* but none from *S. mansoni*. Furthermore, the PCR (and LAMP) method could detect the infection of *S. japonicum* in every stage inside the snail. In fact, PCR could detect potential infection from snails deemed negative for infection by microscopy that were sampled from wild snails collected from endemic areas. LAMP, which is rapid, easy, and safe to use in the field, was able to amplify the schistosomal DNA from a single infected snail in a total of 100 snails without marked inhibitions. PCR and LAMP targeting to 28S rDNA may be useful for monitoring the infection rate of snails in endemic areas and for confirming complete eradications against infected snails in the areas where the new integrated strategy is implemented.

Received January 8, 2010. Accepted for publication April 24, 2010.

Acknowledgments: This work was supported financially by the Grant-in-Aid for Young Scientists (B) from the Japan Society for the Promotion of Science (19790305), Grant-in-Aid for Scientific Research (B) from the Japan Society for the Promotion of Science (18406012), Grant-in-Aid for Scientific Research on Priority Areas from the Japan Society for the Promotion of Science (19041049), Grants-in-Aid from the Ministry of Health, Labor and Welfare of Japan (H18-Shinko-008), Kurozumi Medical Foundation, and the US–Japan Cooperative Medical Science Program.

Authors' addresses: Takashi Kumagai, Section of Environmental Parasitology, Department of International Health Development, Division of Public Health, Graduate School of Medical and Dental Sciences, Tokyo Medical and Dental University, Yushima, Bunkyo-ku, Tokyo, Japan, E-mail: tkuma.vip@tmd.ac.jp. Rieko Furushima-Shimogawara, Section of Environmental Parasitology, Department of International Health Development, Division of Public Health, Graduate School of Medical and Dental Sciences, Tokyo Medical and Dental University, Yushima, Bunkyo-ku, Tokyo, Japan, E-mail: rfuru.vip@tmd.ac.jp. Hiroshi Ohmae, Department of Parasitology, National Institute of Infectious Diseases, Toyama, Shinjyuku-ku, Tokyo, Japan, E-mail: h-ohmae@nih.go.jp. Tian-Ping Wang, Anhui Institute of Parasitic Diseases, Wuhu, China, E-mail: wangtianping@hotmail.com. Shaohong Lu, Institute of Parasitic Diseases, Zhejiang Academy of Medical Sciences, Hangzhou, China, E-mail: llsshh2003@163.com. Rui Chen, Institute of Parasitic Diseases, Zhejiang Academy of Medical Sciences, Hangzhou, China, E-mail: chenrui@163.com. Liyong Wen, Institute of Parasitic Diseases, Zhejiang Academy of Medical Sciences,

Hangzhou, China, E-mail: wenliyonghz@hotmail.com. Nobuo Ohta, Section of Environmental Parasitology, Department of International Health Development, Division of Public Health, Graduate School of Medical and Dental Sciences, Tokyo Medical and Dental University, Yushima, Bunkyo-ku, Tokyo, Japan, E-mail: matata.vip@tmd.ac.jp.

REFERENCES

1. Ross AG, Bartley PB, Sleigh AC, Olds GR, Li Y, Williams GM, McManus DP, 2002. Schistosomiasis. *N Engl J Med 346:* 1212–1219.
2. Liang S, Yang C, Zhong B, Qiu D, 2006. Re-emerging schistosomiasis in hilly and mountainous areas of Sichuan, China. *Bull World Health Organ 84:* 139–144.
3. Ross AG, Sleigh AC, Li Y, Davis GM, Williams GM, Jiang Z, Feng Z, McManus DP, 2001. Schistosomiasis in the People's Republic of China: prospects and challenges for the 21st century. *Clin Microbiol Rev 14:* 270–295.
4. Zhou XN, Wang LY, Chen MG, Wu XH, Jiang QW, Chen XY, Zheng J, Utzinger J, 2005. The public health significance and control of schistosomiasis in China—then and now. *Acta Trop 96:* 97–105.
5. Zhou XN, Guo JG, Wu XH, Jiang QW, Zheng J, Dang H, Wang XH, Xu J, Zhu HQ, Wu GL, Li YS, Xu XJ, Chen HG, Wang TP, Zhu YC, Qiu DC, Dong XQ, Zhao GM, Zhang SJ, Zhao NQ, Xia G, Wang LY, Zhang SQ, Lin DD, Chen MG, Hao Y, 2007. Epidemiology of schistosomiasis in the People's Republic of China, 2004. *Emerg Infect Dis 10:* 1470–1477.
6. Li SZ, Luz A, Wang XH, Xu LL, Wang Q, Qian YJ, Wu XH, Guo JG, Xia G, Wang LY, Zhou XN, 2009. Schistosomiasis in China: acute infections during 2005–2008. *Chin Med J 122:* 1009–1014.
7. Wang LD, Chen HG, Guo JG, Zeng XJ, Hong XL, Xiong JJ, Wu XH, Wang XH, Wang LY, Xia G, Hao Y, Chin DP, Zhou XN, 2009. A strategy to control transmission of *Schistosoma japonicum* in China. *N Engl J Med 360:* 121–128.
8. Wang LD, Guo JG, Wu XH, Chen HG, Wang TP, Zhu SP, Zhang ZH, Steinmann P, Yang GJ, Wang SP, Wu ZD, Wang LY, Hao Y, Bergquist R, Utzinger J, Zhou XN, 2009. China's new strategy to block *Schistosoma japonicum* transmission: experiences and impact beyond schistosomiasis. *Trop Med Int Health 14:* 1475–1483.
9. Pontes LA, Dias-Neto E, Rabello A, 2002. Detection by polymerase chain reaction of *Schistosoma mansoni* DNA in human serum and feces. *Am J Trop Med Hyg 66:* 157–162.
10. Hamburger J, He-Na Abbasi I, Ramzy RM, Jourdane J, Ruppel A, 2001. Polymerase chain reaction assay based on a highly repeated sequence of *Schistosoma haematobium*: a potential tool for monitoring schistosome-infested water. *Am J Trop Med Hyg 65:* 907–911.
11. Sandoval N, Siles-Lucas M, Lopez Aban J, Pérez-Arellano JL, Gárate T, Muro A, 2006. *Schistosoma mansoni*: a diagnostic approach to detect acute schistosomiasis infection in a murine model by PCR. *Exp Parasitol 114:* 84–88.
12. Hertel J, Kedves K, Hassan AH, Haberl B, Haas W, 2004. Detection of *Schistosoma mansoni* cercariae in plankton samples by PCR. *Acta Trop 91:* 43–46.
13. Suzuki T, Osada Y, Kumagai T, Hamada A, Okuzawa E, Kanazawa T, 2006. Early detection of *Schistosoma mansoni* infection by touchdown PCR in a mouse model. *Parasitol Int 55:* 213–218.
14. Laha T, Brindley PJ, Smout MJ, Verity CK, McManus DP, Loukas A, 2002. Reverse transcriptase activity and untranslated region sharing of a new RTE-like, non-long terminal repeat retrotransposon from the human blood fluke, *Schistosoma japonicum*. *Int J Parasitol 32:* 1163–1174.
15. Driscoll AJ, Kyle JL, Remais J, 2005. Development of a novel PCR assay capable of detecting a single *Schistosoma japonicum* cercaria recovered from *Oncomelania hupensis*. *Parasitology 131:* 497–500.
16. Xia CM, Rong R, Lu ZX, Shi CJ, Xu J, Zhang HQ, Gong W, Luo W, 2009. *Schistosoma japonicum*: a PCR assay for the early detection and evaluation of treatment in a rabbit model. *Exp Parasitol 121:* 175–179.
17. Hung YW, Remais J, 2008. Quantitative detection of *Schistosoma japonicum* cercariae in water by real-time PCR. *PLoS Negl Trop Dis 2:* e337.
18. Lier T, Johansen MV, Hjelmevoll SO, Vennervald BJ, Simonsen GS, 2008. Real-time PCR for detection of low intensity *Schistosoma japonicum* infections in a pig model. *Acta Trop 105:* 74–80.
19. Sandoval N, Siles-Lucas M, Pérez-Arellano JL, Carranza C, Puente S, López-Abán J, Muro A, 2006. A new PCR-based approach for the specific amplification of DNA from different *Schistosoma* species applicable to human urine samples. *Parasitology 133:* 581–587.
20. Notomi T, Okayama H, Masubuchi H, Yonekawa T, Watanabe K, Amino N, Hase T, 2000. Loop-mediated isothermal amplification of DNA. *Nucleic Acids Res 28:* E63.
21. Han ET, Watanabe R, Sattabongkot J, Khuntirat B, Sirichaisinthop J, Iriko H, Jin L, Takeo S, Tsuboi T, 2007. Detection of four *Plasmodium* species by genus- and species-specific loop-mediated isothermal amplification for clinical diagnosis. *J Clin Microbiol 45:* 2521–2528.
22. Thekisoe OM, Kuboki N, Nambota A, Fujisaki K, Sugimoto C, Igarashi I, Yasuda J, Inoue N, 2007. Species-specific loop-mediated isothermal amplification (LAMP) for diagnosis of trypanosomosis. *Acta Trop 102:* 182–189.
23. Takagi H, Itoh M, Islam MZ, Razzaque A, Ekram AR, Hashighuchi Y, Noiri E, Kimura E, 2009. Sensitive, specific, and rapid detection of *Leishmania donovani* DNA by loop-mediated isothermal amplification. *Am J Trop Med Hyg 81:* 578–582.
24. Nkouawa A, Sako Y, Nakao M, Nakaya K, Ito A, 2009. Loop-mediated isothermal amplification method for differentiation and rapid detection of *Taenia* species. *J Clin Microbiol 47:* 168–174.
25. Xu J, Rong R, Zhang HQ, Shi CJ, Zhu XQ, Xia CM, 2010. Sensitive and rapid detection of *Schistosoma japonicum* DNA by loop-mediated isothermal amplification (LAMP). *Int J Parasitol 40:* 327–331.
26. Hirayama H, Kageyama S, Moriyasu S, Sawai K, Onoe S, Takahashi Y, Katagiri S, Toen K, Watanabe K, Notomi T, Yamashina H, Matsuzaki S, Minamihashi A, 2004. Rapid sexing of bovine pre-implantation embryos using loop-mediated isothermal amplification. *Theriogenology 62:* 887–896.
27. Utzinger J, Zhou XN, Chen MG, Bergquist R, 2005. Conquering schistosomiasis in China: the long march. *Acta Trop 96:* 69–96.
28. Zhou XN, Wang LY, Chen MG, Wang TP, Guo JG, Wu XH, Jiang QW, Zheng J, Chen XY, 2005. An economic evaluation of the national schistosomiasis control programme in China from 1992 to 2000. *Acta Trop 96:* 255–265.
29. van Keulen H, Loverde PT, Bobek LA, Rekosh DM, 1985. Organization of the ribosomal RNA genes in *Schistosoma mansoni*. *Mol Biochem Parasitol 15:* 215–230.
30. Littlewood DT, Johnston DA, 1995. Molecular phylogenetics of the four *Schistosoma* species groups determined with partial 28S ribosomal RNA gene sequences. *Parasitology 111:* 167–175.
31. Das A, Holloway B, Collins WE, Shama VP, Ghosh SK, Sinha S, Hasnain SE, Talwar GP, Lal AA, 1995. Species-specific 18S rRNA gene amplification for the detection of *P. falciparum* and *P. vivax* malaria parasites. *Mol Cell Probes 9:* 161–165.
32. Schönian G, Nasereddin A, Dinse N, Schweynoch C, Schallig HD, Presber W, Jaffe CL, 2003. PCR diagnosis and characterization of *Leishmania* in local and imported clinical samples. *Diagn Microbiol Infect Dis 47:* 349–358.
33. Kojima KK, Fujiwara H, 2005. Long-term inheritance of the 28S rDNA-specific retrotransposon R2. *Mol Biol Evol 22:* 2157–2165.
34. Zhang H, Thekisoe OM, Aboge GO, Kyan H, Yamagishi J, Inoue N, Nishikawa Y, Zakimi S, Xuan X, 2009. *Toxoplasma gondii*: sensitive and rapid detection of infection by loop-mediated isothermal amplification (LAMP) method. *Exp Parasitol 122:* 47–50.
35. Karanis P, Thekisoe O, Kiouptsi K, Ongerth J, Igarashi I, Inoue N, 2007. Development and preliminary evaluation of a loop-mediated isothermal amplification procedure for sensitive detection of *Cryptosporidium* oocysts in fecal and water samples. *Appl Environ Microbiol 73:* 5660–5662.
36. Wang T, Zhang S, Wu W, Zhang G, Lu D, Ornbjerg N, Johansen MV, 2006. Treatment and reinfection of water buffaloes and

cattle infected with *Schistosoma japonicum* in Yangtze River Valley, Anhui province, China. *J Parasitol 92:* 1088–1091.
37. Wang TP, Johansen MV, Zhang SQ, Wang FF, Wu WD, Zhang GH, Pan XP, Ju Y, Ørnbjerg N, 2005. Transmission of *Schistosoma japonicum* by humans and domestic animals in the Yangtze River valley, Anhui province, China. *Acta Trop 96:* 198–204.
38. Aonuma H, Suzuki M, Iseki H, Perera N, Nelson B, Igarashi I, Yagi T, Kanuka H, Fukumoto S, 2008. Rapid identification of *Plasmodium*-carrying mosquitoes using loop-mediated isothermal amplification. *Biochem Biophys Res Commun 376:* 671–676.
39. Aonuma H, Yoshimura A, Perera N, Shinzawa N, Bando H, Oshiro S, Nelson B, Fukumoto S, Kanuka H, 2009. Loop-mediated isothermal amplification applied to filarial parasites detection in the mosquito vectors: *Dirofilaria immitis* as a study model. *Parasit Vectors 2:* 15.

Medical Practice

2010 vol. 27 no. 09

寄生虫とアレルギーの親密な関係

長田良雄

東京 文光堂 本郷

寄生虫とアレルギーの親密な関係

長田良雄
産業医科大学免疫学・寄生虫学／おさだ・よしお

先進諸国におけるアレルギー疾患の増加がいわれて久しい．その原因については，栄養状態の変化・居住環境の変化(密閉された室内環境)・大気汚染などさまざまな説があるが，近年注目されているものとしていわゆる衛生仮説 hygiene hypothesisがある．この説は英国のStrachanの論文[1]すなわち年上の兄弟姉妹の数とアトピーのリスクが逆相関にあるという報告に端を発するもので，「幼少時の"ある程度"不衛生な環境がアレルギー疾患の発症を防ぐ」という概念である．衛生仮説は一般社会でも注目されており，一昨年は某公共放送のテレビ番組で，乳幼児期に牛舎に出入りしていた子供の喘息や花粉症の発症率が低く，その現象には細菌の成分エンドトキシンが関係しているという欧州の研究が紹介された．その影響かどうかは不明だが，「エンドトキシンを浴びよう！」という趣旨の牧場ツアーが企画されたり，「お部屋にエンドトキシンを！」という触れ込みで乾燥牛糞製品が通信販売されたりもしているようだ．

さて，元来の衛生仮説は上記の様に細菌等の微生物とアレルギー疾患に関するもので，従来は「細菌成分によりTh1型免疫応答が刺激される結果，Th2型免疫応答が抑制されアレルギーになりにくくなる」という，いわゆる「Th1-Th2パラダイム」で現象が説明されていた．だが，先進国では自己免疫疾患(主にTh1型またはTh17型の免疫応答)もアレルギー疾患と同様に増加していること[2]に加え，Th2型応答を誘導する寄生蠕虫にもアレルギー疾患や自己免疫疾患に対する予防・改善効果があるという多数の実験的報告がなされるに至り，「Th1-Th2パラダイム」での説明は困難になっている．最近は上記いずれの免疫応答をも抑制し得る制御性T細胞regulatory T cell(Treg)の関与の可能性が注目されているが，メカニズムに関してはなお不明な点が多い．

ところで，寄生蠕虫はヒトにおいて本当にアレルギー疾患を予防あるいは改善する効果を持っているのだろうか？ この点は文献により結果が一定しないため，複数の疫学調査を統合的に分析した論文(メタ分析など)を参照してみる必要がある．調査時点での寄生虫感染状態と皮膚プリックテストおよび喘息リスクに関する多数の横断研究の分析を行った報告[3,4]をみると，その結論は「調査された蠕虫(回虫，鉤虫，鞭虫，住血吸虫)に関する限り，すべて皮膚プリックテスト反応性を低下させている(住血吸虫が最もその効果が高い)」が，「喘息リスクへの影響は蠕虫の種類によって異なる」というものであった．具体的には，鉤虫感染は有意に喘息のリスクを下げていることが判明した(オッズ比0.50)．一方で，回虫感染はリスクを上げており(オッズ比1.34)，鞭虫・糞線虫・蟯虫の感染は有意な影響を与えていなかった．なお鉤虫については，感染強度に比例したリスク低減効果があるとの結果も同時に得られている．よって，少なくともある種の蠕虫については，アレルギー疾患の予防・改善効果の存在が期待される．駆虫介入研究では，駆虫後に皮膚テスト反応性が上昇したとの報告もある(これに反する報告もある)．ただ，日本において寄生蠕虫感染の減少が近年のアレルギー疾患の増加にどの程度関係しているかを論ずるのは難しい．蠕虫感染は1960年代中ごろまでに激減しているのに対しアレルギー疾患はそれ以後に増加し始め近年も継続して増加傾向にあること，乳児期には蠕虫よりむしろ細菌やウイルスへの暴露機会が多いことを考えると，比較的その影響は小さいと考えるのが自然であろう．

比較的病原性の低い寄生蠕虫を"生きたまま"免疫異常疾患の治療に用いる試みは欧米では積極的に行われており，ブタ鞭虫卵が炎症性腸疾患に対

0910-1551/10/ ¥100/頁 /JCOPY

細菌や寄生虫への暴露がアレルギー疾患を予防・改善するという報告がなされている(衛生仮説).
横断研究によると,アレルギー疾患に対する影響は寄生蠕虫の種類によって異なる.
免疫異常疾患やアレルギー疾患に対する寄生蠕虫の臨床応用が試みられている.

して効果があるという結果が得られている[5].さらに今年に入り,喘息に対するアメリカ鉤虫の治験結果(二重盲検試験)が報告された[6].残念ながら有意な改善効果は確認されなかったが,この結果には感染に用いた虫体数が少なかった(10隻)ことも影響しているかもしれない.他の免疫異常疾患に対しても寄生虫の治験が計画・進行中であり,今後も有望な寄生虫と対象疾患が見出され,臨床応用に向かってさらに研究開発が進むことを期待したい.

文 献

1) Strachan, D.P. : Hay fever, hygiene, and household size. BMJ **299** (6710) : 1259-1260, 1989
2) Bach, J.F. : The effect of infections on susceptibility to autoimmune and allergic diseases. N Engl J Med **347** (12) : 911-920, 2002
3) Flohr, C. et al. : Do helminth parasites protect against atopy and allergic disease? Clin Exp Allergy **39** (1) : 20-32, 2009
4) Leonardi-Bee, J. et al. : Asthma and current intestinal parasite infection : systematic review and meta-analysis. Am J Respir Crit Care Med **174** (5) : 514-523, 2006
5) Summers, R.W. et al. : *Trichuris suis* therapy for active ulcerative colitis : a randomized controlled trial. Gastroenterology **128** (4) : 825-832, 2005
6) Feary, J.R. et al. : Experimental hookworm infection : a randomized placebo-controlled tirial in asthma. Clin Exp Allergy **40** (2) : 299-306, 2010

MALARIA JOURNAL

RESEARCH Open Access

Suppressive effect of azithromycin on *Plasmodium berghei* mosquito stage development and apicoplast replication

Shoichi Shimizu[1,2], Yoshio Osada[1], Tamotsu Kanazawa[1], Yoshiya Tanaka[2], Meiji Arai[3*]

Abstract

Background: Azithromycin (AZM) is a macrolide antibiotic that displays an excellent safety profile even in children and pregnant women and has been shown to have anti-malarial activity against blood stage *Plasmodium falciparum*. This study evaluated the transmission-blocking effect of AZM using a rodent malaria model.

Methods: AZM-treated mice infected with *Plasmodium berghei* were exposed to *Anopheles stephensi* mosquitoes, followed by the observation of parasite development at different phases in the mosquito, i.e., ookinetes in the midgut, oocysts on the midgut, and sporozoites in the midgut and salivary glands. Furthermore, to evaluate the effect on organelle replication of each stage, quantitative real-time PCR analysis was performed.

Results: The inhibitory effect of AZM was noticeable in both gametocyte-ookinete transformation in the midgut and sporozoite production in the oocyst, while the latter was most remarkable among all the developmental phases examined. Real-time PCR analysis revealed that AZM suppressed apicoplast replication at the period of sporozoite production in oocysts.

Conclusions: AZM inhibits parasite development in the mosquito stage, probably through the same mechanism as in the liver and blood stages. Such a multi-targeting anti-malarial, along with its safety, would be ideal for mass drug administration in malaria control programmes.

Background

Malaria, caused by protozoan parasites of the genus *Plasmodium* and transmitted by mosquitoes of the genus *Anopheles*, remains one of the world's most important health problems, causing nearly a million deaths per year [1]. Because of the rapid emergence and spread of drug-resistant *Plasmodium falciparum*, the development of alternative control tools is needed urgently [2]. A possible strategy is to block malarial transmission from gametocyte carriers to the vector mosquitoes using a transmission-blocking vaccine [2,3] or a drug that interrupts parasite development in the mosquito vector [4]. The strategy of blocking malarial transmission has been claimed to limit the spread of malaria and to reduce the spread of drug-resistant parasites [5-8].

Considering that very high coverage is essential for a significant impact on malaria transmission, mass drug administration (MDA) for people including children and pregnant women in endemic area is required [6]. In MDA, safety is a paramount issue because the drug will be given to large numbers of non-infected individuals [7]. Thus, only drugs with an excellent safety profile should be considered for MDA. Primaquine, the generally available gametocytocidal drug, has been used previously in MDA [9,10], but its haemolytic effect in glucose-6-phosphate dehydrogenase deficient individuals has made this drug less acceptable for MDA [7,8]. To date, a limited number of drugs or compounds has been confirmed to possess transmission-blocking activity [5,11-13]. Most of them have not been considered for clinical applications due to their toxicity and/or cost of development [12]. Therefore, if licensed antibiotics are proven to have transmission-blocking activity, practical evaluation should be greatly accelerated and their impact should be fully exploited [14].

* Correspondence: marai@med.kagawa-u.ac.jp
[3]Department of International Medical Zoology, Faculty of Medicine, Kagawa University, 1750-1 Ikenobe, Miki-cho, Kita-gun, Kagawa 761-0793, Japan

Azithromycin (AZM), a 15-membered azalide that has been broadly used for the treatment of bacterial infections [15], displays a good safety profile, including in children and pregnant women [2,16,17]. Importantly, AZM was shown to have inhibitory activity against *Plasmodium* spp. both *in vitro* and *in vivo* [15,18-20] and was effective for prophylaxis and treatment against human malaria in field conditions [21-23]. It has been proposed that AZM exerts a "delayed death" effect against blood stage *P. falciparum*, in which the progeny of AZM-treated parasites that inherited non-functional apicoplasts fail to develop, leading to a delayed, but potent anti-malarial effect [24]. Therefore, it was hypothesized that this delayed effect of AZM would also be exerted against parasite development in the mosquito, leading to transmission blockade.

The aim of this study was to evaluate the transmission-blocking activity of AZM using a rodent malaria model, and to investigate whether the apicoplast is the target of AZM in the mosquito stage.

Methods

Parasites and mosquitoes

Plasmodium berghei ANKA strain, clone 2.34 was maintained by cyclic passage in BALB/c mice (Japan SLC, Shizuoka, Japan) and SDA500 strain of *Anopheles stephensi*. For drug treatment and mosquito biting studies, mice infected with the second blood passage parasites after mosquito transmission were used. Cyclic colonies of *An. stephensi* were maintained at University of Occupational and Environmental Health, Japan. Mosquitoes were reared according to the MR4 Methods in *Anopheles* Research Manual [25].

Administration of AZM to *P. berghei*-infected mice

All the animal experiments were performed under the control of the Ethics Committee of Animal Care and Experimentation in accordance with The Guiding Principles of Animal Care Experimentation, The University of Occupational and Environmental Health, Japan and the Japanese Law for Animal Welfare and Care (No. 221). Six-week-old female BALB/c mice (18.5-20.5 g) were infected with *P. berghei* by intraperitoneal injection of 5×10^6 parasitised erythrocytes per mouse. Parasitaemia and mature microgametocytaemia (density of male gametocytes), the latter of which is thought to be a limiting factor for the efficiency of fertilization in the vector mosquito due to the female-biased sex ratio [26,27], were monitored daily by microscopic observation of Giemsa-stained thin blood smears [14]. Four days post-infection, 6-10 infected mice were divided into two groups to match parasitaemia and microgametocytaemia. Mice of the experimental group were given azithromycin (AZM) (LKT Laboratories, St. Paul, MN, USA) suspended in 0.3% carboxymethylcellulose (CMC) (Nacalai Tesque, Kyoto, Japan) at a dose of 400 mg/kg orally and those of the control group were given 0.3% CMC only.

Exflagellation assay

In order to evaluate the effect of AZM on exflagellation (microgametogenesis) activity, 3 μl of tail blood was taken from each infected mouse at 24 hours after drug administration (the same time as blood feeding). The blood sample was immediately mixed with 300 μl of exflagellation medium (RPMI 1640 containing 25 mM HEPES, 25 mM sodium bicarbonate, 20% foetal bovine serum, pH 8.0) and 20 μl of the suspension was loaded onto a Fuchs-Rosenthal haemocytometer (C-Chip DHC-F01, Digital Bio Technology, Seoul, Korea), then incubated at 19°C for 20 minutes. Exflagellation centres were numerated by microscopic observation at ×200 magnifications and expressed as a number of exflagellation events per 10^4 red blood cells (RBCs).

Assessment of sporogonic development

At 24 hours post-drug administration, infected mice were exposed to 300-400 mosquitoes in each group that had emerged 6-8 days before, for 15 minutes at 19°C. Two- to three-hundred engorged mosquitoes in each group were collected and kept at 19°C. At 24 hours post blood feeding, 10-20 mosquitoes in each group were dissected for ookinete counting. The gut contents of each mosquito were mixed with fetal bovine serum on a glass slide. A thin film of the midgut contents was prepared and stained with Giemsa, then the ookinete count was made in a total of 300 observation fields with ×50 oil-immersion objective and ×10 ocular lens as described previously [28]. At 10 days post blood feeding, 10-20 mosquitoes in each group were dissected and the number of oocysts per midgut was determined by light microscopic observation. At 20 days post blood feeding, 30 mosquitoes in each group were dissected for sporozoite numeration. Ten sets of salivary glands and midguts were dissected out and pooled separately in 1.5 ml microtubes, then homogenized in 100 μl PBS. The suspension was loaded onto a haemocytometer, and the number of sporozoites was determined. Three replicates were performed for each experimental set. In another set of experiment, 20 mosquitoes from each group were individually dissected at 20 days post blood feeding, and the prevalence of salivary gland sporozoites was examined.

Quantitative real-time PCR analysis to determine effect of AZM on apicoplast DNA replication

In order to evaluate the effect of AZM-treatment on apicoplast DNA replication, apicoplast DNA/nuclear

DNA ratios were determined by quantitative real-time PCR. Blood stage genomic DNA of *P. berghei* was prepared from the mouse blood collected from 3-5 infected mice by cardiac puncture at 24 or 72 hours post-drug administration. For preparation of mosquito stage genomic DNA, midguts were dissected out and pooled from 20 infected mosquitoes in each group at 5, 10, and 15 days post blood feeding. Genomic DNA was isolated from the parasites by using Get pure DNA Kit-Cell, Tissue (Dojindo Molecular Technologies, Kumamoto, Japan) and Dr. GenTLE Precipitation Carrier (Takara Bio, Shiga, Japan) in accordance with the manufacturer's instructions. The nuclear and organelle-specific genes that we used for quantification of the nuclear DNA, apicoplast DNA, and mitochondrial DNA were *fabI*, *tufA*, and *cytb*, respectively [15,29]. Primers used for the amplification of each gene were designed and checked for specificity by using Primer-BLAST provided by National Center for Biotechnology Information [30]. The accession numbers of each gene and the designed primer sequences are listed in Additional file 1. Quantitative PCR was performed using Fast Real-Time SYBR Green master mix and a StepOnePlus sequence detection system (Applied Biosystems, Foster City, CA, USA) in accordance with the manufacturer's instructions. PCR was performed in duplicate for each sample. DNA samples obtained from blood stage parasites in the control group, which resulted in highest amount of amplified product for each gene, were serially diluted and used as the standard for absolute quantification. Organelle DNA replication was evaluated by comparison of PCR product quantities from organelle DNA with nuclear DNA [31,32]. To confirm specific amplification of desired products, DNA melting curve analysis was performed.

Statistical analysis

Mann-Whitney U test was used to determine statistical differences in parasite number, parasitaemia and microgametocytaemia between the experimental and control groups. *P* values lower than 0.05 were considered significant. All tests were two-tailed. All statistical analyses were performed using Microsoft Excel 2007 (Microsoft Corporation, Tokyo, Japan).

Results

Determination of appropriate timing for blood feeding

It has already been reported that AZM exerts schizontocidal effects against *P. berghei* blood stage four days after drug administration [19]. Thus, to evaluate the effect of AZM against mosquito stage, the earlier timing seems to be appropriate for blood feeding. Therefore, at first, the parasitaemia and microgametocytaemia were checked at 24 hours post-drug administration. No significant difference between AZM-treated mice and control mice was observed in either parasitaemia (median value: 6.0% in AZM-treated mice vs 5.7% in control mice, $P = 0.72$, $n = 20$) or microgametocytaemia (0.031% vs 0.033%, $P = 0.89$, $n = 20$). Then, it was decided to treat mice with AZM 24 hours prior to blood feeding.

Effect of AZM on exflagellation activity of *P. berghei* microgametocytes

To evaluate the effect of AZM on the function of microgametocyte, infected mouse blood was collected at the time of blood feeding (24 hours post-drug administration) and used to test for exflagellation activity. No significant difference of exflagellation events was observed between AZM-treated mice and control mice, suggesting that AZM did not affect the biological function of male gametocytes (Figure 1).

Effect of AZM on mosquito stage development of *P. berghei*

The effect of AZM on parasite development in *An. stephensi* mosquitoes fed on blood of *P. berghei*-infected mice that had been given AZM 24 hours before blood feeding was assessed. Mosquitoes were dissected at 24 hours, 10, and 20 days post blood feeding to determine the levels of ookinetes, oocysts, and sporozoites both in the midgut and salivary glands, respectively. This

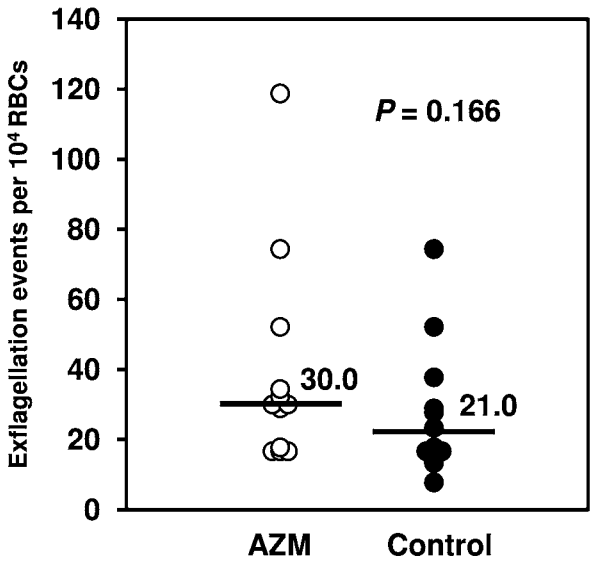

Figure 1 Effect of AZM on exflagellation of *P. berghei* microgametocytes *in vitro*. The number of exflagellation events per 10^4 RBCs was counted *in vitro* 24 hours after administration of AZM (White circle) or CMC (Black circle, as control). Horizontal lines and adjacent numbers represent the median number of exflagellation events in each group. *P* values were determined by Mann-Whitney U test. Combined results of three independent experiments are shown ($n = 12$).

experiment revealed that AZM treatment suppressed parasite development in all the four stages in the mosquito, i.e., reduction of ookinetes in the midgut (50% reduction as compared with the controls, $P = 0.016$, Figure 2A), oocysts on the midgut (45% reduction, $P = 0.003$, Figure 2B), sporozoites both in the midgut (79% reduction, $P < 0.001$, Figure 2C) and in the salivary glands (50% reduction, $P = 0.002$, Figure 2D). In another set of experiment, the prevalence of salivary gland sporozoites was 100% in both groups, indicating that AZM did not reduce the prevalence.

Effect of AZM on replication of *P. berghei* apicoplast

In the case of blood stages, inhibition of apicoplast replication by chemicals has been usually evaluated by the ratio of apicoplast DNA to nuclear DNA [31,32]. In this study, to evaluate the effect of AZM on the replication of *P. berghei* apicoplast, the relative amounts of organellar DNA to nuclear DNA were estimated using real-time PCR. During the blood stage of parasite development, AZM treatment resulted in the suppression of apicoplast replication at 72 hours post-drug administration (1.0 at 24 hours post-drug administration, 0.14 at 72 hours post-drug administration, Figure 3A). This result agreed with previous reports about the effect of AZM [24], clindamycin [31], and 15-deoxyspergualin [32] on *P. falciparum in vitro*, all of which are believed to impair parasite growth by inhibiting apicoplast replication. In the mosquito stage, apicoplast replication in parasites derived from AZM-treated mice was not reduced at 5 days post blood feeding, i.e., 6 days post-drug administration, followed by successive suppressions

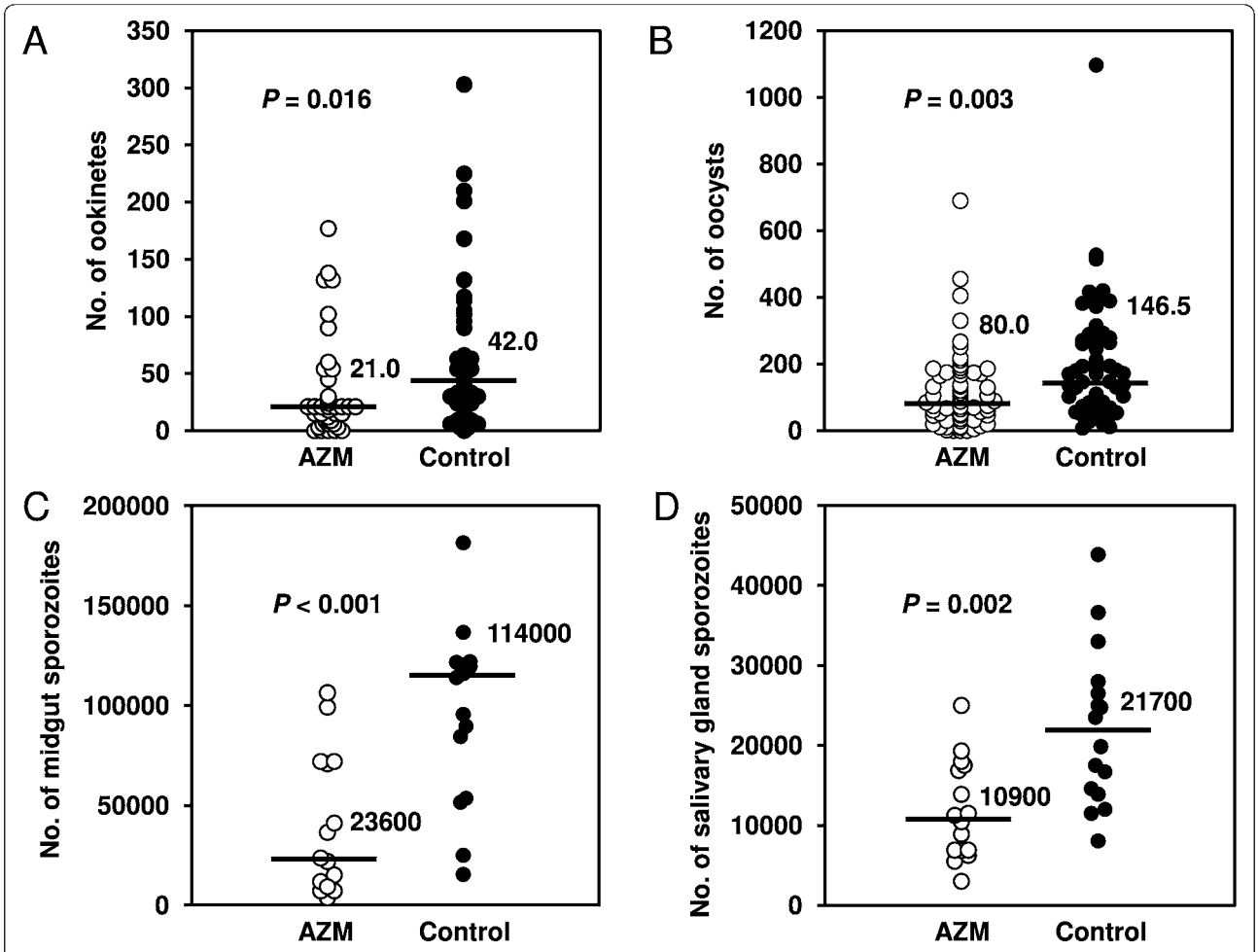

Figure 2 Effect of AZM on *P. berghei* mosquito stage development. Mosquitoes were allowed to feed on blood of *P. berghei*-infected mice that had been given AZM (White circle) or CMC (Black circle) at 24 hours before blood feeding. (A) Ookinete numbers in midguts dissected at 24 hours post blood feeding were determined by microscopy analysis. (B) Oocyst numbers on midguts dissected at 10 days post blood feeding were counted. (C, D) Sporozoite numbers in midgut oocysts (C) and salivary glands (D) were determined at 20 days post blood feeding. Horizontal lines and adjacent numbers represent the medians ($n = 40$ in (A); $n = 60$ in (B); $n = 15$ (calculated from 150 mosquitoes) in (C) and (D)). *P* values were determined by Mann-Whitney U test. Combined results of three to five independent experiments are shown.

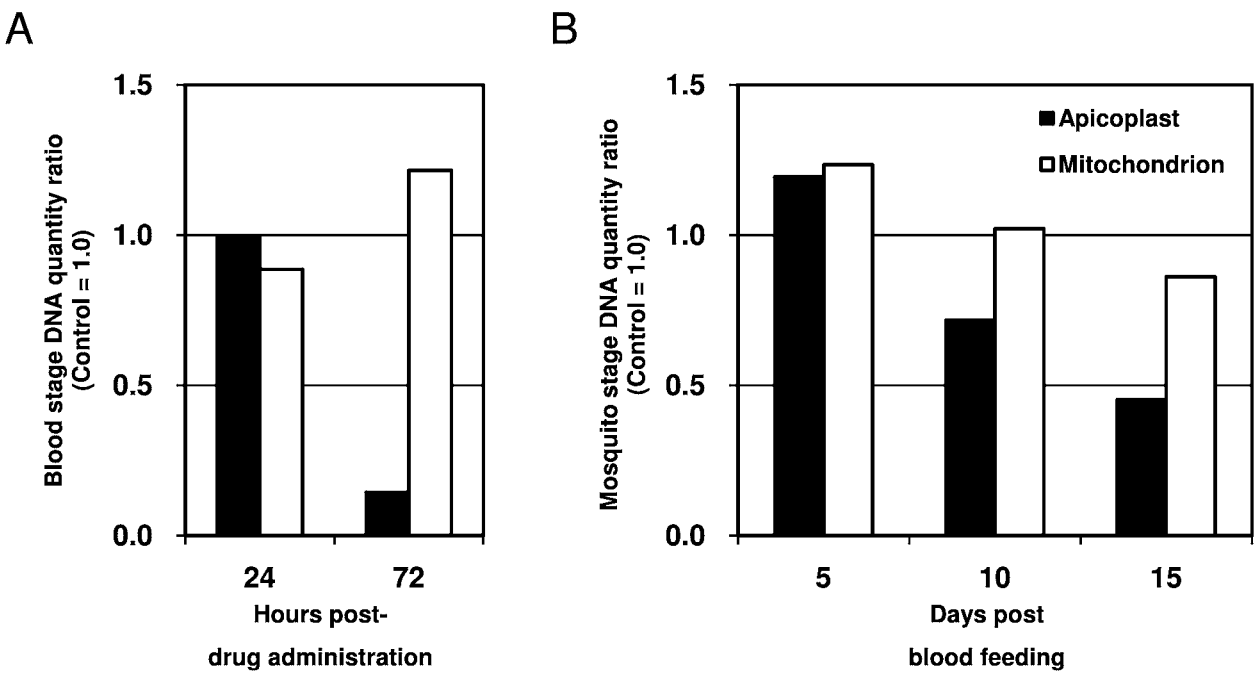

Figure 3 Effect of AZM on replication of *P. berghei* apicoplasts. Ratios of apicoplast DNA/nuclear DNA in AZM-treated parasites were calculated by quantitative real-time PCR, then standardized with the ratio from control parasites, giving ratios of (apicoplast/nuclear DNA ratio in AZM-treated parasites)/(apicoplast/nuclear DNA ratio in control parasites) (Black square). Similarly, the ratios of (mitochondrial/nuclear DNA ratio in AZM-treated parasites)/(mitochondrial/nuclear DNA ratio in control parasites) were calculated (White square). (A) Analysis of blood stage parasites at 24 hours post-drug administration (= the time of blood feeding) and 72 hours post-drug administration. (B) Analysis of mosquito stage parasites at 5, 10, and 15 days post blood feeding. DNA ratio of each control group is 1.0 on the vertical axis. A representative result of four independent experiments is shown.

at 10 days and 15 days post blood feeding (Figure 3B). In contrast, mitochondrial replication was not affected in both the blood and mosquito stages (Figure 3A, B), suggesting that the inhibitory effect of AZM was specific to the apicoplast.

Discussion

It has been demonstrated that AZM inhibits apicoplast replication in blood stage *P. falciparum* [24] and liver stage *P. berghei* [33]. Indeed, combinations of AZM with conventional schizontocides were applied for human malaria cases in the field. They showed good results [22,34,35], whereas AZM monotherapy did not [34]. In this study, it was shown for the first time that AZM inhibits apicoplast replication of *P. berghei* also in the mosquito stage. These findings imply that AZM suppresses parasite growth at three different stages in the life cycle by attacking the same target, apicoplast replication. These data indicate that AZM has a further possibility of blocking malaria transmission.

In the present study, *P. berghei* development was apparently inhibited by AZM treatment at all the phases examined. It is notable that AZM treatment suppressed ookinete formation without affecting exflagellation activity, implying that AZM affected only macrogametocytes (female). This is compatible with the fact that the apicoplast is a maternally inherited organelle [36,37].

Considering the continuous development of parasites in mosquitoes, the reduction of oocysts (45%) was similar to the reduction of ookinetes (50%), suggesting that AZM does not have much effect on oocyst formation from ookinetes. On the other hand, the inhibitory effect of AZM on the mosquito stage was most remarkable in the production of sporozoites (79%). It has been reported in both blood and liver stage schizogony that replication and segregation of apicoplasts proceed during the middle to late stages of serial nuclear divisions and are completed before daughter merozoites are formed [33,38]. These findings allow it to be speculated that in the case of mosquito stage sporogony, apicoplast replication occurs during middle to late stage of nuclear divisions in oocysts, corresponding to around 8 to 15 days post blood feeding for oocyst maturation [39]. Therefore, inhibition of sporozoite production may result from the inhibition of apicoplast replication during the above-mentioned period in oocysts. Taken together, it seems that AZM inhibits mosquito stage development at two different

steps; i.e., gametocyte-ookinete transformation in the midgut and sporozoite production in the oocyst. The latter is probably due to the inhibition of apicoplast replication. Interestingly, the drastic impact observed on midgut sporozoites was diminished at the salivary gland phase. A possible explanation for this discrepancy could be in part attributable to a linear relationship model in which the number of *P. berghei* salivary gland sporozoite per individual *An. stephensi* mosquito linearly related to the number of oocysts per mosquito [40]. Although it describes better at low oocyst numbers (less than 50 per mosquito), according to this model, 45% reduction in oocyst number corresponds to 45% reduction in salivary gland sporozoites, matching well with the pattern observed in the present study. Therefore, the observed change in the reduction rate of parasite number may not be relevant to prolonged impairment of apicoplast replication, but a consequence of the density-dependent transition during late life-stage in the mosquito.

It has been reported that AZM has schizontocidal activity against *P. falciparum* [20], *Plasmodium vivax* [23] and *P. berghei* [19], implying that AZM may reduce transmission, to some extent, by killing progenitor cells of gametocytes. Although available reports on gametocytocidal effect of AZM against human malaria are limited, AZM has been reported to have a small impact on reducing *P. vivax* gametocytes [41], but almost no impact on *P. falciparum* gametocytaemia [42]. The latter case is consistent with the observation that *P. falciparum* gametocytes are resistant to most schizontocidal drugs [27]. In terms of gametocyte reducing activity, the impact of AZM on *P. berghei* gametocytaemia would be similar to that on *P. falciparum*, rather than *P. vivax*. In the present study, we focused on the activity of AZM against mosquito stages of *P. berghei*, and demonstrated that AZM reduces sporozoite burden in salivary glands, independently of its gametocytocidal effect. Coleman *et al* reported that several compounds which had shown transmission-blocking activity against *P. berghei* were also effective against both *P. falciparum* and *P. vivax* [5,12], suggesting that *P. berghei* model would be useful for screening of candidate compounds for a transmission-blocking drug for human malaria. Taken together, AZM would be promising for suppressing mosquito stage development of *P. falciparum* and *P. vivax*, and would deserve further study.

In the present study, AZM treatment resulted in 79% and 50% reduction in sporozoites in the midgut and salivary glands, respectively, whereas prevalence of mosquitoes was not affected. Considering that inocula of only 10 sporozoites in wide range of *Plasmodium* spp. can be infectious to their vertebral hosts, the prevalence rather than the infection intensity of mosquitoes would be a suitable parameter for evaluating any transmission-blocking strategy [40]. However, it has been proposed by Medley *et al* [43] that the impact of transmission-blocking substances appears mainly on reduction in infection intensity, but not on that of prevalence under conditions of high oocyst intensities, whereas a rapid reduction in prevalence occurs under conditions of low oocyst intensities. The authors claim that their data derived from several *Plasmodium* spp. including *P. falciparum* and *P. vivax*, may afford broad applicability. Their observations have been supported by Sinden *et al* [40], who reported a saturating relationship between mean oocyst numbers and mean salivary gland sporozoite numbers, implying that the impact of 50% reduction in oocyst number becomes evident in reduction of salivary gland sporozoite when oocyst burden is low (less than 50 oocysts per mosquito). Furthermore, the authors also demonstrated that a 90% blockade in oocyst numbers gives no effect on prevalence of infected mosquitoes when mean oocyst numbers are high (more than 100), whereas significant reduction in prevalence is expected when oocyst load is very low (less than 10). Taking these information into account, the inhibitory effect of AZM on *P. berghei* development in the mosquito observed under conditions of high parasite load may allow to speculate that AZM would reduce both infection intensity and prevalence of the mosquitoes that fed blood from individuals carrying gametocytes of human malaria parasites under field conditions where parasite loads of *P. falciparum* or *P. vivax* are significantly lower than those in this study [44-46]. In order to examine that possibility, further studies on transmission blocking effect of AZM on *P. berghei* under conditions of low parasite loads are underway.

The dose of AZM administered to mice in this study (400 mg/kg) was much higher than those used for human clinical practice (10-40 mg/kg) [17,19,35,47]. It has been reported that there are significant interspecies difference in pharmacokinetic parameters of AZM between mice and human [48-50]. The dose and peak concentration of AZM required for efficacy in murine models are considerably greater than those in human due to the higher rate of AZM clearance in mice (*e.g.* much shorter half-life and greater clearance rate in mice than in human) [48-50]. Therefore, the results obtained by the murine model in this study do not suggest that administration of 400 mg/kg of AZM would be necessary for suppression of the mosquito stage development of human malaria parasites.

The precise mechanism of the effect of AZM on apicoplast replication has not been fully elucidated. Sidhu *et al* [15] reported an intensive study using selected AZM-resistant *P. falciparum* and proposed that the anti-malarial properties of AZM are a result of its

binding to the apicoplast 50 S ribosomal subunit and inhibiting protein synthesis in this organelle. Therefore, it will be necessary to investigate the inhibitory effect of AZM on the mosquito-stage development in genetically modified *P. berghei* that have various mutations in the genes coding for apicoplast ribosomal proteins. If binding of AZM to the apicoplast ribosomal protein leads to inhibition of both apicoplast replication and sporogony in the mosquito, it could be confirmed that the apicoplast is the target of AZM.

Inhibitory mechanism of AZM on gametocyte-ookinete transformation could not be explained by the suppression of apicoplast replication, because apicoplast does not replicate at this phase. A possible explanation would be that AZM may block the fatty acid synthesis pathway within the apicoplast, causing the parasite to run out of material necessary for the drastic membrane biogenesis and reorganisation to form machinery for motility and invasion, during gametocyte-ookinete transformation [33].

Conclusions

It is a new finding that AZM reduces *Plasmodium* sporozoite production in the mosquito, the mechanism of which would not depend on gametocytocidal effect, but be caused by suppression of apicoplast replication and an uncharacterised effect on gametocyte-ookinete transformation. In conclusion, clear advantages of AZM include; 1) a unique feature of multi-targeting at blood stage (treatment), liver stage (prophylaxis), and mosquito stage (transmission blocking), possibly by a common mechanism of action including the inhibition of apicoplast replication, and 2) an excellent safety profile that allows AZM to be given to children and pregnant women. Both of these advantages would warrant further investigations of AZM, especially on its prevalence-reducing efficacy under conditions of low parasite loads. Thereafter, AZM would be tested for the substantial transmission-blocking activity against human malaria parasites, in the expectation of a new drug which would be effective in reducing malaria morbidity and mortality and inhibit the spread of drug-resistant parasites in malaria endemic areas.

Additional file 1: Primer sets for *Plasmodium berghei* organelle-specific genes
Click here for file
[http://www.biomedcentral.com/content/supplementary/1475-2875-9-73-S1.DOC]

Acknowledgements
We wish to express our thanks to Prof. Motomi Torii, Department of Molecular Parasitology, Ehime University Graduate School of Medicine, Ehime, Japan, for kind advice regarding the maintenance of mosquito colonies. This work was supported by a Grant-in-Aid for Challenging Exploratory Research from Japan Society for the Promotion of Science (No. 20659065 to MA) and a Grant-in-Aid for the Promotion of Occupational Health for the Post Graduate Student of the University of Occupational and Environmental Health, Japan (to SS). We also acknowledge technical assistance by Ms. Masumi Shioda.

Author details
[1]Department of Immunology and Parasitology, University of Occupational and Environmental Health, Japan, 1-1 Iseigaoka, Yahatanishi-ku, Kitakyushu 807-8555, Japan. [2]First Department of Internal Medicine, University of Occupational and Environmental Health, Japan, 1-1 Iseigaoka, Yahatanishi-ku, Kitakyushu 807-8555, Japan. [3]Department of International Medical Zoology, Faculty of Medicine, Kagawa University, 1750-1 Ikenobe, Miki-cho, Kita-gun, Kagawa 761-0793, Japan.

Authors' contributions
SS and MA conceived and designed the experiments. SS and YO performed the experiments. SS, YO, TK, and YT analysed the data. SS and MA wrote the paper. All authors read and approved the final manuscript.

Competing interests
The authors declare that they have no competing interests.

Received: 18 December 2009 Accepted: 10 March 2010
Published: 10 March 2010

References

1. Aregawi M, Cibulskis R, Otten M, Williams R, Dye C: *World Malaria Report 2008* World Health Organization, Geneva 2008.
2. Carter R, Mendis KN, Miller LH, Molineaux L, Saul A: **Malaria transmission-blocking vaccines–how can their development be supported?** *Nat Med* 2000, **6**:241-244.
3. Kaslow DC: **Transmission-blocking vaccines: Uses and current status of development.** *Int J Parasitol* 1997, **27**:183-189.
4. Bucher GA: **Antimalarial drugs and the mosquito transmission of *Plasmodium*.** *Int J Parasitol* 1997, **27**:975-987.
5. Coleman RE, Nath AK, Schneider I, Song GH, Klein TA, Milhous WK: **Prevention of sporogony of *Plasmodium falciparum* and *P. berghei* in *Anopheles stephensi* mosquitoes by transmission-blocking antimalarials.** *Am J Trop Med Hyg* 1994, **50**:646-653.
6. De Martin S, von Seidlein L, Deen JL, Pinder M, Walraven G, Greenwood BM: **Community perceptions of a mass administration of an antimalarial drug combination in The Gambia.** *Trop Med Int Health* 2001, **6**:442-448.
7. von Seidlein L, Greenwood BM: **Mass drug administration of antimalarial drugs.** *Trends Parasitol* 2003, **10**:452-460.
8. White NJ: **The role of anti-malarial drugs in eliminating malaria.** *Malar J* 2008, **7(Suppl 1)**:S8.
9. Doi H, Kaneko A, Panjaitan W, Ishii A: **Chemotherapeutic malaria control operation by single dose or Fansidar plus primaquine in North Sumatra, Indonesia.** *Southeast Asian J Trop Med Public Health* 1989, **20**:341-349.
10. Kaneko A, Taleo G, Kalkoa M, Yamar S, Kobayakawa T, Björkman A: **Malaria eradication on islands.** *Lancet* 2000, **356**:1560-1564.
11. Chotivanich K, Sattabongkot J, Udomsangpetch R, Looareesuwan S, Day NPJ, Coleman RE, White NJ: **Transmission-blocking activities of quinine, primaquine, and artesunate.** *Antimicrob Agents Chemother* 2006, **50**:1927-1930.
12. Coleman RE, Polsa N, Eikarat N, Kollars TM Jr, Sattabongkot J: **Prevention of sporogony of *Plasmodium vivax* in *Anopheles dirus* mosquitoes by transmission-blocking antimalarials.** *Am J Trop Med Hyg* 2001, **65**:214-218.
13. Pukrittayakamee S, Chotivanich K, Chantra A, Clemens R, Looareesuwan S, White NJ: **Activities of artesunate and primaquine against asexual- and sexual-stage parasites in falciparum malaria.** *Antimicrob Agents Chemother* 2004, **48**:1329-1334.
14. Arai M, Alavi YIH, Mendoza J, Billker O, Sinden RE: **Isonicotinic acid hydrazide: an anti-tuberculosis drug inhibits malarial transmission in the mosquito gut.** *Exp Parasitol* 2004, **106**:30-36.
15. Sidhu AB, Sun Q, Nkrumah LJ, Dunne MW, Sacchettini JC, Fidock DA: ***In vitro* efficacy, resistance selection, and structural modeling studies implicate the malarial parasite apicoplast as the target of azithromycin.** *J Biol Chem* 2007, **282**:2494-2504.

16. Sarkar M, Woodland C, Koren G, Einarson AR: **Pregnancy outcome following gestational exposure to azithromycin.** *BMC Pregnancy Childbirth* 2006, **6**:18.
17. Treadway G, Pontani D: **Paediatric safety of azithromycin: worldwide experience.** *J Antimicrob Chemother* 1996, **37(Suppl C)**:143-149.
18. Andersen SL, Ager AL, McGreevy P, Schuster BG, Ellis W, Berman J: **Efficacy of azithromycin as a causal prophylactic agent against murine malaria.** *Antimicrob Agents Chemother* 1994, **38**:1862-1863.
19. Gingras BA, Jensen JB: **Antimalarial activity of azithromycin and erythromycin against *Plasmodium berghei*.** *Am J Trop Med Hyg* 1993, **49**:101-105.
20. Noedl H, Krudsood S, Leowattana W, Tangpukdee N, Thanachartwet W, Looareesuwan S, Miller RS, Fukuda M, Jongsakul K, Yingyuen K, Sriwichai S, Ohrt C, Knirsch C: **In vitro antimalarial activity of azithromycin, artesunate, and quinine in combination and correlation with clinical outcome.** *Antimicrob Agents Chemother* 2007, **51**:651-656.
21. Chico RM, Pittrof R, Greenwood B, Chandramohan D: **Azithromycin-chloroquine and the intermittent preventive treatment of malaria in pregnancy.** *Malar J* 2008, **7**:255.
22. Noedl H, Krudsood S, Chalermratana K, Silachamroon U, Leowattana W, Tangpukdee N, Looareesuwan S, Miller RS, Fukuda M, Jongsakul K, Sriwichai S, Rowan J, Bhattacharyya H, Ohrt C, Knirsch C: **Azithromycin combination therapy with artesunate or quinine for the treatment of uncomplicated *Plasmodium falciparum* malaria in adults: a randomized, phase 2 clinical trial in Thailand.** *Clin Infect Dis* 2006, **43**:1264-1271.
23. Dunne MW, Singh N, Shukla M, Valecha N, Bhattacharyya PC, Patel K, Mohapatra MK, Lakhani J, Devi CU, Adak T, Dev V, Yadav RS, Lele C, Patki K: **A double-blind, randomized study of azithromycin compared to chloroquine for the treatment of *Plasmodium vivax* malaria in India.** *Am J Trop Med Hyg* 2005, **73**:1108-1111.
24. Dahl EL, Rosenthal PJ: **Multiple antibiotics exert delayed effects against the *Plasmodium falciparum* apicoplast.** *Antimicrob Agents Chemother* 2007, **51**:3485-3490.
25. **Methods in *Anopheles* Research Manual.** [http://www.mr4.org/AnophelesProgram/tabid/553/Default.aspx].
26. van Dijk MR, Janse CJ, Thompson J, Waters AP, Braks JA, Dodemont HJ, Stunnenberg HG, van Gemert GJ, Sauerwein RW, Eling W: **A central role for P48/45 in malaria parasite male gamete fertility.** *Cell* 2001, **104**:153-164.
27. Talman AM, Domarle O, McKenzie FE, Ariey F, Robert V: **Gametocytogenesis: the puberty of *Plasmodium falciparum*.** *Malar J* 2004, **3**:24.
28. Arai M, Billker O, Morris HR, Panico M, Delcroix M, Dixon D, Ley SV, Sinden RE: **Both mosquito-derived xanthurenic acid and a host blood-derived factor regulate gametogenesis of *Plasmodium* in the midgut of the mosquito.** *Mol Biochem Parasitol* 2001, **116**:17-24.
29. Vaidya AB, Mather MW: **Mitochondrial evolution and functions in malaria parasites.** *Annu Rev Microbiol* 2009, **63**:249-267.
30. **Primer-BLAST.** [http://www.ncbi.nlm.nih.gov/tools/primer-blast/].
31. Ramya TN, Mishra S, Karmodiya K, Surolia N, Surolia A: **Inhibitors of nonhousekeeping functions of the apicoplast defy delayed death in *Plasmodium falciparum*.** *Antimicrob Agents Chemother* 2007, **51**:307-316.
32. Ramya TN, Karmodiya K, Surolia A, Surolia N: **15-deoxyspergualin primarily targets the trafficking of apicoplast proteins in *Plasmodium falciparum*.** *J Biol Chem* 2007, **282**:6388-6397.
33. Stanway RR, Witt T, Zobiak B, Aepfelbacher M, Heussler VT: **GFP-targeting allows visualization of the apicoplast throughout the life cycle of live malaria parasites.** *Biol Cell* 2009, **101**:415-430.
34. Dunne MW, Singh N, Shukla M, Valecha N, Bhattacharyya PC, Dev V, Patel K, Mohapatra MK, Lakhani J, Benner R, Lele C, Patki K: **A multicenter study of azithromycin, alone and in combination with chloroquine, for the treatment of acute uncomplicated *Plasmodium falciparum* malaria in India.** *J Infect Dis* 2005, **191**:1582-1588.
35. Miller RS, Wongsrichanalai C, Buathong N, McDaniel P, Walsh DS, Knirsch C, Ohrt C: **Effective treatment of uncomplicated *Plasmodium falciparum* malaria with azithromycin-quinine combinations: a randomized, dose-ranging study.** *Am J Trop Med Hyg* 2006, **74**:401-406.
36. Creasey A, Mendis K, Carlton J, Williamson D, Wilson I, Carter R: **Maternal inheritance of extrachromosomal DNA in malaria parasites.** *Mol Biochem Parasitol* 1994, **65**:95-98.
37. Okamoto N, Spurck TP, Goodman CD, McFadden GI: **Apicoplast and mitochondrion in gametocytogenesis of *Plasmodium falciparum*.** *Eukaryot Cell* 2009, **8**:128-132.
38. van Dooren GG, Marti M, Tonkin CJ, Stimmler LM, Cowman AF, McFadden GI: **Development of the endoplasmic reticulum, mitochondrion and apicoplast during the asexual life cycle of *Plasmodium falciparum*.** *Mol Microbiol* 2006, **57**:405-419.
39. Landau I, Boulard Y: **Life cycles and morphology.** *Rodent Malaria* New York: Academic PressKillick-Kenckrick R, Peters W 1978, 53-84.
40. Sinden RE, Dawes EJ, Alavi Y, Waldock J, Finney O, Mendoza J, Butcher GA, Andrews L, Hill AV, Gilbert SC, Basanez MG: **Progression of *Plasmodium berghei* through *Anopheles stephensi* is density-dependent.** *PLoS Pathog* 2007, **3**:e195.
41. Pukrittayakamee S, Imwong M, Singhasivanon P, Stepniewska K, Day NJ, White NJ: **Effects of different antimalarial drugs on gametocyte carriage in *P. vivax* malaria.** *Am J Trop Med Hyg* 2008, **79**:378-384.
42. Rino BE, Van TT, Giovanni F, Franco M: **Azithromycin in the treatment of *Plasmodium falciparum* gametocytes: a preliminary observation.** *J Trop Pediatr* 2000, **46**:56.
43. Medley GF, Sinden RE, Fleck S, Billingsley PF, Tirawanchai N, Rodriguez MH: **Heterogeneity in patterns of malarial oocyst infections in the mosquito vector.** *Parasitology* 1993, **106**:441-449.
44. Awono-Ambene HP, Diawara L, Robert V: **Comparison of direct and membrane feeding methods to infect *Anopheles arabiensis* with *Plasmodium falciparum*.** *Am J Trop Med Hyg J* 2001, **64**:32-34.
45. Ouédraogo AL, Bousema T, Schneider P, de Vlas SJ, Ilboudo-Sanogo E, Cuzin-Ouattara N, Nébié I, Roeffen W, Verhave JP, Luty AJ, Sauerwein R: **Substantial contribution of submicroscopical *Plasmodium falciparum* gametocyte carriage to the infectious reservoir in an area of seasonal transmission.** *PLoS One* 2009, **4**:e8410.
46. Zollner GE, Ponsa N, Garman GW, Poudel S, Bell JA, Sattabongkot J, Coleman RE, Vaughan JA: **Population dynamics of sporogony for *Plasmodium vivax* parasites from western Thailand developing within three species of colonized *Anopheles* mosquitoes.** *Malar J* 2006, **5**:68.
47. Blasi F, Aliberti S, Tarsia P: **Clinical applications of azithromycin microspheres in respiratory tract infections.** *Int J Nanomedicine* 2007, **2**:551-559.
48. Girard AE, Girard D, English AR, Gootz TD, Cimochowski CR, Faiella JA, Haskell SL, Retsema JA: **Pharmacokinetic and *in vivo* studies with azithromycin (CP-62,993), a new macrolide with an extended half-life and excellent tissue distribution.** *Antimicrob Agents Chemother* 1987, **31**:1948-1954.
49. Luke DR, Foulds G, Cohen SF, Levy B: **Safety, toleration, and pharmacokinetics of intravenous azithromycin.** *Antimicrob Agents Chemother* 1996, **40**:2577-2581.
50. Girard D, Finegan SM, Dunne MW, Lame ME: **Enhanced efficacy of single-dose versus multi-dose azithromycin regimens in preclinical infection models.** *J Antimicrob Chemother* 2005, **56**:365-371.

doi:10.1186/1475-2875-9-73
Cite this article as: Shimizu *et al.*: Suppressive effect of azithromycin on *Plasmodium berghei* mosquito stage development and apicoplast replication. *Malaria Journal* 2010 **9**:73.

Khan et al. Parasites & Vectors 2010, 3:114
http://www.parasitesandvectors.com/content/3/1/114

Parasites & Vectors

SHORT REPORT Open Access

Evaluation of rK-39 strip test using urine for diagnosis of visceral leishmaniasis in an endemic area in Bangladesh

Md Gulam Musawwir Khan[1], Mohammad Shafiul Alam[1*], Milka Patracia Podder[2], Makoto Itoh[3], Kazi M Jamil[1], Rashidul Haque[1], Yukiko Wagatsuma[4]

Abstract

Diagnosis of visceral leishmaniasis (VL) by demonstration of parasites in tissue smears obtained from bone marrow, spleen or lymph nodes is risky, painful, and difficult. The rK-39 strip test is widely used for the diagnosis of VL using blood/serum samples in endemic countries. The aim of the study was to evaluate the rK-39 strip test using urine sample as a non-invasive means for the diagnosis of VL. The rk-39 strip test was performed using urine from 100 suspected VL cases along with 25 disease control (malarial febrile cases) and 50 healthy control (from endemic and non-endemic areas). All the VL suspected cases were positive with the rK-39 strip test using serum. The sensitivity and specificity of the rK-39 strip test using urine samples was 95% and 93.3%, respectively, compared to serum based rK-39 test. The findings suggest that the urine based rK-39 test could be a practical and efficient tool for the diagnosis of VL patients in rural areas, particularly where resources are limited.

Introduction

Visceral leishmaniasis (VL) is a serious public health problem in Bangladesh where 20 million people (18% of the total population) are at risk with a trend of rising incidence [1]. Diagnosis of VL still relies on clinical manifestations and microscopic confirmation of parasites from aspirates of lymph nodes, bone marrow, and the spleen. These invasive and painful techniques require skilled personnel and are difficult to implement in resource-limited settings. Several less-invasive serological tests, including indirect fluorescent antibody test (IFAT), enzyme-linked immunosorbent assay (ELISA), and an improved version of direct agglutination test (DAT) have been evaluated for the diagnosis of VL [2-4]. However, a rapid immune-chromatographic test (ICT) based on a recombinant 39-amino acid repeat antigen, conserved in the kinesin region of *Leishmania chagasi* and *Leishmania donovani* (rK-39 strip test), gained popularity for the field screening of kala-azar [5]. The detection of soluble antigen and antibody in urine of VL patients has been reported [6]. A urine-based ELISA method has also been developed to detect anti-*Leishmania donovani* immunoglobulin G (IgG) [7].

Recently, a low molecular weight, heat-stable, and carbohydrate based leishmanial antigen has also been detected in urine of VL patients [8]. A latex agglutination test (KAtex) based on antigen detection in urine of VL cases has been evaluated in different field studies; however, the test showed lower sensitivity in some studies [9,10]. So, the antibody detection tests especially DAT and rK-39 strip test, are still being extensively used in the field-screening of VL.

The study was conducted to determine the potential application of the rK-39 strip test for detecting anti-leishmanial antibody in urine for the preliminary diagnosis of VL infection compared with the serum-based rK-39 test to establish the value of the urine-based rapid test for the primary diagnosis of VL.

Study area and population

In total, 100 suspected VL patients, who were positive with the serum based rK-39 strip test and had fever for at least two weeks, along with other clinical signs [11], were enrolled in this study from Trishal Upazila (sub-

* Correspondence: shafiul@icddrb.org
[1]International Centre for Diarrhoeal Disease Research, Bangladesh (ICDDR,B), 68 Shaheed Tajuddin Ahmed Sharani, Mohakhali, Dhaka 1212, Bangladesh
Full list of author information is available at the end of the article

district) Health Complex (UHC) in Mymensingh district, which is one of the most endemic VL regions in Bangladesh. All the VL subjects were treated free of charge in the UHC as per the National Guideline and the WHO recommendations. To investigate cross-reaction with other diseases, twenty five (25) subjects with malaria were enrolled from a malaria-endemic area. To investigate subclinical infection, twenty five (25) healthy controls were enrolled who lived in the endemic area (Trishal) but did not have a past history of VL. Twenty five (25) healthy controls from non-endemic area were also enrolled for assessing the specificity of the urine rK-39 strip test. The serum rK-39 test was performed again in the field setting, a small laboratory in Trishal with that is near about 300 meters form UHC, whereas the urine rK-39 test was performed in the Parasitology Laboratory, ICDDR,B in Dhaka.

Ethical approval

The Ethical Review Committee (ERC) and Research Review Committee (RRC) of ICDDR,B approved the study.

Sample collection and methods

Finger- prick blood was taken in a capillary tube and transferred to a micro-tube (200 μm). Urine samples were also collected in a tube containing preservative (Na-azide) and stored at 4°C until transporting to the ICDDR,B. The blood sample was then centrifuged for separation of serum at the field laboratory (Trishal) where the rK-39 strip test (Kalaazar Detect™, InBios Inc., USA) was also performed as per the protocol of the manufacturer. Briefly, 1 drop of serum samples was applied to the base of nitro-cellulose strips impregnated with recombinant rK-39 antigen. After being air-dried, 3 drops of the test buffer (phosphate-buffered saline, plus bovine serum albumin) were added, and the strip was placed upright. The appearance of a lower red band (control) indicated the proper functioning of the test while the appearance of an upper red band indicated the presence of anti-rK-39 IgG, signifying a positive test. For urine assay, 3 drops of urine sample were applied directly to the strip without adding any test buffer. In both the cases the strip was observed after 10 minutes for the test band. A skilled laboratory technician performed the urine rK-39 strip test in the Parasitology Laboratory ICDDR,B who also monitored the serum rK-39 strip test at the field level.

Data analysis

Sensitivity and specificity were computed along with 95% confidence interval (CI) using the Epi Info software (version 6.02; CDC, Atlanta, GA, USA). Data were also analyzed by 2×2 contingency tables using the SPSS software (version 10.0) for Windows (release 10.0.1, standard version, 1999; SPSS Inc., Chicago, USA), which enabled us to calculate the kappa coefficient or κ value. Reproducibility was assessed between the field rK-39 serum test and the urine rK-39 test in laboratory settings followed by Landis Koch [12] based on κ value.

Results

The serum rK-39 strip test was positive in 100 enrolled VL subjects whereas all the healthy controls from the endemic area and non-endemic area and all the diseased controls (confirmed malaria subjects) were tested negative. The urine rK-39 strip test was positive in 95 out of the 100 VL subjects and in five out of 25 confirmed malaria patients who were tested negative in serum rK-39 strip test. However, the urine rK-39 was tested negative in all the healthy controls from the VL endemic and non-endemic areas. Thus, the sensitivity and specificity of urine rK-39 was found 95% (95% CI: 88.2-98.1) and 93.3% (95% CI: 84.5-97.5), respectively, considering the serum rK-39 test result as the gold standard (Table 1). Kappa coefficient (κ) for the urine rK-39 strip test was found 0.88.

Discussion

According to the national guideline for the treatment of VL in Bangladesh, suspected kala-azar cases must be confirmed by a positive rK-39 or demonstration of parasite in the tissue (bone marrow/splenic puncture) or by PCR [11]. The ICT based rK-39 antibody test has been used widely in Bangladesh for the diagnosis of VL because of its high sensitivity and specificity [5].

According to the instruction of the manufacturer, this test is performed using serum or plasma for which collection of venous blood or figure- prick is necessary. But our study showed an excellent sensitivity and specificity level for the rK-39 dipstick test using a non-invasive procedure, i.e. urine samples. The sensitivity of the urine rK-39 strip test observed in our study (95%) corroborates the results of the urine-based DAT (90.7%)

Table 1 Comparison of urine and Serum based rK-39 strip test in the diagnosis of clinically suspected VL

Patient type	Serum rK-39 test		Urine rK-39 test	
	+ve	-ve	+ve	-ve
No. of VL case	100	0	95	5
No. of Malaria	0	25	5	20
No. of Non endemic healthy control	0	25	0	25
No. of VL Endemic healthy control	0	25	0	25
Total	100	75	100	75

Urine rK-39 strip sensitivity: 95% (95% CI: 88.2-98.1); specificity: 93.3% (95% CI: 84.5-97.5); kappa (κ): 0.88

and urine ELISA (93.3%) [7]. The sensitivity and specificity of urine rK-39 in our study is within the acceptance level of the serum rK-39 strip test's sensitivity and specificity of specificity targeted (>90%) in the Indian subcontinent [13]. The urine-based rK-39 test has great advantages over the serum-based test because of ease of sample collection without causing any discomfort or pain to the subject. The non-invasive urine collection procedure minimizes the risk of blood-borne infections and facilitates the collection of samples from infants and children. Although, in our study a considerable number of positive test result with malaria (5/25) were noted in urine rK-39 test, but none was found in the healthy control subjects. We suspect this positive urine rK-39 strip test as false-positive as they were tested negative in the serum rk-39 test in the same malaria patient. This kind of false positivity might be raised due to the binding of unknown urinary components with the rK-39 antigen line in the test strip. According to Boelaert *et al.* [14], an ideal VL rapid diagnostic test should achieve a sensitivity level of ≥95% and a specificity level of ≥98% in both field and laboratory settings, and the test results should be interpreted in 30 minutes. The findings of our study showed that the non-invasive urine rK-39 strip test gave results in 10 minutes. The sensitivity of our test was satisfactory; however desired specificity was not achieved. The reproducibility of the urine rK-39 strip test was excellent (κ = 0.88) which corroborates with the reproducibility that had been assessed in a multi-centre evaluation of rK39 strip test with serum conducted in East Africa and the Indian subcontinent [13].

In our study the specificity has probably been overestimated because under real-life conditions there will be many malaria patients among the suspects to be tested. Moreover, half of the healthy controls were from a non-endemic area. The sensitivity may have been overestimated in our study because the comparison was based on rK-39 sero-positive subjects. Another limitation of the rK-39 test is its variable sensitivity and specificity reported in different studies [15-18]. To overcome these limitations, further investigations are required to assess the performance of the urine rK-39 test in a larger field condition with a larger population size, including parasitological confirmed VL subjects to confirm our data.

Conclusion

The urine rK-39 strip test would be a promising non-invasive *point-of-care* tool for the rapid screening of VL in remote rural areas where there is a high prevalence of VL. However, a large scale field evaluation of the urine rK-39 strip test is required before using it as a diagnostic tool for VL patients in different endemic areas. To the best of our knowledge, this is the first study on rK-39 strip test using urine samples.

Acknowledgements

The study was funded by the International Medical Cooperation of the Ministry of Health, Labor and Welfare, Japan (grant number: H19-21-kokui-shitei-015). ICDDR,B acknowledges with gratitude the commitment of the Ministry of Health, Labor and Welfare, Japan to its research efforts.
We are also grateful to Debashis Ghosh and Nazmul Huda for field sampling and AEM Rubayet Elahi and Sharmina Deloer for helping with the laboratory assays and Trishal UHC for providing facilities for subjects enrollment.

Author details

[1]International Centre for Diarrhoeal Disease Research, Bangladesh (ICDDR,B), 68 Shaheed Tajuddin Ahmed Sharani, Mohakhali, Dhaka 1212, Bangladesh. [2]Department of Zoology, University of Dhaka, Dhaka 1000, Bangladesh. [3]Department of Parasitology, Aichi Medical University School of Medicine, Nagakute, Aichi, Japan. [4]Department of Epidemiology, Graduate School of Comprehensive Human Sciences, University of Tsukuba, Ibaraki, Japan.

Authors' contributions

MGMK, MSA, MI, KMJ, RH, and YW have equally contributed in designing the study protocol. MSA was the PI of the project and was responsible for field set up and enrolling patients. MGMK, MSA, and MPP performed laboratory evaluation of the test. MGMK, MSA, and MPP drafted the manuscript. All authors edited, read, and approved the final manuscript.

Competing interests

The authors declare that they have no competing interests.

Received: 9 September 2010 Accepted: 26 November 2010
Published: 26 November 2010

References

1. Bern C, Chowdhury R: **The epidemiology of visceral leishmaniasis in Bangladesh: prospects for improved control.** *Indian J Med Res* 2006, **123**:275-288.
2. Choudhry A, Puri A, Guru PY, Saxena RP, Saxena KC: **An indirect fluorescent antibody (IFA) test for the serodiagnosis of Kala-Azar.** *J Commun Dis* 1992, **24**:32-36.
3. Zijlstra EE, Daifalla NS, Kager PA, Khalil EA, El-Hassan AM, Reed SG, Ghalib HW: **rK39 enzyme-linked immunosorbent assay for diagnosis of *Leishmania donovani* infection.** *Clin Diagn Lab Immunol* 1998, **5**:717-720.
4. Meredith SE, Kroon NC, Sondorp E, Seaman J, Goris MG, van Ingen CW, Oosting H, Schoone GJ, Terpstra WJ, Oskam L: **Leish-KIT, a stable direct agglutination test based on freeze-dried antigen for serodiagnosis of visceral leishmaniasis.** *J Clin Microbiol* 1995, **33**:1742-1745.
5. Sundar S, Reed SG, Singh VP, Kumar PC, Murray HW: **Rapid accurate field diagnosis of Indian visceral leishmaniasis.** *Lancet* 1998, **351**:563-565.
6. Kohanteb J, Ardehali SM, Rezai HR: **Detection of *Leishmania donovani* soluble antigen and antibody in the urine of visceral leishmaniasis patients.** *Trans R Soc Trop Med Hyg* 1987, **81**:578-580.
7. Islam MZ, Itoh M, Shamsuzzaman SM, Mirza R, Matin F, Ahmed I, Shamsuzzaman Choudhury AK, Hossain MA, Qiu XG, Begam N, *et al*: **Diagnosis of visceral leishmaniasis by enzyme-linked immunosorbent assay using urine samples.** *Clin Diagn Lab Immunol* 2002, **9**:789-794.
8. Sarkari B, Chance M, Hommel M: **Antigenuria in visceral leishmaniasis: detection and partial characterisation of a carbohydrate antigen.** *Acta Trop* 2002, **82**:339-348.
9. Attar ZJ, Chance ML, el-Safi S, Carney J, Azazy A, El-Hadi M, Dourado C, Hommel M: **Latex agglutination test for the detection of urinary antigens in visceral leishmaniasis.** *Acta Trop* 2001, **78**:11-16.
10. Rijal S, Boelaert M, Regmi S, Karki BM, Jacquet D, Singh R, Chance ML, Chappuis F, Hommel M, Desjeux P, *et al*: **Evaluation of a urinary antigen-based latex agglutination test in the diagnosis of kala-azar in eastern Nepal.** *Trop Med Int Health* 2004, **9**:724-729.
11. **National Guideline and Training Module for Kala azar Elimination in Bangladesh. Directorate General of Health Services, Ministry of Health and Family Welfare, Government of Bangladesh.** 2008, 1-119.

12. Landis JR, Koch GG: **The measurement of observer agreement for categorical data.** *Biometrics* 1977, **33**:159-174.
13. Boelaert M, El-Safi S, Hailu A, Mukhtar M, Rijal S, Sundar S, Wasunna M, Aseffa A, Mbui J, Menten J, *et al*: **Diagnostic tests for kala-azar: a multi-centre study of the freeze-dried DAT, rK39 strip test and KAtex in East Africa and the Indian subcontinent.** *Trans R Soc Trop Med Hyg* 2008, **102**:32-40.
14. Boelaert M, Bhattacharya S, Chappuis F, El-Safi S, Hailu A, Mondal D, Rijal S, Sundar S, Wasunna M, Peeling RW: **Evaluation of rapid diagnostic tests: visceral leishmaniasis.** *Nature Reviews Microbiology* 2007, **5**:S30-S39.
15. Mandal J, Khurana S, Dubey ML, Bhatia P, Varma N, Malla N: **Evaluation of direct agglutination test, rk39 Test, and ELISA for the diagnosis of visceral leishmaniasis.** *Am J Trop Med Hyg* 2008, **79**:76-78.
16. Boelaert M, Rijal S, Regmi S, Singh R, Karki B, Jacquet D, Chappuis F, Campino L, Desjeux P, Le Ray D, *et al*: **A comparative study of the effectiveness of diagnostic tests for visceral leishmaniasis.** *Am J Trop Med Hyg* 2004, **70**:72-77.
17. Singh S, Kumari V, Singh N: **Predicting kala-azar disease manifestations in asymptomatic patients with latent *Leishmania donovani* infection by detection of antibody against recombinant K39 antigen.** *Clin Diagn Lab Immunol* 2002, **9**:568-572.
18. Veeken H, Ritmeijer K, Seaman J, Davidson R: **Comparison of an rK39 dipstick rapid test with direct agglutination test and splenic aspiration for the diagnosis of kala-azar in Sudan.** *Trop Med Int Health* 2003, **8**:164-167.

doi:10.1186/1756-3305-3-114
Cite this article as: Khan *et al.*: Evaluation of rK-39 strip test using urine for diagnosis of visceral leishmaniasis in an endemic area in Bangladesh. *Parasites & Vectors* 2010 **3**:114.

International Immunology, Vol. 22, No. 3, pp. 157–166
doi:10.1093/intimm/dxp122
Advance Access publication 3 February 2010

IFN-γ is a master regulator of endotoxin shock syndrome in mice primed with heat-killed *Propionibacterium acnes*

Kosuke Kawa[1,2,*], Hiroko Tsutsui[3,*], Ryosuke Uchiyama[3], Junko Kato[3], Kiyoshi Matsui[1], Yoichiro Iwakura[4], Takayuki Matsumoto[1] and **Kenji Nakanishi[2,5]**

[1]Department of Internal Medicine, [2]Department of Immunology and Medical Zoology and
[3]Department of Microbiology, Hyogo College of Medicine, Nishinomiya, Hyogo 663-8501, Japan
[4]Center for Experimental Medicine, Institute of Medical Science, University of Tokyo, Tokyo 108-8639, Japan
[5]Collaborative Development of Innovation Seeds, Japan Science and Technology Corporation, Tokyo 102-8666, Japan

*These authors contributed equally to this study.

Correspondence to: K. Nakanishi; E-mail: nakaken@hyo-med.ac.jp

Transmitting editor: T. Watanabe

Received 5 November 2009, *accepted* 1 December 2009

Abstract

Hyper-coagulation, hypothermia, systemic inflammatory responses and shock are major clinical manifestations of endotoxin shock syndrome in human. As previously reported, mice primed with heat-killed *Propionibacterium acnes* are highly susceptible to the action of LPS to induce tumour necrosis factor (TNF)-α and to that of TNF-α to trigger lethal shock. Here we investigated the mechanisms underlying the *P. acnes*-induced sensitization to LPS and TNF-α and the development of individual symptoms after subsequent challenge with LPS or TNF-α. *Propionibacterium acnes*-primed wild-type (WT) mice, but not naive mice, exhibited hyper-coagulation with elevated levels of thrombin–antithrombin complexes and anti-fibrinolytic plasminogen activator inhibitor 1 in their plasma, hypothermia, systemic inflammatory responses and high mortality rate after LPS or TNF-α challenge. *Propionibacterium acnes* treatment reportedly induces both T_h1 and T_h17 cell development. *Propionibacterium acnes*-primed *Il12p40*$^{-/-}$ and *Ifnγ*$^{-/-}$ mice, while not *Il17A*$^{-/-}$ mice, evaded all these symptoms/signs upon LPS or TNF-α challenge, indicating essential requirement of IL-12–IFN-γ axis for the sensitization to LPS and TNF-α. Furthermore, IFN-γ blockade just before LPS challenge could prevent *P. acnes*-primed WT mice from endotoxin shock syndrome. These results demonstrated requirement of IFN-γ to the development of endotoxin shock and suggested it as a potent therapeutic target for the treatment of septic shock.

Keywords: hyper-coagulation, hypothermia, sepsis, T_h1 cells, TNF-α

Introduction

Disseminated intravascular coagulation (DIC), a status of hyper-coagulation, is commonly associated with septic shock syndrome (1, 2), in which tumour necrosis factor (TNF)-α produced by innate immune cells stimulated with pathogen-associated molecular pattern (PAMP) plays a critical role. Intravenous injection of recombinant human TNF-α activates coagulation system in healthy human and baboon, which is monitored by the elevation of plasma levels of thrombin–antithrombin complexes (TAT) (3, 4). Furthermore, this treatment increases levels of plasminogen activator inhibitor 1 (PAI-1), which promotes a procoagulant status by inhibiting the action of tissue-type plasminogen activator (tPA) to convert plasminogen into fibrinolytic plasmin (3–5). Thus, the balance between PAI-1 and tPA regulates coagulation, and induction of PAI-1 is crucial for the development of prothrombotic state by diminishing plasmin-dependent fibrinolysis. Indeed, plasma PAI-1 levels have been reported to correlate well with the disease severity of septic shock patients with DIC (6–8). We and other investigators reported that formation of intestinal adhesion is also regulated by the balance between PAI-1 and tPA (9, 10). We recently found that the PAI-1 induction is up-regulated by the action of IFN-γ from intestinal NKT cells in post-operative adhesion formation (10). Furthermore, IFN-γ from T_h1 cells was reported to be essential for the formation

of peritonitis-induced intestinal adhesion (11). Thus, it is important to determine whether and how IFN-γ triggers and/or modulates the action of TNF-α to induce hyper-coagulation and other symptoms (12, 13) and high mortality as well (14).

As previously reported, priming with heat-killed *Propionibacterium acnes* (*P. acnes*) renders mice highly susceptible to the lethal effects of LPS (15–17). *Propionibacterium acnes*-primed mice, when challenged with a sub-lethal dose of LPS, develop endotoxin shock syndrome accompanied by high elevation of serum pro-inflammatory cytokines (15, 17, 18). In contrast, *P. acnes*-primed *Il12p40*$^{-/-}$ mice completely escape from such LPS hyper-responsiveness (19). This strongly suggests the importance of IL-12 and/or IL-23 for *P. acnes* priming, as IL-12p40 is their common and essential subunit (20). Since IL-12 induces development of T_h1 cells and IL-23 activates of T_h17 cells (21), it is important to determine whether IL-12p40 contributes to the LPS sensitization, via induction of IFN-γ and/or IL-17.

Here, we showed that IFN-γ induces LPS sensitization and positively regulates the development of major symptoms induced by LPS challenge. Upon challenge with a sub-lethal dose of LPS, *P. acnes*-primed wild-type (WT) mice, but not naive mice, developed severe hypothermia, systemic inflammation and hyper-coagulation with elevation of plasma levels of TAT and PAI-1 and eventually died of shock. In contrast, *P. acnes*-primed *Ifnγ*$^{-/-}$ mice as well as *Il12p40*$^{-/-}$ mice evaded all these symptoms, indicating requirement of IL-12–IFN-γ axis for the LPS sensitization. Besides, *P. acnes*-primed *Ifnγ*$^{-/-}$ mice, contrasting to WT mice, evaded all the symptoms upon challenge with TNF-α, indicating that IFN-γ plays a central role in determining the sensitization to TNF-α as well. Finally we showed that administration of neutralizing anti-IFN-γ mAb at the time of LPS challenge could prevent *P. acnes*-primed WT mice from all the symptoms. These results clearly demonstrated that IFN-γ is a master regulator of endotoxin shock syndrome and suggested that IFN-γ might be a potential therapeutic target for the treatment of serious septic shock syndrome.

Methods

Mice

Ifnγ$^{-/-}$ mice on a BALB/c background (22) and *Il17A*$^{-/-}$ mice on a C57BL/6 (B6) background (23) were described elsewhere. *Il12p40*$^{-/-}$ B6 129 mice (24) were backcrossed with BALB/c mice, and F10 mice were used. BALB/c WT, BALB/c *nu/nu* and B6 WT mice were purchased from Clea Japan (Osaka, Japan). Female mice (8–12 weeks old) were used. All mice were maintained under specific pathogen-free conditions and received human care as outlined in the Guide for the Care and Use of Experimental Animals in Hyogo College of Medicine.

Reagents

LPS from *Escherichia coli* (O55: B5), which selectively activates Toll-like receptor 4 both *in vivo* and *in vitro* (25), were purchased from Sigma (St Louis, MO, USA). Heat-killed *P. acnes* was prepared as described elsewhere (26). Recombinant murine TNF-α was purchased from PeproTech (Rocky Hill, NJ, USA). Hybridoma producing neutralizing anti-IFN-γ mAb (R6A2) was purchased from American Type Culture Collection (ATCC, Livermore, CA). Neutralizing anti-IFN-γ mAb for *in vivo* treatment was prepared as shown previously (26). The culture medium was RPMI 1640 supplemented with 10% heat-inactivated fetal calf serum, 50 μM 2-ME, 2 mM L-glutamine, 100 U ml^{-1} penicillin and 100 μg ml^{-1} streptomycin.

Sequential administration of P. acnes and LPS or TNF-α

Mice were administered intra-peritoneally with heat-killed *P. acnes* (1 mg in 200 μl PBS). At day 5, mice were challenged with various doses of LPS or rTNF-α via a tail vein (26). In some experiments, *P. acnes*-primed mice were administered intra-peritoneally with various doses of anti-IFN-γ mAb 30 min before LPS challenge (27). At the indicated time points, plasma was sampled for measurement of concentrations of various pro-inflammatory cytokines, TAT and PAI-1 according to the method described by Sommeijer *et al.* (28). Briefly, anesthetized mice were administered with 180 μl of 3.2% (w/v) sodium citrate via the vena cava, and 10 s later, plasma was sampled through the same syringe. The rectal temperature was periodically monitored. Survival was monitored until 72 and 24 h after challenge with LPS and TNF-α, respectively. We killed all mice that appeared inactive and lost reactions to a supine position and counted them as dead ones.

Assay for TAT, PAI-1 and cytokines

An ELISA kit for PAI-1 was purchased from Innovative Research Inc. (Novi, MI, USA). ELISA kits for IFN-γ, TNF-α, IL-6 and IL-12p40 were from R&D (San Diego, CA, USA). HMGB-1 ELISA kits were from SinoTest (Sagamihara-shi, Japan). We measured TAT concentrations by a commercially available kit from Enzyme Research Laboratories (South Bend, IN, USA) according to the manufacturer's instruction.

Core body temperature

Rectal temperature readings were performed using a rectal probe digital thermometer (BAT-10; Physitemp, Clifton, NJ, USA). Difference in rectal temperature post and prior to the challenge was calculated and shown as ΔRectal temperature.

Responsiveness of splenocytes to LPS and TNF-α

Splenocytes (2×10^6 ml^{-1}) from variously treated mice with various genotypes were incubated with LPS or rTNF-α *in vitro*. Supernatants were collected for measurement of pro-inflammatory cytokines.

T-cell reconstitution

In total, 2×10^7 splenic T cells from naive WT BALB/c mice, enriched by a nylon wool column method (>90% CD3$^+$) (29), were transferred into naive BALB/c *nu/nu* mice through a tail vein for the T-cell reconstitution, and after 24 h, these T cell-reconstituted *nu/nu* mice were sequentially administered with *P. acnes* and challenged with LPS.

Statistics

All data are shown as the mean ± SD of samples in each experimental group. Five to 10 mice were used for each group. Significance between the experimental and control

groups was examined by the unpaired Student's *t*-test. *P*-values <0.05 were considered significant. Two to three experiments were separately performed, and representative data were shown in each data.

Results

In vivo sensitization to LPS by priming with heat-killed P. acnes

We administered heat-killed *P. acnes* into WT BALB/c mice and challenged them with LPS (2 or 20 μg per head) at day 5 after this pretreatment. Half of the *P. acnes*-primed mice died within 12 h after challenge with 2 μg LPS, while all died after challenge with 20 μg LPS (Fig. 1A), indicating that LPS kills the animals in a dose-dependent manner. In sharp contrast, none of naive mice succumbed to these LPS challenges (Fig. 1A). Thus, *P. acnes*-primed mice are highly susceptible to LPS.

Since hypothermia is an important clinical indicator of sepsis in human (2, 30, 31), we measured rectal temperature of *P. acnes*-primed mice after LPS challenge. Mice challenged with 2 μg LPS showed 9°C diminution at 6 h and gradually recovered thereafter (Fig. 1B). Mice challenged with 20 μg LPS exhibited 12°C reduction without any recovery. PBS treatment instead of LPS challenge did not affect body temperature or mortality rate of *P. acnes*-primed mice (Fig. 1A and B).

Elevation of TAT and PAI-1 after LPS challenge

Endotoxin occasionally induces DIC in septic patients (1), and DIC exacerbates septic shock (6–8). Thus, we measured plasma levels of TAT and PAI-1 in *P. acnes*-primed mice after challenge with 2 μg LPS. Plasma TAT levels were strikingly elevated in *P. acnes*-primed mice with a peak at 4 h after LPS challenge (Fig. 1C). In contrast, naive mice showed only limited elevation of plasma TAT levels (Fig. 1C). Plasma PAI-1 levels were also dramatically elevated in *P. acnes*-primed mice after LPS challenge. Compared with the kinetics of TAT induction, PAI-1 level remained at basal levels until 4 h and sharply increased at 8 h after LPS challenge (Fig. 1C). In contrast, plasma PAI-1 levels remained low in naive mice after LPS challenge (Fig. 1C). *P. acnes* priming alone only modestly increased plasma TAT and PAI-1 levels (Fig. 1C). PAI-1 and tPA mRNA expression

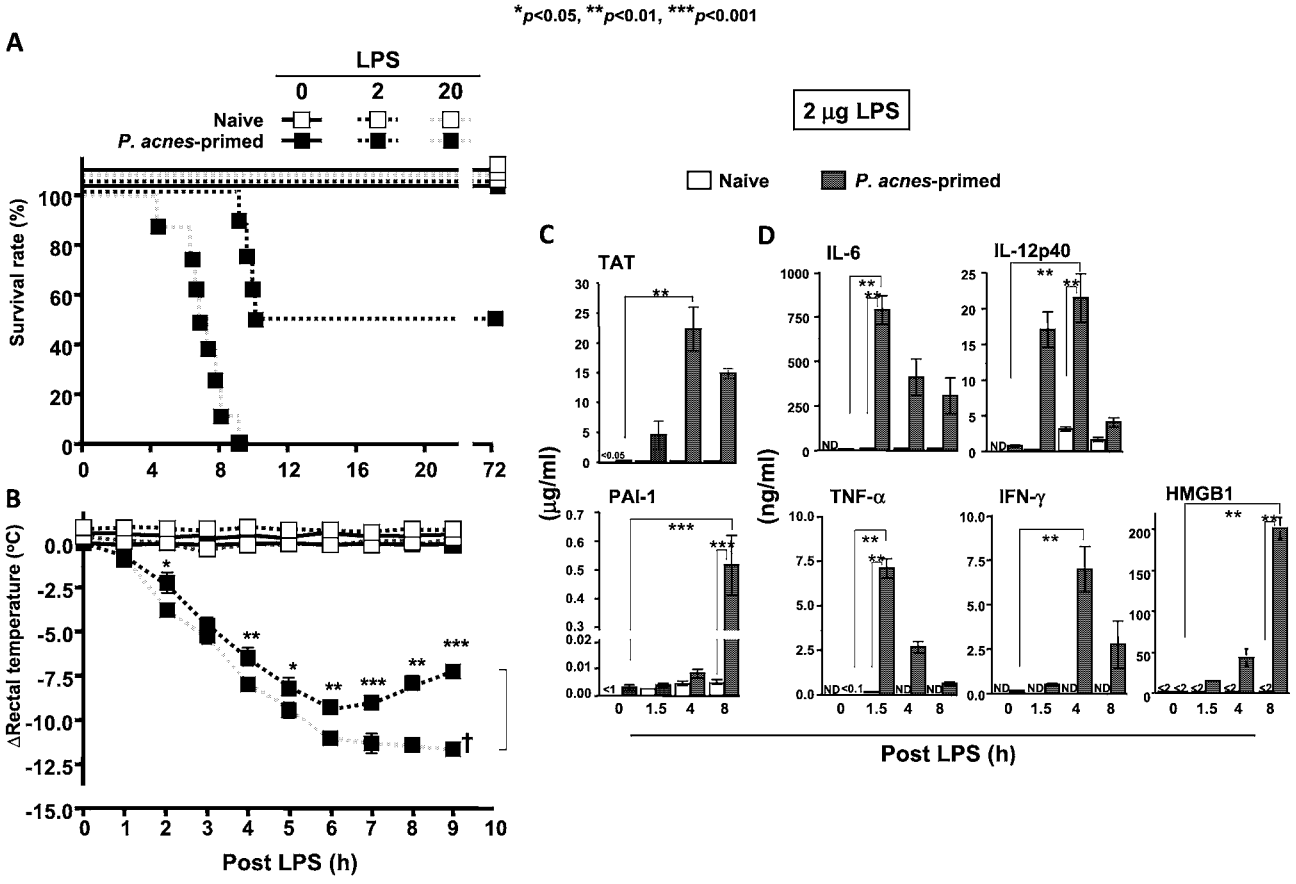

Fig. 1. Increase of the *in vivo* susceptibility to LPS by priming with heat-killed *Propionibacterium acnes*. WT BALB/c mice were administered with heat-killed *P. acnes*. *Propionibacterium acnes*-primed mice were challenged with 20 or 2 μg of LPS. Survival was monitored until 72 h (A). Rectal temperatures were measured, and difference of rectal temperatures at each time point to that before LPS challenge was shown (B). At various time points after LPS challenge, plasma was sampled for measurement of TAT and PAI-1 concentrations (C) and of IL-6, IL-12p40, TNF-α, IFN-γ and HMGB1 levels (D) by ELISA. A dagger indicates the time point at which all the mice die of shock.

levels increased strikingly (50-fold) and modestly (5.5-fold) in the liver of *P. acnes*-primed mice after LPS challenge, respectively (Supplementary Figure 1, available at *International Immunology* Online), suggesting that LPS induces hyper-coagulation status in *P. acnes*-primed mice by much higher induction of PAI-1 than that of tPA.

Induction of production of pro-inflammatory cytokines by LPS challenge

Propionibacterium acnes-primed mice, but not naive mice, promptly increased plasma levels of IL-6 and TNF-α after LPS challenge (Fig. 1D). They started to increase plasma level of IL-12p40 at 1.5 h, increased it further until 4 h and decreased it rapidly thereafter. We also noticed that they start to increase IFN-γ level at 4 h (Fig. 1D), prior to the increase of PAI-1 level (Fig. 1C). Since high-mobility group box protein 1 (HMGB1) is a potent cytokine that mediates severe sepsis at late stage (32–34), we measured plasma HMGB1 level. Like other pro-inflammatory cytokines, plasma HMGB1 level was dramatically elevated after LPS challenge in *P. acnes*-primed mice but not in naive mice (Fig. 1D).

Requirement of IL-12p40 for the LPS sensitization

Previously, we demonstrated that *P. acnes*-primed *Il12p40*$^{-/-}$ mice showed 100% survival after LPS challenge (19). Thus, we examined whether *P. acnes*-primed *Il12p40*$^{-/-}$ mice also evade other symptoms. None of *P. acnes*-primed *Il12p40*$^{-/-}$ mice died of endotoxin shock (Fig. 2A) and developed hypothermia (Fig. 2B) after challenge with 2 μg of LPS, which is 50% lethal dose for *P. acnes*-primed WT mice (Fig. 2A). Furthermore, the elevation of their plasma TAT and PAI-1 levels was very modest (Fig. 2C). This was also the case for TNF-α, IFN-γ or HMGB1 level in the plasma of *P. acnes*-primed *Il12p40*$^{-/-}$ mice at 8 h after LPS challenge (Fig. 2D). Taken together, these results indicated that *P. acnes*-primed *Il12p40*$^{-/-}$ mice are unresponsive to LPS and strongly suggested that IL-12p40 is necessary for the sensitization to LPS. To verify this possibility, we incubated splenocytes from naive or *P. acnes*-primed WT and *Il12p40*$^{-/-}$ mice with LPS and measured pro-inflammatory cytokine levels in their culture supernatants. Compared with those from naive WT mice, splenocytes from *P. acnes*-primed WT mice produced much larger amounts of TNF-α, IL-6 and IFN-γ upon LPS challenge

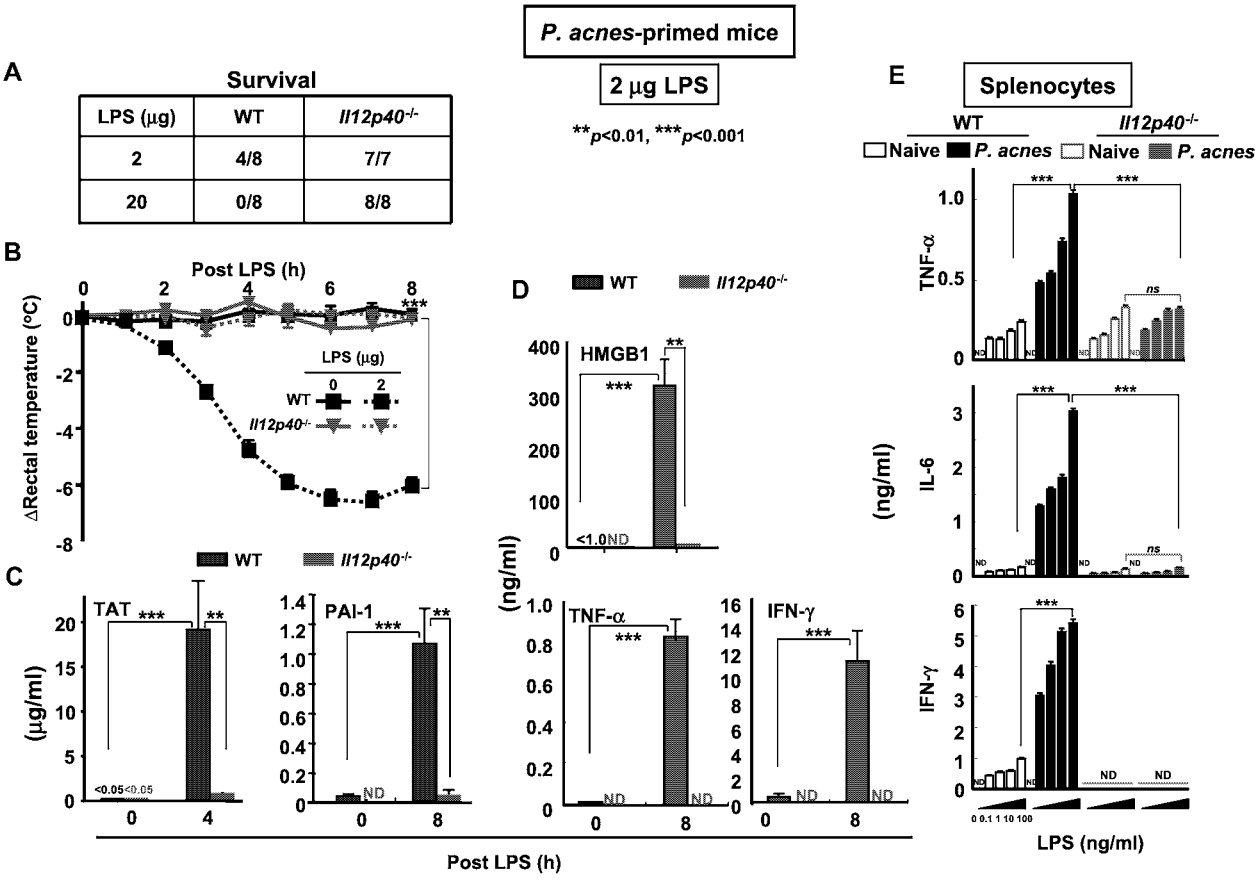

Fig. 2. Requirement of IL-12p40 for *Propionibacterium acnes*-induced LPS sensitization. *Propionibacterium acnes*-primed WT BALB/c mice or Il12p40$^{-/-}$ mice were challenged with 2 μg LPS. Survival rate (A) and rectal temperatures (B) were monitored until 72 and 8 h, respectively. At the indicated time point, plasma was sampled for measurement of TAT and PAI-1 (C) and pro-inflammatory cytokines (D). Splenocytes from naive or *P. acnes*-primed WT or *Il12p40*$^{-/-}$ mice were incubated with LPS *in vitro*, and TNF-α, IL-6 and IFN-γ concentrations in each supernatant were measured by ELISA. The data were shown as mean ± SD of those of splenocytes from four to five mice in each experimental group (E).

in vitro. In contrast, splenocytes from *P. acnes*-primed *Il12p40*$^{-/-}$ mice produced small amounts of these cytokines, like as those from naive WT or *Il12p40*$^{-/-}$ mice (Fig. 2E). These results taken together clearly indicated that IL-12p40 is essentially required for *P. acnes*-induced LPS sensitization.

Importance of T_h1 cells but not T_h17 cells for the LPS sensitization

Since *Il12p40*$^{-/-}$ mice failed to develop T_h1 cell (Supplementary Figure 2, available at *International Immunology* Online) and to become sensitized to LPS after treatment with *P. acnes* (Fig. 2A–E), we next investigated whether T cells are required for the sensitization to LPS. As *nu/nu* mice lack thymic T cells, we examined whether *P. acnes* priming is able to induce *nu/nu* mice to be susceptible to LPS. Expectedly, all *P. acnes*-primed *nu/nu* mice could survive after challenge with 20 μg of LPS that could 100% kill *P. acnes*-primed WT mice, suggesting that thymus-derived T cells are required for the *P. acnes*-induced sensitization to LPS (Fig. 3A). To verify this possibility, we transferred WT splenic T cells into *nu/nu* mice and sequentially treated them with *P. acnes* and 20 μg of LPS. All the *nu/nu* mice reconstituted with thymic T cells, like WT mice, became to succumb to the sequential treatment with *P. acnes* and 20 μg of LPS (Fig. 3B). Collectively, these results strongly suggested the importance of T cells for the *P. acnes*-induced sensitization to LPS.

IL-12p40 is a common and essential subunit of IL-12 and IL-23. As IL-23 can activate T_h17 cells and as *P. acnes*-primed mice reportedly possess T_h17 cells and T_h1 cells both specific for *P. acnes* (35), we examined possible contribution of IL-17 to the LPS sensitization. Upon LPS challenge, *P. acnes*-primed *Il17A*$^{-/-}$ mice showed survival rate and hypothermia comparable to those of WT mice (Fig. 3C and D). Thus, IL-17 is not profoundly involved in the sensitization to LPS.

IL-12 contributes to the sensitization to LPS through induction of IFN-γ

We next investigated whether T_h1 cytokine IFN-γ is essential for the LPS sensitization. Like *Il12p40*$^{-/-}$ mice (Fig. 2), *P. acnes*-primed *Ifnγ*$^{-/-}$ mice evaded the lethality, hypothermia, hyper-coagulation and systemic inflammation after LPS challenge (Fig. 4A and B). They failed to increase production of TAT, PAI-1, TNF-α and HMGB1 after sequential treatment with *P. acnes* and LPS (Fig. 4C and D). Furthermore, *P. acnes* treatment did not increase the responsiveness to LPS of *Ifnγ*$^{-/-}$ splenocytes, as illustrated by the failure of splenocytes from *P. acnes*-primed *Ifnγ*$^{-/-}$ mice to produce large amounts of TNF-α and IL-6 upon challenge with LPS *in vitro* (Fig. 4E). These results indicated requirement of IFN-γ for the LPS sensitization.

As IFN-γ was reported to be capable of sensitizing macrophages to LPS (36), we investigated whether IL-12, like IFN-γ, has the same capacity. To test this, we incubated bone marrow-derived macrophages from WT, *Il12p40*$^{-/-}$ or *Ifnγ*$^{-/-}$ mice with rIL-12 or rIFN-γ. Then, we stimulated them with LPS. We found that pretreatment with IFN-γ, but not IL-12, is able to enhance production of TNF-α and IL-6 from WT, *Il12p40*$^{-/-}$ or *Ifnγ*$^{-/-}$ macrophages upon LPS stimulation (Supplementary Figure 3, available at *International Immunology*

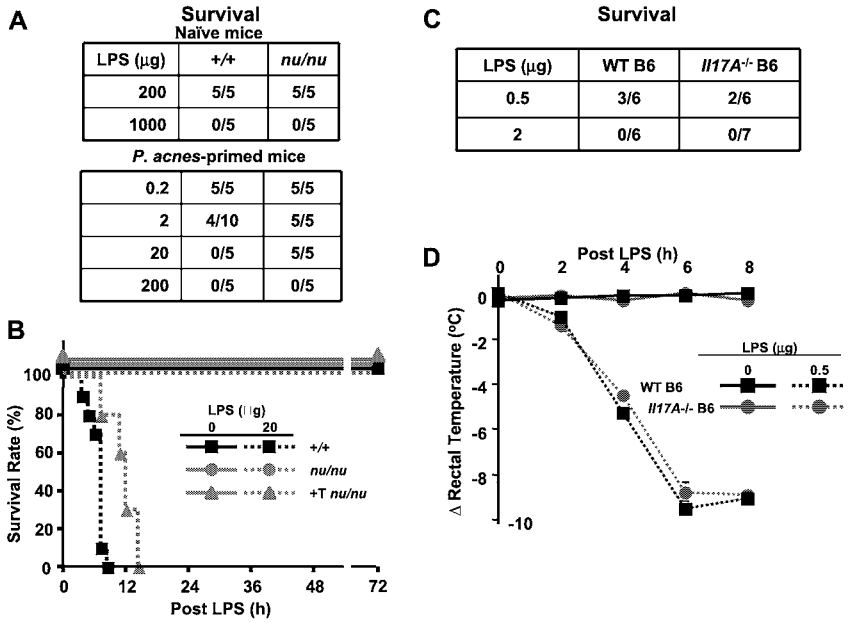

Fig. 3. Importance of T_h1 cells but not T_h17 cells for the LPS sensitization. Naive and *Propionibacterium acnes*-primed BALB/c WT (+/+) mice and nu/nu mice were administered with various doses of LPS, and mouse survival was monitored until 72 h (A). *nu/nu* mice reconstituted with T cells from WT mice were sequentially treated with *P. acnes* and 20 μg LPS (B). WT B6 mice (black symbols) and *Il17A*$^{-/-}$ B6 mice (blue symbols) were treated with *P. acnes* and subsequently challenged with LPS (C and D). The survival rate after 0.5 or 2 μg LPS (C) and body temperature reductions after challenge with 0.5 μg LPS (D) were monitored until 72 and 8 h, respectively.

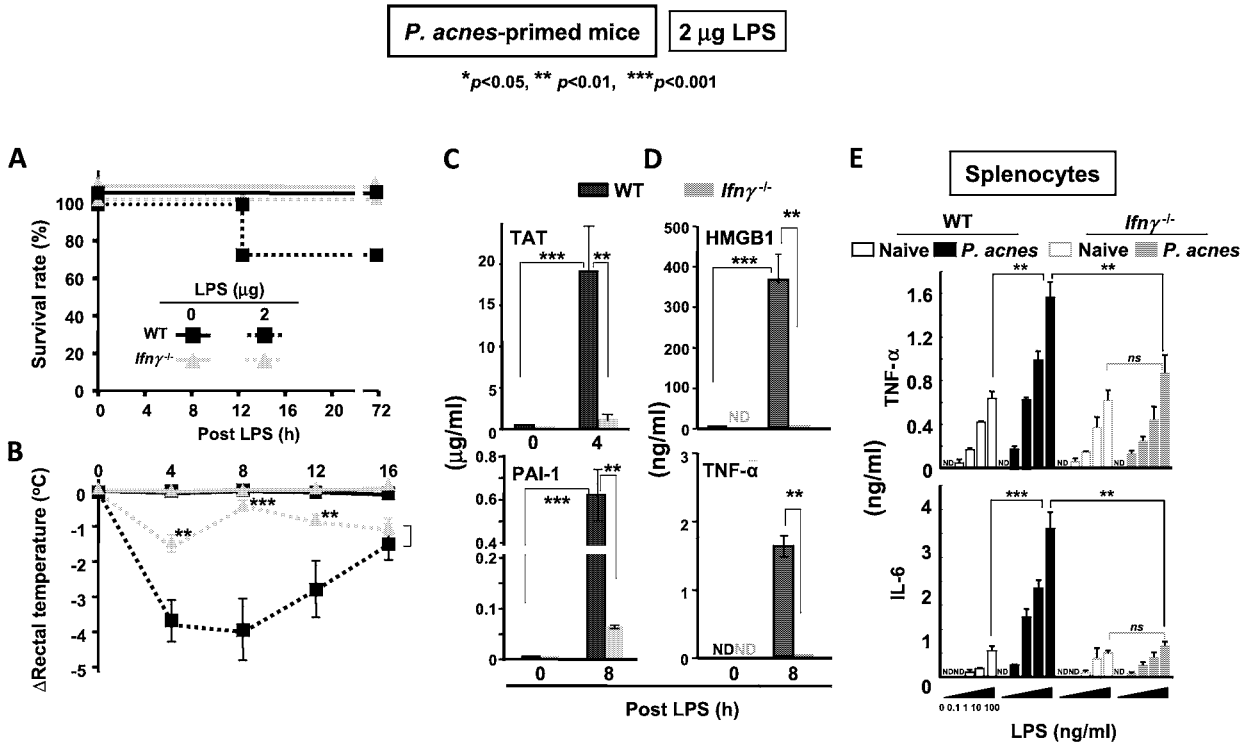

Fig. 4. *Propionibacterium acnes*-primed *Ifnγ*$^{-/-}$ mice were resistant to LPS. *Propionibacterium acnes*-primed WT mice (gray columns or symbols) and *Ifnγ*$^{-/-}$ mice (green columns or symbols) were administered intravenous with 2 μg LPS. Survival rates were monitored (A). Rectal temperatures were measured (B). Plasmas were sampled at 4 h post LPS for measurement of TAT (C), PAI-1(C), TNF-α (D) and HMGB1 (D). Splenocytes from naive or *P. acnes*-primed WT or *Ifnγ*$^{-/-}$ mice were incubated with various doses of LPS *in vitro*, and TNF-α and IL-6 concentrations in each supernatant were measured by ELISA. The data were shown as mean ± SD of those of splenocytes from four to five mice in each experimental group (E).

Online). Thus, IL-12 lacks the potential to directly sensitize macrophages to LPS either in the presence or in the absence of *Ifnγ*, while IFN-γ could fulfill the potential even in the absence of *Il12p40*. The results demonstrated prerequisite of IL-12-induced IFN-γ for the *P. acnes*-induced *in vivo* sensitization to LPS.

Requirement of IFN-γ for the sensitization to TNF-α

Since *P. acnes*-primed WT mice are susceptible to exogenous TNF-α (16), we next investigated whether IFN-γ is also critical for the sensitization to TNF-α. Consistent with our previous report (16), *P. acnes*-primed WT mice showed poor survival after treatment with a sub-lethal dose of TNF-α (Fig. 5A). Moreover, they developed all the symptoms observed in the *P. acnes*-primed mice with endotoxin shock syndrome (Fig. 5B–D), indicating that TNF-α is capable of replacing LPS in induction of each symptom. TNF-α blockade reportedly can protect against lethal outcome of *P. acnes*-primed mice after LPS challenge (37). This report together with our present results strongly suggested that TNF-α is a potent effector cytokine involved in the endotoxin shock syndrome. In sharp contrast, *P. acnes*-primed *Ifnγ*$^{-/-}$ mice were resistant to the lethal effects of TNF-α (Fig. 5A–D), indicating the importance of IFN-γ for the *in vivo* sensitization to TNF-α as well. Taken together, these results demonstrated a central role of IFN-γ in the development of the endotoxin shock syndromes via induction of *in vivo* sensitization to LPS and TNF-α.

IFN-γ also controls LPS challenge phase of endotoxin shock syndrome

We wanted to know whether IFN-γ is also necessary for the development of each symptom or sign during the excitation phase induced by LPS challenge. To test this, we administered neutralizing anti-IFN-γ mAb into *P. acnes*-primed WT mice at 30 min prior to challenge with 20 μg LPS. Neutralizing anti-IFN-γ mAb could rescue the lethal outcome and the serious hypothermia in a dose-dependent manner (Fig. 6A and B). Neutralizing anti-IFN-γ mAb also prevented the hyper-coagulation (Fig. 6C) and elevation of plasma levels of HMGB1 and TNF-α (Fig. 6D). Thus, IFN-γ is important for the development of each symptom during the excitation phase. Collectively, all the results demonstrated that IFN-γ is a master regulator of the endotoxin shock syndrome.

Discussion

Our present study demonstrated the importance of IL-12–IFN-γ axis for the development of endotoxin shock syndrome. In response to heat-killed *P. acnes*, macrophages and dendritic cells release IL-12, which induces and activates T_h1 cells (Supplementary Figure 2, available at

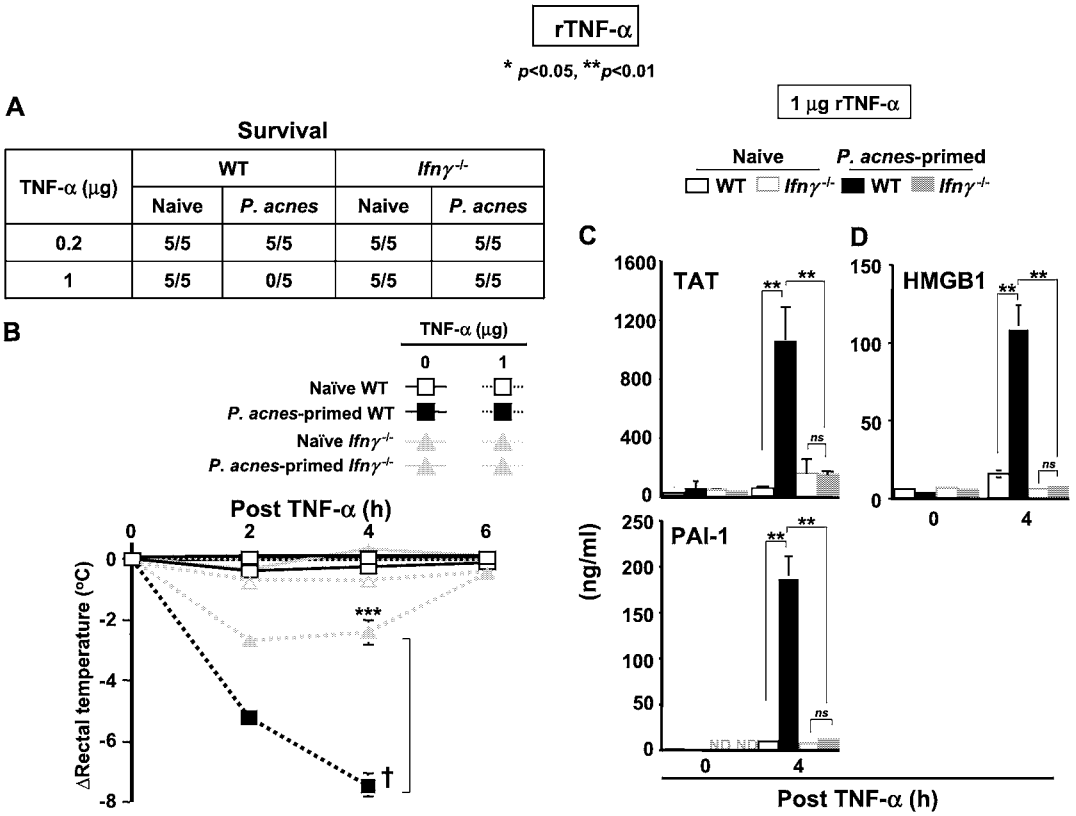

Fig. 5. Importance of IFN-γ for *in vivo* sensitization to TNF-α. *Propionibacterium acnes*-primed or naive WT mice and *Ifnγ*$^{-/-}$ mice were administered intravenous with 0.2 or 1 μg rTNF-α. Survival rates were monitored until 24 h after TNF-α challenge (A). Rectal temperatures were measured (B). Plasmas were sampled at 4 h for measurement of PAI-1 (C) and HMGB1 (D). A dagger indicates the time point at which all the mice die of shock.

International Immunology Online) to produce IFN-γ (38). Resultant IFN-γ prepares macrophages to be susceptible to LPS, which robustly induces TNF-α production (Fig. 7; Supplementary Figure 3, available at *International Immunology* Online). Furthermore, *P. acnes* pretreatment induces mice to be highly susceptible to TNF-α via induction of IFN-γ, which eventually results in their development of hypothermia, hyper-coagulation and lethal shock (Fig. 5). Thus, this IL-12–IFN-γ axis is critical for the *in vivo* sensitization to both LPS and TNF-α. After LPS challenge, IFN-γ-activated macrophages and perhaps dendritic cells produced large amounts of IL-12 and IL-18 (26), which synergistically activate T_h1 cells and NK cells to produce IFN-γ (39, 40) (Fig. 7). This IFN-γ positively regulates the development of lethal outcomes, hypothermia, systemic inflammation and hyper-coagulation by strongly increasing responsiveness to LPS and TNF-α and conceivably by synergistically cooperating with LPS and TNF-α (41) (Figs 6 and 7). Accordingly, IFN-γ is a central cytokine that initiates both the hypersensitization to LPS/TNF-α during *P. acnes* priming phase and the development of endotoxin shock syndrome after LPS challenge (Fig. 7).

This study does not exclude roles of NK cells as a cell source of IFN-γ during the priming and effector phases. However, we found that *P. acnes*-primed *nu/nu* mice are resistant to 20 μg of LPS, which kills 100% *P. acnes*-primed WT mice, and that reconstitution with WT T cells provided *nu/nu* mice with the capacity to develop LPS susceptibility after *P. acnes* treatment (Fig. 3A and B), indicating the importance of T_h1 cells for LPS sensitization. However, we also found that *P. acnes*-primed *nu/nu* mice died of endotoxin shock after challenge with high dose of LPS (200 μg per head) (Fig. 3A), suggesting possible contribution of NK cell production of IFN-γ to the LPS sensitization. Therefore, in the *nu/nu* mice NK cells might, at least partly, participate in the establishment of *P. acnes*-induced sensitization to LPS by production of IFN-γ in response to IL-12 and IL-18.

IL-18 is also a potent IFN-γ-inducing cytokine. However, in contrast to *Il12p40*$^{-/-}$ mice, *Il18*$^{-/-}$ mice shows normal susceptibility to the sequential treatment with *P. acnes* and LPS (19). This is partly due to the facts that IL-18 has little capability to induce T_h1 cell development (40) and that IL-18 does not affect IL-12 production (42). Thus, IL-12 is critically involved in the *P. acnes*-induced LPS sensitization via induction of production of IFN-γ principally from T_h1 cells.

Our present study revealed the importance of IFN-γ even during the excitation phase induced by LPS challenge. IFN-γ blockade 30 min prior to LPS challenge protected against all the endotoxin shock-associated alterations (Fig. 6). Several mechanistic possibilities might explain the involvement of IFN-γ in the development of TNF-α-mediated endotoxin

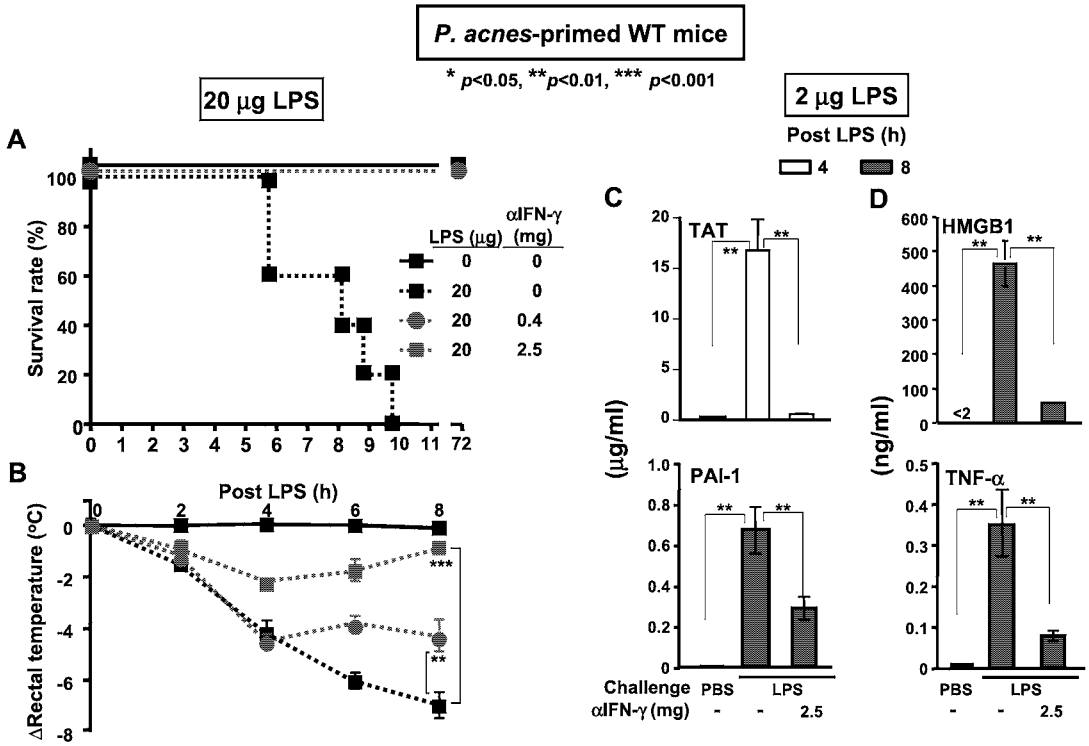

Fig. 6. IFN-γ profoundly controls endotoxin shock syndrome. *Propionibacterium acnes*-primed WT BALB/c mice were administered with various doses of neutralizing anti-IFN-γ 30 min prior to LPS challenge. Survival rate (A) and rectal temperature decrease (B) were monitored. At 4 h (open columns) or 8 h post LPS challenge, plasma was sampled for analysis of hyper-coagulation (TAT and PAI-1 concentrations) (C) and for measurement of HMGB1 and TNF-α concentrations (D).

shock syndrome. First, IFN-γ might modulate production of TNF-α after LPS challenge (Fig. 4E; Supplementary Figure 3, available at *International Immunology* Online). IFN-γ was reported to enhance TNF-α production induced by LPS (41). In fact, IFN-γ blockade significantly hampered plasma increase of TNF-α after LPS challenge (Fig. 6D). Second, although acting on the very late phase of *P. acnes* priming, this IFN-γ blockade may be able to desensitize the established sensitivity to LPS in *P. acnes*-primed WT mice. Third, IFN-γ and TNF-α might synergize for the development of each symptom. It is well established that IFN-γ and TNF-α synergize for production of various cytokines/chemokines, exemplified by IL-6 and CXCL10 (IP-10), via activating nuclear factors, such as STAT-1/IFN regulated factor 1 and NF-κB (41, 43). Likewise, the cooperative activation of these nuclear factors might control production of key factors involved in the development of each symptom.

HMGB1, originally discovered as a nuclear protein, was recently reevaluated as a potent late phase mediator of severe sepsis (32–34). HMGB1 levels are reported to elevate during severe sepsis in humans and animals. Furthermore, HMGB1 blockade prevents septic animals from lethality. We demonstrated that LPS induces an increase in the plasma level of HMGB1 in an IFN-γ-dependent manner (Figs 4D and 6D). As it is capable of inducing production of pro-inflammatory cytokines and chemokines in inflammatory cells, HMGB1 might be another potent target for the treatment of endotoxin shock syndrome.

PAI-1-induced hyper-coagulation seems to be beneficial for host defense against local bacterial invasion. Bacteria have unique proteolytic machinery for their successful invasion into mammalian host. Most important proteolytic proteins are plasminogen activators. Individual bacteria produce their own plasminogen activators, exemplified by streptokinase and staphylokinase produced by Group A *Streptococcus pyogenes* and *Staphylococcus aureus*, respectively. Bacterial plasminogen activators destroy host extracellular matrix barrier, allowing them to invade deeper into the host and finally to establish their infection (44). However, PAI-1-induced fibrin deposition surrounding the initial invasion sites might enclose the destroyed extracellular matrix and protect against bacterial translocation and dissemination by serving as a new barrier, eventually strengthening the efficient bacterial eradication. Therefore, local hyper-coagulation induced by IFN-γ might be regarded as a potent host defense weapon. In other word, immune cells produce IFN-γ, which protects host tissue from bacterial invasion by encapsulating them with thrombus. Thus, PAI-1 might be a potent host defense molecule induced by inflammatory and T_h1 responses. Indeed, *Pai1*$^{-/-}$ mice are highly susceptible to pneumonia induced by airway infection with *Klebsiella pneumoniae*, a Gram-negative bacterium (45).

IFN-γ and TNF-α are essential for host defense against various pathogens by activating phagocytes and inducing inflammation. Upon microbial infection, mammalian host produces appropriate amounts of these cytokines

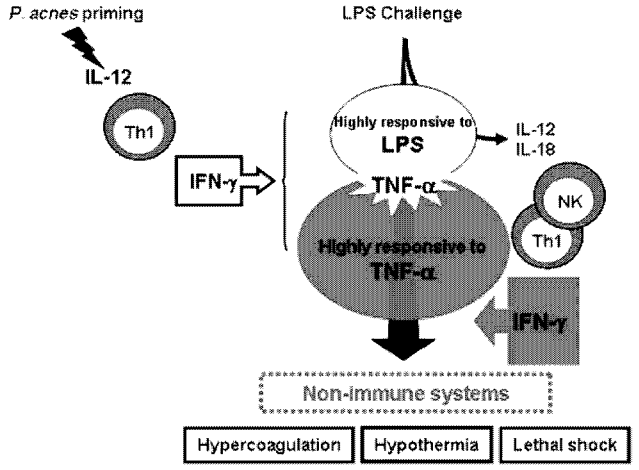

Fig. 7. A proposal model for the endotoxin shock in *Propionibacterium acnes*-primed mice. After priming with heat-killed *P. acnes*, macrophages produce IL-12, which causes T_h1 cell development. IFN-γ produced by the T_h1 cells prime macrophages to be highly susceptible to LPS. Besides, IFN-γ renders mice highly susceptible to TNF-α. After challenge of *P. acnes*-primed mice with LPS, IFN-γ-primed macrophages produce robust IL-12 and IL-18, which then activates T_h1 cells and NK cells to produce a large amount of IFN-γ. The IFN-γ-primed macrophages simultaneously produce enormous TNF-α. TNF-α, in turn, might act on the cells that become highly responsive to TNF-α after *P. acnes* priming to initiate the development of hypothermia, hyper-coagulation, systemic inflammatory responses and lethal shock. IFN-γ positively regulates the development of those clinical symptoms and signs. Thus, IFN-γ is a central factor that primarily controls both *P. acnes*-induced priming phase and the effector phase induced by LPS challenge.

under the proper control of cytokine activation cascades. For example, following *Listeria monocytogenes* infection, mice produce various pro-inflammatory cytokines, including TNF-α, IL-12 and IL-18, via recognizing listerial PAMPs by pattern recognition receptors such as TLR and Nod-like receptor (46, 47). IL-12 and IL-18 then induce production of IFN-γ, which in collaboration with TNF-α efficiently eliminates *L. monocytogenes*. Thus, appropriate amounts of IFN-γ and TNF-α are beneficial for the host. However, dysregulated production of or responsiveness to those cytokines often leads to diseases, exemplified by the endotoxin shock syndrome. Thus, IFN-γ might tip the balance of actions of TNF-α. Furthermore, IFN-γ primarily contributes to the development of severe liver injury induced by activation of a second cell death receptor Fas, as well. *Propionibacterium acnes*-primed mice, but not naive mice, develop massive liver injury after challenge with soluble Fas ligand (48), while *P. acnes*-primed *Ifnγ*$^{-/-}$ mice can evade this injury (our unpublished data). Thus, IFN-γ might play a central role in the development of severe illnesses and syndromes that are caused by activation of cell death receptors.

Endotoxin shock is a life-threatening condition. Thus, it is very important to determine the master regulator of endotoxin shock. Our present study could reveal that IFN-γ is a master regulator of endotoxin shock and neutralization of IFN-γ even just before LPS challenge could rescue animals from endotoxin shock. Many investigators revealed the molecular mechanisms how IFN-γ synergizes with LPS and/or TNF-α for induction of various gene expressions *in vitro* (41). However, it is still to be elucidated how endogenous IFN-γ synergizes with LPS and TNF-α for *in vivo* induction of hypothermia, hyper-coagulation and shock. Although we need extensive efforts to resolve this issue, we believe our data present key information on the treatment of endotoxin shock syndrome.

Supplementary data

Supplementary data are available at *International Immunology* Online.

Funding

Hitech Research Center grant from the Ministry of Education, Culture, Sports, Science and Technology of Japan (Project number 06H025).

Acknowledgements

The authors have no conflicting financial interests to disclose.

References

1 Levi, M. and Ten Cate, H. 1999. Disseminated intravascular coagulation. *N. Engl. J. Med.* 341:586.
2 Russell, J. A. 2006. Management of sepsis. *N. Engl. J. Med.* 355:1699.
3 van der Poll, T., Büller, H. R., ten Cate, H. *et al.* 1990. Activation of coagulation after administration of tumor necrosis factor to normal subjects. *N. Engl. J. Med.* 322:1622.
4 van der Poll, T., Jansen, P. M., Van Zee, K. J. *et al.* 1996. Tumor necrosis factor-alpha induces activation of coagulation and fibrinolysis in baboons through an exclusive effect on the p55 receptor. *Blood* 88:922.
5 Sawdey, M. S. and Loskutoff, D. J. 1991. Regulation of murine type 1 plasminogen activator inhibitor gene expression *in vivo*. *J. Clin. Invest.* 88:1346.
6 Brandtzaeg, P., Joø, G. B., Brusletto, B. and Kierulf, P. 1990. Plasminogen activator inhibitor 1 and 2, alpha-2-antiplasmin, plasminogen, and endotoxin levels in systemic meningococcal disease. *Thromb. Res.* 57:271.
7 García-Segarra, G., Espinosa, G., Tassies, D. *et al.* 2007. Increased mortality in septic shock with the 4G/4G genotype of plasminogen activator inhibitor 1 in patients of white descent. *Intensive Care Med.* 33:1354.
8 Phillippé, J., Offner, F., Declearck, P. J. *et al.* 1991. Fibrinolysis and coagulation in patients with infectious disease and sepsis. *Thromb. Haemost.* 65:291.
9 Holmdahl, L., Eriksson, E., Al-Jabreen, M. and Risberg, B. 1996. Fibrinolysis in human peritoneum during operation. *Surgery* 119:701.
10 Kosaka, H., Yoshimoto, T., Fujimoto, J. and Nakanishi, K. 2008. Interferon-γ is a therapeutic target molecule for prevention of postoperative adhesion formation. *Nat. Med.* 14:437.
11 Chung, D. R., Chitnis, T., Pnzo, R. J., Kasper, D. L., Sayegh, M. H. and Tzianabos, A. O. 2002. $CD4^+$ T cells regulate surgical and postinfectious adhesion formation. *J. Exp. Med.* 195:1471.
12 Ketterhut, I. C., Fiers, W. and Goldberg, A. L. 1987. The toxic effects of tumor necrosis factor *in vivo* and their prevention by cyclooxygenase inhibitors. *Proc. Natl Acad. Sci. USA* 84:4273.
13 Kozak, Conn, C. A., Klir, J. J., Wong, G. H. and Kluger, M. J. 1995. TNF soluble receptor and antiserum against TNF enhance lipopolysaccharide fever in mice. *Am. J. Physiol. Regul. Integr. Comp. Physiol.* 269:R23.
14 Beutler, B. and Cerami, A. 1986. Cachectin and tumour necrosis factor as two sides of the same biological coin. *Nature* 320:584.

15 Mizoguchi, Y., Tsutsui, H., Sakagami, Y. *et al.* 1987. The protective effects of prostaglandin E1 in an experimental massive hepatic necrosis model. *Hepatology* 7:1184.
16 Yoshimoto, T., Nakanishi, K., Hirose, K. *et al.* 1992. High serum IL-6 level reflects susceptible status of the host to endotoxin and IL-1/tumor necrosis factor. *J. Immunol.* 148:3596.
17 Okamura, H., Tsutsui, H., Komatsu, T. *et al.* 1995. Cloning of a new cytokine that induces IFN-γ production by T cells. *Nature* 378:88.
18 Tsutsui, H., Matsui, K., Okamura, H. and Nakanishi, K. 2000. Pathophysiological roles of interleukin-18 for inflammatory liver diseases. *Immunol. Rev.* 174:192.
19 Sakao, Y., Takeda, K., Tsutsui, H. *et al.* 1999. IL-18-deficient mice are resistant to endotoxin-induced liver injury but highly susceptible to endotoxin shock. *Int. Immunol.* 11:471.
20 Oppmann, B., Lesley, R., Blom, B. *et al.* 2000. Novel p19 protein engages IL-12p40 to form a cytokine, IL-23, with biological activities similar as well as distinct from IL-12. *Immunity* 13:715.
21 Korn, T., Bettelli, E., Oukka, M. and Kuchroo, V. K. 2009. IL-17 and Th17 cells. *Annu. Rev. Immunol.* 27:485.
22 Tagawa, Y., Sekikawa, K. and Iwakura, Y. 1997. Suppression of concanavalin A-induced hepatitis in IFN-γ (-/-) mice, but not TNF-α (-/-) mice: role for IFN-γ in activating apoptosis of hepatocytes. *J. Immunol.* 159:1418.
23 Nakae, S., Komiyama, Y., Nambu, A. *et al.* 2002. Antigen-specific T cell sensitization if impaired in IL-17-deficient mice, causing suppression of allergic cellular and humoral responses. *Immunity* 17:375.
24 Takeda, K., Tsutsui, H., Yoshimoto, T. *et al.* 1998. Defective NK cell activity and Th1 response in IL-18-deficient mice. *Immunity* 8:383.
25 Imamura, M., Tsutsui, H., Yasuda, K. *et al.* 2009. Contribution of TIR domain-containing adapter inducing IFN-β-mediated IL-18 release to LPS-induced liver injury in mice. *J. Hepatol.* 51:333.
26 Tsutsui, H., Matsui, K., Kawada, N. *et al.* 1997. IL-18 accounts for both TNF-α- and Fas ligand-mediated hepatotoxic pathways in endotoxin-induced liver injury in mice. *J. Immunol.* 159:3961.
27 Terada, M., Tsutsui, H., Imai, Y. *et al.* 2006. Contribution of IL-18 to atopic-dermatitis-like skin inflammation induced by *Staphylococcus aureus* product in mice. *Proc. Natl Acad. Sci. USA* 103:8816.
28 Sommeijer, D. W., van Oerle, R., Reitsma, P. H. *et al.* 2005. Analysis of blood coagulation in mice: pre-analytical conditions and evaluation of a home-made assay for thrombin-antithrombin complexes. *Thrombosis J.* 3:12.
29 Matsui, K., Yoshimoto, T., Tsutsui, H. *et al.* 1997. *Propionibacterium acnes* treatment diminishes $CD4^+$ $NK1.1^+$ T cells but induces type I T cells in the liver by induction of IL-12 and IL-18 production from Kupffer cells. *J. Immunol.* 159:97.
30 Clemmer, T. P., Fisher, C. J. Jr., Bone, R. C., Slotman, G. J., Metz, C. A. and Thomas, F. O. 1992. Hypothermia in the sepsis syndrome and clinical outcome. The methylprednisolone severe sepsis study group. *Crit. Care Med.* 20:1395.
31 Remick, D. G. and Xioa, H. 2006. Hypothermia and sepsis. *Front. Biosci.* 11:1006.
32 Wang, H., Bloom, O., Zhang, M. *et al.* 1999. HMB-1 as a late mediator of endotoxin lethality in mice. *Science* 285:248.
33 Lotze, M. T. and Tracey, K. J. 2005. High-mobility group box1 protein (HMGB1): nuclear weapon in the immune arsenal. *Nat. Rev. Immunol.* 5:331.
34 Bianchi, M. E. and Manfredi, A. A. 2007. High-mobility group box 1 (HMGB1) protein at the cross roads between innate and adaptive immunity. *Immunol. Rev.* 220:35.
35 Perona-Wright, G., Jenkins, S. J., O'Connor, R. A. *et al.* 2009. A pivotal role for CD40-mediated IL-6 production by dendritic cells during IL-17 induction *in vivo*. *J. Immunol.* 182:2808.
36 Collart, M. A., Belin, J. D., Vassalli, S., de Kossodo, S. and Vassalli, P. 1986. Gamma interferon enhances macrophage transcription of the tumor necrosis factor/cachectin, interleukin 1, and urokinase genes, which are controlled by short-lived repressors. *J. Exp. Med.* 164:2113.
37 Smith, S. R., Calzetta, A., Bankowski, J., Kenworthy-Bott, L. and Terminelli, C. 1993. Lipopolysaccharide-induced cytokine production and mortality in mice treated with *Corynebacterium pervum*. *J. Leuk. Biol.* 54:23.
38 Trinchieri, G. 1995. Interleukin-12: a proinflammatory cytokine with immunoregulatory functions that bridge innate resistance and antigen-specific and adaptive immunity. *Annu. Rev. Immunol.* 13:251.
39 Hyodo, Y., Matsui, K., Hayashi, N. *et al.* 1999. IL-18 up-regulates perforin-mediated NK activity without increasing perforin messenger RNA expression by binding to constitutively expressed IL-18 receptor. *J. Immunol.* 162:1662.
40 Nakanishi, K., Yoshimoto, T., Tsutsui, H. and Okamura, H. 2001. Interleukin-18 regulates both Th1 and Th2 responses. *Annu. Rev. Immunol.* 19:423.
41 Paludan, S. R. 2000. Synergistic action of pro-inflammatory agents: cellular and molecular aspects. *J. Leuk. Biol.* 67:18.
42 Seki, E., Tsutsui, H., Nakano, H. *et al.* 2001. LPS-induced IL-18 secretion from murine Kupffer cells independently of MyD88 that is critically involved in induction of production of IL-12 and IL-1®. *J. Immunol.* 166:2651.
43 Ohmori, Y. and Hamilton, T. A. 1995. The interferon-stimulated response element and a κB site mediate synergistic induction of murine IP-10 gene transcription by IFN-γ and TNF-α. *J. Immunol.* 154:5235.
44 Bergmann, S. and Hammerschmidt, S. 2007. Fibrinolysis and host response in bacterial infections. *Thromb. Haemost.* 98:512.
45 Renckens, R., Roelofs, J. J. T. H., Bonta, P. I. *et al.* 2007. Plasminogen activator inhibitor type 1 is protective during severe Gram-negative pneumonia. *Blood* 109:1593.
46 Seki, E., Tsutsui, H., Tsuji, N. M. *et al.* 2002. Critical roles of myeloid differentiation factor 88-dependent proinflammatory cytokine release in early phase clearance of *Listeria monocytogenes* in mice. *J. Immunol.* 169:3863.
47 Martinon, F. and Tschopp, J. 2007. Inflammatory caspases and inflammasomes: master switches of inflammation. *Cell Death Differ.* 14:10.
48 Tsutsui, H., Kayagaki, N., Kuida, K. *et al.* 1999. Caspase-1-independent, Fas/Fas ligand-mediated IL-18 secretion from macrophages causes acute liver injury in mice. *Immunity* 11:359.

Allergology International. 2010;59:137-141
DOI: 10.2332/allergolint.10-RAI-0208

REVIEW ARTICLE

Importance of IL-18-Induced Super Th1 Cells for the Development of Allergic Inflammation

Kenji Nakanishi[1], Hiroko Tsutsui[2] and Tomohiro Yoshimoto[3]

ABSTRACT

Th1 cells, which express IL-18R, produce IFN-γ in response to Ag and IL-2 and increase further production of IFN-γ upon additional IL-18 stimulation. They simultaneously produce Th2 cytokines (IL-9 and IL-13), GM-CSF and chemokines (RANTES, MIP-1α). Human Th1 cells also produce IFN-γ and IL-13 in response to anti-CD3 and IL-18. Recently, we demonstrated Th1 cells induce intrinsic type atopic asthma and dermatitis by production of Th1- and Th2-cytokines and chemokines. Here, we review the pathological roles of Th1 cells, stimulated with Ag and IL-18 *in vivo*, in the pathogenesis of allergic disorders by production of Th1 and Th2 cytokines and chemokines. Based on this unique function of Ag- plus IL-18-stimulated Th1 cells, we proposed to designate them as "super Th1 cells".

KEY WORDS

allergic inflammation, atopic dermatitis, bronchial asthma, IL-18, super Th1

INTRODUCTION

Bronchial asthma is a complex syndrome characterized by airway hyperresponsiveness (AHR) and reversible airflow obstruction associated with airway inflammation and remodeling and occasional high serum level of IgE.[1-7] Th2 cells have been recognized as inducing bronchial asthma by production of Th2 cytokines.[1-10] Particularly, IL-13 is suggested to play a critical role in induction of AHR, eosinophilic infiltration, goblet cell metaplasia, and lung fibrosis.[9-11] In contrast, Th1 cells had been regarded to inhibit bronchial asthma by production of IFN-γ.[12-14] However, several studies have disclosed the disability of Th1 cell to suppress Th2 cell-induced AHR.[15-19] On the contrary, a combination of Th1 and Th2 cells or their products rather augment each activity to induce airway inflammation and AHR.[15,16,19]

We demonstrated recently that OVA (Ag) plus IL-18 acts on adoptively transferred OVA-specific memory type Th1 cells to induce airway inflammation and AHR in a naive host mouse.[20] Th1 cells, which express IL-18R, produce IFN-γ in response to OVA and increase further IFN-γ production in response to additional IL-18 stimulation.[21] Surprisingly, they simultaneously produce Th2 cytokines (e.g., IL-9 and IL-13), GM-CSF and chemokines (e.g., RANTES and MIP-1) when stimulated with OVA and IL-18.[20] Human Th1 cells also produce IFN-γ and IL-13 in response to anti-CD3 plus IL-18.[22] Recently, we demonstrated Th1 cells induce intrinsic atopic dermatitis by production of Th1 and Th2 cytokines and chemokines.[23] Thus, IL-18 has added its new function to its growing functional list.[24-26] Based on this unique function of Ag-plus IL-18-stimulated Th1 cells, we proposed to designate them as "super Th1 cells".[23]

THE MOLECULAR MECHANISM FOR IL-18 SECRETION

As *Il18*, like *Il1*β, lack leader sequence, *Il18* product pro-IL-18 cannot be secreted, but is stored intracellularly.[24,25,27,28] Many cell types exemplified by macrophages produce pro-IL-18 in the steady state.[24,27,28] Epithelial cells lining host body, such as respiratory epithelial cells, intestinal epithelial cells and keratinocytes can produce pro-IL-18 under normal conditions as well. Pro-IL-18 needs appropriate post-translational processing to become biologically active and to be ex-

[1]Department of Immunology and Medical Zoology, [2]Department of Microbiology and [3]Laboratory of Allergic Diseases, Institute for Advanced Medical Sciences, Hyogo College of Medicine, Hyogo, Japan.
Correspondence: Kenji Nakanishi, MD, Professor, Department of Immunology and Medical Zoology, Hyogo College of Medicine, Nishinomiya, Hyogo 663-8501, Japan.
Email: nakaken@hyo-med.ac.jp
Received 10 March 2010.

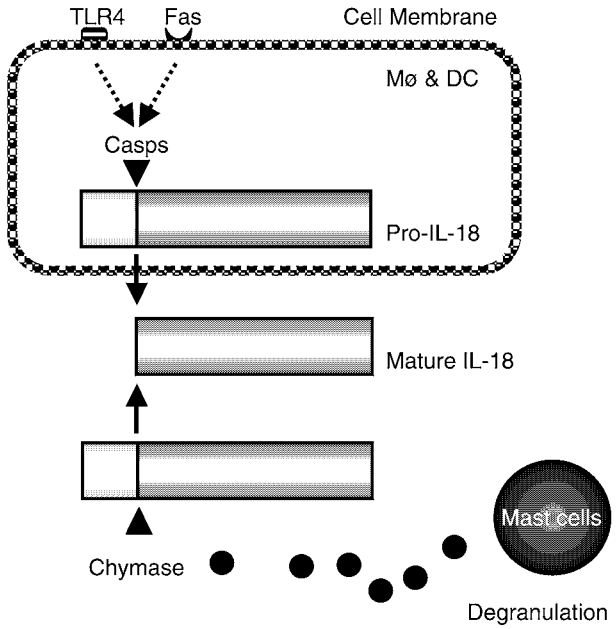

Fig. 1 Mechanisms involved in the processing and releasing IL-18. Macrophages (Mϕ) and dendritic cells are major cell sources of IL-18. The cells constitutively produce pro-IL-18. After stimulation through Toll-like receptor 4 (TLR4) and Fas, caspases (Casps) are activated for appropriately cleavage of proIL-18, resulting in the release of biologically active mature IL-18. Chymase degranulated from activated human mast cells can process pro-IL-18 into biologically active IL-18 as well.

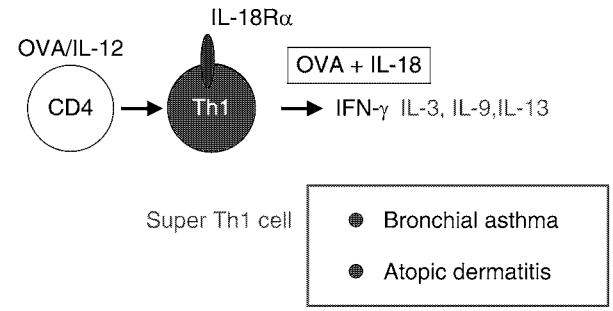

Fig. 2 Super Th1 cells. When they are activated with Ag together with IL-18, Th1 cells become to exert their actions as super Th1 cells by producing both Th1 and Th2 cytokines. Among the cytokines, IFN-γ and IL-13 are critical for the development of AHR and airway fibrosis, respectively.

tracellularly released (Fig.1).[27,28] Caspase 1 (Casp1) is an authentic processing enzyme for IL-18 and IL-1 β.[27] Casp1 is also produced as enzymatically inactive zymogen in the cytoplasm and needs mutual cleavage to become active. Recently, the multiple protein complex named inflammasome is verified to be the platform for Casp1 activation.[29] Inflammasome is composed of Nod-like receptor (NLR), a cytoplasmic sensor, Casp1 activation adaptor ASC, pro-Casp1 and substrates such as pro-IL-18 and pro-IL-1β. Nalp3/NLRP3 is believed to senses extrinsic pathogen-associated molecular patterns (PAMPs). Indeed, after stimulation with LPS, Nalp3 inflammasome is promptly formed, followed by rapid processing of IL-1 β and/or IL-18. Thus, microbial infection induces IL-18 and IL-1β release via activation of Nalp3 inflammasome. For example, in response to TLR4 agonist LPS, hepatic tissue macrophages secrete IL-18 and IL-1β in a manner dependent on Casp1, ASC and Nalp3.[30]

IL-18 processing might occur extracellularly as well. Recent report shows that chymase, an enzyme localized in the granules of mast cells, has capacity to cleave pro-IL-18 into biologically active IL-18 (Fig.1).[31] Since mast cells are accumulated into the skin lesion of mice with AD-like dermatitis,[23,26,32] chymase from the activated mast cells might exacerbate the skin inflammation by enhancing the local release of biologically active IL-18.

Epithelial cells are major cell source of various pro-allergic cytokines, such as IL-18, IL-25, TSLP and IL-33. As they are accumulated preferentially in the inflammatory sites of patients with Th2 type allergic diseases, IL-25, TSLP and IL-33 might be involved in the development of Th2 type allergy.[33-35] By contrast, epithelium-derived IL-18 might trigger infectious type of allergic diseases as described later, although the mechanism for secretion of IL-18 from the epithelial cells are still to be elucidated.[36,37]

SUPER TH1 CELLS AND ASTHMA

IL-18R expression levels determine the intensity of responsiveness to IL-18 and are quite distinct among Th cell subsets.[25,26] Naïve CD4+ T cells and Th2 cells express little IL-18R, while Th1 cells express high levels of it. Consistently, the amount of IL-4 produced by Th2 cells is not affected by additional stimulation with IL-18. In contrast, Th1 cells produce larger amounts of Th1 cytokines such as IFN-γ and TNF-α when additionally stimulated through their IL-18R (Fig.2). From these early studies IL-18 was regarded as the Th1 response-activating cytokine. Our resent study unveiled a second important property of IL-18 in the adaptive immunity. IL-18 has potential to render Th1 cells to produce Th2 cytokines.[20] Upon simultaneous engagement of TCR and IL-18R, Th1 cells become to produce abundant IL-3, IL-13 and IL-9, but still not IL-4, in addition to the Th1 cytokines. They also produce larger amounts of chemokines that can recruit various pro-atopic cells, including granulocytes, macrophages and lymphocytes. We designate these IL-13/IL-9/chemokine-producing Th1 cells as super Th1

cells (Fig.2).

What about *in vivo* role of super Th1 cells? Naïve mice transferred with OVA-specific Th2 cells that are generated from OVA-specific naïve DO11.10 CD4+ cells by *in vitro* incubation under Th2 condition, namely "Passive Th2 mice", expectedly develop asthmatic response upon intranasal OVA challenge.[20] They develop AHR, airway eosinophillia and goblet cell metaplasia of airway epithelial cells. Expectedly, IL-13 blockade can protect against the development of all of those manifestations. In contrast, "Passive Th1 mice", which are generated by the protocol similar to "Passive Th2 mice" except for *in vitro* incubation of naïve OVA-specific CD4+ cells under Th1 condition, do not show any asthmatic signs and/or symptoms after intranasal challenge with OVA alone. However, whenever challenged with OVA together with IL-18, "Passive Th1 mice" start to succumb to AHR, airway eosinophilia and peribronchial fibrosis, suggesting the possible activation of super Th1 cells. In contrast to Th2 type asthma observed in "Passive Th2 mice", IL-13 blockade prevents airway eosinophilic inflammation and peribronchial fibrosis, partly and profoundly, but entirely not AHR.[37] This AHR can be protected by IFN-γ blockade. Thus, super Th1 cells might be involved in the pathogenesis of certain types of allergic disorders by producing both IFN-γ and IL-13.

INFECTIOUS TYPE BRONCHIAL ASTHMA

It is well documented that microbial infection aggravates and/or triggers allergic diseases in human. For example, lower respiratory infection with rhinovirus, a common microbe relevant to cold, or with *Mycoplasma pneumoniae* and *Chlamydophila pneumoniae*, common bacteria causative of community-acquired pneumonia, frequently provokes or exacerbates bronchial asthma in asthmatic patients.[38,39] Lesional skin infection with *Staphylococcus aureus* worsens the disease severity in patients with atopic dermatitis (AD). As microbial infection sometimes evokes IL-18 secretion,[25,26] we may assume that microbial products might cause local release of IL-18, which in turn triggers bronchial asthma by activation of super Th1 cells. As expected, murine bronchial epithelial cells can respond to LPS by releasing IL-18. "Passive Th1 mice" or wild-type mice immunized with OVA in Th1 adjuvant ("Active Th1 mice") show AHR, peribronchial eosinophilic inflammation upon intranasal challenge with OVA in combination with LPS, a cell-wall component of Gram-negative bacteria.[37] In sharp contrast, IL-18 blockade can rescue "Active Th1 mice" from these clinical manifestations after intranasal challenge with OVA and LPS. *Il18*$^{-/-}$ mice immunized with OVA in Th1 adjuvant can evade them after being similarly challenged.[37] Thus, endogenously produced IL-18 and exogenously administered OVA both might activate OVA-specific super Th1 cells, leading to the development of asthmatic manifestations in infectious type of asthma.

ATOPIC DERMATITIS INDUCED BY TOPICAL APPLICATION WITH STAPHYLOCOCCAL PRODUCT

Super Th1 cells are also highlighted in infectious type of AD in mice. Consecutive and topical application of protein A (SpA) purified from cell wall of *Staphylococcus aureus* induces AD-like pruritic dermatitis in mice with genetically impaired skin barrier function, NC/Nga mice.[23] CD4+ T cells purified from draining lymph nodes (DLN) of mice prior to the onset show the characteristics of Th1 cells. These cells produce Th1 cytokines (IFN-γ and TNF-α), but not Th2 cytokine (IL-4 and IL-13) upon TCR engagement. However, CD4+ DLN cells prepared from the mice post onset exhibit the feature as super Th1 cells. Keratinocytes freshly isolated from naive mice release IL-18 in response to SpA *in vitro*,[36] suggesting involvement of IL-18 in the in vivo development into super Th1 cells. In fact, IL-18 blockade and deletion of *Il18* rescue mice from the development of SpA-induced AD-like dermatitis, concomitant with prevention of their super Th1 cell development. Among cytokines produced by super Th1 cells IFN-γ and TNF-α are important. IFN-γ or TNF-α blockade prevents the development of this skin inflammation. Thus, IL-18-dependent super Th1 cell development is important for the development of this dermatitis.

CLINICAL EVIDENCE FOR IL-18

Accumulating evidence suggests positive relationship between IL-18 levels in the lesion or circulation and allergic diseases, such as asthma, allergic rhinitis and AD.[40-42] In particular, after inhalatory challenge test with flour allergens patients with occupational allergic asthma and/or rhinitis show a significant increase in IL-18 levels in nasal lavage fluid. Furthermore, *IL18* polymorphism that ensures higher production of IL-18 upon appropriate stimuli is preferentially accumulated in patients with allergic disorders.[43-45] Although no polymorphisms differed significantly in frequency between the control and adult asthma groups, functional polymorphism in IL-18 is associated with severity of adult bronchial asthma.[46] These results suggest association of IL-18 with allergic disorder in human. However, the molecular mechanism for IL-18 induction of differentiation from Th1 cells into Super Th1 cells is unclear. Nonetheless, possible therapeutics targeting IL-18 might be beneficial for inflammatory type of allergic disorders.

CONCLUDING REMARKS

One may accept that super Th1 cells are activated upon microbial infection of allergic lesion. What is a super Th1 cell subset? Do super Th1 cells, like Th1 cells, require the proper epigenetic regulation? If so,

what is a transcription factor essential for the differentiation into super Th1 cells, like T-bet/STAT4 for Th1 cells (Fig.2)?

Although we need further studies to settle those issues, targeting super Th1 cells and super Th1-associated cytokines might be of value in the therapy of severe, recurrent asthma and perhaps of infectious type allergic diseases. We previously generated human anti-human IL-18 mAb by the gene-manipulating technique.[47] This human-derived mAb targeting human IL-18 might be highlighted as a therapeutic agent against infectious type allergic diseases as well.

ACKNOWLEDGEMENTS

We thank Drs. Nobuki Hayashi (Hyogo College of Medicine) and Hitoshi Mizutani (Mie University School of Medicine) for their enthusiastic discussion.

REFERENCES

1. Bochner BS, Undem BJ, Lichtenstein LM. Immunological aspects of allergic asthma. *Annu Rev Immunol* 1994;**12**: 295-335.
2. Busse WW, Lemanske RJ. Asthma. *N Engl J Med* 2001; **344**:350-62.
3. Cohn L, Elias JA, Chupp GL. Asthma: mechanisms of disease persistence and progression. *Annu Rev Immunol* 2004;**22**:789-815.
4. Davies DE, Wicks J, Powell RM, Puddicombe SM, Holgate ST. Airway remodeling in asthma: new insights. *J Allergy Clin Immunol* 2003;**111**:215-25.
5. Elias JA, Lee CG, Zheng T *et al.* New insights into the pathogenesis of asthma. *J Clin Invest* 2003;**111**:291-7.
6. Umetsu DT, McIntire JJ, Akbari O, Macaubas C, DeKruyff RH. Asthma: an epidemic of dysregulated immunity. *Nat Immunol* 2002;**3**:715-20.
7. Wills-Karp M. Immunologic basis of antigen-induced airway hyperresponsiveness. *Annu Rev Immunol* 1999;**17**: 255-81.
8. Nakamura Y, Ghaffar O, Olivenstein R *et al.* Gene expression of the GATA-3 transcription factor is increased in atopic asthma. *J Allergy Clin Immunol* 1999;**103**:215-22.
9. Kuperman DA, Huang X, Koth LL *et al.* Direct effects of interleukin-13 on epithelial cells cause airway hyperreactivity and mucus overproduction in asthma. *Nat Med* 2002;**8**:885-9.
10. Wills-Karp M, Luyimbazi J, Xu X *et al.* Interleukin-13: central mediator of allergic asthma. *Science* 1998;**282**:2258-61.
11. Wynn T. IL-13 effector functions. *Annu Rev Immunol* 2003;**21**:425-56.
12. Cohn L, Homer RJ, Niu N, Bottomly K. T helper 1 cells and interferon gamma regulate allergic airway inflammation and mucus production. *J Exp Med* 1999;**190**:1309-18.
13. Huang TJ, MacAry PA, Eynott P *et al.* Allergen-specific Th1 cells counteract efferent Th2 cell-dependent bronchial hyperresponsiveness and eosinophilic inflammation partly via IFN-gamma. *J Immunol* 2001;**166**:207-17.
14. Iwamoto I, Nakajima H, Endo H, Yoshida S. Interferon gamma regulates antigen-induced eosinophil recruitment into the mouse airways by inhibiting the infiltration of CD4+ T cells. *J Exp Med* 1993;**177**:573-6.
15. Ford JG, Rennick D, Donaldson DD *et al.* IL-13 and IFN-gamma: interactions in lung inflammation. *J Immunol* 2001;**167**:1769-77.
16. Hansen G, Berry G, DeKruyff RH, Umetsu DT. Allergen-specific Th1 cells fail to counterbalance Th2 cell-induced airway hyperreactivity but cause severe airway inflammation. *J Clin Invest* 1999;**103**:175-83.
17. Li L, Xia Y, Nguyen A, Feng L, Lo D. Th2-induced eotaxin expression and eosinophilia coexist with Th1 responses at the effector stage of lung inflammation. *J Immunol* 1998;**161**:3128-35.
18. Randolph DA, Carruthers CJ, Szabo SJ, Murphy KM, Chaplin DD. Modulation of airway inflammation by passive transfer of allergen-specific Th1 and Th2 cells in a mouse model of asthma. *J Immunol* 1999;**162**:2375-83.
19. Randolph DA, Stephens R, Carruthers CJ, Chaplin DD. Cooperation between Th1 and Th2 cells in a murine model of eosinophilic airway inflammation. *J Clin Invest* 1999;**104**:1021-9.
20. Sugimoto T, Ishikawa Y, Yoshimoto T *et al.* Interleukin 18 acts on memory T helper cells type 1 to induce airway inflammation and hyperresponsiveness in a naive host mouse. *J Exp Med* 2004;**199**:535-45.
21. Yoshimoto T, Takeda K, Tanaka T *et al.* IL-12 upregulates IL-18 receptor expression on T cells, Th1 cells, and B cells: synergism with IL-18 for IFN-gamma production. *J Immunol* 1998;**161**:3400-7.
22. Hata H, Yoshimoto T, Hayashi N, Hada T, Nakanishi K. IL-18 together with anti-CD3 antibody induces human Th1 cells to produce Th1- and Th2-cytokines and IL-8. *Int Immunol* 2004;**16**:1733-9.
23. Terada M, Tsutsui H, Imai Y *et al.* Contribution of IL-18 to atopic-dermatitis-like skin inflammation induced by *Staphylococcus aureus* product in mice. *Proc Natl Acad Sci U S A* 2006;**103**:8816-21.
24. Okamura H, Tsutsui H, Komatsu T *et al.* Cloning of a new cytokine that induces IFN-gamma production by T cells. *Nature* 1995;**378**:88-91.
25. Nakanishi K, Yoshimoto T, Tsutsui H, Okamura H. Interleukin-18 regulates both Th1 and Th2 responses. *Annu Rev Immunol* 2001;**19**:423-74.
26. Tsutsui H, Yoshimoto T, Hayashi N, Mizutani H, Nakanishi K. Induction of allergic inflammation by interleukin-18 in experimental animal models. *Immunol Rev* 2004; **202**:115-38.
27. Gu Y, Kuida K, Tsutsui H *et al.* Activation of interferon-γ inducing factor mediated by interleukin-1β converting enzyme. *Science* 1997;**275**:206-9.
28. Tsutsui H, Kayagaki N, Kuida K *et al.* Caspase-1-independent, Fas/Fas ligand-mediated IL-18 secretion from macrophages causes acute liver injury in mice. *Immunity* 1999;**11**:359-67.
29. Martinon F, Tschopp J. Inflammatory caspases and inflammasomes: master switches of inflammation. *Cell Death Differ* 2007;**14**:10-22.
30. Imamura M, Tsutsui H, Yasuda K *et al.* Contribution of TIR domain-containing adapter inducing IFN-β-mediated IL-18 release to LPS-induced liver injury in mice. *J Hepatol* 2009;**51**:333-41.
31. Omoto Y, Tokime K, Yamanaka K *et al.* Human mast cell chymase cleaves pro-IL-18 and generates a novel and biologically active I-18 fragment. *J Immunol* 2006;**177**:8315-9.
32. Konishi H, Tsutsui H, Murakami T *et al.* IL-18 contributes to the spontaneous development of atopic dermatitis-like inflammatory skin lesion independently of IgE/stat6 under specific pathogen-free conditions. *Proc Natl Acad Sci U S A* 2002;**99**:11340-5.

33. Cohn L, Elias JA, Chupp GL. Asthma: mechanisms of disease persistence and progression. *Annu Rev Immunol* 2004;**22**:789-815.

34. Liu Y-J, Soumelis V, Watanabe N *et al.* TSLP: An epithelial cell cytokine that regulates T cell differentiation by conditioning dendritic cell maturation. *Annu Rev Immunol* 2007;**25**:193-219.

35. Saenz SA, Taylor BC, Artis D. Welcome to the neighborhood: epithelial cell-derived cytokines license innate and adaptive immune responses at mucosal sites. *Immunol Rev* 2008;**226**:172-90.

36. Nakano H, Tsutsui H, Terada M *et al.* Persistent secretion of IL-18 in the skin contributes to IgE response in mice. *Int Immunol* 2003;**15**:611-21.

37. Hayashi N, Yoshimoto T, Izuhara K *et al.* T helper 1 cells stimulated with ovalbumin and IL-18 induce airway hyperresponsiveness and lung fibrosis by IFN-γ and IL-13 production. *Proc Natl Acad Sci U S A* 2007;**104**:14765-70.

38. Gern JE. Rhinovirus and the initiation of asthma. *Curr Opin Allergy Clin Immunol* 2009;**9**:73-8.

39. Sutherland ER, Martin RJ. Asthma and atypical bacterial infection. *Chest* 2007;**132**:1962-6.

40. Wong CK, Ho CY, Ko FWS *et al.* Proinflammatory cytokines (IL-17, IL-6, IL-18 and IL-12) and Th cytokines (IFN-g, IL-4, IL-10 and IL-13) in patients with allergic asthma. *Clin Exp Immunol* 2001;**125**:177-83.

41. Tanaka T, Tsutsui H, Yoshimoto T *et al.* Interleukin-18 is elevated in the sera from patients with atopic dermatitis and from atopic dermatitis model mice, NC/Nga. *Int Arch Allergy Immunol* 2001;**125**:236-40.

42. Krakowiak A, Walusiak J, Krawczyk P *et al.* IL-18 levels in nasal lavage after inhalatory challenge test with flour in bakers diagnosed with occupational asthma. *Int J Occup Med Environ Health* 2008;**21**:165-72.

43. Higa S, Hirano T, Mayumi M *et al.* Association between interleukin-18 gene polymorphism 105A/C and asthma. *Clin Exp Allergy* 2003;**33**:1097-102.

44. Novak N, Kruse S, Potreck J *et al.* Single nucleotide polymorphisms of the IL18 gene are associated with atopic eczema. *J Allergy Clin Immunol* 2005;**115**:828-33.

45. Sebeloba S, Izakovicova-Holla L, Stejskalova A *et al.* Interleukin-18 and its three gene polymorphisms relating to allergic rhinitis. *J Hum Genet* 2007;**52**:152-8.

46. Harada M, Obara K, Hirota T *et al.* A functional polymorphism in IL-18 is associated with severity of bronchial asthma. *Am J Respir Crit Care Med* 2009;**180**:1048-55.

47. Hamasaki T, Hashiguchi S, Ito Y *et al.* Human anti-human IL-18 antibody recognizing the IL-18-binding site 3 with IL-18 signaling blocking activity. *J Biochem* 2005;**138**:433-42.

International Immunology, Vol. 22, No. 7, pp. 561–570
doi:10.1093/intimm/dxq040
Advance Access publication 23 May 2010

Contribution of IL-18 to eosinophilic airway inflammation induced by immunization and challenge with *Staphylococcus aureus* proteins

Mai Kuroda-Morimoto[1,2,3], Hidehisa Tanaka[1,2], Nobuki Hayashi[1,2], Masakiyo Nakahira[1,2], Yasutomo Imai[2,4], Michiko Imamura[2,5], Koubun Yasuda[1,2], Shizue Yumikura-Futatsugi[1,2], Kiyoshi Matsui[2,3], Toshihiro Nakashima[2,6], Kazuhisa Sugimura[2,7], Hiroko Tsutsui[2,8], Hajime Sano[2,3] and **Kenji Nakanishi[1,2]**

[1]Department of Immunology and Medical Zoology, Hyogo College of Medicine, Nishinomiya, Hyogo 663-8501, Japan
[2]Collaborative Development of Innovation Seeds, Japan Science and Technology Corporation, Tokyo 102-8666, Japan
[3]Department of Internal Medicine, [4]Department of Dermatology, and [5]Department of Surgery, Hyogo College of Medicine, Nishinomiya, Hyogo 663-8501, Japan
[6]Chemo-Sera-Therapeutic Research Institute, Kumamoto 869-1298, Japan
[7]Department of Bioengineering, Faculty of Engineering, Kagoshima University, Kagoshima 890-0060, Japan
[8]Department of Microbiology, Hyogo College of Medicine, Nishinomiya, Hyogo 663-8501, Japan

Correspondence to: K. Nakanishi; E-mail: nakaken@hyo-med.ac.jp

Transmitting editor: T. Kurosaki

Received 28 December 2009, *accepted* 6 April 2010

Abstract

We previously reported that intranasal challenge with ovalbumin (OVA) plus IL-18 induces airway hyperresponsiveness (AHR) and eosinophilic airway inflammation in mice with OVA-specific T_h1 cells. These two conditions can be prevented by neutralizing anti-IFN-γ and anti-IL-13 antibodies, respectively. The mice develop AHR and eosinophilic airway inflammation after challenge with OVA plus LPS instead of IL-18 and endogenous IL-18 is known to be involved. In contrast, IL-18 does not facilitate these changes in mice possessing OVA-specific T_h2 cells. Here, we investigated whether IL-18 is involved in the development of asthma in mice immunized and challenged with bacterial proteins. Upon intranasal exposure to protein A (SpA) derived from *Staphylococcus aureus*, mice immunized with SpA exhibited AHR and peribronchial eosinophilic inflammation if IFN-γ or IL-13 were present, respectively. The $CD4^+$ T cells from draining lymph nodes (DLNs) of the SpA-immunized and -challenged mice produced a robust IFN-γ and IL-13 in response to immobilized anti-CD3 antibodies. Treatment with neutralizing anti-IL-18 antibodies prevented asthmatic inflammation concomitant with their impaired potential to express IFN-γ and IL-13. Furthermore, naive mice that received the $CD4^+$ T cells from DLNs of SpA-immunized mice developed airway inflammation depending upon the presence of IL-18. Immunodeficient mice that received human PBMCs, which had been stimulated with SpA *in vitro*, developed dense peribronchial accumulation of human $CD4^+$ T cells upon SpA challenge. Neutralizing anti-human IL-18 antibodies protected against this airway inflammation. These results suggest the importance of IL-18 for the development of asthmatic inflammation associated with airway exposure to bacterial proteins.

Keywords: airway hyperresponsiveness, asthma, eosinophilic inflammation, IL-18, *Staphylococcus aureus*

Introduction

Bronchial asthma is complex syndrome characterized by airway hyperresponsiveness (AHR) and reversible airflow obstruction with airway inflammation and mucus formation (1–8). Bronchial asthma is believed to be mediated by T_h2 cells and their cytokines. IL-13 produced by the T_h2 cells can principally account for almost all the above pathogenic responses (2, 9). However, other subsets of $CD4^+$ T cells, such as T_h1, T_h17, regulatory T (Treg) and CD1d-restricted NKT cells, are now recognized to play a role in the modulation of airway allergic inflammation (10). T_h2 cell-directed therapy has limited

efficacy (11), suggesting that bronchial asthma develops by diverse immunological mechanisms. Respiratory infections caused by bacteria frequently activate the T_h1-cell response through activation of Toll-like receptors (12, 13) and are associated with the initiation and/or exacerbation of bronchial asthma in humans (14, 15). These clinical studies strongly suggest that some types of bronchial asthma may be explained by the activation of T_h1-cell responses. However, intranasal challenge with ovalbumin (OVA) alone cannot evoke asthma in mice carrying OVA-specific T_h1 cells (16, 17), indicating that the T_h1-cell response alone is not sufficient enough to induce these pathological alterations. We have demonstrated that intranasal challenge with exogenous IL-18 or bacterial LPS induces IL-18 production in mice. In conjunction with OVA, this can induce robust asthma in mice immunized with OVA and the T_h1 adjuvant, CFA (16–18). OVA initiates OVA-specific T_h1 cells to produce IFN-γ but not IL-13, whereas OVA with IL-18 is capable of activating these T_h1 cells to produce larger amounts of IFN-γ, as well as IL-13, IL-9 and various chemokines that recruit eosinophils and other leukocytes (16). Persistent stimulation with IL-18 and the antigen alters the T_h1 cells, resulting in them producing both IFN-γ and IL-13 (19). With respect to their potential to produce both pro-inflammatory and pro-atopic cytokines/chemokines, we designated T_h1 cells that were re-stimulated with antigen and IL-18 as super T_h1 cells (16, 18, 19). In asthmatic mice possessing super T_h1 cells, IL-13 is responsible for the eosinophilic airway inflammation and remodeling. AHR is caused by IFN-γ, but not IL-13 (16, 17), which is in contrast to T_h2 cell-initiated asthmatic alterations where IL-13 plays a common and critical role (20, 21). Thus, IL-18 is likely to be involved in the development of bacterial infection-associated asthma. However, it is entirely unknown whether bacteria or their products by themselves can trigger super T_h1 cell type bronchial asthma.

The site of a pathogenic infection often determines the phenotype of infection-associated atopic diseases presumably by recruiting and activating pathogen-specific effector T cells and by inducing IL-18 release from the site. Infection with bacteria such as *Staphylococcus aureus* sometimes exacerbates atopic dermatitis in humans (22). We recently observed that consecutive and topical application of *S. aureus* protein A (SpA) (23) induces atopic dermatitis-like skin alterations in naive NC/Nga mice that have a genetically impaired skin barrier (19). The $CD4^+$ T cells prepared from the DLNs of mice with SpA-induced dermatitis express a cytokine profile characteristic of super T_h1 cells. Administration of neutralizing anti-IL-18 antibodies protects against dermatitis as well as super T_h1-cell development (19). Based on these observations, we assumed that the mice carrying SpA-specific T_h1 cells were highly vulnerable to asthma upon intranasal challenge with SpA. To test this hypothesis, we generated a novel asthmatic inflammation mouse model to determine the requirement of IL-18 in the development of SpA-induced asthma. Severely immunodeficient mice that had been inoculated with SpA-stimulated human PBMCs exhibited airway inflammation following intranasal challenge with SpA. Treatment with neutralizing anti-human IL-18 antibodies prevented this airway inflammation. Thus, IL-18 could be a potential target for the treatment of asthmatic inflammation associated with bacterial infection.

Methods

Animals and reagents

Female BALB/c mice and BALB/c *nu/nu* mice were purchased from CLEA Japan (Osaka, Japan). C57BL/6 background *Rag2*$^{-/-}$*C*$\gamma^{-/-}$ mice were from Taconic Farms (Hudson, NY, USA). All animals were bred and/or maintained in specific pathogen-free conditions at the animal facilities of Hyogo College of Medicine and were used at 6–10 weeks of age. Animal experiments were performed in accordance with the guidelines of the National Institutes of Health, as specified by the animal care policy of Hyogo College of Medicine. SpA from *S. aureus* Cowan I was purchased from CalbioChem (La Jolla, CA, USA). Recombinant murine IL-18 was purchased from MBL (Nagoya, Japan). Anti-mouse CD3ε mAb (2C11), anti-mouse CD4 mAb (GK1), anti-human CD4 mAb (RPA-T4) and anti-human CD45 mAb (HI30) were from BD Biosciences Pharmingen (San Diego, CA, USA). Neutralizing anti-IFN-γ mAb was partly purified from the ascites fluid collected from BALB/c *nu/nu* mice inoculated intraperitoneally with hybridoma 6A2 purchased from the American Type Culture Collection (Manassas, VA, USA) (17, 19). Soluble IL-13Rα2-Fc was purchased from R&D Systems (San Diego, CA, USA) (17, 19). Rabbit polyclonal anti-mouse IL-18 antibodies were prepared in our laboratory (19). We generated a neutralizing anti-human IL-18 mAb as described previously (24).

Induction of asthma

The experimental protocol for asthma induction was the same as described in our previous report except we used SpA instead of OVA (17) (Supplementary Figure 1 is available at *International Immunology* Online). Briefly, BALB/c mice were immunized with SpA (500 μg) in CFA, followed by a boost with SpA in incomplete Freund's adjuvant (IFA) at day 14. For the adoptive cell transfer study, $CD4^+$ T cells isolated from DLNs of the immunized and boosted mice were labeled with 5-carbozyfluorescein diacetate succinimidyl ester (CFSE) and 6-CFSE. The CFSE-labeled cells (1×10^7) were administered intravenously into naive BALB/c mice (17). Two weeks following the SpA boost or after $CD4^+$ T cell transfer, mice were exposed intranasally to 50 μl of SpA (250 μg) in PBS for three consecutive days. In some experiments, neutralizing anti-mouse IL-18 antibodies (500 μg) were injected intraperitoneally into the mice at 1 day before and 1 day after intranasal exposure to SpA (17, 19). Anti-IFN-γ mAb (100 μg) or IL-13R2α-Fc (20 μg) was intranasally administered as outlined previously (17). Mice were sacrificed at 24 h after the final intranasal exposure of SpA.

Invasive measurement of AHR

Invasive measurement of AHR was assessed as an increase in pulmonary resistance (RLung) in response to aerosolized β-methacholine as described previously (17). RLung was measured by Pulmos-II (MIPS, Osaka, Japan) hardware and software (MIPS).

Preparation of $CD4^+$ lymph node cells and lung homogenate

$CD4^+$ T cells from the DLN were purified by magnetic-activated cell sorting (17). Lungs were homogenized with

1 ml of lysis buffer according to the method described previously (19, 25).

Cytoplasmic staining for IFN-γ and IL-13

Cells were isolated from mediastinal lymph nodes of SpA-immunized mice after consecutive 3-day challenge with SpA and were incubated with immobilized anti-CD3 mAb and 100 U ml^{-1} of IL-2 in the presence or absence of rmIL-18 (100 ng ml^{-1}) for 48 h. Cytoplasmic staining of the cells for IFN-γ and IL-13 were performed using antigen-presenting cells (APC)-anti-CD4 mAb (RM4-5), FITC-anti-IFN-γ mAb (XMG1.2) and PE-anti-IL-13 mAb (eBio13A).

Preparation of human PBMCs

PBMCs from healthy volunteers (26) were cultured with 100 μg ml^{-1} of SpA for 4 days. Experimental protocols for the use of human PBMCs were approved by the College Review Board of Hyogo College of Medicine.

Establishment of mice implanted with human PBMCs

SpA-stimulated human PBMCs (1×10^7) were transplanted intravenously into *Rag2*$^{-/-}$*C*$\gamma^{-/-}$ mice (27). One-week post-transplantation, we isolated lymphocytes from the peripheral blood and spleen of the recipient mice and analyzed proportions of human $CD45^+$ cells in each preparation by flow cytometry. We used mice that contained >5% human $CD45^+$ cells in their peripheral blood because they also contained > 10% dual $CD45^+/CD4^+$ cells in their spleen (described below). The mice that received human SpA-stimulated PBMCs were then exposed intranasally to SpA for three consecutive days. In order to block the action of human IL-18, anti-human IL-18 mAb (300 μg) was intranasally administered 1 h before SpA exposure. Twenty-four hours following the final administration of SpA, lungs were sampled for histological and confocal microscopic studies.

Preparation of bronchoalveolar lavage fluid

Bronchoalveolar lavage fluid (BALF) was collected (17) and total cell number was determined in each sample. Cytospin preparations of BALF were stained with Dif-Quik (Baxter Healthcare Corp., Miami, FL, USA). Eosinophils and neutrophils were distinguished from each other by their difference in staining.

Histology

Lung specimens were fixed in 10% buffered formalin and sections were stained with hematoxylin and eosin (17). Fields of view on a microscope were selected at random and printed in large scale to distinguish eosinophils from other cell types. Eosinophils and the total number of nucleated cells in each field of view were counted. The mean ± SD of 10 fields of view per sample were calculated.

Confocal laser microscopic analysis

Frozen sections were fixed and incubated with FITC- or PE-conjugated mAb, followed by evaluation using a laser confocal microscope (model IX81; Olympus, Tokyo, Japan) (19).

Detection of cytokines and chemokines

Concentrations of IL-4, IL-13, tumor necrosis factor-α and IFN-γ in culture supernatants were determined with appropriate ELISA kits (Genzyme, Cambridge, MA, USA). Mouse IL-18 was measured by an ELISA kit from MBL. The concentrations of various mouse chemokines were measured with a Bio-Plex Cytokine assay kit (Bio-Rad, Hercules, CA, USA).

Statistics

Three to five mice were used for each experimental group. Data are expressed as the mean ± SD of triplicate samples. Significance between experimental and control groups was determined via an unpaired Student's *t*-test. A P value <0.05 was considered significant. Two to three experiments were performed per assay, and the representative data were shown.

Results

SpA-induced asthmatic inflammation

We examined whether intranasal challenge with SpA induces asthma-like airway inflammation in SpA-immunized mice. We immunized BALB/c mice subcutaneously with SpA in the T_h1 adjuvant, CFA, followed by a booster with SpA in IFA 2 weeks later. Twenty-eight days after the initial immunization, we administered SpA through a nasal tract for three consecutive days and examined the severity of asthmatic inflammation by measuring AHR, analyzing BALF preparations and lung histology (Supplemental Figure 1 is available at *International Immunology* Online). Invasive measurement of AHR revealed that SpA-immunized mice exhibited substantial AHR upon intranasal SpA challenge (Fig. 1A). None of the mice exhibited AHR after treatment with PBS (Fig. 1A) and naive mice were free from AHR even after SpA challenge (Fig. 1A). Thus, SpA immunization and SpA challenge are both required for the development of AHR. Following intranasal challenge with SpA, SpA-immunized mice demonstrated an increase in the number of eosinophils and neutrophils in BALF (Fig. 1B). These increases were not observed after treatment with PBS (Fig. 1B). The severity of AHR, consistent with our previous observations (16, 17), coincided with the cell numbers of eosinophils in BALF. This was also the case for the density of eosinophilic inflammation around the airway. Histological analysis revealed that only SpA-immunized mice developed severe inflammation around the airway following challenge with SpA, but not with PBS (Fig. 1C, E and F). Furthermore, intranasal challenge with SpA, but not PBS or OVA, induced eosinophilia (Supplementary Figure 2 is available at *International Immunology* Online), suggesting that SpA works in an antigen-specific manner. Naive mice exhibited only modest lung inflammation, if any, after intranasal SpA challenge (Fig. 1D). Eosinophils accumulated around the airway of the SpA-immunized and -challenged mice but not in mice treated with the other combinations of immunogens (Fig. 1J). Taken together, these results indicate that SpA-immunized and -challenged mice fulfill the clinical signs of asthmatic inflammation and are a suitable mouse model for bacterial infection-associated asthma-like inflammatory illnesses.

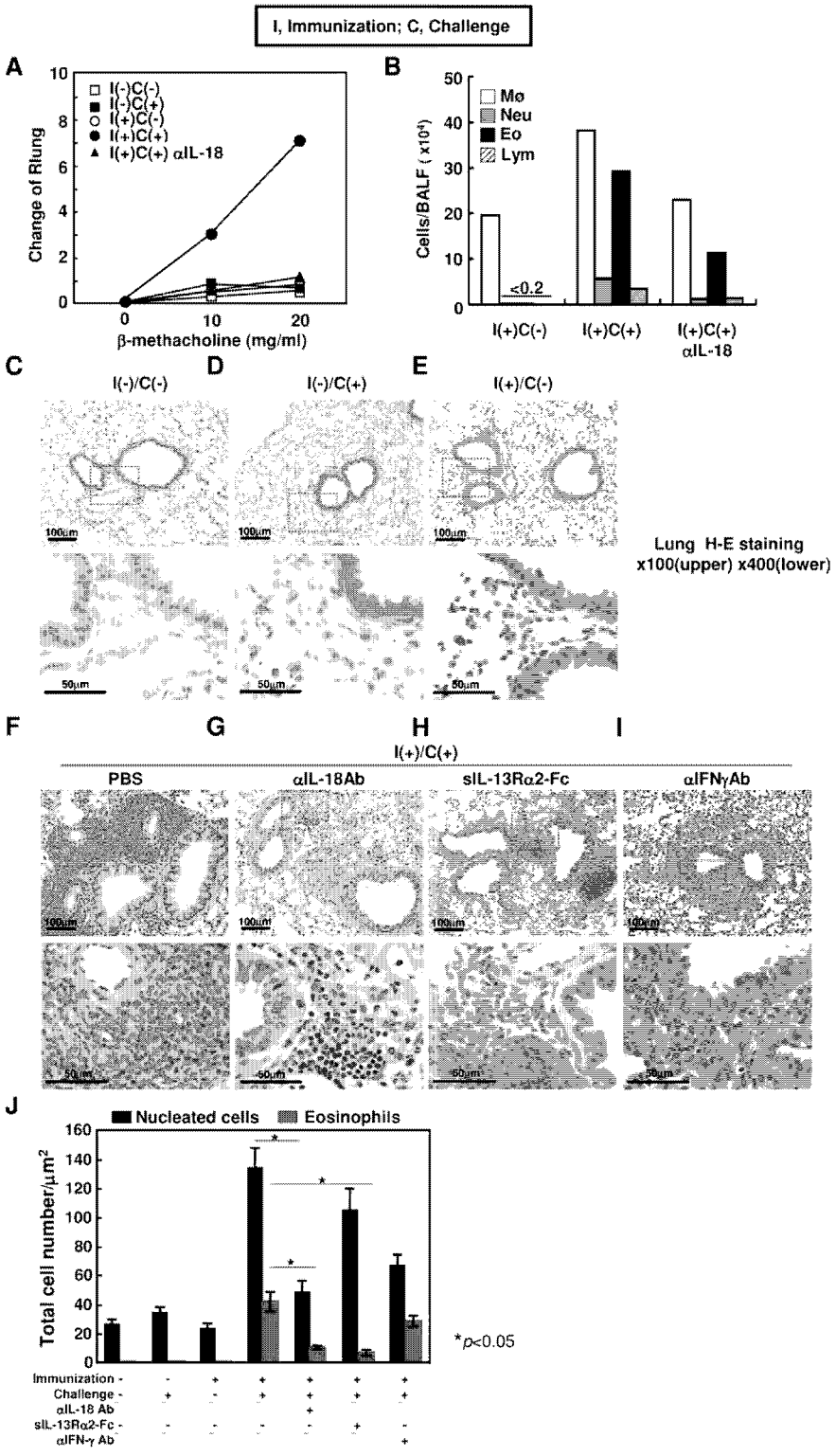

Fig. 1. Requirement of endogenous IL-18 for SpA-induced bronchial asthma. SpA-immunized mice 'I(+)' or naive mice 'I(−)' were intranasally challenged with SpA (250 μg/50 μl) 'C(+)' or PBS (50 μl) 'C(−)'. Neutralizing anti-IL-18 antibodies (500 μg) (A, B, G and J), soluble IL-13R2α-Fc (sIL-13Rα-Fc) (20 μg) (H) or neutralizing anti-IFN-γ (αIFNγ antibody) (100 μg) was administered twice into SpA-immunized mice intravenously, (I) 1 day before or after 3-day intranasal challenge with SpA (αIL-18 antibody). Twenty-four hours after the last SpA challenge, invasive measurement of AHR (A), cellular analysis of BALF (B) and histological analysis of lung specimens (C–I) were performed. (C–I) Upper panels are at low magnifications, and the lower panels are high magnification images of the areas indicated by a red-dotted square in the corresponding

Requirement of IL-18 for SpA-induced asthma

As previously reported, SpA-induced atopic dermatitis develops in an IL-18-dependent manner (19). We investigated whether IL-18 plays a pivotal role in the development of SpA-induced asthmatic inflammation. To test this, we administered neutralizing anti-IL-18 antibodies into the SpA-immunized mice 1 day before and 1 day after the initial intranasal SpA challenge (Supplementary Figure 1 is available at *International Immunology* Online). Administration of neutralizing anti-IL-18 antibodies profoundly reduced AHR (Fig. 1A) and significantly hampered respiratory inflammation and eosinophilia (Fig. 1B, G and J). Consistently (2, 9, 16), blocking the action of IL-13, but not IFN-γ, protected against eosinophilia in the airway (Fig. 1H–J). Conversely and consistently, blockade of IFN-γ, but not of IL-13, prevented AHR (16) (Supplementary Figure 3 is available at *International Immunology* Online). It would appear that endogenous IL-18 seems to be important in the development of SpA-induced asthmatic airway inflammation due to IL-13 production.

Super T_h1-cell differentiation

As IL-13 was profoundly involved in inflammation of the airways (Fig. 1H and J), we examined whether this experimental immunization/challenge protocol induces the development of $CD4^+$ DLN cells into super T_h1 cells or into IL-13-secreting T_h2 cells. We stimulated $CD4^+$ DLN cells with immobilized anti-CD3 mAb and measured the concentrations of T_h2 and super T_h1 cytokines. $CD4^+$ DLN cells from SpA-immunized and -challenged mice produced larger amounts of IFN-γ and IL-13, but little IL-4, compared with SpA-immunized mice without SpA challenge (Fig. 2A), indicating their development into super T_h1 cells, but not T_h2 cells, during intranasal SpA challenge. Furthermore, we examined whether both IL-13 and IFN-γ are produced by a single $CD4^+$ cell isolated from SpA-challenged and SpA-immunized mice. We isolated cells from mediastinal lymph nodes of SpA-challenged and SpA-immunized mice and incubated the cells with plate-bound anti-CD3 in the presence or absence of exogenous IL-18. We found a very small proportion of $IL\text{-}13^+IFN\text{-}\gamma^+$ $CD4^+$ T cells after TCR stimulation alone (Fig. 2B). However, upon TCR and IL-18 stimulation, the proportion of $IL\text{-}13^+IFN\text{-}\gamma^+$ $CD4^+$ T cells was significantly elevated (Fig. 2B), suggesting that super T_h1-cell differentiation occurs in SpA-immunized mice after intranasal challenge with SpA. At the same, this stimulation induced an increase in two other populations: IL-13-produicng cells and IFN-γ-producing cells (Fig. 2B). Thus, three populations, consisting of IL-13-produicng cells, IFN-γ-producing cells and IL-13 plus IFN-γ-producing cells, contribute to induction of SpA-induced bronchial asthma.

Next, we investigated the roles of endogenous IL-18 in super T_h1-cell development. $CD4^+$ DLN cells prepared from the mice additionally treated with anti-IL-18 antibodies produced much less IFN-γ and IL-13 than those from SpA-induced asthmatic mice (Fig. 2A), suggesting the possibility that IL-18 release during SpA challenge participates in super T_h1-cell differentiation. To test this possibility, we examined whether IL-18 is produced in the asthmatic lung. SpA immunization alone failed to induce significant increase in IL-18 concentration within the lung tissue (Fig. 2C). SpA immunization and challenge seemed to increase IL-18 levels significantly in the lung (Fig. 2C). These results suggest that airway constituents such as respiratory epithelial cells and/or alveolar macrophages might release IL-18 in response to SpA.

Induction of chemokines attracting eosinophils and neutrophils in the lungs

As IL-18 is capable of inducing chemokine production from epithelial cells, T_h1 cells and super T_h1 cells (16, 18), we examined whether IL-18 could induce expression of chemokines in the lung, particularly chemokines recruiting eosinophils and neutrophils, during intranasal SpA challenge. Lung homogenates from mice immunized with SpA only contained almost basal amounts of chemokines attracting eosinophils, including CCL5 (RANTES) and CCL11 (Eotaxin), and neutrophils, such as CXCL1 (KC) and CCL2 (MCP-1), when compared with naive mice (Fig. 3). However, it was only after SpA challenge that pulmonary levels of CCL5, CCL11, CCL2 and CXCL1 were significantly elevated (Fig. 3). This was also the case for the chemokines attracting diverse types of leukocytes, such as, CCL3 (MIP-1α) and CCL4 (MIP-1β), as well as the pro-inflammatory cytokines, IL-1β and IL-6 (Fig. 3). In contrast, T_h2 cytokines, IL-4 and IL-5 were not induced after SpA challenge (Fig. 3). As expected, treatment with neutralizing anti-IL-18 antibodies during intranasal exposure to SpA significantly reduced chemokine expression levels (Fig. 3). Thus, the expression of these chemokines could be induced by IL-18.

Importance of SpA-activated super T_h1 cells in the development of airway inflammation

We examined whether super T_h1 cells are effector cells of SpA-induced asthmatic inflammation. To test this, we transferred $CD4^+$ DLN cells from SpA-immunized mice into naive mice, followed by intranasal administration of SpA for three consecutive days. Upon daily exposure to PBS, mice receiving the $CD4^+$ DLN cells demonstrated an intact response to methacholine treatment and evaded airway inflammation (Figs 1A and C and 4A and C). Upon exposure to SpA, these mice exhibited obvious AHR (Fig. 4A) and airway inflammation (Fig. 4C), prompting us to investigate whether donor $CD4^+$ DLN cells migrated into the airway as a response to SpA challenge in order to exert their effector functions. We labeled the donor cells with CFSE, injected them into naive recipient mice and analyzed their localization in the recipient lung after SpA challenge. Many CFSE-labeled cells had migrated into the lung (Fig. 4B). Most of the

upper panels. Upper scale bars indicate 100 μm, while the lower ones represent 50 μm. Lung sections were stained with hematoxylin and eosin (H&E). The mean ± SD of total nucleated cells per square micrometer (black bars) and eosinophils per square micrometer (red bars) in 10 fields of view selected at random are shown (J). Mø, macrophages; Neu, neutrophils; Eo, eosinophils; Lym, lymphocytes. Data are representative of three independent experiments with five mice per group.

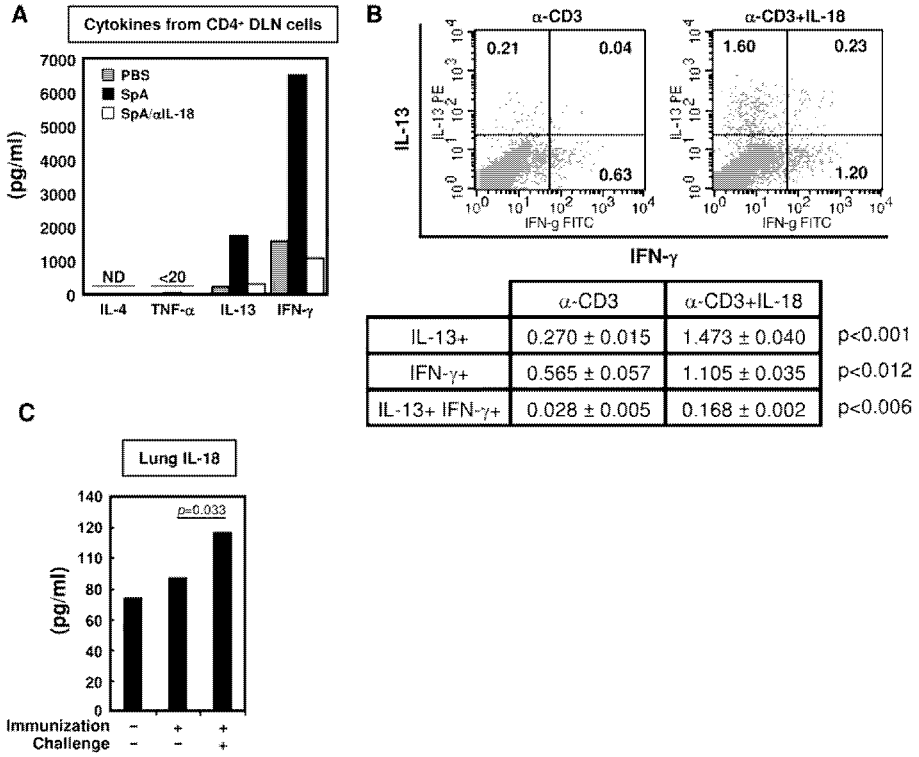

	α-CD3	α-CD3+IL-18	
IL-13+	0.270 ± 0.015	1.473 ± 0.040	p<0.001
IFN-γ+	0.565 ± 0.057	1.105 ± 0.035	p<0.012
IL-13+ IFN-γ+	0.028 ± 0.005	0.168 ± 0.002	p<0.006

Fig. 2. IL-18-dependent differentiation toward super T_h1 cells. (A) DLN cells were prepared from variously treated mice as shown in the legend to Fig. 1A, and $CD4^+$ T cells (1×10^5) were incubated on immobilized anti-CD3ε mAb. Various cytokine concentrations in each supernatant were measured by ELISA. (B) Mediastinal lymph node cells were prepared from SpA-challenged SpA-immunized mice and were incubated with immobilized anti-CD3ε mAb alone (α-CD3) or anti-CD3ε mAb plus IL-18 for 48 h, followed by cytoplasmic staining for IFN-γ and IL-13. (C) Lung homogenates were prepared from naive mice, SpA-immunized mice and SpA-immunized and -challenged mice, for the measurement of IL-18 by ELISA. Data are representative of three independent experiments with five mice in each group.

pulmonary $CD4^+$ T cells co-expressed CFSE (Fig. 4B), indicating that the donor $CD4^+$ T cells but few of the recipient cells, accumulated in the lung. Upon exposure to PBS, few CFSE-labeled cells or $CD4^+$ T cells were observed in the recipient lung (data not shown). These results demonstrate that SpA-specific $CD4^+$ DLN cells migrate and are fully activated after being exposed to SpA, eventually leading to the development of asthmatic inflammation. Blocking the action of IL-18 protected the mice from AHR and airway inflammation (Fig. 4A and C), suggesting that SpA-induced IL-18 in the airway in combination with administered SpA might differentiate the donor cells toward super T_h1 cells, thereby becoming highly pathogenic effector cells.

Involvement of human IL-18 in SpA-induced airway inflammation in transiently humanized mice

Finally, we investigated whether IL-18 is a therapeutic target for the treatment of airway inflammation in humans, associated with bacterial infection. First, we tried to generate mice transiently carrying human immune competent cells. We incubated PBMCs from healthy donors with SpA *in vitro*, transferred them into immunodeficient mice without T cells, B cells and NK cells and investigated whether human PBMCs settled in the recipient mice by calculating proportions of human $CD45^+$ hematopoietic cells (27) in peripheral immune tissues. Human $CD45^+$ cells were robustly observed in the spleen and peripheral blood of the recipient mice at day 7 after PBMC transfer (Fig. 5). About one-third of human $CD45^+$ cells co-expressed the human CD4 marker (Fig. 5).

Like the $CD4^+$ DLN cell-transplanted mice (Fig. 4), the SpA-stimulated humanized mice developed airway inflammation upon intranasal challenge with SpA, concomitant with dense accumulation of human $CD4^+$ T cells around the airway (Fig. 6C and D). This result indicated that SpA-stimulated human $CD4^+$ T cells migrated into the airway and presumably evoked pulmonary inflammation in response to exogenous SpA and endogenous IL-18. Upon PBS exposure, however, the host mice showed weak airway inflammation with modest but apparent accumulation of human $CD4^+$ cells (Fig. 6A and B). We investigated the role of human IL-18 and confirmed that anti-human IL-18 mAb (24) potently neutralized human IL-18 (Supplementary Figure 4 is available at *International Immunology* Online). This mAb prevented SpA-induced airway inflammation in these mice by attenuating airway accumulation of human $CD4^+$ T cells (Fig. 6E and F). Therefore, human cell-derived IL-18 might fully activate human SpA-specific T_h1 cells to become pathogenic effector cells. Indeed, human PBMCs could release super T_h1 cell-inducing cytokines, such as IL-12 and IL-18, and super T_h1 cytokines, such as IL-13 and IFN-γ, in response to SpA *in vitro* (Supplementary Figure 5 is

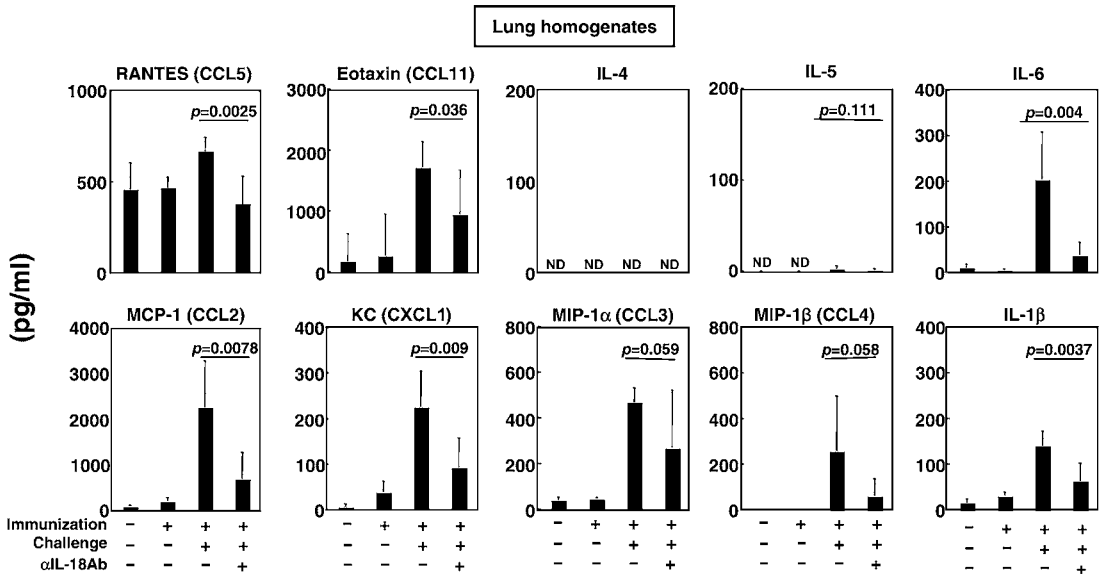

Fig. 3. IL-18 involvement in the induction of chemokines for neutrophils and eosinophils. Lung homogenates were prepared from the mice of three experimental groups (five mice per group) as shown in the legend to Fig. 1A and naive mice (five mice per group). The concentration of CCL2 (MCP-2), CCL3 (MIP1α), CCL4 (MIP1β), CCL5 (RANTES), CCL11 (Eotaxin), CXCL1 (KC), IL-1β, IL-4, IL-5 and IL-6 were measured by BioPlex®. Data are representative of three independent experiments.

available at *International Immunology* Online). Taken together, these results suggest that blocking the action of IL-18 is a potent therapeutic regimen for human airway inflammation initiated and/or exacerbated by bacterial infection.

Discussion

This study showed that endogenous IL-18 is critical for the development of SpA-induced asthmatic inflammation in mice. Upon intranasal exposure to SpA, mice immunized with SpA developed bronchial asthma-like airway inflammation (Fig. 1), concomitant with super T_h1-cell development and elevation of lung pro-inflammatory cytokine/chemokine production (Figs 2A–B and 3). Notably, lung IL-18 levels were significantly elevated in the SpA-induced asthmatic mice (Fig. 2C), and all these responses were prevented by inhibiting the action of IL-18 (Figs 1–3). Thus, IL-18 released from the lung exposed to SpA, together with SpA-presenting APC, might enter into mesenteric lymph node, in which SpA-specific T_h1 cells might develop toward super T_h1 cells. Furthermore, SpA-activated $CD4^+$ T cells, when transferred into naive mice, prepared the host mice to be highly responsive to intranasal administration of SpA, inducing bronchial asthma-like symptoms dependent upon endogenous IL-18 (Fig. 4). Finally, the humanized mice developed airway inflammation in a manner dependent on human IL-18 after intranasal SpA challenge (Fig. 6). IL-18 is important for *S. aureus*-associated asthmatic inflammation in mice and perhaps in humans.

We generated an airway inflammation model of temporally humanized mice by intranasal challenge with the bacterial protein, SpA. *Rag2*$^{-/-}$*Cγ*$^{-/-}$ mice injected with human PBMC transiently possessed human hematopoietic cells in their peripheral lymphoid organs (Fig. 5). Due of their lack of T, B and NK cells, the recipient mice could not recognize human donor cells as antigens. In contrast, human donor cells consisting of those types of lymphocytes had the potential to be activated by recognizing xenogeneic recipient cells in host mice. In fact, mice having received human PBMCs spontaneously exhibited non-specific inflammatory changes in their lungs and livers as compared with control *Rag2*$^{-/-}$*Cγ*$^{-/-}$ mice (Figs 1C and 6A; Supplementary Figure 6 is available at *International Immunology* Online). Despite apparent infiltration with human hematopoietic cells in the steady state (Fig. 6B), the basal lung inflammatory change was minimal (Fig. 6A), and the host mice survived without ill effects until sacrificed. This may be partly due to the inability of host cells to respond to IL-2, IL-4, IL-7, IL-9, IL-15 and IL-21 signals. Therefore, it could be said that these transiently humanized mice have limited inflammatory responses without SpA challenge. However, intranasal SpA challenge induced severe airway inflammation in the mice that received SpA-stimulated PBMCs (Fig. 6C and D). Human $CD4^+$ T cells were densely recruited into airway after SpA challenge (Fig. 6C). Administration of neutralizing anti-human IL-18 significantly inhibited the development of airway inflammation by diminishing the accumulation of the donor cells (Fig. 6E and F). SpA-specific human $CD4^+$ T cells activated by both SpA and IL-18 likely induced the development of airway inflammation by releasing human cytokines and chemokines that recruit human PBMCs. Additionally, some of human chemokines [e.g. CCL5 (RANTES)] might act on murine cells to migrate as well. Further study is required to identify the human factors involved in this airway inflammation. Nonetheless, our results strongly suggest that IL-18 is a potent clinical target for the treatment of bronchial asthma associated with *S. aureus* colonization or infection.

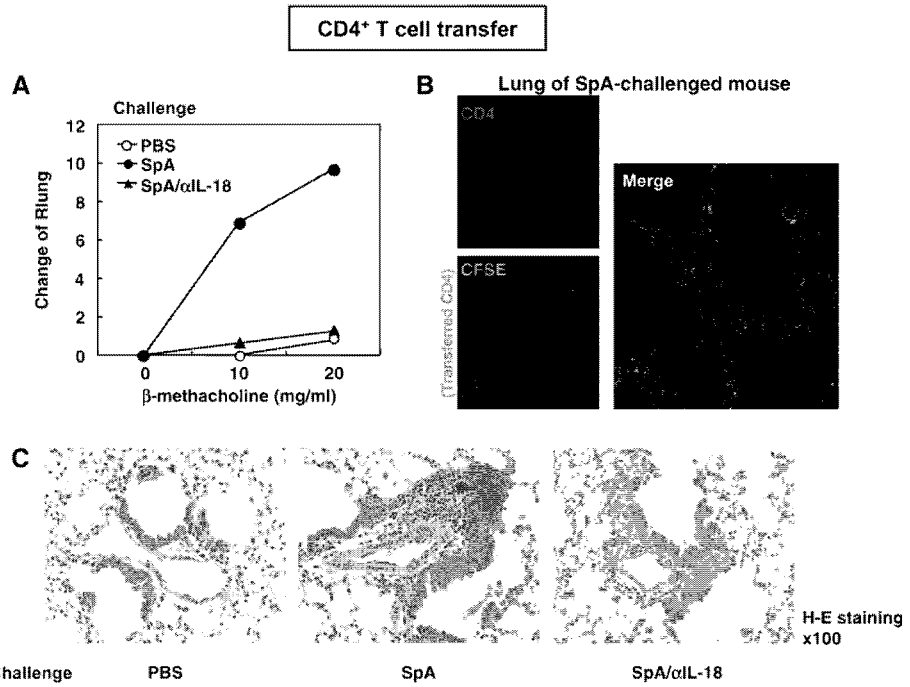

Fig. 4. SpA-sensitized CD4$^+$ T cells can transfer disease susceptibility. CD4$^+$ DLN cells isolated from mice immunized and boosted with SpA were labeled with CFSE and transferred into naive mice (1×10^7 per mouse). Recipient mice received intranasal challenge with SpA (250 μg/50 μl) (SpA), PBS or SpA and neutralizing anti-IL-18 antibodies (500 μg) (SpA/αIL-18). Twenty-four hours after the last SpA challenge, invasive measurement of AHR (A), confocal microscopic analysis for pulmonary CFSE (green) and CD4 (red) expression (B) and histological analysis (H&E) (C) were performed. Data are representative of three independent experiments with five mice.

It is unclear how human T cells recognize SpA in the transiently humanized mice. After *in vitro* stimulation with SpA, human PBMCs produced IFN-γ and IL-13 (Supplementary Figure 3 is available at *International Immunology* Online), and the CD4$^+$ T-cell population expanded (data not shown), suggesting that human APCs possess the potential to present SpA to the CD4$^+$ T cells in order to activate them. It was assumed that APCs included in the human donor cell preparation might serve as APCs for the SpA-specific human effector CD4$^+$ T cells in humanized mice as well. Alternatively, SpA-specific human effector cells might recognize SpA presented by xenogeneic mouse APCs by the mechanisms currently poorly understood.

We did not measure AHR of transiently humanized mice for a number of reasons. First, the recipients are *Rag2*$^{-/-}$*Cγ*$^{-/-}$ mice, which lack responsiveness to IL-2, IL-4, IL-7, IL-9, IL-15 and IL-21. Second, in general, mice are poor responders to human cytokines. Third, C57BL/6 mice, a background of *Rag2*$^{-/-}$*Cγ*$^{-/-}$ mice, are resistant to T_h2 type and super T_h1 cell type asthma (16). Fourth, is that transiently humanized mice are not homogeneous in terms of the degree of repopulation with human CD4$^+$ T cells.

Bronchial asthma is now recognized to have diverse immunopathogenesis. Recently, we demonstrated that intranasal challenge with OVA, plus the IL-18-inducible bacterial LPS, initiates robust bronchial asthma in mice immunized with OVA/CFA. Neutralization of IL-18 during OVA plus LPS challenges inhibits AHR in OVA-specific T_h1 cell-bearing mice, suggesting that OVA plus LPS activates T_h1 cells via endogenous IL-18. In contrast, the role of endogenous IL-18 in allergic T_h2/IgE-dependent asthma is not clearly defined. One report demonstrated only partial contribution of IL-18 to OVA inhalation-induced chronic allergic airway inflammation with remodeling (20). Another report demonstrated that IL-18 does not affect AHR and airway inflammation in allergic bronchial asthma (21), contrasting strikingly to the clear pathological role of endogenous IL-18 in non-allergic super T_h1 cell-dependent asthma (17).

Various types of cells, including macrophages and epithelial cells, can produce IL-18 (28). In this study, we observed elevation of lung IL-18 in the SpA-immunized mice only after intranasal SpA challenge (Fig. 2B), suggesting that IL-18 might be derived from airway constituents, such as respiratory epithelial cells and/or alveolar macrophages. Despite our intensive efforts, we could not observe obvious release of IL-18 from either type of cells after *in vitro* stimulation with SpA.

Recent reports have clearly shown that respiratory epithelial cells play a pivotal role in the development of T_h2 type murine asthma induced by airway exposure to the house dust mite, a common allergen of human asthma (29–31). It was believed that an antigen-specific T_h2-cell response develops only under the limited condition of immunization with the protein in combination with T_h2-cell adjuvant. Beyond this dogma, it was shown that multiple intra-tracheal challenges with house dust mite alone could trigger a T_h2-cell response without prior immunization with antigen/T_h2 adjuvant complex. Mice lacking TLR4 expression on their respiratory epithelial cells, but not hematopoietic cells, were able to evade T_h2 type asthma. Because house dust mites possess intrinsic TLR4 agonists, TLR4 on respiratory

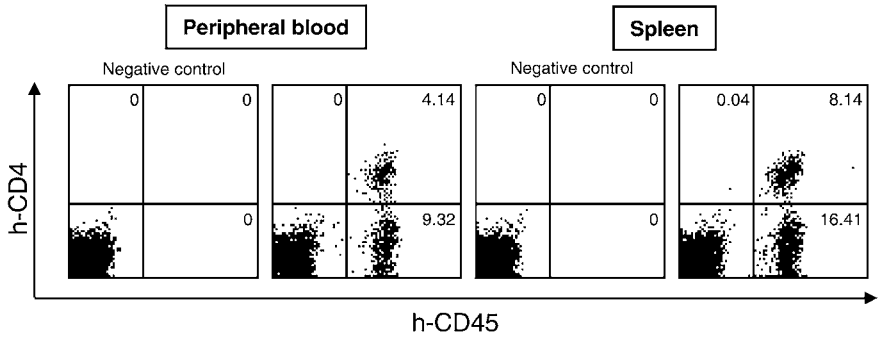

Fig. 5. Mice injected with human PBMCs. Seven days after SpA-stimulated PBMC (1×10^7) were injected into mice, the *Rag2*$^{-/-}$*C*$\gamma^{-/-}$ mice were analyzed for repopulation with human lymphocytes in their peripheral blood and spleen. Cells were incubated with PE-conjugated anti-human CD4 and FITC-labeled anti-human CD45 or a corresponding isotype-matched mAb (negative control). Data are representative of four independent experiments with five mice.

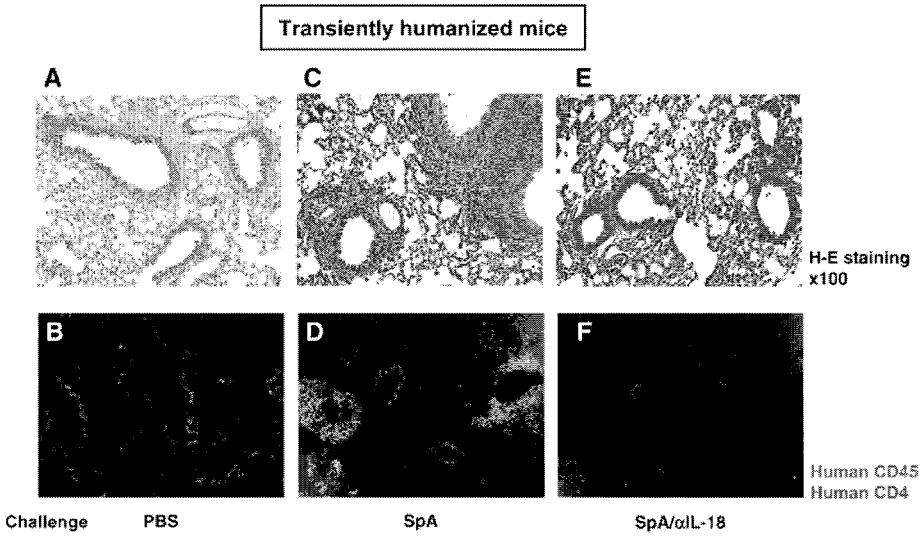

Fig. 6. Blocking the action of human IL-18 prevents SpA-induced airway inflammation in transiently humanized mice. Mice having received SpA-stimulated PBMC (1×10^7) were intranasally treated with PBS (A and B) or challenged with SpA (250 μg/50 μl) (SpA; C and D) or with SpA and neutralizing anti-human IL-18 antibody (300 μg) (SpA/αIL-18; E and F). Twenty-four hours after the last SpA challenge, lung specimens were sampled for histological analysis [hematoxylin and eosin (H&E)] (A, C and E) and for localization analysis of human CD4$^+$CD45$^+$ T cells (B, D and F). Data are representative of two independent experiments with five mice.

epithelial cells might recognize the agonist and produce T_h2-activating cytokines, such as IL-25, TSLP and IL-33 (29, 32, 33), eventually resulting in the development of T_h2 type asthma. As previously reported, daily topical application of SpA without T_h1 adjuvant can induce atopic dermatitis, in which super T_h1-cell development plays a critical role (19). Intriguingly, murine epidermal cells can release super T_h1 cell-activating IL-18 in response to SpA (34). Thus, SpA, like house dust mites in the airway, seems to exert dual actions as a T-cell antigen and adjuvant in the skin. These observations together with our present results suggest that respiratory mucosa and skin, particularly respiratory epithelial cells and epidermal cells, respectively, are the sites required for activation of T_h2 and/or super T_h1 cells. A similar mechanism might also be responsible for the airway asthmatic inflammation induced by SpA.

Accumulated evidence suggests the involvement of IL-18 in atopic diseases in humans. Patients with atopic dermatitis and bronchial asthma have higher levels of serum IL-18 than healthy volunteers (35, 36). In particular, serum IL-18 levels are shown to coincide with the disease severity of atopic dermatitis. Furthermore, gain-of-function polymorphisms of *IL-18* are observed in patients with atopic dermatitis and bronchial asthma (37–39). This implies that IL-18 is preferentially produced after airway and/or dermal colonization with microbes in those patients, eventually leading to the development of exposure site-specific super T_h1 cell-dependent allergic diseases.

Funding

Hitech Research Center grant from the Ministry of Education, Culture, Sports, Science and Technology of Japan (Project number; 06H025).

Acknowledgements

The authors have no conflicting financial interests to disclose.

References

1 Busse, W. W. and Lemanske, R. F. Jr. 2001. Asthma. *N. Engl. J. Med.* 344:350.
2 Wills-Karp, M. 2004. Interleukin-13 in asthma pathogenesis. *Immunol. Rev.* 202:175.
3 Wills-Karp, M. 1999. Immunologic basis of antigen-induced airway hyperresponsiveness. *Annu. Rev. Immunol.* 17:255.
4 Umetsu, D. T., McIntire, J. J., Akbari, O., Macaubas, C. and DeKruyff, R. H. 2002. Asthma: an epidemic of dysregulated immunity. *Nat. Immunol.* 3:715.
5 Anderson, B. 2008. Endotyping asthma: new insights into key pathogenic mechanisms in a complex, heterogenous disease. *Lancet.* 372:1107.
6 Frey, U. and Suki, B. 2008. Complexity of chronic asthma and chronic obstructive pulmonary disease: implications for risk assessment, and disease progression and control. *Lancet.* 372:1088.
7 Kubo, M., Ozaki, A., Tanaka, S., Okamoto, M. and Fukushima, A. 2006. Role of suppressor of cytokine signaling in ocular allergy. *Curr. Opin. Allergy Clin. Immunol.* 6:361.
8 Hoshino, A., Tsuji, T., Maatsuzaki, J. *et al.* 2004. STAT6-mediated signaling in Th2-dependent allergic asthma: critical role for the development of eosinophilia, airway ahyper-responsiveness and mucus hypersecretion, distinct from its role in Th2 differentiation. *Int. Immunol.* 16:1497.
9 Cohn, L., Elias, J. A. and Chupp, G. L. 2004. Asthma: mechanisms of disease persistence and progression. *Annu. Rev. Immunol.* 22:789.
10 Medoff, B. D., Thomas, S. Y. and Luster, A. D. 2008. T cell trafficking in allergic asthma: the ins and outs. *Annu. Rev. Immunol.* 26:205.
11 Bisgaard, H., Hermansen, M. N., Buchvald, F. *et al.* 2007. Childhood asthma after bacterial colonization of the airway in neonates. *N. Engl. J. Med.* 357:1487.
12 Kaisho, T. and Akira, S. 2006. Toll-like receptor function and signaling. *J. Allergy Clin. Immunol.* 117:979.
13 Akira, S., Uematsu, S. and Takeuchi, O. 2006. Pathogen recognition and innate immunity. *Cell* 124:783.
14 Singh, A. M. and Busse, W. W. 2006. Asthma exacerbations 2: aetiology. *Thorax* 61:809.
15 Cosentini, R., Tarsia, P., Canetta, C. *et al.* 2008. Severe asthma exacerbation: role of acute *Chlamydophila pneumoniae* and *Mycoplasma pneumoniae* infection. *Respir. Res.* 9:48.
16 Sugimoto, T., Ishikawa, Y., Yoshimoto, T., Hayashi, N., Fujimoto, J. and Nakanishi, K. 2004. Interleukin 18 acts on memory T helper cells type 1 to induce airway inflammation and hyperresponsiveness in a naive host mouse. *J. Exp. Med.* 199:535.
17 Hayashi, N., Yoshimoto, T., Izuhara, K., Matsui, K., Tanaka, T. and Nakanishi, K. 2007. T helper 1 cells stimulated with ovalbumin and IL-18 induce airway hyperresponsiveness and lung fibrosis by IFN-γ and IL-13 production. *Proc. Natl Acad. Sci. USA* 104:14765.
18 Tsutsui, H., Yoshimoto, T., Hayashi, N., Mizutani, H. and Nakanishi, K. 2004. Induction of allergic inflammation by interleukin-18 in experimental animal models. *Immunol. Rev.* 202:115.
19 Terada, M., Tsutsui, H., Imai, Y. *et al.* 2006. Contribution of IL-18 to atopic-dermatitis-like skin inflammation induced by *Staphylococcus aureus* product in mice. *Proc. Natl Acad. Sci. USA* 103:8816.
20 Yamagata, S., Tomita, K., Sato, R., Niwa, A., Higashino, H. and Tohda, Y. 2008. Interleukin-18-deficient mice exhibit diminished chronic inflammation and airway remodelling in ovalbumin-induced asthma model. *Clin. Exp. Immunol.* 154:295.
21 Hartwig, C., Tschernig, T., Mazzega, M., Braun, A. and Neumann, D. 2008. Endogenous IL-18 in experimentally induced asthma affects cytokine serum levels but is irrelevant for clinical symptoms. *Cytokine* 42:298.
22 Leung, D. Y. and Bieber, T. 2003. Atopic dermatitis. *Lancet* 361:151.
23 Gomez, M. I., Lee, A., Reddy, B. *et al.* 2004. *Staphylococcus aureus* protein A induces airway epithelial inflammatory responses by activating TNFR1. *Nat. Med.* 10:842.
24 Hamasaki, T., Hashiguchi, S., Ito, Y. *et al.* 2005. Human anti-human IL-18 antibody recognizing the IL-18-binding site 3 with IL-18 signaling blocking activity. *J. Biochem.* 138:433.
25 Ishikawa, Y., Yoshimoto, T. and Nakanishi, K. 2006. Contribution of IL-18-induced innate T cell activation to airway inflammation with mucus hypersecretion and airway hyperresponsiveness. *Int. Immunol.* 18:847.
26 Hata, H., Yoshimoto, T., Hayashi, N., Hada, T. and Nakanishi, K. 2004. IL-18 together with anti-CD3 antibody induces human Th1 cells to produce Th1- and Th2-cytokines and IL-8. *Int. Immunol.* 16:1733.
27 Goldman, J. P., Blundell, M. P., Lopes, L., Kinnon, C., DiSanto, J. P. and Thrasher, A. J. 1998. Enhanced human cell engraftment in mice deficient in RAG2 and the common cytokine receptor g chain. *Br. J. Haematol.* 103:335.
28 Nakanishi, K., Yoshimoto, T., Tsutsui, H. and Okamura, H. 2001. Interleukin-18 regulates both Th1 and Th2 responses. *Annu. Rev. Immunol.* 19:423.
29 Kato, A. and Schleimer, R. P. 2007. Beyond inflammation: airway epithelial cells are at the interface of innate and adaptive immunity. *Curr. Opin. Immunol.* 19:711.
30 Hammad, H., Chieppa, M., Perros, F., Willart, M. A., Germain, R. N. and Lambrecht, B. N. 2009. House dust mite allergen induces asthma via Toll-like receptor 4 triggering of airway structural cells. *Nat. Med.* 15:410.
31 Trompette, A., Divanovic, S., Visintin, A. *et al.* 2009. Allergenicity resulting from functional mimicry of a Toll-like receptor complex protein. *Nature* 457:585.
32 Cayrol, C. and Girard, J.-P. 2009. The IL-1-like cytokine IL-33 is activated after maturation by caspase-1. *Proc. Natl Acad. Sci. USA* 106:9021.
33 Saenz, S. A., Taylor, B. C. and Artis, D. 2008. Welcome to the neighborhood: epithelial cell-derived cytokines license innate and adaptive immune responses at mucosal sites. *Immunol. Rev.* 226:172.
34 Nakano, H., Tsutsui, H., Terada, M. *et al.* 2003. Persistent secretion of IL-18 in the skin contributes to IgE response in mice. *Int. Immunol.* 15:611.
35 Tanaka, T., Tsutsui, H., Yoshimoto, T. *et al.* 2001. Interleukin-18 is elevated in the sera from patients with atopic dermatitis and from atopic dermatitis model mice, NC/Nga. *Int. Arch. Allergy Immunol.* 125:236.
36 Tanaka, H., Miyazaki, N., Oashi, K. *et al.* 2001. IL-18 might reflect disease activity in mild and moderate asthma exacerbation. *J. Allergy Clin. Immunol.* 107:331.
37 Higa, S., Hirano, T., Mayumi, M. *et al.* 2003. Association between interleukin-18 gene polymorphism 105A/C and asthma. *Clin. Exp. Allergy* 33:1097.
38 Novak, N., Kruse, S., Potreck, J. *et al.* 2005. Single nucleotide polymorphisms of the IL18 gene are associated with atopic eczema. *J. Allergy Clin. Immunol.* 115:828.
39 Arimitsu, J., Hirano, T., Higa, S. *et al.* 2006. IL-18 gene polymorphisms affect IL-18 production capability by monocytes. *Biochem. Biophys. Res. Comm.* 342:1413.

International Immunology, Vol. 22, No. 6, pp. 479–489
doi:10.1093/intimm/dxq035
Advance Access publication 25 May 2010

Contribution of IL-33 to induction and augmentation of experimental allergic conjunctivitis

Saori Matsuba-Kitamura[1,2,*], Tomohiro Yoshimoto[1,3,4,*], Koubun Yasuda[1,4], Shizue Futatsugi-Yumikura[1], Yuuko Taki[1], Taichiro Muto[1], Tomohiro Ikeda[2], Osamu Mimura[2] and **Kenji Nakanishi[1,4]**

[1]Department of Immunology and Medical Zoology, [2]Department of Ophthalmology and [3]Laboratory of Allergic Diseases, Institute for Advanced Medical Sciences, Hyogo College of Medicine, Nishinomiya, Hyogo 663-8501, Japan
[4]Research for Evolutional Science and Technology, Japan Science and Technology Corporation, Saitama 332-0012, Japan

*These authors contributed equally to this study.

Correspondence to: K. Nakanishi; E-mail: nakaken@hyo-med.ac.jp

Transmitting editor: T. Hamaoka

Received 25 November 2009, *accepted* 15 March 2010

Abstract

IL-33, a member of the IL-1 family of cytokines, is the ligand for ST2 (IL-33Rα chain). IL-33 has the capacity to induce T_h2 cytokine production from T_h2 cells, mast cells and basophils, indicating that IL-33 has the potential to induce T_h2 cytokine-mediated allergic inflammation of the eye. Thus, we tested the pathological role of IL-33 in allergic conjunctivitis (AC). As reported elsewhere, animals immunized with ragweed pollen (RW)/alum and boosted with RW/PBS developed AC promptly (within 15 min) and conjunctival eosinophilic inflammation after a delay (within 24 h) in response to eye drop challenge with RW. Furthermore, RW-immunized mice, when topically challenged with both RW and IL-33, developed more striking eosinophilia in their conjunctiva without exacerbation of the clinical AC score. This *in vivo* IL-33 treatment significantly increased the capacity of T cells in the cervical lymph nodes of RW-immunized mice to produce IL-4, IL-5 and IL-13 upon challenge with anti-CD3 and anti-CD28 antibodies *in vitro*. Furthermore, the infiltrating cells were largely eosinophils and a small proportion of $CD4^+$ T cells, both of which express ST2. We also found that even splenic eosinophils express ST2 and show increased expression in response to IL-5, granulocyte–macrophage colony-stimulating factor (GM-CSF) or IL-33. Eosinophils, stimulated with IL-5 and/or GM-CSF, are responsive to IL-33, which induces production of IL-4 and chemokines. Finally, we showed that conjunctival tissues constitutively express biologically active IL-33, suggesting that IL-33 might play a crucial role in the induction and augmentation of AC.

Keywords: allergen, allergic conjunctivitis, chemokines, eosinophils, eotaxin, eye, IL-33, rodent, ST2, T_h2 cells

Introduction

Allergic conjunctivitis (AC) is a common ocular inflammatory disease. In developed countries, 20–30% of the population has experienced allergies, and 50% of these individuals suffer from ocular allergies (1, 2). AC can occur as mild transient inflammation such as seasonal AC or more severe chronic forms such as vernal keratoconjunctivitis (3, 4). AC is induced by a hypersensitivity response after exposure to an allergen. This response comprises two stages: an IgE-dependent early-phase response (within 15 min after exposure) and a T_h2 cytokine-dependent late-phase (12–24 h after exposure) response. Clinical symptoms and signs, such as itching, conjunctival swelling (chemosis) and congestion, occur as a result of the early-phase response. The late-phase response can involve conjunctival eosinophilic infiltration at 8–24 h after exposure to an allergen. Eosinophilic inflammation is not only a hallmark of AC but also a major cause of tissue injury and remodeling (5). Induction of the late-phase response is dependent on the accumulation of antigen-activated T_h2 cells (6–8), which produce IL-4, IL-5, IL-6, IL-9, IL-13 and chemokines. However, the precise mechanisms by which T_h2 cells promote the pathogenic immune responses in AC are still unclear. Indeed, it has not been clearly demonstrated that antigen-specific T_h2 cells actually infiltrate the conjunctiva. Furthermore, the mechanisms underlying the onset of AC and the progression to severe AC pathologies, such as vernal keratoconjunctivitis, remain unclear.

Recently, IL-33 was cloned and shown to be the ligand of ST2 (9). Initially, IL-33, like other members of the IL-1 family (10), was thought to be changed into its active form after cleavage with caspase-1 (9). However, a very recent study revealed that an even larger (31 kDa) form of IL-33 has strong biological activity and loses its activity after cleavage with caspase-1 (11). Our laboratory and others reported that T_h1 and T_h2 cells preferentially express IL-18Rα chain and ST2, respectively (12–14). In the same way that functional IL-18R is composed of an IL-18Rα and an IL-18Rβ chain (15, 16), functional IL-33R consists of an IL-33Rα (ST2) and an IL-33Rβ (IL-1Rβ) chain (17, 18). Although T_h2 cells preferentially express IL-33R, ST2 deficiency does not affect the development of T_h2 cells *in vitro* (19). Furthermore, inoculation with gastrointestinal nematodes normally induces IgE in $ST2^{-/-}$ mice (19). These results suggest the possibility that IL-33 principally augments allergic inflammation by enhancing T_h2 cytokine production from T_h2 cells (12). However, basophils and mast cells, when stimulated with IL-3 and IL-33, also produce large amounts of T_h2 cytokines (12, 20). Furthermore, we recently demonstrated that administration of IL-33 into naive mice induces ST2/MyD88-dependent airway hyperresponsiveness (AHR), goblet cell hyperplasia and eosinophilia by induction of IL-4, IL-5 and IL-13 in the lungs even in the absence of T cells (12). These results clearly suggest that IL-33 is an important cytokine that induces and augments T_h2 cytokine-mediated allergic inflammation by activation of T_h2 cells and possibly mast cells and basophils.

In this study, we examined the pathological role of IL-33 in the development of AC. Ragweed pollen (RW)-immunized mice develop early-phase AC manifestation and late-phase conjunctival eosinophilic inflammation after challenge with RW. Additional IL-33 challenge significantly increased the late-phase response without affecting the early-phase response. We found that antigen challenge induced recruitment of $ST2^+CD4^+$ T cells and $ST2^+$ eosinophils into the conjunctiva and additional IL-33 challenge significantly enhanced these responses. We also found that IL-5 induced IL-33R expression on eosinophils and that these IL-5-stimulated eosinophils produced IL-4 and chemokines in response to IL-33. Finally, we demonstrated that IL-33 is constitutively expressed in epithelial cells in the conjunctiva, suggesting its important role in induction and augmentation of AC.

Methods

Mice

BALB/c mice were purchased from Charles River Laboratories Japan Inc. (Yokohama, Japan). All animal experiments were performed in accordance with the guidelines of the Institutional Animal Care Committee of Hyogo College of Medicine.

Reagents

Recombinant human IL-33 and recombinant mouse IL-33 (rmIL-33) were made by Hokudo Co., Ltd (Sapporo, Japan) as described in our previous report (12). Purified antibody against mouse CD3 (2C11) was prepared in our laboratory. PE-anti-mouse CD4 (GK1.5), PE-anti-mouse Siglec-F (E50-2440) and biotin-anti-mouse IgE (R35-118) were purchased from BD Biosciences (San Diego, CA, USA). FITC-anti-mouse T1/ST2 was purchased from MD Biosciences (St Paul, MN, USA). Anti-CD28 and anti-CD16/32 were purchased from BioLegend (San Diego, CA, USA). Rat anti-mouse IgE (23G3) and affinity-purified goat anti-mouse IgG1 were purchased from Southern Biotechnology Associates Inc. (Birmingham, AL, USA). RW was purchased from PolyScience (Niles, IL, USA). RW extract was purchased from LSL Co. Ltd. (Tokyo, Japan). Mouse IL-3, IL-5 and granulocyte–macrophage colony-stimulating factor (GM-CSF) were purchased from Genetics Institute Inc. (Cambridge, MA, USA).

Experimental AC by active immunization

Mice were immunized with a mixture of RW (100 μg in 200 μl) and aluminum hydroxide hydrate gel (1 mg in 200 μl) (Sigma Aldrich, St Louis, MO, USA) by subcutaneous (s.c.) injection on day 0 and with RW/PBS (100 μg in 200 μl) by intraperitoneal (i.p.) injection on day 14. A week after the boost, mice (five mice per group) were challenged by topical administration of eye drops of RW (1 mg in 5 μl PBS per eye) or PBS (5 μl per eye). For IL-33 treatment, mice (five mice per group) were treated with IL-33 (1 μg in 5 μl PBS per eye) by topical administration of eye drops 1 h before and 2, 4 and 6 h after challenge with PBS or RW. A clinical score for AC was determined within 15–30 min after eye drop challenge with RW by examining chemosis, redness, lid edema, tearing, discharge and scratching behavior, based on the criteria described by Ozaki *et al.* (8) (Table 1). Two observers, one of who was an experienced ophthalmologist, carried out a blind test to evaluate clinical appearances and photographs. Scratching behavior was monitored for 30 s, and the frequency of scratching was counted and evaluated as follows: one to three times, mild; four to six times, moderate, and more than seven times, severe. The final AC score was calculated as the sum of the values for both eyes for each mouse. After 24 h, eyes were isolated for histological analysis, and the number of infiltrating cells was counted in the conjunctiva.

In vitro cytokine production

Cervical lymph node cells were isolated from mice and cultured at 2×10^5 0.2 ml^{-1} per well under stimulation with immobilized anti-CD3 and anti-CD28 (each 5 μg ml^{-1} for coating) in RPMI 1640 supplemented with 10% fetal bovine serum, 2-ME (50 μM), L-glutamine (2 mM), penicillin (100 U ml^{-1}) and

Table 1. Clinical evaluation of AC

	Absent	Mild	Moderate	Severe
Chemosis	0	1	2	3
Conjunctival redness	0	1	2	3
Lid edema	0	1	2	3
Tear and discharge	0	1	2	3
Scratching	0	1	2	3

Animals were examined clinically for signs of an early-phase response 15 min after topical application of RW. Chemosis, conjunctival redness, lid edema, tearing and discharge and scratching behavior were graded based on the grading table. Clinical appearances were evaluated blind by two observers. A score was given for each eye, and the final results show the sum of these scores for both eyes of each mouse. Scores shown in the figures are the average values for each mouse.

streptomycin (100 μg ml^{-1}). After 48 h stimulation, supernatants were harvested and the concentration of IL-4, IL-5 and IL-13 was tested using an ELISA kit. Eosinophils (1 × 10^5 0.2 ml^{-1} per well), sorted as described below, were stimulated with medium alone, IL-5 (40 ng ml^{-1}) and/or IL-33 (100 ng ml^{-1}) in the presence or absence of GM-CSF (50 ng ml^{-1}) for 24 h. Supernatants were harvested and tested for cytokines and chemokines using the Bio-Plex System (Bio-Rad, Hercules, CA, USA) as previously described (12).

Flow cytometry and cell purification

Spleen cells (2 × 10^6 ml^{-1}) from naive BALB/c mice were stimulated with medium alone, IL-5 (40 ng ml^{-1}) and/or IL-33 (100 ng ml^{-1}) in the presence or absence of GM-CSF (50 ng ml^{-1}) in 24-well plates for 24 h. After incubation, cells were harvested and examined for their expression of IL-33Rα chain and gated as side $scatter^{high}$ (SSC^{high}), $Siglec\text{-}F^+$, non-B and non-T cells by FACSCalibur (BD Biosciences). For preparation of splenic eosinophils, spleen cells from BALB/c mice were first depleted of $Thy1.2^+$ T cells and $B220^+$ cells using the MACS system (Miltenyi Biotec, Bergisch Gladbach, Germany) and then residual cells were stained and separated into $Siglec\text{-}F^+$ $CCR3^+$ cells using a fluorescence cell sorter (FACS Aria; BD Biosciences). The purity of sorted eosinophils was >99%.

ELISA assay

ELISA kits for IL-4, IL-5, IL-6, IL-13 and eotaxin (R&D Systems Inc., Minneapolis, MN, USA) were used. To measure IL-33 protein levels, we constructed an ELISA system to quantify mouse IL-33 protein levels. We made polyclonal rabbit IgG antibody to IL-33, which were further purified using a cyanogen bromide-activated Sepharose 4B column conjugated with rmIL-33 (10 mg). A 96-well plate (Coster 9018; Corning Incorporated, Corning, NY, USA) was coated with this affinity-purified anti-IL-33 polyclonal antibody and blocked with StartingBlock™ blocking buffer (Thermo Scientific, Rockford, IL, USA). Mouse IL-33 was detected with biotin-conjugated IL-33 mAb (clone; Nessy-1, AXXORA, San Diego, CA, USA) and streptavidin–HRP (BD Biosciences). The ELISA system was specific for mouse IL-33 and did not detect any other cytokines tested, including mouse IL-1β, IL-2, IL-4, IL-12, IL-18, tumor necrosis factor-α, IFN-γ, GM-CSF and human IL-33. IL-33 levels were determined by standard curves obtained using known amounts of rmIL-33. Total IgE was measured by ELISA as described previously (21). To detect RW-specific IgE in sera, biotin-conjugated RW extract was prepared in our laboratory.

Bioassay for mouse IL-33

Sorted bone marrow-derived basophils (10^5 0.2 ml^{-1} per well), obtained as described previously (12), were stimulated in the presence of IL-3 (20 U ml^{-1}) with rmIL-33 (0–100 ng ml^{-1}) or the soluble fraction (0–320 μg ml^{-1}) of homogenized conjunctival tissue with or without affinity-purified anti-IL-33 polyclonal antibody (20 μg ml). After 24 h, supernatants were harvested and tested for IL-6 by ELISA.

Homogenized conjunctival tissue

Bulbar conjunctiva, palpebral conjunctiva and the eyelid were isolated from each mouse and homogenized with PBS using Bead Smash 12 (Wakenyaku, Kyoto, Japan) for 1 min, five times. The homogenates were then centrifuged at 20 000 *g* for 5 min at 4°C. Supernatants (soluble fraction) were harvested and stored at −80°C prior to use.

Histology

Eyes were enucleated from mice, fixed in 4% PFA, embedded in paraffin, cut into 4-μm vertical plane sections including the optic nerve and stained with hematoxylin and eosin. Cytospan preparations of sorted $Siglec\text{-}F^+$ $CCR3^+$ (eosinophils) cells were stained with Wright–Giemsa.

Confocal microscopy

Frozen sections from freshly isolated conjunctival specimens were fixed and incubated with FITC-anti-mouse T1/ST2 and PE-anti-mouse CD4 or FITC-anti-mouse T1/ST2 and PE-anti-mouse Siglec-F at 4°C overnight. For IL-33 protein staining, samples were incubated in 4% PFA PBS (Wako, Osaka, Japan) at 4°C overnight. Paraffin-embedded sections (4-μm thick) of the conjunctiva were deparaffinized, heated in a microwave (500 W for 5 min, three times) in citrate buffer (pH 6.0) for antigen retrieval and then cooled at room temperature for 50 min before blocking. The sections were incubated in PBS containing 1.0% BSA and 0.05% Tween 20 for blocking. The sections were incubated with purified anti-IL-33 polyclonal antibody (rabbit IgG), at 4°C overnight, and then secondary antibody, biotin-conjugated goat antibody against rabbit IgG (Vector Laboratory, Burlingame, CA, USA), at room temperature for 30 min. Sections were then stained with a tertiary antibody, Alexa Fluor 555-conjugated streptavidin (Invitrogen, Carlsbad, CA, USA), at room temperature for 30 min. Coverslips were applied along with mounting medium containing 4′,6-diamidino-2-phenylindole (Invitrogen) and the sections were examined under a microscope Zeiss LSM 510 (Carl Zeiss, Thornwood, NY, USA). Computer software, Zeiss LSM 510 ver. 3.2 (Carl Zeiss), was used for image processing and analysis.

Quantitative real-time PCR

Total RNA was extracted from cervical lymph nodes or conjunctiva using the RNeasy Plus Mini Kit (Qiagen, Germantown, MA, USA) and the cDNA was synthesized using SuperScript III RNase H Reverse Transcriptase (Invitrogen). The expression of the gene was quantified with the TaqMan Gene Expression Assay (Applied Biosystems, Foster, CA, USA). The results were presented as relative expression values standardized with the expression of the gene encoding eukaryotic 18S ribosomal RNA (rRNA) (18S). Specific primers used for quantitative real-time PCR were ST2 (IL1RL1, interleukin 1 receptor-like 1) (Assay ID: Mm00516117_m1), IL-33 (*Il33*) (Assay ID: Mm00505403_m1) and 18S rRNA (*18S*) (Assay ID: Hs99999901_s1).

Statistics

Data are presented as means ± SDs. Statistical comparisons between two experimental groups were determined by the paired Student's *t*-test performed using GraphPad Instat

Software (San Diego, CA, USA). *P*-values <0.05 were considered statistically significant.

Results

Exogenous IL-33 fails to augment RW-induced immediate type AC

We first examined whether exogenous IL-33 has the capacity to enhance the early-phase response of RW-induced allergic inflammation (i.e. AC). We immunized BALB/c mice with RW by sequential s.c. injection of RW/alum, followed by i.p. injection of RW/PBS. Then, we challenged their eyes by topical administration of RW and/or IL-33. At 15 min after challenge, we scored the severity of AC (see Methods) by measuring the degree of chemosis, conjunctival redness, lid edema, tearing, discharge and scratching as described in Table 1. As reported elsewhere (8), naive mice after being challenged with RW developed AC-like manifestations (score, 3.3 ± 1.2) (Fig. 1A), suggesting that RW has the capacity to irritate conjunctiva in a non-specific manner. Compared with non-immunized and subsequently PBS- or RW-challenged control mice, RW-immunized mice developed severe AC (score, 11.6 ± 1.7; $P < 0.001$) (Fig. 1A) at 15 min after the challenge with RW, suggesting that RW challenge induces immediate type AC possibly in an IgE-dependent manner. Indeed, RW-immunized mice displayed RW-specific IgE in their sera (Fig. 1B). Eye drop challenge with RW and/or IL-33 did not change the level of RW-specific IgE in sera. We also found that this additional IL-33 challenge was unable to augment RW-induced AC, suggesting that RW is solely responsible for inducing AC manifestations after the challenge with RW and IL-33, although we cannot exclude the contribution of endogenous IL-33.

Exogenous IL-33 augments RW-driven conjunctival eosinophilic inflammation

We next compared the histological changes in the conjunctiva at 24 h after challenge with RW and/or IL-33 (Fig. 1C). Despite the failure of the additional IL-33 challenge to increase the AC score at 15 min (Fig. 1A), this treatment did significantly augment eosinophilic infiltration in the conjunctiva compared with that induced by RW challenge alone ($P < 0.05$; Fig. 1C and D). Thus, we investigated the mechanism behind exogenous IL-33-augmented eosinophilic infiltration. We compared the capacity of T cells from the cervical lymph nodes of RW-immunized mice at 24 h after challenge with RW and/or IL-33 to produce T_h2 cytokines upon stimulation with anti-CD3 and anti-CD28 antibodies *in vitro* (Fig. 2A). Lymph node cells from RW-immunized mice produced IL-4, IL5 and IL-13 upon stimulation *in vitro* and lymph node cells from RW-immunized and RW-challenged mice produced the same cytokines but at higher levels. Furthermore, additional *in vivo* IL-33 challenge significantly increased the capacity of lymph node cells to produce IL-4, IL-5 and IL-13 upon stimulation *in vitro*, although IL-33 challenge alone failed to do so (Fig. 2A). In addition to T_h2 cytokines, we simultaneously measured GM-CSF production from lymph node cells stimulated with anti-CD3 plus anti-CD28 *in vitro*. Although we could detect GM-CSF in the supernatants of lymph node cells from naive mice, the levels in RW-immunized mice after *in vivo* challenge with RW or RW plus IL-33 were significantly increased upon stimulation with anti-CD3 and anti-CD28 antibodies *in vitro* ($P < 0.01$ and $P < 0.05$, respectively) (Supplementary Figure 1 is available at *International Immunology* Online).

To clarify the mechanism of how RW and IL-33 synergistically increase T_h2 cytokine production, we examined IL-33R expression by cervical lymph node cells in RW-immunized mice after challenge with RW and/or IL-33. We found that RW challenge markedly increased IL-33Rα mRNA expression by lymph node cells ($P < 0.05$; Fig. 2B) and additional IL-33 challenge further increased this mRNA expression ($P < 0.05$; Fig. 2B). Thus, cervical lymph node cells in RW-immunized and RW plus IL-33-challenged mice increased their IL-33 responsiveness by increasing IL-33Rα chain expression. We also examined local levels of eotaxin, a potent chemoattractant for eosinophils (22–24), after challenge with RW and/or IL-33. Although we could detect eotaxin in the supernatants of homogenates of conjunctiva from naive mice, the supernatants from RW-immunized mice showed significantly increased levels of eotaxin after challenge with RW or RW plus IL-33 ($P < 0.05$; Fig. 2C). Taken together, these results strongly indicated that when T_h2 cells in cervical lymph nodes were stimulated with RW or RW plus IL-33, they were able to migrate to the conjunctiva and produce IL-4, IL-5 and IL-13 in the tissue. Then, IL-4 and IL-13 from T_h2 cells were able to act in combination to induce recruitment of eosinophils via eotaxin production in the conjunctival tissue (Fig. 2C).

Accumulation of IL-33Rα chain-positive cells in the conjunctiva of AC mice

Recruitment of T_h2 cells to the site of RW challenge is a key step in induction of AC. Thus, we tested whether topical RW application induces local accumulation of T_h2 cells. Since T_h2 cells express IL-33Rα (ST2) (12, 25), we examined T_h2 cell accumulation by measuring ST2 expression. Topical challenge with PBS or IL-33 alone did not induce accumulation of $ST2^+$ cells, while challenge with RW, particularly when combined with IL-33, induced marked accumulation of $ST2^+$ cells in the conjunctiva of RW-immunized mice. We detected a substantial number of $CD4^+$ T cells in the tissue and found that a large proportion (~70%) expressed ST2 (Fig. 3A). Thus, these challenges induced recruitment of RW-specific T_h2 cells into the conjunctiva. We also detected a much larger number of $ST2^+$ cells lacking CD4 compared with $ST2^+CD4^+$ T cells. By testing the cell type, we found that ~80% of these cells were eosinophils because they expressed Siglec-F (6, 26) (Fig. 3B). Taken together, these results indicated that, upon challenge with RW or RW plus IL-33, RW-specific T_h2 cells infiltrated the conjunctiva and produced IL-4 and IL-13, which in turn induced accumulation of $ST2^+$ eosinophils via local induction of eotaxin production in the conjunctiva.

IL-5, GM-CSF or IL-33 stimulation up-regulates the expression of IL-33Rα chain on eosinophils

Since RW challenge induced accumulation of T_h2 cells, which produce IL-4, IL-5, IL-13 and GM-CSF, we next determined

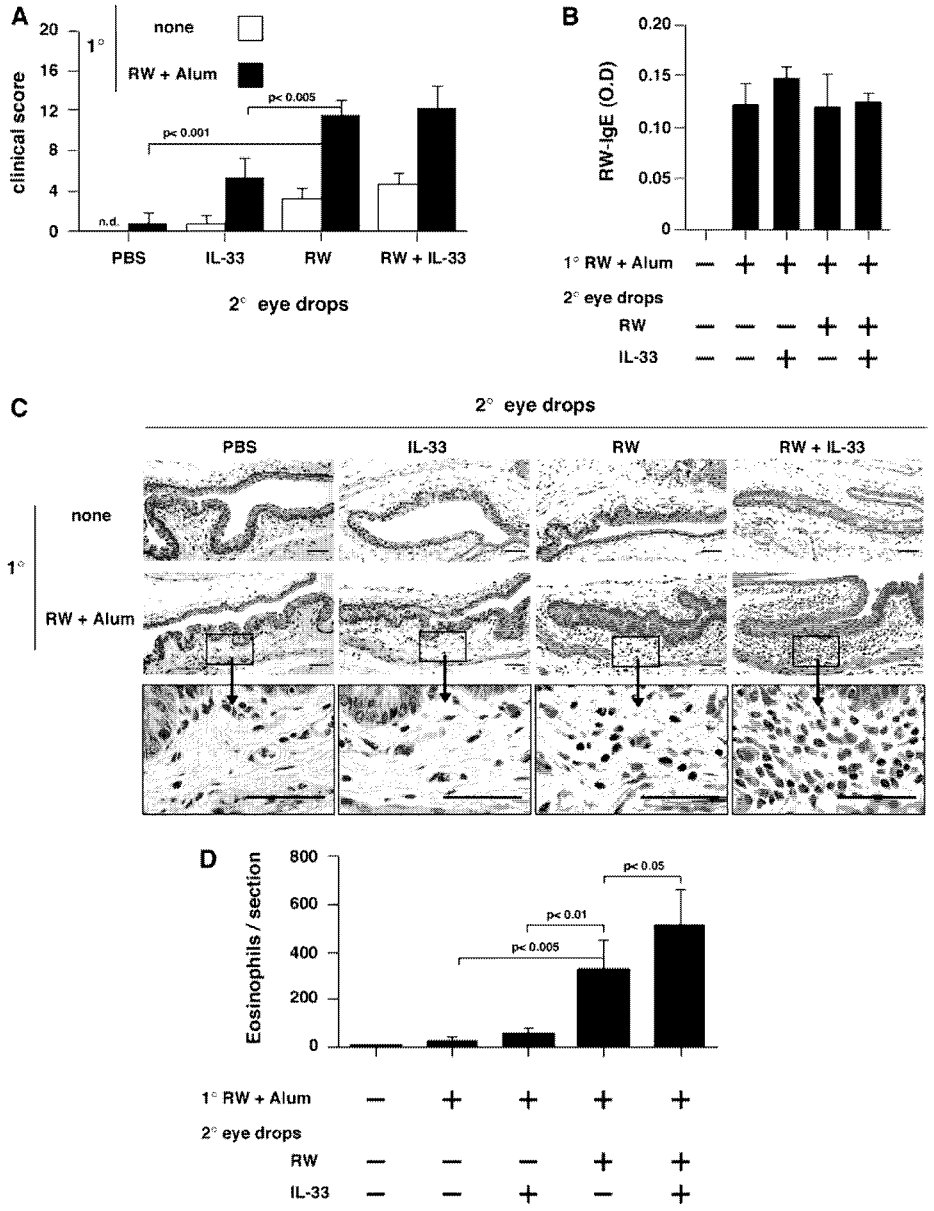

Fig. 1. Induction of AC and conjunctival eosinophilic inflammation by RW or RW plus IL-33 in RW-immunized mice. BALB/c mice were immunized with RW as described in Methods. Naive mice or RW-immunized mice were topically challenged with RW (1 mg 5 μl^{-1} PBS per eye) and/or IL-33 (1 μg 5 μl^{-1} PBS per eye). We administered IL-33 1 h before and 2, 4 and 6 h after challenge with PBS or RW. (A) Clinical score (as described in Methods) in the early-phase response, 15–30 min after challenge. (B) RW-specific IgE levels in the serum. (C) Twenty-four hours after challenge, eyes were enucleated from each group of mice (five mice per group), fixed in PFA, cut into 4-μm vertical plane sections including the optic nerve and stained with hematoxylin and eosin. Representative results from three independent experiments are shown; scale bar, 50 μm. (D) The number of eosinophils in the conjunctiva was counted. Results are shown as the mean ± SD of five animals per group and are representative of more than three independent experiments; n.d., not detected. Statistical differences between samples were determined using the Student's *t*-test (A and D).

which of these cytokines were responsible for inducing ST2 expression on eosinophils. We prepared splenic cells from naive mice and cultured them with medium alone or with IL-5, IL-33 or a combination of IL-5 and IL-33, in the presence or absence of GM-CSF for 24 h. We then compared IL-33Rα expression by eosinophils cultured under these various conditions. We selected eosinophils by gating SSC^{high}, Siglec-F^{+}, non-B and non-T cell fractions. Eosinophils cultured alone expressed IL-33Rα (23.6%). Neither IL-4 nor IL-13 stimulation increased IL-33Rα expression (data not shown). However,

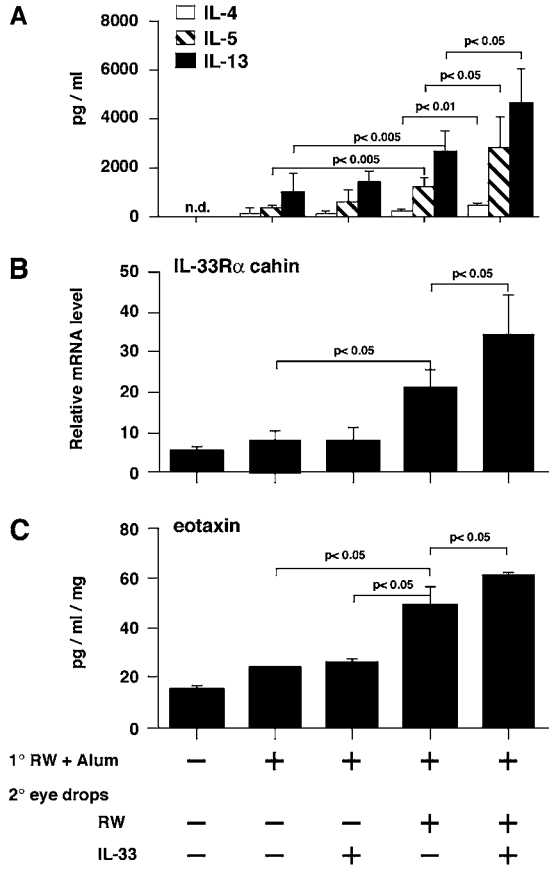

Fig. 2. Enhancement of T_h2 cytokine production and IL-33R expression by cervical lymph node cells after eye drop challenge with RW or RW plus IL-33. BALB/c mice were immunized with RW and topically challenged with RW (1 mg 5 μl^{-1} PBS per eye) and/or IL-33 (1 μg 5 μl^{-1} PBS per eye). Cervical lymph nodes cells were isolated from mice 24 h after challenge. Cell suspensions were cultured at 2×10^5 0.2 ml^{-1} per well under stimulation with immobilized anti-CD3 and anti-CD28 antibodies (each 5 μg ml^{-1} for coating). After 48 h of culture, supernatants were harvested and tested for IL-4, IL-5 and IL-13 by ELISA (A). The relative mRNA expression levels of IL-33Rα chain were determined by real-time PCR (B). (C) At 24 h post-challenge, eyes were enucleated from mice, homogenized and centrifuged as described in Methods. The obtained supernatants were tested for eotaxin by ELISA. Results shown are the mean ± SD of five animals per group and are representative of more than three independent experiments; n.d., not detected. Statistical differences between samples were determined using the Student's *t*-test.

stimulation with IL-5, IL-33 or IL-5 plus IL-33 strongly increased IL-33Rα expression (70.5, 69.8 and 84.7%, respectively) (Fig. 4A). Furthermore, stimulation with GM-CSF or GM-CSF plus IL-33 or with the combination of GM-CSF, IL-5 and IL-33 also strongly up-regulated IL-33Rα expression (66.0, 79.2 and 86.2%, respectively) (Fig. 4A). Thus, T_h2 cytokines, IL-4 and IL-13, play a critical role in recruitment of eosinophils via eotaxin production from conjunctival tissue and IL-5 and GM-CSF induce ST2 expression on eosinophils.

Next, we examined whether eosinophils become responsive to IL-33 after stimulation with IL-5, GM-CSF or IL-5 plus GM-CSF. We highly purified Siglec-F^+CCR3^+ cells by cell sorting (Fig. 4B) and light and electron microscopic examination revealed that sorted Siglec-F^+CCR3^+ cells were mature eosinophils (27) (Fig. 4C). We examined the IL-33 responsiveness of these cells by measuring their production of cytokines, IL-4 and IL-13, and chemokines, MIP-1α and MIP-1β. Stimulation with IL-5, IL-33 or GM-CSF alone only modestly induced eosinophils to produce IL-4 and chemokines. However, when eosinophils were stimulated with IL-33 in the presence of IL-5 and/or GM-CSF, they could produce substantial amounts of cytokine (IL-4) and chemokines (MIP-1α and MIP-1β) (Fig. 4D). However, compared with basophils or mast cells (12, 20), eosinophils only modestly produced IL-13 in response to IL-33 (Fig. 4D). Thus, activated eosinophils alone further increase accumulation of eosinophils by production of IL-4, which induces eotaxin in the tissue, and MIP-1α and MIP-1β, potent chemoattractants for eosinophils (24, 28–30). Taken together, these results indicated that eosinophils might induce inflammation of conjunctiva when stimulated with IL-5, GM-CSF and IL-33 by the production of cytokines, chemokines and possibly chemical mediators.

IL-33 production by conjunctiva

We finally examined whether conjunctiva contains biologically active IL-33. It has been reported that IL-33 is constitutively expressed in the nucleus of endothelial and epithelial cells (31, 32). Immunohistochemical analysis revealed that IL-33 is constitutively expressed in the nucleus of epithelial cells of the conjunctiva of naive mice (Fig. 5A). Measurement of IL-33 mRNA expression indicated that the conjunctiva of naive mice constitutively expressed IL-33 mRNA and increased this message moderately after challenge with topical RW (Fig. 5B). We also found that naive mice possess IL-33 protein in their conjunctiva (Fig. 5C) and also increase this protein content moderately after topical RW application (Fig. 5C). These results strongly suggested that IL-33 is constitutively expressed in conjunctiva and topical RW administration weakly but significantly increased IL-33 levels. Next, we examined whether this IL-33 protein was biologically active. For this purpose, we measured the capacity of IL-33 to induce production of IL-6 from bone marrow-derived basophils. Basophils incubated with IL-3 produced IL-6 in a dose-responsive manner upon challenge with various doses of IL-33 *in vitro* (12). Addition of anti-IL-33 antibody completely inhibited IL-6 production (Fig. 5D). We simultaneously stimulated basophils in the presence of IL-3 with various doses of supernatant from the homogenized conjunctiva of naive mice or RW-challenged mice. Basophils produced IL-6 in a dose-responsive manner in response to these supernatants. Addition of anti-IL-33 antibody completely inhibited IL-6 production, suggesting that these homogenates contain functionally active IL-33 (Fig. 5D). From the results of this bioassay, we could also estimate the level of biologically active IL-33 in the homogenized conjunctiva from naive mice and RW-challenged mice and revealed that they have similar IL-33 activity (naive mice, 23.7 ng mg^{-1} protein, and RW-challenged mice, 25.5 ng mg^{-1} protein).

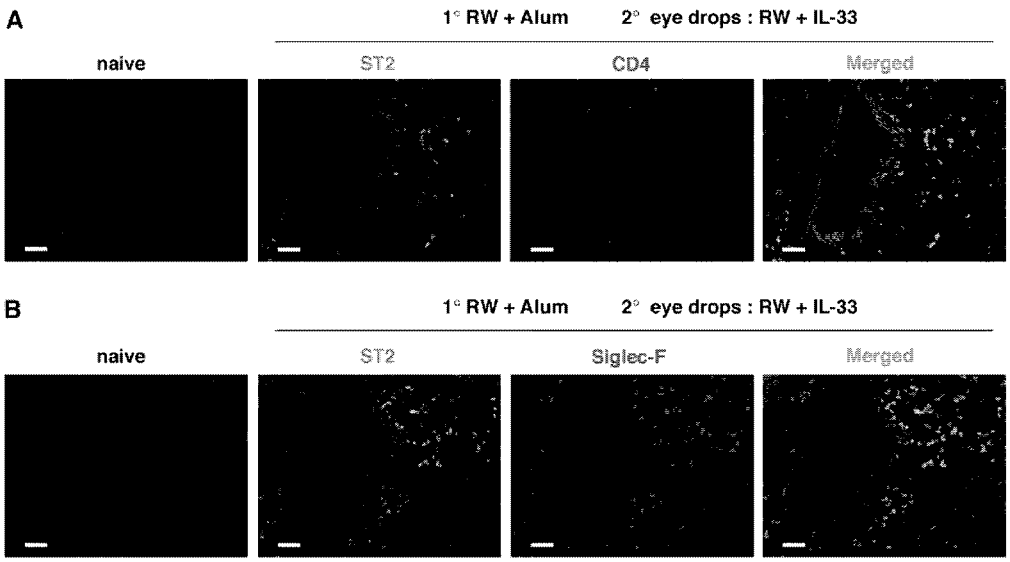

Fig. 3. Confocal microscopic examination of IL-33Rα chain$^+$ cells in the conjunctiva tissue of RW-immunized mice after challenge with RW and/or IL-33. BALB/c mice were immunized with RW and topically challenged with RW (1 mg 5 μl^{-1} PBS per eye) and IL-33 (1 μg 5 μl^{-1} PBS per eye). At 24 h post-challenge, eyes were enucleated from naive and treated mice (five mice per group) and frozen. Frozen sections were fixed and incubated with antibodies to mouse ST2 and CD4 (A) or mouse ST2 and Siglec-F (B) and then examined by confocal microscopy. (A) CD4, red; ST2, green, and co-localization, yellow (merged). (B) Siglec-F, red; ST2, green, and co-localization, yellow (merged); scale bar, 50 μm. Representative results from two independent experiments are shown.

Discussion

The findings of previous studies strongly suggest that IL-33 is a powerful inducer of allergic inflammation (9, 12, 33–35). IL-33 stimulates antigen-stimulated T_h2 cells to increase production of IL-4 modestly and IL-5 and IL-13 strongly (9, 12). IL-33 also induces mouse basophils and mast cells, which express IL-33R abundantly, to produce IL-4, IL-6, IL-9, IL-13, GM-CSF and chemokines (RANTES, MIP-1α, MIP-1β and MCP-1) (12). Intranasal administration of IL-33 induces AHR, goblet cell hyperplasia and eosinophilia in the lungs of mice even in the absence of acquired immunity, and this effect is entirely dependent on ST2, MyD88 and IL-13 (12). Human basophils also produce IL-4, IL-8 and IL-13 in response to IL-3 plus IL-33 (36, 37). These results indicate an important role for IL-33 and ST2 in allergic inflammatory responses.

We have shown previously that the serum level of IL-33 is significantly elevated in patients with Japanese cedar pollinosis (35). In addition, IL-33 is reported to be markedly elevated in the sera of patients during anaphylactic shock (34). We have also shown a significant association between Japanese cedar pollinosis susceptibility and IL-33 polymorphism (rs1929992) (35). This was the first demonstration of the involvement of IL-33 in human allergic diseases. Subsequent studies also revealed that single-nucleotide polymorphisms within the genes encoding the ST2/IL-33Rα chain (rs1420101 on 2q12) and IL-33 (rs3939286 on 9p24) were significantly associated with blood eosinophil counts and allergic asthma (38). These studies prompted us to study the role of IL-33 in experimental AC.

In this study, we first demonstrated that RW challenge induced AC promptly and then eosinophilic inflammation in the conjunctiva of RW-immunized mice (Fig. 1A). Next, we demonstrated that additional IL-33 challenge significantly increased eosinophilic infiltration in the conjunctiva of RW-immunized mice at 24 h after challenge (Fig. 1C). Then, we investigated the mechanism of IL-33 activity and found that additional *in vivo* IL-33 treatment increased the capacity of T_h2 cells in regional lymph nodes of RW-immunized mice to produce T_h2 cytokines in response to anti-CD3 and anti-CD28 antibodies *in vitro* (Fig. 2A). Although further studies are required, we can speculate that IL-33, applied topically, and dendritic cells, pulsed with RW peptide, reach cervical lymph nodes via the afferent lymphatic vessel and in combination induce and activate RW-specific T_h2 cells. We also found that cells in cervical lymph nodes increase their expression of IL-33Rα chain after challenge with RW or RW plus IL-33 (Fig. 2B), suggesting that antigenic stimulation, particularly with IL-33, up-regulates expression of IL-33Rα chain. We detected substantial numbers of IL-33Rα$^+$ CD4$^+$ T cells in the conjunctiva suggesting that T_h2 cells, after challenge with RW or RW plus IL-33, migrate from cervical lymph nodes to the conjunctiva and play a critical role in the development of experimental AC (Fig. 3A).

Another striking future of this experimental AC model is the massive infiltration of IL-33Rα$^+$ eosinophils in the conjunctiva (Fig. 3B). This finding indicates that T_h2 cells are responsible for inducing recruitment of IL-33Rα$^+$ eosinophils in the conjunctiva. We found that topical application of RW and IL-33 strongly induces local production of eotaxin,

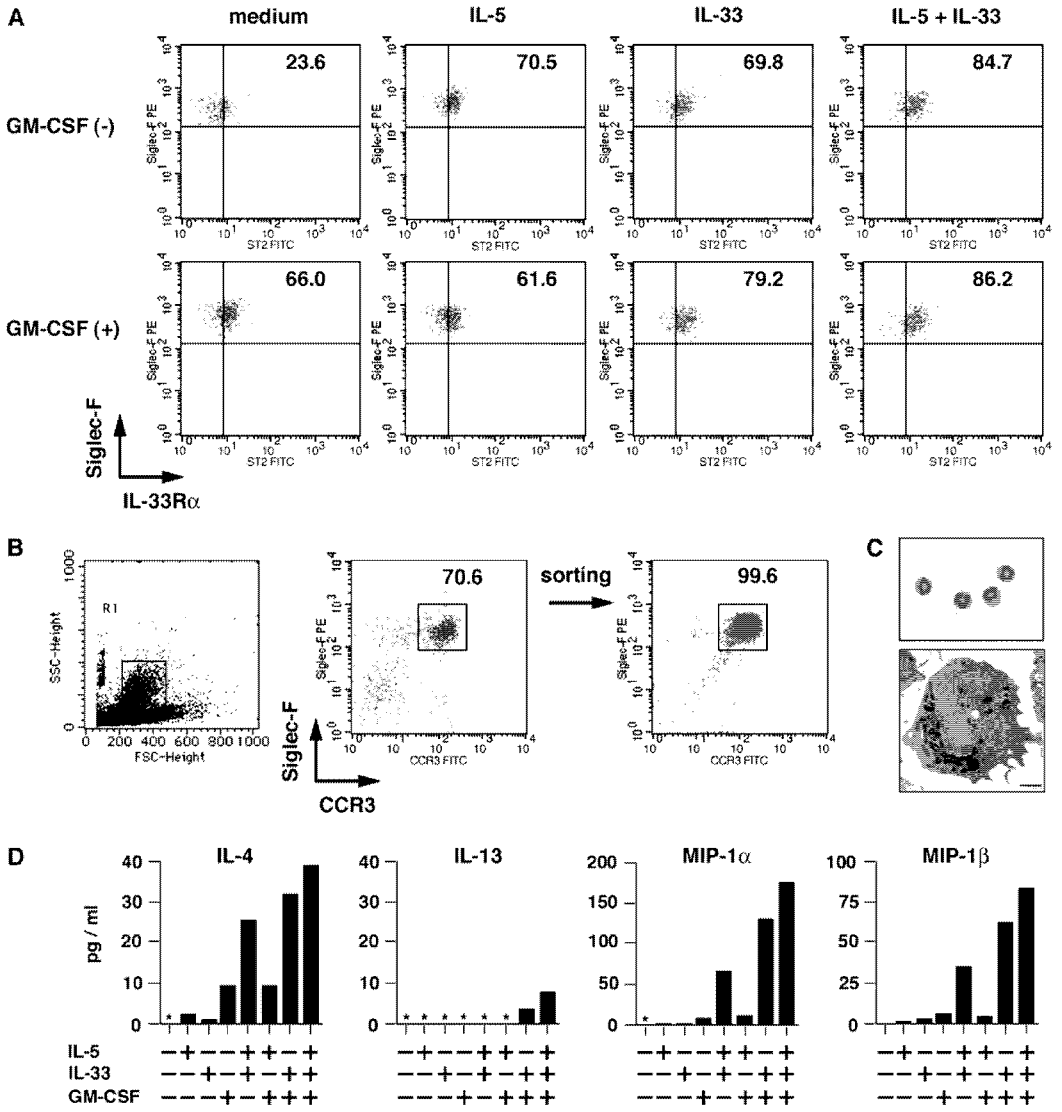

Fig. 4. Eosinophils stimulated with IL-5 increase IL-33Rα chain expression and become responsive to IL-33. (A) Spleen cells (2×10^6 ml^{-1}) from naive BALB/c mice were stimulated with medium alone, IL-5 (40 ng ml^{-1}) and/or IL-33 (100 ng ml^{-1}) in the presence or absence of GM-CSF (50 ng ml^{-1}) in 24-well plates for 24 h. Cultured cells, gated as SSC^{high}, Siglec-F$^+$, non-B and non-T cells, were examined for expression of IL-33Rα chain by flow cytometry. Numbers indicate the percentage of Siglec-F$^+$ IL-33Rα chain$^+$ cells. (B) Flow cytometric analysis of the expression of SSC and forward scatter (left) or Siglec-F and CCR3 (middle) by freshly prepared splenic non-B and non-T cells from naive BALB/c mice. Expression of Siglec-F and CCR3 by sorted cells is also shown (right). The numbers above the outlined areas indicate the percentage of Siglec-F$^+$ CCR3$^+$ cells. (C) Sorted Siglec-F$^+$ CCR3$^+$ (eosinophils) cell populations were stained by Wright–Giemsa staining (×100) (upper) and subjected to electron microscopic examination (lower); scale bar, 1 μm. (D) The sorted eosinophils (1×10^5 0.2 ml^{-1} per well) were stimulated with medium alone, IL-5 (40 ng ml^{-1}) and/or IL-33 (100 ng ml^{-1}) in the presence or absence of GM-CSF (50 ng ml^{-1}) for 24 h. Supernatants were harvested and tested for IL-4, IL-13, MIP-1α and MIP-1β using the Bio-Plex System. Asterisk indicates not detected. Representative results from three (A) or two (C–D) independent experiments are shown.

a chemoattractant for eosinophils, in the conjunctiva. Since IL-4 or IL-13 are known to induce production of eotaxin by fibroblasts (22–24), we propose that T_h2 cells induce recruitment of eosinophils by production of IL-4 and IL-13 in the conjunctiva. It is also important to determine which T_h2 cytokine can up-regulate IL-33Rα expression on eosinophils. We found that IL-5 strongly up-regulated IL-33Rα expression on eosinophils (Fig. 4A). Furthermore, IL-33 along with IL-5 stimulated eosinophils to produce IL-4, MIP-1α and MIP-1β (Fig. 4D). We also demonstrated that, like IL-5, GM-CSF strongly up-regulates IL-33Rα expression on eosinophils and IL-33 along with GM-CSF stimulates eosinophils to produce IL-4, MIP-1α and MIP-1β (Fig. 4A and D). Interestingly, IL-33 is able to up-regulate its own receptor (Fig. 4A).

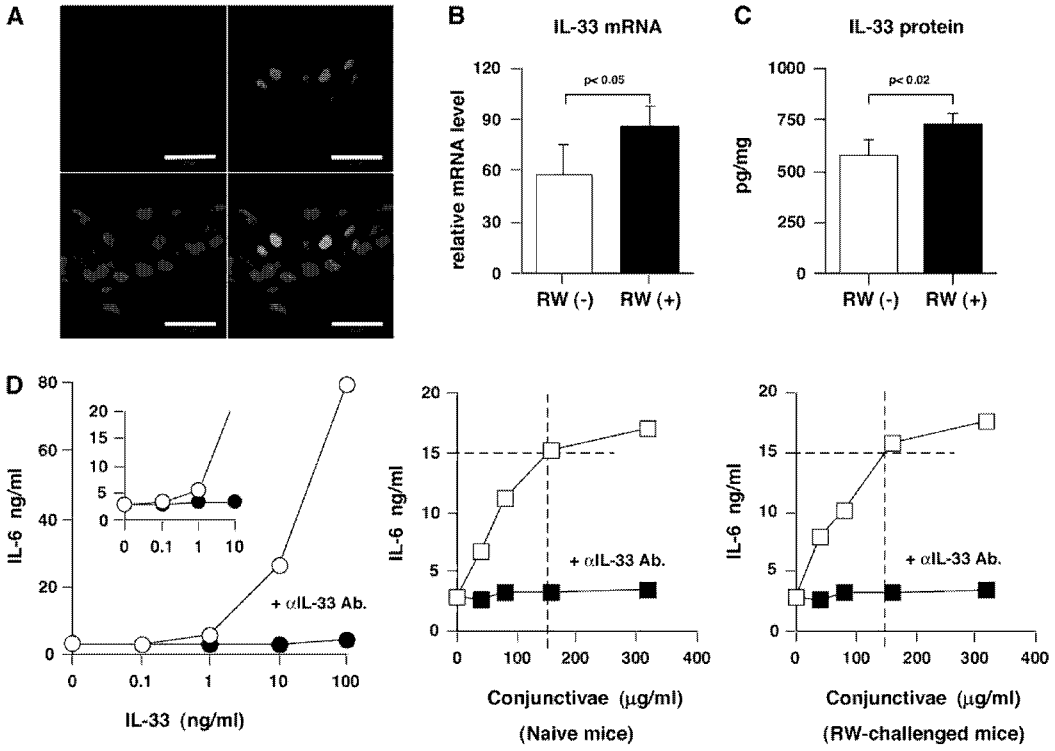

Fig. 5. Expression of IL-33 by the conjunctiva of mice before and after eye drop challenge with RW. (A) Eyes were enucleated from naive BALB/c mice, fixed in 4% PFA, embedded in paraffin and cut into 4-μm vertical plane sections including the optic nerve. Immunofluorescence staining was performed using an anti-IL-33 polyclonal antibody made in our laboratory. IL-33 expression was detected by red staining and DNA was counterstained with 4′,6-diamidino-2-phenylindole (blue); scale bar, 20 μm. (B and C) IL-33 mRNA and protein levels in the conjunctival tissue of naive or eye drop-challenged mice (1 mg 5 μl^{-1} PBS per eye, every 2 h, three times). At 24 h post-challenge, the conjunctiva was isolated from each group of mice. Relative IL-33 mRNA expression was measured by real-time PCR (B). IL-33 protein from homogenized conjunctiva was measured by ELISA (C). Results show the mean ± SD of five animals per group and are representative of two independent experiments. Statistical differences between samples were determined using the Student's *t*-test (B and C). (D) Bone marrow-derived basophils were cultured with rmIL-33 (0–100 ng ml^{-1}) or the soluble fraction from homogenized conjunctiva (0–320 mg ml^{-1}) from naive or RW-challenged mice, as described above for part B and C, in the presence or absence of anti-IL-33 polyclonal antibody (10 μg ml^{-1}) for 24 h. Supernatants were harvested and tested for IL-6 production by ELISA. Representative results from two independent experiments are shown.

However, IL-33 alone cannot induce production of IL-4 and chemokines. The receptors for IL-5 and GM-CSF are composed of a ligand-binding chain and a signal-transducing common β chain. Taken together, these results strongly indicated that two distinct signals, a common β-mediated signal (by IL-5 and/or GM-CSF) and an ST2/MyD88-mediated signal (by IL-33), are essential for induction of cytokine and chemokine production from eosinophils. A recent study indicated that ST2 expression by T_h2 cells is regulated by GATA3 and STAT5 (39). IL-5 and GM-CSF are both STAT5 activators (40). These findings indicated that IL-33 and STAT5 activators increase ST2 expression not only by T_h2 cells but also by eosinophils. Thus, our data strongly indicated that T_h2 cytokines play a crucial role in the recruitment and activation of eosinophils.

In contrast to murine splenic eosinophils, as shown in this report, freshly isolated human peripheral blood eosinophils do not express ST2 on their cell surface, although they express ST2 mRNA (41, 42). However, human peripheral blood eosinophils start to express ST2 molecules on their cell surface after incubation with medium alone for 24 h and ST2 expression is increased further after incubation with GM-CSF (41) but not with IL-33 (42). Human eosinophils can produce IL-8 when stimulated with IL-33 in the presence of IL-5 or GM-CSF (36, 41). Furthermore, IL-33 potently activates and induces superoxide production and degranulation in human eosinophils (41). It is intriguing to speculate that topical challenge with RW and IL-33 which in combination stimulate T_h2 cells to produce T_h2 cytokines in the conjunctiva and IL-5 from T_h2 cells in combination with IL-33 stimulate these IL-33Rα$^+$ eosinophils in the conjunctiva to produce cytokines, chemokines and eosinophil-derived cationic proteins, resulting in the exacerbation of AC.

Recent studies by our laboratory and others (43–45) suggest the importance of basophils in the induction of the T_h2 response against protease antigens, antigen–IgE complexes or intestinal parasites. Based on the findings of these studies, we could suspect that RW–IgE complexes might enhance uptake of RW by basophils via the receptor Fc epsilon receptor I and the resulting RW-pulsed basophils

might induce or enhance development of RW-specific T_h2 cells *in vivo*. Thus, it is crucial to clarify the antigen-presenting cell function of basophils in the induction of pollen-specific T_h2 cells in RW-immunized mice.

We further revealed that IL-33 is constitutively expressed in epithelial cells in the conjunctiva of normal mice by immunohistochemical staining (Fig. 5A). Furthermore, a biological assay of IL-33 clearly revealed that biologically active IL-33 is constitutively expressed in the conjunctiva (Fig. 5D) and that the level of this molecule is significantly increased by exposure of the conjunctiva to RW (Fig. 5B and C). In general, members of the IL-1 cytokine family, including IL-1α, IL-1β and IL-18, are widely expressed in hematopoietic cells and are important for inflammatory responses and host defenses (16, 46). In addition, human IL-33 is expressed in the nucleus of epithelial cells, including those of the skin and gastrointestinal tract, where pathogens, allergens and other environmental agents are frequently encountered (32). Thus, IL-33, in a similar way to the prototype 'alarmin' high-mobility group box 1 (47), may work as an endogenous danger signal (32, 48). Indeed, IL-33 can be released after endothelial cell damage or injury (11). Pollen grains contain allergen proteins, enzymes (49) and bioactive lipids (50), the latter two of which might be involved in the pathogenesis of allergic diseases via an IgE-independent mechanism. Furthermore, RW releases serine and cysteine endopeptidases (51, 52). In addition, RW contains nicotinamide adenine dinucleotide phosphate oxidase that can generate reactive oxygen species in the epithelial cells of the conjunctiva (53). Thus, IL-33 could be increased and released when epithelial cells are stimulated or damaged by RW-derived serine and cysteine endopeptidases or by RW-mediated oxidative stress. It is possible that scratching further induces the production of IL-33 from conjunctiva. Once IL-33 is released by epithelial cells, like exogenous IL-33, this endogenous IL-33 together with RW-pulsed dendritic cells enters lymph nodes via the afferent lymphatic vessel and stimulates RW-specific T_h2 cells to develop into cells that migrate and produce IL-4, IL-5 and IL-13 in the conjunctiva. Thus, our results strongly suggest the contribution of endogenous IL-33 to the activation of T_h2 cells and eosinophils, which in combination induce AC. In this way, IL-33 might represent an important therapeutic target for the treatment of AC.

Supplementary data

Supplementary Figure 1 is available at *International Immunology* Online.

Funding

Grant-in-Aid for Scientific Research on Priority Areas and a Hi-Tech Research Center grant from the Ministry of Education, Culture, Sports, Science and Technology of Japan and a Grant-in-Aid for Scientific Research (No. 19390121) from the Japan Society for the Promotion of Science and the Ministry of Health.

References

1 Bielory, L. 2000. Allergic and immunologic disorders of the eye. Part II: ocular allergy. *J. Allergy Clin. Immunol.* 106:1019.
2 Stahl, J. L. and Barney, N. P. 2004. Ocular allergic disease. *Curr. Opin. Allergy Clin. Immunol.* 4:455.
3 Calonge, M. 1999. Classification of ocular atopic/allergic disorders and conditions: an unsolved problem. *Acta Ophthalmol. Scand. Suppl.* 228:10.
4 Niederkorn, J. Y. 2008. Immune regulatory mechanisms in allergic conjunctivitis: insights from mouse models. *Curr. Opin. Allergy Clin. Immunol.* 8:472.
5 Miyazaki, D., Tominaga, T., Yakura, K. *et al.* 2008. Conjunctival mast cell as a mediator of eosinophilic response in ocular allergy. *Mol. Vis.* 14:1525.
6 Carreras, I., Carreras, B., McGrath, L., Rice, A. and Easty, D. L. 1993. Activated T cells in an animal model of allergic conjunctivitis. *Br. J. Ophthalmol.* 77:509.
7 Magone, M. T., Chan, C. C., Rizzo, L. V., Kozhich, A. T. and Whitcup, S. M. 1998. A novel murine model of allergic conjunctivitis. *Clin. Immunol. Immunopathol.* 87:75.
8 Ozaki, A., Seki, Y., Fukushima, A. and Kubo, M. 2005. The control of allergic conjunctivitis by suppressor of cytokine signaling (SOCS)3 and SOCS5 in a murine model. *J. Immunol.* 175:5489.
9 Schmitz, J., Owyang, A., Oldham, E. *et al.* 2005. IL-33, an interleukin-1-like cytokine that signals via the IL-1 receptor-related protein ST2 and induces T helper type 2-associated cytokines. *Immunity* 23:479.
10 Arend, W. P., Palmer, G. and Gabay, C. 2008. IL-1, IL-18, and IL-33 families of cytokines. *Immunol. Rev.* 223:20.
11 Cayrol, C. and Girard, J. P. 2009. The IL-1-like cytokine IL-33 is inactivated after maturation by caspase-1. *Proc. Natl Acad. Sci. USA* 106:9021.
12 Kondo, Y., Yoshimoto, T., Yasuda, K. *et al.* 2008. Administration of IL-33 induces airway hyperresponsiveness and goblet cell hyperplasia in the lungs in the absence of adaptive immune system. *Int. Immunol.* 20:791.
13 Xu, D., Chan, W. L., Leung, B. P. *et al.* 1998. Selective expression and functions of interleukin 18 receptor on T helper (Th) type 1 but not Th2 cells. *J. Exp. Med.* 188:1485.
14 Yoshimoto, T., Takeda, K., Tanaka, T. *et al.* 1998. IL-12 up-regulates IL-18 receptor expression on T cells, Th1 cells, and B cells: synergism with IL-18 for IFN-gamma production. *J. Immunol.* 161:3400.
15 Born, T. L., Thomassen, E., Bird, T. A. and Sims, J. E. 1998. Cloning of a novel receptor subunit, AcPL, required for interleukin-18 signaling. *J. Biol. Chem.* 273:29445.
16 Nakanishi, K., Yoshimoto, T., Tsutsui, H. and Okamura, H. 2001. Interleukin-18 regulates both Th1 and Th2 responses. *Annu. Rev. Immunol.* 19:423.
17 Ali, S., Huber, M., Kollewe, C., Bischoff, S. C., Falk, W. and Martin, M. U. 2007. IL-1 receptor accessory protein is essential for IL-33-induced activation of T lymphocytes and mast cells. *Proc. Natl Acad. Sci. USA* 104:18660.
18 Chackerian, A. A., Oldham, E. R., Murphy, E. E., Schmitz, J., Pflanz, S. and Kastelein, R. A. 2007. IL-1 receptor accessory protein and ST2 comprise the IL-33 receptor complex. *J. Immunol.* 179:2551.
19 Hoshino, K., Kashiwamura, S., Kuribayashi, K. *et al.* 1999. The absence of interleukin 1 receptor-related T1/ST2 does not affect T helper cell type 2 development and its effector function. *J. Exp. Med.* 190:1541.
20 Ho, L. H., Ohno, T., Oboki, K. *et al.* 2007. IL-33 induces IL-13 production by mouse mast cells independently of IgE-FcepsilonRI signals. *J. Leukoc. Biol.* 82:1481.
21 Yoshimoto, T., Bendelac, A., Hu-Li, J. and Paul, W. E. 1995. Defective IgE production by SJL mice is linked to the absence of CD4+, NK1.1+ T cells that promptly produce interleukin 4. *Proc. Natl Acad. Sci. USA* 92:11931.
22 Andrews, A. L., Bucchieri, F., Arima, K. *et al.* 2007. Effect of IL-13 receptor alpha2 levels on the biological activity of IL-13 variant R110Q. *J. Allergy Clin. Immunol.* 120:91.
23 Fujisawa, T., Kato, Y., Atsuta, J. *et al.* 2000. Chemokine production by the BEAS-2B human bronchial epithelial cells: differential regulation of eotaxin, IL-8, and RANTES by TH2- and TH1-derived cytokines. *J. Allergy Clin. Immunol.* 105:126.

24 Ishikawa, Y., Yoshimoto, T. and Nakanishi, K. 2006. Contribution of IL-18-induced innate T cell activation to airway inflammation with mucus hypersecretion and airway hyperresponsiveness. *Int. Immunol.* 18:847.
25 Lohning, M., Stroehmann, A., Coyle, A. J. *et al.* 1998. T1/ST2 is preferentially expressed on murine Th2 cells, independent of interleukin 4, interleukin 5, and interleukin 10, and important for Th2 effector function. *Proc. Natl Acad. Sci. USA* 95:6930.
26 Zhang, M., Angata, T., Cho, J. Y., Miller, M., Broide, D. H. and Varki, A. 2007. Defining the *in vivo* function of Siglec-F, a CD33-related Siglec expressed on mouse eosinophils. *Blood* 109:4280.
27 Kitaura, M., Nakajima, T., Imai, T. *et al.* 1996. Molecular cloning of human eotaxin, an eosinophil-selective CC chemokine, and identification of a specific eosinophil eotaxin receptor, CC chemokine receptor 3. *J. Biol. Chem.* 271:7725.
28 Lukacs, N. W., Standiford, T. J., Chensue, S. W., Kunkel, R. G., Strieter, R. M. and Kunkel, S. L. 1996. C-C chemokine-induced eosinophil chemotaxis during allergic airway inflammation. *J. Leukoc. Biol.* 60:573.
29 Lukacs, N. W., Strieter, R. M., Shaklee, C. L., Chensue, S. W. and Kunkel, S. L. 1995. Macrophage inflammatory protein-1 alpha influences eosinophil recruitment in antigen-specific airway inflammation. *Eur. J. Immunol.* 25:245.
30 Lukacs, N. W., Strieter, R. M., Warmington, K., Lincoln, P., Chensue, S. W. and Kunkel, S. L. 1997. Differential recruitment of leukocyte populations and alteration of airway hyperreactivity by C-C family chemokines in allergic airway inflammation. *J. Immunol.* 158:4398.
31 Carriere, V., Roussel, L., Ortega, N. *et al.* 2007. IL-33, the IL-1-like cytokine ligand for ST2 receptor, is a chromatin-associated nuclear factor *in vivo*. *Proc. Natl Acad. Sci. USA* 104:282.
32 Moussion, C., Ortega, N. and Girard, J. P. 2008. The IL-1-like cytokine IL-33 is constitutively expressed in the nucleus of endothelial cells and epithelial cells *in vivo*: a novel 'alarmin'? *PLoS One* 3:e3331.
33 Hayakawa, H., Hayakawa, M., Kume, A. and Tominaga, S. 2007. Soluble ST2 blocks interleukin-33 signaling in allergic airway inflammation. *J. Biol. Chem.* 282:26369.
34 Pushparaj, P. N., Tay, H. K., H'Ng, S. *et al.* 2009. The cytokine interleukin-33 mediates anaphylactic shock. *Proc. Natl Acad. Sci. USA* 106:9773.
35 Sakashita, M., Yoshimoto, T., Hirota, T. *et al.* 2008. Association of serum interleukin-33 level and the interleukin-33 genetic variant with Japanese cedar pollinosis. *Clin. Exp. Allergy* 38:1875.
36 Pecaric-Petkovic, T., Didichenko, S. A., Kaempfer, S., Spiegl, N. and Dahinden, C. A. 2009. Human basophils and eosinophils are the direct target leukocytes of the novel IL-1 family member IL-33. *Blood* 113:1526.
37 Smithgall, M. D., Comeau, M. R., Yoon, B. R., Kaufman, D., Armitage, R. and Smith, D. E. 2008. IL-33 amplifies both Th1- and Th2-type responses through its activity on human basophils, allergen-reactive Th2 cells, iNKT and NK cells. *Int. Immunol.* 20:1019.
38 Gudbjartsson, D. F., Bjornsdottir, U. S., Halapi, E. *et al.* 2009. Sequence variants affecting eosinophil numbers associate with asthma and myocardial infarction. *Nat. Genet.* 41:342.
39 Guo, L., Wei, G., Zhu, J. *et al.* 2009. IL-1 family members and STAT activators induce cytokine production by Th2, Th17, and Th1 cells. *Proc. Natl Acad. Sci. USA* 106:13463.
40 Mui, A. L., Wakao, H., O'Farrell, A. M., Harada, N. and Miyajima, A. 1995. Interleukin-3, granulocyte-macrophage colony stimulating factor and interleukin-5 transduce signals through two STAT5 homologs. *EMBO J.* 14:1166.
41 Cherry, W. B., Yoon, J., Bartemes, K. R., Iijima, K. and Kita, H. 2008. A novel IL-1 family cytokine, IL-33, potently activates human eosinophils. *J. Allergy Clin. Immunol.* 121:1484.
42 Suzukawa, M., Koketsu, R., Iikura, M. *et al.* 2008. Interleukin-33 enhances adhesion, CD11b expression and survival in human eosinophils. *Lab. Invest.* 88:1245.
43 Perrigoue, J. G., Saenz, S. A., Siracusa, M. C. *et al.* 2009. MHC class II-dependent basophil-CD4+ T cell interactions promote T(H)2 cytokine-dependent immunity. *Nat. Immunol.* 10:697.
44 Sokol, C. L., Chu, N. Q., Yu, S., Nish, S. A., Laufer, T. M. and Medzhitov, R. 2009. Basophils function as antigen-presenting cells for an allergen-induced T helper type 2 response. *Nat. Immunol.* 10:713.
45 Yoshimoto, T., Yasuda, K., Tanaka, H. *et al.* 2009. Basophils contribute to T(H)2-IgE responses *in vivo* via IL-4 production and presentation of peptide-MHC class II complexes to CD4+ T cells. *Nat. Immunol.* 10:706.
46 Dinarello, C. A. 2009. Immunological and inflammatory functions of the interleukin-1 family. *Annu. Rev. Immunol.* 27:519.
47 Bianchi, M. E. 2007. DAMPs, PAMPs and alarmins: all we need to know about danger. *J. Leukoc. Biol.* 81:1.
48 Haraldsen, G., Balogh, J., Pollheimer, J., Sponheim, J. and Kuchler, A. M. 2009. Interleukin-33-cytokine of dual function or novel alarmin? *Trends Immunol.* 30:227.
49 Bagarozzi, D. A. Jr and Travis, J. 1998. Ragweed pollen proteolytic enzymes: possible roles in allergies and asthma. *Phytochemistry* 47:593.
50 Traidl-Hoffmann, C., Kasche, A., Jakob, T. *et al.* 2002. Lipid mediators from pollen act as chemoattractants and activators of polymorphonuclear granulocytes. *J. Allergy Clin. Immunol.* 109:831.
51 Gunawan, H., Takai, T., Ikeda, S., Okumura, K. and Ogawa, H. 2008. Protease activity of allergenic pollen of cedar, cypress, juniper, birch and ragweed. *Allergol. Int.* 57:83.
52 Gunawan, H., Takai, T., Kamijo, S. *et al.* 2008. Characterization of proteases, proteins, and eicosanoid-like substances in soluble extracts from allergenic pollen grains. *Int. Arch. Allergy Immunol.* 147:276.
53 Bacsi, A., Dharajiya, N., Choudhury, B. K., Sur, S. and Boldogh, I. 2005. Effect of pollen-mediated oxidative stress on immediate hypersensitivity reactions and late-phase inflammation in allergic conjunctivitis. *J. Allergy Clin. Immunol.* 116:836.

 DOI 10.1002/eji.201040588 Eur. J. Immunol. 2010. 40: 1836–1842

Review Series 14th IGI

European Journal of Immunology

Basophils are potent antigen-presenting cells that selectively induce Th2 cells

Kenji Nakanishi[1,2]

[1] Department of Immunology and Medical Zoology, Hyogo College of Medicine, Nishinomiya, Hyogo, Japan
[2] Collaborative Development of Innovatioin Seeds, Japan Science and Technology Corporation, Saitama, Japan

Basophils and mast cells are important effector cells in helminth-infected host and IgE-mediated allergic inflammation. Although they have the same progenitors, basophils and mast cells complete their terminal differentiation in the bone marrow and peripheral tissues, respectively, and only basophils circulate in the blood. Although it is recognized that basophils are important for Th2 responses, and it is also well established that IL-4 is required for Th2 differentiation from naïve $CD4^+$ T cells, the nature of the cells that produce "early" IL-4, remained elusive until recently. Three groups independently demonstrated that basophils are the predominant APC in inducing Th2 response against helminth parasites and allergens. Basophils express MHC class II and CD80/86, have the potential to take-up and process protein Ag (particularly Ag–IgE complex) and to present peptide in the context of MHC class II, and to produce IL-4. These Ag-pulsed basophils induce the development of Th2 cells both *in vitro* and *in vivo*. Thus, basophils contribute to Th2/IgE response by the production of IL-4 and presentation of MHC class II/peptide complex to naïve $CD4^+$ T cells, in contrast to the Th1-inducing action of DC. In this review, we summarize what is known regarding basophil function in allergy and parasite infection, examine the novel Ag-presenting function of basophils and discuss potential clinical implications of this finding.

Key words: Ag–IgE complex · Basophils · Helminth infection · Th2 response

Introduction

Mast cells, basophils and eosinophils are key effector cells in response to parasite infection and allergic inflammation [1–5]. Basophils and eosinophils are granulocytes, which mature in the bone marrow, circulate in the blood and are recruited to allergic inflammatory sites [3–5]. In contrast, progenitors of mast cells migrate from the bone marrow to the peripheral tissues and undergo their terminal differentiation *in situ*; mast cells that complete their differentiation in the skin or intestine develop into connective tissue mast cells and mucosal mast cells, respectively [1, 2]. Mast cells and basophils express the high-affinity receptor for IgE and, upon crosslinking of FcεR1-bound IgE with multivalent Ag, rapidly produce diverse preformed mediators, cytokines (*e.g.* IL-4 and IL-13) and lipid mediators, leading to the induction of immediate-type hypersensitivity [1–5]. Here, the author reviews the major functions of basophils as effector cells in the development of allergic inflammation and their novel function as Th2-inducing APC in helminth infection and allergy.

Correspondence: Prof. Kenji Nakanishi
e-mail: nakaken@hyo-med.ac.jp

Basophil development and its role in allergy

As mentioned, mast cells, basophils and eosinophils are the key innate effector cells involved in parasite-induced immune responses and allergic inflammation. Basophils are short-lived cells that account for less than 1% of circulating granulocytes in the blood. In contrast, mast cells are located in the tissue and mast cell progenitors have the potential to proliferate locally in the tissue in response to IL-3, IL-4 and IL-9, resulting in local mastocytosis.

A study by Arinobu *et al.* [6] has identified a common progenitor of basophils and mast cell precursor (BMCP), which arise from the granulocyte/monocyte progenitor (GMP). Eosinophil precursor also arises from GMP. The development from GMP to eosinophil precursor and BMCP, and from BMCP to basophil precursor or MCP, are regulated by the level and order of expression of transcription factors, C/EBPα and GATA-2 [6]. Morphologically, basophils and eosinophils have lobulated nucleus and secretory granules in the cytoplasm. Mast cells are round cells with a non-segmented nucleus and intracellular granules. Although basophils and mast cells are heterogeneous in their development and morphology, they are regarded to share a pathological role in allergic responses, as demonstrated by their potential to produce cytokines, vasoactive histamine and lipid mediators after FcεR1 crosslinkage [1–5]. Thus, individuals with atopy, after repeated exposure to a particular Ag such as pollen, exhibit immediate-type hypersensitivity. Furthermore, there is tight correlation between FcεR1 expression on basophils and IgE level in human peripheral blood [7], suggesting a positive feedback mechanism for the IgE-mediated immediate-type hypersensitivity reaction [8, 9]. Thus, once individuals with atopy start to produce IgE, they develop progressive allergic inflammation by increasing production of IgE and expression of FcεR1 on effector cells.

Basophil activation in parasitic infection and allergic inflammation: Role of IL-3

There appears to be at least two major pathways of basophil activation during allergic inflammation, one involving Ag/IgE signaling and the other that is mediated by PAMP and soluble mediators such as IL-18 and IL-33.

An important cytokine involved in both pathways of basophil activation is IL-3. IL-3 is not only an important growth factor for mast cells and basophils, IL-3 stimulation also induces basophil production of IL-4. Furthermore, basophils, when stimulated with a combination of IL-3 and crosslinking of FcεR1 by Ag, strongly produce IL-4 and IL-13, suggesting the importance of crosstalk between IL-3-mediated signaling and FcεR1-mediated signaling for IL-4 and IL-13 production. Furthermore, FcR common γ-chain (FcγR) may also be important in basophil activation. Recently, Hida *et al.* [10] demonstrated that basophils lacking FcγR could proliferate normally but failed to produce IL-4 in response to IL-3, suggesting that FcγR-mediated IL-3 signal is crucial in IL-4 production by basophils.

The effect of IL-3 can also be observed in IgE-independent basophil IL-4 production. We previously demonstrated that basophils express IL-18R and IL-33R and produce IL-4, IL-6, IL-13 and chemical mediators when stimulated with IL-3 plus IL-18/IL-33 *in vitro* (Fig. 1, left panel) [11, 12]. These results suggest the potential of basophils to induce allergic inflammation in an IgE-independent manner (innate-type allergic inflammation). Mouse basophils also express TLR1, TLR2, TLR4 and TLR6 and produce Th2 cytokines including IL-4 and IL-13 in response to stimulation with TLR ligands plus IL-3 [13].

Thus, as stated, there are at least two major basophils activation pathways during allergic inflammation. One is an Ag/IgE-dependent pathway responsible for "acquired-type allergic inflammation" and the other is an IL-18, IL-33 or PAMP-dependent pathway responsible for "innate-type allergic inflammation."

IL-3 is also important for generation and peripheral accumulation of basophils during parasitic infections [14]. Infection of wild-type mice with *Strongyloides venezuelensis* or *Nippostrongylus brasiliensis* causes accumulation of basophils in the liver and spleen of the host [15]; however, this accumulation is not observed in IL-3-deficient mice [14]. Thus, IL-3 produced by Th2 cells is critically involved in generation, accumulation and activation of basophils.

In terms of the interactions between allergic inflammation and parasitic infection, we showed previously that nasal administration of IL-18 or IL-33 induces bronchial asthma entirely independently of allergen and IgE [12, 16]. As these cytokines are stored in the epithelial cells, infection with pathogens, including helminth parasites, bacteria, fungi and viruses or exposure to allergens, can induce the release of IL-18 and IL-33 from epithelial cells, causing IL-18 and/or IL-33-mediated allergic inflammation (Fig. 2), which is dependent on IL-18R and/or IL-33R and the adapter protein MyD88 pathway (Fig. 1). Basophils and mast cells also produce Th2 cytokines in response to parasite Ag (*e.g.* IPSE-α-1, a soluble glycoprotein Ag from eggs of *Schistosoma mansoni* and has been shown to stimulate basophils in an IgE-specific but Ag-nonspecific manner [17]). Basophils and mast cells may also respond to other parasite Ag, suggesting their role in defense against intestinal nematode such as *S. venezuelensis*, *N. brasiliensis* or *Trichuris muris*. Eosinophils are also effector cells of parasite infection – they defend against the tissue stage of helminth that is too large to be phagocytosed. IgE antibodies that bind to the surface of helminths activate eosinophils to produce granule content such as the major basic protein, which is highly toxic to helminths. Recruitment of eosinophils is also a well-known late hallmark of allergic inflammation and contributes to pathological processes in allergic diseases. Thus, basophils, mast cells and eosinophils are major effector granulocytes in parasitic infection and allergic inflammation.

Basophils in chronic allergic inflammation and systemic anaphylactic shock

Recent studies suggest that basophils also induce IgE-mediated chronic allergic inflammation and IgG1-mediated systemic anaphylactic shock [4, 18, 19]. Mukai *et al.* demonstrated that a single injection of multivalent Ag in the ear of mice passively sensitized with Ag-specific IgE induces immediate-phase, late-phase and delayed-onset of ear swelling characterized by infiltration with basophils and eosinophils [18]. Mast cell-deficient mice did not develop immediate- and late-phase ear swelling, suggesting mast cells are responsible for inducing these ear swellings. In contrast, depletion of basophils in wild-type mice diminished delayed-onset of ear swelling and eosinophilic infiltration. Moreover, transfer of basophils into FcεR1-deficient mouse showed that basophils are responsible for inducing delayed-onset ear swelling that is

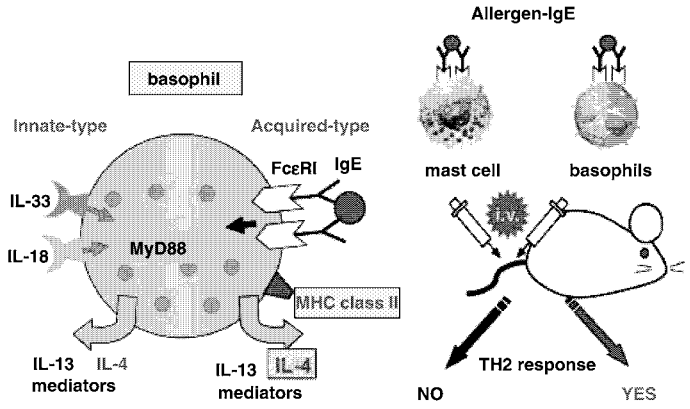

Basophils are APC that can specifically induce Th2 cells.

Figure 1. Basophils are effectors cells and also inducers of Th2 response *in vivo*. Basophils, which produce IL-4, IL-13, and other mediators when stimulated with IL-3 plus Ag/IgE complex (acquired-type activation) also produce these cytokines and mediators, when stimulated with IL-3 plus IL-18 or IL-3 plus IL-33 (innate-type allergy). Furthermore, intravenous administration of basophils (but not mast cells) pulsed with allergen induce the development of Th2 cells in the peripheral lymphoid organs.

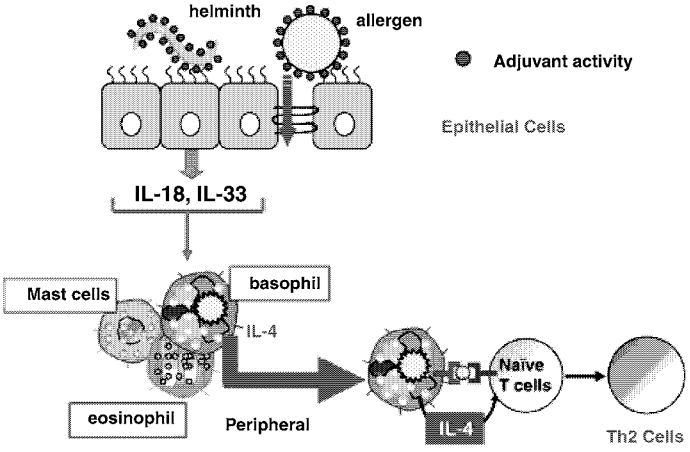

Figure 2. Interaction between epithelial cells and basophils. IL-18 or IL-33 derived from epithelial cells stimulated with helminth or allergen induces mast cells, basophils and eosinophils to produce Th2 cytokines, chemokines and chemical mediators. Among these granulocytes, basophils strongly produce IL-4 in response to IL-18 or IL-33. Basophils also uptake and process allergen and express allergen-derived peptide with MHC class II. These basophils prime Th2 responses in an MHC class II-dependent and IL-4-dependent manner.

associated with marked eosinophilic infiltration. Therefore, basophils seem to induce delayed-onset or chronic allergic inflammation by recruiting eosinophils [18].

It is well documented that mast cells and IgE are crucially involved in the development of systemic anaphylaxis. Interestingly, mice deficient for mast cells or IgE nevertheless develop systemic anaphylaxis, suggesting that an alternative pathway may be involved. Tsujimura *et al.* [19] clearly demonstrated that basophils and IgG1 induce mast cell-independent systemic anaphylaxis.

Role of Th cells in allergy and infection

Allergen-activated Th2 cells produce cytokines that induce allergen-specific IgE production by B cells and recruitment of mast cells, eosinophils and basophils to the site of allergic inflammation. Helminth infection also induces Th2 responses, resulting in high levels of IgE and recruitment of mast cells, eosinophils and basophils to the infected organ. Naïve $CD4^+$ T cells develop into Th1, Th2, Th17 cells and Treg upon activation by appropriate combination of antigenic signal, costimulation and cytokine signals by APC and accessory cells [20]. IFN-γ and IL-12 induce the development of Th1 cells, which are characterized by a high-level production of IFN-γ and are indispensable for eradication of intracellular pathogens [21]. IL-4 triggers the differentiation of Th2 cells [22]. Th2 cells are critically involved in clearing extracellular multi-cellular parasites such as helminths and in helping B cells to produce antibodies. Th2 cells are also involved in the pathogenesis of allergic inflammation. Th17 cells play an important role for the defense against extracellular pathogens and fungi [23]. Differentiation of Th17 cells is induced by TGF-β and IL-6 in the mouse and by TGF-β and IL-6 or IL-21 in the human [23] (see also review on IL-6 in this issue [24]). Treg can be induced by TGF-β and are involved in maintaining immune tolerance [25].

The initial source of the differentiation factors for both Th1 and Th2 cells are cells of the innate immune system responding to microbial Ag, parasitic Ag, or allergens. DC recognize bacteria through TLR and mature to express costimulatory molecules CD80/86 and to produce IL-12 and IL-18, favoring development of Th1 cells [26–28]. Thus, DC infected with intracellular bacteria induce Th1 cells.

Of particular importance to allergic inflammation and parasite infections is the nature of APC involved in polarizing Th2 responses. Ag-pulsed DC can also induce the development of Ag-specific naïve $CD4^+$ T cells into Th2 cells under the presence of IL-4 *in vitro* [20]; however, the APC involved in the development of Th2 response under physiological conditions remains uncertain. Several reports indicate that there are several pathways for the differentiation of naïve $CD4^+$ T cells into Th2 cells [29–33]. The Notch-ligand Jagged 1 and Jagged 2 on DC can trigger Th2 differentiation independently of IL-4 and STAT6 signaling [29]. Epithelial cells-derived cytokine, thymic stromal lymphopoetin (TSLP), activates DC to express OX40L, which induces the development of Th2 cells [30]. Aluminum adjuvant also induces Th2-cell differentiation, although exact mechanism remains uncertain [31]. In addition, M2 macrophages (also known as alternatively activated macrophages), eosinophils and mast cells are also important for the development of Th2 cells [32, 33].

Previous studies suggested that basophils may be critical in Th2 immunity. Min and colleagues [34] showed that naïve $CD4^+$ T cells stimulated with peptide-pulsed DC develop into Th2 cells when cultured with basophils from wild-type mice but not from IL-4-deficient mice. As both DC and basophils are added to the same culture, it was initially considered that DC deliver antigenic-specific signal and basophils promote the development of Th2 response by providing early IL-4 signal to Ag-activated $CD4^+$ T cells. It was also previously reported that helminth infection induces the development of Th2 cells and accumulation of basophils in the spleens and livers of host mice [15], suggesting that the relationship between Th2 cells and basophils may be more direct. *In vivo*, mice deficient in interferon-regulatory factor 2 show expansion of basophil and spontaneous Th2 differentiation [35], suggesting promotion of Th2 immune response by basophils. Furthermore, this Th2 differentiation is markedly reduced by the introduction of mutation in the gene-encoding c-Kit, because this mutation reduces the number of basophils [35]. Thus, although indirect evidence support the role of basophils in Th2 immunity, it is important to formally prove that basophils produce "early" IL-4, required for the development of naïve $CD4^+$ T cells into Th2 cells. Recently, three groups independently demonstrated that basophils and not DC, are the critical APC involved in Th2 differentiation *in vivo* [36–38].

Th2 development: Basophils as IL-4 provider

Medzhitov and colleagues [39] previously reported that basophils are important for the development of Th2 cells in response to papain. At day 3 after papain stimulation, basophils migrated into the T-cell zones of the draining lymph nodes, in which the basophils produce IL-4 and/or TSLP, which promote Th2 differentiation *in vivo*. Papain is a cysteine protease hydrolate enzyme from papaya that mimics the activity of proteases secreted by helminth parasites. Depletion of basophils with antibody against FcεR1 diminishes the development of Th2 cells, suggesting that basophils are involved in Th2 cell differentiation. This study [39] strongly indicates that basophils are critically involved in Th2 responses by their unique function to produce early IL-4 and TSLP in response to papain or bromelain. It remains uncertain, however, whether basophil-derived IL-4 is indeed involved in the development of Th2 cells in response to stimuli other than protease allergens.

Basophils as Th2-inducing APC

Data from our group also supported a role of basophils in Th2 responses – we reported that IL-18 and IL-33 synergize with IL-3 to strongly induce basophil, but not mast cell, production of IL-4 and IL-13 *in vitro*, respectively [11, 12] (Fig. 1, left panel), suggesting a role of basophils in promoting Th2 response by producing IL-4. Furthermore, basophils are shown to be an important regulator of Th2 responses *in vivo*, particularly in helminth-infected mice [3, 15]. As the size of helminths is too large to be phagocytosed directly by DC, it is more likely that DC take up Ag shed or secreted by parasites and present the Ag on MHC class II complex to naïves T cells in the context of IL-4 from parasite Ag-stimulated basophils. Although this is a persuasive hypothesis, the exact role of basophils in Th2 development remains to be formally demonstrated.

As noted, three groups independently demonstrated that contrary to our intuition, DC are not required for the development of Th2 responses to protease allergens, helminthic parasites or complexes of Ag and IgE [36–38]. All three groups demonstrated that basophils express MHC class II, CD80/86 and produce IL-4. Two groups showed that basophils induce Th2 cells in the absence of DC [36, 38]. Our group demonstrated that administration of Ag-pulsed basophils but not Ag-pulsed DC or mast cells selectively induces Th2 cells *in vivo* [37] (Fig. 1, right panel). Together, the three studies [36–38] suggest that basophils induce allergen or helminth-induced Th2 response by functioning as Th2-inducing APC. Artis and colleagues [36], using MHC II^{CD11c} transgenic mice, where MHC class II expression is restricted to $CD11c^+$ DC, demonstrated that these mice, when inoculated with *T. muris*, fail to develop Th2 response and to expel helminths. MHC II^{CD11c} transgenic mice do not secrete intestinal goblet-specific immune effector molecule resistin-like molecule β, which is induced by Th2 cells. Artis and colleagues [36] simultaneously demonstrated that this infection induced the development of Th1 cells, suggesting that $CD11c^+$ cells are required for the generation of Th1 cells; basophils, on the other hand, are dominant Th2-inducing APC that express IL-4 and MHC class II, as supported by depletion of basophils *in vivo*, which led to impaired protective Th2 immunity to *T. muris* in wild-type

mice. Contrary to these findings, however, Min and colleagues [14] demonstrated that basophil depletion in *N. brasiliensis*-infected mice did not affect the development of Th2 cells, suggesting that *N. brasiliensis* infection induces Th2 immunity even in the absence of basophils. We therefore need further studies to reconcile this apparent discrepancy.

Medzhitov and colleagues [38] demonstrated that skin DC are dispensable for mounting Th2 responses to papain. This group previously reported that, as with injection of the soluble Ag of *S. mannsoni* eggs, papain rapidly induces recruitment of basophils to the lymph node [39]. In the lymph nodes, basophils secrete IL-4 and TSLP, which are critically involved in the development of Ag-specific Th2 cells. Given that this treatment simultaneously induced recruitment of DC, Medzhitov and colleagues [39] initially considered that basophils function as accessory cells and DC present Ag in the presence of IL-4 from basophils. In the follow-up study, Medzhitov and colleagues [38] very clearly demonstrated that skin DC are not required for the development of Th2 cells in the draining lymph nodes. In this study [38], papain was injected into the ear, where skin DC capture Ag and present Ag-derived peptides to naïve T cells in the draining lymph nodes. If skin DC capture Ag and present it at the lymph node, rapid removal of this Ag-pulsed DC by prompt excision of the injection site should inhibit the Th2 response; however, this treatment failed to inhibit development of Th2 cells, suggesting that Ag capture by skin DC is not required for induction of papain-specific Th2 development. Instead, soluble papain can directly enter lymph nodes from injection site. Furthermore, selective depletion of $CD11c^+$ DC did not inhibit Th2 development to papain, although mice failed to develop Th1 responses. Artis's [36] and Medzhitov's [38] groups used the same strategy to deplete DC, using the CD11c-restricted diphteria toxin receptor mice, in which CD11c-expressing DC are efficiently depleted upon delivery of diphteria toxin, the two groups demonstrated that DC depletion only inhibited the development of Th1 cells without affecting the development of Th2 response. These results strongly indicated that other type/s of APC might be required for Th2 cytokine-dependent immune response. Medzhitov's group [38] demonstrated that OVA-pulsed basophils induce the development of OVA-specific naïve $CD4^+$ T cells into Th2 cells *in vitro*. They also show basophils can uptake, process and present soluble Ag. They further demonstrated that adoptive transfer of OVA-pulsed basophils induced Th2 response in MHC class II-deficient mice.

Basophils produce IL-4 and IL-13 upon stimulation with Ag/IgE complex. In addition, our *in vitro* studies demonstrated that, among mast cells and basophils, only basophils strongly produce IL-4 and IL-13 in response to IL-3 and IL-18 or IL-33 [11, 12]. These data suggest a role of basophils in the development of Th2 cells. These observations led us to examine the possibility whether basophils directly induce the development of Th2 cells, instead of functioning as accessory cells *in vitro* [37].

Splenic basophils from mice inoculated with *S. venezuelensis* produce large amounts of IL-4, IL-6 and IL-13 in the medium even in the absence of exogenous IL-3. In contrast, splenic basophils from naïve mice produce small amounts of IL-4, IL-6 and IL-13 only in IL-3-containing medium. Furthermore, basophils from infected mice express MHC class II and strongly induce the development of OVA-specific naïve $CD4^+$ T cells into Th2 cells *in vitro* in the presence of OVA peptide, IL-2 and IL-3 without IL-4 (neutral culture condition). Thus, we initially regarded only basophils from infected mice as potent APC; however, we soon found that splenic basophils from naïve mice also express comparable level of MHC class II and have the capacity to strongly induce the development of Th2 cells *in vitro* under neutral conditions [37]. We next examined bone marrow basophils and showed that these also have the potential to induce the development of Th2 cells. We purified basophils from bone marrow cells cultured with IL-3 for 10 days. Similar to splenic basophils, bone marrow basophils express MHC class II, CD80, CD86 and CD62L. Furthermore, bone marrow basophils can take-up and process protein Ag and express peptide in association with MHC class II. In particular, bone marrow basophils can efficiently uptake a low dose of Ag/IgE complex, and present Ag/MHC class II and produce IL-4, suggesting that they are potent Th2-inducing APC.

We also demonstrated that i.v. administration of OVA-pulsed basophils, which we prepared by culturing basophils with DNP–OVA and anti-DNP–IgE complexes, strongly induce OVA-specific Th2 cells in the spleen of naïve mouse (Fig. 1, right panel). We found that basophils' APC activity was enhanced when pulsed with DNP-OVA in the presence of anti-DNP IgE. In contrast, i.v. administration of OVA-pulsed DC failed to induce Th2 cells, although this treatment induced IFN-γ-producing Th1 cells. Thus, basophils are potent Th2-inducing APC *in vivo*. We transferred only $0.25–0.5 \times 10^6$ basophils and found dramatic induction of Th2 responses. We have also demonstrated that single i.v. administration of low-dose DNP–OVA/anti-DNP–IgE complex into naïve mice rapidly and preferentially induced OVA-specific Th2 cells in an endogenous basophil-dependent manner. Such sensitized mice promptly produced OVA-specific IgG1 antibody in response to i.v. administration of soluble OVA. Furthermore, IL-3 treatment prepares mice to be highly susceptible to Th2-inducing action of IgE complex by increasing the number of basophils.

Clinical implication: Basophils as a potential therapeutic target

Animals respond to allergen exposure by producing Ag-specific IgE. Such sensitized individuals, upon re-exposure to the same allergens, increase the production of IgE, which form allergen–IgE complexes by binding to allergens. These IgE complexes are captured by basophils that develop into Th2-inducing APC and present allergen-derived peptide with MHC class II and provide IL-4 to naïve $CD4^+$ T cells. Thus, basophils play a very important role in amplification of Th2-IgE responses, suggesting that they may be an important therapeutic target and depletion of basophils by antibody such as anti-FcεR1 might be an effective

therapeutic pathway. Published work has suggested that anti-IgE therapy is effective for Th2-IgE diseases [40]. The effect of anti-IgE therapy is believed to interfere with IgE-mediated activation of mast cells and basophils; however, on the basis of our research, another consequence of this antibody therapy might be the inhibition of basophil development into Th2-inducing APC, adding another rationale for anti-IgE therapy.

Concluding remarks

Basophils can uptake intact proteins and process them into peptides. Thus, basophils have the potential to induce primary Th2 response (Fig. 2). FcεR1 has a dominant effect during the memory phase of the Th2 response, because FcεR1 has the capacity to bind a very small amount of Ag–IgE complex and to present Ag-derived peptide with MHC class II. Denzel *et al.* [41, 42] reported that basophils bind large amounts of intact Ag *via* FcεR1-bound IgE. These basophils activate $CD4^+$ T cells to enhance Ag-specific B-cell memory responses (proliferation and Ig production) by presenting Ag and secretion of IL-4 and IL-6, suggesting that activated basophils induce and activate Th2-type cells, which help B cell proliferation and IgG1 production.

Atopic individuals are characterized by increased number of basophils at sites of allergic inflammation [43–45]. Although human mature basophils lack HLA-DR, we have demonstrated that some of them re-express HLA-DR when stimulated with IL-3 [37]. Given that IL-3 and other factors may be present at high concentrations at the site of allergic inflammation, accumulated basophils might re-express HLA-DR. Once the immune system of individuals with atopy start to produce Ag-specific IgE, they can steadily increase the amounts Ag and Ag-specific IgE complex. This allows basophils to take up Ag–IgE complex and become potent Th2 cell-inducing APC and induce progressive allergic inflammation in these individuals. Antibody therapy against IgE or basophils might be effective, because depletion of IgE or basophils could diminish basophil-dependent induction of Th2 cells.

Acknowledgements: Supported by The Japanese Ministry of Education, Culture, Sports, Science and Technology (Grant-in-Aid for Scientific Research on Priority Areas 18073016 and Hitech Research Center Grant)

Conflict of interest: The author declares no financial or commercial conflict of interest.

References

1 **Galli, S. J., Grimbaldeston, M. and Tsai, M.,** Immunomodulatory mast cells: negative, as well as positive, regulators of immunity. *Nat. Rev. Immunol.* 2008. **8**: 478–486.

2 **Galli, S. J., Kalesnikoff, J., Grimbaldeston, M. A., Piliponsky, A. M., Williams, C. M. and Tsai, M.,** Mast cells as "tunable" effector and immunoregulatory cells: recent advances. *Annu. Rev. Immunol.* 2005. **23**: 749–786.

3 **Min, B.,** Basophils: what they 'can do' versus what they 'actually do'. *Nat. Immunol.* 2008. **9**: 1333–1339.

4 **Karasuyama, H., Mukai, K., Tsujimura, Y. and Obata, K.,** Newly discovered roles for basophils: a neglected minority gains new respect. *Nat. Rev. Immunol.* 2008. **9**: 9–13.

5 **Sullivan, B. M. and Locksley, R. M.,** Basophils: a nonredundant contributor to host immunity. *Immunity* 2009. **30**: 12–20.

6 **Arinobu, Y., Iwasaki, H., Gurish, M. F., Mizuno, S., Shigematsu, H., Ozawa, H., Tenen, D. G. *et al.*,** Developmental checkpoints of the basophil/mast cell lineages in adult murine hematopoiesis. *Proc. Natl. Acad. Sci. USA* 2005. **102**: 18105–18110.

7 **Saini, S. S., Klion, A. D., Holland, S. M., Hamilton, R. G., Bochner, B. S. and Macglashan, D. W., Jr.,** The relationship between serum IgE and surface levels of FcepsilonR on human leukocytes in various diseases: correlation of expression with FcepsilonRI on basophils but not on monocytes or eosinophils. *J. Allergy Clin. Immunol.* 2000. **106**: 514–520.

8 **Lantz, C. S., Yamaguchi, M., Oettgen, H. C., Katona, I. M., Miyajima, I., Kinet, J. P. and Galli, S. J.,** IgE regulates mouse basophil Fc epsilon RI expression *in vivo*. *J. Immunol.* 1997. **158**: 2517–2521.

9 **Yamaguchi, M., Lantz, C. S., Oettgen, H. C., Katona, I. M., Fleming, T., Miyajima, I., Kinet, J. P., Galli, S. J.,** IgE enhances mouse mast cell Fc(epsilon)RI expression *in vitro* and *in vivo*: evidence for a novel amplification mechanism in IgE-dependent reactions. *J. Exp. Med.* 1997. **185**: 663–672.

10 **Hida, S., Yamasaki, S., Sakamoto, Y., Takamoto, M., Obata, K., Takai, T., Karasuyama, H. *et al.*,** Fc receptor gamma-chain, a constitutive component of the IL-3 receptor, is required for IL-3-induced IL-4 production in basophils. *Nat. Immunol.* 2009. **10**: 214–222.

11 **Yoshimoto, T., Tsutsui, H., Tominaga, K., Hoshino, K., Okamura, H., Akira, S., Paul, W. E. *et al.*,** IL-18, although antiallergic when administered with IL-12, stimulates IL-4 and histamine release by basophils. *Proc. Natl. Acad. Sci. USA* 1999. **96**: 13962–13966.

12 **Kondo, Y., Kondo, Y., Yoshimoto, T., Yasuda, K., Futatsugi-Yumikura, S., Morimoto, M., Hayashi, N. *et al.*,** Administration of IL-33 induces airway hyperresponsiveness and goblet cell hyperplasia in the lungs in the absence of adaptive immune system. *Int. Immunol.* 2008. **20**: 791–800.

13 **Yoshimoto, T. and Nakanishi, K.,** Roles of IL-18 in basophils and mast cells. *Allergol. Int.* 2006. **55**: 105–113.

14 **Kim, S., Prout, M., Ramshaw, H., Lopez, A. F., LeGros, G. and Min, B.,** Cutting edge: basophils are transiently recruited into the draining lymph nodes during helminth infection *via* IL-3, but infection-induced Th2 immunity can develop without basophil lymph node recruitment or IL-3. *J. Immunol.* 2010. **184**: 1143–1147.

15 **Min, B., Prout, M., Hu-Li, J., Zhu, J., Jankovic, D., Morgan, E. S., Urban, J. F., Jr. *et al.*,** Basophils produce IL-4 and accumulate in tissues after infection with a Th2-inducing parasite. *J. Exp. Med.* 2004. **200**: 507–517.

16 **Ishikawa, Y., Yoshimoto, T. and Nakanishi, K.,** Contribution of IL-18-induced innate T cell activation to airway inflammation with mucus hypersecretion and airway hyperresponsiveness. *Int. Immunol.* 2006. **18**: 847–855.

17 **Schramm, G., Mohrs, K., Wodrich, M., Doenhoff, M. J., Pearce, E. J., Haas, H. and Mohrs, M.,** Cutting edge: IPSE/alpha-1, a glycoprotein from *Schistosoma mansoni* eggs, induces IgE-dependent, antigen-independent

IL-4 production by murine basophils *in vivo*. *J. Immunol.* 2007. **178**: 6023–6027.

18 **Mukai, K., Matsuoka, K., Taya, C., Suzuki, H., Yokozeki, H., Nishioka, K., Hirokawa, K. *et al.***, Basophils play a critical role in the development of IgE-mediated chronic allergic inflammation independently of T cells and mast cells. *Immunity* 2005. **23**: 191–202.

19 **Tsujimura, Y., Obata, K., Mukai, K., Shindou, H., Yoshida, M., Nishikado, H., Kawano, Y. *et al.***, Basophils play a pivotal role in immunoglobulin-G-mediated but not immunoglobulin-E-mediated systemic anaphylaxis. *Immunity* 2008. **28**: 581–589.

20 **Zhu, J. and Paul, W. E.**, CD4 T cells: fates, functions, and faults. *Blood* 2008. **112**: 1557–1569.

21 **Trinchieri, G.**, Interleukin-12 and the regulation of innate resistance and adaptive immunity. *Nat. Rev. Immunol.* 2003. **3**: 133–146.

22 **Seder, R. A. and Paul, W. E.**, Acquisition of lymphokine-producing phenotype by CD4+T cells. *Annu. Rev. Immunol.* 1994. **12**: 635–673.

23 **Korn, T., Bettelli, E., Oukka, M. and Kuchroo, K.**, IL-17 and Th17 cells. *Annu. Rev. Immunol.* 2009. **27**: 485–518.

24 **Kimura, A. and Kishimoto, T.**, IL-6: Regulator of Treg/Th17 balance. *Eur. J. Immunol.* 2010. **40**: 1830–1835.

25 **Sakaguchi, S., Yamaguchi, T., Nomura, T. and Ono, M.**, Regulatory T cells and immune tolerance. *Cell* 2008. **133**: 775–787.

26 **Takeda, K., Kaisho, T. and Akira, S.**, Toll-like receptors. *Annu. Rev. Immunol.* 2003. **21**: 335–376.

27 **Nakanishi, K., Yoshimoto, T., Tsutsui, H. and Okamura, H.**, Interleukin-18 is a unique cytokine that stimulates both Th1 and Th2 responses depending on its cytokine milieu. *Cytokine Growth Factor Rev.* 2001. **12**: 53–72.

28 **Nakanishi, K., Yoshimoto, T., Tsutsui, H. and Okamura, H.**, Interleukin-18 regulates both Th1 and Th2 responses. *Annu. Rev. Immunol.* 2001. **19**: 423–474.

29 **Amsen, D., Antov, A. and Flavell, R. A.**, The different faces of Notch in T-helper-cell differentiation. *Nat. Rev. Immunol.* 2009. **9**: 116–124.

30 **Ito, T., Wang, Y. H., Duramad, O., Hori, T., Delespesse, G. J., Watanabe, N., Qin, F. X. *et al.***, TSLP-activated dendritic cells induce an inflammatory T helper type 2 cell response through OX40 ligand. *J. Exp. Med.* 2005. **202**: 1213–1223.

31 **Aimanianda, V., Haensler, J., Lacroix-Desmazes, S., Kaveri, S. V. and Bayry, J.**, Novel cellular and molecular mechanisms of induction of immune responses by aluminum adjuvants. *Trends Pharmacol. Sci.* 2009. **30**: 287–295.

32 **Anderson, C. F. and Mosser, D. M.**, A novel phenotype for an activated macrophage: the type 2 activated macrophage. *J. Leukoc. Biol.* 2002. **72**: 101–106.

33 **Padigel, U. M., Hess, J. A., Lee, J. J., Lok, J. B., Nolan, T. J., Schad, G. A. and Abraham, D.**, Eosinophils act as antigen-presenting cells to induce immunity to *Strongyloides stercoralis* in mice. *J. Infect. Dis.* 2007. **196**: 1844–1851.

34 **Oh, K., Shen, T., Le Gros, G. and Min, B.**, Induction of Th2 type immunity in a mouse system reveals a novel immunoregulatory role of basophils. *Blood* 2007. **109**: 2921–2927.

35 **Hida, S., Tadachi, M., Saito, T. and Taki, S.**, Negative control of basophil expansion by IRF-2 critical for the regulation of Th1/Th2 balance. *Blood* 2005. **106**: 2011–2017.

36 **Perrigoue, J. G., Saenz, S. A., Siracusa, M. C., Allenspach, E. J., Taylor, B. C., Giacomin, P. R., Nair, M. G. *et al.***, MHC class II-dependent basophil-$CD4^+$ T cell interactions promote Th2 cytokine-dependent immunity. *Nat. Immunol.* 2009. **10**: 697–705.

37 **Yoshimoto, T., Yasuda, K., Tanaka, H., Nakahira, M., Imai, Y., Fujimori, Y. and Nakanishi, K.**, Basophils contribute to Th2-IgE responses *in vivo* via IL-4 production and presentation of peptide-MHC class II complexes to $CD4^+$ T cells. *Nat. Immunol.* 2009. **10**: 706–712.

38 **Sokol, C. L., Chu, N. Q., Yu, S., Nish, S. A., Laufer, T. M. and Medzhitov, R.**, Basophils function as antigen-presenting cells for an allergen-induced T helper type 2 response. *Nat. Immunol.* 2009. **10**: 713–720.

39 **Sokol, C. L., Barton, G. M., Farr, A. G. and Medzhitov, R.**, A mechanism for the initiation of allergen-induced T helper type 2 responses. *Nat. Immunol.* 2008. **9**: 310–318.

40 **Adcock, I. M., Caramori, G. and Chung, K. F.**, New targets for drug development in asthma. *Lancet* 2008. **372**: 1073–1087.

41 **Denzel, A. Maus, U. A., Rodriguez-Gomez, M., Moll, C., Nidermeier, M., Winter, C., Maus, R., *et al.***, Basophils enhance immunological memory responses. *Nat. Immunol.* 2008. **9**: 733–742.

42 **Gauvreau, G. M., Lee, J. M., Watson, R. M., Irani, A. M., Schwartz, L. B., and O'Byrne, P. M.**, Increased numbers of both airway basophils and mast cells in sputum after allergen inhalation challenge of atopic asthmatics. *Am. J. Respir. Crit. Care Med.* 2000. **161**: 1473–1478.

43 **Irani, A. M., Huang, C., Xia, H. Z., Kepley, C., Nafie, A., Fouda, E. D., Craig, S., *et al.***, Immunohistochemical detection of human basophils in late-phase skin reactions. *J. Allergy Clin. Immunol.* 1998. **101**: 354–362.

44 **Koshino, T., Arai, Y., Miyamoto, Y., Sano, Y., Itami, M., Teshima, S., Hirai, K., *et al.***, Airway basophil and mast cell density in patients with bronchial asthma: relationship to bronchial hyperresponsiveness. *J. Asthma* 1996. **33**: 89–95.

45 **Macfarlane, A. J., Kon, O. M., Smith, S. J., Zeibecoglou, K., Khan, L. N., Barata, L. T., McEuen, A. R., *et al.***, Basophils, eosinophils, and mast cells in atopic and nonatopic asthma and in late-phase allergic reactions in the lung and skin. *J. Allergy Clin. Immunol.* 2000. **105**: 99–107.

Abbreviations: **BMCP:** basophils and mast cell precursor · **FcγR:** FcR common γ-chain · **GMP:** granulocyte/monocyte progenitor · **TSLP:** thymic stromal lymphopoetin

Full correspondence: Prof. Kenji Nakanishi, Department of Immunology and Medical Zoology, Hyogo College of Medicine, 1-1 Mukogawa-cho, Nishinomiya, Hyogo 663-8501 Japan
Fax: +81-798-40-5423
e-mail: nakaken@hyo-med.ac.jp

Received: 16/4/2010
Revised: 17/5/2010
Accepted: 18/5/2010

Hepatology Research

Hepatology Research 2010; **40**: 823–831 doi: 10.1111/j.1872-034X.2010.00670.x

Original Article

Crucial role of impaired Kupffer cell phagocytosis on the decreased Sonazoid-enhanced echogenicity in a liver of a nonalchoholic steatohepatitis rat model

Shohei Yoshikawa,[1] Hiroko Iijima,[1] Masaki Saito,[1] Hironori Tanaka,[1] Hiroyasu Imanishi,[1] Naoki Yoshimoto,[2] Tomohiro Yoshimoto,[3] Shizue Futatsugi-Yumikura,[4] Kenji Nakanishi,[4] Tohru Tsujimura,[5] Takashi Nishigami,[5] Atsushi Kudo,[6] Shigeki Arii[6] and Shuhei Nishiguchi[1]

[1]*Division of Hepatobiliary and Pancreatic Diseases, Department of Internal Medicine, Hyogo College of Medicine,* [2]*Ultrasound Imaging Center, Hyogo College of Medicine,* [3]*Laboratory of Allergic Diseases, Institute for Advanced Medical Sciences, Hyogo College of Medicine,* [4]*Department of Immunology and Medical Zoology, Hyogo College of Medicine,* [5]*Department of Pathology, Hyogo College of Medicine, and* [6]*Department of Hepatobiliary Pancreatic Surgery, Tokyo Medical and Dental University, Tokyo, Japan*

Aims: To evaluate the dynamics of Kupffer cell (KC) phagocytosis by performing both *in vivo* and *in vitro* studies using Sonazoid (GE Healthcare, Oslo) in a rat nonalcoholic steatohepatitis (NASH) model.

Methods: Contrast enhanced ultrasonography (CEUS) was performed on a rat NASH model induced by a methionine choline deficient diet (MCDD) and control rats, and Sonazoid was used to measure the signal intensity in the liver parenchyma. The uptake of Sonazoid by the KCs was observed by intravital microscopy. Their phagocytic capability was evaluated *in vitro* using isolated and cultured KCs. The uptake of fluorescein isothiocyanate (FITC)-labeled latex beads was observed and quantitatively analyzed by flow cytometry.

Results: In the MCDD group, liver parenchymal enhancement was reduced 20 min after the Sonazoid injection. Microscopic observation of the isolated and cultured KCs revealed that the number of phagocytosed Sonazoid microbubbles was significantly decreased. Confocal laser scanning microscopic (CLSM) observation showed a decrease in the uptake of the latex beads. A decreased phagocytic capacity in the MCDD group was suggested by the quantitative analysis using flow cytometry, as well as by intravital microscopy.

Conclusions: CEUS with Sonazoid is a powerful evaluation tool to diagnose NASH from an early stage of the disease.

Key words: Kupffer cells, nonalcoholic steatohepatitis, phagocytosis, Sonazoid, ultrasound contrast agents.

INTRODUCTION

NONALCOHOLIC FATTY LIVER disease (NAFLD) has been increasing as the incidence of obesity and metabolic syndrome has been rising. Nonalcoholic steatohepatitis (NASH) draws particular attention due to the risk of progression to cirrhosis and hepatocellular carcinoma.[1–3] Liver biopsy has been considered to be the only way to definitively diagnose NASH[4,5] because diagnosis using imaging modalities is believed to be impossible.[6] In a recent study, magnetic resonance imaging was used for the quantification of the liver fat content and the evaluation of hepatic fibrosis, but it was still inadequate to replace liver biopsy.[7] Liver biopsy is not necessarily recommended for all NAFLD patients because of the risks of the procedure.

We have previously reported the usefulness of contrast enhancement ultrasound (CEUS) in the diagnosis of NASH with a contrast agent, Levovist, which is phagocytosed by the Kupffer cells (KC) in the liver.[8,9] In the liver parenchyma of NASH patients, the accumulation of Levovist microbubbles decreased remarkably 5 min after Levovist injection (especially by 20 min).

Correspondence: Dr Hiroko Iijima, Division of Hepatobiliary and Pancreatic Diseases, Department of Internal Medicine, Hyogo College of Medicine, 1-1 Mukogawa-cho, Nishinomiya, Hyogo 663-8501, Japan. Email: hiroko-i@hyo-med.ac.jp
Received 15 January 2009; revision 17 February 2010; accepted 19 January 2010.

Tsujimoto *et al.* demonstrated reduced contrast effect and phagocytic activity *in vitro* in a rat model prepared by a choline-deficient l-amino acid-defined (CDAA) diet.[10] However, they did not prove it *in vivo* in a rat model that the decreased parenchymal enhancement with Levovist was attributed to phagocytosis by KCs. Sonazoid (GE Healthcare, Oslo) has also been proven to be phagocytosed by KCs.[11,12] We performed CEUS using Sonazoid on a rat NASH model prepared by a methionine choline deficient diet (MCDD)[13] to evaluate the parenchymal enhancement. The phagocytosis of Sonazoid by phagocytic cells was observed *in vivo* in real time by intravital microscopy. To evaluate and prove Sonazoid phagocytosis *in vitro*, isolated and cultured KCs were observed and compared between the MCDD and control groups. Moreover, to evaluate the phagocytic capacity of KCs, the uptake of fluorescein isothiocyanate (FITC)-labeled latex beads was observed and a quantitative analysis was performed using flow cytometry.

METHODS

Animals

THIS STUDY PROTOCOL was approved by the Animal care committee of the Hyogo College of Medicine, and was performed in conformity with their institutional guidelines.

Male Wistar rats (190–200 g; SLC Japan, Tokyo), were housed in the animal facility of the Hyogo College of Medicine and kept at a controlled temperature of 23 ± 1~2°C under 12 h light/12 h dark cycles. Animals for the NASH model were given free access to tap water and MCDD (Oriental Yeast, Tokyo). Animals in the control group had free access to tap water and a normal laboratory diet (MF diet; Oriental Yeast). Animals on the 2nd, 4th and 8th weeks of the diet were used. For observation by intravital microscopy, 25% urethane (Wako Pure Chemical Industries, Osaka) subcutaneous anesthesia was used; and for other observations, isoflurane (Takeda Pharmaceutical, Tokyo) inhalation anesthesia was used.

Histological examination

The liver tissues were fixed in 10% formalin, and then stained with hematoxylin and eosin or Azan. Then, the degree of steatosis, inflammation and fibrosis were assessed from the tissues using the Brunt's histological grading and scoring system.

Preparation of contrast agents and latex beads

The contrast agent Sonazoid and 2.6% FITC-labeled latex beads (Polyscience, Warrington, PA) with diameters of 1 μm and 2 μm, were used. They were diluted with distilled water to 1×10^9 microbubbles/mL and 1×10^9 beads/mL, respectively.

Contrast enhanced ultrasound using Sonazoid

Sonazoid at 0.015 μL (approximately 1.5×10^4 microbubbles)/100g body was injected into the caudal vein after being diluted with distilled water to a total volume of 500 μL.

CEUS was performed by a Toshiba Aplio (Toshiba Medical Systems, Tokyo) with a 7.5 MHz linear transducer. Following conventional B-mode imaging, images were obtained in Advanced Dynamic Flow (ADF) mode with a high mechanical index (MI) of 1.0 to cause destructions of the Sonazoid bubbles. The images were obtained at a focus depth of 3 cm from the body surface at a frame rate of 10 frames/second.

Scanning was performed in various planes of the liver at 20 and 50 min after the Sonazoid injection. This scanning time was based on evidence that the Kupffer phase started at approximately 20 min after the Sonazoid injection when the washout of Sonazoid from the hepatic vein was observed in a healthy volunteer.[14] On the 2nd, 4th, and 8th weeks of the diet, CEUS was performed on four animals from each group to see if any differences in parenchymal enhancement could be detected depending on the duration of the diet. CEUS using ADF was performed at 20 min after the Sonazoid injection to measure the parenchymal intensity within the region of interest (ROI), which was randomly set in the depth within the focus area. The average signal intensity in the liver parenchyma was then calculated after it was converted to sound pressure using the antilog calculation. Scanned images were recorded separately as ADF signals and gray scale signals.

Intravital microscopic observation of phagocytosis by Kupffer cells

Animals in both groups were opened under anesthesia to expose their livers, and were placed in a prone position on a 3 cm diameter transplant platform. A 23 gauge indwelling cannula was inserted into the caudal vein, and 500 μL of 150 μL/100 g Sonazoid diluted with distilled water was administered.

Preparation and phagocytosis of Kupffer cells – *in vitro* study

KCs were isolated from animals in both groups with the previously published procedure: After anesthetizing the animals by isofluran inhalation, the portal vein was cannulated with a 20-gauge needle and the inferior vena cava was opened and a perfusion circuit was created.

Briefly, liver non-parenchymal cells were isolated by the pronase-collagenase method as previously described,[15] and eluted fractions were collected using a Beckman J6-MC centrifuge (Beckman Coulter, Fullerton, CA). The cells were washed, and re-suspended in Roswell Park Memorial Institute (RPMI) 1640 supplemented with 10% fetal bovine serum containing 2-ME (50 μM), L-glutamine (2 mM), penicillin (100 U/mL) and streptomycin (100 μg/mL), plated onto plastic dishes 3.5 cm in diameter, and incubated for 24 h. The plastic adherent cells (1×10^6/mL) were then incubated with 3×10^5 Microbubble/ml Sonazoid for 30 min. After washing the plates with culture medium, the uptake of Sonazoid by the isolated KCs was observed by inverted microscopy (TE300-HM-2; Nikon, Tokyo) in a micro-incubator at 37°C in 5% CO_2. The microscopic images were recorded by image analyzing software (Aquacosmos; Hamamatsu Photonics, Shizuoka). The Sonazoid microbubbles phagocytosed by the KCs were then counted.

Observation of phagocytosis by Kupffer cells – *in vivo* study

Confocal laser scanning microscopy (CLSM)

Latex beads (diameter: 2 μm, concentration: 1×10^8/kg) were administered through the caudal vein of animals from both groups. At 60 min after injection, the animals were sacrificed by anesthesia overdose to prepare frozen sections of the liver. The frozen sections were observed by CLSM (LSM510; Carl Zeiss, Jena).

Flow cytometric quantitative analysis of phagocytic capacity of Kupffer cells

Prior to the experiment, we determined the gating area of KCs fraction using purified KCs according to their forward scatter (FSC) and side scatter (SSC) on a flow cytometer. Once the gated area for KCs was determined, it was used for the rest of the experiments. Aliquots of 1×10^8/kg of FITC-labeled latex beads (diameters: 1 μm and 2 μm) were injected in both groups. At 1 h after injection, KCs isolated by the above-mentioned procedure were cultured for 24 h in an incubator at 37°C in 5% CO_2 to purify the KC fraction and reduce the contaminated cells. Following several washes with phosphate buffered saline (PBS), KCs adhered to the bottom of the dishes were detached with 0.25% Trypsin ethylenediaminetetraacetic acid (EDTA; Invitrogen, Tokyo). They were then centrifuged, and RPMI was added to the sediment to make a total volume of 1 mL in a culture tube. KCs in the tube were then analyzed by flow cytometry. The equipment used was a FACScan (BD Bioscience, San Jose, CA).

Statistics

The statistical significance of the signal intensity change in both groups was evaluated using a repeated measures analysis of variance (ANOVA) test. The Kruskal–Wallis test and Scheffe's *F*-test were performed for a comparison of the phagocytic capacity of isolated and cultured KCs between both groups. All data were analyzed by a statistical software package (SPSS, Chicago, IL).

RESULTS

Changes in liver histology

THE HISTOLOGICAL CHANGES were found as follows: the MCDD-2wk group revealed inflammation and steatosis, but no fibrosis. The MCDD-4wk group showed inflammation, steatosis and slight fibrosis, which was equivalent to grade 2/stage 2 of Blunt's grading/staging system. Inflammation and steatosis were found in the MCDD-8wk group, and their fibrosis was more severe than the one in the MCDD-4wk group, and was corresponding to Blunt's grade 2 /stage 3.

Sonazoid CEUS examination

The signal intensity decreased after Sonazoid injection in the MCDD group as compared to the control group. The quantification of the signal intensity at 20 min after injection is shown in Figure 1. The parenchymal intensity in the control group was −5.0 and −5.5 at 20 and 50 min after Sonazoid injection, respectively, but was −13.0 and −13.3 in the MCDD-4wk group, respectively. In the control group, the intensity decreased slightly to −3.5dB, −4.8dB and −5.5dB on the 2nd, 4th and 8th weeks of administration, respectively. In contrast, in the MCDD group, the intensity decreased according to the duration of the diet administration as to −11.5dB, −13.0dB and −20.5dB on the 2nd, 4th and 8th weeks, respectively; this was a significant difference between the groups ($P < 0.05$) (Figs 1,2).

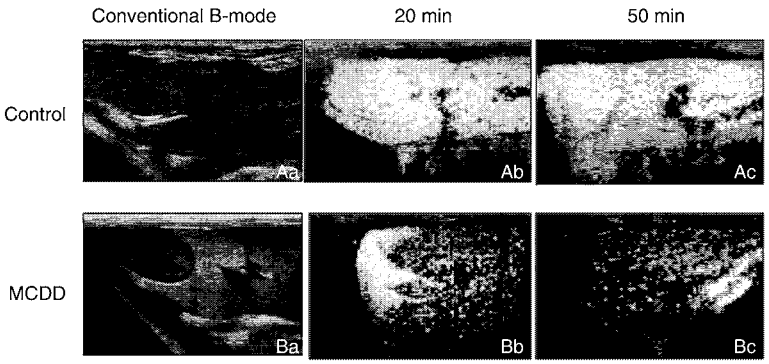

Figure 1 Abdominal US B-mode images (Aa, Ba) and Sonazoid CEUS images (Ab, Ac, Bb, Bc) of control rats (Aa-c) and MCDD-4wk fed rats (Ba-c). The hepato-renal echo contrast was greater in the MCDD rat group as compared with the control group. The livers in the control rats were clearly enhanced until 50 min after injection. In contrast, the enhancement of the liver decreased in the MCDD rats at both 20 and 50 min after injection.

Time course change of Sonazoid phagocytosis observed by intravital microscopy

Five animals from each group were compared. Particles appeared on the sinusoidal wall were observed almost simultaneously at Sonazoid administration, and then the uptake of Sonazoid by phagocytic cells on the sinusoidal wall was recorded using a fixed camera in the view area of the portal vein before Sonazoid injection until 30 min after injection (Fig. 3). The time course was observed by intravital microscopy for 30 min after the Sonazoid injection, and showed that the number of Sonazoid microbubbles phagocytosed by the KCs kept increasing in the control group. However, in the MCDD group, only several Sonazoid microbubbles were phagocytosed by the KCs (Fig. 4).

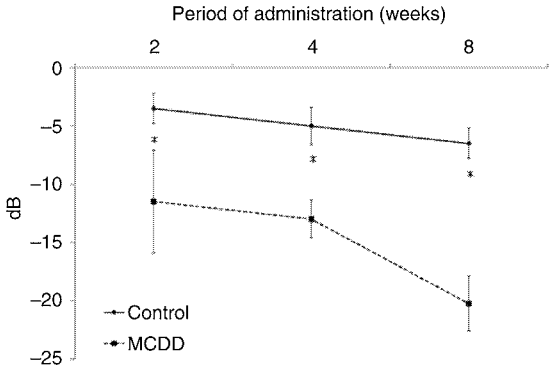

Figure 2 Liver parenchymal intensity (dB) of Sonazoid CEUS on control and MCDD rats at 2 weeks, 4 weeks and 8 weeks of diet administration. The vertical axis is the signal intensity (dB) and the horizontal axis is the duration of diet administration. The parenchymal intensity in the MCDD group showed a decrease as compared with the control group at −11.5dB, −13dB and −20.5dB at the 2nd, 4th, and 8th weeks after administration, respectively ($P < 0.05$).

Phagocytosis of FITC-labeled latex beads by Kupffer cells – *in vivo*

CLSM observations

The number of FITC-labeled latex beads phagocytosed by the KCs and stained as fluorescent green was compared between the two groups. The number of fluorescent-green phagocytosed latex beads in the MCDD group decreased in comparison with the control group, and this suggested decreased phagocytic capacity of the Kupffer cells in the MCDD group (Fig. 5).

Phagocytosis of isolated Kupffer cells – *in vitro*

The inverted microscopic observation of isolated and cultured KCs with Sonazoid is shown in Figure 6. Significant differences were found between the control group and each week of the MCDD groups, and also between the MCDD-2wk and MCDD-8wk groups and between the MCDD-4wk and MCDD-8wk groups ($P < 0.01$) (Fig. 6).

Phagocytosis capability by flow cytometric analysis

Flow cytometric analysis was performed to quantify the phagocytic capacity of isolated and cultured KCs, which were treated with fluorescent latex beads. The phagocytosis rate in the control group was 88%, and many latex beads were ingested. In contrast, the rate was 61% in the MCDD-2wk (B), 37% in the MCDD-4wk (C) and 27% in the MCDD-8wk (D) groups, where the phagocytic capacity had decreased in proportion to the duration

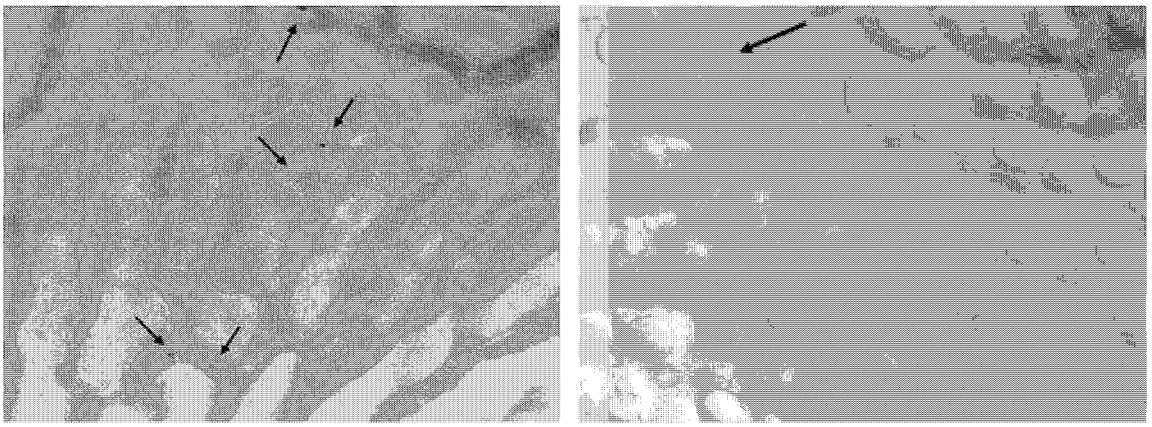

Figure 3 Intravital microscopic observation at 30 min after Sonazoid injection. A number of Sonazoid were phagocytosed by phagocytic cells in the control group; whereas a couple of them were phagocytosed in the MCDD-2wk group.

of the MCDD administration. The phagocytosis index (expressed by the number of KCs which phagocytosed beads/the total number of KCs) in the MCDD group was also lower than in the control groups at every duration of the MCDD administration (Fig. 7). This finding revealed that the phagocytic capacity started to decrease at the early stages of the disease, and kept on decreasing week by week.

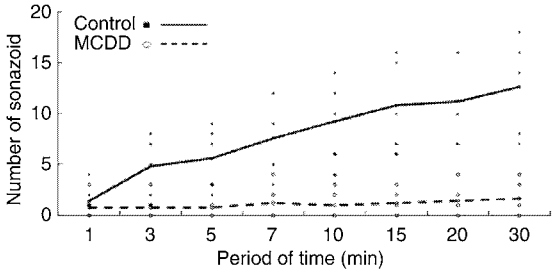

Figure 4 Time-course change in the phagocytosis of Sonazoid. The number of Sonazoid microbubbles phagocytosed by the KCs was plotted at 1, 3, 5, 7, 10, 15, 20 and 30 min after the Sonazoid injection. The control group is shown with a solid line and the MCDD-2wk group is shown with a broken line. Significant difference was seen in the two groups ($P < 0.001$). In the control group, the phagocytosis of Sonazoid increased up to 30 min after Sonazoid injection. In the MCDD-2wk group, only a couple of Sonazoid microbubbles were phagocytosed over a couple min after the injection.

DISCUSSION

NASH HAS BEEN increasing worldwide, and is the most common form of non-alcoholic/non-viral liver disease in the United States and European countries.[16] NAFLD was once considered a benign, reversible condition, and therefore was often left untreated. However, since NASH was introduced by Ludwig, a strong risk of this disease progressing to cirrhosis and hepatocellular carcinoma has been identified.[1–3] In the United States, an estimate shows about 30% of the population has NAFLD, and about 10% of these NAFLD patients has NASH.[17] In countries other than the United States, many people are believed to be developing NASH as their diets become Westernized.[18]

Ultrasonography is used for various organs as a non-invasive diagnostic modality. Ultrasound diagnosis with an intravenous contrast agent is also widely used, and has become indispensable especially in diagnosing the liver diseases.[19,20] The sonographic features of NAFLD including NASH are a high-level echo, a bright liver, vascular blurring, deep attenuation and hepatorenal contrast.[21–24] Abdominal computerized tomography (CT), which provides a more objective assessment, diagnoses NAFLD when the liver to spleen ratio (L/S ratio) is less than 0.9.[25] Thus, the diagnosis of NAFLD could be easily made by these imaging modalities, although distinguishing NASH from NAFLD is considered to be difficult by means of only imaging modalities and blood tests or an invasive liver biopsy is

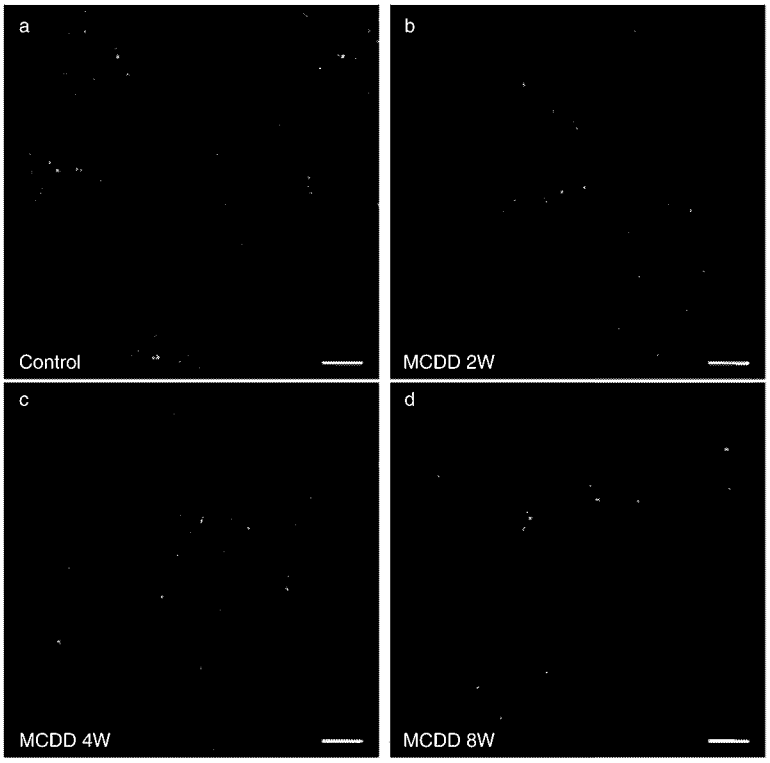

Figure 5 The animals were sacrificed at 60 min after fluorescent latex beads injection and were observed by CLSM. Many latex beads were observed in the control rats (shown in A) as compared with the MCDD rats (in B-D). The fluorescent agent of the latex beads is recognized as green.

required.[4–6] Given the prevalence of NAFLD patients, which has been reported to be as high as 30% of adults who get a medical checkup,[4–6] establishing non-invasive and reliable methods for diagnosing NASH is urgently needed. In the past, we have reported the usefulness of CEUS diagnosis using Levovist to distinguish NASH from NAFLD[9] because it is not realistic to perform liver biopsies for so many NAFLD patients. The diagnosis is made possible by the fact that the liver parenchymal enhancement significantly decreases in NASH patients at 20 min after Levovist injection during the delayed parenchymal phase. One suspected reason for this is the decreased phagocytic capacity of KCs in NASH.[9] Levovist was proven to be phagocytosed by KCs.[11] Furthermore, a study using latex beads on a rat NASH model prepared by a CDAA diet also showed reduced KC phagocytic function, with no changes in the KC numbers, in which the decreased parenchymal contrast effect was possibly attributed to a decrease in the phagocytic capability of KCs, although it did not prove that Levovist itself was phagocytosed by KCs.[10] Moreover, a recent study reported that the engulfment of erythrocytes by KCs was observed by electron microscopy in a rat NASH model induced by a high-fat diet.[26]

Sonazoid is a microbubble with a diameter of 2–4 μm, and contains perfulbutane gas. It has a phospholipid shell which is negatively charged on its surface, and is known to be phagocytosed by liver macrophages, the KCs.[27,28] A report showed that 99% of Sonazoid and 47% of Levovist microbubbles were phagocytosed by isolated and cultured rat KCs;[11] In other words, Sonazoid is expected to be more readily phagocytosed than Levovist. In the present study, the time-course change of KC phagocytosis was investigated by performing CEUS on both MCDD and control rats using Sonazoid by intravital microscopy, and by analyzing isolated and cultured KCs. Sonazoid CEUS performed on a rat NASH model at 20 and 50 min after Sonazoid injection showed a significant decrease in enhancement at 50 min (Fig. 1). Using intravital microscopic observation, the Sonazoid continued to be phagocytosed in the control group, whereas in the MCDD group, the number of phagocytosed Sonazoid

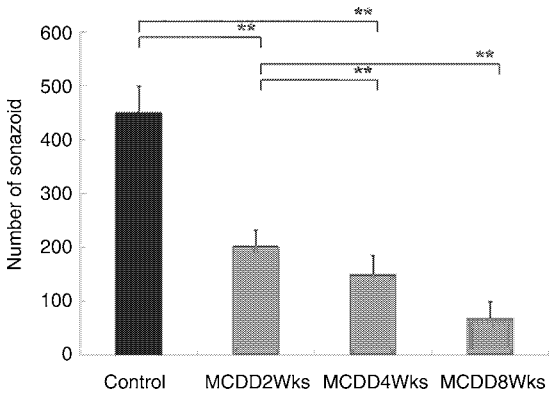

Figure 6 The number of Sonazoid microbubbles phagocytosed by isolated KCs in the control group and the MCDD-2wk, 4wk and 8wk groups were observed by inverted microscopy. After Sonazoid was added, the isolated KCs were cultured before observation. The number of Sonazoid microbubbles phagocytosed by 10 KCs in the control group was 450.5 ± 48.5, whereas 204.1 ± 28.7, 150.9 ± 34.2, and 69.7 ± 29.1 microbubbles were phagocytosed in the MCDD-2wk, 4wk and 8wk groups, respectively (mean ± standard deviation). Significant differences were found between the control group and each week of the MCDD groups, and also between the MCDD-2wk and MCDD-8wk groups and between the MCDD-4wk and MCDD-8wk groups ($P < 0.01$).

microbubbles by phagocytic cells was few after injection. Considering that most of phagocytic cells on sinusoidal wall are KCs, it is reasonable to think contrast agent is phagocytosed by KCs in hepatic sinusoids. Time-course observation also showed the number of phagocytosed microbubbles by phagocytic cells did not increase in the MCDD group (Fig. 4). This finding suggests that the phagocytic capability of KCs may start to decrease during the early stage of NASH, and that could enable the diagnosis of NASH at an early stage of fibrosis. To demonstrate these findings using isolated and cultured KCs, the number of phagocytosed Sonazoid microbubbles decreased in the MCDD rats (Fig. 6). In addition, the number of phagocytosed Sonazoid or latex beads tended to decrease in proportion to the duration of the MCDD administration (Fig. 5). In NASH patients, fibrosis is often detected at a late stage of the disease, because NASH is usually monitored as NAFLD. However, by using Sonazoid CEUS, the diagnosis of NASH could be possible at an early stage, and this represents a groundbreaking development in NASH treatment.

Our study also suggested the clinical usefulness of Sonazoid CEUS in the diagnosis of NASH by demonstrating that: (i) parenchymal enhancement was decreased in the delayed parenchymal phase; and (ii) the phagocytic capacity of Kupffer cells was lowered as the duration of MCDD administration increased. Considering that Sonazoid is specifically phagocytosed by Kupffer cells, the quantification of phagocytic capacity should also be possible.

Some studies have reported the narrowed sinusoids seen in steatosis and steahohepatitis disturb the hepatic microcirculation.[29–31] In particular, the sinusoidal space of a NAFLD animal model was reduced by up to 50 % of the size of healthy control animals.[31] In order to preclude the possibility that the lowered liver parenchymal enhancement was caused by a circulatory disturbance of the contrast agent, latex beads with a diameter of 1 μm, which is smaller than the diameter of Sonazoid (2 μm), were used in the present *in vivo* study, since the width of a normal sinusoid is approximately 5 μm. We performed CEUS with Levovist (4 mL/body) at one minute after Levovist intravenous injection in the early vascular phase to see if decreased parenchymal enhancement was associated with the narrowed sinusoids. Additionally, the parenchymal enhancement of fatty liver patients, NASH patients and healthy volunteers at 1 min after Levovist injection showed a similar intensity in the liver parenchyma in the early vascular phase (Fig. 8). These results demonstrated that the decreased enhancement of liver parenchyma was not due to the narrowed sinusoids or circulatory disturbances.

As shown above, our results suggested decreased Sonazoid-enhanced echogenicity was mainly due to impaired KC phagocytosis, although narrowed sinusoids could be present in MCDD rats due to fatty liver. Sonazoid CEUS could become a useful tool to distinguish NASH patients from many NAFLD patients.

ACKNOWLEDGEMENTS

THIS STUDY WAS supported by a Grant-in-Aid for Scientific Research from the Ministry of Education, Culture, Sports, Science and Technology of Japan, nos. 19500428 and 21300194 and a Grant-in-Aid for Researchers, Hyogo College of Medicine.

We thank all of our colleagues in the Division of Hepatobiliary and Pancreatic Medicine, Ms Sayaka Fujii and Ms Mayumi Yamada, for providing support for our experiments, and the technicians in the Ultrasound Imaging Center.

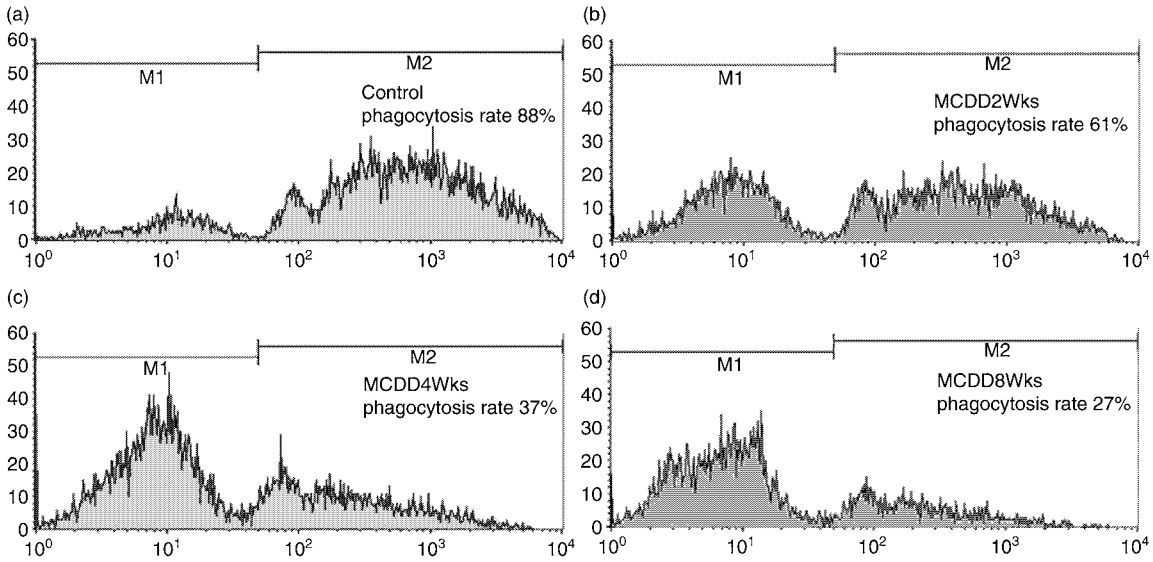

Figure 7 Flow cytometric analysis of isolated and cultured KCs after being treated with fluorescent latex beads. The vertical axis is the KC count and the horizontal axis is the fluorescent intensity. M1 is the number of KCs which did not phagocytose any beads, and M2 is the number of KCs which phagocytosed beads. The phagocytosis rate was calculated by M2/M1 + M2 (the total number of KCs). The phagocytosis rate in the control group was 88% and many latex beads were ingested, whereas the rate was 61 % in the MCDD-2wk (B), 37% in the MCDD-4wk (C) and 27% in the MCDD-8wk (D) groups, where the phagocytic capacity was decreased in proportion to the duration of MCDD administration.

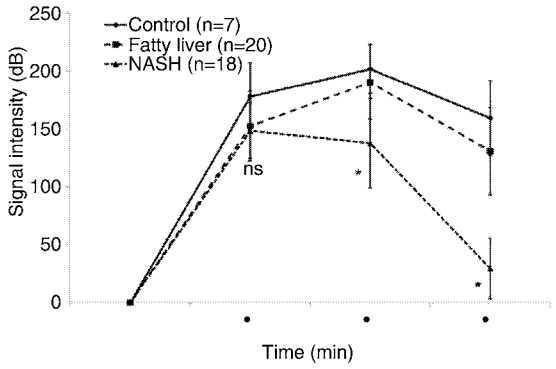

Figure 8 Parenchymal signal intensity in the early vascular phase and the delayed parenchymal phase of Levovist CEUS was evaluated in seven controls (healthy volunteers), 20 fatty liver patients and 18 NASH patients. At 1 min after the Levovist injection, the signal intensity was 178.1 ± 29.3 in the controls, 152.4 ± 30.0 in the fatty liver patients and 148.5 ± 23.6 in the NASH patients (mean ± standard deviation) and no significant differences were observed. However, at 5 and 20 min after injection, there was a significant decrease in the signal intensity in the NASH group.

REFERENCES

1 Ludwig J, Viggiano TR, McGill DB, Oh BJ. Nonalcoholic steatohepatitis: Mayo Clinic experiences with a hitherto unnamed disease. *Mayo Clin Proc* 1980; **55**: 434–8.
2 Bugianesi E, Leone N, Vanni E *et al.* Expanding the natural history of nonalcoholic steatohepatitis: from cryptogenic cirrhosis to hepatocellular carcinoma. *Gastroenterology* 2002; **123**: 134–40.
3 Shimada M, Hashimoto E, Taniai M *et al.* Hepatocellular carcinoma in patients with non-alcoholic steatohepatitis. *J Hepatol* 2002; **37**: 154–60.
4 Saadeh S, Younossi ZM, Remer EM *et al.* The utility of radiological imaging in nonalcoholic fatty liver disease. *Gastroenterology* 2002; **123**: 745–50.
5 Brunt EM, Janney CG, Di Bisceglie AM, Neuschwander-Tetri BA, Bacon BR. Nonalcoholic steatohepatitis: a proposal for grading and staging the histological lesions. *Am J Gastroentero* 1999; **94**: 2467–74.
6 Matteoni CA, Younossi ZM, Gramlich T, Boparai N, Liu YC, McCullough AJ. Nonalcoholic fatty liver disease: a spectrum of clinical and pathological severity. *Gastroenterology* 1999; **116**: 1413–9.
7 Schwenzer NF, Springer F, Schraml C, Stefan N, Machann J, Schick F. Non-invasive assessment and quantification of

liver steatosis by ultrasound, computed tomography and magnetic resonance. *J Hepatol* 2009; **51**: 433–5.
8 Iijima H, Moriyasu F, Miyahara T, Yanagisawa K. Ultrasound contrast agent, Levovist microbubbles are phagocytosed by Kupffer cells-In vitro and in vivo studies. *Hepatol Res* 2006; **35**: 235–7.
9 Iijima H, Moriyasu F, Tsuchiya K, Suzuki S, Yoshida M. Decrease in accumulation of ultrasound contrast microbubbles in non-alcoholic steatohepatitis. *Hepatol Res* 2007; **37**: 722–30.
10 Tsujimoto T, Kawaratani H, Kitazawa T *et al.* Decreased phagocytic activity of Kupffer cells in a rat nonalcoholic steatohepatitis model. *World J Gastroenterol* 2008; **14**: 6036–43.
11 Yanagisawa K, Moriyasu F, Miyahara T, Yuki M, Iijima H. Phagocytosis of ultrasound contrast agent microbubbles by Kupffer cells. *Ultrasound Med Biol* 2007; **33**: 318–25.
12 Watanabe R, Matsumura M, Munemasa T, Fujimaki M, Suematsu M. Mechanism of hepatic parenchyma-specific contrast of microbubble-based contrast agent for ultrasonography: microscopic studies in rat liver. *Invest Radiol* 2007; **42**: 643–51.
13 Weltman MD, Farrell GC, Liddle C. Increased hepatocyte CYP2E1 expression in a rat nutritional model of hepatic steatosis with inflammation. *Gastroenterology* 1996; **111**: 1645–53.
14 Sasaki S, Iijima H, Moriyasu F, Hidehiko W. Definition of contrast enhancement phases of the liver using a perfluoro-based microbubble agent. *Ultrasound Med Biol* 2009; **35**: 1819–27.
15 Tsutsui H, Mizoguchi Y, Morisawa S. Importance of direct hepatocytolysls by liver macrophages in experimental fulminant hepatitls. *Hepatogastroenterology* 1992; **39**: 553–9.
16 Skelly MM, James PD, Ryder SD. Findings on liver biopsy to investigate abnormal liver function tests in the absence of diagnostic serology. *J Hepatol* 2001; **35**: 195–9.
17 Green RM. NASH:hepatic metabolism and not simply the metabolic syndrome. *Hepatology* 2003; **38**: 14–7.
18 Charlton M. Nonalcoholic fatty liver disease: a review of current understanding and future impact. *Clin Gastroenterol Hepatol* 2004; **2**: 1048–58.
19 Harvey CJ, Blomley MJ, Eckersley RJ, Heckemann RA, Butler-Barnes J, Cosgrove DO. Pulse-inversion mode imaging of liver specific microbubbles: improved detection of subcentimetre metastases. *Lancet* 2000; **355**: 807–8.
20 Gaiani S, Celli N, Piscaglia F *et al.* Usefulness of contrast-enhanced perfusional sonography in the assessment of hepatocellular carcinoma hypervascular at spiral computed tomography. *J Hepatol* 2004; **41**: 421–6.
21 Taylor KJ, Carpenter DA, Hill CR, McCready VR. Gray scale ultrasound imaging. The anatomy and pathology of the liver. *Radiology* 1976; **119**: 415–23.
22 Joseph AE, Dewbury KC, McGuire PG. Ultrasound in the detection of chronic liver disease (the 'bright liver'). *Br J Radiol* 1979; **52**: 184–8.
23 Foster KJ, Dewbury KC, Griffith AH, Wright R. The accuracy of ultrasound in the detection of fatty infiltration of the liver. *Br J Radiol* 1980; **53**: 440–2.
24 Yajima Y, Ohta K, Narui T, Abe R, Suzuki H, Ohtsuki M. Ultrasonographical diagnosis of fatty liver: significance of the liver-kidney contrast. *Tohoku J Exp Med* 1983; **139**: 43–50.
25 Ricci C, Longo R, Gioulis E *et al.* Noninvasive in vivo quantitative assessment of fat content in human liver. *J Hepatol* 1997; **27**: 108–13.
26 Otogawa K, Kinoshita K, Fujii H *et al.* Erythrophagocytosis by liver macrophages (Kupffer cells) promotes oxidative stress, inflammation, and fibrosis in a rabbit model of steatohepatitis: implications for the pathogenesis of human nonalcoholic steatohepatitis. *Am J Pathol* 2007; **170**: 967–80.
27 Sontum PC, Ostensen J, Dyrstad K, Hoff L. Acoustic properties of NC100100 and their relation with the microbubble size distribution. *Invest Radiol* 1999; **34**: 268–75.
28 Sontum PC. Physicochemical characteristics of Sonazoid, a new contrast agent for ultrasound imaging. *Ultrasound Med Biol* 2008; **34**: 824–33.
29 Ijaz S, Yang W, Winslet MC, Seifalian AM. Impairment of hepatic microcirculation in fatty liver. *Microcirculation* 2003; **10**: 447–56.
30 McCuskey RS, Ito Y, Robertson GR, McCuskey MK, Perry M, Farrell GC. Hepatic microvascular dysfunction during evolution of dietary steatohepatitis in mice. *Hepatology* 2004; **40**: 386–93.
31 Farrell GC, Teoh NC, McCuskey RS. Hepatic microcirculation in fatty liver disease. *Anat Rec (Hoboken)* 2008; **291**: 684–92.

Hindawi Publishing Corporation
Gastroenterology Research and Practice
Volume 2010, Article ID 641865, 11 pages
doi:10.1155/2010/641865

Review Article

The TLR4/TRIF-Mediated Activation of NLRP3 Inflammasome Underlies Endotoxin-Induced Liver Injury in Mice

Hiroko Tsutsui,[1] Michiko Imamura,[1,2,3,4] Jiro Fujimoto,[2] and Kenji Nakanishi[3]

[1] *Department of Microbiology, Hyogo College of Medicine, 1-1, Mukogawa-cho, Nishinomiya 663-8501, Japan*
[2] *Department of Surgery, Hyogo College of Medicine, 1-1, Mukogawa-cho, Nishinomiya 663-8501, Japan*
[3] *Department of Immunology & Medical Zooloty, Hyogo College of Medicine, 1-1, Mukogawa-cho, Nishinomiya 663-8501, Japan*
[4] *Cancer Center, Hyogo College of Medicine, Nishinomiya, Japan*

Correspondence should be addressed to Hiroko Tsutsui, gorichan@hyo-med.ac.jp

Received 11 March 2010; Accepted 22 April 2010

Academic Editor: Ekihiro Seki

Administration of heat-killed *Propionibacterium acnes* renders mice highly susceptible to LPS. After LPS challenge *P. acnes*-primed mice promptly show hypothermia, hypercoagulation (disseminated intravascular coagulation), elevation of serum proinflammatory cytokine levels, and high mortality. The surviving mice develop liver injury. As previously reported, IL-18 plays a pivotal role in the development of this liver injury. Many cell types including macrophages constitutively store IL-18 as biologically inactive precursor (pro) form. Upon appropriate stimulation exemplified by TLR4 engagement, the cells secrete biologically active IL-18 by cleaving pro-IL-18 with caspase-1. Caspase-1 is also constitutively produced as a zymogen in macrophages. Recently, NLRP3, a cytoplasmic pathogen sensor, has been demonstrated to be involved in the activation of caspase-1. Here, we review the molecular mechanisms for the liver injuries, particularly focusing on the TLR4/NLRP3-mediated caspase-1 activation process, with a brief introduction of the mechanism underlying *P. acnes*-induced sensitization to LPS.

1. Introduction

TLR, topics of this issue, is an extracellular sensor family of pathogen-associated molecular patterns (PAMPs) [1, 2]. As described by Yamamoto et al. in this special issue, TLR1, TLR2, TLR4, TLR5, TLR6, and TLR11 are expressed on the cell surface, while TLR3, TLR7, TLR8, and TLR9 are expressed on the membrane of endosome, which is a transport vesicle originated from the cell membrane to trap and transport the extracellular macromolecules into the inside of the cells. Besides, mammalian host possess cytoplasmic sensors consisting of at least two families, RIG-I-like receptor (RLR) and Nod-like receptor (NLR) families [3–5]. After sensing intracellular, virus-derived double-stranded (ds) RNA, RLR members relay a signal to activate inflammatory responses for viral clearance via induction of proinflammatory cytokines and type 1 IFNs [6, 7]. Some of the NLR family members are associated with the cytoplasmic formation and activation of inflammasome. Inflammasome is a multiple protein complex and is regarded as the platform for activation of caspase-1 [8, 9]. Caspase-1 is produced as enzymatically inactive precursors (pro) and requires appropriate cleavage to become active. Macrophages including Kupffer cells constitutively produce procaspase-1 and accomplish caspase-1 activation in the inflammasomes after being stimulated [10–12]. Caspase-1 cleaves biologically inactive pro-IL-1β and pro-IL-18, leading to extracellular release of the corresponding active forms. Many cell types including Kupffer cells produce and store pro-IL-18 in the steady state, while they start to produce pro-IL-1β only after activation with appropriate stimuli [13–15]. Thus, the inflammasomes contribute to the secretion of IL-18 and IL-1β via activation of caspase-1.

Inflammasome is composed of certain member of NLR and procaspase 1 [5, 8, 9] (Figure 1). NLR family members are divided into two groups. One is an NLRP group possessing pyrin domain (PYD), and the other is an NLRC group lacking PYD but possessing caspase recruitment domain (CARD) [19]. NLRP1 (Nalp1), NLRP3 (Nalp3), and NLRC4 (Ipaf) have been demonstrated to nucleate the

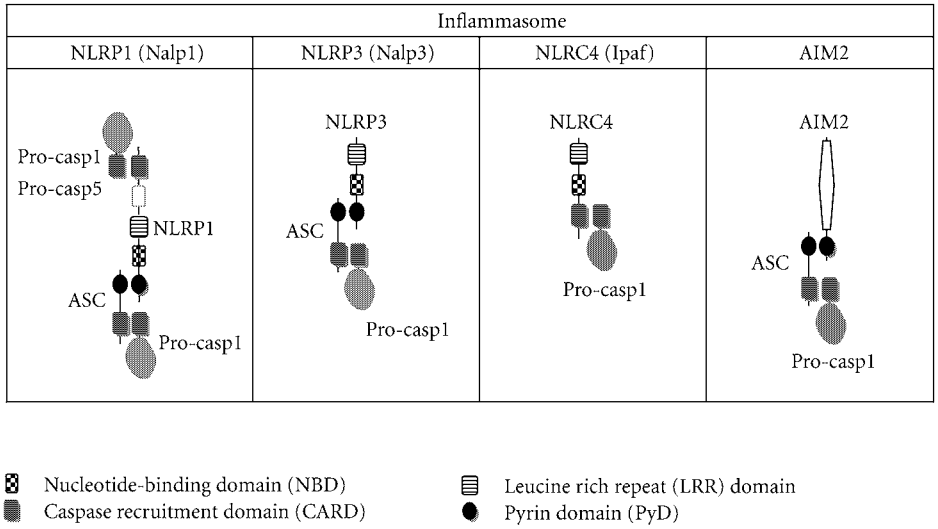

FIGURE 1: Inflammasome constituents. There have been reported at least four types of inflammasomes, NLRP1 (Nalp1), NLRP3 (Nalp3), NLRC4 (Ipaf), and AIM2 inflammasomes. NLR is subdivided into two groups, PYD-possessing group, namely, NLRP and PYD-lacking group NLRC. After exposure of cells to the corresponding stimuli, these NLRs and AIM2 are believed to be self-oligomerized. As it contains CARD at an N-terminus and PYD at a C-terminus, self-oligomerized NLRP1 can recruit procaspase (casp)-1 and procaspase-5 by action of its CARD and also assembly procaspase-1 with help from ASC that possesses both PYD and CARD. Self-oligomerized NLRP3 recruits procaspase-1 by interposing ASC between them. In contrast, self-oligomerized NLRC4 recruits procaspase-1 by directly interacting CARD of procaspase-1 with its CARD. AIM2, belonging a different protein family, is also believed to be self-oligomerized after recognition of double-stranded DNA and recruits procaspase-1 with help from ASC. NLR, Nod-like receptor; CARD, caspase recruitment domain; PYD, pyrin domain.

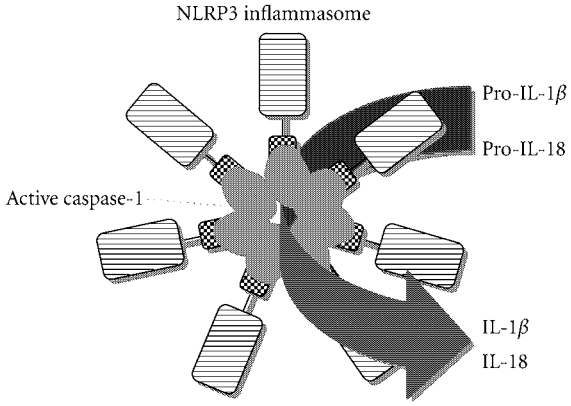

FIGURE 2: A possible schema for IL-18/IL-1β processing by the inflammasome. After appropriate stimulation, the NLRP3 inflammasome is activated to induce active caspase-1, which eventually results in conversion of pro-IL-18/pro-IL-1β into biologically active IL-18/IL-1β.

inflammasomes [5, 19]. In the inflammasome these NLRs are believed to sense cytoplasmic PAMPs exemplified by LPS presumably via their leucine rich repeat (LRR) domain. LRR domain of NLRP3 can recognize all of the TLR agonists except for TLR5 agonist, flagellin of bacterial flagellum, while that of NLRC4 senses flagellin [20]. After being stimulated the NLRs are self-oligomerized by binding each other using their nucleotide-binding domain (NBD). Self-oligomerized NLRP1 directly recruits procaspase-1 by homophilic protein-protein interaction between its N-terminal CARD and CARD of procaspase1 and/or procaspase-5 [8]. ASC consisting of PYD and CARD is regarded as an adapter protein for caspase-1 activation. The NLRP1 can bind to PYD of ASC by its PYD domain at C-terminus, and CARD of ASC eventually recruits procaspase-1 by CARD-CARD interaction (Figure 1). The same scenario can be sketched for the recruitment of procaspase-1 around the oligomerized NLRP3-ASC complexes (Figure 1). NLRC4 has CARD but not PYD. Upon appropriate stimulation of NLRC4, procaspase-1 is recruited onto NLRC4 directly by CARD-CARD interaction (Figure 1). Recently, AIM2, belonging to a different protein family namely PYHIN, was reported to activate caspase-1 by sensing cytoplasmic ds-DNA [7, 21–25]. After recognition of ds-DNA by HIN 200 domain of it, AIM2 might be self-oligomerized for recruitment of procaspase-1 by similarly interposing ASC between these two proteins (Figure 1). Recruitment of procaspase-1 into these inflammasomes is likely to activate caspase-1, leading to conversion from pro-IL-18 and pro-IL-1β into active IL-18 and IL-1β [26] (Figure 2).

As previously reported, mice having received heat-killed *Propionibacterium acnes* are highly susceptible to LPS [27–30]. *P. acnes*-primed mice suffer from liver injuries after LPS challenge. However, administration of neutralizing anti-IL-18 antibodies (Abs) just before LPS challenge can prevent *P. acnes*-primed mice from the liver injury [17]. Besides, *Il18*$^{-/-}$ mice are resistant to the *P. acnes*/LPS treatment [18]. Thus, IL-18 is important for the development of liver injuries.

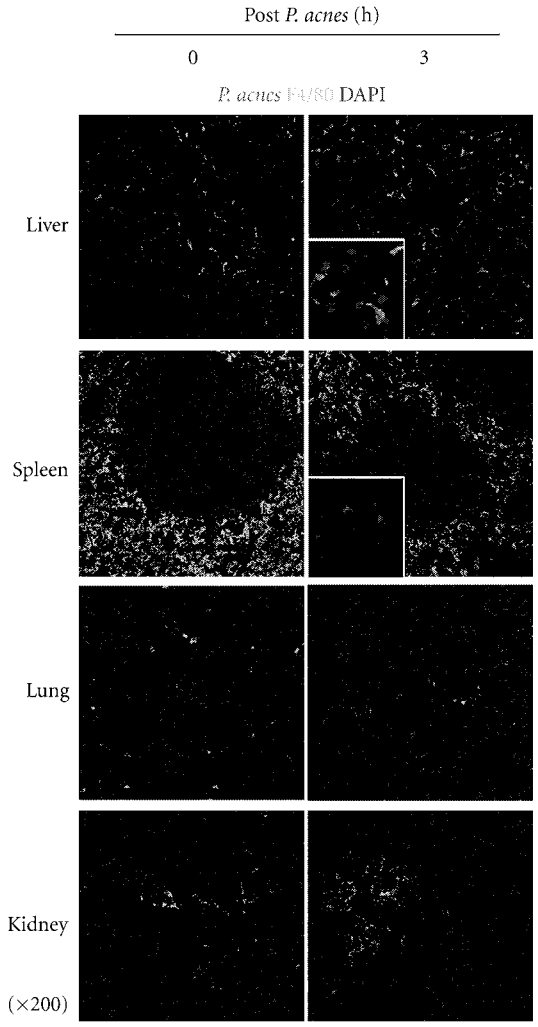

FIGURE 3: Kupffer cells promptly capture heat-killed *P. acnes*. Cy3-labeled, heat-killed *P. acnes* (red) were administered into naïve wild-type mice through a tail vein, and at 3 h tissue specimens were sampled. Frozen tissue slices were incubated with anti-F4/80 mAb (green) and DAPI for detecting macrophages and cell nuclei, respectively. F4/80$^+$ cells (Kupffer cells) capture *P. acnes*, while both F4/80$^+$ and F4/80$^-$ cells ingest them in the spleen. In contrast to live and spleen, both lung and kidney rarely contain *P. acnes*. Magnification of insets is x800.

Here, we review the mechanisms for the *P. acnes*/LPS-induced liver injuries, particularly focusing on those how active IL-18 is released. Prior to addressing this, we would like to introduce the cellular and molecular mechanisms by which pretreatment with *P. acnes* render mice highly susceptible to LPS.

2. Endotoxin Shock Syndrome in *P. acnes*/LPS-Treated Mice

Hypothermia, hypercoagulation (disseminated intravascular coagulation; DIC), high lethality, and tissue injuries are major clinical manifestations of endotoxin shock syndrome [30–35]. After challenge with a subclinical dose of LPS, naïve wild-type (WT) mice do not show these signs (Table 1). In contrast, mice having received heat-killed *P. acnes* 7 days before are highly susceptible to LPS. *P. acnes*-primed mice, but not naïve mice, show obvious and gradual reduction of rectal temperature, serum elevation of proinflammatory cytokines including IL-6, IFN-γ, and TNF-α, high mortality and liver injuries after challenge with the same subclinical dose of LPS [18, 30, 32]. LD_{50} to LPS in *P. acnes*-primed mice is a thousandth or less of that in naïve mice [30]. Furthermore, they exhibit severe hypercoagulation status, which is monitored by plasma levels of coagulation indicator, thrombin antithrombin complexes (TAT), and anti-fibrinolytic protein, plasminogen activator type 1 (PAI-1) that potently inhibits fibrinolysis by blocking conversion from plasminogen into fibrinolytic plasmin [32, 36]. *P. acnes*-primed mice, but not naïve mice, tremendously increase plasma levels of TAT and PAI-1 after LPS challenge [32]. Thus, *P. acnes* treatment powerfully sensitizes mice to LPS.

3. Kupffer Cell Ingestion of Heat-killed *P. acnes*

P. acnes, a Gram-positive bacterium, is often detectable on human skin and has been believed to be relevant to various inflammatory diseases, such as synovitis, acne, pustulosis, hyperostosis, and osteitis (SAPHO) and sarcoidosis [37]. What happens in mice treated with heat-killed *P. acnes*? To address this, we labeled heat-killed *P. acnes* by Cy3, injected them into WT mice through a tail vein, and sampled various tissue specimens at 3 h. We examined tissue distribution of Cy3$^+$ particles by confocal microscopic analyses. Expectedly, heat-killed *P. acnes* are accumulated in the liver and spleen, whereas they were almost absent in the lung and kidney (Figure 3). F4/80$^+$ cells principally capture *P. acnes* in the liver, while both F4/80$^-$ cells and F4/80$^+$ cells ingest them in the spleen (Figure 3).

At day 7 after *P. acnes* treatment tremendous hepatosplenomegaly is observed (Figure 4(a)). The liver doubles its normal weight, whereas weight of spleen achieve more than 5 times (Figure 4(b)). In contrast to the liver and spleen, weight of kidney or lung remains unchanged. In the liver, the dense granulomas primarily consisting of F4/80$^+$ macrophages develop, in the center of which *P. acnes*-ingested F4/80$^+$ Kupffer cells are localized (Figure 4(c)), suggesting that *P. acnes*-ingested F4/80$^+$ Kupffer cells might recruit many F4/80$^+$ macrophages. Immunostaining using rhodamine-conjugated anti-F4/80 mAb followed by counterstaining with hematoxylin reveals that abundant F4/80$^+$ cells are present in the hepatic granulomas [38]. In contrast to the liver, obvious accumulation of F4/80$^+$ cells around *P. acnes* is absent in the spleen (Figure 4(c)). Many dendritic cells were reported to compose the hepatic granulomas as well [39, 40]. *P. acnes* treatment increases hepatic F4/80$^+$ cell number to 30 times and more of that in naïve mice, while the splenic F4/80$^+$ cell number reaches only less than 5 times (Figure 4(d)). Furthermore,

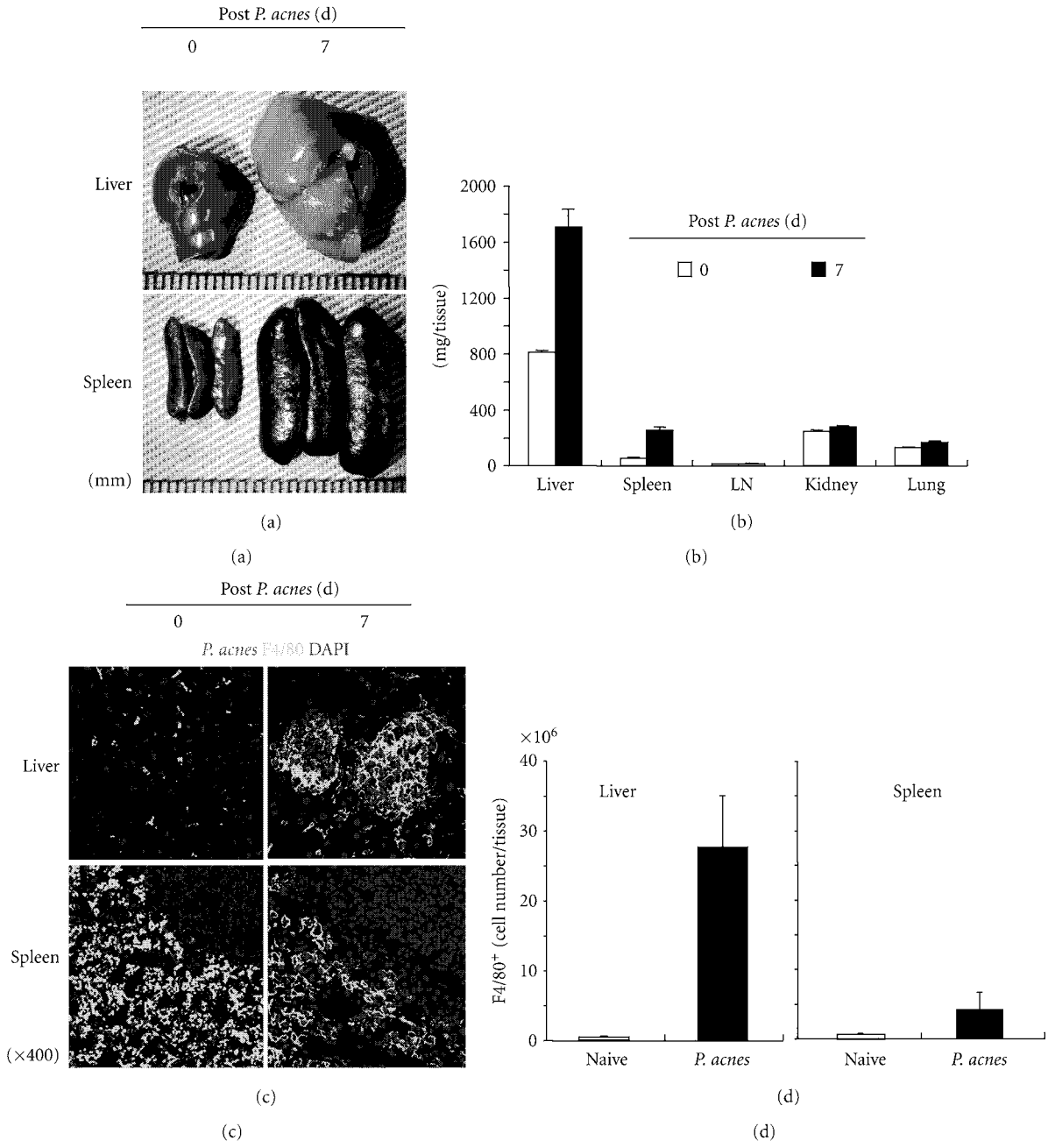

FIGURE 4: Hepatosplenomegaly and hepatic granulomas in *P. acnes*-primed mice. Wild-type mice received Cy3-labeled, heat-killed *P. acnes*, and at day 7 various tissues were removed and weighed (a, b). The liver slices were stained with anti-F4/80 mAb and DAPI for detecting macrophages and cell nuclei, respectively (c). Kupffer cells and splenocytes were prepared from *P. acnes*-primed (closed) or naïve mice (open). After staining with anti-F4/80 mAb, proportion of $F4/80^+$ cells were determined by FACS, and total $F4/80^+$ cell number was counted.

splenic macrophages from *P. acnes*-primed mice produce much higher levels of proinflammatory cytokines including TNF-α in response to LPS than do those from naïve mice [32]. This is also the case for Kupffer cells. Thus, *P. acnes* treatment induces both numerical increase and qualitative alteration of macrophages in the liver and spleen. This may implicate the importance of macrophages for the accomplishment of the LPS sensitization by *P. acnes* treatment.

4. Requirement of Macrophages for the Sensitization to LPS Induced by *P. acnes* Treatment

Depletion of macrophages rescues *P. acnes*-primed mice from the liver injury and high mortality induced by the subsequent challenge with LPS [38] (Table 1). This clearly demonstrates the indispensability of macrophages for the *P. acnes*-induced sensitization to LPS. Intravenous injection of

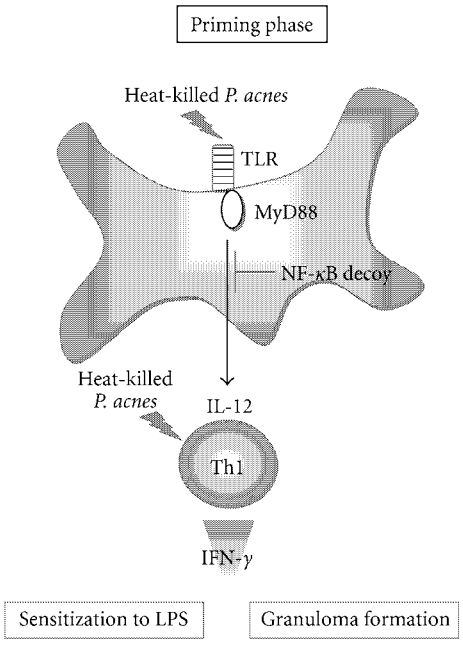

FIGURE 5: Molecular and cellular mechanisms underlying *P. acnes*-induced sensitization to LPS. After recognition of heat-killed *P. acnes*, cytoplasmic domain of TLR9 recruits MyD88 and relays a signal for nuclear translocation of NF-κB, eventually resulting in various gene expressions including IL-12 production. IL-12 is involved in the development of *P. acnes*-specific Th1 cells, which produce robust IFN-γ in response to *P. acnes*. IL-12 also activates hepatic NK cells to release IFN-γ. IFN-γ derived from Th1 cells and NK cells sensitize mice to LPS and induce their dense hepatic granuloma formation. Administration of NF-κB decoy profoundly inhibits both the LPS sensitization and the hepatic granuloma formations [16].

clodronate liposome depletes macrophages in mice, while control PBS liposome do not affect them [41]. These two groups of mice are treated with *P. acnes*, followed by LPS challenge at day 7. The *P. acnes*-primed mice depleted of macrophages show phenotypes similar to naïve mice after LPS challenge [38]. They lack liver injury and 100% survive (Table 1). *P. acnes*-primed mice receiving PBS liposome, however, show the susceptibility to LPS similar to that in *P. acnes*-primed mice [38]. Thus, macrophages are necessarily required for the *P. acnes*-induced sensitization to LPS.

5. Importance of MyD88-IL-12-IFN-γ Axis for the Sensitization to LPS

It is well established that IFN-γ can potently prime macrophages to efficiently respond to LPS [42]. IFN-γ-primed macrophages produce much larger amounts of TNF-α and IL-6 than naïve cells [32]. Furthermore, Th1 cell differentiation occurs both in the liver and spleen after *P. acnes* treatment in a manner dependent on IL-12, a prototype cytokine for Th1 cell differentiation [32, 43]. Splenocytes and splenic $CD4^+$ T cells from *P. acnes*-primed WT mice produce a large amount of IFN-γ but entirely not IL-4 in response to heat-killed *P. acnes* and immobilized anti-CD3 mAb, respectively [18, 32]. Besides, splenic $CD4^+$ T cells from *P. acnes*-primed $Il12p40^{-/-}$ mice do not differentiate into Th1 cells [18, 44]. Hepatic $CD4^+$ T cells differentiate toward Th1 cells as well, which is totally inhibited by the treatment with neutralizing anti-IL-12 monoclonal antibody (mAb) [45]. IL-12 directly activates hepatic NK cells to produce IFN-γ [46, 47]. Furthermore, hepatic NK cells are numerically increased and acquire the high responsiveness to LPS during *P. acnes* priming phase [48]. From these observations together, one may assume the importance of IL-12-IFN-γ axis for the development of LPS sensitization via induction of Th1 cells. Expectedly, *P. acnes*-primed $Ifn\gamma^{-/-}$ mice, $Il12p40^{-/-}$ mice or mice with inherited unresponsiveness to IL-12 are resistant to LPS, in terms of lack of hypothermia, hypercoagulation or high mortality [32, 49] (Table 2). In addition, neither $Ifn\gamma^{-/-}$ nor $Il12p40^{-/-}$ mice form dense hepatic granulomas after *P. acnes* treatment [18, 50] (Table 2). Thus, IL-12-IFN-γ axis is critical for the LPS sensitization.

As they cannot actively enter into inside of cells, heat-killed *P. acnes* are likely to be recognized by extracellular sensor TLR. As expected, MyD88, which is a key signal adapter molecule of the major TLR signal pathway [2], is essentially required for the development of hepatic granulomas after *P. acnes* priming, strongly suggesting critical role of TLR/MyD88 pathway in the development of *P. acnes*-induced LPS sensitization. $Myd88^{-/-}$ mice lack hepatic granuloma formation after *P. acnes* treatment, and after LPS challenge *P. acnes*-primed $Myd88^{-/-}$ mice do not suffer from the mortality or liver injuries [38, 51] (Table 2, Figure 5). The MyD88-mediated pathway activates nuclear translocation of NF-κB [2]. It is intriguingly to note that administration of NF-κB decoy during *P. acnes* priming phase completely abrogates the hepatic granuloma formation and the sensitization to LPS in WT mice [16]. This strengthens further the importance of the MyD88-mediated pathway for the LPS sensitization. Among TLR members, TLR9 that senses bacterial unmethylated CpG DNA, but not TLR2 that recognize bacterial cell wall product peptidoglycan, was clearly verified to be required for the LPS sensitization by *P. acnes* priming [52, 53]. Indeed, *P. acnes*-primed $Tlr2^{-/-}$ mice are comparably susceptible to LPS as *P. acnes*-primed WT mice, although *P. acnes* possess abundant TLR2 ligands in their cell walls (52). In contrast, *P. acnes*-primed $Tlr9^{-/-}$ mice, like $Myd88^{-/-}$mice, fail to develop hepatic granulomas and become susceptible to LPS [53]. This suggests that unmethylated CpG-DNA of *P. acnes* is pivotal for the sensitization to LPS at least by *P. acnes*-priming. Taken together, these observations strongly suggest that the MyD88-IL-12-IFN-γ axis plays a pivotal role in the hepatic granuloma formation and sensitization to LPS (Figure 5).

Upon challenge with TNF-α instead of LPS, *P. acnes*-primed WT mice show the manifestations/signs similar to those of endotoxin shock syndrome [29, 30, 32], indicating that TNF-α is an effector cytokine and that *P. acnes* treatment tremendously facilitates responsiveness to TNF-α. TNF-α-challenged, *P. acnes*-primed mice, but not naïve mice,

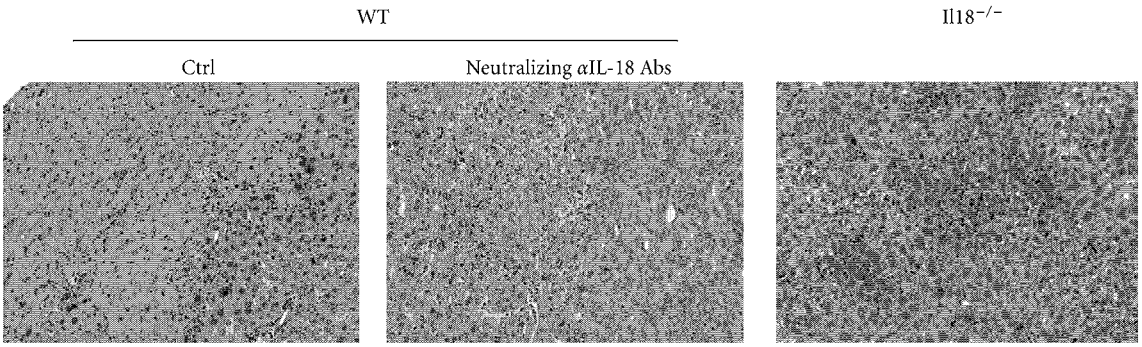

FIGURE 6: Importance of IL-18 for the development of *P. acnes*/LPS-induced liver injury. *P. acnes*-primed wild-type (WT) showed liver necrosis after LPS challenge. However, treatment with neutralizing anti-IL-18 just before LPS challenge could protect against this liver injuries [17]. Furthermore, *Il18*$^{-/-}$ mice were resistant to the sequential treatment with *P. acnes* and LPS [18].

TABLE 1: Clinical manifestations upon LPS challenge. Naïve mice, *P. acnes*-primed mice, and *P. acnes*-primed mice depleted of macrophages (Mø) were challenged with LPS, and hypothermia, hypercoagulation, lethality and liver injuries were monitored by measurement of rectal temperature[a], measurement of plasma TAT/PAI-1 levels[b] and histological analyses[d].

Mice		Systemic alterations			Liver injury[d]
		Hypothermia[a]	Hypercoagulation[b]	Lethality (%)[c]	
Naïve		−	±	0	−
P. acnes-primed	Mø-sufficient[e]	+++	+++	100	+++
	Mø-ablated[f]	ND	ND	0	−

[a]+++ indicates more than 5°C reduction of rectal temperature after LPS challenge; − indicates less than 1°C of it.
[b]+++ indicates more than 10 μg/ml of plasma TAT levels; − indicates normal range of them (< 50 ng/ml); ± indicates less than 200 ng/ml.
[c]Mice were monitored for 48 h after LPS challenge.
[d]+++ indicates more than 300 IU of serum ALT levels; − indicates normal range of them (< 50 IU).
[e] *P. acnes*-primed mice were treated twice with PBS liposome.
[f] *P. acnes*-primed mice were treated twice with clodronate liposome to deplete macrophages.
ND; not done

suffer from hypothermia with exceptionally high plasma levels of plasma TAT and PAI-1 and show high mortality. Consistently, *P. acnes*-primed *Ifnγ*$^{-/-}$ mice are resistant to TNF-α as well [32]. Thus, *P. acnes* treatment renders mice highly susceptible to LPS for TNF-α production and also to TNF-α itself via induction of IFN-γ production.

6. Importance of IFN-γ for the Systemic Endotoxin Shock Manifestations after LPS Challenge

Administration of neutralizing anti-IFN-γ mAb just before LPS challenge could partly rescue *P. acnes*-primed mice from hypothermia, hypercoagulation, and high mortality [32], demonstrating the importance of endogenous IFN-γ for the accomplishment of LPS phase as well. Taken together, IFN-γ is a master regulator of the systemic endotoxin shock syndrome by induction of the sensitization to LPS and activation of the LPS phase.

7. IL-18 Is Necessary and Sufficient for the Development of Liver Injuries

Upon LPS challenge many *P. acnes*-primed WT mice shortly died, and the surviving mice suffer from liver injuries later (Figure 6). Blockade of IL-18 or genetic depletion of *Il18* can protect against the liver damages [17, 54] (Figure 6). Upon LPS challenge *P. acnes*-primed *Il18*$^{-/-}$ mice having normally dense hepatic granulomas develop the endotoxin shock syndrome comparably as *P. acnes*-primed WT mice [18]. In contrast, the surviving *Il18*$^{-/-}$ mice evade the liver injuries [18] (Figure 6). These results indicate that IL-18 is necessary for the development of this liver injury. Furthermore, administration of IL-18 causes liver injuries in *P. acnes*-primed WT mice but not naïve mice [55]. Therefore, IL-18 is necessary and sufficient for *P. acnes*/LPS-induced liver injury.

IL-18 is capable of inducing hepatocytotoxic TNF-α directly in many cell types [13]. NK cells and Th1 cells, but not naïve CD4$^+$ T cells, express IL-18R [47, 56]. During *P. acnes* priming phase, naïve CD4$^+$ T cells differentiate into *P. acnes*-specific Th1 cells as described above. Therefore, IL-18 activates both NK cells and *P. acnes*-specific Th1 cells to produce robust IFN-γ, which in turn might fully activate Kupffer cells and hepatic macrophages to further produce TNF-α [54]. In addition, IL-18 has potent capacity to induce and upregulate Fas ligand expression on NK cells enough to kill Fas-expressing hepatocytes [54]. Thus, endogenous IL-18 participates in the liver injuries through induction of proinflammatory cytokines and cell death-inducing protein.

Table 2: Importance of IL-12-IFN-γ axis for in vivo LPS sensitization by *P. acnes* treatment. Mice with various genotypes were sequentially administered with *P. acnes* and LPS. At day 7 after *P. acnes* priming, hepatic granuloma formation was determined by histological analyses.

P. acnes-primed mice	Sensitization phase	LPS phase				
	Granuloma formation[a]	Hypothermia[b]	Hypercoagulation[c]	Serum TNF-α[d]	Lethality[e]	Liver injury[f]
WT	+++	+++	+++	+++	100	+++
Il12p40$^{-/-}$	−	−	−	−	0	−
Ifn$\gamma^{-/-}$	−	−	−	−	0	−

[a]+++ indicates that 20% and more area of the liver section is occupied by granulomas; − indicates no granulomas.
[b]+++ indicates more than 5°C reduction of rectal temperature after LPS challenge; − indicates less than 1°C of it.
[c]+++ indicates more than 10 μg/mL of plasma TAT levels; − indicates normal range of them (< 50 ng/mL); ± indicates < 50 ng/mL and > 200 ng/mL.
[d]+++ indicates more than 5 ng/mL; − indicates less than 0.1 ng/mL.
[e]Mice were monitored for 48 h after LPS challenge.
[f]+++ indicates more than 300 IU of serum ALT levels; − indicates normal range of them (< 50 IU).

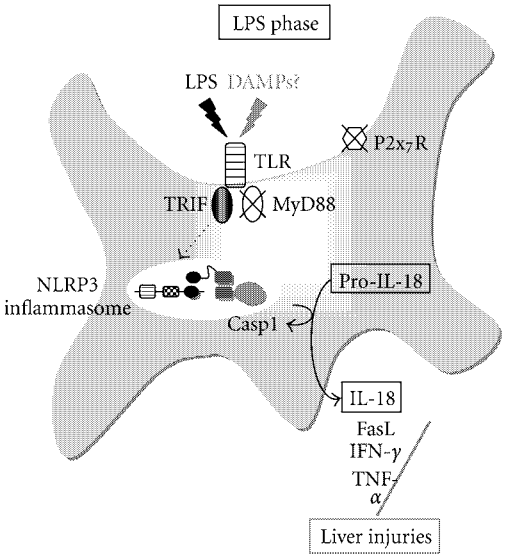

Figure 7: Molecular and cellular mechanisms for LPS phase. After challenge of *P. acnes*-primed wild-type mice with LPS, TLR4 is activated via TRIF for activation of NLRP3 inflammasome, which eventually leads to cleavage of procaspase-1 into its active form caspase-1. Active caspase-1, then, processes pro-IL-18 into active IL-18 for extracellular release. IL-18 upregulates both hepatotoxic Fas ligand (FasL) expression and TNF-α production. DAMPs and alarmin released from the injured hepatocytes might further activate the Kupffer cells, eventually resulting in the acceleration of inflammatory responses. DAMPs, damage-associated molecular patterns.

8. Kupffer Cells Secrete IL-18 in a Manner Dependent on TRIF and the NLRP3 Inflammasome

Many investigators use peritoneal exudate cells (PEC) prepared from the mice administered intraperitoneally with thioglycorate or bone marrow-derived macrophages (BMM) by incubation of bone marrow cells with recombinant monocyte colony-stimulating factor as conventional murine macrophages. These two types of macrophages cannot secrete IL-1β or IL-18 after stimulation with LPS alone. However, LPS-primed PEC or BMM can secrete robust IL-1β and IL-18 upon subsequent stimulation with exogenous ATP in a TLR4- and caspase-1-dependent fashion [57, 58]. From these observations the following possibilities have been believed. First, TLR4-mediated signal pathway cannot activate caspase-1. Second, ATP signaling via its cell surface receptor P2x$_7$R is a central event required for the caspase-1 activation in LPS-stimulated macrophages. Third, the TLR4-mediated signal pathway is only required for induction of proIL-1β production. We also confirmed the absence of IL-1β or IL-18 release from LPS-activated PEC or BMM. In contrast to these PEC and BMM, WT Kupffer cells can release substantial amounts of IL-1β and IL-18 in response to LPS or synthetic lipid A (active center of LPS) alone [15, 38, 54, 59] (Table 3), strongly suggesting involvement of the TLR4 signaling in release of IL-1β and IL-18. As LPS-stimulated caspase-1-deficient Kupffer cells do not secrete IL-1β or IL-18 [11, 12], caspase-1 is an essential processing enzyme of such IL-1β and IL-18. In fact, western blotting analyses reveal active form of caspase-1 in the lipid A-stimulated WT Kupffer cells [38] (Table 3). Expectedly, *Tlr4*$^{-/-}$ Kupffer cells fail to activate caspase-1 upon stimulation with lipid A [38]. Thus, Kupffer cells seem to be different from PEC or BMM in the ability to activate caspase-1 upon TLR4 engagement. However, it is still to be elucidated how Kupffer cells acquire the potential to activate caspase-1 in response to TLR4 agonists alone.

The TLR4 signaling is relayed by the MyD88- and TRIF-mediated pathways [2]. *Myd88*$^{-/-}$ Kupffer cells stimulated with TLR4 agonists show normal caspase-1 activation [38]. As the *Myd88*$^{-/-}$ Kupffer cells cannot produce pro-IL-1β, eventually resulting in lack of mature IL-1β secretion [38] (Table 3). In contrast to proIL-1β, pro-IL-18 is constitutively stored in *Myd88*$^{-/-}$ Kupffer cells as well as WT cells [15]. Therefore, it is convincing that *Myd88*$^{-/-}$ Kupffer cells cultured with LPS can secrete IL-18 [15, 38] (Table 3). *Trif*$^{-/-}$ Kupffer cells show the reverse phenomena. Despite of their normal production of pro-IL-1β and pro-IL-18, *Trif*$^{-/-}$ Kupffer cells cannot release IL-1β or IL-18 due to their inability to activate caspase-1 [38]. These results demonstrate a pivotal role of TRIF but not

Table 3: Requirement of MyD88 and TRIF for LPS sensitization and Caspase-1 activation, respectively. Mice with various genotypes were sequentially treated with *P. acnes* and LPS, and liver specimens and sera were sampled for histological analyses and measurement of IL-18/IL-1β levels by ELISA, respectively. Kupffer cells were incubated with LPS for 4 h, and each supernatant was collected for western blotting analyses and ELISA. Naïve mice have no hepatic granulomas or injuries, and their serum IL-18 and iL-1β were undetectable. Naïve Kupffer cells released no IL-18 and IL-1β.

Genotype	Sensitization phase	Response to LPS				
		In vivo		LPS-stimulated Kupffer cells		
				Western blotting analyses		ELISA
	Granuloma formation[a]	Liver injury[b]	Serum IL-18/IL-1β[c](ELISA)	ProIL-1β production[d]	Active Casp1[e]	IL-1β/IL-18 release[f]
WT	+++	+++	+++	+++	+++	+++
Tlr4$^{-/-}$	+++	–	–	–	–	–
Myd88$^{-/-}$	–	–	–	–	+++	++[g]
Trif$^{-/-}$	+++	–	–	+++	–	–
Casp1$^{-/-}$	+++	–	–	+++	–	–
Asc$^{-/-}$	+++	–	–	+++	–	–
Nlrp3$^{-/-}$	+++	–	–	ND	ND	–
P2x7r$^{-/-}$	+++	+++	+++	+++	+++	+++

[a]+++ indicates that 20% and more area of the liver section is occupied by granulomas; – indicates no granulomas.
[b]+++ indicates more than 300 IU of serum ALT levels; – indicates normal range of them (< 50 IU).
[c]+++ indicates more than 1000 and 50 pg/mL of serum IL-18 and IL-1β levels, respectively; – indicates normal range of them.
[d]+++ indicates 10 times and more pro-IL-1β density in cell lysates; – indicates the absence of pro-IL-1β.
[e]+++ indicates the presence of active Caspase-1 (Casp1) in supernatant; – indicates the absence of it.
[f]+++ indicates more than 100 pg/mL; – indicates undetectable levels.
[g]++ indicates more than 50 pg/mL of IL-18, but undetectable IL-1β.
ND; not done

MyD88 in the TLR4-mediated caspase-1 activation (Table 3, Figure 7).

Asc$^{-/-}$ Kupffer cells have the phenotype similar to *Caspase1*$^{-/-}$ cells [38, 60], suggesting that NLRP3 or AIM2 inflammasome or unidentified one that needs ASC protein (Figure 1) is involved in the caspase-1 activation. Lipid A-stimulated *Nlrp3*$^{-/-}$ Kupffer cells fail to secrete IL-18 or IL-1β [38]. Therefore, the NLRP3 inflammasome activation is necessary for the TLR4-mediated casapse-1 activation (Table 3, Figure 7).

These results cannot exclude the possibility that the TRIF-mediated pathway might cause extracellular release of ATP and that this self-derived ATP might activate the NLRP3 inflammasome in LPS-stimulated Kupffer cells [57, 58]. Unexpectedly, *P2x7r*$^{-/-}$ Kupffer cells show normal caspase-1 activation and normal release of IL-1β and IL-18 [38]. These results demonstrate the dispensability of endogenous ATP/P2x$_7$R-mediated pathway for the TLR4/TRIF/NLRP3-mediated caspase-1 activation (Table 3, Figure 7).

Although we now know the importance of the NLRP3 inflammasome, the precise mechanisms by which the TRIF-mediated signal pathway activates the NLRP3 inflammasome is unclear. It is also unknown whether NLRP3 protein directly recognizes TLR4 agonists. If so, how do the TLR4 agonists translocate into the inside of Kupffer cells? Alternatively, does TRIF-mediated pathway trigger synthesis of cytoplasmic NLRP3 agonist? If so, what is the NLRP3 agonist? And, how about the molecular mechanisms for the TRIF-induced NLRP3 agonist? We need further extensive studies to address these key queries.

9. Requirement of NLRP3 Inflammasome Activation for the Liver Injury

The capacity to activate caspase-1 reflects on the development of liver injury [38, 60]. Expectedly, *P. acnes*-primed *Tlr4*$^{-/-}$ mice, although manifesting normal levels of hepatic granuloma formation, can avoid the liver injury after LPS challenge accompanied by lack of serum elevation of IL-18 (Table 3, Figure 7). Since they fail to develop hepatic granulomas, *P. acnes*-primed *Myd88*$^{-/-}$ mice lack the production of robust IL-18 after *P. acnes* priming, presumably resulting in escape from the liver injury (Table 3, Figure 7). This demonstrates again requirement of MyD88 for the *P. acnes*-induced LPS sensitization. Conversely, *P. acnes*-primed *Trif*$^{-/-}$ mice, *Caspase1*$^{-/-}$ mice, *Asc*$^{-/-}$ mice and *Nlrp3*$^{-/-}$ mice all have normal dense granulomas in their livers, but fail to develop liver injury after LPS challenge, concomitant with the absence of the serum IL-18 increase (Table 3, Figure 7). *P2x7r*$^{-/-}$ mice have comparable phenotype as WT mice (Table 3, Figure 7), demonstrating dispensability of endogenous ATP/P2x$_7$R pathway for the liver injuries. Thus, the TLR4/TRIF-mediated activation of NLRP3 inflammasome is critical for the development of the *P. acnes*/LPS-induced liver injuries via activation of caspase-1 for maturation and release of IL-18.

10. Methods

10.1. Mice. C57BL/6 mice were purchased from Clea Japan (Osaka, Japan). Female mice (8–12-week-old) were used for this study. Mice were maintained under specific pathogen-free conditions, and received humane care as outlined in the Guide for the Care and Use of Experimental Animals in Hyogo College of Medicine.

10.2. Reagents. Monoclonal antibody (mA) against F4/80 of mouse macrophage was purchased from BMA (Augst, Switzerland). DAPI was from KPL (Gaitherburg, MD).

10.3. Treatment with P. acnes. Heat-killed *P. acnes* were labeled with or without Cy3 (GE, Buchinghamshire, UK) according to the manufacture's instruction and were injected into mice through a tail vein. At the indicated time points various tissues and tissue specimens were sampled for weighing and analysis of the cellularity by confocal microscopy, respectively.

10.4. Confocal Microscopic Analysis. Frozen sections of various tissues were incubated with mAb against F4/80, biotinylated antirat IgG, and then Alexa Fluor 488-conjugated streptavidin (Molecular Probes). Nuclei were stained by DAPI. The immunostaining of each section was evaluated using a laser scanning confocal microscopy [61, 62].

10.5. Flowcytometry [61]. Spleen cells and Kupffer cells were isolated from variously treated WT B6 mice [55]. Cells were incubated with APC-conjugated anti-F4/80 mAb.

11. Closing Remarks

PAMPs evoke innate immune responses by activating pattern recognition receptors (PRRs), such as TLR, NLR, and RLR. Similarly, injured host cells release endogenous "damage"-associated molecular patterns (DAMPs) that induce similar responses via recognition by PRRs [63–65]. For example, high-mobility group box1 protein (HMGB1) that is localized in the nuclei of various cell types in the steady state becomes to be extracellularly released upon stimulation of the cells with death stress. HMGB1, then, initiates innate immune responses via activating TLR4 [66]. Mitochondria are endosymbionts derived from certain bacteria during the evolution of life. Therefore, it is plausible that mitochondria possess DAMPs homologous to its ancestral PAMPs. Very recently, this was verified [67]. Mitochondrion possesses unmethylated CpG-DNA and formyl peptides similar to bacterial N-formylated proteins, which are recognized by PRRs expressed on neutrophils, TLR9, and formyl peptide receptor, respectively. Intravenous injection of the mitochondrial DAMPs causes systemic inflammatory responses and lung injuries [67]. As trauma patients have elevated serum levels of these mitochondrial DAMPs, sterile injury-induced systemic inflammatory response syndrome (SIRS), often occurring after severe trauma, might undergo in response to endogenous mitochondrial DAMPs derived from the injured cells [67]. In addition to DAMPs, self-derived "alarmin" is proposed as another potent inflaming molecules. "Alarmin" is compartmentalized in certain organelle in the steady state. Once damaged, cells begin to actively secrete "alarmin", which in turn triggers inflammatory responses. Intraperitoneal injection of dying cells was reported to be able to trigger peritonitis with dense neutrophil recruitment in an IL-1α/IL-1R-dependent manner [68]. Furthermore, administration of acetoaminophen, a common antipyretic, causes massive liver injury with sterile neutrophilic inflammation in a manner dependent on IL-1α presumably derived from the damaged hepatocytes as well [68]. Thus, dying cell-derived IL-1α is regarded as alarmin. Like IL-1α, IL-33 is localized in the cell nuclei in the steady state and is believed to be secreted after stimulation of the cells with death stress [69]. Histone proteins derived from cell nuclei play a role as alarmin as well [70]. These endogenous DAMPs and alarmin might accelerate liver injuries induced by exogenous PAMPs and might become novel therapeutic targets for severe sepsis with organ failures.

Acknowledgment

This work was supported in part by a Hitec Research Center Grant from the Ministry of Education, Culture, Sports, Science and Technology of Japan and by Grants from the Naito Foundation and the Japanese Foundation for Applied Enzymology. The authors would like to thank Ms Mitani for an excellent technique.

References

[1] C. A. Janeway Jr. and R. Medzhitov, "Innate immune recognition," *Annual Review of Immunology*, vol. 20, pp. 197–216, 2002.

[2] S. Akira, S. Uematsu, and O. Takeuchi, "Pathogen recognition and innate immunity," *Cell*, vol. 124, no. 4, pp. 783–801, 2006.

[3] A. Komuro, D. Bamming, and C. M. Horvath, "Negative regulation of cytoplasmic RNA-mediated antiviral signaling," *Cytokine*, vol. 43, no. 3, pp. 350–358, 2008.

[4] M. S. Lee and Y.-J. Kim, "Signaling pathways downstream of pattern-recognition receptors and their cross talk," *Annual Review of Biochemistry*, vol. 76, pp. 447–480, 2007.

[5] A. Stutz, D. T. Golenbock, and E. Latz, "Inflammasomes: too big to miss," *Journal of Clinical Investigation*, vol. 119, no. 12, pp. 3502–3511, 2009.

[6] S.-Y. Zhang, S. Boisson-Dupuis, A. Chapgier, et al., "Inborn errors of interferon (IFN)-mediated immunity in humans: insights into the respective roles of IFN-α/β, IFN-γ, and IFN-λ in host defense," *Immunological Reviews*, vol. 226, no. 1, pp. 29–40, 2008.

[7] V. Hornung and E. Latz, "Intracellular DNA recognition," *Nature Reviews Immunology*, vol. 10, no. 2, pp. 123–130, 2010.

[8] F. Martinon, K. Burns, and J. Tschopp, "The Inflammasome: a molecular platform triggering activation of inflammatory caspases and processing of proIL-β," *Molecular Cell*, vol. 10, no. 2, pp. 417–426, 2002.

[9] J. Tschopp, F. Martinon, and K. Burns, "NALPs: a novel protein family involved in inflammation," *Nature Reviews*, vol. 4, no. 2, pp. 95–104, 2003.

[10] K. Kuida, J. A. Lippke, G. Ku, et al., "Altered cytokine export and apoptosis in mice deficient in interleukin-1β converting enzyme," *Science*, vol. 267, no. 5206, pp. 2000–2003, 1995.

[11] Y. Gu, K. Kuida, H. Tsutsui, et al., "Activation of interferon-γ inducing factor mediated by interleukin-1β converting enzyme," *Science*, vol. 275, no. 5297, pp. 206–209, 1997.

[12] T. Ghayur, S. Banerjee, M. Hugunin, et al., "Caspase-1 processes IFN-γ-inducing factor and regulates LPS-induced IFN-γ production," *Nature*, vol. 386, no. 6625, pp. 619–623, 1997.

[13] K. Nakanishi, T. Yoshimoto, H. Tsutsui, and H. Okamura, "Interleukin-18 regulates both Th1 and Th2 responses," *Annual Review of Immunology*, vol. 19, pp. 423–474, 2001.

[14] H. Tsutsui, T. Yoshimoto, N. Hayashi, H. Mizutani, and K. Nakanishi, "Induction of allergic inflammation by interleukin-18 in experimental animal models," *Immunological Reviews*, vol. 202, pp. 115–138, 2004.

[15] E. Seki, H. Tsutsui, H. Nakano, et al., "Lipopolysaccharide-induced IL-18 secretion from murine Kupffer cells independently of myeloid differentiation factor 88 that is critically involved in induction of production of IL-12 and IL-1β," *Journal of Immunology*, vol. 166, no. 4, pp. 2651–2657, 2001.

[16] I. Ogushi, Y. Iimuro, E. Seki, et al., "Nuclear factor κB decoy oligodeoxynucleotides prevent endotoxin-induced fatal liver failure in a murine model," *Hepatology*, vol. 38, no. 2, pp. 335–344, 2003.

[17] H. Okamura, H. Tsutsui, T. Komatsu, et al., "Cloning of a new cytokine that induces IFN-γ production by T cells," *Nature*, vol. 378, no. 6552, pp. 88–91, 1995.

[18] Y. Sakao, K. Takeda, H. Tsutsui, et al., "IL-18-deficient mice are resistant to endotoxin-induced liver injury but highly susceptible to endotoxin shock," *International Immunology*, vol. 11, no. 3, pp. 471–480, 1999.

[19] J. P.-Y. Ting, R. C. Lovering, E. S. Alnemri, et al., "The NLR gene family: a standard nomenclature," *Immunity*, vol. 28, no. 3, pp. 285–287, 2008.

[20] T.-D. Kanneganti, M. Lamkanfi, Y.-G. Kim, et al., "Pannexin-1-mediated recognition of bacterial molecules activates the cryopyrin inflammasome independent of Toll-like receptor signaling," *Immunity*, vol. 26, no. 4, pp. 433–443, 2007.

[21] D. A. Muruve, V. Pétrilli, A. K. Zaiss, et al., "The inflammasome recognizes cytosolic microbial and host DNA and triggers an innate immune response," *Nature*, vol. 452, no. 7183, pp. 103–107, 2008.

[22] V. Hornung, A. Ablasser, M. Charrel-Dennis, et al., "AIM2 recognizes cytosolic dsDNA and forms a caspase-1-activating inflammasome with ASC," *Nature*, vol. 458, no. 7237, pp. 514–518, 2009.

[23] T. Fernandes-Alnemri, J.-W. Yu, P. Datta, J. Wu, and E. S. Alnemri, "AIM2 activates the inflammasome and cell death in response to cytoplasmic DNA," *Nature*, vol. 458, no. 7237, pp. 509–513, 2009.

[24] T. Bürckstümmer, C. Baumann, S. Blüml, et al., "An orthogonal proteomic-genomic screen identifies AIM2 as a cytoplasmic DNA sensor for the inflammasome," *Nature Immunology*, vol. 10, no. 3, pp. 266–272, 2009.

[25] T. L. Roberts, A. Idris, J. A. Dunn, et al., "HIN-200 proteins regulate caspase activation in response to foreign cytoplasmic DNA," *Science*, vol. 323, no. 5917, pp. 1057–1060, 2009.

[26] F. Martinon, A. Mayor, and J. Tschopp, "The inflammasomes: guardians of the body," *Annual Review of Immunology*, vol. 27, pp. 229–265, 2009.

[27] J. Ferluga and A. C. Allison, "Role of mononuclear infiltrating cells in pathogenesis of hepatitis," *The Lancet*, vol. 1, no. 8090, pp. 610–611, 1978.

[28] Y. Mizoguchi, H. Tsutsui, K. Miyajima, et al., "The protective effects of prostaglandin E1 in an experimental massive hepatic cell necrosis model," *Hepatology*, vol. 7, no. 6, pp. 1184–1188, 1987.

[29] H. Tsutsui, Y. Mizoguchi, and S. Morisawa, "Importance of direct hepatocytolysis by liver macrophages in experimental fulminant hepatitis," *Hepato-Gastroenterology*, vol. 39, no. 6, pp. 553–559, 1992.

[30] T. Yoshimoto, K. Nakanishi, S. Hirose, et al., "High serum IL-6 level reflects susceptible status of the host to endotoxin and IL-1/tumor necrosis factor," *Journal of Immunology*, vol. 148, no. 11, pp. 3596–3603, 1992.

[31] J. A. Russell, "Management of sepsis," *The New England Journal of Medicine*, vol. 355, no. 16, pp. 1699–1713, 2006.

[32] K. Kawa, H. Tsutsui, R. Uchiyama, et al., "IFN-γ is a master regulator of endotoxin shock syndrome in mice primed with heat-killed *Propionibacterium acnes*," *International Immunology*, vol. 22, no. 3, pp. 157–166, 2010.

[33] T. P. Clemmer, C. J. Fisher Jr., R. C. Bone, et al., "Hypothermia in the sepsis syndrome and clinical outcome. The Methylprednisolone Severe Sepsis Study Group," *Critical Care Medicine*, vol. 20, no. 10, pp. 1395–1401, 1992.

[34] D. G. Remick and H. Xioa, "Hypothermia and sepsis," *Frontiers in Bioscience*, vol. 11, no. 1, pp. 1006–1013, 2006.

[35] M. Levi and H. Ten Cate, "Disseminated intravascular coagulation," *The New England Journal of Medicine*, vol. 341, no. 8, pp. 586–592, 1999.

[36] M. S. Sawdey and D. J. Loskutoff, "Regulation of murine type 1 plasminogen activator inhibitor gene expression in vivo. Tissue specificity and induction by lipopolysaccharide, tumor necrosis factor-α, and transforming growth factor-β," *Journal of Clinical Investigation*, vol. 88, no. 4, pp. 1346–1353, 1991.

[37] L. Romics Jr., A. Dolganiuc, K. Kodys, et al., "Selective priming to toll-like receptor 4 (TLR4), not TLR2, ligands by *P. acnes* involves up-regulation of MD-2 in mice," *Hepatology*, vol. 40, no. 3, pp. 555–564, 2004.

[38] M. Imamura, H. Tsutsui, K. Yasuda, et al., "Contribution of TIR domain-containing adapter inducing IFN-β-mediated IL-18 release to LPS-induced liver injury in mice," *Journal of Hepatology*, vol. 51, no. 2, pp. 333–341, 2009.

[39] H. Yoneyama, K. Matsuno, Y. Zhang, et al., "Regulation by chemokines of circulating dendritic cell precursors, and the formation of portal tract-associated lymphoid tissue, in a granulomatous liver disease," *Journal of Experimental Medicine*, vol. 193, no. 1, pp. 35–49, 2001.

[40] H. Yoneyama, S. Narumi, Y. Zhang, et al., "Pivotal role of dendritic cell-derived CXCL10 in the retention of T helper cell 1 lymphocytes in secondary lymph nodes," *Journal of Experimental Medicine*, vol. 195, no. 10, pp. 1257–1266, 2002.

[41] N. Van Rooijen and A. Sanders, "Elimination, blocking, and activation of macrophages: three of a kind?" *Journal of Leukocyte Biology*, vol. 62, no. 6, pp. 702–709, 1997.

[42] M. A. Collart, D. Belin, J.-D. Vassalli, S. de Kossodo, and P. Vassalli, "γ interferon enhances macrophages transcription of the tumor necrosis factor/cachectin, interleukin 1, and urokinase genes, which are controlled by short-lived repressors," *Journal of Experimental Medicine*, vol. 164, no. 6, pp. 2113–2118, 1986.

[43] K. Takeda, H. Tsutsui, T. Yoshimoto, et al., "Defective NK cell activity and Th1 response in IL-18-deficient mice," *Immunity*, vol. 8, no. 3, pp. 383–390, 1998.

[44] A. Kumanogoh, T. Shikina, K. Suzuki, et al., "Nonredundant roles of Sema4A in the immune system: defective T cell priming and Th1/Th2 regulation in Sema4A-deficient mice," *Immunity*, vol. 22, no. 3, pp. 305–316, 2005.

[45] K. Matsui, T. Yoshimoto, H. Tsutsui, et al., "*Propionibacterium acnes* treatment diminishes $CD4^+NK1.1^+$ T cells but induces type I T cells in the liver by induction of IL-12 and IL-18 production from Kupffer cells," *Journal of Immunology*, vol. 159, no. 1, pp. 97–106, 1997.

[46] G. Trinchieri, "Interleukin-12: a proinflammatory cytokine with immunoregulatory functions that bridge innate resistance and antigen-specific adaptive immunity," *Annual Review of Immunology*, vol. 13, pp. 251–276, 1995.

[47] Y. Hyodo, K. Matsui, N. Hayashi, et al., "IL-18 up-regulates perforin-mediated NK activity without increasing perforin messenger RNA expression by binding to constitutively expressed IL-18 receptor," *Journal of Immunology*, vol. 162, no. 3, pp. 1662–1668, 1999.

[48] J. Sawaki, H. Tsutsui, N. Hayashi, et al., "Type 1 cytokine/chemokine production by mouse NK cells following activation of their TLR/MyD88-mediated pathways," *International Immunology*, vol. 19, no. 3, pp. 311–320, 2007.

[49] T. Merlin, A. Sing, P. J. Nielsen, C. Galanos, and M. A. Freudenberg, "Inherited IL-12 unresponsiveness contributes to the high LPS resistance of the Lps^d C57BL/10ScCr mouse," *Journal of Immunology*, vol. 166, no. 1, pp. 566–573, 2001.

[50] H. Tsuji, N. Mukaida, A. Harada, et al., "Alleviation of lipopolysaccharide-induced acute liver injury in Propionibacterium aches-primed IFN-γ-deficient mice by a concomitant reduction of TNF-α, IL-12, and IL-18 production," *Journal of Immunology*, vol. 162, no. 2, pp. 1049–1055, 1999.

[51] I. Hritz, A. Velayudham, A. Dolganiuc, et al., "Bone Marrow-derived immune cells mediate sensitization to liver injury in a myeloid differentiation factor 88-dependent fashion," *Hepatology*, vol. 48, no. 4, pp. 1342–1347, 2008.

[52] L. Romics Jr., A. Dolganiuc, A. Velayudham, et al., "Toll-like receptor 2 mediates inflammatory cytokine induction but not sensitization for liver injury by *Propionibacterium acnes*," *Journal of Leukocyte Biology*, vol. 78, no. 6, pp. 1255–1264, 2005.

[53] C. Kalis, M. Gumenscheimer, N. Freudenberg, et al., "Requirement for TLR9 in the immunomodulatory activity of *Propionibacterium acnes*," *Journal of Immunology*, vol. 174, no. 7, pp. 4295–4300, 2005.

[54] H. Tsutsui, K. Matsui, N. Kawada, et al., "IL-18 accounts for both TNF-α- and Fas ligand-mediated hepatotoxic pathways in endotoxin-induced liver injury in mice," *Journal of Immunology*, vol. 159, no. 8, pp. 3961–3967, 1997.

[55] H. Tsutsui, N. Kayagaki, K. Kuida, et al., "Caspase-1-independent, Fas/Fas ligand-mediated IL-18 secretion from macrophages causes acute liver injury in mice," *Immunity*, vol. 11, no. 3, pp. 359–367, 1999.

[56] T. Yoshimoto, K. Takeda, T. Tanaka, et al., "IL-12 up-regulates IL-18 receptor expression on T cells, Th1 cells, and B cells: synergism with IL-18 for IFN-γ production," *Journal of Immunology*, vol. 161, no. 7, pp. 3400–3407, 1998.

[57] S. Mariathasan and D. M. Monack, "Inflammasome adaptors and sensors: intracellular regulators of infection and inflammation," *Nature Reviews Immunology*, vol. 7, no. 1, pp. 31–40, 2007.

[58] F. Martinon and J. Tschopp, "Inflammatory caspases and inflammasomes: master switches of inflammation," *Cell Death and Differentiation*, vol. 14, no. 1, pp. 10–22, 2007.

[59] K. Matsui, H. Tsutsui, and K. Nakanishi, "Pathophysiological roles for IL-18 in inflammatory arthritis," *Expert Opinion on Therapeutic Targets*, vol. 7, no. 6, pp. 701–724, 2003.

[60] M. Yamamoto, K. Yaginuma, H. Tsutsui, et al., "ASC is essential for LPS-induced activation of procaspase-1 independently of TLR-associated signal adaptor molecules," *Genes to Cells*, vol. 9, no. 11, pp. 1055–1067, 2004.

[61] M. Terada, H. Tsutsui, Y. Imai, et al., "Contribution of IL-18 to atopic-dermatitis-like skin inflammation induced by *Staphylococcus aureus* product in mice," *Proceedings of the National Academy of Sciences of the United States of America*, vol. 103, no. 23, pp. 8816–8821, 2006.

[62] E. Seki, Y. Kondo, Y. Iimuro, et al., "Demonstration of cooperative contribution of MET- and EGFR-mediated STAT3 phosphorylation to liver regeneration by exogenous suppressor of cytokine signalings," *Journal of Hepatology*, vol. 48, no. 2, pp. 237–245, 2008.

[63] P. Matzinger, "The danger model: a renewed sense of self," *Science*, vol. 296, no. 5566, pp. 301–305, 2002.

[64] A. Rubartelli and M. T. Lotze, "Inside, outside, upside down: damage-associated molecular-pattern molecules (DAMPs) and redox," *Trends in Immunology*, vol. 28, no. 10, pp. 429–436, 2007.

[65] M. T. Lotze, H. J. Zeh, A. Rubartelli, et al., "The grateful dead: damage-associated molecular pattern molecules and reduction/oxidation regulate immunity," *Immunological Reviews*, vol. 220, no. 1, pp. 60–81, 2007.

[66] M. T. Lotze and K. J. Tracey, "High-mobility group box 1 protein (HMGB1): nuclear weapon in the immune arsenal," *Nature Reviews Immunology*, vol. 5, no. 4, pp. 331–342, 2005.

[67] Q. Zhang, M. Raoof, Y. Chen, et al., "Circulating mitochondrial DAMPs cause inflammatory responses to injury," *Nature*, vol. 464, no. 1, pp. 104–107, 2010.

[68] C.-J. Chen, H. Kono, D. Golenbock, G. Reed, S. Akira, and K. L. Rock, "Identification of a key pathway required for the sterile inflammatory response triggered by dying cells," *Nature Medicine*, vol. 13, no. 7, pp. 851–856, 2007.

[69] G. Haraldsen, J. Balogh, J. Pollheimer, J. Sponheim, and A. M. Küchler, "Interleukin-33-cytokine of dual function or novel alarmin?" *Trends in Immunology*, vol. 30, no. 5, pp. 227–233, 2009.

[70] J. Xu, X. Zhang, R. Pelayo, et al., "Extracellular histones are major mediators of death in sepsis," *Nature Medicine*, vol. 15, no. 11, pp. 1318–1321, 2009.

nature immunology

The Jmjd3-*Irf4* axis regulates M2 macrophage polarization and host responses against helminth infection

Takashi Satoh[1,2,8], Osamu Takeuchi[1,2,8], Alexis Vandenbon[3], Koubun Yasuda[4], Yoshiaki Tanaka[5], Yutaro Kumagai[1,2], Tohru Miyake[1,2], Kazufumi Matsushita[1,2], Toshihiko Okazaki[1], Tatsuya Saitoh[1,2], Kiri Honma[6], Toshifumi Matsuyama[6], Katsuyuki Yui[6], Tohru Tsujimura[7], Daron M Standley[3], Kenji Nakanishi[4], Kenta Nakai[6] & Shizuo Akira[1,2]

Polarization of macrophages to M1 or M2 cells is important for mounting responses against bacterial and helminth infections, respectively. Jumonji domain containing-3 (Jmjd3), a histone 3 Lys27 (H3K27) demethylase, has been implicated in the activation of macrophages. Here we show that Jmjd3 is essential for M2 macrophage polarization in response to helminth infection and chitin, though Jmjd3 is dispensable for M1 responses. Furthermore, *Jmjd3* (also known as *Kdm6b*) is essential for proper bone marrow macrophage differentiation, and this function depends on demethylase activity of Jmjd3. *Jmjd3* deficiency affected trimethylation of H3K27 in only a limited number of genes. Among them, we identified *Irf4* as encoding a key transcription factor that controls M2 macrophage polarization. Collectively, these results show that Jmjd3-mediated H3K27 demethylation is crucial for regulating M2 macrophage development leading to anti-helminth host responses.

Innate immune cells such as macrophages sense the presence of microbial infection through pattern-recognition receptors and mount anti-microbial responses[1–3]. The Toll-like receptor (TLR) family is one of the best-characterized PRR families recognizing various pathogens such as bacteria, viruses, protozoa and fungi. TLRs are crucial in evoking innate immune responses to infection by various pathogens, leading to production of inflammatory mediators, including proinflammatory cytokines, chemokines and interferons.

Macrophages are functionally polarized into M1 and M2 cells in response to infection with microorganisms and host mediators[4,5]. M1 macrophages produce large amounts of nitric oxide by expressing inducible nitric oxide synthase (iNOS) and tumor necrosis factor (TNF), and are essential for clearing bacterial, viral and fungal infections[6]. Other macrophages, called alternatively activated macrophages or M2 macrophages, have an important role in responses to parasite infection, tissue remodeling, angiogenesis and tumor progression. M2 macrophages are characterized by their high expression of arginase-1 (*Arg1*), chitinase-like Ym1 (*Chi3l3*), found in inflammatory zone-1 (*Fizz1*, also called *Retnla*) mannose receptor (*Mrc1* encoding MR, also known as CD206), and chemokines such as CCL17 and CCL24 (refs. 7–11). The PRR system responsible for the recognition of helminth infection and M2 polarization has yet to be identified.

Cytokines and growth factors have been implicated in the reprogramming of M1 and M2 macrophages. Whereas interferon-γ (IFN-γ), produced by activated T cells and TLR ligands, induces M1 macrophage generation, stimulation of macrophages with interleukin-4 (IL-4) or IL-13 induces M2-type macrophages[4,5]. In addition, immune complexes, IL-10 and glucocorticoid or secosteroid hormones are also known to generate M2 macrophages. Among growth factors, treatment of bone marrow cells with granulocyte-macrophage colony-stimulating factor (GM-CSF) and macrophage colony-stimulating factor (M-CSF) leads to generation of M1 and M2 cells, respectively[12–15].

TLRs trigger intracellular signaling pathways, inducing activation of a set of transcription factors, such as NF-κB, AP-1, C/EBPβ, PU.1 and interferon-regulatory factors (IRFs)[1,16]. These transcription factors cooperatively upregulate the expression of multiple genes such as proinflammatory cytokines, leading to M1 macrophage polarization. Proteins induced by TLR signaling are known to modulate inflammatory responses. IκBζ, an IκB family member, positively regulates certain genes such as *Il6* by interacting with NF-κBp50 or inducing histone modification[17,18], whereas ATF3 negatively regulates expression[19]. In contrast, transcription factors such as STAT6 and peroxisome proliferator-activated receptor-γ (PPARγ) are involved in polarization of M2 macrophages[5,20].

[1]Laboratory of Host Defense, World Premiere Initiative Immunology Frontier Research Center, Osaka University, Osaka, Japan. [2]Research Institute for Microbial Diseases, Osaka University, Osaka, Japan. [3]Laboratory of Systems Immunology, World Premiere International Immunology Frontier Research Center, Osaka University, Osaka, Japan. [4]Department of Immunology and Medical Zoology, Hyogo College of Medicine, Hyogo, Japan. [5]Laboratory of Functional Analysis *In Silico*, Human Genome Center, Institute of Medical Science, University of Tokyo, Tokyo, Japan. [6]Department of Molecular Microbiology and Immunology, Graduate School of Biomedical Sciences, Nagasaki University, Nagasaki, Japan. [7]Department of Pathology, Hyogo College of Medicine, Hyogo, Japan. [8]These authors contributed equally to this work. Correspondence should be addressed to S.A. (sakira@biken.osaka-u.ac.jp).

Received 19 March; accepted 22 July; published online 22 August 2010; doi:10.1038/ni.1920

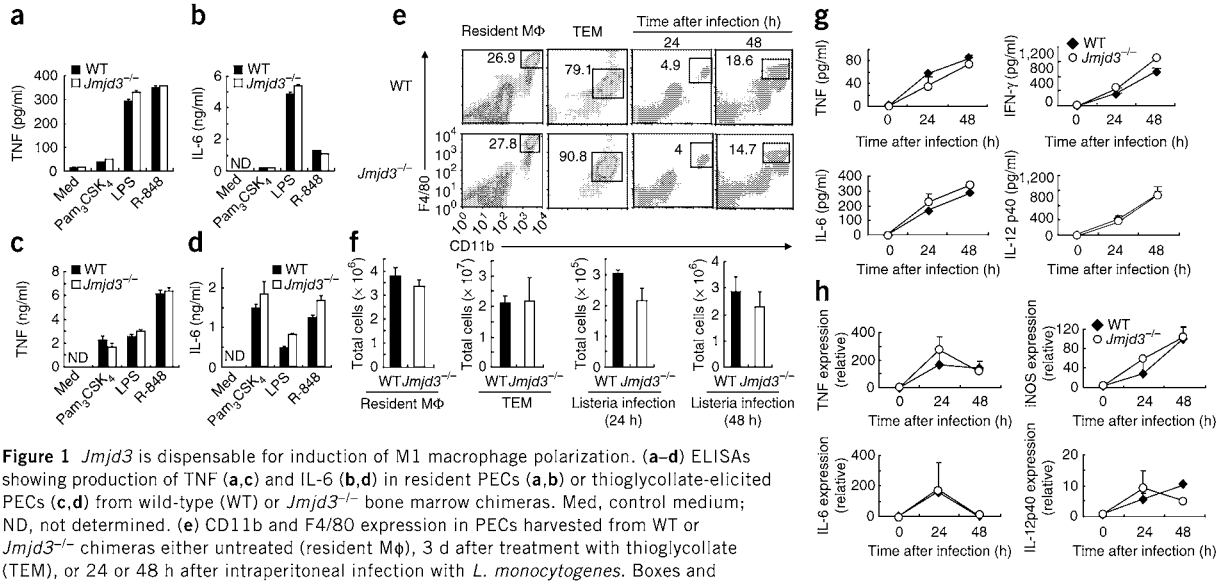

Figure 1 *Jmjd3* is dispensable for induction of M1 macrophage polarization. (**a–d**) ELISAs showing production of TNF (**a**,**c**) and IL-6 (**b**,**d**) in resident PECs (**a**,**b**) or thioglycollate-elicited PECs (**c**,**d**) from wild-type (WT) or *Jmjd3*$^{-/-}$ bone marrow chimeras. Med, control medium; ND, not determined. (**e**) CD11b and F4/80 expression in PECs harvested from WT or *Jmjd3*$^{-/-}$ chimeras either untreated (resident Mϕ), 3 d after treatment with thioglycollate (TEM), or 24 or 48 h after intraperitoneal infection with *L. monocytogenes*. Boxes and numbers indicate percentage of F4/80^{+}CD11b^{+} cells in total PECs. (**f**) Numbers of F4/80^{+}CD11b^{+} macrophages in PECs harvested from WT or *Jmjd3*$^{-/-}$ chimeras either untreated, 3 d after thioglycollate treatment or 24 or 48 h after intraperitoneal infection with *L. monocytogenes*. (**g**) ELISAs showing concentrations of TNF, IL-6, IFN-γ and IL-12p40 in the sera of WT or *Jmjd3*$^{-/-}$ chimeras infected with *L. monocytogenes*. (**h**) Quantitative PCR analysis showing expression of TNF, IL-6, IL-12p40 and iNOS mRNAs (relative to 18S rRNA) in PECs in mice infected with *L. monocytogenes*. Results are representative of four (**c–f**) or two (**a**,**b**,**g**,**h**) independent experiments (error bars indicate s.d.).

In addition to regulation by transcription factors, epigenetic regulation is essential for controlling proper gene expression[16]. Histone modifications, particularly at the N-terminal tails, and dynamic chromatin remodeling have been shown to be important for controlling sets of genes. In the case of histone modification, trimethylation of H3K4 is associated with active gene transcription, whereas trimethylation of H3K9, H3K27 and H4K20 is linked to silencing of gene expression[16,21,22]. The methylation of H3K27 is mediated by the Polycomb repressive complex-2 (PRC2), composed of Ezh2, Suz12 and Eed (ref. 23). Proteins harboring a Jumonji-C (JmjC) domain, such as Jmjd3, Utx and Uty, are known to act as H3K27 demethylases, catalyzing the conversion of H3K27me3 (trimethylated) to H3K27me1 (monomethylated)[24–26].

It has been reported that the expression of *Jmjd3* is induced in macrophages by TLR stimuli in an NF-κB–dependent fashion[26]. *Jmjd3* has also been identified as an early TLR-inducible gene in mouse macrophages by microarray analysis[27]. H3K27 trimethylation is implicated in the silencing of gene expression, and it has been shown that Jmjd3 is recruited to transcription start sites (TSSs) that have abundant RNA polymerase II and H3K4me3 (ref. 28). Jmjd3 is reported to fine-tune macrophage activation by controlling *Bmp2* and *Hox* expression[26]. Furthermore, Jmjd3 has been linked to the control of development through the regulation of *Hox*, and to oncogenesis through promotion of the expression of *Ink4a*[29,30]. Here we report the role of Jmjd3 *in vivo* in controlling M2 macrophage polarization and identify *Irf4* as a Jmjd3 target gene crucial for the regulation of macrophages.

RESULTS

Generation of *Jmjd3*$^{-/-}$ mice

To investigate the functional roles of Jmjd3 in immune responses *in vivo*, we generated *Jmjd3*$^{-/-}$ mice (**Supplementary Fig. 1a,b**). Reverse-transcription PCR analysis showed that the expression of *Jmjd3* was abrogated in *Jmjd3*$^{-/-}$ mouse embryonic fibroblasts (**Supplementary Fig. 1c**). *Jmjd3*$^{-/-}$ mice died perinatally, and adult *Jmjd3*$^{-/-}$ mice were not obtained (**Supplementary Fig. 2a**). Histological examination revealed that alveolar cell walls were thickened with tissues, and almost no air space was observed in lungs of *Jmjd3*$^{-/-}$ neonates (**Supplementary Fig. 2b**), suggesting that the postnatal lethal phenotype of *Jmjd3*$^{-/-}$ mice is due to premature development of lung tissues. To analyze the role of *Jmjd3* in hematopoietic cells, we obtained fetal liver cells from *Jmjd3*$^{-/-}$ E15.5 embryos and established bone marrow–chimeric mice. Flow cytometry revealed that populations of T cells, B cells, conventional dendritic cells, plasmacytoid dendritic cells, natural killer cells, neutrophils, F4/80^{+}CD11b^{+} macrophages and Ly6C^{hi}CD11b^{+} inflammatory monocytes in the spleen were similar between wild-type and *Jmjd3*$^{-/-}$ chimeras (**Supplementary Fig. 3**). Proliferative responses of splenic T and B cells to mitogens and antigen receptor stimuli were also not altered (**Supplementary Fig. 4**). Furthermore, *Jmjd3*$^{-/-}$ splenic T cells differentiated into either type 1 or type 2 helper T cells (T_H1 and T_H2) produced normal amounts of IFN-γ or IL-4, respectively (**Supplementary Fig. 5**). These results indicate that T cells lacking *Jmjd3* are capable of differentiating into T_H1 and T_H2 cells in response to cytokines.

Jmjd3 is dispensable for M1 macrophages

As *Jmjd3* is a TLR-inducible gene in macrophages, we first examined cytokine production of peritoneally resident and thioglycollate-elicited peritoneal exudate cells (PECs) in response to TLR ligands including lipopeptide (Pam_3CSK_4, a TLR2 ligand), lipopolysaccharide (LPS, a TLR4 ligand), imidazoquinoline analog (R-848, a TLR7 ligand) and oligonucleotide with a CpG motif (CpG-DNA, a TLR9 ligand). Production of TNF and IL-6 in response to TLR ligands did not differ between wild-type and *Jmjd3*$^{-/-}$ tissue-resident macrophages and thioglycollate-elicited PECs (**Fig. 1a–d**). PECs elicited

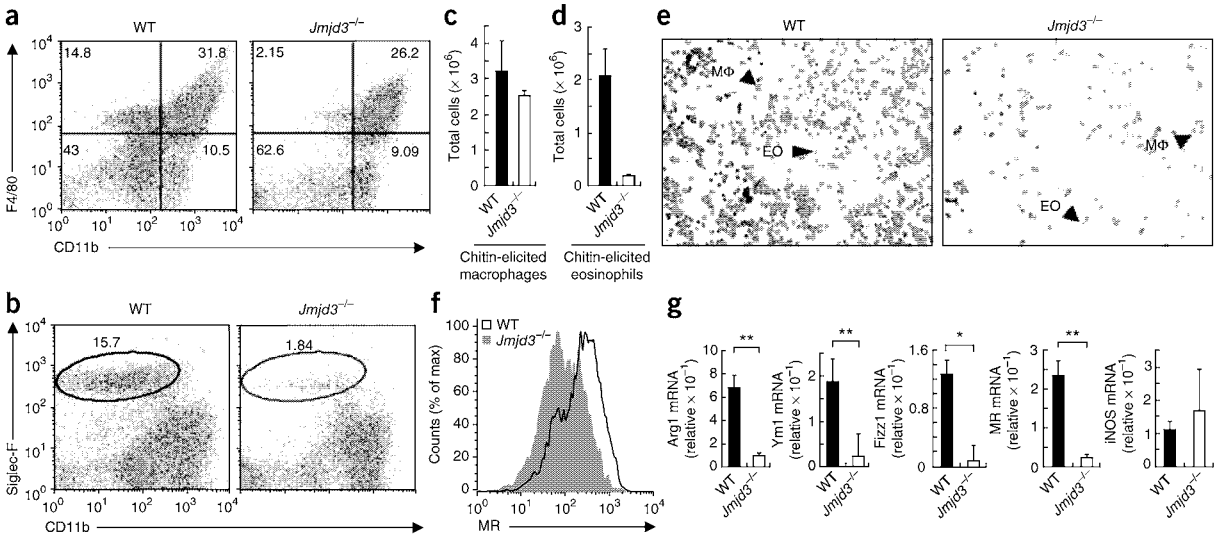

Figure 2 Crucial role of *Jmjd3* in M2 macrophage polarization in response to chitin administration. (**a**,**b**) Expression of CD11b and either F4/80 (**a**) or Siglec-F (**b**) in PECs harvested from wild-type (WT) or *Jmjd3*$^{-/-}$ chimeric mice 2 d after peritoneal injection with chitin. Quadrants and numbers in **a** indicate percentage of cells in each gate (F4/80$^+$CD11b$^+$, F4/80$^+$CD11b$^-$, F4/80$^-$CD11b$^+$ and F4/80$^-$CD11b$^-$); circles and numbers in **b** indicate percentage of Siglec-F$^+$ eosinophils in total PECs. (**c**,**d**) Numbers of F4/80$^+$CD11b$^+$ macrophages (**c**) or Siglec-F$^+$ eosinophils (**d**) in PECs harvested from WT or *Jmjd3*$^{-/-}$ chimeric mice 2 d after peritoneal injection with chitin. (**e**) Cell types within PEC population from chitin-treated mice, stained with Diff-Quick in cytospin centrifuges. Mϕ, macrophages; EO, eosinophils. (**f**) Surface MR expression on peritoneal F4/80$^+$CD11b$^+$ macrophages from chitin-treated mice. Graph shows MR expression on macrophages on horizontal axis. (**g**) Quantitative PCR showing expression of Arg1, Ym1, Fizz1, MR and iNOS mRNAs (relative to 18S rRNA). Total RNA was prepared from PECs 48 h after administration of chitin. $^*P < 0.05$; $^{**}P < 0.01$ (two-tailed Student's *t*-test). Results are representative of five (**a**–**d**), two (**e**) or three (**f**,**g**) independent experiments (error bars indicate s.d.).

by peptone treatment of wild-type or *Jmjd3*$^{-/-}$ chimeras also produced similar amounts of TNF and IL-6 in response to TLR ligand stimulation (**Supplementary Fig. 6a**). Flow cytometry revealed that the proportions of F4/80$^+$CD11b$^+$Gr1$^-$ cells among resident and thioglycollate-elicited PECs did not differ between wild-type and *Jmjd3*$^{-/-}$ chimeras (**Fig. 1e** and **Supplementary Fig. 7**). The total number of peritoneally resident macrophages, thioglycollate-elicited macrophages and peptone-elicited macrophages was not changed in *Jmjd3*$^{-/-}$ chimeras (**Fig. 1f** and **Supplementary Fig. 6b**). We then examined the role of Jmjd3 in M1 macrophage polarization in response to *Listeria monocytogenes* infection. When *L. monocytogenes* was inoculated intraperitoneally, production of proinflammatory cytokines in the sera was similar in wild-type and *Jmjd3*$^{-/-}$ chimeras (**Fig. 1g**). F4/80$^+$CD11b$^+$Gr1$^+$ macrophages, F4/80^{int}CD11b$^+$Gr1^{hi} neutrophils, and F4/80$^-$CD11b^{int}B220$^+$ and F4/80$^-$CD11b$^-$B220$^+$ B cells were examined in PECs prepared from *L. monocytogenes*–infected mice (**Supplementary Fig. 8**). The number of macrophages recruited to the peritoneal cavity was similar in wild-type and *Jmjd3*$^{-/-}$ chimeras (**Fig. 1e**,**f**). Furthermore, the expression of genes encoding TNF, IL-6, IL-12p40 and iNOS in PECs were similarly upregulated (**Fig. 1h**). Collectively, these data suggest that Jmjd3 is not involved in the generation and recruitment of M1 macrophages in response to inflammatory reagents and bacterial infection *in vivo*.

Jmjd3 is needed for M2 polarization to chitin

Chitin is a polymerized sugar and a structural component of helminths, arthropods and fungi[31]. It has been shown that chitin administration recruits macrophages with the M2 phenotype to the site of administration, which are important for subsequent recruitment of eosinophils[32,33]. Indeed, we found that intraperitoneal administration of chitin recruited F4/80$^+$CD11b$^+$ macrophages (**Fig. 2a**), Siglec-F$^+$CCR3$^+$CD4$^-$ eosinophils and CD11b^{int}B220$^+$ B cells to the peritoneal cavity after 48 h in wild-type mice (**Fig. 2b** and **Supplementary Fig. 9**). Whereas the number of chitin-elicited F4/80$^+$CD11b$^+$ macrophages was similar between wild-type and *Jmjd3*$^{-/-}$ chimeras (**Fig. 2c**), the recruitment of eosinophils was severely impaired in *Jmjd3*$^{-/-}$ chimeras (**Fig. 2b–e**). Furthermore, the expression of MR on chitin-elicited macrophages was severely impaired in *Jmjd3*$^{-/-}$ chimeras (**Fig. 2f**). Chitin-elicited macrophages, but not eosinophils or B cells, expressed high levels of mRNA encoding Arg1, Ym1, Fizz1 and MR, the hallmarks of M2 macrophages (**Supplementary Fig. 10**). The expression of genes encoding Arg1, Ym1, Fizz1 and MR was considerably lower in chitin-induced PECs obtained from *Jmjd3*$^{-/-}$ chimeras compared with wild-type controls, whereas expression of the gene encoding iNOS, associated with M1 macrophages, was not altered (**Fig. 2g**). Of note, the numbers of eosinophils circulating in the blood were similar in wild-type and *Jmjd3*$^{-/-}$ chimeric mice, suggesting that eosinophil development was not impaired by *Jmjd3* deficiency (data not shown). Together, these results suggest Jmjd3 is necessary for M2 macrophage polarization in response to chitin administration.

Role of *Jmjd3* in helminth infection

Next we investigated whether Jmjd3 contributes to the responses against helminth infection *in vivo*. We used the *Nippostrongylus brasiliensis* infection model, which induces a strong type 2 immune response in the lung. Bronchoalveolar lavage (BAL) staining 5 and 13 d after infection revealed that macrophages were similarly recruited to the lung in wild-type and *Jmjd3*$^{-/-}$ bone marrow chimeras (**Fig. 3a**,**b**).

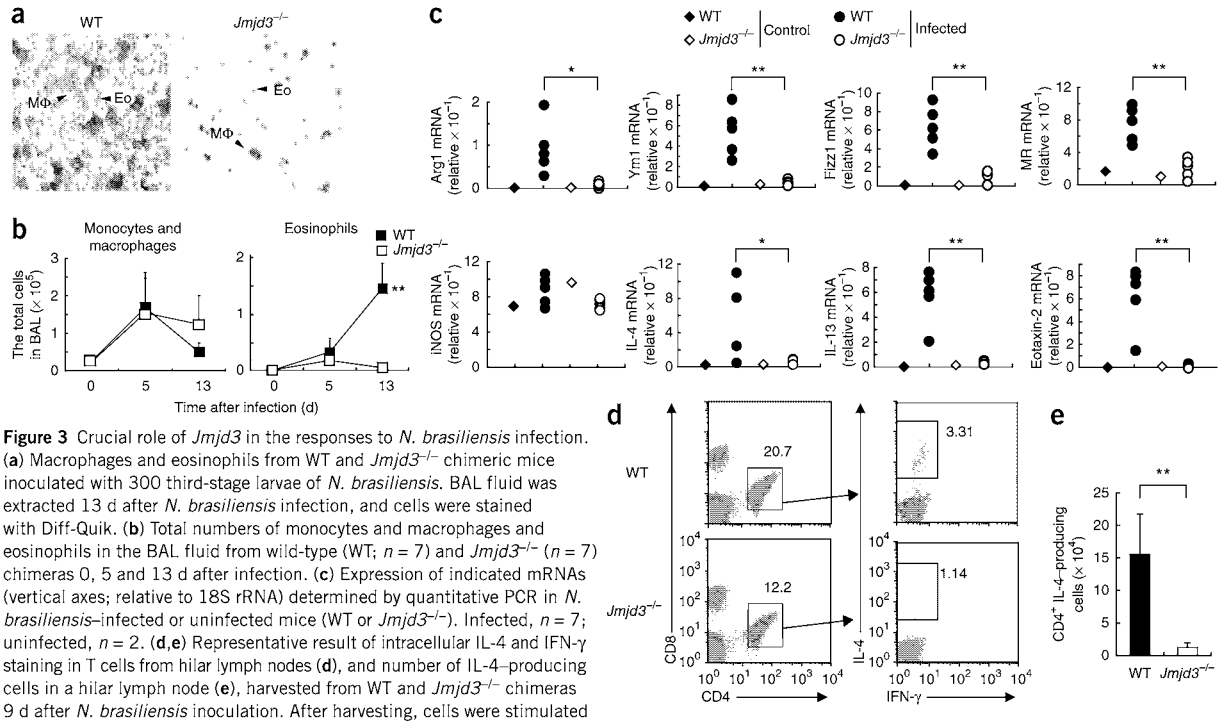

Figure 3 Crucial role of *Jmjd3* in the responses to *N. brasiliensis* infection. (**a**) Macrophages and eosinophils from WT and *Jmjd3*$^{-/-}$ chimeric mice inoculated with 300 third-stage larvae of *N. brasiliensis*. BAL fluid was extracted 13 d after *N. brasiliensis* infection, and cells were stained with Diff-Quik. (**b**) Total numbers of monocytes and macrophages and eosinophils in the BAL fluid from wild-type (WT; $n = 7$) and *Jmjd3*$^{-/-}$ ($n = 7$) chimeras 0, 5 and 13 d after infection. (**c**) Expression of indicated mRNAs (vertical axes; relative to 18S rRNA) determined by quantitative PCR in *N. brasiliensis*–infected or uninfected mice (WT or *Jmjd3*$^{-/-}$). Infected, $n = 7$; uninfected, $n = 2$. (**d**,**e**) Representative result of intracellular IL-4 and IFN-γ staining in T cells from hilar lymph nodes (**d**), and number of IL-4–producing cells in a hilar lymph node (**e**), harvested from WT and *Jmjd3*$^{-/-}$ chimeras 9 d after *N. brasiliensis* inoculation. After harvesting, cells were stimulated with CD3 and CD28 for 4 h, and CD4, CD8, IL-4 and IFN-γ expression were determined. Boxes and numbers indicate percentages of CD4$^+$ cells in hilar lymph node cells and IL-4–producing cells in CD4$^+$ cells. $^*P < 0.05$; $^{**}P < 0.01$ (two-tailed Student's *t*-test). Results are representative of two experiments with four mice per group (**a**,**b**), a single experiment with seven mice per group (**c**) or a single experiment with five mice (**d**,**e**) (error bars indicate s.d.).

However, the recruitment of eosinophils was severely impaired in *Jmjd3*$^{-/-}$ chimeric mice (**Fig. 3b**). To investigate the characteristics of recruited macrophages, we extracted RNA from lung tissue 5 d after *N. brasiliensis* infection. M2 markers such as Arg1, Ym1, Fizz1 and MR were barely expressed in *Jmjd3*$^{-/-}$ chimeras (**Fig. 3c**). Furthermore, induction of genes encoding the eosinophil-recruiting chemokine eotaxin-2 and the T_H2-inducing cytokines IL-4 and IL-13 was severely impaired in *Jmjd3*$^{-/-}$ chimeric mice (**Fig. 3c**). Thus, we

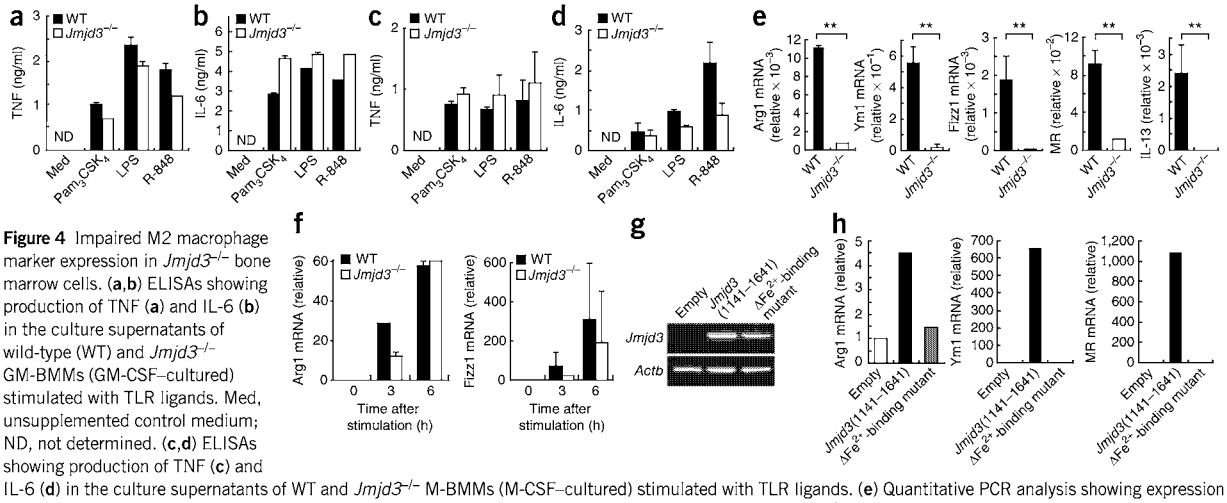

Figure 4 Impaired M2 macrophage marker expression in *Jmjd3*$^{-/-}$ bone marrow cells. (**a**,**b**) ELISAs showing production of TNF (**a**) and IL-6 (**b**) in the culture supernatants of wild-type (WT) and *Jmjd3*$^{-/-}$ GM-BMMs (GM-CSF–cultured) stimulated with TLR ligands. Med, unsupplemented control medium; ND, not determined. (**c**,**d**) ELISAs showing production of TNF (**c**) and IL-6 (**d**) in the culture supernatants of WT and *Jmjd3*$^{-/-}$ M-BMMs (M-CSF–cultured) stimulated with TLR ligands. (**e**) Quantitative PCR analysis showing expression of Arg1, Ym1, Fizz1, MR and IL-13 mRNAs (relative to 18S rRNA) in total RNA prepared from WT and *Jmjd3*$^{-/-}$ M-BMMs. (**f**) Quantitative PCR analysis showing expression of Arg1 and Fizz1 mRNAs (relative to 18S rRNA) in total RNA prepared from WT and *Jmjd3*$^{-/-}$ M-BMMs stimulated with IL-4 (10 ng/ml). (**g**,**h**) Reverse-transcription PCR showing expression of *Jmjd3* cDNA, with *Actb* cDNA as an expression control (**g**), and quantitative PCR showing expression of Arg1, Ym1 and MR mRNAs (relative to empty-vector control; **h**), in total RNA of *Jmjd3*$^{-/-}$ M-BMMs generated from bone marrow cells infected with retroviruses expressing WT Jmjd3 (amino acid residues 1141–1641) or its iron binding–deficient mutant. Results are representative of four (**a**–**d**), three (**e**,**f**) or two (**g**,**h**) independent experiments (error bars indicate s.d.).

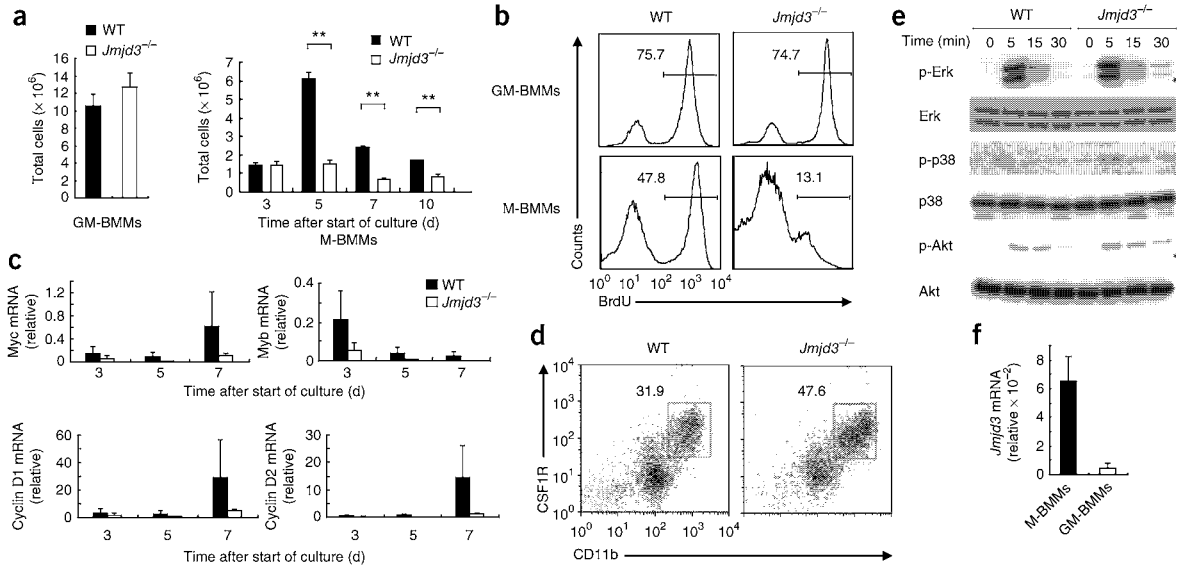

Figure 5 *Jmjd3* is required for the cell-cycle progression of M-BMMs. (**a**) Numbers of GM-BMMs and M-BMMs generated from wild-type (WT) and *Jmjd3*$^{-/-}$ bone marrow cells. Bone marrow cells from WT and *Jmjd3*$^{-/-}$ chimeras were cultured in the presence of GM-CSF for 5 d or M-CSF for time indicated (horizontal axis), and the number of adherent CD11b^{+} cells was counted. (**b**) Incorporation of BrdU in WT and *Jmjd3*$^{-/-}$ GM-BMMs and M-BMMs incubated in the presence of BrdU for 24 h. Incorporation was examined by intracellular staining with anti-BrdU. (**c**) Quantitative PCR showing expression of mRNAs encoding c-Myc, c-Myb, cyclin D1 and cyclin D2 (relative to 18S rRNA) in WT and *Jmjd3*$^{-/-}$ M-BMMs. (**d**) Surface expression of colony stimulating receptor (CSF1R) and CD11b on WT and *Jmjd3*$^{-/-}$ M-BMMs. Boxes and numbers indicate percentages of CSF1R-expressing M-BMMs. (**e**) Expression of phosphorylated (p-) and unphosphorylated Erk, p38 and Akt in WT and *Jmjd3*$^{-/-}$ M-BMMs stimulated with M-CSF (50 ng/ml). Cells were starved for 4 h before stimulation, and cell lysates were subjected to immunoblot analysis with antibodies to p-Erk, p-p38 and p-Akt. The membrane was stripped and reprobed for expression of Erk, p38 and Akt. (**f**) Quantitative PCR showing Jmjd3 mRNA expression (relative to 18S rRNA) by M-BMMs and GM-BMMs. $^{*}P < 0.05$; $^{**}P < 0.01$ (two-tailed Student's *t*-test). Results are representative of four (**a**), three (**b**,**f**) or two (**c**–**e**) independent experiments (error bars indicate s.d.).

investigated the activation of T cells in the pulmonary lymph nodes 9 d after *N. brasiliensis* infection. Whereas CD4^{+} T cells prepared from wild-type pulmonary lymph nodes expressed IL-4, but not IFN-γ, the frequency of IL-4–producing CD4^{+} T cells was severely impaired in pulmonary T cells prepared from *Jmjd3*$^{-/-}$ chimeric mice, suggesting that Jmjd3-mediated M2 macrophage activation is crucial for *N. brasiliensis* to induce T_H2 responses in the lung (**Fig. 3d,e**). However, histological changes in the intestine were not severely impaired in *Jmjd3*$^{-/-}$ chimeric mice (data not shown). Collectively, our results demonstrate that Jmjd3 is essential for mounting immune responses to helminth infection, directing M2 macrophage polarization in the lung but not in the small intestine.

Role of *Jmjd3* in M2 macrophage generation in response to M-CSF

Numerous studies have shown that GM-CSF induces M1 macrophages from bone marrow cells and M-CSF induces M2 macrophages from bone marrow cells[12–15]. When we used GM-CSF to generate macrophages, similar amounts of TNF and IL-6 were produced in wild-type and *Jmjd3*$^{-/-}$ chimeras in response to TLR ligands from adherent CD11b^{+} macrophages (termed GM-BMMs, for GM-CSF–induced bone marrow–derived macrophages; **Fig. 4a,b**). In contrast, production of IL-6, but not TNF, in response to TLR ligand stimulation was partially impaired in *Jmjd3*$^{-/-}$ bone marrow cultured in the presence of M-CSF (M-BMMs; **Fig. 4c,d**). Furthermore, the expression of genes encoding Arg1, Ym1, Fizz1, MR and IL-13 was severely impaired in M-BMMs from *Jmjd3*$^{-/-}$ chimeras (**Fig. 4e**), which indicates that *Jmjd3* is crucial for expression of hallmark M2 genes in M-BMMs. Jmjd3 is involved in the response of macrophages to IL-4 stimulation[34]; nevertheless, Arg1 and Fizz1 gene expression were similar after IL-4 stimulation in wild-type and *Jmjd3*$^{-/-}$ M-BMMs (**Fig. 4f**), suggesting that the responses to IL-4 were not impaired in *Jmjd3*$^{-/-}$ M-BMMs. We then used microarray analysis to examine the gene expression profiles in wild-type and *Jmjd3*$^{-/-}$ M-BMMs with or without LPS stimulation. The expression of 1,371 genes was more than 50% lower in unstimulated *Jmjd3*$^{-/-}$ M-BMMs compared with wild-type (**Supplementary Table 1**). In addition to *Arg1*, *Chi3l3* and *Fizz1*, the expression of cytokine genes such as *Il2*, *Il3*, *Il4*, *Il5* and *Il13*, as well as that of chemokine genes such as *Ccl1*, *Ccl17*, *Ccl22* and *Ccl24*, was severely impaired in *Jmjd3*$^{-/-}$ M-BMMs (**Supplementary Table 1**). The expression of 2,188 genes was more than twofold higher in wild-type M-BMMs in response to LPS stimulation, and that of 436 genes was reduced by over 50% in LPS-stimulated *Jmjd3*$^{-/-}$ M-BMMs (**Supplementary Table 2**). For example, the expression of *Il6* and *Il12b* was partially impaired in *Jmjd3*$^{-/-}$ M-BMMs, consistent with a previous report (**Supplementary Table 2**). Therefore, Jmjd3 is important for inducing expression of a large set of genes, and some of these are related to M2 macrophage polarization in M-BMMs.

In addition to its JmjC domain, Jmjd3 contains a putative tetratricopeptide repeat domain in the N terminus. We therefore examined whether the demethylase activity of Jmjd3 is needed for the defect in M2 macrophage marker expression. We retrovirally expressed the C-terminal part of Jmjd3, containing the JmjC domain (amino acid residues 1141–1641), or its iron binding–deficient mutant (A1388H) in *Jmjd3*$^{-/-}$ bone marrow cells and then induced M-BMMs (**Fig. 4g**).

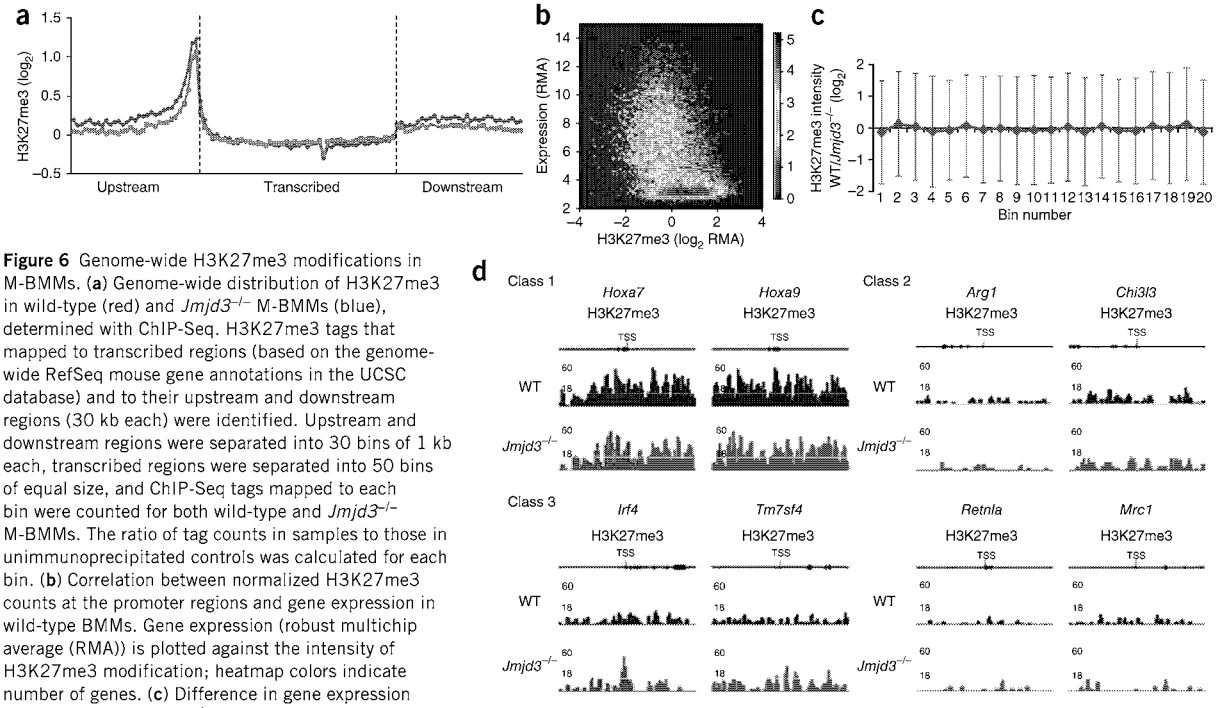

Figure 6 Genome-wide H3K27me3 modifications in M-BMMs. (**a**) Genome-wide distribution of H3K27me3 in wild-type (red) and *Jmjd3*$^{-/-}$ M-BMMs (blue), determined with ChIP-Seq. H3K27me3 tags that mapped to transcribed regions (based on the genome-wide RefSeq mouse gene annotations in the UCSC database) and to their upstream and downstream regions (30 kb each) were identified. Upstream and downstream regions were separated into 30 bins of 1 kb each, transcribed regions were separated into 50 bins of equal size, and ChIP-Seq tags mapped to each bin were counted for both wild-type and *Jmjd3*$^{-/-}$ M-BMMs. The ratio of tag counts in samples to those in unimmunoprecipitated controls was calculated for each bin. (**b**) Correlation between normalized H3K27me3 counts at the promoter regions and gene expression in wild-type BMMs. Gene expression (robust multichip average (RMA)) is plotted against the intensity of H3K27me3 modification; heatmap colors indicate number of genes. (**c**) Difference in gene expression between WT and *Jmjd3*$^{-/-}$ M-BMMs does not correlate with H3K27me3 levels. We classified RefSeq genes into 20 bins sorted by their expression difference between WT and *Jmjd3*$^{-/-}$ cells. Bins are numbered from low to high WT/*Jmjd3*$^{-/-}$ expression ratio. The average H3K27 modification intensity was calculated in each bin. (**d**) H3K27me3 modifications of wild-type (WT, blue) and *Jmjd3*$^{-/-}$ (red) cells on class 1 genes (*Hoxa7* and *Hoxa9*), class 2 genes (*Arg1*, *Chi3l3* for Ym1, *Fizz1*, *Mrc1* for MR) and class 3 genes (*Irf4* and *Tm7sf4*). Gray lines indicate the threshold tag counts for WT (18 tags) and *Jmjd3*$^{-/-}$ M-BMMs (18 tags) corresponding to a false discovery rate of 1×10^{-6}.

The A1388H mutation has been shown to abrogate the H3K27 demethylase activity of Jmjd3 (ref. 26). Expression of the C-terminal part of Jmjd3 was sufficient to upregulate M2 marker genes such as *Arg1*, *Chi3l3* and *Mrc1* (**Fig. 4h**). In contrast, the expression of *Jmjd3* (A1388H) did not increase the expression of M2 marker genes, which indicates that the H3K27me3 demethylase activity of Jmjd3 is necessary and sufficient for expression of M2 marker genes in M-BMMs.

M-BMMs require *Jmjd3* for cell cycle progression

In addition to the impaired M2 marker expression, the total number of M-BMM cells in *Jmjd3*$^{-/-}$ chimeras was considerably lower than in the wild type at days 5 and 7 of culture with M-CSF (**Fig. 5a**), although the number of GM-BMM cells (M1) was not altered. We found 5-bromodeoxyuridine (BrdU) incorporation, a measure of cell division, was severely impaired in *Jmjd3*$^{-/-}$ M-BMMs compared with wild-type cells (**Fig. 5b**), whereas wild-type and *Jmjd3*$^{-/-}$ GM-BMMs incorporated BrdU similarly. These results indicate that Jmjd3 controls cell-cycle progression in response to M-CSF stimulation. Expression of cell cycle–regulatory proteins (c-Myc, c-Myb, cyclin D1 and cyclin D2) was impaired in *Jmjd3*$^{-/-}$ M-BMMs at day 5 of culture (**Fig. 5c**); however, the surface expression of M-CSF receptor (CSF-1R) was normal in *Jmjd3*$^{-/-}$ M-BMMs (**Fig. 5d**). Furthermore, *Jmjd3* deficiency did not affect activation of the intracellular signaling molecules Erk, p38 and Akt, as indicated by their phosphorylation in M-BMMs (**Fig. 5e**), implying that the cell proliferation defects in *Jmjd3*$^{-/-}$ M-BMMs are not due to less activation of MAP kinases or Akt. The expression of *Jmjd3* in M-BMMs was much higher than that in GM-BMMs (**Fig. 5f**), suggesting that differential expression of *Jmjd3* in M-BMMs and GM-BMMs determines the contribution of Jmjd3 to their proliferation. Together, these data indicate that Jmjd3 performs a key step in the generation of M-BMMs, but not GM-BMMs, by controlling cell proliferation downstream of CSF-1R signaling.

Genome-wide analysis of H3K27me3 controlled by Jmjd3

Next we analyzed the genome-wide distribution of H3K27 trimethylation in wild-type and *Jmjd3*$^{-/-}$ M-BMMs by chromatin immunoprecipitation–sequencing (ChIP-Seq) analysis. We obtained an overall picture of the H3K27me3 distribution in transcribed regions (based on the genome-wide RefSeq mouse gene annotations in the University of California, Santa Cruz database) and in regions 30 kb upstream and 30 kb downstream. High levels of H3K27me3 tags were detected surrounding TSSs in M-BMMs from wild-type and *Jmjd3*$^{-/-}$ chimeras (**Fig. 6a**). In contrast, H3K27me3 levels were low in transcribed loci compared with upstream and downstream regions (**Fig. 6a**). Notably, H3K27me3 signals at the promoter and downstream regions were higher in *Jmjd3*$^{-/-}$ M-BMMs compared with wild-type cells.

We then compared the gene expression data obtained by microarray experiments with H3K27 methylation status. Overall, H3K27me3 levels in regions close to the TSS (−5 to +1 kb) correlated negatively with gene expression in M-BMMs (correlation coefficient −0.441; **Fig. 6b**). Next, we sorted genes by their ratio of expression in wild-type and *Jmjd3*$^{-/-}$ M-BMMs and examined H3K27me3 levels. However, we did not detect a correlation between H3K27me3 status and the difference in gene expression in wild-type compared with *Jmjd3*$^{-/-}$ M-BMMs (**Fig. 6c**). These data suggest that only small numbers of genes were affected by the absence of *Jmjd3*, and most loci are regulated by Utx or by both Jmjd3 and Utx.

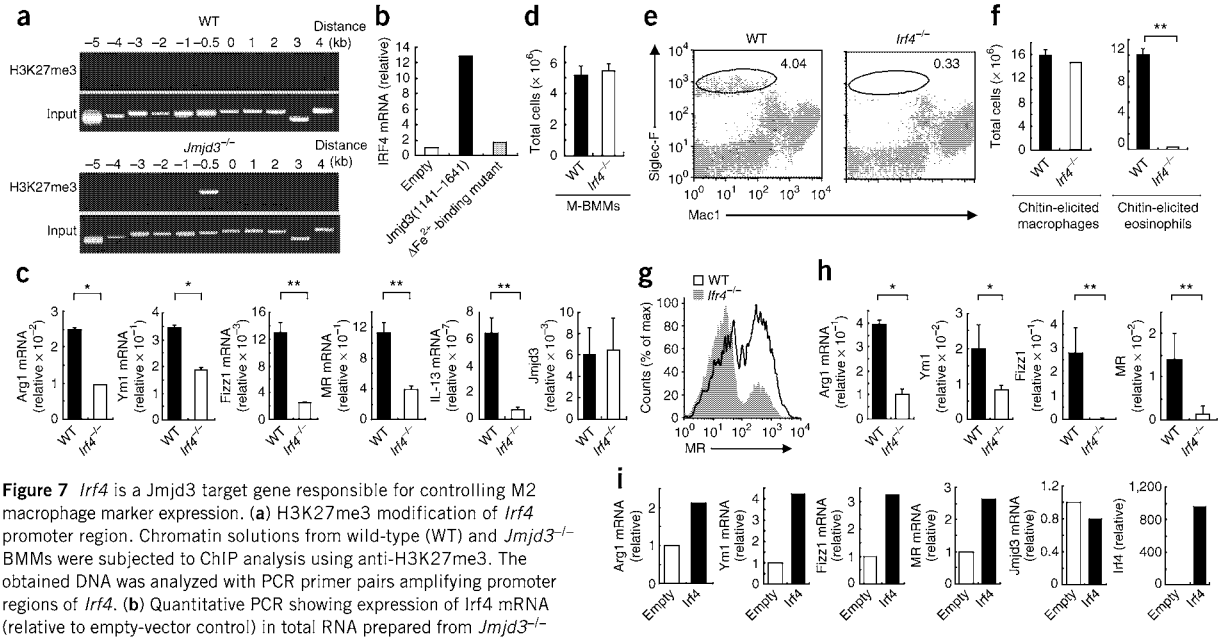

Figure 7 *Irf4* is a Jmjd3 target gene responsible for controlling M2 macrophage marker expression. (**a**) H3K27me3 modification of *Irf4* promoter region. Chromatin solutions from wild-type (WT) and *Jmjd3*$^{-/-}$ BMMs were subjected to ChIP analysis using anti-H3K27me3. The obtained DNA was analyzed with PCR primer pairs amplifying promoter regions of *Irf4*. (**b**) Quantitative PCR showing expression of Irf4 mRNA (relative to empty-vector control) in total RNA prepared from *Jmjd3*$^{-/-}$ M-BMMs retrovirally reconstituted with WT Jmjd3 (amino acid residues 1141–1641) or its iron binding–deficient mutant. (**c**) Quantitative PCR showing expression of M2 markers and Jmjd3 in bone marrow cells from WT and *Irf4*$^{-/-}$ mice cultured in the presence of M-CSF for 5 d. (**d**) Numbers of M-BMMs obtained from wild-type and *Irf4*$^{-/-}$ mice. (**e–g**) Macrophage and eosinophil recruitment (**e**), numbers of macrophages and eosinophils (**f**) and expression of MR (**g**) in macrophages from chitin-elicited PECs. WT and *Irf4*$^{-/-}$ mice were intraperitoneally treated with chitin, and PECs were prepared 48 h after treatment. Graph in **g** shows percentage of macrophages with the MR expression levels indicated on horizontal axis. (**h**) Quantitative PCR showing expression of M2 markers (relative to 18S rRNA) in total RNA prepared from PECs obtained from chitin-treated WT and *Irf4*$^{-/-}$ mice. (**i**) Quantitative PCR showing expression of M2 markers and Jmjd3 (relative to empty-vector control) in *Jmjd3*$^{-/-}$ M-BMMs in which Irf4 was ectopically expressed using retrovirus. $^{*}P < 0.05$; $^{**}P < 0.01$ (two-tailed Student's *t*-test). Results are representative of two (**a**,**b**,**i**) or three (**c–h**) independent experiments (error bars indicate s.d.).

Given the higher concentration of H3K27me3 tags in the region near the TSS, and the lack of overall correlation between expression changes and tag numbers, we focused on the promoter regions of individual genes that showed H3K27me3 peaks. We looked for peaks in wild-type and *Jmjd3*$^{-/-}$ M-BMM samples and divided the genome-wide set of genes into three different classes depending on H3K27me3 status (**Fig. 6d**). Class 1 genes harbored an H3K27me3 peak in wild-type M-BMMs. Class 2 genes did not have an H3K27me3 peak in either wild-type or *Jmjd3*$^{-/-}$ M-BMMs. Class 3 genes such as *Irf4* and *Tm7sf4* had an H3K27me3 peak in *Jmjd3*$^{-/-}$ but not in wild-type M-BMMs. We generated a table of 500 genes differentially expressed in wild-type and *Jmjd3*$^{-/-}$ M-BMMs, comparing H3K27 methylation status and gene expression from the microarray data (**Supplementary Table 3**).

Although *Hox* genes, such as *Hoxa7*, *Hoxa9* and *Tlx1* (also called *Hox11*), and *Bmp2* have been reported to be regulated by Jmjd3 (ref. 26), the H3K27 of their loci were highly trimethylated in M-BMMs both in the presence and absence of *Jmjd3*, and they therefore were assigned to class 1 (**Fig. 6d** and **Supplementary Table 3**). Furthermore, *Hox* and *Bmp2* gene expression was not lower in *Jmjd3*$^{-/-}$ M-BMMs (**Supplementary Table 3**), which indicates that these genes are not crucially regulated by Jmjd3 in M-BMMs. Furthermore, M2 marker genes, such as *Arg1*, *Chi3l3*, *Rentla* and *Mrc1*, were all in class 2, which indicates that their expression is not directly regulated by Jmjd3 (**Fig. 6d** and **Supplementary Table 3**). Thus, we proposed that transcription factors directly regulated by Jmjd3-mediated demethylation are responsible for the polarization of macrophages. When we searched genes categorized in class 3, we found *Irf4* and *Cebpb*. In particular, the promoter region close to the TSS of *Irf4* had a high H3K27me3 signal in *Jmjd3*$^{-/-}$ but not in wild-type M-BMMs (**Fig. 6d**).

Identification of *Irf4* as a Jmjd3 target gene

We confirmed by ChIP analysis that H3K27 at the promoter region of *Irf4* is differentially methylated in wild-type and *Jmjd3*$^{-/-}$ macrophages (**Fig. 7a**). Furthermore, when we retrovirally expressed the C-terminal region of Jmjd3 or its mutant in *Jmjd3*$^{-/-}$ macrophages, we found the expression of *Irf4* was demethylase activity dependent (**Fig. 7b**). These results demonstrate that *Irf4* is one of the Jmjd3 target genes in M-BMMs. Therefore, we examined the contribution of Irf4 to expression of mRNAs encoding Arg1, Ym1, Fizz1 and MR by using *Irf4*$^{-/-}$ mice. Induction of M2-related genes was severely impaired in *Irf4*$^{-/-}$ M-BMMs; in contrast, the expression of *Jmjd3* was similar between wild-type and *Irf4*$^{-/-}$ M-BMMs (**Fig. 7c**). Notably, the number of M-BMM cells was not lower in *Irf4*$^{-/-}$ mice (**Fig. 7d**). When chitin was administered peritoneally, recruitment of eosinophils, but not macrophages, was severely impaired in *Irf4*$^{-/-}$ mice (**Fig. 7e,f**). MR expression in chitin-elicited peritoneal macrophages was greatly impaired in *Irf4*$^{-/-}$ mice (**Fig. 7g**). In addition, the mRNA expression of the M2 macrophage markers encoding Arg1, Ym1, Fizz1 and MR was severely impaired in chitin-induced macrophages from *Irf4*$^{-/-}$ mice (**Fig. 7h**). These results demonstrate that Irf4 is crucial for the polarization of macrophages to M2 in M-BMMs and *in vivo* in response to chitin administration.

We then retrovirally expressed Irf4 in *Jmjd3*$^{-/-}$ M-BMMs and examined the expression of M2 marker genes (**Fig. 7i**). The expression

of Irf4 upregulated mRNAs encoding Arg1, Ym1, Fizz1 and MR in *Jmjd3*$^{-/-}$ M-BMMs, though the expression of Jmjd3 was unaltered (**Fig. 7i**). These results suggest that Irf4 contributes to the expression of M2 marker genes downstream of Jmjd3.

DISCUSSION

Here we focused on the role of Jmjd3 in macrophages mounting antibacterial and anti-parasitic responses. Whereas Jmjd3 was dispensable for M1 macrophage polarization, mice lacking *Jmjd3* did not mount proper M2 responses against helminth infection or chitin administration. Furthermore, bone marrow macrophages induced by M-CSF showed demethylase activity–dependent defects in expressing various genes, including M2 macrophage markers. Nevertheless, only a subset of genes had H3K27me3 levels differentially regulated by the presence or absence of *Jmjd3*. Among these genes, we found *Irf4* to be one of the direct targets of Jmjd3-mediated demethylation. Finally, we found that Irf4 is a transcription factor crucial for the induction of M2 macrophage responses.

Although *Jmjd3* is a TLR-inducible gene, *Jmjd3*$^{-/-}$ mice showed vigorous M1 macrophage activation in response to *Listeria* inoculation. These results suggest that *Jmjd3* is not essential for generating and recruiting M1 macrophages to bacterial infections. Our data are consistent with a previous report showing that gene expression in response to LPS stimulation is only modestly changed in macrophages lacking *Jmjd3* and that Jmjd3 in this case fine-tunes the transcriptional output[28]. TLR signaling upregulates genes involved not only in the promotion of inflammation, but also in termination or tissue remodeling. For instance, ATF3 and Zc3h12a are rapidly induced in response to TLR stimulation and inhibit inflammatory cytokine production[19,27]. It has been shown that M2 macrophages promote tissue remodeling as well as T_H2 responses. Thus, it is possible that *Jmjd3* induction functions as part of a feedback mechanism acting to repair inflammatory damage caused by TLR stimulation.

Chitin is an abundant structural component of helminths, crustaceans and fungi, and administration of chitin strongly induces M2 macrophage activation. Intraperitoneal administration of chitin recruited M2 macrophages and eosinophils in a Jmjd3- and Irf4-dependent fashion. These results indicate that the Jmjd3-*Irf4* axis is essential for M2 macrophage polarization to helminth infection.

However, addition of chitin to the macrophage culture did not stimulate the cells to upregulate M2 marker gene expression in our experiments (data not shown). Although TLR2 has been reported to mediate acute inflammation in response to chitin, another study has shown that chitin-mediated M2 macrophage activation is independent of MyD88, an adaptor molecule used by all TLRs (refs. 32,35). Currently, the mechanism by which chitin activates macrophages is not well understood. Moreover, it is still not clear what unique role Jmjd3 carries out in the generation of M2 macrophages in response to chitin and helminth infection. The identification of the chitin receptor(s) in the future will be vital for clarifying mechanisms of innate immune activation in response to helminth infection.

Jmjd3$^{-/-}$ mice also showed severe defects in recruiting M2 macrophages in response to *N. brasiliensis* infection. Although it is unknown which components of *N. brasiliensis* activate innate immune cells, Jmjd3-mediated H3K27me3 demethylation seems to be essential for macrophage responses to this parasite. Further studies are needed to identify the role of Jmjd3 in controlling infection with other helminths pathogenic to humans. M2 macrophages are known to be important for tumor cell survival and tissue remodeling in response to inflammation, in addition to the response against helminth infection[36]. Thus, it would be interesting to use this mouse model to explore how epigenetic regulation in macrophages promotes cancer progression or wound healing.

A previous report has found that *Jmjd3* expression is upregulated in response to IL-4 and that H3K27me3 levels decrease in response to IL-4 stimulation[34]. We observed that although M-BMMs and chitin-induced peritoneal macrophages showed severe defects in M2 macrophage marker expression in the absence of *Jmjd3*, *Jmjd3*$^{-/-}$ M-BMMs were capable of upregulating expression of genes representative of M2 macrophages in response to IL-4 stimulation. These findings suggest that IL-4 acts independently of Jmjd3-mediated H3K27 demethylation to promote M2 polarization. The same report[34] showed that H3K27me3 levels of various M2 marker genes were directly controlled by Jmjd3 to activate transcription. In contrast, our ChIP-Seq data demonstrate that H3K27me3 levels of most M2 marker genes, such as *Arg1*, are not changed in the absence of *Jmjd3*. Furthermore, deficiency in *Irf4*, one of the Jmjd3 target genes, resulted in defective M2 responses to chitin administration or M-CSF culture. Thus, it is more likely that Jmjd3 secondarily regulates M2 macrophage polarization by controlling expression of a set of transcription factors.

In addition to M2 marker gene expression, M-BMMs lacking *Jmjd3* showed proliferation defects in response to M-CSF stimulation. This is not due to impaired M-CSF receptor expression or defective activation of initial signaling molecules. Although the expression of genes involved in cell-cycle progression, such as those encoding c-Myc, cyclin D1 and cyclin D2, was impaired in *Jmjd3*$^{-/-}$ M-BMMs, H3K27me3 levels of these genes did not differ between wild-type and *Jmjd3*$^{-/-}$ M-BMMs. Furthermore, *Irf4*$^{-/-}$ M-BMMs did not show a defect in cell cycling (data not shown). Thus, it is possible that other Jmjd3 target genes are responsible for controlling the proliferation of M-BMMs.

ChIP-Seq analysis revealed that, in general, differences between wild-type and *Jmjd3*$^{-/-}$ M-BMM H3K27me3 levels at gene promoter regions were subtle. Nevertheless, gene expression profiles examined by microarray analysis were substantially different in wild-type and *Jmjd3*$^{-/-}$ M-BMMs, and the responses to chitin or helminth infection *in vivo* were severely impaired in *Jmjd3*$^{-/-}$ mice. Although it has been shown that *Hoxa* and *Bmp2* genes are potential targets of Jmjd3 (ref. 26), the expression of these genes was not lower in *Jmjd3*$^{-/-}$ cells, and the H3K27me3 levels were similar between wild-type and *Jmjd3*$^{-/-}$ M-BMMs. These results suggest that other H3K27 demethylases such as Utx and Uty compensate for the lack of *Jmjd3* in macrophages.

However, we identified Irf4 as one direct Jmjd3-specific target transcription factor. Irf4 has been shown to be involved in T_H2 cell polarization as well as in plasma cell differentiation and class-switch recombination in B cells[37,38]. It has also been reported that Irf4 functions in regulatory T cells to regulate T_H2 responses[39]. Indeed, *Irf4*$^{-/-}$ mice have been found to show defective T_H2 responses to *N. brasiliensis* infection[40]. Given that *Irf4*$^{-/-}$ mice did not induce M2 macrophages in response to chitin administration in our experiments, it is likely that the defects of macrophages in *Irf4*$^{-/-}$ mice also contribute to their abnormal responses to *N. brasiliensis* infection. In macrophages, Irf4 functions as a negative regulator of TLR signaling by associating with MyD88 (refs. 41,42).

Jmjd3$^{-/-}$ mice showed neonatal death due to a developmental defect in lung tissue. Although Jmjd3 directly regulated the expression of *Irf4* in macrophages, *Irf4*$^{-/-}$ mice did not show a developmental defect. Thus, Jmjd3 controls genes other than *Irf4* in the lung tissues for proper tissue development, and we focused solely on the role of this molecule in macrophages.

It is tempting to speculate that the change in epigenetic status is crucial for determining macrophage polarization. Future development of procedures to specifically regulate Jmjd3 demethylase activity might be useful for manipulating macrophages to mount anti-helminth host defenses and tissue repair.

METHODS

Methods and any associated references are available in the online version of the paper at http://www.nature.com/natureimmunology/.

Accession codes. GEO: microarray data, GSE23180; ChIP-Seq data, GSE23297.

Note: Supplementary information is available on the Nature Immunology website.

ACKNOWLEDGMENTS

We thank all the colleagues in our laboratory, E. Kamada for secretarial assistance and Y. Fujiwara, M. Kumagai, R. Abe, N. Kitagaki and S. Yumikura for technical assistance. This work was supported by the Special Coordination Funds of the Japanese Ministry of Education, Culture, Sports, Science and Technology, and grants from the Ministry of Health, Labour and Welfare in Japan, the Global Center of Excellence Programs of Osaka University and Nagasaki University and the US National Institutes of Health (P01 AI070167). Computational time was provided by the Super Computer System at the Human Genome Center, Institute of Medical Science, The University of Tokyo. A.V. was partly supported by a Japanese government scholarship.

AUTHOR CONTRIBUTIONS

T. Satoh and O.T. designed and performed experiments. Y.K., T. Miyake, K.M., T.O. and T. Saitoh performed experiments. A.V., Y.T., D.M.S. and K. Nakai analyzed ChIP-Seq data. K. Yasuda and K. Nakanishi performed *N. brasiliensis* infection experiments. K.H., T. Matsuyama and K. Yui provided *Irf4*$^{-/-}$ mice. T.T. performed histological examination. O.T., T. Satoh and S.A. wrote the manuscript. S.A. supervised the project. A.V. and K.Y. contributed equally to this work.

COMPETING FINANCIAL INTERESTS

The authors declare no competing financial interest.

Published online at http://www.nature.com/natureimmunology/.
Reprints and permissions information is available online at http://npg.nature.com/reprintsandpermissions/.

1. Takeuchi, O. & Akira, S. Pattern recognition receptors and inflammation. *Cell* **140**, 805–820 (2010).
2. Medzhitov, R. Origin and physiological roles of inflammation. *Nature* **454**, 428–435 (2008).
3. Beutler, B. Microbe sensing, positive feedback loops, and the pathogenesis of inflammatory diseases. *Immunol. Rev.* **227**, 248–263 (2009).
4. Mantovani, A., Sozzani, S., Locati, M., Allavena, P. & Sica, A. Macrophage polarization: tumor-associated macrophages as a paradigm for polarized M2 mononuclear phagocytes. *Trends Immunol.* **23**, 549–555 (2002).
5. Gordon, S. Alternative activation of macrophages. *Nat. Rev. Immunol.* **3**, 23–35 (2003).
6. Benoit, M., Desnues, B. & Mege, J.L. Macrophage polarization in bacterial infections. *J. Immunol.* **181**, 3733–3739 (2008).
7. Bronte, V. & Zanovello, P. Regulation of immune responses by L-arginine metabolism. *Nat. Rev. Immunol.* **5**, 641–654 (2005).
8. Nair, M.G., Guild, K.J. & Artis, D. Novel effector molecules in type 2 inflammation: lessons drawn from helminth infection and allergy. *J. Immunol.* **177**, 1393–1399 (2006).
9. Nair, M.G. *et al.* Chitinase and Fizz family members are a generalized feature of nematode infection with selective upregulation of Ym1 and Fizz1 by antigen-presenting cells. *Infect. Immun.* **73**, 385–394 (2005).
10. Stein, M., Keshav, S., Harris, N. & Gordon, S. Interleukin 4 potently enhances murine macrophage mannose receptor activity: a marker of alternative immunologic macrophage activation. *J. Exp. Med.* **176**, 287–292 (1992).
11. Mantovani, A. *et al.* The chemokine system in diverse forms of macrophage activation and polarization. *Trends Immunol.* **25**, 677–686 (2004).
12. Verreck, F.A. *et al.* Human IL-23-producing type 1 macrophages promote but IL-10-producing type 2 macrophages subvert immunity to (myco)bacteria. *Proc. Natl. Acad. Sci. USA* **101**, 4560–4565 (2004).
13. Martinez, F.O., Gordon, S., Locati, M. & Mantovani, A. Transcriptional profiling of the human monocyte-to-macrophage differentiation and polarization: new molecules and patterns of gene expression. *J. Immunol.* **177**, 7303–7311 (2006).
14. Fleetwood, A.J., Lawrence, T., Hamilton, J.A. & Cook, A.D. Granulocyte-macrophage colony-stimulating factor (CSF) and macrophage CSF-dependent macrophage phenotypes display differences in cytokine profiles and transcription factor activities: implications for CSF blockade in inflammation. *J. Immunol.* **178**, 5245–5252 (2007).
15. Fleetwood, A.J., Dinh, H., Cook, A.D., Hertzog, P.J. & Hamilton, J.A. GM-CSF- and M-CSF-dependent macrophage phenotypes display differential dependence on type I interferon signaling. *J. Leukoc. Biol.* **86**, 411–421 (2009).
16. Medzhitov, R. & Horng, T. Transcriptional control of the inflammatory response. *Nat. Rev. Immunol.* **9**, 692–703 (2009).
17. Yamamoto, M. *et al.* Regulation of Toll/IL-1-receptor-mediated gene expression by the inducible nuclear protein IκBζ. *Nature* **430**, 218–222 (2004).
18. Kayama, H. *et al.* Class-specific regulation of pro-inflammatory genes by MyD88 pathways and IκBζ. *J. Biol. Chem.* **283**, 12468–12477 (2008).
19. Gilchrist, M. *et al.* Systems biology approaches identify ATF3 as a negative regulator of Toll-like receptor 4. *Nature* **441**, 173–178 (2006).
20. Charo, I.F. Macrophage polarization and insulin resistance: PPARγ in control. *Cell Metab.* **6**, 96–98 (2007).
21. Wei, G. *et al.* Global mapping of H3K4me3 and H3K27me3 reveals specificity and plasticity in lineage fate determination of differentiating CD4+ T cells. *Immunity* **30**, 155–167 (2009).
22. Barski, A. *et al.* High-resolution profiling of histone methylations in the human genome. *Cell* **129**, 823–837 (2007).
23. Schuettengruber, B., Chourrout, D., Vervoort, M., Leblanc, B. & Cavalli, G. Genome regulation by polycomb and trithorax proteins. *Cell* **128**, 735–745 (2007).
24. Hong, S. *et al.* Identification of JmjC domain-containing UTX and JMJD3 as histone H3 lysine 27 demethylases. *Proc. Natl. Acad. Sci. USA* **104**, 18439–18444 (2007).
25. Lan, F. *et al.* A histone H3 lysine 27 demethylase regulates animal posterior development. *Nature* **449**, 689–694 (2007).
26. De Santa, F. *et al.* The histone H3 lysine-27 demethylase Jmjd3 links inflammation to inhibition of polycomb-mediated gene silencing. *Cell* **130**, 1083–1094 (2007).
27. Matsushita, K. *et al.* Zc3h12a is an RNase essential for controlling immune responses by regulating mRNA decay. *Nature* **458**, 1185–1190 (2009).
28. De Santa, F. *et al.* Jmjd3 contributes to the control of gene expression in LPS-activated macrophages. *EMBO J.* **28**, 3341–3352 (2009).
29. Barradas, M. *et al.* Histone demethylase JMJD3 contributes to epigenetic control of INK4a/ARF by oncogenic RAS. *Genes Dev.* **23**, 1177–1182 (2009).
30. Agger, K. *et al.* The H3K27me3 demethylase JMJD3 contributes to the activation of the INK4A-ARF locus in response to oncogene- and stress-induced senescence. *Genes Dev.* **23**, 1171–1176 (2009).
31. Bowman, S.M. & Free, S.J. The structure and synthesis of the fungal cell wall. *Bioessays* **28**, 799–808 (2006).
32. Reese, T.A. *et al.* Chitin induces accumulation in tissue of innate immune cells associated with allergy. *Nature* **447**, 92–96 (2007).
33. Kreider, T., Anthony, R.M., Urban, J.F. Jr. & Gause, W.C. Alternatively activated macrophages in helminth infections. *Curr. Opin. Immunol.* **19**, 448–453 (2007).
34. Ishii, M. *et al.* Epigenetic regulation of the alternatively activated macrophage phenotype. *Blood* **114**, 3244–3254 (2009).
35. Da Silva, C.A., Hartl, D., Liu, W., Lee, C.G. & Elias, J.A. TLR-2 and IL-17A in chitin-induced macrophage activation and acute inflammation. *J. Immunol.* **181**, 4279–4286 (2008).
36. Mantovani, A. & Sica, A. Macrophages, innate immunity and cancer: balance, tolerance, and diversity. *Curr. Opin. Immunol.* **22**, 231–237 (2010).
37. Ahyi, A.N., Chang, H.C., Dent, A.L., Nutt, S.L. & Kaplan, M.H. IFN regulatory factor 4 regulates the expression of a subset of T_H2 cytokines. *J. Immunol.* **183**, 1598–1606 (2009).
38. Klein, U. *et al.* Transcription factor IRF4 controls plasma cell differentiation and class-switch recombination. *Nat. Immunol.* **7**, 773–782 (2006).
39. Zheng, Y. *et al.* Regulatory T-cell suppressor program co-opts transcription factor IRF4 to control T_H2 responses. *Nature* **458**, 351–356 (2009).
40. Honma, K. *et al.* Interferon regulatory factor 4 differentially regulates the production of T_H2 cytokines in naive vs. effector/memory CD4+ T cells. *Proc. Natl. Acad. Sci. USA* **105**, 15890–15895 (2008).
41. Honma, K. *et al.* Interferon regulatory factor 4 negatively regulates the production of proinflammatory cytokines by macrophages in response to LPS. *Proc. Natl. Acad. Sci. USA* **102**, 16001–16006 (2005).
42. Negishi, H. *et al.* Negative regulation of Toll-like-receptor signaling by IRF-4. *Proc. Natl. Acad. Sci. USA* **102**, 15989–15994 (2005).

ONLINE METHODS

Generation of *Jmjd3*$^{-/-}$ mice. The *Jmjd3* gene was isolated from genomic DNA extracted from embryonic stem cells (GSI-I) by PCR. The targeting vector was constructed by replacing a 4-kb fragment encoding the *Jmjd3* open reading frame (exons 14–21, including exons encoding the JmjC domain) with a neomycin-resistance gene cassette (*neo*), and herpes simplex virus thymidine kinase was inserted into the genomic fragment for negative selection. After the targeting vector was transfected into embryonic stem cells, G418 and gancyclovir doubly-resistant colonies were selected and screened by PCR; recombination was further confirmed by Southern blotting. These homologous-recombinant clones were microinjected into blastocysts derived from C57BL/6 mice and were transferred to pseudopregnant females. Matings of chimeric male mice to C57BL/6 female mice resulted in transmission of the mutant allele to the germline. Resulting *Jmjd3*$^{+/-}$ mice were intercrossed to generate *Jmjd3*$^{-/-}$ mice. All animal experiments were done with the approval of the Animal Research Committee of the Research Institute for Microbial Diseases, Osaka University.

Mice, cells and reagents. *Irf4*$^{-/-}$ mice were prepared as described[41]. Bone marrow–derived macrophages were generated in RPMI-1640 medium containing 10% (vol/vol) FCS, 50 μM 2-mercaptoethanol and 10 ng/ml GM-CSF (PeproTech) or 10 ng/ml M-CSF (PeproTech). Pam_3CSK_4 and R-848 were prepared as described[27]. LPS (*Salmonella minnesota* Re595) was from Sigma.

Generation of bone marrow–chimeric mice. Fetal liver cells were prepared from wild-type and *Jmjd3*$^{-/-}$ embryos (embryonic day 15.5). The cell suspensions were intravenously injected into lethally irradiated CD45.1 C57BL/6 mice. The chimeric mice were given neomycin and ampicillin in their drinking water for 4 weeks. The mice were analyzed at least 8 weeks after reconstitution. More than 90% of splenocytes from chimeric mice were CD45.2 positive.

Quantitative PCR analysis. Total RNA was isolated with TRIzol (Invitrogen), and reverse transcription was performed with ReverTra Ace (Toyobo) according to the manufacturer's instructions. For quantitative PCR, cDNA fragments were amplified by Realtime PCR Master Mix (Toyobo); fluorescence from the TaqMan probe for each cytokine was detected by a 7500 real-time PCR system (Applied Biosystems). To determine the relative induction of cytokine mRNA in response to various stimuli, the mRNA expression level of each gene was normalized to the expression level of 18S rRNA. The experiments were repeated at least twice.

Immunoblot analysis. M-BMMs were cultured for 4 h in medium without M-CSF (PeproTech) and then were collected and replated. M-BMMs were stimulated with M-CSF for times indicated in **Figure 5e** and were lysed with lysis buffer (20 mM Tris-HCl, pH 7.5, 150 mM NaCl, 1 mM EDTA and 1% (vol/vol) Nonidet P-40) containing complete mini protease inhibitor cocktail (Roche). Cell lysates were separated by standard SDS-PAGE and analyzed by immunoblot. Antibodies to the following proteins were used: phosphorylated Erk (Cell Signaling no. 9101), phosphorylated Akt (Cell Signaling 9271), phosphorylated p38 (Cell Signaling 9211), Akt (Cell Signaling 9272), p38 (Santa Cruz C-20), Erk (Santa Cruz K-23) and β-actin (Santa Cruz C-11).

Flow cytometry. Antibodies for flow cytometry were purchased from BD Biosciences and eBioscience. Cells were washed in ice-cold flow-cytometry buffer (2% (vol/vol) FCS and 2 mM EDTA in PBS, pH 7.5), then incubated with each antibody for 15 min and washed twice with flow-cytometry buffer. Intracellular cytokines were stained with Cytofix/Cytoperm Plus Fixation/Permeabilization Kit (BD Biosciences) according to the manufacturer's instructions. Data were acquired on a FACSCalibur flow cytometer (BD Biosciences) and analyzed with FlowJo (Tree Star).

Construction of *Jmjd3* expression plasmids. *Jmjd3* cDNA (corresponding to amino acid residues 1141–1641) was obtained by PCR from a mouse cDNA library, and a point mutation resulting in the A1388H substitution in the JmjC domain was introduced by site-directed mutagenesis (Stratagene). The full or mutated *Jmjd3* cDNAs were cloned into the pMRX-ires-puro vector for retrovirus production[43].

Retroviral transduction. Bone marrow cells were isolated from *Jmjd3*$^{-/-}$ mice that had been injected intraperitoneally 4 d earlier with 5 mg of 5-fluorouracil (Nacalai Tesque). Cells were cultured in stem cell medium (RPMI supplemented with 15% (vol/vol) FCS, 10 mM sodium pyruvate, 2 μM L-glutamine, 50 μM β-mercaptoethanol, 100 U/ml penicillin, 100 g/ml streptomycin, 100 ng/ml stem cell factor, 10 ng/ml IL-6 and 10 ng/ml IL-3). Then, 48 h later, these cells were transduced with retroviral supernatant (supplemented with stem cell factor, IL-6, IL-3 and 10 ng/ml of polybrene) on two successive days. Virus was produced by PlatE packaging cells transfected with various plasmids. After the second transduction, cells were washed and resuspended in macrophage growth medium (RPMI-1640 medium supplemented with 10% (vol/vol) FCS, 50 μM β-mercaptoethanol, 100 U/ml penicillin, 100 μg/ml streptomycin and 20 ng/ml M-CSF). After 3.5 d in culture, cells were washed once and macrophage growth medium with 2.5 μg/ml puromycin (InvivoGen) was added. The cells were cultivated for 2 d after changing of the medium and then were analyzed.

Chitin administration. Chitin (Sigma) was washed three times in PBS and then sonicated with a UR-20P device (Tomy) for 30 min on ice. After filtration with 100 μM cell strainer, chitin was diluted in 50 ml PBS. About 800 ng chitin was intraperitoneally injected, and PECs were collected 2 d after administration.

Responses to *N. brasiliensis* infection. Wild-type and *Jmjd3*$^{-/-}$ fetal liver–chimeric mice were subcutaneously inoculated with 300 third-stage larvae of *N. brasiliensis* 8 weeks after fetal liver transfer. On day 5 after infection, *N. brasiliensis*–inoculated mice were killed and perfused with PBS, and total RNAs from lungs were extracted. RNA was subjected to quantitative PCR for the analysis of expression of various genes. Nine days after infection, hilar lymph nodes were harvested, a single-cell suspension was prepared and cell numbers were counted. The lymph node cells were stimulated with anti-CD3 and anti-CD28. They were stained with CD4 and treated with cytofix (BD Biosciences), then stained with anti–IL-4 and anti–IFN-γ. Next, the cells were examined by flow cytometry. BAL was performed at 5 and 13 d after *N. brasiliensis* infection, and macrophages and eosinophils were enumerated on cytospin smears stained with Diff-Quick (Baxter Healthcare).

Microarray and chromatin immunoprecipitation–sequencing analysis. Microarray and ChIP-Seq protocols and data analysis are described in **Supplementary Methods**.

Statistics. Statistical significance was calculated with the two-tailed Student's *t*-test.

43. Saitoh, T. *et al.* TWEAK induces NF-κB2 p100 processing and long lasting NF-κB activation. *J. Biol. Chem.* **278**, 36005–36012 (2003).

doi:10.1038/ni.1920

Available online at www.sciencedirect.com
ScienceDirect
Current Opinion in Immunology

Basophils as APC in Th2 response in allergic inflammation and parasite infection

Kenji Nakanishi[1,2]

Basophils are important effector cells, which contribute to protection against helminths and execute proinflammatory effector function during allergic inflammation. Basophils are also regulators of Th2 responses in helminth-infected hosts and in allergen-injected animals. Recently, three groups using different experimental systems have shown that basophils are antigen-presenting cells (APC), which induce Th2 cells both *in vitro* and *in vivo*. Basophils express MHC class II and CD80/86, have the potential to take-up and process protein antigen (Ag), particularly Ag-IgE complexes, and to present peptide with MHC class II and produce IL-4. However, relevance of basophils as Th2 cell-inducing APC *in vivo* has been challenged by several recent reports that favor the concept that basophils and DC cooperate or basophils merely amplify DC-driven Th2 cell differentiation. In this review, I summarize and discuss the data on the role of basophils as Th2 cell-inducing APC in allergy and parasite infection.

Addresses
[1] Department of Immunology and Medical Zoology, Hyogo College of Medicine, 1-1 Mukogawa-cho, Nishinomiya, Hyogo 663-8501 Japan
[2] Collaborative Development of Innovatioin Seeds, Japan Science and Technology Corporation, Saitama 332-0012, Japan

Corresponding author: Nakanishi, Kenji (nakaken@hyo-med.ac.jp)

Current Opinion in Immunology 2010, **22**:814–820

This review comes from a themed issue on
Allergy and hypersensitivity
Edited by Marsha Wills-Karp and Martien Kapsenberg

Available online 20th November 2010

0952-7915/$ – see front matter

DOI 10.1016/j.coi.2010.10.018

Introduction

Mast cells, basophils, and eosinophils are important effector cells in helminth infection and allergic inflammation [1,2,3•,4•,5]. Basophils are rare circulating cells, accounting for less than 1% of total circulating granulocytes. Basophils, mast cells, and eosinophils arise from the same progenitor. Basophils and eosinophils complete their terminal differentiation in bone marrow. By contrast, mast cells migrate as immature cells from the bone marrow to the peripheral tissues, where they undergo their terminal differentiation [1,2]. Mast cells that complete their differentiation in the skin or in the intestine develop into connective tissue mast cells (CTMCs) and mucosal mast cells (MMCs), respectively. Circulating basophils share several features with tissue-resident mast cells. Both cell types constitutively express FcεR1 and contain basophilic granules in the cytoplasm, and upon cross-linking of FcεR1-bound IgE with multivalent antigens, immediately release various kinds of effector molecules such as histamine and lipid mediators, and Th2-associated cytokines such as IL-4, IL-5, and IL-13, causing immediate type hypersensitivity [1,2,3•,4•,5]. Eosinophils also express FcεR1 and induce allergic inflammation by production of chemical mediators when stimulated with cross-linking of FcεR1-bound IgE with antigen. Owing to scarcity of cell number, paucity of specific basophil markers, and their functional similarity to mast cells, basophils have been simply regarded as effector cells of the Th2 immune response [3•,4•,5].

IL-3 is a growth factor for basophils. Furthermore, IL-3 is required for optimal basophil IL-4 and IL-13 production. FcR common γ-chain (FcRγ) is a widely expressed adapter, which bears an immunoreceptor tyrosine-based activation motif (ITAM) [6]. This adapter protein is known to associate with various FcR including FcεR1. Recent study by Hida and colleagues demonstrated that basophils lacking FcRγ could proliferate normally but failed to produce IL-4 in response to IL-3, suggesting that FcRγ-mediated IL-3 signal is crucially involved in induction of IL-4 production by basophils [7]. Now it is well recognized that basophils strongly produce IL-4 and IL-13 when stimulated with cross-linking of FcεR1 and IL-3.

The effect of IL-3 is also found in IgE-independent basophil IL-4 production [5,8,9•]. Basophils express IL-18R and IL-33R and very strongly produce IL-4 and IL-13 when stimulated with IL-18 or IL-33 in the presence of IL-3 *in vitro* [8,9•]. Basophils also express Toll-like receptor (TLR)1, TLR2, TLR4, and TLR6 and produce Th2 cytokines in response to IL-3 plus corresponding TLR ligands[10]. Thus, there are at least two major activation pathways for basophil IL-4 production. One is the Ag/IgE complex-induced activation pathway responsible for 'acquired-type allergic inflammation' and the other is the IL-18, IL-33, or pathogen associated molecular pattern (PAMP)-induced activation pathway responsible for 'innate type allergic inflammation'. Here, I review the major function of basophils as effectors cells in the development of allergic inflammation and the recently found novel function of basophils as Th2 cell-inducing APC in allergy and helminth infection.

Development of basophils, mast cells and eosinophils

Blood circulating basophils are mature cells with a life span of about 60 h. Injection of IL-3 increases basophil generation in bone marrow, resulting in an increase in the number of circulating basophils. By contrast, mast cells in the peripheral tissue have the potential to proliferate in response to IL-3 and IL-9 *in situ*. Thus, intestinal helminth infection induces intestinal mast cell hyperplasia in an IL-3-dependent manner. A study of the development of mouse eosinophils, basophils, and mast cells has identified that granulocyte/monocyte progenitor (GMP) is a common progenitor of basophils, mast cells, and eosinophils [11]. Both basophil/mast cell precursors (BMCP) and eosinophil precursor (EoP) arise from GMP. Development from GMP to EoP and BMCP, and from BMCP to basophil precursors (BaP) and mast cell precursors (MCP), are regulated by the level and order of expression of transcription factors, C/EBPα, and, GATA-2 [11]. However, in the case of development of human granulocytes, common myeloid progenitor (CMP) develops into GMP and EoP, which then develop into basophils/mast cells and eosinophils, respectively [11].

The major function of basophils as effector cells

Although basophils and mast cells are regarded as important effector cells in allergic response by their potential to promptly produce chemical mediators and cytokines after FcεR1 cross-linkage [1,2,3•,4•,5], recent studies suggest that basophils also induce IgE-mediated chronic allergic inflammation and IgG1-mediated systemic anaphylactic shock [4•,12,13•]. Karasuyama and colleagues demonstrated that a single injection of multivalent antigen in the ear of mice passively sensitized with antigen-specific IgE, elicits immediate-phase, late-phase, and delayed onset of ear swelling characterized by infiltration with basophils and eosinophils (chronic allergic inflammation) [12]. They showed that mast cell-deficient mice only developed chronic allergic inflammation, while basophil-depleted mice failed to develop it, suggesting that basophils are responsible for inducing chronic allergic inflammation. Very recently, a study by Voehringer and colleagues has confirmed this observation by using basophil-deficient mice (*Mcp8Cre*), which constitutively lack more than 90% of basophils [14••]. Furthermore, they demonstrated that reconstitution of *Mcpt8Cre* mice with bone marrow basophils restored this IgE-mediated chronic allergic inflammation response [14••]. These results strongly indicate that basophils are required and sufficient to induce IgE-mediated chronic allergic inflammation by recruiting eosinophils [12,14••].

It is well documented that mast cells and IgE are crucially involved in the development of systemic anaphylaxis. However, interestingly, mice deficient for mast cells, IgE, or FcεR1α chain still develop systemic anaphylaxis, indicating involvement of an alternative pathway. FcRγ-deficient mice that lack the expression of FcεR1 and stimulatory FcγR do not develop systemic anaphylaxis, suggesting that IgG also plays a crucial role in induction of systemic anaphylaxis. Karasuyama and colleagues demonstrated that basophils and IgG1 contribute to certain type of mast cell-independent systemic anaphylaxis [13•]. They demonstrated that basophils released a large amount of platelet-activating fator (PAF) when stimulated with allergen-IgG1 immune complexes. Based on this result, they speculated that basophils induce systemic anaphylaxis through the release of PAF that is 30,000 times more potent than histamine [13•]. However, basophil-ablated *Mcpt8Cre* mice are shown to normally develop IgE or IgG1-dependent systemic anaphylaxis, suggesting the possibility that basophils play a minor role in an induction of systemic anaphylaxis [14••]. In a previous study, Finkelman and colleagues reported that macrophages play a major role in IgG-mediated systemic anaphylaxis through the release of PAF [15]. These results suggest that both basophils and macrophage contribute to IgG1-mediated systemic anaphylaxis. However, further research is needed to determine which cell contributes most strongly to this IgG-mediated anaphylaxis.

Th subset

Naïve $CD4^+$ T cells develop into Th1, Th2, Th17, and Treg cells, when they are given antigenic signals, co-stimulatory signals, and appropriate cytokine signals by APC and accessory cells [16]. IFN-γ, IL-12, and T-bet control development of Th1 cells, which are highly effective in clearance of intracellular pathogens by the production of IFN-γ [16,17]. IL-4 and GATA-3 control development of Th2 cells [16,18], which produce IL-4, IL-5, IL-6, IL-9, and IL-13. These Th2 cytokines are important for the development of allergic inflammation and clearance of helminth infections via the induction of IgE production, activation of mast cells, basophils, and eosinophils. Th17 cell subset is important for the development of autoimmune diseases and for the clearance of extracellular pathogens and fungi by producing IL-17 [19]. Differentiation of Th17 cells is induced by TGFβ and IL-6 in the mouse and by TGFβ and IL-6/IL-21 in the human. Treg cells are induced by TGFβ and are essential for immune tolerance and regulation of allergy and autoimmunity [20].

It is well recognized that DCs play a central role in initiation of activation and differentiation of Th subsets. DCs sense microbes through TLRs and mature to express co-stimulatory molecules CD80/86 and to produce the cytokines that provide the appropiate instructive signal for the development of Th1, Th17, and Treg cells [19–21]. Antigen-pulsed DC also induce the development of Th2 cells under the influence of IL-4 *in vitro* [16]. Furthermore, several reports indicate the presence of

other pathways for the differentiation of naïve $CD4^+$ T cells into Th2 cells [22–26]. DCs cannot produce IL-4, however DCs have the potential to induce Th2 cells via expression of the Notch ligand Jagged 1 and Jagged2 [22]. DCs also induce Th2 cells by expressing OX-40L after being stimulated with thymic stromal lymphopoetin (TSLP) [23]. Aluminum adjuvant induces Th2 cell differentiation, although the exact mechanism still remains uncertain [24]. In addition, M2 macrophages (also known as alternatively activated macrophages), as well as eosinophils and mast cells are also important for the development of Th2 cells [25,26]. Thus, it is important to determine which cell types help DCs to induce the development of Th2 cells.

Th2 development: basophils as accessory cells that produce early IL-4

Min *et al.* reported that naïve $CD4^+$ T cells stimulated with peptide-pulsed DCs could develop into Th2 cells when co-cultured with basophils from wild type mice but not from IL-4-deficient mice [27••]. As DCs and basophils are added to the same culture, it was initially interpreted that DC deliver antigenic-specific signal, and basophils provide IL-4 for the development of Th2 cells. In *in vivo* studies, mice deficient in interferon-regulatory factor 2 (IRF2) or Lyn have increased numbers of basophils and exhibit spontaneous Th2 differentiation under steady state conditions [28,29]. However, introduction of mutation in the gene encoding c-Kit inhibits this spontaneous Th2 differentiation by reducing the number of basophils [28]. Thus, basophils might be required for the development of naïve $CD4^+$ T cells into Th2 cells *in vivo*. Medzhitov and colleagues showed that basophils are important in initiation of the development of Th2 cells in response to the protease allergen, papain [30••,31]. At day 3 after subcutaneous papain injection, basophils enter and transiently reside in the T cell zones of the draining lymph nodes, where basophils are stimulated to produce IL-4 and/or TSLP, which promote Th2 differentiation *in vivo*. Basophils are also necessary for Th2 differentiation in the mice infected with *T. muris* [32]. Depletion of basophils with antibody against FcεR1 diminished the development of Th2 cells in both models of Th2 cell differentiation, suggesting that basophils are involved in Th2 cell differentiation by production of 'early IL-4' [31,32]. Furthermore, basophil production of IL-4 and IL-6 promotes the development of IL-10-producing $CD8^+$ T cells *in vivo* [33], suggesting that basophils play important roles for the functional differentiation of $CD4^+$ T cells and $CD8^+$ T cells.

Induction of Th2 cells by basophils pulsed with Ag/IgE complex

Basophils promptly produce IL-4 and IL-13 when they are stimulated with Ag/IgE complex or with IL-18 and/or IL-33 in the presence of IL-3 [5,8,9•,10]. Thus, if basophils express MHC class II and CD80/86, we could speculate that basophils also have the potential to induce the development of Th2 cells. Three groups independently demonstrated that basophils constitutively express MHC class II, as well as co-stimulatory molecules such as CD40, CD80, and CD86 [31,32,34]. These groups further demonstrated that basophils are potent APCs [31,32,34]. We have reported that basophils have the capacity to induce Th2 differentiation both *in vitro* and *in vivo* [34].

We prepared splenic basophils from mice inoculated with *S. venezuelensis*, as helminth infection markedly induces an increase in the number of basophils in the spleen and liver [35]. Basophils from infected mice have the capacity to strongly produce IL-4, IL-6, and IL-13 in medium alone, even without IL-3 [34]. Furthermore, they express MHC class II and CD80/86 and induce the development of OVA-specific naïve $CD4^+$ T cells into Th2 cells *in vitro* in the presence of OVA peptide, IL-2 and IL-3 without IL-4 (neutral culture condition) [34]. Thus, we initially regarded only those basophils derived from infected mice to be potent Th2 cell-inducing APC. However, we quickly learned that splenic basophils derived from naïve mice also produce IL-4, IL-6, and IL-13 in IL-3-containing medium [34]. Compared to the amount of cytokines produced by basophils from infected animals, the amount of cytokines produced by basophils from naïve mice is relatively low. Furthermore, they need the presence of IL-3 in the culture medium to produce these cytokine [7,34]. Nevertheless, splenic basophils from naïve mice express comparable levels of MHC class II and CD80/86 and have the capacity to induce the development of Th2 cells *in vitro* under neutral conditions. Thus, both types of basophils are potent APC that strongly induce Th2 cells *in vitro*.

We next tested whether bone marrow basophils also have the potential to induce the development of Th2 cells. We found that they express MHC class II, CD80, CD86, and CD62L, and take-up allergen such as OVA, and process them into small peptides [34]. Since they express FcεR1 abundantly, we speculated that they can take up a low dose of Ag/IgE complex, present Ag/MHC class II, and produce IL-4. Thus, we examined whether basophils become very potent Th2 cell-inducing APC, when Ag is provided as Ag/IgE complexes [34].

We prepared OVA-pulsed basophils by culturing basophils with DNP-OVA and anti-DNP IgE complexes. Then, we intravenously (iv) administered 0.25 or 0.5 million OVA-pulsed basophils to naïve mice. This treatment strongly induced OVA-specific Th2 cells in the spleen of naïve mice. By contrast, iv administration of OVA-pulsed DCs or mast cells failed to induce Th2 cells, although OVA-pulsed DCs induced IFN-γ producing Th1 cells. Thus, basophils are very potent Th2 cell-inducing APC even *in vivo*. We next tested whether

endogenous basophils are crucially involved in the development of Th2 cells *in vivo* by injecting DNP-OVA/anti-DNP IgE complexes into naïve mice. We found that a single iv administration of low dose DNP-OVA/anti-DNP IgE complexes into naïve mice rapidly and preferentially induced OVA-specific Th2 cells. This induction of OVA-specific Th2 by injection of Ag/IgE complex is strongly inhibited by depletion of basophils through injection of anti-FcεR1 antibody [34]. Furthermore, IL-3 treatment renders mice highly susceptible to Th2 cell-inducing action of IgE complex by increasing the number of basophils [34]. Taken together, these results strongly indicate that basophils are also potent Th2 cell-inducing APC *in vivo*.

Atopic individuals are characterized by increased numbers of basophils at sites of allergic inflammation [36–38]. Human mature basophils lack, or only weakly express, HLA-DR but have the potential to display increased HLA-DR expression when stimulated with IL-3 [34]. As levels of IL-3 and other factors may be increased at sites of allergic inflammation, we speculated that accumulated basophils might increase their HLA-DR expression and, thus, play a role as APC in peripheral tissues and augment Th2/IgE response.

To test our hypothesis, we injected Ag/IgE complexes into naïve mice, and, indeed, showed that this treatment efficiently induced Ag-specific Th2 cells *in vivo* [34]. Since naïve mice do not possess Ag-specific IgE, we speculate that this Ag/IgE complex-dependent induction of Ag-specific Th2 cell via basophils mainly account for the mechanism how repetitive exposure to allergen augment allergic inflammation. Once atopic individuals start to produce antigen-specific IgE, their concentration of Ag/Ag-specific IgE complexes may steadily increase. Subsequently, these complexes might be efficiently taken up by basophils via the FcεR1, resulting in these basophils becoming potent Th2 cell-inducing APC, which induce progressive allergic inflammation by enhancing Th2/IgE responses in these individuals. Furthermore, Ag/IgE stimulation upregulates the expression of FcεR1 on basophils [39,40]. Indeed, there is tight correlation between FcεR1 expression on basophils, and IgE levels in human peripheral blood [41], suggesting a positive feedback mechanism for IgE-mediated immediate type hypersensitivity. Furthermore, Denzel *et al.* reported that basophils could bind large amounts of antigens via FcεR1-bound IgE and produce IL-4 and IL-6, cytokines that are known to be required for antibody production in the spleen [42]. These basophils also activate Th2 type T cells, which help B cell proliferation and IgG1 production. Depletion of basophils decreased production of IgG1 [42]. Thus, Ag/IgE complexes and basophils play a crucial role in progression of allergic disease, and, therefore, antibody therapy against IgE or basophils might be an effective therapeutic means of treating persistent allergic disease.

Basophils as Th2 cell-inducing APC in allergy and helminth-infected hosts

Two groups revealed that basophils induce Th2 cells in the absence of DCs *in vivo* [31,32]. These studies suggest that basophils are involved in allergen-induced or helminth-induced Th2 responses by functioning as Th2 cell-inducing APC [31,32]. Artis and colleagues, by using MHC II^{CD11c} transgenic mice, where MHC class II expression is restricted to $CD11c^+$ DCs, demonstrated that these mice, when inoculated with *T. muris*, fail to develop Th2 responses or expel helminths [32]. They simultaneously demonstrated that this infection induced the development of Th1 cells, suggesting that $CD11c^+$ cells are required for the generation of Th1 cells. Then, they demonstrated that basophils are dominant Th2 cell-inducing APCs that express IL-4 and MHC class II. They proved this by the evidence that depletion of basophils *in vivo* reduced protective Th2 cell response to *T. muris* in wild type mice [32]. However, Min and colleagues have demonstrated that basophil depletion in *N. brasiliensis*-infected mice does not affect the development of Th2 cells, suggesting that basophils may not be essential for Th2 differentiation in mice infected with the murine hookworm, *N. brasiliensis* [43]. Nevertheless, this infection induces recruitment of basophils into the draining lymph nodes with similar kinetics as those in other models, suggesting that basophils are not required for protection against primary *N. brasiliensis* infection. However, interestingly, basophils are essential for protection against secondary *N. brasiliensis* infection, even in the absence of mast cells and $CD4^+$ T cells, which are both required for efficient worm expulsion during primary infection with *N. brasiliensis* [44]. A recent study by Voehringer and colleagues has demonstrated that *Mcpt8Cre* mice with constitutive and selective depletion of basophils, normally develop Th2 cells, a IgG1/IgE response, and eosinophilia upon infection with *N. brasiliensis* [14••]. However, they further demonstrated that basophils are essential for protection against secondary *N. brasiliensis* infection [14••,44]. These observations suggest a complex role for basophils in host defense against parasites, and also underline the complexity of regulation of acquired Th2 immunity by innate cells.

Medzhitov and colleagues also demonstrated that skin DCs are not required for mounting Th2 responses to papain. They previously reported that, like injection of the soluble antigens of *S. mansoni* eggs, papain injections rapidly induce recruitment of basophils to the lymph node [30••,31]. As this treatment simultaneously induces recruitment of DC, they initially considered that basophils function as accessory cells, and DC present Ag in the presence of basophil-derived IL-4. However, they

have demonstrated that skin DC are not required for the development of Th2 cells in draining lymph nodes [31]. They subcutaneously injected papain into the ear, where skin DCs capture antigens and present Ag-derived peptides to naïve T cells at draining lymph nodes. If skin DCs capture antigens and present this in the lymph node, rapid removal of these Ag-pulsed DCs by prompt excision of the injection site should inhibit Th2 response. However, this treatment failed to inhibit development of Th2 cells, suggesting that Ag captured by skin DC is not required for induction of papain-specific Th2 development. They demonstrated that soluble papain can directly enter lymph nodes from the injection site. Furthermore, selective depletion of $CD11c^+$ DCs did not inhibit Th2 development to papain, suggesting the presence of Th2-inducing APC other than DCs in the lymph nodes. Medzhitov and colleagues, as well as Artis and colleagues used CD11c-restricted diphteria toxin receptor mice, in which CD11c-expressing DC are efficiently depleted upon delivery of diphteria toxin [31,32]. They demonstrated that DC depletion only inhibited the development of Th1 cells without affecting the development of Th2 response. These results strongly indicate that other types of APC might be required for Th2 cytokine-dependent immune responses. Subsequently, they identified basophils as another type of Th2 cell-inducing APC, as this papain-induced Th2 cell differentiation could be blocked by the depletion of basophils by means of anti-FcεR1 antibody MAR-1 [31]. They have clearly shown that basophils can take up, process, and present soluble antigens. Furthermore, they demonstrated that basophils form immune synapses with T cells within 60 min of co-culture [31]. Finally, they demonstrated that adoptive transfer of OVA-pulsed basophils induced Th2 response in MHC class II-deficient mice.

The above-mentioned studies showed that basophils are potent APCs that preferentially induce Th2 cells both *in vitro* and *in vivo*. Mice deficient in the Src family tyrosine kinase, Lyn, have increased numbers of basophils, exhibit spontaneous Th2 differentiation, and produce IgE autoantibodies against various autoantigens, including dsDNA, that cause lupus-like nephritis in Lyn−/− mice [29]. Thus, basophils regulate not only allergic diseases and anti-helminth immunity but also autoimmune diseases.

Following studies

However, recent studies questioned the role of basophils as Th2 cell-inducing APCs. Tang *et al.* suggested that DCs and basophils cooperatively induce a Th2 cell response against papain [45]. Phythian-Adams *et al.* reported that depletion of $CD11c^+$ DCs during the priming stage of Th2 response against the helminth *Schistosoma mansoni* severely impaired Th2 induction, while basophil depletion using MAR-1 antibody had no measurable effect, underlining the important role of DCs in the development of Th2 response against helminth infection [46]. Furthermore, Hammad *et al.* demonstrated that Th2 responses against house dust mite are initiated by FcεR1-expressing inflammatory DCs, which is amplified by basophils [47]. Voehringer and colleagues examined basophil function using newly developed basophil-ablated mice. In this model they could not find the evidence that basophils are required for Th2 cell differentiation *in vivo* [14••]. They speculated that antibody-mediated depletion of basophils with MAR-1 (anti-FcεR1) may simultaneously deplete FcεR1 expressing inflammatory DCs [47]. They also suggested bystander effects of antibody-treatment, including activation of mast cells and macrophages, as well as the formation of immune complexes.

Conclusion

The data on the role of basophils as APCs are confusing but the issue is still interesting. As we reported previously [34], basophils pulsed with Ag/IgE complexes have potent Th2 cell-inducing APC activity both *in vitro* and *in vivo*. Basophils take-up intact OVA and present OVA-peptide in conjunction with MHC class II to OVA-peptide specific naïve $CD4^+$ T cells. Furthermore, when injected into naïve animal, these Ag-pulsed basophils also exhibited Th2 cell-inducing APC activity *in vivo*. However, their role as initiating cells of primary Th2 response might be minor. I suspect their important role for secondary Th2 response. Nevertheless, since basophils often show strong protective effect against helminth infection, they are still very interesting cells. To fully understand the role of basophils in Th2-mediated anti-helminth immunity, we definitively need further studies of these cells *in vivo*.

References and recommended reading

Papers of particular interest published within the period of review have been highlighted as:

- • of special interest
- •• of outstanding interest

1. Galli SJ, Tsai M, Piliponsky AM: **The development of allergic inflammation.** *Naure* 2008, **454**:445-454.

2. Galli SJ, Kalesnikoff J, Grimbaldeston MA, Piliponsky AM, Williams CM, Tsai M: **Mast cells as "tunable" effector and immunoregulatory cells: recent advances.** *Annu Rev Immunol* 2005, **23**:749-786.

3. • Min B: **Basophils: what they 'can do' versus what they 'actually do'.** *Nat Immunol* 2008, **9**:1333-1339.
This is the comprehensive review of basophils and highlight the importance of basophils in immune response, parasite infection, and allergic inflammation. Potential involvement of basophils in clinical setting is also discussed.

4. • Karasuyama H, Mukai K, Tsujimura Y, Obata K: **Newly discovered roles for basophils: a neglected minority gains new respect.** *Nat Rev Immunol* 2008, **9**:9-13.
This review summarized newly discovered novel roles for basophils in allergic response and clearly showed that the basophils are functionally distinct from mast cells.

5. Sullivan BM, Locksley RM: **Basophils: a nonredundant contributor to host immunity**. *Immunity* 2009, **30**:12-20.

6. Malbec O, Daëron M: **The mast cell IgG receptors and their roles in tissue inflammation**. *Immunol Rev* 2007, **217**:206-221.

7. Hida S, Yamasaki S, Sakamoto Y, Takamoto M, Obata K, Takai T, Karasuyama H, Sugane K, Saito T, Taki S: **Fc receptor gamma-chain, a constitutive component of the IL-3 receptor, is required for IL-3-induced IL-4 production in basophils**. *Nat Immunol* 2009, **10**:214-222.
This paper showed the first time the requirement of cross-talk between FcRγ and IL-3R for basophil IL-4 production. FcRγ constititutively associates with the common β chain of IL-3R and transduce IL-3 activation signal by recruiting Syk.

8. Yoshimoto T, Tsutsui H, Tominaga K, Hoshino K, Okamura H, Akira S, Paul WE, Nakanishi K: **IL-18, although antiallergic when administered with IL-12, stimulates IL-4 and histamine release by basophils**. *Proc Natl Acad Sci USA* 1999, **96**:13962-13966.

9. • Kondo Y, Yoshimoto T, Yasuda K, Futatsugi-Yumikura S, Morimoto M, Hayashi N, Hoshino T, Fujimoto J, Nakanishi K: **Administration of IL-33 induces airway hyperresponsiveness and goblet cell hyperplasia in the lungs in the absence of adaptive immune system**. *Int Immunol* 2008, **20**:791-800.
This paper showed the first time that basophils simultaneously express IL-18R and IL-33R and strongly produce IL-4 and IL-13 when stimulated with IL-18 and/or IL-33 together with IL-3. IL-33 administration induces IL-13-dependent airway hyperresponsiveness and goblet cell hyperplasia in SCID mice, suggesting the presence and involvement of IL-33-responsive innate cells in allergic inflammation.

10. Yoshimoto T, Nakanishi K: **Roles of IL-18 in basophils and mast cells**. *Allergol Int* 2006, **55**:105-113.

11. Arinobu Y, Iwasaki H, Akashi K: **Origin of basophils and mast cells**. *Allergol Int* 2009, **58**:21-28.

12. Mukai K, Matsuoka K, Taya C, Suzuki H, Yokozeki H, Nishioka K, Hirokawa K, Etori M, Yamashita M, Kubota T *et al.*: **Basophils play a critical role in the development of IgE-mediated chronic allergic inflammation independently of T cells and mast cells**. *Immunity* 2005, **23**:191-202.

13. • Tsujimura Y, Obata K, Mukai K, Shindou H, Yoshida M, Nishikado H, Kawano Y, Minegishi Y, Shimizu T, Karasuyama H: **Basophils play a pivotal role in immunoglobulin-G-mediated but not immunoglobulin-E-mediated systemic anaphylaxis**. *Immunity* 2008, **28**:581-589.
Basophils are dispensable for IgE-mediated anaphylactic shock but are indispensable for IgG1-mediated systemic anaphylaxis. Thus, basophils play a crucial role in IgG1-mediated anaphylaxis.

14. •• Ohnmacht C, Schwartz C, Panzer M, Schiedewitz I, Naumann R, Voehringer D: **Basophils orchestrate chronic allergic dermatitis and protective immunity against helminths**. *Immunity* 2010, **33**:364-374.
Newly discovered functions of basophils *in vivo* are mainly obtained from mice depleted of basophils by using monoclonal antibody specific for FcεR1 (MAR-1) or CD200R3(Ba103). The possibility that basophils and/or nonbasophils are activated by the Ab treatment has been concerned. Thus, establishement of basophil-deficient mice has been eagerly needed. These authors performed analysis of the functions of basophils *in vivo* and questioned the importance of basophils-induced systemic anaphylaxis and Th2 cell-inducing APC function of basophils *in vivo*.

15. Strait RT, Morris SC, Yang M, Qu XW, Finkelman FD: **Pathways of anaphylaxis in the mouse**. *J Allergy Clin Immunol* 2002, **109**:658-668.

16. Zhu J, Paul WE: **CD4 T cells: fates, functions, and faults**. *Blood* 2008, **112**:1557-1569.

17. Trinchieri G: **Interleukin-12 and the regulation of innate resistance and adaptive immunity**. *Nat Rev Immunol* 2003, **3**:133-146.

18. Seder RA, Paul WE: **Acquisition of lymphokine-producing phenotype by CD4+ T cells**. *Annu Rev Immunol* 1994, **12**:635-673.

19. Korn T, Bettelli E, Oukka M, Kuchroo K: **IL-17 and Th17 cells**. *Annu Rev Immunol* 2009, **27**:485-518.

20. Sakaguchi S, Yamaguchi T, Nomura T, Ono M: **Regulatory T cells and immune tolerance**. *Cell* 2008, **133**:775-787.

21. Takeda K, Kaisho T, Akira S: **Toll-like receptors**. *Annu Rev Immunol* 2003, **21**:335-376.

22. Amsen D, Antov A, Flavell RA: **The different faces of Notch in T-helper-cell differentiation**. *Nat Rev Immunol* 2009, **9**:116-124.

23. Ito T, Yang M, Wang YH, Lande R, Gregorio J, Perng OA, Qin XF, Liu YJ, Gilliet M: **TSLP-activated dendritic cells induce an inflammatory T helper type 2 cell response through OX40 ligand**. *J Exp Med* 2005, **202**:1213-1223.

24. Aimanianda V, Haensler J, Lacroix-Desmazes S, Kaveri SV, Bayry J: **Novel cellular and molecular mechanisms of induction of immune responses by aluminum adjuvants**. *Trends Pharmacol Sci* 2009, **30**:287-295.

25. Anderson CF, Mosser DM: **A novel phenotype for an activated macrophage: the type 2 activated macrophage**. *J Leukoc Biol* 2002, **72**:101-106.

26. Padigel UM, Hess JA, Lee JJ, Lok JB, Nolan TJ, Schad GA, Abraham D: **Eosinophils act as antigen-presenting cells to induce immunity to Strongyloides stercoratis in mice**. *J Infect Dis* 2007, **196**:1844-1851.

27. •• Oh K, Shen T, Le Gros G, Min B: **Induction of Th2 type immunity in a mouse system reveals a novel immunoregulatory role of basophils**. *Blood* 2007, **109**:2921-2927.
In general, naïve CD4+ T cells stimulated with Ag-pulsed DCs develop into Th1 cells. However, in this report, authors showed that basophils have the capacity to induce the development of naïve CD4+ T cells stimulated with Ag-pulsed DCs into Th2 cells by production of IL-4, which simultaneously inhibits development of Th1 cells.

28. Hida S, Tadachi M, Saito T, Taki S: **Negative control of basophil expansion by IRF-2 critical for the regulation of Th1/Th2 balance**. *Blood* 2005, **106**:2011-2017.

29. Charles N, Hardwick D, Daugas E, Illei GG, Rivera J: **Basophils and the T helper 2 environment can promote the development of lupus nephritis**. *Nat Med* 2010, **16**:701-707.
This paper showed that activation of basophils by complexes of autoantigen/autoantigen-reactive IgE causes their homing to lymph nodes, where they promote Th2 cell differentiation and enhance the production of autoantibodies, causing lupus-like nephritis in Lyn−/− mice.

30. •• Sokol CL, Barton GM, Farr AG, Medzhitov R: **A mechanism for the initiation of allergen-induced T helper type 2 responses**. *Nat Immunol* 2008, **9**:310-318.
This paper showed the mechanisms how innate immune cells senses protein allergens and induce the development of Th2 cells *in vivo*. Basophils were recruited to lymph node in response to subcutaneous injection of protease allergens (e.g. papain) or schstosome soluble egg antigens. Then, basophils were directly activated to produce IL-4 and TSLP, which in combination induce Th2 cell differentiation *in vivo*.

31. Sokol CL, Chu NQ, Yu S, Nish SA, Laufer TM, Medzhitov R: **Basophils function as antigen-presenting cells for an allergen-induced T helper type 2 response**. *Nat Immunol* 2009, **10**:713-720.

32. Perrigoue JG, Saenz SA, Siracusa MC, Allenspach EJ, Taylor BC, Giacomin PR, Nair MG, Du Y, Zaph C, van Rooijen N *et al.*: **MHC class II-dependent basophil-CD4$^+$ T cell interactions promote Th2 cytokine-dependent immunity**. *Nat Immunol* 2009, **10**:697-705.

33. Kim S, Shen T, Min B: **Basophils can directly present or cross-present antigen to CD8 lymphocytes and alter CD8 T cell differentiation into IL-10-producing phenotypes**. *J Immunol* 2009, **183**:3033-3039.

34. Yoshimoto T, Yasuda K, Tanaka H, Nakahira M, Imai Y, Fujimori Y, Nakanishi K: **Basophils contribute to Th2-IgE responses in vivo vai IL-4 production and presentation of peptide-MHC class II complexes to CD4$^+$ T cells**. *Nat Immunol* 2009, **10**:706-712.

35. Min B, Prout M, Hu-Li J, Zhu J, Jankovic D, Morgan ES, Urban JF Jr, Dvorak AM, Finkelman FD, LeGros G *et al.*: **Basophils produce IL-4 and accumulate in tissues after infection with a Th2-inducing parasite**. *J Exp Med* 2004, **200**:507-517.

36. Irani AM, Huang C, Xia HZ, Kepley C, Nafie A, Fouda ED, Craig S, Zweiman B, Schwartz LB: **Immunohistochemical detection of human basophils in late-phase skin reactions**. *J Allergy Clin Immunol* 1998, **101**:354-362.

37. Koshino T, Arai Y, Miyamoto Y, Sano Y, Itami M, Teshima S, Hirai K, Takaishi T, Ito K, Morita Y: **Airway basophil and mast cell density in patients with bronchial asthma: relationship to bronchial hyperresponsiveness**. *J Asthma* 1996, **33**:89-95.

38. Macfarlane AJ, Kon OM, Smith SJ, Zeibecoglou K, Khan LN, Barata LT, McEuen AR, Buckley MG, Walls AF, Meng Q *et al.*: **Basophils, eosinophils, and mast cells in atopic and nonatopic asthma and in late-phase allergic reactions in the lung and skin**. *J Allergy Clin Immunol* 2000, **105**:99-107.

39. Lantz CS, Yamaguchi M, Oettgen HC, Katona IM, Miyajima I, Kinet JP, Galli SJ: **IgE regulates mouse basophil Fc epsilon RI expression in vivo**. *J Immunol* 1997, **158**:2517-2521.

40. Yamaguchi M, Lantz CS, Oettgen HC, Katona IM, Fleming T, Miyajima I, Kinet JP, Galli SJ: **IgE enhances mouse mast cell Fc(epsilon)RI expression in vitro and in vivo: evidence for a novel amplification mechanism in IgE-dependent reactions**. *J Exp Med* 1997, **185**:663-672.

41. Saini SS, Klion AD, Holland SM, Hamilton RG, Bochner BS, Macglashan DW Jr: **The relationship between serum IgE and surface levels of FcepsilonR on human leukocytes in various diseases: correlation of expression with FcepsilonRI on basophils but not on monocytes or eosinophils**. *J Allergy Clin Immunol* 2000, **106**:514-520.

42. Denzel A, Maus UA, Rodriguez Gomez M, Moll C, Niedermeier M, Winter C, Maus R, Hollingshead S, Briles DE, Kunz-Schughart LA *et al.*: **Basophils enhance immunological memory responses**. *Nat Immunol* 2008, **9**:733-742.

43. Kim S, Prout M, Ramshaw H, Lopez AF, LeGros G, Min B: **Cutting edge: basophils are transiently recruited into the draining lymph nodes during helminth infection via IL-3, but infection-induced Th2 immunity can develop without basophil lymph node recruitment or IL-3**. *J Immunol* 2010, **184**:1143-1147.

44. Ohnmacht C, Voehringer D: **Basophils protect against reinfection with hookworms independently of mast cells and memory Th2 cells**. *J Immunol* 2010, **184**:344-350.

45. Tang H, Cao W, Kasturi SP, Ravindran R, Nakaya HI, Kundu K, Murthy N, Kepler TB, Malissen B, Pulendran B: **The T helper type 2 response to cysteine proteases requires dendritic cell-basophil cooperation via ROS-mediated signaling**. *Nat Immunol* 2010, **11**:608-617.

46. Phythian-Adams AT, Cook PC, Lundie RJ, Jones LH, Smith KA, Barr TA, Hochweller K, Anderton SM, Hämmerling GJ, Maizels RM *et al.*: **CD11c depletion severely disrupts Th2 induction and development in vivo**. *J Exp Med* 2010, **207**:2089-2096.

47. Hammad H, Plantinga M, Deswarte K, Pouliot P, Willart MA, Kool M, Muskens F: **Lambrecht BN:Inflammatory dendritic cells – not basophils – are necessary and sufficient for induction of Th2 immunity to inhaled house dust mite allergen**. *J Exp Med* 2010, **207**:2097-2111.

Acta Med. Okayama, 2010
Vol. 64, No. 4, pp. 233-241

Acta Medica Okayama
http://escholarship.lib.okayama-u.ac.jp/amo/

Original Article

Production of a Transgenic Mosquito Expressing Circumsporozoite Protein, a Malarial Protein, in the Salivary Gland of *Anopheles stephensi* (Diptera: Culicidae)

Hiroyuki Matsuoka*, Tsunetaka Ikezawa, and Makoto Hirai

Division of Medical Zoology, Jichi Medical University, Shimotsuke, Tochigi 329-0498, Japan

We are producing a transgenic mosquito, a flying syringe, to deliver a vaccine protein to human beings via the saliva the mosquito deposits in the skin while biting. The mosquito produces a vaccine protein in the salivary gland (SG) and deposits the protein into the host's skin when it takes the host's blood. We chose circumsporozoite protein (CSP), currently the most promising malaria vaccine candidate, to be expressed in the SG of *Anopheles stephensi*. To transform the mosquitoes, plasmid containing the CSP gene under the promoter of female SG-specific gene, as well as the green fluorescent protein (GFP) gene under the promoter of 3xP3 as a selection marker in the eyes, was injected into more than 400 eggs. As a result, five strains of GFP-expressing mosquitoes were established, and successful CSP expression in the SG was confirmed in one strain. The estimated amount of CSP in the SG of the strain was 40 ng per mosquito. We allowed the CSP-expressing mosquitoes to feed on mice to induce the production of anti-CSP antibody. However, the mice did not develop anti-CSP antibody even after transgenic mosquitoes had bitten them several times. We consider that CSP in the SG was not secreted properly into the saliva. Further techniques and trials are required in order to realize vaccine-delivering mosquitoes.

Key words: malaria, salivary gland, flying syringe, transgenic mosquito, vaccine

Mosquitoes are nuisance to human beings because they puncture the skin to obtain blood, which they use for their eggs. They deposit saliva in the skin when they take blood, and this causes itching [1]. They also transmit pathogens of diseases such as malaria, filarisis, yellow fever, and dengue fever. People have long tried to prevent mosquitoes from biting using mosquito nets [2] and repellents [3]. Moreover, people have attacked mosquitoes with insecticides to eliminate them [4, 5]. These struggles have continued not only in developing countries but also in advanced countries.

In the last 30 years, developments in genetic engineering have allowed us to add new genes to wild-type cells or to remove protein genes from them [6]. These technologies were used at first in bacteria or yeast to obtain recombinant proteins for experiments and to understand the mechanisms of protein molecules. More recently, many transgenic experiments have been applied to plants and animals, including vertebrates and insects. Recombinant-DNA-modified soybean, cotton, and corn are widely adopted and harvested around the world [7]. Transgenic mice, sheep, dogs, zebra fish, flies, silkworms, and so on have appeared in laboratories as well [8-12]. The objectives of genetic engineering in animals are

Received December 24, 2009; accepted April 27, 2010.
*Corresponding author. Phone:+81-285-58-7339; Fax:+81-285-44-6489
E-mail:hiroyuki@jichi.ac.jp (H. Matsuoka)

several: to understand cell differentiation, to find molecules responsible for causing specific diseases, and to speed up the production of meat, fish, and silk.

Some attempts have been made to create transgenic mosquitoes to make them non-vectors of germs or to reduce the germs' transmission ability [13, 14]. Anopheline mosquitoes are the primary targets for transgenes, because they transmit malaria parasites. Some laboratories, including ours, have succeeded in producing transgenic mosquitoes with lower levels of malaria parasites in the digestive tract after blood meals on malaria-infected animals [15, 16]. The goal of those attempts is to control disease transmission through genetic modification of the mosquitoes [17].

We here present a new attempt to produce a useful protein in the mosquito salivary gland (SG) by adding a new gene to a mosquito chromosome. When mosquitoes attach to the skin surface, they try to find blood vessels from which they can take blood. At that time, they first deposit their saliva in the skin [1]. Mosquito saliva contains many molecules, such as vasodilators, platelet inhibitors, an anesthetic substance, and so on [18]. These substances dilate the blood vessel, allowing the mosquito to insert its proboscis into the vessel. A mosquito can have a blood meal without the blood coagulating and without being noticed. On the other hand, humans develop anti-saliva protein antibodies after experiencing several mosquito bites [19, 20]. Our idea is to put a gene encoding a useful protein into a mosquito chromosome, causing it to make the useful protein in its saliva and to inject the protein, via the saliva, into animals or human beings upon blood feeding. We expect that the host would develop antibodies to the recombinant protein as a reaction. If these transgenic (TG) mosquitoes, whose saliva contains a vaccine protein against a disease, were spread in an area where people are suffering from the disease, people who are daily bitten by them would develop antibodies to the vaccine protein, ultimately vaccinating the community from the disease. In this situation, mosquitoes would play the role of vaccine deliverers [21].

In field conditions of malaria-endemic areas, for instance, nearly 100 mosquitoes bite an individual per night, but more than 50% of the mosquitoes are nulliparous females (non-oviposit females) [22]. Even in malaria-holoendemic areas, the percentage of mosquitoes infected with malaria parasites in the SG is less than 4% among collected Anopheline mosquitoes [23]. Indeed, it is important to reduce malaria-infective mosquitoes, but people in malaria-endemic areas are bitten by thousands of non-infective mosquitoes each year. These non-infective mosquitoes could work as vaccine distributors.

We discovered one molecule of a platelet inhibitor in the SG of a model mosquito, *Anopheles stephensi*, cloned the gene, and named it the Anopheline antiplatelet protein (AAPP) [24]. This molecule is expressed only in the female SG. We used the upper stream area of the AAPP gene (*aapp*) as a promoter for the vaccine protein. For the vaccine protein, we chose circumsporozoite protein (CSP) of the malaria parasite. This molecule has been studied as a malaria vaccine candidate [25, 26]. In a rodent malaria model, a monoclonal antibody to CSP neutralizes the infectivity of sporozoite, an infective form of malaria parasite from the mosquito [27], and a synthetic peptide induces sufficient antibodies to protect immunized mice from sporozoite challenge [28]. CSP is now thought to be a promising vaccine candidate molecule [29], and recombinant proteins composed of CSP are being evaluated in malaria-endemic areas [30]. Thus, we decided to produce a TG mosquito containing the promoter area of *aapp* followed by the CSP gene (*csp*). We expected that the TG mosquitoes would express CSP in the SG and inject the recombinant CSP (rCSP) into the skin of mice when the TG mosquitoes fed on them.

Materials and Methods

Mosquitoes, mice, and parasites. *Anopheles stephensi* SDA 500 strain was reared in our laboratory under conditions of 26℃ room temperature, 50–70% relative humidity, and light control of 14 h bright and 10 hours dark. Female BALB/c mice were purchased from SLC (Shizuoka, Japan). A rodent malaria parasite, *Plasmodium berghei* ANKA strain, was maintained by cyclical passage through BALB/c mice and *An. stephensi* mosquitoes.

Recombinant CSP of P. berghei (rPbCSP). The rPbCSP was expressed as His-tagged at the C-terminal by the baculovirus expression system, and purified with a nickel column (Qiagen, Hilden, Germany) as described elsewhere [31]. The rPbCSP is expressed with two molecular weight sizes, 70 and

82kDa [31]. When mice are immunized with rPbCSP three times, they become protected against parasite challenge (unpublished data). The protein concentration of rPbCSP was measured using a Bio-Rad Protein Assay Kit (Bio-Rad Laboratories, Hercules, CA, USA). Bovine serum immunoglobulin was used as a standard for the protein concentration.

Preparation of anti-CSP antibody. For anti-CSP antibody production, 0.5ml of rPbCSP solution (50μg/ml) and 0.5ml of alum, $Al(OH)_3$ (16mg/ml), were well mixed and 0.2ml was injected intraperitoneally into each of four BALB/c mice. Injection was done 3 times at intervals of 2 weeks. Anti-CSP antibody was monitored by ELISA, as shown below, and the mice were sacrificed to take their sera. The sera were used as the anti-CSP antibody.

Preparation of anti-saliva antibody. To prepare anti-saliva antibody, 4 female BALB/c mice were each bitten by 100 female mosquitoes every 2 weeks for a 10-week period (5 biting sessions). Development of an anti-saliva antibody in the mice was confirmed by ELISA as shown below, and sera were taken from the mice. The sera were used as the anti-saliva antibody.

Evaluation for antibody titer by ELISA. For the evaluation of anti-CSP antibody, 8 wells of a 96-well assay plate were coated with 100μl of rPbCSP (1μg/ml) in 0.05M carbonate buffer (pH9.6), and 8 wells were filled with 100μl of carbonate buffer without antigen. The plate was incubated at 4℃ overnight.

For the evaluation of anti-saliva antibody, 10 pairs of SG were collected from female mosquitoes, destroyed in 1.0ml of carbonate buffer by sonication (1 sec × 5 times), and centrifuged (8,000rpm for 3min). The supernatant was used as the SG antigen. Eight wells were each coated with 100μl of SG antigen.

Two microliters of blood was collected from the tail of each mouse 7 days after the injection of rPbCSP or mosquito biting. The blood was mixed with 0.8ml of phosphate-buffered saline containing 1% bovine serum albumin (BSA/PBS) and centrifuged at 8,000rpm for 3min. The supernatant was used as an 800-fold-diluted serum.

After the antigen solution was removed and washed twice, the wells of an ELISA plate were blocked with 150μl of 1% BSA/PBS for 30min. After removing the blocking solution, 100μl of the mouse serum diluted 800-fold was distributed into each of 2 antigen wells and 2 no-antigen wells and incubated for 2h. As the second antibody, rabbit anti-mouse IgG conjugated with horseradish peroxidase (HRP) (Bio-Rad Laboratories) diluted 3,000-fold was distributed into each of the same wells and incubated for 1h. After the plate was washed, the substrate solution, a mixture of 0.04% 2,2'-azino-bis(3-ethylbenzthiazoline-6-sulfonic acid) (ABTS) (Sigma-Aldrich, St. Louis, MO, USA), 0.05% H_2O_2 in 0.05M phosphate, and 0.1M citrate buffer (pH4.5) was added. After 20–60min, a green color appeared. The absorption was measured at a wavelength of 405 nm by a microplate reader, Spectra Max M5 (Molecular Devices, Tokyo, Japan). The mean absorbance of antigen wells minus the mean absorbance of no-antigen wells was taken as the OD value for the antigen.

Plasmid construction (Fig. 1). The anopheline anti-platelet protein gene (*aapp*) promoter region and its signal peptide coding region of *An. stephensi* [24] (1,746bp) were amplified with a primer pair of AAPP-F-*AscI* (5'-*GGCGCGCC*TTATAAGACGGAG CTCATTGTCGCTCGTC-3') and AAPP-R-*SmaI* (5'-*CCCGGG*CGGCCGTGCGGATACGATCAGCGC AAGGC-3'), then cloned into the pCR-BluntII TOPO vector (Invitrogen, Carlsbad, CA, USA) (plasmid a). The open reading frame of the *P. berghei CSP* gene without a signal peptide coding region or a C-terminal GPI-anchor domain coding region was amplified with a primer pair of PbCS-F-*SmaI* (5'-*CCCGGG*CAAAAT AAAATCATCCAAGCCCAAAGGAAC-3') and PbCS-R-*SpeI* (5'-*ACTAGT*TATTTATCCATTTTAC AAATTTCAGTATCAATATC-3'), then cloned into the vector (plasmid b). The 3' non-coding region of the AAPP gene was amplified with a primer pair of 3UTR-F-*SpeI* (5'-*ACTAGT*GAAACACACCGTTAA CGACAC-3') and 3UTR-R-*XbaI* (5'-*TCTAGA*TATTC AAAGGTCCACAAATGTC-3'), then cloned into the vector (plasmid c). The inserts of plasmids a, b, and c were serially cloned into the pENTR4 vector (Invitrogen) (donor vector).

The pBac [3xP3-EGFP] vector [11] and helper plasmid were kindly provided by Professor A. S. Raikhel (Department of Entomology, University of California at Riverside, USA). The pBac [3xP3-EGFP] vector was digested with *AscI*, blunted with a

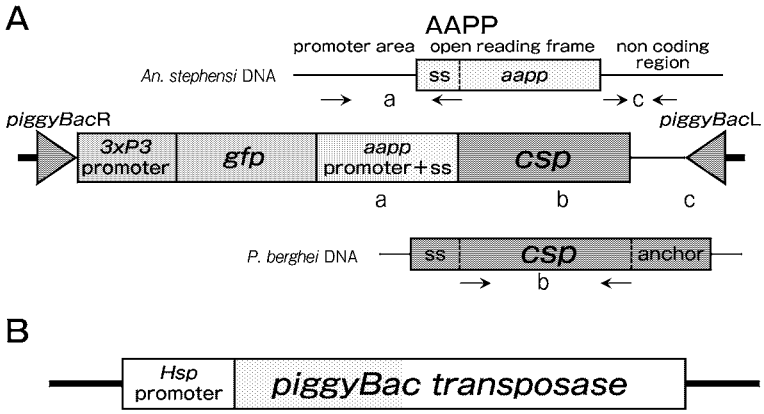

Fig. 1 Construction of plasmids injected into mosquito eggs. A, Two DNA fragments (a and c) were amplified from *A. stephensi* DNA. One DNA fragment (b) was amplified from *P. berghei* DNA. Three fragments were inserted in tandem in a plasmid vector downstream from the GFP gene. A promoter, 3*xP3*, was adopted to induce GFP expression in the eyes of mosquitoes as a selection marker. AAPP: anopheline anti-platelet protein. ss: signal sequence. CSP: circumsporozoite protein; B, To improve uptake of the recombinant plasmid in the mosquito chromosome, a piggyback helper plasmid was added when microinjection was performed. Hsp: heat-shock protein.

Klenow fragment, and dephosphorylated. The reading frame cassette A (Invitrogen) was then cloned into the vector (destination vector). The insert in the donor vector was cloned into the destination vector by Gateway LR clonase reaction (Invitrogen). The resulting plasmid (pBac-AAPP-PbCSP: Fig. 1A) was expected to drive CSP gene expression under the AAPP promoter. The pBac-AAPP-PbCSP plasmid was mixed with piggyBac helper (Fig. 1B) and microinjected into the eggs of *A. stephensi* as described below.

Microinjection of the plasmids into mosquito eggs. The mosquito microinjection was performed as described elsewhere [32]. In brief, blood-fed *An. stephensi* mosquitoes were allowed to lay eggs on a wet filter sheet 72–84 h after a blood meal. Eggs were laid and injected with plasmids within 90 min after oviposition. Injection was done by glass needles (Eppendorf, Hamburg, Germany) with a mixture of the pBac-AAPP-PbCSP (500 ng/μl) and piggyBac helper (300 ng/μl) in injection buffer (5 mM KCl, 0.1 mM Na_2HPO_4, pH 6.8). After injection, the eggs were placed in water and observed for hatching. Hatched larvae were analyzed on a fluorescence microscope at a wavelength of 490 nm to detect GFP expression.

Selection of transgenic mosquito. We selected GFP-expressing larvae and made them emerge (G0). One G0 adult female (or male) expressing GFP was put in a cage containing 5 wild-type males (or females). After mating and blood feeding, each female was allowed to lay eggs individually. Hatched larvae were observed under a fluorescence microscope, and GFP-expressing larvae were isolated as a G1 strain. Among the same batch of G1, mosquitoes were allowed to mate, feed, and lay eggs. Hatched larvae were observed and GFP-expressing larvae were isolated as the G2 of the strain.

Selection of CSP-expressing strain. Ten pairs of SG were collected from G2 female adults in each strain, destroyed in 1.0 ml of carbonate buffer by sonication (1 sec × 5 times), and centrifuged (8,000 rpm for 3 min). The supernatant was used as the SG antigen. Then, 100 μl of SG antigen was distributed into each of four wells of an ELISA plate and allowed to stand at 4℃ overnight. After blocking with 1% BSA/PBS, anti-CSP antibody diluted 800-fold was poured into 2 wells, and normal mouse serum diluted 800-fold was poured into 2 other wells. Incubation with the secondary antibody and the subsequent procedures were the same as described above.

Western blotting. Ten pairs of salivary glands were collected from both TG female mosquitoes and wild-type female mosquitoes. Samples were separated on a 10% SDS-polyacrylamide gel under reducing conditions (with 2% 2-mercaptoethanol), transferred onto a nitrocellulose (NC) sheet, and probed with mouse anti-CSP antibody diluted 800-fold. The NC sheet was next incubated with anti-mouse IgG conju-

gated with HRP (Bio-Rad Laboratories) diluted 3,000 fold, then reacted with substrate, SuperSignal West Pico Chemiluminescent Substrate (Thermo Fisher Scientific, Rockford, IL, USA). Positive bands were visualized in a Lumino Image Analyzer (LAS-1000) (Fuji Film, Tokyo, Japan).

Immunization of mice via biting by CSP-expressing transgenic mosquitoes. Two female BALB/c mice were bitten by each of 50 TG female mosquitoes every 2 weeks over a 10-week period (5 biting sessions). Two other mice were bitten by wild-type female mosquitoes under the same protocol. Two microliters of mouse blood was collected from the tail vein 7 days after the final mosquito biting. Antibody assay to CSP and SG was carried out by ELISA as described above.

Comparison of CSP contents in the SG before and after blood feeding. A pair of SG of the TG female mosquitoes before blood feeding was transferred in 0.5 ml of carbonate buffer, destroyed, and centrifuged as above. Another TG female mosquito was dissected within 10 min after full blood feeding, and a pair of SG were isolated and treated as described above. Each antigen solution was added to 4 wells, 100 μl per well. Anti-CSP antibody (800-fold) was reacted with the 2 wells and anti-saliva antibody (800-fold) was reacted with the other 2 wells. Incubation with the secondary antibody and the subsequent procedures were the same as described above. Eight SG samples in each group were tested.

Results and Discussion

Isolation of TG mosquito. We injected recombinant plasmid into 461 mosquito eggs, from which 109 larvae hatched and 103 adults emerged (G0 adults: 56 males and 47 females). We crossed these G0 males with wild-type females and allowed them to lay eggs. We also crossed G0 females with wild-type males and allowed them to lay eggs. GFP-expressing larvae were selected and allowed to emerge. From the G0 male group we established 1 strain, and from the G0 female group we established 4 strains. The rate of establishment for 5 strains from the 461 egg injections (1.1%) was reasonable compared with our previous experiments [16, 33] and with the results obtained by other groups [15, 32].

As shown in Fig. 2, larvae and adult TG mosquitoes expressed GFP in the eyes as expected, because the *3xP3* promoter works specifically in the eyes [11]. Unexpectedly, GFP was expressed not only in the eyes but also in the SG (Fig. 2C). 3xP3 marker protein is typically used for *Drosophila* (a small fly) transgenesis, and expression of a transgene in the SG of *Drosophila* has not been confirmed. Thus, this is the first observation that the *3xP3* promoter works in the SG of a mosquito. The SG cells may contain some transcriptional factors to attach to the *3xP3* promoter. GFP expression in female SG was observed among all strains of CS1 to CS5. In the SG, the highest expression of GFP was observed in the distal region of the lateral lobes in all SGs (Fig. 2C). In contrast, GFP was not always expressed in the median lobes. This tendency was similar to the results of a previous report [33].

Recombinant CSP expression in the SG. We expected that rCSP would be expressed in the SG of TG mosquitoes. ELISA was performed to confirm rCSP expression. Ten pairs of SG from each strain of TG female mosquitoes were collected and used as ELISA antigens. Only one of the 5 strains (CS2) showed strong reactivity against anti-CSP antibody (Fig. 3). This means that the *3x3P* promoter worked in all 5 strains, but that the *aapp* promoter worked only in strain CS2. The exact reason for this is unknown, but may be related to the insertion site in the mosquito chromosome. The insertion site may allow the *3xP3* promoter, but not the *aapp* promoter, to work. A possible explanation for this is that some of the transcriptional factors that attach to the *aapp* promoter to start AAPP expression react mostly with the intrinsic *aapp* promoter. The inserted *aapp* promoter cannot react with these factors, and thus rCSP may be expressed in only small amounts.

Western blotting analysis and estimation of rCSP expression. Western blotting was performed with 10 pairs of SG dissected from transgenic mosquitoes of the CS2 strain. A band of 38 kDa reacted with anti-CSP in the TG mosquito lane (Fig. 4). The molecular size was as we expected for rCSP. This indicates that we succeeded in producing a foreign protein of rCSP in the mosquito SG. A comparison of the density of the 38 kDa band with those of the positive control bands of a series of different amounts of rPbCSP revealed that the amount of rCSP in the CS2 lane was equivalent (in reactivity

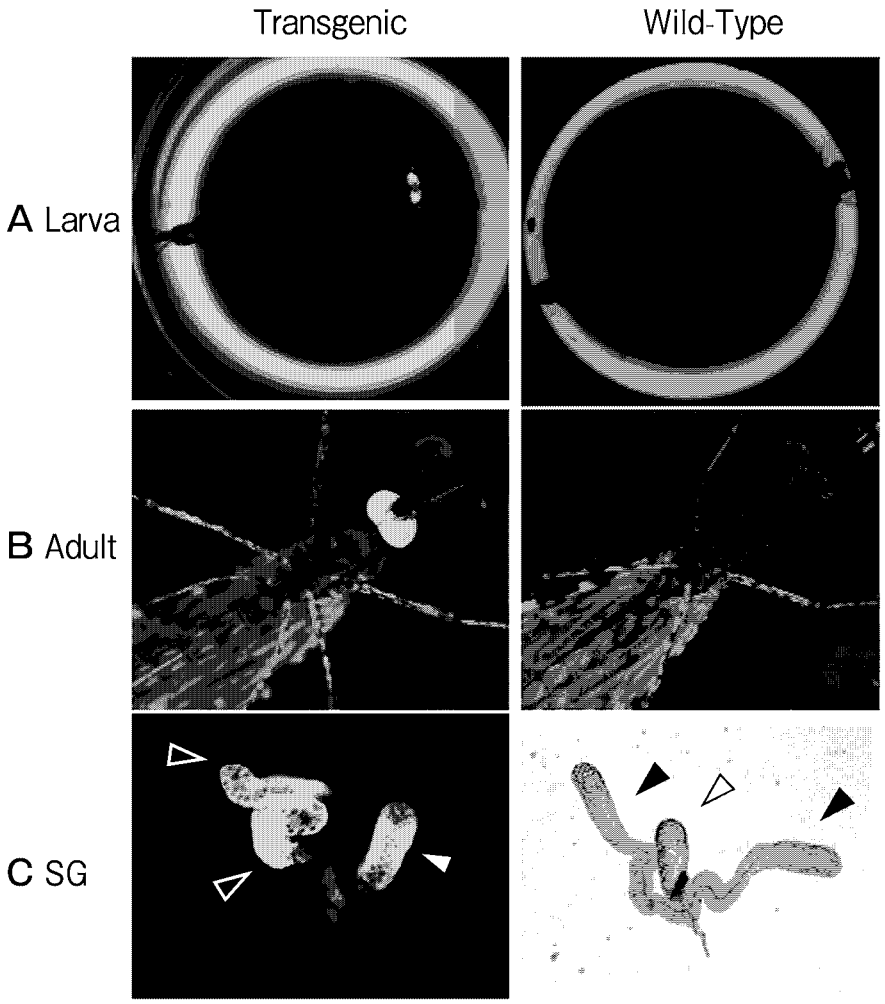

Fig. 2 Transgenic mosquito of *A. stephensi* expressing GFP. **A**, Larvae expressing GFP in the eyes. Since each larva was placed into its own wells of a 96-well plate, auto-fluorescence appeared from the well edge; **B**, Adult female expressing GFP in the eyes; **C**, Unexpectedly, GFP was expressed in the SG of transgenic mosquitoes. As a reference, the SG of a wild-type mosquito was taken at the phase condition. Arrow heads (▶) show the lateral lobes of SG, and the other arrow heads (▷) show the median lobes of SG. No GFP expression was observed in the SG of wild-type mosquitoes.

with the anti-CSP antibody) to 400ng rPbCSP. This, in turn, indicated that approximately 40ng of rCSP was expressed in one pair of SG in the TG mosquito.

Besides the 38kDa band, some other faint bands appeared in the CS2 lane. The molecular sizes of these bands were 26, 48, 64, and 80kDa. Even in the reducing conditions (with 2% 2-mercaptoethanol), some intermolecular re-binding may have occurred. There is another possibility that rCSP binds to some molecules of the SG components such as ubiquitins, proteosome-associated cofactors [34].

Anti-CSP antibody in mice bitten by TG mosquitoes. Two Female BALB/c mice were each bitten by 50 TG female mosquitoes of the CS2 strain every 2 weeks over a 10-week period. The mice developed anti-SG antibody but did not develop anti-CSP antibody (Fig. 5). In our prediction, 20% of rCSP (about 8ng of rCSP per mosquito) in the SG should be injected into a mouse during a single blood feeding. In each blood feeding, a mouse received 50 TG mosquito bites and received a total of 400ng of rCSP in the skin. As these blood feedings were conducted 5 times, each mouse was injected with 2,000ng of rCSP. From these injections, the mice

should have developed anti-CSP antibody in the serum. However, no antibody against rPbCSP was detected in the mice. Only anti-SG antibody was detected in the mouse serum. In our experience, 2 injections each of 1,000 ng rPbCSP are sufficient to develop anti-rPbCSP in mice (unpublished observation). Thus, we consider the possibility that rCSP was not secreted as we had expected in the saliva of the TG mosquito and thus was not injected into the skin during blood feeding.

Comparison of CSP contents in the SG before and after blood feeding. We performed ELISA with antigens of the SG before and after blood feeding. The amount of rCSP in the SG after blood feeding did not decrease, although the amount of total saliva protein did decrease (Fig. 6). This indicates that the TG mosquitoes consume a lot of saliva during blood feeding and that the saliva does not contain rCSP.

We used the *aapp* promoter for rCSP expression

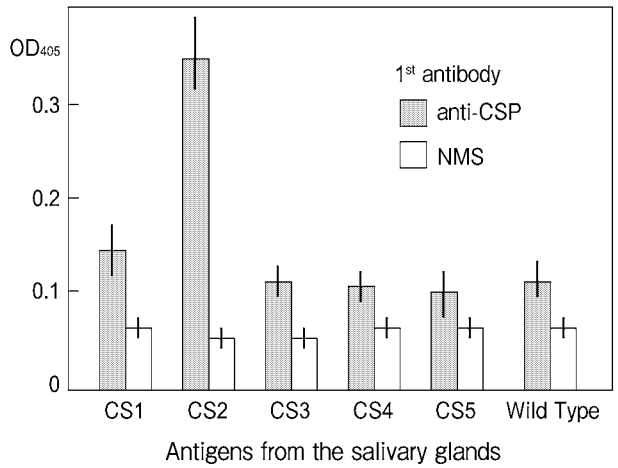

Fig. 3 Evaluation of CSP expression in SG among 5 mosquito strains. SG was taken from the 5 strains and tested as an antigen. Anti-CSP was used as the first antibody. SG from the CS2 strain reacted highly to anti-CSP. NMS (normal mouse serum) was used as a control antibody. The test was conducted 3 times.

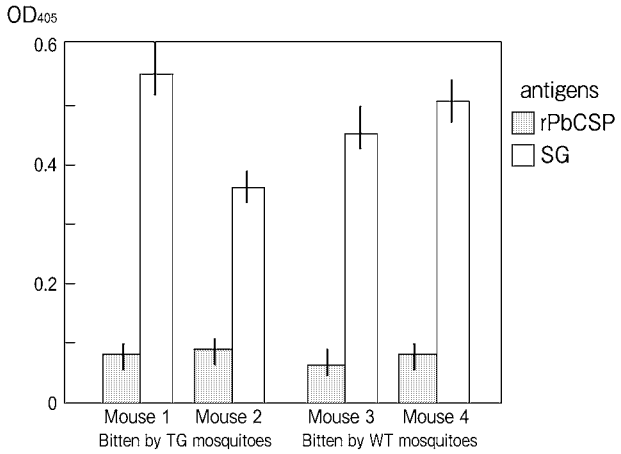

Fig. 5 Anti-CSP antibody and anti-saliva antibody evaluated by ELISA. Mice 1 and 2, which were bitten by TG mosquitoes of the CS2 strain, did not develop anti-CSP antibody. All 4 mice developed anti-saliva antibody. The test was conducted 3 times.

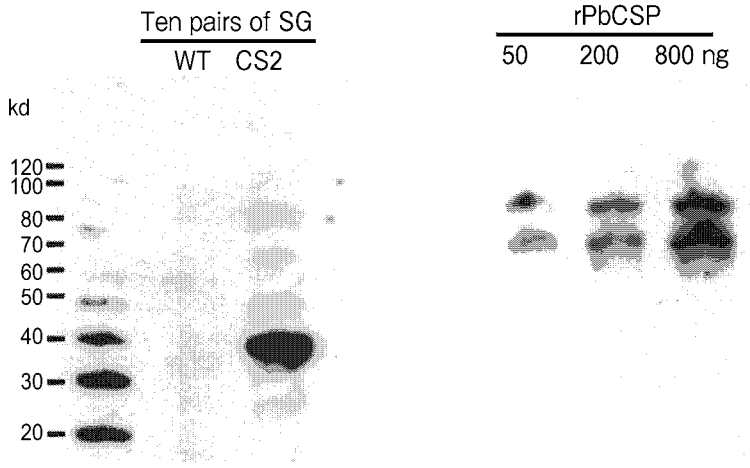

Fig. 4 Western blotting analysis of CS2 strain salivary glands. A 38 kDa band appeared after the reaction with anti-CSP antibody. The left lane contains molecular weight markers. Series of rPbCSP (70 kDa and 82 kDa) with different amounts were run on the same gel in the right 3 lanes.

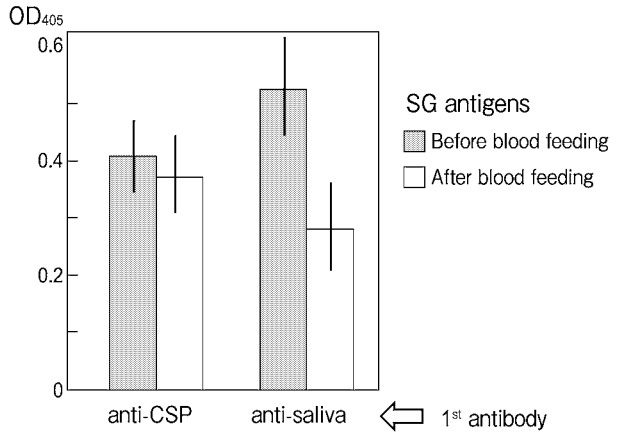

Fig. 6 Comparison of CSP contents in the SG before and after blood feeding. Both SG antigens (n = 8) were filled in the ELISA plate. The reactivity of anti-CSP to both SGs was similar, whereas the reactivity of anti-saliva to the SGs after blood feeding was significantly reduced ($p < 0.05$).

because AAPP was confirmed to be secreted in the saliva and injected into the skin during blood feeding [24]. However, we obtained the disappointing result that the TG mosquito did not properly release the foreign protein into the mouse skin. One possible explanation is that rCSP may have been captured by some components of the SG cells, such as ubiquitins [35]. As shown in Fig. 4, rCSP was expressed as some larger molecules in Western blot analysis. This figure suggests the possibility of "captured rCSP" in the SG. According to this hypothesis, rCSP cannot be secreted in the saliva because of its molecular characteristics, even if it has a secretion signal. We are preparing a new construct using the *aapp* promoter and *aapp* secretion signal with other foreign protein genes to test this hypothesis.

In summary, we presented a transgenic mosquito expressing a foreign protein in the SG. The expressed protein was rCSP, a promising malaria vaccine candidate protein. The amount of rCSP in one pair of SG was estimated to be 40ng. If 20% of rCSP in the SG is injected into a mouse during a single blood feeding band there are 50 mosquito bites on the mouse, 8 × 50ng of CSP should be injected and anti-CSP antibody should be developed in the mouse after several episodes of blood feeding. Since we did not succeed in preparing such a TG mosquito, we will develop new constructs for producing alternative TG mosquitoes.

Acknowledgments. This work was supported by a grant from the Bill & Melinda Gates Foundation through the Grand Challenges Exploration Initiative to HM as well as by a grant-in-aid from the Japanese Ministry of Education, Culture, Sports, Science, and Technology (16590344 to HM). Some items of the experimental apparatus were subsidized by JKA through its promotional funds from Keirin Racing.

References

1. Clements AN: The adult salivary glands and their secretions; in The Biology of Mosquitoes, Chapman & Hall, London (1992) pp 251-262.
2. Baume CA and Marin MC: Intra-household mosquito net use in Ethiopia, Ghana, Mali, Nigeria, Senegal, and Zambia: Are nets being used? Who in the household uses them? Am J Trop Med Hyg (2007) 77: 963-971.
3. Fradin MS and Day JF: Comparative efficacy of insect repellents against mosquito bites. N Engl J Med (2002) 347: 13-18.
4. Vine JM: Malaria control with DDT on a national scale—Greece, 1946. Proc Roy Soc Med (1947) 40: 841-848.
5. Hemingway J, Field L and Vontas J: An overvew of insecticide resistance. Science (2002) 298: 96-97.
6. Sambrook J, Fritsch EF and Maniatis T: Molecular Cloning: A Laboratory Manual. 2nd Ed, Cold Spring Harbor Laboratory Press, New York (1989) vol. 1-3.
7. Miller HI and Carter CA: Genetically engineered wheat, redux. Trend Biotech (2010) 28: 1-2.
8. Glaser S, Anastassiadis K and Stewart AF: Current issues in mouse genome engineering. Nat Genet (2005) 37: 1187-1193.
9 Lee BC, Kim MK, Jang G, Oh HJ, Yada F, Kim HJ, Shamin MH, Kim JJ, Kang SK, Schatten G and Hwang WS: Dogs cloned from adult somatic cells. Nature (2005) 436: 641-642.
10. Lieschke GJ and Currie PD: Animal models of human disease: zebrafish swim into view. Nat Rev Genetics (2007) 8: 353-367.
11. Horn C, Jaunich B and Wimmer EA: Highly sensitive, fluorescent transformation marker for *Drosophila transgenesis*. Dev Genes Evol (2000) 210: 623-629.
12. Goldsmith MR, Shimada T and Abe H: The genetics and genomics of the silkworm, *Bobyx mori*. Ann Rev Entomol (2004) 50: 71-100.
13. Alphey L, Beard CB, Billingsley P, Coetzee M, Crisanti A, Curtis C, Eggleston P, Godfray C, Hemingway J, Jacobs-Lorena M, James AA, Kafatos FC, Mukwaya LG, Paton M, Powell JR, Schneider W, Scott TW, Sina B, Sinden R, Sinkins S, Spielman A, Toure Y and Collins FH: Malaria control with genetically manipulated insect vectors. Science (2002) 298: 119-121.
14. Nirmala X and James AA: Engineering Plasmodium-refractory phenotypes in mosquitoes. Trends Parasitol (2003) 19: 384-387.
15. Ito J, Ghosh A, Moreira LA, Wimmer EA and Jacobs-Lorena M: Transgenic anopheline mosquitoes impaired in transmission of a malaria parasite. Nature (2002) 417: 452-455.
16. Yoshida S, Shimada Y, Kondoh D, Kouzuma Y, Ghosh AK, Jacobs-Lorena M and Sinden RE: Hemolytic C-type lectin CEL-III from sea cucumber expressed in transgenic mosquitoes impairs malaria parasite development. PLoS Pathogens (2007) 3: 1962-1970.
17. James AA: Control of disease transmission through genetic modification of mosquitoes; in Insect Transgenesis, Handler AM and James AA eds, CRC Press, Roca Raton, Florida (2000) pp 319-

333.
18. James AA: Molecular and biochemical analyses of the salivary glands of vector mosquitoes. Bull Inst Pasteur (1994) 92: 133-150.
19. Penneys NS, Nayar JK, Bernstein H, Knight JW and Leonardi C: Mosquito salivary gland antigens identified by circulating human antibodies. Arch Dermatol (1989) 125: 219-222.
20. Matsuoka H, Matsubara H, Waidhet P, Hashimoto T, Ishii A, Sato Y, Ando K and Chinzei Y: Depletion of salivary gland proteins in *Anopheles stephensi* (Diptera: Culicidae) on blood feeding, and induction of antibody to the proteins in mice being fed. Med Ent Zool (1997) 48: 211-218.
21. Crampton JM, Stowell SL, Karras M and Sinden RE: Model systems to evaluate the use of transgenic haematophagous insects to deliver protective vaccines. Parassitologia (1999) 41: 473-477.
22. Harada M, Ikeshoji T and Suguri S: Comparative study of the effect of using insecticide-impregnated bed nets and indoor residual spraying on malaria control in the Solomon Islands; in Malaria Research in The Solomon Islands, Ishii A, Nihei N and Sasa M eds, Inter Group Corporation, Tokyo (1998) pp 120-125.
23. Molineaux L and Gramiccia: The Garki Project - Research on the epidemiology and control of malaria in the Sudan savanna of West Africa. The World Health Organization, Geneva (1980) pp 53-108.
24. Yoshida S, Sudo T, Niimi M, Tao L, Sun B, Kambayashi J, Watanabe H, Luo E and Matsuoka H: Inhibition of collagen-induced platelet aggregation by anopheline antiplatelet protein, a saliva protein from a malaria vector mosquito. Blood (2008) 111: 2007-2014.
25. Nardin EH, Nussenzweig V, Nussenzweig R, Collins WE, Harinasta KT, Tapchaisri P and Chomcharn Y: Cirumsporozoite proteins of human malaria parasites *Plasmodium falciparum* and *Plasmodium vivax*. J Exp Med (1982) 156: 20-30.
26. Dame JB, Williams JL, McCutchan TF, Weber JL, Wirtz RA, Hockmeyer WT, Maloy WL, Haynes JD, Schneider I, Roberts D, Sanders GS, Reddy EP, Diggs CL and Miller LH: Structure of the gene encoding the immunodominant surface antigen on the sporozoite of the human malaria parasite *Plasmodium falciparum*. Science (1984) 225: 593-599.
27. Eichinger DJ, Arnot DE, Tam JP, Nussenzweig V and Enea V: Circumsporozoite protein of *P. berghei*: Gene cloning and identification of the immunodominant epitopes. Mol Cell Biol (1986) 6: 3965-3972.
28. Zavala F, Tam JP, Barr PJ, Romero PJ, Ley V, Nussenzweig RS and Nussenzweig V: Synthetic peptide vaccine confers protection against murine malaria. J Exp Med (1987) 166: 1591-1596.
29. Stoute JA, Slaoui M, Heppner DG, Momin P, Kester KE, Desmons P, Wellde BT, Garcon N, Krzych U and Marchand M: A preliminary evaluation of a recombinant circumsporozoite protein vaccine against *Plasmodium falciparum* malaria. N Engl J Med (1997) 336: 86-91.
30. Bejon P, Lusingu J, Olotu A, Leach A, Lievens M, Vekemans J, Mshamu S, Lang T, Gould J, Dubois MC, Demoitié MA, Stallaert JF, Vansadia P, Carter T, Njuguna P, Awuondo KO, Malabeja A, Abdul O, Gesase S, Mturi N, Drakeley CJ, Savarese B, Villafana T, Ballou WR, Cohen J, Riley EM, Lemnge MM, Marsh K and von Seidlein L: Efficacy of RTS, S/AS01E vaccine against malaria in children 5 to 17 months of age. New Engl J Med (2008) 359: 2521-2532.
31. Yoshida S, Kondoh D, Arai E, Matsuoka H, Seki C, Tanaka T, Okada M and Ishii A: Baculovirus virions displaying *Plasmodium berghei* circumsporozoite protein protect mice against malaria sporozoite infection. Virol (2003) 316: 161-170.
32. Catteruccia F, Nolan T, Loukeris TG, Blass C, Savakis C, Kafatos FC and Crisanti A: Stable germline transformation of the malaria mosquito *Anopheles stephensi*. Nature (2000) 405: 959-962.
33. Yoshida S and Watanabe H: Robust salivary gland-specific transgene expression in *Anopheles stephensi* mosquito. Insect Mol Biol (2006) 15: 403-410.
34. Hochstrasser H: Ubiquitin, proteasomes, and the regulation of intracellular protein degradation. Curr Opin Cell Biol (1995) 7: 215-223.
35. Fallon AM and Witthuhn BA: Proteasome activity in a naïve mosquito cell line infected *Walbachia pipientis* wAlbB. In Vitro Cell Dev Biol (2009) 45: 460-466.

European Journal of Immunology

Involvement of CD8$^+$ T cells in protective immunity against murine blood-stage infection with *Plasmodium yoelii* 17XL strain

Takashi Imai[1,2], Jianying Shen[1], Bin Chou[1], Xuefeng Duan[1], Liping Tu[1], Kohhei Tetsutani[1], Chikako Moriya[1], Hidekazu Ishida[1], Shinjiro Hamano[1], Chikako Shimokawa[1], Hajime Hisaeda[1] and Kunisuke Himeno[1]

[1] Department of Microbiology and Immunology, Graduate School of Medical Sciences, Kyushu University, Fukuoka, Japan
[2] Laboratory for Immunochaperones, RIKEN Research Center for Allergy and Immunology, Kanagawa, Japan

When developing malaria vaccines, the most crucial step is to elucidate the mechanisms involved in protective immunity against the parasites. We found that CD8$^+$ T cells contribute to protective immunity against infection with blood-stage parasites of *Plasmodium yoelii*. Infection of C57BL/6 mice with *P. yoelii* 17XL was lethal, while all mice infected with a low-virulence strain of the parasite 17XNL acquired complete resistance against re-infection with *P. yoelii* 17XL. However, the host mice transferred with CD8$^+$ T cells from mice primed only with *P. yoelii* 17XNL failed to acquire protective immunity. On the other hand, the irradiated host mice were completely resistant to *P. yoelii* 17XL infection, showing no grade of parasitemia when adoptively transferred with CD8$^+$ T cells from immune mice that survived infection with both *P. yoelii* XNL and, subsequently, *P. yoelii* 17XL. These protective CD8$^+$ T cells from immune WT mice had the potential to generate IFN-γ, perforin (PFN) and granzyme B. When mice deficient in IFN-γ were used as donor mice for CD8$^+$ T cells, protective immunity in the host mice was fully abrogated, and the immunity was profoundly attenuated in PFN-deficient mice. Thus, CD8$^+$ T cells producing IFN-γ and PFN appear to be involved in protective immunity against infection with blood-stage malaria.

Key words: CD8 T cells · Immune responses · Infectious diseases · Malaria · Memory cells

Supporting Information available online

Introduction

Malaria is one of the main global infectious diseases, and results in 300–500 million clinical cases and one million deaths annually, mostly among young children in sub-Saharan Africa (http://rbm.who.int/wmr2005/[1]). The development of resistance to drugs in parasites and vectors poses one of the greatest threats to malaria control and has been linked to recent increases in malaria morbidity and mortality, so vaccine development is urgently required. To achieve this purpose, it is essential to elucidate the detailed protective mechanisms of the hosts against infection.

Correspondence: Dr. Takashi Imai
e-mail: t-imai@rcai.riken.jp

Antibodies and T cells play crucial roles in protective immunity against malaria parasites. Antibodies specific for merozoites prevent invasion of those parasites into RBC [2–5]. These antibodies, attached to the parasites or parasitized RBC, lyse the parasites and RBC in a complement-dependent manner. Another function of these antibodies is to mediate phagocytosis and digestion by monocytes/macrophages [3–5]. $CD4^+$ T cells act as Th cells for B-cell differentiation and antibody production; on the other hand, Th cells activate phagocytosing macrophages and kill the parasites. Thus, $CD4^+$ T cells should play key roles in protective immunity against both liver and blood-stage malaria. Strangely, however, clinical vaccine trials using antigenic peptide for malaria have resulted in failure in some cases [6], despite the fact that activation of $CD4^+$ T cells and antibody production have been efficiently induced in vaccine trials.

$CD8^+$ T cells have been proposed to be essential for protective immunity against liver-stage malaria [2–5]. On the other hand, several studies have concluded that $CD8^+$ T cells do not contribute to protective immunity against blood-stage parasites, mainly because of the absence of MHC class I molecules on infected erythrocytes, by which antigens are presented to $CD8^+$ T cells [7–10]. For example, Vimetz *et al.* have reported that adoptive transfer of $CD8^+$ T cells from immune animals does not confer protective immunity to blood-stage infection in the host [7]. However, some studies have stressed the existence of $CD8^+$ T cells specific for blood-stage malaria parasites. First, $CD8^+$ T-cell clones that proliferate and produce IFN-γ in response to blood-stage malarial antigens in an HLA-restricted manner are generated in patients who live in a malaria-endemic area [11]. Second, experimental infections of non-immune volunteers with an ultra-low dose of infected RBC induce immunity to subsequent challenge in the absence of detectable antibody responses. Those who acquire immunity show proliferative responses in $CD8^+$ T cells [12].

There are few studies showing that $CD8^+$ T cells protect against blood-stage parasites. However, there are some reports in murine models that $CD8^+$ T cells contribute to the pathology of experimental cerebral malaria. Mice that are depleted in, or do not have, $CD8^+$ T cells, are protected against experimental cerebral malaria [13]. $CD8^+$ T cells might contribute *via* perforin (PFN)-dependent destruction of cerebral microvasculor endothelial cells [14]. These malaria Ag-specific $CD8^+$ T cells are induced by cross-presentation from dendritic cells [15]. In the present study, we evaluated the contribution of $CD8^+$ T cells in immunity against blood-stage parasites.

Results

$CD8^+$ T cells from *Plasmodium yoelii* 17XNL-recovered mice fail to transfer protection against PyL

We infected C57BL/6 mice with the blood-stage form of the rodent malaria parasite *P. yoelii* 17X, which has two substrains. One substrain, PyL, is highly virulent in mice and causes lethal infection; the other, PyNL, causes a self-limiting, non-lethal infection [16]. Mice infected with 25 000 PyNL-parasitized RBC (PyNL-pRBC) spontaneously recovered within 4 wk of infection (data not shown). Mice that recovered from infection with PyNL (PyNL-recovered mice) were then infected with PyL. These mice were highly resistant to the lethal infection and allowed no parasite growth, while control mice showed rapid parasite growth and died within 10 days (Fig. 1A). Thus, infection with PyNL functions as a live vaccination against lethal infection with PyL. To examine the involvement of $CD8^+$ T cells in protective immunity to blood-stage infection with PyL, we injected PyNL-recovered mice with anti-CD8 mAb to deplete $CD8^+$ T cells prior to infection with PyL. However, depletion of $CD8^+$ T cells, as well as $CD4^+$ T cells, did not attenuate protection in PyNL-recovered mice (data not shown). We next performed adoptive transfer experiments. $CD8^+$ T cells purified from PyNL-recovered mice were transferred to the syngeneic recipient mice. In order to exclude the influence of host lymphocytes, we irradiated the recipients with 5.5 Gy of γ radiation. One week after cell transfer, these mice were infected with PyL. These recipient mice failed to control infection with PyL, similar to those transferred with $CD8^+$ T cells from uninfected control mice (Fig. 1B). These results were very similar to those of previous studies [6–9], which indicates that $CD8^+$ T cells do not contribute to protection against blood-stage malaria parasites.

$CD8^+$ T cells from highly immunized mice transfer protection against PyL

PyNL-recovered mice showed sterile immunity against infection with PyL. However, $CD8^+$ T cells from these mice did not transfer protection to the recipient mice. Several factors, such as presence or absence of antibodies in the circulation, might account for this discrepancy. Among these factors, we speculate that $CD8^+$ T cells

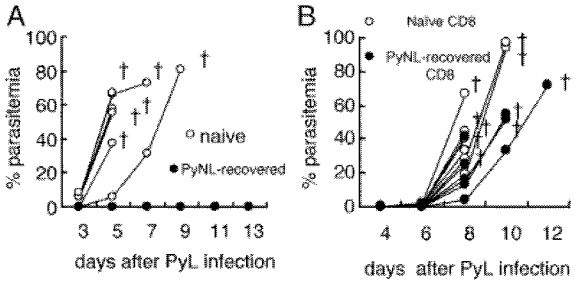

Figure 1. $CD8^+$ T cells from PyNL-recovered mice failed to transfer protection against PyL. (A) The kinetics of parasitemia in PyNL-recovered (closed circles) or naive (open circles) mice were monitored after infection with 25 000 PyL-pRBC. (B) $CD8^+$ T cells (8×10^6) purified from PyNL-recovered (closed circles) or naive (open circles) mice were transferred to the syngeneic irradiated recipient mice, followed by infection with PyL. Each symbol represents a value from an individual mouse. Daggers indicate death. Similar results were obtained from at least four experiments.

are hardly activated during primary infection, as prime-boost regimens are commonly used to fully activate antigen-specific $CD8^+$ T cells [17]. To assess this possibility, PyNL-recovered mice were further infected twice with PyL (immune mice, Fig. 2A). Although PyNL-recovered mice showed no signs of infection, or even parasite growth, when boosted with PyL as shown in Fig. 1A, serum antibodies specific for PyL were significantly increased after the boosts (Fig. 2B), which indicates successful reactivation of parasite-specific immunity. $CD4^+$ or $CD8^+$ T cells purified from immune mice were transferred to irradiated recipients, which were subsequently infected with PyL and monitored for the course of infection (Fig. 2C and D). All recipients transferred with $CD4^+$ or $CD8^+$ T cells from control mice died as parasites grew. Mice that received $CD4^+$ T cells from immune mice showed low parasitemia and survived with no parasite recrudescence (Fig. 2C). Surprisingly, $CD8^+$ T cells from immune mice transferred protection against infection with PyL as well as $CD4^+$ T cells (Fig. 2D). Furthermore, transfer of $CD8^+$ T cells from immune mice also conferred protection against PyL in RAG2 KO recipient mice (Supporting Information Fig. S1B). To exclude the possibility that small contaminating population of other cells was responsible for the protection, we sorted the three groups of cells from immune mice for adoptive transfer experiment, using MACS cell separation system; the first group was $CD8^+$ cells, the second was $CD4^-$ (CD4 depleted, negative selection) $CD8^+$ cells and last one was $CD4^-$ $CD8^-$ (CD4, CD8 depleted, negative selection) cells. Although $CD4^-$ $CD8^+$ T cells from immune mice transferred protection against infection with PyL, mice depleted of both CD4 and CD8 T cells failed to control the infection and died from high parasitemia (Supporting Information Fig. S1A), confirming that contaminants do not contribute to protection. These results clearly demonstrate that $CD8^+$ T cells play a protective role against blood-stage malaria parasites.

Immunophenotype characterization of $CD8^+$ T cells in immune mice

Mice that received $CD8^+$ T cells from immune mice showed low parasitemia and survived with no parasite recrudescence. This protective immunity against malaria parasites might induce activation of $CD8^+$ T cells and generate memory $CD8^+$ T cells. We analyzed the phenotype of $CD8^+$ T cells. Naive T cells express CD62L (L-selectin), which is known to be a homing receptor, and shed this molecule to migrate from lymphoid organs to inflammatory sites after activation [18]. CD44 appears to be the most reliable marker that is expressed at high levels in all memory T cells of mice, irrespective of their activation status [19]. $CD8^+$ T cells can be classified into three groups according to their expression patterns of CD62L and CD44: $CD62L^{hi}CD44^{lo}$, $CD62L^{hi}CD44^{hi}$ and $CD62L^{lo}CD44^{hi}$ patterns represent naive, central memory, and effector memory phenotypes, respectively [19]. Spleen cells from recipient mice transferred with the

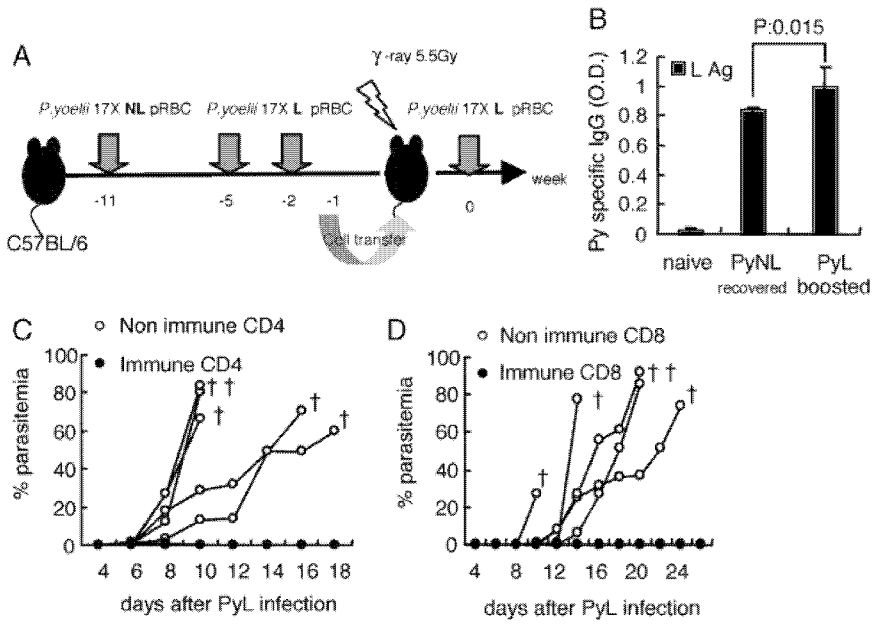

Figure 2. $CD8^+$ T cells from highly immunized mice transferred protection against PyL. (A) Protocol of immunization, cell transfer and challenge infection. (B) Antibody titers specific for malaria parasites in sera collected from mice were measured. Data are the means+SD of OD_{415} values of 200-fold-diluted sera from six mice in each group. Parasitemia of the recipients transferred with $CD4^+$ (C) or with $CD8^+$ (D) T cells purified from control (open circles) or immune (closed circles) mice were evaluated as in Fig. 1B. One representative of at least two repeated experiments is shown. Daggers indicate death.

indicated cells were analyzed 7 days after infection with PyL (Fig. 3A right panels). Cells from the recipients left uninfected were also analyzed (Fig. 3A left panels). Immune mice contained twice as many CD62L^{lo} and effector memory CD8$^+$ T cells than naive control mice (Fig. 3A). Also, the numbers of CD8$^+$ T cells expressing CD30, which is known to be a marker of memory T cells, increased in immune mice by as much as 16.7% *versus* 5.8% in naive mice (data not shown). In response to infection with PyL, the numbers of effector memory CD8$^+$ T cells predominantly increased in recipients transferred with CD8$^+$ T cells from immune mice (Fig. 3A). Furthermore, infection of these mice markedly increased the numbers of CD8$^+$ T cells that express granzyme B, PFN or IFN-γ, all of which are important molecules for the protective role of CD8$^+$ T cells. In sharp contrast, infection of recipients transferred with CD8$^+$ T cells from non-immune mice did not affect the expression of these molecules (Fig. 3B), although CD8$^+$ T cells were slightly activated, as evaluated by an increase in the size of the CD62L^{lo} population (Fig. 3A). These results demonstrate that the immunization protocol can effectively generate memory CD8$^+$ T cells that respond quickly to become effector cells.

IFN-γ from CD8$^+$ T cells is important to protect against infection with PyL

We evaluated the role of IFN-γ in protective immunity mediated by CD8$^+$ T cells. IFN-γ is a pro-inflammatory cytokine that is intimately involved in the innate and acquired immune responses. This cytokine has important roles in immunity against blood-stage malaria, because a previous study has demonstrated that IFN-γ KO mice are highly susceptible to infection with *Plasmodium chabaudi* AS-pRBC [20]. First, the irradiated recipients transferred with CD8$^+$ T cells from immune mice were treated with neutralizing antibodies to IFN-γ prior to infection with PyL. The recipients injected with anti-IFN-γ suffered from high parasitemia and died quickly, while those injected with irrelevant antibodies showed only a slight increase in parasitemia (Fig. 4A). To confirm the importance of IFN-γ secreted from CD8$^+$ T cells, we employed IFN-γ KO mice as immune donors, because the recipient-derived cells might have secreted the cytokine. IFN-γ KO mice were much more susceptible to infection with PyNL, and 25–50% of these mice survived (data not shown). However, once recovered from the infection, IFN-γ KO mice acquired sterile immunity to infection with PyL. CD8$^+$ T cells from immune IFN-γ KO mice were transferred to the irradiated recipients prior to infection with PyL. The recipients transferred with CD8$^+$ T cells from immune IFN-γ KO mice failed to control the infection similar to those transferred with CD4$^+$ T cells from immune IFN-γ KO mice (Fig. 4B). These results suggest that IFN-γ is important to CD8$^+$ T-cell-mediated protection against blood-stage malaria.

Macrophages play essential roles in CD8$^+$ T-cell-mediated protection against PyL

Among the pivotal roles of IFN-γ, activation of macrophages is supposed to be one of the major mechanisms for activating anti-malarial immunity. Macrophages play a critical role in innate immunity against malaria due to their ability to phagocytose pRBC in the absence of cytophilic or opsonizing parasite-specific antibodies [21]. In adaptive immunity, upon

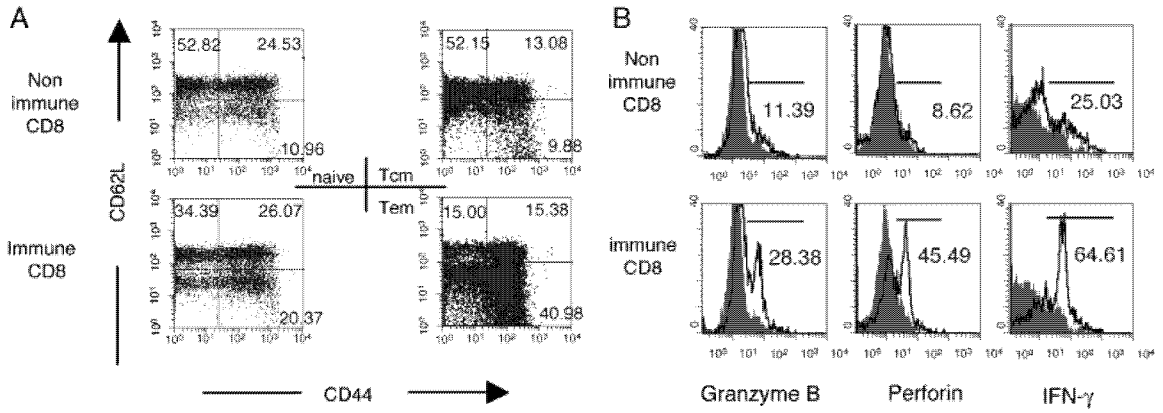

Figure 3. Immunophenotype and expression of effector molecules of protective CD8$^+$ T cells. (A) Spleen cells from recipient mice transferred with the indicated cells were analyzed 7 days after infection with PyL (right panels). Cells from the recipients left uninfected were also analyzed (left panels). Gated CD8$^+$ T cells from mice were classified into central memory (Tcm), effector memory (Tem) and naive cells by staining with CD62L and CD44. Numbers represent the percentage of cells in the corresponding quadrants. (B) Spleen cells from recipient mice transferred with non-immune (upper panel) or immune (lower panel) CD8$^+$ T cells were collected 7 days after PyL infection. Expression of granzyme B, PFN and IFN-γ in CD8$^+$ T cells from spleen was analyzed by intracellular staining with the corresponding antibodies. The expression profiles of CD8$^+$ T cells from the infected recipients (solid lines) were plotted over those of CD8$^+$ T cells from uninfected naive mice (shaded areas). Numbers indicate the percentages of CD8$^+$ T cells positive for the indicated marker in infected recipients. The percentages of CD8$^+$ T cells from uninfected mice positive for granzyme B, PFN, and IFN-γ were 4.6, 9.5 and 11.5 %, respectively.

stimulation with IFN-γ, macrophages function as effector cells that can mediate antibody-dependent cellular inhibition or the production of anti-parasitic molecules. Thus, we evaluated the role of macrophages in irradiated recipients transferred with $CD8^+$ T cells from immune mice. Carrageenan (CGN), a sulfate polygalactose preferentially phagocytosed but undigested in macrophages, was administered to the recipients to impair macrophages [22]. This manipulation completely abolished the protective ability of $CD8^+$ T cells (Fig. 4C). These results indicate that macrophages, presumably activated by IFN-γ secreted from $CD8^+$ T cells, are responsible for parasite eradication in recipient mouse transferred with immune $CD8^+$ T cells. Indeed, the potential of macrophages for phagocytosing pRBC was profoundly impaired in recipients transferred with $CD8^+$ T cells from immune IFN-γ KO mice compared with those from recipients transferred with immune WT mice (Fig. 4D).

PFN from $CD8^+$ T cells contribute partially to protection against PyL

$CD8^+$ T cells from immune mice expressed effector molecules related to cytotoxicity. We investigated the involvement of these molecules in the mechanism of protective immunity induced by $CD8^+$ T cells against blood-stage parasites. PFN KO mice were infected with PyNL. PFN KO mice were more susceptible to infection with PyNL than WT mice, and only half of them survived (Fig. 5A), which suggests that PFN has a protective role. Mice surviving infection with PyNL were resistant to boosting with PyL to the same degree as WT mice, and we employed these mice as immune mice. We compared the activation and phenotype of $CD8^+$ T cell from immune WT and immune PFN KO mice that were subsequently used in the adoptive transfer experiments (Supporting Information Fig. S2A). The activation maker (CD62L lo cells) was almost the same between WT and

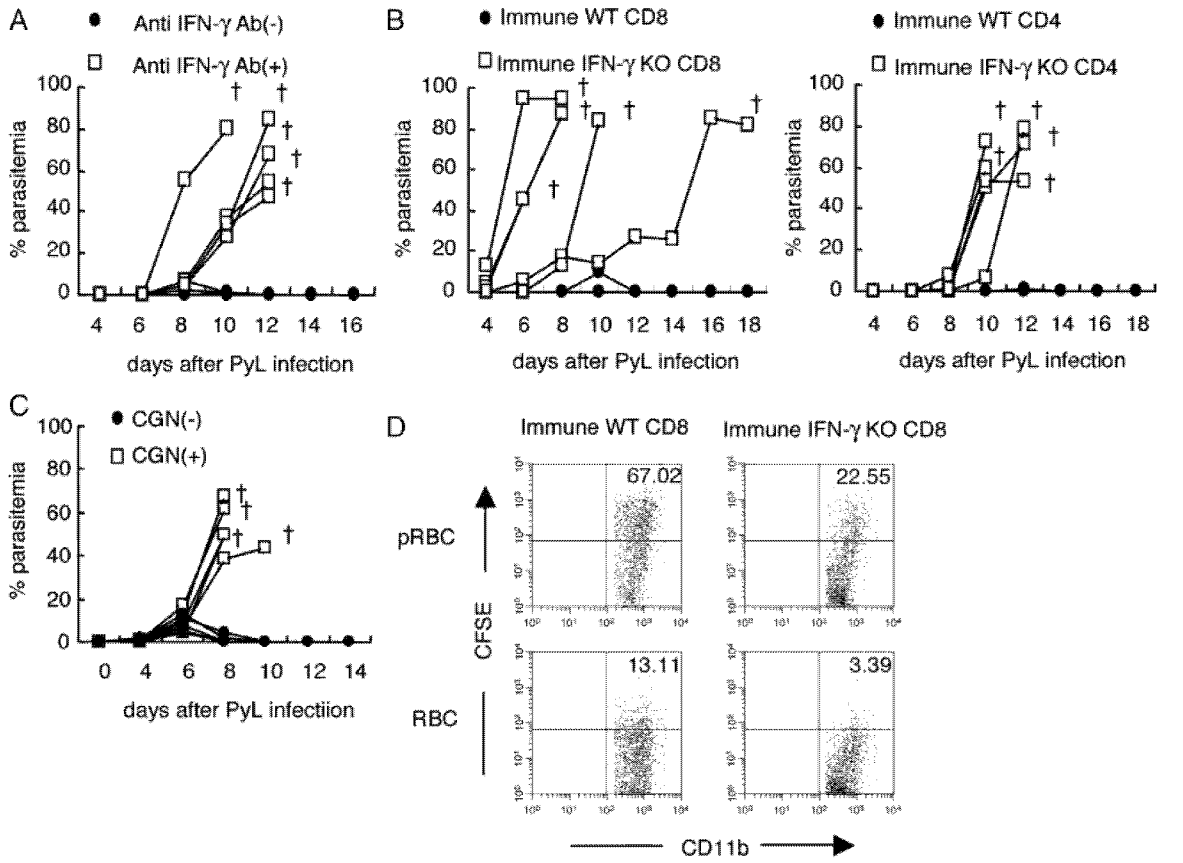

Figure 4. IFN-γ from $CD8^+$ T cells was essential for protection against blood-stage malaria. (A) Parasitemia in recipients transferred with immune $CD8^+$ T cells treated with anti-IFN-γ (open squares) or irrelevant antibodies (closed circles) was evaluated as in Fig. 1B. (B) $CD8^+$ (left panel) or $CD4^+$ (right panel) T cells from IFN-γ KO (open squares) or WT (closed circles) mice were transferred to the irradiated recipients, followed by infection with PyL. (C) Macrophages played an essential role in $CD8^+$ T-cell-mediated protection against PyL. The irradiated recipients transferred with $CD8^+$ T cells from immune mice were treated with CGN to impair macrophage function (open squares), and parasitemia was evaluated. Daggers indicate death. (D) Macrophage uptake assay. Splenic CD11b macrophages were removed from day 7 post-PyL-infected recipients that were transferred with $CD8^+$ T cells from immune WT or immune IFN-γ KO mice. Macrophages were co-cultured with CFSE-labeled pRBC or RBC. The percentage of $CD11b^+$ cells undergoing phagocytosis is presented. One representative of at least two repeated experiments is shown.

PFN KO (Supporting Information Fig. S2C). Furthermore, the number of transferred effector memory cells that are thought to be a key player in protection against infection was also the same between WT and PFN KO (Supporting Information Fig. S2B). These results indicated that activation and phenotype of transplanted immune PFN KO $CD8^+$ T cells are very similar to immune WT $CD8^+$ T cells even though PFN KO mouse are susceptible to PyNL infection. When infected with PyL, the irradiated recipients transferred with $CD8^+$ T cells from immune PFN KO mice showed higher parasitemia at an early stage of infection than those transferred with $CD8^+$ T cells from immune WT mice, and some mice in the former group failed to control the challenge infection (Fig. 5B). However, $CD4^+$ T cells from these donors protected recipients from infection with PyL, similar to those from immune WT mice (Fig. 5B). These results indicate that the cytotoxicity-related molecule PFN contribute, at least in part, to the protective immunity to blood-stage malaria infection conferred by $CD8^+$ T cells.

Discussion

In the present study, we found that $CD8^+$ T cells play roles in the protective immunity against blood-stage infection with highly virulent *P. yoelii* in C57BL/6 mice. Irradiated naive mice transferred with $CD8^+$ T cells from these mice were resistant to infection with PyL. IFN-γ and macrophages were essential for the protective immunity dependent on $CD8^+$ T cells. Additionally, cytotoxicity-related molecules expressed by $CD8^+$ T cells, such as PFN, appeared to also contribute to this protective immunity. It is noteworthy that the protective immunity mediated by $CD8^+$ T cells was not acquired when recipient mice were treated with CGN, a macrophage blocker, after challenge with the parasite. Based on those observations, the role of $CD8^+$ T cells in protective immunity would be exerted by a two-step mechanism. As a first step, these T cells would activate macrophages through the release of IFN-γ. These macrophages should potently phagocytize the infected erythrocytes and digest them. If the parasites were not completely eliminated by the first step mechanism, $CD8^+$ T cells might kill the infected macrophages *via* the PFN-granzyme system in the second step.

We used irradiated or RAG2-deficient mice as recipients for transfer with immune CD8 T cells. It is well established that T cells transferred into such immunodeficient hosts will expand in a non-physiologic manner (homeostatic proliferation) that may result in artificial activation [23]. Moreover, irradiated hosts likely represent a highly inflammatory environment, "hormesis effects" [24]. Similarly, RAG-deficient mice have robust innate immune systems to partially compensate for the lack of adaptive immunity [25]. It is quite possible that these unexpected effects are responsible for the protection observed here. However, only $CD8^+$ T cells from immune mice but not from naive mice (even after a single infection) were potent in transferring protection. These results clearly indicate that protection through the transfer of immune $CD8^+$ T cells is unlikely due to hormesis or homeostatic proliferation and is antigen-specific. In terms of antigen specificity, we determined whether immune $CD8^+$ T cells transfer protection against an irrelevant protozoan parasite, *Toxoplasma gondii*. Mice transferred with immune $CD8^+$ T cells were susceptible

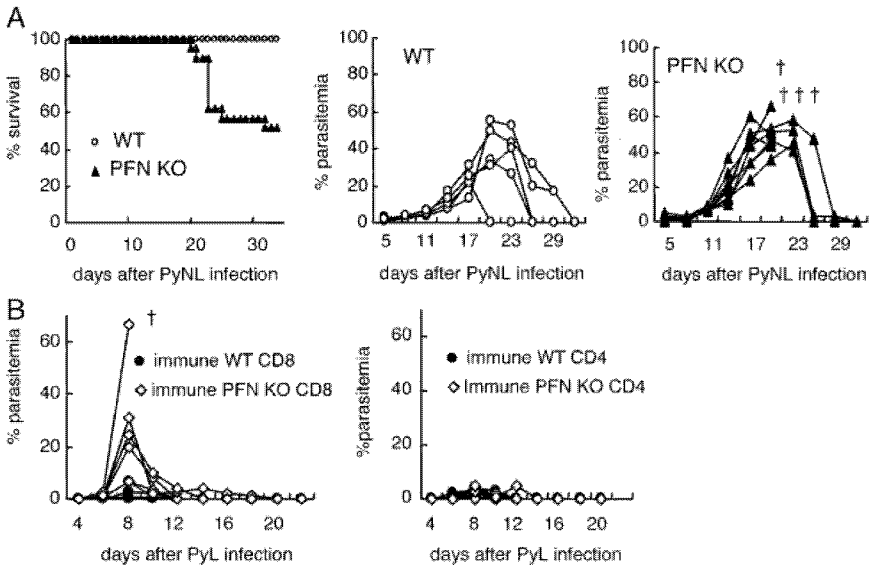

Figure 5. Molecules associated with CTL activity partially contributed to protection against blood-stage malaria. (A) Survival rates and parasitemia in PFN KO (closed triangles) mice were monitored after infection with 25 000 PyNL-pRBC. (B) The recipient mice transferred with $CD8^+$ or $CD4^+$ T cells from immune PFN KO mice were infected with PyL, and parasitemia was evaluated as in Fig. 1B. One representative of at least two repeated experiments is shown. Daggers indicate death.

to the infection similar to those with naive $CD8^+$ T cells (data not shown).

Malaria parasites reside within RBC to evade host immunity. Merozoite-specific antibodies in the circulation readily bind to free merozoites and may inhibit invasion of the parasites into RBC, but these antibodies cannot reach merozoites once they have invaded RBC. Furthermore, blood-stage parasites should escape recognition by $CD8^+$ T cells since RBC do not express MHC class I molecules on their surface, leading to the conclusion that $CD8^+$ T cells could not contribute to protective immunity against blood-stage parasites [6–9].

RBC have no MHC class I molecules. Nevertheless, $CD8^+$ T cells specific for malaria antigens are activated during blood-stage malaria [10, 11]. Taken together with our observation that the numbers of activated $CD8^+$ T cells increased after infection with PyL, antigens derived from malaria parasites must be presented on MHC class I molecules on APC including macrophages. The activation mechanism of $CD8^+$ T cells may be explained by cross-presentation of APC that have engulfed pRBC as other particle antigens [26].

$CD8^+$ T-cell-dependent protective immune responses have been shown to correlate well with IFN-γ production and cytotoxic activity. Our results showed important roles of IFN-γ in protection mediated by $CD8^+$ T cells. Macrophages were also important in this protection, strongly suggesting that $CD8^+$ T cells contribute to the elimination of blood-stage parasites by activating macrophages with IFN-γ, and that the activated macrophages would phagocytose and digest pRBC.

On the other hand, cytotoxic activity exerted by PFN might play some roles in the protective immunity in the late stage of the protective immunity. Macrophages activated with IFN-γ phagocytose antigen abundantly, and are exhausted after phagocytosis reaches its limit [27]. As a final step, $CD8^+$ T cells direct pRBC-phagocytosed monocytes/macrophages to undergo apoptosis *via* the PFN-granzyme B pathway, and completely eliminate them. A previous study reported that $CD8^+$ T cells mediate loss of macrophages in the spleen, which is the most important organ for removal of pRBC by macrophages [28]. Thus, cytotoxic activity exerted by PFN and granzyme B in $CD8^+$ T cells might be directed to these macrophages, resulting in the elimination of parasites and recruitment of fresh macrophages.

Although great efforts have been made to develop vaccines against malaria, practical vaccine strategies have not yet been established. One of the causes for this failure may be that host protective immunity and the immune evasion mechanisms of the parasites have not been fully understood. We clearly showed the involvement of $CD8^+$ T cells in protective immunity against blood-stage infection. In addition, blood-stage parasites seem to evade $CD8^+$ T cell immunity. That is, dendritic cells that interact with pRBC selectively impair the cell cycles of $CD8^+$ T cells, but not $CD4^+$ T cells [29]. In developing vaccines for blood-stage malaria, establishment of strategies for activating $CD8^+$ T cells specific for the parasites or infected erythrocytes may be essential.

Materials and Methods

Mice and parasites

C57BL/6 mice were obtained from Kyudo (Tosu, Japan), RAG2-deficient mice were obtained from Central Laboratory of Experimental Animals (Kawasaki, Japan), PFN-deficient mice were obtained from Jackson Immuno Research Laboratories (West Grove, PA, USA), IFN-γ-deficient mice were provided by Dr. A. Nakane (Hirosaki University), and Ly5.1C57BL/6 mice were obtained from Sankyo Lab Service (Tokyo, Japan) with the permission of Dr. H. Nakauchi (Tokyo University). Age- and sex-matched groups of WT and mutant mice were used. All experiments using mice were reviewed by the Committee for Ethics on Animal Experiments in the Faculty of Medicine, and carried out under the control of the Guidelines for Animal Experiments in the Faculty of Medicine, Kyushu University and the Law (No. 105) and Notification (No. 6) of the Government. Blood-stage parasites of PyL or PyNL, generous gifts from Dr. M Torii (Ehime University) and Dr. K. Yui (Nagasaki University), were obtained after fresh passage through a donor mouse 2–3 days after inoculation with frozen stock. Mice were infected with 25 000 pRBC i.p., which were purified as previously described, and used for infection.

Determination of parasitemia

Blood samples were collected from the experimental mice by bleeding *via* the tail vein at the time indicated. Thin blood films were prepared and fixed with methanol followed by staining with Giemsa solution (Sigma-Aldrich, St. Louis, MO, USA). Parasitemia was determined by counting the percentages of pRBC under a microscope.

Reagents

FITC-, PE-, and PE-Cy5-anti-CD8, FITC-anti-CD4, FITC-anti-CD62L, PE-anti-CD30, PE-anti-granzyme B, and FITC-anti-PFN (eBioscience, San Diego, CA, USA) were used for flow cytometry. Purified anti-CD16/32 (2.4G2) antibodies were obtained from eBioscience. Anti-PE- and anti-FITC microbeads (Miltenyi Biotech, Bergisch Gladbach, Germany) were used for MACS cell purification. mAb to IFN-γ (R4-6A2) purified from the ascites fluid of hybridoma-injected athymic nude mice was used for *in vivo* treatment. CGN type IV (Wako, Osaka, Japan) was used for macrophage blockade.

Purification of cells and adoptive transfer

Spleens were aseptically removed from mice and prepared as single-cell suspensions. RBC were lysed with NH_4Cl, and the cells

were washed twice in fresh medium. $CD4^+$ or $CD8^+$ T cells were purified with positive selection using a MACS cell separation system (Miltenyi Biotech) according to the manufacturer's protocols; in some experiments negative and positive selection were done. The purity of the separated cells was usually >95%. Eight million purified cells were adoptively transferred i.v. to syngeneic recipients that had been irradiated with 5.5 Gy of γ-radiation (GammaCell) or to RAG2 KO mice.

Determination of antibodies specific for PyL

Serum antibodies specific for PyL were measured by ELISA. The 96-well microtiter plates were coated with 50 μL PyL antigen solution (5 μg/mL). Diluted serum samples were added to the wells, and then incubated at room temperature for 2 h. PyL-specific antibodies were detected by horseradish peroxidase-conjugated anti-mouse IgG (Zymed, San Francisco, CA, USA). Enzymatic activity was visualized using a substrate. Absorbance at 415 nm was measured using a spectrophotometer.

Flow cytometry

Spleen cell suspensions were stained with combinations of fluorochrome-labeled antibodies. For intracellular staining, cells were stimulated with 50 ng/mL PMA and 1 μg/mL calcium ionophore in the presence of 1 μg/mL brefeldin A, in complete medium at 37°C for 5 h. These cells were then incubated with anti-CD16/32 (Fc-block) and stained with surface markers, followed by fixation with 4% paraformaldehyde and permeabilization with 0.1% saponin. Then, the cells were stained with second antibodies. Stained cells were analyzed by a FACS Calibur cytometer (Becton Dickinson, San Jose, CA, USA), and the data were analyzed using CellQuest Pro software (Becton Dickinson).

In vivo neutralization of IFN-γ and macrophage inhibition

To neutralize IFN-γ, mice received i.p. injection with 500 μg of anti-IFN-γ antibody 1 day prior to infection, and every 2 wk thereafter. To impair macrophages [22], mice were injected i.p. with 1 mg CGN on 2, 5, 8, 11 and 14 days after infection.

Macrophage uptake assay

The macrophage phagocytosis assay was a modification of a previous method [26]. To stain pRBC or normal RBC, cells (10^7 cells/mL) were incubated with 10 μM CFSE (Molecular Probes, CA, USA) in PBS for 15 min at 37°C. CFSE staining was stopped by adding excess complete medium and washing cells three times with medium. $CD8^+$ T cells from immune WT or immune IFN-γ KO mice were transferred to the recipients. Splenic CD11b macrophages were then removed from mice at day 7 post PyL infection for a macrophage uptake assay. Splenic $CD11b^+$ cells were purified with positive selection using an MACS cell separation system (Miltenyi Biotech) according to the manufacturer's protocols. Splenic CD11b macrophages (10^6 cells/well) were seeded with CFSE-labeled pRBC or normal RBC in a 1:20 ratio, at a final volume of 200 μL for 4 h at 37°C. Following co-culture, non-ingested RBC were removed by lysis with NH_4Cl lysing buffer, and the remaining macrophages were washed twice with PBS, FcR-blocked and then stained with PE-labeled anti-CD11b mAb, in sorting buffer consisting of PBS with 1% FBS and 0.05% sodium azide (Sigma-Aldrich, St. Louis, MO, USA). The capacity of macrophages to uptake CFSE-labeled pRBC or normal RBC was analyzed by a FACS Calibur cytometer (Becton Dickinson), and the data were analyzed using CellQuest Pro software (Becton Dickinson).

Statistical analysis

Statistical evaluation of differences between experimental groups was done by analysis of variance and two-tailed unpaired Student's *t*-tests; $p<0.05$ was considered statistically significant

Acknowledgements: This work was supported by grants from the Ministry of Education, Science Sport and Culture of Japan to K.H. (18015040, 19590429), to H.H. (18590400, 19041056), and from The Uehara Memorial Foundation to H.H.

Conflict of interest: The authors declare no financial or commercial conflict of interest.

References

1 **WHO World malaria report.** 2005. http://rbm.who.int/wmr.

2 **Hafalla, J. C., Cockburn, I. A. and Zavala, F.,** Protective and pathogenic roles of CD8+T cells during malaria infection. *Parasite Immunol.* 2006. **28**: 15–24.

3 **Wizel, B., Houghten, R. A., Parker, K. C., Coligan, J. E., Church, P., Gordon, D. M., Ballou, W. R. and Hoffman, S. L.,** Irradiated sporozoite vaccine induces HLA-B8-restricted cytotoxic T lymphocyte responses against two overlapping epitopes of the Plasmodium falciparum sporozoite surface protein 2. *J. Exp. Med.* 1995. **182**: 1435–1445.

4 **Marsh, K. and Kinyanjui, S.,** Immune effector mechanisms in malaria. *Parasite Immunol.* 2006. **28**: 51–60.

5 **Good, M. F. and Doolan, D. L.,** Immune effector mechanisms in malaria. *Curr. Opin. Immunol.* 1999. **11**: 412–419.

6 **Herrera, S., Herrera, M. A., Corredor, A., Rosero, F., Clavijo, C. and Guerrero, R.,** Failure of a synthetic vaccine to protect Aotus lemurinus against asexual blood stages of *Plasmodium falciparum*. *Am. J. Trop. Med. Hyg.* 1992. **47**: 682–690.

7 **Vinetz, J. M., Kumar, S., Good, M. F., Fowlkes, B. J., Berzofsky, J. A. and Miller, L. H.,** Adoptive transfer of CD8+T cells from immune animals does

not transfer immunity to blood stage *Plasmodium yoelii* malaria. *J. Immunol.* 1990. **144**: 1069–1074.

8 **Jayawardena, A. N., Murphy, D. B., Janeway, C. A. and Gershon, R. K.,** T cell-mediated immunity in malaria I The Ly phenotype of T cells mediating resistance to *Plasmodium yoelii*. *J. Immunol.* 1982. **129**: 377–381.

9 **Suss, G., Eichmann, K., Kury, E., Linke, A. and Langhorne, J.,** Roles of CD4- and CD8-bearing T lymphocytes in the immune response to the erythrocytic stages of *Plasmodium chabaudi*. *Infect. Immun.* 1988. **56**: 3081–3088.

10 **van der Heyde, H. C., Manning, D. D., Roopenian, D. C. and Weidanz, W. P.,** Resolution of blood-stage malarial infections in CD8+cell-deficient beta 2-m0/0 mice. *J. Immunol.* 1993. **151**: 3187–3191.

11 **Sinigaglia, F., Richard, J. and Pink, L.,** Human T lymphocyte clones specific for malaria (Plasmodium falciparum) antigens. *EMBO J.* 1985. **4**: 3819–3822.

12 **Pombo, D. J., Lawrence, G., Hirunpetcharat, C., Rzepczyk, C., Bryden, M., Cloonan, N., Anderson, K. *et al.*,** Immunity to malaria after administration of ultra-low doses of red cells infected with Plasmodium falciparum. *Lancet* 2002. **360**: 610–617.

13 **Belnoue, E., Kayibanda, M., Vigario, A. M., Deschemin, J. C., van Rooijen, N., Viguier, M., Snounou, G. and Renia, L.,** On the pathogenic role of brain-sequestered alphabeta CD8+T cells in experimental cerebral malaria. *J. Immunol.* 2002. **169**: 6369–6375.

14 **Nitcheu, J., Bonduelle, O., Combadiere, C., Tefit, M., Seilhean, D., Mazier, D. and Combadiere, B.,** Perforin-dependent brain-infiltrating cytotoxic CD8+T lymphocytes mediate experimental cerebral malaria pathogenesis. *J. Immunol.* 2003. **170**: 2221–2228.

15 **Lundie, R. J., de Koning-Ward, T. F., Davey, G. M., Nie, C. Q., Hansen, D. S., Lau, L. S., Mintern, J. D. *et al.*,** Blood-stage Plasmodium infection induces CD8+T lymphocytes to parasite-expressed antigens, largely regulated by CD8alpha+dendritic cells. *Proc. Natl. Acad. Sci. USA* 2008. **105**: 14509–14514.

16 **Langhorne, J.,** The immune response to the blood stages of Plasmodium in animal models. *Immunol. Lett.* 1994. **41**: 99–102.

17 **Schneider, J., Gilbert, S. C., Hannan, C. M., Degano, P., Prieur, E., Sheu, E. G., Plebanski, M. and Hill, A. V.,** Induction of CD8+T cells using heterologous prime-boost immunisation strategies. *Immunol. Rev.* 1999. **170**: 29–38.

18 **Williams, M. A. and Bevan, M. J.,** Effector and memory CTL differentiation. *Annu. Rev. Immunol.* 2007. **25**: 171–192.

19 **Krishnan, L., Gurnani, K., Dicaire, C. J., van Faassen, H., Zafer, A., Kirschning, C. J., Sad, S. and Sprott, G. D.,** Rapid clonal expansion and prolonged maintenance of memory CD8+T cells of the effector (CD44highCD62Llow) and central (CD44highCD62Lhigh) phenotype by an archaeosome adjuvant independent of TLR2. *J. Immunol.* 2007. **178**: 2396–2406.

20 **Su, Z. and Stevenson, M. M.,** Central role of endogenous gamma interferon in protective immunity against blood-stage Plasmodium chabaudi AS infection. *Infect. Immun.* 2000. **68**: 4399–4406.

21 **Shear, H. L., Nussenzweig, R. S. and Bianco, C.,** Immune phagocytosis in murine malaria. *J. Exp. Med.* 1979. **149**: 1288–1298.

22 **Zhang, M., Hisaeda, H., Sakai, T., Ishikawa, H., Hao, Y. P., Nakano, Y., Ito, Y. and Himeno, K.,** Macrophages expressing heat-shock protein 65 play an essential role in protection of mice infected with *Plasmodium yoelii*. *Immunology* 1999. **97**: 611–615.

23 **Brown, I. E., Blank, C., Kline, J., Kacha, A. K. and Gajewski, T. F.,** Homeostatic proliferation as an isolated variable reverses CD8+T cell anergy and promotes tumor rejection. *J. Immunol.* 2006. **177**: 4521–4529.

24 **Ren, H., Shen, J., Tomiyama-Miyaji, C., Watanabe, M., Kainuma, E., Inoue, M., Kuwano, Y. and Abo, T.,** Augmentation of innate immunity by low-dose irradiation. *Cell Immunol.* 2006. **244**: 50–56.

25 **Grundy, M. A. and Sentman, C. L.,** Immunodeficient mice have elevated numbers of NK cells in non-lymphoid tissues. *Exp. Cell Res.* 2006. **312**: 3920–3926.

26 **Ing, R., Segura, M., Thawani, N., Tam, M. and Stevenson, M. M.,** Interaction of mouse dendritic cells and malaria-infected erythrocytes: uptake, maturation, and antigen presentation. *J. Immunol.* 2006. **176**: 441–450.

27 **Cannon, G. J. and Swanson, J. A.,** The macrophage capacity for phagocytosis. *J. Cell Sci.* 1992. **101**: 907–913.

28 **Beattie, L., Engwerda, C. R., Wykes, M. and Good, M. F.,** CD8+ T lymphocyte-mediated loss of marginal metallophilic macrophages following infection with Plasmodium chabaudi chabaudi AS. *J. Immunol.* 2006. **177**: 2518–2526.

29 **Pouniotis, D. S., Proudfoot, O., Bogdanoska, V., Scalzo, K., Kovacevic, S., Coppel, R. L. and Plebanski, M.,** Selectively impaired CD8+but not CD4+ T cell cycle arrest during priming as a consequence of dendritic cell interaction with plasmodium-infected red cells. *J. Immunol.* 2005. **175**: 3525–3533.

Abbreviations: **CGN:** carrageenan · **PFN:** perforin · **pRBC:** parasitized RBC · **PyNL:** *P. yoelii* 17XNL

Full correspondence: Dr. Takashi Imai, Laboratory for Immunochaperones, RIKEN Research Center for Allergy and Immunology, Kanagawa, Japan
Fax:+81-92-642-6118
e-mail: t-imai@rcai.riken.jp

Received: 16/4/2009
Revised: 30/11/2009
Accepted: 7/1/2010
Accepted article online: 25/1/2010

Biochemical and Biophysical Research Communications 402 (2010) 790–795

Contents lists available at ScienceDirect

Biochemical and Biophysical Research Communications

journal homepage: www.elsevier.com/locate/ybbrc

Development of experimental cerebral malaria is independent of IL-23 and IL-17

Hidekazu Ishida [a,b], Chikako Matsuzaki-Moriya [a], Takashi Imai [b], Kunio Yanagisawa [b], Yoshihisa Nojima [c], Kazutomo Suzue [b], Makoto Hirai [b], Yoichiro Iwakura [d], Akihiko Yoshimura [e], Shinjiro Hamano [f], Chikako Shimokawa [f], Hajime Hisaeda [b,*]

[a] Department of Microbiology and Immunology, Graduate School of Medical Sciences, Kyushu University, Fukuoka 812-8582, Japan
[b] Department of Parasitology, Gunma University, Graduate School of Medicine, Gunma 371-8511, Japan
[c] Department of Medicine and Clinical Science, Gunma University, Graduate School of Medicine, Gunma 371-8511, Japan
[d] Center for Experimental Medicine, Institute of Medical Science, The University of Tokyo, Tokyo 108-8639, Japan
[e] Department of Microbiology and Immunology, School of Medicine, Keio University, Tokyo 160-8582, Japan
[f] Department of Parasitology, Institute of Tropical Medicine, Nagasaki University, Nagasaki 852-8523, Japan

ARTICLE INFO

Article history:
Received 21 October 2010
Available online 29 October 2010

Keywords:
Cerebral malaria
IL-23
IL-17
Immune responses
Malaria

ABSTRACT

Cerebral malaria (CM) is the most severe complication of *Plasmodium* infection. Although inappropriate immune responses to *Plasmodium falciparum* are reported as the major causes of CM, the precise mechanisms for development remain unclear. IL-23 and IL-17 have critical roles in the onset of autoimmunity and inflammatory diseases triggered by microbial infections. Thus, we investigated the influence of IL-23 and IL-17 on experimental CM (ECM) using *Plasmodium berghei* ANKA infection of C57BL/6 mice. Both IL-23 deficient mice and wild-type (WT) mice developed ECM. IL-17 deficient mice also developed ECM, while IL-17 producing cells other than $CD4^+$ T cells (Th17) were increased in WT mice that developed ECM. In conclusion, this study showed that IL-23 and IL-17 are not involved in ECM development.

1. Introduction

Malaria is a major life-threatening parasitic disease. Each year, 500 million cases and 2 million deaths are reported and 40% of the world's population is at risk of malaria infection [1]. Cerebral malaria (CM) associated with *Plasmodium falciparum* infection is responsible for almost all malaria deaths and is characterized by impaired consciousness/coma and generalized convulsions [2,3]. Approximately 1% of *P. falciparum* infected patients develop CM. The majority of these cases occur in young children in sub-Saharan Africa, of which, 10–20% are fatal and the remaining survivors acquire permanent neurological damage [4,5]. Histologically, multifocal capillary obstruction with parasitized red blood cells (RBC) and leukocytes is observed in brain tissue from patients that die of CM [6] and suggests *P. falciparum* infection may trigger vascular and immune system dysfunction. However, the precise mechanisms causing CM are not fully understood.

After the discovery of $CD4^+$ T cells producing IL-17 (Th17), a new subset of effector T helper cells, the immune responses involving IL-23 and IL-17 have been investigated in detail. IL-23 is a heterodimeric cytokine comprised of a p40 subunit and a unique p19 subunit [7]. Recently, it was revealed that IL-23 is critical for the development of Th17 [8] and for immune cell activation [9,10]. IL-17 is a proinflammatory cytokine secreted by immune cells and mediates granulopoiesis, infiltration of neutrophils and recruitment of T cells into peripheral tissues via the induction of chemokine and cytokine expression [11,12].

Many studies using *IL-23 p19*$^{-/-}$ mice (P19KO) and *IL-17*$^{-/-}$ mice (17KO) suggest that IL-23 and IL-17 play a critical role in the onset of autoimmune diseases, such as experimental autoimmune encephalitis, collagen induced arthritis and inflammatory bowel diseases [7,13–15]. Furthermore, as both cytokines contribute to the development of arthritis caused by *Borrelia burgdorferi* infection [16] and brain damage caused by *Toxoplasma gondii* infection [17], IL-23 and IL-17 may be associated with the immunopathology triggered by microorganism infection.

Infection of susceptible mouse strains with *Plasmodium berghei* ANKA (PbA) allows for the development of experimental CM (ECM) that shares some characteristics with CM. Immune cells, including T cells, antigen-presenting cells (APC), NK cells and neutrophils, play critical roles in the development of ECM [18–21]. During infection, these cells activate and cooperate with each other to allow T cell migration into brain. This results in blood–brain barrier (BBB) disruption and is a key pathological feature of ECM. IL-23 is

Abbreviations: IL-23, Interleukin-23; IL-17, Interleukin-17; RBC, red blood cell; Th, T helper cells; NK cells, natural killer cells; Treg, regulatory T cell.

* Corresponding author. Address: Department of Parasitology, Gunma University, Graduate School of Medicine, 3-39-22, Showa-machi, Maebashi, Gunma 371-8511, Japan. Fax: +81 27 220 8025.
E-mail address: hisa@med.gunma-u.ac.jp (H. Hisaeda).

0006-291X/$ - see front matter © 2010 Elsevier Inc. All rights reserved.
doi:10.1016/j.bbrc.2010.10.114

strongly associated with activation of APC and NK cells and also with development of Th17 that is capable BBB disruption [8–10]. IL-17 is involved in the activation and recruitment of neutrophils [11] and upregulation of CXCL 9, 10, and 11, which are ligands of CXCR3 essential for the migration of $CD8^+$ T cells into brain [12,22]. Given these findings, it is possible that IL-23 and/or IL-17 may contribute to development of ECM.

We therefore examined the role of IL-23 and IL-17 in ECM development using P19KO and 17KO mice. Our results demonstrated that P19KO mice developed ECM similarly to wild-type (WT) mice. 17KO mice also developed ECM while IL-17-producing cells other than $CD4^+$ T cells increased in WT mice during ECM. Thus, our results conclude that IL-23 and IL-17 may not be involved in ECM development.

2. Materials and methods

2.1. Mice and parasites

C57BL/6 mice were purchased from Kyudo (Tosu, Japan). Age and sex-matched groups of WT mice, P19KO mice and 17KO mice were used for experiments. All experiments that involved mice were reviewed by the Committee for Ethics on Animal Experiments in the Faculty of Medicine and were conducted under the control of the Guidelines for Animal Experiments in the Faculty of Medicine, Kyushu University and the Law (No. 105) and Notification (No. 6) of the Government. Blood-stage parasites of *P. berghei* ANKA (PbA) were a generous gift from Dr. M. Torii (Ehime University), obtained after fresh passage through a donor mouse, 2–3 days after inoculation with frozen stock. Mice were infected with 50,000 parasitized RBC (pRBC) via intraperitoneal injection.

2.2. Determination of parasitemia

Blood samples were collected from the tail vein of experimental mice at the time indicated. Thin blood films were prepared and fixed with methanol before being stained with Giemsa solution (Sigma–Aldrich, St. Louis, MO, USA). Parasitemia was determined by counting the percentage of infected RBC (pRBC) using light microscopy.

2.3. Preparation of brain-sequestered leukocytes (BSL) and spleen cells

BSL were prepared according to the previously described methods [23,24]. Briefly, sacrificed mice were intracardially perfused with PBS to remove both circulating, nonadherent RBC and leukocytes from the brain. The brain was then removed and crushed in RPMI1640 supplemented with 100 IU/mL penicillin, 100 mg/mL streptomycin, 20 mM HEPES, 2 mM L-glutamine, 100 mM 2-mercaptoethanol and 10% inactivated fetal bovine serum (complete medium). The tissue suspension was centrifuged at 400 *g* for 5 min and the pellet was resuspended with HEPES buffer, supplemented with 0.05% collagenase (Roche Applied Science, Indianapolis, IN, USA) and 2 U of DNase (Sigma–Aldrich, St. Louis, MO, USA)/ml. The mixture was stirred at room temperature for 60 min, then passed through a sterile gauze and centrifuged at 80 *g* for 30 s to remove debris. The supernatant was deposited on a 30% Percoll (Sigma–Aldrich, St. Louis, MO, USA) to remove brain cells and centrifuged at 1400 *g* for 10 min. The pellet was resuspended with medium to form single-cell suspensions. Residual RBC in single-cell suspensions prepared from the brain and spleen were lysed with NH_4Cl. Cells were then washed twice with fresh medium before being used for experiments. $CD4^+$ cells were purified with positive selection using a MACS cell separation system (Miltenyi Biotech) according to the manufacturer's protocols. Separated cell purity was generally >95%.

2.4. Real-time RT-PCR

Total RNA was extracted from BSL, spleen cells and $CD4^+$ cells before being reverse-transcribed to cDNA. mRNA that encoded genes of interest was quantified from cDNA by evaluating SYBR Green dye incorporation (Takara, Tokyo, Japan) using a real-time PCR system GeneAmp7000 thermal cycler (Applied Biosystems, Foster City, CA, USA). PCR was performed according to the manufacturer's protocols. Expression levels of target genes were determined as the difference of Ct between the β-actin-encoding gene and target gene using the following formula: $\Delta Ct = Ct_{\text{target gene}} - Ct_{\text{reference gene}}$. PCR primers used were as follows: for IL-23p19, 5′-TGGCTGTG CCTAGGAGTAGCA-3′ and 5′-TTCATCCTCTTCTTCTCTTAGTAGATTC ATA-3′; for IL-17, 5′-TCATCTGTGTCTCTGATGCTGTTG-3′ and 5′-TCG CTGCCTTCACTGT-3′; for RORγt, 5′-AGCAGTGTAATGTGGCCTAC-3′ and 5′- GCACTTCTGCATGTAGACTG-3′; and for β-actin, 5′-TGGAAT CCTGTGGCATCCATGAAAC-3′ and 5′-TAAAACGCAGCTCAGTAACAG TCCG-3′.

2.5. Flow cytometry

BSL and spleen cells were stained with a combination of fluorochrome-labeled antibodies. For intracellular staining, cells were stimulated with 50 ng/ml PMA and 500 ng/ml calcium ionophore in the presence of Golgi plug (BD Bioscience, San Jose, CA, USA), in complete medium at 37 °C for 4 h. Cells were then incubated with anti-CD16/32 (Fc-block) and stained with FITC-anti-CD4 (eBioscience, San Diego, CA, USA) followed by fixation/permeabilization with BD cytofix/cytoperm (BD Bioscience, San Jose, CA, USA) according to manufacturer's protocols. Cells were stained with PE-anti-IL-17 or PE-anti-IFN-γ (BD Bioscience, San Jose, CA, USA) and analyzed using a FACS Caliber cytometer (Becton Dickinson, San Jose, CA, USA). Data were analyzed using CellQuest Pro software (Becton Dickinson).

2.6. Histology

For histological analysis of cerebral pathology, brains from mice developing ECM were perfused with PBS and carefully removed and fixed in formaldehyde solution (4 v/v%). The 5-μm tissue sections were prepared and stained with hematoxylin and eosin (HE).

2.7. Statistical analysis

Statistical differences between experimental groups were evaluated using a two-tailed unpaired Student's *t*-test. Survival analysis was determined using Kaplan Meier survival analysis. $P < 0.05$ was considered statistically significant.

3. Results and discussion

3.1. IL-23 is not involved in the onset of ECM

C57BL/6 mice infected with PbA developed ECM that was characterized by neurological manifestations, such as ataxia, paralysis (monoplegia, hemiplegia and tetraplegia) and coma as early as 7 or 8 days after infection, and death occurred between 7 and 10 days after infection [25]. We first investigated the expression of IL-23 during ECM to assess the involvement of IL-23. BSL and spleen cells were collected and p19 mRNA expression was analyzed by quantitative RT-PCR. No significant difference in the expression of p19 mRNA was observed between mice developing ECM and uninfected control mice (Fig. 1A and B). Thus, PbA infection of mice did not induce IL-23 in both tissues sampled. Furthermore, to directly investigate the contribution of IL-23 to the

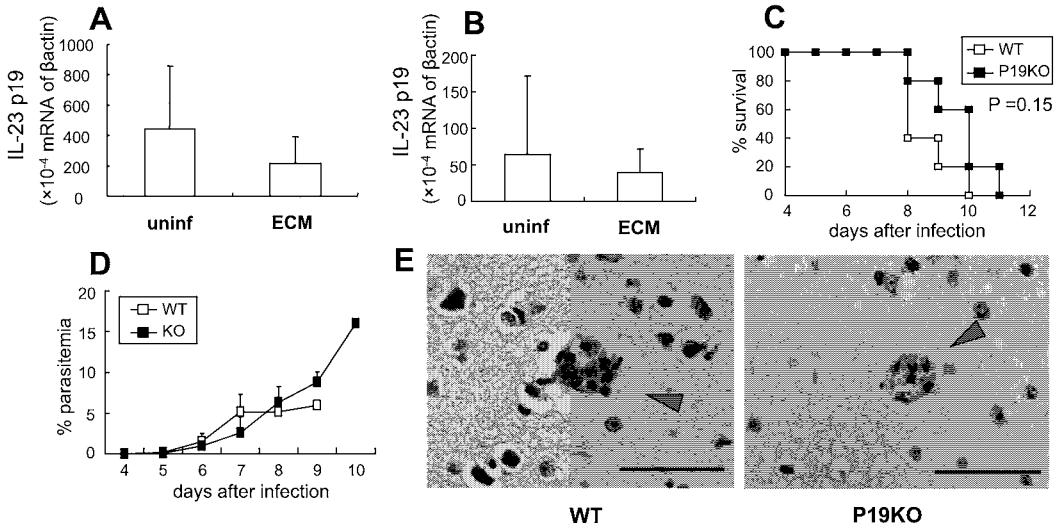

Fig. 1. ECM induced by PbA infection was independent of IL-23. mRNA encoding IL-23p19 in BSL (A) and spleen cells (B) isolated from mice developing ECM was quantified using RT-PCR. Values are relative to amounts of mRNA encoding β-actin. Data represent the mean ± SD of four mice. Survival rates (C) or parasitemia (D) of WT and P19KO mice infected with 50,000 PbA-pRBC were monitored. Each group is comprised of five mice. One representative of at least two repeated experiments is shown. Brains from WT (left panel) and P19KO mice (right panel) developing ECM were analyzed for histological examination (E). Representative histological sections from areas around the blood vessels of cerebrum with HE staining are shown (original magnification, ×1000). Arrowheads indicate accumulation of mononuclear cells and erythrocytes. Scale bars equal 50 μm.

development of ECM, P19KO mice were infected with PbA. Infected P19KO as well as WT mice showed severe neurological symptoms and died within 11 days when the parasitemia was lower than 10% (Fig. 1C, D), suggesting that P19KO mice developed ECM. To confirm development of ECM in these mutants, histological analyses of brains isolated from P19KO mice developing ECM were performed. Both P19KO and WT mice showed cerebral blood vessels sequestered with mononuclear cells and erythrocytes, a typical sing of ECM induced by PbA (Fig. 1E). No sequestered vessel was observed before infection (data not shown). These results clearly demonstrated that the development of ECM does not require IL-23.

3.2. IL-17 does not contribute to ECM development

To assess whether IL-17 contributes to ECM, we analyzed IL-17 producing cells using flow cytometry. IL-17 producing cells were increased in the brain and spleen of mice developing CM when compared to uninfected control mice (Fig. 2A and C). The emergence of Th17 during ECM was also investigated as an assessment of IL-17 production. Mice that developed ECM showed a higher frequency and absolute number of $CD4^+$ IFN-γ^+ Th1 cells (IFN-γ^+ $CD4^+$ cells (Th1)) in the brain and spleen when compared to uninfected control mice (Fig. 2B and C), which supported previous study [26]. By contrast, there were no differences in the frequency and absolute number of Th17 between mice that developed ECM and uninfected control mice (Fig. 2A and C). Furthermore, we analyzed the expression of mRNAs encoding IL-17 and a "master-regulator" transcription factor of Th17, RORγt, in $CD4^+$ cells purified from BSL and spleen cells. Mice that developed ECM showed lower mRNA expression levels compared to uninfected mice (Fig. 3A and B). These results demonstrate that IL-17-producing cells other than Th17 developed during ECM. Finally, to directly investigate the contribution of IL-17 to onset of ECM, 17KO mice were infected with PbA. Both infected 17KO mice and infected WT mice developed neurological symptoms and died (Fig. 4A) and produced no differences in parasitemia kinetics (Fig. 4B). Histological examination of brain sections revealed that 17KO as well as WT mice showed leukocyte-packed vessels (Fig. 4C). These results demonstrate that the development of ECM is independent of IL-17.

3.3. General discussion

As observed during our study, infection with PbA did not induce the expression of IL-23 and a lack of IL-23 did not affect the develop ECM. Moreover, IL-17 deficient mice also develop ECM, while IL-17 producing cells increased in WT mice affected with ECM. These results suggest that both cytokines are unnecessary for the development of ECM.

Th17 development was not observed during infection with PbA primarily because IL-23, which is critical for Th17 expansion, was not secreted. We confirmed that expression of mRNA encoding IL-17 or RORγt in $CD4^+$ T cells decreased in mice that developed ECM and that the frequency and cell number of Th17 were not increased. In addition, environments under malaria infection favor to induce Treg [29,30], consequently might disturb Th17 differentiation as a counter-regulatory action [31]. By contrast, we observed that the frequency of Th1 was increased in WT mice that developed ECM (Supplementary Fig. 1). Expression of mRNA encoding T-bet or IFN-γ in $CD4^+$ T cells from mice that developed ECM were higher than those from uninfected mice (data not shown). These findings suggested that Th1 rather than Th17 may be of importance in ECM development and supports previous suggestions that Th1 are dominant during ECM [26].

IL-17 is known to suppress pathogenic Th1 responses during inflammatory bowel disease [27,28], suggesting that augmented induction of Th1 covers or compensates lack of IL-17-mediated pathogenesis in ECM development. However, there was no difference between WT and 17KO mice in Th1 induced by infection with PbA (Supplementary Fig. 1). Given these results, it appears that IL-17 does not suppress Th1 responses during ECM and thus does not contribute to ECM development.

In addition to the ECM produced by PbA infection, hepatic injury observed in mice infected with *P. berghei* NK65 (PbNK) is also reported to be immunopathological [1,32]. Our preliminary results revealed that P19KO mice or 17KO mice infected with PbNK displayed elevated serum levels of enzymes released from the damaged hepatocytes, as was the case for WT mice (data not shown). Thus, these cytokines do not appear to be involved in ECM development or liver injury by infection with PbNK. Immunopathologies

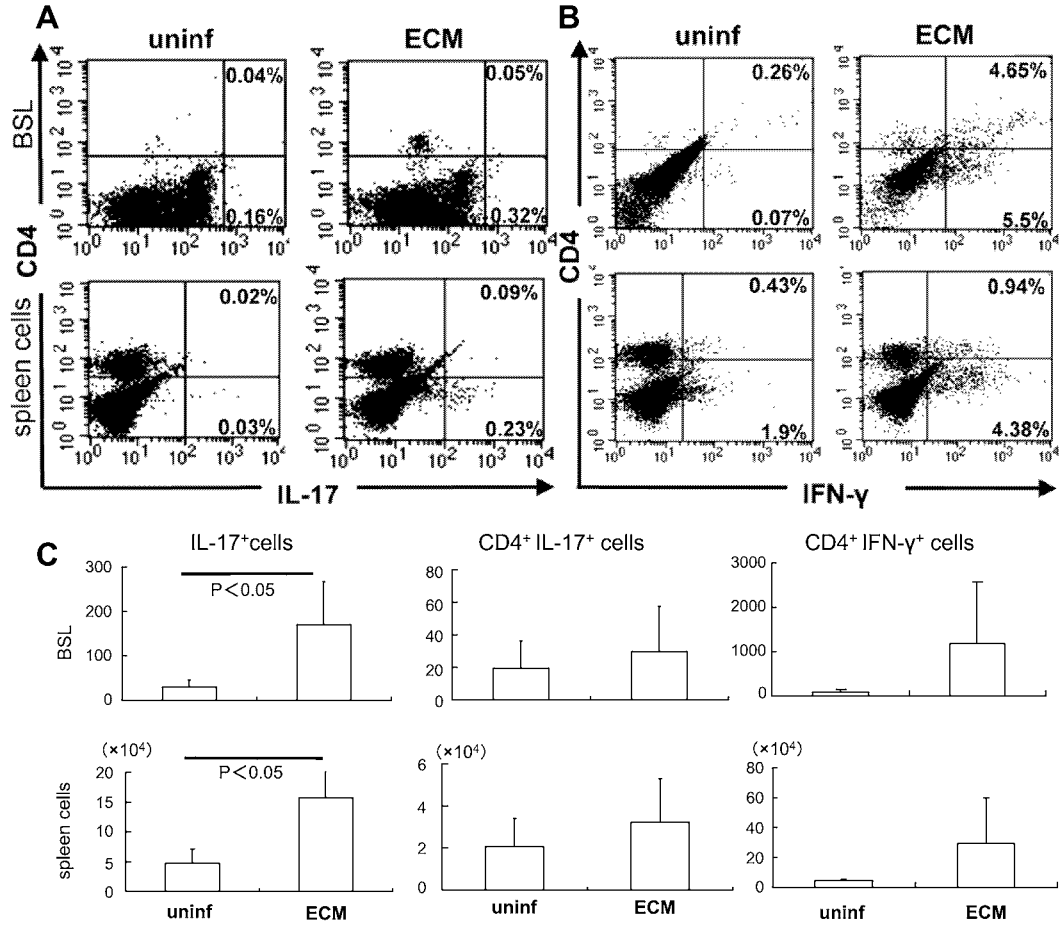

Fig. 2. Induction of IL-17-producing cells during infection with PbA. BSL (upper panel) or spleen cells (lower panel) isolated from mice that developed ECM were analyzed for IL-17 (A) and IFN-γ (B) production. Gated lymphocytes were plotted for CD4 and each cytokine. The numbers indicate the percentage of quadrants. Absolute numbers of the indicated cells were also shown (C). Data represent the mean ± SD of five mice. One representative of at least two repeated experiments is shown.

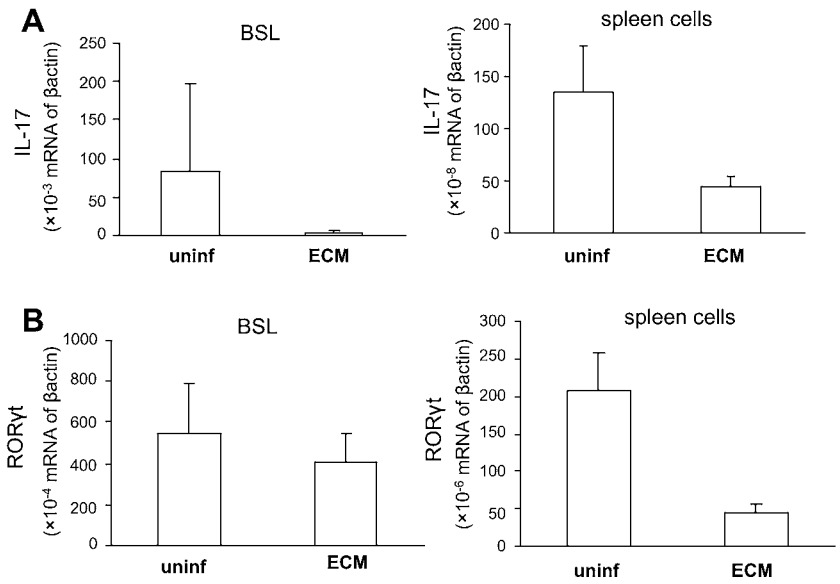

Fig. 3. Induction of Th17 in mice infected with PbA. CD4⁺ cells were purified from BSL and spleen cells of mice developing ECM and analyzed for the expression of mRNA encoding IL-17 (A) and RORγt (B) as in Fig. 1A. One representative of at least two repeated experiments is shown.

induced by malaria parasites may therefore be independent of IL-23 and IL-17, unlike other infectious diseases.

IL-23 and IL-17 are reported to be protective against some infections [33], yet are responsible for inflammatory pathologies

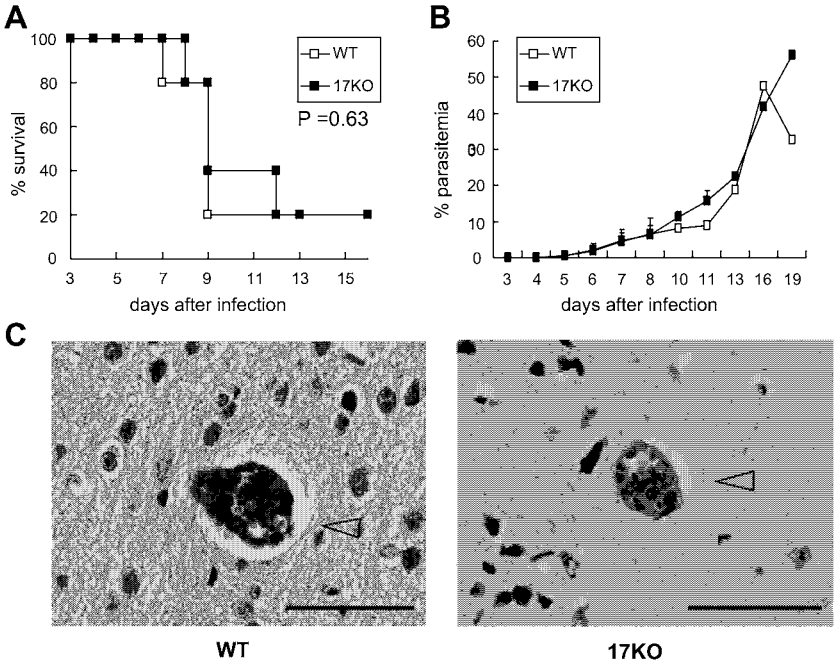

Fig. 4. ECM induced by PbA infection was independent of IL-17. Survival rates (A) or parasitemia (B) of WT and 17KO mice infected with 50,000 PbA-pRBC were monitored as in Fig. 1C. Histological analysis of brain sections of WT (left panels) and 17KO mice (right panels) developing ECM was performed as in Fig. 1E.

in other situations. Parasitemia in P19KO or 17KO mice infected with PbA was similar to that in infected WT mice. These findings suggest that IL-23 and IL-17 do not contribute to the reduction of parasite burdens in mice infected with PbA. However, those cytokines have protective effects against infection with PbNK65 and the lack of IL-23 shortened the survival of infected mice. IL-23 also has anti-protozoan effects against *Plasmodium yoelii* XL (manuscript in preparation). The protective effects of IL-23 and IL-17 during malaria therefore appear to dependent on the species and strain of malaria parasites.

In conclusion, IL-23 and IL-17 are not critical for the development of ECM, a complicated pathology that is produced in association with various immune cells, cytokines and chemokines. It would also be of interest to investigate whether similar results could be achieved using human patients. Such insights will potentially further our understanding CM pathogenesis and help establish new therapeutic strategies.

Acknowledgments

The authors thank Rumiko Koitabashi for handling and support with brain sections. This work was supported by grants from the Ministry of Education, Science Sport and Culture of Japan to H.H. (20390121, 21022036).

Appendix A. Supplementary data

Supplementary data associated with this article can be found, in the online version, at doi:10.1016/j.bbrc.2010.10.114.

References

[1] M.F. Good, H. Xu, M. Wykes, C.R. Engwerda, Development and regulation of cell-mediated immune responses to the blood stages of malaria: implications for vaccine research, Annu. Rev. Immunol. 23 (2005) 69–99.
[2] G.G. MacPherson, M.J. Warrell, N.J. White, S. Looareesuwan, D.A. Warrell, Human cerebral malaria. A quantitative ultrastructural analysis of parasitized erythrocyte sequestration, Am. J. Pathol. 119 (1985) 385–401.
[3] L.H. Miller, D.I. Baruch, K. Marsh, O.K. Doumbo, The pathogenic basis of malaria, Nature 415 (2002) 673–679.
[4] Roll Back Malaria: spotlight on Africa, TDR News (2000) 10, 15.
[5] R.W. Snow, J.F. Trape, K. Marsh, The past, present and future of childhood malaria mortality in Africa, Trends Parasitol. 17 (2001) 593–597.
[6] H.C. van der Heyde, J. Nolan, V. Combes, I. Gramaglia, G.E. Grau, A unified hypothesis for the genesis of cerebral malaria: sequestration, inflammation and hemostasis leading to microcirculatory dysfunction, Trends Parasitol. 22 (2006) 503–508.
[7] R.A. Kastelein, C.A. Hunter, D.J. Cua, Discovery and biology of IL-23 and IL-27: related but functionally distinct regulators of inflammation, Annu. Rev. Immunol. 25 (2007) 221–242.
[8] E. Bettelli, T. Korn, M. Oukka, V.K. Kuchroo, Induction and effector functions of T(H)17 cells, Nature 453 (2008) 1051–1057.
[9] C.L. Langrish, B.S. McKenzie, N.J. Wilson, R. de Waal Malefyt, R.A. Kastelein, D.J. Cua, IL-12 and IL-23: master regulators of innate and adaptive immunity, Immunol. Rev. 202 (2004) 96–105.
[10] W. Sun, X. He, Z. Guo, Q. Wang, X. Li, J. Rayner, L. Zhang, J. Wang, X. Cao, IL-12p40-overexpressing immature dendritic cells induce T cell hyporesponsiveness in vitro but accelerate allograft rejection in vivo: role of NK cell activation and interferon-gamma production, Immunol. Lett. 94 (2004) 191–199.
[11] C.T. Weaver, R.D. Hatton, P.R. Mangan, L.E. Harrington, IL-17 family cytokines and the expanding diversity of effector T cell lineages, Annu. Rev. Immunol. 25 (2007) 821–852.
[12] S.A. Khader, G.K. Bell, J.E. Pearl, J.J. Fountain, J. Rangel-Moreno, G.E. Cilley, F. Shen, S.M. Eaton, S.L. Gaffen, S.L. Swain, R.M. Locksley, L. Haynes, T.D. Randall, A.M. Cooper, IL-23 and IL-17 in the establishment of protective pulmonary $CD4^+$ T cell responses after vaccination and during mycobacterium tuberculosis challenge, Nat. Immunol. 8 (2007) 369–377.
[13] W. Ouyang, J.K. Kolls, Y. Zheng, The biological functions of T helper 17 cell effector cytokines in inflammation, Immunity 28 (2008) 454–467.
[14] E. Bettelli, M. Oukka, V.K. Kuchroo, T(H)-17 cells in the circle of immunity and autoimmunity, Nat. Immunol. 8 (2007) 345–350.
[15] C.M. Tato, D.J. Cua, Reconciling id, ego, and superego within interleukin-23, Immunol. Rev. 226 (2008) 103–111.
[16] J. Knauer, S. Siegemund, U. Muller, S. Al-Robaiy, R.A. Kastelein, G. Alber, R.K. Straubinger, Borrelia burgdorferi potently activates bone marrow-derived conventional dendritic cells for production of IL-23 required for IL-17 release by T cells, FEMS Immunol. Med. Microbiol. 49 (2007) 353–363.
[17] J.S. Stumhofer, A. Laurence, E.H. Wilson, E. Huang, C.M. Tato, L.M. Johnson, A.V. Villarino, Q. Huang, A. Yoshimura, D. Sehy, C.J. Saris, J.J. O'Shea, L. Hennighausen, M. Ernst, C.A. Hunter, Interleukin 27 negatively regulates the development of interleukin 17-producing T helper cells during chronic inflammation of the central nervous system, Nat. Immunol. 7 (2006) 937–945.
[18] D.S. Hansen, N.J. Bernard, C.Q. Nie, L. Schofield, NK cells stimulate recruitment of $CXCR3^+$ T cells to the brain during *Plasmodium berghei*-mediated cerebral malaria, J. Immunol. 178 (2007) 5779–5788.

[19] C. Engwerda, E. Belnoue, A.C. Gruner, L. Renia, Experimental models of cerebral malaria, Curr. Top. Microbiol. Immunol. 297 (2005) 103–143.
[20] L. Chen, Z. Zhang, F. Sendo, Neutrophils play a critical role in the pathogenesis of experimental cerebral malaria, Clin. Exp. Immunol. 120 (2000) 125–133.
[21] S. deWalick, F.H. Amante, K.A. McSweeney, L.M. Randall, A.C. Stanley, A. Haque, R.D. Kuns, K.P. MacDonald, G.R. Hill, C.R. Engwerda, Cutting edge: conventional dendritic cells are the critical APC required for the induction of experimental cerebral malaria, J. Immunol. 178 (2007) 6033–6037.
[22] J. Miu, A.J. Mitchell, M. Muller, S.L. Carter, P.M. Manders, J.A. McQuillan, B.M. Saunders, H.J. Ball, B. Lu, I.L. Campbell, N.H. Hunt, Chemokine gene expression during fatal murine cerebral malaria and protection due to CXCR3 deficiency, J. Immunol. 180 (2008) 1217–1230.
[23] E. Belnoue, M. Kayibanda, A.M. Vigario, J.C. Deschemin, N. van Rooijen, M. Viguier, G. Snounou, L. Renia, On the pathogenic role of brain-sequestered alphabeta CD8$^+$ T cells in experimental cerebral malaria, J. Immunol. 169 (2002) 6369–6375.
[24] T. Voza, A.M. Vigario, E. Belnoue, A.C. Gruner, J.C. Deschemin, M. Kayibanda, F. Delmas, C.J. Janse, B. Franke-Fayard, A.P. Waters, I. Landau, G. Snounou, L. Renia, Species-specific inhibition of cerebral malaria in mice coinfected with *Plasmodium* spp., Infect. Immun. 73 (2005) 4777–4786.
[25] J. Hearn, N. Rayment, D.N. Landon, D.R. Katz, J.B. de Souza, Immunopathology of cerebral malaria: morphological evidence of parasite sequestration in murine brain microvasculature, Infect. Immun. 68 (2000) 5364–5376.
[26] N.H. Hunt, G.E. Grau, Cytokines: accelerators and brakes in the pathogenesis of cerebral malaria, Trends Immunol. 24 (2003) 491–499.
[27] C.L. Maynard, C.T. Weaver, Intestinal effector T cells in health and disease, Immunity 31 (2009) 389–400.
[28] W. O'Connor Jr., M. Kamanaka, C.J. Booth, T. Town, S. Nakae, Y. Iwakura, J.K. Kolls, R.A. Flavell, A protective function for interleukin 17A in T cell-mediated intestinal inflammation, Nat. Immunol. 10 (2009) 603–609.
[29] H. Hisaeda, Y. Maekawa, D. Iwakawa, H. Okada, K. Himeno, K. Kishihara, S. Tsukumo, K. Yasutomo, Escape of malaria parasites from host immunity requires CD4$^+$ CD25$^+$ regulatory T cells, Nat. Med. 10 (2004) 29–30.
[30] T.T. Long, S. Nakazawa, S. Onizuka, M.C. Huaman, H. Kanbara, Influence of CD4$^+$ CD25$^+$ T cells on *Plasmodium berghei* NK65 infection in BALB/c mice, Int. J. Parasitol. 33 (2003) 175–183.
[31] E. Bettelli, Y. Carrier, W. Gao, T. Korn, T.B. Strom, M. Oukka, H.L. Weiner, V.K. Kuchroo, Reciprocal developmental pathways for the generation of pathogenic effector TH17 and regulatory T cells, Nature 441 (2006) 235–238.
[32] A. Bhalla, V. Suri, V. Singh, Malarial hepatopathy, J. Postgrad. Med. 52 (2006) 315–320.
[33] F.L. van de Veerdonk, M.S. Gresnigt, B.J. Kullberg, J.W. van der Meer, L.A. Joosten, M.G. Netea, Th17 responses and host defense against microorganisms: an overview, BMB Rep. 42 (2009) 776–787.

International Immunology Advance Access published February 5, 2010

International Immunology 2010; 1 of 11
doi:10.1093/intimm/dxp126

Transient role of $CD4^+CD25^+$ regulatory T cells in mycobacterial infection in mice

Yuriko Ozeki[1,2], Isamu Sugawara[3], Tadashi Udagawa[3], Toshiaki Aoki[3], Mayuko Osada-Oka[1], Yoshitaka Tateishi[1], Hajime Hisaeda[4], Yuji Nishiuchi[5], Nobuyuki Harada[3], Kazuo Kobayashi[6] and **Sohkichi Matsumoto[1]**

[1]Department of Bacteriology, Osaka City University Graduate School of Medicine, 1-4-3 Abeno-ku, Osaka 545-8585, Japan
[2]Sonoda Women's University, 7-29-1 Minamitsukaguchi-cho, Amagasaki, Hyogo 661-8520, Japan
[3]Mycobacterial Reference Center, The Research Institute of Tuberculosis, 3-1-24 Matsuyama Kiyose-shi Tokyo, 204-8533, Japan
[4]Department of Microbiology and Immunology, Graduate School of Medical Sciences, Kyushu University, 3-1-1 Maidashi, Higashi-ku, Fukuoka 812-8582, Japan
[5]Peptide Institute Inc., Protein Research Foundation, Minoh-shi, Osaka 562-8686, Japan
[6]Department of Immunology, National Institute of Infectious Diseases, Toyama 1-23-1, Shinjuku-ku, Tokyo 162-8640, Japan

Correspondence to: S. Matsumoto and Y. Ozeki; E-mail. sohkichi@med.osaka-cu.ac.jp and yuriozeki@med.osaka-cu.ac.jp

Transmitting editor: S. Koyasu

Received 22 April 2009, *accepted* 22 December 2009

Abstract

$CD4^+CD25^+$ regulatory T (Treg) cells cause immune suppression by inhibiting T cell effector functions and play pivotal roles not only in self-tolerance but also in immune response to parasitic microbial pathogens. Mycobacteria are major parasitic bacterial pathogens, but the role of $CD4^+CD25^+$ Treg cells in mycobacterial infection is not yet defined. In this study we found that, at the early stage of infection, depletion of $CD25^+$ cells reduced both bacterial load and granuloma formation in mice infected with *Mycobacterium tuberculosis* strains, such as *M. tuberculosis* Erdman or *M. tuberculosis* Kurono. However, at a later stage of infection, bacterial burden and histopathology were similar regardless of depletion of $CD25^+$ cells. Severe combined immunodeficient (SCID) mice reconstituted with $CD4^+CD25^-$ T cells alone or a combination of $CD4^+CD25^+$ and $CD4^+CD25^-$ T cells showed similar bacterial loads and survival kinetics after infection with *M. tuberculosis* Erdman. Consistent with *in vivo* data, *in vitro* studies revealed that mycobacterial antigens, purified protein derivative of tuberculin (PPD), failed to induce the suppressive function of $CD4^+CD25^+$ Treg cells to $CD4^+CD25^-$ effector T cells, as demonstrated by the lack of response of $CD4^+CD25^+$ T cells to PPD, in mice chronically infected with *Mycobacterium bovis* bacillus Calmette–Guérin and *M. tuberculosis*. Our data show that $CD4^+CD25^+$ Treg cells have a transient effect at the early stage of mycobacterial infection but, contrary to the expectation, have little impact on the overall course of infection.

Keywords: bacterial, T cells, rodent, inflammation, lung

Introduction

Mycobacteria are intracellular bacterial pathogens, which persistently infect eukaryotes, including mammals, and cause diseases not only following primary infection but also by reactivation from latent state. Several species of mycobacteria, such as *Mycobacterium tuberculosis* and *Mycobacterium bovis*, are known to cause human tuberculosis. The World Health Organization estimates that *M. tuberculosis* infects one-third of the world's population and is responsible for 2 million deaths each year (1). While the infection remains latent in 95% of the infected cases of *M. tuberculosis*, 5–10% of those who initially controlled the infection later develop active disease at some stage during their lifetime. To suppress intracellular growth of mycobacteria, macrophage activation by IFN-gamma is critical in both mice (2, 3) and humans (2, 3).

The important role of the $CD4^+CD25^+$ regulatory T (Treg) cells in immune response has recently been recognized. This T cell subset maintains immunologic self-tolerance and suppresses the onset of autoimmune diseases (4). The vast majority of Treg cells constitutively express CD25/IL-2 receptor alpha chain in the physiological state (5, 6). $CD4^+CD25^+$ Treg cells also express cytotoxic T-lymphocyte-associated protein 4 (CTLA-4; 7, 8), glucocorticoid-induced tumor necrosis factor receptor (GITR; 9, 10) and the transcription factor,

FoxP3 (11, 12). Some subsets of $CD4^+CD25^+$ Treg cells also produce effector cytokines, such as IL-10 and transforming growth factor (TGF)-β (13, 14). The defining feature of $CD4^+CD25^+$ Treg cells is their ability to inhibit the proliferation of T cells and IFN-gamma production through cell–cell contact (15, 16), possibly mediated by CTLA-4, and/or through the production of immunosuppressive cytokines, such as TGF-β and IL-10 (13, 14).

Recently, it has been reported that $CD4^+CD25^+$ Treg cells are also involved in suppressive immune responses during several infectious diseases. Depletion of $CD4^+CD25^+$ Treg cells enhances anti-microbial activity against diverse pathogens including the protozoan *Leishmania major* and *Plasmodium yoelii*, viruses such as HIV and Herpes simplex virus and bacteria such as *Helicobacter pylori* (17–21).

In spite of suggested importance of $CD4^+CD25^+$ Treg cells in parasitic pathogens, the knowledge in mycobacterial infection remains controversial (22–25). Kursar *et al.* and Scott-Browne *et al.* showed that Treg cells prevented protective immunity against *M. tuberculosis* infection by utilizing reconstituted and chimeric mice, respectively (22, 25). In contrast, Quinn *et al.* suggested minor role of $CD4^+CD25^+$ in both *Mycobacterium bovis* bacillus Calmette Guérin (BCG)-induced protection and natural mycobacterial infection (23, 24). In order to elucidate the roles of $CD4^+CD25^+$ Treg cells in mycobacterial infection more precisely, we carried out the experiments using Treg-deleted mice by antibody to CD25 molecule and SCID mice reconstituted with T cell subsets. We found that mycobacterial antigen-specific $CD4^+CD25^+$ Treg cells were hardly developed after mycobacterial infection in mice and therefore the function of $CD4^+CD25^+$ Treg cells was limited after the infection was established. Thus, $CD4^+CD25^+$ Treg cells have little impact on the overall course of mycobacterial infection.

Methods

Mice

Specific pathogen-free, female DBA/2 mice aged 6 weeks were purchased from Japan SLC (Shizuoka, Japan). BALB/c and SCID/BALB/c mice were purchased from Japan CLEA (Tokyo, Japan). All mice were maintained under specific pathogen-free conditions in the animal facilities of Osaka City University Graduate School of Medicine and in a biosafety-level-3 facility at The Research Institute of Tuberculosis according to the standard guidelines for animal experiments at each institute with approval of their ethical committees.

Depletion of $CD4^+CD25^+$ cells

A hybridoma cell line expressing anti-mouse CD25 monoclonal IgM [a monoclonal antibody against mouse CD25 (7D4), American Type Culture Collection, Manassas, VA, USA] was expanded as ascites in pristine-primed SCID mice (Wako, Osaka, Japan). The Ig-rich fraction was obtained by 30% ammonium sulfate precipitation of ascitic fluid followed by dialysis in PBS. An isotype-matched control IgM was purchased from eBioscience (San Diego, CA, USA). The protein concentration was determined by Bradford's method using BSA (Sigma–Aldrich, St Louis, MO, USA) as a standard. For depletion of $CD25^+$ cells in early stage of infection, mice were injected with 1 mg of 7D4 or control IgM intraperitoneally (i.p.) 1 day before, and then 3 and 10 days after *M. tuberculosis* infection. For depletion of $CD25^+$ cells in late stage of infection, mice were injected (i.p.) with 1 mg of 7D4 or control IgM at 60, 65 and 70 days after *M. tuberculosis* infection. Depletion of $CD4^+CD25^+$ cells was assessed by flow cytometry using a FACScan (Becton Dickinson, Franklin Lakes, NJ, USA). Peripheral blood leukocytes (PBLs) were obtained by incubation with 0.83% ammonium chloride solution at 37°C for 5 min to induce erythrocyte lysis. PBLs or splenocytes were stained with PE-conjugated anti-CD4 mAb (GK1.5, eBioscience) and FITC-conjugated anti-CD25 mAb (PC61, eBioscience). The data were analyzed by flow cytometry with using Cellquest™ software (Becton Dickinson).

Bacteria and infection

Mycobacterium bovis BCG Tokyo, *M. tuberculosis* H37Rv, *M. tuberculosis* Kurono (ATCC 35812) and *M. tuberculosis* Erdman were grown in 7H9 medium (Difco, Detroit, MI, USA) supplemented with 10% BSA, dextrose and catalase enrichment (Difco) and 0.05% Tween 80 at 37°C to mid-logarithmic phase, then stored in frozen aliquots as previously described (26). For infection with *M. tuberculosis* Kurono and *M. tuberculosis* Erdman, the nebulizer of a Middlebrook airborne infection apparatus (Glas-col, Terre Haute, IN, USA) was filled with 5 ml PBS containing 5×10^6 colony-forming units (CFU) of bacteria and the mice were airborne infected for 90 min by Glas-Col aerosol generator. This procedure deposits ~10 CFU of bacteria into the lungs. At 0, 3 and 5 weeks (and also 2 weeks in some experiments) post-infection, three to five mice per group were euthanized and the lungs, livers and spleens were harvested. The organs were homogenized in 1 ml sterile distilled water using a mortar and pestle and serial dilutions were plated onto Middlebrook 7H11 agar containing oleic acid, dextrose, albumin and catalase enrichment (Difco) (7H11-OADC agar). Bacterial numbers were counted using CFU after culturing at 37°C for 20–30 days. To investigate the role of $CD4^+CD25^+$ Treg cells in the late stage of infection, mice were airborne-infected with *M. tuberculosis* H37Rv as the same method described above and $CD25^+$ cells were depleted by 7D4 treatment on days 60, 65, and 70. At 75 days post-infection, eight mice per group were euthanized and bacterial numbers in lungs and spleens were determined by CFU count and histological evaluation were performed as the same procedures described above.

Isolation of $CD4^+CD25^+$ T cells and $CD4^+CD25^-$ T cells

BALB/c mice were infected i.p. with 5×10^4 CFU of *M. bovis* BCG Tokyo. $CD4^+CD25^+$ T cells and $CD4^+CD25^-$ T cells were purified from spleens of normal mice or chronically BCG-infected (>6 months post-infection) BALB/c mice using $CD4^+CD25^+$ regulatory T cell isolation kit (Miltenyl Biotec, Bergisch Gladgach, Germany) after depleting erythrocytes with 0.83% ammonium chloride solution. Obtained cells were labeled with PE-conjugated anti-CD25 mAb, stained with FITC-conjugated anti-CD4 mAb (eBioscience) and analyzed

by flow cytometer. The purity of selected populations was confirmed as >96%. Expression of foxp3 in the $CD4^+CD25^+$ T cell population was confirmed using flow cytometer after intracellular staining with anti-FITC-conjugated anti-mouse foxp3 mAb (eBioscience). $CD4^+CD25^+$ T cells stained by this procedure were >90% foxp3-positive. Non-$CD4^+$ cells of normal mice retained in the MACS separation column were flushed out and incubated for >2 h. Attached cells were used as antigen-presenting cells (APCs) after treatment with 20-Gy radiation. T cell populations and APCs were also isolated from DBA/2 mice chronically infected with *M. tuberculosis* as the similar procedure with BCG-infected mice described above. However, in this case, to obtain APCs, spleen cells of normal DBA/2 mice were incubated for >2 h and attached cells were treated with mitomycin C (50 μg zml^{-1}) for 30 min at 37°C instead of radiation.

In vitro T cell proliferation assay and measurement of cytokines

$CD4^+CD25^+$ T cells and $CD4^+CD25^-$ T cells were prepared to be 1×10^6 cells ml^{-1}. Various ratios of $CD4^+CD25^+$ T cells and $CD4^+CD25^-$ T cells were cultured for 5 or 7 days with 10 μg ml^{-1} of purified protein derivative of tuberculin (PPD) or anti-CD3 mAb (CEDARLANE, Canada) in the presence of 1×10^5 cells ml^{-1} of APC in 96-well plates in RPMI 1640 supplemented with 10% FCS, 2 mM L-glutamine, penicillin (100 U ml^{-1}), streptomycin (100 mg ml^{-1}) and 50 mM 2-mercaptoethanol. Proliferation was evaluated by pulsing cells with 1 μCi (37 kBq) per well [^{3}H]thymidine ([^{3}H]TdR) for 6 h and [^{3}H]TdR incorporation measured using a scintillation counter. In the experiments to analyze the function of T cells derived from *M. tuberculosis*-infected mice, proliferation was evaluated by incorporation of 5-bromo-2′-deoxyuridine (BrdU) using a commercially available kit (Cell proliferation ELISA, BrdU colorimetoric, Roche, Germany). Production of IFN-gamma, IL-10, IL-2 and IL-6 in the culture supernatant was measured using a commercially available ELISA kit (R&D System, Minneapolis, MN, USA).

Transfer of T cell population into SCID mice

$CD4^+CD25^+$ T cells and $CD4^+CD25^-$ T cells were purified from the spleens of BALB/c mice chronically infected with BCG using $CD4^+CD25^+$ Treg cell isolation kit. Totally, 7.5×10^5 $CD4^+CD25^-$ T cells or 7.5×10^5 $CD4^+CD25^+$ T cells either alone or in combination (7.5×10^5 $CD4^+CD25^-$ T cells and 7.5×10^4 $CD4^+CD25^+$ T cells) were transferred intravenously to cognate SCID mice (17). One day after transfer, recipient mice were infected aerogenically with *M. tuberculosis* Erdman as described above. Three weeks post-infection, five to eight mice were euthanized and bacterial burden was counted. The survival time course of seven mice per group was observed for up to 165 days post-infection.

Neutralization of IL-6 in culture supernatant

$CD4^+CD25^-$ T cells, $CD4^+CD25^+$ T cells and APCs were isolated from chronically BCG-infected mice according to the procedures described above. Anti-mouse IL-6-neutralizing mAb (Biolegend, San Diego, CA, USA) or isotype-matched control antibody (Southern Biotech, Birmingham, AL, USA) was added to the culture of $CD4^+CD25^-$ effector T cells either alone or in combination with $CD4^+CD25^+$ T cells at concentration of 0.02 μg ml^{-1} and cultured for 4 days in the presence of PPD or anti-CD3 mAb. IFN-gamma production and [^{3}H]TdR incorporation were measured after 4 days incubation.

Transfer of culture medium

T cell subsets were obtained from chronically BCG-infected mice as described above. $CD4^+CD25^-$ T cells/$CD4^+CD25^+$ T cells/APCs (1:0:0.1) or $CD4^+CD25^-$ T cells/$CD4^+CD25^+$ T cells/APCs (1:1:0.1) were cultured with PPD or anti-CD3 mAb for 7 days and each culture supernatant stored at −80°C until later use. Freshly isolated $CD4^+CD25^-$ T cells/$CD4^+CD25^+$ cells/APCs (1:0:0.1) or $CD4^+CD25^-$ T cells/$CD4^+CD25^+$ T cells/APCs (1:1:0.1) were cultured with stored supernatant:new medium (1:1) in the presence or absence of anti-CD3 mAb. On day 4, [^{3}H]TdR incorporation was measured as described above.

In vitro activation of $CD4^+CD25^+$ T cells

$CD4^+CD25^+$ T cells isolated from chronically infected BALB/c mice with BCG or *M. tuberculosis* H37Rv were incubated with Dynabeads Mouse CD3/CD28 T cell Expander (Invitrogen, Norway) at a bead:cell ratio of 2:1 adding 2000 U ml^{-1} of recombinant mouse IL-2 according to the manufacturer's protocol. Two days after incubation, the beads were

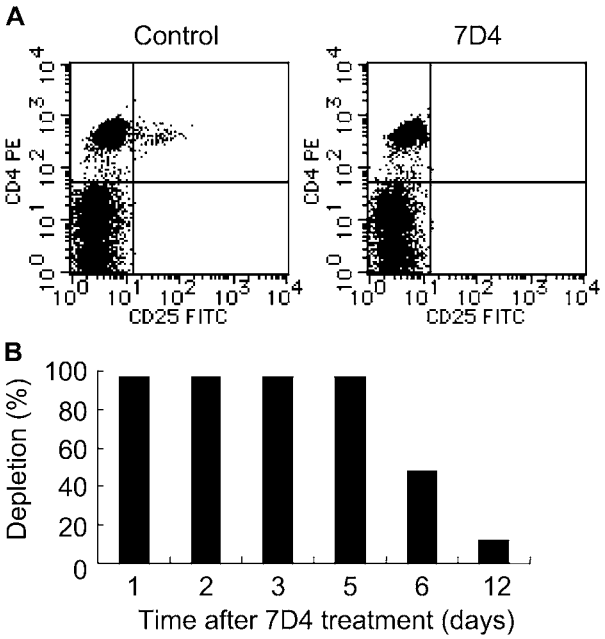

Fig. 1. Selective loss of $CD4^+CD25^+$ T cells by treatment with anti-CD25 mAb, 7D4. (A) Flow cytometric analysis of PBLs obtained from i.p.-injected mice with 1 mg of anti-CD25 mAb (7D4) or control IgM (control) 1 day after injection. Cells were stained with FITC-conjugated anti-CD25 mAb (PC61) and PE-conjugated anti-CD4 mAb (GK1.5). (B) Time course of the level of depletion of $CD4^+CD25^+$ T cell in PBL after a single dose of 7D4. Data are expressed as percent depleted relative to the $CD4^+CD25^+$ cell population in control IgM-treated mice. Data are mean of three mice per time point.

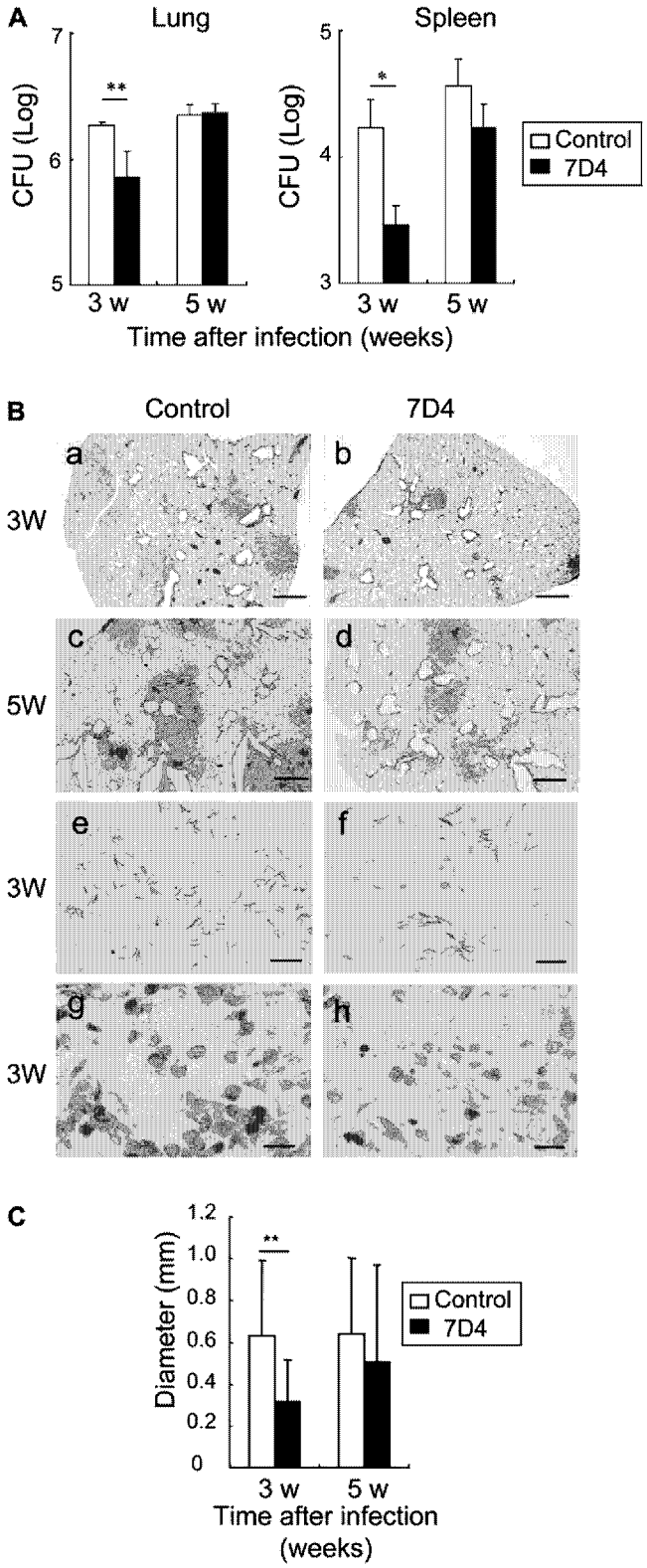

Fig. 2. The effect of $CD25^+$ cell depletion in *Mycobacterium tuberculosis* Kurono infection in mice. DBA/2 mice treated with 1 mg of 7D4, anti-CD25 mAb or control IgM were aerogenically infected with 5×10^6 CFU of *M. tuberculosis* Kurono. (A) Bacterial numbers were counted in lungs (left panel) and spleens (right panel) of mice treated with control IgM (open bars) or with 7D4, anti-CD25 mAb (closed bars). (B) Histopathological features of lungs from *M. tuberculosis* Kurono-infected mice. Lung sections were stained with H&E (a–d), Ziehl–Neelsen (e and f) and Giemsa (g and h). Granulomas mainly consisted of epithelioid macrophages (g and h). Numerous acid-fast bacteria were observed in granulomas of both control IgM-treated and anti-CD25 mAb-treated (7D4) mice. (a, c, e and g) Lungs sections from mice treated with control IgM. (b, d, f and h) Lungs sections from mice treated with 7D4. (a, b and e–h) Three weeks after infection. (c and d) Five weeks after infection. Bars, 500 μm (a–d), 10 μm (e-h). (C) The diameter of granulomatous lesions was measured in the lung sections from mice treated with control IgM (open bars) or with 7D4, anti-CD25 mAb (closed bars). Bars represent mean ±standard deviation of three to five mice. $*P < 0.05$ versus control mice; $**P < 0.01$ versus control mice.

removed from $CD4^+CD25^+$ T cells by magnet. After washing with medium, cells were used as activated $CD4^+CD25^+$ T cells. Freshly isolated $CD4^+CD25^-$ effector T cells were incubated with activated $CD4^+CD25^+$ T cells in the presence of PPD.

Histological analysis

Tissues were removed from mice at various intervals, fixed in 10% formalin and embedded in paraffin blocks. Sections (5 μm) were stained with hematoxylin and eosin (H&E), Ziehl–Neelsen or Giemsa methods. To evaluate the intensity of inflammatory response of the lung, the mean diameters of pulmonary granulomas were measured in three sections per mouse using Microanalyzer (Poladigital, Tokyo, Japan).

Statistical analysis

Results were analyzed by one-way analysis of variance (ANOVA) by SAS system R.8.1. Data were expressed as mean values ± standard deviation and considered significant if $P < 0.05$.

Results

Depletion of $CD25^+$ cells in early stage of infection causes transient effect on in vivo growth of M. tuberculosis Kurono and M. tuberculosis Erdman

7D4 is a mAb against mouse CD25. Administration of 1 mg 7D4 into a mouse resulted in the loss of >96% of $CD4^+CD25^+$ T cells in the peripheral blood and spleens (Fig. 1A). Loss of $CD25^+$ cells maintained at least for 5 days after 7D4 treatment (Fig. 1B). Depletion of $CD25^+$ cells by 7D4 protects mice from death caused by infection of *Plasmodium yoelii*, suggesting a role for $CD4^+CD25^+$ Treg cells in exacerbating malaria (21).

Using 7D4, we first depleted $CD25^+$ cells of DBA/2 mice and then infected animals with 5×10^6 CFU/mouse of *M. tuberculosis* Kurono, which was clinically isolated strain in Japan, by airborne infection. Bacterial load in lung and spleen, and histopathology of the lung were monitored at 3 and 5 weeks post-infection. *Mycobacterium tuberculosis* Kurono multiplied to approximately 2×10^6 CFU per lung 3 weeks post-challenge and maintained these bacterial numbers 5 weeks post-challenge. In spleens, we detected 2×10^4 and 3×10^4 CFU per organ 3 and 5 weeks

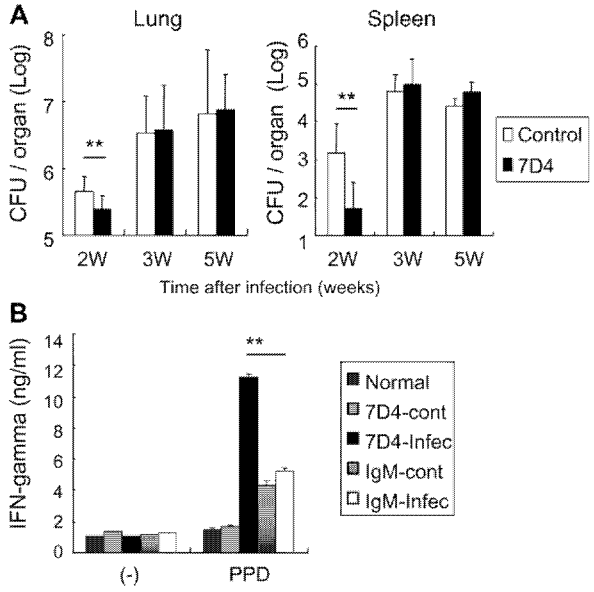

Fig. 3. The effect of CD25$^+$ cell depletion in *Mycobacterium tuberculosis* Erdman infection. (A) Control IgM-treated mice (open bars) and 7D4 anti-CD25 antibody-treated-mice (closed bars) were aerogenically infected with 5 × 10^6 CFU of *M. tuberculosis* Erdman. Bacterial numbers of lungs and spleens were measured at 2, 3 and 5 weeks post-infection. $^{**}P < 0.01$ versus control mice. (B) CD4$^+$ T cells from non-infected mice with 7D4 treatment (7D4-cont), *M. tuberculosis*-infected mice with 7D4 treatment (7D4-Infec), non-infected mice with control IgM treatment (IgM-cont) or *M. tuberculosis*-infected mice with control IgM treatment (IgM-Infec) were cultured with APC in the presence (PPD) or absence (−) of 10 μg ml^{-1} PPD for 7 days. Production of IFN-gamma in the culture supernatants was analyzed. $^{**}P < 0.01$: *Mycobacterium tuberculosis*-infected mice with control IgM treatment (IgM-Infec) versus *M. tuberculosis*-infected mice with 7D4 treatment (7D4-Infec).

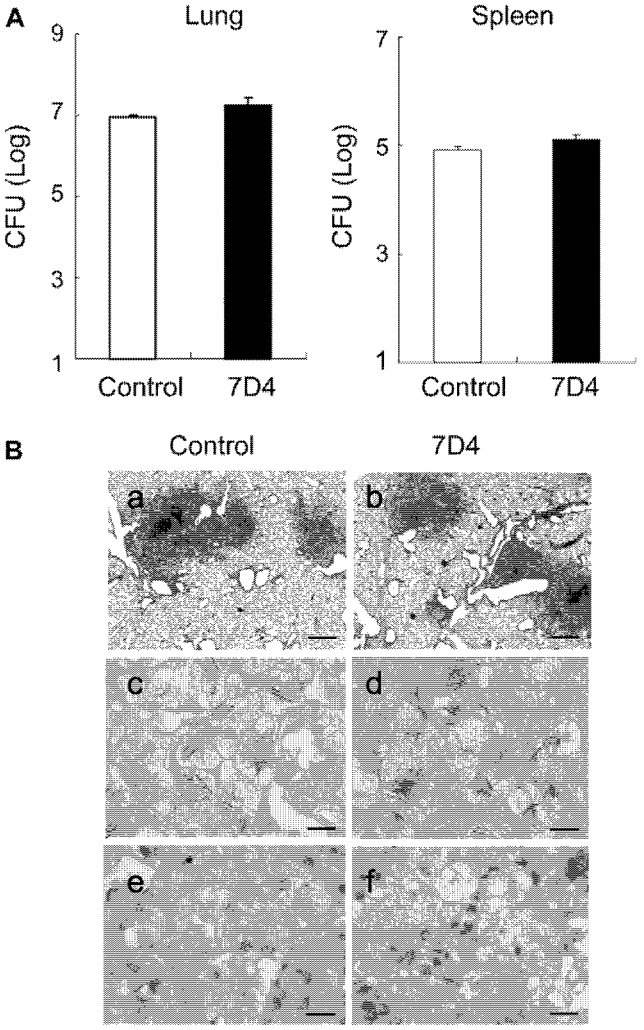

Fig. 4. The effect of depletion of CD25$^+$ cell in chronically infected mice with *M. tuberculosis*. DBA/2 mice were aerogenically infected with 5 × 10^6 CFU of *M. tuberculosis* H37Rv. Two months after infection, mice were treated with 1 mg of 7D4 or control IgM three times with 4 days interval. Five days later from final treatment, mice were sacrificed and analyzed. (A) Bacterial numbers in lungs (left panel) and spleens (right panel) of mice treated with control IgM (open bars) or 7D4 (closed bars). (B) Lung sections were stained with H&E (a and b), Ziehl–Neelsen (c and d) and Giemsa (e and f). Granulomas mainly consisted epithelioid macrophages (e and f). Numerous acid-fast bacteria were observed in granulomas of both control IgM- and 7D4-treated mice. (a, c and e) Lungs sections from mice treated with control IgM. (b, d and f) Lungs sections from mice treated with 7D4. Bars, 500 μm (a and b), 10 μm (c–f). Bars represent mean ±standard deviation of eight mice.

post-challenge, respectively (Fig. 2A). Depletion of CD25$^+$ cells resulted in significantly lower bacterial number in both lung and spleen 3 weeks after challenge; however, this effect became marginal 5 weeks post-challenge (Fig. 2A). Numerous bacteria were observed in granulomas of 7D4-treated and control mice after infection (Fig. 2B, e and f), consistent with higher bacterial burdens revealed by plating of organ homogenates (Fig. 2A). Histological examination of the lung correlated with the CFU results; 3 weeks post-infection, depletion of CD25$^+$ cells resulted in decreased granuloma formation compared with mice treated with control IgM, but normalized 5 weeks after challenge [Fig. 2B(a–d) and C]. Histopathology showed that granuloma cellular composition did not differ between 7D4-treated mice and control mice, which consisted predominately of epithelioid macrophages (Fig. 2B, g and h). Thus in *M. tuberculosis* Kurono infection, the effect of CD25$^+$ cell depletion was limited to the early phase of infection only.

To determine whether the transient effect of CD25$^+$ cells is specific for *M. tuberculosis* Kurono, we performed similar experiments employing another commonly used mycobacterial strain, *M. tuberculosis* Erdman. Similar results were observed in bacterial burdens: 7D4-treated mice revealed significantly lower bacterial numbers than those of IgM-treated mice at early stage (2 weeks post-infection), but not 3 weeks or 5 weeks post-challenge (Fig. 3A). Splenic CD4$^+$ T cells derived from 7D4-treated mice at this time point produced significantly higher levels of IFN-gamma than those of IgM-treated mice when stimulated with PPD (Fig. 3B).

We also examined the effects of depletion of CD25$^+$ cells on the survival of another mycobacterial strain, *Mycobacterium bovis* bacillus Calmette-Guérin (BCG). DBA/2 or BALB/c mice depleted of CD25$^+$ cells by 7D4 were challenged with BCG intravenously and the survival of BCG in the lungs

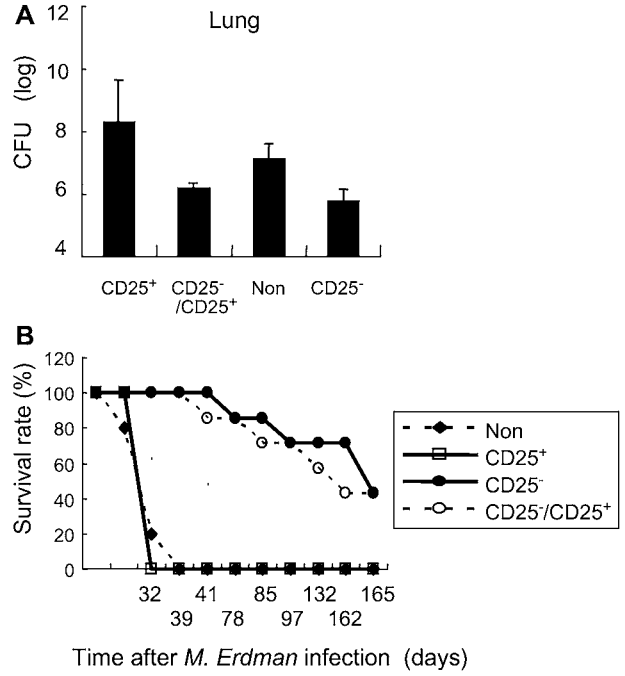

Fig. 5. Bacterial burden and survival kinetics of reconstituted SCID mice with T cell subsets after infection of *Mycobacterium tuberculosis* Erdman. (A) T cell subsets were isolated from spleens of chronically BCG-infected mice. SCID mice were reconstituted with 7.5×10^5 of $CD4^+CD25^+$ T cells only ($CD25^+$), 7.5×10^5 of $CD4^+CD25^-$ T cells and 7.5×10^4 of $CD4^+CD25^+$ T cells ($CD25^-/CD25^+$), untransferred (Non), and 7.5×10^5 of $CD4^+CD25^-$ T cells only ($CD25^-$). One day after reconstitution, naive or T cell subset-reconstituted SCID mice were aerogenically infected with 5×10^6 CFU *M. tuberculosis* Erdman. (B) Survival rates of naive or reconstituted SCID mice after infection. Time course of survival was examined up to 165 days post-infection. Five to eight mice per group were analyzed.

post-challenge was monitored. Unlike *M. tuberculosis*, there was no marked increase in BCG levels in the mouse lungs. Depletion of $CD25^+$ cells did not alter the survival ratio of BCG in the lungs of DBA/2 and BALB/c mice 3 and 5 weeks post-infection, although *in vitro* stimulation with PPD, lymphocytes derived from 7D4-treated mice at 3 weeks after challenge produced higher amount of IFN-gamma than those from control IgM-treated mice (data not shown).

Depletion of $CD25^+$ cells in the chronic stage of infection does not affect the bacterial burdens and pathology

We next examined the effects of depletion of $CD25^+$ cells in the late stage of mycobacterial infection. DBA/2 mice were airborne-infected with *M. tuberculosis* H37Rv and $CD25^+$ cells were depleted by 7D4 treatment after 60, 65 and 70 days later. Five days later from the final treatment of 7D4, we analyzed the bacterial burden and histology in the organs. Bacterial numbers of lungs and spleens in 7D4-treated mice were rather slightly higher than those in control IgM-treated mice; however, significant differences were not observed (Fig. 4A). Pulmonary granuloma formation was conspicuous in both 7D4-treated mice and control IgM-treated mice (Fig. 4B, a and b). Cellular composition of granuloma did not differ between 7D4-treated mice and control mice and numerous bacteria were observed in both groups of mice (Fig. 4B, c–f).

$CD4^+CD25^+$ T cells do not suppress protection induced by $CD4^+CD25^-$ T cells against M. tuberculosis infection in reconstituted mice

To further evaluate the role of $CD4^+CD25^+$ Treg cells in mycobacterial infection at late stage (after developing acquired immunity), the following experiment was conducted. $CD4^+CD25^-$ T cells and $CD4^+CD25^+$ T cells were purified from chronically BCG-infected mice: >90% of the $CD4^+CD25^+$ T cells obtained expressed FoxP3 as estimated by FACScan (data not shown). Each T cell subset, either alone or in combination, was then transferred into SCID mice and mice were infected with *M. tuberculosis* Erdman by airborne exposure. Three weeks post-infection, the bacterial number in lungs (Fig. 5A) and survival kinetics of mice (Fig. 5B) were analyzed.

Observed increases in *M. tuberculosis* were similar in both naive SCID mice and SCID mice reconstituted with $CD4^+CD25^+$ T cells alone, suggesting that $CD4^+CD25^+$ T cells offer no protection against *M. tuberculosis*. In contrast, SCID mice reconstituted with $CD4^+CD25^-$ T cells controlled *M. tuberculosis* infection, at a similar level to that of mice reconstituted with the combination of $CD4^+CD25^-$ T cells and $CD4^+CD25^+$ T cells (Fig. 5A). The survival kinetics showed similar outcomes between mice reconstituted with $CD4^+CD25^-$ T cells plus $CD4^+CD25^+$ T cells and $CD4^+CD25^-$ effector T cells alone (Fig. 5B). These data suggest that the role of $CD4^+CD25^+$ Treg cells in host protection is marginal against *M. tuberculosis* in the overall course of infection (Fig. 5B).

Stimulation with mycobacterial antigens fails to express the function of $CD4^+CD25^+$ Treg cells in vitro

To ascertain why $CD4^+CD25^+$ Treg cells have only a minor role in the late stage of mycobacterial infection, we compared the action of $CD4^+CD25^+$ T cells to $CD4^+CD25^-$ T cells *in vitro*. $CD4^+CD25^+$ and $CD4^+CD25^-$ T cells were isolated from normal mice or mice chronically infected with BCG or *M. tuberculosis* and stimulated with PPD or anti-CD3 mAb in the presence of APCs. $CD4^+CD25^+$ T cells alone showed characteristics of Treg cells, which neither proliferate nor produce cytokines in response to neither PPD nor anti-CD3 mAb (Fig. 6, A–J and a–e). Culture experiments using a combination of $CD4^+CD25^+$ and $CD4^+CD25^-$ T cells showed that $CD4^+CD25^+$ T cells derived from both normal and infected mice suppressed proliferation of $CD4^+CD25^-$ T cells and production of cytokines, such as IFN-gamma and IL-10, in a dose-dependent manner following stimulation with anti-CD3 mAb, showing the characteristics in Treg cells. However, following stimulation with PPD, $CD4^+CD25^+$ T cells failed to suppress both proliferation and production of cytokines. In contrast, IL-2 production was suppressed in a dose-dependent manner in the presence of PPD. Definitive IL-6 production was observed when $CD4^+CD25^-$ T cells were incubated alone or combination with $CD4^+CD25^+$ T cells in the presence of PPD (Fig. 6, I, J and e).

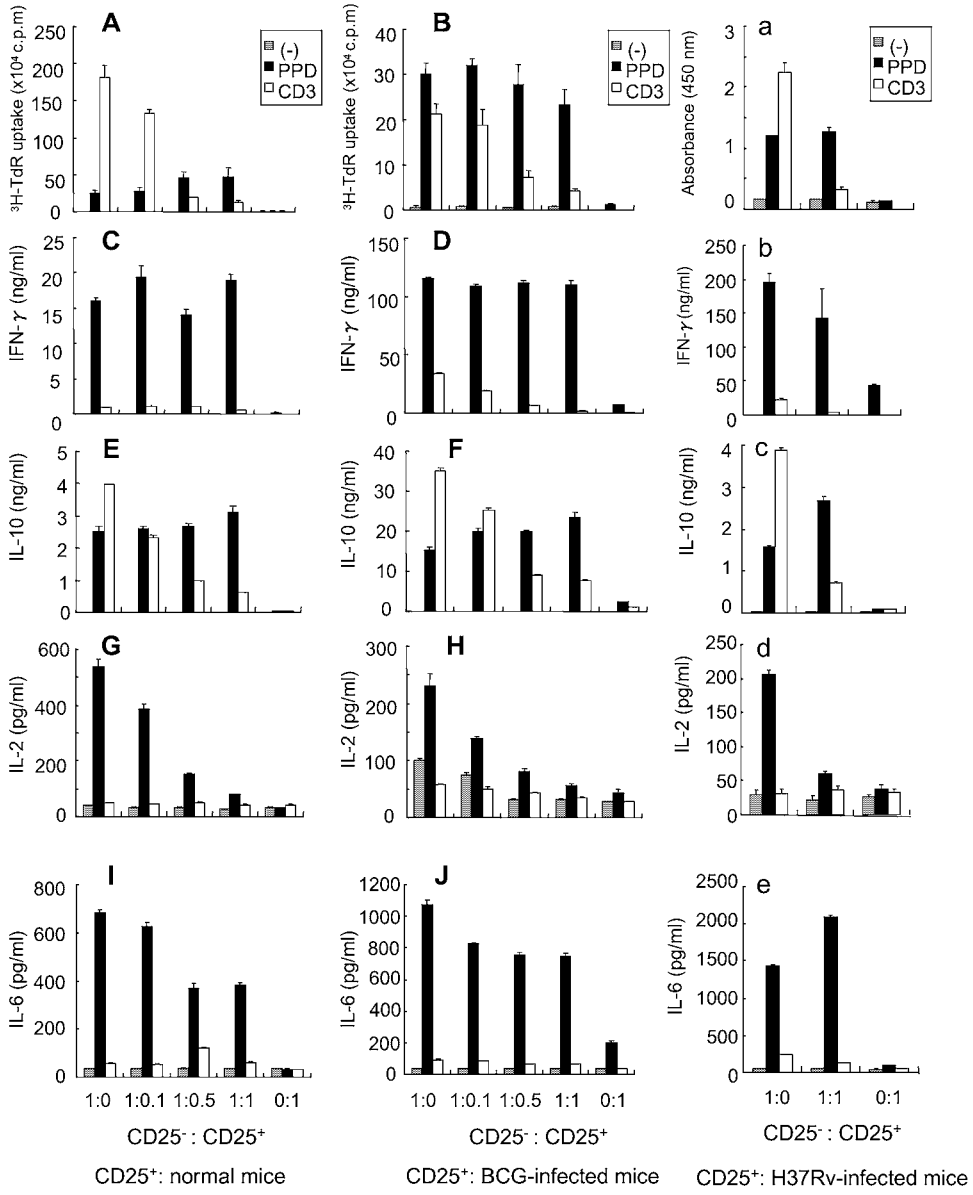

Fig. 6. Stimulation of CD4$^+$CD25$^+$ T cells by PPD fails to suppress the function of PPD-activated CD4$^+$CD25$^-$ T cells. CD4$^+$CD25$^+$ T cells (CD25$^+$) purified from normal (A, C, E, G and I) mice or mice chronically infected with BCG (B, D, F, H and J) or *Mycobacterium tuberculosis* (a–e) were co-cultured with CD4$^+$CD25$^-$ effector T cells (CD25$^-$) purified from mice chronically infected with BCG or *M. tuberculosis* at various ratios with T cell-depleted irradiated spleen cells (APCs) in the presence of PPD (PPD), or anti-CD3 mAb (CD3), or alone (–). Proliferative responses were analyzed at day 5 (A, B and a). Cytokine production in culture supernatants was measured at day 7 (C, E, I, J and b–e) or day 5 (D, F, G and H).

Soluble mediators are not suppressive factors of CD4$^+$CD25$^+$ Treg cell function when stimulated with PPD

Because IL-6 allows effector T cells to overcome suppression by CD4$^+$CD25$^+$ Treg cells (27), we considered the possibility that IL-6 inhibits the function of CD4$^+$CD25$^+$ Treg cells when stimulated with *M. tuberculosis*-derived mycobacterial antigen, PPD. Therefore, we neutralized IL-6 by neutralizing mAb; however, neutralization of IL-6 did not recover suppressive activity of CD4$^+$CD25$^+$ Treg cells (Fig. 7A and B).

To determine whether soluble factors beside IL-6 abrogate the suppressive function of CD4$^+$CD25$^+$ Treg cells upon PPD stimulation, we examined the effects of soluble factors released from T cells and APCs. The culture supernatants from CD4$^+$CD25$^+$ T cells cultured with both CD4$^+$CD25$^-$ T cells and APCs in the presence of PPD or anti-CD3 mAb were collected and then transferred to fresh culture of CD4$^+$CD25$^-$ T cells, CD4$^+$CD25$^+$ T cells and APCs in the presence or absence of anti-CD3 mAb. The proliferative response of CD4$^+$CD25$^-$ effector T cells was analyzed by incorporation of [^{3}H]TdR. The results showed that the supernatants of combined CD4$^+$CD25$^-$ and CD4$^+$CD25$^+$ T cell culture failed to diminish suppressive activity of proliferative response of CD4$^+$CD25$^-$ T cells by CD4$^+$CD25$^+$ T cell stimulated with anti-CD3 mAb (Fig. 8). These results show

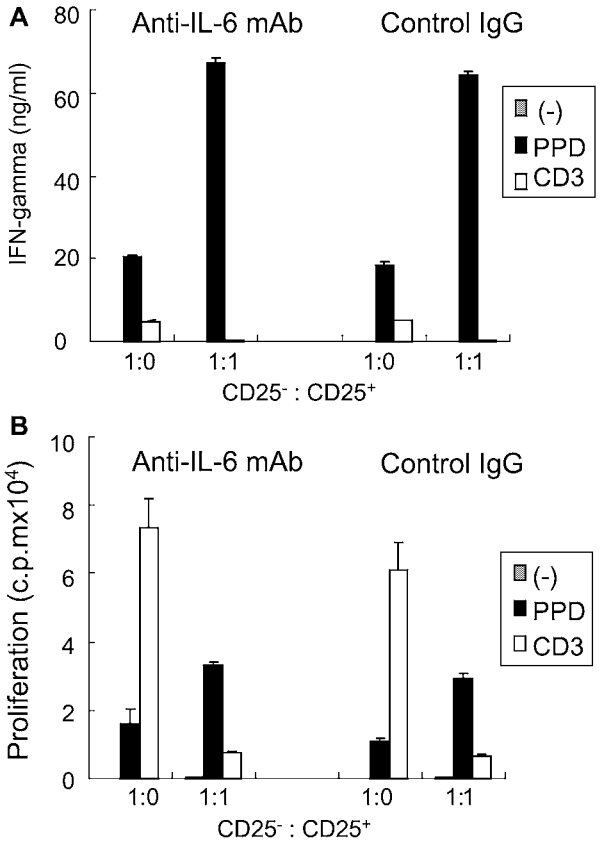

Fig. 7. Neutralization of IL-6 does not affect the $CD4^+CD25^+$ T cell-mediated suppression of the function of effector T cells. $CD4^+CD25^-$ T cells and $CD4^+CD25^+$ T cells were isolated from mice chronically infected with BCG. $CD4^+CD25^-$ effector T cells alone (1:0) or combination of $CD4^+CD25^-$ effector T cells and $CD4^+CD25^+$ T cells (1:1) were cultured with APCs in the presence of PPD (PPD), anti-CD3 mAb (CD3) or absence of these (–). In each well, 0.02 μg ml^{-1} of anti-IL-6 mAb or control IgG were added. IFN-gamma production in culture supernatant (A) and proliferative responses of T cells (B) were analyzed at day 4.

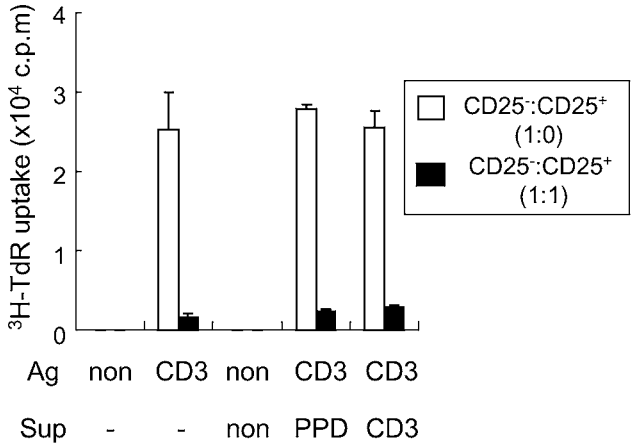

Fig. 8. Soluble mediators upon PPD stimulation do not abrogate $CD4^+CD25^+$ T cell-mediated suppression. $CD4^+CD25^-$ effector T cells ($CD25^-$) and $CD4^+CD25^+$ T cells ($CD25^+$) were isolated from spleens of chronically BCG-infected mice. $CD4^+CD25^-$ T cells/$CD4^+CD25^+$ T cells/APC (1:0:0.1) or $CD4^+CD25^-$ T cells/$CD4^+CD25^+$ cells/APC (1:1:0.1) were cultured with PPD (Sup, PPD), anti-CD3 mAb (Sup, CD3) or alone (Sup, non), for 7 days. Each culture supernatant was stored. Freshly isolated $CD4^+CD25^-$ T cells/$CD4^+CD25^+$ cells/APC (1:0:0.1) or $CD4^+CD25^-$ T cells/$CD4^+CD25^+$ cells/APC (1:1:0.1) were cultured 1:1stored supernatant: fresh culture medium in the presence (Ag, CD3) or absence (Ag, non) of anti-CD3 mAb. Proliferative responses were analyzed at day 4.

that the defective function of $CD4^+CD25^+$ Treg cells following PPD stimulation was not dependent on soluble factors released from T cells and APCs.

Activated $CD4^+CD25^+$ Treg cells suppress the function of PPD-stimulated $CD4^+CD25^-$ effector T cells

Two possibilities could explain the lack of effect of PPD-stimulated $CD4^+CD25^+$ Treg cells on the function of $CD4^+$ $CD25^-$ T cells. First, that activated $CD4^+CD25^+$ Treg cells fail to suppress the function of $CD4^+CD25^-$ T cells by mycobacterial antigens, and second that $CD4^+CD25^+$ Treg cells are not activated by mycobacterial antigens at the late stage of infection. To investigate these possibilities, we purified $CD4^+CD25^+$ T cells from chronically infected mice with BCG or *M. tuberculosis*, then activated *in vitro* with anti-CD3/CD28 mAb-coated beads in the presence of recombinant IL-2. The cells were then cultured with $CD4^+CD25^-$ T cells derived from BCG- or *M. tuberculosis*-infected mice in the presence of PPD. We found that activated $CD4^+CD25^+$ T cells unequivocally suppressed both proliferation and production of IFN-gamma of $CD4^+CD25^-$ T cells stimulated with PPD (Figs 9 and 10). Thus, our data show that both BCG and *M. tuberculosis* infection activate antigen-specific $CD4^+CD25^-$ effector T cells, but not $CD4^+CD25^+$ Treg cells, at the late stage of infection.

Discussion

$CD4^+CD25^+$ Treg cells play a pivotal role in self-tolerance and autoimmune diseases and also in the progression of infectious diseases. It has been shown that $CD4^+CD25^+$ Treg cells are preventive against eradication of persistent pathogens, such as *Leishmania* protozoa, herpes simplex virus and HIV (17–20). Mycobacteria are major parasitic bacteria for eukaryotes (28). In this study, we investigated the role of $CD4^+CD25^+$ Treg cells in mycobacteria infection in mice.

We first studied the effects of Treg cell depletion against infection of mycobacteria. At the early stage of infection, depletion of $CD25^+$ cells significantly suppressed the growth of virulent *M. tuberculosis* strains, such as Kurono and Erdman, suggesting a role for $CD4^+CD25^+$ Treg cells in exacerbation of tuberculosis at the early stage of infection. This is consistent with the previous study performed by Kursar *et al.* (22). This effect of $CD4^+CD25^+$ Treg cells is presumably mediated through naturally occurring $CD4^+CD25^+$ Treg cells, which can be activated through Toll-like receptor (TLR)-mediated signaling (29–32). Mycobacterial DNA [TLR9 ligand (33)] and lipoproteins [TLR2 ligand (34)] may participate in activation of naturally occurring $CD4^+CD25^+$ Treg cells at this stage.

Two to three weeks post-infection, acquired immunity is evident (35). IFN-gamma producing T-helper 1 cells (T_h1) are major effectors in suppressing intracellular survival of

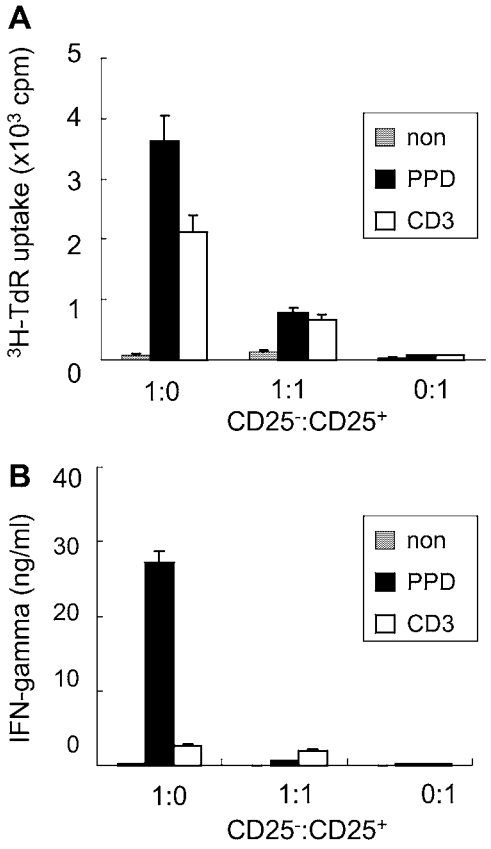

Fig. 9. *In vitro* activation of CD4$^+$CD25$^+$ T cells derived from BCG-infected mice inhibits the function of PPD-stimulated CD4$^+$CD25$^-$ effector T cells. CD4$^+$CD25$^+$ T cells obtained from chronically BCG-infected mice were activated by incubation with anti-CD3/CD28 mAb-coated beads at a bead:cell ratio 2:1 in the presence of 2000 U ml^{-1} of recombinant mouse IL-2 for 48 h. Activated CD4$^+$CD25$^+$ T cells were co-cultured with freshly isolated CD4$^+$CD25$^-$ effector T cells in the presence of PPD (filled column), anti-CD3 mAb (open column) or alone (gray column). (A) Proliferation of CD4$^+$CD25$^-$ effector T cells wase analyzed at day 4. (B) IFN-gamma production in the culture supernatant as measured at day 7.

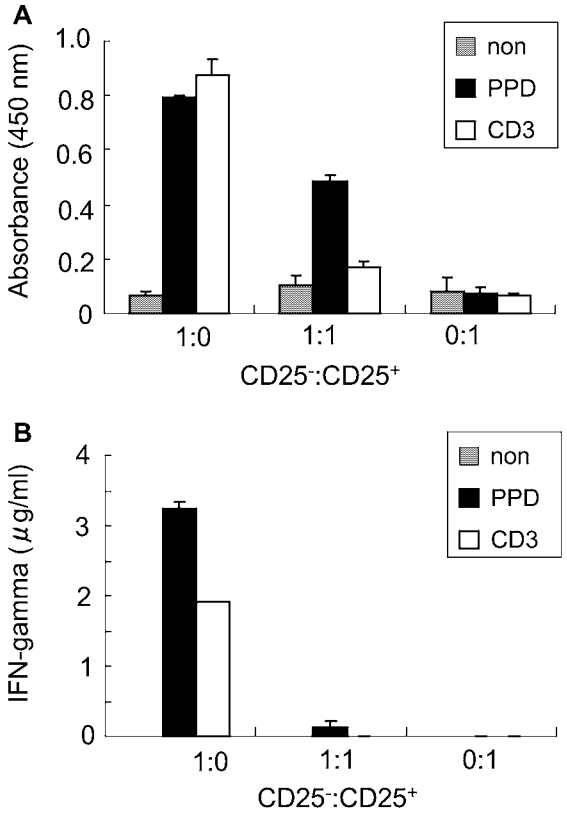

Fig. 10. *In vitro* activation of CD4$^+$CD25$^+$ T cells derived from *Mycobacterium tuberculosis*-infected mice inhibit the function of PPD-stimulated CD4$^+$CD25$^-$ effector T cells. CD4$^+$CD25$^+$ T cells obtained from chronically *M. tuberculosis* H37Rv-infected mice were activated by incubation with anti-CD3/CD28 mAb-coated beads at a bead:cell ratio of 2:1 in the presence of 2000 U ml^{-1} of recombinant mouse IL-2 for 48 h. Activated CD4$^+$CD25$^+$ T cells were co-cultured with freshly isolated CD4$^+$CD25$^-$ effector T cells in the presence of PPD (filled column), anti-CD3 mAb (open column) or alone (gray column). (A) Proliferation of CD4$^+$CD25$^-$ effector T cells was analyzed at day 4. (B) IFN-gamma production in the culture supernatant as measured at day 7.

mycobacteria (36–38). In the CD25$^+$ cell-depletion experiments, the advantages of CD25$^+$ cell depletion were diminished 3 and 5 weeks after the challenge of *M. tuberculosis* Erdman and Kurono, respectively (Figs 2 and 3). We also found that persistence of BCG in mice is not altered by depletion of CD25$^+$ cells by 7D4 (data not shown). These data can be explained by the short-action profile of antibodies. However, we could not find any effect of depletion of CD25$^+$ cells at the chronic stage of infection (Fig. 4), when bacterial numbers were sustained at the same level (39). Similar results were obtained using another anti-CD25 mAb PC6C1, which causes significant reduction of the number of persistent *Leishmania major* in mice by suppressing CD4$^+$CD25$^+$ Treg cells (personal communication with Dr Alan Sher). Furthermore, our *in vivo* experiments in reconstituted SCID mice further suggest that the role of CD4$^+$CD25$^+$ Treg is minimal after infection is established (Fig. 5). The survival kinetics of mice reconstituted with CD4$^+$CD25$^-$ T cells alone are comparable to those in mice reconstituted with both CD4$^+$CD25$^-$ effector T cells and CD4$^+$CD25$^+$ Treg cells (10:1). These data indicate that CD4$^+$CD25$^+$ Treg cells have no impact on the overall outcome of *M. tuberculosis* infection. Kursar *et al.* suggested that CD4$^+$CD25$^+$ Treg cells prevent the bactericidal immune response based on data analyzed in RAG-KO mice reconstituted with each T cell subset (22). However, they reconstituted mice with T cells from naive animals at an unphysiological ratio of CD4$^+$CD25$^-$ T cells to CD4$^+$CD25$^+$ T cells (2:1). These differences may explain the discrepancy between studies.

In order to elucidate the cellular mechanisms of the minimal effect of CD4$^+$CD25$^+$ Treg cells in *M. tuberculosis* infection after the infection was established, we evaluated the function of CD4$^+$CD25$^+$ Treg cells *in vitro*. We activated each population of CD4$^+$ T cells derived from naive and BCG- or *M. tuberculosis*-chronically infected mice with anti-CD3 mAb or *M. tuberculosis*-derived antigens, PPD. BCG has >99.5% identical genome with that of *M. tuberculosis* (40) and therefore BCG and *M. tuberculosis* share almost identical antigens. CD4$^+$CD25$^+$ T cells suppressed anti-CD3-induced

activation (proliferation, production of IFN-gamma and IL-10) of $CD4^+CD25^-$ effector T cells whereas, reflecting our *in vivo* data, PPD stimulation failed to suppress the function of $CD4^+CD25^-$ effector T cells. Both $CD4^+CD25^-$ and $CD4^+CD25^+$ T cells consume IL-2 to proliferate or maintain the state but only $CD25^+CD25^-$ effector T cells produce IL-2. Thus, the level of IL-2 inversely correlated with the number of $CD4^+CD25^+$ T cells (Fig. 6G, H and d) is considered the results of consumption of IL-2 by $CD4^+CD25^+$ T cells but not functional suppression.

One of mechanisms of diminished Treg cell function is mediated by IL-6, which is produced by activated APC through TCR signaling (27). We observed obvious production of IL-6 with PPD stimulation, although which cells produced IL-6 was unknown (Fig. 6, I, J and e). However, neither IL-6 nor other soluble factors released from cells were involved in the non-functional property of $CD4^+CD25^+$ Treg cells following PPD stimulation (Fig. 8). An explanation for this phenomenon is that PPD-specific $CD4^+CD25^+$ Treg cells are not activated at the late stage of mycobacterial infection because $CD4^+CD25^+$ Treg cells activated by anti-CD3/CD28 suppress the function of $CD4^+CD25^-$ effector T cells following stimulation with PPD (Figs 9 and 10).

With the exception of one recent study on herpes simplex virus infection (41), $CD4^+CD25^+$ Treg cells are thought to support parasite persistence in the host by inhibiting the function of effector T cells by a variety of mechanisms. According to this theory, several reports regarding mycobacterial infection have suggested a role for $CD4^+CD25^+$ Treg cells in disease progression and establishment of latent infection (22, 25, 42). However, our findings refute this theory, because $CD4^+CD25^+$ cells did not affect the total infectious load of *M. tuberculosis* in mice (Fig. 5) and mycobacterial infection did not activate mycobacteria-specific $CD4^+CD25^+$ Treg cells (Figs 6, 9 and 10). Several reports showed that FoxP3-positive Treg cells are found in the site of infection with BCG or *M. tuberculosis* (23, 25, 42). However, we consider that these Treg cells are unresponsive to mycobacterial antigens, rather than responding to self-antigens in the disrupted tissues of the infectious legion (43).

In contrast, $CD4^+CD25^+$ Treg cells responding to parasite antigens are activated during infection of *Leishmania* (17, 44) and *Plasmodium* (21). These parasites more closely resemble mammals in the history of evolution; therefore, it can be speculated that they express antigens similar to mammalian self-antigens, which leads to activation of self-antigen-reactive $CD4^+CD25^+$ Treg cells (43). This may be a possible reason for the discrepancy of the host response to mycobacteria versus protozoa. The host must recognize pathogens to survive and mycobacteria represent major bacterial pathogens for vertebrates. In our study, the fact that effector T cells are activated in response to mycobacterial antigens, while suppressive $CD4^+CD25^+$ Treg cells are comparatively silent, is rational based on the host's need to protect itself from mycobacterial infection.

Funding

Japan Health Sciences Foundation; Ministry of Health, Labour and Welfare (Research on Emerging and Re-emerging Infectious Diseases, Health Sciences Research Grants); Ministry of Education, Culture, Sports, Science and Technology; Osaka City University Urban Research; Biochemical Tokyo Research Foundation, and The United States-Japan Cooperative Medical Science Program Against Tuberculosis Leprosy.

Acknowledgements

We would like to thank Dr Toshiki Tamura and Dr Hidefumi Kojima for their advice and Mr Satoru Iwatani for technical support of FACS analysis. We also thank Dr Saburo Yamamoto and Miss Sara Matsumoto for heartfelt encouragement. The authors have no conflicting financial interests.

References

1 Dye, C., Scheele, S., Dolin, P., Pathania, V. and Raviglione, M. C. 1999. Consensus statement. Global burden of tuberculosis: estimated incidence, prevalence, and mortality by country. WHO Global Surveillance and Monitoring Project. *JAMA* 282:677.
2 Jouanguy, E., Altare, F., Lamhamedi, S. *et al.* 1996. Interferon-gamma-receptor deficiency in an infant with fatal bacille Calmette-Guerin infection. *N. Engl. J. Med.* 335:1956.
3 Newport, M. J., Huxley, C. M., Huston, S. *et al.* 1996. A mutation in the interferon-gamma-receptor gene and susceptibility to mycobacterial infection. *N. Engl. J. Med.* 335:1941.
4 Sakaguchi, S. 2000. Regulatory T cells: key controllers of immunologic self-tolerance. *Cell* 101:455.
5 Sakaguchi, S. 2004. Naturally arising CD4+ regulatory t cells for immunologic self-tolerance and negative control of immune responses. *Annu. Rev. Immunol.* 22:531.
6 Shevach, E. M. 2001. Certified professionals: CD4(+)CD25(+) suppressor T cells. *J. Exp. Med.* 193:F41.
7 Read, S., Malmstrom, V. and Powrie, F. 2000. Cytotoxic T lymphocyte-associated antigen 4 plays an essential role in the function of CD25(+)CD4(+) regulatory cells that control intestinal inflammation. *J. Exp. Med.* 192:295.
8 Takahashi, T., Tagami, T., Yamazaki, S. *et al.* 2000. Immunologic self-tolerance maintained by CD25(+)CD4(+) regulatory T cells constitutively expressing cytotoxic T lymphocyte-associated antigen 4. *J. Exp. Med.* 192:303.
9 Shimizu, J., Yamazaki, S., Takahashi, T., Ishida, Y. and Sakaguchi, S. 2002. Stimulation of CD25(+)CD4(+) regulatory T cells through GITR breaks immunological self-tolerance. *Nat. Immunol.* 3:135.
10 McHugh, R. S., Whitters, M. J., Piccirillo, C. A. *et al.* 2002. CD4(+)CD25(+) immunoregulatory T cells: gene expression analysis reveals a functional role for the glucocorticoid-induced TNF receptor. *Immunity* 16:311.
11 Hori, S., Nomura, T. and Sakaguchi, S. 2003. Control of regulatory T cell development by the transcription factor Foxp3. *Science* 299:1057.
12 Sakaguchi, S., Yamaguchi, T., Nomura, T. and Ono, M. 2008. Regulatory T cells and immune tolerance. *Cell* 133:775.
13 Asseman, C., Mauze, S., Leach, M. W., Coffman, R. L. and Powrie, F. 1999. An essential role for interleukin 10 in the function of regulatory T cells that inhibit intestinal inflammation. *J. Exp. Med.* 190:995.
14 Gorelik, L. and Flavell, R. A. 2000. Abrogation of TGFbeta signaling in T cells leads to spontaneous T cell differentiation and autoimmune disease. *Immunity* 12:171.
15 Takahashi, T., Kuniyasu, Y., Toda, M. *et al.* 1998. Immunologic self-tolerance maintained by CD25+CD4+ naturally anergic and suppressive T cells: induction of autoimmune disease by breaking their anergic/suppressive state. *Int. Immunol.* 10:1969.
16 Thornton, A. M. and Shevach, E. M. 1998. CD4+CD25+ immunoregulatory T cells suppress polyclonal T cell activation *in vitro* by inhibiting interleukin 2 production. *J. Exp. Med.* 188:287.
17 Belkaid, Y., Piccirillo, C. A., Mendez, S., Shevach, E. M. and Sacks, D. L. 2002. CD4+CD25+ regulatory T cells control Leishmania major persistence and immunity. *Nature* 420:502.
18 Suvas, S., Kumaraguru, U., Pack, C. D., Lee, S. and Rouse, B. T. 2003. CD4+CD25+ T cells regulate virus-specific primary and memory CD8+ T cell responses. *J. Exp. Med.* 198:889.

19 Aandahl, E. M., Michaelsson, J., Moretto, W. J., Hecht, F. M. and Nixon, D. F. 2004. Human CD4+ CD25+ regulatory T cells control T-cell responses to human immunodeficiency virus and cytomegalovirus antigens. *J. Virol.* 78:2454.
20 Lundgren, A., Suri-Payer, E., Enarsson, K. *et al.* 2003. Helicobacter pylori-specific $CD4^+$ CD25high regulatory T cells suppress memory T-cell responses to H. pylori in infected individuals CD4 T cell activation by myelin oligodendrocyte glycoprotein is suppressed by adult but not cord blood $CD25^+$ T cells. *Infect. Immun.* 71:1755.
21 Hisaeda, H., Maekawa, Y., Iwakawa, D. *et al.* 2004. Escape of malaria parasites from host immunity requires $CD4^+$ $CD25^+$ regulatory T cells. *Nat. Med.* 10:29.
22 Kursar, M., Koch, M., Mittrucker, H. W. *et al.* 2007. Cutting Edge: regulatory T cells prevent efficient clearance of Mycobacterium tuberculosis. *J. Immunol.* 178:2661.
23 Quinn, K. M., McHugh, R. S., Rich, F. J. *et al.* 2006. Inactivation of CD4+ CD25+ regulatory T cells during early mycobacterial infection increases cytokine production but does not affect pathogen load. *Immunol. Cell Biol.* 84:467.
24 Quinn, K. M., Rich, F. J., Goldsack, L. M. *et al.* 2008. Accelerating the secondary immune response by inactivating CD4(+)CD25(+) T regulatory cells prior to BCG vaccination does not enhance protection against tuberculosis. *Eur. J. Immunol.* 38:695.
25 Scott-Browne, J. P., Shafiani, S., Tucker-Heard, G. *et al.* 2007. Expansion and function of Foxp3-expressing T regulatory cells during tuberculosis. *J. Exp. Med.* 204:2159.
26 Kaneko, H., Yamada, H., Mizuno, S. *et al.* 1999. Role of tumor necrosis factor-alpha in *Mycobacterium*-induced granuloma formation in tumor necrosis factor-alpha-deficient mice. *Lab. Invest.* 79:379.
27 Pasare, C. and Medzhitov, R. 2003. Toll pathway-dependent blockade of CD4+CD25+ T cell-mediated suppression by dendritic cells. *Science* 299:1033.
28 Flynn, J. L. and Chan, J. 2001. Immunology of tuberculosis. *Annu. Rev. Immunol.* 19:93.
29 Caramalho, I., Lopes-Carvalho, T., Ostler, D., Zelenay, S., Haury, M. and Demengeot, J. 2003. Regulatory T cells selectively express toll-like receptors and are activated by lipopolysaccharide. *J. Exp. Med.* 197:403.
30 Crellin, N. K., Garcia, R. V., Hadisfar, O., Allan, S. E., Steiner, T. S. and Levings, M. K. 2005. Human CD4+ T cells express TLR5 and its ligand flagellin enhances the suppressive capacity and expression of FOXP3 in CD4+CD25+ T regulatory cells. *J. Immunol.* 175:8051.
31 Peng, G., Guo, Z., Kiniwa, Y. *et al.* 2005. Toll-like receptor 8-mediated reversal of CD4+ regulatory T cell function. *Science* 309:1380.
32 Sutmuller, R. P., den Brok, M. H., Kramer, M. *et al.* 2006. Toll-like receptor 2 controls expansion and function of regulatory T cells. *J. Clin. Invest.* 116:485.
33 Bafica, A., Scanga, C. A., Feng, C. G., Leifer, C., Cheever, A. and Sher, A. 2005. TLR9 regulates Th1 responses and cooperates with TLR2 in mediating optimal resistance to *Mycobacterium tuberculosis*. *J. Exp. Med.* 202:1715.
34 Thoma-Uszynski, S., Stenger, S., Takeuchi, O. *et al.* 2001. Induction of direct antimicrobial activity through mammalian toll-like receptors. *Science* 291:1544.
35 North, R. J. and Jung, Y. J. 2004. Immunity to tuberculosis. *Annu. Rev. Immunol.* 22:599.
36 Flynn, J. L., Chan, J., Triebold, K. J., Dalton, D. K., Stewart, T. A. and Bloom, B. R. 1993. An essential role for interferon gamma in resistance to *Mycobacterium tuberculosis* infection. *J. Exp. Med.* 178:2249.
37 Cooper, A. M., Dalton, D. K., Stewart, T. A., Griffin, J. P., Russell, D. G. and Orme, I. M. 1993. Disseminated tuberculosis in interferon gamma gene-disrupted mice. *J. Exp. Med.* 178:2243.
38 Scanga, C. A., Mohan, V. P., Yu, K. *et al.* 2000. Depletion of CD4(+) T cells causes reactivation of murine persistent tuberculosis despite continued expression of interferon gamma and nitric oxide synthase 2. *J. Exp. Med.* 192:347.
39 Jung, Y. J., LaCourse, R., Ryan, L. and North, R. J. 2002. Evidence inconsistent with a negative influence of T helper 2 cells on protection afforded by a dominant T helper 1 response against Mycobacterium tuberculosis lung infection in mice. *Infect. Immun.* 70:6436.
40 Behr, M. A., Wilson, M. A., Gill, W. P. *et al.* 1999. Comparative genomics of BCG vaccines by whole-genome DNA microarray. *Science* 284:1520.
41 Lund, J. M., Hsing, L., Pham, T. T. and Rudensky, A. Y. 2008. Coordination of early protective immunity to viral infection by regulatory T cells. *Science* 320:1220.
42 Roberts, T., Beyers, N., Aguirre, A. and Walzl, G. 2007. Immunosuppression during active tuberculosis is characterized by decreased interferon- gamma production and CD25 expression with elevated forkhead box P3, transforming growth factor-beta, and interleukin-4 mRNA levels. *J. Infect. Dis.* 195:870.
43 Nishikawa, H., Kato, T., Tawara, I. *et al.* 2005. Definition of target antigens for naturally occurring CD4(+) CD25(+) regulatory T cells. *J. Exp. Med.* 201:681.
44 Mendez, S., Reckling, S. K., Piccirillo, C. A., Sacks, D. and Belkaid, Y. 2004. Role for CD4(+) CD25(+) regulatory T cells in reactivation of persistent leishmaniasis and control of concomitant immunity. *J. Exp. Med.* 200:201.

Biochemical and Biophysical Research Communications 392 (2010) 277–282

Contents lists available at ScienceDirect

Biochemical and Biophysical Research Communications

journal homepage: www.elsevier.com/locate/ybbrc

Genetic immunization based on the ubiquitin-fusion degradation pathway against *Trypanosoma cruzi*

Bin Chou [a,b], Kenji Hiromatsu [a,*], Hajime Hisaeda [b], Xuefeng Duan [b], Takashi Imai [b], Shigeo Murata [c], Keiji Tanaka [c], Kunisuke Himeno [b]

[a] *Department of Microbiology and Immunology, Faculty of Medicine, Fukuoka University, 7-45-1 Nanakuma, Jonan-ku, Fukuoka 814-0180, Japan*
[b] *Department of Parasitology, Graduate School of Medical Science, Kyushu University, Fukuoka 812-8582, Japan*
[c] *Department of Molecular Oncology, The Tokyo Metropolitan Institute of Medical Science, Tokyo 113-8613, Japan*

ARTICLE INFO

Article history:
Received 15 December 2009
Available online 7 January 2010

Keywords:
Amastigote surface protein-2
Trypanosoma cruzi
DNA vaccine
Ubiquitin-fusion degradation

ABSTRACT

Cytotoxic $CD8^+$ T cells are particularly important to the development of protective immunity against the intracellular protozoan parasite, *Trypanosoma cruzi*, the etiological agent of Chagas disease. We have developed a new effective strategy of genetic immunization by activating $CD8^+$ T cells through the ubiquitin-fusion degradation (UFD) pathway. We constructed expression plasmids encoding the amastigote surface protein-2 (ASP-2) of *T. cruzi*. To induce the UFD pathway, a chimeric gene encoding ubiquitin fused to ASP-2 (pUB-ASP-2) was constructed. Mice immunized with pUB-ASP-2 presented lower parasitemia and longer survival period, compared with mice immunized with pASP-2 alone. Depletion of $CD8^+$ T cells abolished protection against *T. cruzi* in mice immunized with pUB-ASP-2 while depletion of $CD4^+$ T cells did not influence the effective immunity. Mice deficient in LMP2 or LMP7, subunits of immunoproteasomes, were not able to develop protective immunity induced. These results suggest that ubiquitin-fused antigens expressed in antigen-presenting cells were effectively degraded via the UFD pathway, and subsequently activated $CD8^+$ T cells. Consequently, immunization with pUB-ASP-2 was able to induce potent protective immunity against infection of *T. cruzi*.

Introduction

Trypanosoma cruzi is an intracellular protozoan hemoflagellate parasite of humans and many other mammals. It is also the etiological pathogen of Chagas disease. Patients infected with *T. cruzi* have been treated with many kinds of drugs, but those therapies are hardly effective in chronically infected individuals. Furthermore, parasites that are naturally resistant to chemotherapy have been reported in various regions of Latin America [1].

T cell-mediated immunity, especially via $CD8^+$ cytotoxic T lymphocytes (CTL), has been demonstrated to play a crucial role in resolving *T. cruzi* infection in humans and mice [2]. Antigens recognized by $CD8^+$ T cells are first processed by the ubiquitin proteasome system (UPS) [3]. $CD8^+$ T cells then recognize antigenic epitopes presented by major histocompatibility complex (MHC) class I molecules on the surface of infected host cells. As a result, *T. cruzi* is cleared by cytolysis of parasite-infected host cells [4]. Activation of $CD8^+$ T cells requires antigen-processing through the UPS prior to presentation in association with MHC class I molecules [5].

Recently, it was reported that an artificially fused mono-ubiquitin and antigenic protein was readily directed to the proteasome, and those antigenic peptides are then effectively presented on antigen-presenting cells (APCs). This virtual pathway of UPS was named the ubiquitin-fusion degradation (UFD) pathway [6]. This immunization strategy is effective in maximizing $CD8^+$ T cell-responses against those antigenic peptides. We previously reported that immunization with naked DNA encoding an antigen artificially fused to a mono-ubiquitin is an efficient strategy for the induction of antigen-specific immunity mediated by $CD8^+$ T cells [7].

A number of antigens of *T. cruzi* recognized by the immune system have been defined at the molecular level in the last decade [8,9]. Genetic immunization strategies have recently become popular and attractive for prophylaxis and therapy against infection of *T. cruzi*. It has been shown that amastigote surface protein-2 (ASP-2) is one of the targets for $CD8^+$ T cells and contains CTL epitopes such as the H-$2K^b$ restricted VNHRFTLV [10]. Based on these facts, we developed a new strategy for genetic immunization employing

Abbreviations: *T. cruzi*, *Trypanosoma cruzi*; UFD, ubiquitin-fusion degradation; ASP-2, amastigote surface protein-2; UPS, ubiquitin proteasome system

* Corresponding author. Fax: +81 92 801 9390.
E-mail address: khiromatsu@fukuoka-u.ac.jp (K. Hiromatsu).

0006-291X/$ - see front matter © 2010 Elsevier Inc. All rights reserved.
doi:10.1016/j.bbrc.2009.12.166

the UFD pathway. Expression plasmids encoding ASP-2 fused to a mono-ubiquitin (pUB-ASP-2) were constructed. Mice immunized with pUB-ASP-2 exhibited a low parasitemia and survived longer compared with mice in the control group; while immunization with pASP-2 alone was scarcely effective. $CD8^+$ T cells exerted ASP-2 specific cytotoxic activities and IFN-γ secretion. Application of the UFD pathway for genetic immunization was confirmed by using immunoproteasome deficient mice such as PA28α/β, LMP2 or LMP7 KO mice.

Materials and methods

Animals and parasites. Female 8-week old C57BL/6 (B6) mice were purchased from Seac Yoshitomi (Fukuoka, Japan). Proteasome activator PA28 knockout ($PA28\alpha/\beta^{-/-}$) and immunoproteasome subunit LMP2 or LMP7 knockout ($LMP2^{-/-}$ or $LMP7^{-/-}$) mice were B6 background. The Tulahuen strain of *T. cruzi* was maintained by weekly passage in B6 mice.

Cloning and sequencing. Total RNA was isolated from liver sections obtained from *T. cruzi* infected B6 mice and reverse-transcribed to cDNA. ASP-2 cDNA was amplified by PCR using sense, 5′-ATGCTCTCACGTGTTGCTGCTGTC-3′, and antisense 5′-TTA GTCGCCACCGTTTCCTTTTTTATCG-3′ primers. Specific oligonucleotides were designed on the basis of the previously published nucleotide sequence of *asp-2* [11]. The resulting amplicon was ligated into a pGEM-T easy vector (Promega, USA) and transformed into DH5α *Escherichia coli* (Invitrogen, USA). Clones containing inserts of the expected size were selected. Sequencing was initially performed using SP6 and T 7 primers, the sequences of which were present in the flanking regions of the pGEM-T easy vector. Subsequently, to complete sequencing of each clone, new oligonucleotides were designed to cover the entire sequence.

DNA and predicted amino acid sequences were analyzed using the Lasergene 7.1 software package (DNASTAR Inc., USA). Sequence alignments were produced using Clustal V. Analysis for potential secretory signal peptides (SP) was performed at the SignalP website (http://www.cbs.dtu.dk/services/SignalP/).

Plasmids. A plasmid encoding ASP-2 (aa65–703, signal peptide deleted) and tagged with His residues (pASP-2) was constructed by amplifying *asp-2* from clone 2 using the following primers: 5′-GCATCCTCGAGATGGCTGTGGAGGGTAAGTCCGGG-3′, 5′-GTCATCTTAAGTTAGTGATGGTGGTGATGGTGGTCGCCACCGTTTCCTTTTTTATCG-3′. PCR products were treated with enzymes and inserted into the XhoI and AflII sites of the pcDNA3.1(−) vector (Invitrogen, USA). The pUB vector we made previously was used to construct pUB-ASP-2 (aa65–703, SP deleted) and tagged with His [7]. The gene *asp-2*, was cut from pASP-2 and inserted into the XhoI and AflII sites of the pUB vector.

In vivo gene transfer and challenge of T. cruzi. As described previously, a Helios Gene Gun (BioRad, USA) was used [12]. Protocols of immunization and infection with *T. cruzi* trypomastigotes were same with previous description [12].

In vitro transfection and Western blotting. Protocols of transfection and Western immunoblotting were same as described previously [12,13].

Cytotoxicity assay, ELISA and flow cytometry. Protocols of cytotoxicity assay, ELISA and flow cytometry were same as described previously [12,13].

Statistical analysis. Data are expressed as mean ± SEM. Differences between experimental groups within each experiment were analyzed by using the unpaired Student's *t*-test and were considered significant when the *p*-value was <0.05. Survival differences between experimental groups within each experiment were analyzed by using the log-rank test and were considered significant when the *p*-value was <0.05.

Results

Construction of plasmids encoding ASP-2 or UB-ASP-2

The *asp-2* gene is polymorphic, as its sequence is different even in the same strains of *T. cruzi* [14]. In this study, we obtained four clones of the *asp-2* gene from the Tulahuen strain and picked up one particular clone (clone 2: GenBank Accession No. GU445326). Compared with the original sequence of the Brazil strain (GenBank Accession No. U77951) and the sequence of the Tulahuen strain (GenBank Accession No. EF579921), the amino acid sequence of ASP-2 used in this study contained the ASP box motif (SxDxGxTW) and the VTV box motif (VTVxNVxLYNR) (Fig. 1A). The amino acid identity of ASP-2 used in this study compared with the Brazil strain is 89.8%, and 83.1% when compared with the Tulahuen strain. The H-$2K^b$ restricted CTL epitope (aa553–560, VNHSFTLV) contains a single amino acid change when compared with the Brazil strain [15], and two amino acid changes when compared with the Tulahuen strain [14]. ASP-2 and UB-ASP-2 expression plasmids were constructed as described in the materials and methods section (Fig. 1B). Construction of pASP-2 and pUB-ASP-2 was confirmed by DNA sequencing. The expression of ASP-2 or the fusion protein UB-ASP-2 was confirmed by Western immunoblotting after transfection of COS7 cells with these plasmids; a specific band was detected in lysates from cells transfected with pASP-2 or pUB-ASP-2 (Fig. 1C).

Anti-parasite immunity against T. cruzi was induced by immunization with pUB-ASP-2

CTL epitopes are produced through the ubiquitin–proteasome pathway and we expected that antigen presentation of MHC class I-associated ASP-2 peptides to $CD8^+$ T cells would become significantly more efficient following immunization with pUB-ASP-2. To verify this, B6 mice were immunized with pcDNA, pASP-2 or pUB-ASP-2 into the abdominal skin by using a gene-gun system four times, at two-week intervals. Two weeks following the last immunization, mice were challenged with 1000 blood-derived *T. cruzi* trypomastigotes by subcutaneous injection at the base of the tail. Mice immunized with pUB-ASP-2 developed a lower parasitemia than control pcDNA immunized groups (Fig. 2A); survival was also prolonged by immunization with pUB-ASP-2 (Fig. 2B). Six out of seven pUB-ASP-2 immunized mice survived until the end of the experiment. Mice immunized with pASP-2 did not develop a protective response suggesting that artificial fusion of the gene encoding mono-ubiquitin and the ASP-2 protein was required for the induction of immunity.

Immune response following immunization with pUB-ASP-2

To investigate the mechanism of protective immunity conferred by immunization with pUB-ASP-2, spleen cells separated from mice immunized with pcDNA, pASP-2 or pUB-ASP-2, were co-cultured with the non-specific stimulator PMA. Production of intracellular IFN-γ and Granzyme b (GZM-b) by T cells was analyzed using flow cytometry. Intracellular IFN-γ and GZM-b was strongly induced in $CD8^+$ T cells of mice immunized with pUB-ASP-2 (Fig. 3A). The absolute number of both IFN-γ^+CD8^+ T cells and GZM-b^+CD8^+ T cells in the spleen was significantly higher in pUB-ASP-2 immunized mice (Fig. 3B). There was no significant difference in the IFN-γ and GZM-b secretion level of $CD4^+$ T cells. Production of IFN-γ and GZM-b in $CD4^+$ T cells was at almost the same level in mice treated with pcDNA, pASP-2 or pUB-ASP-2 (data not shown). These results indicate that immunization with pUB-ASP-2 promotes $CD8^+$ T cell activation, and enhances the expression level of IFN-γ and GZM-b in $CD8^+$ T cells.

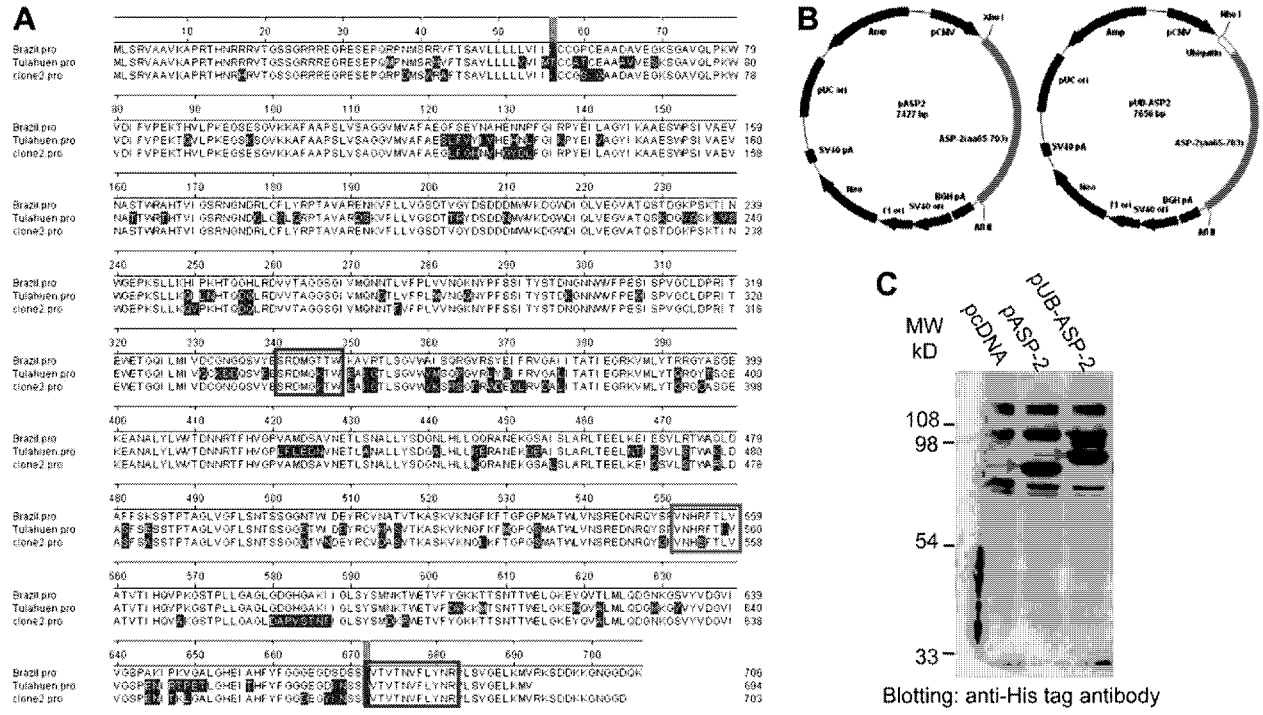

Fig. 1. Sequence of ASP-2, plasmid construction and expression *in vivo*. (A) Predicted amino acid sequence of ASP-2 clone 2 (GenBank Accession No. GU445326) and comparison with predicted amino acid sequences of Brazil (GenBank Accession No. U77951) and Tulahuen (GenBank Accession No. EF579921) strains. Letters marked in red are different from the original sequence of the Brazil strain. Letters highlighted in blue indicate the ASP box motif (SxDxGxTW) and the VTV box motif (VTVxNVxLYNR). Letters highlighted with a red box indicate the H-2K^b restricted CTL epitope. (B) Schematic representation of pASP-2 (upper panel) and pUB-ASP-2 (lower panel). (C) Expression of ASP-2 or UB-ASP-2 in COS7 cells. Sizes of the molecular weight markers are shown on the left.

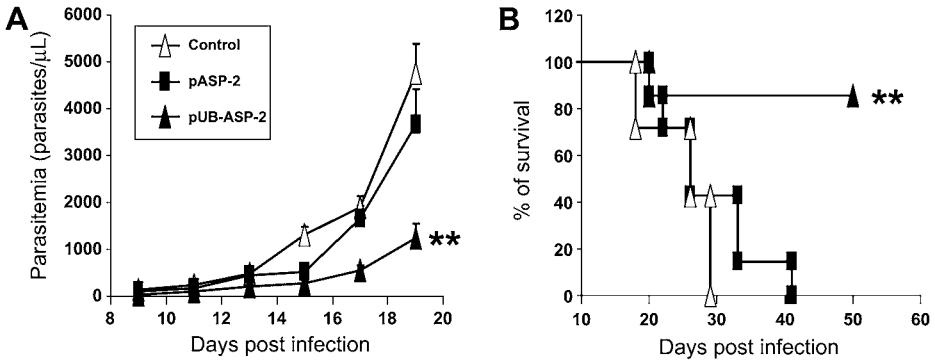

Fig. 2. Induction of anti-parasite immunity by immunization with pUB-ASP-2. C57BL/6 mice were immunized with pcDNA (open triangles), pASP-2 (closed squares) or pUB-ASP-2 (closed triangles), and then challenged with 1000 blood-derived *T. cruzi* trypomastigotes. Mice were scored on the basis of parasitemia (A) and survival (B). (A) Each value represents the mean ± SEM from seven mice in each group. $^{**}p < 0.02$ compared with other groups by the Student's *t*-test. (B) Results are expressed as the percentages of surviving mice in groups of seven. $^{**}p < 0.02$ compared with other groups by the log-rank test.

Antigen-specific CD8$^+$ T cells are activated by immunization with pUB-ASP-2

To confirm that these activated CD8$^+$ T cells were specific to ASP-2, we cultured splenocytes with the ASP-2 CTL epitope (VNHSFTLV) and then measured the production of IFN-γ and GZM-b by performing intracellular FACS. As expected, the percentage and absolute cell number of IFN-γ$^+$ or GZM-b$^+$ CD8$^+$ T cells in pUB-ASP-2 immunized mice were significantly higher than in mice immunized with pcDNA or pASP-2 (Fig. 3C and D). No differences in production of IFN-γ and GZM-b were seen in CD4$^+$ T cells between the control and immunized mice (data not shown).

The amount of secreted IFN-γ in supernatants from spleen cells stimulated with the ASP-2 epitopes was measured by ELISA. The production of IFN-γ in the supernatant from mice immunized with pUB-ASP-2 was significantly higher than those from mice immunized with pcDNA or pASP-2 (Fig. 3E).

To clarify the ASP-2 specific cytotoxic activity of CD8$^+$ T cells, we examined the CTL activity of CD8$^+$ T cells isolated from mice immunized with pUB-ASP-2. Compared with other immunized groups, CTL activities of CD8$^+$ T cells isolated from mice immunized with pUB-ASP-2 were prominent in H-2^b-bearing EL4 cells pulsed with ASP-2 epitopes (Fig. 3F). This clearly demonstrated that ASP-2 specific CD8$^+$ T cells were specifically activated by immunization with pUB-ASP-2.

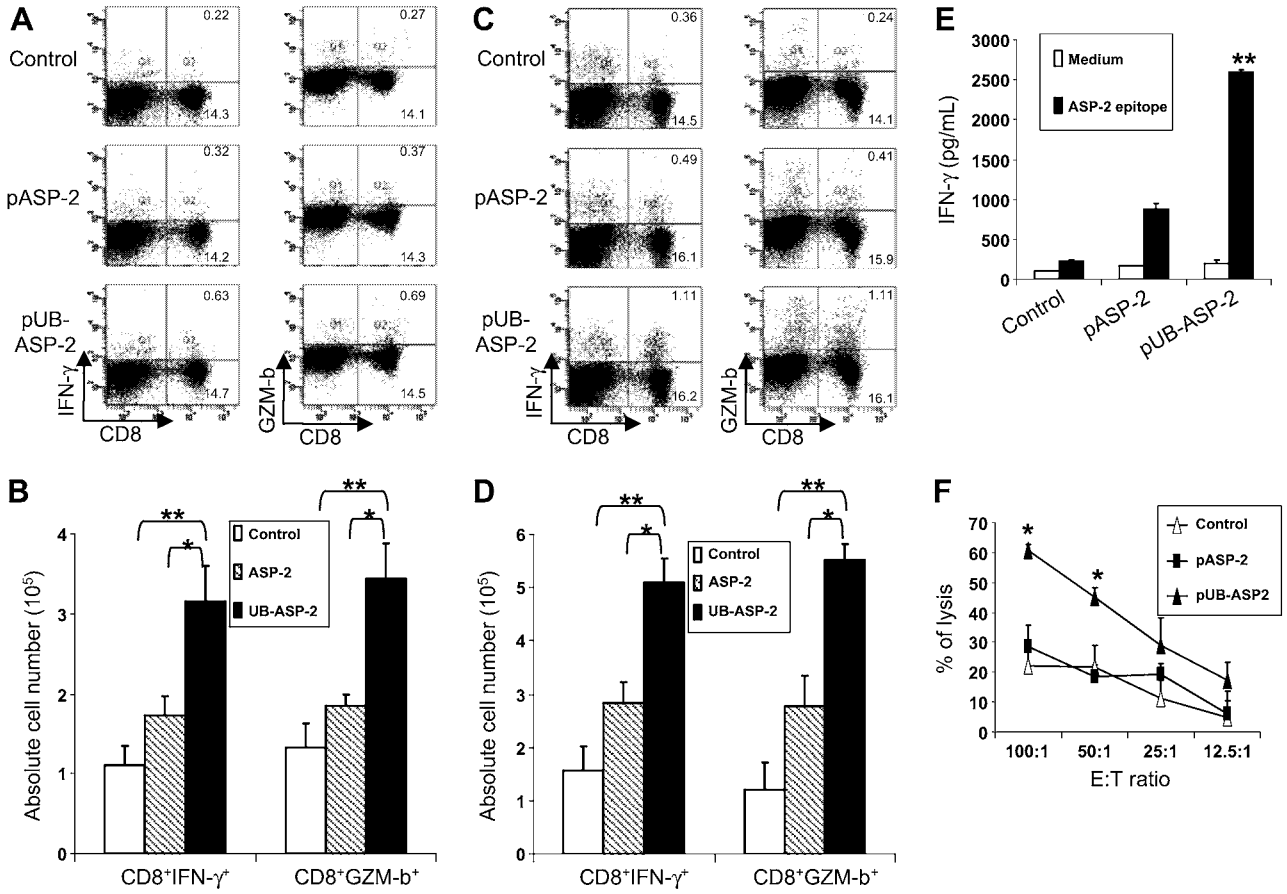

Fig. 3. Functional analysis of splenocytes in mice immunized with pUB-ASP-2. Immunized mice were sacrificed 10 days after the last booster injection. (A and B) Spleen cells were isolated and re-stimulated with PMA for 4 h *in vitro*. (A) Percentage of IFN-γ or Granzyme b positive cells was measured using a FACScan flow cytometer. (B) Total cell number is also indicated. $^{**}p < 0.02$ compared with control group by the Student's *t*-test. $^{*}p < 0.05$ compared with the pASP-2 group by the Student's *t*-test. (C–F) Spleen cells were isolated and re-stimulated with CTL epitope for 4 days *in vitro*. (C) Percentage of IFN-γ or Granzyme b positive cells was measured using FACScan flow cytometer. (D) Total cell number is also indicated. $^{**}p < 0.02$ compared with control group by the Student's *t*-test. $^{*}p < 0.05$ compared with the pASP-2 group by the Student's *t*-test. (E) IFN-γ secretion in the supernatant was measured. $^{**}p < 0.02$ compared with other groups by the Student's *t*-test. (F) CTL activity of $CD8^+$ T cells was measured. $^{*}p < 0.05$ compared with other groups by the Student's *t*-test.

Anti-parasite immunity induced by pUB-ASP-2 was dependent on $CD8^+$ T cells

To assess the role of $CD8^+$ T cells *in vivo*, we depleted $CD4^+$ or $CD8^+$ T cells by treatment with specific antibodies one day before infection with *T. cruzi*. Mice depleted of $CD8^+$ T cells showed a higher parasitemia compared with control mice (Fig. 4A) and died earlier than mice in other groups (Fig. 4B). $CD4^+$ T cells were not required for the effector phase to clear and resist infection with *T. cruzi* as evaluated by parasitemia and survival rate, indicating the efficiency of immunization with pUB-ASP-2 was solely dependent upon $CD8^+$ T cells *in vivo*. These results are also consistent with what we previously reported regarding a DNA vaccine against *T. cruzi* using TSA-1 as a target gene [12].

Degradation of UB-ASP-2 is dependent on proteasome in vitro

Physical binding between ASP-2 with mono-ubiquitin was crucial for the activation of ASP-2 specific $CD8^+$ T cells. This finding indicates that after artificial binding of mono-ubiquitin to ASP-2, the *ub-asp-2* gene products are rapidly degraded by the proteasome through the UFD pathway. Thus, ASP-2 epitopes are efficiently presented to MHC class I molecules, resulting in effective induction of $CD8^+$ T cells specific for the CTL epitope in ASP-2. These hypotheses were confirmed by our Western immunoblotting results. COS7 cells transfected with plasmids in the presence of the proteasome inhibitor MG-132, significantly repressed degradation of UB-ASP-2 proteins, resulting in an accumulation of UB-ASP-2 proteins (Fig. 4C). There was no difference in the amount of ASP-2 proteins present in cells whether MG-132 was present or absent. As shown in Fig. 4D, normalized to HSP90, the detectable amount of UB-ASP-2 proteins was approximately 40% lower without MG-132. These results clearly indicate that fusion of ASP-2 with a mono-ubiquitin renders the chimeric protein susceptible to degradation via the UFD pathway and the increased production of ASP-2 epitopes via the UFD pathway leads to efficient antigen presentation to $CD8^+$ T cells.

The critical role of the immunoproteasome in induction of protective immunity by pUB-ASP-2

We used mice deficient in the proteasome regulator PA28 complex (α/β) or the immunoproteasome subunits LMP2 or LMP7 to clarify whether induction of anti-parasite immunity by pUB-ASP-2 immunization is dependent on the immunoproteasome through the UFD pathway *in vivo* [16–18]. Protection against *T. cruzi* induced by pUB-ASP-2 was completely abolished in LMP2 or LMP7 knockout (KO) mice. These KO mice immunized with pUB-ASP-2 or pcDNA3.1 had a similar survival rate (Fig. 4E). Survival time was prolonged in PA28α/β KO mice immunized with pUB-ASP-2 after *T. cruzi* infection, but decreased when compared with wild-type mice immunized with pUB-ASP-2 (Fig. 4E). These data indi-

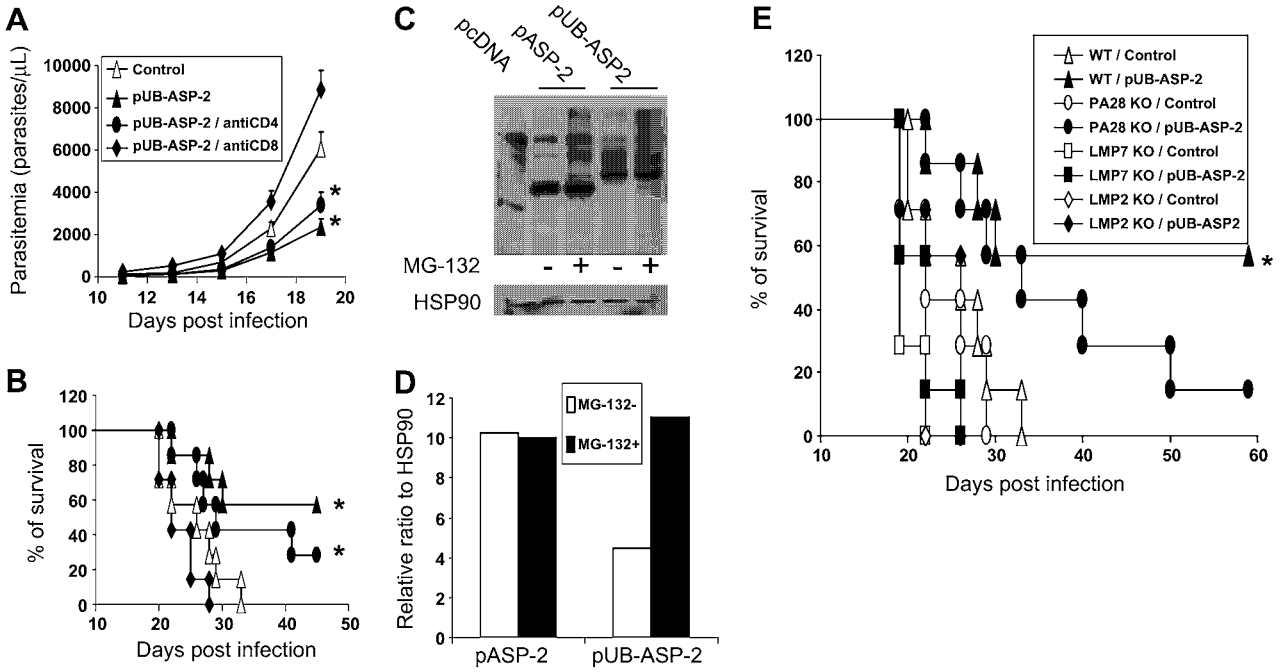

Fig. 4. Effects of immunization with pUB-ASP-2 were dependent on $CD8^+$ T cells *in vivo*; and critical involvement of the proteasome in the processing of UB-ASP-2 proteins *in vitro* and the effect of immunization with pUB-ASP-2 *in vivo*. (A and B) Mice were immunized with pUB-ASP-2 three times and treated with anti-CD4 (500 μg/mice) or anti-CD8 (500 μg/mice) depletion antibodies at one day before the challenge with *T. cruzi*. (A) Parasitemia levels of each group of mice. $^*p < 0.05$ compared with the control group by the Student's *t*-test. (B) The survival of each group of mice. $^*p < 0.05$ compared with the control group by the log-rank test. (C) COS7 cells transfected with pcDNA3.1(−), pASP-2 or pUB-ASP-2 were cultured with or without MG-132. Cell lysates were used for Western immunoblotting and proteins detected with an anti-His antibody (upper panel) or anti-HSP90 antibody (lower panel). (D) Relative expression to HSP90 was calculated using densitometry. (E) Survival rate of immunoproteasome subunit deficient mice. PA28α/β$^{-/-}$, LMP2$^{-/-}$ and LMP7$^{-/-}$ mice were immunized with the control plasmid pcDNA3.1 or pUB-ASP-2. $^*p < 0.05$ compared with the wild type/control group by the log-rank test.

cate that immunoproteasomes play critical roles in producing ASP-2 epitopes and thus activating ASP-2 specific $CD8^+$ T cells by immunization with pUB-ASP-2.

Discussion

$CD8^+$ T cells are important for host resistance against *T. cruzi* infection [2] as they are intracellular protozoan parasites. Many antigenic peptides of *T. cruzi* have been identified as potential vaccine candidates in the last decade [8,9], including the peptides of the *T. cruzi* trans-sialidase family and the trans-sialidase-like family. Trypomastigote surface antigen-1 (TSA-1), a member of the *T. cruzi* trans-sialidase family is expressed on the trypomastigote, but not on the amastigote of *T. cruzi*. In mammalian hosts, *T. cruzi* cycles between extracellular, non-replicative trypomastigotes circulating in the blood and intracellular replicative amastigotes. Extracellular trypomastigote appears to be an inappropriate target for $CD8^+$ T cells since the protozoa itself does not express MHC class I molecules. ASP-2 is a recognized antigen of the intracellular amastigote of *T. cruzi*, and includes the CTL epitopes on APCs. In the present study, we employed ASP-2 as the candidate protein for immunization and inducing specific activated $CD8^+$ T cells.

Endogenous antigens are processed by the proteasome after being polyubiquitinated [5]. This type of antigen processing has been accepted as the ubiquitin–proteasome system (UPS) [3]. Antigenic peptides fused with a mono-ubiquitin will be effectively directed to be poly-ubiquitination and the fusion protein then introduced to the UPS and degraded. This virtual route for the UPS is known as the UFD pathway [6]. Based on this mechanism, we developed a novel immunization strategy to activate antigen-specific $CD8^+$ T cells by inducing the UFD pathway [7]. We constructed the plasmid pUB-ASP-2, encoding the ASP-2 protein fused to a mono-ubiquitin. Using an *in vitro* system, we confirmed that ASP-2 artificially fused with ubiquitin was degraded to a large extent in COS7 cells. The detectable amount of UB-ASP-2 in COS7 cells transfected with pUB-ASP-2 was lower than that of ASP-2 in COS7 cells transfected with pASP-2. In the presence of the proteasome inhibitor, MG-132, the degradation of UB-ASP-2 was inhibited. The detectable amount of UB-ASP-2 in pUB-ASP-2 transfected COS7 cells was similar to the levels of ASP-2 in pASP-2 transfected COS7 cells in the presence of MG-132. In accordance with our previous report [7], the UFD pathway plays a central role in removing the CTL epitopes of ASP-2 by degrading the ubiquitinated ASP-2 protein. Subsequently, those CTL epitopes are directed to MHC class I molecules in the endoplasmic reticulum resulting in the activation of ASP-2-specific $CD8^+$ T cells.

In this study, immunization with a plasmid encoding ASP-2 fused to a mono-ubiquitin, induced a very strong protective immunity against *T. cruzi* infection when compared with immunization with ASP-2 alone. ASP-2 specific CTL activity was induced in mice immunized with pUB-ASP-2, and ASP-2 specific production of IFN-γ and GZM-b in $CD8^+$ T cells were also enhanced compared with pASP-2 immunized mice. This protective immunity was ablated in mice where $CD8^+$ but not $CD4^+$ T cells were depleted. Therefore, application of ASP-2 fused with a mono-ubiquitin appeared to be an efficient strategy to induce a $CD8^+$ T cell mediated immune response against *T. cruzi* by activating the UFD pathway.

The immunomodulatory cytokine IFN-γ, which is mainly secreted by activated $CD8^+$ T cells, Th1 cells and NK cells, enhances antigen presentation by modifying proteasome regulators and subunits, in addition to upregulating MHC and TAP genes. IFN-γ regulates the expression of PA28α and PA28β, which form the heptameric proteasome activator complex PA28 [19]. This heteromultimer is able to bind to the α rings of the 20S core proteasome, enhancing proteolytic activity of the proteasome. Studies *in vitro*

have shown that purified PA28α/β can enhance coordinated dual cleavage of the 20S proteasome, resulting in an augmented output and liberation of peptides [20]. IFN-γ also alters the quality of protease activity in the proteasome by incorporating three IFN-γ inducible catalytic subunits, LMP2, LMP7 and MECL-1, to replace the constitutive catalytic subunits (γ/δ, X/MB1 and Z, respectively) in the 20S core proteasome during biogenesis [21]. The 20S core proteasome incorporating LMP2, LMP7 and MECL-1 is known as the immunoproteasome [3]. This IFN-γ inducible immunoproteasome is more favorable than the constitutive proteasome for antigen presentation as subunits induced by IFN-γ stimulate cleavage of hydrophobic, basic and branched chain residues instead of acidic ones [22,23]. To confirm utilization of the UFD pathway is indispensable for $CD8^+$ T cell induction of protective immunity, mice deficient in immunoproteasome subunits were used. The effects of immunization with pUB-ASP-2 was severely impaired in LMP2/7 KO mice, and partially repressed in PA28α/β KO mice. It was thought that the capacity to generate CTL epitopes of ASP-2 was decreased in PA28α/β KO mice, although our results indicate these epitopes were still generated. Both LMP2 and LMP7 have specific cleavage activity after basic or hydrophobic residues of peptides, therefore LMP2 and LMP7 KO mice should not produce ASP-2 epitopes and consequently not activate $CD8^+$ T cells.

In the present study, we immunized mice with plasmids encoding ASP-2 without a signal peptide to minimize the effects of $CD4^+$ T cells, and to diminish the production of ASP-2 specific antibodies in mice after immunization with plasmids. It is interesting that mice immunized with pUB-ASP-2 and treated with anti-CD4 antibodies are still resistant to *T. cruzi* infection. These data indicate that $CD8^+$ T cell-mediated anti-parasite immunity was induced using a novel immunization strategy without the support of $CD4^+$ T cells. It is appealing to apply this strategy of immunization with HIV patients because their $CD4^+$ T cell function is defective [24].

Acknowledgments

This work was supported by grants-in-aid from the Ministry of Education, Science, Sport and Culture of Japan (15019075, 15025255, 15390136, 15659265).

References

[1] E.L. Camandaroba, E.A. Reis, M.S. Goncalves, M.G. Reis, S.G. Andrade, *Trypanosoma cruzi*: susceptibility to chemotherapy with benznidazole of clones isolated from the highly resistant Colombian strain, Rev. Soc. Bras. Med. Trop. 36 (2003) 201–209.
[2] Z. Brener, R.T. Gazzinelli, Immunological control of *Trypanosoma cruzi* infection and pathogenesis of Chagas' disease, Int. Arch. Allergy Immunol. 114 (1997) 103–110.
[3] K. Tanaka, M. Kasahara, The MHC class I ligand-generating system: roles of immunoproteasomes and the interferon-gamma-inducible proteasome activator PA28, Immunol. Rev. 163 (1998) 161–176.
[4] R.L. Tarleton, L. Zhang, Chagas disease etiology: autoimmunity or parasite persistence?, Parasitol Today 15 (1999) 94–99.
[5] C.M. Pickart, Mechanisms underlying ubiquitination, Annu. Rev. Biochem. 70 (2001) 503–533.
[6] E.S. Johnson, P.C. Ma, I.M. Ota, A. Varshavsky, A proteolytic pathway that recognizes ubiquitin as a degradation signal, J. Biol. Chem. 270 (1995) 17442–17456.
[7] M. Zhang, C. Obata, H. Hisaeda, K. Ishii, S. Murata, T. Chiba, K. Tanaka, Y. Li, M. Furue, B. Chou, T. Imai, X. Duan, K. Himeno, A novel DNA vaccine based on ubiquitin-proteasome pathway targeting 'self'-antigens expressed in melanoma/melanocyte, Gene Ther. 12 (2005) 1049–1057.
[8] V.A. Campo, C.A. Buscaglia, J.M. Di Noia, A.C. Frasch, Immunocharacterization of the mucin-type proteins from the intracellular stage of *Trypanosoma cruzi*, Microbes Infect. 8 (2006) 401–409.
[9] B. Wizel, M. Nunes, R.L. Tarleton, Identification of *Trypanosoma cruzi* trans-sialidase family members as targets of protective CD8+ TC1 responses, J. Immunol. 159 (1997) 6120–6130.
[10] H.P. Low, M.A. Santos, B. Wizel, R.L. Tarleton, Amastigote surface proteins of *Trypanosoma cruzi* are targets for CD8+ CTL, J. Immunol. 160 (1998) 1817–1823.
[11] H.P. Low, R.L. Tarleton, Molecular cloning of the gene encoding the 83 kDa amastigote surface protein and its identification as a member of the *Trypanosoma cruzi* sialidase superfamily, Mol. Biochem. Parasitol. 88 (1997) 137–149.
[12] B. Chou, H. Hisaeda, J. Shen, X. Duan, T. Imai, L. Tu, S. Murata, K. Tanaka, K. Himeno, Critical contribution of immunoproteasomes in the induction of protective immunity against *Trypanosoma cruzi* in mice vaccinated with a plasmid encoding a CTL epitope fused to green fluorescence protein, Microbes Infect. 10 (2008) 241–250.
[13] M. Zhang, K. Ishii, H. Hisaeda, S. Murata, T. Chiba, K. Tanaka, Y. Li, C. Obata, M. Furue, K. Himeno, Ubiquitin-fusion degradation pathway plays an indispensable role in naked DNA vaccination with a chimeric gene encoding a syngeneic cytotoxic T lymphocyte epitope of melanocyte and green fluorescent protein, Immunology 112 (2004) 567–574.
[14] C. Claser, N.M. Espindola, G. Sasso, A.J. Vaz, S.B. Boscardin, M.M. Rodrigues, Immunologically relevant strain polymorphism in the Amastigote Surface Protein 2 of *Trypanosoma cruzi*, Microbes Infect. 9 (2007) 1011–1019.
[15] A.V. Machado, J.E. Cardoso, C. Claser, M.M. Rodrigues, R.T. Gazzinelli, O. Bruna-Romero, Long-term protective immunity induced against *Trypanosoma cruzi* infection after vaccination with recombinant adenoviruses encoding amastigote surface protein-2 and trans-sialidase, Hum. Gene Ther. 17 (2006) 898–908.
[16] H.J. Fehling, W. Swat, C. Laplace, R. Kuhn, K. Rajewsky, U. Muller, H. von Boehmer, MHC class I expression in mice lacking the proteasome subunit LMP-7, Science 265 (1994) 1234–1237.
[17] L. Van Kaer, P.G. Ashton-Rickardt, M. Eichelberger, M. Gaczynska, K. Nagashima, K.L. Rock, A.L. Goldberg, P.C. Doherty, S. Tonegawa, Altered peptidase and viral-specific T cell response in LMP2 mutant mice, Immunity 1 (1994) 533–541.
[18] S. Murata, H. Udono, N. Tanahashi, N. Hamada, K. Watanabe, K. Adachi, T. Yamano, K. Yui, N. Kobayashi, M. Kasahara, K. Tanaka, T. Chiba, Immunoproteasome assembly and antigen presentation in mice lacking both PA28alpha and PA28beta, Embo J. 20 (2001) 5898–5907.
[19] M. Rechsteiner, C. Realini, V. Ustrell, The proteasome activator 11 S REG (PA28) and class I antigen presentation, Biochem. J. 345 (Pt 1) (2000) 1–15.
[20] M. Groettrup, A. Soza, M. Eggers, L. Kuehn, T.P. Dick, H. Schild, H.G. Rammensee, U.H. Koszinowski, P.M. Kloetzel, A role for the proteasome regulator PA28alpha in antigen presentation, Nature 381 (1996) 166–168.
[21] P.M. Kloetzel, F. Ossendorp, Proteasome and peptidase function in MHC-class-I-mediated antigen presentation, Curr. Opin. Immunol. 16 (2004) 76–81.
[22] J. Driscoll, M.G. Brown, D. Finley, J.J. Monaco, MHC-linked LMP gene products specifically alter peptidase activities of the proteasome, Nature 365 (1993) 262–264.
[23] M. Gaczynska, K.L. Rock, A.L. Goldberg, Gamma-interferon and expression of MHC genes regulate peptide hydrolysis by proteasomes, Nature 365 (1993) 264–267.
[24] A.K. Vaidian, L.M. Weiss, H.B. Tanowitz, Chagas' disease and AIDS, Kinetoplastid Biol. Dis. 3 (2004) 2.

International Immunology, Vol. 22, No. 12, pp. 941–952
doi:10.1093/intimm/dxq448
Advance Access publication 8 November 2010

Production of IFN-γ by CD4$^+$ T cells in response to malaria antigens is IL-2 dependent

Daisuke Kimura[1], Mana Miyakoda[1], Kiri Honma[1], Yoshisada Shibata[2,3], Masao Yuda[4], Yasuo Chinzei[4] and Katsuyuki Yui[1,3]

[1]Division of Immunology, Department of Molecular Microbiology and Immunology
[2]Atomic Bomb Disease Institute and [3]Global COE program, Graduate School of Biomedical Sciences, Nagasaki University, 1-12-4, Sakamoto, Nagasaki 852-8523, Japan
[4]Department of Medical Zoology, School of Medicine, Mie University, 2-174, Edobashi, Tsu 514-8507, Japan

Correspondence to: K. Yui; E-mail: katsu@nagasaki-u.ac.jp

Received 14 July 2010, *accepted* 1 October 2010

Abstract

T-cell immune responses are critical for protection of the host and for disease pathogenesis during infection with *Plasmodium* species. We examined the regulation of CD4$^+$ T-cell cytokine responses during infection with *Plasmodium berghei* ANKA (PbA). CD4$^+$ T cells from PbA-infected mice produced IFN-γ, IL-4 and IL-10 in response to TCR stimulation at levels higher than those from uninfected mice. This altered cytokine response was dependent on parasitemia. To examine the specificity of the response, mice were adoptively transferred with CD4$^+$ T cells from OT-II TCR transgenic mice and were infected with PbA expressing OVA. Unexpectedly, CD4$^+$ T cells from the OT-II-transferred wild-type PbA-infected mice showed high levels of IFN-γ production after stimulation with OVA and the cells producing IFN-γ were not OT-II but were host CD4$^+$ T cells. Further investigation revealed that host CD4$^+$ T cells produced IFN-γ in response to IL-2 produced by activated OT-II cells. This IFN-γ response was completely inhibited by anti-CD25 mAbs, and this effect was not due to the block of the survival signals provided by IL-2. Furthermore, IFN-γ production by CD4$^+$ T cells in response to PbA antigens was dependent on IL-2. These findings suggest the importance of IL-2 levels during infection with malaria parasites and indicate that CD4$^+$ T cells can produce IFN-γ without TCR engagement via a bystander mechanism in response to IL-2 produced by other activated CD4$^+$ T cells.

Keywords: cytokine, mouse, parasite

Introduction

Malaria is caused by infection of RBCs with parasites of the *Plasmodium* species and remains one of the crucial threats to public health in the world. The critical roles of cellular immunity in protection against the blood stage of malaria infection have been demonstrated in early studies using thymectomized rats and mice depleted of B cells by anti-μ chain antibody treatment (1–3). These studies were confirmed using mice that were rendered B cell deficient by targeted disruption of Ig gene (4, 5). It was also shown that protective immunity can be transferred to naive hosts by adoptive transfer of immune CD4$^+$ T cells (6). IFN-γ produced by T cells as well as NK cells plays a central role in regulating the protective immune response against blood-stage malaria infection (3, 7–9). Mice deficient in IFN-γ or its receptor showed delayed development of protective immunity and high mortality rate after infection with *Plasmodium chabaudi* (10). However, as with other protective immunity, production of this potent cytokine is not always beneficial but rather is harmful for the host in some cases. Pregnant IFN-$\gamma^{-/-}$ mice showed a delay in malaria-induced fetal loss relative to wild-type controls, although these mice experienced a more severe course of infection (11). Neutralization of IFN-γ with its specific mAb early after infection with *Plasmodium berghei* ANKA (PbA) prevented cerebral malaria (12). These studies point to the importance of regulation of IFN-γ levels during malaria infection in order to establish antiparasite immune protection, while maintaining minimum pathogenesis. However, little is known about the regulation of conventional CD4$^+$ T-cell function with respect to IFN-γ production during infection with *Plasmodium* species.

We have examined the cytokine production of CD4$^+$ T cells from mice infected with PbA. These T cells produced little

IL-2 and a large amount of IFN-γ, IL-4 and IL-10 in response to TCR stimulation. Further study indicated that the production of IFN-γ by $CD4^+$ T cells from the infected mice does not necessarily require direct TCR engagement. Rather, these $CD4^+$ T cells produced IFN-γ, IL-4 and IL-10 in response to IL-2. Furthermore, IFN-γ production by $CD4^+$ T cells in response to malaria antigen was dependent on IL-2.

Methods

Mice and P. berghei infection

OT-II transgenic mice expressing the TCR specific for $OVA_{323-339}$/I-A^b were kindly provided by Dr H. Kosaka (Osaka University, Japan) (13), B6.SJL-Ptprc congenic (B6.Ly5.1) mice ($CD45.1^+$) by Dr Y. Takahama (Tokushima University, Japan), Rag-$2^{-/-}$ mice by Dr Y. Yoshikai (Kyushu University, Fukuoka, Japan) (14) and MyD88$^{-/-}$ and TRIF$^{-/-}$ mice by Dr K. Takeda and Dr S. Akira (Osaka University, Japan) (15,16). C57BL/6 (B6) mice were purchased from SLC (Hamamatsu, Japan). OT-II and B6.Ly5.1 mice were bred and offspring were intercrossed to obtain CD45.1 OT-II mice. Rag-$2^{-/-}$ mice and CD45.1 OT-II mice were intercrossed to obtain CD45.1 Rag-$2^{-/-}$ OT-II mice. These mice were maintained in the Laboratory Animal Center for Animal Research at Nagasaki University and were used at the age of 8–14 weeks. OVA-PbA was described previously (17). Mice were infected with wild-type PbA (WT-PbA) or OVA-PbA by intra-peritoneal injection of parasitized RBCs (10^4 infected RBC), monitored by microscopic examination of standard blood films and were sacrificed when parasitemia reached 3.7–15.0% (days 6–8). The animal experiments reported herein were conducted according to the Guidelines of the Laboratory Animal Center for Biomedical Research at Nagasaki University.

Adoptive transfer and flow cytometry

For adoptive transfer, $CD4^+$ T cells were purified using anti-CD4 IMag (BD Biosciences, San Diego, CA, USA), labeled with 5,6-carboxyfluorescein diacetate succinimidyl ester (CFSE) (Invitrogen, Carlsbad, CA, USA) at the final concentration of 15 mM and were injected into the tail vein of B6.Ly5.1 or B6 mice ($0.5–1 \times 10^7$ per mice). After infection with PbA and parasitemia reached 3%, spleen cells were prepared, stained with biotin-anti-CD45.2 plus streptavidin-Cy5 and PE-anti-CD4 mAb and analyzed using FACScan (BD Biosciences) (Fig. 3A). For all other analysis, spleen cells were stained with PE-Cy7-anti-CD45.1 (or anti-CD45.2), PE-Cy7- or allophycocyanin-anti-CD4, PE-anti-CD69, FITC- or PE-anti-CD25, FITC–streptavidin plus biotin-anti-CD122 or PE-anti-CD122, PE-anti-CD62L, FITC-anti-CD44, FITC-anti-TCRβ or allophycocyanin–streptavidin plus biotin-anti-NK1.1 mAb and analyzed using FACSCanto II (BD Biosciences). For cell sorting, purified $CD4^+$ T cells were stained with a combination of allophycocyanin-anti-CD4, FITC-anti-CD44 and PE-anti-CD62L (Fig. 2) or by a combination of PE-anti-CD4, PE-Cy7-anti-CD45.1 and allophycocyanin-anti-CD45.2 mAb (Fig. 4) and were sorted using FACSAria II (BD Biosciences).

For intracellular cytokine staining, $CD4^+$ T cells were stimulated with anti-TCR mAb (H57-597, 10 μg ml^{-1}), dendritic cells (DC) pulsed with $OVA_{323-339}$ (10 μg ml^{-1}) or recombinant IL-2 (10 ng ml^{-1}) for total of 12–24 h with an addition of monensin during the final 6 h. After blocking Fc receptor with mAb (2.4G2), cells were stained with PE-Cy7-anti-CD45.1, allophycocyanin-anti-CD4, FITC-anti-CD44, FITC-anti-CD25, allophycocyanin–streptavidin or FITC–streptavidin, biotin-anti-CD122, biotin-anti-NK1.1 or FITC-anti-TCRβ, fixed, permeabilized and were stained with PE-anti-Foxp3, PE-anti-IL-2, PE-anti-IL-4, FITC- or PE-anti-IL-10, Alexaflour 488- or PE-anti-IFN-γ mAb according to the manufacturer's instructions (BD Biosciences). The ratios of viable cells were determined by staining cells with FITC–annexin V and 7-aminoactinomycin D (7AAD).

Cell culture and ELISA

$CD4^+$ T cells ($2–3 \times 10^5$) were cultured for 24–48 h in 96-well plates coated with anti-TCR mAb (H57-597, 3–5 μg ml^{-1}) or in the presence of recombinant IL-2 (10 ng ml^{-1}), IL-7 (10 ng ml^{-1}), IL-12 (0.01–3 ng ml^{-1}) (Pepro Tec, London, UK) or IL-18 (0.1–30 ng ml^{-1}) (MBL, Nagoya, Japan). For stimulation with protein antigens, $CD4^+$ T cells ($2–3 \times 10^5$) were cultured with DC ($1–3 \times 10^4$) pulsed with $OVA_{323-339}$ (3 μg ml^{-1}), streptococcal enterotoxin B (SEB, 2 μg ml^{-1}) (Toxin Tec, Sarasota, FL, USA) or crude malaria antigen (6.6×10^7 RBCs ml^{-1}). Crude malaria antigens were prepared using blood samples collected from PbA-infected Rag2$^{-/-}$ mice (parasitemia ~45%). After washing, RBCs were suspended in PBS at a final concentration of 1×10^9 RBCs ml^{-1} and were lysed by five freeze–thaw cycles as described previously (17). DCs (>95%) were prepared from B6 spleen cells using anti-CD11c magnetic-activated cell sorting (MACS) microbeads and autoMACS (Miltenyi Biotech, Gladbach, Germany). IL-12 and IL-18 were neutralized using specific mAbs C17.8 (10 μg ml^{-1}) and 93-10C (5 μg ml^{-1}; MBL), respectively. To prepare NK1.1$^-$CD4$^+$ T cells, splenocytes were depleted of NK1.1$^+$ cells using autoMACS prior to $CD4^+$ T-cell purification.

Transwell experiments were performed in 24-well plates with pore size 0.4-μM cell culture inserts (BD Biosciences). OT-II $CD4^+$ T cells (2×10^5) were cultured in the bottom chamber in the presence and absence of DC (1×10^5) pulsed with $OVA_{323-339}$ (3 μg ml^{-1}). Responder $CD4^+$ T cells (1.8×10^6) were cultured in the top chamber. After 48 h in culture, supernatant was recovered from both upper and lower chambers.

In the experiments using OT-II culture supernatant, OT-II $CD4^+$ T cells (1×10^4) and DC (1×10^4) pulsed with $OVA_{323-339}$ were cultured for 48 h in 96-well plate, and the supernatant was collected. The level of IL-12 and IL-18 in the supernatant was 17.5 ± 2.3 pg ml^{-1} and 9.1 ± 8.1 pg ml^{-1}, respectively. This supernatant (50 μl) was added in culture (the total volume of 200 μl). Thus, the final concentration of IL-12 and IL-18 contained in the supernatant was ~4.4 pg ml^{-1} and ~2.3 pg ml^{-1}, respectively. Inhibition of IL-2 receptor (CD25) was performed using a combination of 3C7 (5 μg ml^{-1}) and PC61.5 (5μg ml^{-1}) (18, 19).

The levels of cytokines in the supernatants were determined by a sandwich ELISA according to the manufacturer's directions using the following mAbs; JES6-1A12 and

biotin-JES6-5H4 for IL-2, 11B11 and biotin-BVD6-24G2 for IL-4 and R4-6A2 and biotin-XMG1.2 for IFN-γ (all mAbs were from e-Bioscience, San Diego, CA, USA). The levels of IL-10, IL-12p70 (e-Bioscience), IL-18 (MBL) and transforming growth factor-β (Promega, Madison, WI, USA) were determined using a manufacturer's cytokine ELISA kits.

Real-time reverse transcription–PCR

The mRNA expression was determined by an automated real-time reverse transcription–PCR system using the ABI PRISM 7900HT Sequence Detection System (Applied Biosystems, Foster City, CA, USA) as described previously (20). RNA was converted to cDNA and amplified by PCR in the PCR reaction buffer containing the double stranded DNA-specific fluorescent dye SYBR Green. Sequences of primers used for IFN-γ, IL-4, T-bet, GATA3 and G3PDH are indicated (21–23). Primers for IL-10 was 5′-TGACTGGCATGAGGATCAGC-3′ and 5′-AGTCCGCAGCTCTAGGAGCA-3′. The mRNA levels were determined as the ratio of the each DNA to G3PDH.

Statistical analysis

Except for the frequency or count data, comparison of the distributions of measurements among groups was based on the logarithmic values of the measurements. In comparison of two groups, *t*-test was used, while in comparison of three or more groups, overall comparison was first made by analysis of variance (ANOVA) for one-way or two-way data at the significance level of 0.05, and if significant, each pair of the groups was compared by *t*-test with the significance level determined by Bonferroni procedure controlling the family-wise error rate <0.05. Procedures of ANOVA and *t*-test in the SAS® system were used for the calculations.

Results

Up-regulation of cytokine production in CD4⁺ cells from PbA-infected mice

To determine the function of CD4⁺ T cells during infection with malaria parasites, CD4⁺ cells from mice uninfected or infected with PbA were stimulated with DC pulsed with superantigen, SEB or with plate-coated anti-TCR mAb (Fig. 1A). CD4⁺ cells from PbA-infected mice showed increased production of IFN-γ, IL-4 and IL-10 in response to TCR stimulation, while the production of IL-2 was severely impaired. The reduction in IL-2 production by T cells in infected mice was consistent with previous studies (24, 25). To examine whether the same cells produced IFN-γ, IL-4 and IL-10 simultaneously, we performed intracellular cytokine staining (Fig. 1B). Approximately 50% of IL-10-producing cells produced IFN-γ, and ~80% of IL-4-producing cells produced IL-10, indicating that a significant number of cells produced multiple cytokines. We focused further studies on the mechanism of up-regulation of IFN-γ, IL-4 and IL-10 in PbA-infected mice. These CD4⁺ cells expressed much higher levels of IFN-γ, IL-4 and IL-10 mRNA than those from naive mice after anti-TCR stimulation (Fig. 1C). However, these CD4⁺ cells did not express increased levels of T-bet or GATA-3 (Fig. 1C), key transcription factors of T_h1 and T_h2 differentiation (26), respectively, suggesting that the up-regulation of cytokine production was not due to the differentiation toward T_h1 or T_h2 lineages. Recently, it was shown that CD4⁺ T cells from post-septic model mice expressed a reduced level of IL-2 and increased levels of other cytokine genes including IFN-γ, IL-4 and IL-10 after stimulation with anti-CD3 mAb and that they exhibited decreased capacity to commit to either T_h1 or T_h2 lineages (27). Thus, this type of altered cytokine responses is not unique to PbA infection.

Next, C57BL/6 mice were infected with PbA for 0–8 days, and the levels of parasitemia as well as cytokine production by CD4⁺ cells in response to anti-TCR mAb were monitored in individual mice (Fig. 2A). Parasitemia became detectable (~0.1%) 4 days after infection. After 5 days, when the level of parasitemia reached ~1%, the production of IFN-γ was greatly up-regulated. However, after 3 days of chloroquine treatment, parasitemia became undetectable and IFN-γ production by CD4⁺ cells was reduced (Fig. 2B), indicating that the altered cytokine response by CD4⁺ cells was dependent on parasitemia. We next examined whether IFN-γ-producing cells were naive or effector/memory (E/M) cells. The proportion of E/M-type cells ($CD62L^{low}CD44^{high}$) increased in CD4⁺ cells of PbA-infected mice (42.8%) when compared with those from uninfected mice (20.7%) (Fig. 2C). Naive ($CD62L^{high}CD44^{low}$) and E/M-type cells were purified by cell sorting and were evaluated for their IFN-γ production. E/M-type CD4⁺ T cells from PbA-infected mice produced IFN-γ at levels much higher than those from uninfected mice or naive CD4⁺ T cells in response to anti-TCR mAb.

Antigen specificity of CD4⁺ cells producing high levels of IFN-γ

To determine whether the PbA-specific CD4⁺ T cells mediated high IFN-γ production, we used recombinant PbA that express OVA (OVA-PbA) (17). C57BL/6 mice were adoptively transferred with CFSE-labeled CD4⁺ cells from OVA-specific TCR transgenic mice, OT-II, and were infected with WT-PbA or OVA-PbA (Fig. 3). The proportion of OT-II cells was increased in mice infected with OVA-PbA (2.1%) when compared with mice not infected (0.3%) or infected with WT-PbA (0.4%). OT-II cells divided 2–3 times and up-regulated activation markers CD69 and CD25 in the OVA-PbA-infected host (Fig. 3B), suggesting the specific activation of OT-II cells in response to OVA-PbA. However, total CD4⁺ cell population from mice infected with either WT- or OVA-PbA produced IFN-γ at levels much higher than those from uninfected mice after co-culture with DC pulsed with $OVA_{323-339}$ (Fig. 3C). Intracellular cytokine staining showed that significant numbers of host CD4⁺ cells, and not OT-II cells, produced IFN-γ in response to $OVA_{323-339}$-pulsed DC (Fig. 3D). To confirm this observation, OT-II and host CD4⁺ cells were purified by sorting and examined for production of IFN-γ in response to $OVA_{323-339}$-pulsed DC (Fig. 4). Host CD4⁺ cells from infected mice did not produce significant levels of IFN-γ by themselves, indicating that these cells did not directly respond to $OVA_{323-339}$. When they were mixed with OT-II cells either from infected or uninfected mice, high levels of IFN-γ were detected, suggesting that CD4⁺ cells from infected mice produced IFN-γ in cooperation with activated OT-II cells.

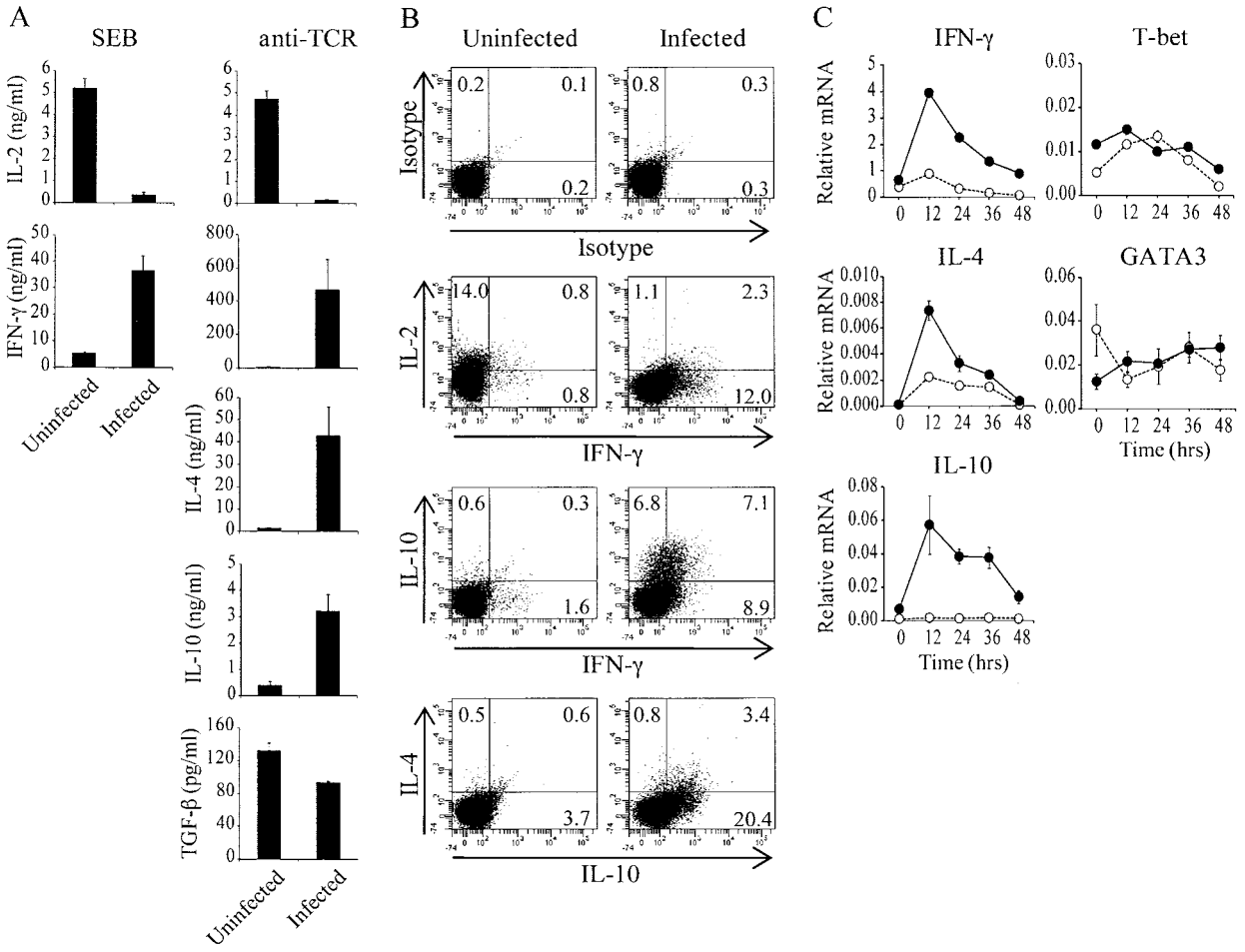

Fig. 1. CD4⁺ T cells from PbA-infected mice produce high levels of IFN-γ, IL-4 and IL-10 in response to TCR stimulation. (A) CD4⁺ T cells from mice not infected or infected with PbA for 7 days (parasitemia 6.4–7.8%) were cultured in the presence of DC (1×10^4) pulsed with SEB or on plates coated with anti-TCR mAb. The levels of IL-2, IFN-γ, IL-4, IL-10 and transforming growth factor-β in the supernatant were determined by ELISA. A significant difference was observed for all parameters between uninfected and infected mice ($P < 0.005$). Representative data of two similar results are shown. (B) CD4⁺ T cells from mice not infected or infected with PbA for 6 days (parasitemia 5.1–8.0%) were stimulated with plate-coated anti-TCR mAb for 12 h and the expression of IL-2, IFN-γ, IL-4 and IL-10 was determined by intracellular cytokine staining. Numbers in each quadrant represent percentages of cells. (C) CD4⁺ T cells (5×10^5 per well) from mice not infected or infected with PbA for 7 days (parasitemia 3.7–5.6%) were stimulated with plate-coated anti-TCR mAb for 0–48 h. The levels of mRNA in uninfected (open circles) and PbA-infected mice (closed circles) were determined by real-time reverse transcription–PCR. Representative data of two similar experiments are shown.

CD4⁺ cells from PbA-infected mice produce high levels of IFN-γ in response to a soluble mediator produced by OT-II

To determine whether IFN-γ response of CD4⁺ cells from PbA-infected mice was mediated by the cognate interaction with OT-II or by soluble factor(s), two methods were used: Transwell culture and the addition of culture supernatant. When CD4⁺ cells from PbA-infected mice were cultured in the upper chamber and OT-II/$OVA_{323-339}$-pulsed DC in the lower chamber, CD4⁺ cells produced IFN-γ at levels similar to co-culture (Fig. 5A). Reproducible results were observed when the cells in upper and lower chambers were exchanged (data not shown). Culture supernatant from OT-II/$OVA_{323-339}$-pulsed DC stimulated IFN-γ production by CD4⁺ T cells from PbA-infected mice (Fig. 5B). These results suggest that CD4⁺ cells from PbA-infected mice produced IFN-γ without direct TCR engagement and that this response was mediated by soluble factor(s) produced by OT-II/$OVA_{323-339}$-pulsed DC.

The major cytokines that are known to promote CD4⁺ T cell production of IFN-γ are IL-12 and IL-18 (28, 29). A combination of these two cytokines can stimulate IFN-γ production of CD4⁺ T cells without TCR engagement (30–32). Although these cytokines were able to stimulate IFN-γ production of CD4⁺ cells from PbA-infected mice (Fig. 6), the levels of IL-12 and IL-18 detected in the culture supernatant of the OT-II/$OVA_{323-339}$-pulsed DC were 17.5 pg ml^{-1} and 9.1 pg ml^{-1}, respectively, and was not sufficient to promote IFN-γ production (Fig. 6A and B). In addition, a saturating concentration of anti-IL-12 mAb did not inhibit IFN-γ production by CD4⁺ cells co-cultured with OT-II/$OVA_{323-339}$-pulsed DC or with their supernatant. Since signal transduction through the IL-18 receptor depends on MyD88, the response of CD4⁺ cells from MyD88 KO mice was also examined. CD4⁺ cells of the PbA-infected MyD88/Trif double KO mice produced IFN-γ at levels similar to CD4⁺ cells from PbA-infected B6 mice in the presence of culture supernatant from OT-II/

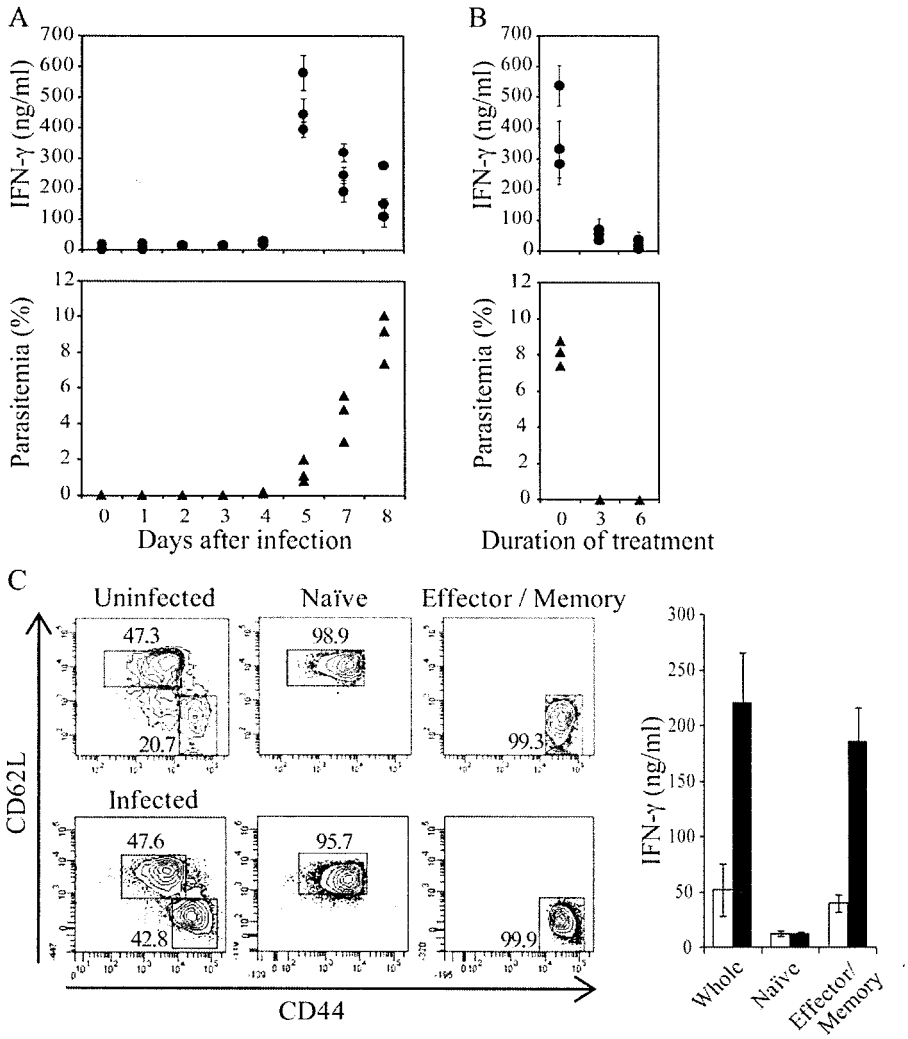

Fig. 2. Correlation between parasitemia levels and production of IFN-γ by CD4⁺ T cells. (A) Mice (three mice per group) were infected with PbA and the level of parasitemia (closed triangles) was determined. CD4⁺ T cells prepared from each mouse were stimulated with plate-coated anti-TCR mAb and IFN-γ levels in the supernatant were determined by ELISA (closed circles). Values shown are the means ± SD from each mouse. (B) After 7 days of infection (parasitemia 7.4–8.8%), mice were treated daily with chloroquine for 6days. The levels of parasitemia (closed triangles) and IFN-γ production of CD4⁺ T cells (closed circles) were determined. Representative data of two similar results are shown. (C) Naive ($CD62L^{high}CD44^{low}$) and E/M ($CD62L^{low}CD44^{high}$) CD4⁺ T cells were purified from uninfected (open bar) and infected for 7 days (parasitemia 8.6%) (closed bar) B6 mice by cell sorting and were stimulated on plates coated with anti-TCR mAb. The levels of IFN-γ in the supernatant were determined by ELISA. A significant difference in the levels of IFN-γ was observed between uninfected and infected mice for whole and E/M cells ($P < 0.05$), while no difference was observed for naive cells. Either for uninfected or infected mice, the levels of IFN-γ were significantly higher in whole and E/M cells than in naive cells, while no significant difference was observed in the levels of IFN-γ between whole and E/M cells. Representative data of three similar results are shown.

$OVA_{323-339}$-pulsed DC. Saturating concentrations of anti-IL-12 and anti-IL-18 mAb did not have significant inhibitory effects (Fig. 6). Thus, the soluble mediator produced by OT-II/$OVA_{323-339}$-pulsed DC, which stimulated IFN-γ production by CD4⁺ cells, was neither IL-12 nor IL-18.

IL-2 stimulates IFN-γ production of CD4⁺ cells from PbA-infected mice

Our study using different types of TCR transgenic T cells suggested that CD4⁺ T cells, and not CD8⁺ T cells, produced the stimulating factor (data not shown). Therefore, we examined whether IL-2 can stimulate IFN-γ production. OT-II cells produced IL-2 at a concentration of 9.76 ± 1.26 ng ml^{-1} in the supernatant. This concentration was sufficient to induce the production of IFN-γ, IL-4 and IL-10 in CD4⁺ cells from PbA-infected mice without TCR engagement, and the response was IL-2 dose dependent (Fig. 7A and B). To confirm the effect of IL-2 on cytokine production, we used cocktails of anti-CD25 mAbs to inhibit IL-2 receptor signaling and supplemented the culture with IL-7, which supported the survival of CD4⁺ T cells in the absence of IL-2 signals. Anti-CD25 mAbs completely inhibited the production of IFN-γ by CD4⁺ cells from PbA-infected mice in response to the supernatant of OT-II cells or during co-culture with OT-II/$OVA_{323-339}$-pulsed DC, and this effect was not due to the inhibition of survival signal since the viability of CD4⁺ cells

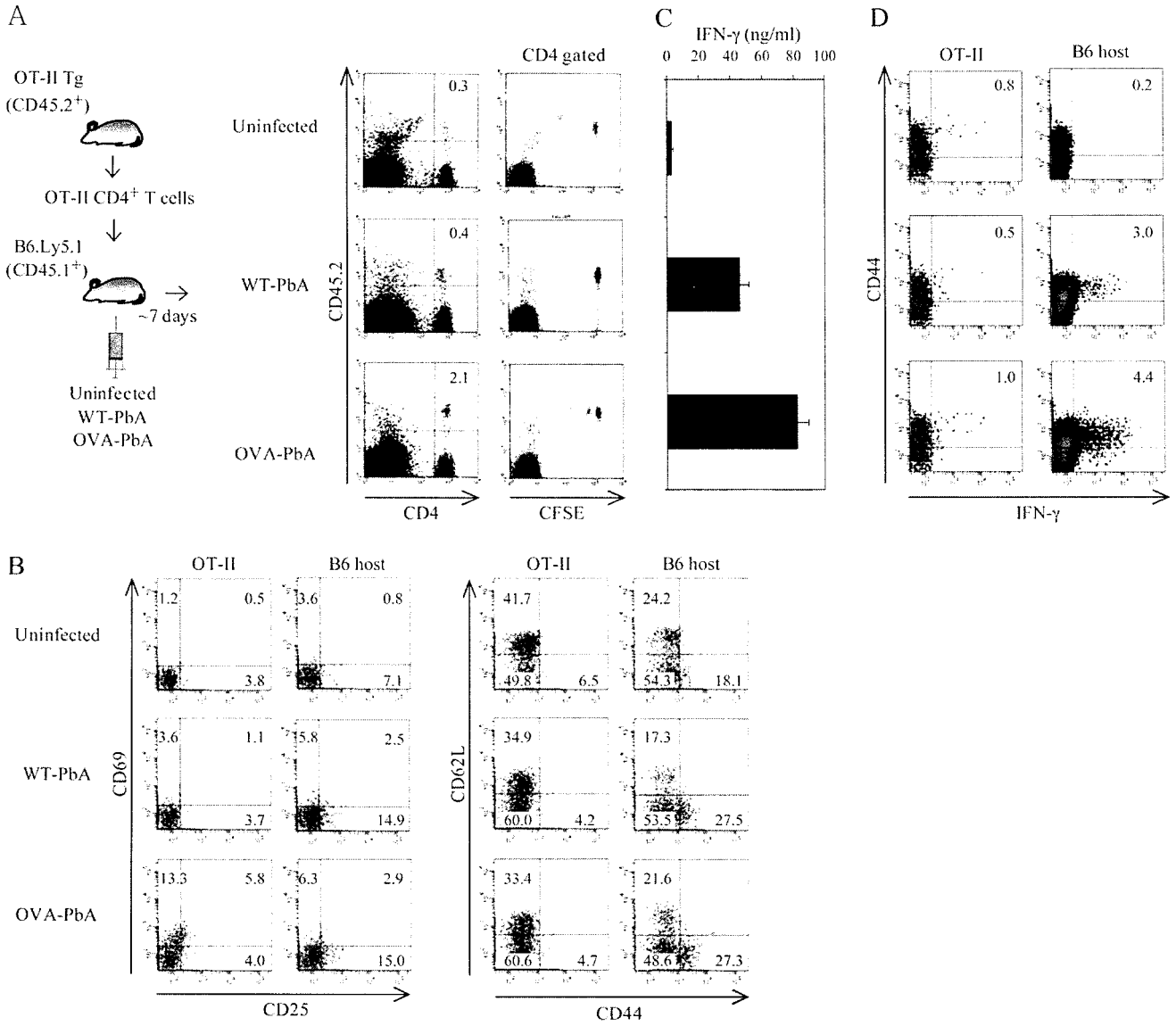

Fig. 3. Proliferation and cytokine production of CD4⁺ T cells in mice after infection with OVA-PbA. B6.Ly5.1 (CD45.1⁺) (A) or B6 (B–D) mice were adoptively transferred with CFSE-labeled OT-II (A, CD45.2⁺, 1 × 10^7) or CD45.1 OT-II cells (B–D, 3 × 10^7), respectively, and were uninfected or infected with WT- or OVA-PbA. (A) Seven days later (parasitemia 13.6–15.0%), spleen cells were analyzed using flow cytometry. The numbers in the right upper corner represent the proportions of OT-II (CD45.2⁺CD4⁺) cells. Representative data of four similar results are shown. (B) Seven days after adoptive transfer of CD45.1 OT-II cells (parasitemia 3.8–4.2%), spleen cells were stained with allophycocyanin-anti-CD4, PE-Cy7-anti-CD45.1, PE-anti-CD69, FITC-anti-CD25, PE-anti-CD62L and FITC-anti-CD44 mAbs. FACS profiles of OT-II (CD45.1⁺CD4⁺) and host B6 (CD45.1⁻CD4⁺)-gated populations are shown. The number in each quadrant represents the proportion of each population. (C) CD4⁺ T cells were stimulated with dendritic cells pulsed with $OVA_{323-339}$. The proportion of OT-II in total CD4⁺ T cells was 3.7–5.9%. The levels of IFN-γ were significantly higher both in WT-PbA-infected mice and in OVA-PbA-infected mice than in uninfected mice ($P < 0.05$). Representative data of six similar results are shown. (D) After 8 days of infection (parasitemia 9.0%), CD4⁺ T cells were purified, stimulated with DC pulsed with $OVA_{323-339}$ for 24 h and the production of IFN-γ was analyzed by intracellular cytokine staining of CD45.1⁺CD4⁺ (OT-II cells, left panels) and CD45.2⁺CD4⁺ (B6 host cells, right panels) gated populations. Representative data of three similar results are shown.

was not impaired (Fig. 7B). Other common γ-chain family cytokines such as IL-4, IL-7 and IL-15 did not have this effect (data not shown). Therefore, we concluded that IL-2 produced by OT-II cells was responsible for IFN-γ production by CD4⁺ cells from PbA-infected mice.

We examined the expression of the IL-2 receptor on CD4⁺ spleen cells. Purified CD4⁺ cell population contained minor population of NK1.1⁺TCRβ⁺ NKT cells (4.9%) and NK1.1⁻TCRβ⁺ conventional T cells (92.2%) (Fig. 8A). The proportion of NKT cells was increased to 9.2% in CD4⁺ cells after infection with PbA. In uninfected mice, 8.5 and 5.6% of CD4⁺ T (CD4⁺NK1.1⁻) cells expressed IL-2 receptor α- and β-chains, respectively. These levels increased in PbA-infected mice to 24.0 and 17.3%, respectively. Similarly, the expression of IL-2 receptor α- and β-chains increased in CD4⁺ NKT (CD4⁺NK1.1⁺) cells from 16.5 to 28.8% and from 18.0 to 30.6% in PbA-infected mice, respectively. The majority of CD4⁺CD25⁺ cells in uninfected mice was Foxp3⁺

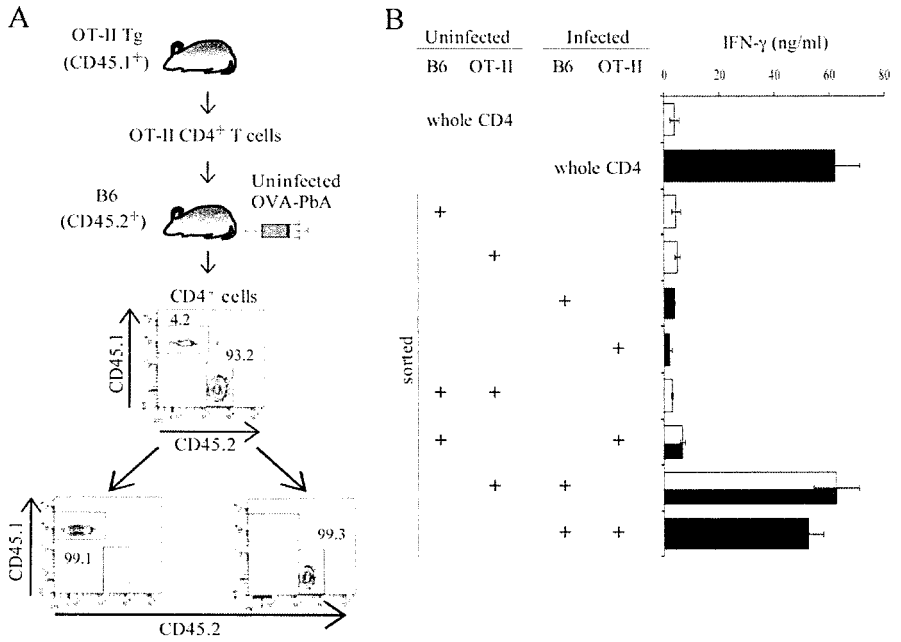

Fig. 4. Cooperation of CD4⁺ T cells from PbA-infected mice and OT-II cells in producing IFN-γ. B6 mice were adoptively transferred with CD45.1 Rag-2$^{-/-}$ OT-II cells (1×10^7) and were infected or not infected with OVA-PbA. After 7 days (parasitemia 6.7%), OT-II and host B6 CD4⁺ T cells were purified by cell sorting from uninfected (open bar) and infected (closed bar) mice and were cultured in the presence of DC (1×10^4) pulsed with $OVA_{323\ 339}$. The number of OT-II (2×10^4) and host CD4⁺ T cells (1.8×10^5) in culture was determined to reflect the original *in vivo* ratio of these cells. Addition of OT-II cells from uninfected or infected mice showed a significantly larger effects in increasing IFN-γ levels in infected B6 cells than in uninfected B6 cells ($P < 0.05$). Representative data of three similar results are shown.

regulatory T cells, and this population did not increase in PbA-infected mice, while the proportion of CD25⁺Foxp3⁻CD4⁺ T cells increased by ~6.5% (Fig. 8B). These CD4⁺ cells were cultured in the presence of IL-2 for 24 h and IFN-γ expression was examined by intracellular cytokine staining (Fig 8C). Despite their expression of IL-2 receptor, significant numbers of CD4⁺ T cells and NKT cells that produce IFN-γ were not detected in uninfected mice, indicating that CD4⁺Foxp3⁺ cells did not produce IFN-γ in response to IL-2. In contrast, 4.8 and 10.4% of CD4⁺ T and NKT cells from PbA-infected mice, respectively, produced IFN-γ in response to IL-2. Since the majority of CD4⁺ cells is NK1.1⁻ conventional T cells, these cells are the main population of CD4⁺ cells that produce IFN-γ in response to IL-2. Taken together, CD4⁺Foxp3⁻ conventional T cells, which were activated and expressed IL-2 receptor during *Plasmodium* infection, produced IFN-γ in response to IL-2. In addition, we were able to show that CD4⁺ NK T cells in PbA-infected mice also produced IFN-γ in response to IL-2.

Finally, we examined whether IFN-γ production by CD4⁺ T cells in response to TCR ligand was dependent on IL-2 (Fig. 9). CD4⁺ T cells (CD4⁺NK1.1⁻ cells) were purified from mice before and after infection with PbA. IFN-γ production by these CD4⁺ T cells was examined in the presence and absence of anti-CD25 mAbs and IL-7, which supported the survival. CD4⁺ T cells from uninfected mice produced IFN-γ in response to anti-TCR mAb, although the level was lower than that of infected mice. This response was almost completely inhibited by anti-CD25 mAbs. CD4⁺ T cells from PbA-infected mice produced IFN-γ in response to PbA antigen, and this response was also inhibited by anti-CD25 mAbs. The inhibitory effects of anti-CD25 mAbs were not due to the inhibition of survival singal, as shown previously (Fig. 7B). In contrast, IFN-γ production of the same CD4⁺ T cells in response to anti-TCR mAb was not inhibited by anti-CD25 mAbs. Thus, CD4⁺ T cells from PbA-infected mice produced IFN-γ in IL-2-dependent manner in response to malaria antigens. However, these CD4⁺ T cells produced IFN-γ in IL-2-independent manner in response to anti-TCR mAb.

Discussion

CD4⁺ T cells of E/M phenotype produced high levels of IFN-γ, IL-4 and IL-10 in response to TCR occupancy during infection with PbA. Using adoptive transfer of OT-II cells, we unexpectedly found that CD4⁺ T cells from PbA-infected mice, not OT-II cells, produced high levels of IFN-γ in response to $OVA_{323-339}$-pulsed DC. Further investigation revealed that CD4⁺ T cells from PbA-infected mice produced IFN-γ, IL-4 and IL-10 in response to IL-2 without TCR occupancy (Fig. 10). To our knowledge, this is the first report that IL-2 can stimulate the production of IFN-γ by conventional αβT cells. The IL-2 receptor is expressed on two types of CD4⁺ T cells, recently activated CD4⁺ cells and Foxp3⁺ regulatory T cells. It is likely that CD4⁺ T cells that were activated and induced to express IL-2 receptor by malaria antigens during infection produced IFN-γ in response to IL-2 *in vitro* since ligation of the IL-2 receptor expressed on CD4⁺Foxp3⁺ T cells of uninfected mice did not induce IFN-γ production. IL-2 receptor expression in conventional CD4⁺ T cells, however, is not sufficient for IL-2-dependent IFN-γ production. CD4⁺CD25⁺Foxp3⁻ T cells that were pre-activated *in vitro*

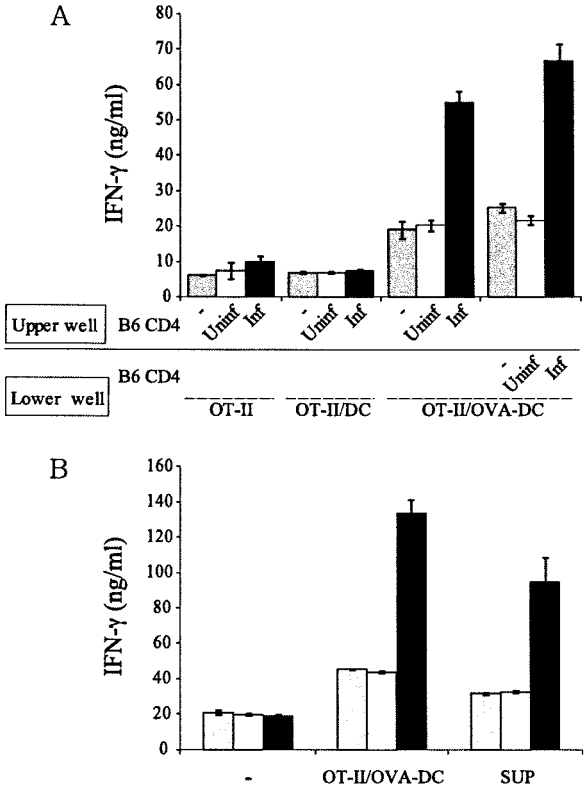

Fig. 5. CD4⁺ T cells from PbA-infected mice produce IFN-γ in response to a soluble factor produced by OT-II/$OVA_{323\ 339}$-pulsed DC. (A) CD4⁺ T cells from mice uninfected (open bar) or PbA-infected for 8 days (parasitemia 5.8–8.8%, closed bar) or no cells (gray bar) were placed in the upper or lower chamber of a Transwell plate, and OT-II cells were placed in the lower chamber in the presence and absence of DC pulsed with or without $OVA_{323\ 339}$. In the group with OT-II/OVA-DC in lower well, the levels of IFN-γ in CD4⁺ T cells were significantly higher in those from infected mice than in those from uninfected mice irrespective of whether T cells were in upper well or lower well ($P < 0.05$). Representative data of three similar results are shown. (B) CD4⁺ T cells from mice uninfected (open bar) or infected for 6 days (parasitemia 4.0–5.7%, closed bar) or no cells (gray bar) were cultured in the presence (OT-II/OVA-DC) and absence (–) of OT-II cells and DC pulsed with $OVA_{323\ 339}$ or in the presence of supernatant from OT-II cells stimulated with $OVA_{323\ 339}$-pulsed DC (SUP). Either in group with OT-II/OVA-DC or with OVA-DC, the levels of IFN-γ were significantly higher in CD4⁺ T cells from infected mice than in those from uninfected mice ($P < 0.05$). Representative data of four similar results are shown.

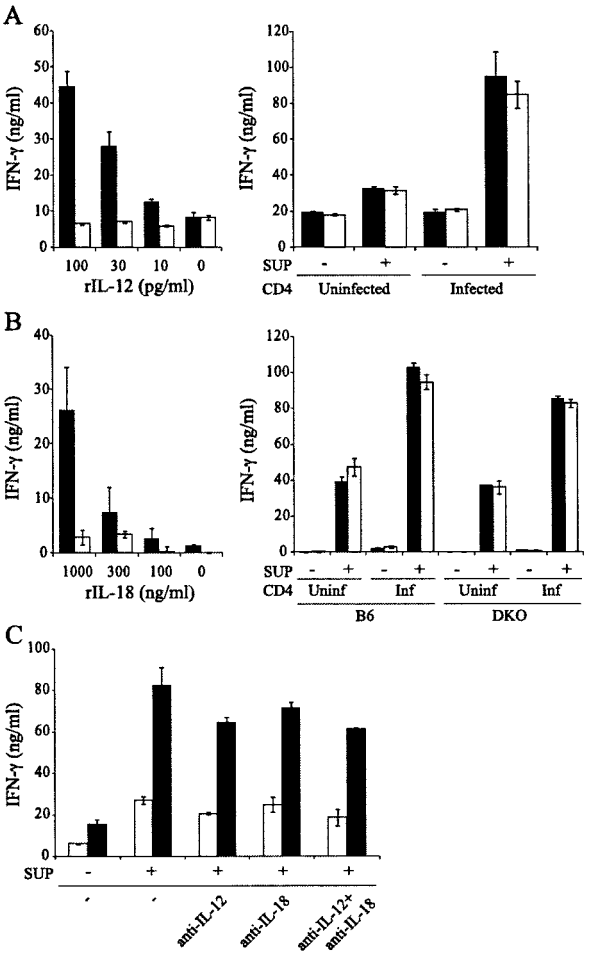

Fig. 6. The soluble mediator that stimulates IFN-γ production of CD4⁺ T cells from PbA-infected mice is not IL-12 or IL-18. (A and B, left) CD4⁺ T cells from the infected mice for 7 days (parasitemia 5.2–7.7%) were cultured in the presence of varying concentrations of recombinant IL-12 or IL-18 with (open bar) and without (closed bar) anti-IL-12 mAb or anti-IL-18 mAb, respectively. In CD4⁺ T cells from the infected mice, IFN-γ was produced significantly depending on the levels of recombinant IL (rIL)-12 ($P < 0.05$), while the production was blocked by anti-IL-12 mAb. Although a similar dose–response was suggested for rIL-18, the level of IFN-γ at 1000 (nanograms per milliliter) was significantly higher ($P < 0.05$) compared with that at 100 or 0 (nanograms per milliliter). (A, right) CD4⁺ T cells from uninfected or infected mice were cultured in the presence and absence of supernatant of OT-II/$OVA_{323\ 339}$-pulsed DC (SUP) with (open bar) and without (closed bar) anti-IL-12 mAb. In the presence of SUP, no significant difference was observed in the levels of IFN-γ between CD4⁺ T cells with or without anti-IL-12 mAb. Representative data of two similar results are shown. (B, right) CD4⁺ T cells from uninfected or infected B6 or $MyD88^{-/-}TRIF^{-/-}$ double knockout mice were cultured in the presence and absence of SUP with (open bar) and without (closed bar) anti-IL-18 mAb. In both of CD4⁺ T cells from B6 and DKO mice, the levels of IFN-γ significantly increased in the presence of SUP irrespective of whether the mice were infected or uninfected and of with or without anti-IL-18 ($P < 0.05$). However, no significant decrease with anti-IL-18 mAb was observed in the levels of IFN-γ. (C) CD4⁺ T cells from B6 mice uninfected and infected for 7 days (parasitemia 7.6%) were cultured in the presence (+) and absence (–) of SUP with (closed bar) and without (open bar) anti-IL-12, anti-IL-18 mAb or both. In CD4⁺ T cells either from uninfected or infected mice, the levels of IFN-γ significantly increased with SUP ($P < 0.05$). However, single or simultaneous effects of anti-IL-12 and anti-IL-18 mAbs in blocking the increase were not significant. Representative data of two similar results are shown.

with anti-TCR mAb to induce the expression of IL-2 receptor did not produce IFN-γ in response to IL-2, consistent with previous studies (data not shown) (33). It is intriguing that some cells produce IFN-γ in response to IL-2 and others do not. One possibility is that CD4⁺ T cells have different components of the IL-2 receptor α-, β- and γ-chains forming high and intermediate affinity receptors, in which some of the α-chains (CD25) are located in microdomains of the plasma membrane (34). Signaling events induced by IL-2 may vary depending on the structure of the IL-2 receptor as well as association with other components, such as lipid rafts (35). Alternatively, the signaling module of CD4⁺ T cells may vary between types of T cells and may depend on the nature of stimulation. For example, IL-12 and IL-18 induce GADD45β,

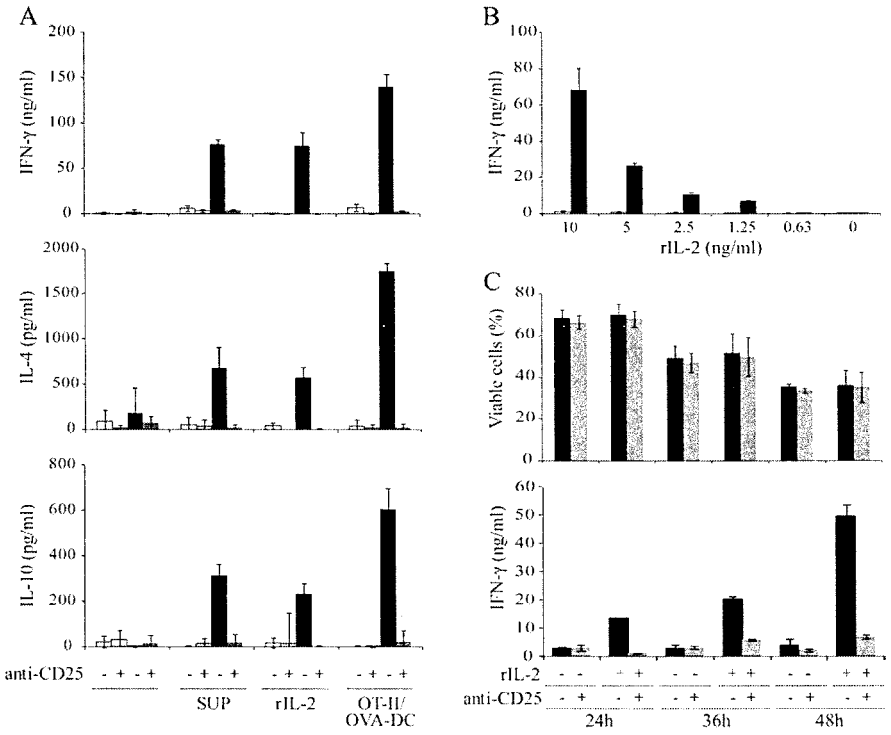

Fig. 7. IL-2 stimulates CD4⁺ T cells from PbA-infected mice to produce IFN-γ, IL-4 and IL-10. (A) CD4⁺ T cells from infected (8 days, parasitemia 9.8 %, closed bar) and uninfected (open bar) mice were stimulated with the supernatant from the OT-II/$OVA_{323\ 339}$-pulsed DC (SUP), recombinant IL-2 (rIL-2) or co-cultured with OT-II and $OVA_{323\ 339}$-pulsed DC (OT-II/OVA-DC) in the presence (+) and absence (−) of anti-CD25 mAbs. In CD4⁺ T cells from PbA-infected mice, addition of SUP, rIL-2 or OT-II/OVA-DC significantly increased the levels of IFN-γ, IL-4 and IL-10 ($P < 0.05$) and such an increase was significantly blocked by anti-CD25 mAbs ($P < 0.05$). Representative data of three similar results are shown. (B) CD4⁺ T cells from infected (7 days, parasitemia 6.6%, closed bar) and uninfected (open bar) mice were cultured in the presence of varying concentrations of recombinant IL-2. The levels of IFN-γ in the culture supernatant were determined by ELISA. In CD4⁺ T cells from infected mice, the levels of IFN-γ significantly increased with IL-2 equal to or exceeding 1.25 ng ml^{-1} ($P < 0.05$). (C) CD4⁺ T cells from the infected (7 days, parasitemia 5.2–7.7%) mice were cultured with (gray bar) and without (closed bar) anti-CD25 mAbs for 24–48 h. The proportions of viable (Annexin V^-7AAD^-) cells were determined by staining with annexin V and 7-aminoactinomycin D (7AAD). The levels of IFN-γ in the culture supernatant were determined by ELISA. At each time point, no significant difference was observed in the frequency of viable cells between cells with and without anti-CD25 mAbs for either with or without rIL-2. Representative data of four similar results are shown.

an activator of MEKK4, which leads to p38 mitogen-activated protein kinase (MAPK) activation (32). In combination with other signaling pathways, the activation of this GADD45β-MEKK4-p38 MAPK pathway leads to IFN-γ production in CD4⁺ T cells without TCR engagement (30–32). Further study is required to investigate the expression of GADD45β or other signaling molecules in the IFN-γ activation pathway by CD4⁺ T cells from PbA-infected mice.

In addition to CD4⁺ T cells, we have shown that CD4⁺ NKT cells from PbA-infected mice also produced IFN-γ in response to IL-2. It was previously reported that IL-2 induces IFN-γ production by human NK cells, Vγ9Vδ2 T cells and NKT cells (33,36). In these studies, human cells were purified and stimulated *in vitro* with their appropriate ligands to induce expression of CD25. Unlike typical IL-2 signaling pathway, the addition of IL-2 activated not only Stat3 and Stat5 pathways but also Stat4 leading to the induction of IFN-γ production in NK, Vγ9Vδ2 T and NKT cells. NK cells are important sources of IFN-γ during early response to *Plasmodium* infection (7). In human studies, it was shown that NK cells from malaria-naive donors produced IFN-γ in response to *Plasmodium falciparum*-infected RBCs *in vitro* (37). Recently, it was shown that this NK response is dependent on IL-2 produced by CD4⁺ T cells (38). In this study, we have shown that mouse CD4⁺ T and NKT cells are able to produce IFN-γ in response to IL-2 under certain conditions. It will be intriguing to investigate whether CD4⁺ T cells from PbA-infected mice utilize signaling pathway similar to human NK, Vγ9Vδ2 T and NKT cells (33, 36) in producing IFN-γ in response to IL-2.

We have also shown that production of IFN-γ by CD4⁺ T cells from the infected mice in response to PbA was almost completely inhibited by anti-CD25 mAbs, indicating that these PbA-specific T cells produced IFN-γ in an IL-2-dependent manner. The effect of anti-CD25 mAbs was not due to the inhibition of survival signal since the culture was supplemented with IL-7, and we did not detect any significant differences between CD4⁺ T cells culture with and without anti-CD25 mAbs. Interestingly, CD4⁺ T cells showed differential dependencies on IL-2 when stimulated with anti-TCR mAb. IFN-γ production by CD4⁺ T cells in response to anti-TCR mAb was IL-2 prior to PbA infection but was IL-2 dependent during infection. Thus, the IL-2 dependency of the IFN-γ response by CD4⁺ T cells varied depending on the source of T cells as well as the nature of the TCR ligand. It is possible that the requirement of IL-2 for IFN-γ production differs

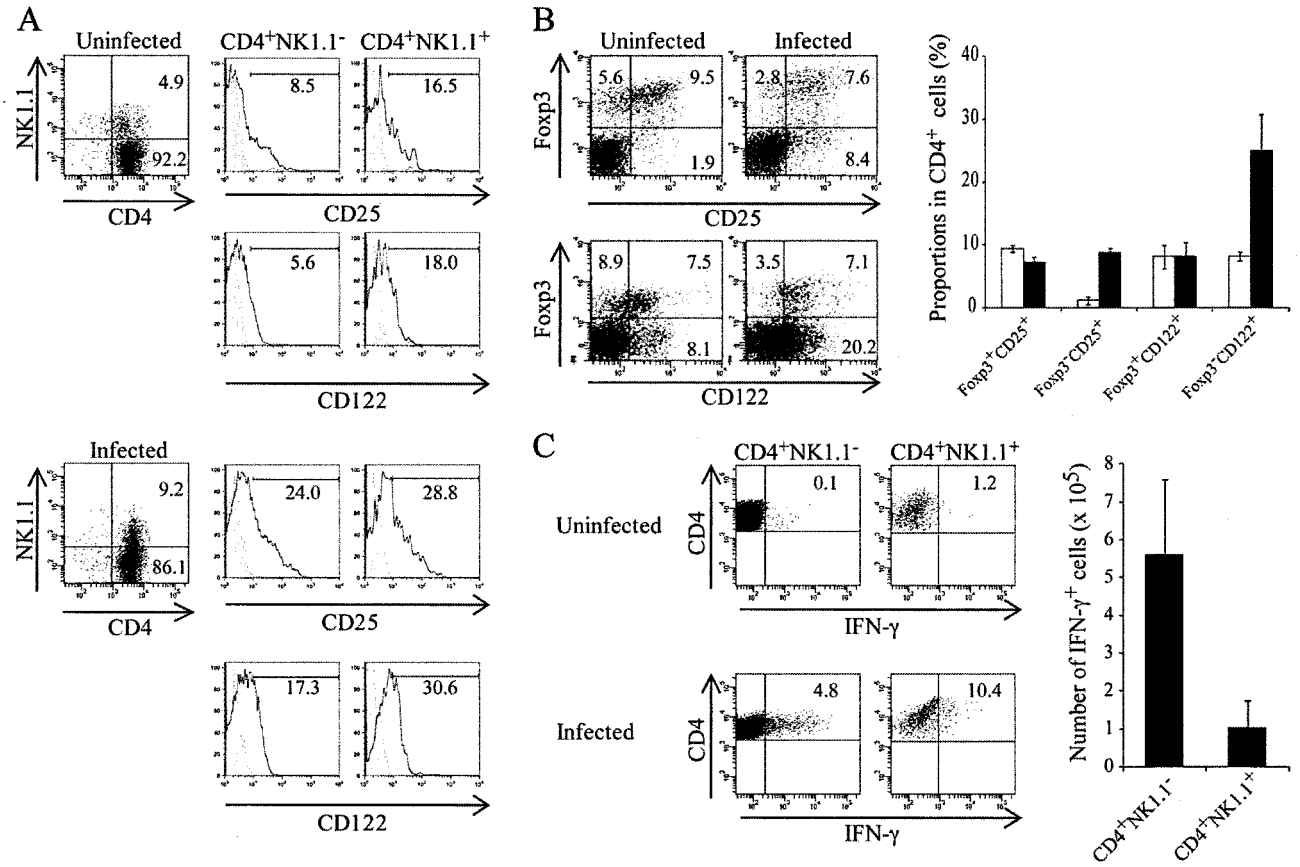

Fig. 8. CD4⁺ T cells from PbA-infected mice express high levels of IL-2 receptor. (A) Spleen cells from B6 mice uninfected or infected for 8 days with PbA (parasitemia 6.7–13.1%) were stained with PE-Cy7-anti-CD4, allophycocyanin–streptavidin plus biotin-anti-NK1.1, FITC-anti-TCRβ and PE-anti-CD25 or PE-anti-CD122 mAbs. The expression of CD25 and CD122 is shown for CD4⁺NK1.1⁺TCR⁺ and CD4⁺NK1.1⁻TCR⁺ gated populations. (B) Spleen cells from B6 mice uninfected or infected for 7 days with PbA (parasitemia 4.4–4.9%) were stained with PE-Cy7-anti-CD4, FITC-anti-CD25, FITC–streptavidin plus biotin-anti-CD122 and with PE-anti-Foxp3 mAbs, and the profiles of CD4⁺ gated populations are shown (left). The number represents the proportion of cells in each region within total CD4⁺ cells from uninfected (open bar) and PbA-infected (closed bar) mice. The experiments were repeated five times and the mean ± SD of each subpopulation within CD4⁺ cells are shown (right). The proportions of Foxp3⁻CD25⁺ cells and Foxp3⁻CD122⁺ cells significantly increased in infected mice than in uninfected mice. (C) CD4⁺ cells from B6 mice infected or uninfected with PbA were stimulated with IL-2 for 24 h, stained with PE-Cy7-anti-CD4, allophycocyanin–streptavidin plus biotin-anti-NK1.1, FITC-anti-TCRβ and with PE-anti-IFN-γ mAb. Numbers in the right quadrant represent the proportion of IFN-γ-producing cells in total CD4⁺ cells for CD4⁺NK1.1⁺TCR⁺ and CD4⁺NK1.1⁻TCR⁺ gated populations (left). Representative data of four similar results are shown. The number of IFN-γ-producing cells in each spleen was calculated from four mice in each group (right). The number of IFN-γ-producing cells was significantly larger in CD4⁺NK1.1⁻TCR⁺ gated population than in CD4⁺NK1.1⁺TCR⁺ gated population ($P < 0.001$).

between T cell types; effector CD4⁺ T cells that were induced during the active infection produce IFN-γ in an IL-2-independent manner, while naive or memory CD4⁺ T cells produce IFN-γ in an IL-2-dependent manner. Alternatively, the *in vivo* environment may influence the IL-2 dependency of CD4⁺ T cell response. During PbA-infection, innate immune responses are activated, which produce a variety of cytokines. This inflammatory environment may compensate for the IL-2 requirement and condition the IFN-γ response of T cells.

IFN-γ plays important roles in regulating the protective immune response against blood-stage malaria infection and in the pathogenesis of cerebral malaria (3, 39). The data presented here indicate that the level of IFN-γ production by CD4⁺ T cells is critically dependent on the level of IL-2 production during infection with malaria parasites. However, we and others have shown that the production of IL-2 in response to TCR occupancy was severely impaired in CD4⁺ T cells in mice infected with PbA and in patients with acute *P. falciparum* infection in Thailand (this study, 24, 25). While molecular mechanisms underlying the reduction in IL-2 production are not clearly understood, regulation of the levels of IFN-γ production during severe malaria infection may be important to reduce the pathogenesis caused by excessive IFN-γ. Regulation of IFN-γ may also be beneficial for the parasite since it can escape immune attack by activated immune effector mechanisms, including macrophages. In fact, it is reported that treatment of *Plasmodium yoelii* infected mice with exogenous IL-2 restored IFN-γ and other cytokine expression and was associated with diminution of parasitemia, although the survival rate did not improve in this study (40). Finally, it is likely that this type of IL-2 dependency of IFN-γ production is also induced during infection with *P. falciparum,* the human malaria parasite, as well as in other infectious diseases or immune disorders. Increased

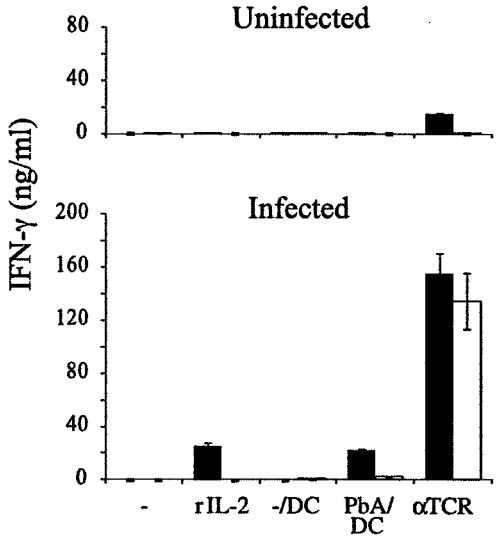

Fig. 9. IFN-γ production of CD4⁺ T cells from PbA-infected mice in response to malaria antigen is IL-2 dependent. CD4⁺NK1.1⁻ T cells from mice uninfected or infected for 7 days (parasitemia 10.6 %) were cultured in the absence (–) and presence of IL-2 [recombinant IL (rIL)-2], DC (DC), DC pulsed with soluble malaria antigen (PbA/DC) or anti-TCR mAb (αTCR) with (open bar) and without (closed bar) anti-CD25 mAbs (A). In T cells from uninfected mice, the level of IFN-γ was significantly lower for PbA/DC and anti-TCR mAb in those with anti-CD25 mAbs than in those without anti-CD25 mAbs ($P < 0.05$). On the other hand, in T cells from infected mice, although the level of IFN-γ was significantly lower for rIL-2 and PbA/DC in those with anti-CD25 mAbs than in those without anti-CD25 mAbs ($P < 0.05$), no such significant difference was observed for anti-TCR mAb. Representative data of three similar results are shown.

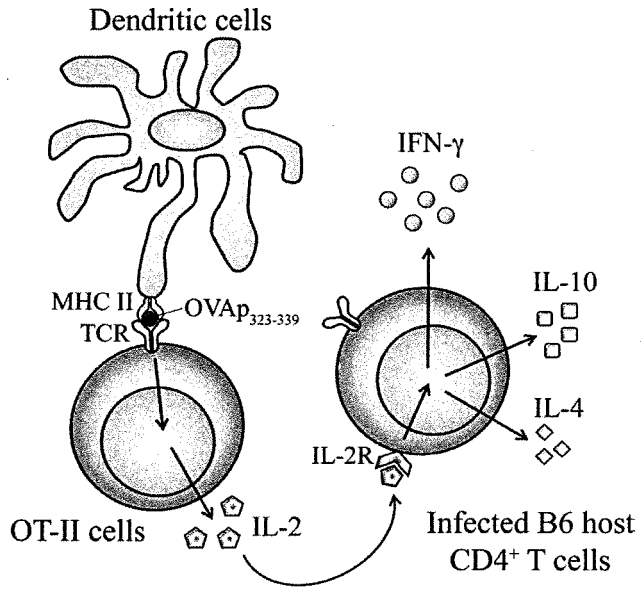

Fig. 10. A model of the production of IFN-γ, IL-4 and IL-10 by CD4⁺ T cells from PbA-infected mice. CD4⁺ T cells from B6 mice that were transferred with OT-II cells and were infected with PbA produced IFN-γ, IL-4 and IL-10 in response to DC pulsed with $OVA_{323-339}$ *in vitro*.

understanding of the molecular mechanisms underlying regulation of the cytokine network during infection should suggest methods to prevent the pathogenesis of malaria infection as well as other immune disorders and also enhance the protective immune response.

Funding

Grants-in-Aid from the Ministry of Education, Science, Sports and Culture, Japan (21390125 and 21790408); Global COE program, Nagasaki University; by the president's discretionary fund of Nagasaki University.

Acknowledgements

We thank Dr H. Kosaka, Dr Y. Takahama, Dr K. Takeda and Dr S. Akira for providing mice; M. Ueda, T. Ikeda and K. Kimura for their technical assistance.

References

1 Brown, I. N., Allison, A. C. and Taylor, R. B. 1968. *Plasmodium berghei* infections in thymectomized rats. *Nature* 219:292.
2 Grun, J. L. and Weidanz, W. P. 1981. Immunity to *Plasmodium chabaudi* adami in the B-cell-deficient mouse. *Nature* 290:143.
3 Good, M. F., Xu, H., Wykes, M. and Engwerda, C. R. 2005. Development and regulation of cell-mediated immune responses to the blood stages of malaria: implications for vaccine research. *Annu. Rev. Immunol.* 23:69.
4 van der Heyde, H. C., Huszar, D., Woodhouse, C., Manning, D. D. and Weidanz, W. P. 1994. The resolution of acute malaria in a definitive model of B cell deficiency, the JHD mouse. *J. Immunol.* 152:4557.
5 von der Weid, T., Honarvar, N. and Langhorne, J. 1996. Gene-targeted mice lacking B cells are unable to eliminate a blood stage malaria infection. *J. Immunol.* 156:2510.
6 Taylor-Robinson, A. W., Phillips, R. S., Severn, A., Moncada, S. and Liew, F. Y. 1993. The role of TH1 and TH2 cells in a rodent malaria infection. *Science* 260:1931.
7 Stevenson, M. M. and Riley, E. M. 2004. Innate immunity to malaria. *Nat. Rev. Immunol.* 4:169.
8 De Souza, J. B., Williamson, K. H., Otani, T. and Playfair, J. H. 1997. Early γ-interferon responses in lethal and nonlethal murine blood-stage malaria. *Infect. Immun.* 65:1593.
9 Langhorne, J., Meding, S. J., Eichmann, K. and Gillard, S. S. 1989. The response of CD4⁺ T cells to *Plasmodium chabaudi chabaudi*. *Immunol. Rev.* 112:71.
10 Su, Z. and Stevenson, M. M. 2000. Central role of endogenous gamma interferon in protective immunity against blood-stage *Plasmodium chabaudi* AS infection. *Infect. Immun.* 68:4399.
11 Poovassery, J. S., Sarr, D., Smith, G., Nagy, T. and Moore, J. M. 2009. Malaria-induced murine pregnancy failure: distinct roles for IFN-γ and TNF. *J. Immunol.* 183:5342.
12 Grau, G. E., Heremans, H., Piguet, P. F. *et al.* 1989. Monoclonal antibody against interferon γ can prevent experimental cerebral malaria and its associated overproduction of tumor necrosis factor. *Proc. Natl Acad. Sci. USA* 86:5572.
13 Barnden, M. J., Allison, J., Heath, W. R. and Carbone, F. R. 1998. Defective TCR expression in transgenic mice constructed using cDNA-based α- and β-chain genes under the control of heterologous regulatory elements. *Immunol. Cell Biol.* 76:34.
14 Shinkai, Y., Rathbun, G., Lam, K. P. *et al.* 1992. RAG-2-deficient mice lack mature lymphocytes owing to inability to initiate V(D)J rearrangement. *Cell* 68:855.
15 Adachi, O., Kawai, T., Takeda, K. *et al.* 1998. Targeted disruption of the MyD88 gene results in loss of IL-1- and IL-18-mediated function. *Immunity* 9:143.
16 Yamamoto, M., Sato, S., Hemmi, H. *et al.* 2003. TRAM is specifically involved in the Toll-like receptor 4-mediated MyD88-independent signaling pathway. *Nat. Immunol.* 4:1144.
17 Miyakoda, M., Kimura, D., Yuda, M. *et al.* 2008. Malaria-specific and nonspecific activation of CD8⁺ T cells during blood stage of *Plasmodium berghei* infection. *J. Immunol.* 181:1420.
18 Ortega, G., Robb, R. J., Shevach, E. M. and Malek, T. R. 1984. The murine IL 2 receptor. I. Monoclonal antibodies that define distinct

functional epitopes on activated T cells and react with activated B cells. *J. Immunol.* 133:1970.
19 Lowenthal, J. W., Corthesy, P., Tougne, C., Lees, R., MacDonald, H. R. and Nabholz, M. 1985. High and low affinity IL 2 receptors: analysis by IL 2 dissociation rate and reactivity with monoclonal anti-receptor antibody PC61. *J. Immunol.* 135:3988.
20 Kawabata, Y., Udono, H., Honma, K. *et al.* 2002. Merozoite surface protein 1-specific immune response is protective against exoerythrocytic forms of *Plasmodium yoelii*. *Infect. Immun.* 70:6075.
21 Tominaga, N., Ohkusu-Tsukada, K., Udono, H., Abe, R., Matsuyama, T. and Yui, K. 2003. Development of Th1 and not Th2 immune responses in mice lacking IFN-regulatory factor-4. *Int. Immunol.* 15:1.
22 Honma, K., Udono, H., Kohno, T. *et al.* 2005. Interferon regulatory factor 4 negatively regulates the production of proinflammatory cytokines by macrophages in response to LPS. *Proc. Natl Acad. Sci. USA* 102:16001.
23 Honma, K., Kimura, D., Tominaga, N., Miyakoda, M., Matsuyama, T. and Yui, K. 2008. Interferon regulatory factor 4 differentially regulates the production of Th2 cytokines in naive vs. effector/memory CD4⁺ T cells. *Proc. Natl Acad. Sci. USA* 105:15890.
24 Luyendyk, J., Olivas, O. R., Ginger, L. A. and Avery, A. C. 2002. Antigen-presenting cell function during *Plasmodium yoelii* infection. *Infect. Immun.* 70:2941.
25 Ho, M., Webster, H. K., Green, B., Looareesuwan, S., Kongchareon, S. and White, N. J. 1988. Defective production of and response to IL-2 in acute human *falciparum* malaria. *J. Immunol.* 141:2755.
26 Szabo, S. J., Sullivan, B. M., Peng, S. L. and Glimcher, L. H. 2003. Molecular mechanisms regulating Th1 immune responses. *Annu. Rev. Immunol.* 21:713.
27 Carson, W. F.t, Cavassani, K. A. and Ito, T. 2003. Impaired CD4⁺ T-cell proliferation and effector function correlates with repressive histone methylation events in a mouse model of severe sepsis. *Eur. J. Immunol.* 40:998.
28 Trinchieri, G. 1995. Interleukin-12: a proinflammatory cytokine with immunoregulatory functions that bridge innate resistance and antigen-specific adaptive immunity. *Annu. Rev. Immunol.* 13:251.
29 Nakanishi, K., Yoshimoto, T., Tsutsui, H. and Okamura, H. 2001. Interleukin-18 regulates both Th1 and Th2 responses. *Annu. Rev. Immunol.* 19:423.
30 Robinson, D., Shibuya, K., Mui, A. *et al.* 1997. IGIF does not drive Th1 development but synergizes with IL-12 for interferon-γ production and activates IRAK and NFκB. *Immunity* 7:571.
31 Yoshimoto, T., Takeda, K., Tanaka, T. *et al.* 1998. IL-12 up-regulates IL-18 receptor expression on T cells, Th1 cells, and B cells: synergism with IL-18 for IFN-γ production. *J. Immunol.* 161:3400.
32 Yang, J., Zhu, H., Murphy, T. L., Ouyang, W. and Murphy, K. M. 2001. IL-18-stimulated GADD45 β required in cytokine-induced, but not TCR-induced, IFN-γ production. *Nat. Immunol.* 2:157.
33 Bessoles, S., Fouret, F., Dudal, S., Besra, G. S., Sanchez, F. and Lafont, V. 2008. IL-2 triggers specific signaling pathways in human NKT cells leading to the production of pro- and anti-inflammatory cytokines. *J. Leukoc. Biol.* 84:224.
34 Ellery, J. M. and Nicholls, P. J. 2002. Possible mechanism for the alpha subunit of the interleukin-2 receptor (CD25) to influence interleukin-2 receptor signal transduction. *Immunol. Cell Biol.* 80:351.
35 Tsujino, S., Miyazaki, T., Kawahara, A., Maeda, M., Taniguchi, T. and Fujii, H. 1999. Critical role of the membrane-proximal, proline-rich motif of the interleukin-2 receptor γc chain in the Jak3-independent signal transduction. *Genes Cells* 4:363.
36 Lafont, V., Loisel, S., Liautard, J. *et al.* 2003. Specific signaling pathways triggered by IL-2 in human Vγ9Vδ2 T cells: an amalgamation of NK and αβ T cell signaling. *J. Immunol.* 171:5225.
37 Artavanis-Tsakonas, K. and Riley, E. M. 2002. Innate immune response to malaria: rapid induction of IFN-γ from human NK cells by live *Plasmodium falciparum*-infected erythrocytes. *J. Immunol.* 169:2956.
38 Horowitz, A., Newman, K. C., Evans, J. H., Korbel, D. S., Davis, D. M. and Riley, E. M. 2002. Cross-talk between T cells and NK cells generates rapid effector responses to *Plasmodium falciparum*-infected erythrocytes. *J. Immunol.* 184:6043.
39 Yanez, D. M., Manning, D. D., Cooley, A. J., Weidanz, W. P. and van der Heyde, H. C. 1996. Participation of lymphocyte subpopulations in the pathogenesis of experimental murine cerebral malaria. *J. Immunol.* 157:1620.
40 Lucas, B., Kasper, L. H., Smith, K. and Haque, A. 1996. *In vivo* treatment with interleukin 2 reduces parasitemia and restores IFN-γ gene expression and T-cell proliferation during acute murine malaria. *C R Acad. Sci. III* 319:705.

MALARIA JOURNAL

ORAL PRESENTATION Open Access

Complete abrogation of sporozoite-induced sterile immunity by blood stage parasites of homologous and heterologous malaria species

Megumi Inoue[1*], Jianxia Tang[1], Osamu Kaneko[1], Katsuyuki Yui[2], Richard Culleton[1]

From Parasite to Prevention: Advances in the understanding of malaria
Edinburgh, UK. 20-22 October 2010

Immunisation of mice and humans with attenuated sporozoites has been shown to confer sterile immunity against infection. There are ongoing efforts to develop a vaccine based on this system. Attenuation of sporozoites may be achieved via irradiation, genetic modification, or through the use of drugs targeting the blood stage parasite. Recently, it has been shown that the administration of chloroquine, a drug that acts exclusively against the erythrocytic stages of malaria parasites, concurrently with live sporozoites can induce sterile immunity against homologous challenge with *Plasmodium falciparum* sporozoites in humans. However, it is not known whether the protection achieved against *P. falciparum* will also protect against other species of human malaria parasites, which are almost always endemic in the same region. Given the high amount of antigen diversity within malaria parasite species, coupled with the large evolutionary distances between the human species, it seems unlikely that immunity to heterologous species would be achieved. Of concern is whether the development of an acute blood stage infection of a heterologous species may abrogate the immunity achieved against the vaccine target species. This phenomenon would have serious consequences for the deployment of an attenuated sporozoite vaccine in a multispecies endemic area.

Here, we describe the results of experiments aimed at determining whether immunity achieved against one species of malaria parasite by sporozoite immunisation is protective against a secondary species, and whether the development of acute blood stage infections of the heterologous species abrogates the immunity achieved against the vaccine target species. As such experiments are currently impossible using human malaria parasite species, we have used the rodent malaria parasite species *Plasmodium vinckei* and *Plasmodium yoelii*. These two species were selected as they offer the widest possible evolutionary distance between rodent malaria parasites, although they are still much more closely related than any two of the human species. We found that although there was some cross protection between the species following sporozoite immunisation in conjunction with mefloquine treatment, the major component of this immunity was species specific. Mice immunised with *P. yoelii* sporozoites were completely protected against the development of blood stage infection following *P. yoelii* sporozoite challenge, whereas they were completely susceptible to infection with *P. vinckei*. Crucially, we found that the development of a blood stage infection of either species completely removed the sterile protection achieved *via* sporozoite immunisation.

Author details
[1]Department of Protozoology, Institute of Tropical Medicine, Nagasaki University, 1-12-4 Sakamoto Nagasaki 852-8523, Japan. [2]Department of Molecular Microbiology and Immunology, Graduate School of Biomedical Sciences, Nagasaki University, 1-12-4 Sakamoto Nagasaki 852-8523, Japan.

Published: 20 October 2010

doi:10.1186/1475-2875-9-S2-O19
Cite this article as: Inoue *et al.*: Complete abrogation of sporozoite-induced sterile immunity by blood stage parasites of homologous and heterologous malaria species. *Malaria Journal* 2010 9(Suppl 2):O19.

[1]Department of Protozoology, Institute of Tropical Medicine, Nagasaki University, 1-12-4 Sakamoto Nagasaki 852-8523, Japan
Full list of author information is available at the end of the article

Am. J. Trop. Med. Hyg., 84(2), 2011, pp. 292–297
doi:10.4269/ajtmh.2011.10-0432

Genetic Polymorphism of *Plasmodium vivax msp1p*, a Paralog of Merozoite Surface Protein 1, from Worldwide Isolates

Yue Wang,† Osamu Kaneko,† Jetsumon Sattabongkot, Jun-Hu Chen, Feng Lu, Jong-Yil Chai, Satoru Takeo, Takafumi Tsuboi, Francisco J. Ayala, Yong Chen, Chae Seung Lim, and Eun-Taek Han*

Department of Parasitology, Kangwon National University College of Medicine, Chuncheon, Gangwon-do, Republic of Korea; Institute of Parasitic Diseases, Zhejiang Academy of Medical Sciences, Hangzhou, People's Republic of China; Department of Protozoology, Institute of Tropical Medicine and the Global Center of Excellence Program, Nagasaki University, Nagasaki, Japan; Department of Entomology, Armed Forces Research Institute of Medical Sciences, Bangkok, Thailand; Jiangsu Institute of Parasitic Diseases, Wuxi, People's Republic of China; Department of Parasitology and Tropical Medicine, Seoul National University College of Medicine, Seoul, Republic of Korea; Cell-Free Science and Technology Research Center, Ehime University, Ehime, Japan; Department of Ecology and Evolutionary Biology, University of California, Irvine, California; Zhejiang Medical College and Zhejiang Academy of Medical Sciences, Hangzhou, People's Republic of China; Department of Laboratory Medicine, College of Medicine, Korea University, Seoul, Republic of Korea

Abstract. *Plasmodium vivax msp1p*, a paralog of the candidate vaccine antigen *P. vivax* merozoite surface protein 1, possesses a signal peptide at its N-terminus and two epidermal growth factor–like domains at its C-terminus with a glycosylphosphatidylinositol attachment site. The *msp1p* gene locus may have originated by a duplication of the *msp1* gene locus in a common ancestor of the analyzed *Plasmodium* species and lost from *P. yoelii*, *P. berghei*, and *P. falciparum* during their evolutionary history. Full-length sequences of the *msp1p* gene were generally highly conserved; they had a few amino acid substitutions, one highly polymorphic E/Q-rich region, and a single-to-triple hepta-peptide repeat motif. Twenty-one distinguishable allelic types (A1–A21) of the E/Q-rich region were identified from worldwide isolates. Among them, four types were detected in isolates from South Korea. The length polymorphism of the E/Q-rich region might be useful as a genetic marker for population structure studies in malaria-endemic areas.

INTRODUCTION

Among the species of malarial parasite that infect humans, *Plasmodium vivax* is the most globally prevalent and threatens almost 40% of the world's population, resulting in approximately 250 million clinical infections each year.[1] Although *P. vivax* malaria had been considered relatively benign, compared with that of *P. falciparum*, this view is now being challenged. Additionally, resistance to chloroquine is appearing in countries where malaria is endemic.[2] Thus, there are good reasons to pursue an effective *P. vivax* vaccine.[3] In this regard and in contrast to *P. falciparum*, research into *P. vivax* is limited, due in part to difficulties in culturing blood-stage parasites *in vitro*.[4] Nevertheless, several *P. vivax* vaccine candidates from different parasitic stages have been characterized.[5] Among them, various merozoite surface proteins (MSPs), apical membrane protein-1, duffy binding protein, Pvs25, Pvs28, circumsporozoite protein, and thrombospondin-related anonymous protein have been studied.[5]

Merozoite surface proteins have been characterized and are highly immunogenic in natural infection.[6–9] Among them, several major vaccine candidate antigens (including MSP1, MSP4, MSP5, MSP8, and MSP10) are either known or presumed glycosylphosphatidylinositol (GPI)–anchored membrane proteins. *Plasmodium vivax* MSP1 is the largest and most abundant protein on the *P. vivax* merozoite surface.[5,10] The gene that encodes this protein (*Pvmsp1*) is highly polymorphic and consists of a mosaic of conserved and variable blocks with numerous recombination sites distributed throughout the gene. However, the fragment that encodes the 19-kDa C-terminal epidermal growth factor (EGF)–like domain is relatively conserved.[11] This gene has been used as a polymorphic marker for investigations of the genetic structure of *P. vivax* populations and in molecular epidemiology.[12]

With the completion of *P. vivax* genome sequencing, GPI-anchored proteins of *P. vivax* have been predicted by comparison with validated *P. falciparum* GPI-anchored proteins.[13,14] *Plasmodium vivax msp1p* (*Pvmsp1p*), a novel paralog of the *Pvmsp1* gene, was found immediately upstream of *Pvmsp1*.[14] This gene is predicted to encode a 1,854-amino-acid protein (predicted molecular mass of 215 kDa) with an N-terminal signal sequence, C-terminal EGF-like domains, and a GPI-attachment motif (Figure 1).[14] The functions of this molecule remain unknown. Thus, we have analyzed available genomic data from PlasmoDB (http://www.plasmodb.org/) to search for distinctive pattern of diversity in *msp1p* and *msp1* genes among *Plasmodium* species. We have also assessed the nature and extent of polymorphisms in PvMSP1P from worldwide isolates and laboratory lines of *P. vivax*.

MATERIALS AND METHODS

Gene sequences. The following sequences of malarial parasites were used for the analyses: human *P. falciparum* PfMSP1 (CAA27070), PfMSP8 (PFE0120c), and PfMSP10 (PFF0995c), and *P. vivax* PvMSP1 (PVX_099980), PvMSP8 (PVX_097625), PvMSP10 (PVX_114145), and PvMSP1P (PVX_099975); rodent malaria *P. berghei* PbMSP1 (AAC28871), PbMSP8 (PBANKA_110220), and PbMSP10 (PBANKA_111960), *P. yoelii* PyMSP1 (PY05748), and *P. chabaudi* PchMSP1 (PCAS_083080); primate malaria *P. knowlesi* PkMSP1 (PKH_072850) and PkMSP1P (PKH_072840), *P. reichenowi* PrMSP1 (CAH10285), and *P. cynomolgi* PcyMSP1 (BAI82251); and avian malaria *P. gallinaceum* PgMSP1 (CAH10838). The *P. gallinaceum* sequence database (http://www.sanger.ac.uk/) was used to search for homologs of PvMSP1P and PvMSP10.

Blood samples and DNA preparation. Blood samples were collected, after informed consent had been obtained, from 81

*Address correspondence to Eun-Taek Han, Department of Parasitology, Kangwon National University College of Medicine, Hyoja2-dong, Chuncheon, Gangwon-do 200-701, Republic of Korea. E-mail: ethan@kangwon.ac.kr
†These authors contributed equally to this article.

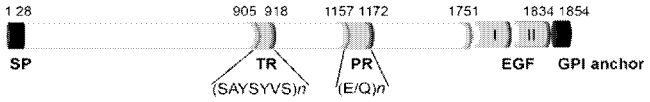

FIGURE 1. Schematic diagram of the *Plasmodium vivax* merozoite surface protein 1 paralog. A putative signal peptide (SP), the epidermal growth factor (EGF)–like domains, and the glycosylphosphatidylinositol (GPI)–anchor attachment site are indicated. TR = tandem repeat region of hepta-peptide; PR = polymorphic E/Q rich region. White color indicates region conserved among strains.

symptomatic patients diagnosed by microscopic examination with *P. vivax* infection at Korea University Ansan Hospital, local health centers, and clinics in Gyeonggi and Gangwon provinces, Republic of Korea. Genomic DNA was purified from 200 μL of whole blood by using a QIAamp DNA Blood Mini Kit (QIAGEN, Valencia, CA), according to the manufacturer's protocol. Genomic DNA of *P. vivax* isolates (n = 33) obtained from Thailand (n = 26), Indonesia (n = 3), India (n = 1), Papua New Guinea (n = 1), Western Samoa (n = 1), and Pakistan (n = 1), and nine *P. vivax* laboratory lines (Africa Mauritania, New Guinea, Honduras III, Brazil I, Salvador I, Vietnam IV, Indonesia I, India VII, and Columbia Rio Meta) were used for polymerase chain reaction (PCR).

Amplification and sequencing of target genes. Genomic DNA from 20 isolates from the Republic of Korea and 9 isolates from other locations was used for amplification of the *Pvmsp1p* full-length gene. Primers SeqF1 (5′-TGC ATA TTC ATA CGC GTG TGT-3′) and SeqR8 (5′-GGC TGC CCC TAA CTT AGC A-3′) were designed based on the *Pvmsp1p* sequence of the *P. vivax* Sal I strain. These were used to amplify DNA fragments from 90 basepairs upstream to 80 basepairs downstream of the *Pvmsp1p* coding sequence by using LA Taq DNA polymerase (TaKaRa, Tokyo, Japan). The PCR amplification was performed on a MyCycler Thermal Cycler (Bio-Rad, Hercules, CA) by using the following temperature profile: 94°C for 2 minutes; 35 cycles at 94°C for 30 seconds, 64°C for 30 seconds, 72°C for 6 minutes; and a final extension at 72°C for 10 minutes.

Both strands of the PCR products were directly sequenced by using a series of sequencing forward primers (SeqF1; SeqF2: 5′-ATC AAC CGG AAG AAC TCC CT-3′; SeqF3: 5′-CAA AGG GAG AAG AAA AAA ATG TAC C-3′; SeqF4: 5′-GGT GAG CTA ATC GAA CGG G-3′; SeqF5: 5′-TGG GGC GCA CAT AAC CT-3′; SeqF6: 5′-CCC GTC TAC TCC AAG GAT GTG ATA AG-3′; SeqF7: 5′-TGA AGT GCA ACA CGT GGA AT-3′; SeqF8: 5′-GTG GAC TAC TAC GGG CTA AGG A-3′ and SeqF9: 5′-ATT CTC TAT GCA GAC AAG GAG GTG-3′) and reverse primers (SeqR1: 5′-AAG GCA GGA TTA GAG AGG ACG; SeqR2: 5′-CGC ACG TTT AGG TGG TAG TC-3′; SeqR3: 5′-AGC GTC AAA TCG TGG CAG-3′; SeqR4: 5′-TTC GTG ATG ATC GCG TTG GTT AGC AG-3′; SeqR5: 5′-TCC CCG ATG AAG AAA TAT GC-3′; SeqR6: 5′-ACT GCA GAT GGA TGG TCA TCT-3′; SeqR7: 5′-AAC TGC ATC GCG TCC GTA T-3′; and SeqR8) using an ABI Prism 377 DNA sequencer (Genotech, Seoul, South Korea).

Analysis of the full-length gene sequences showed one highly polymorphic region. This region was amplified by PCR from genomic DNA of 61 samples form the Republic of Korea and 24 samples from other locations, as well as nine laboratory strains, and sequenced. To examine variable tandem repeat regions, as found in the *Pvmsp1p* gene sequence, primers (TR-F: 5′-CCT ACA CGG GAT GGG AGA T-3′ and TR-R: 5′-CGG AGA GCG AGT TCG TGA T-3′) were used to amplify a 200-basepair fragment encompassing this region from 33 worldwide isolates and 9 laboratory lines.

Data analysis. Sequence data were submitted to GenBank under accession numbers GU556592–GU556620. Amino acid sequence alignments were constructed using the MUSCLE program, with manual corrections.[15] The number of nonsynonymous substitutions per nonsynonymous site (dN) and the number of synonymous substitutions per synonymous site (dS) were computed by using the Nei-Gojobori method[16] with the Jukes-Cantor correction, as implemented in the MEGA 4 program.[17] An unrooted tree was constructed by the neighbor-joining method with the Jones-Taylor-Thornton amino acid substitution model,[18] accompanied by bootstrap analysis with 1,000 replicates for the neighbor-joining method and 100 for the maximum parsimony method implemented in PHYLIP version 3.68 after excluding insertions/deletions (indels) and unreliable amino acid sites.[19]

RESULTS

An MSP1P homolog can be found in the *P. vivax* and *P. knowlesi* genome databases, but not in the *P. falciparum*, *P. yoelii*, or *P. berghei* genome databases. To investigate the evolutionary relationship of MSP1P with other MSPs, we searched for *Pvmsp1p* homologs in the available *Plasmodium* genome database and analyzed their relationship with MSP1 by using the distantly related MSP8 and MSP10 sequences as outgroups. A TBLASTN search of the *P. gallinaceum* sequence database (http://www.sanger.ac.uk) was conducted by using the PvMSP1P amino acid sequence as a query. This search identified a contig (28a.d000006175.Contig1) that contained a putative partial sequence of the *Pgmsp1p* gene (encoding the C-terminal end included EGF-like domains) (Figure 2). Based on the BLOSUM matrix, the amino acid sequence identity/similarity of the EGF-like domains to those of PvMSP1P and PkMSP1P were 56/71% and 58/75%, respectively (Figure 3A). The identity/similarity of the N-terminal region of this gene

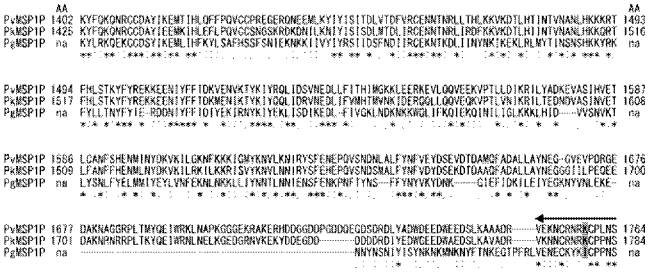

FIGURE 2. Alignment of the partial amino acid sequences of *Plasmodium vivax* merozoite surface protein 1 paralog (PvMSP1P), *P. knowlesi* merozoite surface protein 1 paralog (PkMSP1P), and *P. gallinaceum* merozoite surface protein 1 paralog (PgMSP1P). Dashes indicate deletions. Cys residues with light areas indicate Cys residues conserved among all sequences and those with dark areas and the arrowhead indicate the additional two Cys residues conserved among MSP8, MSP10, MSP1P, and Pf/Pr/PgMSP1 (Figure 3). Asterisks, dots, and colons under the alignment indicate identical, conserved, and semi-conserved substitutions, respectively, based on BLOSUM. The glycosylphosphatidylinositol (GPI) modification site is indicated with arrowhead.

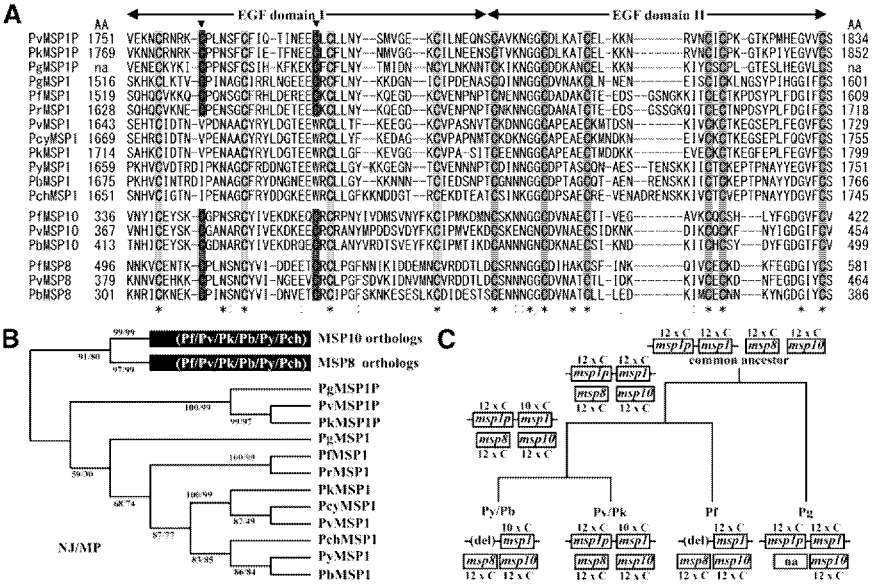

FIGURE 3. Relationship between *Plasmodium vivax* merozoite surface protein 1 paralog (MSP1P) and other *Plasmodium* merozoite surface proteins possessing epidermal growth factor (EGF)–like domains. **A**, Amino acid sequence alignment of the EGF-like domains of *Plasmodium* MSP1, MSP8, MSP10, and MSP1P. Dashes indicate a deletion. Cys residues with light areas indicate Cys residues conserved among all sequences and those with dark areas masks and the arrowhead indicate the additional two Cys residues conserved among MSP8, MSP10, MSP1P, and Pf/Pr/PgMSP1. Asterisks, dots, and colons under the alignment indicate identical, conserved, and semi-conserved substitutions, respectively, based on BLOSUM. **B**, Unrooted dendrograms of the EGF-like region of MSP1, MSP8, MSP10, and MSP1P amino acid sequences. Trees were constructed by the neighbor-joining and maximum parsimony methods using amino acid positions 1759, 1782, 1783, 1784, 1785, 1786, 1787, 1812, 1813, 1814, 1815, 1822, 1823, and 1824 (after *P. vivax* MSP1P amino acid sequence) after excluding indel and unreliable sites. Numbers on branches indicate bootstrap values. **C**, Schematic diagram of the proposed evolutionary history of the *msp1p* gene locus in *Plasmodium* spp. The *msp1p* gene locus was generated by duplication of the *msp1* gene locus in the common ancestor of known *Plasmodium* species. This locus was then deleted in *P. yoelii*, *P. berghei,* and *P. falciparum*. Sequences of *P. falciparum* PfMSP1 (CAA27070), PfMSP8 (PFE0120c) and PfMSP10 (PFF0995c); *P. vivax* PvMSP1 (PVX_099980), PvMSP1P (PVX_099975), PvMSP8 (PVX_097625) and PvMSP10 (PVX_114145); *P. knowlesi* PkMSP1 (PKH_072850) and PkMSP1P (PKH_072840); *P. berghei* PbMSP1 (AAC28871), PbMSP8 (PBANKA_110220) and PbMSP10 (PBANKA_111960); *P. reichenowi* PrMSP1 (CAH10285); *P. gallinaceum* PgMSP1 (CAH10838), PgMSP1P (encoded in 28a.d000006175.Contig1), PgMSP10 (encoded in 28a.d000005716.Contig1); *P. cynomolgi* PcyMSP1 (BAI82251); *P. yoelii* PyMSP1 (PY05748); and *P. chabaudi* PchMSP1 (PCAS_083080) were used.

product to the corresponding region of PvMSP1P (amino acid positions 1,402–1,675) and PkMSP1P (1,425–1,699) were 37/60% and 39/61%, respectively (Figure 2), where the similarity with PgMSP1 was less than 30%. This gene product formed a single clade with Pv/PkMSP1P with high bootstrap values (99–100%; Figure 3B), confirming that this gene was *Pgmsp1p*. Thus, *P. gallinaceum*, *P. vivax*, and *P. knowlesi* have both *msp1* and *msp1p* in their genome and PvMSP1P has weak homology with PvMSP1. This finding, in turn, suggests that the *msp1* and *msp1p* gene loci were generated by a gene duplication event prior to diversification of these parasite species. Because rodent malaria parasite species form a single clade with *P. vivax* and *P. knowlesi*, the lack of a *msp1p* homolog in the *P. yoelii* and *P. berghei* genomes is likely caused by deletion of the *msp1p* gene locus during their evolution. Deletion of this gene locus may also have occurred in *P. falciparum* (Figure 2C).

In a previous study, Carlton and others reported that the PvMSP1P EGF-like domains contained extra two Cys residues absent in PvMSP1 and rodent malaria parasite MSP1, but present in PfMSP1 (Figure 3A).[14] This finding suggested that PvMSP1P might be evolutionarily closer to PfMSP1 than to PvMSP1. However, this appears not to be so for three reasons. First, the dendrogram using EGF-like domains indicated that PvMSP1P formed one clade with PkMSP1P and PgMSP1P and was separated from the MSP1 clade (Figure 3B). Second, beside the EGF-like domains, N-terminal side of the PgMSP1P showed greater similarity to Pv/PkMSP1P (> 60%) than PgMSP1 (< 30%). Third, EGF-like domains of the distantly related MSP8 and MSP10 proteins contain two extra Cys residues, similar to MSP1P and Pf/Pr/PgMSP1. This finding indicates that the common ancestral protein of these MSPs possessed 12 Cys residues (Figure 3A). Collectively, these data suggest that the two Cys sites of the first MSP1 EGF-like domain in *P. vivax*, *P. knowlesi*, *P. yoelii*, and *P. berghei* were substituted with other amino acids during their evolution.

To assess the global genetic diversity of the *Pvmsp1p* gene, we determined the *Pvmsp1p* full-length sequence of 20 isolates of *P. vivax* from the Republic of Korea and 9 strains of *P. vivax* from other locations worldwide. One highly polymorphic glutamate (Glu, E)/glutamine (Gln, Q)-rich region and a polymorphic hepta-peptide motif (SAYSYVS) with number variation (single to triple) were detected. There was no amino acid polymorphism in the EGF-like domains (Figure 1). No diversifying selection was detected, and there was no significant excess of dN over dS.

To determine the repeat variation of the hepta-peptide motif, additional genomic DNA from *P. vivax* worldwide, isolates and laboratory strains was amplified by PCR. All field isolates and laboratory strains had double repeats of this hepta-peptide motif, except for the isolates from Western Samoa (triple repeats) and Pakistan (single repeat). Outside of one E/Q-rich region and the hepta-peptide motif, the sequences were highly conserved with relatively few amino acid substitutions (Table 1).

TABLE 1

Amino acid polymorphisms in the full-length *Plasmodium* merozoite surface protein 1 paralog sequence of *P. vivax* isolates from various locations*

Positions of amino acids	Isolate	
2 3 5 5 7 //* 1 1 1 1 1 1 1 1 8 9 0 1 5 // 2 3 3 4 5 5 7 7 9 9 8 7 5 // 3 2 8 0 4 5 0 6 // 2 0 6 4 6 3 3 7	No. (%)	Sources
A R E R S // S R E Q Q E P D		Salvador I (PVX_099975)
· · · · · // · · · · · · · ·	9 (31.0)	South Korea, Thailand, Pakistan, India
· · · · · // · · · · · · T ·	8 (27.6)	South Korea, Papua New Guinea
· · · · I // · · · · · · · ·	3 (10.3)	South Korea
· · · · I // · · · · · · T ·	4 (13.8)	South Korea
· · · · I // · · K · · K · ·	1 (3.4)	Western Samoa
· · · · · // · · K · · · · E	1 (3.4)	Indonesia
V · · K · // · · · · · · · ·	1 (3.4)	Thailand
· · K · · // · · · · · · · ·	1 (3.4)	Thailand
· Q · · I // N L · K H · · ·	1 (3.4)	Thailand
Total	29 (100)	

* / / = region included hepta-repeat and E/Q-rich sequences.

Of these substitutions, only the S755I or P1686T (or both) mutations were found in 15 of the isolates from the Republic of Korea and Papua New Guinea, whereas more mutants were found in the worldwide isolates (Table 1).

A short and highly diverse region, composed of Glu and Gln as 3–5 Glu residues, followed by one or several basic E/Q*n* (n = 1–6) units, was found in the *Pvmsp1p* gene. Twenty-one distinguishable allelic types (A1–A21) were identified in 127 isolates (clones), based on a comparison with corresponding regions in the *P. vivax* Sal I strain (Table 2). Type A1 had an identical sequence to that of the Sal I strain, which was found in only two laboratory strains, from Central and South America. Type A2 predominated (33.1%, 42 of 127) in all *P. vivax* samples, and in the Korean (35.8%, 29 of 81), Thai (26.7%, 8 of 30), Pacific (67%, 2 of 3), and African isolates (100%, 1 of 1), which share 96.7% amino acid identity with type A1. The 81 Korean isolates appeared to have limited diversity because only four genotypes (allelic types A2, A7, A20, A21) were found, whereas isolates from other locations worldwide, and laboratory strains, showed 20 allelic types (the exception being A21). Interestingly, type A21 was detected only in Korean isolates (18.5%, 15 of 81).

Polymerase chain reaction amplification resulted in two or three target bands in each of three Thai isolates, which suggested multi-clone infection. To confirm this finding, PCR products of the polymorphic region amplified from these samples was cloned and sequenced. Three types (A2, A16, A20) were detected from the Thai T21 isolate, two (A7, A15) from isolate T25, and two (A19, A20) from isolate T29.

DISCUSSION

We have assessed the evolutionary relationship of the *msp1p* gene with other *msp* genes and propose that a duplication event (*msp1* and *msp1p*) occurred before the diversification of the clades in *P. vivax* and *P. gallinaceum*. This account requires two independent deletions of *msp1p*, one in the rodent lineage (after its divergence from the primate lineage to *P. knowlesi* and *P. vivax*) and another deletion in the lineage to *P. falciparum* (after its divergence from the primate lineage to *P. knowlesi* and *P. vivax*). We also propose that the common ancestor of *P. vivax*, *P. knowlesi*, *P. yoelii*, and *P. berghei* possessed MSP1 that had 12 Cys residues in the first EGF-like domain, and that two Cys sites were substituted to other amino acids during their evolution. We further investigated the genetic diversity of the *Pvmsp1p* gene in isolates from locations worldwide, including the Republic of Korea. We found an E/Q-rich polymorphic region, a hepta repeat region, and several polymorphic sites. However, no diversifying selection was apparent by comparing *d*N and *d*S. Although the molecular data (e.g., size, molecular mass, number, location of Cys residue) were similar to those of PvMSP1, PvMSP1P is not polymorphic and appears to not be under noticeable host immune pressure. However, the repeat-length polymorphism of the E/G-rich region may prove useful as a genetic marker for epidemiologic studies.

High conservation of the double EGF-like domains was also detected in other merozoite surface proteins, such as MSP1 and MSP4. These are involved in putative ligand-receptor interactions during erythrocyte invasion by merozoites.[20,21] Thus, the lack of variation in the C-terminus sequence of PvMSP1P, especially the high conservation of the double EGF-like domains, suggests that these regions play an important role in this process.

The overall nucleotide diversity of *Pvmsp1p* is much lower than that of other *P. vivax* antigens, such as MSP1, MSP3β, and apical membrane antigen 1.[20,22,23] In the PvMSP1P sequences, the E/Q-rich region was shown to be highly polymorphic (21 allelic types in 127 clones/isolates). In the cases of PvMSP1 and Pfs230 (AF269242), the E/Q-rich region was also highly polymorphic and represented the principal source of genetic diversity.[24,25] In a low-complexity region analysis of *Plasmodium*,[26] Gln appeared with a somewhat higher frequency in the repetitive than in the non-repetitive motifs. The E/Q-rich regions and repeat motif of PvMSP1P and Pfs230 were located in a low-complexity region.[27] These low-complexity regions harbor tandem repeats identified in *Plasmodium* and correspond to species-specific and rapidly diverging regions.[26]

This variation in E/Q-rich regions and the number of repeats could be generated by slipped-strand mispairing mechanisms. These result in duplication, deletion, or mutation of certain repeat units.[28,29] The tandem repeat regions of PvMSP1P may result from rapid diversification, which enables the parasite to evade the immune response of the host by antigenic polymorphism.[26]

Finally, the highly polymorphic E/Q-rich region sequence of PvMSP1P might be useful as a genetic marker for studies on the population structure and dynamics of *P. vivax* in malaria-endemic areas.

TABLE 2

Allelic types of the E/Q-rich region of *Plasmodium* merozoite surface protein 1 paralog and geographic prevalence of each *P. vivax* isolate from various locations*

Allelic types	Amino acid sequence variation of E/Q rich region sequence	No. (%) following sources							GenBank accession no.
		South Korea	Thailand	Asia†	Pacific region	Central and South America	Africa	Total	
	1157 1174								
Sal I	EE—EQQQ—————EQEQQEQQQQKK							PVX_099975	
A1	· ·—· · · ·————· · · · · · · · · · · ·					2 (50.0)		2 (1.6)	GU556592
A2	· ·E—· · · ·————· · · · · · · · · · · ·	29 (35.8)	8 (26.6)	2 (25.0)	2 (66.6)		1 (100)	42 (33.1)	GU556607
A3	· ·EE· · · ·————· · · · · · · · · · · ·		2 (6.7)					2 (1.6)	GU556593
A4	· ·—· · · ·EQ————· · · · · · · · · · · ·		1 (3.3)					1 (0.8)	GU556594
A5	· ·—· · · ·-QEQQ————· · · · · · · · · · · ·		1 (3.3)					1 (0.8)	GU556595
A6	· ·E—· · · ·EQEQQ————· · · · · · · · · · · ·		2 (6.7)					2 (1.6)	GU556596
A7	· ·—· · · ·EQEQQ————· · · · · · · · · · · ·	18 (22.2)	1 (3.3)					19 (15.0)	GU556597
A8	· ·E————EQ————· · · · · · · · · · · ·		5 (16.7)	1 (12.5)				6 (4.7)	GU556617
A9	· ·E—· · · ·EQEQQ———-Q-· · · · · · · · · · · ·				1 (33.3)	1 (25.0)		2 (1.6)	GU556598
A10	· ·—· · · ·————· · —· · · · · · · ·			1 (12.5)				1 (0.8)	GU556599
A11	· ·E———— -EQQ————· · · · · · · · · · · ·					1 (25.0)		1 (0.8)	GU556600
A12	· ·—· · · ·EQEQQ—EQQ-· · · · · · · · · · · ·			1 (12.5)				1 (0.8)	GU556601
A13	· ·————EQ——EQ——-· · · · · · · · · · · ·			1 (12.5)				1 (0.8)	GU556616
A14	· ·E—· · · ·EQEQQ—EQQ-· · · · · · · · · · · ·			1 (12.5)				1 (0.8)	GU556602
A15	· ·E————————————· · · · · · · ·		1 (3.3)					1 (0.8)	GU556619
A16	· ·E—· · · ·EQEQQEQEQQ-· · · · · · · · · · · ·		1 (3.3)					1 (0.8)	GU556618
A17	· ·—· · · ·————————-EQQ———· ·		2 (6.7)					2 (1.6)	GU556603
A18	· ·—· · · ·EQEQQQQEQQQ--· · · · · · · · · · · ·		2 (6.7)	1 (12.5)				3 (2.4)	GU556604
A19	· ·—· · · ·————————· · · ·————· ·		2 (6.7)					2 (1.6)	GU556605
A20	· ·E—· · · ·————————· · · ·————· ·	19 (23.5)	2 (6.7)					21 (16.5)	GU556611
A21	· ·E—· · · ·EQ———EQQQ· · · ·————· ·	15 (18.5)						15 (11.8)	GU556606
	Total	81 (100)	30‡ (100)	8 (100)	3 (100)	4 (100)	1 (100)	127 (100)	

* Dots and dashes represent identical residues and deletions, respectively.
† Asia except South Korea and Thailand.
‡ Including four clones found in mixed infection from Thailand isolates.

Received July 30, 2010. Accepted for publication October 7, 2010.

Acknowledgment: We thank A. Escalante for providing the *P. vivax* DNA samples of laboratory strain used in this study.

Financial support: This study was supported by National Research Foundation of Korea grant (2009-075103) from the Korean government.

Disclaimer: The views of the authors do not purport to reflect the position of the U.S. Department of the Army or Department of Defense.

Authors' addresses: Yue Wang and Jun-Hu Chen, Department of Parasitology, Kangwon National University College of Medicine, Chuncheon, Gangwon-do 200-701, Republic of Korea and Institute of Parasitic Diseases, Zhejiang Academy of Medical Sciences, Hangzhou 310013, People's Republic of China, E-mails: wangyuerr@yahoo.com.cn and hzjunhuchen@yahoo.com.cn. Osamu Kaneko, Department of Protozoology, Institute of Tropical Medicine, Nagasaki University, 1-12-4 Sakamoto, Nagasaki, Japan, E-mail: okaneko@nagasaki-u.ac.jp. Jetsumon Sattabongkot, Department of Entomology, Armed Forces Research Institute of Medical Science, Bangkok 10400, Thailand, E-mail: JetsumonP@afrims.org. Feng Lu, Department of Parasitology, Kangwon National University College of Medicine, Chuncheon, Gangwon-do 200-701, Republic of Korea and Jiangsu Institute of Parasitic Diseases, Wuxi 214064, People's Republic of China, E-mail: lufeng981@hotmail.com. Jong-Yil Chai, Department of Parasitology and Tropical Medicine, Seoul National University College of Medicine, Seoul, Republic of Korea, E-mail: cjy@snu.ac.kr. Satoru Takeo and Takafumi Tsuboi, Cell-Free Science and Technology Research Center, Ehime University, 3 Bunkyo-cho, Matsuyama, Ehime 790-8577, Japan, E-mails: tsuboi@ccr.ehime-u.ac.jp and stakeo@ccr.ehime-u.ac.jp. Francisco J. Ayala, Department of Ecology and Evolutionary Biology, University of California, Irvine, CA, E-mail: fjayala@uci.edu. Yong Chen, Zhejiang Medical College, Hangzhou 310053, and Zhejiang Academy of Medical Sciences, Hangzhou 310013, People's Republic of China, E-mail: cyong93@yahoo.com.cn. Chae Seung Lim, Department of Laboratory Medicine, College of Medicine, Korea University, Seoul 152-703, Republic of Korea, E-mail: malarim@korea.ac.kr. Eun-Taek Han, Department of Parasitology, Kangwon National University College of Medicine, Chuncheon, Gangwon-do 200-701, Republic of Korea, E-mail: ethan@kangwon.ac.kr.

REFERENCES

1. Price RN, Tjitra E, Guerra CA, Yeung S, White NJ, Anstey NM, 2007. Vivax malaria: neglected and not benign. *Am J Trop Med Hyg 77:* 79–87.
2. Mueller I, Galinski MR, Baird JK, Carlton JM, Kochar DK, Alonso PL, del Portillo HA, 2009. Key gaps in the knowledge of *Plasmodium vivax*, a neglected human malaria parasite. *Lancet Infect Dis 9:* 555–566.
3. Herrera S, Corradin G, Arevalo-Herrera M, 2007. An update on the search for a *Plasmodium vivax* vaccine. *Trends Parasitol 23:* 122–128.
4. Udomsangpetch R, Kaneko O, Chotivanich K, Sattabongkot J, 2008. Cultivation of *Plasmodium vivax*. *Trends Parasitol 24:* 85–88.
5. Galinski MR, Barnwell JW, 2008. *Plasmodium vivax*: who cares? *Malar J 7 (Suppl 1):* S9.
6. Black CG, Barnwell JW, Huber CS, Galinski MR, Coppel RL, 2002. The *Plasmodium vivax* homologues of merozoite surface proteins 4 and 5 from *Plasmodium falciparum* are expressed at different locations in the merozoite. *Mol Biochem Parasitol 120:* 215–224.
7. Perez-Leal O, Sierra AY, Barrero CA, Moncada C, Martinez P, Cortes J, Lopez Y, Torres E, Salazar LM, Patarroyo MA, 2004. *Plasmodium vivax* merozoite surface protein 8 cloning, expression, and characterisation. *Biochem Biophys Res Commun 324:* 1393–1399.
8. Perez-Leal O, Sierra AY, Barrero CA, Moncada C, Martinez P, Cortes J, Lopez Y, Salazar LM, Hoebeke J, Patarroyo MA, 2005. Identifying and characterising the *Plasmodium falciparum* merozoite surface protein 10 *Plasmodium vivax* homologue. *Biochem Biophys Res Commun 331:* 1178–1184.
9. de Oliveira CI, Wunderlich G, Levitus G, Soares IS, Rodrigues MM, Tsuji M, del Portillo HA, 1999. Antigenic properties of the merozoite surface protein 1 gene of *Plasmodium vivax*. *Vaccine 17:* 2959–2968.
10. Udagama PV, Gamage-Mendis AC, David PH, Peiris JS, Perera KL, Mendis KN, Carter R, 1990. Genetic complexity of *Plasmodium vivax* parasites in individual human infections analyzed with monoclonal antibodies against variant epitopes on a single parasite protein. *Am J Trop Med Hyg 42:* 104–110.
11. Putaporntip C, Jongwutiwes S, Sakihama N, Ferreira MU, Kho WG, Kaneko A, Kanbara H, Hattori T, Tanabe K, 2002. Mosaic organization and heterogeneity in frequency of allelic recombination of the *Plasmodium vivax* merozoite surface protein-1 locus. *Proc Natl Acad Sci U S A 99:* 16348–16353.
12. Cui L, Escalante AA, Imwong M, Snounou G, 2003. The genetic diversity of *Plasmodium vivax* populations. *Trends Parasitol 19:* 220–226.
13. Gilson PR, Nebl T, Vukcevic D, Moritz RL, Sargeant T, Speed TP, Schofield L, Crabb BS, 2006. Identification and stoichiometry of glycosylphosphatidylinositol-anchored membrane proteins of the human malaria parasite *Plasmodium falciparum*. *Mol Cell Proteomics 5:* 1286–1299.
14. Carlton JM, Adams JH, Silva JC, Bidwell SL, Lorenzi H, Caler E, Crabtree J, Angiuoli SV, Merino EF, Amedeo P, Cheng Q, Coulson RM, Crabb BS, Del Portillo HA, Essien K, Feldblyum TV, Fernandez-Becerra C, Gilson PR, Gueye AH, Guo X, Kang'a S, Kooij TW, Korsinczky M, Meyer EV, Nene V, Paulsen I, White O, Ralph SA, Ren Q, Sargeant TJ, Salzberg SL, Stoeckert CJ, Sullivan SA, Yamamoto MM, Hoffman SL, Wortman JR, Gardner MJ, Galinski MR, Barnwell JW, Fraser-Liggett CM, 2008. Comparative genomics of the neglected human malaria parasite *Plasmodium vivax*. *Nature 455:* 757–763.
15. Edgar RC, 2004. MUSCLE: multiple sequence alignment with high accuracy and high throughput. *Nucleic Acids Res 32:* 1792–1797.
16. Nei M, Gojobori T, 1986. Simple methods for estimating the numbers of synonymous and nonsynonymous nucleotide substitutions. *Mol Biol Evol 3:* 418–426.
17. Tamura K, Dudley J, Nei M, Kumar S, 2007. MEGA4: Molecular Evolutionary Genetics Analysis (MEGA) software version 4.0. *Mol Biol Evol 24:* 1596–1299.
18. Jones DT, Taylor WR, Thornton JM, 1992. The rapid generation of mutation data matrices from protein sequences. *Comput Appl Biosci 8:* 275–282.
19. Felsenstein J, 1993. *PHYLIP (Phylogeny Inference Package) Version 3.5c*. Seattle, WA: Department of Genetics, University of Washington.
20. Thakur A, Alam MT, Sharma YD, 2008. Genetic diversity in the C-terminal 42 kDa region of merozoite surface protein-1 of *Plasmodium vivax* (PvMSP-1(42)) among Indian isolates. *Acta Trop 108:* 58–63.
21. Putaporntip C, Jongwutiwes S, Ferreira MU, Kanbara H, Udomsangpetch R, Cui L, 2009. Limited global diversity of the *Plasmodium vivax* merozoite surface protein 4 gene. *Infect Genet Evol 9:* 821–826.
22. Thakur A, Alam MT, Bora H, Kaur P, Sharma YD, 2008. *Plasmodium vivax*: sequence polymorphism and effect of natural selection at apical membrane antigen 1 (PvAMA1) among Indian population. *Gene 419:* 35–42.
23. Rayner JC, Huber CS, Feldman D, Ingravallo P, Galinski MR, Barnwell JW, 2004. *Plasmodium vivax* merozoite surface protein PvMSP-3 beta is radically polymorphic through mutation and large insertions and deletions. *Infect Genet Evol 4:* 309–319.
24. Leclerc MC, Menegon M, Cligny A, Noyer JL, Mammadov S, Aliyev N, Gasimov E, Majori G, Severini C, 2004. Genetic diversity of *Plasmodium vivax* isolates from Azerbaijan. *Malar J 3:* 40.
25. Niederwieser I, Felger I, Beck HP, 2001. Limited polymorphism in *Plasmodium falciparum* sexual-stage antigens. *Am J Trop Med Hyg 64:* 9–11.
26. Brocchieri L, 2001. Low-complexity regions in *Plasmodium* proteins: in search of a function. *Genome Res 11:* 195–197.
27. Aurrecoechea C, Brestelli J, Brunk BP, Dommer J, Fischer S, Gajria B, Gao X, Gingle A, Grant G, Harb OS, Heiges M, Innamorato F, Iodice J, Kissinger JC, Kraemer E, Li W, Miller JA, Nayak V, Pennington C, Pinney DF, Roos DS, Ross C, Stoeckert CJ Jr, Treatman C, Wang H, 2009. PlasmoDB: a functional genomic database for malaria parasites. *Nucleic Acids Res 37:* D539–D543.
28. Pizzi E, Frontali C, 2001. Low-complexity regions in *Plasmodium falciparum* proteins. *Genome Res 11:* 218–229.
29. Tanabe K, Sakihama N, Kaneko A, 2004. Stable SNPs in malaria antigen genes in isolated populations. *Science 303:* 493.

Am. J. Trop. Med. Hyg., 84(1), 2011, pp. 107–108
doi:10.4269/ajtmh.2011.10-0291

Case Report: Expansion of Visceral Leishmaniasis to the Western Hilly Part of Nepal

Basu Dev Pandey,* Sher Bahadur Pun, Osamu Kaneko, Kishor Pandey, and Kenji Hirayama

Sukraraj Tropical and Infectious Diseases Hospital, Kathmandu, Nepal; Everest International Clinic and Research Center, Kathmandu, Nepal; Department of Protozoology, Institute of Tropical Medicine (NEKKEN) and the Global Center of Excellence Program, Nagasaki University, Nagasaki, Japan; Department of Immunogenetics, Institute of Tropical Medicine (NEKKEN) and the Global Center of Excellence Program, Nagasaki University, Nagasaki, Japan

Abstract. We report the first case of visceral leishmaniasis (VL) from the non-endemic western hilly region of Nepal. The patient presented with a history of high-grade fever, abdominal distension, anemia, and weight loss. The case was confirmed as VL by microscopical detection of the *Leishmania* species amastigote in bone marrow aspiration and by a positive result for the rK39 test. The patient was treated with 0.5–1.0 mg/kg of Amphotericin B for 14 days (total of 405 mg), and amastigotes were negative on discharge. Five months later, this patient again developed fever, abdominal distension, and anemia. Clinical and hematological examinations suggested a relapse of VL. The patient was treated with 1 mg/kg of Amphotericin B for 18 days (total of 515 mg) and was clinically improved on discharge.

INTRODUCTION

Visceral leishmaniasis (VL), known as kala-azar in Nepal and India, is a deadly vector-borne disease, which is endemic in Bangladesh, India, and Nepal in South Asia with estimated more than 60% of all VL cases worldwide, primarily affecting in rural areas.[1,2] In Nepal, 5.7 million people are estimated to be at risk and mainly confined to 13 districts southeast of the Terai region, which borders the VL endemic districts of Bihar state in India (Figure 1).[3] A total of 23,368 cases with 311 deaths have been reported between 1980 and 2007.[3] The disease is highly endemic in rural poor areas where most deaths are reported. People residing in these areas have little knowledge about the disease; hence, VL cases may be underestimated in these regions. Treatment failure with pentavalent antimonial (sodium stibogluconate [SSG]) has been reported in the recent years in Nepal,[4] and as a result, liposomal Amphotericin B is currently recommended by National Program of Nepal for kala-azar treatment. Not only is the emergence and spread of drug resistance troubling, but VL cases have been recently reported from the regions that were previously considered to be non-endemic in Nepal.

CASE REPORT

Here, we describe a 13-year-old male from Doti who was referred to Sukraraj Tropical and Infectious Disease Hospital (STIDH), Kathmandu, from Nepalgunj Medical College in February 2009. The patient attended several clinics and hospitals in Nepalgunj, including India, with chief complains of high grade fever for 3 months associated with chills and rigors in 2004 before hospitalization. The patient had no history of travel to India or VL endemic regions of Nepal before fever started. Fever subsided, and general conditions were improved after locally treated with antipyretics and antibiotics followed by anti-malarial treatment. However, within 1 year, the patient was admitted to Nepalgunj Medical College with chief complains of fever, abdominal distension, and weight loss. The patient went under clinical and laboratory examinations for 12 days in the medical college. A provisional diagnosis of VL was made based on the positive result of the rK39 dipstick test (InSure; InBios Int, Seattle, WA). The patient was referred to STIDH for further investigation and definite diagnosis.

The patient was found to be anemic, and the spleen size was approximately 5 cm below the left costal margin at the time of admission. Initial hematological examination showed a white blood cell count of 5,100/mm^3, hemoglobin level of 5.8 g/dL, and total neutrophil count of 56%, with a lymphocyte of 44%. Random glucose level was 88 mg/dL, with blood urea of 17 mg/dL and serum creatinine of 0.8 mg/dL. *Leishmania* species amastigotes were found in the bone marrow aspiration smear, and rK39 test was positive, confirming *Leishmania* infection. Human immunodeficiency virus (HIV) infection was excluded by the negative result of the rapid diagnosis test (Determine HIV-1/2 kit; Abbott, Minato-Ku, Tokyo, Japan), and tuberculosis was excluded by the negative observation of the chest X-ray examination as well Tuberculin Purified Protein Derivative (PPD) test for this disease. The patient was treated with Amphotericin B with the initial dose of 0.5 mg/kg body weight, which was gradually increased to 1 mg/kg for 14 days, with total dose of 405 mg. The patient was given a transfusion of six units of whole blood during treatment and was clinically improved as indicated by the absence of fever, shrinking spleen size, and absence of amastigote. The patient was free from symptoms for about 5 months after treatment.

The patient revisited STIDH in July 2009, with chief complaints of fever and abdominal distension. Physical examination revealed anemia and splenomegaly measuring 8 cm in size below the left costal margin. Ultrasonography of abdominal revealed gross hepato-splenomegaly with the liver size of 17.6 cm, and spleen size of 18.7 cm. Laboratory examinations showed renal function, and platelets count was within normal range but the hemoglobin level (7 mg/dL) was decreased. Although amastigotes were not found in the bone marrow smear, a relapse case of VL was suspected based on the clinical features, decreased hemoglobin level, and previous VL history. The patient was treated with Amphotericin B (1 mg/kg body weight) for 18 days with a total dose of 515 mg. The patient was given a transfusion of 2 units of whole blood during treatment and was clinically improved with increased hemoglobin level of 7.4 mg/dL within 1 week and decreased spleen size by about 4 cm on discharge.

*Address correspondence to Basu Dev Pandey, Sukraraj Tropical and Infectious Diseases Hospital and Everest International Clinic and Research Center, Teku Road, Kathmandu, Nepal 9045. E-mail: basupandey@wlink.com.np

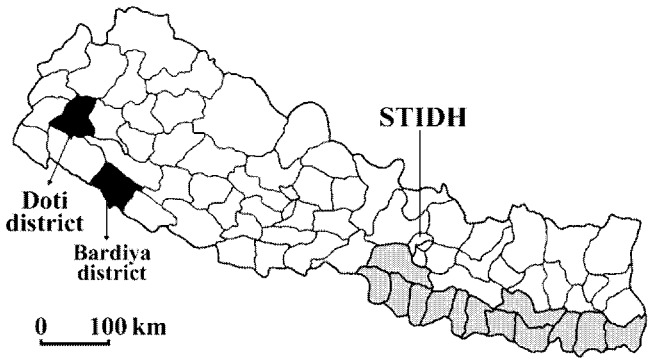

FIGURE 1. District maps of Nepal. Districts endemic for leishmaniasis are indicated in grey. The VL patient reported resides in the hilly district Doti (black). The Bardiya district, where a suspected miltefosine-resistant VL case was previously reported, is indicated (black). STIDH indicates the Sukraraj Tropical and Infectious Disease Hospital.

DISCUSSION

This is the first report of VL from the non-endemic far western hilly region of Nepal. Nepal is geographically divided into three areas: the Mountain, Hills, and Terai regions. VL transmission generally occurs in plain Terai region, with an altitude of a maximum of 305 m. However, cases have been increasingly reported from hilly regions of India and the eastern part of Nepal in the recent years.[2,5] VL has been considered to be a disease of low altitude and is usually found below the altitude of 600 m (2,000 ft) above sea level.[6] In the present report, however, VL is found in the hilly, far western region at an altitude of 1,113 m (3,654 feet) above sea level. VL cases from hilly regions above the altitude of 1,000 m have been reported in India,[7,8] which could be because of the improved monitor system, changes in seasonal climate over the past years, and potential changes of geographical distribution of the vectors. Previously, we have reported a VL case from midwestern region of Nepal.[9] However, it was unclear if this patient was infected with VL in this region because of the history of traveling to India. In this study, however, the patient had no history of traveling to India or VL endemic regions of Nepal, suggesting that VL was expanding into newer areas. The transmission of the *Leishmania donovani* needs a vector sandfly and potentially, reservoir animals; however, this information in the hilly region of Nepal, including the Doti district, is not available. Active VL and entomological surveillance are warranted in the far western region of Nepal to confirm this point. The patient reported in this study showed VL symptoms within 1 year after the complete standard VL treatment; however, treatment with the same drug, Amphotericin B, was able to cure this patient, suggesting that the relapse was likely not caused by the drug resistance of the parasites. The precise reason of the relapse is unclear and not the major point in this study. VL is a major health problem in Nepal and is endemic in 13 districts of the eastern and central Terai region. According to annual health report of the Department of Health Services in Nepal, VL incidence has shown to be 2.67 per 10,000 people at risk in 2006–2007.[2] The VL elimination program aims at reducing incidence to 1 per 10,000 at risk by the year 2015. An increasing trend of sporadic VL cases from other parts (non-endemic regions) of the country like Doti could challenge the aim of the VL elimination program. In addition, findings of drug resistance reports from newer areas could be another obstacle in reducing the morbidity and mortality rate in the long term in Nepal. Thus, policy makers should give a high priority in expanding active VL surveillance network in the newly parasite-detected areas to achieve the realistic goal by the year 2015.

Received May 21, 2010. Accepted for publication September 5, 2010.

Acknowledgments: We gratefully thank to the director and staff of the Sukraraj Tropical and Infectious Diseases Hospital for providing care to the patients and facility. We would also like to thank Mr. Kiran Pandey at the Everest International Clinic and Research Center, Kathmandu, Nepal, for his technical support. Assessment and treatment of patients was carried out in accordance with standard clinical procedures at the Sukraraj Tropical and Infectious Diseases Hospital, Kathmandu, Nepal. Informed consent was obtained from the patients for their assessment, treatment, and publication of the case report. B.D.P. performed the clinical evaluation and management of the cases; B.D.P. and S.B.P. drafted the manuscript, and O.K., K.P., and K.H. revised the paper. All authors read and approved the final manuscript.

Financial support: This study was supported in part by Grants-in-Aid from Ministry of Education, Culture, Sports, Science and Technology (MEXT), the Global Center of Excellence (COE) Program at Nagasaki University (to O.K. and K.H.), and the National Bio-Resource Project (NBRP) of MEXT, Japan (to K.H.).

Authors' addresses: Basu Dev Pandey and Sher Bahadur Pun, Sukraraj Tropical and Infectious Diseases Hospital and Everest International Clinic and Research Center, Kathmandu, Nepal, E-mails: basupandey@wlink.com.np and drsherbdr@yahoo.com. Osamu Kaneko, Department of Protozoology, Institute of Tropical Medicine (NEKKEN) and the Global Center of Excellence Program, Nagasaki University, Nagasaki, Japan, E-mail: okaneko@nagasaki-u.ac.jp. Kishor Pandey, Everest International Clinic and Research Center, Kathmandu, Nepal, E-mail: pandey_kishor@hotmail.com. Kenji Hirayama, Department of Immunogenetics, Institute of Tropical Medicine (NEKKEN) and the Global Center of Excellence Program, Nagasaki University, Nagasaki, Japan, E-mail: hiraken@nagasaki-u.ac.jp.

REFERENCES

1. Pandey K, Pant S, Kanbara H, Shuaibu MN, Mallik AK, Pandey BD, Kaneko O, Yanagi T, 2008. Molecular detection of *Leishmania* parasites from whole bodies of sandflies collected in Nepal. *Parasitol Res 108:* 293–297.
2. World Health Organization, 2005. Regional technical advisory group on kala-azar elimination. Proceedings of the 1st Meeting, December 20–23, 2004; New Delhi, India.
3. Department of Health Sciences, 2007. *Annual Report on Nepal.* Kathmandu, Nepal, 145–148.
4. Rijal S, Chappuis F, Singh R, Bovier PA, Acharya P, Karki BM, Das ML, Desjues P, Loutan L, Koirala S, 2003. Treatment of visceral leishmaniasis in south-eastern Nepal: decreasing efficacy of sodium stiboglucanate and need for the policy to limit further decline. *Trans R Soc Trop Med Hyg 97:* 350–354.
5. Joshi S, Bajracharya BL, Baral MR, 2006. Kala-azar (visceral leishmaniasis) from Khotang. *Kathmandu Univ Med J 4:* 232–234.
6. Park K, 2007. Leishmaniasis. Park K, ed. *Park's Text Book of Preventive and Social Medicine*, 6th ed. Jabalpur, India: Banarsidas Bhanot, 256–258.
7. Verma SK, Ahmed S, Shirazi N, Kusum A, Kaushik RM, Barthwal SP, 2007. Sodium stibogluconate-sensitive visceral leishmaniasis in the non-endemic hilly region of Uttarkhand, India. *Trans R Soc Trop Med Hyg 101:* 730–732.
8. Mahajan SK, Machhan P, Kanga A, Thakur S, Sharma A, Prasher BS, Pal LS, 2004. Kala-azar at high altitude. *J Commun Dis 36:* 117–120.
9. Pandey BD, Pandey K, Kaneko O, Yanagi T, Hirayama K, 2009. Relapse of visceral leishmaniasis after miltefosine treatment in a Nepalese patient. *Am J Trop Med Hyg 80:* 580–582.

Parasitol Res (2010) 107:727–730
DOI 10.1007/s00436-010-1920-0

SHORT COMMUNICATION

Diagnosis of visceral leishmaniasis by polymerase chain reaction of DNA extracted from Giemsa's solution-stained slides

Kishor Pandey · Basu Dev Pandey · Arun Kumar Mallik · Osamu Kaneko · Haruki Uemura · Hiroji Kanbara · Tetsuo Yanagi · Kenji Hirayama

Received: 30 April 2010 / Accepted: 7 May 2010 / Published online: 25 May 2010

Abstract Visceral leishmaniasis (VL) is caused by the protozoan parasite *Leishmania donovani* and is a potentially fatal disease in endemic areas of the world. Nepal is an endemic area in which VL causes major public health problems in the lowland areas of the southeast regions. The aim of the present study was to evaluate the sensitivity of polymerase chain reaction (PCR) amplification for the detection of *Leishmania* DNA from Giemsa's solution-stained bone marrow slides. Bone marrow samples were aspirated from a total of 115 VL suspected patients and used to prepare smears on glass slides and for the initiation of in vitro culture. Bone marrow slides were used for microscopic observation, DNA extraction, and subsequent PCR amplification. PCR analysis showed that all the positive samples were of *Leishmania* parasites. The PCR assay also showed a higher sensitivity (69%) than microscopic examination (57%) and culture (21%). In addition, PCR was able to detect VL in 12% of samples which were negative by microscopy. PCR of DNA extracted from Giemsa's solution-stained bone marrow slides is a suitable tool for confirming diagnosis in patients with VL and may also be useful in the diagnosis of difficult cases. Bone marrow smears are easily stored and can be easily sent to research centers where PCR is available. This makes PCR a good option for diagnosis in the field.

K. Pandey (✉) · K. Hirayama
Department of Immunogenetics, Institute of Tropical Medicine (NEKKEN) and the Global COE Program, Nagasaki University, 1-12-4 Sakamoto,
Nagasaki 852-8523, Japan
e-mail: pandey_kishor@hotmail.com

K. Hirayama
e-mail: hiraken@nagasaki-u.ac.jp

B. D. Pandey
Sukraraj Tropical and Infectious Diseases Hospital,
Kathmandu, Nepal
e-mail: basupandey@wlink.com.np

A. K. Mallik
Janakpur Zonal Hospital,
Janakpur, Nepal
e-mail: ak_mallik@yahoo.com

O. Kaneko · H. Uemura · H. Kanbara
Department of Protozoology, Institute of Tropical Medicine (NEKKEN) and the Global COE Program, Nagasaki University, 1-12-4 Sakamoto,
Nagasaki 852-8523, Japan

O. Kaneko
e-mail: okaneko@nagasaki-u.ac.jp

H. Uemura
e-mail: uemura@nagasaki.net-u.ac.jp

T. Yanagi
Animal Research Center for Tropical Infections,
Institute of Tropical Medicine, Nagasaki University,
1-12-4 Sakamoto,
Nagasaki 852-8523, Japan
e-mail: tyanagi@tm.nagasaki-u.ac.jp

Introduction

Visceral leishmaniasis (VL) is a parasitic disease caused by the protozoan parasite *Leishmania donovani* and is transmitted by sand fly vectors. VL has been reported from 51 countries around the world and has an annual incidence of 500,000 cases. VL is responsible for about 59,000 deaths per year and 2.4 million disability-adjusted life years are lost worldwide. India, Nepal, and Bangladesh account for 300,000 cases annually, and thus account for 60% of the total global burden of this disease. In Nepal,

VL causes major public health problems as well as mortality in the lowland areas of the southeast regions which border Bihar Indian state, a known VL endemic area. Early treatment is a major pillar of the current VL elimination program, which has been launched by the governments of India (Aransay et al. 2000), Nepal, and Bangladesh (Sundar et al. 2008; Al-Jawabreh et al. 2003).

The gold standard method for VL diagnosis is microscopical examination of *L. donovani* bodies in bone marrow aspirates. Such detection of *Leishmania* parasites in a clinical sample is necessary to confirm a suspected case of VL. The most common method for VL diagnosis is direct detection of parasites, either by microscopical examination or in vitro cultivation, for which sensitivity is low (Herwaldt 1999). Other methods for diagnosis of VL, such as parasitological or serological tests, are difficult even in well-equipped hospitals (Sundar 2003; da Silva 2005). As an alternative at the district level, serological tests (direct agglutination test or rK39 immunochromatographic test) were used. The minimum basis for starting treatment for VL is positivity for rK39 immunochromatographic test. The serodiagnosis is negative in the early acute stage of the disease and do not differentiate between active, past, or subclinical infection. It remains positive well beyond the time of cure, thus limiting their use for the diagnosis of relapses or reinfection (Chappuis et al. 2007). Thus, improved tools for the diagnosis of VL are needed. Molecular methods including polymerase chain reaction (PCR)-based techniques have proven to be highly sensitive and specific as they analyze parasite DNA and may be applied to a variety of clinically obtained samples (Marfurt et al. 2003; Bensoussan et al. 2006; Schallig and Oskam 2002; Reithinger and Dujardin 2007; Brustoloni et al. 2007) For clinical samples, Giemsa's solution-stained bone marrow smears on glass slides are potentially very valuable sources of DNA for PCR-based diagnosis. Firstly, PCR diagnosis using DNA extracted from Giemsa's solution-stained bone marrow slides is a suitable tool to confirm diagnosis in patients with VL and is useful in the diagnosis of difficult cases. Secondly, historical slides or archived materials may be assessed, thus allowing retrospective studies. Lastly, bone marrow smears can be easily stored and sent to research centers where PCR diagnosis can be readily achieved.

A number of PCR-based diagnoses from Giemsa's solution-stained samples on glass slides have been previously reported, including blood smears for *Plasmodium* spp. (Li et al. 1997), for cutaneous Leishmaniasis (Motazedian et al. 2002), and fecal smears containing *Cryptosporidium parvum* (Amar et al. 2001). However, PCR-based *Leishmania* diagnosis from bone marrow smears on glass slides have not been widely applied, although we have recently described the use of this strategy to confirm VL infection of a Nepali patient (Pandey et al. 2009) Thus, in the present study, we have investigated the sensitivity of PCR diagnosis from bone marrow samples obtained from clinically suspected VL patients in comparison with microscopy and parasite culture.

Material and methods

Sample collection

Bone marrow samples were collected from clinically suspected VL patients on the basis of clinical history (continuous fever for 2 weeks, headache, and splenomegaly) in Nepal during 2003–2005. Bone marrow was aspirated by sternal puncture and used for smear preparation and to initiate *Leishmania* culture. Bone marrow smears were fixed with methanol and stained with Giemsa's solution. More than 100 microscopic fields were observed in order to detect the parasite. The slides were kept at room temperature and brought to Japan for further analysis. Informed consent from each of the patients was obtained after an explanation of the uses of bone marrow aspirates. The research protocol was approved by the Ethical Committee of Nagasaki University.

DNA extraction

After shipping to Japan, all bone marrow smear samples were re-examined microscopically for *Leishmania* parasite infection. Then, Giemsa's solution-stained smears were wiped with fresh paper wipes (Kimwipe wipers S-200; Kimberly-Clark, Dallas, TX) to remove immersion oil, wetted with sterile phosphate-buffered saline, and scraped with a sterile scalpel. The DNA was extracted by using the DNeasy Blood and Tissue Kit (Qiagen, Valencia, CA) according to the manufacturer's instructions, yielding a final elution volume of 25 μl. Two different reference strains of *L. donovani*, Dd8 Indian strain (accession no. Y11401) and T4 Nepalese strain (accession no AB458390), were used as positive controls for PCR amplification.

PCR amplification

We selected the conserved region of minicircle kinetoplast DNA because its copy number is more than 10^4 per parasite, maximizing the possibility of detection (Akkafa et al. 2008; Smyth et al. 1992; Salotra et al. 2001). PCR analysis consisted of two steps, the details of which were given previously (Aransay et al. 2000; Pandey et al. 2008). Briefly, first-round PCR amplification was carried out in a total of 10 μl reaction mixture with primers LINR4 (5′-

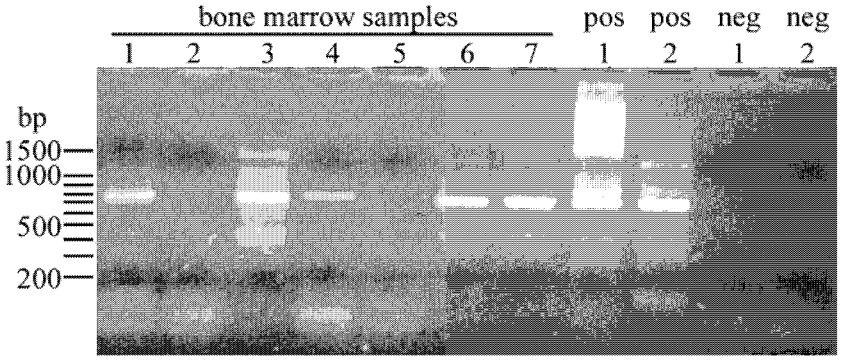

Fig. 1 PCR amplification of the *Leishmania* DNA obtained from Giemsa's solution-stained smears on glass slides. *Lanes 1–7* bone marrow samples, *pos1* and *pos2* DNA from cultured *Leishmania* parasite, *neg1* DNA from mouse bone marrow without *Leishmania* infection, *neg2* without DNA template. In this experiment, *sample numbers 1, 3, 4, 6,* and *7* were judged to be positive for *Leishmania* infection

GGGGTTGGTGTAAAATAGGG-3′) and LIN17 (5′-TTTGAACGGGATTTCTG-3′) and 2 μl of DNA solution. The second-round seminested PCR was carried out in a 20-μl reaction mixture volume as for the first round by adding primer LIN19 (5′-CAGAACGCCCCTACCCG-3′) and 1 μl of the first PCR product. Two negative controls and two positive controls were set for each experiment. The first negative control was normal mouse bone marrow and the other was DNA-negative reaction mixture. Two positive controls contained DNA from cultured *L. donovani* parasites. Ten microliters of the PCR-amplified products were subjected to 2% agarose gel electrophoresis, stained with ethidium bromide, and visualized under UV light. A 100-bp DNA ladder was used as a marker.

Results and discussion

Microscopical examination, parasite culture, and PCR diagnosis using bone marrow smears were performed for 115 samples obtained from clinically suspected VL patients. Samples which produced a 720-bp band following PCR amplification and electrophoresis were judged to be positive for VL. Figure 1 shows an example of an agarose gel electrophoresis image. The positive controls produced the expected 720-bp band which was absent from the negative controls. Among 115 samples, *Leishmania* DNA was successfully detected in 79 samples. PCR diagnosis showed the highest sensitivity (79 positive/115 samples, 68.7%) compared to microscopical examination (65/115, 56.5%) and parasite culture (20/115, 21%; Table 1). All samples positive by microscopic examination or parasite culture for *Leishmania* infection were positive by PCR diagnosis and all negative samples by PCR diagnosis were negative by other methods.

Despite its high sensitivity and specificity, PCR diagnosis may have limitations in VL diagnosis. PCR diagnosis alone cannot differentiate between asymptomatic and acute infections of VL (Deborggraeve et al. 2008), thus this method may be used only for the confirmation of suspected cases of acute VL. Currently, asymptotic VL patients in endemic regions are not treated with (Kennedy 1984) drugs because the available drugs for VL are highly toxic and their unnecessary use may stimulate the emergence and spread of drug-resistant parasite strains. However, it should be noted that PCR diagnosis of *Leishmania* DNA in asymptomatic VL patients is beneficial for epidemiological studies.

Table 1 Comparison of PCR amplification, microscopical examination, and parasite culture to diagnose visceral leishmaniasis

	Total	Microscopy		Culture	
		(+)	(−)	(+)	(−)
PCR diagnosis (+)	79 (68.7%)	65	14	20	59
PCR diagnosis (−)	36 (31.3%)	0	36	0	36
Total	115	65 (56.5%)	50 (43.5%)	20 (21.0%)	95 (79.0%)

Acknowledgement We thank Richard Culleton for proofreading the manuscript. KP is a recipient of a Ph.D. scholarship from the Ministry of Education, Culture, Sports, Science and Technology (MEXT) of Japan. This study was supported in part by Grants-in-Aid from MEXT, the Global COE Program at Nagasaki University (to KH and OK), and the National Bio-Resource Project (NBRP) of MEXT, Japan (to KH).

References

Aransay AM, Scoulica E, Tselentis Y (2000) Detection and identification of *Leishmania* DNA within naturally infected sand flies by seminested PCR on minicircle kinetoplastic DNA. Appl Environ Microbiol 66:1933–1938

Sundar S, Mondal D, Rijal S et al (2008) Implementation research to support the initiative on the elimination of kala azar from Bangladesh, India and Nepal—the challenges for diagnosis and treatment. Trop Med Int Health 13:2–5

Al-Jawabreh A, Barghuthy F, Schnur LF, Jacobson RL, Schonian G, Abdeen Z (2003) Epidemiology of cutaneous leishmaniasis in the endemic area of Jericho, Palestine. East Mediterr Health J 9:805–815

Herwaldt BL (1999) Leishmaniasis. Lancet 354:1191–1199

Sundar S (2003) Diagnosis of kala-azar—an important stride. J Assoc Physicians India 51:753–755

da Silva LJ (2005) Vianna and the discovery of *Leishmania braziliensis*: the role of Brazilian parasitologists in the identification of Bauru's ulcer as American leishmaniasis. Parassitologia 47:335–341

Chappuis F, Sundar S, Hailu A et al (2007) Visceral leishmaniasis: what are the needs for diagnosis, treatment and control? Nat Rev Microbiol 5:873–882

Marfurt J, Nasereddin A, Niederwieser I, Jaffe CL, Beck HP, Felger I (2003) Identification and differentiation of *Leishmania* species in clinical samples by PCR amplification of the miniexon sequence and subsequent restriction fragment length polymorphism analysis. J Clin Microbiol 41:3147–3153

Bensoussan E, Nasereddin A, Jonas F, Schnur LF, Jaffe CL (2006) Comparison of PCR assays for diagnosis of cutaneous leishmaniasis. J Clin Microbiol 44:1435–1439

Schallig HD, Oskam L (2002) Molecular biological applications in the diagnosis and control of leishmaniasis and parasite identification. Trop Med Int Health 7:641–651

Reithinger R, Dujardin JC (2007) Molecular diagnosis of leishmaniasis: current status and future applications. J Clin Microbiol 45:21–25

Brustoloni YM, Lima RB, da Cunha RV et al (2007) Sensitivity and specificity of polymerase chain reaction in Giemsa-stained slides for diagnosis of visceral leishmaniasis in children. Mem Inst Oswaldo Cruz 102:497–500

Li J, Wirtz RA, McCutchan TF (1997) Analysis of malaria parasite RNA from decade-old Giemsa-stained blood smears and dried mosquitoes. Am J Trop Med Hyg 57:727–731

Motazedian H, Karamian M, Noyes HA, Ardehali S (2002) DNA extraction and amplification of *Leishmania* from archived, Giemsa-stained slides, for the diagnosis of cutaneous leishmaniasis by PCR. Ann Trop Med Parasitol 96:31–34

Amar C, Pedraza-Diaz S, McLauchlin J (2001) Extraction and genotyping of *Cryptosporidium parvum* DNA from fecal smears on glass slides stained conventionally for direct microscope examination. J Clin Microbiol 39:401–403

Pandey BD, Pandey K, Kaneko O, Yanagi T, Hirayama K (2009) Relapse of visceral leishmaniasis after miltefosine treatment in a Nepalese patient. Am J Trop Med Hyg 80:580–582

Akkafa F, Dilmec F, Alpua Z (2008) Identification of *Leishmania* parasites in clinical samples obtained from cutaneous leishmaniasis patients using PCR-RFLP technique in endemic region, Sanliurfa province, in Turkey. Parasitol Res 103:583–586

Smyth AJ, Ghosh A, Hassan MQ et al (1992) Rapid and sensitive detection of *Leishmania* kinetoplast DNA from spleen and blood samples of kala-azar patients. Parasitology 105(Pt 2):183–192

Salotra P, Sreenivas G, Pogue GP et al (2001) Development of a species-specific PCR assay for detection of *Leishmania donovani* in clinical samples from patients with kala-azar and post-kala-azar dermal leishmaniasis. J Clin Microbiol 39:849–854

Pandey K, Pant S, Kanbara H et al (2008) Molecular detection of *Leishmania* parasites from whole bodies of sandflies collected in Nepal. Parasitol Res 103:293–297

Deborggraeve S, Laurent T, Espinosa D et al (2008) A simplified and standardized polymerase chain reaction format for the diagnosis of leishmaniasis. J Infect Dis 198:1565–1572

Kennedy WP (1984) Novel identification of differences in the kinetoplast DNA of *Leishmania* isolates by recombinant DNA techniques and in situ hybridisation. Mol Biochem Parasitol 12:313–325

Selective accumulation of rhodacyanine in plasmodial mitochondria is related to the growth inhibition of malaria parasites†

Daiki Morisaki,[a] Hye-Sook Kim,[b] Hiroshi Inoue,[a] Hiroki Terauchi,[a] Shusuke Kuge,[a] Akira Naganuma,[a] Yusuke Wataya,[b] Hidetoshi Tokuyama,[a] Masataka Ihara*[ac] and Kiyosei Takasu*[ad]

Received 25th January 2010, Accepted 12th February 2010
DOI: 10.1039/c0sc00125b

Fluorescent rhodacyanines, which display antimalarial activity *in vitro* and *in vivo*, stain plasmodial parasites at the erythrocytic stage. A good correlation between the antimalarial activity and the accumulation of the dyes is observed. A fused-rhodacyanine, which displays a strong fluorescent property itself, was designed as a new probe for plasmodial parasites. It appears to be specifically localized in the parasitic mitochondria.

Introduction

Malaria, which is caused by the infection of *Plasmodium* spp., is one of the most serious tropical diseases. The gravest problem is that the parasites rapidly develop resistance to antimalarial drugs.[1] Particularly, the efficacy of clinically available antimalarials, such as chloroquine (CQ), primaquine, and pyrimethamine, is dramatically decreasing. The development of new antimalarials with novel molecular skeletons and displaying different mechanisms of action against plasmodial parasites to existing drugs is required.[2,3] Recently, we reported that rhodacyanines **1**[4] (Fig. 1), which are structurally unrelated to those compounds commonly used as chemotherapeutics for malaria treatment, show a strong *in vitro* antimalarial activity against *P. falciparum*.[5] Further studies have revealed that they are highly active against chloroquine-resistant strains and that several of them display good *in vivo* efficacy (*P. berghei* mouse models).[6] It is noteworthy that some of the *in vivo* active compounds showed no significant acute toxicity. However, no information on the biological mode of action of antimalarial rhodacyanines has been reported. We describe herein the intracellular behavior of rhodacyanines in the malaria-infected erythrocytes. Furthermore, we report on the good correlation between the antimalarial activity of the rhodacyanines and their accumulation effect in the parasitic mitochondrion.

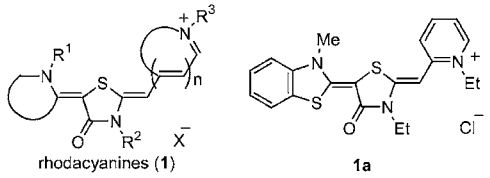

Fig. 1 Rhodacyanines: general structure (left) and representative compound **1a** (right).

Results and discussion

At the outset of our study, the intracellular distribution of **1a**[4] (EC_{50} = 21 nM against *P. falciparum* K1 strain, selective index = >5000 *in vitro*) was examined. Rhodacyanine **1a** itself shows weak fluorescence in response to irradiation with visible light (λ_{ex} = 495 nm, λ_{em} = 516 nm, $\Phi = 2.1 \times 10^{-4}$ in MeOH). Upon the addition of **1a** (final concentration: 5×10^{-6} M) onto cultured human erythrocytes infected with *P. falciparum* and after stirring for 2 h, the cells were fixed as a thin-layered smear on a glass plate and stained using the Diff-Quik® method. In the bright-field image, mature parasites in malaria-infected erythrocytes could be recognized by the optically dense, and brown-black staining of hemozoin in their digestive vacuoles (Fig. 2a). In contrast, fluorescent microscopic observation (through an FITC filter) reveals that **1a**, which is visualized as a red spot, is selectively accumulated in malaria parasites (Fig. 2b). Non-infected host erythrocytes are not stained by **1a**. Additionally, we noted that the selective accumulation can be clearly observed in the living cells (unfixed erythrocytes on the glass plate). Essentially, the accumulation is irreversible; the fluorescent localization is maintained after the treatment with **1a** in infected

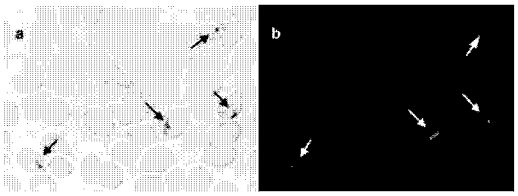

Fig. 2 Microscopic images of the intracellular distribution of **1a** in *P. falciparum*-infected erythrocytes. (a) Bright-field image; parasitic hemozoins (black arrows). (b) Fluorescent image through an FITC filter; **1a** (white arrows).

[a]*Graduate School of Pharmaceutical Sciences, Tohoku University, Aobayama, Sendai 980-8578, Japan*
[b]*Faculty of Pharmaceutical Sciences, Okayama University, Tsushima, Okayama 700-8530, Japan*
[c]*Faculty of Pharmaceutical Sciences, Hoshi University, 2-4-41 Ebara, Tokyo 142-8501, Japan. E-mail: m-ihara@hoshi.ac.jp*
[d]*Graduate School of Pharmaceutical Sciences, Kyoto University, Yoshida, Sakyo-ku, Kyoto 505-8501, Japan. E-mail: kay-t@pharm.kyoto-u.ac.jp; Fax: +81-75-753-4610; Tel: +81-75-753-4610*

† Electronic supplementary information (ESI) available: Color graphics of the accumulation study and characterization data for all new compounds. See DOI: 10.1039/c0sc00125b/

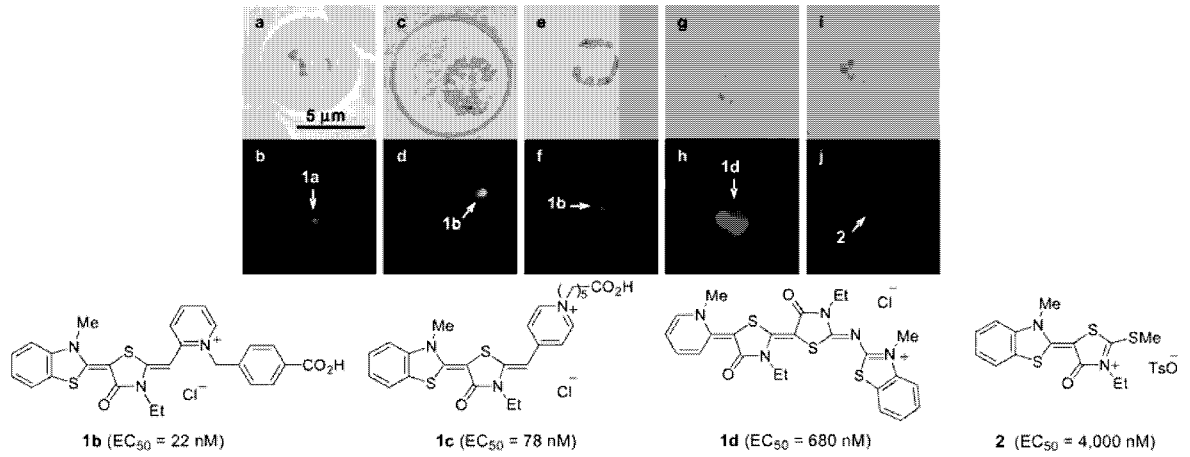

Fig. 3 Accumulation of **1a** (a, b), **1b** (c, d), **1c** (e, f), **1d** (g, h) and **2** (i, j). The final concentration of the rhodacyanines was 5.0×10^{-6} M. Bright-field images (a, c, e, g, i) and fluorescent images through an FITC filter (b, d, f, h, j).

erythrocytes, after washing with PBS (phosphate buffered saline) several times.

The fluorescence distribution of several rhodacyanines and their analogues in the malaria-infected erythrocytes was examined using *P. berghei*. In accordance with the results found for *P. falciparum*, **1a** selectively localizes in the same specific subcellular sites (organelles) of the parasites (Fig. 3a, b).[7] Rhodacyanines displaying strong antimalarial activity, such as **1b** (EC_{50} = 22 nM against *P. falciparum*) also exhibited specific localization. Their fluorescence can be observed as sharp spots (Fig. 3c, d). In contrast, less active compounds like **1d** (EC_{50} = 680 nM) do not show specific concentration into an organelle and instead leach away into the parasitic cytoplasm (Fig. 3g, h), although they still remain in the plasmodial cells (no fluorescence was observed in the erythrocyte cytoplasm). Compound **1c** (EC_{50} = 78 nM against *P. falciparum*) with an intermediate activity shows less specific localization (Fig. 3e, f) compared with **1a** and **1b**. No specific accumulation was observed for much less active compounds like **2** (EC_{50} = 4000 nM; Fig. 3i, j). These observations indicate that there is a good correlation between antimalarial activity and specific accumulation.

Next, we attempted to determine the plasmodial subcellular sites into which the rhodacyanines were selectively accumulated. A multiple-stain experiment with **1a**, DAPI (4′,6-diamino-2-phenylindole; selective staining agent for nuclei) and Diff-Quik® showed that **1a** accumulated in all of the parasitic organelles, except for the nucleus and food vacuoles. However, further investigation could not be carried out owing to the weak fluorescence and/or staining abilities of **1a**.

In order to shed light on the more detailed mechanism, stronger fluorescent probe candidates should be synthesized. We envisaged that fixation of flexible bonds to rhodacyanines would give compounds of improved fluorescent ability due to suppression of energy loss from the excited state to the ground state by vibrational transitions. In this regard, we designed four classes of rhodacyanines **3–6**, which have a fused ring skeleton. The synthetic route to a series of rhodacyanines is shown in Scheme 1.[8] Preparation of **3** started from cyclization of alcohol **7**, followed by condensation with **9** and successive ion exchange. Rhodacyanine **4**, which possesses a pyrrolothiazolinone skeleton as a central core, was synthesized through a 7 step sequence synthesis from **7**. Rhodacyanine **5**, in which rhodanine and pyridine rings are interlocked by an ethylene tether, were synthesized from **14** in 7 steps. Compound **6** was synthesized from ethyl 2-methylnicotinate (**18**). Reaction of 3-aminomethyl-2-methylpyridine (**19**), which was prepared from **18** in three steps, yields rhodanine **20** on treatment with carbon disulfide and methyl bromoacetate in the presence of triethylamine. Then **20** was coupled with methylthiobenzothiazolium salt (**12**) to give **21** in a 69% yield (2 step yield, from **19**). *N*-Methylation of **21** with methyl iodide followed by treatment with methyl triflate in the presence of triethylamine and an ion exchange process afforded fused-rhodacyanine **6** in 42% yield (3 steps).

The antimalarial activity and fluorescent properties of fused-rhodacyanines **3–6** are summarized in Table 1. *In vitro* antimalarial activities (EC_{50}) of **3–6** were shown to be comparable to that of the original rhodacyanine **1a**. Their selective toxicities were excellent as well. As expected, the fluorescence intensities of the new probes are improved over that of **1a**. Especially, compounds **5** and **6** show a 70-fold increase in fluorescence intensity compared to **1a**, and a significant red shift of the fluorescent emission was observed (excitation: λ_{ex} = 495 nm).

With the probes **3–6** in hand, their fluorescent accumulation effects were examined using the *P. berghei* strain. The results are shown in Fig. 4. It is noteworthy that the fluorescence localization of **6** into parasitic organelles can be clearly detected, even upon treatment with a 100-fold less amount of **6** (final concentration; 5×10^{-8} M) compared to the original rhodacyanine **1a**. Double stain experiments of the *P. berghei*-infected erythrocytes co-incubated with **6** and a selective fluorescent marker of subcellular organelle, were performed. As markers of nuclei and mitochondria, DAPI and MitoTracker Red CMXRos® were used, respectively. Microscopic images are shown in Fig. 5 and 6. The studies indicated that rhodacyanine **6** and DAPI were selectively accumulated in different organelles, respectively

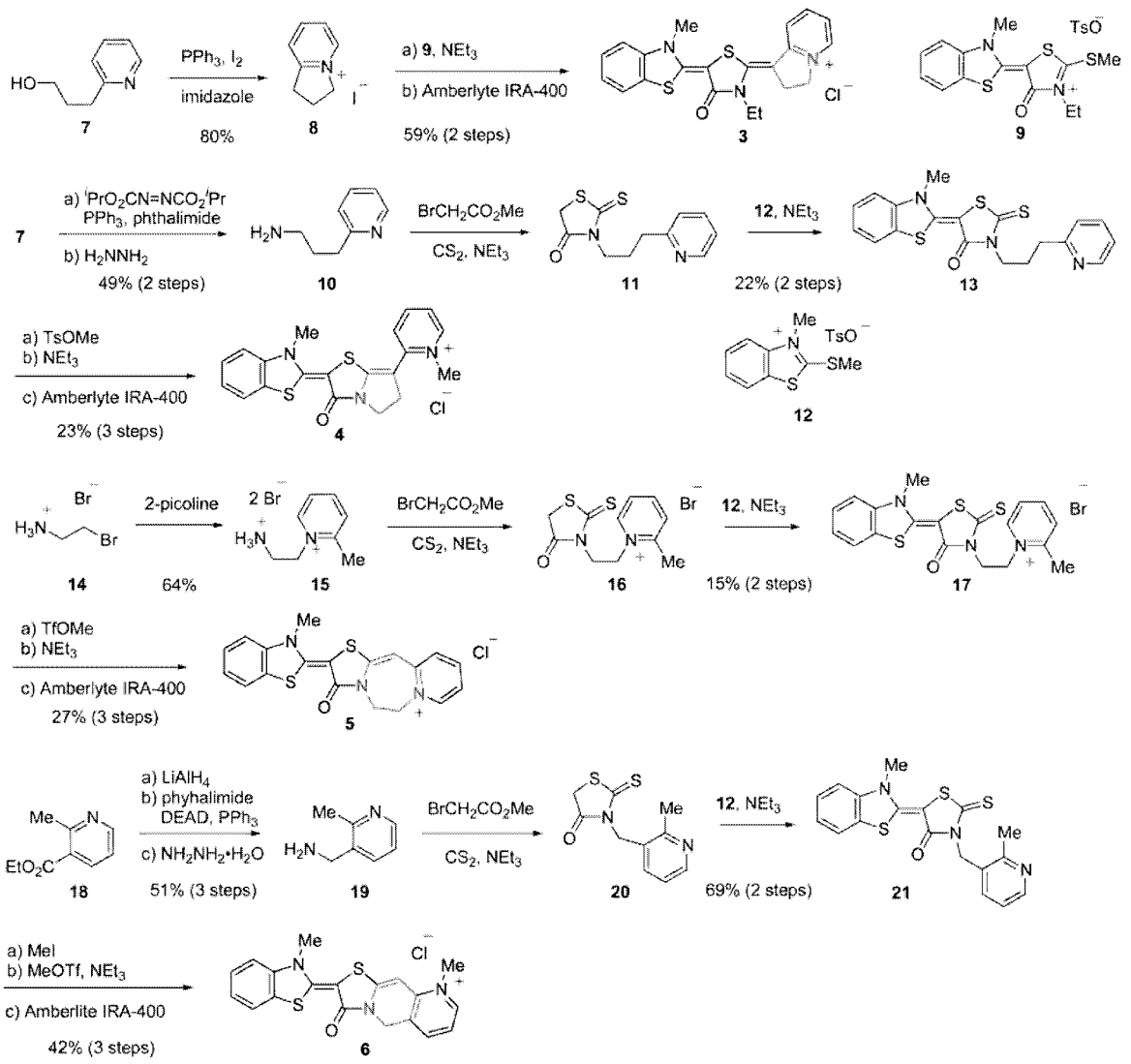

Scheme 1 Synthesis of fused-rhodacyanines **3–6**.

Table 1 *In vitro* antimalarial activity and fluorescent properties of tested compounds

Probe	EC_{50}/nM[a]	Selectivity[b]	λ_{em}/nm[c]	Φ_F[d]
1a	21	>5000	516	2.1×10^{-4}
3	46	3500	548	4.7×10^{-4}
4	64	2300	516	2.9×10^{-3}
5	46	>5000	576	1.4×10^{-2}
6	65	>5000	563	1.4×10^{-2}

[a] *In vitro* antiplasmodial activity against *P. falciparum* K1. [b] Selective toxicity, EC_{50} value for L-6/EC_{50} for *P. falciparum*. Cytotoxicity was evaluated using rat skeletal myoblast L-6 cells representing a model of a host. [c] Maximum with highest wavelength of emission spectra (excitation: λ_{ex} = 495 nm) in MeOH (1.0×10^{-6} M) at 20 °C. [d] Determined relative to fluorescein.

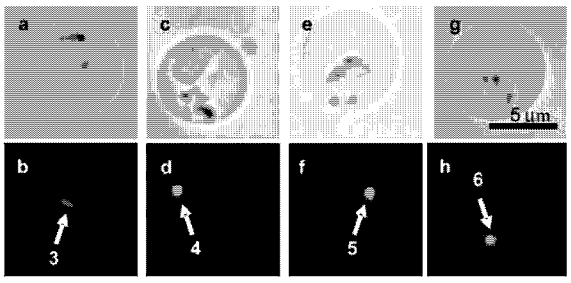

Fig. 4 Accumulation of fused rhodacyanines **3** (a, b), **4** (c, d), **5** (e, f) and **6** (g, h). Their final concentrations were 5.0×10^{-6} M (**3**, **4**), 1.0×10^{-6} M (**5**) and 5.0×10^{-8} M (**6**). Bright-field images (a, c, e, g) and fluorescent images through an FITC filter (b, d, f, h).

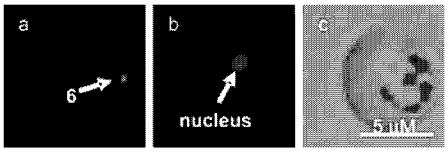

Fig. 5 Fluorescent microscopic images of the intracellular distribution of **6** and DAPI in *P. berghei*-infected erythrocytes, (a) through an FITC filter; **6** (green spot); (b) though a DAPI filter, parasitic nucleus stained by DAPI; (c) superimposed.

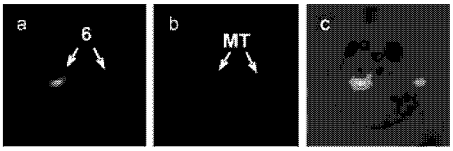

Fig. 6 Fluorescent microscopic images of the intracellular distribution of **6** and CMXRos® in *P. berghei*-infected erythrocytes, (a) through an FITC filter; **6** (green spots); (b) through a Y7 filter, mitochondria (MT) stained by CMXRos® (red spots); (c) superimposed.

(Fig. 5). In contrast, fluorescence localization of **6** is clearly consistent with that of CMXRos (Fig. 6). Thus, we concluded that rhodacyanines selectively accumulate in the plasmodial mitochondria. Fused-rhodacyanine **6** could be used as a visible diagnostic probe for plasmodial mitochondria.[9]

The selective uptake of rhodacyanines in mitochondria is consistent with the DLC (π-delocalized lipophilic cation) hypothesis,[10] which is our starting point for the drug design. The conceptual term DLC was originally proposed by Chen *et al.* in their anticancer research work. It has subsequently been reported that several DLC compounds exhibit selective antitumor activity due to their selective accumulation in the mitochondria of carcinoma cells. This accumulation depends on the mitochondrial membrane potential (negative inside). Our results in this study suggest the DLC hypothesis would also be applicable to antimalarial drug design.[11] It is noteworthy that rhodacyanines are found to display strong antileishmanial activity against *Leishmania* spp.,[12] which are related parasitic protozoa to *Plasmodium* spp. The uptake of rhodacyanines in mitochondria might be a key role in the inhibition of related protozoal diseases.

Conclusions

In summary, we have found that antimalarial rhodacyanines selectively accumulate in erythrocytic plasmodial mitochondria. Furthermore, there is good correlation between their accumulation and antimalarial activity. Thus, the accumulation effect will have a dominant influence on the inhibition of plasmodial growth. It is noteworthy that the newly synthesized rhodacyanine **6** could be applied as a probe for plasmodial parasites as well as their mitochondria since it displays strong fluorescent properties and almost no cytotoxicity. Further studies are undergoing to understand the biological mechanism of action of rhodacyanines in detail.

Acknowledgements

We thank Mr Marcel Kaiser and Prof. Reto Brun for the determination of the EC_{50} values of the synthetic compounds against *P. falciparum* K1. This work was financially supported by Grants-in-Aid from the Intelligent Cosmos Foundation and Japan Science and Technology Agency (JST).

Notes and references

1 (*a*) W. Peters, *Br. Med. Bull.*, 1982, **38**, 187; (*b*) W. H. Wernsdorfer and D. Payne, *Pharmacol. Ther.*, 1991, **50**, 95.
2 P. J. Rosenthal and L. H. Miller, in *Antimalarial Chemotherapy*, ed. P. J. Rosenthal, Humana Press, Totowa, 2001, pp. 3–15.
3 (*a*) M.-L. Go, *Med. Res. Rev.*, 2003, **23**, 456; (*b*) R. G. Ridley, *Nature*, 2002, **415**, 686; (*c*) A. M. Thayer, *Chem. Eng. News*, 2005, **83**(43), 69.
4 M. Kawakami, K. Koya, T. Ukai, N. Tatsuta, A. Ikegawa, K. Ogawa, T. Shishido and L. B. Chen, *J. Med. Chem.*, 1998, **41**, 130.
5 K. Takasu, H. Inoue, H.-S. Kim, M. Suzuki, T. Shishido, Y. Wataya and M. Ihara, *J. Med. Chem.*, 2002, **45**, 995.
6 (*a*) K. Takasu, K. Pudhom, M. Kaiser, R. Brun and M. Ihara, *J. Med. Chem.*, 2006, **49**, 4795; (*b*) K. Pudhom, K. Kasai, H. Terauchi, H. Inoue, M. Kaiser, R. Brun, M. Ihara and K. Takasu, *Bioorg. Med. Chem.*, 2006, **14**, 8550; (*c*) K. Pudhom, J.-F. Ge, C. Arai, M. Yang, M. Kaiser, S. Wittlin, R. Brun, I. Itoh and M. Ihara, *Heterocycles*, 2009, **77**, 207.
7 After verifying similar accumulation effects, we mainly used rodent malaria, *P. berghei*, instead of human malaria, *P. falciparum*, for safety reasons.
8 Syntheses of fused-rhodacyanines **3–5** have been reported in a preliminary communication: K. Takasu, D. Morisaki, M. Kaiser, R. Brun and M. Ihara, *Heterocycles*, 2005, **66**, 161.
9 Although several low-molecular weight compounds have been reported to be visible diagnostic agents for plasmodial parasites, almost all of those stain the parasitic nucleus or cytoplasm. To the best of our knowledge, it has been reported that parasitic mitochondria can be stained only by rhodamine 123, see: (*a*) K. Tanabe, *J. Protozool.*, 1983, **30**, 707; (*b*) A. A. Divo, T. G. Geary, J. B. Jensen and H. Ginsburg, *J. Protozool.*, 1985, **32**, 442.
10 L. B. Chen, *Annu. Rev. Cell Biol.*, 1988, **4**, 155.
11 K. Takasu, T. Shimogama, C. Saiin, H.-S. Kim, Y. Wataya, R. Brun and M. Ihara, *Chem. Pharm. Bull.*, 2005, **53**, 653.
12 (*a*) K. Takasu, H. Terauchi, H. Inoue, M. Takahashi, S. Sekita and M. Ihara, *Heterocycles*, 2004, **54**, 215; (*b*) M. Yang, C. Arai, A. Baker Md, J. Lu, J.-F. Ge, K. Pudhom, K. Takasu, K. Kasai, M. Kaiser, R. Brun, V. Yardley, I. Itoh and M. Ihara, *J. Med. Chem.*, 2010, **53**, 368.

HETEROCYCLES, Vol. 81, No. 5, 2010, pp. 1193 - 1229. © The Japan Institute of Heterocyclic Chemistry
Received, 19th January, 2010, Accepted, 1st March, 2010, Published online, 2nd March, 2010
DOI: 10.3987/COM-10-11912

GERANYL DERIVATIVES OF ISOQUINOLINE ALKALOIDS SHOW INCREASED BIOLOGICAL ACTIVITIES

Yumi Nishiyama,[a] Kinuko Iwasa,[*,a] Suguru Okada,[a] Sousuke Takeuchi,[a] Masataka Moriyasu,[a] Miyoko Kamigauchi,[a] Junko Koyama,[a] Atsuko Takeuchi,[a] Harukuni Tokuda,[b] Hye-Sook Kim,[c] Yusuke Wataya,[c] Kazuyoshi Takeda,[d] Yi-Nan Liu,[e] Pei-Chi Wu,[e] Kenneth F. Bastow,[e] Toshiyuki Akiyama,[e] and Kuo-Hsiung Lee[e]

[a]Kobe Pharmaceutical University, 4-19-1 Motoyamakita, Higashinada-ku, Kobe-shi 658-8558, Japan, [b]Department of Biochemistry and Molecular Biology, Kyoto Prefectural University of Medicine, Kawaramachi-dori, Kamigyo-ku, Kyoto 602-0841, Japan, [c]Faculty of Pharmaceutical Science, Okayama University, Tsushima, Okayama 700, Japan, [d]Yokohama College of Pharmacy, 601 Matanocyo, Hodogayaku, Yokohama-shi 245-0066 Japan, [e]Natural Products Research Laboratories, Eshelman School of Pharmacy, University of North Carolina, Chapel Hill, NC 27599-7360, USA

Abstract – Three types of isoquinoline alkaloids were tested for antimicrobial, cytotoxic, anti-malarial, anti-oxidant, and anti-HIV activities, as well as inhibitory activity against Epstein-Barr virus early antigen (EBV-EA) activation induced by 12-*O*-tetradecanoylphorbol-13-acetate (TPA) in Raji cells. *N*- or *O*-Geranylation contributed to increased potency in four types of activities except anti-HIV and anti-oxidant. Some types of alkaloids may be useful as lead compounds for developing potential chemotherapeutic agents. *N*,*N*-Geranylated salsolinol was significantly active in three different assays, antimicrobial, cytotoxic, and EBV-EA, and may be a most useful compound.

INTRODUCTION

A number of aromatic prenyltransferases, responsible for prenyl group attachment, have only recently been isolated and characterized.[1-4] Aromatic prenyltransferases catalyze the transfer of a C_5

(dimethylallyl), C_{10} (geranyl) or C_{15} (farnesyl) prenyl group derived from the corresponding isoprenyl diphosphate metabolites onto a variety of electron-rich aromatic acceptors. Prenyl groups appear in a wide variety of bioactive natural products of microbial and plant origin, including amino acids, stilbenes, alkaloids, polyketides and phenylpropanoids such as flavonoids, creating natural product hybrids with altered or enhanced bioactivities. For example, prenylated indole alkaloids containing both aromatic and isoprenoid moieties, are widely distributed in terrestrial and marine organisms.[5] Prenylation appears in many cases to provide a higher level of bioactivity compared to the nonprenylated precursors and sometimes to cause biological activities distinct from those of the parent compounds.[6,7] Thus, prenylated compounds represent a new frontier for the development of novel drugs, in particular, anti-microbial, anti-oxidant, anti-inflammatory, anti-viral, and anti-cancer agents. We have previously tested the antimicrobial, antimalarial, cytotoxic, anti-HIV, and anti-oxidant activities and inhibitory effects on EBV-EA induction of isoquinoline alkaloids.[8,9] Some of the tested isoquinolines showed significant activities in these assays. It was expected that addition of the prenyl group to the isoquinoline alkaloids [simple isoquinolines, 1-benzylisoquinolines, and protoberberines] would increase their potency compared with that of the parent compounds in some assays. In this paper, we describe the synthesis of *N*- and *N*,*N*-geranyl, and *O*- and *O*,*O*-geranyl derivatives of isoquinoline alkaloids and compare their activities with those of non-prenylated compounds in five assays: antimicrobial activity, antimalarial activity, cytotoxicity evaluation,[10] inhibitory effects on EBV-EA induction,[11] free radical scavenging activity, and anti-HIV activity.[12]

RESULTS AND DISCUSSIONS

Chemistry. Geranylation of **(±)**-salsolinol (**1**)[8] with geranyl bromide and sodium hydride in *N*,*N*-dimethylformamide has been previously described to give the *N*- and *N*,*N*-geranyl derivatives (**2**, **3**).[13] **(±)**-*N*-Methylsalsolinol (**4**) and quaternary **(±)**-*N*,*N*-dimethylsalsolinol (**5**) has been prepared from **(±)-carnegine.**[13] Geranylation of **5** by the same methods gave the *O*- and *O*,*O*-geranyl derivatives (**6**-**8**) (Scheme 1). Geranylation of **(±)**-tetrahydropapaveroline (**9**)[9] gave the *N*- and *N*,*N*-geranyl derivatives (**10** and **11**), and **(±)**-*N*-methylpapaveroline (**12**) produced the *O*,*O*-geranyl derivative (**13**) (Scheme 2). Geranylation of **(±)**-2,3,9,10-tetrademethyltetrahydropalmatine (**14**)[9] afforded the *N*-geranyl derivatives (**15** and **16**) and **(±)**-2,3,10,11-tetrademethylpseudotetrahydropalmatine (**17**)[9] gave the *N*-geranyl derivative (**18**) (Scheme 3). Each geranylated compound was purified by preparative HPLC of the reaction mixtures using NH_4OAc (0.05% TFA)-MeOH (0.05% TFA).

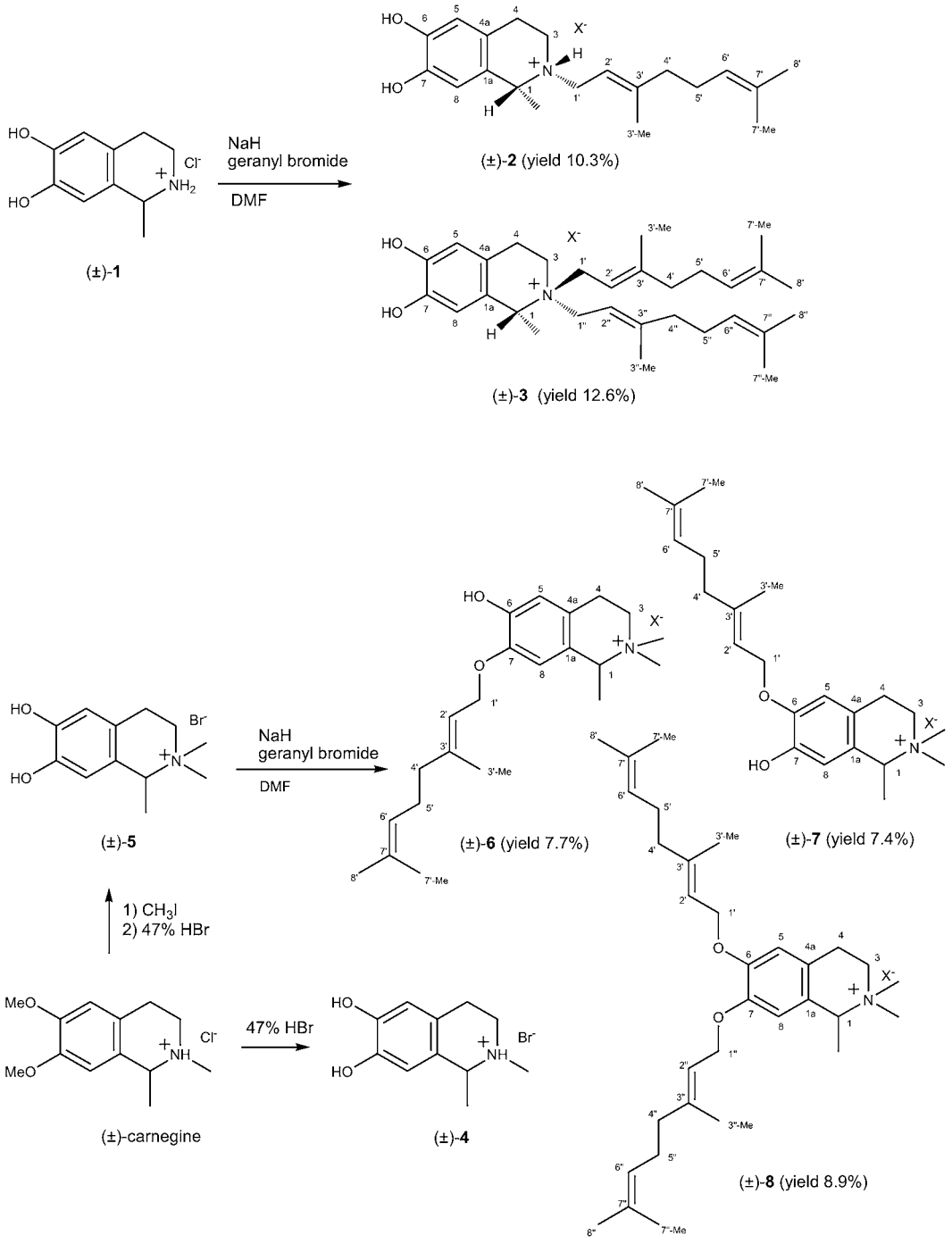

Scheme 1. *N*-geranylation of simple isoquinolines

The HPLC of the reaction mixture in geranylation of salsolinol (**1**) is shown in Figure 1 (I). The peaks a_1 and b_1 were determined to be **(±)-***N*-geranylsalsolinol (**2**) and **(±)-***N*,*N*-digeranylsalsolinol (**3**), respectively (Scheme 1). Their structures, including the stereostructure, have been previously described:[13] orientation of the C (1)-methyl group is quasi-axial in **2** and **3** and that of the *N*-geranyl group is quasi-equatorial in **2**.

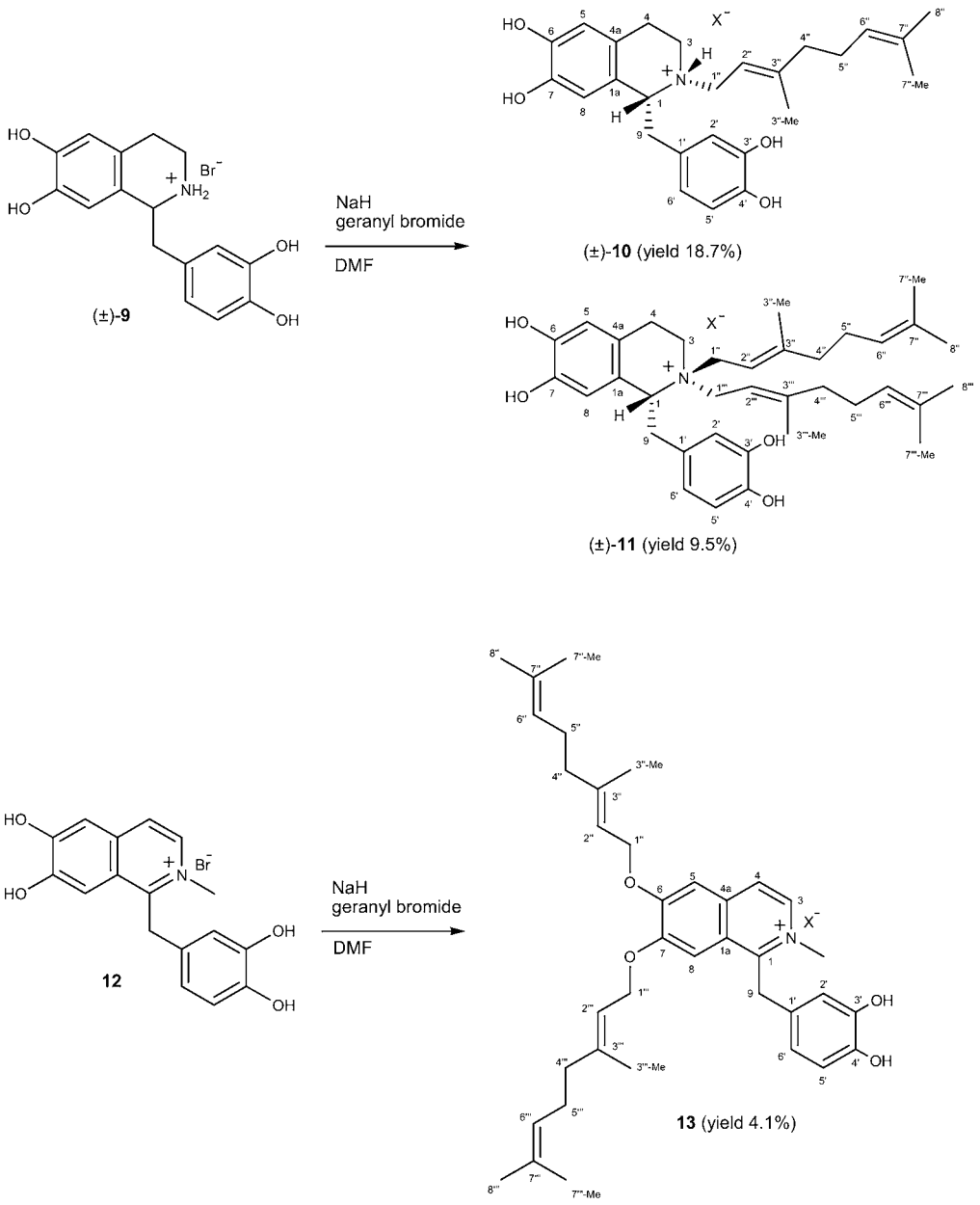

Scheme 2. *N*-geranylation of 1-benzylisoquinolines

These stereostructures were identical with the optimized geometry of **2** and **3** calculated. The optimized geometry and molecular orbital of **2** and **3** were calculated by the DFT (Density Function Theory) method using the Materials Studio DMol3 package of Accelrys Inc.[14,15] (Figure 1) and they may be necessary to clarify the biological activities' mechanisms.

HPLC of the reaction mixture in geranylation of **(±)**-*N*,*N*-dimethylsalsolinol (**5**) is shown in Figure 1. Compounds **6**-**8**, corresponding to the peaks a_2, b_2, and c_2, respectively, (Figure 1, II) were separated and purified by preparative HPLC. The molecular formula of compound **6** was determined to be $C_{22}H_{34}NO_2$ by analysis of its HRSIMS ($[M]^+$, *m/z* 344.2606), which indicates the presence of one geranyl group.

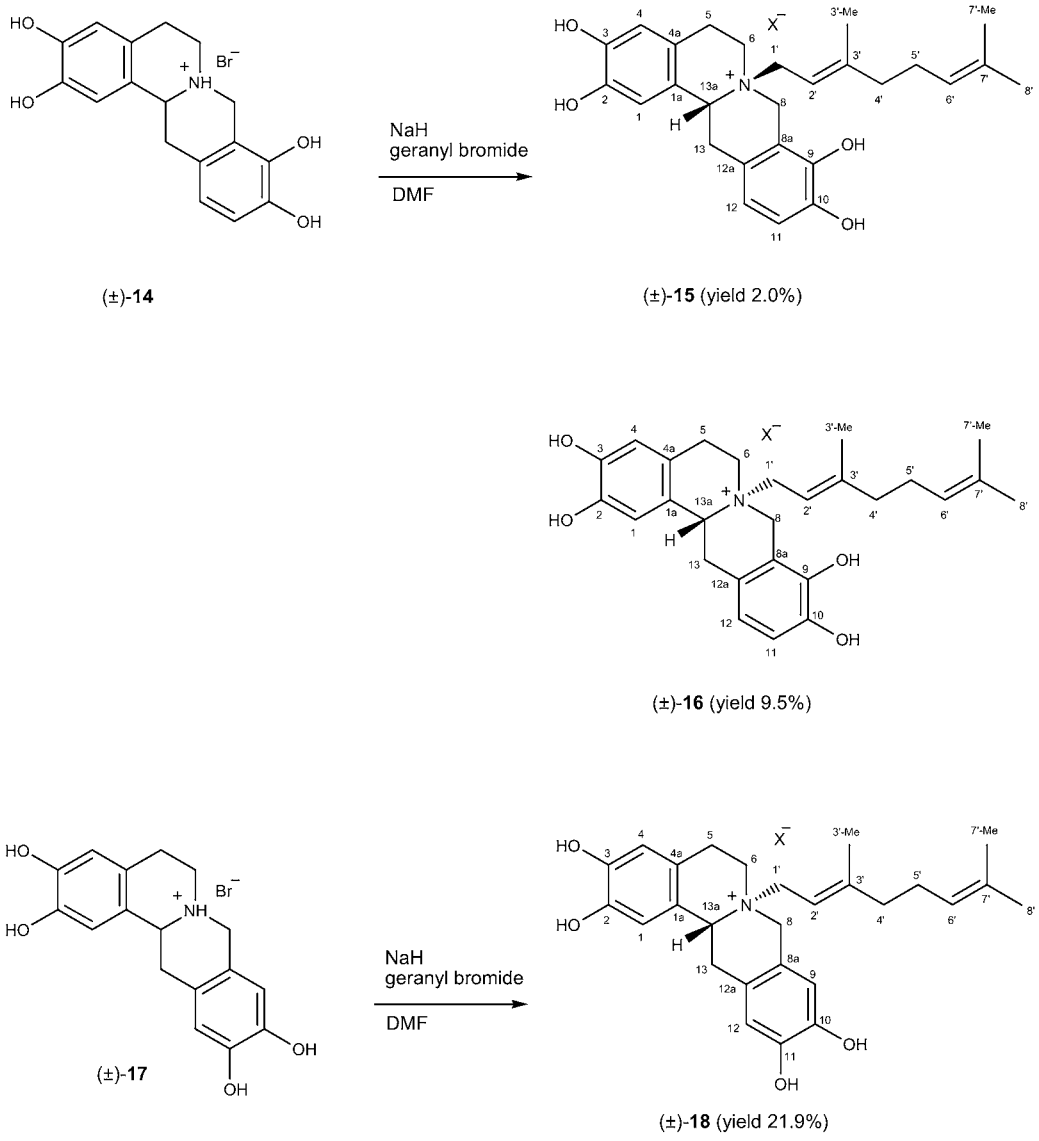

Scheme 3. *N*-geranylation of tetrahydroprotoberberines

The ^{1}H NMR spectrum displays two aromatic proton singlets at δ 6.68 and 6.74, a methine proton at δ 4.57 (q, J = 6.5 Hz), two methylene groups [δ 3.77 (1H), 3.55 (1H), and 3.08 (2H)], two *N*-methyl proton signals [δ 3.17 (3H) and 3.14 (3H)], and a methyl proton signal [δ1.69 (3H, d, J = 6.5 Hz)], characteristic of the isoquinoline moiety, and three methyl proton signals at δ 1.75 (3H, s), 1.65 (3H, s), and 1.59 (3H, s), two olefinic protons at δ 5.48 (1H, t, J = 6.5 Hz) and 5.09 (1H, t, J = 6.5 Hz), and three methylene groups [δ 4.62 (2H, d, J = 6.5), δ 2.12 (2H, m), and δ 2.09 (2H, m)], assignable to the geranyl group. The olefinic protons at δ 5.48 and 5.09 show COSY coupling to the methylene protons at δ 4.62 and 2.12, respectively, which led to the assignment of H-2' (δ 5.48) and H-6' (δ 5.09), respectively. The methylene protons at δ 4.62 and 2.12 were assigned to H_2-1' and H_2-5', respectively.

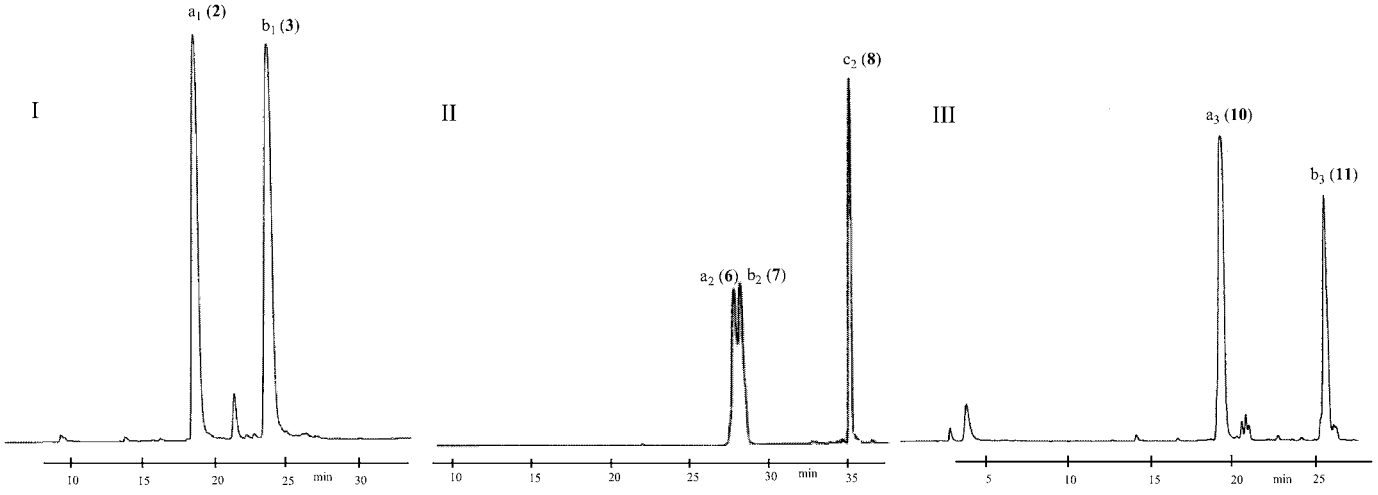

Figure 1. Analytical scale HPLC chromatograms of geranylated products of I: salsolinol (**1**), II: *N*, *N*-dimethylsalsolinol (**5**), and III: tetrahydropapaveroline (**9**) Column: Cosmosil 5C18-ARII (6.0 x 150 mm); Eluent: A:0.1M NH4OAc (0.05% TFA), B:MeOH (0.05% TFA), I and II [A/B: 80/20 (initial) 0/100 (30 min)]; III [A/B: 75/25 (initial) 50/50 (10 min) 0/100 (30 min)]; Flow rate: 1 mL/min; Detector: UV(280 nm)

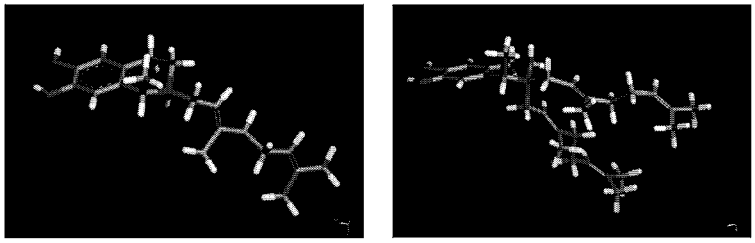

Optimized geometry of *N*-geranylsalsolinol (**2**) E=-986.0139433 Ha (BLYP/DNP)

Optimized geometry of *N*,*N*-digeranylsalsolinol (**3**) E=-1376.8807811 Ha (BLYP/DNP)

The NOE correlations between an aromatic proton at δ 6.74 and a proton at δ 4.57 (H-1) indicated that this aromatic proton was assigned as H-8. The aromatic proton at δ 6.68, which was correlated with the methylene protons at δ 3.08 (H_2-4) was assigned as H-5. NOE correlations were also observed between the aromatic proton at δ 6.74 (H-8) and methylene protons at δ 4.62 (H-1'), indicating that a geranyl group was attached to oxygen at C-7. Based on the above evidence, compound **6** was indicated to be 7-*O*-geranyl-*N*, *N*-dimethylsalsolinol (Scheme 1). Moreover, the ^{13}C NMR spectrum of **6** supports this assignment, with signals corresponding to 22 carbons, including two protonated olefinic carbons (δ 124.90; 120.94), two protonated aromatic carbons (δ 116.01; 113.25), six quaternary carbons (δ 148.79; 147.83; 142.30; 132.63; 124.39; 122.17), five methylene carbons (δ 67.06; 56.86; 40.61; 27.41; 24.30), a methine carbon (δ 69.51), two *N*-methyl carbons (δ 51.50; 50.11) and four methyl carbons (δ 25.84; 18.63; 17.72; 16.69). The carbon signal at δ 147.83 (C-7) displays HMBC correlations with the proton signal at δ 4.62 (H-1'), confirming 7-*O*-geranylation, which was already suggested by the NOE correlation between H-8 and H-1'. On the basis of these data, the structure of **6**

was established to be **(±)**-7-*O*-geranyl-*N*,*N*-dimethylsalsolinol.

The molecular formula of compound **7** was determined to be $C_{22}H_{34}NO_2$ by analysis of its HRSIMS ($[M]^+$, *m/z* 344.2603), which indicated the presence of one geranyl group. The ^1H NMR spectrum is almost the same with that of **6**. The NOE correlations between the aromatic proton at δ 6.66 and δ 4.55 (H-1) and the aromatic proton at δ 6.79 and the methylene protons at δ 3.12 (H_2-4) indicate that the aromatic protons at δ 6.66 and 6.79 were assigned to H-8 and H-5, respectively. NOE correlations were also observed between the aromatic proton at δ 6.79 (H-5) and methylene protons at δ 4.63 (H-1'), indicating that a geranyl group is attached to oxygen at C-6. Based on the above evidence, compound **7** was found to be 6-*O*-geranyl-*N*,*N*-dimethylsalsolinol (Scheme 1). Moreover, the ^{13}C NMR spectrum of **7** supports this structure, with signals corresponding to 22 carbons. The carbon signal at δ 148.62 (C-6) display HMBC correlations with the proton signal at δ 4.63 (H-1'), confirming 6-*O*-geranylation, which was suggested by the NOE correlation between H-5 and H-1'. On the basis of these data, the structure of **7** was confirmed to be **(±)**-6-*O*-geranyl-*N*,*N*-dimethylsalsolinol.

The molecular formula of compound **8** was determined to be $C_{32}H_{50}NO_2$ by analysis of its HRSIMS ($[M]^+$, *m/z* 480.3858), which indicated the presence of two geranyl groups. The ^1H NMR spectrum displays two aromatic protons as singlets at δ 6.83 and 6.79, a methine proton at δ 4.54 (q, J = 6.5 Hz), two methylene groups [δ 3.79 (1H), 3.57 (1H), and 3.14 (2H)], two *N*-methyl groups [δ 3.17 (3H) and 3.15 (3H)], and a methyl proton signal [δ 1.69 (3H, d, J = 6.5 Hz)], characteristic of an isoquinoline moiety, and six methyl proton signals at δ 1.66 (6H, s), 1.60 (6H, s), 1.736 (3H, s), and 1.742 (3H, s), four olefinic protons at δ 5.48 (2H) and 5.10 (2H), and six methylene groups [δ 4.58 (2H), 4.59 (2H), 2.12 (4H, m), and δ 2.07 (4H)], assignable to two geranyl groups. The aromatic proton at δ6.83 shows NOE correlations with both methylene protons at δ 3.14 (H-4) and 4.58 (or 4.59, H-1'). This aromatic proton was assigned H-5. Therefore, the geranyl group is attached to the oxygen at C-6. The aromatic proton at δ 6.79 displays NOE correlations with protons at δ 4.54 (H-1), 4.59 (or 4.58, H-1''), and 1.69 (1-Me) indicating that this aromatic proton was H-8. This indicated that the other geranyl group is attached to the oxygen at C-7. From these data, the structure of **8** was deduced to be 6, 7-*O*-digeranyl-*N*,*N*-dimethylsalsolinol (Scheme 1). The ^{13}C NMR spectrum of **8** supports this structure.

Assignments of ^1H and ^{13}C signals of **6-8** were made by 1D and 2D (^1H-^1H COSY, NOESY, HSQC, and HMBC) spectroscopic data. The geometry of the disubstituted olefinic bonds (between 2' and 3' or 2'' and 3'') was determined to be *E* on the basis of the NOE correlation between H-2' and H-4'or H-2'' and H-4'', respectively. The NOE correlations between H-1 and both quasi-equatorial and quasi-axial *N*-methyl groups indicate the quasi-equatorial orientation of H-1, that is, quasi-axial orientation of the methyl group at C-1. These stereostructures were identical with the optimized geometry of **6-8**

calculated.

HPLC of the reaction mixture in geranylation (Scheme 2) of **(±)**-tetrahydropapaveroline (**9**) is shown in Figure 1 (III). The compounds corresponding to the peaks a_3 and b_3 (Figure 1, III) (**10** and **11**) were purified by prep. HPLC of the reaction mixture. The molecular formula of compound **10** (peak a_3) was determined to be $C_{26}H_{34}NO_4$ by analysis of its HRSIMS ($[M + H]^+$, *m/z* 424.2494), which indicates the presence of one geranyl group. The ^1H NMR spectrum displays two aromatic proton singlets at δ 6.65 and 6.18, a methine proton at δ 4.42 (1H, t, J = 6.5 Hz), two methylene groups [δ 3.68 (1H), 3.38 (1H), and 2.97 (2H)] arisen from the isoquinoline moiety, three aromatic protons at δ 6.75 (1H, d, J = 8.5 Hz), 6.50 (1H, brd, J = 8.5 Hz), and 6.58 (1H, brs), methylene protons [δ 3.04 (1H) and 3.14 (1H)] characteristic of a benzyl group, and three methyl proton signals at δ 1.70 (3H, s), 1.64 (3H, s), and 1.57 (3H, s), two olefinic protons at δ 5.26 (1H, m) and 5.12 (1H, m), and three methylene groups [δ 3.83 (1H), δ 3.71 (1H), and δ 2.18 (4H)], assignable to a geranyl group. The NOE correlations between the methylene protons (H-1'') of the geranyl group and both the methine proton (H-1) of the isoquinoline structure and the methylene protons (H-9) of the benzyl group indicate that the geranyl group was attached to nitrogen. Based on the these evidences, compound **10** was established to be **(±)**-*N*-geranyltetrahydropapaveroline (Scheme 2). The ^{13}C NMR spectrum of **10** supports this structure, with signals corresponding to 24 carbons (two carbons overlap), including two protonated olefinic carbons (δ 124.56; 114.15), five protonated aromatic carbons (δ 121.87; 117.67; 116.76; 116.12; 115.75), nine quaternary carbons (δ 149.65; 147.30; 146.92; 146.04; 145.65; 133.29; 121.93; 121.87x2), six methylene carbons (δ 51.86; 44.80; 40.74x2; 27.14; 22.90), a methine carbon (δ 63.01), and three methyl carbons (δ 25.94; 17.84; 16.80). Assignments of ^1H and ^{13}C signals of **10** were made by 1D and 2D (^1H-^1H COSY, NOESY, HSQC, and HMBC) spectroscopic data. The geometry of the disubstituted olefinic bond (between 2'' and 3'') was determined to be *E* on the basis of the NOE correlation between H-2'' and H-4''. The geranyl group may be a quasi-equatorial orientation, because a methylene proton (H-1'') of the geranyl group displayed NOE correlations with both the methine proton (H-1) of the isoquinoline structure and the methylene protons (H-9) of the benzyl group. Therefore, the benzyl group is considered to be quasi-axial orientation. The upfield shift (+ 3.6 ppm) at C-3 in **10** compared with *N*-methylsalsolinol (**4**) is interpreted as being due to larger steric compression by the quasi-axial benzyl group at C-1 in **10** than that by the quasi-axial methyl group at C-1 in **4**.

The molecular formula of compound **11** (peak b_3) was determined to be $C_{36}H_{50}NO_4$ by analysis of its HRSIMS ($[M]^+$, *m/z* 560.3746), which indicates the presence of two geranyl groups. The ^1H NMR and ^{13}C NMR spectra of **11** display the signals due to the 1-benzyltetrahydroisoquinoline structure and two sets of signals due to two geranyl groups. The protons at δ 3.78 (H-1") and 4.13 (H-1"') show HMBC

correlations with carbons at δ 58.30 (C-1''') and 55.79 (C-1''), respectively. Furthermore, HMBC correlations were observed from protons at δ 3.96 (H-1'') and δ 4.13 (H-1''') to the carbon at δ 52.01 (C-3). The proton at δ 4.20 (H-1''') also shows a correlation with the carbon at δ 70.72 (C-1). It was concluded that both geranyl groups are attached to nitrogen on the basis of these HMBC correlations, as well as by NOE correlations between H-1 (δ 4.42) and H-1'' (δ 3.96), H-3 (δ 3.53) and H-1''' (δ 4.20), and H-3 (δ 3.68) and H-1''' (δ 4.13 and δ 4.20), respectively. Assignments of ^{1}H and ^{13}C signals of **11** were made by 1D and 2D (^{1}H-^{1}H COSY, NOESY, HSQC, and HMBC) spectroscopic data. Based on these evidences, compound **11** was determined to be **(±)-*N*,*N*-digeranyltetrahydropapaveroline** (Scheme 2). The geometries of the disubstituted olefinic bonds (between 2'' and 3'' and between 2''' and 3''') were determined to be *E* on the basis of the NOE correlations between H-2'' and H-4'', and H-2''' and H-4''', respectively. NOE correlations were observed between the proton at δ 4.20 (H-1''') and H_2-3 at δ 3.68 and 3.53 (quasi-axial and quasi-equatorial protons), indicating that C-1''' of the geranyl group is a quasi-equatorial orientation. The quasi-equatorial orientation of the proton at C-1 was suggested by the NOE correlations between the methine proton at δ 4.42 (H-1) and the proton (δ 3.96) of C-1'' of the quasi-axial geranyl group. Therefore, the orientation of the benzyl group is quasi-axial. This was suggested from the fact that the upfield shift (+ 4.1 ppm) at C-3 in **11** compared with *N*, *N*-dimethylsalsolinol (**5**) arises from larger steric compression by the quasi-axial benzyl group at C-1 in **11** than that by the quasi-axial methyl group at C-1 in **5**.

HPLC of the reaction mixture in geranylation (Scheme 2) of *N*-methylpapaveroline (**12**) is shown in Figure 2 (I). Some compounds (peaks a_4, b_4, and d_4) in the reaction mixture changed during prep.

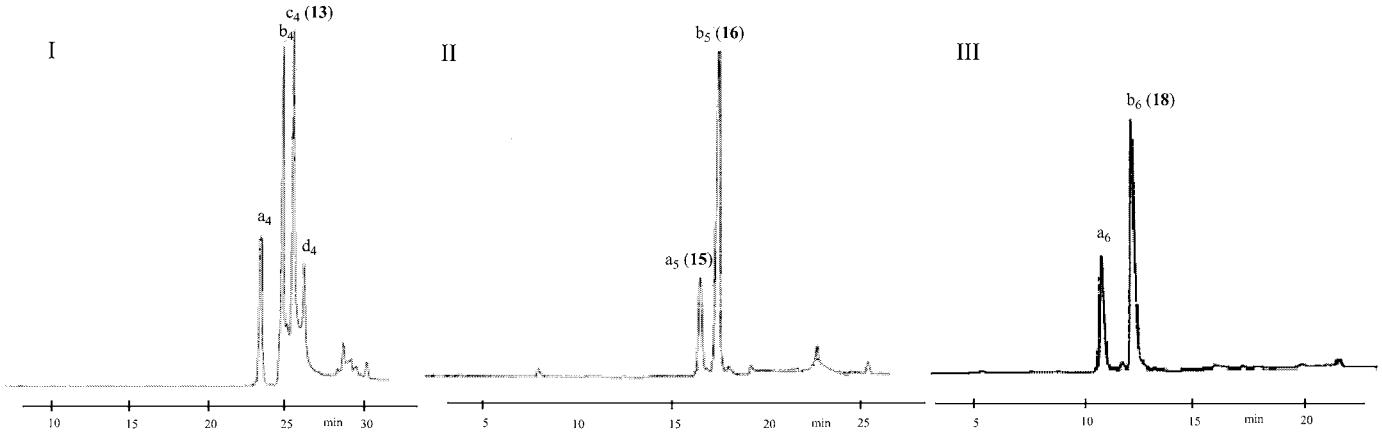

Figure 2. Analytical scale HPLC chromatograms of products obtained by geranylation of I: *N*-methylpapaveroline (**12**), II: 2, 3, 9, 10-tetrademethyltetrahydropalmatine (**14**), and III: 2, 3, 10, 11-tetrademethylpseudotetrahydropalmatine (**17**) Column: Cosmosil $5C_{18}$-ARII (6.0 x 150 mm); Eluent: A:0.1M NH_4OAc (0.05% TFA), B:MeOH (0.05% TFA), I [A/B: 75/25 (initial) 50/50 (10 min) 0/100 (30 min)], II and III [A/B: 80/20 (initial) 0/100 (20 min); Flow rate: 1 mL/min; Detector: UV(280 nm)

HPLC and were not purified. Only peak c_4 was purified by prep. HPLC. The molecular formula of compound **13** (peak c_4) was determined to be $C_{37}H_{48}NO_4$ by analysis of its HRSIMS ($[M]^+$, *m/z* 570.3592), which indicates the presence of two geranyl groups. The ^1H NMR spectrum displays two aromatic protons as doublets at δ 8.32 and 8.08 (J = 7.0 Hz), two aromatic protons as singlets at δ 7.70 and 7.60 originating in the isoquinoline moiety, three aromatic protons at δ 6.71 (1H, d, J = 8.5 Hz), 6.36 (1H, dd, J = 8.5, 1.5 Hz), and 6.49 (1H, d, 1.5 Hz), a methylene proton at δ 4.83 (2H) characteristic of a benzyl group, six methyl proton signals at δ 1.83 (3H, s), 1.70 (3H, s), 1.61 (3H, s), 1.59 (3H, s), 1.58 (3H, s), and 1.55 (3H, s), four olefinic protons at δ 5.58 (1H), 5.39 (1H), 5.09 (1H), and 5.02 (1H), and six methylene groups [δ 4.90 (2H), 4.80 (2H), 2.15 (2H), 2.13 (2H), 2.05 (2H), and 1.98 (2H)], assignable to two geranyl groups. The aromatic proton at δ 7.60 shows NOE correlations with both protons at δ 8.08 (H-4) and 4.90 (H-1''). Thus, the proton at δ 7.60 was assigned to H-5. Therefore, the geranyl group is attached to the oxygen at C-6. The aromatic proton at δ 7.70 displays NOE correlations with protons at δ 4.80 (H-1'''), indicating that this proton is H-8. This indicates that the other geranyl group is attached to the oxygen at C-7. Based on these evidences, compound **13** was identified as *O*,*O*-digeranylpapaveroline (Scheme 2). Moreover, the ^{13}C NMR spectrum of **13** shows four protonated olefinic carbons (δ 124.91; 124.84; 119.65; 119.32), seven protonated aromatic carbons (δ 136.61; 123.58; 120.39; 117.14; 116.13; 108.15; 108.08), 12 quaternary carbons (δ 158.86; 156.93; 154.18; 147.50; 146.17; 144.48; 143.93; 137.50; 132.81; 132.63; 126.47; 125.62), seven methylene carbons (δ 67.71; 67.33; 40.63; 40.46; 34.96; 27.30; 27.29), one *N*-methyl carbon (δ 46.28), and six methyl carbons (δ 25.91; 25.87; 17.82; 17.81; 16.88; 16.84). The carbon signal at δ 158.86 (C-6) displayed HMBC correlations with the proton signal at δ 4.90 (H-1''), confirming 6-*O*-geranylation, which was also suggested by the NOE correlation between H-5 and H-1''. The carbon signal at δ 154.18 (C-7) displayed HMBC correlations with the proton signal at δ 4.80 (H-1'''), confirming 7-*O*-geranylation, which was corroborated by the NOE correlation between H-8 and H-1'''. Assignments of ^1H and ^{13}C signals of **13** were made by 1D and 2D (^1H-^1H COSY, NOESY, HSQC, and HMBC) spectroscopic data. On the basis of this evidence, the structure of **13** was established to be *O*, *O*-digeranylpapaveroline (Scheme 2). The geometries of the disubstituted olefinic bonds (between 2'' and 3'' and between 2''' and 3''') were determined to be *E* on the basis of the NOE correlation between H-2'' and H-4'', and between 2''' and 3''', respectively.

HPLC of the reaction mixture in geranylation (Scheme 3) of 2, 3, 9, 10-tetrademethyltetrahydropalmatine (**14**) is shown in Figure 2 (II). The compounds corresponding to peaks a_5 and b_5 (Figure 2, II) (**15** and **16**) were purified by prep. HPLC. The molecular formula of compound **15** (peak a_5) was determined to be $C_{27}H_{34}NO_4$ by analysis of its HRSIMS ($[M]^+$, *m/z* 436.2486), which indicates the presence of one

geranyl group. The ^{1}H NMR spectrum displays two aromatic proton singlets at δ 6.72 and 6.66, two aromatic proton doublets at δ 6.78 (1H, d, J = 8.0 Hz), 6.57 (1H, d, J = 8.0 Hz), methine and methylene protons at δ 4.58 (3H, brs), three methylene groups [δ 3.81 (1H), 3.54 (1H), 3.28 (1H), 3.18 (2H), 3.12 (1H)] arising from the protoberberine moiety and three methyl proton signals at δ 1.65 (3H, s), 1.59 (3H, s), and 1.58 (3H, s), two olefinic protons at δ 5.44 (1H, t, J = 8.0 Hz) and 5.08 (1H, brs), and three methylene groups [δ 4.08 (2H), 2.22 (2H), and 2.20 (2H)], assignable to the geranyl group. The NOE correlations between a methylene proton (δ 4.08, H-1') of the geranyl group and the protons at δ 4.58 (H-8 and/or H-13a) indicate that the geranyl group is attached to nitrogen. Based on these evidences, compound **15** was determined to be *N*-geranyl-2, 3, 9, 10-tetrademethyltetrahydropalmatinium salt. The ^{13}C NMR spectrum of **15** supports this structure, with signals corresponding to 26 (one carbon was overlapped) carbons including four protonated aromatic carbons (δ 119.69; 116.59x2; 114.52), eight quaternary carbons (δ 147.66; 146.25; 144.85; 143.60; 124.76; 121.90; 120.93; 114.80), four methylene carbons (δ 57.06; 51.66; 34.89; 23.75), and a methine carbon (δ 64.34) which arise from the tetrahydroprotoberberine structure, and two protonated olefinic carbons (δ 124.12; 111.74), two quaternary carbons (δ 152.82; 133.47), three methylene carbons (δ 59.93; 41.04; 26.97), three methyl groups (δ 25.78; 17.79; 16.94) assignable to the geranyl group. Assignments of ^{1}H and ^{13}C signals of **15** were made by 1D and 2D (^{1}H-^{1}H COSY, NOESY, HSQC, and HMBC) spectroscopic data. On the basis of these data, the structure of **15** was established to be **(±)-***N*-geranyl-2,3,9,10-tetrademethyl-tetrahydropalmatinium salt with the B/C-*cis* form as described later (Scheme 3).

The molecular formula of compound **16** (peak b_5) was determined to be $C_{27}H_{34}NO_4$ by analysis of its HRSIMS ($[M]^+$, *m/z* 436.2484), which indicates the presence of one geranyl group. The ^{1}H NMR spectrum displays two aromatic proton singlets at δ 6.84 and 6.71, two aromatic proton doublets at δ 6.85 and 6.77 (J = 8.2 Hz), a methine proton at δ 5.07 (1H, dd, J = 12.5, 5.0 Hz), and four methylene groups [δ 4.72 (1H, d, J = 15.5 Hz), 4.17 (1H, d, J = 15.5 Hz), 3.89 (1H), 3.83 (1H), 3.69 (1H), 3.26 (1H), 3.20 (1H), and 3.05 (1H)] which arise from the tetrahydroprotoberberine structure, and three methyl proton signals at δ 1.72 (3H, s), 1.66 (3H, s), and 1.33 (3H, s), two olefinic protons at δ 5.44 (1H, dd, J = 9.0, 5.5 Hz) and 5.14 (1H, brs), and three methylene groups [δ 3.86 (1H, m), 3.61 (1H, m), and δ 2.20 (4H, m)], assignable to the geranyl group. The NOE correlation between one of the methylene protons (δ 3.86, H-1') of the geranyl group and one of the methylene protons (δ 4.72, H-8) indicates that the geranyl group is attached to nitrogen. Based on these evidences, compound **16** was postulated to be the isomer of *N*-geranyl-2,3,9,10-tetrademethyltetrahydropalmatininium salt (**15**). Moreover, the ^{13}C NMR spectrum of **16** supports this structure, with signals corresponding to 27 carbons, including four protonated

aromatic carbons (δ 120.60; 116.84; 116.15; 113.45), eight quaternary carbons (δ 147.37; 146.63, 44.95; 143.66, 122.77; 122.43; 122.06; 115.38), four methylene carbons (δ 58.43; 57.62; 29.60; 24.48), and a methine carbon (δ 68.21) which arise from the tetrahydroprotoberberine structure, and two protonated olefinic carbons (δ 124.71; 114.42), two quaternary carbons (δ 153.83; 133.45), three methylene carbons (δ 46.96; 41.14; 27.10) and three methyl groups (δ 25.97; 17.89; 16.0) assignable to the geranyl group. The proton signals (H-1') at δ 3.86 and 3.61 display HMBC correlations with the carbons at δ 57.62 (C-8) and δ 58.43 (C-6), respectively, confirming *N*-geranylation, which was also suggested by the NOE correlation between H-8 and H-1'. Assignments of ^{1}H and ^{13}C signals of **16** were made by 1D and 2D (^{1}H-^{1}H COSY, NOESY, HSQC, and HMBC) spectroscopic data. On the basis of these evidences, the structure of **16** was confirmed to be **(±)**-*N*-geranyl-2,3,9,10-tetrademethyltetrahydropalmatininium salt with the B/C-*trans* form as described below (Scheme 3).

Compounds **15** and **16** are stereoisomers of the B/C ring juncture. The chemical shifts of C-6 in **15** and **16** are 51.66 and 58.43 ppm, respectively. The upfield shift of C-6 in **15** compared with **16** is interpreted as being due to steric compression in the B/C-*cis* form because C (6)-H and C (13a)-C (13) bonds are 1, 3-diaxial in the B/C-*cis* form. The chemical shifts at C-13 in **15** and **16** are 34.89 and 29.60 ppm, respectively. The upfield shift of C-13 in **16** compared with **15** arises from steric interaction (1,3-diaxial) between C (13)-H and the *N*-(C-1') bonds in the B/C-*trans* form. Compounds **15** and **16** were established to be **(±)**-*cis*- and *trans*-*N*-geranyl-2,3,9,10-tetrademethyltetrahydropalmatininium salts (Scheme 3). The geometry of the disubstituted olefinic bond (between 2' and 3') was determined to be *E* in both compounds on the basis of the NOE correlation between H-2' and H-4'.

The HPLC of the reaction mixture in geranylation (Scheme 3) of 2,3,10,11-tetrademethylpseudo-tetrahydropalmatine (**17**) is shown in Figure 2 (III). Compound **18**, which corresponds to peak b_6 (Figure 2, III), was purified by prep. HPLC, although a_6 was not purified. The molecular formula of compound **18** was determined to be $C_{27}H_{34}NO_4$ by analysis of its HRSIMS ($[M]^+$, *m/z* 436.2487), which indicates the presence of one geranyl group. The ^{1}H NMR spectrum displays four aromatic proton singlets at δ 6.83, 6.81, 6.70, 6.55, a methine proton at δ 5.07 and four methylene groups [δ 4.39 (1H), 4.34 (1H), 3.85 (1H), 3.78 (1H), 3.63 (1H), 3.25 (1H), 3.15 (1H), and 3.04 (1H)] which arise from the protoberberine skeleton and three methyl proton signals at δ 1.73 (3H, s), 1.67 (3H, s), and 1.32 (3H, s), two olefinic protons at δ 5.44 (1H) and 5.12 (1H), and three methylene groups [δ 3.87 (1H), 3.64 (1H), and δ 2.20 (4H)], assignable to the geranyl group. From a comparison of the ^{1}H NMR spectrum with that of compounds **15** and **16**, compound **18** was postulated to be *N*-geranyl-2,3,10,11-tetrademethyl-pseudotetrahydropalmatinium salt with a B/C-*cis* or B/C-*trans* junction. The ^{13}C NMR spectrum of **18** displays signals corresponding to 27 carbons, including four protonated aromatic carbons

(δ 116.26; 116.15; 114.17; 113.46), eight quaternary carbons (δ 147.62; 146.69; 146.63; 147.39; 122.72; 122.53; 122.05; 118.26), four methylene carbons (δ 61.61; 58.27; 29.83; 24.38), a methine carbon (δ 68.55) arising from the tetrahydroprotoberberine structure, and two protonated olefinic carbons (δ 124.86; 111.41), two quaternary carbons (δ 152.91; 133.27), three methylene carbons (δ 46.69; 41.01; 27.04), and three methyl groups (δ 26.0; 17.91; 16.79) assignable to the geranyl group. Compound **18** was identified as **(±)-***trans*-*N*-geranyl-2,3,10,11-tetrademethylpseudotetrahydropalmatinium salt (Scheme 3) from comparison of the chemical shifts of C-6 (δ 58.27) and C-13a (δ 68.55) with those (δ 51.66 and 64.34) in **15** (B/C-*cis*) and those (δ 58.43 and 68.21) in **16** (B/C-*trans*). The geometry of the disubstituted olefinic bond (between 2' and 3') was determined to be *E* on the basis of the NOE correlation between H-2' and H-4'. Assignments of ^{1}H and ^{13}C signals of **18** were made by 1D and 2D (^{1}H-^{1}H COSY, NOESY, HSQC, and HMBC) spectroscopic data.

Antimicrobial activity.

The synthetic simple isoquinolines [salsolinol (**1**), *N*-geranylsalsolinol (**2**), *N*,*N*-digeranylsalsolinol (**3**), *N*-methylsalsolinol (**4**), *N*,*N*-dimethylsalsolinol (**5**), 7-*O*-geranylsalsolinol (**6**), 6-*O*-geranylsalsolinol (**7**), and 6,7-*O*-digeranylsalsolinol (**8**)], the synthetic 1-benzylisoquinolines [tetrahydropapaveroline (**9**), *N*-geranyl- and *N*,*N*-digeranyltetrahydropapaveroline (**10** and **11**), *N*-methylpapaveroline (**12**), and *O*, *O*-digeranyl-*N*-methylpapaveroline (**13**)], and the synthetic tetrahydroprotoberberines [2,3,9,10-tetrademethyltetrahydropalmatine (**14**), *cis*- and *trans*-*N*-geranyl-2,3,9,10-tetrademethyltetrahydropalmatinium salts (**15** and **16**), 2,3,10,11-tetrademethylpseudotetrahydropalmatine (**17**), and *trans*-*N*-geranyl-2,3,10,11-tetrademethylpseudotetrahydropalmatininium salt (**18**)] were tested against *Staphylococcus aureus* (Gram-positive) and *Escherichia coli* (Gram-negative) by the liquid dilution method. The minimum inhibitory concentrations (MIC) are presented in Table 1. The results for **1**-**5** have already been published.[13]

N-Geranylation increases the activity against both bacteria compared with salsolinol (**1**), *N*-methylsalsolinol (**4**), and *N*,*N*-dimethylsalsolinol (**5**), which are inactive. Notably, *N*,*N*-digeranylated salsolinol (**3**) displays significant activity (7.8 μg/mL) against *S. aureus*. Thus, according to these data, *N*-quaternization by *N*-geranylation (**3**), not simply *N*-alkylation (**5**), appears to be important for enhanced antimicrobial activity.

Table 1. Antibacterial activity of several 1soquinoline-type alkaloids **1-18**

group	compound	MIC (μg/mL)[a]	
		Staphylococcus aureus ATCC25923	*Escherichia coli* ATCC25922
simple isoquinolines	**1**[b]	> 1000	> 1000
	2[b]	≧ 62.5	≧ 1000
	3[b]	≧ 7.8	≧ 31.3
	4[b]	> 1000	> 1000
	5[b]	> 1000	> 1000
	6	62.5	> 250
	7	62.5	> 250
	8	250	> 250
1-benzylisoquinolines	**9**	> 250	> 250
	10	≧ 250	> 250
	11	≧ 125	> 250
	12	> 250	> 250
	13	≧ 125	> 250
protoberberines	**14**	> 250	> 250
	15	≧ 250	> 250
	16	≧ 250	≧ 250
	17	> 250	> 250
	18	> 250	> 250
	Benzalkonium chlloride	3.9	15.7
	Benzethonium chloride	7.8	7.8

Enhancement of activity against *S. aureus* was observed in *O*-gerany isoquinolines (**6-8**). Enhanced activity was not observed in *N*- or *O*-geranylation of 1-benzylisoquinolines and tetrahydroprotoberberines.

Cytotoxicity evaluation.

The synthetic simple isoquinolines (**1-8**), 1-benzylisoquinolines (**9-13**), and tetrahydroprotoberberines (**14-18**) were assayed for *in vitro* cytotoxicity against five human tumor cell lines, including lung carcinoma (A-549), prostate carcinoma (DU145), epidermoid carcinoma of the nasopharynx (KB), a drug-resistant KB-subline (KBvin), and human promyelocytic leukemia (HL-60). The cytotoxicity data are given as an ED_{50} value for each cell line, the concentration of a compound that caused a 50% reduction in absorbance at 562 nm relative to untreated cells using SRB[10] and MTT[16] and/or WST-8 assays (HL60 is a non-adherent cell line; therefore, the SRB assay could not be used with it), and are shown in Tables 2 and 3. The results for **1-5** have already been published.[13]

The parent salsolinol (**1**), *N*-methylsalsolinol (**4**), and *N*,*N*-dimethylsalsolinol (**5**) showed no activity in SRB and MTT assays, and *N*-geranylsalsolinol (**2**) showed either weak or no activity against all cell lines in both assays. In comparison, *N*,*N*-digeranylsalsolinol (**3**) showed especially increased activity against DU-145, KB, and HL-60 cell lines. Compound **3** exhibited the highest potency (1.2 μg/mL) against the HL-60 cell line, and also displayed high activity (0.77 μg/mL) against this cell line in the WST-8 assay (Table 3).[17] Thus, *N*-geranylation, particularly digeranylation, increased cytotoxicity, while *N*-methylation, either mono or di, had no effect. The increase in cytotoxicity was found in *O*- and *O*,*O*-digeranyl compounds (**6-8**) compared with the parent *N*,*N*-dimethylsalsolinol (**5**) in the SRB assay, though activity of *O*,*O*-digeranyl compounds (**8**) was weaker than that of *N*,*N*-digeranylsalsolinol (**3**). Thus, from these data, *N*-quaternization by *N*-geranylation, not simply *N*-alkylation, appears to be important for enhanced cytotoxicity.

In 1-benzyltetrahydroisoquinoline, *N*- and *N*,*N*-digeranylations of tetrahydropapaveroline (**9**) increased remarkably the activity against three or four cell lines tested in the SRB assay. Compounds **10** and **11** showed a broad spectrum of activity. It was demonstrated that *N*-geranylation in the 1-benzyltetrahydroisoquinoline-type alkaloids contributes especially to the increase in cytotoxicity. The increase in cytotoxicity by *N*,*N*-digeranylations (**11**) compared with *N*-geranylation (**10**) was not observed to be distinct from that of the simple isoquinolines.

An increase in cytotoxicity was found in the *O*,*O*-digeranyl derivative (**13**) of papaveroline (**12**), except for the KBvin cell line in SRB and MTT assays. Compound **13** exhibited high potency (1.49 μg/mL) against the HL-60 cell line, and also displayed high activity (1.24 μg/mL) against this cell line in the WST-8 assay.[17]

Table 2. *In vitro* cytotoxic activity of several isoquinoline-type alkaloids **1-18** against various human tumor cell lines

group[a]	compound	cell line[b] A-549	DU-145	KB	KBvin	HL-60
		ED_{50} (μg/mL)[c]-SRB				
	1[d]	NA[e]	NA	NA	NA	ND[e]
	2[d]	7.75	7.75	10.1	5.64	ND
	3[d]	5.72	3.84	3.28	NA	ND
	4[d]	> 20	> 20	> 20	> 20	ND
I	**5**[d]	> 20	> 20	> 20	> 20	ND
	6	> 20	12.4	12.8	> 20	ND
	7	7.12	13.9	7.70	> 20	ND
	8	8.90	11.5	7.60	> 20	ND
	9	NA	NA	NA	NA	ND
	10	1.31	3.56	3.38	3.60	ND
II	**11**	1.34	2.00	2.35	7.96	ND
	12	11.95	7.46	8.05	5.07	ND
	13	6.25	5.89	5.37	NA	ND
	14	6.05	2.88	5.40	1.45	ND
	15	7.40	3.29	5.87	3.19	ND
III	**16**	3.63	3.26	5.70	1.33	ND
	17	NA	NA	14.6	NA	ND
	18	9.68	2.31	2.90	NA	ND
	Taxol[f]	2.91	1.91	3.10	> 850	ND
		ED_{50} (μg/mL)[c] –MTT[g]				
	1[d]	NA	NA	NA	NA	NA
I	**2**[d]	NA	NA	NA	NA	NA

	3[d]	15.8	3.28	5.70	NA	1.20
II	**12**	NA	NA	NA	NA	12.3
	13	7.50	5.26	6.43	NA	1.49

[a]I: simple isoquinolines, II: 1-benzylisoquinolines, III: protoberberines
[b]A-549: lung carcinoma, DU-145: prostate carcinoma , KB: epidermoid carcinoma of the nasopharynx, KBvin: drug-resistant, HL-60: human promyelocytic leukemia.
[c]Cytotoxicity as ED_{50} for each cell line, the concentration of compound that causes a 50% reduction in adsorbance at 562 nm relative to unreated cells using the SRB or MTT assay. Pure compound is considered to be significantly active when its $ED_{50} < 4.0$ μg/mL.
[d]These data have already been prepared.[13] [e]NA: no activity (if it does not have 50% inhibition at 20 μg/mL, we suggest it has no activity); ND: not determined; [f]ng/mL; [g]Different time of treatment (because of long doubling time in HL-60): 24 hr for A-549, DU-145, KB, and KBvin; 72 hr for HL-60 in MTT assay

In 2,3,9,10-tetrademethyltetrahydropalmatine (**14**), an increase in cytotoxicity by *N*-geranylation (**15**, **16**) of the stereostructure was not observed in almost all cell lines, while in the *N*-geranyl derivative (**18**) with a B/C-*trans* junction of 2,3,10,11-tetrademethylpseudotetrahydropalmatine (**17**), the activity increased, except for the KBvin cell line. Contrary to this, compounds **15** and **16** displayed higher activity than **18** against the HL-60 cell line.

Comparing the activity between the compounds and the cell lines, *N*- and *N*,*N*-geranyl derivatives (**10** and **11**) of the 1-benzyltetrahydroisoquinolines and *N*-geranyl compound (**16**, tetrahydroprotoberberine) with a B/C-*trans* junction showed high potency (1.31-3.63 μg/mL) in three or four cell lines. The *N*,*N*- and *N*-geranylated compounds (**3**, simple isoquinoline and **18**, tetrahydroprotoberberine) displayed high activity (2.31-3.84 μg/mL) in DU145 and KB cell lines. 2,3,9,10-Tetrademethyltetrahydroprotoberberine (**14**-**16**) exhibited high potency (1.33-3.19 μg/mL) in the KBvin cell line, independent of the presence of the geranyl group. In both MTT and WST-8 assays, only two *N*,*N*- and *O*,*O*-geranylated compounds (**3**, simple isoquinoline and **13**, 1-benzylisoquinoline) displayed high activity in the HL-60 cell line. It was suggested that the structures of the test samples had a strong effect on the HL-60 cell line.

Table 3. *In vitro* cytotoxic activity of several isoquinolines-type alkaloids**1-4** and **9-18** against HL-60

group	compound	IC_{50} value (μg/mL)-WST-8
simple isoquinolines	**1**	7.17
	2	7.33
	3	0.77
	4	5.09
1-benzylisoquinolines	**9**	6.99
	10	4.78
	11	7.32
	12	3.68
	13	1.24
protoberberines	**14**	>20
	15	8.05
	16	12.38
	17	6.15
	18	16.3

Inhibitory effects on EBV-EA induction.

The Epstein-Barr virus early antigen (EBV-EA) activation assay is considered to be an effective indicator for the evaluation of anti-tumor-promoting activity.[11] The inhibitory effects of simple isoquinolines (**1-8**), 1-benzylisoquinolines (**9-13**), and tetrahydroprotoberberines (**14-18**) on EBV-EA activation induced by 12-*O*-tetradecanoylphorbol-13-acetate (TPA) in Raji cells were examined as a primary screening of anti-tumor-promoting activity.

Table 4. Inhibitory effects of several isoquinoline-type alkaloids **1**–**18** on TPA Induced EBV-EA activation (100%)[a]

group	compound	concentration (mol ratio/32 pmol TPA) 1000	500	100	10	IC_{50}[b]
		% to control (% viability)				
simple isoquinolines	**1**[c]	12.0 (60)	37.6	79.0	100	384
	2[c]	3.1 (70)	24.3	71.6	97.4	350
	3[c]	0 (70)	20.6	69.3	91.7	296
	4[c]	9.3 (60)	36.8	78.8	100	372
	5[c]	8.7 (60)	35.1	78.0	100	369
	6	8.9 (60)	36.8	69.8	98.7	371
	7	8.0 (60)	36.1	69.0	98.0	369
	8	5.3 (60)	32.6	67.3	96.5	335
1-benzylisoquinolines	**9**	13.9 (60)	37.5	76.9	100	387
	10	11.8 (60)	36.1	75.4	100	380
	11	8.9 (60)	35.0	74.3	100	369
	12	15.0 (60)	39.2	80.6	100	410
	13	9.1 (60)	31.2	72.4	100	323
protoberberines	**14**	0 (60)	25.8	76.8	96.9	321
	15	0 (60)	23.2	74.2	94.3	307
	16	0 (60)	23.7	74.8	94.7	308
	17	0 (60)	23.7	71.5	94.0	305
	18	0 (60)	23.2	71.1	93.8	303
	Ginsenoside-Rg1	0 (80)	32.5	72.6	91.0	310
	β-Carotene	9.1 (60)	34.3	82.7	100	400

[a]Values represent percentages relative to the positive control value. TPA (32 pmol, 20 ng) = 100%. Values in parentheses are viability percentages of Raji cell. [b]IC_{50} represents the mol ratio to TPA that inhibits 50% of positive control (100%) activated with 32 pmol of TPA.

[c]These data have been published.[13]

The inhibitory effects of the test compounds on TPA-induced EBV-EA activation, their effects on the viability of Raji cells, and the 50% inhibitory concentration (IC_{50}) values are shown in Table 4. The results for **1-5** have already been published.[13]

All simple isoquinolines (**1-8**) displayed stronger inhibition (IC_{50} 296-384) than that of the reference β-carotene (IC_{50} 400), which has been studied extensively in cancer chemoprevention using animal models.[18] The inhibitory activity was more increased by geranylation than by methylation on nitrogen (compared with **3** and **5**). Therefore, *N*-geranylation but not *N*-dimethylation appears to be important for enhanced activity. *N*,*N*-Digeranylsalsolinol (**3**) displayed the strongest inhibition (IC_{50} 296), and its activity was higher than that of ginsenoside-Rg1, which is known as a strong anti-tumor-promoter.[19]

The 6,7-*O*-digeranylated derivative (**8**) had increased activity (IC_{50} 335) compared with the parent compound (**5**), though 6- and 7-*O*-geranylation (**6** and **7**) scarcely affected the activity. Thus, these compounds, especially *N*,*N*- and *O*,*O*-digeranylated derivatives, appear to be useful leads for further development of potential cancer chemopreventive agents.

There was little increase in inhibition by *N*-, and *N*,*N*-geranylation (**10** and **11**) of tetrahydropapaveroline (**9**). Increased inhibition (IC_{50} 323) was observed in *O*, *O*-geranylation (**13**) of papaveroline (**12**). All tetrahydroprotoberberines (**14-18**) displayed strong inhibition (IC_{50} 303-321) comparable to ginsenoside-Rg1 (IC_{50} 310), independent of whether the compound has the geranyl group or not. They might be valuable antitumor promoters. In 2, 3, 9, 10-tetrademethyltetrahydropalmatine (**14**), there was little increase in inhibition by *N*-geranylation (**15**, **16**) independent of the stereostructure.

In simple isoquinolines and 1-benzylisoquinolines, digeranylated derivatives (**3**, **8**, and **13**) displayed potent activity, suggesting that relative lipophilicity of the geranyl groups may contribute to the inhibitory effect.

Free radical scavenging activity.

Several human illnesses, such as cancer, diabetes, atherosclerosis, etc., can be linked to the damaging action of reactive free radicals.[20] The ability of three types of compounds (**1**–**18**) to scavenge 1,1-diphenyl-2-picrylhydrazyl (DPPH) free radicals was examined; the results are presented in Table 5. The results for **1-3** have already been published[13]. To evaluate the free radical scavenging activity of these compounds, the concentration required to scavenge DPPH free radicals by 50% (SC_{50}) was determined.

The antioxidant α-tocopherol was used as a reference compound. Compounds **1-3** displayed similar potency and were more active than α-tocopherol. 6-*O*- or 7-*O*-Geranylation (**6** or **7**) of **5** reduced the activity and 6,7-*O*-digeranylation (**8**) further reduced the activity.

Table 5. Radical scavenging activity of several isoquinoline-type alkaloids **1-18**

group	compound	SC_{50} (μM)[a]
simple isoquinolines	**1**[b]	12.0
	2[b]	17.0
	3[b]	11.5
	4	32.1
	5	31.3
	6	40.7
	7	41.1
	8	57.7
1-benzylisoquinolines	**9**	2.64
	10	7.81
	11	6.47
	12	2.95
	13	9.94
protoberberines	**14**	5.53
	15	8.39
	16	3.81
	17	6.04
	18	5.36
	α-tocopherol	24.3

[a]The compound concentration showing radical scavenging efficacy of 50% was defined as SC_{50}.
[b]These data have already been prepared.[13]

All 1-benzyltetrahydroisoquinolines (**9-13**) are more active than α-tocopherol. *N*-Geranylation (**10**, **11**) of 1-benzyltetrahydroisoquinoline (**9**) reduced the activity. The activity also decreased by *O*,*O*-digeranylation (**13**) of papaveroline (**12**). All tetrahydroprotoberberines (**14-18**) proved to be more active than α-tocopherol; increased activity by *N*-geranylation was small.

In all three types of isoquinoline alkaloids, the activity was reduced by *N*- or *O*-geranylation. Obviously the phenolic hydroxyl groups on the aromatic rings strongly influenced the activity, without an affect of the geranyl group.

Antimalarial activity.

The simple isoquinolines (**1-3**), 1-benzylisoquinolines (**12**, **13**), and tetrahydroprotoberberines (**14**, **16-18**) were tested *in vitro* against human malaria parasite, *Plasmodium falciparum* FCR-3. The antimalarial activity of each compound was determined as a percentage of reduction compare of control. The compound concentration required to inhibit cell growth by 50% was expressed as EC_{50}. To evaluate the toxicity of the compounds for mammalian cells, the concentration causing a 50% growth reduction (IC_{50}) of mouse mammary FM3A cells, a model of the host, was determined. The IC_{50}/EC_{50} ratios for the compounds were calculated as an evaluation of antimalarial activity. The results are presented in Table 6. In three types of isoquinoline derivatives, *N*-geranylation increased the inhibitory activity; however, the geranylated derivatives of the simple isoquinolines and 1-benzylisoquinolines showed only slight inhibitory activity and no selectivity. Only *N*-geranyl derivatives (**16** and **18**) of the tetrahydroprotoberberines inhibited *P. falciparum* with EC_{50} values in the order of 10^{-7} M. This is an increase antimalarial activity compared with the parentcompounds (**14** and **17**), and their selectivity indexes were > 15. Compounds **16** and **18** were potent antimalarial agents with higher selectivity indexes compared with the other test compounds.

In addition, *N*-geranyl derivatives, **16** and **18**, it is noted that the selectivity of the compounds (selectivity; >15) was comparable to that of mefloquine (selectivity; 90). It means that these compounds have safety for human clinical treatment of malaria if these compounds developed new antiamalrial drug.

Table 6. *In vitro* antimararial activity of several isoquinoline-type alkaloids **1**-**3**, **12**-**14**, and **16**-**18**

group	compound	50 % inhibitory concentration (μM)[a] *Plasmodium falciparum* FCR-3 EC_{50} (growth %)	Mouse mammary cells FM3A IC_{50} (growth %)	selectivity index[b] IC_{50} / EC_{50}
simple isoquinolines	**1**	>27 (100 %)	9.0	-
	2	5.3	0.08	-
	3	3.4	0.45	-
1-benzylisoquinolines	**12**	5.1	2.9	-
	13	3.6	1.5	-
protoberberines	**14**	>17 (100 %)	>8.3 (73 %)	-
	16	0.33	>4.9 (69 %)	>15
	17	9.5	8.1	-
	18	0.53	>7.7 (69 %)	>15
	Mefloquine	0.032	2.9	91

[a]The 50 % inhibitory concentration was defined by comparison with drug-free controls incubated under same condition.

[b]In vitro selectivity index was estimated from the ratio (IC_{50} / EC_{50}) of the drug concentrations necessary to inhibit the growth rate of cells to 50 % of the growth value between the malaria parasites
and mouse mammary FM3A cells which served as a model host.

Table 7. Anti-HIV activity of several isoquinoline-type alkaloids **1-18**

group	compound	IC_{50}(μg/mL)[a]	EC_{50} (μg/mL)[b]
simple isoquinoline type	**1**[c]	>25	>2.5
	2[c]	20.23	>2.5
	3[c]	10.68	>2.5
	4	>25	>2.5
	5	>25	>25
1-benzylisoquinoline type	**9**	19.69	>2.5
	10	24.59	>2.5
	11	18.02	>2.5
	12	>25	>2.5
	13	17.95	>2.5
protoberberine type	**14**	>25	>2.5
	15	19.84	>2.5
	16	>25	>25
	17	18.13	22.54
	18	>25	>25
	AZT[d]	500	0.014

[a]The agent concentration that inhibited H9 cell growth by 50%. [b]The agent concentration that inhibited viral replication in H9 cell by 50%. [c]These data have already been prepared.[13]

[d]Azidothymidine

Anti-HIV activity.

The isoquinoline alkaloids (**1-4** and **9-18**) were tested against HIV-1 replication in H9 lymphocytes in order to evaluate their anti-HIV activity. However, none of them displayed anti-HIV activity (Table 7). Interestingly, results in the anti-HIV assay did not parallel those in the antimicrobial and cytotoxicity assays.

Conclusions.

In summary, three types of isoquinoline alkaloids (**1-18**) were tested for antimicrobial, cytotoxic, anti-malarial, anti-oxidant, and anti-HIV activities, as well as inhibitory activity against Epstein-Barr virus early antigen (EBV-EA) activation induced by 12-*O*-tetradecanoylphorbol-13-acetate (TPA) in Raji cells. *N*- or *O*-Geranylation contributed to increased potency in four types of activities except anti-HIV and anti-oxidant. *N*,*N*-Geranylation of salsolinol (simple isoquinoline, **1**) strongly increased the potency in antimicrobial activity. *N*,*N*- and *N*-Geranylations of tetrahydropapaveroline (1-benzylisoquinoline, **9**) strongly enhanced cytotoxic activity. *N*,*N*-Geranylation of **1** and *N*-geranylation of **17** (2,3,10,11-oxygenated protoberberine) increased the same activity to a lesser extent. *N*,*N*-Geranylation of **1** and *O*,*O*-geranylation of papaveroline (1-benzylisoquinoline, **11**) strongly increased cytotoxic activity against the HL-60 cell line. *N*,*N*-Geranylsalsolinol (**3**) showed potent inhibitory effects on EBV-EA induction compared with those of the parent compound (**1**). *O*,*O*-Geranylation of **5** (simple isoquinoline) and *N*,*N*-geranylation of **11** (1-benzylisoquinoline) enhanced the inhibitory activity. The protoberberines (**14-18**) tested also displayed strong inhibitory activity. *N*-Geranylation of 2,3,9,10- and 2,3,10,11-oxygenated protoberberines increased the antimalarial activity. Among the tested biological activities of the isoquinolines **1-18**, *N*,*N*-geranylation of salsolinol (**1**) strongly increased potency in three assays, antimicrobial and cytotoxic activities and inhibitory effects on EBV-EA induction, while *N*-geranylation increased the same activities to a lesser extent. However, *N*,*N*- and *N*-methylation did not increase the activities in these assays. These simple *N*-geranylated isoquinolines also have free radical scavenging activity. These findings indicate that the *N*-geranyl group plays an important role in mediating these biological activities.

Compound **3** shows antimicrobial, cytotoxic, and inhibitory effects on EBV-EA induction, compounds **10**, **11**, **13**, and **18** are cytotoxic, **8**, **13**, and **14-18** inhibit EBV-EA induction, and **16** and **18** display antimalarial activity. In the present studies, we have identified new biologically active *N*- or *O*-geranylated isoquinolines, which may be considered as lead structures for developing potential chemotherapeutic agents. It was first suggested that the addition of a geranyl residue to isoquinoline skeletons may contribute to the enhancement of the biological activities of isoquinoline alkaloids.

EXPERIMENTAL

General procedures. Conventional ^{1}H NMR, NOESY, COSY, HMBC, and HMQC spectra were obtained on a Varian VXR-500 spectrometer (^{1}H: 500 MHz) using CD_3OD solvent, except where noted, with TMS as int. standard. ^{13}C NMR and DEPT spectra were measured on a Varian VXR-500 spectrometer (125 MHz). Mass spectra were determined on a Hitachi M-4100 instrument at 75 eV. The secondary ion mass spectra (SIMS) were measured using glycerol as matrix. HPLC and prep. HPLC analyses were performed using a Hitachi M-6200 intelligent pump (1 mL/min) and Hitachi M-6250 or Jasco PU-2089 intelligent pump (6 mL/min), respectively, and a Hitachi L-4000 UV detector (280 nm). Cosmosil 5C$_{18}$-AR reversed-phase column of small (4.6 i.d. X 150 mm) and large (20 i.d. X 250 mm) sizes were used for HPLC and prep. HPLC, respectively. Analyses with a Hitachi HPLC system were made using a solvent system, (A) 0.1M NH4OAc (0.05% TFA) / (B) MeOH (0.05% TFA) under the following gradient conditions: A/B, initial (75/25), 10 min (50/50), 30 min (20/80) or initial (80/20), 30 min (0/100) or initial (80/20), 20 min (0/100) (flow rate 1 mL/min). Prep. HPLC analyses for purification were performed using a solvent system, (A) H_2O (0.05% TFA) / (B) MeOH (0.05% TFA) under the following gradient conditions: A/B 50/50 to 0/100, 30 to 60 min (flow rate 6 mL/min). (±)-Tetrahydropapaverine hydrochloride and azidothymidine (AZT) were purchased (Sigma). (±)-Salsolinol (**1**),[8] (±)-carnegine,[9] (±)-*N*-methylpapaveroline (**11**),[9] (±)-2,3,9,10-tetrademethyl-tetrahydropalmatine (**14**),[9] and (±)-2, 3, 10, 11-tetrademethylpseudotetrahydropalmatine (**17**)[9] have previously been prepared.

Optimized geometry and molecular orbital were calculated by the DFT Method (Density Function Theory) using the Materials Studio DMol3 package of Accelrys Inc.[14,15] First, optimized geometry was obtained using the Perdew-Wong LDA functional (PWC)[21] and double numerical plus d-functional (DND) basis set. Second, the optimized geometry obtained was further calculated for molecular orbitals using the Becke exchange plus Lee-Young-Parr correlation (BLYP)[22, 23] and the double numerical plus polarization (DNP) basis set.

Preparations of (±)-*N*- and (±)-*N*,*N*-geranylsalsolinol (2 and 3). To a stirred suspension of sodium hydride (245 mg, 10.2 mmol) in DMF (15 mL) at room temperature under N_2 (±)-salsolinol hydrochloride[8] (**1**, 1 g, 4.65 mmol) was added by portions followed by a catalytic amount of hydroquinone. The mixture was stirred for 30 min. Geranyl bromide (953 mg, 4.39 mmol) was added dropwise and the mixture was stirred for 2 h. NaH (245 mg, 10.2 mmol) and geranyl bromide (953 mg, 4.39 mmol) were added again, and the mixture was stirred for 2 h. After decomposition of excess NaH with MeOH (1 mL), the mixture was poured onto ice-water and extracted with Et_2O followed by $CHCl_3$. Et_2O and $CHCl_3$ were separately dried and evaporated. The $CHCl_3$ extract was subjected to prep.

HPLC [0.1M NH_4OAc (0.05% TFA) / MeOH (0.05% TFA) (A/B) initial 60/40, 0/100 (30 min)] to give (±)-*N*-geranylsalsolinol (**2**, 205.7 mg, yield 10.3%) and (±)-*N*,*N*-geranylsalsolinol (**3**, 329.9 mg; yield 12.6%) as trifluoroacetate. **2**: SIMS *m/z* $[M + H]^+$ 316; HRMS *m/z* $[M + H]^+$ 316.2257 ($C_{20}H_{30}NO_2$ requires 316.2271). **3**: SIMS *m/z* $[M]^+$ 452; HRMS *m/z* $[M]^+$ 452.3527 ($C_{30}H_{46}NO_2$ requires 452.3523). The ^1H and ^{13}C NMR spectral data of these compounds have been previously presented.[13]

Preparation of (±)-*N*-methylsalsolinol (4). Carnegine-HCl (500 mg, 1.94 mmol) in 47% HBr (2 ml) was refluxed for 2 h at 130° in an oil bath. The solvent was evaporated *in vacuo*, the residue in MeOH was crystallized to give (±)-*N*-methylsalsolinol-HBr (**4**, 398.5 mg, yield 64.8%). SIMS *m/z* $[M + H]^+$ 194; HRMS *m/z* $[M + H]^+$ 194.1201 ($C_{11}H_{16}NO_2$ requires 194.1176). The ^1H and ^{13}C NMR spectral data of **4** have been previously presented.[13]

Preparation of (±)-*N*,*N*-dimethylsalsolinol (5). A solution of carnegine-HCl (3.1 g, 12.06 mmol) and CH_3I (1 ml) in MeOH (25 ml) and $(Me)_2CO$ (25 ml) in a glass-stoppered bottle was heated for 75 min at 110 °C in a oil bath. The solvent was evaporated *in vacuo*, the residue was crystallized in $(Me)_2CO$-Et_2O to give *N*-methylcarnegine iodide (4.75 g, yield 86.5%). The iodide (3.8 g) in 47% HBr (10 ml) was refluxed for 1 h at 140 °C in an oil bath. The solvent was evaporated *in vacuo*, the residue was crystallized in $(Me)_2CO$-Et_2O to give (±)-*N*,*N*-dimethylsalsolinol bromide (**5**, 2.97 g, yield 98.5%). SIMS *m/z* $[M]^+$ 208; HRMS *m/z* $[M]^+$ 208.1350 ($C_{12}H_{18}NO_2$ requires 208.1336). The ^1H and ^{13}C NMR spectral data of **5** have been previously presented.[13]

Preparations of (±)-7-*O*-geranyl-, (±)-6-*O*-geranyl-, and (±)-6,7-*O*-digeranyl-*N*,*N*-dimethylsalsolinol (6-8). To a stirred suspension of NaH (260 mg, 10.8 mmol) in DMF (15 mL) at rt under N_2 (±)-*N*,*N*-dimethylsalsolinol hydrobromide (**5**, 1 g, 3.47 mmol) was added portionwise followed by a catalytic amount of hydroquinone. The mixture was stirred for 30 min. Geranyl bromide (1 g, 4.61 mmol) was added dropwise and the whole mixture was stirred for 3 h. After decomposition of excess NaH with MeOH (1 mL), the mixture was poured onto ice-water and extracted with $CHCl_3$. The combined organic layer was dried and evaporated. The $CHCl_3$ extract was subjected to prep. HPLC [0.1M NH_4OAc (0.05% TFA)/MeOH (0.05% TFA) (A/B) initial 100/0, 0/100 (540 min)] to give (±)-7-*O*-geranyl-*N*,*N*-dimethylsalsolinol (**6**, 102.2 mg, yield 7.7%), (±)-6-*O*-geranyl-*N*,*N*-dimethylsalsolinol (**7**, 98.8 mg, yield 7.4%) and (±)-6,7-*O*-digeranyl-*N*,*N*-dimethylsalsolinol (**8**, 154.2 mg, yield 8.9%) as trifluoroacetates. **6**: ^1H NMR (500 MHz, CD_3OD) δ 6.68 (1H, s, H-5), 6.74 (1H, s, H-8), 5.48 (1H, t, J = 6.5 Hz, H-2′), 5.09 (1H, t, J = 6.5 Hz, H-6′), 4.62 (2H, d, J = 6.5 Hz, H-1′), 4.57 (1H, q, J = 6.5 Hz, H-1), 3.77 (1H, dt, J = 12.5, 8.0 Hz, Hax′-3), 3.55 (1H, dt, J = 12.5, 5.0 Hz, Heq′-3), 3.17 (3H, s, ax′NMe), 3.14 (3H, s, eq′NMe), 3.08 (2H, m, H-4), 2.12 (2H, m, H-5′), 2.09 (2H, m, H-4′), 1.75 (3H, s, 3′-Me), 1.69 (3H, d, J = 6.5 Hz, Me-1), 1.65 (3H, s, 8′), 1.59 (3H, s, 7′-Me); ^{13}C NMR (125 MHz,

CD_3OD) δ 148.79 (C-6), 147.83 (C-7), 142.30 (C-3′), 132.63 (C-7′), 124.90 (C-6′), 124.39 (C-1a), 122.17 (C-4a), 120.94 (C-2′), 116.01 (C-5), 113.25 (C-8), 69.51 (C-1), 67.06 (C-1′), 56.86 (C-3), 51.50 (eq′NMe), 50.11 (ax′NMe), 40.61 (C-4′), 27.41 (C-5′), 25.84 (C-8′), 24.30 (C-4), 18.63 (C-1-Me), 17.72 (7′-Me), 16.69 (3′-Me); SIMS *m/z* $[M]^+$ 344; HRMS *m/z* $[M + H]^+$ 344.2606 ($C_{22}H_{34}NO_2$ requires 344.2588), *m/z* $[M\text{-}C_{10}H_{16}]^+$ 208.1355 ($C_{12}H_{18}NO_2$ requires 208.1338) ; **7**: ^1H NMR (500 MHz, CD_3OD) δ 6.79 (1H, s, H-5), 6.66 (1H, s, H-8), 5.50 (1H, m, H-2′), 5.10 (1H, m, H-6′), 4.63 (2H, d, *J* = 6.5 Hz, H-1′), 4.55 (1H, q, *J* = 6.5 Hz, H-1), 3.78 (1H, dt, *J* = 12.5, 7.5 Hz, Hax′-3), 3.56 (1H, dt, *J* = 12.5, 6.0 Hz, Heq′-3), 3.17 (3H, s, ax′NMe), 3.13 (3H, s, eq′NMe), 3.12 (2H, m, H-4), 2.12 (2H, m, H-5′), 2.07 (2H, m, H-4′), 1.75 (3H, s, 3′-Me), 1.67 (3H, d, *J* = 6.5 Hz, Me-1), 1.65 (3H, s, Me-8′), 1.60 (3H, s, 7′-Me); ^{13}C NMR (125 MHz, CD_3OD) δ 148.62 (C-6), 147.90 (C-7), 142.26 (C-3′), 132.63 (C-7′), 124.90 (C-6′), 124.39 (C-1a), 122.17 (C-4a), 120.94 (C-2′), 116.01 (C-5), 113.25 (C-8), 69.36 (C-1), 66.86 (C-1′), 57.19 (C-3), 51.58 (eq′NMe), 49.80 (ax′NMe), 40.62 (C-4′), 27.39 (C-5′), 25.86 (C-8′), 24.51 (C-4), 18.36 (C-1-Me), 17.74 (7′-Me), 16.67 (3′-Me); SIMS *m/z* $[M]^+$ 344; HRMS *m/z* $[M + H]^+$ 344.2603 ($C_{22}H_{34}NO_2$ requires 344.2588), *m/z* $[M\text{-}C_{10}H_{16}]^+$ 208.1317 ($C_{12}H_{18}NO_2$ requires 208.1338); **8**: ^1H NMR (500 MHz, CD_3OD) δ 6.83 (1H, s, H-5), 6.79 (1H, s, H-8), 5.48 (2H, m, H-2′, H-2′′), 5.10 (2H, m, H-6′, H-6′′), 4.59 (2H, m, H-1′′), 4.58 (2H, m, H-1′), 4.54 (1H, q, *J* = 6.5 Hz, H-1), 3.79 (1H, dt, *J* = 12.5, 8.0 Hz, Hax′-3), 3.57 (1H, dt, *J* = 12.5, 5.0 Hz, Heq′-3), 3.17 (3H, s, ax′NMe), 3.15 (3H, s, eq′NMe), 3.14 (2H, m, H-4), 2.12 (4H, m, H-5′, H-5′′), 2.07 (4H, m, H-4′, H-4′′), 1.742 (3H, s, 3′′-Me), 1.736 (3H, s, 3′-Me), 1.69 (3H, d, *J* = 6.5 Hz, Me-1), 1.66 (6H, s, 8′, 8′′), 1.60 (6H, s, 7′-Me, 7′′-Me); ^{13}C NMR (125 MHz, CD_3OD) δ 150.79 (C-6), 149.78 (C-7), 142.58(C-3′′), 142.56 (C-3′), 132.68 (C-7′), 125.09 (C-1a), 124.96 (C-6′), 122.33 (C-4a), 120.94 (C-2′′), 120.85 (C-2′), 115.05 (C-5), 114.41 (C-8), 69.60 (C-1), 67.38 (C-1′), 67.04 (C-1′′), 56.83 (C-3), 51.55 (eq′NMe), 50.25 (ax′NMe), 40.66 (C-4′, C-4′′), 27.48 (C-5′), 27.44 (C-5′′), 25.93 (C-8′), 24.56 (C-4), 18.63 (C-1-Me), 17.81 (7′-Me), 16.77 (3′-Me), 16.74 (3′′-Me); SIMS *m/z* $[M]^+$ 480; HRMS *m/z* $[M]^+$ 480.3858 ($C_{32}H_{50}NO_2$ requires 480.3837), *m/z* $[M\text{-}C_{10}H_{16}]^+$ 344.2586 ($C_{22}H_{34}NO_2$ requires 344.2588).

Preparation of (±)-tetrahydropapaveroline (9). A solution of (±)-tetrahydropapaverine hydrochloride (Sigma, 2 g, 5.26 mmol) in 47% HBr (10 ml) was refluxed for 2.5 h. The solvent was evaporated *in vacuo*. The crystalline product was recrystallized from MeOH to give (±)-tetrahydropapaveroline hydrobromide **9** (1.84 g, yield 95.1%) which was identified by comparing its ^1H NMR and HPLC with data of an authentic sample.

Preparations of (±)-*N*- and (±)-*N*,*N*-digeranyltetrahydropapaveroline (10 and 11). To a stirred suspension of NaH (65 mg, 2.71 mmol) in DMF (15 mL) at rt under N_2 (±)-tetrahydropapaveroline hydrobromide (**9**, 1 g, 2.72 mmol) was added portionwise followed by a catalytic amount of

hydroquinone. The mixture was stirred for 30 min. Geranyl bromide (590 mg, 2.72 mmol) was added dropwise, and the mixture was stirred for 10 h. Geranyl bromide (295 mg, 1.36 mmol) was added dropwise and the mixture was further stirred for 12 h. After decomposition of excess NaH with MeOH (1 mL), the mixture was poured onto ice-water and extracted with Et_2O followed by $CHCl_3$. The Et_2O and $CHCl_3$ phases were separately dried and evaporated. The $CHCl_3$ extract was subjected to prep. HPLC [0.1M NH_4OAc (0.05% TFA)/MeOH (0.05% TFA) (A/B) initial 80/20, 0/100 (60 min)] to give (±)-*N*-geranyltetrahydropapaveroline (**10**, 274 mg, yield 18.7%) and (±)-*N*,*N*-digeranyltetrahydropapaveroline (**11**, 175 mg, yield 9.5%) as trifluoroacetate. **10**: ^{1}H NMR (500 MHz, CD_3OD) δ 6.75 (1H, d, *J* = 8.5 Hz H-5′), 6.65 (1H, s, H-5), 6.58 (1H, brs, H-2′), 6.50 (1H, brd, *J* = 8.5 Hz, H-6′), 6.18 (1H, s, H-8), 5.26 (1H, m, H-2′′), 5.12 (1H, m, H-6′′), 4.42 (1H, t, *J* = 6.5 Hz, H-1), 3.83 (1H, dd, *J* = 13.0, 8.5 Hz, H-1′′), 3.71 (1H, m, H-1′′), 3.68 (1H, m, H-3), 3.38 (1H, m, H-3), 3.14 (1H, m, H-9), 3.04 (1H, m, H-9), 2.97 (2H, m, H-4), 2.18 (4H, s, H-4′′, H-5′′), 2.12 (2H, m, H-5′), 2.07 (2H, m, H-4′), 1.70 (3H, s, Me-8′′), 1.64 (3H, s, 7′′-Me), 1.57 (3H, s, 3′′-Me); ^{13}C NMR (125 MHz, CD_3OD) δ 149.65 (C-3′′), 147.30 (C-6), 146.92 (C-3′), 146.04 (C-4′), 145.65 (C-7), 133.29 (C-7′′), 127.63 (C-1′), 124.56 (C-6′′), 121.93 (C-4a), 121.87 (C-1[a], C-6′), 117.67 (C-2′), 116.76 (C-5′), 116.12 (C-5), 115.75 (C-8), 114.15 (C-2′′), 63.01 (C-1), 51.86 (C-1′′), 44.80 (C-3), 40.74 (C-4′′, C-9), 27.14 (C-5′′), 25.94 (C-8′′), 22.90 (C-4), 17.84 (7′′-Me), 16.80 (3′′-Me); SIMS *m/z* $[M + H]^+$ 424; HRMS *m/z* $[M + H]^+$ 424.2494 ($C_{26}H_{34}NO_4$ requires 424.2482); **11**: ^{1}H NMR (500 MHz, CD_3OD) δ 6.67 (1H, d, *J* = 8.0 Hz H-5′), 6.64 (1H, s, H-5), 6.38 (1H, brs, H-2′), 6.30 (1H, dd, *J* = 8.0, 2.0 Hz, H-6′), 5.89 (1H, s, H-8), 5.61 (1H, d, *J* = 7.0 Hz H-2′′′), 5.42 (1H, t, *J* = 7.0 Hz, H-2′′), 5.15 (1H, m, H-6′′′) 4.99 (1H, m, H-6′′), 4.42 (1H, dd, *J* = 9.5, 3.0 Hz, H-1), 4.20 (1H, dd, *J* = 14.5, 7.0 Hz, H-1′′′) 4.13 (1H, dd, *J* = 14.5, 7.0 Hz, H-1′′′), 3.96 (1H, dd, *J* = 14.5, 9.0 Hz, H-1′′), 3.78 (1H, dd, *J* = 14.5, 6.0 Hz, H-1′′), 3.68 (1H, m, Hax′-3), 3.53 (1H, m, Heq′-3), 3.45 (1H, dd, *J* = 13.5, 3.5 Hz, H-9), 2.88 (1H, dd, *J* = 13.5, 9.5 Hz, H-9), 2.97 (2H, m, H-4), 2.28 (4H, s, H-4′′′, H-5′′′), 2.18 (4H, s, H-4′′, H-5′′), 2.07 (2H, m, H-4′), 1.85 (3H, s, 3′′′-Me), 1.69 (3H, s, Me-8′′), 1.68 (3H, s, Me-8′′′), 1.65 (3H, s, 7′′′-Me), 1.62 (3H, s, 7′′-Me) , 1.46 (3H, s, 3′′-Me); ^{13}C NMR (125 MHz, CD_3OD) δ 151.18 (C-3′′), 150.09 (C-3′′′), 147.52 (C-6), 146.65 (C-3′), 145.82 (C-4′), 145.24 (C-7), 133.37 (C-7′′), 133.32 (C-7′′′), 127.88 (C-1′), 124.70 (C-6′′), 124.65 (C-6′′′), 121.42 (C-4a), 122.52 (C-1a), 122.25 (C-6′), 118.04 (C-2′), 116.51 (C-5′), 115.85 (C-5), 116.81 (C-8), 112.11 (C-2′′, C-2′′′), 70.72 (C-1), 58.30 (C-1′′′), 55.79 (C-1′′), 52.01 (C-3), 41.06 (C-4′′, C-4′′′), 38.32 (C-9), 27.14 (C-5′′′), 27.05 (C-5′′), 25.98 or 25.99 (C-8′′or C-8′′′), 24.0 (C-4), 17.87 or 17.89 (7′′-Me or 7′′′-Me), 17.28 (3′′′-Me), 16.90 (3′′-Me);SIMS *m/z* $[M]^+$ 560; HRMS *m/z* $[M]^+$ 560.3746 ($C_{36}H_{50}NO_4$ requires 560.3746), *m/z* $[M\text{-}C_{10}H_{16}]^+$ 424.2498 ($C_{26}H_{34}NO_2$ requires 424.2482).

Preparation of 6,7-*O*,*O*-digeranyl-*N*-methylpapaveroline (13). To a stirred suspension of NaH (115

mg, 4.79 mmol) in DMF (15 mL) at rt under N_2 *N*-methylpapaveroline bromide[9] (**12**, 1 g, 2.66 mmol) was added portionwise followed by a catalytic amount of hydroquinone. The mixture was stirred for 30 min. Geranyl bromide (240 mg, 1.11 mmol) was added dropwise and the mixture was stirred for 10 h. Geranyl bromide (295 mg, 1.36 mmol) and NaH (70 mg, 2.92 mmol) were added dropwise and the mixture was stirred for a further 5 h. The reaction mixture was treated and separated by prep. HPLC as described in preparation of **10** and **11** to give 6,7-*O*,*O*-digeranyl-*N*-methylpapaveroline (**13**, 31 mg; yield 4.1%) as trifluoroacetate. **13**: ^{1}H NMR (500 MHz, CD_3OD) δ 8.32 (1H, d, J = 7.0 Hz, H-3), 8.08 (1H, d, J = 7.0 Hz, H-4), 7.70 (1H, s, H-8), 7.60 (1H, s, H-5), 6.71 (1H, d, J = 8.5 Hz, H-5′), 6.49 (1H, d, J = 1.5 Hz, H-2′), 6.36 (1H, dd, J = 8.5, 1.5 Hz, H-6′), 5.58 (1H, t, J = 6.5 Hz, H-2′′), 5.39 (1H, t, J = 6.5 Hz, H-2′′′), 5.09 (1H, m, H-6′′), 5.02 (1H, m, H-6′′′), 4.90 (2H, d, J = 6.5 Hz, H-1′′), 4.83 (2H, s, H-9), 4.80 (2H, d, J = 6.5 Hz, H-1′′′), 4.30 (3H, s, N-Me), 2.15 (H-5′′), 2.13 (4H, s, H-4′′), 2.05 (2H, m, H-5′′′), 1.98 (2H, m, H-4′′′), 1.83 (3H, s, 3′′-Me), 1.70 (3H, s, 3′′′-Me), 1.61 (3H, s, 8′′), 1.59 (3H, s, 8′′′), 1.58 (3H, s, 7′′-Me), 1.55 (3H, s, 7′′′-Me); ^{13}C NMR (125 MHz, CD_3OD) δ 158.86 (C-6), 156.93 (C-1), 154.18 (C-7), 147.50 (C-3′), 146.17 (C-4′), 144.48 (C-3′′), 143.93 (C-3′′′), 137.50 (C-4a), 136.61 (C-3), 132.81 (C-7′′), 132.63 (C-7′′′), 126.47 (C-1′), 125.62 (C-1a), 124.91 or 124.84 (C-6′′or C-6′′′), 123.58 (C-4), 120.39 (C-6′), 119.65 (C-2′′′), 119.32 (C-2′′), 117.14 (C-5′), 116.13 (C-2′), 108.15 (C-8), 108.08 (C-5), 67.71 (C-1′′), 67.33 (C-1′′′), 46.28 (N-Me), 40.63 (C-4′′) , 40.46 (C-4′′′), 34.96 (C-9), 27.30 or 27.29 (C-5′′or C-5′′′), 25.91 (C-8′′), 25.87 (C-8′′′), 17.82 or 17.81 (7′′ or 7′′′-Me), 16.88 or 16.84 (3′′ or 3′′′-Me); SIMS *m/z* $[M]^+$ 570; HRMS *m/z* $[M]^+$ 570.3592 ($C_{37}H_{48}NO_4$ requires 570.3583).

Preparations of (±)-(*cis*) and (±)-(*trans*)-*N*-geranyl-2,3,9,10-tetrademethyltetrahydropalmatinium salts (15 and 16). To a stirred suspension of NaH (126 mg, 5.25 mmol) in DMF (15 mL) at room temperature under N_2 (±)-2,3,9,10-tetrademethyltetrahydropalmatine hydrobromide[9] (**14**, 1 g, 2.63 mmol) was added by portion followed by a catalytic amount of hydroquinone. The mixture was stirred for 30 min. Geranyl bromide (571 mg, 2.38 mmol) was added dropwise and the mixture was stirred for 2.5 h. Geranyl bromide (220 mg, 1.01 mmol) and NaH (50 mg, 2.08 mmol) were added again and the mixture was further stirred for 2.5 h. After decomposition of excess NaH with MeOH (1 mL), the mixture was poured onto ice-water and extracted with Et_2O followed by $CHCl_3$. The Et_2O and $CHCl_3$ phases were separately dried and evaporated. The $CHCl_3$ extract was subjected to preparative HPLC [0.1M NH_4OAc (0.05% TFA)/MeOH (0.05% TFA) (A/B) initial 60/40, 0/100 (30 min)] to give (±)-(*cis*)-*N*-geranyl-2,3,9,10-tetrademethyltetrahydropalmatinium salt (**15**, 29.5 mg, yield 2.0%) and (±)-(*trans*)-*N*-geranyl-2,3,9,10-tetrademethyltetrahydropalmatinium salt (**16**, 137.6 mg, yield 9.5%) as trifluoroacetates. **15**: ^{1}H NMR (500 MHz, CD_3OD) δ 6.78 (1H, d, J = 8.0 Hz, H-11), 6.72 (1H, s, H-4), 6.66 (1H, s, H-1), 6.57

(1H, d, J = 8.0 Hz, H-12), 5.44 (1H, t, J = 8.0 Hz, H-2′), 5.08 (1H, brs, H-6′), 4.58 (3H, brs, H-8, H-13a), 4.08 (2H, m, H-1′), 3.81 (1H, m, H-6), 3.54 (1H, m, H-6), 3.28 (1H, m, H-13), 3.18 (2H, m, H-5), 3.12 (1H, m, H-13), 2.22 (2H, m, H-4′), 2.20 (2H, m, H-5′), 1.65 (3H, s, 3′-Me), 1.59 (3H, s, 8′), 1.58 (3H, s, 7′-Me); ^{13}C NMR (125 MHz, CD_3OD) δ 152.82 (C-3′), 147.66 (C-3), 146.25 (C-2), 144.85 (C-10), 143.60 (C-9), 133.47 (C-7′), 124.76 (C-1a), 124.12 (C-6′), 121.90 (C-12a), 120.93 (C-4a), 119.69 (C-12), 116.59 (C-4, C-11), 114.80 (C-8a), 114.52 (C-1), 111.74 (C-2′), 64.34 (C-13a), 59.93 (C-1′), 57.06 (C-8), 51.66 (C-6), 41.04 (C-4′), 34.89 (C-13), 26.97 (C-5′), 25.78 (C-8′), 23.75 (C-5), 17.79 (7′-Me), 16.94 (3′-Me);SIMS *m/z* $[M]^+$ 436; HRMS *m/z* $[M]^+$ 436.2486 ($C_{27}H_{34}NO_4$ requires 436.2482), *m/z* $[M\text{-}C_{10}H_{16}]^+$ 300.1230 ($C_{17}H_{18}NO_4$ requires 300.1235); **16**: ^{1}H NMR (500 MHz, CD_3OD) δ 6.85 (1H, d, J = 8.2 Hz, H-11), 6.84 (1H, s, H-1), 6.77 (1H, d, J = 8.2 Hz, H-12), 6.71 (1H, s, H-4), 5.44 (1H, dd, J = 9.5, 5.5 Hz, H-2′), 5.14 (1H, brs, H-6′), 5.07 (1H, dd, J = 12.5, 5.0 Hz, H-13a), 4.72 (1H, d, J = 15.5 Hz, H-8), 4.17 (1H, d, J = 15.5 Hz, H-8), 3.89 (1H, m, H-6), 3.86 (1H, m, H-1′), 3.83 (1H, m, H-13), 3.69 (1H, m, H-6), 3.61 (1H, m, H-1′), 3.54 (1H, m, H-6), 3.26 (1H, m, H-5), 3.20 (1H, dd, J = 12.5, 5.0 Hz, H-13), 3.05 (1H, brs, H-5), 2.20 (4H, m, H-4′, H-5′), 1.72 (3H, s, 8′), 1.66 (3H, s, 7′-Me), 1.33 (3H, s, 3′-Me); ^{13}C NMR (125 MHz, CD_3OD) δ 153.83 (C-3′), 147.37 (C-3), 146.63 (C-2), 144.95 (C-10), 143.66 (C-9), 133.45 (C-7′), 124.71 (C-6′), 122.77 (C-4a), 122.43 (C-12a), 122.06 (C-1a), 120.60 (C-12), 116.84 (C-11), 116.15 (C-4), 115.38 (C-8a), 113.45 (C-1), 111.42 (C-2′), 68.21 (C-13a), 58.43 (C-6), 57.62 (C-8), 46.96 (C-1′), 41.14 (C-4′), 29.60 (C-13), 27.10 (C-5′), 25.97 (C-8′), 24.48 (C-5), 17.79 (7′-Me), 16.0 (3′-Me);SIMS *m/z* $[M]^+$ 436; HRMS *m/z* $[M]^+$ 436.2484 ($C_{27}H_{34}NO_4$ requires 436.2482), *m/z* $[M\text{-}C_{10}H_{16}]^+$ 300.1230 ($C_{17}H_{18}NO_4$ requires 300.1235).

Preparation of (±)-(*trans*)-*N*-geranyl-2,3,10,11-tetrademethylpseudotetrahydropalmatinium salts (18). To a stirred suspension of NaH (130 mg, 5.42 mmol) in DMF (15 mL) at room temperature under N_2 (±)-2, 3, 10, 11-tetrademethylpseudotetrahydropalmatine hydrobromide[9] (**17**, 1 g, 2.63 mmol) was added by portions followed by a catalytic amount of hydroquinone. The mixture was stirred for 30 min. Geranyl bromide (580 mg, 2.67 mmol) was added dropwise and the mixture was stirred for 4.5 h. After decomposition of excess NaH with MeOH (1 mL), the mixture was poured onto ice-water. The precipitated crystals (703 mg) were subjected to prep. HPLC [0.1M NH_4OAc (0.05% TFA)/MeOH (0.05% TFA) (A/B) initial 60/40, 0/100 (30 min)] to give (±)-(*trans*)-*N*-geranyl-2,3,10,11-tetrademethylpseudotetrahydropalmatinium trifluoroacetate (**18**; 318.8 mg; yield 21.9%). **18**: ^{1}H NMR (500 MHz, CD_3OD) δ 6.83 (1H, s, H-1), 6.81 (1H, s, H-12), 6.70 (1H, s, H-4), 6.55 (1H, s, H-9), 5.44 (1H, m, H-2′), 5.12 (1H, brs, H-6′), 5.07 (1H, m, H-13a), 4.39 (1H, d, J = 15.0 Hz, H-8), 4.34 (1H, d, J = 15.0 Hz, H-8), 3.87 (1H, m, H-1′), 3.85 (1H, m, H-6), 3.78 (1H, m, H-13), 3.64 (1H, m, H-1′), 3.63 (1H, m, H-6), 3.25 (1H, m, H-5), 3.15 (1H, d, J = 13.0 Hz, H-13), 3.04 (1H, m, H-5), 2.20 (4H, m, H-4′, H-5′),

1.73 (3H, s, 8′), 1.67 (3H, s, 7′-Me), 1.32 (3H, s, 3′-Me); ^{13}C NMR (125 MHz, CD_3OD) δ 152.91 (C-3′), 147.62 (C-11), 147.39 (C-3), 146.69 (C-10), 146.63 (C-2), 133.27 (C-7′), 124.86 (C-6′), 122.72 (C-4a), 122.53 (C-12a), 122.05 (C-1a), 118.26 (C-8a), 116.26 (C-12), 116.15 (C-4), 114.17 (C-9), 113.46 (C-1), 111.41 (C-2′), 68.55 (C-13a), 61.61 (C-8), 58.27 (C-6), 46.69 (C-1′), 41.01 (C-4′), 29.83 (C-13), 27.04 (C-5′), 26.0 (C-8′), 24.38 (C-5), 17.91 (7′-Me), 16.79 (3′-Me); SIMS *m/z* $[M]^+$ 436; HRMS *m/z* $[M]^+$ 436.2487 ($C_{27}H_{34}NO_4$ requires 436.2482), *m/z* $[M\text{-}C_{10}H_{16}]^+$ 300.1241 ($C_{17}H_{18}NO_4$ requires 300.1235).

Antimicrobial assay. Antibacterial activities against *E. coli* (ATCC 25923) and *S. aureus* (ATCC 25922) were determined by means of the minimum inhibitory concentration (MIC) using the two-fold serial broth dilution test[7] in liquid nutrient medium and 24-well microplates. MIC was defined as the lowest concentration of the test substance which did not induce visible growth in comparison with a blank experiment. The substances were dissolved in DMSO (final concentration 2.5%). Dilutions with the test medium furnished concentrations from 3.9-250 μg/mL. Benzalkonium and benzethonium chloride were used as standards. The several 24-well plates in which each well contained an appropriate growth medium with a different concentration of the respective test samples were incubated with the test organism. The 24-well plate was incubated at 37°C for 24 h for bacteria. Bacteria tested were preliminarily cultivated in 3% nutrient broth ('Nissui', Japan) at 37°C. All experiments were run in duplicate or triplicate.

***In vitro* cytotoxicity assay (SRB assay).** Cytotoxicity was evaluated using a standard HTCL assay. The assay was carried out according to the standard SRB assay procedure described by Rubinstein *et al.*[10] Samples were tested first by prescreening against KB at 40, 4, and 0.4 μg/mL for a two-day exposure period. Active compounds that inhibited KB cell growth ≥ 40% relative to control at 4 μg/mL were re-tested in a dose-response study against an HTCL panel. Drug stock solutions were prepared in DMSO, and the final solvent concentration was 2% DMSO (v/v), a concentration without effect on cell replication. The human tumor cell line panel constituted of lung carcinoma (A-549), prostate carcinoma (DU-145), epidermoid carcinoma of the nasopharynx (KB), and KBvin (drug resistant), and human promyelocytic leukemia (HL-60). Cells were cultured at 37°C in RPMI-1640 with 100 μg/mL kanamycin and 10% (v/v) fetal bovine serum in a humidified atmosphere containing 5% CO_2. Initial seeding densities varied among the cell lines to ensure a final absorbance reading in control cultures in the range 1-2.5 A_{562} units. Drug exposure was for 3 days, and the ED_{50} value (μg/mL), the drug concentration that reduced the absorbance by 50%, was interpolated from dose-response data. Each test was performed in triplicate, and absorbance readings varied no more than 5%. ED_{50} values determined in independent tests varied no more than 30%.

***In vitro* cytotoxicity assay (MTT assay).** All cell lines were propagated in RPMI-1640 medium

supplemented with 10% (v/v) FBS, 100 U/mL penicillin and 100 μg/mL streptomycin at 37°C in a humidified atmosphere of 5% CO_2 and 95% air. Cell viability was measured by the MTT [3-(4,5-dimethythiazol-2-yl)-2,5-diphenyltetrazolium bromide] colorimetric method. Cells were seeded at densities of 5,000–10,000 cells/well in 96-well tissue culture plates. On day two, cells were treated with test compounds for another 72 h. After drug treatment, attached cells were incubated with MTT (0.5 mg/mL, 1 h) and subsequently solubilized in DMSO. The absorbancy at 550 nm was then measured using a microplate reader. The ED_{50} (μg/mL) is the concentration of agent that reduced cell viability by 50% under the experimental conditions.

***In vitro* cytotoxicity assay (WST-8 assay).** *Cell Cultures.* Human promyelocytic leukemia HL-60 cells were purchased from Dainippon Pharmaceutical Co., Ltd., and maintained in RPMI-1640 medium (Sigma), supplemented with 10% heat-inactivated fetal bovine serum (Sigma) and 2 mM L-glutamine (Sigma) at 37 °C in a humidified atmosphere containing 5% CO_2. The doubling time of cells was approximately 24 h. *WST-8 Assay.*[17] The test compounds were dissolved in DMSO at 50 mM and stored at -20°C. These stock solutions were further diluted with medium from 50 to 0.6 μM prior to use. The final concentrations of DMSO in the culture medium were less than 0.1%. 0.1% DMSO-treated cells were used as the control for all experiments. Cytotoxic effects of test compounds on HL-60 cells were detected by the WST-8 assay. HL-60 cells were plated at 5×10^3 cells/90 μL medium/well into 96-well plates. After overnight growth, cells were treated with various concentrations of test samples for 48 h. Following incubation with test compounds, cell viability was assayed with a Cell Counting Kit-8 (Dojindo Molecular Technologies). Ten microliters of WST-8 solution (5 mM) was added to each well and then incubated for 3 h. The relative viability of cells was determined by measuring the absorbance at 450 nm (reference at 650 nm) with a micro plate reader Anthos Lucy 2 (Aloka Co., Ltd.,). The IC_{50} (μg/mL) is the concentration of agent that reduced cell viability by 50% under the experimental conditions.

***In vitro* EBV-EA activation experiment.**[24] The inhibition of EBV-EA activation was assayed using Raji cells (virus non-producer) which were cultivated in 8% FBS RPMI 1640 medium. The indicator Raji cells (1×10^6 cells/ml) were incubated at 37 °C for 48 h in 1 ml of the medium containing *n*-butyric acid (4 mM, inducer), 32 pmol of TPA (20 ng/ml in DMSO), and 32, 16, 3.2, and 0.32 nmol of the test compound (DMSO solution). Smears were made from the cell suspension. The activated cells were stained by high-titer EBV-EA positive sera from nasopharyngeal carcinoma (NPC) patients and detected by a conventional indirect immunofluorescence technique. In each assay, at least 500 cells were counted, and the experiments were repeated three times. The average extent of EA induction was compared with that of positive control experiments with *n*-butyric acid (4 mM) plus TPA (32 pmol) in which EA

induction was ordinarily around 40%. In this screening method, the cell viability required for the judgment of inhibitory effects was more than 60%.

Determination of the scavenging effect on DPPH radicals.[25] Ethanol (100 μl) was added to individual wells of a 96-well plate. The test compounds were dissolved in DMSO and diluted with EtOH to adjust to 500 μM concentration. The final solvent concentration was 0.25% DMSO (v/v). The sample solution (100 μl) was added to individuals by the 2-fold dilution, and EtOH solution (100 μl) of DPPH radical (final concentration was 100 μM) was also added. The final concentration of the test compounds was from 0.24 to 250 μM. A control sample containing EtOH solution (100 μl) of DPPH radical and EtOH (100 μl) was prepared in the 96-well plate, which was incubated at 25 °C for 30 min in the dark. After incubation, the decrease in absorbance was determined by measuring the optical density change at 550 nm with a microplate luminescence reader Lucy 2 (ALOKA). The radical-scavenging activity expressed as % inhibition against DPPH radical, was calculated according to Yen and Duh (1994): % Inhibition = $[(A_B-A_A)/A_B]\times100$, (A_A is the absorbance of the tested sample after 30 min; A_B is the absorbance of the blank sample). The data presented are the average from two or three independent experiments.

***In vitro* antimalaria screening.** *Parasites.* In all of the studies described in this report, *P. falciparum* strain FCR-3(ATCC 30932) was used.[26, 27] Human serum and erythrocytes were obtained from healthy donors, stored at 4°C and used within 10-14 days from donation. Parasites were cultured in 10% heat inactivated A^+ human erythrocytes and suspended at a 5% hematocrit in RPMI 1640 medium (Gibco, NY) which contained 50 mg of gentamicin per liter, and 10% group A^+ human serum and was buffered with 25 mM *N*-2-hydroxyethylpiperazine-*N'*-2-ethansulfonic acid (HEPES, pH 7.4) and 25 mM $NaHCO_3$. Cultures were maintained at 37 °C in a gas mixture of 5% O_2-5% CO_2-90% nitrogen.[28] *Drug testing.* Various concentrations of compounds, suspended in 10 μl of distilled water, were added to individual wells of a 24-well plate. Erythrocytes with 0.3% parasitemia were added to each well in 990 μl of culture medium to give a final hematocrit of 3%. The plates were incubated at 37 °C for 72 h under 5% O_2-5% CO_2-90% nitrogen. Parasite morphology in drug-treated culture after 72 hrs was measured by staining with Giemsa, and the number of parasitized red blood cells per 10,000 erythrocytes was counted and growth rates were calculated. All compounds were run in duplicate at each concentration. Drug-free control cultures were run simultaneously. All data points represent means of at least two experimental tests. The 50% inhibitory concentration (EC_{50}) was defined by comparison with drug-free controls incubated under the same conditions.[29,30] *Mammalian cells.* A wild-type mouse FM3A cell line (subclone F-28-7) was supplied by the Health Sciences Research Resources Bank (Osaka, Japan).

FM3A cells were maintained in suspension culture at 37°C in a 5% CO_2 atmosphere in plastic bottles containing ES medium (Nissui Pharmaceutical Co., Ltd., Tokyo, Japan) supplemented with 2% heat-inactivated fetal bovine serum (Gibco, NY).[31, 32] *Toxicity to mammalian cells.* The cell line grew with a doubling time of about 12 h. Before being exposed to drugs, cells were seeded at 990 μl of a density of 5×10^4 cells/ml, and various concentrations of compounds dispensed in 10 μl of distilled water were added to individual wells of a 24-well plate. The plates were incubated at 37 °C in a 5% CO_2 atmosphere for 48 hrs. Cell numbers were measured using a blood cell counter CC-108 (Toa Medical Electric Co., Japan). All data points represent means of at least two experimental tests. The 50% inhibitory concentration (IC_{50}) is defined by comparison with that of drug-free controls incubated under the same conditions. Cell growth inhibition is the index of cytotoxicity including cytostatic activity of the test compounds. *Selective toxicity.* Selective toxicity was estimated from the ratio (IC_{50}/EC_{50}) of the drug concentrations necessary to inhibit the growth rate of cells to 50% of the growth value between the malaria parasites and mouse mammary FM3A cells which served as a model host.[33]

Anti-HIV assay. The T cell line H9 was maintained in continuous culture with complete medium (RPMI 1640 with 10% fetal calf serum [FCS] supplemented with L-glutamine) at 5% CO_2 and 37 °C. Aliquots of this cell line were used in experiments only when in the log-phase of growth. Test samples were first dissolved in DMSO. The following are the final drug concentrations routinely used for screening: 100, 20, 4, and 0.8 μg/mL. For active agents, additional dilutions are prepared for subsequent testing so that accurate EC_{50} values (see definition below) could be achieved. As the test samples were being prepared, an aliquot of H9 cells was infected with HIV-1 (IIIB isolate), while another aliquot was mock-infected with complete medium. The mock-infected sample was used for toxicity determinations (IC_{50}, see definition below). The stock virus used for these studies typically had a $TCID_{50}$ value of 10^4 Infectious Units (IU)/mL. The appropriate amount of virus for a multiplicity of infection between 0.1 and 0.01 IU/cell was added to the first aliquot of cells. The other aliquot of cells received only culture medium and was then incubated under identical conditions to the HIV-infected cells. After 4 h incubation at 37 °C and 5% CO_2, both cell populations were washed three times with fresh medium and then added to the appropriate wells of a 24-well plate containing various concentrations of the test drug or culture medium (positive infected control/negative-control drug). In addition, AZT was also assayed during each experiment as a positive-control drug. The plates were incubated at 37 °C and 5% CO_2 for 4 days. Cell-free supernatants were collected on day 4 and tested by an in-house p24 antigen ELISA assay; p24 antigen is a core protein of HIV and, therefore, is an indirect measure of virus present in the supernatants. Toxicity was determined by performing cell counts by a coulter counter on the mock-infected cells, which had received either culture medium (no toxicity), test sample or AZT. If a

test sample had suppressive capability and was not toxic, its effects wre reported in the following terms: IC_{50}, the concentration of test sample that was toxic to 50% of the mock-infected cells; EC_{50}, the concentration of the test sample that was able to suppress HIV replication by 50%; and therapeutic index (TI), the ratio of IC_{50} to EC_{50}.

ACKNOWLEGEMENT

This work was supported in part by a grant from the National Cancer Institute Grant CA-17625 awarded to K. H. Lee.

REFERENCES.

1. F. Pojer, E. Wemakor, B. Kammerer, H. Chen, C. T. Walsh, S.-M. Li, and L. Heide, *Proc. Natl. Acad. Sci.*, 2003, USA 100, 2316.
2. D. J. Edwards and W. H. Gerwick, *J. Am. Chem. Soc.*, 2004, **126**, 11432.
3. T. Kuzuyama, J. P. Noel, and S. B. Richard, *Nature,* 2005, **435**, 983.
4. M. Tello, T. Kuzuyama, L. Heide, J. P. Noel, S. B. Richard, *Cell Mol. Life Sci.*, 2008, **65**, 1459.
5. S.-M. Li, *Phytochemistry*, 2009, **70**, 1746.
6. T. Usui, M. Kondoh, C. B. Cui, T. Mayumi, and H. Osada, *Biochem. J.*, 1998, **333**, 543.
7. B. Botta, A. Vitali, P. Menendez, D. Misiti, and M. G. Delle, *Curr. Med. Chem.*, 2005, **12**, 717.
8. K. Iwasa, M. Moriyasu, Y. Tachibana, H.-S Kim, Y. Wataya, W. Wiegrebe, K. F. Bastow, L. M. Cosentino, M. Kozuka, and K. H. Lee, *Bioorg. Med. Chem.*, 2001, **9**, 2871.
9. W. H. Cui, K. Iwasa, H. Tokuda, A. Kashihara, Y. Mitani, T. Hasegawa, Y. Nishiyama, M. Moriyasu, H. Nishino, M. Hanaoka, C. Mukai, and K. Takeda, *Phytochemistry*, 2006, **67**, 70.
10. L. V. Rubinstein, R. H. Shoemaker, K. D. Paull, R. M. Simo, R. S. Tosini, P. Skehan, P. A.Scudiero, A. Monks, and M. R. Boyd, *J. Natl. Cancer Inst.*, 1990, **82**, 1113.
11. Y. Ito, S. Yanase, J. Fujita, T. Harayama, T. Takashima, and H. Imanaka, *Cancer Lett.*, 1981, **13**, 29.
12. Y. Kashiwada, F. Hashimoto, L. M. Cosentino, C. H. Chen, P. E. Garrett, and K. H. Lee, *J. Med. Chem.*, 1996, **39**, 1016.
13. K. Iwasa, S. Okada, Y. Nishiyama, S. Takeuchi, M. Moriyasu, C. Tode, M. Sugiura, A. Takeuchi, H. Tokuda, K. Takeda, Y.-N. Liu, P-.C. Wu, K. F. Bastow, T. Akiyama, and K. H. Lee, *Heterocycles*, 2009, **77**, 1355.
14. B. Delley, *J. Chem. Phys.*, 1990, **92**, 508.
15. B. Delley, *J. Chem. Phys.*, 2000, **113**, 7756.
16. T. Mosmann, *J. Immunol. Methods*, 1983, **16**, 55.

17. M. Ishiyama, Y. Miyazono, K. Sasamoto, Y. Ohkura, and K. Ueno, *Taranta*, 1997, **44**, 1299.
18. A. Murakami, H. Ohigashi, and K. Koshimizu, *Biosci. Biotechnol. Biochem.*, 1996, **60**, 1.
19. K. Yasukawa, M. Takido, T. Matsumoto, M. Takeuchi, and S. Nakagawa, *Oncology*, 1991, **48**, 72.
20. T. Konoshima, M. Takasaki, M. Kozuka, T. Nagao, H. Okabe, N. Irino, T. Nakasumi, H. Tokuda, and H. Nishino, *Biol. Pharm. Bull.*, 1995, **18**, 284.
21. J. P. Perdew and Y. Wang, *Phys. Rev. B*, 1992, **45**, 13244.
22. A. D. Becke, *J. Chem. Phys.*, 1988, **88**, 2547.
23. C. Lee, W. Yang, and R. G. Parr, *Phys. Rev. B,* 1988, **37**, 786.
24. Y. Takemura, M. Ju-ichi, C. Ito, H. Furukawa, and H. Tokuda, *Planta Med.*, 1995, **61**, 366.
25. M. S. Blois, *Nature*, 1958, **181**, 1199.
26. W. Trager and J. B. Jensen, *Science,* 1976, **193**, 673.
27. J. B. Jensen, W. Trager, and J. Doherty, *Exp. Parasitol*, 1979, **48**, 36.
28. R. W. Winter, K. A. Cornell, L. L. Johnson, M. Ignatushchenko, D. J. Hinrivhs, and M. K. Riscoe, *Antimicrob Agents Chemother.*, 1996, **40**, 1408.
29. A. V. O. Ofulla, V. C. N. Okoye, B. Khan, J. I. Githure, C. R. Roberts, A. J. Johnson, and S. K. Martin, *Am. J. Trop. Med. Hyg.*, 1993, **49**, 335.
30. H. Asahi and T. Kanazawa, *Parasitology*, 1994, **109**, 397.
31. A. Yoshioka, S. Tanaka, O. Hiraoka, Y. Koyama, Y. Hirota, D. Ayusawa, T. Seno, C. Garrett, and Y. Wataya, *J. Biol. Chem.*, 1987, **262**, 8235.
32. Y. Wataya and O. Hiraoka, *Biochem. Biophys. Res. Commun,* 1984, **123**, 677.
33. I. S. Shin, H. Tanifuji, Y. Arata, Y. Morizawa, T. Nakayama, and Y. Wataya, *Parasitol. Res.*, 1995, **81**, 622.

the FEBS Journal

Association of RNase L with a Ras GTPase-activating-like protein IQGAP1 in mediating the apoptosis of a human cancer cell-line

Akira Sato[1], Tomoharu Naito[1], Akiko Hiramoto[1], Kazato Goda[1], Takuya Omi[1], Yukio Kitade[2], Takuma Sasaki[3], Akira Matsuda[4], Masakazu Fukushima[1], Yusuke Wataya[1] and Hye-Sook Kim[1]

1 Department of Molecular Drug Informatics, Faculty of Pharmaceutical Sciences, Okayama University, Japan
2 Department of Biomolecular Science, Faculty of Engineering, Gifu University, Japan
3 Department of Bioorganic Chemistry, School of Pharmacy, Aichi Gakuin University, Nagoya, Japan
4 Department of Medicinal Chemistry, Faculty of Pharmaceutical Sciences, Hokkaido University, Sapporo, Japan

Keywords
apoptosis; ECyd; focused proteomics; IQGAP1; RNase L

Correspondence
H.-S. Kim, Faculty of Pharmaceutical Sciences, Okayama University, Tsushima, Okayama 700-8530, Japan
Fax: +81 86 251 7974
Tel: +81 86 251 7975
E-mail: hskim @cc.okayama-u.ac.jp

Note
Akira Sato and Tomoharu Naito contributed equally to this work

(Received 14 April 2010, revised 28 July 2010, accepted 26 August 2010)

doi:10.1111/j.1742-4658.2010.07833.x

Mammalian intracellular ribonuclease L (RNase L) is a latent endoribonuclease that functions against viral infections as an apoptosis-inducing protein, and its activity requires intracellular 5′-end-triphosphorylated-2′,5′ oligoadenylates (2-5A) as an activator. Previously, we showed that RNase L can be activated in human cancer cell line HT1080 by an RNA polymerase I inhibitor, 1-(3-*C*-ethynyl-β-D-*ribo*-pentofuranosyl)cytosine (3′-ethynylcytidine; ECyd). In ECyd-treated cells, knockdown of the RNase L resulted in a marked decrease in c-jun N-terminal kinase (JNK) phosphorylation, thereby inhibiting apoptosis. We investigate RNase L binding partners by focused proteomic approach using immunoprecipitation with anti-RNase L IgG and mass spectrometry. We found that the IQ motif-containing Ras GTPase-activating-like protein 1 (IQGAP1) can associate with RNase L, and that phosphorylation occurs on the IQGAP1. ECyd-induced JNK phosphorylation and apoptosis were inhibited when IQGAP1 was knocked down with a small interfering RNA. These results raise the interesting possibility that the RNase L–IQGAP1 association may regulate JNK phosphorylation in RNase L-madiated apoptosis. It is likely IQGAP1 works as a regulator in apoptosis.

Structured digital abstract

- MINT-7990574: *RNaseL* (uniprotkb:Q05823) *physically interacts* (MI:0914) with *Kinesin-like protein KIF23* (uniprotkb:Q02241) and *Ras GTPase-activating-like protein IQGAP1* (uniprotkb:P46940) by *anti bait coimmunoprecipitation* (MI:0006)
- MINT-7990598: *RNaseL* (uniprotkb:Q05823) *physically interacts* (MI:0915) with *IQGAP1* (uniprotkb:P46940) by *anti bait coimmunoprecipitation* (MI:0006)

Introduction

A cellular RNA-hydrolysing enzyme RNase L has an intriguing function in inducing cell death. This mammalian protein is a latent endonuclease that can work against viral infections by inducing apoptotic death of the infected cell [1,2]. This particular role of the nuclease is a current focus of attention for many

Abbreviations
2-5A, 5′-end-triphosphorylated-2′,5′ oligoadenylates; ECyd, 1-(3-*C*-ethynyl-β-D-*ribo*-pentofuranosyl)cytosine (3′-ethynylcytidine); IQGAP1, IQ motif-containing Ras GTPase-activating-like protein 1; JNK, c-jun N-terminal kinase; siRNA, small interfering RNA.

laboratories [3–9]. In order to initiate the apoptosis, RNase L has to be activated by intracellular 5′-end-triphosphorylated-2′,5′-oligoadenylates (2-5A). In this activation, 2-5A binds to RNase L at its N-terminal ankyrin repeat domain, the 2-5A–RNase L complex then causes damage to the mitochondrial membrane, eventually leading to apoptotic cell death. Elucidation of the details in this intracellular event is important, for this 2-5A-RNase L pathway is implicated in responses to not only viral infections, but also several types of external stimuli [1,3–9]. We are particularly interested in the possibility of clarifying a case of an anticancer drug action in terms of the 2-5A-RNase L pathway. An RNA synthesis inhibitor, 1-(3-*C*-ethynyl-β-D-*ribo*-pentofuranosyl)cytosine (3′-ethynylcytidine; ECyd), has been shown to exhibit cancer cell-selective toxicity by causing apoptotic cell death [10–12]. Our recent work has shown that activated RNase L is involved in this process and that the events ensuing the RNase L activation are c-jun N-terminal kinase (JNK) activation, followed by mitochondrial membrane damage, leading to cell apoptosis [13].

We have attempted to find specific cellular proteins that have affinities to RNase L with a view to elucidating the mechanism of the apoptotic process. We performed this investigation using focused proteomic means, i.e. coimmunoprecipitation with an anti-RNase L IgG, coupled with analysis by nano-LC MS/MS to identify the coprecipitated proteins. Here, we describe the identification of IQ motif-containing Ras GTPase-activating-like protein 1 (IQGAP1), which bears a strong affinity to RNase L. Furthermore, we found that the IQGAP1–RNase L complex has newly incorporated phosphate group(s) on the IQGAP1.

Participation of IQGAP1 in this apoptotic cell death was verified using small interfering (si)RNA knockdown experiments. Administration of an siRNA targeting the RNase L gene effectively prevented apoptosis, and administration of siRNA against IQGAP1 had the same effect. Based on these results, we now propose a process in which the partnership between RNase L and IQGAP1 operates for apoptosis.

Results and Discussion

Identification of RNase L binding protein

We recently reported that siRNA-mediated knockdown of RNase L markedly decreased the phosphorylation of JNK and inhibited apoptosis in ECyd-treated HT1080 cells [13]. This suggested that RNase L might possess a phosphorylating function. It is known that the RNase L molecule has a kinase homology domain [1,2], the function of which remains unknown. It is possible, therefore, that the JNK might be bound to and then phosphorylated by RNase L. This supposition led us to investigate whether JNK might be bound to an RNase L that has been fixed on an antibody against RNase L. Thus, we performed immunoprecipitation of ECyd-treated HT1080 cell lysate by adding an anti-RNase L IgG. As a control, we used a lysate from cells not treated with ECyd. The precipitates were solubilized and analysed by SDS gel electrophoresis. The results are shown in Fig. 1 (with Fig. S1). We cut out 15 protein bands as having different intensities between the anti-RNase L IgG immunoprecipitants (RNase L binding proteins; Fig. 1, lane 2 and/or lane 4) and the Protein G agarose precipitation for nonspecific binders (Protein G agarose beads binding proteins; Fig. 1, lane 1 and/or lane 3). The marked bands (no. 1–8 and 2′-8′) were those that had been strongly bound to RNase L (Fig. 1, lanes 2 and 4). In the proteomic analysis using nano LC-MS/MS, no JNK was detected among the binders. Instead, six proteins (i.e. myosin-9, IQGAP1, myosin-IE, immunoglobulin protein and kinesin-like protein KIF23, in addition to RNase L) were identified in these 15 bands. We also obtained complementary data for the identification of the focused protein bands based on MS/MS experiments (Table 1). Myosin-9 was present in the band 1 and also in the Protein G precipitations lane (nonspecific binding protein). Myosin-i.e and its isoform were present in bands 3–6 and 3′–6′. The myosin-IE might have been directly recognized by anti-RNase L IgG (Fig. 2B, pointed by an asterisk). Thus, we consider that the myosin-9 and myosin-IE were non-specifically bound to Protein G agarose beads. In this experiment, RNase L was identified in bands 8 and 8′. Therefore, we thought that IQGAP1 may be a specific RNase L binding partner, as found in bands 2 and 2′.

IQGAP1 is a 190 kDa molecular scaffold containing several domains that are required to interact with numerous proteins [14–16]. These motifs include a calponin homology domain (calcium-binding domain of calponin), four IQ (Ile–Gln) motifs and a Ras GTPase-related domain. Known targets for IQGAP1 include calmodulin, Cdc42, Rac1, actin, β-catenin, E-cadherin, S100B, CLIP-170, MEK1/2 and ERK1/2. Through interactions with these proteins, IQGAP1 participates in multiple cellular activities, including transcription, cell–cell adhesion and regulation of the cytoskeleton [14–16]. In addition, Li *et al.* [17] reported that IQGAP1 is highly phosphorylated in human cells and that IQGAP1 is a target for protein kinase C.

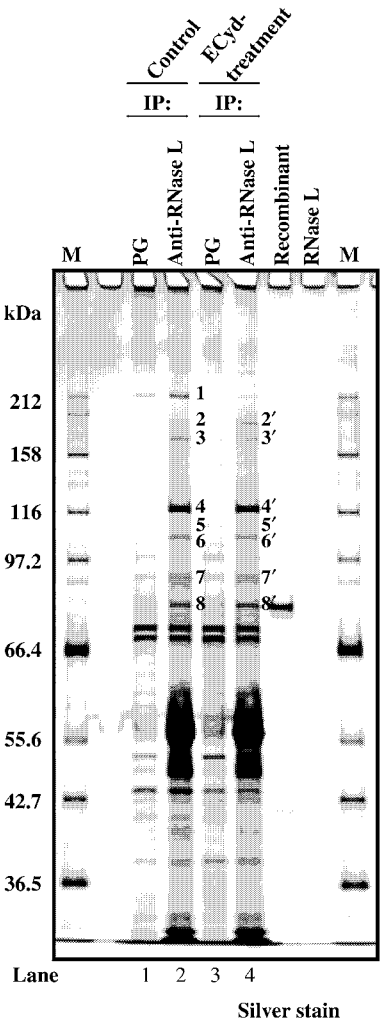

Fig. 1. Identification of RNase L binding proteins. Immunoprecipitation (IP) was done for RNase L from HT1080 cell extracts that had been treated with or without ECyd 1.3 μM for 24 h. Samples were loaded on 7.5% (w/v) SDS/PAGE and analysed by silver staining. The proteins analysed (bands 1–8 and 2′–8′) were excised from the silver-stained gel and digested in gel with trypsin. Extracted peptides were analysed by nano LC-MS/MS. PG; IP with Protein G only. Anti-RNase L; IP with anti-RNase L IgG. M; Protein size marker. All identified proteins are presented in Table 1.

To compare the RNase L–IQGAP1 association between ECyd-treated and -untreated cells, western blotting was performed with anti-IQGAP1 and anti-RNase L IgG individually. The intensities of both total IQGAP1 and total RNase L protein bands were not different between ECyd-treated and -untreated cells (Fig. 2A). It is notable, however, that the level of the IQGAP1 associated with RNase L was increased significantly in ECyd-treated cells (Fig. 2B). We measured the ratio of IQGAP1 associated with RNase L to total IQGAP1, and the results showed that 12% and 5% of total IQGAP1 was associated with RNase L in ECyd-treated cells and untreated cells, respectively (Fig. 2A,B).

To validate the interaction between RNase L and IQGAP1, we analysed the effect of RNase L knockdown on the association with these proteins. In the transfection with the RNase L-siRNA, the protein-band intensity of RNase L was decreased both in the cell lysate (A6) and in the immunoprecipitates (B6). The IQGAP1 in the immunoprecipitates was increased in ECyd-treated cells (B1, B2). The intensity of the IQGAP1 protein band in the immunoprecipitates of ECyd-treated RNase L knocked-down cells became the same as that in the untreated stage (B1, B2, B3). Interestingly, the IQGAP1 protein band in the whole-cell lysate was not different between the Ecyd treatment (A2) and RNase L knockdown (A3). siRNA with a four-base mismatch sequence (mismatch-siRNA; nonsilencing siRNA) had no effect on the interaction or the protein level (data not shown). These findings suggest that the association of RNase L and IQGAP1 was enhanced by ECyd treatment.

Phosphorylation of IQGAP1 after treatment with ECyd

We investigated the phosphorylation levels of endogenous IQGAP1 in ECyd-treated cells by using [^{32}P]-orthophosphate uptake experiments. Proteins were extracted from the cells and immunoprecipitated with anti-RNase-L IgG. From the resulting precipitate, proteins were eluted and resolved by PAGE. After transferring onto poly(vinylidene difluoride) membranes, the proteins were visualized by means of autoradiography. For comparison, whole-cell lysate without immunoprecipitation was submitted to the same analysis. The ^{32}P-labelled protein band was found in the position of IQGAP1 from ECyd-treated whole-cell lysates (Fig. 3A). The ^{32}P-labelled protein band was not detected in cells without ECyd treatment (Fig. 3A). However, immunoprecipitate experiments demonstrated that IQGAP1 associated with activated RNase L was labelled and the labelling with [^{32}P]-orthophosphate was high (fivefold higher: control, 15.70 ± 0.01; ECyd, 84.50 ± 3.82) in ECyd-treated cells but not in untreated cells (Fig. 3B).

Next, we investigated the mechanisms of IQGAPI phosphorylation regulated by RNase L in ECyd-treated cells. High levels in expression of IQGAP1 and RNase L were observed for cells in the untreated, in 2-5A-treated or ECyd-treated stages (Fig. 4A, lanes 1–3). However, the protein levels of phosphorylated

Table 1. Identification of RNase L binding protein.

Band no.	Identified protein	Accession no.[a]	Distinct peptides[b]	Score[c]	Sequence coverage	Theoretical M_r	Theoretical pI
1	Myosin-9	P35579	90	1452.88	49	226402.2	5.5
2	Ras GTPase-activating-like protein IQGAP1	P46940	35	434.16	25	189252.9	6.08
3	Myosin-IE	Q12965	15	184.38	17	127041.6	9.01
4	Myosin-IE	Q12965	48	714.46	44	127041.6	9.01
5	Myosin-IE	Q12965	10	132.27	11	127041.6	9.01
6	Myosin-IE	Q12965	12	165.84	15	127041.6	9.01
	Kinesin-like protein KIF23	Q02241	15	198.87	22	98106	8.69
7	Not identified[d]	–	–	–	–	–	–
8	2-5A-dependent ribonuclease (RNaseL)	Q05823	18	204.41	22	83533.2	6.2
2′	Ras GTPase-activating-like protein IQGAP1	P46940	27	357.81	20	189252.9	6.08
3′	Myosin-IE	Q12965	17	231.56	19	127041.6	9.01
4′	Myosin-IE	Q12965	42	640.24	41	127041.6	9.01
5′	Myosin-IE	Q12965	6	78.28	7	127041.6	9.01
6′	Myosin-IE	Q12965	12	189.97	17	127041.6	9.01
	Kinesin-like protein KIF23	Q02241	7	118.22	11	98106	8.69
7′	Not identified	–	–	–	–	–	–
8′	2-5A-dependent ribonuclease (RNaseL)	Q05823	26	353.11	33	83533.2	6.2

[a] Accession number from Swiss-prot protein database. [b] Number of matched peptides that in the an *in silico* the protein sequence. [c] Mill MS proteomic workbench prpbability-based peptide score calculated for MS/MS results. [d] No specific proteins were identifiable in MS/MS experiments.

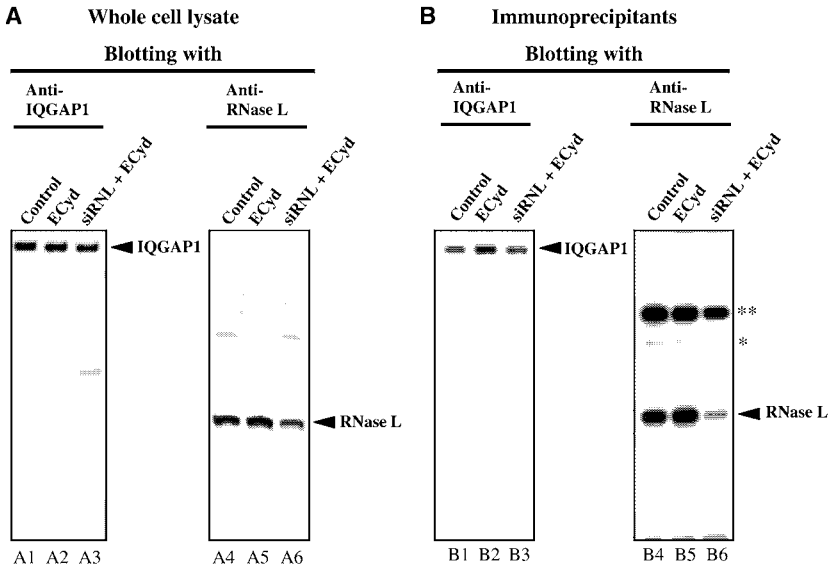

Fig. 2. Association of RNase L and IQGAP1. (A) Western blotting of whole-cell lysate. (B) Western blotting of immunoprecipitants. HT1080 cells (1.2×10^5) were transfected with RNase L-siRNA 5 nM in the presence of Lipofectamine 2000 2 $\mu g \cdot mL^{-1}$ for 24 h according to the manufacturer's protocol (Invitrogen), and then treated with ECyd 1.3 μM for 32 h. After ECyd treatment, cell lysates were immunoprecipitated with anti-RNase L IgG (B). Western blotting (WB) was probed with anti-RNase L and anti-IQGAP1 IgG, individually. The asterisks indicated nonspecific coimmunoprecipitated bands that cross-reacted with anti-RNase L IgG. Data are representative of at least three independent experiments. Control; Lipofectamine-only treatment, ECyd; ECyd treatment, siRNL+ECyd; RNase L-siRNA + ECyd treatment.

IQGAP1 in the immunoprecipitates were significantly higher both in 2-5A-treated and ECyd-treated cells in comparison with the control (Fig. 4A, lanes 4–6). In addition, the knockdown of RNase L markedly decreased total and phosphorylated IQGAP1 protein levels in the immunoprecipitates (Fig. 4B, lanes 3, 7).

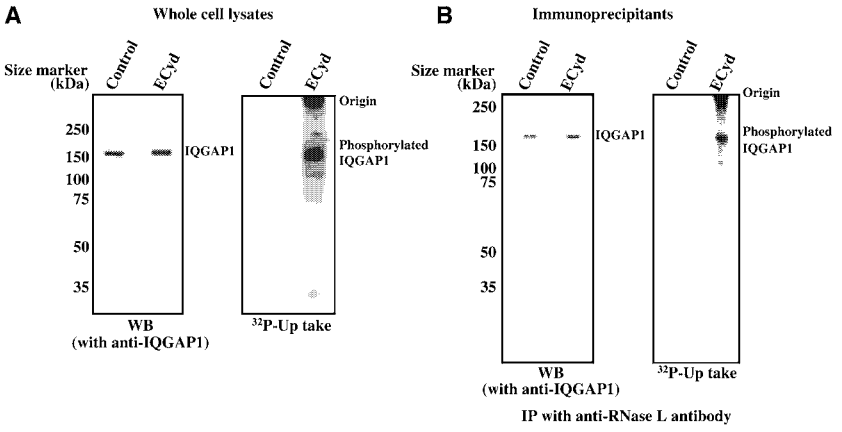

Fig. 3. Phosphorylation of IQGAP1 in ECyd-treated cells. HT1080 cells were incubated with [^{32}P]-orthophosphate in the presence of ECyd. Cells were solubilized and immunoprecipited with anti-RNase L IgG. (A) Analysis of whole-cell lysates: (left) western blotting with anti-IQGAP1 IgG, (right) ^{32}P-radioactivity. (B) Analysis of immunoprecipitants: (left) western blotting with anti-IQGAP1 IgG, (right) ^{32}P-radioactivity. The data represent three independent experiments.

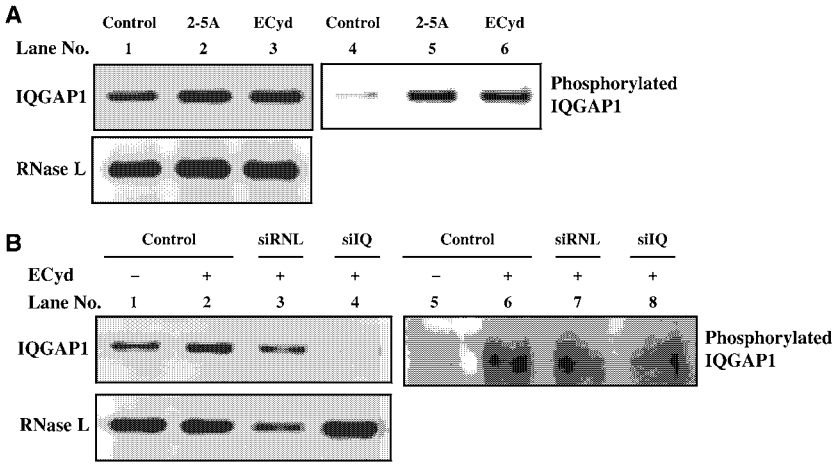

Fig. 4. Participation of RNase L in phosphorylating IQGAP1. (A) HT1080 cells were transfected with 2-5A(pApApA) 1 μM for 6 h (lanes 2, 5) and treated with ECyd 1.3 μM for 24 h (lanes 3, 6). Cell lysates were immunoprecipitated with anti-RNase L IgG, the precipitate was solubilized and the solution was submitted to gel electrophoresis. Western blotting was carried out with anti-IQGAP1 (upper left), anti-RNase L (lower left), and anti-phosphoserine/threonine/tyrosine sera (upper right). (B) HT1080 cells were transfected with siRNL; RNase L-siRNA 5 nM (lanes 3, 7) or siIQ; IQGAP1-siRNA 10 nM (lanes 4, 8) in the presence of Lipofectamine 2000 2 μg·mL^{-1} for 24 h, prior to ECyd 1.3 μM treatment. Cell lysates were immunoprecipitated with anti-RNase L IgG, the precipitate was solubilized and the solution was submitted to gel electrophoresis. Western blotting was carried out with anti-IQGAP1 (upper left) anti-RNase L (lower left), and anti-phosphoserine/threonine/tyrosine sera (upper right). The data represent three independent experiments.

Transfection of IQGAP1 siRNA led to decreases in both total IQGAP1 and phosphorylated IQGAP1 without affecting RNase L expression (Fig. 4B, lanes 4, 8).

In total, these results indicate that ECyd treatment can result in a distinctive increase in the proportion of phosphorylated IQGAP1 in the RNase L–IQGAP1 complex.

Prevention of ECyd-induced JNK phosphorylation and apoptosis by knocking down IQGAP1

The possibility that IQGAP1 functions to transmit apoptosis signals from RNase L to the JNK pathway was investigated. First, we explored the effect of IQGAP1 knockdown in ECyd-induced apoptosis. With ECyd-treated cells, expression of IQGAP1 was suppressed on administration of IQGAP1 siRNA and the number of apoptotic cells decreased, as measured by the TUNEL assay. Thus, we observed that the knockdown efficacy for IQGAP1 protein was > 60% by IQGAP1 siRNA transfection compared with that by mismatch-siRNA transfection (Figs 5A and S2). The number of ECyd-induced apoptotic cells was drastically decreased when IQGAP1 was knocked-down. By contrast, mismatch-siRNA transfection had no effect on ECyd-induced apoptosis (Fig. 5B,C). Next, in order to analyse the effect of IQGAP1 on

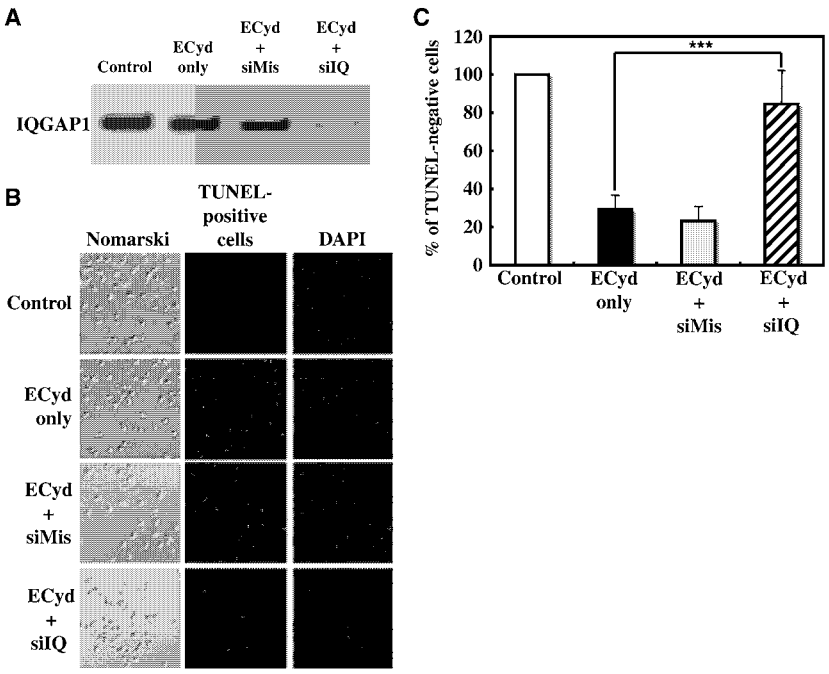

Fig. 5. Suppression of apoptosis in ECyd-treated cells with siRNA against IQGAP1. (A) HT1080 cells were transfected with siIQ; IQGAP1-siRNA 10 nM and siMis; mismatch-siRNA 10 nM in the presence of Lipofectamine 2000 2 $\mu g \cdot mL^{-1}$ for 24 h, and then treated with ECyd 1.3 μM for 32 h followed by western blot analysis. (B) Detection of apoptotic cells using the TUNEL assay. Apoptotic cells are shown in the green panel. Nuclei were stained with 4′,6-diamidino-2-phenylindole dihydrochloride. (C) Bar graph shows the percentage of TUNEL-negative cells in ECyd-treated HT1080 cells with or without siIQ transfection. $***P < 0.05$ total number of cells was counted at least 300 cells. Control, Lipofectamine 2000 treated cells.

the phosphorylation of JNK in HT1080 cells, siRNA for IQGAP1 was used to knockdown the IQGAP1 protein expression. The level of phosphorylated JNK was decreased in knocked-down cells, whereas the JNK-phosphorylation remained high in both the ECyd-only and ECyd-plus-mismatch-siRNA treatments. However, the fluorescence levels that represented the total JNK were the same in all of these treatments (Fig. 6). These findings indicate that IQGAP1 contributes to ECyd-induced JNK phosphorylation and apoptosis. Therefore, we consider that the association with RNase L and IQGAP1 plays a critical role in the apoptotic signaling pathway. Li *et al.* [9] suggested that JNK is an essential molecule in the apoptosis mediated by RNase L. Our recent work demonstrated that the knockdown of the RNase L in the ECyd-treated HT1080 cells dramatically decreased the phosphorylation of JNK, thereby inhibiting mitochondria-mediated apoptosis [13]. Therefore, the complex of IQGAP1 and RNase L may be regulating JNK phosphorylation in the RNase L-mediated apoptosis. Given the report of the IQGAP1 phosphorylation by protein kinase C [17], we think it possible that the observed IQGAP1 phosphorylation in the apoptosis may be mediated by either protein kinase C or/and by other proteins (e.g. RNase L). We are currently investigating the kinase activity of RNase L using *in vitro* assays (details to be published elsewhere). It is important to further investigate the mechanisms involved in this 'RNase L controlled IQGAP1 JNK phosphorylation' in apoptosis.

Conclusions

We have demonstrated that RNase L interacts with a partner, IQGAP1, and that this interaction is involved in promoting ECyd-induced apoptosis. In addition, we have shown that in this process IQGAP1 phosphorylation is enhanced. As the scheme in Fig. 7 indicates, we consider that the ECyd-induced apoptotic signal pathway is mediated by an RNase L–IQGAP1 association.

Materials and methods

Materials

ECyd was synthesized as described previously [10]. Lipofectamine 2000 was purchased from Invitrogen (Carlsbad, CA, USA). Human recombinant RNase L was prepared as described by Yoshimura *et al.* [18] and 2-5A was synthesized according to Lesiak and Torrence [19]. The IQGAP1 and phosphoserine/threonine/tyrosine antibodies were from Upstate Biotechnology (Lake Placid, NY, USA) and Abcam (Cambridge, UK), respectively. Preparation of mAb to human RNase L and synthesis of siRNA were performed as reported previously [20]. The siRNA against RNase L (RNase L-siRNA) and the control siRNA with four-base mismatch (mismatch-siRNA) used were as follows: RNase L-siRNA, 5′-GCUGUUCAAAACGAAGAUGTT-3′ 3′-TTCGACAAGUUUUGCUUCUAC-5′; mismatch-siRNA, 5′-GCUAUUCUAAAGGAAUAUGTT-3′ 3′-TTCGAUAAGAUUUCCUUAUAC-5′. The TT dinucleotide attached to

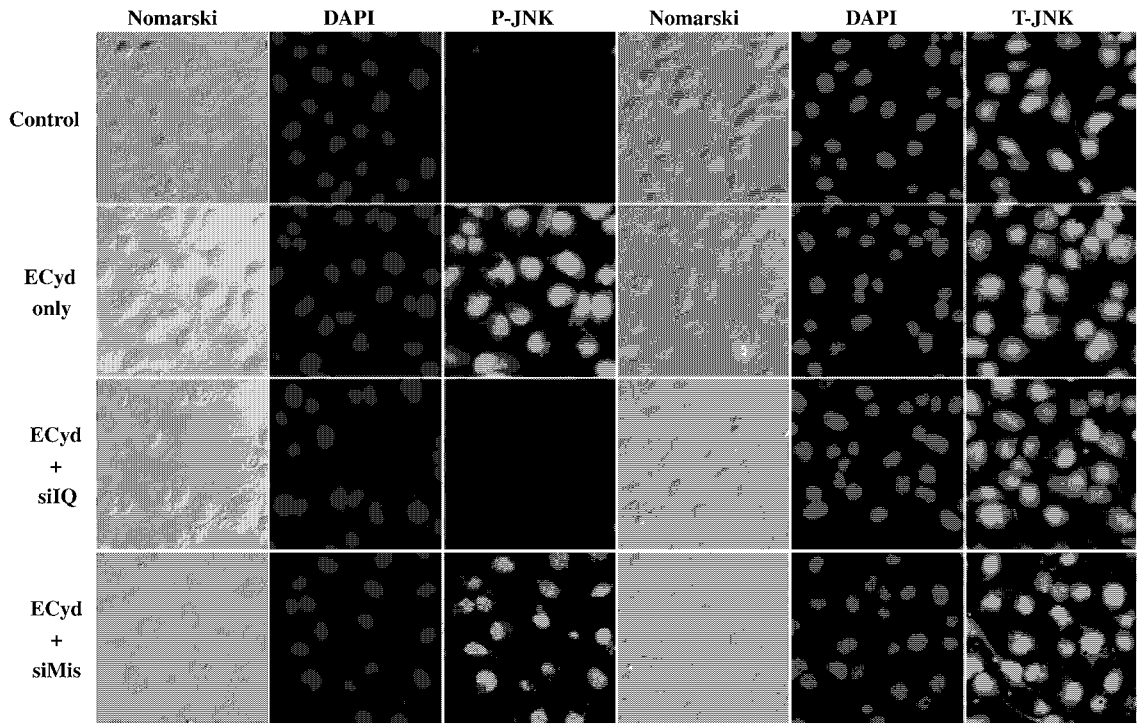

Fig. 6. Inhibition of JNK phosphorylation in ECyd-treated cells with siRNA against IQGAP1. HT1080 cells were transfected with siIQ; IQGAP1-siRNA 10 nM and siMis; mismatch-siRNA 10 nM in the presence of Lipofectamine 2000 2 $\mu g \cdot mL^{-1}$ for 24 h, and then treated with ECyd 1.3 μM for 24 h followed by immunofluorescence staining. Phosphorylated JNK (P-JNK) and total JNK (T-JNK) were detected by immunofluorescence with specific antiboby (Cell Signaling Technology). Nuclei were stained with 4′,6-diamidino-2-phenylindole dihydrochloride. Green fluorescence represents IF: P-JNK and T-JNK. Control indicates lipofectamine-only treated cells. The set of data in a given column were obtained from image-photos taken with a fixed exposure time.

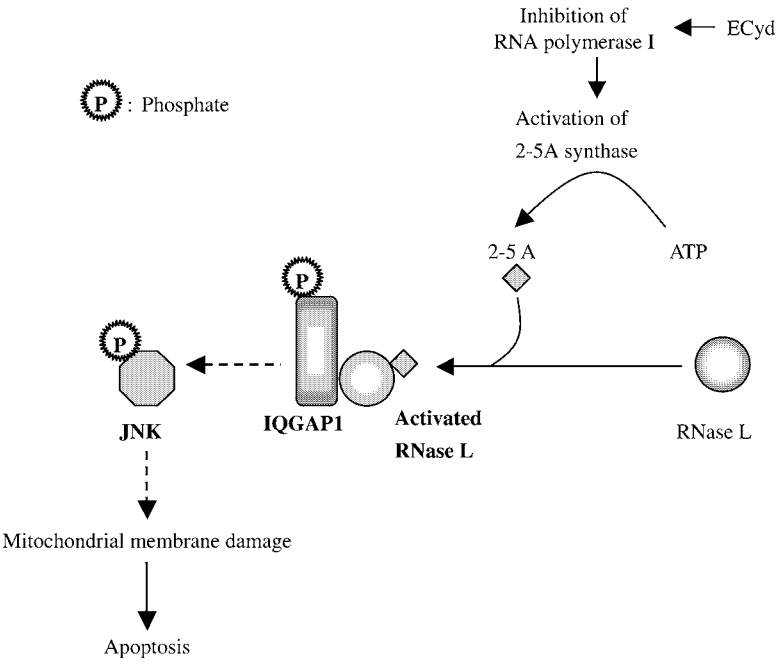

Fig. 7. Scheme of apoptotic signal pathway mediated by RNase L–IQGAP1 association in ECyd-treated cells. ECyd, an RNA polymerase I inhibitor, has potent cytotoxic activity against human cancer cells. In ECyd-treated cells, RNase L is activated and involved in JNK phosphorylation, which then induces mitochondria-dependent apoptosis. In the cell-death mechanisms, we hypothesize that RNase L mediates the phosphorylation of IQGAP1, the phosphate is then transferred to JNK, and the JNK-phosphorylation triggers apoptosis.

each of these oligonucleotides at their 3′-overhang was a 2′-deoxythymidine dimer with a carbamate linkage. It is known that carbamate internucleoside linkages enhance the siRNA silencing activities [20]. The IQGAP1-siRNA (Hs_IQGAP1_5_HP Validated siRNA, Catalog number SI02655268) and Nonsilencing-siRNA (AllStars Negative Control siRNA, Catalog number 1027280) were purchased from Qiagen (Hilden, Germany). ^{32}P-Orthophosphate, carrier-free, was from Perkin–Elmer (Waltham, MA, USA).

Cell culture and transfection for gene silencing

The human fibrosarcoma HT1080 cell line (American Type Culture Collection, Rockville, MD, USA) was cultured as described previously [11,12]. Transfection of siRNAs into HT1080 cells for silencing genes was performed as described previously, by administration with Lipofectamine 2000 [13,20,21].

Immunoprecipitation

HT1080 cells were gently lysed with RIPA buffer (50 mM Tris/HCl, pH 8.0, with 150 mM sodium chloride, 1.0% NP-40, 0.5% sodium deoxycholate and 0.1% SDS; Product number R0278; Sigma-Aldrich, St. Louis, MO, USA) with protease and phosphatase inhibitors (Sigma-Aldrich) for 30 min on ice and then centrifuged at 15 000 ***g*** at 4 °C for 15 min. The supernatant collected as cell lysate ($\sim 3 \times 10^6$ cells equivalent) was treated with 30 μL Protein G–Sepharose beads (ImmunoPure Immobilized Protein-G plus; Pierce, Rockford, IL, USA) to remove nonspecific binding proteins, and then incubated with 5 μg of anti-RNase L IgG at 4 °C for 4 h. The lysate was then incubated with an additional 30 μL of Protein G agarose beads at 4 °C for 12 h. The immunoprecipitated complexes were washed three times with RIPA buffer supplemented with protease and phosphatase inhibitors (Sigma-Aldrich). RNase L–protein complexes were eluted from the beads by heating at 95 °C for 5 min in 1 × SDS/sample buffer (62.5 mM Tris/HCl, pH 6.8, 25% glycerol, 2% SDS, 0.01% Bromophenol Blue; #161-0737; Bio-Rad, Hercules, CA, USA) supplemented with 5% β-mercaptoethanol and used for western blot analysis. This immunoprecipitation procedure was based on *Current Protocols in Molecular Biology* [22].

Western blotting

HT1080 cells were suspended in 20 mM Hepes (pH 7.5), 10 mM potassium acetate, 15 mM magnesium acetate, 1 mM dithiothreitol, 1 mM phenylmethanesulfonylfluoride, 10 μg·mL^{-1} aprotinin and 0.5% (v/v) Nonidet P-40, and homogenized by Dounce homogenizer on ice. Insoluble materials were removed by centrifugation at 10 000 ***g***, at 4 °C for 10 min. Proteins in soluble fractions were separated on 7.5% polyacrylamide SDS/gels, and transferred to poly(vinylidene difluoride) membranes (Millipore, Bedford, MA, USA). For detection of IQGAP1, HT1080 cells were gently lysed with RIPA buffer supplemented with protease and phosphatase inhibitors for 30 min on ice, and then the mixture was centrifuged at 15 000 ***g*** at 4 °C for 15 min. The supernatant was diluted with an equal amount of 2 × SDS sample buffer supplemented with 10% β-mercaptoethanol. This sample was boiled for 5 min, and proteins (20 μg) were separated by 12.5% PAGE. Western blotting was carried out with individual antibodies. The secondary antibody used was horseradish peroxidase-conjugated anti-mouse IgG (GE Healthcare, Little Chalfont, Buckinghamshire, UK). The protein bands were visualized using an ECL-plus western blotting detection system (GE Healthcare). Protein expression was quantified using VersaDoc imaging system (Bio-Rad).

HPLC-Chip-MS/MS

Tryptic digestion of proteins and MS analysis were carried out as described previously [23]. HPLC-Chip-MS/MS experiments were performed using an Agilent 1100 LC/MSD-Trap-XCT series system. The ionization system was the Chip Cube using HPLC-Chip-MS. The chip was automatically loaded and positioned into the MS nanospray chamber. The chip contained a Zorbax 300SB-C_{18} (40 nL, 5 μm) enrichment column and a Zorbax 300SB-C_{18} (43 mm × 75 μm, 5 μm) analysis column. The sample loading into the enrichment column was performed at a flow rate of 4 μL·min^{-1} with a 0.1% HCOOH in H_2O. LC gradient (mobile phase A: 0.1% HCOOH in H_2O; mobile phase B: 0.1% HCOOH and 10% H_2O in CH_3CN) was delivered at a flow rate of 300 nL·min^{-1}. Tryptic peptides were eluted from the reversed-phase column into the mass spectrometer using a linear gradient elution of 4–85% phase B over 40 min. The capillary voltage was set to 1850 V, the flow at 4 L·min^{-1}, and the temperature of the drying gas at 300 °C.

Database searches were performed against the Swiss-Prot database (release 51.3 of 12 December 2006) using a spectrum Mill MS proteomic workbench offered by Agilent (software version; A. 03. 020. 060). The search parameters were set so that they allowed the peptide mass tolerance at ± 2.5 Da and the fragment ion tolerance at ± 0.7 Da. The allowance also included matching peptides containing one miscleavage, selection of species (*Homo sapiens*), fixed modification of carbamidomethylated cysteines, and a variable modification of methionine oxidation. Identification of proteins was validated when at least two peptide sequences matched with the database sequences, with concomitant occurrence of the peptide score > 11.

Radiolabelling and protein fractionation

HT1080 cells were rinsed twice with phosphate-free RPMI 1640 medium containing BSA (which had been dial-

ysed overnight against phosphate-free RPMI 1640). The cells were incubated with ECyd in the phosphate-free RPMI 1640 at 37 °C for 14 h, and then with 1 mCi·mL^{-1} ^{32}P-orthophosphate (^{32}P-Pi) at 37 °C for 2 h. Cells were rinsed twice with NaCl/P_i and then lysed with RIPA buffer. The cell lysate was centrifuged at 15 000 ***g*** at 4 °C for 10 min, and the supernatant was collected for immunoprecipitation with anti-RNase L IgG (see below). Immunoprecipitated samples were submitted to SDS/PAGE (7.5% acrylamide gel). The gels were then wrapped in thin plastic films and exposed to a phospho-imager screen for recording their radioactivities. The recorded imaging plates were scanned with BAS1800II (FUJIFILM, Tokyo, Japan).

TUNEL assays for cell viability

The assays were carried out according to the TdT-mediated dUTP-biotin Nick End Labeling (TUNEL) protocol (#TB235; Promega, Madison, WI, USA) as described previously [13].

Immunofluorescence

After ECyd treatment, HT1080 cells were placed on coverglass plates. The cells were washed three times with NaCl/P_i and fixed with 3% formaldehyde in NaCl/P_i for 10 min. After fixation, cells were washed twice with NaCl/P_i, and were made permeable by treatment with 0.2% Triton X-100 in cold NaCl/P_i for 5 min. The slides were then incubated with NaCl/P_i containing 0.5% BSA as a blocking agent against nonspecific surface adsorption of antibodies for 30 min prior to treatment for 1 h with 1 μg·mL^{-1} anti-phosphorylated-JNK or anti-total-JNK serum (Cell Signaling Technology, Beverly, MA, USA). The cells were then incubated with 5 μg·mL^{-1} fluorescein-labelled goat anti-mouse IgG and 1 μg·mL^{-1} 4′,6-diamidino-2-phenylindole dihydrochloride for 30 min. Cells were washed three times with NaCl/P_i and covered with PermaFluor aqueous mounting medium (Invitrogen, Eugene, OR, USA). Stained cells were observed with an Olympus BX60 microscope (Olympus, Tokyo, Japan) fitted with appropriate fluorescence filters.

Acknowledgements

The authors thank Dr Hikoya Hayatsu (Faculty of Pharmaceutical Sciences, Okayama University) for helpful discussions. This research was partially supported by the Ministry of Education, Culture, Sports, Science and Technology for Exploratory Research (18659029, YW).

References

1 Bisbal C & Silverman RH (2007) Diverse functions of RNase L and implications in pathology. *Biochimie* **89**, 789–798.

2 Townsend HL, Jha BK, Han JQ, Maluf NK, Silverman RH & Barton DJ (2008) A viral RNA competitively inhibits the antiviral endoribonuclease domain of RNase L. *RNA* **14**, 1026–1036.

3 Castelli JC, Hassel BA, Wood KA, Li XL, Amemiya K, Dalakas MC, Torrence PF & Youle RJ (1997) A study of the interferon antiviral mechanism: apoptosis activation by the 2-5A system. *J Exp Med* **186**, 967–972.

4 Díaz-Guerra M, Rivas C & Esteban M (1997) Activation of the IFN-inducible enzyme RNase L causes apoptosis of animal cells. *Virology* **236**, 354–363.

5 Zhou A, Paranjape J, Brown TL, Nie H, Naik S, Dong B, Chang A, Trapp B, Fairchild R, Colmenares C *et al.* (1997) Interferon action and apoptosis are defective in mice devoid of 2′,5′-oligoadenylate-dependent RNase. *EMBO J* **16**, 6355–6363.

6 Zhou A, Paranjape JM, Hassel BA, Nie H, Shah S, Galinski B & Silverman RH (1998) Impact of RNase L overexpression on viral and cellular growth and death. *J Interferon Cytokine Res* **18**, 953–961.

7 Castelli JC, Hassel BA, Maran A, Paranjape J, Hewitt JA, Li XL, Hsu YT, Silverman RH & Youle RJ (1998) The role of 2′-5′-oligoadenylate-activated ribonuclease L in apoptosis. *Cell Death Differ* **5**, 313–320.

8 Rusch L, Zhou A & Silverman RH (2000) Caspase-dependent apoptosis by 2′,5′-oligoadenylate activation of RNase L is enhanced by IFN-beta. *J Interferon Cytokine Res* **18**, 1091–1100.

9 Li G, Xiang Y, Sabapathy K & Silverman RH (2004) An apoptotic signaling pathway in the interferon antiviral response mediated by RNase L and c-Jun NH_2-terminal kinase. *J Biol Chem* **279**, 1123–1131.

10 Hattori H, Tanaka M, Fukushima M, Sasaki T & Matsuda A (1996) Nucleosides and nucleotides. 158. 1-(3-C-ethynyl-beta-D-ribo-pentofuranosyl)-cytosine, 1-(3-C-ethynyl-beta-D-ribo-pentofuranosyl)uracil, and their nucleobase analogues as new potential multifunctional antitumor nucleosides with a broad spectrum of activity. *J Med Chem* **30**, 5005–5011.

11 Takatori S, Tsutsumi S, Hidaka M, Kanda H, Matsuda A, Fukushima M & Wataya Y (1998) The characterization of cell death induced by 1-(3-*C*-ethynyl-beta-D-*ribo*-pentofuranosyl) cytosine (ECyd) in FM3A cells. *Nucleosides Nucleotides* **17**, 1309–1317.

12 Takatori S, Kanda H, Takenaka K, Wataya Y, Matsuda A, Fukushima M, Shimamoto Y, Tanaka M & Sasaki T (1999) Antitumor mechanisms and metabolism of the novel antitumor nucleoside analogues, 1-(3-*C*-ethynyl-beta-D-*ribo*-pentofuranosyl)cytosine and 1-(3-*C*-ethynyl-beta-D-*ribo*-pentofuranosyl)uracil. *Cancer Chemother Pharmacol* **44**, 97–104.

13 Naito T, Yokogawa T, Takatori S, Goda K, Hiramoto A, Sato A, Kitade Y, Sasaki T, Matsuda A, Fukushima M *et al.* (2009) Role of RNase L in apoptosis induced by 1-(3-*C*-ethynyl-beta-D-*ribo*-pentofuranosyl)cytosine. *Cancer Chemother Pharmacol* **63**, 837–850.
14 Brown MD & Sacks DB (2006) IQGAP1 in cellular signaling: bridging the GAP. *Trends Cell Biol* **16**, 242–249.
15 Johnson M, Sharma M & Henderson BR (2009) IQGAP1 regulation and roles in cancer. *Cell Signal* **21**, 1471–1478.
16 White CD, Brown MD & Sacks DB (2009) IQGAPs in cancer: a family of scaffold proteins underlying tumorigenesis. *FEBS Lett* **583**, 1817–1824.
17 Li Z, McNulty DE, Marler KJ, Lim L, Hall C, Annan RS & Sacks DB (2005) IQGAP1 promotes neurite outgrowth in a phosphorylation-dependent manner. *J Biol Chem* **280**, 13871–13878.
18 Yoshimura A, Nakanishi M, Yatome C & Kitade Y (2002) Comparative study on the biological properties of 2′,5′-oligoadenylate derivatives with purified human RNase L expressed in *E. coli*. *J Biochem* **132**, 643–648.
19 Lesiak K & Torrence PF (1986) Synthesis and biological activities of oligo(8-bromoadenylates) as analogues of 5′-O-triphosphoadenylyl(2′-5′)adenylyl(2′-5′)adenosine. *J Med Chem* **29**, 1015–1022.
20 Ueno Y, Naito T, Kawada K, Shibata A, Kim HS, Wataya Y & Kitade Y (2005) Synthesis of novel siRNAs having thymidine dimers consisting of a carbamate or a urea linkage at their 3′ overhang regions and their ability to suppress human RNase L protein expression. *Biochem Biophys Res Commun* **330**, 1168–1175.
21 Ueno Y, Kawada K, Naito T, Shibata A, Yoshikawa K, Kim HS, Wataya Y & Kitade Y (2008) Synthesis and silencing properties of siRNAs possessing lipophilic groups at their 3′-termini. *Bioorg Med Chem* **16**, 7698–7704.
22 Ausubel FM, Brent R, Kingston RE, Moore DD, Seidman JG, Smith JA & Struhl K (1999) *Current Protocols in Molecular Biology*, Vol. 2, *Immunoprecipitation*, Unit 10.16.1–10.16.29. John Wiley & Sons, Inc.
23 Sato A, Satake A, Hiramoto A, Wataya Y & Kim HS (2010) Protein expression profiles of necrosis and apoptosis induced by 5-fluoro-2′-deoxyuridine in mouse cancer cells. *J Proteome Res* **9**, 2329–2338.

Supporting information

The following supplementary material is available:
Fig. S1. Isolation of RNase L-binding proteins.
Fig. S2. Knockdown of IQGAP1 by RNA interference.

This supplementary material can be found in the online version of this article.

Please note: As a service to our authors and readers, this journal provides supporting information supplied by the authors. Such materials are peer-reviewed and may be re-organized for online delivery, but are not copy-edited or typeset. Technical support issues arising from supporting information (other than missing files) should be addressed to the authors.

research articles Journal of proteome research

Protein Expression Profiles of Necrosis and Apoptosis Induced by 5-Fluoro-2′-deoxyuridine in Mouse Cancer Cells

Akira Sato, Akito Satake, Akiko Hiramoto, Yusuke Wataya, and Hye-Sook Kim*

Faculty of Pharmaceutical Sciences, Okayama University, Tsushima, Okayama 700-8530, Japan

Received November 17, 2009

We have investigated the molecular mechanisms regulating the necrosis and apoptosis that occur on treatment of mouse mammary tumor FM3A cells with 5-fluoro-2′-deoxyuridine (FUdR), a potent anticancer agent, using the original clone F28-7 and its variant F28-7-A cells. Previously, we reported an interesting observation that FUdR induces a necrotic morphology in F28-7 but an apoptotic morphology in F28-7-A cells. We have now analyzed the protein expression profiles of these FUdR-induced necrosis and apoptosis. Thus, proteome analysis of these clones by two-dimensional gel electrophoresis and mass spectrometry showed that the cytoplasmic intermediate filament protein, cytokeratin-19, is expressed at a significantly higher level in F28-7 than in F28-7-A cells. This strong expression was detected both in untreated and FUdR-treated stages of F28-7 cells. We interpreted this phenomenon as suggesting that cytokeratin-19 possesses a function in leading the cell to apoptosis. We performed a knockdown of cytokeratin-19 expression in F28-7 cells by use of the small interfering RNA technique. Indeed, a lowering of the cytokeratin-19 expression down to the level in F28-7-A occurred, and the FUdR-induced death morphology of this knockdown F28-7 was apoptosis, instead of the necrosis usually observable in the FUdR-treated F28-7. It is known that the cytoskeletal protein cytokeratin-19 undergoes caspase-mediated degradation during apoptosis. Our present finding provides an interesting possibility that cytokeratin-19 may have a key role in regulating cell-death morphology.

Keywords: apoptosis • cell death • cytokeratin-19 • 5-fluoro-2′-deoxyuridine (FUdR) • intermediate filament • lamin B1 • necrosis • proteome analysis • siRNA

Introduction

Transcriptome and proteome analyses have been performed extensively to identify candidate genes and proteins involved in biological processes. A technique well suited for the analysis of protein compositions, modifications, and translocations is proteome analysis based on two-dimensional gel electrophoresis (2-DE) and mass spectrometry.[1] In cancer research, the subject of cell death is important for achieving therapeutic induction of cancer-cell-selective death. Among these two major forms of cell death, apoptosis and necrosis, apoptosis has received a proportionately greater degree of attention than has necrosis.[2,3] Proteome analysis has been used extensively to study apoptosis in cells, and more than 100 proteins have been identified as participants in the apoptosis.[4] However, this approach has been seldom applied for studies of necrosis.

We have investigated the molecular mechanisms regulating necrosis and apoptosis that occur on treatment of mouse mammary tumor FM3A cells with 5-fluoro-2′-deoxyuridine (FUdR), using the original clone F28-7 and its variant F28-7-A cells.[5,6] FUdR, a potent anticancer agent, exerts its effect by inhibiting thymidylate synthase, an essential machinery for DNA synthesis in cell proliferation (see ref 7 and references therein). Previously, we reported that the treatment can induce in F28-7 cells a breakdown of DNA into chromosome-sized fragments leading to necrosis, and that it can induce in F28-7-A more extensive DNA cleavage into oligonucleosome-sized fragments and subsequent development of apoptosis.[5] Through our recent studies on the gene expression profiles during the cell-death induced by FUdR, we proposed possible mechanisms associated with the necrosis and apoptosis.[6]

We have aimed at gaining more comprehensive insights into the cellular mechanisms activated during necrosis and apoptosis. The proteome of a cell is highly dependent on the conditions to which the cell is exposed and may respond in a quite complex manner. Current development of proteomics has now enabled us to analyze the protein expression profiles of necrosis induced by FUdR in F28-7 cells and those of apoptosis in F28-7-A cells. Here, we describe the patterns of differentially expressed proteins between these cells, as revealed by the proteome analysis. Also, phenotypic screening by use of small interfering RNAs (siRNAs) led to detection of a number of differentially expressed proteins in these cells. Using this approach, we identified two new regulators of the cell death: the nuclear inner membrane protein lamin B1[8] and the cytoplasmic intermediate filament-protein cytokeratin-19 (this report). A knockdown of cytokeratin-19 expression in F28-7 cells was performed by use of the siRNA technique, resulting in a decreased expression of cytokeratin-19 down to the level

* To whom correspondence should be addressed. Corresponding author: Dr. Hye-Sook Kim, Faculty of Pharmaceutical Sciences, Okayama University, Tsushima, Okayama 700-8530, Japan. Tel., +81-86-251-7975; Fax, +81-86-251-7974; E-mail, hskim@cc.okayama-u.ac.jp.

10.1021/pr9010537

Published on Web 02/15/2010

in F28-7-A which is prone to apoptotic death. Remarkably, the FUdR-induced death morphology of this knocked-down F28-7 was apoptosis, clearly different from the necrosis that occurs in the FUdR-treated original F28-7.

Materials and Methods

Reagents, Antibodies, Cell, and Cell Culture. 5-Fluoro-2′-deoxyuridine (FUdR) was obtained from Sigma. FUdR was stored as 2 mM stocks in HPLC-grade water at −20 °C. 4′,6-Diamidino-2-phenylindole dihydrochloride (DAPI) was from Invitrogen. A set of four siRNAs against cytokeratin-19 mRNA was used: Mm_Krt1−19_1 FlexiTube siRNA, Catalog number SIO1085735; Mm_Krt1−19_2 FlexiTube siRNA, Catalog number SIO1085742; Mm_Krt1−19_3 FlexiTube siRNA, Catalog number SIO1085749; and Mm_Krt1−19_4 FlexiTube siRNA, Catalog number SIO1085756. AllStars Negative Control siRNA, Catalog number 1027280, was used as a nonsilencing siRNA. These siRNAs were obtained from Qiagen. The primary antibodies, rabbit polyclonal antihuman keratin-19 (K19) and rabbit polyclonal antikeratin-8 antibody, were from ANASPEC. Rabbit polyclonal anti-Annexin-A1 antibody and rabbit polyclonal antiglyceraldehyde-3-phosphate dehydrogenase (GAPDH) antibody were from Abcam and Trevigen, respectively. The secondary antibodies; antimouse IgG horseradish peroxidase-linked whole antibody and antirabbit IgG horseradish peroxidase-linked whole antibody were from GE Healthcare.

Original-type F28-7 clone and variant F28-7-A clone of mouse mammary tumor FM3A cells used in the study have been described previously.[5] The cells were cultured in ES medium (Nissui Pharmaceuticals), supplemented with 2% fetal bovine serum (Gibco) and 0.03% L-glutamine (Wako), in a humidified atmosphere with 5% CO_2 at 37 °C. Under these conditions, the doubling time of both F28-7 and F28-7-A cells was approximately 12 h.

F28-7 and F28-7-A cells (approximately 5×10^5 cells/mL) were treated with 1 μM FUdR. Cell viability was estimated with a hemocytometer by means of trypan blue-exclusion.

Two-Dimensional Gel Electrophoresis (2-DE). Cells were cultured, collected, and washed in ice-cold phosphate-buffered saline (PBS) and then lysed in 1.5 mL of Ready Prep Rehydration/Sample buffer (8 M urea, 2% CHAPS, 50 mM DTT, 0.001% bromophenol blue, and 0.2% w/v Bio-Lyte 3/10 ampholytes) prepared according to the manufacturer's instructions (Bio-Rad), with supplemental addition of Protease-Inhibitor Cocktail for Mammalian Cell (Sigma). The cells were sonicated on ice using Branson sonifier 250, then the lysate was left at room temperature for 30 min. The cell lysate was centrifuged at 10 000× *g* for 15 min at room temperature and the supernatant containing the solubilized proteins was used directly or stored at −80 °C prior to use. Protein concentrations were determined using the Lowry-method-oriented RCDC protein assay reagent (Bio-Rad). Protein samples from at least three independent experiments were collected for 2-DE analysis. The proteins were separated by large 2-DE (gel size 18 cm × 20 cm). Briefly, samples containing 200 μg of protein in 350 μL Rehydration/Sample buffer were loaded on the immobilized pH gradient (IPG) strips (ReadyStrips IPG Strips, 17 cm, pH range 3−10 nonlinear: Bio-Rad). Active rehydration and isoelectric focusing (IEF) were performed at 20 °C using PROTEAN IEF Cell (Bio-Rad). After active rehydration (50 V) for at least 12 h, IEF was performed in three steps, that is, conditioning (15 min at 250 V), voltage ramping (250−10,000 V in 2 h), and focusing (5 h at 10 000 V). The current was set at <50 μA per strip. Samples were subjected to reduction/alkylation prior to second dimension electrophoresis. Thus, the strips were incubated for 20 min in an equilibration buffer containing 2% (w/v) DTT, 6 M urea, 2% (w/v) SDS, 375 mM Tris, pH 8.8, and 20% (w/v) glycerol, then for 10 min in the same solution substituting DTT with 2.5% (w/v) iodoacetamide (Bio-Rad). Both of these steps were performed at room temperature. The strip was then sealed on top of the SDS-polyacrylamide gel using a 1% agarose solution. The run on the second dimension was carried out on an 12% polyacrylamide gel (Bio-Rad). Electrophoresis was performed at 20 °C for the first 30 min at 16 mA per gel, followed by 5 h at 24 mA per gel, on a PROTEAN II XL Cell system (Bio-Rad). Gels were fixed for 30 min in 7% acetic acid containing 10% ethanol and stained in the dark at room temperature for at least 16 h with 250 mL per gel of SYPRO Ruby stain (Bio-Rad). Gels were destained in 7% acetic acid containing 10% methanol for 1 h and scanned with the Molecular Imager FX (Bio-Rad).

Image Analysis. After scanning, the gel images were analyzed using PDQuest software, version 7.1.1 (Bio-Rad). Scanned gel images were processed to remove backgrounds and to automatically detect spots. For all spot intensity calculations, normalized values were used. Normalization of spot intensity was done so that the total sum of intensities in a gel would be equal to 1 000 000, and normalized spot intensities were expressed in ppm. The Student's *t*-test was performed, comparing protein expression in the SYPRO Ruby-stained 2D gels of F28-7 and F28-7-A cells in untreated or FUdR-treated stage ($n = 3$, $p < 0.05$).

Tryptic Digestion. Protein spots to be identified were excised from the 2-DE gels using an EXQuest Spot Cutter (Bio-Rad) and placed into a 96-well microtiter plate. The gels were washed twice with water, shrunk with acetonitrile, and dried in a SpeedVac. Then, samples were digested with 12.5 ng/μL porcine methylated trypsin (Promega) in 40 mM ammonium bicarbonate for at least 4 h at 37 °C.

MALDI-TOF MS, MALDI-TOF/TOF MS, and LC−MS/MS Analyses. The mass spectra were recorded by using Autoflex, Autoflex-III (Bruker Daltonics, Bremen, Germany), and HPLC-Chip-MS (Agilent Technologies, Santa Clara, CA). For MALDI-TOF MS and MALDI-TOF/TOF MS analyses, 2 μL of extracted peptides was spotted onto a Prespotted AnchorChip target-plate (Bruker Daltonics #227463) for MALDI-TOF analysis. MALDI MS measurements were performed in the mass range of 650−2600 Da on Autoflex and Autoflex-III mass spectrometers, set to reflectron mode, after calibration using a mixture of Anchor-spotted calibration standards (Bruker Daltonics). Mass spectra were determined as the sum of 200 laser shots. Also, the HPLC-Chip-IT-MS/MS experiments were performed on an Agilent 1100 LC/MSD-Trap-XCT series system. The ionization system was the Chip Cube using HPLC-Chip-MS. The chip was automatically loaded and positioned into the MS nanospray chamber. The chip contained a Zorbax 300SB-C_{18} (40 nL, 5 μm) enrichment column and a Zorbax 300SB-C_{18} (43 mm × 75 μm, 5 μm) analysis column. The sample loading into the enrichment column was performed at a flow rate set at 4 μL/min with a 0.1% HCOOH in H_2O. LC gradient (mobile phase-A: 0.1% HCOOH in H_2O; mobile phase-B: 0.1% HCOOH and 10% H_2O in CH_3CN) was delivered with the flow rate set at 300 nL/min. Tryptic peptides were eluted from the reversed-phase column into the mass spectrometer using a linear gradient elution of 4−85% phase-B over 40 min. The capillary

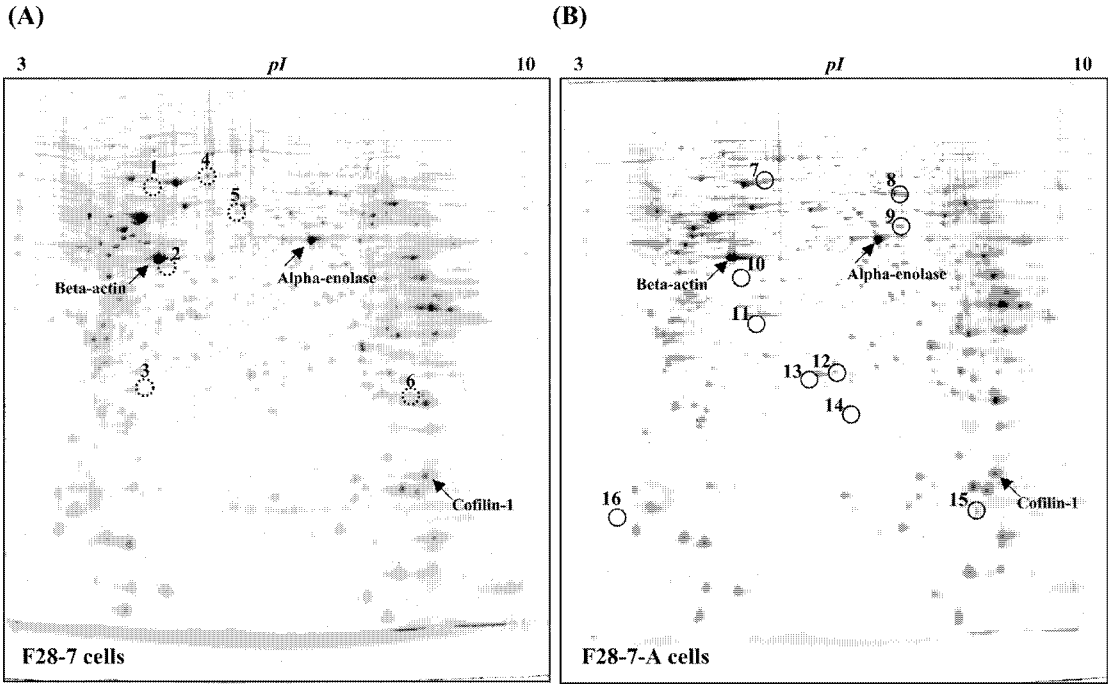

Figure 1. Sypro Ruby-stained 2D gels of F28-7 and F28-7-A cells in untreated stage. (A) Proteome 2D-map of F28-7 cells (two additional independent experiments gave essentially identical results). (B) Proteome 2D-map of F28-7-A cells (reproducibility confirmed; $n = 3$). Whole cell lysates were prepared from F28-7 and F28-7-A cells, and the individual lysates were focused on a pH 3–10 nonlinear range IPG strip and then separated on a 12.5% SDS-PAGE gel, stained, and visualized as described under "Experimental Procedures". The spots 1–6 displayed in the 2D-map of F28-7 cells (A) gave corresponding spots of lower intensities for F28-7-A (B). The spots 7–16 displayed in the 2D proteome map of F28-7-A cells (B) gave corresponding spots of lower intensities for F28-7 cells (A). Protein spots are identified by MALDI-TOF/MS, and nano LC–MS/MS.

voltage was set to 1850 V and the flow and the temperature of the drying gas were 4 L/min and 300 °C, respectively.

Database Searching. With MALDI-TOF/MS analysis, the proteins were identified by the peptide mass fingerprinting (PMF) and/or MS/MS ion search using MASCOT search engine (version 2.2.6; Matrix Science, London, UK). The Swiss-Prot database (release 57.13 of 19-Jan-2010; 514 212 sequences; 180 900 945 residues) was used for the searches. For PMF analysis, the peptide masses were exported to Biotools software version 3.2 (Autoflex, Bruker Daltonics) and used to perform a MASCOT search engine. Search parameters allowed a mass deviation of ±150 ppm, matching peptides containing one miscleavage, selection of species (*Mus musculus*), fixed modification of carbamidomethylated cysteines, and a variable modification of oxidized methionines. MASCOT protein scores greater than 48 were considered as significant ($p < 0.05$). In the MS/MS analysis, search parameters were set so that they allowed the peptide mass tolerance at ±150 ppm, and the fragment ion tolerance at ±0.5 Da. The allowance also included matching peptides containing one miscleavage, selection of species (*Mus musculus*), fixed modification of carbamidomethylated cysteines, and a variable modification of oxidized methionines. MASCOT protein scores (based on MS/MS spectra) of greater than 54 were considered statistically significant ($p < 0.05$). The individual MS/MS spectra with a statistically significant (confidence interval >95%) ion score were accepted. In the PMF and MS/MS ion search, the significance threshold for positive identification was determined by the Mascot Search program.

For HPLC-Chip/MS analysis, database searches were performed against the Swiss-Prot database (release 57.12 of 15-Dec-2009; 513 877 sequences; 180 750 753 residues) using a spectrum Mill MS proteomic workbench offered by Agilent (Software version Rev A. 03. 03. 084. SR4). The search parameters were set so that they allowed the peptide mass tolerance at ±2.5 Da, and the fragment ion tolerance at ±0.7 Da. The allowance also included matching peptides containing one miscleavage, selection of species (*Mus musculus*), fixed modification of carbamidomethylated cysteines, and a variable modification of methionine oxidation. Identification of proteins was validated when at least two peptide sequences matched with the database sequences, with concomitant occurrence of the peptide score greater than 11.

All MS and MS/MS spectra obtained were searched against the mouse protein database, which was collected from the Swiss-Prot (*Mus musculus*, 16 214 sequences) database.

The molecular masses and isoelectric points were calculated by employing the software Compute p*I*/MW (www.expasy.ch/tool/pi_tool.html).

Western Blot Analysis. Cells were washed in ice-cold PBS and then whole cell lysates were prepared using Laemmili sample buffer (Bio-Rad). Proteins (5×10^4 cells per lane) were subsequently fractionated under reducing conditions by 7.5% SDS-polyacrylamide gel electrophoresis and blotted onto a polyvinylidene difluoride membrane (Millipore). The membrane was then blocked against nonspecific binding by treatment for 1 h with 5% bovine serum albumin in Tris-buffered saline containing 0.1% Tween 20, and then immunoblotted overnight at 4 °C using the respective primary antibody. Next, the membrane was incubated for 1 h at room temperature with a horseradish peroxidase-conjugated antimouse IgG or antirabbit IgG secondary antibody, and the protein bands were visualized using an ECL plus Western blotting detection system (GE Healthcare). Protein expression

Table 1. Differential Protein-Spots from F28-7 and F28-7-A

spot no.	fold difference[a]	accession no.[b]	protein name	biological process (function)	theoretical p*I*	theoretical MW (Da)
			Spots stronger in F28-7 than in F28-7-A			
1	2.4	P14733	Lamin B1	Chromatin modificaton	5.11	66785.60
2[c]	3.3	P19001	Keratin, type I cytoskeletal 19 (Cytokeratin-19)	Cytoskeleton organization	5.28	44541.80
3	5.0	P10107	Annexin A1	Signal transduction	6.97	38734.30
4	2.0	P38647	Stress-70 protein, mitochondrial (GRP 75)	Protein folding	5.91	73528.33
5	2.0	P11679	Keratin, type II cytoskeletal 8	Cytoskeleton organization	5.70	54565.31
6	2.5	P19157	Glutathione S-transferase P1	Glutathione metabolism	7.69	23609.18
			Spots weaker in F28-7 than in F28-7-A			
7	0.2	P38647	Stress-70 protein, mitochondrial (GRP 75)	Protein folding	5.91	73528.33
8	0.6	P48678	Lamin-A/C	Chromatin modificaton	6.54	74237.57
		Q60864	Stress-induced phosphoprotein 1	Stress response	6.40	62582.11
		Q9CWJ9	Bifunctional purine biosynthesis protein PURH	Purine nucleotide biosynthesis	6.30	64217.38
9	0.4	Q9JLJ2	4-trimethylaminobutyraldehyde dehydrogenase (Aldehyde dehydrogenase 9A1)	Carnitine metabolism	6.63	53514.72
		P50431	Serine hydroxymethyltransferase, cytosolic	Glycine metabolism	6.47	52584.87
		Q8C1B7	Septin-11	Cell cycle	6.24	49694.64
10	0.6	Q9CQM9	Glutaredoxin-3	Redox homeostasis	5.42	37778.38
		Q8BK64	Activator of 90 kDa heat shock protein ATPase homologue 1 (AHA1)	Protein folding	5.41	38117.13
11	0.3	Q9QZH3	Peptidyl-prolyl cis−trans isomerase E	Protein folding	5.41	33448.85
12	0.6	O08807	Peroxiredoxin 4	Redox homeostasis	6.67	31052.52
13	0.5	Q60631	Growth factor receptor-bound protein 2	Signal transduction	5.89	25238.41
14	0.4	Q99LP6	GrpE protein homologue 1, mitochondrial	Protein folding	8.58	24307.02
		Q99LX0	Protein DJ-1	Protein folding	6.32	20021.31
15	0.3	P50446	Keratin, type II cytoskeletal 6A	Cytoskeletone organization	8.04	59335.12
16	0.4	Q8CGP5	Histone H2A type 1-F	Chromatin modificaton	11.05	14161.53

[a] Fold difference (F28-7/F28-7-A cells) > 1.5 or ≤ 0.6. [b] Swiss-prot primary accession number. [c] See graphic below. Bold-lettered peptide sequences indicate the identified peptides by MS/MS experiments in MALDI-TOF and/or nano-LC−MS/MS.

Spot No. 2

Keratin, type I cytoskeletal 19 (P19001)

MTSYSYR**QTS AMSSFGGTGG GSVRIGSGGV FR**APSIHGGS GGRGVSVSST R**FVTSSSGSY GGVRGGSFSG TLAVSDGLLS GNEKITMQNL NDRLASYLDK** VR**ALEQANGE LEVK**IRDWYQ KQGPGPSR**DY NHYFK**TIEDL R**DKILGATID NSKIVLQIDN ARLAADDFR**T KFETEHALRL SVEADINGLR R**VLDELTLAR** TDLEMQIESL KEELAYLKK**N HEEEITALRS** QVGGQVSVEV DSTPGVDLAK ILSEMR**SQYE IMAEKNRKDA EATYLARIEE LNTQVAVHSE QIQISKTEVT DLRRTLQGLE IELQSQLSMK AALEGTLAET EAR**YGVQLSQ IQSVISGFEA QLSDVRADIE RQNQEYKQLM DIK**SRLEQEI ATYRSLLEGQ EAHYNNLPTP KAI**

was quantified using VersaDoc imaging system (Bio-Rad). The following antibodies were used: anticytokeratin-19 antibody (1:200), anti-GAPDH antibody (1:10 000), antimouse IgG horseradish peroxidase-linked whole antibody (1:20 000), and antirabbit IgG horseradish peroxidase-linked whole antibody (1:20 000).

Transfection. Exponentially growing 2×10^5 cells were suspended in 75 μL siPORT electroporation buffer (Ambion) containing cytokeratin-19 siRNA cocktail or nonsilencing siRNA (final concentration 8×10^{-7} M) and introduced into 0.1 cm gap electroporation cuvette (Bio-Rad). The cytokeratin-19 siRNA cocktail was prepared by mixing Mm_Krt1−19_1, Mm_Krt1−19_2, Mm_Krt1−19_3, and Mm_Krt1−19_4 Flexi-Tube siRNAs. Cells were then electroporated using the Bio-Rad Gene Pulser Xcell at voltage 0.15 kV, pulse length 1000 μs, and number of pulse 1. After electroporation, cells were plated at 5×10^4 cells/mL in fresh ES medium in tissue culture flasks. Forty-eight hours after the electroporation, cells were used for further experiments.

Results

Protein Expression Analysis of Mouse Mammary Tumor FM3A Cells F28-7 and F28-7-A. Cell lysates were analyzed using 2-DE to detect changes in the proteome of F28-7 and F28-7-A cells. Figure 1A and B show typical two-dimensional gels of F28-7 and F28-7-A cell-lysates. Approximately 1800 protein spots per gel were detected within a pI range of 3−10 and a relative molecular mass range of 10−150 kDa. These data were reproducible in two additional independent experiments using newly cultured cells. With a 1.5-fold cutoff, that is, either >1.5 or <0.6, the analysis picked up 16 spots as having different intensities between F28-7 and F28-7-A. Spots 1−6 (Figure 1A) gave higher intensities in F28-7 than in F28-7-A; and Spots 7−16 (Figure 1B) gave lower intensities in F28-7 than in F28-7-A. Twenty-two proteins were identified in these 16 spots by MS analysis using MALDI-TOF/MS and nano LC−MS/MS. Of these 22 proteins, 6 were consistently higher and 16 were consistently lower in abundance in the F28-7 cells. Table 1 lists the names

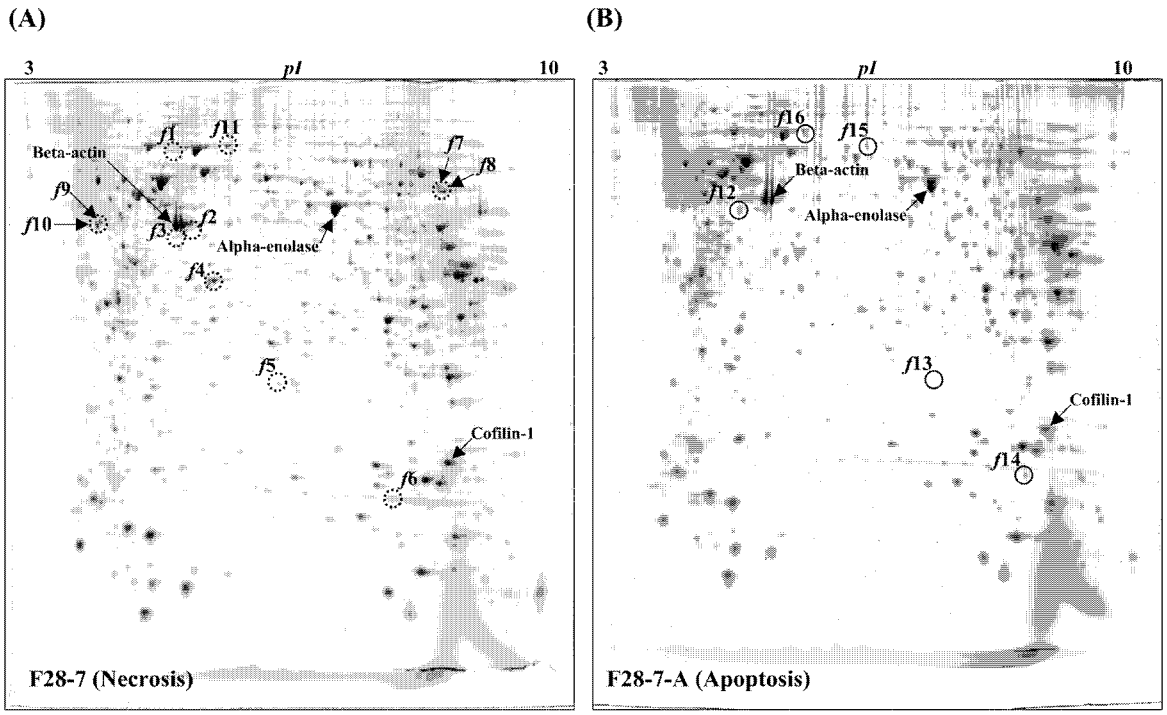

Figure 2. Sypro Ruby-stained 2D gels of FUdR-induced necrosis in F28-7 and apoptosis in F28-7-A cells. (A) Proteome 2D-map of F28-7 cells undergoing FUdR-induced necrosis (reproducibility confirmed; $n = 3$). (B) Proteome 2D-map of F28-7-A cells undergoing FUdR-induced apoptosis (reproducibility confirmed; $n = 3$). F28-7 and F28-7-A cells were treated with 1 μM FUdR for 16 h. Whole cell lysates were prepared and they were individually focused on a pH 3−10 nonlinear range IPG strip and then separated on a 12.5% SDS-PAGE gel, stained, and visualized as described under Materials and Methods. The spots *f*1−*f*11 displayed in the 2D-map of F28-7 cells (A) gave corresponding spots of lower intensities for F28-7-A (B). The spots *f*12−*f*16 displayed in the 2D proteome map of F28-7-A cells (B) gave spots of lower intensities for F28-7 (A). Protein spots are identified by MALDI-TOF MS, MALDI-TOF/TOF MS, and nano-LC−MS/MS.

of these identified proteins, their Swiss-prot database accession numbers, spot designation, reported isoelectric points and molecular weight values, along with associated biological processes (functions). In addition, data were obtained for the identification of the focused protein spots based on peptide mass fingerprint and MS/MS experiments (see Supplementary Tables 1 and 2, Supporting Information). The functions associated with these proteins include chromatin modification, cytoskeleton organization, signal transduction, glutathione metabolism, stress response, purine nucleotide biosynthesis, carnitine metabolism, redox homeostasis, and protein folding. These identified proteins are those functioning at various stages of important biological processes.

The accuracy of the proteome results was confirmed using traditional immunological techniques. Thus, we analyzed the expression levels of the identified proteins by Western blotting. The analysis showed that the relative levels of cytokeratin-19, cytokeratin-8, and annexin A1 in F28-7, in comparison to those in F28-7-A cells, were 33.3, 5.0, and 10.0, respectively (Supplementary Figure 1, Supporting Information). The high expressions of these proteins in Western blotting conform with the results of proteome analysis.

Protein Expression Analysis of FUdR-Induced Necrosis and Apoptosis. Next, we examined the effect of FUdR-treatment on the proteome profiles. F28-7 and F28-7-A cells were treated with 1 μM FUdR for 16 h. The treatment with FUdR caused induction of necrosis in F28-7 and apoptosis in F28-7-A cells.[5] We previously found that the release of cytochrome c from mitochondria into both the cytoplasm and the nucleus induced apoptosis but not necrosis.[6] This key phenomenon occurred at 16 h after treatment with FUdR. Therefore, we performed proteome analysis at the 16 h. Cell lysates were analyzed using 2-DE to detect changes in the necrosis and apoptosis cell-proteomes. Figure 2A and B shows typical two-dimensional gels of the necrosis and apoptosis cell-lysates. Approximately 1800 protein spots per gel were reproducibly detected. Using a 1.5-fold cutoff, the analysis identified 16 altered protein spots: 11 high intensity spots and 5 low intensity spots in necrosis (F28-7) compared to apoptosis cells (F28-7-A), which accounted for about 1% of the total number of detectable proteins. Twenty-four proteins were identified in these 16 spots by MS analysis using MALDI-TOF MS, MALDI-TOF/TOF MS, and nano-LC−MS/MS. The expression levels of the 24 proteins were significantly different between the necrosis and apoptosis cells. Among them, 13 proteins were consistently higher and 11 proteins were consistently lower in abundance in the necrosis cells. Table 2 lists the names and features of the 24 proteins. In addition, a complete list of data is available for the identification of the focused protein spots based on peptide mass fingerprints and MS/MS experiments (see Supplementary Tables 1 and 3, Supporting Information). The protein functions thus found to differ between necrosis and apoptosis were chromatin modification, cytoskeleton organization, glycolysis, ATP biosynthesis, glycine metabolism, protein folding, and galactose metabolism. Remarkably, a number of the mitochondrial proteins exhibited the differential expressions. These proteins include pyruvate dehydrogenase E1 component subunit beta, ATP synthase subunit alpha, stress-70 protein (GRP75), peptidyl-tRNA hydrolase 2, and pyruvate kinase isozyme M1/M2. Furthermore, proteins corresponding to

Table 2. Differential Protein Spots from FUdR-treated-F28-7 and -F28-7-A

spot no.	fold difference[a]	accession no.[b]	protein name	biological process (function)	theoretical p*I*	theoretical MW (Da)
			Spots stronger in F28-7 than in F28-7-A			
*f*1	1.7	P14733	Lamin B1	Chromatin modificaton	5.11	66785.60
*f*2[c]	5.0	P19001	Keratin, type I cytoskeletal 19 (Cytokeratin-19)	Cytoskeleton organization	5.28	44541.80
*f*3[d]	5.0	P19001	Keratin, type I cytoskeletal 19 (Cytokeratin-19)	Cytoskeleton organization	5.28	44541.80
*f*4	2.0	O35639	Annexin A3	Unknown (Calcium ion binding)	5.33	36371.00
		Q9D051	Pyruvate dehydrogenase E1 component subunit beta, mitochondrial	Glycolysis	6.41	38937.09
		Q9CSU0	Regulation of nuclear pre-mRNA domain-containing protein 1B	Unknown (Unknown)	5.73	36883.74
*f*5	5.0	P97861	Keratin, type II cuticular Hb6	Cytoskeleton organization	5.63	53251.26
*f*6	3.3	Q9D2U9	Histone H2B type 3-A	Chromosome organization	10.37	13994.20
		Q9CZX8	40S ribosomal protein S19	Translation	10.41	16085.49
*f*7	Specific in F28−7	Q03265	ATP synthase subunit alpha, mitochondrial	ATP biosynthesis	9.22	59752.60
		Q9CY58	Plasminogen activator inhibitor 1 RNA-binding protein	Unknown (RNA binding)	8.60	44714.12
		P50431	Serine hydroxymethyltransferase, cytosolic	Glycine metabolism	6.47	52584.87
*f*8	Specific in F28-7	Q03265	ATP synthase subunit alpha, mitochondrial	ATP biosynthesis	9.22	59752.60
		Q9CY58	Plasminogen activator inhibitor 1 RNA-binding protein	Unknown (RNA binding)	8.60	44714.12
*f*9	2.0	O35887	Calumenin	Unknown (Calcium ion binding)	4.49	37063.72
*f*10	2.5	O35887	Calumenin	Unknown (Calcium ion binding)	4.49	37063.72
*f*11	1.7	P38647	Stress-70 protein, mitochondrial (GRP 75)	Protein folding	5.91	73528.33
			Spots weaker in F28-7 than in F28-7-A			
*f*12	0.6	Q9R0N0	Galactokinase	Galactose metabolism	5.17	42176.08
		Q9JHJ0	Tropomodulin-3	Cytoskeleton organization	5.02	39502.72
*f*13	0.6	P11983	T-complex protein 1 subunit alpha B (TCP-1-alpha)	Protein folding	5.82	60448.64
		Q9R0N0	Galactokinase	Galactose metabolism	5.17	42176.08
		P02535	Keratin, type I cytoskeletal 10 (Cytokeratin-10)	Cytoskeleton organization	5.04	57769.85
		Q8R2Y8	Peptidyl-tRNA hydrolase 2, mitochondrial	Translation (Hydrolase)	6.95	19526.56
		O35639	Annexin A3	Unknown (Calcium ion binding)	5.33	36371.00
*f*14	0.1	Q8R2Y8	Peptidyl-tRNA hydrolase 2, mitochondrial	Translation (Hydrolase)	6.95	19526.56
*f*15	0.4	P11983	T-complex protein 1 subunit alpha B (TCP-1-alpha)	Protein folding	5.82	60448.64
		P42932	T-complex protein 1 subunit theta (TCP-1-theta)	Protein folding	5.44	59555.48
		P52480	Pyruvate kinase isozyme M1/M2	Glycolysis	7.17	57844.89
		Q61781	Keratin, type I cytoskeletal 14 (Cytokeratin-14)	Cytoskeleton organization	5.10	52866.97
		P80316	T-complex protein 1 subunit epsilon	Protein folding	5.72	59624.08
*f*16	0.5	P38647	Stress-70 protein, mitochondrial (GRP 75)	Protein folding	5.91	73528.33

[a] Fold change (FUdR-treated F28-7/FUdR-treated F28-7-A cells) > 1.5 or ≤ 0.6. [b] Swiss-prot primary accession number. [c] See graphic below. Bold-lettered peptide sequences indicate the identified peptides by MS/MS experiments in MALDI-TOF and/or nano-LC−MS/MS. [d] See graphic below. Bold-lettered peptide sequences indicate the identified peptides by MS/MS experiments in MALDI-TOF and/or nano-LC−MS/MS.

Spot No. *f*2

Keratin, type I cytoskeletal 19 (P19001)

MTSYSYR**QTS AMSSFGGTGG GSVRIGSGGV FRAPSIHGGS GGR**GVSVSST R**FVTSSSGSY GGVRGGSFSG TLAVSDGLLS GNEKITMQNL NDRLASYLDK** VR**ALEQANGE LEVK**IRDWYQ KQGPGPSR**DY NHYFK**TIEDL RDK**ILGATID NSKIVLQIDN ARLAADDFRT KFETEHALRL SVEADINGLR RVLDELTLAR TDLEMQIESL KEELAYLKKN HEEEITALRS QVGGQVSVEV DSTPGVDLAK ILSEMRSQYE IMAEK**NR**KDA EATYLARIEE LNTQVAVHSE QIQISKTEVT DLRRTLQGLE IELQSQLSMK AALEGTLAET EAR**YGVQLSQ IQSVISGFEA QLSDVRADIE RQNQEYKQLM DIK**SRLEQEI ATYR**SLLEGQ EAHYNNLPTP KAI

Spot No. *f*3

Keratin, type I cytoskeletal 19 (P19001)

MTSYSYR**QTS AMSSFGGTGG GSVRIGSGGV FR**APSIHGGS GGRGVSVSST R**FVTSSSGSY GGVRGGSFSG TLAVSDGLLS GNEKITMQNL NDRLASYLDK** VR**ALEQANGE LEVK**IRDWYQ KQGPGPSR**DY NHYFK**TIEDL RDK**ILGATID NSKIVLQIDN ARLAADDFRT KFETEHALRL** SVEADINGLR R**VLDELTLAR** TDLEMQIESL KEELAYLKK**N HEEEITALRS** QVGGQVSVEV DSTPGVDLAK ILSEMR**SQYE IMAEK**NRK**DA EATYLAR**IEE LNTQVAVHSE QIQISK**TEVT DLR**RTLQGLE IELQSQLSMK **AALEGTLAET EAR**YGVQLSQ IQSVISGFEA QLSDVRADIE RQNQEYKQLM DIKSR**LEQEI ATYR**SLLEGQ EAHYNNLPTP KAI

chromatin and cytoskeleton-organization showed differential expressions. These proteins include lamin B1, keratin type I cytoskeletal 19 (cytokeratin-19), keratin type II cuticular Hb6, histone H2B type 3-A, keratin type I cytoskeletal 10 (cytokeratin-10), and keratin type I cytoskeletal 14 (cytokeratin-14), all of them being those involved in the maintenance of nuclear and cell morphology. Interestingly, lamin B1 and cytokeratin-19 were higher (1.7, 5.0, respectively) in F28-7 (necrosis cells), compared to F28-7-A cells (apoptosis cells) in this FUdR-treatment (Table 2 and Figure 3). At the untreated stage also,

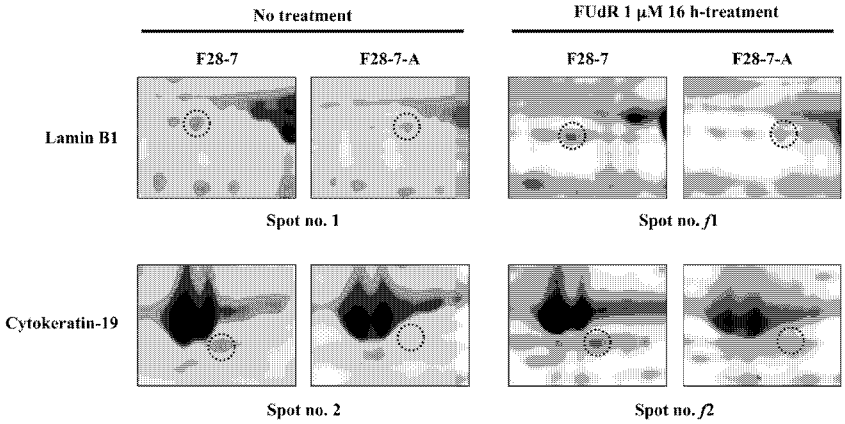

Figure 3. Selected regions of two-dimensional gels illustrating individual protein expression changes following FUdR treatment. Pictures showing enlarged areas for lamin B1 (spot 1 and spot *f*1), and cytokeratin-19 (spot 2 and spot *f*2).

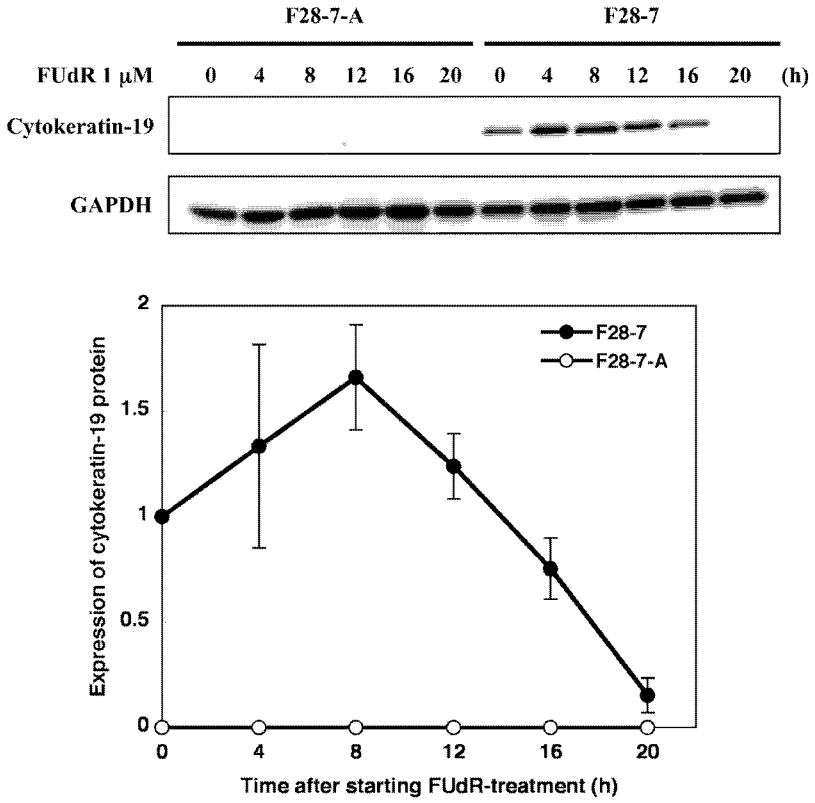

Figure 4. Western blot validation of cytokeratin-19 protein expression. Whole cell lysates were prepared from F28-7 and F28-7-A cells in untreated (0 h) and FUdR-treated stages (4, 8, 12, 16 h). Expression of cytokeratin-19 and GAPDH proteins were examined by Western blot analysis. Expression of GAPDH was used as an internal control. The patterns shown are results obtained in one experiment. Two additional experiments gave similar results. Expression of cytokeratin-19 protein is represented by the density of cytokeratin-19/GAPDH protein band relative to the zero-time value with F28-7 cells (●). The values for F28-7-A (○) were null at all data points. Results are averages of three independent experiments with error bars showing the ±SD in triplicates.

lamin B1 and cytokeratin-19 were higher (2.5, and 3.3, respectively) in F28-7, compared to F28-7-A (Table 1 and Figure 3). Therefore, we interpreted this as suggesting that lamin B1 and cytokeratin-19 could be regulators in the FUdR-induced necrosis and apoptosis.

Modulation of FUdR-Induced Cell Death by Silencing Cytokeratin-19 Expression. As described above, lamin B1 and cytokeratin-19 are strongly expressed in F28-7, as compared with those in F28-7-A, both in untreated- and FUdR-treated-stages. Our previous work showed that the knockdown of lamin B1 by siRNA technique can cause a shift from FUdR-induced necrosis to apoptosis.[8] In addition, we previously reported that the cytokeratin-19 mRNA was strongly expressed in FUdR-induced necrosis, as compared with those in FUdR-induced apoptosis, by using cDNA microarray technology.[6] The possibility that cytokeratin-19 may also be associated with these differential patterns of cell death morphology was, therefore, investigated.

First, we analyzed the expression levels of cytokeratin-19, using Western blotting. As shown in Figure 4, the cytokeratin-19 protein was detected for F28-7 but not for F28-7-A cells. The level of cytokeratin-19 protein was indeed higher in F28-7 than in F28-7-A both before and after the FUdR-treatment. In the F28-7 cells, the expression of cytokeratin-19 protein

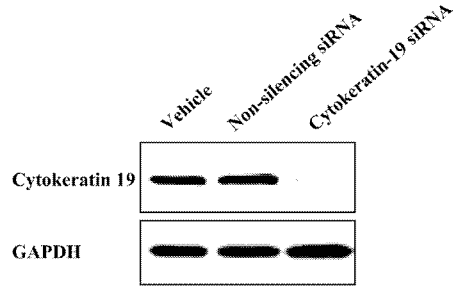

Figure 5. Knockdown of cytokeratin-19 by RNA interference. F28-7 cells were transfected with nonsilencing siRNA and with cytokeratin-19 siRNA cocktail. Forty-eight hours after the transfection, the levels of expression of cytokeratin-19 and those of GAPDH, an internal control, were examined by Western blot analysis. These results are representative of three independent experiments.

continued to increase until eight-hours of the FUdR-treatment, then decreased gradually, until it reached near to the zero level at 20 h.

Next, to test if a lowering of endogenously expressed cytokeratin-19 in F28-7 cells can modulate FUdR-induced necrosis, we carried out a knockdown of the expression in F28-7 cells by using cytokeratin-19 siRNA. Western blot analysis performed for cell extracts at 48 h after the siRNA-transfection at a greater-than-80% efficiency indicated that the treatment reduced the cytokeratin-19 protein levels, while the glyceraldehyde-3-phosphate dehydrogenase (GAPDH) protein levels as a control showed no change (Figure 5). The level of cytokeratin-19 protein expression in F28-7 became as low as that in F28-7-A cells. Thus, the knockdown efficacy was more than 70% in cytokeratin-19 siRNA cocktail-transfected cells, compared to that in the vehicle- and nonsilencing siRNA-transfected cells. Another control experiment in which a nonsilencing siRNA was administered showed no effect on the expression of cytokeratin-19 or GAPDH. The cell viability at 48 h after the transfection was 95.5 ± 0.9% ($n = 3$) with the vehicle, 98.9 ± 0.7% ($n = 3$) with the nonsilencing siRNA, and 99.1 ± 0.6% ($n = 3$) in the cytokeratin-19 siRNA cocktail-transfected cells. The knockdown of cytokeratin-19 in the F28-7 cells did not change the cell viability. In addition, either the nonsilencing siRNA or the cytokeratin-19 siRNA cocktail alone had no effect on the cell morphology, that is, the morphology-change required subsequent FUdR-treatment (Figure 6, upper diagram).

We explored the morphology in the cytokeratin-19 knocked-down F28-7 cells on treatment with 1 μM FUdR. The necrotic morphology in F28-7 and apoptotic morphology in F28-7-A cells were characteristically observed at 21 h after treatment with FUdR. At the 21 h, the controls given vehicle or nonsilencing siRNA showed the cytoplasmic swelling, a feature of necrosis, and the cytokeratin-19 siRNA cocktail-transfected cells, in contrast, showed a typical apoptotic morphology; the membrane blebbing and the formation of apoptotic bodies (Figure 6, bottom diagram). At this point of treatment, the cell viability was 26.7 ± 1.6% ($n = 3$) with the vehicle, 26.6 ± 1.9% ($n = 3$) with the nonsilencing siRNA, and 28.0 ± 1.1% ($n = 3$) with the cytokeratin-19 siRNA cocktail transfection. These results indicate that the knockdown of cytokeratin-19 caused the cells a shift from necrosis to apoptosis, without changing the viability-levels. We confirmed, by microscopic inspection, that almost all the dying cells underwent apoptotic morphologies after the cytokeratin-19 siRNA cocktail transfection with subsequent FUdR treatment.

Discussion

We believe that depending on intracellular environment, for example proteome status, a cell is destined to necrosis or to apoptosis. Our previous reports to sort out candidate regulators for the cell death-pathways from the microarray data, however, have been unsuccessful.[6] This time, with the use of proteome analysis, we have shown that at the untreated and FUdR-treated stages the nuclear and the cytoplasmic intermediate filament-proteins, lamin B1 and cytokeratin-19, are higher in F28-7 than in F28-7-A cells. Consequently, we focused on these proteins as candidate cell death-regulators of FUdR-induced necrosis and apoptosis. Thus, in our recent publication,[8] we reported that a knockdown of lamin B1 by its siRNA induced a shift from necrosis to apoptosis in F28-7 cells, thereby proposing that lamin B1 could be such a regulator. Lamin B1 is one of the nuclear lamins and a key structural component of the lamina, an intermediate filament meshwork that lies beneath the inner nuclear membrane. It is known that the nuclear lamins play a crucial role in fundamental cellular processes, including nuclear organization, chromatin segregation, DNA

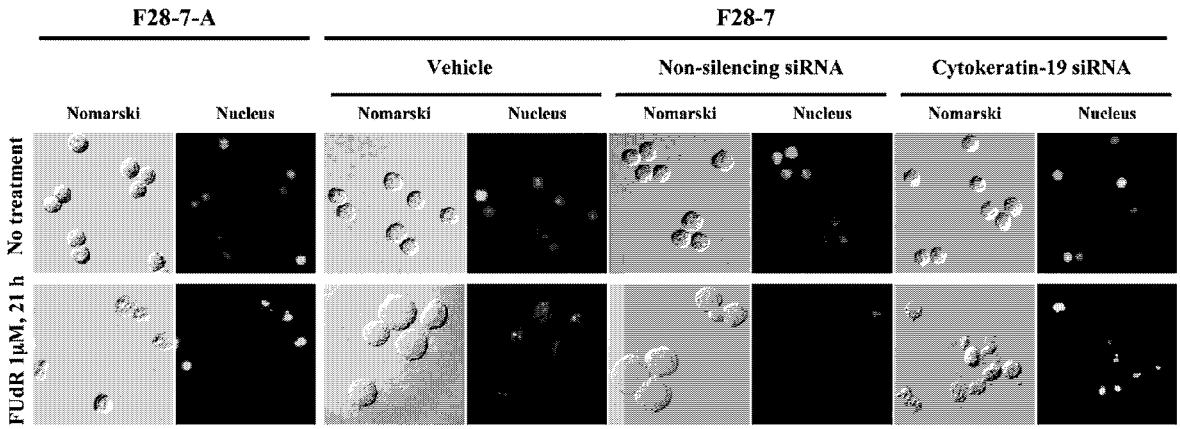

Figure 6. Knockdown of cytokeratin-19 shifts FUdR-induced cell-death morphology from necrosis to apoptosis. Forty-eight hours after transfection with the vehicle, the nonsilencing siRNA, or the cytokeratin-19 siRNA cocktail, the F28-7 cells were treated with or without 1 μM FUdR for 21 h and then stained with DAPI as described under Materials and Methods. Morphological changes were analyzed under a fluorescence microscope at ×400 magnification. Two additional experiments gave similar results.

replication, and gene expression.[9−13] Using the same strategy as with lamin B1, we have shown here that a knockdown of cytokeratin-19 in F28-7 results in a shift from necrosis to apoptosis for the FUdR-induced cell-death, leading us to propose that cytokeratin-19 functions, either directly or indirectly, in regulating the cell death-morphology. Both of those proteins, lamin B1 and cytokeratin-19, are constituents of cellular intermediate filaments. Intermediate filaments, together with actin microfilaments and tublin microtubles, comprise the three major cytoskeletal networks that are found in most eukaryotic cells.[14] Keratins, which are the largest intermediate filament protein subgroup, can be divided into acidic type-I (K9−K20) and basic type-II (K1−K8).[15] Keratin networks are highly dynamic; keratins are reorganized during cell differentiation, mitosis and apoptosis, and they play important cytoprotective and structural support roles for the cells.[16,17] Cytokeratin-19 is a member in the largest cytoplasmic intermediate filament-protein subgroup, constituting a key structural component of the cytoskeletal proteins.[18,19] Previous reports have indicated that cytokeratin-19 undergoes caspase-mediated degradation during apoptosis.[20−22] However, participation of cytokeratin-19 in regulation of necrosis and apoptosis has not been documented. Our data suggest that strong expressions of nuclear and cytoplasmic intermediate filament-proteins, lamin B1 and cytokeratin-19, are important in necrosis, and poor expressions of these proteins lead to apoptosis. In addition, it is known that nuclear and cytoplasmic intermediate filament-proteins (e.g., lamin B1, cytokeratin-8, cytokeratin-18, cytokeratin-19, and vimentin) are caspase substrates, which undergo caspase-mediated cleavage during apoptosis.[20−24] It seems that a decrease of these intermediate filament-proteins gives greater flexibility in nucleus and cell-structure, thereby leading to apoptosis.

As described above, the proteome analysis revealed differently expressed proteins (see Tables 1 and 2). Most of these proteins are for the first time revealed as being differently expressed in necrosis and apoptosis. These proteins need to be investigated further to determine whether they are directly involved in the FUdR-induced necrosis and apoptosis at all.

In our proteome analysis, several proteins (e.g., stress-70 protein, galactokinase, annexin A3 and ATP synthase subunit alpha) were detectable in different spots, most likely as a consequence of post-translational modifications or differential mRNA splicings.

Our recent work revealed that a release of cytochrome c from mitochondria into the cytoplasm and nucleus occurs in the apoptosis but not in the necrosis.[6] Reports from other laboratories have shown that mitochondria play a role in mediating both necrosis and apoptosis.[25−27] Interestingly, a number of the mitochondrial proteins exhibit differential expressions in F28-7 and F28-7-A cells either in the untreated stages or in the FUdR-treated stages. Among these proteins, a member of the molecular chaperone Heat shock protein 70 (HSP70) family, stress-70 protein (GRP75), was found to be present in Spot 4 in Figure 1A and Spot 7 in Figure 1B. It is known that GRP75 receives phosphorylation and/or acetylation as post-translational modifications.[28,29] We propose that an expression change, that can involve post-translational modification, of these mitochondria-localized proteins play an important role prior to the release of cytochrome c, a role decisive in determining the FUdR-induced death morphology.

Previously, we demonstrated that an inhibition of HSP90, a well-documented chaperone, causes in F28-7 a shift from necrosis to apoptosis in FUdR-induced cell-killing.[6] HSP90 is probably one of key regulators in the necrosis and apoptosis, and it would be interesting to explore the relationship between the presently found activities of cytokeratin-19 and lamin B1, the filament constituents, and the role of the ubiquitous cell-component HSP90 in the cell death.

Finally, our present work shows that these cell-death models and the approach by proteome analysis coupled with usage of interfering RNAs provide a useful methodology in studying molecular mechanisms of necrosis and apoptosis.

Acknowledgment. We thank Dr. Hikoya Hayatsu (Faculty of Pharmaceutical Sciences, Okayama University) for helpful discussions. This research was partly supported by Grant-in-Aid for Young Scientists (B) from the Ministry of Education, Culture, Sports, Science and Technology (21790078, A.S.).

Supporting Information Available: Supplementary Figure 1 and Tables 1−3. This material is available free of charge via the Internet at http://pubs.acs.org.

References

(1) Klose, J.; Kobalz, U. Two-dimensional electrophoresis of proteins: an updated protocol and implications for a functional analysis of the genome. *Electrophoresis* **1995**, *16*, 1034–1059.
(2) Farber, E. Programmed cell death: necrosis versus apoptosis. *Mod. Pathol.* **1994**, *7*, 605–609.
(3) Kerr, J. F. Shrinkage necrosis: a distinct mode of cellular death. *J. Pathol.* **1971**, *105*, 13–20.
(4) Thiede, B.; Rudel, T. Proteome analysis of apoptotic cells. *Mass Spectrom. Rev.* **2004**, *23*, 333–349.
(5) Kakutani, T.; Ebara, Y.; Kanja, K.; Hidaka, M.; et al. Different modes of cell death induced by 5-fluoro-2′-deoxyuridine in two clones of the mouse mammary tumor FM3A cell line. *Biochem. Biophys. Res. Commun.* **1998**, *247*, 773–779.
(6) Sato, A.; Hiramoto, A.; Uchikubo, Y.; Miyazaki, E.; et al. Gene expression profiles of necrosis and apoptosis induced by 5-fluoro-2′-deoxyuridine. *Genomics* **2008**, *92*, 9–17.
(7) Yoshioka, A.; Tanaka, S.; Hiraoka, O.; Koyama, Y.; et al. Deoxyribonucleoside triphosphate imbalance. 5-Fluorodeoxyuridine-induced DNA double strand breaks in mouse FM3A cells and the mechanism of cell death. *J. Biol. Chem.* **1987**, *262*, 8235–8241.
(8) Sato, A.; Hiramoto, A.; Satake, A.; Miyazaki, E.; et al. Association of nuclear membrane protein lamin B1 with necrosis and apoptosis in cell death induced by 5-fluoro-2′-deoxyuridine. *Nucleosides Nucleotides Nucleic Acids* **2008**, *27*, 433–438.
(9) Cohen, M.; Lee, K. K.; Wilson, K. L.; Gruenbaum, Y. Transcriptional repression, apoptosis, human disease and the functional evolution of the nuclear lamina. *Trends Biochem. Sci.* **2001**, *26*, 41–47.
(10) Wilson, K. L.; Zastrow, M. S.; Lee, K. K. Lamins and disease: insights into nuclear infrastructure. *Cell* **2001**, *104*, 647–650.
(11) Goldman, R. D.; Gruenbaum, Y.; Moir, R. D.; Shumaker, D. K.; et al. Nuclear lamins: building blocks of nuclear architecture. *Genes Dev.* **2002**, *16*, 533–547.
(12) Burke, B.; Stewart, C. L. Life at the edge: the nuclear envelope and human disease. *Nat. Rev. Mol. Cell Biol.* **2002**, *3*, 575–585.
(13) Hutchison, C. J. Lamins: building blocks or regulators of gene expression. *Nat. Rev. Mol. Cell Biol.* **2002**, *3*, 848–858.
(14) Ku, N. O.; Zhou, X.; Toivola, D. M.; Omary, M. B. The cytoskeleton of digestive epithelia in health and disease. *Am. J. Physiol.* **1999**, *277*, G1108–1137.
(15) Schweizer, J.; Bowden, P. E.; Coulombe, P. A.; Langbein, L.; et al. New consensus nomenclature for mammalian keratins. *J. Cell Biol.* **2006**, *174*, 169–174.
(16) Omary, M. B.; Coulombe, P. A.; McLean, W. H. Intermediate filament proteins and their associated diseases. *N. Engl. J. Med.* **2004**, *351*, 2087–2100.

(17) Omary, M. B.; Ku, N. O.; Tao, G. Z.; Toivola, D. M.; et al. Heads and tails" of intermediate filament phosphorylation: multiple sites and functional insights. *Trends Biochem. Sci.* **2006**, *31*, 383–394.
(18) Wu, Y. J.; Rheinwald, J. G. A new small (40 kd) keratin filament protein made by some cultured human squamous cell carcinomas. *Cell* **1981**, *25*, 627–635.
(19) Moll, R.; von Bassewitz, D. B.; Schulz, U.; Franke, W. W. An unusual type of cytokeratin filament in cells of a human cloacogenic carcinoma derived from the anorectal transition zone. *Differentiation* **1982**, *22*, 25–40.
(20) Ku, N. O.; Liao, J.; Omary, M. B. Apoptosis generates stable fragments of human type I keratins. *J. Biol. Chem.* **1997**, *272*, 33197–33203.
(21) Ku, N. O.; Omary, M. B. Effect of mutation and phosphorylation of type I keratins on their caspase-mediated degradation. *J. Biol. Chem.* **2001**, *2276*, 26792–26798.
(22) Oshima, R. G. Apoptosis and keratin intermediate filaments. *Cell Death Differ.* **2001**, *9*, 486–492.
(23) Kawahara, A.; Enari, M.; Talanian, R. V.; Wong, W. W.; et al. Fas-induced DNA fragmentation and proteolysis of nuclear proteins. *Genes Cells* **1998**, *3*, 297–306.
(24) Byun, Y.; Chen, F.; Chang, R.; Trivedi, M.; et al. Caspase cleavage of vimentin disrupts intermediate filaments and promotes apoptosis. *Cell Death Differ.* **2001**, *8*, 443–450.
(25) Tsujimoto, Y. Cell death regulation by the Bcl-2 protein family in the mitochondria. *J. Cell. Physiol.* **2003**, *195*, 158–167.
(26) Green, D. R.; Kroemer, G. The pathophysiology of mitochondrial cell death. *Science* **2004**, *305*, 626–629.
(27) Nakagawa, T.; Shimizu, S.; Watanabe, T.; Yamaguchi, O.; et al. Cyclophilin D-dependent mitochondrial permeability transition regulates some necrotic but not apoptotic cell death. *Nature* **2005**, *434*, 652–658.
(28) Rikova, K.; Guo, A.; Zeng, Q.; Possemato, A.; et al. Global survey of phosphotyrosine signaling identifies oncogenic kinases in lung cancer. *Cell* **2007**, *131*, 1190–1203.
(29) Matsuoka, S.; Ballif, B. A.; Smogorzewska, A.; McDonald, E. R.; et al. ATM and ATR substrate analysis reveals extensive protein networks responsive to DNA damage. *Science* **2007**, *316*, 1160–1166.

PR9010537

Transmission of the bacterium occurs primarily through bites from arthropods, including the dog tick (*Dermacentor variabilis*), the wood tick (*D. andersoni*), the lone star tick (*Amblyomma americanum*), and the deer fly (*Chrysops* spp.). In addition, contact with infected animals, most commonly rabbits, wild rodents, and cats, is another common route of transmission to humans (*1*,*6*).

Tularemia occurs in various animal species. Lagomorphs, rodents, and sheep are most susceptible; infected animals are frequently found dead or moribund. Carnivores are less susceptible; however, feline tularemia occurs sporadically, and human infections associated with bites and scratches from infected cats have been recognized (*7*). In addition to arthropod bites, contact with infected dead rabbits or their tissues appears to be the most common source of human infection. A wide variety of case reports have been published describing unique incidences of rabbit–human transmission, including a lawn mower aerosolizing rabbit nests along with their occupants (*8*), consumption of undercooked rabbit meat (*9*), and contact with a "lucky" rabbit's foot (*10*).

The purpose of this report is to alert veterinarians, veterinary laboratory personnel, and public health officials that rabbit tularemia can be easily overlooked on gross examination in animals displaying lesions of hepatic coccidiosis, a common disease of the wild rabbit. Therefore, all rabbits submitted for postmortem examinations should be regarded as potentially infected with tularemia, particularly during seasons when vectors are active.

Dae Young Kim, Thomas J. Reilly, Susan K. Schommer, and Sean T. Spagnoli

Author affiliation: University of Missouri, Columbia, Missouri, USA

DOI: 10.3201/eid1612.101013

References

1. Foley JE, Nieto NC. Tularemia. Vet Microbiol. 2010;140:332–8. DOI: 10.1016/j.vetmic.2009.07.017
2. Hobbs RP, Twigg LE. Coccidia (*Eimeria* spp.) of wild rabbits in southwestern Australia. Aust Vet J. 1998;76:209–10. DOI: 10.1111/j.1751-0813.1998.tb10131.x
3. Ellis J, Oyston PC, Green M, Titball RW. Tularemia. Clin Microbiol Rev. 2002;15:631–46. DOI: 10.1128/CMR.15.4.631-646.2002
4. Long GW, Oprandy JJ, Narayanan RB, Fortier AH, Porter KR, Nacy CA. Detection of *Francisella tularensis* in blood by polymerase chain reaction. J Clin Microbiol. 1993;31:152–4.
5. Centers for Disease Control and Prevention. Reported tularemia cases by state—United States, 2000–2008 [cited 2010 Jun 23]. http://www.cdc.gov/tularemia/Surveillance/Tul_CasesbyState.html
6. Farlow J, Wagner DM, Dukerich M, Stanley M, Chu M, Kubota K, et al. *Francisella tularensis* in the United States. Emerg Infect Dis. 2005;11:1835–41.
7. Arav-Boger R. Cat-bite tularemia in a seventeen-year-old girl treated with ciprofloxacin. Pediatr Infect Dis J. 2000;19:583–4. DOI: 10.1097/00006454-200006000-00024
8. Agger WA. Tularemia, lawn mowers, and rabbits' nests. J Clin Microbiol. 2005;43:4304. DOI: 10.1128/JCM.43.8.4304-4305.2005
9. Jansen A, Schmidt W, Schneider T. Rabbit's revenge. Lancet Infect Dis. 2003;3:348. DOI: 10.1016/S1473-3099(03)00656-X
10. Ryan-Poirier K, Whitehead PY, Leggiadro RJ. An unlucky rabbit's foot? Pediatrics. 1990;85:598–600.

Address for correspondence: Dae Young Kim, Veterinary Medical Diagnostic Laboratory, College of Veterinary Medicine, University of Missouri, 1600 E Rollins St, Columbia, MO 65211, USA; email: kimdy@missouri.edu

Imported Leishmaniasis in Dogs, US Military Bases, Japan

To the Editor: Leishmaniasis is found in canids in ≈50 of the 88 countries where leishmaniases are found in humans (*1*). In Japan, 2 cases of imported canine leishmaniasis have been documented in dogs from Spain (*2*,*3*). We report 2 cases of leishmaniasis in dogs in which dermatitis developed mainly on the face. Leishmaniasis was diagnosed from results of a serologic rk39 test, followed by PCR of skin lesion specimens for the *Leishmania* spp.–specific small subunit (SSU) rRNA gene. Because the dogs had lived on a US military base in Sicily, Italy, for 3 years before their owners were transfered to Japan, the animals were likely infected with *L. infantum* in Italy.

Animal 1 was a 6-year-old female dog that had lived in Sicily for 3 years, since 2003, and had been brought to Japan in September 2006. While she lived in Italy, she had exhibited alopecic, pruritic, and crusty skin lesions, mainly around the face and on the forearms and hind legs.

In November 2006, the dog was brought to the US Army Veterinary Command's Zama Veterinary Treatment Facility with dermatitis (online Appendix Figure, panel A, www.cdc.gov/EID/content/16/12/2017-appF.htm) and additional signs of kidney failure. A serum specimen was positive by the rk39 dipstick test for diagnosis of visceral leishmaniasis (Kalazar Detect; InBios, Seattle, WA, USA). A skin punch biopsy specimen was obtained for cultures and PCR for the parasites in December 2006. Cultures of 4 skin specimens were all negative, probably because of cool transportation of the samples for 1.5 days before the cultures were started. The dog's condition was treated with ketoconazole and then allopurinol. The

skin conditions initially improved, but the lesions did not completely resolve (online Apendix Figure, panels B–D). In May 2008, the dog was humanely killed because of central vestibular disease with unknown cause. A necropsy was not performed.

Animal 2 was a 12-year-old male dog that had also lived in Sicily for 3 years since 2000, and was brought to Yokosuka Base in Japan in 2003. In January 2004, the dog was positive for visceral leishmaniasis by the rk39 test; no particular clinical signs were observed.

In March 2007, the dog was referred to Zama Veterinary Treatment Facility with pruritic alopecia on the dorsum and head, and a skin punch biopsy specimen was obtained for histopathologic evaluation. The presence of amastigotes of *Leishmania* species within areas of dermal inflammation was confirmed at the Armed Forces Institute of Pathology (Washington, DC, USA). In April 2007, a second skin punch biopsy specimen was obtained for PCR.

PCR was performed for the *Leishmania*-specific SSU rRNA gene (*4*). For primary PCR, primers R221 (5′-GGTTCCTTTCCTGATTTACG-3′) and R332 (5′-GGCCGGTAAAGGCC GAATAG-3′) were used. For nested PCR, primers R223 (5′-TCCCA TCGCAACCTCGGTT-3′) and R333 (5′-AAAGCGGGCGCGGTG CTG-3′) were used. In the primary reaction, the expected PCR products of ≈603 bp were detected in 2 of 4 skin DNA specimens from patient 1 and 1 of 5 skin DNA specimens from patient 2 (Figure, panel A, lanes 2, 3, 9). In the nested reaction, the expected PCR products of ≈359 bp were seen in all 4 specimens from patient 1 and in 4 of 5 specimens from patient 2 (Figure, panel B, lanes 1–4, and 5, 6, 8, 9); some bands were faint. The nucleotide sequences (288 bp) of the nested PCR product of patient 1 were 100% identical to those of patient 2 and sequences of the SSU rRNA gene of *L. infantum* (IPT1 strain, used as a positive control), *L. infantum* (M81429), *L. donovani* (M80295), and *L. chagasi* (M81430).

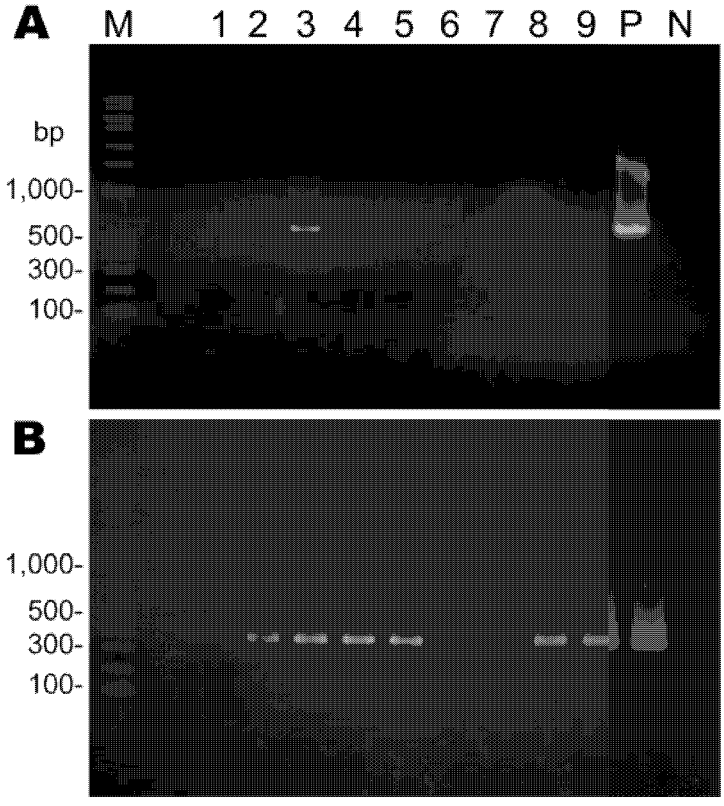

Figure. PCR amplification of the *Leishmania* spp.–specific small subunit rRNA gene from skin biopsy specimens from infected dogs, Japan. DNA samples (100–200 ng) were subjected to primary PCR (A), followed by nested PCR (B). Lanes 1–4, skin DNA samples from patient 1; lanes 5–9, skin DNA samples from patient 2; M, DNA molecular marker; P, positive control; N, negative control.

Global warming, which causes changes in the distribution of the sand fly vectors, and human-produced risk factors, such as travel, migration, and urbanization, may increase the incidence of leishmaniasis (*5*). Military mobility and operations are also a major risk factor for leishmaniasis in humans and canids (*6*). In Japan, of >300 kala-azar (visceral leishmaniasis) patients reported, 218 were soldiers who returned from the People's Republic of China before and after World War II (*7*). In the present study, 2 dogs infected with *L. infantum* had been brought to Japan from Italy by US military families.

Dog-to-dog transmission by direct contact with contaminated blood through biting may explain the recent outbreaks of leishmaniasis in foxhounds in North America (*8*). In Japan, although no sandfly species that could transmit leishmania have been reported (*7*), direct dog-to-dog transmission of leishmaniasis can occur. *Babesia gibsoni* infection is prevalent among fighting dogs in Japan, likely because of the transmission of infected erythrocytes through biting (*9*). Greater sharing of information and of diagnostic procedures is required in Japan because few medical and veterinary practitioners have experience with leishmaniasis patients.

This study was supported in part by grants from the Global Center of Excellence program for International Collaboration Centers for Zoonosis Control and grant no. 183801780 from the Ministry

of Education, Culture, Sport, Science and Technology of Japan.

Yuta Kawamura, Isao Yoshikawa, and Ken Katakura

Author affiliations: Hokkaido University Graduate School of Veterinary Medicine, Sapporo, Hokkaido, Japan (Y. Kawamura, K. Katakura); and US Army Japan District Veterinary Command–Zama Branch Kangawa, Japan (I. Yoshikawa)

DOI: 10.3201/eid1612.100389

References

1. Alvar J, Cañavate C, Molina R, Moreno J, Nieto J. Canine leishmaniasis. Adv Parasitol. 2004;57:1–88. DOI: 10.1016/S0065-308X(04)57001-X
2. Namikawa K, Watanabe M, Lynch J, Sugaki Y, Kitai T, Sunaga F, et al. A canine case of *Leishmania infantum* infection in Japan. Jpn J Vet Dermatol. 2006;12:11–5. DOI: 10.2736/jjvd.12.11
3. Takahashi N, Naya T, Watari T, Matsumoto Y, Matsumoto Y, Tsujimoto H, et al. An imported case of canine cutaneous leishmaniasis in Japan. Jpn J Vet Dermatol. 1997;3:25–7.
4. Van Eys GJ, Schoone GJ, Kroon NC, Ebeling SB. Sequence analysis of small subunit ribosomal RNA genes and its use for detection and identification of *Leishmania* parasites. Mol Biochem Parasitol. 1992;51:133–42. DOI: 10.1016/0166-6851(92)90208-2
5. Desjeux P. The increase in risk factors for leishmaniasis worldwide. Trans R Soc Trop Med Hyg. 2001;95:239–43. DOI: 10.1016/S0035-9203(01)90223-8
6. Coleman RE, Bukert DA, Putma JL, Sherwood V, Caci JB, Jennings BT, et al. Impact of Phlebotomine sand flies on U.S. military operations at Talli air base, Iraq: 1. background, military situation, and development of a "leishmaniasis control program." J Med Entomol. 2006;43:647–62. DOI: 10.1603/0022-2585(2006)43[647:IOPSFO]2.0.CO;2
7. Katakura K. Molecular epidemiology of leishmaniasis in Asia (focus on cutaneous infections). Curr Opin Infect Dis. 2009;22:126–30. DOI: 10.1097/QCO.0b013e3283229ff2'
8. Duprey ZH, Steurer FJ, Rooney JA, Kirchhoff LV, Jackson JE, Rowton ED, et al. Canine visceral leishmaniasis, United States and Canada, 2000–2003. Emerg Infect Dis. 2006;12:440–6.
9. Miyama T, Sakata Y, Shimada Y, Ogino S, Watanabe M, Itamoto K, et al. Epidemiological survey of *Babesia gibsoni* infection in dogs in eastern Japan. J Vet Med Sci. 2003;67:467–71. DOI: 10.1292/jvms.67.467

Address for correspondence: Ken Katakura, Laboratory of Parasitology, Department of Disease Control, Graduate School of Veterinary Medicine, Hokkaido University, Kita 18 Nishi 9, Kita-ku Sapporo 060-0818, Hokkaido, Japan; email: kenkata@vetmed.hokudai.ac.jp

Serologic Evidence of Pandemic (H1N1) 2009 Infection in Dogs, Italy

To the Editor: Until recently, the general consensus has been that dogs are poorly susceptible to natural infection with influenza A viruses; however, since the recent upsurge of influenza A circulating subtypes H5N1 and H1N1 viruses, cases of natural infection in dogs have apparently increased. Thus, the role of these animals is being reconsidered in the transmission and spread of influenza viruses (*1–3*).

In April 2009, the most recent of the human influenza A pandemics, pandemic (H1N1) 2009, was detected in Mexico. The virus rapidly spread worldwide, within weeks of its first isolation. To date, pandemic (H1N1) 2009 has primarily infected humans, although transmission from infected humans to other animals, including pigs, turkeys, ferrets, cats, and dogs has been reported (*4*,*5*).

In Italy (population ≈58 million), the first human cases of pandemic (H1N1) 2009 were reported in May 2009; confirmed cases peaked during the second week of November 2009 (week 46) (*6*). As of May 9, 2010, Italy had recorded an estimated 5,582,000 cases of pandemic (H1N1) 2009. In Italy as well, the population has ≈7 million companion dogs and ≈7.5 million cats (*7*). Because of the close contact between persons and their companion animals, we initiated this serologic study to determine whether evidence of pandemic (H1N1) 2009 transmission could be found in companion animals in Italy.

We tested serum specimens from dogs (n = 964) and cats (n = 97), originally submitted to the Istituto Zooprofilattico Sperimentale delle Venezie in Legnaro, Italy, from October through December 2009 (weeks 41–53), for assessment of rabies vaccine efficacy. An average of 70 samples were tested per week; the highest number of samples (n = 106) was tested for week 51 and the lowest (n = 25) for week 53. Testing for antibody to influenza A nucleoprotein was performed by using a commercially available competitive ELISA (cELISA) (ID Screen Influenza A Antibody Competition Assay; ID Vet, Montpellier, France), according to the manufacturer's instructions. Previous work from our laboratory has assigned a sensitivity of 93.98% and specificity of 98.71% to this cELISA for the testing of canine serum samples (*8*). In total, 29 serum specimens tested at a 1:10 dilution, all from dogs, were positive after a second confirmatory screening. None of the 97 feline serum samples were positive by cELISA.

The cELISA-positive serum specimens were then treated with receptor-destroying enzyme (RDE; Sigma-Aldrich, St. Louis, MO, USA) (1 part serum: 3 parts RDE) for 16 h at 37°C, followed by heat inactivation at 56°C for 30 min. We then tested the specimens by the hemagglutination inhibition (HI) test against the pandemic virus A/Verona/Italy/2810/2009 (H1N1), A/swine/Italy/711/2006 (H1N1), and H3N8 (A/canine/Florida/2004) by using 0.5% chicken erythrocytes and standard methods (*9*). Seven serum samples (nos. 4410, 4438, 4444, 4460, 4517, 4520, 4681) were positive by HI

NOTE *Parasitology*

Evaluation of Myanmar Medicinal Plant Extracts for Antitrypanosomal and Cytotoxic Activities

Saw BAWM[1)], Saruda TIWANANTHAGORN[1)], Kyaw San LIN[2)], Junichi HIROTA[1)], Takao IRIE[1)], Lat Lat HTUN[2)], Ni Ni MAW[3)], Tin Tin MYAING[2)], Nyunt PHAY[4)], Satoshi MIYAZAKI[1)], Tatsuya SAKURAI[1)], Yuzaburo OKU[1)], Hideyuki MATSUURA[5)] and Ken KATAKURA[1)]*

[1)]*Laboratory of Parasitology, Department of Disease Control, Graduate School of Veterinary Medicine, Hokkaido University, Kita 18, Nishi 9, Kita-ku, Sapporo 060–0818, Japan,* [2)]*Department of Pharmacology and Parasitology, University of Veterinary Science, Yezin, Naypyitaw, Myanmar,* [3)]*Livestock Breeding and Veterinary Department, Naypyitaw, Myanmar,* [4)]*Pathein University, Pathein, Myanmar and* [5)]*Laboratory of Bioorganic Chemistry, Division of Applied Bioscience, Graduate School of Agriculture, Hokkaido University, Kita 9, Nishi 9, Kita-ku, Sapporo 060–8589, Japan*

(Received 11 November 2009/Accepted 6 December 2009/Published online in J-STAGE 22 December 2009)

ABSTRACT. Current chemotherapeutic options for African trypanosomiasis in humans and livestock are very limited. In the present study, a total of 71 medicinal plant specimens from 60 plant species collected in Myanmar were screened for antitrypanosomal activity against trypomastigotes of *Trypanosoma evansi* and cytotoxicity against MRC-5 cells *in vitro*. The methanol extract of dried rootbark of *Vitis repens* showed the highest antitrypanosomal activity with IC_{50} value of 8.6 ± 1.5 μg/m*l* and the highest selectivity index of 24.4. The extracts of *Brucea javanica, Vitex arborea, Eucalyptus globulus* and *Jatropha podagrica* had also remarkable activity with IC_{50} values and selectivity indices in the range of 27.2–52.6 μg/ml and 11.4–15.1 respectively.

KEY WORDS: antitrypanosomal activity, Myanmar medicinal plants, *Trypanosoma evansi*, *Vitis repens*.

J. Vet. Med. Sci. 72(4): 525–528, 2010

Tsetse-transmitted African trypanosomiasis, such as sleeping sickness in humans and nagana in cattle, are causing serious problems to human health and animal production in Africa. A wasting disease called surra by *Trypanosoma evansi* infection is not restricted to Africa and distributed worldwide, because the parasite is mechanically transmitted by blood-sucking insects such as *Tabanus* and *Stomoxys* species. *T. evansi* is pathogenic to a wide variety of animals, including equines, camels, cattle, buffaloes, goats, sheep, pigs, and dogs, causing great economic losses in livestock industries in Asia [3, 9]. However, current chemotherapeutic options for trypanosomiasis in humans and livestock are very limited and far from ideal. Existing trypanocidal drugs have to be administered by injection. The drugs have been associated with severe side-effects and ineffectiveness against drug resistant parasites. Therefore, research for developing of new drugs, which are safe, effective, cheap, easy-to-administer, and possess novel mechanism of action, is urgently needed [6, 7, 10].

Myanmar is abundant plant resources and Myanmar peoples have inherited their own traditional medicine to maintain their health and treat various ailments including malaria, diarrhea and fever for over millennia of history [14]. Recently, we reported that quassinoids isolated from the fruits of an Asian medicinal plant, *Brucea javanica*, showed remarkable antibabesial and antitrypanosomal activities [2, 11, 16], suggesting a promise use of medicinal plant extracts for protozoan diseases in livestock. In the present study, the *in vitro* antitrypanosomal and cytotoxic activities of crude extracts of medicinal plants in Myanmar were evaluated.

A total of 55 fresh plant specimens from 45 plant species were collected at the National Herbal Park in Naypyitaw and the National Botanical Garden in Pyin-oo-lwin, Myanmar in January 2009 (Table 1). Species identification was done by Mr. Hla Myint and Dr. Kyaw Kyaw Swe at each Institute. These fresh plants were cut into small pieces with scissors and preserved in 70% ethanol immediately after collection. Seven dry plant specimens from seven plant species were prepared at Pathein University after identification of the plant species. Nine dry plant specimens from nine plant species were obtained at Thein-gyi market in Yangon. Only *Andrographis paniculata* overlapped in both the fresh (stem and twigs with leaves) and dry (leaf and stem) samples.

Fresh plant specimens (15–30 g) were extracted with 40 m*l* of 70% ethanol for two weeks. Dry plant specimens (10–20 g), except the powder of *Brucea javanica* fruits, were also cut into small pieces. These dry samples were extracted with 40 m*l* of 70% methanol for 7 days at room temperature. The choice for use of ethanol for fresh sample extraction was due to the availability and low toxicity at the time of collecting plant samples. We used methanol for dry sample extraction because methanol was scored slightly higher than ethanol for the screening of antimicrobial components from plants [5]. The extracts were passed through a filter paper (Advantec Toyo Kaisha, Ltd., Tokyo, Japan) and concentrated in a rotary evaporator at 37°C, yielding dried crude extracts in the range of 0.7–28.0% weight of the starting

* CORRESPONDENCE TO: KATAKURA, K., Laboratory of Parasitology, Department of Disease Control, Graduate School of Veterinary Medicine, Hokkaido University, Kita 18, Nishi 9, Kita-ku, Sapporo 060–0818, Japan.
e-mail: kenkata@vetmed.hokudai.ac.jp

Table 1. *In vitro* antitrypanosomal and cytotoxic activities of crude plant extracts

Scientific name (family name)	Parts	% yield of extracts	IC_{50} ($\mu g/ml$) Antitrypanosomal *T. evansi*	IC_{50} ($\mu g/ml$) Cytotoxicity MRC-5	SI	Traditional uses
Fresh Sample						
Adhatoda vasica Nees. (Acanthaceae)	L	4.8	458.1 ± 189.1	nd		Pulmonary diseases, dry cough
Ageratum conyzoides Linn. (Compositae)	L	2.9	440.6 ± 75.3	nd		Antibacterial
Alpinia officinarum Hance. (Zingiberaceae)	R	5.4	242.2 ± 20.5	nd		Anti-diuretics, aches etc.
Alstonia scholaris R. Br. (Apocyanaceae)	L	1.0	391.7 ± 5.8	nd		Antiseptic, amoebic dysentery
Andrographis paniculata Nees. (Acanthaceae)	STL	1.1	467.4 ± 8.8	nd		Malaria, antipyretic, tonic
Artemesia annua Linn. (Compositae)	L	4.3	316.2 ± 99.4	nd		Malaria
Artemesia annua	Fl	0.8	326.9 ± 47.3	nd		Malaria
Artemesia vulgaris Linn. (Compositae)	LS	16.9	196.9 ± 112.5	nd		Malaria
Asparagus racemosus Willd. (Liliaceae)	R	14.2	325.9 ± 125.6	nd		Diarrhoea, fever, blood tonic
Azadirachta indica (Meliaceae)	L	7.9	167.8 ± 12.5	nd		Diabetes, malaria, skin diseases
Barleria prionitis Linn. (Acanthaceae)	L	4.4	>1000	nd		Diuretic, oedema, pile
Barleria prionitis	L	4.2	252.4 ± 23.9	nd		
Blumea balsamifera DC. (Compositae)	L	2.0	429.5 ± 19.4	nd		Gastric disease, arthritis
Crinum latifolium Linn. (Amaryllidaceae)	L	1.9	443.1 ± 103.9	nd		Dysentry, diarrhoea
Crinum pratense Herb. (Amaryllidaceae)	L	2.3	251.8 ± 72.1	nd		Gonorrhoea, arthritis, dilatation of pupil
Crinum sp.	L	2.7	400.1 ± 51.6	nd		Malaria, dysentery
Curcuma comosa (Zingiberaceae)	Rh	3.6	236.9 ± 6.6	nd		
Elettaria cardamomum Maton. (Zingiberaceae)	L	3.1	157.9 ± 15.8	nd		Dysentery, malaria and diarrhoea
Eucalyptus globulus Labill. (Myrtaceae)	L	0.7	51.1 ± 1.5	622.95 ± 299.7	12.2	Malaria
Euonymus kachinensis (Celastraceae)	L	3.8	232.2 ± 62.2	nd		Relief poisons, sore, antimicrobial
Eupatorium odoratum Linn. (Compositae)	L	9.4	414.7 ± 89.8	nd		Antiseptic, anti tumor
Euphorbia hirta Linn. (Euphorbiaceae)	L	3.1	118.7 ± 7.1	nd		Antimicrobial
Euphorbia longana (Euphorbiaceae)	LFl	5.1	280.3 ± 69.2	nd		Diarrhoea
Holarrhena antidysenterica Wall. (Apocynaceae)	L	1.7	180.6 ± 54.8	nd		Amoebic dysentery, diarrhoea, astringent
Hydrocotyle asiatica Linn. (Umbelliferae)	L	5.3	590.9 ± 25.9	nd		Longevity, leprosy
Ichnocarpus frutescens R.Br. (Apocyanaceae)	L	2.4	205.5 ± 86.1	nd		Tonic, effective on the heart, gallbladder
Jatropha podagrica HK. (Euphorbiaceae)	L	3.5	736.5 ± 186.1	nd		Pulmonary and gastrointestinal diseases
Jatropha podagrica	F	3.7	52.3 ± 13.5	652.7 ± 202.9	12.5	
Kalanchoe laciniata DC. (Crassulaceae)	LT	3.1	396.3 ± 46.5	nd		Dysentery, diarrhoea
Mansonia gagei Drummond. (Sterculiaceae)	L	2.9	789.6 ± 80.8	nd		Fever, dysentery
Morinda angustifolia Roxb. (Rubiaceae)	L	3.5	330.3 ± 11.0	nd		Fever, tonic, dysentery, diarrhoea
Ocimum sanctum Linn. (Labiatae)	LFl	1.8	578.0 ± 251.3	nd		Deodorant, headache, cough
Origanum majorana Linn. (Labiatae)	L	1.9	287.6 ± 73.0	nd		Antimicrobial, anti inflammation, diuretic
Orthosiphon aristatus (Blume) Miq. (Labiatae)	L	3.0	495.0 ± 51.1	nd		Diabetes, arthritis, diuretics
Orthosiphon stamineus (Labiatae)	L	2.6	144.7 ± 36.4	628.9 ± 66.8	4.3	Diabetes, arthritis, diuretics
Physalis peruviana Linn. (Solanaceae)	F	5.4	625.1 ± 86.4	nd		Fever
Piper attenuatum Buch. Ham. (Piperaceae)	L	5.5	282.8 ± 141.9	nd		Malaria
Piper attenuatum	F	5.1	469.6 ± 4.1	nd		
Piper nigrum Linn. (Piperaceae)	L	2.5	170.8 ± 49.4	nd		Malaria
Plumbago rosea Linn. (Plumbaginaceae)	L	1.7	554.5 ± 144.7	nd		Dysmenorrhea, amenorrhea
Plumbago rosea	Fl	2.1	156.7 ± 68.8	557.05 ± 269.4	3.6	
Plumbago zeylanica Linn. (Plumbaginaceae)	L	1.7	268.8 ± 0.9	nd		Leucoderma, scabies, anthelmintic
Rhoeo discolor Hance. (Commelinaceae)	L	1.8	75.8 ± 16.0	424.9 ± 160.0	5.6	Dysentry, diarrhoea
Rhoeo discolor	Fl	1.5	135.5 ± 34.0	>1000		
Rhoeo sp.	L	5.8	808.1 ± 16.1	nd		
Rhoeo sp.	Fl	2.1	490.3 ± 77.2	nd		
Sansevieria cylindrica (Liliaceae)	LT	6.2	208.6 ± 29.5	nd		Dysentry, diarrhoea
Sansevieria zeylanica Wild. (Liliaceae)	LT	1.7	255.6 ± 56.9	nd		Anti venom
Sansevieria zeylanica	L	4.8	400.8 ± 116.4	nd		
Saxifraga virginiensis (Saxifragaceae)	LS	1.8	255.6 ± 27.5	nd		Diuretic, oedema,
Talinum patens L. Wild. (Portulacaceae)	L	1.6	244.6 ± 128.2	nd		Fever, dysentery
Zingiber officinale Rosc. (Zingiberaceae)	L	2.5	305.2 ± 141.8	nd		Asthma, hiccough, cholera, earache
Zingiber officinale	R	2.4	358.6 ± 208.6	nd		
Zizyphus rugosa Lank. (Rhamnaceae)	F	11.8	373.8 ± 145.7	nd		Diarrhoea, tachycardia, skin infection
Zizyphus rugosa	S	0.7	257.6 ± 56.8	nd		

Table 1. *In vitro* antitrypanosomal and cytotoxic activities of crude plant extracts (continued)

Scientific name (family name)	Parts	% yield of extracts	IC_{50} (μg/m*l*)		SI	Traditional uses
			Antitrypanosomal	Cytotoxicity		
			T. evansi	MRC-5		
Dry Sample						
From Pathein						
Crataeva religiosa Forst. (Capparidaceae)	LS	4.0	107.1 ± 11.6	691 ± 489.3	6.4	Tumour, as tonic agent, urinary disorders
Eichomia crassipes (Pontederiaceae)	LS	4.2	157.8 ± 47.6	nd		Malaria, fever
Oldenlandia diffusa Willd. (Rubiaceae)	LS	10.0	504.8 ± 21.7	nd		Toothache, haemoptysis, menorrhagia
Phyllanthus niruri Linn. (Euphorbiaceae)	LS	5.9	336.9 ± 53.5	nd		Fever, dysentery
Phyllanthus simplex Retz. (Euphorbiaceae)	LS	2.2	96.1 ± 34.6	98.8 ± 26.0	1.0	Fever, dysentery
Vernonia cenerea Less. (Compositae)	LS	11.5	789.8 ± 2.6	nd		Fever
Vitex arborea Desf. (Verbenaceae)	LS	10.4	48.6 ± 10.9	735.15 ± 374.5	15.1	Fever
From Yangon						
Andrographis sp.	LS	28.0	616.2 ± 0.1	nd		Malaria, antipyretic, tonic
Andrographis paniculata	LS	19.6	54.7 ± 33.1	55.1 ± 20.0	1.0	
Brucea javanica (L.) Merr. (Simaroubaceae)	F	12.5	27.2 ± 7.9	309.15 ± 1.6	11.4	Dysentery, tumor, malaria
Cinnamomum tamala F. Nees. (Lauraceae)	B	17.0	445.9 ± 75.5	nd		Dysentery, antiseptic
Combretum acuminatum (Combretaceae)	Rh	14.0	90.7 ± 11.6	853.15 ± 39.3	9.4	Malaria, dysentery
Gentiana kurroo Royle. (Gentianaceae)	R	10.0	155.3 ± 80.1	nd		To promote digestion, urinary disorders
Tacca pinnatifida Forst. (Taccaceae)	R	4.7	208.4 ± 153.5	nd		Fever
Vitis repens Wight & Arn. (Vitaceae)	RB	2.3	8.6 ± 1.5	209.9 ± 125.5	24.4	Ulcers, hepatitis and jaundice, tumor
Withania somnifera Dunal. (Solanaceae)	SB	4.0	353.2 ± 174.8	nd		Inflammation, diuretic, aphradisiac
Reference drug						
Diminazene aceturate			0.01140 ± 0.001	>1000		

Plant part: L, leaf; R, root; STL, stem and twigs with leaves; F, fruit; Fl, flower; LFl, leaf and flower; LS, leaf and stem; LT, leaf and twig; Rh, rhizomes; RB, rootbark; SB, stembark. nd, not determined.

materials (Table 1). The extracts were dissolved in DMSO and diluted with HMI-9 medium [2] with 0.5% DMSO before use.

Antitrypanosomal activity test was performed in 96-well microtiter plates [2]. Trypomastigotes of bloodstream-form of *Trypanosoma evansi* (H3 strain, isolated from deer in Thailand) were used in this study. Each well contained plant extracts (1.9–1,000 μg/m*l*) and 5×10^4 parasites/m*l* in 100 μl of HMI-9 medium. Diminazene aceturate (Sigma, St. Louis, MO, U.S.A.) was used as a standard trypanocidal drug. Plates were incubated at 37°C in 5% CO_2 in air for 72 hr. Six hours before the end of incubation, 10 μl of Alamar Blue® (TREK Diagnostic Systems, Cleveland, OH, U.S.A.) was added to the cultures, and absorbance at 570 and 600 nm was measured using a plate reader (SpectraMax M5-H, Molecular Devices, Sunnyvale, CA, U.S.A.). IC_{50} (inhibitory concentration, 50%) value was calculated by computerized probit analysis. All tests were performed twice or three times, with each plant extract concentration in triplicate. Cytotoxicity assay against MRC-5 cells (human diploid lung fibroblast cell line, purchased from RIKEN Cell Bank, Tsukuba, Japan) was similarly carried out in 96-well culture plates containing a concentration of 2.5×10^4 cells/m*l* and plant extracts (concentrations of 3.9–1,000 μg/m*l*) in 100 μl of MEM medium (SAFC Biosciences, Lenexa, KS, U.S.A.) supplemented with 3% HEPES (Sigma) and 10% heat inactivated FBS (fetal bovine serum, Gibco, Carlsbad, CA, U.S.A.). After 6 days incubation at 37°C in 5% CO_2 in air, 10 μl Alamar Blue® was added to each well for 6 hr, followed by colorimetric readings, and IC_{50} values were calculated as described above. The selectivity index (SI) was determined by dividing the IC_{50} value for MRC-5 cells by the IC_{50} value for trypanosomes.

The plant species name, plant part used, yield of extract, antitrypanosomal activity, cytotoxicity, SI value and traditional use of 71 plant materials from 60 plant species collected in Myanmar are summarized in Table 1. When IC_{50} values of plant extracts against *T. evansi* were <100 μg/m*l*, cytotoxicity tests against MRC-5 cells were performed. Additionally, some other extracts showing IC_{50} values of 100–200 μg/m*l* were also examined for their cytotoxic activities. As far as we know, except for *Brucea javanica, Andrographis paniculata* and *Plumbago zeylanica*, these plant species were examined for their antiprotozoal activities for the first time. Antiprotozoal activities of medicinal plant crude extracts were classified into four categories, highly active ($IC_{50} \leq 10$ μg/m*l*), active ($IC_{50}>10 \leq 50$ μg/m*l*), moderately active ($IC_{50}>50 \leq 100$ μg/m*l*, and non-active ($IC_{50}>100$ μg/m*l*) [13]. When plant extracts showed SI≥10, these samples are considered to have good selectivity and will be considered for further bio-guided fractionation. According to these criteria, the dry plant extract from rootbark of *Vitis repens* Wight & Arn. (Vitaceae) showed high activity against *T. evansi* (IC_{50}=8.6 μg/m*l*) with good selectivity (SI=24.4). This plant species has been used for the treatment of ulcers, hepatitis/jaundice, and hypertension in Myanmar. The genus Vitis commonly contains various oligomers of resveratrol, such as vitisinols A–D, (+)-σ-viniferin, (–) viniferal, ampelopsin C, miyabenol A, (+)-vitisin A, and (+)-vitisin C [8]. These compounds are of great

interest in further investigation for the antiprotozoal activities.

Brucea javanica (L.) Merr. is widely distributed throughout Asia, where the fruits have been used for various ailments, including cancer, amoebic dysentery, and malaria. Quassinoids isolated from this plant had inhibitory activity against not only *Plasmodium falciparum* [12] but also *Babesia gibsoni in vitro* [16] and *in vivo* [11] as well as against *T. evansi in vitro* [2]. In this study, crude extract from the fruits of *B. javanica* showed the second strongest activity against *T. evansi* (IC_{50}=27.2 ± 7.9 μg/ml) and good selectivity (SI=11.4), confirming the previous studies. Further studies are required whether these extracts and quassinoids are also effective against *T. brucei* subspecies.

Vitex arborea Desf. (Verbenaceae) is a small to medium-sized evergreen tree distributed in Asia. In Myanmar, this plant is used for the treatment of fever and diarrhea. The methanol extract from leaf/stem of *Vitex arborea* showed IC_{50} of 48.6 ± 10.9 μg/ml and SI of 15.1, but there are no reports of isolated compounds from this plant species. *Jatropha podagrica* (Euphorbiaceae) is a shrub commonly found in Africa, Asia, and Latin America. The major constituents of *Jatropha* species are diterpenoids, which have shown antibacterial activity [1] as well as leishmanicidal and trypanocidal activity [15]. Recently, it has been reported that one xanthone isolated from the roots of *Andrographis paniculata* showed good *in vitro* activity (IC_{50}=4.6 μg/ml) against *T. brucei* brucei [4]. The methanol extract from the leaves and stem of this plant species showed IC_{50} value of 54.7 ± 33.1 μg/ml, but selectivity index was very low (SI=1) in this study.

In conclusion, the present study revealed that some medicinal plants in Myanmar may offer a potential use for the treatment of *Trypanosoma evansi* infection. Further studies including determination and purification of active compounds in these most promising plant extracts will be carried out.

ACKNOWLEDGMENT(S). We thank Mr. Maung Maung Nyunt, Dr. Aung Gyi, Dr. Myint Thein and all staffs of Livestock Breeding and Veterinary Department and of the University of Veterinary Science, Myanmar, and Mr. Hla Myint of Department of Traditional Medicinal, Ministry of Health, Myanmar and Dr. Kyaw Kyaw Swe for assistance in the collection and identification of plant samples. We also wish to thank Miss E. Tanaka of Hokkaido University for cytotoxic assay. This work was supported in part by the Global COE program, "Establishment of International Collaboration Centers for Zoonosis Control" from MEXT, Japan.

REFERENCES

1. Aiyelaagbe, O. O., Adesogan, K., Ekundayo, O. and Gloer, J. B. 2007. Antibacterial diterpenoids from *Jatropha podagrica* Hook. *Phytochemistry* **68**: 2420–2425.
2. Bawm, S., Matsuura, H., Elkhateeb, A., Nabeta, K., Subeki, Nonaka, N., Oku, Y. and Katakura, K. 2008. *In vitro* antitrypanosomal activities of quassinoid compounds from the fruits of a medicinal plant, *Brucea javanica*. *Vet. Parasitol.* **158**: 288–294.
3. Brun, R., Hecker, H. and Lun, Z.-R. 1998. *Trypanosoma evansi* and *T. equiperdum*: distribution, biology, treatment and phylogenetic relationship (a review). *Vet. Parasitol.* **79**: 95–107.
4. Dua, V. K., Verma, G. and Dash, A. P. 2009. *In vitro* antiprotozoal activity of some xanthones isolated from the roots of *Andrographis paniculata*. *Phytother. Res.* **23**: 126–128.
5. Eloff, J. N. 1998. Which extractant should be used for the screening and isolation of antimicrobial components from plants? *J. Ethnopharmacol.* **60**: 1–8.
6. Hoet, S., Opperdoes, F., Brun, R. and Quetin-Leclercq, J. 2004. Natural products active against African trypanosomes: a step towards new drugs. *Nat. Prod. Rep.* **21**: 353–364.
7. Kibona, S. N., Matemba, L., Kaboya, J. S. and Lubega, G. W. 2006. Drug-resistance of *Trypanosoma b. rhodesiense* isolates from Tanzania. *Trop. Med. Int. Health* **11**: 144–155.
8. Li, W. W., Li, B. G. and Chen, Y. Z. 1998. Flexuosol A, a new tetrastilbene from *Vitis flexuosa*. *J. Nat. Prod.* **61**: 646–647.
9. Luckins, A. G. 1988. *Trypanosoma evansi* in Asia. *Parasitol. Today* **4**: 137–142.
10. Matovu, E., Seebeck, T., Enyaru, J. and Kamisnky, R. 2001. Drug resistance in *T. brucei* spp., the causative agents of sleeping sickness in man and nagana in cattle. *Microbes Infect.* **3**: 763–770.
11. Nakao, R., Mizukami, C., Kawamura, Y., Subeki, Bawm, S., Yamasaki, M., Maede, Y., Matsuura, H., Nabeta, K., Nonaka, N., Oku, Y. and Katakura, K. 2009. Evaluation of efficacy of bruceine A, a natural quassinoid compound extracted from a medicinal plant, *Brucea javanica*, for canine babesiasis. *J. Vet. Med. Sci.* **71**: 33–41.
12. O'Neill, M. J., Bray, D. H., Boardman, P., Phillipson, J. D., Warhurst, D. C., Peters, W. and Suffness, M. 1986. Plants as sources of antimalarial drugs: *in vitro* antimalarial activities of some quassinoids. *Antimicrob. Agents Chemother.* **30**: 101–104.
13. Osorio, E., Arango, G. J., Jiménez, N., Alzate, F., Ruiz, G., Gutiérrez, D., Paco, M. A., Giménez, A. and Robledo, S. 2007. Antiprotozoal and cytotoxic activities *in vitro* of Colombian Annonaceae. *J. Ethnopharmacol.* **111**: 630–635.
14. Soe, K. and Ngwe, T. M. 2004. Medicinal Plants of Myanmar: Identification and Uses of Some 100 Commonly Used Species Series (1), Forest Resource Environment Development and Conservation Association, Yangon.
15. Schmeda-Hirschmann, G., Razmilic, I., Sauvain, M., Moretti, C., Muñoz, V., Ruiz, E., Balanza, E. and Fournet, A. 1996. Antiprotozoal activity of jatrogrossidione from *Jatropha grossidentata* and jatrophone from *Jatropha isabelli*. *Phytother. Res.* **10**: 375–378.
16. Subeki, Matsuura, H., Takahashi, K., Nabeta, K., Yamasaki, M., Maede, Y. and Katakura, K. 2007. Screening of Indonesian medicinal plant extracts for anti-babesial activity and isolation of new quassinoids from *Brucea javanica*. *J. Nat. Prod.* **70:** 1654–1657.

Parasitology International 59 (2010) 647–652

Contents lists available at ScienceDirect

Parasitology International

journal homepage: www.elsevier.com/locate/parint

Short communication

Gene silencing in *Echinococcus multilocularis* protoscoleces using RNA interference

Chiaki Mizukami [a], Markus Spiliotis [b], Bruno Gottstein [b], Kinpei Yagi [c], Ken Katakura [a], Yuzaburo Oku [a,*]

[a] *Laboratory of Parasitology, Department of Disease Control, Graduate School of Veterinary Medicine, Hokkaido University, Sapporo 060-0818, Japan*
[b] *Institute of Parasitology, University of Berne, Länggass-Strasse 122, CH-3001 Berne, Switzerland*
[c] *Hokkaido Institute of Public Health, Sapporo 060-0819, Japan*

ARTICLE INFO

Article history:
Received 15 April 2010
Received in revised form 23 August 2010
Accepted 24 August 2010
Available online 9 September 2010

Keywords:
Cestode
Echinococcus multilocularis
Protoscolex
RNAi
siRNA

ABSTRACT

We investigated the potential of gene silencing in *Echinococcus multilocularis* protoscoleces using RNA interference (RNAi). For the introduction of siRNA, soaking and electroporation were first examined for their effects on the viability of protoscoleces and their efficacy for siRNA introduction. Consequently, electroporation using 100 V and 800 μF showed the optimal results. This electroporation procedure was then evaluated for its ability to induce RNAi in protoscoleces using siRNAs targeting the *14-3-3* and *elp* genes. It was found that the levels of *14-3-3* and *elp* mRNA in *14-3-3* siRNA- and *elp* siRNA-treated protoscoleces were reduced to 21.8 ± 2.6 and 35.5 ± 0.4% of those of the untreated control by day 3, respectively. Moreover, the target proteins significantly decreased in the siRNA-treated samples by day 15. In the analysis of viability, the untreated control, electroporation control, *14-3-3* siRNA-treated, and *elp* siRNA-treated samples displayed 98.4 ± 1.4, 83.0 ± 2.5, 58.0 ± 23.0, and 55.1 ± 14.6% viability, respectively, on day 15. In conclusion, we successfully demonstrated that RNAi mediated the knock-down of target gene expression in *E. multilocularis* protoscoleces at both the transcriptional and translational levels.

Larval stage infection with *Echinococcus multilocularis* causes alveolar echinococcosis, one of the most lethal helminthic infections in humans, demonstrating a greater than 90% fatality rate in untreated patients [1]. Recently, *E. multilocularis* has emerged as a model experimental research system given its interesting characteristics, including its continuous active proliferation and underlying molecular mechanisms of host-parasite interactions [2], in addition to the availability of well-developed *in vivo* maintenance methods using mice and gerbils and *in vitro* cultivation systems [3]. Studies in this organism are also facilitated by available genetic information, such as cDNA sequences and genomic databases (i.e., http://fullmal.hgc.jp/em/; http://www.sanger.ac.uk/Projects/Echinococcus/), long-term *in vitro* cultivation techniques of primary cells, and the ability to transiently transfect cells using plasmids and *Listeria monocytogenes* [4]. However, no methods have been established so far, that allow to knock-out or knock-down the expression of specific genes in *E. multilocularis*.

In this study, we investigated the potential of gene silencing in *E. multilocularis* protoscoleces using RNA interference (RNAi). RNAi is a mechanism in which the degradation of mRNA is induced by complementary short interfering RNA (siRNA) through intracellular mechanisms that have been widely conserved during evolution; as a consequence of these events, gene expression can be effectively suppressed [5]. An advantage of RNAi is its ability to provide information regarding gene function in a relatively quick and easy manner [6], and represents a promising technique for gene function analysis that has been successfully applied in numerous organisms to date. In the phylum Platyhelminthes, RNAi was achieved via soaking and electroporation processes for the introduction of siRNA in schistosomules [7–9], *Fasciola hepatica* [10], and planaria [11]. Among cestodes, Pierson et al. recently reported successful RNAi in adult worms of *Moniezia expansa* using dsRNA [12]. It was therefore expected that this technique could also be applied to *E. multilocularis*, which would greatly facilitate the investigation of gene function and identification of essential gene products of this deadly parasite, and should help to provide important knowledge for the control of echinococcosis.

The protoscoleces of *E. multilocularis* can be isolated in large quantities from fertile metacestode tissues obtained from laboratory animals, and can subsequently be easily maintained *in vitro* for several weeks. Interestingly, protoscoleces are able to develop into either adults or larval vesicles [13]. Thus, protoscoleces represent an attractive research material to study the mechanisms and factors involved in several developmental stages of this parasite.

The *14-3-3* (GenBank accession no. U63643) and *elp* (AJ012663) genes of *E. multilocularis*, which encode for 14-3-3 and antigen II/3, respectively, served as the model target genes in this study. The 14-3-3 proteins constitute a family of conserved ubiquitous eukaryotic proteins that are involved in a number of important cellular processes, including signal transduction, cell-cycle control, apoptosis, stress response, and malignant transformation [14]. In *E. multilocularis*, one 14-3-3 isoform has been published so far which is similar to the zeta isoform in higher eukaryotes and is highly expressed at the metacestode stage and mainly localizes to the germinal layer of cysts

* Corresponding author. Tel./fax: +81 11 706 5196.
E-mail address: oku@vetmed.hokudai.ac.jp (Y. Oku).

1383-5769/$ – see front matter © 2010 Elsevier Ireland Ltd. All rights reserved.
doi:10.1016/j.parint.2010.08.010

and the apical structures in both invaginated and evaginated protoscoleces [15]. The protein encoded by the *elp* gene, which has been referred to as antigen II/3, Em10, or Em18, is expressed in both *E. multilocularis* adult and metacestode stages and has been used as an important diagnostic antigen [16]. Antigen II/3 shares homology with the mammalian ezrin, radixin, and moesin (ERM) protein family [17] that is involved in several key processes related to cellular architecture maintenance, including cell–cell adhesion, membrane trafficking, microvillus formation, transmembrane signaling, and cell division [18]. In *E. multilocularis*, antigen II/3 localizes within the germinal layer and parenchymal cells of protoscoleces and on the surface of calcareous corpuscles (Fig. 1 of [19]). Matsumoto et al. reported that the combination of 14-3-3 and antigen II/3 expression could be used as a molecular marker of viability and growth activity in *E. multilocularis* [20].

All experiments in this study were performed using protoscoleces isolated from the *E. multilocularis* Nemuro strain maintained at the Hokkaido Institute of Public Health (Sapporo, Japan). To isolate protoscoleces, larval cyst masses isolated from cotton rats (*Sigmodon hispidus*) were minced, passed through a sieve (100-μm mesh size), and then washed repeatedly with 0.85% physiological saline until host materials were thoroughly removed. The protoscoleces were then treated with 0.5% hydrochloric acid and 0.5% pepsin dissolved in 0.85% physiological saline for 30 min to digest any remaining host tissue (this treatment can be a stimulus for differentiation to adults), and were subsequently cultured in CMRL1066 medium (Gibco) supplemented with 10% fetal calf serum (Gibco), 200 U/ml penicillin G, and 200 μg/ml streptomycin (Gibco) in culture flasks for 1–2 days at 37 °C in the presence of 100% N_2.

For the RNAi experiments, we attempted to select suitable conditions in which protoscoleces could maintain high viability. The negative control RNAi experiments were performed using fluorescently labeled (FAM-labeled negative control #1 siRNA, Ambion) and negative control (Silencer negative control #1 siRNA, Ambion) siRNAs. The sequence of negative control #1 siRNA was unknown, as it is proprietary information of Ambion; however, the company states that the siRNA does not specifically target any human, mouse, or rat gene. To determine the suitable conditions for siRNA introduction, soaking and electroporation were tested without siRNA. Soaking was performed with 1–30 μl transfection reagent (NeoFX, Ambion) in 100 μl culture medium and electroporation was performed at 100–400 V (100-V intervals) and 100–1,000 μF (100-μF intervals) to examine their effects on the viability of the protoscoleces. The results of these tests revealed that protoscoleces exhibited greater than 80% viability 3 days after either soaking with 0–10 μl transfection reagent or electroporation at 100 V with 100–800 μF or 200 V with 100 μF.

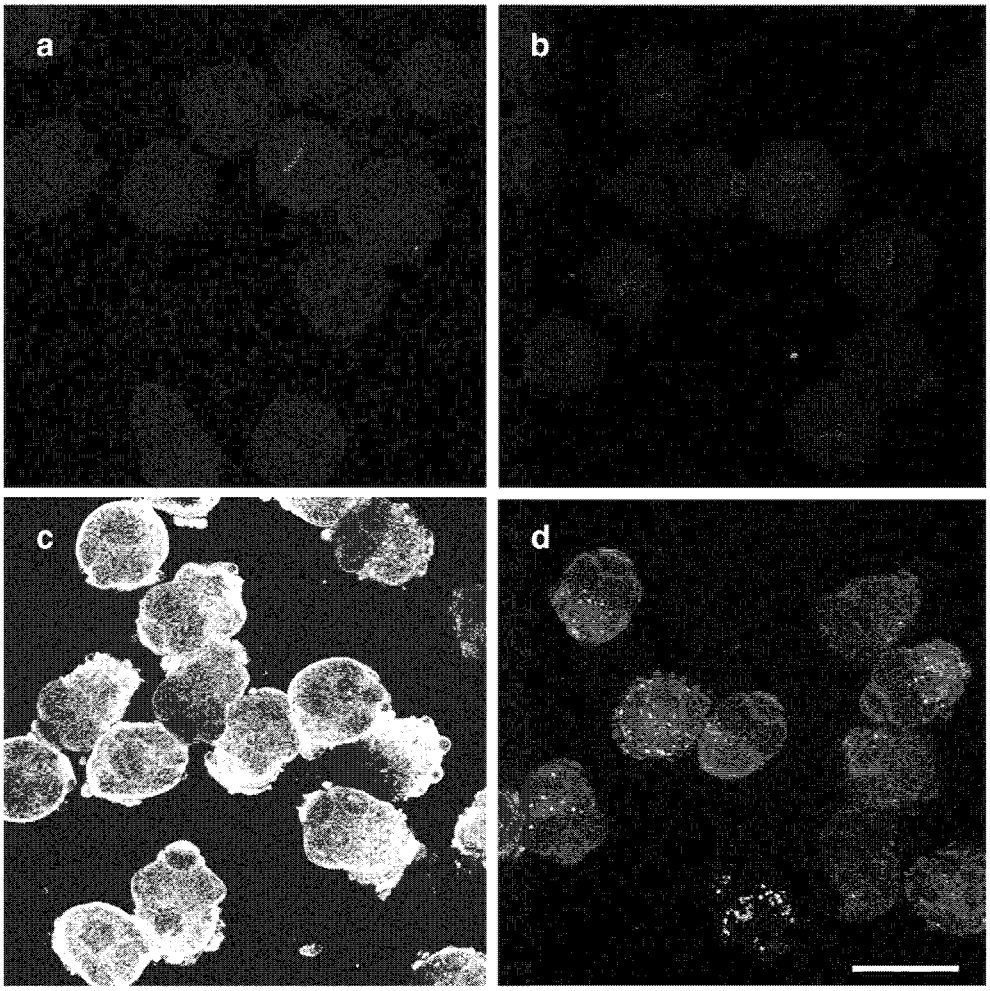

Fig. 1. Localization of fluorescently labeled siRNA following soaking or electroporation. Parasites untreated (a) or treated with fluorescently labeled siRNA via soaking in transfection reagent (b) or electroporation (c and d) were observed by confocal microscopy. At 30 min after electroporation, strong fluorescence was detected in the parasites (c). Diminished fluorescence and several bright spots were observed in protoscoleces 2 h after electroporation (d). No fluorescence was detected in the parasites of the untreated control (a) or parasites treated by soaking (b) 30 min after treatment. The scale bar indicates 200 μm.

The three promising candidate conditions, soaking with 10 μl transfection reagent, and electroporation with 100 V–800 μF and 200 V–100 μF, were tested for their efficacy of siRNA introduction using fluorescently labeled siRNA. For soaking, 100 μl culture medium containing approximately 2,000 protoscoleces was placed in a 24-well plate, and the fluorescently labeled siRNA (5 μM final concentration) alone or with 10 μl transfection reagent (NeoFX, Ambion) was then added to each well. The parasites were incubated at 37 °C in the presence of 5% CO_2 in the dark. For electroporation, 100 μl electroporation buffer (Ambion) containing approximately 2,000 protoscoleces was placed in a 4-mm cuvette, and the fluorescently labeled siRNA was added to give a final concentration of 5 μM. Electroporation was performed at 100 V–800 μF or 200 V–100 μF using an exponential decay pulse (Gene Pulser II, Bio-Rad). After incubation at 37 °C for 10 min, the buffer containing protoscoleces was transferred into 1 ml culture medium, which was then further incubated at 37 °C in 24-well plates in the presence of 5% CO_2 in the dark. At 30 min and 2 h after treatment, the parasites were washed with PBS and viewed under a fluorescent microscope (FV500, Olympus) to evaluate the efficacy of the three treatment conditions.

As expected, fluorescence was not detected in the untreated parasites (Fig. 1a). Surprisingly, fluorescence was also undetectable in the parasites treated by soaking with (Fig. 1b) or without transfection reagent (data not shown). We had previously hypothesized that the tegument, the surface syncytial structure that covers the entire body of the protoscolex and is involved in the active transport of extrasomatic low molecular weight nutrients [21], would be suitable for the absorption of siRNA. However, soaking proved to be unsuccessful for the introduction of siRNA into the parasites. In contrast, in the parasites treated by electroporation at 100 V–800 μF, strong fluorescence was detected 30 min after treatment (Fig. 1c), although the fluorescence decreased 2 h after treatment (Fig. 1d). Electroporation at 200 V–100 μF showed a very similar result to the 100 V–800 μF conditions (data not shown). The reason for the loss of fluorescence at 2 h after treatment is unknown. Krautz-Peterson et al. reported successful gene suppression in schistosomules using RNAi, although a similar reduction in fluorescence was observed in the method they used [9]. According to our present results, the electroporation condition of 100 V–800 μF was selected for the introduction of siRNA into protoscoleces in the subsequent experiments.

We next examined the efficacy of RNAi with the selected electroporation conditions. The respective target sequences were determined using the BLOCK-iT RNAi Designer software (https://rnaidesigner.invitrogen.com/rnaiexpress/), and the resulting 23 nt designed siRNA duplexes were obtained from Sigma-Aldrich at a concentration of 100 μM. The sequence of the siRNA targeting *14-3-3 zeta* was 5'-GCU CGU CGU UCA UCG UGG AGA AU-3' without a overhang, and that targeting *elp* was 5'-AAC CUU UCU AAG ACU GGA UAA GA-3' without a overhang. To analyze the effects of siRNA introduction into *E. multilocularis*, four sample groups of protoscoleces were prepared: untreated controls, electroporation controls, *14-3-3* siRNA-treated samples, and *elp* siRNA-treated samples. One hundred microliters of electroporation buffer (Ambion) containing approximately 2,000 protoscoleces was placed in a 4-mm cuvette for each sample. siRNA targeting *14-3-3* or *elp* at a final concentration of 3 μM was added to each cuvette of the 14-3-3 or *elp* siRNA-treated sample group, respectively. The negative control siRNA (Silencer negative control #1 siRNA, Ambion) was added to all of the electroporation controls at a final concentrations of 3 μM. Electroporation was then performed at 100 V–800 μF using an exponential decay pulse (Gene Pulser II, Bio-Rad). After incubation at 37 °C for 10 min, the buffer containing protoscoleces was transferred into 1 ml culture medium in the well of a 24-well plate. For the untreated controls, 2,000 protoscoleces were directly transferred from flasks into 1 ml culture medium. All samples were further incubated at 37 °C in the presence of 5% CO_2 in the dark and half of the medium was changed every 3 days. The analyses were performed in triplicate for each group.

The RNAi effects on mRNA levels were evaluated using real-time RT-PCR. For the analyses, total RNA was first extracted from all groups at day 0 and 3 after electroporation using TRIzol reagent (Invitrogen), and cDNA was then synthesized from 200 ng RNA in a total volume of 10 μl using the PrimeScript RT Reagent Kit (Takara) according to the manufacturer's instructions. Real-time PCR was carried out using 2 μl of 1:100 cDNA dilution, SYBR Premix Ex Taq II (Takara) and the following primer sets: *14-3-3 zeta* forward 5'-AAC TTG CTA TCC GTT GC-3', reverse 5'-CAC CTT CTT AAG GTA AAT GTC-3'; *elp* forward 5'-GTG AAG TCT GGT ACT TCG-3', reverse 5'-ATC CAG TCT TAG AAA GGT TG-3'; *actin 2* forward 5'-TCA ATC CTA AAG CCA ATC-3', reverse 5'-CGT ACA ACG ACA GCA C-3' for *emactin2* (XvEMb06047 from our cDNA library, http://fullmal.hgc.jp/em/); *14-3-3 epsilon* forward 5'-ATC TTA ATG ATG AAT CCG CTC CTG- 3', reverse 5'-GTT CAT CGC CCT CAT CCT TG- 3' for *14-3-3 epsilon* (Emmg-5f10.q1k, http://www.sanger.ac.uk/Projects/Echinococcus/). All samples were run in triplicate and underwent 40 amplification cycles at 95 °C for 5 s and 60 °C for 31 s using a StepOne Real-Time PCR System (Applied Biosystems). The amount of each cDNA was then calculated using standard curves and compared to the relative amounts of *emactin2*, an endogenous standard. Each relative amount was subsequently normalized to the untreated control at day 0. Statistical analyses using one-way ANOVA and Tukey's multiple comparison test were then performed.

The results of the real-time RT-PCR analyses revealed that *14-3-3 zeta* mRNA reduced to 21.8 ± 2.6% of the untreated control levels in *14-3-3* siRNA-treated protoscoleces by day 3, which was significantly ($P<0.01$) lower than the levels of the untreated control, electroporation control, and *elp* siRNA-treated samples (Fig. 2a). The levels of *elp* mRNA were also low in *elp* siRNA-treated protoscoleces, decreasing to 35.5 ± 0.4% of the untreated control levels by day 3, whereas the *elp* mRNA levels in the electroporation control and *14-3-3* siRNA-treated samples were 64.6 ± 19 and 57.5 ± 1.7% of the untreated control; however, ANOVA analyses suggested that the differences were not statistically significant (Fig. 2c). No significant reduction was observed in *14-3-3 epsilon* mRNA in any sample (Fig. 2b), even though *14-3-3 epsilon* mRNA contained a sequence which matches 21 of the 23 siRNA bases targeting the 14-3-3 zeta protein. This result suggested that as few as two base differences ensures the specificity of siRNA in *E. multilocularis*. All target mRNAs showed modest reductions in the electroporation controls; however, no statistical differences were observed between the untreated and electroporation controls.

The RNAi effects on protein expression levels were evaluated using western blot analysis. The treated protoscoleces were collected on day 3, 6, 10, and 15 after electroporation and homogenized using a hand homogenizer (23 M-R25, Nippon Genetics). Fifty microliters of radioimmunoprecipitation assay (RIPA) buffer containing 25 mM Tris, 150 mM NaCl, 5 mM EDTA, 1% sodium deoxycholate, 1% Triton X-100, and 0.1% SDS (pH 7.5) was added, and the specimens were treated by repeated freezing and thawing. Fifty microliters of 2× SDS sample buffer (100 mM Tris, 4% SDS, 12% 2-mercaptoethanol, 20% glycerol, and a few drops of bromphenol blue (BPB) solution (pH 6.8)) was added to the samples, which were then heated at 90 °C for 10 min and centrifuged at 20,000×*g* for 10 min. Extracted proteins were size separated on 12% acrylamide gels and transferred to polyvinylidene fluoride (PVDF) membranes. Detection of the specific proteins was performed using rabbit anti-14-3-3 [22], rabbit anti-antigen II/3 [20], and rabbit anti-actin (anti-beta-actin (NT), AnaSpec) antibodies as the primary antibodies, and goat anti-rabbit antibody (anti-rabbit IgG AP conjugate, Promega) as the secondary antibody. In the western blot obtained under reducing conditions, we identified a specific 27-kDa protein with the anti-14-3-3 antibody, 65-kDa and 52-kDa proteins with the anti-antigen II/3 antibody, and a 42-kDa protein with the anti-actin antibody. The detection of two II/3 protein bands has been reported previously by Felleisen & Gottstein, who speculated that

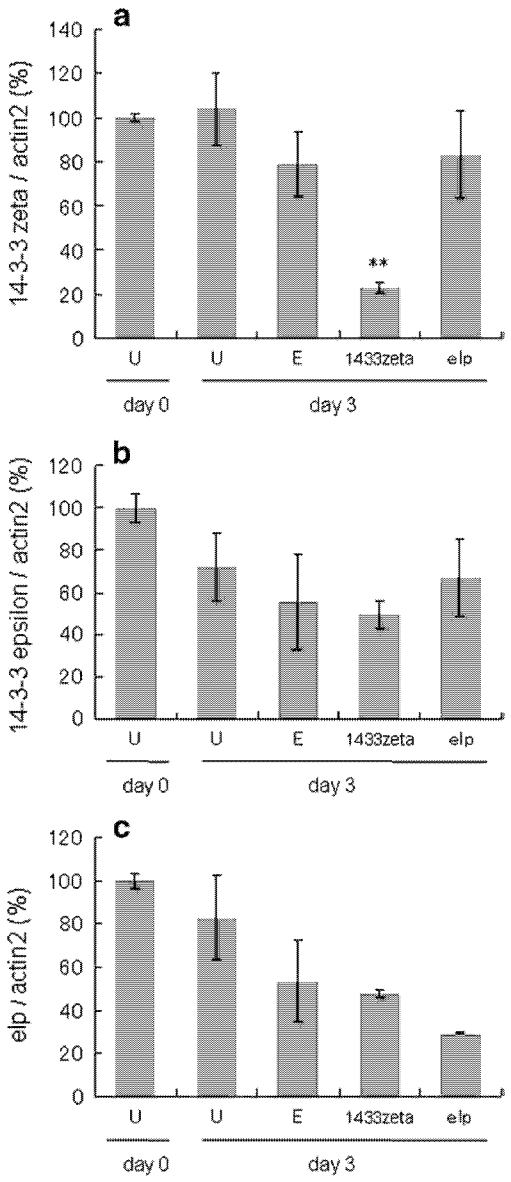

Fig. 2. RNAi effects on mRNA levels in *E. multilocularis* protoscoleces. Relative amounts of each mRNA were detected using real-time RT-PCR. *14-3-3 zeta* mRNA significantly reduced to 21.8 ± 2.6% of the untreated control levels in *14-3-3* siRNA-treated protoscoleces by day 3 (a). No significant reduction was observed in *14-3-3 epsilon* mRNA in any sample (b). The *elp* mRNA levels were lowered in *elp* siRNA-treated protoscoleces, reducing to 35.5 ± 0.4% of the untreated control by day 3. The electroporation control and *14-3-3* siRNA-treated samples showed *elp* mRNA levels of 64.6 ± 19 and 57.5 ± 1.7%, respectively, of the untreated controls. However, ANOVA analyses suggested that the differences between the siRNA-treated samples were not statistically significant (c). U: untreated control; E: electroporation control. Bars represent the standard deviation. $^{**}P<0.01$.

the 52-kDa protein could potentially be a processing or degradation product of the 65-kDa protein [19]. The PVDF membranes were air dried and scanned (Fig. 3a, b), and densitometry analyses were carried out using Photoshop 6.0 (Adobe). The values of the 14-3-3- and II/3-protein blots were normalized to those of actin and then transformed to set the untreated control of each day as 100%. The data were analyzed statistically using one-way ANOVA and Tukey's multiple comparison test. It was revealed that 14-3-3 protein gradually decreased to 41.6 ± 9.7, 39.7 ± 11.7, and 22.1 ± 7.1% of the untreated control levels by day 6, 10, and 15, respectively, in the *14-3-3* siRNA-treated samples. In the electroporation controls, 14-3-3 protein displayed a modest reduction compared to the untreated control from day 6 to 15 (70.0 ± 29.1 (day 6), 64.2 ± 15.0 (day 10), and 72.2 ± 5.2% (day 15) of the untreated control). Statistical analysis indicated that 14-3-3 protein was significantly reduced in siRNA-treated samples by day 15 (Fig. 3c). The densitometry analyses also demonstrated that the II/3-upper protein (65 kDa) levels were reduced to 88.2 ± 33.0, 87.2 ± 6.7, 59.6 ± 4.6, and 68.7 ± 4.6% of the untreated control by day 3, 6, 10, and 15, respectively, in the *elp* siRNA-treated samples. No reduction was observed in electroporation controls. Statistical analysis showed that II/3-upper protein was significantly reduced in the *elp* siRNA-treated samples by day 15 (Fig. 3d). The expression of the II/3-lower protein (52 kDa) was also decreased, with levels of 69.9 ± 5.5, 46.4 ± 5.2, 34.3 ± 2.7, and 26.2 ± 1.8% of untreated control observed by day 3, 6, 10, and 15, respectively, in the *elp* siRNA-treated samples. A modest effect was observed in the electroporation control by day 10 and 15, as the II/3-lower protein decreased to 78.5 ± 29.8 and 62.2 ± 6.0%, respectively, of the untreated control levels. Statistical analysis indicated that II/3-lower protein (52 kDa) was significantly reduced in the siRNA-treated samples on day 6 and 15 (Fig. 3e).

When a comparison was made with the electroporation controls that were set as 100%, the 14-3-3, II/3-upper (65 kDa), and II/3-lower (52 kDa) proteins reduced to 30.6 ± 9.9, 60.8 ± 4.0, and 42.1 ± 3.0%, respectively, in the corresponding siRNA-treated samples by day 15. It is speculated that the anti-14-3-3 antibody likely does not distinguish between the 14-3-3 isoforms, as it detected 14-3-3 isoforms other than what were targeted by the 14-3-3 zeta siRNA, indicating it is highly possible that 14-3-3 zeta itself was reduced to a greater extent than shown in these experiments. The results presented here suggest that RNAi did not uniformly affect the target genes in *E. multilocularis* protoscoleces. In this study, the knock-down of *14-3-3* was the most effective. The observed differences in the efficiency of RNAi on the *14-3-3* and *elp* (antigen II/3) mRNA and resulting protein levels may be due to differences of protein distribution within cells. It was previously reported that 14-3-3 protein mainly localizes in the apical region, pad and adjacent structures, and suckers of protoscoleces [15], whereas antigen II/3 localizes within the germinal layer and in the periphery of individual cell conglomerates inside of protoscoleces [19]. As shown in Fig. 1, it appeared that the amount of siRNA introduced into the surface structures was larger than that found in the internal regions of protoscoleces. It is therefore possible that more siRNA was delivered to cells actively producing 14-3-3 than to those cells producing antigen II/3. In addition to this speculation, the properties and stability of the target mRNAs and proteins may be involved in the difference knock-down efficiencies between the two proteins. The II/3-upper protein (65 kDa) seemed to be less sensitive to both electroporation and siRNA than the lower protein (52 kDa). Although the reason for the difference is unknown, again, the individual properties and stability of the two protein forms may be involved. Unexpectedly, we also observed protein reduction in a few of the electroporation control samples, suggesting that the electroporation treatment could affect the protein expression to a certain degree. It is considered that the reductions were a result of the electroporation procedure itself and were not caused by off-target effects of the negative control siRNA, since it was suggested that a mismatch of two nucleotides could ensure the specificity of siRNA (Fig. 2a and b), and a similar reduction was observed after electroporation without siRNA (data not shown). The differences of the electroporation treatment effects on the protein levels were likely due to differences in localization, stability, or other characteristics of these proteins. In future studies, it may be necessary to consider that observed reductions of target proteins in siRNA-treated samples would include effects by electroporation treatment, in addition to the RNAi effect, and appropriate controls should therefore be included.

Finally, the effects of siRNA introduction by electroporation on the viability of the protoscoleces were evaluated in all samples on day 3, 6, 10, and 15. Viability was calculated by counting the number of living protoscoleces that exhibited a clear appearance and that contained

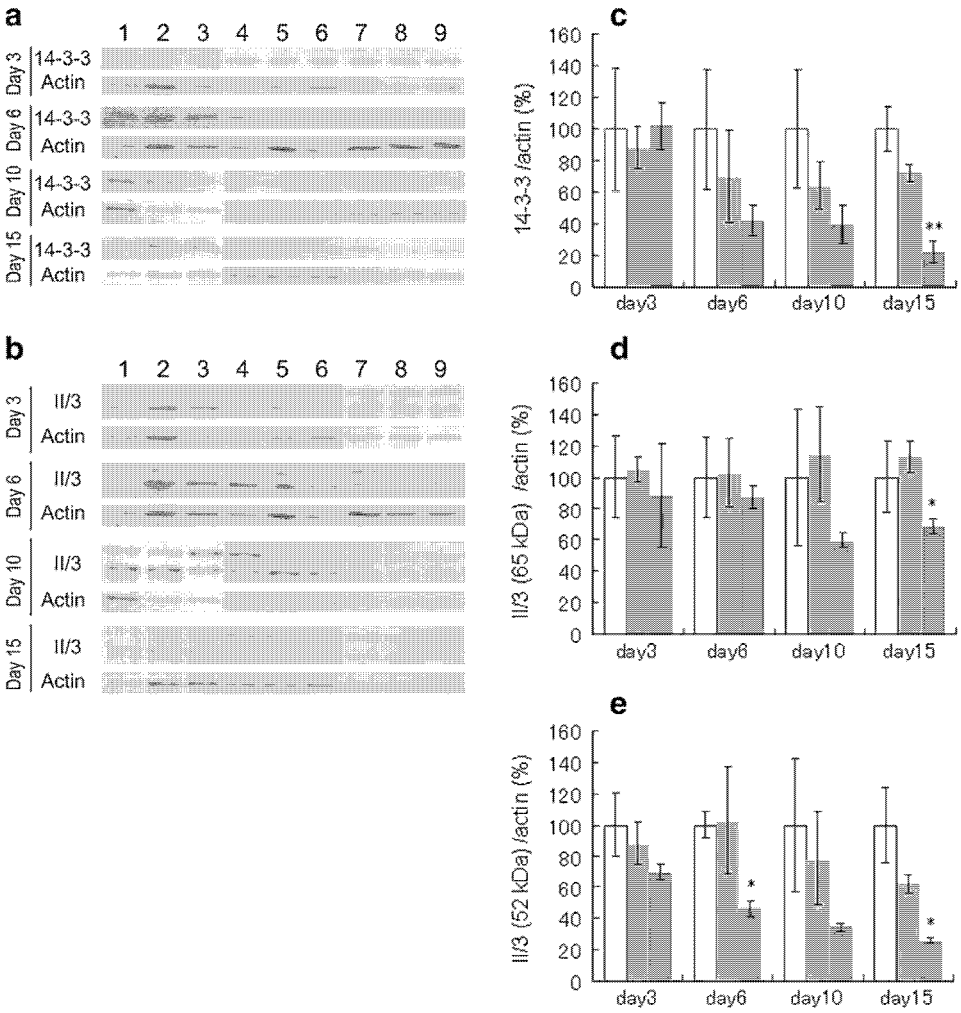

Fig. 3. RNAi effects on protein expression levels in *E. multilocularis* protoscoleces. Detection of 14-3-3, II/3 (*elp*), and actin was performed by western blotting. Untreated control (a and b, lanes 1–3), electroporation control (a and b, lanes 4–6), samples treated with siRNA targeting *14-3-3 zeta* (a, lanes 7–9), samples treated with siRNA targeting *elp* (b, lanes 7–9). The 14-3-3- and II/3-protein blots were evaluated by densitometry analyses. The values were normalized to those of actin and then transformed to set the untreated control levels of each day as 100%. The data were analyzed statistically by using one-way ANOVA and Tukey's multiple comparison test. 14-3-3 protein decreased to 41.6 ± 9.7, 39.7 ± 11.7, and 22.1 ± 7.1% of untreated control levels at day 6, 10, and 15, respectively, in the *14-3-3* siRNA-treated samples. (c). II/3-upper protein was reduced to 88.2 ± 33.0, 87.2 ± 6.7, 59.6 ± 4.6, and 68.7 ± 4.6% of the untreated control by day 3, 6, 10, and 15, respectively, in the *elp* siRNA-treated samples. No reduction was observed in the electroporation controls (d). II/3-lower protein decreased to 69.9 ± 5.5, 46.4 ± 5.2, 34.3 ± 2.7, and 26.2 ± 1.8% of the untreated control by day 3, 6, 10, and 15, respectively, in the *elp* siRNA-treated samples (e). $^{*}P<0.05$, $^{**}P<0.01$.

transparent structures and the number of dead protoscoleces that appeared opaque and demonstrated a rough surface and damaged inner structures. On day 3 and 6, no significant reduction of viability was observed in siRNA-treated samples. By day 10, the untreated control, electroporation control (silencer negative siRNA-treated), *14-3-3* siRNA-treated, and *elp* siRNA-treated samples displayed 94.6 ± 3.4, 86.5 ± 1.4, 80.1 ± 3.0, and 78.4 ± 4.0% viability, respectively, and by day 15, viabilities of 98.4 ± 1.4, 83.0 ± 2.5, 58.0 ± 23.0, and 55.1 ± 14.6%, respectively, were observed. The data of each day were analyzed by one-way ANOVA and Tukey's multiple comparison test, and a significant siRNA effect was found only between the controls (untreated and electroporation controls) and *elp* siRNA-treated samples on day 10. Despite the lack of statistical significance, the observed trend of decreasing viability in *14-3-3* and *elp* siRNA-treated protoscoleces indicates that these two proteins play important roles in essential cellular activities [14,18]. The 14-3-3 zeta protein is consider to have high potential as a vaccine candidate to larval echinococcosis [23], and a DNA vaccine consisting of *TEG-Tsag*, which is a homolog to *elp*, displayed significant levels of protection in a *Taenia crassiceps* murine model of cysticercosis [24].

In morphological observation, several protoscoleces increased in length and others swelled after the 15-day culture in both the control and treated groups. Although the number of swelled protoscoleces increased by a certain degree in samples treated by electroporation (controls and siRNA-treated), no clear difference was found by microscopic observation between the electroporation controls and siRNA-treated protoscoleces.

In conclusion, we demonstrated the potential of gene silencing in *E. multilocularis* protoscoleces using an RNAi method involving electroporation that induced reductions of target mRNA, target protein, and viability in *E. multilocularis* protoscoleces. Despite its successful application, further improvements to this method may be necessary, as it required relatively high concentrations of siRNA (3 or 5 μM), RNAi effects were not observed until several days after siRNA introduction, and the electroporation treatment may cause reductions in the levels of certain proteins. Nevertheless, this method represents a powerful tool for investigating gene function and identifying essential gene products in *E. multilocularis* protoscoleces.

Care of experimental animals

All animal experiments were carried out in accordance with the ethical guidelines of Hokkaido University and Hokkaido Prefecture.

Acknowledgements

We thank Dr. Jun Matsumoto (Nihon University) and Dr. Nariaki Nonaka (University of Miyazaki) for many helpful suggestions regarding the experiments. This study was supported by a Grant-in-Aid for Scientific Research from the Ministry of Education, Culture, Sports, Science and Technology of Japan (Grant no. 20380164), a Grant for Research on New Influenza, Emerging and Re-emerging Infectious Diseases from the Ministry of Health, Labour and Welfare of Japan, and a grant from the Swiss National Science Foundation (grant no. 3100A0-111780).

References

[1] Craig PS, Rogan MT, Allan JC. Detection, screening and community epidemiology of taeniid cestode zoonoses: cystic echinococcosis, alveolar echinococcosis and neurocysticercosis. Adv Parasitol 1996;38:169–250.
[2] Brehm K, Spiliotis M. The influence of host hormones and cytokines on *Echinococcus multilocularis* signalling and development. Parasite 2008;15:286–90.
[3] Brehm K, Spiliotis M. Recent advances in the in vitro cultivation and genetic manipulation of *Echinococcus multilocularis* metacestodes and germinal cells. Exp Parasitol 2008;119:506–15.
[4] Spiliotis M, Lechner S, Tappe D, Scheller C, Krohne G, Brehm K. Transient transfection of *Echinococcus multilocularis* primary cells and complete in vitro regeneration of metacestode vesicles. Int J Parasitol 2008;38:1025–39.
[5] Kurreck J. RNA interference: from basic research to therapeutic applications. Angew Chem Int Ed Engl 2009;48:1378–98.
[6] Cottrell TR, Doering TL. Silence of the strands: RNA interference in eukaryotic pathogens. Trends Microbiol 2003;11:37–43.
[7] Boyle JP, Wu XJ, Shoemaker CB, Yoshino TP. Using RNA interference to manipulate endogenous gene expression in *Schistosoma mansoni* sporocysts. Mol Biochem Parasitol 2003;128:205–15.
[8] Correnti JM, Brindley PJ, Pearce EJ. Long-term suppression of cathepsin B levels by RNA interference retards schistosome growth. Mol Biochem Parasitol 2005;143:209–15.
[9] Krautz-Peterson G, Radwanska M, Ndegwa D, Shoemaker CB, Skelly PJ. Optimizing gene suppression in schistosomes using RNA interference. Mol Biochem Parasitol 2007;153:194–202.
[10] McGonigle L, Mousley A, Marks NJ, Brennan GP, Dalton JP, Spithill TW, et al. The silencing of cysteine proteases in *Fasciola hepatica* newly excysted juveniles using RNA interference reduces gut penetration. Int J Parasitol 2008;38:149–55.
[11] Pineda D, Rossi L, Batistoni R, Salvetti A, Marsal M, Gremigni V, et al. The genetic network of prototypic planarian eye regeneration is Pax6 independent. Development 2002;129:1423–34.
[12] Pierson L, Mousley A, Devine L, Marks NJ, Day TA, Maule AG. RNA interference in a cestode reveals specific silencing of selected highly expressed gene transcripts. Int J Parasitol 2009;40:605–15.
[13] Gottstein B. Molecular and immunological diagnosis of echinococcosis. Clin Microbiol Rev 1992;5:248–61.
[14] van Hemert MJ, Steensma HY, van Heusden GP. 14-3-3 proteins: key regulators of cell division, signalling and apoptosis. Bioessays 2001;23:936–46.
[15] Siles-Lucas Mdel M, Gottstein B. The 14-3-3 protein: a key molecule in parasites as in other organisms. Trends Parasitol 2003;19:575–81.
[16] Gottstein B, Jacquier P, Bresson-Hadni S, Eckert J. Improved primary immunodiagnosis of alveolar echinococcosis in humans by an enzyme-linked immunosorbent assay using the Em2plus antigen. J Clin Microbiol 1993;31:373–6.
[17] Brehm K, Jensen K, Frosch P, Frosch M. Characterization of the genomic locus expressing the ERM-like protein of *Echinococcus multilocularis*. Mol Biochem Parasitol 1999;100:147–52.
[18] Louvet-Vallee S. ERM proteins: from cellular architecture to cell signaling. Biol Cell 2000;92:305–16.
[19] Felleisen R, Gottstein B. *Echinococcus multilocularis*: molecular and immunochemical characterization of diagnostic antigen II/3-10. Parasitology 1993;107(Pt 3):335–42.
[20] Matsumoto J, Muller N, Hemphill A, Oku Y, Kamiya M, Gottstein B. 14-3-3- and II/3-10-gene expression as molecular markers to address viability and growth activity of *Echinococcus multilocularis* metacestodes. Parasitology 2006;132:83–94.
[21] Halton DW. Nutritional adaptations to parasitism within the platyhelminthes. Int J Parasitol 1997;27:693–704.
[22] Siles-Lucas M, Felleisen RS, Hemphill A, Wilson W, Gottstein B. Stage-specific expression of the 14-3-3 gene in *Echinococcus multilocularis*. Mol Biochem Parasitol 1998;91:281–93.
[23] Siles-Lucas M, Merli M, Gottstein B. 14-3-3 proteins in *Echinococcus*: their role and potential as protective antigens. Exp Parasitol 2008;119:516–23.
[24] Rosas G, Fragoso G, Garate T, Hernández B, Ferrero P, Foster-Cuevas M, et al. Protective immunity against *Taenia crassiceps* murine cysticercosis induced by DNA vaccination with a *Taenia saginata* tegument antigen. Microbes Infect 2002;4:1417–26.

ARTICLE IN PRESS
PARINT-00817; No of Pages 9
Parasitology International xxx (2010) xxx–xxx
Contents lists available at ScienceDirect
Parasitology International
journal homepage: www.elsevier.com/locate/parint

Transcripts analysis of infective larvae of an intestinal nematode, *Strongyloides venezuelensis*

Ayako Yoshida [a], Eiji Nagayasu [a], Anna Nishimaki [a], Akira Sawaguchi [b], Sayaka Yanagawa [a], Haruhiko Maruyama [a,*]

[a] Department of Infectious Diseases, Division of Parasitology, Faculty of Medicine, University of Miyazaki, Miyazaki, Japan
[b] Department of Anatomy, Division of Ultrastructural Cell Biology, Faculty of Medicine, University of Miyazaki, Miyazaki, Japan

ARTICLE INFO

Article history:
Received 14 April 2010
Received in revised form 4 October 2010
Accepted 27 October 2010
Available online xxxx

Keywords:
Strongyloides
Nematode
Infective larva
EST

ABSTRACT

Free-living infective larvae of *Strongyloides* nematodes fulfill a number of requirements for the successful infection. They need to endure a long wait in harsh environmental conditions, like temperature, salinity, and pH, which might change drastically from time to time. Infective larvae also have to deal with pathogens and potentially hazardous free-living microbes in the environment. In addition, infective larvae must recognize the adequate host properly, and start skin penetration as quickly as possible. All these tasks are essentially important for the survival of *Strongyloides* nematodes, however, our knowledge is extremely limited in any one of these aspects. In order to understand how *Strongyloides* infective larvae meet these requirements, we examined transcripts of infective larvae by randomly sequencing cDNA clones constructed from *S. venezuelensis* infective larvae. After assembling successfully sequenced clones, we obtained 162 unique singletons and contigs, of which 84 had been significantly annotated. Annotated genes included those for respiratory enzymes, heat-shock proteins, neuromuscular proteins, proteases, and immunodominant antigens. Genes for lipase, small heat-shock protein, globin-like protein and cytochrome *c* oxidase were most abundantly transcribed, though genes of unknown functions were also abundantly transcribed. There were no hits found against NCBI or NEMABASE4 for 37 (22.3%) EST out of the total 162 EST. Although most of the transcripts were not infective larva-specific, the expression of respiration related proteins was most actively transcribed in the infective larva stage. The expression of astacin-like metalloprotease, small heat-shock protein, *S. stercoralis* L3Nie antigen homologue, and one unannotated and 2 novel genes was highly specific for the infective larva stage.

1. Introduction

Strongyloidiasis is endemic in tropical and subtropical regions, such as Southeast Asia, Latin-America, and sub-Saharan Africa, and endemic foci are present in temperate countries as well, e.g. Mediterranean coast of Spain, southern United States, and Satsunann-Ryukyu Islands in Japan [1–3]. Hundreds of millions of people have been possibly affected globally, though no precise estimate is available.

The key for the control of strongyloidiasis is in the infective larva because the infection starts with this stage of the worm. Free-living infective larvae develop from eggs deposited by free-living females in the soil or parasitic females in the infected host. Infective larvae then wait a host to be infected for some time in the external environment. Considering the life of infective larvae, they obviously face a number of hard tasks before they finally find the host.

First, they are required to endure physical and chemical conditions among them. Temperature, salinity, and pH might change drastically during the wait and chemical compounds could contaminate their surroundings. Second, they have to get rid of or get along with pathogens and potentially hazardous free-living microbes. Among them are various kinds of viruses, bacteria, parasites, and fungi. Infective larvae should be equipped with a kind of defense mechanisms as free-living nematodes are [4,5]. Otherwise they would be heavily infected before they infect the host. In addition to the protection against a number of environmental factors, they must recognize appropriate host animals and start skin penetration as quickly as possible. Failure in host-finding and infection processes would result in the extinction of the species.

Strongyloides infective larvae definitely have solutions to all of the problems and situations described above, however, little is known about their survival and infection strategies [6]. It would be of great scientific and practical significance to understand the biological processes taking place in *Strongyloides* infective larvae. For example, because infection control cannot be done solely with a mass treatment of humans and animals due to the adverse side effects of drugs on biological diversity, new strategies to control the infection have to be explored based on the biology of the nematodes [7,8].

* Corresponding author. 5200 Kihara, Kiyotake, Miyazaki 889-1692, Japan. Tel.: +81 985 85 0990; fax: +81 985 84 3887.
E-mail address: hikomaru@med.miyazaki-u.ac.jp (H. Maruyama).

1383-5769/$ – see front matter © 2010 Elsevier Ireland Ltd. All rights reserved.
doi:10.1016/j.parint.2010.10.007

Please cite this article as: Yoshida A, et al, Transcripts analysis of infective larvae of an intestinal nematode, *Strongyloides venezuelensis*, Parasitol Int (2010), doi:10.1016/j.parint.2010.10.007

In the present study, we examined the transcripts of infective larvae by randomly sequencing cDNA clones to clarify the biological processes activated in *S. venezuelensis* infective larvae. We found that the transcripts for respiratory enzymes, heat-shock proteins, neuromuscular proteins, proteases for infection, and an autophagy-related protein were observed. In addition, infective larvae of *S. venezuelensis* abundantly expressed genes which cannot be found in nucleotide databases with significant match. Further analysis of these molecules of unknown functions would greatly facilitate our understanding of the survival strategy of *Strongyloides* nematodes.

2. Materials and methods

2.1. Parasites and animals

Strongyloides venezuelensis has been maintained in male Wistar rats in the Division of Parasitology, Department of Infectious Diseases, University of Miyazaki [9]. ICR mice and Wistar rats were purchased from Kyudo (Kumamoto, Japan). All animals were kept and handled under the approval of the Animal Experiment Committee, University of Miyazaki. The third-stage infective larvae (L3i) were obtained from faecal culture by the filter paper method [10]. L3i were used right after they emerged from the feces (2–3 days after starting faecal culture). Parasitic adult female worms were collected from infected rats 8–10 days post infection (p.i.) [11].

Preparation of larvae in different developmental stages was carried out as previously described [12]. Lung-stage larvae (LL3) were collected as follows; male ICR mice were subcutaneously inoculated with 30,000 L3i, and lungs were removed 72–75 h p.i., homogenized with a Polytron PT-MR3000 (Kinematica AG, Littau, Switzerland) at 20,000 rpm for a few seconds. Lung homogenates were wrapped with Kimwipe papers and incubated in phosphate-buffered saline (PBS) at 37 °C for 1.5 h and emerging worms were collected. Since *S. venezuelensis* has been reported to molt twice in the intestinal mucosa, we designated lung larvae as LL3 [13]. For the preparation of tissue-migrating larvae (L3tm), L3i were injected into the peritoneal cavity of ICR mice, and recovered 20 h p.i. from the peritoneal cavity.

Collected worms were washed with sterile distilled water or PBS extensively, pelleted at the bottom of 2 ml centrifuge tubes then stored at −80 °C until used for RNA preparation (see below).

2.2. cDNA library construction

Infective larvae were homogenized in TRIzol reagent (Invitrogen, Carlsbad, CA, USA) with glass beads for 1.5–2.5 min by a Mini-BeadBeater (Bio Spec Products, Bartlesville, OK, USA), followed by total RNA purification according to the manufacturer's instruction. After treatment with DNaseI (Promega, Madison, WI), poly $(A)^+$ RNA was purified with GenElute mRNA Miniprep Kit (Sigma, Saint Louis, MO).

A cDNA library was constructed using a SMART cDNA library construction kit (Clontech, Mountain View, CA). Reverse transcription (RT) of purified poly $(A)^+$ RNA was performed using MMLV reverse transcriptase with the SMART IV oligonucleotide primer and the CDS III/3′ PCR primer provided in the kit. Double-stranded cDNA (ds-cDNA) was synthesized by long distance PCR with the 5′ PCR primer and the CDS III/3′ PCR primer using the Advantage 2 PCR kit (Clontech). The ds-cDNA was treated with proteinase K and then digested with *Sfi*I. After size fractionation, cDNA was ligated to *Sfi*I-digested pDNR-LIB. The ligation product was then transformed into *Escherichia coli* ElectroMAX DH10B electrocompetent cells (Invitrogen).

2.3. DNA sequencing

Clones were transferred to LB agar plates containing 50 μg/ml chloramphenicol and grown for 20 h prior to colony direct PCR. Insert DNA was amplified from 500 randomly selected clones with a M13 primer set, and PCR products were purified with Post-Reaction Purification Columns (Sigma). Single-pass sequencing was performed from the 5′-end only using M13 forward primer (5′-GTAAAAC-GACGGCCAGT-3′) in ABI PRISM 3130×l Genetic Analyzer (Applied Biosystems, Carlsbad, CA), using ABI PRISM Big-Dye Terminator v3.1 Cycle sequencing kit (Applied Biosystems, Foster City, CA, USA).

2.4. EST processing, contig assembly and analysis

All ESTs were edited out flanking vector and adaptor sequences. After removing rRNA sequences, high quality ESTs longer than 250 bp (408 sequences) were assembled into clusters of contiguous sequences by using Sequencher software (Gene Codes, Ann Arbor, MI, USA). Reads with more than 99% identity were assembled into the same contig. The consensus sequences of contigs and singletons

Table 1
Primer sequences for real-time PCR.

NCBI accession	Associated annotation	Forward primer (5′→3′)	Reverse primer (5′→3′)	Expected product size
HO652180	FMRFamide-related peptide	CATTCACCATCCGAGGTTACTT	GCAAGGGCTTGTTGTAGGG	115
HO652210	Cytochrome P450	GGGAAAAAGAATATGTGCAGGA	TGATAACACCAGAATCGGATGA	132
HO652258	NADH dehydrogenase subunit 6	TGTTGGTTGTTTTGCCAGTT	CCATAACCACAAAAATTCCACTT	99
HO652261	Poly(A)-binding protein	GGTGTCAATGCAGGACAAGTTA	TTGGATAATTCTGTGGGTTTCC	94
HO652553	Hsp90	CCAAGAGGATGCTGGTGATT	TCGAGACAATGCCGACTGTA	84
HO652574	L3Nie Ag (SvL3Nie-2)	GAACCAGAAAAATAAATTGGGAGA	ACTTCATCGTACCAACCTTTTACTCC	87
HO652576	Astacin-like metalloproteinase	GGTGTTGTTACACCCCAAGC	AACAACAATATATTAGTGCAATCGTT	145
HP429054	Globin-like protein	TCCGGAAATGGCAGATTATT	AGGCGGAAGAAACACTGAAA	111
HP429055	Novel[a] (SVC L3ist-1)	TAACCTAAATACTATCTTTTACAATTCC	CAATTCAGTTAATTTCCCTCCA	89
HP429056	Novel[a] (SVC L3ist-2)	TGGAGAGAAATTAACTGAATTGTTGG	TTTTCAATGTTTTTATGCAGGTTC	114
HP429057	*S. stercoralis* Hsp20 (SvHsp-Ss2)	TGGGATTGGCCTTTAAGTCA	GCAGTGAATGTCAATTTTGTCC	147
HP429058	*None*[b] *(PTC 00570_1)*	CGTAGAGGATCCACTGGACA	CATTGATACCAGTATCCATTACAGAGG	85
HP429059	*A. suum* Hsp20 (SvHsp20-As1)	TTTCCTTCCGCCATTCCTAT	TTGAAACGCCCTCATCTCTAA	108
HP429060	Lipase, class 2	TGCAAGTGTGGTAAAGATTGCACATGT	CCTCACAACATTTTGATTCAGCACAGC	88
HP429062	Cytochrome *c* oxidase subunit I	TGCTGGTGGTAATCCTTTGA	ATCCCAAGGGTTCCAAAAAC	151
HP429068	L3Nie Ag (SvL3Nie-1)	CTTGCAGCAAAAGCACAAAA	CAATGGTGAACCAAATGCAA	117
HP429073	*None*[c] *(FC810578.1)*	TGGCCATGGTATGTAGCAAT	ACCCCTAAATGATAGAATGCAGTTGA	131
HP429091	*S. stercoralis* Hsp20 (SvHsp-Ss1)	TTGTGATTGGCCACTTAATGTA	CCTGAATATCCTGTGGGTCAA	113
AB453330.1	18S rebosomal RNA	CCAGCTTTCCAAGTGCATAA	CATCCAAGATGCTCATTACACA	86

[a] Novel; No hits were found in major databases.
[b] Hits were found in NEMABASE4 with no associated annotation.
[c] No hit in NEMABASE4. Match was found in NCBI EST database.

Please cite this article as: Yoshida A, et al. Transcripts analysis of infective larvae of an intestinal nematode, *Strongyloides venezuelensis*, Parasitol Int (2010), doi:10.1016/j.parint.2010.10.007

Table 2
S. venezuelensis L3 ESTs with significant annotation by homology search against NEMABASE4.

S. venezuelensis (singleton/contig)		Top hit in Nembase4 (tblastx)				
NCBI accession	Length (bp)	Identifier	Organism	Clade	E-value	Associated annotation
HO652177	601	SSC02297_1	*S. stercoralis*	IV	4.00E−87	Proteasome, subunit alpha/beta
HO652179	576	CRC00223_1	*C. remanei*	V	5.00E−11	RNA recognition motif, RNP-1
HO652180	585	SSC04545_1	*S. stercoralis*	IV	6.00E−45	FMRFamide-related peptide
HO652192	348	SSC00140_1	*S. stercoralis*	IV	3.00E−27	FMRFamide-related peptide
HO652206	292	ACC15350_1	*A. caninum*	V	7.00E−19	Ammonium transporter
HO652209	759	HBC05087_1	*H. bacteriophora*	V	3.00E−83	Cytochrome b/b6
HO652210	406	SRC01426_1	*S. ratti*	IV	4.00E−51	Cytochrome P450
HO652222	427	SSC01666_1	*S. stercoralis*	IV	1.00E−48	Hydroxytetrahydrobiopterindehydratase
HO652225	342	CJC00147_1	*C. japonica*	V	3.00E−15	Signal recognition particle, SRP9 subunit
HO652234	761	SRC00984_2	*S. ratti*	IV	1.00E−153	Ras small GTPase, Ras type
HO652237	564	SSC03440_1	*S. stercoralis*	IV	3.00E−48	LUC7 related
HO652242	636	MJC01056_1	*M. javanica*	IV	2.00E−17	DNA repair protein (XPGC)/yeast Rad
HO652258	389	CSC00005_1	*Caenorhabditis sp.*	V	1.00E−09	NAD Hdehydrogenase (ubiquinone)
HO652261	713	SRC00248_1	*S. ratti*	IV	1.00E−128	Poly(A)-binding protein
HO652283	707	SRC07549_1	*S. ratti*	IV	1.00E−108	Calcium-binding EF-hand
HO652285	867	XIC01943_1	*X. index*	I	2.00E−89	beta-1,4-mannosyltransferase activity
HO652301	574	SRC00826_1	*S. ratti*	IV	7.00E−38	Histone H1/H5
HO652303	620	PTC01840_1	*P. trichosuri*	IV	4.00E−88	NIF system FeS cluster assembly, NifU, N-terminal
HO652319	687	SRC01269_1	*S. ratti*	IV	1.00E−111	Neural proliferation differentiation control-1
HO652339	828	SSC00792_1	*S. stercoralis*	IV	1.00E−103	Klarsicht/ANC-1/syne-1 homology
HO652341	817	LSC00488_1	*L. sigmodontis*	III	4.00E−90	Neurotransmitter-gated ion-channel
HO652363	569	PTC00864_1	*P. trichosuri*	IV	2.00E−99	Isocitrate lyase and phosphorylmutase
HO652371	689	AYC01701_1	*A. ceylanicum*	V	1.00E−31	HSP20-like chaperone
HO652385	324	SRC00573_1	*S. ratti*	IV	2.00E−53	Ribosome maturation protein SBDS, N-terminal
HO652387	837	HGC09675_1	*H. glycines*	IV	8.00E−90	Peptidase C2, calpain
HO652391	682	SSC00507_1	*S. stercoralis*	IV	6.00E−71	Basic helix-loop-helix dimerisation region bHLH
HO652393	304	SRC06206_1	*S. ratti*	IV	1.00E−11	Lysosome-associated membrane glycoprotein (Lamp)/CD68
HO652397	702	SSC03354_1	*S. stercoralis*	IV	4.00E−80	Ankyrin
HO652402	806	SRC01740_1	*S. ratti*	IV	1.00E−105	TRAF-like
HO652403	702	SSC01995_1	*S. stercoralis*	IV	1.00E−36	NLI interacting factor
HO652411	638	AAC00359_1	*A. cantonensis*	V	4.00E−39	Neurotransmitter-gated ion-channel
HO652429	713	SRC03434_1	*S. ratti*	IV	1.00E−96	Alpha/beta hydrolase fold-1
HO652446	591	PTC02320_1	*P. trichosuri*	IV	6.00E−45	Zinc finger, C3HC4 RING-type
HO652452	642	ACC01684_2	*A. caninum*	V	7.00E−42	Globin-like
HO652470	681	PTC01361_1	*P. trichosuri*	IV	2.00E−23	Bicarbonate transporter, eukaryotic
HO652471	586	SRC00877_1	*S. ratti*	IV	2.00E−99	NADH:ubiquinone oxidoreductase, 51 kDa subunit
HO652478	385	SSC01554_1	*S. stercoralis*	IV	2.00E−41	Neuroendocrine 7B2 precursor
HO652504	687	CRC01991_1	*C. remanei*	V	1.00E−47	Oxysterol-binding protein
HO652510	481	SSC05747_1	*S. stercoralis*	IV	1.00E−44	Barrier to autointegration factor, BAF
HO652512	799	SRC00306_1	*S. ratti*	IV	1.00E−152	14-3-3 protein
HO652514	263	SRC02616_1	*S. ratti*	IV	2.00E−50	C2 calcium-dependent membrane targeting
HO652517	526	SSC02701_1	*S. stercoralis*	IV	1.00E−75	Histone H2B
HO652520	545	CBC03783_1	*C. brenneri*	V	2.00E−41	Glycosyl transferase, group 1
HO652521	479	CSC01296_1	*Caenorhabditis sp.*	V	1.00E−21	RhoGAP
HO652553	286	SSC00283_1	*S. stercoralis*	IV	4.00E−29	Heat-shock protein Hsp90
HO652559	336	SSC02701_1	*S. stercoralis*	IV	5.00E−36	Histone H2B
HO652574	361	SRC08538_1	*S. ratti*	IV	9.00E−31	L3Nie Ag (SvL3Nie-2)
HO652576	666	SSC00003_1	*S. stercoralis*	IV	1.00E−86	Astacin-like metalloproteinase
HO652580	406	MHC11486_1	*M. hapla*	IV	1.00E−07	Amino acid/polyamine transporter I
HP429054	589	HBC06265_1	*H. bacteriophora*	V	3.00E−47	Globin-like protein
HP429057	461	SSC01535_1	*S. stercoralis*	IV	3.00E−19	S. stercoralis Hsp20 (SvHsp20-Ss2)
HP429059	565	ASC17349_1	*A. suum*	III	2.00E−23	A. suum Hsp20 (SvHsp20-As1)
HP429060	508	SSC00303_1	*S. stercoralis*	IV	2.00E−15	Lipase, class 2
HP429061	455	SSC00007_1	*S. stercoralis*	IV	7.00E−68	Aminotransferase, class I and II
HP429062	1558	OOC00027_4	*O. ostertagi*	V	0	Cytochrome *c* oxidase, subunit I
HP429068	655	SRC08538_1	*S. ratti*	IV	7.00E−70	L3Nie Ag (SvL3Nie-1)
HP429076	762	SSC02252_1	*S. stercoralis*	IV	1.00E−122	EF-hand
HP429077	441	SRC00553_1	*S. ratti*	IV	1.00E−35	Calcium-binding EF-hand
HP429078	524	TLC00048_1	*T. leonina*	III	3.00E−62	Cytochrome *c* oxidase, subunit III
HP429079	628	SRC00445_1	*S. ratti*	IV	6.00E−97	EF-hand
HP429083	889	SSC00456_1	*S. stercoralis*	IV	1.00E−70	Proteinase inhibitor I33, aspin
HP429085	863	CJC01127_2	*C. japonica*	V	5.00E−45	NADH:ubiquinone/plastoquinone oxidoreductase
HP429086	480	ASC00025_17	*A. suum*	III	4.00E−76	Cytochrome *c* oxidase subunit II C-terminal
HP429088	417	SRC04160_1	*S. ratti*	IV	4.00E−42	Light chain 3 (LC3)
HP429091	661	SSC01535_1	*S. stercoralis*	IV	4.00E−78	S. stercoralis Hsp20 (SvHsp20-Ss1)
HP429092	1322	SSC05809_1	*S. stercoralis*	IV	2.00E−62	Methyltransferase type 11
HP429094	277	NAC00065_1	*N. americanus*	V	3.00E−16	Cytochrome b/b6, C-terminal
HP429095	589	ASC24228_1	*A. suum*	III	2.00E−19	ATPase, F0 complex, subunit A

Genus designations used in the table are as follows: *A. caninum*; *Ancylostoma caninum*, *A. cantonensis*; *Angiostrongylus cantonensis*, *A. ceylanicum*; *Ancylostoma ceylanicum*, *A. suum*; *Acaris suum*, *C. brenneri*; *Caenorhabditis brenneri*, *C. japonica*; *Caenorhabditis japonica*, *C. remanei*; *Caenorhabditis remanei*, *H. bacteriophora*; *Heterorhabditis bacteriophora*, *H. glycines*; *Heterodera glycines*, *L. sigmodontis*; *Litomosoides sigmodontis*, *M. hapla*; *Meloidogyne hapla*, *M. javanica*; *Meloidogyne javanica*, *N. americanus*; *Necator americanus*, *O. ostertagi*; *Ostertagia ostertagi*, *P. trichosuri*; *Parastrongyloides trichosuri*, *S. ratti*; *Strongyloides ratti*, *S. stercoralis*; *Strongyloides stercoralis*, *T. leonina*; *Toxascaris leonina*, *X. index*; *Xiphinema index*.

Please cite this article as: Yoshida A, et al, Transcripts analysis of infective larvae of an intestinal nematode, *Strongyloides venezuelensis*, Parasitol Int (2010), doi:10.1016/j.parint.2010.10.007

Table 3
S. venezuelensis L3 ESTs with significant annotation against NCBI non-redundant protein database.

S. venezuelensis (singleton/contig)		Top hit in the NCBI non-redundant protein database (blastx)				Top hit in Nembase4 (tblastx)			
NCBI accession	Length (bp)	NCBI accession	Best identity descriptor	Organism	E-value	Identifier	Organism	Clade	E-value
HO652462	820	NP_501872.1	hypothetical protein F01G10.6	*C. elegans*	3.00E−12	N/F[a]	–	–	–
HO652207	396	XP_002636737.1	Hypothetical protein CBG23460	*C. briggsae*	4.00E−15	PTC02337_1	*P. trichosuri*	IV	2.00E−21
HO652218	448	XP_002633793.1	Hypothetical protein CBG03485	*C. briggsae*	6.00E−22	HCC05184_1	*H. contortus*	V	4.00E−33
HO652251	849	XP_002632491.1	CBR-CCG-1 protein	*C. briggsae*	2.00E−49	SRC00347_1	*S. ratti*	IV	1.00E−140
HO652337	409	XP_001892281.1	hypothetical protein	*B. malayi*	6.00E−38	PPC05674_1	*P. pacificus*[b]	V	8.00E−50
HO652351	463	XP_002631908.1	hypothetical protein CBG07885	*C. briggsae*	2.00E−37	PTC00166_1	*P. trichosuri*	IV	5.00E−53
HO652377	395	XP_001902589.1	putative salt tolerance protein	*B. malayi*	5.00E−19	PTC04384_1	*P. trichosuri*	IV	4.00E−61
HO652412	835	XP_002645282.1	CBR-AJM-1 protein	*C. briggsae*	3.00E−09	SSC03769_1	*S. stercoralis*	IV	8.00E−65
HO652449	581	NP_499054.1	TransThyretin-Related family domain family member (ttr-5)	*C. elegans*	9.00E−33	SRC01281_1	*S. ratti*	IV	2.00E−84
HO652459	286	NP_510509.2	hypothetical protein F09B12.3	*C. elegans*	1.00E−14	SRC04118_1	*S. ratti*	IV	2.00E−34
HO652491	650	XP_001902568.1	hypothetical protein Bm1_55555	*B. malayi*	1.00E−27	SSC01022_1	*S. stercoralis*	IV	2.00E−85
HO652499	797	NP_505173.2	hypothetical protein F52E1.13	*C. elegans*	3.00E−43	CRC02974_1	*C. remanei*	V	5.00E−20
HO652537	528	NP_499054.1	TransThyretin-Related family domain family member (ttr-5)	*C. elegans*	2.00E−30	SRC01281_1	*S. ratti*	IV	4.00E−78
HO652548	533	XP_002646626.1	Hypothetical protein CBG11056	*C. briggsae*	8.00E−10	SRC02345_1	*S. ratti*	IV	3.00E−57
HP429066	2081	NP_492698.2	hypothetical protein ZC247.1	*C. elegans*	1.00E−71	SSC03002_1	*S. stercoralis*	IV	6.00E−72
HP429084	856	CAR63582.1	Conserved Cystein/Glycine domain protein	*A. cantonensis*	1.00E−41	SRC00347_1	*S. ratti*	IV	1.00E−129

S. venezuelensis L3i ESTs that did not hit in NEMABASE4 or ESTs which had matches to NEMABASE4 ESTs without annotation, were further analysed against NCBI non-redundant protein database. Sixteen EST were given annotation by this search.
[a] N/F: no hit in NEMABASE4.
[b] *Pristionchus pacificus*.

comprised the unique sequences, which were compared against NEMBASE4 (http://www.nematodes.org/ nembase4/), using tBLASTx. ESTs that did not hit were further compared with the National Center for Biotechnology Information (NCBI) non-redundant protein database using BLASTx (cut-off: E<1e−5), and NCBI EST database using BLASTn (cut-off: E<1e−10). The sequences of the transcripts in the

Hsp20

```
SvHsp20-Ss1    1:MAANNNNPSDSTDSSTXSNEEHHXERTXSYY-APSKKDDKSSAFVFSTLLEXGKDQIVCD 59
SvHsp20-Ss2    1:----------------------------N-FTMSTSS-E-------K-L-VW-------D 14
SvHsp20-As1    1:IKXLR-------------H------RCVFPSAIPMLIHTTNSI--LNDLESSLNPRHVXS 39
                                           .       .       .      *         . .

SvHsp20-Ss1   60:WPLNVKNDGLFKSKELNDKITLTLDCRXFDPQDIQVSVXGERVGIHCEHPKRKNSTT-CE 118
SvHsp20-Ss2   15:WPLSHSEDGVFTSKEIDGKIGITVDCKLFKDKEVNVIVDKDKIDIHCLHEEVEKSGLVCK 74
SvHsp20-As1   40:LKIIRDEGVSITNEGISLKFDVSQ----FKXEELSINVVDGVLVIEGKHEQMDDGKGIVS 95
                 ...   ... ......  *.  . ..  *.  .  . *      *.. *.    .   .

SvHsp20-Ss1  119:RKISRTYKXPQCYDINTLQHKVNSSGELII---------TANRTXRT---           156
SvHsp20-Ss2   75:REISRCYRLPATLDPKTVKHSLKN-GELII---------TVEK--KA---           109
SvHsp20-As1   96:RHFIRKFRLPENLKAEDIKSELSKEGMLAIEGKCLDHEKTKVKSIPIDVK           145
                 * ..* ...*  ..  . .. .   *.*.*         *  .
```

L3Nie

```
SvL3Nie-1      1:FDISKYKGNNKFSNKIFDQIWKGYNYDSDKQNKFVDMKRRFLLETNKYRRAQGVPNLVVD 60


SvL3Nie-1     61:SGLAAKAQKYAEYLAQIRQLVHDRRNSIEKTGENLAFGSPLISHLAVKKWYDEIELYDFN 120
SvL3Nie-2      1:                          NQKNKLGENLAFASPRIAHIGVKGWYDEVKDYNFN 35
                                              * ****** ** * *  ** ****   * **

SvL3Nie-1    121:RPGFSSATGHFTQLVWKDSRKAGFGVAVSSDGKGVYVVCKYTPPGNYNNKYSENVKRLSA 180
SvL3Nie-2     36:KQGFRHGIGHFTQLVWKSSSKVGCGVA--AGSKGVFTVCKYSPAGNLMGAFEKNVSPKKA 93
                    **    ********* * * * ***     ***  **** * **       **    *

SvL3Nie-1    181:TKPSSKPKRRS
```

Fig. 1. Comparison of predicted amino acid sequences between three Hsp20s and two L3Nie antigens. In *S. venezuelensis* ESTs, three different Hsp20 and two L3Nie were found. In order to clarify the difference between these ESTs, they were aligned against each other by using the GENETYX-WIN software (GENETYX CORPORATION, Tokyo, Japan). Identical residues are marked with an asterisk, and conserved residues between two Hsp20s are marked with a dot. SvHsp20-Ss1 showed 40% identity to SvHsp20-Ss2. SvHsp20-As1 was found to have 29% identity with SvHsp20-Ss2, but no significant similarity with SvHsp20-Ss1. Identity between SvL3Nie-1 and 2 was 56%. Accession numbers for each genes: SvHSP20-Ss1; HP429091, SvHSP20-Ss2; HP429057, SvHSP20-As1; HP429059, SvL3Nie-1; HP429068, SvL3Nie-2; HO652574.

Please cite this article as: Yoshida A, et al. Transcripts analysis of infective larvae of an intestinal nematode, *Strongyloides venezuelensis*, Parasitol Int (2010), doi:10.1016/j.parint.2010.10.007

present study have been deposited into the GenBank under accession numbers HO652177–HO652584 and HP429054–HP429095.

2.5. Reverse transcriptase-polymerase chain reaction (RT-PCR)

RT-PCR was performed with worms of different developmental stages; infective larvae (L3i), tissue-migrating larvae (L3tm), lung larvae (LL3), and parasitic adult worms. For RNA isolation, worms were crushed manually using a freeze-crushing apparatus (SK Mill, Tokken, Chiba, Japan), followed by isolation with TRIzol reagent. After treatment with DNase I (Ambion, Austin, TX, USA), concentration of RNA was measured using a Quant-iT assay kit (Invitrogen). cDNA was synthesized from 1 μg of total RNA by reverse transcription in 100 μl reaction using PrimeScript 1st strand cDNA Synthesis Kit (Takara Bio, Shiga, Japan).

For 63 selected genes, PCR primers were designed to have theoretical Tm of 57–63 °C and amplicon sizes of 200–500 bp. One microliter of the prepared cDNA preparation was used for PCR amplification. The amplification program was as follows; initial denaturation at 94 °C for 2 min, 30 cycles of denaturation at 94 °C for 45 s, annealing 58 °C for 45 s and elongation at 68 °C for 30 s, followed by a final extension at 68 °C for 7 min. Five microliter of the PCR products was mixed with 1 μl of EZ-VISION DNA dye/buffer (AMRESCO, Solon, OH, USA), run on 1% agarose gel, then visualized by UV transillumination and photographed.

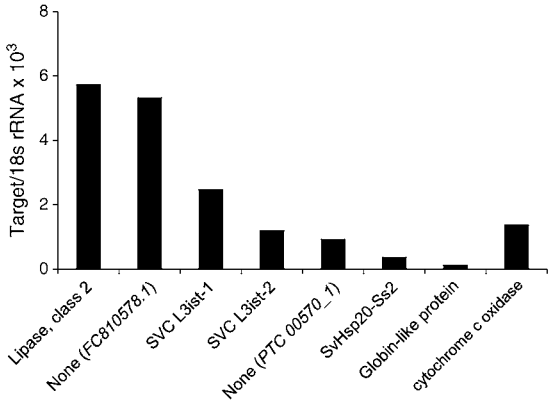

Fig. 2. Expression analysis of abundant transcripts in infective larvae. Quantification of transcripts was achieved by real-time PCR using gene-specific primer sets for the top 8 sequences (Table 4). The gene for a class 2 lipase was the most abundantly transcribed in L3i, which was followed by novel genes of unknown functions. The target values were normalized to 18S rRNA expression. Accession numbers for each genes: lipase; HP429060, *FC810578.1*; HP429073, SVC L3ist-1; HP429055, SVC L3ist-2; , HP429056, *PTC 00570_1*; HP429058, SvHsp20-Ss2; HP429057, Globin-like protein; HP429054, cytochrome *c* oxidase; HP429062.

2.6. Real-time PCR analyses

Expression of selected transcripts was analyzed in real-time PCR. The regions amplified with each primer sets were shown in Table 1. Total RNA was extracted from different stages of larvae as described above, and cDNA was generated from 400 ng of RNA using Prime-Script 1st strand cDNA Synthesis Kit (Takara Bio). Real-time PCR was then performed with an ABI PRISM 7000 Sequence Detection Systems and a Power SYBR Green PCR Master Mix (Applied Biosystems). Relative quantification was assessed by normalizing the amount of the target transcript to 18S ribosomal RNA gene.

3. Results

A cDNA library was constructed from infective larvae of *S. venezuelensis*. A total of 500 clones were sequenced producing 408 high quality ESTs (250 bp cut-off) with an average of 490 ± 164 bp. Assembling the 408 ESTs resulted in 42 contigs (288 ESTs) and 120

Table 4
The most abundant transcripts in *S. venezuelensis* L3i cDNA library.

S. venezuelensis (singleton/contig)		Blast top hit against NEMABASE4			
NCBI accession	Number of clones	Identifier	Organism	E-value	Associated annotation
HP429060	38	SSC00303_1	*S. stercoralis*	2.00E−15	Lipase, class 2
HP429056	33	Novel[a] (SVC L3ist-2)	–	–	–
HP429054	29	HBC06265_1	*H. bacteriophora*	3.00E−47	Globin-like protein
HP429055	27	Novel[a] (SVC L3ist-1)	–	–	–
HP429057	26	SSC01535_1	*S. stercoralis*	3.00E−19	S. stercoralis Hsp20 (SvHsp20-Ss2)
HP429073	14	FC810578.1[b]	*S. ratti*	5.00E−13	None
HP429058	10	PTC00570_1	*P. trichosuri*	3.00E−29	None
HP429062	8	OOC00027_4	*O. ostertagi*	0	Cytochrome *c* oxidase, subunit I
HP429064	7	Novel[a]	–	–	–
HP429079	6	SRC00445_1	*S. ratti*	6.00E−97	EF-hand
HP429066	5	SSC03002_1	*S. stercoralis*	6.00E−72	None
HP429070	5	SRC01349_1	*S. ratti*	2.00E−19	None
HP429075	5	SSC00031_1	*S. stercoralis*	5.00E−70	None
HP429076	4	SSC02252_1	*S. stercoralis*	1.00E−122	EF-hand
HP429085	4	CJC01127_2	*C. japonica*	5.00E−45	NADH:ubiquinone/plastoquinone oxidoreductase
HP429072	4	SRC01349_1	*S. ratti*	2.00E−22	None
HP429067	4	Novel[a]	–	–	–
HP429069	4	Novel[a]	–	–	–
HP429059	3	ASC17349_1	*A. suum*	2.00E−23	A. suum Hsp20 (SvHsp20-As1)
HP429068	3	SRC08538_1	*S. ratti*	7.00E−70	L3Nie Ag (SvL3Nie-1)
HP429084	3	SRC00347_1	*S. ratti*	1.00E−129	None
HP429081	3	SRC07826_1	*S. ratti*	4.00E−37	None
HP429074	3	SSC04537_1	*S. stercoralis*	2.00E−07	None
HP429087	3	Novel[a]	–	–	–
HP429065	3	Novel[a]	–	–	–

[a] Novel; No hits were found in major public databases.
[b] All hits shown here were found against Nembase4 except for FC810578.1, which was found a match in NCBI EST database only.

Please cite this article as: Yoshida A, et al, Transcripts analysis of infective larvae of an intestinal nematode, *Strongyloides venezuelensis*, Parasitol Int (2010), doi:10.1016/j.parint.2010.10.007

singletons. tBLASTx analysis against NEMABASE4, a comprehensive resource for nematode transcriptome analysis holding 679,480 nematode EST, resulted in 114 (70.4%) *S. venezuelensis* L3i ESTs showing significant (E<1e−5) matches to nematode EST, in which associated annotation was given to 68 sequences (Table 2).

S. venezuelensis L3i ESTs that did not hit in NEMABASE4 and the ones which had matches to NEMABASE4 ESTs without annotation, were further analyzed by BLASTx against the NCBI non-redundant protein databases. This search yielded 16 more genes with description (Table 3). Thus in total, 84 ESTs resulted in significant annotation against the major public databases. It should be noted that most of the hits in NEMABASE4 were genes of clade IV nematode, and a majority of the clade IV hits were with genes from *Strongyloides* (Tables 2 and 3).

Some *S. venezuelensis* L3i ESTs shown in Table 2 hit the same sequences in databases. For example, HP429091 and HP429057 hit *S. stercoralis* Hsp20 (SSC01535_1), and HP429068 and HO652574 hit *S. ratti* L3Nie Ag (SRC08538_1). Sequence alignment of these ESTs revealed that they differed significantly from each other (Fig. 1). Therefore, they were considered as different gene products and designated as shown in Fig. 1.

Of 162 *S. venezuelensis* L3i ESTs, 47 gave no hits in NCBI databases or NEMABASE4 in BLASTx and tBLASTx, respectively. We compared these sequences with NCBI EST division in BLASTn to find 7 more hits (E<1e−10). Thus of 162 unique sequences, 37 (22.3%) had no hits against NCBI or NEMABASE4, indicating that these were novel genes.

Matched transcripts with significant annotation (84 sequences) could be grouped into some categories: genes for proteins involved in oxidative phosphorylation, structural proteins, heat-shock proteins, neuromuscular proteins, and immunodominant proteins. Interesting transcripts were also found such as calpain (HO652387, Table 2), astacin-like metalloproteinase (HO652576, Table 2), salt tolerance protein (HO652377, Table 3), DNA repair protein (HO652242, Table 2), and autophagy-related LC3 (HP429088, Table 2).

The most abundant transcripts in *S. venezuelensis* infective larva, estimated from the frequency of clones, contained class 2 lipase, globin-like protein, and small heat-shock protein 20, SvHsp20-Ss2, similar to *S. stercoralis* Hsp20. However, a number of abundant transcripts had no hits even against NCBI EST using BLASTn (Table 4), suggesting that infective larvae probably express a number of species-specific genes. In order to examine the relative amount of expression of these seemingly abundant transcripts in L3i, we performed real-time PCR for the top 8 sequences containing 4 unannotated ESTs. We found that the gene for a class 2 lipase was the most abundantly transcribed in L3i, which was followed by novel genes and genes of unknown functions (Fig. 2). Two genes, *S. venezuelensis* L3i-specific transcript 1 and 2 (SVC L3ist-1 and SVC L3ist-2), had no hits in nucleotide databases by BLASTn analysis, indicating that these were novel genes.

Because infective larvae have to survive stressful environment, we examined in real-time PCR the gene expression of heat-shock proteins and energy-related proteins in different developmental stages. Expression profile of the heat-shock proteins differed from each other. As shown in Table 2, we obtained one Hsp90 and three Hsp20

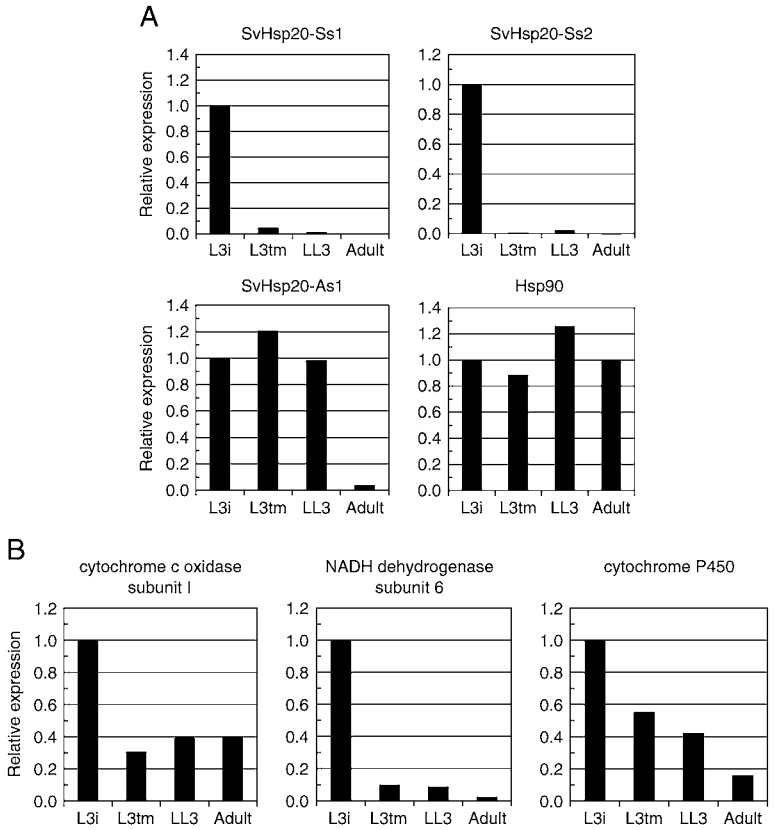

Fig. 3. Comparison of mRNA expression in developmental stages. Real-time PCR was performed with infective larvae (L3i), tissue-migrating larvae (L3tm), lung larvae (LL3) and adult female worms. (A) Expression profile of the heat-shock proteins. Hsp90 was evenly expressed through all developmental stages, while the expression of SvHsp20-As1 was decreased in adult worm. SvHsp20-Ss1 was expressed only in the infective larva stage differed from each other. (B) Gene expression of energy-related proteins. Genes, including cytochrome *c* oxidase subunit I, NADH dehydrogenase subunit 6, and cytochrome P450, were most actively transcribed in the infective larva stage. Relative expression of the target genes was assessed by normalizing to 18S rRNA expression. Gene expression in L3i was defined as 1.0. Accession numbers for each genes: SvHsp20-Ss1; HP429091, SvHsp20-Ss2; HP429057, SvHsp20-As1; HP429059, Hsp90; HO652553, cytochrome *c* oxidase; HP429062, NADH dehydrogenase; HO652258, cytochrome P450; HO652210.

Please cite this article as: Yoshida A, et al. Transcripts analysis of infective larvae of an intestinal nematode, *Strongyloides venezuelensis*, Parasitol Int (2010), doi:10.1016/j.parint.2010.10.007

sequences. Since these three Hsp20 (HP429091, HP429057, and HP429059) differed significantly from each other (Fig. 1), they were referred to as SvHsp20-Ss1, SvHsp20-Ss2, and SvHsp20-As1, respectively. While Hsp90 was expressed evenly from infective larvae to parasitic adult females, the expression of SvHsp20-As1 decreased when the worms reached maturity. In contrast, SvHsp20-Ss1 and SvHsp20-Ss2 were expressed only in the infective larva stage (Fig. 3A).

Genes for spiration-related proteins, including cytochrome *c* oxidase subunit I (HP429062), NADH dehydrogenase (HO652258), and cytochrome P450 (HO652210), were most actively transcribed in the infective larva stage (Fig. 3B), suggesting that infective larvae are active in producing ATP by oxidative phosphorylation. In fact, infective larvae had batteries of well-developed mitochondria immediately under the muscular layer demonstrated by transmission electron microscopy (data not shown).

In order to identify L3i-specific transcripts, which could be the clues to the elucidation of the survival strategy of infective larvae, we compared the expression pattern along the developmental stages of 62 genes by RT-PCR, containing 57 annotated and 5 non-annotated but highly abundant genes listed in Table 4. cDNA was prepared from infective larvae (L3i), tissue-migrating larvae (L3tm), lung larvae (LL3), and parasitic adult female worms, was amplified in PCR followed by the examination on agarose gel. PCR products were successfully obtained for 52 transcripts, revealing 7 transcripts being specific for infective larva stage (Table 5).

To confirm the stage specificity of these genes, we examined the expression in real-time PCR. Among 7 L3i specific transcripts listed in Table 5, the specific expression of SvHsp20-Ss1 and SvHsp20-Ss2, has been already demonstrated in Fig. 3. As shown in Fig. 4, the expression of the remaining 5 genes was highly specific as well for infective larvae. In addition to SvHsp20-Ss1 and SvHsp20-Ss2, L3i-specific transcripts were astacin-like metalloprotease, SvL3Nie-2, an unannotated gene (*PTC 00570_1*), and two novel transcripts (SVC L3ist-1 and SVC L3ist-2). Quite interestingly, SvL3Nie-1, which is similar to SvL3Nie-2, showed different expression patterns with SvL3Nie-2. SvL3Nie-1 was expressed constitutively from L3i to tissue-migrating L3tm stage (Fig. 4).

Table 5
Expression of transcripts along developmental stages.

S. venezuelensis (singleton/contig)		Best identity descriptor
Expression	NCBI accession	
L3i only	HO652574	SvL3Nie-2
	HO652576	Astacin-like metalloproteinase
	HP429055	Novel[a] (SVC L3ist-1)
	HP429056	Novel[a] (SVC L3ist-2)
	HP429057	SvHsp20-Ss2
	HP429058	None (PTC 00570_1)[b]
	HP429091	SvHsp20-Ss1
L3i to L3tm	HP429068	SvL3Nie-1
L3i to LL3	HO652180	FMRFamide-related peptide
	HO652403	NLI interacting factor
	HO652411	Neurotransmitter-gated ion-channel
	HP429054	Globin-like protein
	HP429059	SvHsp20-As1
	HP429061	Aminotransferase, class I and II
	HP429076	EF-hand
	HP429077	Calcium-binding EF-hand
	HP429088	Light chain 3 (LC3)
L3i to adult	HO652177	Proteasome, subunit alpha/beta
	HO652206	Ammonium transporter
	HO652234	Ras small GTPase, Ras type
	HO652242	DNA repair protein (XPGC)/yeast Rad
	HO652251	C. briggsae CBR-CCG-1 protein[c]
	HO652258	NADH dehydrogenase subunit 6
	HO652261	Poly(A)-binding protein
	HO652285	beta-1,4-mannosyltransferase activity
	HO652301	Histone H1/H5
	HO652303	NIF system FeS cluster assembly, NifU, N-terminal
	HO652319	Neural proliferation differentiation control-1
	HO652339	Klarsicht/ANC-1/syne-1 homology
	HO652341	Neurotransmitter-gated ion-channel
	HO652363	Isocitrate lyase and phosphorylmutase
	HO652371	HSP20-like chaperone
	HO652385	Ribosome maturation protein SBDS, N-terminal
	HO652387	Peptidase C2, calpain
	HO652397	Ankyrin
	HO652412	*C. briggsae* CBR-AJM-1 protein[c]
	HO652449	TransThyretin-Related family domain family member[c]
	HO652459	hypothetical protein F09B12.3[c]
	HO652470	Bicarbonate transporter, eukaryotic
	HO652504	Oxysterol-binding protein
	HO652510	Barrier to autointegration factor, BAF
	HO652514	C2 calcium-dependent membrane targeting
	HO652517	Histone H2B
	HO652520	Glycosyl transferase, group 1
	HO652537	TransThyretin-Related family domain family member[c]
	HO652553	Heat-shock protein Hsp90
	HP429060	Lipase, class 2
	HP429062	Cytochrome *c* oxidase, subunit I
	HP429073	None[b]
	HP429083	Proteinase inhibitor I33, aspin
	HP429084	Putative conserved cystein/glycine domain protein[c]
	HP429092	Methyltransferase type 11

[a] Novel; No hits were found in major databases.
[b] Hits were found in NEMABASE4 with no associated annotation.
[c] Hits were found in NEMABASE4 without associated annotation. Annotation was given in NCBI NR protein database.

4. Discussion

Most cases of strongyloidiasis are subclinical, and chronic infections remain unrecognized for decades [14]. However, it might turn life-threatening when the patients are on immunosuppressive drugs [15] or have co-infections with HTLV-1 [16–18]. In severe strongyloidiasis, large numbers of infective larvae penetrate skin and intestinal mucosa causing disseminated infections. Understanding the biology of infective larvae would lead us to find a novel strategy for the control of severe infections.

Our present study on transcripts of *S. venezuelensis* infective larva revealed interesting features of their biology. First, in the present cDNA library, clones coding for lipase appeared repeatedly. Representation in a cDNA library generally reflects the abundance in the original transcriptome [19], and the real-time PCR results confirmed lipase as one of the most actively transcribed genes (Fig. 2). It appears that infective larvae of *S. venezuelensis* possibly degrade stored lipid for energy generation. Because infective larvae do not feed during wait [20], and express both an autophagosome marker LC3 (HP429088 in Table 2) and a proteasome protein (HO652177 in Table 2), infective larvae possibly depend on both the ubiquitin–proteasome system and autophagy processes for the energy sources. Recent study has revealed that autophagy regulates intracellular lipid metabolism [21], which is evoked when animals are under starvation [22–24].

Transcripts for several different heat-shock proteins were found in *S. venezuelensis* infective larvae cDNA. Hsp90, an evolutionarily conserved indispensable molecular chaperone, is involved in the folding, stabilization, activation, and assembly of a wide range of cellular proteins, playing a central role in many biological processes [25]. In *C. elegans*, Hsp90 is upregulated in dauer larvae, to which infective larvae of parasitic nematodes are often compared [26]. Our present study demonstrated that Hsp90 is abundantly and constitutively transcribed throughout the life of *S. venezuelensis* (Fig. 3A). In spite of a number of similarities between infective larvae and dauer larvae, recent comparative genomics between *C. elegans* and

Please cite this article as: Yoshida A, et al, Transcripts analysis of infective larvae of an intestinal nematode, *Strongyloides venezuelensis*, Parasitol Int (2010), doi:10.1016/j.parint.2010.10.007

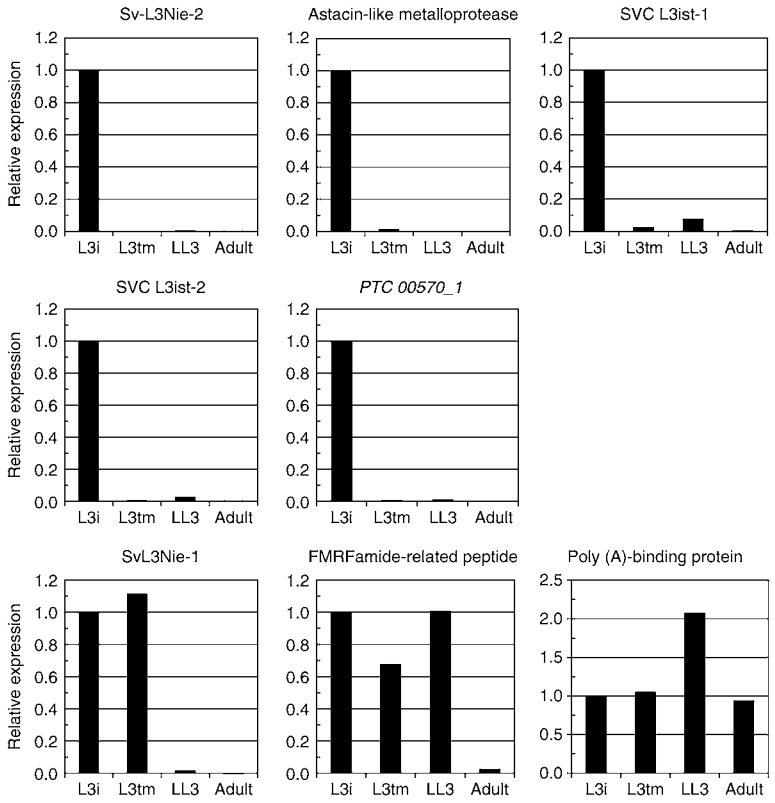

Fig. 4. Quantitative analysis of mRNA expression for infective larvae (L3i) specific transcripts. Quantitative real-time PCR validated the specific expression of six genes in infective L3 larvae. Relative expression of the target genes was assessed by normalizing to 18S rRNA expression. Gene expression in L3i was defined as 1.0. Accession number for genes analysed are as follows: Sv-L3Nie-2; HO652574, Astacin-like metalloprotease; HO652576, SVC L3ist-1 (novel gene); HP429055, SVC L3ist-2 (novel gene); HP429056, *PTC 00570_1*; HP429058, Sv-L3Nie-1; HP429068, FMR Famide-related peptide; HO652180, Poly (A)-binding protein; HO652261.

S. stercoralis has failed uncover evidence of an L3i/dauer expression signature conserved between the two species [27].

On the other hand, interesting expression patterns were observed in small heat-shock proteins, Hsp20. We found that infective larvae of *S. venezuelensis* had at least three Hsp20s, which were significantly different not only in the sequence but in the expression pattern along the developmental stages as well (Fig. 3A). In mammals, Hsp20 protects cells from the aggregation of denatured proteins, and is abundantly expressed in smooth muscle cells and cardiomyocytes [28,29]. In parasitic nematodes, small heat-shock proteins have been reported to have a role in muscle cells and muscle contraction [30]. Therefore these Hsp20 might be involved in different muscular functions, or they might have totally different roles in *S. venezuelensis*.

Upon infection, infective larvae must penetrate skin as quickly as possible. Infective larvae of *S. venezuelensis* have a zinc metalloprotease activity, which has been assumed to play a major role in skin penetration [12]. This metalloprotease activity at 40 kDa is presumably a *S. venezuelensis* homologue of Ss40 of *S. stercoralis*, a zinc metalloprotease deployed by infective larvae [31,32]. Recent study identified an astacin-like metalloprotease transcript in infective larvae of *S. stercoralis*, which has been referred to as 'strongylastacin' [33], to which one of the transcripts in the present study (HO652576) is highly homologous. The expression of this transcript is specific for infective larva stage, which perfectly matches to the metalloprotease activity previously reported [12].

The most significant results in this study were that the substantial portion of transcripts of *S. venezuelensis* infective larvae contained novel sequences. Especially, novel transcripts, SVC L3ist-1 and SVC L3ist-2, were abundantly expressed and they were infective larva-specific (Table 5, Fig. 4). We could not find similar sequences in public nucleotide databases, even against NEMABESE4, the most comprehensive resource for nematode EST analysis. Because NEMABESE4 contains EST data on *S. stercoralis* as well as *S. ratti*, these two transcripts should be not only stage-specific but species-specific molecules. Transcriptome analysis of *Ancylostoma caninum* has revealed that more than 80% of infective larva-specific transcripts (66 out of 78) are species-specific [34]. Comparative genomics among hookworms and *Srtongyloides* nematodes, that produce tissue penetrating infective larvae, should be one of the most exciting issues in the field of parasitology.

Apart from the biology of *S. venezuelensis* infective larvae, we could identify transcripts for candidate antigens for immunodiagnosis. We found two different transcripts homologous to *S. stercoralis* L3Nie antigen (SvL3Nie-1 and SvL3Nie-2) and proteinase inhibitor I33, which is similar to *Onchocerca volvulus* immunodominant antigen Ov33 (HP429083). L3Nie antigen is a member of the Ancylostoma Secretory Protein family, which was cloned with a patient serum [35], and has been shown to be useful in the diagnosis of strongyloidiasis [36]. Ov33, on the other hand, is recognized by more than 90% of onchocerciasis patient sera and has been used for immunodiagnosis as a single protein or fusion protein [37,38]. Gold standard for the diagnosis method for strongyloidiasis is the stool examination, however, the sensitivity of detecting larvae is not enough especially for chronic infections in immunocompetent hosts [39,40]. Because Ov33 homologue and L3Nie antigen appear to be abundantly transcribed in larvae, the combined use of the two antigens in immunodiagnosis might improve the sensitivity and specificity

Please cite this article as: Yoshida A, et al. Transcripts analysis of infective larvae of an intestinal nematode, *Strongyloides venezuelensis*, Parasitol Int (2010), doi:10.1016/j.parint.2010.10.007

significantly. Therefore further analysis is required of these antigens with strongyloidiasis patient sera.

5. Conclusions

A total of 408 EST were obtained from a cDNA library of *S. venezuelensis* infective larvae. Most abundant transcripts are those for lipase, respiration enzymes, and heat-shock proteins, however they contained 37 novel sequences which cannot be found in public nucleotide databases. Of seven transcripts which are infective larvae stage-specific, three have been unannotated and two were novel. Further research on these novel genes will clarify the biology of the infective larva.

Acknowledgements

This work was supported by grants from the Ministry of Education, Culture, Sports, Science and Technology of Japan (Grant-in-Aid for Scientific Research C 21590466, Grant-in-Aid for Scientific Research on Priority Areas 'Matrix of Infection Phenomena' 21022041), the Ministry of Health, Labour and Welfare (H20-Shinko-Ippan-016, H21-Kokui-Shitei-004), and the Japan Health Sciences Foundation (KHA2031).

References

[1] Román-Sánchez P, Pastor-Guzmán A, Moreno-Guillén S, Igual-Adell R, Suñer-Generoso S, Tornero-Estébanez C. High prevalence of *Strongyloides stercoralis* among farm workers on the Mediterranean coast of Spain: analysis of the predictive factors of infection in developed countries. Am J Trop Med Hyg 2003;69:336–40.
[2] Safdar A, Malathum K, Rodriguez SJ, Husni R, Rolston KV. Strongyloidiasis in patients at a comprehensive cancer center in the United States. Cancer 2004;100:1531–6.
[3] Hirata T, Uchima N, Kishimoto K, Zaha O, Kinjo N, Hokama A, et al. Impairment of host immune response against *Strongyloides stercoralis* by human T cell lymphotropic virus type 1 infection. Am J Trop Med Hyg 2006;74:246–9.
[4] Couillault C, Pujol N, Reboul J, Sabatier L, Guichou JF, Kohara Y, et al. TLR-independent control of innate immunity in *Caenorhabditis elegans* by the TIR domain adaptor protein TIR-1, an ortholog of human SARM. Nat Immunol 2004;5:488–94.
[5] Pujol N, Zugasti O, Wong D, Couillault C, Kurz CL, Schulenburg H, et al. Anti-fungal innate immunity in *C. elegans* is enhanced by evolutionary diversification of antimicrobial peptides. PLoS Pathog 2008;4:e1000105.
[6] Hotez PJ, Bethony J, Bottazzi ME, Brooker S, Diemert D, Loukas A. New technologies for the control of human hookworm infection. Trends Parasitol 2006;22:327–31.
[7] Suarez VH. Helminthic control on grazing ruminants and environmental risks in South America. Vet Res 2002;33:563–73.
[8] De Lange HJ, Lahr J, Van der Pol JJ, Wessels Y, Faber JH. Ecological vulnerability in wildlife: an expert judgment and multicriteria analysis tool using ecological traits to assess relative impact of pollutants. Environ Toxicol Chem 2009;28:2233–40.
[9] Maruyama H, Nawa Y, Ohta N. *Strongyloides venezuelensis*: binding of orally secreted adhesion substances to sulfated carbohydrates. Exp Parasitol 1998;89:16–20.
[10] Korenaga M, Nawa Y, Mimori T, Tada I. *Strongyloides ratti*: the role of enteral antigenic stimuli by adult worms in the generation of protective immunity in rats. Exp Parasitol 1983;55:358.
[11] Maruyama H, Yabu Y, Yoshida A, Nawa Y, Ohta N. A role of mast cell glycosaminoglycans for the immunological expulsion of intestinal nematode, *Strongyloides venezuelensis*. J Immunol 2000;164:3749–54.
[12] Maruyama H, Nishimaki A, Takuma Y, Kurimoto M, Suzuki T, Sakatoku Y, et al. Successive changes in tissue migration capacity of developing larvae of an intestinal nematode, *Strongyloides venezuelensis*. Parasitology 2006;132:1–8.
[13] Wertheim G. Growth and development of *Strongyloides venezuelensis* Brumpt, 1934 in the albino rat. Parasitology 1970;61:381–8.
[14] Gill GV, Welch E, Bailey JW, Bell DR, Beeching NJ. Chronic *Strongyloides stercoralis* infection in former British Far East prisoners of war. Q J Med 2004;97:789–95.
[15] Keiser PB, Nutman TB. *Strongyloides stercoralis* in the immunocompromised population. Clin Microbiol Rev 2004;17:208–17.
[16] Yamaguchi K, Takatsuki K. Adult T cell leukaemia-lymphoma. Baillières Clin Haematol 1993;6:899–915.
[17] Verdonck K, González E, Van Dooren S, Vandamme AM, Vanham G, Gotuzzo E. Human T-lymphotropic virus 1: recent knowledge about an ancient infection. Lancet Infect Dis 2007;7:266–81.
[18] Marcos LA, Terashima A, Dupont HL. Strongyloides hyperinfection syndrome: an emerging global infectious disease. Trans R Soc Trop Med Hyg 2008;102:314–8.
[19] Audic S, Claverie JM. The significance of digital gene expression profiles. Genome Res 1997;7:986–95.
[20] Ashton FT, Zhu X, Boston R, Lok JB, Schad GA. *Strongyloides stercoralis*: amphidial neuron pair ASJ triggers significant resumption of development by infective larvae under host-mimicking in vitro conditions. Exp Parasitol 2007;115:92–7.
[21] Singh R, Kaushik S, Wang Y, Xiang Y, Novak I, Komatsu M, et al. Autophagy regulates lipid metabolism. Nature 2009;458:1131–5.
[22] Mizushima N, Yamamoto A, Matsui M, Yoshimori T, Ohsumi Y. In vivo analysis of autophagy in response to nutrient starvation using transgenic mice expressing a fluorescent autophagosome marker. Mol Biol Cell 2004;15:1101–11.
[23] Kuma A, Hatano M, Matsui M, Yamamoto A, Nakaya H, Yoshimori T, et al. The role of autophagy during the early neonatal starvation period. Nature 2004;432:1032–6.
[24] Shibata M, Yoshimura K, Tamura H, Ueno T, Nishimura T, Inoue T, et al. LC3, a microtubule-associated protein1A/B light chain3, is involved in cytoplasmic lipid droplet formation. Biochem Biophys Res Commun 2010;393:274–9.
[25] Nollen EA, Morimoto RI. Chaperoning signaling pathways: molecular chaperones as stress-sensing 'heat shock' proteins. J Cell Sci 2002;115:2809–16.
[26] Ogawa A, Streit A, Antebi A, Sommer RJ. A conserved endocrine mechanism controls the formation of dauer and infective larvae in nematodes. Curr Biol 2009;19:67–71.
[27] Mitreva M, McCarter JP, Martin J, Dante M, Wylie T, Chiapelli B, et al. Comparative genomics of gene expression in the parasitic and free-living nematodes *Strongyloides stercoralis* and *Caenorhabditis elegans*. Genome Res 2004;14:209–20.
[28] Fan GC, Ren X, Qian J, Yuan Q, Nicolaou P, Wang Y, et al. Novel cardioprotective role of a small heat-shock protein, Hsp20, against ischemia/reperfusion injury. Circulation 2005;111:1792–9.
[29] Salinthone S, Tyagi M, Gerthoffer WT. Small heat shock proteins in smooth muscle. Pharmacol Ther 2008;119:44–54.
[30] Raghavan N, Ghosh I, Eisinger WS, Pastrana D, Scott AL. Developmentally regulated expression of a unique small heat shock protein in *Brugia malayi*. Mol Biochem Parasitol 1999;104:233–46.
[31] McKerrow JH, Brindley P, Brown M, Gam A, Stanton C, Neva FA. *Strongyloides stercoralis*: identification of a protease that facilitates penetration of the skin by the infective larvae. Exp Parasitol 1990;70:134–43.
[32] Brindley PJ, Gam AL, McKerrow JH, Neva FA. Ss40: the zinc endopeptidase secreted by infective larvae of *Strongyloides stercoralis*. Exp Parasitol 1995;80:1–7.
[33] Gomez Gallego S, Loukas A, Slade RW, Neva FA, Varatharajalu R, Nutman TB, et al. Identification of an astacin-like metallo-proteinase transcript from the infective larvae of *Strongyloides stercoralis*. Parasitol Int 2005;54:123–33.
[34] Wang Z, Abubucker S, Martin J, Wilson RK, Hawdon J, Mitreva M. *Ancylostoma caninum* transcriptome and exploring nematode parasitic adaptation. BMC Genomics 2010;11:307.
[35] Ravi V, Ramachandran S, Thompson RW, Andersen JF, Neva FA. Characterization of a recombinant immunodiagnostic antigen (NIE) from *Strongyloides stercoralis* L3-stage larvae. Mol Biochem Parasitol 2002;125:73–81.
[36] Ramanathan R, Burbelo PD, Groot S, Iadarola MJ, Neva FA, Nutman TB. A luciferase immunoprecipitation systems assay enhances the sensitivity and specificity of diagnosis of *Strongyloides stercoralis* infection. J Infect Dis 2008;198:444–51.
[37] Lucius R, Kern A, Seeber F, Pogonka T, Willenbucher J, Taylor HR, et al. Specific and sensitive immunodiagnosis of onchocerciasis with a recombinant 33 kD *Onchocerca volvulus* protein (Ov33). Trop Med Parasitol 1992;43:139–45.
[38] Nde PN, Pogonka T, Bradley JE, Titanji VP, Lucius R. Sensitive and specific serodiagnosis of onchocerciasis with recombinant hybrid proteins. Am J Trop Med Hyg 2002;66:566–71.
[39] Sato Y, Kobayashi J, Toma H, Shiroma Y. Efficacy of stool examination for detection of *Strongyloides* infection. Am J Trop Med Hyg 1995;53:248–50.
[40] Siddiqui AA, Berk SL. Diagnosis of *Strongyloides stercoralis* infection. Clin Infect Dis 2001;33:1040–7.

Please cite this article as: Yoshida A, et al. Transcripts analysis of infective larvae of an intestinal nematode, *Strongyloides venezuelensis*, Parasitol Int (2010), doi:10.1016/j.parint.2010.10.007

Parasitology International 59 (2010) 477–480

Contents lists available at ScienceDirect

Parasitology International

journal homepage: www.elsevier.com/locate/parint

Case report

Zoonotic filariasis caused by *Onchocerca dewittei japonica* in a resident of Hiroshima Prefecture, Honshu, Japan

Shigehiko Uni [a,*], Tomoyuki Boda [b], Koichi Daisaku [b], Yoshihiro Ikura [c], Haruhiko Maruyama [d], Hideo Hasegawa [e], Masako Fukuda [f,g], Hiroyuki Takaoka [g], Odile Bain [h]

[a] *Department of Medical Zoology, Osaka City University Medical School, Abeno-ku, Osaka 545-8585, Japan*
[b] *Shobara Red Cross Hospital, Shobara, Hiroshima 727-0013, Japan*
[c] *Department of Pathology, Osaka City University Medical School, Abeno-ku, Osaka 545-8585, Japan*
[d] *Department of Infectious Diseases, Division of Parasitology, Faculty of Medicine, University of Miyazaki, Miyazaki 889-1692, Japan*
[e] *Department of Biology, Faculty of Medicine, Oita University, Oita 879-5593, Japan*
[f] *Research Promotion Project, Oita University, Oita 879-5593, Japan*
[g] *Department of Infectious Disease Control, Faculty of Medicine, Oita University, Oita 879-5593, Japan*
[h] *Parasitologie comparée, UMR 7205 CNRS, Muséum National d'Histoire Naturelle, 75231 Paris, France*

ARTICLE INFO

Article history:
Received 13 May 2010
Accepted 21 May 2010
Available online 31 May 2010

Keywords:
Zoonotic onchocerciasis
Onchocerca dewittei japonica
Filarioidea
Cuticular characteristics
Wild boar
Japan

ABSTRACT

A female of *Onchocerca* sp. was found to be the probable causative agent of a subcutaneous nodule in the left knee of a 70-year-old man in a rural area of Hiroshima Prefecture, Honshu, the main island of Japan. We compared the characteristics of the agent with the features of the four previously suspected species found in cattle and horses in various parts of the world, as well as *O. lupi* and *O. jakutensis* that were suspected or proved, respectively, in zoonotic cases in Europe. In addition, the morphologic characteristics of this parasite were compared with those of the four *Onchocerca* species found in wild animals in Japan. Based on such characteristics as the large triangle ridges, the considerable distance between any two adjacent ridges, and the absence of inner cuticular striae in the longitudinal sections, we found the causative agent in the present case to be identical to the female of *Onchocerca dewittei japonica*. All five previous cases of zoonotic onchocerciasis in Japan had been found in Oita, Kyushu, the main southern island. This human case caused by *O. dewittei japonica* suggests that zoonotic onchocerciasis is liable to occur in rural areas in Japan where wild boar, *Simulium* vectors, and humans overlap.

1. Introduction

Zoonotic filariasis is an infection found in humans which is caused by filarioids of animals [1]. Numerous human cases caused by members of the genus *Dirofilaria* have been found throughout the world [2]. In contrast, human cases caused by *Onchocerca* species parasitic in animals are rare; the first of 15 cases known to date was reported in Ukraine in 1965. Five human cases in Europe, five in Japan, four in North America, and one on the Arabian Peninsula have been discovered worldwide [3–18].

In zoonotic onchocerciasis, the causative agents suspected are *O. gutturosa* Neumann, 1910 from cattle and *O. cervicalis* Railliet and Henry, 1910 from horses [3–8,13]. Much more recently, in Japan, *Onchocerca dewittei japonica* Uni et al., 2001;[19] from wild boar was identified in four of the most recent five cases in Oita, Kyushu, the main southern island of Japan [9,12,14,15]. In retrospect, *O. lupi* found from dogs was suspected to be responsible for subconjunctival infections [3,11] in which the causative agent could not be unambiguously determined in Europe [20]. Finally, *Onchocerca* of the red deer, *O. jakutensis* (Guvanov, 1964) was identified in a patient in Austria [17].

Here we present a new case of a zoonotic onchocerciasis found from a patient living in a rural area of Hiroshima Prefecture in Honshu, the main island of Japan.

2. Case study

The patient, a 70-year-old man living in Fuchu City, Hiroshima Prefecture, found a nodule on the left knee in the beginning of the year 2009 and reported feeling pain in the nodule in May 2009. The nodule, 2 cm in diameter, was surgically removed from the subcutaneous connective tissue at the knee at the Shobara Red Cross Hospital in Hiroshima Prefecture in July 2009. The mass excised (1 × 2 cm) was fixed in 4% paraformaldehyde for 24 h and embedded in paraffin, a routine process. The sections were stained with hematoxylin and eosin. Histologic sections examined: S3-1, S3-2, S3-4, and S7-9.

A coiled worm was found in the nodule and several longitudinal, oblique, and transverse sections of the main part of the body (midbody) of the worm were examined with a microscope (Fig. 1; 1–5). The worm

* Corresponding author. Tel.: +81 6 66453760; fax: +81 6 66453762.
E-mail address: uni@med.osaka-cu.ac.jp (S. Uni).

1383-5769/$ – see front matter © 2010 Elsevier Ireland Ltd. All rights reserved.
doi:10.1016/j.parint.2010.05.006

was a female with its uteri in which microfilariae or embryos were not seen (Fig. 1; 1 and 4). In addition, a section of the thin anterior part, 83 μm wide, with the esophagus and a section of the posterior part of the worm, 125 μm wide, were found. Thus, this nodule was occupied by one female adult.

In the longitudinal sections of the worm (Fig. 1; 2), the external transverse ridges were salient on the cuticle and the distance between two adjacent ridges in the main body is shown in Table 1. Our examination revealed two adjoining ridges of one side indicated by two arrows; an arrowhead indicated a small overlapping ridge of the other side (Fig. 1; 2). The distance between the ridges was therefore measured on the ridges of the one side. The ridges formed a sharp triangle (Fig. 1; 3). The cuticle was divided into two main parts of equal thickness and no inner striae were found on the middle line (Fig. 1; 3).

In the transverse sections of the main body, the cuticle was composed of four layers, the muscle cells were 42–52 in number, and the two lateral chords were large. No inner projections of the cuticle were found at the lateral chords. The transverse sections of the midbody were round and lateral thickening of the cuticle was not seen (Fig. 1; 4). The differences of the thickness of the cuticle can be seen at the ridge in Fig. 1; 5. The difference (30 μm) between the thick cuticle (55 μm) and the thin cuticle (25 μm) corresponded to the height of the ridges of *O. dewittei japonica* (Table 1).

Regarding the histologic reaction of the host, the worm was surrounded with eosinophilic exudate in the center of the granuloma while away from the center, macrophages, neutrophils, eosinophils, and lymphocytes had infiltrated the granulomatous tissue (Fig. 1; 1). Macrophages and eosinophils intensively accumulated around some sections of disintegrating parts of the worm (Fig. 1; 5) but neutrophils were very scarce.

The patient, a farmer, lives in a rural area near mountains inhabited by wild boar. He has never been outside Japan and had not visited Oita, Kyushu, within the past several years. He has not raised pets such as

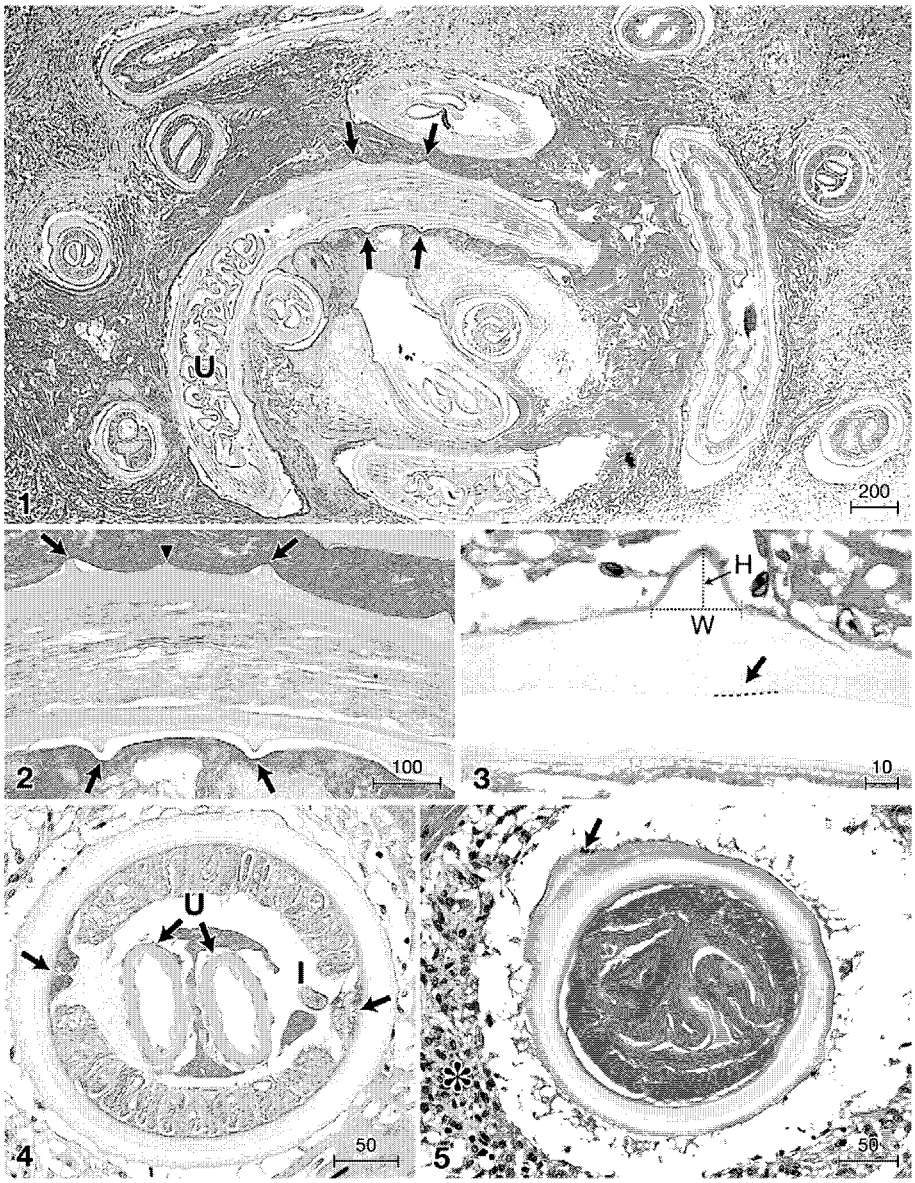

Fig. 1. Histologic sections of a female *Onchocerca dewittei japonica*, found in a nodule excised from the left knee of a 70-year-old man. The sections are stained with hematoxylin and eosin. Bars, micrometers. 1. A coiled female with transverse ridges (arrows) on the cuticle and the uteri (U) in the pseudocoelom. 2. The salient transverse ridges (arrows) of one side and a small ridge (an arrowhead) of the other side (semicircular ridges are overlapping at the lateral field, see text). 3. The triangle ridge in the longitudinal section: height (H) and width (W), and the lack of the inner striae at the dotted line with an arrow in the cuticle. 4. The transverse section at the midbody with thick cuticle, muscle cells, and two large lateral chords (arrows). Two empty uteri (U) and intestine (I) in the pseudocoelom. 5. In the transverse section, a thick portion of the cuticle indicates the ridge (an arrow). The section is intensively surrounded by macrophages (*).

Table 1
Comparison of histologic characteristics of *Onchocerca* sp. found from a human nodule with females of *Onchocerca* species known in Japan.

	Onchocerca sp. (present study)	*O. gutturosa*	*O. lienalis*	*O. skrjabini*	*O. eberhardi*	*O. suzukii*	*O. dewittei japonica*
Body width at midbody	270–310	170–250**, 140–225***, 200–300*****	180–200**,180–220****, 150–220*****	170–300	60–170	228–430	180–310
Distance between 2 adjacent ridges	210–280	50–75**, 70–80***, 87–166*****	30–40**, 25–45****, 60*****	48–55	25–40	No ridges	185–290
Shape of ridges (H/W)* in longitudinal sections	Triangle (13–25/23–28)	Rounded ridges (5/12**, 4–5/5–10***, 10–13/26*****)	Small, rounded ridges (3/15–23*****)	Small ridges (6/12)	Small, rounded ridges (3/8)	No ridges	Triangle (8–23/23–30)
Thickness of cuticle without ridges	30–40	30**, 25–35***	12–17****, 10*****	20–30	28–32	15–50	10–32
Number of inner striae between 2 adjacent ridges	None	3**, 4–8***, 2–4*****	2**, ****, *****	3–4	2	None	None
Size of lateral chords (H/W)* in transverse sections	13–25/42–55	13/54****	16–21/52–63****	15–25/50–88	10/38	5–37/125–132	10–18/45–63
Number of muscle cells per quadrant	8–15	2–4****	5–7******	2–3	1–2	8–13	8–22
Height of muscle cells	38–43	40****	31****	25–40	15–18	30–38	45–50
Diameter of intestine	15–18	20–34****	26****	38–68	15–20	20–48	15–17
Host(s)	Human	Cattle	Cattle	Deer and serows	Deer	Serows	Wild boar
Histologic sections and references	Sections (S3-1, S3-2, S3-4, S7-9) from a human	**[5]; ***[22]; ****[23]; *****[24]	**[5]; ****[23]; ***** [24]; ******[14]	Sections (YG2-31) from a serow	Sections (S57-F3) from a deer	Sections (YG2-35) from a serow	Sections (B57-1) from a wild boar

Dimensions in micrometers.
*H/W: height/width.

dogs and cats. Immunologic deficiency was not found in his laboratory examination at the hospital.

3. Discussion

In the longitudinal sections, the presence of the transverse ridges on the cuticle of the worm appeared to be typical of a female of the species among the genus *Onchocerca*: 28 species and one subspecies (*O. dewittei japonica*) with the ridges on the cuticle of the female worms and three species without the ridges [21].

The present causative agent can be distinguished from *O. gutturosa* and *O. lienalis*, the two species found in cattle. In these species, the ridges (evident in the posterior part in *O. lienalis*) are rounded, not triangular; the distance between adjacent ridges is smaller; and the females possess inner striae in the cuticle (Table 1), [5,22–24]. In addition, the female of *O. lienalis* has fine, irregular longitudinal striations on the outer surface [23]. The females of *O. cervicalis* and *O. reticulata* from horses have the inner striae in the cuticle and shorter distance between adjoining ridges than that of the causative agent [22]. These four *Onchocerca* species from domestic animals can therefore be excluded from consideration as the causative agent in this case.

The present agent was distinguished from *O. lupi* and *O. jakutensis* in such characteristics as the distance between ridges, the shapes of the ridges, and the inner striae [20,25].

To compare the causative agent with the *Onchocerca* species already found from wild ungulates in Japan, we used portions of the collections of the histologic sections made from females of *Onchocerca* species in the Department of Medical Zoology, Osaka City University Medical School (Table 1) and published descriptions of these species. In Table 1, *O. skrjabini* Rukhlyadev, 1964, taken from a serow, is distinguished from the present human-case causative agent, owing to great differences in such principal characteristics as the distance between adjacent ridges, shape of the ridges, and the inner striae in the cuticle [26,27]. *Onchocerca eberhardi* Uni et al., 2007 taken from a sika deer differs from the causative agent in the diameter of the midbody as well as such characteristics as the distance between the ridges, the shape of ridges, and the inner striae [21]. In *O. suzukii* Yagi et al., 1994 taken from a serow, the transverse ridges are absent on the cuticle [27].

On the contrary, *O. dewittei japonica* taken from a wild boar was found to be identical to the present human-case causative agent in the distance between adjacent ridges, the shape of the ridges, the lack of inner striae in the cuticle, and other dimensions such as the body width, number of muscle cells, and size of lateral chords (Table 1) [19]. Therefore, comparison of the causative agent of the human case with the *Onchocerca* species, either outside Japan or present in Japan, indicated that the agent was a female adult of *O. dewittei japonica*.

Detailed examinations of the histologic sections of *O. dewittei japonica* found both in a human (the present study) and from wild boar now allow us to identify retrospectively this species as the causative agent of the first human case in Japan [7,8] which had been suspected as *O. gutturosa* or *O. cervicalis*. Uni et al. [19] described the ridges of *O. dewittei japonica* female as semicircular, with double thickness of the cuticle on the transverse sections. Thus, the difference in the cuticular thickness has a specific value to suggest the presence of salient ridges in transverse sections. In the slightly oblique section shown in their Fig. 3 of the first human case [7], it is our consideration that the difference (24 μm) between the thick cuticle (36 μm) (with the transverse ridge) and the thin cuticle (12 μm) (without ridges) corresponds to the height (8–23 μm) of ridges on *O. dewittei japonica* rather than that (4–13 μm) of those on *O. gutturosa* (Table 1). The difference in the cuticular thickness therefore indicates that the causative agent in the first human case found was *O. dewittei japonica* also, but this species had not yet discovered from wild boar at that time.

Wolbachia bacterial endosymbionts were found in *O. dewittei japonica* [28, Casiraghi et al., ongoing work]. It is indicated that (1) *Wolbachia* stimulate neutrophil infiltration in onchocercomata caused by *Wolbachia*-positive filariae and that (2) eosinophils accumulate to kill the parasites after elimination of the *Wolbachia* by antibiotics [29,30]. Histologic examination showed that, rather than neutrophils, macrophages and eosinophils were abundant around the sections of the worm. The endosymbionts appear to have been destroyed in the altered parts of

the worm; the neutrophils appear to have already been replaced with eosinophils in the course of the death of the parasite in the immunological environment.

Until now, all four known cases of zoonotic onchocerciasis caused by *O. dewittei japonica* parasites found in wild boar (plus probably an earlier case, examined in retrospect) were limited only to Oita, Kyushu. However, the present findings indicate that zoonotic onchocerciasis has occurred in at least one other island of Japan as well. The prevalence of *O. dewittei japonica* in wild boar, as measured by the presence of microfilariae in skin snips, was high in and near Hiroshima Prefecture: 78% (31/40) of wild boar were found to harbor this filarioid in Shimane Prefecture adjoining Hiroshima Prefecture, examined between 2005 and 2006, and was close to the prevalence of the parasites (40/45, or 89%) in wild boar in Oita, Kyushu, in 2003. In Wakayama Prefecture, located in the west-central part of Honshu, 77% (23/30) of wild boar harbored this filarioid in 2007. Thus, as in Kyushu, almost all wild boar over one year old in the western part of Honshu examined, were found to harbor *O. dewittei japonica* (Uni et al., unpublished data).

Having obtained experimentally the infective larvae of *O. dewittei japonica* from several kinds of black flies [31], and having identified as *O. dewittei japonica* the larvae from black flies caught in Oita, Fukuda et al. suggested that *Simulium bidentatum* is a vector in the transmission of the zoonotic onchocerciasis caused by *O. dewittei japonica* in Oita [32]. The black fly inhabits Honshu and Shikoku as well as Kyushu and bites both animals and humans. In the present case, DNA sequences of the mitochondrial *CO1* gene obtained from the causative agent, embedded in paraffin for histologic examination, showed high similarities to those of *O. dewittei japonica* [33, Fukuda et al., in preparation].

In Japan, the habitat of the wild boar (estimated population: several hundred thousands) has recently broadened in the western part of Honshu, Shikoku, and Awaji-shima Island as well as Kyushu, because the annual snowfall has decreased, rice fields left unused by migration of segments of the work forces away from rural areas are favorable habitat for wild boar, and the population of hunters has largely decreased [34]. Therefore, the present human-host case caused by *O. dewittei japonica* suggests that zoonotic onchocerciasis is now liable to occur in other rural areas in Japan, or wherever wild boar and humans are in close proximity and the *Simulium* vectors are known, as well as in Oita.

Acknowledgements

We thank Prof. Kenichi Wakasa, Department of Diagnostic Pathology, Osaka City University Medical School, for comments about the histologic sections of the human case. We thank Mr. J. L. Yohay for reading the manuscript.

References

[1] Orihel T, Eberhard ML. Zoonotic filariasis. Clin Microbiol Rev 1998;11:366–81.
[2] Pampiglione S, Rivasi F. Human dirofilariasis due to *Dirofilaria* (*Nochotiella*) *repens*: an update of world literature from 1995 to 2000. Parassitologia 2000;42:231–54.
[3] Azarova NS, Miretsky OY, Sonin MD. The first instance of detection of nematode *Onchocerca* Diesing, 1841 in a person in the USSR. Med Parazitol (Mosk) 1965;34: 156–8 (In Russian).
[4] Siegenthaler R, Gubler R. Paraarticuläres Nematodengranulom (einheimische *Onchocerca*). Schweiz Med Wochenschr 1965;95:1102–4.
[5] Beaver PC, Horner GS, Bilos JZ. Zoonotic onchocercosis in a resident of Illiois and observations on the identification of *Onchocerca* species. Am J Trop Med Hyg 1974;23:595–607.
[6] Ali-Khan Z. Tissue pathology and comparative microanatomy of *Onchocerca* from a resident of Ontario and other enzootic *Onchocerca* species from Canada and the U.S.A. Ann Trop Med Parasitol 1977;71:469–82.
[7] Beaver PC, Yoshimura H, Takayasu S, Hashimoto H, Little MD. Zoonotic *Onchocerca* in a Japanese child. Am J Trop Med Hyg 1989;40:298–300.
[8] Hashimoto H, Murakami I, Fujiwara S, Takayasu S, Takaoka H, Uga S, et al. A human case of zoonotic onchocerciasis in Japan. J Dermatol 1990;17:52–5.
[9] Takaoka H, Bain O, Tajimi S, Kashima K, Nakayama I, Korenaga M, et al. Second case of zoonotic *Onchocerca* infection in a resident of Oita in Japan. Parasite 1996;3: 179–82.
[10] Burr Jr WE, Brown MF, Eberhard ML. Zoonotic *Onchocerca* (Nematoda: Filarioidea) in the cornea of a Colorado resident. Ophthalmology 1998;105:1494–7.
[11] Pampiglione S, Vakalis N, Lyssimachou A, Kouppari G, Orihel TC. Subconjunctival zoonotic *Onchocerca* in an Albanian man. Ann Trop Med Parasitol 2001;95: 827–32.
[12] Takaoka H, Bain O, Uni S, Korenaga M, Tada K, Ichikawa H, et al. Human infection with *Onchocerca dewittei japonica*, a parasite from wild boar in Oita, Japan. Parasite 2001;8:261–3.
[13] Wright RW, Neafie RC, McLean M, Markman AW. Zoonotic onchocerciasis of the shoulder: a case report. J Bone Joint Surg 2002;84:627–9.
[14] Takaoka H, Bain O, Uni S, Korenaga M, Kozek WJ, Shirasaka C, et al. Zoonotic onchocerciasis caused by a parasite from wild boar in Oita, Japan. A comprehensive analysis of morphological characteristics of the worms for its diagnosis. Parasite 2004;11:285–92.
[15] Takaoka H, Yanagi T, Daa T, Anzai S, Aoki C, Fukuda M, et al. An *Onchocerca* species of wild boar found in the subcutaneous nodule of a resident of Oita, Japan. Parasitol Int 2005;54:91–3.
[16] Sallo F, Eberhard ML, Fok E, Baska F, Hatvani I. Zoonotic intravitreal *Onchocerca* in Hungary. Ophthalmology 2005;112:502–4.
[17] Koehsler M, Soleiman A, Aspöck H, Auer H, Walochnik J. *Onchocerca jakutensis* filariasis in humans. Emerg Infect Dis 2007;13:1749–52.
[18] Hira PR, Al-Buloushi A, Khalid N, Iqbal J, Bain O, Eberhard ML. Case report: zoonotic filariasis in the Arabian Peninsula: autochthonous onchocerciasis and dirofilariasis. Am J Trop Med Hyg 2008;79:739–41.
[19] Uni S, Bain O, Takaoka H, Miyashita M, Suzuki Y. *Onchocerca dewittei japonica* n. subsp., a common parasite from wild boar in Kyushu Island, Japan. Parasite 2001;8:215–22.
[20] Sréter T, Széll Z, Egyed Z, Varga I. Subconjuncival zoonotic onchocerciasis in man: aberrant infection with *Onchocerca lupi*? Ann Trop Med Parasitol 2002;96: 497–502.
[21] Uni S, Bain O, Agatsuma T, Harada M, Torii H, Fukuda M, et al. *Onchocerca eberhardi* n. sp. (Nematoda: Filarioidea) from sika deer in Japan; relationships between species parasitic in cervids and bovids in the Holarctic region. Parasite 2007;14: 199–211.
[22] Bain O. Redescription de cinq espèces d'onchocerques. Ann Parasitol Hum Comp 1975;50:763–88.
[23] Bain O, Petit G, Poulain B. Validité des deux espèces *Onchocerca lienalis* et *O. gutturosa*, chez les bovins. Ann Parasitol Hum Comp 1978;53:421–30.
[24] Eberhard ML. Studies on the *Onchocerca* (Nematoda: Filarioidea) found in cattle in the United States. I. Systematics of *O. gutturosa* and *O. lienalis* with a description of *O. stilesi* sp. n. J Parasitol 1979;65:379–88.
[25] Demiaszkiewicz AW. Redescription of *Onchocerca jakutensis* (Gubanov, 1964) (Nematoda, Filaroidea). Acta Parasitol 1993;38:124–7.
[26] Uni S, Suzuki Y, Katsumi A, Kimata I, Iseki M, Bain O. Taxonomy and pathology of filarial parasites from Japanese serows (*Capricornis crispus*). Proc 9th Int Cong Parasitol; 1998. p. 681–4.
[27] Yagi K, Bain O, Shoho C. *Onchocerca suzukii* n. sp. and *O. skrjabini* (= *O. tarsicola*) from a relict bovid, *Capricornis crispus*, in Japan. Parasite 1994;1:349–56.
[28] Bain O, Casiraghi M, Martin C, Uni S. The Nematoda Filarioidea: critical analysis linking molecular and traditional approaches. Parasite 2008;15:342–8.
[29] Brattig NW, Büttner DW, Hoerauf A. Neutrophil accumulation around *Onchocerca* worms and chemotaxis of neutrophils are dependent on *Wolbachia* endobacteria. Microbes Infect 2001;3:439–46.
[30] Nfon CK, Makepeace BL, Njongmeta LM, Tanya VN, Bain O, Trees AJ. Eosinophils contribute to killing of adult *Onchocerca ochengi* within onchocercomata following elimination of *Wolbachia*. Microbes Infect 2006;8:2698–705.
[31] Fukuda M, Takaoka H, Uni S, Bain O. Infective larvae of five *Onchocerca* species from experimentally infected *Simulium* species in an area of zoonotic onchocerciasis in Japan. Parasite 2008;15:111–9.
[32] Fukuda M, Otsuka Y, Uni S, Bain O, Takaoka H. Molecular identification of infective larvae of three species of *Onchocerca* found in wild-caught females of *Simulium bidentatum* in Japan. Parasite 2010;17:39–45.
[33] Fukuda M, Uni S, Boda T, Daisaku K, Hasegawa H, Otsuka Y, et al. A case of zoonotic onchocerciasis in Hiroshima: identification of the causative agent by mitochondrial DNA analysis of paraffin-embedded specimens. Med Entomol Zool 2010;61: 62 (Suppl.).
[34] Kodera Y. *Sus scrofa* Linnaeus, 1758. In: Ohdachi SD, Ishibashi Y, Iwasa MA, Saitoh T, editors. The wild mammals of Japan. Kyoto: Shoukadoh; 2009. p. 304–5.

Molecular Biology and Evolution

Research article

Divergence of the Mitochondrial Genome Structure in the Apicomplexan Parasites, Babesia and Theileria

Kenji Hikosaka,[1] Yoh-ichi Watanabe,[2] Naotoshi Tsuji,[3] Kiyoshi Kita,[2] Hiroe Kishine,[4] Nobuko Arisue,[5] Nirianne Marie Q. Palacpac,[5] Shin-ichiro Kawazu,[6] Hiromi Sawai,[1] Toshihiro Horii,[5] Ikuo Igarashi,[6] and Kazuyuki Tanabe[1,*]

[1]Laboratory of Malariology, International Research Center of Infectious Diseases, Research Institute for Microbial Diseases, Osaka University, Suita, Osaka, Japan

[2]Department of Biomedical Chemistry, Graduate School of Medicine, The University of Tokyo, Bunkyo-ku, Tokyo, Japan

[3]Laboratory of Parasitic Diseases, National Institute of Animal Health, National Agriculture and Food Research Organization, Tsukuba, Ibaraki, Japan

[4]Department of Molecular Biology, Research Institute for Microbial Diseases, Osaka University, Suita, Osaka, Japan

[5]Department of Molecular Protozoology, Research Institute for Microbial Diseases, Osaka University, Suita, Osaka, Japan

[6]National Research Center for Protozoan Diseases, Obihiro University of Agriculture and Veterinary Medicine, Obihiro, Hokkaido, Japan

***Corresponding author:** E-mail: kztanabe@biken.osaka-u.ac.jp.

Associate editor: Richard Thomas

Abstract

Mitochondrial (mt) genomes from diverse phylogenetic groups vary considerably in size, structure, and organization. The genus Plasmodium, causative agent of malaria, of the phylum Apicomplexa, has the smallest mt genome in the form of a circular and/or tandemly repeated linear element of 6 kb, encoding only three protein genes (*cox1*, *cox3*, and *cob*). The closely related genera Babesia and Theileria also have small mt genomes (6.6 kb) that are monomeric linear with an organization distinct from Plasmodium. To elucidate the structural divergence and evolution of mt genomes between Babesia/Theileria and Plasmodium, we determined five new sequences from *Babesia bigemina*, *B. caballi*, *B. gibsoni*, *Theileria orientalis*, and *T. equi*. Together with previously reported sequences of *B. bovis*, *T. annulata*, and *T. parva*, all eight Babesia and Theileria mt genomes are linear molecules with terminal inverted repeats (TIRs) on both ends containing three protein-coding genes (*cox1*, *cox3*, and *cob*) and six large subunit (LSU) ribosomal RNA (rRNA) gene fragments. The organization and transcriptional direction of protein-coding genes and the rRNA gene fragments were completely conserved in the four Babesia species. In contrast, notable variation occurred in the four Theileria species. Although the genome structures of *T. annulata* and *T. parva* were nearly identical to those of Babesia, an inversion in the 3-kb central region was found in *T. orientalis*. Moreover, the *T. equi* mt genome is the largest (8.2 kb) and most divergent with unusually long TIR sequences, in which *cox3* and two LSU rRNA gene fragments are located. The *T. equi* mt genome showed little synteny to the other species. These results suggest that the Theileria mt genome is highly diverse with lineage-specific evolution in two Theileria species: genome inversion in *T. orientalis* and gene-embedded long TIR in *T. equi*.

Key words: mitochondrion, mitochondrial genome, Babesia, Theileria, Plasmodium, Apicomplexa.

Introduction

Mitochondria, organelles essential for energy transduction and cellular functions, are present in almost all eukaryotes. Like nuclear genomes of eukaryotes, mitochondrial (mt) genomes from diverse phylogenetic groups vary considerably in size, structure, and organization as well as in the number of genes (Gray et al. 2004). The largest mt genome is found in land plants, in which the size ranges from 180 to 2,400 kb (Ward et al. 1981; Palmer et al. 1992), and the smallest is the 6-kb genome of the genus Plasmodium, causative agents of malaria. Plasmodium belongs to the phylum Apicomplexa, which includes >5,000 species, all of which are parasites of clinical or economic importance (Levine 1988). Veterinary and opportunistic pathogens include Babesia, which causes babesiosis in ruminants and humans; Theileria, causal agents for tropical theileriosis and East Coast fever in cattle; Cryptosporidium, responsible for cryptosporidiosis in humans and animals; and Toxoplasma, causing toxoplasmosis in immunocompromised patients and congenitally infected fetuses.

Relatively few apicomplexan mt genomes have been studied, and available data suggest that they are remarkably diverse in structure and genome organization. In Plasmodium, the mt genome is in the form of a circular and/or tandemly repeated, predominantly linear 6-kb element (Preiser et al. 1996; Wilson and Williamson 1997). The 6-kb element encodes only three mt protein-coding genes (cytochrome *c* oxidase subunits I and III: *cox1* and *cox3* and cytochrome *b*: *cob*) in addition to large subunit (LSU) and small subunit (SSU) ribosomal RNAs (rRNAs). The two rRNA genes are extensively fragmented and rearranged with 20 identified rRNA pieces, and curiously, no transfer RNA genes have

yet been identified (Feagin et al. 1997). The mt genomes of closely related apicomplexan parasites Babesia and Theileria (Lau 2009) are 6.6 kb in size and monomeric linear molecules with terminal inverted repeats (TIRs), indicative of telomeres (Kairo et al. 1994; Brayton et al. 2007). Similar to Plasmodium, mt genomes of Babesia and Theileria contain the three protein-coding genes, but gene order and transcriptional direction are clearly different from Plasmodium (Kairo et al. 1994; Brayton et al. 2007). Thus, the mt genomes of Plasmodium and Babesia/Theileria are structurally highly divergent regardless of their close relatedness (Kuo et al. 2008). For *Toxoplasma gondii*, the mt genome remains to be isolated and analyzed, although multiple copies of partial mt genes (*cox1* and *cob*) were found to be scattered throughout the nuclear genome (Ossorio et al. 1991). In *Cryptosporidium parvum*, the mitochondrion is degenerative and lacks any DNA (Abrahamsen et al. 2004). Clearly, the phylum Apicomplexa provides interesting materials to further understand the evolution of mt genomes.

It remains unknown how the remarkable structural divergence between Plasmodium and Babesia/Theileria mentioned above was generated. Gathering enough data set will also help provide further insights on the extent at which the mt genomes have evolved in the different genera as well as in the phylum. In this study, we determined five new mt genome sequences from Babesia and Theileria species. Analyses of the genome structures show that although the mt genome structure is conserved in Babesia species, it varies notably in both size and genome organization in Theileria species, with lineage-specific evolution in two Theileria species: genome inversion in *T. orientalis* and gene-embedded long TIR in *T. equi*.

Materials and Methods

Parasite Species

Mitochondrial genome sequences were determined from the following seven parasite species: *Babesia bigemina* (Kochinda stock) (Fujinaga et al. 1980), *B. caballi* (USDA strain) (Avarzed et al. 1997), *B. gibsoni* (National Research Center for Protozoan Diseases strain) (Ishimine et al. 1978), *B. bovis* (Miyama stock) (Fujinaga et al. 1980), *Theileria orientalis* (Ikeda stock) (Kim et al. 2004), *T. equi* (USDA strain) (Avarzed et al. 1998), and *T. parva* (Muguga stock) (Kairo et al. 1994). Their host animals are cattle for *B. bigemina*, *B. bovis*, *T. orientalis*, and *T. parva*; horses for *B. caballi* and *T. equi*; and dogs for *B. gibsoni* (supplementary table S1, Supplementary Material online).

DNA Sequencing

Parasite genomic DNA was extracted from animal bloods infected with *B. bigemina*, *B. gibsoni*, *B. bovis*, *T. orientalis*, and *T. parva*, and from cultures of *B. caballi* and *T. equi*, using QIAamp DNA Blood Mini Kit (QIAGEN, Hilden, Germany) according to the manufacturer's instructions. Nucleotide sequences of the mt genomes were determined by direct sequencing of polymerase chain reaction (PCR) products using specific primers (supplementary table S2a, Supplementary Material online). The primers were designed by aligning reported mt genome sequences of *B. bovis* (DDBL/EMBL/GenBank accession number EU075182), *T. parva* (Z23263), and *T. annulata* (NW_001091933). Amplification was carried out in a 20 μl reaction mixture containing 0.2 μM each of forward and reverse primers, 400 μM each of deoxynucleotide triphosphate (dNTP), 1 U of LA-Taq (Takara, Shiga, Japan), 2 μl of 10× PCR buffer, 2.5 mM of $MgCl_2$, and 1 μl of genomic DNA. PCR conditions were as follows: initial denaturation at 94 °C for 1 min and amplification for 40 cycles at 94 °C for 30 s, 55–68 °C (depending on primers used) for 30 s, and 72 °C for 1–6 min (depending on amplicon size, 1 min/kb), followed by a final extension at 72 °C for 10 min.

Sequences of the *T. equi* mt telomeric regions were determined by using the terminal deoxynucleotidyl transferase (TdT) tailing method (Bah et al. 2004) with some modifications. Briefly, the 3′ end was tailed with cytosine by initial denaturation of genomic DNA (150 ng) for 5 min at 95 °C and then incubated for 30 min at 37 °C in a reaction mixture containing 200 μM deoxycytidine triphosphate, 1 U of TdT (Takara), 20 mM Tris–HCl (pH 8.4), 50 mM KCl, and 1.5 mM $MgCl_2$, followed by heat inactivation of TdT at 65 °C for 10 min. The first PCR was done in a 50 μl reaction mixture containing 2 μl of the tailed DNA fragments, 1.25 U of AmpliTaq DNA Polymerase (Applied Biosystems, Foster City, CA), 2.5 mM $MgCl_2$, 200 μM dNTPs, 0.4 μM of an mt genome–specific primer (supplementary table S2b, Supplementary Material online), and a selective anchor primer (5′-CTACTACTACTAGGCCACGCGTCGACTAGTACGGGGGGGGGGGGGGG-3′). Initial denaturation was at 95 °C for 2 min, followed by 40 cycles at 94 °C for 30 s and 62 °C for 3 min, and with a final extension step at 72 °C for 10 min. The second PCR was performed using 1 μl of the first PCR product in a 50 μl reaction mixture mentioned above, containing a nested primer (supplementary table S2b, Supplementary Material online) and a universal amplification primer (5′-CTACTACTACTAGGCCACGCGTCGACTAGTAC-3′). The second PCR amplification was at 95 °C for 2 min, and 25 cycles of 94 °C for 30 s, 62 °C for 2 min, followed by an extension step at 72 °C for 10 min. This method would not work for the other Babesia and Theileria samples. It can be surmised that relatively high (A + T) content in TIRs of the other samples may have caused some problems. Multiple palindromes in TIR reported for *T. parva* (Shukla and Nene 1998) may also be contributing factors in the difficulty to determine telomeric sequences. In *T. equi*, unlike other Babesia and Theileria species, the TIR has a relatively low (A + T) content with no apparent multiple palindromes and, surprisingly, contains *cox3* and two fragments of rRNA gene (see Results).

TIR sequences of other Babesia and Theileria species were determined using an "inverted PCR," in which primers leading toward telomere ends (supplementary table S2b, Supplementary Material online) were used. We assumed that small inverted sequences, probably present in TIRs as reported for *T. parva* (Shukla and Nene 1998), could

self-anneal in opposite direction, enabling amplification of two telomeric regions encompassed by two outward primers when *Taq* polymerase with an exonuclease activity, that could excise unpaired bases (such as LA-Taq), was used. This inverted PCR successfully amplified specific DNA bands for all (Babesia and Theileria) but one species (i.e., *T. equi*) examined here.

PCR products were purified using QIAquick PCR Purification Kit (QIAGEN). DNA sequencing was performed directly from two independent PCR products using the BigDye Terminator v3.1 Cycle Sequencing Kit (Applied Biosystems) and an ABI 3130 Genetic Analyzer (Applied Biosystems). Sequencing primers were designed to cover target regions in both directions. DDBL/EMBL/GenBank accession numbers of sequences obtained in this study are given in supplementary table S1 (Supplementary Material online). The *T. parva* sequence obtained here has a 24-bp inconsistency with the reported *T. parva* sequence (Z23263). The *B. bovis* sequence in this study has a 7-bp difference from the reported *B. bovis* sequence (EU075182). These differences may be due to polymorphism because uncloned stock (*T. parva*) and different parasite strains (*B. bovis*) were used. We used our sequences of *T. parva* and *B. bovis* for analysis.

Gene Annotation

Nucleotide sequences of obtained mt genomes from Babesia and Theileria species and their deduced amino acid sequences were aligned together with reported sequences from *B. bovis* (EU075182), *T. parva* (Z23263), and *T. annulata* (NW_001091933) by ClustalW (Thompson et al. 1994). Alignment was manually corrected. Protein-coding genes were predicted using previously annotated sequences from *T. parva* and *B. bovis*.

To identify putative rRNA genes, mitochondrial DNA (mtDNA) sequences or annotated rRNA gene fragments from *B. bovis* (EU075182) and *T. parva* (Z23263) were used as queries under the suggested algorithm parameters (Freyhult et al. 2007) in NCBI BLAST 2.2 (Altschul et al. 1990). In silico analysis was also done with Probalign beta version 1.2 (Roshan et al. 2008) and SSEARCH 3.5 (Pearson 1991) using known rRNA gene fragments and suggested advanced search options (Freyhult et al. 2007; Roshan et al. 2008). Newly identified candidate rRNA genes were, likewise, used as input sequences. The information from sequence alignments using ClustalW (Thompson et al. 1994) and putative base-pairings between fragments proposed for *T. parva* mitochondrial ribosomal RNA fragments (Kairo et al. 1994) were considered in assigning the termini of the candidate genes. Similar searches using some of the rRNA fragment sequences from *Plasmodium falciparum* (Feagin et al. 1997) detected additional candidate gene regions.

Southern Blot Hybridization

Genomic DNA of *B. gibsoni*, *T. orientalis*, and *T. equi*, either undigested or digested with *Pvu*II, *Hind*III, or *Xho*I, was electrophoresed on 0.8% agarose gels in Tris–acetate–ethylenediaminetetraacetic acid (40 mM Tris–acetate and 1 mM ethylenediaminetetraacetic acid) and then transferred to a positively charged nylon membrane (Amersham Hybond-N+; GE Healthcare, Little Chalfont, England). PCR products amplified specifically from *B. gibsoni*, *T. orientalis*, and *T. equi* genomic DNA (supplementary table S2c, Supplementary Material online) were labeled with digoxigenin-deoxyuridine triphosphate using the DIG High Prime DNA Labeling and Detection Starter Kit II (Roche Diagnostics, Rotkreuz, Switzerland). The digoxigenin-labeled DNA probes were used for overnight hybridization. Blots were washed twice with 2× saline–sodium citrate (SSC) and 0.1% sodium dodecyl sulfate (SDS) and twice with 0.5× SSC and 0.1% SDS at 65 °C for 15 min. Hybridization signals were detected using the Detection Starter Kit II.

RNA Preparation and Analysis

Transcription of *cox1*, *cox3*, and *cob* in *B. gibsoni*, *T. orientalis*, and *T. equi* was analyzed by reverse transcriptase-PCR (RT-PCR). Total RNA was extracted with RNeasy Mini Kit (QIAGEN). DNase I treatment was done to remove any residual DNA before cDNA synthesis. Using specific primers (supplementary table S2d, Supplementary Material online), cDNA synthesis and DNA amplification were carried out using PrimeScript High Fidelity RT-PCR Kit (Takara). RNA extracts that were not treated with reverse transcriptase gave no PCR products.

For northern blot analysis, total RNA including short RNAs from *B. gibsoni* was prepared with mirVana miRNA Isolation Kit (Ambion, Austin, TX). Total RNA (10 μg) was subjected to 8.3 M urea-12% (w/v) polyacrylamide gel electrophoresis. After electrophoresis, the gel was stained with ethidium bromide and photographed. RNA was electroblotted on Biodyne Plus (Pall, Glen Cove, NY) using a semi-dry blotter NA-1515B (Nihon Eido, Tokyo, Japan) according to the manufacturer's protocol. The blotted membrane was ultraviolet treated for cross-linking (Brown et al. 2004) and incubated in hybridization solution (200 mM sodium phosphate [pH 7.2]-7% [w/v] SDS) for 30 min at 37 °C. The oligo probe was 5′ labeled with T4 polynucleotide kinase and [γ-^{32}P] adenosine triphosphate according to the enzyme supplier's instruction (Takara) and purified based on Brown et al. (2004). After overnight hybridization at 37 °C, the membrane was then washed twice with 2× SSC-0.5% (w/v) SDS at 37 °C, twice at 47 °C, and finally twice with 0.2× SSC-0.5% (w/v) SDS at 47 °C. The membrane was exposed to an Imaging Plate (Fujifilm, Tokyo, Japan), and the plate was scanned with a BAS2500 Bioimaging Analyzer (Fujifilm).

Phylogenetic Analysis

The concatenated amino acid sequences of *cox1* and *cob* were used for phylogenetic analysis. (Sequences of *cox3* were not used due to very high divergence in Babesia/ Theileria species [see Results].) The data set of 834 amino acid positions, comprising 474 COX1 and 360 COB amino acids, was analyzed using the PROML program in PHYLIP version

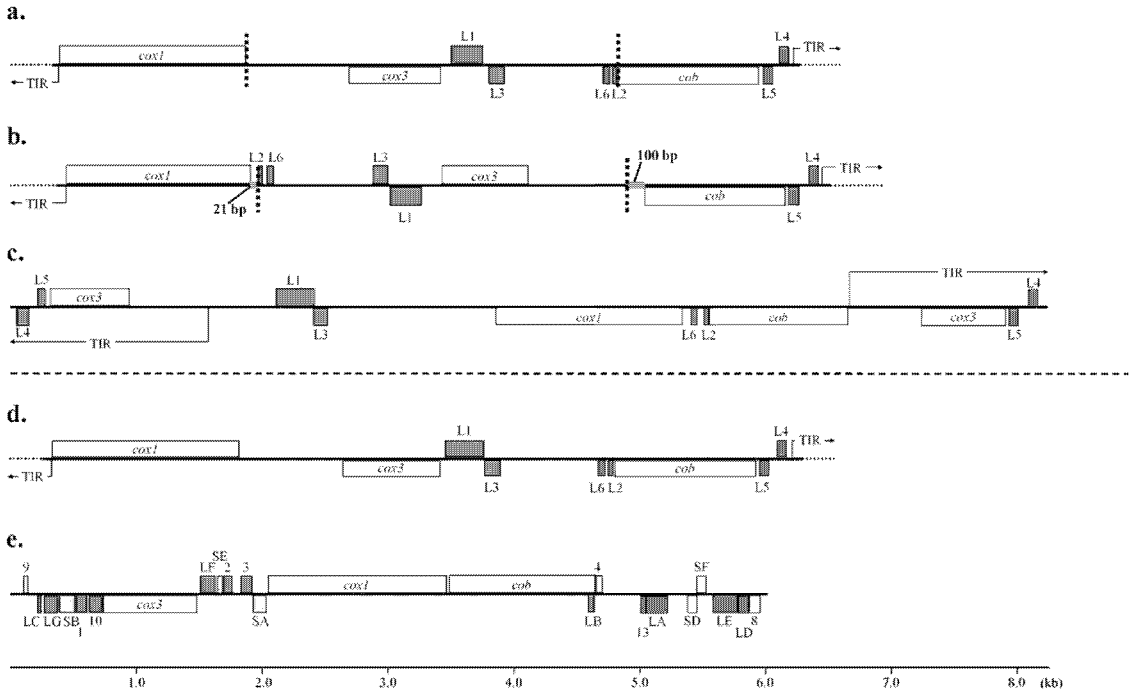

FIG. 1. Structure of the mitochondrial genomes of *Babesia gibsoni* (*a*), *Theileria orientalis* (*b*), and *T. equi* (*c*). Mitochondrial (mt) genome structure was completely conserved among *B. gibsoni*, *B. bigemina* (not shown), *B. caballi* (not shown), *B. bovis* (not shown), and *T. parva* (*d*). The *T. orientalis* mt genome has an inversion in the 3-kb central region. The *T. equi* mt genome has a relatively long TIR and contains a *cox3* gene and rRNA gene fragments. Shown for comparison is the mt genome of *Plasmodium falciparum* (*e*) (Feagin et al. 1997). Genes shown above the bold line in each genome are transcribed left to right and those below are transcribed from right to left. Two small gray lines in the *T. orientalis* genome indicate an inversion. Vertical broken lines indicate the boundaries of the 3-kb inversion. Dark and light gray boxes indicate fragments of LSU and SSU rRNA genes, respectively. *cox1*, cytochrome *c* oxidase subunit I; *cox3*, cytochrome *c* oxidase subunit III; *cob*, cytochrome *b*.

3.68 (Felsenstein and Churchill 1996) under the Jones, Taylor, and Thornton model (Jones et al. 1992) with the amino acid frequencies of the data set used to infer the maximum likelihood (ML) tree. Corresponding sequence of *P. falciparum* was used as an outgroup. To take the evolutionary rate heterogeneity, the R option was set to utilize discrete Γ distribution with eight categories for approximating the site rate distribution. CODEML program in PAML version 4.2 (Yang 2007) was used to estimate the Γ shape parameter value α. Bootstrap analysis was done by applying PROML to 100 resampled data sets produced by SEQBOOT program in PHYLIP. Bootstrap proportion (BP) values were calculated for internal branches of the inferred ML tree using CONSENSE in PHYLIP.

LSU sequences (592 sites in total: 265 bp for LSU1; 35 bp for LSU2; 111 bp for LSU3; 82 bp for LSU4; 64 bp for LSU5; and 35 bp for LSU6) were analyzed using the ML method performed with PAUP* 4.0 b10 (Swofford 2002). The appropriate nucleotide substitution model was first determined using the Modeltest (version 3.7) estimations, including both the proportion of invariable sites and the Γ shape parameter (Posada and Crandall 1998). For branch support of the ML tree, bootstrap probability was estimated from 1,000 heuristic replicates with single random addition replicates. All trees were reconstructed with TreeView 1.6.6 (Page 1996). For statistical comparisons among the ML best tree and its alternatives, *P* values of Kishino–Hasegawa (KH) test (Kishino and Hasegawa 1989) and Simodaira–Hasegawa (SH) test (Shimodaira and Hasegawa 1999) were obtained.

Results

Mitochondrial Genome Organization

We obtained 5.8- to 5.9-kb sequences from each of *B. bigemina*, *B. caballi*, *B. gibsoni*, and *B. bovis*, in which three protein-coding genes, *cox1*, *cox3*, and *cob*, and five fragments of the LSU rRNA gene were identified (fig. 1*a*). TIR sequences were also found on both ends of the predicted linear mt genomes. Although full-length sequences of TIRs were not successfully determined, the size of the TIR was inferred to be 440–450 bp from results of Southern blot hybridization analysis (see below). Additionally, we identified one LSU fragment of rRNA gene, LSU6, that showed a high sequence similarity to the 3′ part of RNA10 of the *P. falciparum* rRNA gene fragment (Feagin et al. 1997) (underlined sequence in the following *B. gibsoni* LSU sequence are identical nucleotides to *P. falciparum*

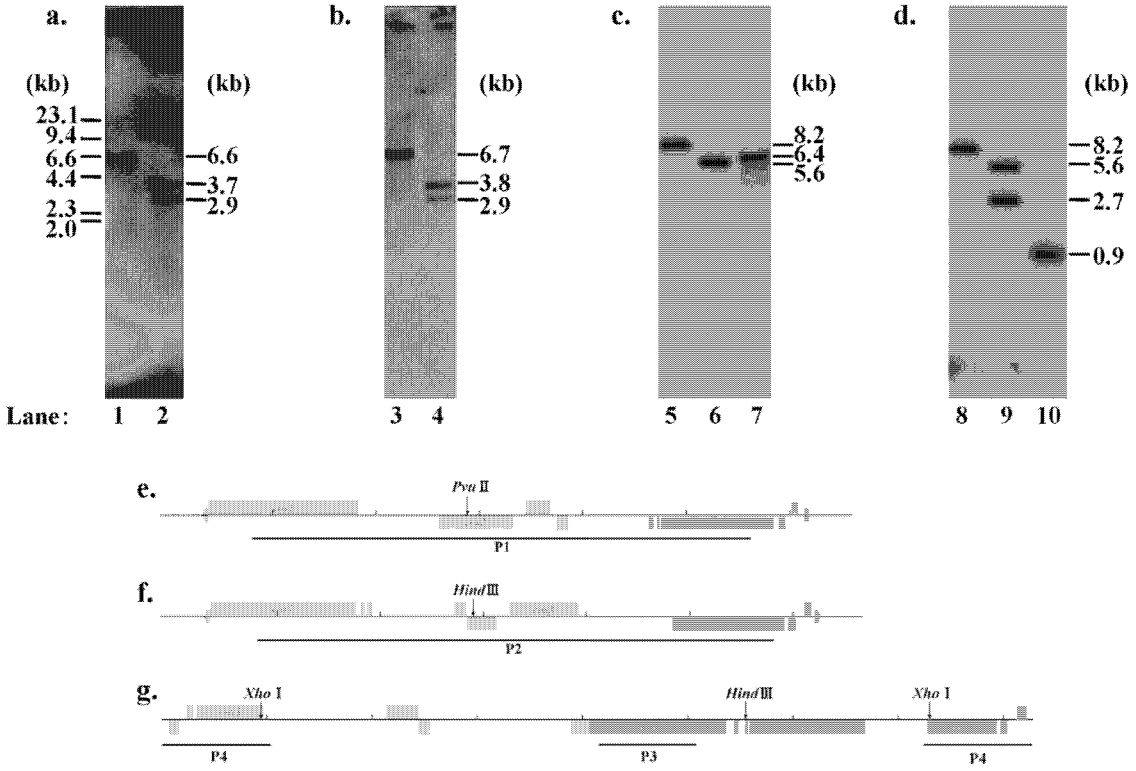

FIG. 2. Monomeric linear structure of the mitochondrial genomes of *Babesia gibsoni*, *Theileria orientalis*, and *T. equi*. Genomic DNA of *B. gibsoni* (*a*), *T. orientalis* (*b*), and *T. equi* (*c* and *d*) was hybridized with a *B. gibsoni* probe P1 (*e*), a *T. orientalis* probe P2 (*f*), and *T. equi* probes P3 and P4 (*g*), respectively. Undigested DNA (lanes 1, 3, 5, and 8) or DNA digested with *Pvu*II (lane 2), *Hind*III (lanes 4, 6, and 9), or *Xho*I (lanes 7 and 10) was fractionated on 0.8% agarose gels.

RNA10: 5′-ATAGCCGGAGTACGTAAGGAATAGGAAA-GATTAACCGCTATCA-3′). The organization and predicted transcriptional direction of the three protein-coding genes and the six LSU rRNA gene fragments were completely conserved among *B. bigemina*, *B. caballi*, *B. gibsoni*, *B. bovis*, *T. parva*, and *T. annulata* (fig. 1*a*). Southern blots probed with a 4.9-kb portion (P1) of the *B. gibsoni* mt genome produced a clear signal at 6.6 kb against *B. gibsoni* genomic DNA and two bands at 3.7 and 2.9 kb against DNA digested with *Pvu*II (fig. 2*a* and *e*). The sizes of the two bands were identical to those predicted from the sequence. These results confirm the monomeric linear 6.6 kb of *B. gibsoni* mt genome similar to that reported for *T. parva* and *T. annulata* (Hall et al. 1990; Kairo et al. 1994).

Interestingly, the *T. orientalis* mt genome, aside from having three protein-coding genes, six rRNA gene fragments, and TIRs similar to four Babesia species, *T. parva*, and *T. annulata* (fig. 1*b*) showed an inversion at the 3.0-kb central region containing *cox3*, LSU1, LSU3, LSU6, and LSU2. No sequences that potentially form secondary structures such as a hairpin structure were apparent near the boundaries of this inverted sequence, but instead, unique insertions of 21–22 and 84–102 bp were noted (fig. 1*b*), making the *T. orientalis* mt genome slightly longer (112–168 bp) than the other six Babesia and Theileria mt genomes (supplementary table S3, Supplementary Material online). As predicted from the sequence, southern hybridization using a *T. orientalis* probe (P2) that spans the central 5.0-kb region yielded a band at 6.7 kb against undigested DNA and two bands at 3.8 and 2.9 kb against *Hind*III-digested DNA (fig. 2*b* and *f*). From these results, the *T. orientalis* mt genome shows a 6.7-kb monomeric linear structure.

Strikingly distinctive from all other mt genomes described above is *T. equi*. First, the size of the *T. equi* genome is 8.2 kb, that is, 1.6–1.7 kb longer than that of other species. Second, TIR sequences are large (1,563 bp), compared with the 440–450 bp TIRs of the other seven species, and, interestingly, contained *cox3* and two LSU rRNA gene fragments, LSU4 and LSU5. TIR sequences on both ends showed complete identity. Third, the protein-coding genes and rRNA gene fragments showed little synteny to other species (fig. 1*c*). Hybridization with a probe corresponding to a 1.0-kb region in *cox1* (P3) produced a band at 8.2 kb against undigested DNA, a band at 5.6 kb against *Hind*III-digested DNA, and a band at 6.4 kb against *Xho*I-digested DNA (fig. 2*c* and *g*). Another *T. equi* probe using a 1-kb region in the TIR (P4) produced a band at 8.2 kb against undigested DNA, two bands at 5.6 and 2.7 kb against *Hind*III-digested DNA, and a band at 0.9 kb against

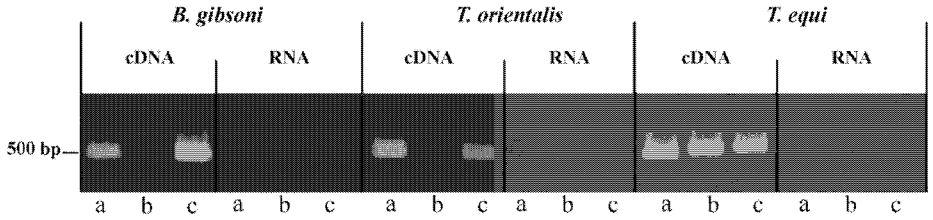

FIG. 3. Transcription of the three protein-coding genes *cox1* (*a*), *cox3* (*b*), and *cob* (*c*) in the mitochondrial genome of *Babesia gibsoni*, *Theileria orientalis*, and *T. equi*. See Materials and Methods for details.

*Xho*I-digested DNA (fig. 2*d* and *g*). The sizes of these bands match the predicted *T. equi* sequence, indicating an 8.2-kb monomeric linear structure of the *T. equi* mt genome.

Transcription

RT-PCR using three separate primer sets targeting about 500-bp sequences of *cox1*, *cox3*, and *cob* of *B. gibsoni* gave the expected transcript size using cDNA but not using RNA (fig. 3). Similarly, expected PCR sized fragments were obtained using primers specific to *T. orientalis* or *T. equi* for *cox1*, *cox3*, and *cob*. Results confirm the transcription of the three protein-coding genes, including *cox3* in the 3-kb inverted region of *T. orientalis* and *cox3* in TIR of *T. equi*.

Transcription of LSU6 was confirmed by northern blot analysis. Probing with two oligonucleotides (18-mer and 23-mer at the 5′ and 3′ end, respectively) complementary to LSU6 against *B. gibsoni* total RNA produced approximately 90-nt RNA signal (fig. 4), suggesting that the LSU6 was actually transcribed and the corresponding stable transcript existed as a short RNA fragment. Due to extreme difficulties in obtaining an adequate amount of parasites from infected hosts and/or in vitro culture limitations for *B. bigemina*, *B. caballi*, *T. orientalis*, and *T. equi*, we were unable to perform additional northern blot analyses. Together with the report of Kairo et al. (1994) on the transcription of the three protein-coding genes and five known LSU rRNA gene fragments (LSU1–LSU5) in *T. parva*, however, these results suggest that both protein genes and rRNA gene fragments are transcribed in Babesia and Theileria.

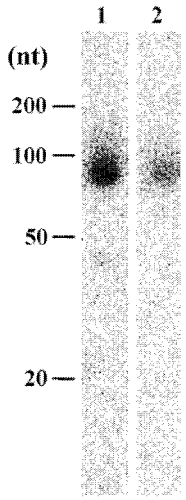

FIG. 4. Transcription of the *Babesia gibsoni* mt genome LSU6. *B. gibsoni* total RNA was probed with oligonucleotides complementary to the putative LSU6 fragment. Probe sequences: lane 1, TGATAGCGGTTAATCTTTCCTAT; lane 2, CTTACGTACTCCGGCTAT. Positions and sizes (in nucleotides [nt]) of marker RNAs (DynaMarker RNA Low II; BioDynamics Laboratory) are shown.

Sequence Similarity and Phylogeny

cox1 and *cob* pairwise sequence similarity scores among *B. bovis*, *B. bigemina*, *B. caballi*, *B. gibsoni*, *T. parva*, *T. orientalis*, *T. annulata*, and *T. equi* were comparable: 67–88% for *cox1* and 60–85% for *cob* at the amino acid sequence level (supplementary table S4, Supplementary Material online). Conserved sequence regions in COX1 and COB correspond to the 12 and 9 transmembrane domains as inferred from bovine COX1 (SWISS-PROT protein database accession number P00396) and COB (P00157), respectively, in which multiple heme-binding histidine residues that form catalytic sites are perfectly conserved (Widger et al. 1984; Yun et al. 1991; Castresana et al. 1994; Ferguson-Miller and Babcock 1996). For *cox3*, pairwise sequence similarity was relatively low, and *T. equi cox3* in particular has considerably low similarity to *cox3* of other species (37–41% compared with the 57–80% similarity of other *cox3* in Babesia and Theileria species). Nevertheless, the predicted *T. equi* COX3 amino acid sequence shows seven transmembrane domains (from I to VII) and the C-terminal hydrophobic domain VII (P00415) that are highly conserved among a wide variety of organisms from prokaryotes to plants (Haltia et al. 1991). In contrast to these protein-coding genes, pairwise sequence similarity of six LSUs was very high, 75–96% among all the Babesia and Theileria species examined here (supplementary table S5, Supplementary Material online).

The ML tree was inferred from concatenated COX1 and COB amino acid sequences using *P. falciparum* as an outgroup (fig. 5). Monophyletic relationships were observed with high BP values (98%) for 1) *B. bovis*, *B. bigemina*, *B. caballi*, and *B. gibsoni* and 2) *T. annulata*, *T. parva*, and *T. orientalis*. *Theileria equi* was located at the branch

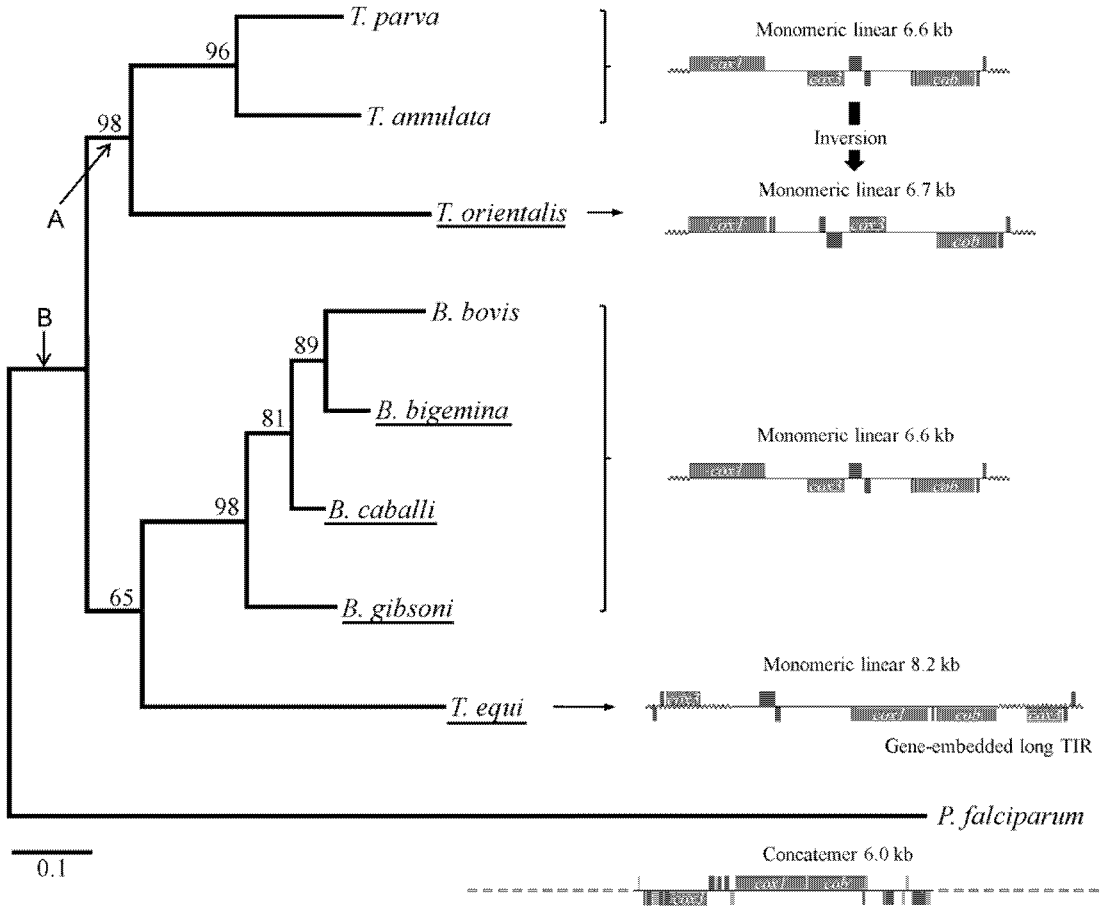

FIG. 5. The ML phylogenetic tree of the two mitochondrial protein-coding genes, *cox1* and *cob*, from eight Babesia and Theileria species. *Plasmodium falciparum* was used as an outgroup. Concatenated amino acid sequences (834 sites) were used with 1,000 heuristic replicates under a Jones, Taylor, and Thornton model ($\alpha = 0.72$). The numbers shown along nodes represent bootstrap values. Arrows, A and B, indicate alternative positions of the *Theileria equi* sequence, whose possibilities were statistically compared by the SH and KH tests. Five parasite sequences obtained in this study are underlined.

leading to the common ancestor of Babesia species with moderate BP value (65%). The other possible branching positions of *T. equi* at the ancestral branch of Theileria (arrow A in fig. 5) or at the ancestral branch of Theileria and Babesia (arrow B in fig. 5) were, however, not rejected by either the KH or the SH tests (supplementary table S6, Supplementary Material online), thus indicating that the evolutionary position of *T. equi* is yet unclear with the present data set.

The ML tree constructed using LSU sequences was basically the same as that of *cox1* and *cob* (supplementary fig. S1, Supplementary Material online), although, in this case, unrooted trees were compared because an appropriate outgroup species is not available for LSU. Monophyletic relationships of the four Babesia species and of *T. annulata*, *T. parva*, and *T. orientalis* were supported with high BP values. Within the clade of Babesia, however, the relationship between *B. bovis*, *B. bigemina*, and *B. caballi* was not supported with high BP values and not highly consistent to that in the *cox1/cob* tree. Notably, when the data set of LSU was applied to the two topologies, one for the *cox1/cob* tree and the other for the LSU tree, the two trees were not significantly different (data not shown), suggesting that the relationship of the three Babesia species was not clearly separable using the LSU sequences.

Partial TIR sequences (47–1,563 bp) (supplementary table S3, Supplementary Material online) were highly divergent among all eight Babesia and Theileria species examined here. In noncoding regions excluding TIR, we identified 14 sequence regions that were highly similar among all the Babesia and Theileria species (fig. 6 and supplementary tables S7 and S8, Supplementary Material online). Pairwise sequence similarity of these 14 regions ranged from 81% to 97%, values comparable with LSUs. The array and direction of the 14 regions were well conserved among (including the inverted region of *T. orientalis*), but one, species. *Theileria equi* was the exception, in which case the 14 regions were extensively

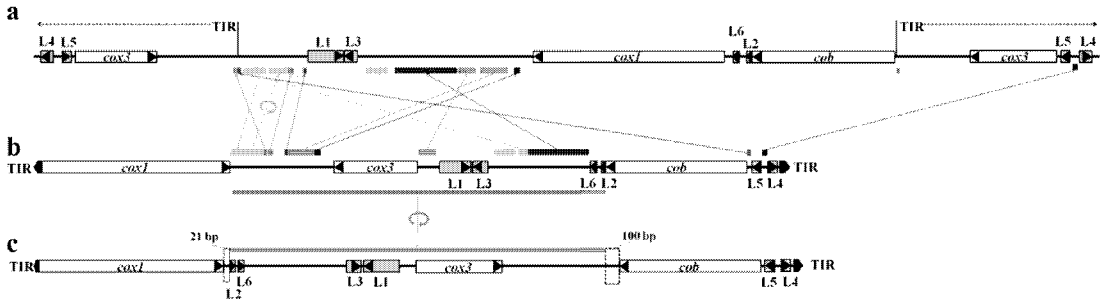

FIG. 6. Arrangement of small noncoding sequence regions in the mitochondrial genome highly conserved between *Theileria equi* (*a*), *Babesia gibsoni* (*b*), and *T. orientalis* (*c*). Those sequences are indicated by matched colored bars and arrows. A 3.0-kb inversion in the *T. orientalis* mt genome is shown by green bars with a circular arrow in (*b*) and (*c*). *cox1*, cytochrome *c* oxidase subunit I; *cox3*, cytochrome *c* oxidase subunit III; *cob*, cytochrome *b*.

rearranged (fig. 6). Within species, these 14 regions did not show sequence similarity to each other.

Discussion

This study presents for the first time evidence of the highly divergent mt genomes in the genus Theileria and a high conservation in the genus Babesia. *Theileria annulata* and *T. parva* have an mt genome structure nearly identical to that of Babesia, whereas the mt genomes of *T. orientalis* and *T. equi* were clearly distinctive: a large genomic region is inverted in *T. orientalis*, and in *T. equi*, there occurs an unusually long TIR, containing *cox3* and two LSU rRNA gene fragments. The phylogenetic tree of *cox1*/*cob* showed two separate clades: one for three Theileria species (*T. parva*, *T. annulata*, and *T. orientalis*) and another for four Babesia species. The mt genome structures of these Theileria species are highly conserved. This suggests that an inversion event occurred specifically in the *T. orientalis* lineage after divergence from a common ancestor of *T. annulata*, *T. parva*, and *T. orientalis*. The phylogenetic position of *T. equi* was not clearly determined in the *cox1*/*cob* tree. This unclear positioning of *T. equi* is consistent with the tree based on 18S rRNA gene, a nuclear genome gene (Criado-Fornelio et al. 2003). Thus, it remains to be solved whether a common ancestor of *T. equi*, the Theileria clades, and Babesia clades possessed an mt genome with gene-embedded long TIR. Phylogenetic separation of *T. equi* from Theileria clade as well as the identical life cycle, namely, the presence of schizogony in lymphocytes and lack of transovarial transmission by vector (Uilenberg 2006), suggests that, most likely, the mt genome of the common ancestor contained a long TIR.

Compared with moderate sequence similarity in *cox1* and *cob* of Theileria and Babesia species, *cox3* is highly divergent. Similarly, *cox3* is more divergent than *cox1* and *cob* in Plasmodium species (Wilson and Williamson 1997; Perkins 2008). COB is a subunit of complex III, essential for electron transfer in the mitochondrial respiratory chain (Xia et al. 1997). COX1 (subunit I) (and also COX2 [subunit II]), which contains heme and copper and is essential for electron transfer, is 1 of 13 subunits of cytochrome *c* oxidase (complex IV), a terminal oxidase in the respiratory chain (Castresana et al. 1994). COX3, which is not directly involved in the electron transport, is considered to stabilize the complex of COX1 and COX2 (Haltia et al. 1991; Tsukihara et al. 1996). Such an accessory role of COX3 in the function of cytochrome *c* oxidase may relax constraints, causing acceleration of evolutionary rate and low sequence similarity.

In addition to the five previously known LSU rRNA gene fragments (LSU1–LSU5) (Kairo et al. 1994; Brayton et al. 2007), we newly identified an LSU fragment, LSU6, in all Babesia and Theileria species, whose transcription was confirmed by northern blot analysis. Kairo et al. (1994) have previously mapped LSU1–LSU5 (by comparative secondary structure modeling) to the 3′ half of *Escherichia coli* 23S (LSU) rRNA. LSU5 and 5′ region of LSU1 form the domain IV of LSU, whereas 3′ region of LSU1, LSU2, LSU3, and LSU4 forms the domain V of the LSU, which contains the peptidyl transferase center. We mapped the newly identified LSU6 to positions 2640–2670, which forms a part of the domain VI (alpha-sarcin/ricin stem loop) of the LSU. Contrary to the other LSU fragments, the borders of LSU6 were unclear because the flanking sequences have no recognizable complementarities to other fragments. In addition to LSU6, we found a small sequence region in all Babesia and Theileria mtDNA, which showed a high sequence similarity to a small subunit fragment (SSUF) of the *P. falciparum* rRNA gene. We were not, however, able to confirm transcription of the SSUF (data not shown), although the region is regarded as one of the highly similar noncoding regions (supplementary table S7, Supplementary Material online). The mtDNA of Babesia/Theileria still contains large unannotated sequence regions (about one-third sequence regions of the genome), and those sequences are highly conserved among parasite species of the two genera (supplementary table S8, Supplementary Material online). It is thus likely that unidentified rRNA gene fragments as well as other genes exist in these regions. Comprehensive and detailed mtDNA transcript analysis of Babesia/Theileria would be required for further identification of genes and gene fragments as was done for *P. falciparum* (Feagin et al. 1997).

The observed high divergence of TIR sequences among Babesia and Theileria species was not surprising because no universal signature has been reported for TIR sequences of linear mt genomes from several unicellular flagellates: *Polytomella capuana*, *Po. parva*, and *Chlamydomonas reinhardtii* in the Reinhardtii clade of chlorophycean green algae (Smith and Lee 2008). Inverted complementary sequences at both ends of a linear mt genome are believed to play important roles in replication and stabilization (Nosek and Tomaska 2003). In TIR, small repeats with forward and reverse directions frequently occur, which are likely to form secondary structure. In general, sequence regions containing small repeats diverge rapidly compared with nonrepeat sequences. As a consequence, little sequence conservation is expected in TIR of a linear mt genome. An exception is *T. equi* TIR, in which sequence regions of *cox3* and two LSU rRNA gene fragments are relatively conserved, perhaps due to functional constraints.

In conclusion, our studies show the remarkable structural diversity in the mt genomes of Theileria species, in contrast to the highly conserved genome among Babesia species. The finding of a high structural divergence of the *T. equi* mt genome from other Babesia and Theileria species suggests the occurrence of lineage-specific evolution of mt genomes within the closely related Babesia and Theileria genera. Further investigations into mt genomes of other Theileria species and other related genera, such as those that belong to the Archaeopiroplasmids group, should provide insights into the evolutionary origin of a major structural divergence between Plasmodium (circular/concatemer genome) and Babesia/Theileria (linear genome) in the same phylum Apicomplexa.

Supplementary Material

Supplementary material, tables S1–S8, and figure S1 are available at *Molecular Biology and Evolution* online (http://www.mbe.oxfordjournals.org/).

Acknowledgments

We wish to thank T. Toyama for technical advice and H. Inokuma for kindly providing parasite samples. This work was supported by Grant-in-Aids for Scientific Research from the Ministry of Education, Culture, Sports, Science and Technology of Japan (18073013) and from Japan Society for Promotion of Sciences (18GS03140013 and 20390120).

References

Abrahamsen MS, Templeton TJ, Enomoto S, et al. (20 co-authors). 2004. Complete genome sequence of the apicomplexan, *Cryptosporidium parvum*. *Science* 304:441–445.

Altschul SF, Gish W, Miller W, Myers EW, Lipman DJ. 1990. Basic local alignment search tool. *J Mol Biol.* 215:403–410.

Avarzed A, Igarashi I, De Waal DT, et al. (12 co-authors). 1998. Monoclonal antibody against *Babesia equi*: characterization and potential application of antigen for serodiagnosis. *J Clin Microbiol.* 36:1835–1839.

Avarzed A, Igarashi I, Kanemaru T, Hirumi K, Omata Y, Saito A, Oyamada T, Nagasawa H, Toyoda Y, Suzuki N. 1997. Improved in vitro cultivation of *Babesia caballi*. *J Vet Med Sci.* 59:479–481.

Bah A, Bachand F, Clair E, Autexier C, Wellinger RJ. 2004. Humanized telomeres and an attempt to express a functional human telomerase in yeast. *Nucleic Acids Res.* 32:1917–1927.

Brayton KA, Lau AO, Herndon DR, et al. (28 co-authors). 2007. Genome sequence of *Babesia bovis* and comparative analysis of apicomplexan hemoprotozoa. *PLoS Pathog.* 3:1401–1413.

Brown T, Mackey K, Du T. 2004. Analysis of RNA by northern and slot blot hybridization. *Curr Protoc Mol Biol.* 4.9:1–19.

Castresana J, Lubben M, Saraste M, Higgins DG. 1994. Evolution of cytochrome oxidase, an enzyme older than atmospheric oxygen. *Embo J.* 13:2516–2525.

Criado-Fornelio A, Martinez-Marcos A, Buling-Sarana A, Barba-Carretero JC. 2003. Molecular studies on *Babesia*, *Theileria* and *Hepatozoon* in southern Europe. Part II. Phylogenetic analysis and evolutionary history. *Vet Parasitol.* 114:173–194.

Feagin JE, Mericle BL, Werner E, Morris M. 1997. Identification of additional rRNA fragments encoded by the *Plasmodium falciparum* 6 kb element. *Nucleic Acids Res.* 25:438–446.

Felsenstein J, Churchill GA. 1996. A hidden Markov model approach to variation among sites in rate of evolution. *Mol Biol Evol.* 13:93–104.

Ferguson-Miller S, Babcock GT. 1996. Heme/copper terminal oxidases. *Chem Rev.* 96:2889–2908.

Freyhult EK, Bollback JP, Gardner PP. 2007. Exploring genomic dark matter: a critical assessment of the performance of homology search methods on noncoding RNA. *Genome Res.* 17:117–125.

Fujinaga T, Minami T, Ishihara T. 1980. Serological relationship between a large *Babesia* found in Japanese cattle and *Babesia major*, *B. bigemina* and *B. bovis*. *Res Vet Sci.* 29:230–234.

Gray MW, Lang BF, Burger G. 2004. Mitochondria of protists. *Annu Rev Genet.* 38:477–524.

Hall R, Coggins L, McKellar S, Shiels B, Tait A. 1990. Characterisation of an extrachromosomal DNA element from *Theileria annulata*. *Mol Biochem Parasitol.* 38:253–260.

Haltia T, Saraste M, Wikstrom M. 1991. Subunit III of cytochrome *c* oxidase is not involved in proton translocation: a site-directed mutagenesis study. *Embo J.* 10:2015–2021.

Ishimine T, Makimura S, Kitazawa S, Tamura S, Suzuki N. 1978. Pathophysiological findings on blood of beagles experimentally infected with *B. gibsoni*. *Jpn J Trop Med Hyg.* 6:15–26.

Jones DT, Taylor WR, Thornton JM. 1992. The rapid generation of mutation data matrices from protein sequences. *Comput Appl Biosci.* 8:275–282.

Kairo A, Fairlamb AH, Gobright E, Nene V. 1994. A 7.1 kb linear DNA molecule of *Theileria parva* has scrambled rDNA sequences and open reading frames for mitochondrially encoded proteins. *Embo J.* 13:898–905.

Kim JY, Yokoyama N, Kumar S, Inoue N, Inaba M, Fujisaki K, Sugimoto C. 2004. Identification of a piroplasm protein of *Theileria orientalis* that binds to bovine erythrocyte band 3. *Mol Biochem Parasitol.* 137:193–200.

Kishino H, Hasegawa M. 1989. Evaluation of the maximum likelihood estimate of the evolutionary tree topologies from DNA sequence data, and the branching order in hominoidea. *J Mol Evol.* 29:170–179.

Kuo CH, Wares JP, Kissinger JC. 2008. The apicomplexan whole-genome phylogeny: an analysis of incongruence among gene trees. *Mol Biol Evol.* 25:2689–2698.

Lau AO. 2009. An overview of the *Babesia*, *Plasmodium* and *Theileria* genomes: a comparative perspective. *Mol Biochem Parasitol.* 164:1–8.

Levine ND. 1988. Progress in taxonomy of the apicomplexan protozoa. *J Protozool.* 35:518–520.

Nosek J, Tomaska L. 2003. Mitochondrial genome diversity: evolution of the molecular architecture and replication strategy. *Curr Genet.* 44:73–84.

Ossorio PN, Sibley LD, Boothroyd JC. 1991. Mitochondrial-like DNA sequences flanked by direct and inverted repeats in the nuclear genome of *Toxoplasma gondii*. *J Mol Biol.* 222:525–536.

Page RD. 1996. TreeView: an application to display phylogenetic trees on personal computers. *Comput Appl Biosci.* 12:357–358.

Palmer JD, Soltis D, Soltis P. 1992. Large size and complex structure of mitochondrial DNA in two nonflowering land plants. *Curr Genet.* 21:125–129.

Pearson WR. 1991. Searching protein sequence libraries: comparison of the sensitivity and selectivity of the Smith-Waterman and FASTA algorithms. *Genomics* 11:635–650.

Perkins SL. 2008. Molecular systematics of the three mitochondrial protein-coding genes of malaria parasites: corroborative and new evidence for the origins of human malaria. *Mitochondrial DNA.* 19:471–478.

Posada D, Crandall KA. 1998. MODELTEST: testing the model of DNA substitution. *Bioinformatics* 14:817–818.

Preiser PR, Wilson RJ, Moore PW, McCready S, Hajibagheri MA, Blight KJ, Strath M, Williamson DH. 1996. Recombination associated with replication of malarial mitochondrial DNA. *Embo J.* 15:684–693.

Roshan U, Chikkagoudar S, Livesay DR. 2008. Searching for evolutionary distant RNA homologs within genomic sequences using partition function posterior probabilities. *BMC Bioinformatics.* 9:61.

Shimodaira H, Hasegawa M. 1999. Multiple comparisons of log-likelihoods with applications to phylogenetic inference. *Mol Biol Evol.* 16:1114–1116.

Shukla GC, Nene V. 1998. Telomeric features of *Theileria parva* mitochondrial DNA derived from cycle sequence data of total genomic DNA. *Mol Biochem Parasitol.* 95:159–163.

Smith DR, Lee RW. 2008. Mitochondrial genome of the colorless green alga *Polytomella capuana*: a linear molecule with an unprecedented GC content. *Mol Biol Evol.* 25:487–496.

Swofford DL. 2002. PAUP*: phylogenetic analysis using parsimony (and other methods). Sunderland (MA): Sinauer Associates.

Thompson JD, Higgins DG, Gibson TJ. 1994. CLUSTAL W: improving the sensitivity of progressive multiple sequence alignment through sequence weighting, position-specific gap penalties and weight matrix choice. *Nucleic Acids Res.* 22:4673–4680.

Tsukihara T, Aoyama H, Yamashita E, Tomizaki T, Yamaguchi H, Shinzawa-Itoh K, Nakashima R, Yaono R, Yoshikawa S. 1996. The whole structure of the 13-subunit oxidized cytochrome c oxidase at 2.8 A. *Science* 272:1136–1144.

Uilenberg G. 2006. Babesia—a historical overview. *Vet Parasitol.* 138:3–10.

Ward BL, Anderson RS, Bendich AJ. 1981. The mitochondrial genome is large and variable in a family of plants (Cucurbitaceae). *Cell* 25:793–803.

Widger WR, Cramer WA, Herrmann RG, Trebst A. 1984. Sequence homology and structural similarity between cytochrome *b* of mitochondrial complex III and the chloroplast b_6-*f* complex: position of the cytochrome *b* hemes in the membrane. *Proc Natl Acad Sci USA.* 81:674–678.

Wilson RJ, Williamson DH. 1997. Extrachromosomal DNA in the Apicomplexa. *Microbiol Mol Biol Rev.* 61:1–16.

Xia D, Yu CA, Kim H, Xia JZ, Kachurin AM, Zhang L, Yu L, Deisenhofer J. 1997. Crystal structure of the cytochrome bc_1complex from bovine heart mitochondria. *Science* 277:60–66.

Yang Z. 2007. PAML 4: phylogenetic analysis by maximum likelihood. *Mol Biol Evol.* 24:1586–1591.

Yun CH, Crofts AR, Gennis RB. 1991. Assignment of the histidine axial ligands to the cytochrome $b_H$and cytochrome $b_L$components of the bc_1complex from *Rhodobacter sphaeroides* by site-directed mutagenesis. *Biochemistry* 30:6747–6754.

Parasitology International 59 (2010) 278–282

Contents lists available at ScienceDirect

Parasitology International

journal homepage: www.elsevier.com/locate/parint

Short communication

Inhibitory effect of terpene nerolidol on the growth of *Babesia* parasites

Mahmoud AbouLaila [a,b], Thillaiampalam Sivakumar [a,c], Naoaki Yokoyama [a], Ikuo Igarashi [a,*]

[a] National Research Center for Protozoan Diseases, Obihiro University of Agriculture and Veterinary Medicine, Inada-cho, Obihiro, Hokkaido 080-8555, Japan
[b] Department of Parasitology, Faculty of Veterinary Medicine, Minoufiya University, Sadat City, Minoufiya, Egypt
[c] Veterinary Research Institute, Gannoruwa, Peradeniya, Sri Lanka

ARTICLE INFO

Article history:
Received 26 July 2009
Received in revised form 25 January 2010
Accepted 16 February 2010
Available online 21 February 2010

Keywords:
Nerolidol
Babesia
In vitro
In vivo

ABSTRACT

Nerolidol is a sesquiterpene present in the essential oils of many plants, approved by the U.S. FDA as a food flavoring agent. Nerolidol interferes with the isoprenoid biosynthetic pathway in the apicoplast of *P. falciparum*. In the present study, the *in vitro* growth of four *Babesia* species was significantly ($P<0.05$) inhibited in the presence of nerolidol (IC_{50}s values = 21 ± 1, 29.6 ± 3, 26.9 ± 2, and 23.1 ± 1 μM for *B. bovis*, *B. bigemina*, *B. ovata*, and *B. caballi*, respectively). Parasites from treated cultures failed to grow in the subsequent viability test at a concentration of 50 μM. Nerolidol significantly ($P<0.05$) inhibited the growth of *B. microti* at the dosage of 10 and 100 mg/kg BW, while the inhibition was low compared with the high doses used. Therefore, nerolidol could not be used as a chemotherapeutic drug for babesiosis.

Babesia, a tick-born protozoan parasite, is one of the major pathogens that infect erythrocytes in a wide range of wild and economically valuable animals, such as cattle and horses. The clinical symptoms of babesiosis include malaise, fever, hemolytic anemia, jaundice, hemoglobinuria, and edema in the infected animals. *Babesia* parasites are prevalent worldwide, mainly in tropical and sub-tropical areas. Serious economic damage in the livestock industry has been caused by *Babesia* infections in such areas [1,2]. Several babesicidal drugs that have been in use for years have proven to be ineffective owing to problems related to their toxicity and the development of resistant parasites [3,4]. Therefore, the development of new drugs that have a chemotherapeutic effect against babesiosis with high specificity to the parasites and low toxicity to the hosts has been desired.

The apicoplast was acquired by horizontal transfer (secondary endosymbiosis) from a eukaryotic alga [5] and has been identified in many apicomplexan parasites, including *Babesia* [6]. The apicoplast is essential for long term parasite viability and has been an attractive target for development of parasiticidal drug therapies as the biosynthetic pathways represented therein are of cyanobacterial origin and differ substantially from corresponding pathways in the mammalian host [7,8]. The apicoplast has synthetic pathways such as fatty acid biosynthesis and isoprenoid biosynthetic pathways. In apicomplexan parasites, synthesis of isopentenyl diphosphate (IPP), the universal isoprenoid precursor, has long been assumed to proceed exclusively via the acetate/mevalonate (MVA) ubiquitous pathway, a pathway that is absent from malaria parasites [9]. However, an alternative MVA-independent pathway for the formation of isopentenyl diphosphate (IPP) occurs in bacteria, algae and chloroplasts of higher plants [9]. The initial step of this MVA-independent pathway is the formation of 1-deoxy-D-xylulose4-phosphate (DOXP) by condensation of pyruvate and glyceraldehyde-3-phosphate, catalyzed by DOXP synthase. In the second step, DOXP reductoisomerase synthesizes 2-C-methyl-D-erythritol-4-phosphate (with 2-C-methyl-D-erythrose-4-phosphate as an intermediate), in a single step, by intramolecular rearrangement followed by a reduction process [9]. IPP is the basic five-carbon building block (C_5) that forms the next member of the series. Two C_5 units condense to form geranyl pyrophosphate (C_{10}), which condenses with another molecule of IPP to form farnesyl pyrophosphate (FPP) (C_{15}). FPP is incorporated in the formation of prenylated proteins, ubiquinones (Coenzyme Q), and dolichols [9]. Isoprenoid biosynthesis in malaria parasites operates by a different mechanism than that in humans; therefore, could be a promising target for drug therapy [9]. While in most eukaryotic cells, the isoprenoid biosynthesis is achieved through a mevalonate dependent pathway which generates essential metabolic products in addition to cholesterol and ergosterol, such as the dolichols, which are present in all membranes in variable amounts and, in a modified phosphorylated form, are required for the asparagine-linked glycosylation of proteins. The pathway also generates the isoprene side chains attached to the benzoquinone ring of ubiquinone, prenyl groups transferred to prenylated proteins, and prenylated transfer RNAs [9]. *Leishmania* species cannot synthesize cholesterol de novo but are able to produce ergosterol through the mevalonate pathway [10]. In addition to ergosterol, other products of the mevalonate pathway have been identified in *Leishmania*: coenzyme Q9 (CoQ9) was detected as the predominant species of ubiquinone in promastigotes and amastigotes of *L. amazonensis*, whereas CoQ7 and CoQ8 were also identified in promastigotes [11]; prenylated proteins were observed in *Leishmania mexicana*

* Corresponding author. Tel.: +81 155 49 5641; fax: +81 155 49 5643.
E-mail address: igarcpmi@obihiro.ac.jp (I. Igarashi).

1383-5769/$ – see front matter © 2010 Elsevier Ireland Ltd. All rights reserved.
doi:10.1016/j.parint.2010.02.006

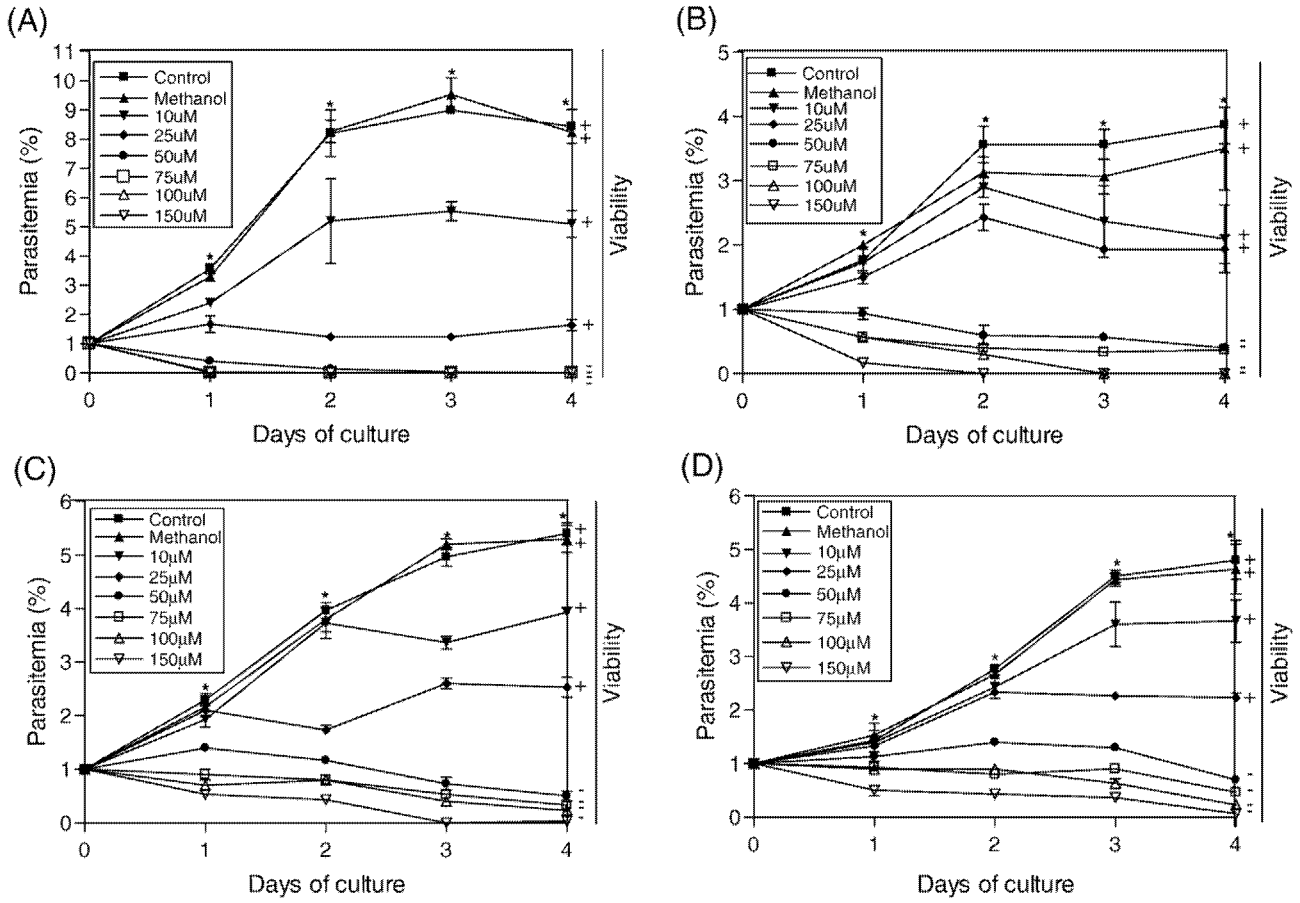

Fig. 1. Inhibitory effect of different concentrations of nerolidol on the *in vitro* growth of *B. bovis* (panel A), *B. bigemina* (panel B), *B. ovata* (panel C), and *B. caballi* (panel D). Each value represents the mean ± standard deviation in triplicate. These curves represent the mean of three experiments carried out in triplicate. *, statistically significant differences (student's *t* test, $P<0.05$) between 10 µM (panels A and B) and 25 µM (panels C and D) treated cultures and the control. Parasite viability was monitored in subcultures without nerolidol for 10 days (±, viable cells and −, dead cells).

after incorporation of labeled mevalonate, and phosphorylated dolichol has been detected as a sugar donor for glycosylation of proteins in *L. mexicana* [12]. The isoprenoid biosynthetic pathway is the only active pathway in *B. bovis* apicoplast, and is similar to that of *P. falciparum* [13]. Therefore, the blockade of the mevalonate independent pathway in the apicoplast could potentially have serious effects for *Babesia* parasites.

Nerolidol is a sesquiterpene present in essential oils of several plants, approved by the U.S. Food and Drug Administration as a food flavoring agent, it has been tested as a skin penetration enhancer for the transdermal delivery of therapeutic drugs [14]. In *Leishmania amazonensis*, nerolidol inhibited the isoprenoid biosynthesis, as shown by reduced incorporation of mevalonic acid (MVA) or acetic acid precursors into dolichol, ergosterol, and ubiquinone, in treated promastigotes due to the blockage of an early step in the mevalonate pathway [14], while in *P. falciparum*, nerolidol interferes with the isoprenoid biosynthetic pathway of the apicoplast leading to the interference with the biosynthesis of the dolichols, with the isoprenic chain of ubiquinones, and with protein isoprenylation of the parasites [15]. Nerolidol have leishmanicidal [14], and antimalarial [15,16] activities. The aim of this study was to evaluate the inhibitory effect of nerolidol on the growth of *Babesia* parasites.

B. bovis Texas strain, *B. bigemina* Argentina strain, *B. ovata* Miyake strain, and *B. caballi* U.S. Department of Agriculture strain were used in this study. Parasites were grown in a micro-aerophilous stationary phase culture system using bovine (for bovine *Babesia*) or equine (for *B. caballi*) erythrocytes (RBC) and sera as described previously [17,18]. GIT medium alone was used to test the effect of nerolidol without serum on *B. bovis* and *B. caballi* [19]. The overlaying medium was replaced daily with a fresh medium, and the infected RBC were passaged every 3 days [20]. Nerolidol (a mixture of *cis*- and *trans*-nerolidol) was purchased from Sigma-Aldrich (St. Louis, MO). A 20 mM stock solution prepared in methanol was used for *in vitro* experiments.

The *in vitro* growth inhibition assay for nerolidol followed the methods previously described [17,21] with some modifications. Parasite-infected RBC were diluted with uninfected RBC to obtain an RBC pack with 1% parasitemia. Twenty microliters of RBC with 1% parasitemia was dispensed to a 96-well microtiter plate together with 200 µl of the culture medium containing the indicated concentration of nerolidol (10, 25, 50, 75, 100, and 150 µM), and then incubated at 37 °C in a humified multi-gas water-jacketed incubator. For the control, cultures without the drug and another containing only methanol similar to the highest concentration

Table 1
The IC_{50} values of nerolidol for *Babesia* parasites and mammalian cells.

Organism	IC_{50} (µM)[a]
B. bovis	21 ± 1
B. bigemina	29.6 ± 3
B. ovata	26.9 ± 2
B. caballi	23.1 ± 1
J774.A1 macrophages[b]	125.69 ± 14.40
Human foreskin fibroblasts[b]	134.94 ± 32.19

[a] IC_{50} values expressed as nerolidol concentration are in micromolar of the growth medium and were determined on day 3 of *in vitro* culture using a curve fitting technique. IC_{50} values represent the mean and standard deviation of 3 separate experiments.

[b] The IC_{50} values for mammalian cells reported by Arruda et al. [14].

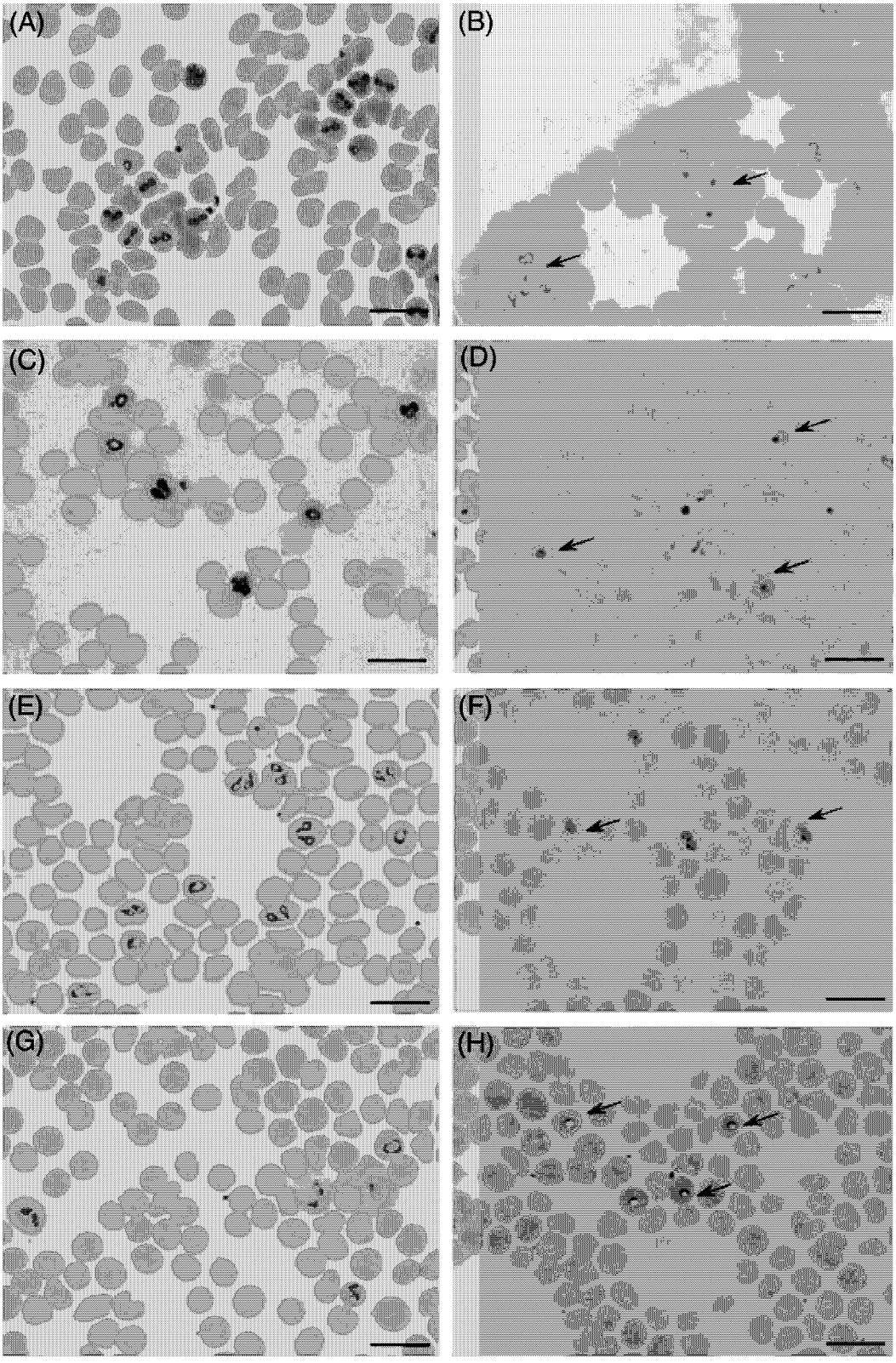

Fig. 2. Light micrographs of nerolidol-treated *Babesia* parasites in an *in vitro* culture. Micrographs were taken on day 3 of the experiments for 10 μ M treated cultures. *B. bovis*: control (panel A), and treated (panel B). *B. bigemina*: control (panel C), and treated (panel D). *B. ovata*: control (panel E), and treated (panel F). *B. caballi*: control (panel G), and treated (panel H). The drug-treated cultures showed a higher number of degenerated and swollen parasites than the control cultures. Scale bars = 10 μm.

used in drug were prepared. The experiments were carried out in triplicate for each drug concentration for 3 separate trails for a period of four days. The culture medium was replaced daily with 200 μl of a fresh medium containing the appropriate concentration of the drug. Parasitemia was monitored daily by counting the parasitized RBC to approximately 1000 RBC in Giemsia-stained thin blood smears. After the fourth day of treatment, 6 μl of each of the control and nerolidol-treated (at the various concentrations) RBC was mixed with 14 μl of

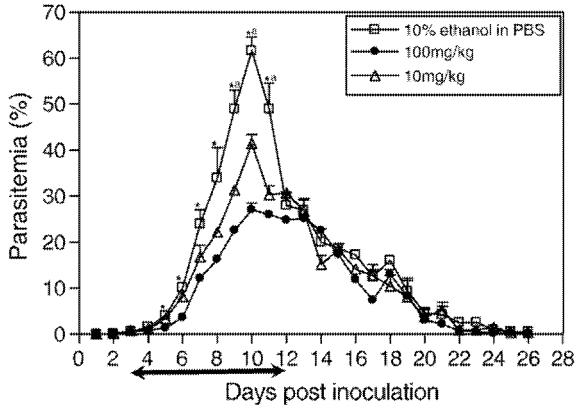

Fig. 3. Inhibitory effect of nerolidol (10 and 100 mg/kg) on the *in vivo* growth of *B. microti* for observations of 5 mice in each group. Each value represents the mean ± standard deviation of two separate experiments.* and [a], statistically significant differences ($P<0.05$) between 100 mg/kg and 10 mg/kg treated groups, and the control group, respectively. The double head arrow (↔) indicates the nerolidol intraperitoneal injection period.

parasite-free RBC and suspended in fresh growth medium without nerolidol supplementation. The plates were incubated for the next 10 days. The culture medium was replaced daily, and parasite recrudescence was determined by light microscopy to evaluate the parasite viability [20]. The values of a 50% inhibitory concentration (IC_{50}) of nerolidol against all parasites were calculat/ed based on parasitemia observed at 3 days after drug treatment by interpolation after curve fitting technique.

The *in vivo* growth inhibition assay for nerolidol was carried out two times according to the method previously described [14,20] with some modifications. Fifteen 8-week-old female BALB/c mice (CLEA Japan, Tokyo, Japan) were divided into 3 groups each contain five mice and intraperitoneally inoculated with 1×10^6 Munich strain *B. microti*-infected RBC that was maintained by passage in the blood of BALB/c mice [22]. Nerolidol was administered at a dose rate of 10 and 100 mg/kg after dissolving in 0.3 ml 10% ethanol in 0.01 M phosphate buffer (pH 7.4) for the first and second groups respectively. The third group was only administered 0.3 ml 10% ethanol in 0.01 M phosphate buffer (pH 7.4) as a control. When the infected mice showed about 1% parasitemia, all groups underwent daily intraperitoneal injections from days 3 to 12 post-infection. The levels of parasitemia in all mice were monitored daily until 26 days post-infection by examination of stained thin blood smears prepared from venous tail blood. All animal experiments were conducted in accordance with the Standard Relating to the Care and Management of Experimental Animals promulgated by the National Research Center for Protozoan Diseases, Obihiro University of Agriculture and Veterinary Medicine, Hokkaido, Japan.

JMP statistical software (version 5.1., SAS institute Inc., USA) was used to compare means of parasitemia percentage in the *in vitro* and *in vivo* studies using the independent Student's *t* test and considered to be significantly different when $P<0.05$.

The *in vitro* growth was significantly inhibited ($P<0.05$) at 10 μM (for *B. bovis*, and *B. bigemina*) (Fig. 1A, B), and at 25 μM (for *B. ovata*, and *B. caballi*) (Fig. 1C, D). The parasites' growth was completely suppressed at 50 μM (for *B. bigemina*), and at 75 μM (for *B. bovis*, *B. ovata*, and *B. caballi*). The calculated IC_{50}s values of nerolidol on the third day of culture for the growth of *B. bovis*, *B. bigemina*, *B. ovata*, and *B. caballi* were 21 ± 1, 29.6 ± 3, 26.9 ± 2, and 23.1 ± 1 μM, respectively (Table 1). *B. bovis is* more susceptible to nerolidol compared to other species of *Babesia*. Complete clearance was observed on the third (for *B. bovis*, *B. bigemina*, and *B. ovata*), and the fourth (for *B. caballi*) days of drug treatment. Subsequent cultivation of the parasites without the drug for a 10-day period showed no regrowth of the four species at 50 μM (Fig. 1) as shown by light microscopy. The serum has no effect on the inhibition of nerolidol to *Babesia* species as indicated from the use of GIT medium without serum for *B. bovis* and *B. caballi* (data not shown). The addition of only methanol to the culture had no influence on the growth. The effective doses of nerolidol for the growth inhibition of *Babesia* parasites were lower than the effective doses of heparin [20], and in nearly similar level to those of other drugs that had been tested as babesicidal drugs [21,23–27]. While they have medium level between those reported for *P. falciparum* [15] and *L. amazonensis* [14]. The average IC_{50} values of nerolidol for *Babesia* parasites were low compared with nerolidol IC_{50} values for mammalian cells (125.69 ± 14.40 μM; J774.A1 macrophages and 134.94 ± 32.19 μM; human foreskin fibroblast) [14]. The light microscope study showed that the drug affected the morphology of the parasite in treated cultures of *B. bovis* (Fig. 2B), *B. bigemina* (Fig. 2D), *B. ovata* (Fig. 2F), and *B. caballi* (Fig. 2H). The drug-treated cultures showed high number of degenerated and swollen parasites without cytoplasm compared to the control cultures. Based on light microscopic observations of the changes in the host cell shape, size, and color, nerolidol was non-toxic to erythrocytes.

The effect of nerolidol on the course of *B. microti* in mice was revealed. In the treated groups the level of parasitemia increased significantly (Student's *t* test, $P<0.05$) more slowly than the control, achieving peak parasitemia of 27 and 41.3% in the presence of 100 mg/kg and 10 mg/kg on day 10 post inoculation. In contrast, in the control group, the peak parasitemia was 58.3% (10% ethanol in PBS) on day 10 post inoculation (Fig. 3). The difference in growth inhibition (Student's *t* test, $P<0.05$) between 10 and 100 mg/kg and the control groups was significant on days 9–11 and days 5–11 PI, respectively. There was a significant difference between the 2 used doses of nerolidol ($P<0.05$) from days 5 to 11 PI, but the difference in the growth inhibition between the two doses was low (Fig. 2). The overall inhibition was moderate relative to the high doses used, while the inhibitory effect on *L. amazonensis* was low [14], this may be due to the differences in the life cycle, and pathogenicity of the two parasites. Toxic effects were not observed on mice after intraperitoneal administration of nerolidol; this is in good agreement with what was reported by Arruda et al. [14], where the mice injected with 100 mg/kg nerolidol for 12 days did not show any signs of toxicity. The half life of nerolidol may be very short; therefore, this may lead to its degradation and consequently low effect and no toxic signs even at high doses on the host.

The presence of an active isoprenoid pathway for the biosynthesis of dolichol of 11 and 12 isoprenic units was reported in *L. amazonensis* promastigotes [14] and in *P. falciparum* [28]. Dolichols composed of 11 to 13 isoprene units had been previously characterized in *Trypanosoma brucei* [29], and side chain of the 8 and 9 isoprenic units attached to benzoquinone rings of ubiquinones in *P. falciparum* [30]. While in the mammalian cells, the isoprenic chains of dolichols and ubiquinones comprise 20 to 22 and 10 isoprenic units, respectively [31]. In *Babesia* parasites, the presence of an active isoprenoid pathway was reported [13], while the structure of the dolichol and the side chain attached to the benzoquinone rings of ubiquinones are not known and need further studies.

In *Leishmania amazonensis*, nerolidol inhibited the isoprenoid biosynthesis, as shown by inhibiting incorporation of mevalonic acid (MVA) or acetic acid precursors into dolichol, ergosterol, ubiquinone, and by inhibiting the synthesis of geraniol, farnesol, and the putative hexaprenol intermediate in treated promastigotes due to the blockage of an early step in the mevalonate pathway [14], while in *P. falciparum*, nerolidol interferes with the isoprenoid biosynthetic pathway of the apicoplast leading to the interference with the biosynthesis of the dolichols, with the isoprenic chain of ubiquinones, and with protein isoprenylation of the parasites [15]. *B. bovis* has active isoprenoid pathway which is similar to that of *P. falciparum* [13]; therefore, the mechanism of inhibition for *Babesia* parasites may be similar to that of *P. falciparum* which requires further studies.

In conclusion, the results of the present study showed that nerolidol effectively inhibited the *in vitro* growth of *Babesia* parasites, while its *in vivo* effect on *B. microti* was weak in spite of the high doses

used. Therefore, nerolidol could not be used for the treatment of babesiosis.

Acknowledgements

This study was supported by Grants from the Promotion of Basic Research Activities for Innovative Biosciences (PROBRAIN), the 21st Century COE Program (A-1), Ministry of Education, Culture, Sports, Science, and Technology, Japan, the Japan International Cooperation Agency (JICA), and The Ministry of Higher Education Egypt.

References

[1] Homer MJ, Aguilar-Delfin I, Telford III SR, Krause PJ, Persing DH. Babesiosis. Clin Microbiol Rev 2000;13:451–69.
[2] Kuttler KL. Worldwide impact of babesiosis. In: Ristic M, editor. Babesiosis of domestic animals and man. Boca Raton: CRC Press Inc.; 1988. p. 1–22.
[3] Bork S, Yokoyama N, Igarashi I. Recent advances in the chemotherapy of babesiosis by Asian scientist: toxoplasmosis and babesiosis in Asia. Asian Parasitol 2005;4: 233–42.
[4] Vial HJ, Gorenflot A. Chemotherapy against babesiosis. Vet Parasitol 2006;138: 147–60.
[5] Gleeson MT. The plastid in Apicomplexa: what use is it? Int J Parasitol 2000;30: 1053–70.
[6] Wilson RJ, Williamson DH. Extrachromosomal DNA in the Apicomplexa. Microbiol Mol Biol Rev 1997;61:1–16.
[7] Fichera ME, Roos DS. A plastid organelle as a drug target in apicomplexan parasites. Nature 1997;390:407–9.
[8] Vaishnava S, Striepen B. The cell biology of secondary endosymbiosis—how parasites build, divide, and segregate the apicoplast. Mol Microbiol 2006;61: 1380–7.
[9] Jomaa H, Wiesner J, Sanderbrand S, Altincicek B, Weidemeyer C, Hintz M, et al. Inhibitors of the nonmevalonate pathway of isoprenoid biosynthesis as antimalarial drugs. Science 1999;285:1573–6.
[10] Goad LJ, Holz Jr GG, Beach DH. Sterols of *Leishmania* species: implications for biosynthesis. Mol Biochem Parasitol 1984;10:161–70.
[11] Ellis JE, Setchell KD, Kaneshiro ES. Detection of ubiquinone in parasitic and free-living protozoa, including species devoid of mitochondria. Mol Biochem Parasitol 1994;65:213–24.
[12] Yokoyama K, Trobridge P, Bruckner FS, Scholten J, Stuart KD, Voorhis WCV, et al. The effects of protein farnesyltransferase inhibitors on trypanosomatids: inhibition of protein farnesylation and cell growth. Mol Biochem Parasitol 1998;94:87–97.
[13] Brayton K, Lau A, Herndon D, Hannick L, Kappmeyer L, Berens S, et al. Genome sequence of *Babesia bovis* and comparative analysis of apicomplexan hemoprotozoa. PLoS Pathog 2007;3:1401–13.
[14] Arruda D, D'Alexandri F, Katzin A, Uliana S. Antileishmanial activity of the terpene Nerolidol. Antimicrob Agents Chemother 2005;49:1679–87.
[15] Rodrigues Goulart H, Kimura E, Peres V, Couto A, Aquino Duarte F, Katzin A. Terpenes arrest parasite development and inhibit biosynthesis of isoprenoids in *Plasmodium falciparum*. Antimicrob Agents Chemother 2004;48:2502–9.
[16] Lopes N, Kato M, Andrade E, Maia J, Yoshida M, Planchart A, et al. Antimalarial use of volatile oil from leaves of *Virola surinamensis* (Rol.) Warb. by Waiapi Amazon Indians. J Ethnopharmacol 1999;67:313–9.
[17] Avarzed A, Igarashi I, Kanemaru T, Hirumi K, Omata Y, Saito A, et al. Improved in vitro cultivation of *Babesia caballi*. J Vet Med Sci 1997;59:479–81.
[18] Igarashi I, Njonge FK, Kaneko Y, Nakamura Y. *Babesia bigemina*: *in vitro* and *in vivo* effects of curdlan sulfate on the growth of parasites. Exp Parasitol 1998;90:290–3.
[19] Bork S, Okamura M, Matsuo T, Kumar S, Yokoyama N, Igarashi I. Host serum modifies the drug susceptibility of *Babesia bovis in vitro*. Parasitology 2005;130: 489–92.
[20] Bork S, Yokoyama N, Ikehara Y, Kumar S, Sugimoto C, Igarashi I. Growth-inhibitory effect of heparin on *Babesia* parasites. Antimicrob Agents Chemother 2004;48: 236–41.
[21] Bork S, Yokoyama N, Matsuo T, Claveria FG, Fujisaki K, Igarashi I. Growth inhibitory effect of triclosan on equine and bovine *Babesia* parasites. Am J Trop Med Hyg 2003;68:34–40.
[22] Nishisaka M, Yokoyama N, Xuan X, Inoue N, Nagasawa H, Fujisaki K, et al. Characterization of the gene encoding a protective antigen from *Babesia microti* identified it as the η subunit of chaperonin-containing T-complex protein 1. Int J Parasitol 2001;31:1673–9.
[23] Bork S, Yokoyama N, Matsuo T, Claveria FG, Fujisaki K, Igarashi I. Clotrimazole, ketoconazole, and clodinafop-propargyl as potent growth inhibitors of equine *Babesia* parasites during *in vitro* culture. J Parasitol 2003;89:604–6.
[24] Bork S, Yokoyama N, Matsuo T, Claveria FG, Fujisaki K, Igarashi I. Clotrimazole, ketoconazole, and clodinafop-propargyl inhibit the *in vitro* growth of *Babesia bigemina* and *Babesia bovis* (Phylum Apicomplexa). Parasitology 2003;127:311–5.
[25] Bork S, Das S, Okubo K, Yokoyama N, Igarashi I. Effects of protein kinase inhibitors on the *in vitro* growth of *Babesia bovis*. Parasitology 2006;132:775–9.
[26] Nagai A, Yokoyama N, Matsuo T, Bork S, Hirata H, Xuan X, et al. Growth-inhibitory effects of artesunate, pyrimethamine, and pamaquine against *Babesia equi* and *Babesia caballi* in *in vitro* cultures. Antimicrob Agents Chemother 2003;47:800–3.
[27] Nakamura K, Yokoyama N, Igarashi I. Cyclin-dependent kinase inhibitors block erythrocyte invasion and intraerythrocytic development of *Babesia bovis in vitro*. Parasitology 2007;135:1–7.
[28] Couto AS, Kimura EA, Peres VJ, Uhrig ML, Katzin AM. Active isoprenoid pathway in the intra-erythrocytic stages of *Plasmodium falciparum*: presence of dolichols of 11 and 12 isoprene units. Biochem J 1999;341:629–37.
[29] Löw P, Dallner G, Mayor S, Cohen S, Chait BT, Menon AK. The mevalonate pathway in the bloodstream forms of *Trypanosoma brucei*. J Biol Chem 1991;266:19250–7.
[30] Parodi AJ, Martin-Barrientos J, Engel JC. Glycoprotein assembly in *Leishmania mexicana*. Biochem Biophys Res Commun 1984;118:1–7.
[31] Kellogg BA, Poulter CD. Chain elongation in the isoprenoid biosynthetic pathway. Curr Opin Chem Biol 1997;1:570–8.

Veterinary Parasitology 170 (2010) 193–196

Contents lists available at ScienceDirect

Veterinary Parasitology

journal homepage: www.elsevier.com/locate/vetpar

Seroprevalence of *Babesia* infections of dairy cows in northern Thailand

Hiroshi Iseki[a], Lijia Zhou[a], Chulmin Kim[a], Tawin Inpankaew[b], Chainirun Sununta[c], Naoaki Yokoyama[a], Xuenan Xuan[a], Sathaporn Jittapalapong[b], Ikuo Igarashi[a,*]

[a] *National Research Center for Protozoan Diseases, Obihiro University of Agriculture and Veterinary Medicine, Inada-cho, Obihiro, Hokkaido 080-8555, Japan*
[b] *Department of Parasitology, Kasetsart University, Bangkok, Thailand*
[c] *Chiang Rai Provincial Office, Department of Livestock Development, Chiang Rai, Thailand*

ARTICLE INFO

Article history:
Received 3 November 2009
Received in revised form 18 February 2010
Accepted 24 February 2010

Keywords:
Babesia bovis
Babesia bigemina
Indirect fluorescent-antibody test (IFAT)
Dairy cows
Enzyme-linked immunosorbent assay (ELISA)
Western blot
Thailand

ABSTRACT

The present study was conducted to demonstrate the epidemiological distribution of bovine babesiosis in the northern regions of Thailand. A total of 700 serum samples of dairy cows in the northern provinces (Chiang Rai, Chiang Mai, Lumpang, and Mae Hong Sorn) were tested for antibodies against *Babesia bovis* and *B. bigemina*. Species-specific enzyme-linked (rRAP-1/CTs) were performed. According to the results, 517 (73.8%) and 484 (69.1%) were positive for *B. bovis* and *B. bigemina*, respectively. In addition, 370 (52.9%) were positive for mixed infections by both ELISAs. On the other hand, all samples were also examined by the indirect fluorescent-antibody test (IFAT) with *B. bovis*- and *B. bigemina*-infected blood smears. According to the IFAT, 482 (68.8%) and 531 (75.8%) were positive for these infections, respectively. The overall concordances between the ELISA and IFAT techniques were 93.6% and 90.7% for *B. bovis* and *B. bigemina* infections, respectively. These results indicated that *babesia* infections are widespread in the northern parts of Thailand. To our knowledge, this is the first report describing the epidemiology of *Babesia* infections using rRAP-1/CT-based ELISAs in these areas.

1. Introduction

Bovine babesiosis is known as one of the most economically important diseases in tropical and subtropical regions (McCosker, 1981). This tick-borne disease is mainly caused by two intraerythrocytic protozoan parasites, *Babesia bovis* and *B. bigemina*. The clinical signs induced by these parasites are characterized by fever, anemia, and hemoglobinuria in the infected cattle (de Vos and Potgieter, 1994). However, the disease caused by *B. bovis* is more severe than that by *B. bigemina* (Ristic, 1981). Acute infections are usually diagnosed by a microscopic examination of blood smears, whereas subclinical infections have been identified serologically (Weiland and Reiter, 1988). Therefore, differential diagnosis between *B. bovis* and *B. bigemina* infections will lead to a better understanding of their epidemiology, and the species-specific distribution in the field will provide useful information to establish a control program of these diseases (de Vos and Potgieter, 1994).

Thailand is a developing agricultural country located in Southeast Asia. In this country, livestock development, particularly for dairy cows, has been hampered by persistently low production of milk and meat due to many infectious pathogens, including *Babesia*. In 1990, 428 cattle sera of 12 provinces in Thailand were tested for the antibodies of bovine babesiosis by the IFAT (Nishikawa et al., 1990). The prevalence of antibodies to *B. bovis* and *B. bigemina* was 74.5% (Nishikawa et al., 1990); however, there are only a few reports of bovine babesiosis in Thailand. Therefore, further reliable information is needed to reduce losses to animal owners due to these diseases.

The objective of the present study is to determine the prevalence of *Babesia* infections among dairy cows in northern provinces of Thailand using the IFAT and

* Corresponding author. Tel.: +81 155 49 5641; fax: +81 155 49 5643.
E-mail address: igarcpmi@obihiro.ac.jp (I. Igarashi).

0304-4017/$ – see front matter © 2010 Elsevier B.V. All rights reserved.
doi:10.1016/j.vetpar.2010.02.038

Table 1
Comparison of ELISA and IFAT in the detection of anti-*B.bovis* or *B. bigemina*-specific antibodies[a].

Provinces	Total	*B. bovis*				*B. bigemina*			
		ELISA		IFAT		ELISA		IFAT	
		+	–	+	–	+	–	+	–
Chiang Rai	392	284(72.4)	108(27.6)	269(68.6)	123(31.4)	257(65.5)	135(34.5)	283(72.1)	109(27.9)
Chiang Mai	150	126(84)	24(16)	111(74)	39(26)	107(71.3)	43(28.7)	123(82)	27(18)
Lumpang	100	91(91)	9(9)	89(89)	11(11)	85(85)	15(15)	95(95)	5(5)
Mae HongSorn	58	16(27.5)	42(72.5)	13(22.4)	45(77.6)	35(60.3)	23(39.7)	30(51.7)	28(48.3)
Total	700	517(73.8)	183(26.2)	482(68.8)	218(31.2)	484(69.1)	216(30.9)	531(75.9)	169(24.1)

[a] Values in parenthesis are in percentage.

the enzyme-linked immunosorbent assay (ELISA) with recombinant rhoptry-associated protein-1 (RAP-1) of each parasite (Boonchit et al., 2004, 2006).

2. Materials and methods

2.1. Preparation of recombinant antigens

The rRAP-1/CT, which consisted of a C-terminal portion of *B. bovis* and *B. bigemina* RAP-1, were prepared as previously described (Boonchit et al., 2004, 2006). Briefly, a gene encoding the *B. bovis* and *B. bigemina* RAP-1/CTs (C-terminal portion of the RAP-1) were expressed as an rRAP-1/CT fused with glutathione S-transferase (GST) in *E. coli*. Recombinant RAP-1/CT in an elution buffer (50 mM Tris–HCl, pH 7.5, 100 mM NaCl, and 2 mM EDTA) was used without thrombin protease, and rRAP-1/CT was obtained as a GST-fused protein according to the manufacturer's instructions (Amersham Pharmacia Biotech, Little Chalfont, UK). GST was used as control antigen in ELISA.

2.2. ELISA and IFAT

The purified proteins were subjected to species-specific diagnostic ELISAs (Boonchit et al., 2004, 2006). By optimization with 30 non-infected bovine sera, cutoffs for the OD at 415 nm in *B. bovis* and *B. bigemina* ELISAs were determined to be 0.07 and 0.096, respectively. The IFAT was also performed as previously described (Boonchit et al., 2004, 2006).

2.3. Sera

For the present investigation, 700 bovine sera were collected from 55 small dairy farms located in Chiang Rai (392), Chiang Mai (150), Lumpang (100), and Mae Hong Sorn provinces (58) in northern Thailand and stored at −20 °C until used.

2.4. Statistical analysis

The results of the ELISA were compared with those of the IFAT, and the percentages of overall concordance were calculated (percent concordance (%) = number of concordances between the ELISA and the standard IFAT reference × 100/number of tested samples) (Kim et al., 2007). The prevalence of *B. bovis* and *B. bigemina* according to the ELISA in each province was statistically analyzed employing Pearson's chi-square test $P<0.05$ as the values representing a significant difference. The chi-square test was applied to compare the rates of seropositivity among age groups, study sites, and gender. The statistical significance in this study was defined as $P<0.05$.

3. Results

According to ELISA, the prevalence of *B. bovis* and *B. bigemina* infection in Thailand was 73.8% (517/700) and 69.1% (484/700), respectively (Table 1). The percentages of *B. bovis*-positive sera in the four provinces, i.e., Chiang Rai, Chiang Mai, Lumpang, and Mae Hong Sorn, were 72.4% (284/392), 84% (126/150), 91% (91/100), and 27.5% (16/58), respectively. On the other hand, *B. bigemina*-positive sera represented 65.5% (257/392), 71.3% (107/150), 85% (85/100), and 60.3% (35/58), respectively. Mixed infections of *B. bovis* and *B. bigemina* were also determined to be 48.7% (191/392), 60.7% (91/150), 77% (77/100), and 18.9% (11/58), respectively. The rate of *B. bovis*-infected animals was significantly higher in Lumpang than in Chiang Rai ($P<0.01$); it was also significantly higher in Chiang Mai than in Chiang Rai ($P<0.01$) (Fig. 1A and C). In contrast, the rate of *B. bovis*-infected animals was significantly lower in Mae Hong Sorn than in the other three provinces ($P<0.01$). These results indicated that the rate of *B. bovis*-infected animals is highly different in the four provinces. On the other hand, the rate of *B. bigemina*-infected animals was significantly higher in Lumpang than in Chiang Rai ($P<0.01$), Chiang Mai ($P<0.05$), and Mae Hong Sorn ($P<0.01$) (Fig. 1B and D). The results of the ELISA were compared with those of the IFAT to evaluate the sensitivity and specificity of the ELISA for the detection of the specific antibodies to each parasite in Thailand. According to the IFAT, the overall prevalence for *B. bovis* and *B. bigemina* infections was determined to be 68.8% (482/700) and 75.9% (531/700), respectively (Table 1). The *B. bovis*-positive rates of four provinces were 68.6% (269/392), 74% (111/150), 89% (89/100), and 22.4% (13/58) in Chiang Rai, Chiang Mai, Lumpang, and Mae Hong Sorn, respectively. Moreover, *B. bigemina*-positive rates showed 72.1% (283/392), 82% (123/150), 95% (95/100), and 51.7% (30/58) in Chiang Rai, Chiang Mai, Lumpang, and Mae Hong Sorn, respectively. In addition, the prevalence of *B. bovis* and *B. bigemina* infections varied in different age groups, ranging from 68.4% to 93.8% and 45.5% to 88.2%, respectively (Table 2).

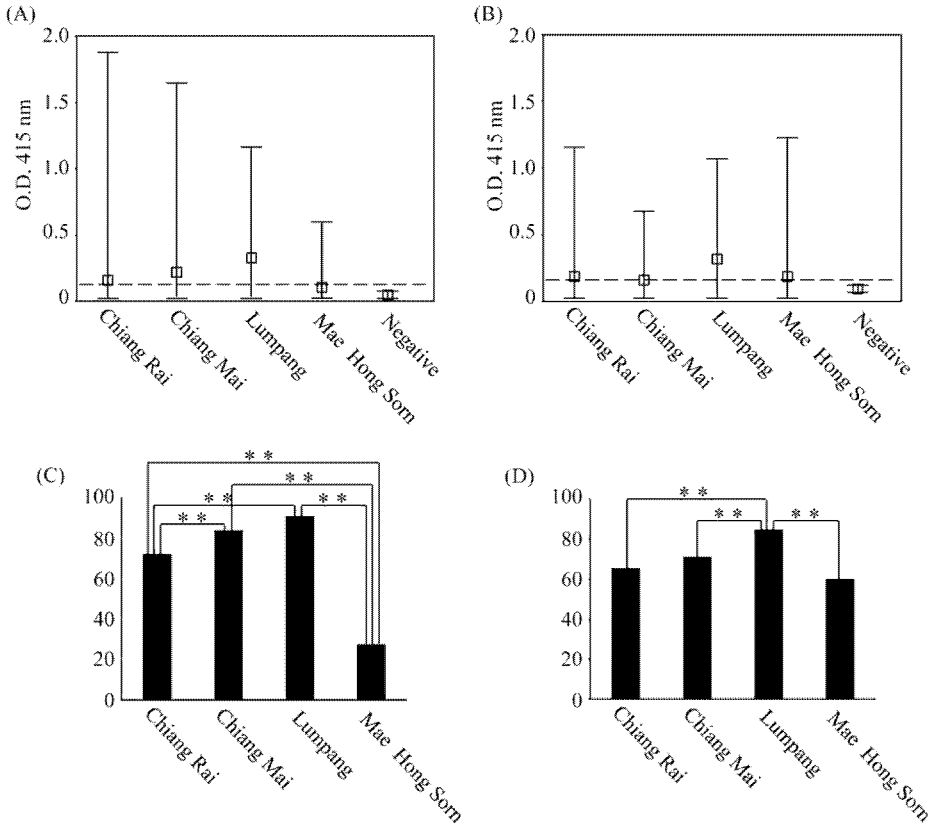

Fig. 1. ELISA O.D. values distribution of *B. bovis* (A) and *B. bigemina* (B) seroprevalence and sero-positive prevalence of *B. bovis* (C) and *B. bigemina* (D) in four different regions in Thailand. Maximum and minimum values (bars) and median values (boxes) from the ELISA are shown in panels A and B. The cutoff line was defined as the mean value plus the threefold standard deviation of the optical density (OD) obtained from 30 uninfected serum samples. These represent the OD at 415 nm of *B. bovis*-infected sera and *B. bigemina*-infected sera; Chiang Rai ($n = 392$), Chiang Mai ($n = 150$), Lumpang ($n = 100$), and Mae Hong Sorn ($n = 58$). The asterisks indicate significant differences in each region (**$P < 0.01$).

4. Discussion

The overall concordances of the ELISA and the IFAT were determined to be 93.6% and 90.7% for *B. bovis* and *B. bigemina* infections, respectively, when the results of the IFAT were used as the reference standard. The prevalence of *B. bovis*-positive animals in the ELISA was higher than that in the IFAT; in contrast, the rate of *B. bigemina*-positive animals in the ELISA was lower than that in the IFAT. This contradiction could be explained by a report in which *B. bigemina*-infected sera had cross-reactivity against *B. bovis*-infected sera (Morzaria et al., 1992).

Resistance to babesiosis is influenced by several factors, including the age of the animal (Ristic, 1981). Therefore, we analyzed the relationship between the prevalence of *B. bovis* and *B. bigemina* and the age of the examined cattle. However, there were no statistically significant differences between the age group and the infection rates,

Table 2
Seroprevalence of *B. bovis* and *B. bigemina* in different age groups of dairy cows[a].

Provinces	Age (year)	No. of animals	No. of positives (seroprevalence (%))	
			B. bovis	*B. bigemina*
ChiangRai	1	0	0	0
	1–5	212	145(68.4)	141(66.5)
	>5	180	134(74.4)	116(64.4)
Chiang Mai	1	11	10(90.9)	5(45.5)
	1-5	96	81(84.4)	71(74)
	>5	43	36(83.7)	33(76.7)
Lumpang	1	7	6(85.7)	6(85.7)
	1-5	76	64(84.2)	67(88.2)
	>5	17	15(93.8)	13(76.5)

[a] Values in parenthesis are in percentage.

except for a group of *B. bigemina*-infected cattle in Chiang Mai. In Chiang Mai, a significant difference was obtained in the infection rate between <1-year and 1–5-year groups ($P < 0.05$). Calves can receive anti-*Babesia* antibodies via the colostrum immediately after birth from immune mothers, which is considered to be a challenge during the first month of life (James, 1988). Most cattle develop lasting immunity after recovering; while this immunity is not absolute, it may last for life, even in the absence of re-infection (de Vos and Potgieter, 1994). Further epidemiological surveys on antibodies would give some interesting information on the control of both bovine babesiosis.

We believe that the epidemiological data obtained in the present study will contribute to establish a plan and strategy to control or diminish bovine babesiosis in the northern regions of Thailand. The prevalence of bovine babesiosis in Thailand suggests that an endemic stability might be present in the studied areas. In addition, our data will be beneficial for provincial veterinarians to understand current epidemiological status of the infections and will help Thai farmers reduce losses from this disease.

Acknowledgments

This study was supported by Grants-in-Aid for Scientific Research from the Japan Society for the Promotion of Science (JSPS) and the Program for the Promotion of Basic Research Activities for Innovative Biosciences (PROBRAIN), Japan. This project was financially supported by the Faculty of Veterinary Medicine, Kasetsart University Research Development Institute (KURDI), the Japan International Cooperation Agency (JICA), and the Program of Founding Research Center for Emerging and Re-emerging Infectious Diseases, Ministry of Education, Culture, Sports, Science, and Technology (MEXT), Japan.

References

Boonchit, S., Alhassan, A., Chan, B., Xuan, X., Yokoyama, N., Ooshiro, M., Goff, W.L., Waghela, S.D., Wagner, G., Igarashi, I., 2006. Expression of C-terminal truncated and full-length *Babesia bigemina* rhoptry-associated protein 1 and their potential use in enzyme-linked immunosorbent assay. Vet. Parasitol. 137, 28–35.

Boonchit, S., Xuan, X., Yokoyama, N., Goff, W.L., Waghela, S.D., Wagner, G., Igarashi, I., 2004. Improved enzyme-linked immunosorbent assay using C-terminal truncated recombinant antigens of *Babesia bovis* rhoptry-associated protein-1 for detection of specific antibodies. J. Clin. Microbiol. 42, 1601–1604.

de Vos, A.J., Potgieter, F.T., 1994. Bovine babesiosis. In: Coetzer, J.A.W., Thomson, G.R., Tustin, R.C. (Eds.), Infectious Diseases of Livestock. Oxford University Press, Cape Town, South Africa, pp. 278–294.

James, M.A., 1988. Immunology of babesiosis. In: Ristic, M. (Ed.), Babesiosis of Domestic Animal and Man. CRC Press, Boca Raton, FL, pp. 119–130.

Kim, C., Alhassan, A., Verdida, R.A., Yokoyama, N., Xuan, X., Fujisaki, K., Kawazu, S., Igarashi, I., 2007. Development of two immunochromatographic tests for the serodiagnosis of bovine babesiosis. Vet. Parasitol. 148, 137–143.

McCosker, P.J., 1981. The global importance of babesiosis. In: Ristic, M., Kreier, J.P. (Eds.), Babesiosis. Academic Press, New York, NY, pp. 1–24.

Morzaria, S., Katende, J., Kairo, A., Nene, V., Musoke, A., 1992. New methods for the diagnosis of *Babesia bigemina* infection. Mem. Inst. Oswaldo Cruz 87 (Suppl. 3), 201–205.

Nishikawa, H., Sarathan, N., Tantasuwan, D., Neramitmansuk, P., 1990. Serological survey of trypanosomiasis and babesiosis in cattle and buffaloes in Thailand. In: Proceedings of the Seventh FAVA Congress, November, pp. 4–7.

Ristic, M., 1981. Babesiosis. In: Ristic, M., MacIntyre, I. (Eds.), Disease of Cattle in the Tropics. Martinus Nijhof Publishers, The Hague, The Netherlands, pp. 443–468.

Weiland, G., Reiter, I., 1988. Methods for serological response to *Babesia*. In: Ristic, M. (Ed.), Babesiosis of Domestic Animal and Man. CRC Press, Boca Raton, FL, pp. 143–158.

Veterinary Parasitology 172 (2010) 65–70

Contents lists available at ScienceDirect

Veterinary Parasitology

journal homepage: www.elsevier.com/locate/vetpar

Development and evaluation of two nested PCR assays for the detection of *Babesia bovis* from cattle blood

Mahmoud AbouLaila, Naoaki Yokoyama, Ikuo Igarashi*

National Research Center for Protozoan Diseases, Obihiro University of Agriculture and Veterinary Medicine, Inada-Cho, Obihiro, Hokkaido 080-8555, Japan

ARTICLE INFO

Article history:
Received 18 July 2009
Received in revised form 6 April 2010
Accepted 9 April 2010

Keywords:
Nested PCR
B. bovis
Detection
Blood
Cattle

ABSTRACT

We developed and evaluated two nested polymerase chain reaction (nPCR) assays for the diagnosis of *Babesia bovis* infection in cattle based on two membrane protein genes from *B. bovis*, BBOV_IV005650 (BV5650) and BBO_IV008970 (BV8970). The specificities and sensitivities of the tests were compared with *B. bovis* Rhoptery associated protein 1 gene (RAP-1) nPCR. The specificity of the tests was 100% for *B. bovis* DNA. The sensitivities of nPCR to *B. bovis* from the *in vitro* cultured parasites were as low as 10^{-8}%, 10^{-6}%, and 10^{-7}% parasitemia for BV5650, BV8970, and RAP-1 nPCR, respectively. The nPCR detected as little as 1 fg genomic DNA per test for BV5650 and 100 fg per test for both BV8970 and RAP-1 genes. For field applications, the sensitivity was evaluated to a total of 165 field samples from Ghana, Mongolia, Brazil and Japan. The nPCR assay of BV5650 was the most sensitive for the detection of *B. bovis* from the field samples. The BV5650 nPCR assay provides a good diagnostic tool for laboratory diagnostic assessment of *B. bovis* infection in cattle worldwide.

1. Introduction

Babesia bovis is a tick-transmitted protozoan parasite of cattle. The disease is considered one of the most important tick-borne diseases of cattle worldwide, and of the 1.2×10^9 cattle in the world, over 500 million of these cattle are potentially at risk of having bovine babesiosis (McCosker, 1981). The clinical signs of *B. bovis* infection are fever, hemoglobinuria, acute anemia, and cerebral or nervous signs (Homer et al., 2000). Animals that survive *B. bovis* infection generally become low-level carriers of the parasite and serve as a reservoir for transmission (Mahoney, 1969).

Routine clinical diagnosis for babesiosis is usually based on the microscopic detection of parasites from collected blood smears. The detection had been considered to be the "gold standard" for the diagnosis of babesiosis (Böse et al., 1995). However, the technique is relatively laborious when large numbers of blood smear samples must be simultaneously quantified. Furthermore, it is extremely difficult to detect parasites in blood smears during low parasitemia as in the case of carrier animals (Almeria et al., 2001). Alternative techniques have been developed for the laboratory diagnosis of babesiosis. For example, many serological diagnostic tests have been developed for the detection of specific antibodies to bovine *Babesia* parasites, such as the complement fixation test (CFT), the indirect hemaglutination (IHA) test, the latex agglutination test (LAT), the indirect fluorescent antibody test (IFAT), the enzyme-linked immunosorbent assay (ELISA) (Weiland and Reiter, 1988; Boonchit et al., 2006; Goff et al., 2006), and immunochromatographic test (ICT) (Kim et al., 2008). However, the antibodies cannot always be detected in long-term carriers despite the presence of the parasite, and the lack of discrimination between previous exposure and current infections (Wagner et al., 1992). Fur-

* Corresponding author at: Research Unit for Molecular Diagnosis, National Research Center for Protozoan Diseases, Obihiro University of Agriculture and Veterinary Medicine, Nishi 2-13, Inada-Cho, Obihiro, Hokkaido 080-8555, Japan. Tel.: +81 155 49 5641; fax: +81 155 49 5643.
E-mail address: igarcpmi@obihiro.ac.jp (I. Igarashi).

0304-4017/$ – see front matter © 2010 Elsevier B.V. All rights reserved.
doi:10.1016/j.vetpar.2010.04.011

thermore, cross-reactivity of the antibodies against other *Babesia* species has limited the specificity of serological tests (Papadopoulos et al., 1996; Passos et al., 1998).

Polymerase chain reaction (PCR) assays for the diagnostic detection of *Babesia* parasites have the potential to provide rapid results with high specificity and sensitivity, in particular nested PCR assay (Fahrimal et al., 1992; Smeenk et al., 2000; Almeria et al., 2001; Gayo et al., 2003; Oliveira-Sequeira et al., 2005; Costa-Júnior et al., 2006; Martins et al., 2008). These PCR assays have various advantages over the microscopic and serological diagnostic test. For example, PCR diagnosis is possible in animals as young as 1 month of age, and the data obtained by PCR assays refer to the current prevalence, in contrast to the data obtained by serological assays (Wagner et al., 1992). In addition, the sensitivity of these assays for detecting bovine babesiosis has been shown to be higher than that of microscopic detection methods (Fahrimal et al., 1992; Figueroa et al., 1993; Almeria et al., 2001).

Completion of the genome sequence of *B. bovis* resulted in a large number of candidate genes for designing new PCR methods (Brayton et al., 2007). The search for new genes is required for the diagnosis of *B. bovis* infection. We chose two membrane protein genes, BBOV_IV005650 (BV5650) and BBOV_IV008970 (BV8970), from *B. bovis* genome sequence database to be used in the nested PCR assay. These two genes are unique for *B. bovis* and have no homologues either in *B. bigemina* genome sequence database or in the other apicomplexan parasites (Brayton et al., 2007). Unlike other apical complex proteins (e.g., Rhoptry-Associated Protein 1), which are conserved among *Babesia* species, the genes encoding BBOV_IV005650 (BV5650) and BBOV_IV008970 (BV8970) have not been detected in *B. bigemina* genome sequence (www.sanger.ac.uk). Therefore, the use of these genes for the diagnosis of *B. bovis* infection may increase the specificity, and sensitivity of the PCR. The aim of this study was to evaluate the diagnostic efficiency of the nested PCR assays based on these two membrane protein genes for diagnosis of *B. bovis* compared with the Rhoptry-Associated Protein 1 (RAP-1) nested PCR used in the previous studies.

2. Materials and methods

2.1. Parasites

The Texas strain of *B. bovis* (Hines et al., 1995) was maintained in purified bovine red blood cells (RBC) with a microaerophilic stationary-phase culture system (Bork et al., 2003a). Medium M199 (Sigma–Aldrich, Tokyo, Japan) was supplemented with 40% normal bovine serum to prepare the culture medium for the parasites.

2.2. DNA extraction

B. bovis-infected RBC were washed three times with cold phosphate-buffered saline (PBS) by centrifuging at $1000 \times g$ for 5 min at 4 °C and resuspended in PBS. The infected RBC were serially diluted 10-fold with normal RBC to adjust the parasite concentrations from 2.7×10^{-2} (parasitemia: 0.0000000001%) to 2.7×10^{6} (parasitemia: 1%) infected RBC/200 μl of the total RBC. Also another concentration of 7×10^{7} (5.2%) infected RBC/200 μl of total RBC was prepared (as positive control). Then all the dilutions separately subjected to DNA extraction with a QIAamp DNA Blood Mini Kit (QIAGEN, Tokyo, Japan). The purified DNA samples were used as templates for the subsequent PCR method. Genomic DNA was extracted from cultured parasites with 5% parasitemia as mentioned above for measuring the sensitivity of the primers to genomic DNA (Alhassan et al., 2005). The DNA measured spectrophotometrically and diluted 10-fold from 200 ng/μl to 2 fg/μl. DNA from the field samples were extracted from blood-spotted filter papers (Abe and Konomi, 1998; da Silva et al., 2004). Briefly, the spotted filter papers were cut out with a 2-mm hole puncher (2.0-mm Harris Micro Punch; Whatman, Middlesex, UK). DNA samples were extracted from the cut portion containing the spotted blood using a QIAamp DNA Mini Kit (QIAGEN). As negative controls, distilled water, extracted DNA samples of normal bovine blood and other cultured parasites (*B. bigemina*, *Theileria parva*, *Trypanosoma conglonse*, and *Neospora caninum*) were prepared as described above.

2.3. PCR and nested PCR amplifications

PCR and nested PCR (nPCR) amplifications were carried out with the developed primers specific to *B. bovis*, BBOV_IV005650 (BV5650) and BBOV_IV008970 (BV8970) membrane protein genes, Gene Bank accession numbers of XM_001610444, and XM_001610769, respectively (Table 1). The published pairs of species-specific primers for the detection of *B. bovis* (Figueroa et al., 1993) were used as a control for the developed primers. PCR was performed in 25 μl of a mixture containing 0.5 μl of the extracted DNA template, 50 pmol of each primer, 200 μM of each dNTP, and 1.25 U of Taq Gold DNA polymerase (Applied Biosystems, Foster City, CA, USA) in a PCR buffer (Applied Biosystems). The reactions were performed at the following temperatures: initial denaturation at 95 °C for 5 min to activate the Taq Gold DNA polymerase, followed by 35 cycles (1 min of denaturation at 94 °C, 1 min of annealing (at 57.5 °C for BV897 and at 64.5 °C for BV565), 1 min of extension at 72 °C), and 10 min of final extension at 72 °C in a Gene Amp PCR system 9700 (Applied Biosystems). The amplified PCR products of 0.5 μl were used for the subsequent nPCR with a limited annealing temperature at 57 °C. The PCR and nPCR conditions for *B. bovis* RAP-1 follow the method previously described (Figueroa et al., 1993). Cross-contamination was prevented by using plugged tips, performing the PCR in a separate room from that used for DNA extraction. The PCR and nested PCR products were subjected to electrophoresis in 2% agarose gel and then visualized under an ultraviolet (UV) light after staining with ethidium bromide (Sigma-Aldrich).

2.4. DNA sequencing

Positive DNA products from the specificity test (PCR, and nPCR), and from field samples nPCR were purified after 2% agarose gel electrophoresis using QIAquick Gel Extraction Kit (Qiagen K.K., Tokyo, Japan) and then cloned into a

Table 1
Primers sets developed for *B. bovis* DNA amplification in the present study.

Target gene	Assay	Primers	Sequences (5′→3′)	Amplicons size
BV5650[a]	PCR	F	ccggaattccaaatggcaacaaaggttga	720
		R	ccgctcgagggagcagcgtattacttcctcacgt	
	nPCR	F1	cgaggatttggtagacctcatc	561
		R1	cgtaaaatgtgtacaactattt	
BV8970[b]	PCR	F	ccggaattcacggaagagccgctagatgta	590
		R	ccgctcgagtcataatcagcctcggtgaaagc	
	nPCR	F1	cgctccgtagatgtggtgtcc	420
		R1	actatcatcagagtcggaatca	

[a] BBOV_IV005650 gene.
[b] BBOV_IV008970 gene.

pCR2.1® cloning vector using The Original TA Cloning Kit (Invitrogen, Carlsbad, CA, USA). The nucleotide sequences of inserts were determined using a Big Dye Terminator Kit (Applied Biosystems Japan, Ltd.) with ABI PRISM 3100™ genetic analyzer (Applied Biosystems Japan, Ltd.). The Genetyx 7 package (Software Development Co., Ltd., Tokyo, Japan) was used to align the determined sequences.

2.5. Field samples

FTA cards were used to collect 40, 24, and 81 field blood samples from cattle living in Ghana, Mongolia, and Brazil, respectively. DNA samples were extracted from the FTA cards as described above. Moreover, 20 blood samples were collected from Japan (a region considered free of *B. bovis* infections) and the DNA was extracted with a QIAamp DNA Blood Mini Kit (QIAGEN, Tokyo, Japan).

3. Results

3.1. Specificities of PCR and nested PCR methods

The species-specific PCR primers for *B. bovis* specifically produced the positive amplicons of 720 bp for BV5650, 590 bp for BV8970, and 356 bp for RAP-1 genes of only *B. bovis* DNA. The nested primers targeted 561 bp for BV5650, 420 bp for BV8970, and 291 bp for RAP-1 genes only from *B. bovis* DNA. There was no amplification for DNA from *B. bigemina*, *Theileria parva*, *Trypanosoma conglonse*, and *Neospora caninum* that were used as negative controls. In order to confirm the nucleotide sequences of PCR and nested PCR products, the amplified DNA products were purified from the positive reactions and cloned into the vector. The determined sequences of all DNA fragments were 100% identical to the reported ones of BBOV_IV005650, BBOV_IV008970, and *B. bovis* RAP-1 genes (Gene Bank accession numbers: XM_001610444, XM_001610769 and AF027149, respectively) (data not shown).

3.2. Sensitivities of the PCR and nested PCR methods

3.2.1. Sensitivities to DNA extracted from diluted infected RBC

To evaluate the sensitivities of the PCR and nested PCR methods of the newly developed primers, *B. bovis* DNA samples were extracted from a 10-fold serial dilution of the culture and then subjected to the PCR and nested PCR methods. In addition, the detection limits of the PCR and nested PCR methods were compared to those of PCR and nPCR methods of RAP-1 gene. In the PCR methods (Fig. 1), positive band of 720 bp (Panel A, lane 10) was detected from the dilution of 0.00000001% parasitemia (2.7×10^{-2} infected RBC) for BV5650. Positive bands of 590 bp (Panel B, lane 4), and 356 bp (Panel C, lane 4) were detected from the dilution of 0.01% parasitemia (2.7×10^{4} infected RBC) for BV8970, and RAP-1 genes, respectively. Subsequently, in the nPCR methods (Fig. 2), specific band of 561 bp was observed from the dilution of 0.00000001% parasitemia (2.7×10^{-2} infected RBC) for BV5650 gene (Panel A, lane 10). Specific bands of 420 bp from the dilution of 0.000001% parasitemia (2.7×10^{0} infected RBC) for BV8970 gene (Panel B, lane 8), and of 291 bp from the dilution of 0.0000001% parasitemia (2.7×10^{-1} infected RBC) for RAP-1 gene (Panel C, lane 9) were detected, respectively.

3.2.2. Sensitivities to 10-fold diluted genomic DNA

We evaluated the sensitivities of the PCR and nested PCR methods of the newly developed primers for the genomic DNA of *B. bovis*. DNA was diluted 10-fold and then subjected to the PCR and nested PCR methods. The detection limit for the PCR was 10 fg genomic DNA per test for BV5650, while it detected 10 ng for both BV8970, and RAP-1 genes (data not shown). The nPCR (Fig. 3) detected as low as 1 fg genomic DNA per test for BV5650 (Panel A, lane 9), 100 fg per test for both BV8970 (Panel B, lane 7), and RAP-1 (Panel C, lane 7) genes.

3.3. Detection of B. bovis from field samples by PCR and nPCR methods

Field blood samples collected from cattle living in Ghana, Mongolia, and Brazil were surveyed using the PCR and nPCR methods in order to demonstrate the field utility of these methods as a diagnostic tool for epidemiological studies. Forty, 24, 20, and 81 field blood samples were collected from Ghana, Mongolia, Japan, and Brazil, respectively. The PCR of BV5650 detected *B. bovis* DNA in 70% (28/40), 54.2% (13/24), and 27.2% (22/81) of the samples from Ghana, Mongolia, and Brazil, respectively (Table 2). The PCR of *B. bovis* RAP-1 only detected *B. bovis* DNA in 2.5%

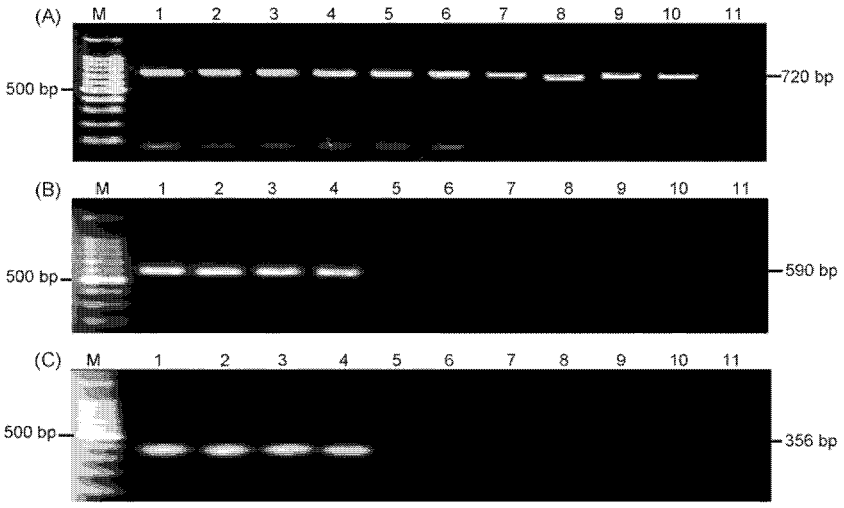

Fig. 1. Sensitivities of the PCR methods. PCR methods were carried out using the extracted DNAs from dilutions of infected RBC in the *in vitro* culture. BV5650 PCR (F and R) (Panel A), BV8970 PCR (F and R) (Panel B), and *B. bovis* RAP-1 (F and R) (Panel C) primers. In all panels, lane 1, 7×10^7; lanes 2–10, 2.7×10^6, 2.7×10^5, 2.7×10^4, 2.7×10^3, 2.7×10^2, 2.7×10^1, 2.7×10^0, 2.7×10^{-1}, and 2.7×10^{-2} infected RBC; and lane 11, bovine DNA. Lane M shows a 100-bp ladder size marker and the band of 500 bp is indicated on the left. The size of the positive bands is indicated on the right.

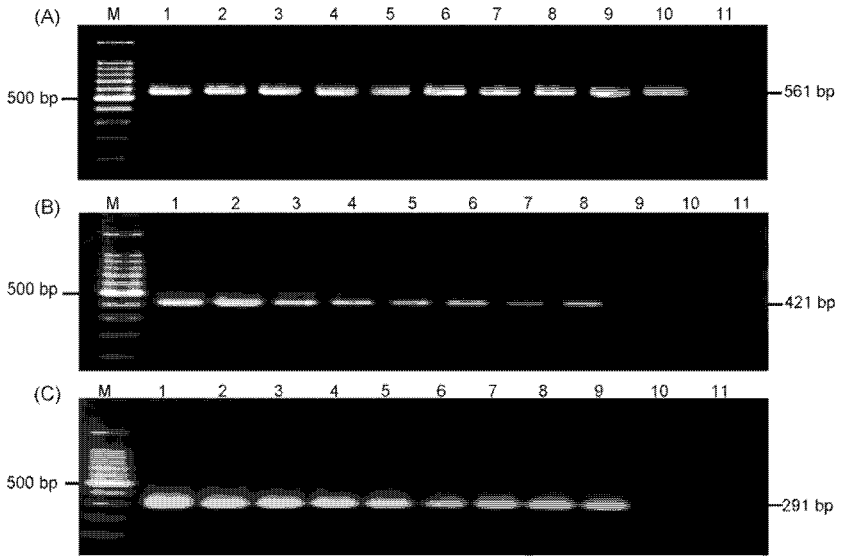

Fig. 2. Sensitivities of the nPCR methods. nPCR methods were carried out using the extracted DNAs from dilutions of infected RBC in the *in vitro* culture. BV5650 nPCR (F1 and R1) (Panel A), BV8970 nPCR (F1 and R1) (Panel B), and *bovis* RAP-1 nPCR (Panel C) primers. In all panels, lane 1, 7×10^7; lanes 2–10, 2.7×10^6, 2.7×10^5, 2.7×10^4, 2.7×10^3, 2.7×10^2, 2.7×10^1, 2.7×10^0, 2.7×10^{-1}, and 2.7×10^{-2} infected RBC; and lane 11, bovine DNA. Lane M shows a 100-bp ladder size marker and the band of 500 bp is indicated on the left. The size of the positive bands is indicated on the right.

Table 2
Comparison of the positive numbers among conventional PCR and nested PCR methods for *B. bovis* detection from field bovine blood samples collected from Ghana, Mongolia, Brazil, and Japan.

Country	Number	BV5650[a]		BV8970[b]		BVRAP-1[c]	
		Positive numbers (%)					
		nPCR	PCR	nPCR	PCR		
Ghana	40	28 (70)	33(82.5)	0 (0)	15(37.5)	0 (0)	10 (25)
Mongolia	24	13(54.2)	22(91.7)	0 (0)	2(8.33)	0 (0)	13(54.2)
Brazil	81	22(27.2)	52(64.2)	0 (0)	17 (21)	2(2.5)	31(38.2)
Japan	20	0	0 (0)	0 (0)	0 (0)	0 (0)	0 (0)

[a] BV5650 is BBOV_IV005650 gene.
[b] BV8970 is BBOV_IV008970 gene.
[c] *B. bovis* RAP-1 gene.

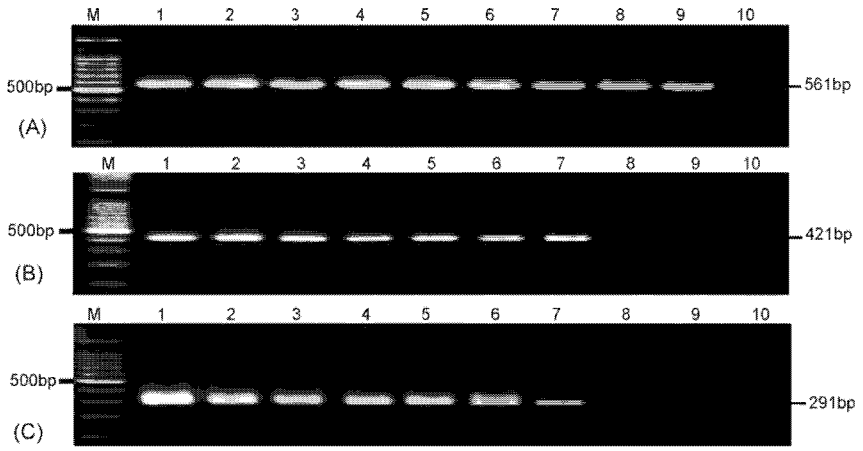

Fig. 3. Sensitivities of the nPCR methods. The nPCR methods were carried out using the 10-fold diluted genomic DNA extracted from the *in vitro* culture. BV5650 nPCR (F1 and R1) (Panel A), BV8970 nPCR (F1 and R1) (Panel B), and *bovis* RAP-1 nPCR (Panel C) primers. In all panels, lane 1, 100 ng; lane 9, 1 fg; and lane 10, bovine DNA. Lane M shows a 100-bp ladder size marker and the band of 500 bp is indicated on the left. The size of the positive bands is indicated on the right.

(2/81) of the samples from Brazil while the PCR of BV8970 could not detect *B. bovis* in any of the samples from the three countries (Table 2). Subsequently, the nPCR detection rates for *B. bovis* by BV5650 nPCR were 82.5% (33/40), 91.7% (22/24), and 64.2% (52/81) in Ghana, Mongolia, and Brazil, respectively (Table 2). BV8970 nPCR detected *B. bovis* in 37.5% (15/40), 8.33% (2/24), and 21% (17/81) of the samples from Ghana, Mongolia, and Brazil, respectively (Table 2). *B. bovis* RAP-1 nPCR detected *B. bovis* in 25% (10/40), 54.2% (13/24), and 38% (31/81) of the samples from Ghana, Mongolia, and Brazil, respectively. The BV5650, BV8970, and *B. bovis* RAP-1 PCR and nPCR could not detect *B. bovis* in any of the samples from Japan (Table 2). The sequences of the positive nested DNA fragments were almost 100% identical to the reported ones of BBOV_IV005650, BBOV_IV008970, and 99% identical to the *B. bovis* RAP-1 genes (Gene Bank accession numbers: XM_001610444, XM_001610769, and AF027149, respectively) (supplementary data).

4. Discussion

In this report, we described the successful development of two nested PCR methods for the detection of *B. bovis*. In the methods, sets of the designed primers specifically amplified the target DNAs derived from the respective BV5650 and BV8970 membrane protein genes. The specificity of the new primers was in agreement with that of *B. bovis* RAP-1 gene in PCR and nPCR methods.

The PCR and nPCR methods of BV5650 gene were more sensitive than the PCR and nPCR of BV8970, and *B. bovis* RAP-1 genes, respectively. They provide the detection of 10^{-8}% parasitemia (0.027 parasite) per test for DNA extracted from diluted infected RBC. The PCR and nPCR methods of BV5650 gene permitted the detection of 10 fg and 1 fg/test of the genomic DNA, respectively. The PCR and nPCR methods of BV5650 gene were more sensitive than the PCR and nPCR methods of BV8970, and *B. bovis* RAP-1 genes.

The detection rates for the field samples collected from Ghana, Mongolia, Japan, and Brazil were assessed. The PCR method of BV5650 gene had the highest positive numbers of the total samples tested. The nPCR method of the BV5650 gene also had the highest positive numbers of the total samples tested. The high number of positive samples detected by BV5650 nPCR were consistent with that were detected by spherical body protein 2 gene nPCR primers for the samples from Ghana (36/40), Mongolia (23/24), and Brazil (67/81) (AbouLaila et al., 2010). The high number of positive samples detected by BV5650 nPCR may be due to the presence of several gene copies in the genome. However, further studies are required to confirm this hypothesis. The sequence conservation among strains may also be a factor for these high positive numbers. While the *B. bovis* RAP-1 has two nearly identical copies (Norimine et al., 2002).

There are several reported methods describing the detection of *B. bovis*, but only some of them have been tested with random field samples: the nPCR (Figueroa et al., 1993; Almeria et al., 2001; Gayo et al., 2003; Oliveira et al., 2005; Costa-Júnior et al., 2006; Goff et al., 2006), the RLB (Gubbels et al., 1999; Brígido et al., 2004; Oura et al., 2004), the LAMP assay (Iseki et al., 2007), and recently the semi-inested hot-start PCR (Martins et al., 2008). The sensitivity of our nPCR is higher than reported sensitivities in previous studies using the nPCR of around 10^{-7}% parasitemia (Oliveira-Sequeira et al., 2005), 10^{-6}% parasitemia (Costa-Júnior et al., 2006), and 10^{-4}% parasitemia (Iseki et al., 2007).

The high positive numbers by our nPCR for *B. bovis* in the field samples from Brazil, and Ghana were consistent with that was detected by Oliveira-Sequeira et al. (2005), and the LAMP test by Iseki et al. (2007), respectively indicating high prevalence of babesiosis caused by *B. bovis* infection in both countries. To our knowledge, this is the first molecular detection of *B. bovis* from Mongolia. High detection rates of *B. bovis* by nPCR indicate that not only equine babesiosis (Boldbaatar et al., 2005), but also bovine babesiosis caused by *B. bovis* infection are prevalent in Mongolia.

In conclusion, we developed two nPCR-based methods for the detection of *B. bovis* from cattle blood. The BV5650 nPCR assay has higher levels of sensitivity than BV8970

nPCR; therefore, BV5650 nPCR method provides a good diagnostic tool for laboratory diagnostic assessment of *B. bovis* infection in cattle worldwide.

Acknowledgements

This study was supported by Grants-in-Aid for Scientific Research from the Japanese Society for the Promotion of Science, Grants from the Promotion of Basic Research Activities for Innovative Biosciences (PROBRAIN), the 21st Century COE Program (A-1), Ministry of Education, Culture, Sports, Science, and Technology, Japan, and the Ministry of Higher Education and Scientific Research, Egypt.

Appendix A. Supplementary data

Supplementary data associated with this article can be found, in the online version, at doi:10.1016/j.vetpar.2010.04.011.

References

Abe, K., Konomi, N., 1998. Hepatitis C virus RNA in dried serum spotted onto filter paper is stable at room temperature. J. Clin. Microbiol. 36, 3070–3072.

AbouLaila, M., Yokoyama, N., Igarashi, I., 2010. Development and evaluation of a nested PCR based on spherical body protein 2 gene for the diagnosis of *Babesia bovis* infection. Vet. Parasitol. 139, 45–50.

Alhassan, A., Pumidonming, W., Okamura, M., Hirata, H., Battsetseg, B., Fujisaki, K., Yokoyama, N., Igarashi, I., 2005. Development of a single-round and multiplex PCR method for the simultaneous detection of *Babesia caballi* and *Babesia equi* in horse blood. Vet. Parasitol. 129, 43–49.

Almeria, S., Castella, J., Ferrer, D., Ortuno, A., Estrada-Pena, A., Gutierrez, J.F., 2001. Bovine piroplasms in Minorca (Balearic Islands Spain): a comparison of PCR-based and light microscopy detection. Vet. Parasitol. 99, 249–259.

Boldbaatar, D., Xuan, X., Battsetseg, B., Igarashi, I., Battur, B., Batsukh, Z., Bayambaa, B., Fujisaki, K., 2005. Epidemiological study of equine piroplasmosis in Mongolia. Vet. Parasitol. 127, 29–32.

Boonchit, S., Alhassan, A., Chan, B., Xuan, X., Yokoyama, N., Ooshiro, M., Goff, W.L., Waghela, S.D., Wagner, G., Igarashi, I., 2006. Expression of C-terminal truncated and full-length *Babesia bigemina* rhoptry-associated protein 1 and their potential use in enzyme-linked immunosorbent assay. Vet. Parasitol. 137, 28–35.

Bork, S., Yokoyama, N., Matsuo, T., Claveria, F.G., Fujisaki, K., Igarashi, I., 2003a. Growth inhibitory effect of triclosan on equine and bovine *Babesia* parasites. Am. J. Trop. Med. Hyg. 68, 334–340.

Böse, R., Jorgensen, W.K., Dalgliesh, R.J., Friedhoff, K.T., De vos, A.J., 1995. Current state and future trends in the diagnosis of babesiosis. Vet. Parasitol. 57, 61–74.

Brayton, K., Lau, A., Herndon, D., Hannick, L., Kappmeyer, L., Berens, S., et al., 2007. Genome sequence of *Babesia bovis* and comparative analysis of Apicomplexan Hemoprotozoa. PLoS Pathogens 3, 1401–1413.

Brígido, C., da Fonseca, I.P., Parreira, R., Fazendeiro, I., do Rosaírio, V.E., Centeno-Lima, S., 2004. Molecular and phylogenetic characterization of *Theileria* spp. parasites in autochthonous bovines (Mirandesa breed) in Portugal. Vet. Parasitol. 123, 17–23.

Costa-Júnior, L.M., Rabelo, É.M.L., Filho, O.A.M., Ribeiro, M.F.B., 2006. Comparison of different direct diagnostic methods to identify *Babesia bovis* and *Babesia bigemina* in animals vaccinated with live attenuated parasites. Vet. Parasitol. 139, 231–236.

da Silva, E.S., Gontijo, C.M., Pacheco Rda, S., Brazil, R.P., 2004. Diagnosis of human visceral leishmaniasis by PCR using blood samples spotted on filter paper. Genet. Mol. Res. 3, 251–257.

Fahrimal, Y., Goff, W.L., Jasmer, D.P., 1992. Detection of *Babesia bovis* carrier cattle by using polymerase chain reaction amplification of parasite DNA. J. Clin. Microbiol. 30, 1374–1379.

Figueroa, J.V., Chieves, L.P., Johnson, G.S., Buening, G.M., 1993. Multiplex polymerase chain reaction based assay for the detection of *Babesia bigemina*, *Babesia bovis* and *Anaplasma marginale* DNA in bovine blood. Vet. Parasitol. 50, 69–81.

Gayo, V., Romito, M., Nel, L.H., Solari, M.A., Viljoen, G.J., 2003. PCR-based detection of the transovarial transmission of Uruguayan *Babesia bovis* and *Babesia bigemina* vaccine strains. Onderstepoort. J. Vet. Res. 70, 197–204.

Goff, W.L., Molloy, J.B., Johnson, W.C., Suarez, C.E., Pino, I., Rhalem, A., Sahibi, H., Ceci, L., Carelli, G., Adams, D.S., McGuire, T.C., Knowles, D.P., McElwain, T.F., 2006. Validation of a competitive enzyme-linked immunosorbent assay for detection of antibodies against *Babesia bovis*. Clin. Vaccine Immunol. 13, 1212–1216.

Gubbels, J.M., de Vos, A.P., van der Weide, M., Viseras, J., Schouls, L.M., de Vries, E., Jongejan, F., 1999. Simultaneous detection of bovine *Theileria* and *Babesia* species by reverse line blot hybridization. J. Clin. Microbiol. 37, 1782–1789.

Hines, S., Palmer, G., Brown, W., McElwain, T., Suarez, C., Vidotto, O., Rice-Ficht, A., 1995. Genetic and antigenic characterization of *Babesia bovis* merozoite spherical body protein Bb-1. Mol. Biochem. Parasit. 69, 149–159.

Homer, M.J., Aguilar-Delfin, I., Telford III, S.R., Krause, P.J., Persing, D.H., 2000. Babesiosis. Clin. Microbiol. Rev. 13, 451–469.

Iseki, H., Alhassan, A., Ohta, N., Thekiose, O.M., Yokoyama, N., Inoue, N., Nambota, A., Yasuda, J., Igarashi, I., 2007. Development of a multiplex loop-mediated isothermal amplification (mLAMP) method for the simultaneous detection of bovine *Babesia* parasites. J. Microbiol. Methods 71, 281–287.

Kim, C.M., Blanco, L.B., Alhassan, A., Iseki, H., Yokoyama, N., Xuan, X., Igarashi, I., 2008. Development of a rapid immunochromatographic test for simultaneous serodiagnosis of bovine babesioses caused by *Babesia bovis* and *Babesia bigemina*. Am. J. Trop. Med. Hyg. 78, 117–121.

Mahoney, D.F., 1969. Bovine babesiosis: a study of factors concerned in transmission. Ann. Trop. Parasitol. 63, 1–14.

Martins, T.M., Pedro, O.C., Caldeira, R.A., do Rosário, V.E., Neves, L., Domingos, A., 2008. Detection of bovine babesiosis in Mozambique by a novel seminested hot-start PCR method. Vet. Parasitol. 153, 225–230.

McCosker, P.J., 1981. The global importance of babesiosis. In: Ristic, M., Kreier, J.P. (Eds.), Babesiosis. Academic Press, New York, NY, pp. 1–24.

Norimine, J., Suarez, C.E., McElwain, T.F., Florin-Christensen, M., Brown, W.C., 2002. Immunodominant epitopes in *Babesia bovis* Rhoptry-Associated Protein 1 that elicit memory CD4+–T-lymphocyte responses in *B. bovis*-immune individuals are located in the amino-terminal domain. Infect. Immun. 70, 2039–2048.

Oliveira, M.C.S., Oliveira-Sequeira, T.C.G., Araujo Jr., J.P., Amarante, A.F.T., Oliveira, H.N., 2005. *Babesia* spp. infection in *Boophilus microplus* engorged females and eggs in Sao Paulo State. Brazil. Vet. Parasitol. 130, 61–67.

Oliveira-Sequeira, T.C., Oliveira, M.C., Araujo Jr., J.P., Amarante, A.F., 2005. PCR-based detection of *Babesia bovis* and *Babesia bigemina* in their natural host *Boophilus microplus* and cattle. Int. J. Parasitol. 35, 105–111.

Oura, C.A.L., Bishop, R.P., Wampande, E.M., Lubega, G.W., Tait, A., 2004. Application of a reverse line blot assay to the study of haemoparasites in cattle in Uganda. Int. J. Parasitol. 34, 603–613.

Papadopoulos, B., Perie, N.M., Uilenberg, G., 1996. Piroplasms of domestic animals in the Macedonia region of Greece. 1. Serological cross-reactions. Vet. Parasitol. 63, 41–56.

Passos, L.M.F., Bell-Sakyi, L., Brown, C.G.D., 1998. Immunochemical characterization of *in vitro* culture-derived antigens of *Babesia bovis* and *Babesia bigemina*. Vet. Parasitol. 76, 239–249.

Smeenk, I., Kelly, P.J., Wray, K., Musuka, G., Trees, A.J., Jongejan, F., 2000. *Babesia bovis* and *B. bigemina* DNA detected in cattle and ticks from Zimbabwe by polymerase chain reaction. J. S. Afr. Vet. Assoc. 71, 21–24.

Wagner, G., Cruz, D., Holman, P., Waghela, S., Perrone, J., Shompole, S., Rurangirwa, F., 1992. Non-immunologic methods of diagnosis of babesiosis. Mem. Inst. Oswaldo Cruz 87, 193–199.

Weiland, G., Reiter, I., 1988. Methods for serological response to babesia. In: Ristic, M. (Ed.), Babesiosis of Domestic Animal and Man. CRC Press, Boca Raton, FL, pp. 143–158.

JOURNAL OF CLINICAL MICROBIOLOGY, July 2010, p. 2509–2514 Vol. 48, No. 7
0095-1137/10/$12.00 doi:10.1128/JCM.00331-10

Evaluation of a Loop-Mediated Isothermal Amplification Method as a Tool for Diagnosis of Infection by the Zoonotic Simian Malaria Parasite *Plasmodium knowlesi*[▽]

Hiroshi Iseki,[1] Satoru Kawai,[2]* Nobuyuki Takahashi,[1] Makoto Hirai,[3] Kazuyuki Tanabe,[4] Naoaki Yokoyama,[1] and Ikuo Igarashi[1]

National Research Center for Protozoan Diseases, Obihiro University of Agriculture and Veterinary Medicine, Obihiro, Hokkaido, Japan[1]; Center for Tropical Medicine and Parasitology, Dokkyo Medical University, Mibu, Tochigi, Japan[2]; Department of Parasitology, Gunma University Graduate School of Medicine, Maebashi, Gunma, Japan[3]; and Laboratory of Malariology, Research Institute for Microbial Diseases, Osaka University, Suita, Osaka, Japan[4]

Received 18 February 2010/Returned for modification 9 April 2010/Accepted 26 April 2010

Loop-mediated isothermal amplification (LAMP) is a novel method that rapidly amplifies target DNA with high specificity under isothermal conditions. It has been applied as a diagnostic tool for several infectious diseases, including viral, bacterial, and parasitic diseases. In the present study, we developed a LAMP method for the molecular diagnosis of *Plasmodium knowlesi* infection (*Pk*LAMP) and evaluated its sensitivity, specificity, and clinical applicability. We designed three sets of *Pk*LAMP primers for the species-specific β-tubulin gene. The primer sets for *Pk*LAMP specifically amplified the autologous DNA extracts of *P. knowlesi*, and the sensitivity of the test was 100-fold that of single-PCR assay. These results indicate that our *Pk*LAMP method can be used to efficiently distinguish between *P. knowlesi* and other malaria parasites. To evaluate the feasibility of using *in vivo* materials, comparisons of *Pk*LAMP and the conventional nested PCR (nPCR) method and microscopic examination were made with blood samples from two experimentally infected monkeys. These studies showed that *P. knowlesi* infection can be identified much earlier with *Pk*LAMP than with nPCR and microscopy. Moreover, the detection performance of *Pk*LAMP using whole blood as the template was identical to that of *Pk*LAMP when genomic DNA extracts were used. These results suggest that the *Pk*LAMP method is a promising tool for molecular diagnosis of *P. knowlesi* infection in areas of endemicity.

Naturally acquired human infections with a macaque malaria parasite, *Plasmodium knowlesi*, have now been referred to as the fifth human malaria (4, 17). In fact, recent studies have shown that naturally occurring *P. knowlesi* malaria cases are not rare and are widely distributed in Southeast Asia, particularly in forested areas inhabited by the natural macaque host and vectors such as the *Anopheles leucophyrus* group (4, 5, 16).

Until recently, numerous cases of *P. knowlesi* infections in humans may have been misdiagnosed as ordinary *Plasmodium malariae* malaria (4, 5, 16), since the morphological characteristics of the blood stages of *P. knowlesi* parasites are similar to those of *P. malariae*, and it can be easily misidentified as *P. malariae* on microscopic examination (16). Moreover, our recent study showed that some commercial rapid malaria diagnostic tests based on the detection of parasite lactate dehydrogenase enzyme (pLDH) are unable to distinguish between human malaria parasites and *P. knowlesi*, since certain antibodies to pLDH that were thought to be specific for *Plasmodium falciparum* and *Plasmodium vivax* also bind to *P. knowlesi* (9). Although the development of a PCR diagnostic method has been essential to solving these problems of misdiagnosis, PCR assays are not a simple method of detection and are not a viable option for routine diagnosis.

Loop-mediated isothermal amplification (LAMP) has been developed as a novel method to amplify DNA with high specificity and simplicity (13). It consists simply of incubating a mixture of the target gene, four or six different primers, *Bst* DNA polymerase, and substrates. The significant advantages of the LAMP method are (i) high amplification efficiency under isothermal conditions (63 to 65°C) and (ii) visual judgment based on the turbidity or fluorescence of the reaction mixture, which is kept in the reaction tube (10, 12). LAMP has thus emerged as a powerful tool to facilitate genetic testing for the rapid diagnosis of several infectious diseases, including viral, bacterial, and parasitic diseases (8, 11). Although the detection performances of LAMP for four human malaria parasites have been assessed in clinical and epidemiological settings, the LAMP method has not yet been evaluated for the diagnosis of *P. knowlesi* infection (3, 7, 14). In the present study, we developed a LAMP method for diagnosis of *P. knowlesi* infection (*Pk*LAMP) and evaluated its sensitivity, specificity, and clinical applicability using blood samples obtained from experimentally *P. knowlesi*-infected monkeys.

MATERIALS AND METHODS

Specific primers for *Pk*LAMP. The LAMP method requires a set of four specific primers: a forward inner primer (FIP), a backward inner primer (BIP), and two outer primers (F3 and B3), which recognize a total of six distinct nucleotide sequences (B1, B2, B3, F1, F2, and F3) on the target gene (10, 12, 13).

* Corresponding author. Mailing address: Center for Tropical Medicine and Parasitology, Dokkyo Medical University, Mibu, Tochigi 321-0293, Japan. Phone: 81 282 87 2134. Fax: 81 282 86 6431. E-mail: skawai@dokkyomed.ac.jp.

[▽] Published ahead of print on 5 May 2010.

A

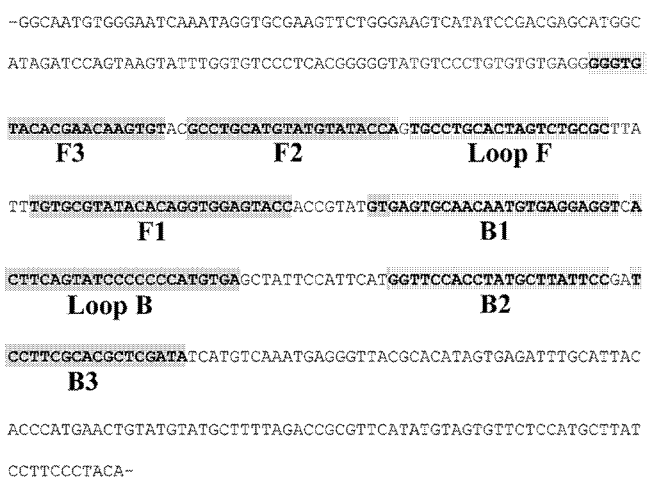

B

Primer	Type	Sequence *
Knowlesi-F3	F3	5′-GGGTGTACACGAACAAGTGT-3′
Knowlesi-B3	B3c	5′-TATCGAGCGTGCGAAGGA-3′
Knowlesi-FIP	F1c-F2	5′-GGTACTCCACCTGTGTATACGCACAGAATTCCGCCTGCATGTATGTATACCAG-3′
Knowlesi-BIP	B1-B2c	5′-GTGAGTGCAACAATGTGAGGAGGTGAATTCCGGAATAAGCATAGGTGGAACC-3′
Knowlesi-FLP	Loop F	5′-GCGCAGACTAGTGCAGGCA-3′
Knowlesi-BLP	Loop B	5′-ACTTCAGTATCCCCCCCATGTGA-3′

*Underlining indicates a restriction enzyme site of *Eco R* I.

FIG. 1. Locations and sequences of LAMP targets and priming sites for the *P. knowlesi* β-tubulin gene. (A) Locations of priming sites of the *Pk*LAMP primer set in the reference sequence (GenBank accession number AY639984) are indicated by gray shading. (B) Primer sets used for amplification of the *P. knowlesi* β-tubulin gene in LAMP.

Since it has been demonstrated that additional loop primers increase the amplification efficiency, loop primers for each target gene were also synthesized. The specific primers for *P. knowlesi* were designed against species-specific β-tubulin gene sequences (GenBank accession number AY639984) (Fig. 1A). For easy confirmation of the amplified sequences, we modified the FIP and BIP by inserting a restriction enzyme (EcoRI) cleavage site between the F1 complementary sequence and F2 and between the B1 complementary sequence and B2, respectively, as shown in Fig. 1B.

***Pk*LAMP procedures.** The *Pk*LAMP reaction was performed as described previously (10, 12, 13). Briefly, the reaction was performed with 25 μl of a mixture containing 1 μl of the extracted DNA template, 40 pmol each of the FIP and BIP, 5 pmol each of the F3 and B3 primers, 20 pmol each of the forward loop primer (FLP) and backward loop primer (BLP), and 1 μl of fluorescent detection reagent (Eiken Chemical Co., Ltd., Tokyo, Japan) with Loopamp DNA amplification kit (Eiken Chemical Co., Ltd., Tokyo, Japan). The *Pk*LAMP reaction was performed as described above with each of the specific primers. In a conventional heat block, the mixture was incubated at 66°C (temperatures of 47 to 72°C were also tested) for 60 min, and the reaction was then terminated by heating the mixture at 80°C for 5 min. For the initial validation study, *Pk*LAMP was confirmed with real-time monitoring of the increase of turbidity using a Loopamp real-time turbidimeter (LA-200; Teramecs, Kyoto, Japan). To confirm the amplified DNA products of each parasite, 1 μg/μl of the product was digested with the EcoRI at 37°C for 1 h. The nontreated and EcoRI-digested LAMP products were subjected to electrophoresis on a 2% agarose gel and then visualized under UV light after staining with ethidium bromide (Sigma). Digested LAMP DNA products were purified after 2% agarose gel electrophoresis and then cloned into a pCRII cloning vector using a TA cloning kit (Invitrogen, Carlsbad, CA). The nucleotide sequences of inserts were determined using a Big Dye Terminator kit (Applied Biosystems Japan, Ltd.) with an automated DNA sequencer (ABI Prism 3100 genetic analyzer; Applied Biosystems Japan, Ltd.). The Genetyx 7 package (Software Development Co., Ltd., Tokyo, Japan) was used to align the determined sequences. For the challenge infections, the amplified products in the reaction tube were directly detected with the naked eye using Loopamp fluorescent detection reagent (Eiken Chemical Co., Ltd.) according to the manufacturer's instructions.

Specificity of *Pk*LAMP primers. Specificity of the *Pk*LAMP primers was tested using genomic DNAs (gDNAs) of various *Plasmodium* species in a gel electrophoresis and fluorescent analysis. The gDNAs of *P. falciparum*, *P. vivax*, *P. malariae*, and *P. ovale* were kindly provided by Takefumi Tsuboi of Ehime University of Japan. Blood samples infected with *P. inui*, *P. simiovale*, *P. fieldi*, *P. fragile*, *P. hylobati*, and *P. gonderi* were obtained from American Type Culture Collection (ATCC), and gDNAs of these parasites were extracted from frozen infected blood with a QIAamp DNA blood mini kit (Qiagen, Tokyo, Japan) according to the manufacturer's instructions. *P. coatneyi*- and *P. cynomolgi*-infected blood samples were obtained from experimentally infected monkeys and were subjected to DNA extraction with the QIAamp DNA blood mini kit. These purified DNA samples were used as templates for the subsequent *Pk*LAMP and single-PCR assays. As a negative control, DNA extracted from normal monkey blood was prepared as described above.

Sensitivity tests for *Pk*LAMP and single PCR. For sensitivity testing, the *Pk*LAMP reaction was tested using 10-fold serial dilutions of plasmid DNA containing the target sequence by cloning from *P. knowlesi* H strain genomic DNA and compared against results of the single-PCR assay using F3 and B3 primers. PCR amplification was performed in 25 μl of a mixture containing 1 μl of the extracted DNA template, 50 pmol of each primer, 200 μM each deoxynucleoside triphosphate (dNTP), and 1.25 U of *Taq* Gold DNA polymerase (Applied Biosystems, Foster City, CA) in a PCR buffer (Applied Biosystems). The reaction was performed for 35 cycles under the following conditions: 10 min

at 95°C to activate the *Taq* Gold DNA polymerase, 1 min of denaturation at 94°C, 1 min of annealing at 60°C, 1 min of extension at 72°C, and 10 min of final extension at 72°C in a Gene Amp PCR system 9700 (Applied Biosystems). The PCR products were subjected to agarose gel electrophoresis and then visualized as described above.

Evaluation of *Pk*LAMP using blood samples from infected monkeys. *Pk*LAMP was evaluated for fluorescence detection of *P. knowlesi* target DNA using blood samples obtained from experimentally *P. knowlesi*-infected monkeys. Two monkeys, J58 (male) and J64 (male), which were 3-year-old Japanese macaques (*Macaca fuscata*) weighing 4.2 kg and 4.7 kg, respectively, were used in this experiment. Both monkeys were second-generation offspring bred in captivity. The investigators adhered to the Guidelines for the Use of Experimental Animals authorized by the Japanese Association for Laboratory Animal Science. Monkey J58 was inoculated intravenously with 1×10^8 fresh *P. knowlesi* H strain (ATCC 30158) parasitized red blood cells (PRBCs) obtained from another infected Japanese macaque. Monkey J64 was inoculated intravenously with frozen *P. knowlesi* Hackeri strain (ATCC 30153)-infected blood obtained from the ATCC. After infection, Giemsa-stained thin blood films were prepared daily from peripheral blood obtained by ear prick, and parasitemia in the infected monkeys was monitored by microscopic examination. Heparinized blood samples for *Pk*LAMP assay were obtained daily from the infected monkeys during the course of infection. The infected blood samples were subjected to DNA extraction with a QIAamp DNA blood mini kit (Qiagen) as described above. The DNA extracts and whole blood samples were frozen at −80°C until use.

Comparison of *Pk*LAMP and nested PCR using DNA extracts and whole blood as template. We compared the sensitivities of *Pk*LAMP and conventional nested PCR (nPCR) assays using DNA extract of *P. knowlesi* and whole blood obtained from two infected monkeys during the course of infection. The nPCR assay, based on the *Plasmodium* DNA sequence of the small-subunit (SSU) rRNA gene, was performed according to a standard protocol as described previously (15). The nest 1 reaction was carried out in a 50-μl reaction mixture containing 2× PCR master mix (Ampli*Taq* Gold PCR master mix; Applied Biosystems), 250 nM each primer (rPLU1 and rPLU5) (15), and 2 μl of DNA template. The reaction mixture for nest 1 PCR amplification was placed in a thermal cycler (TP600; Takara Bio Inc., Shiga, Japan) at 95°C for 5 min for initial denaturation. This was followed by 40 cycles of 94°C for 30 s, 55°C for 60 s, and 72°C for 120 s for amplification and then 72°C for 10 min for final extension. Nest 2 PCR amplification was performed in a 20-μl reaction mixture containing 2× PCR master mix (Applied Biosystems), 250 nM each primer (Pmk8 and Pmkr9) (16), and 2 μl of the nest 1 PCR products used as DNA templates. the reaction mixture for nest 2 PCR amplification was placed in a thermal cycler (TP600) at 95°C for 5 min for initial denaturation. This was followed by 40 cycles of 94°C for 30 s, 60°C for 60 s, and 72°C for 60 s for amplification and then 72°C for 10 min for final extension. Nest 2 PCR products were electrophoresed separately on a 2% agarose gel and illuminated with UV light.

RESULTS

Specificity of *Pk*LAMP primers. The specificity of the *Pk*LAMP primers was investigated by using various *Plasmodium* gDNAs as templates for *Pk*LAMP. As shown in Fig. 2A, a typical ladder pattern was detected in *P. knowlesi* DNA (lane 1) but not in the DNAs of other *Plasmodium* species. Moreover, fluorescent detection was also specifically obtained in the reaction tube including gDNA of *P. knowlesi*, as shown in Fig. 2B. The sizes of the *Pk*LAMP fragments digested by EcoRI were identical to the predicted sizes for the parasite (data not shown). To evaluate the accuracy and robustness of the LAMP method, the *Pk*LAMP reaction was carried out in a water bath at 47 to 72°C separately. Positive ladder patterns were observed at 48 to 71°C and strongly at 56 to 70°C. These findings demonstrated that a set of species-specific primers was highly specific for the detection of the corresponding parasite in *Pk*LAMP. To confirm the nucleotide sequences of the LAMP products, the amplified and digested DNA products were purified from the positive controls and cloned into a vector. The determined sequences of the DNA fragments were completely identical to the reported ones (data not shown) (*P. knowlesi*, accession no. AY639984).

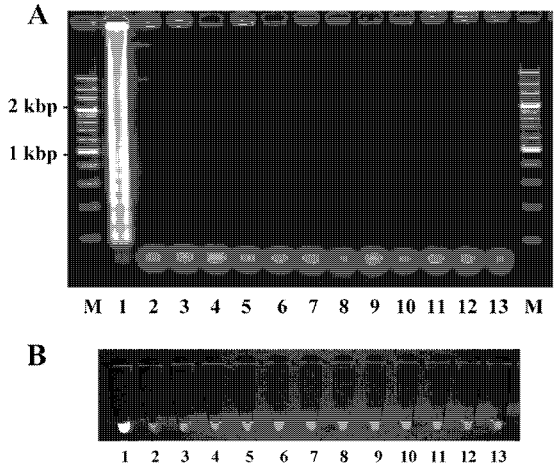

FIG. 2. Specificity of *Pk*LAMP for *P. knowlesi*. (A) Agarose gel electrophoresis of LAMP products from genomic DNAs of 13 *Plasmodium* spp. and ethidium bromide staining. (B) Visual detection of LAMP products under UV light using the Loopamp fluorescent detection reagent. Lanes M, 200-bp ladder size markers; lanes 1, *P. knowlesi*; lanes 2, *P. falciparum*; lanes 3, *P. malariae*; lanes 4, *P. vivax*; lanes 5, *P. ovale*; lanes 6, *P. coatneyi*; lanes 7, *P. cynomolgi*; lanes 8, *P. inui*; lanes 9, *P. simiovale*; lanes 10, *P. fieldi*; lanes 11, *P. fragile*; lanes 12, *P. gonderi*; lanes 13, *P. hylobati*.

Sensitivity of *Pk*LAMP reaction. To examine the sensitivity of *Pk*LAMP, three *Pk*LAMP detection methods were compared with conventional single PCR using two outer primers, F3 and B3, for the detection of *P. knowlesi* β-tubulin gene. As shown in Fig. 3A, amplification by real-time *Pk*LAMP was obtained in reaction tubes containing from 10^8 to 10^2 copies/μl of the DNA template in a 60-min reaction with a turbidity assay. On gel electrophoresis analysis, the amplified products also showed ladder-like patterns from 10^8 to 10^2 copies/μl (Fig. 3B). The amplified products in these positive reaction tubes were also visually detectable using the Loopamp fluorescent detection reagent, as shown in Fig. 3C. In contrast, the limit of detection for PCR using the F3 and B3 primers was 10^8 to 10^4 copies/μl (Fig. 3D). Therefore, it appeared that the sensitivity of the *Pk*LAMP, regardless of the detection method, was 100-fold higher than that of the single-PCR assay.

Evaluation of *Pk*LAMP and nPCR using DNA extracts and whole blood samples as templates. The course of infection of *Macaca* monkeys experimentally infected with *P. knowlesi* was monitored by *Pk*LAMP and nPCR for detecting parasite DNA (Table 1). Both monkeys infected with *P. knowlesi* developed a fulminating acute infection, and they finally became lethargic and severely withdrawn just before autopsy. In monkey J58 inoculated with fresh PRBCs of *P. knowlesi* strain H, the parasites in the peripheral blood were first detected by microscopy on day 1; parasite densities then increased to around 10% within 3 days after infection. *P. knowlesi* DNA could be detected by *Pk*LAMP as well as nPCR assay on all days during the course of infection (Table 1). In monkey J64 inoculated with frozen PRBCs of *P. knowlesi* strain Hackeri, the parasites were first detected by microscopy on day 6; parasite densities then increased sharply to around 58% within 9 days after

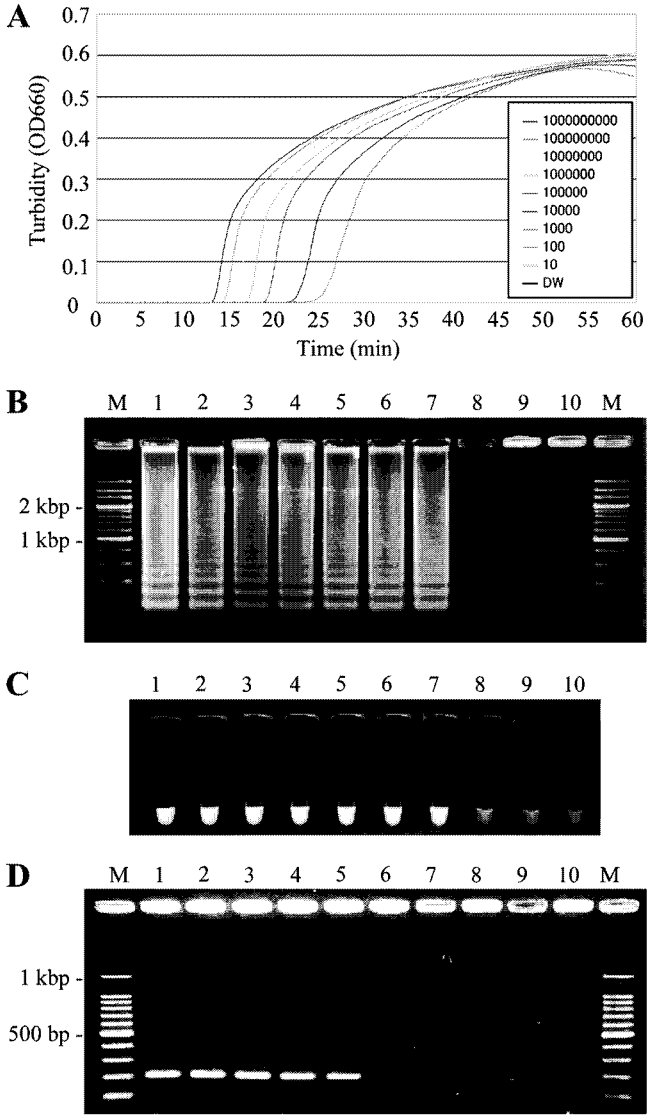

FIG. 3. Comparison of sensitivities of three methods of detection of *Pk*LAMP and conventional single PCR for the detection of the *P. knowlesi* β-tubulin gene. Template DNA was prepared on serial dilutions of plasmid DNA (10^8 copies to 1 copy per reaction) containing a β-tubulin gene for each assay. (A) Real-time LAMP assay monitored by real-time measurement of turbidity. OD_{660}, optical density at 660 nm. (B) Agarose gel electrophoresis of LAMP products. (C) Visual detection of LAMP products under UV light using the Loopamp fluorescent detection reagent. (D) Agarose gel electrophoresis of single-PCR products using the F3 and B3 primers. Lanes M, 200-bp ladder size markers (A) and 100-bp ladder size markers (B); lanes 1 to 9, 10^8 copies to 1 copy of plasmid; lanes 10, distilled water (B to D).

infection. *P. knowlesi* DNA could be detected by *Pk*LAMP throughout the course of infection, while the earliest detection of parasite DNA by the nPCR assay was on the third day after infection (Table 1).

We also compared the amplification efficiencies of *Pk*LAMP and nPCR using frozen whole blood as a template. As shown in Table 1, *Pk*LAMP could amplify the target from whole blood with an efficiency similar to that with DNA extracts throughout the course of infection. These results clearly indicate that *Pk*LAMP could detect even the target DNA from nonpurified whole blood. In contrast, nPCR assay using whole blood from J58 and J64 could amplify parasite DNA only on day 3 and day 9, respectively, when parasite densities were markedly increased in the blood (Table 1).

DISCUSSION

The diagnosis of malaria at regional clinics in areas of endemicity has been performed mainly by microscopic examination of blood smears because of its ease and rapid application. However, the morphology of the asexual stages of the zoonotic simian *Plasmodium* parasites substantially resembles that of human parasites, particularly on thick blood films, and laboratory technicians are trained to recognize only the four species of human parasites (16). In fact, numerous human cases of *P. knowlesi* infection have been misdiagnosed by microscopy as *P. malariae* due to their morphological similarities (4, 5, 16). The application of DNA amplification to the diagnosis of malaria can solve these problems. Amplification of parasite DNA using a specific PCR has been applied to various *Plasmodium* species, including four human malarial parasites and *P. knowlesi* (5, 15, 16). However, despite the excellent specificity and sensitivity of PCR and real-time PCR, these methods require complicated procedures and sophisticated instrumentation such as a thermal cycler, and they are often impractical under conditions requiring field diagnosis. In this regard, the LAMP method has the advantages of simplicity, specificity, and sensitivity compared to other molecular diagnostic methods. Thus, the LAMP method is a promising candidate for wide use in regional clinics and under field conditions.

In the present study, we successfully developed a LAMP method for detecting *P. knowlesi* infection, using a primer set that targets the β-tubulin genes of parasites. The specificity of the primers was evaluated using nine species of simian malaria parasites and four species of human malaria parasites. The results showed that the primer set for *Pk*LAMP amplified only the autologous DNA samples of *P. knowlesi* in typical ladder bands. In contrast, no ladder bands were obtained from any other control. These findings indicate that this primer set is specific for *P. knowlesi* and can be used to examine for *P. knowlesi* malaria as well as to distinguish between it and other types of malaria. The sensitivity of the test was evaluated, and the results showed that *Pk*LAMP was 100-fold more sensitive than single-PCR assay using the F3 and B3 primers. Moreover, the present study showed that an isothermal reaction time of 1 h was enough to amplify 10^9 copies of the target DNA in reaction tubes containing from 10^8 to 10^2 copies/μl of the DNA template and that results could be easily judged by visual inspection of the turbidity or fluorescence of the reaction mixture (10, 13). These results suggest that the *Pk*LAMP assay is reliable and useful for the diagnosis of *P. knowlesi* malaria.

To evaluate the feasibility of using *in vivo* materials, comparisons of *Pk*LAMP and the conventional nested PCR method and microscopic examination were made with blood samples from two infected monkeys. These studies validated *Pk*LAMP as an alternative molecular diagnostic tool, which can be used in the diagnosis of early and advanced infections of *P. knowlesi*. Early species identification in the diagnosis of malaria is very important in preventing disease progression. In particular, early

TABLE 1. Comparison of *Pk*LAMP with nPCR and microscopic examination for detection of *P. knowlesi* in two infected monkeys[a]

Day after infection	Monkey J58					Monkey J64				
	Parasitemia (%)	*Pk*LAMP result with:		nPCR result with:		Parasitemia (%)	*Pk*LAMP result with:		nPCR result with:	
		DNA extract	Whole blood	DNA extract	Whole blood		DNA extract	Whole blood	DNA extract	Whole blood
0	−	−	−	−	−	−	−	−	−	−
1	<0.01	+	+	+	−	−	+	+	−	−
2	0.2	+	+	+	−	−	+	+	−	−
3	10.8 (autopsy)	+	+	+	+	−	+	+	+	−
4						−	+	+	+	−
5						−	+	+	+	−
6						0.01	+	+	+	−
7						0.1	+	+	+	−
8						2.0	+	+	+	−
9						58.0 (autopsy)	+	+	+	+

[a] Monkeys J58 and J64 were infected with *P. knowlesi* strains H and Hackeri, respectively.

identification of *P. knowlesi* infection is essential, since the unique 24-h asexual replication cycle among human and simian malaria parasites can rapidly result in high levels of parasitemia with a fatal outcome in humans (4, 5). Although nPCR and sequencing have been applied to species identification for malaria diagnosis, a more rapid diagnostic test such as *Pk*LAMP would be a convenient and powerful tool for enabling the delivery of prompt and adequate medical treatment.

The present study also assessed the detection performance of *Pk*LAMP with different DNA template preparations, including frozen whole blood or genomic DNA extracts. The detection efficiency of *Pk*LAMP using whole blood was identical to that of *Pk*LAMP when gDNA extracts were used as the template. However, the detection performance of nPCR using the whole-blood templates was quite poor. It appears that this is due to blood components, such as myoglobin, hem-blood protein complexes, and immunoglobulin G, that inactivate the *Taq* DNA polymerase used in standard PCR (1). In contrast, such inhibitors do not affect the *Bst* polymerase used in LAMP (6). According to previous reports, the specificity and sensitivity of detection appear to be unaffected by LAMP processing conditions or sample type, including whole blood, filter paper- or card-processed blood, serum, sputum, and crudely processed tissue samples (8). Furthermore, Poon et al. have reported that *P. falciparum* DNA was detected by LAMP using a promising simple DNA template method of preparation from heat-treated blood (14). Further improvement of template production methods for *Pk*LAMP will be required to optimize and simplify template preparation.

In conclusion, *Pk*LAMP can be considered an efficient candidate for the molecular diagnosis of *P. knowlesi* infection in areas of endemicity. Thekisoe et al. reported that LAMP reagents are stable at ambient temperature for up to 2 weeks (16a). In addition, a recent study of the LAMP method showed that it is able to detect both *Plasmodium* oocysts and sporozoites from an "all-in-one" template using whole mosquito bodies (2). These observations further emphasize the potential usefulness of the LAMP method as a diagnostic and new epidemiological surveillance tool for malaria. Our studies will also provide a powerful method for the diagnosis and monitoring of *P. knowlesi* infection in the field.

ACKNOWLEDGMENTS

We are grateful to Mayumi Ohshita and Mayu Tanaka at the Center for Tropical Medicine and Parasitology, Dokkyo Medical University, for technical support.

This study was supported in part by the following four grants: (i) a grant from the program for Promotion of Fundamental Studies in Health Sciences (no. 04-09) from the National Institute of Biomedical Innovation, (ii) a grant from the Promotion of Basic Research Activities for Innovative Biosciences program (PROBRAIN), (iii) a grant from the 21st Century COE Program (A-1) of the Ministry of Education, Culture, Sports, Science, and Technology of Japan, and (iv) a cooperative research grant (2007-19-3) from the National Research Center for Protozoan Diseases, Obihiro University of Agriculture and Veterinary Medicine.

REFERENCES

1. **Akane, A., H. Matsubara, S. Nakamura, S. Takahashi, and K. Kimura.** 1994. Identification of the heme compound copurified with deoxyribonucleic acid (DNA) from bloodstains, a major inhibitor of polymerase chain reaction (PCR) amplification. J. Forensic Sci. **39:**362–372.
2. **Aonuma, H., M. Suzuki, H. Iseki, N. Perera, B. Nelson, I. Igarashi, T. Yagi, H. Kanuka, and S. Fukumoto.** 2008. Rapid identification of *Plasmodium*-carrying mosquitoes using loop-mediated isothermal amplification. Biochem. Biophys. Res. Commun. **376:**671–675.
3. **Chen, J.-H., F. Lu, C. S. Lim, J.-Y. Kim, H.-J. Ahn, I.-B. Suh, S. Takeo, T. Tsuboi, J. Sattabongkot, and E.-T. Han.** 2010. Detection of *Plasmodium vivax* infection in the Republic of Korea by loop-mediated isothermal amplification (LAMP). Acta Trop. **113:**61–65.
4. **Cox-Singh, J., and B. Singh.** 2008. Knowlesi malaria: newly emergent and of public health importance. Trend Parasitol. **24:**406–410.
5. **Cox-Singh, J., T. M. E. Davis, L. Kim-Sung, S. S. G. Shamsul, A. Matusop, S. Ratnam, H. A. Rahman, D. J. Conway, and B. Singh.** 2008. *Plasmodium knowlesi* malaria in humans is widely distributed and potentially life-threatening. Clin. Infect. Dis. **46:**165–171.
6. **Grab, D. J., J. Lonsdale-Eccles, and N. Inoue.** 2005. LAMP for tedpoles. Nat. Methods **2:**635.
7. **Han, E. T., R. Watanabe, J. Sattabongkot, B. Khuntirat, J. Sirichaisinthop, H. Iriko, L. Jin, S. Takeo, and T. Tsuboi.** 2007. Detection of four *Plasmodium* species by genus- and species-specific loop-mediated isothermal amplification for clinical diagnosis. J. Clin. Microbiol. **45:**2521–2528.
8. **Karanis, P., and J. Ongerth.** 2009. LAMP—a powerful and flexible tool for monitoring microbial pathogens. Trends Parasitol. **25:**498–499.
9. **Kawai, S., M. Hirai, K. Haruki, K. Tanabe, and Y. Chigusa.** 2009. Cross-reactivity in rapid diagnostic tests between human malaria and zoonotic simian malaria parasite *Plasmodium knowlesi* infections. Parasitol. Int. **58:** 300–302.
10. **Mori, Y., K. Nagamine, N. Tomita, and T. Notomi.** 2001. Detection of loop-mediated isothermal amplification reaction by turbidity derived from magnesium pyrophosphate formation. Biochem. Biophys. Res. Commun. **289:**150–154.
11. **Mori, Y., and T. Notomi.** 2009. Loop-mediated isothermal amplification (LAMP): a rapid accurate, and cost-effective diagnostic method for infectious diseases. J. Infect. Chemother. **15:**62–69.

12. **Nagamine, K., T. Hase, and T. Notomi.** 2002. Accelerated reaction by loop-mediated isothermal amplification using loop primers. Mol. Cell Probes **16:**223–229.
13. **Notomi, T., H. Okayama, H. Masubuchi, T. Yonekawa, K. Watanabe, N. Amino, and T. Hase.** 2000. Loop-mediated isothermal amplification of DNA. Nucleic Acids Res. **28:**e63.
14. **Poon, L. L. M., B. W. Y. Wong, E. H. T. Ma, K. H. Chan, L. M. C. Chow, W. Abeyewickreme, N. Tangpukdee, K. Y. Yuen, Y. Guan, S. Looareesuwan, and M. Peiris.** 2006. Sensitive and inexpensive molecular test for falciparum malaria: detecting *Plasmodium falciparum* DNA directly from heat-treated blood by loop-mediated isothermal amplification. Clin. Chem. **52:**303–306.
15. **Singh, B., A. Bobogare, J. Cox-Singh, G. Snounou, H. S. Adullah, and H. A. Rahman.** 1999. A genus- and species-specific nested polymerase chain reaction malaria detection assay for epidemiologic studies. Am. J. Trop. Med. Hyg. **60:**687–692.
16. **Singh, B., L. Kim-Sung, A. Matusop, A. Radhakrishnan, S. S. G. Shamsul, J. Cox-Singh, A. Thomas, and D. J. Conway.** 2004. A large focus of naturally aquired *Plasmodium knowlesi* infections in human beings. Lancet **363:**1017–1024.
16a. **Thekisoe, O. M. M., R. S. B. Bazie, A. M. Coronel-Servian, C. Sugimoto, S.-I. Kawazu, and N. Inoue.** 2009. Stability of loop-mediated isothermal amplification (LAMP) reagents and its amplification efficiency on crude trypanosome DNA templates. J. Vet. Med. Sci. **71:**471–475.
17. **White, N. J.** 2008. *Plasmodium knowlesi*: the fifth human malaria parasite. Clin. Infect. Dis. **46:**172–173.

Parasitology International 59 (2010) 481–486

Contents lists available at ScienceDirect

Parasitology International

journal homepage: www.elsevier.com/locate/parint

Short communication

Artesunate, a potential drug for treatment of *Babesia* infection

Youn-Kyoung Goo [a], M. Alaa Terkawi [a], Honglin Jia [a], G. Oluga Aboge [a], Hideo Ooka [a], Bryce Nelson [a], Suk Kim [b], Fujiko Sunaga [c], Kazuhiko Namikawa [c], Ikuo Igarashi [a], Yoshifumi Nishikawa [a], Xuenan Xuan [a,*]

[a] National Research Center for Protozoan Diseases, Obihiro University of Agriculture and Veterinary Medicine, Obihiro, Hokkaido 080-8555, Japan
[b] College of Veterinary Medicine & Research Institute of Life Science, Gyeongsang National University, Jinju, Gyeongnam 660-701, Republic of Korea
[c] School of Veterinary Medicine, Azabu University, Sagamihara, Kanagawa 229-8501, Japan

ARTICLE INFO

Article history:
Received 30 September 2009
Received in revised form 30 May 2010
Accepted 3 June 2010
Available online 9 June 2010

Keywords:
Artesunate
Babesia bovis
Babesia gibsoni
Babesia microti

ABSTRACT

The effects of artesunate, a water-soluble artemisinin derivative, against *Babesia* species, including *Babesia bovis*, *Babesia gibsoni* and *Babesia microti* were studied. Cultures of *B. bovis* and *B. gibsoni* were treated with 0.26, 2.6, 26 and 260 μM artesunate, showing inhibition of parasite growth at concentrations equal to and greater than 2.6 μM artesunate by days 3 post-treatment for *B. gibsoni* and *B. bovis* in a dose-dependent manner. Consistent with *in vitro* experiments, artesunate was effective in the treatment of mice infected with *B. microti* at doses equal to and greater than 10 mg/kg of body weight on days 8–10 post-infection. Taken together, these results suggest that artesunate could be a potential drug against *Babesia* infection.

Babesiosis is a parasitic disease caused by intraerythrocytic protozoa of the genus *Babesia* and transmitted by ticks to their vertebrate hosts. The disease is recognized to be of veterinary importance in cattle, horses, and dogs and is highlighted as an emerging zoonosis in humans. Symptoms can include a malaria-like syndrome, including fever, haemolytic anemia, and hemoglobinuria, and clinical cases appear suddenly and severe [1]. There are a number of babesiacides, but only a few drugs are currently available such as imidocarb dipropionate (Imizol®, Schering-Plough Animal Health) and diminazene aceturate (Berenil®, Intervet India Pvt. Ltd.) for animals, such as cattle, horses, and dogs, and quinine, clindamycin and atovaquone (Mepron®, Glaxo Welcome) for humans [2]. However, an increasing number of resistant parasites to commercial drugs are appearing, adverse effects of drugs are well documented, and the long term persistence of low level parasitemia after treatment still necessitate development of an effective treatment.

Artemisinin and its derivatives, such as artesunate, artemether, arteether, and dihydroartemisinin, are the most potent antimalarial drugs available throughout the world [3]. The artemisinin derivatives act rapidly on the parasites leading to their quick elimination thereby rendering these derivatives effective against severe malaria. Furthermore, parasites are slow to develop resistance and these derivatives exhibit high efficacy against all asexual stages of *Plasmodium falciparum* with rare adverse effects [4–7].

Among artemisinin derivatives, artesunate, a water-soluble half-ester succinate derivative, has been the most commonly used derivative for more than 15 years; many clinicians feel that parenteral administration of artesunate is the most effective treatment for severe malaria [8,9]. Since *Babesia* species share a similar life cycle, as well as clinical symptoms, with *Plasmodium* species, coupled with the previously observed growth-inhibitory effect of artesunate on *Babesia* (*Theileria*) *equi* and *B. caballi in vitro* and on *B. microti* in hamster [10,11], we tested whether artesunate inhibited the growth of other *Babesia* species. In previous studies, the significant growth-inhibitory effects of atovaquone and diminazene aceturate were shown on *B. microti* and *B. divergens* and on *B. rodhani*, *B. divergens* and *B. bovis*, respectively [12–18]. Therefore, atovaquone and diminazene aceturate were used to compare an efficacy of artesunate against *Babesia* parasites. With this in mind, we evaluated the efficacy of artesunate against *B. bovis* for cattle and *B. gibsoni* for dogs *in vitro*, and *B. microti* for mice and humans *in vivo* and compared these growth-inhibitory effects with those of currently available drugs, such as atovaquone and diminazene aceturate.

For *in vitro* assays, solutions of 156 mM artesunate (Guangxi, China), 26 mM atovaquone (Toronto Research Chemical Inc., Canada) and 260 mM diminazene aceturate (Kanto Chemical Co., Inc., Japan) added to growth media were prepared. The Texas T2B strain of *B. bovis* and NRCPD strain of *B. gibsoni* were maintained in bovine and canine RBC as previously established methods [19,20]. The *in vitro* growth-inhibitory assay was carried out in 48-well tissue culture plates by modified methods described previously [10]. Initial *Babesia* parasite cultures containing 1% infected erythrocytes were prepared from cultures that had reached 3 to 5% parasitemia by mixing with

* Corresponding author. Tel.: +81 155 49 5648; fax: +81 155 49 5643.
E-mail address: gen@obihiro.ac.jp (X. Xuan).

1383-5769/$ – see front matter © 2010 Elsevier Ireland Ltd. All rights reserved.
doi:10.1016/j.parint.2010.06.004

uninfected bovine and canine RBC. To each well, 50 μl of infected erythrocytes were added to 450 μl of growth medium containing either 0.26, 2.6, 26 and 260 μM of one of the drugs (artesunate, atovaquone or diminazene aceturate). Evaluation of growth-inhibitory effects of each drug and concentration was performed for each parasite species and monitored in triplicate and in three independent trials. Culture plates were kept in a humidified 5% CO_2 incubator at 37 °C. Per well, 250 μl of the culture medium with the indicated concentration of drug was replaced daily for 4 days. Thereafter, to demonstrate whether the inhibitory effect was maintained after withdrawal of treatment, parasite cultures were subcultured with uninfected bovine and canine RBC as described above and parasite re-growth was monitored for another two days. Parasitemia in Giemsa-stained culture smears was calculated from eight to ten microscopic fields covering approximately 2000 cells.

B. bovis and *B. gibsoni* were grown *in vitro* beginning at 1% parasitemia in the presence of the aforementioned concentrations of artesunate, atovaquone and diminazene aceturate, and parasitemia was compared to a control. Statistical significance between the mean parasitemia of a control group and that of each group treated with drugs was determined using one-way ANOVA and Tukey's tests using the JMP Version 8 Program (SAS Institute Inc., USA). Beginning at day 2 post-treatment significant growth inhibition ($P<0.05$) of *B. bovis* was observed in groups treated with equal to and greater than 2.6 μM artesunate (Fig. 1A). Moreover, this growth-inhibitory effect was maintained in equal to and greater than 2.6 μM artesunate even after withdrawal of the treatment at day 4. Upon comparison of the growth-inhibitory effect against three drugs on *B. bovis*, it appears that artesunate may be moderately effective than atovaquone but less than diminazene aceturate at day 4 post-treatment (Fig. 1A versus 1B and C, respectively). These results could be explained by their mechanisms acting to parasites. Diminazene aceturate binds to the AT-rich domains of the DNA double helices, which leads to an interference with the activities of the eukaryotic type II topoisomerase enzyme and finally causes death of parasites [21,22]. On the other hand, atovaquone suppresses electron flow in mitochondrion of parasites by inhibition of binding between ubiquinone and cytochrome bc_1 [23]. In addition, artesunate inhibits sarcoplasmic/endoplasmic reticulum Ca^{2+}-ATPase (SERCA) responsible for the maintenance of calcium ion concentrations, which is related to the generation of calcium-mediated signaling and the invasion of parasites to erythrocytes, thereby inhibiting the parasite growth [24].

Artesunate was also found to be effective against *B. gibsoni*, where significant growth inhibition ($P<0.05$) was observed at 26 and 260 μM from day 1 post-treatment. Moreover, this significant difference was observed in all test concentrations at day 3 post-treatment (Fig. 2A). Furthermore, upon withdrawal of the treatment, reemergence of the parasite failed to occur in concentrations equal to and greater than 2.6 μM artesunate. As with *B. bovis*, artesunate was found to be less effective than diminazene aceturate in suppressing the growth of *B. gibsoni* (Fig. 2). Regarding the efficacy of artesunate and atovaquone, while 2.6 μM artesunate could rather effectively inhibit parasite growth than 2.6 μM atovaquone, 26 μM atovaquone was more effective than 26 μM artesunate on *B. gibsoni*. Therefore, it is difficult to conclude which drug is more effective in the growth inhibition of *B. gibsoni*.

The growth inhibition of both *B. bovis* and *B. gibsoni* exhibited a dose dependence and therefore the half maximal inhibitory concentration (IC_{50}) for each parasite was calculated as the concentration required for a 50% reduction in the mean parasitemia of drug-treated groups by a comparison with that of control groups at day 4 post-treatment. The IC_{50} was calculated using non-linear curve-fitting of the percent inhibitions against various concentrations of three drugs by a calculation software (Sigma Plot, Japan). Although the IC_{50} values for diminazene aceturate (*B. bovis*, 24.82 ± 2.37 nM; *B. gibsoni*, 41.93 ± 2.32 nM) suggested this drug to be more effective than artesunate (*B. bovis*, 372.2 ± 24.32 nM; *B. gibsoni*, 924.0 ± 97.26 nM) in treatment of both *B. bovis* and *B. gibsoni*, previous attempts at using diminazene aceturate for treatment of babesiosis failed due to its toxicity to kidney, brain, and liver which can result in serious side-effects such as weakness, paralysis, lack of responsiveness to stimuli in the central nervous system especially in dogs as well as humans [25–27]. Moreover, due to these side-effects, the diminazene aceturate was recently withdrawn from the market in Japan, and this drug is not approved by the Food and Drug Administration (FDA) in the U.S.A. [28]. In contrast to diminazene aceturate, few significant side-effects of artesunate have been reported in more than two million patients treated with artesunate [3,6]. Therefore, artesunate could be a preferential choice for the treatment of *B. bovis* and *B. gibsoni* based on these results.

In order to determine anti-babesial effects of artesunate against *B. microti*, female 6-week-old BALB/c mice (Japan CLEA, Japan) were used in an experimental infection study. Moreover, atovaquone was tested in parallel on mice infected with *B. microti* as a currently available anti-babesial drug in order to compare its anti-babesial effects with artesunate. Infection was initiated by intraperitoneal (i.p.) injection of 1×10^7 *B. microti* Munich strain infected erythrocytes isolated from a mouse with 40.7% parasitemia. Infected mice were divided into 8 groups as follows: control groups were either administered 5% sodium bicarbonate (SB) for artesunate or phosphate buffered saline (PBS) for atovaquone intramuscularly. Experimental groups were divided as 1, 10 or 50 mg/kg of body weight of artesunate (AR1, AR10 and AR50, respectively) or atovaquone (AT1, AT10 and AT50, respectively) and subsequently administrated 0.2 ml of the indicated doses of artesunate or atovaquone dissolved in 5% sodium bicarbonate or PBS, respectively, by intramuscular route. The doses of atovaquone for this study were decided based on previous studies in which 50–100 mg/kg of body weight of atovaquone inhibited the growth of *B. microti* in hamster and Mongolian gerbil [13,14]. Parasitemia was monitored by examination of Giemsa-stained, thin blood smears using a light microscope. The body weight of mice was measured every 2 days and each mouse was given the indicated doses of the drug once per day for 6 consecutive days beginning 2 days post-infection. The infected erythrocytes appeared in peripheral blood of all mice on day 2 post-infection and thus treatment was started from day 2 post-infection. In Fig. 3A, peak parasitemia (35.5%) was observed in SB on day 10 post-infection. In contrast, lower parasitemia was observed in AR10 as well as AR50. Statistical significance of mean parasitemia between SB or PBS and each experimental group was determined using ANOVA and Tukey's tests using the JMP Version 8 program (SAS Institute Inc., USA). Significant differences ($P<0.05$) between SB and experimental AR50 and AR10 groups were observed on days 8–10 post-infection. Although artesunate failed to eradicate parasites and parasitemia increased up to 19.6% and 24.7% (standard deviation: ±6.32 and ±9.34) for AR10 and AR50 after the cessation of the treatment, respectively, artesunate not only inhibited the growth of the parasites but also delayed the increase of parasitemia, indicating that artesunate could be used for controlling *B. microti* infection. Moreover, artesunate was able to suppress more effectively the increase in parasitemia compared to atovaquone which showed significant inhibition ($P<0.05$) between PBS group and AT50 only at day 11 post-infection. Atovaquone did not effectively inhibit parasite growth in BALB/c mice, which is different from previous studies in gerbils and hamsters. Although mice, gerbils and hamsters are closely related in aspect of taxonomy, species differences in pharmacokinetics might affect absorption, distribution, metabolism and excretion of drugs [29,30]. The efficacy of artesunate could be improved by a combination with another effective babesiacide. Indeed, the combination of artesunate with other drugs has been advocated to malaria patients to prevent drug resistant parasites and to improve its efficacy by using drugs which have the different mode of action [31].

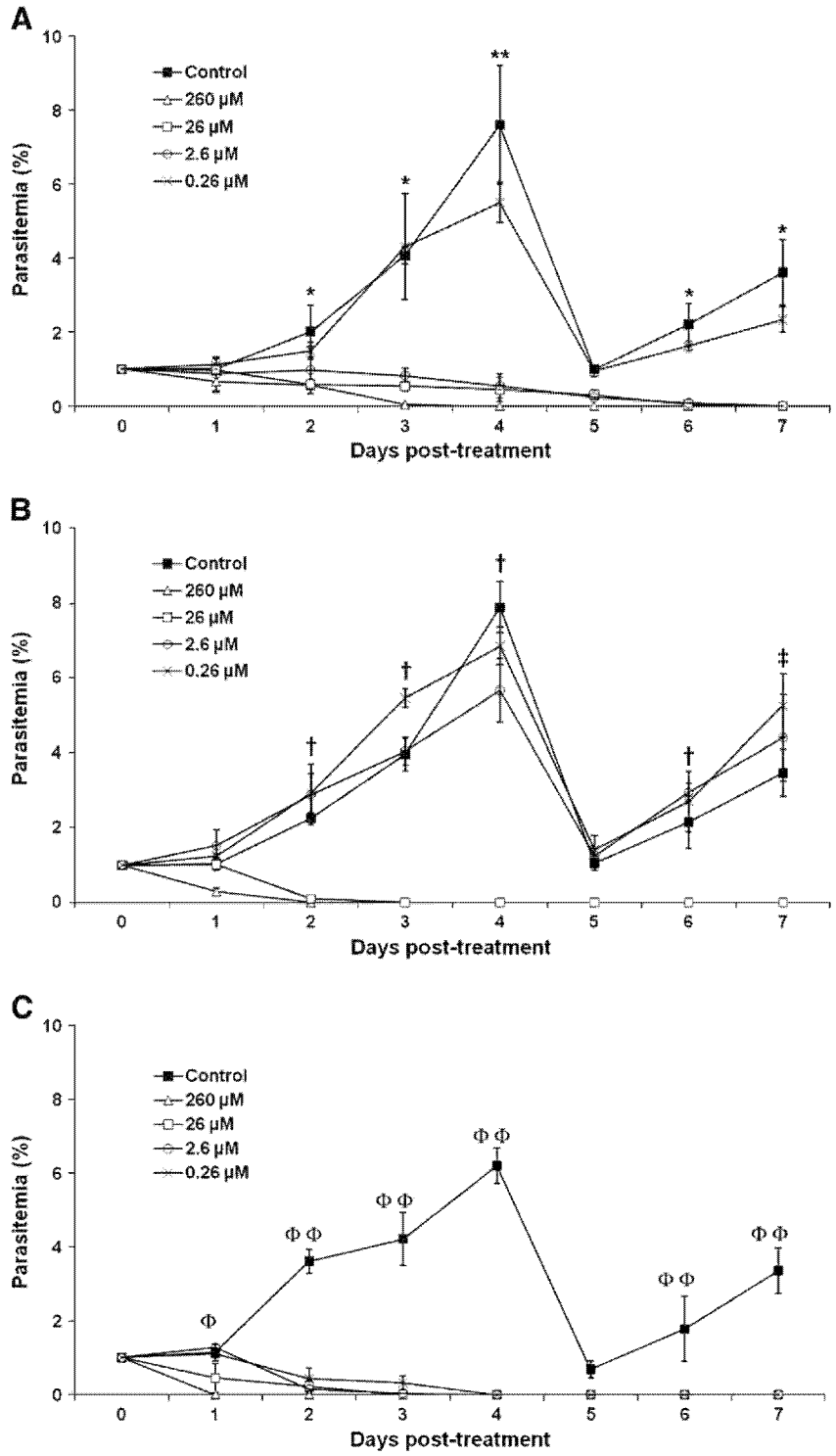

Fig. 1. Growth curves of *B. bovis in vitro* cultures treated with 0.26, 2.6, 26 and 260 μM of artesunate (A), atovaquone (B) and diminazene aceturate (C). Cultures started at 1% parasitemia and Giemsa-stained thin blood smears were prepared to determine daily parasitemia. (A) *, significant difference ($P<0.05$) between control group and groups tested with 2.6, 26 and 260 μM of artesunate; **, significant difference ($P<0.05$) between control group and all groups tested with artesunate. (B) †, significant difference ($P<0.05$) between control group and groups tested with 26 and 260 μM of atovaquone; ‡, significant difference ($P<0.05$) between control group and all groups tested with atovaquone. (C) Φ, significant difference ($P<0.05$) between control group and groups tested with 26 and 260 μM of diminazene aceturate; ΦΦ, significant difference ($P<0.05$) between control group and all groups tested with diminazene aceturate (the error bars, standard deviations).

This study has used a mouse model to evaluate the efficacy of artesunate against *B. microti* which causes rodent and human babesiosis. These results might help to discover a drug used for humans infected with *B. microti*. Therefore, an i.m. artesunate regimen was selected to treat *B. microti* infection since a prompt treatment is required to treat these infections that occur suddenly and severely in humans. While i.v. administration is also recommended for patients in severe condition, particularly those in comas, venous access may not be possible where only basic health care facilities exist. In addition, even when the drugs can be administered by i.v., patient discomfort and inconvenience, as well as risks such as overhydration and thrombophlebitis may make i.v. less attractive than i.m. [32].

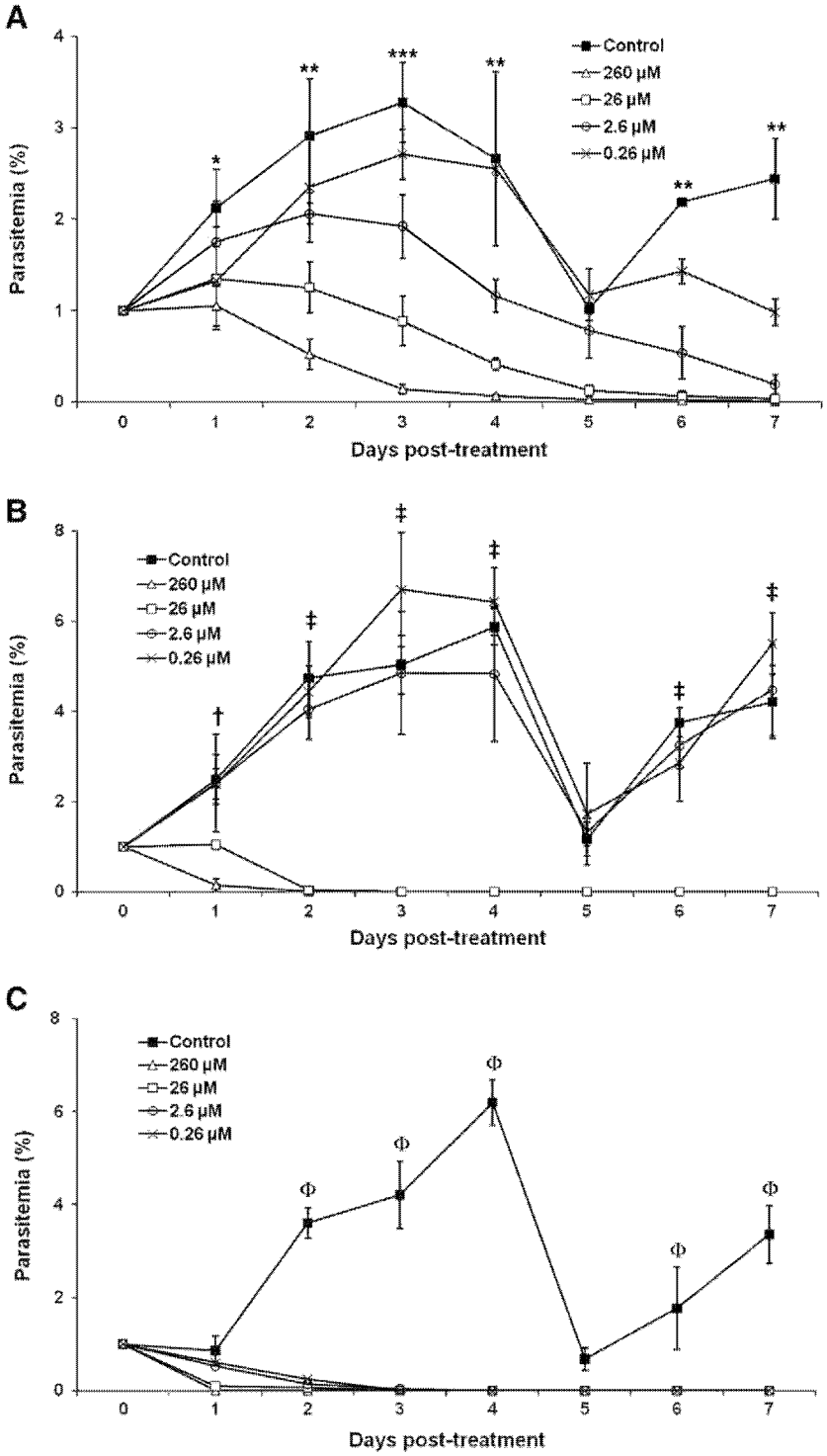

Fig. 2. Growth curves of *B. gibsoni in vitro* culture treated with 0.26, 2.6, 26 and 260 μM of artesunate (A), atovaquone (B) and diminazene aceturate (C). Cultures started at 1% parasitemia and Giemsa-stained thin blood smears were prepared to determine daily parasitemia. (A) *, significant difference ($P<0.05$) between control group and groups tested with 26 and 260 μM of artesunate; **, significant difference ($P<0.05$) between control group and groups tested with 2.6, 26 and 260 μM of artesunate; ***, significant difference ($P<0.05$) between control group and all tested groups with artesunate. (B) †, significant difference ($P<0.05$) between control group and groups tested with 260 μM of atovaquone; ‡, significant difference ($P<0.05$) between control group and groups tested with 26 and 260 μM of atovaquone. (C) Φ, significant difference ($P<0.05$) between control group and all groups tested with diminazene aceturate (the error bars, standard deviations).

Although i.m. administration of the oil-soluble antimalarial artemisinins could damage brain stem centers mainly involved in auditory processing and vestibular reflexes [33–35], artesunate, a water-soluble artemisinin derivative, has shown to cause less neurotoxic effects [36]. Mice treated with artesunate here displayed neither decrease in body weight on day 12 post-infection compared to that on day 1 post-infection (data not shown) nor clinical abnormalities such as gait and equilibrium disturbances, suggesting that doses between 1–50 mg/kg of body weight of artesunate were not responsible for neurotoxicity.

In conclusion, we have demonstrated that artesunate inhibits the growth of *B. bovis* and *B. gibsoni in vitro* and i.m. administration of

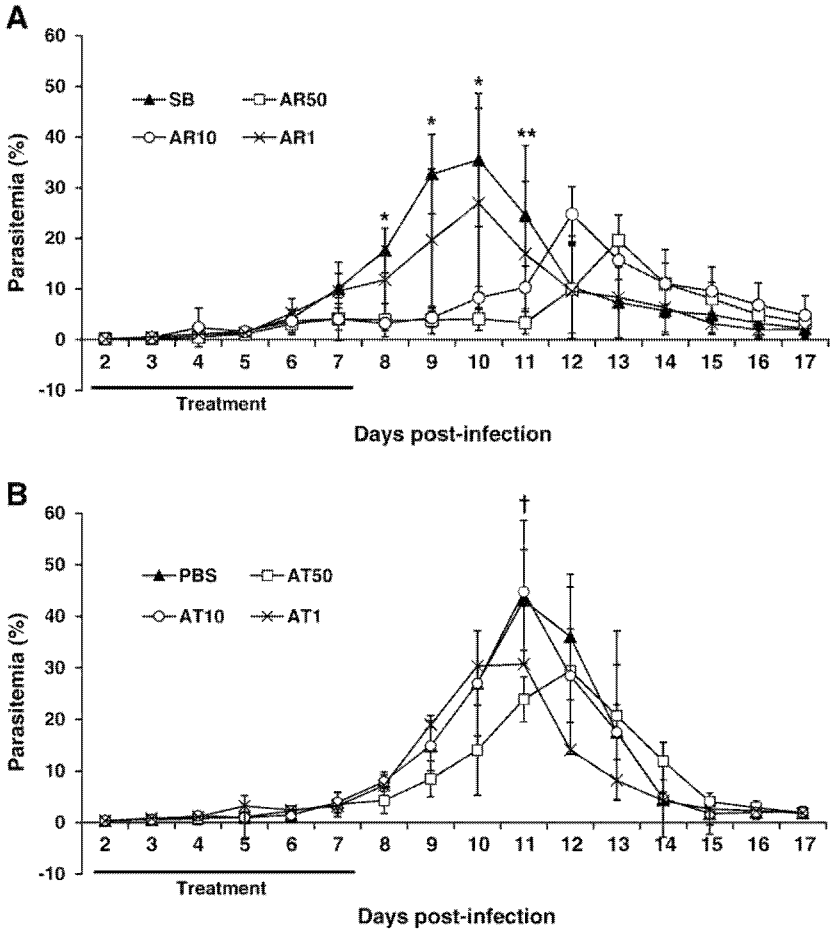

Fig. 3. Course of parasitemia in artesunate (A) and atovaquone (B) treated mice infected with *B. microti*. *B. microti* infected mice were treated with artesunate or atovaquone for 6 days, from day 2 to day 7 post-infection, and Giemsa-stained thin blood smears were prepared to determine daily parasitemia. (A) Artesunate treatment in mice infected with *B. microti*. SB, group for 5% sodium bicarbonate; AR50, group for 50 mg/kg of body weight of artesunate; AR10, group for 10 mg/kg of body weight of artesunate; AR1, group for 1 mg/kg of body weight of artesunate. *, significant difference ($P<0.05$) between SB and tested groups, AR50 and AR10; **, significant difference ($P<0.05$) between SB and AR50. (B) Atovaquone treatment in mice infected with *B. microti*. PBS, group for phosphate buffered saline; AT50, group for 50 mg/kg of body weight of atovaquone; AT10, group for 10 mg/kg of body weight of atovaquone; AT1, group for 1 mg/kg of body weight of atovaquone. †, significant difference ($P<0.05$) between PBS and AT50 (the error bars, standard deviations).

artesunate suppressed growth of *B. microti in vivo* without side-effects, suggesting that artesunate could be a potential drug for *Babesia* infection. However, *in vivo* experiments for *B. microti* indicated possible recrudescence of parasite growth after cessation of artesunate treatment.

Acknowledgments

This study was supported by a grant from The 21st Century COE Program (A-1) and a Grant-in-Aid for Scientific Research, both from the Ministry of Education, Culture, Sports, Science, and Technology of Japan. We wish to thank Dr Navarrete A. Ian for help with the statistical analysis.

References

[1] Homer MJ, Aguilar-Delfin I, Telford 3rd SR, Krause PJ, Persing DH. Babesiosis. Clin Microbiol Rev 2000;13:451–69.
[2] Vial HJ, Gorenflot A. Chemotherapy against babesiosis. Vet Parasitol 2006;138:147–60.
[3] Hien TT, White NJ. Qinghaosu. Lancet 1993;341:603–8.
[4] ter Kuile F, White NJ, Holloway P, Pasvol G, Krishna S. *Plasmodium falciparum*: *in vitro* studies of the pharmacodynamic properties of drugs used for the treatment of severe malaria. Exp Parasitol 1993;76:85–95.
[5] McGready R, Cho T, Cho JJ, Simpson JA, Luxemburger C, Dubowitz L, et al. Artemisinin derivatives in the treatment of falciparum malaria in pregnancy. Trans R Soc Trop Med Hyg 1998;92:430–3.
[6] Price R, van Vugt M, Phaipun L, Luxemburger C, Simpson J, McGready R, et al. Adverse effects in patients with acute falciparum malaria treated with artemisinin derivatives. Am J Trop Med Hyg 1999;60:547–55.
[7] Golenser J, Waknine JH, Krugliak M, Hunt NH, Grau GE. Current perspectives on the mechanism of action of artemisinins. Int J Parasitol 2006;36:1427–41.
[8] Nontprasert A, Nosten-Bertrand M, Pukrittayakamee S, Vanijanonta S, Angus BJ, White NJ. Assessment of the neurotoxicity of parenteral artemisinin derivatives in mice. Am J Trop Med Hyg 1998;59:519–22.
[9] Ashley EA, White NJ. Artemisinin-based combinations. Curr Opin Infect Dis 2005;18:531–6.
[10] Nagai A, Yokoyama N, Matsuo T, Bork S, Hirata H, Xuan X, et al. Growth-inhibitory effects of artesunate, pyrimethamine, and pamaquine against *Babesia equi* and *Babesia caballi* in *in vitro* cultures. Antimicrob Agents Chemother 2003;47:800–3.
[11] Marley SE, Eberhard ML, Steurer FJ, Ellis WL, McGreevy PB, Ruebush 2nd TK. Evaluation of selected antiprotozoal drugs in the *Babesia microti*-hamster model. Antimicrob Agents Chemother 1997;41:91–4.
[12] Pudney M, Gray JS. Therapeutic efficacy of atovaquone against the bovine intraerythrocytic parasite, *Babesia divergens*. J Parasitol 1997;83:307–10.
[13] Gray JS, Pudney M. Activity of atovaquone against *Babesia microti* in the Mongolian gerbil, *Meriones unguiculatus*. J Parasitol 1999;85:723–8.
[14] Wittner M, Lederman J, Tanowitz HB, Rosenbaum GS, Weiss LM. Atovaquone in the treatment of *Babesia microti* infections in hamsters. Am J Trop Med Hyg 1996;55:219–22.
[15] Hughes WT, Oz HS. Successful prevention and treatment of babesiosis with atovaquone. J Infect Dis 1995;172:1042–6.
[16] Akiba M, Saeki H, Ishii T, Yamamoto S, Ueda K. Immunological changes in *Babesia rodhaini* infected BALB/c mice after treated with anti-babesial drug; diminazene diaceturate. J Vet Med Sci 1991;53:371–7.
[17] Yeruham I, Avidar Y, Aroch I, Hadani A. Intra-uterine infection with *Babesia bovis* in a 2-day-old calf. J Vet Med B Infect Dis Vet Public Health 2003;50:60–2.

[18] Gray JS. Chemotherapy of *Babesia divergens* in the gerbil, *Meriones unguiculatus*. Res Vet Sci 1983;35:318–24.
[19] Levy MG, Ristic M. Babesia bovis: continuous cultivation in a microaerophilous stationary phase culture. Science 1980;207:1218–20.
[20] Sunaga F, Namikawa K, Kanno Y. Continuous in vitro culture of erythrocytic stages of *Babesia gibsoni* and virulence of the cultivated parasite. J Vet Med Sci 2002;64:571–5.
[21] Portugal J. Berenil acts as a poison of topoisomerase II. FEBS Lett 1994;344:136–8.
[22] Kuttle KL, Johnson LW. Chemoprophylactic activity of imidocarb, diminazene and oxytetracycline against *Babesia bovis* and *B. bigemina*. Vet Parasitol 1986;21: 107–18.
[23] Fry M, Pudney M. Site of action of the antimalarial hydroxynaphthoquinone, 2-[trans-4-(4′-chlorophenyl) cyclohexyl]-3-hydroxy-1, 4-naphthoquinone (566C80). Biochem Pharmacol 1992;43:1545–53.
[24] Eckstein-Ludwig U, Webb RJ, Van Goethem ID, Lee AG, Kimura M, O'Neill PM, et al. Artemisinins target the SERCA of *Plasmodium falciparum*. Nature 2003;424: 957–61.
[25] Ruebush 2nd TK, Rubin RH, Wolpow ER, Cassaday PB, Schultz MG. Neurologic complications following the treatment of human *Babesia microti* infection with diminazene aceturate. Am J Trop Med Hyg 1979;28:184–9.
[26] Milner RJ, Reyers F, Taylor JH, van der Berg JS. The effect of diminazene aceturate in cholinesterase activity in dogs with canine babesiosis. J S Afr Vet Assoc 1997;68: 111–3.
[27] Taboada J. Babesiosis pp. 473–481. *In*: Infectious diseases of the dog and cat (Creene, C.E. ed.), Saunders, Philadelphia, PA.
[28] Farwell GE, Legrand EK, Cobb CC. Clinical observations on *Babesia gibsoni* and *Babesia canis* infections in dogs. J Am Vet Med Assoc 1982;180:507–11.
[29] Anari MR, Creighton MD, Ngui JS, Tschirret-Guth RA, Teffera Y, Doss GA, et al. Species differences in metabolism and pharmacokinetics of a sphingosine–phosphate receptor agonist in rats and dogs: formation of a unique glutathione adduct in the rat. Drug Metab Dispos 2006;34:1367–75.
[30] Parke DV. Species differences in pharmacokinetics. Vet Res Commun 1983;7: 285–300.
[31] Whegang SY, Tahar R, Foumane VN, Soula G, Gwet H, Thalabard JC, et al. Efficacy of non-artemisinin- and artemisinin-based combination therapies for uncomplicated falciparum malaria in Cameroon. Malar J 2010;9:56.
[32] Ilett KF, Batty KT, Powell SM, Binh TQ, Thu le TA, Phuong HL, et al. The pharmacokinetic properties of intramuscular artesunate and rectal dihydroartemisinin in uncomplicated falciparum malaria. Br J Clin Pharmacol 2002;53:23–30.
[33] Brewer TG, Grate SJ, Peggins JO, Weina PJ, Petras JM, Levine BS, et al. Fatal neurotoxicity of arteether and artemether. Am J Trop Med Hyg 1994;51:251–9.
[34] Brewer TG, Peggins JO, Grate SJ, Petras JM, Levine BS, Weina PJ, et al. Neurotoxicity in animals due to arteether and artemether. Trans R Soc Trop Med Hyg 1994;88:33–6.
[35] Petras JM, Kyle DE, Gettayacamin M, Young GD, Bauman RA, Webster HK, et al. Arteether: risks of two-week administration in *Macaca mulatta*. Am J Trop Med Hyg 1997;56:390–6.
[36] Nontprasert A, Pukrittayakamee S, Dondorp AM, Clemens R, Looareesuwan S, White NJ. Neuropathologic toxicity of artemisinin derivatives in a mouse model. Am J Trop Med Hyg 2002;67:423–9.

Experimental Parasitology 127 (2011) 287–293

Contents lists available at ScienceDirect

Experimental Parasitology

journal homepage: www.elsevier.com/locate/yexpr

Research Brief

Babesia microti: Molecular and antigenic characterizations of a novel 94-kDa protein (BmP94)

Hideo Ooka, Mohamad Alaa Terkawi, Youn-Kyoung Goo, Yuzi Luo, Yan Li, Junya Yamagishi, Yoshifumi Nishikawa, Ikuo Igarashi, Xuenan Xuan *

National Research Center for Protozoan Diseases, Obihiro University of Agriculture and Veterinary Medicine, Obihiro, Hokkaido 080-8555, Japan

ARTICLE INFO

Article history:
Received 1 February 2010
Received in revised form 7 June 2010
Accepted 15 June 2010
Available online 25 June 2010

Keywords:
Babesia microti
BmP94
ELISA
Vaccination

ABSTRACT

A novel gene, *BmP94*, encoding 94-kDa protein of *Babesia microti* was identified by immunoscreening of the cDNA expression library. The full-length of *BmP94* was expressed in *Escherichia coli* (rBmP94), which resulted in insoluble form with low yield, and the truncated hydrophilic C-terminus region of the gene was expressed as a soluble protein (rBmP94/CT) with improved productivity. Antiserum raised against rBmP94/CT recognized the 94-kDa native protein in the parasite extract by Western blot analysis. Next, an ELISA using rBmP94/CT was evaluated for diagnostic use, and it demonstrated high sensitivity and specificity when tested with the sera from mice experimentally infected with *B. microti* and closely related parasites. Moreover, the immunoprotective property of rBmP94/CT as a subunit vaccine was evaluated in BALB/c mice against a *B. microti* challenge, but no significant protection was observed. Our data suggest that the immunodominant antigen BmP94 could be a promising candidate for diagnostic use for human babesiosis.

1. Introduction

Babesia microti is a tick-transmitted intraerythrocytic parasite considered to be the primary etiological agent of human babesiosis. Human babesiosis caused by *B. microti* was first recognized as an endemic disease in North America and has recently emerged in Europe and East Asia (Homer et al., 2000; Saito-Ito et al., 2000; Hildebrandt et al., 2007). Infection usually causes asymptomatic to mild flu-like clinical manifestations including fever, sweat, chills, malaise, myalgia, and anemia (Homer et al., 2000). Severe symptoms, however, have been seen among patients who are immune-compromised, splenectomised, infants, or elderly (Homer et al., 2000; Leiby, 2006). The bite of an infected hard-bodied tick, *Ixodes scapularis*, is known to be the primary mode of transmission. Some cases, however, have occurred via transfusion of infected blood (Saito-Ito et al., 2000; Leiby, 2006; Tonnetti et al., 2009). Currently, the Red Cross and other blood donation agencies prohibit people with a history of babesiosis from donating blood (Vannier and Krause, 2009). Accordingly, there is an urgent and rational need to develop an effective means for the control including diagnosis and prevention of babesiosis.

Microscopic identification using a Giemsa-stained thin blood smear has been considered the standard technique for *Babesia* diagnosis, but the method has some limitations in the chronic stage of infection where the parasitemia is low. Polymerase chain reaction (PCR) has recently been used for detecting *B. microti* infection with high sensitivity and specificity (Persing et al., 1992). PCR, however, requires specialized laboratory equipment and facilities in addition to well-trained laboratory personnel. Alternatively, the indirect fluorescent-antibody test (IFAT) and enzyme-linked immunosorbent assay (ELISA) with whole parasite have been utilized for serological diagnosis of *Babesia* infection. However, the poor quality of the antigens and occasional cross-reactions with other *Babesia* species resulting in false-positive reactions have limited their application (Bose et al., 1995). Recombinant proteins derived from parasites provide better options because they are usually available in pure forms and offer higher specificity than whole parasite (Tebele et al., 2000; Boonchit et al., 2006). Several antigens have been isolated from *B. microti* and evaluated as candidates for serodiagnosis in ELISA (Lodes et al., 2000; Homer et al., 2003). Thus far, however, no reliable and appropriately sensitive antigen for human use has been reported. Using ELISA along with recombinant protein needs to be considered as a measure for screening blood donors for silent *Babesia* infection prior to transfusion (Leiby, 2006). Therefore, further studies are desired to establish an effective ELISA method with a suitable recombinant antigen that can detect the infection with different *B. microti* strains.

On the other hand, over the past decade, several attempts have been undertaken to develop an anti-*Babesia* vaccine. However, no vaccine has been proven yet to be completely effective

* Corresponding author. Fax: +81 155 49 5643.
E-mail address: gen@obihiro.ac.jp (X. Xuan).

0014-4894/$ - see front matter © 2010 Elsevier Inc. All rights reserved.
doi:10.1016/j.exppara.2010.06.018

for preventing the infection (Brown and Palmer, 1999; Brown et al., 2006a). Recently, the development of subunit vaccines has moved towards recombinant proteins (Brown et al., 2006a; Shkap et al., 2007), but from an immunological point of view, the immunodominant antigens identified by protective serum could be candidates for a subunit vaccine (Jia et al., 2008). With this in mind, the present paper demonstrates the molecular and immunogenic characterizations of an immunodominant antigen of *B. microti* identified by immunoscreening of the cDNA expression library with acutely *B. microti*-infected sera. Results indicate promise of recombinant *Escherichia coli*-expressed BmP94 as a potential serodiagnostic antigen, but not a vaccine candidate for *B. microti* infection in mouse model.

2. Materials and methods

2.1. Parasites and experimental animals

The *B. microti* Munich strain, Australian strain of *Babesia rodhaini* (kindly provided by the Kyusyu Branch of the National Institute of Animal Health, Japan) and *Plasmodium berghei* ANKA strain were maintained in BALB/c mice (Clea, Tokyo, Japan) by serial passaging. Infections were initiated by an intraperitoneal (i.p.) injection of infected erythrocytes (Igarashi et al., 1993; Inoue et al., 2006). Blood was harvested during the acute stage for either sera or infected erythrocytes preparation. BALB/c and ICR mice (Clea, Tokyo, Japan) were used for the infection and immunization experiments. All animal experiments described in this article were conducted in accordance with the Guiding Principles for the Care and Use of Research Animals promulgated by Obihiro University of Agriculture and Veterinary Medicine.

2.2. Immunoscreening of the cDNA expression library

The cDNA library of *B. microti* merozoites (10^7 PFU) previously constructed (Nishisaka et al., 2001) was immunoscreened with the serum from acutely *B. microti*-infected BALB/c mice, and the cDNA inserts of positive clones were sequenced using an automated sequencer (ABI PRISM 3100 Genetic Analyzer, Applied Biosystems, Foster City, CA, USA). Complete nucleotide sequences of identical cDNAs were analyzed using a basic local alignment search tool (BLAST) accessed through the National Center for Biotechnology Information (NCBI, http://www.ncbi.nlm.nih.gov). A cDNA clone encoding the 94-kDa protein (BmP94) was found as the most frequent gene and was thus selected for further study. The presence and location of a putative N-terminal signal peptide in the *BmP94* sequence were predicted using the SignalP server (http://www.cbs.dtu.dk/services/SignalP/). The presence of functional motifs and domains was predicted using the MyHits domain search database (http://myhits.isb-sib.ch/cgi-bin/motif_scan).

2.3. Southern blot analysis

Genomic DNA of *B. microti* was extracted from the erythrocytic stages of the parasite and digested overnight with *Acc*I, *Bam*HI, *Sac*I, and *Sca*I. The DNA samples were separated on 0.8% (w/v) agarose gel and transferred to a nylon membrane (Hybond-N^+, Amersham-Buchler, Munich, Germany). The blots were pre-hybridized at 56 °C for 6 h and probed overnight with a full-length of *BmP94* cDNA labeled with alkaline phosphatase (Amersham Pharmacia Biotech, Little Chalfont, Buckinghamshire, UK).

2.4. Cloning, expression, and purification of recombinant BmP94 and BmP94/CT

The entire fragments encoding BmP94 without a signal peptide and its hydrophilic C-terminal region (618–863 amino acids, BmP94/CT), determined by software analysis (DNASTAR; NetWell Corporation, Tokyo, Japan), were amplified using primer sets: 5′-CAGGATCCGAATTTGTTGACCTACA-3′ and 5′-GACTCGAGATCTTAA ACAGATTGTTGCGG-3′; 5′-ATGGATCCAGCGATAATGAAACGCCCG CA-3′ and 5′-GACTCGAGATCTTAAACAGATTGTTGCGG-3′, respectively. According to the manufacturer's instructions, the PCR products were inserted into the pGEX-4T-3 vector (Amersham Pharmacia Biotech, Piscataway, NJ, USA) using the *Bam*HI and *Xho*I sites and expressed in an *E. coli* DH5α strain. A fresh 10 ml overnight culture of transformed *E. coli* was grown in 1 l of LB base broth containing 50 μg/ml of ampicillin at 37 °C with shaking at 250 rpm until the optical density (OD) at 600 nm reached to 0.5. The expression of the proteins were induced by 1–5 mM-beta-galactoside (IPTG) followed by incubation at 27 °C overnight. The *E. coli* culture was centrifuged at 8000*g* for 15 min, the cell pellet was then suspended in TNE buffer (50 mM Tris–HCl, pH 8.0, 100 mM NaCl, 2 mM EDTA, 1% Triton X-100) containing 50 mg/ml lysozyme, 1% (w/v) *N*-Lauroylsarcosine sodium and protease inhibitors. The recombinant proteins were purified from the soluble fractions using glutathione-Sepharose 4B beads, according to the manufacturer's instructions (Amersham Pharmacia Biotech, Piscataway, NJ, USA).

2.5. Production of anti-rBmP94/CT serum

Six-week-old ICR mice were immunized i.p. with 200 μg of the purified rBmP94/CT protein emulsified in 200 μl of Freund's complete adjuvant (Difco Laboratories, Detroit, MI, USA). Two boosters were given i.p. at 14 day intervals using the same amount of antigen emulsified in Freund's incomplete adjuvant (Difco, Detroit, MI, USA). Sera were collected two weeks after the last booster and checked for specific antibodies by IFAT.

2.6. IFAT and confocal laser microscopic observation

B. microti-parasitized erythrocytes were coated on IFAT slides, dried, and fixed in absolute acetone for 10 min. For confocal microscopic observation, thin blood smears of *B. microti*-infected erythrocytes were fixed with absolute methanol at −20 °C for 30 min. Standard IFAT protocol was employed to localize the protein (Terkawi et al., 2007). Briefly, the anti-rBmP94/CT serum was applied as the first antibody on the fixed smears and incubated in a moist chamber at 37 °C for 1 h. After washing four times with phosphate-buffered saline containing 0.05% Tween 20 (PBST), Alexa-Fluor® 488-conjugated goat anti-mouse immunoglobin G (IgG) (Molecular Probes, Eugene, OR, USA) was applied as a secondary antibody (1:200) and then incubated at 37 °C for 1 h. The slides were washed four times with PBST and incubated with 2.5 μg/ml propidium iodide (PI) (Molecular Probes, Eugene, OR, USA) containing 50 μg/ml RNase (Qiagen, Hilden, Germany) at 37 °C for 10 min. After washing with PBS twice, the glass slides were mounted by adding 10 μl of a 50% glycerol-PBS (v/v) solution and covered with a glass cover slip. The slides were examined using a confocal laser scanning microscope (TCSNT, Leica, Heidelberg, Germany).

2.7. Sodium dodecyl sulfate–polyacrylamide gel electrophoresis (SDS–PAGE) and Western blot analysis

Protein expressions were verified by SDS–PAGE stained with Coomassie blue, and their antigenicities were confirmed by Western blot analysis (Xuan et al., 1996). *B. microti*-infected erythro-

cytes obtained from infected mice at the peak of parasitemia were haemolysed with 0.15% saponin. After centrifugation, the pellet was washed four times with cold PBS, resuspended in PBS, sonicated and lastly precipitated with acetone (Terkawi et al., 2009). Native BmP94 was identified in the parasites extract by Western blot analysis. Proteins in the extract were size-separated by electrophoresis in 10% SDS–PAGE and electroblotted onto a nitrocellulose membrane. The membrane was blocked with phosphate-buffered saline containing 0.05% Tween 20 (PBST) plus 5% skim milk and probed with anti-rBmP94/CT serum as a primary antibody. After washing with phosphate-buffered saline containing 0.05% Tween 20 (PBST), a secondary antibody, horseradish peroxidase-conjugated to anti-mouse IgG (Bethyl, Montgomery, TX, USA), was applied. Finally, bands were visualized by using 3,3′-diaminobenzidine tetrahydrochloride (Nacalai Tesque, Inc., Kyoto, Japan) and H_2O_2.

2.8. ELISA

The standard ELISA was performed as previously described (Terkawi et al., 2007). Briefly, microtiter plates (Nunc, Roskilde, Denmark) were coated overnight at 4 °C with 1 μg/ml of the rBmP94, 0.45 μg/ml of the rBmP94/CT, and 0.22 μg/ml of the control GST emulsified in a coating buffer (0.05 M carbonate buffer, pH 9.6). The plates were then blocked with PBS containing 3% (w/v) skim milk for 1 h at 37 °C. After washing, the plates were incubated with serum samples. The bound antibody was detected by treatment with horseradish peroxidase (HRP)-conjugated (Bethyl, Montgomery, TX, USA) to anti-mouse IgG (1:6000) and ABTS [2,2′-azinobis (3-ethylbenzthiazolinesulfonic acid)] (Sigma, St. Louis, MO, USA). The color was allowed to develop at room temperature. Optical density (OD) was measured by an MTP-500 microplate reader (Corona Electric, Hitachinaka-shi, Japan) at 415 nm. The positive cut-off value was calculated as the mean OD value of the serum samples from specific pathogen-free mice plus threefold of their standard deviation.

2.9. Vaccination and challenge infection

A total of 15 female BALB/c (six-week-old) mice were divided into three groups ($n = 5$). Two hundred micrograms of purified rBmP94/CT emulsified in 100 μl of Freund's complete adjuvant

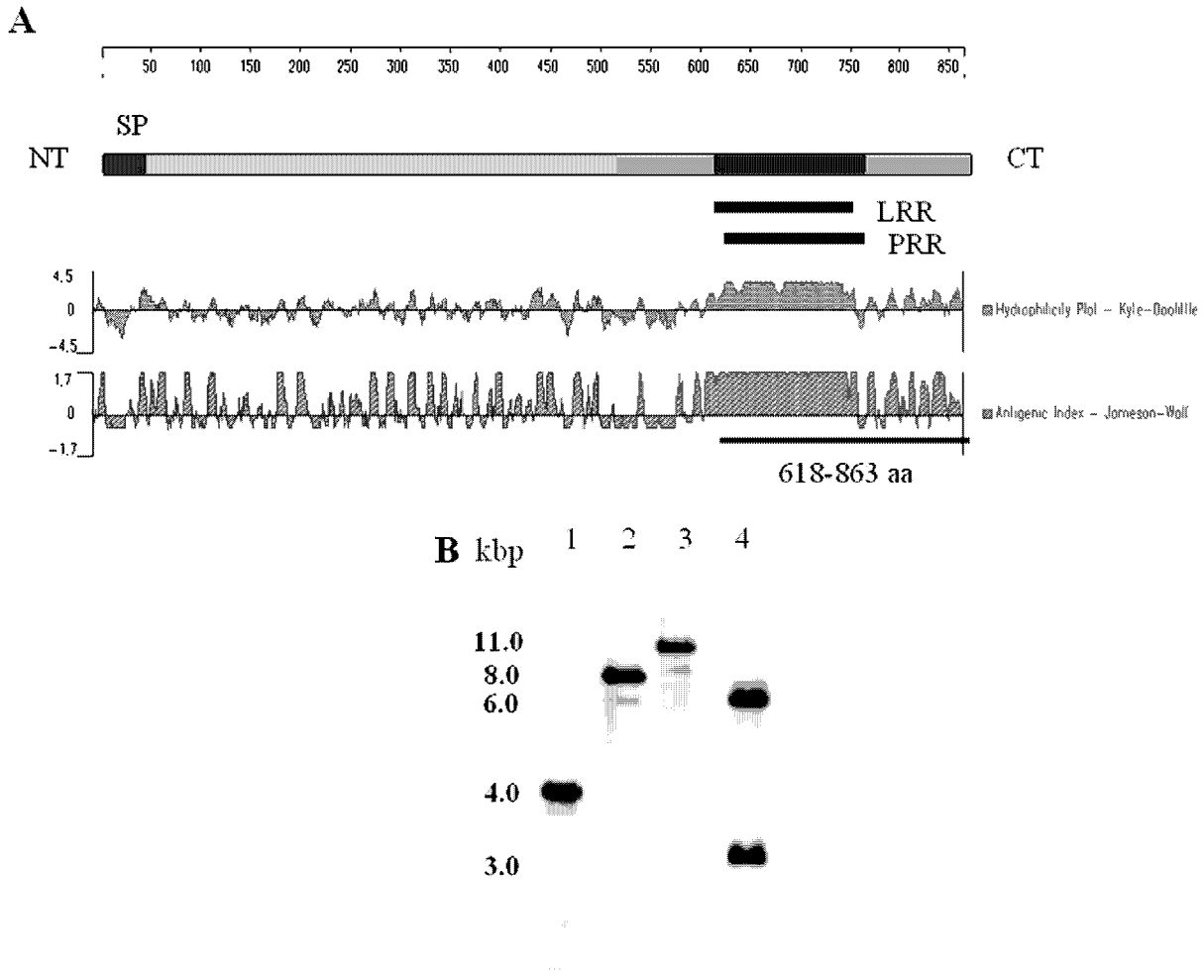

Fig. 1. (A) Schematic representation of the protein structure of BmP94 (upper), and software analysis of the hydrophilicity (middle) and antigenicity (lower) of BmP94 (DNASTAR; NetWell Corporation, Tokyo, Japan). The truncation region for rBmP94/CT is underlined. NT, N-terminus; CT, C-terminus; SP, signal peptide (1–39 amino acids); LRR, lysine-rich region (618–741 amino acids); PRR, proline-rich region (630–744 amino acids). (B) Southern blot analysis of genomic DNA of *Babesia microti* digested with different restriction enzymes, *Acc*I (lane 1), *Bam*HI (lane 2), *Sac*I (lane 3), and *Sca*I (lane 4), and hybridized with specific probe of the BmP94 gene.

was administered i.p. and followed by two additional boosters with the same amount of antigen in Freund's incomplete adjuvant at 14 day intervals. This group was designated as a test group. Control group mice received either GST protein or no immunization. Two weeks after the last boosting, the mice were challenged i.p. with 1×10^7 *B. microti*-infected erythrocytes. Parasitemias were monitored daily for 30 days by examination of Giemsa-stained smears. The antibody responses were determined before challenge. The blood samples were collected from tail bleeds using hematocrit capillary tubes (Hirschmann® laborgerate, Eberstadt, Germany).

2.10. Statistical analysis

One-way analysis of variance (ANOVA) was used to compare the means of all variables. The mean values were considered statistically different when $P < 0.05$.

2.11. Nucleotide sequence accession number

The complete sequence of the *BmP94* gene has been submitted to the GenBank with the accession number (AB540023).

3. Results and discussion

The emergence of human babesiosis caused by *B. microti* and the increase of immunocompromised patients' population in the world emphasize the need to search for effectively preventive means. Within this context, the present study demonstrates the identification of a novel *B. microti* antigen and the evaluation of its potential use for diagnosis and vaccination in rodent model. The cDNA library of *B. microti* was screened with sera from mice acutely infected with *B. microti*. A total of 164 positive clones were obtained, isolated, sequenced, and then subjected to BLAST analysis. Eighty-five clones that showed high reactivity with the sera were found to contain cDNA encoding novel amino acid sequences which were later designated as the *BmP94* gene. The full-length of *BmP94* contained an open reading frame of 2589 nucleotides encoding a polypeptide of 863 amino acid residues with a calculated molecular mass of 93.92-kDa and an isoelectric point of 6.1. The hydrophobic region at the N-terminus of *BmP94* showed the characteristics of a signal peptide, and the most likely cleavage site was predicted to be between 39 and 40 amino acids. In addition, the C-terminus of BmP94 contained a lysine-rich region (618–741 amino acids) and a proline-rich region (630–744 amino acids) that were predicted to be highly hydrophilic and antigenic (Fig. 1A) and thus determined to be the target region for further truncation (618–863 amino acids). Southern blot analysis of the genomic DNA probed with the *BmP94* gene demonstrated a single hybridizing band, after DNA digestion with *Acc*I, *Bam*HI, and *Sac*I, that cut outside the *BmP94* gene (Fig. 1B, lanes 1–3). On the other hand, the enzymes that cut a single site within the gene yielded two hybridizing bands (Fig. 1B, lane 4, *Sca*I). These results revealed that the genomic DNA of *B. microti* contains a single copy of the *BmP94* gene. Thereafter, the rBmP94 lacking an N-terminus signal peptide and truncated rBmP94/C-terminal region (618–863 amino acids) were expressed in *E. coli* as GST-fusion protein with a molecular mass of 120-kDa and 54-kDa, respectively, including a 26-kDa GST tag (Fig. 2). Sera from mice experimentally infected with *B. microti* reacted with the rBmP94 and rBmP94/CT by Western blot analysis (Fig. 2) indicating the antigenicity of the recombinant proteins. Notably, the expression of rBmP94/CT was increased in amount more than 10 times as compared to the expression of non-truncated rBmP94 (Fig. 2C), likely due to the hydrophobic nature of the BmP94′ N-termini that would lead to significant amounts of insoluble forms. The improvement in productivity enabled the immunization of mice and production of specific antiserum. Mouse-raised anti-rBmP94/CT serum specifically reacted with 94-kDa protein in *B. microti* extract by Western blot analysis (Fig. 3A, lane 1), and the observed molecular size of BmP94 was consistent with the expected molecular weight. The same serum was further used to know the localization of the protein in the *B. microti* merozoites by IFAT (Fig. 3B). Confocal microscopic observation of extracellular parasites and intracellular parasites demonstrated the expression of the BmP94 with various developmental stages of merozoites (Fig. 3B, a–h). However, weak or no reaction was sometimes observed with dividing form (Fig. 3B, e and f), suggesting that BmP94 probably expresses in a stage-dependent manner. Although, the fluorescence was consistently observed within the cytosol of parasites, the conclusive localization of the BmP94 needs further investigation using electron microscopic examination.

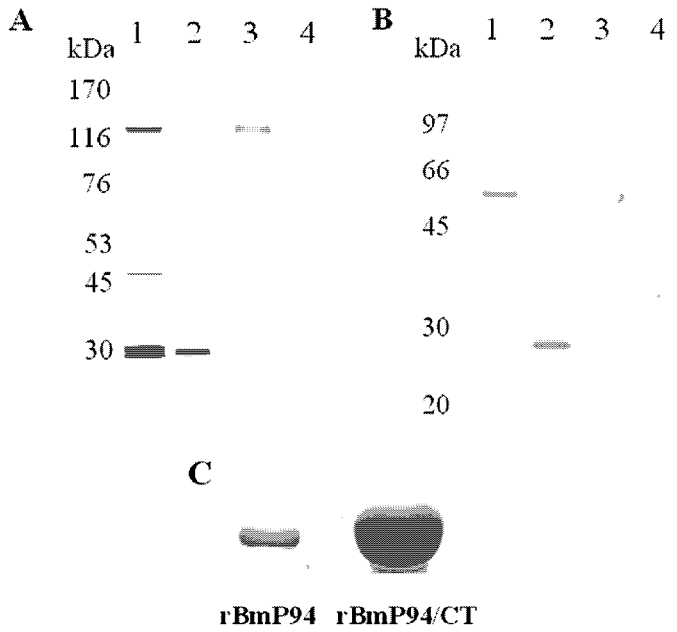

Fig. 2. SDS–PAGE and Western blot analysis of recombinant BmP94 (120-kDa), recombinant BmP94/CT (54-kDa), and GST (26-kDa). (A) Recombinant BmP94 (lanes 1 and 3) and GST (lanes 2 and 4), stained with amido black (lanes 1 and 2) and probed with *Babesia microti*-infected mouse serum (lanes 3 and 4), the bands around 45-kDa, 27-kDa, and 25-kDa appeared in SDS–PAGE might be degraded forms of the proteins due to stress response of the host cell. (B) Recombinant BmP94/CT (lanes 1 and 3) and GST (lanes 2 and 4), stained with amido black (lanes 1 and 2) and probed with *B. microti*-infected mouse serum (lanes 3 and 4); (C) Comparison of productivity between insoluble rBmP94 and soluble rBmP94/CT from the same amount of *Escherichia coli*.

The antigenicity of the rBmP94 was evaluated using ELISA with variously *B. microti*-infected sera. Sera from *B. microti*-infected mice showed a highly specific reaction as evidenced by high ODs, whereas sera from infected mice with closely related parasites, *B. rodhaini* and *P. berghei*, showed a clear negative reaction ($OD < 0.1$). These revealed the specificity of rBmP94-ELISA in detection of the infection (Fig. 4A). Interestingly, rBmP94/CT-ELISA demonstrated a similar specificity when tested with the same sera (Fig. 4A). Next, the sensitivity of ELISA using rBmP94 and rBmP94/CT was examined by testing sera obtained sequentially after infection of mice infected with *B. microti*. Although the antibody responses to rBmP94 were detectable two days earlier than the antibody to rBmP94/CT, no significant differences in the OD values were observed during the acute and chronic stages (Fig. 4B). The slight difference might be due to the presence of antigenic regions found in the N-terminus (Fig. 1). However, the improvement in productivity together with similar diagnostic properties of the

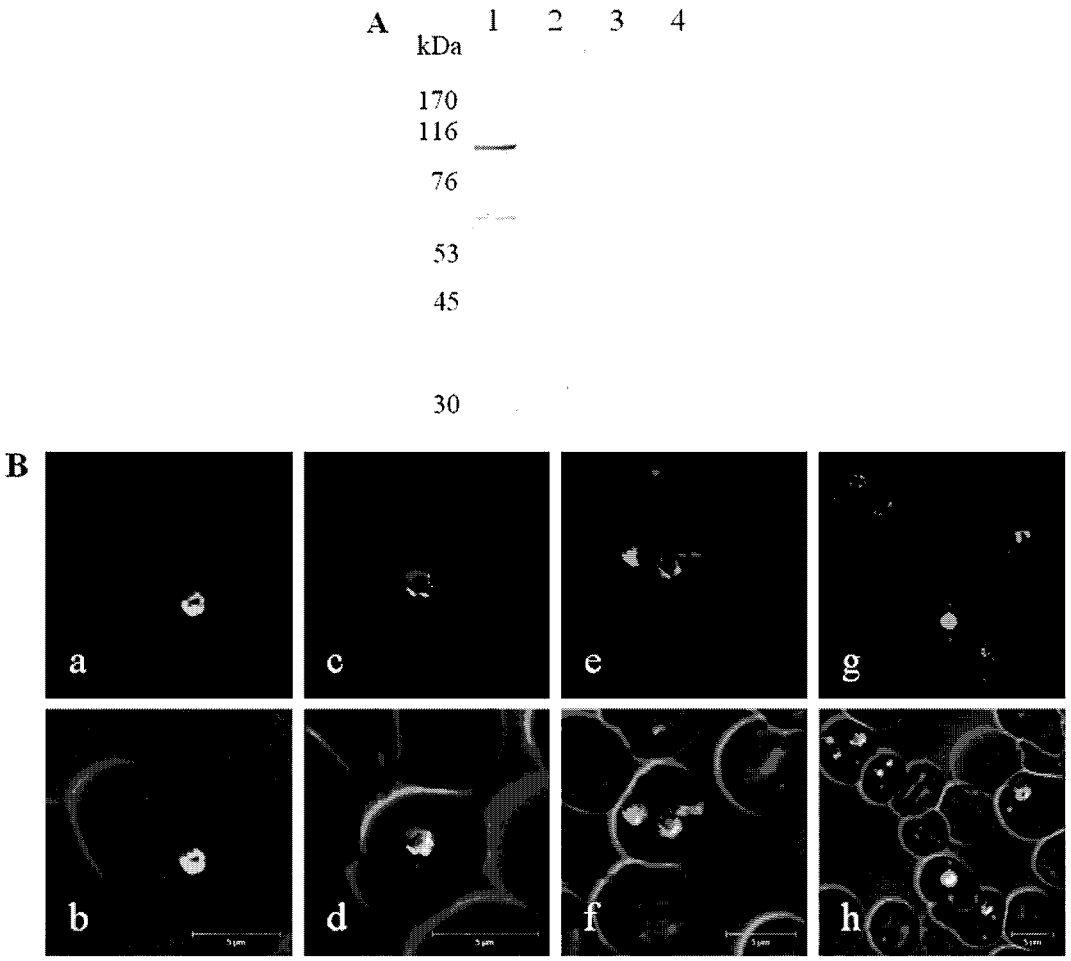

Fig. 3. Western blot and immunofluorescence microscopy analyses of native BmP94. (A) *Babesia microti*-infected erythrocytes (lanes 1 and 3) and erythrocytes from healthy mice (lanes 2 and 4) probed with anti-rBmP94/CT serum (lanes 1 and 2) or normal mouse serum (lanes 3 and 4). Apparent minor bands; 60-kDa and 26-kDa might be degraded forms of the native protein. (B) Immunofluorescence microscopy analysis. Methanol-fixed smears of *B. microti*-infected RBC were preincubated with the anti-rBmP94/CT serum, visualized with Alexa-Fluor® 488-conjugated IgG secondary antibody and propidium iodide (PI) staining, and finally examined with confocal laser microscopy. The specific reaction of the protein and anti-rBmP94/CT serum is green, and the nucleus is red. Panels a–h, the reactivity of antiserum with extracellular and intracellular *B. microti* merozoites. Panels a, c, e, and g, the overlaid image of fluorescent reactivity and red PI staining of nuclei; b, d, f, and h, the overlaid image of fluorescent green reactivity and red PI staining on phase-contrast images of the parasites. Bars, 5 μm.

full-length protein indicates the success of the truncation strategy of rBmP94/CT. Several recombinant merozoite antigens have been identified as immunodominant and have diagnostic significance in various *Babesia* species. Likewise, recombinant BmN1-17 derived from *B. microti* MN1 strain has been documented to be highly sensitive (98%) in detection the infection of human positive sera (Homer et al., 2003). However, none of these identified antigens were evaluated with *B. microti* Munich strain infected sera and our study is the first report about ELISA development based on Munich strain that considered potentially as agent for human babesiosis. Although our data did not show the performance of rBmP94 with human sera, the high sensitivity and specificity of the antigen in mouse model were promising enough to pursue development of a reliable serodiagnostic reagent for detection of *B. microti* infection. Further study including the examination of rBmP94-ELISA with different strains of *B. microti*-infected sera is required to obtain the conclusive remark of rBmP94 as antigen for serodiagnosic use.

The high antigenicity combined with high yield of rBmP94/CT was motivating to evaluate its potential as a vaccine candidate. The immunization regime induced highly specific antibodies (IFAT titers, 1:25,600) in mice that received rBmP94/CT but not in mice that received GST or the control mice (data not shown). The mice were then challenged and parasitemia was monitored for 30 days post-infection. All mice developed parasitemia as early as 2 days post-challenge, and peak levels were observed at day 8; no significant differences were observed between the test and control groups (data not shown). Although the vaccination was not protective, further study including different delivery schemes such as liposome vaccination, DNA vaccination, and virus vector vaccination might be necessary to attain the protective properties of this molecule. The failure in protection could support the concept that immunodominant antigens serologically identified are not necessarily protective (Brown et al., 2006b). However, several reports documented the usefulness of serological screening to identify subunit vaccine candidates. For example, immunization with ribosomal phosphoprotein P0 delayed the onset of *B. microti* infection and significantly reduced the peripheral parasitemia (Terkawi et al., 2007). In support of this, immunization with HSP-70 elicited significant protection against *B. microti* challenge infection (Terkawi et al., 2009).

In summary, we have identified and characterized a novel BmP94 antigen by immunoscreening of the *B. microti* cDNA library and evaluated its potential for serodiagnosis and as a subunit vaccine. The high specificity and sensitivity of ELISA-rBmP94/CT were promising enough to pursue development of a reliable serodiagnostic reagent for detection of infection in the mouse model.

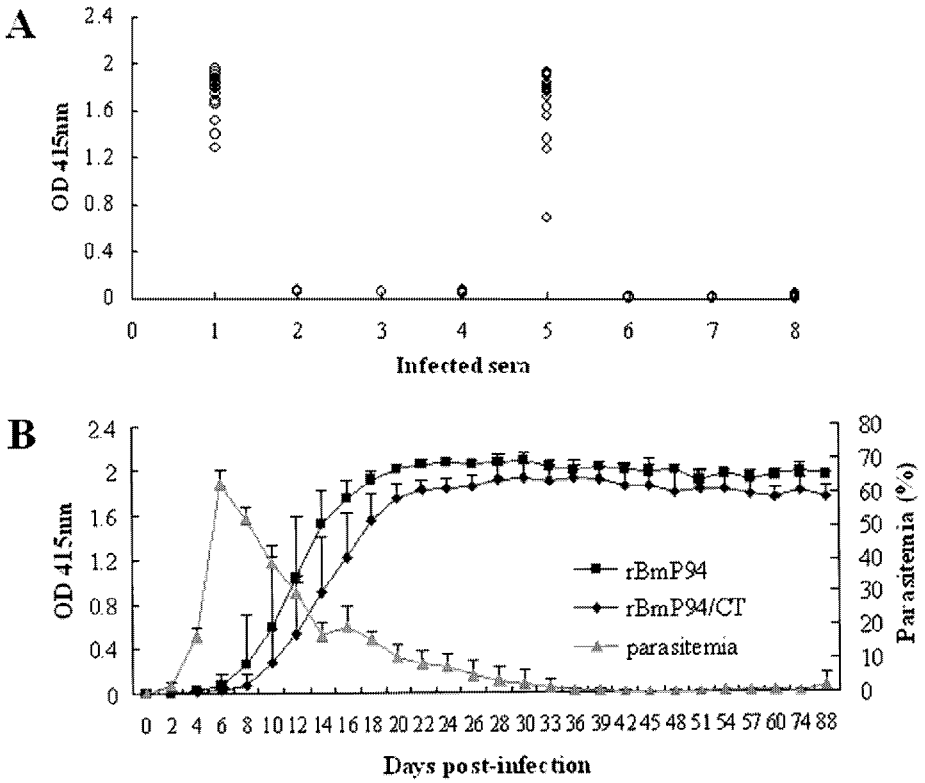

Fig. 4. Evaluation of rBmP94- and rBmP94/CT-ELISA. (A) The reactivity of rBmP94 (lanes 1–4) and rBmP94/CT (lanes 5–8) with B. microti - and closely related parasite-infected mice sera. Lanes 1 and 5: *Babesia microti*-infected mouse sera (n = 18); lanes 2 and 6: *Babesia rodhaini*-infected mouse sera (n = 6); lanes 3 and 7: *Plasmodium berghei*-infected mouse sera (n = 6); lanes 4 and 8: specific pathogen-free mouse sera (n = 12). (B) Sensitivity of rBmP94 (0.1 μg / well) and rBmP94/CT (0.045 μg / well) with serial serum samples from mice experimentally infected with *B. microti* (n = 5). The parasitemia was determined by microscopic examination. Each point represents the mean ± the standard deviation.

Immunization with rBmP94/CT combined with Freund's adjuvant was not significantly protective against challenge infection, although induced high titer of specific antibody. These findings should hopefully provide a basis for future work that could exploit this protein as antigen for diagnostic use.

Acknowledgments

This work was supported by a Grant-in-Aid for Scientific Research from the Ministry of Education, Culture, Sports, Science, and Technology, Japan.

References

Boonchit, S., Alhassan, A., Chan, B., Xuan, X., Yokoyama, N., Ooshiro, M., Goff, W.L., Waghela, S.D., Wagner, G., Igarashi, I., 2006. Expression of C-terminal truncated and full-length *Babesia bigemina* rhoptry-associated protein 1 and their potential use in enzyme-linked immunosorbent assay. Veterinary Parasitology 137, 28–35.

Bose, R., Jorgensen, W.K., Dalgliesh, R.J., Friedhoff, K.T., De Vos, A.J., 1995. Current state and future trends in the diagnosis of babesiosis. Veterinary Parasitology 57, 61–74.

Brown, W.C., Palmer, G.H., 1999. Designing blood-stage vaccines against *Babesia bovis* and *B. Bigemina*. Parasitology Today 15, 275–281.

Brown, W.C., Norimine, J., Goff, W.L., Suarez, C.E., McElwain, T.F., 2006a. Prospects for recombinant vaccines against *Babesia bovis* and related parasites. Parasite Immunology 28, 315–327.

Brown, W.C., Norimine, J., Knowles, D.P., Goff, W.L., 2006b. Immune control of *Babesia bovis* infection. Veterinary Parasitology 138, 75–87.

Hildebrandt, A., Hunfeld, K.-P., Baier, M., Krumbholz, A., Sachse, S., Lorenzen, T., Kiehntopf, M., Fricke, H.-J., Straube, E., 2007. First confirmed autochthonous case of human *Babesia microti* infection in Europe. European Journal of Clinical Microbiology and Infectious Diseases 26, 595–601.

Homer, M.J., Aguilar-Delfin, I., Telford, S.R., Krause, P.J., Persing, D.H., 2000. Babesiosis. Clinical Microbiology Reviews 13, 451–469.

Homer, M.J., Lodes, M.J., Reynolds, L.D., Zhang, Y., Douglass, J.F., McNeill, P.D., Houghton, R.L., Persing, D.H., 2003. Identification and characterization of putative secreted antigens from *Babesia microti*. Journal of Clinical Microbiology 41, 723–729.

Igarashi, I., Hosomi, T., Kaidoh, T., Omata, Y., Saito, A., Suzuki, N., Aikawa, M., 1993. Comparison of damage to kidneys and liver caused by lethal *Babesia rodhaini* infection and non-lethal *Babesia microti* infection in mice. Journal of Protozoology Research 3, 144–155.

Inoue, M., Xuan, X., Fujisaki, K., Igarashi, I., Suzuki, H., 2006. Short report: role of type I/II scavenger receptors in malarial infection in C57BL/6J mice. American Journal of Tropical Medicine and Hygiene 75, 178–181.

Jia, H., Terkawi, M.A., Aboge, G.O., Goo, Y.K., Zhou, J., Lee, E.G., Nishikawa, Y., Igarashi, I., Fujisaki, K., Xuan, X., 2008. *Babesia gibsoni*: Identification of an immunodominant, interspersed repeat antigen. Experimental Parasitology 118, 146–149.

Leiby, D.A., 2006. Babesiosis and blood transfusion: flying under the radar. Vox Sanguinis 90, 157–165.

Lodes, M.J., Houghton, R.L., Bruinsma, E.S., Mohamath, R., Reynolds, L.D., Benson, D.R., Krause, P.J., Reed, S.G., Persing, D.H., 2000. Serological expression cloning of novel immunoreactive antigens of *Babesia miroti*. Infection and Immunity 68, 2783–2790.

Nishisaka, M., Yokoyama, N., Xuan, X., Inoue, N., Nagasawa, H., Fujisaki, K., Mikami, T., Igarashi, I., 2001. Characterisation of the gene encoding a protective antigen from *Babesia microti* identified it as the eta subunit of chaperonin containing T-complex protein1. International Journal for Parasitology 31, 1673–1679.

Persing, D.H., Mathiesen, D., Marshall, W.F., Telford, S.R., Spielman, A., Thomford, J.W., Conrad, P.A., 1992. Detection of *Babesia microti* by polymerase chain reaction. Journal of Clinical Microbiology 30, 2097–2103.

Saito-Ito, A., Tsuji, M., Wei, Q., He, S., Matsui, T., Kohsaki, M., Arai, S., Kamiyama, T., Hioki, K., Ishihara, C., 2000. Transfusion-acquired, autochthonous human babesiosis in Japan: isolation of *Babesia microti*-like parasites with hu-RBC-SCID mice. Journal of Clinical Microbiology 38, 4511–4516.

Shkap, V., De Vos, A.J., Zweygarth, E., Jongejan, F., 2007. Attenuated vaccines for tropical theileriosis, babesiosis and heartwater: the continuing necessity. Trends in Parasitology 23, 420–426.

Tebele, N., Skilton, R.A., Katende, J., Wells, C.W., Nene, V., McElwain, T., Morzaria, S.P., Musoke, A.J., 2000. Cloning, characterization, and expression of a 200-kilodalton diagnostic antigen of *Babesia bigemina*. Journal of Clinical Microbiology 38, 2240–2247.

Terkawi, M.A., Jia, H., Zhou, J., Lee, E.G., Igarashi, I., Fujisaki, K., Nishikawa, Y., Xuan, X., 2007. *Babesia gibsoni* ribosomal phosphoprotein P0 induces cross-protective immunity against *B. microti* infection in mice. Vaccine 25, 2027–2035.

Terkawi, M.A., Aboge, G., Jia, H., Goo, Y.K., Ooka, H., Yamagishi, J., Nishikawa, Y., Yokoyama, N., Igarashi, I., Kawazu, S.I., Fujisaki, K., Xuan, X., 2009. Molecular and immunological characterization of *Babesia gibsoni* and *Babesia microti* heat shock protein-70. Parasite Immunology 31, 328–340.

Tonnetti, L., Eder, A.F., Dy, B., Kennedy, J., Pisciotto, P., Benjamin, R.J., Leiby, D.A., 2009. Transfusion-transmitted *Babesia microti* identified through hemovigilance. Transfusion 49, 2557–2563.

Vannier, E., Krause, P.J., 2009. Update on babesiosis. Interdisciplinary Perspectives on Infectious Diseases 2009, 984568.

Xuan, X., Maeda, K., Mikami, T., Otsuka, H., 1996. Characterization of canine herpesvirus glycoprotein C expressed by a recombinant baculovirus in insect cells. Virus Research 46, 57–64.

CLINICAL AND VACCINE IMMUNOLOGY, Feb. 2011, p. 337–342 Vol. 18, No. 2
1556-6811/11/$12.00 doi:10.1128/CVI.00388-10

Spherical Body Protein 4 Is a New Serological Antigen for Global Detection of *Babesia bovis* Infection in Cattle[▽]

Mohamad Alaa Terkawi, Nguyen Xuan Huyen, Putut Eko Wibowo, Faasoa Junior Seuseu, Mahmoud Aboulaila, Akio Ueno, Youn-Kyoung Goo, Naoaki Yokoyama, Xuenan Xuan, and Ikuo Igarashi*

National Research Center for Protozoan Diseases, Obihiro University of Agriculture and Veterinary Medicine, Inada-cho, Obihiro, Hokkaido 080-8555, Japan

Received 27 August 2010/Returned for modification 29 September 2010/Accepted 22 November 2010

Five *Babesia bovis* recombinant proteins, including merozoite surface antigen 2c (BbMSA-2c), C-terminal rhoptry-associated protein 1 (BbRAP-1/CT), truncated thrombospondin-related anonymous protein (BbTRAP-T), spherical body protein 1 (BbSBP-1), and spherical body protein 4 (BbSBP-4), were evaluated as diagnostic antigens to detect the infection in cattle. The recombinant proteins were highly antigenic when tested with experimentally *B. bovis*-infected bovine serum in Western blot analysis. Furthermore, five antisera that had been raised against each of the recombinant proteins reacted specifically with the corresponding authentic protein, as determined in Western blot analysis. Next, enzyme-linked immunosorbent assays (ELISAs) using these recombinant proteins were evaluated for diagnostic use, and the sensitivity and specificity of each protein were demonstrated with a series of serum samples from experimentally *B. bovis*-infected cattle. Furthermore, a total of 669 field serum samples collected from cattle in regions of *B. bovis* endemicity in seven countries were tested with the ELISAs, and the results were compared to those of an indirect fluorescent antibody test (IFAT), as a reference. Among five recombinant antigens, recombinant BbSBP-4 (rBbSBP-4) had the highest concordance rate (85.3%) and kappa value (0.705), indicating its reliability in the detection of specific antibodies to *B. bovis* in cattle, even in different geographical regions. Overall, we have successfully developed an ELISA based on rBbSBP-4 as a new serological antigen for a practical and sensitive test which will be applicable for epidemiologic survey and control programs in the future.

Bovine babesiosis is an economically important tick-borne disease in tropical and subtropical areas of the world (3). The disease is caused by hemoprotozoan parasites of the genus *Babesia*, namely, *B. bovis*, *B. bigemina*, *B. beliceri*, *B. divergens*, *B. major*, *B. ovata*, *B. occultans*, and *B. jakimovi* (28). Among them, *B. bovis* and *B. bigemina* are the most important species, and they are usually found together in most areas of endemicity (22, 31). Although *B. bovis* and *B. bigemina* are phylogenetically related and transmitted by *Rhipicephalus* (*Boophilus*) *microplus*, they cause remarkably different diseases in cattle (3). Infection by *B. bovis* is more severe than that of *B. bigemina*, due to the sequestration of infected erythrocytes in the microcapillaries of the kidneys, lungs, and brain, resulting in organ failure and systemic shock that leads to death. Cattle that survive *B. bovis* infection generally become carriers of the parasite and serve as reservoirs for transmission to other animals (3). Thus, highly sensitive and specific diagnostic tools are required to detect the carrier animals and to differentiate this infection from other closely related ones. Such diagnostic tests must lead to a better understanding of the protozoan epidemiology, providing useful information for disease management and control strategies (10).

A large number of serological tests have been developed for the detection of specific antibodies to bovine *Babesia* parasites for epidemiological surveys as well as for the identification of carrier animals (2, 7, 30). Among these assays, the indirect immunofluorescent antibody test (IFAT) is the most sensitive, but cross-reactivity with other *Babesia* spp., subjective interpretation, and low throughput have limited its usefulness (8). In contrast, enzyme-linked immunosorbent assays (ELISAs) can be used as a routine diagnostic test or as a screening test for epidemiologic studies. Although a number of diagnostic ELISAs have been developed, several problems regarding the sensitivity and specificity remain, related mostly to the characteristics and preparation of the antigens. For example, crude antigens have been used to detect the antibodies to *Babesia* parasites, but the poor purification quality of the antigen and the potential cross-reactivity with other protozoan parasites have impeded their application. Such crude antigens frequently contain host cell components, which may affect the accuracy of test results by increasing the nonspecific background (7–9, 21, 29). On the other hand, recombinant proteins derived from the parasites could become alternative sources of antigens, allowing a better standardization of the tests with high specificity and sensitivity (7, 8). Despite the potential advantages of using recombinant antigens in serological tests, their sensitivity needs to be significantly improved (29). Therefore, further research to identify new antigen makers is extremely desirable.

Babesia parasites are defined by the common characteristic structures of the apical complex, which consists of rhoptries, micronemes, and spherical body organelles. Proteins derived from these organelles, coupled with the membrane component of parasites, are believed to have critical functions in parasite

* Corresponding author. Mailing address: National Research Center for Protozoan Diseases, Obihiro University of Agriculture and Veterinary Medicine, Inada-cho, Obihiro, Hokkaido 080-8555, Japan. Phone: 81-155-49-5641. Fax: 81-155-49-5643. E-mail: igarcpmi@obihiro.ac.jp.

▽ Published ahead of print on 1 December 2010.

survival and growth (34). These proteins include (i) variable merozoite surface antigens (VMSAs) (4), which are believed to play key roles in the initial attachment of merozoites and sporozoites during their invasion (34), (ii) microneme and rhoptry proteins, including apical membrane antigen 1 (AMA-1), thrombospondin-related anonymous protein (TRAP), and rhoptry-associated protein 1 (RAP-1), which seem to be involved in the formation of a tight junction between merozoites and erythrocytes (RBC) (11), and (iii) spherical body proteins (SBPs), which have roles in stabilizing the environment after invasion and in aiding parasite growth (14, 26). Importantly, they have been suggested as promising candidates for developing subunit vaccines or diagnostic antigens (34).

With this in mind, we validated five ELISAs with different recombinant proteins, including merozoite surface antigen 2c (BbMSA-2c) (19), C-terminal rhoptry-associated protein 1 (BbRAP-1/CT) (6), thrombospondin-related anonymous protein (BbTRAP) (11), spherical body protein 1 (BbSBP-1) (16), and spherical body protein 4 (BbSBP-4) (M. A. Terkawi, F. J. Seuseu, P. E. Wibowo, N. X. Huyen, M. Aboulaila, N. Yokoyama, X. Xuan, and I. Igarashi, submitted for publication), and then evaluated their potential application for the diagnostic detection of specific antibodies to *B. bovis*. The results indicate the promising use of an ELISA with rBbSBP-4 antigen as a global diagnostic marker for the detection of *B. bovis* infection.

MATERIALS AND METHODS

Parasites. The Texas strain of *B. bovis* and the Argentina strain of *B. bigemina* were continuously cultured with bovine erythrocytes (RBC) by using a microaerophilous stationary-phase culturing system (1, 15, 20). The cultured parasite was harvested when the parasitemia reached 8 to 10%.

Expression and purification of recombinant proteins and production of polyclonal antibodies. The DNA fragments encoding *B. bovis* merozoite surface antigen 2c (BbMSA-2c; GenBank accession number AY052542) (19), the C-terminal region of rhoptry-associated protein 1 (BbRAP-1/CT [388 to 490 amino acids {aa}]; AF030062) (5, 6), full-length or truncated thrombospondin-related anonymous protein (BbTRAP or BbTRAP-T [321 to 561 aa]; AY486102) (11), spherical body protein 1 (BbSBP-1; AAC37226) (16), and spherical body protein 4 (BbSBP-4; AB594813) (Terkawi et al., submitted) were amplified from a *B. bovis* cDNA phage expression library by standard PCRs using gene-specific primers (Table 1). The amplified DNA fragments were cloned into a pGEX-4T1 plasmid vector (Amersham Pharmacia Biotech, Madison, CA) using the suitable restriction enzyme sites and then expressed as glutathione *S*-transferase (GST) fusion genes in the *Escherichia coli* DH-5α strain (Amersham Pharmacia Biotech). The recombinant proteins were purified from the soluble fractions of *E. coli* lysates using glutathione-Sepharose 4B beads (Amersham Pharmacia Biotech) and then analyzed by SDS-PAGE and Western blot analysis, as described previously (26).

Thereafter, each of the antisera for recombinant proteins was prepared in 6-week-old BALB/c mice (n = 5) according to the standard protocol (25). Briefly, mice were intraperitoneally (i.p.) immunized with 100 μg of each recombinant protein emulsified in Freund's complete adjuvant (Sigma, St. Louis, MO). Two boosters were given i.p. using 50 μg of the same proteins emulsified in Freund's incomplete adjuvant (Sigma) at 14-day intervals. Sera were collected 2 weeks after the last booster and then checked for the production of specific antibodies using the IFAT and Western blotting.

SDS-PAGE and Western blotting. The expressed recombinant proteins were verified by sodium dodecyl sulfate-polyacrylamide gel electrophoresis (SDS-PAGE) with subsequent Coomassie blue staining, while their antigenicities were confirmed with Western blot analysis. To identify the authentic parasite proteins, the *B. bovis*-infected RBC were obtained from the *in vitro* culture, washed three times with cold phosphate-buffered saline (PBS), and then lysed with 0.25% saponin. The pellet was washed four times with cold PBS, resuspended in PBS, disrupted three times by a freeze-thaw cycle in liquid nitrogen, and then sonicated in an ice slurry (Terkawi et al., submitted). The protein concentrations of lysates were determined by a bicinchoninic acid (BCA) protein assay kit (Pierce Biotechnology, Rockford, IL) and finally stored at −80°C until use. The extracted proteins were separated in 12% SDS-PAGE and then electroblotted onto a nitrocellulose membrane (32). The membrane was blocked with 0.05% Tween 20 in PBS (PBS-T) plus 5% skimmed milk and probed with the indicated protein-specific primary antibodies. After the membrane was washed with PBS-T, a secondary antibody, horseradish peroxidase (HRP)-conjugated anti-bovine or -mouse immunoglobulin G (IgG) antibody (Bethyl Laboratories, Montgomery, TX), was applied. Finally, reacted bands were visualized using a solution containing 3-diaminobenzidine tetrahydrochloride (DAB) and H_2O_2 (Dojindo, Tokyo, Japan).

TABLE 1. Gene-specific primers for amplifying *BbMSA-2c*, *BbRAP-1/CT*, *BbTRAP-T*, *BbSBP-1*, and *BbSBP-4*

Gene	Oligonucleotide primer[a]
BbMSA-2c	5′-CGGAATTCATGGTGTCTTTAACATAATAACC-3′
	5′-TAGCGGCCGCGAATGCAGAGAGAACGAAGTAGCAG-3′
BbRAP-1/CT	5′-ACGGATCCGAGTTTTTCAGGGAA-3′
	5′-ACCTCGAGAAACTCATGTATGAT-3′
BbTRAP-T	5′-AGAATTCGAACCAAGCCGTGCTACACCG-3′
	5′-ACTCGAGCTATTGTTTTTCGCCCTCGTAG-3′
BbSBP-1	5′-GCGAATTCAACGAAGCTGAGGTATCTCAG-3′
	5′-GGCTCGAGTTAGTCTAGCATCTGTATTTT-3′
BbSBP-4	5′-AGGAATTCGAGGAGGAGGAAACTGATGAG-3′
	5′-GCCTCGAGTTATTCCTCAATGTCGGCTGT-3′

[a] Each oligonucleotide primer includes restriction enzyme sites at the 5′ end (underlined), which are EcoRI and NotI for *BbMSA-2c*, BamHI and XhoI for *BbRAP-1/CT*, and EcoRI and XhoI for *BbTRAP-T*, *BbSBP-1*, and *BbSBP-4*.

Bovine sera. Positive serum samples were collected from cattle experimentally infected with *B. bovis* (n = 25) or *B. bigemina* (n = 30) (National Institute of Animal Health, Tsukuba, Ibaraki, Japan) or with *Theileria orientalis* (n = 6) (Obihiro University of Agriculture and Veterinary Medicine, Japan), while non-*Babesia*-infected control sera (n = 50) were obtained from healthy cattle that had been bred at Obihiro University of Agriculture and Veterinary Medicine, Washington State University (Pullman, WA), and Texas A&M University (College Station, TX) (19). Field bovine sera were collected from Brazil (n = 108), Ghana (n = 80), China (n = 100), Thailand (n = 100), Mongolia (n = 81), South Korea (n = 100), and Hokkaido, Japan (n = 100) (1, 5, 18).

ELISAs. Standard enzyme-linked immunosorbent assays (ELISAs) were performed in the present study as described previously (25). Briefly, 96-well microtiter plates (Nunc, Roskilde, Denmark) were coated overnight at 4°C with 100 μl of each recombinant protein at a concentration of 2 μg/ml per well in a coating buffer (50 mM carbonate-bicarbonate buffer, pH 9.6). The plates were washed once with 0.05% Tween 20-PBS (PBS-T) and then incubated with 100 μl of a blocking solution (3% skim milk in PBS) for 1 h at 37°C. After the antigen-coated wells were washed once with PBS-T, they were incubated with 50 μl of the serum samples diluted 1:100 with the blocking solution for 1 h at 37°C. The plates were washed six times with PBS-T and then incubated with 50 μl of HRP-conjugated sheep anti-bovine IgG antibody (Bethyl) diluted 1:4,000 with the blocking solution for 1 h at 37°C as a secondary antibody. The plates were washed six times as described above, and 100 μl of a substrate solution [0.1 M citric acid, 0.2 M sodium phosphate, 0.3 mg/ml of 2,2′-azide-bis (3-ethylbenzthiazoline-6-sulfonic acid) (Sigma), and 0.01% of 30% H_2O_2] was then added to each well. After incubation for 1 h at room temperature (RT), the optical density (OD) was measured with an MTP-500 microplate reader (Corona Electric, Tokyo, Japan) at a wavelength of 415 nm. The cutoff points were calculated by the receiver operating characteristic (ROC) analysis with MedCalc statistical software (version 11.4; http://www.medcalc.be) for each recombinant protein with 50 non-*Babesia*-infected bovine sera (12, 13).

IFAT. The *B. bovis*-infected RBC were coated on indirect fluorescent antibody test (IFAT) slides (Matsunami Glass Ind., Ltd., Osaka, Japan), dried, and then fixed in absolute acetone for 20 min for standard IFAT observation (4). Briefly,

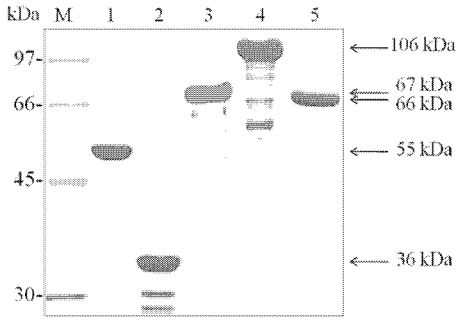

FIG. 1. Successful expression of recombinant proteins in *E. coli*. Twelve percent SDS-polyacrylamide gel electrophoresis (SDS-PAGE) of recombinant protein stained with Coomassie blue. Lanes: M, molecular mass marker; 1, rBbMSA-2c; 2, rBbRAP-1/CT; 3, rBbTRAP-T; 4, rBbSBP-1; 5, rBbSBP-4. The size of each recombinant protein is indicated on the right.

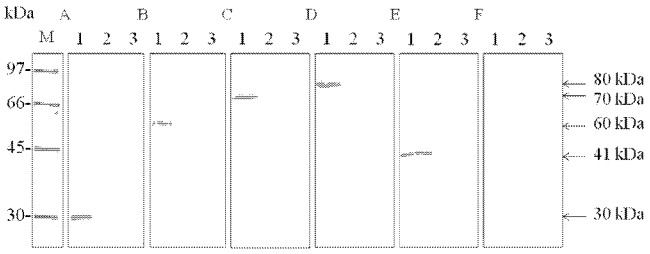

FIG. 3. Western blot analysis of authentic proteins with antisera against different recombinant proteins. BbMSA-2c (A), BbRAP-1 (B), BbTRAP (C), BbSBP-1 (D), and BbSBP-4 (E) were detected on the lysate of *B. bovis* parasites (lanes 1) but not on *B. bigemina* (lanes 2) and noninfected bovine RBC (lanes 3). The reactivity of the lysates was also examined with anti-GST serum (F) as a negative control.

a 10-μl field serum sample diluted in PBS (1:100) was applied as the first antibody on the fixed smears and then incubated for 1 h at 37°C in a moist chamber. After the slides were washed with PBS three times, fluorescein isothiocyanate (FITC)-conjugated sheep anti-bovine IgG antibody (Bethyl Laboratories, Montgomery, TX) was applied as a secondary antibody (1:250), and incubation proceeded for 1 h at 37°C. Propidium iodide (PI) (Molecular Probes) was used to stain the parasite's nuclei (26). After the glass slides were washed with PBS twice, they were mounted by adding 10 μl of a 50% (vol/vol) glycerol-PBS solution and covering them with glass coverslips and examined using a fluorescent microscope (E400 Eclipse; Nikon, Kawasaki, Japan).

Statistical analysis. The results of ELISAs were compared with those of the IFAT to calculate the percentages of agreement, the sensitivity and specificity (18), and the kappa values; thus, the strength of agreement between the ELISA and the IFAT was considered the kappa value: fair (0.21 to 0.40), moderate (0.41 to 0.60), and substantial (0.61 to 0.8) (http://faculty.vassar.edu/lowry/VassarStats.html).

RESULTS

Production of recombinant proteins. The genes encoding BbMSA-2c, BbRAP-1/CT, BbTRAP-T, BbSBP-1, and BbSBP-4 were successfully expressed as soluble GST fusion proteins in *E. coli* with molecular masses of 55, 36, 66, 106, and 67 kDa, respectively (Fig. 1). Sera collected from cattle experimentally infected with *B. bovis* specifically reacted to all the recombinant proteins but not to the control GST protein in Western blot analysis (data not shown), suggesting their high antigenicity with the infected sera. Because full-length BbTRAP resulted in a low yield in the soluble fraction, only rBbTRAP-T was used for further validation (data not shown). Thereafter, five different antisera raised against each recombinant protein were used to identify the native proteins derived from *B. bovis*. Confocal microscopic observation of the IFAT demonstrated strong reactivity of each antiserum with both intra- and extraerythrocytic parasites of *B. bovis* (Fig. 2). Western blot analysis of *B. bovis* lysate probing these antisera revealed 30-, 60-, 70-, 80-, and 41-kDa proteins of BbMSA-2c, BbRAP-1, BbTRAP, BbSBP-1, and BbSBP-4, respectively (Fig. 3, lanes 1). All sizes of the authentic *B. bovis* proteins were consistent with the expected molecular weights for each mature protein. In contrast, these antisera did not cross-react with the lysate of *B. bigemina*-infected erythrocytes or normal bovine erythrocytes (Fig. 3, lanes 2 and 3, respectively).

Application of the recombinant proteins for serological diagnoses. The specificity and sensitivity of rBbMSA-2c, rBbRAP-1/CT, rBbTRAP-T, rBbSBP-1, and rBbSBP-4 were evaluated in a standard ELISA with experimentally infected and negative-control bovine sera. The cutoff OD values were determined to be 0.14, 0.20, 0.217, 0.173, and 0.11, respectively, for rBbMSA-2c, rBbRAP-1/CT, rBbTRAP-T, rBbSBP-1, and rBbSBP-4 using ROC analysis with 50 negative-control sera (Fig. 4). Notably, the ELISAs based on these recombinant proteins succeeded in clearly differentiating between *B. bovis*-infected sera and either the negative-control sera or B. *bigemina*-infected and *T. orientalis*-infected sera. All 25 *B. bovis*-

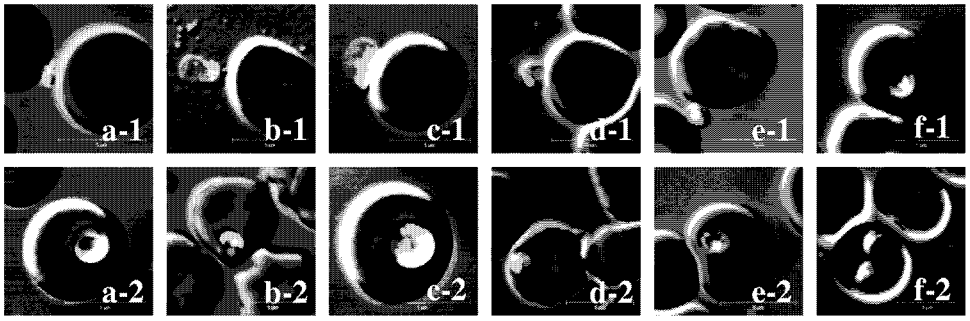

FIG. 2. Reactivity of each antiserum with *B. bovis* parasites by the IFAT. Confocal laser microscopic observation of extracellular (a-1 to e-1) and intracellular *B. bovis* parasites (a-2 to f-2). Thin blood smears of *B. bovis*-infected RBC fixed with absolute methanol were probed with each antiserum: a, anti-rBbMSA-2c; b, anti-rBbRAP-1/CT; c, anti-rBbTRAP-T; d, anti-rBbSBP-1; e, anti-rBbSBP-4; f, anti-GST. Specific immunofluorescent reaction (green) and nuclear staining (red) were observed.

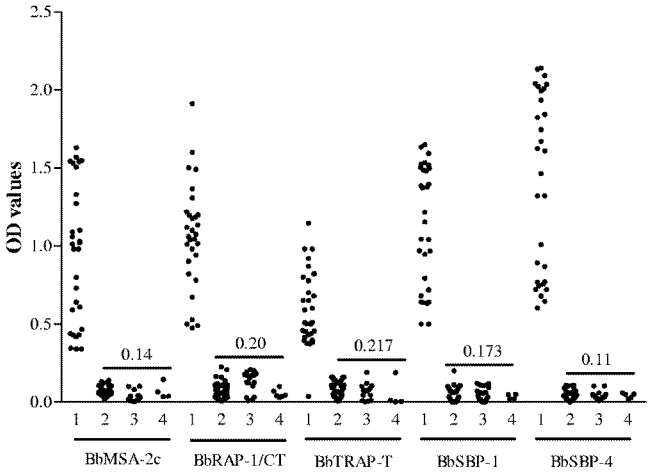

FIG. 4. Reactivity of ELISA using recombinant proteins with bovine sera. Lane 1, experimentally *B. bovis*-infected sera; lane 2, experimentally *B. bigemina*-infected sera; lane 3, noninfected bovine sera; lane 4, *Theileria orientalis*-infected sera. The cutoff of each recombinant protein is indicated by a bar.

infected serum samples tested had higher ODs than the cutoff value, contrary to the 30 *B. bigemina*-infected sera and 6 *Theileria orientalis*-infected sera, which had ODs lower than the cutoff values (Fig. 4). Although all recombinant proteins demonstrated good performance as ELISA antigens capable of identifying the experimental infection, rBbSBP-4 seemed to be the best due to its high OD values with *B. bovis*-infected sera and its lower OD values with normal bovine sera or *B. bigemina*- and *T. orientalis*-infected sera. Of note, rBbTRAP-T showed low OD values with *B. bovis*-infected sera. Furthermore, many samples were near the cutoff, and one sample was below, which indicates the low potential of rBbTRAP-T as a diagnostic antigen.

The diagnostic performances of these recombinant proteins were also evaluated with 669 field samples collected from areas of *B. bovis* endemicity, including Brazil (108 samples), Ghana (80 samples), China (100 samples), Thailand (100 samples), and Mongolia (81 samples), and areas where *B. bovis* is nonendemic, including South Korea (100 samples) and Hokkaido, Japan (100 samples). In addition, their results were compared to those of the IFAT, as a reference test (Table 2). None of the antigens showed a reaction, as tested using ELISAs and the IFAT with serum samples derived from areas where *B. bovis* is nonendemic (data not shown). On the other hand, the specificity and sensitivity of ELISAs with serum samples derived from the areas of endemicity ranged from 54.85% (rBbTRAP-T) to 96.01% (rBbSBP-4) and from 23.45% (rBbTRAP-T) to 96.43% (rBbSBP-4), respectively (Table 3). Next, the results were statistically compared to IFAT data. The agreement (con-

TABLE 2. Summary of ELISA results with recombinant proteins and IFAT results with field sera collected from different areas of *B. bovis* endemicity

Site or IFAT result	No. of IFAT samples	No. of ELISA samples									
		MSA-2c		RAP-1/CT		TRAP-T		SBP-1		SBP-4	
		+	−	+	−	+	−	+	−	+	−
Brazil											
+	80	52	28	35	45	10	70	74	6	78	2
−	28	2	26	0	28	1	27	8	20	4	24
Total	108	54	54	35	73	11	97	82	26	82	26
Ghana											
+	41	24	17	13	28	16	25	27	14	32	31
−	39	6	33	3	36	1	38	8	31	8	9
Total	80	30	50	16	64	17	63	35	45	40	40
China											
+	36	22	14	21	15	3	33	22	14	34	2
−	64	9	55	6	58	1	63	9	55	6	58
Total	100	31	69	27	73	4	96	31	69	40	60
Thailand											
+	57	45	12	34	23	10	47	38	19	51	6
−	43	16	27	16	27	2	41	14	29	11	32
Total	100	61	39	50	50	12	88	52	48	62	38
Mongolia											
+	29	17	12	18	11	9	20	16	13	18	11
−	52	11	41	10	42	4	48	6	46	10	42
Total	81	28	53	28	53	13	68	22	59	28	53
Overall											
+	243	160	83	121	122	48	195	177	66	213	30
−	226	44	182	35	191	9	217	45	181	39	187
Total	469	204	265	156	313	57	412	222	247	252	217

TABLE 3. The specificity and sensitivity of ELISAs and comparison of ELISA and IFAT results

Parameter	BbMSA	BbRAP-1CT	BbTRAP-T	BbSBP-1	BbSBP-4
Specificity (%)	85.3	72.3	54.85	91.49	96.01
Sensitivity (%)	83.95	64.2	23.45	91.35	96.43
Concordance (%)	72.9	66.53	56.5	76.33	85.3
Kappa value	0.461	0.339	0.153	0.528	0.705

cordance) between the IFAT and the ELISA was calculated to be 56.5% (rBbTRAP-T), 66.53% (rBbRAP-1CT), 72.9% (rBbMSA-2c), 76.33% (rBbSBP-1), and 85.3% (rBbSBP-4), and the kappa values were determined to be 0.153, 0.339, 0.461, 0.528, and 0.705, respectively (Table 3). These results revealed that rBbSBP-4 is the best diagnostic antigen assayed in the ELISA for the detection of a specific antibody to *B. bovis* among five antigens examined.

DISCUSSION

The global impact of bovine babesiosis has spurred an interest in developing effective diagnostic strategies that could lead to better management of the control of infection. *B. bovis* infection can be diagnosed directly by microscopic examination or PCR and indirectly with several serological methods (31). Although all of these tests have shortcomings, the serological tests, particularly the ELISA, seems to be the most practical and economical for epidemiological investigation (2, 7, 8). Indeed, the ELISA offers greater sensitivity, objectivity, and capacity for quick adaptation to test a large number of sera than any of the existing serological tests. The crude antigen prepared from merozoites has been utilized traditionally for serological detection; however, recombinant protein can be an alternative source, allowing better standardization of the test while reducing the cost of the massive production of the parasite (7, 9, 21). At this point, many recombinant antigens have been evaluated for diagnostic ELISAs; however, their sensitivities in diverse geographic areas have not produced perfect results. Therefore, further research on new antigens is extremely desirable for the development of a standard global assay. Within this context, we have validated five ELISAs utilizing deferent recombinant proteins and evaluated their usefulness for global application.

Although the ELISAs based on recombinant proteins differentiated clearly between experimentally *B. bovis*-infected and other closely related protozoan-infected bovine sera, their performances using field bovine sera varied, especially in comparison to IFAT results. Of note, rBbSBP-4 demonstrated the best performance, with high specificity, sensitivity, and agreement rates with the IFAT. These might be due to the fact that BbSBP-4 is a unique protein that has no significant homology with other apicomplexan parasites and is highly conserved among different geographic isolates from Asia, Africa, and South America (Terkawi et al., submitted). In addition, BbSBP-4 was found to shed within the cytoplasm of infected RBC in the late developmental stage of the parasites and was, subsequently, detected as an exoantigen in the supernatant of an *in vitro* culture (Terkawi et al., submitted). The secretion nature of BbSBP-4 may make the molecule very immunogenic during infection and allow direct interaction with host immune cells. On the other hand, rBbSBP-1 showed good diagnostic performance, with promising specificity and sensitivity for the detection of infection. Indeed, BbSBP-1 has been documented to be an immunodominant 80-kDa merozoite protein located in the spherical bodies, detected within the cytoplasmic face of the infected RBC membrane shortly after the invasion, and capable of eliciting the proliferation of both $CD4^+$ and $CD8^+$ T lymphocytes (16, 27). The better performance of rBbSBP-4 than of rBbSBP-1 in diagnosis might be due to the characteristics of the native protein which is found abundantly in the cytosol of infected host cells in the late stage of division of the parasites and, consequently, in the supernatant of the culture (Terkawi et al., submitted). This allows a direct and longer exposure to host immune cells (17). Moreover, the analyses of the determinant's composition based on an *in silico* epitope are necessary to understand antigenic attributes of these molecules. Further study including the combination of the two antigens on the basis of their B- and T-cell epitopes in the ELISA might be valuable, providing more accurate diagnostic tools for the detection of *B. bovis* infection.

A major membrane protein, BbMSA-2c, is a member of the complex VMSA genes and is known as a promising diagnostic antigen (19). Members of this family, however, exhibit high sequence variability among geographically distant strains (23). This might be the reason for the lower antigenicity of rBbMSA-2c for the detection of infection and might limit its potential for global diagnosis. The rhoptry-associated protein 1 (RAP-1) occurs in all *Babesia* species, has significant sequence homology with other apical complex proteins, and includes neutralization-sensitive B-cell and T-cell epitopes (24). BbRAP-1 is known as an exoantigen that is detected within the cytoplasm of infected RBC at the early stage of infection and persists shortly before disappearing at the ring stage (26, 27, 33). The full-length protein has been documented to be unsuitable for diagnosis due to the high conservation of 300 amino acids at the N-terminal region, which causes cross-reactivity with other *Babesia* spp. On the contrary, the C terminus presents distinct sequences with low identities with other *Babesia* RAP-1s and can serve as a species-specific diagnostic antigen (5, 6, 26). Therefore, the C terminus of BbRAP-1 has been used broadly as an antigen for serodiagnosis and epidemiological surveys, with high reliability (6, 18). However, our data have shown that this antigen had good performance with samples from Asia but not with those from Ghana and Brazil. In support of this, Boonchit et al. (5) have noted that rBbRAP-1CT has better performance for the detection of infection in Mongolian than Brazilian serum samples. The low sensitivity of rBbRAP-1CT is probably due to diversity in the sequences encoding the C-terminal region among geographically distant strains. Unexpectedly, rBbTRAP-T showed the lowest specificity and sensitivity with field serum samples, indicating that this antigen is not suitable for the development of a serological test. In a related study, rBgTRAP was noted as the best antigen for the detection of infection with *B. gibsoni* in canine sera (14, 26). The discrepancies in performance might be due to differences in the host and immune responses as well as the low identical homology between the genes in the species.

Serological diagnosis of *Babesia* infection is usually based on the detection of the antibodies against asexual blood-stage parasites. Although the IFAT has been a reliable serological

test in recent decades, it is time-consuming and subjective. Additionally, it cannot be automated, and results are largely influenced by the degree of training of the technician. Recently, the competitive ELISA (cELISA) with the C terminus of the rhoptry-associated protein 1 has been validated and undergone interlaboratory validation under OIE standards (12, 13). Despite the high specificity and sensitivity of the cELISA with *B. bovis*-infected sera from different geographic regions, the assay has shown a limitation in detecting the early stage of infection. Indeed, the IFAT could detect specific antibodies in experimentally *B. bovis*-infected sera about 2 days before the cELISA (12). Moreover, Goff et al. (13) have noted that samples with low OD values (near the cutoff point) in the cELISA should be repeated for further confirmation. These may affect the accuracy of the diagnosis in epidemiological investigation, particularly with carrier animals that have low antibody titers. Therefore, there is a need to continue research on the development of effective diagnostic assays. In the present study, we attempted to develop an indirect ELISA for the diagnosis of *B. bovis* infection. Our results demonstrated the usefulness of an ELISA utilizing rBbSBP-4 for the serological detection of *B. bovis* infection in cattle from different geographic regions of the world. The ELISA with rBbSBP-4 provides a more practical and sensitive tool than the standard IFAT and thus will be applicable for epidemiological surveys and control of the disease. Further investigations including a direct comparison of this ELISA with the previously validated cELISA (13) are required to achieve better diagnosis of *B. bovis* infection in the future.

ACKNOWLEDGMENTS

This work was supported by a grant from the Global COE Program (J02) and a Grant-in-Aid for Scientific Research (B-19405044), both from the Ministry of Education, Culture, Sports, Science, and Technology, Japan, and a program for the Promotion of Basic Research Activities for Innovative Bioscience (PROBRAIN).

M.A.T. was supported by a research grant fellowship from the Japanese Society for the Promotion of Science (JSPS) for young scientists. N.X.H., P.E.W., and F.J.S. were supported by Japan International Cooperation Agency (JICA).

REFERENCES

1. **Altangerel, K., et al.** 2009. Evaluation of *Babesia bigemina* 200 kDa recombinant antigen in enzyme-linked immunosorbent assay. Parasitol. Res. **105:** 249–254.
2. **Araújo, F. R., et al.** 1998. Comparison between enzyme-linked immunosorbent assay, indirect fluorescent antibody and rapid conglutination test in detecting antibodies against *Babesia bovis*. Vet. Parasitol. **74:**101–108.
3. **Bock, R., L. Jackson, A. de Vos, and W. Jorgensen.** 2004. Babesiosis of cattle. Parasitology **129:**247–269.
4. **Bono, M. F., et al.** 2008. Efficiency of a recombinant MSA-2c-based ELISA to establish the persistence of antibodies in cattle vaccinated with *Babesia bovis*. Vet. Parasitol. **157:**203–210.
5. **Boonchit, S., et al.** 2002. Evaluation of an enzyme-linked immunosorbent assay with recombinant rhoptry-associated protein-1 antigen of *Babesia bovis* for the detection of specific antibodies in cattle. J. Clin. Microbiol. **40:**3771–3775.
6. **Boonchit, S., et al.** 2004. Improved enzyme-linked immunosorbent assay using C-terminal truncated recombinant antigens of *Babesia bovis* rhoptry-associated protein-1 for detection of specific antibodies in cattle. J. Clin. Microbiol. **42:**1601–1604.
7. **Böse, R., R. H. Jacobson, K. R. Gale, D. J. Waltisbuhl, and I. G. Wright.** 1990. An improved ELISA for detection of antibodies against *Babesia bovis* using either a native or a recombinant *B. bovis* antigen. Parasitol. Res. **76:**648–652.
8. **Böse, R., W. K. Jorgensen, R. J. Dalgliesh, K. T. Friedhoff, and A. J. de Vos.** 1995. Current state and future trends in diagnosis of babesiosis. Vet. Parasitol. **57:**61–74.
9. **de Echaide, S. T., et al.** 1995. Evaluation of enzyme-linked immunosorbent assay kit to detect *Babesia bovis* antibodies in cattle. Prev. Vet. Med. **24:**277–283.
10. **de Vos, A. J., and F. T. Potgieter.** 1994. Bovine babesiosis, p. 278–294. *In* J. A. W. Coetzer, G. R. Thomson, and R. C. Tustin (ed.), Infectious diseases of livestock. Oxford University Press, Cape Town, South Africa.
11. **Gaffar, F. R., A. P. Yatsuda, F. F. Franssen, and E. de Vries.** 2004. A *Babesia bovis* merozoite protein with a domain architecture highly similar to the thrombospondin-related anonymous protein (TRAP) present in *Plasmodium* sporozoites. Mol. Biochem. Parasitol. **136:**25–34.
12. **Goff, W. L., et al.** 2003. Competitive enzyme-linked immunosorbent assay based on a rhoptry-associated protein 1 epitope specifically identifies *Babesia bovis*-infected cattle. Clin. Diagn. Lab. Immunol. **10:**38–43.
13. **Goff, W. L., et al.** 2006. Validation of a competitive enzyme-linked immunosorbent assay for detection of antibodies against *Babesia bovis*. Clin. Vaccine Immunol. **13:**1212–1216.
14. **Goo, Y. K., et al.** 2008. *Babesia gibsoni*: serodiagnosis of infection in dogs by an enzyme-linked immunosorbent assay with recombinant BgTRAP. Exp. Parasitol. **118:**555–560.
15. **Hines, S. A., G. H. Palmer, D. P. Jasmer, T. C. McGuire, and T. F. McElwain.** 1992. Neutralization-sensitive merozoite surface antigens of *Babesia bovis* encoded by members of a polymorphic gene family. Mol. Biochem. Parasitol. **55:**85–94.
16. **Hines, S. A., et al.** 1995. Genetic and antigenic characterization of *Babesia bovis* merozoite spherical body protein Bb-1. Mol. Biochem. Parasitol. **69:** 149–159.
17. **Homer, M. J., et al.** 2003. Identification and characterization of putative secreted antigens from *Babesia microti*. J. Clin. Microbiol. **41:**723–729.
18. **Iseki, H., et al.** 2010. Seroprevalence of *Babesia* infections of dairy cows in northern Thailand. Vet. Parasitol. **170:**193–196.
19. **Kim, C. M., et al.** 2008. Development of a rapid immunochromatographic test for simultaneous serodiagnosis of bovine babesiosis caused by *Babesia bovis* and *Babesia bigemina*. Am. J. Trop. Med. Hyg. **78:**117–121.
20. **Levy, M. G., and M. Ristic.** 1980. *Babesia bovis*: continuous cultivation in a microaerophilus stationary phase culture. Science **204:**1218–1220.
21. **Machado, R. Z., et al.** 1997. An enzyme-linked immunosorbent assay (ELISA) for the detection of antibodies against *Babesia bovis* in cattle. Vet. Parasitol. **71:**17–26.
22. **McCosker, P. J.** 1981. The global importance of babesiosis, p. 1–24. *In* M. Ristic and J. P. Kreier (ed.), Babesiosis. Academic Press, Inc., New York, NY.
23. **Palmer, G. H., et al.** 1991. Strain variation of *Babesia bovis* merozoite surface-exposed epitopes. Infect. Immun. **59:**3340–3342.
24. **Suarez, C. E., et al.** 1991. Characterization of the gene encoding a 60-kilodalton *Babesia bovis* merozoite protein with conserved and surface exposed epitopes. Mol. Biochem. Parasitol. **46:**45–52.
25. **Terkawi, M. A., et al.** 2007. *Babesia gibsoni* ribosomal phosphoprotein P0 induces cross-protective immunity against *B. microti* infection in mice. Vaccine **25:**2027–2035.
26. **Terkawi, M. A., et al.** 2009. Molecular characterizations of three distinct *Babesia gibsoni* rhoptry-associated protein-1s (RAP-1s). Parasitology **136:** 1147–1160.
27. **Tetzlaff, C. L., A. C. Rice-Ficht, V. M. Woods, and W. C. Brown.** 1992. Induction of proliferative responses of T cells from *Babesia bovis*-immune cattle with a recombinant 77-kilodalton merozoite protein (Bb-1). Infect. Immun. **60:**644–652.
28. **Uilenberg, G.** 2006. *Babesia*—a historical overview. Vet. Parasitol. **138:**3–10.
29. **Waltisbuhl, D. J., I. G. Goodger, I. G. Wright, M. A. Commins, and D. F. Mahoney.** 1987. An enzyme-linked immunosorbent assay to diagnose *Babesia bovis* infection in cattle. Parasitol. Res. **73:**126–131.
30. **Weiland, G., and I. Reiter.** 1988. Methods for serological response to *Babesia*, p. 143–158. *In* M. Ristic. (ed.), Babesiosis of domestic animals and man. CRC Press, Inc., Boca Raton, FL.
31. **World Organization for Animal Health (OIE).** 2008. Chapter 2.3.8, Bovine babesiosis. *In* Manual of diagnostic tests and vaccines for terrestrial animals. OIE, Paris, France. http://www.oie.int/fr/normes/mmanual/A_00059.htm.
32. **Xuan, X., et al.** 2001. Expression of *Babesia equi* merozoite antigen 1 in insect cells by a recombinant baculovirus and evaluation of its diagnostic potential in an enzyme-linked immunosorbent assay. J. Clin. Microbiol. **39:**705–709.
33. **Yokoyama, N., et al.** 2002. Cellular localization of *Babesia bovis* merozoite rhoptry-associated protein 1 and its erythrocyte-binding activity. Infect. Immun. **70:**5822–5826.
34. **Yokoyama, N., M. Okamura, and I. Igarashi.** 2006. Erythrocyte invasion by *Babesia* parasites: current advances in the elucidation of the molecular interactions between the protozoan ligands and host receptors in the invasion stage. Vet. Parasitol. **138:**22–32.

PROTIST, in press

Compartmentalization of a Glycolytic Enzyme in *Diplonema*, a Non-kinetoplastid Euglenozoan

Takashi Makiuchi[a,1], Takeshi Annoura[a,2], Muneaki Hashimoto[a], Tetsuo Hashimoto[b], Takashi Aoki[a], and Takeshi Nara[a,3].

[a]Department of Molecular and Cellular Parasitology, Juntendo University School of Medicine, 2-1-1 Hongo, Bunkyo-ku, Tokyo 113-8421, Japan
[b]Institute of Biological Sciences, University of Tsukuba, 1-1-1 Tennoudai, Tsukuba, Ibaraki 305-8572, Japan

Running title: Glycosome-like Organelles in Diplonemids

[1]Current address: Department of Parasitology, National Institute of Infectious Diseases, 1-23-1 Toyama, Shinjuku-ku, Tokyo 162-8640, Japan
[2]Current address: Leiden Malaria Research Group, Department of Parasitology, Centre for Infectious Diseases, Leiden University Medical Center, LUMC, L4-Q, Albinusdreef 2, 2333 ZA Leiden, Netherlands.
[3]Corresponding author; Fax +81 3 5800 0476
e-mail tnara@juntendo.ac.jp (T. Nara)

Abstract

Glycosomes are peroxisome-related organelles containing glycolytic enzymes that have been found only in kinetoplastids. We show here that a glycolytic enzyme is compartmentalized in diplonemids, the sister group of kinetoplastids. We found that, similar to kinetoplastid aldolases, the fructose 1,6-bisphosphate aldolase of *Diplonema papillatum* possesses a type 2-peroxisomal targeting signal. Western blotting showed that this aldolase was present predominantly in the membrane/organellar fraction. Immunofluorescence analysis showed that this aldolase had a scattered distribution in the cytosol, suggesting its compartmentalization. In contrast, orotidine-5'-monophosphate decarboxylase, a non-glycolytic glycosomal enzyme in kinetoplastids, was shown to be a cytosolic enzyme in *D. papillatum*. Since euglenoids, the earliest diverging branch of Euglenozoa, do not possess glycolytic compartments, these findings suggest that the routing of glycolytic enzymes into peroxisomes may have occurred in a common ancestor of diplonemids and kinetoplastids, followed by diversification of these newly established organelles in each of these euglenozoan lineages.

Key Words: Euglenozoa; evolution; glycosome; kinetoplastids; peroxisome; trypanosomatids.

Introduction

Peroxisomes are cellular compartments surrounded by a single membrane and present in almost all eukaryotes. These specialized organelles are involved in the oxidation of various organic substrates using molecular oxygen. This process results in the generation of toxic hydrogen peroxide, which must be

detoxified by catalase. Peroxisomes participate in important metabolic pathways, including the β-oxidation of fatty acids, free radical detoxification, and purine/pyrimidine degradation (Gabaldón et al. 2006; Parsons et al. 2001; Schlüter et al. 2006).

The physiological functions and enzymatic contents of peroxisomes vary across species and often among growth conditions (Michels et al. 2005; Parsons et al. 2001). For example, glyoxysomes, the specialized form of peroxisomes found in germinating plant seeds, contain enzymes of the glyoxylate cycle, whereas peroxisomes of leaves contain enzymes of the glycolate pathway, a difference regarded as a typical example of organellar diversification (Gabaldón 2010; Hayashi et al. 2000; Tolbert et al. 1968).

The protistan group Euglenozoa includes three major lineages, euglenoids, diplonemids, and kinetoplastids, with euglenoids constituting the earliest branch followed by the separation of the diplonemid and kinetoplastid lineages (Cavalier-Smith 1981; Simpson et al. 2002; Simpson and Roger 2004). Kinetoplastids consist of bodonids and trypanosomatids, the latter of which include medically important pathogens, such as *Trypanosoma brucei*, which causes sleeping sickness (African Trypanosomiasis); *T. cruzi*, which causes Chagas disease (American Trypanosomiasis) and *Leishmania* spp., which cause leishmaniasis.

The presence of peroxisomes in euglenoids is not fully understood. *Euglena* possesses peroxisome-like particles but lacks catalase activity (Collins and Merrett 1975; Graves et al. 1971; Shigeoka et al. 1980). In contrast, kinetoplastids possess unique peroxisome like-organelles, called glycosomes, characterized by compartmentalization of most of the glycolytic pathway (Michels et al. 2006; Opperdoes and Borst 1977; Opperdoes et al. 1988). In addition, glycosomes contain other metabolic enzymes, such as most of the enzymes of the purine salvage pathway and the last two enzymes of the de novo pyrimidine biosynthetic pathway, orotate phosphoribosyltransferase (OPRT) and orotidine-5'-monophosphate decarboxylase (OMPDC) (Hammond and Gutteridge 1982; Michels et al. 2000). These findings highlight the unique evolution of peroxisomes in the kinetoplastid lineage.

The evolutionary trail by which peroxisomes gave rise to glycosomes in kinetoplastids, however, remains unclear, due largely to the lack of biochemical and genetic information regarding the nature of peroxisomes and peroxisome-related organelles in diplonemids, the closest relatives of kinetoplastids. We previously reported that the structure of the *OPRT* and *OMPDC* genes varies among euglenozoan lineages (Makiuchi et al. 2007; Makiuchi et al. 2008). Euglenoids possess a *OMPDC-OPRT* fusion gene, with the OMPDC activity present in the cytosol (Walther et al. 1980). In contrast, kinetoplastids possess an inversely fused *OMPDC-OPRT* gene, with the OMPDC-OPRT fusion protein having a peroxisome-targeting signal (C-terminal PTS1), suggesting that it is localized in glycosomes. In the diplonemid, *Diplonema papillatum*, the subcellular localization of OMPDC (and putative OPRT) has not yet been determined. We found that *D. papillatum OMPDC* is a stand-alone gene, lacking the consensus sequence of a PTS, suggesting that the protein is localized in the cytosol (Makiuchi et al. 2008).

In the present study, we examined whether glycosome-associated enzymes are compartmentalized in diplonemids. We characterized two enzymes, the glycolytic fructose 1,6-bisphosphate aldolase (ALD) and OMPDC in *D. papillatum*. We demonstrate that a consensus sequence of an N-terminal PTS2 is present in ALD of *D. papillatum*, suggesting that this enzyme is localized in peroxisomes, as is that of trypanosomatids. Phylogenetic analysis showed monophyly of trypanosomatid and diplonemid ALDs. Biochemical analysis showed the different distributions of ALD and OMPDC, predominantly in the membrane-rich and cytosolic fractions, respectively. Immunofluorescence analysis showed that *D. papillatum* ALD has a scattered pattern of distribution, whereas OMPDC has a uniform pattern of distribution. Our findings may provide insights into the distinct evolution of peroxisome like-organelles in the different euglenozoan lineages.

Results

Presence of a Peroxisomal Targeting Signal in *D. papillatum* ALD

ALD is a glycosomal enzyme in trypanosomatids (Hart et al. 1984; Taylor and Gutteridge 1987). Full-length ALD cDNA of *D. papillatum* (GenBank™ AB550707) was cloned based on its partial sequence registered in the TBest database (http://tbestdb.bcm.umontreal.ca/searches/login.php). In general, ALDs can be divided into two

classes, Class I and Class II; Class I aldolases are present in vertebrates, plants and a number of protists and prokaryotes (see Fig. 2), whereas Class II aldolases are present in fungi, several protists and many prokaryotes (Rutter 1964). We found that the amino acid sequence of *D. papillatum* ALD showed identities of 63%, 45%, 48%, and 50% with the Class I ALDs of trypanosomatids, *Euglena gracilis* (euglenoids), *Arabidopsis thaliana* (plants), and humans (animals), respectively.

D. papillatum ALD is comprised of 374 amino acids and has an estimated molecular weight of 41 kD. The amino acid residues constituting the active site of class-I ALD are fully conserved in *D. papillatum* ALD (St-Jean et al. 2005). Indeed, recombinant *D. papillatum* ALD expressed in *Escherichia coli* was able to catalyze the formation of glyceraldehyde-3-phosphate and dihydroxyacetone phosphate from the substrate, fructose-1,6-bisphospate (data not shown). The most striking feature of *D. papillatum* ALD is the presence of a consensus N-terminal peroxisomal targeting signal (PTS2) present in trypanosomatid ALDs (Gabaldón 2010; Michels et al. 2005), suggesting that *D. papillatum* ALD is likely to localize in peroxisome-related compartments (Fig. 1A).

D. papillatum ALD Has a Common Evolutionary Origin as Glycosomal ALDs of Kinetoplastids

We examined whether the targeting of ALD to peroxisome-related organelles occurred in the common ancestor of diplonemids and kinetoplastids or evolved independently in each lineage. Phylogenetic analysis of Class I ALDs clearly showed monophyly of diplonemid and trypanosomatid ALDs within the eukaryotic clade with strong bootstrap support (Fig. 2). The evolutionary origin of euglenoid Class I ALD is unclear, due mainly to the lack of resolution. It is worth noting that euglenoids possess both Class I (plastid) and Class II (cytosolic) ALDs (Plaumann et al. 1997). The finding, that euglenoid Class I ALD did not fall into the diplonemid/kinetoplastid clade, suggests their different origin, the former originating probably from a secondary endosymbiont (an algal lineage) that gave rise to the plasmid. We conclude that the addition of PTS2 to ALD may have occurred in the common ancestor of diplonemids and kinetoplastids after separation of the euglenoid lineage.

Evidence of Compartmentalization of *D. papillatum* ALD

Trypanosomatid OMPDC is fused with orotate phosphoribosyltransferase (OPRT) as OMPDC-OPRT and possesses a C-terminal PTS (PTS1), whereas *D. papillatum* OMPDC is a stand-alone enzyme lacking PTSs (Makiuchi et al. 2008). Since PTS2 is present in *D. papillatum* ALD, the ALD and OMPDC may be localized differently in diplonemids. To determine their cellular localizations, we performed western blot analysis of the *D. papillatum* subcellular fractions using specific antibodies to *D. papillatum* ALD and OMPDC (Fig. 1B).

We first confirmed the specificity of the antibody raised against *D. papillatum* ALD by western blotting (Fig. 1B, left). Immunoprecipitates of extracts of both *D. papillatum* and *T. cruzi* using anti-DpALD antibody showed bands at 41 kD, as expected, which were confirmed as aldolase by LC-MS/MS analysis (Supplementary Table S1)

D. papillatum ALD was detected predominantly in the membrane-rich fraction (105,000 ×*g* sediment, lane 3, middle) but not in the cytosolic fraction (105,000 ×*g* supernatant; lane 2, middle). In contrast, OMPDC was detected predominantly in the cytosolic fraction (105,000 ×*g* supernatant; lane 2, right). These results suggest that, in *D. papillatum,* ALD is membrane-associated and likely to be localized in peroxisome-related organelles, whereas OMPDC is a cytosolic protein.

Different Subcellular Distributions of ALD and OPMDC in *D. papillatum*

We further examined the localization of ALD and OMPDC by indirect immunofluorescence analysis. ALD was detected as "*dots*" in both *D. papillatum* and *T. cruzi* (Fig. 3). Confocal fluorescence microscopy showed that the fluorescence signals of mitochondrial DNA and ALD did not merge (Fig. 3, bottom), suggesting that ALD is not a mitochondrial protein and that ALD is compartmentalized into peroxisome-related organelles in both species. In contrast, *D. papillatum* OMPDC was detected throughout the cells and did not co-localize with ALD, again suggesting that OMPDC is a cytosolic protein. Taken together, these findings suggest that, in *D. papillatum,* ALD and OMPDC are separately localized in peroxisome-related compartments and the cytosol, respectively.

Discussion

This is the first report suggesting that, in diplonemids, a glycolytic enzyme is

compartmentalized in peroxisome-related organelles. At present, the biochemical properties of glycolytic enzymes in diplonemids are largely unknown; only partial nucleotide sequences for the fifth enzyme, glyceraldehyde 3-phosphate dehydrogenase (GAPDH), have been cloned but their cellular localization is unknown (Qian and Keeling 2001).

The presence of PTS suggested that peroxisomes are most likely to be the ALD-associated organelles. The presence of ALD in other organelles, such as the mitochondrion and endoplasmic reticulum, is unlikely. The mitochondrion of *D. papillatum* is large and highly branched throughout the cell (Marande et al. 2005). We found, however, that the fluorescence signal of mitochondrial DNA did not co-localize with that of ALD. Moreover, the predicted signal sequences by MitoProt (http://ihg2.helmholtz-muenchen.de/ihg/mitoprot.html) and SignalP (http://www.cbs.dtu.dk/services/SignalP/) indicated that it was unlikely that *D. papillatum* ALD had been imported into the mitochondrion (probability, 0.1330) or endoplasmic reticulum (probability, 0.000).

Glycosomes contain the first seven of the ten enzymes of glycolysis (Michels et al. 2006). In general, the accumulation or compartmentalization of enzymes involved in a metabolic pathway is advantageous for concerted metabolism. This may occur by the formation of enzyme complexes or the fusion of functionally related enzymes. This, however, does not seem true for glycosomes. The compartmentalization of glycolytic enzymes appears physiologically critical for trypanosomatids, especially because hexokinase and 6-phosphofructokinase, the allosteric enzymes that regulate glycolysis in canonical eukaryotes and catalyze the reactions upstream of ALD, are insensitive to their allosteric inhibitors (Michels et al. 2006). The occurrence of these enzymes in the cytosol may result in the accumulation of toxic glycolytic intermediates and the consumption of cytosolic ATP (Bakker et al. 2000). The compartmentalization of glycolytic enzymes may have resulted in the feedback regulation of hexokinase and 6-phosphofructokinase becoming redundant and finally lost, causing their compartmentalization to be critical.

Notably, OMPDC is localized differently in kinetoplastids and diplonemids. Glycosomes also contain enzymes involved in gluconeogenesis, nucleotide biosynthesis, and sugar-nucleotide biosynthesis (Michels et al. 2006). One sugar-nucleotide, UDP-GlcNAc, has been predicted to be an important metabolite in the synthesis of glycosylphosphatidylinositol (GPI)-anchored glycoproteins, which are essential components in trypanosomatids (Ferguson 1999; Stokes et al. 2008). It is important to know whether the enzymes of non-glycolysis pathways became compartmentalized in a common ancestor of diplonemids/kinetoplastids.

We previously showed that, after separation of the kinetoplastid and diplonemid lineages, a common ancestor of kinetoplastids acquired the OMPDC gene by lateral gene transfer, and that this gene subsequently fused with the OPRT gene (Makiuchi et al. 2008). Thus, glycolytic enzymes likely accumulated in the peroxisomes of a common ancestor of kinetoplastids and diplonemids. After the separation of the kinetoplastid lineage, the compartmentalization of other enzymes, including OMPDC (-OPRT fusion), into peroxisome-derived organelles may have occurred, resulting in the formation of glycosomes.

It is worth noting that glycosomes of the parasitic bodonids, *Trypanoplasma borreli* and *Cryptobia salmositica,* possess catalase activity, an authentic peroxisome marker enzyme (Ardelli et al. 2000; Opperdoes et al. 1988). In conjunction with the notion that trypanosomatids are monophyletic and nested within the bodonid clade, stepwise evolution of peroxisome-related organelles in each lineage may have occurred in association with the acquisition and/or loss of the related genes in a lineage-specific manner.

Our findings not only unite kinetoplastids and diplonemids at the level of peroxisome evolution but provide evidence of the diversification of these organelles in Euglenozoa. Further identification of the enzymes involved in the specialized peroxisomes of both lineages would clarify their physiological and biochemical importance.

Methods

Organisms: An axenic culture of *D. papillatum* (ATCC 50162) was routinely maintained as described (Makiuchi et al. 2008). *T. cruzi* Tulahuen strain was maintained in LIT medium (Annoura et al. 2005).

cDNA cloning of the *ALD* gene from *D. papillatum*: The full-length *D. papillatum* ALD cDNA was obtained by 5'- and 3'-RACEs using the partial sequence of a putative *ALD* gene (GenBank™; EC842358, TBestDB;

DPL00001327) registered in the TBest database and the following primer sets: for 5'-RACE, 5'-CGTCGAACTTCTGGGTAAGG-3' (cDNA synthesis), 5'-GCTACAGTTTCTGTACTTTATTG-3' (sense PCR primer, spliced-leader specific), and 5'-ATGACACCGCTGATGTACTG-3' (antisense primer) (Sturm et al. 2001); for 3'-RACE, 5'-AATAAAGCGGCCGCGGATCCAATTTTTTTT TTTTTTTTVN-3' (cDNA synthesis), 5'-GCTGCGACAAGCGCTTCAAG-3' (amplification of the sense strand), 5'-AGACGCTACCGTGCCCTGAT-3' (sense PCR primer), and 5'-AATAAAGCGGCCGCGGATCCAA-3' (antisense primer). Finally, the full-length ALD cDNA was PCR amplified using the primers 5'-CACCATGTCTGCCCGTATCGAAGTCCTGA-3' (sense) and 5'-CTAGTAGGTGTTGCCCTTGATGTAC-3' (antisense) and *D. papillatum* cDNA as a template.

Phylogenetic analysis: All sequence data, with the exception of that of *D. papillatum* ALD cloned by us and first reported here, were collected from public sequence databases by taxonomic and BLAST searches. The sequences reported in this paper appear in the DDBJ/EMBL/GenBank databases under accession number AB550707 for *Diplonema papillatum* ALD mRNA. Multiple alignment of ALD sequences was obtained using CLUSTAL W (Thompson et al. 1994), with the alignment corrected by manual inspection. Unambiguously aligned positions were selected and used for phylogenetic analyses, which were performed by the maximum likelihood (ML), maximum parsimony (MP), and distance matrix (DM) methods implemented in the PHYLIP3.69 package, and by the ML method in the PAML package (Felsenstein ; Yang 1997). With 33 taxa, 310 unambiguously aligned amino acid sites were used for analysis, corresponding to residues 81-105, 107-157, 166-174, 179-225, 240-250, 255-260, 265-281, 290-308 and 317-361 of the *D. papillatum* sequence.

Expression of recombinant *D. papillatum* ALD and OMPDC: The full-length PCR products for the *ALD* and *OMPDC* genes of *D. papillatum* were subcloned in the pET151 expression vector (Invitrogen), which allows N-terminal fusion with His_6-tag, and sequenced. After transformation of *Escherichia coli* BL21-CodonPlus® (DE3)-RP cells (STRATAGENE®, Agilent Technologies, Inc., CA, USA) with the plasmids, expression of ALD and OMPDC was induced by incubation at 25°C in the presence of IPTG. The recombinant proteins were affinity-purified with His•Bind® resin (Novagen, EMD Biosciences, Inc., Madison, WI, USA), equilibrated with phosphate-buffered saline (PBS, pH 7.2), cleaved with AcTEV™ Protease (Invitrogen) to remove the tag and, finally purified further on a His•Bind® column.

Antibodies: Female BALB/c mice were immunized with 100 μg recombinant ALD, and female Japanese white rabbits were immunized with 200 μg OMPDC, each in Freund's complete adjuvant, followed by booster injections with the same antigens in Freund's incomplete adjuvant. IgG was purified from each antiserum using HiTrap™ Protein G HP (GE Healthcare).

Subcellular fractionation, immunoprecipitation, and Western blotting: *D. papillatum* cells were washed once with artificial seawater and twice with 25 mM Tris-HCl/10 mM KCl/1 mM EDTA/250 mM sucrose (pH 7.4). The cells were homogenized in the latter buffer containing a protease inhibitor cocktail (Complete Mini, Roche Diagnostics K.K., Tokyo, Japan) using a cell disruption bomb (Parr Instrument Company, Moline, IL, USA) at 250 psi for 10 min. The homogenates were centrifuged twice at 1,000 ×*g* for 10 min and the supernatant was centrifuged at 105,000 × *g* for 1 hour. The resulting pellet and supernatant were defined as the membrane-rich and cytosolic fractions, respectively. For immunoprecipitation, the cells were harvested by centrifugation at 1,700 ×*g* for 10 min at 4 °C and washed once with PBS (pH 7.2) by centrifugation at 1,700 ×*g* for 10 min at 4 °C. Using an ultrasonicator, the cells were lysed in 10 mM Tris-HCl/150 mM NaCl/1 % TritonX-100/0.5 % NP-40 (pH 8.0) supplemented with the protease inhibitor cocktail. The cell lysates, each containing 140 μg protein, were incubated with the antibody and precipitated using Protein G Magnetic Beads (New England Biolabs, Beverly, MA). The resulting precipitates were separated by SDS-PAGE and transferred to PVDF membranes, which were incubated with the corresponding antibody. Antibody reactions were visualized using alkaline phosphatase-conjugated secondary antibody and a chemiluminescent substrate (CSPD, Roche Diagnostics).

Immunofluorescence microscopy: *D. papillatum* cells were allowed to adhere onto poly-L-lysine coated slides for 15 min in a humidity chamber at 4 °C. After removal of unbound cells, the bound cells were fixed for 25 min with 4% paraformaldehyde and permeabilized in PBS containing 0.5% Triton-X 100 for 10 min at 4 °C. The slides were

incubated in blocking solution (PBS containing 0.05% Tween 20 and 1% BSA) for 30 min, and subsequently with the specific antibody in blocking solution for 90 min at room temperature. After washing with PBS, the slides were incubated with secondary antibodies and counterstained for 10 min with Hoechst 33342 for immunofluorescence microscopy or Hoechst 33258 for confocal laser microscopy. The localization of each enzyme was assessed by fluorescence microscopy.

Acknowledgements

We thank Tsutomu Fujimura, Reiko Mineki, and Hikari Taka of the Division of Proteomics and Biomolecular Science, Biomedical Research Center at Juntendo University Graduate School of Medicine, for mass-spectrometric analysis. This work was supported in part by grants-in-aid for scientific research Nos. 20790327, 18890188 (to T. Annoura) and 19590436 (to T. Nara) and by 21st Century COE Research (to T. Annoura, T. Makiuchi and T. Aoki) from the Ministry of Education, Sports, Culture, Science, and Technology of Japan.

Appendix A. Supplementary materials

Supplementary information is available at Protist online (http://www.elsevier.de/protist).

References

Annoura T, Nara T, Makiuchi T, Hashimoto T, Aoki T (2005) The origin of dihydroorotate dehydrogenase genes of kinetoplastids, with special reference to their biological significance and adaptation to anaerobic, parasitic conditions. J Mol Evol **60**: 113-127

Ardelli BF, Witt JD, Woo PT (2000) Identification of glycosomes and metabolic end products in pathogenic and nonpathogenic strains of *Cryptobia salmositica* (Kinetoplastida: Bodonidae). Dis Aquat Organ **42**: 41-51

Bakker BM, Mensonides FI, Teusink B, van Hoek P, Michels PA, Westerhoff HV (2000) Compartmentation protects trypanosomes from the dangerous design of glycolysis. Proc Natl Acad Sci USA **97**: 2087-2092

Cavalier-Smith T (1981) Eukaryote kingdoms: seven or nine? Biosystems **14**: 461-481

Collins N, Merrett MJ (1975) The localization of glycollate-pathway enzymes in *Euglena*. Biochem J **148**: 321-328

Felsenstein J. *PHYLIP*. Available from: http://evolution.gs.washington.edu/phylip.html.

Ferguson MA (1999) The structure, biosynthesis and functions of glycosylphosphatidylinositol anchors, and the contributions of trypanosome research. J Cell Sci **112 (Pt 17)**: 2799-2809

Gabaldón T (2010) Peroxisome diversity and evolution. Philos Trans R Soc Lond B Biol Sci **365**: 765-773

Gabaldón T, Snel B, van Zimmeren F, Hemrika W, Tabak H, Huynen MA (2006) Origin and evolution of the peroxisomal proteome. Biol Direct **1**: 8

Graves LB, Jr., Hanzely L, Trelease RN (1971) The occurrence and fine structural characterization of microbodies in *Euglena gracilis*. Protoplasma **72**: 141-152

Hammond DJ, Gutteridge WE (1982) UMP synthesis in the kinetoplastida. Biochim Biophys Acta **718**: 1-10

Hart DT, Misset O, Edwards SW, Opperdoes FR (1984) A comparison of the glycosomes (microbodies) isolated from *Trypanosoma brucei* bloodstream form and cultured procyclic trypomastigotes. Mol Biochem Parasitol **12**: 25-35

Hayashi M, Toriyama K, Kondo M, Kato A, Mano S, De Bellis L, Hayashi-Ishimaru Y, Yamaguchi K, Hayashi H, Nishimura M (2000) Functional transformation of plant peroxisomes. Cell Biochem Biophys **32**: 295-304

Makiuchi T, Nara T, Annoura T, Hashimoto T, Aoki T (2007) Occurrence of multiple, independent gene fusion events for the fifth and sixth enzymes of pyrimidine biosynthesis in different eukaryotic groups. Gene **394**: 78-86

Makiuchi T, Annoura T, Hashimoto T, Murata E, Aoki T, Nara T (2008) Evolutionary analysis of synteny and gene fusion for pyrimidine biosynthetic enzymes in Euglenozoa: an extraordinary gap between kinetoplastids and diplonemids. Protist **159**: 459-470

Marande W, Lukeš J, Burger G (2005) Unique mitochondrial genome structure in diplonemids, the sister group of kinetoplastids. Eukaryot Cell **4**: 1137-1146

Michels PA, Hannaert V, Bringaud F (2000) Metabolic aspects of glycosomes in trypanosomatidae - new data and views. Parasitol Today **16**: 482-489

Michels PA, Bringaud F, Herman M, Hannaert V (2006) Metabolic functions of glycosomes in trypanosomatids. Biochim Biophys Acta **1763**: 1463-1477

Michels PA, Moyersoen J, Krazy H, Galland N, Herman M, Hannaert V (2005) Peroxisomes, glyoxysomes and glycosomes (review). Mol Membr Biol **22**: 133-145

Opperdoes FR, Borst P (1977) Localization of nine glycolytic enzymes in a microbody-like organelle in *Trypanosoma brucei*: the glycosome. FEBS Lett **80**: 360-364

Opperdoes FR, Nohynkova E, Van Schaftingen E, Lambeir AM, Veenhuis M, Van Roy J (1988) Demonstration of glycosomes (microbodies) in the Bodonid flagellate *Trypanoplasma borelli* (Protozoa, Kinetoplastida). Mol Biochem Parasitol **30**: 155-163

Parsons M, Furuya T, Pal S, Kessler P (2001) Biogenesis and function of peroxisomes and glycosomes. Mol Biochem Parasitol **115**: 19-28

Plaumann M, Pelzer-Reith B, Martin WF, Schnarrenberger C (1997) Multiple recruitment of class-I aldolase to chloroplasts and eubacterial origin of eukaryotic class-II aldolases revealed by cDNAs from *Euglena gracilis*. Curr Genet **31**: 430-438

Qian Q, Keeling PJ (2001) Diplonemid glyceraldehyde-3-phosphate dehydrogenase (GAPDH) and prokaryote-to-eukaryote lateral gene transfer. Protist **152**: 193-201

Rutter WJ (1964) Evolution of Aldolase. Fed Proc **23**: 1248-1257

Schlüter A, Fourcade S, Ripp R, Mandel JL, Poch O, Pujol A (2006) The evolutionary origin of peroxisomes: an ER-peroxisome connection. Mol Biol Evol **23**: 838-845

Shigeoka S, Nakano Y, Kitaoka S (1980) Metabolism of hydrogen peroxide in *Euglena gracilis* Z by L-ascorbic acid peroxidase. Biochem J **186**: 377-380

Simpson AG, Roger AJ (2004) Protein phylogenies robustly resolve the deep-level relationships within Euglenozoa. Mol Phylogenet Evol **30**: 201-212

Simpson AG, Lukeš J, Roger AJ (2002) The evolutionary history of kinetoplastids and their kinetoplasts. Mol Biol Evol **19**: 2071-2083

St-Jean M, Lafrance-Vanasse J, Liotard B, Sygusch J (2005) High resolution reaction intermediates of rabbit muscle fructose-1,6-bisphosphate aldolase: substrate cleavage and induced fit. J Biol Chem **280**: 27262-27270

Stokes MJ, Guther ML, Turnock DC, Prescott AR, Martin KL, Alphey MS, Ferguson MA (2008) The synthesis of UDP-N-acetylglucosamine is essential for bloodstream form *Trypanosoma brucei* in vitro and in vivo and UDP-N-acetylglucosamine starvation reveals a hierarchy in parasite protein glycosylation. J Biol Chem **283**: 16147-16161

Sturm NR, Maslov DA, Grisard EC, Campbell DA (2001) *Diplonema* spp. possess spliced leader RNA genes similar to the Kinetoplastida. J Eukaryot Microbiol **48**: 325-331

Taylor MB, Gutteridge WE (1987) *Trypanosoma cruzi*: subcellular distribution of glycolytic and some related enzymes of epimastigotes. Exp Parasitol **63**: 84-97

Thompson JD, Higgins DG, Gibson TJ (1994) CLUSTAL W: improving the sensitivity of progressive multiple sequence alignment through sequence weighting, position-specific gap penalties and weight matrix choice. Nucleic Acids Res **22**: 4673-4680

Tolbert NE, Oeser A, Kisaki T, Hageman RH, Yamazaki RK (1968) Peroxisomes from spinach leaves containing enzymes related to glycolate metabolism. J Biol Chem **243**: 5179-5184

Walther R, Wasternack C, Helbing D, Lippmann G (1980) Pyrimidine metabolizing enzymes in *Euglena gracilis*: Synthesis and localization of OPRTase, ODCase and β -ureidopropionase. Biochem Physiol Pflanzen **175**: 764-771

Yang Z (1997) PAML: a program package for phylogenetic analysis by maximum likelihood. Comput Appl Biosci **13**: 555-556

Figure Legends

Figure 1. Characterization of aldolase (ALD) of *Diplonema papillatum*. (**A**) Amino acid sequence alignment of Class I fructose-1,6-bisphosphate aldolases. The asterisks indicate the same or equivalent amino acids. The N-terminal peroxisomal targeting signals (PTS2), consisting of a consensus nonapeptide (R/K)-(L/V/I)-X_5-(Q/H)-(L/A), are shaded. (**B**) Western blot analysis of ALD (41 kD) (left and middle panels) and orotidine-5'-monophosphate decarboxylase (OMPDC, 25 kD) (right panel) of *D. papillatum*. The anti-ALD antibody specifically recognizes ALD of *Trypanosoma cruzi* (Tc) and *D. papillatum* (Dp) (left panel). The crude cell lysate (lane 1), supernatant (lane 2) and precipitate (lane 3) of a 105,000 × *g* preparation were reacted with the specific antibodies. The arrow and arrowheads indicate the bands for ALD (41 kD) and the precipitated antibodies, respectively.

Figure 2. Phylogenetic reconstruction of Class I fructose-1,6-bisphosphatae aldolase (ALD). The consensus maximum likelihood (ML) tree of ALD inferred by the JTT model taking across-site rate heterogeneity into consideration. The α-value of the Γ shape parameter used in the analysis was 0.85937. Bootstrap proportions (BPs) by the ML method are attached to the internal branches. Branches with less than 50% BP support are unmarked. For the four nodes, BP values determined by the distance matrix (DM) and maximum parsimony (MP) methods are also shown.

Figure 3. Indirect immunofluorescence analyses of *T. cruzi* and *D. papillatum*. *T. cruzi* (Tc, top) and *D. papillatum* (Dp, middle) were fixed, reacted with anti-*D. papillatum* ALD antibody, conjugated with Alexa Fluor 488, and counterstained with Hoechst 33342. Localization of ALD and OMPDC in *D. papillatum* cells was assessed by confocal microscopy (bottom, counterstained with Hoechst 33258). Neither pre-immune sera nor the antiserum absorbed with the corresponding antigens showed any fluorescent signal. DIC, differential interference contrast image; Merged, merged image. Scale bar = 5 μm.

Makiuchi *et al.* Figure 1.

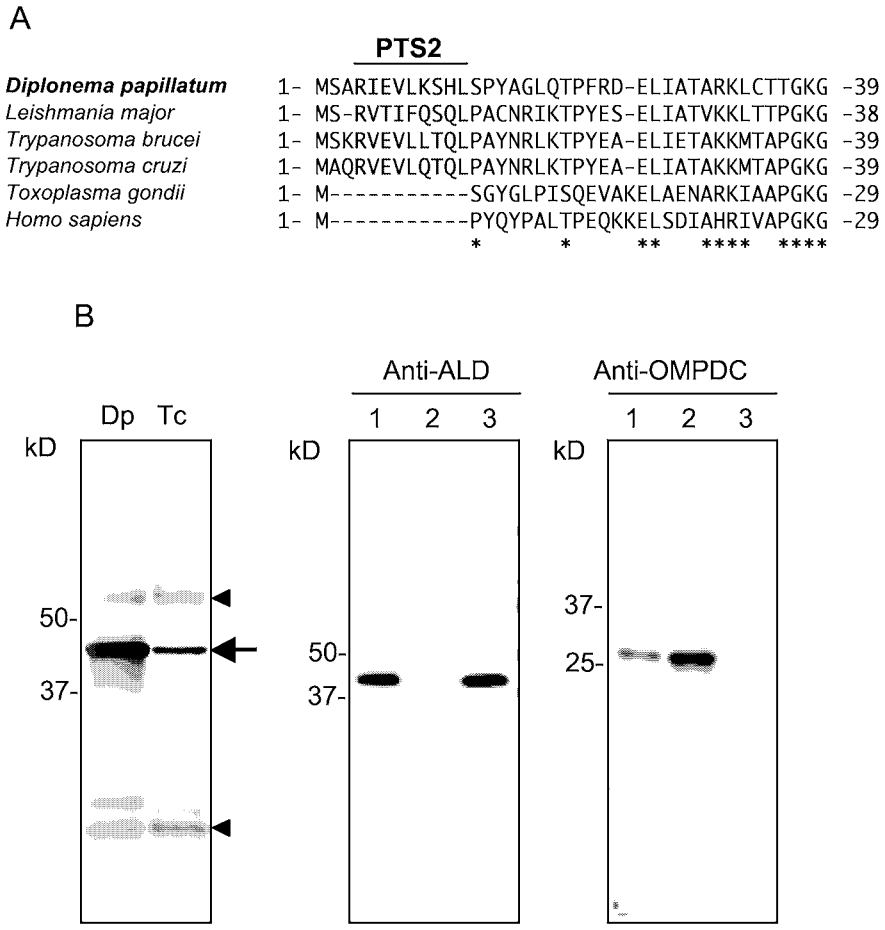

Makiuchi *et al.* Figure 2.

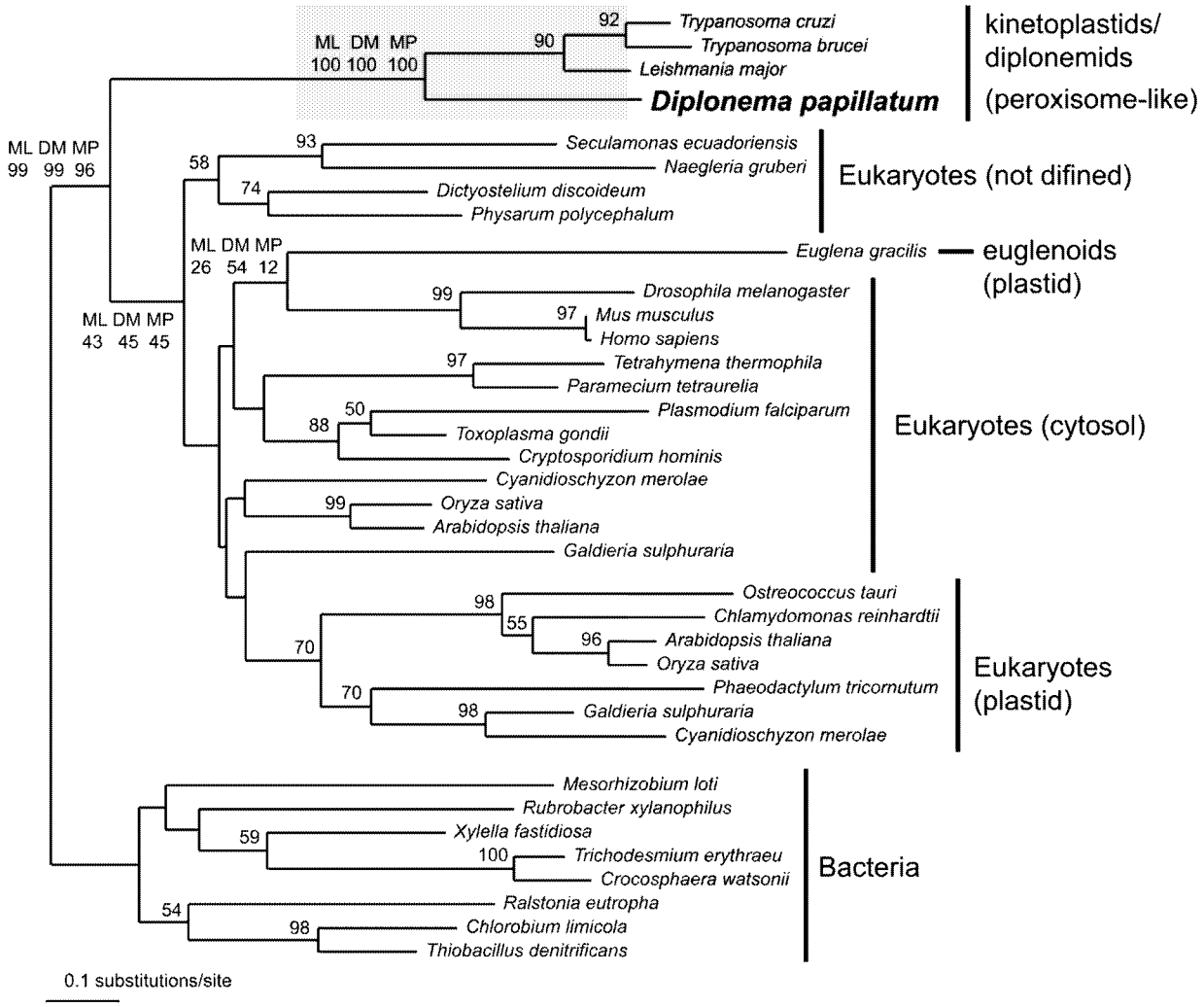

Makiuchi *et al.* Figure 3.

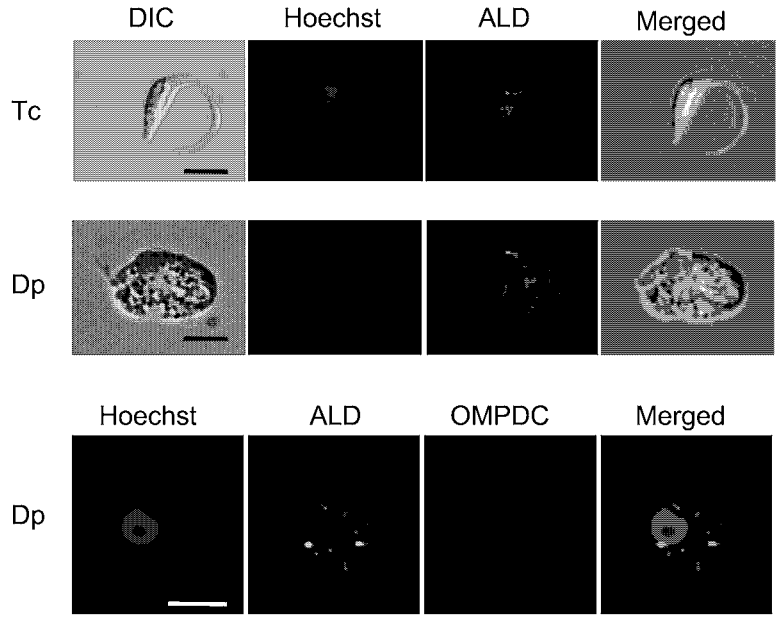

Supplementary Materials and Methods

In-gel digestion and liquid chromatography-tandem mass spectrometry (LC-MS/MS)

In-gel trypsin digestion of SDS–PAGE bands of interest was performed as described (Mineki et al. 2002). The protein(s) in each band were digested with trypsin, eluted from the gel, and dissolved in 10 μl 1% formic acid. Mass spectrometry was performed using an AB-QSTAR pulsar *i* hybrid (Applied Biosystems, Inc., Framingham, CA) and a micro-liquid chromatograph (Magic 2002; Michrom Bioresources, Inc., Abum, CA) equipped with a 0.2-mm ID × 50 mm Magic C18 column. The amino acid sequences of the peptides were assessed by LC-MS/MS, with a Mascot search engine (www.matrixscience.com/search_form_select.html) used for all peptide mass mapping and MS/MS ion searching against the proteome database, NCBInr.

References

Mineki R, Taka H, Fujimura T, Kikkawa M, Shindo N, Murayama K (2002) In situ alkylation with acrylamide for identification of cysteinyl residues in proteins during one- and two-dimensional sodium dodecyl sulphate-polyacrylamide gel electrophoresis. Proteomics **2**: 1672-1681

Supplementary Table S1. Amino acid sequences of polypeptides, identified by liquid chromatography-tandem mass spectrometry, specific for *D. papillatum* and *T. cruzi* native ALDs.

Species	Sequence	*Mr* (expt)	*Mr* (calc)
D. papillatum	^{32}KLCTTGK^{38}	820.42	820.45
	^{39}GLLAADESQGSCDK^{52}	1463.61	1463.66
	^{39}GLLAADESQGSCDKR^{53}	1619.68	1619.76
	^{54}FKPIGLPNNEENR^{66}	1526.75	1526.78
	^{102}SFPELCNSLGIVPGIK^{117}	1743.83	1743.92
	^{118}TDKGLVDAVGGAPGEQATQGLDNYEK^{143}	2632.17	2632.26
	^{121}GLVDAVGGAPGEQATQGLDNYEK^{143}	2288.01	2288.09
	^{121}GLVDAVGGAPGEQATQGLDNYEKR^{144}	2444.11	2444.19
	^{184}YAQLSQK^{190}	836.40	836.44
	^{191}QGLVPIVEPEVMIDGNHDIAACQAVSQR^{218}	3042.58	3042.49
	^{219}VWAEVVR^{225}	857.45	857.48
	^{262}ATLTTLAR^{269}	845.46	845.50
	^{316}ALQASALK^{323}	800.43	800.48
	^{324}AWGGKEENK^{332}	1017.44	1017.49
	^{345}MNSLATLGK^{353}	933.47	933.50
	^{354}YNPGEDSK^{361}	908.34	908.39
	^{365}ESLYIK^{370}	751.38	751.41
T. cruzi	^{20}TPHEAELIATAK^{31}	1279.68	1279.68
	^{32}KMTAPGK^{38}	747.39	747.39
	^{33}MTAPGK^{38}	603.30	603.31
	^{54}FAPLGLSNTEEHR^{66}	1469.71	1469.73
	^{97}ASTGETFVQLLQR^{109}	1448.78	1448.76
	^{110}KGVVPGIK^{117}	796.52	796.52
	^{111}GVVPGIK^{117}	668.43	668.42
	^{118}TDMGLNPLVEGAEGEQMTGGLDGYVER^{144}	2853.28	2853.28
	^{148}YYSLGCR^{154}	931.43	931.42
	^{160}NVYK^{163}	522.28	522.28
	^{164}IQNGTVSEAAVR^{175}	1243.66	1243.65
	^{176}FNAETLAR^{183}	920.47	920.47
	^{254}ATPGQVAQYTVSTLAR^{269}	1661.89	1661.87
	^{308}LTFSYAR^{314}	856.44	856.44
	^{315}ALQSSALK^{322}	816.47	816.47
	^{328}DSGIAAGR^{335}	745.37	745.37
	^{337}AFMHRAK^{341}	660.32	660.32
	^{342}AKMNSLAQLGR^{352}	1203.67	1203.64
	^{344}MNSLAQLGR^{352}	988.50	988.51
	^{356}AEDDKESHSLYVAGNSY^{372}	1883.82	1883.82

Mr (expt) and *Mr* (calc) denote the experimentally determined and calculated molecular masses, respectively. Delta values (experimental minus calculated) of less than ±0.1 are considered highly specific.

Oncogene (2010), 1–11

www.nature.com/onc

ORIGINAL ARTICLE

Osteopontin-mediated enhanced hyaluronan binding induces multidrug resistance in mesothelioma cells

K Tajima[1,2], R Ohashi[1,2], Y Sekido[3], T Hida[3], T Nara[4], M Hashimoto[4], S Iwakami[5], K Minakata[1,2], T Yae[1,6], F Takahashi[1,2], H Saya[6] and K Takahashi[1,2]

[1]Department of Respiratory Medicine, Juntendo University, School of Medicine, Bunkyo-Ku, Tokyo, Japan; [2]Research Institute for Diseases of Old Ages, Juntendo University, School of Medicine, Bunkyo-Ku, Tokyo, Japan; [3]Division of Molecular Oncology, Aichi Cancer Center Research Institute, Chikusa-ku, Nagoya, Japan; [4]Department of Molecular and Cellular Parasitology, Juntendo University, School of Medicine, Bunkyo-Ku, Tokyo, Japan; [5]Department of Respiratory Medicine, Juntendo University Shizuoka Hospital, Shizuoka, Japan and [6]Division of Gene Regulation Institute for Advanced Medical Research School of Medicine, Keio University, Shinjuku-Ku, Tokyo, Japan

Malignant pleural mesothelioma (MPM) is resistant to chemotherapy and thus shows a dismal prognosis. Osteopontin (OPN), a secreted noncollagenous and phosphoprotein, is suggested to be involved in the pathogenesis of MPM. However, the precise role of OPN, especially in the multidrug resistance of MPM, remains to be elucidated. We therefore established stable transfectants (ACC-MESO-1/OPN), which constitutively express OPN, to determine its role in the chemoresistance observed in MPM. The introduction of the OPN gene provides MPM cells with upregulated multidrug resistance through the mechanism of enhanced hyaluronate (HA) binding. The expression of CD44 variant isoforms, which inhibit HA binding, significantly decreased in ACC–MESO–1/OPN cells in comparison to control transfectants. Interestingly, the inhibition of the HA-CD44 interaction abrogated multidrug resistance in the ACC–MESO–1/OPN, thus suggesting the involvement of the surviving signal emanating from the HA-CD44 interaction. An enhanced level of the p-Akt in ACC–MESO–1/OPN cells was observed, and was diminished by CD44 siRNA. Inhibition of the Akt phosphorylation increased in number of the cells underwent apoptosis induced by NVB, VP-16 and GEM. Collectively, these results indicate that OPN is strongly involved in multidrug resistance by enhancing the CD44 binding to HA.
Oncogene advance online publication, 18 January 2010; doi:10.1038/onc.2009.478

Keywords: osteopontin; mesothelioma; multidrug resistance; hyaluronan; CD44

Introduction

Malignant pleural mesothelioma (MPM) is an extremely aggressive tumor, which has been shown to be resistant to all conventional therapeutic regimens. A surgical resection is possible in only a minority of patients, and fewer than 15% of these patients live beyond 5 years (Sugarbaker *et al.*, 1996; Boutin *et al.*, 1998; Rusch and Venkatraman, 1999). For those who are not treated with a curative resection, the median survival has been reported to be 6 months (Ruffie, 1991; De Pangher Manzini *et al.*, 1993). As a result, chemotherapy is still the mainstay of disease therapy. Various drugs including doxorubicin, cyclophosphamide, cisplatin (CDDP), carboplatin, gemcitabine (GEM), and pemetrexed have been tested in different combinations (Samson *et al.*, 1987; Chahinian *et al.*, 1993; White *et al.*, 2000; Kindler *et al.*, 2001; Hughes *et al.*, 2002). However, the limited combinations of these agents have marginally provided some clinical benefit because of multidrug resistance. Moreover, none of the molecular targeting agents have shown any of their clinical benefit in the patients with MPM (Moore *et al.*, 2007; Jackman *et al.*, 2008). Therefore, it is hoped that a better understanding of the mechanism of the multidrug resistance in MPM may provide the rationale for the development of new therapeutic strategies.

Drug resistance arises in numerous ways, such as through a decreased access to or uptake of drugs, the activation of repair and detoxification mechanisms, and an increased drug efflux. Among these numerous mechanisms, resistance against anti-cancer agents has been recently reported upon cell adhesion to the extracellular matrix (ECM) (Damiano *et al.*, 1999; Elliott and Sethi, 2002; Hazlehurst *et al.*, 2003), thus suggesting that tumor–microenvironment interaction regulates the sensitivity of anti-cancer agents. For instance, it has been reported that small cell lung cancer cells, myeloma cells, glioma cells and colon cancer cells were protected from apoptosis induced by various anticancer agents when the cells were plated on ECM (Damiano *et al.*, 1999; Sethi *et al.*, 1999; Uhm *et al.*, 1999; Kouniavsky *et al.*, 2002). MPM cells are surrounded by pleural effusion, which contains a variety of ECM including hyaluronate (HA) and osteopontin (OPN) (Thylen *et al.*, 1997; Pass *et al.*, 2005; Grigoriu *et al.*, 2007). The ability to grow in pleural fluid suggests

Correspondence: Dr K Tajima, Department of Respiratory Medicine, Juntendo University, School of Medicine, 2-1-1 Hongo, Bunkyo-Ku, Tokyo 113-8421, Japan.
E-mail: tajiken@juntendo.ac.jp
Received 31 March 2009; revised 25 October 2009; accepted 2 November 2009

that the MPM cells are capable of surviving and proliferating against apoptosis under the influence of this particular microenvironment. These findings indicate that the biological function of MPM appears to be strictly regulated by the interaction with ECM.

OPN, a secreted noncollagenous, phosphoprotein, functions as both an ECM component and cytokine through the binding to its receptors; integrin and CD44 (Denhardt *et al.*, 2001). OPN has been associated with cancer progression, metastasis and apoptosis (Rangaswami *et al.*, 2006). Several studies have revealed elevated levels of OPN in serum and pleural effusion to be observed in patients with MPM (Pass *et al.*, 2005; Grigoriu *et al.*, 2007), thus suggesting the involvement of OPN in the pathogenesis of MPM. In fact, OPN was recently demonstrated to mediate MPM cell proliferation and migration (Ohashi *et al.*, 2009). OPN has also been reported to be involved in resistance to chemotherapy of mouse breast cancer cells by inhibiting apoptosis (Graessmann *et al.*, 2007). However, the role of OPN especially in multidrug resistance in MPM has not yet been clarified.

HA is a linear glycosaminoglycan, which is ubiquitously distributed in the ECM, and interacts with cell surface receptors including CD44 (Toole, 2004). HA facilitates cell adhesion, cell motility, cellular proliferation and tumor progression (Lokeshwar *et al.*, 1997). An increased HA production was found to upregulate drug resistance in cancer cells (Misra *et al.*, 2003). It is therefore possible that the effect of CD44 binding to HA on cell-survival signaling might alter drug resistance. In fact, HA–CD44 interaction was recently revealed to have a pivotal role in the chemoresistance in non-small cell lung cancer cells (Ohashi *et al.*, 2007). Very interestingly, recent studies have strongly supported the notion that the OPN could modulate the CD44 isoform expression, which closely regulates HA binding. For instance, Khan *et al.* (2005) reported that OPN modulates the specific CD44 isoform expression to facilitate breast cancer cell migration. Moreover, an overexpression of endogenous OPN results in increased hyaruronan synthase 2 activities, thus leading to an increased HA production and an enhanced anchorage-independent growth (Cook *et al.*, 2006).

Based on these findings, we hypothesized that OPN could regulate chemosensitivity through the alteration of CD44 binding to HA. We also discuss the potential mechanisms of the multidrug resistance in MPM.

Results

Generation of stable transfectant that secretes OPN

BMGNeo–OPN and BMGNeo were transfected into the ACC-MESO-1 cells and we thus obtained two stable OPN-overexpressing clones (ACC-MESO-1/OPN#7 and ACC-MESO-1/OPN#8) and two control clones (ACC-MESO-1/Neo#1 and ACC-MESO-1/Neo#2). To verify the secretion of OPN protein from the transfectant, we conducted the ELISA for OPN. As shown in Figure 1a, ELISA demonstrated the ACC-MESO-1/OPN cells to secrete significant amounts of OPN.

Transfection with OPN gene result in increased multidrug resistance

The IC_{50} of NVB against OPN7 cells and OPN8 cells were 3.87 ± 0.47 ng/ml and 4.56 ± 0.89 ng/ml, respectively, whereas those against Neo1 cells, Neo2 cells and parental cells were 1.70 ± 0.04 ng/ml, 1.97 ± 0.71 ng/ml and 1.91 ± 0.11 ng/ml, respectively (Figure 1b). The IC_{50} of VP16 against OPN7 cells and OPN8 cells were 8.71 ± 0.34 μM and 15.76 ± 1.49 μM, respectively, whereas those against Neo1 cells, Neo2 cells and parental cells were 4.47 ± 1.51 μM, 3.69 ± 1.00 μM and 2.17 ± 0.19 μM, respectively (Figure 1c). As IC_{50} never reached at any concentration of GEM in OPN transfectants, we could not show the IC_{50} regarding OPN transfectants. The IC_{50} of GEM against Neo1 cells, Neo2 cells and parental cells were 0.05 ± 0.002 μM, 0.03 ± 0.02 μM and 0.04 ± 0.018 μM, respectively (Figure 1d). The IC_{50} of CDDP against OPN7 cells and OPN8 cells were 6.44 ± 0.18 μg/ml and 5.85 ± 0.40 μg/ml, respectively, whereas those against Neo1 cells, Neo2 cells and parental cells were 12.00 ± 1.52 μg/ml, 11.56 ± 2.68 μg/ml and 3.39 ± 1.68 μg/ml, respectively (Figure 1e). These results indicate that the ACC-MESO-1/OPN cells were more resistant to NVB, VP-16 and GEM than the ACC-MESO-1/Neo or parental cells, whereas ACC-MESO-1/OPN cells did not demonstrate resistance to CDDP. We next evaluated the amount of apoptotic cells (Figure 1f). We observed that ACC-MESO-1/OPN cells were more significantly resistant to apoptosis mediated by anticancer agents than ACC-MESO-1/Neo cells. These data indicate that the transfection with OPN gene thus resulted in an increased multidrug resistance. Moreover, transfection with OPN gene also increased resistance to apoptosis induced by NVB, VP-16 and GEM.

OPN regulates cell adhesion to HA

To evaluate the effect of OPN transfected to ACC-MESO-1 cells on OPN or HA binding, an *in vitro* cell adhesion assay was performed using ACC-MESO-1/OPN, ACC-MESO-1/Neo and parental cells. The cells were investigated for adhesion to OPN, HA or BSA (Figure 2a). Interestingly, the ratio of adherence to HA (percent-specific adhesion to HA/percent-specific adhesion to BSA) of ACC-MESO-1/OPN cells was significantly greater than that of the ACC-MESO-1/Neo and parental cells, whereas neither ACC-MESO-1/OPN cells nor ACC-MESO-1/Neo cells demonstrated adherence to OPN (Table 1). To investigate whether the silencing of the OPN expression abrogates enhanced adhesion to HA, we downregulated the OPN expression in ACC-MESO-1/OPN#8 cells by siRNA. siRNA transfection downregulated the OPN expression by $>80\%$ (Figure 2b) and then we next performed an adhesion assay. As expected, the silencing of OPN expression in ACC-MESO-1/OPN#8 cells decreased the adhesion to HA (Figure 2c). These results therefore suggest that OPN regulates the cell adhesion to HA.

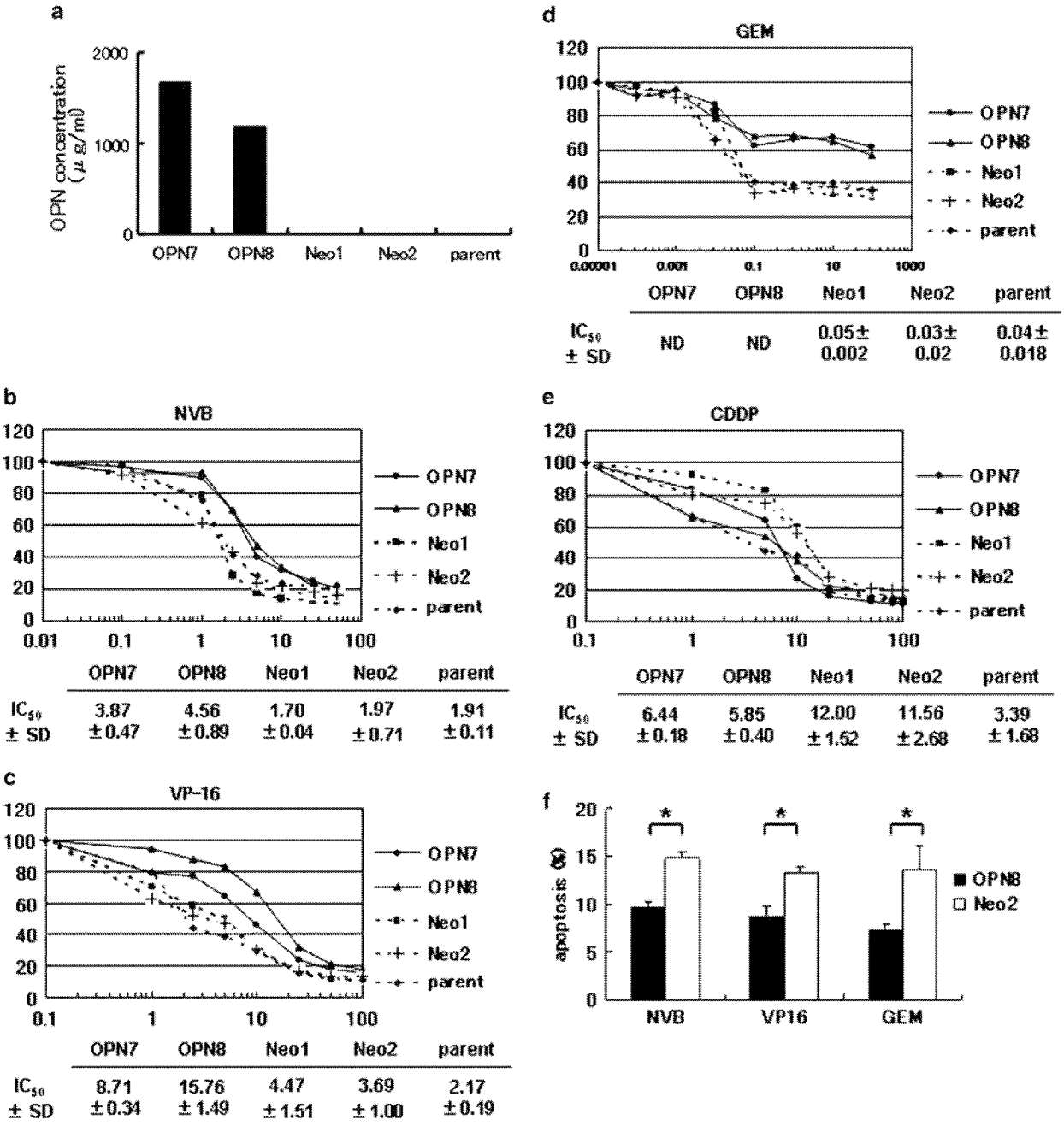

Figure 1 Establishment of ACC-MESO-1 cells transfected with an empty vector (ACC-MESO-1/Neo) or OPN gene (ACC-MESO-1/OPN). (**a**) OPN protein secretion was determined with ELISA. *In vitro* chemosensitivity assay. Both ACC-MESO-1/OPN and ACC-MESO-1/Neo clones were cultured in the absence or the presence of various concentration of vinorelbin (VNB; **b**), etoposide (VP-16; **c**), gemcitabine (GEM; **d**), and cisplatin (CDDP; **e**). Data are representative of the findings of one of three independent experiments with similar results. IC_{50}s are presented as the mean ± s.d. in triplicates. ND: not determined. (**f**) Apoptosis induction was evaluated by Annexin V staining method. ACC-MESO-1/OPN#8 cells were cultured in the presence of VNB (2.5 ng/ml), VP-16 (10 μM) and GEM (0.1 μM). Closed and open squares indicate ACC-MESO-1/OPN#8 and ACC-MESO-1/Neo#2, respectively. Data are presented as the mean ± s.d. of apoptotic cells of three independent experiments. $^*P<0.05$ vs OPN8.

Expression of CD44 and CD44 variant isoforms

As ACC-MESO-1/OPN cells showed an enhanced adhesion to HA, we therefore compared the expression levels of CD44, a principle receptor for HA, on the surface of ACC-MESO-1/OPN, ACC-MESO-1/Neo and parental cells with FACScan. As shown in Figure 3a, there was no difference in the total CD44 surface expression among ACC-MESO-1/OPN, ACC-MESO-1/Neo and parental cells. As certain CD44 variant isoforms have been reported to display significantly less HA binding than CD44s (Iida and Bourguignon, 1997), we next examined the expression pattern

of the CD44 variant isoforms using RT–PCR (Figure 3b) and western blotting (Figure 3c). It was noteworthy that the fragment of CD44s, which was expected to exhibit a PCR amplification product of 375 bp and several other larger fragments were expressed in each clone, thus suggesting the presence of alternatively spliced transcripts (Figure 3b). To identify these larger fragments, a direct DNA sequence analysis was performed. The 550 bp product corresponds to exon14 (v10), whereas the 750 bp product corresponds to exons12, 13 and 14 (v8, v9 and v10, respectively) (data not shown). CD44 protein expression was analyzed by western blotting using BU52. The expression of high molecular weight CD44 variant isoforms was significantly decreased in the ACC-MESO-1/OPN cells in comparison compared to that of the ACC-MESO-1/Neo and parental cells (Figure 3c). To determine whether exogenous OPN regulates the expression of CD44 variant isoforms on ACC-MESO-1 cells, a western blot analysis was performed to evaluate the CD44 isoform expression on the ACC-MESO-1 cells cultured on OPN and BSA. The expression of high molecular weight CD44 variant isoforms significantly decreased in the ACC-MESO-1 cells cultured on OPN compared with that of the ACC-MESO-1 cells cultured on BSA (Figure 3d).

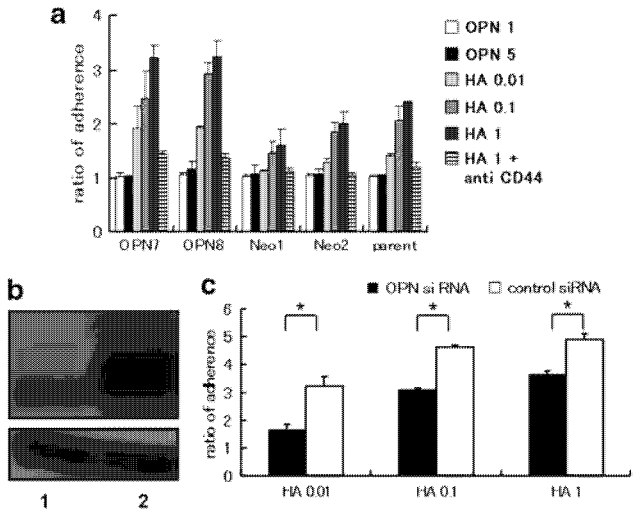

Figure 2 Adhesion assay. *In vitro cell* adhesion assay of ACC-MESO-1/OPN cells and ACC-MESO-1/Neo cells. (**a**) ACC-MESO-1/OPN, ACC-MESO-1/Neo or parental cells, were allowed to adhere to wells coated with OPN (1, 5 μg/ml), HA (0.01, 0.1, 1 mg/ml) or BSA (10 mg/ml) in the presence or absence of anti-CD44 antibody (BU75, 1 μg/ml). Data are presented as the mean ± s.d. in triplicates. (**b**) OPN expression by ACC-MESO-1/OPN cells transfected with OPN siRNA (lane 1) or negative control siRNA (lane 2). OPN protein expression was detected by western blotting. Bottom panel shows β-actin expression as loading control. (**c**) *In vitro* cell adhesion assay was performed using ACC-MESO-1/OPN OPN#8 siRNA and ACC-MESO-1/OPN#8 control siRNA. Closed and open squares indicate OPN siRNA and control siRNA, respectively. Data are presented as the mean ± s.d. in triplicates. $^{*}P<0.05$ vs control siRNA.

Downregulation of CD44v10 expression increases the multidrug resistance

To investigate whether the downregulation of the CD44v10 expression is involved in the mechanism of the multidrug resistance, we downregulated the CD44v10 expression in ACC-MESO-1 cells by siRNA. siRNA transfection downregulated the CD44v10 expression by >80% and then a chemosensitivity assay was performed (Figure 4a). The IC_{50} of NVB against the ACC-MESO-1 cells transfected with CD44v10 siRNA was 17.47 ± 7.00 ng/ml, whereas those against the cells transfected with control siRNA was 2.54 ± 0.31 ng/ml (Figure 4b). The IC_{50} of NVB against the ACC-MESO-1 cells transfected with CD44v10 siRNA was significantly higher than that against the cells transfected with control siRNA ($P<0.05$). The IC_{50} of VP16 against the ACC-MESO-1 cells transfected with CD44v10 siRNA was 10.53 ± 0.11 μM, whereas those against the cells transfected with control siRNA was 2.36 ± 0.20 μM (Figure 4c). The IC_{50} of VP-16 against the ACC-MESO-1 cells transfected with CD44v10 siRNA was significantly higher than that against the cells transfected with control siRNA ($P<0.05$). As IC_{50} was never

Table 1 The ratio of adherence to HA and OPN (percent-specific adhesion to HA or OPN/percent-specific adhesion to BSA)[a]

	OPN 1	*OPN 5*	*HA 0.01*	*HA 0.1*	*HA 1*
OPN7	1.02 ± 0.09	1.00 ± 0.02	1.92 ± 0.40*	2.47 ± 0.48^{+}	3.21 ± 0.24$^{\#,\#\#,\#\#\#}$
OPN8	1.05 ± 0.03	1.15 ± 0.15	1.93 ± 0.01*,**,***	2.93 ± 0.22$^{+,++,+++}$	3.25 ± 0.30$^{\#,\#\#,\#\#\#}$
Neo1	1.02 ± 0.03	1.08 ± 0.15	1.11 ± 0.01	1.45 ± 0.22	1.60 ± 0.30
Neo2	1.03 ± 0.05	1.08 ± 0.09	1.29 ± 0.06	1.85 ± 0.18	2.00 ± 0.21
Parent	1.01 ± 0.05	1.03 ± 0.03	1.40 ± 0.02	2.07 ± 0.24	2.39 ± 0.01

[a]Data are presented as the mean ± s.d. in triplicates.
$^{*}P<0.05$ vs Neo1 cells treated with HA 0.01.
$^{**}P<0.05$ vs Neo2 cells treated with HA 0.01.
$^{***}P<0.05$ vs parent cells treated with HA 0.01.
$^{\#}P<0.05$ vs Neo1 cells treated with HA 1.
$^{\#\#}P<0.05$ vs Neo2 cells treated with HA 1.
$^{\#\#\#}P<0.05$ vs parent cells treated with HA 1.
$^{+}P<0.05$ vs Neo1 cells treated with HA 0.1.
$^{++}P<0.05$ vs Neo2 cells treated with HA 0.1.
$^{+++}P<0.05$ vs parent cells treated with HA 0.1.

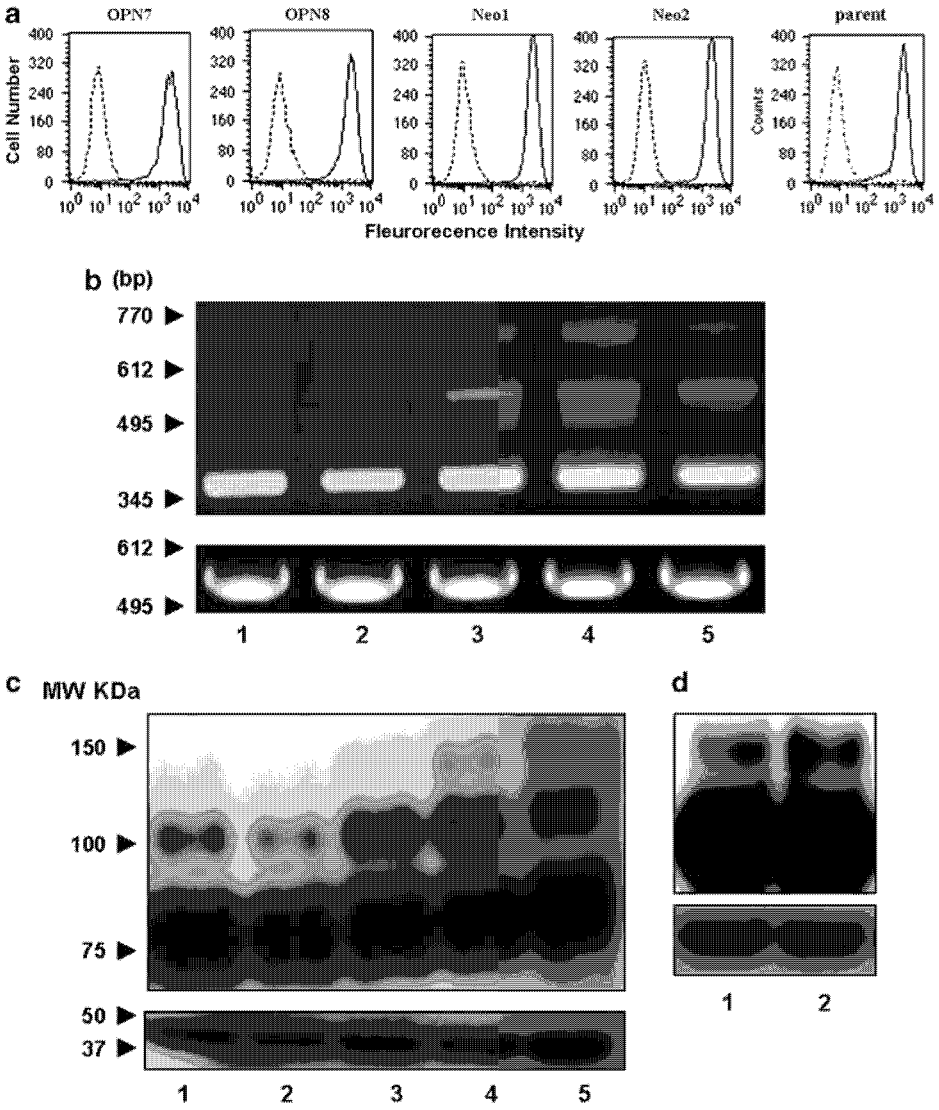

Figure 3 The expression of CD44 and CD44variant forms on ACC-MESO-1/OPN, ACC-MESO-1/Neo and parental cells. (**a**) To determine the CD44 expression, ACC-MESO-1/OPN, ACC-MESO-1/Neo and parental cells were incubated with monoclonal anti-CD44 (BU52, 1 μg/ml) antibody and analyzed with FACScan. (**b**) CD44 mRNA expression by ACC-MESO-1/OPN#7 (lane 1), ACC-MESO-1/OPN#8 (lane 2), ACC-MESO-1/Neo#1 (lane 3), ACC-MESO-1/Neo#2 (lane 4) and ACC-MESO-1 cells (lane 5) were shown. A bottom panel of each set shows β-actin expression as a control. DNA size markers are shown on the left side. (**c**) The expression of CD44s and variants on ACC-MESO-1/OPN#7 (lane 1), ACC-MESO-1/OPN#8 (lane 2), ACC-MESO-1/Neo#1 (lane 3), ACC-MESO-1/Neo#2 (lane 4) and ACC-MESO-1 (lane 5) were assessed by western blotting with anti-CD44 antibody (BU52). A bottom panel shows β-actin expression as loading control. The molecular weight size markers are indicated on the left side. (**d**) The expression of CD44s and variants on ACC-MESO-1 cells cultured on OPN (lane 1) and BSA (lane 2). CD44 protein expression was detected by western blotting. Bottom panel shows β-actin expression as loading control.

reached at any concentration of GEM in the ACC-MESO-1 cells transfected with CD44v10 siRNA, we could not show the IC_{50} against these cells. The IC_{50} of GEM against the cells transfected with control siRNA was $0.08 \pm 0.009\,\mu M$ (Figure 4d). As expected, the silencing of the CD44v10 expression in ACC-MESO-1 cells increases the multidrug resistance. The silencing of CD44v10 expression in ACC-MESO-1 cells also increases adhesion to HA (data not shown). These results suggest that the downregulation of CD44v10, accompanied by the enhanced adhesion to HA, is involved in the multidrug resistance.

Inhibition of the HA–CD44 interaction abrogated multidrug resistance and resistance to apoptosis

To determine whether HA–CD44 interaction is involved in the mechanism of the multidrug resistance, the expression of CD44 in ACC-MESO-1/OPN and ACC-MESO-1/Neo cells were downregulated by siRNA. siRNA transfection downregulated the CD44 expression by >70% and then a chemosensitivity assay was performed (Figure 5a). The IC_{50} of NVB against the OPN8 cells transfected with CD44 siRNA, OPN8 cells transfected with control siRNA, Neo2 cells transfected with CD44 siRNA and Neo2 cells transfected with

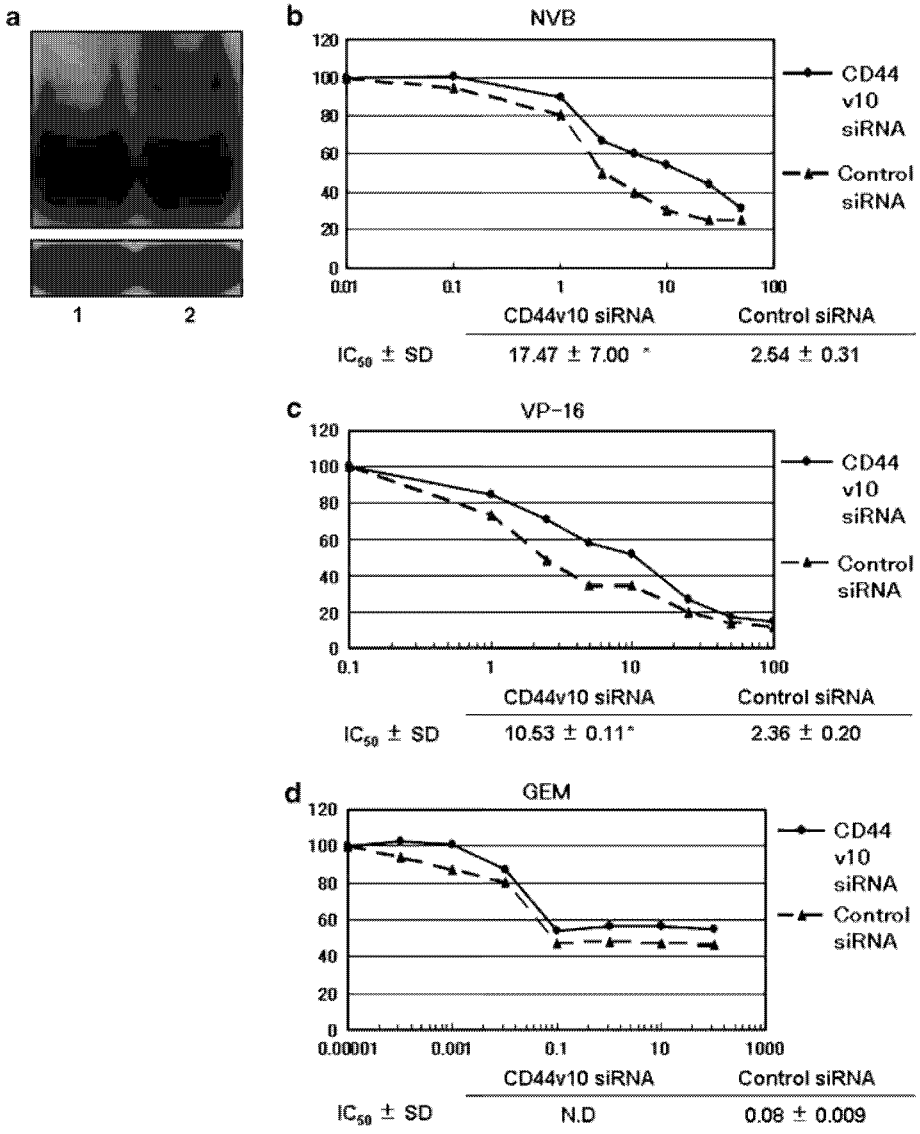

Figure 4 Effect of CD44v10 downregulation by siRNA on chemosensitivity of ACC-MESO-1 cells. (**a**) CD44v10 expression of ACC-MESO-1 cells transfected with CD44v10 siRNA (lane 1) or negative control siRNA (lane 2). A bottom panel shows β-actin expression as loading control. ACC-MESO-1 CD44 siRNA and negative control siRNA cells were cultured in the absence or the presence of various concentrations of vinorelbin (VNB; **b**), etoposide (VP-16; **c**) and gemcitabine (GEM; **d**). IC_{50}s are presented as the mean ± s.d. in triplicates. $^*P<0.05$ vs control siRNA. ND, not determined.

control siRNA were 1.10 ± 0.11 ng/ml, 5.33 ± 0.49 ng/ml, 1.65 ± 0.13 ng/ml and 1.61 ± 0.20 ng/ml, respectively (Figure 5b). The IC_{50} of VP-16 against the OPN8 cells transfected with CD44 siRNA, OPN8 cells transfected with control siRNA, Neo2 cells transfected with CD44 siRNA and Neo2 cells transfected with control siRNA were 17.54 ± 0.74 μM, 19.95 ± 1.05 μM, 11.52 ± 0.26 μM and 12.95 ± 0.75 μM, respectively (Figure 5c). As IC_{50} was never reached at any concentration of GEM in the OPN8 cells transfected with CD44 siRNA and control siRNA, we could not show the IC_{50} regarding the OPN8 cells. The IC_{50} of GEM against the Neo2 cells transfected with CD44 siRNA and Neo2 cells transfected with control siRNA were 0.07 ± 0.009 μM and 0.06 ± 0.008 μM, respectively (Figure 5d). As expected, the silencing of the CD44 expression in ACC-MESO-1/OPN#8 cells abrogated the multidrug resistance and increased apoptotic cells in number (Figure 5e). In contrast, silencing of CD44 expression did not influence the chemosensitivity in ACC-MESO-1/Neo#2 cells. ACC-MESO-1/OPN cells in the absence or the presence of BU75 were also cultured with VNB, VP-16 and GEM. As shown in Figure 5f, inhibition of the HA–CD44 interaction increased apoptosis and abrogated resistance to apoptosis. To confirm that the resistance to apoptosis was mediated by overexpression of OPN, we downregulated OPN expression by siRNA and performed the same experiment (Figure 5g). We again observed the downregulation of OPN expression to increase apoptosis. These results together with Figure 3c suggest that OPN-mediated alteration in HA–CD44 binding is involved in the mechanism of multidrug

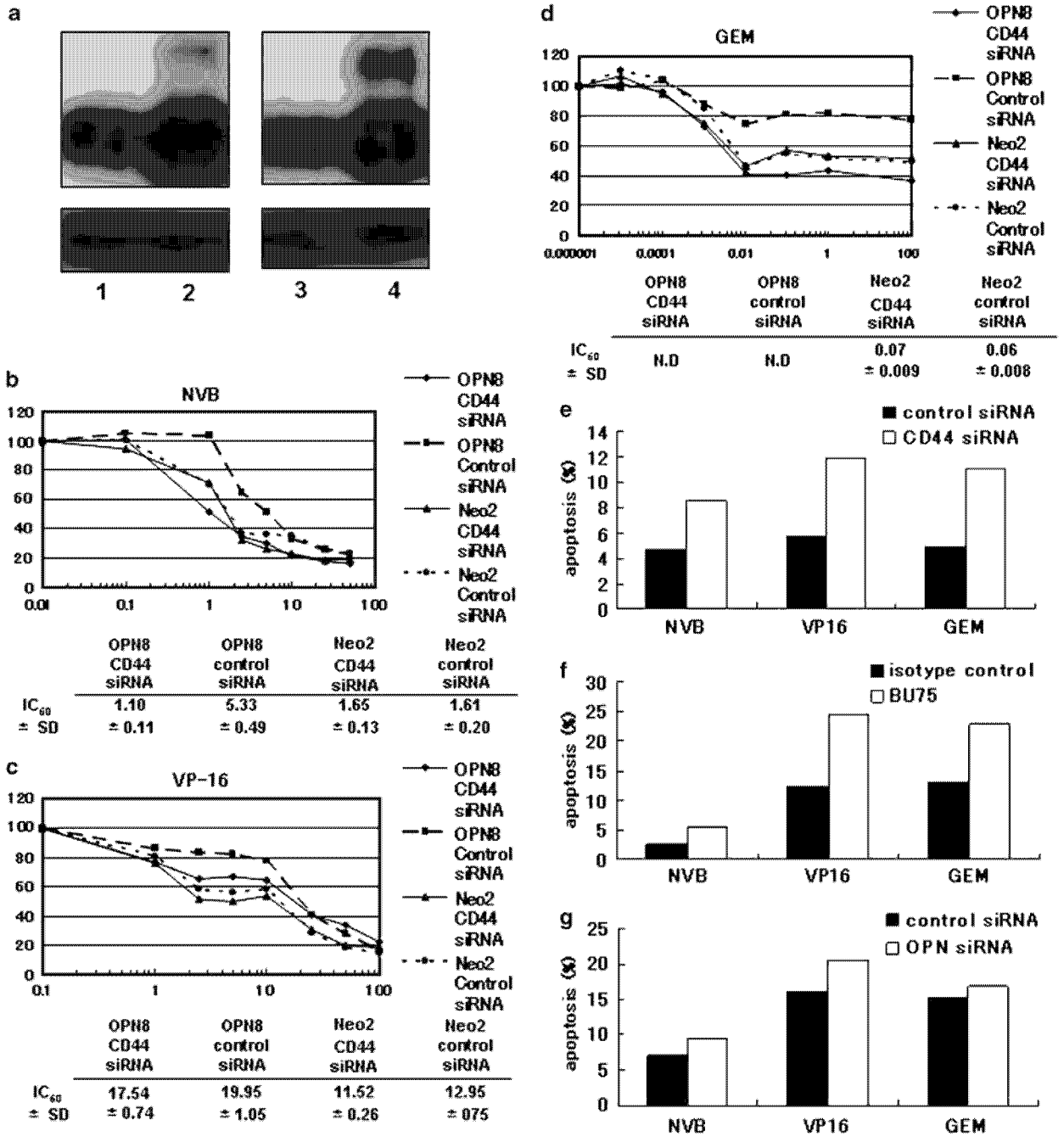

Figure 5 The effect of CD44 downregulation by siRNA on chemosensitivity of ACC-MESO-1/OPN and ACC-MESO-1/Neo cells. (**a**) The CD44 expression of ACC-MESO-1/OPN#8 or ACC-MESO-1/Neo#2 cells transfected with CD44 siRNA (lane 1, 3) or negative control siRNA (lane 2, 4). A bottom panel shows β-actin expression as loading control. ACC-MESO-1/OPN#8 or ACC-MESO-1/Neo#2 CD44 siRNA and negative control siRNA cells were cultured in the absence or the presence of various concentrations of vinorelbin (VNB; **b**), etoposide (VP-16; **c**) and gemcitabine (GEM; **d**). IC_{50}s are presented as the mean ± s.d. in triplicates. ND: not determined. (**e**) Effect of CD44 downregulation by siRNA on apoptosis of ACC-MESO-1/OPN cells exposed to indicate chemotherapeutic agents. Apoptosis was evaluated by the Annexin V staining method. ACC-MESO-1/OPN#8 cells treated with CD44 siRNA or negative control siRNA were cultured in the presence of VNB (2.5 ng/ml), VP-16 (10 μM) and GEM (0.1 μM). Closed and open squares indicate the percentage of apoptotic cells treated with negative control siRNA or CD44 siRNA, respectively. (**f**) The effect of anti-CD44 antibody (BU75) on apoptosis of ACC-MESO-1/OPN cells exposed to indicated chemotherapeutic agents. Apoptosis was evaluated by Annexin V staining method. ACC-MESO-1/OPN#8 cells were incubated with BU75 (1 μg/ml) or isotype control mouse IgG2a (1 μg/ml) in the presence of VNB (2.5 ng/ml), VP-16 (10 μM) and GEM (0.1 μM). Closed and open squares indicate the percentage of apoptotic cells treated with isotype control mouse IgG2a or BU75, respectively. (**g**) ACC-MESO-1/OPN#8 treated with OPN siRNA or negative control siRNA cells were cultured in the presence of VNB (2.5 ng/ml), VP-16 (10 μM) and GEM (0.1 μM). Closed and open squares indicate the percentage of apoptotic cells treated with negative control siRNA or OPN siRNA, respectively. All results (**e**–**g**) are representative ones of three independent experiments with similar results.

resistance and resistance to apoptosis induced by NVB, VP-16 and GEM.

CD44-mediated resistance to apoptosis involves the Akt survival pathway

As the Akt pathway is a well-characterized kinase that promotes cellular survival and several researchers have already shown that HA activates the PI3k–Akt signaling pathway (Sohara *et al*., 2001; Ghatak *et al*., 2002; Zoltan-Jones *et al*., 2003), we therefore investigated whether the survival signal emanating from the HA–CD44 interaction is mediated by the activation of the Akt pathway. To assess Akt phosphorylation, immunoblotting with anti-Akt and phospho-Akt-specific antibodies was carried out in ACC-MESO-1/OPN and ACC-MESO-1/Neo cells (Figure 6a). As expected, the enhanced level of phosphorylation of Akt (p-Akt) was observed in the ACC-MESO-1/OPN cells. To investigate whether the HA–CD44 interaction mediates p-Akt, the CD44 expression was thus downregulated by siRNA and then the p-Akt expression was assessed. As shown in Figure 6b, the elevation of p-Akt in the ACC-MESO-1/OPN cells decreased by the downregulation of CD44. To substantiate the functional role of Akt activation in the resistance to apoptosis, Akt inhibitor (LY294002) was used to block Akt activation.

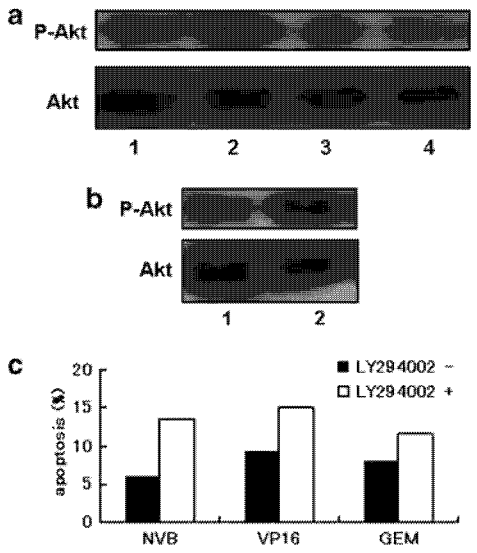

Figure 6 Effect of OPN upregulation or CD44 downregulation on phosphorylated Akt expression. (**a**) Expression of phosphorylated Akt and total Akt in ACC-MESO-1/OPN#7 (lane 1), ACC-MESO-1/OPN#8 (lane 2), ACC-MESO-1/Neo#1 (lane 3) and ACC-MESO-1/Neo#2 cells (lane 4) were determined by a western blot analysis. (**b**) ACC-MESO-1/OPN#8 cells were transfected with CD44 siRNA (lane 1) or negative control siRNA (lane 2). The expression of phosphorylated Akt and total Akt were determined by western blot analysis. (**c**) ACC-MESO-1/OPN#eight cells were incubated with or without LY294002 (10 μM) in the presence of VNB (2.5 ng/ml), VP-16 (10 μM) and GEM (0.1 μM). The percentage of apoptotic cells was determined by Annexin V staining method. Closed and open squares indicate the percentage of apoptotic cells treated without and with LY294002, respectively. The results are representative of three independent experiments with similar results.

ACC-MESO-1/OPN cells with or without LY294002 were cultured in the presence of VNB, VP-16 and GEM and apoptosis was detected by Annexin V (Figure 6c). As expected, the inhibition of the Akt phosphorylation increased the number of cells that underwent apoptosis. These results suggest that the activation of the Akt survival pathway, induced through the CD44, is therefore involved in the resistance to apoptosis induced by NVB, VP-16 and GEM.

Discussion

We here demonstrated that OPN provides MPM cells with an increased multidrug resistance and resistance to apoptosis to anti-cancer agents through HA–CD44 interaction. OPN-mediated alteration in CD44 binding to HA appears to have an important role in obtaining multidrug resistance by ACC-MESO-1/OPN cells.

In this study, the transfection of the OPN gene mediated the upregulation of HA binding in MPM cells. In contrast, the silencing of the OPN gene in ACC-MESO-1/OPN cells abrogated an enhanced adhesion to HA. These results indicate that OPN either directly or indirectly regulates HA binding. How does OPN gene transfer confer enhanced HA binding? First of all, we quantified and compared the amount of HA secreted into medium by both OPN transfectants. As opposed to our hypothesis, there was no difference in the amount of secreted HA (data not shown). In contrast, the expression of high molecular weight CD44 variant isoforms containing v8-10 and v10 was significantly reduced in ACC-MESO-1/OPN cells in comparison with control transfectants, whereas total CD44 expression levels on both transfectants are equivalent. As Iida and Bourguignon, (1997) demonstrated that cells coexpressing both transfected CD44v10 and endogeneous CD44s display a significant reduction in HA-mediated cell adhesion in comparison with parental cells expressing only CD44s, OPN-mediated enhanced HA binding in this study appears to be attributable to the downregulation of the CD44 variant isoforms, but not to the upregulation of CD44 expression.

Recent studies have revealed that HA strongly promotes anchorage-independent growth and that the resistance of cancer cells to growth arrest and apoptosis under anchorage-independent conditions is dependent on the constitutive interactions between HA and CD44 (Li and Heldin, 2001; Zoltan-Jones *et al*., 2003). The treatment of tumor cells with hyaluronidase was observed to increase the activities of various chemotherapeutic agents. In contrast, an increased HA production has been reported to induce resistance in drug-sensitive tumors (Misra *et al*., 2003). In our study, ACC-MESO-1/OPN cells which showed an enhanced adhesion to HA obtained multidrug resistance, and a disruption of HA–CD44 interaction by siRNA or neutralizing anti-CD44 antibody abrogated the resistance to apoptosis. Several groups have revealed that HA activates the PI3K–Akt signaling pathway through CD44, thereby

promoting cell survival (Sohara *et al.*, 2001; Ghatak *et al.*, 2002; Zoltan-Jones *et al.*, 2003). In fact, hyaluronan oligomers (oHA), which compete for endogenous polymeric HA, suppresses the PI3K/Akt cell survival pathway and retains chemosensitivity to anti-cancer agents (Cordo Russo *et al.*, 2008). In our study, the downregulation of the CD44 expression by siRNA suppressed Akt phosphorylation and increased apoptotic cells in number by the treatment with anti-cancer agents. These results suggested that OPN-induced resistance to apoptosis in the mesothelioma is mediated by the PI3K/Akt signaling pathway.

Khan *et al.* (2005) demonstrated that OPN upregulates the CD44v6, nine expressions, which have a key role in cancer metastasis, and the upregulation of variant CD44 isoforms has been reported to facilitate breast cancer cell migration . In contrast, OPN gene transfer in MPM cells reduced the CD44v8-10, ten expressions, and the downregulation of these variant CD44 isoforms confers chemoresistance of MPM in this study. The difference in OPN-induced alteration of CD44 isoforms may reflect the difference in the cell type between breast cancer and MPM. In MPM, local invasiveness is characteristic, whereas distant metastasis is infrequently observed. Such invasive growth requires ECM for MPM cells as previously reported (Li and Heldin, 2001). Moreover, the acquisition of chemoresistance by HA–CD44 interaction could be advantage for MPM cells to protect themselves by anti-cancer agents. These ideas are supported by previous reports which demonstrated MPM to be associated with elevated levels of OPN and HA in the pleural effusion (Thylen *et al.*, 1997; Pass *et al.*, 2005; Grigoriu *et al.*, 2007).

In this study, ACC-MESO-1/OPN cells, which showed an enhanced HA binding were shown to be more resistant to anti-cancer agents, NVB, VP-16 and GEM. These agents confer antitumor ability by a different mechanism. NVB binds to tubulin and inhibits its polymerization to form microtubules. VP-16 acts through inhibition of DNA topoisomerase II. GEM requires intracellular activation to its triphosphate derivative dFdCTP, which incorporates into DNA and then inhibits DNA synthesis. However, whether resistance to these three agents is mediated by the same mechanism still remains to be elucidated. We found the inhibition of the Akt phosphorylation by LY294002 to increase the number of cells that underwent apoptosis by the treatment with all three agents. These results suggested that the activation of the Akt survival pathway, induced through the CD44, may therefore be involved in the resistance to these three agents. Although, there still remains the question of what downstream events of the Akt pathway are involved in multidrug resistance, the inhibition of HA–CD44 or Akt pathway in combination with conventional agents may be more useful than conventional chemotherapy in the treatment of MPM.

To confirm that these findings can be generalized, we also examined other mesothelioma cell lines, such as H28 and ACC-MESO-4. Unfortunately, all mesothelioma cell lines tested, except ACC-MESO-1, expressed significant mRNA amounts of OPN by RT–PCR (data not shown). We therefore tried to downregulate the OPN expression in H28, which secreted significant amounts of OPN, by siRNA or miRNA to evaluate the role of OPN in chemoresistance. However, we were unable to establish stable transfectant by miRNA. siRNA transfection also could not downregulate the OPN expression. Although our data, in which OPN is involved in the chemoresistance, is promising, we still need to confirm that these results can be generalized by using animal models in the future.

In summary, we herein demonstrated that OPN mediated the alteration in HA–CD44 binding and that HA–CD44 interaction therefore has an important role in the acquisition of multidrug resistance by MPM. These results highlight the potential importance of OPN, which modulates HA–CD44 interaction, as a therapeutic target in multidrug resistance in patients with MPM.

Materials and methods

Cell lines

The human mesothelioma cell lines, ACC-MESO-1 cells were established at the Aich Cancer Center Research Institute (Nagoya, Japan) (Usami *et al.*, 2006). The cells were maintained in RPMI-1640 (Kohjin Bio, Sakado-city, Saitama Japan) containing 10% fetal calf serum (FCS), penicillin (100 U/ml) and streptomycin (100 μg/ml) at 37 °C in 5% CO_2 atmosphere. The cells were routinely tested for Mycoplasma contamination using the MycoAlert Mycoplasma Detection Kit (Cambrex, Rockland, ME, USA).

Reagents

The monoclonal anti-CD44 antibody (BU52), which is directed against epitopes common to all CD44 isoforms and the monoclonal anti-CD44 antibody (BU75), which blocks hyaluronate (HA) binding to CD44, were purchased from Ancell Corp (Bayport, MN, USA). The rabbit anti-Osteopontin (OPN) polyclonal antibody was purchased from Immuno-Biological and Laboratories (Gunma, Japan). The rabbit anti-Akt polyclonal antibody and the rabbit anti-phospho-Akt antibody were purchased from Cell Signaling Technology (Beverly, MA, USA). LY294002 was purchased from Sigma Chemicals (St Louis, MO, USA). To evaluate cell viability, the Cell Counting Kit-8 was purchased from Wako (Osaka, Japan).

Transfection

We have previously described the eukaryotic cDNA expression vector BMG Neo, conferring neomycin resistance, and BMGNeo containing the murine OPN cDNA was designated as BMGNeo–OPN (Takahashi *et al.*, 2002). BMGNeo and BMGNeo–OPN were transfected into ACC-MESO-1 cells using Lipofectamine 2000 Reagent (Invitrogen Corporation, Camarillo, CA, USA) according to the manufacture's instructions. The cells were selected with medium containing 0.5 mg/ml of 418 sulfate (Geneticin; Invitrogen Corporation). Several clones were isolated with limiting dilution. The resulting selected and isolated cells transfected with BMGNeo–OPN and BMGNeo were designated as ACC-MESO-1/OPN and ACC-MESO-1/Neo, respectively.

Detection of CD44 transcription by reverse transcriptase–polymerase chain reaction
The expression of CD44 mRNA was assessed by RT–PCR. TaKaRa FastPure RNA kit (Takara, Japan) was used to extract RNA according to the manufacturer. cDNA was synthesized using SuperscriptIII reverse transcriptase (Invitrogen Corporation). To detect CD44 variant isoform expression, the sense primer; 5′-GACAAGTTTTGGTGGCACGCA-3′, and antisense primer; 5′-TCAGATCCATGAGTGGTATGGG AC-3′ were used. This amplifies the intervening region of the transcripts including any inserted exons of the variant (CD44v) region. Amplifications for β-actin (sense primer, 5′-AGAAA ATCTGGCACCACACC-3′; antisense primer, 5′-AGGAGG GAAGGCTGGAAGAG-3′) were performed in TaKaRa-ExTaq polymerase (Takara, Japan). The PCR conditions were 2 min at 95 °C; 25 cycles of 1 min at 95 °C, 1 min at 55 °C, and 1 min at 72 °C, followed by a 7-min incubation at 72 °C.

Sequence
RT-PCR was performed under the same conditions as described above. The PCR products were purified by using MinElute (Qiagen, Maryland, MD, USA). Sequencing was performed using commercial reagents and an automated sequencer (ABI Prism BigDye Terminator v1.1 Cycle Sequencing Kit and ABI 3130 Genetic Analyzer; both Applied Biosystems, Foster city, CA, USA).

Detection of OPN protein secretion by ELISA
To determine OPN secretion in culture supernatant, a commercial ELISA kit (Immuno-Biological and Laboratories) was used according to the manufacture's instructions. Briefly, ACC-MESO-1/OPN and ACC-MESO-1/Neo were plated at 5×10^5 cells/well in 6-well 35 mm culture plates in 3 ml medium with 10% FCS. After 24 h, the culture medium was replaced with a medium containing 1% FCS for an additional 48 h. The culture supernatants were collected and subjected to an ELISA analysis.

In vitro *chemosensitivity assay*
The ells (2.0×10^3) were seeded onto 96-well microtiter plates in the absence or the presence of various concentration of chemotherapeutic agents including vinorelbine (VNB, Kyowa Hakko, Tokyo, Japan), etoposide (VP-16, Sigma), gemcitabine (GEM, Eli Lilly, Kobe, Japan) and cisplatin (CDDP, LKT Laboratories, St Paul, MN, USA). After 72 h of incubation, 10 μl of Cell Counting Kit-8 was added to each well. Four hours later, the optical density was measured at 450 nm with a microplate reader (Bio-Rad, Richmond, CA, USA). The results are expressed as the percentage of cell viability.

Adhesion assay
Ninety-six-well flat bottom plates (Corning Incorporated, Corning, New York, USA) were coated with recombinant OPN (1 and 5 μg/ml) or HA (0.01, 0.1 and 1 mg/ml) or 10 mg/ml BSA in PBS overnight at 4 °C. The following procedures were previously described (Takahashi *et al*., 2003).

RNA interference assay
ACC-MESO-1/OPN cells were transfected with 5 nM OPN siRNA using Hiperfect Transfection Reagent (Qiagen) or 10 nM CD44 and CD44v10 siRNA using Lipofectamine RNAiMAX (Invitrogen Corporation) according to the manufacturer's instructions. A knockdown efficacy was evaluated by Western bloting. Small interfering RNAs directed against OPN (spp1) (Mm_Spp1_1_HP siRNA), CD44 (5′-AAAUGG UCGCUACAGCAUCTT-3′), CD44v10 (5′-CACACGAAGG AAAGCAGGACCUUCA-3′) and a negative control (Allstars Negative Control siRNA) were purchased from either Qiagen or Invitrogen. The ACC-MESO-1/OPN cells transfected with siRNA for OPN, CD44 and negative control siRNA were designated as ACC-MESO-1/OPN OPN siRNA, ACC-MESO-1/OPN CD44 siRNA and ACC-MESO-1/OPN control siRNA, respectively.

Western bloting
For the Western blot analyses, the cells were homogenized in lysis buffer (50 mM Tris, pH 8.0, 150 mM NaCl, 0.02% NaN3, 1 mM phenylmethylsulfonylfluoride, 1 μg/ml aprotinin, 1% Triton-X-100). Samples containing equal amounts of protein were separated on acrylamide gels and transferred to a nitrocellulose filter with electroblotting. The filters were blocked for 1 h in PBS containing 0.1% Tween-20 (PBS-T) and 5% dry milk, washed in PBS-T, and then incubated with BU52 (1:500), rabbit anti-Osteopontin polyclonal antibody (1:500), rabbit anti-Akt polyclonal antibody (1:1000), rabbit anti-phospho-Akt antibody (1:1000) and monoclonal anti-β-actin antibody (1:4000) at 4 °C overnight. The filters were again washed and then incubated with horseradish-peroxidase-conjugated anti-mouse IgG or anti-rabbit IgG antibody (Amersham Pharmacia Biotech, Buckinghamshire, UK) for 1 h. Filters were then washed in PBS-T, and specific proteins were detected using the enhanced chemiluminescence system (Amersham Pharmacia Biotech).

Flowcytometric analysis
The adherent cells were detached from plates with 0.05% EDTA in PBS and were washed in PBS containing 0.1% BSA. Then, the cells (5×10^5) were incubated with BU52 (1 μg/ml) in PBS containing 0.1% BSA at 4 °C for 30 min. After washing the cells, the cells were incubated with fluorescent-labeled anti-mouse IgG (Chemicon, Temecula, CA, USA). The Propidium Iodide (Sigma) was added to final concentration of 10 μg/ml to exclude dead cells. Fluorescence was analyzed with a FACScan (Becton-Dickson Co., Mountain view, CA, USA).

Evaluation of apoptosis by Annexin V
ACC-MESO-1/OPN cells transfected with CD44 siRNA, OPN siRNA and negative control cells were treated with VNB, VP-16, or GEM for 48 h in the presence or absence of LY294002. Cells were harvested and the Annexin V-FITC –PI Kit (Sigma Inc.) was used according to the manufacturer's instructions. Early-stage apoptotic cells were Annexin positive and PI negative (right lower quadrant) and late-stage apoptotic cells were labeled by positivity with Annexin V and PI (right upper quadrant). The percentage of apoptotic cells was assessed by adding the percentage of cells in the two right quadrants.

Statistics
A statistical analysis was performed with an analysis of variance (ANOVA). The differences between the means were considered to be statistically significant at $P<0.05$.

Conflict of interest

The authors declare no conflict of interest.

Acknowledgements

This work was supported in part by a Grants-in-Aid for Cancer Research from the Ministry of Education, Culture, Sports, Science and Technology of Japan (K.T. No 19590914).

References

Boutin C, Schlesser M, Frenay C, Astoul P. (1998). Malignant pleural mesothelioma. *Eur Respir J* **12**: 972–981.

Chahinian AP, Antman K, Goutsou M, Corson JM, Suzuki Y, Modeas C *et al.* (1993). Randomized phase II trial of cisplatin with mitomycin or doxorubicin for malignant mesothelioma by the Cancer and Leukemia Group B. *J Clin Oncol* **11**: 1559–1565.

Cook AC, Chambers AF, Turley EA, Tuck AB. (2006). Osteopontin induction of hyaluronan synthase 2 expression promotes breast cancer malignancy. *J Biol Chem* **281**: 24381–24389.

Cordo Russo RI, Garcia MG, Alaniz L, Blanco G, Alvarez E, Hajos SE. (2008). Hyaluronan oligosaccharides sensitize lymphoma resistant cell lines to vincristine by modulating P-glycoprotein activity and PI3K/Akt pathway. *Int J Cancer* **122**: 1012–1018.

Damiano JS, Cress AE, Hazlehurst LA, Shtil AA, Dalton WS. (1999). Cell adhesion mediated drug resistance (CAM-DR): role of integrins and resistance to apoptosis in human myeloma cell lines. *Blood* **93**: 1658–1667.

De Pangher Manzini V, Brollo A, Franceschi S, De Matthaeis M, Talamini R, Bianchi C. (1993). Prognostic factors of malignant mesothelioma of the pleura. *Cancer* **72**: 410–417.

Denhardt DT, Noda M, O'Regan AW, Pavlin D, Berman JS. (2001). Osteopontin as a means to cope with environmental insults: regulation of inflammation, tissue remodeling, and cell survival. *J Clin Invest* **107**: 1055–1061.

Elliott T, Sethi T. (2002). Integrins and extracellular matrix: a novel mechanism of multidrug resistance. *Expert Rev Anticancer Ther* **2**: 449–459.

Ghatak S, Misra S, Toole BP. (2002). Hyaluronan oligosaccharides inhibit anchorage-independent growth of tumor cells by suppressing the phosphoinositide 3-kinase/Akt cell survival pathway. *J Biol Chem* **277**: 38013–38020.

Graessmann M, Berg B, Fuchs B, Klein A, Graessmann A. (2007). Chemotherapy resistance of mouse WAP-SVT/t breast cancer cells is mediated by osteopontin, inhibiting apoptosis downstream of caspase-3. *Oncogene* **26**: 2840–2850.

Grigoriu BD, Scherpereel A, Devos P, Chahine B, Letourneux M, Lebailly P *et al.* (2007). Utility of osteopontin and serum mesothelin in malignant pleural mesothelioma diagnosis and prognosis assessment. *Clin Cancer Res* **13**: 2928–2935.

Hazlehurst LA, Landowski TH, Dalton WS. (2003). Role of the tumor microenvironment in mediating *de novo* resistance to drugs and physiological mediators of cell death. *Oncogene* **22**: 7396–7402.

Hughes A, Calvert P, Azzabi A, Plummer R, Johnson R, Rusthoven J *et al.* (2002). Phase I clinical and pharmacokinetic study of pemetrexed and carboplatin in patients with malignant pleural mesothelioma. *J Clin Oncol* **20**: 3533–3544.

Iida N, Bourguignon LY. (1997). Coexpression of CD44 variant (v10/ex14) and CD44S in human mammary epithelial cells promotes tumorigenesis. *J Cell Physiol* **171**: 152–160.

Jackman DM, Kindler HL, Yeap BY, Fidias P, Salgia R, Lucca J *et al.* (2008). Erlotinib plus bevacizumab in previously treated patients with malignant pleural mesothelioma. *Cancer* **113**: 808–814.

Khan SA, Cook AC, Kappil M, Gunthert U, Chambers AF, Tuck AB *et al.* (2005). Enhanced cell surface CD44 variant (v6, v9) expression by osteopontin in breast cancer epithelial cells facilitates tumor cell migration: novel post-transcriptional, post-translational regulation. *Clin Exp Metastasis* **22**: 663–673.

Kindler HL, Millard F, Herndon II JE, Vogelzang NJ, Suzuki Y, Green MR. (2001). Gemcitabine for malignant mesothelioma: a phase II trial by the Cancer and Leukemia Group B. *Lung Cancer* **31**: 311–317.

Kouniavsky G, Khaikin M, Zvibel I, Zippel D, Brill S, Halpern Z *et al.* (2002). Stromal extracellular matrix reduces chemotherapy-induced apoptosis in colon cancer cell lines. *Clin Exp Metastasis* **19**: 55–60.

Li Y, Heldin P. (2001). Hyaluronan production increases the malignant properties of mesothelioma cells. *Br J Cancer* **85**: 600–607.

Lokeshwar VB, Obek C, Soloway MS, Block NL. (1997). Tumor-associated hyaluronic acid: a new sensitive and specific urine marker for bladder cancer. *Cancer Res* **57**: 773–777.

Misra S, Ghatak S, Zoltan-Jones A, Toole BP. (2003). Regulation of multidrug resistance in cancer cells by hyaluronan. *J Biol Chem* **278**: 25285–25288.

Moore MJ, Goldstein D, Hamm J, Figer A, Hecht JR, Gallinger S *et al.* (2007). Erlotinib plus gemcitabine compared with gemcitabine alone in patients with advanced pancreatic cancer: a phase III trial of the National Cancer Institute of Canada Clinical Trials Group. *J Clin Oncol* **25**: 1960–1966.

Ohashi R, Tajima K, Takahashi F, Cui R, Gu T, Shimizu K *et al.* (2009). Osteopontin modulates malignant pleural mesothelioma cell functions *in vitro*. *Anticancer Res* **29**: 2205–2214.

Ohashi R, Takahashi F, Cui R, Yoshioka M, Gu T, Sasaki S *et al.* (2007). Interaction between CD44 and hyaluronate induces chemoresistance in non-small cell lung cancer cell. *Cancer Lett* **252**: 225–234.

Pass HI, Lott D, Lonardo F, Harbut M, Liu Z, Tang N *et al.* (2005). Asbestos exposure, pleural mesothelioma, and serum osteopontin levels. *N Engl J Med* **353**: 1564–1573.

Rangaswami H, Bulbule A, Kundu GC. (2006). Osteopontin: role in cell signaling and cancer progression. *Trends Cell Biol* **16**: 79–87.

Ruffie PA. (1991). Pleural mesothelioma. *Curr Opin Oncol* **3**: 328–334.

Rusch VW, Venkatraman ES. (1999). Important prognostic factors in patients with malignant pleural mesothelioma, managed surgically. *Ann Thorac Surg* **68**: 1799–1804.

Samson MK, Wasser LP, Borden EC, Wanebo HJ, Creech RH, Phillips M *et al.* (1987). Randomized comparison of cyclophosphamide, imidazole carboxamide, and adriamycin versus cyclophosphamide and adriamycin in patients with advanced stage malignant mesothelioma: a Sarcoma Intergroup Study. *J Clin Oncol* **5**: 86–91.

Sethi T, Rintoul RC, Moore SM, MacKinnon AC, Salter D, Choo C *et al.* (1999). Extracellular matrix proteins protect small cell lung cancer cells against apoptosis: a mechanism for small cell lung cancer growth and drug resistance *in vivo*. *Nat Med* **5**: 662–668.

Sohara Y, Ishiguro N, Machida K, Kurata H, Thant AA, Senga T *et al.* (2001). Hyaluronan activates cell motility of v-Src-transformed cells via Ras-mitogen-activated protein kinase and phosphoinositide 3-kinase-Akt in a tumor-specific manner. *Mol Biol Cell* **12**: 1859–1868.

Sugarbaker DJ, Garcia JP, Richards WG, Harpole Jr DH, Healy-Baldini E, DeCamp Jr MM *et al.* (1996). Extrapleural pneumonectomy in the multimodality therapy of malignant pleural mesothelioma. Results in 120 consecutive patients. *Ann Surg* **224**: 288–294; discussion 294–6.

Takahashi F, Akutagawa S, Fukumoto H, Tsukiyama S, Ohe Y, Takahashi K *et al.* (2002). Osteopontin induces angiogenesis of murine neuroblastoma cells in mice. *Int J Cancer* **98**: 707–712.

Takahashi K, Takahashi F, Hirama M, Tanabe KK, Fukuchi Y. (2003). Restoration of CD44S in non-small cell lung cancer cells enhanced their susceptibility to the macrophage cytotoxicity. *Lung Cancer* **41**: 145–153.

Thylen A, Levin-Jacobsen AM, Hjerpe A, Martensson G. (1997). Immunohistochemical differences between hyaluronan- and non-hyaluronan-producing malignant mesothelioma. *Eur Respir J* **10**: 404–408.

Toole BP. (2004). Hyaluronan: from extracellular glue to pericellular cue. *Nat Rev Cancer* **4**: 528–539.

Uhm JH, Dooley NP, Kyritsis AP, Rao JS, Gladson CL. (1999). Vitronectin, a glioma-derived extracellular matrix protein, protects tumor cells from apoptotic death. *Clin Cancer Res* **5**: 1587–1594.

Usami N, Fukui T, Kondo M, Taniguchi T, Yokoyama T, Mori S *et al.* (2006). Establishment and characterization of four malignant pleural mesothelioma cell lines from Japanese patients. *Cancer Sci* **97**: 387–394.

White SC, Anderson H, Jayson GC, Ashcroft L, Ranson M, Thatcher N. (2000). Randomised phase II study of cisplatin-etoposide versus infusional carboplatin in advanced non-small-cell lung cancer and mesothelioma. *Ann Oncol* **11**: 201–206.

Zoltan-Jones A, Huang L, Ghatak S, Toole BP. (2003). Elevated hyaluronan production induces mesenchymal and transformed properties in epithelial cells. *J Biol Chem* **278**: 45801–45810.

Gurbadam et al. Parasites & Vectors 2010, 3:8
http://www.parasitesandvectors.com/content/3/1/8

Parasites & Vectors

MEETING REPORT Open Access

Mongolian and Japanese Joint Conference on "Echinococcosis: diagnosis, treatment and prevention in Mongolia" June 4, 2009

A Gurbadam[1], D Nyamkhuu[2], G Nyamkhuu[3], A Tsendjav[4], O Sergelen[1], B Narantuya[3], Z Batsukh[5], G Battsetseg[5], B Oyun-Erdene[6], B Uranchimeg[6], D Otgonbaatar[7], D Temuulen[1], E Bayarmaa[1], D Abmed[2], S Tsogtsaikhan[1], A Usukhbayar[1], K Smirmaul[8], J Gereltuya[8], A Ito[9*]

Abstract

The first Mongolian-Japanese Joint Conference on "Echinococcosis: diagnosis, treatment and prevention in Mongolia" was held in Ulaanbaatar on June 4th, 2009. It was the first chance for Mongolian experts (clinicians, pathologists, parasitologists, biologists, epidemiologists, veterinarians and others working on echinococcosis) joined together. Increase in the number of cystic echinococcosis (CE) cases year by year was stressed. CE in children may be more than adult cases. Alveolar echinococcosis was suspected chronic malignant hepatic tumors or abscesses. Main discussion was as to how to introduce modern diagnostic tools for pre-surgical diagnosis, how to establish the national system for the data base of echinococcosis with the establishment of a network system by experts from different areas. The importance of molecular identification of the parasites in domestic and wild animals was also stressed.

Report

D Nyamkhuu, D Otgonbaatar, G Nyamkhuu, O Sergelen, A Gurbadam, Z Batsukh, K Smirmaul and A Ito had often been discussing on how to establish the reference center on echinococcosis in Mongolia from 2004. Ito visited Ulaanbaatar for the first time in May 1995 as one of the parasitology delegates from the United States with Cross from the Uniformed Services University of Health Sciences in Bethesda, Maryland. At that time, Goosh, Head of the Department of Surgery at the Mongolian National Medical University (= Health Sciences University of Mongolia (HSUM) from 2003) explained the situation of echinococcosis in Mongolia. He concluded that most cases of echinococcosis in Mongolia were cystic echinococcosis (CE), since the life style of Mongolians was nomadic. Only 5 alveolar echinococcosis (AE) cases were confirmed before 1995. However, there is no published record, mainly due to the collapse of the Soviet Union. Clinical cases of echinococcosis in Mongolia were managed by surgeons. In 1950, 7.8% of all surgical patients in Mongolia were CE, whereas it was 1.9% in 1990 [1]. Also, Davaatseren and others reported that CE was the cause for 18% of the surgical cases in the First Hospital of Ulaanbaatar (i.e. SCCH) in 1993 [2,3].

After the Soviet Union collapsed in 1990, control programs for deworming dogs in Russia and former Soviet Union controlled states were also affected. Therefore, a resurgence of CE through the increase in number of dogs infected with *E. granulosus* was expected to become a serious public health risk for the people in these areas including Mongolia [3,4].

On June 4, 2009, Gurbadam and Temuulen at the Department of Medical Biology and Histology, HSUM, set up the first Mongolian-Japanese Joint Conference on "Echinococcosis: diagnosis, treatment and prevention in Mongolia" at HSUM when Ito visited Ulaanbaatar. It was the first chance for 19 Mongolian experts involved in echinococcosis to join together. There has been no other such meeting where clinicians, pathologists, parasitologists, biologists, epidemiologists, veterinarians and others working on echinococcosis in Mongolia joined together. Surgeons working in HSUM, SCCH, SRCMCH, pathologists from CP, HSUM, SCCH,

* Correspondence: akiraito@asahikawa-med.ac.jp
[9]Asahikawa Medical College (AMC), Asahikawa, Japan

immunologists, biologists, parasitologists from HSUM, and veterinarians from IVM and V.E.T. Net Mongolia NGO and a medical official, Luo from WHO/WPRO Ulaanbaatar as an observer attended.

The meeting was chaired by Gurbadam and opened with welcome remarks by the Dean, Batbaatar, School of Biomedicine, HSUM. Nyamkhuu, Director General of NCCD explained the historical background on the action plan towards the establishment of a national reference center for control of echinococcosis in Mongolia.

Two speakers gave special lectures. The first speaker was Ito. His topics were the "Recent advances in serodiagnosis on echinococcosis" and "Discussion on the new bilateral proposal on the establishment of centers for control of echinococcosis in Mongolia". He briefly explained three main topics. The first was the life cycles of *Echinococcus granulosus* and *E. multilocularis* along with their geographic distribution in the world [5]. The second was the recent advances in serodiagnosis of AE using recombinant Em18 with data from international joint projects with German [6], French and Swiss groups (unpublished) and Japanese [7]. The third topic was the similar approach using recombinant AgB8/1 for CE. The importance of the combination of abdominal imaging and serology was stressed according to recommendations from WHO (2001) [8]. The representative stressed the importance of a depository of the case records in Mongolia. Then, Naymkhuu from SCCH explained the most recent 5 AE cases in Mongolia (1982, 2002, 2006, 2007, 2009) [9]. Pre-surgical diagnoses for all AE cases were suspected chronic malignant hepatic tumors or abscesses. There was no application of serology for pre-surgical diagnosis. Ito showed antibody responses in AE case 4 (2007) and stressed that he expected strong positive responses in case 5 (2009) when he could check it after the meeting. [It has become evident that case 5 shows very strong antibody responses to RecEm18, the most sensitive and specific marker for the presence of active AE lesions [6,7,9,10]. Furthermore, haplotype network analysis of the most recent 3 histopathological specimens has revealed the presence of the two, Asian and Inner Mongolian genotypes reported by Nakao and others [5] in Mongolia [10]. Therefore, it is a very interesting area on the geographic distribution of the two genotypes of *E. multilocularis* in Mongolia and may be also in Russia and China. Also, there are many domestic and wild animals which may become intermediate hosts for *E. granulosus sensu lato* [11]. Therefore, molecular approaches on *Echinococcus* spp. and their host spectra will become interesting and important for genetic diversity, geographic distribution and co-evolution of *Echinococcus* spp. in Mongolia, Russia and China [5].

The second speaker was Tsendjav from SRCMCH. He summarized 25 pediatric CE cases from 2008 (19 in 2008, 6 from Jan until May 2009; 15 boys and 10 girls including 4 children under the age of 5-years) at SRCMCH. All participants stressed that the number of CE cases had been increasing year by year.

Through open discussion, Narantuya from SCCH summarized a total of 144 (63 males and 81 females) CE cases (1989-2009 June). In 2008 and 2009 until June, 13 and 11 cases, respectively, were surgically confirmed to be CE at SCCH. There is a tendency to see more CE cases year by year. Among them, 98 cases had liver cysts (68.1%). Sergelen from HSUM explained 9 complicated CE cases with surgery out of UB in 2008. Therefore, we had at least 22 CE cases in 2008 in Mongolia. So, pediatric CE cases in UB in 2008 were more than adult CE cases in UB. It suggests that adult cases are more asymptomatic than pediatric cases. However, we in Mongolia have had no idea how to record the cases and how to educate people especially school children how dogs are high risk for transmission of this disease. We all discussed how to keep the database and share among the experts in Mongolia systematically. NCCD will establish the reference center for human cases with closer contact with Word Health Organization (WHO/WPRO) in Ulaanbaatar, whereas IVM will report animal cases and notify the Food and Agricultural Organization of the United Nations (FAO) in Ulaanbaatar. As echinococcosis is a zoonosis, periodical exchange of mutual information will become a great benefit for launching the active strategy for control and prevention of echinococcosis in Mongolia. The specimens from humans and animals may be deposited at CIDNF. Pediatric cases should be reported not only to Ministry of Health, Mongolia but also to the United Nations Children's Fund (UNICEF) in Ulaanbaatar in order to save children's lives.

Although this meeting was a bilateral meeting on echinococcosis, similar approaches for discussion on the strategy for future control of echinococcosis will become important especially in countries in former Soviet Union, Russia and China [4,12-14].

Author details
[1]Health Science University of Mongolia (HSUM), Ulaanbaatar, Mongolia. [2]National Center of Communicable Diseases (NCCD), Ministry of Health, Ulaanbaatar, Mongolia. [3]State Central Clinical Hospital (SCCH), Ulaanbaatar, Mongolia. [4]State Research Center on Maternal and Child Health (SRCMCH), Ulaanbaatar, Mongolia. [5]Institute of Veterinary Medicine (IVM), Ulaanbaatar, Mongolia. [6]Pathology Center (PC), Ministry of Health, Ulaanbaatar, Mongolia. [7]Center of Infectious Diseases with Natural Foci (CIDNF), Ministry of Health, Ulaanbaatar, Mongolia. [8]Mongolia V.E.T NET, Ulaanbaatar, Mongolia. [9]Asahikawa Medical College (AMC), Asahikawa, Japan.

Received: 25 January 2010
Accepted: 8 February 2010 Published: 8 February 2010

References

1. Spira AM: **Saturday, May 13, 1995. Ulaanbaatar: Infectious Disease Department, National Medical University of Mongolia.** *Journal of the Citizen Ambassador Program Parasitology Delegation to the People's Republic of China and Mongolia May 7 to 20, 1995* 7-8.
2. Davaatseren N, Otogondalai A, Nyamkhuu G, Rusher AH: **Management of echinococcosis in Mongolia.** *J Ark Med Soc* 1995, **92**:122-125.
3. Ebright JR, Altantsetseg T, Oyungerel R: **Emerging infectious diseases in Mongolia.** *Emerg Infect Dis* 2003, **9**:1509-1515.
4. Torgerson P, Shaikenov B: **Echinococcosis in Central Asia: Problems and Solutions.** Almaty: INTAS Network Project 01-1505 2004.
5. Nakao M, Xiao N, Okamoto M, Yanagida T, Sako Y, Ito A: **Geographic pattern of genetic variation in the fox tapeworm *Echinococcus multilocularis*.** *Parasitol Int* 2009, **58**:384-389.
6. Tappe D, Frosch M, Sako Y, Itoh S, Grüner B, Reuter S, Nakao M, Ito A, Kern P: **Close relationship between clinical regression and specific serology in the follow-up of patients with alveolar echinococcosis in different clinical stages.** *Am J Trop Med Hyg* 2009, **80**:792-797.
7. Ishikawa Y, Sako Y, Itoh S, Ohtake T, Kohgo Y, Matsuno T, Ohsaki Y, Miyokawa N, Nakao M, Nakaya K, Ito A: **Serological monitoring of progression of alveolar echinococcosis with multi-organ involvement using recombinant Em18.** *J Clin Microbiol* 2009, **47**:3191-3196.
8. Eckert J, Gemmell MA, Meslin FX, Pawlowski ZS: **WHO/OIE Manual on Echinococcosis in Humans and Animals: a Public Health Problem of Global Concern.** Paris: World Organisation for Animal Health 2001.
9. Ito A, Agvaandaram G, Bat-Ochir OE, Chuluunbaatar B, Gonchigsenghe N, Yanagida T, Sako Y, Myadagsuren N, Dorjsuren T, Nakaya K, Nakao M, Ishikawa Y, Davvajav A, Dulmaa N: **Histopathological, serological and molecular confirmation of indigenous alveolar echinococcosis cases in Mongolia.** *Am J Trop Med Hyg* 2010.
10. Ito A, Nakao M, Sako Y: **Echinococcosis: serological detection of patients and molecular identification of parasites.** *Future Microbiol* 2007, **2**:439-449.
11. Nakao M, McManus DP, Schantz PM, Craig PS, Ito A: **A molecular phylogeny of the genus *Echinococcus* inferred from complete mitochondrial genomes.** *Parasitology* 2007, **134**:713-722.
12. Craig PS, Li T, Qiu J, Zhen R, Wang Q, Giraudoux P, Ito A, Heath D, Warnock B, Schantz P, Yang W: **Echinococcosis and Tibetan communities.** *Emerg Infect Dis* 2008, **14**:1674-1675.
13. Ito A, Urbani C, Qiu J, Vuitton DA, Qiu D, Heath DD, Craig PS, Feng Z, Schantz PM: **Control of echinococcosis and cysticercosis: a public health challenge to international cooperation in China.** *Acta Trop* 2003, **86**:3-17.
14. Craig PS, Deshan L, MacPherson SN, Dazhong S, Reynold D, Barnish G, Gottstein B, Zhirong W: **A large focus of alveolar echinococcosis in central China.** *Lancet* 1992, **340**:826-831.

doi:10.1186/1756-3305-3-8
Cite this article as: Gurbadam *et al.*: Mongolian and Japanese Joint Conference on "Echinococcosis: diagnosis, treatment and prevention in Mongolia" June 4, 2009. *Parasites & Vectors* 2010 **3**:8.

CLINICAL AND VACCINE IMMUNOLOGY, Mar. 2010, p. 470–475 Vol. 17, No. 3
1556-6811/10/$12.00 doi:10.1128/CVI.00466-09

Specific IgG Responses to Recombinant Antigen B and Em18 in Cystic and Alveolar Echinococcosis in China[▽]

Tiaoying Li,[1,2,3]* Akira Ito,[2] Xingwang Chen,[1] Yasuhito Sako,[2] Jiamin Qiu,[1] Ning Xiao,[1] Dongchuan Qiu,[1] Minoru Nakao,[2] Tetsuya Yanagida,[2] and Philip S. Craig[3]

Institute of Parasitic Diseases, Sichuan Centers for Disease Control and Prevention, Sichuan Province, People's Republic of China[1]; Department of Parasitology, Asahikawa Medical College, Midorigaoka Higashi 2-1-1-1, Asahikawa 078-8510, Japan[2]; and Cestode Zoonoses Research Group, Parasitology and Disease Center, Biomedical Sciences Research Institute, School of Environment and Life Sciences, University of Salford, Salford M54 WT, Greater Manchester, United Kingdom[3]

Received 4 November 2009/Returned for modification 7 December 2009 Accepted 22 December 2009

An understanding of the correlation of the specific antibody responses and the disease phase is essential in evaluating diagnostic values of immunological tests in human echinococcosis. In this study, 422 echinococcosis patients diagnosed by ultrasonography, including 246 with cystic echinococcosis (CE), 173 with alveolar echinococcosis (AE), and 3 with dual infection, were tested for specific IgG in sera against recombinant AgB (rAgB) and recombinant Em18 (rEm18) in an enzyme-linked immunosorbent assay. As a result, rAgB-specific antibody was detected in 77.6% of CE and 86.1% of AE patients, while rEm18-specific antibody was present in 28.9% of CE and 87.3% of AE patients. Additionally, all three patients with dual infection exhibited specific antibodies responding to rAgB and rEm18. Further analysis revealed that rAgB-specific antibody was elevated in a significantly greater proportion (87.3%) of CE patients with cysts at active or transitional stages (CE1, CE2, or CE3), compared to 54.8% of other patients with cysts at an early or an inactive stage (CL or CE4 or CE5). Furthermore, rAgB-specific antibody was detected in 95.6% of CE2 cases, which was statistically greater than that (73.7%) in CE1 patients. Although rEm18-specific antibody was elevated in 28.9% of CE patients, the positive reaction was much weaker in CE than in AE cases. Serum levels and concentrations of rEm18-specific antibody were further indicated to be strongly disease phase correlated in AE patients, with positive rates of 97.4% in cases with alveolar lesions containing central necrosis and 66.7% in patients with early alveolar lesions that measured ≤5 cm.

Humans acquire the infection of echinococcosis by accidental ingestion of eggs excreted with feces of carnivores harboring the adult worms of *Echinococcus* spp. The eggs hatch in the small intestine of humans, releasing the oncosphere, which migrates via the portal system into various organs and then develops into the metacestode stage. The larval parasite can establish itself in any part of the human body but most frequently does so in the liver (32). Diagnosis of human echinococcosis is primarily based on the pathognomonic features in images obtained using imaging techniques including ultrasonography, computed tomography (CT), and magnetic resonance imaging (MRI). Of these techniques, B-ultrasound is much more widely applied, as CT and MRI are too expensive and largely inaccessible in most areas where echinococcosis is endemic. Criteria for classification of cystic echinococcosis (CE) and alveolar echinococcosis (AE) have been proposed based on stage-specific ultrasound images (20, 36). Briefly, on the basis of conformational features of cysts, CE lesions are differentiated into six types: CL, CE1, CE2, CE3, CE4, and CE5. The CL type refers to a cystic lesion of a parasite origin and without a clear rim, indicating the parasite is at a very early stage of development. The CE1 type describes a unilocular simple cyst with uniform anechoic content and, importantly, with a visible wall, while the CE2 type is characterized by multivesicular, multiseptated cysts in which daughter cysts may partially or completely fill the unilocular mother cyst. The presence of CE1 or CE2 cysts is indicative of an active stage of the disease. The CE3 type is distinguished by detachment of the cyst membrane and/or partial degeneration of cyst content, suggestive of a transitional parasite. A CE4 or CE5 type of cyst shows an involution, with a necrotic or inactive parasite, with the features of complete degeneration of cyst content for CE4 and a calcified cyst wall for CE5 (36). In contrast, AE lesions are characterized by a nonhomogenous hyperechoic tumor-like structure with a poorly defined verge and containing scattered calcifications and/or a central necrotic cavity (1), and they are further differentiated into three types and eight subtypes based on the features and sizes of lesions, including AE1, AE2, and AE3 (20). In detail, AE1 refers to alveolar lesions measuring ≤5 cm, normally without central necrosis detected, and the type is differentiated further as AE1s (single lesion) and AE1m (multiple lesion) subtypes and indicates an early stage of the disease. Alveolar lesions that measure >5 cm and ≤10 cm are classified as AE2 and include three subtypes, recorded as AE2s (single lesion), AE2m (multiple lesions), and AE2f (presence of central necrotic fluid, regardless of the number of lesions), suggestive of a developing parasite, while AE lesions that measure >10 cm in diameter are confirmed as AE3, indicative of an advanced stage of the disease; this type

* Corresponding author. Mailing address: Institute of Parasitic Diseases, Sichuan Centers for Disease Control and Prevention, 6 Zhongxue Lu, Chengdu 610041, Sichuan Province, China. Phone: 86-28-85589532. Fax: 86-28-85589563. E-mail: litiaoying@sina.com.

▽ Published ahead of print on 30 December 2009.

includes three subtypes, i.e., AE3s (single lesion), AE3m (multiple lesions), and AE3f (presence of central necrotic fluid).

Meanwhile, several antigens, such as antigen B (AgB) (15, 23, 24, 26) for cystic echinococcosis and for *Echinococcus multilocularis* Em2a (8), II/3 (34), II/3-10 (27), EM10 (5), EM4 (9), and Em18 (12, 30), have been confirmed to be of potential use in serodiagnosis of human echinococcosis. However, relatively little information about the correlation between the specific antibody levels in humans and disease pathology or stage is available (29).

In this study, serum levels and concentrations of specific IgG antibodies in human CE and AE patients at different stages were determined by enzyme-linked immunosorbent assay (ELISA) using recombinant antigen B (rAgB) and recombinant Em18 (rEm18) as antigens.

MATERIALS AND METHODS

Serum samples. A total of 422 serum samples were collected from 422 individuals with confirmative ultrasound images of echinococcal lesions during 2001 to 2008 in Tibetan communities of northwest Sichuan (23). We also performed all ultrasound examinations. Of these 422 individuals, 246 were diagnosed as CE, 173 as AE, and 3 as dual infection with both CE and AE. According to the criteria for classification of ultrasound images of cystic echinococcosis (36), 5 of the 246 CE cases were determined to have CL cysts of a parasitic origin (CL cysts of nonparasite origin were excluded in this study), 57 had CE1-type cysts, 68 had cysts belonging to the CE2 type, 39 had CE3 cysts, and 68 had CE4 or CE5 cysts. Two or more cystic lesions belonging to different types were concurrently observed in nine additional cases. Of 173 AE cases, 21 were classified as AE1, 54 as AE2 (without necrotic cavity), 20 as AE3 (without necrosis), and an additional 78 were grouped as AEf, including AE2f and AE3f. Serum samples were stored at −20°C until tested.

rAgB and rEm18 ELISAs. The rAgB and rEm18 antigens were prepared as described previously (26, 30). Each serum sample was analyzed in an ELISA for specific IgG antibody responses to rAgB and rEm18 as reported previously (26, 30), with a minor alteration. In the assays, a 100-μl volume was applied throughout unless otherwise stated and phosphate-buffered saline (PBS) containing 0.05% Tween 20 was employed as the washing buffer (PBST), while casein buffer (1% casein in 20 mM Tris-HCl [pH 7.6] containing 150 mM NaCl) was used as diluting solution of serum and conjugate and also as blocking solution. PBS was employed to dilute antigens. Briefly, 96-well microtiter plates (Maxisorp; Nunc, Roskilde, Denmark) were coated with diluted antigen at a protein concentration of 0.5 μg/ml for rAgB and 1.0 μg/ml for rEm18 and incubated at 4°C overnight. After wells were rinsed three times with PBST, 300 μl of blocking solution was added to each well. Plates were incubated at 37°C for 1 h and washed five times. Serum samples diluted at 1:100 were added in duplicate wells and incubated at 37°C for 1 h. After washing five times, plates were incubated with rec-protein G-peroxidase conjugate (Invitrogen, Camarillo, CA) at a 1:4,000 dilution at 37°C for 1 h. Plates were washed five times and incubated with substrate solution [0.4 mM 2,2'-azino-bis(3-ethylbenzthiazoline-6-sulfonic acid) (ABTS) in 0.1 M citric acid buffer and 0.2 M Na_2HPO_4] at room temperature for 30 min. The color reaction was stopped by application of 1% SDS in each well. The optical density (OD) was determined at 405 nm with a microplate ELISA reader (model 450; Bio-Rad Laboratories, Hercules, CA).

The cutoff points were determined as the mean optical density of 30 serum samples obtained from healthy donors plus 3 standard deviations (SD).

Statistical analyses. A chi-square test was used for comparing sensitivities among patients grouped on the basis of the type of echinococcal lesion, and the Kruskal-Wallis H rank sum test was applied to compare ELISA OD values for multiple groups of patients with lesions at different stages, whereas the Wilcoxon rank sum test was used to compare OD values between two groups of patients. *P* values equal to or less than 0.05 were considered indicative of statistical significance.

RESULTS

The cutoff values (mean OD plus 3 SD) derived from analysis of negative-control sera ($n = 30$) were 0.048 for rAgB and 0.076 for rEm18.

TABLE 1. Results of ELISAs with rAgB and rEm18 as antigens in 246 CE patients

Cyst type(s)	No. of patients examined	No. (%) of patients with positive response to:	
		rAgB	rEm18
CL	5	2 (40.0)	0 (0)
CE1	57	42 (73.7)	16 (28.1)
CE2	68	65 (95.6)	31 (45.6)
CE3	39	35 (89.7)	14 (35.9)
CE4/CE5[a]	68	38 (55.9)	7 (10.3)
Mixed	9	9 (100.0)	3 (33.3)
Total	246	191 (77.6)	71 (28.9)

[a] The patients with CE4 or CE5 cysts (indicative of inactive parasites) were grouped together.

CE. (i) rAgB ELISA. Of the 246 CE cases, a total of 77.6% (191) showed a positive IgG antibody response to rAgB, and the patients with positive reactions had a median OD of 0.640. However, patients with CL or CE4/CE5 cysts exhibited lower activities than those with CE1, CE2, or CE3 cysts. That is, 2 of 5 patients with CL cysts and 55.9% (38/68) of persons with CE4/CE5 cysts responded to rAgB, whereas specific antibody was detected in 73.7% (42/57) of CE1 cases, 95.6% (65/68) of CE2 cases, 89.7% (35/39) of CE3 cases, and in all 9 patients with mixed types of cysts (Table 1). Further analysis revealed that antibody activity against rAgB was significantly different between CE patients with cysts at the early CL or inactive CE4/CE5 stage (40/73; 54.8%) and patients with active or transitional cysts (CE1, CE2, or CE3; 151/173; 87.3%) ($\chi^2 = 31.09$; $P = 0.000$). Moreover, OD values in patients with active or transitional cysts were greater than those in patients with early or inactive cysts ($P = 0.000$) (Fig. 1A). Additionally, CE1 patients had a significantly lower positive rate (73.7%) than CE2 patients (95.6%; $\chi^2 = 11.97$; $P = 0.005$) (Table 1), and the difference in mean OD values was also significant ($P = 0.000$) (Fig. 1A).

(ii) rEm18 ELISA. Sera from CE patients were also tested using rEm18 as antigen. Of the 246 CE cases, 28.9% (71) showed a positive response to rEm18, and all the cases with seropositivity had an OD median of 0.135. Antibody levels against rEm18 varied among patients with different types of cysts. That is, all 5 patients with CL cysts showed a negative response, while specific antibody was detected in 45.6% (31/68) of CE2 patients, 35.9% (14/39) of CE3 cases, 3 of 9 CE cases with mixed types of cysts, 28.1% (16/57) of CE1 patients, and 10.3% (7/68) of CE4/CE5 cases (Table 1). However, reactions with rEm18 in CE patients were generally weak, with respective OD medians for each group (in parentheses), as follows: CL (0.008), CE1 (0.021), CE2 (0.063), mixed (0.051), CE3 (0.052), and CE4/5 (0.027) (Fig. 1C). The difference was significant ($P = 0.000$).

Of the 71 CE cases with a positive response to rEm18, all except 4 also exhibited specific antibody to rAgB at a rather high level (median, 0.994) (Fig. 1E). The four negative sera consisted of CE1 (two), CE3 (one), and CE4/CE5 (one).

AE. (i) rAgB ELISA. In 173 AE patients, 149 (86.1%) contained protein G binding antibodies (IgG) that recognized rAgB from *Echinococcus granulosus*, with an OD median of

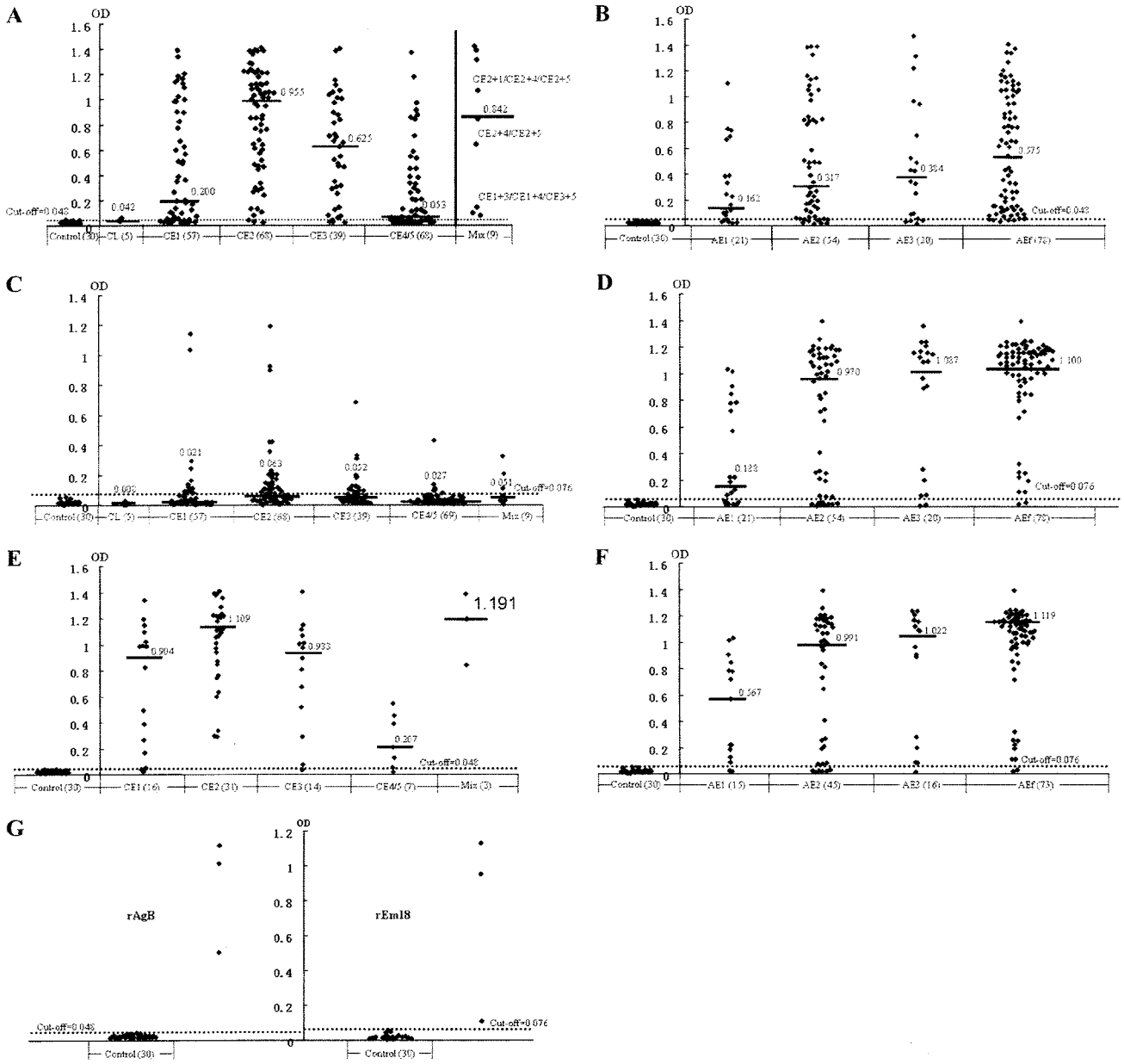

FIG. 1. Results of rAgB and rEm18 ELISAs for CE and AE patients with echinococcal lesions at different stages. (A) rAgB ELISA in 246 CE cases; (B) rAgB ELISA in 173 AE cases; (C) rEm18 ELISA in 246 CE cases; (D) rEm18 ELISA in 173 AE cases; (E) rAgB ELISA in 71 CE cases with a positive response to rEm18; (F) rEm18 ELISA in 149 AE cases with a positive response to rAgB; (G) rAgB and rEM18 ELISAs for 3 cases with dual infections of both CE and AE. The dashed lines indicate the cutoff values, and black bars refer to OD medians. Controls were healthy persons. The numbers in parentheses indicate numbers of tested cases or persons.

0.489 for the positive cases. Serum levels and concentrations of specific antibody were shown to be elevated in patients with late-stage disease (AE2, AE3, or AEf) (Fig. 1B). That is, 93.6% (73/78) of AEf patients exhibited a positive antibody response, while positive responses were observed in 83.3% (45/54) for AE2, 80.0% (16/20) for AE3, and 71.4% (15/21) for AE1 patients (Table 2). Further analysis revealed that the differences in the positive rates were significant ($\chi^2 = 8.41$; $P = 0.0382$).

TABLE 2. Results of ELISAs with rAgB and rEm18 as antigens in 173 AE patients

Cyst type	No. of patients examined	No. (%) of patients with positive response to:	
		rAgB	rEm18
AE1	21	15 (71.4)	14 (66.7)
AE2	54	45 (83.3)	43 (79.6)
AE3	20	16 (80.0)	18 (90.0)
AEf	78	71 (91.0)	76 (97.4)
Total	173	147 (85.0)	151 (87.3)

(ii) rEm18 ELISA. Of the same 173 AE cases, 87.3% (151) exhibited a specific antibody response to rEm18, with an OD median of 1.068 for the positive cases. Antibody levels and concentrations were observed to be greatly elevated with advanced disease (Fig. 1D). That is, 14 (66.7%) of 21 patients with AE1-type lesions showed positive reactions, while 79.6% (43/54) of AE2 and 90.0% (18/20) of AE3 cases exhibited specific antibody, and the positive rate reached 97.4% (76/78) in patients with AEf-type lesions (Table 2). The positive rates proved to be significantly different ($\chi^2 = 18.27$; $P < 0.0005$). In addition, the differences in OD medians between those patients at different stages (AE1, AE2, AE3, or AEf) were also significant ($\chi^2 = 32.265$; $P = 0.000$).

Of the 149 AE patients with a positive response to rAgB, 136 (91.3%) exhibited specific antibody to rEm18 (Fig. 1F). In other words, AE patients with a positive response to rEm18 were more likely to react with rAgB (136/151; 90.1%) than AE patients with a negative response to rEm18 (13/22; 59.1%) ($\chi^2 = 15.33$; $P < 0.0001$).

As expected, a much greater proportion of AE patients (87.3%) exhibited rEm18-specific antibodies than CE patients (28.9%; $\chi^2 = 138.83$; $P = 0.000$). Similarly, rEm18 ELISA OD values of AE patients (OD median, 1.029) were significantly higher than those of CE patients (OD median, 0.036; $P = 0.000$). In contrast, antibody activities with rAgB in CE patients (77.6%) or AE patients (86.1%) were different ($\chi^2 = 4.77$; $P = 0.0290$), but the difference in OD medians was not significant ($P = 0.473$).

Cases with dual infection. All three cases with dual CE/AE infection showed positive responses to both rAgB and rEm18 (Fig. 1G).

DISCUSSION

rAgB and rEm18 have recently been produced and have proved to be highly useful for serodiagnosis of human echinococcosis, with a high sensitivity and 100% specificity (26, 30, 37). Our current study focused on testing the sensitivity, and the results indicated that rAgB detected *Echinococcus* genus-specific antibodies, because both CE and AE patients were seropositive at similar levels, whereas rEm18 antigen exhibited higher *E. multilocularis* species specificity, with 87.3% of AE cases classified as seropositive and, by contrast, only weak reactions observed in 28.9% of CE patients. In addition, specific IgG antibody levels and concentrations measured against rAgB and rEm18 proved to be strongly correlated with disease stage in CE and AE cases, respectively.

Both human CE and AE are highly endemic in northwest Sichuan Province, China (21, 22), where a large number of echinococcosis cases at different stages were detected in the field through mass screening programs by portable ultrasound scan, which permitted us to analyze the correlation of specific antibody response and disease stage. Considering the natural history of cystic echinococcosis, cysts are classified into six types: CL (refers to cysts of a parasitic origin) and CE1, CE2, CE3, CE4, and CE5, indicating the different pathological/growth activities of the parasite in human hosts (36). Diagnosis of CE is currently primarily based on the imaging features of the cysts, but specific serology is also important as a complementary diagnostic tool. As one of the most important immunogenic antigens, *E. granulosus* native AgB detects about 80% to 90% of CE cases (15, 19, 24, 25), while rAgB has shown a similar diagnostic value, with positive reactions in about 70% to 90% of CE cases (26, 28, 33). Our current study revealed that rAgB had a similar positive rate (77.6%) in CE patients, and rAgB-specific antibody levels and concentrations in CE patients were strongly associated with the cyst type; i.e., when the parasite was at a very early (CL) or inactive (CE4 or CE5) stage, the specific IgG antibodies were present at a significantly lower concentration in a small proportion of patients, with a seropositive rate of 54.8% and an OD median of 0.050, compared to 87.3% seropositive and an OD median of 0.648 when the parasite was in an active (CE1 or CE2) or transitional (CE3) stage of development. Similar observations were made previously for ultrasound-confirmed CE cases detected in community studies (2, 3) and for hospitalized patients (28). Interestingly, patients with CE1 cysts in our study showed a markedly lower seropositivity (73.7%) and lower OD (median, 0.2) with rAgB than patients with CE2 cysts (95.6% seropositive and 0.995 OD median); this was probably caused by different structural features of the cysts, which can lead to the release of fewer antigens, including antigen B in the blood circulation, in CE1 cases than in CE2 cases. However, a similar seropositivity with native AgB in CE1 and CE2 cases was reported by Ortona et al. (28); this discrepancy might arise from differences in the time of serum sampling (before or after surgical or chemotherapeutic intervention), but it may be because CE2 and CE3 were revised in the original Gharbi classification (7, 35) before the WHO recommendation to change these criteria were published (36). In our study, 86.1% of AE sera were also recognized by rAgB, which was exceptionally higher than that where AE is exclusively endemic (approximately 40.0%), as reported previously (15, 19, 26). One possibility is that these AE cases might be coinfected with CE in other organs, such as the lung. However, a more likely probability is that rAgB applied in our study refers to rAg8/1 from *E. granulosus* protoscoleces (rEgAgB8/1), which is 92.6% homologous at the amino acid level to AgB8/1 from *E. multilocularis* metacestodes (EmAgB8/1) (26). These two antigens have been shown to have very similar immunoreactive regions which are thought to stimulate human hosts to produce similar IgG antibodies in CE and AE patients, respectively (26). Therefore, rAgB, although from *E. granulosus*, can bind IgG antibodies in both CE and AE sera to a similar level.

Several *E. multilocularis* antigens, such as EM10 (5), II/3 (34), II/3-10 (27), and EM4 (10), have proved to have potential for use in differential serodiagnosis of AE from CE. Em18 from *E. multilocularis* protoscoleces was confirmed to be a fragment of EM10 (30) and demonstrated its usefulness for highly sensitive and specific diagnosis of AE (12, 13, 14, 17, 18). In the current study, 87.3% of AE patients exhibited a specific antibody response to rEm18, which was identical to results of a previous report (30) but was lower than the results from other studies in which rEm18 detected almost 100% of AE cases (16, 37). This discrepancy is probably caused by the differences of the disease stages, as our study indicated the rEm18-specific antibody levels and concentrations in AE patients were strongly correlated with the stage of alveolar lesions. When the disease became aggravated, with the lesion changing from AE1 to AE2, AE3, or AEf, antibody activities

against rEm18 were significantly elevated, from 66.7% to 97.4%, and concurrently serum concentrations of specific antibody also evidently increased with the OD value, changing from 0.188 to 1.100. This observation indicates that Em18 can be highly useful for assessing the parasite activities in human AE patients following interventional measures. Similar results have recently been published in which rEm18 serology was shown to be reliable for monitoring the progression of AE (11, 31). A much greater proportion (28.9%) of CE cases were observed to exhibit specific antibody against rEm18 than those (3% to 13%) described in previous studies (16, 18, 30, 37), in which positive patients were found to have complicated or multiple cysts. In the current study, CE patients with all types of cysts except for CL were observed to respond to rEm18; of these, cases with CE2 (45.6%) were most likely to have specific antibody compared to the other groups (ranging from 10.3% to 35.9%). Nevertheless, all the seropositive reactions in CE patients were much weaker than in AE patients (OD medians, 0.135 versus 1.068). Similar results were obtained with antigens EM10 or II/3, described in previous studies (4, 6), in which AE patients were found to have raised specific antibody to EM10 more frequently than CE patients, despite there being a protein with a high level of homology to EM10 expressed by *E. granulosus* metacestodes. The significant differences in activities with rEm18 or EM10 in AE and CE patients may be partially attributable to different pathological features of metacestodes of *E. multilocularis* and *E. granulosus*. The *E. granulosus* metacestode grows in a cyst with a double wall by endogenous budding. Conversely, the *E. multilocularis* metacestode grows via exogenous budding, and it therefore has intimate contact with host tissues (32).

ACKNOWLEDGMENTS

The study was supported by grant number RO1 TW001565 from the Fogarty International Center of NIH to P.S.C.; by the International Joint Research Project of the Japan Society for the Promotion of Science (JSPS 17256002 and 21256003), the JSPS—Asia/Africa Scientific Platform Fund (2006-2011), and the Infection Matrix Fund from the Ministry of Education, Japan, to A.I.; and by the Invitation Fund by Japan China Medical Association to M.N. This study was also supported in part by the Sichuan Provincial Department of Health, China, a Ph.D. split-site studentship (to T.L.) between the University of Salford, United Kingdom, and SIPD/Sichuan CDC, China.

REFERENCES

1. **Bresson-Hadni, S., E. Delabrousse, O. Blagosklonov, B. Bartholomot, S. Koch, J. P. Miguet, G. A. Mantion, and D. A. Vuitton.** 2006. Imaging aspects and non-surgical interventional treatment in human alveolar echinococcosis. Parasitol. Int. **55**(Suppl.):S267–S272.
2. **Cohen, H., E. Paolillo, R. Bonifacino, B. Botta, L. Parada, P. Cabrera, K. Snowden, R. Gasser, R. Tessier, L. Dibarboure, H. Wen, J. C. Allan, H. Soto de Alfaro, M. T. Rogan, and P. S. Craig.** 1998. Human cystic echinococcosis in a Uruguayan community: a sonographic, serologic, and epidemiologic study. Am. J. Trop. Med. Hyg. **59:**620–627.
3. **Daeki, A. O., P. S. Craig, and M. K. Shambesh.** 2000. IgG-subclass antibody responses and the natural history of hepatic cystic echinococcosis in asymptomatic patients. Ann. Trop. Med. Parasitol. **94:**319–328.
4. **Felleisen, R., and B. Gottstein.** 1994. Comparative analysis of full-length antigen II/3 from *Echinococcus multilocularis* and *E. granulosus*. Parasitology **109:**223–232.
5. **Frosch, P. M., M. Frosch, T. Pfister, V. Schaad, and D. Bitter-Suermann.** 1991. Cloning and characterization of an immunodominant major surface antigen of *Echinococcus multilocularis*. Mol. Biochem. Parasitol. **48:**121–130.
6. **Frosch, P. M., F. Muhlschlegel, L. Sygulla, M. Hartmann, and M. Frosch.** 1994. Identification of a cDNA clone from the larval stage of *Echinococcus granulosus* with homologies to the *E. multilocularis* antigen EM10-expressing cDNA clone. Parasitol. Res. **80:**703–705.
7. **Gharbi, H. A., B. Hassine, M. W. Braunner, and K. Dupuch.** 1981. Ultrasound examination of hydatid liver. Radiology **139:**459–463.
8. **Gottstein, B.** 1985. Purification and characterization of a specific antigen from *Echinococcus multilocularis*. Parasite Immunol. **7:**201–212.
9. **Hemmings, L., and D. P. McManus.** 1989. The isolation, by differential antibody screening, of *Echinococcus multilocularis* antigen gene clones with potential for immunodiagnosis. Mol. Biochem. Parasitol. **33:**171–182.
10. **Hemmings, L., and D. P. McManus.** 1991. The diagnostic value and molecular characterization of an *Echinococcus multilocularis* antigen gene clone. Mol. Biochem. Parasitol. **44:**56–62.
11. **Ishikawa, Y., Y. Sako, S. Itoh, T. Ohtake, Y. Kohgo, T. Matuno, Y. Ohsaki, N. Miyokawa, M. Nakao, K. Nakaya, and A. Ito.** 2009. Serological monitoring of progression of alveolar echinococcosis with multi-organ involvement using recombinant Em18. J. Clin. Microbiol. **47:**3191–3196.
12. **Ito, A., M. Nakao, H. Kutsumi, M. W. Lightowlers, M. Itoh, and S. Sato.** 1993. Serodiagnosis of alveolar hydatid disease by Western blotting. Trans. R. Soc. Trop. Med. Hyg. **87:**170–172.
13. **Ito, A., P. M. Schantz, and J. F. Wilson.** 1995. Em18, a new serodiagnostic marker for differentiation of active and inactive cases of alveolar hydatid disease. Am. J. Trop. Med. Hyg. **52:**41–44.
14. **Ito, A., L. Ma, M. Itoh, S. Y. Cho, Y. Kong, S. Y. Kang, T. Horii, X. L. Pang, M. Okamoto, T. Yamashita, M. W. Lightowlers, X. G. Wang, and Y. H. Liu.** 1997. Immunodiagnosis of alveolar echinococcosis by enzyme-linked immunosorbent assay using a partially purified Em18/16 enriched fraction. Clin. Diagn. Lab. Immunol. **4:**57–59.
15. **Ito, A., L. Ma, P. M. Schantz, B. Gottstein, Y. H. Liu, J. J. Chai, S. K. Abdelhafez, N. Altintas, D. D. Joshi, M. W. Lightowlers, and Z. S. Pawlowski.** 1999. Differential serodiagnosis for cystic and alveolar echinococcosis using fractions of *Echinococcus granulosus* cyst fluid (antigen B) and *Echinococcus multilocularis* protoscolex (Em18). Am. J. Trop. Med. Hyg. **60:**188–192.
16. **Ito, A., N. Xiao, M. Liance, M. O. Sato, Y. Sako, W. Mamuti, Y. Ishikawa, M. Nakao, H. Yamasaki, K. Nakaya, K. Bardonnet, S. Bresson-Hadni, and D. A. Vuitton.** 2002. Evaluation of an enzyme-linked immunosorbent assay (ELISA) with affinity-purified Em18 and an ELISA with recombinant Em18 for differential diagnosis of alveolar echinococcosis: results of a blind test. J. Clin. Microbiol. **40:**4161–4165.
17. **Ito, A., M. Nakao, and Y. Sako.** 2007. Echinococcosis: serological detection of patients and molecular identification of parasites. Future Microbiol. **2:**439–449.
18. **Jiang, L., H. Wen, and A. Ito.** 2001. Immunodiagnostic differentiation of alveolar and cystic echinococcosis using ELISA test with 18-kDa antigen extracted from *Echinococcus* protoscoleces. Trans. R. Soc. Trop. Med. Hyg. **95:**285–288.
19. **Leggatt, G. R., W. Yang, and D. P. McManus.** 1992. Serological evaluation of the 12 kDa subunit of antigen B in *Echinococcus granulosus* cyst fluid by immunoblot analysis. Trans. R. Soc. Trop. Med. Hyg. **86:**1–4.
20. **Li, T., J. Qiu, P. S. Craig, A. Ito, W. Yang, D. A. Vuitton, N. Xiao, X. Chen, W. Yu, and P. M. Schantz.** 2004. Review of 311 cases of alveolar echinococcosis and criteria for the classification of hepatic ultrasound images. Southeast Asian J. Trop. Med. Public Health **35**(Suppl.):1–5.
21. **Li, T., J. Qiu, W. Yang, P. S. Craig, X. Chen, N. Xiao, A. Ito, P. Giraudoux, W. Mamuti, W. Yu, and P. M. Schantz.** 2005. Echinococcosis in Tibetan populations, western Sichuan Province, China. Emerg. Infect. Dis. **11:**1866–1873.
22. **Li, T., X. Chen, Z. Ren, J. Qiu, D. Qiu, N. Xiao, A. Ito, H. Wang, P. Giraudoux, Y. Sako, M. Nakao, and P. S. Craig.** Widespread co-endemicity of human cystic and alveolar echinococcosis on the eastern Tibetan Plateau, China. Acta Trop., in press.
23. **Lightowlers, M. W., D. Liu, A. Haralambous, and M. D. Rickard.** 1989. Subunit composition and specificity of major cyst fluid antigens of *Echinococcus granulosus*. Mol. Biochem. Parasitol. **37:**171–182.
24. **Maddison, S. E., S. B. Slemenda, P. M. Schantz, J. A. Fried, M. Wilson, and V. C. W. Tsang.** 1989. A specific diagnostic antigen of *Echinococcus granulosus* with an apparent molecular weight of 8 kDa. Am. J. Trop. Med. Hyg. **40:**377–383.
25. **Mamuti, W., H. Yamasaki, Y. Sako, K. Nakaya, M. Nakao, M. W. Lightowlers, and A. Ito.** 2002. Usefulness of hydatid cyst fluid of *Echinococcus granulosus* developed in mice with secondary infection for serodiagnosis of cystic echinococcosis in humans. Clin. Diagn. Lab. Immunol. **9:**573–576.
26. **Mamuti, W., H. Yamasaki, Y. Sako, M. Nakao, N. Xiao, K. Nakaya, N. Sato, D. A. Vuitton, R. Piarroux, M. W. Lightowlers, P. S. Craig, and A. Ito.** 2004. Molecular cloning, expression, and serological evaluation of an 8-kilodalton subunit of antigen B from *Echinococcus multilocularis*. J. Clin. Microbiol. **42:**1082–1088.
27. **Muller, N., B. Gottstein, M. Vogel, K. Flury, and T. Seebeck.** 1989. Application of a recombinant *Echinococcus multilocularis* antigen in an enzyme-linked immunosorbent assay for immunodiagnosis of human alveolar echinococcosis. Mol. Biochem. Parasitol. **36:**151–159.
28. **Ortona, E., R. Rigano, P. Margutti, S. Notargiacomo, S. Ioppolo, S. Vaccari, S. Barca, B. Buttari, E. Profumo, A. Teggi, and A. Siracusano.** 2000. Native

and recombinant antigens in the immunodiagnosis of human cystic echinococcosis. Parasite Immunol. **22:**553–559.

29. **Rogan, M. T., and P. S. Craig.** 2001. Immunological approaches for transmission and epidemiological studies in cestode zoonoses: the role of serology in human infection, p. 135–145. *In* P. S. Craig (ed.), Tapeworm zoonoses, an emergent and global problem. NATO Science Series. IOS Press. Amsterdam, The Netherlands.
30. **Sako, Y., M. Nakao, K. Nakaya, H. Yamasaki, B. Gottstein, M. W. Lightowers, P. M. Schantz, and A. Ito.** 2002. Alveolar echinococcosis: characterization of diagnostic antigen Em18 and serological evaluation of recombinant Em18. J. Clin. Microbiol. **40:**2760–2765.
31. **Tappe, D., M. Frosch, Y. Sako, S. Itoh, B. Grüner, S. Reuter, M. Nakao, A. Ito, and P. Kern.** 2009. Close relationship between clinical regression and specific serology in the follow-up of patients with alveolar echinococcosis in different clinical stages. Am. J. Trop. Med. Hyg. **80:**792–797.
32. **Thompson, R. C. A.** 1995. Biology and systematics of *Echinococcus*, p. 1–50. *In* R. C. A. Thompson and A. J. Lymbery (ed.), *Echinococcus* and hydatid disease. CAB International, Wallingford, United Kingdom.
33. **Virginio, V. G., A. Hernandez, M. B. Rott, K. M. Monteiro, A. F. Zandonai, A. Nieto, A. Zaha, and H. B. Ferreira.** 2003. A set of recombinant antigens from *Echinococcus granulosus* with potential for use in the immunodiagnosis of human cystic hydatid disease. Clin. Exp. Immunol. **132:**309–315.
34. **Vogel, M., B. Gottstein, N. Muller, and T. Seebeck.** 1988. Production of a recombinant antigen of *Echinococcus multilocularis* with high immunodiagnostic sensitivity and specificity. Mol. Biochem. Parasitol. **31:**117–125.
35. **Wang, Y., X. Zhang, B. Bartholomot, B. Liu, J. Luo, T. Li, X. Wen, H. Zheng, H. Zhou, H. Wen, N. Davaadori, L. Gambolt, T. Mukhar, K. al-Qaoud, S. Abdel-Hafez, P. Giraudoux, D. A. Vuitton, A. Fraser, M. T. Rogan, and P. S. Craig.** 2003. Classification, follow-up and recurrence of hepatic cystic echinococcosis using ultrasound images. Trans. R. Soc. Trop. Med. Hyg. **97:**203–211.
36. **WHO Informal Working Group.** 2003. International classification of ultrasound images in cystic echinococcosis for application in clinical and field epidemiological settings. Acta Trop. **85:**253–261.
37. **Xiao, N., W. Mamuti, H. Yamasaki, Y. Sako, M. Nakao, K. Nakaya, B. Gottstein, P. M. Schantz, M. W. Lightowlers, P. S. Craig, and A. Ito.** 2003. Evaluation of use of recombinant Em18 and affinity-purified Em18 for serological differentiation of alveolar echinococcosis from cystic echinococcosis and other parasitic infections. J. Clin. Microbiol. **41:**3351–3353.

Am. J. Trop. Med. Hyg., 82(2), 2010, pp. 266–269
doi:10.4269/ajtmh.2010.09-0520

Short Report: Histopathological, Serological, and Molecular Confirmation of Indigenous Alveolar Echinococcosis Cases in Mongolia

Akira Ito,* Gurbadam Agvaandaram, Oyun-Erdene Bat-Ochir, Batsaikhan Chuluunbaatar, Nyamkhuu Gonchigsenghe, Tetsuya Yanagida, Yasuhito Sako, Narankhajid Myadagsuren, Temuulen Dorjsuren, Kazuhiro Nakaya, Minoru Nakao, Yuji Ishikawa, Abmed Davaajav, and Nyamkhuu Dulmaa

Asahikawa Medical College, Asahikawa, Japan; Health Sciences, University of Mongolia, Ulaanbaatar, Mongolia; Center of Pathology, Ministry of Health, Ulaanbaatar, Mongolia; State Central Clinical Hospital, Ulaanbaatar, Mongolia; National Center for Communicable Diseases, Ministry of Health, Ulaanbaatar, Mongolia

Abstract. Alveolar echinococcosis cases diagnosed histopathologically in 2002, 2006, 2007, and 2009 in Ulaanbaatar, Mongolia were reconfirmed by evaluating the cytochrome *c* oxidase subunit I gene of mitochondrial DNA. The most recent three cases using paraffin-embedded and ethanol-fixed specimens revealed that one was of the "Asian" haplotype, whereas two others were of the "Inner Mongolian" type. All patients were born in the western provinces of Mongolia, they never resided outside of Mongolia, and they were given a preliminary diagnosis of malignant hepatic tumor or abscess. The most recent two cases were also confirmed serologically to be active alveolar echinococcosis.

Alveolar echinococcosis (AE), often misdiagnosed as hepatocellular carcinoma, is caused by the accidental ingestion of eggs of the fox tapeworm, *Echinococcus multilocularis*. AE is one of the most lethal parasitic zoonoses and is prevalent in most areas of the Northern Hemisphere. Endemic areas include parts of North America (Canada, Alaska, and some of the lower contiguous states of the United States),[1] Asia (Russia and other states of the former Soviet Union,[1,2] China,[1,3–5] and Japan[1,6]), and the majority of Europe.[1,7] One of the largest known foci of AE is in China.[1,3–5] Although *E. multilocularis* has been reported from Russia[1,2] and China,[1,3–5] only two AE cases have previously been reported from Mongolia (the first case in 1982 and the second in 2002).[8,9]

Recently, we have confirmed three additional indigenous AE cases at the State Central Clinical Hospital (SCCH) in Ulaanbaatar (UB), Mongolia in 2006, 2007, and 2009 with ethical approvals in Mongolia. Here, we summarize the three most recent AE cases as well as the case from 2002. Cases were confirmed by histopathological observation (Figure 1), serology (Figure 2), and molecular analysis based on cytochrome *c* oxidase subunit I (*cox1*) of mitochondrial DNA (Figure 3).

Case 2, a 28-year-old policeman born in Orkhon-Uul province, was admitted to the SCCH in 2002. Pre-surgical diagnosis was a suspected chronic liver abscess. During surgery, the patient died of heart failure. Post-mortem diagnosis was hepatic AE with a 13.8 × 7.7-cm lesion on the right lobe of the liver.

Case 3, a 25-year-old disabled man born in Uvs province but living in UB since 1995, was admitted to the SCCH in 2006. He had a 15 × 9.5-cm lesion on the right lobe of the liver with invasion to the diaphragm. The lesion was not resectable, and he died 5 days post-operatively from liver failure. Post-mortem diagnosis was hepatic AE.

Case 4, a 22-year-old female student born in Khovd province, was admitted to the SCCH in May 2007. She had a 7 × 7.5-cm lesion on the left lobe of the liver and a 4 × 4.5-cm lesion on the upper lobe of the left lung. The hepatic lesion was resected but was deemed too large for radical resection, and therefore, the pulmonary cyst was left without surgical treatment. Histopathology revealed hepatic AE (Figure 1).

Case 5, a 20-year-old unemployed female born in Bayan-Ulgii province, was admitted to the SCCH in January 2009 with hepatic and pulmonary lesions. She had a 6.3 × 6.2-cm lesion on the right lobe of the liver. Histopathology revealed hepatic AE. Among the five confirmed AE cases in Mongolia, three patients (cases 1–3) died before, during, or within 1 week of surgery because of the advanced stage of disease.[8]

A serum sample from case 4 was obtained in September 2008, 1 year after surgery, without any clinical background information. Serology (Figure 2) was carried out by immunoblot (IB; Figure 2A) and a commercially available rapid immunochromatography (ICT) kit[10] (Figures 2B–C) using a recombinant Em18 (RecEm18).[11,12] Case 4 showed very strong antibody responses to RecEm18, the highly specific diagnostic antigen for detection of active AE by both IB and ICT.[10–15] This finding indicates that this woman still had active lesions, because serology becomes negative within 1 year of successful radical resection.[12,13] A pre-surgical serum sample from case 5 also showed very strong antibody responses to RecEm18 in IB and ICT, suggesting that AE could have been easily confirmed if serology was introduced for diagnosis before surgery. Antibody responses in case 4 seemed to be much stronger than that in case 5 when we tested these sera by the rapid ICT kit (Figure 2B–C), because the strength of the band is a quantitative result (Sako Y and others, unpublished data). All known Mongolian AE cases,[8,9,16] including the three most recent cases, were diagnosed as malignant hepatic tumors or abscesses before surgery, but they were confirmed as AE after histopathological examination.

A formalin-fixed specimen was evaluated for the case diagnosed in 2002 (case 2), paraffin-embedded specimens were evaluated for the cases diagnosed in 2006 and 2007 (cases 3 and 4), and an ethanol-fixed specimen was evaluated for the case diagnosed in 2009 (case 5). No specimen was available from the 1982 case (case 1) because of the sociopolitical crisis that occurred around 1990.

A DNA tissue kit (Qiagen, Hilden, Germany) was used for extracting DNA from each specimen. For paraffin-embedded specimens, histological sections were processed using xylene and ethanol for paraffin removal and were then rehydrated before DNA extraction. Because of the degradation of DNA, it is difficult to obtain long-fragment DNA from formalin-fixed tissues. Thus, for cases 2–4, we performed polymerase chain reaction (PCR) using primer pairs, which can amplify small

*Address correspondence to Akira Ito, Department of Parasitology, Asahikawa Medical College, Midorigaoka Higashi 2-1-1-1, Asahikawa 078-8510, Japan. E-mail: akiraito@asahikawa-med.ac.jp

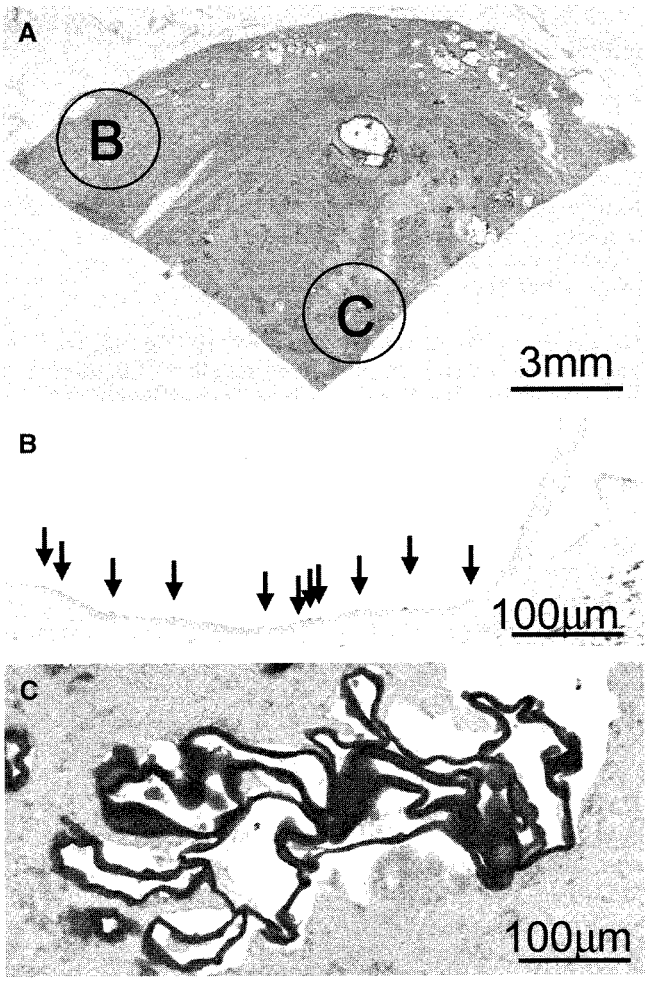

FIGURE 1. Histopathological pictures of AE case 4 showing (**A**) characteristic laminated layers of *E. multilocularis* (Periodic Acid Schiff [PAS] staining), (**B**) active outer lesion with germinal cells and germinal layer (Hematoxylin staining), and (**C**) inactive or necrotic inner lesion without germinal cell or germinal layer but PAS-positive laminated layers (PAS staining). This figure appears in color at www.ajtmh.org.

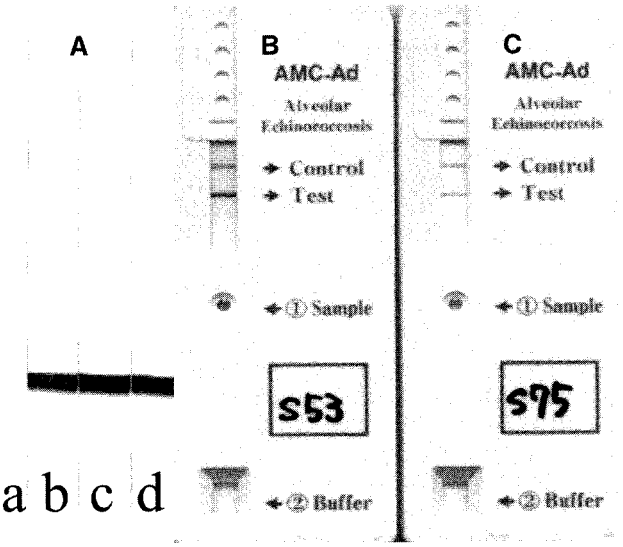

FIGURE 2. Immunoblot and immunochromatographic figures of the two AE cases in Mongolia using a recombinant Em18.[11,12] (**A**) Immunoblot figures. Lane a, shows a pooled negative control serum in 1:50 dilution, lane b, shows confirmed AE serum in 1:1000 dilution, and lanes c and d show sera from cases 4 and 5, respectively, in 1:20 dilution. (**B** and **C**) Immunochromatographic figures of cases 4 and 5, respectively.[10]

(100–200 bp) fragments of *cox1*. For case 5, complete *cox1* was amplified. Some of the primers were already reported elsewhere,[17] and others were newly designed for the present study (Table 1).

All PCRs were performed in 20-μL volumes containing 0.5 units of Ex Taq Hot Start Version (TaKaRa, Ohtsu, Japan), 0.2 mM of dNTP, 1 × Ex Taq Buffer with a final $MgCl_2$ concentration of 2.0 mM, 15 pmol of each primer, and 1.0 μL of genomic DNA. PCR amplification consisted of initial denaturation at 95°C for 2 minutes, 35 cycles of 95°C for 15 seconds, 53°C for 15 seconds, and 72°C for 20 seconds, and a terminal extension at 72°C for 1 minute. PCR products were directly sequenced, and the obtained sequences were concatenated. Partial *cox1* sequences (1,543 bp) from cases 3 and 4 and a complete *cox1* sequence (1,608 bp) from case 5 were obtained. To estimate the genealogical relationship among the haplotypes in the world, the statistical parsimony network of *cox1* haplotypes was constructed by TCS 1.21.[18] Mitochondrial DNA studies have already revealed that isolates of *E. multilocularis* occur in the Northern Hemisphere, and they are divided into four clades: European, Asian, North American, and Inner Mongolian.[17] Case 4 was of the "Asian" type, whereas cases 3 and 5 were of the "Inner Mongolian" type (Figure 3). Case 2 was also confirmed as AE based on *cox1* sequence, but it was not included in the haplotype network analysis because of the short sequence (659 bp).

All AE cases confirmed from the western parts of Mongolia, which are located between Russia and China where highly endemic AE foci were previously described by WHO,[1] had no history of going abroad and were concluded to be indigenous AE cases. This leads to the hypothesis that there may be one large focus of AE in the mountainous region that includes parts of Mongolia, China, and Russia.

The coexistence of the Asian and North American haplotypes was reported from the St. Lawrence Island in the Bering Sea, and a evolutionary scenario in which distinct parasite populations derived from glacial refugia have been maintained by indigenous host mammals was discussed.[17] The present results indicate that human AE cases in Mongolia show additional and different coexistence of the Asian and Inner Mongolian haplotypes. Therefore, further studies on the genetic diversities of the parasite through identification of the natural intermediate and definitive host animals in Mongolia are necessary and essential to discuss the evolution of this parasite.[1,17] Surveillance of *E. multilocularis* in humans and animals, such as rodents (intermediate hosts), red foxes (*Vulpes vulpes*), corsac foxes (*Vulpes corsac*),[19] wolves, and dogs (definitive hosts), is currently under discussion between the National Center for Communicable Diseases in Mongolia and Asahikawa Medical College in Japan.

Received September 4, 2009. Accepted for publication October 26, 2009.

Acknowledgment: We thank Dr. Christine Budke for editing this manuscript.

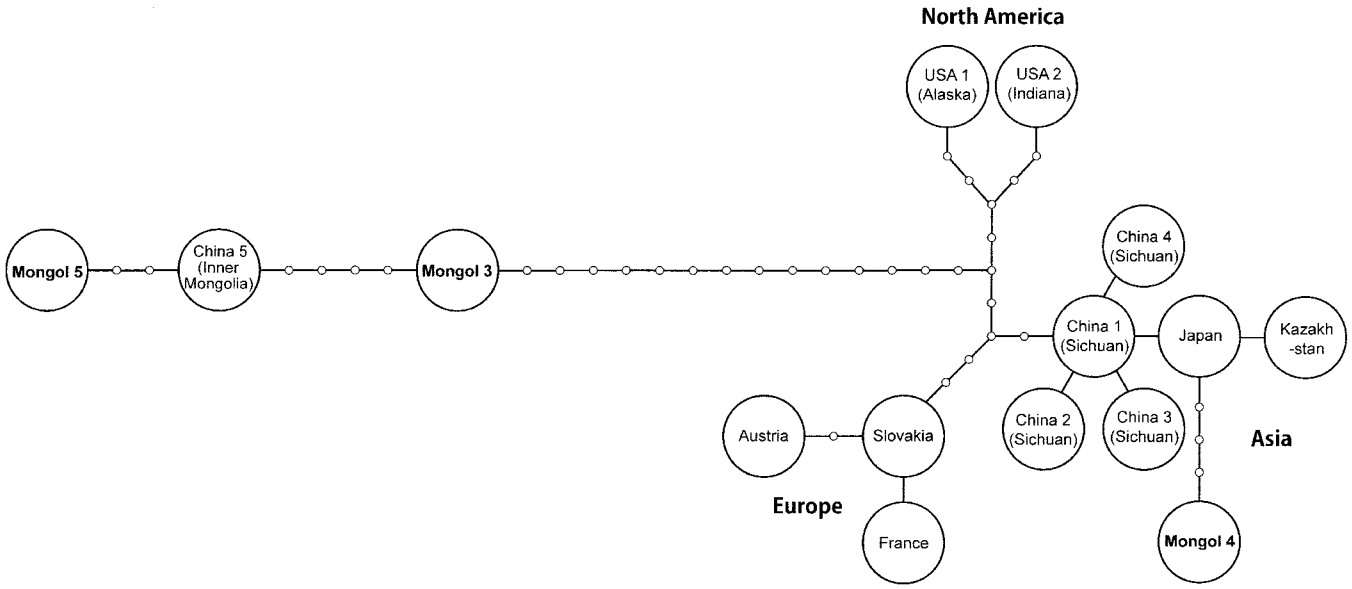

FIGURE 3. Haplotype network constructed with the program TCS 1.21[18] based on 1543 base pairs of *cox1* sequences.[17] Each node indicates a mutational change, and the geographic names inside circles represent the origins of haplotypes. GenBank accession numbers of each sequence used in the present study are as follows: Austria (AB461412), France (AB461413), Slovakia (AB461414), Kazakhstan (AB461415), Japan (AB461416), China 1 (AB461417), China 2 (AB477010), China 3 (AB477011), China 4 (AB477012), USA 1 (AB461418), USA 2 (AB461419), China 5 (AB461420), Mongol 2 (AB510022), Mongol 3 (AB510023), Mongol 4 (AB510024), and Mongol 5 (AB510025).

Financial support: This study was supported in part by a Grant-in-Aid for international research projects on cestode zoonoses in Asia (17256002, 21256003) and by the Asia-Africa Science Platform Fund (2006-2011) from the Japan Society for the Promotion of Science (to A.I.). N.M. received a World Health Organization/Special Programme for Research and Training in Tropical Diseases (WHO/TDR) Grant (200075162). Nucleotide sequence data reported in this paper are available in the DNA Data Bank of Japan/GenBank/European Molecular Biology Laboratory (DDBJ/GenBank/EMBL) databases under accession numbers AB510022 (Mongol 2), AB510023 (Mongol 3), AB510024 (Mongol 4), and AB510025 (Mongol 5).

TABLE 1

Primers used for the amplification of *cox1* gene fragments of *E. multilocularis*

Primers	Sequence (5′ to 3′)	Positions	Reference
Em *cox1* F1	gactttctctttggttggtgtaag	tRNA-ser	17
Em *cox1* F11	tgtgattaggtagttgggtattga	11–34	PS
Em *cox1* F100	ttaagttttagtttgttgattcgtg	100–124	PS
Em *cox1* F9	tgactaatcatggtataataatgatc	182–207	PS
Em *cox1* F400	tcttcttcatatttttctaggagtag	400–425	PS
Em *cox1* F500	gtactttgtatagtgtttttatgact	500–525	PS
Em *cox1* F4	gttttggctgctgctattactatgc	601–625	PS
Em *cox1* F2	gtttatgttttgattctgcctggatt	727–752	PS
Em *cox1* F5	tgggttggatgtgaagacggcggt	885–908	PS
Em *cox1* F1000	aagagtgatcctattttgtggtgggt	1000–1025	PS
Em *cox1* F1100	ttttacacgatacttgatttgtggtg	1100–1125	PS
Em *cox1* F6	attactggtttgaggttgaataagt	1201–1225	PS
Em *cox1* F10	cctatgcattattttggtttatgtg	1282–1306	PS
Em *cox1* F7	tcttttatatctgcgtttagtgggtg	1375–1400	PS
Em *cox1* R1	aacctaaacaaccaacttcacag	*rrnL*	17
Em *cox1* R11	gtaattatgtatttgctgttggttag	1583–1608	PS
Em *cox1* R10	tagtggattatttaatgagtcctgta	1475–1500	PS
Em *cox1* R1400	cttttatatctgcgtttagtgggtg	1376–1400	PS
Em *cox1* R9	tatgtgggttgcctcgtcgtgtgtg	1301–1325	PS
Em *cox1* R1200	ttatgtttatttgatggtgaccgttg	1175–1200	PS
Em *cox1* R4	cgatacttgatttgtggtggctcat	1107–1131	PS
Em *cox1* R8	atgttgcttaattctagtgtaaata	976–1000	PS
Em *cox1* R7	gtttgggttttatggtttgttgttt	801–825	PS
Em *cox1* R2	ttcagcatatgttttggttttttgg	692–716	PS
Em *cox1* R600	tattttattgttagtgacgttgcct	576–600	PS
Em *cox1* R400	tggttggacttttttatcctccattgt	375–400	PS
Em *cox1* R12	ggtggtttgtctgatttgaatttgcc	268–293	PS
Em *cox1* R200	tttttggtgactaatcatggtataat	175–200	PS

PS = present study; tRNA-ser = tRNA gene for serine; *rrnL* = large subunit ribosomal RNA.

Authors' addresses: Akira Ito, Tetsuya Yanagida, Yasuhito Sako, Minoru Nakao, and Yuji Ishikawa, Department of Parasitology, Asahikawa Medical College, Asahikawa, 078-8510, Japan, E-mails: akiraito@asahikawa-med.ac.jp, yanagida@asahikawa-med.ac.jp, yasusako@asahikawa-med.ac.jp, nakao@asahikawa-med.ac.jp, and iyuji@mvc.biglobe.ne.jp. Gurbadam Agvaandaram, Narankhajid Myadagsuren, and Temuulen Dorjsuren, Department of Medical Biology and Histology, School of Biomedicine, Health Sciences University of Mongolia, Ulaanbaatar 210648, Mongolia, E-mails: agurbadam@yahoo.com, narankhajid@yahoo.com, and dtemuulen@yahoo.com. Oyun-Erdene Bat-Ochir and Batsaikhan Chuluunbaatar, Center of Pathology, Ministry of Health, Ulaanbaatar 210648, Mongolia, E-mails: oerdene@yahoo.com and info@pathologycenter.emoh.mn. Nyamkhuu Gonchigsenghe, Department of Surgery, State Central Clinical Hospital, Ulaanbaatar 210648, Mongolia, E-mail: davka64@yahoo.com. Kazuhiro Nakaya, Animal Laboratory for Medical Research, Asahikawa Medical College, Asahikawa, 078-8510, Japan, E-mail: nky48@asahikawa-med.ac.jp. Abmed Davaajav and Nyamkhuu Dulmaa, National Center for Communicable Diseases, Ministry of Health, Ulaanbaatar 210648, Mongolia, E-mails: abmed99@yahoo.com and dnyamkhuu@nccd.gov.mn.

REFERENCES

1. Eckert J, Schantz PM, Gasser RB, Torgerson PR, Bessonov AS, Movsessian SO, Thakur A, Grimm F, Nikogossian MA, 2001. Geographic distribution and prevalence. Eckert J, Gemmell MA, Meslin FX, Pawlowski ZS, eds. *WHO/OIE Manual on Echinococcosis in Humans and Animals: A Public Health Problem of Global Concern.* Paris: World Organization for Animal Health, 100–142.
2. Bessonov AS, 1998. *Echinococcus multilocularis* infection in Russia and neighboring countries. *Helminthologia 35:* 73–78.
3. Craig PS, Deshan L, MacPherson CN, Dazhong S, Reynolds D, Barnish G, Gottstein B, Zhorong W, 1992. A large focus of alveolar echinococcosis in central China. *Lancet 340:* 826–831.
4. Ito A, Urbani C, Qiu JM, Vuitton DA, Qiu DC, Heath DD, Craig PS, Zheng F, Schantz PM, 2003. Control of echinococcosis and

cysticercosis: a public health challenge to international cooperation in China. *Acta Trop 86:* 3–17.
5. Craig PS, The Echinococcosis Working Group in China, 2006. Epidemiology of human alveolar echinococcosis in China. *Parasitol Int 55:* S221–S225.
6. Ito A, Romig T, Takahashi K, 2003. Perspective on control options for *Echinococcus multilocularis* with particular reference to Japan. *Parasitology 127:* S159–S172.
7. Romig T, Dinkel A, Mackenstedt U, 2006. The present situation of echinococcosis in Europe. *Parasitol Int 55:* S187–S191.
8. Galtsog L, Enkhtsetseg O, Gurbadam A, Narankhajid M, Temuulen D, 2002. First case of *Alveococcus multilocularis* was diagnosed in Mongolia. *Mongolian Med Sci J 122:* 27–30.
9. Ebright JR, Altantsetseg T, Oyungerel R, 2003. Emerging infectious diseases in Mongolia. *Emerg Infect Dis 9:* 1509–1515.
10. Sako Y, Fukuda K, Kobayashi Y, Ito A, 2009. Development of an immunochromatographic test to detect antibodies against recombinant Em18 for diagnosis of alveolar echinococcosis. *J Clin Microbiol 47:* 252–254.
11. Sako Y, Nakao M, Nakaya K, Yamasaki H, Gottstein B, Lightowlers MW, Schantz PM, Ito A, 2002. Alveolar echinococcosis: characterization of diagnostic antigen Em18 and serological evaluation of recombinant Em18. *J Clin Microbiol 40:* 2760–2765.
12. Ito A, Nakao M, Sako Y, 2007. Echinococcosis: serological detection of patients and molecular identification of parasites. *Future Microbiol 2:* 439–449.
13. Tappe D, Frosch M, Sako Y, Itoh S, Grüner B, Reuter S, Nakao M, Ito A, Kern P, 2009. Close relationship between clinical regression and specific serology in the follow-up of patients with alveolar echinococcosis in different clinical stages. *Am J Trop Med Hyg 80:* 792–797.
14. Fujimoto N, Ito A, Ishikawa Y, Inoue M, Suzuki Y, Ohhira M, Ohtake T, Kohgo Y, 2005. Usefulness of recombinant Em18-ELISA to evaluate efficacy of treatment in patients with alveolar echinococcosis. *J Gastroenterol 40:* 426–431.
15. Ishikawa Y, Sako Y, Itoh S, Ohtake T, Kohgo Y, Matsuno T, Ohsaki Y, Miyokawa N, Nakao M, Nakaya K, Ito A, 2009. Serological monitoring of progression of alveolar echinococcosis with multi-organ involvement using recombinant Em18. *J Clin Microbiol 47:* 3191–3196.
16. Davaatseren N, Otogondalai A, Nyamkhuu G, Susher AH, 1995. Management of echinococcosis in Mongolia. *J Ark Med Soc 92:* 122–125.
17. Nakao M, Xiao N, Okamoto M, Yanagida T, Sako Y, Ito A, 2009. Geographic patterns of genetic variation in the fox tapeworm *Echinococcus multilocularis*. *Parasitol Int 58:* 384–389.
18. Clement M, Posada D, Crandall KA, 2000. TCS: a computer program to estimate gene genealogies. *Mol Ecol 9:* 1657–1659.
19. Tang CT, Wang YH, Peng WF, Tang L, Chen D, 2006. Alveolar *Echinococcus* species from *Vulpes corsac* in Hulunbeier, Inner Mongolia, China, and differential development of the metacestodes in experimental rodents. *J Parasitol 92:* 719–724.

Acta Tropica 113 (2010) 248–256

Contents lists available at ScienceDirect

Acta Tropica

journal homepage: www.elsevier.com/locate/actatropica

Widespread co-endemicity of human cystic and alveolar echinococcosis on the eastern Tibetan Plateau, northwest Sichuan/southeast Qinghai, China

Tiaoying Li[a,d,f,*], Xingwang Chen[a], Ren Zhen[b], Jiamin Qiu[a], Dongchuan Qiu[a], Ning Xiao[a], Akira Ito[d], Hu Wang[c], Patrick Giraudoux[e], Yasuhito Sako[d], Minoru Nakao[d], Philip S. Craig[f]

[a] Institute of Parasitic Diseases, Sichuan Centers for Disease Control and Prevention, Sichuan Province, People's Republic of China
[b] Aba Military Hospital, Maerkang, Sichuan Province, People's Republic of China
[c] Qinghai Provincial Institute of Endemic Disease Control, Qinghai Province, People's Republic of China
[d] Department of Parasitology, Asahikawa Medical College, Asahikawa, Japan
[e] Department of Chrono-environment, UMR UFC/CNRS 6249, USCINRA, Université de Franche-Comté, 25030 Besancon Cedex, France
[f] Cestode Zoonoses Research Group and School of Environment and Life Sciences, University of Salford, Salford, UK

ARTICLE INFO

Article history:
Received 21 May 2009
Received in revised form 28 October 2009
Accepted 17 November 2009
Available online 24 November 2009

Keywords:
Cystic echinococcosis
Alveolar echinococcosis
Ultrasound
Prevalence
Tibetan
Sichuan Province
Qinghai Province

ABSTRACT

Cystic echinococcosis (CE) or hydatid disease is known to be cosmopolitan in its global distribution, while alveolar echinococcosis (AE) is a much rarer though more pathogenic hepatic parasitic disease restricted to the northern hemisphere. Both forms of human echinococcosis are known to occur on the Tibetan Plateau, but the epidemiological characteristics remain poorly understood. In our current study, abdominal ultrasound screening programs for echinococcosis were conducted in 31 Tibetan townships in Ganze and Aba Tibetan Autonomous Prefectures of northwest Sichuan Province during 2001–2008. Hospital records (1992–2006) in a major regional treatment centre for echinococcosis in Sichuan Province were also reviewed. Of 10,186 local residents examined by portable ultrasound scan, 645 (6.3%) were diagnosed with echinococcosis: a prevalence of 3.2% for CE, 3.1% for AE and 0.04% for dual infection (both CE and AE). Human cystic and alveolar echinococcosis in pastoral areas was highly co-endemic, in comparison to much lower prevalences in semi-pastoral or farming regions. The high ultrasound prevalence in these co-endemic areas in northwest Sichuan Province was also reflected in the hospital study, and hospital records furthermore indicated another possible highly co-endemic focus in Guoluo Prefecture of Qinghai Province, located at the border of northwest Sichuan. These chronic cestode zoonoses constitute an unparalleled major public health problem for pastoral Tibetan communities, and pose great difficulties for adequate treatment access and effective transmission control in such remote regions.

1. Introduction

Human echinococcosis refers to infection with the larval (metacestode) stage of zoonotic cestodes (tapeworms) belonging to the genus *Echinococcus*. Four main species were recognized until recently, namely, *Echinococcus granulosus*, *E. multilocularis*, *E. oligarthrus* and *E. vogeli* (Rausch and Bernstein, 1997; Kumaratilake and Thompson, 1982). A new (fifth) species of *Echinococcus*, named *E. shiquicus*, has recently been described by our team in wildlife hosts from the eastern Tibetan Plateau, China (Xiao et al., 2005), however its infectivity to humans is unknown (Li et al., 2008). All the classic four recognized *Echinococcus* species of carnivores can infect humans (i.e. zoonotic) and may cause three clinical forms of echinococcosis, i.e. cystic echinococcosis (CE) caused by *E. granulosus*, alveolar echinococcosis (AE) caused by *E. multilocularis*, or polycystic echinococcosis due to *E. vogeli* or *E. oligarthrus*. The distribution of *E. granulosus* is cosmopolitan and is the predominant cause of human echinococcosis worldwide (McManus, 2002). Transmission of *E. oligarthrus* and *E. vogeli* is restricted to Central and South America where sporadic cases may occur, especially due to the latter species (D'Alessandro, 1997). *E. multilocularis* is also a relatively rare parasitic disease in humans and is restricted to the Northern Hemisphere, with primary transmission in wildlife (cycling between foxes and rodents). Human AE cases have however occurred more frequently in foci in Alaska, northern and central Europe, Central Asia, Siberia, China and Japan (Craig, 2003).

In China, human CE has been demonstrated to be widespread in at least 21 of its 31 provinces, but was more prevalent in the following northwest Provinces or Autonomous regions: Qinghai, Gansu, Sichuan, Ningxia, Xinjiang, Inner Mongolia, Tibet and Yunnan (Shi, 1997; Wen and Yang, 1997; Craig, 2004). From the 1990s active mass screening surveys using portable ultrasound began to reveal very high prevalence rates of human alveolar echinococcosis in several agricultural counties of Gansu and Ningxia provinces

* Corresponding author. Tel.: +86 28 85589532; fax: +86 28 85589563.
E-mail address: litiaoying@sina.com (T. Li).

0001-706X/$ – see front matter © 2009 Elsevier B.V. All rights reserved.
doi:10.1016/j.actatropica.2009.11.006

(Craig et al., 1992; Yang et al., 2006), and more surprisingly in pastoral Tibetan communities in western Sichuan Province (Li et al., 2005).

With the aim of understanding the epidemiology of human echinococcosis (both CE and AE) in Tibetan communities of the eastern Tibetan Plateau, mass screening programs for echinococcosis were conducted in 31 Tibetan townships located in western Sichuan Province. In addition, hospital records of echinococcosis patients post-operatively confirmed were reviewed from one of the main treatment centres in the region.

2. Materials and methods

2.1. Study sites

Parts of populations in a total of 31 townships, located in Ganze and Aba Tibetan Autonomous Prefectures of northwest Sichuan were screened by mass ultrasound. Participants in the study were selected on a voluntary basis. The involved townships included 24 pastoral townships within Ganze and located in the counties of Shiqu, Seda, Baiyu, Ganzi, Dege or Yajiang, where altitudes ranged from 3700 m to 4500 m, and the main occupation of local residents was raising yaks and sheep/goats as the primary source of income. In addition, three farming (primary agricultural) townships were selected from Yajiang and Danba Counties (Ganze Prefecture) and Maerkang County (Aba Prefecture), with altitudes varying from 2010 m to 2680 m. Four semi-pastoral townships were also included and were located in Rangtang County (Aba Prefecture), with altitudes ranging from 3451 m to 3600 m, where local people subsisted on both agricultural and livestock grazing (Fig. 1). Screening programs for abdominal echinococcosis using portable ultrasound (GE, LOGIQ α100, Wuxi, China) were performed in Spring or early Winter during 2001–2008 in the selected sites. In cooperation with County level Centers for Disease Control (CDC) and local health administrators (cadres), information about the purpose of the screening program was spread to the villagers and townships. Volunteers were self-selected by informed consent and were assured free diagnosis and medical treatment with long-term albendazole drug therapy for echinococcosis if diagnosis was indicated. Recommendation was also provided for possible surgical intervention (cyst/lesion removal or drainage) if appropriate. Persons with other infections or medical conditions were examined and referred to local health clinics for further investigation or treatment.

2.2. Questionnaire

For each self-selected participant a questionnaire was completed using Tibetan registration auxillaries, designed to obtain information on demographics, animal ownership and potential risk factors for echinococcosis including the source of drinking water, dog ownership, the frequency of dog contact, ownership of fox skin products etc.

2.3. Criteria for diagnosis and classification of echinococcosis

Diagnosis and classification of cystic echinococcosis (CE) was made using portable ultrasound according to the criteria proposed by the World Health Organization Informal Working Group on Echinococcosis for CE (Pawlowski et al., 2001). On the basis of conformational features of cysts, CE lesions (primarily in the liver) were differentiated into six types including CL, CE1, CE2, CE3, CE4, and CE5. In this study, CL cysts of a parasitic origin were exclusively counted, and CL cysts of a non-parasitic origin were excluded by comprehensive analysis of other factors, particularly such as the patient age, and partially by further observation during follow-up. In general, the CL type refers to a cystic lesion without clear rim indicating the parasite is at an early stage of development if the cyst is of a parasitic origin, while the presence of CE1 or CE2 is suggestive of active stages of the disease, while CE3 suggests the parasite is at

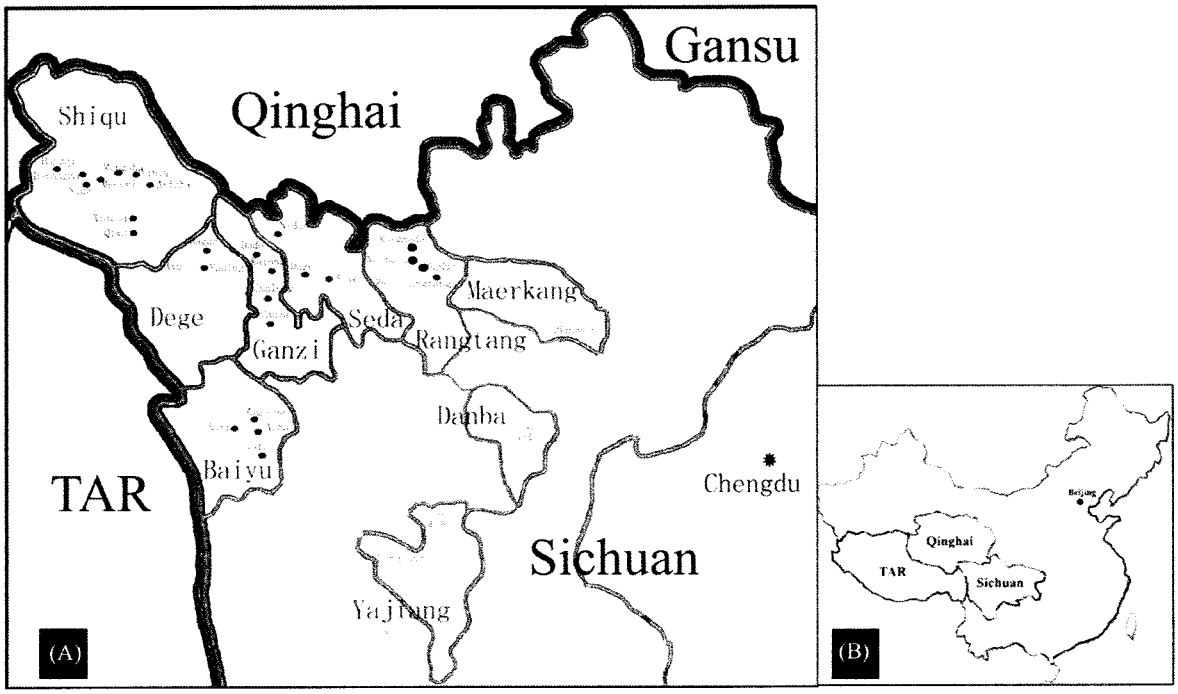

Fig. 1. Study sites of mass screening programs for abdominal echinococcosis by B-ultrasound in Sichuan Province, China. (A) Localities of study sites—(●) townships with detection of AE cases; (○) townships with detection of CE cases; (◒) townships with detection of both CE and AE cases; (⊗) townships without echinococcosis cases detected. (B) China map with the locality of Beijing (capital), Sichuan Province, Qinghai Province and Tibetan Autonomous Region (TAR).

a transitional stage, and CE4 or CE5 implies an involution, necrotic or inactive parasite (Pawlowski et al., 2001).

Diagnosis of AE was dependent on detection of distinctive tumour-like lesions in the liver characterized by a non-homogeneous hyperechoic structure and with poorly defined verge, containing scattered calcifications, and/or a central necrotic cavity with a hyperechoic pseudoliquid structure (Pawlowski et al., 2001; Bresson-Hadni et al., 2006) and further classification was based on the criteria proposed previously (Li et al., 2004) and the PNM system (Kern et al., 2006). Briefly, on the basis of the features and the size of lesions, AE lesions were classified into three types and eight subtypes which indicated different stages of the disease. AE lesions ≤5 cm, normally without central necrosis detected, were confirmed as AE1 and differentiated further as, AE1s (single lesion) and AE1m (multiple lesions), which indicated an early stage of the disease. Alveolar lesions measured >5 cm ≤ 10 cm were classified as AE2 including three subtypes recorded as AE2s (single lesion), AE2m (multiple lesions) and AE2f (presence of central necrotic fluid, regardless of the number of lesions), suggestive of a developing parasite, while AE lesions measured >10 cm at diameter were confirmed as AE3 indicative of an advanced stage of the disease, which include three subtypes, i.e. AE3s (single lesion), AE3m (multiple lesions) and AE3f (presence of central necrotic fluid, regardless of the number of lesions).

2.4. Serology

Persons with confirmative or suspected CE/AE lesions or with other space-occupying lesions in the liver were asked to give a five ml venous blood sample for detection of *Echinococcus* antibodies using ELISA with recombinant AgB as antigen for CE or AE, and ELISA with recombinant Em18 antigen for AE, as described elsewhere (Sako et al., 2002; Xiao et al., 2003; Mamuti et al., 2004).

2.5. Hospital study

All patients who were treated surgically for echinococcosis in Aba Military Hospital (located in Maerkang, Aba Prefecture, Sichuan Province) (Fig. 5) during 1992–2006, and post-operatively confirmed by histopathology as echinococcosis, were included in this study ($n = 1312$). Further information about age, gender, domicile, ethnicity, and post-operative diagnosis, etc was collected. This hospital has 200 beds of which 95% are used to admit non-military patients.

Diagnosis of echinococcosis before operation was made by abdominal B-ultrasound examination and/or computed tomography (CT) (Ren et al., 2008). Post-operative confirmation was made by histopathology, as well as by PCR and DNA sequencing of isolates for some cases (Li et al., 2008). Briefly, morphological identification of CE infection was based on the observation of the structure of cystic lesions characterized by unilocular cysts with a thick laminated layer, presence of a germinal layer, and/or brood capsules with protoscoleces. For AE histopathology, the presence of large numbers of vesicles with different sizes and shapes with a thin laminated layer, and concurrence of distinct hyperplasia of fibro-connective tissue and cellular infiltration of eosinophils, lymphocytes and plasma cells, resulted in a diagnosis.

Table 1
Prevalence of human echinococcosis at township levels by ultrasound scanning in northwest Sichuan Province.

County	Township	No. examined	CE (*n*) %	AE (*n*) %	Dual infection	Total %
Shiqu	Niga	475	4.00(19)	4.00(19)	0	8.00
	Mengsha	356	9.55(34)	7.02(25)	1	16.85
	Yiniu	631	3.33(21)	9.35(59)	0	12.68
	Arizha	381	5.51(21)	8.14(31)	1	13.91
	Xiazha	584	7.02(41)	4.79(28)	0	11.82
	Qiwu	349	6.88(24)	1.72(6)	0	8.60
	Derongma	108	10.19(11)	4.63(5)	0	14.81
	Mengyi	100	14.00(14)	7.00(7)	0	21.00
	Hongqi	212	11.32(24)	5.66(12)	1	17.45
Ganzi	Kalong	549	0.91(5)	3.83(21)	0	4.74
	Chalong	614	2.61(16)	6.35(39)	0	8.96
	Chaza	116	2.59(3)	2.59(3)	0	5.17
	Dade	123	1.63(2)	3.25(4)	0	4.88
Seda	Daze	310	2.58(8)	3.23(10)	1	6.13
	Niduo	229	3.93(9)	1.75(4)	0	5.68
	Seke	492	0.61(3)	1.42(7)	0	2.03
Baiyu	Maqiong	302	3.97(12)	1.66(5)	0	5.63
	Nata	271	1.48(4)	2.58(7)	0	4.06
	Acha	258	3.10(8)	0.78(2)	0	3.88
	Anzi	119	1.68(2)	2.52(3)	0	4.20
Rangtang	Gaduo	274	0(0)	1.82(5)	0	1.82
	Nanmuda	145	0(0)	1.38(2)	0	1.38
	Rongmuda	162	0(0)	0.62(1)	0	0.62
	Zhongrangtang	94	1.06(1)	2.13(2)	0	3.19
Dege	Dagun	269	3.35(9)	0.37(1)	0	3.72
	Yading	198	7.07(14)	1.52(3)	0	8.59
	Axu	117	5.13(6)	0(0)	0	5.13
Yajiang	Honglong	610	2.30(14)	0(0)	0	2.30
	Waduo	584	0(0)	0(0)	0	0.00
Maerkang	Zhuokeji	571	0.88(5)	0(0)	0	0.88
Danba	Badi	583	0(0)	0(0)	0	0
Total		10186	3.24(330)	3.05(311)	4	6.33

2.6. Statistical analysis

Data were analyzed using Epi InfoTM (version 3.5; Centers for Disease Control and Prevention, Atlanta, GA), statistical significance was set at $p < 0.01$.

3. Results

3.1. Mass screening using ultrasound

A total of 10,186 participants originating from Tibetan communities of 31 townships in nine counties in Sichuan Province were registered by questionnaire and examined by abdominal ultrasound. Population sample (age ranged from 1 to 92 years; median 32.8 years) comprised 50.4% (5133) females and 49.6% (5053) males. Persons of Tibetan ethnicity comprised 96.1% of the sampled population. The other participants listed their ethnicity as Han (3.9%). Questionnaire data revealed 46.9% (4781) were herdsmen who raised livestock including yaks, sheep and/or goats as the primary source of their income. Other listed occupations included student (19.1%), farmer (12.2%), part-time herdsman (4.5%), public servant (7.4%), preschooler (3.6%), and other (6.3%).

3.1.1. Prevalence of human echinococcosis

Of 10,186 volunteers examined by abdominal ultrasound scanning, 311 (3.1%) were confirmed to have AE infection, 330 (3.2%) to have CE, and 4 (0.04%) individuals to have dual infection with both CE and AE (Table 1; Figs. 2 and 3).

Of 315 persons with a confirmative image of AE lesions (including four persons with dual infection), 74 (23.5%) had hepatic lesions of AE1 type (67 AE1s and 7 AE1m), 142 (45.1%) had AE2 lesions in the liver (75 AE2s, 20 AE2m and 47 AE2f), while hepatic lesions characterized by AE3 were detected in 99 (31.4%) individuals (34 AE3s, 3 AE3m and 62 AE3f) (Table 2). In addition, 136 single AE lesions were located in the right hepatic lobe, and 36 were in the left hepatic lobe. Involvement of both lobes was observed in 79 AE cases. More than one alveolar lesion was detected in the liver in the remaining 64 cases.

Of 334 persons who presented with cystic images indicative of CE cysts (including 4 cases with dual infection), nine (2.7%) were detected to have CL type lesions, 103 (30.8%) were classified to have CE1 lesions, 98 (29.3%) had CE2 cysts, 12 (3.6%) had CE3 lesions, 80 (24.0%) and 17 (5.1%) had CE4 or CE5 type cysts, respectively. Furthermore, multiple CE lesions with mixed type cysts were detected in an additional 15 cases (4.5%), i.e. 5 patients with CE1 and CE2 cysts, 3 with CE1 and CE4 cysts, 5 with CE2 and CE4 cysts, 1 with CE2 and CE5 cysts, and 1 with CE3 and CE5 type cysts (Table 2). In addition to the liver, one or more CE cystic lesions were identified in the peritoneal cavity in 24 patients, 7 cases in the spleen and 1 case in the kidney.

3.1.2. Echinococcosis prevalence at township level

Of 7773 volunteers originating from 24 pastoral townships that were examined by ultrasound, 324 (4.2%) were confirmed to have CE infection, 301 (3.9%) to have hepatic AE infection, and 4 (0.04%) persons presented with dual infection (both CE and AE). The overall prevalence of echinococcosis in pastoral townships ranged from 2.0% (10/492) in Seke Township, Seda County to 21.0% (21/100) in Mengyi Township, Shiqu County. The highest AE prevalence (9.4%, 59/631) was recorded in Yiniu Township of Shiqu County, and the highest CE prevalence (14.0%, 14/100) was recorded in Mengyi also in Shiqu County. No AE cases were detected in Honglong Township,

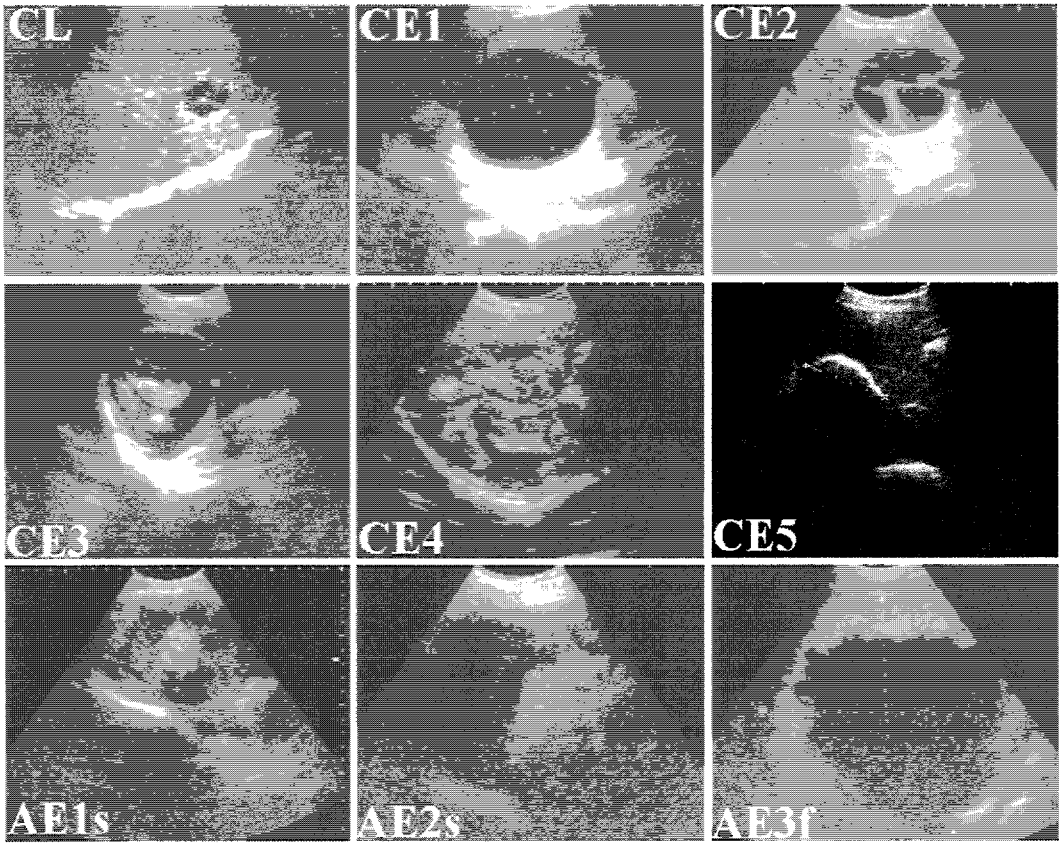

Fig. 2. Ultrasound images of different types of hepatic echinococcal lesions in patients detected in northwest Sichuan.

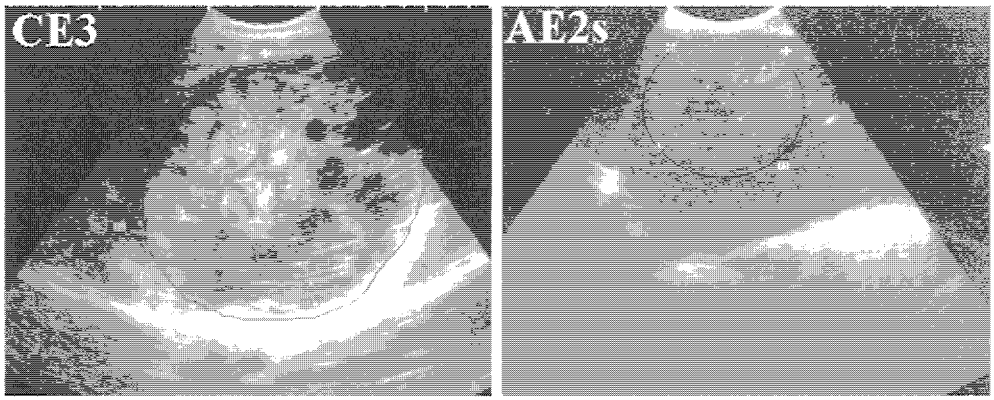

Fig. 3. Hepatic ultrasound images of the patient with dual infection (both CE and AE) in northwest Sichuan Province. CE and AE lesions were marked by a circle, respectively.

Yajiang County, however CE prevalence was 2.3% (Table 1). Therefore, both human cystic and alveolar echinococcosis was shown to be highly co-endemic in 23 of 24 pastoral townships studied in western Sichuan (Table 1).

In contrast, a much lower prevalence of human echinococcosis was recorded in farming or semi-farming townships, i.e. only 5 CE cases (3 CE4 and 2 CE5 advanced type cysts) were detected in 3 farming townships, with a prevalence of 0.3% (5/1738). Furthermore, only 0.1% (1/675) and 1.5% (10/675) of local people in 4 semi-farming townships had CE or AE infection, respectively (Table 1).

3.1.3. Prevalence by gender and age

Of 645 persons with an evidence of abdominal echinococcosis, 394 (CE = 212, AE = 179, dual infection = 3) were female, and 251 (CE = 118, AE = 132, dual infection = 1) were male. In other words, the prevalence of echinococcosis (CE or AE) in females was 7.7% (394/5133) (4.1% for CE, 3.5% for AE and 0.1% for dual infection), and 5.0% (251/5053) for male (2.3% for CE, 2.6% for AE and 0.02% for dual infection). Statistical analysis revealed that the prevalence of echinococcosis in females (7.7%) was significantly higher than that for males (5.0%) ($\chi^2 = 31.49$, $p < 0.01$).

Among the 645 persons with abdominal detectable *Echinococcus* lesions, the average age was 40.9 years. The youngest patient with CE was 3 years and the oldest was 81 years, and the average age of CE cases detected by ultrasound was 38.6 years ($n = 330$). However, age specific prevalence of CE cyst type varied. The average age of subgroup population with CE cysts at an early stage (CL) lesions was 11.3 years ($n = 9$), while average age group with CE cystic lesions at active stages (CE1, CE2), at transitional stages (CE3) or inactive stages (CE4, CE5), was 38.2 years ($n = 201$), 36.3 years ($n = 12$) and 43.5 years ($n = 97$), respectively. The average age of persons diagnosed in the communities with hepatic AE was 43.4 years (age range 6–81 years). The subgroup of cases with early AE1 lesions had an average age of 39.7 years ($n = 74$), while the mean age of the population with AE2 lesions was 44.7 years ($n = 142$), and 44.0 years for the subgroup with advanced AE3 lesions ($n = 99$). In addition, the average age for 4 persons with dual infection was 39.8 years (ranging 11–66 years).

For human AE prevalence showed an increase with age, which peaked at the >60 years group (6.5%). Further analysis revealed a significant difference of AE prevalence between age groups ($\chi^2 = 108.91$, $p < 0.01$, 6 degrees of freedom). For abdominal CE prevalence peaked at 5.0% in the >40 to ≤50 years age group, and then decreased. The four persons with dual CE and AE infection were detected across the age cohort (Fig. 4).

3.1.4. Prevalence of echinococcosis by occupation

Herdsman had the highest risk for abdominal echinococcosis infection, with a total prevalence of 10.6% (505/4781) (5.5% for CE and 5.0% for AE). Farmers had the lowest prevalence of 0.4% (5/1245) (0.4% for CE). For other occupations, the prevalence was recorded as 2.2% (10/453) for part-time herdsman (0.2% for CE and 2.0% for AE), 1.7% (34/1944) for students (0.9% for CE, 0.8% for AE and 0.05% for dual infection), 1.9% (7/371) for preschooler (1.6% for CE and 0.3% for AE), 3.9% (29/749) for public servants (2.0% for CE and 1.9% for AE), and 8.6% (55/643) for others (3.6% for CE, 4.8% for AE and 0.2% for dual infection). The prevalence for both CE and AE combined proved to be of statistical significance between occupations ($\chi^2 = 325.28$, $p < 0.01$, 6 degrees of freedom).

3.2. Serology

A total of 191 (77.6%) CE sera and 147 (85.0%) AE sera showed positive response to *E. granulosus* recombinant antigen B (rAgB), while 28.9% (71/246) CE sera and 87.3% (151/173) AE sera were recognized by *E. multilocularis* recombinant Em18 (rEm18). Moreover, significant differences of seropositivities with ELISA-rAgB

Table 2
Ultrasonic classification of echinococcal lesions in 649 cases (including 4 patients with dual infection) in northwest Sichuan Province.

Subtype of AE	No. cases	Proportion %	Subtype of CE	No. cases	Proportion %
AE1s	67	21.27	CL	9	2.69
AE1m	7	2.22	CE1	103	30.84
AE2s	75	23.81	CE2	98	29.34
AE2m	20	6.35	CE3	12	3.60
AE2f	47	14.92	CE4	80	23.95
AE3s	34	10.80	CE5	17	5.09
AE3m	3	0.95	Mix	15	4.49
AE3f	62	19.68			
Total	315	100.00		334	100.00

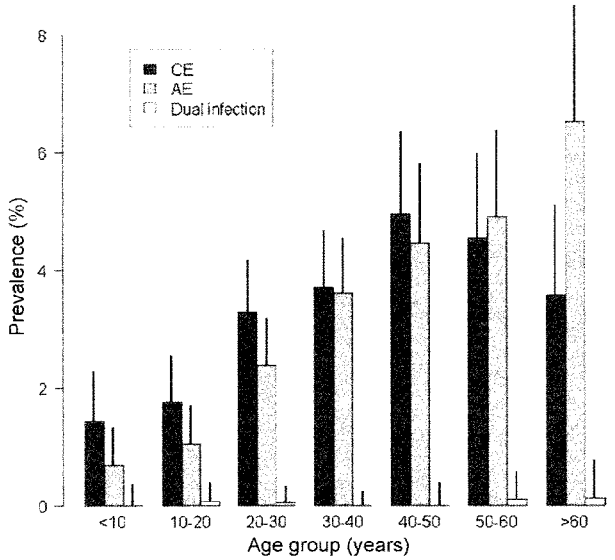

Fig. 4. Prevalence of echinococcosis by age groups in northwest Sichuan Province.

or ELISA-rEm18 were observed in CE/AE cases with echinococcal lesions at different stages. Detailed description of the serology profiles will be reported elsewhere (Li et al., unpublished data).

3.3. Aba hospital study

During 1992–2006, records were identified for 1312 patients (male = 719, female = 593) with post-operatively confirmed echinococcosis in Aba Military Hospital. The majority 79.6% (n = 1044) were confirmed as CE, and 268 as AE infection. Persons of Tibetan ethnicity comprised 97.4% (1278/1312) of these patients, and all the others were Han Chinese. The mean age of 1292 patients (information about age was not available for the other 20 patients) was 42.8 years, ranging from 4 to 81 years. The youngest CE case was 4 years old and the oldest 81 years, with a mean age of 42.9 years (n = 1027). While the average age of AE cases was 42.5 years (n = 265), with an age range of 8–79 years. The main treatment used for CE was endocystectomy, and for AE cases resection of total/partial alveolar lesion.

Of 1044 patients treated with CE infection, 84.8% (885) had cystic lesions located in the liver, 11.7% (122) in the abdominal cavity or pelvic cavity, and 1.6% (17) in both abdominal cavity and pelvic cavity as well as the liver. Involvement of other organs or tissues was also recorded: spleen CE (1 case), subcutaneous CE (8 cases), lung (4 cases), brain (3 cases), vertebra (2 cases), bone (1 case), and eye (1 case).

Of 268 AE cases treated, alveolar lesions were detected only in the liver in 93.7% (251) of patients. In the remaining 17 AE patients, other organs were also involved, i.e. the brain (5 cases), lung (5 cases), brain and lung (1 case), vertebra (5 cases) and bladder (1 case).

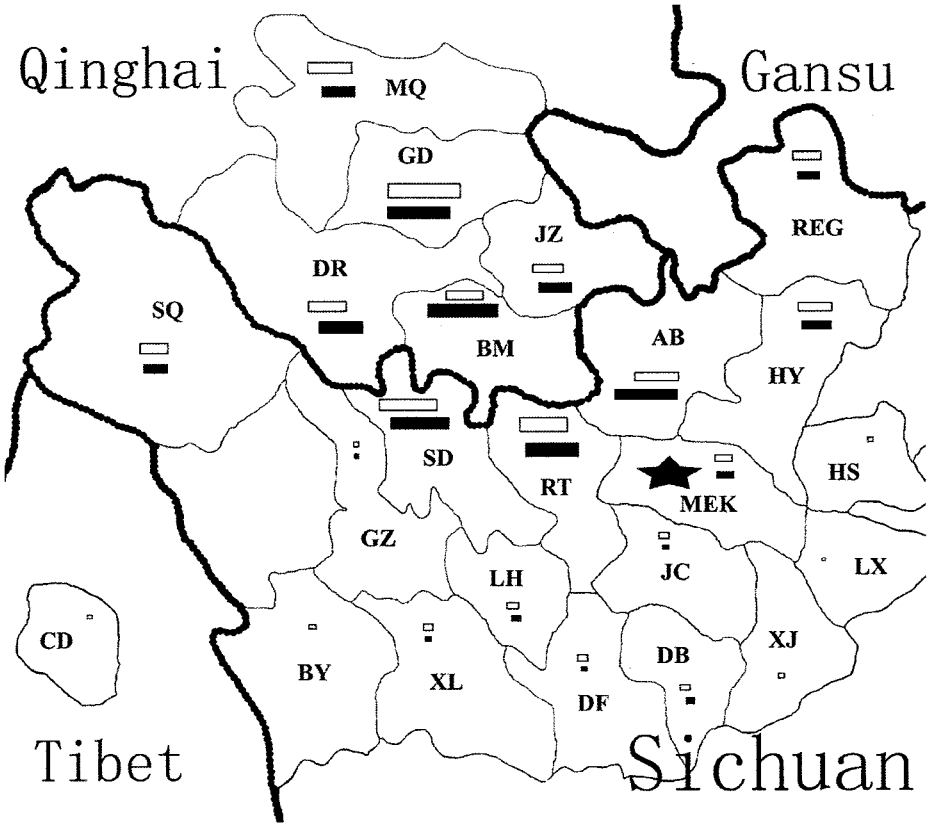

Fig. 5. Geographic distribution of 1312 human cases of echinococcosis post-operatively confirmed during 1992–2006 in Aba Army Hospital; Solid and open bars indicate AE and CE cases, respectively. The length of bars shows approximate proportion of each disease in the county. Symbol (*) shows the locality of Aba Army Hospital. Full name of each county is shown as follows: SQ = Shiqu, GZ = Ganzi, SD = Seda, BY = Baiyu, XL = Xinlong, LH = Luhuo, DF = Daofu, DB = Danba, RT = Rangtang, AB = Aba, REG = Ruoergai, MEK = Maerkang, HY = Hongyuan, HS = Heishui, LX = Lixian, XJ = Xiaojin, JC = Jinchuan, BM = Banma, JZ = Jiuzhi, GD = Gande, MQ = Maqin, DR = Dari, CD = Changdu.

The majority (99.9%) of the 1312 echinococcosis patients treated at Aba Military Hospital lived in Sichuan or Qinghai provinces, and only one CE patient came from the Tibetan Autonomous Region (Changdu County) (Fig. 2). For 1044 CE cases, 56.5% (590) originated from 17 counties of Sichuan Province. The remaining 453 (43.4%) CE cases came from 5 counties of Guoluo Prefecture of Qinghai Province (Fig. 5). Of 268 AE cases treated at Aba Military Hospital, 150 (56.0%) resided in 13 counties of Sichuan Province, while 118 (44.0%) AE cases lived in the same 5 counties of Guoluo Prefecture, Qinghai Province, i.e. Banma, Dari, Gande, Jiuzhi, and Maqin counties (Fig. 5).

4. Discussion

Human cystic echinococcosis (CE) caused by *E. granulosus*, results in more lost DALYs (disability adjusted life years) globally than that due to onchocerciasis or Chagas disease (Budke et al., 2006), with the greatest echinococcosis burden in Central Asia and China (Craig et al., 2007). The Chinese Ministry of Health carried out a national survey in 2002 for 8 important parasitic diseases, and found the prevalence of human CE was highest (2.5%) in Tibetan communities (Craig et al., 2008). In western China human alveolar echinococcosis, caused by *E. multilocularis*, is also endemic albeit with a more focal distribution than CE and generally considered mainly to be a zoonotic disease in poor Han or Hui upland agricultural communities (Craig et al., 1992; Yang et al., 2006). Human CE and AE cause chronic cystic or vesicular lesions respectively, which may eventually be highly pathogenic and very difficult to treat (WHO, 1996; McManus et al., 2003).

We now demonstrate the occurrence of a major co-endemic focus of human CE/AE in Tibetan pastoral communities present in northwest Sichuan and southeast Qinghai at the eastern edge of the Tibetan Plateau. The average total ultrasound prevalence of human abdominal echinococcosis in 10,186 persons screened in two Tibetan Autonomous Prefectures of northwest Sichuan was 8.1% (4.2% for CE, 3.9% for AE, and 0.05% for dual CE/AE infection). The highest co-endemicity (10.6% total prevalence) at community level occurred in pastoralists (herdsmen occupation), in which approximately half the cases detected were due to the most pathogenic form AE. Human echinococcosis cases were also detected after mass screening in agricultural/semi-farming Tibetan communities but with significantly lower ultrasound prevalence (<0.5% for either disease). This high co-endemicity for CE and AE at pastoral community level in northwest Sichuan, was also verified by examination of hospital records in one important treatment centre in Aba Tibetan Autonomous Prefecture, and also identified CE and AE cases originating from another highly co-endemic pastoral region, i.e. Guoluo Tibetan Autonomous Prefecture in Qinghai Province (Han et al., 2006; Yu et al., 2008), which borders northwest Sichuan.

A total of 645 cases of human cystic ($n = 330$) and alveolar ($n = 311$) echinococcosis, as well as 4 mixed CE/AE cases, were identified by mass ultrasound screening in 8 counties of west Sichuan Province, i.e. counties of Shiqu, Seda, Ganze, Baiyu, Dege, Yajiang, Rangtang and Maerkang. Patient records from Aba Military Hospital in Maerkang (Sichuan) between 1992 and 2006, for 1312 confirmed echinococcosis cases ($n = 1044$ CE, $n = 268$ AE), identified patient domicile in an additional 5 counties in neighbouring Qinghai Province, i.e. counties of Banma, Dari, Jiuzhi, Gande and Maqin. More detailed analysis of these hospital cases has been reported elsewhere (Ren et al., 2008).

Western China has long been known to be endemic for human cystic echinococcosis (CE) (Craig et al., 1991), however the distribution of human alveolar echinococcosis (AE) the most pathogenic form, appears more focal with apparent hotspots in Gansu, Ningxia, Xinjiang, Qinghai and Sichuan provinces/regions, some of which are also co-endemic for CE (Craig et al., 1992; Yang et al., 2006; Li et al., 2005; Han et al., 2006; Yu et al., 2008; Schantz et al., 2003; Zhou et al., 2000). Human CE and AE are co-endemic in only a few other world regions, notably eastern Turkey, Central Asia and Siberia (Craig, 2003). The current study now identifies a geographic area on the eastern edge of the Tibetan Plateau of approximately 313,200 km^2 involving at least 11 pastoral counties over 2 adjacent provinces, with the greatest levels of co-endemicity of human CE and AE so far described worldwide.

In Tibetan pastoral communities, domestic dogs are kept in large numbers to guard property and livestock, and are usually tied during daytime and released at night. As Tibetan Buddhism forbids killing animals including dogs, with exception of food provision, large populations of stray dogs exist especially around temples. During the livestock slaughtering season (October to December), dogs (both owned and stray) are frequently fed with raw offal (including livers and lungs of yaks, sheep or goats) by herdsman. In addition, dogs may also prey on small mammals in around townships and adjacent pastures. A necropsy study of stray dogs in Ganze Prefecture revealed a 29.5% prevalence for *E. granulosus* and 11.5% for *E. multilocularis* (Qiu et al., 1989). A recent diagnostic purgation study in Shiqu County identified 8% of owned dogs infected with *E. granulosus* and 12% with *E. multilocularis* infection (Budke et al., 2005). The Tibetan fox (*Vulpes ferrilata*) appears to be the main sylvatic definitive host of both *E. multilocularis* and *E. shiquicus* in these pastoral areas (Qiu et al., 1995; Xiao et al., 2005), and ownership of fox skins was shown to be a risk factor for human AE (Wang et al., 2006). To date however, there is no evidence that human echinococcosis can be caused by *E. shiquicus* (Li et al., 2008). Yaks as well as sheep and goats appear to be key intermediate hosts for transmission of *E. granulosus* on the Tibetan Plateau (He and Liu, 2000). In addition, the high altitude grassland is abundant in small mammal communities, and up to 5 species (in the genera *Microtus*, *Cricetulus* and *Ochotona*) have so far been identified as possible key reservoir intermediate hosts of *E. multilocularis* (Giraudoux et al., 2006). The involvement of dogs as well as foxes in transmission of *E. multilocularis*, the diversity of small mammal potential hosts, landscape/habitat ecology of small mammals, together with poor hygiene and other risk behaviors (Li et al., 2005; Wang et al., 2006), seem to be major factors contributing to the high prevalence of both human cystic and alveolar echinococcosis in pastoral areas of the eastern Tibetan Plateau.

Landscape ecology suitable for transmission of *E. multilocularis* can vary over short distances (10 km) (Giraudoux et al., 2003). An interesting observation in the current study was the absence of AE cases detected in one pastoral township (Honglong in Yajiang County), where altitude (4168 m), average number of dogs owned (1.2) and livestock ownership, was similar to other pastoral townships with high human AE prevalence (e.g. Yiniu Township in Shiqu County at 4200 m and average 2.9 dogs owned per household). Subtle differences in landscape ecology could affect suitable habitat for potential small mammal hosts and their population dynamics which enable transmission of *E. multilocularis* (Giraudoux et al., 2003).

Although a human CE prevalence of 0.3% (mean age = 61.6 years) was found after ultrasound screening in farming areas, all cysts were confirmed by ultrasound to be involutive or inactive, i.e. CE4 or CE5 types, which may indicate less recent transmission of *E. granulosus* in those non-pastoral areas. Furthermore, no human AE cases were detected by mass screening in such farming areas. By contrast, upland farming/agricultural communities have been identified as important AE foci in some other parts of China (Craig et al., 1992) as well as in Europe (Giraudoux et al., 2003). In mixed farm-

ing/pastoral Tibetan areas both CE and AE were detected during screening, but the prevalence was lower (0.2% for CE and 1.5% for AE), in comparison with the higher altitude pastoral regions. Traditionally, females in Tibetan communities are usually responsible for home chores, such as feeding dogs and collecting yak dung for fuel. Women may therefore have more opportunities to be exposed to environments contaminated by *Echinococcus* spp eggs, resulting in the significantly higher prevalence we observed in females. Older age groups of either sex, are at greater risk probably because they have more opportunities for exposure over time.

Portable ultrasound has been applied for community screening for abdominal echinococcosis in China since the early 1990s (Craig et al., 1992; Yang et al., 2006). Cases identified in remote rural areas have benefited from early diagnosis (Bartholomot et al., 2002; Li et al., 2005), which improves chances for better treatment and prognosis. Classification of ultrasound images of CE based on the criteria proposed by WHO provided information about the stage of this disease as well as choice of treatment procedures (WHO IWG, 2003). In the current study, patients with diagnosis of CE cysts that were classified on ultrasound image as CL (of a parasitic origin), CE1, CE2 or CE3, were considered to be active and growing and therefore recommended for either long-term oral albendazole therapy (6 months) with periodic follow-up, and/or for surgical treatment (endocystectomy or percutaneous approaches). Conversely, for patients with CE4 or CE5 hydatid cysts indicative of an involutive or inactive parasite, no positive therapy was considered necessary, rather a 'wait and watch' approach was adopted (Kern, 2003). For classification of alveolar echinococcosis cases the PNM system proposed by the WHO Informal Working Group for clinical settings (Kern et al., 2006) was applied. In addition, criteria for the classification of ultrasound images of alveolar echinococcosis was proposed by us for application in resource poor community settings (Li et al., 2004). In the current study, 31.4% of AE cases detected were categorized as AE3 (lesions measured >10 cm), indicative of an advanced stage with poor prognosis, because of impossibility of radical removal of alveolar lesions and poor efficacy of albendazole on late stage lesions (Pawlowski et al., 2001; Kern et al., 2006). AE cases that exhibited a lesion with a central necrotic cavity was detected in a total of 109 AE patients classified as AE2 or AE3, however, the presence of central necrosis was more frequent in cases with AE3 lesions (62.6%, 62/99) compared to those with AE2 type lesions (33.1%, 47/142) ($\chi^2 = 20.45$, $p < 0.01$). We also identified 4 cases that exhibited dual hepatic infection with both cystic and alveolar echinococcosis in the current study; an unusual and complicated clinical situation, and though rare, has been previously reported in western China (Wen et al., 1992; Yang et al., 2008).

In conclusion, a large co-endemic focus of human cystic and alveolar echinococcosis has been confirmed on the eastern Tibetan Plateau within Tibetan communities, primarily covering the border region of northwest Sichuan and southeast Qinghai, with an overall combined CE/AE prevalence of 6.3%. Prevalence was significantly higher in pastoral communities (8.1%) compared to that in semi-pastoral (1.6%) or farming communities (0.3%). Further active screening programmes and early surgical and/or medical interventions, particularly for alveolar echinococcosis, are imperative to reduce the public health impact of human echinococcosis in this remote resource-poor region of western China.

Finally, the initiation in 2006 of a national echinococcosis control programme (focused on dog dosing with praziquantel and active mass screening) which has so far covered 114 counties in western China, may succeed in interrupting transmission and reducing the public health impact of echinococcosis, but needs to be permanently implemented in these co-endemic areas of the eastern Tibetan Plateau.

Acknowledgements

The study was supported by Grant Number RO1 TW001565 from the Fogarty International Center of NIH. The content is solely the responsibility of the authors and doesn't necessarily represent the official views of the Fogarty International Center or the National Institutes of Health. The funders had no role in the study design, data collection and analysis, decision to publish, or preparation of the manuscript. This study was also supported in part by Sichuan Provincial Department of Health, China, a PhD split-site studentship (to TL) between the University of Salford, UK and SIPD/Sichuan CDC, China, the Japan Society for the Promotion of Science (JSPS) to AI (17256002, 21256003) and the Japan–China Medical Exchange Program from JSPS to MN.

References

Bartholomot, G., Vuitton, D.A., Harraga, S., Snida, Z., Giraudoux, P., Barnish, G., Wang, Y.H., MacPherson, C.N., Craig, P.S., 2002. Combined ultrasound and serologic screening for hepatic alveolar echinococcosis in central China. Am. J. Trop. Med. Hyg. 66, 23–29.

Bresson-Hadni, S., Delabrousse, E., Blagosklonov, O., Bartholomot, B., Koch, S., Miguet, J.P., Andre Mantion, G., Vuitton, D.A., 2006. Imaging aspects and non-surgical interventional treatment in human alveolar echinococcosis. Parasitol. Int. 55S, S267–S272.

Budke, C.M., Campos-Ponce, M., Qian, W., Torgerson, P.R., 2005. A canine purgation study and risk factor analysis for echinococcosis in a high endemic region of the Tibetan plateau. Vet. Parasitol. 127, 43–49.

Budke, C.M., Deplazes, P., Torgerson, P.R., 2006. Global socioeconomic impact of cystic echinococcosis. Emerg. Infect. Dis. 12, 296–303.

Craig, P.S., 2003. *Echinococcus multilocularis*. Curr. Opin. Infect. Dis. 16, 437–444.

Craig, P.S., 2004. Epidemiology of echinococcosis in China. Southeast Asian J. Trop. Med. Public Health 35, 1–13.

Craig, P.S., Budke, C.M., Schantz, P.M., Li, T., Qiu, J., Yang, Y., Zeyhle, E., Rogan, M.T., Ito, A., 2007. Human echinococcosis: a neglected disease? Trop. Med. Health 35, 283–292.

Craig, P.S., Deshan, L., MacPherson, C.N., Dazhong, S., Reynolds, D., Barnish, G., Gottstein, B., Zhirong, W., 1992. A large focus of alveolar echinococcosis in central China. Lancet 340, 826–831.

Craig, P.S., Li, T., Qiu, J., Ren, Z., Wang, Q., Giraudoux, P., Ito, A., Heath, D., Warnock, B., Schantz, P., Yang, W., 2008. Echinococcosis and Tibetan communities. Emerg. Infect. Dis. 14, 1674–1675.

Craig, P.S., Liu, D., Ding, Z., 1991. Hydatid disease in China. Parasitol. Today 7, 46–50.

D'Alessandro, A., 1997. Polycystic echinococcosis in tropical America: *Echinococcus vogeli* and *E. oligarthrus*. Acta Trop. 67, 43–65.

Giraudoux, P., Craig, P.S., Delattre, P., Bao, G., Bartholomot, B., Harraga, S., Quere, J.P., Raoul, F., Wang, Y., Shi, D., Vuitton, D.A., 2003. Interactions between landscape changes and host communities can regulate *Echinococcus multilocularis* transmission. Parasitology 127 (Suppl), S121–S131.

Giraudoux, P., Pleydell, D., Raoul, F., Quéré, J.P., Wang, Q., Yang, Y., Vuitton, D.A., Qiu, J., Yang, W., Craig, P.S., 2006. Transmission ecology of *Echinococcus multilocularis*: what are the ranges of parasite stability among various host communities in China. Parasitol. Int. 55 (Suppl), S237–S246.

Han, X., Wang, H., Qiu, J., Ma, X., Cai, H., Liu, P., Ding, Q., Dai, N., Ito, A., Craig, P.S., 2006. Epidemiological study of cystic and alveolar echinococcosis in Banma County of Qinghai Province, China. Zhongguo Ji Sheng Chong Xue Yu Ji Sheng Chong Bing Za Zhi 22, 189–190.

He, J., Liu, F., 2000. Study on echinococcosal infection in livestock and small mammals in Tibetan regions of western Sichuan, China. Zhongguo Ji Sheng Chong Xue Yu Ji Sheng Chong Bing Za Zhi 16, 62–65.

Kern, P., 2003. *Echinococcus granulosus* infection: clinical presentation, medical treatment and outcome. Langenbecks Arch. Surg. 388, 413–420.

Kern, P., Wen, H., Sato, N., Vuitton, D.A., Gruener, B., Shao, Y., Delabrousse, E., Kratzer, W., Bresson-Hadni, S., 2006. WHO classification of alveolar echinococcosis: principles and application. Parasitol. Int. 55 (Suppl), S283–S287.

Kumaratilake, L.M., Thompson, R.C., 1982. A review of the taxonomy and speciation of the genus Echinococcus Rudolphi 1801. Z. Parasitenkd. 68, 121–146.

Li, T., Ito, A., Nakaya, K., Qiu, J., Nakao, M., Ren, Z., Xiao, N., Chen, X., Giraudoux, P., Craig, P.S., 2008. Species identification of human echinococcosis using histopathology and genotyping in northwestern China. Trans. R. Soc. Trop. Med. Hyg. 102, 585–590.

Li, T., Qiu, J., Craig, P.S., Ito, A., Yang, W., Vuitton, D.A., Xiao, N., Chen, X., Yu, W., Schantz, P.M., 2004. Review of 311 cases of alveolar echinococcosis and criteria for the classification of hepatic ultrasound images. Southeast Asian J. Trop. Med. Public Health 35 (Suppl 1), 1–5.

Li, T., Qiu, J., Yang, W., Craig, P.S., Chen, W., Xiao, N., Ito, A., Giraudoux, P., Mamuti, W., Yu, W., Schantz, P.M., 2005. Echinococcosis in Tibetan populations, western Sichuan Province, China. Emerg. Infect. Dis. 11, 1866–1873.

Mamuti, W., Yamasaki, H., Sako, Y., Nakao, M., Xiao, N., Nakaya, K., Sato, N., Vuitton, D.A., Piarroux, R., Lightowlers, M.W., Craig, P.S., Ito, A., 2004. Molecular cloning, expression, and serological evaluation of an 8-kilodalton

subunit of antigen B from *Echinococcus multilocularis*. J. Clin. Microbiol. 42, 1082–1088.
McManus, D.P., 2002. The molecular epidemiology of *Echinococcus granulosus* and cystic hydatid disease. Trans. R. Soc. Trop. Med. Hyg. 96 (Suppl 1), S151–S157.
McManus, D.P., Zhang, W., Li, J., Bartley, P.B., 2003. Echinococcosis. Lancet 362, 1295–1304.
Pawlowski, Z.S., Eckert, J., Vuitton, D.A., Ammann, R.W., Kern, P., Craig, P.S., Dar, K.F., De Rosa, F., Filice, C., Gottstein, B., Grimm, F., Macpherson, C.N.L., Sato, N., Todorov, T., Uchino, J., von Sinner, W., Wen, H., 2001. Echinococcosis in humans: clinical aspects, diagnosis and treatment. In: Eckert, J., Gemmell, M., Meslin, F.-X., Pawlowski, Z. (Eds.), WHO/OIE Manual on Echinococcosis In Humans and Animals: A Public Health Problem of Global Concern. World Organisation for Animal Health, Paris, pp. 20–59.
Qiu, J., Chen, X., Ren, M., Luo, C., 1995. Epidemiological study on alveolar echinococcosis on the Tibetan Plateau. Shi Yong Ji Sheng Chong Bing Za Zhi 3, 106–108.
Qiu, J., Qiu, D., Luo, C., Zhu, Y., Chen, X., 1989. Survey on infective agent of alveolar echinococcosis in Ganzi Prefecture and experimental research in animal. Zhongguo Ji Sheng Chong Xue Yu Ji Sheng Chong Bing Za Zhi 5, 38–40.
Rausch, R.L., Bernstein, J.J., 1997. *Echinococcus vogeli* sp. n. (Cestoda: Taeniidae) from the bush dog *Speothos venaticus* (Lund). Z. Prakt. Anasth. Wiederbeleb. Intensivther. 23, 25–34.
Ren, Z., Li, T., Liao, W., Chen, X., Zhao, X., Xiao, N., Yu, X., Zhang, X., Ito, A., Qiu, J., Giraudoux, P., Craig, P.S., 2008. Review and analysis of epidemiological data of 1312 post-operated cases of echinococcosis on the Tibetan Plateau, China. Ji Sheng Chong Bing Yu Gan Rang Xing Ji bing Za Zhi 6, 117–120.
Sako, Y., Nakao, M., Nakaya, K., Yamasaki, H., Gottstein, B., Lightowers, M.W., Schantz, P.M., Ito, A., 2002. Alveolar echinococcosis: characterization of diagnostic antigen Em18 and serological evaluation of recombinant Em18. J. Clin. Microbiol. 40, 2760–2765.
Schantz, P.M., Wang, H., Qiu, J., Liu, F.J., Saito, E., Emshoff, A., Ito, A., Roberts, J.M., Delker, C., 2003. Echinococcosis on the Tibetan Plateau: prevalence and risk factors for cystic and alveolar echinococcosis in Tibetan populations in Qinghai Province, China. Parasitology 127 (Suppl), S109–S120.
Shi, D., 1997. Epidemiology and transmission of cystic echinococcosis: China. Arch. Int. Hydatid. 32, 50–54.
Wang, Q., Qiu, J., Yang, W., Schantz, P.M., Raoul, F., Craig, P.S., Giraudoux, P., Vuitton, D.A., 2006. Socioeconomic and behavior risk factors of human alveolar echinococcosis in Tibetan communities in Sichuan, People's Republic of China. Am. J. Trop. Med. Hyg. 74, 856–862.
Wen, H., Tian, W.L., Zou, P.F., Xiang, M.X., 1992. A rare case of mixed cystic and alveolar hydatidosis. Trans. R. Soc. Trop. Med. Hyg. 86, 290–291.
Wen, H., Yang, W.G., 1997. Public health importance of cystic echinococcosis in China. Acta. Trop. 67, 133–145.
WHO, WHO Informal Working Group on Echinococcosis, 1996. Guildelines for treatment of cystic and alveolar echinococcosis. Bull. WHO 74, 1295–1304.
WHO IWG, 2003. International classification of ultrasound images in cystic echinococcosis for application in clinical and field epidemiological settings. Acta Trop. 85, 253–261.
Xiao, N., Mamuti, W., Yamasaki, H., Sako, Y., Nakao, M., Nakaya, K., Gottstein, B., Schantz, P.M., Lightowlers, M.W., Craig, P.S., Ito, A., 2003. Evaluation of use of recombinant Em18 and affinity-purified Em18 for serological differentiation of alveolar echinococcosis from cystic echinococcosis and other parasitic infections. J. Clin. Microbiol. 41, 3351–3353.
Xiao, N., Qiu, J., Nakao, M., Li, T., Yang, W., Chen, X., Schantz, P.M., Craig, P.S., Ito, A., 2005. *Echinococcus shiquicus* n. sp., a taeniid cestode from Tibetan fox and plateau pika in China. Int. J. Parasitol. 35, 693–701.
Yang, Y.R., Craig, P.S., Sun, T., Vuitton, D.A., Giraudoux, P., Jones, M.K., Williams, G.M., McManus, D.P., 2008. Echinococcosis in Ningxia Hui Autonomous Region, northwest China. Trans. R. Soc. Trop. Med. Hyg. 102, 319–328.
Yang, Y.R., Sun, T., Li, Z., Zhang, J., Teng, J., Liu, X., Liu, R., Zhao, R., Jones, M.K., Wang, Y., Wen, H., Feng, X., Zhao, Q., Zhao, Y., Shi, D., Bartholomot, B., Vuitton, D.A., Pleydell, D., Giraudoux, P., Ito, A., Danson, M.F., Boufana, B., Craig, P.S., Williams, G.M., McManus, D.P., 2006. Community surveys and risk factor analysis of human alveolar and cystic echinococcosis in Ningxia Hui Autonomous Region, China. Bull. World Health Organ. 84, 714–721.
Yu, S.H., Wang, H., Wu, X.H., Ma, X., Liu, P.Y., Liu, Y.F., Zhao, Y.M., Morishima, Y., Kawanaka, M., 2008. Cystic and alveolar echinococcosis: an epidemiological survey in a Tibetan population in southeast Qinghai, China. Jpn. J. Infect. Dis. 61, 242–246.
Zhou, H.X., Chai, S.X., Craig, P.S., Delattre, P., Quere, J.P., Raoul, F., Vuitton, D.A., Wen, H., Giraudoux, P., 2000. Epidemiology of alveolar echinococcosis in Xinjiang Uygur autonomous region, China: a preliminary analysis. Ann. Trop. Med. Parasitol. 94, 715–729.

Acta Tropica 114 (2010) 1–16

Contents lists available at ScienceDirect

Acta Tropica

journal homepage: www.elsevier.com/locate/actatropica

Review

Expert consensus for the diagnosis and treatment of cystic and alveolar echinococcosis in humans☆

Enrico Brunetti[a,*,1], Peter Kern[b], Dominique Angèle Vuitton[c], Writing Panel for the WHO-IWGE[2]

[a] Division of Infectious and Tropical Diseases, University of Pavia, IRCCS S.Matteo Hospital Foundation, WHO Collaborating Center for Clinical Management of Cystic Echinococcosis, 27100 Pavia, Italy
[b] Comprehensive Infectious Diseases Centre, University Hospitals, Albert-Einstein-Allee 23, 89081 Ulm, Germany
[c] WHO Collaborating Centre for Prevention and Treatment of Human Echinococcosis, CHU de Besançon/Université de Franche-Comté, 25030 Besançon, France

ARTICLE INFO

Article history:
Received 23 August 2009
Received in revised form 2 November 2009
Accepted 4 November 2009
Available online 30 November 2009

Keywords:
Echinococcosis
Hydatid disease
Cystic echinococcosis
Alveolar echinococcosis
Diagnosis
Treatment
Ultrasound, imaging techniques

ABSTRACT

The earlier recommendations of the WHO-Informal Working Group on Echinococcosis (WHO-IWGE) for the treatment of human echinococcosis have had considerable impact in different settings worldwide, but the last major revision was published more than 10 years ago. Advances in classification and treatment of echinococcosis prompted experts from different continents to review the current literature, discuss recent achievements and provide a consensus on diagnosis, treatment and follow-up. Among the recognized species, two are of medical importance – *Echinococcus granulosus* and *Echinococcus multilocularis* – causing cystic echinococcosis (CE) and alveolar echinococcosis (AE), respectively.

For CE, consensus has been obtained on an image-based, stage-specific approach, which is helpful for choosing one of the following options: (1) percutaneous treatment, (2) surgery, (3) anti-infective drug treatment or (4) watch and wait. Clinical decision-making depends also on setting-specific aspects. The usage of an imaging-based classification system is highly recommended.

For AE, early diagnosis and radical (tumour-like) surgery followed by anti-infective prophylaxis with albendazole remains one of the key elements. However, most patients with AE are diagnosed at a later stage, when radical surgery (distance of larval to liver tissue of >2 cm) cannot be achieved. The backbone of AE treatment remains the continuous medical treatment with albendazole, and if necessary, individualized interventional measures. With this approach, the prognosis can be improved for the majority of patients with AE.

The consensus of experts under the aegis of the WHO-IWGE will help promote studies that provide missing evidence to be included in the next update.

Contents

1. Introduction 2
2. Methodology for the preparation of the document 2
3. Cystic echinococcosis (CE) 2
   3.1. Organ location 2
   3.2. Course of infection 3
   3.3. Diagnosis 3
      3.3.1. Imaging 3
      3.3.2. Direct assessment of *E. granulosus* and its viability 4
      3.3.3. E. Granulosus serology 4
      3.3.4. CE case definition 4

☆ This document is an abridged version of a more detailed text that will be published online on the WHO website.

* Corresponding author.
E-mail addresses: selim@unipv.it (E. Brunetti), peter.kern@uni-ulm.de (P. Kern), dvuitton@univ-fcomte.fr (D.A. Vuitton).
[1] Tel.: +39 0382 502799/502159; fax: +39 0382 502296.
[2] WHO-Informal Working Group on Echinococcosis.

0001-706X/$ – see front matter © 2009 Elsevier B.V. All rights reserved.
doi:10.1016/j.actatropica.2009.11.001

3.4. Treatment 5
3.4.1. General indications for treatment: a stage-specific approach 5
3.4.2. Surgery for abdominal cysts 5
3.4.3. PERCUTANEOUS TREATMENTS (PTs) 6
3.4.4. Antiparasitic drug treatment 7
3.4.5. Watch and Wait approach 7
3.4.6. Management of cysts in extra-hepatic sites and specific situations 8
3.5. Strength of recommendation: B Quality of Evidence: III 8
3.5.1. Monitoring of CE patients 8
4. Alveolar echinococcosis 8
4.1. Organ location 8
4.2. Course of infection 8
4.3. Diagnosis 8
4.3.1. Imaging 8
4.3.2. Direct assessment of *E. multilocularis* and its viability 9
4.3.3. WHO classification of AE 9
4.3.4. E. Multilocularis *serology* 9
4.3.5. AE case definition 9
4.4. Treatment 10
4.4.1. General indications for treatment 10
4.4.2. Antiparasitic drug treatment 10
4.4.3. Surgery 11
4.4.4. Endoscopic and percutaneous interventions (EPI) 12
4.4.5. Monitoring of patients with AE 12
Acknowledgements 12
Appendix A. List of experts 13
References 14

1. Introduction

Human echinococcosis is a zoonosis caused by larval forms (metacestodes) of *Echinococcus* (*E.*) tapeworms found in the small intestine of carnivores. Among the recognized species, two are of medical importance – *E. granulosus* and *E. multilocularis* – causing cystic echinococcosis (CE) and alveolar echinococcosis (AE) in humans, respectively. This expert consensus is a follow-up to the Guidelines published in 1996 by the WHO-Informal Working Group on Echinococcosis (WHO-IWGE) (WHO-IWGE, 1996). Readers are referred for detailed information and scientific discussion to WHO reports (WHO/OIE, 2001) and published reviews (Junghanss et al., 2008; McManus et al., 2003; Craig et al., 2007). In endemic areas, the annual incidence of CE ranges from <1 to 200 per 100,000 inhabitants (WHO/OIE, 2001); that of AE ranges from 0.03 to 1.2 per 100,000 inhabitants (Schweiger et al., 2007) but may be significantly higher in certain endemic foci (WHO/OIE, 2001; Craig, 2003). Human CE remains highly endemic in pastoral communities, particularly in regions of South America, the Mediterranean littoral, Eastern Europe, the Near and Middle East, East Africa, Central Asia, China and Russia. The distribution of human AE cases is more restricted but is an important public health concern in parts of central and eastern Europe, the Near East, Russia, China and northern Japan (WHO/OIE, 2001). The estimated minimum global human burden of CE averages 285,000 disability-adjusted life years (DALYs) or an annual loss of US $194,000,000 (Budke, 2006). In untreated or inadequately treated AE, mortality is >90% within 10–15 years of diagnosis (Torgerson et al., 2008). The mortality rate from CE (about 2–4%) is lower than that from AE, but it may increase considerably if medical treatment and care are inadequate.

2. Methodology for the preparation of the document

The process was initiated by the subgroup "Standardization/Classification" of the WHO-IWGE (chaired by Peter Kern, Ulm, Germany and Enrico Brunetti, Pavia, Italy) and discussed in Chengdu, P.R.China, May 2006 and Athens, Greece, May 2007. An expert meeting of the WHO-IWGE aimed to reach a consensus on the clinical management of patients with CE and AE was organized at the Saline Royale d'Arc-et-Senans and in Besançon, France, by Prof. D.A. Vuitton, Prof. S. Bresson-Hadni, Prof. G. Mantion, WHO Collaborating Centre for Prevention and Treatment of Human Echinococcosis, Besançon, France and Prof. Hao Wen, Urumqi, P.R.China, Xinjiang/China Key Lab of Basic and Clinical Research on Echinococcosis, and was chaired by Prof. P. Craig, Salford, UK Coordinator, WHO-IWGE, and by Dr. F.-X. Meslin, Division of Emerging Diseases, World Health Organization, Geneva; Switzerland. Rapporteurs of the different subsections and nominees by the WHO supported the writing panel. A final consensus was achieved by e-mail in February 2009.

Papers covering the subject were obtained by a Medline search of the literature published in English on this subject.

Key words were "echinococcal cysts," "hydatid cysts," "hydatid disease," "cystic echinococcosis," "alveolar echinococcosis," "liver transplant," "hydatidosis," "hydatid," "surgery," "mebendazole," "albendazole," "praziquantel," "chemotherapy," "PAIR," "percutaneous treatment," "percutaneous drainage," and "ultrasound." Papers published from 1980 to 2008 were included. The authors' files were used as well. Levels of recommendations given in this document follow the "Guide to Practice Guidelines" of the Infectious Diseases Society of America (Kish, 2001; Table 1).

3. Cystic echinococcosis (CE)

3.1. Organ location

In primary CE, metacestodes – the larval forms of the parasite – may develop in almost any organ. Up to 80% patients have a single organ involved and a solitary cyst localized to the liver (4/5) or lungs (1/5). The liver/lung ratio may vary from 2 to 1 to 7 to 1 or more (Larrieu and Frider, 2001). *E. granulosus* germinal layer generates brood capsules and protoscoleces into a central cavity filled with a clear "hydatid" fluid; it is surrounded first by an acellular laminated layer, then by the host reaction. "Daughter" vesicles of variable size may be present inside or outside the "mother" cyst (Fig. 1).

Table 1
Infectious Diseases Society of America grading system (strength of recommendation and quality of evidence).

Strength of recommendation	
A	Good evidence to support a recommendation for use
B	Moderate evidence to support a recommendation for use
C	Poor evidence to support a recommendation
D	Moderate evidence to support a recommendation against use
E	Good evidence to support recommendation against use
Quality of evidence	
I	Evidence from ≥1 properly randomized, controlled trial
II	Evidence from ≥1 well-designed clinical trial, without randomization; from cohort or case-controlled analytic studies; from multiple time series; or from dramatic results from uncontrolled experiments
III	Evidence from opinions of respected authorities, based on clinical experience, descriptive studies, or reports of committees

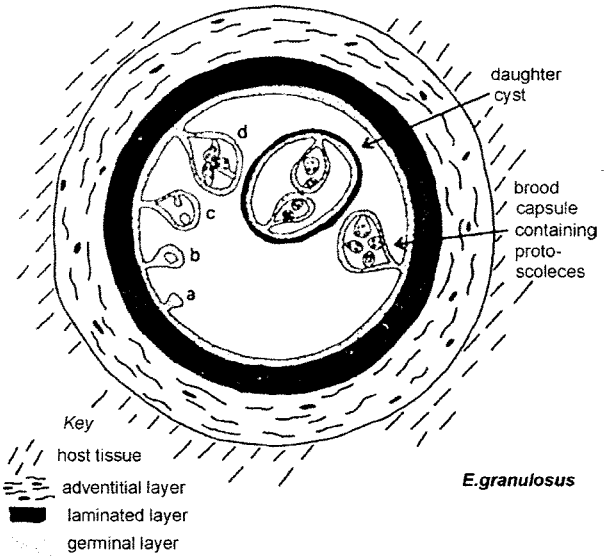

Fig. 1. Diagrammatic representation of structure of the echinococcal cyst.

3.2. Course of infection

Ultrasound (US) surveys have shown that cysts may grow 1–50 mm per year or persist without changes for years. They may also spontaneously rupture or collapse or disappear (Romig et al., 1986; Frider et al., 1999; Wang et al., 2006; Mufit et al., 1998). The sequence of cyst changes during the natural history is still unclear (Rogan et al., 2006). Liver cysts appear to grow at a lower rate than lung cysts (Larrieu and Frider, 2001). Clinical symptoms usually occur when the cyst compresses or ruptures into neighbouring structures.

3.3. Diagnosis

The diagnosis of CE is based on clinical findings, imaging techniques, and serology. Proof of the presence of protoscoleces may be given by microscopic examination of the fluid and histology.

3.3.1. Imaging

A. US examination and WHO classification

US examination is the basis of CE diagnosis in abdominal locations, at both the individual and population levels (Macpherson and Milner, 2003). US may visualize cysts in other organ locations, including lung when cysts are peripherally located (El Fortia et al., 2006).

In 1995, the WHO-IWGE developed a standardised classification that could be applied in all settings to replace the plethora of previous classifications and allow a natural grouping of the cysts into three relevant groups: active (CE1 and 2), transitional (CE3) and inactive (CE4 and 5) (WHO and Echinococcosis, 2003). WHO-IWGE classification is the basis for the present Guidelines (Fig. 2); it differs from Gharbi's classification introduced in 1981 (Gharbi et al., 1981) by adding a "cystic lesion" (CL) stage (undifferentiated), and by reversing the order of CE Types 2 and 3 (Fig. 3). CE3 transitional cysts may be differentiated into CE3a (with detached endocyst) and CE3b (predominantly solid with daughter vesicles) (Junghanss et al., 2008). CE1 and CE3a are early stages and CE4 and CE5 late stages.

B. Imaging techniques other than US

Conventional radiography is useful to diagnose thoracic and bone involvement.

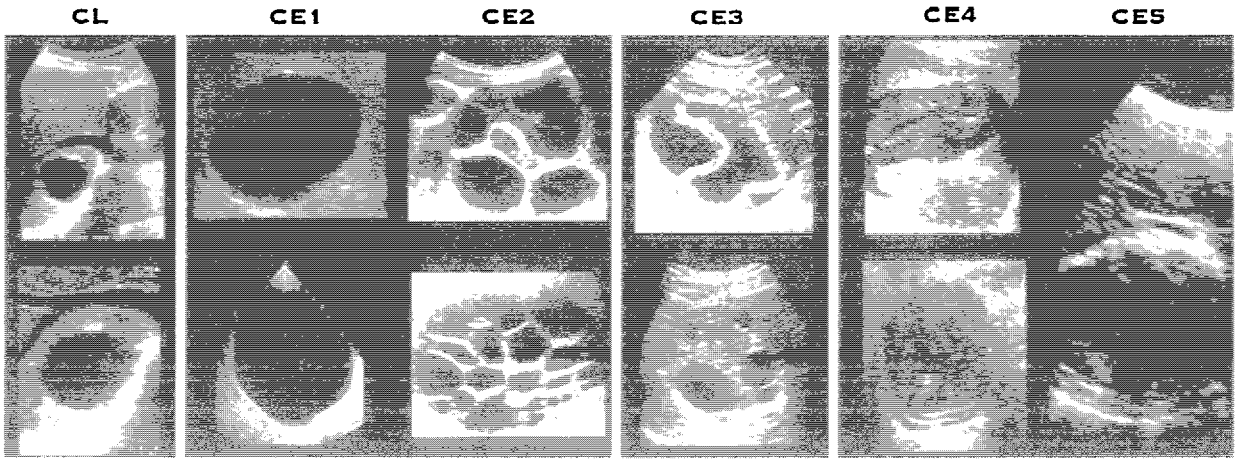

Fig. 2. WHO-IWGE standardized classification.

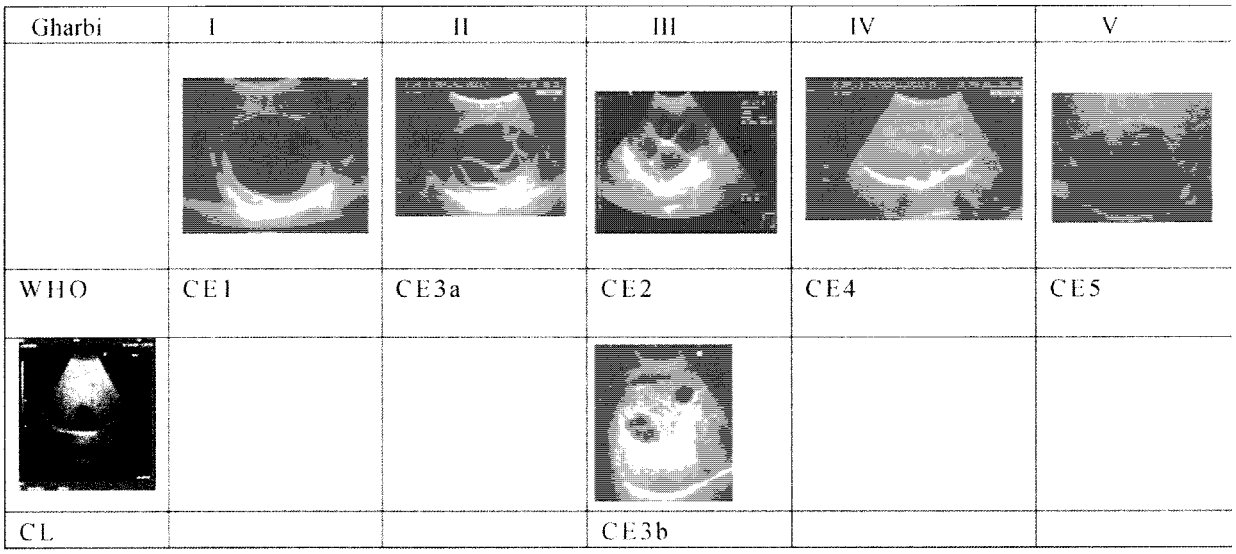

Fig. 3. Comparison of Gharbi's and WHO-IWGE ultrasound classification. CL, as a potentially parasitic cyst, was not in Gharbi's. WHO CE3b had not been explicitly described by Gharbi. CE3b might be classified as Type III, although in the original Gharbi paper there was no distinction between multivesiculated (honeycomb-like) cysts and cysts with daughter cysts in solid matrix.

Computed tomography (CT), and *magnetic resonance (MR) imaging*, with one T2-weighted imaging sequence and if possible cholangiopancreatography (MRCP) are indicated in (1) subdiaphragmatic location, (2) disseminated disease, (3) extra-abdominal location, (4) in complicated cysts (abscess, cysto-biliary fistulae) and (5) pre-surgical evaluation. Whenever possible, MR imaging should be preferred to CT due to better visualization of liquid areas within the matrix (Hosch et al., 2008).

3.3.2. Direct assessment of E. granulosus and its viability

Microscope examination of protoscoleces after cyst fluid aspiration using vital staining gives evidence for the parasitic nature and viability of a cyst (WHO/OIE, 2001). Detection of parasitic antigens gives no indication of viability. Presence of calcification is not reliable as an indicator of non-viability: more frequent in CE4 and CE5, it may be observed at all stages (Hosch et al., 2007). MR spectroscopy has been evaluated to assess cyst viability in fluids taken surgically or percutaneously (Hosch et al., 2008). *In vivo* evaluation of cyst viability has already been performed using MR spectroscopy in cysts that do not move with respiration such as brain cysts (Seckin et al., 2008) and might become possible for other locations in the future (Hosch et al., 2008).

3.3.3. E. Granulosus serology

Sensitivity of serum antibody detection using indirect hemagglutination, ELISA, or latex agglutination, with hydatid cyst fluid antigens, ranges between 85 and 98% for liver cysts, 50–60% for lung cysts and 90–100% for multiple organ cysts (Siracusano and Bruschi, 2006; Ito and Craig, 2003; Siles-Lucas and Gottstein, 2001). Specificity of all tests is limited by cross-reactions due to other cestode infections (*E. multilocularis* and *Taenia solium*), some other helminth diseases, malignancies, liver cirrhosis and presence of anti-P1 antibodies. Confirmatory tests must be used (arc-5 test; Antigen B (AgB) 8 kDa/12 kDa subunits or EgAgB8/1 immunoblotting) in dubious cases (Siracusano and Bruschi, 2006; Ito and Craig, 2003). Immunoblotting may be used as a first-line test and is best for differential diagnosis (Akisu et al., 2006). Mass screening in populations at risk optimally deploys US and serology (Macpherson and Milner, 2003).

Detection of parasite-specific IgE or IgG4 has no significant diagnostic advantage. Both, as well as eosinophil count, are more elevated after rupture/leakage of cysts (Khabiri et al., 2006).

3.3.4. CE case definition

The International Classification of Diseases and Related Health Problems ICD10 (10th Revision Version for 2007; http://www.who.int/classifications/icd/en) subclassifies:

B67.0 E. granulosus, liver infection
B67.1 E. granulosus, lung infection
B67.2 E. granulosus, bone infection
B67.3 E. granulosus, other organs and multiple site infection
B67.4 E. granulosus, unspecified infection

ICD 9 codes are also listed as they are still used in many countries:

122.0 E. granulosus, liver infection
122.1 E. granulosus, lung infection
122.2 E. granulosus, thyroid infection
122.3 E. granulosus infection, other
122.4 E. granulosus, unspecified infection

A. Clinical criteria

At least one of the following three:

1. A slowly growing or static cystic mass(es) (signs and symptoms vary with cyst location, size, type and number) diagnosed by imaging techniques.
2. Anaphylactic reactions due to ruptured or leaking cysts.
3. Incidental finding of a cyst by imaging techniques in asymptomatic carriers or detected by screening strategies.

B. Diagnostic criteria

1. Typical organ lesion(s) detected by imaging techniques (e.g. US, CT-scan, plain film radiography, MR imaging).

2. Specific serum antibodies assessed by high-sensitivity serological tests, confirmed by a separate high specificity serological test.
3. Histopathology or parasitology compatible with cystic echinococcosis (e.g. direct visualization of the protoscolex or hooklets in cyst fluid).
4. Detection of pathognomonic macroscopic morphology of cyst(s) in surgical specimens.

C. Possible versus probable versus confirmed case

Possible case. Any patient with a clinical or epidemiological history, *and* imaging findings *or* serology positive for CE.

Probable case. Any patient with the combination of clinical history, epidemiological history, imaging findings *and* serology positive for CE on two tests.

Confirmed case. The above, plus either (1) demonstration of protoscoleces or their components, using direct microscopy or molecular biology, in the cyst contents aspirated by percutaneous puncture or at surgery, or (2) changes in US appearance, e. g. detachment of the endocyst in a CE1 cyst, thus moving to a CE3a stage, or solidification of a CE2 or CE3b, thus changing to a CE4 stage, after administration of ABZ (at least 3 months) or spontaneous.

3.4. Treatment

There is no "best" treatment option for CE and no clinical trial has compared all the different treatment modalities, including "Watch and Wait." Treatment indications are complex and are based on cyst characteristics, available medical/surgical expertise and equipment, and adherence of patients to long-term monitoring. Because treatment involves a variety of options and requires specific clinical experience, patients should be referred to recognized, reference and national/regional CE treatment centres, whenever available.

3.4.1. General indications for treatment: a stage-specific approach

The opinion of WHO-IWGE experts with regard to a stage-specific approach is summarized in Table 2. Radical surgery aims to remove cysts completely. Percutaneous treatments (PT) and antiparasitic treatment with benzimidazoles (BMZ) represent alternatives to surgery. Cyst type (according to US classification), size, location and presence/absence of complications are the basis for decision-making (Menezes da Silva, 2003). For complicated cysts and cysts with multiple locations, a staging system similar to that used for AE has been proposed (Kjossev and Losanoff, 2005), however it should be tested prospectively in larger series of patients and various settings before final validation.

3.4.2. Surgery for abdominal cysts

A. Indications

Surgery should be carefully evaluated against other options before choosing this treatment. It is the first choice for complicated cysts. In the liver, it is indicated for: (1) removal of large CE2-CE3b cysts with multiple daughter vesicles, (2) single liver cysts, situated superficially, that may rupture spontaneously or as a result of trauma when PTs are not available, (3) infected cysts, again, when PTs are not available, (4) cysts communicating with the biliary tree (as alternative to PT) and (5) cysts exerting pressure on adjacent vital organs.

B. Contraindications

Surgery is contraindicated in patients to whom general contraindications for surgery apply, inactive asymptomatic cysts, difficult to access cysts, and very small cysts.

C. Choice of surgical technique

Parasitic material should be removed as much as possible. However, the more radical the intervention, the higher the operative risk, but with the likelihood of fewer relapses, and vice versa (Aydin et al., 2008). Laparoscopic surgery is a technical option in selected cases but the risk of complications including spillage has never been fully evaluated (Baskaran and Patnaik, 2004).

Total removal of the cyst is usually described as "pericystectomy." "Closed total pericystectomy" removes the cyst without opening it, and "open total pericystectomy" sterilizes the metacestode with protoscolicidal agents, evacuates the contents of the cyst, then removes the pericystic tissue. A cleavage plane between the inner layer of the host's reaction facing towards the parasite and the outer layer, or adventitia, described by Peng and co-workers, limits the damage to liver parenchyma when dissecting around the cyst and allows safer removal of the cyst (Peng et al., 2002). Based

Table 2
Suggested stage-specific approach to *uncomplicated* cystic echinococcosis of the liver.

WHO classification	Surgery	Percutaneous treatment	Drug therapy	Suggested	Resources setting
CE1				<5 cm ABZ	*Optimal*
				PAIR	*Minimal*
		√	√	>5 cm PAIR + ABZ	*Optimal*
				PAIR	*Minimal*
CE2			√	Other PT + ABZ	*Optimal*
	√	√			
				Other PT	*Minimal*
CE3a				<5 cm ABZ	*Optimal*
		√	√	PAIR	*Minimal*
				>5 cm PAIR + ABZ	*Optimal*
				PAIR	*Minimal*
CE3b				Non-PAIR PT + ABZ	*Optimal*
	√	√	√		
				Non-PAIR PT	*Minimal*
CE4				*Watch and Wait*	*Optimal*[a]
CE5				*Watch and Wait*	*Optimal*[a]

[a] "Minimal" may not be applicable here because in low resources, remote endemic areas, it may be impossible or too expensive to travel to the nearest hospital just to get a diagnosis.

on these anatomical considerations, such an operation should be more adequately named "total cystectomy."

Partial cystectomy, in which the cyst content is sterilized and removed after opening, with the pericyst partially resected, is especially suited for endemic areas where the operations are performed by general surgeons. No special equipment is required and liver tissue is neither entered nor resected. However, the risk of secondary echinococcosis from protoscolex dissemination is higher than with total pericystectomy or total cystectomy.

D. Prevention of protoscolex spillage; choice of protoscolicides

Any effort made to avoid fluid spillage is recommended, including protection of peritoneal tissues and organs with protoscolicide-soaked surgical drapes and injection of protoscolicide into the cyst before opening. At present, 20% hypertonic saline is recommended (WHO/OIE, 2001). Saline should be in contact with the germinal layer for at least 15 min, and its use avoided when communication between the cyst and the bile ducts is found, to avoid the risk of chemically-induced sclerosing cholangitis. A series of compounds are protoscolicidal in vitro, including ivermectin, praziquantel (PZQ) and BMZ. However, they should be further studied in humans for efficacy and safety (Hokelek et al.,2002; Bygott and Chiodini, 2009; Dziri et al., 2009).

Peri-operative BMZ may reduce cyst pressure and decrease the risk of secondary CE. The length of administration usually ranges between 1 day before and 1 month after surgery but has never been formally evaluated. A recent paper comparing different peri-operative ABZ regimens concluded that ABZ is an effective adjuvant therapy in surgical treatment of liver CE (Arif et al., 2008), but the question of what is the best timing remains unanswered. Adjunctive PZQ might be helpful, but this needs confirmation (Cobo et al., 1998).

E. Management of cysto-biliary fistulas

Cyst diameter is a factor associated with a high risk of biliary-cyst communication in clinically asymptomatic patients. With a cyst diameter of 7.5 cm as a cut-off point, a 79%, likelihood to find a cysto-biliary fistula was calculated (Aydin et al., 2008). Thus, surgeons operating on cysts larger than 7.5 cm should be prepared to deal with this complication. Sphincterotomy alone is not an adequate treatment (Aydin et al., 2008). Biliary communication can be detected, located and classified intra-operatively by using dye or radio-opaque markers. During surgery, most communications can be managed with suture. However, biliary-intestinal anastomosis or liver resection are sometimes necessary. If post-operative bile leakage occurs, patience is advised. Operative management should be avoided whenever possible. The chances of spontaneous closure of fistulae from cysts with a calcified wall are small.

F. Benefits

Surgery may cure the patient completely but does not totally prevent recurrence. Given the dearth of clinical trials, the level of evidence is low for the surgical treatment of complicated liver CE and disseminated CE (Dziri et al., 2004). Standardized terminology and procedures should be agreed upon by surgeons for the techniques to be compared.

G. Risks

The risks include those associated with any surgical intervention, anaphylactic reactions, and secondary CE owing to spillage of viable parasite material. Operative mortality varies from 0.5% to 4%, but may be higher if surgical and medical facilities are inadequate (WHO/OIE, 2001; Junghanss et al., 2008).

H. Medical requirements

The medical staff must have experience in treating CE and the surgical ward must be adequately equipped.

Strength of recommendation: B Quality of Evidence: III

3.4.3. PERCUTANEOUS TREATMENTS (PTs)

PTs can broadly be divided into: (1) those aiming at the destruction of the germinal layer (PAIR) and (2) those aiming at the evacuation of the entire endocyst (also known as Modified Catheterization Techniques).

PAIR (Puncture, aspiration, injection, re-aspiration)

A. Indications

PAIR is a minimally invasive technique used in the treatment of cysts in the liver and other abdominal locations (WHO-IWGE, 2003a,b). It is indicated for inoperable patients and those who refuse surgery, in cases of relapse after surgery or failure to respond to BMZ alone. Best results with PAIR + BMZ are achieved in >5 cm CE1 and CE3a cysts where it may be the first-line treatment (Khuroo et al., 1993). In pregnant women with symptomatic cysts and in children aged <3 years, the risk of BMZ must be carefully assessed (Ustunsoz et al., 2008).

B. Contraindications

PAIR is contraindicated for CE2 and CE3b, for CE4 and CE5, and for lung cysts. Biliary fistulae contraindicate protoscolicide use.

C. Principle and technique

PAIR includes: (1) percutaneous puncture of cysts using US guidance, (2) aspiration of cyst fluid, (3) injection of protoscolicide for 10–15 min and (4) re-aspiration of the fluid (WHO-IWGE, 2003a,b). Safety assessment lies on data from more than 4000 PAIRs over a period of more than 20 years. CE2 and CE3b cysts treated by PAIR tend to relapse (Junghanss et al., 2008). Communication with bile ducts should be assessed by analyzing cyst fluid for bilirubin or by injecting contrast medium into the cyst cavity before the "injection" step (WHO-IWGE, 2003a,b). Giant (>10 cm) cysts are best treated with continuous catheter drainage until the daily output falls below 10 mL (Men et al., 2006).

D. Choice of protoscolicides; prevention of protoscolex spillage

Protoscolicides used in PAIR are mainly 20% NaCl and 95% ethanol. Transhepatic cyst puncture prevents peritoneal protoscolex spillage. Prophylaxis with ABZ 4 h before and 1 month after PAIR is mandatory (WHO-IWGE, 2003a,b; Morris and Taylor, 1988).

E. Benefits

PAIR confirms the diagnosis and removes parasitic material. It is minimally invasive, less risky and usually less expensive than surgery (Smego et al., 2003).

F. Risks

Risks include those associated with any liver PTs, biliary fistulae after intracystic decompression, sclerosing cholangitis should the scolecidal agent reach the biliary vessels persistence of exophytic daughter vesicles, anaphylactic reactions, and secondary echinococcosis. Specific complications are no more frequent after PAIR than after surgery (Ustunsoz et al., 1999).

G. Medical requirements

PAIR should only be performed by experienced physicians with drugs and resuscitation equipment to manage anaphylactic shock at hand and a surgical back-up team.

OTHER PERCUTANEOUS TREATMENTS

These are reserved to cysts that are difficult to drain or tend to relapse after PAIR (CE2 and CE3b). These procedures aim to remove the entire endocyst and daughter cysts from the cyst cavity. Large-bore catheters (Haddad et al., 2000; Schipper et al., 2002) and cutting devices together with an aspiration apparatus have been successfully employed (Saremi and McNamara, 1995). Among more than 1000 patients, rates of short- and medium-term success are satisfactory with minimal complications (Vuitton et al., 2002; Wang et al., 1994). These techniques have also been successfully employed for CE2 cysts located outside the abdomen (Akhan et al., 2007). However, long-term evaluation is still not available, therefore caution is advised before drawing reliable conclusions.

Strength of recommendation: B Quality of Evidence: III

3.4.4. Antiparasitic drug treatment

A. Indications

BMZ are indicated for inoperable patients with liver or lung CE; patients with multiple cysts in two or more organs, or peritoneal cysts. Small (<5 cm) CE1 and CE3a cysts in the liver and lung respond favourably to BMZ alone (Dogru et al., 2005; Vutova et al., 1999). BMZ should be used to prevent recurrence following surgery or PAIR (Arif et al., 2008).

B. Contraindications

BMZ are contraindicated in cysts at risk of rupture and in early pregnancy. ABZ has been proven teratogenic in rats and rabbits. Physiological exposure to ABZ and its principal metabolite, ABZ sulfoxide, in early human pregnancy is substantially lower (perhaps 10–100 times) than in the animal species in which teratogenic or embryotoxic effects have been recorded. Therefore, the risk of fetal exposure from the recommended therapeutic dose is probably very small. Despite the fact that no abnormal birth outcome has been observed following ABZ administration during pregnancy, treatment of gravid or potentially gravid females should be avoided, unless the benefit of treatment significantly outweighs the potential risk to the developing fetus (Bradley and Horton, 2001).

BMZ must be used with caution in patients with chronic hepatic disease and avoided in those with bone-marrow depression. Inactive or calcified asymptomatic cysts should not be treated unless they are complicated.

BMZ alone are not effective in large cysts (over 10 cm), as their effect is extremely slow in cysts with large volumes of fluid.

C. Drugs: benzimidazoles

Albendazole (ABZ) is currently the drug of choice to treat CE, either alone or together with PT (Franchi et al., 1999). Given orally, at a dosage of 10–15 mg/kg/day, in two divided doses, with a fat-rich meal to increase its bioavailability, it should be administered continuously, without the monthly treatment interruptions recommended in the 1980s (Franchi et al., 1999). Treatment interruptions were felt to be required because of the limited long-term toxicity data available in the early days of use (Junghanss et al., 2008). However, optimal dosage and optimal duration have never been formally assessed. Alternatively, mebendazole (MBZ), the first BMZ tested successfully against *Echinococcus*, may be used at a dosage of 40–50 mg/kg body weight daily, in three divided doses with fat-rich meals, if ABZ is not available or not tolerated (WHO-IWGE, 1996; Franchi et al., 1999).

D. Other drugs

PZQ 40 mg/kg once a week in combination with ABZ seems more effective in killing protoscoleces than ABZ alone (Cobo et al., 1998). The usefulness of PZQ in avoiding secondary echinococcosis needs further study.

E. Benefits

BMZ can be used in patients of any age. However, there is little experience with children under-6 years old; it is less limited by the patient's status than surgery. Standard dosage-ABZ for 3–6 months produces an average of 30% cure. The number of patients with clinical or US improvement increases with longer durations of treatment while the proportion of patients with cure does not significantly change (Vutova et al., 1999; Franchi et al., 1999). ABZ is more effective in young patients and for small CE1 and CE3a cysts. BMZ are less effective for CE2 and CE3b (Vutova et al., 1999; Franchi et al., 1999). The importance of cyst stage and size in determining response to treatment was recently confirmed by a systematic review in which data relative to 1159 liver and peritoneal cysts were analyzed (Stojkovic et al., 2009).

Randomized controlled trials that compare standardized benzimidazole therapy on responsive cyst stages with the other treatment modalities are needed to draw reliable conclusions.

F. Risks

Adverse effects of BMZ include hepatotoxicity, severe leucopenia, thrombocytopenia and alopecia (Junghanss et al., 2008). Increase in aminotransferase levels may be due to drug-related efficacy or to real drug-related toxicity. Risks include embryotoxicity and teratogenicity, which have been observed in laboratory animals (Bradley and Horton, 2001).

G. Medical requirements

Hospitalization is not necessary but regular follow-up is required. Costs of BMZ and repeated examinations may be prohibitive in countries with limited resources.

H. Pharmacovigilance

Recommandations for pharmacovigilance are given below under "Monitoring of CE patients" and 4.4.2 F.

Strength of recommendation: B Quality of Evidence: III

3.4.5. Watch and Wait approach

Some cysts do not require any treatment if uncomplicated, namely, CE4 and CE5 (CL cysts should not be treated, until their parasitic nature has been proven). Long-term follow-up of patients

with US imaging has increased clinicians' confidence that in selected cases, i.e. when inactive cysts are not complicated, treatment can be put on hold (Junghanss et al., 2008).

This approach deserves formal evaluation.

Strength of recommendation: B Quality of Evidence: III

3.4.6. Management of cysts in extra-hepatic sites and specific situations

Because of the lower frequency of CE in extra-hepatic sites, the strength of recommendation is even lower than for treatment of hepatic CE.

A. Lung

The presentation of pulmonary CE varies widely, making a uniform treatment recommendation impossible. BMZ used alone showed good efficacy on small, uncomplicated lung cysts. BMZ should be avoided pre-operatively in larger lung cysts. Surgery aims at removing the parasite and treating associated pathology. It should be as conservative as possible. Radical procedures are required for extended parenchymal involvement, severe pulmonary suppuration, and complications (Isitmangil et al., 2002).

B. Bone

Bone involvement accounts for 0.5–2% of the total number of cases and is potentially the most debilitating form of CE. The most effective treatment is radical resection of the affected bone (Zlitni et al., 2001). Multiple recurrences with the need for repeated surgical procedures, in addition to the presence of serious complications such as spinal involvement, fistulae, acute and chronic osteomyelitis, have an extremely poor prognosis. When the hip is involved, broad resections should be carried out, with the implantation of a prosthetic hip absolutely contraindicated. CE in bone is less sensitive to ABZ than cysts at other sites and high dosage and long-term administration (years) are indicated.

C. Heart

Cardiac involvement accounts for 0.5–2% of total cases with 10% of cases showing various symptoms. Surgery is the treatment of choice (Thameur et al., 2001). Venous filters are used to prevent dissemination. If complete removal of the cysts is possible, the prognosis is good, with a low rate of recurrence.

D. Disseminated disease

When cysts are widespread, usually after cyst rupture, spontaneously or during surgery, a surgical approach is often impractical (Chawla et al., 2003). If the cysts are very large or located in or near vital organs the treatment should be combined surgery and ABZ, despite its palliative nature. However, medical treatment alone with ABZ, maintained for an indefinite length of time, is the only option available in most cases, with an acceptable response (reduction in the number and/or size of lesions) (Chawla et al., 2003). Discontinuation is often associated with recurrence.

3.5. Strength of recommendation: B Quality of Evidence: III

3.5.1. Monitoring of CE patients

Follow-up visits, including US examination should be done every 3–6 months initially and every year once the situation is stable. Leukocyte counts and aminotransferase measurements are necessary at monthly intervals to detect adverse reactions. Oral drug doses can be adapted to individual patients in order to achieve adequate serum levels but only a few laboratories have the capability to determine ABZ sulfoxide or MBZ plasma drug levels (WHO-IWGE, 1996) (see also section on AE).

One of the major problems of CE is the frequency of relapses. Serological markers to assess relapses have been widely studied, but while the persistence of raised antibody levels or a further increase may be suggestive of residual disease or recurrence, this may happen even when cysts have been successfully removed with surgery (Galitza et al., 2006). This may be confusing even to experienced clinicians. New antigens seem to be promising in improving the performance of serology in post-treatment monitoring (Ben Nouir et al., 2008).

4. Alveolar echinococcosis

4.1. Organ location

Initially, metacestodes of *E. multilocularis* develop almost exclusively in the liver, predominantly in the right lobe, from foci of a few millimeters to areas of 15–20 cm or more in diameter, sometimes with central necrosis (WHO-IWGE, 1996; WHO/OIE, 2001). *E. multilocularis* does not form cysts as *E. granulosus* does. From the liver, the larva spreads to other organs by infiltration or metastasis formation. Primary extra-hepatic locations of *E. multilocularis* are rare (Kern et al., 2003).

4.2. Course of infection

AE is characterized by an initial asymptomatic incubation period of 5–15 years and a subsequent chronic course. The symptoms are primarily cholestatic jaundice (1/3 cases) and/or abdominal pain (1/3 cases). In 1/3 of patients, AE is found incidentally on investigation of various symptoms such as: fatigue and weight loss, hepatomegaly and abnormal US or routine laboratory findings (WHO-IWGE, 1996; WHO/OIE, 2001). Mortality is high in non-treated patients but in Europe treatment has changed average life expectancy at diagnosis from 3 years in the 1970s to 20 years in 2005 (Torgerson et al., 2008). Under the influence of the host's defense mechanisms, the larva can degenerate and die; calcified dead lesions can be identified during mass screening programmes (Rausch et al., 1987; Bresson-Hadni et al., 1994; Gottstein et al., 2001; Romig et al., 1999).

4.3. Diagnosis

Diagnosis of alveolar echinococcosis is based on clinical findings and epidemiological data, imaging techniques, histopathology and/or nucleic acid detection, and serology.

4.3.1. Imaging

A. Ultrasound examination

As for CE, US examination is the basis of AE diagnosis in abdominal locations, at the individual and population levels, but needs an experienced examiner (Bartholomot et al., 2002; Romig et al., 1999). Typical findings (70% of cases) include (1) juxtaposition of hyper- and hypoechogenic areas in a pseudo-tumour with irregular limits and scattered calcification and (2) pseudo-cystic appearances due to a large area of central necrosis surrounded by an irregular hyperechogenic ring. Less typical features (30% of cases) include (1) haemangioma-like hyperechogenic nodules as the initial lesion and (2) a small calcified lesion due either to a dead or a small-sized developing parasite (Bresson-Hadni et al., 2000, 2006). US

with colour Doppler provides information on biliary and vascular involvement.

B. Imaging techniques other than US

CT gives an anatomical and morphological characterization of lesions and best depicts the characteristic pattern of calcification (WHO/OIE, 2001). In cases of diagnostic uncertainty, MR imaging may show the multivesicular morphology of the lesions, thereby supporting the diagnosis (Bresson-Hadni et al., 2006) and is the best technique to study extension to adjacent structures. For pre-operative evaluation, MRCP has replaced percutaneous cholangiography to study the relationship between the AE lesion and the biliary tree (Bresson-Hadni et al., 2006). Initial radiological examination to exclude pulmonary and cerebral AE is recommended.

4.3.2. Direct assessment of E. multilocularis and its viability

Histopathological examination shows the parasitic vesicles delineated by a Periodic-Acid-Schiff (PAS)+ laminated layer. The periparasitic granuloma is composed of epithelioid cells lining the parasitic vesicles, macrophages, fibroblasts and myofibroblasts, giant multinucleated cells, and various cells of the nonspecific immune response, usually surrounded by lymphocytes. Also present are collagen and other extracellular matrix protein deposits (Yamasaki et al., 2007).

Polymerase chain reaction (PCR) can detect *Echinococcus*-specific nucleic acids in tissue specimens resected or biopsied from patients and RT-PCR may assess viability (Ito and Craig, 2003; Yamasaki et al., 2007). However, a negative result on a thin needle aspiration sample does not rule out disease and a negative finding using RT-PCR does not indicate complete inactivity of a lesion (Yamasaki et al., 2007).

[^{18}F]Fluoro-Deoxyglucose-Positron-Emission-Tomography (FDG-PET) scanning indirectly demarcates areas of parasitic activity. If combined with CT (PET/CT), or MRI (PET/MRI), it may show active lesions at a time when clinical symptoms are absent and recurring disease not yet detectable by conventional imaging (Reuter et al., 2004; Stumpe et al., 2007). However, lack of detectable metabolic activity does not mean parasite death, but indicates suppressed periparasitic inflammatory activity (Stumpe et al., 2007). Delayed PET image acquisition (3 h after FDG injection) improves the assessment of primary and metastatic liver lesions (Bresson-Hadni et al., 2006).

4.3.3. WHO classification of AE

The WHO-IWGE PNM classification system, based on imaging findings, has been established as the international benchmark for standardized evaluation of diagnostic and therapeutic measures (WHO/OIE, 2001; Kern et al., 2006). It denotes the extension of the parasitic mass in the liver (P), the involvement of neighbouring organs (N), and metastases (M) (Table 3). PNM classification should improve the quality control of current treatment strategies in single centres and uniform evaluation of multicentre studies.

4.3.4. E. Multilocularis serology

As for CE, immunodiagnosis represents a valuable diagnostic tool to confirm the nature (and species) of the etiological agent (WHO-IWGE, 1996; WHO/OIE, 2001; Ito and Craig, 2003). The use of purified and/or recombinant, or *in vitro*-produced *E. multilocularis* antigens (Em2, Em2+, Em18; for complete list, see WHO-IWGE, 1996; Ito and Craig, 2003) has a high diagnostic sensitivity of 90–100%, with a specificity of 95–100%. Most of the purified antigens allow discrimination between AE and CE in 80–95% of cases. Immunoblotting tests may be used for confirmation or as a first-line investigation if easily available. For AE screening, a combined approach using US and serology discriminates different infection status among seropositive individuals: (1) patients with active hepatic lesions, (2) individuals presenting with fully calcified lesions and (3) individuals presenting with no detectable lesion at all. The latter two variants refer to persons exposed to infection but in whom the parasite has not become established or does not progress (Vuitton et al., 2006).

Table 3
PNM classification of alveolar echinococcosis.

P	Hepatic localisation of the parasite
PX	Primary tumour cannot be assessed
P0	No detectable tumour in the liver
P1	Peripheral lesions without proximal vascular and/or biliar involvement
P2	Central lesions with proximal vascular and/or biliar involvement of one lobe[a]
P3	Central lesions with hilar vascular or biliar involvement of both lobes and/or with involvement of two hepatic veins
P4	Any liver lesion with extension along the vessels[b] and the biliary tree
N	Extra-hepatic involvement of neighbouring organs [diaphragm, lung, pleura, pericardium, heart, gastric and duodenal wall, adrenal glands, peritoneum, retroperitoneum, parietal wall (muscles, skin, bone), pancreas, regional lymph nodes, liver ligaments, kidney]
NX	Not evaluable
N0	No regional involvement
N1	Regional involvement of contiguous organs or tissues
M	The absence or presence of distant metastasis [lung, distant lymph nodes, spleen, CNS, orbital, bone, skin, muscle, kidney, distant peritoneum and retroperitoneum]
MX	Not completely evaluated
M0	No metastasis[c]
M1	Metastasis

[a] For classification, the plane projecting between the bed of the gall bladder and the inferior vena cava divides the liver in two lobes.
[b] Vessels mean inferior vena cava, portal vein and arteries.
[c] Chest X-ray and cerebral CT negative.

4.3.5. AE case definition

The International Classification of Diseases and Related Health Problems ICD10 (10th Revision Version for 2007; http://www.who.int/classifications/icd/en) subclassifies:

B67.5 E. multilocularis, liver infection
B67.6 E. multilocularis, other organs and multiple site infection
B67.7 E. multilocularis, unspecified infection

ICD 9 codes are also listed as they are still used in many countries:

122.5 E. multilocularis, liver infection
122.6 E. multilocularis infection, other
122.7 E. multilocularis infection, unspecified

A. Clinical criteria

At least the following: a slowly growing tumour (signs and symptoms vary with tumour location, size and type (solid, partly multivesicular, with central necrosis)), diagnosed by imaging techniques.

B. Diagnostic criteria

At least one of the following four:

1. Typical organ lesions detected by imaging techniques (e.g. abdominal US, CT, MR).

2. Detection of *Echinococcus* spp. specific serum antibodies by high-sensitivity serological tests and confirmed by a high specificity serological test.
3. Histopathology compatible with AE.
4. Detection of *E. multilocularis* nucleic acid sequence(s) in a clinical specimen.

C. Possible versus probable versus confirmed case

Possible case. Any patient with clinical and epidemiological history and imaging findings or serology positive for AE.

Probable case. Any patient with clinical and epidemiological history, and imaging findings and serology positive for AE with two tests.

Confirmed case. The above, plus (1) histopathology compatible with AE and/or (2) detection of *E. multilocularis* nucleic acid sequence(s) in a clinical specimen.

4.4. Treatment

Treatment should be planned in a multidisciplinary discussion, taking all elements of available pre-treatment imaging into account. In addition to chemotherapy, early diagnosis, improved surgery, and medical care of the patients have contributed to the success of treatment and to the increase in patients' survival time during the past 3 decades (Bresson-Hadni et al., 2000; Kadry et al., 2005; Buttenschoen et al., 2009a; Torgerson et al., 2008). Patients should be referred to recognised national/regional AE treatment centres whenever available, or treated under the guidance of such centres.

4.4.1. General indications for treatment

The following principles should be followed: (1) BMZ are mandatory in all patients, temporarily after complete resection of the lesions, and for life in all other cases, (2) interventional procedures should be preferred to palliative surgery whenever possible and (3) radical surgery is the first choice in all cases suitable for total resection of the lesion(s). A consensus view of a number of experts on a stage-specific approach is summarized in Table 4.

4.4.2. Antiparasitic drug treatment

A. Indications

Long-term BMZ treatment for several years is mandatory in all inoperable AE patients and following surgical resection of the parasite lesions. Since residual parasite tissue may remain undetected at radical surgery, including liver transplantation (LT), BMZ should be given for at least 2 years and these patients monitored for a minimum of 10 years for possible recurrence (Reuter et al., 2000). Pre-surgical BMZ administration is not recommended except in the case of LT.

B. Contraindications

In view of the severity of AE, there are only a few contraindications for medical treatment and they are mostly due to life-threatening side effects. In some instances (e.g. pregnant women) certain precautions are necessary (see Contraindications in Section 3).

C. Drugs: BMZ

ABZ is given orally at a dosage of 10–15 mg/kg/day, in 2 divided doses, with fat-rich meals. In practice, a daily dose of 800 mg is given to adults, divided in two doses. Continuous ABZ treatment of AE is well tolerated and has been used for more than 20 years in some patients. Intermittent treatment should no longer be used. Occasionally, ABZ has been given in higher doses of 20 mg/kg/day for up to 4.5 years. Alternatively, if ABZ is not available or not well tolerated, MBZ may be given at daily doses of 40–50 mg/kg/day split into three divided doses with fat-rich meals. For details on the pharmacology of BMZ, see (WHO-IWGE, 1996).

Strength of recommendation: B Quality of Evidence: III

D. Other drugs

Based on experimental data, PZQ has no place in the treatment of human AE (Marchiondo et al., 1994).

Table 4
Stage-specific approach to alveolar echinococcosis.

WHO classification	Surgery	Interventional treatment	Drug therapy	Suggested	Resources setting
P1N0M0				Radical resection (R0)	*Optimal*
	√		√	BMZ for 2 years PET/CT controls	
				Radical resection (R0)	*Minimal*
				BMZ for 3 months	
P2N0M0			√	Radical resection (R0)	*Optimal*
				BMZ for 2 years	
	√			Radical resection (R0)	*Minimal*
				BMZ for 3 months	
P3N0M0			√	BMZ continuously	*Optimal*
				PET/CT/MRI scan initially and in 2 years intervals	
				BMZ continuously	*Minimal*
P3N1M0		√	√	BMZ continuously + PET/CT/MRI scan initially and in 2 years intervals	*Optimal*
				Surgery, if indicated	*Minimal*
P4N0M0		√	√	BMZ continuously + PET/CT/MRI scan initially and in 2 years intervals	*Optimal*
				Surgery, if indicated	*Minimal*
P4N1M1		√	√	BMZ continuously + PET/CT/MRI scan initially and in 2 years intervals	*Optimal*
				Surgery, if indicated	*Minimal*

Conventional and liposomal amphothericin B have been used as a salvage treatment in a few patients who did not tolerate BMZ (Reuter et al., 2003).

Nitazoxanide had no efficacy in a recent pilot trial (Kern et al., 2008).

New ABZ formulations such as liposomes and nanoparticles seem to improve ABZ bioavailability. Randomized, controlled trials are necessary to draw definitive conclusions on efficacy and side-effects of these new formulations.

E. Benefits

Controlled, but non-randomized studies showed that long-term BMZ improved the 10-year survival rate in non-radically operated AE patients compared to untreated historical control patients from 6–25% to 80–83%, respectively, and prevented recurrences after radical surgery (Ammann and Eckert, 1996; Torgerson et al., 2008).

F. Risks

The same risks for BMZ described in Section 3 exist for their use in AE. Although no systematic evaluation has been performed, long-term administration does not seem to increase such risks or to generate resistance.

G. Medical requirements

Hospitalization is not needed but regular medical and laboratory checks for adverse reactions and efficacy are necessary. The costs of anthelmintics and repeated medical examinations are high. Reference centres should be used to monitor drug levels and specific antibodies, and for specialised imaging techniques (such as PET/CT or MR scans).

C. Pharmacovigilance

Examinations for adverse reactions are necessary initially every 2 weeks (first 3 months), then monthly (first year), then every 3 months. As BMZ administration is crucial in all cases of AE, if an increase above 5 times the upper limit of normal (ULN) of aminotransferases is observed, the following steps are recommended: (1) check for other causes of the increase (other medication, viral hepatitis, AE-related biliary obstruction or liver abscess), (2) monitor drug levels, (3) if ABZ sulfoxide plasma levels are higher than the recommended range of concentrations (1–3 μmol/L, 4 h after morning drug intake), decrease ABZ dosage and shift to the alternative BMZ (MBZ if ABZ and vice versa) and (4) if an increase over 5 × ULN persists, consult a reference centre. Decrease of leukocyte count under 1.0 × 109/L indicates BMZ toxicity and warrants treatment withdrawal.

4.4.3. Surgery

Radical resection is the primary goal. Excision of the entire parasitic lesion should follow the rules of tumour surgery, classified according to the quality of resection: R0: no residue; R1: microscopic residue; R2: macroscopic residue. Non-radical liver surgery, previously regarded as beneficial for reducing the parasitic mass, does not appear currently to offer advantages over conservative treatment (Kadry et al., 2005; Buttenschoen et al., 2009). Lesions not confined to the liver are not a contraindication to surgery *per se*, but curative procedures have to meet the criteria for R0-resections as well. Lesions in other organs (e.g. brain) should be managed either by surgery or by alternative measures. Irrespective of the type of procedure, concomitant BMZ treatment is mandatory for at least 2 years. No staging system can judge "resectability" but the WHO-IWGE PNM classification (Kern et al., 2006) gives a rough estimation and enables comparison of results from different groups. Each case should be discussed in an interdisciplinary context.

A. Indications

Whenever possible complete resection of AE lesions should be performed. The potential for resection and whether there is disease dissemination must be assessed carefully by pre-operative imaging techniques. LT should be reserved for patients with very advanced forms of the disease as salvage therapy.

B. Contraindications

In principle, radical surgery should be avoided when R0-resection is not achievable. Palliative surgery is almost always contraindicated; the few exceptions should be discussed thoroughly. LT is contraindicated in the presence of extra-hepatic locations and if immunosuppressive drugs and/or BMZ are contraindicated.

C. Choice of surgical technique

Radical surgery is the treatment of choice (R0-resection). As the parasite's growth resembles a malignant tumour, procedures and techniques recommended in oncological surgery, with a 2 cm safety margin are logical (Marchiondo et al., 1994; Sato et al., 1997; Uchino et al., 1993). Post-operative BMZ and long-term follow-up are mandatory in all cases (Table 4).

Palliative surgery should be avoided whenever possible. However, the diversity of AE manifestations sometimes results in individual solutions. R1- or even R2-resections might be necessary to effectively deal with a septic focus if R0-resection is impossible and/or if percutaneous or endoscopic drainage, which should be attempted first, is not effective (Buttenschoen et al., 2009b). Palliative resection combined with BMZ has proven to be effective in treating skin lesions.

Strength of recommendation: B Quality of Evidence: III

D. Liver transplantation

LT has been performed in approximately 60 patients in the world, with inoperable lesions and/or chronic liver failure (Koch et al., 2003). Immunosuppression favours re-growth of larval remnants and formation or increase in size of metastases (Vuitton et al., 2006). The conditions to qualify a patient for LT are: (1) severe liver insufficiency (secondary biliary cirrhosis or Budd-Chiari syndrome) or recurrent life-threatening cholangitis, (2) inability to perform radical liver resection and (3) absence of extra-hepatic AE locations: cases with residual AE in lung or abdominal cavity should be regarded as exceptional indications, balancing all the pros and cons (Scheuring et al., 2003).

E. Benefits

Radical surgery may cure the patient. Palliative surgery has very little benefit, except in rare selected cases. In highly selected cases, LT may save AE patients' lives. In a study by Bresson-Hadni et al., 5-year survival was 71% and 5-year survival without recurrence was 58%, which is better than in LT for hepatocellular carcinoma (Bresson-Hadni et al., 2003). Long-term survival (over 15 years) is possible in patients with residual or recurrent lesions under BMZ treatment.

F. Risks

The risks include those associated with any surgical intervention and specifically possible damage to major vessels along with the immunosuppression and chronic bacterial infection often observed in AE patients. Invisible or unrecognized parasitic remnants may re-grow and disseminate to other organs even after years have passed.

Strength of recommendation: C Quality of Evidence: II

G. Medical requirements

Hospitalization in a surgical ward with easy access to blood supply facilities is mandatory. The surgical team should be experienced in major (liver) surgery and in treating AE. LT requires a highly specialized team and equipment. Supportive medical care includes post-transplantation follow-up, adjustment of immunosuppressive drugs, and diagnosis and management of complications of the immunosuppressive regimen combined with continuous chemotherapy with BMZ.

4.4.4. Endoscopic and percutaneous interventions (EPI)

A number of local complications may occur for which interventional procedures have to be considered (Bresson-Hadni et al., 2006).

A. Indications

EPIs are indicated for complications if surgery is felt to be too high a risk and total resection of the lesions cannot be safely performed. Main indications include liver abscess due to bacterial infection of necrotic lesions, jaundice due to bile duct obstruction with or without acute cholangitis, hepatic or portal vein thrombosis and bleeding of oesophageal varices secondary to portal hypertension.

B. Contraindications

EPIs may spread parasite material and should be avoided if post-interventional BMZ is not possible.

C. Principle and techniques

Percutaneous bile or abscess drainage has now advantageously replaced palliative surgery with jejuno-biliary anastomosis to treat life-threatening cholangitis or liver abscess (Bresson-Hadni et al., 2000, 2006). However, bile drainage necessitates a permanent external drain, generally for life, and regular changing to prevent obstruction.

Endoscopic dilation of bile duct strictures followed by insertion of multiple plastic stents is an interesting alternative to PI since it immediately allows internal bile drainage (Bresson-Hadni et al., 2006). Additional treatment with ursodeoxycholic acid (UDCA) is given in some centres; its usefulness in preventing stent obstruction should be studied prospectively.

D. Benefits

EPIs together with BMZ avoid palliative surgery and can improve life expectancy and quality of life of AE patients. In addition, radical resection which was not possible initially may become feasible following the shrinkage of a necrotic cavity after percutaneous drainage.

E. Risks

Risks of EPIs include haemorrhage (for all procedures) and internal bile leakage or prolonged bile leakage through an external drain for bile duct drainage.

F. Medical requirements

Short-term hospitalization is usually necessary. Specific equipment that allows US (and/or CT) guidance of PI and/or an appropriate endoscope is required. In addition, medical professionals with a large experience of such procedures are essential to their success.

Strength of recommendation: B Quality of Evidence: III

4.4.5. Monitoring of patients with AE

After initiation of any type of treatment, long-term follow-up by US at shorter intervals and CT and/or MRI at intervals of 2–3 years, should be planned. Progression is documented by enlargement of lesions over time.

Determination of ABZ sulfoxide blood levels, 4 h after the morning dose, is recommended 1, 4 and 12 weeks after starting treatment, and 2–4 weeks after each dose adjustment with an estimated therapeutic range of 0.65–3 μmol/L. ABZ dosage should be reduced if 2 sequential measurements are above 10 μmol/L. Monitoring of MBZ plasma level is possible; plasma levels should be over 250 nmol/L (WHO-IWGE, 1996).

Complete surgical removal of the lesions results in a rapid decrease of anti-Em2- and anti-Em18-antibodies which subsequently become undetectable (Scheuring et al., 2003). Interpretation of serological results in patients treated with BMZ without radical resection is more complex (Tappe et al., 2009). Presence of anti-II/3-10/Em18-antibodies is more likely to reflect the presence of a viable metacestode with disappearance of such antibodies indicating lesions dying-out (Ammann et al., 2004).

BMZ are only parasitostatic and many studies have demonstrated that they do not kill *E. multilocularis* metacestodes (WHO-IWGE, 1996). After several years of BMZ administration, however, the question of treatment interruption may be raised, in the absence of progression of the lesions assessed by conventional imaging, and indirect assessment of viability using PET/CT (Reuter et al., 2004; Stumpe et al., 2007). Although it does not provide direct evidence of *E. multilocularis* viability, and recurrence may occur, this technique, together with the follow-up of specific serum antibodies, may support decision-making and follow-up after BMZ withdrawal in highly selected patients.

Acknowledgements

We gratefully acknowledge the support of François-Xavier Meslin, Department of Neglected Tropical Diseaes, WHO, of the Universitè de Franche-Comté, and of the Paul-Ehrlich-Gesellschaft für Chemotherapie e.V. EB is grateful to Sam Goblirsch, MD, for careful revision of English language of the final draft.

Appendix A. List of experts

Argentina	Bernardo Frider	Division of Internal Medicine-Hepatology; Argerich Hospital, Government of Buenos Aires City, Associated to the University of Buenos Aires, 1171 Buenos Aires, Argentina	frider@bigfoot.com
Bulgaria	Kirien Kjossev	Department of General Surgery; Military Medical Academy, Sofia, Bulgaria	kirien@abv.bg
	Vladimir Prandjev	Department of Neurosurgery; Military Medical Academy, Sofia, Bulgaria	prandjev@hotmail.com
France	Karine Bardonnet	CCOMS; Dept of Biochemistry; University Hospital, 25030 Besançon, France	kbardonnet@chu-besancon.fr
	Brigitte Bartholomot	CCOMS; Centre de Radiologie des Deux-Princesses, 25000 Besançon, France	brigitte.bartholomot@wanadoo.fr
	Oleg Blagosklonov	CCOMS; Dept of Nuclear Medicine; University Hospital, 25030 Besançon, France	oleg.blagosklonov@univ-fcomte.fr
	Franck Boué	Agence Française de Sécurité Sanitaire des Aliments ; Technopôle Agricole et Vétérinaire, 54220 Malzéville, France	f.boue@afssa.fr
	Solange Bresson-Hadni	CCOMS; Dept of Digestive and Cancer Surgery; University Hospital, 25030 Besançon, France	dr.bresson.hadni@wanadoo.fr; ccoms@chu-besancon.fr
	Eric Delabrousse	CCOMS; Dept of Radiology A; University Hospital, 25030 Besançon, France	e.delabrousse@chu-besancon.fr
	Alain Gérard	Dept of Infectious Diseases; University Hospital Brabois, 54500 Vandoeuvre les Nancy, France	a.gerard@chu-nancy.fr
	Patrick Giraudoux	CCOMS; UMR Chrono-Environnement; Université de Franche-Comté, 25030 Besançon	patrick.giraudoux@univ-fcomte.fr
	Jenny Knapp	CCOMS; UMR Chrono-Environnement; Université de Franche-Comté, 25030 Besançon	patrick.giraudoux@univ-fcomte.fr
	Georges Mantion	CCOMS; Dept of Digestive and Cancer Surgery; University Hospital, 25030 Besançon, France	gmantion@univ-fcomte.fr
	Laurence Millon	CCOMS; Dept of Parasitology; University Hospital, and UMR Chrono-Environnement; Université de Franche-Comté, 25030 Besançon	laurence.millon@univ-fcomte.fr
	Martine Piarroux	CCOMS; FrancEchino Network; University Hospital, 25030 Besançon	mpiarroux@yahoo.fr
	Renaud Piarroux	Dept of Parasitology; University Hospital La Timone, 13385 Marseille cedex 5, France	Renaud.Piarroux@mail.ap-hm.fr
	Francis Raoul	CCOMS; UMR Chrono-Environnement; Université de Franche-Comté, 25030 Besançon	francis.raoul@univ-fcomte.fr
	Anne-Laure Rayssac and Carine Richou	CCOMS; Dept of Hepatology; University Hospital, 25030 Besançon	crichou@chu-besancon.fr
	Dominique A Vuitton	CCOMS; EA 3181; Université de Franche-Comté, 25030 Besançon	dominique.vuitton@univ-fcomte.fr
	Jérôme Watelet	Dept of Gastroenterology; University Hospital Brabois, 54500 Vandoeuvre les Nancy, France	j.watelet@chu-nancy.fr
Germany	Holger Barth	Dept of Surgery; University Hospital, 89081 Ulm, Germany	Holger.Barth@uni-ulm.de
	Klaus Buttenschön	Dept of Surgery; University Hospital, 89081 Ulm, Germany	klaus.buttenschoen@uniklinik-ulm.de
	Waldemar Hosch	Dept of Radiology; University Hospital; 69120 Heidelberg, Germany	waldemar.hosch@urz.uni-heidelberg.de
	Thomas Junghanss	Section of Clinical Tropical Medicine; University Hospital; 69120 Heidelberg	Thomas.Junghanss@urz.uni-heidelberg.de
	Peter Kern	Sektion Infektiologie und Klinische Immunologie; University Hospital, 89081 Ulm, Germany	peter.kern@uniklinik-ulm.de
	Stefan Reuter	Sektion Infektiologie und Klinische Immunologie, University Hospital, 89081 Ulm, Germany	stefan.reuter@uniklinik-ulm.de
	Hanns M Seitz	Henri-Spaakstr. 161, 53123 Bonn, Germany	seitz@parasit.meb.uni-bonn.de
Iraq	Nadham Mahdi	College of Medicine; University of Basrah, 1565 BASRAH, Iraq	nadhammahdi@yahoo.com
Italy	Giorgio Battelli	Dipartimento di Sanità Pubblica Veterinaria e Patologia Animale; Facoltà di Medicina veterinaria, 40064 Ozzano Emilia (Bologna), Italia	giorgio.battelli@unibo.it
	Enrico Brunetti	Division of Infectious and Tropical Diseases; IRCCS S. Mateo, Pavia University, Pavia, Italy	selim@unipv.it
	Carlo Filice	Division of Infectious and Tropical Diseases; IRCCS S. Mateo, Pavia University, Pavia, Italy	carfil@unipv.it
	Antonella Teggi	Dipartimento di Malattie Infettive; Ospedale Sant'Andrea, University "La Sapienza", 00189 Rome, Italy	spec.trop@tiscali.it
Japan	Akira Ito	Dept of Parasitology; Asahikawa University, 078-8510 Asahikawa, Japan	akiraito@asahikawa-med.ac.jp
	Naoki Sato	Dept of Digestive Surgery; University Hospital, 060-8638 Sapporo, Japan	naoki-sa@med.hokudai.ac.jp
Marocco	Mustapha Benazzouz	Unité d'Hépato-Gastro-Entérologie, Médecine C, Hopital Ibn Sina, BP1005 Rabat, Morocco	benazmusta@menara.ma
Netherlands	Hans G Schipper	Department of Infectious Diseases, Tropical Medicine, and AIDS; Academic Medical Centre, 1105 AZ, Amsterdam,The Netherlands	h.g.schipper@amc.uva.nl
PR China	Fang Ping He	Dept of Hepatology; Key Lab for basic and clinical research on echinococcosis; Xinjiang Medical University 1st Teaching Hospital, 830054 Urumqi, China	hefp2009@163.com
	Wen Ya Liu	Dept of Radiology; Xinjiang Medical University 1st Teaching Hospital, 830054 Urumqi, China	wenyaliu2002@yahoo.com.cn
	Xiao Mei Lu	Dept of Clinical research; Key Lab for basic and clinical research on echinococcosis; Xinjiang Medical University 1st Teaching Hospital, 830054 Urumqi, China	luxiaomei88@163.com
	Shu Mei Ma	Dept of Parasitology; Qinghai Medical College, Xinning, Qinghai,	

Appendix A (*Continued*)

PR China	mashumei411@sohu.com		
	XinYu Peng	Dept of Surgery; Shihezi University Medical College; 832008 Shihezi, Xinjiang, China	pengxy2000@yahoo.com
	Ying Mei Shao	Dept of Digestive and Hepatic Surgery; Key Lab for basic and clinical research on echinococcosis; Xinjiang Medical University 1st Teaching Hospital, 830054 Urumqi, China	shaoym@lzu.edu.cn
	Jian Hua Wang	Dept of Pharmacology; Xinjiang Medical University, 830054 Urumqi, China	jhw716@163.com
	Yun Hai Wang	Dept of Digestive and Hepatic Surgery; Key Lab for basic and clinical research on echinococcosis; 1st Teaching Hospital of Xinjiang Medical University; Urumqi, China	yunhai_wang@hotmail.com
	Hao Wen	Dept of Digestive and Hepatic Surgery; Key Lab for basic and clinical research on echinococcosis; 1st Teaching Hospital of Xinjiang Medical University; Urumqi, China	dr.wenhao@163.com
	Yu Rong Yang	Molecular Parasitology Laboratory; Queensland Institute of Medical Research, Brisbane, Q4006, Australia (and Ningxia Medical College, Yinshuan, China)	yurongY@qimr.edu.au
Perù	Hector H. Garcia	Laboratorio de Parasitologia; Universidad Peruana Cayetano Heredia, SMP, Lima, Peru	hgarcia@jhsph.edu
Portugal	Antonio Menezes da Silva	Dept of Surgery, Hospital Pulido Valente Alameda das Linhas de Torres, 1600 Lisbon, Portugal	mensilvapt@yahoo.com
Romania	Carmen Cretu	Parasitology Department; "Carol Davila" University of Medicine and Pharmacy, 020027, Bucharest, Romania	michaelacarmen.cretu@gmail.com
Serbia	Miroslav Milicevic	Institute for Digestive Diseases; First Surgical Clinic University of Belgrade Clinical Centre, 11000 Belgrade, Serbia	machak@sbb.co.yu
Spain	Rogelio Lopez-Velez	Medicina Tropical y Parasitología Clínica; Servicio de Enfermedades Infecciosas; Hospital Ramón y Cajal. 28034 Madrid, Spain	rlopezvelez.hrc@salud.madrid.org
Switzerland	Bruno Gottstein	Parasitology Institute; Bern University, 3012 Bern, Switzerland	bruno.gottstein@ipa.unibe.ch
	Beat Müllhaupt	Departement für Innere Medizin, Gastroenterologie; Universitätsspital, 8091 Zürich, Switzerland	beat.muellhaupt@usz.ch
Tunisia	Chadli Dziri	Division of General Surgery, Department of Emergency; Hôpital Charles Nicolle, 1006 Tunis, Tunisia	chadli.dziri@planet.tn
Turkey	Okan Akhan	Radyoloji AD, Hacettepe Universitesi, 06100 Ankara, Turkey	akhano@tr.net
	Erbug Keskin	Dept of Paediatric Surgery; University of Cukurova, 01330 Adana, Turkey	erbug@erbug.net
West Indies	Calum Macpherson	Dept of parasitology; St George's University St George's, Grenada, WI	cmacpherson@sgu.edu
USA	Peter M.S. Schantz	Division of Parasitic Diseases; National Center For Infectious Diseases, Centers For Disease Control and Prevention, Atlanta, GA 30341, USA	p.schantz@comcast.net
UK	Peter Chiodini	Department of Clinical Parasitology; Hospital for Tropical Diseases, London WC1E 6JB, UK	peter.chiodini@uclh.nhs.uk
	Philip S. Craig	Biosciences Research Institute; School of Environment & Life Sciences; University of Salford, Salford M5 4WT, UK	p.s.craig@salford.ac.uk
	John Horton	24 The Paddock, Hitchin, Herts. SG4 9EF, UK	Phone: +44-1462-624081; mobile: +44-7881815363 hedgepigs@aol.com
	Michael Rogan	Biosciences Research Institute; School of Environment & Life Sciences; University of Salford, Salford M5 4WT, UK	M.T.Rogan@salford.ac.uk
UN/WHO	Albis Gabrielli	NTD Department, World Health Organisation, 1211 Genève	gabrielli@who.int
	François-Xavier Meslin	NTD Department, World Health Organisation, 1211 Genève	meslin@who.int

References

Akhan, O., Gumus, B., Akinci, D., Karcaaltincaba, M., Ozmen, M., 2007. Diagnosis and percutaneous treatment of soft-tissue hydatid cysts. Cardiovasc. Intervent. Radiol. 30, 419–425.

Akisu, C., Delibas, S.B., Bicmen, C., Ozkoc, S., Aksoy, U., Turgay, N., 2006. Comparative evaluation of western blotting in hepatic and pulmonary cystic echinococcosis. Parasite 13, 321–326.

Ammann, R.W., Eckert, J., 1996. Cestodes. *Echinococcus*. Gastroenterol. Clin. North Am. 25, 655–689.

Ammann, R.W., Renner, E.C., Gottstein, B., Grimm, F., Eckert, J., Renner, E.L., 2004. Immunosurveillance of alveolar echinococcosis by specific humoral and cellular immune tests: long-term analysis of the Swiss chemotherapy trial (1976–2001). J. Hepatol. 41, 551–559.

Arif, S.H., Shams Ul, B., Wani, N.A., Zargar, S.A., Wani, M.A., Tabassum, R., Hussain, Z., Baba, A.A., Lone, R.A., 2008. Albendazole as an adjuvant to the standard surgical management of hydatid cyst liver. Int. J. Surg. 6, 448–451.

Aydin, U., Yazici, P., Onen, Z., Ozsoy, M., Zeytunlu, M., Kilic, M., Coker, A., 2008. The optimal treatment of hydatid cyst of the liver: radical surgery with a significant reduced risk of recurrence. Turk. J. Gastroenterol. 19, 33–39.

Bartholomot, G., Vuitton, D.A., Harraga, S., Shida, Z., Giraudoux, P., Barnish, G., Wang, Y.H., MacPherson, C.N., Craig, P.S., 2002. Combined ultrasound and serologic screening for hepatic alveolar echinococcosis in central China. Am. J. Trop. Med. Hyg. 66, 23–29.

Baskaran, V., Patnaik, P.K., 2004. Feasibility and safety of laparoscopic management of hydatid disease of the liver. JSLS 8, 359–363.

Ben Nouir, N., Nunez, S., Gianinazzi, C., Gorcii, M., Muller, N., Nouri, A., Babba, H., Gottstein, B., 2008. Assessment of *Echinococcus granulosus* somatic protoscolex antigens for serological follow-up of young patients surgically treated for cystic echinococcosis. J. Clin. Microbiol. 46, 1631–1640.

Bradley, M., Horton, J., 2001. Assessing the risk of benzimidazole therapy during pregnancy. Trans. R. Soc. Trop. Med. Hyg. 95, 72–73.

Bresson-Hadni, S., Delabrousse, E., Blagosklonov, O., Bartholomot, B., Koch, S., Miguet, J.P., Mantion, G., Vuitton, D.A., 2006. Imaging aspects and non-surgical interventional treatment in human alveolar echinococcosis. Parasitol. Int. 55 (Suppl.), S267–S272.

Bresson-Hadni, S., Koch, S., Miguet, J.P., Gillet, M., Mantion, G.A., Heyd, B., Vuitton, D.A., 2003. Indications and results of liver transplantation for *Echinococcus* alveolar infection: an overview. Langenbecks Arch. Surg. 388, 231–238.

Bresson-Hadni, S., Laplante, J.J., Lenys, D., Rohmer, P., Gottstein, B., Jacquier, P., Mercet, P., Meyer, J.P., Miguet, J.P., Vuitton, D.A., 1994. Seroepidemiologic screening of *Echinococcus multilocularis* infection in a European area endemic for alveolar echinococcosis. Am. J. Trop. Med. Hyg. 51, 837–846.

Bresson-Hadni, S., Vuitton, D.A., Bartholomot, B., Heyd, B., Godart, D., Meyer, J.P., Hrusovsky, S., Becker, M.C., Mantion, G., Lenys, D., Miguet, J.P., 2000. A twenty-year history of alveolar echinococcosis: analysis of a series of 117 patients from eastern France. Eur. J. Gastroenterol. Hepatol. 12, 327–336.

Budke, C.M., 2006. Global socioeconomic impact of cystic echinococcosis. Emerg. Infect. Dis. 12, 296–303.

Buttenschoen, K., Carli Buttenschoen, D., Gruener, B., Kern, P., Beger, H.G., Henne-Bruns, D., Reuter, S., 2009. Long-term experience on surgical treatment of alveolar echinococcosis. Langenbecks Arch. Surg. 394, 698.

Buttenschoen, K., Carli Buttenschoen, D., Gruener, B., Kern, P., Beger, H.G., Henne-Bruns, D., Reuter, S., 2009a. Long-term experience on surgical treatment of alveolar echinococcosis. Langenbecks Arch. Surg. 394, 689–698.

Buttenschoen, K., Gruener, B., Carli Buttenschoen, D., Reuter, S., Henne-Bruns, D., Kern, P., 2009b. Palliative operation for the treatment of alveolar echinococcosis. Langenbecks Arch. Surg. 394, 199–204.

Bygott, J.M., Chiodini, P.L., 2009. Praziquantel: neglected drug? Ineffective treatment? Or therapeutic choice in cystic hydatid disease? Acta Trop. 111, 95–101.

Chawla, A., Maheshwari, M., Parmar, H., Hira, P., Hanchate, V., 2003. Imaging features of disseminated peritoneal hydatidosis before and after medical treatment. Clin. Radiol. 58, 818–820.
Cobo, F., Yarnoz, C., Sesma, B., Fraile, P., Aizcorbe, M., Trujillo, R., Diaz-de-Liano, A., Ciga, M.A., 1998. Albendazole plus praziquantel versus albendazole alone as a pre-operative treatment in intra-abdominal hydatisosis caused by *Echinococcus granulosus*. Trop. Med. Int. Health 3, 462–466.
Craig, P., 2003. *Echinococcus multilocularis*. Curr. Opin. Infect. Dis. 16, 437–444.
Craig, P., Budke, C.M., Schantz, P.M., Tiaoying, L., Qiu, J.Y.Y., Zehyle, E., Rogan, M.T., Ito, A., 2007. Human echinococcosis: a neglected disease? Trop. Med. Health 35, 283–292.
Dogru, D., Kiper, N., Ozcelik, U., Yalcin, E., Gocmen, A., 2005. Medical treatment of pulmonary hydatid disease: for which child? Parasitol. Int. 54, 135–138.
Dziri, C., Haouet, K., Fingerhut, A., 2004. Treatment of hydatid cyst of the liver: where is the evidence? World J. Surg. 28, 731–736.
Dziri, C., Haouet, K., Fingerhut, A., Zaouche, A., 2009. Management of cystic echinococcosis complications and dissemination: where is the evidence? World J. Surg. 33, 1266–1273.
El Fortia, M., El Gatit, A., Bendaoud, M., 2006. Ultrasound wall-sign in pulmonary echinococcosis (new application). Ultraschall Med. 27, 553–557.
Franchi, C., Di Vico, B., Teggi, A., 1999. Long-term evaluation of patients with hydatidosis treated with benzimidazole carbamates. Clin. Infect. Dis. 29, 304–309.
Frider, B., Larrieu, E., Odriozola, M., 1999. Long-term outcome of asymptomatic liver hydatidosis. J. Hepatol. 30, 228–231.
Galitza, Z., Bazarsky, E., Sneier, R., Peiser, J., El-On, J., 2006. Repeated treatment of cystic echinococcosis in patients with a long-term immunological response after successful surgical cyst removal. Trans. R. Soc. Trop. Med. Hyg. 100, 126–133.
Gharbi, H.A., Hassine, W., Brauner, M.W., Dupuch, K., 1981. Ultrasound examination of the hydatic liver. Radiology 139, 459–463.
Gottstein, B., Saucy, F., Deplazes, P., Reichen, J., Demierre, G., Busato, A., Zuercher, C., Pugin, P., 2001. Is high prevalence of *Echinococcus multilocularis* in wild and domestic animals associated with disease incidence in humans? Emerg. Infect. Dis. 7, 408–412.
Haddad, M.C., Sammak, B.M., Al-Karawi, M., 2000. Percutaneous treatment of heterogenous predominantly solid echopattern echinococcal cysts of the liver. Cardiovasc. Intervent. Radiol. 23, 121–125.
Hosch, W., Junghanss, T., Stojkovic, M., Brunetti, E., Heye, T., Kauffmann, G.W., Hull, W.E., 2008. Metabolic viability assessment of cystic echinococcosis using high-field 1H MRS of cyst contents. NMR Biomed. 21, 734–754.
Hosch, W., Stojkovic, M., Janisch, T., Kauffmann, G.W., Junghanss, T., 2007. The role of calcification for staging cystic echinococcosis (CE). Eur. Radiol. 17, 2538–2545.
Isitmangil, T., Sebit, S., Tunc, H., Gorur, R., Erdik, O., Kunter, E., Toker, A., Balkanli, K., Ozturk, O.Y., 2002. Clinical experience of surgical therapy in 207 patients with thoracic hydatidosis over a 12-year-period. Swiss Med. Wkly. 132, 548–552.
Ito, A., Craig, P.S., 2003. Immunodiagnostic and molecular approaches for the detection of taeniid cestode infections. Trends Parasitol. 19, 377–381.
Junghanss, T., Menezes da Silva, A., Horton, J., Chiodini, P.L., Brunetti, E., 2008. Clinical management of cystic echinococcosis: state of the art, problems, and perspectives. Am. J. Trop. Med. Hyg. 79, 301–311.
Kadry, Z., Renner, E.C., Bachmann, L.M., Attigah, N., Renner, E.L., Ammann, R.W., Clavien, P.A., 2005. Evaluation of treatment and long-term follow-up in patients with hepatic alveolar echinococcosis. Br. J. Surg. 92, 1110–1116.
Kern, P., Abboud, P., Kern, W., Stich, A., Bresson-Hadni, S., Guerin, B., Buttenschoen, K., Gruener, B., Reuter, S., Hemphill, A., 2008. Critical appraisal of nitazoxanide for the treatment of alveolar echinococcosis. Am. J. Trop. Med. Hyg. 79, 119.
Kern, P., Bardonnet, K., Renner, E., Auer, H., Pawlowski, Z., Ammann, R.W., Vuitton, D.A., 2003. European echinococcosis registry: human alveolar echinococcosis, Europe, 1982–2000. Emerg. Infect. Dis. 9, 343–349.
Kern, P., Wen, H., Sato, N., Vuitton, D.A., Gruener, B., Shao, Y., Delabrousse, E., Kratzer, W., Bresson-Hadni, S., 2006. WHO classification of alveolar echinococcosis: principles and application. Parasitol. Int. 55 (Suppl.), S283–S287.
Khabiri, A.R., Bagheri, F., Assmar, M., Siavashi, M.R., 2006. Analysis of specific IgE and IgG subclass antibodies for diagnosis of *Echinococcus granulosus*. Parasite Immunol. 28, 357–362.
Khuroo, M.S., Dar, M.Y., Yattoo, G.N., Zargar, S.A., Javaid, G., Khan, B.A., Boda, M.I., 1993. Percutaneous drainage versus albendazole therapy in hepatic hydatidosis: a prospective, randomized study. Gastroenterology 104, 1452–1459.
Kish, M.A., 2001. Guide to development of practice guidelines. Clin. Infect. Dis. 32, 851–854.
Kjossev, K.T., Losanoff, J.E., 2005. Classification of hydatid liver cysts. J. Gastroenterol. Hepatol. 20, 352–359.
Koch, S., Bresson-Hadni, S., Miguet, J.P., Crumbach, J.P., Gillet, M., Mantion, G.A., Heyd, B., Vuitton, D.A., Minello, A., Kurtz, S., 2003. Experience of liver transplantation for incurable alveolar echinococcosis: a 45-case European collaborative report. Transplantation 75, 856–863.
Larrieu, E.J., Frider, B., 2001. Human cystic echinococcosis: contributions to the natural history of the disease. Ann. Trop. Med. Parasitol. 95, 679–687.
Macpherson, C.N., Milner, R., 2003. Performance characteristics and quality control of community based ultrasound surveys for cystic and alveolar echinococcosis. Acta Trop. 85, 203–209.
Marchiondo, A.A., Ming, R., Andersen, F.L., Slusser, J.H., Conder, G.A., 1994. Enhanced larval cyst growth of *Echinococcus multilocularis* in praziquantel-treated jirds (*Meriones unguiculatus*). Am. J. Trop. Med. Hyg. 50, 120–127.
McManus, D.P., Zhang, W., Li, J., Bartley, P.B., 2003. Echinococcosis. Lancet 362, 1295–1304.
Men, S., Yucesoy, C., Edguer, T.R., Hekimoglu, B., 2006. Percutaneous treatment of giant abdominal hydatid cysts: long-term results. Surg. Endosc. 20, 1600–1606.
Menezes da Silva, A., 2003. Hydatid cyst of the liver-criteria for the selection of appropriate treatment. Acta Trop. 85, 237–242.
Morris, D.L., Taylor, D.H., 1988. Optimal timing of post-operative albendazole prophylaxis in *E. granulosus*. Ann. Trop. Med. Parasitol. 82, 65–66.
Mufit, K., Nejat, I., Mercan, S., Ibrahim, K., Mete, U.Y., Yuksel, K., 1998. Growth of multiple hydatid cysts evaluated by computed tomography. J. Clin. Neurosci. 5, 215–217.
Peng, X., Zhang, S., Niu, J.H., 2002. Total subadventitial cystectomy for the treatment of 30 patients with hepatic hydatid cysts. Chin. J. Gen. Surg. 17, 529–530.
Rausch, R.L., Wilson, J.F., Schantz, P.M., McMahon, B.J., 1987. Spontaneous death of *Echinococcus multilocularis*: cases diagnosed serologically (by Em2 ELISA) and clinical significance. Am. J. Trop. Med. Hyg. 36, 576–585.
Reuter, S., Buck, A., Grebe, O., Nussle-Kugele, K., Kern, P., Manfras, B.J., 2003. Salvage treatment with amphotericin B in progressive human alveolar echinococcosis. Antimicrob. Agents Chemother. 47, 3586–3591.
Reuter, S., Buck, A., Manfras, B., Kratzer, W., Seitz, H.M., Darge, K., Reske, S.N., Kern, P., 2004. Structured treatment interruption in patients with alveolar echinococcosis. Hepatology 39, 509–517.
Reuter, S., Jensen, B., Buttenschoen, K., Kratzer, W., Kern, P., 2000. Benzimidazoles in the treatment of alveolar echinococcosis: a comparative study and review of the literature. J. Antimicrob. Chemother. 46, 451–456.
Rogan, M.T., Hai, W.Y., Richardson, R., Zeyhle, E., Craig, P.S., 2006. Hydatid cysts: does every picture tell a story? Trends Parasitol. 22, 431–438.
Romig, T., Kratzer, W., Kimmig, P., Frosch, M., Gaus, W., Flegel, W.A., Gottstein, B., Lucius, R., Beckh, K., Kern, P., 1999. An epidemiologic survey of human alveolar echinococcosis in southwestern Germany. Romerstein Study Group. Am. J. Trop. Med. Hyg. 61, 566–573.
Romig, T., Zeyhle, E., Macpherson, C.N., Rees, P.H., Were, J.B., 1986. Cyst growth and spontaneous cure in hydatid disease. Lancet 1, 861.
Saremi, F., McNamara, T.O., 1995. Hydatid cysts of the liver: long-term results of percutaneous treatment using a cutting instrument. Am. J. Roentgenol. 165, 1163–1167.
Sato, N., Namieno, T., Furuya, K., Takahashi, H., Yamashita, K., Uchino, J., Suzuki, K., 1997. Contribution of mass screening system to resectability of hepatic lesions involving *Echinococcus multilocularis*. J. Gastroenterol. 32, 351–354.
Scheuring, U.J., Seitz, H.M., Wellmann, A., Hartlapp, J.H., Tappe, D., Brehm, K., Spengler, U., Sauerbruch, T., Rockstroh, J.K., 2003. Long-term benzimidazole treatment of alveolar echinococcosis with hematogenic subcutaneous and bone dissemination. Med. Microbiol. Immunol. (Berl.) 192, 193–195.
Schipper, H.G., Lameris, J.S., van Delden, O.M., Rauws, E.A., Kager, P.A., 2002. Percutaneous evacuation (PEVAC) of multivesicular echinococcal cysts with or without cystobiliary fistulas which contain non-drainable material: first results of a modified PAIR method. Gut 50, 718–723.
Schweiger, A., Ammann, R.W., Candinas, D., Clavien, P.A., Eckert, J., Gottstein, B., Halkic, N., Muellhaupt, B., Prinz, B.M., Reichen, J., Tarr, P.E., Torgerson, P.R., Deplazes, P., 2007. Human alveolar echinococcosis after fox population increase, Switzerland. Emerg. Infect. Dis. 13, 878–882.
Seckin, H., Yagmurlu, B., Yigitkanli, K., Kars, H.Z., 2008. Metabolic changes during successful medical therapy for brain hydatid cyst: case report. Surg. Neurol. 70, 186–189.
Siles-Lucas, M.M., Gottstein, B.B., 2001. Molecular tools for the diagnosis of cystic and alveolar echinococcosis. Trop. Med. Int. Health 6, 463–475.
Siracusano, A., Bruschi, F., 2006. Cystic echinococcosis: progress and limits in epidemiology and immunodiagnosis. Parassitologia 48, 65–66.
Smego Jr., R.A., Bhatti, S., Khaliq, A.A., Beg, M.A., 2003. Percutaneous aspiration-injection-reaspiration drainage plus albendazole or mebendazole for hepatic cystic echinococcosis: a meta-analysis. Clin. Infect. Dis. 37, 1073–1083.
Stojkovic, M., Zwahlen, M., Teggi, A., Vutova, K., Cretu, C.M., Virdone, R., Nicolaidou, P., Cobanoglu, N., Junghanss, T., 2009. Treatment response of cystic echinococcosis to benzimidazoles: a systematic review. PLoS Negl. Trop. Dis. 3, e524.
Stumpe, K.D., Renner-Schneiter, E.C., Kuenzle, A.K., Grimm, F., Kadry, Z., Clavien, P.A., Deplazes, P., von Schulthess, G.K., Muellhaupt, B., Ammann, R.W., Renner, E.L., 2007. F-18-fluorodeoxyglucose (FDG) positron-emission tomography of *Echinococcus multilocularis* liver lesions: prospective evaluation of its value for diagnosis and follow-up during benzimidazole therapy. Infection 35, 11–18.
Tappe, D., Frosch, M., Sako, Y., Itoh, S., Gruener, B., Reuter, S., Nakao, M., Ito, A., Kern, P., 2009. Close relationship between clinical regression and specific serology in the follow-up of patients with alveolar echinococcosis in different clinical stages. Am. J. Trop. Med. Hyg. 80, 792–797.
Thameur, H., Abdelmoula, S., Chenik, S., Bey, M., Ziadi, M., Mestiri, T., Mechmeche, R., Chaouch, H., 2001. Cardiopericardial hydatid cysts. World J. Surg. 25, 58–67.
Torgerson, P.R., Schweiger, A., Deplazes, P., Pohar, M., Reichen, J., Ammann, R.W., Tarr, P.E., Halkik, N., Mullhaupt, B., 2008. Alveolar echinococcosis: from a deadly disease to a well-controlled infection. Relative survival and economic analysis in Switzerland over the last 35 years. J. Hepatol. 49, 72–77.
Uchino, J., Sato, N., Nakajima, Y., Matsushita, M., Takahashi, M., Une, Y., 1993. Treatment. In: Uchino, J., Sato, N. (Eds.), Alveolar Echinococcosis of the Liver. Hokkaido University School of Medicine, Sapporo.
Ustunsoz, B., Akhan, O., Kamiloglu, M.A., Somuncu, I., Ugurel, M.S., Cetiner, S., 1999. Percutaneous treatment of hydatid cysts of the liver: long-term results. Am. J. Roentgenol. 172, 91–96.
Ustunsoz, B., Ugurel, M.S., Uzar, A.I., Duru, N.K., 2008. Percutaneous treatment of hepatic hydatid cyst in pregnancy: long-term results. Arch. Gynecol. Obstet. 277, 547–550.

Vuitton, D., Zhang, S.L., Yang, Y., Godot, V., Beurton, I., Mantion, G., Bresson-Hadni, S., 2006. Survival strategy of *Echinococcus multilocularis* in the human host. Parasitol. Int. 55(Suppl.), S51–S55.

Vuitton, D.A., Zhi Wang, X., Li Feng, S., Cheng Shen, J., Shou Li, Y., Li, S.F., Ke Tang, Q., 2002. PAIR-derived US-guided techniques for the treatment of cystic echinococcosis: a Chinese experience (e-letter). Gut.

Vutova, K., Mechkov, G., Vachkov, P., Petkov, R., Georgiev, P., Handjiev, S., Ivanov, A., Todorov, T., 1999. Effect of mebendazole on human cystic echinococcosis: the role of dosage and treatment duration. Ann. Trop. Med. Parasitol. 93, 357–365.

Wang, X., Li, Y., Feng, S., 1994. [Clinical treatment of hepatic and abdominal hydatid cyst by percutaneous puncture, drainage and curettage] Zhongguo Ji Sheng Chong Xue Yu Ji Sheng Chong Bing Za Zhi 12, 285–287.

Wang, Y., He, T., Wen, X., Li, T., Waili, A., Zhang, W., Xu, X., Vuitton, D.A., Rogan, M.T., Wen, H., Craig, P.S., 2006. Post-survey follow-up for human cystic echinococcosis in northwest China. Acta Trop. 98, 43–51.

WHO-Informal Working Group on Echinococcosis, 1996. Guidelines for treatment of cystic and alveolar echinococcosis in humans. Bull. WHO 74, 231–242.

WHO/OIE Manual on Echinococcosis, 2001. Echinococcosis in Humans and Animals: A Public Health Problem of Global Concern. World Organisation for Animal Health (Office International des Epizooties) and World Health Organisation.

WHO-Informal Working Group on Echinococcosis, 2003a. PAIR: Puncture, Aspiration, Injection, Re-Aspiration. An Option for the Treatment of Cystic Echinococcosis. WHO, Geneva.

WHO-Informal Working Group on Echinococcosis, 2003b. International classification of ultrasound images in cystic echinococcosis for application in clinical and field epidemiological settings. Acta Trop. 85, 253–261.

Yamasaki, H., Nakaya, K., Nakao, M., Sako, Y.A.I., 2007. Significance of molecular diagnosis using histopathological specimens in cestode zoonoses. Trop. Med. Health 35, 307–321.

Zlitni, M., Ezzaouia, K., Lebib, H., Karray, M., Kooli, M., Mestiri, M., 2001. Hydatid cyst of bone: diagnosis and treatment. World J. Surg. 25, 75–82.

Neurocysticercosis: Assessing Where the Infection Was Acquired From

Tetsuya Yanagida, PhD,* Izumi Yuzawa, MD,† Durga D. Joshi, PhD,‡ Yasuhito Sako, PhD,* Minoru Nakao, PhD,* Kazuhiro Nakaya, PhD,§ Nobuyuki Kawano, MD,‖ Hidehiro Oka, MD,† Kiyotaka Fujii, MD,† and Akira Ito, PhD*

*Department of Parasitology, Asahikawa Medical College, Hokkaido, Japan; †Department of Neurosurgery, School of Medicine, Kitasato University, Kanagawa, Japan; ‡National Zoonoses and Food-Hygiene Research Center, Kathmandu, Nepal; §Animal Laboratory for Medical Research, Asahikawa Medical College, Hokkaido, Japan; ‖Isobe Clinic, Kanagawa, Japan

DOI: 10.1111/j.1708-8305.2010.00409.x

Histopathological specimen of a neurocysticercosis patient, who had been living in several endemic countries, was retrospectively analyzed for assessing the origin of the infection. Mitochondrial DNA analysis strongly suggested that the patient became infected with the parasite in Nepal at least 10 years before the onset of the disease.

The pork tapeworm *Taenia solium* is one of the most important human parasites because of its pathogenicity. It causes two types of human infection: (1) teniasis, intestinal infection of adult worms, caused by eating undercooked pork contaminated with cysticerci (larval stage) and (2) cysticercosis, tissue infection of cysticerci throughout the body, acquired by ingesting the eggs. Neurocysticercosis (NCC), cysticercosis in the central nervous system, is a lethal and rather common parasitic disease in many developing countries where pork is consumed. However, the recent increase in the number of immigrants and tourists is spreading the disease into the more developed countries and the communities where eating pork is forbidden.[1–3] Thus, it is important to ascertain the origin of the infection to assess the risk factors in nonendemic areas.[4]

The Study

In August 1996, a 46-year-old Japanese man complained of a dull headache during his stay in Jakarta, Indonesia, and he had a medical examination at the local hospital in Manila, Philippines on the way back to Japan. Cerebral computer tomography (CT) showed a putative brain tumor in the left temporal lobe. Then he came back to Japan and was admitted to Kitasato University Hospital. By CT scanning, a small solitary cystic lesion with ring enhancement was observed at the cerebral surface of the left temporal lobe. He showed no other neurological abnormalities, and his blood/stool tests were within the normal range. In September, the patient was operated and a well-encapsulated cyst of about 1 cm in diameter was surgically resected. Histopathological examination revealed it to be a viable cysticercus of *T. solium*.[5] He recovered well and came back to his job 19 days after the operation. NCC with solitary cyst was later confirmed serologically using highly specific antigens at Asahikawa Medical College.[6]

Where did the patient become infected? Because teniasis/cysticercosis is not endemic in Japan, it was assumed that he acquired the parasite outside of Japan. He had been an overseas technical advisor for 12 years since 1970s, and visited Indonesia, Nigeria, Nepal, and Malaysia, where NCC cases have been reported.[7] Because the patient had lived in Indonesia for 6 years just before the onset of the disease (1990–1996), we suspected that he had been infected with the parasite there. To solve the puzzle, we retrospectively analyzed cytochrome *c* oxidase I (*cox1*) of mitochondrial DNA (mtDNA) using the formalin-fixed and paraffin-embedded histological specimen prepared from the patient. Based on the phylogenetic analysis using

Corresponding Author: Tetsuya Yanagida, PhD, Department of Parasitology, Asahikawa Medical College, Hokkaido 078-8510, Japan. E-mail: yanagida@asahikawa-med.ac.jp

Table 1 Primers used for the amplification of *cox1* gene fragments of *Taenia solium*

Primers	Sequence (5′ to 3′)	Positions	Reference
Tsol cox1/F00	atggttttattagtgcgtc	1–19	PS
Tsol cox1/F100	taagttttagtttattaattcgtgt	101–125	PS
Tsol cox1/F180	gattactaaccatggtataataatg	179–204	PS
Tsol cox1/F300	ctttaagtgcatggttgtt	305–323	PS
Tsol cox1/F380	ggacttttacccacctttatcatct	379–405	PS
Tsol cox1/F500	tatgtacattatatagagtttttatgact	497–525	PS
Taenia cox F3	tatttgatcgtaaatttagttctgcgtt	629–656	9
Tsol cox1/F850	tttaggaagaagtgtgtgagg	846–866	PS
Tsol cox1/F950	gattaaggtttttacttggc	951–970	PS
Tsol cox1/F1080	tctgcttgtgtattagataaagt	1078–1100	PS
Tsol cox1/F1170	ttatgtttgtttggtggtga	1175–1194	PS
Tsol cox1/F1290	ttttgggttgtgtgggtta	1293–1311	PS
Tsol cox1/F1420	gagagtcagttgttaatcgtaaa	1421–1443	PS
Tsol cox1/R1620	ctaaaagaccattccacacgcgaatac	1620–1594	PS
Taenia cox R6	acaggactcataaaaaaattcaccaaaca	1502–1474	9
Tsol cox1/R1370	acagtagacaccatttttaattcaatt	1370–1345	PS
Tsol cox1/R1280	cattttcattatgttatgtcattagggtc	1282–1253	PS
Tsol cox1/R1150	atgacataacataatgaaaatgagca	1150–1125	PS
Tsol cox1/R1050	aaatgtaaacaatactataaacga	1053–1029	PS
Taenia cox R4	attatcatagtaacagaactaaaaaatac	935–907	9
Tsol cox1/830	agcaaacaataacccataa	828–809	PS
Taenia cox R3	gatgaccaaaaaatcaaaacatatgttg	721–694	9
Tsol cox1/R600	aggtaaagtaaccaataacaagatag	600–575	PS
Tsol cox1/R500	atgtacatataaaattaatagaactaaa	505–478	PS
Tsol cox1/R400	taaaggtgggtaaaaagtcc	399–380	PS
Tsol cox1/R280	atccgataatcctcttatca	282–263	PS
Tsol cox1/R190	ttagtaatcaaaaatttataacaatcc	188–162	PS

PS = present study.

mtDNA sequences, *T. solium* can be divided into two genotypes, Asian and African/Latin American.[8] Histological sections were processed by using xylene and ethanol for paraffin removal and were then rehydrated. DNA was extracted with DNeasy tissue kit (Qiagen, Germany). Because of the degradation of DNA, it is difficult to obtain long-fragment DNA from formalin-fixed materials. So we performed polymerase chain reaction (PCR) using primer pairs that can amplify 100 to 200 base pair (bp) fragments. Some of the primers were already reported elsewhere[9] and others were newly designed for the present study (Table 1). PCR products were directly sequenced and the obtained sequences were concatenated and compared with *cox1* sequences available in GenBank database. The following sequences (with GenBank accession numbers) were used for comparison: China 1 (AB066485), China 2 (AB066486), Korea (DQ089663), Thailand (AB066487), Papua (= former Irian Jaya) (AB066488), Bali (AB271234), India (AB066489), Mexico/Peru/Cameroon (AB066490), Ecuador/Bolivia (AB066491), Brazil (AB066492), Tanzania/Mozambique (AB066493). Because no *cox1* sequence of *T. solium* from Nepal, one of the countries where the patient had stayed before (1978–1979, 1984–1986), had been deposited to the database, we collected cysticerci from pigs in three different localities of Nepal (Sunsari, Moranga, and Kathmandu) for *cox1* analysis. One cysticercus was selected from each locality and processed as described in the previous study.[8] As a result, we obtained a partial *cox1* sequence (1570 bp) from the patient (AB494702) and two slightly different sequences of complete *cox1* (1620 bp) from Nepal (Nepal 1: Sunsari, AB491985, Nepal 2: Moranga and Kathmandu, AB491986). The sequence from the patient was identical to one of the two Nepal haplotypes, which was obtained from Sunsari direct. To estimate the genealogical relationship among the haplotypes in the world, we conducted the parsimony network analysis based on the partial *cox1* sequences (1570 bp) with the program TCS version 1.2.[10] As a result, the haplotypes were clearly divided into two geographical groups as previously reported,[8] and the one from the patient was placed into the Asian group (Figure 1). The haplotype from Bali was not included in the haplotype network analysis because only a short sequence (1188 bp) was available in GenBank; however, it was obviously different from all of the others. The result strongly suggests that the patient became infected with *T. solium* not in Indonesia, but in Nepal, an endemic country for cysticercosis.[11] Our result also indicates that he acquired infection before 1986, the last visit to Nepal, and it means that cysticercus had survived in the patient's brain for at least 10 years.

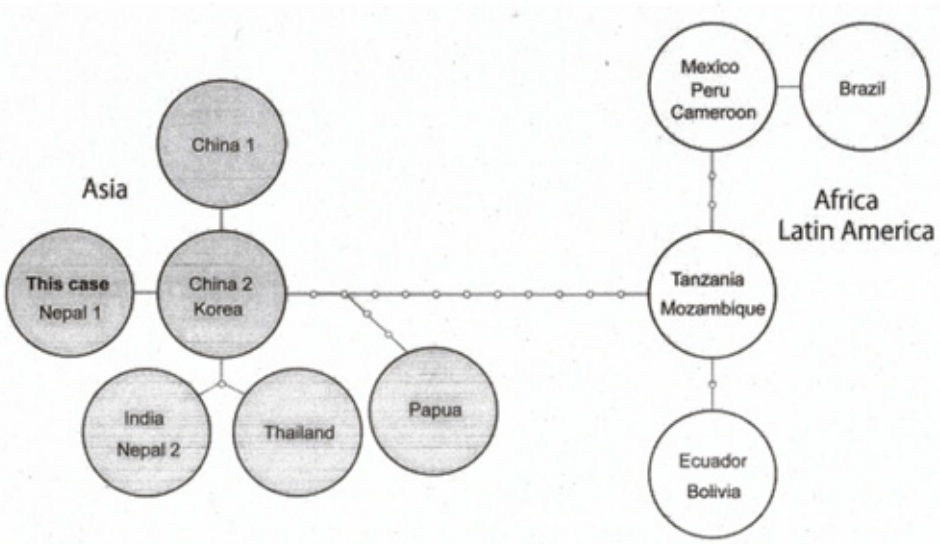

Figure 1 The statistical parsimony networks of *cox1* haplotypes based on 1570 bp sequences. Circles represent haplotypes and each node indicates one mutation step.

Conclusion

As NCC is caused by ingesting the eggs of *T. solium*, even only one teniasis patient can easily disperse this serious disease. Therefore, it is important for disease control and prevention to know where, when, and how the patient acquired NCC, especially in nonendemic countries. As shown in the present study, molecular analysis using *cox1* gene can be a powerful tool for assessing where the patient became infected with *T. solium*, especially in the case of patients who traveled to multiple endemic countries, or who had never visited such contaminated regions. Another mtDNA gene ie, cytochrome *b* has also been demonstrated to serve as a marker for molecular subtyping of *T. solium*.[8] However, we still lack the genetic information from many of the endemic regions. A more globally extensive collection of the specimens, from both domestic pigs and human patient, is needed to make a more detailed genotype map of *T. solium*.

Acknowledgments

This work was supported by the Asia/Africa Science Platform Fund (2006-2011) and International Joint Research Project (17256002, 21256003) from the Japan Society for the Promotion of Science to A. Ito.

Declaration of Interests

The authors state they have no conflicts of interest to declare.

References

1. Schantz PM, Moore AC, Munoz JL, et al. Neurocysticercosis in an Orthodox Jewish community in New York City. N Engl J Med 1992; 327:692–695.
2. Ibrahim N, Azman Ali R, Basri H, et al. Neurocysticercosis in a Malaysian Muslim. Neurol J Southeast Asia 2003; 8:45–48.
3. Schantz PM, Wilkins PP, Tsang VCW. Immigrants, imaging and immunoblots: the emergence of neurocysticercosis as a significant public health problem. In: Scheld WM, Craig WA, Hughes JM, eds. Emerging infections. Vol 2, Washington, DC: ASM Press, 1998: 213–242.
4. Ito A, Nakao M, Wandra T. Human taeniasis and cysticercosis in Asia. Lancet 2003; 362:1918–1920.
5. Yuzawa I, Kawano N, Suzuki S, et al. A case of solitary cerebral cysticercosis. Jpn J Neurosurg 2000; 9:364–369.
6. Ito A, Nakao M, Ito Y, et al. Neurocysticercosis case with a single cyst in the brain showing dramatic drop in specific antibody titers within 1 year after curative surgical resection. Parasitol Int 1999; 48:95–99.
7. Murrell KD. Epidemiology of taeniasis and cysticercosis. In: Murrell KD ed. WHO/FAO/OIE Guidelines for the surveillance, prevention and control of taeniosis/cysticercosis. Paris: OIE, 2005:27–43.
8. Nakao M, Okamoto M, Sako Y, et al. A phylogenetic hypothesis for the distribution of two genotypes of the pig tapeworm *Taenia solium* worldwide. Parasitology 2002; 124:657–662.
9. Yamasaki H, Nakao M, Sako Y, et al. Molecular identification of *Taenia solium* cysticercus genotype in the histopathological specimens. Southeast Asian J Trop Med Public Health 2005; 36(Suppl):S131–S134.
10. Clement M, Posada D, Crandall KA. TCS: a computer program to estimate gene genealogies. Mol Ecol. 2000; 9:1657–1659.
11. Amatya BM, Kimula Y. Cysticercosis in Nepal: a histopathologic study of sixty-two cases. Am J Surg Pathol 1999; 23:1276–1279.

International Journal for Parasitology 40 (2010) 379–385

Contents lists available at ScienceDirect

International Journal for Parasitology

journal homepage: www.elsevier.com/locate/ijpara

Genetic polymorphisms of *Echinococcus* tapeworms in China as determined by mitochondrial and nuclear DNA sequences ☆

Minoru Nakao [a,*], Tiaoying Li [a,b], Xiumin Han [a,c], Xiumin Ma [a,d,e], Ning Xiao [a,b], Jiamin Qiu [b], Hu Wang [c], Tetsuya Yanagida [a], Wulamu Mamuti [a,d], Hao Wen [e], Pedro L. Moro [f], Patrick Giraudoux [g], Philip S. Craig [h], Akira Ito [a]

[a] *Department of Parasitology, Asahikawa Medical College, Asahikawa, Hokkaido 078-8510, Japan*
[b] *Institute of Parasitic Diseases, Sichuan Center for Disease Control and Prevention, Chengdu 610041, China*
[c] *Qinghai Province Institute for Endemic Disease Control, Xining, Qinghai 811602, China*
[d] *Department of Parasitology and Microbiology, Xinjiang Medical University, Urumqi 830054, China*
[e] *Xinjiang Hydatid Clinical Research Institute, The First Affiliated Hospital of Xinjiang Medical University, Urumqi 830054, China*
[f] *Immunization Safety Office, Division of Healthcare Quality Promotion, Centers for Disease Control and Prevention, Atlanta, GA 30333, USA*
[g] *Department of Chrono-environment, UMR UFC/CNRS 6249 aff. INRA, Université de Franche-Comté, Besançon, France*
[h] *Cestode Zoonoses Research Group, Bioscience Research Institute and School of Environment and Life Sciences, University of Salford, Great Manchester M5 4WT, UK*

ARTICLE INFO

Article history:
Received 23 July 2009
Received in revised form 14 September 2009
Accepted 15 September 2009

Keywords:
Echinococcus
Mitochondrial DNA
Genetic diversity
Population genetic structure
China

ABSTRACT

The genetic polymorphisms of *Echinococcus* spp. in the eastern Tibetan Plateau and the Xinjiang Uyghur Autonomous Region were evaluated by DNA sequencing analyses of genes for mitochondrial cytochrome *c* oxidase subunit 1 (*cox1*) and nuclear elongation factor-1 alpha (*ef1a*). We collected 68 isolates of *Echinococcus granulosus* sensu stricto (s.s.) from Xinjiang and 113 isolates of *E. granulosus* s. s., 49 isolates of *Echinococcus multilocularis* and 34 isolates of *Echinococcus shiquicus* from the Tibetan Plateau. The results of molecular identification by mitochondrial and nuclear markers were identical, suggesting the infrequency of introgressive hybridization. A considerable intraspecific variation was detected in mitochondrial *cox1* sequences. The parsimonious network of *cox1* haplotypes showed star-like features in *E. granulosus* s. s. and *E. multilocularis*, but a divergent feature in *E. shiquicus*. The *cox1* neutrality indexes computed by Tajima's *D* and Fu's Fs tests showed high negative values in *E. granulosus* s. s. and *E. multilocularis*, indicating significant deviations from neutrality. In contrast, the low positive values of both tests were obtained in *E. shiquicus*. These results suggest the following hypotheses: (i) recent founder effects arose in *E. granulosus* and *E. multilocularis* after introducing particular individuals into the endemic areas by anthropogenic movement or natural migration of host mammals, and (ii) the ancestor of *E. shiquicus* was segregated into the Tibetan Plateau by colonising alpine mammals and its mitochondrial locus has evolved without bottleneck effects.

1. Introduction

Metacestodes of the dog tapeworm *Echinococcus granulosus* sensu stricto (s.s.) and the fox tapeworm *Echinococcus multilocularis* are highly pathogenic to humans, and cause cystic and alveolar echinococcoses, respectively. Humans become infected through oral ingestion of eggs derived from faeces of canine definitive hosts. Sheep are a main intermediate host for *E. granulosus* s. s., whereas arvicoline rodents serve as intermediate hosts for *E. multilocularis* (Eckert and Deplazes, 2004). Besides the main two species, *Echinococcus equinus*, *Echinococcus ortleppi*, *Echinococcus canadensis*, *Echinococcus felidis*, *Echinococcus shiquicus*, *Echinococcus vogeli* and *Echinococcus oligarthrus* have been regarded as valid by recent phylogenetic studies (Xiao et al., 2005; Nakao et al., 2007; Hüttner et al., 2008). However, the species status of *E. canadensis* is still debatable (Thompson, 2008).

In China, *E. granulosus* s. s. and *E. multilocularis* are widespread in western, northern and central parts of the country (Wang et al., 2008), and hyperendemic foci exist within pastoral areas of the eastern Tibetan Plateau (Schantz et al., 2003; Li et al., 2008) and the Xinjiang Uyghur Autonomous Region (Wang et al., 2001). Both endemic regions are geographically separated by the Kunlum mountains and the Taklamakan Desert. The alpine steppe of the Tibetan Plateau supports human pastoral activity for the raising of yak and sheep. In Xinjiang, nomads and semi-nomads keep

☆ Nucleotide sequence data reported in this paper are available in DDBJ/EMBL/GenBank databases under the Accession Nos. AB491414–AB491471.

* Corresponding author. Tel.: +81 166 68 2422; fax: +81 166 68 2429.
E-mail address: nakao@asahikawa-med.ac.jp (M. Nakao).

0020-7519/$36.00 © 2009 Australian Society for Parasitology Inc. Published by Elsevier Ltd. All rights reserved.
doi:10.1016/j.ijpara.2009.09.006

livestock on low-altitude grassland. This type of sheep husbandry system, including the use of pastoral dogs, is essential to maintain the synanthropic cycle of *E. granulosus* s. s. In contrast, the rodent fauna of grassland and the migration of foxes are key factors in establishing the endemic foci of *E. multilocularis* (Giraudoux et al., 2006). Human infections with *E. multilocularis* are extremely frequent in the Tibetan communities of Sichuan province (Craig, 2006), and the role of dogs in the communities is important to infections (Wang et al., 2006). Thus, the life-cycle of *E. multilocularis* is altered to be synanthropic in hyperendemic areas.

Species of *Echinococcus* prevailing in China have been clarified by molecular taxonomic studies using mtDNA markers (McManus et al., 1994; Zhang et al., 1998; Yang et al., 2005; Bart et al., 2006; Xiao et al., 2004, 2005, 2006; Ma et al., 2008; Li et al., 2008). The molecular identification of *Echinococcus* isolates from various origins showed the following host–parasite relationships in China: (i) domestic mammals (sheep, cattle, goats, yaks and dogs) for *E. granulosus* s. s., (ii) domestic mammals (camels, cattle and dogs) for *E. canadensis* (G6 genotype), (iii) wildlife (voles, hares, pikas, red foxes and Tibetan foxes) and domestic mammals (dogs) for *E. multilocularis* and (iv) wildlife (pikas and Tibetan foxes) for *E. shiquicus*. Human infections have been confirmed for all species except *E. shiquicus*. Interestingly, *E. canadensis* G6 has been found only in Xinjiang (Zhang et al., 1998) and *E. shiquicus* seems to be restricted in the Tibetan Plateau (Xiao et al., 2005). All of the epidemiological information provides a basis to consider the natural history of *Echinococcus* in China. Previous studies demonstrated that intraspecific mtDNA variations occurred in *E. granulosus* s. s. (Yang et al., 2005; Bart et al., 2006; Ma et al., 2008), *E. multilocularis* (Yang et al., 2005) and *E. shiquicus* (Xiao et al., 2005). However, the genetic populations of *Echinococcus* spp. in China have never been characterised in an evolutionary context.

In this study, the genetic diversities of *E. granulosus* s. s., *E. multilocularis* and *E. shiquicus* were explored by using mtDNA and nDNA markers. We sampled the isolates of *E. granulosus* s. s. from Xinjiang and the isolates of all three species from the eastern Tibetan Plateau. The main purpose of this study was to evaluate the population genetic structures of the three species. The resultant data and epidemiological information enabled us to suggest evolutionary hypotheses on how the parasites have spread in China.

2. Materials and methods

2.1. Isolates collected

An *Echinococcus* isolate was defined as a unilocular cyst or a separated alveolar cyst from an intermediate host. During the period from 2002 to 2007, the larval isolates of *Echinococcus* spp. from various hosts were collected in the eastern Tibetan Plateau (Qinghai and Sichuan provinces) and the Xinjiang Uyghur Autonomous Region. Table 1 summarises the number and origin of isolates examined in the two localities. For *E. granulosus* s. s., 113 isolates in the highlands and 68 isolates in the lowlands were treated as two separate populations. On the other hand, 49 isolates of *E. multilocularis* and 34 isolates of *E. shiquicus* were obtained only from the highlands. One isolate in the lowlands was identified as *E. canadensis* G6 genotype. In addition, 57 isolates of *E. granulosus* s. s. in Peru (Moro et al., 2009) served as a foreign control for population genetic analyses. The species identification of those isolates was validated by DNA sequencing described below.

2.2. PCR amplification and sequencing

The genomic DNA of each isolate was prepared from ethanol-preserved larval cysts by using a DNeasy blood and tissue kit (Qiagen), and used as a template for PCR. Partial fragments of a mitochondrial gene for cytochrome *c* oxidase subunit 1 (*cox1*) and a nuclear gene for elongation factor-1 alpha (*ef1a*) were amplified by PCR using specific primers reported previously (Nakao et al., 2000; Moro et al., 2009). The PCR mixture was prepared in a 25 μl final volume containing 1 μl template DNA, 200 μM of each dNTP, 0.2 μM of each primer, 0.5 U of Ex-*Taq* polymerase (Takara) and the manufacturer-supplied reaction buffer. Thermal reactions were performed for 35 cycles of 94 °C for 30 s, 55 °C for 30 s and 72 °C for 60 s. Amplified DNA fragments were purified with QIAquick spin columns (Qiagen), and sequenced directly with a BigDye terminator cycle sequencing kit (Applied Biosystems). The resultant sequence ladders were read by an ABI PRISM 377 genetic analyzer (Applied Biosystems).

2.3. Data analysis

In each species of *Echinococcus*, multiple alignments in NEXUS format were made manually by editing the plain text files of nucleotide sequences. Amino acid sequences were inferred from the nucleotide sequences by echinoderm mitochondrial genetic code (Nakao et al., 2000; Telford et al., 2000) or standard genetic code. Percentage divergence values of nucleotide sequences were determined using the MEGA4 package (Tamura et al., 2007) using Kimura's two parameter model (Kimura, 1980) with a γ-shaped parameter ($a = 0.5$). The identification of haplotypes and the drawing of their networks were executed by TCS 1.2 software (Clement et al., 2000) using statistical parsimony (Templeton et al., 1992). The network estimation was run at a 95% connection limit.

Population diversity indexes (number of haplotypes, haplotype diversity and nucleotide diversity) were calculated using DnaSP 4.5

Table 1
Number of *Echinococcus* isolates used for this study.

Species and localities	Origins of larval isolates						
	Human	Sheep	Yak	Rodent[a]	Hare[b]	Pika[c]	Total
Echinococcus granulosus							
Qinghai & Sichuan	37	57	19	0	0	0	113
Xinjiang	54	14	0	0	0	0	68
Total	91	71	19	0	0	0	181
Echinococcus multilocularis							
Qinghai & Sichuan	20	0	0	26	1	2	49
Echinococcus shiquicus							
Qinghai & Sichuan	0	0	0	0	0	34	34
Echinococcus canadensis (G6)							
Xinjiang	1	0	0	0	0	0	1

[a] *Microtus fuscus*, *Microtus limnophilus* and *Cricetulus kamensis*.
[b] *Lepus oiostolus*.
[c] *Ochotona curzoniae*.

software (Rozas et al., 2003). The population genetics package Arlequin 3.1 (Excoffier et al., 2005) was employed to calculate the neutrality indexes of Tajima's *D* (Tajima, 1989) and Fu's Fs (Fu, 1997). The degree of gene flow between two populations was estimated using a pairwise fixation index (Fst) as determined by the Arlequin package. The three geographic populations of *E. granulosus* s. s. from Xinjiang, the eastern Tibetan Plateau and Peru (out of China) were used to compute the Fst values.

3. Results

3.1. Variations in nucleotide sequences

In our targeted regions of *Echinococcus* DNA, deletion or insertion mutations were not observed, even in different species. The total numbers of nucleotides examined were therefore stable in mitochondrial *cox1* (789 sites) and nuclear *ef1a* (656 sites). The *cox1* sequences could be amplified in all of the isolates of *E. granulosus* s. s. ($n = 181$), *E. multilocularis* ($n = 49$), *E. shiquicus* ($n = 34$) and *E. canadensis* G6 ($n = 1$). However, the PCR positive rate of *ef1a* was relatively lower than that of *cox1*, probably due to the low copy number of the nuclear gene. Each *Echinococcus* sp. retained the species-specific nucleotide sequences of *cox1* and *ef1a* (Table 2).

Considerable intraspecific variations were detected only in the mtDNA sequences of *cox1* (Table 1), indicating its primary use for population genetic analyses. Synonymous substitutions exceeded non-synonymous substitutions in the *cox1* sequences of *E. granulosus* s. s. and *E. shiquicus*. Out of all of the point mutations, 24 sites (49.0%) of *E. granulosus* s. s., one site (25.0%) of *E. multilocularis* and 11 sites (64.7%) of *E. shiquicus* were parsimony informative. Relatively to *E. shiquicus*, singleton substitutions were abundant in *E. granulosus* s. s. and *E. multilocularis*. The pairwise divergence of the *cox1* sequences was computed among individual isolates at an intraspecific level. The maximum values of the divergence were 0.9% in *E. granulosus* s. s., 0.3% in *E. multilocularis* and 1.5% in *E. shiquicus*. The autochthonous species *E. shiquicus* appeared to have the most variable mtDNA.

3.2. Haplotype networks

In *E. granulosus* s. s., 43 mtDNA haplotypes were found in 181 isolates from Xinjiang and the eastern Tibetan Plateau (Qinghai and Sichuan). To discern a genealogical relationship among the haplotypes, we constructed a statistical parsimony network. As shown in Fig. 1, each of the two regions possessed geographically specific haplotypes. The network, however, showed a star-like expansion, and one common haplotype (G01) occupied the centre of the network. The numbers of mutational steps between the common haplotype and the others ranged from one to five, and the frequency of the common haplotype was 53.6% in the population. A similar star-like network was observed in the Peruvian population of *E. granulosus* s. s. (Fig. 2A). Five mtDNA haplotypes were detected in the 57 Peruvian isolates (Moro et al., 2009), but the majority of the isolates (93.0%) belonged to the haplotype G01, which was the most common in the Chinese populations. A single-nucleotide variation was identified between members of the five haplotypes, three of which were geographically specific to Peru.

We detected five mtDNA haplotypes in 49 isolates of *E. multilocularis* from the eastern Tibetan Plateau. These were illustrated as a star-like network with one major haplotype (M01), which comprised 89.8% of the isolates examined (Fig. 2B). All variations found in the five haplotypes were single-nucleotide polymorphisms. As opposed to the convergent networks of *E. granulosus* s. s. and *E. multilocularis*, a divergent network was found in *E. shiquicus* (Fig. 2C). Although 10 mtDNA haplotypes were detected in 34 isolates of *E. shiquicus*, major haplotypes were absent in the population. The maximum number of mutational steps was 13 in the network of *E. shiquicus*.

Table 2
Number of nucleotide substitutions in mitochondrial cytochrome *c* oxidase subunit 1 (*cox1*) and nuclear elongation factor-1 alpha (*ef1a*) genes amplified from *Echinococcus* spp. in China.

Species	*cox1* (789)			*ef1a* (656)		
	n	*S*	NS	*n*	*S*	NS
Echinococcus granulosus	181	30	19	122	0	0
Echinococcus multilocularis	49	1	3	38	0	0
Echinococcus shiquicus	34	16	1	30	3	0

Number of the total nucleotide sites examined is shown in parentheses. Abbreviations are number of isolates examined (*n*), synonymous substitutions (*S*) and non-synonymous substitutions (NS).

3.3. Diversity and neutrality indexes

Diversity indexes for *Echinococcus* populations in each locality were calculated using the data set of *cox1* (Table 3). In the Chinese populations of *Echinococcus* spp., both values of haplotype and nucleotide diversities were the highest in *E. shiquicus* but the lowest in *E. multilocularis*. In the case of *E. granulosus* s. s., the Peruvian population showed the lowest values compared with the Chinese populations. The high levels of haplotype diversity were kept in the Chinese populations of *E. granulosus* s. s., but their nucleotide diversity was relatively low because of the richness of single-nucleotide substitutions.

Neutrality indexes calculated by Tajima's *D* and Fu's Fs tests are also shown in Table 3. The highly negative values were recorded in the Chinese populations of *E. granulosus* s. s. and *E. multilocularis*, indicating a significant deviation from neutrality. The Peruvian population of *E. granulosus* s. s. also showed significant negative values. By contrast, relatively low positive values were obtained in the population of *E. shiquicus*, which kept highly polymorphic mtDNA.

3.4. Fixation index for the populations of E. granulosus s. s

Using the data set of mtDNA, the values of the pairwise fixation index (Fst) were computed to estimate the degree of gene flow among three geographic populations of *E. granulosus* s. s in China and Peru (Table 4). Since one common haplotype existed predominantly in the three localities, the Fst values between the populations were very small, ranging from 0.036 to 0.009. These low values implied that the populations were not genetically differentiated from one another.

4. Discussion

Echinococcoses caused by *E. granulosus* s. s. and *E. multilocularis* lead to considerable social and economic losses in the endemic communities of the eastern Tibetan Plateau (Budke et al., 2005). Furthermore, *E. shiquicus* has been recently discovered in the plateau (Xiao et al., 2005). Information on the population genetic structures of these sympatric species is necessary to better understand the process of intra- and interspecific gene flows, and may provide a foundation for future epidemiological studies on the transmission dynamics of the parasites. In the present study, mtDNA revealed the basic structures of *Echinococcus* populations in the eastern Tibetan Plateau.

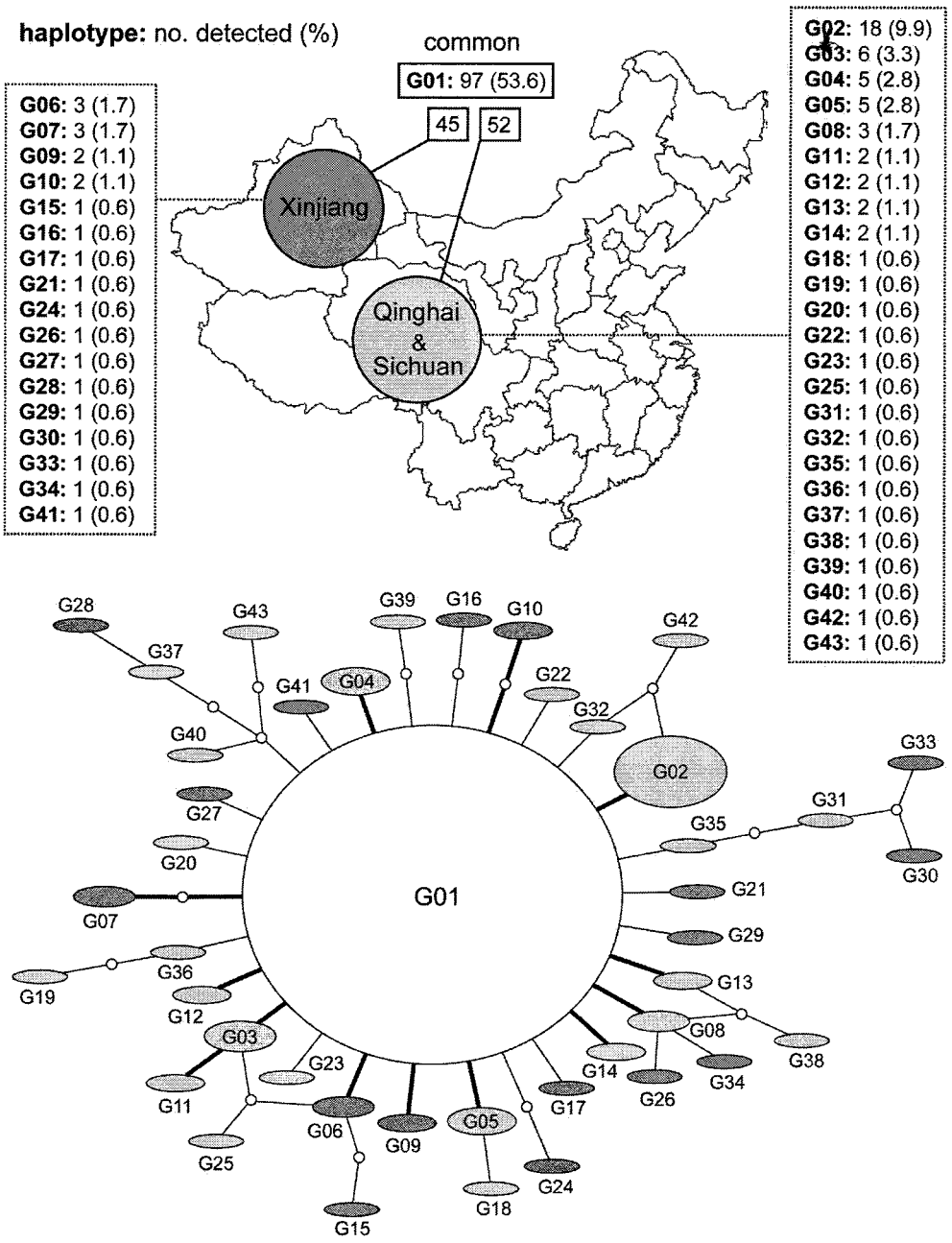

Fig. 1. Frequencies of mitochondrial cytochrome *c* oxidase subunit 1 (*cox1*) haplotypes in Chinese *Echinococcus granulosus* and their network based on statistical parsimony. In the network, the size of ovals indicates the frequency of the haplotypes. Small circles show hypothetical haplotypes. The haplotypes whose frequencies are more than 1% are connected with bold lines. Dark ovals represent the haplotypes found in Xinjiang, whereas the localities of grey ovals are Qinghai and Sichuan. A white oval shows the common haplotype.

We chose the protein-coding gene *cox1* as a marker for *Echinococcus* mtDNA. In other organisms, the mitochondrial control region has been generally used to infer genealogical relationships. However, the corresponding mtDNA regions of *Echinococcus* spp. contain highly repetitive sequences, which are unsuitable for phylogenetic studies (Nakao et al., 2007). The *cox1* gene of *Echinococcus* spp. has already been shown to be a promising candidate for the classification of intra- and interspecific variants even in the short sequence (366 nucleotide sites) (Bowles et al., 1992). In this study, we determined the relatively long sequence of *cox1* (789 nucleotide sites), and detected a sufficient number of haplotypes to analyse the population genetic structures of each species. The haplotypes are only loosely correlated with the intraspecific genotypes of *E. granulosus s. s.* (G1, G2 and G3) and *E. multilocularis* (M1 and M2) defined by Bowles et al. (1992). The negative selection of the *cox1* for the purging of deleterious mutations has been demonstrated by the codon-based *Z*-test (Tamura et al., 2007) using the corresponding sequences of *E. granulosus* s. s., *E. multilocularis*, *E. equinus*, *E. ortleppi*, *E. canadensis*, *E. felidis*, *E. vogeli* and *E. oligarthrus* (M. Nakao, unpublished data). The fragments of the nuclear gene *ef1a* were also sequenced in this study, but their species-specific sequences were not polymorphic at an intraspecific level. The results of species identification by the mitochondrial and nuclear markers were identical, suggesting the infrequency of introgressive hybridization among the sympatric species.

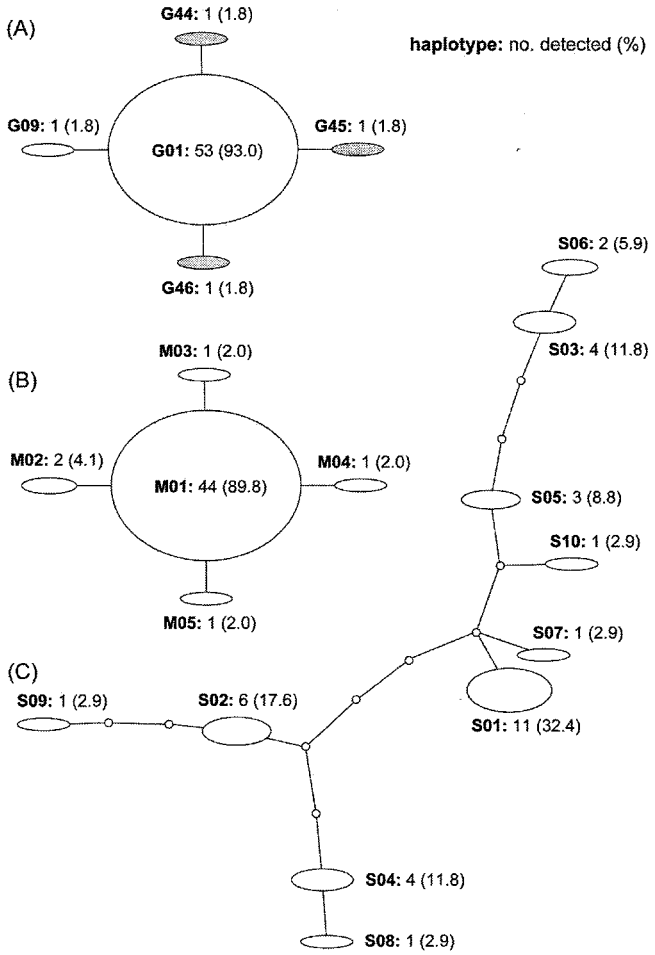

Fig. 2. The statistical parsimony networks of mitochondrial cytochrome *c* oxidase subunit 1 (*cox1*) haplotypes in *Echinococcus* spp. The size of ovals indicates the frequency of the haplotypes. Small circles show hypothetical haplotypes. (A) The Peruvian population of *Echinococcous granulosus* sensu stricto. Grey ovals represent the haplotypes specific to Peru. (B) The Tibetan population of *Echinococcus multilocularis*. (C) The Tibetan population of *Echinococcus shiquicus*.

The *cox1* haplotypes of *E. granulosus* s. s. found in this study did not show an apparent phylogeographic structuring in China. The parsimony network analysis revealed that the haplotypes exhibit a star-like expansion from a main founder haplotype, suggesting that the populations of eastern Tibet and Xinjiang are not fully differentiated from each other. It is noteworthy that the same founder was predominant in the Peruvian population. It seems unlikely that mutations of the founder haplotype are advantageous because the amino acid sequence deduced from the founder is the same as those from other minor haplotypes. The common genetic structure between geographically unrelated populations enables us to speculate that one particular lineage of *E. granulosus* s. s. is widespread globally. The genetic non-differentiation between the local populations is also demonstrated by extreme low values of the fixation index Fst. Furthermore, the significant negative values of the neutrality indexes Tajima's *D* and Fu's Fs suggest that bottleneck events might occur in the recent past. It is most likely that demographic expansions of the parasite occurred after introducing particular individuals into the endemic areas by anthropogenic movements of host mammals (sheep and dogs).

It is assumed that *E. granulosus* s. s. was introduced into South America from Europe through livestock importation after the colonial period. The higher values of haplotype and nucleotide diversities in the Chinese populations of *E. granulosus* s. s. suggest that China historically preceded Peru in the time of initial founder introduction. One could speculate that bottleneck events might also occur in the ancestral population of *E. granulosus* s. s. during the colonisation of domestic sheep as an intermediate host. Archaeological and genetic evidence suggest that sheep were domesticated in the Ancient Near East (Pedrosa et al., 2005), but the genealogical survey of Chinese domestic sheep showed the possibility that additional domestication events occurred independently in other regions (Chen et al., 2006). The lack of archaeoparasitological data does not permit us to infer how and when the parasite invaded China. However, the Ancient Near East is one possible candidate for the cradle of *E. granulosus* s. s. The population genetic structures of *E. granulosus* s. s. should be compared in various endemic areas to clarify its ancestral origin and the process of its worldwide dispersal.

Our previous study has already indicated the rarity of mtDNA polymorphism in the Tibetan population of *E. multilocularis* (Xiao et al., 2005). The present study furthermore revealed that a particular *cox1* sequence was positioned as a basal haplotype, suggesting that a founder effect arose in the population. Our recent phylogeographic study on *E. multilocularis* showed that the worldwide iso-

Table 4
Pairwise fixation index (Fst values) between *Echinococcus granulosus* sub-populations calculated from the nucleotide data set of mitochondrial cytochrome *c* oxidase subunit 1 (*cox1*) gene.

	1	2
1. Qinghai & Sichuan		
2. Xinjiang	0.031[a]	
3. Out of China (Peru)	0.036[a]	0.009

[a] Significant *P* values ($P < 0.01$).

Table 3
Diversity and neutrality indexes for *Echinococcus* populations calculated from the nucleotide data set of mitochondrial cytochrome *c* oxidase subunit 1 (*cox1*) gene.

Species and localities	Diversity				Neutrality	
	n	Hn	Hd ± S.D.	π ± S.D.	*D*	Fs
Echinococcus granulosus						
Qinghai & Sichuan	113	26	0.760 ± 0.038	0.0017 ± 0.0002	−2.323[a]	−26.023[a]
Xinjiang	68	18	0.562 ± 0.073	0.0015 ± 0.0003	−2.456[a]	−15.762[a]
Total (China)	181	43	0.702 ± 0.038	0.0017 ± 0.0002	−2.536[a]	−61.569[a]
Out of China (Peru)	57	5	0.137 ± 0.062	0.0002 ± 0.0001	−1.849[a]	−5.889[a]
Echinococcus multilocularis						
Qinghai & Sichuan	49	5	0.195 ± 0.075	0.0003 ± 0.0001	−1.765[a]	−4.788[a]
Echinococcus shiquicus						
Qinghai & Sichuan	34	10	0.847 ± 0.040	0.0055 ± 0.0004	0.164	0.258

Abbreviations are number of isolates examined (*n*), number of haplotypes (Hn), haplotype diversity (Hd), nucleotide diversity (π), Tajima's *D* (*D*) and Fu's Fs (Fs).
[a] Significant *P* values ($P < 0.01$).

lates were classified into European, Asian and North American clades except the Inner Mongolia isolates from the corsac fox *Vulpes corsac* (Nakao et al., 2009). The geographic clustering indicates a possibility that genetic changes occurred in *E. multilocularis* after the fragmentation of the population during the Pleistocene ice ages. The red fox *Vulpes vulpes*, which has a flexible ability to adapt to various environments, extended its distributional range in the Holarctic region, and might play an essential role in introducing *E. multilocularis* into new areas. It seems likely that an epidemic of the parasite in the eastern Tibetan Plateau was initiated by natural migration of red foxes in the recent past.

The Tibetan indigenous species *E. shiquicus* showed a quite different pattern of population genetic structure when compared with *E. granulosus* s. s. and *E. multilocularis*. Statistical neutrality tests and haplotype network analyses suggest a possibility that the mitochondrial locus of *E. shiquicus* has evolved without bottleneck effects. Our previous report clarified that *E. shiquicus* utilises the Tibetan fox *Vulpes ferrilata* as a definitive host and the plateau pika *Ochotona curzoniae* as an intermediate host (Xiao et al., 2005). Both the autochthonous mammals are adapted to the high altitude steppe but do not survive in lowlands. We can therefore consider that *E. shiquicus* has been segregated in the plateau since the parasite's ancestor colonised the alpine mammals. The lasting geographic segregation seems to be a cause for extraordinary richness of polymorphism in Tibetan *E. shiquicus*.

Diploid organisms having a mixed sexual and asexual reproduction system show different patterns from theoretical population genetic models (Prugnolle et al., 2005). The adult tapeworms of *Echinococcus* are hermaphroditic, and self-fertilisation mainly occurs in the small intestine of canine definitive hosts (Haag et al., 1999). The larvae furthermore proliferate asexually in the viscera of intermediate hosts, and the clonal offspring develop into adults in a definitive host. The biphasic reproduction of *Echinococcus* spp. may strongly affect their population genetic structures and promote a very low genetic variability of nuclear loci. In this study we used a haploid maternally inherited mtDNA marker to examine the population genetic structure of *Echinococcus* because of the lack of appropriate nuclear markers. A panel of single-locus nuclear markers is required for further population genetic studies to elucidate the evolutionary backgrounds of *Echinococcus* worldwide.

Acknowledgments

This study was supported by the US National Institutes of Health Funds (the NIH/NSF Ecology and Infectious Diseases Program, # TWO 1565, Principal Investigator: P.S. Craig), the Japan Society for the Promotion of Science (JSPS) (17256002, 21256003) and JSPS-Asia/Africa Science Platform Fund (2006–2011) to A. Ito. The content is solely the responsibility of the authors and does not necessarily represent the official views of the Fogarty International Center or the National Institutes of Health. The authors thank many colleagues and field workers who collected the isolates of *E. granulosus* s. s., *E. multilocularis* and *E. shiquicus* in China.

References

Bart, J.M., Abdukader, M., Zhang, Y.L., Lin, R.Y., Wang, Y.H., Nakao, M., Ito, A., Craig, P.S., Piarroux, R., Vuitton, D.A., Wen, H., 2006. Genotyping of human cystic echinococcosis in Xinjiang, PR China. Parasitology 133, 571–579.

Bowles, J., Blair, D., McManus, D.P., 1992. Genetic variants within the genus *Echinococcus* identified by mitochondrial DNA sequencing. Mol. Biochem. Parasitol. 54, 165–173.

Budke, C.M., Jiamin, Q., Qian, W., Torgerson, P.R., 2005. Economic effects of echinococcosis in a disease-endemic region of the Tibetan Plateau. Am. J. Trop. Med. Hyg. 73, 2–10.

Chen, S.Y., Duan, Z.Y., Sha, T., Xiangyu, J., Wu, S.F., Zhang, Y.P., 2006. Origin, genetic diversity, and population structure of Chinese domestic sheep. Gene 376, 216–223.

Clement, M., Posada, D., Crandall, K., 2000. TCS: a computer program to estimate gene genealogies. Mol. Ecol. 9, 1657–1660.

Craig, P.S., 2006. Epidemiology of human alveolar echinococcosis in China. Parasitol. Int. 55, S221–S225.

Eckert, J., Deplazes, P., 2004. Biological, epidemiological, and clinical aspects of echinococcosis, a zoonosis of increasing concern. Clin. Microbiol. Rev. 17, 107–135.

Excoffier, L., Laval, G., Schneider, S., 2005. Arlequin ver. 3.0: an integrated software package for population genetics data analysis. Evol. Bioinform. Online 1, 47–50.

Fu, Y.X., 1997. Statistical tests of neutrality of mutations against population growth, hitchhiking and background selection. Genetics 147, 915–925.

Giraudoux, P., Pleydell, D., Raoul, F., Quéré, J.P., Wang, Q., Yang, Y., Vuitton, D.A., Qiu, J., Yang, W., Craig, P.S., 2006. Transmission ecology of *Echinococcus multilocularis*: what are the ranges of parasite stability among various host communities in China? Parasitol. Int. 55, S237–S246.

Haag, K.L., Araújo, A.M., Gottstein, B., Siles-Lucas, M., Thompson, R.C., Zaha, A., 1999. Breeding systems in *Echinococcus granulosus* (Cestoda; Taeniidae): selfing or outcrossing? Parasitology 118, 63–71.

Hüttner, M., Nakao, M., Wassermann, T., Siefert, L., Boomker, J.D., Dinkel, A., Sako, Y., Mackenstedt, U., Romig, T., Ito, A., 2008. Genetic characterization and phylogenetic position of *Echinococcus felidis* (Cestoda: Taeniidae) from the African lion. Int. J. Parasitol. 38, 861–868.

Kimura, M., 1980. A simple method for estimating evolutionary rates of base substitutions through comparative studies of nucleotide sequences. J. Mol. Evol. 16, 111–120.

Li, T., Ito, A., Nakaya, K., Qiu, J., Nakao, M., Zhen, R., Xiao, N., Chen, X., Giraudoux, P., Craig, P.S., 2008. Species identification of human echinococcosis using histopathology and genotyping in northwestern China. Trans. R. Soc. Trop. Med. Hyg. 102, 585–590.

Ma, S.M., Maillard, S., Zhao, H.L., Huang, X., Wang, H., Geng, P.L., Bart, J.M., Piarroux, R., 2008. Assessment of *Echinococcus granulosus* polymorphism in Qinghai province, People's Republic of China. Parasitol. Res. 102, 1201–1206.

McManus, D.P., Ding, Z., Bowles, J., 1994. A molecular genetic survey indicates the presence of a single, homogeneous strain of *Echinococcus granulosus* in northwestern China. Acta Trop. 56, 7–14.

Moro, P., Nakao, M., Ito, A., Schantz, P.M., Cavero, C., Cabrera, L., 2009. Molecular identification of *Echinococcus* isolates from Peru. Parasitol. Int. 58, 184–186.

Nakao, M., McManus, D.P., Schantz, P.M., Craig, P.S., Ito, A., 2007. A molecular phylogeny of the genus *Echinococcus* inferred from complete mitochondrial genomes. Parasitology 134, 713–722.

Nakao, M., Sako, Y., Yokoyama, N., Fukunaga, M., Ito, A., 2000. Mitochondrial genetic code in cestodes. Mol. Biochem. Parasitol. 111, 415–424.

Nakao, M., Xiao, N., Okamoto, M., Yanagida, T., Sako, Y., Ito, A., 2009. Geographic pattern of genetic variation in the fox tapeworm *Echinococcus multilocularis*. Parasitol. Int. 58, 384–389.

Pedrosa, S., Uzun, M., Arranz, J.J., Gutiérrez-Gil, B., San Primitivo, F., Bayón, Y., 2005. Evidence of three maternal lineages in Near Eastern sheep supporting multiple domestication events. Proc. Biol. Sci. 272, 2211–2217.

Prugnolle, F., Liu, H., Meeûs, T., Balloux, F., 2005. Population genetics of complex life-cycle parasites: an illustration with trematodes. Int. J. Parasitol. 35, 255–263.

Rozas, J., Sánchez-DelBarrio, J.C., Messeguer, X., Rozas, R., 2003. DnaSP, DNA polymorphism analyses by the coalescent and other methods. Bioinformatics 19, 2496–2497.

Schantz, P.M., Wang, H., Qiu, J., Liu, F.J., Saito, E., Emshoff, A., Ito, A., Roberts, J.M., Delker, C., 2003. Echinococcosis on the Tibetan Plateau: prevalence and risk factors for cystic and alveolar echinococcosis in Tibetan populations in Qinghai Province, China. Parasitology 127, S109–S120.

Tajima, F., 1989. Statistical method for testing the neutral mutation hypothesis by DNA polymorphism. Genetics 123, 585–595.

Tamura, K., Dudley, J., Nei, M., Kumar, S., 2007. MEGA4: Molecular Evolutionary Genetics Analysis (MEGA) software version 4.0.. Mol. Biol. Evol. 24, 1596–1599.

Telford, M.J., Herniou, E.A., Russell, R.B., Littlewood, D.T., 2000. Changes in mitochondrial genetic codes as phylogenetic characters: two examples from the flatworms. Proc. Natl. Acad. Sci. USA 97, 11359–11364.

Templeton, A.R., Crandall, K.A., Sing, C.F., 1992. A cladistic analysis of phenotypic associations with haplotypes inferred from restriction endonuclease mapping and DNA sequence data. III. Cladogram estimation. Genetics 132, 619–633.

Thompson, R.C.A., 2008. The taxonomy, phylogeny and transmission of *Echinococcus*. Exp. Parasitol. 119, 439–446.

Wang, Q., Qiu, J., Yang, W., Schantz, P.M., Raoul, F., Craig, P.S., Giraudoux, P., Vuitton, D.A., 2006. Socioeconomic and behavior risk factors of human alveolar echinococcosis in Tibetan communities in Sichuan, People's Republic of China. Am. J. Trop. Med. Hyg. 74, 856–862.

Wang, Y.H., Rogan, M.T., Vuitton, D.A., Wen, H., Bartholomot, B., Macpherson, C.N., Zou, P.F., Ding, Z.X., Zhou, H.X., Zhang, X.F., Luo, J., Xiong, H.B., Fu, Y., McVie, A., Giraudoux, P., Yang, W.G., Craig, P.S., 2001. Cystic echinococcosis in semi-nomadic pastoral communities in north-west China. Trans. R. Soc. Trop. Med. Hyg. 95, 153–158.

Wang, Z., Wang, X., Liu, X., 2008. Echinococcosis in China, a review of the epidemiology of *Echinococcus* spp.. Ecohealth 5, 115–126.

Yang, Y.R., Rosenzvit, M.C., Zhang, L.H., Zhang, J.Z., McManus, D.P., 2005. Molecular study of *Echinococcus* in west-central China. Parasitology 131, 547–555.

Xiao, N., Li, T.Y., Qiu, J.M., Nakao, M., Chen, X.W., Nakaya, K., Yamasaki, H., Schantz, P.M., Craig, P.S., Ito, A., 2004. The Tibetan hare *Lepus oiostolus*: a novel intermediate host for *Echinococcus multilocularis*. Parasitol. Res. 92, 352–353.

Xiao, N., Nakao, M., Qiu, J., Budke, C.M., Giraudoux, P., Craig, P.S., Ito, A., 2006. Dual infection of animal hosts with different *Echinococcus* species in the eastern Qinghai–Tibet plateau region of China. Am. J. Trop. Med. Hyg. 75, 292–294.

Xiao, N., Qiu, J., Nakao, M., Li, T., Yang, W., Chen, X., Schantz, P.M., Craig, P.S., Ito, A., 2005. *Echinococcus shiquicus* n. sp., a taeniid cestode from Tibetan fox and plateau pika in China. Int. J. Parasitol. 35, 693–701.

Zhang, L.H., Chai, J.J., Jiao, W., Osman, Y., McManus, D.P., 1998. Mitochondrial genomic markers confirm the presence of the camel strain (G6 genotype) of *Echinococcus granulosus* in north-western China. Parasitology 116, 29–33.

Parasitology International 59 (2010) 70–74

Contents lists available at ScienceDirect

Parasitology International

journal homepage: www.elsevier.com/locate/parint

Evidence of hybridization between *Taenia saginata* and *Taenia asiatica*

Munehiro Okamoto [a,*], Minoru Nakao [b], David Blair [c], Malinee T. Anantaphruti [d], Jitra Waikagul [d], Akira Ito [b]

[a] Department of Parasitology, School of Veterinary Medicine, Faculty of Agriculture, Tottori University, Japan
[b] Department of Parasitology, Asahikawa Medical College, Japan
[c] School of Marine and Tropical Biology, James Cook University, Townsville, Queensland, Australia
[d] Department of Helminthology, Faculty of Tropical Medicine, Mahidol University, Thailand

ARTICLE INFO

Article history:
Received 22 June 2009
Received in revised form 17 October 2009
Accepted 19 October 2009
Available online 27 October 2009

Keywords:
Taenia asiatica
Taenia saginata
Outcrossing
Hybridization

ABSTRACT

There has long been a debate as to the specific status of the cestode *Taenia asiatica*, with some people regarding it as a distinct species and some preferring to recognize it as a strain of *Taenia saginata*. The balance of current opinion seems to be that *T. asiatica* is a distinct species. In this study we performed an allelic analysis to explore the possibility of gene exchange between these closely related taxa. In total, 38 taeniid tapeworms were collected from humans living in many localities including Kanchanaburi Province, Thailand where the two species are sympatric. A mitochondrial DNA (mtDNA)-based multiplex PCR tentatively identified those parasites as *T. asiatica* ($n=20$) and *T. saginata* ($n=18$). Phylogenetic analyses of a mitochondrial cytochrome c oxidase subunit 1 (*cox1*) gene and two nuclear loci, for elongation factor-1 alpha (*ef1*) and ezrin-radixin-moesin (ERM)-like protein (*elp*), assigned all except two individual parasites to the species indicated by multiplex PCR. The two exceptional individuals, from Kanchanaburi Province, showed a discrepancy between the mtDNA and nuclear DNA phylogenies. In spite of their possession of sequences typical of the *T. saginata cox1* gene, both were homozygous at the *elp* locus for one of the alleles found in *T. asiatica*. At the *ef1* locus, one individual was homozygous for the allele found at high frequency in *T. asiatica* while the other was homozygous for the major allele in *T. saginata*. These findings are evidence of occasional hybridization between the two species, although the possibility of retention of ancestral polymorphism cannot be excluded.

1. Introduction

The family Taeniidae consists of only two genera, *Taenia* and *Echinococcus*. These distinctive tapeworms mature in carnivorous mammals worldwide and several species occur in humans, sometimes causing severe disease. There have been many studies on the morphology and genetics of members of these genera, yet there is still debate about the number of species in each genus and the best means of distinguishing them. In *Echinococcus*, molecular studies based largely on mitochondrial but partially on nuclear genes support the recognition of several distinct species [1–6]. Similar studies on members of *Taenia* [7] have also used mitochondrial sequences to aid recognition of species. Under the biological species concept, distinct species are not expected to exchange genes, or to do so very rarely [8]. Evidence for hybridization is often found by study of nuclear loci and comparison of these with mitochondrial data. Introgression (the infiltration of genes from the gene pool of one species into that of another) can be inferred from the finding of mitochondrial sequences typical of one species in an organism with the nuclear alleles of another. Alternatively, hybridization can be demonstrated by the presence of nuclear alleles in a single individual that are typical of more than one species. Evidence of gene exchange between species of *Echinococcus* has been noted [9,10], thus potentially rekindling the debate about species boundaries in this genus. No such study has explored the question of gene exchange between species in the genus *Taenia*. In this paper, we provide the first evidence that this can occur.

Three human *Taenia* species are found in the Asia-Pacific region: *Taenia solium* (pork tapeworm), *Taenia saginata* (beef tapeworm) and *Taenia asiatica* [11]. The larval stages of these *Taenia* species have been identified as *Cysticercus cellulosae*, *Cysticercus bovis* and *Cysticercus viscerotropica*, respectively [12]. Humans may harbor adult worms after consuming raw or under-cooked pork, beef or viscera of swine, respectively, contaminated with metacestodes of these species. It is important to discriminate among these three taxa, since ingestion of *T. solium* eggs by humans may result in neurocysticercosis, a serious public health problem in many areas worldwide [11,13]. *T. saginata* and *T. asiatica* are morphologically very similar, as are their mitochondrial DNA sequences [14]. On the other hand, the two taxa clearly differ in biological features including host specificity and organotropism [12]. Mitochondrial DNA (mtDNA) sequence data are

* Corresponding author. Department of Parasitology, School of Veterinary Medicine, Faculty of Agriculture, Tottori University, 4-101 Koyama-cho Minami, Tottori-shi, Tottori 680-8553, Japan. Tel./fax: +81 857 31 5639.
E-mail address: mokamoto@muses.tottori-u.ac.jp (M. Okamoto).

1383-5769/$ – see front matter © 2009 Elsevier Ireland Ltd. All rights reserved.
doi:10.1016/j.parint.2009.10.007

frequently used to distinguish between these species, but nuclear gene markers have not been used previously. In this study, genotyping at two nuclear loci was carried out to explore the possibility of gene exchange between *T. saginata* and *T. asiatica* in a locality where they are sympatric.

2. Materials and methods

2.1. Parasite samples

Adult tapeworms, which were morphologically similar to *T. saginata*, were collected from humans. In the end, 38 samples from 11 nations (Brazil, Ecuador, Ethiopia, Japan, South Korea, Philippines, China, Taiwan, Cambodia, Thailand and Indonesia) were used in this study. Of these, 15 samples were collected from small villages in Kanchanaburi Province, Thailand. These areas are unique, since the three species of human *Taenia* were identified as sympatrically endemic during surveys in 2002–2005 [16].

2.2. DNA preparation

Genomic DNA was individually extracted from mature or immature proglottids using a QIAamp DNA Mini Kit or a DNeasy tissue kit (QIAGEN, Germany) in accordance with the manufacturer's instructions, and then used as a template for polymerase chain reaction (PCR).

2.3. Multiplex PCR for Taenia species identification

Multiplex PCR based on the mitochondrial cytochrome *c* oxidase subunit 1 (*cox1*) gene is an easy method for identification of human taeniid cestodes [16–18]. Samples were first screened by this method for the tentative identification of species. According to the results, the code "Tasi" (*T. asiatica*) or "Tsag" (*T. saginata*) was added to the sample ID. It is important to note that this code refers to the identification from the mitochondrial genome.

2.4. DNA sequencing and data analysis

Multiplex PCR yields products of taxon-specific lengths that can be visualized in a gel. For finer genetic discrimination, the complete sequence of the *cox1* gene was obtained for each individual. Partial sequences of two nuclear genes, elongation factor-1-alpha (*ef1*) and ezrin/radixin/moesin-like protein (*elp*), were also obtained. Primer pairs listed in Table 1 were used for the PCR amplification and sequencing of those genes.

PCR was carried out in 15 μl reaction mixtures containing 1 μl template, 200 μM of each dNTP, 0.2 μM of each primer, 0.3 U of *Ex Taq* polymerase (TaKaRa, Japan) and the manufacturer-supplied reaction buffer. Thermal cycling was performed for 35 cycles of denaturation (94°C for 30 s), annealing (66°C: *cox1*, 60°C: *ef1*, 65°C: *elp*, for 30 s), and extension (72°C for 80–90 s). The PCR products were purified using MinElute PCR Purification Kits (QIAGEN). Direct sequencing was performed with a Dye Terminator Cycle Sequencing Kit and an ABI PRISM 3100 Generic Analyzer (Applied Biosystems, USA). At least two independent PCR products were used for sequencing. Samples that could not be directly sequenced were subjected to cloning using a TOPO TA Cloning Kit (invitrogen, USA), and more than ten clones were sequenced per sample.

DNA sequences were aligned using the CLUSTAL W computer program [19]. Phylogenetic trees were constructed by the neighbor-joining (NJ) method [20] using the MEGA4.0 computer program [21]. Evolutionary distances were computed using the Maximum Composite Likelihood Method [22]. Each of the phylogenetic trees was evaluated using a bootstrap test based on 1000 resamplings [23]. Sequences of *Taenia solium* from Kanchanaburi Province were used as outgroups (AB066487 for *cox1*, AB505027 for *ef1* and AB505025 for *elp*) to indicate the location of the root of the ingroup. For presentation purposes, the long branch leading to the outgroup is not shown for any tree.

Table 1
Primer pairs used for PCR.

Target genes	Primer names	Sequences (5′ – 3′)
cox1 (mt DNA)	Tsag_cox1/F	GAGGAAATTGTGAAGTTACTGCTA
	Tsag_cox1/R	ATGATGCAAAAGGCAAATAAACCT
ef1 (nuclear DNA)	Tae_ef1/F4	TGTGGTGGAATCGATAAAAGG
	Tae_ef1/R4	TCGATCTCATGTCACGAACG
elp (nuclear DNA)	Tsag_elp/F	CGTATGGAGAATGAACAGAAACTG
	Tsag_elp/R	CTGTGCATCGTGTTTCTCACGCAT

cox1: cytochrome *c* oxidase subunit 1.
ef1: elongation factor-1-alpha.
elp: ezrin/radixin/moesin-like protein.

3. Results

The mtDNA-based multiplex PCR tentatively assigned our samples to *T. asiatica* ($n = 20$) or *T. saginata* ($n = 18$). The phylogenetic tree inferred from complete mitochondrial *cox1* gene sequences (1620 bp) clearly identified two main and rather uniform clusters, agreeing with the results of the multiplex PCR (Fig. 1a). Although pairwise differences between "Tasi" and "Tsag" occurred at approximately 70 sites in the *cox1* gene, variations within each cluster were very small. In the case of the nuclear genes, introns were included in the fragments sequenced. The *ef1* gene fragment was 1095–1096 bp in length (60–61 bp introns and 1035 bp exons) and the *elp* gene sequences consisted of 1162–1164 bp (902–904 bp intron and 260 bp exons).

At the *ef1* locus, we found three alleles (*ef1A*, *ef1B* and *ef1C* — Fig. 1b). Two of these alleles were identified in "Tasi" (*ef1A*, *ef1B*), differing from each other at only a single site in an exon. Most of the samples were homozygous at this locus, but TasiA190 and TasiA210 were heterozygous. We found no variation in "Tsag" sequences (*ef1C*), with the exception of sample TsagA199, which was homozygous for an allele (*ef1A*) found at high frequency in "Tasi". The *ef1C* sequence differed from the other two alleles at 6–8 sites. Four alleles were found at the *elp* locus (*elpA*, *elpB*, *elpC* and *elpD* — Fig. 1c). The first two of these occurred in "Tasi" (*elpA*, *elpB*) and three in "Tsag" (*elpA*, *elpC*, *elpD*). Allele *elpA* thus occurred in both "Tasi" and "Tsag". Alleles *elpA* and *elpB* differed at 1–2 sites, as did *elpC* and *elpD*. Differences between these two pairs of alleles occurred at 6–7 sites. Samples TasiT010 and TsagA201 were heterozygous at this locus. Samples TsagA199 and TsagT017 were homozygous for *elpA*, the major allele found in "Tasi" (Fig. 1c).

For comparison, *ef1* and *elp* genes of *T. solium* both differ from their orthologs in *T. asiatica* and *T. saginata* at 47–50 sites (data not shown). This highlights the close relationship between the last two taxa. The mtDNA classification of all samples and their genotypes at the two nuclear loci are summarized in Table 2.

Nucleotide sequences from *Taenia* species in this study have been deposited into DDBJ/EMBL/GenBank databases under accession numbers AB465211–AB465248 for the *cox1* gene, AB462851–AB462890 for the *ef1* gene and AB462811–AB462850 for the *elp* gene.

4. Discussion

We examined the nucleotide sequences of one mitochondrial gene (*cox1*) and of alleles at two nuclear loci (*ef1* and *elp*) from taeniid worms, which had been tentatively identified as *T. asiatica* or *T. saginata* using multiplex PCR. Phylogenetic analyses of a mitochondrial gene and

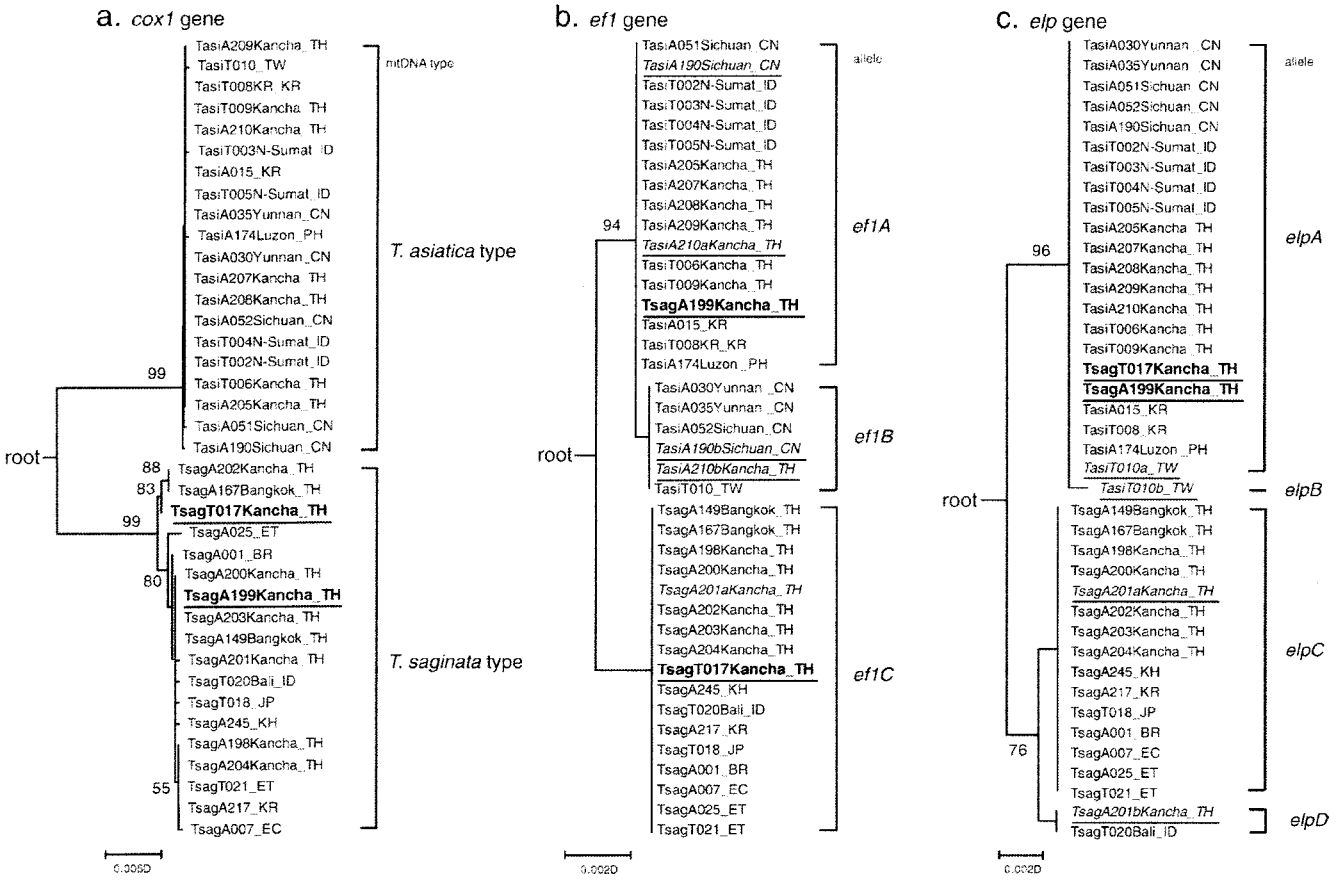

Fig. 1. Neighbor-joining phylogenetic trees of the mitochondrial cytochrome c oxidase subunit I gene (1a: *cox1*), nuclear genes for elongation factor-1-alpha (1b: *ef1*), and ezrin-radixin/moesin-like protein (1c: *elp*). Samples in italic type represent heterozygotes that displayed two alleles. Samples in bold type showed contradictions in the phylogeny between the mitochondrial gene and one or both of the nuclear genes. Numbers on the nodes represent bootstrap values. Each scale bar represents the evolutionary distances. The number after the species code (e.g. A030 or T002) identifies the sample ID used in the Asahikawa Medical College or Tottori University. Each sample code is followed by a locality name (absent from some) and country name (abbreviated). Abbreviations of country names are as follow: BR, Brazil; CN, China; EC, Ecuador; ET, Ethiopia; ID, Indonesia; JP, Japan; KH, Cambodia; KR, South Korea; PH, Philippines; TH, Thailand; TW, Taiwan. See the text for abbreviations of mitochondrial types and alleles.

two nuclear genes yielded trees consisting of two rather uniform clusters in each case. We regard the two clusters as corresponding to *T. asiatica* and *T. saginata*. The considerable difference between the mitochondrial lineages indicates a long period of separation between *T. asiatica* and *T. saginata*. Nuclear alleles *ef1A*, *ef1B*, *elpA* and *elpB* all occurred in *T. asiatica* even where it was not sympatric with *T. saginata*. We therefore regard these alleles as originating with that species. Similarly, *ef1C*, *elpC* and *elpD* were found in individuals of *T. saginata* from parts of the world where *T. asiatica* is not known. Regardless of the species identified, most individuals are homozygous at the nuclear loci. This is to be expected because taeniids are primarily self-fertilizers [24,25], a mating system that will lead to increase homozygosity. Some outcrossing has been demonstrated in *Echinococcus* species and should partially counter the trend towards increasing homozygosity [9]. The presence of a few heterozygous individuals in our study suggests that outcrossing also occurs in *Taenia* species. As shown in Table 2, these individuals are the samples TasiA210 and TasiA190 (heterozygous at *ef1*), TasiT010 (heterozygous at *elp*) and TsagA201 (heterozygous at *elp*).

Two individuals with mitochondrial genomes of the *T. saginata* type possessed at least some alleles typical of *T. asiatica*, suggesting a hybrid origin. TsagA199 has alleles typical of *T. asiatica* at both nuclear loci and TsagT017 displayed such allele at one locus (Table 2). Given the genotypes we observed in our other samples, neither of these individuals could have been an F1 hybrid because they were homozygous at both nuclear loci. Assuming descent from a hybrid ancestor, the observed genotypes could have arisen in two different ways. The presence of a mitochondrial genome of one species in the nuclear environment of another suggests mitochondrial introgression – past hybridization followed by backcrossing into the

Table 2
Samples used, their geographical origins and genotypes.[a]

Samples	mtDNA type	Genotype at *ef1* locus	Genotype at *elp* locus
14 samples[b]	*T. asiatica* type	*ef1A/ef1A*	*elpA/elpA*
3 samples[b]		*ef1B/ef1B*	*elpA/elpA*
TasiA190 Sichuan, China		*ef1A/ef1B*	*elpA/elpA*
TasiA210 Kanchanaburi, Thailand		*ef1A/ef1B*	*elpA/elpA*
TasiT010 Taiwan		*ef1B/ef1B*	*elpA/elpB*
14 samples[b]	*T. saginata* type	*ef1C/ef1C*	*elpC/elpC*
TsagT020 Bali, Indonesia		*ef1C/ef1C*	*elpD/elpD*
TsagA201 Kanchanaburi, Thailand		*ef1C/ef1C*	*elpC/elpD*
TsagT017 Kanchanaburi, Thailand		*ef1C/ef1C*	*elpA/elpA*
TsagA199 Kanchanaburi, Thailand		*ef1A/ef1A*	*elpA/elpA*

[a] See the text for abbreviations of mitochondrial haplotypes and alleles. The number after the species code (e.g. A190 or T010) identifies the sample ID used in the Asahikawa Medical College or Tottori University.
[b] See Fig. 1 for further details of geographical origins of samples.

paternal species and eventual dilution and loss of alleles inherited from the maternal species. It is possible that TsagA199 is a case of mitochondrial introgression. If so, additional nuclear loci in this individual should prove to be from *T. asiatica*. Alternatively, genotypes seen in both TsagA199 and TsagT017 could have arisen from a hybrid ancestor by selfing. The F1 hybrid would have been heterozygous at both loci. Its haploid gametes, however, following self-fertilization, could produce zygotes with the observed genotypes, each with a frequency of one-sixteenth in the next generation (F2). Further generations of selfing would eventually produce worms fixed at every locus for an allele from one parent species or the other. Testing between these two scenarios will simply require genotyping of additional nuclear loci in "pure" *T. saginata* and *T. asiatica* and in worms of supposed hybrid origin. The first scenario (mitochondrial introgression) requires many generations of backcrossing, unlikely in a taxon that predominantly self-fertilizes. The second scenario is therefore the more plausible.

In many animal taxa, hybrids are sterile. That is not the case for at least one of the worms studied here. When severe combined immunodeficiency (SCID) mice were infected with the eggs from TsagT017, mature cysticerci developed [26], demonstrating that the eggs had been fertilized and were viable. In addition, two of the cysticerci were homozygous at the *elp* locus and also at the cathepsin L-like cysteine peptidase locus, with each possessing the major allele found in *T. asiatica* [26]. In the second scenario above, the likelihood of a single egg from the F1 hybrid (F2) having such a genotype is also one-sixteenth. Thus, the hybrid-derived offspring observed in this study may not be from the F2 generation but from later generations.

Since hybrid-derived worms have been found only in Kanchanaburi Province, Thailand, where the two species are sympatrically endemic now, it is highly likely that hybridization between *T. asiatica* and *T. saginata* is an event in progress. However, it may not be very common: we observed hybrid-derived offspring in 13.3% of samples (2 cases/15 samples collected from Kanchanaburi). The difference of intermediate hosts utilized by *T. asiatica* and *T. saginata* may reduce the opportunity of a simultaneous infection with these two species. In fact, we have never found a mixed infection with *T. asiatica* and *T. saginata* in Kanchanaburi, although *T. asiatica* and *T. solium* were simultaneously found in humans because pig is the common intermediate host for both parasites [16].

Although we propose occasional crossing between *T. asiatica* and *T. saginata* as an explanation for our observations, it is also possible that ancestral polymorphism has been retained in what are actually two reproductively isolated species [9]. We argue that this is unlikely because self-fertilization by taeniid tapeworms will lead to rapid loss of some alleles and fixation of others. In addition, sequences of *ef1A* and *elpA* in "TsagA199" or "TsagT017" were identical with those in "Tasi", in introns as well as exons. Complete identity, especially in introns, would not be expected if there had been no gene exchange for long periods of time. Nevertheless, the possibility of retention of ancestral polymorphism cannot be completely dismissed by the present data.

When proglottids or eggs of taeniid cestodes are detected in human feces, the accurate identification of species is now dependent on specific PCR or the sequencing analysis of mtDNA [17,18,27]. The species of intermediate host is then inferred from the taeniid species identified. The occurrence of gene exchange between *T. saginata* and *T. asiatica* indicates that the intermediate host inferred from analysis of the mtDNA may not always be the correct one. In addition, the intermediate host cannot be identified from analysis of nuclear genes such as *ef1* and *elp* alone. Unless the gene or genes that regulate host specificity can be identified, the intermediate host should not be deduced based solely on DNA analysis in sympatric endemic areas. The inability to identify intermediate hosts accurately continues to be a significant epidemiological problem. It is necessary now to examine the genotypes of cysticerci from intermediate hosts (cattle and pigs) in sympatric endemic areas.

The results of this study strongly suggest that reproductive isolation is still incomplete between *T. saginata* and *T. asiatica*, and that hybrid breakdown does not occur. Although *T. asiatica* is still able to hybridize with *T. saginata*, each taxon has its own biological identity [12,15]. Biomedical researchers need more pragmatic approaches that can be understood by non-specialists [25]. At the very least, medical or veterinary researchers should not equate *T. asiatica* with *T. saginata*. Further population genetic studies are necessary to better understand the close relationship between these species. In particular, the finding of F1 hybrids is required to exclude the possibility of ancestral polymorphism.

Acknowledgements

This study was supported in part by Grant-in-Aid for Scientific Research from the Japan Society of Promotion of Science (JSPS) to M. Okamoto (18406008, 21406009) and to A. Ito (17256002, 21256003), by the Asia-Africa Science Platform Fund from JSPS to A. Ito (2006–2011) and by JSPS-Japan China Bilateral Medical Joint Project on Taeniasis/Cysticercosis to M. Nakao (2009–2010). The authors thank the many colleagues and field workers who collected taeniid worms, especially Qiu DC, Li TY, Mamuti W, Eom KS, deLeon WU, Wandra T, Sutisna P, Depary AA, Benitez-Ortiz W, Nunes CM, Fan PC, Yoonuan T, Sato M, Tachi E and Suzuki Y.

References

[1] Xiao N, Qiu J, Nakao M, Li T, Yang W, Chen X, et al. *Echinococcus shiquicus* n. sp., a taeniid cestode from Tibetan fox and plateau pika in China. Int J Parasitol 2005;35:693–701.
[2] Nakao M, McManus DP, Shantz PM, Craig PS, Ito A. A molecular phylogeny of the genus *Echinococcus* inferred from complete mitochondrial genomes. Parasitology 2007;134:713–22.
[3] Hüttner M, Nakao M, Wassermann, Siefert L, Boomker JDF, Dinkel A, et al. Genetic characterization and phylogenetic position of *Echinococcus felidis* Ortlepp, 1937 (Cestoda: Taeniidae) from the African lion. Int J Parasitol 2008;38:861–8.
[4] Thompson RCA, McManus DP. Towards a taxonomic revision of the genus *Echinococcus*. Trends Parasitol 2002;18:452–7.
[5] Thompson RCA. The taxonomy, phylogeny and transmission of *Echinococcus*. Exp Parasitol 2008;119:439–46.
[6] Saarma U, Jõgisalu I, Moks E, Varcasia A, Lavikainen A, Oksanen A, et al. A novel phylogeny for the genus *Echinococcus*, based on nuclear data, challenges relationships based on mitochondrial evidence. Parasitology 2009;136:317–28.
[7] Lavikainen A, Haukisalmi V, Lehtinen MJ, Henttonen H, Oksanen A, Meri A. A phylogeny of members of the family Taeniidae based on the mitochondrial *cox1* and *nad1* gene data. Parasitology 2008;135:1457–67.
[8] Mayr E. What is a species, and what is not? Philos Sci 1996;63:262–77.
[9] Badaraco JL, Ayala FJ, Bart JM, Gottstein B, Haag KL. Using mitochondrial and nuclear markers to evaluate the degree of genetic cohesion among *Echinococcus* populations. Exp Parasitol 2008;119:453–9.
[10] Haag KL, Gottstein B, Ayala FJ. The EG95 antigen of *Echinococcus* spp. contains positively selected amino acids, which may influence host specificity and vaccine efficacy. PLoS ONE 2009;4:e5362.
[11] Ito A, Nakao M, Wandra T. Human taeniasis and cysticercosis in Asia. Lancet 2003;362:1918–20.
[12] Eom KS. What is Asian *Taenia*? Parasitol Int 2006;55 suple:S137–41.
[13] McManus DP. *Taenia* in the gastrointestinal tract. N Engl J Med 2008;358:311.
[14] Bowles J, McManus DP. Genetic characterization of the Asian *Taenia*, a newly described taeniid cestode of humans. Am J Trop Med Hyg 1994;50:33–44.
[15] Hoberg EP. Phylogeny of *Taenia*: Species definitions and origins of human parasites. Parasitol Int 2006;55 suple:S23–30.
[16] Anantaphruti MT, Yamasaki H, Nakao M, Waikagul J, Watthanakulpanich D, Nuamtanon S, et al. Sympatric occurrence of *Taenia solium*, *T. saginata*, and *T. asiatica*, Thailand. Emerg Infect Dis 2007;13:1413–6.
[17] Yamasaki H, Allan JC, Sato MO, Nakao M, Sako Y, Nakaya K, et al. DNA differential diagnosis of taeniasis and cysticercosis by multiplex PCR. J Clin Microbiol 2004;42:548–53.
[18] Jeon HK, Chai JY, Kong Y, Waikagul J, Insisiengmay B, Rim HJ, et al. Differential diagnosis of *Taenia asiatica* using multiplex PCR. Exp Parasitol 2009;121:151–6.
[19] Thompson JD, Higgins DG, Gibson TJ. CLUSTAL W: improving the sensitivity of progressive multiple sequence alignment through sequence weighting, position-specific gap penalties and weight matrix choice. Nucleic Acids Res 1994;22:4673–80.
[20] Saitou N, Nei M. The neighbor-joining method: a new method for reconstruction phylogenetic trees. Mol Biol Evol 1987;4:406–25.
[21] Tamura K, Dudley J, Nei M, Kumar S. MEGA4: molecular evolutionary genetics analysis (MEGA) software version 4.0. Mol Biol Evol 2007;24:1596–9.

[22] Tamura K, Nei M, Kumar S. Prospects for inferring very large phylogenies by using the neighbor-joining method. PNAS 2004;101:11030–5.
[23] Felsenstein J. Confidence limits on phylogenies: an approach using the bootstrap. Evolution 1985;39:783–91.
[24] De Meeus T, Durand P, Renaud F. Species concept: what for? Trend Parasitol 2003;19:425–7.
[25] Tibayrenc M. The species concept in parasites and other pathogens: a pragmatic approach? Trend Parasitol 2006;22:66–70.
[26] Nkouawa A, Sako Y, Nakao M, Nakaya K, Ito A. Loop-mediated isothermal amplification method for differentiation and rapid detection of *Taenia* Species. J Clin Microbiol 2009;47:168–74.
[27] Eom KS, Jeon HK, Kong Y, Hwang UW, Li X, Xu L, et al. Identification of *Taenia asiatica* in China: molecular, morphological, and epidemiological analysis of a Luzhai isolate. J Parasitol 2002;88:758–64.

Parasitology International 59 (2010) 326–330

Contents lists available at ScienceDirect

Parasitology International

journal homepage: www.elsevier.com/locate/parint

Molecular and serological survey on taeniasis and cysticercosis in Kanchanaburi Province, Thailand

Malinee T. Anantaphruti [a,b,*,1], Munehiro Okamoto [c,1], Tippayarat Yoonuan [a], Surapol Saguankiat [a], Teera Kusolsuk [a], Megumi Sato [a], Marcello O. Sato [b], Yasuhito Sako [b], Jitra Waikagul [a], Akira Ito [b,1]

[a] Department of Helminthology, Faculty of Tropical Medicine, Mahidol University, Thailand
[b] Department of Parasitology, Asahikawa Medical College, Asahikawa 078-8510, Japan
[c] Department of Parasitology, School of Veterinary Medicine, Faculty of Agriculture, Tottori University, Tottori 680-8553, Japan

ARTICLE INFO

Article history:
Received 9 February 2010
Received in revised form 17 March 2010
Accepted 18 March 2010
Available online 7 April 2010

Keywords:
Taeniasis
Cysticercosis
Molecular diagnosis
ELISA
Immunoblot
Kanchanaburi, Thailand

ABSTRACT

A community-based field survey on taeniasis and cysticercosis was performed in two villages in Thong Pha Phum District, Kanchanaburi Province, central Thailand, where 3 *Taenia* species, *T. solium*, *T. saginata* and *T. asiatica*, are sympatrically occurring. Four (0.6%) out of 667 stool samples were egg-positive for *Taenia* sp. by Kato–Katz technique. Three out of those four persons and other three persons who were *Taenia* egg-negative but having a recent (<1 year) history of discharging worms in stool were treated with niclosamide. One *Taenia* egg-positive woman was not treated because of severe ascites. After treatment, three persons expelled long strobilae with scolices and two persons expelled strobilae without scolex. One *Taenia* egg-positive person did not expel any worms post-treatment. Among 5 persons, four expelled a single worm, whereas one expelled multiple worms, may be 6 worms but not confirmed by detection of scolices. One scolex was armed with hooklets, whereas 2 others did not. Multiplex PCR of 10 expelled proglottids (including 6 estimated worms from one patient) revealed that one sample was *T. solium*, one *T. saginata*, and 8 *T. asiatica*. A total of 159 residents agreed to receive a serological test for cysticercosis. By ELISA using partially purified glycoprotein antigen, 9 cases, 5 and 4 from villages A and B respectively, were found to be sero-positive. The five and an additional sample on the border line from village A were evaluated using confirmative immunoblot using recombinant chimeric antigen. Among the six samples, four including the border line sample were confirmed to be cysticercosis by immunoblotting. One of the 4 persons had neurological symptoms with nodular lesions in the brain by computed tomography. These 4 confirmed or suspected cysticercosis cases were free of *T. solium* worms, but two of them including confirmed NCC case had a past (>1 year) history of expelling proglottids in the stool.

1. Introduction

A nationwide stool survey in Thailand by the Ministry of Public Health revealed 1–2% of taeniasis infection in the north and northeast of the country, with <1% in the central region, and almost none in the south [1]. It has been reported that human cases of *Taenia saginata* are rather common [2] but those of *Taenia solium* are few [3]. However, cysticercosis cases have often been found in hospital records [4,5]. Until 2007, there was no evidence of the occurrence of *Taenia asiatica* in Thailand. Through the field work from 2002 until 2005 in Thong Pha Phum District, Kanchanaburi Province, Thailand, close to the Myanmar border, both *T. solium* and *T. saginata* were found in the same area. By using molecular approaches [6], the morphologically identified *T. saginata* in this area included not only *T. saginata* but also *T. asiatica* and, therefore, three *Taenia* species, *T. asiatica*, *T. saginata* and *T. solium* sympatrically occurred there [7].

As cysticercosis of *T. solium* is one of the most lethal parasitic diseases and difficult to prevent the spread of it in the community [8,9], we were keen to control cysticercosis at the community basis. Since three *Taenia* species were found to be endemic in this area, Kanchanaburi Province [7], we applied serological screening of cysticercosis and molecular identification of *Taenia* worms from patients to draw precise epidemiology of taeniasis and cysticercosis in this area.

2. Materials and methods

2.1. Study community

The study area was Thong Pha Phum District, 150 km northwest of Kanchanaburi, a province in central Thailand, 130 km west of Bangkok.

* Corresponding author. Department of Helminthology, Faculty of Tropical Medicine, Mahidol University, 420/6 Ratchawithi Road, Ratchathewee, Bangkok 10400, Thailand. Tel./fax: +66 2 643 5600.
E-mail address: tmmtr@mahidol.ac.th (M.T. Anantaphruti).
[1] These authors equally contributed for the preparation of the paper.

1383-5769/$ – see front matter © 2010 Published by Elsevier Ireland Ltd.
doi:10.1016/j.parint.2010.03.007

Table 1
Fecal egg examination for intestinal helminths in Kanchanaburi Province, Thailand.

Village	No. examined	No. positive (%)	Parasites species (%)[a]				
			Hookworm	*Ascaris*	*Trichuris*	*Taenia*	Others
Village A	265	76 (28.7)	70 (26.4)	2 (0.8)	6 (2.3)	2 (0.8)	1 (0.4)[b]
Village B	402	113 (28.1)	88 (21.9)	2 (0.5)	29 (7.2)	2 (0.5)	6 (1.5)[c]
Total	667	189 (28.3)	158 (23.7)	4 (0.6)	35 (5.2)	4 (0.6)	7 (1.1)

[a] Some cases have multiple infections.
[b] *Enterobius vermicularis*.
[c] Intestinal trematodes suspected to be belonging to Heterophyidae.

The area was composed largely of highlands and a water reservoir south of Vajiralongkorn Dam. The study sites were 2 rural villages A and B close to the Thai–Myanmar border. Sympatric occurrence of 3 human *Taenia* species was previously confirmed in the same district including village A [7], whereas there was no information in village B. As people in village A purchased piglets from village B, we chose village B for the second year survey. The villages were surrounded in the south by a water basin, and in the others by heavy forest behind the partial plain area. Communication to and from nearby villages and district centers is limited to travel by boat. Each village has about 800–1000 residents. The majority of the population is Karen in origin with Mon, Myanmar, Lao, and Thai minorities. A number of residents are legal or illegal immigrants mainly from Myanmar. Therefore, actual village names are not specified. The main economical activities are agriculture and fishery. The study was approved by the Ethics Committee of the Faculty of Tropical Medicine, Mahidol University, Thailand. Informed consents were obtained at the time of stool and blood collections.

2.2. Fecal egg examination for intestinal helminths including Taenia spp.

The survey was conducted in December 2006 (village A) and November 2007 (village B). Stool samples were collected from residents aged ≥5 years, of both sexes, who were willing to participate in the study. Community members with histories/memories on *Taenia* proglottids in their stools were encouraged to receive examination. Kato–Katz stool examination was applied for microscopic detection of helminth eggs [10]. Three fecal *Taenia* eggs-positive persons and 3 other persons who had a recent (<1 year) history of discharging worm segments in their stools were treated with 2 g niclosamide early in the morning pre-meal followed by saturated magnesium sulfate (60 ml) 2 h post treatment. Four to five whole bowel movements were collected to detect the worms. Evacuated *Taenia* segments from each carrier were fixed in 80% ethanol for molecular study. All scolices expelled were fixed in 10% formalin for staining and morphological study. A part of individual fecal samples were kept frozen in Eppendorf tubes for DNA analysis.

2.3. Molecular study

Frozen stool samples and *Taenia* segments expelled from the participants kept in 80% ethanol were analyzed by multiplex PCR at Asahikawa Medical College (AMC), Japan. DNA was extracted from worms and stool by using DNeasy tissue kit and QIAamp DNA Stool Mini kit (Qiagen, Hilden, Germany), respectively. Cytochrome c oxidase subunit 1 (*cox1*) gene in mitochondrial DNA of the worms and eggs in stool were PCR-amplified and analyzed [6].

2.4. Serological tests for cysticercosis

Blood samples were obtained from 159 (114 of 8–66 years old from village A and 45 of 8–80 years old from village B) out of 667 residents who provided fecal samples. The serum samples were tested at AMC, Japan, for cysticercosis by ELISA using partially purified glycoprotein antigens (GPsAg) by preparative isoelectric focusing of *T. solium* cysts [11]. The cut-off ELISA value was 3 times of the optical density of pooled healthy control sera. Then, ELISA-positive samples were examined by immunoblot using recombinant chimeric antigens (RecAg) prepared from *T. solium* metacestodes [12].

3. Results

3.1. Intestinal helminth infections and taeniasis

A total of 667 (265 and 402 from villages A and B) stool samples were examined. The results for intestinal helminth infections were similar in the 2 villages (Table 1). *Taenia* eggs were found in 4 persons (2 each from villages A and B). Three other persons from village A had a recent history of discharging proglottids in their stools. Among these 7 persons being suspected of having taeniasis, 6 (nos. 1–6 in Table 2) of them were treated with 2 g niclosamide followed by purgatives. One patient was not treated because of severe ascites. Three participants (nos. 3–5) expelled strobilae with a single scolex each and 2 others (nos. 2, and 6) expelled those without scolices. One patient (no. 6) expelled big biomass, which was estimated as 6 worms

Table 2
Summary of the taeniasis cases from Kanchanaburi Province, Thailand, detected by various methods.

Village	Carriers (age in years, gender)	Helminth eggs-positive	*Taenia* egg-positive	History of expelled proglottids	No. of worms expelled		Multiplex PCR	
					Scolex	Proglottids	Segments	Feces
A	1 (32, male)	Hookworm[a]	+	–	0	0	ND	*T. saginata*
	2 (40, female)	–	+	–	0	1	*T. asiatica*	*T. asiatica*
	3 (44, male)	–	–	+	With hooks	1	*T. solium*	*T. solium*
	4 (35, male)	–	–	+	No hook	1	*T. saginata*	*T. saginata*
	5 (33, female)	ND	ND	+	No hook	1	*T. asiatica*	No band[b]
B	6 (30, female)	–	+	+	0	6[c]	*T. asiatica*	*T. asiatica*
	7 (76, female)[d]	Hookworm[a]	+	+	ND	ND	ND	*T. asiatica*

ND – not done.
[a] Numbers of eggs/gram of feces were 3450 (carrier 1) and 60 (carrier 7).
[b] The stool for coproDNA was collected only after given magnesium salt.
[c] Estimated due to the sizes of the strobilae.
[d] No treatment due to her severe ascites.

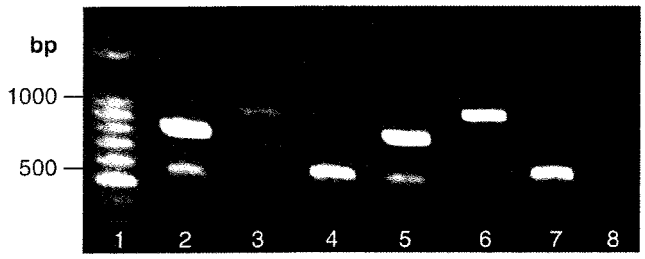

Fig. 1. Multiplex PCR of *Taenia* worms from 3 carriers from village A. Lane 1: DNA markers, Lane 2: *T. saginata* control, Lane 3: *T solium* control, Lane 4: *T. asiatica* control. Lane 5: carrier no. 4, Lane 6: carrier no. 3, Lane 7: carrier no. 5, Lane 8: negative control.

based on the sizes of the strobilae. One of the 3 scolices had hooklets on the rostellum. One *Taenia* egg-positive person (no. 1) did not expel any worms within 5 bowel movements of a day post-treatment.

3.2. Molecular identification of Taenia species

The identification of taeniid worms was carried out by multiplex PCR (Fig. 1, Table 2). The segment from a worm with hooklets on the scolex was identified as *T. solium* (carrier no. 3). Segments from worms without hooklets on the scolex were *T. saginata* and *T. asiatica* (carrier nos. 4 and 5). All other worms including 6 estimated worms from one person were *T. asiatica*.

The 22 available stool samples including those of all 5 and 2 taeniasis patients from villages A and B, respectively (Table 2) were analyzed also by multiplex PCR. Six fecal samples from *Taenia* carriers (nos. 1–4, 6–7) exclusively showed coproDNA-positive results, whereas no. 5 was negative. CoproDNA results from 4 carriers (nos. 2–4, 6) showed the same results from multiplex PCR using the worms.

3.3. Serological tests for cysticercosis and clinical follow-up

Five of 114 people of 8–66 years old from village A and 4 of 45 people of 8–80 years old from village B were sero-positive by ELISA using GPsAg. Five ELISA positives and 1 additional border line case from village A were checked by confirmative immunoblot using RecAg. Three of the five ELISA positives and one border line case showed the specific diagnostic band (Fig. 2). The sample on the border line showed the weakest but visible band. Two of the 4 ELISA positive samples from village B were also positive with RecAg immunoblotting (data not shown). All seven *Taenia* worm/egg-positive cases listed in Table 2 were sero-negative by ELISA, suggesting no person being suffered from taeniasis and cysticercosis simultaneously.

The clinical histories of these 4 serologically confirmed cysticercosis cases from village A were reviewed, and 3 persons underwent brain CT examination. Due to political problem, one patient could not go out from the village. The 42 year-old woman, (lane 3, Fig. 2), had

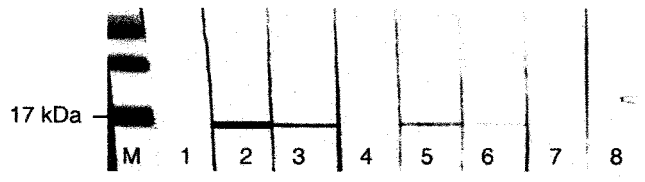

Fig. 2. Immunoblot using RecAg for 6 persons of village A including 5 ELISA-GPsAg positive (lanes 3–7) and one ELISA-GPsAg border line sample (lane 8). Lane M: prestained protein markers to confirm the quality of transblotting and molecular sizes, lane 1: negative control, lane 2: positive control, lanes 3–8: sera from 6 persons suspected by ELISA using GPsAg. Lanes 3, 5, 6 and 8 were positive. Lane 3 was symptomatic NCC case.

clinical symptoms related to neurocysticercosis (NCC), *i.e.* headache, stiff neck, seizure, and vomiting. Brain CT images showed small ill-marginated hypodense areas in the left frontal lobe, at the cortical medullary junction close to the brain surface at left frontal lobe, with minute nodular contrast enhancement (Fig. 3). This person had a past (>1 years ago) history of expelling proglottids. Two other persons were clinically normal and showed no obvious CT-image abnormality.

4. Discussion

Through this study in the two villages in Kanchanaburi Province, central Thailand, we have found a total of 7 *Taenia* carriers (Table 2) detected by fecal egg examination and deworming with molecular speciation by multiplex PCR for worms and/or stool samples. Among those 7 cases, 5 (nos. 2–6, Table 2) were confirmed by treatment with niclosamide. The *Taenia* species were *T. solium* ($n=1$), *T. saginata* ($n=1$) and *T. asiatica* ($n=8$ from 3 carriers). Two persons (nos. 1 and 7) were *Taenia* egg-positive by microscopic examination and coproDNA, the latter method have proven that one (no. 1) was positive for *T. saginata* and the other (no. 7) for *T. asiatica*. However, the no. 1 did not expel any worms after niclosamide treatment and the no. 7 was not treated due to her serious ascites. The present results reconfirmed our previous finding of the sympatric occurrence of three *Taenia* species in village A [7]. In the present study, two worm carriers in village B had *T. asiatica* only.

Serological screening for cysticercosis by ELISA revealed that 9 persons (5 in village A and 4 in village B) were sero-positive against GPsAg. Among them, 5 persons were clearly positive by immunoblot using RecAg (Fig. 2). At the moment, ELISA using GPsAg is recommended for screening of cysticercosis, and the immunoblot using RecAg is strongly recommended for the confirmative serodiagnosis [12,13], since immunoblot using RecAg is 100% specific to *T. solium* cysticercosis [12,14]. Among the immunoblot positive cases, one woman was confirmed to be symptomatic NCC, whereas the others showed no critical clinical abnormalities. Therefore, we concluded that these other cases of antibody-positive to RecAg by immunoblot were asymptomatic cysticercosis cases. As subcutaneous cysticercosis (SCC) is also common clinical manifestation of cysticercosis in Asia, we have to be keen to check SCC as well as NCC. Since identification of cysticercosis cases is not always easy without histopathological specimens [13,15], combination of both radio-imaging figures and serology using highly reliable antigens are the essential tools for screening and diagnosis [8,16].

In this study, all persons including the confirmed and suspected cysticercosis were not taeniasis carriers. However, two of them including confirmed NCC case had a history of expelling proglottids in feces which ceased more than one year ago, suggesting that these two persons might have been infected with *T. solium* in the past. As the carrier of *T. solium* is the highest risk person for cysticercosis, we should pay attention not only for the carriers themselves but also for their family members and neighbors to detect hidden cases of cysticercosis [17–19].

In contrast to the diagnosis for cysticercosis, detection of taeniasis cases is rather easy, since we can detect eggs or proglottids in feces. However, detection of eggs under microscope is not sensitive enough [20]. History of expulsion of proglottids is, in general, not always clear or reliable, especially for *T. solium*, and is highly variable in the communities [21]. In the present study, however, 4 of 6 *Taenia* carriers had a history of expulsion of proglottids (Table 2) and they expelled either *T. solium* (no. 3), *T. saginata* (no. 4) or *T. asiatica* (nos. 5, and 6) after niclosamide treatment. Therefore, the carriers' memories were highly reliable in these villages. Speciation of *Taenia* worms can be easily done by molecular tools. Even the carriers who did not expel worms were diagnosed at species level by coproDNA test (no. 1). Therefore, coproDNA test is expected to be more sensitive than microscopic detection of eggs so far [6]. Nonetheless, multiplex PCR is

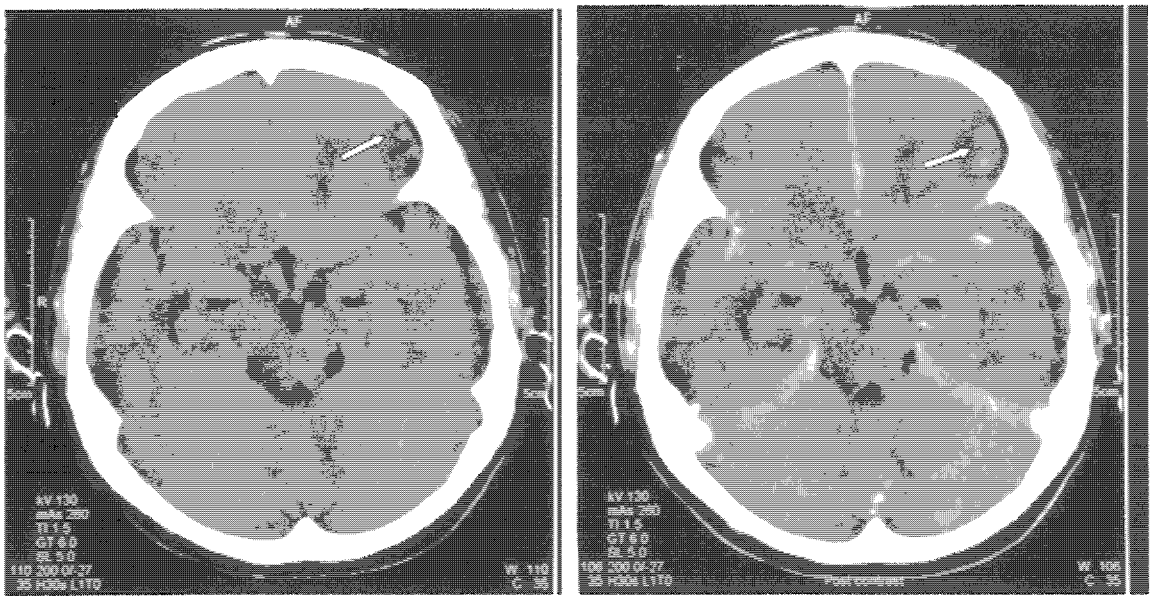

Fig. 3. CT image of 42 year-old woman with clinical symptoms related to neurocysticercosis. A: a poorly defined low attenuation area is noted (arrow) in left frontal gray–white matter junction in non contrast scans. B: Small ring enhancement is noted (arrows) with perifocal edema in contrast enhanced scans. Cysticercosis is one of the differential diagnosis (other possibility include: brain abscess, brain metastasis and granulomatous lesion).

not always applicable in the rural communities where we cannot expect stable electric power supply. Moreover, fecal samples may contain some inhibitors against multiplex PCR [22]. In order to clear these problems, introduction of a new molecular tool, loop-mediated isothermal amplification (LAMP) method [23] should be considered in near future.

In the present study, we found 2 carriers of *T. asiatica* in village B, and 5 carriers of 3 *Taenia* species in village A where the hybrid worms of *T. saginata* and *T. asiatica* have been found [24]. Further studies are necessary to clarify the biological background as to where and how such hybrid *Taenia* is produced. Also, more extensive survey, treatment and prevention are necessary in such areas where sympatric distribution of two or more *Taenia* species is observed.

Acknowledgements

The project was carried out with financial supports from 1) the Asia/Africa Sciences Platform Fund of the Japan Society for the Promotion of Science (JSPS) (2006–2011) and 2) Grant-in-Aid for Scientific Research from JSPS (17256002, 21256003) to A. Ito and (18406008, 21406009) to M. Okamoto. Thanks to Dr. Jirapong Dowreang, radiologist of the Hospital for Tropical Diseases of Faculty of Tropical Medicine for suggestion on computerized tomography (CT) images of Fig. 3. We sincerely thank Dr. Yukifumi Nawa, consultant of Faculty of Tropical Medicine, for his comments and suggestions for improving of the manuscript. Special thanks to the Faculty of Tropical Medicine, Mahidol University for encouragement and facilities in this work.

References

[1] Jongsuksantigul P, Chaeychomsri W, Techamontrikul P, Jeradit P, Suratanavanit P. Studies on prevalence and intensity of intestinal helminthiasis and opisthorchiasis in Thailand. J Trop Med Parasitol 1992;15:80–95 [in Thai with English abstract].
[2] Charoenlarp P, Radomyos P, Bunnag D. The optimum dose of Puag-Haad in the treatment of taeniasis. J Med Assoc Thai 1989;72:71–3.
[3] Anantaphruti MT. Human taeniasis in Thailand. In: Ito A, Wen H, Yamasaki H, editors. Taeniasis/Cysticercosis and Echinococcosis in Asia. Asian Parasitology/Japan: AAA Committee The Federation of Asian Parasitologists; 2005. p. 89–98.
[4] Jitsukon N, Towanabut S. Neurocysticercosis at Prasat Neurological Hospital. Bull Dept Med Serv 1989;14:289–300 [in Thai with English abstract].
[5] Techathuvanan S. Cysticercosis: 5-year review at Rajavithi Hospital. J Rajavithi Hosp 1997;8:33–41 [in Thai with English abstract].
[6] Yamasaki H, Allan JC, Sato MO, Nakao M, Sako Y, Nakaya K, et al. DNA differential diagnosis of taeniasis and cysticercosis by multiplex PCR. J Clin Microbiol 2004;42:548–53.
[7] Anantaphruti MT, Yamasaki H, Nakao M, Waikagul J, Watthanakulpanich D, Nuamtanong S, et al. Sympatric occurrence of *Taenia solium*, *T. saginata*, and *T. asiatica*, Thailand. Emerg Infect Dis 2007;13:1413–6.
[8] Schantz PM. Progress in diagnosis, treatment and elimination of echinococcosis and cysticercosis. Parasitol Int 2006;55:S7–13.
[9] Schantz PM, Wilkins PP, Tsang VC. Immigrants, imaging, and immunoblots: the emergence of neurocysticercosis as a significant public health problem. In: Scheld WM, Craig WA, Hughes JM, editors. Emerging Infections, 2. Washington DC: ASM Press; 1998. p. 213–42.
[10] Katz N, Chaves A, Pellegrino J. A simple device for quantitative stool thick-smear technique in schistosomiasis mansoni. Rev Inst Med Trop Sao Paulo 1972;14:397–400.
[11] Ito A, Plancarte A, Ma L, Kong Y, Flisser A, Cho SY, et al. Novel antigens for neurocysticercosis: simple method for preparation and evaluation for serodiagnosis. Am J Trop Med Hyg 1998;59:291–4.
[12] Sako Y, Nakao M, Ikejima T, Piao XZ, Nakaya K, Ito A. Molecular characterization and diagnostic value of *Taenia solium* low-molecular-weight antigen genes. J Clin Microbiol 2000;38:4439–44.
[13] Ito A, Takayanagui OM, Sako Y, Sato MO, Odashima NS, Yamasaki H, et al. Neurocysticercosis: clinical manifestation, neuroimaging, serology and molecular confirmation of histopathologic specimens. Southeast Asian J Trop Med Public Health 2006;37(Suppl 3):74–81.
[14] Sato MO, Sako Y, Nakao M, Yamasaki H, Nakaya K, Ito A. Evaluation of purified *Taenia solium* glycoproteins and recombinant antigens in the serologic detection of human and swine cysticercosis. J Infect Dis 2006;194:1783–90.
[15] Yamasaki H, Nagase T, Kiyoshige Y, Suzuki M, Nakaya K, Itoh Y, et al. A case of intramuscular cysticercosis diagnosed definitively by mitochondrial DNA analysis of extremely calcified cysts. Parasitol Int 2006;55:127–30.
[16] Ito A, Craig PS. Immunodiagnostic and molecular approaches for the detection of taeniid cestode infections. Trends Parasitol 2003;19:377–81.
[17] Sarti E, Schantz PM, Plancarte A, Wilson M, Gutierrez OI, Aguilera J, et al. Epidemiological investigation of *Taenia solium* taeniasis and cysticercosis in a rural village of Michoacan State, Mexico. Trans R Soc Trop Med Hyg 1994;68:49–52.
[18] Hira PR, Francis I, Abdella NA, Gupta R, Al-Ali FM, Gover S, et al. Cysticercosis: imported and autochthonous infections in Kuwait. Trans R Soc Trop Med Hyg 2004;98:233–9.
[19] Huisa B, Menacho LA, Rodriguez S, Bustos JA, Gilman R, Tsang VC, et al. Taeniasis and cysticercosis in housemaids working in affluent neighborhoods in Lima, Peru. Am J Trop Med Hyg 2005;73:496–500.

[20] Schantz P, Sarti E. Diagnostic methods and epidemiologic surveillance of *Taenia solium* infection. Acta Leidensia 1989;57:153–63.
[21] Wandra T, Sutisna P, Dharmawan NS, Margono SS, Sudewi R, Suroso T, et al. High prevalence of *Taenia saginata* taeniasis and status of *Taenia solium* cysticercosis in Bali, Indonesia, 2002–2004. Trans R Soc Trop Med Hyg 2006;100:346–53.
[22] Kaneko H, Kawana T, Fukushima E, Suzutani T. Tolerance of loop-mediated isothermal amplification to a culture medium and biological substances. J Biochem Biophys Methods 2007;70:499–501.
[23] Nkouawa A, Sako Y, Nakao M, Nakaya K, Ito A. Loop-mediated isothermal amplification method for differentiation and rapid detection of *Taenia* species. J Clin Microbiol 2009;47:168–74.
[24] Okamoto M, Nakao M, Blair D, Anantaphruti MT, Waikagul J, Ito A. Evidence of hybridization between *Taenia saginata* and *Taenia asiatica*. Parasitol Int 2010;59:70–4.

Serological Studies of Neurologic Helminthic Infections in Rural Areas of Southwest Cameroon: Toxocariasis, Cysticercosis and Paragonimiasis

Agathe Nkouawa[1,2], Yasuhito Sako[1], Sonoyo Itoh[1], Alida Kouojip-Mabou[3], Christ Nadège Nganou[4], Yasuaki Saijo[5], Jenny Knapp[1], Hiroshi Yamasaki[6], Minoru Nakao[1], Kazuhiro Nakaya[7], Roger Moyou-Somo[2,4], Akira Ito[1]*

1 Department of Parasitology, Asahikawa Medical College, Asahikawa, Hokkaido, Japan, **2** Medical Research Center, Institute of Medical Research and Medicinal Plants Studies (IMPM), Ministry of Scientific Research and Innovation, Yaoundé, Cameroon, **3** Cité des Palmiers Health District, Douala, Cameroon, **4** Department of Parasitology and Infectious Diseases, Faculty of Medicine and Biomedical Sciences, University of Yaounde I, Yaoundé, Cameroon, **5** Division of Community Medicine and Epidemiology, Department of Health Science, Asahikawa Medical College, Asahikawa, Hokkaido, Japan, **6** Department of Parasitology, National Institute of Infectious Diseases, Tokyo, Japan, **7** Animal Laboratory for Medical Research, Asahikawa Medical College, Asahikawa, Hokkaido, Japan

Abstract

Background: Both epilepsy and paragonimiasis had been known to be endemic in Southwest Cameroon. A total of 188 people (168 and 20 with and without symptoms confirmed by clinicians, respectively, 84.6% under 20 years old) were selected on a voluntary basis. Among 14 people (8.3%) with history of epilepsy, only one suffered from paragonimiasis. Therefore, we challenged to check antibody responses to highly specific diagnostic recombinant antigens for two other helminthic diseases, cysticercosis and toxocariasis, expected to be involved in neurological diseases. Soil-transmitted helminthic infections were also examined.

Methodology/Principal Findings: Fecal samples were collected exclusively from the 168 people. Eggs of *Ascaris lumbricoides*, *Trichuris trichiura* and hookworms were found from 56 (33.3%), 72 (42.8%), and 19 (11.3%) persons, respectively. Serology revealed that 61 (36.3%), 25 (14.9%) and 2 (1.2%) of 168 persons showed specific antibody responses to toxocariasis, paragonimiasis and cysticercosis, respectively. By contrast, 20 people without any symptoms as well as additional 20 people from Japan showed no antibody responses. Among the 14 persons with epilepsy, 5 persons were seropositive to the antigen specific to *Toxocara*, and one of them was simultaneously positive to the antigens of *Paragonimus*. The fact that 2 children with no history of epilepsy were serologically confirmed to have cysticercosis strongly suggests that serological survey for cysticercosis in children is expected to be useful for early detection of asymptomatic cysticercosis in endemic areas.

Conclusions/Significance: Among persons surveyed, toxocariasis was more common than paragonimiasis, but cysticercosis was very rare. However, the fact that 2 children were serologically confirmed to have cysticercosis was very important, since it strongly suggests that serology for cysticercosis is useful and feasible for detection of asymptomatic cysticercotic children in endemic areas for the early treatment.

Citation: Nkouawa A, Sako Y, Itoh S, Kouojip-Mabou A, Nganou CN, et al. (2010) Serological Studies of Neurologic Helminthic Infections in Rural Areas of Southwest Cameroon: Toxocariasis, Cysticercosis and Paragonimiasis. PLoS Negl Trop Dis 4(7): e732. doi:10.1371/journal.pntd.0000732

Editor: Joseph M. Vinetz, University of California San Diego School of Medicine, United States of America

Received January 13, 2010; **Accepted** May 12, 2010; **Published** July 6, 2010

Funding: This work was supported by the special fund for International Leadership in Science and Technology from Ministry of Education, Culture, Sports, Science and Technology, Japan; International Collaboration Research Fund from the Japan Society for the Promotion of Science (JSPS) (17256002, 21256003) and JSPS-Asia/Africa Science Platform Fund (2006–2011) to A.I. and by the Cameroon Institute of Medical Research and Medicinal Plants Studies. The funders had no role in study design, data collection and analysis, decision to publish, or preparation of the manuscript.

Competing Interests: The authors have declared that no competing interests exist.

* E-mail: akiraito@asahikawa-med.ac.jp

Introduction

Parasitic infections are serious public health problems in many developing countries [1,2]. These diseases can affect various tissues and organs including the brain leading to neurological dysfunction. Cysticercosis caused by *Taenia solium* metacestodes has been assumed to be the most common parasitic infection of the brain worldwide including Cameroon [3–5]. As cysticercosis is one of the major causative agents of the late-onset of epilepsy, the major work on cysticercosis has been carried out for adults but not for children in endemic areas, and other causative agents of epilepsy still remain unclear. Therefore, we were lead to obtain more information on the causative agents of epilepsy in developing countries, since many helminthic diseases including toxocariasis, paragonimiasis, onchocerciasis etc., and also protozoan diseases including malaria, toxoplasmosis and others may cause epilepsy [4–6]. Among these neglected helminthic diseases, toxocariasis is expected to have cosmopolitan distribution, since dogs and cats

Author Summary

A total of 188 people (168 and 20 with and without symptoms confirmed by clinicians, respectively, 84.6% under 20 years old) were selected on a voluntary basis in Cameroon. Soil transmitted helminthic infections were prevalent among persons surveyed as is common in developing countries, since eggs of *Ascaris lumbricoides*, *Trichuris trichiura* and hookworms were found from 56 (33.3%), 72 (42.8%) and 19 (11.3%) persons, respectively. Serological analyses revealed that 61 (36.3%), 25 (14.9%) and 2 (1.2%) persons were positive to the diagnostic antigens specific for toxocariasis, paragonimiasis and cysticercosis, respectively. Among 14 people with epilepsy, 5 persons were seropositive to the antigen of *Toxocara* and one of them was simultaneously positive to the antigens of *Paragonimus*. Serological confirmation of cysticercosis in two children is very important, and we suggest that further serologic surveys of cysticercosis be carried out in both children and adults in this area for the promotion of a better quality of life including control and early treatment.

are companion animals with close contact with people in the world [7,8]. Although there are no data on the prevalence of human toxocariasis in Cameroon, its prevalence in dogs in Cameroon is high [9]. Simultaneously, there is poor information on cysticercosis in children in Cameroon, although it seems to be rather common in the adult population [4,5].

Tombel health district in South West Province in Cameroon (Figure 1) is known as an endemic focus of epilepsy and is also highly endemic for paragonimiasis [10,11]. Our previous report in this area showed that 8.3% of enrolled people (14/168) suffered from epilepsy but only one of the epileptic patients simultaneously suffered from paragonimiasis [11]. Therefore, we concluded that paragonimiasis was not the major cause of epilepsy in children in this area.

In this study, we used the same 188 samples examined for paragonimiasis [11] and additional 20 samples from Japan, where cysticercosis and paragonimiasis have long been eradicated and toxocariasis is very rare [12], as healthy controls. We performed serosurveys using highly specific recombinant antigens for toxocariasis and cysticercosis, and simultaneously analyzed the unpublished data on microscopic observation of soil-transmitted helminthic (STH) infections. Serological data on paragonimiasis for this study were modified from published data [11]. Although onchocerciasis was known to be endemic in Cameroon and might be involved in neurological disorder, we could not examine simply because the lack of serological tools [13,14].

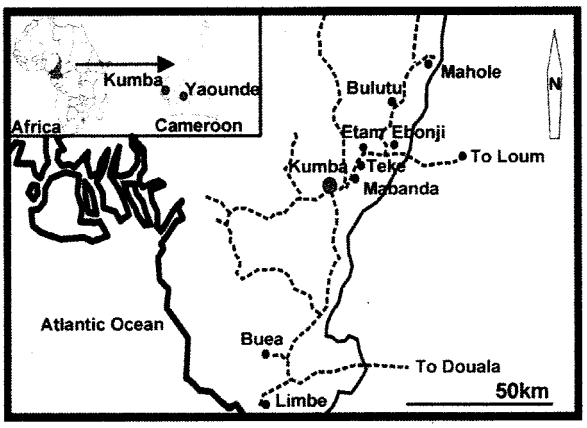

Figure 1. Locations of Bulutu, Ebonji, Etam and Teke in Tombel sub-Division, Southwest Province, Cameroon.
doi:10.1371/journal.pntd.0000732.g001

Materials and Methods

Study sites

Four villages in rural areas, Bulutu, Ebonji, Etam and Teke, were selected for this study. They are located in the Tombel Health District (50,000–100,000 inhabitants) in the rain forest zone about 40 km northwest of Kumba, Manengouba Department, South West Province of Cameroon (4°3′N, 9°3′W). The annual average temperature is 24°C and the relative humidity varies from 52% to 74%. Agriculture is the principal economic activity; hunting and fishing are also practiced (Figure 1).

Ethical statement

The survey, approved by the National Ethics Committee of Cameroon, was conducted in the general population in January 2004 and February 2006 in villages mentioned above.

Human samples

The chief of each village was informed about the study and participants or parents/guardians were asked to give informed consent for participation. A total of 188 people ranged in age from 4 to 78 years (14.9±7.8 years in males and 13.1±6.1 years in females) were examined by clinicians and were asked whether they had experienced symptoms such as cough, haemoptysis, headache, epilepsy, chest pain, and eye disorder and whether they consumed raw and/or undercooked fresh water crabs or pork. Our study population with symptoms ranged from 0–10 years (80 persons), 11–20 years (63 persons), and >21 years (25 persons). Following the questionnaire, serum, sputum and fecal samples were collected from 168 people who accepted to participate to the study voluntarily (28, 52, 55 and 33 from Bulutu, Ebonji, Etam, and Teke villages, respectively). By contrast, 20 healthy persons [5 persons from each village including 11 females and 9 males ranged from 6 to 34 years (13.0±3.7 in males and 15.1±7.5 in females)] confirmed by clinicians donated serum samples exclusively; these serum samples were used as expected healthy controls. An additional 20 serum samples from students at Asahikawa Medical College (AMC), Japan, were used as confirmed healthy controls. Sputum was examined for eggs of *P. africanus* [11]. Fecal samples were examined by flotation techniques for the presence of eggs to provide a diagnosis of helminthic infections.

Serology

A total of 208 serum samples were examined by ELISA. A recombinant antigen of *T. canis* second-stage larvae (0.5 μg/ml) was used for toxocaraisis [15]. Glycoproteins (GPs) (1.0 μg/ml) from *T. solium* cyst fluid purified by preparative isoelectric focusing (pH 9.2–9.6) were used for screening of cysticercosis by ELISA [16]. Immunoblot using a recombinant chimeric antigen, 100% specific to cysticercosis (0.5 μg/mini gel) was applied for serological confirmation of cysticercosis [16–19]. Somatic antigens of *P. africanus* adult worms (5μg/ml), which showed few cross reactivity with other parasitic infections were used for paragonimiasis [11]. Briefly, 96-well microtiter plates (Maxisorp; Nunc, Roskilde, Denmark) were coated with each of the antigens described above in PBS and incubated at 4°C overnight. The

plates were probed with diluted serum samples. Serum dilutions were in 1:200 with bicarbonate buffer for toxocariasis, and 1:100 and 1:200 with blocking buffer for cysticercosis and paragonimiasis, respectively, according to the original papers for these diseases described above. Peroxidase-conjugated rec-Protein G (Zymed, San Francisco, USA) diluted in 1:1000 with blocking buffer was added into each well. Peroxidase activity was revealed by adding 0.4 mmol/l 2,2-azino-bis 3 ethybenz-thiazoline-6-sulphonic acid in 0.1 mol/l sodium citrate buffer, pH 4.7 containing 0.003% H_2O_2 at room temperature. The optical density (OD) was monitored at 405 nm on a microplate reader (ImmunoMini, model NJ-2300; Nalgene Nunc International, Tokyo, Japan). The cut-off value was calculated for each antigen based on the means+3SD of 40 healthy donors from the local areas in Cameroon (n = 20) and from Japan (n = 20).

Statistical analyses

To obtain adjusted odds ratios (ORs) of paragonimiasis and toxocariasis seropositivities for each symptom, we performed multivariate logistic regression analysis adjusted for age (−10, 11–20, 21year) and sex. Because the number of cysticercosis seropositivity was rather small (n = 3), we did not analyze the ORs of cysticercosis seropositivity. For all statistical analyses, a 5% level of significance was applied. All statistical analyses were conducted using SPSS for Windows version 18.0 (SPSS, Inc., Chicago, U.S.A.).

Results and Discussion

In this study, the samples used for paragonimiasis [11] were also tested for toxocariasis and cysticercosis and also the data of STHs were analyzed. The enrolled persons (168: 78 males and 90 females) were diagnosed suffering from cough (n = 135, 80.3%), haemoptysis (n = 18, 11.3%), chest pain (n = 80, 47.6%), epilepsy (n = 14, 8.3%), visual impairment (n = 30, 17.8%) and headache (n = 106, 63.0%) and had histories of eating raw or undercooked crabs (n = 137, 81.5%) or pork (n = 135, 80.3%). Microscopic examination revealed *Paragonimus* eggs in sputum from 16 (9.5%) persons but no eggs from feces [11], whereas *A. lumbricoides*, *T. trichiura*, and hookworms were found in feces from 56 [33.3%; 30 (53.5%) males and 26 (46.4%) females], 72 [42.8%; 38 (52.7%) males and 34 (47.2%) in females] and 19 [11.3%; 14 (73.6%) males and 5 (26.3%) females] persons, respectively. Among these helminthic infections, hookworm infection exclusively showed statistically significant difference between the genders ($p<0.05$). The difference in prevalence between males and females for hookworm infection may be due to the barefoot roaming behavior of males but further investigation of this topic is needed. The highest multiple infections were found in 3 kids infected with 3 STHs and were simultaneously seropositive for paragonimiasis and toxocariasis as well.

ELISA for diagnosis of toxocariasis, paragonimiasis and cysticercosis indicated that 61 [36.3%; 31 (50.8%) males and 30 (49.1%) females], 25 [14.9%; 10 (40%) males and 15 (60%) females] [11], and 3 [1.8%; 2 boys of 13 and 11 year-old, and one girl, 4 year-old] persons were positive (Figure 2). Persons with cough and haemoptysis were more likely to have paragonimiasis (Table 1, OR = 7.19 and 2.28 respectively, $p<0.001$), whereas there was a relative risk with other symptoms. As none of the symptoms were specific for toxocariasis, the probability to have the infection was equally likely in exposed and control group as OR values were close to 1 (Table 1). The likelihood for cysticercosis to occur was not included due to the low number of seropositive persons. Nonetheless, there were crucial differences in antibody

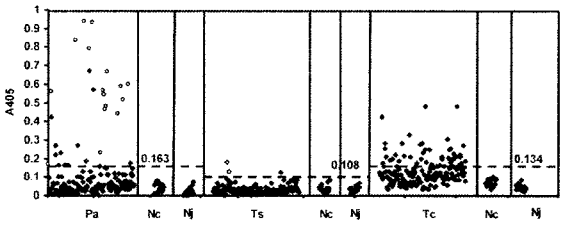

Figure 2. ELISA results for paragonimiasis (Pa), cysticercosis (Ts) and toxocariasis (Tc) from 208 persons. The surveyed persons (n = 208) include 168 and 40 (20 persons from Cameroon (Nc) and 20 from Japan (Nj)) with and without symptoms, respectively. ○, samples with *Paragonimus* eggs in the sputum. Serology could detect more cases than microscopical examination of sputum and was expected to be more sensitive for detection of paragonimiasis including immature adult stage [11]. ◇, samples positive against the recombinant antigen 100% specific to cysticercosis by immunoblot [17]. The broken line denotes the respective cut-off value for each disease and each cut-off value is shown.
doi:10.1371/journal.pntd.0000732.g002

responses between the two groups. Furthermore, there was no difference in OD values between healthy controls from endemic Cameroon and from non-endemic, Japan where we expected no positive samples from students at AMC. Therefore, we concluded that the serological findings indicated specific responses to these three helminthic infections. The ELISA system applied for paragonimiasis in this study was much more sensitive for diagnosis than detection of eggs as already shown (Figure 2) [11]. As it has already been shown that the ELISA for toxocariasis in this study showed no cross-reactions with ascariasis patients in Asia and Latin America [20,21], we consider that it is highly specific to toxocariasis. As children are the most risky population for toxocariasis and the prevalence of *T. canis* in dogs in Cameroon was very high [9], we expected that 61 persons (36.3%) were really exposed to eggs of *Toxocara* [22,23]. Among these seropositive persons, 11 persons were concluded to have dual infection of both *Toxocara* and *Paragonimus*.

Table 1. Odds ratio of positive serological test for each symptom among 188 subjects.

Type of symptom	Serological test	Odds ratio*	95%CI	P value
Headache	Paragonimiasis	1.22	0.52–2.87	0.999
	Toxocariasis	1.12	0.60–2.08	0.729
Haemoptysis	Paragonimiasis	7.19	2.68–19.30	<0.001
	Toxocariasis	0.99	0.40–2.46	0.977
Cough	Paragonimiasis	2.28	0.50–10.29	0.284
	Toxocariasis	1.97	0.75–5.16	0.167
Chest pain	Paragonimiasis	1.44	0.61–3.43	0.406
	Toxocariasis	1.33	0.71–2.48	0.371
Eye disorder	Paragonimiasis	0.91	0.23–3.64	0.910
	Toxocariasis	1.38	0.06–4.31	0.521
Epilepsy	Paragonimiasis	0.51	0.52–3.70	0.539
	Toxocariasis	1.30	0.39–4.28	0.667

*Adjusted for age (−10y, 11–20y, >21y) and sex.
doi:10.1371/journal.pntd.0000732.t001

Three children (1.7%) showing weak responses to the GPs of *T. solium* by ELISA (Figure 2) were further analyzed using the recombinant antigen for serological confirmation of cysticercosis, since there are no false positive antibody responses to the recombinant antigen by immunoblot [17–19]. Two of them showing higher OD values by ELISA (Figure 2) exhibited positive response with the recombinant antigen by immunoblot (Figure 3) [17,18]. Therefore, these two cases are considered as asymptomatic cysticercosis and are important targets for cysticercosis studies in the future. We believe that further epidemiological surveys for neurocysticercosis in the adult population should be carried out in the same areas, since 1) the late-onset epilepsy due to cysticercosis is expected to be detectable more common from senior people [3–6,24,25], 2) cysticercosis prevalence in Cameroon ranges from 2.5% to 13% [4,5] and 3) more than the half of epileptic adult patients show antibodies against cysticercosis in West and North West regions in Cameroon using the same serology [5].

In Papua, Indonesia, one of the most serious endemic areas of cysticercosis in the world, more than 80% and 70% of people over 18 years old, who had history of epileptic seizures with or without subcutaneous nodules, were confirmed as having cysticerci, respectively [26,27]. Approximately 30% of asymptomatic healthy people were serologically identified as positive for cysticercosis and follow up investigations revealed that many of them had detectable subcutaneous nodules. Furthermore, the most recent retrospective study using molecular tools has revealed that a cysticercus of *T. solium* survived at least for 10 years in a patient's brain [28].

According to these data mentioned above, the most important implication on cysticercosis from this serological study is that asymptomatic cysticercosis can be detected from children in endemic areas. Therefore, introduction of serological screening of children becomes highly informative for detection of asymptomatic cases and for getting better and early treatment for them [29]. Follow-up studies on these 2 boys using neuroimaging tools are necessary for further evaluation. We recommend highly reliable serological screening for cysticercosis for all pupils in the primary school, if possible, or all teenagers at least in highly endemic areas. As risk factors associated with human cysticercosis include the occurrence of cysticercosis in pigs, detection of adult worm carriers should be investigated. For the future survey of taeniasis carriers, both copro-ELISA [30] and copro-DNA tests [31] are expected to be introduced in this area, Cameroon, and in any other areas where cysticercosis is highly endemic.

Figure 3. Immunoblot using the recombinant antigen of the 3 samples showing weak positive response by ELISA. Sera were in 1:20 dilutions. Lane 1: negative control, lane 2: positive control, lanes 3–5: samples exhibited weak positive response by ELISA. Lanes 3 and 4 corresponding to the samples showing higher OD value by ELISA were positive to the recombinant antigen by immunoblot.
doi:10.1371/journal.pntd.0000732.g003

Participants in the study were selected on a voluntary basis and may not be representative for the population as the whole but the numbers of children younger than 20 years were approximately 84.6% of surveyed persons. Therefore, the results are highly informative as a preliminary study identifying areas for further investigation of all these helminthic infections in this area.

In conclusion, toxocariasis, paragonimiasis and cysticercosis have been serologically confirmed among surveyed persons. Five of 14 epilepsy cases were sero-positive for toxocariasis. Correlation between epilepsy and these helminthic infections should be further evaluated, since screening of children for these parasitic diseases may become more important and feasible for the early treatment and prevention of these infections and promotion of better quality of life in the future.

Acknowledgments

We sincerely thank PM Schantz for his crucial comments and suggestions and for amendment of the manuscript.

Author Contributions

Conceived and designed the experiments: RMS AI. Performed the experiments: AN YS SI. Analyzed the data: AN YS YS JK AI. Contributed reagents/materials/analysis tools: YS SI AKM CNN HY MN KN RMS AI. Wrote the paper: AN YS AI.

References

1. Stephenson LS, Latham MC, Ottesen EA (2000) Malnutrition and parasitic helminth infections. Parasitology 121: SupplS23–S38.
2. WHO (2002) The world health report 2002: reducing risks, promoting healthy life. Geneva: World Health Organization.
3. Garcia HH, Pretell EJ, Gilman RH, Martinez SM, Moulton LH, et al. (2004) A trial of antiparasitic treatment to reduce the rate of seizures due to cerebral cysticercosis. N Engl J Med 350: 249–258.
4. Nguekam JP, Zoli AP, Zogo PO, Kamga AC, Speybroeck N, et al. (2003) A seroepidemiological study of human cysticercosis in West Cameroon. Trop Med Int Health 8: 144–149.
5. Zoli AP, Nguekam, Shey-Njila O, Nforninwe DN, Speybroeck N, et al. (2003) Neurocysticercosis and epilepsy in Cameroon. Trans R Soc Trop Med Hyg 97: 683–686.
6. Garcia HH, Modi M (2008) Helminthic parasites and seizures. Epilepsia 49 Suppl 6: 25–32.
7. Nicoletti A, Sofia V, Mantella A, Vitale G, Contrafatto D, et al. (2008) Epilepsy and toxocariasis: a case-control study in Italy. Epilepsia 49: 594–599.
8. Bachli H, Minet JC, Gratzl O (2004) Cerebral toxocariasis: a possible cause of epileptic seizure in children. Childs Nerv Syst 20: 468–472.
9. Komtangi MC, Mpoame M, Payne VK, Ngufor MN (2005) Prevalence of gastrointestinal helminths of dogs in Dschang, Cameroon. J Cameroon Acad Sci 5: 11–14.
10. Moyou-Somo R, Tagni-Zukam D (2003) Paragonimiasis in Cameroon: clinicoradiologic features and treatment outcome. Med Trop (Mars) 63: 163–167.
11. Nkouawa A, Okamoto M, Mabou AK, Edinga E, Yamasaki H, et al. (2009) Paragonimiasis in Cameroon: molecular identification, serodiagnosis and clinical manifestations. Trans R Soc Trop Med Hyg 103: 255–261.
12. Akao N, Ohta N (2007) Toxocariasis in Japan. Parasitol Int 56: 87–93.
13. Esum M, Wanji S, Tendongfor N, Enyong P (2001) Co-endemicity of loiasis and onchocerciasis in the South West Province of Cameroon: implications for mass treatment with ivermectin. Trans R Soc Trop Med Hyg 95: 673–676.
14. Oye JE, Kuper H (2007) Prevalence and causes of blindness and visual impairment in Limbe urban area, South West Province, Cameroon. Br J Ophthalmol 91: 1435–1439.
15. Yamasaki H, Araki K, Lim PK, Zasmy N, Mak JW, et al. (2000) Development of a highly specific recombinant *Toxocara canis* second-stage larva excretory-secretory antigen for immunodiagnosis of human toxocariasis. J Clin Microbiol 38: 1409–1413.
16. Ito A, Plancarte A, Ma L, Kong Y, Flisser A, et al. (1998) Novel antigens for neurocysticercosis: simple method for preparation and evaluation for serodiagnosis. Am J Trop Med Hyg 59: 291–294.
17. Sako Y, Nakao M, Ikejima T, Piao XZ, Nakaya K, et al. (2000) Molecular characterization and diagnostic value of *Taenia solium* low-molecular-weight antigen genes. J Clin Microbiol 38: 4439–4444.
18. Sato MO, Sako Y, Nakao M, Yamasaki H, Nakaya K, et al. (2006) Evaluation of purified *Taenia solium* glycoproteins and recombinant antigens in the serologic detection of human and swine cysticercosis. J Infect Dis 194: 1783–1790.
19. Sudewi AAR, Wandra T, Artha A, Nkouawa A, Ito A (2008) *Taenia solium* cysticercosis in Bali, Indonesia: serology and mtDNA analysis. Trans R Soc Trop Med Hyg 102: 96–98.
20. Yamasaki H, Taib R, Watanabe Y, Mak JW, Zasmy N, et al. (1998) Molecular characterization of a cDNA encoding an excretory-secretory antigen from *Toxocara canis* second-stage larvae and its application to the immunodiagnosis of human toxocariasis. Parasitol Int 47: 171–181.

21. De Andrade Lima Coelho R, De Carvalho LB, Jr., Perez EP, Araki K, Takeuchi T, et al. (2005) Prevalence of toxocariasis in northeastern Brazil based on serology using recombinant *Toxocara canis* antigen. Am J Trop Med Hyg 72: 103–107.
22. Fernando SD, Wickramasinghe VP, Kapilananda GM, Devasurendra RL, Amarasooriya JD, et al. (2007) Epidemiological aspects and risk factors of toxocariasis in a pediatric population in Sri Lanka. Southeast Asian J Trop Med Public Health 38: 983 990.
23. Sviben M, Cavlek TV, Missoni EM, Galinovic GM (2009) Seroprevalence of *Toxocara canis* infection among asymptomatic children with eosinophilia in Croatia. J Helminthol 83: 1 3.
24. Schantz PM, Wilkins PP, Tsang VCW (1998) Immigrants, imaging, and immunoblots: the emergence of neurocysticercosis as a significant public health problem. In: Scheld WM, Craig WA, Hughes JM, eds. Emerging Infection 2. Washington, USA: AMS. pp 213 242.
25. Ito A, Takayanagui OM, Sako Y, Sato MO, Odashima NS, et al. (2006) Neurocysticercosis: clinical manifestation, neuroimaging, serology and molecular confirmation of histopathologic specimens. Southeast Asian J Trop Med Public Health 37: Suppl(3)74–81.
26. Wandra T, Ito A, Yamasaki H, Suroso T, Margono SS (2003) *Taenia solium*, cysticercosis, Irian Jaya, Indonesia. Emerg Infect Dis 9: 884–885.
27. Ito A, Wandra T, Yamasaki H, Nakao M, Sako Y, et al. (2004) Cysticercosis/taeniasis in Asia and the Pacific. Vector-Borne Zoonotic Dis 4: 95–107.
28. Yanagida T, Yuzawa I, Joshi D, Sako Y, Nakao M, et al. (2010) Neurocysticercosis: assessing where the infection was acquired from. J Travel Med 17: 206–208.
29. Prabhakar S, Singh G (2002) Paediatric neurocysticercosis. In: Singh G, Prabhakar S, eds. *Taenia solium* Cysticercosis. Oxon, UK: CAB International. pp 257–262.
30. Guezala MC, Rodriguez S, Zamora H, Garcia HH, Gonzalez AE, et al. (2009) Development of a species-specific coproantigen ELISA for human *Taenia solium* taeniasis. Am J Trop Med Hyg 81: 433 437.
31. Nkouawa A, Sako Y, Nakao M, Nakaya K, Ito A (2009) Loop-mediated isothermal amplification method for differentiation and rapid detection of *Taenia* species. J Clin Microbiol 47: 168 174.

JOURNAL OF CLINICAL MICROBIOLOGY, Sept. 2010, p. 3350–3352 Vol. 48, No. 9
0095-1137/10/$12.00 doi:10.1128/JCM.00697-10

Evaluation of a Loop-Mediated Isothermal Amplification Method Using Fecal Specimens for Differential Detection of *Taenia* Species from Humans▽‡

Agathe Nkouawa,[1,2]† Yasuhito Sako,[1]†* Tiaoying Li,[3] Xingwang Chen,[3] Toni Wandra,[4] I. Kadek Swastika,[5] Minoru Nakao,[1] Tetsuya Yanagida,[1] Kazuhiro Nakaya,[6] Dongchuan Qiu,[3] and Akira Ito[1]†

Department of Parasitology[1] and Animal Laboratory for Medical Research,[6] Asahikawa Medical College, Asahikawa, Japan; Medical Research Center, Institute of Medical Research and Study of Medicinal Plants (IMPM), Yaoundé, Cameroon[2]; Institute of Parasitic Diseases, Sichuan Centers for Disease Control and Prevention, Chengdu, Sichuan Province, People's Republic of China[3]; Directorate General of Disease Control and Environmental Health, Ministry of Health, Jakarta, Indonesia[4]; and Department of Parasitology, Faculty of Medicine, University of Udayana, Bali, Indonesia[5]

Received 6 April 2010/Returned for modification 14 June 2010/Accepted 2 July 2010

We compared the performance of loop-mediated isothermal amplification (LAMP) with that of a multiplex PCR method for differential detection of human *Taenia* parasites in fecal specimens from taeniasis patients. The LAMP method, with no false positives, showed a higher sensitivity (88.4%) than the multiplex PCR (37.2%). Thus, it is expected that the LAMP method has a high value for molecular diagnosis of taeniasis.

Differential detection of *Taenia* species (*Taenia saginata*, *T. asiatica*, and *T. solium*) is a key point for control and prevention of taeniasis/cysticercosis in areas where *Taenia* disease is endemic. The identification of the carriers of *T. solium* tapeworms is most important for the prevention of cysticercosis, the most severe *Taenia* disease. Diagnosis of taeniasis by stool examination to detect taeniid eggs, the most common method, lacks both sensitivity and specificity because the eggs of *Taenia* species are morphologically indistinguishable. Moreover, *Taenia* species identification relying on comparative morphology of proglottids also lacks specificity.

The coproantigen detection method has proved to be a useful application in epidemiological surveys (1, 5), but this method is genus specific, not species specific. Recently, a *T. solium*-specific coproantigen enzyme-linked immunosorbent assay (ELISA) has been developed and shown to be potentially useful for mass screening (4). However, this test fails to identify *T. saginata* and *T. asiatica* taeniasis patients. Therefore, molecular tools are more reliable for differential identifications of taeniid parasites. Several PCR technique-based detection methods for *Taenia* species in fecal samples, including the multiplex PCR method with mitochondrial DNA (18), the PCR-restriction fragment length polymorphism method with mitochondrial DNA (15, 16), and the nested-PCR method with the Tso31 gene encoding the *T. solium* oncosphere-specific protein (10), have been reported. We have recently developed a loop-mediated isothermal amplification (LAMP) method targeting cytochrome *c* oxidase subunit 1 (cox1) and cathepsin L-like cysteine peptidase (clp) genes for differential detection of *Taenia* species (13). This method utilizes a *Bst* DNA polymerase with strand replacement activity and four primers that recognize six sequences on the target DNA under isothermal conditions. This method has proved to be simple and highly sensitive and specific for differential detection of *Taenia* species by using DNA prepared from proglottids, cysticerci, and fecal samples of taeniasis patients (12) without using sophisticated and expensive equipment. In the present study, we evaluated its sensitivity and specificity with fecal specimens from taeniasis patients by comparison of the results obtained by the LAMP method with those obtained by the multiplex PCR method.

Thirty-six fecal samples were collected in China from 26 *T. saginata* taeniasis patients, 5 *T. asiatica* taeniasis patients, and 5 *T. solium* taeniasis patients, and 7 fecal samples from Indonesia were obtained from *T. saginata* taeniasis patients after ethical approvals were received from the local health bureaus in both countries. The fecal samples were collected from patients prior to treatment with antiparasitic drugs to expel the worm, and both fecal samples and recovered parasites were stored in 70% ethanol for further analysis. The expelled tapeworm from each patient was identified by multiplex PCR (18). In addition, taeniid egg-negative fecal samples ($n = 11$) from persons without a history of tapeworm expulsion were used as negative controls. Copro-DNAs were extracted by using the QIAamp DNA stool Mini kit (Qiagen, Hilden, Germany) as described previously (13), and the extracted DNA was stored at −20°C until use. Moreover, to confirm the specificity of the LAMP method, DNAs prepared from parasite tissues of *Ascaris lumbricoides*, *Enterobius vermicularis*, *Hymenolepis nana*, and hookworms by using the DNeasy tissue kit (Qiagen) were used. Multiplex PCR and LAMP reactions were carried out as described previously (13, 18). In the multiplex PCR, the diagnostic DNA fragments with sizes of 827, 269, 720, and 984 bp were produced in *T. saginata*, *T. asiatica*, American/African

* Corresponding author. Mailing address: Department of Parasitology, Asahikawa Medical College, Midorigaoka Higashi 2-1-1-1, Asahikawa 078-8510, Hokkaido, Japan. Phone: 81-166-68-2421. Fax: 81-166-68-2429. E-mail: yasusako@asahikawa-med.ac.jp.
† These authors contributed equally to this work.
▽ Published ahead of print on 14 July 2010.
‡ The authors have paid a fee to allow immediate free access to this article.

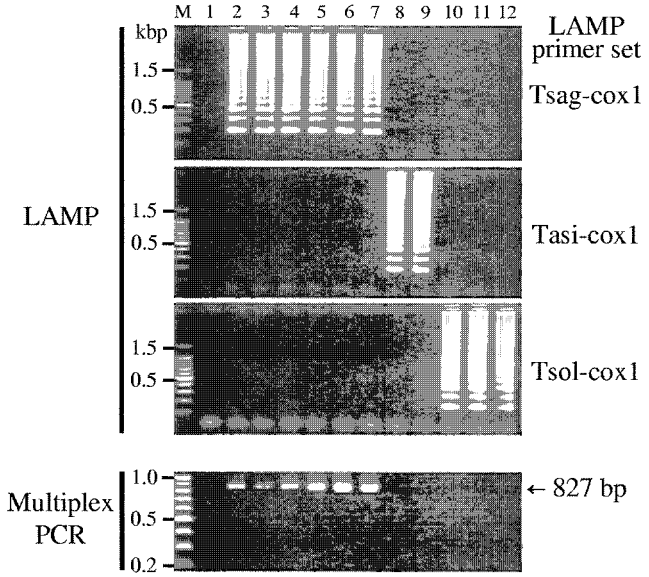

FIG. 1. Differential detection of human *Taenia* species by LAMP with cox1 primer sets and multiplex PCR. The figure shows a representative subset of the data. Lane M, 100-bp DNA ladder marker (Promega); lane 1, negative control without DNA; lanes 2 to 12, copro-DNA from each taeniasis patient. Tsag, *T. saginata*; Tasi, *T. asiatica*; Tsol, *T. solium*.

genotype *T. solium*, and Asian genotype *T. solium*, respectively. To verify the specificity of LAMP amplification, the sequences of LAMP amplicons were determined. Briefly, the LAMP products were digested with HinfI (37°C) or ApoI (50°C) enzymes (New England Biolabs, Beverly, MA) and purified by using the NucleoSpin ExTract kit (Macherey-Nagel, Düren, Germany). The digested products were cloned into the pGEM-T vector (Promega, Madison, WI), after filling in sticky ends to provide blunt-ended DNA and the addition of adenine to the ends by *Taq* DNA polymerase. The ligation mixtures were used to transform *Escherichia coli* DH5α, and each colony was analyzed by PCR using vector primers. The PCR products were sequenced as described previously (13). McNemar's test was applied to compare the sensitivities of LAMP and multiplex PCR.

Figure 1 shows the results of LAMP with cox1 primer sets and multiplex PCR, and Table 1 shows results for all methods with all samples. The LAMP products appeared as a ladder-like pattern on the agarose gel due to their characteristic stem-loop structure. The LAMP with cox1 primer sets could differentially detect target DNA in 37 out of 43 (86.0%) samples, which had *T. saginata* (n = 30), *T. asiatica* (n = 4), and *T. solium* (n = 3). The LAMP with clp primer sets differentially detected target DNA in 13 (30.2%) samples, which had *T. saginata* (n = 11), *T. asiatica* (n = 1), and *T. solium* (n = 1). No amplification from negative control fecal samples was observed by LAMP with cox1 and clp primer sets or by multiplex PCR (data not shown). All samples positive by LAMP with clp primer sets were positive by LAMP with cox1 primer sets except one sample. The differences between detection rates for the cox1 gene and the clp gene may be responsible for the number of copies of each target gene within samples, since a large amount of mitochondrial DNA exists in a cell, and the amount of mitochondrial DNA is one criterion for selection as a target DNA for detection. Although the cox1 gene was targeted, multiplex PCR could differentially identify *Taenia* parasites in only 16 samples, 1 sample after the first PCR and 15 samples after the second PCR. The samples negative by the multiplex PCR method were also negative by PCR using one individual primer set specific to each parasite cox1 gene (data not shown). The LAMP products from the multiplex PCR-negative samples were confirmed to be specific for *Taenia* parasites by sequencing (data no shown), which indicated the high sensitivity of the LAMP methods. *Taq* DNA polymerase used in PCR is often inactivated by inhibitors present in biological samples, which sometimes cause problems related to sensitivity and reproducibility. Due to the tolerance of the *Bst* DNA polymerase to inhibitors, in contrast to the *Taq* DNA polymerase, LAMP appears as a gold standard method to detect pathogens in fecal samples (2, 3, 7–9, 17, 19). The fact that LAMP is less affected by inhibitory substances in biological materials (6) is of great advantage when using fecal specimens that are known to contain a large amount of inhibitors.

Distribution of other intestinal helminthic parasites in areas where taeniasis is endemic raises the possibility of a mixed infection with *Taenia* and other helminthic parasites. Thus, the specificity of the LAMP method was assessed with DNAs extracted from parasites such as *Hymenolepis nana*, *Enterobius vermicularis*, *Ascaris lumbricoides*, and hookworms. All DNAs from these parasites were negative by LAMP with cox1 and clp primer sets (data not shown). LAMP has been shown to be a highly specific method because the amplification occurs when the four primers specifically recognize the six regions within the target sequence, a unique feature of LAMP (11, 14).

Other interesting advantages of LAMP are as follows: (i) it is possible to distinguish a positive LAMP reaction from a negative LAMP reaction by visual endpoint judgment of the turbidity caused by magnesium pyrophosphate as a by-product of the reaction, and (ii) the LAMP method, performed within 90 min, is faster than the multiplex PCR, which takes at least 4 h for completion of the two-round PCR, because LAMP is carried out under isothermal conditions by using a simple incubator, such as a water bath or a block heater.

In this study, we demonstrated that the LAMP method for identification of taeniid DNA in fecal specimens is more sen-

TABLE 1. Results of LAMP and multiplex PCR

Taenia sp.	No. of samples examined	No. of samples positive by method with indicated primer type(s)			
		LAMP			Multiplex PCR (cox1)
		cox1	clp	cox1 and/or clp	
T. saginata[a]	33	30	11	30	16
T. asiatica	5	4	1	4	0
T. solium	5	3	1[b]	4	0
Total	43	37	13	38	16

[a] For *T. saginata* samples, significant differences were observed between LAMP with cox1 and LAMP with clp and between LAMP with cox1 and multiplex PCR ($P < 0.001$).

[b] This sample was negative by LAMP with cox1 primer sets.

sitive, easier, and faster than the multiplex PCR method. In addition to these findings, the simplicity and cost-effectiveness of LAMP may make it easily applicable for a clinical practice as well as an epidemiological survey in areas of disease endemicity, especially developing countries. Therefore, the LAMP method as a molecular diagnosis tool will provide the successful control and prevention of taeniasis/cysticercosis in areas of endemicity.

This work was supported by the special fund for the leadership in science and technology in Asia from the Ministry of Education, Culture, Sports, Science and Technology, Japan, by the International Collaboration Research Fund from the Japan Society for the Promotion of Science (JSPS) (grant no. 17256002), by the JSPS Asia/Africa Science Platform Fund (support to A.I.), by the JSPS Japan-China Medical Exchange Program, and by the Japan-China Medical Association Fund (support to M.N.).

REFERENCES

1. **Allan, J. C., and P. S. Craig.** 2006. Coproantigens in taeniasis and echinococcosis. Parasitol. Int. **55**(Suppl.):S75–S80.
2. **Fukuda, S., Y. Sasaki, M. Kuwayama, and K. Miyazaki.** 2007. Simultaneous detection and genogroup-screening test for norovirus genogroups I and II from fecal specimens in single tube by reverse transcription-loop-mediated isothermal amplification assay. Microbiol. Immunol. **51**:547–550.
3. **Fukuda, S., S. Takao, M. Kuwayama, Y. Shimazu, and K. Miyazaki.** 2006. Rapid detection of norovirus from fecal specimens by real-time reverse transcription-loop-mediated isothermal amplification assay. J. Clin. Microbiol. **44**:1376–1381.
4. **Guezala, M. C., S. Rodriguez, H. Zamora, H. H. Garcia, A. E. Gonzalez, A. Tembo, J. C. Allan, and P. S. Craig.** 2009. Development of a species-specific coproantigen ELISA for human *Taenia solium* taeniasis. Am. J. Trop. Med. Hyg. **81**:433–437.
5. **Ito, A., and P. S. Craig.** 2003. Immunodiagnostic and molecular approaches for the detection of taeniid cestode infections. Trends Parasitol. **19**:377–381.
6. **Kaneko, H., T. Kawana, E. Fukushima, and T. Suzutani.** 2007. Tolerance of loop-mediated isothermal amplification to a culture medium and biological substances. J. Biochem. Biophys. Methods **70**:499–501.
7. **Karanis, P., O. Thekisoe, K. Kiouptsi, J. Ongerth, I. Igarashi, and N. Inoue.** 2007. Development and preliminary evaluation of a loop-mediated isothermal amplification procedure for sensitive detection of *Cryptosporidium* oocysts in fecal and water samples. Appl. Environ. Microbiol. **73**:5660–5662.
8. **Kato, H., T. Yokoyama, and Y. Arakawa.** 2005. Rapid and simple method for detecting the toxin B gene of *Clostridium difficile* in stool specimens by loop-mediated isothermal amplification. J. Clin. Microbiol. **43**:6108–6112.
9. **Liang, S. Y., Y. H. Chan, K. T. Hsia, J. L. Lee, M. C. Kuo, K. Y. Hwa, C. W. Chan, T. Y. Chiang, J. S. Chen, F. T. Wu, and D. D. Ji.** 2009. Development of loop-mediated isothermal amplification assay for detection of *Entamoeba histolytica*. J. Clin. Microbiol. **47**:1892–1895.
10. **Mayta, H., R. H. Gilman, E. Prendergast, J. P. Castillo, Y. O. Tinoco, H. H. Garcia, A. E. Gonzalez, and C. R. Sterling.** 2008. Nested PCR for specific diagnosis of *Taenia solium* taeniasis. J. Clin. Microbiol. **46**:286–289.
11. **Mori, Y., and T. Notomi.** 2009. Loop-mediated isothermal amplification (LAMP): a rapid, accurate, and cost-effective diagnostic method for infectious diseases. J. Infect. Chemother. **15**:62–69.
12. **Nakao, M., T. Yanagida, M. Okamoto, J. Knapp, A. Nkouawa, Y. Sako, and A. Ito.** 2010. State-of-the-art *Echinococcus* and *Taenia*: phylogenetic taxonomy of human-pathogenic tapeworms and its application to molecular diagnosis. Infect. Genet. Evol. **10**:444–452.
13. **Nkouawa, A., Y. Sako, M. Nakao, K. Nakaya, and A. Ito.** 2009. Loop-mediated isothermal amplification method for differentiation and rapid detection of *Taenia* species. J. Clin. Microbiol. **47**:168–174.
14. **Notomi, T., H. Okayama, H. Masubuchi, T. Yonekawa, K. Watanabe, N. Amino, and T. Hase.** 2000. Loop-mediated isothermal amplification of DNA. Nucleic Acids Res. **28**:e63.
15. **Nunes, C. M., A. K. Dias, F. E. Dias, S. M. Aoki, H. B. de Paula, L. G. Lima, and J. F. Garcia.** 2005. *Taenia saginata*: differential diagnosis of human taeniasis by polymerase chain reaction-restriction fragment length polymorphism assay. Exp. Parasitol. **110**:412–415.
16. **Nunes, C. M., L. G. Lima, C. S. Manoel, R. N. Pereira, M. M. Nakano, and J. F. Garcia.** 2003. *Taenia saginata*: polymerase chain reaction for taeniasis diagnosis in human fecal samples. Exp. Parasitol. **104**:67–69.
17. **Plutzer, J., and P. Karanis.** 2009. Rapid identification of *Giardia duodenalis* by loop-mediated isothermal amplification (LAMP) from faecal and environmental samples and comparative findings by PCR and real-time PCR methods. Parasitol. Res. **104**:1527–1533.
18. **Yamasaki, H., J. C. Allan, M. O. Sato, M. Nakao, Y. Sako, K. Nakaya, D. Qiu, W. Mamuti, P. S. Craig, and A. Ito.** 2004. DNA differential diagnosis of taeniasis and cysticercosis by multiplex PCR. J. Clin. Microbiol. **42**:548–553.
19. **Yoda, T., Y. Suzuki, K. Yamazaki, N. Sakon, M. Kanki, I. Aoyama, and T. Tsukamoto.** 2007. Evaluation and application of reverse transcription loop-mediated isothermal amplification for detection of noroviruses. J. Med. Virol. **79**:326–334.

Infection, Genetics and Evolution 10 (2010) 444–452

Contents lists available at ScienceDirect

Infection, Genetics and Evolution

journal homepage: www.elsevier.com/locate/meegid

Review

State-of-the-art *Echinococcus* and *Taenia*: Phylogenetic taxonomy of human-pathogenic tapeworms and its application to molecular diagnosis

Minoru Nakao [a], Tetsuya Yanagida [a], Munehiro Okamoto [b], Jenny Knapp [a], Agathe Nkouawa [a], Yasuhito Sako [a], Akira Ito [a,*]

[a] Department of Parasitology, Asahikawa Medical College, Midorigaoka Higashi 2-1-1-1, Asahikawa 078-8510, Japan
[b] Department of Parasitology, School of Veterinary Medicine, Faculty of Agriculture, Tottori University, Tottori 680-8553, Japan

ARTICLE INFO

Article history:
Received 26 January 2010
Accepted 26 January 2010
Available online 2 February 2010

Keywords:
Echinococcus
Taenia
Phylogeny
Molecular diagnosis

ABSTRACT

The taxonomy of tapeworms belonging to the family Taeniidae has been controversial because of the paucity of adult phenotypic characters and the great plasticity of larvae in intermediate hosts. The family consists of the medically important two genera *Echinococcus* and *Taenia*, which are closely related to each other. Cladistic approaches using the molecular data of DNA and the numerical data of morphologic characters are clarifying phylogenetic relationships among the members of these genera. The nucleotide data of worldwide taeniid parasites accumulated in public DNA databases may provide a basis for the development of molecular diagnostic tools, and make it possible to identify the parasites, at least the human *Taenia* spp. by non-morphologists. Furthermore, the detection of intraspecific genetic variations prompts evolutionary and ecological studies to address fundamental questions of parasite distributional patterns. Here, we introduce the recent advances of taeniid phylogeny and its application to molecular diagnosis.

Contents

1. Introduction 444
2. Basic knowledge of taeniid parasites 445
3. Phylogeny of *Echinococcus* spp. 446
4. Phylogeny of human *Taenia* and the closest relatives 447
5. Molecular clinical diagnosis 448
6. Molecular epidemiology and ecology 449
7. Perspectives of taeniid phylogeny 449
Acknowledgements 450
References 450

1. Introduction

The combination of morphological taxonomy, molecular genetics and evolutionary ecology is required to better understand the biodiversity of parasitic organisms. Fundamental information on their phenotypic and genotypic characteristics is especially important to control human and animal parasitic diseases. Moreover, regional and global phylogeographic surveys establish a basis of understanding for the evolutionary history of parasites.

The species identification of pathogenic organisms is essential for the diagnosis and treatment of infectious diseases. Multicellular parasites have traditionally been classified by morphological taxonomists, who provide a prerequisite fund of knowledge to differentiate etiologic agents isolated from humans and animals. However, the delineation of sibling or cryptic species is a difficult issue in morphological taxonomy. In addition to identifying species, exploring intraspecific variations has become a scientific imperative to characterize the local populations of parasites. The knowledge of parasite diversity at intraspecific level is necessary to understand the difference of clinical manifestations, and become a basis for the development of vaccines and immunodiagnostic antigens.

* Corresponding author. Tel.: +81 166 68 2420; fax: +81 166 68 2429.
E-mail address: akiraito@asahikawa-med.ac.jp (A. Ito).

1567-1348/$ – see front matter © 2010 Elsevier B.V. All rights reserved.
doi:10.1016/j.meegid.2010.01.011

The classification of tapeworms belonging to the family Taeniidae has been controversial because of the paucity of adult phenotypic characters and the great plasticity of larvae developed in various intermediate hosts. Recent advances on biochemical tools for DNA amplification and sequencing have provided a basis for the development of molecular taxonomy. Database catalogs known as "DNA barcoding" (Hebert et al., 2003) make it possible to identify parasites by non-morphologists. A DNA-based approach to the identification of parasites has also prompted the fields of molecular epidemiology and ecology. In this review, we deal especially with the phylogenetic taxonomy of human taeniid tapeworms and summarize the molecular diagnosis of the parasites.

2. Basic knowledge of taeniid parasites

Table 1 shows a brief list of human-pathogenic taeniid species and their closest relatives. The family Taeniidae is a medically important group of tapeworms constituted of the two genera *Echinococcus* Rudolphi 1801 and *Taenia* Linnaeus 1758. Two mammalian hosts showing predator–prey relationships are necessary to maintain the life cycle of the parasites. Carnivores are mostly definitive hosts for hermaphroditic adults, and herbivorous mammals serve as intermediate hosts for bladder larvae. When the intermediate hosts are eaten by the definitive hosts, ingested scolices attach to the intestinal mucosa and develop into adult tapeworms consisting of a chain of proglottids with genital organs. The gravid proglottids containing embryonated eggs are released into external environment. The intermediate hosts orally ingest the eggs, and hatched oncospheres invade various tissues to develop into fluid-filled bladder larvae. The larvae of both hydatid (*Echinococcus* spp.) and coenurus (*Taenia* spp.) enlarge their sizes in connection with the asexual reproduction of scolices in the bladders, whereas cysticercus (*Taenia* spp.) containing an invaginated scolex is mostly regarded as a non-multiplying larva.

All *Echinococcus* spp. are tiny tapeworms within several millimeters in length, but numerous tapeworms are parasitic on a canine definitive host because of the predation of infected animals containing many protoscolices. Medically important pathogens are the dog tapeworm *Echinococcus granulosus* sensu stricto (s. s.) and the fox tapeworm *Echinococcus multilocularis* (Eckert and Deplazes, 2004). Humans are vulnerable to the larval infestation through oral ingestion of eggs derived from feces of canine definitive hosts. Cystic echinococcosis caused by *E. granulosus* s. s. occurs worldwide, particularly in African, Asian and South American countries, whereas alveolar echinococcosis by *E. multilocularis* is restricted in the endemic areas of the Northern Hemisphere. Because sheep is a main intermediate host for *E. granulosus* s. s., a pastoral environment in which working dogs ingest the viscera of sheep is essential for maintaining the synanthropic cycle of the parasites. In human cystic echinococcosis, the liver and lungs are main target organs, and it takes many years to enlarge the spherical hydatid larvae. Alveolar echinococcosis caused by *E. multilocularis* exhibits a contrast to cystic echinococcosis. The parasite principally utilizes foxes as definitive hosts and voles as intermediate hosts, but humans are involved as an aberrant host. In humans, alveolar hydatid usually occurs in the liver, and minute vesicles proliferate slowly in the manner of exogenous budding. The invasive larval development is lethal to humans and animals. The disease is hyperendemic in the Tibetan communities of China (Schantz et al., 2003; Craig et al., 1992, 2008; Craig, 2006), but sporadically occurs even in industrialized European countries (Romig et al., 2006) and in Japan (Ito et al., 2003a).

Among the members of the genus *Taenia*, only *Taenia solium*, *Taenia saginata* and *Taenia asiatica* use humans as a definitive host. The latter species was formerly treated as a geographic race of *T.*

Table 1
Human-pathogenic species of the family Taeniidae and their closest relatives.

Species (genotype)[a]	Human infections[b]	Main hosts for		Distribution[c]
		Adult	Larva	
The genus *Echinococcus*				
E. granulosus (G1)	Common*	Dog	Sheep	Cosmopolitan
E. equinus (G4)	Unknown	Dog	Horse	PA
E. ortleppi (G5)	Rare*	Dog	Cattle	PA, ET and NT
E. canadensis (G6, G7)	Rare*	Dog	Camel, pig	PA, ET and NT
E. canadensis (G8, G10)	Rare*	Wolf	Cervid	PA and NA
E. felidis	Unknown	Lion	Warthog?	ET
E. multilocularis	Common*	Fox	Rodents	PA and NA
E. shiquicus	Unknown	Fox	Pika	PA (Tibet)
E. oligarthrus	Very rare*	Wild felids	Rodents	NT
E. vogeli	Not rare*	Bush dog	Rodents	NT
The genus *Taenia*				
T. saginata	Common#	Human	Cattle	Cosmopolitan
T. asiatica	Common#	Human	Pig	OR and PA (Asia)
T. solium	Common#,*	Human	Pig	Cosmopolitan
T. multiceps	Rare*	Canids	Ungulates	Cosmopolitan
T. serialis serialis	Rare*	Canids	Lagomorphs	Cosmopolitan
T. serialis brauni	Rare*	Canids	Lagomorphs	ET
T. crassiceps	Very rare*	Canids	Rodents	PA and NA
T. taeniaeformis	Very rare*	Felids	Rodents	Cosmopolitan
T. hyaenae	Unknown	Hyena	Ungulates	ET
T. crocutae	Unknown	Hyena	Ungulates	ET
T. simbae	Unknown	Felids	Ungulates	ET

[a] Data of each species are mainly taken from Verster (1969), Gasser et al. (1999), Loos-Frank (2000), Hoberg (2006), McManus and Thompson (2003), Xiao et al. (2005), Hüttner et al. (2008, 2009), Lavikainen et al. (2008), Moks et al. (2008), Saarma et al. (2009) and D'Alessandro and Rausch (2008). The genotypes G6 and G7 of *E. canadensis* were considered as a distinct species, namely *E. intermedius* (Thompson, 2008). The final taxonomic revision awaits the completion of ongoing studies.

[b] Asterisks indicate the accidental invasion of larvae into internal tissues, and hash marks denote the parasitism of adults in the small intestine. The categories of "very rare", "rare", "not rare" mean "few", "around 10 or more", and "around 100 or more" records have been reported, respectively.

[c] The areas are shown as zoogeographic regions; ET, Ethiopian; NA, Nearctic; NT, Neotropical; OR, Oriental; PA, Palearctic.

saginata, but now is considered as a distinct species (Eom and Rim, 1993). The human *Taenia* spp. attain a length of several meters. Swine serve as an intermediate host for *T. solium* and *T. asiatica*, while cattle do the intermediate host for *T. saginata*. Both *T. solium* and *T. saginata* are distributed worldwide through the trade of livestock and the migration of humans. The most severe illness is caused by *T. solium* because its larvae also parasitize human tissues such as subcutis, muscle and brain, resulting in cysticercosis (Ito et al., 2006; Sinha and Sharma, 2009). Eggs released from the tapeworm carriers cause cysticercosis to themselves (autoinfection) and other persons.

3. Phylogeny of *Echinococcus* spp.

Since *E. granulosus* was historically considered as the cause of both unilocular and alveolar echinococcosis, the species validity of *E. multilocularis* had been uncertain until 1950s. Following the discovery of alveolar cysts from microtine voles on St. Lawrence island, Alaska, Rausch and Schiller (1954) described the new species *Echinococcus sibiricensis* and considered it to be a causative agent for alveolar echinococcosis. However, Vogel (1957) directly demonstrated *E. multilocularis* to be a valid taxon, based on the morphological observation of adult tapeworms originated from the alveolar lesions of human cases in Germany. The Alaskan *E. sibiricensis*, therefore, was regarded as a synonym of *E. multilocularis*. The etiologic agent of alveolar echinococcosis in Russia was formerly described as *Alveococcus multilocularis* (Lukashenko, 1968), but this revision was not accepted widely. After the evaluation of *E. multilocularis*, the taxonomic status of *E. granulosus* still remained controversial because morphologically similar taxa were inadequately proposed based mainly on the host specificity (Williams and Sweatman, 1963; Verster, 1965). Rausch (1967) regarded most of them as synonyms of *E. granulosus*, and a subsequent classification permitted only four morphospecies, namely *E. granulosus*, *E. multilocularis*, *Echinococcus oligarthrus* and *Echinococcus vogeli* (Rausch and Bernstein, 1972). From ecological and epidemiological standpoints, *E. granulosus* was divided into "strains", depending on the usage of particular ungulates as intermediate hosts (Thompson et al., 1995).

The amplification of DNA fragments by polymerase chain reaction (PCR) has greatly accelerated taxonomic studies on parasites. In the early phase of the studies, universal PCR primers were designed from the conserved regions of DNA. Mitochondrial DNA (mtDNA) is always a major target to differentiate closely related taxa because of its rapid evolution (Brown et al., 1979). Molecular analyses using the mtDNA sequences of genes for cytochrome *c* oxidase subunit 1 (cox1) and NADH dehydrogenase subunit 1 (nad1) showed that *E. multilocularis*, *E. vogeli* and *E. oligarthrus* maintain their genetic identities and that *E. granulosus* can be divided into mainly 10 genotypes (G1–G10), corresponding to the strain definition (Bowles et al., 1992; Bowles and McManus, 1993; Scott et al., 1997; Lavikainen et al., 2003). Recent taxonomic revisions indicated that *E. granulosus* was an oversimplified species in which four or five cryptic species were intermixed (Thompson and McManus, 2002; Nakao et al., 2007). Reviving the names of synonyms and subspecies, the species has been split into *E. granulosus* s. s. (genotypes G1–G3), *Echinococcus equinus* (G4), *Echinococcus ortleppi* (G5) and *Echinococcus canadensis* (G6–G10). However, the species status of *E. canadensis* is still controversial. Thompson (2008) stated his opinion that the genotypes G6 and G7 (pig and camel strains) should be separated into *Echinococcus intermedius*. However, this nomenclature seems to be unsuitable because the original description of *E. intermedius* did not make a reference to the specificity of its intermediate hosts (López-Neyra and Soler Planas, 1943). No one has seen any study which could morphologically, genetically or ecologically connect with G6/G7 (the pig and camel strains) to *E. intermedius* (described form dogs). Therefore, comparative genetic studies on the genotypes G6–G10 are prerequisite for the taxonomic reconsideration of *E. canadensis* in order to clear the discrepancies among the papers (Le et al., 2002; Nakao et al., 2007; Lavikainen et al., 2008; Moks et al., 2008; Thompson, 2008; Saarma et al., 2009). As G9 reported by Scott et al. (1997) has not been confirmed yet (Kedra et al., 1999) or we have no chance to examine it, we do not deal with it.

Other valid species recently confirmed are *Echinococcus shiquicus* from the Tibetan fox (Xiao et al., 2005) and *Echinococcus felidis* from the African lion (Hüttner et al., 2008). Although their pathogenicity to humans is still unknown, both species are very important in reconstructing the phylogeny of *Echinococcus*. Recently, Tang et al. (2007) described a new species of *Echinococcus russicensis* from the corsac fox in Inner Mongolia. However, a comparative genetic study regarded it as a synonym of *E. multilocularis* (Nakao et al., 2009; Ito et al., 2010).

Bowles et al. (1995) at first analyzed the phylogenetic relationships among species and strains of *Echinococcus* using the sequence data of mtDNA (cox1 and nad1) and nuclear DNA (ribosomal ITS1). The results showed that *E. granulosus* was a species complex containing at least three evolutionarily diverse groups and that the Neotropical species *E. vogeli* and *E. oligarthrus* appeared distinct from the other species and strains. However, the data was less informative for inferring the phylogenetic position of *E. multilocularis* due to the short mtDNA sequences examined and the heterogeneous sequences of ITS1 observed in a single isolate.

The sequencing of complete mitochondrial genomes was greatly valuable in phylogenetic studies on *Echinococcus*. The comparison of the genomes of *E. granulosus* (sheep and horse strains) (Le et al., 2002) and *E. multilocularis* (Nakao et al., 2002b) triggered off a taxonomic revision (Thompson and McManus, 2002). Subsequently, a robust phylogenetic tree was reconstructed from the mitochondrial genomes of representative taxa (Nakao et al., 2007). The tree provides the following topics: (1) the Neotropical species *E. oligarthrus* and *E. vogeli* are basal lineages; (2) *E. multilocularis* and *E. shiquicus* are sister species; (3) *E. granulosus* s. s. is distantly related to *E. equinus*; (4) *E. ortleppi* and the genotypes G6, G7 and G8 are a monophyletic group. In particular, the close relationship of the G6, G7 and G8 suggested that these genotypes (camel, pig and cervid strains, respectively) should be unified into *E. canadensis*. Furthermore, Hüttner et al. (2008) showed that *E. granulosus* s. s. and *E. felidis* are sister species. These phylogenetic interrelationships (Nakao et al., 2007; Hüttner et al., 2008) are summarized in Fig. 1a. However, it is a little bit different from Lavikainen et al. (2008).

On the contrary, Saarma et al. (2009) presented a novel phylogenetic tree for *Echinococcus*, based on the DNA sequences of nuclear genes from published data (Xiao et al., 2005; Hüttner et al., 2008). The tree was inferred from the concatenated DNA data set of genes for elongation factor 1 alpha (ef1a), ezrin-radixin-moesin-like protein (elp), transforming growth factor beta receptor kinase (tgf), thioredoxin peroxidase (th) and calreticulin (cal). Although there was no sequence data of tgf, th and cal in the taxa of *E. ortleppi*, *E. shiquicus*, *E. felidis*, *E. vogeli* and *E. oligarthrus*, the full nuclear phylogeny was based at least on two genes, ef1a and elp, which provided large proportion of the phylogenetic signals. When compared with the result of mitochondrial genes, the nuclear tree showed the translocation of *E. multilocularis* and *E. shiquicus* into basal nodes (Fig. 1b). Further studies on these genotypes especially G5–G10 in Europe are important to get better resolution in the future.

Most recently, a new standpoint of phylogeny for *Echinococcus* was presented by using the EG95 antigen gene (eg95), which may influence host specificity by positively selected amino acids (Haag et al., 2009). The antigen is highly expressed in oncospheres

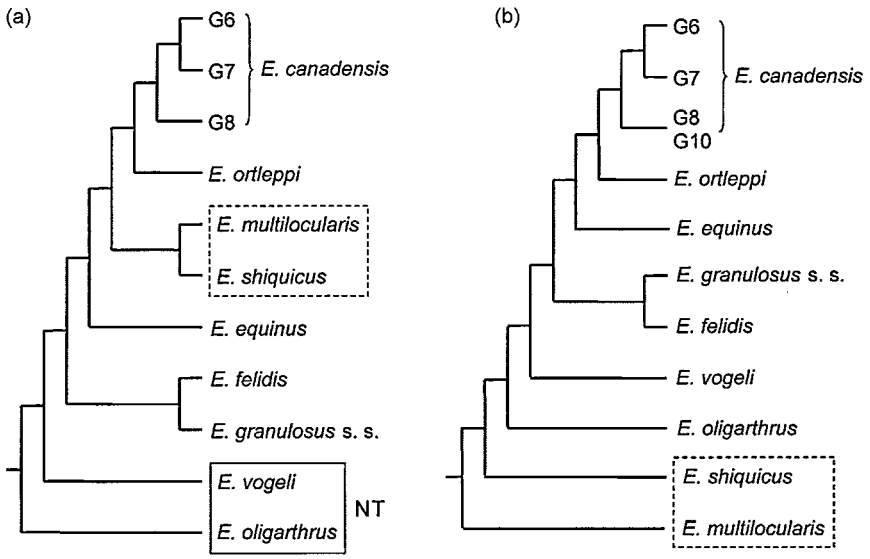

Fig. 1. Phylogenetic relationships of *Echinococcus* tapeworms summarized from recent publications. (a) The cladogram inferred by the nucleotide data of mitochondrial genes (Nakao et al., 2007; Hüttner et al., 2008). Neotropical (NT) species are surrounded by solid line. (b) The cladogram inferred by the nucleotide data of nuclear genes (Saarma et al., 2009). The translocation of taxa is shown by dotted line.

invading into the intermediate hosts, and mainly used as a vaccine for sheep. The evolution of EG95 isoforms was convergent with regard to the number of beta-sheets and alpha-helices, and a phylogenetic association existed between the degree of intermediate host specificity and the number of eg95 variants identified for each species.

4. Phylogeny of human *Taenia* and the closest relatives

Verster (1969) surveyed 70 *Taenia* spp., and showed 32 species to be valid. She divided the valid species into two groups, based on the arrangement of the genital ducts. The ducts of the group I pass between lateral excretory canals, but those of the group II pass the canals ventrally. The group I included human *Taenia* and other species infecting modern canines and felines with the exception of *Taenia taeniaeformis*. The group II consisted of *T. taeniaeformis* and other species infecting the primitive carnivores belonging to the families Viverridae and Mustelidae (e.g., *Taenia martis*, *Taenia mustelae* and *Taenia parva*). Formerly, several genera had been described within the family Taeniidae. The genera Multiceps Goeze 1782, Hydatigera Lamarck 1861 and Tetratirotaenia Abuladse 1964 were characterized with their larval morphology, whereas the genera Taeniarhynchus Weinland 1858, Monordotaenia Little 1967 and Fossor Honess 1937 were differentiated from *Taenia* only by the variations of adult rostellar hooks. All of these genera were treated as *Taenia* in the Verster's monograph. Currently, 42 species have been recognized within this genus (Eom and Rim, 1993; Loos-Frank, 2000; Rausch, 2003a; Hoberg, 2006).

Monophyly of *Taenia* spp. was demonstrated by a numerical taxonomic analysis using 26 morphological characters and 1 organotropic character in larval stage (Hoberg et al., 2000). The comprehensive phylogenetic tree including nearly all species of *Taenia* demonstrated that the above-mentioned old genera should be unified into *Taenia* as synonyms. As concerns human *Taenia* spp., the tree clarified that *T. solium* is distantly related to the sister species pair *T. saginata* and *T. asiatica*. It was also demonstrated that the zoonotic species *Taenia multiceps*, *Taenia serialis*, *Taenia crassiceps* and *T. taeniaeformis* (see Table 1) have no direct relation to the human *Taenia* spp. The phylogenetic structures of *Taenia* spp. supported the "out of Africa" view of human evolution and suggested a dietary change from herbivory to carnivory, which occurred among early hominids (Hoberg et al., 2001; Hoberg, 2006). As summarized in Fig. 2a, the obligate human parasite *T. solium* is connected directly with *Taenia hyaenae* and *Taenia crocutae*, the African tapeworms in hyenas. Moreover, the other human parasites *T. saginata* and *T. asiatica* are close relatives of *Taenia simbae*, the African tapeworm in lion. These phylogenetic relationships and divergence data analyses showed that taeniid tapeworms colonized hominids twice independently in Africa, and that the occurrence of human *Taenia* spp. predated the domestication events of pigs and cattle (Clutton-Brock, 1999; Larson et al., 2005). Thus, the phylogeny of *Taenia* spp. is also attractive to paleoanthropologists for its implication to ancient hominid lifeforms. However, the hypothesis of Hoberg et al. (2001) is totally dependent on the morphological data of *Taenia*, particularly the African species *T. hyaenae*, *T. crocutae* and *T. simbae*. The DNA profiles of those species are completely unknown because of the difficulties involved in sampling from African wildlife. Molecular phylogenetic studies are required to verify the "out of Africa" hypothesis for human *Taenia*.

Using the short mtDNA sequences of cox1 gene, Okamoto et al. (1995) initiated the molecular phylogenetic analysis of *Taenia* tapeworms. However, the phylogenetic position of human *Taenia* was not clarified because of the small number of taxa examined. Partial mtDNA sequences of cox1 and nad1 genes allowed to make phylogenetic trees in which three species of human *Taenia* were included (Gasser et al., 1999; Zhang et al., 2007). The trees clearly show that *T. saginata* and *T. asiatica* are closely related to each other, and that *T. solium* is distant from them. Furthermore, von Nickisch-Rosenegk et al. (1999) reconstructed a taeniid phylogenetic tree using the partial mtDNA sequences of small subunit rRNA gene (rrnS). The tree shows that *Taenia* spp. are divided into two groups, corresponding to the morphological division of Verster (1969). The basal nodes of the tree were occupied by the group of *T. taeniaeformis*, *T. martis*, *T. mustelae* and *T. parva*, which mainly utilizes primitive carnivores as definitive hosts, suggesting that *Taenia* had coevolved with carnivores. The arrangement of genital ducts in proglottid indicated by Verster (1969) seems to be a synapomorphic character in the evolution of *Taenia* spp. Using relatively many taxa of the genera *Taenia* and *Echinococcus*, a more reliable phylogenetic tree has recently been reconstructed from the concatenated mtDNA data set of nad1 and cox1 genes

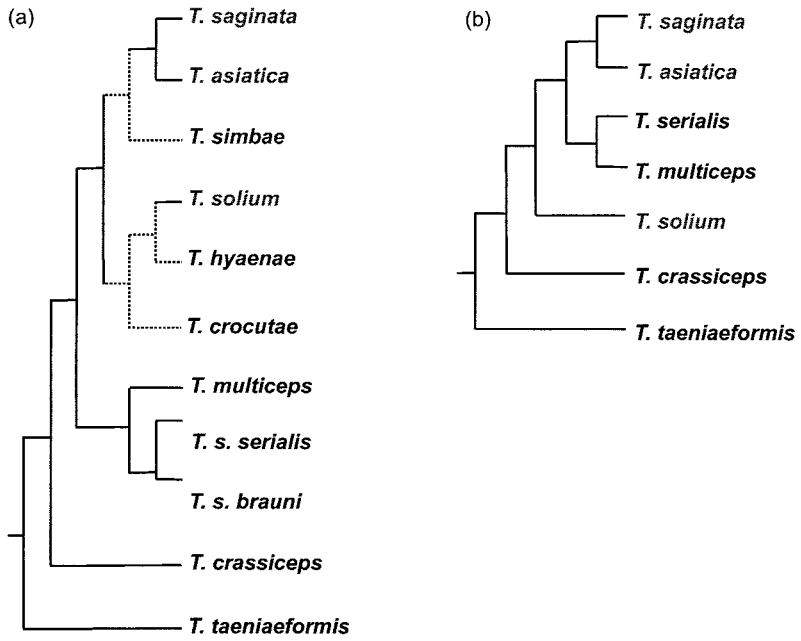

Fig. 2. Phylogenetic relationships of human-pathogenic *Taenia* spp. and their closest relatives. Closed circles indicate human intestinal parasites, while zoonotic species are marked with open circles. (a) The cladogram summarized from the data of numerical morphological analysis (Hoberg et al., 2001; Hoberg, 2006). Dotted branches indicate African lineage. (b) The cladogram summarized from the data of molecular analysis using the nucleotide sequences of mitochondrial genes (von Nickisch-Rosenegk et al., 1999; Gasser et al., 1999; Zhang et al., 2007; Lavikainen et al., 2008). Species in red are human *Taenia*. Species in blue are African species. (For interpretation of the references to color in this figure legend, the reader is referred to the web version of the article.)

(Lavikainen et al., 2008). Although it is a new challenge to reconstruct molecular phylogenetic tree on the two genera (Lavikainen et al., 2008), it is still preliminary and more data using more extensive mitochondrial and nuclear genes. Nevertheless, the tree shows that *Echinococcus* is a monophyletic genus but *Taenia* is paraphyletic because of the remarkable genetic similarity of *T. mustelae* to *Echinococcus*. Also in the numerical taxonomic analysis by Hoberg (2006), this strange species was the most divergent among *Taenia* taxa. These data may imply that a new genus will be described for *T. mustelae* and its relatives. Based on the published data, a molecular phylogenetic relationship among medically important *Taenia* spp. is summarized in Fig. 2b. Unfortunately, this tree is less informative than the morphology-based tree (Fig. 2a) because of the lack of taxa originated from African wildlife. However, the molecular tree showed that the enzootic species *T. serialis* and *T. multiceps* are genetically related to the human-pathogenic species *T. saginata* and *T. asiatica*. The phylotaxonomy of *Taenia* other than human *Taenia* spp. is still in its infancy and needs serious further investigation.

The complete DNA sequences of mitochondrial genomes have been determined in all species of human *Taenia* (Nakao et al., 2003a; Jeon et al., 2005, 2007). Gene arrangements in the genomes are totally identical with one another. However, the pairwise comparison of sequence divergence clearly shows that *T. solium* is distantly related to *T. saginata* and *T. asiatica*. The overall sequence difference between *T. saginata* and *T. asiatica* was 4.6%, while that between *T. saginata* and *T. solium* was 11% (Jeon et al., 2007). The sequence divergence of mitochondrial genes is frequently used as a yardstick for closely related species. For instance, most of congeneric species showed greater than 2% divergence (Hebert et al., 2003). This criterion supports the species validity of *T. asiatica*.

5. Molecular clinical diagnosis

The clinical diagnosis of echinococcosis in humans has been carried out based on the morphological characteristics of macro and microstructures, which are classified into cystic, alveolar and polycystic forms (Eckert and Deplazes, 2004). The pathological identification of the causative species is difficult in the cases of aberrant forms. Such lesions should be subjected to molecular diagnosis for species identification. However, simple differential tests have not been developed for the etiologic agents of *Echinococcus* because there are too many species and genotypes to easily confirm their genetic identity. At present time, clinical samples taken at biopsy are subjected to PCR, and the amplified fragments of mitochondrial and nuclear DNA are subsequently sequenced (Scott et al., 1997; Kedra et al., 1999; McManus et al., 2002; Kamenetzky et al., 2002; McManus and Thompson, 2003; Yang et al., 2005). Sequence homology search in public DNA databases via internet is the easiest way to identify the species and genotypes. PCR-based single-strand conformation polymorphism (SSCP) and restriction fragment length polymorphism (RFLP) analyses were tentatively performed at local scale, where the number of target species was limited (Zhang et al., 1999; Dinkel et al., 2004; Li et al., 2008).

In human *Taenia* infections, patients excrete proglottids and eggs together with feces. The parasite debris of tegumental turnover is also excreted into feces. The genetic identification of these parasite samples is a main purpose for molecular diagnosis. In the view of public health, detecting the carriers of *T. solium* tapeworms is the most important for the prevention of cysticercosis. The carriers discharge characteristic proglottids, but the morphological identification of fecal eggs is practically impossible. Molecular diagnosis, therefore, is needed to clarify causative species. Before the widespread use of PCR technique, Southern blot hybridization using specific DNA probes was utilized to distinguish between *T. solium* and *T. saginata* (Rishi and McManus, 1987; Flisser et al., 1988; Chapman et al., 1995). The assay was highly sensitive and specific, but the isotope-labeled probes were impractical in actual use. The method of PCR-RFLP was subsequently developed to diagnose both human taeniases, based on the sequence variations of nuclear DNA (Mayta et al., 2000; González

et al., 2002) and mtDNA (Rodriguez-Hidalgo et al., 2002). Among the forms of cestode larvae in human cerebral tissue, a proliferating acephalous form is referred to as "racemose" which could be either a larva of *T. multiceps*, *T. serialis*, *T. solium* or unknown *Taenia*. The sequence comparison of parasite DNA clearly reveals that the racemose is an aberrant larva of *T. solium* (Chung et al., 2005; Hinojosa-Juarez et al., 2008).

The widespread distribution of *T. asiatica* in Asian countries prompted us to genetically differentiate it from *T. saginata* (Ito et al., 2003b). Because of the close relationship between *T. asiatica* and *T. saginata*, variable mtDNA was selected as a target for PCR amplification. Based on the richness of thymine-base in cestode mtDNA, a base excision sequence scanning thymine-base method clearly differentiated *T. asiatica* from *T. saginata* and *T. solium* (Yamasaki et al., 2002). The differentiation method of the three human pathogens was further improved to a multiplex PCR method (Yamasaki et al., 2004a), which is applicable to the detection of *Taenia*-specific DNA in feces (copro-DNA). The molecular tools for identification or differentiation of human *Taenia* spp. and genotypes of *T. solium* (Nakao et al., 2002a,b) were overviewed by Ito et al. (2009). The multiplex PCR method is very simple, but requires a thermocycler in modern laboratories. For field use, a loop-mediated isothermal amplification (LAMP) method without using the PCR machine was developed to classify the human taeniid tapeworms (Nkouawa et al., 2009). Positive reactions of the LAMP can be confirmed by naked eyes without electrophoresis (Ito et al., in press).

6. Molecular epidemiology and ecology

Since echinococcosis and taeniasis are zoonotic diseases, prevalence data in both human and animal populations are essential for epidemiological surveillance in various endemic areas. In particular, the accurate diagnosis of definitive hosts (canines for *Echinococcus* and humans for *Taenia*) provides a key information to control the diseases. Immunological methods to detect copro-antigens or serum antibodies are applied for mass screening (Ito and Craig, 2003; Ito et al., 2007; Torgerson and Deplazes, 2009), but the immunodiagnosis is generally unable to differentiate pathogens at species level. In contrast, molecular diagnostic tools can provide differential data even in sympatric areas where several congeneric species coexist (Li et al., 2008). Furthermore, intraspecific variations detected by the molecular tools prompt evolutionary and ecological studies to address fundamental questions of parasite distributional patterns.

Stool examinations to detect taeniid eggs lack accuracy for epidemiological applications because eggs of all species belonging to the family Taeniidae are morphologically indistinguishable. Since canines serve as definitive hosts for many species of taeniid tapeworms, a PCR-based differentiation assay is required for canine surveys to confirm *Echinococcus* infections at species level. The detection of copro-antigens by enzyme-linked immunosorbent assay (ELISA) is now the best method for mass screening, and copro-PCR should be conducted for confirmatory purposes of antigen-positive samples (Torgerson and Deplazes, 2009). The sensitivity and specificity of PCR to detect *Echinococcus* DNA from canine feces have been evaluated under various conditions (Dinkel et al., 1998; Stefanić et al., 2004; Trachsel et al., 2007).

In ecological studies on *Echinococcus* spp., genetic markers are still needed to trace their spatial spread in synanthropic and non-synanthropic habitats. A commonly applied marker for the assessment of population genetic structures is highly polymorphic microsatellite, consisting of short tandemly repeated DNA. Single locus microsatellite markers are especially important in analyzing the kinship of parasites. Although the single locus markers have been isolated from *E. multilocularis* (Nakao et al., 2003b) and *E. granulosus* (Bartholomei-Santos et al., 2003), but their total number is insufficient for ecological use. Bart et al. (2006) found a microsatellite within anonymous multicopy DNA from a genomic library of *E. multilocularis*. This multi-loci microsatellite marker has been widely used to classify *E. multilocularis* individuals into genotypes (Knapp et al., 2009). However, a panel of single locus microsatellite markers should be prepared to depict the high-resolution genetic structures of *Echinococcus* populations. A haploid maternally inherited mtDNA marker has been alternatively used for population genetic studies. A mtDNA-based phylogeographic study demonstrated that *E. multilocularis* populations are generally divided into European, Asian and North American clades (Nakao et al., 2009). It seems likely that those clades were caused by the vicariance of foxes in the Pleistocene ice ages. Moreover, the statistical parsimony network of mtDNA haplotypes illustrated that recent founder effects arose in the Chinese populations of *E. granulosus* s. s. and *E. multilocularis*, whereas *E. shiquicus* which requires the Tibetan fox and plateau pika as the definitive and intermediate host, respectively (Xiao et al., 2005) were completely different from the former two species (Nakao et al., 2010).

A minimal genetic variability within *T. solium* populations was at first found in the short nucleotide sequences of a mitochondrial gene for cox1 and a nuclear gene for the diagnostic antigen Ts14 (Hancock et al., 2001). However, another survey using the complete nucleotide sequences of mitochondrial genes for cox1 and cob revealed that *T. solium* is divided into two main geographic clades (Nakao et al., 2002a). The one is widely distributed in Latin America and Africa, but the other is restricted in Asia. Such a geographic pattern suggests a possibility that *T. solium* was introduced recently into Latin America and Africa from Europe during the colonial age, which started 500 years ago, and that the tapeworm of another origin independently spread in Asia. Recently, this hypothesis was further supported by a new analysis of published data (Martinez-Hernandez et al., 2009). Population genetic studies using random amplified polymorphic DNA (RAPD) show that the local population of *T. solium* maintains a clonal structure, and suggest that the occurrence of local lineages is due to genetic recombination under limited gene flow (Vega et al., 2003; Maravilla et al., 2003). Microsatellite markers have not been isolated from human *Taenia* in spite of their usefulness (Campbell et al., 2006).

Parasite specimens and pathological tissues have been kept for long time in museums, hospitals and institutional laboratories. Molecular retrospective analyses using formalin-fixed or paraffin-embedded samples are important for studying the natural history of past epidemics. The success of PCR is uncertain in the long-term preserved samples because their genomic DNA is highly fragmented by formalin or other preservatives. Short DNA less than 300 base pairs can be generally amplified by using the fragmented DNA as a template for PCR (Schneider et al., 2008). A molecular retrospective study demonstrated the sympatric distribution of three human *Taenia* spp. in Thailand (Anantaphruti et al., 2007) and in Korea (Jeon et al., 2008). A similar PCR diagnosis was also performed in the clinical cases of cysticercosis (Yamasaki et al., 2004b; Yanagida et al., in press) and echinococcosis (Yamasaki et al., 2008).

7. Perspectives of taeniid phylogeny

In metazoan animals, Ernst Mayr's biological species concept (BSC) defines species as "groups of actually or potentially interbreeding natural populations, which are reproductively isolated from other such groups" (de Queiroz, 2005). However, modern molecular systematics develops the phylogenetic species concept (PSC) defining species as the smallest set whose members are descended from a common ancestor (Nixon and Wheeler, 1990). The monophyly-based PSC is less restrictive than the classic

BSC, in possible hybridization between closely related species. The strict application of the classic BSC to taeniid tapeworms may preclude the reliable detection of species.

The members of taeniid tapeworms have unique reproduction systems. The adult tapeworms of human *Taenia* spp. are hermaphroditic, and most infected persons harbor a single adult, suggesting that selfing is a main breeding manner. The reproduction system of *Echinococcus* spp. is more complex. Selfing also occurs in the adults, and asexual reproduction further occurs in the larval stage. These breeding manners are responsible for the genetic uniformity of local populations (Lymbery, 1992; Haag et al., 1999). Recently, Badaraco et al. (2008) indicated a possibility that gene introgression occurs infrequently among *E. granulosus* s. s., *E. ortleppi* and *E. canadensis*. Our research group also found the possible cases of gene introgression between *T. saginata* and *T. asiatica* (Nkouawa et al., 2009; Okamoto et al., 2010). These observations strongly suggest that reproductive isolation is incomplete among closely related species.

In the case of the sympatric species *T. saginata* and *T. asiatica*, "subspecies" is unsuitable for them because this category is for intraspecific populations which evolved allopatrically. The concept of "semispecies" (incipient species showing incomplete reproductive isolation) (Mayr, 1978), therefore, seems the most suitable for them. However, the semispecies is not a rank of the Linnaean taxonomic system. The populations of semispecies must be classified as the same species or different species. Biomedical researchers need pragmatic approaches to species concepts (Tibayrenc, 2006). Since each of *T. saginata* and *T. asiatica* maintains an identity on host specificity, both parasites should not be equated even though they can crossbreed.

As mentioned above, the classification of *E. canadensis* including the genotypes G6-G10 is a debatable issue. Although mitochondrial DNA markers can differentiate among the genotypes (Bowles et al., 1995; Lavikainen et al., 2003), their population genetic structures must be evaluated by using several nuclear DNA markers. The monophyly of genetic variants and the cessation of gene flow are critical points in considering the validity of species. In case the genotypes G6 and G7 (camel and pig strains) keep particular haplotypes at nuclear loci, they should be ranked as a distinct species as mentioned by Nakao et al. (2007) and Thompson (2008). If nuclear haplotypes are relatively common in all members of the genotypes, a rank of subspecies can be used to recognize their minor biological differences because the genotypes G8 and G10 (cervid strains) are ecologically and geographically segregated from the other genotypes by colonizing sylvan wildlife (Rausch, 2003b).

Concerning the phylogeny of the genus *Taenia*, the genetic makeups of the African species *T. hyaenae*, *T. crocutae* and *T. simbae* are absolutely necessary to clarify the evolutionary history of human *Taenia* spp. Chronological analyses based on the molecular phylogeny of the tapeworms may lead to a new paradigm in considering human evolution.

Acknowledgements

Author's works presented in this review were supported by the Japan Society for the Promotion of Science (JSPS) (14256001, 17256002, 21256003 to AI; 16500277, 18406008, 21406009 to MO), JSPS-Asia/Africa Science Platform Fund (2006–2011) to AI, and JSPS-Japan/China bilateral medical joint project on taeniasis/cysticercosis to MN (2009–2010).

References

Anantaphruti, M.T., Yamasaki, H., Nakao, M., Waikagul, J., Watthanakulpanich, D., Nuamtanong, S., Maipanich, W., Pubampen, S., Sanguankiat, S., Muennoo, C., Nakaya, K., Sato, M.O., Sako, Y., Okamoto, M., Ito, A., 2007. Sympatric occurrence of *Taenia solium*, *T. saginata*, and *T. asiatica*, Thailand. Emerg. Infect. Dis. 13, 1413–1416.

Badaraco, J.L., Ayala, F.J., Bart, J.M., Gottstein, B., Haag, K.L., 2008. Using mitochondrial and nuclear markers to evaluate the degree of genetic cohesion among *Echinococcus* populations. Exp. Parasitol. 119, 453–459.

Bart, J.M., Knapp, J., Gottstein, B., El-Garch, F., Giraudoux, P., Glowatzki, M.L., Berthoud, H., Maillard, S., Piarroux, R., 2006. EmsB, a tandem repeated multiloci microsatellite, new tool to investigate the genetic diversity of *Echinococcus multilocularis*. Infect. Genet. Evol. 6, 390–400.

Bartholomei-Santos, M.L., Heinzelmann, L.S., Oliveira, R.P., Chemale, G., Gutierrez, A.M., Kamenetzky, L., Haag, K.L., Zaha, A., 2003. Isolation and characterization of microsatellites from the tapeworm *Echinococcus granulosus*. Parasitology 126, 599–605.

Bowles, J., Blair, D., McManus, D.P., 1992. Genetic variants within the genus *Echinococcus* identified by mitochondrial DNA sequencing. Mol. Biochem. Parasitol. 54, 165–173.

Bowles, J., Blair, D., McManus, D.P., 1995. A molecular phylogeny of the genus *Echinococcus*. Parasitology 110, 317–328.

Bowles, J., McManus, D.P., 1993. NADH dehydrogenase 1 gene sequences compared for species and strains of the genus *Echinococcus*. Int. J. Parasitol. 23, 969–972.

Brown, W.M., George Jr., M., Wilson, A.C., 1979. Rapid evolution of animal mitochondrial DNA. Proc. Natl. Acad. Sci. U.S.A. 76, 1967–1971.

Campbell, G., Garcia, H.H., Nakao, M., Ito, A., Craig, P.S., 2006. Genetic variation in *Taenia solium*. Parasitol. Int. 55 (Suppl.), S121–S126.

Chapman, A., Vallejo, V., Mossie, K.G., Ortiz, D., Agabian, N., Flisser, A., 1995. Isolation and characterization of species-specific DNA probes from *Taenia solium* and *Taenia saginata* and their use in an egg detection assay. J. Clin. Microbiol. 33, 1283–1288.

Chung, J.Y., Kho, W.G., Hwang, S.Y., Je, E.Y., Chung, Y.T., Kim, T.S., Eom, K.S., Sohn, W.M., Cho, S.Y., Kong, Y., 2005. Molecular determination of the origin of acephalic cysticercus. Parasitology 130, 239–246.

Clutton-Brock, J., 1999. A Natural History of Domesticated Mammals. Cambridge University Press, pp. 1–237.

Craig, P.S., Deshan, L., MacPherson, S.N., Dazhong, S., Reynold, D., Barnish, G., Gottstein, B., Zhrong, W., 1992. A large focus of alveolar echinococcosis in central China. Lancet 340, 826–831.

Craig, P.S., Li, T., Qiu, J., Zhen, R., Wang, Q., Giraudoux, P., Ito, A., Heath, D., Warnock, B., Schantz, P., Yang, W., 2008. Echinococcoses and Tibetan communities. Emerg. Infect. Dis. 14, 1674–1675.

Craig, P.S., the Echinococcosis Working Group in China, 2006. Epidemiology of human alveolar echinococcosis in China. Parasitol. Int. 55 (Suppl.), S221–S225.

D'Alessandro, A., Rausch, R.L., 2008. New aspects of neotropical polycystic (*Echinococcus vogeli*) and unicystic (*Echinococcus oligarthrus*) echinococcosis. Clin. Microbiol. Rev. 21, 380–401.

de Queiroz, K., 2005. Ernst Mayr and the modern concept of species. Proc. Natl. Acad. Sci. U.S.A. 102 (Suppl. 1), 6600–6607.

Dinkel, A., Njoroge, E.M., Zimmermann, A., Wälz, M., Zeyhle, E., Elmahdi, I.E., Mackenstedt, U., Romig, T., 2004. A PCR system for detection of species and genotypes of the *Echinococcus granulosus*-complex, with reference to the epidemiological situation in eastern Africa. Int. J. Parasitol. 34, 645–653.

Dinkel, A., von Nickisch-Rosenegk, M., Bilger, B., Merli, M., Lucius, R., Romig, T., 1998. Detection of *Echinococcus multilocularis* in the definitive host: coprodiagnosis by PCR as an alternative to necropsy. J. Clin. Microbiol. 36, 1871–1876.

Eckert, J., Deplazes, P., 2004. Biological, epidemiological, and clinical aspects of echinococcosis, a zoonosis of increasing concern. Clin. Microbiol. Rev. 17, 107–135.

Eom, K.S., Rim, H.J., 1993. Morphologic descriptions of *Taenia asiatica* sp. n. Korean J. Parasitol. 31, 1–6.

Flisser, A., Reid, A., Garcia-Zepeda, E., McManus, D.P., 1988. Specific detection of *Taenia saginata* eggs by DNA hybridisation. Lancet 332, 1429–1430.

Gasser, R.B., Zhu, X., McManus, D.P., 1999. NADH dehydrogenase subunit 1 and cytochrome *c* oxidase subunit I sequences compared for members of the genus *Taenia* (Cestoda). Int. J. Parasitol. 29, 1965–1970.

González, L.M., Montero, E., Puente, S., López-Velez, R., Hernández, M., Sciutto, E., Harrison, L.J., Parkhouse, R.M., Gárate, T., 2002. PCR tools for the differential diagnosis of *Taenia saginata* and *Taenia solium* taeniasis/cysticercosis from different geographical locations. Diagn. Microbiol. Infect. Dis. 42, 243–249.

Haag, K.L., Araújo, A.M., Gottstein, B., Siles-Lucas, M., Thompson, R.C.A., Zaha, A., 1999. Breeding systems in *Echinococcus granulosus* (Cestoda; Taeniidae): selfing or outcrossing? Parasitology 118, 63–71.

Haag, K.L., Gottstein, B., Ayala, F.J., 2009. The EG95 antigen of *Echinococcus* spp. contains positively selected amino acids, which may influence host specificity and vaccine efficacy. PLoS One 4, e5362.

Hancock, K., Broughel, D.E., Moura, I.N., Khan, A., Pieniazek, N.J., Gonzalez, A.E., Garcia, H.H., Gilman, R.H., Tsang, V.C., 2001. Sequence variation in the cytochrome oxidase I, internal transcribed spacer 1, and Ts14 diagnostic antigen sequences of *Taenia solium* isolates from South and Central America, India, and Asia. Int. J. Parasitol. 31, 1601–1607.

Hebert, P.D., Ratnasingham, S., deWaard, J.R., 2003. Barcoding animal life: cytochrome *c* oxidase subunit 1 divergences among closely related species. Proc. R. Soc. Lond. B (Suppl.) 270, S96–S99.

Hinojosa-Juarez, A.C., Sandoval-Balanzario, M., McManus, D.P., Monroy-Ostria, A., 2008. Genetic similarity between cysticerci of *Taenia solium* isolated from human brain and from pigs. Infect. Genet. Evol. 8, 653–656.

Hoberg, E.P., 2006. Phylogeny of *Taenia*: species definitions and origins of human parasites. Parasitol. Int. 55 (Suppl.), S23–S30.

Hoberg, E.P., Alkire, N.L., de Queiroz, A., Jones, A., 2001. Out of Africa: origins of the *Taenia* tapeworms in humans. Proc. R. Soc. Lond. B 268, 781–787.

Hoberg, E.P., Jones, A., Rausch, R.L., Eom, K.S., Gardner, S.L., 2000. A phylogenetic hypothesis for species of the genus *Taenia* (Eucestoda: Taeniidae). J. Parasitol. 86, 89–98.

Hüttner, M., Nakao, M., Wassermann, T., Siefert, L., Boomker, J.D., Dinkel, A., Sako, Y., Mackenstedt, U., Romig, T., Ito, A., 2008. Genetic characterization and phylogenetic position of *Echinococcus felidis* (Cestoda: Taeniidae) from the African lion. Int. J. Parasitol. 38, 861–868.

Hüttner, M., Siefert, L., Mackenstedt, U., Romig, T., 2009. A survey of *Echinococcus* species in wild carnivores and livestock in East Africa. Int. J. Parasitol. 39, 1269–1276.

Ito, A., Craig, P.S., 2003. Immunodiagnostic and molecular approaches for the detection of taeniid cestode infections. Trends Parasitol. 19, 377–381.

Ito, A., Agvaandaram, G., Bat-Ochir, O., Chuluunbaatar, B., Gonchigsenghe, N., Yanagida, T., Sako, Y., Myadagsuren, N., Dorjsuren, T., Nakaya, K., Nakao, M., Ishikawa, Y., Davaajav, A., Dulmaa, N., 2010. Histopathological, serological and molecular analyses of alveolar echinococcosis cases in Mongolia. Am. J. Trop. Med. Hyg. 82, 266–269.

Ito, A., Nakao, M., Sako, Y., 2007. Echinococcosis: serological detection of patients and molecular identification of parasites. Future Microbiol. 2, 439–449.

Ito, A., Nakao, M., Wandra, T., 2003b. Human taeniasis and cysticercosis in Asia. Lancet 362, 1918–1920.

Ito, A., Nakao, M., Okamoto, M., Sako, Y., Yanagida, T., Nkouawa, A., Nakaya, K., in press. Taeniasis and cysticercosis: serological detection of patients and animals, and molecular identification of parasites. Future Microbiol.

Ito, A., Nakao, M., Sako, Y., Nakaya, K., Yanagida, T., Okamoto, M., 2009. Chapter 62 *Taenia*. In: Liu, D. (Ed.), Molecular Detection of Foodborne Pathogens. CRC Press, pp. 839–850.

Ito, A., Romig, T., Takahashi, K., 2003a. Perspective on control options for *Echinococcus multilocularis* with particular reference to Japan. Parasitology 127, S159–S172.

Ito, A., Takayanagui, O.M., Sako, Y., Sato, M.O., Odashima, N.S., Yamasaki, H., Nakaya, K., Nakao, M., 2006. Neurocysticercosis: clinical manifestation, neuroimaging, serology and molecular confirmation of histopathologic specimens. Southeast Asian J. Trop. Med. Public Health 37 (Suppl. 3), 74–81.

Jeon, H.K., Kim, K.H., Chai, J.Y., Yang, H.J., Rim, H.J., Eom, K.S., 2008. Sympatric distribution of three human *Taenia* tapeworms collected between 1935 and 2005 in Korea. Korean J. Parasitol. 46, 235–241.

Jeon, H.K., Kim, K.H., Eom, K.S., 2007. Complete sequence of the mitochondrial genome of *Taenia saginata*: comparison with *T. solium* and *T. asiatica*. Parasitol. Int. 56, 243–246.

Jeon, H.K., Lee, K.H., Kim, K.H., Hwang, U.W., Eom, K.S., 2005. Complete sequence and structure of the mitochondrial genome of the human tapeworm, *Taenia asiatica* (Platyhelminthes; Cestoda). Parasitology 130, 717–726.

Kamenetzky, L., Gutierrez, A.M., Canova, S.G., Haag, K.L., Guarnera, E.A., Parra, A., García, G.E., Rosenzvit, M.C., 2002. Several strains of *Echinococcus granulosus* infect livestock and humans in Argentina. Infect. Genet. Evol. 2, 129–136.

Kedra, A.H., Swiderski, Z., Tkach, V.V., Dubinsky, P., Pawlowski, Z., Stefaniak, J., Pawlowski, J., 1999. Genetic analysis of *Echinococcus granulosus* from humans and pigs in Poland, Slovakia and Ukraine. A multicenter study. Acta Parasitol. 44, 248–254.

Knapp, J., Bart, J.M., Giraudoux, P., Glowatzki, M.L., Breyer, I., Raoul, F., Deplazes, P., Duscher, G., Martinek, K., Dubinsky, P., Guislain, M.H., Cliquet, F., Romig, T., Malczewski, A., Gottstein, B., Piarroux, R., 2009. Genetic diversity of the cestode *Echinococcus multilocularis* in red foxes at a continental scale in Europe. PLoS Negl. Trop. Dis. 3, e452.

Larson, G., Dobney, K., Albarella, U., Fang, M., Matisoo-Smith, E., Robins, J., Lowden, S., Finlayson, H., Brand, T., Wilerslev, E., Rowley-Conwy, P., Andersson, L., Cooper, A., 2005. Worldwide phylogeography of wild boar reveals multiple centers of pig domestication. Science 307, 1618–1621.

Lavikainen, A., Haukisalmi, V., Lehtinen, M.J., Henttonen, H., Oksanen, A., Meri, S., 2008. A phylogeny of members of the family Taeniidae based on the mitochondrial cox1 and nad1 gene data. Parasitology 135, 1457–1467.

Lavikainen, A., Lehtinen, M.J., Meri, T., Hirvelä-Koski, V., Meri, S., 2003. Molecular genetic characterization of the Fennoscandian cervid strain, a new genotypic group (G10) of *Echinococcus granulosus*. Parasitology 127, 207–215.

Le, T.H., Pearson, M.S., Blair, D., Dai, N., Zhang, L.H., McManus, D.P., 2002. Complete mitochondrial genomes confirm the distinctiveness of the horse-dog and sheep-dog strains of *Echinococcus granulosus*. Parasitology 124, 97–112.

Li, T., Ito, A., Nakaya, K., Qiu, J., Nakao, M., Zhen, R., Xiao, N., Chen, X., Giraudoux, P., Craig, P.S., 2008. Species identification of human echinococcosis using histopathology and genotyping in northwestern China. Trans. R. Soc. Trop. Med. Hyg. 102, 585–590.

Loos-Frank, B., 2000. An up-date of Verster's (1969) 'Taxonomic revision of the genus *Taenia* Linnaeus' (Cestoda) in table format. Syst. Parasitol. 45, 155–183.

López-Neyra, C.R., Soler Planas, M.A., 1943. Revision del genero *Echinococcus* Rud y descripción de una especie nueva parárita intestinal del perro en Almería. Rev. Ibér. Parasitol. 3, 169–194.

Lukashenko, N.P., 1968. Comparative biologic and pathologic studies of *Alveococcus multilocularis*. Arch. Environ. Health. 17, 676–680.

Lymbery, A.J., 1992. Interbreeding, monophyly and the genetic yardstick: species concepts in parasites. Parasitol. Today 8, 208–211.

Maravilla, P., Souza, V., Valera, A., Romero-Valdovinos, M., Lopez-Vidal, Y., Dominguez-Alpizar, J.L., Ambrosio, J., Kawa, S., Flisser, A., 2003. Detection of genetic variation in *Taenia solium*. J. Parasitol. 89, 1250–1254.

Martinez-Hernandez, F., Jimenez-Gonzalez, D.E., Chenillo, P., Alonso-Fernandez, C., Maravilla, P., Flisser, A., 2009. Geographical widespread of two lineages of *Taenia solium* due to human migrations: can population genetic analysis strengthen this hypothesis? Infect. Genet. Evol. 9, 1108–1114.

Mayr, E., 1978. Origin and history of some terms in systematic and evolutionary biology. Syst. Zool. 27, 83–88.

Mayta, H., Talley, A., Gilman, R.H., Jimenez, J., Verastegui, M., Ruiz, M., Garcia, H.H., Gonzalez, A.E., 2000. Differentiating *Taenia solium* and *Taenia saginata* infections by simple hematoxylin–eosin staining and PCR-restriction enzyme analysis. J. Clin. Microbiol. 38, 133–137.

McManus, D.P., Thompson, R.C.A., 2003. Molecular epidemiology of cystic echinococcosis. Parasitology 127, S37–S51.

McManus, D.P., Zhang, L., Castrodale, L.J., Le, T.H., Pearson, M., Blair, D., 2002. Short report: molecular genetic characterization of an unusually severe case of hydatid disease in Alaska caused by the cervid strain of *Echinococcus granulosus*. Am. J. Trop. Med. Hyg. 67, 296–298.

Moks, E., Jõgisalu, I., Valdmann, H., Saarma, U., 2008. First report of *Echinococcus granulosus* G8 in Eurasia and a reappraisal of the phylogenetic relationships of 'genotypes' G5–G10. Parasitology 135, 647–654.

Nakao, M., McManus, D.P., Schantz, P.M., Craig, P.S., Ito, A., 2007. A molecular phylogeny of the genus *Echinococcus* inferred from complete mitochondrial genomes. Parasitology 134, 713–722.

Nakao, M., Li, T., Han, X., Ma, X., Xiao, N., Qiu, J., Wang, H., Yanagida, T., Mamuti, W., Wen, H., Moro, P.L., Giraudoux, P., Craig, P.S., Ito, A., 2010. Genetic polymorphisms of *Echinococcus* tapeworms in China as determined by mitochondrial and nuclear DNA sequences. Int. J. Parasitol. 40, 379–385.

Nakao, M., Okamoto, M., Sako, Y., Yamasaki, H., Nakaya, K., Ito, A., 2002a. A phylogenetic hypothesis for the distribution of two genotypes of the pig tapeworm *Taenia solium* worldwide. Parasitology 124, 657–662.

Nakao, M., Sako, Y., Ito, A., 2003a. The mitochondrial genome of the tapeworm *Taenia solium*: a finding of the abbreviated stop codon U. J. Parasitol. 89, 633–635.

Nakao, M., Sako, Y., Ito, A., 2003b. Isolation of polymorphic microsatellite loci from the tapeworm *Echinococcus multilocularis*. Infect. Genet. Evol. 3, 159–163.

Nakao, M., Yokoyama, N., Sako, Y., Fukunaga, M., Ito, A., 2002b. The complete mitochondrial DNA sequence of the cestode *Echinococcus multilocularis* (Cyclophyllidea: Taeniidae). Mitochondrion 1, 497–509.

Nakao, M., Xiao, N., Okamoto, M., Yanagida, T., Sako, Y., Ito, A., 2009. Geographic pattern of genetic variation in the fox tapeworm *Echinococcus multilocularis*. Parasitol. Int. 58, 384–389.

Nixon, K.C., Wheeler, Q.D., 1990. An amplification of the phylogenetic species concept. Cladistics 6, 211–223.

Nkouawa, A., Sako, Y., Nakao, M., Nakaya, K., Ito, A., 2009. Loop-mediated isothermal amplification method for differentiation and rapid detection of *Taenia* species. J. Clin. Microbiol. 47, 168–174.

Okamoto, M., Bessho, Y., Kamiya, M., Kurosawa, T., Horii, T., 1995. Phylogenetic relationships within *Taenia taeniaeformis* variants and other taeniid cestodes inferred from the nucleotide sequence of the cytochrome *c* oxidase subunit I gene. Parasitol. Res. 81, 451–458.

Okamoto, M., Nakao, M., Blair, D., Anantaphruti, M.T., Waikagul, J., Ito, A., 2010. Evidence of hybridization between *Taenia saginata* and *Taenia asiatica*. Parasitol. Int. 59, 70–74.

Rausch, R.L., 1967. A consideration of intraspecific categories in the genus *Echinococcus* Rudolphi, 1801 (Cestoda: Taeniidae). J. Parasitol. 53, 484–491.

Rausch, R.L., 2003a. *Taenia pencei* n. sp. from the Ringtail, *Bassariscus astutus* (Carnivora: Procyonidae), in Texas, U.S.A. Comp. Parasitol. 70, 1–10.

Rausch, R.L., 2003b. Cystic echinococcosis in the Arctic and Sub-Arctic. Parasitology 127 (Suppl.), S73–S85.

Rausch, R.L., Bernstein, J.J., 1972. *Echinococcus vogeli* sp. n. (Cestoda: Taeniidae) from the bush dog, *Speothos venaticus* (Lund). Z. Tropenmed. Parasitol. 23, 25–34.

Rausch, R., Schiller, E.L., 1954. Studies on the helminth fauna of Alaska. XXIV. *Echinococcus sibiricensis* n. sp., from St. Lawrence Island. J. Parasitol. 40, 659–662.

Rishi, A.K., McManus, D.P., 1987. DNA probes which unambiguously distinguish *Taenia solium* from *T. saginata*. Lancet 330, 1275–1276.

Rodriguez-Hidalgo, R., Geysen, D., Benítez-Ortiz, W., Geerts, S., Brandt, J., 2002. Comparison of conventional techniques to differentiate between *Taenia solium* and *Taenia saginata* and an improved polymerase chain reaction-restriction fragment length polymorphism assay using a mitochondrial 12S rDNA fragment. J. Parasitol. 88, 1007–1011.

Romig, T., Dinkel, A., Mackenstedt, U., 2006. The present situation of echinococcosis in Europe. Parasitol. Int. 55 (Suppl.), S187–S191.

Saarma, U., Jõgisalu, I., Moks, E., Varcasia, A., Lavikainen, A., Oksanen, A., Simsek, S., Andresiuk, V., Denegri, G., González, L.M., Ferrer, E., Gárate, T., Rinaldi, L., Maravilla, P., 2009. A novel phylogeny for the genus *Echinococcus*, based on nuclear data, challenges relationships based on mitochondrial evidence. Parasitology 136, 317–328.

Schantz, P.M., Wang, H., Qiu, J., Liu, F.J., Saito, E., Emshoff, A., Ito, A., Roberts, J.M., Delker, C., 2003. Echinococcosis on the Tibetan Plateau: prevalence and risk factors for cystic and alveolar echinococcosis in Tibetan populations in Qinghai Province, China. Parasitology 127, S109–S120.

Schneider, R., Gollackner, B., Edel, B., Schmid, K., Wrba, F., Tucek, G., Walochnik, J., Auer, H., 2008. Development of a new PCR protocol for the detection of species and genotypes (strains) of *Echinococcus* in formalin-fixed, paraffin-embedded tissues. Int. J. Parasitol. 38, 1065–1071.

Scott, J.C., Stefaniak, J., Pawlowski, Z.S., McManus, D.P., 1997. Molecular genetic analysis of human cystic hydatid cases from Poland: identification of a new genotypic group (G9) of *Echinococcus granulosus*. Parasitology 114, 37–43.

Sinha, S., Sharma, B.S., 2009. Neurocysticercosis: a review of current status and management. J. Clin. Neurosci. 16, 867–876.

Stefanić, S., Shaikenov, B.S., Deplazes, P., Dinkel, A., Torgerson, P.R., Mathis, A., 2004. Polymerase chain reaction for detection of patent infections of *Echinococcus granulosus* ("sheep strain") in naturally infected dogs. Parasitol. Res. 92, 347–351.

Tang, C., Cui, G., Qian, Y., Kang, Y., Wang, Y., Peng, W., Lu, H., Chen, D., 2007. Studies on the alveolar *Echinococcus* species in northward Daxingan mountains, Inner Mongolia, China. III. *Echinococcus russicensis* sp. nov. Chin. J. Zoonoses 23, 957–963.

Thompson, R.C.A., 2008. The taxonomy, phylogeny and transmission of *Echinococcus*. Exp. Parasitol. 119, 439–446.

Thompson, R.C.A., McManus, D.P., 2002. Towards a taxonomic revision of the genus *Echinococcus*. Trends Parasitol. 18, 452–457.

Thompson, R.C.A., Lymbery, A.J., Constantine, C.C., 1995. Variation in *Echinococcus*: towards a taxonomic revision of the genus. Adv. Parasitol. 35, 145–176.

Tibayrenc, M., 2006. The species concept in parasites and other pathogens: a pragmatic approach? Trends Parasitol. 22, 66–70.

Torgerson, P.R., Deplazes, P., 2009. Echinococcosis: diagnosis and diagnostic interpretation in population studies. Trends Parasitol. 25, 164–170.

Trachsel, D., Deplazes, P., Mathis, A., 2007. Identification of taeniid eggs in the faeces from carnivores based on multiplex PCR using targets in mitochondrial DNA. Parasitology 134, 911–920.

Vega, R., Piñero, D., Ramanankandrasana, B., Dumas, M., Bouteille, B., Fleury, A., Sciutto, E., Larralde, C., Fragoso, G., 2003. Population genetic structure of *Taenia solium* from Madagascar and Mexico: implications for clinical profile diversity and immunological technology. Int. J. Parasitol. 33, 1479–1485.

Verster, A., 1965. Review of *Echinococcus* species in South Africa. Onderstepoort J. Vet. Res. 32, 7–118.

Verster, A., 1969. A taxonomic revision of the genus *Taenia* Linnaeus, 1758s. str. Onderstepoort J. Vet. Res. 36, 3–58.

Vogel, H., 1957. Ueber den *Echinococcus multilocularis* Süddeutschlands. I. Das Bandwurmstadium von Stämmen menschlicher und tierischer Herkunft. Z. Tropenmed. Parasitology 8, 404–454.

von Nickisch-Rosenegk, M., Silva-Gonzalez, R., Lucius, R., 1999. Modification of universal 12S rDNA primers for specific amplification of contaminated *Taenia* spp. (Cestoda) gDNA enabling phylogenetic studies. Parasitol. Res. 85, 819–825.

Williams, R.J., Sweatman, G.K., 1963. On the transmission, biology and morphology of *Echinococcus granulosus equinus*, a new subspecies of hydatid tapeworm in horses in Great Britain. Parasitology 53, 391–407.

Xiao, N., Qiu, J., Nakao, M., Li, T., Yang, W., Chen, X., Schantz, P.M., Craig, P.S., Ito, A., 2005. *Echinococcus shiquicus* n. sp., a taeniid cestode from Tibetan fox and plateau pika in China. Int. J. Parasitol. 35, 693–701.

Yamasaki, H., Allan, J.C., Sato, M.O., Nakao, M., Sako, Y., Nakaya, K., Qiu, D., Mamuti, W., Craig, P.S., Ito, A., 2004a. DNA differential diagnosis of taeniasis and cysticercosis by multiplex PCR. J. Clin. Microbiol. 42, 548–553.

Yamasaki, H., Matsunaga, S., Yamamura, K., Chang, C.C., Kawamura, S., Sako, Y., Nakao, M., Nakaya, K., Ito, A., 2004b. Solitary neurocysticercosis case caused by Asian genotype of *Taenia solium* confirmed by mitochondrial DNA analysis. J. Clin. Microbiol. 42, 3891–3893.

Yamasaki, H., Nakao, M., Nakaya, K., Schantz, P.M., Ito, A., 2008. Genetic analysis of *Echinococcus multilocularis* originating from a patient with alveolar echinococcosis occurring in Minnesota in 1977. Am. J. Trop. Med. Hyg. 79, 245–247.

Yamasaki, H., Nakao, M., Sako, Y., Nakaya, K., Sato, M.O., Mamuti, W., Okamoto, M., Ito, A., 2002. DNA differential diagnosis of human taeniid cestodes by base excision sequence scanning thymine-base reader analysis with mitochondrial genes. J. Clin. Microbiol. 40, 3818–3821.

Yanagida, T., Yuzawa, I., Joshi, D.D., Sako, Y., Nakao, M., Nakaya, K., Kawano, N., Oka, H., Fujii, K., Ito, A., in press. Neurocysticercosis: assessing where the infection was acquired? J. Travel Med.

Yang, Y.R., Rosenzvit, M.C., Zhang, L.H., Zhang, J.Z., McManus, D.P., 2005. Molecular study of *Echinococcus* in west-central China. Parasitology 131, 547–555.

Zhang, L., Gasser, R.B., Zhu, X., McManus, D.P., 1999. Screening for different genotypes of *Echinococcus granulosus* within China and Argentina by single-strand conformation polymorphism (SSCP) analysis. Trans. R. Soc. Trop. Med. Hyg. 93, 329–334.

Zhang, L., Hu, M., Jones, A., Allsopp, B.A., Beveridge, I., Schindler, A.R., Gasser, R.B., 2007. Characterization of *Taenia madoquae* and *Taenia regis* from carnivores in Kenya using genetic markers in nuclear and mitochondrial DNA, and their relationships with other selected taeniids. Mol. Cell. Probes 21, 379–385.

CLINICAL AND VACCINE IMMUNOLOGY, June 2010, p. 944–948 Vol. 17, No. 6
1556-6811/10/$12.00 doi:10.1128/CVI.00026-10

Immunoglobulin G Subclass Responses to Recombinant Em18 in the Follow-Up of Patients with Alveolar Echinococcosis in Different Clinical Stages[▽]

Dennis Tappe,[1]*§ Yasuhito Sako,[2]§ Sonoyo Itoh,[2] Matthias Frosch,[1] Beate Grüner,[3] Peter Kern,[3] and Akira Ito[2]§

Institute of Hygiene and Microbiology, Josef-Schneider-Str. 2, 97080 Würzburg,[1] and Comprehensive Infectious Diseases Center, Division of Infectious Diseases and Clinical Immunology, University Hospital and Medical Center Ulm, Albert-Einstein-Allee 23, 89081 Ulm,[3] Germany, and Department of Parasitology, Asahikawa Medical College, Midorigaoka Higashi 2-1-1-1, Asahikawa 078-8510, Japan[2]

Received 13 January 2010/Returned for modification 15 March 2010/Accepted 2 April 2010

In this study, we compared the sequential responses of immunoglobulin G (IgG) subclasses to the diagnostic antigen Em18 in sera from patients with alveolar echinococcosis. A total of 225 sera from 36 patients at different clinical stages according to the WHO-PNM staging system were tested. The antibody responses were measured for cohorts with resected and unresected parasitic lesions by enzyme-linked immunosorbent assays (ELISA). Total IgG and, to a lesser extent, IgG4 antibody levels against Em18 correlated with all PNM stages before treatment, whereas levels of IgG2 were low and IgG3 was undetectable. Antibody kinetics, however, depended on the treatment rather than on the PNM stage. For some patients, after curative surgery, IgG1 antibodies dropped below the cutoff earlier than other antibodies, followed by total IgG and IgG4 within 18 months. For some patients with recurrences after surgery, IgG1 and IgG4 reappeared, whereas patients with unresectable lesions but stable disease showed steady declines in the levels of all antibodies, and IgG1 became undetectable in some patients. Additional testing of IgE responses to Em18 showed constantly low levels at all stages and in all cohorts.

Alveolar echinococcosis (AE) is caused by the vesicular larval stage of the fox tapeworm *Echinococcus multilocularis*. The helminth causes dangerous infections characterized by infiltrative growth of the larvae in the livers of natural intermediate hosts such as rodents, and rarely in humans. Metastasis formation may also occur. AE is staged according to the World Health Organization (WHO)-PNM (P, parasitic mass in the liver; N, involvement of neighboring organs; M, metastasis) system (10). Radical resection of parasitic lesions is the preferred treatment (1), but most patients are inoperable at the time of diagnosis (5, 13). In a recent serological study, immunoglobulin G (IgG) antibodies directed against Em18, Em10, and Em2plus antigen compositions showed a close relationship between the clinical status and the treatment of patients with AE (16). In direct comparison, antibodies against Em18 demonstrated the greatest dynamic changeability in all patients, cohorts, and PNM stages, irrespective of the individual treatment. Moreover, Em18 indices had shown the best correlation with the PNM stages prior to treatment. These results prompted us to further investigate the IgG subclass and additionally the IgE response against this diagnostic antigen in patients with either resected or unresectable parasitic lesions.

* Corresponding author. Mailing address: Institute of Hygiene and Microbiology, Josef-Schneider-Str. 2, 97080 Würzburg, Germany. Phone: 49-931-201-46036. Fax: 49-931-201-46445. E-mail: dtappe@hygiene.uni-wuerzburg.de.

§ D.T., Y.S., and A.I. contributed equally to this work.

▽ Published ahead of print on 14 April 2010.

MATERIALS AND METHODS

Patients. All patients described in this study were seen at the University Hospital and Medical Center Ulm, Ulm, Germany. A total of 36 patients (225 sera) with a history of hepatic AE and a follow-up period of 1.5 to 6.5 years were included in the study. The patients (age range, 17 to 86 years; mean age, 51.2 years; sex ratio [male to female], 0.57:1) were assigned to different clinical WHO-PNM stages of the disease. All patients had acquired AE in Germany and received benzimidazole therapy. Thirteen patients had curatively resected lesions; 4 had recurrences after surgery; 1 had a palliative resection only; 16 had unresectable lesions but stable disease; and 2 had apparently dead, fully calcified lesions (Table 1). All serum samples were tested at the Department of Parasitology, Asahikawa Medical College, Asahikawa, Japan, in a blind test. The classification of curative resection, stable disease, progressive disease, or the presence of an apparently dead, fully calcified lesion was established by magnetic resonance imaging based on lesion size and morphology at the respective follow-up intervals. Ethical approval was obtained from the University of Ulm.

Methods. For the Em18 enzyme-linked immunosorbent assay (ELISA), recombinant Em18 antigen (14) was used to coat microtiter plates at a concentration of 100 ng/well. Patients' sera were tested at dilutions of 1:100 for total IgG and IgG subclasses, and 1:10 for IgE, after preabsorption of the wells with 1% casein in 20 mM Tris-HCl (pH 7.4)–150 mM NaCl buffer. Serum IgG bound to echinococcal antigens were detected with horseradish peroxidase (HRP)-conjugated protein G (Zymed) as a secondary antibody by using 2,2′-azinobis(3-ethylbenzthiazolinesulfonic acid) (ABTS; Sigma, Germany) as a chromogenic substrate. For the detection of recombinant Em18-specific IgE and IgG subclasses, HRP-conjugated mouse monoclonal anti-human IgE, IgG1, IgG2, IgG3, or IgG4 antibodies (Zymed) were used. Absorbance was measured after 30 min at 405 nm with a reference wavelength of 630 nm. For the calculation of the cutoff, the mean value of the absorbances of 31 sera from healthy blood donors was added to 3 times the standard deviation (SD) for total IgG and to 5 times the SD for the IgG subclasses and IgE. The index of the individual serum sample was calculated by dividing the sample's absorbance by the cutoff.

Statistical analysis. Statistical analyses were performed with the free software environment "R" for statistical computing. Nonparametric data were analyzed using Spearman's rank test for the correlation of the clinical stage and the ELISA

TABLE 1. Characteristics of patients with alveolar echinococcosis included in the study

Patient no.	Stage	PNM code[a]	Status[a]	Age (yr)[b]	Sex	Follow-up duration (yr)
1	I	P1N0M0	Curative resection	62	F	5.5
2	I	P1N0M0	Curative resection	24	F	5
3	I	P1N0M0	Curative resection	22	F	4
4	I	P1N0M0	Curative resection	33	F	2
5	I	P1N0M0	Apparently dead, fully calcified lesion	58	M	4
6	I	P1N0M0	Unresectable, stable disease	61	M	3.5
7	II	P2N0M0	Curative resection	38	F	3
8	II	P2N0M0	Unresectable, stable disease	71	M	6
9	II	P2N0M0	Unresectable, stable disease	68	F	5.5
10	II	P2N0M0	Unresectable, stable disease	59	F	6.5
11	II	P2N0M0	Unresectable, stable disease	60	F	6
12	II	P2N0M0	Curative resection	41	F	2.5
13	II	P2N0M0	Recurrence after resection	74	F	2.5
14	II	P2N0M0	Unresectable, stable disease	75	M	3
15	IIIa	P3N0M0	Curative resection	25	F	4.5
16	IIIa	P3N0M0	Curative resection	62	M	5.5
17	IIIa	P3N0M0	Recurrence after resection	17	F	3.5
18	IIIa	P3N0M0	Unresectable, stable disease	69	F	6
19	IIIa	P3N0M0	Unresectable, stable disease	39	F	4
20	IIIa	P3N0M0	Apparently dead, fully calcified lesion	57	F	6
21	IIIa	P3N0M0	Unresectable, stable disease	43	M	2
22	IIIa	P3N0M0	Recurrence after resection	19	F	3
23	IIIb	P4N0M0	Unresectable, stable disease	60	F	5
24	IIIb	P3N1M0	Unresectable, stable disease	49	F	5.5
25	IIIb	P2N1M0	Recurrence after resection	50	M	5
26	IIIb	P3N1M0	Progression after palliative resection	32	M	6
27	IIIb	P4N0M0	Unresectable, stable disease	57	M	3
28	IIIb	P4N0M0	Unresectable, stable disease	86	F	5.5
29	IV	P4N1M0	Curative resection	56	F	6.5
30	IV	P4N1M0	Curative resection	30	M	3
31	IV	P4N1M0	Curative resection	72	F	3
32	IV	P4N1M0	Unresectable, stable disease	71	F	5.5
33	IV	P4N1M0	Curative resection	52	M	2.5
34	IV	P4N1M0	Curative resection	63	F	1.5
35	IV	P4N1M0	Unresectable, stable disease	34	M	2.5
36	IV	P4N1M0	Unresectable, stable disease	54	M	4

[a] As assessed either by imaging alone (apparently dead lesion, progressive disease, and stable disease) or by imaging and histology (curative resection).
[b] At the time when the first blood sample was drawn.

index of the respective antibody (subclass) responses. P values of <0.005 were regarded as significant.

RESULTS

The height of the ELISA index of the antibodies tested showed a weak correlation of total IgG and IgG4 with all clinical PNM stages (stages I to IV) prior to treatment (Fig. 1a). IgG4 showed a close-to-linear correlation only with the first three stages (stages I to IIIa). The correlation of IgG1 was poor. Since IgE and IgG2 antibodies showed weak reactivities, and IgG3 antibodies were undetectable, no correlation with the clinical stage could be established for these isotypes/subclasses at all. The clinical PNM stage had no influence on the kinetics of antibody levels *per se*. Rather, antibody levels depended on the treatment the patients underwent at each stage (Fig. 1b and c).

In the cohort of 13 patients who underwent curative resection, levels of all antibodies decreased rapidly after resection of the parasitic lesions. Antibody levels dropped below the cutoff level after some time (Fig. 1b). The index of IgG4 directed against Em18 showed the most marked decline of all antibody (sub)types during the first follow-up interval in all patients and PNM stages in this cohort (Fig. 1b). IgG1 antibodies were the first to drop below the cutoff in some patients, followed by total IgG and IgG4. IgG1 fell below the cutoff in 8 patients (patients 2, 7, 12, 15, 16, 29, 33, and 34) after 30, 12, 24, 6, 12, 12, 6, and 6 months, respectively; total IgG fell below the cutoff in 6 patients (patients 2, 7, 12, 15, 29, and 34) at 54, 12, 24, 6, 12, and 18 months, respectively; and IgG4 fell below the cutoff in 6 patients (patients 2, 7, 12, 15, 29, and 34) after 30, 12, 24, 6, 48, and 18 months, respectively. In some patients, seroreversion in different assays was seen at the same time. Once seroreversion was seen, antibodies remained undetectable throughout the observation period. Follow-up imaging demonstrated that the drop below the cutoff level reflected serologically the clinical regression in this patient cohort.

In the 5 patients with noncurative resection, antibody levels of total IgG, IgG1, and IgG4 against Em18 decreased at first but increased again during the follow-up period. Total IgG never fell below the cutoff level, whereas IgG1 became negative in 2 patients (patients 22 and 26) after 6 and 36 months and increased again after 24 and 54 months, respectively. IgG4 became negative in 1 patient (patient 22) and showed the same kinetics as IgG1 in this patient. Re-

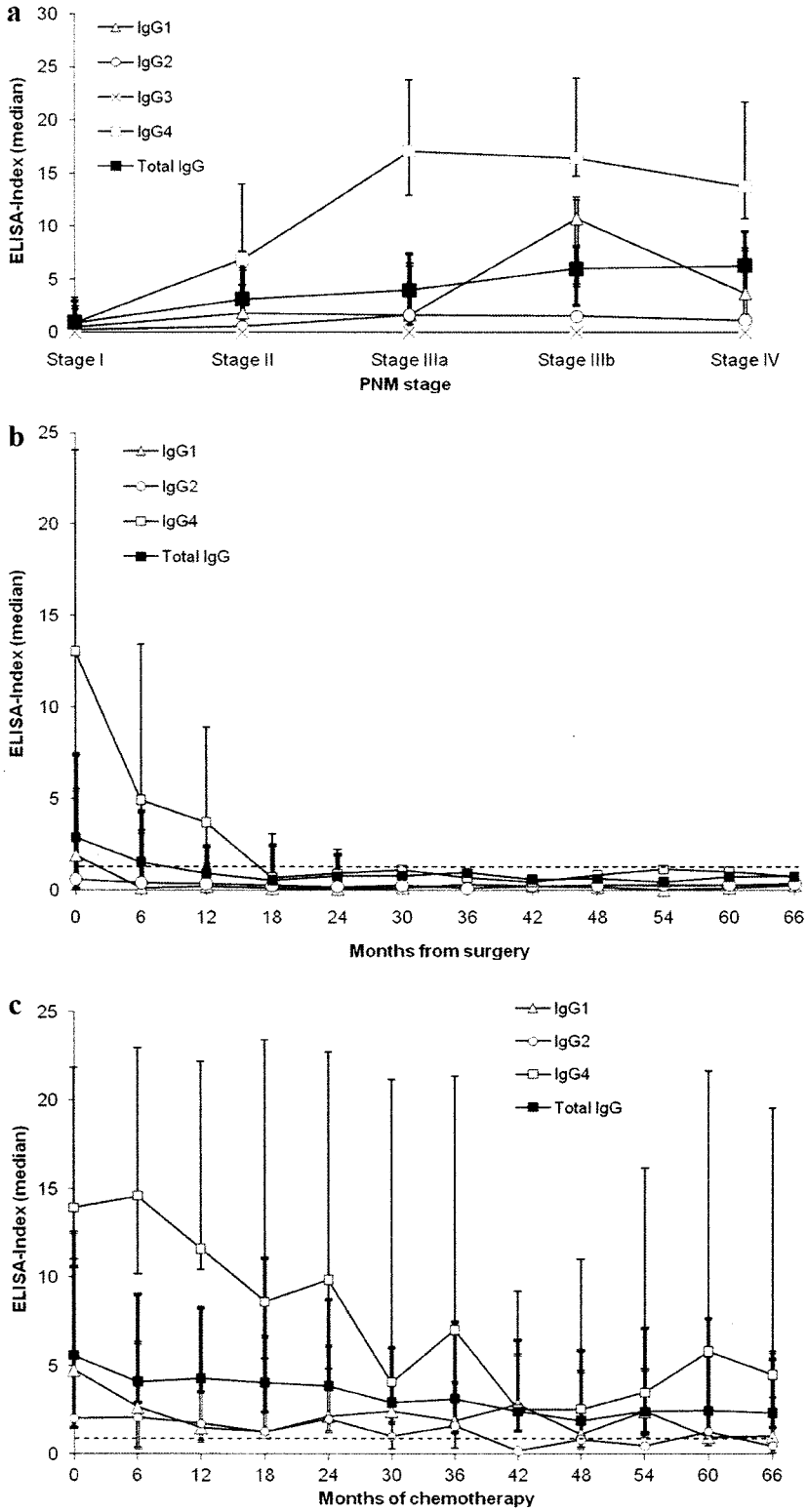

FIG. 1. (a) Correlation of the PNM stage and the ELISA-index prior to treatment. Median index values of the respective antibodies against Em18 are displayed for each PNM stage. The highest median index in all stages was demonstrated for IgG4, whereas IgG3 was completely unreactive. The lowest positive median indices in all stages were demonstrated for IgE (data not shown) and IgG2. A constant increase in the median values of the total IgG index in parallel with the clinical stage is visible. IgG4 indices showed a close-to-linear increase for stages I to IIIa only. Error bars represent ranges for total IgG (bold lines), IgG4 (thin single lines), and IgG1 (thin double lines). Spearman's rank correlation coefficients (ρ) for total IgG, IgG4, and IgG1 with all PNM stages (stages I to IV) were 0.532 ($P, <0.001$), 0.499 ($P, <0.002$), and 0.358 ($P, <0.05$).

currence was demonstrated by follow-up imaging in all patients.

In the cohort of 16 patients with unresectable lesions and stable disease under benzimidazole therapy, total-IgG, IgG1, IgG2, and IgG4 levels showed slow but steady declines (Fig. 1c). IgE levels were very low. No differences in antibody kinetics between different PNM stages in this patient cohort were observed. Overall, the IgG4 index demonstrated the most pronounced decrease in all patients and PNM stages of this cohort. Total IgG showed the smoothest decline, whereas IgG1 and IgG4 displayed undulating decreases. IgG1, IgG2, and IgG4 antibodies dropped below the cutoff in 5 patients (patients 8, 10, 11, 18, and 19) after 12, 36, 72, 18, and 42 months, respectively; in 2 patients (patients 11 and 32) after 12 and 42 months, respectively; and in 1 patient (patient 11) after 72 months. Once seroreversion was seen, antibodies remained undetectable throughout the observation period. The decrease in the antibody levels paralleled serologically the clinically stable disease in this patient cohort as assessed by follow-up imaging.

In the 2 patients with apparently dead lesions, levels of all antibodies against Em18 either were completely below the cutoff or showed a steady decline until total IgG, IgG1, and IgG4 became undetectable at the same time (data not shown). The apparently dead, fully calcified lesions correlated with no detectable growth during follow-up imaging. Testing of IgE responses to Em18 showed constantly low levels in all stages and cohorts (data not shown).

DISCUSSION

In this study, we performed a serological follow-up of patients with AE grouped according to the WHO-PNM staging system. The recombinant diagnostic antigen Em18 was used in different ELISAs, which measured total IgG, IgG subclasses, and IgE in a German patient cohort. Six different assays were run in parallel. In a previous study, the height of antibody levels prior to treatment was dependent on the PNM stage, and indices of anti-Em18 IgG showed the highest correlation of all antigen compositions used (16). Here, a similar correlation was shown for total IgG against Em18. When the IgG subclass responses were analyzed, however, only IgG4 displayed a comparable correlation with all clinical PNM stages before treatment was begun. IgG4 also exhibited the highest ELISA indices in all patient subcohorts and stages, suggesting a higher diagnostic sensitivity than those for other subclasses or total IgG (7). Accordingly, earlier studies have shown that IgG4 was the predominant IgG subclass responding to Em18 (8). In another study, IgG4 and IgG1 isotype levels were significantly elevated in the sera of AE patients (18), and these isotypes also displayed the most sensitive antibody response to a crude parasite extract containing a 17.5- to 18-kDa antigen in an ELISA (18) and immunoblot analysis (4, 20). In our study, IgG1 levels against Em18 were also increased at all clinical stages, whereas IgG2 demonstrated the lowest positive median indices at all stages, and IgG3 was completely undetectable. Since Em18 is a pure protein antigen, and IgG2 has often been associated with anticarbohydrate immune responses in humans (17), it is understandable that only a low IgG2 response was obtained. Why IgG3 was undetectable in our study is less clear. A greater-than-expected proportion of carbohydrate-specific IgG antibody responses in humans can have a non-IgG2 subclass origin (17), possibly also encompassing IgG3. Hypothetically, a suppression of IgG3 responses toward this diagnostic antigen by the parasite might also be possible. In a previous study by others, the sensitivities of IgG2 and IgG3 directed against a crude parasite extract were also significantly lower than those of the other IgG subclasses in AE patients (19). Levels of IgE in response to Em18 were very low in all stages and patient cohorts. These data indicate that Em18 is a good candidate for parasite-specific total-IgG, IgG4, and IgG1 analysis of AE patients at all WHO stages. Em18 might be an unsuitable antigen for IgE and IgG2 testing, and an unsuitable antigen as a pure protein for IgG3 serology as well.

In the follow-up investigations, IgG4 antibodies against Em18 demonstrated the greatest dynamic changeability in all patients, cohorts, and PNM stages, irrespective of the individual treatment. The data obtained from the patient cohort with curatively resected lesions are consistent with previous findings that antibodies directed against various antigen compositions, including Em18, can drop below the cutoff (2, 6, 15, 16). In this study, IgG1 antibodies were the first to drop below the cutoff, followed by total IgG and IgG4 at 6-month intervals, reflecting the curative resection. In contrast, in a previous follow-up study of cured or improved patients, levels of IgG4 antibodies directed against a crude parasite extract tended to decrease earlier than total-IgG levels (18). However, IgG4 antibodies became negative 1 year after successful treatment, as seen in our study.

For patients with recurrences, the initial decrease in the levels of total IgG against Em18, followed by a later increase, has previously been demonstrated in other studies using total IgG in the Em18 ELISA (6, 16), Em18 Western blotting (12), and other assays with different diagnostic antigens (16). Levels of IgG1 and IgG4 against Em18 followed these kinetics, but these antibodies became intermittently negative in a few patients in this study. Accordingly, specific IgG4 responses to a crude antigen extract reappeared in recurrences, as shown in a survey by others (18).

respectively. (b) Antibody profiles of patients after curative resection. Median index values from all assays (except those for IgG3 and IgE) for 13 patients at different clinical stages are presented. Rapid declines in the antibody indices of total IgG, IgG1, and IgG4 are clearly visible. Error bars represent ranges (until month 24) for total IgG, IgG4, and IgG1 as explained for panel a. Serological data were accumulated for intervals of 6 months. At each given interval, data from 2 to 13 patients were available. The cutoff level is 1, represented by the dashed line. The time of resection is month zero. (c) Antibody profiles of patients with stable disease and unresectable lesions. Median index values from all assays (except those for IgG3 and IgE) for 16 patients at different clinical stages are presented. A slow decline in the antibody indices is visible. Error bars represent ranges for total IgG, IgG4, and IgG1 as explained for panel a. Serological data were accumulated for intervals of 6 months. At each given interval, data from 5 to 16 patients were available. The cutoff level is 1, represented by the dashed line. The start of chemotherapy is at month zero.

Our results for the patient cohort with unresectable lesions and stable AE are consistent with previous findings that levels of antibody against Em18 (6, 12, 16), and also other diagnostic antigens (2, 12, 16), decrease slowly under antiparasitic chemotherapy. In our study, total IgG against Em18 showed the smoothest decline, whereas median indices of IgG1 and IgG4 demonstrated undulating decreases over time. In a previous study by others, levels of IgG1 and IgG4 against Em18 fell to zero in some patients treated with albendazole (12), whereas these IgG subclasses showed unchanged levels against a crude parasite antigen extract in patients with stabilized AE (18). In our study, seroreversion was also demonstrable for IgG1 in some patients and for IgG2 and IgG4 in a few patients. Most patients were at an early stage of the disease (stage II). In this patient group, a regression of lesions toward nonviability of the parasite might be possible. However, the observation period might not have been long enough to demonstrate seroreversion in the other IgG subclasses or total IgG.

The kinetics of antibody levels in patients who have apparently dead and fully calcified lesions were very similar to those for the cohort with stable disease, and the results are consistent with those of a previous report (16).

Whether the IgG subclass effect described here is directly related to the Em18 antigen or is a more general effect of AE serology remains to be elucidated. However, several previous studies found that the recombinant Em18 antigen may be one of the best antigens for AE serology (3, 9, 11, 14, 16). Antibody responses to recombinant proteins are much clearer, and thus easier to analyze, than responses to native proteins, since the latter may contain variable epitopes, which may lead to more complex immunological responses.

In conclusion, our data indicate that the diagnostic antigen Em18 is suitable for parasite-specific serology employing total-IgG, IgG1, and IgG4 assays. Total IgG and IgG4 mirror the clinical PNM stage best before treatment. IgG4 shows the greatest changes in all patient cohorts, clinical stages, and treatments; therefore, IgG4 might be the most sensitive antibody subclass for AE serology employing the Em18 antigen. IgG1 antibody kinetics reflect curative resection, recurrence, and possibly the death of the parasite better than any other antibody (sub)class directed against Em18.

ACKNOWLEDGMENTS

We thank Christoph Schoen (Germany) for assistance with the statistical analysis.

Serology in Japan was financially supported in part by the Infection Matrix Fund (2007 to 2008) and the Hokkaido Translational Research Project (2007 to 2012) from the Ministry of Education, Japan, and by the Japan Society for the Promotion of Science (21256003) (to A.I.).

REFERENCES

1. **Ammann, R. W., and J. Eckert.** 1996. Cestodes. *Echinococcus*. Gastroenterol. Clin. North Am. **25:**655–689.
2. **Ammann, R. W., E. C. Renner, B. Gottstein, F. Grimm, J. Eckert, and E. L. Renner; Swiss Echinococcosis Study Group.** 2004. Immunosurveillance of alveolar echinococcosis by specific humoral and cellular immune tests: long-term analysis of the Swiss chemotherapy trial (1976–2001). J. Hepatol. **41:** 551–559.
3. **Bart, J. M., M. Piarroux, Y. Sako, F. Grenouillet, S. Bresson-Hadni, R. Piarroux, and A. Ito.** 2007. Comparison of several commercial serologic kits and Em18 serology for detection of human alveolar echinococcosis. Diagn. Microbiol. Infect. Dis. **59:**93–95.
4. **Dreweck, C. M., C. G. Lüder, P. T. Soboslay, and P. Kern.** 1997. Subclass-specific serological reactivity and IgG4-specific antigen recognition in human echinococcosis. Trop. Med. Int. Health **2:**779–787.
5. **Eckert, J., P. Jacquier, D. Baumann, and P. A. Raeber.** 1995. Echinokokkose des Menschen in der Schweiz, 1984–1992. Schweiz. Med. Wochenschr. **125:** 1989–1998.
6. **Fujimoto, Y., A. Ito, Y. Ishikawa, M. Inoue, Y. Suzuki, M. Ohhira, T. Ohtake, and Y. Kohgo.** 2005. Usefulness of recombinant Em18-ELISA to evaluate efficacy of treatment in patients with alveolar echinococcosis. J. Gastroenterol. **40:**426–431.
7. **Ishikawa, Y., Y. Sako, S. Itoh, T. Ohtake, Y. Kohgo, T. Matuno, Y. Ohsaki, N. Miyokawa, M. Nakao, K. Nakaya, and A. Ito.** 2009. Serological monitoring of progression of alveolar echinococcosis with multiorgan involvement by use of recombinant Em18. J. Clin. Microbiol. **47:**3191–3196.
8. **Ito, A., P. M. Schantz, and J. F. Wilson.** 1995. Em18, a new serodiagnostic marker for differentiation of active and inactive cases of alveolar hydatid disease. Am. J. Trop. Med. Hyg. **52:**41–44.
9. **Ito, A., N. Xiao, M. Liance, M. O. Sato, Y. Sako, W. Mamuti, Y. Ishikawa, M. Nakao, H. Yamasaki, K. Nakaya, K. Bardonnet, S. Bresson-Hadni, and D. A. Vuitton.** 2002. Evaluation of an enzyme-linked immunosorbent assay (ELISA) with affinity-purified Em18 and an ELISA with recombinant Em18 for differential diagnosis of alveolar echinococcosis: results of a blind test. J. Clin. Microbiol. **40:**4161–4165.
10. **Kern, P., H. Wen, N. Sato, D. A. Vuitton, B. Grüner, Y. Shao, E. Delabrousse, W. Kratzer, and S. Bresson-Hadni.** 2006. WHO classification of alveolar echinococcosis: principles and application. Parasitol. Int. **55:**S283–S287.
11. **Li, T., A. Ito, X. Chen, Y. Sako, J. Qiu, N. Xiao, D. Qiu, M. Nakao, T. Yanagida, and P. S. Craig.** 2010. Specific IgG responses to recombinant antigen B and Em18 in cystic and alveolar echinococcosis in China. Clin. Vaccine Immunol. **17:**470–475.
12. **Ma, L., A. Ito, Y. H. Liu, X. G. Wang, Y. G. Yao, D. G. Yu, and Y. T. Chen.** 1997. Alveolar echinococcosis: Em2 plus-ELISA and Em18-Western blots for follow-up after treatment with albendazole. Trans. R. Soc. Trop. Med. Hyg. **91:**476–478.
13. **Reuter, S., A. Buck, O. Grebe, K. Nussle-Kugele, P. Kern, and B. J. Manfras.** 2003. Salvage treatment with amphotericin B in progressive human alveolar echinococcosis. Antimicrob. Agents Chemother. **47:**3586–3591.
14. **Sako, Y., M. Nakao, K. Nakaya, H. Yamasaki, B. Gottstein, M. W. Lightowlers, P. M. Schantz, and A. Ito.** 2002. Alveolar echinococcosis: characterization of diagnostic antigen Em18 and serological evaluation of recombinant Em18. J. Clin. Microbiol. **40:**2760–2765.
15. **Schantz, P. M., J. F. Wilson, S. P. Wahlquist, L. P. Boss, and R. L. Rausch.** 1983. Serologic tests for diagnosis and post-treatment evaluation of patients with alveolar hydatid disease (*Echinococcus multilocularis*). Am. J. Trop. Med. Hyg. **32:**1381–1386.
16. **Tappe, D., M. Frosch, Y. Sako, S. Itoh, B. Grüner, S. Reuter, M. Nakao, A. Ito, and P. Kern.** 2009. Close relationship between clinical regression and specific serology in the follow-up of patients with alveolar echinococcosis in different clinical stages. Am. J. Trop. Med. Hyg. **80:**792–797.
17. **von Gunten, S., D. F. Smith, R. D. Cummings, S. Riedel, S. Miescher, A. Schaub, R. G. Hamilton, and B. S. Bochner.** 2009. Intravenous immunoglobulin contains a broad repertoire of anticarbohydrate antibodies that is not restricted to the IgG2 subclass. J. Allergy Clin. Immunol. **123:**1268–1276.
18. **Wen, H., S. Bresson-Hadni, D. A. Vuitton, D. Lenys, B. M. Yang, Z. X. Ding, and P. S. Craig.** 1995. Analysis of immunoglobulin G subclass in the serum antibody responses of alveolar echinococcosis patients after surgical treatment and chemotherapy as an aid to assessing the outcome. Trans. R. Soc. Trop. Med. Hyg. **89:**692–697.
19. **Wen, H., and P. S. Craig.** 1994. Immunoglobulin G subclass responses in human cystic and alveolar echinococcosis. Am. J. Trop. Med. Hyg. **51:**741–748.
20. **Wen, H., P. S. Craig, A. Ito, D. A. Vuitton, S. Bresson-Hadni, J. C. Allan, M. Rogan, E. Paolillo, and M. Shambesh.** 1995. Immunoblot evaluation of IgG and IgG subclass antibody responses for immunodiagnosis of human alveolar echinococcosis. Ann. Trop. Med. Parasitol. **89:**485–495.

Parasitology International 60 (2011) 108–110

Contents lists available at ScienceDirect

Parasitology International

journal homepage: www.elsevier.com/locate/parint

Short communication

A possible nuclear DNA marker to differentiate the two geographic genotypes of *Taenia solium* tapeworms

Marcello Otake Sato [a,b,*], Yasuhito Sako [b], Minoru Nakao [b], Toni Wandra [b,c], Kazuhiro Nakaya [b], Tetsuya Yanagida [b], Akira Ito [b]

[a] Escola de Medicina, Universidade Federal do Tocantins, Palmas-TO 77001-090, Brazil
[b] Department of Parasitology, Asahikawa Medical University, Asahikawa 078-8510, Japan
[c] Directorate General Disease Control and Environmental Health, Ministry of Health, Jakarta 10560, Indonesia

ARTICLE INFO

Article history:
Received 22 July 2010
Received in revised form 22 September 2010
Accepted 15 November 2010
Available online 23 November 2010

Keywords:
Taenia solium
Nuclear DNA marker
Genotyping

ABSTRACT

Cysticercosis caused by infection with embryonated eggs of the pork tapeworm *Taenia solium* is an important cause of neurological disease worldwide. Based on the phylogenetic analysis of mitochondrial DNA, the pathogen has been divided into two geographic clades, corresponding to Afro-American and Asian genotypes. In this study the genotyping of *T. solium* was carried out by using the nuclear DNA sequences of the immunodiagnostic antigen genes *Ag1V1* and *Ag2*. The two geographic genotypes were supported by the *Ag2* sequences, especially showing unique substitutions in each of the genotypes. It seems likely that the *Ag2* may be a novel nuclear DNA marker to distinguish the two geographic genotypes of *T. solium*.

The larval stage of the pork tapeworm *Taenia solium* is responsible for cysticercosis. Humans are accidentally infected with *T. solium* by ingestion of embryonated eggs excreted with feces of symptomatic and asymptomatic carriers harboring the adult tapeworm in the intestinal tract. The hatched embryos migrate throughout the body of humans and swine, invade mostly skeletal muscle and encyst to form larval cysticerci. The larvae can also reach subcutaneous tissue, eyes and the central nervous system, resulting in neurocysticercosis (NCC). Among human tapeworms, *T. solium* is the most important as the pathogen of emergent or re-emergent zoonosis because the NCC causes focal neurological deficits and seizures in endemic countries [1,2]. The diagnosis of cysticercosis has been done by clinical criteria, computed tomography (CT), nuclear magnetic resonance (NMR) imaging and serology [3,4]. Glycoproteins in the cyst fluid of *T. solium* have been widely used as crude antigens for serodiagnosis [5,6]. Recombinant antigens have been used for the diagnosis of cysticercosis. We demonstrated that the chimeric recombinant protein Ag1V1/Ag2 is a superior antigen for immunodiagnosis in humans and animals [7–11]. Each of the *Ag1V1* and *Ag2* is a gene encoding a low molecular weight backbone protein of the cystic glycoproteins. Our previous phylogenetic analysis of mitochondrial DNA (mtDNA) revealed that *T. solium* individuals can be divided into two geographic clades, corresponding to Afro-American and Asian genotypes [12]. During the analysis process of Western blotting, we also noticed that the banding profiles of crude glycoproteins differ among cyst fluids from geographically different origins [13,14]. In the present study, we evaluated the usefulness of *Ag1V1* and *Ag2* as a nuclear DNA marker to characterize the local isolates of *T. solium*.

A total of 7 geographic samples of *T. solium* cysticerci collected from Indonesia (Papua, former Irian Jaya), India, China, Brazil, Tanzania, Cameroon and South Africa in 1996 through 2001 were examined for this study. All the samples were obtained from muscles of domesticated pigs [14] and were preserved in 70% ethanol until DNA extraction. Genomic DNA was extracted from a single cysticercus by using a spin column kit (DNeasy tissue kit, QIAGEN). Each of *Ag1V1* and *Ag2* genes was amplified by polymerase chain reaction (PCR). Two sets of PCR primers were designed from the cDNA sequences of *Ag1V1* and *Ag2*. The primer pair Ag1V1F (5′-CTC GCT CTC ACT GTA TTC GT-3′) and Ag1V1R (5′-TTG ACA AGT TAA GCA GTT TT-3′) allowed us to amplify the genomic sequence of *Ag1V1*. The amplicons of *Ag2* were obtained by using the primer pair Ag2F (5′-CTC GCT CTC AGT GTT TTC GT-3′) and Ag2R (5′-TTG ACA AGT TAA GCA GCT TC-3′). PCR was carried out in a 50 μl reaction mixture containing 1 μl of template DNA (approximately 100 ng), each dNTP at 200 μM each primer, 1U of DNA polymerase (PrimeSTAR, TaKaRa Biomedicals) and the manufacturer-supplied reaction buffer. For PCR amplification, we employed 30 thermal cycles (94 °C for 30 s, 50 °C for 5 s and 72 °C for 30 s) for both genes. Prior to DNA sequencing, each amplified product was purified by using a PCR clean-up kit (NucleoSpin, Macherey-Nagel). The Bigdye terminator cycle sequencing kit and the ABI PRISM 377 genetic analyzer (Applied Biosystems) were used as recommended by the manufacturer. DNAs were directly sequenced by using PCR primers. In

* Corresponding author. Escola de Medicina, Universidade Federal do Tocantins, Av: NS 15 ALC NO 14, 109 Norte Campus Universitário de Palmas, Palmas, TO CEP77001-090, Brazil. Tel.: +55 63 32328273; fax: +55 63 32328158.
E-mail address: otake@uft.edu.br (M.O. Sato).

1383-5769/$ – see front matter © 2010 Elsevier Ireland Ltd. All rights reserved.
doi:10.1016/j.parint.2010.11.004

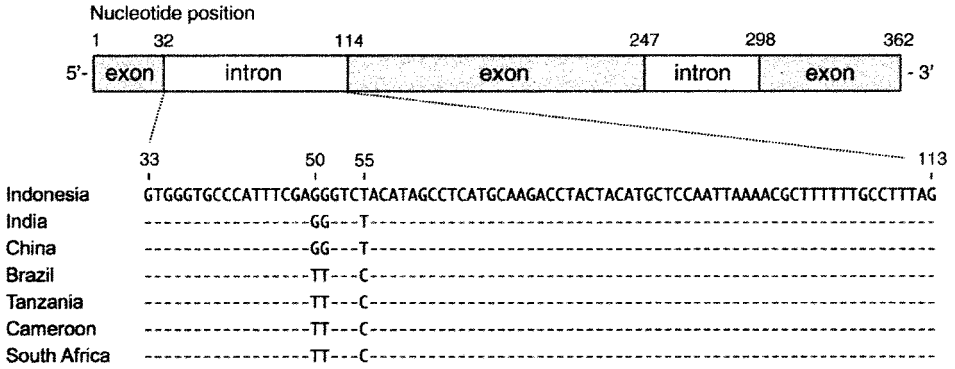

Fig. 1. The exon–intron structure of genomic PCR products for *Ag2* and their multiple alignment showing nucleotide substitutions. The Asian isolates of *T. solium* are originated from Indonesia, India and China, and the Afro-American isolates from Brazil, Tanzania, Cameroon and South Africa.

the case of low amounts of PCR products, the amplicons were subcloned into pGEM-T plasmid vector (Promega) by using an adenine tailing kit (Qiagen). Insert DNAs in the plasmid were read by T7 promoter primer (5′-ATT ATG CTG AGT GAT ATC CC-3′).

As demonstrated by Sato et al. [14], the diagnostic antigen genes *Ag1V1* and *Ag2* are universally present in *T. solium* isolates from Asia, Africa and America. In this study we could amplify the 379 bp fragments of *Ag1V1* and the 362 bp fragments of *Ag2* from all of the isolates examined. After sequencing, we found 3 haplotypes in *Ag1V1* and 2 haplotypes in *Ag2*. Both of the genomic sequences included 2 introns. The nucleotide sequences of *Ag1V1* (DDBJ/EMBL/GenBank accession nos. AB263426–AB263432) contained 2 substitution sites in the second exon and 1 substitution site in the first intron. All of them were transitional changes from thymine to cytosine bases. The two point mutations, which were observed at position 183 in the Brazilian isolate and at position 223 in the Chinese isolate, caused amino acid changes. Although these mutations had no geographic characteristics, more studies on the genetic polymorphisms of *T. solium* in Brazil and China are necessary to determine whether *Ag1V1* is usable as a genetic marker at local level.

As contrasted with *Ag1V1*, the sequences of *Ag2* (AB263419–AB263425) were geographically informative in classifying the isolates. The exon sequences were completely identical among the isolates examined. However, there were 3 substitutions in the first intron. As shown in Fig. 1, transversional substitutions (G and T) occurred at positions 50 and 51, and a transitional substitution (T and C) further occurred at position 55. All of the point mutations were highly correlated with the Afro-American and Asian genotypes of *T. solium*, which were defined from the sequences of mtDNA [12].

The observation of parasitic material is the most important step for diagnosis in parasitology. However, morphological identification is usually difficult in the case that specimens are just a piece of the entire material [15]. The development of DNA markers for *T. solium* worldwide allows us to design a useful tool for diagnosis even if all the morphological characteristics are lost. Based on the sequences of mtDNA, PCR-based techniques such as base excision sequence scanning thymine-base reader analysis, multiplex PCR and DNA sequencing have been used for the molecular identification of adult tapeworms and metacestodes, particularly in differentiating the Afro-American and Asian genotypes of *T. solium* [10,14–16]. However, nuclear DNA markers are still required for the phylogeographic studies of *T. solium* because the maternally inherited haploid mtDNA is unsuitable to use as an ideal marker for population genetics. As shown in this study, the nuclear *Ag2* gene may serve as an alternative DNA marker to determine the geographic genotypes of *T. solium* specimens.

The identification of the genotypes is an important issue on travel medicine programs. In some cases the endemic areas of *T. solium* have natural resources that attract outer people who can become worm carriers for non-endemic areas [9]. Tracking geographic areas where taeniasis/cysticercosis patients became infected may be achieved by examining the genetic polymorphism of *T. solium* [17]. Recently, the coexistence of the Afro-American and Asian genotypes has been found in Madagascar [18]. The nuclear DNA marker of *Ag2* may be useful to detect cross-hybridization events between the two genotypes.

In conclusion, we found a possible nuclear DNA marker to differentiate the geographic genotypes of *T. solium*. More nuclear markers are needed to examine the population genetic structures of *T. solium* worldwide. A panel of the genetic markers will depict the evolutionary tracks of the parasite and humans.

Acknowledgements

This study was supported in part by Grant-in-Aid for Scientific Research from the Japan Society for Promotion of Science (JSPS) (21256003), by the Asia-Africa Scientific Platform Fund (2006–2011), by the Special Cooperation Fund for Promoting Science & Technology, Ministry of Education, Japan (2010–2012) to A. Ito and the National Council for Scientific and Technological Development (CNPq) (502001/2009-7) to M.O. Sato.

References

[1] Schantz PM, Wilkins PP, Tsang VCW. Immigrants, imaging and immunoblots: the emergence of neurocysticercosis as a significant public health problem. In: Scheld WM, Craig WA, Hughes JM, editors. Emerging Infections, 2. Washington, DC: ASM Press; 1998. p. 213–42.
[2] Ito A, Yamasaki H, Nakao M, Sako Y, Okamoto M, Sato MO, et al. Multiple genotypes of *Taenia solium*—ramifications for diagnosis, treatment and control. Acta Trop 2003;87:95–101.
[3] Takayanagui OM, Odashima NS. Clinical aspects of neurocysticercosis. Parasitol Int 2006;55:S111–5.
[4] Ito A, Takayanagui OM, Sako Y, Sato MO, Odashima NS, Yamasaki H, et al. Neurocysticercosis: clinical manifestation, neuroimaging, serology and molecular confirmation of histopathologic specimens. Southeast Asian J Trop Med Public Health 2006;37(Suppl 3):74–81.
[5] Tsang VC, Brand JA, Boyer AE. An enzyme-linked immunoelectrotransfer blot assay and glycoprotein antigens for diagnosing human cysticercosis (*Taenia solium*). J Infect Dis 1989;159:50–9.
[6] Ito A, Plancarte A, Ma L, Kong Y, Flisser A, Cho SY, et al. Novel antigens for neurocysticercosis: simple method for preparation and evaluation for serodiagnosis. Am J Trop Med Hyg 1998;59:291–4.
[7] Sako Y, Nakao M, Ikejima T, Piao XZ, Nakaya K, Ito A. Molecular characterization and diagnostic value of *Taenia solium* low-molecular-weight antigen genes. J Clin Microbiol 2000;38:4439–44.
[8] Ito A, Putra MI, Subahar R, Sato MO, Okamoto M, Sako Y, et al. Dogs as alternative intermediate hosts of *Taenia solium* in Papua (Irian Jaya), Indonesia confirmed by highly specific ELISA and immunoblot using native and recombinant antigens and mitochondrial DNA analysis. J Helminthol 2002;76:311–4.
[9] Sato MO, Yamasaki H, Sako Y, Nakao M, Nakaya K, Plancarte A, et al. Evaluation of tongue inspection and serology for diagnosis of *Taenia solium* cysticercosis in swine: usefulness of ELISA using purified glycoproteins and recombinant antigen. Vet Parasitol 2003;111:309–22.

[10] Sato MO, Cavalcante TV, Sako Y, Nakao M, Yamasaki H, Yatsuda AP, et al. Evidence and potential for transmission of human and swine *Taenia solium* cysticercosis in the Piracuruca region, Piauí, Brazil. Am J Trop Med Hyg 2006;75:933–5.
[11] Sako Y, Nakao M, Nakaya K, Yamasaki H, Ito A. Recombinant antigens for serodiagnosis of cysticercosis and echinococcosis. Parasitol Int 2006;55(Suppl):S69–73.
[12] Nakao M, Okamoto M, Sako Y, Yamasaki H, Nakaya K, Ito A. A phylogenetic hypothesis for the distribution of two genotypes of the pig tapeworm *Taenia solium* worldwide. Parasitology 2002;124:657–62.
[13] Ito A, Nakao M, Okamoto M, Sako Y, Yamasaki H. Mitochondrial DNA of *Taenia solium* cysticercosis: from basic to applied science. In: Singh G, Prabhakar S, editors. *Taenia solium* from Basic to Clinical Science. Wallingford, UK: CABI Publishing; 2002. p. 47–55.
[14] Sato MO, Sako Y, Nakao M, Yamasaki H, Nakaya K, Ito A. Evaluation of purified *Taenia solium* glycoproteins and recombinant antigens in the serologic detection of human and swine cysticercosis. J Infect Dis 2006;194:1783–90.
[15] Yamasaki H, Allan JC, Sato MO, Nakao M, Sako Y, Nakaya K, et al. DNA differential diagnosis of taeniasis and cysticercosis by multiplex PCR. J Clin Microbiol 2004;42:548–53.
[16] Yamasaki H, Nakao M, Sako Y, Nakaya K, Sato MO, Mamuti W, et al. DNA differential diagnosis of human taeniid cestodes by base excision sequence scanning thymine-base reader analysis with mitochondrial genes. J Clin Microbiol 2002;40:3818–21.
[17] Yanagida T, Yuzawa I, Joshi DD, Sako Y, Nakao M, Nakaya K, et al. Neurocysticercosis: assessing where the infection was acquired from. J Travel Med 2010;17:206–8.
[18] Michelet L, Carod JF, Rakontondrazaka M, Ma L, Gay F, Dauga C. The pig tapeworm *Taenia solium*, the cause of cysticercosis: biogeographic (temporal and spacial) origins in Madagascar. Mol Phylogenet Evol 2010;55:744–50.

Experimental Parasitology xxx (2010) xxx–xxx

Contents lists available at ScienceDirect

Experimental Parasitology

journal homepage: www.elsevier.com/locate/yexpr

Echinococcus multilocularis: Identification and functional characterization of cathepsin B-like peptidases from metacestode ☆

Yasuhito Sako [a,*], Kazuhiro Nakaya [b], Akira Ito [a]

[a] *Department of Parasitology, Asahikawa Medical University, Midorigaoka Higashi 2-1, Asahikawa, 078-8510 Hokkaido, Japan*
[b] *Animal Laboratory for Medical Research, Asahikawa Medical University, Midorigaoka Higashi 2-1, Asahikawa, 078-8510 Hokkaido, Japan*

ARTICLE INFO

Article history:
Received 14 September 2010
Received in revised form 12 November 2010
Accepted 16 November 2010
Available online xxxx

Keywords:
Cestode
Echinococcus multilocularis
Metacestode
Cathepsin B-like peptidase
Recombinant enzyme
Host proteins

ABSTRACT

Cysteine peptidases have potent activities in the pathogenesis of various parasitic infections, and are considered as targets for chemotherapy and antigens for vaccine. In this study, two cathepsin B-like cysteine peptidases (EmCBP1 and EmCBP2) from *Echinococcus multilocularis* metacestodes were identified and characterized. Immunoblot analyses demonstrated that EmCBP1 and EmCBP2 were present in excretory/secretory products and extracts of *E. multilocularis* metacestodes. By immunohistochemistry, EmCBP1 and EmCBP2 were shown to localize to the germinal layer, the brood capsule and the protoscolex. Recombinant EmCBP1 and EmCBP2 expressed in *Pichia pastoris*, at optimum pH 5.5, exhibited substrate preferences for Z-Phe-Arg-MCA, Z-Val-Val-Arg-MCA, and Z-Leu-Arg-MCA, and low levels of hydrolysis of Z-Arg-Arg-MCA. Furthermore, recombinant enzymes degraded IgG, albumin, type I and IV collagens, and fibronectin. These results suggested that EmCBP1 and EmCBP2 may play key roles in protein digestion for parasites' nutrition and in parasite–host interactions.

1. Introduction

Alveolar echinococcosis (AE), caused by the larval stage of *Echinococcus multilocularis*, is a serious parasitic disease of humans in countries of the higher latitudes of Northern Hemisphere. In the previous decade, a lot of new data have been published on prevalence of *E. multilocularis* in final and intermediate hosts in areas where it had previously not been recorded (Eckert et al., 2000; Ito et al., 2010). Humans are accidentally infected with *E. multilocularis* by ingestion of eggs excreted with the feces of carnivores harboring adult tapeworm of this species. It is thought that humans become exposed to *E. multilocularis* by handling of infected definitive hosts, or by ingestion of food and water contaminated with eggs. Oncospheres hatched from eggs in the small intestine of humans migrate via the portal system into various organs, mainly liver and differentiate and develop into the metacestode stage. The metacestodes propagate asexually like a tumor leading to organ dysfunction. Since clinical symptoms usually do not become evident until 10 or more years after initial parasite infection, early diagnosis and treatment especially during asymptomatic period are important for reduction of morbidity and mortality (McManus et al., 2003). About one third of patients have cholestatic jaundice and about one third of patients have epigastric pain. In the remaining patients, *E. multilocularis* infections are incidentally detected during medical examination for symptoms such as fatigue, weight loss, hepatomegaly (Pawlowski et al., 2001). In addition to surgical removal of alveolar hydatid cyst, treatment with antiparasitic agents, benzimidazole derivatives, is the most important for AE therapy. However, these drugs have parasitostatic activity rather than parasitocidal activity, and side-effects such as liver damage are often observed with long-term administration (Kern, 2006). Thus, it is urgent to develop novel reliable chemotherapeutic agents.

Cysteine peptidases belonging to clan CA family C1 (Rawlings et al., 2004; http://merops.sanger.ac.uk/) besides their housekeeping functions such as protein turnover in parasite cells are involved in evasion from host immune responses, essential nutrient uptake, and tissue penetration, by degrading host proteins, including immunoglobulin, complement components, kininogen, haemoglobin, albumin, and extracellular matrix proteins (reviewed by Sajid and McKerrow 2002; Dalton et al., 2003; Caffrey et al., 2004; Rosenthal, 2004; McKerrow et al., 2006; Robinson et al., 2008; Smooker et al., 2010). Furthermore, some cysteine peptidases have activities to stimulate human eosinophils to induce degranulation (Shin et al., 2005), deplete CD4 positive human lymphocytes *in vitro* (Molinari et al., 2000), induce apoptosis in human CD4 positive cells (Tato et al., 2004), by interacting with host cells via unknown mechanisms. Therefore, cysteine peptidases of parasites are considered as important targets for chemotherapy and/or

☆ *Note*: The nucleotide sequence data reported in this study are available in the GenBank, EMBL, and DDBJ databases under accession numbers AB586072 (EmCBP1) and AB586073 (EmCBP2).

* Corresponding author. Fax: +81 166 68 2429.
E-mail address: yasusako@asahikawa-med.ac.jp (Y. Sako).

0014-4894/$ - see front matter © 2010 Elsevier Inc. All rights reserved.
doi:10.1016/j.exppara.2010.11.005

Please cite this article in press as: Sako, Y., et al. *Echinococcus multilocularis*: Identification and functional characterization of cathepsin B-like peptidases from metacestode. Exp. Parasitol. (2010), doi:10.1016/j.exppara.2010.11.005

immunoprophylaxis (Dalton et al., 2003; Barr et al., 2005; Abdulla et al., 2007; Alcala-Canto et al., 2007).

E. multilocularis metacestodes survive for many years in human host, which leads us to consider peptidases as important parasite components to evade from host immune responses and to uptake nutrient. However, precise characterization of *E. multilocularis* peptidases essential to develop enzyme inhibitors has been hampered by the difficulty of obtaining pure parasite materials, since parasite materials obtained from laboratory animals are contaminated with numerous host cells resulting from that *E. multilocularis* infiltrate and proliferate by exogenous budding of the germinative cells in host tissue (Thompson, 1995). Recently, we have succeeded in cloning of cathepsin L-like peptidase genes (EmCLP1 and EmCLP2) from *E. multilocularis* metacestodes, which enabled us to prepare a large amount of parasite enzymes for detailed characterizations (Sako et al., 2007). Activities of recombinant EmCLP1 and EmCLP2 to degrade human IgG, bovine albumin, type I and type IV collagen and fibronectin have been demonstrated, which suggests their important roles in parasite growth and survival in the host. In the present study, we have identified two genes encoding cathepsin B-like cysteine peptidases from *E. multilocularis* metacestodes. Immunoblot analyses with monoclonal antibody detected both enzymes in crude metacestode extract and ES products, and immunohistochemical studies revealed that both enzymes are expressed in the germinal layer, the brood capsule, and the protoscolex. Moreover, enzymatic activities against synthetic peptide substrates and macromolecule proteins were also characterized by using recombinant active enzymes expressed in *Pichia pastoris*.

2. Materials and methods

2.1. Animals

Animal procedures and management protocols in this study were approved by the Ethics Committee of Asahikawa Medical University, Asahikawa, Japan.

2.2. Preparation of parasite material

E. multilocularis (Furano isolate, Hokkaido, Japan) metacestode tissue was obtained from non-obese diabetic severe combined immunodeficiency (NOD/Shi-*scid*) mice infected by intraperitoneal passage of metacestodes (Nakaya et al., 2006). Microvesicle and protoscolex suspensions were prepared by pressing metacestode tissue through a 300 μm metal mesh with PBS. The microvesicles and protoscoleces were washed five to seven times with PBS, and then used for preparation of metacestode crude lysate and excretory/secretory (ES) products. Because NOD/Shi-*scid* mice had little inflammatory response, isolation of microvesicles and protoscoleces with less host components, which are commonly found in those from immunocompetent mice, could be done efficiently.

To prepare metacestode crude lysate, microvesicles and protoscoleces were homogenized with three times volume of lysis buffer consisting of 20 mM Tris–HCl, pH 7.4, 150 mM NaCl, and 1.0% 3-[(3-cholamidopropyl)dimethylammonia]-1-propanesulfonic acid (CHAPS) in the presence of peptidase inhibitors (protease inhibitor cocktail for mammalian tissues, Sigma–Aldrich). After one freeze–thaw cycle and centrifugation at 10,000g for 30 min at 4 °C, the supernatant was recovered and kept at −80 °C until use.

To obtain ES products, microvesicles and protoscoleces were cultured in RPMI-1640 medium supplemented with 100 U/ml penicillin and 100 μg/ml streptomycin at 37 °C for 12 h. Few dead microvesicles and protoscoleces were found under a microscopic examination at the end of cultivation, which indicated that the contamination of intracellular proteins released into the medium supernatant as a result of parasite death had been almost completely avoided. The medium supernatant containing ES products was carefully collected and was passed through a disposable chromatography column (Econo-Pac column, Bio-Rad) with a porous bed support (a 30 μm pore size) to remove minor microvesicle and protoscolex contaminants. After filtration through 0.45 μm filter membrane (Millipore), the medium supernatant was concentrated by using an Amicon Ultra-15 Centrifugal Filter Unit with a cutoff size of 5 kDa (Millipore) and kept at −80 °C until use.

2.3. Cloning of EmCBP1 and EmCBP2 genes

Total RNA was isolated from freshly prepared *E. multilocularis* metacestodes using Trizol reagent (Gibco BRL) according to the manufacture's instruction. After purification of Poly(A)$^+$ RNA by using oligo(dT)-latex beads (TaKaRa), cDNA available in 5′ and 3′ rapid amplification of cDNA end (RACE) method was synthesized from 1 μg of purified poly(A) $^+$ RNA by using the GeneRacer Kit (Invitrogen).

3′ RACE were performed with degenerated forward primers designed from the consensus sequences flanking the active site residues of eukaryotic cysteine peptidases and 3′ RACE primer.

The forward primer (5′-CAGGGTCAGTGYGGNTCNTGYTGG-3′) and GeneRacer 3′ primer (5′-GCTGTCAACGATACGCTACGTAACG-3′) were used in the first round PCR, and the forward primer (5′-CAGTGCGGTTCNTGYTGGGCNTTY-3′) and GeneRacer 3′ Nested primer (5′-CGCTACGTAACGGCATGACAGTG-3′) were used in the nested PCR. PCR reactions were performed in a 50 μl of reaction mixture containing 1 × *Ex Taq* Buffer, 2.0 mM $MgCl_2$, 0.2 μM of each primer, 0.2 mM of each dNTP, 5 ng of cDNA and 0.5 units of *EX Taq* DNA polymerase (TaKaRa) and cycling conditions were 30 s at 94 °C (first cycle: 2 min at 94 °C), 30 s at 50 °C and 30 s at 72 °C for 30 cycles. The PCR products were separated in a 1.0% agarose gel, the DNA fragments were recovered and cloned into pGEM T-vector (Promega), and plasmid clones were sequenced. To obtain sequence upstream of EmCBP1 and EmCBP2 genes, 5′ RACE was performed using gene-specific primer (5′-CGTACCATCACTGCTC TCCCGCTTACTGTC-3′ for EmCBP1gene, 5′-TGCAACCAAAGCCACAG AATAAGCC-3′ for EmCBP2 gene) and GeneRacer 5′ primer (5′-CG ACTGGAGCACGAGGACACTGA-3′) with annealing temperature of 60 °C. Finally, full-length cDNAs of the EmCBP1 and EmCBP2 genes were cloned by PCR using a high-fidelity DNA polymerase, Phusion DNA polymerase (Finnzymes), and primers directed to both the UTR ends.

2.4. Expression of the mature region of EmCBP1 and EmCBP2 in Escherichia coli and purification

The mature enzyme region of EmCBP1 or EmCBP2 was amplified by PCR with primer sets containing a restriction enzyme (underlined) recognition sequence added to 5′ end to facilitate cloning of the PCR products. The primers used were: 5′-GGGAATTC CTGCCGGCATCTTTTGATCCC-3′ (mCBP1/F), 5′-GGGTCGACTAGTT TTGTGGGATACCTGC-3′ (CBP1/R), 5′-GGGAATTCCTTCCCTCAGAAT TTGACGCA-3′ (mCBP2/F), 5′-GGGTCGACTCACTTCCTTATTTTTGGA ATACC-3′ (CBP2/R). The PCR reactions were performed with cDNA clones as templates. The PCR products were digested with *Eco*RI and *Sal*I, cloned into bacterial expression vector pET-30a(+) (Novagen) for producing a fusion protein with His tag. The cloned plasmids were transfected into *E. coli* BL21(DE3)pLysS strain. Expression of recombinant proteins was induced by addition of 1 mM isopropyl-β-D-thiogalactoside (IPTG) to the culture. Recombinant proteins were purified using Ni-NTA beads (Qiagen) under denaturation conditions. Protein concentration was determined by BCA protein assay kit (Pierce).

Please cite this article in press as: Sako, Y., et al. *Echinococcus multilocularis*: Identification and functional characterization of cathepsin B-like peptidases from metacestode. Exp. Parasitol. (2010), doi:10.1016/j.exppara.2010.11.005

2.5. Production of monoclonal antibodies

Female BALB/c mice were immunized by intraperitoneally (i.p.) injection of 50 μg of *E. coli*-expressed recombinant EmCBP1 (eEmCBP1) or EmCBP2 (eEmCBP2) emulsified in Freund's complete adjuvant. Three weeks later the procedure was repeated but with Freund's incomplete adjuvant. Three days before the fusion, the mice were i.p. boosted with 50 μg antigens in PBS. Spleen cells of mice were fused with NS-1 myeloma cells. The antibody-secreting hybridomas were screened by ELISA with eEmCBP1 or eEmCBP2. Hybridomas selected were cloned by limit dilution at least twice.

2.6. SDS–PAGE and immunoblot analysis

Proteins were treated with a SDS sample buffer (62.5 mM Tris–HCl, pH 6.8, 2.0% SDS, 50 mM dithiothreitol and 10.0% glycerol) at 100 °C for 5 min and separated in a 7.5% or 12.5% polyacrylamide gel. For immunoblot analysis, the separated proteins were transferred onto a polyvinylidene difluoride (PVDF) membrane sheet (Millipore). The sheet was blocked with blocking solution (20 mM Tris–HCl, pH 7.6, 150 mM NaCl, 1.0% casein, 0.1% Tween 20) and probed with monoclonal antibody followed by alkaline phosphatase-conjugated anti-mouse IgG antibody (Novagen). Nitroblue tetrazolium/5-bromo-4-chloro-3-indoyl phosphate was used for color development.

2.7. Immunohistochemistry

Parasite tissues and livers from infected-NOD/Shi-*scid* mice were washed once with PBS and fixed with 2.0% paraformaldehyde in PBS overnight at 4 °C and then embedded in paraffin. Sections of 5 μm were produced and were transferred to slides. After antigen retrieval using HistoVT One (Nacalai Tesque), sections were treated with peroxidase blocking solution (0.3% H_2O_2 in methanol) for 30 min. Then, sections were washed with PBS, blocked using blocking solution for 1 h and incubated overnight at 4 °C with monoclonal antibody. After three washing with PBS, the sections were incubated with peroxidase-conjugated anti-mouse IgG antibody (ImmPRESS REAGENT, Vector laboratories) for 30 min at room temperature. After four washing with PBS, the sections were incubated with 3-amino-9-ethylcarbazole. All sections were counterstained with hematoxylin.

2.8. Expression of EmCBP1 and EmCBP2 in P. pastoris

The pro-mature coding region of EmCBP1 or EmCBP2 was amplified by PCR with primer sets containing a restriction enzyme (underlined) recognition sequence. The primers used were: 5′-CGGAATTCA GTACTGTGACCAGCGCAATTGG-3′ (proCLP1/F), 5′-ATGCGGCCGCTA GTTTTGTGGGATACCTGC-3′ (PIC CLP1/R), 5′-CGGAATTCAGAAAACC TCATCAGAGCGAC-3′ (proCLP2/F), 5′-ATGCGGCCGCTCACTTCCTTA TTTTTGGAATACC-3′ (PIC CBP2/R). The PCR reactions were carried out as mentioned above. The PCR products were digested with *Eco*RI and *Not*I and cloned into yeast expression vector pPICZα A (Invitrogen), and subsequently linearized with *Pme*I and electroporated into *P. pastoris* KM71 host cells. Yeast transformants were cultured in 500 ml of buffered-glycerol complex medium (1.0% yeast extract, 2.0% peptone, 1.34% yeast nitrogen base, 4×10^{-5}% biotin, 1.0% glycerol, and 100 mM potassium phosphate, pH 6.0) at 28 °C for 2 days and collected by centrifugation at 1000*g* for 5 min, and protein expressions were induced by resuspending the cells in 100 ml of buffered-methanol minimal medium (1.34% yeast nitrogen base, 4×10^{-5}% biotin, 1.0% methanol, and 100 mM potassium phosphate, pH 6.0) at 28 °C for 3 days. Due to the presence of an α-factor leader peptide sequence, recombinant proteins were secreted into expression medium. The culture medium containing recombinant EmCBP1 (yEmCBP1) or EmCBP2 (yEmCBP2) was collected, concentrated using an Amicon stirred cell with a YM-10 membrane and dialyzed against 50 mM sodium acetate buffer (pH 4.5) containing 2.5 mM EDTA. For purification of active form of yEmCBP1, dialysate was directly loaded on a HisTrap SP XL cation-exchange column pre-equilibrated with 50 mM sodium acetate buffer (pH 4.5) containing 2.5 mM EDTA after activation at 37 °C for 1 h in the presence of 10 mM L-cysteine and proteins were eluted by use of a linear salt gradient (0–1.0 M NaCl). For purification of active form of yEmCBP2, the conversion of pro-form into active enzyme was accomplished by treatment with pepsin. After addition of porcine pepsin (Sigma–Aldrich) at a final concentration of 0.5 mg/ml, the activation mixture was incubated at 37 °C for 4 h. The activated yEmCBP2 was purified as mentioned above. Recombinant proteins were treated with peptide:*N*-glycosidase F (PNGase F, New England Biolabs) under denaturing conditions to remove any N-linked oligosaccharides to determine whether recombinant proteins were glycosylated.

2.9. Irreversible active site-labelling of yEmCBP1 and yEmCBP2

A biotinylated dipeptidyl fluoromethylketone (Biotin-Phe-Ala-FMK, MP Biomedicals), a cysteine peptidase inhibitor, was used for active-site labelling. Briefly, the purified enzyme was incubated for 30 min at room temperature with 10 μM biotin-Phe-Ala-FMK in 100 mM sodium acetate buffer (pH 5.5) containing 2.5 mM EDTA, 0.1% CHAPS and 10 mM L-cystine. Labelled proteins were detected with alkaline phosphatase-conjugated streptavidin (Novagen).

2.10. Substrate specificity and kinetic measurements of yEmCBP1 and yEmCBP2

Peptidase activity was characterized by using peptidyl-4-methylcoumarin-7-amide (MCA) as substrates. The standard assay volume was 200 μl, using 100 mM sodium acetate buffer (pH 5.5) containing 0.1% CHAPS, 2.5 mM EDTA and 10 mM L-cysteine. Substrates were added to a final concentration of 2 μM, or other concentration as required. Assays were performed at room temperature. The amount of 7-amino-4-methylcoumarin (AMC) released was measured by the fluorometer (VersaFluor Fluorometer, Bio-Rad) at an excitation wavelength of 370 nm and an emission wavelength of 460 nm.

For determination of the optimum pH of recombinant enzyme activity, 100 mM citrate–phosphate buffer (pH 3.0–8.0) containing 250 mM NaCl, 0.1% CHAPS, 2.5 mM EDTA and 10 mM L-cystine, were used. Substrate specificities were investigated using benzyloxycarbonyl (Z)-Phe-Arg-MCA, Z-Arg-Arg-MCA, Z-Leu-Arg-MCA, Z-Gly-Pro-Arg-MCA, and Z-Val-Val-Arg-MCA at a concentration of 2 μM. The values of K_m and V_{max} for Z-Phe-Arg-MCA and Z-Arg-Arg-MCA were determined by a nonlinear regression analysis. The molar concentration of active recombinant enzymes was determined by active-site titration using the Z-Phe-Arg-MCA and cysteine peptidase inhibitor *trans*-epoxysuccinyl-L-leucylamido(4-guanidino)butane (E-64) as described by Barrett and Kirschke (1981). All peptidyl-MCA substrates used were purchased from Peptide Institute, Japan.

2.11. Inactivation kinetics of yEmCTB1 and yEmCTB2

Inactivation of recombinant enzyme was performed in 100 mM citrate–phosphate buffer (pH 6.5, 7.0, and 7.5) containing 250 mM NaCl, 0.1% CHAPS, 2.5 mM EDTA, and 10 mM L-cystine in the presence of 50 μM Z-Phe-Arg-MCA. Progress of the reaction was monitored continuously by the fluorescence of the released products for 30 min. All progress curves obtained were exponential, and could be best fitted to the following first-order relationship (Eq. 1):

Please cite this article in press as: Sako, Y., et al. *Echinococcus multilocularis*: Identification and functional characterization of cathepsin B-like peptidases from metacestode. Exp. Parasitol. (2010), doi:10.1016/j.exppara.2010.11.005

$$P = P_{\infty}(1 - e^{k_{obs}t})$$

where P and P_{∞} are the product concentration at a given or infinite time, respectively, and k_{obs} is the observed first-order inactivation rate constant. And half-lives were calculated as $t_{1/2} = \ln 2/k_{obs}$.

2.12. Protein substrate digestion

Human IgG, human serum albumin (HSA), soluble calf skin type I collagen, human placenta type IV collagen, and bovine plasma fibronectin were used as protein substrates. All protein substrates used were purchased from Sigma–Aldrich, Japan. Active recombinant enzyme (0.2 μM) was incubated with 0.2 mg/ml of each protein substrate in 100 mM sodium acetate buffer (pH 5.5) containing 2.5 mM EDTA and 10 mM L-cysteine at 37 °C for 4 h. The digestion reaction was stopped by the adding of SDS–PAGE sample buffer. Protein substrate digests were subjected to SDS–PAGE and degradation products were visualized by Coomassie Blue staining.

3. Results

3.1. Primary structure of EmCBP1 and EmCBP2

Following PCR with degenerate primers and sequencing analysis of 48 PCR product clones, a total of four different partial genes encoding cysteine peptidases were obtained from *E. multilocularis* metacestode cDNA. Database search of the deduced amino acid sequences of individual clones revealed that two clones are identical to EmCLP1 and EmCL2 (Sako et al., 2007), respectively, and other two clones show high homology to cathepsin B-like peptidases. Rapid amplification of cDNA ends (RACE) was performed to obtain the full-length of two novel cysteine peptidase cDNAs, termed EmCBP1 and EmCBP2, respectively.

As shown in Fig. 1, EmCBP1 consists of a 18-residue putative signal sequence predicted by the method of Nielsen et al. (1997), a 77-residue propeptide and the 256-residue mature enzyme. EmCBP2 consists of a 16-residue putative signal sequence, a 67-residue propeptide and the 255-residue mature enzyme. Comparison of EmCBP1 with EmCBP2 revealed an amino acid identity of 60.5% (65.6% for the mature region only). The catalytic triad residues are conserved with other crucial residues shaping an oxyanion hole (Menard et al., 1991), and the occluding loop region (Musil et al., 1991) responsible for peptidyldipeptidase activity, a unique feature of cathepsin B, is also present in the mature enzyme. The predicted molecular masses of the mature EmCBP1 and EmCBP2 are 28,241 and 28,140 Da, respectively. In mature region, EmCBP1 has one putative N-linked glycosylation site at position 116.

3.2. Detection of EmCBP1 and EmCBP2 in E. multilocularis

Immunoblot analyses of *E. multilocularis* metacestode crude lysate (Fig. 2, lanes 1) and ES products (lanes 2) were performed. Anti-EmCBP1 monoclonal antibody recognized proteins of 24.5

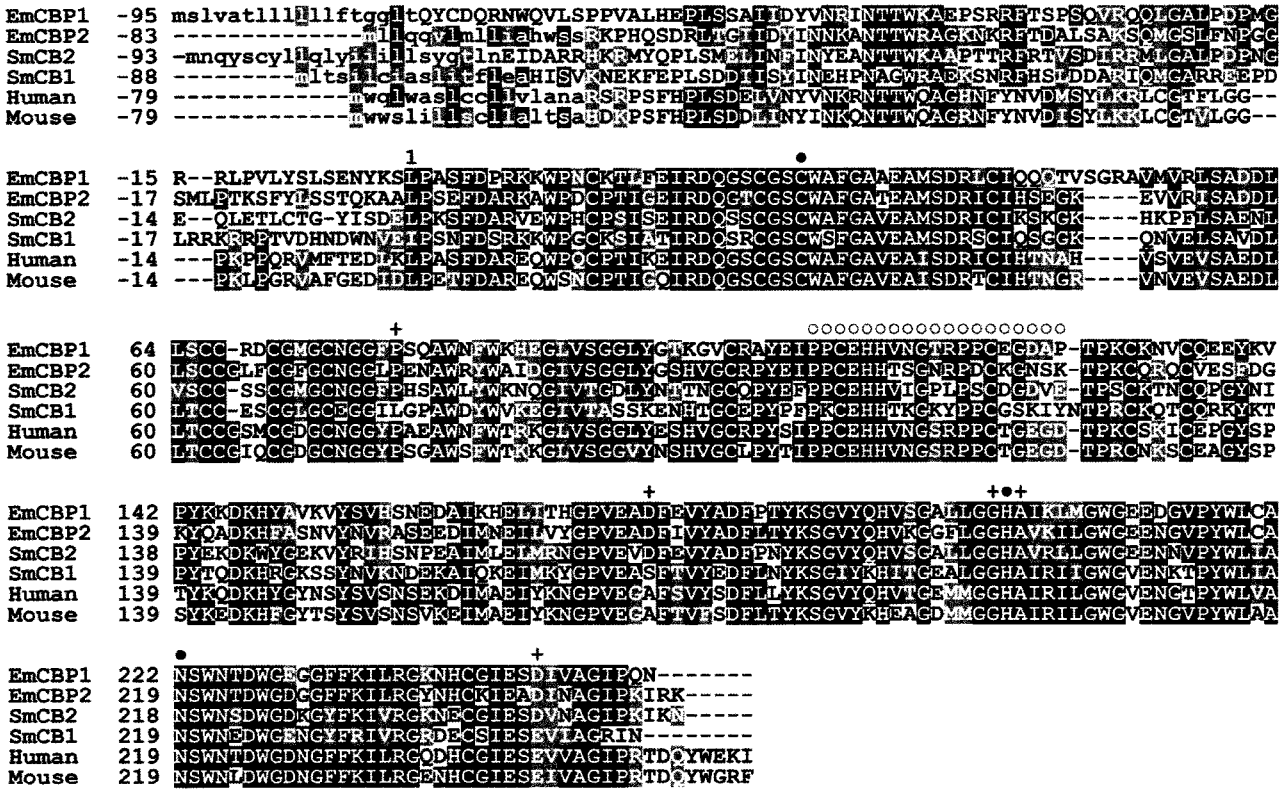

Fig. 1. Comparison of the deduced amino acid sequences of EmCBP1 and EmCBP2 with other cathepsin B enzymes. The alignment was generated using Clustal W server (http://www.ch.embnet.org/software/ClustalW.html) together with BOXSHADE server (http://www.ch.embnet.org/software/BOX_form.html). Gaps were introduced to maximize the alignment. Conserved residues are highlighted: identical, similar and unrelated residues with black, gray, and white backgrounds. Predicted signal sequence is written in lower case and closed circles (●) represent active site residues. Amino acid residues forming substrate binding pockets (McGrath, 1999) are indicated by plus signs (+), and the occluding loop unique to cathepsin B is indicated by open circles (○). Aligned amino acid sequences are *Schistosoma mansoni* cathepsin B (SmCB2, AJ312106), *Schistosoma mansoni* cathepsin B (SmCB1, AAA29865), human cathepsin B (Human, NP_001899), and mouse cathepsin B (Mouse, 1701299A).

Please cite this article in press as: Sako, Y., et al. *Echinococcus multilocularis*: Identification and functional characterization of cathepsin B-like peptidases from metacestode. Exp. Parasitol. (2010), doi:10.1016/j.exppara.2010.11.005

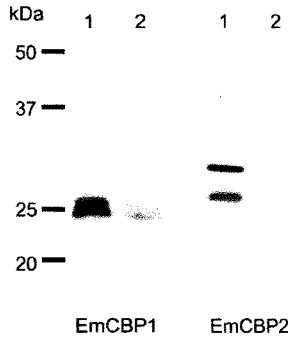

Fig. 2. Immunoblot analyses of *E. multilocularis* metacestodes extracts and ES products. Extracts of *E. multilocularis* metacestodes (lanes 1), and ES products (lanes 2) were probed with anti-EmCBP1 (left) and anti-EmCBP2 (right) monoclonal antibody. Molecular size markers are indicated on the left.

and 25.5 kDa in lysate and ES products, and anti-EmCBP2 monoclonal antibody recognized proteins of 27.0 and 29.9 kDa in lysate and ES products. Isotype-matched negative control monoclonal antibody did not bind to any of these bands (data not shown).

Furthermore, immunohistochemical studies were performed to investigate the localizations of EmCBP1 and EmCBP2 in metacestode. As shown in Fig. 3, the germinal layer, the brood capsule, and the protoscolex were stained. No signals were obtained for the acellular laminated layer of parasite.

3.3. Expression of EmCBP1 and EmCBP2 in yeast

To generate functional peptidases for *in vitro* studies, recombinant EmCBP1(yEmCBP1) and EmCBP2 (yEmCBP2) were expressed in yeast using the *P. pastoris* system and the α-pheromone signal sequence for extracellular secretion. The culture supernatant was collected after 3 days of cultivation and was 20-fold concentrated. The hydrolysis activity of the supernatant treated with and without pepsin in the presence of a reducing agent L-cysteine against Z-Phe-Arg-MCA was tested to determine optimal activation conditions of recombinant enzymes before purification (Fig. 4A). yEmCBP1 was activated at pH 4.5 after 1 h without the pepsin treatment. In contrast, removal of pro-region by pepsin was required for activation of yEmCBP2 (Fig. 4A). The activated recombinant enzyme purified by cation-exchange chromatography as a single peak was analyzed by SDS–PAGE followed by Coomassie Blue staining and immunoblotting (Fig. 4B and C). The purified yEmCBP1 migrated as a broad band between 25 and 50 kDa, and the purified yEmCBP2 migrated as a single band of approximately 27.0 kDa. Treating yEmCBP1 with PNGase F converted the broad band to two bands at 30 and 25.6 kDa (Fig. 4C, lanes 1 and 2), whereas no change in size of yEmCBP2 was observed (Fig. 4C, lanes 3 and 4), which indicated that yEmCBP1 was glycosylated. Analyses using the probe, biotin-Z-Phe-Ala-FMK, able to label specifically active cysteine peptidases revealed that in yEmCBP1 enzymes ranging from 30 to 50 kDa, detected as a 30 kDa band after treated with PNGase F, are active (Fig. 4D, lanes 1 and 2). No active enzyme bands except the 27-kDa enzyme were detected in yEmCBP2 (Fig. 4D, lanes 3 and 4). The labelling of active enzymes with biotin-Phe-Ala-FMK failed by pre-treatment with a cysteine inhibitor, E64 (data not shown).

3.4. Activity of yEmCBP1 and yEmCBP2 against peptidyl-MCA substrates

The substrate specificity of the yEmCBP1 and yEmCBP2 was characterized by using several peptide substrates varying at P2 position (Fig. 5). yEmCBP1 preferred substrates with Phe > Val > Leu at P2 position at an acidic pH optimum of 5.5. Substrate with Pro or Arg at P2 position was also hydrolyzed, but less efficiently. The pH optimum for hydrolyzing substrate with Arg at P2 was shifted to 7.5. yEmCBP2 showed similar features to those of yEmCBP1 except that a marked shifting of the pH optimum for hydrolyzing substrate with Arg at P2 was not observed. yEmCBP2 hydrolyzed peptidyl-MCA substrates more efficiently than yEmCBP1.

Kinetic parameters for hydrolysis of Z-Phe-Arg-MCA (suitable substrate for cathepsin L and B) and Z-Arg-Arg-MCA (cathepsin B-selective substrate) were summarized in Table 1. yEmCBP1 and yEmCBP2 had greater k_{cat}/K_m value for Z-Phe-Arg-MCA over Z-Arg-Arg-MCA. Difference in k_{cat}/K_m values between two substrates for yEmCBP1 and yEmCBP2 was 93- and 137-fold, respectively.

3.5. Inactivation kinetics of yEmCBP1 and yEmCBP2

The kinetics of the pH-induced inactivation of yEmCBP1 and yEmCBP2 were studies at pH 6.5, 7.0, and 7.5, and the reaction between enzymes and substrates (Z-Phe-Arg-MCA) was monitored continuously (Fig. 6 and Table 2). The inactivation of yEmCBP1 at pH 6.5 or 7.0 was not observed during monitoring period and its half-time at pH 7.5 was approximately 318 s. The half-time of yEmCBP2 shortened, from approximately 1689 to 10 s, with increasing pH.

3.6. Degradation of macromolecules by yEmCBP1 and yEmCBP2

To investigate the ability of yEmCBP1 and yEmCBP2 to degrade macromolecules, protein digestion analyses were performed (Fig. 7). In these studies, human IgG and human serum albumin

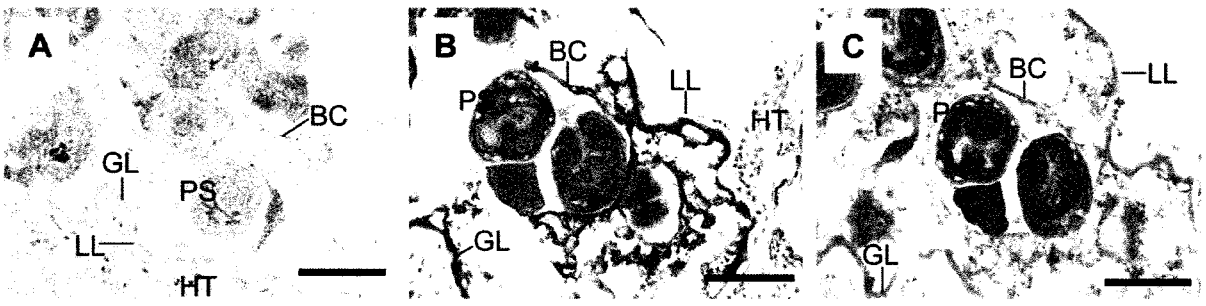

Fig. 3. Immunohistochemical detection of EmCBP1 and EmCBP2 in *E. multilocularis* metacestodes. Parasite tissues (A, B, and C) were isolated and paraffin-sections were produced. The sections were probed with anti-EmCBP1 (B), anti-EmCBP2 (C) and isotype-matched negative control (A) monoclonal antibody. The following structures are indicated: PS, protoscolex; GL, germinal layer; BC, brood capsule; LL, laminated layer; HT, host tissue. Scale bar = 100 μm.

Please cite this article in press as: Sako, Y., et al. *Echinococcus multilocularis*: Identification and functional characterization of cathepsin B-like peptidases from metacestode. Exp. Parasitol. (2010), doi:10.1016/j.exppara.2010.11.005

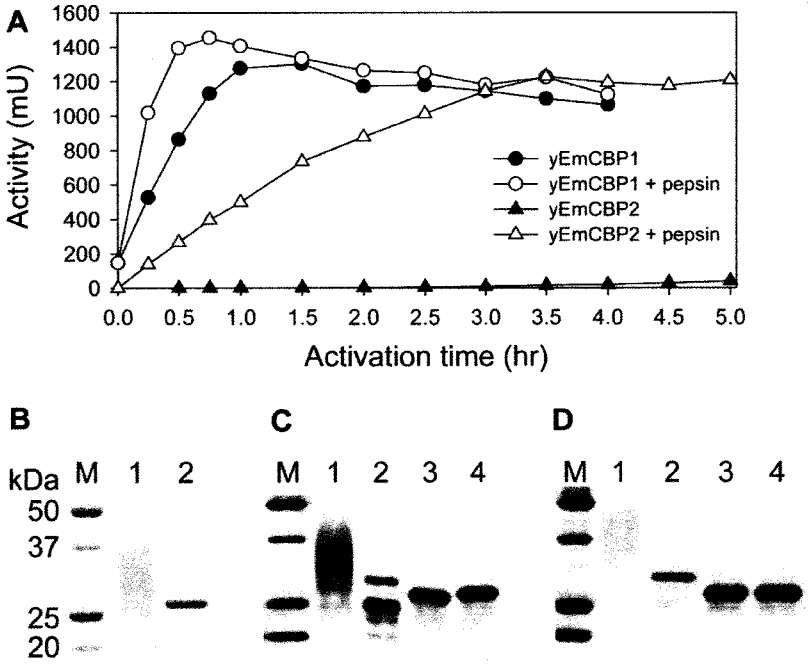

Fig. 4. Expression, purification and active-site labelling of yEmCBP1 and yEmCBP2. (A) Time-dependent activations with and without the pepsin treatment. Aliquots were withdrawn from the incubation mixture at the indicated time points, and the activities were monitored with 50 μM Z-Phe-Arg-MCA. (B) Purified recombinant enzymes were subjected to SDS–PAGE and stained with Coomassie blue. Lane 1, yEmCBP1; lane 2, yEmCBP2. (C) Immunoblot analyses of purified recombinant enzymes before (lanes 1 and 3) and after (lanes 2 and 4) deglycosylation by the treatment with PNGase F. yEmCBP1 (lanes 1 and 2) and yEmCBP2 (lanes 3 and 4) were detected by using monoclonal antibody specific for each protein. (D) Detection of active recombinant enzymes by labelling of purified recombinant proteins with the cysteine peptidase-specific probe, biotin-Phe-Ala-FMK. After labelling, aliquots of recombinant enzymes were treated with (lanes 2 and 4) and without (lanes 1 and 3) PNGase F. yEmCBP1 (lanes 1 and 2) and yEmCBP2 (lanes 3 and 4) were detected with alkaline phosphate-conjugated streptavidin. Molecular size markers are indicated on the left.

as humoral molecules and type I and type IV collagens and fibronectin as extracellular matrix molecules were chosen. All protein substrates used in this study were readily hydrolyzed by yEmCBP1 and yEmCBP2. All degradations of protein substrates were completely inhibited by adding a cysteine peptidase inhibitor, E-64 (data not shown).

4. Discussion

Numerous studies have demonstrated that cysteine peptidases from protozoa, trematode and nematode parasites are involved in various functions including nutrient uptake, disruption of the immune system, invasion and penetration into host tissues, which leads us strongly to consider them as a likely target for the chemotherapy (reviewed by Sajid and McKerrow, 2002; Dalton et al., 2003; Caffrey et al., 2004; Rosenthal, 2004; McKerrow et al., 2006; Robinson et al., 2008; Smooker et al., 2010). By contrast, few characterizations of peptidases including cysteine peptidases of cestodes *E. multilocularis* and *Echinococcus granulosus* have been described (McManus and Barrett, 1985; Marco and Nieto, 1991; Sako et al., 2007). In this study, two cathepsin B-like cysteine peptidases, EmCBP1 and EmCBP2, from *E. multilocularis* metacestode were identified, functionally expressed and characterized.

Sequencing analyses revealed that EmCBP1 and EmCBP2 have a catalytic triad (Cys, His, and Asn) and an oxyanion hole (Menard et al., 1991) those are characteristic features of clan CA family C1 cysteine peptidase. The occluding loop that is responsible for peptidyldipeptidase activity (Musil et al., 1991) and is a feature distinguishing cathepsin B from other cysteine peptidases is also conserved. RT-PCR analyses using EmCBP1 and EmCBP2-specific primer, in addition to the fact that EmCBP1 and EmCBP2 were found in the database of *E. multilocularis* whole genome project (http://www.sanger.ac.uk/resources/downloads/helminths/echinococcus-multilocularis.html), demonstrated that the genes obtained were originated from *E. multilocularis*, not from mouse used for preparation of parasite materials (data not shown).

Immunoblot and immunohistochemical experiments demonstrated that EmCBP1 and EmCBP2 were expressed in the germinal layer, the brood capsule and the protoscolex of larva and that some portions of both enzymes were secreted. The sizes, 24.5 and 25.5 kDa, of proteins detected by anti-EmCBP1 monoclonal antibody were smaller than the predicted size, 28.4 kDa. Cathepsin B is synthesized as an inactive 43 kDa pro-form and is processed to a single-chain form (31 kDa) or a two-chain form (heavy chain of 25 kDa and light chain of 5 kDa) to be activated (Towatari et al., 1979). It is possible that EmCBP1 consists of a heavy chain and light chain linking by a disulphide bond, and the protein bands detected by monoclonal antibody might be derived from the heavy chains. Anti-EmCBP2 monoclonal antibody recognized protein of 27.0 and 29.9 kDa in lysate and ES products. The latter protein might be intermediate forms of proenzyme. Determinations of N-terminal amino acid sequences of purified native EmCBP1 and EmCBP2 must be carried out.

The expressions of the active recombinant EmCBP1 and EmCBP2 were conducted by the use of the *P. pastoris* expression system. yEmCBP1 was successfully activated at pH 4.5 and purified. Because of the existence of one N-glycosylation site in mature enzyme, yEmCBP1 was glycosylated and detected as a broad band with 25–50 kDa range in size after purification. Some portion of yEmCBP1, detected as a 25.6 kDa-protein by immunoblot analysis after treated with PNGase F, could not be labelled efficiently with active enzyme-specific probe, biotin-Phe-Ala-FMK, which indi-

Please cite this article in press as: Sako, Y., et al. *Echinococcus multilocularis*: Identification and functional characterization of cathepsin B-like peptidases from metacestode. Exp. Parasitol. (2010), doi:10.1016/j.exppara.2010.11.005

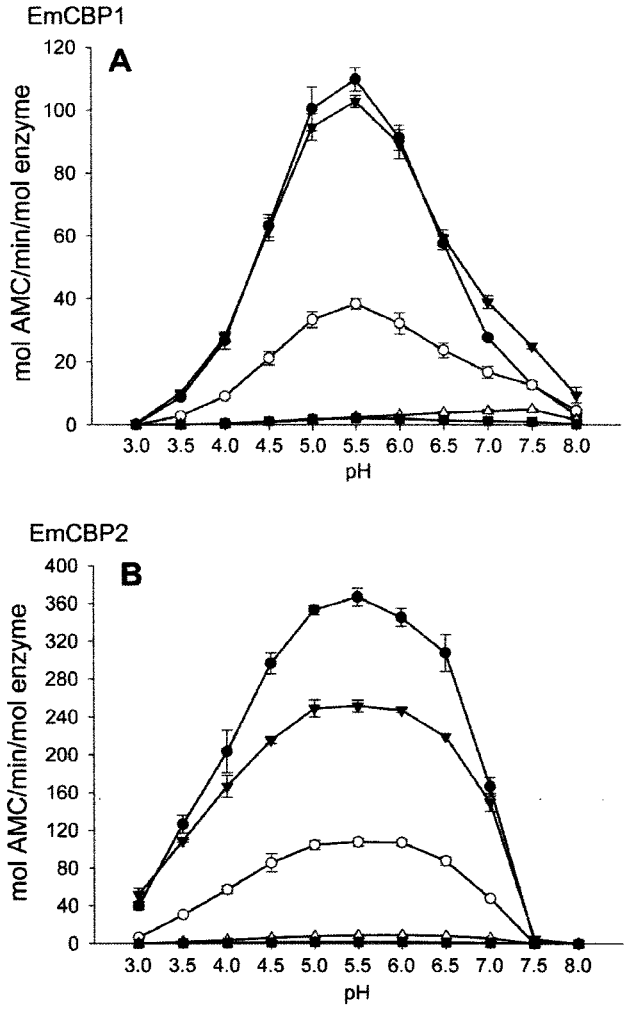

Fig. 5. pH optima and S2 subsite specificity of yEmCBP1 and yEmCBP2. Five substrates, Z-Phe-Arg-MCA (closed circles), Z-Val-Val-Arg-MCA (closed triangles), Z-Leu-Arg-MCA (open circles), Z-Gly-Pro-Arg-MCA (closed squares), and Z-Arg-Arg-MCA (open triangles) were tested at a final concentration of 2 μM. The standard deviation of three experiments is indicated.

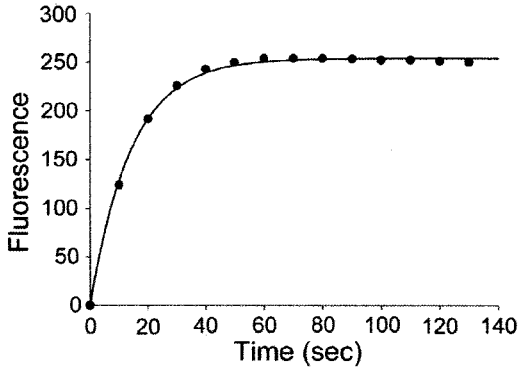

Fig. 6. Progress curve for the inactivation of yEmCBP2 at pH 7.5. Substrate, Z-Phe-Arg-MCA, was tested at a final concentration of 50 μM, and progress of the reaction was monitored continuously by the fluorescence of the released products. The solid line is the theoretical first-order curve calculated using Eq. 1.

Table 2
Effect of pH on the rate of inactivation of yEmCBP1 and yEmCBP2.[a]

	pH	$10^3 \times k_{obs}$ (s^{-1})	$t_{1/2}$ (s)
yEmCBP1	6.5	Nob[b]	Nob
	7.0	Nob	Nob
	7.5	2.18 ± 0.02	317.69 ± 3.40
yEmCBP2	6.5	0.41 ± 0.01	1689.29 ± 61.11
	7.0	6.79 ± 0.48	102.32 ± 7.20
	7.5	70.52 ± 2.23	9.83 ± 0.31

[a] The best estimates for the observed inactivation rate constant, k_{obs}, are given by nonlinear regression analysis. Corresponding half-lives were calculated using following relation ship: $t_{1/2} = \ln 2/k_{obs}$. Inactivation was investigated in the presence of 50 μM Z-Phe-Arg-MCA.
[b] Nob = not observed during incubation.

cated that they were inactive enzyme. This may be due to miss-folding, the oxidation, or the autodegradation of the mature enzyme during expression and purification. Activation of yEmBP2 was unsuccessful under the same condition of yEmCBP1 activation. Alternative activation condition in the presence of negatively charged glycosaminoglycan with dextran sulfate which facilitates autocatalytic activation (Barlic-Maganja et al., 1998) was tested but resulted in unsuccessful (data not shown). However, active yEmCBP2 could be obtained by *trans*-processing with pepsin, resulting in a single 27 kDa-protein.

In cysteine peptidases belonging to clan CA, the S2 subsite is substantial substrate-binding pocket for determination of substrate specificity (McGrath, 1999). The substrate specificity of the yEmCBP1 and yEmCBP2 was characterized by the use of several peptide substrates varying at P2 position. Both enzymes preferred substrates with Phe > Val > Leu at P2 position at an acidic pH optimum of 5.5, and cathepsin B-selective substrate Z-Arg-Arg-MCA was less hydrolyzed. Kinetic parameters for hydrolysis of Z-Phe-Arg-MCA and Z-Arg-Arg-MCA revealed that there were 93- and 137-fold-differences in k_{cat}/K_m values for yEmCBP1 and yEmCBP2, respectively. Similar preference has been observed in a cathepsin B isoform (SmCB2) of *Schistosoma mansoni*, not other isoform (SmCB1) (Caffrey et al., 2002). By contrast, the difference reported for mammalian cathepsin B is smaller than 10-fold (Hasnain et al., 1992; Wang et al., 1998). EmCBP1, EmCBP2 and SmCB2 have a negatively charged residue Asp at position 173 (mouse cathepsin B

Table 1
Kinetic parameters for hydrolysis of peptidyl-MCA substrates by yEmCBP1 and yEmCBP2.[a]

	Substrate	K_m (μM)	k_{cat} (s^{-1})	k_{cat}/K_m ($mM^{-1}\ s^{-1}$)
yEmCBP1	Z-Phe-Arg-MCA	20.45 ± 1.23	33.23 ± 1.01	1626.71 ± 48.67
	Z-Arg-Arg-MCA	747.67 ± 41.15	13.05 ± 0.63	17.46 ± 0.11
yEmCBP2	Z-Phe-Arg-MCA	27.17 ± 0.82	71.68 ± 1.52	2638.40 ± 23.29
	Z-Arg-Arg-MCA	1124.47 ± 76.15	21.57 ± 1.05	19.19 ± 0.36

[a] The K_m and V_{max} values were calculated by a nonlinear regression analysis of substrate concentration versus peptidase velocity. The k_{cat} values were calculated from V_{max} and the molar concentration of active enzyme titrated with Z-Phe-Arg-MCA and cysteine peptidase inhibitor E-64.

Please cite this article in press as: Sako, Y., et al. *Echinococcus multilocularis*: Identification and functional characterization of cathepsin B-like peptidases from metacestode. Exp. Parasitol. (2010), doi:10.1016/j.exppara.2010.11.005

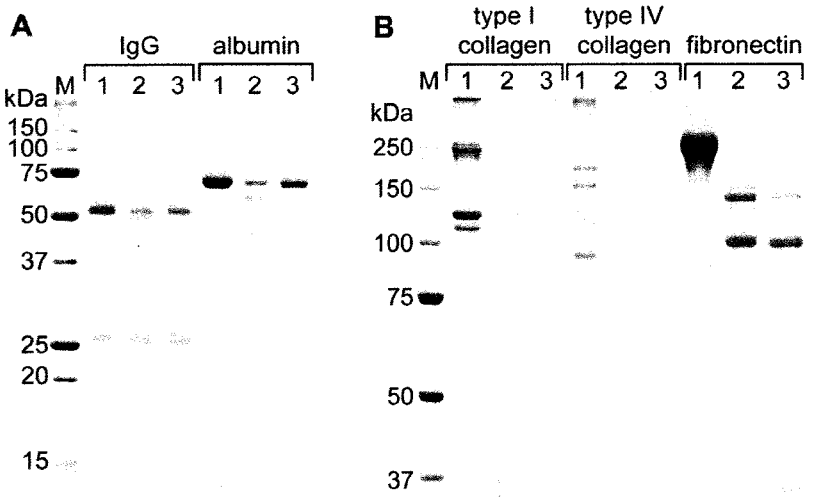

Fig. 7. Degradation of macromolecules by yEmCBP1 and yEmCBP2. Humoral molecules (A) and extracellular matrix molecules (B) were incubated with yEmCBP1 or yEmCBP2 at 37 °C for 4 h at pH 5.5. Protein substrate digests were subjected to SDS–PAGE and degradation products were visualized by Coomassie Blue staining. Each substrate was incubated with none of enzyme (lanes 1), yEmCBP1 (lanes 2), and yEmCBP2 (lanes 3). Molecular size markers are indicated on the left.

numbering) involving in S2 subsite formation, whereas mammalian cathepsin B from human, mouse, rat, and bovine and SmCB1 have an uncharged residue, Ala and Ser, respectively, without other substantial differences. Therefore, the possibility that the negatively charged residue Asp participates in the substrate preference is raised. Further analyses by using recombinant enzymes in which Asp is replaced with Ala are necessary to confirm this possibility.

The facts that at acidic condition yEmCBP1 and yEmCBP2 were stable, active and had broad specificity against host proteins including immunoglobulin, albumin, collagens, and fibronectin, suggested that these enzymes are lysosomal enzymes and are involved in protein digestion for parasites' nutrition. Additionally, the possibility that yEmCBP1 and yEmCBP2 act as extracellular enzymes was raised since both enzymes were detected in ES products. However, yEmCBP1 and yEmCBP2, especially latter, were unstable at neutral or slightly alkaline pH close to physiological pH similarly to mammal papain-like cysteine peptidases except for cathepsin S (Turk et al., 2000). Since the echinococcal cyst fluid has a neutral pH, EmCBP1 and EmCBP2 secreted into cyst fluid might lose their enzymatic activity. In contrast, EmCBP1 and EmCBP2 secreted outside of parasite cysts might not lose their enzymatic activity, because it is known that the host inflammatory responses can lead to tissue acidification (Kellum et al., 2004) and cathepsin B secreted from some kind of tumor cells becomes stable at alkaline pH by interacting with heparin and heparan sulfate (Almeida et al., 2001; Roshy et al., 2003). The activities of cysteine peptidases secreted into host tissues to degrade extracellular matrix molecules, e.g., collagen and fibronectin, have been described in several nematode and trematode parasites (Berasain et al., 1997; Rhoads and Fetterer, 1997; Smooker et al., 2010), and these characters seem to be implicated in migration of parasite through host tissues. Because the larva of *E. multilocularis* infiltrates and proliferates indefinitely by exogenous budding of the cellular germinal layer (Thompson, 1995), the ability of EmCBP1 and EmCBP2 to degrade extracellular matrix molecules might be involved in pathogenesis of *E. multilocularis*. Inhibition analyses of EmCBP1 and EmCBP2 by specific inhibitors or genetic knock out of enzymes would be needed to confirm such a role of peptidases *in vivo*.

In conclusion, we identified and characterized two novel cathepsin B-like peptidases from *E. multilocularis* metacestodes. The enzymes may play a primary role in protein digestion for parasites' nutrition. Thus, the inactivation of these enzymes may impair the survival of the parasite in the host. Further studies are needed to provide a greater understanding of the biological significance of EmCBP1 and EmCBP2 in parasite–host interactions.

Acknowledgements

This study was supported in part by the Japan Society for the Promotion of Science (JSPS) (21256003), JSPS-Asia/Africa Science Platform Fund (2006–2011) and by the Special Coordination Fund for Promoting Science & Technology (2010–2012) by Ministry of Education, Japan.

References

Abdulla, M.H., Lim, K.C., Sajid, M., McKerrow, J.H., Caffrey, C.R., 2007. Schistosomiasis mansoni: novel chemotherapy using a cysteine protease inhibitor. PLoS Medicine 4, e14.

Alcala-Canto, Y., Ibarra-Velarde, F., Sumano-Lopez, H., Gracia-Mora, J., Alberti-Navarro, A., 2007. Effect of a cysteine protease inhibitor on *Fasciola hepatica* (liver fluke) fecundity, egg viability, parasite burden, and size in experimentally infected sheep. Parasitology Research 100, 461–465.

Almeida, P.C., Nantes, I.L., Chagas, J.R., Rizzi, C.C., Faljoni-Alario, A., Carmona, E., Juliano, L., Nader, H.B., Tersariol, I.L., 2001. Cathepsin B activity regulation. Heparin-like glycosaminogylcans protect human cathepsin B from alkaline pH-induced inactivation. The Journal of Biological Chemistry 276, 944–951.

Barlic-Maganja, D., Dolinar, M., Turk, V., 1998. The influence of Ala205 on the specificity of cathepsin L produced by dextran sulfate assisted activation of the recombinant proenzyme. Biological Chemistry 379, 1449–1452.

Barr, S.C., Warner, K.L., Kornreic, B.G., Piscitelli, J., Wolfe, A., Benet, L., McKerrow, J.H., 2005. A cysteine protease inhibitor protects dogs from cardiac damage during infection by *Trypanosoma cruzi*. Antimicrobial Agents and Chemotherapy 49, 5160–5161.

Berasain, P., Goni, F., McGonigle, S., Dowd, A., Dalton, J.P., Frangione, B., Carmona, C., 1997. Proteinases secreted by *Fasciola hepatica* degrade extracellular matrix and basement membrane components. Journal of Parasitology 83, 1–5.

Barrett, A.J., Kirschke, H., 1981. Cathepsin B, Cathepsin H, and cathepsin L. Methods in Enzymology 80, 535–561.

Caffrey, C.R., McKerrow, J.H., Salter, J.P., Sajid, M., 2004. Blood 'n' guts: an update on schistosome digestive peptidases. Trends in Parasitology 20, 241–248.

Caffrey, C.R., Salter, J.P., Lucas, K.D., Khiem, D., Hsieh, I., Lim, K.C., Ruppel, A., McKerrow, J.H., Sajid, M., 2002. SmCB2, a novel tegumental cathepsin B from adult *Schistosoma mansoni*. Molecular and Biochemical Parasitology 121, 49–61.

Dalton, J.P., Neill, S.O., Stack, C., Collins, P., Walshe, A., Sekiya, M., Doyle, S., Mulcahy, G., Hoyle, D., Khaznadji, E., Moiré, N., Brennan, G., Mousley, A., Kreshchenko, N., Maule, A.G., Donnelly, S.M., 2003. *Fasciola hepatica* cathepsin L-like proteases: biology, function, and potential in the development of first generation liver fluke vaccines. International Journal for Parasitology 33, 1173–1181.

Eckert, J., Conraths, F.J., Tackmann, K., 2000. Echinococcosis: an emerging or re-emerging zoonosis? International Journal for Parasitology 30, 1283–1294.

Hasnain, S., Hirama, T., Tam, A., Mort, J.S., 1992. Characterization of recombinant rat cathepsin B and nonglycosylated mutants expressed in yeast. New insights into the pH dependence of cathepsin B-catalyzed hydrolyses. The Journal of Biological Chemistry 267, 4713–4721.

Please cite this article in press as: Sako, Y., et al. *Echinococcus multilocularis*: Identification and functional characterization of cathepsin B-like peptidases from metacestode. Exp. Parasitol. (2010), doi:10.1016/j.exppara.2010.11.005

Ito, A., Agvaandaram, G., Bat-Ochir, O.-E., Chuluunbaatar, B., Gonchigsenghe, N., Yanagida, T., Sako, Y., Myadagsuren, N., Dorjsuren, T., Nakaya, K., Nakao, M., Ishikawa, Y., Davaajav, A., Dulmaa, N., 2010. Histopathological, serological, and molecular confirmation of indigenous alveolar echinococcosis cases in Mongolia. American Journal of Tropical Medicine and Hygiene 82, 266–269.

Kellum, J.A., Song, M., Li, J., 2004. Science review: extracellular acidosis and the immune response: clinical and physiologic implications. Critical Care 8, 331–336.

Kern, P., 2006. Medical treatment of echinococcosis under the guidance of Good Clinical Practice (GCP/ICH). Parasitology International 55 Suppl, S273–S282.

Marco, M., Nieto, A., 1991. Metalloproteinases in the larvae of *Echinococcus granulosus*. International Journal for Parasitology 21, 743–746.

McGrath, M.E., 1999. The lysosomal cysteine proteases. Annual Review of Biophysics and Biomolecular Structure 28, 181–204.

McKerrow, J.H., Caffrey, C., Kelly, B., Loke, P., Sajid, M., 2006. Proteases in parasitic diseases. Annual Review of Pathology 1, 497–536.

McManus, D.P., Barrett, N.J., 1985. Isolation, fractionation and partial characterization of the tegumental surface from protoscoleces of the hydatid organism, *Echinococcus granulosus*. Parasitology 90, 111–129.

McManus, D.P., Zhang, W., Li, J., Bartley, P.B., 2003. Echinococcosis. Lancet 362, 1295–1304.

Menard, R., Carriere, J., Laflamme, P., Plouffe, C., Khouri, H.E., Vernet, T., Tessier, D.C., Thomas, D.Y., Storer, A.C., 1991. Contribution of the glutamine 19 side chain to transition-state stabilization in the oxyanion hole of papain. Biochemistry 30, 8924–8928.

Molinari, J.L., Mejia, H., White Jr., A.C., Garrido, E., Borgonio, V.M., Baig, S., Tato, P., 2000. *Taenia solium*: a cysteine protease secreted by metacestodes depletes human CD4 lymphocytes *in vitro*. Experimental Parasitology 94, 133–142.

Musil, D., Zucic, D., Turk, D., Engh, R.A., Mayr, I., Huber, R., Popovic, T., Turk, V., Towatari, T., Katunuma, N., Bode, W., 1991. The refined 2.15 A X-ray crystal structure of human liver cathepsin B: the structural basis for its specificity. The EMBO Journal 10, 2321–2330.

Nakaya, K., Mamuti, W., Xiao, N., Sato, M.O., Wandra, T., Nakao, M., Sako, Y., Yamasaki, H., Ishikawa, Y., Craig, P.S., Schantz, P.M., Ito, A., 2006. Usefulness of severe combined immunodeficiency (scid) and inbred mice for studies of cysticercosis and echinococcosis. Parasitology International 55 Suppl, S91–S97.

Nielsen, H., Engelbrecht, J., Brunak, S., von Heijne, G., 1997. Identification of prokaryotic and eukaryotic signal peptides and prediction of their cleavage sites. Protein Engineering 10, 1–6.

Pawlowski, Z.S., Eckert, J., Vuitton, D.A., Ammann, R.W., Kern, P., Craig, P.S., Far, K.F., De Rosa, F., Filice, C., Gottstein, B., Grimm, F., Macpherson, C.N.L., Sato, N., Todorov, Uchino, J., von Sinner, W., Wen, H., 2001. Echinococcosis in humans: clinical aspects, diagnosis and treatment. In: Eckert, J., Gemmell, M.A., Meslin, F.-X., Pawlowski, Z.S. (Eds.), WHO/OIE manual on echinococcosis in humans and animals: a public health problem of global concern. World Organization for Animal Health, Paris, France, pp. 20–71.

Rawlings, N.D., Tolle, D.P., Barrett, A.J., 2004. MEROPS: the peptidase database. Nucleic Acids Research 32, D160–D164.

Rhoads, M.L., Fetterer, R.H., 1997. Extracellular matrix: a tool for defining the extracorporeal function of parasite proteases. Parasitology Today 13, 119–122.

Robinson, M.W., Dalton, J.P., Donnelly, S., 2008. Helminth pathogen cathepsin proteases: it's a family affair. Trends in Biochemical Sciences 33, 601–608.

Rosenthal, P.J., 2004. Cysteine proteases of malaria parasites. International Journal for Parasitology 34, 1489–1499.

Roshy, S., Sloane, B.F., Moin, K., 2003. Pericellular cathepsin B and malignant progression. Cancer and Metastasis Reviews 22, 271–286.

Sajid, M., McKerrow, J.H., 2002. Cysteine proteases of parasitic organisms. Molecular and Biochemical Parasitology 120, 1–21.

Sako, Y., Yamasaki, H., Nakaya, K., Nakao, M., Ito, A., 2007. Cloning and characterization of cathepsin L-like peptidases of *Echinococcus multilocularis* metacestodes. Molecular and Biochemical Parasitology 154, 181–189.

Shin, M.H., Chung, Y.B., Kita, H., 2005. Degranulation of human eosinophils induced by *Paragonimus westermani*-secreted protease. Korean Journal of Parasitology 43, 33–37.

Smooker, P.M., Jayaraj, R., Pike, R.N., Spithill, T.W., 2010. Cathepsin B proteases of flukes: the key to facilitating parasite control? Trends in Parasitology 26, 506–514.

Tato, P., Fernández, A.M., Solano, S., Borgonio, V., Garrido, E., Sepúlveda, J., Molinari, J.L., 2004. A cysteine protease from *Taenia solium* metacestodes induce apoptosis in human CD4+ T-cells. Parasitology Research 92, 197–204.

Thompson, R.C.A., 1995. Biology and systematics of *Echinococcus*. In: Thompson, R.C.A., Lymbery, A.J. (Eds.), *Echinococcus* and Hydatid Disease. CAB International, Wallingford, UK, pp. 1–50.

Towatari, T., Kawabata, Y., Katunuma, N., 1979. Crystallization and properties of cathepsin B from rat liver. European Journal of Biochemistry 102, 279–289.

Turk, B., Turk, D., Turk, V., 2000. Lysosomal cysteine proteases: more than scavengers. Biochimica et Biophysica Acta 1477, 98–111.

Wang, B., Shi, G.P., Yao, P.M., Li, Z., Chapman, H.A., Bromme, D., 1998. Human cathepsin F. Molecular cloning, functional expression, tissue localization, and enzymatic characterization. The Journal of Biological Chemistry 273, 32000–32008.

Please cite this article in press as: Sako, Y., et al. *Echinococcus multilocularis*: Identification and functional characterization of cathepsin B-like peptidases from metacestode. Exp. Parasitol. (2010), doi:10.1016/j.exppara.2010.11.005

CHAPTER 51

Cysticercosis and taeniosis: *Taenia solium, Taenia saginata* and *Taenia asiatica*

Ana Flisser, Philip S. Craig and Akira Ito

Summary

The pork and beef tapeworms, *Taenia solium* and *Taenia saginata* respectively, are taeniid cestodes and major food-borne or meat-borne zoonoses. Human tapeworms and swine cysticerci have been known since Egyptian and Greek cultures. Nevertheless their association as part of the life cycle of the same parasite was only demonstrated during the nineteenth century. Kuchenmeister fed convicts with cysticerci excised from pork meat and found adult tapeworms in the intestine after autopsy, while van Beneden fed *T. solium* eggs to pigs and found numerous cysticerci in muscles after slaughter (Grove 1990).

T. solium is the only causative agent of neurocysticercosis in humans and is, therefore, the more important of these species in public health. This chapter describes classical aspects of the morphology of the parasites as well as clinical aspects of the diseases they cause. Most importantly, detailed explanations of taxonomic aspects, specially related to the newly recognized *Taenia asiatica* are given. Furthermore, the epidemiology and transmission dynamics of the parasites, as well as intervention measures such as health education, mass drug treatment and vaccination, are described in detail. The chapter concludes with considerations on the surveillance and a discussion on prospects for the control of these cestode zoonoses.

Taxonomy

The classification of human *Taenia* is as follows:

Kingdom: Animalia,

Phylum: Platyhelminthes,

Class: Cestoidea,

Subclass: Eucestoda,

Order: Cyclophyllidea,

Family: Taeniidae,

Genus: *Taenia*,

Species: *Taenia solium* Linnaeus (1758),

Species: *Taenia saginata* Goeze (1782),

Species: *Taenia asiatica* Eom and Rim (1993).

Taeniidae are mammalian parasites with adults found in carnivores and larvae in herbivores. In the adult parasite, the scolex, which is the anchorage organ aided by suckers, usually bears 2 rows of hooks that rarely are absent. The genital pore is irregularly alternated along the strobila with a single set of reproductive organs in each proglottid. Eggs have a radial striated appearance because of the embryophore formed by embryophoric blocks.

Adult *Taenia solium* and *Taenia saginata* are found in the human intestine. The larval stage or metacestode (cysticercus) is found in pigs (*T. solium*) and bovines (*T. saginata*).

Taenia asiatica has been recognized in Asia and the Pacific. Adult tapeworms appear to be *T. saginata* but infected people eat pork rather than beef (Huang *et al.* 1966; Kosin *et al.* 1972; Fan 1988). It has been called the Asian *Taenia* and expected to be a new species (Fan 1988; reviewed by Simanjuntak *et al.* 1997). Subsequent molecular studies revealed very small differences from *T. saginata* and it was classified as a subspecies of *T. saginata* (*T. saginata asiatica*, Fan *et al.* 1995), which used different intermediate hosts distributed in Asia and the Pacific (Fan 1988, 1995; McManus and Bowles 1994). Later, it was described as *Taenia asiatica*, an independent but sister species of *T. saginata* (reviewed by Ito *et al.* 2003; Eom 2006; Hoberg 2006). Separate species are believed to be valid as *T. saginata* and *T asiatica* are distribute sympatrically but to data no hybrids between the two have been identified which would be expected if they were subspecies or strains of the same species. However, the numbers of specimens to date examined is small. (Hoberg 2006). Fig. 51.1 illustrates a summary of the molecular phylogeny of taeniid cestodes (modified from Okamoto *et al.* 2007).

Molecular phylogeny

Molecular tools have been used to further characterize the 3 human *Taenia* species (McManus and Ito 2005) and their epidemiology and possible origin. Mitochondrial DNA data strongly suggest that *T. saginata* and *T. asiatica* are very closely related to each other and

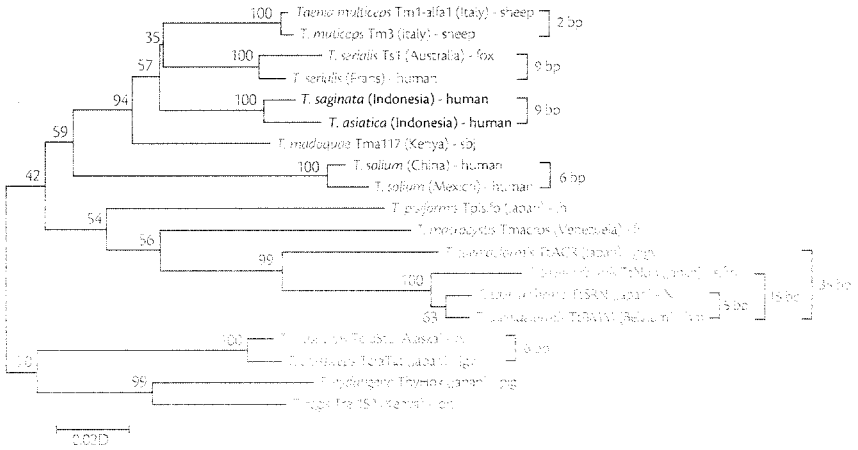

Fig. 51.1 Molecular phylogeny of genus *Taenia*.
Modified from Okamoto *et al.* (1995)

that *T. solium* is divided into two genotypes, the Asian and the American/African genotypes (Fig. 51.2). Minor diversity within the genotypes has been demonstrated in samples from Peru and Mexico (Nakao *et al.* 2002; Campbell *et al.* 2006; Maravilla *et al.* 2003, 2008; Sudewi *et al.* 2008). Molecular phylogenic studies (Sudewi *et al.* 2008) suggest that *T. solium* in Papua originated elsewhere in Asia rather than from nearby Bali as suggested by Gadjusek (1978).

T. saginata mitochondrial DNA analysis shows large variations (Rodriguez-Hidalgo *et al.* 2002; Myadagsuren *et al.* 2007) pointing to a higher complexity of this parasite than that of *T. solium*.

T. solium emerged in Africa several millions years ago as a parasite of early hominids that probably evolved from parasites of hyaeniids (Hoberg 2001, 2006).

Detection of parasite DNA using faecal samples and multiplex PCR for identification of human *Taenia* should be used in endemic areas for *T. solium*, *T. saginata* and *T. asiatica*, because their sympatric distribution may complicate surveillance of cysticercosis control (Ananthaphruti *et al.* 2007).

Morphology

Tapeworm

Tapeworms are flat long helminths: adults measuring 1.5 to 10 m. The head or scolex, has four suckers and a rostellum, which may be armed with hooks (*T. solium*), unarmed (*T. saginata*) or have a sunken or unarmed rostellum (*T. asiatica*, Fig. 51.3). Hooks are organized as a two row crown of 22 to 32 hooks that ranges in size from 159 to 173 μm. The most conspicuous part of the tapeworm is the chain of segments that forms the strobila. It has the appearance of a ribbon and is constituted by more than a thousand proglottids (proper name for segments). Tapeworms do not have digestive organs, thus feed passively through their tegument. In contrast they have a well formed excretory system that contains numerous collecting ducts and flame cells. Proglottids develop from the neck region behind the scolex. Proximal proglottids are immature, they are followed by mature ones that contain several

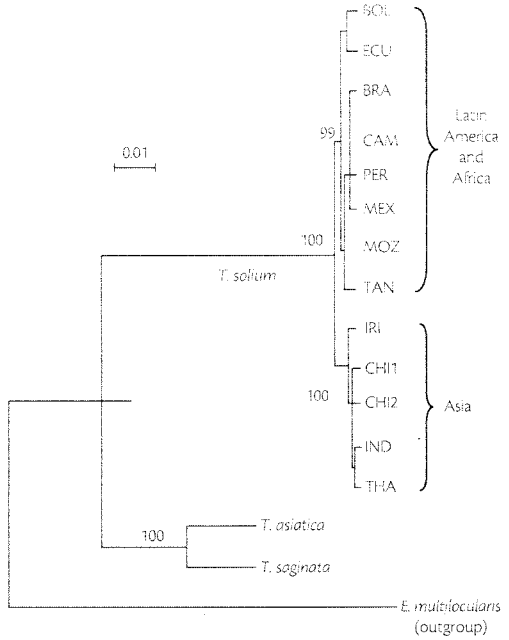

Fig. 51.2 Two genotypes of *T. solium* in the world. The neighbour-joining phylogenetic tree of taeniid tapeworms inferred from the complete nucleotide sequences of mitochondrial *cox1* gene. The scale bar represents the estimated number of nucleotide substitutions per nucleotide site. The isolates of *T. solium* were obtained from Bolivia (BOL), Ecuador (ECU), Brazil (BRA), Cameroon (CAM), Peru (PER), Mexico (MEX), Mozambique (MOZ), Tanzania (TAN), Irian Jaya (IRI), China (CHI1 and CHI2), India (IND) and Thailand (THA).
Modified from Nakao *et al.* (2002)

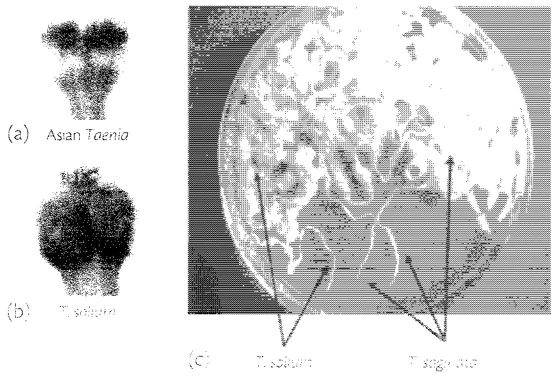

Fig. 51.3 Three *Taenia* worms of two species were expelled from one woman in Kanchanaburi, Thailand in 2004 (2 *T. solium* and 1 Asian *Taenia*) and from one Tibetan girl in 2007 (2 *T. saginata* and 1 *T. solium*). Fig. (a) and (b) show the scolex of one of the 2 *T. solium* and one Asian *Taenia* from Kanchanaburi which were confirmed by DNA analysis. Fig. (b) was morphologically identified to be *T. saginata*, since there was no evidence on the distribution of Asian *Taenia* in Thailand before this study. Fig (c) shows two *T. saginata* and one *T. solium* from a Tibetan girl (Dr Li TY unpublished data). In these areas, three species have been confirmed to be occurring sympatrically.
[illegible]

hundred testes and two to three ovary lobes per segment. Tapeworms are hermaphrodites; self-fertilization occurs and eggs develop in the multi-branched sac-like uterus of gravid proglottids, at the end of the strobila, which contain between 50,000 and 80,000 eggs per gravid segment. Distal proglottids become bigger, measuring from a couple of mm to up to 2 cm long. *T. solium* has 7–14 lateral uterine branches in the proglottid whilst *T. saginata* has 14–32. This feature is very important for species identification when the scolex cannot be found (Eom and Rim 1993; Fan *et al.* 1995; Flisser *et al.* 2004a; Andreassen 2005).

The adult tapeworm dwells in the human small intestine. An autoradiographic analysis of the germinative tissue in evaginated cysticerci identified stem cells that proliferate continuously, differentiate and migrate to the tegument, constituting the main process by which these worms grow (Merchant *et al.* 1998). Adult *T. solium* has been established experimentally in one gibbon, one chacma baboon, many golden hamsters and, recently, in gerbils and chinchillas (Verster 1965; 1974; Cadigan *et al.* 1967; Maravilla *et al.* 1998). Experimentally infected hamsters develop mature segments and, when rodents are immunosuppressed with steroids, long lasting gut infections (1–3 months) are attained, pre-gravid proglottids develop in hamsters and in gerbils, while gravid proglottids and mature eggs may develop in chinchillas (Maravilla *et al.* 1998). The inflammatory, humoral and cellular immune responses have been characterized in non immunosuppressed hamsters (Avila *et al.* 2006). Experimental infections with adult *T. saginata* have been established in immunosuppressed golden hamsters without obtaining mature or gravid proglottids (Verster 1974) but their study has not been followed.

Eggs

Eggs are spherical, range in size from 20 to 50 μm and are morphologically indistinguishable from eggs of other taeniid species. Each egg contains an embryo, which is a multi-cellular structure that has six hooks, therefore it is also named hexacanth embryo or oncosphere. When eggs are released from the definitive host, many are fully embryonated and infective whilst others are at different stages of maturation and not infective. The embryophore appears as a rigid structure that protects the oncosphere while the egg is in the environment, making eggs extremely resistant. When eggs are ingested by the intermediate host, the cementing substance that joins embryophoric blocks is susceptible to enzymatic digestion which allows the oncosphere to be released (Laclette *et al.* 1982; Fan *et al.* 1995). Aided by their hooks and by enzymes released in vesicles, the oncospheres invade the intestinal mucosa and, after circulating, develop in the intermediate host.

Cysticercus

T. solium cysticerci have been identified in liver, brain and skeletal muscles of pigs six days after infection measuring around 0.3 mm. By 60 to 70 days after infection cysticerci have a fully developed scolex and measured between 6 to 9 mm (Yoshino 1933a, b, c). The mature cysticercus is usually spherical or oval, white or yellow, measures 0.5 and 1.5 cm and has a translucent bladder wall, through which the scolex can be seen. Young cysticerci have minimal inflammatory reaction surrounding them, while older parasites or those that are in pigs that were treated with a cestocidal drug, have an intense reaction that includes eosinophils, lymphocytes and macrophages (Flisser *et al.* 1990a; Aluja and Vargas 1989; Aluja *et al.* 1998). Cysticerci have two chambers: an inner one contains the scolex and the spiral canal and is surrounded by an outer compartment that contains the vesicular fluid, usually less than 0.5 ml. When a cysticercus is ingested by the definitive host, the first event that takes place is the widening of the pore of the bladder wall for the scolex and neck to emerge, leaving the bladder wall and vesicular fluid to disintegrate in the digestive tract of the definitive host (Rabiela *et al.* 2000).

T. solium cysticerci may also establish in humans causing cysticercosis in the central nervous system, eye, striated and heart muscle and subcutaneous tissue. Two morphological types of metacestodes develop in humans: cellulose and racemose. The cellulose cysticercus is as previously described and is present in swine and in humans. This type of cysticercus is generally separated from the host tissue by a thin collagenous capsule, within which it remains alive (Escobar 1983; Aluja and Vargas 1988; Aluja *et al.* 1998). The racemose cysticercus appears either as a large, round or lobulated bladder circumscribed by a delicate wall, or resembles a cluster of grapes, it measures up to 10 or even 20 cm and may contain 60 ml fluid. Cellulose cysticerci grow and transform into racemose in spacious areas such as basal cisterns, especially optic, carotid, Sylvian and peduncular cisterns. The most important characteristics of this type of cysticercus is that usually the scolex cannot be seen, in some cases only detailed histological studies reveal its remains (Berman *et al.* 1981; Jung *et al.* 1981; Rabiela *et al.* 1989).

T. saginata cysticerci, (cysticercus bovis), is an oval bladder less than 1cm long, fluid filled and containing the invaginated scolex but does not have hooks. Cysticerci lodge in the skeletal muscle of cattle and sporadic reports of unarmed cysticerci in llamas, pronghorn, oryx, topi and other antelopes, bushbucks, gazelles, wildebeest, oryx and giraffes, have appeared in the literature (Nelson *et al.* 1965; Pawlowski and Schultz 1972; Gemmell *et al.* 1983). Intermediate host acquire the infection when grazing on contaminated pasture.

T. asiatica cysticerci are smaller than those of *T. saginata* measuring approximately 2–3 mm in diameter. Both metacetodes have a scolex with a round rostellum surrounded by four symmetrically placed conspicuous suckers, while *T. asiatica* has two rows of rudimentary hooklets, considered as a wart-like formation that usually do not develop into morphologically identifiable hooks. *T. asiatica* cysticerci are found in domestic pigs and wild boar (Fan *et al.* 1995) and develop in liver but not in muscle. Most importantly, *T. asiatica* does not appear to cause cysticercosis in humans. This supports the hypothesis that it is a sister species of *T. saginata*. Both *T. saginata* and *T. asiatica* may be found sympatrically in Asia and the Pacific (Flisser *et al.* 2004; Ito *et al.* 2008). The main features of tapeworms, cysticerci and eggs are shown in Table 51.1.

Table 51.1 Morphological characteristics of human tapeworms

	Taenia solium	*Taenia saginata*	*Taenia asiatica*
Entire body			
Length (m)	1–5	4–12	1–8
Width (mm)	7–10	12–14	9–12
Proglottids (number)	700–1,000	1000–1,500	200–1,200
Scolex			
Diameter (mm)	0.6–1.0	1.5–2.0	0.2–2.0
Suckers (number)	4	4	4
Rostellum	Present	Absent	Present, small
Hooks (number)	22–32	Absent	Vestigial***
Mature proglottid			
Testes (number)	350–600	800–1,200	300–1,200
Ovary (number of lobes)	3	2	2
Vaginal sphincter	Absent	Present	Present
Length (mm)	2.1–2.5	2.1–4.5	
Width (mm)	2.8–3.5	3.1–6.7	
Gravid proglottid			
Uterus (number of branches)	7–11	14–32	12–26
Posterior protuberance	Absent	Present	Present
Length (mm)	3.1–10	10–20	4–22
Width (mm)	3.8–8.7	6.5–9.5	3–12
Cysticercus			
Size (mm)	8–15*	6–10	0.4–3.5
Fluid contents (ml)	<0.5**	NR	NR
Hooks in scolex	Present	Absent	Rudimentary
Egg			
Size (μm)	26–34	26–34	16–45
Hooks (number)	6	6	6

* In humans racemose type cysticerci measure up to 20 cm.
** In humans racemose type cysticerci contain up to 60 ml.
*** Hooks are sunken and rudimentaryNR–not reported.

Life cycle

Life cycles of the human *Taenia* are shown in Fig. 51.4. When a person ingests raw or semi-cooked pork or beef with viable cysticerci, the scolex evaginates and attaches to the intestinal mucosa in the upper third section of the small intestine (duodenum-jejunum). Gravid proglottids are released with faeces and/or spontaneously, starting at 8–12 weeks after infection. Although some sources state that tapeworms can survive for about 25 years, published original articles indicate that *T. saginata* can be found in the intestine of the host for approximately two years. Recent experience indicates that *T. solium* remains for shorter periods. Tapeworms release a few gravid proglottids, full of eggs, daily or 2–3 times per week (Andreassen 2005; Flisser *et al.* 2005a, 2006).

When swine or cattle ingest eggs, bile and enzymes disaggregate the embryophoric blocks and digest the oncospheral membrane. Cysticerci establish primarily in skeletal and cardiac muscle, as well as in the brain of pigs, a process that takes approximately 12 weeks. They remain viable for at least one year, when pigs are usually sent to slaughter. In cattle, cysticerci are usually calcified in adult animals, indicating that for *T. saginata* cysticercus life span is short. The main distinguishing feature of the life cycle of *T. asiatica* compared to *T. saginata* is the viscerotropic nature of cysticerci in pigs (especially to the liver), in contrast to the musculotropic cysticerci of *T. saginata* in cattle. Metacestodes from beef and swine become infective to humans about 8 to 10 weeks post-infection. Humans only acquire cysticercosis when they consume eggs in food handled by people infected by adult *T. solium* or through the faecal oral route (Eom and Rim 1993; Fan *et al.* 1995, Eom 2006).

Clinical aspects

Intestinal taeniosis

Intestinal taeniosis, caused by *T. solium* or *T. saginata*, is normally non pathogenic. It is identified because proglottids are frequently released (Craig and Ito 2007). Observations on a total of 3,100 affected people, show that by far the most frequent symptom is the discharge of proglottids (93%) (Pawlowski and Schultz 1972). This is a distinctive sign because of a sensation in the rectum followed by a crawling sensation in the perianal region and the thighs due to the discharge and movement of the proglottids. Up to 35% of tapeworm carriers felt abdominal pain and/or nausea. Weight loss only occurred in 21%, change in appetite in 17% and 15% reported headaches. In Ethiopia, 18 of 26 *T. saginata* carriers reported independent migration of segments from the anus (Tesfa-Yohannes 1990). Voluntary self-infections of humans with cysticerci of *T. saginata* reported release of 5–15 segments per day starting 10–12 weeks post infection (Craig and Ito 2007). As a result of worm migration to unusual sites or due to mechanical effects, various rare acute conditions or complications may occur, including appendicitis, invasion of the pancreatic and bile ducts, intestinal obstruction and perforation, vomiting of proglottids, or even vaginal bleeding due to a tapeworm in the uterus (reviewed in Flisser 1995, Jongwutiwes *et al.* 2004, Ahsan *et al.* 2005, Liu *et al.* 2005, Karanikas *et al.* 2007). Of greater importance in avoiding *T. solium* adult infections is that the tapeworm carrier is the main risk factor for acquiring cysticercosis (Flisser and Gyorkos 2007).

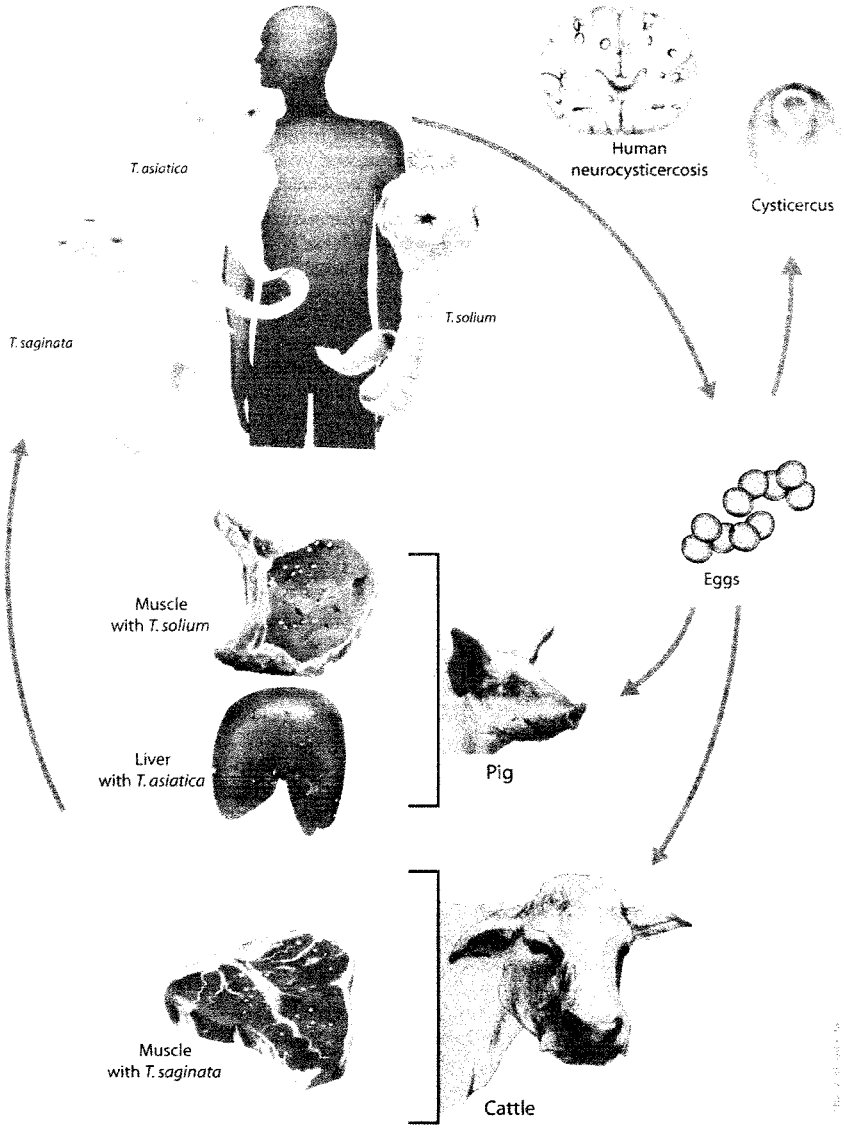

Fig. 51.4 Life cycle of human tapeworms.

Taeniosis has been diagnosed for over a half a century by detecting eggs in stools under microscopy or proglottids with the naked eye (Hall *et al.* 1981). These approaches are not very sensitive because they depend on the natural release of segments and on technical expertise. Coproantigens are parasite-specific products present in host faeces that can be detected by immunologic techniques. These products are associated with adult parasite metabolism and are present independently of eggs or proglottids. In addition, they are undetectable in the faeces shortly after removal of the adult worms and therefore can indicate treatment success. Detecting human taeniosis by an enzyme-linked immunosorbent assay (ELISA), without necessarily observing eggs in the stool, represents a significant advance in diagnosis. The assay can detect as little as 35 ng protein/ml of adult parasite antigen products. The sensitivity depends on the assay format employed and the quality of the immunized rabbit serum used. A high titre rabbit serum offers a higher sensitivity. Rabbit anti-*Taenia* antiserum is not commercially available at this time so that antibody titres and avidity may vary. Coproantigen detection by ELISA have already been applied for screening of taeniosis (including *T. asiatica*) in several field studies (Flisser 2002a; Allan and Craig 2006; Wandra *et al.* 2006b; Flisser and Gyorkos 2007).

Neurocysticercosis

Neurocysticercosis (NCC) is due to the development of *T. solium* cysticerci in the human central nervous system, where parasites can be found in the parenchyma, the subarachnoid tissue, and the ventricles. Clinical manifestations are polymorphic and depend on the location, number and development or involution stages of the parasites as well as characteristics of the immune response of the host. The most important sign is epilepsy that occurs mainly when cysticerci are lodged in the brain parenchyma. Extraparenchymal cysticerci can cause hydrocephalus due to mechanical obstruction of ventricular circulation of cerebrospinal fluid or to inflammatory reaction in basal cisterns. Symptoms usually occur after the cyst has initiated its degenerative process and are due mainly to the inflammatory response they induce or to residual scarring. In contrast, living cysticerci induce minimal inflammation, and can stay in this condition for several years because parasites evade the immune response. When the immune response becomes exacerbated it produces a cascade of immunological mechanisms that cause parasite death, but also severe damage to the neighbouring structures in the host, especially to basal blood vessels. These include dense collagen walls around cysticerci, astrocitic gliosis, microglia and capillary vessel proliferation. When cysticerci start to degenerate they have an appearance of colloidal, whitish vesicles, this stage is followed by a granulomatous one and finally parasites become calcified due to mineralization of the nodule, with surrounding intense gliosis and multinucleated giant cells, typical of a chronic inflammatory reaction to a foreign body Parasites in different stages of involution are frequently found in the same brain, which suggests either recurrent infections, parasites with different survival abilities or different immune response in different parasites or sites in the brain (Escobar *et al.* 1983; Sotelo and Del Brutto 2000; Medina-Escutia *et al.* 2001; Saenz *et al.* 2006).

Diagnosis of NCC is based on two types of techniques. Imaging techniques (computed tomography, CT, and magnetic resonance, MR) allow the definition of the number, stage, location and extension of the lesions. Immunologic assays identify anticysticercus antibodies and parasite antigens. Based on these techniques and epidemiologic data, several criteria have been established for diagnosis.

1) Absolute, when there is a histological demonstration of the parasite from biopsy of a brain or spinal cord lesion, cystic lesions showing the scolex on CT or MR, and direct visualization of subretinal parasites by funduscopic examination.
2) Major, when there are lesions highly suggestive of NCC on imaging studies, positive western blot in serum for the detection of anticysticercus antibodies, resolution of intracranial cystic lesions after therapy with praziquantel or albendazole, and spontaneous resolution of small single enhancing lesions.
3) Minor, when there are lesions compatible with neurocysticercosis on imaging studies, clinical manifestations suggestive of NCC, positive ELISA for detection of anticysticercus antibodies or cysticercus antigens, and cysticercosis outside the central nervous system.
4) Epidemiologic, when there is evidence of a household contact with *T. solium*, individuals coming from or living in an area where cysticercosis is endemic, history of frequent travel to disease-endemic areas. Interpretation of these criteria allows two degrees of diagnostic certainty. Definitive diagnosis is in patients who have one absolute criterion or in those who have two major plus one minor and one epidemiologic criterion. Probable diagnosis, in patients who have one major plus two minor criteria, or one major plus one minor and one epidemiologic criterion, and in those who have three minor plus one epidemiologic criterion (Del Brutto *et al.* 2001).

In imaging studies, a parenchymal living cysticercus generally is small, round and hypodense (CT) or hypointense (MR). When the parasite is colloidal, an external ring of inflammation appears with contrast fluid. A hyperdense (CT) or hyperintense (MR) invaginated scolex can be seen in both cases. Big living or colloidal cysticerci, up to 5 cm diameter, can be found in the subarachnoidal space or in the ventricles. Calcified parasites are round (hyperdense) and are better detected by CT (Sotelo and Del Brutto 2002, Amara *et al.* 2003; Arriada *et al.* 2003; Ito *et al.* 2006). For immunodiagnostic purposes currently the best technique is immunoblot using a semi-purified fraction obtained from a crude extract of cysticerci with a lentil-lectin column. Seven glycoprotein (GP) bands (with molecular masses of 50, 39–42, 24, 21, 18, 14 and 13 kDa) show 100% specificity for the detection of human cysticercosis. Sensitivity is related to the number of cysticerci in the brain and their viability: 98% sensitivity was found with three or more cysticerci, while only 65% sensitivity was obtained with one or two parasites (Tsang *et al.* 1989; Wilson *et al.* 1991). Also immunoblot has been standardized using GP purified by preparative isoelectrofocusing, which allow successfully using them also in ELISA with almost complete sensitivity and specificity (Ito *et al.* 1998, 2002a, 2006; Sako *et al.* 2000; Sato *et al.* 2003, 2006).

Treatment of NCC includes cestocidal drugs (praziquantel and albendazole) to kill living parasites and surgical procedures to remove intraventricular or subarachnoidal cysticerci or to place a ventricular shunt. Drugs to control symptoms are frequently used in order to reduce inflammation (corticoids), to control convulsive crisis (antiepileptics) or to reduce pain (analgesics). Pharmacokinetic and toxicological studies performed in humans with either cestocidal drug have shown that these agents have a fast absorption and, in general, lack toxic effects. Efficacy of cestocidal treatment is measured by the reduction in the number and size of cysticerci seen in CT or MR, by clinical improvement, elimination of corticoids or anticonvulsants and by the correction of ventricular dilatation. The most frequent surgical intervention is placement of ventricular shunts to deviate the cerebrospinal fluid to the peritoneal cavity in order to control hydrocephalus. Solitary intraventricular cysticerci can by surgically removed, nowadays even by endoscopy, in order to rapidly improve the patient's health (Bergsneider *et al.* 2000; Del Brutto *et al.* 2001; Colli *et al.* 2002; Sotelo and Del Brutto 2002; Psarros *et al.* 2003; Jung *et al.* 2008; Suri *et al.* 2008).

As with *T. saginata*, no proven cases have been reported of human cysticercosis caused by *T. asiatica*, and although the possibility remains it is probably unlikely. At least one study failed to experimentally infect non-human primates (baboons) dosed orally with eggs of *T. asiatica* (Fall *et al.* 1995).

Epidemiology

The family Taeniidae comprises around 33 species of tapeworms including the 3 human species. For *Taenia* of non-human hosts,

studies of host ecology and transmission biology are most important, while for the human *Taenia* species human behaviour, husbandry practices and socio-economic risk factors contribute to transmission, therefore epidemiological studies are essential.

Taenia solium

T. solium and human cysticercosis are widely distributed, with highest transmission in Latin America, India and Southeast (SE) Asia (WHO 1983). Studies indicate under-recognized but significant transmission of the parasite in several countries of sub-Saharan Africa (Geerts *et al.* 2002), Papua, Indonesia (Gajdusek 1978; Simanjuntak *et al.* 1997; Margono *et al.* 2006; Wandra *et al.* 2007) and of China and SE Asia (Simanjuntak *et al.* 1997; Roman *et al.* 2000; Singh *et al.* 2002; Craig and Ito 2007; Li *et al.* 2007). Nevertheless no global burden for human cysticercosis has yet been calculated (Carabin *et al.* 2005). Epidemiologic studies estimate 5–6 million cases worldwide (Craig *et al.* 1996), including at least 400,000 symptomatic cases in Latin America (Bern *et al.* 1999), 1.5–3 million cases in sub-Saharan Africa (A. L. Willingham personal communication), and 3 million cysticercosis cases estimated for China (Li *et al.* 2007). Furthermore, due to migration there are many neurological cases in developed countries, such as USA, and also recently, tapeworm carriers in the USA and Muslim countries have expanded interest in cysticercosis proposing it as an emerging infectious disease (Schantz *et al.* 1998, Flisser *et al.* 2004a). The economic impact of human and porcine cysticercosis, both in monetary burden and societal losses, is significant (Carabin *et al.* 2005, Rajkotia *et al.* 2007). There has been a formal proposal to declare NCC an international reportable disease (Roman *et al.* 2000), and *T. solium* has been included in a priority list of six human diseases (polio, mumps, rubella, dracunculiasis, lymphatic filariasis and cysticercosis) targeted for global eradication (ITFDE 1993; WHO/DFID-AHP 2006).

The epidemiology of *T. solium* taeniosis/cysticercosis is primarily linked to three main transmission features that must occur in an endemic community:

1) Keeping/raising pigs that have access to human faeces,
2) Lack of latrines or latrines accessible by pigs,
3) Eating undercooked or raw pork as part of local cuisine and/or because of poor cooking.

Human cysticercosis (including neurocysticercosis) is caused only by ingestion of the microscopic eggs or gravid proglottids. Main transmission pathways for human cysticercosis occur when eggs contaminate the hands a tapeworm carrier which increases the chance of self-infection as up to 30% of neurocysticercosis patients report a history of taeniosis (Gilman *et al.* 2000). Eggs may contaminate persons that have contact with a tapeworm carrier, or contaminate food prepared by a carrier, or contaminate vegetables close to indiscriminate sites of human defecation, or vegetables may be contaminated by eggs via human faeces as fertilizer (the latter practice remains common in parts of China and south east Asia). Other possible routes for egg contamination in humans may occur, such as deliberate use of proglottids as traditional medicaments (for example in South Africa) (Heinz and Macnab 1965). Note therefore that absence of pork eating may not prevent occurrence of human cysticercosis in a *T. solium* endemic area or even infection in low-risk groups, as long as at least one tapeworm carrier occurs in a household or local community (Schantz *et al.* 1992, WHO/FAO/OIE 2005).

In endemic communities in Latin America prevalence of human taeniosis based on microscopy/coproantigen ELISA is usually below 3%, porcine cysticercosis seropositivity or tongue palpation prevalence range from 1–>50%, and human cysticercosis seropositivity from 3–25% (Allan *et al.* 1996; Garcia-Noval *et al.* 1996; Rodriguez-Canul *et al.* 1999; Flisser *et al.* 2003; Garcia *et al.* 2003a, b; Flisser and Gyorkos 2007). The incidence of epilepsy/seizures/convulsions (the main symptom of neurocysticercosis) was 18–29 per 1,000 in Central American communities, of which 40% of cases may have detectable lesions compatible with NCC. However, there is not always a clear association between seropositivity and seizure history and/or a CT scan positive image (Garcia-Noval *et al.* 2001, 2002). Official abattoir slaughter rates for porcine cysticercosis, while useful in identification of potential hotspots, are usually of little practical value because most pigs from poor rural endemic communities are slaughtered at home or within a village setting. For example, in one highly endemic *T. solium* area of SW China, only 1.3% of pigs slaughtered at abattoirs were positive by meat inspection (Li *et al.* 2007). Epidemiological studies in Latin America, especially in Mexico, Guatemala, Honduras, Ecuador, Bolivia and Peru, have helped to identify major risk factors for taeniosis and human and porcine cysticercosis in rural endemic communities in that region. These are summarized below.

Risk of human taeniosis

These include eating undercooked pork, living in a household with infected pigs, female, age 10–39 years, Taenia carriers in the household and seropositivity for anti-cysticercus antibodies (Sarti *et al.* 1988, 1992, 1997, 2000; Allan *et al.* 1996a; Rodriguez-Canul *et al.* 1999; Garcia *et al.* 2003b).

Risk of human cysticercosis

A history of taeniosis (Gilman *et al.* 2000); person older than 10 years (Garcia *et al.* 1995, 946 patients); presence of a tapeworm carrier (person who is taeniid egg positive, coproantigen positive, and/or passed proglottids) in a household/family or in a neighbouring house or housing cluster (Sarti *et al.* 1988, 1994, 2000; Diaz-Camacho *et al.* 1990; Sanchez *et al.* 1998; Garcia-Noval *et al.* 1999; Garcia *et al.* 2003b); raising pigs; presence of cysticercosis positive pigs (tongue palpation, immunoblot seropositive, or necropsy positive) in a household (Garcia *et al.* 2003b); presence in family/household of a person with a history of late-onset (>18 years of age) seizures/epilepsy; immunoblot seropositive for antibobodies against low molecular weight (< 50KDa) *T. solium* metacestode glycoproteins (Garcia-Noval *et al.* 1996; Garcia *et al.* 2003b).

Risk of porcine cysticercosis

Presence of a human tapeworm carrier in a household (Sarti *et al.* 1988; Lescano *et al.* 2007); lack of latrine (Sarti *et al.* 1994; Allan *et al.* 1996b; Vazquez *et al.* 2001); presence of free-range backyard or wandering pigs in communities that practice home-slaughter (Rodriguez-Canul *et al.* 1998; 1999); a seropositive pig within 50–500 metres of a house with a *Taenia* carrier (Lescano *et al.* 2007).

Whilst transmission of *T. solium* occurs mainly in rural areas of under-developed regions where pig ownership is high (Flisser *et al.* 2004), transmission or outbreaks of human cysticercosis have also been described in urban foci in endemic countries such as

Ecuador and Peru (Goodman *et al.* 1999; Huisa *et al.* 2005). Furthermore, serological surveys revealed 12–15% cysticercosis seropositivity in soldiers living in Tegucigalpa (capital city of Honduras) and in Mexico City (Sanchez *et al.* 1998; Garcia-Garcia *et al.* 1999). Also, NCC cases have occurred in extremely low risk individuals in affluent households in New York City as a result of transmission of *T. solium* eggs from tapeworm positive housemaids (Schantz *et al.* 1992).

As previously discussed, recent molecular genotypic analysis of mitochondrial DNA extracted from *T. solium* isolates from different world regions, indicated two main genotypes, clades or strains, i.e. an Asian type and an African/Latin American type (Nakao *et al.* 2002). These have since been confirmed in several studies. However, it is not yet clear if the two genotypes exhibit differing epidemiology, transmission patterns or pathology (Craig and Ito 2007).

Taenia saginata

The human beef tapeworm, *T. saginata*, is the commonest taeniid of humans with an estimated 60,000–70,000 carriers worldwide (Flisser and Craig 2005; Craig and Ito 2007). In highly endemic regions, for example Ethiopia, Bali and Tibet, 22–27% prevalences of human *T. saginata* taeniosis have been recorded (Li *et al.* 2006; Wandra *et al.* 2006a, b; Craig and Ito 2007). In Europe and Australia beef tapeworm infection remains endemic, albeit at low prevalence (usually <0.05%), probably maintained in part due to the practice of application of sewage sludge on to pastures (Rickard *et al.* 1977; Cabaret *et al.* 2002; Boone *et al.* 2007). Human cysticercosis cannot be caused by ingestion of *T. saginata* eggs and therefore the public health impact for this parasite is limited to gut infection of humans (taeniosis). Consequently the epidemiology of this tapeworm species chiefly concerns transmission from human carriers to cattle, yak or other bovines. Bovine cysticercosis is however of economic importance because it may be responsible for condemnation or downgrading of meat, and even prevent development of potential beef export markets in resource-poor economies (Kebede 2008).

The risk factor for human *T. saginata* taeniosis is eating raw or under-cooked beef. Therefore *T. saginata* is more prevalent in communities or populations where dietary practices or cuisines include under-cooked and/or raw beef. For example in Sichuan and Yunnan provinces of SW China, and in Bali, Indonesia, raw beef is a delicacy. Consequently in their rural populations *T. saginata* taeniosis prevalence may be >20% (Li *et al.* 2006; Wandra *et al.* 2006b). In Bali, Indonesia 56/60 cases of suspected *T. saginata* were detected by questionnaire in a community study (n = 398) and confirmed as *T. saginata* by PCR. Males had a significantly higher prevalence and the risk age group was 30–44 years (Wandra *et al.* 2006). A similar cross-sectional epidemiological study (n = 661) in a Tibetan area of western Sichuan Province (China) found that 31% of persons reported a history of proglottid expulsion, and 18 of 21 proglottid positives tested by PCR were confirmed as *T. saginata* and three as *T. asiatica*. Of the 21 faecal samples from *Taenia* carriers 18 were also coproantigen ELISA positive (Li *et al.* 2007). In these 2 studies risk factors for taeniosis were consumption of raw beef, a history of passing proglottids in the previous 1–2 years, owning cattle/yak, poor hygiene/hand-washing and low level of education. Mean age of first infection (anamnesis) in 26 *T. saginata* cases treated in Addis Ababa was 12.2 years (Tesfa-Yohannes 1990).

Taenia asiatica

Taenia asiatica has been found in Taiwan, Korea, China, Vietnam, Philippines, Indonesia and Thailand. It is expected to also occur in Lao PD, Cambodia and Myanmar (Ito *et al.* 2007, 2008). *T. asiatica* was only described formally as a new tapeworm of humans in 1993 (Eom and Rim 1993). Prior to that its occurrence in rural communities of south east Asia was attributed to *T. saginata*, to which it closely resembles morphologically, but was often described in patients that consumed raw pig liver but not beef (Isobe 1922; Huang *et al.* 1966; Chao *et al.* 1979; Fan 1988; Fan *et al.* 1990; Eom and Rim 1993; Ito *et al.* 2003). It appears that spontaneous release of motile segments occurs in *T. asiatica* infections in the same way as for *T. saginata* and similarly therefore *T. asiatica* carriers are usually aware of their infection (Craig and Ito 2007; Wandra *et al.* 2007).

There have been relatively few epidemiological studies in known *T. asiatica* endemic communities, because previous studies were unable to differentiate *T. asiatica* and *T. saginata*, and so the majority of infections were classed as *T. saginata* (Eom and Rim 2001; Ito *et al.* 2003). One recent specific epidemiologic study on *T. asiatica* was undertaken in a rural Batak ethnic community in Ambarita village on Samosir Island, Lake Toba, Sumatra (Wandra *et al.* 2006). A total of 240 persons were voluntarily registered and answered a questionnaire, which indicated eight persons with a history of passing proglottids, and six (2.5% total prevalence) of these passed *T. asiatica* tapeworms (confirmed by PCR). Interestingly all six cases were coproparasitologically negative for *Taenia* eggs, but four that were tested by coproantigen ELISA were positive. Risk factors for *T. asiatica* taeniosis in the Lake Toba community were: consumption of pork (only 2.5% of population ate beef), home slaughter of pigs, predilection for raw pig liver and lack of sanitary facilities (Wandra *et al.* 2006, 2007). Since experimental infections in pigs performed with eggs from *T. asiatica* (Lake Toba isolate) developed cysticerci in the liver and not in the muscles or other locations (Fan *et al.* 1990, 2006), it is likely that in parts of Southeast Asia the distribution of *T. asiatica* and *T. solium* will be sympatric. This appears to be the case, at least, in Tibetan and Bai ethnic groups in SW China (Li *et al.* 2006) and in Karen ethnic communities on the Thai-Myanmar border (Anantaphruti *et al.* 2007). In the latter study in Kanchanaburi Province Thailand, all three human *Taenia* species occurred in those communities where under-cooked pork and beef were consumed, and at least one dual infection with *T. solium* and *T. asiatica* adult tapeworms was confirmed after DNA analysis (Fig. 51.3).

Transmission dynamics

There have been relatively few quantitative studies in relation to the transmission dynamics of the human *Taenia* spp. In contrast, a significant number of experimental and field studies were used to construct transmission models for the common taeniid species of livestock. Animal studies with *Taenia* species can be used to understand transmission dynamics of *T. solium* (Lawson and Gemmell 1989).

At any one time a *Taenia* parasite population will be in one of three states: the egg, the metacestode (cysticercus), or the adult; all three states can happen simultaneously in one community and even in the same human host in the case of *T. solium*. The effects of environmental factors such as temperature, humidity, dispersal (rain, arthropods) on eggs in the environment were important in

consideration of transmission of dog-sheep taeniid species (Lawson and Gemmell, 1983). For *T. solium* however the rapid direct ingestion of human faeces by pigs is common so that eggs may not be exposed for long periods in an endemic environment (Martinez-Maya *et al.* 2000). A recent study based on experimental pig infections further indicates that pig-pig transmission may occur through coprophagy ie. pig-human coprophagy followed by pig-pig coprophagy (Gonzalez *et al.* 2006). The distribution of cestode larvae in the pig intermediate host is usually over-dispersed, with acquired immunity stimulated by egg/oncosphere challenge and age-specific resistance also occurring probably within 15 days (Gemmell *et al.* 1987) the duration of immunity is not clear but probably lasts three months in the absence of egg challenge (Kyvsgaard *et al.* 2007). Pigs may be protected against *T. solium* egg infection from probably as little as 10 eggs, and immunity can be passively transferred from pregnant sow to new born piglets to provide up to 2–4 months protection (Gemmell *et al.* 1987; Gonzalez *et al.* 2002). In humans the biotic potential of a gravid adult *T. solium* tapeworm is relatively high with possibly 200,000 eggs passed per day, though the size (approximately 2–3 m) and life-span (probably months to a few years) of this species appears to be significantly below that for *T. saginata* (Allan *et al.* 1996a; Flisser 2006; Craig and Ito 2007). The basic reproductive number (Ro) for *T. solium* has been assumed to be close to one (Gonzalez *et al.* 2002), nevertheless a relatively low prevalence (~1%) of human taeniosis can still sustain transmission of *T. solium* (WHO/FAO/OIE, 2005). In addition to these parasite factors, transmission dynamics of *T. solium* will be affected by human/pig interrelations, pig behaviour, human sanitary habits and local socio-economic factors (Lawson and Gemmell 1989; Sarti *et al.* 1997; Gonzalez *et al.* 2002; Kyvsgaard *et al.* 2007). Knowledge of the transmission dynamics will assist in development of rational intervention simulations and control programs.

Prevention and control

In theory it should be relatively easy to prevent the occurrence of human taeniosis/cysticercosis and to break the parasitic life-cycle of the three human *Taenia* species. This is because humans are the only natural definitive host, and domestic pigs and cattle, the only important intermediate hosts. Consequently *T. solium* was added to the list of eradicable diseases (ITFDE 1993; Schantz *et al.* 1993). However, in practice it will be very difficult to implement control measures in poor rural areas of developing countries in which *T. solium* is highly endemic and where sanitation is poor or absent, where there exists cultural preference for under-cooked pork, where home-slaughter is the norm, and where pigs are bred unpenned and allowed to roam free. Furthermore, pork is the most popular meat consumed worldwide with at least 300 million pigs in endemic regions (Flisser *et al.* 2003, 2006). The demand for household pig rearing and pork protein is growing rapidly in resource-poor regions which will increase the transmission potential of *T. solium* and the probability of exposure to human taeniosis/cysticercosis (Lekule and Kyvsgaard 2003; WHO/DFID-AHP, 2006).

Prevention and control of cysticercosis/taeniosis can be considered as a long-term horizontal approach eg, improved sanitation, husbandry, slaughter regulations, meat inspection, and general education. Education is making a difference in Mexico. But control measures can be more focused or vertically directed interventions that aim to break the transmission cycle over shorter periods. There are 4 main options for such directed shorter-term intervention approaches:

1) Directed health/husbandry education,
2) Mass treatment against human taeniosis,
3) Mass chemotherapy against porcine cysticercosis,
4) Anti-cysticercosis livestock vaccines.

Of course combinations of some of the above interventions are likely to further improve control efficacy, especially against *T. solium*. In addition appropriate surveillance methods and systems, including modern computer simulations to model cost-effective intervention approaches, are required at local and regional scales to measure control effect and monitor progress.

Animal husbandry, meat inspection, sanitation and socio-economic development

Pork 'measles' was known in ancient Greece and described by Aristotle. Furthermore pork vendors in ancient Rome had to guarantee that pig meat was free of measles. In the Middle Ages the Ausburg Charter of 1276 stated, '*If a butcher kills a measly hog, he shall sell it to no one without a statement of this fact*' (Discussed in Viljoen 1937). An understanding of the life-cycle of *T. solium* after its elucidation and publication by Kuchenmeister in Germany in 1855, quickly resulted in formal recommendations about the dangers of eating under-cooked pork, and also clarified why the infection was rare in Jewish and Muslim communities (Grove 1990). Over the next 100 years the prevalence of human and porcine cysticercosis slowly declined across Western Europe, primarily through gradual improvements in sanitation, the adoption of formal meat inspection measures, less consumption of raw pork (in part because of historic out-breaks of trichinellosis in continental Europe), and the move to more intensive rearing of pigs (Grove 1990; WHO/FAO/OIE 2005). Endemic foci of *T. solium* however remain today in parts of rural Portugal and Spain where free-range pig husbandry is still not uncommon (Overbosch 2002; WHO/FAO/OIE 2005).

The connection between bovine cysticercosis ('beef measles') and an outbreak of human taeniosis in soldiers in South Africa was noted by Knox in 1819 and, following these observations, the role of cattle in the life-cycle of *T. saginata* was elucidated in 1861 by Leuckart (Viljoen 1937). Several authors by the late ninetienth and early twentieth centuries already advocated the inspection of slaughtered cattle, treatment of measly beef by freezing (-10°C for 2–6 days), and cooking or heating infected beef (Grove 1990). For *T. solium*, cysticerci are killed at -20°C for 1–3 days (Sotelo *et al.* 1986; Garcia *et al.* 2007) and proper salting of pork (12–24 hours) is also effective (Rodriguez-Canul *et al.* 2002). In most of Europe the prevalence of *T. saginata* taeniosis has declined to levels below 0.1% (range 0.01–2%), while prevalence of bovine cysticercosis at meat inspection ranges between 0.02 and 7% (Cabaret *et al.*, 2002). Improved sanitation in Europe has no doubt reduced the likelihood of direct contamination of grazing pastures. However indiscriminate defecation by campers, walkers, travellers etc, and the use of treated urban sewage sludge to irrigate pastures, has probably maintained transmission of *T. saginata* in several parts of the developed world (Rickard *et al.* 1977; Cabaret *et al.* 2002). In Switzerland during 2005 and 2006, 119 farms with infected cattle were identified at slaughter as compared to 66 randomly selected

farms with cattle slaughtered in the same period but with no evidence or history of infection. The presence of a railway line or a car park close to areas grazed by cattle, leisure activities around these areas, use of purchased roughage and organized public activities on farms attracting visitors, were the risk factors, pointing to outdoor defecation by tapeworm carriers (Flutsch *et al.* 2008).

Routine meat inspection usually involves up to five knife cuts in specific sites on the carcass (e.g. masseters, upper foreleg, hind-leg, heart, tongue). However >30% of infected cattle or pig carcasses (especially with light infections) may not be detected by these methods (WHO/FAO/OIE 2005; Phiri *et al.* 2006; Geysen *et al.* 2007). Restraint or corralling of pigs in resource-poor settings is effective in preventing ingestion of human faeces (Vazquez *et al.* 2001). In practice this is not easy to implement because of economic constraints. Furthermore in parts on India, Indonesia and China pigs are restrained or penned deliberately under or close to latrines so that they are able to remove human faecal waste from the household environment (PS Craig, unpublished observation). Backyard-free-roaming pigs or semi-confined household pigs in southern Mexico had significantly higher *T. solium* seropositive rates compared to more intensively farmed animals (Sarti *et al.* 1994, 1997, 2000; Rodriguez-Canul *et al.* 1998). Reports of restraint of pigs that were normally free-roaming have indicated decrease in swine cysticercosis rates in Peru and China (Bern *et al.* 1999; Vazquez *et al.* 2001; Pawlowski *et al.* 2005).

Health education

Humans can acquire cysticercosis after accidentally ingesting *T. solium* eggs. Furthermore, the prevalence of taeniosis among patients with neurocysticercosis is higher than previously reported. In addition, a clear association between the presence of taeniosis and the severity of neurocysticercosis was seen, since most massive cerebral infections (with more than 100 cysticerci) were present in patients who harboured the adult tapeworm in the intestine. Therefore, the perception that tapeworms are silent guests, causing no harm to humans, is erroneous and tapeworm carriers should be regarded as potential risks to themselves and to those living in their close environment (Gilman *et al.* 2000). Consequently, an important risk factor is the presence of a tapeworm carrier in the household or neighbourhood (Sarti *et al.* 1988; Flisser 2002b, Flisser and Gyorkos 2007). A study performed in a Mexican municipality with around 750,000 inhabitants showed that self-identification of tapeworm carriers is a feasible tool for control of *T. solium* (Flisser *et al.* 2005b). Also, identified tapeworm carriers can be treated with a high degree of efficacy (Jeri *et al.* 2004).

Health education in relation to taeniosis/cysticercosis could, in theory, lead to the acquisition of appropriate knowledge required to understand the life-cycle of the parasite. That knowledge could result in a change in risk-behaviours and/or husbandry practices that help propagate transmission, with a resultant reduction in human and livestock infection/exposure indices. There are only a few modern examples of specific education programmes in relation to *T. solium*, and very few, if any, reported for *T. saginata* or *T. asiatica*. In the late 1980s and early 1990s community based epidemiologic studies on *T. solium* in Mexico began to identify some of the sociological/behavioural risk factors for human and porcine infection (Sarti *et al.* 1988, 1992; Schantz *et al.* 1994). As a consequence, two educational intervention programs were developed and applied to rural communities in Mexico. In Guerrero State, 131 families were given health education about the parasite and associated risk factors, and after two years 76% of children but only 2% of adults acquired specific knowledge. Disappointingly the pre-intervention prevalence of tongue palpable cysticerci in one year old pigs increased from 6% to 11% (Keilbach *et al.* 1989). In Morelos State, a rural population (n = 1,931) was subjected to intense health education which used knowledge acquisition questionnaires, tongue palpation with immunoblot serology in pigs, and microscopy and coproantigen rates in humans, as pre-intervention and post-intervention indicators of transmission. Although there was no significant difference in human taeniosis rates before and after the educational programme, health education increased villagers' knowledge about the parasite and transmission, despite an apparent lack of observed major behavioural changes. Nevertheless in this case there was significantly reduced porcine infection and exposure rates after six months (Sarti *et al.* 1997), which remained up to 42 months (A Flisser, unpublished observations).

A health education intervention trial was also recently applied in north eastern Tanzania-but differed from the Mexican one in that the study was a randomized control programme (n = 827 households, including 418 as household controls), targeted towards pig husbandry including building proper pig pens, as well as pit latrines, and safe disposal of human faeces; sentinel pigs were employed as transmission indicators over a one year period. Similar to the Morelos study, despite significant gain in knowledge acquisition, there was no improvement in observed risk practices amongst targeted or control households. However the porcine incidence rate based on tongue palpation and circulating antigen testing in sentinel pigs (given to each family) was significantly lower in the health education intervention household group, as was reported pork consumption (Ngowi *et al.* 2008). Long-term follow-up was not reported and it remains to be seen whether public health education alone could provide sustained decrease in transmission of *T. solium* in resource-poor communities in Latin America, Sub Saharan Africa or elsewhere. Interestingly rigorous health education programmes for cystic echinococcosis in resource-rich countries/regions were not always effective for long-term sustained reduction of transmission of *Echinococcus granulosus* (Craig and Larrieu 2006).

Taeniosis mass drug treatment

The life-cycles of *T. solium*, *T. saginata* and *Taenia asiatica* involve humans as the only obligatory definitive host. Therefore, effective anthelmintic mass treatment of human populations in endemic areas could result in control of transmission or even elimination of the parasite (Pawlowski 1990). Furthermore, the provision of annual or sub-annual mass treatment for school age children using albendazole for gastrointestinal nematode and other infections has been very successful in reducing the burden of chronic helminth infections in under-developed regions (Molyneux *et al.* 2005; Flisser *et al.* 2008). Consequently, the approach of mass treatment against human taeniosis has gained support. Furthermore, effective tapeworm treatment could remove any (or more than one) of the three *Taenia* species (as well as *Hymenolepis nana*) where they are sympatric (Allan *et al.* 2002; WHO/FAO/OIE 2005; Anantaphruti *et al.* 2007; Craig and Ito 2007).

There are several factors to consider in relation to mass treatment for human taeniosis however, that are different from directly transmitted gastrointestinal nematodes.

1) The age-specific prevalence of *T. solium* taeniosis is distributed mainly above the school-age group (ie. >15 years old) (Allan *et al.* 1996b; Sarti *et al.* 1997, 2000, Garcia *et al.* 2003b), and thus targeted treatment to schools would not be so effective.

2) The prevalence of human *T. solium* taeniosis is usually below 3.5% in endemic communities and therefore very high population coverage is required.

3) Pigs if untreated, act as a reservoir of infection back to the human population.

4) The most effective anthelmintic drug against human taeniosis is praziquantel (not albendazole the preferred drug in mass-treatment of gastrointestinal nematodes), but this drug is also used to treat neurocysticercosis and therefore has the potential to cause cerebral inflammation in asymptomatic neurocysticercosis cases. Despite that risk for mass administration of praziquantel such clinical effects have to date only rarely been reported (Cruz *et al.* 1989; Flisser *et al.*1993). In relation to praziquantel safety, that drug has been extensively used in China and Africa at higher dosage for mass treatment campaigns against schistosomosis without apparent adverse effects on asymptomatic neurocysticercosis (Pawlowski 2006).

At the present time (2008) only six studies have been reported internationally since 1989 in which mass drug administration was used to control *T. solium* transmission, and all of these were carried out in Latin America (summarized in Table 51.2). Five of these studies used praziquantel and one niclosamide as the taenicidal agent. Niclosamide is slightly less efficacious (85–90%) than praziquantel (>95%) and is five times more expensive and has a more limited shelf-life (Pawlowski *et al.* 2005). Niclosamide however has the advantage that the drug is poorly absorbed from the gut and therefore would not cause potential inadvertent effects on asymptomatic neurocysticercosis. Also *Taenia* tapeworms are usually passed intact after niclosamide treatment which facilitates identification (Allan *et al.* 1996b, 2002).

The endemic *T. solium* rural populations targeted ranged in size from <400 in Sinaloa Mexico to 10,000 in the Loja/El Oro region of south Ecuador. Follow-up occurred at various periods from four to 40 months but the average was one year. Pre and post intervention surveillance was mainly based on human taeniosis prevalence (stool examination and/or coproantigen test), and porcine cysticercosis prevalence/incidence in pig cohorts born after the intervention (necropsy, tongue palpation and/or serology). In one study in Peru the pig population was also subjected to mass treatment with the drug oxfendazole (Garcia *et al.* 2006). Other factors, such as health education and changes in behaviour as well as improved sanitation and pig husbandry may have occurred in parallel as a result of the programme design, or indirectly occurred in the community, and thus could have influenced the effect of taeniosis mass-treatment (Allan *et al.* 2002). Five of the six mass treatment programmes (see Table 51.2), where human taeniosis was monitored, showed a statistically significant decrease in the prevalence of taeniosis within one year of mass treatment, with no taeniosis cases being detected post-intervention in three of those studies (Cruz *et al.* 1989; Keilbach *et al.* 1989; Diaz-Camacho *et al.* 1991). In all but one intervention study, porcine cysticercosis rates were also significantly reduced after 1–3.5 years follow-up, but pig infection was not eliminated (Sarti *et al.* 2000). Even when two rounds of oxfendazole dosing of pigs was included with a taeniosis mass treatment program for the human population, the parasite persisted in the pig population despite significant decrease in porcine seroprevalence and seroconversion rates (Garcia *et al.* 2006).

Taenicidal drug coverage of the human population was never above 70–90% in these six mass treatment programmes and therefore persistence of a handful of tapeworm carriers in a treated community could still maintain transmission because of the high biotic potential of the parasite. Nevertheless these studies demonstrate that at least short-term reduction (within one year) in transmission of *T. solium* may occur after taeniosis mass-treatment. Long term assessments have not been carried out except in Morelos (Mexico) where 42 months after mass administration with a single dose of praziquantel, human taeniosis prevalence remained 56% below the pre-intervention rate, pig tongue palpation rates were 52% lower and the seroprevalence of human cysticercus antibodies was 75% reduced (Sarti *et al.* 2000). In this study 5mg/kg instead of 10 mg/pg praziquantel were used (as recommended by WHO, Pawlowski 1990), and therefore drug efficacy was 50% instead of 95%. Mass treatment alone will therefore probably not be enough to interrupt transmission of *T. solium*, which appears to return to pre-intervention levels within 2–3 years (Garcia *et al.* 2007). Therefore options should consider more frequent drug administration and ensure that >95% of the population is treated (Gonzalez *et al.* 2002). Alternatively specific identification and treatment of tapeworm carriers should be also considered (Flisser *et al.* 2005b).

Mass treatment for *T. saginata* taeniosis is unlikely to be cost-effective because this parasite does not cause sufficient economic or public health impacts. However in some regions where *T. saginata* is common, self-medication on a large scale may occur; for example in Addis Ababa (Ethiopia) where >80% of the adult population regularly take taenicidal drugs (Tesfa-Yohannes 1990; Pawlowski 2006). Prophylactic use of taenicidal drugs by workers in cattle feed-lots may also reduce the risk of local outbreaks of bovine cysticercosis in both developed and resource-poor settings (Dorny *et al.* 2002).

Anthelmintic mass drug treatment of livestock

The possibility to use anti-metacestode drugs to control the transmission of *T. solium* from pigs to humans has also been investigated. Both praziquantel and albendazole can affect the viability of *T. solium* cysticerci in pigs, and the latter was 100% effective in killing muscle cysticerci (non viable cysts were present) though viable cysts remained in the brain (Flisser *et al.* 1989; Peniche-Cardenas *et al.* 2002). Praziquantel was highly effective even at one day treatment (Torres *et al.* 1992). The overall efficacy of both drugs, however, was not as great as oxfendazole for treatment of porcine cysticercosis (Gonzalez *et al.* 1996), although this latter drug was used at a higher dose than the one commercially available. A single dose (30mg/kg) of oxfendazole caused cyst death and disappearance within 3 months of treating infected pigs, and pigs also appeared refractory to further infection for another 3 months (Gonzalez *et al.* 1996; 2001). In rural Latin America and in other resource-poor regions, pigs are usually about 9 months old at slaughter, so a single dose of oxfendazole or praziquantel (or better two doses at 3 months and 6 months) could in theory keep pigs free of cysticerci for that period with the added advantage of full economic return on the carcass (Torres *et al.* 1992; Gonzalez *et al.* 2003).

Table 51.2 Summary of 6 control programmes for *T. solium* in rural communities in Latin America where mass treatment of human taeniosis was applied

Country (site/start year of programme)	Human Pop.	Drug mg/kg, no. doses (% cover)	Follow-up period	Taen-iasis pre-(%)	Taen-iasis post-(%)	Pig Cystic. pre-(%)	Pig Cystic. post- (%)	Ref.
Ecuador (Loja/1986)	10,000	PZQ 5mg/kg, x1 (76%)	1 year	1.6 °	0 (n = 539)	11.4*	2.6 (n = 113)	Cruz *et al.* (1989)
Mexico (Guerrero/1986)	530	PZQ 5mg/kg, x1 (60%)	4mths-1year	3.2 °	0	6** (n = 440)	11	Keilbach *et al.* (1989)
Mexico (Sinaloa/1989)	339	PZQ 10mg/kg, x1 (71%)	1 year	1.3°	0 (n = 238)	ND	ND	Camacho *et al.* (1991)
Mexico (Morelos/1991)	1865	PZQ 5mg/kg, x1 (87%)	3.5 yrs	1.1++	0.5 (n = 605)	1.2** 4.8+	0.6 3.4	Sarti *et al.* (2000)
Guatemala (Santa Gertrudis/1994)	1582	Niclosamide 1gm, x1 (75%)	10 months	3.5++	1.0	55+	? (n = 330)	Allan *et al.* (1997)
Peru (Quilcas/1996)	2100	PZQ 5mg/kg, x1 (75%)	18 months	ND	ND	0.5?+^ plus OXF	0.40	Garcia *et al.* (2006)

° Stool exam/worm recovery; ++ coproantigen/worm recovery; * pig necropsy;
** pig tongue palpation; + pig serology; ^ total mean seroprevalence plus OXF additional treatments of two rounds oxfendazole in pigs (n = 31 [?] at 30mg/kg PZQ praziquantel

Despite these results, an intervention trial that used mass administration of oxfendazole to pigs in parallel with mass praziquantel administration to the human population in Peru, reduced transmission but did not eliminate human taeniosis or porcine cysticercosis after 18 months (Garcia *et al.* 2006).

Cysticercosis vaccines for livestock

The marked protective immune response of sheep and cattle to experimental egg challenge or vaccination with oncosphere antigen extracts of various *Taenia* species, lead the development of protective sub-unit vaccines against cysticercosis and echinococcosis (Lightowlers and Gauci 2001; Lightowlers 2003; 2006; reviewed by Flisser and Lightowlers 2008). In 1989 the first recombinant subunit anti-parasite vaccine (To45W) was developed, and this was for *Taenia ovis*, the cause of ovine cysticercosis, a non-zoonotic metacestode disease of economic importance (Johnson *et al.* 1989). Following that success, which was based on the use of a recombinant oncosphere peptide antigen, the homologous genes were identified in *T. saginata* and the expressed peptides (TSA-9/TSA-18) given intramuscularly with adjuvant to cattle resulted in 99% protection against oral challenge with *T. saginata* eggs (Lightowlers *et al.* 1996). Efforts were subsequently directed towards the scaling-up of both vaccines (for ovine and bovine cysticercosis) for production such that adequate quantities and quality-controlled vaccines are available for practical use (Lightowlers 2006).

A parallel approach using the homologous genes was subsequently adopted for development of a *T. solium* recombinant subunit oncosphere vaccine (TSOL18) against porcine cysticercosis which gave 99.5–100% protection against experimental egg challenge infection of pigs (Flisser *et al.* 2004b; Gonzalez *et al.* 2005). There are other putative anti-infection vaccines for *T. solium* cysticercosis (Flisser and Lightowlers 2001; Hernandez *et al.* 2007), but it is likely that TSOL18 will provide the most effective protective vaccine in pigs for further assessment and eventual incorporation into *T. solium* control programmes (Gonzalez *et al.* 2003; Pawlowski *et al.* 2005). The more difficult proposition for the therapeutic vaccination of intermediate hosts against already established taeniid larval cysts has been considered but remains largely experimental (Bogh *et al.* 1988; Craig and Zumbuehl 1988; Evans 2002).

Surveillance methods

Prevention and control of any infectious/parasitic disease cannot be reliably undertaken without appropriate surveillance tools. Several approaches and tools have been developed for taeniosis/cysticercosis, especially in relation to epidemiological and intervention studies for *T. solium*. Surveillance is important in the human population for taeniosis and cysticercosis, and in the pig population for cysticercosis. In addition, health education acquisition by the target population can be measured by questionnaires and observational studies. A number of diagnostic or detection methods have been developed for *T. solium* (Schantz and Sarti 1989; Garcia *et al.* 2003a).

Taeniosis

Clinical out-patient records are not very useful for human taeniosis because many people self-treat within the community. Self-identification by tapeworm carriers is also of variable value, but most reliable for *T. saginata* or *T. asiatica* because of the frequency of anamnesis in carriers (i.e. spontaneous escape of motile segments), but contradictory data have been published for *T. solium* (Hall *et al.* 1981; Flisser *et al.* 2005b; Wandra *et al.*2006b). Use of questionnaire and demonstration of proglottid recognition has been reported to be useful in identification of human *T. saginata* and *T. asiatica*, but also for *T. solium* taeniosis carriers (Fan *et al.* 1992; Wandra *et al.* 2006a; Flisser *et al.* 2005b). Stool microscopy for detection of *Taenia* spp eggs and coproantigen ELISA for *Taenia* spp faecal antigen detection, have overall been most effective methods for surveillance of human taeniosis, the latter test being up to

2–3 times more sensitive and more efficient for testing large numbers of stool samples (Allan *et al.* 1996a; Allan and Craig 2006). Specificity for taeniosis detection can be achieved by copro-PCR for DNA detection (Yamasaki *et al.* 2004) or at post-purge by morphological criterion of intact proglottids or by DNA confirmation (Ito and Craig 2003; Li *et al.* 2006). The logistics of collecting stool samples while treating/purging positive persons is rather complex and not without difficulty, but is the best approach for active mass screening for *T. solium* taeniosis (Garcia-Noval *et al.* 1996). In order to improve sampling efficiency, a species specific serological test for *T. solium* taeniosis has been developed. However antibodies from prior tapeworm exposures may not be differentiated from current infection so sensitivity will be lower (Wilkins *et al.* 1999).

Porcine and bovine cysticercosis

Slaughter-house or slaughter-slab records are not very reliable, especially in resource-poor rural areas, because of the sensitivity limitations of meat inspection, and also the preference for households to slaughter at home or in small butchers without inspection. This is especially the case for pig infection data collection. Better approaches, though more expensive, include the purchase by a control/surveillance authority, of a sample of pigs of different ages from within the community and to undertake their own rigorous necropsy of the entire carcass. Also the use of sentinel pigs can be effective in measuring active transmission and monitoring environmental contamination (Gonzalez *et al.* 1994; Ngowi *et al.* 2008). Serodiagnostic tests for porcine and bovine cysticercosis have been developed based on specific serum antibody or circulating antigen detection (Craig and Rickard 1980; Gonzalez *et al.* 1990; Dorny *et al.* 2004; WHO/FAO/OIE 2005; Abuseir *et al.* 2007). Antibody tests based on recognition of low molecular weight *T. solium* metacestode glycoproteins show high specificity in immunoblots for both human and porcine cysticercosis, and even for dog cysticercosis, and have also been purified or cloned for high through-put screening ELISAs (Ito *et al.* 2002; Hancock *et al.* 2006; Sato *et al.* 2006; Flisser and Gyorkos 2007). The surveillance value of porcine serology in several epidemiological studies has in general been shown to be very useful and an important indicator of transmission before and after application of control intervention (Allan *et al.* 1996b, 1998; Sarti *et al.* 1997, 2000; Rodriguez-Canul *et al.* 1998; Flisser 2002a; Garcia *et al.* 2003b, c, 2006; Sato *et al.* 2003; Flisser and Gyorkos 2007; Lescano *et al.* 2007). The advantage of circulating antigen detection rather than serum antibodies is its association with current viable cyst infection, and these assays have been particularly useful in seroepidemiological studies of bovine cysticercosis where both infection prevalence and intensity are usually lower than in porcine cysticercosis (Onyango-Abuge *et al.* 1996; Dorny *et al.* 2000). Serum antigen ELISA for porcine cysticercosis likewise has proved useful in some epidemiological studies on *T. solium* (Sikasunge *et al.* 2008) as well as for human cysticercosis (Aranda-Alvarez *et al.* 1995; Correa *et al.* 1999). Surveys for *T. asiatica* cysticercosis in pigs are more difficult at routine meat inspection because of the small cyst size (2–3mm) in the liver and also lower prevalence rates than for *T. solium* cysticercosis, for example 0.01% viable cysts of *T. asiatica* were found in >25,000 pigs inspected in Chongju, Korea (Eom and Rim 2001). Currently there is no serological test available for *T. asiatica* porcine cysticercosis.

Human cysticercosis

Hospital records for neurocysticercosis have proved useful in establishing public health impact, the burden of disease, and in advocating surveillance and control both historically and currently (Roman *et al.* 2000; Flisser 2002a, Garcia *et al.* 2007; Li *et al.* 2007). In highly endemic communities prevalence of epilepsy, with serological and/or CT image confirmation is also an important indicator of disease burden due to neurocysticercosis (Schantz *et al.* 1994; Garcia-Noval *et al.* 1999; Carabin *et al.* 2005). Active mass screening is probably the most effective way to establish true prevalence of human cysticercosis and should comprise the following: questionnaire (including history of convulsions, taeniosis), brief clinical examination (presence skin nodules, headache, epilepsy, other symptoms of neurocysticercosis) and blood sample for serology using a species-specific test. Ideally individuals with clinical data related to cysticercosis and/or seropositive persons should also be followed up by an imaging technique of the brain to confirm presence of neurocysticercosis. In one study a proportion of healthy persons (ie. clinically normal, circulating antibody/antigen seronegative, taeniosis negative, no reports of history of convulsions, etc) were also shown to have CT images of brain lesions (usually calcified) indicative of neurocysticercosis (Garcia-Noval *et al.* 2001). Furthermore, some seropositive persons may sero-revert over a period of months/years and thus specific anti-*T. solium* cysticercosis antibodies may also be transient (Garcia *et al.* 2001; Meza *et al.* 2003). Interpretation of the results of such comprehensive mass screenings can be difficult, so long-term follow-up studies are recommended.

Prospects/options for control

Of the three human *Taenia* species, *T. solium* is by far the most important from a public health perspective and it has recently been considered priority for control by several international agencies (ITFDE 1993; Roman *et al.* 2000; WHO/FAO/OIE 2005; WHO/DFID-AHP 2006). Because *T. solium* is both a food-borne zoonoses and a sanitary-associated transmitted parasite, active control measures need to target both humans and pigs, and therefore requires intersectoral cooperation between medical and veterinary services (Pawlowski *et al.* 2005; Willingham and Engels 2006). A combination of several measures, including mass treatment of humans, mass treatment of pigs, porcine vaccination, economic incentives and health education, with application of appropriate surveillance tools, carried out under the direction of an integrated control authority, is likely to be most effective approach for control of transmission of *T. solium* over short time periods (<10 years). In the coming decades rural developments in sanitation, poverty reduction and improvements in pig husbandry and local economies will probably increase chances for the control of *T. solium*.

Application of quantitative models using parasite transmission parameters and cost-benefit analysis has only recently been developed for computer-assisted simulations of intervention measures against *T. solium*. Such models are still relatively crude because of the lack of accurate hard data for several transmission parameters including the biotic potential of the parasite, its basic reproductive number, role of immunity in pigs and humans, longevity of adult tapeworms, human taeniosis reinfection rates, survival of eggs in the environment, etc. (Sciutto *et al.* 2008). Despite the need for further data, informed prior assumptions can be made especially

using Bayesian/stochastic statistical approaches (Basanez *et al.* 2004), so that groups/packages of interventions for *T. solium* control have been modelled to identify optimal cost-effective options (Gonzalez *et al.* 2002; Kyvsgaard *et al.* 2007).

Two simplified transmission intervention simulation models assessed the following 4 main interventions against *T. solium*:

1) Horizontal-type measures (latrines, meat inspection, proper cooking),
2) Mass treatment of humans for taeniosis,
3) Mass treatment of humans and pigs,
4) Identification and targeted treatment of taeniosis carriers and pig vaccination (TSOL18).

The simulations used hypothetical communities of 1,000 or 2,000 individuals with interventions over a period of 5 years or 10 years. Assumptions were that the Ro for the parasite was between 1–1.75, the vaccine was 100% protective against porcine cysticercosis (with 90% cover) and mass drug treatment had 100% cover in humans and 90% in pigs. In summary, the most important findings of the simulations were:

1) Human mass treatment can result in short-term significant reduction in transmission (within 48 months) but was insufficient alone to eliminate transmission which returned to pre-control levels unless more than 11 interventions occurred at 90 day intervals with 100% cover (probably unachievable).
2) If mass treatment (or targeted treatment) of humans was followed by at least 2 treatments of pigs, or followed by porcine vaccination, then significant reduction in transmission was possible within 5 years.
3) Horizontal measures required 5–10 years to result in significant reductions in human and porcine rates but infection still remained at low prevalence (~0.5% human taeniosis; ~10% porcine cysticercosis (Gonzalez *et al.* 2002; Kyvsgaard *et al.* 2007).

A multiple intervention approach against *T. solium* appears to have the biggest chance of reducing transmission as judged by the few real intervention programmes and these were supported by the simulation models. Cost-benefit analysis showed that economic considerations are likely to be very important in whether a Ministry of Agriculture and/or Health decides to support a long-term costly intervention (Lawson and Gemmell 1989; Gonzalez *et al.* 2002; Flisser *et al.* 2003, 2006). The health and economic benefits, logistics of scale and out-reach achieved by combining interventions for several zoonotic diseases (especially the group of so called neglected zoonotic diseases i.e. cysticercosis, brucellosis, anthrax, rabies, echinococcosis, zoonotic trypanosomiasis, zoonotic mycobacterium infections) as well as possibly other infectious diseases (Zinstaag *et al.* 2005) has gained support for the route to more effective disease control and poverty-reduction in resource-poor regions of the world (WHO/DFID-AHP 2006).

Acknowledgements

The authors dedicate this chapter to the memory of Dr P. C. Fan, who worked at the Department of Parasitology, Institute of Tropical Medicine, National Yang-Ming University School of Medicine, Taipei, Taiwan, and passed away on September 2nd, 2008.

References

Abuseir, S. *et al.* (2007). Evaluation of a serological method for the detection of *Taenia saginata* cysticercosis using serum and meat juice samples. *Parasit. Res.*, **101:** 131–37.

Ahsan, S. *et al.* (2006). A case of *Taenia saginata* (tapeworm) infestation of the uterus presenting with abnormal vaginal bleeding. *J. Pak. Med. Ass.*, **56:** 377–78.

Allan, J.C. and Craig, P.S. (2006). Coproantigens in taeniasis and echinococcosis. *Parasit. Intern.*, **55:** S75–80.

Allan, J.C. *et al.* (1996a). Epidemiology of intestinal taeniasis in four rural Guatemalan communities. *Ann. Trop. Med. Parasit.*, **90:** 157–65.

Allan, J.C. *et al.* (1996b). Epidemiology of *Taenia solium* taeniasis and cysticercosis in two rural Guatemalan communities. *Am. J. Trop. Med. Hyg.*, **55:** 282–89.

Allan, J.C. *et al.* (2002). Control of *Taenia solium* with emphasis on treatment of taeniosis. In: G. Singh and S. Prabhakar (eds.) *Taenia solium cysticercosis from basic to clinical science*, pp. 414–20. Wallingford, UK: CABI Publishing.

Aluja, A.S. and Vargas, G. (1988). The histopathology of porcine cysticercosis. *Vet. Parasit.*, **28:** 65–77.

Aluja, A.S. *et al.* (1998). *Taenia solium* cysticercosis in young pigs: age of first infection, histological characteristics of the infection and antibody response. *Vet. Parasit.*, **76:** 71–79.

Amara, L. *et al.* (2003). Unusual manifestations of neurocysticercosis in MR imaging: analysis of 172 cases. *Arqu. Neuropsiqui.*, **61:** 533–41.

Anantaphruti, M.T. *et al.* (2007). Sympatric occurrence of *Taenia solium*, *T.saginata*, and *T.asiatica*, in Thailand. *Emerg. Infect. Dis.*, **13:** 1413–16.

Andreassen, J. (2005). Intestinal tapeworms. In: F.E.G. Cox, *et al.* (eds.) *Topley & Wilson's Microbiology and Microbial Infections* pp. 658–76. London: Hodder Arnold.

Aranda-Alvarez, J.G. *et al.* (1995). Human cysticercosis: risk factors associated with circulating serum antigens in an open community of San Luis Potosi, México. *Ann. Trop. Med. Parasit.*, **89:** 689–92.

Arriada, M.N. *et al.* (2003). Imaging features of sellar cysticercosis. *Am. J. Neuroradiol.*, **24:** 1386–89.

Avila, G. *et al.* (2006). Laboratory animal models for human *Taenia solium*. *Parasit. Intern.*, **55:** S99–S103.

Bassanez, M.G. *et al.* (2004). Bayesian statistics for parasitologists. *Trends in Parasit.*, **20:** 85–91.

Bergsneider, M. *et al.* (2000). Endoscopic management of cysticercal cysts within the lateral and third ventricles. *J. Neurosurg.*, **92:** 14–23.

Berman, J.D. *et al.* (1981). Cysticercosis of 60 milliliter volume in human brain. *Am. J. Trop. Med. Hyg.*, **30:** 616–19.

Bern, C. *et al.* (1999). Magnitude of the disease burden from neurocysticercosis in a developing country. *Clin. Infect. Dis.*, **29:** 1203–09.

Bogh, H.O. *et al.* (1988). Studies on stage-specific immunity against *Taenia taeniaeformis* metacestodes in mice. *Parasite Immun.*, **10:** 255–64.

Cabaret, J. *et al.* (2002). The use of urban sewage sludge on pastures: the cysticercosis threat. *Vet. Res.*, **33:** 575–97.

Cadigan, F.C. *et al.* (1967). The lar gibbon as definitive and intermediate host of *Taenia solium*. *J. Parasit.*, **53:** 844.

Campbell, G. *et al.* (2006). Genetic variation in *Taenia solium*. *Parasit. Intern.*, **55:** S121–26.

Chao, D. *et al.* (1979). *Taenia saginata* (?) among Taiwan aborigines is probably a new species. *Chinese J. Microbiol.*, **12:** 108–09.

Carabin, H. *et al.* (2005). Methods for assessing the burden of parasitic zoonoses: echinococcosis and cysticercosis. *Trends in Parasit.*, **21:** 327–33.

Colli, B.O. *et al.* (2002). Surgical treatment of cerebral cysticercosis: long-term results and prognostic factors. *Neurosurg. Focus*, **12:** e3.

Correa, D. *et al.* (1999). Antigens and antibodies in sera from human cases of epilepsy or taeniasis from an area of Mexico where *Taenia solium* cysticercosis is endemic. *Ann. Trop. Med. Parasit.*, **93:** 69–74.

Craig, P.S. and Ito, A. (2007). Intestinal cestodes. *Curr. Opin. Infect. Dis.*, **20:** 524–32.

Craig, P.S. and Larrieu, E. (2006). Control of cystic echinococcosis/hydatidosis: 1863–2002. *Adv. Parasit.*, **61:** 443–508.

Craig, P.S. and Rickard, M.D. (1980). Evaluation of 'crude' antigen prepared from *Taenia saginata* for the serological diagnosis of *T.saginata* cysticercosis in cattle using the enzyme-linked immunosorbent assay (ELISA). *Zeitsch. Parasitenk.*, **61:** 287–97.

Craig, P.S. and Zumbuehl, O. (1988). Immunization against experimental rabbit cysticercosis using liposome-associated antigen preparations. *J. Helminthol.*, **62:** 58–62.

Craig, P.S. *et al.* (1996). Detection, screening and community epidemiology of taeniid cestode zoonoses: cystic echinococcosis, alveolar echinococcosis and neurocysticercosis. *Adv. Parasit.*, **38:** 169–250.

Craig, P.S. *et al.* (2007). Human echinococcosis: a neglected disease? *Trop. Med. Health*, **35:** 283–92.

Cruz, M. *et al.* (1989). Operational studies on the control of *Taenia solium* taeniasis/cysticercosis in Ecuador. *Bull. WHO*, **67:** 401–07.

Del Brutto, O.H. *et al.* (2001). Proposed diagnostic criteria for neurocysticercosis. *Neurology*, **57:** 177–83.

Diaz-Camacho, S. *et al.* (1990). Serology as an indicator of *Taenia solium* tapeworm infection in a rural community in Mexico. *Trans. R. Soc. Trop. Med. Hyg.*, **84:** 563–66.

Diaz Camacho, S.P. *et al.* (1991). Epidemiologic study and control of *Taenia solium* infections with praziquantel in a rural village of Mexico. *Am. J. Trop. Med. Hyg.*, **45:** 522–31.

Dorny, P. *et al.* (2000). Sero-epidemiological study of *Taenia saginata* cysticercosis in Belgian cattle. *Vet. Parasit.*, **88:** 43–49.

Dorny, P. *et al.* (2002). A sero-epidemiological study of bovine cysticercosis in Zambia. *Vet. Parasit.*, **10:** 211–15.

Dorny, P. *et al.* (2004). A Bayesian approach for estimating values for prevalence and diagnostic test characteristics of porcine cysticercosis. *Intern. J. Parasit.*, **34:** 569–76.

Eom, K.S. (2006). What is Asian *Taenia*? *Parasit. Intern.*, **55:** S137–S141.

Eom, K.S. and Rim, H.J. (1993). Morphologic descriptions of *Taenia asiatica* sp.n. *Korean J. Parasit.*, **31:** 1–6.

Eom, K.S. and Rim, H.J. (2001). Epidemiological understanding of *Taenia* tapeworm infections with special reference to Taenia asiatica in Korea. *Korean J. Parasit.*, **39:** 267–83.

Escobar, A. (1983). The pathology of neurocysticercosis. In: E. Palacios, *et al.* (eds.) *Cysticercosis of the Central Nervous System*, pp. 27–54. IL, USA: Springfield.

Evans, C.A.W. (2002). *Taenia solium* vaccination: present status and future prospects. In: G. Singh and S. Prabhakar (eds.) *Taenia solium cysticercosis from basic to clinical science*, pp. 421–29. Wallingford, UK: CABI Publishing.

Fall, E.H. *et al.* (1995). Failure of experimental infections of baboons (*Papio hamadryas*) with the eggs of Asian *Taenia*. *J. Helminthol.*, **69:** 367–68.

Fan, P.C. (1988). Taiwan *Taenia* and taeniasis. *Parasit. Today*, **4:** 86–88.

Fan, P.C. (1995). The history of taeniasis saginata in Taiwan before world war II. *Yonsei Rep. Trop. Med.*, **26:** 13–17.

Fan, P.C. *et al.* (1990). Pig as an experimental intermediate host of *Taenia saginata* (Ethiopia and Madagascar strains). *Ann. Trop. Med. Parasit.*, **84:** 93–94.

Fan, P.C. *et al.* (1992). Clinical manifestations of taeniasis in Taiwan aborigines. *J. Helminthol.*, **66:** 118–23.

Fan, P.C. *et al.* (1995). Morphological description of *Taenia saginata asiatica* (Cyclophyllidea: Taeniidae) from man in Asia. *J. Helminthol.*, **69:** 299–303.

Fan, P.C. *et al.* (2006). Pig as a favourable animal for *Taenia saginata asiatica* infection. *Kaohsiung J. Med. Sci.*, **22:** 1–12.

Flisser, A. (1995). *Taenia solium, Taenia saginata* and *Hymenolepis nana*. In: M. J. G. Farthing *et al.* (eds.) *Enteric infections 2: Intestinal Helminths*, pp. 173–89. London: Chapman and Hall Medical.

Flisser, A. (2002a). Epidemiological studies of taeniosis and cysticercosis in Latin America. In: P. Craig and Z. Pawlowski (eds.) *Cestode Zoonoses: Echinococcosis and cysticercosis, an emergent and global problem*, Vol. 341, pp. 3–11. NATO Science Series. Amsterdam: IOS Press.

Flisser, A. (2002b). Risk factors and control measures for taeniosis/cysticercosis. In: P. Craig and Z. Pawlowski (eds.) *Cestode Zoonoses: Echinococcosis and cysticercosis, an emergent and global problem*, Vol. 341, pp. 335–42, NATO Science Series. Amsterdam: IOS Press.

Flisser, A. (2006). Where are the tapeworms? *Parasit. Intern.*, **55:** S117–S20.

Flisser, A., and Craig, P.S. (2005). Larval cestodes. In: F.E.G. Cox *et al.* (eds.) *Topley & Wilson's Microbiology and Microbial Infections*, 10th edn, Vol. 5, pp. 677–712. London: Arnold Hodder.

Flisser, A. and Gyorkos, T. (2007). Contribution of immunodiagnostic tests to epidemiological/intervention studies of cysticercosis/taeniosis in Mexico. *Parasite Immun.*, **29:** 637–49.

Flisser, A. and Lightowlers, M.W. (2001). Vaccination against *Taenia solium* cysticercosis. *Memor. Instituto Oswaldo Cruz*, **96:** 353–56.

Flisser, A. *et al.* (1990). Praziquantel treatment of porcine brain and muscle *Taenia solium* cysticercosis. 1. Radiological, physiological and histopathological studies. *Parasit. Res.*, **76:** 263–69.

Flisser, A. *et al.* (1993). Neurological symptoms in occult neurocysticercosis after single taenicidal dose of praziquantel. *Lancet*, **342:** 748.

Flisser, A. *et al.* (2003). Neurocysticercosis: regional status, epidemiology, impact and control measures in the Americas. *Acta Trop.*, **87:** 43–51.

Flisser, A. *et al.* (2004a). Portrait of human tapeworms. *J. Parasit.*, **80:** 914–16.

Flisser, A. *et al.* (2004b). Induction of protection against porcine cysticercosis by vaccination with recombinant oncosphere antigens. *Infect. Immun.*, **72:** 5292–97.

Flisser A. *et al.* (2005a). Biology of *Taenia solium, Taenia saginata* and *Taenia saginata asiatica*. In: K.D. Murrell (ed.) *WHO/FAO/OIE Guidelines for the surveillance, prevention and control of taeniosis/cysticercosis*, pp. 1–9. Paris: OIE.

Flisser, A. *et al.* (2005b). Evaluation of a self-detection tool for tapeworm carriers for use in public health. *Am. J. Trop. Med. Hyg.*, **72:** 510–12.

Flisser, A. *et al.* (2006). Control of the taeniosis/cysticercosis complex: future developments. *Veterinary Parasit.*, **139:** 283–92.

Flisser, A. *et al.* (2008). Using national health weeks to deliver deworming to children: lessons from Mexico. *J. Epidem. Comm. Health*, **62:** 314–17.

Flütsch, F. *et al.* (2008). Case-control study to identify risk factors for bovine cysticercosis on farms in Switzerland. *Parasit.*, **135:** 641–46.

Gajdusek, D.C. (1978). Introduction of *Taenia solium* into West New Guinea with a note on an epidemic of burns from cysticercosis epilepsy in the Ekari people of the Wissel Lakes area. *Papua New Guinea Med. J.*, **21:** 329–42.

Garcia, H.H. *et al.* (1995). Factors associated with *T.solium* cysticercosis. Analysis of 946 Peruvian neurologic patients. *Am. J. Trop. Med. Hyg.*, **52:** 147–50.

Garcia, H.H. *et al.* (2001). Transient antibody response in *Taenia solium* infection in field conditions-a major contributor to high seroprevalence. *Am. J. Trop. Med. Hyg.*, **65:** 31–32.

Garcia, H.H. *et al.* (2002). Current consensus guidelines for treatment of neurocysticercosis. *Clin. Microbiol. Rev.*, **15:** 747–56.

Garcia, H.H. *et al.* (2003a). *Taenia solium* cysticercosis. *Lancet*, **361:** 547–56.

Garcia, H.H. *et al.* (2003b). Hyperendemic human and porcine *Taenia solium* infection in Peru. *Am. J. Trop. Med. Hyg.*, **68:** 268–75.

Garcia, H.H. *et al.* (2003c). Diagnosis, treatment and control of *Taenia solium* cysticercosis. *Curr. Opin. Infect. Dis.*, **16:** 411–19.

Garcia, H.H. *et al.* (2006). Combined human and porcine mass chemotherapy for the control of *T.solium*. *Am. J. Trop. Med. Hyg.*, **74:** 850–55.

Garcia, H.H. *et al.* (2007). Strategies for the elimination of taeniasis/cysticercosis. *J. Neurolog. Sci.*, **262:** 153–57.

Garcia-Garcia, M.D.L. *et al.* (1999). Prevalence and risk of cysticercosis and taeniasis in an urban population of soldiers and their relatives. *Am. J. Trop. Med. Hyg.*, **61:** 386–89.

Garcia-Noval, J. *et al.* (1996). Epidemiology of *Taenia solium* taeniasis and cysticercosis in two rural Guatemalan communities. *Am. J. Trop. Med. Hyg.*, **55:** 282–89.

Garcia-Noval, J. *et al.* (2001). An epidemiological study of epilepsy and epileptic seizures in two rural Guatemalan communities. *Ann. Trop. Med. Parasit.*, **95:** 167–75.

Garcia-Noval, J. *et al.* (2002). *Taenia solium* taeniasis and cysticercosis in Central America. In: G. Singh, and S. Prabhakar, (eds.) *Taenia solium cysticercosis from basic to clinical science*, (pp. 91–100. Wallingford, UK: CABI Publishing.

Gemmell, M.A. *et al.* (1987). Population dynamics in echinococcosis and cysticercosis: evaluation of the biological parameters of *Taenia hydatigena* and *T.ovis* and comparison with those of *Echinococcus granulosus*. *Parasit.*, **94:** 161–80.

Geerts, S. *et al.* (2001). *Taenia solium* cysticercosis in Africa: an under-recognised problem. In: P. Craig, and Z. Pawlowski (eds.) *Cestode zoonoses: echinococcosis and cysticercosis. An emergent and global problem*. Vol. 341, pp. 13–23. NATO Science Series. Amsterdam: IOS Press.

Geysen, D. *et al.* (2007). Validation of meat inspection results for *Taenia saginata* cysticercosis by PCR-restriction fragment length polymorphism. *J. Food Product.*, **70:** 236–40.

Gilman R.H. *et al.* (2000). Prevalence of taeniosis among patients with neurocysticercosis is related to severity of infection. *Neurology*, **55:** 1062.

Gonzalez, A.E. *et al.* (1990). Prevalence and comparison of serologic assays, necropsy, and tongue palpation for the diagnosis of porcine cysticercosis in Peru. *Am. J. Trop. Med. Hyg.*, **43:** 194–99.

Gonzalez, A.E. *et al.* (1994). Use of sentinel pigs to monitor environmental *Taenia solium* contamination. *Am. J. Trop. Med. Hyg.*, **51:** 847–50.

Gonzalez, A.E. *et al.* (1996). Effective, single-dose treatment of porcine cysticercosis with oxfendazole. *Am. J. Trop. Med. Hyg.*, **54:** 391–94.

Gonzalez, A.E. *et al.* (2001). Protection of pigs with cysticercosis from further infections after treatment with oxfendazole. *Am. J. Trop. Med. Hyg.*, **65:** 15–18.

Gonzalez, A.E. *et al.* (2002). Use of a simulation model to evaluate control programmes against *Taenia solium* cysticercosis. In: G. Singh and S. Prabhakar (eds.) *Taenia solium cysticercosis. From basic to clinical science*, pp. 437–48. Wallingford, UK: CABI Publishing.

Gonzalez, A.E. *et al.* (2003). Control of *Taenia solium*. *Acta Trop.*, **87:** 103–09.

Gonzalez, A.E. *et al.* (2005). Short report: vaccination of pigs to control human neurocysticercosis. *Am. J. Trop. Med. Hyg.*, **72:** 837–39.

Gonzalez, A.E. *et al.* (2006). Transmission dynamics of *Taenia solium* and potential for pig-to-pig transmission. *Parasit. Intern.*, **55:** S131–35.

Goodman, K.A. *et al.* (1999). Case-control study of seropositivity for cysticercosis in Cuenca, Ecuador. *Am. J. Trop. Med. Hyg.*, **60:** 70–74.

Grove, D.I. (1990). *A history of human helminthology*. In: G. Singh and S. Prabhakar (ed.) *Taenia solium and taeniasis solium and cysticercosis*, pp. 355–84. Wallingford, UK: CAB International.

Hall, A. *et al.* (1981). *Taenia saginata* (Cestoda) in western Kenya: the reliability of faecal examinations in diagnosis. *Parasitology*, **83:** 91–101.

Hancock, K. *et al.* (2006). Characterization and cloning of T24, a *Taenia solium* antigen diagnostic for cysticercosis. *Mol. Biochem. Parasit.*, **147:** 109–17.

Heinz, H.J. and Macnab, G.M. (1965). Cysticercosis in the Bantu of South Africa. *South African J. Med. Sci.*, **30:** 19–31.

Hernandez, M. *et al.* (2007). A new highly effective anticysticercosis vaccine expressed in transgenic papaya. *Vaccine*, **25:** 4252–60.

Hoberg, E.P. *et al.* (2001). Out of Africa: origin of the *Taenia* tapeworms in humans. *Proc. R. Soc. London B*, **268:** 781–87.

Hoberg, E.P. (2006). Phylogeny of *Taenia*: Species definitions and origins of human parasites. *Parasit. Intern.*, **55:** S23–30.

Huang, S.W. *et al.* (1966). Studies on *Taenia* species prevalence among the aborigines in Wulai District. *Bull. Instit. Zool. Acad. Sinica*, **5:** 87–91.

Huisa, B.N. *et al.* (2005). Taeniasis and cysticercosis housemaids working in affluent neighborhoods in Lima, Peru. *Am. J. Trop. Med. Hyg.*, **73:** 496–500.

Isobe, M. (1922). On the development of a *Taenia saginata* (?) (Report I). *J. Med. Ass. Form.*, **222:** 161–78.

ITFDE, International Task force for Disease Eradication (1993). Recommendations of the International Task Force for Disease Eradication. *Morb. Mort. Wkly. Rep.*, **42:** RR–16, 1–46.

Ito, A. and Craig, P.S. (2003). Immunodiagnostic and molecular approaches for the detection of taeniid cestode infections. *Trends in Parasit.*, **19:** 377–81.

Ito, A. *et al.* (1998). Novel antigens for neurocysticercosis: simple method for preparation and evaluation for serodiagnosis. *Am. J. Trop. Med. Hyg.*, **59:** 291–94.

Ito, A. *et al.* (2002). Dogs as alternative intermediate hosts of *Taenia solium* in Papua (Irian Jaya), Indonesia confirmed by highly specific ELISA and immunoblot using native and recombinant antigens and mitochondrial DNA analysis. *J. Helminthol.*, **76:** 311–14.

Ito, A. *et al.* (2003). Human taeniasis and cysticercosis in Asia. *Lancet*, **362:** 1918–20.

Ito, A. *et al.* (2006). Neurocysticercosis: clinical manifestation, neuroimaging, serology and molecular confirmation of histopathologic specimens. *Southeast Asian J. Trop. Med. Pub. Health*, **37** (Suppl 3): 74–81.

Ito, A. *et al.* (2007). The present situation of taeniasis and cysticercosis in Asia and the Pacific. *Southeast Asian J. Trop. Med. Pub. Health*, **38** (S1): 119–24.

Ito, A. *et al.* (2008). Molecular and immunological diagnosis of taeniasis and cysticercosis in Asia and the Pacific. *Southeast Asian J. Trop. Med. Pub. Health*, **39** (S1): 37–47.

Ieri, C. *et al.* (2004). Species identification after treatment of human taeniasis. *Lancet*, **363:** 949–50.

Johnson, K.S. *et al.* (1989). Vaccination against ovine cysticercosis using a defined recombinant antigen. *Nature*, **338:** 585–87.

Jongwutiwes, S. *et al.* (2004). Jejunal perforation caused by morphologically abnormal *Taenia saginata* infection. *J. Infect.*, **49:** 324–28.

Jung, R.C. *et al.* (1981). Racemose cysticercus in human brain. A case report. *Am. J. Trop. Med. Hyg.*, **30:** 620–24.

Jung, H. *et al.* (2008). Medical treatment for neurocysticercosis: drugs, indications and perspectives. *Curr. Topics Med. Chem.*, **8:** 424–33.

Karanikas, I.D. *et al.* (2007). Taenia saginata: a rare cause of bowel obstruction. *Trans. R. Soc. Trop. Med. Hyg.*, **101:** 527–28.

Kebede, N. (2008). Cysticercosis of slaughtered cattle in northwestern Ethiopia. *Res. Vet. Sci.*, **85:** 522–26.

Keilbach, N.M. *et al.* (1989). A program to control taeniasis-cysticercosis (*T.solium*): experiences in a Mexican village. *Acta Leid.*, **57:** 181–89.

Kosin, E. *et al.* (1972). Taeniasis di Pulau Samosir. *Maj. Kedok. Universitat.*, **3:** 5–11.

Kyvsgaard, N.C. *et al.* (2007). Simulating transmission and control of *Taenia solium* infections using a Reed-Frost stochastic model. *Intern. J. Parasit.*, **37:** 547–58.

Laclette, J.P. *et al.* (1982). *Ultrastructure of the surrounding envelopes of Taenia solium eggs*. In: A. Flisser et al. (eds.) *Cysticercosis. Present state of knowledge and perspectives*, pp. 375–87. NY: Academic Press.

Lawson, J.R. and Gemmell, M.A. (1983). Hydatidosis and cysticercosis: the dynamics of transmission. *Adv. Parasit.*, **22:** 261–308.

Lawson, J.R. and Gemmell, M.A. (1989). The ovine cysticercosis as models for research into the epidemiology and control of the human and porcine cysticercosis *Taenia solium*: II. The application of control. *Acta Leiden.*, **57:** 173–80.

Lekule, F.P. and Kyvsgaard, N.C. (2003). Improving pig husbandry in tropical resource-poor communities and its potential to reduce risk of porcine cysticercosis. *Acta Trop.*, **87:** 111–17.

Lescano, A.G. *et al.* (2007). Swine cysticercosis hotspots surrounding *Taenia solium* tapeworm carriers. *Am. J. Trop. Med. Hyg.*, **76:** 376–83.

Li, T. *et al.* (2006). Taeniasis/cysticercosis in a Tibetan population in Sichuan Province, China. *Acta Trop.*, **100:** 223–31.

Li, T. *et al.* (2007). Taeniasis/cysticercosis in China. *Southeast Asian J. Trop. Med. Pub. Health*, **38** (Suppl 1): 1–9.

Lightowlers, M.W. (2003). Vaccines for prevention of cysticercosis. *Acta Trop.*, **87:** 129–35.

Lightowlers, M.W. (2006). Vaccines against cysticercosis and hydatidosis: foundations in taeniid cestode immunology. *Parasit. Intern.*, **55:** S30–43.

Lightowlers, M.W. and Gauci, C.G. (2001). Vaccines against cysticercosis and hydatidosis. *Veterinary Parasit.*, **101:** 337–52.

Lightowlers, M.W. *et al.* (1996). Taenia saginata: vaccination against cysticercosis in cattle with recombinant oncosphere antigens. *Experim. Parasit.*, **84:** 330–38.

Liu, Y.M. *et al.* (2005). Acute pancreatitis caused by tapeworm in the biliary tract. *Am. J. Trop. Med. Hyg.*, **73:** 377–80.

Maravilla, P. *et al.* (1998). Comparative development of *Taenia solium* in experimental models. *J. Parasit.*, **84:** 882–86.

Maravilla, P. *et al.* (2003). Detection of genetic variation in *Taenia solium*. *J. Parasit.*, **89:** 1250–54.

Maravilla, P. *et al.* (2008). Genetic polymorphism in *Taenia solium* cysticerci recovered from experimental infections in pigs. *Infect. Genet. Evol.*, **8:** 213–16.

Margono, S.S. *et al.* (2006). Taeniasis/cysticercosis in Papua (Irian Jaya), Indonesia. *Parasit. Intern.*, **55:** S143–48.

Martinez-Maya, J.I. *et al.* (2000). Failure to incriminate domestic flies (Diptera: Muscidae) as mechanical vectors of *Taenia* eggs (Cyclophillidea: Taeniidae) in rural Mexico. *J. Med. Entom.*, **37:** 489–91.

McManus, D.P. (2006). Molecular discrimination of taeniid cestodes. *Parasit. Intern.*, **55:** S31–37.

McManus, D.P. and Bowles J. (1994). Asian (Taiwan) *Taenia*: species or strain. *Parasit. Today*, **10:** 273–75.

McManus, D.P. and Ito, A. (2005). Application of molecular techniques for identification of human *Taenia* spp. In: K.D. Murrell (ed.) *WHO/FAO/OIE Guidelines for the surveillance, prevention and control of taeniosis/cysticercosis*, pp. 52–55. Paris: OIE.

Medina-Escutia, E. *et al.* (2001). Cellular immune response and Th1/Th2 cytokines in human neurocysticercosis: Lack of immune suppression. *Parasitology*, **87:** 587–90.

Merchant, M.T. *et al.* (1998). *Taenia solium* description of the intestinal implantation sites in experimental hamster infections. *J. Parasit.*, **84:** 681–85.

Meza-Lucas, A. *et al.* (2003). Limited and short-lasting humoral response in *Taenia solium:* seropositive households compared with patients with neurocysticercosis. *Am. J. Trop. Med. Hyg.*, **69:** 223–27.

Molyneux, D.H. *et al.* (2005). Rapid-impact interventions: how a policy of integrated control for Africa's neglected tropical diseases could benefit the poor. *PloS Med.*, **2:** 101–07.

Myadagsuren, N. *et al.* (2007). Taeniasis in Mongolia, 2002–2006. *Am. J. Trop. Med. Hyg.*, **77:** 342–46.

Nakao, M. *et al.* (2002). A phylogenetic hypothesis for the distribution of 2 genotypes of the pig tapeworm *Taenia solium* worldwide. *Parasitology*, **124:** 657–62.

Nelson, G.S. *et al.* (1965). The significance of wild animals in the transmission of cestodes of medical importance in Kenya. *Trans. R. Soc. Trop. Med. Hyg.*, **59:** 507–24.

Ngowi, H.A. *et al.* (2008). A health-education intervention trial to reduce porcine cysticercosis in Mbulu District, Tanzania. *Prevent. Vet. Med.*, **85:** 52–67.

Okamoto, M. *et al.* (1995). Phylogeneitic relationships within *Taenia taeniaeformis* variants and other taeniid cestodes inferred from the nucleotide sequence of the cytochrome c oxidase subunit I gene. *Parasitol. Res.*, **81:** 451–58.

Okamoto, M. *et al.* (2007). Asian *Taenia*: species or subspecies? *Southeast Asian J. Trop. Med. Pub. Health*, **38**S1: 125–30.

Overbosch, D. *et al.* (2002). Neurocysticercosis in Europe. In: P. Craig and Z. Pawlowski (eds.) *Cestode zoonoses: echinococcosis and cysticercosis. An emergent and global problem*, Vol. 5, pp. 33–40, NATO Science Series. Amsterdam: IOS Press.

Pawlowski, Z. (1990). Perspectives on the control of *Taenia solium*. *Parasit. Today*, **6:** 371–73.

Pawlowski, Z. (2006). Role of chemotherapy of taeniasis in prevention of neurocysticercosis. *Parasit. Intern.*, **55:** S105–09.

Pawlowski, Z. *et al.* (2005). Control of taeniasis/cysticercosis: from research towards implementation. *Intern. J. Parasit.*, **35:** 1221–32.

Pawlowski, Z. and Schultz, M.G. (1972). Taeniasis and cysticercosis (*Taenia saginata*). *Adv. Parasit.*, **10:** 269–343.

Peniche-Cardenas, A. *et al.* (2002). Chemotherapy of porcine cysticercosis with albendazole sulphoxide. *Vet. Parasit.*, **108:** 63–73.

Phiri, I.K. *et al.* (2006). Assesssment of routine inspection methods for porcine cysticercosis in Zambian village pigs. *J. Helminthol.*, **80:** 69–72.

Psarros, T.G. *et al.* (2003). Endoscopic management of supratentorial ventricular neurocysticercosis: case series and review of the literature. *Mini. Invas. Neurosurg.*, **46:** 331–334.

Rabiela, M.T. *et al.* (1989). Morphological types of *Taenia solium* cysticerci. *Parasit. Today*, **5:** 357–59.

Rabiela, M.T. *et al.* (2000). Evagination of *Taenia solium* cysticerci: a histologic and electron microscopy study. *Arch. Med. Res.*, **31:** 603–07.

Rajkotia, Y. *et al.* (2007). Economic burden of neurocysticercosis: results from Peru. *Trans. R. Soc. Trop. Med. Hyg.*, **101:** 840–46.

Rickard, M.D. *et al.* (1977). The prevalence of cysticerci of *Taenia saginata* in cattle reared on sewage-irrigated pasture. *Med. J. Aus.*, **1:** 525–27.

Rodriguez-Canul, R. *et al.* (1998). Application of an immunoassay to determine risk factors associated with porcine cysticercosis in rural areas of Yucatan, Mexico. *Vet. Parasit.*, **79:** 165–80.

Rodriguez-Canul, R. *et al.* (1999). Epidemiological study of *Taenia solium* taeniasis/cysticercosis in a rural village in Yucatan State, Mexico. *Ann. Trop. Med. Parasit.*, **93:** 57–67.

Rodriguez-Canul, R. *et al.* (2002). *Taenia solium* metacestode viability in infected pork after preparation with salt pickling or cooking methods common in Yucatan, Mexico. *J. Food Prod.*, **65:** 666–69.

Rodriguez-Hidalgo, R. *et al.* (2002). Comparison of conventional techniques to differentiate between *Taenia solium* and *Taenia saginata* and an improved polymerase chain reaction-restriction fragment length polymorphism assay using a mitochondrial 12S r DNA fragment. *J. Parasit.*, **88:** 1007–11.

Roman, G. *et al.* (2000). A proposal to declare neurocysticercosis an international reportable disease. *Bull. WHO*, **78:** 399–406.

Saenz, B. *et al.* (2006). Neurocysticercosis: clinical, radiologic, and inflammatory differences between children and adults. *Pediat. Infect. Dis. J.*, **25:** 801–03.

Sako, Y. *et al.* (2000). Molecular characterization and diagnostic value of *Taenia solium* low-molecular-weight antigen genes. *J. Clin. Microbiol.*, **38:** 4439–44.

Sanchez, A.L. *et al.* (1998). Prevalence of taeniasis and cysticercosis in a population of urban residence in Honduras. *Acta Trop.*, **69:** 141–49.

Sarti, E. *et al.* (1988). *Taenia solium* taeniasis and cysticercosis in a Mexican village. *Trop. Med. Parasit.*, **39:** 194–98.

Sarti, E. *et al.* (1992). Prevalence and risk factors for *Taenia solium* taeniasis and cysticercosis in humans and pigs in a village in Morelos, Mexico. *Am. J. Trop. Med. Hyg.*, **46:** 677–85.

Sarti, E. *et al.* (1994). Epidemiologic investigation of *Taenia solium* taeniasis and cysticercosis in a rural village of Michoacan State, Mexico. *Trans. R. Soc. Trop. Med. Hyg.*, **88:** 49–52.

Sarti, E. *et al.* (1997). Development and evaluation of a health education intervention against *Taenia solium* in a rural community in Mexico. *Am. J. Trop. Med. Hyg.*, **56:** 127–32.

Sarti, E. *et al.* (2000). Mass treatment against human taeniasis for the control of cysticercosis: a population-based intervention study. *Trans. R. Soc. Trop. Med. Hyg.*, **94:** 85–89.

Sato, M.O. *et al.* (2003). Evaluation of tongue inspection and serology for diagnosis of *Taenia solium* cysticercosis in swine: usefulness of ELISA using purified glycoproteins and recombinant antigen. *Vet. Parasit.*, **111:** 309–22.

Sato, M.O. *et al.* (2006). Evaluation of purified *Taenia solium* glycoproteins and recombinant antigens in the serologic detection of human and swine cysticercosis. *J. Infect. Dis.*, **194:** 1783–90.

Schantz, P.M. and Sarti, E. (1989). Diagnostic methods and epidemiologic surveillance of *Taenia solium* infection. *Acta Leiden.*, **57:** 153–63.

Schantz, P.M. *et al.* (1992). Neurocysticercosis in an orthodox Jewish community in New York City. *N. Eng. J. Med.*, **327:** 692–95.

Schantz, P.M. *et al.* (1993). Potential eradicability of taeniasis and cysticercosis. *Bull. PAHO*, **27:** 397–403.

Schantz, P.M. *et al.* (1994). Community-based epidemiological investigations of cysticercosis due to *Taenia solium*: comparison of serological screening tests and clinical findings in two populations in Mexico. *Clin. Infect. Dis.*, **18:** 879–85.

Sciutto, E. *et al.* (2008). Vaccines against cysticercosis. *Curr. Topics Med. Chem.*, **8:** 415–23.

Sikasunge, C.S. *et al.* (2007). Risk factors associated with porcine cysticercosis in selected districts of Eastern and Southern provinces of Zambia. *Vet. Parasit.*, **143:** 59–66.

Simanjuntak, G.M. *et al.* (1997). Taeniasis/cysticercosis in Indonesia as an emerging disease. *Parasit. Today*, **13:** 321–23.

Singh, G. *et al.* (2002). *Taenia solium* taeniasis and cysticercosis in Asia. In: G. Singh and S. Prabhakar (eds.) *Taenia solium cysticercosis*, pp. 111–27. Oxon, UK: CAB International.

Sotelo, J. and Del Brutto, O.H. (2000). Brain cysticercosis. *Arch. Med. Res.*, **31:** 3–14.

Sotelo, J. and Del Brutto, O.H. (2002). Review of neurocysticercosis. *Neurosurg. Focus*, **12:** e1.

Sotelo, J. *et al.* (1986). Freezing of infested pork muscle kills cysticerci. *J. Am. Med. Ass.*, **256:** 893–94.

Sudewi, A.A. *et al.* (2008). *Taenia solium* cysticercosis in Bali, Indonesia: serology and mtDNA analysis. *Trans. R. Soc. Trop. Med. Hyg.*, **102:** 96–98.

Suri A. *et al.* (2008). Transventricular, transaqueductal scope-in-scope endoscopic excision of fourth ventricular neurocysticercosis: a series of 13 cases and a review. *J. Neurosurg. Ped.*, **1:** 35–39.

Tesfa-Yohannes, T. (1990). Effectiveness of praziquantel against *Taenia saginata* infections in Ethiopia. *Ann. Trop. Med. Parasit.*, **84:** 581–85.

Torres, A. *et al.* (1992). Praziquantel treatment of porcine brain and muscle *Taenia solium* cysticercosis. *3. Effect of 1-day treatment. Parasit. Res.*, **78:** 161–64.

Tsang, V.C.W. *et al.* (1998). An enzyme-linked immunoelectrotransfer blot assay by glycoprotein antigens for diagnosing human cysticercosis (*Taenia solium*). *J. Infect. Dis.*, **159:** 50–59.

Vázquez-Flores, S. *et al.* (2001). Hygiene and restraint of pigs associated with absence of *Taenia solium* cysticercosis in a rural community of Mexico. *Salud Pública de México*, **43:** 574–76.

Verster, A. (1965). *Taenia solium* Linnaeus (1758) in the chacma babbon. Papio ursinus, (Kerr 1792). *J. South Afri. Vet. Med. Ass.*, **36:** 580.

Verster, A. (1974). The golden hamster as a definitive host of *Taenia solium* and *Taenia saginata*. *Onderstepoort J. Vet. Res.*, **41:** 23–28.

Viljoen, N.F. (1937). Cysticercosis in swine and bovines, with special reference to South African conditions. *Onderstepoort J. Vet. Sci. Anim. Indust.*, **9:** 337–570.

Wandra, T. *et al.* (2006a). High prevalence of *Taenia saginata* taeniasis and status of *Taenia solium* cysticercosis in Bali, Indonesia, 2002–2004. *Trans. R. Soc. Trop. Med. Hyg.*, **100:** 346–53.

Wandra, T. *et al.* (2006b). Taeniasis and cysticercosis in Bali and North Sumatra, Indonesia. *Parasit. Intern.*, **55:** S155–60.

Wandra, T. *et al.* (2007). Current situation of taeniasis and cysticercosis in Indonesia. *Trop. Med. Health*, **35:** 323–28.

WHO (1983). *Guidelines for surveillance, prevention and control of taeniasis/cysticercosis*, (eds. M. Gemmell, Z. Matyas, Z. Pawlowski, and E.J.L. Soulsby), VPH/83.49, pp. 207. Geneva: World Health Organization.

WHO/DFID-AHP (2006). *The control of neglected zoonotic diseases*. WHO/SDE/POS/2006. pp. 1, 54. Geneva: World Health Organization.

WHO/FAO/OIE (2005). *Guidelines for the surveillance, prevention and control of taeniosis/cysticercosis*. (ed. K.D. Murrell), pp. 139. Paris: OIE.

Wilson, M. *et al.* (1991). Clinical evaluation of the cysticercosis enzyme linked immunoelectrotransfer blot in patients with neurocysticercosis. *J. Infect. Dis.*, **164:** 1007–08.

Wilkins, P.P. *et al.* (1999). Development of a serologic assay to detect *Taenia solium* taeniasis. *Am. J. Trop. Med. Hyg.*, **60:** 199–204.

Willingham, A.L. and Engels, D. (2006). Control of *Taenia solium* cysticercosis/taeniosis. *Adv. Parasit.*, **61:** 509–66.

Yamasaki, H. *et al.* (2004). DNA differential diagnosis of taeniasis and cysticercosis by multiplex PCR. *J. Clin. Microbiol.*, **42:** 548–53.

Yoshino, K. (1933a). Studies on the post-embryonal development of *Taenia solium*. Part I. On the hatching of the egg of *Taenia solium*. *J. Med. Ass. Form.*, **32:** 139–41.

Yoshino, K. (1933b). Studies on the post-embryonal development of *Taenia solium*. Part II. On the migration course of the oncosphere of Taenia solium within the intermediate host. *J. Med. Ass. Form.*, **32:** 155–58.

Yoshino, K. (1933c). Studies on the post-embryonal development of *Taenia solium*. Part III. On the development of cysticercus cellulosae within the definite intermediate host. *J. Med. Ass. Form.*, **32:** 166–69.

Zinsstag, J. *et al.* (2005). Potential of cooperation between human and animal health to strengthen health systems. *Lancet*, **366:** 2142–45.